

361-17

313

Physics Abstracts

ISSN 0036-8091

Science Abstracts Series A

1st July 1983

Abstracts 59523-64571

UNIVERSITY
JUL 8 1983
LIBRARY

inspec
The Institution of Electrical Engineers

Q

1

S3

V. 86

1983

NO. 1211

N/c

Se

PHYSICS ABSTRACTS

Physics Abstracts is one of a series of abstracts publications produced by INSPEC. Published twice monthly by the Institution of Electrical Engineers, it forms the world's major English-language abstracting service for the physics community.

SUBJECT SCOPE & COVERAGE

Physics Abstracts covers the whole field of physics. An impression of its scope can be gained from the classification scheme. The information contained in *Physics Abstracts* is derived from a wide range of sources including journals, reports, books, dissertations and conference papers published in all countries and languages of the world.

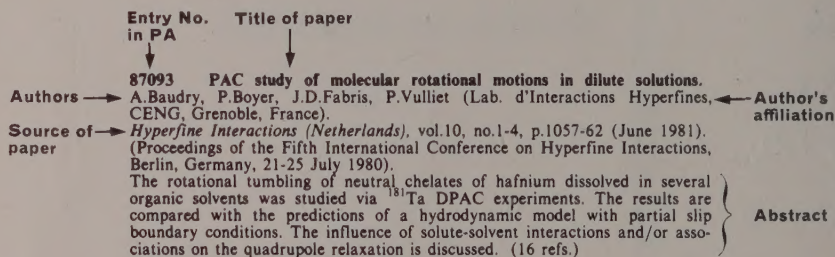
The number of items included is currently running at over 100,000 per year.

JOURNALS SCANNED

A list of the journals scanned for the INSPEC services is published with the twice-yearly author indexes to *Physics Abstracts*. Additions and amendments to this list are included in *Physics Abstracts* towards the end of the first issue for each month.

FORM OF ENTRY

All entries in *Physics Abstracts* follow the same basic pattern. The following example identifies the individual parts of a typical entry for an article from a journal.



Entries for other types of material differ mainly in the reference to the source, e.g., a report will refer to the report series and the number of the individual report. A conference paper on the other hand will normally refer to the title, place and date of the conference at which the paper was given.

SUBJECT ARRANGEMENT & SUBJECT GUIDE

The abstracts are arranged by subject in accordance with the scheme in the CLASSIFICATION and CONTENTS which appears opposite. The page number for the start of each subject section is given. An alphabetical index to the scheme—the SUBJECT GUIDE—follows the CLASSIFICATION and CONTENTS.

SUBJECT INDEXES

Detailed twice-yearly subject indexes to the individual entries are provided separately, covering the periods January-June and July-December. In these SUBJECT INDEXES each major concept occurring in each paper abstracted is indexed under headings drawn from the INSPEC Thesaurus.

AUTHOR INDEX

At the end of each issue, an alphabetical index of authors is provided showing the entry number of the items written by them. These indexes are cumulated every six months and, with the addition of the title of the individual papers, are published separately to cover the periods January-June and July-December of each year.

SUBSIDIARY INDEXES

Where appropriate, the following subsidiary indexes are included for the convenience of users:

Bibliography index of articles where a significant list of references or bibliography is contained.

Book index of books received and abstracted.

Corporate Author index where a corporate organisation rather than an individual is responsible for publication. This index includes all reports.

Conference index with reference to individual papers.

Subscription prices and ordering procedure are shown on the inside back cover.

PHYSICS ABSTRACTS is published twice monthly by the Institution of Electrical Engineers in association with the Institute of Electrical and Electronics Engineers Inc. Printed by Unwin Brothers Limited, The Gresham Press, Old Woking, Surrey. 2nd Class postage paid at Piscataway, N.J. 08854, USA. POSTMASTER: Send address changes to INSPEC/IEEE SERVICE CENTER, 445 Hoes Lane, Piscataway, N.J. 08854.

© 1983. THE INSTITUTION OF ELECTRICAL ENGINEERS. All rights reserved. No part of this publication may be reproduced, stored in a retrieval system, or transmitted, in any form or by any means, electronic, mechanical, photocopying, recording or otherwise without the prior permission of the Institution of Electrical Engineers.

CLASSIFICATION AND CONTENTS

The abstracts are arranged by subject in accordance with the following scheme. The page number for each section is given. The CLASSIFICATION AND CONTENTS is followed by an alphabetical guide to the scheme, the SUBJECT GUIDE.

The classification scheme is the result of cooperation between INSPEC, the American Institute of Physics, the European Physical Society and the Physics Working Group of the ICSU-AB.

0000	GENERAL	4751	0620H	Measurement standards and calibration	4767
			0620J	Determination of fundamental constants	4767
0100	COMMUNICATION, EDUCATION, HISTORY, AND PHILOSOPHY	4751	0630	Measurement of basic variables	4768
0110	Announcements, news, and organizational activities	—	0630C	Spatial variables measurement	4768
0130	Physics literature and publications	4751	0630E	Mass and density measurement	4768
0130B	Publications of lectures (advanced institutes, summer schools, etc.)	—	0630F	Time and frequency measurement	4768
0130C	Conference proceedings	4751	0630G	Velocity, acceleration and rotation measurement	4768
0130E	Monographs, and collections	4752	0630L	Measurement of basic electromagnetic variables	4768
0130K	Handbooks, dictionaries, tables and data compilation	—	0650	Data handling and computation	4768
0130M	Textbooks for graduates and researchers	4752	0660	Laboratory techniques	4769
0130P	Textbooks for undergraduates	4753	0670	General instrumentation	4769
0130R	Surveys and tutorial papers; resource letters	4753	0690	Other topics in measurement science, general laboratory techniques and instrumentation systems	—
0130T	Bibliographies	4754			
0140	Education	4754	0700	SPECIFIC INSTRUMENTATION AND TECHNIQUES OF GENERAL USE IN PHYSICS	4769
0150	Educational aids	4754	0710	Mechanical instruments and measurement methods	4769
0155	General Physics	—	0720	Thermal instruments and techniques	4769
0160	Biographical, historical, and personal notes	—	0720D	Thermometry	4769
0165	History of science	4754	0720F	Calorimetry	4770
0170	Philosophy of science	4755	0720H	Furnaces	4770
0175	Science and society	4755	0720K	High-temperature techniques and instrumentation; pyrometry	4770
0190	Other topics of general interest	—	0720M	Cryogenics	4770
			0725	Hygrometry	4770
0200	MATHEMATICAL METHODS IN PHYSICS	4755	0730	Vacuum production and techniques	4770
0210	Algebra, set theory, and graph theory	4755	0730C	Vacuum pumps	—
0220	Group theory	4755	0730D	Vacuum meters	4770
0230	Function theory, analysis	4755	0735	High pressure production and techniques	4770
0240	Geometry, differential geometry, and topology	4756	0750	Electrical instruments and techniques	4771
0250	Probability theory, stochastic processes, and statistics	4756	0755	Magnetic instruments and techniques	4771
0260	Numerical approximation and analysis	4756	0758	Magnetic resonance spectrometers, auxiliary instruments and techniques	4771
0270	Computational techniques	4756	0760	Optical instruments and techniques	4772
0290	Other topics in mathematical methods in physics	—	0760D	Photometry and radiometry	4773
			0760F	Polarimetry and ellipsometry	4773
0300	CLASSICAL AND QUANTUM PHYSICS; MECHANICS AND FIELDS	4756	0760H	Refractometry and reflectometry	4773
0320	Classical mechanics of discrete systems: general mathematical aspects	4756	0760L	Interferometry	4773
0330	Special relativity	4756	0760P	Optical microscopy	4774
0340	Classical mechanics of continuous media: general mathematical aspects	4757	0762	Detection of radiation (bolometers, photoelectric cells, i.r. and submillimetre waves detection)	4774
0340D	Mathematical theory of elasticity	4757	0765	Optical spectroscopy and spectrometers	4774
0340G	Fluid dynamics: general mathematical aspects	4757	0765E	UV and visible spectroscopy and spectrometers	4775
0340K	Waves and wave propagation: general mathematical aspects	4757	0765G	IR spectroscopy and spectrometers	4775
0350	Classical field theory	—	0768	Photography, photographic instruments and techniques	4776
0365	Quantum theory; quantum mechanics	4757	0775	Mass spectrometers and mass spectrometry techniques	4776
0370	Theory of quantized fields	—	0777	Particle beam production and handling; targets	4776
0380	General theory of scattering	4759	0780	Electron and ion microscopes and techniques	4777
			0785	X-ray, gamma-ray instruments and techniques	4778
			0790	Other topics in specialised instrumentation	4778
0400	RELATIVITY AND GRAVITATION	4759	1000	THE PHYSICS OF ELEMENTARY PARTICLES AND FIELDS	4778
0420	General relativity	4759			
0430	Gravitational waves and radiation: theory	4760	1100	GENERAL THEORY OF FIELDS AND PARTICLES	4778
0440	Continuous media; electromagnetic and other mixed gravitational systems	4760	1110	Field theory	4778
0450	Unified field theories and other theories of gravitation	4760	1120	S-matrix theory	4780
0460	Quantum theory of gravitation	4761	1130	Symmetry and conservation laws	4780
0465	Supergravity	4761	1140	Currents and their properties	—
0480	Experimental tests of general relativity and observations of gravitational radiation	4761	1150	Dispersion relations and sum rules	4782
0490	Other topics in relativity and gravitation	—	1160	Complex angular momentum; Regge formalism	—
			1180	Relativistic scattering theory	4782
			1190	Other topics in general field and particle theory	—
0500	STATISTICAL PHYSICS AND THERMODYNAMICS	4761	1200	SPECIFIC THEORIES AND INTERACTION MODELS; PARTICLE SYSTEMATICS	4782
0520	Statistical mechanics	4761	1210	Unified field theories and models	4782
0530	Quantum statistical mechanics	4762	1220	Models of electromagnetic interactions	4783
0540	Fluctuation phenomena, random processes, and Brownian motion	4762	1220D	Specific calculations and limits of quantum electrodynamics	4783
0550	Lattice theory and statistics; Ising problems	4765	1220F	Experimental tests of quantum electrodynamics	4783
0560	Transport processes: theory	4766	1225	Models for gravitational interactions	—
0570	Thermodynamics	4767	1230	Models of weak interactions	4783
0590	Other topics in statistical physics and thermodynamics	—	1235	Composite models of particles	4783
			1235C	General properties of quantum chromodynamics (dynamics, confinement, etc.)	4783
0600	MEASUREMENT SCIENCE, GENERAL LABORATORY TECHNIQUES, AND INSTRUMENTATION SYSTEMS	4767	1235E	Applications of quantum chromodynamics to particle properties and reactions	4784
0620	Metrology	4767	1235H	Phenomenological composite models of particle structure and reactions (partons, bags, etc.)	4785
0620D	Measurement and error theory	4767	1235K	Other composite models	4785
0620F	Units	—			

	page		page		
1240	Models of strong interactions	4786	2360	alpha decay	4797
1240E	Statistical models	4786	2390	Other topics in nuclear decay and radioactivity	—
1240F	Bootstrap models	—			
1240H	Duality and dual models	4786	2400	NUCLEAR REACTIONS AND SCATTERING:	
1240K	Hadron classification schemes	—		GENERAL	4797
1240M	Complex angular momentum plane; Regge poles and cuts (Reggeons)	—	2410	Nuclear reaction and scattering models and methods	4797
1240P	Absorptive, optical, and eikonal models	—	2410H	Optical and diffraction models	4798
1240Q	Potential models	4786	2430	Resonance reactions and scattering	4798
1240R	Peripheral models (one or more particle exchange)	—	2450	Direct reactions	4798
1240S	Multiperipheral and multi-Regge models	4786	2460	Statistical theory and fluctuations	4798
1240V	Vector-meson dominance	4786	2470	Polarization in reactions and scattering	4798
1270	Hadron mass formulas	4786	2475	General properties of fission	4799
1290	Miscellaneous theoretical ideas and models	4786	2490	Other topics in nuclear reactions and scattering, general	—
1300	SPECIFIC REACTIONS AND PHENOMENOLOGY	4787	2500	NUCLEAR REACTIONS AND SCATTERING:	
1310	Weak and electromagnetic interactions of leptons	4787		SPECIFIC REACTIONS	4799
1315	Neutrino interactions	4787	2510	Nuclear reactions and scattering involving few-nucleon systems	4799
1320	Leptonic and semileptonic decays of mesons	4787	2520	Photonuclear reactions and photon scattering	4799
1325	Hadronic decays of mesons	4787	2530	Lepton-induced reactions and scattering	4799
1330	Decays of baryons	4787	2540	Nucleon-induced reactions and scattering	4799
1335	Decays of leptons	—	2550	^2H - and ^3H -induced reactions and scattering	4800
1340	Electromagnetic processes and properties	4787	2560	^3He - and ^4He -induced reactions and scattering	4800
1340D	Electromagnetic mass differences	—	2570	Heavy ion induced reactions and scattering	4800
1340F	Electromagnetic form factors; electric and magnetic moments	4787	2580	Meson- and hyperon-induced reactions and scattering	4801
1340H	Electromagnetic decays	4788	2585	Fission reactions	4802
1340K	Electromagnetic corrections to strong and weak interaction processes	4788	2588	Fusion reactions	4802
1360	Photon and charged-lepton interactions with hadrons	4788	2590	Other topics in nuclear reactions and scattering: specific reactions	4802
1360F	Elastic and Compton scattering	4788			
1360H	Total and inclusive cross sections	4788	2700	PROPERTIES OF SPECIFIC NUCLEI LISTED BY	
1360K	Meson production	4788		MASS RANGES	4802
1360M	Meson-resonance production	4788	2710	$A \leq 5$	4802
1360P	Baryon and baryon resonance production	—	2720	$6 \leq A \leq 19$	4803
1365	Hadron production by electron-positron collisions	4788	2730	$20 \leq A \leq 38$	4803
1375	Hadron-induced low- and intermediate-energy reactions and scattering, energy ≤ 10 GeV	4789	2740	$39 \leq A \leq 58$	4803
1375C	Nucleon-nucleon interactions, including antinucleon, deuteron, etc. (energy ≤ 10 GeV)	4789	2750	$59 \leq A \leq 89$	4803
1375E	Hyperon-nucleon interactions (energy ≤ 10 GeV)	—	2760	$90 \leq A \leq 149$	4803
1375G	Pion-baryon interactions (energy ≤ 10 GeV)	4789	2770	$150 \leq A \leq 189$	4803
1375J	Kaon-baryon interactions (energy ≤ 10 GeV)	4789	2780	$190 \leq A \leq 219$	4803
1375L	Meson-meson interactions (energy ≤ 10 GeV)	4789	2790	$220 \leq A$	4803
1385	Hadron-induced high- and super-high-energy interactions, energy > 10 GeV	4789	2800	NUCLEAR ENGINEERING AND NUCLEAR	
1385D	Elastic scattering (energy > 10 GeV)	4789		POWER STUDIES	4804
1385F	Inelastic scattering, two-particle final states (energy > 10 GeV)	4790	2820	Neutron physics	4804
1385H	Inelastic scattering, many-particle final states (energy > 10 GeV)	4790	2841	Fission reactor theory and design	4804
1385K	Inclusive reactions, including total cross sections, (energy > 10 GeV)	4790	2842	Fission reactor materials	4804
1385M	Cosmic ray interactions	—	2842H	Fuel preparation and reprocessing	4812
1388	Polarisation in interactions and scattering	4790	2843	Fission reactor operation	4813
1390	Other topics in specific reactions and phenomenology of elementary particles	4791	2844	Fission reactor protection systems, safety and accidents	4814
			2850	Fission reactor types and applications	4817
			2852	Fusion reactors	4817
			2858	Integrated reactor systems	4823
			2870	Nuclear explosions	4823
			2880	Radiation technology, including shielding	4823
			2890	Other topics in nuclear engineering and nuclear power studies	4823
1400	PROPERTIES OF SPECIFIC PARTICLES AND RESONANCES	4791	2900	EXPERIMENTAL METHODS AND INSTRUMENTATION FOR	
1420	Baryons and baryon resonances	4791		ELEMENTARY-PARTICLE AND NUCLEAR	
1440	Mesons and meson resonances	4792		PHYSICS	4823
1460	Leptons	4792	2910	Preacceleration (injection)	—
1480	Other and hypothetical particles	4792	2915	Electrostatic and linear particle accelerators	4823
			2920	Cyclic accelerators and storage facilities	4824
2000	NUCLEAR PHYSICS	4792	2925	Particle sources and targets, preparation and technology	4825
2100	NUCLEAR STRUCTURE	4792	2930	Radiation spectrometers and spectroscopic techniques	4827
2110	General and average properties of nuclei; properties of nuclear energy levels	4792	2940	Radiation detectors	4827
2110D	Binding energy and masses	4793	2960	Counting circuits and nuclear electronics	4828
2110F	Shape, charge, radius and form factors	4793	2970	Radiation measurement, detection and counting	4829
2110H	Spin, parity, and isobaric spin	4793	2975	Polarization analysis	—
2110J	Spectroscopic factors	4793	2980	Nuclear information processing	—
2110K	Electromagnetic moments	4793	2990	Other topics in high-energy and nuclear experimental methods and instrumentation	4829
2110M	Level density and structure	4793			
2130	Nuclear forces	4794	3000	ATOMIC AND MOLECULAR PHYSICS	4829
2140	Few-nucleon systems	4794			
2160	Nuclear-structure models and methods	4794	3100	THEORY OF ATOMS AND MOLECULES	4829
2160C	Shell model	4794	3110	General theory of structure, transitions and chemical binding	4829
2160E	Collective models	4795	3115	General mathematical and computational developments	4830
2160F	Models based on group theory	4795	3120	Specific calculations and results	4830
2160G	Cluster models	4795	3120D	Complete ab initio calculations (exact or nearly exact calculations on small species)	—
2160J	Hartree-Fock and random-phase approximations	4795	3120E	Ab initio LCAO and GO SCF calculations	4831
2165	Nuclear matter	4795	3120G	Other accurate, or nearly ab initio calculations (DIM method, SAMO method, etc.)	4831
2180	Hypernuclei	4795	3120L	Statistical model calculations (Thomas-Fermi and Thomas-Fermi-Dirac models)	—
2190	Other topics in nuclear structure	—	3120N	Semi-empirical NDO calculations (CNDO, INDO, MINDO, PCIO methods, etc.)	4832
2300	RADIOACTIVITY AND ELECTROMAGNETIC TRANSITIONS	4796			
2320	Electromagnetic transitions	4796			
2320C	Lifetimes and transition probabilities	4796			
2320N	Internal conversion and extranuclear effects	—			
2340	beta decay; electron and muon capture	4796			

	page		page
3120P	Other semi-empirical calculations (Hückel, generalized Hückel, PPP methods, etc.)	4832	3500 PROPERTIES OF ATOMS AND MOLECULES; INSTRUMENTS AND TECHNIQUES
3120R	Valence bond calculations (ab initio or not)	—	3510 Atoms
3120T	Electron correlation and CI calculations	4832	3510B Atomic masses, mass spectra, abundances, and isotopes
3120W	Empirical methods (nonquantum methods for conformations, as Wiberg method, Westheimer method, etc.)	—	3510D Electric and magnetic moments, polarizability
3130	Corrections to electronic structure	4833	3510F Relativistic corrections, fine- and hyperfine-structure constants
3150	Excited states	4834	3510H Ionization potentials, electron affinities
3170	Effects of molecular interactions on electronic structure	4835	3510W Weak interactions
3170D	Environmental and solvent effects	4835	3520 Molecules
3170F	Potential-energy surfaces for collisions	4835	3520B General molecular conformation and symmetry; stereochemistry
3170H	Time-dependent phenomena: excitation and relaxation processes, and reaction rates	4835	3520D Interatomic distances and angles
3170K	Molecular solids	4836	3520G Bond strengths, dissociation energies, hydrogen bonding, etc.
3190	Other topics in the theory of atoms and molecules	4836	3520J Barrier heights (internal rotation, inversion); rotational isomerism, conformational dynamics
3200	ATOMIC SPECTRA AND INTERACTIONS WITH PHOTONS	4836	3520M Electric and magnetic moments (and derivatives), polarizability, and magnetic susceptibility
3220	Atomic spectra grouped by wavelength ranges	4836	3520P Rotation, vibration, and vibration-rotation constants
3220B	Radiofrequency, microwave, and infrared spectra	4836	3520S Hyperfine and fine-structure constants
3220J	Visible and ultraviolet spectra	4836	3520V Ionization potentials, electron affinities, molecular core binding energy
3220R	X-ray spectra	4836	3520W Weak interactions
3250	Fluorescence, phosphorescence	4837	3520X Mass spectra
3260	Zeeman and Stark effects	4837	3520Y Correlation times in molecular dynamics
3270	Spectral line shapes and intensities	4837	3580 Atomic and molecular measurements and techniques
3280	Photon interactions with atoms	4838	
3280B	Level crossing and optical pumping	4838	
3280D	Autoionization	4839	
3280F	Photoionization and photodetachment	4839	
3280H	Auger effect and inner-shell ionization	—	
3280K	Multiphoton processes	4839	
3290	Other topics in atomic spectra and interactions with photons	4840	
3300	MOLECULAR SPECTRA AND INTERACTIONS WITH PHOTONS	4840	4000 CLASSICAL AREAS OF PHENOMENOLOGY
3310	Calculation of molecular spectra	4840	
3320	Molecular spectra grouped by wavelength ranges	4841	4100 ELECTRICITY AND MAGNETISM; FIELDS AND CHARGED PARTICLES
3320B	Radiofrequency and microwave spectra	4842	4110 Classical electromagnetism
3320E	Infrared spectra	4842	4110D Electrostatics, magnetostatics
3320F	Raman and Rayleigh spectra	4843	4110F Steady-state electromagnetic fields; electromagnetic induction
3320K	Visible spectra	4844	4110H Electromagnetic waves: theory
3320L	Ultraviolet spectra	4845	4170 Particles in electromagnetic fields: classical aspects
3320N	Vacuum ultraviolet spectra	4845	4180 Particle beams and particle optics
3320R	X-ray spectra	4845	4180D Electron beams and electron optics
3325	Nuclear magnetic resonance and relaxation; nuclear quadrupole resonance (NQR)	4845	4180G Ion beams and ion optics
3330	Electron paramagnetic resonance and relaxation	4846	4190 Other topics in electricity and magnetism
3335	Double resonances and other multiple resonances	4847	
3335H	MODR and PMDR (microwave optical double resonance and phosphorescence microwave double resonance)	4847	4200 OPTICS
3340	Mössbauer spectra	4847	4210 Propagation and transmission in homogeneous media
3345	Magneto-optical and electro-optical spectra; dichroism	4847	4220 Propagation and transmission in inhomogeneous media
3345B	Zeeman and Stark effects	4848	4230 Optical information, image formation and analysis
3345C	Magnetic circular dichroism	4848	4240 Holography
3350	Fluorescence, phosphorescence; radiationless transitions (intersystem crossing, internal conversion)	4848	4250 Quantum optics
3365	Photoelectron spectra	4852	4252 Masers
3370	Intensities and shapes of molecular spectral lines and bands	4853	4255 Lasing processes
3380	Photon interactions with molecules	4853	4255B General theory of lasing action
3380B	Level crossing and optical pumping	4853	4255D CO ₂ lasers
3380E	Autoionization, photoionization, and photodetachment	4854	4255F Inert gas lasers
3380G	Diffuse spectra; predissociation, photodissociation	4854	4255H Lasing action in other gas lasers
3380K	Multiphoton processes	4856	4255K Chemical lasers
3390	Other topics in molecular spectra and interactions with photons	4856	4255M Lasing action in liquids and organic dyes
3400	ATOMIC AND MOLECULAR COLLISION PROCESSES AND INTERACTIONS	4856	4255P Lasing action in semiconductors with junctions
3410	General theories and models	4856	4255R Lasing action in other solids
3420	Interatomic and intermolecular potentials and forces	4857	4255T Free electron lasers
3440	Elastic scattering of atoms and molecules	4857	4260 Laser systems and laser beam applications
3450	Inelastic scattering of atoms and molecules	4859	4260B Design of specific laser systems
3450E	Rotational and vibrational energy transfer	4861	4260D Laser resonators and cavities
3450H	Electronic excitation and ionization (inc. beam-foil excitation and ionization)	4861	4260F Laser beam modulation
3450L	Chemical reactions, energy disposal, and angular distribution, as studied by atomic and molecular beams	4863	4260H Optical problems related to properties and interactions of laser beams
3470	Charge transfer	4863	4260K Optical problems related to applications of laser beams
3480	Electron scattering	4864	4265 Nonlinear optics
3480B	Elastic scattering of electrons by atoms and molecules	4864	4265B General theory
3480D	Atomic excitation and ionization by electron impact	4865	4265C Stimulated Raman, Brillouin and Rayleigh scattering; parametric oscillations and harmonic generation
3480G	Molecular excitation, ionization, and dissociation by electron impact	4866	4265F Phase conjugation
3490	Other topics in atomic and molecular collision processes and interactions	—	4265G Photon echoes, self-induced transparency, optical saturation and related effects
			4265J Beam trapping, self focusing, thermal blooming, and related effects
			4270 Optical materials
			4270C Glass
			4270G Light-sensitive materials
			4272 Optical sources and standards
			4278 Optical lens and mirror systems
			4278H Coatings
			4280 Optical devices, techniques and applications

	page		page
4280B	<i>Spatial filters, zone plates</i>	42887	4755K <i>Multiphase flows</i>
4280C	<i>Spectral and other filters</i>	42887	4755M <i>Flow through porous media</i>
4280D	<i>Monochromators</i>	42887	4760 <i>Flows in ducts, channels, and conduits</i>
4280E	<i>Shutters, windows, diaphragms, deflectors, choppers</i>	42887	4765 <i>Magnetohydrodynamics and electrohydrodynamics</i>
4280F	<i>Gratings, echelles</i>	42887	4770 <i>Reactive, radiative, or nonequilibrium flows</i>
4280K	<i>Optical beam modulators</i>	42887	4775 <i>Relativistic fluid dynamics</i>
4280L	<i>Optical waveguides</i>	42887	4780 <i>Instrumentation for fluid dynamics</i>
4280M	<i>Fibre optics</i>	42888	4790 <i>Other topics in fluid dynamics</i>
4280Q	<i>Image detectors, convertors, and intensifiers</i>	42889	
4280S	<i>Optical communications devices</i>	42889	5000 FLUIDS, PLASMAS AND ELECTRIC DISCHARGES
4282	<i>Integrated optics</i>	42889	
4285	<i>Optical testing and workshop techniques</i>	42890	5100 KINETIC AND TRANSPORT THEORY OF FLUIDS; PHYSICAL PROPERTIES OF GASES
4290	<i>Other topics in optics</i>	42890	5110 <i>Kinetic and transport theory</i>
		5120 <i>Viscosity and diffusion: experimental</i>	4910
4300	ACOUSTICS	4890	5130 <i>Thermal properties of gases</i>
4320	<i>General linear acoustics</i>	4890	5140 <i>Acoustical properties of gases; ultrasonic relaxation</i>
4325	<i>Nonlinear acoustics and macrosonics</i>	4891	5150 <i>Electrical phenomena in gases</i>
4328	<i>Aeroacoustics and atmospheric sound</i>	4892	5160 <i>Magnetic phenomena in gases</i>
4330	<i>Underwater sound</i>	4892	5170 <i>Optical phenomena in gases</i>
4335	<i>Ultrasonics, quantum acoustics, and physical effects of sound</i>	4892	5190 <i>Other topics in the physics of fluids</i>
4340	<i>Mechanical vibrations and shock</i>	4892	
4345	<i>Statistical studies of acoustical response</i>	—	5200 THE PHYSICS OF PLASMAS AND ELECTRIC DISCHARGES
4350	<i>Noise, its effects and control</i>	4893	5220 <i>Elementary processes in plasma</i>
4355	<i>Architectural acoustics</i>	4893	5220F <i>Electron collisions</i>
4360	<i>Acoustic signal processing</i>	4893	5220H <i>Atomic, molecular, heavy-particle collisions</i>
4363	<i>Acoustic holography</i>	—	5225 <i>Plasma basic properties</i>
4370	<i>Speech communication</i>	4893	5225F <i>Transport properties</i>
4375	<i>Music and musical instruments</i>	4893	5225P <i>Emission, absorption, and scattering of radiation</i>
4385	<i>Acoustical measurements and instrumentation</i>	4893	5230 <i>Plasma flow; magnetohydrodynamics</i>
4388	<i>Transduction; devices for the generation and reproduction of sound</i>	4894	5235 <i>Waves, oscillations, and instabilities in plasma</i>
4390	<i>Other topics in acoustics</i>	—	5235R <i>Plasma turbulence</i>
		5235T <i>Shock waves</i>	4915
4400	HEAT FLOW, THERMAL AND THERMODYNAMIC PROCESSES	4894	5240 <i>Plasma interactions</i>
4410	<i>Heat conduction (models, phenomenological description)</i>	4894	5240D <i>Electromagnetic wave propagation in plasma</i>
4425	<i>Convective and constrained heat transfer</i>	4895	5240F <i>Antennas in plasma; plasma-filled wave guides</i>
4430	<i>Heat transfer in inhomogeneous media and through interfaces</i>	4895	5240H <i>Solid-plasma interactions</i>
4440	<i>Radiative heat transfer</i>	4896	5240K <i>Sheaths</i>
4450	<i>Thermal properties of matter (phenomenology, experimental techniques)</i>	4896	5240M <i>Beam interactions in plasma</i>
4460	<i>Thermodynamic processes (phenomenology, experimental techniques)</i>	4896	5250 <i>Plasma production and heating</i>
4490	<i>Other topics in heat flow, thermal and thermodynamic processes</i>	—	5250J <i>Plasma production and heating by laser beams</i>
		4897	5250L <i>Plasma production and heating by shock wave and wire explosion</i>
4600	MECHANICS, ELASTICITY, RHEOLOGY	4897	5255 <i>Plasma equilibrium and confinement</i>
4610	<i>Mechanics of discrete systems</i>	4897	5260 <i>Relativistic plasma</i>
4620	<i>Continuum mechanics</i>	4897	5265 <i>Plasma simulation</i>
4630	<i>Mechanics of solids and rheology</i>	4897	5270 <i>Plasma diagnostic techniques and instrumentation</i>
4630C	<i>Static elasticity</i>	4897	5275 <i>Plasma devices and applications</i>
4630J	<i>Viscoelasticity, plasticity, viscoplasticity, creep, and stress relaxation</i>	4898	5280 <i>Electric discharges</i>
4630L	<i>Static buckling and instability</i>	4898	5290 <i>Other topics in plasma physics and electric discharges</i>
4630M	<i>Vibrations, aeroelasticity, hydroelasticity, mechanical waves, and shocks</i>	4899	
4630N	<i>Fracture mechanics, fatigue, and cracks</i>	4900	6000 CONDENSED MATTER: STRUCTURE, THERMAL AND MECHANICAL PROPERTIES
4630P	<i>Friction, wear, adherence, hardness, mechanical contacts</i>	4901	
4630R	<i>Measurement methods and techniques</i>	4901	6100 STRUCTURE OF LIQUIDS AND SOLIDS; CRYSTALLOGRAPHY
4660	<i>Rheology of fluids and pastes</i>	4901	6110 <i>X-ray determination of structures</i>
4690	<i>Other topics in mechanics, elasticity, and rheology</i>	—	6110D <i>Theories of diffraction and scattering</i>
		4902	6110F <i>Experimental techniques</i>
4700	FLUID DYNAMICS	4902	6112 <i>Neutron determination of structures</i>
4710	<i>General theory</i>	4902	6114 <i>Electron determination of structures</i>
4715	<i>Laminar flows</i>	4902	6114D <i>Theories of diffraction and scattering</i>
4715C	<i>Laminar boundary layers</i>	4902	6114F <i>Experimental diffraction and scattering</i>
4715F	<i>Stability of laminar flows</i>	4902	6114H <i>Low-energy electron diffraction (LEED) and reflection High-energy electron diffraction (RHEED)</i>
4720	<i>Hydrodynamic stability</i>	4902	6116 <i>Other determination of structures</i>
4725	<i>Turbulent flows, convection, and heat transfer</i>	4903	6116D <i>Electron microscopy determinations</i>
4725C	<i>Isotropic turbulence</i>	4903	6116F <i>Field-ion microscopy determinations</i>
4725F	<i>Boundary layer and shear turbulence</i>	4903	6116N <i>EPR and NMR determinations</i>
4725J	<i>Turbulent diffusion</i>	4903	6120 <i>Classical, semiclassical, and quantum theories of liquid structure</i>
4725M	<i>Noise (turbulence generated)</i>	4903	6125 <i>Studies of specific liquid structures</i>
4725Q	<i>Convection and heat transfer</i>	4904	6125M <i>Liquid metals</i>
4725R	<i>Wakes</i>	4904	6130 <i>Liquid crystals</i>
4730	<i>Rotational flow and vorticity</i>	4904	6140 <i>Amorphous and polymeric materials</i>
4735	<i>Waves</i>	4905	6140D <i>Glasses</i>
4740	<i>Compressible flows; shock and detonation phenomena</i>	4905	6140K <i>Polymers, elastomers, and plastics</i>
4740D	<i>General subsonic flows</i>	—	6150 <i>Crystalline state</i>
4740H	<i>Transonic flows</i>	4905	6150C <i>Physics of crystal growth</i>
4740K	<i>Supersonic and hypersonic flows</i>	4906	6150E <i>Crystal symmetry; models and space groups, and crystalline systems and classes</i>
4740N	<i>Shock-wave interactions</i>	4906	6150J <i>Crystal morphology and orientation</i>
4745	<i>Rarefied gas dynamics</i>	4906	6150K <i>Crystallographic aspects of polymorphic and order-disorder transformations</i>
4750	<i>Non-Newtonian dynamics</i>	4906	6150L <i>Crystal binding</i>
4755	<i>Nonhomogeneous flows</i>	4906	6155 <i>Specific structure of elements and alloys</i>
4755B	<i>Cavitation</i>	4906	6155D <i>Nonmetallic elements</i>
4755C	<i>Jets</i>	4906	6155F <i>Metallic elements</i>
4755E	<i>Nozzles</i>	4907	6155H <i>Alloys</i>
4755H	<i>Stratified flows</i>	4907	6160 <i>Specific structure of inorganic compounds</i>
		4907	6165 <i>Specific structure of organic compounds</i>
			6170 <i>Defects in crystals</i>

		page			page
6170B	Interstitials and vacancies	4936	6630D	Theory of diffusion and ionic conduction in solids	4960
6170D	Colour centres	4936	6630F	Self-diffusion in metals, semimetals, and alloys	4960
6170E	Other point defects	4936	6630H	Self-diffusion and ionic conduction in nonmetals	4960
6170G	Dislocations: theory	4936	6630J	Diffusion, migration, and displacement of impurities	4961
6170J	Etch pits, decoration, transmission electron-microscopy and other direct observations of dislocations	4937	6630L	Diffusion, migration, and displacement of other defects	4962
6170L	Slip, creep, internal friction and other indirect evidence of dislocations	4938	6630N	Chemical interdiffusion	4962
6170N	Grain and twin boundaries	4938	6630Q	Electromigration	—
6170P	Stacking faults, stacking fault tetrahedra and other planar or extended defects	4939	6660	Thermal conduction in nonmetallic liquids	4963
6170R	Crystal impurities: general	4939	6670	Nonelectronic thermal conduction and heat-pulse propagation in nonmetallic solids	4963
6170T	Doping and implantation of impurities	4939	6690	Other topics in nonelectronic transport properties	—
6170W	Impurity concentration, distribution, and gradients	4940	6700	QUANTUM FLUIDS AND SOLIDS; LIQUID AND SOLID HELIUM	4964
6170Y	Interaction between different crystal structure defects	4940	6720	Quantum effects on the structure and dynamics of nondegenerate fluids	—
6180	Radiation damage and other irradiation effects	4941	6740	Boson degeneracy and superfluidity of helium-4	4964
6180B	Laser beams	4941	6750	Fermi fluids; liquid helium-3	4964
6180C	X-rays	4942	6760	Mixed systems; liquid helium 3-4 mixtures	4964
6180E	Gamma rays	4942	6770	Films	4964
6180F	Electrons and positrons	4942	6780	Solid helium and related quantum crystals	4964
6180H	Neutrons	4943	6790	Other topics in quantum fluids and solids (e.g. neutron-star matter)	4964
6180J	Ions	4943	6800	SURFACES AND INTERFACES; THIN FILMS AND WHISKERS	4965
6180L	Atoms and molecules	—	6810	Fluid surfaces and interfaces with fluids	4965
6180M	Channelling, blocking and energy loss of particles	4945	6815	Liquid thin films	4965
6190	Other topics in structure of liquids and solids	—	6820	Solid surface structure	4965
6200	MECHANICAL AND ACOUSTIC PROPERTIES OF CONDENSED MATTER	4945	6825	Mechanical and acoustical properties of solid surfaces and interfaces	4966
6210	Mechanical properties of liquids	4945	6830	Dynamics of solid surfaces and interface vibrations	4966
6220	Mechanical properties of solids (related to microscopic structure)	4945	6840	Surface energy of solids; thermodynamic properties	4967
6220D	Elastic constants	4945	6845	Solid-fluid interface processes	4967
6220F	Deformation and plasticity	4946	6848	Solid-solid interfaces	4971
6220H	Creep	4947	6855	Thin film growth, structure, and epitaxy	4971
6220M	Fatigue, brittleness, fracture, and cracks	4947	6860	Physical properties of thin films, nonelectronic	4974
6220P	Tribology	4948	6870	Whiskers and dendrites: growth, structure, and nonelectronic properties	4974
6230	Mechanical and elastic waves	4948	6890	Other topics in the structure and nonelectronic properties of surfaces and thin films	—
6240	Anelasticity, internal friction, and damping	4949	7000	CONDENSED MATTER: ELECTRONIC STRUCTURE, ELECTRICAL, MAGNETIC, AND OPTICAL PROPERTIES	4974
6250	High-pressure and shock-wave effects in solids	4949	7100	ELECTRON STATES	4974
6260	Acoustic properties of liquids	4949	7110	General theories and computational techniques	4974
6265	Acoustic properties of solids	4949	7120	Electronic density of states determinations	4974
6280	Ultrasonic relaxation	4950	7125	Nonlocalized single-particle electronic states	4975
6290	Other topics in mechanical and acoustical properties of condensed matter	4950	7125C	Techniques of band-structure calculation (general theory, applications of group theory, analytic continuation, etc)	4975
6300	LATTICE DYNAMICS AND CRYSTAL STATISTICS	4950	7125H	Measurement of Fermi surface parameters	4975
6310	General theory	4950	7125J	Effective mass and g-factors	4975
6320	Phonons and vibrations in crystal lattices	4950	7125L	Electron energy states in liquid metals	—
6320D	Phonon states and bands, normal modes, and phonon dispersion	4950	7125M	Electron energy states in amorphous and glassy solids	4975
6320H	Phonon-phonon interactions	—	7125P	Band structure of crystalline metals	4976
6320K	Phonon-electron interactions	4951	7125R	Band structure of crystalline elemental semiconductors	4976
6320M	Phonon-defect interactions	4951	7125T	Band structure of crystalline semiconductor compounds and insulators	4976
6320P	Localized modes	4951	7130	Metal-insulator transitions	4976
6350	Vibrational states in disordered systems	—	7135	Excitons and related phenomena	4976
6370	Statistical mechanics of lattice vibrations	4951	7136	Polaritons	4977
6375	Statistical mechanics of displacive phase-transitions	4951	7138	Polarons and electron-phonon interactions	4977
6390	Other topics in lattice dynamics and crystal statistics	4951	7145	Collective effects	4977
6400	EQUATIONS OF STATE, PHASE EQUILIBRIA, AND PHASE TRANSITIONS	4951	7145G	Exchange, correlation, dielectric and magnetic functions, plasmons	4978
6410	General theory of equations of state and phase equilibria	4951	7145J	Fermi-Thomas model	—
6430	Equations of state of specific substances	4952	7145N	Calculations of total electronic binding energy	4978
6460	General studies of phase transitions	4952	7150	Localized single-particle electronic states	4978
6470	Phase equilibria, phase transitions, and critical points	4952	7155	Impurity and defect levels	4978
6470D	Solid-liquid transitions	4953	7155J	Localization in disordered structures	4980
6470F	Liquid-vapour transitions	4953	7165	Positron states	—
6470H	Solid-vapour transitions	4954	7170	Level splitting and interactions	4980
6470J	Liquid-liquid transitions	4954	7170C	Crystal and ligand fields	4980
6470K	Solid-solid transitions	4954	7170E	Spin-orbit coupling, Zeeman, Stark and strain splitting	4980
6470M	Transitions in liquid crystals	4955	7170G	Exchange interactions	—
6470P	Glass transitions	4956	7170J	Nuclear states and interactions	4980
6475	Solubility, segregation, and mixing	4956	7190	Other topics in electron states	—
6480	Other phase properties of systems	4958	7200	ELECTRONIC TRANSPORT IN CONDENSED MATTER	4981
6490	Other topics in equations of state, phase equilibria, and phase transitions	—	7210	Theory of electronic transport; scattering mechanisms	4981
6500	THERMAL PROPERTIES OF CONDENSED MATTER	4958	7215	Electronic conduction in metals and alloys	4981
6520	Heat capacities of liquids	4958	7215C	Electrical and thermal conduction in amorphous and liquid metals and alloys	4981
6540	Heat capacities of solids	4958	7215E	Electrical and thermal conduction in crystalline metals and alloys	4981
6550	Thermodynamic properties and entropy	4958			
6570	Thermal expansion and thermomechanical effects	4959			
6590	Other topics in thermal properties of condensed matter	4959			
6600	TRANSPORT PROPERTIES OF CONDENSED MATTER (NONELECTRONIC)	4959			
6610	Diffusion and ionic conduction in liquids	4959			
6620	Diffusive momentum transport	4960			
6630	Diffusion in solids	4960			

	page		page		
7215G	Galvanomagnetic and other magnetotransport effects	4982	7510J	Heisenberg and other quantized localized spin models	4995
7215H	Thermomagnetic effects	—	7510L	Band and itinerant models	4995
7215J	Thermoelectric effects	4982	7520	Diamagnetism and paramagnetism	4995
7215L	Relaxation times and mean free paths	—	7520C	Nonmetals	4995
7215N	Collective modes, e.g. in one-dimensional conductors	4982	7520E	Metals and alloys	4995
7215Q	Scattering mechanisms and Kondo effect	4982	7520H	Local moment in dilute alloys; Kondo effect	4995
7220	Conductivity phenomena in semiconductors and insulators	4982	7525	Spin arrangements in magnetically ordered materials (neutron studies, etc)	4995
7220D	General theory, scattering mechanisms	4983	7530	Magnetically ordered materials, other intrinsic properties	4996
7220F	Low-field transport and mobility; piezoresistance	4983	7530C	Saturation moments and magnetic susceptibility	4996
7220H	High-field and nonlinear effects	4984	7530D	Spin waves	4997
7220J	Charge carriers: generation, recombination, lifetime, and trapping	4984	7530E	Exchange and superexchange interactions	4997
7220M	Galvanomagnetic and other magnetotransport effects	4984	7530G	Anisotropy	4998
7220N	Thermomagnetic effects	4985	7530H	Magnetic impurity interactions	4999
7220P	Thermoelectric effects	4985	7530K	Magnetic phase boundaries	4999
7230	High-frequency effects; plasma effects	4985	7530S	Magnetocaloric effect	5000
7240	Photoconduction and photovoltaic effects; photoelectric effects	4986	7540	Critical-point effects, specific heats, short-range order	5001
7250	Acoustoelectric effects	4987	7540D	Ising and other classical spin models	5003
7255	Magnetoacoustic effects	—	7540F	Heisenberg and other quantized spin models	5004
7260	Mixed conductivity and conductivity transitions	4987	7550	Studies of specific magnetic materials	5004
7270	Noise processes and phenomena	4987	7550B	Ferromagnetism of Fe and its alloys	5004
7280	Conductivity of specific semiconductors and insulators	4987	7550C	Ferromagnetism of other metals	5005
7280C	Elemental semiconductors	4987	7550D	Ferromagnetism of nonmetals	5005
7280E	III-V and II-VI semiconductors	4987	7550E	Antiferromagnetics	5006
7280G	Transition-metal compounds	4988	7550G	Ferrimagnetics	5006
7280J	Other crystalline inorganic semiconductors	4988	7550K	Amorphous magnetic materials	5006
7280L	Organic semiconductors	4988	7550M	Magnetic liquids	5007
7280N	Amorphous and glassy semiconductors	4988	7560	Domain effects, magnetization curves, and hysteresis	5007
7280P	Liquid semiconductors	—	7560C	Domain walls and domain structure	5007
7290	Other topics in electronic transport in condensed matter	4988	7560E	Magnetization curves, hysteresis, Barkhausen and related effects	5008
			7560G	High coercivity materials	5009
			7560J	Fine-particle systems	5009
			7560L	Magnetic aftereffects	5010
			7560N	Magnetic annealing and temperature-hysteresis effects	5010
7300	ELECTRONIC STRUCTURE AND ELECTRICAL PROPERTIES OF SURFACES, INTERFACES, AND THIN FILMS	4988	7570	Magnetic films and plates	5010
7320	Electronic surface states	4988	7570K	Domain structure (magnetic bubbles)	5013
7325	Surface conductivity	4989	7580	Magnetomechanical and magnetoelectric effects, magnetostriction	5014
7330	Surface double layers, Schottky barriers, and work functions	4989	7590	Other topics in magnetic properties and materials	5015
7340	Interfaces	4990	7600	MAGNETIC RESONANCES AND RELAXATION IN CONDENSED MATTER; MÖSSBAUER EFFECT	5015
7340B	Static electrification	4990	7620	General theory of resonances and relaxation	—
7340G	Tunnelling: general	—	7630	Electron paramagnetic resonance and relaxation	5015
7340J	Metal-to-metal contacts	—	7630D	Ions and impurities: general	5015
7340L	Semiconductor-to-semiconductor contacts, p-n junctions, and heterojunctions	4990	7630F	Iron group (3d) ions and impurities (Ti-Cu)	5015
7340M	Semiconductor-electrolyte contacts	4990	7630H	Platinum and palladium group (4d and 5d) ions and impurities (Zr-Ag and Hf-Au)	—
7340N	Metal-nonmetal contacts	4991	7630K	Rare-earth ions and impurities	5016
7340Q	Metal-insulator-semiconductor structures	4991	7630L	Other ions and impurities	—
7340R	Metal-insulator-metal structures	4991	7630M	Colour centres and other defects	5016
7340S	Metal-semiconductor-metal structures	4991	7630P	Conduction electrons	—
7360	Electronic properties of thin films	4992	7630R	Free radicals	5016
7360D	Metallic thin films	4992	7640	Diamagnetic and cyclotron resonances	5016
7360F	Semiconductor films	4992	7650	Ferromagnetic, antiferromagnetic, and ferrimagnetic resonances; spin wave resonance	5016
7360H	Insulating thin films	4993	7660	Nuclear magnetic resonance and relaxation	5016
7360K	Superconducting films	4993	7660C	Chemical and Knight shifts	5017
7390	Other topics in electrical properties of surfaces, interfaces, and thin films	—	7660E	Relaxation effects	5017
			7660G	Quadrupole resonance	5017
7400	SUPERCONDUCTIVITY	4993	7660L	Spin echoes	5018
7410	Occurrence, critical temperature	4993	7670	Magnetic double resonances and cross effects	5018
7420	Theory	4993	7670D	Electron-nuclear double resonance (ENDOR)	5018
7420F	BCS theory and its applications	—	7670E	Dynamical nuclear polarization	—
7430	General properties	4993	7670F	Double nuclear magnetic resonance (DNMR)	5018
7430C	Magnetization curves, Meissner effect, penetration depth	4993	7670H	Optical double magnetic resonance (ODMR)	5018
7430E	Thermodynamic properties; thermal conductivity	—	7670K	Electron double resonance (ELDOR)	—
7430G	Response to electromagnetic fields, nuclear magnetic resonance, ultrasonic attenuation	4993	7680	Mössbauer effect; other gamma-ray spectroscopy	5018
7440	Fluctuations and critical effects	4993	7690	Other topics in magnetic resonances and relaxation	5020
7450	Proximity effects, tunnelling phenomena, and Josephson effect	4993	7700	DIELECTRIC PROPERTIES AND MATERIALS	5020
7455	Type-I superconductivity	—	7720	Permittivity	5020
7460	Type-II superconductivity	4994	7730	Polarization and depolarization effects	5021
7460E	Mixed state, H_{c2} , surface sheath	4994	7740	Dielectric loss and relaxation	5021
7460G	Flux pinning; fluxon-defect interactions	4994	7750	Dielectric breakdown and space-charge effects	5022
7460J	Critical currents	4994	7755	Dielectric thin films	5022
7470	Superconducting materials	4994	7760	Piezoelectricity and electrostriction	5022
7470D	Material effects on T_c , K , critical currents	4994	7770	Pyroelectric and electrocaloric effects	5022
7470G	Type-I superconductors (non transition metals)	4994	7780	Ferroelectricity and antiferroelectricity	5022
7470L	Type-II superconductors (transition metals, alloys and compounds)	4994	7780B	Transitions and Curie point	5022
7470N	Dirty superconductors	—	7780D	Domain structure and effects; hysteresis	5023
7470P	Materials for high-field applications	—	7785	Electrical resonances	—
7490	Other topics in superconductivity	—	7790	Other topics in dielectric properties and materials	5023
			7800	OPTICAL PROPERTIES AND CONDENSED MATTER SPECTROSCOPY AND OTHER INTERACTIONS OF MATTER WITH PARTICLES AND RADIATION	5023
7500	MAGNETIC PROPERTIES AND MATERIALS	4994			
7510	General theory and models of magnetic ordering	4994	7820	Optical properties and materials	5023
7510D	Crystal-field theory and spin Hamiltonians	4994	7820B	General theory (for pure homogeneous materials)	5023
7510H	Ising and other classical spin models	4994			

		page		page	
7820D	Optical constants and parameters	5024	8140E	Cold working, work hardening; annealing, recovery and recrystallisation; textures	5056
7820E	Optical rotatory power	5025	8140G	Other heat and thermomechanical treatments	5057
7820F	Birefringence	5025	8140J	Elasticity and anelasticity	5059
7820H	Piezo-, elasto- and acousto-optical effects	5025	8140L	Deformation, plasticity and creep	5059
7820J	Electro-optical effects	5025	8140N	Fatigue, embrittlement, and fracture	5062
7820L	Magneto-optical effects	5026	8140P	Friction, lubrication, and wear	5066
7820N	Thermo-optical effects	5027	8140R	Electrical and magnetic properties (related to treatment conditions)	5067
7830	Infrared and Raman spectra and scattering	5027	8140T	Optical properties (related to treatment conditions)	5067
7835	Brillouin and Rayleigh scattering	5031	8160	Corrosion, oxidation and surface treatments	5067
7840	Visible and ultraviolet spectra	5031	8160B	Metals and alloys	5068
7845	Stimulated emission	5032	8170	Materials testing	5070
7850	Impurity and defect absorption in solids	5032	8190	Other topics in materials science	5071
7855	Photoluminescence	5033			
7860	Other luminescence spectra and radiative recombination	5035	8200	PHYSICAL CHEMISTRY	5072
7860F	Electroluminescence	5035	8220	Chemical kinetics	5072
7860H	Cathodoluminescence, ionoluminescence	5035	8220K	Potential energy surfaces for chemical reactions	5072
7860K	Thermoluminescence	5036	8220M	Nonequilibrium kinetics	5072
7860M	Sonoluminescence, triboluminescence	—	8220R	Energy distribution and transfer, relaxation	5072
7860P	Chemiluminescence	5036	8230	Specific chemical reactions; reaction mechanisms	5072
7865	Optical properties of thin films	5036	8235	Polymer reactions and polymerization	5075
7870	Other interactions of matter with particles and radiation	5037	8240	Chemical kinetics and reactions: special regimes	5076
7870B	Positron annihilation	5037	8240D	Atomic and molecular beam reactions	—
7870C	X-ray scattering	—	8240T	Chemiluminescence and chemical laser kinetics	5076
7870D	X-ray absorption and absorption edges	5037	8245	Electrochemistry and electrophoresis	5076
7870E	X-ray emission threshold and fluorescence	5038	8250	Photochemistry and radiation chemistry	5077
7870G	Microwave and radiofrequency interactions	—	8250E	Photodissociation, photoionization as studied by luminescence and radiationless transitions	5078
7890	Other topics in optical properties of condensed matter and other interactions of matter with particles and radiation	—	8255	Radiochemistry	5078
			8260	Chemical thermodynamics	5078
			8265	Surface processes	5079
			8270	Disperse systems	5080
			8280	Chemical analysis and related physical methods of analysis	5081
7900	ELECTRON AND ION EMISSION BY LIQUIDS AND SOLIDS; IMPACT PHENOMENA	5038	8290	Other topics in physical chemistry	5083
7920	Impact phenomena	5038			
7920D	Laser-light impact phenomena	5038	8600	ENERGY RESEARCH AND ENVIRONMENTAL SCIENCE	5083
7920F	Electron impact: Auger emission	5038	8610	Energy resources and their utilisation	5083
7920H	Electron impact: secondary emission	—	8610B	Fossil and other fuels	5083
7920K	Other electron impact phenomena	5038	8610D	Wind energy	5083
7920N	Atom, molecule, and ion impact	5040	8610F	Tidal and flow energy	5084
7920R	Atomic and molecular beam interactions	5041	8610H	Geothermal energy	5084
7940	Thermionic emission	—	8610K	Solar energy	5084
7960	Photoemission and photoelectron spectra	5041	8610N	Nuclear energy	5084
7970	Field emission and field ionization	5042	8610Z	Other topics	5085
7975	Exoelectron emission	5043	8630	Energy conversion	5085
7980	Resonance tunnelling	—	8630D	Electrochemical conversion: general	5085
7990	Other topics in emission and impact phenomena in condensed matter	5043	8630E	Primary cells	—
			8630F	Secondary cells	5085
8000	CROSS-DISCIPLINARY PHYSICS AND RELATED AREAS OF SCIENCE AND TECHNOLOGY	5043	8630G	Fuel cells	—
8100	MATERIALS SCIENCE	5043	8630J	Photoelectric conversion: solar cells and arrays	5085
8110	Methods of crystal growth and purification	5043	8630K	Photoelectrochemical conversion	5089
8110B	Growth from vapour	5043	8630L	Electroosmotic and magnetohydrodynamic conversion	5089
8110D	Growth from solutions	5043	8630M	Thermoelectric conversion	—
8110F	Growth from melts	5043	8630N	Thermionic conversion	—
8110H	Zone melting and zone refining	5044	8630P	Photosynthesis	—
8110J	Growth from solid phases	5044	8630Q	Chemical energy conversion	5089
8115	Methods of thin film deposition	5044	8630R	Thermal energy conversion (heat engines and heat pumps)	5089
8115C	Deposition by cathodic sputtering	5044	8630S	Photothermal conversion	5090
8115G	Vacuum deposition	5045	8630Z	Other topics	—
8115H	Chemical vapour deposition	5045	8640	Energy storage (secondary energy)	5090
8115J	Ion plating and other vapour deposition	5046	8640C	Storage in mechanical energy	5090
8115L	Deposition from liquid phases (melts and solutions)	5046	8640F	Storage in thermal energy	5090
8120	Other methods of preparation of materials	5047	8640H	Storage in chemical energy	5090
8120C	Vacuum methods	—	8640K	Hydrogen storage and technology	5090
8120E	Powder techniques, compaction and sintering	5047	8640Z	Other topics	—
8120G	Specific metals and alloys (compacts, pseudoalloys)	5048	8660	Requirement for energy: ecological aspects	—
8120J	Dispersion-fibre-, and platelet-reinforced metal-based composites	5049	8670	Environmental science	5091
8120L	Ceramics and refractories	5049	8670C	Soil	5091
8120N	Cermets, ceramic and refractory composites	5051	8670E	Water	5091
8120P	Glasses	5052	8670G	Atmosphere	5092
8120Q	Glass-based composites, vitroceramics	5052	8670J	Noise	5093
8120S	Polymers	5052	8670L	Measurement techniques in environmental science	5093
8120T	Reinforced polymers and polymer-based composites	5052	8670Z	Other topics	5093
			8690	Other topics in energy research and environmental science	—
8130	Phase diagrams and microstructures developed by solidification and solid-solid phase transformations	5052	8700	BIOPHYSICS, MEDICAL PHYSICS, AND BIOMEDICAL ENGINEERING	5093
8130B	Phase diagrams of metals and alloys	5052	8710	General, theoretical, and mathematical biophysics	5093
8130D	Phase diagrams of other materials	5053	8715	Molecular biophysics	5094
8130F	Solidification	5053	8715B	Structure, configuration, conformation, and active sites at the biomolecular level	5094
8130H	Constant-composition solid-solid phase transformations: polymorphic, massive, and order-disorder	5054	8715M	Interactions with radiations at the biomolecular level	5095
8130K	Martensitic transformations	5055	8716	Biothermics	5095
8130M	Precipitation	5055	8720	Membrane biophysics	5096
8140	Treatment of materials and its effects on microstructures and properties	5056	8725	Cellular biophysics	5096
8140C	Solid solution hardening, precipitation hardening, dispersion hardening	5056	8725D	Biological transport: cellular and subcellular transmembrane physics	5097
			8730	Biophysics of neurophysiological processes	5098

	page		page
8732	Physiological optics, vision	5098	9460 Interplanetary space
8732C	<i>Anatomy and optics of the eye</i>	5099	9480 Aerospace facilities and techniques; space research
8732E	<i>Physiology of the eye; nerve structure and function</i>	5099	9490 Other topics in space physics
8732L	<i>Light detection; adaptation and discrimination</i>	5099	
8732N	<i>Colour detection; adaptation and discrimination</i>	5099	9500 FUNDAMENTAL ASTRONOMY AND
8732S	<i>Psychophysics of vision, visual perception, binocular vision</i>	5100	ASTROPHYSICS, INSTRUMENTATION AND
8734	Audition	5101	TECHNIQUES AND ASTRONOMICAL
8736	Speech	5101	OBSERVATIONS
8738	Mechano- and chemio-ceptions	5101	5143
8740	Biomagnetism	5102	5143 Fundamental astronomy
8745	Biomechanics, biorheology, biological fluid dynamics	5102	5143 <i>Celestial mechanics</i>
8750	Biological effects of radiations	5104	5143 Fundamental aspects of astrophysics
8750B	<i>Interactions of biosystems with radiations</i>	5104	5145 Observatories
8750C	<i>Bioacoustics (sonic and ultrasonic effects on living matter)</i>	5104	5145 Astronomical instruments
8750E	<i>Bio-optics (effects of microwaves, light, laser and other electromagnetic waves)</i>	5104	5145 Auxiliary and recording instruments
8750G	<i>Ionizing radiations (u.v., X-ray, gamma-ray; particle radiation effects)</i>	5105	5146 Other instrumentation and techniques
8760	Medical and biomedical uses of fields, radiations, and radioactivity	5106	5146 Techniques of observation and reduction
8760B	<i>Sonic and ultrasonic radiation</i>	5106	5146 Astronomical observations (listed by techniques of observation)
8760D	<i>Electric and magnetic fields (d.c. and pulsed)</i>	5106	5146 <i>Radio and radar</i>
8760G	<i>Laser beams, microwaves, and other electromagnetic waves</i>	5106	5146 <i>Far infrared (bolometric, photoconductive)</i>
8760J	<i>Corpuscular radiation and radioisotopes</i>	5107	5147 <i>Photographic region (near infrared, visible, and normal ultraviolet)</i>
8760L	<i>Preparation of radioactive materials for medical and biomedical uses</i>	5109	5147 <i>Space ultraviolet</i>
8760M	<i>Radiation dosimetry</i>	5109	5147 <i>X-ray</i>
8760P	<i>Radiation protection</i>	5111	5147 <i>gamma-ray and elementary particle</i>
8760R	<i>Radioactive pollution</i>	5111	5147 <i>Other (inc. gravitational radiation, magnetograms, etc)</i>
8765	Aerospace biophysics and medical physics (effects of accelerations, weightlessness and environment)	—	5147 Catalogues, atlases etc
8770	Biomedical engineering	5111	5147 Other topics in astronomy and astrophysics
8770E	<i>Diagnostic methods and instrumentation</i>	5112	9600 SOLAR SYSTEM
8770G	<i>Patient care and treatment</i>	5112	9610 General, solar nebula, and cosmogony
8770J	<i>Prosthetics and other practical applications</i>	5113	9620 Moon
8780	Biophysical instrumentation and techniques	5113	9630 Planets and satellites
8790	Other topics in biophysics, medical physics, and biomedical engineering	5114	9630D <i>Mercury</i>
9000	GEOPHYSICS, ASTRONOMY AND ASTROPHYSICS	5114	9630E <i>Venus</i>
9100	SOLID EARTH GEOPHYSICS	5114	9630G <i>Mars</i>
9110	Geodesy and gravity	5114	9630H <i>Asteroids</i>
9125	Geomagnetism and palaeomagnetism; geoelectricity	5115	9630K <i>Jupiter</i>
9130	Seismology	5116	9630M <i>Saturn</i>
9135	Earth's interior structure and properties	5119	9630T <i>Other planets</i>
9140	Volcanology	5121	9650 Other objects in the planetary system
9145	Physics of plate tectonics	5121	9650D <i>Interplanetary matter, magnetic and electric fields</i>
9150	Marine geology and geophysics	5123	9650G <i>Comets</i>
9160	Physical properties of rocks and minerals	5124	9650K <i>Meteors, showers and meteoroids</i>
9165	Geophysical aspects of geology, mineralogy and petrology	5124	9650M <i>Meteorites, micrometeorites</i>
9190	Other topics in solid Earth geophysics	5125	9660 Solar physics
9200	HYDROSPHERIC AND ATMOSPHERIC GEOPHYSICS	5125	9690 Other topics on the solar system
9210	Physics of the oceans	5125	9700 STARS
9220	Interdisciplinary aspects of oceanography	5126	9710 Stellar characteristics
9240	Hydrology and glaciology	5126	9720 Normal stars (by class); general or individual
9260	Meteorology	5127	9730 Variable and peculiar stars
9260S	<i>Climatology</i>	5132	9760 Late stages of stellar evolution
9265	Atmospheric optics	5132	9760B <i>Supernovae</i>
9290	Other topics in hydrospheric and atmospheric geophysics	5132	9760G <i>Pulsars</i>
9300	GEOPHYSICAL OBSERVATIONS, INSTRUMENTATION, AND TECHNIQUES	5132	9760J <i>Neutron stars</i>
9330	Information related to geographical regions	5132	9760L <i>Black holes</i>
9355	International organizations, national and international programs	5134	9780 Binary and multiple stars
9365	Data acquisition and storage	—	9790 Other topics in stellar astronomy
9385	Instrumentation and techniques for geophysical research	5134	9800 STELLAR SYSTEMS; GALACTIC AND EXTRAGALACTIC OBJECTS AND SYSTEMS; THE UNIVERSE
9400	AERONOMY AND SPACE PHYSICS	5137	9810 Stellar dynamics
9410	Physics of the neutral atmosphere	5137	9820 Stellar clusters and associations
9410Q	<i>Airglow and nightglow</i>	5137	9840 Interstellar matter; and nebulae
9410S	<i>Aurora</i>	5137	9850 The Galaxy, extragalactic objects and systems
9420	Physics of the ionosphere	5137	9850K <i>Groups, clusters, superclusters</i>
9430	Physics of the magnetosphere	5139	9870 Other objects and background radiations of unknown origin and distances
9440	Cosmic rays	5140	9870D <i>Discrete radio sources</i>
9440C	<i>Origin and propagation outside the solar system</i>	5140	9870J <i>Quasars</i>
9440E	<i>Interplanetary propagation and effects</i>	—	9870L <i>IR sources</i>
9440H	<i>Energetic solar particles and photons</i>	5141	9870Q <i>X-ray and gamma-ray sources</i>
9440K	<i>Solar modulation and geophysical effects</i>	—	9870S <i>Cosmic ray sources</i>
9440L	<i>Composition and energy spectra</i>	5141	9870V <i>Background radiations</i>
9440N	<i>Extensive air showers</i>	—	9880 Cosmology
9440R	<i>High-energy interactions</i>	5141	9890 Other topics in galactic and extragalactic astronomy
9440T	<i>Muons and neutrinos</i>	5141	
9440V	<i>Cosmic-ray effects in meteorites and terrestrial matter</i>	5141	

AUTHOR INDEX

xvii

followed by

SUBSIDIARY INDEXES

SUBJECT GUIDE

The SUBJECT GUIDE is an alphabetical index to subjects covered in the classification scheme, by which the abstracts are arranged. The numbers given are classification codes. The CLASSIFICATION AND CONTENTS, which precede the Guide, gives the page number for each section.

	Classification		Classification		Classification
A mesons	1440	Atomic polarisability	3510D	Boson systems	0530
Ab initio calculations	3120	Atomic spectra	32	Boundary layer flow	4715C, 4725F
Aberrations	4180, 4230, 4278	Atomic structure	31, 3510	Boundary layer turbulence	4725F
Abrasion	4630P, 6220P, 8140P	Atomic transitions	3110	Brain	87
Absorptive models	1240P	Atoms	30	Bremsstrahlung	0350, 41, 7870
Acceleration measurement	0630G	Audition	8734	Brillouin spectra	3320F, 4265C, 5170, 7835
Accumulation layers	7320, 7340Q	Auger effect	3280H, 7920F, 7920N, 7960, 8260	Brillouin zones	6320, 7125
Acoustic devices	4385	Aurora	9410S	Brink model	2160G
Acoustic holography	4363	Autoionisation	3280D, 3380E	Brittleness	4630N, 6220M, 8140N
Acoustic noise	4350, 4360, 4388, 8670J	Axial vector currents	1140	Brownian motion	0540
Acoustic nuclear magnetic resonance	7660	Axiomatic field theory	1110	Bubble chambers	2940
Acoustic paramagnetic resonance	7630			Buckling	4630L, 6220F, 8140L
Acoustic properties of gases	5140				
Acoustic properties of liquids	6260				
Acoustic properties of solids	6265				
Acoustic signal processing	4360				
Acoustic wave propagation	4320, 4325, 5140, 6260, 6265				
Acoustics	43	B mesons	1440	C invariance	1130
Acousto-optical effects	5140, 5170, 7820H	Background radiation	9870V	Calibration	0620H
Acoustoelectric effects	4388, 5140, 5150, 7250	Band model of magnetism	7510L	Calorimetry	0720F
Adaptive optics	42	Band structure	7125	Cameras	0768
Adherence	4630P	Barkhausen effect	7560E	Capillarity	6810
Adhesion	4630P, 6825, 8190	Barrier heights	3520J	Carbon dioxide lasers	4255D, 4260
Adsorption	6845, 8265	Baryon-baryon interactions	1375C, 1375E, 1385	Cardiology	87
Aerodynamics	4740	Baryon-baryon scattering	1375C, 1375E, 1385	Carrier density	7220
Aeroelasticity	4630C, 4630M	Baryon decays	1330	Carrier lifetime	7220J
Aeronomy	94	Baryon electric moment	1340F, 1420	Carrier mobility	7220
Aerosols	4755K, 8270, 92	Baryon-kaon interactions	1375J, 1385	Casting	8120, 8130F
Aerospace	9480, 9555	Baryon-kaon scattering	1375J, 1385	Catalogues	9585
Aerospace biophysics	8765	Baryon magnetic moment	1340F, 1420	Cathodochromism	7820
Ageing	8140G	Baryon mass	1420	Cathodoluminescence	7860H
Airglow	9410Q	Baryon parity	1420	Cavitation	4755B
Algebra	0210	Baryon-pion interactions	1375G, 1385	Celestial mechanics	0320, 9510C
Alpha decay	2360	Baryon-pion scattering	1375G, 1385	Cells (electric)	8630D
Alpha particle-nucleus reactions	2560	Baryon-pion production	1360P, 1365, 1375, 1385	Cellular biophysics	8725
Alpha particle-nucleus scattering	2560	Baryon resonance production	1360P, 1365, 1375, 1385	Ceramic preparation	8120L, 8120N
Alpha particle spectroscopy	2930			Ceramics	81
Alpha particles	2140, 2710	Baryon resonances	1420	Cermets	81
Amorphous semiconductors	6140, 7125M, 7220, 7280N	Baryon spin	1420	CESR	7630P
Amorphous state	6140, 81	Baryons	1420	Chalcogenide glasses	6140D, 7280N
Anderson model	7110, 7125M, 7155	BCS theory	2160, 7420F	Channel flow	4760
Anelasticity	4630J, 6240, 8140J	Beam-foil excitation	3450H	Channelling	6180M
Anemometers	4780, 9385	Beam-foil ionisation	3450H	Chaos	0540
Angular measurement	0630C	Beam handling equipment	2925	Charge density waves	7145, 7215N
Annealing	8140E, 8140G	Beam handling techniques	2925	Charge exchange	3470
Anodisation	8160, 8245	Bending	4630J, 6220F, 8140L	Charge ordered states	7145, 7150
Antiferromagnetism	7530	Beta decay	2340	Charge transfer	3470
Antiferroelectric materials	7780	Beta ray spectroscopy	2930	Charge transfer reactions	8230
Antiferromagnetic properties of substances	75, 7550E	Betatron	2920	Charge transfer states	31, 7170C
Antiferromagnetic resonance	7650	Bethe-Salpeter equations	1110	Charm particles	1420, 1440
Antiphase boundaries	81	Bi-metric gravity theories	0450	Chemical analysis	8280
Antiphase domains	81	Bibliographies	0130T	Chemical binding	3110, 3520G
Antireflection coatings	4270, 4278H, 4280	Binary stars	9780	Chemical energy conversion	8630Q
Appearance potential spectroscopy	0785, 7870E	Binding energy	31, 3520V, 6150L	Chemical energy storage	8640H
APW calculations	7110, 7125C	Bio-optics	8750E, 8760G	Chemical kinetics	8220
Architectural acoustics	4355	Bioacoustics	8738, 8750B, 8750C, 8760B	Chemical lasers	4255K, 4260, 8240
Artificial limbs	8770J	Biocommunications	87	Chemical reactions	3450L, 8230, 8235, 8240
Artificial organs	8770J	Biocontrol	8710	Chemical shifts	3325, 7660C
Association	6120, 6125, 8230	Biocybernetics	8710	Chemical thermodynamics	8260
Asteroids	9630H	Bioelectric phenomena	8730, 8732E	Chemical vapour deposition	6855, 8115H
Astroarchaeology	9590	Bioenergy conversion	8630Z	Chemiluminescence	5170, 7860P, 8240
Astrometry	95, 9555	Biography	0150	Chemioception	8738
Astronomical instruments	95	Biological effects of radiation	8750	Chemisorption	6845, 8265
Astronomy and astrophysics	95, 96, 97, 98	Biological fluid dynamics	8745	Cherenkov detectors	2940
Atlases	9585	Biological techniques and instruments	8780	Cherenkov radiation	41
Atmospheric acoustics	4328	Biology	87	Chiral symmetries	1130
Atmospheric optics	9265	Biomagnetism	8740, 8760D	Cholesteric liquid crystals	6130, 6470M
Atmospherics	9260, 94	Biomass	8630Z	CI calculations	3120T
Atom beam reactions	8240D	Biomechanics	8745	CIDEP	3330
Atom-surface impact	34, 7920N, 7920R	Biomedical engineering	8770	CIDNP	3325
Atomic beams	3440, 3450, 3580, 8240D	Biomedical equipment	8770	Cinematography	0768
Atomic clusters	3640	Biomedical measurement	8770	Claddings	8160
Atomic collisions	34	Biomedical ultrasonics	8760G	Classical field theory	0350
Atomic electric moments	3510D	Biomedical uses of radiation and radioactivity	8760	Classical mechanics	0320, 0340
Atomic electron correlations	3120T	Biomembrane transport	8720, 8725D	Classical statistical mechanics	0520
Atomic electron impact excitation	3480	Biomembranes	8720	Clebsch-Gordon coefficients	0365
Atomic electron impact ionization	3480	Biomolecular effects of radiation	8715M, 8750	Climatology	9260
Atomic excited states	3150	Biomolecular structure	3620, 8715B	Cloud chambers	2940
Atomic fine structure	3510F	Biophysical techniques and instruments	8780	Clouds	9260
Atomic fluorescence	3250	Biophysics	87	Cluster approximation	7110, 7125M
Atomic forces	3420	Biorheology	8745	CNDO calculations	3120N
Atomic hyperfine interactions	3130	Biothermics	8716	CO ₂ lasers	4255D, 4260
Atomic hyperfine structure	3510F	Biotransport	8725D, 8745	Coal	8610B
Atomic inelastic collisions	3450	Birefringence	4210, 4220, 7820F	Coating techniques	6855, 8115, 8160
Atomic magnetic moments	3510D	Black holes	9760L	Coatings	6855, 8115, 8160
Atomic mass	3510B	Blood	87	Coercivity	7560, 7780
Atomic orbital calculations	3120	Bolometers	0720, 0762	Coherent antiStokes Raman scattering	3320F, 4265C, 7830
Atomic orbitals	3120	Boltzmann equation	0560	Cold working	8140E
Atomic phosphorescence	3250	Bond angles	3520D	Collective accelerators	2915
Atomic physics	30	Bond lengths	3520D	Colloids	4755K, 8270
		Bond strength	3520G	Colorimetry	0760D
		Bonds (chemical)	31, 3520G, 6150L	Colour centre lasers	4255R, 4260, 6170D
		Bone	87	Colour centres	6170D, 7155, 7630M, 7850
		Bootstrapping	1150, 1240F	Colour model	1235C
		Bose-Einstein statistics	0530	Colour vision	8732N
				Comets	9650G

Classification	Classification	Classification
Commensurate-incommensurate transformations 0570, 6460, 6470K, 7780B	Dictionaries 0130K	Electrojet 94
Compaction 8120E	Dielectric function 7145G, 7820D	Electroluminescence 7860F
Complex angular momentum plane 1160	Dielectric hysteresis 7780D	Electrolysis 8245, 8630D
Composite material preparation 8120J, 8120N, 8120Q, 8120T	Dielectric losses 7740	Electrolytic polishing 8160, 8170
Composite materials 81	Dielectric measurement 0750	Electromagnetic corrections 1340H
Composite particle models 1235	Dielectric polarisation 5150, 7730	Electromagnetic decays 1340H
Compressibility 4630J, 51, 6210, 6220F, 8140L	Dielectric properties of substances 77	Electromagnetic fields 4110
Compressible flow 4740	Dielectric relaxation 5150, 7740	Electromagnetic induction 4110F
Compton effect 1360F, 6180C, 6180E, 7870	Dielectric resonance 7785	Electromagnetic interaction models 1220
Computerised tomography 8760J, 8770E	Dielectric thin films 7755	Electromagnetic wave propagation 4110H
Configuration interactions 3120T	Differential geometry 0240	Electromagnetic waves in plasma 5240D
Conformational dynamics 3520J	Diffraction gratings 4280F	Electromagnetism 0350, 4110
Conservation laws 1130	Diffraction models 1240S	Electromigration 6610, 6630Q
Constrained heat transfer 4425	Diffuse spectra 3380G	Electron affinity 3510H, 3520V
Contact lenses 8732, 8770J	Diffusion 0560	Electron beam deposition 8115G
Continuous media mechanics 4620, 4630	Diffusion in gases 5110, 5120	Electron beam effects 51, 6180F
Convection 0560, 4425, 4725Q, 5130	Diffusion in liquids 6610	Electron beams 4180D
Conversion electron spectra 2320N	Diffusion in solids 6630	Electron capture decay 2340
Correlation times 3520Y	DIM method 3120G	Electron diffraction crystallography 6114
Corrosion 8160, 8160B	Dingle temperature 7125, 7520	Electron-electron interactions 1310, 1365
Corrosion protective coatings 8160, 8160B	Diode lasers 4255P, 4260	Electron-electron scattering 1310
Corrosion testing 8170	Dirac equation 0365	Electron emission 79
Cosmic dust 9840	Direct nuclear reactions 2450	Electron energy states (condensed matter) 71
Cosmic ray interactions 1385M, 9440	Discharges (electric) 5280	Electron field emission 7970
Cosmic ray-nucleus reactions 2590, 9440R	Disclinations 6130, 6170G, 6170J, 6170L	Electron gas 0530, 7145
Cosmic rays 9440, 9870S	Discrete system mechanics 4610	Electron-hadron interactions 1360
Cosmogony 9610	Dislocations 6170G, 6170J, 6170L	Electron-hadron scattering 1360F
Cosmology 9880	Disperse systems 8270	Electron-hole drops 7135, 7855
Cottrell atmospheres 6170G, 6170J, 6170L	Dispersion hardening 8140C	Electron-hole recombination 7220J
Couette flow 4730	Dispersion relations 0210, 1120, 1150	Electron impact 3480, 7920
Coupled channel theory 2410	Displacive transformations 6375, 6470K, 7780B	Electron lenses 4180D
CP invariance 1130	Dissociation 3380G, 3480G, 8230	Electron microscopes 0780
CPA calculations 6350, 7110, 7125	Dissociation energies 3520G	Electron microscopy 0780, 6116D
CPT invariance 1130	Distorted wave Born approximations 2410	Electron-nucleus reactions 2530
Crack detection 8170	Distributed Bragg reflector lasers 4260, 4282	Electron-nucleus scattering 2530
Cracks 4630N, 6220M, 8140N	Distributed feedback lasers 4260, 4282	Electron-phonon interactions 6320K, 7138, 72, 7420
Crazing 6220M, 8140N, 8160	Domains 8130, 8140	Electron-positron interactions 1310, 1365
Creep 4630J, 6170L, 6220H, 8140L	Doping profiles 6170W	Electron-positron scattering 1310
Creep testing 8170	Dosimeters 2940, 2970	Electron probe analysis 8280
Critical points 0570, 6460, 6470, 8260	Dosimetry 2880, 8760M	Electron radiation 41
Crossing symmetries 1150	Double NMR 3335, 7670F	Electron ring accelerators 2915
Cryogenics 0720M	Double resonances 3335, 7670	Electron scattering 3480
Crystal binding 6150L	Drawing (mechanical) 6220F, 8120, 8140L	Electron sources 2925
Crystal defects 6170	Drift chambers 2940	Electron spectra 3365, 3480, 79
Crystal field theory 7170C, 7510D	Dual models 1240H	Electron spectroscopy 0780, 2930, 3365, 79, 8280
Crystal growth 6150C, 8110	Duct flow 4760	Electron spin polarisation 75
Crystal growth from melt 6150C, 8110F	Ductility 4630J, 6220F, 8140L	Electron traps 7155, 7220J
Crystal growth from solution 6150C, 8110D	Dye lasers 4255M, 4260	Electronic conduction in thin films 7360
Crystal growth from vapour 6150C, 8110B	Dynamic nuclear polarisation 3335, 7670E	Electronic density of states 7120
Crystal hyperfine field interactions 7170, 7510D	Dynamic testing 8170	Electronic excitation 3450H
Crystal inclusions 6170, 8130, 8140	Dynamical symmetries 1130	Electronic ionisation 3450H
Crystal microstructure 6170, 6480, 8130, 8140	Dynamics 0320	Electrons 1460
Crystal morphology 6150J	Ear 8734	Electrophoresis 8245
Crystal purification 8110	Earth 90	Electrophoretic coatings 6855, 8115L, 8160
Crystal structure 61	Earthquakes 9130	Electrophysiology 8730, 8732E
Crystal structure of alloys 6155H	ECG 8730, 8770	Electroplating 8115L, 8160
Crystal structure of elements 6155D, 6155F	Echelles 4280F	Electropolishing 8160, 8170
Crystal structure of inorganic compounds 6160	Eclipses 95, 9620, 9660	Electrostatic accelerators 2915
Crystal structure of organic compounds 6165	Ecology 8660	Electrostatic coatings 8115, 8160
Crystal surface and interface vibrations 6830	Education 0140, 0150	Electrostatic lenses 4180
Crystal symmetry 6150E	Educational aids 0150	Electrostatics 4110D
Crystallisation 6140, 6150C, 6470D	Educational computer use 0150	Electrostriction 7760
Crystallographic shear 6170P	EEG 8730, 8770	Electroviscous effect 6210, 6620, 8270
Crystallography 61	Eikonal models 1240P	Elemental abundance 3510B
Curie temperature 7530K, 7540, 7780B	Einstein equation 0420	Elemental semiconductors 7220, 7280C
Current algebra 1140	Einstein-Maxwell fields 0440, 0450	Elementary particle electric moments 1340F
CVD coatings 6855, 8115H, 8160	Elastic constants 6220D	Elementary particle form factors 1340F
Cyclic accelerators 2920	Elastic deformation 4630C, 6220F, 8140J	Elementary particle inclusive interactions 1310, 1360H, 1365, 1385K
Cyclotron resonance 7125, 7640	Elastic waves 0340K, 4630M, 6230	Elementary particle magnetic moments 1340F
Cyclotrons 2920	Elasticity 0340D, 4630C, 6220, 8140J	Elementary particle polarisation 1388
	Elastomers 3620, 6140K, 81	Elementary particle symmetries 1130
	ELDOR 3335, 7670K	Ellipsometry 0760F
	Election correlations 3120T	Embrittlement 6220M, 8140N
D mesons 1440	Electrets 7730	Emissivity 6590
De Haas-van Alphen effect 7125	Electric breakdown 5280, 7750	ENDOR 3335, 7670D
Debye temperature 6370	Electric charge 4110D	Energy conversion 8630
Debye-Waller factors 6370	Electric discharges 5280	Energy gap 7125, 74
Decomposition 6475, 8130	Electric domains 7780D	Energy loss of particles 2970, 6180M
Deep levels 7155	Electric fields 4110	Energy range relationships 2970
Defect electron energy states 7155	Electric moments 2110K	Energy research 86
Defibrillators 8770G, 8770J	Electrical conductivity of gases 5150	Energy resources 8610
Deformation 0340, 4630, 6220F, 8140L	Electrical conductivity of liquids 6610, 72	Energy storage 8640
Degenerate semiconductors 7220, 7280	Electrical conductivity of solids 72	Enthalpy 0570, 6550, 8260
Dendrites 6870	Electrical conductivity transitions 7260	Entropy 0570, 5130, 6550
Dendritic structure 8130, 8140	Electrical phenomena in gases 5150	Epitaxial growth 6855, 8115
Densitometry 0768	Electrical properties of substances 5150, 72, 8140R	Epitaxial layers 6855, 6860
Density measurement 0630E	Electrical variables measurement 0750	EPR 3330, 7630
Density of liquids 6210	Electricity 41	Equations of state 0570, 5110, 6410, 6430
Density of solids 6220, 8190	Electro-optical effects 3345, 5170, 7820J	Eta meson resonances 1440
Desorption 6845, 8265	Electrocardiography 8730, 8770	Eta mesons 1440
Detonation 4740, 8240	Electrochemical analysis 8280	Etching 6170J, 8160, 8170
Deuteron-nucleon interactions 1375C, 1385	Electrochemical energy conversion 8630D	Euclidean field theory 1110
Deuteron-nucleon scattering 1375C, 1385	Electrochemistry 8245	Eutectic structure 8130, 8140
Deuteron-nucleus reactions 2550	Electrodeposition 6855, 8115L, 8160, 8245	Evaporation 6470F
Deuteron-nucleus scattering 2550	Electrodynamics 0350, 4170	Evolution (biological) 8790
Deuterons 2140, 2710	Electroencephalography 8730, 8770	EXAFS 3220R, 3320R, 7870D
Diamagnetic properties of substances 5160, 7520	Electroforming 8120, 8245	Exchange interactions (electron) 7170G, 7530E
Dibaryons 1420	Electrogasdynamic conversion 8630L	Excimer lasers 4255F, 4255H, 4260
Dichroism 3345, 7820F	Electrohydrodynamics 4765	

	Classification		Classification		Classification
Excitons	7135	Gamma-ray sources	2925	Helium 3-nucleus reactions	2560
Exoelectron emission	7975	Gamma-ray sources (astronomical)	9870Q	Helium 3-nucleus scattering	2560
Exosphere	94	Gamma-ray spectra	2320, 7680	Higgs bosons	1480
Exotic atoms	3610	Gamma-ray spectroscopy	2930	High-energy cosmic ray interactions	1385M, 9440
Exotic molecules	3610	Gamma ray transitions	2320	High field effects	7220H
Explosions	4740, 4770, 8240	Garnets	7550G	High-frequency effects	7230
Extraterrestrial life	8790, 9590	Gas lasers	4255D, 4255F, 4255H, 4260	High pressure effects in solids	6250
Eye	8732	Gases	50	High pressure techniques	0735
Eye anatomy and optics	8732C	Gauge field theory	1110	High temperature techniques	0720K
Eye physiology	8732E	Gegenschein	9650D	History	0160, 0165
		Geiger counters	2940	Hodoscopes	2970
F mesons	1440	Gels	8270	Hole traps	7155, 7220J
Faddeev equation	1180	General relativity	0420	Holography	4240
Fallout	2870, 2880, 9260, 94	Generalised Huckel calculations	3120P	Hopping conduction	7220F
Faraday effect	7820L	Generator coordinate method	2160E	Hot carriers	7220H, 7230
Fatigue	4630N, 6220M, 8140N	Geodesy	9110	Hot working	8140G
Fatigue testing	8170	Geoelectricity	9125	Hubbard model	7110, 7510L
Fermi-Dirac statistics	0530	Geographical regions	9330	Huckel calculations	3120P
Fermi level	7125	Geology	9165	Humidity	51, 9260
Fermi surface	7125H	Geometrical optics	42	Hybrid reactors	2858
Fermion systems	0530	Geometry	0240	Hydroelasticity	4630C, 4630M
Ferrimagnetic properties of substances		Geophysical equipment	9385	Hydroelectric power	8610F
	75, 7550G	Geophysics	91, 92, 93	Hydrogen bonds	3520G
Ferrimagnetic resonance	7650	Geothermal energy	8610H	Hydrogen economy	8640K
Ferrites	7550G	Giant stars	9720	Hydrogen embrittlement	6220M, 8140N, 8160
Ferroacoustic resonance	7125, 7255, 7580	Ginzburg-Landau theory	7420	Hydrogen power	8640K
Ferroelectric semiconductors	7220, 7780	Glaciology	9240	Hydrogen production	8640K
Ferroelectricity	7780	Glass	4270C, 6140D, 81	Hydrogen storage	8640K
Ferromagnetic properties of substances		Glass preparation	8120P, 8120Q	Hydrology	9240
	75, 7550B, 7550C, 7550D	Glass transitions	6470P	Hydrosphere	92
Ferromagnetic resonance	7650	Glauber model	2410H	Hygrometry	0725
Few nucleon systems	2140	Glauber scattering	1180	Hypernuclei	2180
Fibre optics	4280M	Glueons	1480	Hyperon decays	1330
Fibre reinforced composites	81	GO calculations	3120	Hyperon-kaon interactions	1375I, 1385
Field emission electron microscopy		Graded Lie algebras	1130	Hyperon-kaon scattering	1375I, 1385
	0780, 6116D	Grain boundaries	6170N, 8130, 8140	Hyperon-nucleon interactions	1375E, 1385
Field emission ion microscopy	0780, 6116F	Grain size	8130, 8140	Hyperon-nucleon scattering	1375E, 1385
Field ion emission	7970	Granular structure	81	Hyperon-nucleus reactions	2580
Filtration	4755M	Graph theory	0210	Hyperon-nucleus scattering	2580
Fission breeder reactors	2850	Gravimeters	9385	Hyperon-pion interactions	1375G, 1385
Fission counters	2940	Gravitation	04, 9530	Hyperon-pion scattering	1375G, 1385
Fission-fusion reactor systems	2858	Gravitational collapse	0440, 9530, 9760	Hyperon resonances	1420
Fission power reactors	2850	Gravitational constants	0490	Hyperons	1420
Fission reactor design	2841	Gravitational experiments	0480	Hyperonic flows	4740K
Fission reactor fuel	2842	Gravitational interaction models	1225	Hypothetical particles	1480
Fission reactor fuel preparation	2842H	Gravitational radiation	0430, 0480		
Fission reactor fuel reprocessing	2842H	Gravitational waves	0430, 0480		
Fission reactor materials	2842	Gravity	0320, 9110		
Fission reactor operation	2843	Grinding	4285, 8120, 8160	II-VI semiconductors	7220, 7280E
Fission reactor safety	2844	Group theory	0220, 0365, 1130	III-V semiconductors	7220, 7280E
Fission reactor theory	2841	Guided electromagnetic wave propagation	0320, 4110H	III-VI semiconductors	7220, 7280
Fission reactor waste	2842	Guided light propagation	4280L	Image converters, detectors & intensifiers	4280Q
Fission research reactors	2850	Gunn effect	7220H	Image processing	4230, 9575
Flames	8240			Impact ionisation	7220H
Flexoelectricity	6130, 7760	H I regions	9840	Impurities	6170R, 6170T, 6170W
Flow	47	H II regions	9840	Impurity and defect absorption spectra of solids	7850
Flow birefringence	5170, 7820F	Hadron calorimeters	2970	Impurity electron states	7155
Flow instrumentation	4780	Hadron classification schemes	1240K	Inclusions	6170, 8130, 8140
Flow measurement	4780	Hadron-electron interactions	1360	Indeterminacy	0365
Flow separation	4755	Hadron-electron scattering	1360F	INDO calculations	3120N
Flow stability	4720	Hadron-hadron interactions	1375, 1385	INDOR	3335
Flow through porous media	4755M	Hadron-hadron scattering	1375, 1385	Inert gas lasers	4255F, 4260
Flowmeters	4780	Hadron-muon interactions	1360	Infrared astronomy	95
Fluctuations	0540	Hadron-muon scattering	1360F	Infrared detectors	0730, 0762
Fluid dynamics	0340Q, 47	Hadron-nucleus reactions	2540, 2580	Infrared imaging	0720, 4280Q, 8760G
Fluid kinetic theory	5110	Hadron-nucleus scattering	2540, 2580	Infrared sources (astronomical)	9870L
Fluid mechanics	0340Q, 47	Hadron-photon interactions	1360	Infrared spectra	3220B, 3320E, 7830
Fluid rheology	4660	Hadron-photon scattering	1360F	Injection lasers	4255P, 4260
Fluid transport theory	5110	Hadronic decays	1325, 1330	Injector acceleration	2910
Fluorescence	3250, 3350, 7855	Haemodynamics	8745	Inner-shell ionisation	3280H
Fluxmeters	0755	Half lives	23	Instrumentation	06, 07
Foams	8270	Hall effect	7215G, 7220M	Insulating thin films	7360H
Folding models	2410H	Hardening	8140C, 8140E, 8160	Integral radiation detectors	2970
Forming processes	8120	Hardness	4630P, 6220M, 6825, 8140N	Integrated optics	4282
Fossil fuels	8610B	Hardness testing	8170	Interacting boson model	2160E, 2160F
Fourier transform optics	4230	Harmonic generation	4265C, 4325, 4360	Interatomic angles	3520D
Fracture	4630N, 6220M, 8140N	Harmonic oscillators	0365	Interatomic distances	3520D
Fracture toughness testing	8170	Hartree-Fock approximation	2160J, 3120D, 3120G, 7110	Interatomic forces	3420
Fragmentation reactions	2450	Hawking effects	0460	Interatomic potentials	3420
Free-electron approximation	7110, 7125C	Health hazards	8750, 8760R, 8790	Interface phenomena	68, 7340
Free electron lasers	4255T, 4260	Health physics	8760	Interferometry	0760L, 9575
Free energy	0570, 5130, 64, 6550	Hearing	8734	Intergalactic matter	9850
Free molecular flows	4745	Hearing aids	8734, 8770J	Intermediate boson decay	1390
Free radicals	30, 7630R, 8230, 8250	Heat capacity	4450	Intermediate bosons	1230, 1480
Frenkel defects	6170B	Heat conduction	4410	Intermediate state	7455
Friction	4630P, 6220P, 8140P	Heat engines	8630R	Intermolecular forces	3420
Fuel cells	8630G	Heat exchanges	8630R	Intermolecular mechanics	3420
Functional analysis	0230	Heat flow	44	Intermolecular potentials	3420
Functions	0230	Heat pumps	8630R	Internal conversion	3250
Fusion reactions	2588	Heat radiation	4440	Internal friction	6170L, 6240, 8140J
Fusion reactor plasma confinement	5255	Heat transfer	44, 4725Q	Internal rotation	3520J
Fusion reactors	2852	Heat treatment	8140Q	Internal stresses	4630, 6220, 8140
		Heavily doped semiconductors	7220, 7280	Internal symmetries	1130
Galaxies	9850	Heavy ion-nucleus reactions	2570	Interplanetary matter	9460, 9650D
Galaxy	9850	Heavy ion-nucleus scattering	2570	Interstellar matter	9840
Galvanomagnetic effects	7215G, 7220M	Heavy leptons	1460	Interstitials	6170B
Gamma ray angular distributions	2320	Heavy particle spectroscopy	2930	Inversion	3520J
Gamma ray astronomy	95	Heisenberg model	7510J, 7540F	Inversion layers	7320, 7340Q
Gamma-ray effects	5170, 6180E	Helicity	1130	Ion-atom collisions	34
Gamma-ray lasers	4255	Helicons	7230	Ion beam effects	6180J
Gamma ray mixing ratios	2320			Ion beams	4180G

	Classification
Ion emission	79
Ion implantation	6170T, 6180J
Ion lasers	4255F, 4255H, 4260
Ion microscopes	0780
Ion microscopy	0780, 6116F
Ion-molecule collisions	34
Ion optics	4180G
Ion plating	8115J, 8160
Ion pumps	0730C
Ion recombination	34
Ion sources	0777, 2925
Ion-surface impact	7920N
Ionic conduction in solids	6630
Ionisation	52, 5280, 79
Ionisation counters	2940
Ionisation gauges	0730D
Ionisation potentials	3510H, 3520V
Ionoluminescence	7860H
Ionosphere	9420
Irreversible thermodynamics	0570
Ising lattices	0550
Ising model	7510H, 7540D
Isobaric analog resonances	2430
Isobaric analog states	2430
Isotope effects	3130
Isotope enrichment	2842H
Isotope separation	2842H, 3510B
Isotopes	30, 3510B
Isotropic turbulence	4725C
IV-VI semiconductors	7220, 7280

Jahn-Teller effect	3130, 7170C
Jets	4755C
Josephson effect	7450
Joule-Thomson effect	5130
Junction lasers	4255P, 4260
Jupiter	9630K
K-harmonics model	2160G
Kaon absorption	2580
Kaon-baryon interactions	1375J, 1385
Kaon-baryon scattering	1375J, 1385
Kaon capture	2580
Kaon decays	1320, 1325
Kaon-nucleus reactions	2580
Kaon-nucleus scattering	2580
Kaons	1440
Kapitza resistance	6740, 6830
Kidney	87
Kinetic theory	0520
KKR calculations	7110, 7125C
Knight shift	7660C
Knock-on reactions	2450
Knudsen flow	4745
Kondo effect	7215Q, 7520H
Kronig-Penney model	7110, 7125C

Laboratory apparatus and techniques	0150, 0660, 0670, 07
Laminar flows	4715
Laminates	81
Landau levels	7145
Laser accessories	4260
Laser beam applications	4260K
Laser beam effects	4260H, 6180B, 7920D
Laser beam modulation	4260F
Laser beam properties	4260H
Laser cavity resonators	4260D
Laser system design	4260B
Laser theory	4255B
Laser velocimeters	0630G, 4260K, 4780
Lasers	4255, 4260
Latent heat	0570, 64, 6550, 8260
Lattice constants	6150, 6155, 6160, 6165
Lattice dynamics	63
Lattice energy	6150L
Lattice field theory	1110
Lattice localised modes	6320P
Lattice phonons	6320
Lattice theory and statistics	0550
LCAO calculations	3120, 7110
Least squares analysis	0250
Lee model	1110
Lenses	4278
Lepton decays	1335
Lepton electromagnetic interactions	1310
Lepton-lepton scattering	1310
Lepton mass	1460
Lepton-nucleus reactions	2530
Lepton-nucleus scattering	2530
Lepton parity	1460
Lepton spin	1460
Lepton weak interactions	1310
Leptonic decays	1320, 1330, 1335
Leptons	1460
Level crossing	3280B, 3380B
Light	42
Light absorption	4210, 4220, 5170, 78
Light coherence	4210, 4220, 4250

Light interference	4210, 4220
Light interferometry	0760L
Light modulation	4260F, 4280K
Light polarisation	4210, 4220
Light propagation	4210, 4220
Light scattering	4210, 4220, 5170, 78
Light sensitive materials	4270G
Light sources	4272
Light transmission	4210, 4220
Lightning	9260
Linear accelerators	2915
Lipid bilayers	8720, 8725
Liquid crystal phase transformations	6130, 6470M
Liquid crystals	6130
Liquid helium 3-4 mixtures	6760
Liquid helium-3	6750
Liquid helium	67
Liquid lasers	4255M, 4260
Liquid metal embrittlement	6220M, 8140N, 8160
Liquid phase epitaxial growth	6855, 8115L
Liquid semiconductors	6125, 7120, 7220, 7280P
Liquid structure	6120, 6125
Liquid theory	6120, 6130
Liquid-vapour transformations	6470F
Liver	87
Localized electron states	7150
Lorentz invariance	1130
Lorentz transformation	0330
Low energy electron diffraction	6114H, 6820
Low mass nuclear reactions	2510
Low temperature techniques	0720M
LPE	6855, 8115L
Lubrication	4630P, 6220P, 8140P
Luminescence	3250, 3350, 7855, 7860
Lung	87

Mach number	4740
Macromolecules	3620
Magnetic aftereffect	7560L
Magnetic anisotropy	7530G
Magnetic annealing	7560N, 8140E
Magnetic breakdown	7125H
Magnetic bubbles	7570K
Magnetic circular dichroism	3345C, 7820L
Magnetic cooling	0720M, 7530S
Magnetic domains	7560C, 7570K
Magnetic fields	4110
Magnetic hysteresis	7560E
Magnetic lenses	4180
Magnetic materials	75, 7550
Magnetic monopoles	1480
Magnetic phenomena in gases	5160
Magnetic properties of substances	5160, 75, 8140R
Magnetic relaxation	5160, 76
Magnetic resonance	3220B, 3325, 76
Magnetic resonance spectrometers	0758
Magnetic semiconductors	7220, 75
Magnetic storms	9430
Magnetic thin films	7570
Magnetic transitions	7530K, 7540
Magnetic traps	5255
Magnetic variables measurement	0755
Magnetisation	7430C, 7560
Magnetism	41, 5160, 75
Magneto-optical effects	3345, 5160, 5170, 7820L

Magnetoacoustic effects	5140, 5160, 7125, 7255, 7580
Magnetocaloric effects	7530S
Magnetocardiography	8740, 8760D
Magnetoelastic effects	7580
Magnetolectric effects	5150, 5160, 7580
Magnetohydrodynamic conversion	5230, 8630L
Magnetohydrodynamic waves	4765, 5235, 7230
Magnetohydrodynamics	4765, 5230
Magnetomechanical effects	7580
Magnetometers	0755, 9385
Magnetoresistance	7215G, 7220M
Magnetosphere	9430
Magnetostatic waves	75
Magnetostatics	4110D
Magnetostriiction	7580
Magnetrons	0750
Magnons	7530D, 7650
Majorana-Weyl fields	0450
Mandelstam representation	1150
Many-body problems	05, 9510C
Many-body reaction theory	2410
Marine geology	9150
Markov processes	0540
Mars	9630G
Martensitic transformations	6470K, 8130K
Masers	4252
Mass differences	1340D
Mass formulae	1240K, 1270
Mass spectra	3510B, 3520X
Mass spectrometers	0775

Mass spectroscopic chemical analysis	Classification 8280
Mass transfer	0560
Materials preparation	8120
Materials science	81
Materials testing	8170
Mathematical computing	0270
Mathematics	02
Maxwell equations	0350, 4110
MBE	6855, 8115G
Measurement	06
Mechanical birefringence	4210, 7820F
Mechanical contact	4630P
Mechanical energy storage	8640C
Mechanical impact	4630P
Mechanical properties of substances	4630, 4660, 62, 8140
Mechanical property measurement	4630R
Mechanical strength	4630, 6220, 8140
Mechanical testing	8170
Mechanical waves	4630M, 6230
Mechanics	0320, 0340, 46
Mechanoreception	8738
Medical diagnosis	8770E
Medical effects of radiation	8750
Medical physics	87
Medical uses of radiation and radioactivity	8760
Medicine	87
Meissner effect	7430C
Melting	6470D
Membrane biophysics	8720
Membranes	5120, 6610, 8265, 8720, 8725
Mercury (planet)	9630D
Meson absorption	2580
Meson capture	2580
Meson decays	1320, 1325
Meson electric moments	1340F, 1440
Meson magnetic moments	1340F, 1440
Meson mass	1440
Meson-meson interactions	1375L, 1385
Meson-meson scattering	1375L, 1385
Meson-nucleon interactions	1375, 1385
Meson-nucleon scattering	1375, 1385
Meson-nucleus reactions	2580
Meson-nucleus scattering	2580
Meson parity	1440
Meson production	1360K, 1365, 1375, 1385
Meson resonance production	1360M, 1365, 1375, 1385
Meson resonances	1440
Meson spin	1440
Mesons	1440
Mesosphere	9260
Metal corrosion	8160B
Metal-insulator boundaries	7340N
Metal-insulator-metal structures	7340R
Metal-insulator-semiconductor structures	7340Q
Metal-insulator transition	7130
Metal oxidation	8160B
Metal-semiconductor-metal structure	7340S
Metallography	8170
Metallurgy	81
Metamagnetism	7530K
Meteorites	9650M
Meteorology	9260
Meteors	9650K
Microphones	4385, 4388
Microscopes	0760P
Microtrons	2920
Microwave-optical double resonance	3335H, 7670H
Microwave spectra	3220B, 3320B, 7870G
Microwave spectrometers	0758, 0765
Mictomagnetism	7540
MINDO calculations	3120N
Mineralogy	9160
Mirrors	4278
Mixed conductivity	7260
Mixed state	7460E
Mixed valence states	7170C
Mixing	6475
Moderators	2842
Moire fringes	0760, 4210
Molecular beam epitaxial growth	6855, 8115G
Molecular beam reactions	8240D
Molecular beams	3440, 3450, 3580, 8240D
Molecular biophysics	8715
Molecular clusters	3640
Molecular collisions	34
Molecular configurations	3520B
Molecular dissociation	3380G, 3480G
Molecular dynamics	3520Y
Molecular electric moments	3520M
Molecular electron correlations	3120T
Molecular electron impact ionisation	3480G
Molecular electronic states	31
Molecular fine structure	3520S
Molecular fluorescence	3350
Molecular hyperfine interactions	3130
Molecular hyperfine structure	3520S
Molecular inelastic collisions	3450
Molecular magnetic moments	3520M

	Classification		Classification		Classification
Molecular magnetic susceptibility	3520M	Nonhomogeneous flows	4755	Oil	8610B
Molecular moments	3520M	Nonlinear acoustics	4325	Omega mesons	1440
Molecular nuclear coupling	3325	Nonlinear field theory	1110	One-dimensional conductivity	7215N
Molecular orbitals	3120	Nonlinear optics	4265	One-meson exchange models	1240R
Molecular orbitals calculations	3120	Nonlinear optics theory	4265B	Opalescence	7820
Molecular phosphorescence	3350	Nonlinear symmetries	1130	Optical beam splitters	4280
Molecular photodissociation	3380G	Nonlocal field theories	1110	Optical bistability	4265, 4280
Molecular physics	30	Normalising	8140G	Optical choppers	4280E
Molecular polarisability	3520M	Novae	9730	Optical coatings	4270, 4278H, 4280
Molecular predissociation	3380G	Nozzles	4755E	Optical coherent transients	4265G
Molecular rotation	3310, 3520P	NQR	3325, 7660G	Optical collimators	4280
Molecular rotation-vibration	3310, 3450E, 3520P	Nuclear backbending	2110, 2110H	Optical communication devices	4280S
Molecular solids	3170K	Nuclear binding energy	2110D	Optical constants	5170, 7820D
Molecular spectra	3320	Nuclear bombardment target	2925	Optical couplers	4280L, 4280M
Molecular structure	31, 3520B	Nuclear charge	2110F	Optical deflectors	4280E
Molecular symmetry	3520B	Nuclear chemistry	8255	Optical design techniques	4278, 4280
Molecular transitions	3110	Nuclear cluster model	2160G	Optical diaphragms	4280E
Molecular vibration	3310, 3520P, 6320, 7830	Nuclear collective levels	2110	Optical dispersion	4210, 4220, 5170, 7820
Molecule-surface impact	34, 7920N, 7920R	Nuclear collective models	2160E	Optical double resonance	3335, 7670H
Molecules	30	Nuclear collective resonances	2430	Optical elements	4278, 4280
Monochromators	0785, 4280D	Nuclear Coulomb effects	2110	Optical fabrication	4285
Monolayers	6845, 8265	Nuclear cranking model	2160E	Optical fibres	4280M
Monte Carlo methods	0250	Nuclear decay	23	Optical films	4270, 4278, 4280, 7865
Moon	9620	Nuclear deformation	2110F	Optical filters	4280B, 4280C
Morin temperature	7530K, 7540	Nuclear electric moments	2110K	Optical frequency conversion	4265C
Mossbauer effect	2430, 2520, 3340, 7680	Nuclear electromagnetic transitions	2320	Optical glass	4270C
Muffin-tin potential	7110, 7125C	Nuclear electronics	2960	Optical gratings	4280F
Multi-Regge models	1240S	Nuclear emulsions	2940	Optical harmonic generation	4265C
Multiperipheral models	1240S	Nuclear energy	8610N	Optical images	4230
Multiphase flow	4755K	Nuclear energy level lifetimes	2320C	Optical information processing	4230
Multiphoton spectra	3280K, 3380K	Nuclear energy level schemes	2110, 2110M	Optical instruments	0760, 4278, 4280
Multiple stars	9780	Nuclear energy level transitions	2320	Optical Kerr effect	4265J
Multiwire proportional chambers	2940	Nuclear energy levels	2110, 2110M	Optical materials	4270
Muon absorption	2530	Nuclear energy states	2110, 2110M	Optical model	1240P
Muon capture	2340, 2530	Nuclear engineering	28	Optical modulation	4260F, 4280K
Muon-hadron interactions	1360	Nuclear engineering computing	2841, 2980	Optical monochromators	4280D
Muon-hadron scattering	1360F	Nuclear explosions	2870	Optical parametric devices	4265C
Muon-nucleus reactions	2530	Nuclear fireballs	2460	Optical phase conjugation	4265F
Muon-nucleus scattering	2530	Nuclear fission	2475, 2585	Optical phenomena in gases	5170
Muon spin rotation	7690	Nuclear forces	2130	Optical prisms	4278, 4280
Muons	1460	Nuclear form factors	2110F	Optical projectors	4278
Muscle	87	Nuclear g-factors	2110K	Optical properties of substances	5170, 78, 8140T
Musical acoustics	4375	Nuclear giant resonances	2430	Optical pumping	3280B, 3380B, 4255, 7845
		Nuclear hole states	2110	Optical rangefinders	4280
N/D method	1150	Nuclear information processing	2980	Optical resolving power	4230
NDT	8170	Nuclear instrument control	2980	Optical rotation	4210, 7820E
Nebulae	9840	Nuclear instrumentation	2880, 29	Optical saturable absorption	4265G
Neel temperature	7530K, 7540	Nuclear isobaric spin	2110H	Optical saturation	4265G
Negative resistance	7220H	Nuclear magnetic moments	2110K	Optical self-focusing	4265J
Nematic liquid crystals	6130, 6470M	Nuclear magnetic resonance	3320B, 3325, 7430G, 7660	Optical self-induced transparency	4265G
Neptune	9630T	Nuclear mass	2110D	Optical shutters	4280E
Neurophysiology	8730, 8732E	Nuclear matrix elements	2320	Optical sources	4272
Neutral currents	1140, 1230	Nuclear matter	2165	Optical storage	4230, 4240
Neutrino interactions	1315	Nuclear medicine	8760J, 8770	Optical susceptibility	77, 78
Neutrino-nucleus reactions	2530	Nuclear models	2160	Optical systems	0760, 4278, 4280
Neutrino-nucleus scattering	2530	Nuclear optical model	2410H	Optical telescopes	0760, 4278, 9555
Neutrino scattering	1315	Nuclear Overhauser effect	3335	Optical testing	4278, 4285
Neutrinos	1460	Nuclear parity	2110H	Optical transfer function	4230
Neutron absorption	2540, 2820	Nuclear physics	20	Optical waveguide components	4280L
Neutron diffraction crystallography	6112	Nuclear polarisation in liquids and solids	7660	Optical waveguides	4280L
Neutron diffraction examination of materials	6112, 7525	Nuclear power	28	Optical windows	4280E
Neutron diffusion	2820	Nuclear pumped lasers	4255, 4260	Optical workshop techniques	4285
Neutron effects	51, 6180H	Nuclear quadrupole resonance	3325, 7660G	Optical zone plates	4280B
Neutron-hyperon interactions	1375E, 1385	Nuclear radius	2110F	Optics	0760, 0765, 42
Neutron-hyperon scattering	1375E, 1385	Nuclear reaction models	2410	OPW calculations	7110, 7125C
Neutron induced fission	2540, 2585	Nuclear reactions	24, 25	Orbital calculation methods	3120
Neutron-kaon interactions	1375J, 1385	Nuclear resonance reactions	2430	Order-disorder transformations	6150K, 6460, 6470K, 8130H
Neutron-kaon scattering	1375J, 1385	Nuclear resonances	2430	Orthotics	8770J
Neutron-meson interactions	1375, 1385	Nuclear rotational bands	2110	Otology	8730
Neutron-meson scattering	1385	Nuclear shape	2110F	Overhauser effect	3325
Neutron moderation	2820	Nuclear shell model	2160C	Oxidation	8160, 8160B, 8230
Neutron-neutron interactions	1375C, 1385	Nuclear single particle levels	2110	Ozonosphere	9260
Neutron-neutron scattering	1375C, 1385	Nuclear size	2110H		
Neutron-nucleus reactions	2540	Nuclear spectroscopic factors	2110J		
Neutron-nucleus scattering	2540	Nuclear spin	2110H		
Neutron physics	2820	Nuclear statistical models	2460		
Neutron-pion interactions	1375G, 1385	Nuclear structure	21	P invariance	1130
Neutron-pion scattering	1375G, 1385	Nuclear structure models	2160	p-n junctions	7340L
Neutron-proton interactions	1375C, 1385	Nuclear transition probabilities	2320C	Pacemakers	8770J
Neutron-proton scattering	1375C, 1385	Nucleation	6150C, 64, 6855, 8140	Pade scattering	1180
Neutron radiative capture	2540	Nuclear decays	1330	Palaeomagnetism	9125
Neutron radiography	8170, 8760J	Nucleon-hyperon interactions	1375E, 1385	Paramagnetic properties of substances	5160, 7520
Neutron scattering	2820	Nucleon-hyperon scattering	1375E, 1385	Paramagnetic resonance	3330, 7630
Neutron sources	2925	Nucleon-kaon interactions	1375J, 1385	Partially conserved currents	1140
Neutron spectroscopy	2930	Nucleon-kaon scattering	1375J, 1385	Particle beam diagnostics	2925
Neutron stars	9760J	Nucleon-meson interactions	1375, 1385	Particle beams	4180
Neutron transport	2820	Nucleon-meson scattering	1375, 1385	Particle optics	4180
Neutrons	1420	Nucleon-nucleon interactions	1375C, 1385	Particle telescopes	2970
Nightglow	9410Q	Nucleon-nucleon scattering	1375C, 1385	Particle track visualisation	2940
Nilsson model	2160C	Nucleon-nucleus reactions	2540	Parton models	1235H
NMR	3220B, 3325, 7430G, 7660	Nucleon-nucleus scattering	2540	Passivation	8160
Nomenclature and symbols	01	Nucleon-pion interactions	1375G, 1385	Paste rheology	4660
Nomograms	0260	Nucleon-pion scattering	1375G, 1385	Patient care	8770G
Non-Abelian fields	1110	Nucleons	1420	Patient diagnosis	8770E
Non-Newtonian dynamics	4750	Numerical analysis	0260	Patient monitoring	8770
Non-Newtonian flows	4750	Numerical methods	0260	Patient treatment	8770G
Noncollisional ionisation	3490	Observatories	9545	PCILO calculations	3120N, 3120T
Noncrystalline state structure	6140	Occultations	9510	Peculiar stars	9730
Nondestructive testing	8170	Oceanography	9210	Peierls instability	7130, 7215N
Nonequilibrium flows	4770	Ohmic contacts	7340	Peripheral models	1240R
				Permittivity	5150, 7720
				Petrology	9160, 9165

	Classification
Phase diagrams	6470, 8130B, 8130D
Phase equilibrium	0570, 64, 8130B, 8130D
Phase transformations	0570, 64, 8130
Phi mesons	1440
Philosophy of science	0170
Phonon interactions	6320
Phosphorescence	3250, 3350, 7855
Phosphorescence microwave double resonance	3335H, 7670H
Photoacoustic effect	4388, 6265
Photocapacitance	7240
Photocathodes	7960
Photochemistry	8250
Photochromism	7820
Photoconductivity	7240
Photodetachment	3280F, 3380E
Photodiodelectric effect	7240
Photodisintegration	2520
Photoelasticity	4630C, 4630R, 7820F, 8140J
Photoelectric conversion	8630J
Photoelectricity	7240
Photoelectrochemical conversion	8630K
Photoelectromagnetic effects	7240
Photoelectron spectra	3280F, 3365, 7960
Photoemission	7960
Photofission	2520, 2585
Photography	0768, 8250, 9575
Photoionisation	3280F, 3380E
Photoluminescence	3250, 3350, 7855
Photolysis	8250
Photomagnetic effect	7520, 7590
Photometry	0760D, 9575
Photomultipliers	0760D, 2940
Photon counting	0762, 4250
Photon echo	4265G
Photon-hadron interactions	1360
Photon-hadron scattering	1360F
Photon-nucleus scattering	2520
Photon sources	2925
Photons	1480
Photonuclear reactions	2520
Photoplasticity	4630J, 6220F, 8140L
Photorefractive effect	4240, 4270G, 7820
Photosphere	9660
Photosynthesis	8630P, 8725
Photothermal conversion	8630S
Photovoltaic effects	7240
Physical chemistry	82
Physical optics	42
Physiological models	8710
Physiological optics	8732
Physiology	87
Pick-up reactions	2450
Piezoelectricity	7760
Piezorefractance	7820H
Piezoresistance	7220F
Pinch effect	5255
Pion absorption	2580
Pion-baryon interactions	1375G, 1385
Pion-baryon scattering	1375G, 1385
Pion capture	2580
Pion decays	1320, 1325
Pion-nucleus reactions	2580
Pion-nucleus scattering	2580
Pions	1440
Pipe flow	4760
Plane wave Born approximations	2410
Planetary nebulae	9840
Planets	9630, 9780
Plasma	52
Plasma antennas	5240F
Plasma applications	5275
Plasma arc spraying	5275, 8115, 8160
Plasma beam interactions	5240M
Plasma collision processes	5220F, 5220H
Plasma confinement	5255
Plasma deposited coatings	6855, 8115J, 8160
Plasma deposition	8115J
Plasma devices	5275
Plasma diagnostics	5270
Plasma electromagnetic wave propagation	5240D
Plasma elementary processes	5220
Plasma equilibrium	5255
Plasma-filled waveguides	5240F
Plasma flow	5230
Plasma heating	5250
Plasma heating by laser beam	5250J
Plasma heating by shock wave	5250L
Plasma heating by wire explosion	5250L
Plasma magnetohydrodynamics	5230
Plasma oscillations	5235
Plasma production by laser beam	5250J
Plasma production by shock wave	5250L
Plasma production by wire explosion	5250L
Plasma radiation	5225P
Plasma sheaths	5240K
Plasma shock waves	5235T
Plasma simulation	5265
Plasma sources	5250
Plasma transport processes	5225F
Plasma turbulence	5235R
Plasma-wall interactions	5240H

	Classification
Plasma waves	5235
Plasmons	7145G, 7230
Plastic crystals	6150, 7660
Plastic deformation	4630J, 6220F, 8140L
Plastic detectors	2940
Plasticity	4630J, 6220F, 8140L
Plastics	6140K, 81
Plate tectonics	9145
Pleochroism	3345, 7820F
Pluto	9630T
Pneumodynamics	8745
Poincare invariance	1130
Point contacts	7340
Point defects	6170B, 6170D, 6170E, 7850
Poiseuille flow	4760
Poisson ratio	6220D, 8140J
Polar semiconductors	7220, 7280
Polarimeters	0760F, 2975
Polarimetry	2975
Polarised bombardment targets	2925
Polarised nuclear reactions	2470
Polarised sources	2925
Polaritons	6320, 7136, 7830
Polarography	8280
Polarons	7138
Polishing	4285, 8160, 8170
Pollution	8670, 9220, 9260
Polymer films	6140K, 6855, 81
Polymer melts	4750, 6125
Polymer molecules	3620
Polymer preparation	8120S, 8120T
Polymer reactions	8235
Polymer solutions	4750, 6125
Polymerisation	8235
Polymers	3620, 6140K, 81
Polymorphic transformations	6150K, 6470K, 8130H
Polymorphism	6150K, 6155, 6160, 6165
Pomeranchuk poles	1240M
Population II stars	9720
Population inversion	3280B, 3380B, 4250, 4255, 7845
Porous materials	4755M, 81
Position sensitive detectors	2940
Positron annihilation in liquids and solids	6180F, 7125, 7870B
Positron states	7165
Positrons	1460
Potential energy curves	3190
Potential energy surfaces	3170F, 8220K
Potential models	1240Q
Potts model	0550
Powder metallurgy	8120E, 8120G
Powder spraying	8115, 8160
Powder technology	8120E
Powders	4755K, 8120
PPP calculations	3120P
Pre-equilibrium model	2460
Preacceleration	2910
Precipitation	6475, 8130M, 8260
Precipitation hardening	8140C
Primary cells	8630E
Probability theory	0250
Proportional counters	2940
Prosthetics	8770J
Protective coatings	8160
Proteins	3620, 8715
Proton absorption	2540
Proton-hyperon interactions	1375E, 1385
Proton-hyperon scattering	1375E, 1385
Proton-kaon interactions	1375J, 1385
Proton-kaon scattering	1375I, 1385
Proton magnetic resonance	3325, 7660
Proton-meson interactions	1375, 1385
Proton-meson scattering	1375, 1385
Proton-neutron interactions	1375C, 1385
Proton-neutron scattering	1375C, 1385
Proton-nucleus reactions	2540
Proton-nucleus scattering	2540
Proton-pion interactions	1375G, 1385
Proton-pion scattering	1375G, 1385
Proton-proton interactions	1375C, 1385
Proton-proton scattering	1375C, 1385
Proton radiative capture	2540
Protons	1420
Pseudopotential methods	7110, 7125C
Psi mesons	1440
Pulsars	9760G
Pulsatile flow	4760
Pulse amplifiers	2960
Pulse counting	2960
Pulse height analysers	2960
Pulse shaping circuits	2960
Pyroelectricity	7770
Pyrometers	0720, 0762
Q-switching	4260F
QCD	1235C
QED	1220
Quadrupole moments	2110K, 3520M, 7660
Quantum electrodynamics	1220
Quantum field theory	0370, 1110

	Classification
Quantum fluids	0530, 67
Quantum gravity	0460
Quantum measurement theory	0365
Quantum mechanics	0365
Quantum optics	4250
Quantum statistical mechanics	0530
Quark confinement	1235C
Quark models	1235
Quarks	1480
Quasars	9870J
Quenching (thermal)	8140G
Radiation angular correlations	2970
Radiation belts	9430
Radiation chemistry	8250
Radiation coincidence measurements	2970
Radiation detectors	0762, 2940, 2970
Radiation effects	5190, 6180
Radiation gas dynamics	4770
Radiation hardening	8140C
Radiation measurement	2970
Radiation monitoring	2880, 2940, 2960, 2970, 8760P
Radiation monitoring electronics	2960
Radiation protection	2880, 8760P
Radiation spectrometers	2930
Radiation spectroscopy	2930
Radiation therapy	8760B, 8760G, 8760J, 8770G
Radiative effects	3130
Radiative flows	4770
Radiative transfer	0560, 4440, 9265, 9530, 9710
Radioactive dating	0790, 9385
Radioactive decay periods	23
Radioactive decay schemes	23
Radioactive pollution	8670, 8760R
Radioactive sources	2925
Radioactive tracers	2925, 8760J, 8760L
Radioactive waste	2842
Radioactivity	23, 2880
Radioactivity measurement	2970
Radioastronomy	95
Radiobiology	8750G
Radiochemistry	8255
Radiofrequency spectra	3220B, 3320B, 7870G
Radiofrequency spectrometers	0758, 0765
Radiography	0785, 8170, 8760J, 8770E
Radioisotope scanning and imaging	8760J, 8770E
Radiometry	0760D
Radioresources (astronomical)	9870D
Rain	9260
Raman lasers	4255, 4260, 4265C
Raman spectra	3320F, 7830
Random noise	0250, 7270
Random phase approximations	2160J, 7110, 7145
Random processes	0540
Rarefied gas dynamics	4745
Rayleigh scattering	3320F, 4265C, 7835
Reaction kinetics	8220, 8240
Reactive flows	4770
Recrystallisation	6150C, 8110J, 8140E
Reflection high energy electron diffraction	6114H
Reflectivity	42, 4210, 4220, 5170, 78
Reflectometry	0760H
Refractive index	4110H, 4210, 4220, 5170, 7820D
Refractometers	0760H
Refractories	81
Refractory preparation	8120L, 8120N
Regge poles	1160, 1240M
Relativistic band structure calculations	7110, 7125C
Relativistic effects	3130, 3510F
Relativistic field theory	1110
Relativistic flows	4775
Relativistic mechanics	0330
Relativistic plasmas	5260
Relativistic scattering theory	1180
Relativity	04, 9530
Remote sensing	8670L, 9385
Renormalisable fields	1110
Replica techniques	0780, 6116, 68
Resistance thermometers	0720D
Resource letters	0130R
Reverberation	4355
Reviews	0130R
Rheopexy	4660
Rho mesons	1440
Ring lasers	4260D
Rock magnetism	9160
Rotational energy transfer	3450E
Rotational flow	4730
Rotational isomerism	3520J
RPA calculations	2160J, 7110, 7145
S-matrix theory	1120
SAMO method	3120G

	Classification		Classification		Classification
Satellites	9480, 9630	Spin-spin relaxation	3325, 3330, 76	Thermal conductivity	0570, 0720, 4450, 5130, 6660, 6670, 7215C, 7215E, 7430E
Saturn	9630M	Spin waves	7530D, 7650	Thermal diffusion in gases	5110, 5120
Scaling phenomena	1130	Spinoidal decomposition	6475, 8130	Thermal diffusion in liquids	4725J, 6610
Scanning radiography		Spontaneous fission	2585	Thermal energy conversion	8630R
	0785, 8170, 8760J, 8770E	Spontaneous symmetry breaking	1130	Thermal energy storage	8640F
Scattering	0365, 0380	Spray coating techniques	8115, 8160	Thermal expansion	5130, 6570
SCF calculations	3120, 7110, 7125, 7170	Sputter etching	8160	Thermal processes	44
Schlieren devices	4280	Sputtered coatings	6855, 8115C	Thermal properties	4450
Schottky defects	6170B	Sputtering	7920, 8115C	Thermal properties of gases	5130
Schottky effect	7330, 7940	Stacking faults	6170P	Thermal property measurement	4450
Schrodinger equation	0365	Stark effect	3260, 3345B, 7170E, 7820J, 7830, 7840	Thermal quenching	8140G
Schwinger source theory	1110	Stars	97	Thermally stimulated currents	7220J, 7730
Scintillation counters	2940	Statistical models	1240E	Thermionic conversion	8630N
Second sound	67	Statistical physics	05	Thermionic emission	7940
Secondary cells	8630F	Statistics	0250	Thermo-optical effects	5130, 5170, 7820N
Secondary emission	7920	Stellar clusters	9820	Thermochemistry	82
Segregation	6475, 8130M	Stellar motion	9810	Thermocouples	0720, 0762
Seismology	9130	Stellarators	5255, 5275	Thermodynamic properties	6550
Self-diffusion	51, 66	Stereochemistry	3520B	Thermodynamics	0570, 4460
Self-focusing	4265J	Stimulated Brillouin scattering	4265C	Thermoelasticity	4630C, 4660, 6220D, 8140J
Self-induced transparency	4265G	Stimulated emission	4250, 4255, 7845	Thermoelectric conversion	8630M
Semiconductor counters	2940	Stimulated light scattering	4265C	Thermoelectricity	7215J, 7220P
Semiconductor doping	6170T	Stimulated Raman scattering	4265C	Thermoluminescence	7860K
Semiconductor-electrolyte boundaries	7340M	Stochastic processes	0250, 0540	Thermoluminescent dating	0790, 9385
Semiconductor growth		Storage rings	2920	Thermoluminescent dosimeters	2940, 2970
	6150C, 6855, 8110, 8115	Strain gauges	0710, 4630R	Thermomagnetic effects	7215H, 7220N
Semiconductor-insulator boundaries	7340Q	Strange particles	1420, 1440	Thermomechanical treatment	8140G
Semiconductor junction lasers	4255P, 4260	Stratified flow	4755H	Thermometers	0720D
Semiconductor junctions	7340L	Stratosphere	1480	Thermopiles	0720, 0762
Semiconductor materials	7280	Streamer chambers	2940	Thickness measurement	0630C
Semiconductor metal boundaries	7340N	Stress corrosion cracking	6220M, 8160, 8160B	Thin films	6855, 6860, 7360, 7570, 7755, 7865
Semiconductor thin films	7360F	Stress relaxation	4630J, 6240, 8140J	Thixotropy	4660
Semimicrobial NDO calculations	3120N	Stress/strain relations	46, 6220F, 8140L	Thomas-Fermi-Dirac model	3120L
Semileptonic decays	1320, 1330, 1335	Stripping reactions	2450	Thomas-Fermi model	2160, 3120L, 7145J
Semimetallic thin films	7360F	Strong gravity	0460	Tidal energy	8610F
Sensory aids	8770J	Strong interaction models	1240	Tides	9110, 9210, 9410
Sets	0210	Structure functions	1340F	Time measurement	0630F
Shape memory effects	6220F, 8130K, 8140L	SU ₂ theory	1130	Time-of-flight spectrometers	0775, 2930
Shear modulus	6220D, 8140J	SU ₃ theory	1130	Tokamaks	5275
Shear turbulence	4725F	SU ₄ theory	1130	Topology	0240
Shielding	2842, 2880	Sublimation	6470H	Track chambers	2940
Shock waves	4630M, 4740N, 6250	Subsonic flows	4740D	Transducers	0670, 4388
Sintering	8120E	Substrates	6855, 6860, 8115	Transition radiation	41, 6180, 7870
Size effect	7230, 7360	Sum rules	1150	Transits	9510
Skin effect	7230	Sun	9660	Transonic flows	4740H
Slip	4630J, 6170L, 6220F, 8140L	SU _N theory	1130	Transport processes	0560
Slip flows	4745	Superconducting materials	7470	Triboelectricity	7340B
Slug flow	4755K	Superconducting semiconductors	7470	Triboluminescence	7860M
Smectic liquid crystals	6130, 6470M	Superconducting thin films	7360K	Triplet state	3150, 7135
Societal aspects	0175	Superconductive tunnelling	7450	Triton-nucleus reactions	2550
Solar absorbers	8630S	Supercooling	64	Triton-nucleus scattering	2550
Solar cells	8630J	Superexchange interactions	7530E	Tritons	2140, 2710
Solar collectors	8630S	Superfluidity	0530, 67	Troposphere	9260
Solar energy	8610K	Superfingant stars	9720	Tube flow	4760
Solar energy concentrators	4278, 8610K	Supergravity	0465	Tunnelling	7340, 7450
Solar nebula	9610	Superionic conducting materials	6630	Turbidity	4220, 8270, 9210, 9265
Solar system	96	Superlattices	6155, 6160, 6165, 7340L, 8130, 8140	Turbulence generated noise	4725M
Solar wind	9440H, 9460, 9660	Supernova remnants	9840	Turbulent diffusion	4725J
Solar helium	6780	Supernovae	9760B	Turbulent flows	4725
Solid instability	4630L	Superparamagnetism	75	Twilight	9260, 94
Solid lasers	4255R, 4260	Superradiance	3290, 4250, 7845	Twinning	6170N
Solid-liquid transformations	6470D	Supersonic flows	4740K	Two-phase flow	4755K
Solid rheology	4630	Supersymmetry	1130		
Solid solubility	6475, 8130	Surface acoustic wave devices	4360, 4385, 4388	Ultrasonic absorption	43, 5140, 6260, 6265
Solid solution hardening	8140C	Surface acoustic waves	4320, 4325, 4360, 4388, 6825	Ultrasonic applications	43
Solid state detectors	2940	Surface carrier scattering	7325	Ultrasonic relaxation	5140, 6280
Solid state phase transformations		Surface electron states	7320	Ultrasonic velocity	43, 5140, 6260, 6265
	6470K, 8130H	Surface energy	6810, 6840	Ultrasonic waves	43, 5140, 6260, 6265
Solid-state plasma	7230	Surface hardening	8160, 8160B	Ultraviolet spectra	3220J, 3320L, 3320N, 7840
Solid-vapour transformations	6470H	Surface ionisation	7330, 79	Umklapp process	6320H, 6320K
Solidification	6470D, 8130F	Surface reactions	8270	Underwater sound	4330, 9210
Soils	4755K, 8270	Surface structure	6820	Undulator radiation	4170
Solubility	6475, 8130	Surface tension	6810	Unified field theories	0450, 1210
Solutions	6120, 6125, 6475	Surface texture	6820	Units (measurement)	0620F
Solvent effects	3170D	Surface treatment	8160, 8160B	Upsilon mesons	1440
Sonar	4330, 9210, 9385	Surgery	8770G	Uranus	9630T
Sonoluminescence	7860M	Suspensions	8270		
Sorption	6845, 8265	Synchrocyclotrons	2920	Vacancies (crystal)	6170B
Space charge	52, 5280, 7750	Synchrotron radiation	4170, 4272	Vacuum apparatus	0730
Space groups	6150E	Synchrotrons	2920	Vacuum deposited coatings	6855, 8115G
Space physics	94	Synergetic fission reactor systems	2858	Vacuum deposition	8110B, 8115G, 8115H, 8115J
Space research	9480			Valence bond calculations	3120R
Space-time configurations	04	T invariance	1130	Van de Graaff accelerators	2915
Spallation breeder reactors	2858	Tachyons	1480	Van de Graaff generators	0750
Spallation reactions	2450, 2540	Tandem accelerators	2915	Van der Waals forces	3420
Spark chambers	2940	Teaching	0140, 0150	Vaporisation	6470F
Spatial filters	4280B	Tectonics	9145	Vapour deposited coatings	6855, 8115C, 8115G, 8115H, 8115J
Special relativity	0330	Telescopes	0760, 4278, 9555	Vapour deposition	8110B, 8115C, 8115G, 8115H, 8115J
Specific heat	4450, 5130, 6520, 6540, 7430E, 7540	Tempering	8140G	Vapour phase epitaxial growth	6855, 8115G, 8115H, 8115J
Speckle	4220	Tensile strength	6220F, 8140L	Variable stars	9730
Spectra	32, 3320, 78	Terrestrial atmosphere	9260, 94	Vector meson dominance model	1240V
Spectrochemical analysis	8280	Terrestrial electricity	9125	Velocity measurement	0630G
Spectrophotometers	0760D, 0765	Terrestrial heat	9135	Veneziano model	1240H
Spectroscopy	0758, 0765, 0775, 9575	Textbooks	0130M, 0130P	Venus	9630E
Speech	4370, 8736	Texture	8140E	Vibrating bodies	4630M
Speech communication	4370	Thermal blooming	4265J		
Spheroidizing	8140G				
Spin density waves	75				
Spin glasses	7540				
Spin-lattice relaxation	76				
Spin-orbit interactions	2110, 2160, 31, 7170E				
Spin-phonon interactions	6320, 75, 76				

	Classification
Vibrational energy transfer	3450E
Vibrational states of disordered systems	6350
Vibrations	0320, 0340K, 4340, 4630M
Viscoelasticity	4630J, 4660, 6240, 8140J
Viscometers	4780
Viscoplasticity	4630J, 6220F, 8140L
Viscosity	5110, 5120, 6210, 6620
Viscosity of gases	5120
Visible spectra	3220J, 3320K, 7840
Vision	8732
Visual perception	8732S
Visual pigments	8732L, 8732N
Vitreous state	6140, 81
Vlasov equation	5220, 5225F
Voids (solid)	6170, 6180
Volcanology	9140
Volume measurement	0630C
Vorticity	4730, 6740
VPE	6855, 8115G, 8115H, 8115J

Wakes	4725R
Water wave energy	8610F
Wave energy	8610F
Wave equations	0340K, 0365
Waves	0340G, 0340K, 4735, 4740N
Weak interaction models	1230
Weak interactions (atomic)	3510W

	Classification
Weak interactions (molecular)	3520W
Wear	4630P, 6220P, 8140P
Wear resistant coatings	6220P, 8140P, 8160
Weather analysis	9260
Weighing	0630E
Weinberg-Salam model	1210
Westheimer method	3120W
Wetting	6810, 6845, 81
Whiskers (crystal)	6870
White darfs	9720
Wiberg method	3120W
Wigner functions	0365
Wind	9260, 9410
Wind energy	8610D
Woods-Saxon potentials	2160C
Work function	7330, 7340, 79
Work hardening	8140E

X-ray absorption spectra	3220R, 3320R, 7870D
X-ray apparatus	0785
X-ray astronomy	95
X-ray crystallography	6110
X-ray diffraction	6110
X-ray diffraction examination of materials	6155, 6160, 6165, 6170

	Classification
X-ray effects	6180C
X-ray emission spectra	3220R, 3320R, 7870E
X-ray lasers	4255
X-ray monochromators	0785, 6110F
X-ray scattering	6110, 7870C
X-ray sources	2925
X-ray sources (astronomical)	9870Q
X-ray spectra	3220R, 3320R, 7870D, 7870E
X-ray spectroscopy	2930
Xalpha calculations	3120G

Yang-Mills fields	1110
Yield point	4630J, 6220F, 8140L
Young's modulus	6220D, 8140J
Yrast states	2110

Zeeman effect	3260, 3345B, 7170E, 7820L, 7830, 7840
Zener effect	7220H
Zener relaxation	4630J, 6240, 8140J
Zero sound	67
Zodiacal light	9460, 9650D
Zone melting	8110H
Zone refining	8110H
Zoology	87

Physics Abstracts

1st JULY 1983

Volume 86

Number 1211

00.00 GENERAL

01.00 COMMUNICATION, EDUCATION, HISTORY, AND PHILOSOPHY

01.30 PHYSICS LITERATURE AND PUBLICATIONS

59523 Plutonium recycling scenario in light water reactors. Assessment of the environmental impact in the European Community. Chur, Switzerland: Harwood Academic Publishers (1982), iv+254 pp. [3 7186 0118 4]

The aim of the report is to make a forward assessment of any additional environmental impact of a conceivable plutonium recycling strategy in some light water nuclear power plants in the light of the possible development of nuclear generating capacity in the European Community at the end of the century. The specific studies initiated are as follows: description of a reference mixed oxide fuel fabrication plant; preliminary design for a plutonium oxide storage unit; environmental radiological impact of plutonium recycling in light water reactors; differential environmental impact of reprocessing spent U/Pu mixed-oxide instead of spent uranium fuel; environmental impact of the conversion of plutonium nitrate arising from the reprocessing of mixed-oxide fuel; environmental impact of plutonium transportation for normal transport conditions; and toxicity of plutonium, americium and curium.

01.30C Conference proceedings

59524 Proceedings of Symposium 4 of the COSPAR Twenty-Fourth Plenary Meeting.

Adv. Space Res. (GB), vol.2, no.4 (1982).

Conference held at: Ottawa, Canada. Date 16 May-2 June 1982. The following topics were dealt with: spatial resolution of telescopes in space, IR and submillimetre astronomy techniques and instrumentation, X-ray instruments and missions, far and EUV techniques and instrumentation and solar physics.

59525 Supercritical Fluids. Their Chemistry and Application.

Fluid Phase Equilibria (Netherlands), vol.10, no.2-3 (March 1983).

Conference held at: Cambridge, England. Date 13-15 Sept. 1982. The following topics were dealt with: general theory and predictions of supercritical fluid equilibria; thermophysical properties of supercritical fluids; applications of supercritical fluids including fluid extraction techniques. 21 papers were presented, all of which are published in full in the present proceedings. Abstracts of individual papers can be found under the relevant classification codes in this or other issues.

59526 21st Annual Congress of the South African Association for Physicists in Medicine and Biology (papers in summary form only received).

Health Phys. (GB), vol.44, no.3 (March 1983).

Conference held at: Bloemfontein, South Africa. Date 16-18 March 1981. The topics dealt with included: radiation protection past, present and future; criteria for setting a lower limit to radiation dose; in vivo chest measurements used for routine determinations of U contamination; a national calibration service in radiation dosimetry; physical aspects of neutron dosimetry and the neutron response of a photon detector; a new type of recoil spectrometer for neutron energy spectra measurements; existing and future dosimetry standards; calibration of a remotely controlled afterloading system suitable for brachytherapy; the neutron sensitivity of a GM counter; absorbed doses to a tissue equivalent phantom during pantomographic radiology. 19 papers were presented.

59527 2nd Special Symposium on the National Radiation Environment Indian Association for Radiation Protection (papers in summary form only received).

Health Phys. (GB), vol.44, no.3 (March 1983).

Conference held at: Bombay, India. Date 19-23 Jan. 1981. The topics dealt with included: dosimetry analysis of high natural radioactivity areas of the Indian SW coast; Rn and daughter products in man and his environment; α spectroscopic techniques for field measurement of Rn daughters; the electret system and measuring Rn isotopes and decay products in dwellings; natural contamination in radionuclide detection systems; radiation exposure and resulting risk due to residence and employment in a Rn spa; internal exposure of residents in high background areas; natural radioactivity releases from coal fired and geothermal power plants in Italy; lung exposure to Rn daughters. 20 papers were presented.

59528 1982 IEEE Conference on the Application of Accelerators in Research and Industry.

IEEE Trans. Nucl. Sci. (USA), vol.ns-30, no.2 (April 1983).

Conference held at: Denton, TX, USA. Date 8-10 Nov. 1982. Sponsors: DOE; NSF; D.A.R.P.A.; Naval Surface Weapons Centre; NBS; et al. The following topics were dealt with: accelerator application in: atomic and molecular physics; energy loss; nuclear physics and astrophysics; CTR and related phenomena; trace analysis with ion beams, surface analysis, microprobes; accelerator technology; detectors and spectrometers; accelerator targets; radiological safety aspects, activation and bulk analysis; radiation processing; mineral exploration and geophysics; computed tomography; ion implantation, semiconductors, materials modifications, channeling, sputtering; medical applications, radiotherapy, image applications, radioisotope production. 257 papers were presented, of which 246 are published in full in the present proceedings. Abstracts of individual papers can be found under the relevant classification codes in this or other issues.

59529 Proceedings of the Meeting held by The Astronomical Science Group of Ireland.

Irish Astron. J., vol.15, no.3 (March 1982), [received: April 1983]

Conference held at: Cork, Ireland. Date 22 May 1981. The following topics were dealt with: evolved H II region M16, IR, gamma rays, Cygnus X-3, image intensifiers, R81, P Cygni star, Large Magellanic Cloud, Irish early astronomy.

59530 Proceedings of the Third International Workshop on Railway and Tracked Transit System Noise.

J. Sound & Vib. (GB), vol.87, no.2 (22 March 1983).

Conference held at: Monument, CO, USA. Date 8-10 April 1981. The following topics were dealt with: sources and mechanisms of wheel/rail noise; means for control of wheel/rail noise; other sources of railway noise; elevated structure noise; propagation of railway noise; community response to railway noise; and ground vibration from railway operations. 29 papers were presented, all of which are published in full in the present proceedings.

59531 Proceedings of a Symposium on Random Walks and Their Application to the Physical and Biological Sciences.

J. Stat. Phys. (USA), vol.30, no.2 (Feb. 1983).

Conference held at: Gaithersburg, MD, USA. Date 28 June-1 July 1982. The following topics were dealt with: continuous time random walks from classical dynamics; reaction-diffusion processes; fractal and lacunary stochastic processes; nonexponential decay in relaxation phenomena; exciton motion; relaxation, capture and annihilation; renormalization group approach; hopping and multiple-trapping transport; excitation trapping; diffusion; random walks on inhomogeneous lattices; diffusion-controlled reactions among stationary sinks; stochastic biological locomotion; ligand migration in biomolecules; protein folding; self-avoiding walks; polymers excluded volume; Monte Carlo renormalisation group calculations for polymers; Pearson's random walk; vacancy mechanism in crystals; energy transfer as a random walk; diffusion in concentrated lattice gases; deterministic microscopic dynamics; random walks of dislocations; adsorption kinetics on stepped surfaces; and equilibrium folding pathways for model proteins. 44 papers were presented, of which 29 are published in full in the present proceedings. Abstracts of individual papers can be found under the relevant classification codes in this or other issues.

59532 Proceedings of the Third International Conference on 'Vibrations at Surfaces'.

J. Electron Spectrosc. & Relat. Phenom. (Netherlands), vol.29 (15 Jan. 1983).

Conference held at: Asilomar, CA, USA. Date 1-4 Sept. 1982. The topics chosen for the eight sessions held over a span of 3 days were: (I) vibrational frequency shifts and width-lateral interactions; (II) dynamical processes at surfaces; (III) and (IV) electron loss spectroscopy; (V) Raman and surface enhanced Raman scattering; (VI) infrared absorption and reflection spectroscopy; (VII) beam surface scattering—surface phonons; (VIII) electron tunnelling spectroscopy—surface enhanced Raman studies in electrochemistry. In addition, C.B. Duke presented an introductory keynote surveying progress in the field since the last meeting. In the final session H. Ibach and T. Grimley presented conference overviews and future prospects for the field from an experimental and theoretical perspective. Approximately 102 papers were presented in the present proceedings. Abstracts of individual papers can be found under the relevant classification codes in this or other issues.

59533 RAS Specialist Discussion on Astrophysical Applications of Accretion Disks (Papers in summary form only received).

Observatory (GB), vol.103, no.1053 (April 1983).

Conference held at: London, England. Date 8 Oct. 1982. The following topics were dealt with: accretion discs in regions of star formation; protoplanetary discs; accretion-disc coronae; disc eruptions in cataclysmic variable stars; jets and the giant binary star R Aquarii; alpha-beta accretion discs; the theory of thick accretion discs; and accretion discs in galactic nuclei. 8-papers were presented, of which all are published as abstracts only.

59534 Proceedings of the First International Conference on 'Radiation Effects in Insulators'.

Radiat. Eff. (GB), vol.65, no.1-4 (1982).

Conference held at: Arco, Largo di Garda, Italy. Date 1981. Abstracts of individual papers can be found under the relevant classification codes in this or other issues.

59535 Radiation and the Worker - Where do we go from Here?.

Radiol. Prot. Bull. (GB), no.51, suppl. (March 1983).

Conference held at: London, England. Date 7 Jan. 1983. The following topics were dealt with: scientific and administrative bases of radiological protection; radiation and the law; radiation protection and the unions; radiation protection and the employer. Four papers were presented, all of which are published in the present proceedings as abstracts only.

59536 OFC '83. Sixth Topical Meeting on Optical Fiber Communication (papers in summary form only received).

New York, USA: IEEE (1983), 108 pp.

Conference held at: New Orleans, LA, USA. Date 28 Feb.-2 March 1983. The following topics were dealt with: optical fibre telecommunications; non-oxide fibre materials; undersea systems; fibre design; passive optical components; fibre splicing; cables; single-mode fibres; polarisation; chemical studies; sensors; sources; detectors; transmitters; receivers; fibre strength; fibre drawing; system technology; diode laser noise; telecommunication systems; lightwave systems; fibre fabrication; distribution; local networks; local loop applications; nonlinear optics; radiation effects; and military applications.

59537 Proceedings of the Symposium on Low-Level Waste Disposal. Site Characterization and Monitoring (NUREG/CP-0028).

Oak Ridge, TN, USA: Oak Ridge Nat. Lab. (1982), ix+502 pp.

Conference held at: Arlington, VA, USA. Date 16-17 June 1982. Sponsors: U.S. Nucl. Regul. Comm.; Oak Ridge Nat. Lab. The following topics were dealt with: low level nuclear waste disposal; geological site characterisation; geomechanical properties; hydrologic characterisation; groundwater investigation; surface water quality; air quality; meteorological measurements. 19 papers were presented, all of which are published in full in the present proceedings.

ings. Abstracts of individual papers can be found under the relevant classification codes in this or other issues.

59538 Sintering - Theory and Practice. Proceedings of the 5th International Round Table Conference on Sintering.

Amsterdam, Netherlands: Elsevier (1982), xii+654 pp. [0 444 42122 X]
Conference held at: Portoroz, Yugoslavia. Date 7-10 Sept. 1981. The following topics were dealt with: sintering, theory and kinetics, solid state sintering, liquid phase sintering, activated sintering, hot pressing, powder metallurgy, ceramics sintering, surface energy, solid solution additives, reactive sintering, interfacial segregation, shrinkage, grain growth, densification, sol-gel processes, diffusion during sintering, dimensional changes, grain boundaries, electronic structure, magnetic properties, mechanical properties and electrical properties of sintered materials, geometrical aspects, computer simulation, and sintering of garnets and semiconductors. 86 papers were presented of which all are published in full in the present proceedings. Abstracts of individual papers can be found under the relevant classification codes in this or other issues.

59539 Topics in Ocean Physics. Proceedings of the International School of Physics, 'Enrico Fermi', Course LXXX.

Amsterdam, Netherlands: North-Holland (1982), xvi+554 pp. [0 444 86160 2]
Conference held at: Varenna, Italy. Date 7-19 July 1980. The following topics were dealt with: (1) the dynamics of mesoscale and large-scale flows, (2) nonlinear wave mechanics, (3) mixed-layer physics, and, (4) linear models of ocean surface waves. 21 papers were presented.

59540 Exploration of the Polar Upper Atmosphere. Proceedings of the NATO Advanced Study Institute.

Reidel: Dordrecht, Netherlands (1981), xvi+498 pp. [90 277 1225 5]
Conference held at: Lillehammer, Norway. Date 5-16 May 1980. The following topics were dealt with: the neutral polar atmosphere above the tropopause, the polar ionosphere, optical remote sensing of the polar atmosphere and ionosphere, solar-magnetosphere-polar atmosphere interactions, electric fields and currents at high latitudes, waves and particles in the polar regions, historical exploration of the polar upper atmosphere and applications of polar upper atmosphere research.

59541 Earthquake Prediction. An International Review. Symposium on Earthquake Prediction.

Washington, DC, USA: American Geophys. Union (1981), viii+680 pp. [0 87590 403 3]

Conference held at: Mohonk, NY, USA. Date 12-16 May 1980. The following topics were dealt with: seismicity patterns, recurrence times along major fault zones, seismic precursors and nonseismic precursors, models, laboratory investigations and national programs.

59542 Reevaluations of Dosimetric Factors, Hiroshima and Nagasaki. Proceedings of a Symposium.

Oak Ridge, TN, USA: U.S. Dept. Energy (1982), x+296 pp. [0 87079 398 5]

Conference held at: Germantown, MD, USA. Date 15-16 Sept. 1981. Sponsors: Office Health Environ. Res.; Office Energy Res.; U.S. Dept. Energy. This volume is the result of recent research which indicates that significant revisions may have to be made in the estimates of radiation doses to survivors of the atomic bombs at Hiroshima and Nagasaki. Studies of health effects among these survivors and their correlation with the doses estimated in the late 1950s and early 1960s have provided a fundamental data base for estimating radiation risk. Because of the profound implications of any substantial modifications of the estimated neutron and gamma doses in the two cities, this book explores the current status of research and assesses future directions and priorities. The thirteen papers provide a comprehensive discussion of the many factors that affect the dose estimates, including weapon yields, prompt and delayed neutron and gamma source terms, air transport, and structure and body shielding. Taken as a whole, the volume contains detailed information on the historical perspective, recent developments (notably in significant improvements in source terms and air-transport calculations), and plans for future research efforts.

59543 Stochastic Processes in Quantum Theory and Statistical Physics. Proceedings of the International Workshop.

Berlin, Germany: Springer-Verlag (1982), viii+337 pp. [3 540 11956 6]

Conference held at: Marseille, France. Date 29 June-4 July 1981. The following topics were dealt with: relations of the theory of diffusion processes, jump processes, and random fields with nonrelativistic quantum mechanics, stochastic mechanics, quantum field theory, and gauge field theory; stochastic processes in solid state physics and in equilibrium and nonequilibrium classical and quantum statistical mechanics, noncommutative stochastic processes, stochasticity in classical dynamical systems, and stochastic processes in acoustics and music. Abstracts of individual papers can be found under the relevant classification codes in this or other issues.

01.30E Monographs, and collections

59544 Paleoreconstruction of the continents. M.W.McElhinny, D.A.Valencia [Ed.]

Washington, DC, USA: American Geophysical Union (1981), 194 pp.

The following topics were dealt with: continental fitting, palynology, palaeogeography, palaeoclimatology, glaciation, marine magnetic anomalies, Arctic seafloor structure, and palaeomagnetic studies of: Africa and Madagascar, Australia and Antarctica, India, South America, Japanese islands, southeast and east Asia, northern Europe, southern Europe and Middle East, North America, and the Soviet Union.

59545 Tectonic and geologic evolution of southeast asian seas and islands. D.E.Hayes [Ed.]

Washington, DC, USA: American Geophysical Union (1980), v+326 pp. [0 87590 023 2]

The following topics were dealt with: the tectonic and geological evolution of the Philippines and adjacent seas; the spatial distribution of earthquakes and subducted lithosphere in the Philippine and northeastern Indonesian islands; Eocene oceanic crust in the Celebes Basin; marine magnetic anomalies in the western Philippine Sea; the Central Basin Fault of the West Philippine Basin; the tectonic evolution of the South China Basin; Quaternary sedimentation in the South China Basin; Recent volcanism in the central Philippines; the Sunda Arc and the Molucca Sea; variations in geological structure along the Sunda fore arc; the Molucca Sea collision zone; the lower trench slope off Nias Island in the Sunda Arc; crustal structure across the Mariana island arc; faulting in the Mariana fore arc; palaeomagnetism of Tuk Island and Saipan; volcanic rocks of the Philippine Sea; primitive arc volcanism and a boninite series; back arc spreading and arc volcanism in the Philippine Sea; a palaeomagnetic synthesis for southeast Asia; and heat flow in the east and southeast Asian seas. 18 papers were presented, all of which are published in

full in the present proceedings. Abstracts of individual papers can be found under the relevant classification codes in this or other issues.

59546 Neutron sources. For basic physics and applications. H.H.Barsehall, G.A.Bartholomew, C.B.Bigham, R.C.Bloch, R.M.Brugger, R.E.Chrien, S.Cierjacks, H.Conrads, J.S.Fraser, G.F.Knoll, M.A.Lone, C.A.Uttley, L.Walter, G.B.West, W.L.Whittemore.

Oxford, England: Pergamon (1983), xx+349 pp. [0 08 029351 4]

This book is the second in the Series on Neutron Physics and Nuclear Data in Science and Technology sponsored by the Nuclear Energy Agency Nuclear Data Committee (NEANDC). The development of neutron sources has advanced tremendously in recent decades and they are now a basic tool for all areas of neutron physics research and nuclear applications. In this book, neutron sources are classified according to the technique by which the neutrons are produced. The corresponding chapters are treated separately by different authors. Each chapter itself gives a more or less independent description for the reader who is interested in a particular category of neutron source. This presentation has led to a certain amount of necessary duplication, but the more generally interested reader will also find numerous cross references between chapters. Each chapter includes a short introduction explaining the source characteristics, a description of the neutron production technique, a thorough discussion of the principal source components and of individual design concepts realized in various laboratories and an illustration of typical source parameters and characteristic applications.

59547 Realism and the aim of science. K.R.Popper.

London, England: Hutchinson (1983), xxxix+420 pp.

In Realism and the Aim of Science, Popper formulates and explains his nonjustificationist theory of knowledge. Science—empirical science—aims at true explanatory theories, yet it can never prove, or finally establish, or justify, any of its theories as true, not even if it is, in fact, a true theory. So science must continue to question and to criticize all its theories, even those which happen to be true. But it can give reasons for preferring some theories to others: some theories are better tested (corroborated), they may raise or solve more problems, they may have greater explanatory power, and they may even be able to correct those (apparent) facts which they were designed to explain. Thus although we do not possess a criterion of truth, we do possess something like a criterion of progress for our theories: of progress towards the truth and towards deeper and more powerful theoretical explanations. Popper replaces the utopian aim of justifying our theories by the realistic aim of submitting them to the severest theoretical and empirical criticism which our ingenuity can devise. Testing a theory consists not only in observing, but in ingenious attempts to find out its weak spots: the spots where the theory may be found wanting, the problems it may be unable to solve.

59548 Research and development on radioactive waste management and storage. First annual progress report of the European Community programme 1980-1984.

Chur, Switzerland: Harwood Academic Publishers (1982), 129 pp. [3 7186 0115 X]

This is the first progress report of the European Community's second programme (1980-1984) of research on radioactive waste management and storage (indirect action). It shows the status of the programme on 31 December 1980. The aim of the programme is the joint development and improvement of a management system of radioactive waste produced by the nuclear industry which, at its various stages, ensures the safety and protection of both man and his environment.

59549 Energy reviews. Nuclear power systems. Vol.1. L.A.Melentiev [Ed.]

Chur, Switzerland: Harwood Academic Publishers (1982), ix+334 pp. [3 7186 0071 4]

This volume, the first in the 'Energy Reviews' section of this series, is devoted primarily to the development and operation of the electrical power system in the Soviet Union. The collection begins with an outline of energy trends in the USSR and presents the reasons for the impending fundamental change in the fuel based for electrical power plants in the European regions of the USSR. It was also considered important to have special articles on the following topics: prospects for using new methods of producing electrical power and the development of district heating in the Soviet Union. Another of the papers was prompted by the widespread use in the USSR of mathematical models for designing and managing electrical power systems.

59550 Cellules solaires constitues de couches minces de CdTe polycristallines (Solar cells made from polycrystalline CdTe thin films). Y.Marfaing.

Report EUR 8154 EN-FR, Comm. European Communities, Luxembourg (1982), 75 pp. Contract 206-76 ESF.

The following topics were dealt with: minority carrier diffusion lengths; theoretical and experimental analyses; p-n homojunction characteristics.

01.30M Textbooks for graduates and researchers

59551 Relativistic astrophysics. M.Demianski.

Oxford, England: Pergamon (1981), 300 pp. [0 08 025042 4]

Discusses gravitational fields, relativistic thermodynamics and hydrodynamics, stellar equilibrium and stability in general relativity, rotating stars, neutron stars, pulsars, gravitational collapse and black holes, gravitational waves and cosmology.

59552 Channels of Mars. V.R.Baker.

Bristol, England: Adam Hilger (1982), xiii+198 pp. [0 85274 467 6]

Discusses telescopes, canals and space probes, morphology, channel types and age and distribution, origin, valley patterns and networks, ice, outflow channels, channelled scabland, Earth analogue, catastrophic floods and water.

59553 Superconductivity in ternary compounds. II. Superconductivity and magnetism. M.B.Maple, O.Fischer [Ed.]

Berlin, Germany: Springer-Verlag (1982), xvi+306 pp. [3 540 11814 4]

Considers the problems of the coexistence of superconductivity and magnetism. The topics covered include: the critical fields and critical currents of ternary molybdenum chalcogenides; the superconductivity and magnetism in rare earth rhodium borides and rare earth transition metal stannides; NMR and Mossbauer effect measurements in ternary compounds and the neutron scattering measurements of magnetic ordering in ternary superconductors.

59554 Analysis, manifolds and physics. Revised edition. Y.Choquet-Bruhat, C.DeWitt-Morette, M.Dillard-Bleick.

Amsterdam, Netherlands: North-Holland (1982), xx+630 pp. [0 444 86017 7]

A theoretical physicist needs to be able to use nearly all branches of mathematics and to use them reliably. The authors have written this book to make contemporary mathematics accessible and useful to the physicist. For this reason, the book covers a very large amount of material and brings together several branches of mathematics of interest to physics. It also includes many problems with their solutions. The present edition is a thorough revision of the first. There is a new chapter entitled 'Connections on Principle Fibre

Bundles' which includes sections on holonomy, characteristic classes, invariant curvature integrals and problems on the geometry of gauge fields, monopoles, instantons, spin structure and spin connections. Other additions include a section on the second fundamental form, a section on almost complex and kahlerian manifolds, and a problem on the method of stationary phase. Many paragraphs have been rewritten, and examples and exercises added to ease the study of several chapters. The index has been expanded by more than 150 entries. This reference book, which can also be used as a text, provides an answer to the needs of graduate physical mathematics students and their teachers.

59555 Adsorption on metal surfaces. An integrated approach. J.Benard [Ed.] Y.Berthier, F.Delamare, E.Hondros, M.Huber, P.Marcus, A.Masson, J.Oudar, G.E.Rhead.

Amsterdam, Netherlands: Elsevier (1983), x+338 pp. [0 444 42163 7]
This book makes no claim to be an exhaustive review of the research which has been done on adsorption on metals. The abundance and diversity of this research would have made such a task difficult and probably of limited interest. It is, rather, an attempt at an overall view inspired by the constant preoccupation with bringing together the thermodynamic approach with the atomistic approach to surface and interfacial interactions. The authors cover the following topics: the absolute measurement of the concentration of adsorbates on single-crystal faces, the structure interpretation of diffraction patterns, the specific role of surface defects, and finally the role of equilibria which are established under certain conditions between the bulk metal and its surface. The bibliography at the end of each chapter has been limited to those publications in which the authors' opinions have made a really original and significant contribution on either the experimental or the conceptual level.

01.30P Textbooks for undergraduates

59556 Spectral transform and solitons: Tools to solve and investigate nonlinear evolution equations. Vol.1. F.Calogero, A.Degasperis.
Amsterdam, Netherlands: North-Holland (1982), xviii+514 pp. [0 444 86368 0]

This book presents a novel technique to solve and investigate (certain classes of) nonlinear partial differential equations of evolution. The main motives are the solvability by this technique of many nonlinear evolution equations of great applicative and theoretical interest, and the phenomenology associated with the concept of 'solitons', that is closely related with this technique and has major relevance to various fields of application. This broadness of scope, both in pure and in applied mathematics as well as the dynamical stage of development of this field of enquiry exclude the possibility of providing a systematic and complete coverage of the theory and/or its applications in a single book. This volume focusses on one approach, and leaves out any specific treatment of applications. The guiding thread is the analogy of the spectral transform technique for solving nonlinear evolution equations to the Fourier transform method for solving linear PDEs. The presentation is primarily aimed at students who are approaching this subject for the first time; the book is organized so as to be suitable for self-instruction, or as a textbook (possibly also at the undergraduate level). It will be of use also to the expert researcher, who will find, in addition to a thorough treatment of several topics previously only dealt with in scattered papers, some novel results. (466 refs.)

59557 Probabilistic and statistical aspects of quantum theory. A.S.Holevo.
Amsterdam, Netherlands: North-Holland (1982), x+316 pp. [0 444 86333 8]
The book is accessible to a wide circle of readers, both mathematicians and physicists. It has six chapters dealing with the following subjects: statistical models; mathematics of quantum theory; symmetry groups in quantum mechanics; covariant measurements and optimality; Gaussian states, and unbiased measurements.

59558 Elementary statistical thermodynamics. A problems approach. N.O.Smith.
New York, USA: Plenum (1982), xiv+216 pp. [0 306 41205 5]
This text has been designed to provide an introductory treatment of statistical thermodynamics for all students of chemistry: The author presents a thorough and logical account of the foundations and applications of the subject, in clear steps guiding the neophyte to the point where he or she will be able to apply the elementary material to the calculation of thermodynamic properties by statistical methods. The approach used throughout is problem-based, in the belief that to learn a quantitative subject a student must, above all, work numerical problems in it. An abundance of illustrative examples and problems are provided, with many of the problems fully worked out. Coverage includes the subject of probability developed from first principles, the elementary statistical mechanics of systems of distinguishable particles, the Boltzmann distribution law, the statistical basis of entropy, the statistical treatment of systems of nonlocalized particles and of ideal gases, the calculation of the partition functions for the various kinds of energy (developed at length as an example of how thermodynamic functions are computed), and the subject of chemical equilibrium.

01.30R Surveys and tutorial papers; resource letters

59559 Atmospheric pressure waves generated by solar eclipses. C.A.Reddy (Space Phys. Div., Vikram Sarabhai Space Centre, Trivandrum, India).
Proc. Indian Natl. Sci. Acad. Part A, vol.48, suppl.3, p.356-69 (Oct. 1982). (Symposium on the Total Solar Eclipse of 16 February 1980, New Delhi, India, Jan. 1981).

A review of the present state of knowledge about the solar eclipse-induced pressure perturbations in the atmosphere is presented. The results of experimental measurements on the ground-level pressure perturbations during solar eclipses are critically reviewed and compared with theoretical predictions. The Lamb wave hypothesis of Chimonas (1973) is shown to provide a satisfactory explanation for the ground-level pressure perturbations; but more theoretical modelling work is needed to find out the reasons for the low amplitudes or the non-existence of eclipse-induced pressure perturbations during several observations. It is also pointed out that the ionospheric observations on solar eclipse-induced perturbations in the upper atmosphere are inconclusive in relation to the hypothesis that the gravity waves generated in the stratosphere in the wake of the Moon's shadow can generate ionospheric perturbations. It is concluded that further theoretical work and well-planned measurements from a network of observing stations are needed for further elucidation of the relevant questions. (28 refs.)

Radiation hormesis, public health, and public policy: a commentary See Entry 59583

Precision measurements and fundamental constants See Entry 59755

Flat panel display and projection display See Entry 59770

Taking the measure of temperature... See Entry 59783

Spectroscopy and integral image quality See Entry 59870

Electromagnetic and weak interactions in stochastic space-time: a review See Entry 59961

Technicolor See Entry 59991

Cornerstones of QCD See Entry 59992

The spectroscopy of light mesons See Entry 60006

How the first neutral-current experiments ended See Entry 60034

Comments on recent progress in few particle physics See Entry 60147

Development of material for the JET mechanical structure See Entry 60424

Recent advances in simple valence-bond theory and the theory of hybrid bond orbitals See Entry 60562

Radiative lifetimes of excited states of atoms See Entry 60625

The triatomic rare gas halide excimers See Entry 60738

First observation of bound-continuum transitions in the laser-induced $A^1\Sigma^+_g$ $X^1\Sigma^+_g$ fluorescence of Na_2 See Entry 60802

Effects of a nuclear scattering resonance on bremsstrahlung production and K-shell ionization See Entry 60953

Electron-atom scattering: the state of the experiments See Entry 60988

The threshold laws for electron-atom and positron-atom impact ionization See Entry 60989

Surface electromagnetic fields See Entry 61056

Vibronic solid state lasers: the transition metal ion laser See Entry 61158

Present prospects for continuous coherent ultraviolet sources See Entry 61232

Steady state thermodynamics and spatial correlations See Entry 61472

Kinetics of fluctuations for systems undergoing phase transitions—interfacial approach See Entry 61485

Particle simulation of plasmas See Entry 61692

Lyotropic polymeric liquid crystals See Entry 61778

Polymorphism in polar mesogens. I. Physicochemistry and structure See Entry 61779

Polymorphism in polar mesogens. II. Theoretical aspects See Entry 61780

Polymorphism in polar mesogens. III. Molecular aspect See Entry 61781

Twisted chiral mesophases See Entry 61784

Disc-like molecules and mesogenic polymorphism See Entry 61785

Basic-potential method for studying crystal potential See Entry 61850

Applications of thermoanalytical techniques to the study of crystallization kinetics in glass-forming liquids. I. Theory See Entry 62067

The nematic to smectic-A transition: a theoretical overview See Entry 62098

Multicritical phenomena in liquid crystals See Entry 62099

Review on lattice diffusion of substitutional impurities in iron. A summary report See Entry 62175

Some remarks on the carbon atoms pairs migrational relation in α -Fe-C See Entry 62181

Superflows and superfluidity See Entry 62200

Conference overview, directions and future work and critical issues: theory [surface vibrations] See Entry 62237

Conference overview: experimental [surface vibrations] See Entry 62238

Theoretical studies of molecular adsorption on metal surfaces See Entry 62246

New aspects of the oxygen donor in gallium phosphide See Entry 62365

Solution of the Kondo problem See Entry 62551

Mossbauer spectroscopy and magnetism See Entry 62841

Mossbauer spectroscopy of implanted sources See Entry 62844

Mossbauer studies of valence fluctuations See Entry 62845

^{67}Zn Mossbauer spectroscopy See Entry 62846

Mossbauer spectroscopy with $^{191,193}Ir$ See Entry 62847

Mossbauer spectroscopy with actinide elements See Entry 62848

Experimental techniques for conversion electron Mossbauer spectroscopy See Entry 62849

Transparent conductors—a status review See Entry 63078

High-rate sputter technique See Entry 63158

Experimental investigation of plastic strains of porous solids—a review See Entry 63190

Contemporary development of the science of sintering See Entry 63192

Studies on fabrication of superconducting V_3Ga wires See Entry 63202

On reactions between silicon and nitrogen. I. Mechanisms See Entry 63219

Extrusion and extruders. Historical outline, actual situation and future trends See Entry 63255

Crystallographic aspects of precipitation of supersaturated aluminium-base solid solutions See Entry 63300

Acoustic emission during phase transformations in alloys See Entry 63486

Acoustic emission monitoring See Entry 63489

Vinyl polymerization initiated by reducing compounds of transition metals. I. The polymerizing initiating effect of chromium (II) and titanium (II) compounds See Entry 63548

Synthesis and properties of poly(maleic anhydride) See Entry 63549

A review of some present molecular and submolecular physical concepts in biology See Entry 63769

Structure and function of viroids See Entry 63774

Secondary structures of proteins and peptides in amphiphilic environments (a review) See Entry 63781

Absorbance and fluorescence changes in relation to light-scattering changes in chloroplast thylakoid membranes See Entry 63795

Myopia development in nonhuman primates—a literature review See Entry 63828

Clinical nuclear magnetic resonance imaging See Entry 63918

Functional imaging of the brain See Entry 63940

Scientific and administrative bases of radiological protection See Entry 63983

Biological applications of picosecond spectroscopy See Entry 64015

A review of the paleomagnetism of Australia and Antarctica See Entry 64027

- Paleomagnetism of North America: a brief review See Entry 64034
 Paleomagnetic synthesis for southeast Asia: constraints on plate motions See Entry 64038
 A review of geological evidence for recurrence times of large earthquakes See Entry 64071
 Specification of a soon-to-occur seismic faulting in the Tokai District, central Japan, based upon seismotectonics See Entry 64074
 Long- and intermediate-term seismic precursors to earthquakes—state of the art See Entry 64075
 1980 update of heat flow in the east and southeast Asian seas See Entry 64099
 Atmospheric gravity waves produced by solar eclipses—a review See Entry 64206
 The removal of particulate matter from the atmosphere: the physical mechanisms See Entry 64214
 Airborne γ -ray spectrometry in uranium exploration. Principles and current practice See Entry 64254
 Tracer techniques in hydrology See Entry 64263
 Gamma astronomy of the Sun and study of solar cosmic rays See Entry 64330
 A review of double layer simulations See Entry 64373
 Charged particle reaction cross sections and nucleosynthesis See Entry 64460
 Supernovae. II. The aftermath See Entry 64496

01.30T Bibliographies

- 59560 An atomic spectroscopy bibliography for July-December 1982. D.M.Lawrence (Perkin-Elmer Corp., Norwalk, CT, USA). *At. Spectrosc. (USA)*, vol.4, no.1, p.10-36 (Jan.-Feb. 1983). The author presents a comprehensive atomic spectroscopy bibliography for July-December 1982. (568 refs.)
 59561 Publications concerning microscopic equipment, methods, applications, and related topics. *Microsc. Acta (Germany)*, vol.87, no.2, p.183-226 (March 1983). For previous pt. see *ibid.*, vol.87, no.1, p.53-88, 1983. The topics covered include: image analysis, stereology and morphometry; photometry, fluorometry and densitometry; refractometry; interferometry and measurements of hardness or thickness; lasers and holography; X-ray methods, X-ray and electron diffraction, ion beams; ultrasonics and acoustic microscopy. (875 refs.)
 High-spin molecules: electron spin resonance of manganese halides and sulfide at 4 K See Entry 60764
 The removal of particulate matter from the atmosphere: the physical mechanisms See Entry 64214
 Airborne γ -ray spectrometry in uranium exploration. Principles and current practice See Entry 64254
 Borehole logging for uranium by measurement of natural γ -radiation See Entry 64255
 Tracer techniques in hydrology See Entry 64263
 A comparison of volcanic eruption processes on Earth, Moon, Mars, Io and Venus See Entry 64408

01.40 EDUCATION

- 59562 Science anxiety and science learning. J.V.Mallow (Dept. of Phys., Loyola Univ., Chicago, IL, USA), S.L.Greenburg. *Phys. Teach. (USA)*, vol.21, no.2, p.95-9 (Feb. 1983). Discusses the origins and nature of science anxiety. The authors describe the Science Anxiety Clinic and outline the techniques used therein, including science skills training and psychological interventions. Finally comments on the connection between science anxiety and cognitive processes in science learning are given. (20 refs.)

01.50 EDUCATIONAL AIDS

- 59563 Classroom Moire demonstrator. B.W.Cotterman, P.D.Heimdahl (Dept. of Mech., US Military Acad., West Point, NY, USA). *Exp. Tech. (USA)*, vol.7, no.1, p.38-9 (Jan. 1983). A simple and inexpensive 10-minute visual demonstration of moire fringe analysis for use in a classroom or a large lecture room is described. The moire demonstrator consists of a 3-ft wide by 4-ft high, $1/4$ -in. thick Plexiglas master grille connected to a wooden frame. The master grille is made from strips of electrical tape. The specimen consists of a clear-plastic garbage bag clamped at the top to the frame and at the bottom to a rigid movable support arm. A light bouncing off the view-graph screen placed behind the demonstrator projects the grilles. (no refs.)
 59564 Plastic concave and convex cylindrical mirrors. B.F.Melton, T.W.Mayes (Univ. of North Carolina, Charlotte, NC, USA), R.P.Lemmon. *Phys. Teach. (USA)*, vol.21, no.2, p.195-9 (Feb. 1983). Concave and convex cylindrical mirrors are used widely in optics experiments for introductory physics laboratories. The authors describe the advantages of using longer focal length concave and convex cylindrical mirrors constructed from sheets of flexible, back-surfaced, mirror acrylic plastic. Suggestions for several student experiments, along with typical experimental results, are also presented. (6 refs.)

01.65 HISTORY OF SCIENCE

- 59565 Recollections of the discovery of the Thomas precessional frequency. L.H.Thomas (Univ. of North Carolina, Raleigh, NC, USA). *AIP Conf. Proc. (USA)*, no.95, p.4-12 (1982). (5th High Energy Spin Symposium, Westhampton Beach, NY, USA, Sept. 1982). The author discusses his recollections of early work on the spinning electron and the discovery of the Thomas precessional frequency. (no refs.)
 59566 International Colloquium on the History of Particle Physics. *J. Phys. Colloq. (France)*, vol.43, no.C-8 (Dec. 1982). Conference held at: Paris, France. Date 21-23 July 1982. The following topics were dealt with: cosmic rays, physics with accelerators, strange particles, early cloud chamber expts., ideas and discovery of leptonic property, neutrino physics, Beta decay and the weak interaction, atomic bomb (philosophy), isospin, quantum electrodynamics, chronology of particle physics.

Abstracts of individual papers can be found under the relevant classification codes in this or other issues.

- 59567 The role of cosmic rays in the development of particle physics. C.Peyrou (Div. EP, CERN, Geneva, Switzerland). *J. Phys. Colloq. (France)*, vol.43, no.C-8, p.c8/7-67 (Dec. 1982). (International Colloquium on the History of Particle Physics, Paris, France, 21-23 July 1982). The discoveries of elementary particles in cosmic rays are reviewed. The paper starts with the discovery of the positron in 1932, follows with the discoveries of the light mesons and make an extensive description of the finding of strange particles in cosmic rays. (67 refs.)
 59568 Development of the cosmic ray techniques. B.Rossi (Dept. of Phys., MIT, Cambridge, MA, USA). *J. Phys. Colloq. (France)*, vol.43, no.C-8, p.c8/69-99 (Dec. 1982). (International Colloquium on the History of Particle Physics, Paris, France, 21-23 July 1982). A close relationship exists between the advances of cosmic-ray physics and technical developments. Thus the development of highly sensitive ionization chambers, eventually to become self-recording instruments, was an essential prerequisite of the observations which first suggested, then proved the extraterrestrial origin of the radiation. The invention of the Geiger-Muller counter and of the associated coincidence devices opened the door to the investigation of the physical properties of the local radiation. Also 'c.r. telescopes', made of G.M. counters, discovered the E-W effect, showing that primary c.r. are positively charged particles. The development of cloud-chambers suitable for c.r. observations, and the development of nuclear emulsions were responsible for the discovery of 'new' elementary particles in the local radiation (the positive electron, the μ -meson, the π -meson, the 'strange' particles). New techniques involving the use of very large detector arrays produced important advances in the study of air showers showing that the primary spectrum extends beyond 10^{20} e.v. Finally, the availability of space vehicles, coupled with the development of new suitable detectors made it possible to determine the chemical and isotopic composition of the incident radiation. (25 refs.)
 59569 Early history of physics with accelerators. H.L.Anderson (Los Alamos Nat. Lab., Los Alamos, NM, USA). *J. Phys. Colloq. (France)*, vol.43, no.C-8, p.c8/101-62 (Dec. 1982). (International Colloquium on the History of Particle Physics, Paris, France, 21-23 July 1982). The early history of physics with accelerators is reviewed, with emphasis on three experiments which have had a profound influence on our view of the structure of matter: the Franck-Hertz experiment demonstrating the mechanism of atomic spectra, the Cockcroft-Walton experiment opening practical ways of studying nuclear disintegration, and the discovery of the Δ^{++} isobar of the proton by Fermi and collaborators, revealing structure in the nucleon. Fermi's work is illustrated by pages from his notebooks. (52 refs.)
 59570 Observations on the discovery of the strange particles. G.D.Rochester (Dept. of Phys., Durham Univ., Durham, England). *J. Phys. Colloq. (France)*, vol.43, no.C-8, p.c8/169-75 (Dec. 1982). (International Colloquium on the History of Particle Physics, Paris, France, 21-23 July 1982). Observations on the early history of the discovery of the strange particles, starting in 1940 with the work of L. Janossy and his collaborators on showers of penetrating particles and ending with the confirmation of the Manchester discoveries by C.D. Anderson and his group in Pasadena in 1950. The role of P.M.S. Blackett is emphasised. (11 refs.)
 59571 Early cloud chamber experiments at the Pic-du-Midi. C.C.Butler (Loughborough Univ. of Technol., Loughborough, England). *J. Phys. Colloq. (France)*, vol.43, no.C-8, p.c8/177-84 (Dec. 1982). (International Colloquium on the History of Particle Physics, Paris, France, 21-23 July 1982). The early history of cloud chamber work on strange particles is described. Particular attention is given to the pioneering work of the Manchester group at the Pic-du-Midi in France. The paper concludes with some preliminary remarks on the value of historical studies of the development of main areas of physics. (15 refs.)
 59572 Cosmic rays and particle physics at Berkeley. W.B.Fretter (Univ. of California, Berkeley, CA, USA). *J. Phys. Colloq. (France)*, vol.43, no.C-8, p.c8/191-4 (Dec. 1982). (International Colloquium on the History of Particle Physics, Paris, France, 21-23 July 1982). The author presents a review of work performed at Berkeley using two particular cloud chambers. An explanation of the phenomena observed and the experiments performed with cosmic rays during the years 1935-1960 is also presented. (no refs.)
 59573 Strange particle theory in the cosmic ray period. R.H.Dalitz (Dept. of Theoretical Phys., Oxford, England). *J. Phys. Colloq. (France)*, vol.43, no.C-8, p.c8/195-205 (Dec. 1982). (International Colloquium on the History of Particle Physics, Paris, France, 21-23 July 1982). The author discusses the role of theoretical physicists in strange particle theory during the cosmic ray period. A review of conferences held and theories presented in the development of strange particles is also made. (22 refs.)
 59574 Ideas and nonideas and the discovery of the leptonic property in Rome. O.Piccioni (Dept. of Phys., Univ. of California, San Diego, La Jolla, CA, USA). *J. Phys. Colloq. (France)*, vol.43, no.C-8, p.c8/207-13 (Dec. 1982). (International Colloquium on the History of Particle Physics, Paris, France, 21-23 July 1982). The author presents a summary of his work on muon detection in Rome from 1941. (14 refs.)
 59575 The infancy and youth of neutrino physics: some recollections. B.Pontecorvo (JINR, Dubna, USSR). *J. Phys. Colloq. (France)*, vol.43, no.C-8, p.c8/221-36 (Dec. 1982). (International Colloquium on the History of Particle Physics, Paris, France, 21-23 July 1982). The talk is quite subjective in character, and is in no way complete. It is not a chapter of history of particle physics. It is a collection of a few short stories related to neutrino physics. Two of these, about Pauli and Fermi, touch on subjects already covered by a number of physicists, including the author, in connection with the recent neutrino's fiftieth birthday. A story about Majorana's work on Majorana's fermions, which is following, has been covered much less extensively, at least in English. There follow a few recollections, very personal indeed, related to the experimental and theoretical work of the author in proposing and developing the C1-A method of neutrino detection, in establishing the notion of weak processes and in proposing a new type of weak interaction investigations-high energy neutrino experiments. (41 refs.)

59576 Neutrinos to 1960—personal recollections. F.Reines (Dept. of Phys., Univ. of California, Irvine, CA, USA).

J. Phys. Colloq. (France), vol.43, no.C-8, p.C8/237-60 (Dec. 1982). (International Colloquium on the History of Particle Physics, Paris, France, 21-23 July 1982).

An account is given of the events which led to the detection of the free neutrino starting from the tentative idea to use a nuclear explosion as the neutrino source to the detailed realization of the experiment at a nuclear reactor. The logical requirement for detection of the neutrino at a point remote from its origin is discussed as are some subsequent developments in experimental neutrino physics. (35 refs.)

59577 Beta decay opens the way to weak interactions. E.Amaldi (Istituto di Fisica, Guglielmo Marconi, Roma, Italy).

J. Phys. Colloq. (France), vol.43, no.C-8, p.C8/261-300 (Dec. 1982). (International Colloquium on the History of Particle Physics, Paris, France, 21-23 July 1982).

After a short introduction with some personal recollection, the author summarizes, in Section 2, the main points of Fermi's theory of beta decay and of the neutrino hypothesis first proposed by Pauli. The successive Sections refer to: a few extensions and modifications of this theory (Section 3), various experimental investigations carried out in the 1930s for testing Pauli's hypothesis and Fermi's approach (Section 4), further attempts, refinements and proposals (Section 5) and a few fundamental steps forward such as the discovery of the universality of weak interactions, of parity violation by weak interactions, the 2-component theory of the neutrino and the (V-A) theory of weak interactions (Section 6). Finally Section 7 refers to a few contributions given in the period 1930-1960 to the problem of double beta decay. (103 refs.)

59578 The road to Los Alamos. S.R.Weart (Centre for History of Phys., American Inst. of Phys., New York, NY, USA).

J. Phys. Colloq. (France), vol.43, no.C-8, p.C8/301-21 (Dec. 1982). (International Colloquium on the History of Particle Physics, Paris, France, 21-23 July 1982).

A field of science involves not only pure knowledge, but also images in the public mind. By affecting funding and recruitment into the field, these images help to determine its destination in the world of action. The history of nuclear physics offers an example. By 1938 the field was linked with images of 'transmutation', involving not only scientific methods but images of great improvements for health and wealth, and weapons that would bring world peace or doom. The scientists who went to Los Alamos to build atomic bombs did so chiefly because they wanted to defend themselves against the Nazis, just as others were doing with radar and incendiary bombs. Yet they were also responding to fantastic, but accurate, images that were already deeply established in the public mind; without those images there would have been no atomic bombs. (no refs.)

59579 Isospin. N.Kemmer (Univ. of Edinburgh, Edinburgh, Scotland).

J. Phys. Colloq. (France), vol.43, no.C-8, p.C8/359-93 (Dec. 1982). (International Colloquium on the History of Particle Physics, Paris, France, 21-23 July 1982).

The history of isospin is described, starting from the introduction by Heisenberg (1932) of the concept (ρ -spin), associated with the idea that proton and neutron are two states of the same entity (later to be called 'nucleon'). It is stressed that from the start Heisenberg had the picture of the transmission of proton-neutron interaction by a charged agent (field) in mind. It is shown that, in contrast, Majorana's modification of Heisenberg's interaction scheme rejected the isospin formalism and moved away from a field picture. The introduction of isospin into field theories of nucleon-nucleon interaction is described: the charge independent extension first of the Fermi (β , ν) field (Kemmer, 1937) and then of the Yukawa field (Kemmer, 1938). A brief account is given of the consolidation of the 'symmetric theory' of the isospin of the nucleon-pion system, following the post-war experimental proof of the existence of the pion isotriplet and the improvement in the understanding of field theories in terms of the renormalisation concept. The application of this iso-invariance of the (N- π) system in the description of a wide range of phenomena (weak interactions) is sketched. The first step into nonabelian gauge theory—the Yang-Mills iso-vector gauge field—is briefly described, concluding with brief remarks on the status of isospin within the framework of modern particle theory. (35 refs.)

59580 Strangeness. M.Gell-Mann (Lauritsen Lab. of Phys., California Inst. of Technol., Pasadena, CA, USA).

J. Phys. Colloq. (France), vol.43, no.C-8, p.C8/395-408 (Dec. 1982). (International Colloquium on the History of Particle Physics, Paris, France, 21-23 July 1982).

This paper is not a history of the discovery of the strangeness, but rather a contribution to such a history, consisting of personal reminiscences. The atmosphere and ideas of the period 1951-1953 are described. The author explains the reasons that led him to introduce the concept of the strangeness and how he had to convince people and to overcome oppositions. (11 refs.)

59581 Quantum electrodynamics—an individual view. J.Schwinger (Dept. of Phys., Univ. of California, Los Angeles, CA, USA).

J. Phys. Colloq. (France), vol.43, no.C-8, p.C8/409-23 (Dec. 1982). (International Colloquium on the History of Particle Physics, Paris, France, 21-23 July 1982).

The aim of this report is to describe the development of the quantum electrodynamics in the years from the 1930s to the 1950s. It is based on the way the author saw and participated to this development. Four phases are discussed: preparation (1934-1946); noncovariant relativistic theory (1947); first covariant relativistic theory (1947-1948); second covariant relativistic theory (1949-50). A detailed technical description is presented. The author shows the influence of quantum electrodynamics in other areas of physics. (54 refs.)

59582 An essay of chronology of particle physics until 1965. J.Six (Lab. de l'Accelérateur Lineaire, Univ. Paris-Sud, Orsay, France), X.Artru.

J. Phys. Colloq. (France), vol.43, no.C-8, p.C8/465-93 (Dec. 1982). (International Colloquium on the History of Particle Physics, Paris, France, 21-23 July 1982).

The main developments in elementary particle physics, from the origins to 1965, are presented in a chronological list with three columns: theories, experimental discoveries and technical means. The work mainly focuses on the period 1930-1965, for which are given the references of the original papers. (165 refs.)

01.70 PHILOSOPHY OF SCIENCE

Realism and the aim of science See Entry 59547

The road to Los Alamos See Entry 59578

01.75 SCIENCE AND SOCIETY

59583 Radiation hormesis, public health, and public policy: a commentary. R.J.Hickey, E.J.Bowers, R.C.Clelland (Univ. of Pennsylvania, Philadelphia, PA, USA).

Health Phys. (GB), vol.44, no.3, p.207-19 (March 1983).

Public policy affecting public health regarding effects of low-level ionizing radiations has been, and is being, determined by effects estimates based on linear or other monotonic extrapolation from high-level radiation dose-response data to presumed ecologically realistic low-level exposure effects. Such predictive, unmeasured estimates are very possibly in serious error; they are incompatible with observed low-level dose-response data that indicate a negative correlation between low-level radiation data and health effects, such as cancer mortality rates. Observed negative correlations with low-level radiation data are to be expected on the basis of evidence supporting the validity of the hormesis phenomenon. The ignoring of the hormesis phenomenon seems to constitute a very serious error in modern biomedical science and in preventive medicine. A mathematical model is offered that describes the general shape of certain dose-response functions when radiation hormesis at low-level exposure is taken into consideration along with the well-known detrimental effects of high-level radiation. (77 refs.)

02.00 MATHEMATICAL METHODS IN PHYSICS

Analysis, manifolds and physics. Revised edition See Entry 59554

02.10 ALGEBRA, SET THEORY, AND GRAPH THEORY

59584 Cartesian polytensors. J.Applequist (Dept. of Biochem. & Bio-phys., Iowa State University, Ames, IA, USA).

J. Math. Phys. (USA), vol.24, no.4, p.736-41 (April 1983).

A Cartesian polytensor is defined as a set of Cartesian tensors in a sequence of increasing rank. A matrix formulation of polytensors is given to express arrays of direct tensor products and series of tensor contractions in concise form. The transformation of a polytensor under rotation of coordinate axes is shown to be accomplished by means of an orthogonal matrix. The special properties of compressed polytensors, composed of totally symmetric tensors with redundant component deleted, are demonstrated. The use of polytensors is illustrated by an application to the problem of interactions among polarizable electric charge distributions. (7 refs.)

Affine Maczynski logics on compact convex sets of states See Entry 59607

Calculus on complex Banach spaces See Entry 59608

Scattering matrix of nonspherical particles See Entry 64233

02.20 GROUP THEORY

(for algebraic methods in quantum mechanics, see 03.65; for symmetries in elementary particle physics, see 11.30)

59585 Some character theory for groups of linear and antilinear operators. J.D.Newmarch (Dept. of Phys., Univ. Pertanian Malaysia, Selangor, Malaysia).

J. Math. Phys. (USA), vol.24, no.4, p.742-56 (April 1983).

Elementary group concepts are recast into a form applicable to finite magnetic groups of linear and antilinear operators. Analogs of useful definitions for linear groups such as the Frobenius-Schur invariant, commutator subgroups, and ambivalent classes are considered. These are applied to the 180 magnetic single and double point groups and it is shown that only seven require independent treatment of characters. (37 refs.)

59586 Complementary group with respect to SO(n). G.Couvreux, J.Deenen, C.Quesne (Phys. Theorique et Math., Univ. Libre de Bruxelles, Brussels, Belgium).

J. Math. Phys. (USA), vol.24, no.4, p.779-84 (April 1983).

The authors look for a complementary group with respect to SO(n) within either irreducible representation $\langle \frac{1}{2} \rangle_n$ or $\langle \frac{1}{2} \rangle_{2n-1}^{3/2}$ of the group $Sp(2dn, R)$ of linear canonical transformations in a $2dn$ -dimensional phase space. They prove that (i) such a group is $Sp(2d, R)$ when $n=2q+1$ or $n=2q>2d$; (ii) it is $SU(d, d)$ when $n=2$ and $d>1$; (iii) it does not exist when $n=2$, $d=1$, or $2 < n=2q \leq 2d$. (12 refs.)

59587 Fonction generatrice des facteurs isocscalaires des groupes unitaires (Generating function of isoscalar factors of unitary groups). M.Hage Hassan.

Report LYCEN/8306, Univ. Lyon, France (Feb. 1983), 23 pp. In French.

The author introduces a new schematisation of the elements of the unitary group fundamental representation basis. Using this schematisation as well as two rules which will be established in this work, he finds by an elementary calculus, the generating function of the Gel'fand basis of the unitary group, and the generating function of coupling coefficients. This last generating function allows one to find the one corresponding to SU(n) isoscalar factors. (8 refs.)

On the 3j symmetries See Entry 59611

Weight vector representatives for SO(2N) See Entry 59941

A theorem on orbit structures (strata) of compact linear Lie groups See Entry 59942

Internal labels of degenerate representations See Entry 59943

Analysis of the outer product for the symmetric group See Entry 59944

Luneburg lens: unitary invariance and point characteristic See Entry 61253

02.30 FUNCTION THEORY, ANALYSIS

59588 Continuous and discrete matrix Burgers' hierarchies. D.Levi, O.Ragnisco, M.Bruschini (Istituto di Fisica, Univ. di Roma, Roma, Italy).

Nuovo Cimento B (Italy), vol.74B, ser.2, no.1, p.33-51 (11 March 1983).

The authors derive two hierarchies of matrix nonlinear evolution equations which reduce to the Burgers' hierarchy in the scalar case and can be linearized by a matrix analogue of the Hopf-Cole transformation: for these hierarchies they display the associated class of Backlund transformations and show some special kinds of explicit solutions. Moreover, by exploiting a discrete version of the Hopf-Cole transformation, they are also able to construct

- two hierarchies of linearizable nonlinear difference evolution equations and to derive for them Backlund transformations and explicit solutions. (9 refs.)
Spectral transform and solitons: Tools to solve and investigate nonlinear evolution equations. Vol.1 See Entry 59556
Fonction generatrice des facteurs isocscalaires des groupes unitaires (Generating function of isoscalar factors of unitary groups) See Entry 59587
A decreasing property of solutions of parabolic equations with applications to thermoelasticity See Entry 59595
Existence of global solutions in nonlinear wave equations See Entry 59601
Calculus on complex Banach spaces See Entry 59608
Renormalization group and linear integral equations See Entry 59751
Lie transformations, nonlinear evolution equations, and Painleve forms See Entry 59946
Apparent symmetry breaking and its restoration in path integral variational method See Entry 59956
Numerical solution of two-dimensional static boundary problems for flexible conical shells See Entry 61401
Bending of a plate with a periodic system of cuts See Entry 61409
Stressed state of a square sample for crack resistance tests of sheet materials See Entry 61457
Nonsteady interaction between a die and an elastic medium See Entry 61458
A finite element formulation for steady transonic Euler equations See Entry 61521
Inviscid axisymmetric jet impingement with recirculating stagnation regions See Entry 61535
On the use of the false perturbation method in astronomical practice See Entry 64396

02.40 GEOMETRY, DIFFERENTIAL GEOMETRY, AND TOPOLOGY

(see also 04. Relativity and gravitation)

- The problem of motion in the Kaluza theory See Entry 59645
Generalized curvilinear diffraction gratings. V. Diffraction catastrophes See Entry 61075

02.50 PROBABILITY THEORY, STOCHASTIC PROCESSES, AND STATISTICS

(see also 05. Statistical physics)

- Stochastic jump processes in the phase space representation of quantum mechanics See Entry 59629
Transformation of Wiener integrals and the desingularization of Coulomb problem See Entry 59630
A stochastic picture of spin See Entry 59632
Momentum-position complementarity in stochastic mechanics See Entry 59633
Stochasticity in non-equilibrium statistical mechanics See Entry 59669
Non-commutative martingales and stochastic integrals in Fock space See Entry 59676
Scalar and vector laws of distribution of random quantities See Entry 59680
The power of chaos measured through the spectral analysis of experimental data See Entry 59682
Error estimates of solutions and mean of solutions of stochastic differential systems See Entry 59683
Momentum from sample paths in stochastic mechanics See Entry 59708
Mostly chaos See Entry 59709
One-time characteristic functional in the stochastic quantization See Entry 59717
On the statistical mechanics of surfaces See Entry 59722
A note on irreducibility and ergodicity of symmetric Markov processes See Entry 59723
Stochastic processes in music and art See Entry 59724
Some results on the spectra of random Schrodinger operators and their application to random point interaction models in one and three dimensions See Entry 59739
Stochastic processes and Fermi fields See Entry 59931
Creep of structural elements with random parameters See Entry 61419
Classical S-matrix theory of viscomagnetic production cross section See Entry 61587
Monte Carlo calculation of the erosion rate and ion current at a vacuum arc cathode See Entry 61717
A Monte Carlo study of semi-dilute hard sphere mixtures See Entry 61748
Fractal dimensions and 1/f noise See Entry 62463
Statistical rules of fatigue crack development See Entry 63422

02.60 NUMERICAL APPROXIMATION AND ANALYSIS

- Finite element, boundary element and coupled analysis of unbounded problems in elastostatics See Entry 59593
Variational scattering theory with functionals of fractional form See Entry 59636
Monte Carlo evaluation of functional integrals using coherent-state Slater determinants See Entry 59675
Dual finite-element calculations for static electric and magnetic fields See Entry 61045
Finite-element analysis of topographic waveguides for acoustic surface waves using approximate analytical solutions for substrate region See Entry 61329
Numerical solution of two-dimensional static boundary problems for flexible conical shells See Entry 61401
Analysis of shells with Monge's middle surfaces by a semianalytical finite element method See Entry 61402
Fast convergence modal analysis for continuous systems See Entry 61436

- Numerical ways of solving the problems of vibrations of thin plates subjected to impact loads See Entry 61449
An unsteady interactive separation process See Entry 61491
Numerical solution of transonic stream function equation See Entry 61520
A finite element formulation for steady transonic Euler equations See Entry 61521
Unsteady transonic flow over wings including inviscid/viscous interaction See Entry 61522
Inviscid axisymmetric jet impingement with recirculating stagnation regions See Entry 61535
An empirical initial estimate for the solution of Kepler's equation See Entry 64360

02.70 COMPUTATIONAL TECHNIQUES

(for data handling and computation, see 06.50)

- Standard interfaces for program-modular multiprocessor systems (review) [nuclear physics application] See Entry 60560
Navier-Stokes solution on the CYBER-203 by a pseudospectral technique See Entry 61519

03.00 CLASSICAL AND QUANTUM PHYSICS; MECHANICS AND FIELDS

03.20 CLASSICAL MECHANICS OF DISCRETE SYSTEMS: GENERAL MATHEMATICAL ASPECTS

(for applied classical mechanics of discrete systems, see 46.10; for celestial mechanics, see 95.10)

- 59589 Explicit suspensions of diffeomorphisms—an inverse problem in classical dynamics. P.J.Channell (Los Alamos Univ. Lab., Los Alamos, NM, USA). *J. Math. Phys. (USA)*, vol.24, no.4, p.823-7 (April 1983).
The author presents a set of explicit prescriptions for associating with a given map of R^2 , which is C^2 -isotopic to the identity, a time-dependent vector field whose time-1 map is the given one. Also shown is how to apply additional restrictions to the vector field including that it be periodic in time, Hamiltonian, and of potential form; several examples show numerical verification of the theory. (5 refs.)
Momentum-position complementarity in stochastic mechanics See Entry 59633
Stability theory of synchronized motion in coupled-oscillator systems See Entry 59715
Numerical analysis of flexural vibrations of rotors resting on elastic supports .. See Entry 61398

03.30 SPECIAL RELATIVITY

- 59590 A special relativistic heat engine. W.S.Cariens. *Int. J. Math. & Math. Sci. (India)*, vol.6, no.1, p.193-6 (1983).
Using the concepts of a heat engine from classical thermodynamics and $E=MC^2$ from special relativity, the author constructs a relativistic heat engine. Central to its functioning is the rest mass increase which results from heating a mass; this in turn will increase both its internal energy and its macroscopic kinetic energy. The engine's operation is as follows; a mass is accelerated to a high speed, heat is added from a comoving reservoir to increase its kinetic energy, the new 'heavier' mass is slowed down to its initial speed, and finally it is cooled to repeat the cycle. More work is seen to be produced during deceleration than was absorbed in acceleration. The efficiency of the engine is derived, and seen to be analogous to the corresponding Carnot equation. (5 refs.)
59591 Questions on universal constants and four-dimensional symmetry from a broad viewpoint. I. J.P.Hsu (Space Sci. Lab., NASA/Marshall Space Flight Center, Huntsville, AL, USA). *Nuovo Cimento B (Italy)*, vol.74B, ser.2, no.1, p.67-80 (11 March 1983).
It is demonstrated that there is a flexibility in clock synchronizations and that the four-dimensional symmetry framework can be viewed broadly. A new viewpoint of the four-dimensional framework is discussed on the basis of a common time for all observers who may be in motion relative to each other. Such a common time can be realized by a special method of clock synchronization and it is not absolute in the Newtonian sense. The author suggests that the truly universal constants in physics are $J=0.35 \times 10^{-37}$ g cm and $\bar{e}=1.6 \times 10^{-20}$ e.m.u. rather than \hbar , e (in e.s.u.) and the speed of light because J and \bar{e} are independent of a special arrangement of the measuring apparatus—such as clock synchronizations. (13 refs.)
59592 Are classical tachyons slower-than-light quantum particles?. E.Recamì, G.D.Maccarrone. *Report INFN/AE-83/1*, Ist. Naz. Fis. Nucl., Catania, Italy (4 Jan. 1983), 9 pp.
After having studied the shape that a tachyon T (e.g., intrinsically spherical) would take up, the authors show in an explicit example that the characteristics of classical tachyons are similar to those of the ordinary (slower-than-light) quantum particles. In particular, a realistic tachyon is associated with a 'phase-speed' V ($V^2 > c^2$), but with a 'group-speed' $v=c^2/V$ ($v^2 < c^2$). (13 refs.)

03.40 CLASSICAL MECHANICS OF CONTINUOUS MEDIA: GENERAL MATHEMATICAL ASPECTS

03.40D Mathematical theory of elasticity

(see also 46.20 Continuum mechanics, and 46.30 Mechanics of solids)

59593 Finite element, boundary element and coupled analysis of unbounded problems in elastostatics. G.Beer (Dept. of Civil Engng., Univ. of Queensland, Queensland, Australia).

Int. J. Numer. Methods Eng. (GB), vol.19, no.4, p.567-80 (April 1983).

The implementation of a combined boundary element-finite element analysis capability is discussed. A comparison is then made between the finite element, boundary element and coupled method as applied to unbounded problems in elasticity and plasticity. (19 refs.)

59594 Geometrically nonlinear formulation for the curved shell elements.

K.S.Surana (McDonnell Douglas Automation Co., Saint Louis, MO, USA).

Int. J. Numer. Methods Eng. (GB), vol.19, no.4, p.581-615 (April 1983).

Presents a geometrically nonlinear formulation using total lagrangian approach for the three-dimensional curved shell elements. The basic element geometry is constructed using the coordinates of the middle surface nodes and the mid-surface nodal point normals. The element displacement field is described using three translations of the mid-surface nodes and the two rotations about the local axes. The existing shell element formulations are restricted to small nodal rotations between two successive load increments. The element formulation presented here removes such restrictions. This is accomplished by retaining nonlinear nodal rotation terms in the definition of the displacement field and the consistent derivation of the element properties. The formulation presented here is very general and yet can be made specific by selecting proper nonlinear functions representing the effects of nodal rotations. The element properties are derived and presented in detail. Numerical examples are also presented to demonstrate the behaviour and the accuracy of the elements. (26 refs.)

59595 A decreasing property of solutions of parabolic equations with applications to thermoelasticity. W.A.Day (Hertford College, Univ. of Oxford, Oxford, England).

Q. Appl. Math. (USA), vol.40, no.4, p.468-75 (Jan. 1983).

The object of this paper is to establish a decreasing property of solutions of parabolic equations which satisfy boundary conditions of a somewhat unusual kind. The author begins by illustrating, with the aid of two examples from the quasi-static theory of thermoelasticity, how such problems can arise. The coupled partial differential equations are first considered which describe the behaviour of a slab made of homogeneous and isotropic material. (7 refs.)

On the Lagrangian formulation of continuum mechanicsSee Entry 61403

Finite anti-plane shear of a semi-infinite strip subject to a self-equilibrated end tractionSee Entry 61410

Fast convergence modal analysis for continuous systemsSee Entry 61436

Computation of normal modes from identified complex modesSee Entry 62008

03.40G Fluid dynamics: general mathematical aspects

(see also 47. Fluid dynamics)

59596 On the Burnett and higher order equations of hydrodynamics.

L.S.Garcia-Colin (Dept. of Phys., Univ. Nacional Autonoma de Mexico, Mexico City, Mexico).

Physica A (Netherlands), vol.118A, no.1-3, p.341-9 (March 1983). (Proceedings of the Conference on Nonlinear Fluid Behavior, Boulder, CO, USA, 7-11 June 1982).

Several derivations of the Burnett and high order in the gradients equation of classical hydrodynamics are critically examined. It is clearly pointed out that the two available phenomenological derivations and Grad's (1958) kinetic derivation are compatible with the local equilibrium assumption and the entropy balance equation. Furthermore, the failure to fulfil these requirements when such equations are obtained from the Chapman-Enskog method for solving Boltzmann's equations is accounted for. A comparison with other more microscopic methods to obtain these equations is also provided. (20 refs.)

On the Lagrangian formulation of continuum mechanicsSee Entry 61403

Number of modes governing two-dimensional viscous, incompressible flowsSee Entry 61473

Speed of propagation of infinitesimal disturbances in a relativistic gasSee Entry 61570

03.40K Waves and wave propagation: general mathematical aspects

(see also 46.30M Mechanical and elastic waves, 43.20 General linear acoustics)

59597 Inverse problem for the reduced wave equation with fixed incident field. III. V.H.Weston (Dept. of Math., Purdue Univ., West Lafayette, IN, USA).

J. Math. Phys. (USA), vol.24, no.4, p.828-33 (April 1983).

For pt.II see *ibid.*, vol.22, p.2523 (1981). The inverse problem for the reduced wave equation $\Delta u + k^2 n^2(x)u = 0$, $x \in R^2$, is examined for the case where measurements of the amplitude of the scattered field (produced by a fixed incident field at a single frequency) are obtained at a finite number of points. A strategy is given for the recovering of the phase data through the minimization of a quadratic form involving comparison data. The problem is then reduced to the problem treated in previous papers where the complex-valued quantities $u^*(x_i)$ are known at a finite number of points. A relationship between the smallest eigenvalue of the 'measurement' matrix and $\|k\|_2$ is given. (4 refs.)

59598 On signal velocity for anomalous dispersive waves. F.Mainardi

(Dipartimento di Matematica, Univ. di Bologna, Bologna, Italy).

Nuovo Cimento B (Italy), vol.74B, ser.2, no.1, p.52-8 (11 March 1983).

The concept of signal velocity for dispersive waves is usually identified with that of group velocity. When the dispersion is anomalous, this interpretation is not correct since the group velocity can assume nonphysical values. In this note, by using the steepest-descent method first introduced by Brillouin (1960), the phase velocity is shown to be the signal velocity when the dispersion is anomalous in the full range of frequencies. (8 refs.)

59599 Travelling waves in a dielectric slab with an abrupt change in thickness. F.G.Leppington (Dept. of Math., Imperial Coll., London, England).

Proc. R. Soc. London Ser. A (GB), vol.386, no.1791, p.443-60 (8 April 1983).

If a slab (or tube) of dielectric material of uniform thickness is surrounded by a medium of lower dielectric constant it can support travelling waves that propagate without attenuation. If there is an abrupt change in the slab thickness, reflection and radiation will occur. The author considers the simplest prototype case, in which a transverse magnetic travelling wave, whose length is large compared with slab thickness, encounters such a change in geometry. At points very close to the junction the field is modelled by a quasistatic solution. An outer approximation is calculated, based on the idea of replacing the actual slab by a hypothetical surface of infinitesimal thickness, with appropriate discontinuity conditions. A solution is determined in the form of an inverse Fourier integral, and explicit results are given for the reflection and transmission coefficients. (5 refs.)

59600 An improved solution to the fourth moment equation for intensity fluctuations. C.Macaskill (Dept. of Appl. Math. & Theoretical Phys., Univ. of Cambridge, Cambridge, England).

Proc. R. Soc. London Ser. A (GB), vol.386, no.1791, p.461-74 (8 April 1983).

An approximate solution is presented for the fourth moment equation that describes fluctuations of intensity in a wave propagating through a randomly fluctuating medium. The solution is valid for high frequency or relatively strong fluctuations in the medium. The solution procedure is straightforward and at zero order agrees with previously derived approximate solutions. However, the present method is much more direct and more easily extended to complicated problems. Indeed, the first order correction to this basic solution is also determined and it is found that significantly better agreement with previous numerical work is obtained. In addition, knowledge of the correction term allows approximate estimates to be made for the error involved in using the basic solution. (17 refs.)

59601 Existence of global solutions in nonlinear wave equations. Y.Niwa (Dept. of Math., Univ. of Tokyo, Tokyo, Japan).

Proc. Jpn. Acad. Ser. A (Japan), vol.58, no.9, p.391-4 (Nov. 1982). [received: April 1983] (4 refs.)

59602 Control of wave processes with distributed controls supported on a subregion. J.Lagnese (Dept. of Maths., Georgetown Univ., Washington, DC, USA).

SIAM J. Control & Optimiz. (USA), vol.21, no.1, p.68-85 (Jan. 1983).

It is proved that solutions of one-dimensional wave equations satisfying general boundary conditions at the ends of a bounded interval I can be exactly controlled to any finite energy state by means of distributed controls which vanish outside of any fixed nonempty subinterval of I . An example is given which shows that no such general analogous result can hold in higher dimensions. In this case, for a spherical region, those states are characterized which can be exactly controlled to zero by means of controls supported in an annulus within the region. It is found that very strong controllability obtains when the controls are distributed near the boundary, but that only rather weak controllability is possible with controls supported in an interior annulus. Applications of these results to boundary control problems in annular regions are also discussed. (12 refs.)

59603 Nature of the instability in a system of two weakly coupled waves.

A.P.Kuznetsov (N.G. Chernyshevskii State Univ., Saratov, USSR).

Sov. Tech. Phys. Lett. (USA), vol.8, no.8, p.408-9 (Aug. 1982). Translation of:

Pis'ma v Zh. Tekh. Fiz. (USSR), vol.8, no.15-16, p.941-4 (Aug. 1982).

[received: April 1983]

Studies the nature of the instability in a situation in which it is not clear whether one is dealing with an amplifier or an oscillator. A method is proposed for studying the nature of the instability in multiparameter problems; this method radically shortens the formal mathematical aspect of the analysis. (3 refs.)

Spectral transform and solitons: Tools to solve and investigate nonlinear evolution equations. Vol.1See Entry 59556

Exact solution to the formation and propagation problem of a non-stationary shock wave in bilinear mediaSee Entry 61442

Multi-soliton solutions for a classical ferromagnetic chainSee Entry 62536

03.65 QUANTUM THEORY; QUANTUM MECHANICS

(see also 05.30 Quantum statistical mechanics; for relativistic wave equations, see 11.10)

59604 Exponential factor optimization in characteristic function method for electrically charged particles. M.Demiralp (Dept. of Appl. Math., Marmara Sci. & Industrial Res. Inst., Gebze-Kocaeli, Turkey).

Int. J. Quantum Chem. (USA), vol.23, no.3, p.779-87 (March 1983).

(Proceedings of the Fourth International Congress in Quantum Chemistry, Uppsala, Sweden, 13-20 June 1982).

The simplest basis function on hyperspherical coordinates with an optimization parameter is used to construct the characteristic function for a system of electrically charged particles. The first three coefficients of the serial expansion of the characteristic function in powers of eigenvalue parameter are evaluated in terms of well-known functions. The construction of a Pade table for this expansion with the aid of these coefficients, a theoretical discussion, the optimization of the exponential parameter, evaluation of ground state energies for certain systems, and finally comparison of accuracy increments due to optimization for several systems complete the work. (14 refs.)

59605 Scattering in view of the Titchmarsh-Weyl theory. M.Rittby, N.Elander (Res. Inst. for Phys., Stockholm, Sweden), E.Brandas.

Int. J. Quantum Chem. (USA), vol.23, no.3, p.865-74 (March 1983).

(Proceedings of the Fourth International Congress in Quantum Chemistry, Uppsala, Sweden, 13-20 June 1982).

The Titchmarsh-Weyl theory for a singular second-order differential equation is presented. The equations, however, are arranged such that the theory is immediately applicable to the multichannel formulation. The mathematical basis of the Titchmarsh-Weyl theory (TWT) is outlined and the Titchmarsh-Weyl m function is presented. Relations to the associated Green's function and the spectral function are given. It is shown how some quantities common in scattering theory can be expressed in terms of the TWT. The method of complex rotation is then applied to the TWT to create a complex rotated analog of the Titchmarsh-Weyl theory. This is then extended as exterior complex scaling is introduced. An outline of a proof for the method of exterior complex scaling is presented and some numerical results of the complete theory are given. (32 refs.)

- 59606 Hypervirial theorems for some simple quantum chemistry systems.** F.M.Fernandez, E.A.Castro (INIFTA, Sección Química Teórica, La Plata, Argentina). *Int. J. Quantum Chem. (USA)*, vol.23, no.3, p.915-19 (March 1983). (Proceedings of the Fourth International Congress in Quantum Chemistry, Uppsala, Sweden, 13-20 June 1982).
A very general form of the hypervirial theorems, which can be applied to several quantum systems of great interest for the theoretical quantum chemists is presented. (18 refs.)
- 59607 Affine Maczynski logics on compact convex sets of states.** J.Pykacz (Inst. of Maths., Univ. of Gdansk, Gdansk, Poland). *Int. J. Theor. Phys. (USA)*, vol.22, no.2, p.97-106 (Feb. 1983).
Sets of affine functions satisfying Maczynski orthogonality postulate and defined on compact convex sets of states are examined. Relations between affine Maczynski logics and Boolean algebras when the set of states is a Bauer simplex (classical mechanics, some models of nonlinear quantum mechanics) are studied. It is shown that an affine Maczynski logic defined on a Bauer simplex is a Boolean algebra if it is a sublattice of a lattice consisting of all bounded affine functions defined on the simplex. (10 refs.)
- 59608 Calculus on complex Banach spaces.** J.Pian, C.S.Sharma (Dept. of Maths., Birkbeck Coll., London, England). *Int. J. Theor. Phys. (USA)*, vol.22, no.2, p.107-30 (Feb. 1983).
Using the techniques of modern functional analysis, a variety of new concepts have been developed and new results proved which extend considerably the new calculus on complex Banach spaces developed by Sharma and Rebelo (1975). The distinguishing feature of the new calculus is that in this calculus the more general concept of additivity replaces that of linearity in the Frechet calculus. (9 refs.)
- 59609 Remarks on semiclassical quantization.** P.Pechukas (Dept. of Chem., Columbia Univ., New York, NY, USA). *J. Chem. Phys. (USA)*, vol.78, no.6, pt.2, p.3999-4004 (15 March 1983).
Semiclassical quantization in the basic, or 'primitive', version often predicts a simpler, more highly degenerate energy level spectrum than is observed. This point is illustrated by remarks on two-dimensional systems with threefold and higher rotational symmetry and on perturbations of such systems. For example, according to semiclassical quantization essentially all energy levels of a C_3 system are at least doubly degenerate. Such 'incorrect' degeneracy predictions are to be interpreted as predictions of coalescence of levels in the semiclassical ($\rightarrow 0$) limit, coalescence which may manifest itself in real spectra as an excess of near degeneracies. Finally, a consideration on degeneracy rules out one possible solution to the problem of semiclassical quantization of ergodic systems. (14 refs.)
- 59610 Semiclassical quantization and extraction of eigenfunctions using arbitrary trajectories.** N.de Leon, E.J.Heller (Theoretical Div., Los Alamos Nat. Lab., Los Alamos, NM, USA). *J. Chem. Phys. (USA)*, vol.78, no.6, pt.2, p.4005-17 (15 March 1983).
The authors present in this paper a coordinate independent semiclassical quantization method. They demonstrate that in order to extract accurate eigenvalues and eigenfunctions the trajectory does not necessarily have to reside on the quantizing torus, rather, one can use information obtained on arbitrary tori. Because the method is coordinate independent, no difficulty is encountered in quantizing within classical resonance zones. Furthermore, nearby eigenstates and eigenvalues (nearly in action space) may be extracted from the same trajectory—this is especially convenient when the density of states becomes large. (29 refs.)
- 59611 On the $3j$ symmetries.** J.D.Newmarch (Dept. of Phys., Univ. Pertanian Malaysia, Selangor, Malaysia). *J. Math. Phys. (USA)*, vol.24, no.4, p.757-64 (April 1983).
The symmetric properties of the $3jm$ tensor for any finite or compact linear group are discussed using a wreath product construction. This is shown to provide a complete group theoretic explanation for all symmetry properties whether 'essential' or 'arbitrary'. The link with the similar—but distinct—method of inner plethysms is considered. (26 refs.)
- 59612 Some special $SU(3) \supset R(3)$ Wigner coefficients and their application.** K.T.Hecht, Y.Suzuki (Dept. of Phys. Dept., Univ. of Michigan, Ann Arbor, MI, USA). *J. Math. Phys. (USA)*, vol.24, no.4, p.785-92 (April 1983).
Bargmann space expansions of oscillator functions are used to derive analytic expressions for $SU(3) \supset R(3)$ Wigner coefficients for the couplings $(2,0) \times (0,2) \rightarrow (\lambda_3, \mu_3) L_3=0$ and $(\lambda_{10}) \times (\lambda_{20}) \rightarrow (\lambda_{30}, \mu_{30}) L_3=0$, with arbitrary (λ, μ) . These lead to expansions useful in nuclear cluster problems and are used to give a simple form for the $SU(3)$ -irreducible tensor expansion of a scalar two-body interaction, an application which motivated this investigation. (19 refs.)
- 59613 Operator formalism equivalent to the Feynmann quantization technique.** V.Janis, J.Soucek (Math. Inst., Czechoslovak Acad. of Sci., Prague, Czechoslovakia), V.Soucek. *J. Math. Phys. (USA)*, vol.24, no.4, p.834-8 (April 1983).
The concept of a Fock-Stueckelberg space of quantum states and a procedure of an operator quantization using only Lagrangians (kinematical quantization) are introduced. A propagator operator \mathcal{K} , matrix elements of which are Green's functions, is used, and an equation of motion for it is derived. The authors prove that kinematical quantization is an operator (coordinate-free) form of the Feynmann quantization technique. The Feynman path integral (FPI) is obtained as a spectral representation of the operator \mathcal{K} in a coordinate basis. The connection of a representation of commutation relations in this scheme, the domain of integration in FPI, and causality is mentioned. (12 refs.)
- 59614 Weak dispersion-free states and the hidden variables hypothesis.** P.Ptak (Tech. Univ. of Prague, Czechoslovakia). *J. Math. Phys. (USA)*, vol.24, no.4, p.839-40 (April 1983).
The author investigates dispersion-free states which are additive only on the pairs containing a central element (central-absolutely compatible). The author shows that any logic possesses plenty of such states, in fact, as many as a certain Boolean algebra. The latter result matches the hidden variables conjecture. (13 refs.)
- 59615 A generalization of Cohen's theorem.** R.Groblicki (Dept. of Math., Monash Univ., Clayton, Victoria, Australia). *J. Math. Phys. (USA)*, vol.24, no.4, p.841-3 (April 1983).
The theorem due to L. Cohen (1966, 1968), which implies that quantum mechanics cannot be formulated as a stochastic theory in phase space, is generalized. The assumption that the phase-space representatives of the density operators satisfy the quantum mechanical marginals is replaced by the weaker condition of Ω -representability. (10 refs.)
- 59616 A partial inner product space of analytic functions for resonances.** L.P.Horwitz, E.Katznelson (Dept. of Phys. & Astron., Tel Aviv Univ., Ramat Aviv, Israel). *J. Math. Phys. (USA)*, vol.24, no.4, p.848-59 (April 1983).
Generalized Hilberg spaces $D(\alpha, \beta)$ are defined using analytic continuation of Hardy class functions into a wedge bounded by the angles α, β . Eigenfunctions of isolated complex eigenvalues may be found in $D(\alpha, \beta)$ for operators that have a self-adjoint representation in L^2 . These eigenvalues correspond to resonances in the associated decay problem. A bilinear form between $D(\alpha, \beta)$ and $D(-\beta, -\alpha)$ is defined, which has some of the properties of a Hilbert space scalar product, and it is shown that this form can be used to define a variational principle to obtain the eigenvalue equations. (19 refs.)
- 59617 The generalized anharmonic oscillator in three dimensions: Exact eigenvalues and eigenfunctions.** A.Rampal, K.Datta (Dept. of Phys. & Astron., Univ. of Delhi, Delhi, India). *J. Math. Phys. (USA)*, vol.24, no.4, p.860-6 (April 1983).
The authors study the generalized anharmonic oscillator in three dimensions described by the potentials of the form $\Sigma_{k=1}^{2m+1} b_k r^{2k}$. The asymptotic analysis of the Schrodinger equation yields the leading asymptotic behavior of the energy eigenfunctions in terms of the dominant $(m+1)$ coupling constants b_k , $m+1 \leq k \leq 2m+1$. Using an ansatz which incorporates this asymptotic behavior, they reduce the eigenvalue equation to an $(m+2)$ -term difference equation. The corresponding Hill determinant may be used to factorize with a finite determinant as a factor, if a set of constraints on the couplings is satisfied; an infinite sequence of such sets exists. The exact energy eigenvalues appear as the real roots of the finite factor of the Hill determinant; the corresponding wavefunctions are Gaussian weighted polynomials. The authors consider the potentials $\Sigma_{k=1}^{2m} b_k r^{2k}$ and $\Sigma_{k=1}^{2m} b_k r^{2k}$ explicitly; potentials of the form $\Sigma_{k=1}^{2m} b_k r^{2k} + \Sigma_{k=1}^{2m} b_k r^{2k} + \delta/r$ containing both even and odd terms are also considered. Finally, they show that this method of constructing exact solutions fails for anharmonic potentials of the form $\Sigma_{k=1}^{2m} b_k r^{2k}$, of which the quartic anharmonic oscillator is the simplest example. (9 refs.)
- 59618 On the nonlinear Schrodinger equation and its fluid-dynamical form.** T.F.Nonnenmacher (Center for Studies of Nonlinear Dynamics, La Jolla Inst., La Jolla, CA, USA), G.Dukek, G.Baumann. *Lett. Nuovo Cimento (Italy)*, vol.36, ser.2, no.14, p.453-6 (2 April 1983).
Derives and generalizes the fluid-dynamical form of the nonlinear Schrodinger equation (NLS) $i\hbar\psi_t = -\hbar^2/2m \nabla^2\psi + V(x) + \kappa|\psi|^2\psi$ with $\psi_t = \partial\psi/\partial t$ by starting out with the canonical Poisson-Hamilton formalism. (10 refs.)
- 59619 On the gradient method in quantum mechanics.** G.Fonte (Istituto di Fisica Teorica, Univ. di Catania, Catania, Italy), G.Schiffner. *Nuovo Cimento B (Italy)*, vol.74B, ser.2, no.1, p.1-26 (11 March 1983).
The authors present the gradient method as a numerical procedure for the discrete spectrum of Hamiltonian operators in a version which is more general and has better numerical flexibility than a previous version. They show that the gradient method, in addition to having relationships to the Rayleigh-Schrodinger perturbation theory and to the variational method, has also some advantageous features in comparison with them and even in comparison with the Pade and Borel summability methods. In order to check the numerical efficiency of their procedure, they have applied it to the calculation of the ground-state energy of the anharmonic oscillators $p^2 + x^2 + \beta x^4$ and $p^2 + x^2 + \beta x^8$ for a large range of β . (25 refs.)
- 59620 A generalized treatment of point canonical transformations in the path integral.** H.O.Girotti, T.J.M.Simoes (Inst. de Fisica, Univ. Federal do Rio Grande do Sul, Porto Alegre, Brazil). *Nuovo Cimento B (Italy)*, vol.74B, ser.2, no.1, p.59-66 (11 March 1983).
The authors investigate nonlinear point canonical transformations within the path integral when an arbitrary discrete procedure is used for defining this integral. A complete derivation of the so-called additional potential, entirely carried out within the functional formalism, is given in this general case. They also present an extension of the average method of McLaughlin and Schulman (1971). (12 refs.)
- 59621 A Backlund transformation for a generalised Calogero-Moser system.** J.Gibbons, T.Hermens, S.Wojciechowski (Istituto di Fisica, Univ. di Roma I, Rome, Italy). *Phys. Lett. A (Netherlands)*, vol.94A, no.6-7, p.251-3 (21 March 1983).
A Backlund transformation for a generalised Calogero-Moser system, in which the particles possess extra, internal, degrees of freedom, is given. It is shown to be a canonical transformation and its generating function is given explicitly. The transformation is compared with that of the usual Calogero-Moser system. (4 refs.)
- 59622 Test of the gauge-invariant formulation of quantum mechanics.** Kuo-Ho Yang (Phys. Dept., St. Ambrose Coll., Davenport, IA, USA). *Phys. Lett. A (Netherlands)*, vol.94A, no.6-7, p.259-63 (21 March 1983).
An experiment, based on a spin system in a static and a time-varying magnetic field, is proposed and analyzed to test the conventional and the gauge-invariant formulations of quantum mechanics. The electric-dipole interaction is reviewed to show that these two formulations can produce the same results when the magnetic interaction is neglected. (21 refs.)
- 59623 Quantum correlations do not transmit signals.** T.F.Jordan (Phys. Dept., Univ. of Minnesota, Duluth, MN, USA). *Phys. Lett. A (Netherlands)*, vol.94A, no.6-7, p.264 (21 March 1983).
That signals cannot be transmitted with the correlations observed in the Einstein-Podolsky-Rosen experiments that violate Bell's inequalities is shown to be a simple general property of correlations between separate subsystems of any quantum-mechanical system. It does not depend, for example, on the particular properties of the state of two spin $1/2$ particles with total spin zero. (6 refs.)
- 59624 The nonlinear evolution equations related to the Wadati-Konno-Ichikawa spectral problem.** M.Boiti, F.Pempinelli, G.Z.Tu (Dipartimento di Fisica, Univ. di Lecce, Lecce, Italy). *Prog. Theor. Phys. (Japan)*, vol.69, no.1, p.48-64 (Jan. 1983).
The Wadati-Konno-Ichikawa (WKI) spectral problem is considered and the nonlinear evolution equations (NLEE) related to this problem are explicitly constructed. Together with the integrable NLEE already found by WKI, new pure differential solvable NLEEs are derived. The properties of the integro-differential operator L generating all the considered NLEEs are studied. It is shown that the usually successful procedure used to derive the Backlund transformation does not work with these highly nonlinear evolution equations. (18 refs.)
- 59625 New U -matrix theory in quantum mechanics.** C.C.Lam, P.C.W.Fung (Phys. Dept., Univ. of Hong Kong, Hong Kong). *Phys. Rev. A (USA)*, vol.27, no.4, p.1760-78 (April 1983).
The authors have analyzed Dyson's U -matrix theory of solving the Schrodinger equation in the interaction picture and are able to express the U matrix as a dominant term plus an infinite series involving multiple integrals of time. For a certain rather restrictive class of Hamiltonians, their theory is exact for a general time-dependent problem. For other Hamiltonians, they can only

obtain approximate expressions for their U matrix and hence the wave function. Treating a time-independent problem as a special case of the time-dependent situation with a sudden-switching process, they have shown that a U matrix is exact. To demonstrate the working procedures of their theory, they apply it to study the well-known time-independent charged harmonic-oscillator problem and the more general harmonic oscillator with a time-dependent driving force. Compared with other methods, their new theory appears to lead to a result which contains more information than others due to the inclusion of noncommutability properties of operators in the operator Schrodinger equation. It has been shown that the classical Feynman path-integral formalism can be deduced from quantum mechanics with the use of the Green's-function operator. It is interesting to note that apart from a step function, the Green's-function operator is the same as that of the authors' $U^{(B)}$ matrix, which is the U matrix obtained within the regime of the Schrodinger picture for a time-independent Hamiltonian, as a special case of their general time-dependent treatment. (25 refs.)

59626 Classical limit of an induced harmonic oscillation with radiation damping. T. Toyoda, K. Wildermuth (Inst. für Theoretische Phys., Tübingen, Germany).

Phys. Rev. A (USA), vol.27, no.4, p.1790-802 (April 1983).

The previously proposed method to obtain classical limits of quantized fields using von Neumann-lattice coherent states as basis states for the projection form of the Schrodinger equation (Toyoda and Wildermuth, 1980) is modified in order to take into account the reaction of the radiation field to the charge in a compact manner. The modification is based on the work of Glauber (1965) on the time evolution of coherent states. To illustrate the method, a charged harmonic oscillator with and without initial external electromagnetic field is investigated. (10 refs.)

59627 Example of two distinct potentials without point eigenvalues which have the same scattering operator with the reflection coefficient $\alpha(0) = -1$. H.E. Moses (Center for Atmospheric Res., Univ. of Lowell, Lowell, MA, USA).

Phys. Rev. A (USA), vol.27, no.4, p.2220-1 (April 1983).

Abraham, DeFacio, and Moses and Brownstein (1981) have given examples of pairs of potentials, which support no point eigenvalues, but which have the same scattering operator. These potentials all have δ -function contributions to them. In the present paper, a pair of potentials is given, neither of which has a δ -function contribution, such that they both have the same simple scattering operator. Like the earlier examples, the new potentials violate the range condition of Faddeev (1965) and Deift and Trubowitz (1969) used in the proof of the one-to-one correspondence of potentials to scattering operators. Thus the present example is an addition to the list of long-range potentials with simple eigenfunctions and scattering operators. (4 refs.)

59628 Quantum theory and non-Kolmogorovian probability. L. Accardi (Dipartimento di Matematica, Univ. di Roma, Roma, Italy).

Stochastic Processes in Quantum Theory and Statistical Physics. Proceedings of the International Workshop, Marseille, France, 29 June-4 July 1981 (Berlin, Germany: Springer-Verlag 1982), p.1-12

Gives a progress report on the author's work concerning the classical probabilistic model, in whose framework the quantum statistical model may be described. The author's approach considers that the possibility of describing a set of conditional probabilities within the framework of a given statistical model can be checked using statistical invariants. Two problems are discussed in particular. The description of non-Kolmogorovian models and the computation of statistical invariants relative to a given set of conditional probabilities and to a given probabilistic model. (9 refs.)

59629 Stochastic jump processes in the phase space representation of quantum mechanics. J. Bertrand, G. Rideau (Lab. de Phys. Theorique et Math., Univ. Paris VII, Paris, France).

Stochastic Processes in Quantum Theory and Statistical Physics. Proceedings of the International Workshop, Marseille, France, 29 June-4 July 1981 (Berlin, Germany: Springer-Verlag 1982), p.13-18

Describes the evolution of quantum observables in terms of stochastic jump processes, following a procedure similar to that set up by Maslov (1980) and extended by Ph. Combe et al. To characterize these observables, the authors use the representation by functions on phase space due to Wigner (1966) and restrict it mainly to observables described by bounded continuous functions (belonging to $C(\mathbb{R}^2)$). (4 refs.)

59630 Transformation of Wiener integrals and the desingularization of Coulomb problem. P. Blanchard (Fakultät für Phys., Univ. Bielefeld, Bielefeld, Germany).

Stochastic Processes in Quantum Theory and Statistical Physics. Proceedings of the International Workshop, Marseille, France, 29 June-4 July 1981 (Berlin, Germany: Springer-Verlag 1982), p.19-28

Discusses the correspondence between the Coulomb problem and the harmonic oscillator at the level of stochastic differential equations associated with the corresponding imaginary-time Schrodinger equation that can be solved by the Wiener integral. (7 refs.)

59631 Laplace expansions of conditional Wiener integrals and applications to quantum physics. I. Davies, A. Truman (Dept. of Heriot-Watt Univ., Edinburgh, Scotland).

Stochastic Processes in Quantum Theory and Statistical Physics. Proceedings of the International Workshop, Marseille, France, 29 June-4 July 1981 (Berlin, Germany: Springer-Verlag 1982), p.40-55

Gives an account of rigorous results on the Laplace expansions of conditional Wiener integrals, their proofs, and some of their applications to quantum mechanics. (25 refs.)

59632 A stochastic picture of spin. W.G. Faris (Dept. of Math., Univ. of Arizona, Tucson, AZ, USA).

Stochastic Processes in Quantum Theory and Statistical Physics. Proceedings of the International Workshop, Marseille, France, 29 June-4 July 1981 (Berlin, Germany: Springer-Verlag 1982), p.154-68

Dankel (1970) has shown how to incorporate spin into stochastic mechanics. The author shows how the resulting non-local hidden variable theory gives an appealing picture of spin correlation experiments in which Bell's inequality is violated. (6 refs.)

59633 Momentum-position complementarity in stochastic mechanics. F. Guerra (Istituto Matematico 'G. Castelnuovo', Univ. di Roma, Roma, Italy), L. Morato.

Stochastic Processes in Quantum Theory and Statistical Physics. Proceedings of the International Workshop, Marseille, France, 29 June-4 July 1981 (Berlin, Germany: Springer-Verlag 1982), p.208-15

Investigates and clarifies the role of momentum variables in stochastic mechanics, to see whether some of the canonical transformation theory formalism of classical and quantum mechanics can be transferred and adapted to the stochastic frame. (13 refs.)

59634 Wiener measures for quantum mechanical path integrals. J.R. Klauder (Bell Labs., Murray Hill, NJ, USA), I. Daubechies.

Stochastic Processes in Quantum Theory and Statistical Physics. Proceedings of the International Workshop, Marseille, France, 29 June-4 July 1981 (Berlin, Germany: Springer-Verlag 1982), p.245-7

Shows that it is possible to represent certain quantum mechanical evolution operators by path integrals with mathematically well-defined measures. For the hamiltonians considered, this measure is a Wiener measure on phase space. To achieve this goal the authors exploit the overcompleteness of the coherent states. (3 refs.)

Stochastic Processes in Quantum Theory and Statistical Physics. Proceedings of the International Workshop See Entry 59543

Probabilistic and statistical aspects of quantum theory See Entry 59557

Recollections of the discovery of the Thomas precessional frequency See Entry 59565

On the global variance in the 1-reduced local energy matrix for closed shell fermion systems See Entry 59674

Nonexponential decay in relaxation phenomena See Entry 59687

Momentum from sample paths in stochastic mechanics See Entry 59708

Some results on the spectra of random Schrodinger operators and their application to random point interaction models in one and three dimensions See Entry 59739

The composite particle representation theory. I. The composite particle representation transformation See Entry 59911

Are fractional charges and Dirac monopoles consistent with quantum mechanics? See Entry 59958

A quantum-mechanical explanation of vibronic phenomena in atom-molecule collisions See Entry 60897

Scattering of neutral atoms by a periodic potential: the Morse corrugated potential See Entry 63116

Beyond the Big Bang See Entry 64570

03.80 GENERAL THEORY OF SCATTERING

(see also 11.20 *S-matrix theory*, and 11.80 *Relativistic scattering*)

59635 Long-range interactions in free-free transitions. L. Rosenberg (Dept. of Phys., New York Univ., New York, NY, USA).

Phys. Rev. A (USA), vol.27, no.4, p.1879-86 (April 1983).

The soft-proton approximation for bremsstrahlung derived some time ago by Low (1958) and extended by Feshbach and Yennie (1962) to allow for resonances, is further generalized, in the framework of nonrelativistic scattering theory, to apply to the case where the scattering potential has a long-range Coulomb tail. The derivation is based on an asymptotic evaluation of the matrix element in configuration space in which electric-dipole, magnetic-dipole, and electric-quadrupole components of the particle-field interaction are accounted for. The $M1$ and $E2$ contributions give rise to retardation corrections, of order v/c , to the leading $E1$ term. The Coulomb tail has the effect of introducing certain factors into the approximate bremsstrahlung amplitude which depend logarithmically on the photon frequency. The result obtained here has an immediate application to the problem of Coulomb scattering in a low-frequency laser field and provides a generalization of earlier work based on the electric-dipole approximation. (12 refs.)

59636 Variational scattering theory with functionals of fractional form. J.W. Darweych, M. Horbatsch (Phys. Dept., York Univ., Toronto, Ontario, Canada).

Phys. Rev. A (USA), vol.27, no.4, p.2245-7 (April 1983).

The recently proposed functional of Takatsuka and McKoy (1981), derived from the Schwinger-type Newton functional, is shown to follow from the usual Hulthen-Kohn variational principle. A generalization of their method becomes obvious in this approach and its better convergence is demonstrated on a simple example. (5 refs.)

Scattering of neutral atoms by a periodic potential: the Morse corrugated potential See Entry 63116

04.00 RELATIVITY AND GRAVITATION

(for special relativity, see 03.30; for relativistic astrophysics, see 95.30; for relativistic cosmology, see 98.80)

04.20 GENERAL RELATIVITY

(see also 02.40 *Geometry and topology*)

59637 Prolongation structure, Backlund transformation and principal homogeneous Hilbert problem in general relativity. Guo Han-ying, Wu Ke (Inst. of Theoretical Phys., Acad. Sinica, Beijing, China), Wang Shi-kun.

Commun. Theor. Phys. (China), vol.2, no.1, p.883-98 (1983).

The authors briefly review the prolongation structure theory for nonlinear systems, such as nonlinear evolution equations and soliton equations. They then present a set of new fundamental equations of prolongation structures for nonlinear systems and a criterion of completeness for conservation laws. A general requirement for auto-Backlund transformations is proposed from the point of view of prolongation structure theory and it is shown that the problem of searching for auto-Backlund transformations can be reduced to a principal homogeneous Hilbert problem. The theory is applied to the various solution generating techniques for gravitational fields with two commuting Killing vectors. The authors also introduce principal inverse scattering problems with respect to the principal pseudopotentials (i.e. the W -potentials) for both vacuum and electrovac cases. Finally, they show the solutions of the n -fold Kerr family and n -fold charged Kerr family by solving the corresponding principal homogeneous Hilbert problem. (31 refs.)

59638 The N -fold Kerr family and charged Kerr family solutions. Wang Shi-kun (Inst. of Appl. Math., Acad. Sinica, Beijing, China), Guo Han-ying, Wu Ke.

Commun. Theor. Phys. (China), vol.2, no.1, p.921-7 (1983).

The N -fold Kerr family and charged Kerr family solutions are given by means of the inductive method to solve the principal homogeneous Hilbert problems associated with the principal inverse scattering equations (i.e. the W -equations) for both vacuum and electrovac cases with stationary axial symmetry in general relativity. (9 refs.)

59639 Spherically symmetric conformally-flat perfect fluid distributions of class-1. S.N.Pandey, Y.K.Gupta, S.P.Sharma (Dept. of Maths., Univ. of Roorkee, Roorkee, India).

Indian J. Pure & Appl. Math., vol.14, no.1, p.79-84 (Jan. 1983).

It is well-known that the Schwarzschild interior solution is the most general static spherically symmetric perfect fluid distribution which is of class-1 as well as, conformal to a flat-space-time. The authors have obtained the most general non-static perfect fluid distribution which is conformally flat as well as of class-1. (5 refs.)

59640 Field of a charged particle in the presence of scalar meson fields in general relativity. D.R.K.Reddy, V.U.M.Rao (Dept. of Appl. Math., Andhra Univ., Waltair, India).

J. Aust. Math. Soc. Ser. B (Australia), vol.24, pt.4, p.461-5 (April 1983).

Field equations for coupled gravitational and zero mass scalar fields in the presence of a point charge are obtained with the aid of a static spherically symmetric conformally flat metric. A closed form exact solution of the field equations is presented which may be considered as describing the field of a charged particle at the origin surrounded by the scalar meson field in a conformally flat space-time. (13 refs.)

59641 Numerical relativity. II. Numerical methods for the characteristic initial value problem and the evolution of the vacuum field equations for space-times with two Killing vectors. R.W.Corkill, J.M.Stewart (Dept. of Appl. Math. & Theoretical Phys., Univ. of Cambridge, Cambridge, England). *Proc. R. Soc. London Ser. A (GB)*, vol.386, no.1791, p.373-91 (8 April 1983). For pt.1 see ibid., vol.384, p.427-454 (1982). The authors consider the numerical solution of the characteristic initial value problem in general relativity. Although the equations to be integrated have regular coefficients, the nonlinearity leads to the occurrence of singularities after a finite evolution time. They first discuss some novel techniques for integrating the equations right up to the singularities, and secondly present as examples the numerical evolution of the Schwarzschild and certain colliding plane wave space-times. (10 refs.)

59642 Solutions of Einstein field equations with zero-mass scalar field and conformal scalar field from vacuum solutions of Einstein field equations. V.B.Johri (Dept. of Math., Indian Inst. of Technol., Madras, India), G.K.Goswami, R.C.Srivastava.

Prog. Theor. Phys. (Japan), vol.69, no.1, p.341-3 (Jan. 1983).

Generation technique has been used to obtain solutions of Einstein field equations with zero-mass scalar field and a new class of solutions of Einstein-Maxwell field equations with an ordinary scalar field. (12 refs.)

59643 Maxwellian formalism of incompressible fluid mechanics. M.S.Garrido (CAUTL-INIC, Lisboa, Portugal).

Port. Phys. (Portugal), vol.13, no.3-4, p.233-8 (1982). In French.

Using a Maxwellian formalism, it is shown how to pass from relativistic equations to galilean equations by the condition $c \rightarrow \infty$. (4 refs.)

Some non-static self gravitating fluids in space-times of cylindrical symmetry. See Entry 59646

Kaluza-Klein theories on bundles with homogeneous fibers. I See Entry 59648

Stationary line of N Kerr masses kept apart by gravitational spin-spin interaction See Entry 59652

Comment on 'Schiff's conjecture on gravitation' See Entry 59653

Hamiltonian formulation for a translation gauge theory of gravitation See Entry 59654

Hamiltonian formulation of the gauge theory of gravitation. Pure-gravity case See Entry 59655

A model for quantum gravity: an effective approach to Einstein theory See Entry 59657

The London equations for superconductors in a gravitational field See Entry 62526

Magnetohydrodynamic Universe corresponding to a Kantowski-Sachs metric See Entry 64366

Runaway instability in accretion disks orbiting black holes See Entry 64544

Anisotropic cosmology. Two energy distributions generating a conformal gravitational field associated to the Kantowski-Sachs field See Entry 64561

04.30 GRAVITATIONAL WAVES AND RADIATION: THEORY

59644 Gravitational radiation of plasma in a magnetic field. D.V.Galtsov, Yu.V.Grats, E.Yu.Melkumova.

Ukr. Fiz. Zh. (USSR), vol.28, no.3, p.381-8 (March 1983). In Russian.

Deals with gravitational radiation caused by fluctuations of electromagnetic fields and currents in a magnetoactive plasma. It is shown that collective effects lead to enhancement of the gravitational radiation power per unit volume as compared with the prediction based on the independent particles model. Gravitational radiation substantially increases with relativistic electron beams available. (7 refs.)

Loss of angular momentum in a binary system due to collisionless particles as monopoles or gravitinos: does it exceed the gravitational radiation emission in the binary system PSR 1913+16? See Entry 64498

04.40 CONTINUOUS MEDIA; ELECTROMAGNETIC AND OTHER MIXED GRAVITATIONAL SYSTEMS

59645 The problem of motion in the Kaluza theory. Wu Ke, Guo Han-ying (Inst. of Theoretical Phys., Acad. Sinica, Beijing, China).

Commun. Theor. Phys. (China), vol.1, no.6, p.745-51 (1982).

It is shown that the equations of motion for a charged massive particle are consequences of the field equations in Kaluza unification theory of gravitation and electromagnetism, i.e. the equations of motion for the particle can be deduced from Kaluza field equations, just as that in Einstein's theory of motion of general relativity the equations of motion for a massive particle are consequences of the Einstein equations. Furthermore, the Lorentz equations for a particle moving in the Maxwell electromagnetic field on the Minkowski space-time can also be obtained from the Maxwell equations by means of the Kaluza mechanism of the Maxwell theory. (11 refs.)

59646 Some non-static self gravitating fluids in space-times of cylindrical symmetry. S.R.Roy, S.Narain (Dept. of Maths., Banaras Hindu Univ., Varanasi, India).

Indian J. Pure & Appl. Math., vol.14, no.1, p.96-107 (Jan. 1983).

Einstein's field equations have been solved for cylindrically symmetric non-static space-times where the gravitating matter is a perfect fluid, the coordinates being assumed to be co-moving. (13 refs.)

Spherically symmetric conformally-flat perfect fluid distributions of class-1 See Entry 59639

Solutions of Einstein field equations with zero-mass scalar field and conformal scalar field from vacuum solutions of Einstein field equations See Entry 59642

Maxwellian formalism of incompressible fluid mechanics See Entry 59643

Spontaneous compactification in six-dimensional Einstein-Maxwell theory See Entry 59647

The London equations for superconductors in a gravitational field See Entry 62526

Magnetohydrodynamic Universe corresponding to a Kantowski-Sachs metric See Entry 64366

Runaway instability in accretion disks orbiting black holes See Entry 64544

04.50 UNIFIED FIELD THEORIES AND OTHER THEORIES OF GRAVITATION

59647 Spontaneous compactification in six-dimensional Einstein-Maxwell theory. S.Randjbar-Daemi (Internat. Centre for Theoretical Phys., Trieste, Italy), A.Salam, J.Strathdee.

Nucl. Phys. B, Part. Phys. (Netherlands), vol.B214, no.3, p.491-512 (18 April 1983).

A discrete set of solutions to the classical Einstein-Maxwell equations in six-dimensional space-time is considered. These solutions have the form of a product of four-dimensional constant curvature space-time with a 2-sphere. The Maxwell field has support on the 2-sphere where it represents a monopole of magnetic charge, $n = \pm 1, \pm 2, \dots$. The spectrum of massless and massive states is obtained for the special case of flat 4-space, and the solution is shown to be classically stable. The limiting case where the radius of the 2-sphere becomes small is considered and a dimensionally reduced effective lagrangian for the long range modes is derived. This turns out to be an $SU(2) \times U(1)$ gauge theory with chiral couplings. (11 refs.)

59648 Kaluza-Klein theories on bundles with homogeneous fibers. I. R.Percacci (Istituto di Fisica Teorica, Univ. di Trieste, Trieste, Italy), S.Randjbar-Daemi.

J. Math. Phys. (USA), vol.24, no.4, p.807-14 (April 1983).

The authors analyze some geometric aspects of Kaluza-Klein theories under the assumption that the $(4+d)$ -dimensional space is a bundle over space-time M with fiber G/H . They formulate the most general metric in the bundle which leads, upon dimensional reduction of the Ricci scalar, to a G -gauge invariant Lagrangian. They find that the treatment of Brans-Dicke-like scalars given by some authors is inconsistent with the bundle-theoretic interpretation. (19 refs.)

59649 On a possible new theory of gravitation. M.Borneas. *Naturwissenschaften (Germany)*, vol.70, no.3, p.140 (March 1983).

The scientist not specializing in the physics of gravitation may wonder at the current situation with regard to theoretical views on this problem. On the one hand, there is Einstein's well-known theory and, on the other hand, many sound arguments (Mach's principle, etc.) have been presented which modify Einstein's equation, from Jordan and Brans-Dicke up to many recent works. Most authors propose a supplementary scalar field. However, the gravitation experiments performed hitherto, under usual conditions, specifically in the solar system, have strongly supported Einstein's equation. How then can one get out of this dilemma? The author suggests that a supplementary field exists, but that its contribution under the conditions in the experiments conducted thus far has been negligible. But this might not be the case under different conditions, in other domains of space. (10 refs.)

59650 Remarks on the Brans-Dicke theory of N dimensions. M.Nishioka (Dept. of Phys., Yamaguchi Univ., Yamaguchi, Japan).

Nuovo Cimento B (Italy), vol.74B, ser.2, no.1, p.27-32 (11 March 1983).

A study of the Brans-Dicke theory in vacuum shows that one of the Brans-Dicke equations is represented in terms of the Riemann curvature tensor, the Weyl projective curvature tensor and its covariant derivative. Studying the case that the covariant derivative of the Weyl projective curvature tensor vanishes, the author comments on the relationship between the Brans-Dicke space-time and the constant curvature space-time. (6 refs.)

59651 On the structure of space, time and field. T.Kaneko, H.Sugawara (Nat. Lab. for High Energy Phys., KEK, Ibaraki, Japan).

Prog. Theor. Phys. (Japan), vol.69, no.1, p.262-99 (Jan. 1983).

A unified theory of gravity and other interactions is proposed. The authors are guided by the principle of equivalence of space-time and field and by Mach's principle. Fundamental Lagrangian is assumed to describe the whole Universe on the one hand and local physical phenomena on the other. A condensed scalar field determines both the structure of the Universe and that of the group of grand unification. The Hubble constant and deceleration parameter are related to the grand unification group. One remarkable feature of their theory is the dependence of the gravitational and the gauge coupling constants on the cosmological time. (10 refs.)

59652 Stationary line of N Kerr masses kept apart by gravitational spin-spin interaction. M.Yamazaki (Dept. of Phys., Kanazawa Univ., Kanazawa, Japan).

Phys. Rev. Lett. (USA), vol.50, no.14, p.1027-30 (4 April 1983).

The metric is presented, in terms of six determinants of degree N , in a concise closed form, describing N collinear isolated Kerr masses ($N=1,2,3,\dots$) balanced by their gravitational spin-spin interaction. Two hitherto unnoticed potentials \tilde{L} and \tilde{M} are introduced to evaluate the metric function ω . The conditions for regularity of the metric on the symmetrical axis are presented. (6 refs.)

59653 Comment on 'Schiff's conjecture on gravitation'. Wei-Tou Ni (Dept. of Phys., Nat. Tsing Hua Univ., Hsinchu, Taiwan), A.Coley.

Phys. Rev. Lett. (USA), vol.50, no.15, p.1173-4 (11 April 1983).

Using a general formalism with seven nonmetric degrees of freedom, Coley (1982) has studied the validity of Schiff's conjecture in a spherically symmetric and static (SSS) gravitational field. This adds to the understanding of Schiff's conjecture considerably. In 1960, Schiff conjectured that the Galileo weak equivalence principle (WEP) should imply the Einstein equivalence principle (EEP), and, therefore, imply the universality of gravitational red shift (UGR). The results of Coley's extensive calculations actually show that WEP-EEP (Schiff's conjecture) and hence also that WEP-UGR in SSS gravi-

tational field in his formalism. This demonstrates the importance and usefulness of WEP. (10 refs.)

Solutions of Einstein field equations with zero-mass scalar field and conformal scalar field from vacuum solutions of Einstein field equations

.....See Entry 59642

The problem of motion in the Kaluza theorySee Entry 59645

The production of string loops in an expanding universeSee Entry 64565

04.60 QUANTUM THEORY OF GRAVITATION

59654 Hamiltonian formulation for a translation gauge theory of gravitation. R.De Azeredo Campos, C.G.Oliveira (Dept. de Física, Univ. de Brasília, Brasília, Brazil).

Nuovo Cimento B (Italy), vol.74B, ser.2, no.1, p.83-92 (11 March 1983). Dirac's Hamiltonian methods are applied to a gauge theory of the translation group formulated by Hayashi (1967, 1972, 1973, 1977) as a gravitational theory which stands on microscopical scale. Four constraint equations are obtained, as in general relativity, because of the existence of the space-time translation group, which is a group of invariance of the theory. Propagation equations for the dynamical variables are also derived. (14 refs.)

59655 Hamiltonian formulation of the gauge theory of gravitation. Pure-gravity case. T.Fukuyama (Dept. of Phys., Osaka Univ., Osaka, Japan), K.Kamimura.

Nuovo Cimento B (Italy), vol.74B, ser.2, no.1, p.93-111 (11 March 1983).

The gauge theory of gravitation invariant under O_3 and the general coordinate transformations is formulated by using Dirac's Hamiltonian formalism. The tetrad field is introduced as a connection of the O_3 gauge group. By fixing the boost part of this gauge freedom, the spin connection is eliminated by using second-class constraints. As a result the system is described by the tetrad field with a set of first-class constraints associated to the local Lorentz and the general co-ordinate transformations. (15 refs.)

59656 Schouten manifold with a spinor structure. T.Obata (Dept. of Electrical Engng., Tohoku Univ., Sendai, Japan), H.Oshima.

Prog. Theor. Phys. (Japan), vol.69, no.1, p.314-22 (Jan. 1983).

The authors equip a general Schouten manifold with a spinor structure and further with a spinor metric, a spinor affine connection and a linear isomorphism of the tangent vector space into the spinor space which is a two-dimensional complex vector space. The nonmetrical tensor that measures the failure of the affine connection to preserve the metric can then be expressed in fundamental geometrical objects which are related to the above spinorial objects. They also give a method of reducing the Schouten manifold to special manifolds such as the Weyl-Cartan manifold and the Riemann-Cartan manifold. (11 refs.)

59657 A model for quantum gravity: an effective approach to Einstein theory. A.Aurilia (Dept. of Phys., Univ. of Alberta, Edmonton, Alberta, Canada), M.Martellini.

Phys. Lett. B (Netherlands), vol.123B, no.5, p.303-7 (7 April 1983).

The authors propose a renormalizable and unitary non-abelian gauge theory for gravitational interactions possessing $Sp(4)$ as a partially conserved gauge symmetry. For energies below the Planck mass the theory reproduces Einstein's general relativity which they regard as an effective theory of gravitational interactions. (9 refs.)

On a possible new theory of gravitationSee Entry 59649

On the structure of space, time and fieldSee Entry 59651

A geometric interpretation for certain scalar-tensor gravity theoriesSee Entry 59661

Loss of angular momentum in a binary system due to collisionless particles as monopoles or gravitinos: does it exceed the gravitational radiation emission in the binary system PSR 1913+16?See Entry 64498

04.65 SUPERGRAVITY

59658 Supergravity with one auxiliary spinor. M.F.Sohnius (CERN, Geneva, Switzerland), P.C.West.

Nucl. Phys. B, Part. Phys. (Netherlands), vol.B216, no.1, p.100-24 (25 April 1983).

The authors present an 'intermediate' off-shell version of $N=1$ supergravity and its tensor calculus. The supergravity multiplet has 16+16 field components. The formulation can be constrained to either of the minimal ones with 12+12 components, or enlarged by matter couplings to several 20+20 component versions. Self-coupled to its own axial gauge submultiplet it leads to spontaneous supersymmetry breaking in the form first discussed by Freedman (1977) and to a propagating gauge field. (19 refs.)

59659 Gravitinos on the lattice. G.Maturana, C.P.van den Doel (Dept. of Phys., Univ. of California, Santa Cruz, CA, USA).

Phys. Lett. B (Netherlands), vol.123B, no.5, p.332-4 (7 April 1983).

Studies spin 3/2 fields on the lattice. Species doubling is found to be totally curable with an analogue of Wilson's method (1974) and partially with an analogue of the Kogut-Susskind formalism (1977). Only the latter preserves local supersymmetry but describes at least four species. (12 refs.)

59660 BRST invariance and the stochastic quantization of supergravity. T.Hori (Dept. of Phys., Tokyo Metropolitan Univ., Tokyo, Japan).

Phys. Lett. B (Netherlands), vol.123B, no.6, p.391-5 (14 April 1983).

The quantization of $N=1$ supergravity without auxiliary fields is considered from a stochastic point of view. Using the BRST symmetry properties of a closed algebra, sufficient conditions for the equivalence of the stochastic and the Faddeev-Popov quantization are derived. (11 refs.)

59661 A geometric interpretation for certain scalar-tensor gravity theories. G.F.Chapline (Lawrence Nat. Lab., Univ. of California, Livermore, CA, USA).

Phys. Lett. B (Netherlands), vol.123B, no.6, p.401-6 (14 April 1983).

Dimensional reduction of ten-dimensional $N=1$ supergravity, where the space of extra dimensions is a compact coset space, leads to a class of non-linear σ -models coupled to gravity. Some members of this class contain only spin 2 and spin 0 fields while other members of this class are supersymmetric non-linear σ -models coupled to supergravity. In all cases the scalar field self-coupling constants are simply related to Newton's constant. (12 refs.)

59662 Hierarchies from supergravity. U.Ellwanger (Dept. of Theoretical Phys., Univ. of Oxford, Oxford, England).

Phys. Lett. B (Netherlands), vol.124B, no.1-2, p.34-6 (21 April 1983). Discusses a non-minimal coupling of scalar fields to supergravity. As well as spontaneous local supersymmetry breaking and a vanishing cosmological constant the author can obtain a gravitino mass of ~ 100 GeV without introducing a mass scale different from the Planck scale. (13 refs.)

59663 Fermion masses from supergravity. D.V.Nanopoulos, M.Srednicki (CERN, Geneva, Switzerland).

Phys. Lett. B (Netherlands), vol.124B, no.1-2, p.37-9 (21 April 1983).

The authors suggest that non-renormalizable interactions (contained, for example, in supergravity theories) are the source of the fermion masses for the first two generations. Small Yukawa couplings are not necessary. They find a new mass relation, $m_e/m_\mu = 2/3$ at the grand unification scale, which is consistent (after renormalization) with low energy physics. (12 refs.)

59664 Gauged $n=8$ supergravity and its breaking from spontaneous compactification. B.Biran, F.Englert (Faculte des Sci., Univ. Libre de Bruxelles, Brussels, Belgium), B.de Wit, H.Nicolai.

Phys. Lett. B (Netherlands), vol.124B, no.1-2, p.45-50 (21 April 1983).

Gauged $N=8$ supergravity emerges from spontaneous compactification of eleven-dimensional supergravity on the riemannian S^7 . This is the only non-trivial compactification scheme preserving full supersymmetry. The four-dimensional theory admits a spontaneously broken solution describable as a compactification on the parallelized S^7 ; supersymmetry is completely broken and the local $SO(8)$ group is reduced to G_2 . (13 refs.)

59665 Radiative corrections to the effective potential in $N=1$ supergravity. R.Barbieri (Istituto di Fisica, Univ. Pisa, Pisa, Italy), S.Cecotti.

Z. Phys. C (Germany), vol.17, no.2, p.183-7 (1983).

The authors compute the one loop quadratic divergences to the effective potential of the matter scalars in $N=1$ supergravity. They discuss in some special instances (the Das-Freedman and the Deser-Zumino lagrangians) the problem of supersymmetry gauge invariance. They comment on the relevance of the calculation to model building. (17 refs.)

Natural values of coupling constants and cosmological inflation in a supersymmetric modelSee Entry 64566

04.80 EXPERIMENTAL TESTS OF GENERAL RELATIVITY AND OBSERVATIONS OF GRAVITATIONAL RADIATION

Precision measurements and fundamental constantsSee Entry 59755

05.00 STATISTICAL PHYSICS AND THERMODYNAMICS

(see also 02.50 Probability theory, stochastic processes, and statistics)

05.20 STATISTICAL MECHANICS

59666 Ensemble corrections for the molecular-dynamics ensemble. D.C.Wallace, G.K.Straub (Los Alamos Nat. Lab., Los Alamos, NM, USA).

Phys. Rev. A (USA), vol.27, no.4, p.2201-5 (April 1983).

Expressions are derived which relate the averages of a dynamical variable in the molecular-dynamics ensemble and in the generalized canonical ensemble. Fluctuations in the two ensembles are also related. These results make the full equilibrium theory of classical statistical mechanics accessible to evaluation by molecular-dynamics computations. (13 refs.)

59667 Concerning the description of processes in objects of finite size. Yu.S.Sereda (Res. Inst. for Mech., State Univ., Gorki, USSR).

Sov. Phys.-Tech. Phys. (USA), vol.27, no.9, p.1058-62 (Sept. 1982). Translation of: *Zh. Tekh. Fiz. (USSR)*, vol.52, no.9, p.1725-30 (Sept. 1982).

[received: April 1983]

A beta distribution is proposed for use as a statistical model of real objects. It is shown that the beta distribution and its entropy can describe fairly completely the physical properties of an investigated object and the processes that occur in it in terms of a sequence of states, each of which can deviate from equilibrium. Possible forms and properties of trajectories of processes with monotonic and external entropy changes are discussed. (18 refs.)

59668 The Van Hove limit in classical and quantum mechanics. G.F.Dell'Antonio (Istituto Matematico G. Castelnuovo, Univ. di Roma, Roma, Italy).

Stochastic Processes in Quantum Theory and Statistical Physics. Proceedings of the International Workshop, Marseille, France, 29 June-4 July 1981 (Berlin, Germany: Springer-Verlag 1982), p.75-110

Outlines an approach to describing the motion of a classical or quantum particle in a random medium. In particular the Van Hove limit of small coupling, long time is studied for the momentum distribution in both classical mechanics and quantum theory. (9 refs.)

59669 Stochasticity in non-equilibrium statistical mechanics. G.G.Emch (Dept. of Math., Univ. of Rochester, Rochester, NY, USA).

Stochastic Processes in Quantum Theory and Statistical Physics. Proceedings of the International Workshop, Marseille, France, 29 June-4 July 1981 (Berlin, Germany: Springer-Verlag 1982), p.147-53

Outlines a proposal to incorporate the following areas into one line of research. Hamiltonian systems, the thermodynamical limit, infinite KMS systems, the choice of time scale, dissipative systems, are reduced description, EK systems. Two lines of enquiry are followed which lead to non-equilibrium statistical mechanics. (10 refs.)

Elementary statistical thermodynamics. A problems approachSee Entry 59558

On the Burnett and higher order equations of hydrodynamicsSee Entry 59596

The description of catastrophic changes in tagged particle dynamics by the self-consistent repeated ring equationSee Entry 59710

Dynamical systems with few degrees of freedomSee Entry 59719

All that Brownian motionSee Entry 59721

Path-integral approach to a finite many-body problemSee Entry 59733

The long time tail conundrum in nonequilibrium statistical mechanicsSee Entry 59744

Gas with a nonMaxwellian velocity distributionSee Entry 61589

05.30 QUANTUM STATISTICAL MECHANICS

(see also 67. Quantum fluids, and 71. Electron states in condensed matter)

59670 The Thirring model at a finite fermion density. Y.Okwamoto (Dept. of Engng. & Sci., Hokkaido Univ., Sapporo, Japan). *J. Phys. Soc. Jpn. (Japan)*, vol.52, no.4, p.1081-3 (April 1983). The spectrum of the massless Thirring model at a finite fermion density is examined, using the Bethe ansatz, with the momentum cutoff. The cutoff procedure in this letter is valid for the model within the first order of the coupling constant. (8 refs.)

59671 Magnetic moment of an electron gas in crossed, homogeneous electric and magnetic fields. P.Achuthan, S.Benjamin, K.Venkatesan (Dept. of Math., Indian Inst. of Technol., Madras, India). *J. Phys. A (GB)*, vol.16, no.6, p.1307-13 (21 April 1983). The magnetic properties of a Dirac electron gas in crossed, homogeneous electric (E) and magnetic (H) fields are studied. An explicit expression for the magnetic moment of the gas is obtained. The calculations in the degeneracy limit of the gas show that (i) for values of $E/H > 0.01$ there is a clear suppression of the transition from paramagnetism to diamagnetism, (ii) there is a weakening of the quasi-periodic oscillations of the magnetic moment observed in the $E=0$ case, again for $E/H > 0.01$, and (iii) there is a distinct possibility of spontaneous magnetisation for the values of $E/H > 0.9$. (13 refs.)

59672 Path integration of an action related to an electron gas in a random potential. A.K.Dhara, D.C.Khandekar, S.V.Lawande (Theoretical Reactor Phys. Section, Bhabha Atomic Res. Centre, Bombay, India). *J. Math. Phys. (USA)*, vol.24, no.4, p.844-7 (April 1983). Path integration of an action related to an electron gas in a random potential is performed within the framework of Feynman's polygonal path approach. The exact propagator obtained is simply related to the harmonic oscillator propagator. The integration is direct and does not require the knowledge of an auxiliary measure or the artificial coupling of the system to the external forces. (11 refs.)

59673 Existence theorems for Segal quantization via spectral theory in Krein space. P.Broadbridge (School of Phys. & Geosci., Western Australian Inst. of Technol., South Bentley, WA, Australia). *J. Aust. Math. Soc. Ser. B (Australia)*, vol.24, pt.4, p.439-60 (April 1983). Segal's unitarizing complex structure J is shown, in Fermi-Dirac statistics to be the orthogonal component in the polar decomposition of the real skew adjoint generator of classical dynamics. It is proven that in Bose-Einstein statistics the classical symplectic dynamics cannot be unitarized unless the generator is similar to a real skew adjoint operator. With the classical Hamiltonian strictly positive, J is the pseudo-orthogonal component in the polar decomposition of the generator, using spectral theory in Krein space with indefinite metric. Thus, J can be expressed simply in terms of the projection $E(0)$ onto the subspace of classical solutions with negative frequency. This complements the physicists' experience that conceptual difficulties arise when dynamically invariant separation of positive and negative frequency solutions is impossible. (26 refs.)

59674 On the global variance in the 1-reduced local energy matrix for closed shell fermion systems. G.F.Thomas (Massey Coll., Univ. of Toronto, Toronto, Ontario, Canada). *Phys. Lett. A (Netherlands)*, vol.94A, no.6-7, p.265-8 (21 March 1983). The global variance in the 1-reduced local energy matrix is proposed as a quantitative measure of the error incurred through use of the Roothaan procedure in a limited basis for a closed shell fermion system. Applications are presented for the singlet ground states of a pair of coupled harmonic oscillators and the hydrogen molecule. (17 refs.)

59675 Monte Carlo evaluation of functional integrals using coherent-state Slater determinants. Y.Avishai (Dept. of Phys., Ben Gurion Univ. of the Negev, Beer Sheva, Israel), J.Richert. *Phys. Rev. Lett. (USA)*, vol.50, no.16, p.1175-8 (18 April 1983). The feasibility of using Monte Carlo methods in finite fermion systems has been investigated. The basic tool is a (recently suggested) functional integral representation of $Z = \text{tr}[\exp(-\beta H)]$ using real coherent states of Slater determinants. Conditions for using the discretized (N -point lattice) version as a starting point for Monte Carlo integrations are studied. The limit of large β is achieved only with large \sqrt{N} . For a two-fermion system numerical calculations of the ground-state energy agree fairly well with the exact value. (21 refs.)

59676 Non-commutative martingales and stochastic integrals in Fock space. R.L.Hudson (Dept. of Math., Univ. of Nottingham, Nottingham, England), R.F.Streater. *Stochastic Processes in Quantum Theory and Statistical Physics. Proceedings of the International Workshop, Marseille, France, 29 June-4 July 1981* (Berlin, Germany: Springer-Verlag 1982), p.216-22. Boson Fock space is used to construct some non-commutative martingales, and a definition of stochastic integrals based on exponential vectors is given. It is shown that Ito's formula reduces to the chain rule with Wick ordering. (4 refs.)

59677 Quantum dissipation and stochastic processes. R.Vilela Mendes (Inst. Nacional de Investigacao Cientifica, Lisboa, Portugal). *Stochastic Processes in Quantum Theory and Statistical Physics. Proceedings of the International Workshop, Marseille, France, 29 June-4 July 1981* (Berlin, Germany: Springer-Verlag 1982), p.332-6. A general scheme to quantize dissipative and volume preserving dynamics is reviewed. The operator solutions of two examples are used to derive the stochastic differential equations obeyed by these processes. (7 refs.)

Stochastic Processes in Quantum Theory and Statistical Physics. Proceedings of the International Workshop See Entry 59543

Probabilistic and statistical aspects of quantum theory See Entry 59557

Quantum theory and non-Kolmogorovian probability See Entry 59628

The Van Hove limit in classical and quantum mechanics See Entry 59668

Effect on spin variables and exciton motion on ground-state properties of the 'trion' See Entry 59737

05.40 FLUCTUATION PHENOMENA, RANDOM PROCESSES, AND BROWNIAN MOTION

59678 Noise competition in a nonlinear system. I. Two independent noises. I.I.Fedchenia (Inst. of Phys., Acad. of Sci., Minsk, Belorussian SSR), N.A.Usova. *Z. Phys. B (Germany)*, vol.50, no.3, p.263-7 (1983). A case of two independent noise sources influence on a locked oscillator phase is investigated. It is shown that they affect the system in an opposite way. Probability density, first passage times, $\langle \psi \rangle$ and $\langle \psi^2 \rangle$ are computed. (15 refs.)

59679 Quantum treatment of Brownian motion and influence of dissipation on diffusion in dynamically disordered systems. J.Heinrichs (Inst. de Phys., Univ. of Liege, Liege, Belgium). *Z. Phys. B (Germany)*, vol.50, no.3, p.269-73 (1983). The time-dependent hamiltonian formulation of the Langevin equation is used as a starting point for a quantum treatment of the motion of a free Brownian particle. From an exact solution of the time-dependent Schrodinger equation for the density-matrix in one dimension the author obtains the mean square displacement, $\langle x^2(t) \rangle$, of the Brownian particle, as well as the mean displacement induced by a uniform electric field $E(t)$. While quantum effects are significant for time intervals up to the frictional relaxation time, the long time results are identical to those obtained directly from the solution of the Langevin equation. Next, the author analyses in a similar way the motion of an electron in a dynamically disordered continuum where the effect of a classical friction force (dissipation) is taken into account. The friction effect is described using the phenomenological time-dependent hamiltonian inferred from the Langevin equation and the potential fluctuations are assumed to have a generalised gaussian white-noise form. The final result for $\langle x^2(t) \rangle$ shows a time-dependence similar to that obtained for the case of Brownian motion. (11 refs.)

59680 Scalar and vector laws of distribution of random quantities. V.F.Paramonov. *Izv. VUZ Mashinostr. (USSR)*, no.12, p.120-5 (1982). In Russian. Formulae are derived for the main theoretical laws of distribution of random quantities and their numerical characteristics in vectorial form, when a change is made from a one-parameter distribution to a two-parameter, or vectorial, distribution. The results can be used for theoretical and probabilistic analyses of vectorial dimensional chains, such as determination of overall pulsations, eccentricities and deviation of coordinate axes. (4 refs.) Z.F.V.

59681 Stochastic classical trajectory approach to relaxation phenomena. III. Comparison of trajectory results to quantum mechanical perturbation theory. A.Nitzan, J.C.Tully (Bell Labs, Murray Hill, NJ, USA). *J. Chem. Phys. (USA)*, vol.78, no.6, pt.2, p.3959-63 (15 March 1983). For pt.II see *ibid.*, vol.69, p.2525 (1978). A simple model representing an impurity oscillator coupled anharmonically to a lattice is examined both by quantum mechanical perturbation theory and by stochastic classical trajectory simulations. Energy relaxation rates are computed as a function of temperature. Classical and quantum relaxation rates are found to agree well at high temperatures but, as expected, diverge drastically at low temperatures. If zero-point motion of the lattice is incorporated into the classical calculation, classical and quantum relaxation rates agree quite well for all temperatures, even for $T \rightarrow 0$. This suggests that the stochastic classical trajectory method can provide an accurate description of relaxation phenomena even at very low temperatures. (10 refs.)

59682 The power of chaos measured through the spectral analysis of experimental data. A.Lafon, A.Rossi, C.Vidal (Centre de Recherche Paul Pascal, Domaine Univ., Talence, France). *J. Phys. (France)*, vol.44, no.4, p.505-12 (April 1983). The authors investigate how far the power of chaos might be figured from the power spectrum of a dynamical regime. The numerical simulation of a model allows them to show that an entropy-like function H and the largest Lyapunov characteristic exponent λ both display nearby variations. Accordingly, they suggest one computes this H function, whenever λ cannot be determined. Since this is always the case when experimental time series are involved, a sequence of chaotic regimes exhibited by the Belousov-Zhabotinsky reaction is used to illustrate this point. (18 refs.)

59683 Error estimates of solutions and mean of solutions of stochastic differential systems. G.S.Laddes, M.Sambandham (Dept. of Math., Univ. of Texas, Arlington, TX, USA). *J. Math. Phys. (USA)*, vol.24, no.4, p.815-22 (April 1983). Stochastic differential equations are considered. Estimates in terms of statistical properties are given for the difference between the solutions and solutions of the mean of stochastic differential systems. For this purpose necessary theorems are developed and sufficient conditions are given to obtain error estimates. A few examples are worked out to demonstrate the usefulness of the results. (8 refs.)

59684 From classical dynamics to continuous time random walks. R.Zwanzig (Inst. for Phys. Sci. & Technol., Univ. of Maryland, College Park, MD, USA). *J. Stat. Phys. (USA)*, vol.30, no.2, p.255-62 (Feb. 1983). (Proceedings of a Symposium on Random Walks and Their Application to the Physical and Biological Sciences, Gaithersburg, MD, USA, 28 June-1 July 1982). The migration of a classical dynamical system between regions of configuration space can be treated as a continuous time random walk between these regions. Derivation of a classical analog of the quantum mechanical generalized master equation provides expressions for the waiting time distribution in terms of transition memory functions. A short memory approximation to these memory functions is equivalent to the well-known transition state method. An example is discussed for which this approximation seems reasonable but is entirely wrong. (9 refs.)

59685 Stochastic flows, reaction-diffusion processes, and morphogenesis. J.J.Kozak, M.D.Hatlee, M.K.Musho, P.A.Politiowicz, C.A.Walsh (Dept. of Chem., Univ. of Notre Dame, Notre Dame, IN, USA). *J. Stat. Phys. (USA)*, vol.30, no.2, p.263-71 (Feb. 1983). (Proceedings of a Symposium on Random Walks and Their Application to the Physical and Biological Sciences, Gaithersburg, MD, USA, 28 June-1 July 1982). Recently, an exact procedure has been introduced (C.A. Walsh and J.J. Kozak, 1981) for calculating the expected walk length (n) for a walker undergoing random displacements on a finite or infinite (periodic) d -dimensional lattice with traps (reactive sites). The method (which is based on a classification of the symmetry of the sites surrounding the central deep trap and a coding of the fate of the random walker as it encounters a site of given symmetry) is applied here to several problems in lattice statistics for each of which exact results are presented. First, the authors assess the importance of lattice geometry in influencing the efficiency of reaction-diffusion processes in simple and multiple trap systems by reporting values of $\langle n \rangle$ for square (cubic) versus hexagonal lattices in $d=2, 3$. They then show how the method

may be applied to variable-step (distance-dependent) walks for a single walker on a given lattice and also demonstrate the calculation of the expected walk length (n) for the case of multiple walkers. Finally, they make contact with recent discussions of 'mixing' by showing that the degree of chaos associated with flows in certain lattice systems can be calibrated by monitoring the lattice walks induced by the Poincaré map of a certain parabolic function. (14 refs.)

59686 Fractal and lacunary stochastic processes. B.D.Hughes (Dept. of Chem. Engng. & Materials Sci., Univ. of Minnesota, Minneapolis, MN, USA), E.W.Montroll, M.F.Schlesinger.

J. Stat. Phys. (USA), vol.30, no.2, p.273-83 (Feb. 1983). (Proceedings of a Symposium on Random Walks and Their Application to the Physical and Biological Sciences, Gaithersburg, MD, USA, 28 June-1 July 1982).

Discrete-time random walks simulate diffusion if the single-step probability density function (jump distribution) generating the walk is sufficiently short-ranged. In contrast, walks with long-ranged jump distributions simulate Levy or stable processes. A one-dimensional walk with a self-similar jump distribution (the Weierstrass random walk) and its higher-dimensional generalizations generate fractal trajectories if certain transience criteria are met and lead to simple analogs of deep results on the Hausdorff-Besicovitch dimension of stable processes. The Weierstrass random walk is lacunary (has gaps in the set of allowed steps) and its characteristic function is Weierstrass' nondifferentiable function. Other lacunary random walks with characteristic functions related to Riemann's zeta function and certain number-theoretic functions have very interesting analytic structure. (26 refs.)

59687 Nonexponential decay in relaxation phenomena. A.K.Rajagopal (Dept. of Phys. & Astron., Louisiana State Univ., Baton Rouge, LA, USA), K.L.Ngai, R.W.Rendell, S.Teitler.

J. Stat. Phys. (USA), vol.30, no.2, p.285-92 (Feb. 1983). (Proceedings of a Symposium on Random Walks and Their Application to the Physical and Biological Sciences, Gaithersburg, MD, USA, 28 June-1 July 1982).

A variety of considerations from different points of view including non-Markovian stochastic processes, basic quantum mechanics, and a mechanism based on condensed matter physics, all lead to the fractional exponential decay at long times in relaxation processes. Implications of this decay law and its verifiable predictions in a broad range of phenomena in condensed matter physics are pointed out. (16 refs.)

59688 Master equation techniques for exciton motion, relaxation, capture, and annihilation. V.M.Kenkre (Dept. of Phys. & Astron., Univ. of Rochester, Rochester, NY, USA).

J. Stat. Phys. (USA), vol.30, no.2, p.293-303 (Feb. 1983). (Proceedings of a Symposium on Random Walks and Their Application to the Physical and Biological Sciences, Gaithersburg, MD, USA, 28 June-1 July 1982).

Techniques developed recently for the study of exciton dynamics in molecular solids are discussed. They include master equation methods for the analysis of prerelaxation energy transfer, the generalized master equation approach to coherence in exciton motion, and the defect technique as applied to exciton trapping and annihilation. (31 refs.)

59689 Renormalization group approach to random walks on disordered lattices. J.Machta (Inst. for Phys. Sci. & Technol., Univ. of Maryland, College Park, MD, USA).

J. Stat. Phys. (USA), vol.30, no.2, p.305-14 (Feb. 1983). (Proceedings of a Symposium on Random Walks and Their Application to the Physical and Biological Sciences, Gaithersburg, MD, USA, 28 June-1 July 1982).

One-dimensional random walks with static disorder are analyzed using a real space renormalization group procedure. The presence of disorder leads to a non-Markovian description of the macroscopic behavior of the random walk. The author considers random walks with nearest-neighbour hopping described by a master equation with both on-site and site-to-site disorder in the transition matrix. Site-to-site disorder leads to a generalized diffusion coefficient with a $t^{-3/2}$ long time tail whereas on-site disorder leads to a generalized Burnett coefficient with a $t^{-1/2}$ long time tail. (12 refs.)

59690 Theory of hopping and multiple-trapping transport in disordered systems. B.Movaghar (Hirst Res. Centre, GEC Res. Labs., Wembley, England), M.Gruneirwald, B.Pohlmann, D.Wurtz, W.Schirmacher.

J. Stat. Phys. (USA), vol.30, no.2, p.315-34 (Feb. 1983). (Proceedings of a Symposium on Random Walks and Their Application to the Physical and Biological Sciences, Gaithersburg, MD, USA, 28 June-1 July 1982).

The authors present a general theory to describe equilibrium and nonequilibrium transport properties of systems in which the carriers perform an incoherent motion that can be described by means of a set of master equations. This includes hopping as well as trapping in the localized energy region of amorphous or perturbed crystalline semiconductors. Employing the mathematical analogy between the master equations and the tight binding problem they develop approximation schemes using methods of many-particle physics to derive expressions for the averaged propagator of the carriers and the conductivity tensor. The calculated conductivity and Hall conductivity of hopping systems compare extremely well to computer simulations over the whole range of frequency, density, and temperature. The authors find that in principle hopping can lead to dispersive transport if the times and densities are very low, but actual experimental data are more easily explained in terms of multiple trapping. (49 refs.)

59691 Single and multiple random walks on random lattices: excitation trapping and annihilation simulations. R.Kopelman, J.Hoshen, J.S.Newhouse (Dept. of Chem., Univ. of Michigan, Ann Arbor, MI, USA), P.Argyris.

J. Stat. Phys. (USA), vol.30, no.2, p.335-43 (Feb. 1983). (Proceedings of a Symposium on Random Walks and Their Application to the Physical and Biological Sciences, Gaithersburg, MD, USA, 28 June-1 July 1982).

Random walk simulations of exciton trapping and annihilation on binary and ternary lattices are presented. Single walker visitation efficiencies for ordered and random binary lattices are compared. Interacting multiple random walkers on binary and ternary random lattices are presented in terms of trapping and annihilation efficiencies that are related to experimental observables. A master equation approach, based on Monte Carlo cluster distributions, results in a nonclassical power relationship between the exciton annihilation rate and the exciton density. (17 refs.)

59692 Trapping of excitation in the average T-matrix approximation. D.L.Huber (Dept. of Phys., Univ. of Wisconsin, Madison, WI, USA).

J. Stat. Phys. (USA), vol.30, no.2, p.345-54 (Feb. 1983). (Proceedings of a Symposium on Random Walks and Their Application to the Physical and Biological Sciences, Gaithersburg, MD, USA, 28 June-1 July 1982).

The author investigates the trapping of excitation by a random array of acceptor ions embedded in an assembly of donors. The problem is formulated in terms of coupled rate equations. Exact results for the fraction of excited donors are obtained in the zero and rapid donor-donor transfer limits for arbitrary ratios of the donor to trap concentration. The average T-matrix approximation (ATA) is introduced to interpolate between these limits in situations where the concentration of traps is much less than the concentration of donor ions. In three-dimensional systems the ATA reproduces the

results of earlier calculations in appropriate limits. The extension of the theory to higher trap concentration is discussed, as are problems connected with the application to one- and two-dimensional arrays. (26 refs.)

59693 Diffusion in random one-dimensional systems. J.Bernasconi, W.R.Schneider (Brown Boveri Res. Center, Baden, Switzerland).

J. Stat. Phys. (USA), vol.30, no.2, p.355-62 (Feb. 1983). (Proceedings of a Symposium on Random Walks and Their Application to the Physical and Biological Sciences, Gaithersburg, MD, USA, 28 June-1 July 1982).

Diffusion on the one-dimensional lattice Z is described by a master equation with nearest-neighbour transfer rates (symmetric or asymmetric). The transfer rates associated with bonds are assumed to be independent, equally distributed random variables. Under various conditions on their common distribution the large time behaviour of averaged site probabilities and/or related quantities is exhibited. (9 refs.)

59694 Random walks on inhomogeneous lattices. P.W.Kasteleyn, W.T.F.den Hollander (Inst.-Lorentz voor Theoretische Natuurkunde, Univ. of Leiden, Leiden, Netherlands).

J. Stat. Phys. (USA), vol.30, no.2, p.363-72 (Feb. 1983). (Proceedings of a Symposium on Random Walks and Their Application to the Physical and Biological Sciences, Gaithersburg, MD, USA, 28 June-1 July 1982).

For lattices with two kinds of points ('black' and 'white'), distributed according to a translation-invariant joint probability distribution, the authors study statistical properties of the sequence of consecutive colors encountered by a random walker moving through the lattice. The probability distribution for the single steps of the walk is considered to be independent of the colors of the points. Several exact results are presented which are valid in any number of dimensions and for arbitrary probability distributions for the coloring of the points and the steps of the walk. They are used to derive a few general properties of random walks on lattices containing traps. (10 refs.)

59695 Random walks on random lattices with traps. V.Halpern (Dept. of Phys., Bar-Ilan Univ., Ramat-Gan, Israel).

J. Stat. Phys. (USA), vol.30, no.2, p.373-81 (Feb. 1983). (Proceedings of a Symposium on Random Walks and Their Application to the Physical and Biological Sciences, Gaithersburg, MD, USA, 28 June-1 July 1982).

A critical examination is presented of the continuous time random walk (CTRW) approximation and of frequency-dependent effective transition rate methods for calculating the configurational average of the Laplace transform of the probability $P(s,t|s_0)$ that a particle performing a random walk will be at site s time t after it reached the site s_0 . Some exact results are derived for the form of $P(s,t|s_0)$ at long times, and these indicate that the effective transition rate methods are the better approximation for systems with symmetric effective hopping rates, while the CTRW approximation is better for systems containing traps, i.e., states that are much easier to enter than to leave. The implications of these results for calculations of transient currents and of the AC conductivity for amorphous semiconductors are discussed. (22 refs.)

59696 Diffusion-controlled reactions among stationary sinks. R.I.Cukier (Dept. of Chem., Michigan State Univ., East Lansing, MI, USA).

J. Stat. Phys. (USA), vol.30, no.2, p.383-9 (Feb. 1983). (Proceedings of a Symposium on Random Walks and Their Application to the Physical and Biological Sciences, Gaithersburg, MD, USA, 28 June-1 July 1982).

The author summarizes results of some calculations in diffusion-controlled reaction theory. He derives the transport equation describing a diffusing species which can react with a set of randomly distributed spherical sinks. Both the form of the transport equation and the dependence on sink volume fraction of the reaction rate and the effective diffusion coefficient are discussed. (9 refs.)

59697 From random to self-avoiding walks. C.Domb (Dept. of Phys., Bar-Ilan Univ., Ramat-Gan, Israel).

J. Stat. Phys. (USA), vol.30, no.2, p.425-36 (Feb. 1983). (Proceedings of a Symposium on Random Walks and Their Application to the Physical and Biological Sciences, Gaithersburg, MD, USA, 28 June-1 July 1982).

A brief review is given of the current situation in the theory of self-avoiding walks. The Domb-Joyce model consists of a random walk on a lattice in which each N step configuration has a weighting factor $\prod_{i=0}^{N-1} (1 - \omega_{ij})$. Here i and j are the lattice sites occupied by the i th and j th points of the walk. When $\omega=0$ the model reduces to a standard random walk, and when $\omega=1$ it is a self-avoiding walk. The universality hypothesis of critical phenomena is used to conjecture the behavior of the model as a function of ω for large N . The implications for the theory of dilute polymer solutions is indicated. (20 refs.)

59698 Renormalization group description of polymer excluded volume. K.F.Freed (Dept. of Chem., Univ. of Chicago, Chicago, IL, USA), A.L.Kholodenko.

J. Stat. Phys. (USA), vol.30, no.2, p.437-47 (Feb. 1983). (Proceedings of a Symposium on Random Walks and Their Application to the Physical and Biological Sciences, Gaithersburg, MD, USA, 28 June-1 July 1982).

A description is provided of the chain conformation space renormalization group approach to the treatment of polymer excluded volume. This method is transformed into one of identical form to the t'Hooft-Veltman renormalization method of field theory, thereby enabling comparison with other methods. A summary is provided of recent new results obtained by this technique for the full second-order dependence of the mean square end-to-end distance (R^2) on chain length and excluded volume as well as a calculation of $\langle R^2 \rangle$ for a polyelectrolyte chain with added salt. (21 refs.)

59699 Self-avoiding walks with geometrical constraints. S.G.Whittington (Dept. of Chem., Univ. of Toronto, Toronto, Ontario, Canada).

J. Stat. Phys. (USA), vol.30, no.2, p.449-56 (Feb. 1983). (Proceedings of a Symposium on Random Walks and Their Application to the Physical and Biological Sciences, Gaithersburg, MD, USA, 28 June-1 July 1982).

The author considers self-avoiding walks on a D -dimensional hypercubic lattice, confined to a slab geometry and confined to a half-space. The author presents a proof of the existence of a 'connective constant' for the slab geometry and reviews some corresponding results for the half-space. The way in which scaling arguments can be used to give stronger, but nonrigorous, results is also discussed. (21 refs.)

59700 Monte Carlo renormalization group calculations for polymers. M.Muthukumar (Dept. of Chem., Illinois Inst. of Technol., Chicago, IL, USA).

J. Stat. Phys. (USA), vol.30, no.2, p.457-65 (Feb. 1983). (Proceedings of a Symposium on Random Walks and Their Application to the Physical and Biological Sciences, Gaithersburg, MD, USA, 28 June-1 July 1982).

A simple method based on Wilson's renormalization group ideas is applied to calculate the dynamical critical exponent z for polymer chains in different dynamical regimes. The Doi-Edwards reptating chain does not belong to the same dynamical universality class as the Rouse chain. The earlier results based on $\epsilon(4-d, d \sim \text{space dimensionality})$ expansion for chains with excluded volume effect are recovered without any ϵ expansion. When com-

bined with the Monte Carlo techniques, this method results in a simple scheme for calculating the static and dynamic exponents for a polymer chain with a prescribed dynamics. Numerical results suggest that the slithering snake model of Wall and Mandel (1975) for the dynamics is in a different dynamic universality class than the Rouse chain. (13 refs.)

59701 On Pearson's random walk and some statistical properties of a quasiperiodic observable in a simple quantum model. F.T.Hioe (Dept. of Phys., St. John Fisher Coll., Rochester, NY, USA).

J. Stat. Phys. (USA), vol.30, no.2, p.467-75 (Feb. 1983). (Proceedings of a Symposium on Random Walks and Their Application to the Physical and Biological Sciences, Gaithersburg, MD, USA, 28 June-1 July 1982). The dynamics of the atomic inversion of a quantum model of field-atom interaction is studied from a statistical point of view. The author determines its mean motion and its partial recurrence frequencies. The mathematical analysis used by Lagrange, Wintner, and Weyl in their pioneering studies of the perturbed planetary motion and its connection with the studies of Pearson's random walks are employed. (19 refs.)

59702 Energy transfer as a random walk with long-range steps. A.Blumen, G.Zumofen (Lehrstuhl für Theoretische Chemie, Tech. Univ. München, Garching, Germany).

J. Stat. Phys. (USA), vol.30, no.2, p.487-95 (Feb. 1983). (Proceedings of a Symposium on Random Walks and Their Application to the Physical and Biological Sciences, Gaithersburg, MD, USA, 28 June-1 July 1982). The authors consider the incoherent energy transport in molecular crystals, where the transfer rates stem from Coulombic and exchange interactions. For substitutionally disordered lattices they present in a first passage model the excitation decay due to trapping by randomly distributed traps; the decay is related to the distribution of the number of distinct sites visited during the time t and is expressible through the cumulants of this distribution. The validity domains of approximate decay laws based on the first few cumulants are also discussed. The authors exemplify the findings for dipolar transfer rates between randomly distributed molecules on a square lattice, by comparing the random walk on the random system to its CTRW (continuous time random walk) counterpart. (17 refs.)

59703 Random walk to and interaction with an impurity. P.M.Richards (Sandia Nat. Labs., Albuquerque, NM, USA).

J. Stat. Phys. (USA), vol.30, no.2, p.497-507 (Feb. 1983). (Proceedings of a Symposium on Random Walks and Their Application to the Physical and Biological Sciences, Gaithersburg, MD, USA, 28 June-1 July 1982). A random walker tagged with a spin may conveniently be studied by small amounts of paramagnetic impurities which significantly affect the spin relaxation at concentrations as low as a few parts per million. Examples are found in nuclear magnetic resonance (NMR) and muon spin rotation (μ SR). At low temperature relaxation is determined by the time for the walker to reach an impurity, and thus the impurity acts like a simple trap. Details of the interaction with the impurity are important at higher temperatures, and the relaxation rate is shown to go through a maximum because of this. Special features associated with many returns to the origin, particularly important in one-dimensional walks, and the difference between incoherent (rapidly fluctuating paramagnetic spin) and coherent (stationary paramagnetic spin) returns are discussed. (13 refs.)

59704 Diffusion in concentrated lattice gases. K.W.Kehr (Inst. für Festkörperforschung, KFA, Jülich, Jülich, Germany).

J. Stat. Phys. (USA), vol.30, no.2, p.509-18 (Feb. 1983). (Proceedings of a Symposium on Random Walks and Their Application to the Physical and Biological Sciences, Gaithersburg, MD, USA, 28 June-1 July 1982). The diffusion of many particles on a lattice is an example of a correlated random-walk process. Recently the waiting-time distributions for two consecutive jumps of a tagged particle have been determined numerically and the time-dependent correlations analyzed in detail. The information over these two consecutive jumps is used to determine the position and velocity autocorrelation functions, and very satisfactory results are obtained for three-dimensional lattices. However, the information of the two consecutive jumps is insufficient when the jump rate of the tagged particle is large compared to that of the other particles, and this approximation fails completely in one dimension. For the linear chain, another approximation which accounts for correlation over all jumps is compared with the numerical simulations. (18 refs.)

59705 Stochastic processes originating in deterministic microscopic dynamics. D.Durr, S.Goldstein, J.L.Lebowitz (Dept. of Math., Rutgers Univ., New Brunswick, NJ, USA).

J. Stat. Phys. (USA), vol.30, no.2, p.519-26 (Feb. 1983). (Proceedings of a Symposium on Random Walks and Their Application to the Physical and Biological Sciences, Gaithersburg, MD, USA, 28 June-1 July 1982). The authors investigate the probability distribution of the scaled trajectory of a test particle moving in an equilibrium fluid according to the laws of classical mechanics, i.e. if $Q(t)$ is the displacement of the test particle they let $Q_A(t) = Q(t)/\sqrt{A}$ and consider the distribution of the trajectory $Q_A(t)$ in the limit $A \rightarrow \infty$. The randomness of the motion is due entirely to the randomness of the initial state of the fluid, test particle, or both, and the process is generally non-Markovian. Nevertheless, it can be proven in some cases and the authors expect it to be true in many more than $Q_A(t)$ looks like Brownian motion in the limit $A \rightarrow \infty$. Some results for simple model systems are presented. (13 refs.)

59706 Kinetics of adsorption on stepped surfaces and the determination of surface diffusion constants. C.H.Wu (RCA Labs., Princeton, NJ, USA), E.W.Montroll.

J. Stat. Phys. (USA), vol.30, no.2, p.537-47 (Feb. 1983). (Proceedings of a Symposium on Random Walks and Their Application to the Physical and Biological Sciences, Gaithersburg, MD, USA, 28 June-1 July 1982). Nitrogen adsorption on stepped W(110) surfaces is examined to illustrate a theory of surface kinetics. Experimental findings by Besocke et al. (1979) have shown that nitrogen chemisorbs dissociatively only at the step corner sites of a W(110) surface. Thus the rate of dissociation reveals the mobility of nitrogen and its interaction with the surface. Using continuous-time-random-walk theory, the authors obtain the probability that molecules reach the step corner sites as a function of time. A kinetic model of nitrogen dissociation is proposed to calculate a coverage function that is in good agreement with experiment. The surface diffusion constant of nitrogen molecules is obtained and is in accordance with previous observations that nitrogen molecules are first weakly physisorbed on the W(110) terrace. Finally, the coverage functions for different step densities are predicted. (16 refs.)

59707 Equilibrium folding pathways for model proteins. S.Miyazawa, R.L.Jernigan (Lab. of Math. Biology, Nat. Inst. of Health, Bethesda, MD, USA).

J. Stat. Phys. (USA), vol.30, no.2, p.549-59 (Feb. 1983). (Proceedings of a Symposium on Random Walks and Their Application to the Physical and Biological Sciences, Gaithersburg, MD, USA, 28 June-1 July 1982). Protein conformations have been generated with both a Monte Carlo scheme and a simpler two-state noninteracting globule-coil model. To describe probable folding pathways, either energy or the number of native residues are employed as simple one-dimensional folding-unfolding coordinates. By considering only conformations at each point on these coordinates, it is possible to obtain detailed conformational descriptions of relatively rare intermediates on the folding pathway. Equilibrium folding-unfolding pathways have been constructed by connecting most probable conformations in order along the folding coordinate. Calculations with the noninteracting globule-coil model have been performed with details chosen to correspond to those in the Monte Carlo calculation for pancreatic trypsin inhibitor. (15 refs.)

59708 Momentum from sample paths in stochastic mechanics. D.de Falco, S.de Martino, S.de Siena (Istituto di Fisica, Facoltà di Scienze, Univ. di Salerno, Salerno, Italy).

Lett. Nuovo Cimento (Italy), vol.36, ser.2, no.14, p.457-60 (2 April 1983). According to Shucker's analysis (1978, 80), quantum-mechanical momentum can be read from the asymptotic behaviour of Nelson's sample paths. The authors use the position-momentum-uncertainty product as a measure of the rate of approach to the large time asymptotics. (4 refs.)

59709 Mostly chaos. B.A.Huberman (Xerox Palo Alto Res. Center, Palo Alto, CA, USA).

Physica A (Netherlands), vol.118A, no.1-3, p.323-8 (March 1983). (Proceedings of the Conference on Nonlinear Fluid Behavior, Boulder, CO, USA, 7-11 June 1982).

Summarizes the author's work in the field of deterministic chaos in condensed matter, the universal properties that the author has found, and the interplay between external fluctuations and the intrinsic chaotic dynamics of nonlinear deterministic equations. This latter aspect has also led to a strong analogy between the onset of chaotic behavior and critical phenomena in phase transitions. The author starts by describing work on a problem that is quite pervasive in condensed matter physics, i.e. that of the dynamics of particles in anharmonic potentials when subjected to a time periodic external field. Although there exists a vast literature on the subject, its reliance on perturbative methods prevented the discovery of very unusual effects which are associated with the global properties of the solutions. (19 refs.)

59710 The description of catastrophic changes in tagged particle dynamics by the self-consistent repeated ring equation. T.Keyes, A.J.Masters (Sterling Chem. Lab., New Haven, CT, USA).

Physica A (Netherlands), vol.118A, no.1-3, p.395-406 (March 1983). (Proceedings of the Conference on Nonlinear Fluid Behavior, Boulder, CO, USA, 7-11 June 1982).

The nature of tagged particle motion in random media can change catastrophically as some parameter, most notably the scattered density, is varied. In some systems, the self-diffusion constant vanishes above a critical density, providing a dynamic analog of the static percolation problem. Good theoretical treatments of these phenomena are given by solutions of the nonlinear equations generated by the 'self-consistent repeating ring' approximation. The authors work out the repeated ring approximation for three systems: a random walk on a lattice where randomly chosen are excluded to the walker, the Lorentz gas, and the motion of a light particle in a real fluid. (9 refs.)

59711 A one-dimensional-map model for noise-induced transitions between bistable states. E.A.Celariar, S.Fraser, R.Kapral (Dept. of Chem., Univ. of Toronto, Toronto, Ontario, Canada).

Phys. Lett. A (Netherlands), vol.94A, no.6-7, p.247-50 (21 March 1983). Noise-induced transition processes involving bistable states of far-from-equilibrium systems are studied in terms of a one-dimensional-map model of the dynamics. The simplicity of the map model permits the mechanisms of these transition phenomena to be examined in some detail. (9 refs.)

59712 Diagram technique for calculating long-wave fluctuation effects. I.M.Khalatnikov, V.V.Lebedev, A.I.Sukhorukov (L.D. Landau Inst. for Theoretical Phys., Acad. of Sci., USSR).

Phys. Lett. A (Netherlands), vol.94A, no.6-7, p.271-4 (21 March 1983). The contribution of long-wave fluctuations to macroscopic equations of the hydrodynamical type is studied. The generating functional, enabling one to formulate the standard technique of Feynman diagrams for calculating the fluctuation interaction higher-order effects, is found. It is shown that in the second order of the perturbation theory the diagram technique is equivalent to the kinetic equation for the fluctuation distribution function. (10 refs.)

59713 Correlation time expansion for non-Markovian, Gaussian, stochastic processes. R.F.Fox (School of Phys., Georgia Inst. of Technol., Atlanta, GA, USA).

Phys. Lett. A (Netherlands), vol.94A, no.6-7, p.281-6 (21 March 1983). Ordered operator cumulants and van Kampen's lemma are used to obtain a correlation time expansion for colored noise, stochastic processes. An explicit result to first order in the correlation time is obtained, and confirms the result of Dekker (1982) obtained by application of Novikov's theorem. The operator cumulant approach is much more direct, systematically yielding the desired result, and systematically provided any higher order correction. The origin of each explicit order of correction is accounted for in a natural manner in terms of the cluster property for ordered operator cumulants. (11 refs.)

59714 Path integrals for non-Markovian processes. L.Pesquera, M.A.Rodriguez, E.Santos (Dept. de Física Teórica, Univ. de Santander, Santander, Spain).

Phys. Lett. A (Netherlands), vol.94A, no.6-7, p.287-9 (21 March 1983). The authors obtain a path-integral expression for the conditional probability density of a system submitted to a non-white noise: the Ornstein-Uhlenbeck noise. In this case the function that corresponds to the Onsager-Machlup potential is no longer similar to a Lagrangian due to the non-markovian character of the system. (6 refs.)

59715 Stability theory of synchronized motion in coupled-oscillator systems. H.Fujisaka (Dept. of Phys., Kagoshima Univ., Kagoshima, Japan), T.Yamada.

Prog. Theor. Phys. (Japan), vol.69, no.1, p.32-47 (Jan. 1983). The general stability theory of the synchronized motions of the coupled-oscillator systems is developed with the use of the extended Lyapunov matrix approach. The authors give the explicit formula for a stability parameter of the synchronized state Ψ_{sync} . When the coupling strength is weakened, the coupled system may exhibit several types of non-synchronized motion. In particular, if Ψ_{sync} is chaotic, they always get a transition from chaotic Ψ_{sync} to a certain non-uniform state and finally the non-uniform chaos. Details associated with such transition are investigated for the coupled Lorenz model. As

an application of the theory, they propose a new experimental method to directly measure the positive Lyapunov exponent of intrinsic chaos in reaction systems. (13 refs.)

59716 Intermittency associated with the breakdown of the chaos symmetry. H.Fujisaka, H.Kamifukumoto, M.Inoue (Dept. of Phys., Kagoshima Univ., Kagoshima, Japan).

Prog. Theor. Phys. (Japan), vol.69, no.1, p.333-7 (Jan. 1983).

The intermittency transition associated with the breakdown of the chaos symmetry in one-dimensional dynamics is studied in connection with the Pomeau-Manneville (1979, 1980) intermittency transition. The strong trajectory instability, which is present even in 'laminar' phases, renders a derivation of probabilistic laws possible. (8 refs.)

59717 One-time characteristic functional in the stochastic quantization.

Y.Nakano (Dept. of Phys., Univ. of Alberta, Edmonton, Alberta, Canada).

Prog. Theor. Phys. (Japan), vol.69, no.1, p.361-5 (Jan. 1983).

The author presents a proof for the equivalence between the stochastic quantization and the ordinary one using one-time characteristic functional. It is shown that one cannot apply the scheme to the gauge theories unless one introduces an infinitesimal parameter which assures the relaxation of the stochastic process. (13 refs.)

59718 Coherent spatial structure versus time chaos in a perturbed sine-Gordon system. A.R.Bishop, K.Fesser, P.S.Lomdahl (Theoretical Div., Los Alamos Nat. Lab., Los Alamos, NM, USA), W.C.Kerr, M.B.Williams, S.E.Trullinger.

Phys. Rev. Lett. (USA), vol.50, no.15, p.1095-8 (11 April 1983).

A novel interplay of coherent spatial structure and temporal chaos is reported for the AC driven, damped sine-Gordon system with breather initial conditions and periodic boundary conditions. The competing tendencies of spatial structures to be stable and of single-particle motions to be chaotic can lead to suppression of chaos, spatio-temporal intermittency, and symmetry-breaking tendencies. Dynamic structure factors provide direct evidence for spatial period halving and renormalized-phonon generation in chaotic regimes. (12 refs.)

59719 Dynamical systems with few degrees of freedom. P.Collet (Centre de Phys. Theorique, Ecole Polytech., Palaiseau, France).

Stochastic Processes in Quantum Theory and Statistical Physics. Proceedings of the International Workshop, Marseille, France, 29 June-4 July 1981 (Berlin, Germany: Springer-Verlag 1982), p.29-39

Discusses initially stable systems in which a series of bifurcations take place, the behaviour becomes more complicated and eventually a chaotic state is reached. Routes to turbulence that result from generic bifurcations are described, together with the period doubling route to turbulence. Some remarks about the turbulent behaviour of simple systems are given. (30 refs.)

59720 Periodic orbits of dynamical systems with chaotic behavior. S.De Gregorio (Istituto di Matematica, Univ. di Roma, Roma, Italy), E.Scoppola, B.Tirozzi.

Stochastic Processes in Quantum Theory and Statistical Physics. Proceedings of the International Workshop, Marseille, France, 29 June-4 July 1981 (Berlin, Germany: Springer-Verlag 1982), p.67-74

Explains the method by which the authors have used a modified version of Sinai and Vul's (1980) method to study closed orbits that appear in the Lorenz model and in the five modes model. (4 refs.)

59721 All that Brownian motion. D.Durr (Inst. fur Math., Ruhr-Univ. Bochum, Bochum, W.Germany).

Stochastic Processes in Quantum Theory and Statistical Physics. Proceedings of the International Workshop, Marseille, France, 29 June-4 July 1981 (Berlin, Germany: Springer-Verlag 1982), p.119-35

Presents some recent results in the mathematical rigorous study of nonequilibrium statistical mechanics. These results have been obtained in collaboration with S. Goldstein and J.L. Lebowitz. (9 refs.)

59722 On the statistical mechanics of surfaces. J.Frohlich (IHES, Bures-sur-Yvette, France), C.E.Pfister, T.Spencer.

Stochastic Processes in Quantum Theory and Statistical Physics. Proceedings of the International Workshop, Marseille, France, 29 June-4 July 1981 (Berlin, Germany: Springer-Verlag 1982), p.169-99

Briefly reviews some rigorous results concerning random surfaces and interfaces. Discussed are the interface in the three-dimensional Ising- and rotator model; the solid-on-solid model; self-avoiding random surfaces and string theories; lattice gauge theories. (33 refs.)

59723 A note on irreducibility and ergodicity of symmetric Markov processes. M.Fukushima (Coll. of General Education, Osaka Univ., Osaka, Japan).

Stochastic Processes in Quantum Theory and Statistical Physics. Proceedings of the International Workshop, Marseille, France, 29 June-4 July 1981 (Berlin, Germany: Springer-Verlag 1982), p.200-7

Gives some theorems, proofs, corollaries and remarks concerning ergodicity and irreducibility in symmetric Markov processes. (6 refs.)

59724 Stochastic processes in music and art. J.C.Risset (Lab. de Mecanique et d'Acoustique, CNRS, Marseille, France).

Stochastic Processes in Quantum Theory and Statistical Physics. Proceedings of the International Workshop, Marseille, France, 29 June-4 July 1981 (Berlin, Germany: Springer-Verlag 1982), p.281-8

Describes some examples of music and visual art based on stochastic processes. Musical works in which randomness is used to determine the choice of note etc. are discussed, and a review is given of information theory in the analysis of music. Random processes in visual arts are also included, emphasising work by Julesz and Noll. (50 refs.)

Proceedings of a Symposium on Random Walks and Their Application to the Physical and Biological Sciences See Entry 59531

Stochastic Processes in Quantum Theory and Statistical Physics. Proceedings of the International Workshop See Entry 59543

An improved solution to the fourth moment equation for intensity fluctuations See Entry 59600

Quantum theory and non-Kolmogorovian probability See Entry 59628

Stochastic jump processes in the phase space representation of quantum mechanics See Entry 59629

A stochastic picture of spin See Entry 59632

Stochasticity in non-equilibrium statistical mechanics See Entry 59669

Non-commutative martingales and stochastic integrals in Fock space See Entry 59676

Quantum dissipation and stochastic processes See Entry 59677

Phase transition and fractals See Entry 59734

A comment on the theory of excitation migration in disordered lattices See Entry 59735

Some results on the spectra of random Schrodinger operators and their application to random point interaction models in one and three dimensions See Entry 59739

Large scale behavior of equilibrium time correlation functions for some stochastic Ising models See Entry 59741

The long time tail conundrum in nonequilibrium statistical mechanics See Entry 59744

The diffusion equation and classical mechanics: an elementary formula See Entry 59746

Hopping transport in disordered one-dimensional lattice systems: random walk in a random medium See Entry 59747

Stochastic processes and Fermi fields See Entry 59931

Electronic excited state transport among molecules distributed randomly in a finite volume See Entry 60619

Two-dimensional random coil chains on hexagonal lattices See Entry 61825

Random walk of dislocations following a high-velocity impact See Entry 62027

Random walk properties of lattices and correlation factors for diffusion via the vacancy mechanism in crystals See Entry 62152

Fractal dimensions and $1/f$ noise See Entry 62463

Physics of ligand migration in biomolecules See Entry 63771

Protein folding as a stochastic process See Entry 63778

Stochastic aspects of biological locomotion See Entry 63816

05.50 LATTICE THEORY AND STATISTICS; ISING PROBLEMS

(see also 75.10H Ising models)

59725 A number of the permissible phases for Ising lattice. Liu Jian-min, Gong Chang-de (Dept. of Phys., Nanjing Univ., Nanjing, China).

Commun. Theor. Phys. (China), vol.2, no.1, p.909-11 (1983).

The catastrophe theory is applied to investigating the number of permissible phases for homogeneous-isotropic and homogeneous-anisotropic Ising lattices. (10 refs.)

59726 Electron localization in a finite one-dimensional chain. K.Tanaka, M.Nagaoka, T.Yamabe (Dept. of Hydrocarbon Chem., Kyoto Univ., Kyoto, Japan).

Int. J. Quantum Chem. (USA), vol.23, no.3, p.1101-9 (March 1983).

(Proceedings of the Fourth International Congress in Quantum Chemistry, Uppsala, Sweden, 13-20 June 1982).

The localization characteristics of the electronic wave functions in a finite one-dimensional chain with the diagonal or the off-diagonal disorder of the potentials have been studied. It has been shown that the eigenfunction at the frontier level is relatively 'strong' against the temptation to localize caused by the existence of the random potentials. It has also been pointed out that the spatial behavior of the total density reflects that of the diagonal random potentials, but that under the off-diagonal random potentials the total density is spatially uniform (completely extended). (19 refs.)

59727 Further comments concerning large amplitude motion in an anharmonic chain with nearest neighbor interactions. S.Bradlow, M.A.Collins, S.A.Rice (James Franck Inst., Univ. of Chicago, Chicago, IL, USA).

J. Chem. Phys. (USA), vol.78, no.6, pt.1, p.3344-5 (15 March 1983).

For original paper see Collins and Rice, *ibid.*, vol.77, no.5, p.2607 (1982). In a recent paper Collins and Rice analyzed the semiclassical dynamics of large amplitude motion in a one-dimensional anharmonic atomic lattice with periodic boundary conditions. Their investigation of the perfectly periodic vibrational modes of the chain yielded a surprising result: they found that while the anharmonicity in the potential greatly influenced the shapes of the vibrational modes, it had very little effect on their energies. Collins and Rice, however, calculated the eigenstate energies only for the ground and first excited states of the periodic modes. Because their findings are so striking, the authors have extended their investigation and have examined the effect of the anharmonicity in the potential on mode shape and energy for small k modes up to the fifth excited state. (1 ref.)

59728 Mean-field renormalisation group transformations for geometric phase transitions. K.De'Bell (Dept. of Phys., Dalhousie Univ., Halifax, Nova Scotia, Canada).

J. Phys. A (GB), vol.16, no.6, p.1279-87 (21 April 1983).

It is shown that the mean-field renormalisation group technique of Indekeu et al. (1982) may be applied directly to the self-avoiding walk (SAW) and percolation problems (without reference to the $n \rightarrow 0$ limit of interacting spin systems). Numerical results for the SAW and bond and site percolation (both directed and undirected) problems on the square lattice, obtained by using a variety of small cells, are reported. An isotropic transformation for the percolation problems on the d -dimensional hypercubic lattice is also discussed. (21 refs.)

59729 Two-dimensional iterated mapping for the mean-field theory of the chiral Potts model. H.C.Ottinger (Fakultat fur Phys., Univ. Freiburg, Freiburg, Germany).

J. Phys. C (GB), vol.16, no.10, p.L257-63 (10 April 1983).

It is shown how the solution of the mean-field equations for the chiral Potts model can be reduced to the iteration of an area-preserving two-dimensional mapping. By this method a variety of modulated magnetic phases can be observed. (10 refs.)

59730 Complete devil's staircase in the one-dimensional lattice gas. Comment on 'One-dimensional lattice gas and the universality of the devil's staircase' by S.E. Burkov. S.Aubry (Lab. Leon Brillouin, CEN Saclay, Gif-sur-Yvette, France).

J. Phys. Lett. (France), vol.44, no.7, p.L247-50 (1 April 1983).

The author calculates explicitly the exact form of the complete devil's staircase for the lattice gas model. Thus, it is shown that the behaviour at the commensurate-incommensurate phase transition essentially depends on the long distance interactions. The author questions the assertion of Burkov (see *ibid.*, vol.44, p.L179, 1983) about the universality properties of the devil's staircase. (10 refs.)

59731 Bond-site percolation in 2D packings. D.Bideau, J.P.Troadec, L.Oger (Univ. de Rennes 1, Rennes, France).

J. Phys. Lett. (France), vol.44, no.8, p.L279-83 (15 April 1983). In French.

Considers the problem of site-bond percolation on a triangular lattice modeling a 2D random mixture of discs, an inactive bond corresponding to a lack of contact between two neighbour discs. For a regular triangular lattice a hypothesis about conduction of a cell of the direct lattice and of a cell of the 'rival' one permits the authors to propose some results about percolation three-

sholds and critical lines in good agreement with the known exact results and results of numerical simulations. (19 refs.)

59732 Statistical mechanics of one-dimensional XYZ spin chain, massive Thirring model and quantum sine-Gordon system. M.Imada (Inst. for Solid State Phys., Univ. of Tokyo, Tokyo, Japan), K.Hida, M.Ishikawa. *J. Magn. & Magn. Mater. (Netherlands)*, vol.31-34, pt.3, p.1221-2 (Feb. 1983). (Proceedings of the International Conference on Magnetism, Kyoto, Japan, 6-10 Sept. 1982).

The specific heat is calculated in the massive Thirring/quantum sine-Gordon limit on the one-dimensional XYZ model with the help of the Bethe ansatz approach. The Schottky-type anomaly appears as a contribution from the quantum soliton. The finite-temperature excitations are also discussed for these models. (13 refs.)

59733 Path-integral approach to a finite many-body problem. H.Grinberg, J.Maranon (Dept. de Física, Facultad de Ciencias Exactas, Univ. Nacional de La Plata, La Plata, Argentina). *Phys. Lett. A (Netherlands)*, vol.94A, no.6-7, p.275-80 (21 March 1983). The Feynman path integral is used to show the equivalence between a finite many-body problem (Huckel model) for a nonrelativistic and nonspin molecular system of N electrons and N one-dimensional Ising models. (7 refs.)

59734 Phase transition and fractals. M.Suzuki (Dept. of Phys., Univ. of Tokyo, Tokyo, Japan). *Prog. Theor. Phys. (Japan)*, vol.69, no.1, p.65-76 (Jan. 1983).

A geometrical interpretation of critical phenomena, particularly of the scaling relations on critical exponents, is given by the use of statistical fractal dimensionality. The relation between this geometrical interpretation and the finite size scaling theory is also discussed. The concept of connectivity dimensionality (or generalized fractal topological dimensionality) is introduced to discuss the relation between critical exponents and fractal dimensionalities of some explicit lattices. (19 refs.)

59735 A comment on the theory of excitation migration in disordered lattices. J.Klafter (Corporate Res. Sci. Lab., EXXON Res. & Engng. Co., Linden, NJ, USA), R.Silbey. *Philos. Mag. B (GB)*, vol.47, no.3, p.337-41 (March 1983).

The transport of an excitation on a lattice randomly occupied by guests is considered, emphasizing the dependence on the initial condition. Exact equations are derived for the transport, which can be written as a generalized master equation or as a continuous-time random-walk equation. (6 refs.)

59736 Eigenvalues of two-dimensional harmonic systems with periodic structures. C.C.Shih (Dept. of Phys. & Astron., Univ. of Tennessee, Knoxville, TN, USA). *Phys. Rev. B (USA)*, vol.27, no.6, p.3287-302 (15 March 1983).

A recent technique of amplitude analysis for one-dimensional systems is generalized to a class of two-dimensional harmonic systems with nearest-neighbor interaction and periodic structures. The characteristic equation for the eigenvalues is reduced to a set of polynomial equations of order equal to the number of particles in the unit cell for finite and infinite crystals. Most of the analytic solutions demonstrated cannot be readily obtained by other methods. Numerical examples of precise eigenvalues and eigenvectors for some large but finite lattices (15×12 , 15×21) can also be evaluated very accurately and efficiently. Analytic and numerical examples of several infinite strips are presented using both the fixed-end and cyclic-boundary conditions. (13 refs.)

59737 Effect on spin variables and exciton motion on ground-state properties of the 'trion'. R.Schilling, D.C.Mattis (Dept. of Phys., Univ. of Utah, Salt Lake City, UT, USA). *Phys. Rev. B (USA)*, vol.27, no.6, p.3318-24 (15 March 1983).

Solves a quantum three-body problem involving two holes and a single electron ('trion') in a two-band Hubbard model. The particles' spin and the exciton hopping matrix element are all included. The authors compare the results with those of a previous paper, in which these additional complications were absent, and find broad agreement. There is one novelty: the trion with single holes is always mobile, even in one dimension. (6 refs.)

59738 Critical behavior of the anisotropic n -vector model, self-avoiding rings, and polymerization. P.D.Gujrati (James Franck Inst., Univ. of Chicago, Chicago, IL, USA). *Phys. Rev. B (USA)*, vol.27, no.7, p.4507-10 (1 April 1983).

The author studies the critical behavior of the m -anisotropic n -vector model with n and m both as continuous variables [$0 \leq n, m < 4 - O(\epsilon)$, $\epsilon = 4 - d$, d = dimensionality of space] to first order in ϵ . The limit $n \rightarrow 0$, $m > 0$ of the model is of interest as a model of self-avoiding rings and of polymerization. For $n \geq m$, n, m integers, the critical behavior of the model is known to be that of the isotropic m -vector model, i.e. the $O(m)$ model. Here he proves that the critical behavior of the anisotropic model is always identical with that of the $O(m)$ model for real n, m regardless of whether $n \geq m$ or $n < m$. In particular, he proves that a single self-avoiding ring and a single self-avoiding walk belong to the same universality class of the $O(0)$ model, while polymerization belongs to the universality class of the $O(m)$ model, $m > 0$. (11 refs.)

59739 Some results on the spectra of random Schrodinger operators and their application to random point interaction models in one and three dimensions. W.Kirsch, F.Martinelli (Inst. für Math., Ruhr-Univ. Bochum, Bochum, Germany).

Stochastic Processes in Quantum Theory and Statistical Physics. Proceedings of the International Workshop, Marseille, France, 29 June-4 July 1981 (Berlin, Germany: Springer-Verlag 1982), p.223-44

Schrodinger operators with a random potential occur naturally in the theory of alloys, liquids, solids with impurities and amorphous materials. Several results are given concerning the spectra of random Schrodinger operators H_ω of the form: $H_\omega = H_0 + V_\omega$ on $L^2(\mathbb{R}^d)$ $H_0 = -\Delta$ being the Laplacian and V_ω a function or a quadratic form which depends on ω , a point in a probability space (Ω, \mathcal{F}, P) . In most considerations V_ω is taken as the total potential acting on the quantum particle generated by 'heavy' particles of random 'charges' $q_i(\omega)$ located at the random positions $\xi_i(\omega)$. (32 refs.)

59740 Existence of a first-order phase transition for the Potts model. R.Kotecky (Dept. of Math. Phys., Charles Univ., Povolavka, Praha, Czechoslovakia), S.B.Slosman.

Stochastic Processes in Quantum Theory and Statistical Physics. Proceedings of the International Workshop, Marseille, France, 29 June-4 July 1981 (Berlin, Germany: Springer-Verlag 1982), p.248-53

Sketches a proof that for many-state Potts model an expected discontinuity of the average energy as a function of temperature really occurs. The presentation is based on previous work by the authors, though they give an alternative proof of one part of the statement. (8 refs.)

59741 Large scale behavior of equilibrium time correlation functions for some stochastic Ising models. H.Spohn (Dept. of Math., Rutgers Univ., New Brunswick, NJ, USA).

Stochastic Processes in Quantum Theory and Statistical Physics. Proceedings of the International Workshop, Marseille, France, 29 June-4 July 1981 (Berlin, Germany: Springer-Verlag 1982), p.304-31

Reviews recent rigorous results and an argument, which proves the exponential decay of correlation functions in space-time for a class of stochastic Ising models at high temperature. Brief outlooks are given on the hydrodynamics of stochastic lattice gases and on linearized hydrodynamics for fluids. (25 refs.)

Proceedings of a Symposium on Random Walks and Their Application to the Physical and Biological Sciences See Entry 59531

Stochastic classical trajectory approach to relaxation phenomena. III. Comparison of trajectory results to quantum mechanical perturbation theory See Entry 59681

Stochastic flows, reaction-diffusion processes, and morphogenesis See Entry 59685

Fractal and lacunary stochastic processes See Entry 59686

Nonexponential decay in relaxation phenomena See Entry 59687

Renormalization group approach to random walks on disordered lattices See Entry 59689

Single and multiple random walks on random lattices: excitation trapping and annihilation simulations See Entry 59691

Trapping of excitation in the average T -matrix approximation See Entry 59692

Diffusion in random one-dimensional systems See Entry 59693

Random walks on inhomogeneous lattices See Entry 59694

Random walks on random lattices with traps See Entry 59695

From random to self-avoiding walks See Entry 59697

Self-avoiding walks with geometrical constraints See Entry 59699

Energy transfer as a random walk with long-range steps See Entry 59702

Random walk to and interaction with an impurity See Entry 59703

Diffusion in concentrated lattice gases See Entry 59704

Kinetics of adsorption on stepped surfaces and the determination of surface diffusion constants See Entry 59706

The description of catastrophic changes in tagged particle dynamics by the self-consistent repeated ring equation See Entry 59710

On the statistical mechanics of surfaces See Entry 59722

Hopping transport in disordered one-dimensional lattice systems: random walk in a random medium See Entry 59747

Critical point shifts in films See Entry 59749

Two-dimensional random coil chains on hexagonal lattices See Entry 61825

Determination of the Ising critical temperature of F slices with an application to garnet See Entry 61836

Random walk of dislocations following a high-velocity impact See Entry 62027

Nucleation and growth of nonclassical droplets See Entry 62058

Random walk properties of lattices and correlation factors for diffusion via the vacancy mechanism in crystals See Entry 62152

Cluster decimation derivation of exact percolation-thermal crossover exponent in dilute spin models See Entry 62543

Phase transitions on fractals. I. Quasi-linear lattices See Entry 62650

Stability of Parisi's solution of a spin glass model See Entry 62651

Hidden Mattis phase in annealed system See Entry 62663

Protein folding as a stochastic process See Entry 63778

05.60 TRANSPORT PROCESSES: THEORY

59742 Transport factors in dense media. E.G.Aznakaev. *Dopov. Akad. Nauk UkrSR. Ser. A (USSR)*, no.2, p.44-6 (1983). In Ukrainian.

Kinetic theory methods are applied to discuss processes of mass, momentum and energy transfer in dense continua. Expressions for the transport factors are derived and the author discusses mass, momentum and energy conservation laws. The equation of state is presented and hydrodynamic equations are considered. (3 refs.)

59743 On maximum principles for diffusion in the presence of three diffusion paths. A.I.Lee, J.M.Hill (Dept. of Math., Univ. of Wollongong, Wollongong, NSW, Australia). *J. Aust. Math. Soc. Ser. B (Australia)*, vol.24, pt.4, p.417-23 (April 1983).

Examines maximum principles for systems of parabolic partial differential equations. The particular system under consideration arises from a random walk model. For a more general system, constraints on the various constants are given which guarantee maximum principles. Remarkably, the physical system arising from the random walk model automatically satisfies these constraints. (13 refs.)

59744 The long time tail conundrum in nonequilibrium statistical mechanics. R.F.Fox (School of Phys., Georgia Inst. of Technol., Atlanta, GA, USA). *Physica A (Netherlands)*, vol.118A, no.1-3, p.383-94 (March 1983).

(Proceedings of the Conference on Nonlinear Fluid Behavior, Boulder, CO, USA, 7-11 June 1982).

The existence and significance of long time tails in diffusion processes is discussed from the viewpoints of computer simulation, theory, and experiments. It is argued that the understanding of this phenomenon is not satisfactory for each of these three points of view. (32 refs.)

59745 Large time solution of an inhomogeneous nonlinear diffusion equation. R.E.Gundy (Math. Inst., Univ. of St. Andrews, St. Andrews, Scotland). *Proc. R. Soc. London Ser. A (GB)*, vol.386, no.1791, p.347-72 (8 April 1983).

The paper considers the large time solution of the nonlinear diffusion equation $\rho(x,t)\partial_t u = \partial/\partial x(C(x)u^\beta\partial_x u)$, $\beta > 0$, for initial data with compact support. The asymptotic behaviour of $\rho(x)$ and $C(x)$ as $|x| \rightarrow \infty$ defines a parameter space, and the nature of the solution at large time depends crucially on the location therein. The author examines the nature and uniformity of the asymptotic solutions for $x \in (-x_0, x_0)$ in a restricted region of the entire parameter space, and in certain cases gives the leading error terms. A new integral invariant of the solution is also given. (21 refs.)

59746 The diffusion equation and classical mechanics: an elementary formula. K.D.Elworthy (Inst. of Maths., Univ. of Warwick, Coventry, England), A.Truman.
Stochastic Processes in Quantum Theory and Statistical Physics. Proceedings of the International Workshop, Marseille, France, 29 June-4 July 1981 (Berlin, Germany: Springer-Verlag 1982), p.136-46
Let M be an n -dimensional Riemannian manifold and Δ its Laplace-Beltrami operator. The authors examine the limiting behaviour as $\mu \rightarrow 0$ of the diffusion equation $\partial g_\mu/\partial t = \mu^2/2 + Vg_\mu/\mu^2$ $0 \leq t \leq \infty$ $g_0(x) = T_0(x) \exp[4S_0(x)/\mu^2]$ for $g_\mu: M \rightarrow R$, given $T_0: M \rightarrow R$ and $S_0: M \rightarrow R$. Using the Girsanov formula the authors obtain an exact path integral expression for the minimal solution g_μ to the equation, which shows clearly how the solution behaves in relation to its WKB approximation. It is valid up to the time when caustics appear, if they do, and requires some smoothness conditions on V , S_0 and T_0 . Also given is the first 'post WKB' term when $T_0 \equiv 1$. Also mentioned are some further developments, in particular indicating how to obtain an exact expression for the propagator for a restricted class of manifolds. (20 refs.)

59747 Hopping transport in disordered one-dimensional lattice systems: random walk in a random medium. W.R.Schneider (Brown Boveri Res. Center, Baden, Switzerland).
Stochastic Processes in Quantum Theory and Statistical Physics. Proceedings of the International Workshop, Marseille, France, 29 June-4 July 1981 (Berlin, Germany: Springer-Verlag 1982), p.289-303
The formalism for a particle moving stochastically on a lattice is extended to introduce disorder to the medium. This is achieved by assuming that transfer rates are random. Finite size effects are studied and the large L behaviour of the static diffusion function is discussed. (7 refs.)

Diffusion in random one-dimensional systems See Entry 59693
Diffusion-controlled reactions among stationary sinks See Entry 59696
Diffusion in concentrated lattice gases See Entry 59704
A finite element solution to the group diffusion problems with albedo-type boundary conditions See Entry 60221
Description and discussion of the current state of the knowledge about the Leidenfrost phenomenon See Entry 60353

05.70 THERMODYNAMICS

(see also 44.60 Thermodynamic processes, 64. Equations of state, phase equilibria and phase transitions, 65. Thermal properties of condensed matter; for chemical thermodynamics, see 82.60)

59748 A note on the use of different representations of excess-energies in ternary systems. J.Agren (ManLabs Inc., Cambridge, MA, USA).
CALPHAD: Comput. Coupling Phase Diagrams & Thermochem. (GB), vol.6, no.4, p.279-81 (1982).
It is pointed out that there really is a physical arbitrariness in the Kohler method that underlies the singularity. The Kohler method as applied, by Kaufman for example, to the subregular solution yields a contribution to the total excess-energy from the binary A-B system, $E_{AB} = X_A X_B L_{AB}$, where L_{AB} is the interchange energy. This is also the type of contribution one obtains in a random solution by counting the number of nearest neighbours. As long as L_{AB} is constant there are no problems. When L_{AB} , i.e. the bonding energy between A and B atoms, varies with composition, and this variation is known as the binary case but not in the ternary, the question arises which value one should choose in a ternary solution. (5 refs.)

59749 Critical point shifts in films. H.Nakanishi, M.E.Fisher (Baker Lab., Cornell Univ., Ithaca, NY, USA).
J. Chem. Phys. (USA), vol.78, no.6, pt.1, p.3279-93 (15 March 1983).
Critical behavior in thin films is discussed with attention to the example of phase separation in binary fluid mixtures between parallel plates. The analyses focus on the dependence of the shift in critical temperature ΔT_c , critical field, etc., on the film thickness D , and on the nature of the walls as modeled by a surface field or chemical potential h_1 which acts near the walls and leads to preferential adsorption of one of the bulk phases. Mean field theory for an Ising/lattice-gas model is utilized and the resulting asymptotic scaling functions for the shifts ΔT_c , etc., are computed within Landau theory by analytic and numerical methods. Series analyses for simple cubic lattice Ising model films with $h_1 = 0$ are used to estimate universal features of three-dimensional systems specifically, if $\xi(\Delta T)$ is the bulk correlation length, determined, say, via scattering experiments, at $\Delta T = T - T_c^\infty > 0$ then the shift ratio $D/\xi(\Delta T_c)$ is about 2.89 for $h_1 = 0$ but 4.61 for $h_1 \rightarrow \infty$, compared with mean field values π and 5.0699. Crossover effects for small nonzero h_1 may lead to 10%-15% errors in estimating the exponent for the decay of ΔT_c with D . The relation of the theory to recent experiments and the connection with wetting phenomena are discussed briefly. (30 refs.)

59750 The effective conductivity of a periodic array of spheres. A.S.Sangani, A.Acrivros (Dept. of Chem. Engng., Stanford Univ., Stanford, CA, USA).
Proc. R. Soc. London Ser. A (GB), vol.386, no.1791, p.263-75 (8 April 1983).
The authors consider the problem of determining the effective conductivity k^* of a composite material consisting of equal-sized spheres of conductivity k^* arranged in a cubic array within a homogeneous matrix of unit conductivity. They modify Zuzovskii & Brenner's (1977) method and thereby obtain a set of infinite linear equations for the coefficients of the formal solution equivalent to that derived by McKenzie et al. (1978) using a method originally devised by Rayleigh (1892). On solving these equations they derive expressions for k^* to $O(\epsilon^2)$, (ϵ being the volume fraction of the spheres) for simple, body-centred and face-centred cubic arrays, and also obtain numerical values for k^* over the whole range of α and c . They show that these results for cubic arrays can be used to estimate k^* for random arrays of identical spheres. (29 refs.)

59751 Renormalization group and linear integral equations. W.Klein (Dept. of Phys., Boston Univ., Boston, MA, USA).
Phys. Rev. B (USA), vol.27, no.7, p.4475-8 (1 April 1983).
The author develops a position-space renormalization-group transformation which can be employed to study general linear integral equations. In this Brief Report he employs his method to study one class of such equations pertinent to the equilibrium properties of fluids. The results of applying his method are in excellent agreement with known numerical calculations where they can be compared. He also obtains information about the singular behavior of this type of equation which could not be obtained numerically. (14 refs.)

59752 Phase transitions and the ordered state in models with a continuous set of energy minima in large- N limit. L.Golubovic (Lab. of Theoretical Phys., Inst. of Nuclear Sci., 'Boris Kidric', Vinca, Belgrade, Yugoslavia).
Phys. Rev. B (USA), vol.27, no.7, p.4488-90 (1 April 1983).
The author establishes a uniqueness theorem for equations governing large- N behavior of the N -component order parameter Landau-Ginzburg-Wilson (LGW) model with the general form of the quadratic term. The theorem is used to support some conclusions of a paper of Ling, Friman, and Grinstein (LFG) concerning the LGW model, the excitation spectrum of which has as an absolute minimum a ring $\{q\}$ imbedded in d -dimensional reciprocal space. For this model they prove the nonexistence of phase transitions when $d \leq 3$ and $N = \infty$, which strengthens the statement of LFG that there is no second-order transition in this case. When $d > 3$ and $N = \infty$ there is a second-order transition to a phase, being the superposition of spirals whose wave vectors lie on $\{q\}$, such that the length of the order parameter is spatially independent. They point out that the LGW model does not possess metastable states when $N = \infty$. (8 refs.)

Elementary statistical thermodynamics. A problems approach See Entry 59558
A special relativistic heat engine See Entry 59590
On the Burnett and higher order equations of hydrodynamics See Entry 59596
Complete devil's staircase in the one-dimensional lattice gas. Comment on 'One-dimensional lattice gas and the universality of the devil's staircase' by S.E. Burkov See Entry 59730
Existence of a first-order phase transition for the Potts model See Entry 59740
Steady state thermodynamics and spatial correlations See Entry 61472
Effective spherical potentials for molecular fluid thermodynamics See Entry 61751
Nucleation and growth of nonclassical droplets See Entry 62058
Chiral symmetry breaking in nonequilibrium systems See Entry 63500

06.00 MEASUREMENT SCIENCE, GENERAL LABORATORY TECHNIQUES, AND INSTRUMENTATION SYSTEMS

06.20 METROLOGY

06.20D Measurement and error theory

59753 Information-theoretical treatment of errors and error characteristic factors. G.Hartig (Sektion Elektronik, Humboldt-Univ. zu Berlin, Berlin, Germany).
Feingeräetechnik (Germany), vol.32, no.3, p.99-101 (1983). In German.
Results for the extension of the information-theoretical treatment of errors are presented. Entropy coefficients calculated on the basis of Pearson-distributions are specified both for single error components and also for error additions consisting of two terms. (9 refs.)

59754 Analysis of statistical moments from discontinuously occurring measuring data. A.Rothe (Sektion Elektronik, Humboldt-Univ. zu Berlin, Berlin, Germany).
Feingeräetechnik (Germany), vol.32, no.3, p.102-4 (1983). In German.
An evaluation procedure for data reduction by statistical moments of the second to fourth order is applied. The method developed for this purpose is explained and the obtained results are presented. (6 refs.)

Effect of vertical deflection nonlinearity on the accuracy of measurement of time parameters with an oscilloscope See Entry 59764
Errors combination in acoustical measurements See Entry 61357
Statistical analysis of the error of concentration measurements using an electron-probe microanalyzer See Entry 63619

06.20H Measurement standards and calibration

Frequency calibration using rubidium See Entry 59763
Standardization of the ohm by means of the Hall effect in silicon metal-oxide semiconductor structures at 0.4-0.7K See Entry 59799
Calibration system for satellite and rocket-borne ion mass spectrometers in the energy range from 5 eV/charge to 100 keV/charge See Entry 59875
Standard radiometer for long-lived radionuclide aerosols See Entry 60557

06.20J Determination of fundamental constants

59755 Precision measurements and fundamental constants. F.M.Pipkin (Harvard Univ., Cambridge, MA, USA), R.C.Ritter.
Science (USA), vol.219, no.4587, p.913-21 (25 Feb. 1983).
Recent developments in the techniques for making precision measurements and their use in the determination of the fundamental constants are reviewed. Particularly noteworthy developments are clocks with high stability, the proposed redefinition of the metre in terms of the standard for time, and the increased precision with which electrical standards can be maintained. The relevance of precision measurements to tests of general relativity is briefly discussed. (51 refs.)

06.30 MEASUREMENT OF BASIC VARIABLES

06.30C Spatial variables measurement

(inc. measurement of all variables extending in space e.g. diameter, height, thickness, displacement, surface topography, particle size, area of disperse systems)

59756 A convenient Fizeau interferometer for thin film thickness measurement. J.J.Prabhakaran, G.Balasubramanian, R.P.Riesz (Post-Graduate Dept. of Phys., American Coll., Madurai, India). *CSIO Commun. (India)*, vol.9, no.1, p.40-3 (Jan.-March 1982). [received: March 1983]

A Fizeau interferometer set-up using Tolansky technique for thin film thickness measurement is presented. The interferometer fringes are seen through a microscope in the reflected configuration. The usual problem of aligning the fringes perpendicular to the travelling microscope bed is avoided by using a rotating micrometer eyepiece in the micropiece. The tedious problem of controlling the direction and spacing of the interference fringes is solved with the help of mechanical fingers. As an example, thickness of a thin film was measured using two different wavelength sources. (4 refs.)

59757 Topographic quantification of non-planar localized surfaces. K.Wright, B.Karlsson (Dept. of Engng. Metals, Chalmers Univ. of Technol., Goteborg, Sweden).

J. Microsc. (GB), vol.130, pt.1, p.37-51 (April 1983). The topography of non-planar localized surfaces can be quantified by roughness indices as well as by height and angular distributions of the surface elements. For the roughness indices general relationships between the profile and spatial quantities including overlapping have been established. Some measurement methods are briefly considered. The profile analysis has proved to be a reliable, easy and fast way to characterize the topography of surfaces. (15 refs.)

59758 Testing the accuracy of tensometry. I.Palfalvi. *Minozeg & Megbizhatóság (Hungary)*, vol.16, no.3, p.207-10 (1982). In Hungarian.

The resistance strain gauge is the generally used sensing element of an extensometer. The change of resistance and the elongation are related by the basic equation of tensometry. The author shows that this basic equation was derived on false assumptions and may lead to considerable errors. The theoretical study has been confirmed by industrial and laboratory experiments. (3 refs.)

59759 Non-optical surface topography by projected interference fringes. O.D.Souares (Centro de Física, Univ. do Porto, Porto, Portugal). *Port. Phys. (Portugal)*, vol.13, no.3-4, p.217-31 (1982).

Optical measurement techniques have always played an important role in precision metrology. Surface topography is a topic of great interest to science, technology and industry. Application of the technique of projected interference fringes in non-optical surface topography is described. Details and limitations of the technique are discussed. Prospects associated with the introduction of digital image processing are outlined. (14 refs.)

59760 Using an electron beam to study the surface microrelief of solids. B.N.Vasichev, G.L.Abramov.

Sov. J. Opt. Technol. (USA), vol.49, no.7, p.422-4 (July 1982). Translation of: *Opt.-Mekh. Prom-st. (USSR)*, vol.49, no.7, p.21-3 (July 1982). [received: April 1983]

Images of fractures, obtained by means of a scanning electron microscope are examined by the optical-structure computer analysis method. It is shown that a quantitative analysis of the microrelief of surfaces can be used to identify and evaluate the character of their damage resulting from fractures and mechanical working. (3 refs.)

59761 Error analysis of displacement measurement by correlation techniques. M.Ishibashi, T.Idogawa (Inst. of Appl. Phys., Univ. of Tsukuba, Ibaraki, Japan).

Trans. Inst. Electron. & Commun. Eng. Jpn. Part C (Japan), vol.J66C, no.1, p.100-1 (Jan. 1983). In Japanese.

Error analysis of displacement measurement by correlation techniques using an ITV camera is presented. Main sources of errors, exposure time of the camera and interpolation of discrete correlation functions with estimation-variance, are discussed. Application of the analysis to a typical example shows the existence of optimum sampling interval. (4 refs.)

Precision measurements and fundamental constants See Entry 59755

Analysis of operation of double-beam photometer for monitoring the thickness of thin films See Entry 59827

HS-1 holocamera See Entry 61110

Real-time holographic interferometry of moving objects in oppositely directed beams See Entry 61111

Wegged ultrasonic transducers having thickness extensional vibration See Entry 61371

Detection of deformations obtained by a moire pattern corresponding to a specific grid See Entry 61460

Laser microspeckle technique in displacement measurement near a crack tip See Entry 61462

Speckle-interferometry, a simple method for deformation analysis See Entry 61464

Study of deformed samples using an interferometer attached to the sample See Entry 61469

A microprocessor-based pulse-height analyzer See Entry 61572

X-ray diffraction intensity ratio method for the thickness measurement of ternary heterogeneous epitaxial layers on GaAs substrate See Entry 62281

Optical surface testing with diffused light See Entry 63474

The automatic photoelectric device with a laser interferometer for measuring photographs of limbs in meridian instruments See Entry 64388

06.30E Mass and density measurement

59762 The effective area of a pressure balance with a mixed principle of operation. R.Wisniewski, M.Urbanski, A.Golkowska (Inst. of Phys., Warsaw Tech. Univ., Warszawa, Poland).

High Temp.-High Pressures (GB), vol.14, no.3, p.311-14 (1982). (10th Plansee Seminar on 'Trends in Refractory Metals, Hardmetals, and Special Materials, and their Technology', Reutte, Austria, 1-5 June 1981).

Theory is presented for the variation with pressure of the effective area of a hybrid unit comprising a pressure balance with a simple piston-cylinder assembly combined with a reentrant cylinder. From the formula obtained,

numerical calculations for the pressure dependence of the effective area over the pressure range up to 1 GPa are given. (4 refs.)

06.30F Time and frequency measurement

(for astronomical aspects see 95.70)

59763 Frequency calibration using rubidium.

Qual. Today (GB), p.77 (Feb. 1983).

Describes the Argo Systems AS 210 calibration system developed for the United States Navy which is essentially a lightweight portable secondary standard. The heart of the system is a self-contained rubidium frequency standard (RFS) with 2 parts in 10^{-11} accuracy—one usually associated only with laboratory secondary standards. The practical value of the RFS is its employment on-site at the user's location. Downtime is greatly reduced and there is no need to move equipment away from the operation centres to a laboratory. The AS 210 is made up of a series of modular plug-ins in a water-resistant mainframe. (no refs.)

59764 Effect of vertical deflection nonlinearity on the accuracy of measurement of time parameters with an oscilloscope. V.I.Kimel'bat.

Meas. Tech. (USA), vol.25, no.7, p.614-17 (July 1982). Translation of: *Izmer. Tekh. (USSR)*, vol.25, no.7, p.55-6 (July 1982). [received: Feb. 1983]

The accuracy of time interval measurements on CRTs is frequently significantly affected by the nonlinearity of the vertical deflection channel. The effect of the vertical nonlinearity on the accuracy of measurement of the duration of the pulse and its leading and trailing edges is analysed and formulas are derived which enable evaluation of the significance of the resulting measurement errors. (3 refs.)

Precision measurements and fundamental constants See Entry 59755

06.30G Velocity, acceleration and rotation measurement

(for flow velocity measurement see 47.80)

Optically recording interferometer for velocity measurements with subnanosecond resolution See Entry 59832

06.30L Measurement of basic electromagnetic variables

(see also 07.50 Electrical instruments and techniques)

Measurement of piezoelectric coefficients and permittivity with small specimens See Entry 59796

Survey measurements of the magnetic field of the University of Manitoba spiral ridge cyclotron See Entry 60559

06.50 DATA HANDLING AND COMPUTATION

(see also 02.70 Computational techniques; 29.80 Nuclear information processing; for optical data processing, storage and retrieval see 42.30; for geophysical data acquisition and storage see 93.65)

59765 Application of the ratio method of EXAFS analysis to disordered systems. G.Bunker (Dept. of Phys., Univ. of Washington, Seattle, WA, USA).

Nucl. Instrum. & Methods Phys. Res. (Netherlands), vol.207, no.3, p.437-44 (1 April 1983).

When moderate disorder is present, the cumulant expansion/ratio method approach to EXAFS data analysis offers an attractive alternative to nonlinear least-squares fitting of the data. Analysis by nonlinear fitting, moment expansion, and cumulant expansion are compared, and useful formulae are derived. k -dependent mean free path is also treated. (16 refs.)

59766 Computer modelling of solids. C.R.A.Catlow, A.N.Cormack (Dept. of Chem., Univ. Coll. of London, London, England).

Lab. Microcomput. (GB), vol.1, no.3, p.23-40 (Autumn 1982). Discusses computer applications to the modelling of solids. Examples of work are chosen from: defect studies; structure and nonstoichiometry; superionic solids; high-temperature studies; crystal structure prediction; shear plane systems; surface studies. (18 refs.)

59767 Unleashing a microcomputer in the laboratory. I. K.G.McConnell (Dept. of Engng. Sci. & Mech., Iowa State Univ., Ames, IA, USA), M.Abdelhamid.

Exp. Tech. (USA), vol.7, no.1, p.22-4 (Jan. 1983). PET microcomputers represent a low-cost computational and controlling facility which is being introduced in many laboratories in order to help engineers and scientists carry out their experiments efficiently. Four types of applications where the PET uses the IEEE bus are outlined. Two specific applications of the PET are described, one for measuring the RMS of a random signal, the other in a measurement system employing the Keithley Model 177 digital multimeter. (3 refs.)

59768 CAMAC controller for a conventional and pseudorandom time-of-flight system. A.M.Ducours, C.J.Yashinovitz (Bell Labs., Murray Hill, NJ, USA).

Rev. Sci. Instrum. (USA), vol.54, no.4, p.444-53 (April 1983). Time-of-flight methods are valuable in measurements of the velocity distribution of low-energy atoms and molecules whose energies are difficult to measure directly. A system is described which uses pseudorandom beam chopping and a CAMAC compatible computer interface to provide energy resolution as good as conventional time-of-flight techniques, but with a duty factor of 50%. This system was designed for ice sputtering experiments. (18 refs.)

Inexpensive moderate speed input processor and buffer memory for NMR instrumentation See Entry 59819

Low-cost microprocessor-based photon correlator See Entry 59826

Prospekt-1 program for recovering the neutron spectra of nuclear reactors See Entry 60337

Predict liquid-phase diffusion coefficients See Entry 62138

Improvement of sensitivity of electron energy loss spectroscopy See Entry 63091

Optical surface testing with diffused light See Entry 63474

Complex analysis of experimental adsorption data using KRS 4200 and ES 1040 computersSee Entry 63597

Thermodynamic values evaluation from adsorption isotherms using KRS 4200 computerSee Entry 63598

06.60 LABORATORY TECHNIQUES

Unleashing a microcomputer in the laboratory. ISee Entry 59767

Tunable picosecond pulses around 1.3 μm generated by a synchronously pumped infrared dye laserSee Entry 61174

Measurement of ultrafast phenomena in the femtosecond time domainSee Entry 61176

Generation of femtosecond intense optical pulses and applications to time resolved spectroscopySee Entry 61199

On centering of lenses during cementingSee Entry 61309

Device for fashioning a U-shaped notch in impact specimensSee Entry 63487

Installation for preparing samples for radioisotope-excited X-ray fluorescence analysisSee Entry 63620

06.70 GENERAL INSTRUMENTATION

59769 Errors due to transverse sensitivity in strain gages. *Exp. Tech. (USA)*, vol.7, no.1, p.30-5 (Jan. 1983). Transverse sensitivity in a strain gage refers to the behavior of the gage in responding to strains which are perpendicular to the primary sensing axis of the gage. In plane wire strain gages, transmission of strain into the wire from a direction perpendicular to the wire axis is nearly negligible, but in foil strain gages the transverse sensitivity arises from much more complex phenomena, and it is affected by almost every aspect of grid design and gage construction. Errors due to transverse sensitivity are analysed and methods available for correcting the transverse sensitivity as well as the effects of shear strain are discussed. These include the rise of 'T'-rosette, three-gage rectangular rosette and delta rosette arrangements. (11 refs.)

59770 Flat panel display and projection display. K.Miyaji (Shibaura Inst. of Technol., Tokyo, Japan). *J. Acoust. Soc. Jpn. (Japan)*, vol.38, no.9, p.592-605 (Sept. 1982). In Japanese. Advancement in flat panel display and projection display technology is reviewed. Displays are divided into two categories: (1) active displays using emissive materials and (2) passive displays using nonemissive materials. A flat panel displays there are plasma displays, electroluminescent displays, liquid-crystal displays, electrochromic displays, magnetic particle displays, and cathode-ray tube displays; and projection displays, there are cathode-ray tubes and laser displays. These are briefly described. (30 refs.) *K.B.*

59771 Design and preparation of high-*Q* niobium reentrant cavities for physics measurements. W.C.Oelfke, W.O.Hamilton (Dept. of Phys. & Astron., Louisiana State Univ., Baton Rouge, LA, USA). *Rev. Sci. Instrum. (USA)*, vol.54, no.4, p.410-14 (April 1983). Some techniques are given for the design, construction, and chemical surface treatment of niobium UHF reentrant cavities. These techniques ensure that when these cavities are operated at helium temperatures they will consistently display unloaded *Q* values above 10⁷. (16 refs.)

Taking the measure of temperature.....See Entry 59783

A temperature-variable sample rotating cryostat in high magnetic fieldsSee Entry 59788

A programmable pulse generator [NMR radiospectrometer control]See Entry 59807

Automatic magnetic dichrometer for the λ=10.6 μm range [for free carrier concentration determination]See Entry 59820

System of moving the source in a nuclear gamma resonance spectrometerSee Entry 60531

A simple technique for installing strain gauges on cylindrical surfacesSee Entry 61468

An ion-implanted resistor as thermal transient sensor for the determination of the thermal diffusivity in siliconSee Entry 62194

Thermomagnetic and magnetothermoelectric quality factor of n-Ag₂TeSee Entry 62437

Electrode material for high-temperature oxygen partial pressure electrochemical sensors: strontium-doped lanthanum chromiteSee Entry 63626

Electrocatalytic glucose sensorSee Entry 63629

07.00 SPECIFIC INSTRUMENTATION AND TECHNIQUES OF GENERAL USE IN PHYSICS

(see also within each subdiscipline for specialized instrumentation and techniques)

07.10 MECHANICAL INSTRUMENTS AND MEASUREMENT METHODS

(for measurement in the mechanics of solids and rheology, see 46.30R; for materials testing, see 81.70)

59772 The unsymmetric gyroscope under the influence of a frictional and a magnetic torque. M.Leppert (Sektion Phys., Friedrich-Schiller Univ., Jena, Germany). *Exp. Tech. Phys. (Germany)*, vol.31, no.1, p.59-64 (1983). In German. The stability of the stationary rotations of an unsymmetric gyroscope is investigated for small deviations from spherical symmetry. The motion of the gyroscope which consists of electrically conducting material is influenced by an homogeneous magnetic field and isotropic friction. (9 refs.)

A simple technique for installing strain gauges on cylindrical surfacesSee Entry 61468

07.20 THERMAL INSTRUMENTS AND TECHNIQUES

(see also 44.50 Thermal properties of matter, 44.60 Thermodynamic processes; for radiometry and detection of thermal radiation see 07.60D and 07.62)

59773 Application of infra-red thermography to electrical engineering. Jin-Soo Song. *J. Korean Inst. Electr. Eng.*, vol.31, no.12, p.803-8 (Dec. 1982). In Korean. (6 refs.)

59774 Some special questions of infrared image forming. I.Benko, S.Konczol. *Meres & Autom. (Hungary)*, vol.31, no.2, p.42-6 (1983). In Hungarian. In thermotechnology infrared images are generally used to investigate the surface temperature distribution. However, image forming is influenced by other factors as well. The authors discuss the effect of the spectral sensitivity of image formers is influenced by other factors as well. The authors discuss the effect of the spectral sensitivity of image formers, the emission coefficient of the investigated surface, the direction of the observation and the shape of objects and the role of infrared reflection. Colour-photos show the appearance of the individual factors on the infrared pictures and this enables the suppression of disturbing circumstances in thermal tests. (5 refs.)

59775 Computerized evaluation of schlieren images [temperature field reconstruction]. L.I.Kiss. *Meres & Autom. (Hungary)*, vol.31, no.2, p.51-4 (1983). In Hungarian. Describes computerised methods for determining the temperature field from schlieren images. The methods reconstruct the temperature field using integration, and require algorithms to perform calculations that were previously carried out intuitively or graphically. (5 refs.)

59776 Measurement of the minimum resolvable temperature difference for thermal viewers. I.Kh.Vorakso, N.F.Soboleva. *Sov. J. Opt. Technol. (USA)*, vol.49, no.7, p.461-2 (July 1982). Translation of: *Opt.-Mekh. Prom.-st. (USSR)*, vol.49, no.7, p.57-8 (July 1982). [received: April 1983] An energy parameter is discussed that makes it possible to characterize thermal viewers; this parameter is called the minimum resolvable temperature difference. The results of a measurement of this parameter for the 'Rubin' thermal viewer are presented. (1 ref.)

59777 Performance of a compact cooling unit utilizing air-water mist flow. T.Aihara (Inst. of High Speed Mech. Tohoku Univ., Sendai, Japan), R.Saga. *Trans. ASME. J. Heat Transfer (USA)*, vol.105, no.1, p.18-24 (Feb. 1983). Performance of a new compact cooling unit for semiconductors, being composed of an atomizer, a fan, and a heat-dissipating surface with no fin, has been measured over a wide range of the mass flow rate of spray water, *m*, and the wall heat flux. The heat transfer performance of the present compact, unit with *m*=0 to 1.05 g/s, attains 1.8 to 20 times that of the parallel-plate channel under the same thermal conditions. (24 refs.)

59778 Particulate fouling on the gas-side of finned tube heat exchangers. T.R.Bott, C.R.Bemrose (Dept. of Chem. Engng., Univ. of Birmingham, Birmingham, England). *Trans. ASME. J. Heat Transfer (USA)*, vol.105, no.1, p.178-83 (Feb. 1983). A 0.3-m (12-in.) square vertical wind tunnel has been built to provide air-flows in the range 2.4-5.8 m/s (490-1140 fpm) for fouling studies. Precipitated calcium carbonate dust can be fed into the airstream (which may be heated) prior to a heat exchanger model. The paper reports results on a four-row, four-pass spiral wound finned tube heat exchanger. Fouling tests have been carried out primarily near the extremes of surface heat flux available (1000 W/m² to -700 W/m²). The results have been analyzed by the general method of Kays and London to give an effective nondimensional airside heat transfer parameter (StPr^{1/3}) and a friction factor. Tests have covered the Reynolds number range from 1350 to 3800. Normalization of fouling data to fixed Reynolds numbers has given friction factor curves which increase to an asymptotic level between 1.4 and 2.5 times the initial value, whilst StPr^{2/3} values tend to fall by only 10-20 percent during the same time. (18 refs.)

59779 Evaluation of a method for heat transfer measurements and thermal visualization using a composite of a heater element and liquid crystals. S.A.Hippensteale, L.M.Russell, F.S.Stepka (NASA Lewis Res. Center, Cleveland, OH, USA). *Trans. ASME. J. Heat Transfer (USA)*, vol.105, no.1, p.184-9 (Feb. 1983). Commercially available elements of a composite consisting of a plastic sheet coated with liquid crystal, another sheet with a thin layer of a conducting material (gold or carbon), and copper bus bar strips were evaluated and found to provide a simple, convenient, accurate, and low-cost measuring device for use in heat transfer research. The particular features of the composite is its ability to obtain local heat transfer coefficients and isotherm patterns that provide visual evaluation of the thermal performances of turbine blade cooling configurations. Examples of the use of the composite are presented. (17 refs.)

The AGA thermovision 110 and its applicational possibilitiesSee Entry 59844

An experimental study of free convection heat transfer from a horizontal cylinder in a vertical array set in free space between parallel wallsSee Entry 61379

Heat transfer from interrupted platesSee Entry 61383

Thermal radiation effects in thermal conductivity measurements: analysis and remediesSee Entry 61395

An ion-implanted resistor as thermal transient sensor for the determination of the thermal diffusivity in siliconSee Entry 62194

07.20D Thermometry

59780 Vapour pressure thermometry in high magnetic fields using a Pirani gauge. M.Mori, S.Mase (Dept. of Phys., Kyushu Univ., Fukuoka, Japan). *Cryogenics (GB)*, vol.23, no.4, p.234-5 (April 1983). Vapour pressure thermometry has the advantage of not being affected by magnetic fields. Therefore, a study was carried out of thermometry below 1K using a Pirani pressure gauge in the vapour of He³. Its sensitivity and error in temperature measurements above 0.55K are dV/dT≥K⁻¹ and 0.4% respectively. Additionally, a semiconductor pressure sensor in the vapour of He⁴ was examined for the vapour pressure thermometry. (5 refs.)

59781 Take your IC's temperature. A.S.Joffe. *73 Amat. Radio's Tech. J. (USA)*, no.270, p.70-1 (March 1983). Describes the design of a solid-state centigrade thermometer. This uses a bridge arrangement and 200 μA meter. (no refs.)

59782 A sensitive ^{13}C MR shift thermometer using dysprosium ion in acetate buffer. P.J.Smolenaers, M.T.Kelso, J.K.Beattie (School of Chem., Univ. of Sydney, Sydney, NSW, Australia).

J. Magn. Resonance (USA), vol.52, no.1, p.118-19 (March 1983).
A D₂O solution of $\sim 0.04\text{ M}$ dysprosium nitrate in acetic acid-acetate buffer at pH 5.2 comprises a useful ^{13}C thermometer for aqueous solution spectrometry. The spectrum is simple; at 15 MHz only two resonances from the methyl and carbonyl carbons occur at either end of the normal ^{13}C spectral range. Hence the thermometric spectrum can be acquired simultaneously without complicating the sample spectrum. At 23 MHz the carbonyl resonance is broadened presumably through some exchange process. Addition of 4% V/V *p*-dioxane to the sample generates another peak $\sim 1500\text{ Hz}$ from the acetate methyl resonance. The temperature dependence of the peak separation is large— $\sim 4\text{ Hz deg}^{-1}$ at 23 MHz resulting in a sensitive temperature probe. A disadvantage of this thermometric solution is that each sample batch must be individually calibrated, since small differences in sample composition, especially in the lanthanide concentration, produce large changes in the observed shifts. Once calibrated, however, the solutions appear indefinitely stable in sealed tubes. (13 refs.)

59783 Taking the measure of temperature...

Lab. Equip. Dig. (GB), vol.21, no.3, p.91-7 (March 1983).

This equipment survey provides a brief insight into the wide range of instrumentation available for measuring temperatures from near absolute zero to 3000°C and focuses on hand-held digital versions. (no refs.)

59784 The possibilities of applying holographic interferometry in temperature measurement. R.Postasy.

Meres & Autom. (Hungary), vol.31, no.2, p.59-67 (1983). In Hungarian.

The different traditional optical methods, like the schlieren technology and the Mach-Zehnder interferometry have only a limited applicational possibility in the determination of the temperature distribution of flowing media. With the appearance of holographic interferometry a wider application of interferometry becomes possible. The author outlines the basic principles and advantages of the different holographic interferometric methods related to thermal measurements. As a practical example the studying of heat transfer around a heated cylinder is referred to. (5 refs.)

59785 Distant action thermometer with LED indication. K.Schlenzig.

Radio Fernsehen Elektron. (Germany), vol.32, no.1, p.25-6 (1983). In German.

The described equipment consists in principle of a remotely placed sensor (thermistor), a temperature-voltage converter amplifier (IC type A 277 D), driven by the converter bridge and provides 12 outputs for 12 LEDs type VQA 15. A more elaborate installation for temperature monitoring in an enclosed premise provides additional limit signalization by varying pitch sound signals. A full circuit diagram is reproduced and discussed in some detail. (1 ref.) A.L.

Cooling liquid ^3He to around $100\text{ }\mu\text{K}$ See Entry 62201

07.20F Calorimetry

Measurement of weak laser light absorption in materials transparent to infrared radiation See Entry 59862

A polystyrene-water calorimeter. See Entry 60478

Total radiant power measurement of laser diode by a calorimetric method See Entry 61203

07.20H Furnaces

59786 A new ultrasonic cell for measurement near melting point of metal.

H.Kamioka (Dept. of Phys., Gifu Univ., Gifu, Japan).

Jpn. J. Appl. Phys. Part 1 (Japan), vol.22, no.3, p.437-40 (March 1983).

A new ultrasonic cell for measurements of ultrasonic velocity and attenuation in a metal under both conditions of melting and solidifying processes has been designed. Ultrasonic pulse transmission method has been used in the present work. As an example, by using a new ultrasonic cell, sound velocity of Wood's alloy is measured at and around the melting temperature, and the results for the change of sound velocity in the vicinity of the melting point are reported and discussed.

Magnetic-field-free vapor furnace for photoelectron spectroscopy. I. Temperatures up to 900 K See Entry 59888

07.20K High-temperature techniques and instrumentation; pyrometry

A sensitive ^{13}C MR shift thermometer using dysprosium ion in acetate buffer ... See Entry 59782

A system for determining fluid properties up to 136 MPa and 473 K See Entry 59794

Electrode material for high-temperature oxygen partial pressure electrochemical sensors: strontium-doped lanthanum chromite See Entry 63626

07.20M Cryogenics

59787 Space adapted cryogenics. J.Lizon-Tati (Spacecraft Technol. Dept., ESA, ESTEC, Noordwijk, Netherlands).

Adv. Space Res. (GB), vol.2, no.4, p.85-95 (1982). (Proceedings of Symposium 4 of the COSPAR Twenty-Fourth Plenary Meeting, Ottawa, Canada, 16 May-2 June 1982).

The cooling requirements applicable to scientific and application payloads of space missions currently planned within the next decade are presented as well as the applicability of the various cryogenic techniques to these requirements. The severe constraints imposed by the spacecraft system, the launch vehicle and the space environment on the spaceborne cryogenic payload are commented on. Infrared astronomy is one of the most demanding candidates for space cryogenics and examples of relevant cooling systems currently under development or proposed for near future missions within ESA activities are described. (20 refs.)

59788 A temperature-variable sample rotating cryostat in high magnetic fields. K.Noto, Z.H.Lee, N.Toyota (Res. Inst. for Iron, Steel & Other Metals, Tohoku Univ., Sendai, Japan).

Cryogenics (GB), vol.23, no.4, p.201-2 (April 1983).

A temperature-variable sample rotating cryostat has been developed in order to measure the angular and temperature dependence of the upper critical field in several single crystal Chevrel phase superconductors. In the cryostat, the temperature of the sample can be varied from 2 to 15 K within an accuracy of

$\pm 10\text{ mK}$. The sample can be rotated in an adiabatic vacuum can around a horizontal axis at the centre of superconducting magnets up to 16.5 T within an accuracy of $\pm 1^\circ$. (5 refs.)

59789 Effect of finite thermal conductivity of the separating wall on the performance of counterflow heat exchangers. K.Chowdhury, S.Saranghi (Advanced Inst. for Cryogenic Engng., Indian Inst. of Technol., Kharagpur, India).

Cryogenics (GB), vol.23, no.4, p.212-16 (April 1983).

Axial conduction is a major source of inefficiency in a compact counterflow heat exchanger. Any attempt to reduce axial conduction by using material of low thermal conductivity for the separating wall results in increased resistance to lateral heat flow, thereby reducing the overall thermal efficiency of the heat exchanger. The governing equations including axial conduction and lateral resistance due to the separating wall have been solved and an expression, for the overall efficiency of the heat exchanger has been derived in terms of relevant nondimensional parameters. Computed results have been presented which give the optimum thermal conductivity of the wall material. (6 refs.)

59790 A precision low temperature resistivity measuring cryostat. A.W.Sheikh (Indian Inst. of Technol., Bombay, India), J.Ray, R.S.Sannabhatti, G.Chandra.

Indian J. Cryog., vol.7, no.3, p.143-6 (1982).

A cryostat for electrical resistivity studies for the temperature range of 1.1 K – 300 K has been developed. Resistivity of metallic samples in the form of foils or wires can be measured. The temperature is controlled below 4.2 K within $\pm 5\text{ mK}$ by controlling helium vapour pressure and at higher temperatures within $\pm 30\text{ mK}$. The standard d.c. four-probe technique is used for measuring the sample resistivity ($1\text{ in } 10^6$). (1 ref.)

59791 On the cryostat for TSC measurements. A.Kenjo.

Technol. Rep. Kyushu Univ. (Japan), vol.55, no.4, p.337-41 (Aug. 1982). In Japanese. [received: Feb. 1983]

The usual cryostats for TSC (Thermally Stimulated Current) measurements are made of an evacuated sample cavity immersed in liquid nitrogen. The author constructed a new type of cryostat in which the inner cavity was cooled with liquid nitrogen. This cryostat enables the temperature to be raised at high heating rates as 1.2°C/s with low power and can save an amount of liquid nitrogen. TSC measurements on an Au-doped Si N^+P diode are performed to demonstrate how this crystal is effective in the experiment which requires high heating rates. (4 refs.)

Design and preparation of high- Q niobium reentrant cavities for physics measurements See Entry 59771

Vapour pressure thermometry in high magnetic fields using a Pirani gauge See Entry 59780

Matrix isolation spectroscopy. A method for investigation of chemisorption on model systems of metal catalysts. (Construction, building and testing of an apparatus for producing matrix isolated metal atom clusters) See Entry 59854

Heat transfer in subcooled liquid cryogenics See Entry 61375

The insulation effectiveness of a porous material as measured by the screening technique See Entry 61394

Experience of T-7 operation in plasma experiments See Entry 61708

Cooling liquid ^3He to around $100\text{ }\mu\text{K}$ See Entry 62201

07.25 HYGROMETRY

59792 Hygrometers—meeting the needs of an expanding market.

D.T.Parker (Shaw Moisture Meters, Bradford, England).

J. A. (Belgium), vol.24, no.1, p.29-31 (Jan. 1983).

Manufacturing and chemical processes as well as operating procedures for new equipment, which require an accurate measurement of moisture levels in air, gases and liquids continue to multiply. The article describes how an established manufacturer of moisture meters is keeping pace with the needs of an increasingly demanding market. (no refs.)

07.30 VACUUM PRODUCTION AND TECHNIQUES

(inc. pressures below 1 atmosphere ; see also 47.45 Rarefied gas dynamics; 81.15G Vacuum deposition)

The performance of mechanical scraping tools in ultrahigh vacuum: an XPS study See Entry 63443

Installation for preparing samples for radioisotope-excited X-ray fluorescence analysis See Entry 63620

07.30D Vacuum meters

59793 Construction and performance characteristics of an indigenous nude Bayard Alpert gauge. S.L.Verma, P.K.Naik (Tech. Phys. Div., Bhabha Atomic Res. Centre, Bombay, India).

Vac News (India), vol.13, no.3, p.18-23 (Sept. 1982). [received: March 1983]

The nude Bayard Alpert gauge is a hot cathode ionization gauge for total measurement of pressures between 8×10^{-10} and 1×10^{-4} Torr approximately. In this gauge the envelope is removed and the gauge head is immersed in the vacuum chamber. The sensitivity of NBAG is determined in an ultrahigh vacuum (UHV) system by comparing it with a conventional Bayard Alpert gauge. (9 refs.)

Vapour pressure thermometry in high magnetic fields using a Pirani gauge See Entry 59780

07.35 HIGH PRESSURE PRODUCTION AND TECHNIQUES

(inc. pressures above 1 atmosphere)

59794 A system for determining fluid properties up to 136 MPa and 473 K . R.Simon, R.L.Schmidt (Chevron Oil Field Res. Co., La Habra, CA, USA).

Fluid Phase Equilibria (Netherlands), vol.10, no.2-3, p.233-48 (March 1983). (Supercritical Fluids. Their Chemistry and Application, Cambridge, England, 13-15 Sept. 1982).

The search for oil and gas has extended to deeper reservoirs, with higher pressures and temperatures. Recent discoveries have exceeded 6000 meters , 120 MPa , and 463 K . In order to obtain engineering data and do phase behaviour research at these conditions, Chevron has constructed a system that operates up to 136 MPa and 473 K . This system measures phase quantities, compositions, densities, viscosities, and interfacial tensions. The heart of the

system is a sapphire tube that allows visual observation of the fluids being studied. The paper describes the highlights of the system, includes data on sapphire strength, and presents information on viscosities and interfacial tensions measured by oscillating crystal and photon correlation spectroscopy techniques. (6 refs.)

59795 Generation of high pressure to 10 GPa by means of MASS OB-8 apparatus equipped with X-ray diffraction system. S.Yamamoto, H.Sawamoto, M.Kumazawa (Dept. of Earth Sci., Nagoya Univ., Nagoya, Japan), A.Hasegawa.

High Temp.-High Pressures (GB), vol.14, no.3, p.283-91 (1982). (10th Plan-see Seminar on 'Trends in Refractory Metals, Hardmetals, and Special Materials, and their Technology', Reutte, Austria, 1-5 June 1981). The multiple-anvil-sliding-system (MASS) OB-8 high-pressure apparatus equipped with an X-ray diffraction system is developed. The mechanism and the experimental techniques used for the generation of high pressures and temperatures with the apparatus are described in detail. This novel device enables the generation of pressures of ~10 GPa and temperatures of ~1000°C simultaneously in a volume of ~40 mm³, and the observation of the compressed sample in the pressure cell by means of X-ray diffraction. The in-situ measurement of pressure in the cell, based on the NaCl scale has revealed the detailed nature of the pressure-generating characteristics in this apparatus. One notable feature is the presence of a large hysteresis in the relation between the pressure generated and the external force applied. (13 refs.)

Improved system for energy-dispersive X-ray diffraction with synchrotron radiation See Entry 61731

07.50 ELECTRICAL INSTRUMENTS AND TECHNIQUES

59796 Measurement of piezoelectric coefficients and permittivity with small specimens. A.W.Palmer, A.C.Lynch, A.T.Parish (Dept. of Electrical & Electronic Engng., City Univ., London, England). *IEE Proc. A (GB)*, vol.130, no.3, p.129-33 (May 1983).

Roughly cubical specimens of about 5 mm side can be used for obtaining results which are believed to be correct within 10%. For piezoelectric measurements, alternating mechanical pressure is used to produce a potential difference which is easily amplified and measured. A single specimen can be used for up to nine different measurements in compression and nine in shear; an alternative is the use of two specimens, tested only in compression. Permittivity along various axes can be measured with the same specimens. As an example, lithium niobate has been studied. (5 refs.)

59797 Thermally induced electric oscillations: a novel method of detection of piezoelectricity. A.Miniewicz, M.Samoc, J.Sworakowski, Z.Zboinski (Inst. of Organic & Phys. Chem., Tech. Univ. of Wroclaw, Wroclaw, Poland). *Mater. Sci. (Poland)*, vol.7, no.4, p.441-6 (1981). A new sensitive technique for studying elastic as well as piezoelectric properties of crystals is presented. The method, employing thermally induced electric oscillations (TIEO), has been tested with standard piezoelectrics: quartz and potassium dihydrophosphate. (12 refs.)

59798 Influence of inhomogeneous compensation on the capacitance measurements. A.A.Lebedev, N.A.Sobolev, B.M.Urunbaev (A.F. Ioffe Physico-techn. Inst., Acad. of Sci., Leningrad, USSR). *Sov. Phys.-Semicond. (USA)*, vol.16, no.10, p.1207-8 (Oct. 1982). Translation of: *Fiz. & Tekh. Poluprovodn. (USSR)*, vol.16, no.10, p.1874-7 (Oct. 1982). [received: April 1983]

When the capacitance methods are used to determine the parameters of deep centers or to identify unknown impurities, it is usually assumed that the base of a diode is doped with deep-level impurities uniformly over its area. If a semiconductor is doped with an impurity that does not compensate a crystal, an inhomogeneous distribution of such an impurity does not affect significantly the results of the capacitance measurements because the time constants of the thermal and optical charging of levels are independent of the deep-level density. The authors show on the other hand, in the case of a compensating impurity its inhomogeneous distribution can result in some deviations from the usual relationships. (5 refs.)

59799 Standardization of the ohm by means of the Hall effect in silicon metal-oxide semiconductor structures at 0.4-0.7K. M.A.Vernikov, L.M.Pazinich, V.M.Pudalov, S.G.Semenchinskii (All-Union Sci.-Res. Inst. of Metrological Service, Moscow, USSR). *Sov. Tech. Phys. Lett. (USA)*, vol.8, no.7, p.355-6 (July 1982). Translation of: *Pis'ma v Zh. Tekh. Fiz. (USSR)*, vol.8, no.13-14, p.820-3 (July 1982). [received: April 1983]

The quantum Hall effect in two-dimensional carrier inversion layers has recently attracted considerable research interest. The effect has made it possible to carry out several precise measurements of h/e^2 . Since the quantity h/e^2 has been measured independently of the Hall effect with an accuracy $\sim 10^{-7}$, the authors consider the inverse problem of creating an absolute standard for the ohm on the basis of h/e^2 . Previously measurements have been taken from Si MOS structures in magnetic fields up to 19 T. The authors consider taking measurements at lower temperatures and in weaker fields, ≤ 10 T. They find it realistic under the experimental conditions they describe to reproduce an absolute ohm within $\leq 10^{-7}$, i.e. within an uncertainty smaller by a factor ~ 30 than that for the standard presently in force. (7 refs.)

Precision measurements and fundamental constants See Entry 59755
A precision low temperature resistivity measuring cryostat See Entry 59790
On the cryostat for TSC measurements See Entry 59791
High accuracy measurement of the Hall effect in magnetic materials with an AC lock-in technique See Entry 62401
Precise millimeter-wave measurements of complex refractive index, complex dielectric permittivity and loss tangent of GaAs, Si, SiO₂, Al₂O₃, BeO, Macor, and glass See Entry 62873

07.55 MAGNETIC INSTRUMENTS AND TECHNIQUES

59800 Thin-film fourteen-hole DC SQUID gradiometer. W.Richter, K.Bluthner (Sektion Phys., Friedrich-Schiller Univ., Jena, Germany). *Exp. Tech. Phys. (Germany)*, vol.31, no.1, p.79-87 (1983). In German. A flat thin-film DC SQUID with fourteen holes and a superconducting input line was tested. The fourteen parallel holes with a relative area of 0.9 mm² lead to a SQUID inductance of 0.25 nH. The input line has an inductance of 22 nH and can be matched to a given signal source. The coupling factor between the input line and the SQUID is 0.5. The device is a gradiometer

with a small baseline and works without shielding in a laboratory environment. (15 refs.)

59801 Dynamics of DC-magnets and their application in the instrument manufacture. M.Konsulova. *Feingeraetetechnik (Germany)*, vol.32, no.2, p.64-5 (1983). In German. When a shading ring is laid around a part of the pole area of a DC-magnet the dynamics of the magnet are affected. Experimental and theoretical investigations for the determination of the magnetic fluxes are presented. (4 refs.)

59802 Measurement of Curie temperature and magnetization of ferromagnetic materials employing an RF oscillator. K.V.S.Rama Rao, V.Seshu Bai, C.Ramasastri (Dept. of Phys., Indian Inst. of Technol., Madras, India), N.Weiden, A.Weiss. *J. Magn. & Magn. Mater. (Netherlands)*, vol.36, no.1-2, p.180-6 (1 April 1983).

Details of a method which employs an RF oscillator to determine the Curie temperature and magnetization of ferromagnetic materials have been described. The results obtained in some intermetallic compounds, namely CrFe, Mn₁₁Sb, Mn₁₂Sb, Mn₉₀Co₁₀Sb and Mn₉₀Fe₁₀Sb are presented. (14 refs.)

59803 Analogue resolver for fluxgate magnetometer signals. J.Baxendale. *New Electron. (GB)*, vol.16, no.6, p.25 (22 March 1983). Signals from the two orthogonal coils in a fluxgate magnetometer are conventionally processed by phase-sensitive detection circuits to give two analogue voltages. These are proportional to sine (X) and cosine (X) where X is the magnetometer bearing relative to magnetic North. Describes a method of resolving sin (X) and cos (X) to give bearing, X where an accuracy of $\pm 2^\circ$ is adequate. Four comparators are used to determine the appropriate bearing angle sector and to drive the analogue switches which select the appropriate function and offset. The analogue output is shown scaled from 0-1 V corresponding to a bearing of 45-405°. (no refs.)

59804 Measuring low coercive force using a vibrating sample magnetometer. J.A.Pesch (IBM System Products Div., Rochester, MN, USA). *Rev. Sci. Instrum. (USA)*, vol.54, no.4, p.480-1 (April 1983). The coercive force H_c of commercially pure iron and an 80% NiFe alloy were measured on toroid samples using a hysteresigraph and on nontoroid samples of the same materials using a vibrating sample magnetometer. Within experimental error, the results were equal for each case. Values of H_c appeared to be insensitive to specimen shape. It appears that the demagnetizing field, which for nontoroid specimens affects the gross shape of the hysteresis loop, can be ignored in the region of low-field measurements for these materials. (4 refs.)

59805 Production of strong magnetic fields by shock waves in a medium. S.D.Gilev, A.M.Trubachev (M.A. Lavrent'ev Inst. of Hydrodynamics, Acad. of Sci., Novosibirsk, USSR). *Sov. Tech. Phys. Lett. (USA)*, vol.8, no.8, p.396-7 (Aug. 1982). Translation of: *Pis'ma v Zh. Tekh. Fiz. (USSR)*, vol.8, no.15-16, p.914-17 (Aug. 1982). [received: April 1983]

The experiments showed that this dynamic method for producing the compression region can be used successfully to produce megagauss magnetic fields. The absence of a metal liner automatically solves the problem of creating the initial magnetic flux in the compression region, and the reduction of the number of ignition points makes it possible to substantially reduce the mass of the explosive charge. All these factors serve to simplify the design of the generator and to raise the possibility of using it in laboratory explosion chambers. (6 refs.)

Method for measuring the field from a magnetic recording head in the scanning electron microscope See Entry 59886

Survey measurements of the magnetic field of the University of Manitoba spiral ridge cyclotron See Entry 60559

High accuracy measurement of the Hall effect in magnetic materials with an AC lock-in technique See Entry 62401

07.58 MAGNETIC RESONANCE SPECTROMETERS, AUXILIARY INSTRUMENTS AND TECHNIQUES

(see also 61.16N EPR and NMR determinations)

59806 ORAND—a new NMR double resonance technique for obtaining symmetrically intensive multiplets by off-resonance experiments. H.-J.Osten, R.Radeglia (Akad. der Wissenschaften, Zentralinst. fuer Phys. Chem., Berlin, Germany), A.Illigmann.

Exp. Tech. Phys. (Germany), vol.31, no.1, p.75-8 (1983). In German. Under certain experimental conditions strong intensity asymmetries within the multiplets can appear in off-resonance decoupled PFT NMR spectra. A new measurement technique is presented which removes these asymmetries and simultaneously retains the strengthening of the signals by the nuclear Overhauser effect. (4 refs.)

59807 A programmable pulse generator [NMR radiospectrometer control]. V.P.Zelenin, S.B.Karpov, V.V.Yaroslaytseva (Perm Univ., Perm, USSR). *Instrum. & Exp. Tech. (USA)*, vol.25, no.4, pt.1, p.869-73 (July-Aug. 1982). Translation of: *Prib. & Tekh. Eksp. (USSR)*, vol.25, no.4, p.83-6 (July-Aug. 1982). [received: April 1983]

A simple pulse generator for an NMR radiospectrometer is described that is programmed from an Elektronika 60 microcomputer, which enables one to generate sequences of two, three, or more pulses, including ones with a repeating group of time intervals in order to control the transmitter, receiver, and suppressor in the spectrometer. The length of the time intervals can be varied from 0.5 μ sec to 100 sec. (3 refs.)

59808 Saturation transfer dispersion electron paramagnetic resonance using a balanced cavity: dynamical calibration and biological applications. P.A.Sehr (Inst. de Biologie Phys.-Chimique, Paris, France), C.Mailer, P.F.Devaux. *J. Magn. Resonance (USA)*, vol.52, no.1, p.23-34 (March 1983).

Saturation transfer dispersion electron paramagnetic resonance spectra of biological samples were recorded using a newly developed balanced cavity. With this configuration the U_1' spectrum (first harmonic dispersion 90° out of phase) has a signal-to-noise ratio comparable to that of the conventionally employed first harmonic-in-phase absorption signal (V_1). Spin-Labeled bovine serum albumin in glycerol/water mixtures was used to establish calibration curves of U_1' spectra. The sensitivity of U_1' to isotropic motions extends from 5.10^{-7} to 10^{-4} sec. The potential of U_1' combined with the balanced cavity scheme for the study of the dynamics of membrane bound proteins is also investigated. Cytochrome c oxidase and rhodopsin in disk membranes were used as model systems. The U_1' spectra of satisfactory signal-to-noise ratio can be obtained with one 8-minute scan and a spin concentration as small as 50 μ M in 10 μ l. The calibration curves obtained can be utilized as a first approximation for these anisotropic systems. (24 refs.)

59809 Proton chemical shifts in polycrystalline solids determined by off-resonance decoupling ¹³C CP-MAS NMR. A.Bax, T.A.Early, G.E.Maciel (Dept. of Chem., Colorado State Univ., Fort Collins, CO, USA).

J. Magn. Resonance (USA), vol.52, no.1, p.35-41 (March 1983).

A ¹³C CP-MAS method is described which uses off-resonance decoupling in order to correlate directly bonded ¹³C-¹H pairs in the solid state. An analysis of the experimental results gives ¹H chemical shifts by inspection while at the same time separating various ¹H resonances via the paired ¹³C resonance. An example is shown using *p*-diethoxybenzene. (18 refs.)

59810 Practice of multidimensional stochastic NMR spectroscopy. The derivation of 1D, 2D, and 3D spectra. B.Blumich, D.Ziessow (Tech. Univ. Berlin, Berlin, Germany).

J. Magn. Resonance (USA), vol.52, no.1, p.42-56 (March 1983).

The hardware modifications necessary for the implementation of multidimensional stochastic magnetic resonance (MUDISM) on a conventional FT spectrometer are described and a practical way for the mass storage of the stochastic raw data is shown. Experimental spectra demonstrate different options in the data reduction. (15 refs.)

59811 A simple method for the calibration of the decoupler radiofrequency field strength. A.Bax (Dept. of Chem., Colorado State Univ., Fort Collins, CO, USA).

J. Magn. Resonance (USA), vol.52, no.1, p.76-80 (March 1983).

A simple experiment is proposed which provides a convenient way to calibrate the decoupler radiofrequency field strength over a wide range of magnitudes and with high accuracy. The calibration can be performed on the sample to be investigated and an example is shown for sucrose. (16 refs.)

59812 Pulse sequences utilizing the correlated motion of coupled heteronuclei in the transverse plane of the doubly rotating frame. M.R.Bendall, D.T.Pegg, D.M.Doddrell (School of Sci., Griffith Univ., Nathan, Queensland, Australia).

J. Magn. Resonance (USA), vol.52, no.1, p.81-117 (March 1983).

In terms of the Heisenberg vector model, heteronuclei undergo a correlated motion via scalar coupling when both have their spins simultaneously in the transverse plane of the doubly rotating reference frame. Several pulse sequences are described in terms of ¹H/¹³C systems. A theoretical analysis of the correlated motions is given for methine (CH), methylene (CH₂), and methyl (CH₃) groups for the situation when the ¹H magnetization vectors are initially placed in the transverse plane of the doubly rotating frame and are allowed to precess freely for (2J)⁻¹ sec, where J is the single-bond ¹H-¹³C coupling constant, prior to the carbon polarization transfer vectors being placed in the transverse plane. The analysis is confirmed experimentally using two-dimensional NMR and the usefulness of the sequences for two-dimensional NMR is assessed. The family of sequences is completed with a theoretical study of sequences which employ polarization transfer in addition to the correlated motion. Experimental verification for the one-dimensional use of these sequences, the exclusive polarization transfer sequence (EPT), in editing ¹³C spectra is given. Reverse EPT, the inverse of EPT, is also described and is shown to be useful for editing ¹H spectra. While it is pointed out that the authors expect there to be a correspondence between correlated motion and Schroedinger picture multiple-quantum coherence, the details of this correspondence are not explored. (19 refs.)

59813 Elimination of solvent signals in carbon magnetic resonance spectroscopy. J.Bornais, S.Brownstein, S.Bywater (Div. of Chem., Nat. Res. Council of Canada, Ottawa, Canada).

J. Magn. Resonance (USA), vol.52, no.1, p.120-22 (March 1983).

The problem of a strong or obscuring solvent signal in proton resonance spectroscopy was alleviated by the use of perdeuterated solvents. The practice of stabilizing the magnetic field-frequency ratio for the spectrometer via the deuterium resonance of the solvent followed from the almost routine use of deuterated solvents and was continued for carbon magnetic resonance. Perdeuterated solvents depleted in ¹³C were developed to remove interfering solvent signals in those cases where the reactivity of the reagents restricted the choice of solvent. However, these are expensive and only available for a few solvents. It has recently become possible to distinguish the number of hydrogen atoms directly bonded to a carbon atom by the modulation of the signal of that carbon atom in response solely to an appropriately gated proton decoupling sequence. For most organic molecules the cancellation of signals from secondary and quaternary carbons is not quite complete because of long-range carbon-hydrogen coupling and because of the range of values found for one-bond carbon-hydrogen coupling constants. Therefore very weak signals are often found for them. In perdeuterated molecules the cancellation of the carbon resonance signals should be complete since there is no carbon-hydrogen spin coupling. (8 refs.)

59814 Correlation of isotropic shifts and chemical shift anisotropies by two-dimensional Fourier-Transform magic-angle hopping NMR spectroscopy. A.Bax, M.Szeverenyi, G.E.Mszchiel (Dept. of Chem., Colorado State Univ., Fort Collins, CO, USA).

J. Magn. Resonance (USA), vol.52, no.1, p.147-52 (March 1983).

A two-dimensional (2-D) Fourier transform (FT) technique which presents the isotropic average chemical shift, $\sigma_1 = (\sigma_{11} + \sigma_{22} + \sigma_{33})/3$, in one frequency dimension (F_1) and the static CSA powder pattern along the other frequency axis (F_2) is presented. The experiment is carried out using discrete 'hops' between evolution segments, rather than continuous sample spinning, and no spinning sidebands are produced. As the detection occurs on a static sample, the signal decays more rapidly than in a normal MAS experiment, and sensitivity suffers correspondingly. Preliminary results show the promise for obtaining powder patterns for individual peaks of complex molecules for which a straight forward nonspinning approach would yield only broad bands of inextricably overlapping powder patterns. This and related experiments are under extensive study. (11 refs.)

59815 Selective solvent suppression in ¹H FT NMR using a DANTE pulse: its application in normal and NOE measurements. C.A.G.Haasnoot (Biophys. Dept., Faculty of Sci., Nijmegen, Netherlands).

J. Magn. Resonance (USA), vol.52, no.1, p.153-8 (March 1983).

Strong peaks arising from solvents or impurities often present an arduous problem for NMR spectroscopists. Especially in ¹H FT NMR studies of biological molecules, when low concentrations of solute (e.g. ≤ 1 mM) are to be examined in D₂O solution, the detection of the weak signals of the solute in the presence of the large residual HDO peak poses a severe dynamic range problem. Apart from the resulting sensitivity reduction of signals arising from the solute, the solvent line may also obscure a portion of interest in the spectrum. Many techniques have been developed for eliminating or suppressing a solvent line from the spectrum, one of which is the WEFT (Water Eliminated Fourier Transform) method. Important to note, however, is the normal WEFT constraint that the longitudinal relaxation time T_1 of the solvent must be significantly longer (or shorter) than the relaxation time of the signals of interest. This requirement is not always fulfilled in the case of small molecules and for biological molecules under specific conditions. The self-complementary hexaribonucleotide (r-CGCGCG) may serve as an exam-

ple of the latter difficulty. In aqueous solution this molecule adopts a double helical structure at ambient temperature. The normal spectrum of a 1 mM sample of this compound in D₂O at 25°C is shown. The residual HDO peak is by far the most intense signal in the spectrum. When the sample is properly degassed, the longitudinal relaxation time of the signals of the hexaribonucleotide appears to be similar to that of the residual HDO resonance. This situation is remedied by modifying the method according to a suggestion of Morris and Freeman (1928): instead of a nonselective π pulse, a selective π pulse is applied to the residual HDO resonance. The selective excitation is created by a so called DANTE pulse sequence. For the rest the normal WEFT scheme is followed. (9 refs.)

59816 NMR broadband decoupling with low radiofrequency power. A.J.Shaka, T.Frenkiel, R.Freeman (Phys. Chem. Lab., Oxford Univ., Oxford, England).

J. Magn. Resonance (USA), vol.52, no.1, p.159-63 (March 1983).

For high resolution NMR spectroscopy of carbon-13, it is important to be able to achieve broadband proton decoupling with the minimum dissipation of radiofrequency power in the probe. Otherwise undesirable heating effects can occur, and the resulting convection may degrade resolving power and sensitivity. Radiofrequency power dissipation is proportional to $d(B_2)^2$ where B_2 is the radiofrequency intensity and d is the duty cycle of the irradiation. It is convenient to define a figure of merit Z for decoupling performance $Z = \Delta B_{\max}/(B_2 d^{1/2})$ where ΔB_{\max} defines the range of proton offsets for which the decoupled carbon-13 resonance is at least 80% of its maximum peak height (measured with coherent irradiation at resonance). The first evidence of imperfect decoupling is a small unresolved residual splitting of the carbon-13 resonance, made manifest by a reduction of peak height. The choice of carbon-13 line broadcasting function determines the sensitivity to small imperfections of the decoupling performance. A full width at half height of 2 Hz has been adopted as the practical standard, taken to be reasonably typical for routine carbon-13 spectroscopy. (14 refs.)

59817 EPT with two variable pulse angles, a universal polarization transfer sequence. M.R.Bendall, D.T.Pegg (School of Sci., Griffith Univ., Nathan, Queensland, Australia).

J. Magn. Resonance (USA), vol.52, no.1, p.164-8 (March 1983).

Recently the authors generalized the EPT sequence (Bendall et al. 1982, 1983) to the DEPT and inverse DEPT pulse sequences, which provide the same polarization transfer enhancements as INEPT and inverse INEPT but have advantages over the latter sequences which include less sensitivity to miset delay periods, thus providing more accurate editing of ¹³C and ¹H spectra; distortionless coupled spectra; and fewer pulses in the sequences. However, unlike INEPT, these sequences have so far been restricted to spin-half heteronuclei. They show that DEPT and inverse DEPT are just special cases of a more general pulse sequence, which is applicable to two scalar coupled spin systems, each containing an arbitrary number of nuclei of arbitrary spin, provided the coupling between the two systems can be characterized by a single constant. They call this the universal polarization transfer (UPT) sequence. (9 refs.)

59818 Efficient fast-recovery scheme for NMR pulse spectrometers. N.S.Sullivan, P.Deschamps, P.Neel, J.M.Vaissiere (CENS, Gif-sur-Yvette, France).

Rev. Phys. Appl. (France), vol.18, no.4, p.253-61 (April 1983).

Describes an active damping circuit, which uses a 90° phase-shift feedback loop to dampen the ringing of nuclear resonance probes just after the RF excitation. The damping does not operate during the reception of the nuclear signal and there is therefore no loss in efficiency or in sensitivity as would be the case for permanent damping. The use of a high voltage FET as a gated duplexer to isolate the RF transmitter after the pulse is also described. The circuit damper is especially useful at low frequencies and the authors have been able to reduce the recovery time of a series resonant circuit ($Q=50$) to less than 7 μ s at 3 MHz using this feedback scheme and the gated duplexer. (35 refs.)

59819 Inexpensive moderate speed input processor and buffer memory for NMR instrumentation. S.D.Kunz, A.G.Redfield (Phys. Dept., Brandeis Univ., Waltham, MA, USA).

Rev. Sci. Instrum. (USA), vol.54, no.4, p.503-4 (April 1983).

An inexpensive, moderately fast input converter, adder, and buffer memory is described for use with an NMR instrument. Speed is a few microseconds per 12-bit data point and word length and size are essentially unlimited. (2 refs.)

A sensitive ¹³CMR shift thermometer using dysprosium ion in acetate buffer ...
..... See Entry 59782

Reexamination of a sequence designed to cancel ¹³C signals of protonated carbons ...
..... See Entry 60753

Bismuth NMR spectroscopy: ²⁰⁹Bi and ¹⁹F high-resolution NMR spectra of the hexafluorobismuthate(V) ion ...
..... See Entry 60754

Suppression of the solvent resonance in 2D NMR spectra of proteins in H₂O solution ...
..... See Entry 61031

Optical multiple pulse sequences for multiphoton selective excitation and enhancement of forbidden transitions ...
..... See Entry 61245

07.60 OPTICAL INSTRUMENTS AND TECHNIQUES

[for radiation detection, see 07.62; for spectroscopy and spectrometers, see 07.65; for holography, see 42.40; for optical sources and standards, see 42.72; for optical lens and mirror systems, see 42.78; for optical devices, techniques and applications, see 42.80; for optical testing and workshop techniques, see 42.85; for radiation spectrometers and spectroscopic techniques, see 29.30; for radiation measurement, detection and counting, see 29.70]

59820 Automatic magnetic dichrometer for the $\lambda=10.6 \mu$ m range [for free carrier concentration determination]. G.N.Potikhonov, E.K.Galanov, V.G.Medvedev, O.R.Zudov (Vavilov State Optical Inst., Vavilov, USSR).

Ind. Lab. (USA), vol.48, no.6, p.591-4 (June 1982). Translation of: *Zavod. Lab. (USSR)*, vol.48, no.6, p.55-7 (June 1982). [received: March 1983]

The authors describe a device developed to measure the magnetic circular dichroism in narrow-band semiconductors in the range 77 to 300K. Using this device the free carrier concentrations of these materials can be determined. (6 refs.)

59821 Measuring thin film parameters by inputting light through a prism. A.N.Ageev, E.N.Mokrushina, A.S.Trifonov (A.F. Ioffe Physicotech. Inst., Acad. of Sci., Leningrad, USSR).

Sov. Phys.-Tech. Phys. (USA), vol.27, no.10, p.1255-6 (Oct. 1982). Translation of: *Zh. Tekh. Fiz. (USSR)*, vol.52, no.10, p.2044-6 (Oct. 1982). [received: April 1983]

To achieve maximum measurement accuracy it is necessary to increase the distance between the prism and the film every time a new mode with a higher mode number is investigated. However, this makes it much more difficult to record multimode film spectra. The difficulty can be circumvented by including prism effects on the mode structure in the calculations; the main difficulty here is to find the size of the gap. The authors show that the gap distance can be determined by comparing spectra for the TE- and TM-polarization modes recorded simultaneously. (8 refs.)

Computerized evaluation of schlieren images [temperature field reconstruction] See Entry 59775

Optical method of determining the Curie point displacement in ferroelectric crystals under external effects See Entry 62899

07.60D Photometry and radiometry

(inc. colorimetry; see also 07.62 Detection of radiation)

59822 Truncation error in colorimetric computations. W.Erb, M.Krystek (Phys. Tech. Bundesanstalt, Braunschweig, Germany).

Color Res. & Appl. (USA), vol.8, no.1, p.17-22 (Spring 1983). The wavelength interval 360-830 nm relevant in colorimetric computations is sometimes truncated by the instrument used to measure the spectral characteristics of a material, or the spectral power distribution of a source, or simply by choice. The (systematic) error resulting from this truncation has been derived. Tables are given for the calculation of the truncation error in each case. (4 refs.)

59823 Greyness of process colors. R.H.Gray (Photo Products Dept., E.I. du Pont de Nemours & Co. Inc., Parlin, NJ, USA).

Color Res. & Appl. (USA), vol.8, no.1, p.43-6 (Spring 1983). A method of measuring and comparing the greyness (unwanted spectral absorptions) of process colorants has been developed. The method uses the 1976 CIELAB color space and, in effect, makes a chromatic match of a trial colorant with a reference Cromalin color and then calculates greyness from the difference of their values of CIE 1976 lightness L. (11 refs.)

59824 Determination of optical constants by photometry. L.Ward (Dept. of Appl. Phys., Coventry Polytech., Coventry, England).

J. Phys. D (GB), vol.16, no.4, p.L71-3 (14 April 1983). A recent study of the accuracies of determining the optical constants of thin films, for film thicknesses up to 0.04 λ , has been extended to include film thicknesses up to 0.25 λ , and the results are reported. It is shown that the method may also be applied to bulk materials. (2 refs.)

59825 A converter of monochromatic radiation to electrical voltage. A.Skubis.

Pol. Tech. Rev. (Poland), no.5-6, p.5 (1982). The photocell converter is designed for measuring the power of monochromatic radiation. It is particularly suitable for measuring the power of He-Ne lasers and LED diodes. The converter consists of a measuring probe adapted for hooking up to any analogue or digital indicator, or to a recorder with input impedance greater than 10 k Ω /V and measuring range expressed in mV. Its operation consists in a conversion of the power of monochromatic radiation to an electric voltage by means of a silicon photocell whose resistance is selected in such a way that it is a function of wavelength and photocell efficiency. A patent application for the converter design has been filed at the Polish Patent Office. Its conversion accuracy is 1%, photo-sensitive element diameter 20 mm, wavelength range 0.4...1.1 μ m and radiation power measuring range 15 μ W...50 mW. (no refs.)

59826 Low-cost microprocessor-based photon correlator. N.S.Murthy, D.M.Choudhary (Instrumentation Programme, Reactor Res. Centre, Kalpakam, India).

Rev. Sci. Instrum. (USA), vol.54, no.4, p.476-9 (April 1983). A simple cost-effective microprocessor-based correlator is described which can be used for Gaussian as well as nonGaussian light sources. Error calculations are presented to show that there is no significant improvement in accuracy by adopting 4-bit word length in preference to 3-bit word length. The instrument can also be used in Raman and Raleigh scattering experiments. A few experimental results are presented bringing out the importance of correlation averaging in S/N enhancement. Some autocorrelograms for fluctuations in the scattered light from polystyrene spheres suspended in water are also presented. The instrument can sample 1500 points and calculate 85 correlations in each scan. All the parameters such as number of samples, number of correlations, number of scans, and the sampling time are user programmable. (6 refs.)

59827 Analysis of operation of double-beam photometer for monitoring the thickness of thin films. R.Kh.Fazylyzanov.

Sov. J. Opt. Technol. (USA), vol.49, no.8, p.519-21 (Aug. 1982). Translation of: *Opt.-Mekh. Prom.-st. (USSR)*, vol.49, no.8, p.47-50 (Aug. 1982). [received: April 1983]

The operation of a double-beam photometer for monitoring the thickness of thin films through the use of a control sample, a portion of which was coated with a quarter-wave layer of material, is analyzed. Expressions are given for calculating the errors for monitoring in terms of transmission extreme and by means of the double-beam photometer. The accuracy of the described method for monitoring a one-layer coating is an order of magnitude greater than the accuracy of monitoring in terms of extrema. The photometry procedure for a seven-layer mirror coating is calculated on a mathematical model. (4 refs.)

59828 Circuit diagrams of exposure metering devices for professional film cameras. M.F.Zelener, V.S.Pantelev.

Tekhn. Kino & Telev. (USSR), no.3, p.15-19 (March 1983). In Russian. The basic parameters and circuit diagrams of exposure metering devices used in professional filming equipment are considered. (7 refs.)

Multispectral radiometer to measure crop canopy characteristics See Entry 59856

Photometric errors induced by edge effects on hypersensitized Kodak spectroscopic plates, Type 103a-O See Entry 59866

Total radiant power measurement of laser diode by a calorimetric method See Entry 61203

Photometric apparatus 'Duga' for investigating Polar auroras and tropical arcs from onboard the orbital station 'Salyut-6' See Entry 64349

07.60F Polarimetry and ellipsometry

Surface Raman ellipsometry See Entry 59851

Optical test of the equation of state of an interfacial region See Entry 62217

07.60H Refractometry and reflectometry

59829 Absolute spectral reflectance of mirrors. F.Grumb, T.Wightman (Res. Labs., Eastman Kodak Co., Rochester, NY, USA).

Color Res. & Appl. (USA), vol.8, no.1, p.40-2 (Spring 1983). Describes the techniques for measuring specular (regular) reflectance of mirrors on an absolute basis. Two independent methods of measuring mirrors are described, and data are presented for the two methods of measurement in the range 400-1500 nm. (2 refs.)

59830 An exact technique for mixing of immersion fluids [refractive index matching for photoelastic applications]. S.Singh (G.B. Pant Univ. of Agriculture & Technol., Nainital, India).

Exp. Tech. (USA), vol.7, no.1, p.27-9 (Jan. 1983).

In three-dimensional photoelastic investigations a reliable stress pattern can be achieved by immersing the specimen in a liquid having substantially the same index of refraction as the model. This technique is based upon the effect of concentration of refractive index of solutions. Graphs from which the proportions of the three most commonly mixed immersion fluids can be readily determined to obtain a desired value of the refractive index of the mixture are provided. (10 refs.)

59831 Method of measuring the refractive indices of absorbing media. A.I.Pen'kovskii.

Sov. J. Opt. Technol. (USA), vol.49, no.8, p.510-13 (Aug. 1982). Translation of: *Opt.-Mekh. Prom.-st. (USSR)*, vol.49, no.8, p.38-41 (Aug. 1982). [received: April 1983]

A method is proposed for measuring the refractive indices of absorbing media by means of FTIR [frustrated total internal reflection] without calculating or measuring the absorption. The method is based on the mutual compensation of the effects of the change in the parameters of the light polarization states at the critical incidence angles. (14 refs.)

Multispectral radiometer to measure crop canopy characteristics See Entry 59856

Characterisation of single-mode fibres by near-field measurement See Entry 61288

Precise millimeter-wave measurements of complex refractive index, complex dielectric permittivity and loss tangent of GaAs, Si, SiO₂, Al₂O₃, BeO, Macor, and glass See Entry 62873

A numerical method for determining the complex refractive index from reflectance and transmittance of supported thin films See Entry 63070

07.60L Interferometry

59832 Optically recording interferometer for velocity measurements with subnanosecond resolution. D.D.Bloomquist, S.A.Sheffield (Sandia Nat. Labs., Albuquerque, NM, USA).

J. Appl. Phys. (USA), vol.54, no.4, p.1717-22 (April 1983).

An optically recording velocity interferometer system, called ORVIS, has been developed to measure particle velocity histories in shock wave experiments on condensed matter. The interferometer fringe motion is recorded with a high speed electronic streak camera, rather than with photomultiplier tubes and oscilloscopes as in previous interferometry systems. With this approach, the particle velocity of a witness foil in a detonation wave experiment was measured with 300-ps time resolution. The authors believe that 20-ps time resolution can be achieved with this technique which would represent an improvement of two orders of magnitude over previous measurement techniques. (10 refs.)

59833 Photon-noise limitations in wave-front-folding interferometry. K.Itoh, Y.Ohtsuka (Dept. of Engng. Sci., Faculty of Engng., Hokkaido Univ., Sapporo, Japan).

J. Opt. Soc. Am. (USA), vol.73, no.4, p.479-85 (April 1983).

Statistical errors in mutual intensity, measured by a photon-noise-limited, wave-front-folding interferometer, are studied from the viewpoint of high-resolution imaging through the turbulent atmosphere. The effects of quantum noise in light detection on the modulus and phase measurements are analyzed, and simplified statistical models of normal distributions are derived. The errors that are due to both the photon noise and atmospheric phase-front perturbations are clarified by using the simplified photon-noise models and the so-called log-normal model for the atmospheric perturbations. The conditions under which the conventional method for phase-unwrapping preprocessing can be applied to the interferometric data are studied to specify the limitations of wave-front-folding interferometry. The analysis suggests the possible application of such interferometry to a survey of simple objects, such as binary stars, or to a detailed investigation of solar-surface structures. (27 refs.)

59834 Moire projection and high temperature Moire grid. H.Kockelmann, W.Zugi.

Mater. Test. (Germany), vol.25, no.4, p.120 (April 1983). In German.

In the high temperature region the production of a temperature independent grid of adequate contrast and stretch is important and the avoiding of physical contact with the ancillary optics. Often small apertures and correspondingly long exposures times are necessary, so that vibration free mounting is required. Depending on the temperature of the test piece, different types of grids can be used, say, for temperatures up to 150°C, in the range from 150 to 460°C, and above 460°C, where for extremely large extensions, electrolytically etched grids are useful. (no refs.) R.S.

59835 A Fabry-Perot etalon with one phase-conjugate mirror. M.Nazarathy (Dept. of Electrical Engng., Stanford Univ., Stanford, CA, USA).

Opt. Commun. (Netherlands), vol.45, no.2, p.117-21 (15 March 1983).

A resonating structure composed of a plane-stratified lossless medium and a phase-conjugate mirror with loss or gain is analyzed by means of a scattering matrix method as well as by tracking the multiple reflections to their steady state. The amount of misdirection in the presence of losses or gains in the PCM is explicitly evaluated. (7 refs.)

59836 Acoustic sensitivity of a fiber-optic interferometer. M.M.Butusov, N.V.Ermakova, N.L.Urvantseva.

Opt. & Spectrosc. (USA), vol.53, no.2, p.115-16 (Aug. 1982). Translation of: *Opt. & Spektrosk. (USSR)*, vol.53, no.2, p.193-4 (Aug. 1982). [received: April 1983]

There is a growing interest in the use of fiber-optic sensors (FOS) for measuring constant and variable pressures (in FOPS), since such sensors possess a broad frequency range and are convenient from the viewpoint of system

interconnection. However, sensitivity of a FOPS depends substantially on its construction and the type of fibers used. The most popular FOPS is an analog of the Mach-Zehnder interferometer, which is made by using single-mode fibers. The sensitivity of a phase FOPS is determined by the degree of phase change Φ of the wave passing through the working fiber per unit length per unit change of pressure i.e. M . The specific value of M is determined with known mechanical and optoelastic constants of the fiber material and its coating and is based on the mechanical model of the behavior of a fiber in an elastic medium, the model selection substantially affecting the computed results. Two models, namely the hydrostatic compression model and the balance-loss model have been proposed and yield different expressions for M . The authors have set up an experiment with an aim to verifying one of the models. (10 refs.)

59837 Ring polarization interferometer. Measurement of the flow rates of transparent media. I.A.Rokos, L.A.Rokosova.

Opt. & Spectrosc. (USA), vol.53, no.2, p.186-90 (Aug. 1982). Translation of: *Opt. & Spektrosk. (USSR)*, vol.53, no.2, p.320-7 (Aug. 1982). [received: April 1983]

A ring polarization interferometer with an external modulator is described in which a nonreciprocal element consisting of a combination of quartz plates is used. This enables the effect of distortions of the state of polarization of the beam at the mirrors to be eliminated and also enables the effect of instability of the operating point of the modulator on the accuracy of the measurements to be removed. A ring polarization interferometer can thus be constructed with a threshold sensitivity of 10^{-6} . A method of designing modulation polarization interferometers using the Poincaré sphere is proposed. As an example, a ring polarization interferometer is described for measuring flow rates using the zero-compensation method, the accuracy of which is independent of the density and velocity distribution functions over the flow cross section. (11 refs.)

59838 Use of large reflectors in long-range interference measuring devices. G.V.Merkishin.

Sov. J. Opt. Technol. (USA), vol.49, no.7, p.465-6 (July 1982). Translation of: *Opt.-Mekh. Prom-st. (USSR)*, vol.49, no.7, p.60-2 (July 1982). [received: April 1983]

The field intensity in the Fraunhofer zone is analyzed for the reflection of monochromatic radiation from large triangular-aperture reflectors. It is shown that increasing the dimensions of the reflectors does not lead to a displacement of the interference pattern minima in the central interference region; therefore it can be used to obtain information by means of conventional interference measuring instruments. Increasing the reflector size simplifies considerably the recording of the interference information. (4 refs.)

59839 A fiber-optic rotation transducer. A.B.Bukhman, E.M.Dianov, A.Ya.Karasik, V.A.Kozlov, A.M.Prokhorov.

Telecommun. & Radio Eng. Part 2 (USA), vol.37, no.4, p.87-9 (April 1982). Translation of: *Radiotekhnika, Moskva (USSR)*, vol.37, no.4, p.56-9 (April 1982). [received: April 1983]

A balanced method of measuring rotation velocities in a fiber-optic ring interferometer is described which can be used to measure velocities of rotation as low as 0.3 deg/sec with a single-mode light guide approximately 275 meters long. (16 refs.)

Classroom Moire demonstrator See Entry 59563

A convenient Fizeau interferometer for thin film thickness measurement See Entry 59756

Non-optical surface topography by projected interference fringes See Entry 59759

The possibilities of applying holographic interferometry in temperature measurement See Entry 59784

Measurement of weak laser light absorption in materials transparent to infrared radiation See Entry 59862

Delay in the spontaneous decay of excited atoms in a resonator See Entry 60642

HS-1 holocamera See Entry 61110

Real-time holographic interferometry of moving objects in oppositely directed beams See Entry 61111

Influence of a nonlinear active medium on the structure of natural oscillation modes of a Fabry-Perot interferometer See Entry 61196

Nonlinear optical phenomena in a multiple interferometer See Entry 61225

Nonlinear interferometry in Langmuir-Blodgett multilayers of polydiacetylene See Entry 61226

Design of a new thin-film electro-optic switch See Entry 61304

Detection of deformations obtained by a moire pattern corresponding to a specific grid See Entry 61460

Laser speckle technique in displacement measurement near a crack tip See Entry 61462

Speckle interferometry, a simple method for deformation analysis See Entry 61464

Study of deformed samples using an interferometer attached to the sample See Entry 61469

Space plasma diagnostics See Entry 61705

The automatic photoelectric device with a laser interferometer for measuring photographs of limbs in meridian instruments See Entry 64388

07.60P Optical microscopy

59840 Laser scanning microscope with automatic focusing. W.Deint

(Tech. Forschung K1 2, Wiesbaden, Germany), M.Linke, R.Muller, I.Sander. *Microsc. Acta (Germany)*, vol.87, no.2, p.129-38 (March 1983). In German.

Describes the design and functioning of a novel type of laser scanning microscope which provides pictures in a range of up to 1 cm \times 3 cm with a local resolution of 1 μ m. During the scanning process the profile of the tests item is followed by the optical system, the focus is adjusted over the surface within the depth of focus range. By means of noncontact position measurement by the optical system, the profile of the test item can be recorded with an accuracy of approximately 1 μ m. (4 refs.)

Publications concerning microscopic equipment, methods, applications, and related topics See Entry 59561

Topographic quantification of non-planar localized surfaces See Entry 59757

Monitoring method for axis alignment of single-mode optical fiber and splice-loss estimation See Entry 61308

Methods of in-shop testing of microscope optical-system centering See Entry 61314

07.62 DETECTION OF RADIATION (BOLOMETERS, PHOTOELECTRIC CELLS, I.R. AND SUBMILLIMETRE WAVES DETECTION)

59841 Photoconductive detectors for space IR astronomy. E.T.Young

(Steward Obs., Univ. of Arizona, Tucson, AZ, USA). *Adv. Space Res. (GB)*, vol.2, no.4, p.59-68 (1982). (Proceedings of Symposium 4 of the COSPAR Twenty-Fourth Plenary Meeting, Ottawa, Canada, 16 May-2 June 1982).

Space observations promise greatly improved sensitivity for infrared astronomical observations. The author gives a survey of current discrete infrared detector technology. Emphasis is on impurity-doped silicon and germanium photoconductors, as these devices are the most sensitive detectors available from the middle infrared out to beyond 120 Nm. Following a discussion of the physics of detector operation, a description of fabrication techniques is given. Pre-amplifier designs are briefly considered. Under the low backgrounds expected in cryogenic telescopes, photoconductors exhibit multiple time constants, and the ionizing radiation environment in space can give rise to significant variations in detector responsivity. Techniques for dealing with the two kinds of anomalous behavior found in space-borne applications are discussed. (38 refs.)

59842 Temperature compensation of pyroelectric radiation detectors. G.Hofmann, N.Neumann, T.Hellfeld (Sektion Elektronik-Technol. und Fein-gerätech. Dresden, Dresden, Germany).

Exp. Tech. Phys. (Germany), vol.31, no.1, p.97-9 (1983). In German.

For many cases the temperature stability of the responsivity of pyroelectric radiation detectors can be improved by a suitable choice of the ratio between elements capacity and input capacity of the preamplifier. Some achievements of detectors made of γ -irradiated TGS and γ -irradiated DTGS are presented. (8 refs.)

59843 Effect of electric fields on long-wavelength response of infra-red detectors. D.D.Coon, R.P.G.Karunasiri (Dept. of Phys., Univ. of Pittsburgh, Pittsburgh, PA, USA).

Electron. Lett. (GB), vol.19, no.8, p.284-7 (14 April 1983).

The effect of electric fields on extrinsic semiconductor infrared-detector response at low temperatures is examined quantitatively at wavelengths beyond the zero-field cutoff. General formulas are presented along with numerical results for Si:P and Si:In. These results illustrate the possibility of narrow-bandwidth detection and electronically modulated response. (12 refs.)

59844 The AGA thermovision 110 and its applicational possibilities. D.Benko.

Meres & Autom. (Hungary), vol.31, no.2, p.71-6 (1983). In Hungarian.

From the infrared imaging devices known and used in Hungary, the device AGA 110 is the easiest to carry and handle. It can be used under severe observation circumstances. The sensitivity of the device can be changed to give grey tone image. On the basis of the technical properties it meets very well the requirements of error detection in operation. The author reports about the experiences obtained during the observation of thermic phenomena and the checking of heat losses. (2 refs.)

59845 Thermal imaging system with a two-phase ternary mixture of liquids. J.C.Loulergue, Y.Levy, C.Imbert (IOTA Univ. Paris-Sud, Orsay, France).

Opt. Commun. (Netherlands), vol.45, no.3, p.149-54 (1 April 1983).

A new infrared camera operating between 8 and 12 μ m is described. The thermo-optical properties of two superposed fluid layers are used. It is shown that the modulation of the fluid-fluid interface, due to the infrared image, of a two-phase ternary mixture can be made much larger than with a two-phase binary one. Making this modulation visible, is the principle of a sensitive IR-visible image converter. (17 refs.)

59846 Reconstruction of field statistics from the photocount statistics of an inertial detector. A.S.Arutyunov.

Opt. & Spectrosc. (USA), vol.53, no.2, p.179-81 (Aug. 1982). Translation of: *Opt. & Spektrosk. (USSR)*, vol.53, no.2, p.307-12 (Aug. 1982). [received: April 1983]

An estimate of the relative effect of dead time on photocount statistics is made within the framework of the phenomenological theory of photoelectric recording. The author considers the possibility of a two-stage determination of the statistical characteristics of radiation when using photocounters that are known to be inertial, for which the effect of dead time is important. It is shown that the statistical information obtained by inertial detectors is in principle incomplete. A basis is given for three methods of establishing the photocount statistics of a noninertial detector from the experimental statistics of a real detector. (8 refs.)

59847 Fast pulsed-irradiation detectors using slow photoresistors and photodiodes. V.M.Mkhitaryan, Kh.V.Partamyan (Phys. Res. Inst., Acad. of Sci., Ashtarak, Armenian SSR).

Sov. Phys.-Tech. Phys. (USA), vol.27, no.9, p.1169-70 (Sept. 1982). Translation of: *Zh. Tekh. Fiz. (USSR)*, vol.52, no.9, p.1900-2 (Sept. 1982). [received: April 1983]

It is shown that slow photoresistors and photodiodes can be used as fast pulsed-radiation detectors with time resolutions down to 10^{-10} s, which enables one to overcome the lack of fast detectors for infrared radiation. (3 refs.)

Application of infra-red thermography to electrical engineering See Entry 59773

A converter of monochromatic radiation to electrical voltage See Entry 59825

Rydberg-atom masers. II. Triggering by external radiation and application to millimeter-wave detectors See Entry 61122

Total radiant power measurement of laser diode by a calorimetric method See Entry 61203

Spacecraft attitude sensing based on the Earth's radiation See Entry 64350

Characterisation of the Reticon 100 \times 100 array See Entry 64389

07.65 OPTICAL SPECTROSCOPY AND SPECTROMETERS

(inc. photoacoustic spectroscopy)

59848 A microcomputer based system for stopped-flow kinetics. R.D.Jee

(School of Pharmacy, Univ. of London, London, England).

Lab. Microcomput. (GB), vol.1, no.3, p.5-10 (Autumn 1982).

Discusses apparatus in which data from a stopped-flow chemical kinetics experiment is stored on an oscilloscope and analysed. An interface for transferring data from a Gould Advance OS400 digital storage oscilloscope to a PET microcomputer is described. An Applied Photophysics model 1704

stopped-flow spectrophotometer was used for the kinetic measurements. (2 refs.)

59849 On the interaction operator in the optical spectroscopies. Duckhwan Lee, A.C.Albrecht (Dept. of Chem., Cornell Univ., Ithaca, NY, USA). *J. Chem. Phys. (USA)*, vol.78, no.6, pt.2, p.3382-92 (15 March 1983). The appropriate form for the interaction operator used to formulate electric-dipole spectroscopies of any order is discussed within the gauge-invariant formulation previously developed by K-H. Yang [Ann. Phys. (NY) 101, 62 (1976)]. Both 'active' (absorptive and emissive) and 'passive' (coherent wave-mixing) spectroscopies are examined. Though formally it is the 'position' operator which is the correct one when describing radiation-matter interaction in terms of the 'dark' eigenstates of material, it is found that under certain limiting constraints the 'momentum' operator leads to equivalent results. The demonstration proceeds without recourse to the commutation relation normally used to relate the position and momentum expressions for the spectroscopic parameters, and it applies to both active and passive spectroscopies at any order. However, for any of the multiply resonant (active or passive) spectroscopies, or for detailed line shape considerations in the active spectroscopies, damping effects must be introduced through the density matrix formalism. It appears that as long as damping is important, there are no circumstances under which the momentum operator expressions can match the correct, gauge invariant, position operator expressions for coupling the dark eigenstates. Finally, if the Hamiltonian defining the dark eigenstates is an approximate one, containing a nonlocal potential (such as a Hartree-Fock Hamiltonian), the momentum form of the interaction operator must be modified to include additional (well-defined) terms before the equivalency with the position operator is established. (34 refs.)

59850 Electric-field-induced differential rotational Raman scattering. A.D.Buckingham, R.A.Shatwell (Univ. Chem. Lab., Univ. of Cambridge, Cambridge, England). *J. Chem. Phys. (USA)*, vol.78, no.6, pt.2, p.3393-7 (15 March 1983). An electrostatic field induces a linear change in the intensity of light scattered by a gas in a circularly polarized incident radiation. Differential scattering intensities for *O*, *P*, *Q*, *R*, *S* lines are evaluated for a linear dipolar molecule. The weak *R*(0) line shows a strong differential scattering. In the classical limit, differential scattering comes from molecules initially in the nonrotating *J*=0 state. (13 refs.)

59851 Surface Raman ellipsometry. G.L.Eesley (Dept. of Phys., General Motors Res. Labs., Warren, MI, USA). *J. Electron Spectrosc. & Relat. Phenom. (Netherlands)*, vol.30, p.41 (Feb. 1983). (Proceedings of the Third International Conference on 'Vibrations at Surfaces', Asilomar, CA, USA, 1-4 Sept. 1982). Summary form only given, as follows. A method for achieving the ultrahigh sensitivity required for surface Raman spectroscopy is described. Polarization selective heterodyne detection permits shot-noise limited submonolayer detection with classically noisy picosecond laser sources. Preliminary experimental results show that the polarization selectivity can be used to reduce the overwhelming thermally induced changes in metal surface reflectivity. (no refs.)

59852 Determination of offset between a fixed wavelength laser and an absorption line using frequency modulation spectroscopy. P.Pokrowsky, E.A.Whittaker, G.C.Bjorklund (IBM Res. Lab., San Jose, CA, USA). *Opt. Commun. (Netherlands)*, vol.45, no.3, p.196-200 (1 April 1983). Frequency modulation spectroscopy is used as a new method to determine the detuning or optical frequency offset between a fixed laser line and the center of an adjacent absorption line. Because the offset is measured directly using high precision RF techniques, the accuracy is limited only by the laser linewidth. The method was demonstrated using (a) a dye laser set at a fixed frequency and an etalon resonance and (b) an infrared He-Ne laser and a methane absorption line. (12 refs.)

59853 Fast-scanning Fourier spectrometer online with a computer complex. V.V.Arkipov, V.N.Bodunova, B.V.Vylegzhanin. *Sov. J. Opt. Technol. (USA)*, vol.49, no.7, p.436-7 (July 1982). Translation of: *Opt.-Mekh. Prom.-st. (USSR)*, vol.49, no.7, p.33-4 (July 1982). [received: April 1983] Reports on a fast-scanning Fourier spectrometer, designed to record interferograms and calculate spectra by means of a computer complex (M6000 and M4030 computers) connected to it remotely. The block diagram of the instrument is given and the features of its operating principle are described. The results of a measurement of several spectra along with a demonstration of the metrological capabilities are presented. The latter include an improved signal/noise ratio in the spectrum by a summing of the interferograms and a programmed generation of relative spectra with a single-beam measurement method. (3 refs.)

59854 Matrix isolation spectroscopy. A method for investigation of chemisorption on model systems of metal catalysts. (Construction, building and testing of an apparatus for producing matrix isolated metal atom clusters). M.Seidel, M.Grosch (Sektion Chemie, Friedrich Schiller Univ., Jena, Germany). *Wiss. Z. Friedrich-Schiller-Univ. Jena, Math. Naturwiss. Reihe (Germany)*, vol.31, no.6, p.1065-72 (1982). In German. The authors describe, in addition to considerations of construction, the build-up and testing of equipment for producing matrix isolated metal atoms, metal atom clusters and their reaction products. A minimal temperature 10-15K was obtained on the sample holder. As a result one can use argon as matrix gas. The consumption of cooling liquid permits after cooling the sample holder and matrix preparation, a time of measurement of 4 hours. The electronic spectra of Ni atoms in an Ar, Kr Xe matrix showed a very good coincidence with literature results. (15 refs.)

A system for determining fluid properties up to 136 MPa and 473K See Entry 59794

Low-cost microprocessor-based photon correlator See Entry 59826

Temperature dependence of the Raman linewidth in H₂⁺ See Entry 60733
Generation of femtosecond intense optical pulses and applications to time resolved spectroscopy See Entry 61199

Laser-power fluctuations: an analog signal-correction technique See Entry 61209

Polarization four-photon spectroscopy within the absorption line: role of coherent Rayleigh scattering and of the multilevel nature of molecules See Entry 61234

Optical multiple pulse sequences for multiphoton selective excitation and enhancement of forbidden transitions See Entry 61245

Measurements of a supersonic velocity in a nitrogen flow using inverse Raman spectroscopy See Entry 61582

Space plasma diagnostics See Entry 61705

Surface photoacoustic spectroscopy—a new technique for the study of surface vibrations See Entry 62224

Determination of cubic optical susceptibilities of liquid crystals by coherent four-photon spectroscopy See Entry 62914

07.65E UV and visible spectroscopy and spectrometers

59855 A tunable, single frequency UV source for high resolution spectroscopy in the 293-330 nm range. W.A.Majewski (Fysisch Lab., Katholieke Univ., Nijmegen, Nijmegen, Netherlands). *Opt. Commun. (Netherlands)*, vol.45, no.3, p.201-6 (1 April 1983). An easily tunable, single frequency source of UV radiation is described. The method is based on an intracavity second harmonic generation (SHG) using an angle tuned KIO₃ crystal in a ring dye laser. The 293-330 nm tuning range with maximum obtainable power of 15 mW and spectral linewidth between 180 and 500 kHz has been obtained for one crystal cut. The method described is simpler, more versatile and covers at least a three times broader spectral range than systems using temperature tuned crystals. Several applications to high resolution molecular spectroscopy are discussed. (22 refs.)

59856 Multispectral radiometer to measure crop canopy characteristics. E.J.Brach, P.Poirier (Engng. & Statistical Res. Inst., Agriculture Canada, Ottawa, Ontario, Canada), R.L.Desjardins, D.Lord. *Rev. Sci. Instrum. (USA)*, vol.54, no.4, p.493-500 (April 1983). A spectroradiometer has been designed for the study of crop reflectance characteristics in the spectral range of 400-1000 nm. Since the instrument records the ratio of incoming to reflected radiation the values obtained are independent of variations in solar elevation, and azimuth angle and atmospheric conditions. A filter wheel with four interchangeable interference filters is used for wavelength selection. The spectroradiometer traverses above a crop canopy on a movable track. This makes it possible to compare measurements from various locations several times in an hour, and to study more than one canopy a day. This instrument provides agronomists with data to estimate crop canopy characteristics such as leaf area index (LAI) rapidly and nondestructively. It also measures the variability of canopy reflectance introduced by temporal and spatial factors. (22 refs.)

59857 Possibilities of increasing the resolution of diffraction spectrographs. V.S.Plotnikov, D.A.Zhuravlev. *Sov. J. Opt. Technol. (USA)*, vol.49, no.7, p.401-2 (July 1982). Translation of: *Opt.-Mekh. Prom.-st. (USSR)*, vol.49, no.7, p.1-3 (July 1982). [received: April 1983]

The possibilities of increasing the resolution of spectrographs by using modern echelle-type diffraction gratings are examined. The advisability of using gratings having blaze angles of 70-80° for obtaining high resolution and reducing instrument size is shown. An experimental model of a spectrograph having an actual resolution of 340000-950000 in the UV spectral region, whose construction is based on that of the commercial DFS-8 spectrograph, has been developed and tested. (5 refs.)

59858 Spectroscopic and dynamic studies in the extreme ultraviolet: recent progress and future possibilities. E.E.Marinero (Dept. of Chem., Stanford Univ., Stanford, CA, USA). Topical Meeting on Excimer Lasers, Incline Village, NV, USA, 10-12 Jan. 1983 (Washington, DC, USA: Opt. Soc. America 1983), p.TuCl/1-3 Absorption of VUV and XUV radiation leads not only to highly excited electronic states of a molecular system but also to phenomena such as photofragmentation and photoionization. Progress in this field is reviewed with particular emphasis to the possibilities opened by the advent of XUV and VUV coherent sources. (no refs.)

07.65G IR spectroscopy and spectrometers

59859 Fourier transform infrared reflection-absorption spectroscopy of surface species. W.G.Golden, D.D.Saperstein (IBM Instruments Inc., San Jose, CA, USA).

J. Electron Spectrosc. & Relat. Phenom. (Netherlands), vol.30, p.43-50 (Feb. 1983). (Proceedings of the Third International Conference on 'Vibrations at Surfaces', Asilomar, CA, USA, 1-4 Sept. 1982). The authors have been able to demonstrate progress in Fourier Transform Infrared Reflection-Absorption Spectroscopy (FT-IRRAS) by incorporating a switching circuit into the data acquisition electronics of an air-equilibrated IBM IR/98 FTIR Spectrometer such that it is possible to obtain simultaneously both reference and polarization modulated spectrum. These spectra ratio to produce good discrimination against gas-phase species. The operating principles of this approach and sample FT-IRRAS spectra of monolayer assemblies of cadmium arachidate adsorbed on silver are discussed. (23 refs.)

59860 Electroreflectance vibrational spectroscopy: a new surface analysis technique using diode lasers. D.K.Lambert (Dept. of Phys., General Motors Res. Labs., Warren, MI, USA).

J. Electron Spectrosc. & Relat. Phenom. (Netherlands), vol.30, p.59-64 (Feb. 1983). (Proceedings of the Third International Conference on 'Vibrations at Surfaces', Asilomar, CA, USA, 1-4 Sept. 1982).

A new infrared technique to measure the vibrational spectra of adsorbed molecules is introduced. An infrared active mode of an oriented molecule has a first order Stark effect. Therefore, infrared absorption by oriented adsorbed molecules is modulated by an alternating electric field. The spectra is obtained by measuring this using a diode laser. The advantages and limitations of Electroreflectance Vibrational Spectroscopy (EVS) are discussed. The Stark tuning rate and consequent signal amplitude are calculated for a number of diatomic molecules. Measurements of diode laser intensity noise are used to estimate the signal to noise ratio for comparison with other techniques. (19 refs.)

59861 Intracavity dye-laser photothermal deflection spectroscopy. K.V.Reddy (McDonnell Douglas Res. Labs., McDonnell Douglas Corp., St. Louis, MO, USA).

Rev. Sci. Instrum. (USA), vol.54, no.4, p.422-4 (April 1983). An intracavity, CW, dye-laser photothermal deflection (PTD) technique has been developed for gas-phase vibrational overtone spectroscopy. This new technique has a similar S/N ratio and significantly lower window noise than the intracavity photoacoustic technique under identical conditions. (5 refs.)

59862 Measurement of weak laser light absorption in materials transparent to infrared radiation. N.A.Kirichenko, B.S.Luk'yanchuk, A.N.Sapetskii, E.V.Siskayan (P.N. Lebedev Phys. Inst., Acad. of Sci., Moscow, USSR). *Sov. Phys.-Tech. Phys. (USA)*, vol.27, no.10, p.1305-6 (Oct. 1982). Translation of: *Zh. Tekh. Fiz. (USSR)*, vol.52, no.10, p.2121-2 (Oct. 1982). [received: April 1983]

It has recently become necessary to fabricate materials with low absorptivity to IR laser radiation. This problem also requires that improvements be made in the methods used to measure small absorption coefficients of materials in

the IR spectrum. A highly sensitive technique (the dynamic method) has been suggested based on an unusual combination of calorimetric and interferometric techniques. The absorption coefficient κ is determined by measuring the period t_0 of the first oscillation caused by interference in the transmission of a plane-parallel plate during thermo-optical expansion. The authors find a correction to the equation for absorption which allows for thermal power losses (to first order) and demonstrate that the corrected equation is much more accurate (the error is roughly halved in typical experiments). (2 refs.)

59863 Intracavity laser spectrometer with a dispersive resonator using F_2^- color centers in an LiF crystal. Yu.L.Gusev, S.I.Marennikov, V.I.Serdnyukov, L.N.Sinita (Inst. of Atmospheric Optics, Acad. of Sci., Tomsk, USSR). *Sov. J. Quantum Electron. (USA)*, vol.12, no.10, p.1370-1 (Oct. 1982). Translation of: *Kvantovaya Elektron. (Moskva USSR)*, vol.9, no.10, p.2105-6 (Oct. 1982). [received: April 1983]

An intracavity spectrometer utilizing F_2^- color centers and operating in the range 1.108-1.169 μ was developed. The spectrometer sensitivity was $\sim 10^{-8}$ cm $^{-1}$ and the spectral resolution was < 0.08 cm $^{-1}$. It was used to record the absorption spectrum of atmospheric air. All the recorded lines were due to water vapor. Transparency microwindows were found in the absorption spectrum of the atmosphere at wavelengths 1.108-1.169 μ . (5 refs.)

Multispectral radiometer to measure crop canopy characteristics See Entry 59856

07.68 PHOTOGRAPHY, PHOTOGRAPHIC INSTRUMENTS AND TECHNIQUES

(for light sensitive materials see also 42.70)

59864 Electronic still-picture camera using magnetic bubble memory. K.Ohnishi, K.Murakami, K.Wakui (NHK Tech. Res. Labs., Tokyo, Japan). *ABU Tech. Rev. (Japan)*, no.85, p.31-6 (March 1983).

Outlines the experimental equipment for an electronic still-picture camera developed by NHK. The equipment used a frame transfer CCD as an image pickup device and a magnetic bubble as a recording device for digital recording. A means of electronically controlling the time of integration, which corresponds to the time of exposure in film cameras, and camera characteristics and variations of picture quality during the time of integration are described. (6 refs.)

59865 3M Colour Reversal 640T—a review. G.Ashton. *Br. J. Photogr. (GB)*, vol.130, no.12, p.318-20 (25 March 1983). 3M Colour Reversal 640T film is primarily intended for exposure by tungsten illumination of a colour temperature of 3200K and is said by the manufacturer to be ideal for exposures at low light levels in a wide variety of situations. The author assesses the film characteristics, the characteristic curves, colour balance and colour response and the sharpness and graininess. In testing Colour Reversal 640T film the comparison material chosen was the nearest competitor for speed and tungsten balance, Kodak Ektachrome 160 (Tungsten). (no refs.)

59866 Photometric errors induced by edge effects on hypersensitized Kodak spectroscopic plates, Type 103a-O. M.Bitrán (Dept. of Astron., Univ. of Florida, Gainesville, FL, USA). *AAS Photo-Bull. (USA)*, no.31, p.6-8 (1982).

A program of regular photographic photometry of quasi-stellar objects has been carried on at the Rosemary Hill Observatory since 1968 (Pollock et al., 1979; Pica et al., 1980). The 4X5-inch plates are exposed at the f/4 Newtonian focus of the 76-cm reflector. Nearly all of the regular monitoring is done with Kodak 103a-O plates that are hypersensitized by nitrogen baking followed by soaking in pure hydrogen, after the procedure described by Scott and Smith (1976). On the very earliest plates, ca. 1968, a single 2-inch field was recorded at the geometrical centre of the 4X5-inch plate. Very early on, however, a so-called '2-banger' cassette was designed by H.W. Schrader. Finally, however, the increasing number of exposures that were being made, as well as the sharply rising plate costs led Schrader to design the '4-banger' cassette. Some concern has existed because of the proximity of the fields in the new design to the edges of the plate. Sufficient statistics have accumulated to warrant a search for possible deleterious effects on the photometry. (5 refs.)

59867 Reciprocity failure of hypersensitized and unhyposensitized Kodak Technical Pan Film 2415. A.G.Smith (Dept. of Astron., Univ. of Florida, Gainesville, FL, USA).

AAS Photo-Bull. (USA), no.31, p.9-12 (1982). The sensitivities of hypersensitized and unhyposensitized samples of Kodak Technical Pan Film 2415 have been measured for exposures ranging from 3 sec to 2 hr in duration. Unhyposensitized 2415 film suffers severe low-intensity reciprocity failure over the entire range of exposures. Hydrogenated film, on the other hand, displays little reciprocity failure over the entire 2400:1 range of exposure times. A consequence of this is that the 'gain' from hypersensitization is a marked function of the exposure for which it is measured, varying from less than 3 for 10-sec exposures to 20 for exposures of 2 hr. (5 refs.)

59868 Electronic photo-flash with photoelectric release. G.Skribanowitz. *Radio Fernsehen Elektron. (Germany)*, vol.32, no.1, p.56-78 (1983). In German.

A high-performance flash is described, employing 5XVQA 15 LEDs as wide-angle photo-elements to operate an 80 WS flash tube (XB 81-00). Circuit diagrams of the mains-operated flash unit (ferrite ignition transformer data are included), of the control unit with thyristor switch, and of the built-in LED test circuit are reproduced and discussed. (7 refs.) A.L.

59869 Automatic camera lens focusing systems. R.B.Mitkin, V.A.Karpushin. *Sov. J. Opt. Technol. (USA)*, vol.49, no.7, p.453-8 (July 1982). Translation of: *Opt.-Mekh. Prom.-st. (USSR)*, vol.49, no.7, p.50-5 (July 1982). [received: April 1983]

Various automatic camera lens focusing systems are examined. The specifications of automatic-focusing camera models are given. The principal directions for future development of such systems are indicated. (57 refs.)

59870 Spectroscopy and integral image quality. B.K.Rozhkov. *Sov. J. Opt. Technol. (USA)*, vol.49, no.8, p.521-31 (Aug. 1982). Translation of: *Opt.-Mekh. Prom.-st. (USSR)*, vol.49, no.8, p.50-9 (Aug. 1982). [received: April 1983]

The basic properties of the three-dimensional integral image and the characteristics of the lens-array photographic systems producing these images are examined. Literature data are analyzed. (79 refs.)

59871 A video tape editing system. A.I.Potashnikov, V.A.Studenikin. *Tekh. Kino & Telev. (USSR)*, no.3, p.6-11 (March 1983). In Russian. Considers some problems of using electronic video tape editing in feature film production. An editor developed by NIKFI and intended for filming on loca-

tions is described. The operation procedures and basic technical parameters of the system are given. (6 refs.)

59872 The Mars-2000M and Mars-3000M lighting devices. A.M.Kuritsyn, N.T.Semenikhin.

Tekh. Kino & Telev. (USSR), no.3, p.19-20 (March 1983). In Russian. The Mars-2000M and Mars-3000M lighting devices for filming are described as well as their light and operating characteristics. (2 refs.)

59873 The effect of modulation characteristics on the output of dye silver optical sound tracks in film prints. T.N.Noskova.

Tekh. Kino & Telev. (USSR), no.3, p.21-3 (March 1983). In Russian. An average output spread due to changes in modulation characteristics of film-print dye silver soundtracks was determined experimentally. The relative effect of changes in densitometric parameters of light and dark sound track areas was evaluated when vacuum stibium-caesium photomultipliers or silicon photodiodes are used in motion picture networks. (4 refs.)

59874 Deep UV lithography by using excimer lasers. (Photo-etching characteristics and development of uniform intensity irradiation system). Y.Kawamura, Y.Itagaki, K.Toyoda, S.Namba (Inst. of Phys. & Chem. Res., Wako-shi, Saitama, Japan).

Typical Meeting on Excimer Lasers, Incline Village, NV, USA, 10-12 Jan. 1983 (Washington, DC, USA: Opt. Soc. America 1983), p.WA4/1-3. The photo-etching characteristics of photoresists for excimer lasers were investigated and compared with those of UV lamps. Uniform intensity irradiation system for micro-electronics processing is demonstrated. (8 refs.)

Circuit diagrams of exposure metering devices for professional film cameras See Entry 59828

Thermal imaging system with a two-phase ternary mixture of liquids See Entry 59845

The stability of cesium iodide X-ray photocathodes See Entry 59898

Modulation transfer functions of a lens-array photographic system See Entry 61101

Evaluation of mechanical and physical properties of films under dynamical loading See Entry 61250

PbO/CdS, Se/Cu mixed photoconductor system for electrophotography See Entry 62445

High-speed photographic study of the dynamic properties of ferrite-garnet films with domain diameters less than 0.5 μ m See Entry 62779

Luminescence flash photostimulation spectra of silver chloride See Entry 63045

ASA 1000 and color too See Entry 64399

07.75 MASS SPECTROMETERS AND MASS SPECTROMETRY TECHNIQUES

(for mass spectroscopic chemical analysis, see 82.80)

59875 Calibration system for satellite and rocket-borne ion mass spectrometers in the energy range from 5 eV/charge to 100 keV/charge. A.G.Ghielmetti, H.Balsiger, R.Banninger, P.Eberhardt, J.Geiss, D.T.Young (Phys. Inst., Univ. of Bern, Bern, Switzerland).

Rev. Sci. Instrum. (USA), vol.54, no.4, p.425-36 (April 1983). A new system has been developed for calibration of space plasma analyzers, in particular ion mass spectrometers. The system provides a large-area (~ 250 cm 2), highly parallel ($\pm 0.5^\circ$), and spatially uniform ($\pm 5\%$) beam of ions over the energy per charge range from 5 eV/charge to 100 keV/charge. Other special features include variable energy spread from $\Delta E \sim 1$ eV/charge to ~ 3 keV/charge and multiple charge state ions such as He^{2+} or Xe^{2+} . Among several key ion optical elements are a high-efficiency electron bombardment ion source capable of delivering $\sim 10^{-8}$ A, a 90° crossed electric and magnetic field mass spectrometer designed to produce either a mixed or a mass-selected beam, and a unique beam expansion system which produces the uniform large-area beam. The system also includes automatic beam monitoring and control via a feedback loop, as well as provisions for semiautomatic control of angle and energy analysis. Use of the calibration system during its development phases has made possible the rapid calibration of five complex satellite ion mass spectrometers already flown. Data from one of these calibrations are discussed. (26 refs.)

59876 Criterion for optimizing ion sources produced by electron impact ionization. L.N.Gall' (Inst. of Analytical Instrumentation, Acad. of Sci., Leningrad, USSR).

Sov. Phys.-Tech. Phys. (USA), vol.27, no.10, p.1280-3 (Oct. 1982). Translation of: *Zh. Tekh. Fiz. (USSR)*, vol.52, no.10, p.2086-92 (Oct. 1982). [received: April 1983]

A simple algorithm is given for calculating a figure of merit I_{max} which is used to analyze and optimize ion sources with bulk ionization. The parameter I_{max} is derived using phase space and beam transport techniques and can be used to treat the initial ion distributions in the ionization region, the focusing properties of the ion-optical system in the ion source, and the beam transport conditions in the mass analyzer. The algorithm is used to calculate the parameters of ion source of the Nir type. (5 refs.)

Electrostatic charged particle analyzer with three coaxial cylindrical electrodes. II. Construction of a three-stage system with a central electrode of finite thickness and axis-axis focusing See Entry 59890

Space plasma diagnostics See Entry 61705

Isotopic analysis of nanomole gas samples by means of dynamic flow mass spectrometry See Entry 63625

The application of plasma mass spectroscopy to plasma etching See Entry 63632

07.77 PARTICLE BEAM PRODUCTION AND HANDLING; TARGETS

(see also 29.25 in elementary-particle and nuclear physics, 41.80 Particle beams and particle optics)

59877 Beam-plasma type metal ion source. J.Ishikawa, T.Takagi (Dept. of Electronics, Kyoto Univ., Kyoto, Japan).

Jpn. J. Appl. Phys. Part 1 (Japan), vol.22, no.3, p.534-40 (March 1983). A metal ion source, whose operation is based on a beam-plasma type ion source, has been developed. Heating of a plasma production chamber (1160°C) and generation of axial magnetic field (0.029 T) were both achieved by DC current flow through a solenoid filament. A continuous ion current of 2-3 mA (Ag, Al, Sb, Mn, Pb) was extracted from a single aperture at a low extraction voltage of 5.2 kV; this was due to a high density plasma production by means of beam-plasma discharge and an ion extraction with ion

space-charge compensation by beam electrons and high energy plasma electrons. For the case of silver ion beam, a silver ion with a purity of 99.5% was extracted without a mass analyzer. Normalized emittance and normalized brightness were 1.9×10^{-8} m.rad and 1.1×10^{11} A.rad $^{-2}$ m $^{-2}$, respectively.

59878 Nonlinear multichannel pulse-sharpening line containing ferrite rings with nonrectangular hysteresis loop. V.A.Shvets (Joint Inst. for Nuclear Res., Dubna, USSR).

Instrum. & Exp. Tech. (USA), vol.25, no.4, pt.1, p.908-12 (July-Aug. 1982). Translation of: *Prib. & Tekh. Eksp. (USSR)*, vol.25, no.4, p.116-19 (July-Aug. 1982). [received: April 1983]

The design is discussed and test results reported for a low-impedance nonlinear multichannel pulse-sharpening line using ferrite rings with a nonrectangular hysteresis loop. Minimal rise times of 0.5 nsec for stationary shock waves are shown to be attainable by combining nonlinear pulse-sharpening channels in parallel inside an external coaxial conductor. The dependence of the rise and delay times of the shock wave front as a function of the current amplitude, length of the pulse-sharpening line, demagnetizing current, etc., are given for the bundle of pulse-sharpening lines tested. The assembly (containing 6000 ferrite rings) is designed as a module in the system controlling the high-current electron beam. (9 refs.)

59879 An intense electron beam source. J.Yeheskel, D.Gazit, R.Avida, M.Friedman (Nuclear Res. Center-Negev, Beer-Sheva, Israel).

J. Phys. D (GB), vol.16, no.4, p.499-504 (14 April 1983).

High emission currents were achieved from a line electron thermionic source. The cathode was heated by electron bombardment from a secondary filament. Cathodes were built from massive strip made of tantalum or tungsten. Current densities were further increased by focusing the secondary electrons on to a narrow strip at the bottom of the cathode. The focus was achieved following a numerical model calculation. The design permitted the emitting surface temperature to be further increased, by keeping the cathode partially molten, in a reliable, continuous mode of operation. (5 refs.)

59880 Volume generation of H⁻ ions in plasmas. M.Bacal (Lab. de Phys.

des Milieux Ionisés, Ecole Polytech., Palaiseau, France).

Phys. Scr. (Sweden), vol.T2, no.2, p.467-78 (1982). [received: April 1983] (1982 International Conference on Plasma Physics, Göteborg, Sweden, 9-15 June 1982).

The generation of hydrogen and deuterium negative ions and beams is reviewed, with particular emphasis on volume production in plasmas, which has recently been found to be a useful element of possible high-power negative-ion-based neutral beam systems. The experimental evidence for volume production is based on the measurement of high density (5×10^{10} cm $^{-3}$) and high fractions (10-35%) of H⁻ and D⁻ ions in plasmas, using the photodetachment method, and on measurements of re-vibrational populations using coherent antiStokes Raman scattering (CARS). These measurements are discussed in terms of a theoretical model relying on the assumption that the dominant negative ion production process is the recently discovered dissociative electron attachment to highly vibrationally excited molecules. Photodetachment, CARS and extraction experiments performed in different magnetic multipole configurations are described; they indicate that the magnetic multipole may be a useful device for this application. (14 refs.)

59881 Three-electrode electrostatic deflection plates for low-energy charged beams. R.Grisenti (Istituto per la Ricerca Sci. e Tecnologica, CNR, Trento, Italy), A.Zecca.

Rev. Sci. Instrum. (USA), vol.54, no.4, p.505 (April 1983).

A simple system of electrostatic deflection plates with three electrodes is described. (no refs.)

CAMAC controller for a conventional and pseudorandom time-of-flight system See Entry 59768

Calibration system for satellite and rocket-borne ion mass spectrometers in the energy range from 5 eV/charge to 100 keV/charge See Entry 59875

Stabilization of longitudinal instabilities in heavy-ion storage rings See Entry 60492

Porous tungsten relativistic electron beam cathodes compared with carbon cathodes See Entry 60512

Two-coordinate scintillation hodoscope on the basis of hodoscope photomultipliers See Entry 60541

Using scintillation hodoscopes with hodoscope photomultipliers in particle-momentum measurements and in fast sampling See Entry 60542

Improved system for energy-dispersive X-ray diffraction with synchrotron radiation See Entry 61731

07.80 ELECTRON AND ION MICROSCOPES AND TECHNIQUES

(see also in condensed matter 61.16D Electron microscopy, 61.16F Field ion microscopy)

59882 Three-dimensional profiling with the Sandia nuclear microprobe. B.L.Doyle, N.D.Wing (Sandia Nat. Labs., Albuquerque, NM, USA).

IEEE Trans. Nucl. Sci. (USA), vol.ns-30, no.2, p.1214-19 (April 1983).

(1982 IEEE Conference on the Application of Accelerators in Research and Industry, Denton, TX, USA, 8-10 Nov. 1982).

A nuclear microprobe analysis system attached to Sandia's EN tandem Van de Graaff accelerator is described. A magnetic quadrupole doublet lens is used for the final focus and 2 μ m beam diameters have been obtained. Several illustrative applications of the microprobe, including the first three-dimensional concentration profiles using Rutherford backscattering and elastic recoil detection ever measured, are given. (14 refs.)

59883 Appraisal of a new charge correction method in X-ray photoelectron spectroscopy. S.Kohiki, T.Ohmura, K.Kusao (Materials Res. Lab., Matsushita Electric Industrial Co. Ltd., Moriguchi, Osaka, Japan).

J. Electron Spectrosc. & Relat. Phenom. (Netherlands), vol.31, no.1, p.85-90 (April 1983).

The authors recently reported a new charge correction method in X-ray photoelectron spectroscopy (1983). They showed that the $2p_{3/2}$ binding energy (BE) of Ar implanted in insulating materials was 242.3 eV, and that this could be used to correct for charge shifts. It is expected that the value of BE_R (Ar $2p_{3/2}$, IM) will change with the variation of the detailed mechanism of extraatomic relaxation from ionic to covalent materials. They have studied the validity of the charge-referencing point Ar $2p_{3/2}$ =242.3 eV in insulating materials with varying bond ionicity. The compounds considered (BN, GaP, InP, BeO and NaCl) have been well characterized previously. (22 refs.)

59884 Calibration of transmission electron microscopic mass determination using objects with known mass distribution. P.W.J.Linders, A.L.H.Stols, A.M.Stadhouders (Inst. for Submicroscopic Morphology, Univ. of Nijmegen Medical School, Nijmegen, Netherlands).

J. Microsc. (GB), vol.130, pt.1, p.85-92 (April 1983).

An improved calibration procedure is described for dry mass determination methods, that are based on microdensitometry of transmission electron micrographs. Polystyrene latex spheres, that are supposed to have a homogeneous mass distribution, are used for the calibration procedure. By computer fitting of the theoretically expected mass distribution to the distribution measured in a line through the centre of a sphere, a mass calibration factor is obtained. The number of measurements required for a predetermined calibration accuracy can be decreased considerably as compared to other calibration methods. Accurate calibration and reproducible adjustment of the electron optical magnification are required. (27 refs.)

59885 Determination of the illuminating angle and defocus spread in transmission electron microscopy. M.Tsuiji, R.St. John Manley (Dept. of Chem., McGill Univ., Montreal, Quebec, Canada).

J. Microsc. (GB), vol.130, pt.1, p.93-8 (April 1983).

In high resolution electron microscopy the beam divergence and defocus spread are important factors determining the resolution limit of the microscope. In this paper a straightforward method is proposed to estimate the illuminating angle (beam divergence) and the parameter of defocus spread using optical diffraction patterns from a through focal series of electron micrographs of a thin amorphous film. (18 refs.)

59886 Method for measuring the field from a magnetic recording head in the scanning electron microscope. O.C.Wells (IBM Thomas J. Watson Res. Center, Yorktown Heights, NY, USA).

J. Microsc. (GB), vol.130, pt.1, p.RP1-2 (April 1983).

Describes a field-plotting method in the SEM that is related to the 'Schlieren' imaging technique (Wells and Brunner, Appl. Phys. Lett., vol.42, p.114-6, 1983). (5 refs.)

59887 Study of scattering of gases of high energy electrons (0.5-3 MeV).

J.L.Balladore, D.Lapeyre, J.P.Martinez, J.Trinquier, B.Jouffrey (Lab. d'Optique Electronique, Univ. Paul Sabatier, Toulouse, France).

J. Microsc. & Spectrosc. Electron. (France), vol.7, no.6, p.575-92 (Dec. 1982). In French.

In electron microscopy the possibility of doing experiments in presence of gas is possible by using an environmental cell. In order to establish the conditions in which images should be obtainable with good contrast and resolution, the partial electron scattering cross sections with several gases at different pressures have been determined. (13 refs.)

59888 Magnetic-field-free vapor furnace for photoelectron spectroscopy. I. Temperatures up to 900K. G.Schönhense (Fritz-Haber-Inst., Max-Planck-Gesellschaft, Berlin, Germany).

Rev. Sci. Instrum. (USA), vol.54, no.4, p.419-21 (April 1983).

A vapor furnace producing stable atomic and molecular beams for photoionization experiments is described. During operation the furnace causes no detectable magnetic stray field because it is heated by a stream of hot air. Thus angle- and energy-resolved measurements of photoelectron spin polarization could be done at a kinetic energy as low as 0.5 eV. The high temporal stability of the target beam is demonstrated by means of an angular distribution measurement with mercury atoms. (8 refs.)

59889 Electron gun with a field-emission cathode for use in electron-probe instruments. B.N.Vasichev, Yu.L.Rybakov.

Sov. J. Opt. Technol. (USA), vol.49, no.8, p.516-19 (Aug. 1982). Translation of: *Opt.-Mekh. Prom.-st. (USSR)*, vol.49, no.8, p.44-7 (Aug. 1982). [received: April 1983]

It is shown that the largest emission current density in a given solid angle can be obtained with pulsed electron emission and optimum electron gun construction. A pulsed field emission gun ensures the largest probe current when the probe diameter ranges from 10 to 100 nm. (6 refs.)

59890 Electrostatic charged particle analyzer with three coaxial cylindrical electrodes. II. Construction of a three-stage system with a central electrode of finite thickness and axis-axis focusing. K.A.Men'shikov ('Kvant' Sci. & Industrial Union, Moscow, USSR).

Sov. Phys.-Tech. Phys. (USA), vol.27, no.10, p.1268-71 (Oct. 1982). Translation of: *Zh. Tekh. Fiz. (USSR)*, vol.52, no.10, p.2066-70 (Oct. 1982). [received: April 1983]

For pt.1 see Zh. Tekh. Fiz., vol.51, p.17-21 (1981). Sov. Phys. Tech. Phys., vol.26, p.8-11 (1981). A three-cylinder mirror analyzer is considered which has better optoelectronic characteristics than the widely used cylindrical mirror analyzers. Calculated results are reported for a system with a middle cylinder of thickness greater than or comparable to the distance over which optoelectronic images are smeared by aberration effects. (Such systems are easier to work with and more general than the one considered in pt.1). It is shown that the thickness of the middle cylinder must be minimal for best performance. (3 refs.)

59891 Imaging XPS—a new technique. I. Principles. N.Gurker, M.F.Ebel, H.Ebel (Inst. fur Angewandte und Tech. Phys., Tech. Univ. Wien, Wien, Austria).

Surf. & Interface Anal. (GB), vol.5, no.1, p.13-19 (Feb. 1983).

XPS imaging promises to be a powerful analytic tool because it enables specific information on both elements and bonding to be recorded on a two-dimensional distribution map. The only scanning XPS method to date which has been found to be practical is essentially a scanned-particle-beam method, like scanning AES, and it is only applicable to thin film specimens. The basic ideas of the new imaging XPS technique is presented based on a quite different concept. It will be applicable to any kind of specimen that can be analysed in a conventional XPS system. It makes use of the dispersion properties of a spherical condenser-type spectrometer and applies a two-dimensional electron detection device for decoding the energy and emission position of an analysed photoelectron. Experimental arrangement and theory of operation are presented. (9 refs.)

59892 Trace structure analysis, ptychography, phase tomography. W.Hoppe (Max-Planck-Inst. fur Biochem., Martinsried, Germany).

Ultramicroscopy (Netherlands), vol.10, no.3, p.187-98 (1982).

Three papers dedicated to the author elicit further comment from his own engagement with the three topics—trace structure analysis ptychography and phase tomography. (50 refs.)

59893 Secondary electron imaging as an aid to STEM microanalysis. R.M.Allen (Sandia Nat. Labs., Livermore, CA, USA).

Ultramicroscopy (Netherlands), vol.10, no.3, p.237-45 (1982).

Secondary electron (SEM mode) imaging in a scanning transmission electron microscope (STEM) has been utilized as an aid to the STEM microanalysis of second phase particles in an Alloy 800 foil by identifying particles at the foil surface facing the incident beam and energy dispersive X-ray detector. Such particles were optimally situated for microanalysis because possible

deleterious effects from beam spreading and matrix absorption were eliminated. This was demonstrated by orienting the sample to analyze the particles on the surface of the foil facing away from the beam and X-ray detector, and subsequently, for comparison, reorienting the sample to reanalyze the particles with the foil surface facing beam and detector. Theoretical calculations of the magnitude of the relative change in particle X-ray signal between the two orientations were in good agreement with the experimental observations. SEM imaging also provided surface reference points for parallax-effect measurements of local foil thickness and particle depth within the foil. (18 refs.)

59894 A new electrostatic phase-shifting effect. G.Matteucci, G.F.Missiroli, G.Pozzi (Istituto di Fisica, Univ. di Bologna, Bologna, Italy). *Ultramicroscopy (Netherlands)*, vol.10, no.3, p.247-51 (1982).

The authors investigate the electron optical properties of the electrostatic field arising from a metallic wire, coated with a different metal in the direction perpendicular to the electron beam. By electron interferometry it is shown that the wire introduces a constant phase difference between the interfering beams. (10 refs.)

59895 Periodic images produced by random noise and a filter. T.tanji, H.Hashimoto, H.Tomioka (Dept. of Appl. Phys., Osaka Univ., Osaka, Japan). *Ultramicroscopy (Netherlands)*, vol.10, no.3, p.281-3 (1982).

The optical spatial filtering method has been of value for high resolution electron microscopy, especially the application of noise filters with periodic hole arrays (Dirac combs) which are very useful in eliminating random noise in the micrograph of a periodic object. A filter located in the diffraction plane of the imaging lens may be used to pass mainly those beams diffracted by the periodic structures and hardly any of those scattered by random noise in the object micrograph. The authors show the images of random scatterers, which are formed by using such a filter with a periodic hole array, and which are then compared with a calculation based on the theory of speckle noise. (6 refs.)

59896 Thickness dependence of the STEM ratio image. R.F.Egerton (Dept. of Phys., Univ. of Alberta, Edmonton, Canada). *Ultramicroscopy (Netherlands)*, vol.10, no.3, p.297-9 (1982).

The author investigates the dependence of the ratio signal upon specimen thickness; in particular, the contrast produced by small variations in thickness. Modifications of the technique are then suggested, which should render the image less sensitive to thickness changes, particularly in the case of thicker specimens. (10 refs.)

Proceedings of the Third International Conference on 'Vibrations at Surfaces'

See Entry 59532

Publications concerning microscopic equipment, methods, applications, and related topics

See Entry 59561

Topographic quantification of non-planar localized surfaces

See Entry 59757

Using an electron beam to study the surface microrelief of solids

See Entry 59760

A comparison of techniques for obtaining convergent beam electron diffraction patterns with a JEOL 200CX

See Entry 61738

Crystallographic contrast due to primary ion channelling in the scanning ion microscope

See Entry 62003

Improvement of sensitivity of electron energy loss spectroscopy

See Entry 63091

Indirect determination of the single loss function from plural scattering data

See Entry 63112

Combined vibrational/temperature programmed reaction spectroscopy studies of reaction intermediates on metal surfaces

See Entry 63586

Elemental analysis performed with the Karlsruhe nuclear microprobe

See Entry 63611

Surface spectroscopy using high energy heavy ions

See Entry 63617

Observation and simulation of unstained DNA images in bright field TEM

See Entry 64018

07.85 X-RAY, GAMMA-RAY INSTRUMENTS AND TECHNIQUES

59897 A microprocessor controlled spectrometer for thermal scan Mossbauer spectroscopy. G.Nolle, H.Ullrich, J.B.Muller, J.Hesse (Inst. A fur Phys., Tech. Univ., Braunschweig, Braunschweig, Germany). *Nucl. Instrum. & Methods Phys. Res. (Netherlands)*, vol.207, no.3, p.459-63 (1 April 1983).

To determine the ordering temperature of ferromagnetic alloys using Mossbauer effect, a 'thermal scan' the measurement of counting rate at the center of gravity of the spectrum is necessary. The authors present a low cost micro-computer controlled system, which sets up the temperatures, takes the spectra and evaluates the ordering temperature from a sequence of measurements. As an example the Curie temperatures of disordered FCC FePt-Invar alloys are given. (3 refs.)

59898 The stability of cesium iodide X-ray photocathodes. K.Premaratne, E.R.Dietz, B.L.Henke (Univ. of Hawaii, Honolulu, HI, USA). *Nucl. Instrum. & Methods Phys. Res. (Netherlands)*, vol.207, no.3, p.465-7 (1 April 1983).

For pulsed X-ray measurements as applied, for example, in high temperature plasma diagnostics, it has been established that the cesium iodide photocathode is very efficient for X-ray diode and streak camera applications. Its quantum yield (electrons/incident photon) is ten to one-hundred times higher than that for the gold photocathode in the 100-10000 eV region. The width of its secondary electron energy distribution is appreciably less than that for gold, allowing time resolved, streak camera measurements to be extended into the picosecond region. An experimental study is described which demonstrates that the cesium iodide photocathode quantum yield and secondary electron energy distribution can be stable under practical conditions of preparation, handling, storage and short period exposures to the atmosphere. (10 refs.)

59899 Utilization of MeV Van de Graaff electrons to produce characteristic X-rays for precision measurements. E.G.Kessler, Jr., R.D.Deslattes (Quantum Metrology Group, NBS, Washington, DC, USA). *IEEE Trans. Nucl. Sci. (USA)*, vol.ns-30, no.2, p.991-5 (April 1983). (1982 IEEE Conference on the Application of Accelerators in Research and Industry, Denton, TX, USA, 8-10 Nov. 1982).

Electrons from a 4 MeV Van de Graaff accelerator are used to produce intense sources of characteristic X-rays from a sampling of mid-to-high Z elements. Thick solid targets and high pressure gas samples are bombarded by up to 50 microamperes of 2.5 MeV electrons. The X-rays are viewed in the backward direction to reduce the background resulting from bremsstrahlung radiation. Wavelengths and widths of the X-rays are measured with a precision two-axis flat crystal spectrometer. (19 refs.)

59900 Continuous X-ray-induced Auger electron spectroscopy. J.Cazaux (Lab. de Spectroscopie des Electrons, UER Sci., Reims, France), Tran Minh Duc.

J. Electron Spectrosc. & Relat. Phenom. (Netherlands), vol.31, no.1, p.13-23 (April 1983).

Bremsstrahlung emission from a tungsten anode has been used, for the first time, to obtain X-ray-induced Auger electron spectra (CXAES) in a conventional X-ray photo-electron spectrometer. Auger KLL signal and background intensities obtained from a silicon-aluminium sample have been compared with those obtained under the same experimental conditions but using a standard aluminium anode. For such an aluminium anode, the respective contributions of the bremsstrahlung and the characteristic radiation to the C_{KVV} intensity have also been established. (15 refs.)

Generation of high pressure to 10 GPa by means of MASS OB-8 apparatus equipped with X-ray diffraction system

See Entry 59795

System of moving the source in a nuclear gamma resonance spectrometer

See Entry 60531

A large-area xenon gas scintillation proportional counter (GSPC) with timing information for the detection of low energy X-rays

See Entry 60537

Metallic multilayers: new possibilities in X-UV optics

See Entry 61257

Strain field analysis with the X-ray integration method

See Entry 61467

Improved system for energy-dispersive X-ray diffraction with synchrotron radiation

See Entry 61731

Regional silver content of radiographic film determined by X-ray fluorescence compared with optical densitometry

See Entry 63947

07.90 OTHER TOPICS IN SPECIALISED INSTRUMENTATION

59901 Using the 'C' programming language for interface control.

N.J.Goddard (Dept. of Chem., Imperial Coll., London, England).

Lab. Microcomput. (GB), vol.1, no.3, p.15-22 (Autumn 1982).

Discusses the advantages of various programming languages to replace BASIC for controlling spectroelectrochemical apparatus via a home-made interface. It is shown that C is not only faster than BASIC but is also easier to program and can dispense with assembly language routines. (7 refs.)

Apparatus for examining the sedimentation stability of a filled polymer [using laser radiation]

See Entry 63601

10.00 THE PHYSICS OF ELEMENTARY PARTICLES AND FIELDS

(for cosmic rays, see 94.40; for high energy-experimental techniques and instrumentation, see 29.)

International Colloquium on the History of Particle Physics

An essay of chronology of particle physics until 1965

See Entry 59566

See Entry 59582

11.00 GENERAL THEORY OF FIELDS AND PARTICLES

(see also 03.65 Quantum mechanics, 03.70 Theory of quantized fields, 03.80 General theory of scattering)

11.10 FIELD THEORY

59902 A discussion on the classical solution of gauge theory. Ming Zhong Wang (Chengdu Univ. of Sci. & Technol., Sichuan, China), Ruan Tunan.

AIP Conf. Proc. (USA), no.95, p.362-4 (1982). (5th High Energy Spin Symposium, Westhampton Beach, NY, USA, Sept. 1982).

This paper deals with the classical solutions of pure gauge theory. The authors pay special attention to the problem of the electric solution and point out the fact that the only electric solution which was discovered in 1962 may be wrong. (9 refs.)

59903 Equivalence of stochastic and canonical quantization in perturbation theory. E.Floratos (ITP, Univ. of Bern, Switzerland), J.Iliopoulos.

Nucl. Phys. B, Part. Phys. (Netherlands), vol.B214, no.3, p.392-404 (18 April 1983).

It is shown that the stochastic quantization method introduced by Parisi and Wu (1981) reproduces, order by order, the ordinary perturbation expansion. The proof is valid for any field theory, including gauge theories, provided one considers gauge-invariant quantities. (8 refs.)

59904 First-order equations for gauge fields in spaces of dimension greater than four. E.Corrigan, C.Devchand, D.B.Fairlie (Dept. of Math. Sci., Univ. of Durham, Durham, England), J.Nuyts.

Nucl. Phys. B, Part. Phys. (Netherlands), vol.B214, no.3, p.452-64 (18 April 1983).

Considers the possibility of satisfying the gauge field equations in dimensions greater than four by imposing linear relations amongst the components of the field strength tensor, $F_{\mu\nu}$, generalising the idea of self-duality in four dimensions. (6 refs.)

59905 Towards a semi-classical approximation of the nonlinear σ -model.

A.Poitrascioiu, A.Rouet (Inst. for Advanced Study, Princeton, NJ, USA).

Nucl. Phys. B, Part. Phys. (Netherlands), vol.B214, no.3, p.481-90 (18 April 1983).

The authors consider the contribution of instantons of arbitrary topological charge to the expectation value of any observable in the CP¹ model defined on the sphere S². They replace the integration over one of the parameters of the instantons by an integration over the group of isospin transformations and carry it out explicitly by using the isospin invariance. This allows one to express the results as the expectation value of an observable of a neutral gas

of 2 species of particles, computed in the grand canonical ensemble. The interactions are complicated and involve multi-body forces ($2 \times k$, k being the topological charge). (5 refs.)

59906 A study of 't Hooft and Wilson loops. S.Samuel (Dept. of Phys., Columbia Univ., New York, NY, USA). *Nucl. Phys. B, Part. Phys. (Netherlands)*, vol.B214, no.3, p.532-46 (18 April 1983).

An investigation is undertaken for 't Hooft loop operators in four-dimensional gauge theories. For the first time, a perimeter law is shown to be their behaviour in weak coupling Wilson lattice (and continuum) nonAbelian $SU(N)$ gauge theories for all N . However, it is also argued that this perimeter law is a poor criterion for quark confinement. Rather, it is suggested that non-leading long-distance behavior is what is crucial and relevant in distinguishing nonAbelian from Abelian (and hence confining from nonconfining) theories. A new object, 'the 't Hooft line', is introduced to measure this nonleading behaviour and is computed in strong coupling on the lattice. There, one finds magnetic screening, characterized by a magnetic screening mass, m_σ . It is shown to all orders in strong coupling that m_σ is the glueball mass, a result which is expected to persist in weak coupling and in the continuum. Two further consequences of this work are that pure nonAbelian gauge theories cannot be in a Higgs phase and that in such models that absence of massless physical particles implies confinement. Finally, nonleading behaviour in Wilson loops is examined. The present picture of confinement suggests the absence of van der Waals forces in Yang-Mills theories. (16 refs.)

59907 Vacuum instability criterion in an effective potential approach. A.Amer, A.E. Yaouanc, L.Oliver, O.Pene, J.-C.Raynal (Lab. de Phys. Theorique et Hautes Energies, Orsay, France). *Nucl. Phys. B, Part. Phys. (Netherlands)*, vol.B214, no.2, p.299-316 (11 April 1983).

The authors propose a definition of the effective potential of a fermion bilinear in field theory that allows them to specify the meaning of the Bogoliubov-Valatin variational method. They show the link of this definition with the usual one in terms of external sources. Then, they expose a method to obtain the instability equation of the chiral invariant vacuum from the quark-gluon interaction in QCD. They obtain, for one-gluon exchange in the Coulomb gauge, a critical coupling $4/3\alpha_{crit} = \pi/(3\pi-4)$. For $\alpha_s > \alpha_{crit}$ the chiral invariant vacuum is unstable. This takes into account transverse gluon exchange, and is to be compared with $4/3\alpha_{crit} = 1$ in the Coulomb approximation, a value that can also be obtained by the Bogoliubov-Valatin variation method. (8 refs.)

59908 Auxiliary field-free supersymmetric gauges. I.Antoniadis (Ecole Polytech., Palaiseau, France), E.Floratos. *Nucl. Phys. B, Part. Phys. (Netherlands)*, vol.B214, no.2, p.350-6 (11 April 1983).

The authors find that, in perturbation theory, nonlight-cone axial gauges, $N_A(x)=0$, preserve the supersymmetry remaining in $N=1$ supersymmetric YM theories, after imposing the Wess-Zumino gauge. (11 refs.)

59909 Two-loop β functions for scalar fields: a simplified approach. T.Murphy (Dublin Inst. for Advanced Studies, Dublin, Ireland). *Nucl. Phys. B, Part. Phys. (Netherlands)*, vol.B214, no.2, p.357-68 (11 April 1983).

A new, simplified method for calculating the renormalization group equations for scalar fields is presented. The method is based on the renormalization of the effective potential as a whole. The two-loop equations for a general theory are given, and the example of the adjoint representation of $SU(n)$ is considered in detail. It is found to differ substantially from the more common example of the fundamental representation. (8 refs.)

59910 One-loop renormalisation of superfield Yang-Mills theories. J.W.Juer, D.Storey (Dept. of Phys., Univ. of Southampton, Southampton, England).

Nucl. Phys. B, Part. Phys. (Netherlands), vol.B216, no.1, p.185-208 (25 April 1983).

The authors calculate the one-loop ultraviolet and infrared divergences in superfield Yang-Mills theories to fourth order in the gauge field. The ultraviolet divergences require a non-linear field renormalisation, and graphs with external ghost fields show that a non-linear renormalisation of the gauge-fixing function is also needed. These observations are confirmed by calculations incorporating matter fields, which are used to extend the result to all orders for the special case of $SU(2)$. On the other hand the infrared divergences, which occur in general gauges, are apparently impossible to remove in any acceptable way. (11 refs.)

59911 The composite particle representation theory. I. The composite particle representation transformation. Cheng-Li Wu (Dept. of Phys., Jilin Univ., Changchun, China), Da Hsuan Fang. *Commun. Theor. Phys. (China)*, vol.1, no.6, p.705-24 (1982).

A generalization of the quantum mechanical representation transformation is presented. It is shown that, as an important example, the Boson-expansion method, commonly employed in nuclear physics, corresponds to such a generalized transformation. Using this generalization, the authors were able to construct a special representation called the 'Composite Particle Representation'. In the composite particle representation, the composite particle degrees of freedom are included, as well as the original particle degrees of freedom. The former is introduced in order that the motion of certain particle clusters can be described as separate entities in a many-body system. This representation is shown to be exactly equivalent to the usual quantum mechanical representation which includes only the original particle degrees of freedom. Many applications of this theory are expected, in particular in the study of hadrons from the quark point of view and the Interacting Boson Model in nuclei. (10 refs.)

59912 Lattice formulation of the pure gauge fields on coset space. Ruan Tunan, Jin Sicong, Liu Zuwei (Univ. of Sci. & Technol. of China, Hefei, China).

Commun. Theor. Phys. (China), vol.2, no.1, p.867-76 (1983).

The authors construct a lattice formulation for pure gauge fields in a coset space in the cases of a group with a nontrivial topological property and of a chiral group, and they present a local gauge invariant action of a quark system on a four-dimensional Euclidean space lattice, which has the continuum limit as usual. For nonchiral groups with a trivial topological property, it is shown that the coset pure gauge fields have no influence on the confinement properties of the quark system, by calculating the lattice current-current propagator when the coset pure gauge fields are retained manifestly. (4 refs.)

59913 On realization of the chiral symmetry in the lattice gauge theory containing the $U(1)$ chiral gauge field. An Ying, Chen Shi, Dai Yuan-ben (Inst. of Theoretical Phys., Acad. Sinica, Beijing, China).

Commun. Theor. Phys. (China), vol.2, no.1, p.877-82 (1983).

The authors investigate the lattice gauge theory with a gauge group $U \times V(1)$ where U is a nonAbelian group and $V(1)$ is a chiral Abelian group. In the

strong coupling approximation for the U gauge field they find that the $V(1)$ chiral symmetry is realised through parity doublets of composite fermions for strong $V(1)$ coupling and that it is spontaneously broken through a technicolor-like mechanism for weak $V(1)$ coupling. (7 refs.)

59914 General solution and Lax Pair for 1-D classical massless Thirring model. M.Wadati (Inst. of Phys., Univ. of Tokyo, Tokyo, Japan).

J. Phys. Soc. Jpn. (Japan), vol.52, no.4, p.1084-5 (April 1983).

Classical massless Thirring model in one dimensional space is studied. The general solution and Lax pair are explicitly presented. Both results imply that the system is completely integrable. (1 ref.)

59915 Nonintegrability of the classical Yang-Mills fields. E.S.Nikolaevskii, L.N.Shur (L.D. Landau Inst. of Theoretical Phys., Acad. of Sci., USSR).

JETP Lett. (USA), vol.36, no.5, p.218-21 (5 Sept. 1982). Translation of: *Pis'ma v Zh. Eksp. & Teor. Fiz. (USSR)*, vol.36, no.5, p.176-9 (5 Sept. 1982). [received: April 1983]

It is shown for the particular case of the classical Yang-Mills equations that there is no additional first integral. It is concluded that the original system of equations does not have a complete set of integrals. (9 refs.)

59916 Crossover from the strong-coupling to the weak-coupling regime in the $SU(2)$ -symmetric Thirring model. G.I.Japaridze, A.A.Nersesyan (Inst. of Phys., Acad. of Sci., Tbilisi, Georgian SSR), P.B.Wiegmann.

Phys. Lett. A (Netherlands), vol.94A, no.6-7, p.254-8 (21 March 1983).

Using the exact solution of the Thirring model with broken $SU(2)$ symmetry the authors study a transition from the strong-coupling to the weak-coupling regime taking place on changing the anisotropy parameter. (14 refs.)

59917 On self-dual gauge fields arising from twistor theory. N.M.J.Woodhouse (Wadham Coll., Oxford, England).

Phys. Lett. A (Netherlands), vol.94A, no.6-7, p.269-70 (21 March 1983).

Some simple expressions are given for the solutions to the self-dual Yang-Mills equations associated with certain linear zero-rest-mass fields. (7 refs.)

59918 Unique trajectory method in Migdal renormalization group approach and crossover phenomena. M.Imachi, S.Kawabe, H.Yoneyama (Dept. of Phys., Kyushu Univ., Fukuoka, Japan).

Prog. Theor. Phys. (Japan), vol.69, no.1, p.221-34 (Jan. 1983).

Migdal renormalization group approach, combined with Wilson-Kogut topological argument, is applied to four dimensional lattice gauge theory of finite subgroup $I(120)$ of $SU(2)$. i) A slight but clear crossover from strong coupling regime to weak coupling regime is observed for the Wilson action. ii) For mixed action, of the fundamental and the adjoint representation, a clearer stepwise transition is found at $1 \leq \beta_a \leq 3$ (where β_a denotes the bare inverse coupling constant of the adjoint representation). This stepwise transition changes into crossover for smaller β_a . iii) There are four critical lines in (β_a, β_b) plane starting from a quadrupole point ($\beta_a^* \sim 0.75$, $\beta_b^* \sim 3.2$) where β_b denotes the bare inverse coupling constant of the fundamental representation: $SQ(3)$ critical line; $Z(2)$ critical line; a critical line due to the discreteness of $I(120)$; and a critical line related to crossover. (15 refs.)

59919 On the relation of first-class constraints to gauge degrees of freedom. R.Sugano (Dept. of Phys., Osaka City Univ., Osaka, Japan), T.Kimura.

Prog. Theor. Phys. (Japan), vol.69, no.1, p.252-61 (Jan. 1983).

A further consideration is made to support the proposition, given in a previous paper (1982), that only intrinsic first class constraints are associated with gauge degrees of freedom. The authors' argument is based on the consistency requirement between the Lagrangian and the Hamiltonian formalisms, reducibility conditions of gauge degrees of freedom and gauge fixing conditions in the quantization procedure by means of the Dirac bracket method. (11 refs.)

59920 A spinor reconstruction theorem. Y.Takahashi (Dept. of Phys., Univ. of Alberta, Edmonton, Alberta, Canada).

Prog. Theor. Phys. (Japan), vol.69, no.1, p.369-71 (Jan. 1983).

The reconstructibility of a spinor via the Pieri identities is discussed in non-relativistic as well as relativistic cases. (5 refs.)

59921 Convergent perturbation theory for the scalar $\phi^2 p$ field theories; the Gell-Mann-Low function. B.S.Shaverdyan, A.G.Ushveridze (Inst. of Phys., Acad. of Sci., Tbilisi, Georgian SSR).

Phys. Lett. B (Netherlands), vol.123B, no.5, p.316-18 (7 April 1983).

A method of construction of convergent perturbation theory for the scalar $\phi^2 p$ field theories is proposed. The method can be used for calculations in the strong coupling regime. The behavior of the Gell-Mann-Low function for ϕ^4 field theory is studied. (6 refs.)

59922 Matter field and fermions in $OSP(4/2)$ by dimensional reduction via superspace. R.Delbourgo, R.J.Farmer, P.D.Jarvis (Dept. of Phys., Univ. of Tasmania, Hobart, Australia).

Phys. Lett. B (Netherlands), vol.123B, no.5, p.319-22 (7 April 1983).

Coset space methods are applied to obtain a dimensionally reduced superfield formulation of quantized gauge theory. Matter fields, including fermions are incorporated in the formalism by appropriate tensor or spinor representations of $OSP(4/2)$. (18 refs.)

59923 The ultra-violet finiteness of the $N=4$ Yang-Mills theory. L.Brink (California Inst. of Technol., Pasadena, CA, USA), Ö.Lindgren, B.E.W.Nilson.

Phys. Lett. B (Netherlands), vol.123B, no.5, p.323-8 (7 April 1983).

The $N=4$ supersymmetric Yang-Mills gauge theory was formulated by the authors in a previous paper (1982) in the light-cone gauge. It is described by a scalar complex superfield whose components are the propagating field components of the theory. Here they prove that the theory is ultra-violet finite to all orders in perturbation theory for a specific form of the light-cone gauge. (11 refs.)

59924 Super-self duality for supersymmetric Yang-Mills theory. I.V.Volovich (Steklov Math. Inst., Moscow, USSR).

Phys. Lett. B (Netherlands), vol.123B, no.5, p.329-31 (7 April 1983).

Super-selfduality equations for supersymmetric Yang-Mills theory are proposed. The solution of these equations with the help of super-twistors is presented. (11 refs.)

59925 On the dynamics of tumbling gauge theories. V.P.Gusynin, V.A.Miransky, Yu.A.Sitenko (Inst. for Theoretical Phys., Kiev, USSR).

Phys. Lett. B (Netherlands), vol.123B, no.6, p.407-12 (14 April 1983).

The dynamics of symmetry breaking in gauge theories without fundamental scalars is investigated. The method of determining the way of the vacuum rearrangement in these theories is elaborated. (12 refs.)

59926 Universality violation and large N interpolations. Tian-iun Chen, Chung-i Tan, Xi-te Zheng (Dept. of Phys., Brown Univ., Providence, RI, USA).

Phys. Lett. B (Netherlands), vol.123B, no.6, p.423-7 (14 April 1983).

The restoration of universality based on a large N motivated asymptotically free scaling formula is re-examined. A mixed $SU(N)$ - $SU(N)/Z_2$ system which serves as a counter-example to the reduction scheme of Grossman and Samuel

(1982) is studied. However, a certain general universal pattern for the constant string tension lines is observed. (10 refs.)

59927 The connection between local operators on the lattice and in the continuum and its relation to meson decay constants. G.Martinelli (INFN, Lab. Nazionali di Frascati, Frascati, Italy), Yi-cheng Zhang. *Phys. Lett. B (Netherlands)*, vol.123B, no.6, p.433-6 (14 April 1983).

The authors have computed, at first order in perturbation theory, the relation between lattice and continuum local operators used in Monte Carlo simulations to evaluate the meson decay constants. These corrections, although with the correct sign, are too small to compensate the discrepancy between existing lattice calculations and experimental values. (11 refs.)

59928 Fermion coupled with vortex with dyon excitation. S.Aoyama, Y.Fujimoto (ICTP, Trieste, Italy). *Phys. Lett. B (Netherlands)*, vol.124B, no.1-2, p.740-8 (21 April 1983).

A system of fermions and a vortex with a dyonic excitation is studied in the context of SU(2) gauge theory. Many of the features of the theory turn out to be similar to those obtained by Callan (1982) and Rubakov (1981) in their recent study of the dyon. The main difference is that the number of fermion states is double and thus a new type of scattering can take place. (12 refs.)

59929 Gauge bosons as composites of fermions. K.G.Akdeniz (Theoretical Phys. Inst., Univ. of Istanbul, Istanbul, Turkey), M.Arik, M.Hortacsu, N.K.Pak. *Phys. Lett. B (Netherlands)*, vol.124B, no.1-2, p.79-82 (21 April 1983).

Non-Abelian gauge theories are obtained as effective theories of certain models which at the Lagrangian level contain only spinor fields. (8 refs.)

59930 Spin-isospin mixing without spontaneous symmetry breakdown. A.Mukherjee, P.Roy (Tata Inst. of Fundamental Res., Bombay, India). *Z. Phys. C (Germany)*, vol.17, no.2, p.141-4 (1983).

The phenomenon is demonstrated in an exactly symmetric SU(2) classical gauge theory with a scalar isodoublet of matter fields. Possible implications for chromodynamics are discussed briefly. (12 refs.)

59931 Stochastic processes and Fermi fields. G.F.de Angelis (Centre de Phys. Theorique, CNRS, Marseille, France), D.de Falco.

Stochastic Processes in Quantum Theory and Statistical Physics. Proceedings of the International Workshop, Marseille, France, 29 June-4 July 1981 (Berlin, Germany: Springer-Verlag 1982), p.56-66

Reports on some results pointing to the possibility of introducing ordinary probability in the analysis of Fermi fields. Using a specific example of a Fermi oscillator, the authors give a Feynman-Kac formula for the Hamiltonian subgroup, a path integral representation of the configurational Schwinger functions and a complete characterisation of the dynamics in terms of stochastic field equations. These expressions are given in terms of ordinary numerical valued Markov processes. (5 refs.)

59932 Lagrangians with anticommuting arguments for Dirac fields. P.Kree (Inst. de Math., Univ. de Paris 6, Paris, France).

Stochastic Processes in Quantum Theory and Statistical Physics. Proceedings of the International Workshop, Marseille, France, 29 June-4 July 1981 (Berlin, Germany: Springer-Verlag 1982), p.254-73

Extends classical Lagrangian theory to the case of a free variable π , which can take the value $-$ or $+$ for commuting and anticommuting formulations. The calculus for functionals with anticommuting arguments is developed, used to extend the Euler-Lagrange equations, an action theorem is proved and the results are applied to Dirac fields. (7 refs.)

Operator formalism equivalent to the Feynmann quantization technique See Entry 59613

Field of a charged particle in the presence of scalar meson fields in general relativity See Entry 59640

Spontaneous compactification in six-dimensional Einstein-Maxwell theory See Entry 59647

Kaluza-Klein theories on bundles with homogeneous fibers. I See Entry 59648

On the structure of space, time and field See Entry 59651

Hamiltonian formulation for a translation gauge theory of gravitation See Entry 59654

Hamiltonian formulation of the gauge theory of gravitation. Pure-gravity case See Entry 59655

A model for quantum gravity: an effective approach to Einstein theory See Entry 59657

Supergravity with one auxiliary spinor See Entry 59658

Gravitinos on the lattice See Entry 59659

Magnetic moment of an electron gas in crossed, homogeneous electric and magnetic fields See Entry 59671

One-time characteristic functional in the stochastic quantization See Entry 59717

Coherent spatial structure versus time chaos in a perturbed sine-Gordon system See Entry 59718

On the statistical mechanics of surfaces See Entry 59722

On the nonrelativistic S-matrix See Entry 59933

The one-loop effective potential in superspace See Entry 59938

The relaxed hypermultiplet: an unconstrained $n=2$ superfield theory See Entry 59939

Lie transformations, nonlinear evolution equations, and Painleve forms See Entry 59946

Spontaneous breakdown of supersymmetry due to gauge interactions See Entry 59949

Comment on the proof of existence of the Nicolai mapping for scalar supersymmetric theories See Entry 59951

A class of finite four-dimensional supersymmetric field theories See Entry 59952

A simple component field method for SUSY effective potential calculations See Entry 59953

Electromagnetic and weak interactions in stochastic space-time: a review See Entry 59961

An axial gauge formulation for QED₂ See Entry 59977

The electrodynamics with magnetic monopoles. I. Coulomb-gauge kinematics See Entry 59978

Note on the magnitude of renormalization constants in quantum electrodynamics See Entry 59979

Poincare algebra of QED with Dirac's monopoles See Entry 59980

Scaling mass relations to two loops: an application to toponium See Entry 59981

Large-N quantum chromodynamics at finite temperature See Entry 59985

Dynamical realization of the linear σ -model and bifermion condensates in QCD See Entry 59988

Technicolor See Entry 59991

Pseudoscalar mesons and instantons See Entry 59997

Minimization principle for the unit of electric charge See Entry 60010

Relativistic quarkonium model based on instantaneous ladder BS equation. I. Basic equation and its properties See Entry 60013

Quarkonium bound states and coupling to hadrons See Entry 60015

On the dynamical problems and the fermion spectra in the rishon model See Entry 60018

Generations of composite fermions See Entry 60021

Theory of strings with boundaries: fluctuations, topology and quantum geometry See Entry 60027

An investigation of quark and diquark fragmentation in p and \bar{p} charged current interactions in BEBC See Entry 60033

Three-jets production in broken color gauge symmetry See Entry 60060

Properties of quark matter governed by quantum chromodynamics. I. The screened charge See Entry 60125

Properties of quark matter governed by quantum chromodynamics. II. Renormalization schemes in quark matter See Entry 60126

Neutrinoless double- β decay with quasi-Dirac neutrinos See Entry 60144

11.20 S-MATRIX THEORY

59933 On the nonrelativistic S-matrix. E.F.Hefter (Inst. fur Theoretische Phys., Univ. Hannover, Hannover, Germany).

Prog. Theor. Phys. (Japan), vol.69, no.1, p.329-32 (Jan. 1983).

Attention is drawn to the older literature results from which it follows immediately that the S-matrix for the Korteweg-de Vries equation (KdV) and for the related (stationary multicomponent) nonlinear Schrodinger equation factorizes. (9 refs.)

Exact solution of the Dirac equation in the field of a 't Hooft-Polyakov monopole See Entry 59963

11.30 SYMMETRY AND CONSERVATION LAWS

(see also 02.20 Group theory)

59934 Measurements of CP-violating polarization of muons from K_{s3} decays. R.K.Adair (Yale Univ., New Haven, CT, USA).

AIP Conf. Proc. (USA), no.95, p.130-8 (1982). (5th High Energy Spin Symposium, Westhampton Beach, NY, USA, Sept. 1982).

Two experiments, conducted at Brookhaven National Laboratory, are described which were directed towards the measurements of the polarization normal to the plane of decay of muons produced in K_{s3} decays; measurements were made on the decays of K^+ and K_L^0 mesons. The value of the polarization derived from summing the results of both experiments is $P_n = (-1.85 \pm 3.60) \times 10^{-3}$ in the direction $p_K X p_{\mu}$, where the limits are of the magnitude to be expected from certain interesting models. (11 refs.)

59935 Parity violation in non-weak processes. M.Simonius (Lab. fur Kernphys., ETH, Zurich, Switzerland).

AIP Conf. Proc. (USA), no.95, p.139-49 (1982). (5th High Energy Spin Symposium, Westhampton Beach, NY, USA, Sept. 1982).

Parity violation in non-weak processes is reviewed with emphasis on recent developments. Effects in electron-hadron systems are summarized briefly. Parity violation in purely hadronic systems and the status of its theoretical analysis is treated in more detail. (44 refs.)

59936 Parity nonconservation in proton-water scattering at 800 MeV. D.E.Nagle, J.D.Bowman, R.Carlini, R.E.Mischke (Los Alamos Nat. Lab., Los Alamos, NM, USA), H.Frauenfelder, R.W.Harper, V.Yuan, A.B.McDonald, R.Talaga.

AIP Conf. Proc. (USA), no.95, p.150-5 (1982). (5th High Energy Spin Symposium, Westhampton Beach, NY, USA, Sept. 1982).

A search has been made for parity nonconservation in the scattering of 800 MeV polarized protons from an unpolarized water target. The result for the longitudinal asymmetry is $A_L = +(6.6 \pm 3.2) \times 10^{-7}$. Control runs with Pb, using a thickness that gave equivalent beam broadening from multiple Coulomb scattering, but a factor of ten less nuclear interactions than the water target, gives $A_L = -(0.5 \pm 6.0) \times 10^{-7}$. (11 refs.)

59937 Parity violations in high energy nucleon nucleon scattering. G.Nardulli (Istituto di Fisica, Univ. di Bari, Bari, Italy).

AIP Conf. Proc. (USA), no.95, p.156-8 (1982). (5th High Energy Spin Symposium, Westhampton Beach, NY, USA, Sept. 1982).

It is shown that, using parity violating nucleon wave function effects, large asymmetries in the scattering of polarized nucleons at large energies naturally arise. (7 refs.)

59938 The one-loop effective potential in superspace. M.T.Grisaru (California Inst. of Technol., Pasadena, CA, USA), F.Riva, D.Zanon.

Nucl. Phys. B, Part. Phys. (Netherlands), vol.B214, no.3, p.465-80 (18 April 1983).

Using superfields and supergraphs the authors evaluate the superspace one-loop effective potential for several supersymmetric models: self-interacting chiral superfields, supersymmetric Yang-Mills, and supersymmetric QED. (7 refs.)

59939 The relaxed hypermultiplet: an unconstrained $n=2$ superfield theory. P.S.Howe (CERN, Geneva, Switzerland), K.S.Stelle, P.K.Townsend.

Nucl. Phys. B, Part. Phys. (Netherlands), vol.B214, no.3, p.519-31 (18 April 1983).

The authors present an off-shell version of the hypermultiplet, without a central charge or gauge antisymmetric tensors. They give the unconstrained superfield form of the action and its coupling to $N=2$ super-Yang-Mills theory. This allows an $N=2$ superspace formulation of the $N=4$ super-Yang-Mills theory whose ultraviolet finiteness is then ensured by $N=2$ nonrenormalization theorems. (15 refs.)

59940 Note on extremes of SU(n) Higgs potentials. Cao Chang-qi (DESY, Hamburg, Germany).

Commun. Theor. Phys. (China), vol.2, no.1, p.913-19 (1983).

The problem of symmetry breaking of SU(n) is discussed more completely with Higgs scalar fields belonging to an adjoint representation or an adjoint together with a fundamental one. (2 refs.)

- 59941 Weight vector representatives for $SO(2N)$.** S.K.Soni (Univ. of Pennsylvania, Philadelphia, PA, USA). *J. Math. Phys. (USA)*, vol.24, no.4, p.729-35 (April 1983). Following Mohapatra and Sakita (1980), it is convenient to rewrite the algebra of $2N$ -matrices in terms of N annihilation operators and N creation operators. The author finds them useful in representing vector fields in the spinorial $\sigma_N + \sigma_N^c$ and the irreducible subcomponents of $\sigma_N \times \sigma_N$ and $\sigma_N \times \sigma_N^c$ operators. Though their Dynkin labels are readily accessible, a natural basis for the enumeration of their complete set of weights is given by N positive weights of the vectorial representation. Their subgroup content under $SU(N) \subset SO(2N)$ and $SO(2m) \otimes SO(2N-2m) \subset SO(2N)$ is made obvious by using a simple identity. Conjugation and Yukawa couplings are touched on briefly. (6 refs.)
- 59942 A theorem on orbit structures (strata) of compact linear Lie groups.** G.Sartori (Istituto di Fisica, Univ. di Padova, Padova, Italy). *J. Math. Phys. (USA)*, vol.24, no.4, p.765-8 (April 1983). The author presents a comprehensive constructive proof of a theorem characterizing the tangent space to a stratum (orbit structure) of the Euclidean space R^n , seat of an orthogonal representation of a compact group G . The characterization is made in terms of gradients of a complete set (integrability basis) of G -invariant polynomials. In a recent paper (Abud and Sartori, 1981), the theorem, which may be considered a generalisation of a theorem by Michel (1971), has been shown to be effective in the determination of the equations of the strata and in the determination of natural extrema of G -invariant functions. (10 refs.)
- 59943 Internal labels of degenerate representations.** T.H.Seligman (Div. de Phys. Theorique, Inst. de Phys. Nucleaire, Orsay, France), R.T.Sharp. *J. Math. Phys. (USA)*, vol.24, no.4, p.769-71 (April 1983). An expression for the number of internal labels of degenerate irreducible representations of compact semisimple Lie groups is given in the same spirit as Racah's formula (1965) for the nondegenerate case. (5 refs.)
- 59944 Analysis of the outer product for the symmetric group.** L.J.Somers (Inst. for Theoretical Phys., Univ. of Nijmegen, Nijmegen, Netherlands). *J. Math. Phys. (USA)*, vol.24, no.4, p.772-8 (April 1983). Expressions are derived to write the basis vectors for an irreducible representation μ of the symmetric group in terms of basis vectors for irreducible representations whose outer product yields μ . (7 refs.)
- 59945 Reciprocal transformation for one-dimensional conservation equations.** G.Rosen (Dept. of Phys. Drexel Univ., Philadelphia, PA, USA). *J. Math. Phys. (USA)*, vol.24, no.4, p.793-4 (April 1983). One-dimensional conservation equations (OCE) of the form $\partial n/\partial t + \partial f/\partial x = 0$ with $n=n(x,t) > 0$ and $f=f(n, \partial n/\partial x, \partial^2 n/\partial x^2, \dots)$ admit a symmetric reciprocal transformation $x \rightarrow x^*(x,t)$, $n \rightarrow n^*(x^*,t) \equiv n$, $f \rightarrow f^* \equiv -n^2 f$, which produces an equivalent OCE for n^* in x^* space. Certain OCE of contemporary interest are reciprocal invariant in the sense that $f^* = f(n^*, \partial n^*/\partial x^*, \partial^2 n^*/\partial x^{*2}, \dots)$. There also exists a class of essentially nonlinear OCE for which the reciprocal transformation produces a linear OCE, and thus equations in this class are solvable analytically. (5 refs.)
- 59946 Lie transformations, nonlinear evolution equations, and Painleve forms.** M.Lakshmanan, P.Kaliappan (Dept. of Phys., Univ. of Madras, Madras, India). *J. Math. Phys. (USA)*, vol.24, no.4, p.795-806 (April 1983). The authors present the results of a systematic investigation of invariance properties of a large class of nonlinear evolution equations under a one-parameter continuous (Lie) group of transformations. It is shown that, in general, the corresponding invariant variables (the subclass of which is the usual similarity variables) lead to ordinary differential equations of Painleve type in the case of inverse scattering transform solvable equations as conjectured by Ablowitz, Ramani, and Segur. This is found to be also true for certain higher spatial dimensional versions such as the Kadomtsev-Petviashvili, two dimensional sine-Gordon, and Ernst equations. For the non-solvable equations considered here this invariance study leads to ordinary differential equations with movable critical points. (39 refs.)
- 59947 Supersymmetric equilibrium.** E.Alvarez (Joseph Henry Labs., Princeton Univ., Princeton, NJ, USA), M.B.Gavela. *Lett. Nuovo Cimento (Italy)*, vol.36, ser.2, no.14, p.467-70 (2 April 1983). A generalized canonical ensemble for supersymmetric systems is introduced assuming that the fundamental conserved quantity is the supersymmetric charge. Some relevant thermodynamic quantities are studied. (3 refs.)
- 59948 Spontaneously broken supersymmetry and Poincare invariance.** X.R.Tata, E.C.G.Sudarshan (Dept. of Phys., Univ. of Texas, Austin, TX, USA), J.M.Schechter. *Phys. Lett. B (Netherlands)*, vol.123B, no.5, p.308-10 (7 April 1983). It is argued that the spontaneous breakdown of global supersymmetry is consistent with unbroken Poincare invariance if and only if the supersymmetry algebra $\mathcal{A}=0$ is understood to mean the invariance of the dynamical variables ϕ under the transformations generated by the algebra, i.e. $[\mathcal{A}, \phi]=0$ rather than as an operator equation. It is further argued that this 'weakening' of the algebra does not alter any of the conclusions about supersymmetry quantum field theories that have been obtained using the original (stronger) form of the algebra. (6 refs.)
- 59949 Spontaneous breakdown of supersymmetry due to gauge interactions.** T.Inami (Inst. of Phys., Univ. of Tokyo-Komaba, Tokyo, Japan), C.S.Lim, N.Sakai. *Phys. Lett. B (Netherlands)*, vol.123B, no.5, p.311-15 (7 April 1983). Presents a new type of spontaneous supersymmetry breakdown at the tree level arising from gauge interactions irrespective of the specific forms of the superpotential. Explicit models are considered for groups $SU(N) \times U(1)$. The existence of an unbroken $U(1)$ gauge symmetry is found to be a general feature of this type of model. (13 refs.)
- 59950 Spontaneous breakdown of supersymmetry and charge confinement.** Z.F.Ezawa, A.Iwazaki, M.Sato (Dept. of Phys., Tohoku Univ., Sendai, Japan). *Phys. Lett. B (Netherlands)*, vol.124B, no.1-2, p.40-4 (21 April 1983). It is argued that charges are confined in supersymmetric theories only if supersymmetry is spontaneously broken. The authors demonstrate this explicitly in a 1+1 dimensional model which has both supersymmetric and broken-supersymmetric phases. (6 refs.)
- 59951 Comment on the proof of existence of the Nicolai mapping for scalar supersymmetric theories.** M.F.L.Golterman (Inst. for Theoretical Phys., Utrecht, Netherlands). *Phys. Lett. B (Netherlands)*, vol.124B, no.1-2, p.51-4 (21 April 1983). It is pointed out that there exists a difficulty in the proof of existence of Nicolai's (1980, 81) transformations of the bosonic fields in supersymmetric theories, which has so far not been resolved. Also the generalization of the proof, which was given for the case of one bosonic field, to the case of more fields is not trivial. (4 refs.)
- 59952 A class of finite four-dimensional supersymmetric field theories.** P.S.Howe (Dept. of Math., King's Coll., London, England), K.S.Stelle, P.C.West. *Phys. Lett. B (Netherlands)*, vol.124B, no.1-2, p.55-8 (21 April 1983). A class of $N=2$ supersymmetric models consisting of $N=2$ Yang-Mills coupled to $N=2$ matter is shown to be finite to all orders of perturbation theory. For this to hold, the representation of the matter fields must be chosen to give a vanishing one-loop β -function. General $N=2$ supersymmetric models have a β -function that is determined to all orders in perturbation theory by the one-loop contribution. (15 refs.)
- 59953 A simple component field method for SUSY effective potential calculations.** R.D.C.Miller (GERN, Geneva, Switzerland). *Phys. Lett. B (Netherlands)*, vol.124B, no.1-2, p.59-63 (21 April 1983). S. Weinberg's tadpole method (1973) for the calculation of effective potentials of conventional field theories also provides an attractive means for calculating SUSY effective potentials. The essential trick is to leave the SUSY unconstrained and consider auxiliary field tadpoles. The method is illustrated for the Wess-Zumino model. (13 refs.)
- 59954 The pionino: an argument against the massless gluino.** M.J.Eides, M.J.Vysotsky (Inst. of Theoretical & Experimental Phys., Moscow, USSR). *Phys. Lett. B (Netherlands)*, vol.124B, no.1-2, p.83-4 (21 April 1983). Demonstrates that spontaneous R-invariance breaking in a low energy SUSY theory inevitably leads to an extra light pseudoscalar boson (pionino). As this possibility is experimentally excluded the R-invariance has to be broken explicitly, for example by a lagrangian gluino Majorana mass term. (6 refs.)
- 59955 Non-collinear breaking of collinear symmetries at finite momentum transfer.** J.Pulido (Dept. of Math. Phys., Univ. of Birmingham, Birmingham, England). *Port. Phys. (Portugal)*, vol.13, no.3-4, p.123-36 (1982). The breaking of the $SU(2)_W$ collinear symmetry arising when leaving the forward direction in the scattering processes is studied. The starting point is the null-plane hydrogen atom Hamiltonian of Bell and Ruegg (1975) which exhibits this $SU(2)_W$ symmetry in an approximate form. Introducing an electromagnetic interaction with non-zero momentum transfer photons, it is found that breaking is mainly due to transversely polarized photons. Application to hadron-hadron scattering can only be realistic in the low q^2 exchange sector. (7 refs.)
- 59956 Apparent symmetry breaking and its restoration in path integral variational method.** J.Alfaro, B.Sakita (Phys. Dept., City Univ. of New York, New York, NY, USA). *Z. Phys. C (Germany)*, vol.17, no.2, p.171-3 (1983). If one uses a symmetry broken trial action in path integral variational calculations, one often obtains a set of apparently symmetry broken degenerate solutions. The authors present a variational method to determine whether the symmetry breaking is apparent or not. In order to elaborate the method they study the ground state energy of deep double well potential in detail. (6 refs.)
- Isospin** See Entry 59579
- Some special $SU(3) \supset R(3)$ Wigner coefficients and their application** See Entry 59612
- Supergravity with one auxiliary spinor** See Entry 59658
- Hierarchies from supergravity** See Entry 59662
- Gauged $N=8$ supergravity and its breaking from spontaneous compactification** See Entry 59664
- Radiative corrections to the effective potential in $N=1$ supergravity** See Entry 59665
- A study of 't Hooft and Wilson loops** See Entry 59906
- Auxiliary field-free supersymmetric gauges** See Entry 59908
- Two-loop β functions for scalar fields: a simplified approach** See Entry 59909
- One-loop renormalisation of superfield Yang-Mills theories** See Entry 59910
- Lattice formulation of the pure gauge fields on coset space** See Entry 59912
- On realization of the chiral symmetry in the lattice gauge theory containing the $U(1)$ chiral gauge field** See Entry 59913
- Crossover from the strong-coupling to the weak-coupling regime in the $SU(2)$ -symmetric Thirring model** See Entry 59916
- Unique trajectory method in Migdal renormalization group approach and crossover phenomena** See Entry 59918
- Matter field and fermions in $OSP(4/2)$ by dimensional reduction via superspace** See Entry 59922
- The ultra-violet finiteness of the $N=4$ Yang-Mills theory** See Entry 59923
- Super-self duality for supersymmetric Yang-Mills theory** See Entry 59924
- On the dynamics of tumbling gauge theories** See Entry 59925
- Fermion coupled with vortex with dyon excitation** See Entry 59928
- Spin-isospin mixing without spontaneous symmetry breakdown** See Entry 59930
- A minimal model of spontaneous CP violation with the gauge group $SU(2)_L \times SU(2)_R \times U(1)_{B-L}$** See Entry 59959
- Intermediate mass scales and proton decay** See Entry 59960
- Complex rishon-type unification** See Entry 59964
- Are n - \bar{n} oscillation and proton decay mutually exclusive?** See Entry 59965
- Radiative corrections to the Higgs potential of $SU(5)$** See Entry 59966
- Fermion mass ratios and low energy grand unification** See Entry 59968
- Flavor unification in $SU(8)$** See Entry 59969
- Higgs-boson effects in grand unified theories** See Entry 59970
- Decoupling in theories with spontaneous symmetry breakdown. II. Application to the $SU(5)$ grand unified theory** See Entry 59971
- Penguin diagram in supersymmetric theories** See Entry 59973
- Comment on neutral currents in a supersymmetric $SU(2) \times U(1) \times \tilde{U}(1)$ model** See Entry 59974
- An axial gauge formulation for QED_2** See Entry 59977
- Poincare algebra of QED with Dirac's monopoles** See Entry 59980
- Dynamical realization of the linear σ -model and bifermion condensates in QCD** See Entry 59988
- Technicolor** See Entry 59991
- Pseudoscalar mesons and instantons** See Entry 59997
- CP violation, horizontal symmetry and the Kobayashi-Maskawa matrix** See Entry 59998
- Baryon masses and chiral symmetry breaking** See Entry 59999

- Baryonium and possible supersymmetry between quarks and antiquarks** See Entry 60000
- The mass and mixing of the pseudoscalar glueball** See Entry 60003
- Weak nuclear interactions in a hybrid baryon-quark model: p-p asymmetry** See Entry 60004
- Short-distance structure of hadrons in supersymmetric QCD** .. See Entry 60007
- On the dynamical problems and the fermion spectra in the rishon model** See Entry 60018
- Quarks and leptons as quasi Nambu-Goldstone fermions** See Entry 60022
- Three-jets production in broken color gauge symmetry** See Entry 60060
- Neutrinoless double- β decay with quasi-Dirac neutrinos** See Entry 60144
- A search on the parity-forbidden alpha width of the $E_\alpha=4.753$ MeV ($J^\pi, T=0^+, 1$) level of ^{18}F** See Entry 60145
- Observation of parity nonconservation in the integrated γ spectrum from (π, γ) reactions in Cl, Br, Cd, Sn, and La nuclei** See Entry 60163
- Possible P, T -odd effects in NMR spectroscopy of molecules in a supersymmetric model** See Entry 64566
- The Inflationary Universe lives?** See Entry 64569

11.50 DISPERSION RELATIONS AND SUM RULES

- 59957 What can we learn from sum rules for vertex functions in QCD?** N.S.Craigie (Internat. Centre for Theoretical Phys., Trieste, Italy), J.Stern. *Nucl. Phys. B, Part. Phys. (Netherlands)*, vol.B216, no.1, p.209-43 (25 April 1983).
- The authors demonstrate that the light-cone sum rules for vertex functions based on the operator product expansion and QCD perturbation theory lead to interesting relationships between various non-perturbative parameters associated with hadronic bound states (e.g. vertex couplings and decay constants). They also show that such sum rules provide a valuable means of estimating the matrix elements of the higher spin operators in the meson wave function. (16 refs.)
- Pseudoscalar mesons and instantons** See Entry 59997
- Baryon masses and chiral symmetry breaking** See Entry 59999
- Exponential dependence of the cross sections for deep-inelastic reactions on the quark's transverse momentum** See Entry 60002
- Sum rule analysis of hyperon magnetic moments** See Entry 60046

11.80 RELATIVISTIC SCATTERING THEORY

(see also 03.80 General theory of scattering)

- Energy densities, initial conditions and hydrodynamic equations for ultra-relativistic nucleus-nucleus collisions** See Entry 60025

12.00 SPECIFIC THEORIES AND INTERACTION MODELS; PARTICLE SYSTEMATICS

12.10 UNIFIED FIELD THEORIES AND MODELS

- 59958 Are fractional charges and Dirac monopoles consistent with quantum mechanics?** A.E.Strominger. *Comments Nucl. & Part. Phys. (GB)*, vol.11, no.4, p.149-53 (1983).
- The author reviews the Dirac quantization condition and its extension to grand unified theories in the context of possible recent evidence for monopoles and for fractional charges. The existence of monopoles rules out several previous theoretical explanations of fractional charges and provides strong constraints on alternative explanations. (7 refs.)
- 59959 A minimal model of spontaneous CP violation with the gauge group $SU(2)_H \times SU(2)_R \times U(1)_{B-L}$** D.Chang (Carnegie-Mellon Univ., Pittsburgh, PA, USA). *Nucl. Phys. B, Part. Phys. (Netherlands)*, vol.B214, no.3, p.435-51 (18 April 1983).
- The author proposes and analyzes a minimal model of spontaneous CP violation with the gauge symmetry $SU(2)_H \times SU(2)_R \times U(1)_{B-L}$. It is found that the 'isconjugate relation' of Mohapatra and Pati is no longer valid in this model even for the four-quark case. However, due to a dynamical effect all three of the main superweak predictions ($\eta_{+-} = \eta_{00}$, $\eta_{+-0} = \eta_{000}$ and $\eta_{+-0} = \eta_{+-}$) are approximately true to better than 1%. For the six-quark case, it is found that the Kobayashi-Maskawa phase is calculable and small so that its presence does not appreciably change the phenomenology of the model. (14 refs.)
- 59960 Intermediate mass scales and proton decay** Ling-fong Li, D.G.Unger (Dept. of Phys., Carnegie-Mellon Univ., Pittsburgh, PA, USA). *Nucl. Phys. B, Part. Phys. (Netherlands)*, vol.B214, no.2, p.223-36 (11 April 1983).
- Simple sufficient conditions are obtained for ensuring baryon number conservation at intermediate mass scales between M_W and the grand unification mass in grand unified theories. These conditions are applied to obtain an $SO(14)$ model which can accommodate fractionally charged physical particles and which is consistent with the present experimental limits on the proton lifetime and $\sin^2 \theta_W(M_W)$. (11 refs.)
- 59961 Electromagnetic and weak interactions in stochastic space-time: a review** Kh.Namsrai, M.Dineykhani (Lab. of Theoretical Phys., JINR, Dubna, USSR). *Int. J. Theor. Phys. (USA)*, vol.22, no.2, p.131-92 (Feb. 1983).
- A scheme for a nonlocal theory of quantized fields based on the hypothesis of stochastic space is proposed. Within this scheme the gauge-invariant quantum electrodynamics of particles with spin 0, 1/2, 1 and four-fermion weak interactions are constructed, and nonlocal corrections to the anomalous magnetic moments of leptons and to the Lamb shift are calculated. Some consequences of the neutrino oscillations and the electromagnetic properties of neutrinos are considered in detail. Further the rare decay $K_L^0 \rightarrow \mu^+ \mu^-$ and the mass difference of K_1^0 and K_S^0 mesons are investigated in this model. It is shown that the parameter of nonlocality (elementary length l) of weak interactions which can characterize a domain of unification of weak and electromagnetic interactions is $\sim 10^{-16}$ cm. The low-energy experiments imply that quantum electrodynamics is valid up to distances of order $\sim 10^{-15}$ cm. (116 refs.)

tions is $\sim 10^{-16}$ cm. The low-energy experiments imply that quantum electrodynamics is valid up to distances of order $\sim 10^{-15}$ cm. (116 refs.)

- 59962 Is unification in physics necessary?** N.Dombey (Univ. of Sussex, Brighton, England). *New Sci. (GB)*, vol.97, no.1345, p.451-3 (17 Feb. 1983).
- The possible discovery of the so-called W subatomic particle is discussed. Physicists at CERN have found evidence consistent with the decay of a W particle. The existence of the W, if confirmed, is a crucial step in the verification of the unified theory of the electromagnetic force and the weak nuclear force. Alternative explanations of the experimental data, not involving the standard unified model, are examined. Sakurai and Hung's explanation of the experimental data on weak neutral currents by assuming quantum mixing between the electromagnetic current and the weak neutral current (1978) is discussed, along with Fermi's theory of beta decay (1933), in which neutral currents could exist without the mediation of W or Z particles, and the experiments at the DESY electron storage rings. The author concludes that, although weak and electromagnetic interactions need to be included in precise calculations of atomic properties, the role of W and Z particles is not yet established. (no refs.)
- 59963 Exact solution of the Dirac equation in the field of a 't Hooft-Polyakov monopole** W.J.Marciano, I.J.Muzinich (Dept. of Phys., Brookhaven Nat. Lab., Upton, NY, USA). *Phys. Rev. Lett. (USA)*, vol.50, no.14, p.1035-7 (4 April 1983).
- This paper presents an exact solution of the Dirac equation for an $I=1/2$ fermion in the field of a 't Hooft-Polyakov magnetic monopole (in the Prasad-Sommerfield limit), which is analytic at $r=0$. Helicity conservation restricts the $J=0$ S-matrix to be pure charge exchange. Because of the long-range interaction, the scattering amplitude is enhanced at long wavelengths $\lambda \gg 1/M$ (the monopole structure size). The relevance of the present results for the question of proton decay catalysis is briefly discussed. (17 refs.)
- 59964 Complex rishon-type unification** A.Davidson, J.Sonnenschein (Dept. of Nuclear Phys., Weizmann Inst. of Sci., Rehovot, Israel). *Phys. Lett. B (Netherlands)*, vol.123B, no.5, p.299-302 (7 April 1983).
- Presents a flavor-chiral version of the rishon model. The troublesome $\alpha_C \rightarrow 0$ 't Hooft limit is satisfied in a non-exotic manner. The scheme is $SU(7)$ grand unified. Its uniqueness stems from the fact that a realistic $SU(n)_{HC}$ scenario is $SU(N)$ embeddable only provided $n=3, 4$ (or 5) preons involved. A total number of three quark/lepton families is dictated by the overall renormalizability. The electric charge serves as the fourth color. (13 refs.)
- 59965 Are n- \bar{n} oscillation and proton decay mutually exclusive?** C.C.Hazra, M.K.Parida, U.Sarkar (Post-Graduate Dept. of Phys., Sambalpur Univ., Sambalpur, India). *Phys. Lett. B (Netherlands)*, vol.123B, no.6, p.413-16 (14 April 1983).
- The effects of introducing the Higgs scalars mediating n- \bar{n} oscillation are examined using renormalisation group equations corresponding to a symmetry-breaking chain of $SO(10)$. In contrast to earlier results, it is found that both n- \bar{n} oscillation and proton decay are allowed along with a low-mass (~ 100 GeV) right-handed neutral gauge boson, but without observable parity restoration. (10 refs.)
- 59966 Radiative corrections to the Higgs potential of $SU(5)$** C.M.Fraser (Dept. of Theoretical Phys., Univ. of Oxford, Oxford, England), H.Huffel. *Phys. Lett. B (Netherlands)*, vol.123B, no.6, p.417-22 (14 April 1983).
- The first order radiative corrections to the Higgs potential of the minimal $SU(5)$ model arising from gauge boson loops are calculated. The authors present bounds on the Higgs couplings and masses, derived from the requirement that the $SU(5) \rightarrow SU(3) \times U(1)$ symmetry breaking pattern should persist at the one-loop level. (7 refs.)
- 59967 Monopolic atoms and monopole catalysis of proton decay** L.Bracci, G.Fiorentini (Istituto di Fisica, Pisa, Italy). *Phys. Lett. B (Netherlands)*, vol.124B, no.1-2, p.29-33 (21 April 1983).
- The authors discuss the possibility that magnetic monopoles form electromagnetically bound systems (monopolic atoms) with atomic nuclei. By taking into account the Rubakov effect they find that a monopole passing through matter should catalyze a proton decay every few microns. Bounds on monopole fluxes and densities are derived. (14 refs.)
- 59968 Fermion mass ratios and low energy grand unification** M.Ozer (Internat. Centre for Theoretical Phys., Trieste, Italy). *Phys. Lett. B (Netherlands)*, vol.124B, no.1-2, p.64-6 (21 April 1983).
- Within the framework of the 'naturalness' hypothesis for the Yukawa couplings, fermion mass ratios are shown to require the energy scale for grand unification and the energy scale for $SU(4)_{color}$ breaking to be greater than $10^9 \sim 10^{10}$ GeV. Hence very low energy unification and neutron-antineutron oscillations in grand unified theories are incompatible with the 'naturalness' of the Yukawa couplings and the masses of the Higgs scalars. (22 refs.)
- 59969 Flavor unification in $SU(8)$** K.S.Soh, P.Y.Pac (Dept. of Phys., Seoul Nat. Univ., Seoul, Korea), S.K.Kim. *Phys. Rev. D (USA)*, vol.27, no.7, p.1597-600 (1 April 1983).
- Flavor unification is proposed in the $SU(8)$ gauge group. This model imbeds the Georgi-Glashow $SU_{CG}(5)$ as a subgroup. It is necessary to modify Georgi's second postulate for grand unification so that the left-handed fermion representations are complex with respect to $SU(3) \times SU_W(2) \times U_Y(1) \times U(1)$. There are three families of light quarks, one right-handed isospin-singlet quark with charge $-1/3$, three ordinary lepton families, and one lepton doublet without a right-handed partner. (24 refs.)
- 59970 Higgs-boson effects in grand unified theories** R.N.Mohapatra (Dept. of Phys., City Coll., City Univ. of New York, New York, NY, USA), G.Senjanovic. *Phys. Rev. D (USA)*, vol.27, no.7, p.1601-12 (1 April 1983).
- It is argued that fine tuning of a minimal set of parameters, needed to fix the hierarchy of gauge-boson masses and a knowledge of intermediate symmetry groups, leads to 'natural' mass scales for physical Higgs bosons in grand unified theories. This is applied to $\Delta B=2$ transitions in models based on $SU(5)$, $SO(10)$, $SU(16)$, and $[SU(2M)]^4$. It turns out that the Higgs bosons which mediate $\Delta B=2$ neutron-antineutron and hydrogen-antihydrogen oscillations become superheavy, and so such transitions can be observable only in theories with low unification scales, such as $SU(16)$ and $[SU(8)]^4$, if one adheres to the hypothesis of minimal fine tuning. (26 refs.)
- 59971 Decoupling in theories with spontaneous symmetry breakdown. II. Application to the $SU(5)$ grand unified theory** D.G.C.McKeon, S.B.Phillips (Dept. of Appl. Math., Univ. of Western Ontario, London, Ontario, Canada). *Phys. Rev. D (USA)*, vol.27, no.7, p.1613-21 (1 April 1983).
- For pt.I see ibid., vol.26, no.8, p.2086 (1982). Following a method outlined previously, the Appelquist-Carazzone theorem is applied directly to the problem of breaking the $SU(5)$ grand unified theory down to the standard $SU(3) \times SU(2) \times U(1)$ theory. This is carried out within the context of the mass-independent renormalization scheme, which necessitates the calculation

of the anomalous-mass-dimension matrix of the intermediate vector bosons. A relation between the strong coupling constant and the Weinberg angle is determined. The mass of the leptoquark vector boson is estimated. (17 refs.)

59972 Fractionally charged lepton and low-mass magnetic monopole. D.K.Hong, J.Kim, J.E.Kim, K.S.Soh (Dept. of Phys., Seoul Nat. Univ., Seoul, Korea).

Phys. Rev. D (USA), vol.27, no.7, p.1651-3 (1 April 1983). The authors study an SO(14) model to predict a low-mass magnetic monopole and fractionally charged leptons. The mass of the magnetic monopole is $\approx 2 \times 10^9$ GeV. (17 refs.)

59973 Penguin diagram in supersymmetric theories. S.P.Chia, S.Nandi (Center for Particle Theory, Univ. of Texas, Austin, TX, USA).

Phys. Rev. D (USA), vol.27, no.7, p.1654-6 (1 April 1983). The authors have studied the penguin diagram in supersymmetric SU(3)_C × SU(2) × U(1) theories. It is found that the new penguin diagram introduced by supersymmetry has a structure similar to the usual penguin diagram. Its contribution, though comparable in the case of exact supersymmetry, is shown to be small when supersymmetry is broken. (9 refs.)

59974 Comment on neutral currents in a supersymmetric SU(2) × U(1) × U(1) model. Jin Min Kim, J.Kim, J.E.Kim (Dept. of Phys., Seoul Nat. Univ., Seoul, Korea).

Phys. Rev. D (USA), vol.27, no.7, p.1662-4 (1 April 1983). The authors studied the neutral-current aspects of Weinberg's supersymmetric SU(2) × U(1) × U(1) model. The scalar partner of the singlet superfield (\tilde{Y}_{X^c}) must develop a relatively large vacuum expectation value $\gtrsim 570$ GeV. (7 refs.)

59975 Upper limits to fermion masses in the Glashow-Weinberg-Salam model. R.A.Flores (Dept. of Phys., Univ. of California, Santa Cruz, CA, USA), M.Sher.

Phys. Rev. D (USA), vol.27, no.7, p.1679-82 (1 April 1983). Upper limits on the mass m_f of a fermion in the Glashow-Weinberg-Salam model were previously found by requiring that the vacuum be an absolute minimum of the one-loop Higgs potential for a Higgs-boson mass $m_H \leq 150$ GeV, it was found that $m_f \leq 100$ GeV. The authors note that including the effect of running couplings in the one-loop term enlarges the range of allowed masses based on this constraint. Requiring only that the Universe arrive in the vacuum and stay there for over 10^{10} yr further increases this bound to $m_f \leq 200$ GeV. (14 refs.)

59976 New ideas about neutrino masses. E.Witten (Joseph Henry Lab., Princeton Univ., Princeton, NJ, USA).

Phys. Teach. (USA), vol.21, no.2, p.78-87 (Feb. 1983). Discusses the question of the mass of the neutrino. Neutrino detection experiments and the phenomenon of parity violation in weak interactions are covered. Matter and antimatter concepts are postulated. Experimental prospects for the measurement of mass are given. (no refs.)

Spontaneous compactification in six-dimensional Einstein-Maxwell theorySee Entry 59647

On the structure of space, time and fieldSee Entry 59651

Fermion masses from supergravitySee Entry 59663

On realization of the chiral symmetry in the lattice gauge theory containing the U(1) chiral gauge fieldSee Entry 59913

Spontaneous breakdown of supersymmetry due to gauge interactionsSee Entry 59949

Scaling mass relations to two loops: an application to toponiumSee Entry 59981

TechnicolorSee Entry 59991

Jets and the physics of new heavy quarksSee Entry 60008

Analysis of preon models with a small number of flavors. IISee Entry 60023

How the first neutral-current experiments endedSee Entry 60034

Is proton decay measurable?See Entry 60038

Status of G-2 calculation for the electron and muonSee Entry 60044

Is the local monopole flux enhanced?See Entry 64370

Axions and the primordial monopole problemSee Entry 64567

The Inflationary Universe lives?See Entry 64569

12.20 MODELS OF ELECTROMAGNETIC INTERACTIONS

Quantum electrodynamics—an individual viewSee Entry 59581

12.20D Specific calculations and limits of quantum electrodynamics

59977 An axial gauge formulation for QED₂. Y.Nakawaki (Dept. of Maths & Phys., Setsunan Univ., Osaka, Japan).

Prog. Theor. Phys. (Japan), vol.69, no.1, p.235-51 (Jan. 1983). By choosing background electric field properly, the author remedies the surface-modified action formulation of Halpern and Senjanovic (1977) and of Pak (1978). It is found that if the proper background electric field satisfies an appropriate commutation relation, the Hamiltonian equation agrees with the Lagrange equation in a physical space defined by means of charge Q in $Q(\text{phys})=0$. An operator solution to massless spinor QED₂ is demonstrated to show that the author's formulation is consistent in every respect. Two ways to incorporate chiral transformations to the solution are also exhibited. (8 refs.)

59978 The electrodynamics with magnetic monopoles. I. Coulomb-gauge kinematics. K.Hirata (Inst. of Phys., Univ. of Tsukuba, Ibaraki, Japan).

Prog. Theor. Phys. (Japan), vol.69, no.1, p.300-13 (Jan. 1983). As the first step of establishing a canonical theory of the electrodynamics with electric and magnetic point particles, the author gives kinematical discussions on the vector potential in the Coulomb gauge, which is shown to be compatible with the Lorentz invariance. The present formulation is a refined version of the fiber bundle formulation of Wu and Yang (1975). The author uses (i) the Dirac strings as subsidiary variables and (ii) a background vector potential to separate terms which depend kinematically on monopoles. The authors formulation is more tractable than the Wu-Yang original version. (17 refs.)

59979 Note on the magnitude of renormalization constants in quantum electrodynamics. S.Aramaki (Dept. of Phys., Nagoya Univ., Nagoya, Japan).

Prog. Theor. Phys. (Japan), vol.69, no.1, p.323-8 (Jan. 1983). It is shown that Kallen's (1958) assertion which states that at least one of the renormalization constants in quantum electrodynamics is infinite cannot be

justified because the reasoning of his arguments destroys the covariance and the gauge invariance of the theory. (6 refs.)

59980 Poincare algebra of QED with Dirac's monopoles. K.Hirata (Inst. of Phys., Univ. of Tsukuba, Ibaraki, Japan).

Prog. Theor. Phys. (Japan), vol.69, no.1, p.366-8 (Jan. 1983). The generators of the Poincare algebra are explicitly constructed, in terms of the canonical variables, for the classical and quantum electrodynamics with electric and magnetic point particles. (7 refs.)

Magnetic moment of an electron gas in crossed, homogeneous electric and magnetic fieldsSee Entry 59671

The one-loop effective potential in superspaceSee Entry 59938

Exact solution of the Dirac equation in the field of a 't Hooft-Polyakov monopoleSee Entry 59963

12.20F Experimental tests of quantum electrodynamics

Status of G-2 calculation for the electron and muonSee Entry 60044

12.30 MODELS OF WEAK INTERACTIONS

Is unification in physics necessary?See Entry 59962

Weak nuclear interactions in a hybrid baryon-quark model: p-p asymmetrySee Entry 60004

Anomalous weak charged currents of leptons and quarks in a substructure modelSee Entry 60019

12.35 COMPOSITE MODELS OF PARTICLES

59981 Scaling mass relations to two loops: an application to toponium. G.Kilcup, A.Manoohar (Lyman Lab. of Phys., Harvard Univ., Cambridge, MA, USA).

Phys. Lett. B (Netherlands), vol.123B, no.6, p.441-4 (14 April 1983). The authors present a general analysis of mass scaling using two-loop renormalization group equation including threshold effects. They apply this to calculate the toponium mass to be 33 ± 3 GeV using the mass relation $m_t/m_c = m_t/m_\mu$. (8 refs.)

Observations on the discovery of the strange particlesSee Entry 59570

Early cloud chamber experiments at the Pic-du-MidiSee Entry 59571

Strange particle theory in the cosmic ray periodSee Entry 59573

StrangenessSee Entry 59580

The composite particle representation theory. I. The composite particle representation transformationSee Entry 59911

Universality violation and large N interpolationsSee Entry 59926

12.35C General properties of quantum chromodynamics (dynamics, confinement, etc.)

59982 Wilson coefficients for parton decay at order α_s . Shen-Chang Chao, D.E.Soper.

Nucl. Phys. B, Part. Phys. (Netherlands), vol.B214, no.3, p.405-16 (18 April 1983). Calculates, at order α_s , certain Wilson coefficients that relate to the P_T spread of quark jets in QCD. Also included is a calculation of the quark decay function $d(z)$ in a spacelike axial gauge. (6 refs.)

59983 Towards a transport theory of the quark-gluon plasma: infrared divergences and scalar-meson theory. Sai-Ping Li, L.McLerran (Univ. of Washington, Seattle, WA, USA).

Nucl. Phys. B, Part. Phys. (Netherlands), vol.B214, no.3, p.417-34 (18 April 1983).

The authors consider the transport theory of an ultra-relativistic gas of particles. They study infrared divergences which may appear in a naive perturbation treatment in a massless scalar meson theory. They briefly discuss the potential applications of transport theory for ultra-relativistic nuclear collisions. (25 refs.)

59984 Dynamic chaos, Anderson localization, and confinement. S.M.Apenko, D.A.Kirzhnits, Yu.E.Loikov (P.N. Lebedev Phys. Inst., Acad. of Sci., Moscow, USSR).

JETP Lett. (USA), vol.36, no.5, p.213-15 (5 Sept. 1982). Translation of: *Pisma v Zh. Eksp. & Teor. Fiz. (USSR)*, vol.36, no.5, p.172-4 (5 Sept. 1982). [received: April 1983]

A possible randomization of quantum chromodynamics can give rise to an effect similar to the localization which occurs in disordered macroscopic media. As a result, a discrete energy spectrum corresponding to a linearly increasing potential arises in a quark-antiquark system. (6 refs.)

59985 Large-N quantum chromodynamics at finite temperature. A.Gocksch (Dept. of Phys., New York Univ., New York, NY, USA), F.Neri.

Phys. Rev. Lett. (USA), vol.50, no.15, p.1099-101 (11 April 1983). It is pointed out that at $N \rightarrow \infty$, for finite temperature, the Schwinger-Dyson equations imply that below the deconfining phase transition the Wilson loops are independent of the temperature. This suggests a first-order deconfinement phase transition. (6 refs.)

59986 Role of the phonon in the quantum-chromodynamical plasma. P.Carruthers (Theoretical Div., Los Alamos Nat. Lab., Los Alamos, NM, USA).

Phys. Rev. Lett. (USA), vol.50, no.16, p.1179-80 (18 April 1983). It is observed that a color-neutral scalar phonon mode of velocity $c/\sqrt{3}$ should exist in the QCD plasma. The energy density of the phonons is $3/3/16$ that of noninteracting massless gluons and compensates to a considerable extent for the suppression of gluon modes due to collective plasma effects. (11 refs.)

59987 Estimating gluon condensation. J.Chakrabarti (Dept. of Phys. & Astron., Univ. of Rochester, Rochester, NY, USA).

Phys. Lett. B (Netherlands), vol.123B, no.5, p.339-44 (7 April 1983). The author makes an independent estimate of $\langle 0|G_\mu^a G_\mu^a|0\rangle$ and shows that its value may be higher than previously thought.

59988 Dynamical realization of the linear σ -model and bifermion condensates in QCD. V.P.Gusynin, V.A.Miransky, Yu.A.Sitenko (Inst. for Theoretical Phys., Kiev, USSR).

Phys. Lett. B (Netherlands), vol.123B, no.6, p.428-32 (14 April 1983). The dynamical realization of the linear σ -model in QCD is obtained in the framework of a recently suggested approach to gauge theories without fun-

damental scalars. It is also shown that the chiral condensate formation suppresses the formation of the colour condensates in the QCD vacuum. (15 refs.)

59989 The colourlessness partition function of the quantum quark-gluon gas. M.I.Gorenstein, S.I.Lipskikh, V.K.Petrov, G.M.Zinovjev (Acad. of Sci., Inst. for Theoretical Phys., Kiev, Ukrainian SSR). *Phys. Lett. B (Netherlands)*, vol.123B, no.6, p.437-40 (14 April 1983). The partition function of a quantum gas of quarks and gluons with an additional requirement of colourlessness for such systems is calculated. The effect of this constraint on the thermodynamical properties of the systems is considered. (9 refs.)

59990 Four quark states in additive potentials. J.L.Ballot, J.M.Richard (Div. de Phys. Theorique, Inst. de Phys. Nucleaire, Orsay, France). *Phys. Lett. B (Netherlands)*, vol.123B, no.6, p.449-51 (14 April 1983). Considers the naive model where the quarks interact through two-body forces with colour octet exchange structure. With smooth quasi-logarithmic potentials, collective binding occurs in flavor exotic configurations. For instance $(cc\bar{s}\bar{s}) < 2(cc\bar{s})$. (12 refs.)

59991 Technicolor. R.K.Kaul (Centre for Theoretical Studies, Indian Inst. of Sci., Bangalore, India). *Rev. Mod. Phys. (USA)*, vol.55, no.2, p.449-75 (April 1983). The need for reexamination of the standard model of strong, weak, and electromagnetic interactions is discussed, especially with regard to 't Hooft's criterion of naturalness. It has been argued that theories with fundamental scalar fields tend to be unnatural at relatively low energies. There are two solutions to this problem: (i) a global supersymmetry, which ensures the absence of all the naturalness-violating effects associated with scalar fields, and (ii) composite structure of the scalar fields, which starts showing up at energy scales where unnatural effects would otherwise have appeared. With reference to the second solution, this article reviews the case for dynamical breaking of the gauge symmetry and the technicolor scheme for this article reviews the case for dynamical breaking of the gauge symmetry and the technicolor scheme for the composite Higgs boson. This new interaction, of the scaled-up quantum chromodynamic type, keeps the new set of fermions, the technifermions, together in the Higgs particles. It also provides masses for the electroweak gauge bosons W^\pm and Z^0 through technifermion condensate formation. In order to give masses to the ordinary fermions, a new interaction, the extended technicolor interaction, which would connect the ordinary fermions to the technifermions, is required. The extended technicolor group breaks down spontaneously to the technicolor group, possibly as a result of the 'tumbling' mechanism, which is discussed. In addition, the author presents schemes for the isospin breaking of mass matrices of ordinary quarks in the technicolor models. In generalized technicolor models with more than one doublet of technifermions or with more than one technicolor sector, one has additional low-lying degrees of freedom, the pseudo-Goldstone bosons. The pseudo-Goldstone bosons in the technicolor model of Dimopoulos are reviewed and their masses computed. In this context the vacuum alignment problem is also discussed. An effective Lagrangian is derived describing colorless low-lying degrees of freedom for models with two technicolor sectors in the combined limits of chiral symmetry and large number of colors and technicolors. Finally, the author discusses suppression of flavor-changing neutral currents in the extended technicolor models. (93 refs.)

59992 Cornerstones of QCD. M.R.Pennington (Dept. of Phys., Univ. of Durham, Durham, England). *Rep. Prog. Phys. (GB)*, vol.46, no.4, p.393-513 (April 1983). Quantum chromodynamics is the theory of the strong interactions. When these occur over very short distances, hadronic processes become calculable in a perturbative way. How this happens is reviewed with particular reference to the tests and clues experiments on e^+e^- annihilation and deep inelastic scattering provide, which show this is really so. (294 refs.)

59993 Loop calculations in confined QCD. I. J.Baacke, Y.Igarashi, G.Kasperidus (Inst. für Phys., Univ. of Dortmund, Dortmund, Germany). *Z. Phys. C (Germany)*, vol.17, no.2, p.161-9 (1983). Presents a method for calculating one loop corrections in QCD confined to a spherical cavity with bag boundary conditions. The authors use euclidean Green's functions separated into free space and boundary parts and use old-fashioned perturbation theory. As a first application they calculate that part of the quark selfenergy that gives rise to the confining mirror charge potential in the nonrelativistic approximation. They obtain a weaker potential for relativistic massive quarks. Some consequences are discussed. (16 refs.)

59994 Non-perturbative phenomena in QCD vacuum, hadrons, and quark-gluon plasma. E.V.Shuryak. Report CERN-83-01, CERN, Geneva, Switzerland (1 Feb. 1983), 21 pp. These lectures provide a brief review of recent progress in nonperturbative quantum chromodynamics (QCD). They are intended for non specialists, mainly experimentalists. The main object of discussion, the QCD vacuum, is a rather complicated medium. It may be studied either by infinitesimal probes producing microscopic excitations ($=$ hadrons), or by finite excitations (say, heating some volume to a given temperature T). In the latter case, some qualitative changes (phase transitions) should take place. A summary is given of the extent to which such phenomena can be observed in the laboratory by proton-proton, proton-nucleus, and nucleus-nucleus collisions. (51 refs.)

Vacuum instability criterion in an effective potential approach See Entry 59907

On realization of the chiral symmetry in the lattice gauge theory containing the U(1) chiral gauge field See Entry 59913

Spin-isospin mixing without spontaneous symmetry breakdown See Entry 59930

The pionino: an argument against the massless gluino See Entry 59954

What can we learn from sum rules for vertex functions in QCD? See Entry 59957

Complex rishon-type unification See Entry 59964

Fermion mass ratios and low energy grand unification See Entry 59968

Generations of composite fermions See Entry 60021

Analysis of preon models with a small number of flavors. II See Entry 60023

Composite quarks and leptons and horizontal symmetries See Entry 60024

Second order QCD corrections to $q\bar{q}$ -annihilation into a lepton pair at large transverse momentum See Entry 60079

Some comments about polarization in deep inelastic processes See Entry 60090

Equilibrium composition and neutrino emissivity of interacting quark matter in neutron stars See Entry 64504

12.35E Applications of quantum chromodynamics to particle properties and reactions

59995 A measurement of charge properties of quark jets at PETRA. Ch.Berger, H.Genzel, R.Grignul, W.Lackas, F.Raupach, W.Wagner (Phys. Inst., RWTH Aachen, Aachen, Germany), A.Klovning, E.Lillestøl, J.M.Olsen, H.Ackermann, G.Alexander, G.Bella, J.Burger, L.Criegee, A.Eskreyes, G.Franke, Ch.Gerke, G.Knies, E.Lehmann, U.Michelsen, K.H.Pape, H.D.Reich, J.M.Scarr, B.Stella, U.Timm, G.G.Winter, S.T.Xue, W.Zimmermann, O.Achterberg, V.Blobel, L.Boesten, V.Hepp, H.Kapitzka, B.Koppitz, B.Lewendel, W.Luhrsen, R.Van Staa, H.Spitzer, C.Y.Chang, R.G.Glasser, R.G.Kellogg, K.H.Lau, R.O.Polyvado, B.Sechi-Zorn, J.A.Skard, A.Skuja, G.Welch, G.T.Zorn, A.Backer, F.Barreiro, S.Brandt, K.Derikum, C.Grupen, H.J.Meyer, B.Neumann, M.Rost, K.Stupperich, G.Zech, H.J.Daum, H.Meyer, O.Meyer, D.Schmidt. *Nucl. Phys. B, Part. Phys. (Netherlands)*, vol.B214, no.2, p.189-200 (11 April 1983).

The charge properties of quark jets produced in e^+e^- annihilation at 30 GeV c.m. energy have been investigated with the PLUTO detector. The authors find that the mean absolute value of the jet charge $\langle |Q_{jet}| \rangle = 0.55 \pm 0.25$ is small compared to the expectation from statistical models. Long-range charge correlations are observed. These results indicate that the sign of the primary quark charge can be obtained with high probability from the charge of the jet and its distribution in the jet. (7 refs.)

59996 A realistic model for e^+e^- annihilation including parton bremsstrahlung effects. T.D.Gottschalk (California Inst. of Technol., Pasadena, CA, USA).

Nucl. Phys. B, Part. Phys. (Netherlands), vol.B214, no.2, p.201-22 (11 April 1983).

The recently proposed model of Field and Wolfram (1983) for e^+e^- annihilation, which describes hadronization without using fragmentation functions, is examined and enlarged. Extensions of the original scheme include (i) heavy quark mass effects in the QCD parton shower and the explicit formation of final state heavy hadrons, (ii) a modification of the cluster formation algorithm to combine small mass clusters prior to hadronization and (iii) an enhanced rate of soft gluon production at early times in the parton shower. The last two modifications are fundamental and provide a more sensible separation of long and short distance physics. Initial results of the model agree well with PETRA/PEP data. Some predictions are made for LEP energies. (44 refs.)

59997 Pseudoscalar mesons and instantons. E.V.Shuryak (CERN, Geneva, Switzerland).

Nucl. Phys. B, Part. Phys. (Netherlands), vol.B214, no.2, p.237-52 (11 April 1983).

The author discusses the QCD sum rules for the correlators of pseudoscalar currents with quantum numbers of π , K , η , η' mesons. In the framework of the instanton model of the QCD vacuum suggested earlier, the author calculates SU(3) breaking effects such as K , η masses and η' mixing, as well as the U(1) breaking effect, the η' mass. The author concludes that all these phenomena are very well reproduced by this model. (22 refs.)

59998 CP violation, horizontal symmetry and the Kobayashi-Maskawa matrix. F.Hayot (Dept. of Phys., Univ. of California, Los Angeles, CA, USA).

Nucl. Phys. B, Part. Phys. (Netherlands), vol.B214, no.2, p.253-60 (11 April 1983).

It is pointed out that in order to have CP violation in horizontal, generation mixing, interactions, while the Kobayashi-Maskawa matrix itself is real, a very specific structure is required for the unitary matrices that relate weak to mass eigenstates. Implications for the structure of quark mass matrices are also discussed. (8 refs.)

59999 Baryon masses and chiral symmetry breaking. D.Espriu, P.Pascual, R.Tarrach (Dept. Theoretical Phys., Univ. of Barcelona, Barcelona, Spain).

Nucl. Phys. B, Part. Phys. (Netherlands), vol.B214, no.2, p.285-98 (11 April 1983).

The authors study the $1/2^+$ baryon octet within the ITEP sum rule approach. With only the input of one mixing angle for the interpolating baryon operator, the quark vacuum condensates and the strange quark mass, the best values for the masses are obtained for $\langle \bar{s}s \rangle^{1/3} = 0.93(\mu\mu)^{1/3}$ and $m_s \approx 115$ MeV. They also give results for the $3/2^+$ decuplet. (11 refs.)

60000 Baryonium and possible supersymmetry between quarks and antiquarks. Gao Chong-shou (Dept. of Phys., Beijing Univ., Beijing, China), Ho Tso-hsiu.

Commun. Theor. Phys. (China), vol.1, no.6, p.761-7 (1982).

The possibility that diquark is a stable object in hadrons and there exists a global supersymmetry between quarks and antiquarks is discussed. Mesons, baryons and baryoniums can be classified unitedly in the adjoint representation of the supersymmetry group. The united mass splitting formula is obtained based on the supersymmetry and a naive physical mechanism for symmetry breaking. The mass spectra for baryonium ground states are obtained numerically and may be verified experimentally. Some significant characteristics of baryoniums are discussed and can be used as evident indications of the appearance of baryoniums. (2 refs.)

60001 A phenomenological transition potential $V_{q-\bar{q}q}$ derived from QCD theory. Zhang Zong-ye, Yu You-wen (Inst. of High Energy Phys., Acad. Sinica, Beijing, China).

Commun. Theor. Phys. (China), vol.1, no.6, p.783-6 (1982).

The procedure of the derivation of one gluon exchange quark-quark potential is extended from the case of on-shell to that of off-shell. A phenomenological transition potential between valence quark and sea quark $V_{q-\bar{q}q}$ is obtained. (3 refs.)

60002 Exponential dependence of the cross sections for deep-inelastic reactions on the quark's transverse momentum. B.L.Ioffe (Inst. of Theoretical & Experimental Phys., USSR).

JETP Lett. (USA), vol.36, no.5, p.198-201 (5 Sept. 1982). Translation of: *Pis'ma v Zh. Eksp. & Teor. Fiz. (USSR)*, vol.36, no.5, p.160-2 (5 Sept. 1982). [received: April 1983]

It is shown on the basis of the sum rules of quantum chromodynamics that the cross sections for the production of a quark (or of hadron jets) with a transverse momentum k_\perp in deep-inelastic reactions depends exponentially on k_\perp^2 if k_\perp is not too large. (6 refs.)

60003 The mass and mixing of the pseudoscalar glueball. T.Teshima, S.Oneda (Dept. of Phys. & Astron., Univ. of Maryland, College Park, MD, USA).

Phys. Lett. B (Netherlands), vol.123B, no.6, p.455-9 (14 April 1983).

The pseudoscalar glueball mass and its mixing with the η' are studied in quantum chromodynamics, incorporating the chiral $U(3) \times U(3)$ algebra. The glueball mass is then estimated to be in the range 1.0-1.8 GeV. Identifying

the glueball with $\iota(1440)$, the η' - η and η' -glueball mixing angles are found to be $(10 \pm 2)^\circ$ and $(32 \pm 11)^\circ$, respectively. The two-photon decay of the glueball is also discussed. (14 refs.)

60004 Weak nuclear interactions in a hybrid baryon-quark model: p-p asymmetry. L.S.Kisslinger, G.A.Miller (Dept. of Phys., Univ. of Washington, Seattle, WA, USA).

Phys. Rev. C (USA), vol.27, no.4, p.1602-10 (April 1983).

The hybrid multi-baryon-quark shell model of nuclei is developed for the study of weak interactions in nuclei. Application to the parity violating asymmetry in p - p elastic scattering is carried out. (25 refs.)

60005 Quark contributions to the $pp \rightarrow \pi^+ \pi^-$ reaction. G.A.Miller, L.S.Kisslinger (Dept. of Phys., Univ. of Washington, Seattle, WA, USA).

Phys. Rev. C (USA), vol.27, no.4, p.1669-76 (April 1983).

A six-quark model is used to estimate short distance contributions to the $pp \rightarrow \pi^+ \pi^-$ amplitude. Substantial corrections to typical calculations are obtained. (24 refs.)

60006 The spectroscopy of light mesons. A.T.Filippov (Joint Inst. for Nuclear Res., Dubna, USSR).

Sov. Phys.-Usp. (USA), vol.25, no.6, p.371-91 (June 1982). Translation of: *Usp. Fiz. Nauk (USSR)*, vol.137, no.2, p.201-36 (June 1982). [received: April 1983]

A review is given of the most recent experimental data on light meson resonances together with a phenomenological analysis incorporating all the basic ideas of QCD. The following topics are discussed in greater detail: (1) the scalar meson problem; (2) the axial meson problem; (3) spin-spin and spin-orbit splitting in meson multiplets; (4) SU_3 and OZI (Okubo-Zweig-Iizuka) breaking in meson spectra and decays; (5) SU_3 breaking in Regge trajectories and in radial excitations; (6) quark mixing in isoscalar mesons (η - η' , ω - ϕ , f - f'); (7) experimental determinations of the η - η' mixing angle, and (8) radiative decays of vector and pseudoscalar mesons. (190 refs.)

Cornerstones of QCD See Entry 59992

About the clusterization of partons in the hadron processes See Entry 60009

Energy densities, initial conditions and hydrodynamic equations for ultra-relativistic nucleus-nucleus collisions See Entry 60025

Deep-inelastic neutrino-production of charmed particles See Entry 60035

Quark models of baryon resonances See Entry 60045

Trigluon effects in $q\bar{q}$ photoproduction See Entry 60050

Quark model calculations of nucleon structure functions See Entry 60053

Glueball production in high energy e^+e^- collision See Entry 60057

Single logarithm effects in electron-positron annihilation See Entry 60058

Experimental evidence for differences in $\langle p_\perp \rangle$ between quark jets and gluon jets See Entry 60059

Three-jets production in broken color gauge symmetry See Entry 60060

$J/\psi + \eta'$ production in e^+e^- -annihilation: a perturbative QCD calculation See Entry 60062

Study of πNN vertex from hadron and quark point of view See Entry 60063

Multi-gluon exchange in pp elastic scattering See Entry 60067

A study of the pion-pair produced in the reaction $pp \rightarrow pp\pi^+\pi^-$ at 19 GeV/c in view of the possibility of gluon Bremsstrahlung See Entry 60069

Spin effects in jet fragmentation See Entry 60091

Properties of quark matter governed by quantum chromodynamics. I. The screened charge See Entry 60125

Properties of quark matter governed by quantum chromodynamics. II. Renormalization schemes in quark matter See Entry 60126

12.35H Phenomenological composite models of particle structure and reactions (partons, bags, etc.)

60007 Short-distance structure of hadrons in supersymmetric QCD. C.Kounnas (CERN, Geneva, Switzerland), D.A.Ross.

Nucl. Phys. B, Part. Phys. (Netherlands), vol.B214, no.2, p.317-49 (11 April 1983).

Assuming supersymmetry to be a real symmetry in particle physics, the authors study the short-distance internal structure of nucleons (structure functions at large Q^2). They determine all calculable quantities in the leading logarithm approximation and discuss the $N=1$ supersymmetry relations between them. Further relations are obtained by observing that the $N=1$ supersymmetric Lagrangian becomes $N=2$ supersymmetric if the quarks and squarks are (formally) put into the adjoint representation of $SU(3)$ colour. From the calculated elements of the 4×4 matrix of the Q^2 evolution kernels and knowing the quark and gluon distributions at low Q^2 they are able to determine the quark, squark, gluon, and gluino distributions for Q^2 above the threshold for the production of supersymmetric particles. They find that in the asymptotic limit ($Q^2 \rightarrow \infty$) the quarks carry only $2/3$ of the nucleon's baryon number and the remaining $1/3$ is carried by the squarks. They also find that in this limit 0.32 of the longitudinal nucleon momentum is carried by gluons, 0.08 by gluinos, 0.36 by the quarks and 0.24 by the squarks. (18 refs.)

60008 Jets and the physics of new heavy quarks. J.B.Babcock, R.E.Cutkosky (Dept. of Phys., Carnegie-Mellon Univ., Pittsburgh, PA, USA).

Nucl. Phys. B, Part. Phys. (Netherlands), vol.B216, no.1, p.40-82 (25 April 1983).

The authors have developed methods that can be used to isolate a clean sample of events with pair-produced heavy quarks in e^+e^- collisions. They show that most of the fundamental properties of a given heavy quark, as they would appear in pair production or in weak decays, can be deduced from a careful examination of this purified sample. (39 refs.)

60009 About the clusterization of partons in the hadron processes. Zhu Wei (Dept. of Phys., Normal Univ. of East China, Shanghai, China), Shen Jian-guo.

Commun. Theor. Phys. (China), vol.2, no.1, p.829-41 (1983).

The concepts of two kinds of clusterizations of partons is proposed. In terms of the model of quark recombination and perturbative QCD a set of distribution functions describing the clusterization are separated from the quark fragmentation function, and so some quantitative phenomenological information about the QCD soft processes is obtained. (5 refs.)

60010 Minimization principle for the unit of electric charge. G.Rosen (Dept. of Phys., Drexel Univ., Philadelphia, PA, USA).

Int. J. Theor. Phys. (USA), vol.22, no.2, p.207-8 (Feb. 1983).

The fine-structure constant is given theoretically as $\alpha = (137.03608)^{-1}$ if the eigenvalue of a charge-related operator is minimal for $\pm e/3$ quark states. (2 refs.)

60011 Role of hard and soft quark-nucleon collisions in the A dependence of the production of high- p_t hadrons in interactions with nuclei. S.A.Voloshin, Yu.P.Nikitin (Moscow Engng. Phys. Inst., Moscow, USSR).

JETP Lett. (USA), vol.36, no.5, p.201-4 (5 Sept. 1982). Translation of: *Pis'ma v Zh. Eksp. & Teor. Fiz. (USSR)*, vol.36, no.5, p.163-5 (5 Sept. 1982). [received: April 1983]

A single hard collision and several soft collisions of a quark of the incident hadron with the nucleons of the nucleus play the major role in shaping the A dependence of the production of hadrons with large values of p_t . (6 refs.)

60012 Unitarity with quarks despite confinement: connection between deep inelastic scattering and deep inelastic annihilation processes in the scaling limit. J.L.Alonso, V.Azcoiti (Dept. de Fisica Teorica, Univ. de Zaragoza, Zaragoza, Spain).

Nuovo Cimento A (Italy), vol.74A, ser.2, no.1, p.9-16 (1 March 1983).

The authors prove that in a parton model which incorporates confinement there exists a subtle connection between analyticity of the virtual Compton amplitude and unitarity with quarks. Then they show that the experimental data on νW_2 for pions and νW_2 for nucleons indicate in this model an exactly zero free mass of at least one of the u or d quarks. This turns out, also, to be essential to understand the accepted behaviour of the pion electromagnetic form factor. (15 refs.)

60013 Relativistic quarkonium model based on instantaneous ladder BS equation. I. Basic equation and its properties. T.Murota (Faculty of Engng., Yamaguchi Univ., Kofu, Japan).

Prog. Theor. Phys. (Japan), vol.69, no.1, p.181-210 (Jan. 1983).

Investigates a relativistic quarkonium model based on the instant ladder BS equation, i.e. the Salpeter equation. The interaction is assumed to be a sum of the linear potential and the gluon exchange propagator in the Coulomb gauge under instantaneous approximation. The author studies properties of the Salpeter equation and accumulate kinematical relations. These results will be used in a forthcoming paper in which the mass levels and other properties of the quarkonium predicted by this model will be reported. (11 refs.)

60014 Constituent quark parton model and soft hadronic processes. A.Kobayashi (Lab. of Phys., Niigata Univ., Niigata, Japan).

Prog. Theor. Phys. (Japan), vol.69, no.1, p.351-3 (Jan. 1983).

Small P_T inclusive spectra are studied from a constituent quark parton model. The constituent quark (CQ) is regarded as made of a valence quark and a cloud of quark-antiquark pairs and gluons. The distribution functions of CQ are estimated using a similar version to the Kuti-Weisskopf model. (8 refs.)

60015 Quarkonium bound states and coupling to hadrons. S.Jacobs, K.J.Miller, M.G.Olsson (Dept. of Phys., Univ. of Wisconsin, Madison, WI, USA).

Phys. Rev. Lett. (USA), vol.50, no.16, p.1181-3 (18 April 1983).

An inconsistency is found involving heavy quarkonia energy levels in the usual single-channel potential picture. Coupling to the nearest hadronic channel resolves the difficulty. (12 refs.)

60016 Production of heavy quarks: a nonperturbative approach. F.Halzen (Phys. Dept., Univ. of Wisconsin, Madison, WI, USA), W.-Y.Keung, D.M.Scott.

Phys. Rev. D (USA), vol.27, no.7, p.1631-3 (1 April 1983).

The authors identify a way of producing heavy quarks overlooked by perturbative QCD. It successfully accommodates the data on photoproduction and hadroproduction of heavy quarks. Rates at higher energies are expected to be significantly in excess of those predicted by perturbative QCD. (5 refs.)

60017 Ground-state and P-wave charmed baryons in a consistent quark model with hyperfine interactions. C.S.Kalman, D.Pfeffer (Elementary Particle Phys. Group, Concordia Univ., Montreal, Quebec, Canada).

Phys. Rev. D (USA), vol.27, no.7, p.1648-50 (1 April 1983).

Masses of the various ground-state and negative-parity baryons containing one charmed quark are calculated using a parameter set developed for the non-charmed baryons. The sole additional parameter needed, m_c , is obtained by fitting to the observed mass of $\Lambda_c^{+}/2$. The resulting calculated value of the mass of $\Sigma_c^{+}/2$ is in reasonable agreement with experimental values. (9 refs.)

On the statistical mechanics of surfaces See Entry 59722

A study of 't Hooft and Wilson loops See Entry 59906

Lattice formulation of the pure gauge fields on coset space See Entry 59912

Flavor unification in $SU(8)$ See Entry 59969

Upper limits to fermion masses in the Glashow-Weinberg-Salam model See Entry 59975

Wilson coefficients for parton decay at order α_s See Entry 59982

A phenomenological transition potential $V_{q-q\bar{q}}$ derived from QCD theory See Entry 60001

Recombination model of subquark collision and scaling violation in superhigh energy collision See Entry 60020

Unified fireball model for subquark stratum and possible experiments carried on colliding beam accelerators See Entry 60026

An investigation of quark and diquark fragmentation in νp and $\bar{\nu} p$ charged current interactions in BEBC See Entry 60033

Recoupling matrix elements and decay See Entry 60037

Electromagnetic radii and quark structure of the nucleon See Entry 60039

Electromagnetic form factors and quark structure of the nucleon See Entry 60047

A new method for calculating a quark model with unequal mass and higher angular momentum See Entry 60048

Fire-string decay in high-energy e^-e^+ annihilation: one-particle distributions and scaling violations See Entry 60061

An experimental study of large-angle elastic scattering of charged mesons and antiprotons on protons at 20 and 30 GeV/c incident momenta See Entry 60066

Fire-string formation at high energies: pp versus $\bar{p}p$ See Entry 60071

Neutron fraction in primary cosmic rays inferred from muon charge ratio See Entry 64331

.....

.....

.....

.....

.....

.....

.....

.....

.....

.....

.....

.....

.....

.....

.....

.....

.....

.....

.....

.....

.....

.....

.....

tions. Mechanisms through which exotic particles gain masses are discussed. It is found that exotic particles such as color octet leptons and color sextet quarks may gain masses ranging from 10^1 to 10^3 . Some phenomenological aspects of these exotic particles are discussed. (10 refs.)

60019 Anomalous weak charged currents of leptons and quarks in a substructure model. Huang Tao, Xie Yicheng (Inst. of High Energy Phys., Acad. Sinica, Beijing, China). *Commun. Theor. Phys. (China)*, vol.1, no.6, p.753-9 (1982).

The authors present a general approach to get the anomalous weak charged current of leptons and quarks in a substructure model, in which quarks, leptons and W-bosons are composed of preons (fermions and scalar bosons). They have shown that the $(V+A)$ current can be determined by the structure of leptons and quarks and the anomalous weak current can be very small. (6 refs.)

60020 Recombination model of subquark collision and scaling violation in superhigh energy collision. Gao Chong-shou (Dept. of Phys., Peking Univ., Beijing, China), Po Tso-hsiu.

Commun. Theor. Phys. (China), vol.2, no.1, p.843-55 (1983).

A recombination model of subquarks for superhigh energy collisions is proposed. The new phenomena observed in superhigh energy cosmic ray experiments can be explained naturally via the cascade decay of superfireballs of the subquark stratum from this model. The mean multiplicity, the average transverse momentum, the distributions of both transverse and longitudinal momenta and the inclusive spectrum for the superhigh energy collisions are obtained based on this model. It is shown that if the mean multiplicity of secondary particles increases as S increases according to the power law, a scaling violation should take place. When the behavior of mean multiplicity changes from $S^{1/4}$ to $S^{1/2}$ there will be a significant jump of violation coefficient and the scaling violation will become more significant as S increases. It is also pointed out that the characteristic behavior of the existence of the subquark stratum for the inclusive distribution is almost model-independent and can be treated as a decided experimental verification of the appearance of the subquark stratum, and in particular for accelerator experiments in the near future. (5 refs.)

60021 Generations of composite fermions. S.Kitakado (Toyota Technol. Inst., Nagoya, Japan). *Prog. Theor. Phys. (Japan)*, vol.69, no.1, p.358-60 (Jan. 1983).

It is shown that the peculiar mass patterns of quarks and leptons might be explained by their possible composite structure. The generation number is related to the difference between the numbers are left- and right-handed constituents contained in the composite fermion. A simple model with three generations is constructed. (8 refs.)

60022 Quarks and leptons as quasi Nambu-Goldstone fermions. W.Buchmuller, R.D.Peccei, T.Yanagida (Max-Planck-Inst. fur Phys. und Astrophys., Munich, Germany).

Phys. Lett. B (Netherlands), vol.124B, no.1-2, p.67-73 (21 April 1983).

The authors discuss a new idea for constructing composite quarks and leptons which have (approximately) vanishing mass. They are associated with fermionic partners of Goldstone bosons arising from the spontaneous breakdown of an internal symmetry G_f in a supersymmetric preon theory. For $G_f=SU(5)$ being broken to $SU(3)\times U(1)_{em}$ there arise as quasi Goldstone fermions, naturally and unequivocally, precisely the quarks and leptons of one family. The dynamics of these quasi Goldstone fermions is explored by constructing a general supersymmetric nonlinear effective Lagrangian. By means of a reduced model, it is shown that the first nontrivial interactions of the quasi Goldstone fermions can give rise, in an effective way, to the weak interactions. Issues connected with the incorporation of families in the scheme and the generation of masses, as well as the possible structure of the underlying preon theory are briefly discussed. (20 refs.)

60023 Analysis of preon models with a small number of flavors. II. T.G.Rizzo (Ames Lab., Iowa State Univ., Ames, IA, USA). *Phys. Rev. D (USA)*, vol.27, no.7, p.1622-30 (1 April 1983).

For pt.I see *ibid.*, vol.27, no.1, p.72 (1983). The author extends his analysis of four- and five-flavor preon models to six-flavor preon models; only a single color-triplet preon and three color-singlet preons are allowed by the trace constraints and the composite spectrum. Assuming that the precolor group is either $SU(N)$ or $SO(N)$ he finds three models of each kind which satisfy the anomaly- and asymptotic-freedom constraints along with possessing a reasonable composite spectrum. All these models may be grand unified at some large mass scale far above the precolor scale Δ_{PC} . (12 refs.)

60024 Composite quarks and leptons and horizontal symmetries. F.Bordi (Dept. of Phys., Johns Hopkins Univ., Baltimore, MD, USA), R.Casalbuoni, D.Dominici, R.Gatto.

Z. Phys. C (Germany), vol.17, no.2, p.179-82 (1983).

The authors describe models of composite quarks and leptons in which an explicit generation quantum number is carried by one of the preons. They find several possible solutions for the subcolor and the horizontal groups. (8 refs.)

Gauge bosons as composites of fermions See Entry 59929

Complex rishon-type unification See Entry 59964

Unified fireball model for subquark stratum and possible experiments carried on colliding beam accelerators See Entry 60026

12.40 MODELS OF STRONG INTERACTIONS

The order α_s^2 energy-energy correlation function at small angles See Entry 60056

Rigorous bounds on $\pi\pi$ amplitudes in terms of the D -wave scattering lengths See Entry 60064

Effective range expansion for the pion-pion system See Entry 60065

12.40E Statistical models

60025 Energy densities, initial conditions and hydrodynamic equations for ultra-relativistic nucleus-nucleus collisions. K.Kajantie, L.Mclerran (Res. Inst. for Theoretical Phys., Univ. of Helsinki, Helsinki, Finland).

Nucl. Phys. B, Part. Phys. (Netherlands), vol.B214, no.2, p.261-84 (11 April 1983).

The authors discuss ultra-relativistic nucleus-nucleus collisions using an inside-outside cascade model. The considerations are valid only for $E_{cm}>20$ GeV/nucleon for collisions of nuclei of equal baryon number $A>1$. The time and space development of the cascade are described, and the maximum energy and quark number densities produced in such collisions are analytically estimated. Assuming thermalization immediately after materialization from the cascade, hydrodynamic equations, with source terms corresponding to the hadronic matter materialization, are determined. These equations are valid

globally in the beam and target fragmentation regions, and in the central region, and determine the energy density ϵ , baryon number density, n_B , and local flow velocity of the hadronic matter, u^μ , if an equation of state is given. (31 refs.)

60026 Unified fireball model for subquark stratum and possible experiments carried on colliding beam accelerators. Gao Chong-shou (Dept. of Phys., Peking Univ., China), Ho Tso-hsiu.

Commun. Theor. Phys. (China), vol.2, no.1, p.857-66 (1983).

A unified model based on the mechanisms of scattering and recombination for quarks and subquarks is proposed. The implications of this model for different energy regions are discussed. For the low energy regions, the predictions of this model are consistent with the well-known picture given experimentally. For the superhigh energy region it can be used to explain naturally almost all the new phenomena observed in cosmic ray experiments. The predictions of this model for experiments on the colliding beam accelerators are discussed in detail. These predictions can be verified and used as significant evidence of the existence of these mechanisms. (8 refs.)

Wilson coefficients for parton decay at order α_s See Entry 59982

A measurement of charge properties of quark jets at PETRA See Entry 59995

Jets and the physics of new heavy quarks See Entry 60008

Recombination model of subquark collision and scaling violation in superhigh energy collision See Entry 60020

Forward-backward multiplicity correlations in pp-collisions at $\sqrt{s}=540$ GeV See Entry 60073

Fluctuations in the hadronic temperature in pp, p \bar{p} and $\alpha\alpha$ collisions at ISR energies See Entry 60075

12.40H Duality and dual models

60027 Theory of strings with boundaries: fluctuations, topology and quantum geometry. O.Alvarez (Newman Lab. of Nuclear Studies, Cornell Univ., Ithaca, NY, USA).

Nucl. Phys. B, Part. Phys. (Netherlands), vol.B216, no.1, p.125-84 (25 April 1983).

The author discusses Polyakov's quantization of the string (1981) in the presence of a boundary allowing for an arbitrary topology for the world sheet. In addition to the dynamical conformal factor discovered by Polyakov, there are a finite number of new degrees of freedom if the surface is more complicated than a sphere or a disc. The quantization of the Liouville theory in an arbitrary topology is discussed. A one-loop calculation shows that the model is renormalizable if one performs a mass renormalization and an additive field renormalization. The renormalization group equations have a perturbative infrared unstable fixed point in all topologies. (28 refs.)

On the statistical mechanics of surfaces See Entry 59722

Super-self duality for supersymmetric Yang-Mills theory See Entry 59924

Universality violation and large N interpolations See Entry 59926

The electrostatics with magnetic monopoles. I. Coulomb-gauge kinematics See Entry 59978

12.40Q Potential models

Four quark states in additive potentials See Entry 59990

Quarkonium bound states and coupling to hadrons See Entry 60015

Recoupling matrix elements and decay See Entry 60037

12.40S Multiperipheral and multi-Regge models

(inc. diffraction and diffractive production models)

60028 Dynamic model of the real part of the scattering amplitude at zero angle. I.I.Levintov (Inst. of Theoretical & Experimental Phys., USSR).

JETP Lett. (USA), vol.36, no.5, p.204-8 (5 Sept. 1982). Translation of: Pis'ma v Zh. Eksp. & Teor. Fiz. (USSR), vol.36, no.5, p.165-8 (5 Sept. 1982). [received: April 1983]

The real part of the elastic forward scattering amplitude is examined on the basis of the diffraction dissociation model. In this picture, the positive sign of the real part observed at high energies indicates that $\text{Re } f(0)$ is an entirely peripheral effect, a halo. This conclusion agrees with the available experimental data. (12 refs.)

12.40V Vector-meson dominance

How large is $\sigma(\psi N)$? See Entry 60055

12.70 HADRON MASS FORMULAS

60029 Fit of charmonium and Upsilon spectra by a common potential $V_0+A\log(1+r)$. S.N.Jena (Dept. of Phys., Aska Sci. College, Aska, India).

Phys. Lett. B (Netherlands), vol.123B, no.6, p.445-8 (14 April 1983).

Shows that both charmonium and Upsilon spectra can be simultaneously fitted by a potential of the form $V(r)=-1.71+1.067\log(1+r)$. It is found that the spin-averaged masses, fine-hyperfine splittings and leptonic decay width ratios of these spectra can be well understood without taking into account the short distance part of the potential as suggested by QCD. The author makes several predictions for the bb spectra which could hopefully be tested in the near future. (10 refs.)

Baryon masses and chiral symmetry breaking See Entry 59999

Ground-state and P -wave charmed baryons in a consistent quark model with hyperfine interactions See Entry 60017

12.90 MISCELLANEOUS THEORETICAL IDEAS AND MODELS

60030 Particle-antiparticle annihilation in diffusive motion. D.Toussaint, F.Wilczek (Inst. for Theoretical Phys., Univ. of California, Santa Barbara, CA, USA).

J. Chem. Phys. (USA), vol.78, no.5, p.2642-7 (1 March 1983).

The authors study both numerically and analytically the time development of a system of particles and antiparticles moving diffusively and annihilating irreversibly. The asymptotic behavior is found to depend dramatically on

whether the initial fluctuations are localized or entirely random. Physical examples of each kind are identified. (12 refs.)

13.00 SPECIFIC REACTIONS AND PHENOMENOLOGY

13.10 WEAK AND ELECTROMAGNETIC INTERACTIONS OF LEPTONS

60031 A search for new heavy leptons at PETRA. W.Bartel, D.Cords, G.Dietrich, R.Eichler, R.Felst, D.Haidt, H.Krehbiel, K.Meier, B.Naroska, L.H.O'Neill, J.Olsson, U.Schneekloth, P.Steffen (DESY, Hamburg, Germany), E.Elsen, G.Heinzelmann, H.Kado, A.Petersen, P.Warming, G.Weber, S.Bethke, J.Heintze, K.H.Hellenbrand, R.D.Heuer, J.von Krogh, P.Lennert, S.Kawabata, S.Komamiya, H.Matsumura, T.Nozaiki, H.Rieseberg, A.Wagner, A.Bell, F.Foster, G.Hughes, H.Wriedt, J.Allison, A.H.Ball, G.Bamford, R.Barlow, C.Bowdery, I.P.Duerdodt, I.Glendinning, F.K.Loebinger, A.A.Macbeth, H.McCann, H.E.Mills, P.G.Murphy, P.Rowe, K.Stephens, D.Clarke, M.C.Goddard, R.Marshall, G.F.Pearce, J.Kanzaki, T.Kobayashi, M.Koshiba, M.Minowa, M.Nozaiki, S.Odaka, S.Orito, A.Sato, H.Takeda, Y.Totsuka, Y.Watanabe, S.Yamada, C.Yanagisawa. *Phys. Lett. B (Netherlands)*, vol.123B, no.5, p.553-60 (7 April 1983). Results are presented on a search for new heavy leptons, a sequential heavy lepton L^\pm , and an electro-type neutral heavy lepton E^0 , using the JADE detector at PETRA. No evidence for either of these particles was observed. A lower mass limit for the L^\pm is determined to be 18.0 GeV/c² at 95% CL. Lower mass limits for the E^0 are 24.5 GeV/c² and 22.5 GeV/c² in the case of universal V+A and V-A coupling at the W-e-E vertex, respectively. (15 refs.)

60032 Production of single W bosons in e^+e^- and e^-p collisions. H.Neufeld (Inst. für Theoretische Phys., Univ. Wien, Wien, Austria). *Z. Phys. C (Germany)*, vol.17, no.2, p.145-51 (1983). The production of W bosons in electron-positron colliding beams below the W⁺W⁻ threshold is discussed. The corresponding reactions $e^+e^- \rightarrow l^\pm W^\mp (\nu_l)$ yield total cross-sections of the order of 10^{-37} cm² (for $l=e$) and 10^{-38} cm² (for $l=\mu$). The total cross-sections as well as the angular and energy distributions of the W boson in $e^+e^- \rightarrow e^\pm W^\mp (\nu_e)$ are sensitive to the magnetic moment of the W. So, with this reaction, not only W bosons can be produced but also the gauge nature of the interaction can be tested. The decay $Z^0 \rightarrow l^\pm W^\mp (\nu_l)$ is discussed in view of its observation in e^+e^- experiments. Finally the cross-sections of $e^-p \rightarrow \nu_e W^- X^+$ are computed. They are of the order of 10^{-38} cm² for $\sqrt{s} \approx 200$ GeV. (16 refs.)

13.15 NEUTRINO INTERACTIONS

(inc. interactions involving cosmic rays)

60033 An investigation of quark and diquark fragmentation in νp and $\bar{\nu} p$ charged current interactions in BEBC. P.Allen, H.Grassler, D.Lanske, R.Schulte (III. Phys. Inst., Tech. Hochschule, Aachen, Germany), K.Bockmann, C.Geich-Gimbel, B.Nellen, H.Saarikko, A.Grant, H.Klein, D.R.O.Morrison, P.Schmid, H.Wachsmuth, G.Corrigan, G.Miyatt, D.Radojicic, B.Saitta, J.Wells, M.Aderholz, T.Coghen, N.Schmitz, K.L.Wernhard, W.Witteck. *Nucl. Phys. B, Part. Phys. (Netherlands)*, vol.B214, no.3, p.369-91 (18 April 1983). Distributions of the Feynman x variable have been determined for positive and negative pions in charged current neutrino-proton and antineutrino-proton reactions with hadronic energy $W > 3$ GeV and Bjorken $x_B < 0.1$. The distributions have been corrected for experimental effects such as measurement errors, uncertainties in estimating and neutrino energy and particle misidentification. In the framework of the quark-parton model, the distributions yield information about the fragmentation of forward going u and d quarks and backward going u and d quarks. Approximate Feynman scaling is observed for the invariant Feynman x_F distributions. They can be fitted by a power law of the form $(1 - |x_F|)^n$ as suggested by the dimensional counting rules. Simple isospin relations predicted by the quark-parton model are fulfilled. The fragmentation of diquarks is compared with that of protons into π^\pm . (21 refs.)

60034 How the first neutral-current experiments ended. P.Galison (Lyman Lab. of Phys., Harvard Univ., Cambridge, MA, USA). *Rev. Mod. Phys. (USA)*, vol.55, no.2, p.477-509 (April 1983). At the beginning of the 1970s there seemed little reason to believe that strangeness-conserving neutral currents existed: theoreticians had no pressing need for them and several experiments suggested that they were suppressed if they were present at all. Indeed the two remarkable neutrino experiments that eventually led to their discovery were designed and built for very different purposes, including the search for the vector boson and the investigation of the parton model. In retrospect one knows that certain gauge theories (notably the Weinberg-Salam model) predicted that neutral currents exist. But until 't Hooft and Veltman proved that such theories were renormalizable, little effort was made to test the new theories. After the proof the two experimental groups began to reorient their goals to settle an increasingly central issue of physics. Do neutral currents exist? The author asks here: What kind of evidence and arguments persuaded the participants that they had before them a real effect and not an artifact of the apparatus? What eventually convinced them that their experiment was over? An answer to these questions requires an examination of the organization of the experiments, the nature of the apparatus, and the previous work of the experimentalists. Finally, some general observations are made about the recent evolution of experimental physics. (99 refs.)

60035 Deep-inelastic neutrino-production of charmed particles. I.Stoletnii. *Ukr. Fiz. Zh. (USSR)*, vol.28, no.3, p.321-6 (March 1983). In Russian. The $\nu N \rightarrow \mu\bar{\nu} X$ and $\bar{\nu} N \rightarrow \mu N \rightarrow \mu DDX$ processes are considered. Differential cross-sections of these reactions are calculated in the second order in QCD. Cross-sections of reactions due to antineutrinos are found to exceed those of analogous reactions due to neutrino under the same kinematic conditions. The results obtained also describe the $\nu N \rightarrow \mu\bar{\nu} X$ reaction which can proceed by an analogous mechanism. (15 refs.)

13.20 LEPTONIC AND SEMILEPTONIC DECAYS OF MESONS

The connection between local operators on the lattice and in the continuum and its relation to meson decay constants See Entry 59927
Measurements of CP-violating polarization of muons from $K_{\mu 3}$ decays See Entry 59934
Fit of charmonium and Upsilon spectra by a common potential $V_0 + A \log(1 + r)$ See Entry 60029

13.25 HADRONIC DECAYS OF MESONS

60036 Effective Lagrangian and nonleptonic decays of R mesons. E.Guadagnini (Istituto di Fisica, Univ. of Pisa, Pisa, Italy). *Phys. Scr. (Sweden)*, vol.27, no.2, p.69-71 (Feb. 1983). The author analyzes the structure of the effective low energy Lagrangian which describes the nonleptonic decays of strange mesons. (8 refs.)

60037 Recoupling matrix elements and decay. E.van Beveren (Inst. for Theoretical Phys., Univ. of Nijmegen, Nijmegen, Netherlands). *Z. Phys. C (Germany)*, vol.17, no.2, p.135-40 (1983). Recoupling matrix elements are evaluated in the harmonic oscillator approximation for all possible angular and radial excitations in processes where quarks recombine. A diagrammatic representation is given. Their use is demonstrated in calculating the transition potential for $\rho \rightarrow 2\pi$ in a pair creation model. (6 refs.)

The connection between local operators on the lattice and in the continuum and its relation to meson decay constants See Entry 59927
Search for charmed particles with the heavy liquid bubble chamber BIBC See Entry 60076

13.30 DECAYS OF BARYONS

60038 Is proton decay measurable?. L.P.Horwitz, E.Katznelson (Tel Aviv Univ., Tel Aviv, Israel). *Phys. Rev. Lett. (USA)*, vol.50, no.16, p.1184-6 (18 April 1983). It is shown that nucleon collisions in a heavy nucleus may satisfy the conditions required for the inhibition of proton decay in the framework of the quantum mechanical theory of the decay of unstable systems. (11 refs.)
Intermediate mass scales and proton decay See Entry 59960
Exact solution of the Dirac equation in the field of a 't Hooft-Polyakov monopole See Entry 59963
Are n- \bar{n} oscillation and proton decay mutually exclusive? See Entry 59965
Monopolic atoms and monopole catalysis of proton decay See Entry 59967
Quark models of baryon resonances See Entry 60045

13.40 ELECTROMAGNETIC PROCESSES AND PROPERTIES

60039 Electromagnetic radii and quark structure of the nucleon. G.F.Wolters (Nat. Inst. for Nuclear & High Energy Phys., Amsterdam, Netherlands). *Z. Phys. C (Germany)*, vol.17, no.2, p.129-34 (1983). Electromagnetic radii and the empirical dipole radius of the nucleon are considered in conjunction with probability densities of constituent quarks. Using as input the neutron charge radius and the dipole radius, constraints on the remaining radii lead to deviations of about 15% from values taken from literature. Some modifications of current values are proposed especially concerning proton radii. Implications of radial quark structure of the nucleon are indicated. (23 refs.)

13.40F Electromagnetic form factors; electric and magnetic moments

60040 Magnetic moments of baryons and quarks. L.G.Pondrom (Univ. of Wisconsin, Madison, WI, USA). *AIP Conf. Proc. (USA)*, no.95, p.45-57 (1982). (5th High Energy Spin Symposium, Westhampton Beach, NY, USA, Sept. 1982). New measurements of $\mu(\Sigma^+)$ and $\mu(\Sigma^-)$ reported to this conference are combined in the previous data to give the current status of the baryon magnetic moments. (21 refs.)
60041 Magnetic moments of charged hyperons. R.Handler, R.Grobel, B.Lundberg, L.Pondrom, M.Sheaff, C.Wilkinson (Univ. of Wisconsin, Madison, WI, USA), A.Beretvas, L.Deck, T.Devlin, B.Luk, R.Rameika, P.T.Cox, C.Dukes, J.Dworkin, O.Oversteth, K.Heller. *AIP Conf. Proc. (USA)*, no.95, p.58-63 (1982). (5th High Energy Spin Symposium, Westhampton Beach, NY, USA, Sept. 1982). Measurements of the magnetic moments of the Ξ^+ , Σ^+ and Σ^- baryons are presented. The values found are $\mu(\Xi^+) = -69 \pm 04$, $\mu(\Sigma^+) = 2.31 \pm 027$ and $\mu(\Sigma^-) = -89 \pm 14$ in units μ_N . The Ξ^- and Σ^- results are final, while the Σ^+ value is based on a preliminary analysis of about 22% of the data sample. (2 refs.)
60042 Magnetic moments of the Σ^+ and Σ^- . J.P.Marriner (Fermilab, Batavia, IL, USA), E.W.Anderson, C.Ansenbrandt, J.P.Berge, A.Breakstone, A.E.Brenner, J.Butler, T.Cardello, P.S.Cooper, K.Doroba, J.Elias, J.Lach, P.Laurikainen, J.MacLachlan, E.McCliment, L.J.Teig, J.Thron, Y.W.Wah. *AIP Conf. Proc. (USA)*, no.95, p.64-71 (1982). (5th High Energy Spin Symposium, Westhampton Beach, NY, USA, Sept. 1982). Reports preliminary results from Fermilab experiment E-497 on the magnetic moments of the Σ^+ and Σ^- . The experiment was designed to measure the fluxes and polarizations of the hyperons. It is possible to measure the magnetic moment by measuring the spin precession of a polarized hyperon beam. (6 refs.)
60043 The Σ^- moment experiment at BNL. B.L.Roberts, G.W.Dodson, J.P.Miller, F.O'Brien, D.Tieger (Boston Univ., Boston, MA, USA), R.J.Pow-ers, N.Colella, R.B.Sutton, M.Eckhause, K.Giovanetti, D.W.Hetzog, J.R.Kane, W.Phillips, W.F.Vulcan, R.E.Welsh, R.Wheyley, R.G.Winter, A.R.Kunselman. *AIP Conf. Proc. (USA)*, no.95, p.72-6 (1982). (5th High Energy Spin Symposium, Westhampton Beach, NY, USA, Sept. 1982). A new measurement of the Σ^- magnetic dipole moment has been performed at the Brookhaven AGS using the exotic atom technique. K^- from the C4 line were stopped in a laminar target which consisted of sheets of Pb or W

immersed in a LH_2 bath. Monoenergetic π^+ from the reaction, $K^- + p \rightarrow \Sigma^- + \pi^+$ tagged Σ^- production. The fine-structure splitting in the Σ^- hyperonic X-rays was measured and the authors report here a preliminary value obtained from the $\Sigma^- (N=11, n=10)$ X-ray in $\Sigma^- \text{-Pb}$. The value obtained is: $\mu(\Sigma^-) = -1.097 \mu_N$ with a statistical error of $\pm 0.04 \mu_N$ and an estimated systematic error of $\pm 0.04 \mu_N$. (5 refs.)

60044 Status of G-2 calculation for the electron and muon. T.Kinoshita (Newman Lab., Cornell Univ., Ithaca, NY, USA). *AIP Conf. Proc. (USA)*, no.95, p.281-8 (1982). (5th High Energy Spin Symposium, Westhampton Beach, NY, USA, Sept. 1982). The electron anomalous magnetic moment provides the most precise test of QED. The present precision is such that one must begin to seriously question the validity of theories of condensed-matter physics underlying the determination of α . The muon anomalous magnetic moment will play a very important role in testing gauge theories of electroweak interactions at the one loop level. Electron and muon moments may also provide useful information on the possible internal structure of leptons. Experimental and theoretical works are under way to improve the precision of these tests. Here the author reports on the present status of theoretical progress. (24 refs.)

60045 Quark models of baryon resonances. G.Karl (Guelph Waterloo Graduate Program in Phys., Univ. of Guelph, Guelph, Ontario, Canada). *AIP Conf. Proc. (USA)*, no.95, p.310-15 (1982). (5th High Energy Spin Symposium, Westhampton Beach, NY, USA, Sept. 1982). After a short introduction the author comments on baryon magnetic moments, on the Ω^- electric quadrupole moment, on coupling constants for weak semileptonic decays and on the question of constituent gluons in baryons. (6 refs.)

60046 Sum rule analysis of hyperon magnetic moments. J.Franklin (Temple Univ., Philadelphia, PA, USA). *AIP Conf. Proc. (USA)*, no.95, p.323-5 (1982). (5th High Energy Spin Symposium, Westhampton Beach, NY, USA, Sept. 1982). Sum rules for baryon magnetic moments are tested using accurate new hyperon magnetic moment measurements reported at this conference. The difference ($\Sigma^0 \Sigma^-$) of Σ hyperon moments is inconsistent with the sum rules indicating large $\text{SU}(3)$ breaking non-static contributions to baryon magnetic moments. The new measurement for the Σ^- moment would imply an anomalously small strange quark contribution to the Σ magnetic moment. (11 refs.)

60047 Electromagnetic form factors and quark structure of the nucleon. G.F.Wolters (Nat. Inst. voor Kernfysica en Hoge Energifysica, Amsterdam, Netherlands). *AIP Conf. Proc. (USA)*, no.95, p.326-8 (1982). (5th High Energy Spin Symposium, Westhampton Beach, NY, USA, Sept. 1982). Electromagnetic nucleon form factors are studied as weighted combinations of constituent quark densities in Q-space. Experimentally established deviations from the empirical dipole fit for G_E , G_M , $G_{E,2}$ and the behaviour of $G_{E,2}$ are shown to agree with the sum rule involved. An explanation is offered of the effect in spin-spin asymmetry in hard pp scattering. (6 refs.)

60048 A new method for calculating a quark model with unequal mass and higher angular momentum. Ming Zhong Wang (Chengdu Univ. of Sci. & Technol., Sichuan, China). *AIP Conf. Proc. (USA)*, no.95, p.359-61 (1982). (5th High Energy Spin Symposium, Westhampton Beach, NY, USA, Sept. 1982). A new calculation method, called the complete rotation method, is proposed to research quark models. With this method, the mesonic scalar-scalar and spinor-spinor quark models are generalized to the case where the mass of quark is not equal to that of the anti-quark. In order to maintain the covariance of Bethe-Salpeter equation, the author has posed a four dimensional covariant potential for the physical requirement. With the aid of DJS-6 computer. The author has solved the system of integral equations. Using these wave functions, the quantitative results are in agreement with experiment, not only for the radius of the pion but also for the spacelike electromagnetic form factor of the pion. Other physical quantities are also calculated. The kernel functions of higher angular momentum are partly given. (10 refs.)

Short-distance structure of hadrons in supersymmetric QCD .. See Entry 60007

Unitarity with quarks despite confinement: connection between deep inelastic scattering and deep inelastic annihilation processes in the scaling limit See Entry 60012

Comment on the problem of the off-shell γNN vertex function in ed elastic scattering See Entry 60051

Off-shell γNN vertex function in ed elastic scattering See Entry 60052

Quark model calculations of nucleon structure functions See Entry 60053

Polarized e^+ -polarized p colliding beams: physics issues See Entry 60089

13.40H Electromagnetic decays

60049 Search for axion production in T decay. M.S.Alam, S.E.Csorna, A.Fridman, L.Garren, M.D.Mestayer, R.S.Panvini (Vanderbilt Univ., Nashville, TN, USA), D.Andrews, P.Avery, K.Berkelman, D.G.Cassel, J.W.DeWire, R.Ehrlich, T.Ferguson, R.Galik, M.G.D.Gilchrie, B.Gittelmann, A.M.Halling, D.L.Hartill, D.Herrup, S.Holzner, M.Ito, J.Kandaswamy, V.Kistiakowsky, D.L.Kreinick, Y.Kubota, N.B.Mistry, F.Morrow, E.Nordberg, M.Ogg, R.Perchonok, R.Plunkett, A.Silverman, P.C.Stein, S.Stone, D.Weber, R.Wilke, A.J.Sadoff, C.Bebek, J.Hassard, M.Hempstead, J.M.Izen, K.Kinoshita, W.W.MacKay, F.M.Pipkin, J.Rohlf, R.Wilson, H.Kagan, K.Chadwick, J.Chauveau, P.Ganci, T.Gentile, J.A.Guida, R.Kass, A.C.Melissinos, S.L.Olsen, G.Parkhurst, R.Poling, C.Rosenfeld, G.Rucinski, E.H.Thorndike, J.Green, R.Hicks, F.Sannes, P.Kubic, A.Snyder, R.Stone, A.Chen, M.Goldberg, N.Horwitz, A.Jawahery, M.Jibaly, P.Lipari, G.C.Moneti, G.Trahern, H.Van Hecke. *Phys. Rev. D (USA)*, vol.27, no.7, p.1665-7 (1 April 1983).

The authors have searched for decays of the $T(1S)$ into a single high-energy photon and a noninteracting long-lived particle, using the CLEO detector at the Cornell Electron Storage Ring. An upper limit of 3×10^{-4} (at 90% confidence level) is obtained for the branching ratio for such decays. (10 refs.)

The mass and mixing of the pseudoscalar glueball See Entry 60003

13.40K Electromagnetic corrections to strong and weak interaction processes

Radiative corrections to the Higgs potential of $\text{SU}(5)$ See Entry 59966

13.60 PHOTON AND CHARGED-LEPTON INTERACTIONS WITH HADRONS

(for neutrino interactions, see 13.15)

60050 Triguon effects in $q\bar{q}$ photoproduction. S.Mahmood (Dept. of Phys., Quaid-i-Azam Univ., Islamabad, Pakistan). *Phys. Rev. D (USA)*, vol.27, no.7, p.1634-5 (1 April 1983).

A specific identification of trigluon effects in quark-antiquark pair production by linearly polarized photons is attempted in the hope of testing the non-Abelian character of quantum chromodynamics. (4 refs.)

Production of single W bosons in e^+e^- and e^-p collisions See Entry 60032

Proton polarization in the photodisintegration of the deuteron at γ energies in the range 700-1100 MeV See Entry 60164

13.60F Elastic and Compton scattering

60051 Comment on the problem of the off-shell γNN vertex function in ed elastic scattering. D.Kusno (Dept. of Phys., Univ. of Indonesia, Jakarta, Indonesia). *Phys. Rev. D (USA)*, vol.27, no.7, p.1657-9 (1 April 1983).

It is shown that there is an ambiguity in the form of the off-shell γNN vertex function in ed elastic scattering. The degree of the ambiguity problem might be reduced by the requirement that the vertex be free of kinematic singularities and the off-shell isoscalar nucleon form factors be analytic. (12 refs.)

60052 Off-shell γNN vertex function in ed elastic scattering. F.L.Ridener, Jr., H.S.Song, R.H.Good, Jr. (Dept. of Phys., Pennsylvania State Univ., University Park, PA, USA). *Phys. Rev. D (USA)*, vol.27, no.7, p.1660-1 (1 April 1983).

Some of the arguments about the form of the off-shell γNN vertex function are reviewed, in response to a comment of Kusno's (1983). It is shown that there is no more ambiguity in the γNN vertex function than provided for in the original paper. (2 refs.)

13.60H Total and inclusive cross sections

(inc. deep-inelastic processes)

60053 Quark model calculations of nucleon structure functions. L.S.Celenza, C.M.Shakin (Dept. of Phys., City Univ. of New York, Brooklyn, NY, USA). *Phys. Rev. C (USA)*, vol.27, no.4, p.1561-71 (April 1983).

The authors present calculations of those structure functions of the nucleon which are measured in deep inelastic electron scattering. A quark model which preserves translational invariance is used. The model exhibits scaling and the structure functions satisfy the Callan-Gross relation in the scaling region. It is possible to fit the experimental values of $F_2^p(x) - F_2^n(x)$ using wave functions that correspond to a relatively small region of confinement. The ratio of $F_2^n(x)/F_2^p(x)$ is also calculated. One can explain the deviation of the value of the latter quantity from the value $2/3$ obtained in the simplest quark model by allowing the neutron confinement radius to be about 10 percent larger than the corresponding proton radius. They also discuss the role of this radius modification in explaining the deviation of the ratio of the proton and neutron magnetic moments from the value of $-3/2$ obtained in standard quark models. (11 refs.)

Production of heavy quarks: a nonperturbative approach See Entry 60016

Measurement of the internal spin structure of the proton See Entry 60088

Polarized e^+ -polarized p colliding beams: physics issues See Entry 60089

13.60K Meson production

60054 Backward electroproduction of π^+ mesons in the second and third nucleon resonance region. H.Breuer, V.Burkert, U.Hartfiel, Knop, G., J.Langen, M.Leeen, W.Mehner, R.Sauerwein, D.Schablitzky, G.Schnicke (Phys. Inst., Univ. Bonn, Bonn, Germany), J.Drees, S.Kiontke, K.Koseck, G.Lenzen, M.Renkhoof. *Z. Phys. C (Germany)*, vol.17, no.2, p.121-7 (1983).

The reaction $ep \rightarrow e\pi^+ n$ has been studied in the invariant mass range of $1.44 \leq W \leq 1.83$ GeV. The outgoing pion was detected in the backward direction ($\cos \theta^* \leq -0.94$) with respect to the virtual photon at four-momentum transfers of $0.4 \leq q^2 \leq 0.7$ (GeV/c^2). The values of the helicity-1/2-partial wave amplitudes $A_2(-D_{13}(1520))$ and $A_3(-F_{15}(1688))$ were determined by a phenomenological analysis and compared with single quark transition models. (19 refs.)

13.60M Meson-resonance production

60055 How large is $\sigma(\psi N)$? F.D.Gault, A.B.Rimmer (Phys. Dept., Univ. of Durham, Durham, England). *Nuovo Cimento A (Italy)*, vol.74A, ser.2, no.1, p.1-8 (1 March 1983).

The total cross-section $\sigma(\psi N)$ is deduced, by using the vector-dominance model, from recent data on $d\sigma/dt$ at $t=0$ for the process $\gamma N \rightarrow \psi N$ with photon energies above 40 GeV. This result is compared with a $\sigma(\psi N)$ determination which is independent of the vector-dominance model. The q^2 -dependence of the vector-meson-photon coupling is examined in an analysis of recent data on the decay widths $\psi \rightarrow \gamma \gamma$ and $\psi \rightarrow \psi \gamma$ and the resulting suppression factor is applied to the vector-dominance model prediction of $\sigma(\psi N)$. The lowest value deduced is $\sigma(\psi N) = 7$ mb. (32 refs.)

13.65 HADRON PRODUCTION BY ELECTRON-POSITRON COLLISIONS

60056 The order α_s^2 energy-energy correlation function at small angles. Shen-Chang Chao, D.E.Soper (Inst. of Theoretical Sci., Univ. of Oregon, Eugene, OR, USA), J.C.Collins. *Nucl. Phys. B, Part. Phys. (Netherlands)*, vol.B214, no.3, p.513-18 (18 April 1983).

The coefficients that give the small angle (back-to-back) behavior of the energy-energy correlation function in e^+e^- annihilation are calculated at order α_s^2 from previous all order, small angle formulas. The purpose is to facilitate comparison with all angle, order α_s^2 calculations. (11 refs.)

60057 Glueball production in high energy e^+e^- collision. E.-I.Kawai (Dept. of Phys., Ehime Univ., Matsuyama, Japan). *Prog. Theor. Phys. (Japan)*, vol.69, no.1, p.211-20 (Jan. 1983). Inclusive glueball production via two-photon subprocess in high energy e^+e^- collision is discussed. Formulae for the cross section are shown and then numerically evaluated. It is demonstrated that considerably large cross section is expected with feasible rate for future experiments. (16 refs.)

60058 Single logarithm effects in electron-positron annihilation. J.Kodaira, L.Trentadue (Stanford Linear Accelerator Center, Stanford Univ., Stanford, CA, USA). *Phys. Lett. B (Netherlands)*, vol.123B, no.5, p.335-8 (7 April 1983). Shows that the inclusion of the single logarithmic terms in the perturbative treatment of the energy-energy correlation at large collinearity angles makes the introduction of nonperturbative hadronisation effects crucial to describe the experimental data at the present energies. It is unlikely that further perturbative corrections will change this result. (14 refs.)

60059 Experimental evidence for differences in $\langle p_T \rangle$ between quark jets and gluon jets. W.Bartel, D.Cords, G.Dietrich, P.Dittmann, R.Eichler, R.Felst, D.Haidt, H.Krehbiel, K.Meier, B.Naroska, L.H.O'Neill, J.Olsson, P.Steffen (Deutsches Elektronen-Synchrotron DESY, Hamburg, Germany), E.Elsen, G.Heinzelmann, H.Kado, A.Petersen, P.Warming, G.Weber, S.Bethke, J.Heintze, K.H.Hellenbrand, R.D.Heuer, S.Kawabata, S.Komamiya, J.von Krogh, P.Lennert, H.Matsumura, T.Nozaki, H.Rieseberg, A.Wagner, A.Bell, F.Foster, G.Hughes, H.Wriedt, J.Allison, A.H.Ball, G.Bamford, R.Barlow, C.Bowdery, I.P.Duerdoth, I.Glendinning, F.K.Loebinger, A.A.Macbeth, H.McCann, H.E.Mills, P.G.Murphy, P.Rowe, K.Stephens, D.Clarke, M.C.Goddard, R.Marshall, G.F.Pearce, J.Kanzaki, T.Kobayashi, M.Koshiba, M.Minowa, M.Nozaki, S.Odaka, S.Orito, A.Sato, H.Takeda, Y.Yotsuka, Y.Watanabe, S.Yamada, C.Yanagisawa. *Phys. Lett. B (Netherlands)*, vol.123B, no.6, p.460-6 (14 April 1983). The authors have studied the transverse momentum p_T of particles within jets as a function of jet energy using planar 3-jet final states produced in the reaction $e^+e^- \rightarrow$ hadrons at CM energies of 22 GeV and 29-36.4 GeV. At a given jet energy, the mean value $\langle p_T \rangle$ of the lowest energy jet is found to be larger than that of the other jets. First order QCD simulations indicate that the lowest energy jet has the largest probability of representing the debris of the gluon. (11 refs.)

60060 Three-jets production in broken color gauge symmetry. J.D.Anand, S.N.Biswas, A.Goyal, J.N.Passi (Dept. of Phys. & Astrophys., Univ. of Delhi, Delhi, India). *Phys. Rev. D (USA)*, vol.27, no.7, p.1636-9 (1 April 1983). The authors calculate the cross section for three-jets production in e^+e^- annihilation for arbitrarily polarized beams in the context of the broken color gauge symmetry originally due to Pati and Salam. For values of the gluon mass $m_g^2/q^2 < 10^{-2}$ (q^2 is the square of the center-of-mass energy) they find marked departure of the thrust-axis angular-dependence coefficient from the QCD prediction. (6 refs.)

60061 Fire-string decay in high-energy e^-e^+ annihilation: one-particle distributions and scaling violations. L.Angelini, L.Nitti, M.Pellicoro, G.Preparata (Istituto di Fisica, Univ. di Bari, Bari, Italy), G.Valenti. *Phys. Rev. D (USA)*, vol.27, no.7, p.1668-71 (1 April 1983). The fire-string approach is applied to study the structure of one-particle inclusive distributions and their energy dependence in high-energy e^-e^+ annihilations. Differently from QCD the authors predict sizable scaling violations, which are found to be in good agreement with recent experimental data. (10 refs.)

60062 $J/\psi + \eta'$ production in e^+e^- -annihilation: a perturbative QCD calculation. J.H.Kuhn (Inst. fur Theoretische Phys., E. Technische Hochschule, Aachen, Germany), K.H.Streng. *Z. Phys. C (Germany)*, vol.17, no.2, p.175-8 (1983). The cross section for the reaction $e^+e^- \rightarrow S_1^+ + S_0^-$ is calculated in the framework of perturbative QCD, using the nonrelativistic approximation for the S_1^+ and S_0^- bound states. The model is applied to J/ψ plus η , η' , and ι production. The authors find extremely small rates in contrast to previous estimates based on vector meson dominance and discuss possible reasons for this difference. (6 refs.)

Cornerstones of QCD See Entry 59992
A measurement of charge properties of quark jets at PETRA See Entry 59995
A realistic model for e^+e^- annihilation including parton bremsstrahlung effects See Entry 59996

13.75 HADRON-INDUCED LOW- AND INTERMEDIATE-ENERGY REACTIONS AND SCATTERING, ENERGY ≤ 10 GEV
(for higher energies, see 13.85)

13.75C Nucleon-nucleon interactions, including antinucleon, deuteron, etc. (energy ≤ 10 GeV)
(for N-N interactions in nuclei, see 21.30)

Parity violation in non-weak processes See Entry 59935
Parity nonconservation in proton-water scattering at 800 MeV See Entry 59936
Parity violations in high energy nucleon nucleon scattering See Entry 59937
Weak nuclear interactions in a hybrid baryon-quark model: p-p asymmetry See Entry 60004
Electromagnetic form factors and quark structure of the nucleon See Entry 60047
Hyperon polarization at high P_T in the reactions $\pi^-p \rightarrow K^0\Lambda/\Sigma^0$ and $pp \rightarrow \Lambda\Lambda/\Sigma^0$ between 3 and 12 GeV/c See Entry 60085
Polarization phenomenology in the optimal representation See Entry 60092

13.75G Pion-baryon interactions (energy ≤ 10 GeV)

60063 Study of π NN vertex from hadron and quark point of view. Sa Ban-hao, Zhang Xiao-ze, He Han-xin, Zhuo Yi-Zhong (Inst. of Atomic Energy, Acad. Sinica, Beijing, China). *Commun. Theor. Phys. (China)*, vol.1, no.6, p.699-704 (1982). The authors have identified the first-order mixing amplitude of π NN process described by the hadron model with the second-order mixing amplitude of the same process described by the quark model. Then the expression for the coupling constant f_π of the π NN vertex with different quark wave functions

and gluon propagators in different approximations has been derived. The calculation results of f_π have been compared with experimental data. (7 refs.)
Quark contributions to the $pp \rightarrow \pi^+$ reaction See Entry 60005
Hyperon polarization at high P_T in the reactions $\pi^-p \rightarrow K^0\Lambda/\Sigma^0$ and $pp \rightarrow \Lambda\Lambda/\Sigma^0$ between 3 and 12 GeV/c See Entry 60085
Nucleon-induced pion production on nucleons and nuclei See Entry 60173
Reaction $\pi^+ + d \rightarrow p + p$ at 65 to 140 MeV See Entry 60213

13.75J Kaon-baryon interactions (energy ≤ 10 GeV)

The Σ^- moment experiment at BNL See Entry 60043
Hyperon polarization produced in meson-proton collisions in the beam fragmentation region See Entry 60080

13.75L Meson-meson interactions (energy ≤ 10 GeV)

60064 Rigorous bounds on $\pi\pi$ amplitudes in terms of the D-wave scattering lengths. A.D.Gangal (Fachbereich Phys., Univ. Kaiserslautern, Kaiserslautern, Germany). *Nuovo Cimento A (Italy)*, vol.74A, ser.2, no.1, p.117-27 (1 March 1983). Rigorous bounds on physical-region averages of real parts of $\pi\pi$ amplitudes are obtained in terms of the D-wave scattering lengths. These bounds provide consistency checks on $\pi\pi$ scattering data, the experimental information on which is not in a satisfactory state. An example of the bounds is (in units with $\hbar=c=m_\pi=1$ and $s=(\text{c.m. energy})^2$)
 $-0.013 \leq g = (3/32) \int_0^s ds (s+4)(8-s) \{ -2(g-4)\text{Re}F^{(0)}(s,0) + 3(3s-4)\text{Re}F^{(1)}(s,0) + 5(s-4)\text{Re}F^{(2)}(s,0) \} \leq 0.019$, where $F^{(l)}(s,t)$ is isospin- l $\pi\pi$ amplitudes. From the CERN-Munich experiment, the value of g would be in the range 0.018 ± 0.008 to 0.029 ± 0.007 depending upon the value of the $I=2$, S-wave scattering length. (15 refs.)

60065 Effective range expansion for the pion-pion system. S.K.Adhikari, J.R.A.Torreao (Dept. de Fisica, Univ. Federal de Pernambuco, Recife, PE, Brazil). *Phys. Lett. B (Netherlands)*, vol.123B, no.6, p.452-4 (14 April 1983). For small value of the scattering length a ($|a| \sim 0$) the effective range function $k \cot \delta$ has a pole for small k^2 . In such a case it is advantageous to study an expression of the function $k^{-1} \tan \delta$ which is expected to yield a linear dependence on k^2 for small k^2 . An expansion for the function $k^{-1} \tan \delta$ is derived and is applied to the pion-pion system to extract the S-wave scattering lengths and effective ranges satisfactorily from phase shifts where the usual effective range expansion fails because of the occurrence of subthreshold poles in $k \cot \delta$. (11 refs.)

13.85 HADRON-INDUCED HIGH- AND SUPER-HIGH-ENERGY INTERACTIONS, ENERGY > 10 GEV
(for low energies, see 13.75)

Role of hard and soft quark-nucleon collisions in the A dependence of the production of high- p_T hadrons in interactions with nuclei See Entry 60011
Energy densities, initial conditions and hydrodynamic equations for ultra-relativistic nucleus-nucleus collisions See Entry 60025
Dynamic model of the real part of the scattering amplitude at zero angle See Entry 60028
Nucleon-induced pion production on nucleons and nuclei See Entry 60173

13.85D Elastic scattering (energy > 10 GeV)

60066 An experimental study of large-angle elastic scattering of charged mesons and antiprotons on protons at 20 and 30 GeV/c incident momenta. C.Baglin (LAPP, Annecy, France), R.B.Bock, K.Brobakken, L.Bugge, T.Buran, A.Buzzo, P.J.Carson, V.Causton, M.Coupland, D.G.Davis, B.G.Duff, S.Ferroni, I.Kenyon-Gjerpe, V.Gracco, J.P.Guillaud, J.Haldorsen, J.D.Hansen, P.Helgaker, F.F.Heyman, D.C.Imrie, E.K.Johansson, K.Kirsebom, S.Kooijman, R.Lowndes, A.Lundby, G.J.Lush, M.Macri, R.Mollerud, J.Myrheim, M.Poulet, J.Tavernier, L.Rossi, A.Santroni, B.Schistad, G.Skjelving, S.O.Sorensen, M.Yvert. *Nucl. Phys. B, Part. Phys. (Netherlands)*, vol.B216, no.1, p.1-39 (25 April 1983). A description is given of an experiment to study elastic scattering of π^\pm , K^\pm and \bar{p} on protons at CM scattering angles from 45° to 100° at incident laboratory momenta 20 GeV/c and 30 GeV/c. The corresponding t range is from $-6.2 (\text{GeV}/c)^2$ to $-28 (\text{GeV}/c)^2$. There are no previous observations for these reactions in this t range. High intensity and large geometrical acceptance were required in order to measure the low cross sections. The experiment used a double-arm spectrometer. MWPCs were used for reconstruction, and threshold and differential Cerenkov counters for identification. Scintillation counters, Cerenkov counters and a hadron calorimeter were used in the trigger. The trigger logic utilized specially designed matrices and a hard wired microprocessor. The π^-p elastic scattering cross sections follow approximately the dimensional counting rule from 3.5 GeV/c and up to 30 GeV/c. The cross sections decrease by seven orders of magnitude in this energy range. The data is compared to quark models. None of these models give a comprehensive description of the results. However, some modifications to these models improve their consistency with the data. (38 refs.)
60067 Multi-gluon exchange in pp elastic scattering. A.Donnachie, P.V.Landshoff (Dept. of Appl. Math. & Theoretical Phys., Univ. of Cambridge, Cambridge, England). *Phys. Lett. B (Netherlands)*, vol.123B, no.5, p.345-8 (7 April 1983). pp elastic scattering data over the ISR range of energies are analysed in terms of multi-gluon exchange. At large values of t three-gluon exchange dominates. At small t the dominant mechanism is a version of the Chou-Yang model improved to incorporate multi-gluon effects. All features of the data are described correctly, with very few adjustable parameters. (8 refs.)

60068 Measurement of the Ξ^-p elastic cross section at 102 and 135 GeV/c. S.F. Biagi (Queen Mary Coll., Univ. of London, London, England), M. Bourquin, A.J. Britten, R.M. Brown, H. Burckhardt, A.A. Carter, J.R. Carter, Ch. Dore, P. Extermann, M. Gailloud, C.N.P. Gee, W.M. Gibson, J.C. Gordon, R.J. Gray, P. Igokemenes, W.C. Louis, T. Modis, P. Muhlemann, J. Perrier, Ph. Rosset, B.J. Saunders, P. Schirato, H.W. Siebert, V.J. Smith, D.P. Stickland, K.-P. Streit, J.J. Thresher, R. Weill.

Z. Phys. C (Germany), vol.17, no.2, p.113-19 (1983).

The Ξ^-p differential elastic cross section has been measured in the SPS hyperon beam at 102 and 135 GeV/c. In the range $0.01 < -t < 0.42$ (GeV/c)², the t distributions are found to be compatible with the form $A \exp(Bt)$ where B is 7.7 ± 0.4 (GeV/c)⁻² at 102 GeV/c and 8.2 ± 0.5 (GeV/c)⁻² at 135 GeV/c. The corresponding total elastic cross sections are $\sigma_{el} = 4.9 \pm 0.7$ mb and $\sigma_{el} = 5.6 \pm 0.9$ mb, respectively. These results are compared with the predictions of phenomenological models. (15 refs.)

Parity violations in high energy nucleon nucleon scattering See Entry 59937

Electromagnetic form factors and quark structure of the nucleon See Entry 60047

Polarization in p-p elastic scattering at high energies See Entry 60084

Polarization phenomenology in the optimal representation See Entry 60092

13.85F Inelastic scattering, two-particle final states (energy > 10 GeV)

The Σ^- moment experiment at BNL See Entry 60043

Observation of the polarization in reaction $\pi^- p \rightarrow \eta n$ at 40 GeV/c See Entry 60086

13.85H Inelastic scattering, many-particle final states (energy > 10 GeV)

60069 A study of the pion-pair produced in the reaction $pp \rightarrow pp\pi^+\pi^-$ at 19 GeV/c in view of the possibility of gluon Bremsstrahlung. T. Jacobsen, V. Bakken (Inst. of Phys., Univ. of Oslo, Oslo, Norway).

Phys. Scr. (Sweden), vol.27, no.2, p.65-8 (Feb. 1983).

Presents some experimental results for the production of pion-pairs in proton-proton collisions at 19 GeV/c by analogy to electromagnetic Bremsstrahlung. The observed features are consistent with the concept of gluon Bremsstrahlung. (5 refs.)

13.85K Inclusive reactions, including total cross sections, (energy > 10 GeV)

60070 Charged hyperon production by 400 GeV/c protons. L.J. Teig (Yale Univ., New Haven, CT, USA), E.W. Anderson, C. Ankenbrandt, J.P. Berge, A. Breakstone, A.E. Brenner, J. Butler, T.R. Cardello, P.S. Cooper, K. Doroba, J. Elias, J. Lach, P. Laurikainen, J. MacLachlan, J.P. Marriner, E. McCliment, E.I. Rosenberg, J.L. Thron, Y.W. Wah.

AIP Conf. Proc. (USA), no.95, p.95-101 (1982). (5th High Energy Spin Symposium, Westhampton Beach, NY, USA, Sept. 1982).

Reports preliminary results from Fermilab Experiment B-497 on the x and p_t dependence of charged hyperon and anti-hyperon production by 400 GeV/c protons on a Cu target. (6 refs.)

60071 Fire-string formation at high energies: pp versus $\bar{p}p$. L. Angelini, L. Nitti, M. Pellicoro, G. Preparata (Istituto di Fisica, Univ. di Bari, Bari, Italy), G. Valenti.

Nucl. Phys. B, Part. Phys. (Netherlands), vol.B216, no.1, p.83-99 (25 April 1983).

A comparison of hadron production in pp and $\bar{p}p$ interactions at $\sqrt{s}=53$ GeV has been carried out using the theoretical approach of fire-string formation. The authors find basically no differences between the two processes as clearly indicated by recent experimental information. (15 refs.)

60072 Polarization of Λ^0 hyperons in inclusive production by 12-GeV protons on tungsten. F. Abe, K. Hara, N. Kim, K. Kondo, S. Miyashita, H. Miyata, I. Nakano, T. Sugaya, R. Tanaka, K. Takikawa, Y. Yamamoto, T. Yasuda, K. Yasuoka (Inst. of Phys., Univ. of Tsukuba, Ibaraki, Japan), Y. Asano, Y. Iguchi, S. Mori, Y. Fukui, S. Kurokawa, A. Maki.

Phys. Rev. Lett. (USA), vol.50, no.15, p.1102-5 (11 April 1983).

The authors have measured the polarization of $2.4 \times 10^5 \Lambda^0$ hyperons in inclusive production by 12-GeV protons on tungsten at three production angles, 3.5° , 6.5° , and 9.5° . In terms of Feynman's x_F and transverse momentum of Λ^0 , the kinematical range is $0.3 \leq x_F \leq 0.8$ and $0.4 \leq p_T \leq 1.6$ GeV/c. The observed polarization does not depend strongly on x_F and increases linearly with p_T to 16% at $p_T=1.0$ GeV/c, showing a tendency to level off above that point. (8 refs.)

60073 Forward-backward multiplicity correlations in $\bar{p}p$ -collisions at $\sqrt{s}=540$ GeV. K. Alpgard (Inst. of Phys., Univ. of Stockholm, Stockholm, Sweden), R.E. Ansorge, B. Asman, S. Berglund, K. Berkelman, D. Bertrand, K. Bockmann, C.N. Booth, C. Buffam, L. Burrow, P. Carlson, J.-L. Chevalley, B. Eckart, G. Ekspong, I. Evangelou, J.-P. Fabre, K.A. French, J. Gaudaen, C. Geich-Gimbel, M. Gijzen, K. von Holt, R. Hospes, D. Johnson, K. Jon-and, Th. Kokott, R. Mackenzie, M.N. Maggs, R. Meinke, Th. Muller, H. Mulkens, D.J. Munday, A. Odian, J.G. Rushbrooke, H. Saarikko, T. Saarikko, F. Triantis, Ch. Walck, C.P. Ward, D.R. Ward, G. Weber, A.R. Weidberg, T.O. White, G. Wilquet, Y. Hamdagni.

Phys. Lett. B (Netherlands), vol.123B, no.5, p.361-6 (7 April 1983).

Results on correlations in charged multiplicities are presented using data from the UA5 detector at the CERN SPS collider. Both short-range and long-range correlations are observed. The analysis gives no evidence for intrinsic long-range correlations. The observations are consistent with a physical picture in which small clusters are emitted at random along the rapidity axis in the plateau region. This result may indicate that random soft processes play a dominant role in high energy hadronic collisions. The average cluster size is about 2 charged particles, the same as at ISR energies. No variation of cluster size with multiplicity has been observed. The forward-backward long-range correlation and its energy dependence are related to the ratio of the first two moments, variance/mean, of the multiplicity distributions. (8 refs.)

60074 High- p_T direct photon production at 11° in pp collisions at $\sqrt{s}=63$ GeV. T. Akesson (Univ. of Lund, Lund, Sweden), M.G. Albrow, S. Almedeh, R. Bailey, O. Benary, H. Boggild, O. Botner, H. Brody, V. Burkert, R. Carosi, W. Cleland, D. Cockerill, S. Dagan, E. Dahl-Jensen, I. Dahl-Jensen, G. Damgaard, A. Di Ciacio, W.M. Evans, C.W. Fabjan, P. Frandsen, S. Frankel, W. Frati, H. Gordon, U. Goerlach, A. Hallgren, K.H. Hansen, M. Harris, B. Heck, H.J. Hilke, J.E. Hooper, G. Jarlskog, P. Jeffreys, T. Jensen, G. Kessler, T. Killian, K. Kroeger, J.v.d. Lans, D. Lissauer, B. Lorstad, H. Lubatti, T. Ludlam, I. Manelli, A. Markou, N.A. McCubbin, F. Meyer, U. Mjornmark, R. Moller, W. Molzon, A. Nappi, B.S. Nielsen, A. Nilsson, L.H. Olsen, Y. Oren, G. Pierazzini, L. Rosset, E. Rosso, R.H. Schindler, B. Schistad, I. Stumer, M. Sullivan, J. Thompson, E. Vella, W.J. Willis, M. Winik, W. Witzeling, C. Woody.

Phys. Lett. B (Netherlands), vol.123B, no.5, p.367-72 (7 April 1983).

The production of direct photons has been measured relative to π^0 's in the rapidity range $2.00 < y < 2.75$ in pp collisions at $\sqrt{s}=63$ GeV at the CERN Intersecting Storage Rings. The γ/π^0 ratio increases from $\leq 2\%$ at $p_T=1.5$ GeV/c to $\sim 8\%$ at $p_T=4.25$ GeV/c, similar to the value observed near 90° . The results indicate no strong enhancement of single-photon production due to quark bremsstrahlung in this kinematic region. (11 refs.)

60075 Fluctuations in the hadronic temperature in pp, $p\alpha$ and $\alpha\alpha$ collisions at ISR energies. K. Braune (Univ. Heidelberg, Heidelberg, Germany), A. Breakstone, R. Campanini, G.O. Claesson, H.B. Crawley, G.M. Dallavalle, K. Doroba, D. Drijard, F. Fabbri, M. Faessler, A. Firestone, H.G. Fischer, H. Frehe, S.I.A. Garpmann, W. Geist, G. Giacomelli, R. Gokiel, M. Gorbics, Ch. Gruhn, P. Hanke, M. Heiden, W. Herr, W. Hofmann, P.G. Innocenti, T.J. Ketel, E.E. Kluge, J.W. Lamsa, T. Lohse, W.T. Meyer, G. Mornach, T. Nakada, I. Otterlund, M. Panter, B. Povh, A. Putzer, K. Rauschnabel, B. Rensch, F. Rimondi, R. Sosnowski, J. Spengler, E. Stenlund, T.J.M. Symons, M. Szczekowski, R. Szwed, O. Ullaland, D. Wegener, M. Wunsch.

Phys. Lett. B (Netherlands), vol.123B, no.6, p.467-70 (14 April 1983).

The authors present evidence for fluctuations of the average transverse momentum in pp, $p\alpha$ and $\alpha\alpha$ collisions at ISR energies. In thermodynamical models, this is interpreted as fluctuations in the temperature of hadronic interactions. They find that the effect does not depend on the energy of the collision, however, the fluctuations are smaller for $p\alpha$ and $\alpha\alpha$ reactions than for pp interactions. (9 refs.)

60076 Search for charmed particles with the heavy liquid bubble chamber BIBC. A. Badertscher, B. Hahn, E. Hugentobler, T. Marti, U. Moser, L. Muller, E. Ramseier (Lab. of High Energy Phys., Univ. of Berne, Berne, Switzerland), I. Derado, V. Eckhardt, P. Freund, H.J. Gebauer, T. Kahl, K.P. Pretzl, P. Seyboth, J. Seyerlein, M. Vidal.

Phys. Lett. B (Netherlands), vol.123B, no.6, p.471-6 (14 April 1983).

In a search for short lived particles with a high resolution C_3F_8 bubble chamber and a streamer chamber, 21 charmed meson candidates produced by 340 GeV/c π^- have been identified. The cross section for associated charm production is $(28 \pm 11) \mu\text{b}$ per nucleon assuming a linear A -dependence. The mean lifetimes of the D mesons in units of 10^{-13} s are $\tau(D^0, D^{\pm}) = 4.1_{-1.3}^{+2.0} \pm 0.5$, $\tau(D^{\pm}) = 6.3_{-2.3}^{+4.8} \pm 1.5$. (8 refs.)

60077 Hadron production in π^+ and π^- neon interactions at 30 and 64 GeV/c. C.D. Rees, H.J. Lubatti, K. Moriyasu, D. Rock (Dept. of Phys., Univ. of Washington, Seattle, WA, USA), R. Arnold, J.L. Guyonnet, M. Paty, J.L. Riester, H. Abramowicz, H. Bialkowska, K. Doroba, M. Szeptycka, S. Tkacz, A.K. Wroblewski, A. Ziemiński.

Z. Phys. C (Germany), vol.17, no.2, p.95-103 (1983).

Reports new results on charge multiplicities from π^+ Ne and π^- Ne interactions at 30 and 64 GeV/c. The average number of fast protons is extracted and found to be essentially independent of the number of identified slow protons. (18 refs.)

60078 Particle production in high-energy hadron-nucleus interactions. K. Braune, W. Bruckner, M.A. Faessler, R.W. Frey, P.C. Gugelot, T.J. Ketel, J. Niewisch, S. Otwinowski, B. Povh, E. Stenlund, M. Uhrmacher (Max-Planck Inst. fur Kernphys., Heidelberg, Germany).

Z. Phys. C (Germany), vol.17, no.2, p.105-12 (1983).

The pseudorapidity distributions of fast particles ($\beta > 0.7$) emitted in inelastic hadron interactions with carbon, copper and lead were measured for incoming energies from 50 to 150 GeV at the CERN super proton synchrotron. Their dependence on target mass and projectile obeys (ν)-scaling as expected. Their energy dependence is in contrast with most model predictions. (21 refs.)

60079 Second order QCD corrections to $q\bar{q}$ -annihilation into a lepton pair at large transverse momentum. H. Perlt (Sektion Phys., Karl-Marx-Univ., Leipzig, Germany).

Z. Phys. C (Germany), vol.17, no.2, p.153-60 (1983).

The $\mathcal{O}(\alpha_s^2)$ correction is presented to $q\bar{q}$ -annihilation into a lepton pair at large transverse momentum. The author calculates the corresponding hadron cross section difference $d\sigma/d^4q(p\bar{p} - e^+e^- + x)$ (q is the momentum of the lepton pair system). The correction to this cross section difference is found to be large. This essentially agrees with recently published results by Ellis, Martinelli and Petronzio (1981). Two important approximations are used: the in invariant mass of the two-gluon-system is put to zero, and only valence-quark scattering is considered. (20 refs.)

Constituent quark parton model and soft hadronic processes .. See Entry 60014

Production of heavy quarks: a nonperturbative approach See Entry 60016

Hyperon polarization produced in meson-proton collisions in the beam fragmentation region See Entry 60080

Polarization of inclusively produced hyperons See Entry 60081

Polarized Λ^0 production at KEK See Entry 60082

Σ^+ and Σ^- production polarizations See Entry 60083

Hyperon polarization at high p_T in the reactions $\pi^- p \rightarrow K^0 \Lambda^0/\Sigma^0$ and $\pi^- \Lambda/\Sigma^-$ between 3 and 12 GeV/c See Entry 60085

Search for polarization in Σ^0 hyperons See Entry 60087

13.88 POLARISATION IN INTERACTIONS AND SCATTERING

60080 Hyperon polarization produced in meson-proton collisions in the beam fragmentation region. J.R. Bensinger (Brandeis Univ., Waltham, MA, USA).

AIP Conf. Proc. (USA), no.95, p.77-82 (1982). (5th High Energy Spin Symposium, Westhampton Beach, NY, USA, Sept. 1982).

Presents new data on hyperon polarization in the beam fragmentation region from 2 BNL-MPS experiments. One sees little or no Λ polarization in the reaction $\pi^- p \rightarrow \Lambda X$ at 16 GeV and very substantial Σ^- polarization in the reaction $K^- p \rightarrow \Sigma^- X$. The author also reviews the polarization of hyperons from meson induced reactions and compares them with the proton-proton results. (8 refs.)

60081 Polarization of inclusively produced hyperons. B.Lundberg, G.Bunce, R.Handler, R.Grobel, R.March, P.Martin, L.Pondrom, M.Sheaff, C.Wilkinson (Univ. of Wisconsin, Madison, WI, USA), P.T.Cox, J.Dworkin, E.C.Dukes, O.E.Overseth, P.Skubic, K.Heller, C.James, A.Beretvas, L.Deck, T.Devlin, B.Edelman, R.T.Edwards, K.B.Luk, J.Norem, P.Petersen, R.Rameika, L.Schachinger, G.Thomson, R.Whitman, P.Yamin. *AIP Conf. Proc. (USA)*, no.95, p.83-9 (1982). (5th High Energy Spin Symposium, Westhampton Beach, NY, USA, Sept. 1982).

The authors report here polarization results from a series of Fermilab experiments from the years 1974 through 1980, with some preliminary data from a high p_T polarization experiment completed in February 1982. The Λ polarization has a remarkably simple and interesting behavior when expressed as a function of x_F and p_T . (10 refs.)

60082 Polarized Λ^0 production at KEK. K.Takikawa, F.Abe, K.Hara, N.Kim, K.Kondo, S.Miyashita, H.Miyata, I.Nakano, T.Sugaya, R.Tanaka, Y.Yamamoto, T.Yasuda, K.Yasuoka (Inst. of Phys., Univ. of Tsukuba, Ibaraki, Japan), Y.Asano, Y.Iguchi, S.Mori, Y.Fukui, S.Kurokawa, A.Maki. *AIP Conf. Proc. (USA)*, no.95, p.90-4 (1982). (5th High Energy Spin Symposium, Westhampton Beach, NY, USA, Sept. 1982).

The authors have measured the polarization of Λ^0 hyperons produced inclusively by 12 GeV protons on tungsten at KEK. For moderate x_F ($0.2 < x_F < 0.7$), the polarization is nearly independent of x_F and increases roughly linearly with p_T . As x_F increases beyond 0.7, however, the polarization shows a significant x_F dependence. Some preliminary data were taken on copper and beryllium targets. A future project on Σ^0 polarization at KEK is indicated. (10 refs.)

60083 Σ^+ and Σ^- production polarizations. P.S.Cooper (Yale Univ., New Haven, CT, USA), E.W.Anderson, C.Ankenbrandt, J.P.Berge, A.Breakstone, A.E.Brenner, J.Butler, T.Cardello, K.Doroba, J.Elias, J.Lach, P.Laurikainen, J.MacLachlan, J.Marriner, E.McCliment, L.J.Teig, J.Thron, Y.W.Wah. *AIP Conf. Proc. (USA)*, no.95, p.102-7 (1982). (5th High Energy Spin Symposium, Westhampton Beach, NY, USA, Sept. 1982).

The authors report preliminary results from Fermilab experiment E-497 on the production polarizations of Σ^+ and Σ^- hyperons. Hyperons were produced inclusively at non zero production angles by 400 GeV/c protons incident on a Cu target. The polarization was analyzed by the weak decay asymmetry in the hadronic decay modes $\Sigma^+ \rightarrow p\pi^0$ and $\Sigma^- \rightarrow n\pi^-$. Based upon samples of 38000 Σ^+ and 317000 Σ^- decays they observe polarizations as a function of p_T which average 22% at an X of 0.53 for Σ^+ and 40% at X of 0.68 and 0.78 for Σ^- . The direction of polarization for both Σ^+ and Σ^- is in the direction of $K_p \times K_\pi$ where the K s are the momentum vectors of the incident proton and produced hyperon respectively. This is opposite to the direction of polarization of inclusively produced lambdas. (5 refs.)

60084 Polarization in p-p elastic scattering at high energies. A.M.T.Lin (Randall Lab. of Phys., Univ. of Michigan, Ann Arbor, MI, USA).

AIP Conf. Proc. (USA), no.95, p.108-13 (1982). (5th High Energy Spin Symposium, Westhampton Beach, NY, USA, Sept. 1982).

Some recent data on polarization in p-p elastic scattering are briefly surveyed and their characteristics reviewed. A new 28 GeV/c measurement of A , the analyzing power is presented. A few interesting theories are also briefly discussed. The author plans more measurements of A soon and plans to measure A_{NN} when the polarized beam comes on at the AGS. (25 refs.)

60085 Hyperon polarization at high P_T in the reactions $\pi^- p \rightarrow K^0 \Lambda^0$ and $p\bar{p} \rightarrow \Lambda \Lambda^0$ between 3 and 12 GeV/c. S.Schwarz, L.Bachman, M.Bogdanoski, D.Perrin (Univ. de Neuchatel, Neuchatel, Switzerland), J.Gago, P.Sonderegger, A.de Bellefon, P.Billoir, J.M.Brunet, G.Tristram, A.Volte.

AIP Conf. Proc. (USA), no.95, p.114-17 (1982). (5th High Energy Spin Symposium, Westhampton Beach, NY, USA, Sept. 1982).

The authors have measured Λ and Λ^0 polarizations in exclusive $\pi^- p$ and $p\bar{p}$ reactions at 3-5 GeV/c and in semi-inclusive reactions at 3-12 GeV/c covering transverse momentum values up to 1.5 GeV/c. The main result is a large and negative polarization which may provide a clear and severe test for theoretical models. (11 refs.)

60086 Observation of the polarization in reaction $\pi^- p \rightarrow \eta n$ at 40 GeV/c. V.D.Apokin, I.A.Avvakumov, N.S.Borisov, B.V.Chuiko, Yu.M.Goncharenko, Yu.M.Kazarinov, B.A.Khachaturov, G.G.G.Macharashvili, V.N.Matafonov, Yu.A.Matulenko, A.P.Meschanin, A.I.Misnik, A.B.Neganov, S.B.Nurushev, L.B.Parfenov, A.F.Prudkoglyad, A.I.Saraykin, E.V.Smirnov, V.L.Solovyanov, L.F.Solov'yev, Yu.A.Usov, A.N.Vasilyev (Inst. for High Energy Phys., Serpukhov, USSR).

AIP Conf. Proc. (USA), no.95, p.118-25 (1982). (5th High Energy Spin Symposium, Westhampton Beach, NY, USA, Sept. 1982).

The preliminary results of polarization measurements in reaction $\pi^- + p \rightarrow \eta + n$ at 40 GeV/c for the 4-momentum transfers up to 1 (GeV/c)² are presented. Averaged blue of the polarization in the t-range $0.5 < |t| < 1$ (GeV/c)² is $- (24 \pm 8)\%$. The presented data are in contradiction with existent Regge model predictions. (15 refs.)

60087 Search for polarization in Ξ^0 hyperons. R.Rameika, P.T.Cox, J.Dworkin, O.E.Overseth (Univ. of Michigan, Ann Arbor, MI, USA), K.Heller, C.James, A.Beretvas, L.Deck, T.Devlin, K.B.Luk, P.Petersen, P.Skubic, G.Thomson, R.Whitman, R.Handler, R.Grobel, B.Lundberg, L.Pondrom, M.Sheaff, C.Wilkinson, G.Bunce.

AIP Conf. Proc. (USA), no.95, p.126-9 (1982). (5th High Energy Spin Symposium, Westhampton Beach, NY, USA, Sept. 1982).

Inclusive hyperon production by 400 GeV protons at Fermilab has shown that the hyperons are produced with significant polarization. However no polarization has been seen for Λ s produced at these energies. The authors present the results of a search for Ξ^0 polarization. Ξ^0 hyperons, obtained from two independent experiments, have been analyzed for inclusive polarization. The data consist of 4529 fully reconstructed events and 23500 events obtained from non-target pointing Λ s. In both experiments the hyperons were produced in the inclusive reaction $p + N \rightarrow \Xi^0 + X$. (4 refs.)

60088 Measurement of the internal spin structure of the proton. R.Oppenheim (Yale Univ., New Haven, CT, USA), G.Baum, M.R.Bergstrom, P.R.Bolton, J.E.Cledenin, N.R.DeBotton, S.K.Dhawan, R.A.Fong-Tom, Y.-N.Guo, V.-R.Harsh, V.W.Hughes, K.Kondo, M.S.Lubell, C.-L.Mao, R.H.Miller, S.Miyashita, K.Morimoto, U.F.Moser, I.Nakano, D.A.Palmer, L.Panda, W.Waith, N.Sasao, K.P.Schuler, M.L.Seely, J.Sodja, P.A.Souder, S.J.St. Lorant, K.Takikawa, M.Werlen.

AIP Conf. Proc. (USA), no.95, p.255-8 (1982). (5th High Energy Spin Symposium, Westhampton Beach, NY, USA, Sept. 1982).

The final results of measurements at SLAC of the spin dependent asymmetry in the deep inelastic scattering of longitudinally polarized electrons by longitudinally polarized protons are presented. Data were obtained at a scattering angle of 10° and at incident energies of 16.2 and 22.7 GeV, which cover the kinematic range $0.18 < x < 0.70$ and $3.5 < Q^2 < 10.0$ (GeV/c)². The authors compare the results with various models of proton spin structure and with the Bjorken and Ellis-Jaffe sum rules. (18 refs.)

60089 Polarized e^+ -polarized p colliding beams: physics issues. J.D.Bjorken (Fermi Nat. Accelerator Lab., Batavia, IL, USA).

AIP Conf. Proc. (USA), no.95, p.268-80 (1982). (5th High Energy Spin Symposium, Westhampton Beach, NY, USA, Sept. 1982).

The physics of collisions of polarized electrons with polarized protons at storage-ring energies is examined, with emphasis on polarization asymmetries of structure functions. The usefulness of positron-proton as well as electron-proton collisions is underlined. (14 refs.)

60090 Some comments about polarization in deep inelastic processes. R.P.Bajpai (HP Univ., Simla, India).

AIP Conf. Proc. (USA), no.95, p.335-6 (1982). (5th High Energy Spin Symposium, Westhampton Beach, NY, USA, Sept. 1982). (4 refs.)

60091 Spin effects in jet fragmentation. G.Gustafson (Dept. of Theoretical Phys., Lund Univ., Lund, Sweden).

AIP Conf. Proc. (USA), no.95, p.355-8 (1982). (5th High Energy Spin Symposium, Westhampton Beach, NY, USA, Sept. 1982).

Discusses how the polarization of inclusively produced hyperons can be understood if quarks are produced by a tunneling process in a confined colour-electric field. (7 refs.)

60092 Polarization phenomenology in the optimal representation. G.R.Goldstein (Dept. of Phys., Tufts Univ., Medford, MA, USA), M.J.Moravcsik.

AIP Conf. Proc. (USA), no.95, p.365-6 (1982). (5th High Energy Spin Symposium, Westhampton Beach, NY, USA, Sept. 1982).

The optimal representation for two body scattering provides a general framework with which study the relations between reaction amplitudes and experimental observables. The infinitude of possible coordinate systems allowed therein becomes restricted by various symmetry relations. For example identical particle constraints at 90° in the center of mass facilitate the experimental testing of dynamical models, pp elastic scattering and the question of a dibaryon resonance provides an informative application. In general the remaining freedom in coordinate systems allows the amplitude choices to be tailored to experimental amplitude from data. Alternatively the amplitude choices can be made to reveal dynamical features as illustrated by pp elastic scattering and π photoproduction. (9 refs.)

Measurements of CP-violating polarization of muons from $K_{\mu 3}$ decays See Entry 59934

Parity violation in non-weak processes See Entry 59935

Parity nonconservation in proton-water scattering at 800 MeV See Entry 59936

Parity violations in high energy nucleon nucleon scattering See Entry 59937

Magnetic moments of the Σ^+ and Σ^- See Entry 60042

Electromagnetic form factors and quark structure of the nucleon See Entry 60047

Trigluon effects in $q\bar{q}$ photoproduction See Entry 60050

Polarization of Λ^0 hyperons in inclusive production by 12-GeV protons on tungsten See Entry 60072

Proton polarization in the photodisintegration of the deuteron at γ energies in the range 700-1100 MeV See Entry 60164

13.90 OTHER TOPICS IN SPECIFIC REACTIONS AND PHENOMENOLOGY OF ELEMENTARY PARTICLES

60093 Contact terms in $\gamma\gamma \rightarrow A_2 \pi \rightarrow \rho\pi\pi$ transitions. E.Bagan, A.Bramon, F.Cornet (Dept. de Fisica Teorica, Univ. Autonoma de Barcelona, Barcelona, Spain).

Phys. Rev. D (USA), vol.27, no.7, p.1640-3 (1 April 1983).

The contribution of contact terms (originated by gauge invariance) to the $\gamma\gamma \rightarrow A_2 \pi^+ \pi^- \rightarrow \rho^+ \pi^- \pi^-$ transitions is evaluated. Large cross sections are predicted immediately above threshold. (14 refs.)

The role of cosmic rays in the development of particle physics See Entry 59967

Production of single W bosons in e^+e^- and e^-p collisions See Entry 60032

14.00 PROPERTIES OF SPECIFIC PARTICLES AND RESONANCES

14.20 BARYONS AND BARYON RESONANCES (inc. antiparticles)

Intermediate mass scales and proton decay See Entry 59960

Exact solution of the Dirac equation in the field of a 't Hooft-Polyakov monopole See Entry 59963

Are n - \bar{n} oscillation and proton decay mutually exclusive? See Entry 59965

Monopolic atoms and monopole catalysis of proton decay See Entry 59967

Baryon masses and chiral symmetry breaking See Entry 59999

Short-distance structure of hadrons in supersymmetric QCD See Entry 60007

Ground-state and P -wave charmed baryons in a consistent quark model with hyperfine interactions See Entry 60017

Is proton decay measurable? See Entry 60038

Electromagnetic radii and quark structure of the nucleon See Entry 60039

Magnetic moments of baryons and quarks See Entry 60040

Magnetic moments of charged hyperons See Entry 60041

Magnetic moments of the Σ^+ and Σ^- See Entry 60042

The Σ^- moment experiment at BNL See Entry 60043

Quark models of baryon resonances See Entry 60045

Sum rule analysis of hyperon magnetic moments See Entry 60046

Electromagnetic form factors and quark structure of the nucleon See Entry 60047

Charged hyperon production by 400 GeV/c protons See Entry 60070

Polarization of Λ^0 hyperons in inclusive production by 12-GeV protons on tungsten See Entry 60072

Hyperon polarization produced in meson-proton collisions in the beam fragmentation region See Entry 60080

Polarization of inclusively produced hyperons	See Entry 60081
Polarized Λ^0 production at KEK	See Entry 60082
Σ^+ and Σ^- production polarizations	See Entry 60083
Hyperon polarization at high P_T in the reactions $\pi^- p \rightarrow K^0 \Lambda / \Sigma^0$ and $p p \rightarrow \Lambda \Lambda / \Sigma^0$ between 3 and 12 GeV/c	See Entry 60085
Search for polarization in Ξ^0 hyperons	See Entry 60087
Measurement of the internal spin structure of the proton	See Entry 60088
Some comments about polarization in deep inelastic processes	See Entry 60090
Spin effects in jet fragmentation	See Entry 60091
Polarization phenomenology in the optimal representation	See Entry 60092

14.40 MESONS AND MESON RESONANCES

Scaling mass relations to two loops: an application to toponium	See Entry 59981
Dynamic chaos, Anderson localization, and confinement	See Entry 59984
Four quark states in additive potentials	See Entry 59990
Pseudoscalar mesons and instantons	See Entry 59997
Baryonium and possible supersymmetry between quarks and antiquarks	See Entry 60000
The mass and mixing of the pseudoscalar glueball	See Entry 60003
The spectroscopy of light mesons	See Entry 60006
Short-distance structure of hadrons in supersymmetric QCD	See Entry 60007
Unitarity with quarks despite confinement: connection between deep inelastic scattering and deep inelastic annihilation processes in the scaling limit	See Entry 60012
Fit of charmonium and Upsilon spectra by a common potential $V_0 + A \log(1+r)$	See Entry 60029
Deep-inelastic neutrino production of charmed particles	See Entry 60035
Effective Lagrangian and nonleptonic decays of R mesons	See Entry 60036
Recoupling matrix elements and decay	See Entry 60037
A new method for calculating a quark model with unequal mass and higher angular momentum	See Entry 60048
Search for axion production in T decay	See Entry 60049
How large is $\sigma(\psi N)$?	See Entry 60055
$J/\psi + \eta'$ production in e^+e^- -annihilation: a perturbative QCD calculation	See Entry 60062
Search for charmed particles with the heavy liquid bubble chamber BIBC	See Entry 60076
Observation of the polarization in reaction $\pi^- p \rightarrow \eta n$ at 40 GeV/c	See Entry 60086
Mesons and quarks in nuclear physics	See Entry 60119

14.60 LEPTONS

Ideas and nonideas and the discovery of the leptonic property in Rome	See Entry 59574
The infancy and youth of neutrino physics: some recollections	See Entry 59575
Neutrinos to 1960—personal recollections	See Entry 59576
Beta decay opens the way to weak interactions	See Entry 59577
Measurements of CP-violating polarization of muons from $K_{\mu 3}$ decays	See Entry 59934
Fractionally charged lepton and low-mass magnetic monopole	See Entry 59972
New ideas about neutrino masses	See Entry 59976
Generations of composite fermions	See Entry 60021
Quarks and leptons as quasi Nambu-Goldstone fermions	See Entry 60022
Composite quarks and leptons and horizontal symmetries	See Entry 60024
A search for new heavy leptons at PETRA	See Entry 60031
Status of G-2 calculation for the electron and muon	See Entry 60044
$1/2^+ \rightarrow 1/2^+$ beta decay with neutrino mass effects in the elementary particle treatment of weak interactions	See Entry 60141
Emission of heavy neutrinos in muon capture	See Entry 60143
Neutrinoless double- β decay with quasi-Dirac neutrinos	See Entry 60144

14.80 OTHER AND HYPOTHETICAL PARTICLES

60094 Intrinsic limits for acoustic detection of magnetic monopoles. C.W.Akerlof (Randall Lab. of Phys., Univ. of Michigan, Ann Arbor, MI, USA). <i>Phys. Rev. D (USA)</i> , vol.27, no.7, p.1675-8 (1 April 1983). The total energy and the energy spectral distribution are calculated for a monopole-induced thermoacoustic pulse. The available acoustic energy is not significantly greater than $1/2 kT$ and thus detection of grand-unified-theory monopoles by this technique is practically infeasible. (16 refs.)	
Are classical tachyons slower-than-light quantum particles?	See Entry 59592
A discussion on the classical solution of gauge theory	See Entry 59902
Fermion coupled with vortex with dyon excitation	See Entry 59928
Gauge bosons as composites of fermions	See Entry 59929
The pionino: an argument against the massless gluino	See Entry 59954
Are fractional charges and Dirac monopoles consistent with quantum mechanics?	See Entry 59958
Exact solution of the Dirac equation in the field of a 't Hooft-Polyakov monopole	See Entry 59963
Are n-n oscillation and proton decay mutually exclusive?	See Entry 59965
Monopole atoms and monopole catalysis of proton decay	See Entry 59967
Higgs-boson effects in grand unified theories	See Entry 59970
Decoupling in theories with spontaneous symmetry breakdown. II. Application to the SU(5) grand unified theory	See Entry 59971
Fractionally charged lepton and low-mass magnetic monopole	See Entry 59972

Upper limits to fermion masses in the Glashow-Weinberg-Salam model	See Entry 59975
The electrodynamics with magnetic monopoles. I. Coulomb-gauge kinematics	See Entry 59978
Poincare algebra of QED with Dirac's monopoles	See Entry 59980
Scaling mass relations to two loops: an application to toponium	See Entry 59981
Technicolor	See Entry 59991
Baryonium and possible supersymmetry between quarks and antiquarks	See Entry 60000
Jets and the physics of new heavy quarks	See Entry 60008
Anomalous weak charged currents of leptons and quarks in a substructure model	See Entry 60019
Generations of composite fermions	See Entry 60021
Quarks and leptons as quasi Nambu-Goldstone fermions	See Entry 60022
Composite quarks and leptons and horizontal symmetries	See Entry 60024
Production of single W bosons in e^+e^- and e^-p collisions	See Entry 60032
Magnetic moments of baryons and quarks	See Entry 60040
Search for axion production in T decay	See Entry 60049
Glueball production in high energy e^+e^- collision	See Entry 60057
High- p_T direct photon production at 11° in pp collisions at $\sqrt{s}=63$ GeV	See Entry 60074
Mesons and quarks in nuclear physics	See Entry 60119
Limit on exotic two-body decays of orthopositronium	See Entry 61027
Is the local monopole flux enhanced?	See Entry 64370
Loss of angular momentum in a binary system due to collisionless particles as monopoles or gravitons: does it exceed the gravitational radiation emission in the binary system PSR 1913+16?	See Entry 64498
Axions and the primordial monopole problem	See Entry 64567

20.00 NUCLEAR PHYSICS

21.00 NUCLEAR STRUCTURE

21.10 GENERAL AND AVERAGE PROPERTIES OF NUCLEI; PROPERTIES OF NUCLEAR ENERGY LEVELS

(for properties of specific nuclei listed by mass ranges, see 27.)

60095 Selective population of high-j states via heavy-ion induced transfer reactions. P.D.Bond. <i>Comments Nucl. & Part. Phys. (GB)</i> , vol.11, no.5, p.231-40 (1983). The unique aspects of certain heavy-ion induced transfer reactions to selectively populated high spin single particle states are discussed. The use of these reactions, in conjunction with gamma-ray coincidence work, to find previously unobserved high spin states with simple configurations is demonstrated. (10 refs.)	
60096 Search for the second excited $11/2^-$ state and weak-coupling scheme in ^{117}Sn . M.Sekiguchi, O.Hashimoto, Y.Shida, F.Soga (Inst. for Nuclear Study, Univ. of Tokyo, Tokyo, Japan). <i>J. Phys. Soc. Jpn. (Japan)</i> , vol.52, no.4, p.1134-41 (April 1983). The second excited $11/2^-$ state in ^{117}Sn has been searched for by four different single-neutron transfer reactions, (d,t), (p,d), (d,p) and ($^3\text{He},\alpha$). The state has been found at $E_x=1.589$ MeV, very near to the $13/2^-$ and $15/2^-$ states observed in an in-beam γ -ray study. These very closely degenerate states are possible three members of the quintet of the weak-coupling scheme [$1_{1/2} \times 2^+$] in this nucleus. (24 refs.)	
60097 Mean distribution of single-particle levels in thin-skinned potential wells and the macroscopic level density parameters of nuclei. V.S.Ramamurthy (Bhabha Atomic Res. Centre, Bombay, India), M.Asghar, S.K.Kataria. <i>Nucl. Phys. A (Netherlands)</i> , vol.A398, no.3, p.544-56 (2 May 1983). A general leptodermous expansion for the density of single-particle levels in thin-skinned potential wells is derived and is used to study the finite size corrections to the macroscopic level density parameters of nuclei. With droplet model values for the potential parameters, the calculated level density parameters for nuclei along the β -stability line show systematic deviations from the experimental estimates. Possible reasons for these deviations are also discussed. (17 refs.)	
60098 Role of high multipole pairs in the description of deformed nuclei. P.Catara, A.Insolia (Istituto di Fisica, Univ. di Catania, Catania, Italy), E.Magliione, A.Vitturi. <i>Phys. Lett. B (Netherlands)</i> , vol.123B, no.6, p.375-8 (14 April 1983). The intrinsic wave function associated to the ground state rotational band of axially symmetric deformed nuclei is described as a condensate of a basic collective pair which includes components with all possible angular momenta. The microscopic structure of its pair is determined by a variational procedure within the pairing plus quadrupole model. The effect of the truncation to the components with angular momentum $\Lambda=0, 2$ only, as suggested by the interacting Boson Model, is tested. It is found that this truncation emphasizes the pairing effects with respect to the shape distortion, with major consequences on different physical observables. (7 refs.)	
60099 Excitation of the 6^- particle-hole state with the $^{40}\text{Ca}(p,n)^{40}\text{Sc}$ reaction at 133.5 MeV. B.D.Anderson, J.W.Watson, C.Lebo, A.R.Baldwin, A.Fazely, R.Madey (Dept. of Phys., Kent State Univ., Kent, OH, USA), C.C.Foster. <i>Phys. Lett. B (Netherlands)</i> , vol.123B, no.6, p.383-6 (14 April 1983). A relatively broad (~ 2.5 MeV) state was observed in ^{40}Sc at $E_x=7$ MeV, which is interpreted as the $T=1, 6^-$ stretched state with the dominant configuration $(\pi f_{7/2} \nu d_{5/2})^{-1}$. The strength observed is comparable to the (p,n) excitation of the $T=1, 6^-$ stretched in state ^{28}P , and the width is understood in terms of the spreading and decay widths of the $1d_{5/2}$ strength in ^{40}Sc . (20 refs.)	

60100 On the pairing field in nuclei. R.A.Brogia, A.Winther (Niels Bohr Inst., Univ. of Copenhagen, Copenhagen, Denmark). *Phys. Lett. B (Netherlands)*, vol.124B, no.1-2, p.11-13 (21 April 1983). An approximate form for the non-local pairing transition density and pairing field for pairing vibrations in nuclei is given on the basis of the Thomas-Fermi approximation. (5 refs.)

60101 Nuclear g factors of the $^{17/2-}$ and $^{21/2+}$ isomeric states of ^{91}Mo . P.Raghavan (Rutgers Univ., New Brunswick, NJ, USA), R.S.Raghavan. *Phys. Rev. C (USA)*, vol.27, no.4, p.1532-5 (April 1983). The nuclear g factors of the $^{17/2-}$ and $^{21/2+}$ isomeric states in ^{91}Mo excited by pulsed heavy-ion reactions have been measured by the time-differential perturbed γ -ray angular distribution method. The spin precession of these isomers was observed in the hyperfine field of ^{90}Mo isomer implanted into ferromagnetic Ni. The field was calibrated using a ^{90}Mo isomer of known g factor. The results are $g(^{17/2-}) = +0.531(7)$ and $g(^{21/2+}) = +0.839(8)$, which can be well described in the framework of multiparticle shell model states using effective g factors of single particle states and the additivity relation. (6 refs.)

60102 Shell model calculations using modified Sussex matrix elements for $A \leq 4$. M.R.Meder, J.E.Purcell (Dept. of Phys. & Astron., Georgia State Univ., Atlanta, GA, USA). *Phys. Rev. C (USA)*, vol.27, no.4, p.1790-8 (April 1983). The $^3\text{S}_1$ and $^3\text{S}_1\text{-}^3\text{D}_1$ Sussex matrix elements are modified by the addition of the matrix elements of a potential whose radial form is that of a momentum-dependent delta function. The strength parameters of the potential are found by fitting to the binding energy and quadrupole moment of the deuteron. Shell model calculations in a 4 $\hbar\omega$ model space using the modified matrix elements and a size parameter of 1.5 fm give binding energies of 7.55, 6.79, and 27.77 MeV for ^3H , ^3He , and ^4He , respectively. The energies of the negative parity states in ^3He are also calculated using the modified matrix elements in a 5 $\hbar\omega$ model space. It is found that their calculated absolute energies are much improved as compared to calculations using the unmodified matrix elements. The relative energies of these states are not significantly changed by the modifications, as expected. (19 refs.)

60103 An approximate calculation of the energy spectrum for particular angular momentum states. H.G.Miller, H.P.Schroder (Inst. für Theoretische Phys., Univ. Frankfurt, Frankfurt/Main, Germany). *S. Afr. J. Phys. (S. Africa)*, vol.5, no.4, p.97-9 (1982). Configuration-mixing calculations have been performed in Ne^{20} with a small number of unprojected basis states which are energetically the lowest lying solutions of the constrained Hartree-Fock equations with an angular momentum constraint of the form $\langle J^2 \rangle = J(J+1)$. For $J=6$, the spectrum of the lowest lying states, although shifted downward by about 500 keV, approximates reasonably well the exact level spectrum of the lower lying 6^+ states. (8 refs.)

Energy levels of the odd manganese nuclei from the $(d, ^3\text{He})$ reaction See Entry 60104

Muonic X-ray measurement of the monopole and quadrupole charge parameters of $^{154-158,160}\text{Gd}$ See Entry 60105

Nuclear structure of even lead isotopes by the (p,t) reaction See Entry 60109

Levels in ^{148}Ce from the decay of mass separated ^{148}La See Entry 60111

The composite particle representation theory. II. The composite particle approximation See Entry 60118

Neutron and proton matrix elements for low-lying 2^+ transitions and the probe dependence of the nuclear deformation parameter See Entry 60130

$^{113}\text{In}(\gamma,n)$ reaction isomeric and ground-state cross-sections See Entry 60169

Excited-state giant dipole resonances in (p,γ) : a new probe of single-particle strengths See Entry 60178

Gamow-Teller strength in the $^{18}\text{O}(p,n)^{18}\text{F}$ reaction at 135 MeV See Entry 60179

Structure of ^{209}Bi deduced from the $^{208}\text{Pb}(t,2n\gamma)$ reaction See Entry 60185

Microscopic study on di-nucleus states of $^{16}\text{O}+^{40}\text{Ca}$ and $^{40}\text{Ca}+^{40}\text{Ca}$. I See Entry 60191

$^{12}\text{C}(^{16}\text{O},\alpha)^{24}\text{Mg}^*$ reaction in the energy region $E_{\text{c.m.}} = 26.6$ to 42.9 MeV See Entry 60198

Structure in the $^{12}\text{C}+^{12}\text{C}$ and $^8\text{Be}+^{16}\text{O}$ fission width distribution of ^{24}Mg observed via the reaction $^{12}\text{C}(^{16}\text{O},\alpha)^{24}\text{Mg} \rightarrow X+Y$ See Entry 60199

Quantized ATDHF calculations for subbarrier fusion of heavy ions See Entry 60216

21.10D Binding energy and masses

Shell model calculations using modified Sussex matrix elements for $A \leq 4$ See Entry 60102

Beta-decay energies and masses of $^{103-105}\text{In}$ See Entry 60112

Extended folding potential model for Λ -deuteron system with hard core potential See Entry 60128

Bound states in the pion-nucleus velocity-dependent potential See Entry 60210

Quantized ATDHF calculations for subbarrier fusion of heavy ions See Entry 60216

21.10F Shape, charge, radius and form factors

Role of high multipole pairs in the description of deformed nuclei See Entry 60098

The density dependence and the range of effective projectile-nucleon interaction from optical model analysis See Entry 60115

πN p-wave field theoretical separable model See Entry 60116

Neutron and proton matrix elements for low-lying 2^+ transitions and the probe dependence of the nuclear deformation parameter See Entry 60130

Chew-Low model and the potential description of the πN interaction See Entry 60153

Nuclear structure effects in high momentum transfer reactions See Entry 60154

On the normal modes of vibration in light deformed nuclei See Entry 60158

Deformation effects in aligned ^6Li scattering See Entry 60167

21.10H Spin, parity, and isobaric spin

Search for the second excited $11/2^-$ state and weak-coupling scheme in ^{117}Sn See Entry 60096

Shell model calculations using modified Sussex matrix elements for $A \leq 4$ See Entry 60102

A study of the $^{86}\text{Sr}(^3\text{He,t})^{86}\text{Y}$ reaction See Entry 60106

Level structure of the doubly odd nucleus ^{112}In from the $(p,n\gamma)$ reaction See Entry 60107

Nuclear structure of even lead isotopes by the (p,t) reaction See Entry 60109

Parity nonconserving nuclear forces See Entry 60114

Energy and projectile dependence of nuclear alignment in fusion-evaporation reactions See Entry 60129

The decay of Ag-105g See Entry 60131

Absolute strength determinations of dipole transitions and unique spin-parity assignments in ^{52}Cr and ^{56}Fe See Entry 60132

A search on the parity-forbidden alpha width of the $E_x = 4.753$ MeV ($J^\pi = 0^+, 1$) level of ^{18}F See Entry 60145

Observation of parity nonconservation in the integrated γ spectrum from (n,γ) reactions in Cl, Br, Cd, Sn, and La nuclei See Entry 60163

The photodisintegration of ^{40}Ar See Entry 60170

$^{12}\text{C}(^{16}\text{O},\alpha)^{24}\text{Mg}^*$ reaction in the energy region $E_{\text{c.m.}} = 26.6$ to 42.9 MeV See Entry 60198

Spin flip transitions in ^{13}C and ^{19}F probed with the (π^-, γ) reaction See Entry 60208

Stretched excitations and the spin-dependent part of the pion-nucleon interaction See Entry 60209

21.10J Spectroscopic factors

60104 Energy levels of the odd manganese nuclei from the $(d, ^3\text{He})$ reaction. N.G.Puttaswamy, W.Oelert, A.Djaloeis, C.Mayer-Borick, P.Turek (Inst. für Kernphys., KFA, Jülich, Jülich, Germany). *IEEE Trans. Nucl. Sci. (USA)*, vol.30, no.2, p.1140-2 (April 1983). (1982 IEEE Conference on the Application of Accelerators in Research and Industry, Denton, TX, USA, 8-10 Nov. 1982). The $^{54,56,58}\text{Fe}(d,^3\text{He})^{53,55,57}\text{Mn}$ reactions have been studied at a bombarding energy of 80 MeV. Angular distributions have been measured in the range of 6° to 30° lab. Energy levels up to excitation energies of 9.2 MeV, 7.2 MeV, and 7.4 MeV in ^{53}Mn , ^{55}Mn , and ^{57}Mn , respectively, have been studied. DWBA calculations were employed to extract spectroscopic factors. The results concerning negative-parity levels have been compared with shell-model calculations. For the case of ^{55}Mn , a comparison of the distribution of the experimental and the shell-model $f_{7/2}$ strengths has been made. The spectroscopic strengths for $s_{1/2}$ and $d_{3/2}$ pickup are rather well predicted by QPCC and CVM calculations. (12 refs.)

Investigation of isobaric analog resonances in ^{53}Mn See Entry 60159

21.10K Electromagnetic moments

60105 Muonic X-ray measurement of the monopole and quadrupole charge parameters of $^{154-158,160}\text{Gd}$. D.B.Laubacher, Y.Tanaka, R.M.Steffen (Dept. of Phys., Purdue Univ., West Lafayette, IN, USA), E.B.Shera, M.V.Hoehn. *Phys. Rev. C (USA)*, vol.27, no.4, p.1772-89 (April 1983).

Monopole and quadrupole charge distributions of ^{154}Gd , ^{155}Gd , ^{156}Gd , ^{157}Gd , ^{158}Gd , and ^{160}Gd were investigated by muonic-atom K and L X-ray measurements. The model-independent Barrett charge radii R_k and the isotope shifts ΔR_k were measured, and values of $\langle r^2 \rangle$ and $\Delta \langle r^2 \rangle$ were deduced. A pronounced even-odd staggering effect of the nuclear charge radii was observed for the series $^{156-158}\text{Gd}$. The quadrupole moments of the first excited states of the even-A Gd nuclei were determined to be $Q^{154}(2^+) = -1.82(4)$ e b, $Q^{156}(2^+) = -1.93(4)$ e b, $Q^{158}(2^+) = -2.01(4)$ e b, and $Q^{160}(2^+) = -2.08(4)$ e b, and the quadrupole moments of the $3/2^-$ ground states of the odd-A $^{155,157}\text{Gd}$ nuclei were determined to be $Q^{155}(3/2^-) = 1.27(3)$ e b and $Q^{157}(3/2^-) = 1.35(3)$ e b. Comparison with a separate measurement of the odd-A ground-state quadrupole moments based on the static hyperfine splitting of the muonic M X-rays showed that the model error in the extracted quadrupole moments of these nuclei is less than 2 per cent. The quadrupole moments and the $B(E2)$ values obtained in the present experiment for the low-lying Gd states are in satisfactory agreement with the axially symmetric rotational model. However, the ^{157}Gd nucleus exhibits a considerable softness as indicated by the isomer shift of the 2^+ excited state and by the experimental value of the ratio $Q(2^+)/B(E2:0^+ \rightarrow 2^+)$. (27 refs.)

Nuclear g factors of the $^{17/2-}$ and $^{21/2+}$ isomeric states of ^{91}Mo See Entry 60101

The understanding of nuclear structure through Mossbauer experiments See Entry 62843

21.10M Level density and structure

60106 A study of the $^{86}\text{Sr}(^3\text{He,t})^{86}\text{Y}$ reaction. C.A.Fields, J.J.Kraushaar, R.A.Ristinen, E.Sugarbaker (Dept. of Phys., Univ. of Colorado, Boulder, CO, USA).

Nucl. Phys. A (Netherlands), vol.A398, no.3, p.434-44 (2 May 1983). Low-lying levels of ^{86}Y have been investigated using the $^{86}\text{Sr}(^3\text{He,t})$ reaction at 42.8 MeV. J^π values or limits were assigned to 20 of the 23 levels observed below 1.5 MeV through the use of collective DWBA calculations or experimental $(^3\text{He,t})$ reaction systematics. The particle-hole structure of ^{86}Y is discussed on the basis of these data and the shell model. (25 refs.)

60107 Level structure of the doubly odd nucleus ^{112}In from the $(p,n\gamma)$ reaction. T.Kohn, M.Adachi, H.Taketani (Dept. of Appl. Phys., Tokyo Inst. of Technol., Tokyo, Japan).

Nucl. Phys. A (Netherlands), vol.A398, no.3, p.493-511 (2 May 1983). Properties of the levels in ^{112}In have been studied with the reaction $^{112}\text{Cd}(p,n\gamma)^{112}\text{In}$. The level scheme of ^{112}In below 1300 keV was constructed from the γ -ray excitation functions and $\gamma\gamma$ coincidences. In ^{112}In , 22 excited states were observed and spins and parities of 8 excited states were newly assigned or restricted by comparing the measured angular distributions and linear polarizations of the decaying γ -rays as well as the excitation functions of the residual levels with the predictions of the statistical compound nucleus model. Possible configurations of the low-lying levels are discussed in terms of their decay properties and the systematics of the excited states in the neighbouring doubly odd In isotopes. (15 refs.)

60108 Level density and shell structure: Rosenzweig model revisited. T.Tsukamoto (Dept. of Phys., Tohoku Univ., Sendai, Japan). *Prog. Theor. Phys. (Japan)*, vol.69, no.1, p.344-7 (Jan. 1983).

The exact number of states $C_2(N, E)$ for the Rosenzweig model is computed for $1 \leq g \leq 15$, $1 \leq N \leq 50$ and $E \leq 400$. An approximate (not asymptotic) formula is obtained by numerical fit. It is suggested that the driving force governing mass transfer has little to do with the shell structure. (12 refs.)

60109 Nuclear structure of even lead isotopes by the (p,t) reaction. M.Takahashi, T.Murakami, S.Morita (Dept. of Phys., Tohoku Univ., Sendai, Japan), H.Orihara, Y.Ishizaki, H.Yamaguchi. *Phys. Rev. C (USA)*, vol.27, no.4, p.1454-73 (April 1983).

The $^{208,206,204}\text{Pb}(p,t)^{206,204,202}\text{Pb}$ reactions have been studied at an incident energy of 51.9 MeV. With the aid of distorted-wave Born approximation calculations a number of spin and parity assignments were made. Systematic trends were observed in the experimental excitation energy of individual levels in the residual nuclei and transition strengths for three reactions. These results are compared with predictions from the shell-model wave functions. The overall agreement is satisfactory. (22 refs.)

60110 Excited states of ^{96}Ru . T.A.Walkiewicz (Edinboro State Coll., Edinboro, PA, USA), S.Raman, J.B.McGrory. *Phys. Rev. C (USA)*, vol.27, no.4, p.1710-23 (April 1983).

The nuclear excited states of ^{96}Ru were studied by means of the decays of 9.25-min and 1.55-min ^{96}Rh isomers, and the $^{93}\text{Nb}(^6\text{Li}, 3n\gamma)$ reaction. Approximately 140 γ -rays measured in these experiments were incorporated into a level scheme consisting of approximately 50 excited states. The experimental level scheme is compared with a level scheme calculated on the basis of the shell model. (14 refs.)

60111 Levels in ^{148}Ce from the decay of mass separated ^{148}La . R.L.Gill, M.Shmid, R.E.Chrien, Y.Y.Chu (Brookhaven Nat. Lab., Upton, NY, USA), A.Wolf, D.S.Brenner, K.Sistemich, F.K.Wohn, H.Yamamoto, C.Chung, W.B.Walters. *Phys. Rev. C (USA)*, vol.27, no.4, p.1732-44 (April 1983).

The level scheme of ^{148}Ce populated by β decay of ^{148}La , produced in thermal neutron fission of ^{235}U , has been studied. Ion beams of mass 148 were separated by an online isotope separator and deposited on a movable tape. Gamma-ray singles, γ - γ time, γ - γ angular correlations, and time sequenced γ and β spectra were collected. The half-life for ^{148}La was measured to be 1.05 ± 0.01 s. A level scheme for ^{148}Ce is presented including several members of the ground, β , γ , and octupole bands. The resulting level scheme has been compared with other $N=90$ nuclides and with interacting-boson-approximation-2 calculations. (32 refs.)

60112 Beta-decay energies and masses of $^{103-105}\text{In}$. J.M.Wouters, H.M.Thiersen, J.Aysto, M.D.Cable, P.E.Haustein, R.F.Parry, J.Cerny (Dept. of Chem., Univ. of California, Berkeley, CA, USA).

Phys. Rev. C (USA), vol.27, no.4, p.1745-53 (April 1983). Decay energies of $^{103-105}\text{In}$ have been determined by β - γ coincidence spectroscopy on sources obtained from an online mass separator. Comparisons of the measured decay energies and deduced masses are made with the predictions of several different theoretical models. The ^{103}In mass is found to be more bound by 1 MeV than predicted by most models, which reproduce adequately the masses of the heavier indium isotopes. Systematic trends of the masses and neutron separation energies of the indium isotopes between the closed $N=50$ and 82 shells are presented. (30 refs.)

60113 Cluster (quadrupole-octupole) phonon model: application to ^{89}Y . C.A.Heras (Dept. de Fisica, Univ. de Oriente, Cumana, Venezuela), S.M.Abecasis. *Phys. Rev. C (USA)*, vol.27, no.4, p.1765-71 (April 1983).

A cluster-phonon model is proposed for odd-mass nuclei to describe simultaneously positive- and negative-parity states, in which octupole as well as quadrupole vibrations of the core are allowed. The cluster states include one-particle and two-particle-one-hole excitations. The residual interaction is of the quadrupole-quadrupole plus pairing type. The model is applied to ^{89}Y , whose energy levels, eigenvectors, spectroscopic factors, and electromagnetic properties are computed and compared with experiment. (16 refs.)

Energy levels of the odd manganese nuclei from the (d, ^3He) reaction See Entry 60104

The decay of Ag-105g See Entry 60131

Separable expansions for virtual states and resonances See Entry 60155

Observation of analog and nonanalog transitions in the reaction $^{56}\text{Fe}(\pi^+, \pi^-)^{56}\text{Ni}$ See Entry 60202

Diffraction theory and the double-charge-exchange reaction $^{18}\text{O}(\pi^+, \pi^-)^{18}\text{Ne}$ See Entry 60207

Bound states in the pion-nucleus velocity-dependent potential See Entry 60210

Pion single and double charge exchange in the resonance region: dynamical corrections See Entry 60211

The understanding of nuclear structure through Mossbauer experiments See Entry 62843

21.30 NUCLEAR FORCES

(see also 13.75C Nucleon-nucleon interactions)

60114 Parity nonconserving nuclear forces. E.G.Adelberger. *Comments Nucl. & Part. Phys. (GB)*, vol.11, no.5, p.189-201 (1983).

Recent experimental and theoretical progress in studies of the parity-nonconserving weak NN force is described. Emphasis is placed on results from the two-nucleon system and from simple parity-mixed doublets in light nuclei. (20 refs.)

60115 The density dependence and the range of effective projectile-nucleon interaction from optical model analysis. D.K.Srivastava, D.N.Basu, N.K.Ganguly (Variable Energy Cyclotron Centre, Calcutta, India). *Phys. Lett. B (Netherlands)*, vol.124B, no.1-2, p.6-10 (21 April 1983).

The relations between the geometries of density distributions and potentials obtained by folding these with density dependent forces have been used to obtain empirical estimates of the range and the density dependence of effective proton-, deuteron-, helion-, and alpha-nucleon interactions, from best fit phenomenological optical potentials available in literature, for these projectiles. (23 refs.)

60116 π N p-wave field theoretical separable model. K.Nakano (Theoretische Kernphys., Univ. Hamburg, Hamburg, Germany). *Phys. Rev. C (USA)*, vol.27, no.4, p.1401-4 (April 1983).

A numerically self-consistent solution for the recently proposed field theoretical π N p-wave separable model was found by the method of singular integral equations. The method of solution and form factors are presented. (9 refs.)

60117 Relativistic shell model: momentum-transfer dependence of the effective force in nuclei. L.S.Celenza, W.S.Pong, C.M.Shakin (Dept. of Phys., City Univ. of New York, New York, NY, USA).

Phys. Rev. C (USA), vol.27, no.4, p.1799-806 (April 1983).

The authors calculate the momentum-transfer dependence of the effective nuclear interaction in a conventional model and in a recently developed relativistic model which emphasises self-consistent-field effects. These latter effects lead to major modifications in the $T=0$ interaction for $S=0$ and $S=1$ and less dramatic changes for the $T=1$ interaction. The calculational methods are similar to those used previously and involve considering only the first iteration of the self-consistent field equations. They review these methods of calculation and present some new results for the (off-shell) nucleon self-energy. (12 refs.)

The composite particle representation theory. II. The composite particle approximation See Entry 60118

Atomic final-state interactions in tritium decay See Entry 60142

Separable expansions for virtual states and resonances See Entry 60155

Special features of the alpha induced deuteron breakup See Entry 60182

Bound states in the pion-nucleus velocity-dependent potential See Entry 60210

Effect of the neutron $^3\text{P}_2$ pairing on the π^0 condensation threshold in neutron star matter See Entry 64505

21.40 FEW-NUCLEON SYSTEMS

60118 The composite particle representation theory. II. The composite particle approximation. Cheng-li Wu (Phys. Dept., Jilin Univ., Changchun, China), Da huan Feng. *Commun. Theor. Phys. (China)*, vol.2, no.1, p.811-27 (1983).

For pt.I see *ibid.*, vol.6, p.705 (1982). A method of solving the many-body problem, known as the composite particle approximation, is proposed. It is shown that a many-body system can be simplified to a composite particle system (plus one or more uncorrelated basic particles), if the binding energies of the composite particles are much larger than the excitation energies of the system, and there is domination of the collective mode for the composite particles. The interactions between the composite particles, as well as the interaction between composite and basic particles, can be evaluated from the original particle-particle interactions. Applications of this theory are indicated. (8 refs.)

Shell model calculations using modified Sussex matrix elements for $A \leq 4$ See Entry 60102

Extended folding potential model for Λ -deuteron system with hard core potential See Entry 60128

$1/2^+ \rightarrow 1/2^+$ beta decay with neutrino mass effects in the elementary particle treatment of weak interactions See Entry 60141

21.60 NUCLEAR-STRUCTURE MODELS AND METHODS

(for hadronic atoms and molecules, see 36.10)

60119 Mesons and quarks in nuclear physics. D.S.Koltun. *Comments Nucl. & Part. Phys. (GB)*, vol.11, no.4, p.171-88 (1983).

The discovery of quark degrees of freedom in elementary particles and the concurrent theoretical developments have changed the picture of strong interactions and of the internal structure of the baryons. It is to be expected that these changes will also affect the understanding of nuclei at the subnucleon level, which have previously been the domain of meson theory. The author provides a brief introductory survey, contrasting the role of mesons and quarks in nuclei. (31 refs.)

60120 New class of supersymmetry in nuclei. A.B.Balantekin (Wright Nuclear Structure Lab., Yale Univ., New Haven, CT, USA), I.Bars, R.Bijker, F.Iachello. *Phys. Rev. C (USA)*, vol.27, no.4, p.1761-4 (April 1983).

The authors suggest that a new class of supersymmetry may occur in nuclei. They construct energy formulas and classification schemes for two specific cases of this class. With this addition, supersymmetry considerations may be extended to many nuclei, thus providing a useful tool to analyze the corresponding spectra. (14 refs.)

The composite particle representation theory. II. The composite particle approximation See Entry 60118

A mathematical approach to the nuclear-matter problem See Entry 60127

Extended folding potential model for Λ -deuteron system with hard core potential See Entry 60128

The theorem of Ehrenfest in the theory of direct radiative transitions between unbound states See Entry 60135

21.60C Shell model

Nuclear g factors of the $17/2^-$ and $21/2^+$ isomeric states of ^{91}Mo See Entry 60101

Shell model calculations using modified Sussex matrix elements for $A \leq 4$ See Entry 60102

Energy levels of the odd manganese nuclei from the (d, ^3He) reaction See Entry 60104

A study of the $^{86}\text{Sr}(^3\text{He}, t)^{86}\text{Y}$ reaction See Entry 60106

Level density and shell structure: Rosenzweig model revisited See Entry 60108

Nuclear structure of even lead isotopes by the (p,t) reaction See Entry 60109

Excited states of ^{96}Ru See Entry 60110

Relativistic shell model: momentum-transfer dependence of the effective force in nuclei See Entry 60117

Search for M1 strength in ^{51}V and the difference in $^{51}\text{V}(e, e')$ and $^{51}\text{V}(p, p')$ spectra See Entry 60133

Nuclear structure effects in high momentum transfer reactions See Entry 60154

Microscopic study on di-nucleus states of $^{16}\text{O} + ^{40}\text{Ca}$ and $^{40}\text{Ca} + ^{40}\text{Ca}$. I See Entry 60191

Spin flip transitions in ^{13}C and ^{19}F probed with the (π^-, γ) reaction See Entry 60208

21.60E Collective models

60121 Microscopic study of the interaction between like bosons in IBM-2. I. Allart (Natuurkundig Lab., Vrije Univ., Amsterdam, Netherlands), G. Bonsignori.

Phys. Lett. B (Netherlands), vol.124B, no.1-2, p.1-5 (21 April 1983).
Using the microscopic two-broken-pair model, the authors studied the interaction between neutron bosons in IBM-2 for the $54 \leq N \leq 78$ region. They demonstrate that the empirically observed attraction between d-bosons in the middle of the shell, especially when they couple to $J=0$, is due to large fractions of S'-pair structure in the two-D-pair states. This results is independent of whether one employs a particle-pair, hole-pair or particle-hole pair approach. They suggest that it is worth while to include the seniority changing parameters $\nu \sim 0$ and $\nu \sim 2$ in phenomenological IBM-2 fits nuclei near the edges of the shell. (14 refs.)

60122 The path integral approach for the nuclear collective motion. D. Galetti, S.S. Mizrahi, B.M. Pimentel (Istituto di Fisica Teorica, Sao Paulo, Brazil).

Phys. Scr. (Sweden), vol.27, no.2, p.72-6 (Feb. 1983).
A procedure is developed for treating a nuclear collective motion via the path integral formalism by defining a collective propagator in the 'phase space' of the collective subspace. This collective subspace is projected out of the full many-body Hilbert space by an approach of the Generator Coordinate Method. Under the approximation of quadratic 'momentum' dependence the authors write the propagator in the coordinate representation from which may derive the collective Schrodinger equation in terms of a canonical pair P and Q . (22 refs.)

The composite particle representation theory. I. The composite particle representation transformation See Entry 59911

Mean distribution of single-particle levels in thin-skinned potential wells and the macroscopic level density parameters of nuclei See Entry 60097

Role of high multipole pairs in the description of deformed nuclei See Entry 60098

On the pairing field in nuclei See Entry 60100

Muonic X-ray measurement of the monopole and quadrupole charge parameters of $^{154}\text{Sm}^{160}\text{Cd}$ See Entry 60105

A study of the $^{86}\text{Sr}(^3\text{He},t)^{86}\text{Y}$ reaction See Entry 60106

Levels in ^{140}Ce from the decay of mass separated ^{148}La See Entry 60111

A Jacobi equation on the coset manifold $SO(2N)/U(N)$ and the quasi-particle RPA equation See Entry 60123

On the normal modes of vibration in light deformed nuclei See Entry 60158

The photodisintegration of ^{40}Ar See Entry 60170

Gamow-Teller strength in the $^{18}\text{O}(p,n)^{18}\text{F}$ reaction at 135 MeV See Entry 60179

Microscopic study on di-nucleus states of $^{16}\text{O}+^{40}\text{Ca}$ and $^{40}\text{Ca}+^{40}\text{Ca}$. I See Entry 60191

Giant resonance excitation in the $^{27}\text{Al}(^6\text{Li},^4\text{He})^{27}\text{Si}$ reaction at 93 MeV See Entry 60196

$^{12}\text{C}(^{16}\text{O},\alpha)^{24}\text{Mg}^*$ reaction in the energy region $E_{\text{cm}} = 26.6$ to 42.9 MeV See Entry 60198

Structure in the $^{12}\text{C}+^{12}\text{C}$ and $^8\text{Be}+^{16}\text{O}$ fission width distribution of ^{24}Mg observed via the reaction $^{12}\text{C}(^{16}\text{O},\alpha)^{24}\text{Mg}-X+Y$ See Entry 60199

21.60F Models based on group theory

60123 A Jacobi equation on the coset manifold $SO(2N)/U(N)$ and the quasi-particle RPA equation. S. Nishiyama (Dept. of Phys., Kochi Univ., Kochi, Japan).

Prog. Theor. Phys. (Japan), vol.69, no.1, p.100-12 (Jan. 1983).
Studies the variational properties of the action functional appeared in the time-dependent Hartree-Bogoliubov (TDHB) theory. Through the calculus of the second variation on the coset manifold $SO(2N)/U(N)$, the Jacobi equation is obtained. Assuming the periodic Jacobi field the author derives in a natural way the equation for the quasi-particle random phase approximation (RPA) describing the collective excitation around certain static HB fields. The present method of obtaining the $SO(2N)$ RPA may be useful to get the $SO(2N+1)$ RPA. (13 refs.)

Role of high multipole pairs in the description of deformed nuclei See Entry 60098

Microscopic study of the interaction between like bosons in IBM-2 See Entry 60121

21.60G Cluster models

Some special $SU(3) \supset R(3)$ Wigner coefficients and their application See Entry 59612

Cluster (quadrupole-octupole) phonon model: application to ^{89}Y See Entry 60113

Deformation effects in aligned ^6Li scattering See Entry 60167

Liquid-gas phase instabilities in nuclear systems See Entry 60193

Q-value systematics applied to the absorption of mesons on complex nuclei See Entry 60212

21.60J Hartree-Fock and random-phase approximations

60124 Classical and quantum mechanical aspects of time-dependent Hartree-Fock trajectories. T. Suzuki (Niels Bohr Inst., Univ. of Copenhagen, Copenhagen, Denmark).

Nucl. Phys. A (Netherlands), vol.A398, no.3, p.557-96 (2 May 1983).
In terms of a quantum mechanical representation based on Slater determinants, classical and quantum mechanical aspects of TDHF trajectories are investigated. The invariant integration measure of the determinantal representation is obtained in a general closed form. Phase space structures of the TDHF equation and its solutions are discussed on this basis. The formal classical structures provide a way of finding a semiclassical expression for the quantum mechanical propagator, into which the superposition principle among TDHF trajectories is incorporated. General properties of the semiclassical propagator such as the time translation/reversal symmetry, unitarity, etc. are studied. Two simple Hamiltonian systems are employed as examples which exhibit analytical solutions for the propagator. To illustrate the effects of

superposition of TDHF paths, a system of interacting two-level nuclei is numerically studied and a comparison with the exact result is made. (59 refs.)

An approximate calculation of the energy spectrum for particular angular momentum states See Entry 60103

A Jacobi equation on the coset manifold $SO(2N)/U(N)$ and the quasi-particle RPA equation See Entry 60123

Transition densities for charge-exchange components of giant isovector resonances and the proton-neutron density distributions in nuclei See Entry 60136

Cross section calculations for nucleon- ^{40}Ca and α - ^{40}Ca elastic scattering from microscopic nonlocal optical potentials See Entry 60180

Quantized ATDHF calculations for subbarrier fusion of heavy ions See Entry 60216

21.65 NUCLEAR MATTER

60125 Properties of quark matter governed by quantum chromodynamics. I. The screened charge. V. Soni (Dept. of Theoretical Phys., Univ. of Madras, Madras, India).

Nucl. Phys. B, Part. Phys. (Netherlands), vol.B216, no.1, p.244-66 (25 April 1983).

A genuine screened charge (coupling) is constructed for quark matter, subject to a flavour constraint, governed by quantum chromodynamics. This is achieved by working in the Coulomb gauge, and using an unambiguous renormalization prescription (formulated in terms of the Lie differential equations) to overcome the problems of the previous attempts. Since one must standardize with the vacuum QCD running (experimental) coupling constant at some asymptotic spacelike momentum transfer, $|p_0|$, it is ensured that the matter contribution is negligible at this point by the condition, $\mu \ll |p_0|$, where μ is the matter (flavour) chemical potential. The screened charge (coupling) has the expected property of merging with the vacuum QCD running coupling constant in the ultraviolet ($p^2 \rightarrow \infty$) and going to zero in the infrared ($p^2 \rightarrow 0$), indicative of complete screening above a critical value of μ . The critical length scale at which the screened charge diverges is well below the vacuum QCD scale length and screening always renders the screened charge smaller than its vacuum QCD counterpart. This gives greater access to the long-distance phenomena besides providing a better expansion parameter for perturbative calculations. The richer physical content of the screened charge is pointed out. The quark mass is included and taken to be renormalized on-shell. (11 refs.)

60126 Properties of quark matter governed by quantum chromodynamics. II. Renormalization schemes in quark matter. V. Soni (Dept. of Theoretical Phys., Univ. of Madras, Madras, India).

Nucl. Phys. B, Part. Phys. (Netherlands), vol.B216, no.1, p.267-76 (25 April 1983).

For pt.I see ibid., vol.216, no.1, p.244-66 (1983). Renormalization schemes are examined (in the Coulomb gauge) for quantum chromodynamics in the presence of quark matter. The author demands that the effective coupling constant for all schemes become congruent with the vacuum QCD running coupling constant as the matter chemical potential, μ , goes to zero. Also, to enable one to standardize with the vacuum QCD running coupling constant at some asymptotic momentum transfer, $|p_0|$, the author keeps $\mu \ll |p_0|$, to ensure that the matter contribution is negligible at this point. This means all schemes merge with vacuum QCD at $|p_0|$ and beyond. Two renormalization group invariants are shown to emerge: (i) the effective or invariant charge, g_{inv} , which is, however, scheme dependent and (ii) $g^2(M)/S(M)$, where $S(M)^{-1}$ is the Coulomb propagator, which is scheme independent. The only scheme in which g_{inv}^2 is scheme independent and identical to $g^2(M)/S(M)$ is the screened charged scheme characterised by the normalization of the entire Green function, S^{-1} , to unity. It is concluded that this is the scheme to be used if one wants to identify with the experimental effective coupling in perturbation theory. However, if one does not restrict to perturbation theory all schemes should be allowed. Although the author discusses matter QCD in the Coulomb gauge, the above considerations are quite general to gauge theories in the presence of matter. (3 refs.)

60127 A mathematical approach to the nuclear-matter problem. C. Villi (Istituto di Fisica, Univ. di Padova, Padova, Italy).

Nuovo Cimento A (Italy), vol.74A, ser.2, no.1, p.37-116 (1 March 1983).
Outlines a mathematical scheme for the description of the overall behaviour of infinite nuclear matter: it has been conceived with the pragmatic purpose of providing simple tools for carrying out realistic numerical calculations. To this end the author revives some insufficiently explored aspects of vintage theories, which seem to have been by-passed by recent theoretical developments. (64 refs.)

Effect of the neutron 3P_2 pairing on the π^0 condensation threshold in neutron star matter See Entry 64505

21.80 HYPERNUCLEI

60128 Extended folding potential model for Λ -deuteron system with hard core potential. K. Hasegawa, Y. Yamamoto, H. Bando (Div. of Math. Phys., Fukui Univ., Fukui, Japan).

Prog. Theor. Phys. (Japan), vol.69, no.1, p.171-80 (Jan. 1983).
An extended folding potential model for the Λ -d system is proposed to treat both the bound state and scatterings within the same framework by using hard core potentials. This model is derived by a variational method to take into account interparticle correlations. The Λ -d scattering length and the binding energy of $^{\Lambda}\text{H}$ are calculated with the effective central potential proposed by Dalitz et al. (1972). The present model is proved advantageous not only in handling hard core potentials but also in visualizing the physical structure of the Λ -d system. (9 refs.)

23.00 RADIOACTIVITY AND ELECTROMAGNETIC TRANSITIONS

(see also 82.55 Radiochemistry)

23.20 ELECTROMAGNETIC TRANSITIONS

60129 Energy and projectile dependence of nuclear alignment in fusion-evaporation reactions. V.Zobel, L.Cleeman, J.Eberth, T.Heck, K.Husing, W.Neumann, M.Nolte (Inst. fur Kernphys., Univ. zu Koln, Koln, Germany). *Nucl. Instrum. & Methods Phys. Res. (Netherlands)*, vol.207, no.3, p.389-94 (1 April 1983).

Nuclear alignment attenuation coefficients of excited levels in ^{67}Ga have been measured via the reactions $^{64}\text{Zn}+\alpha$ and $^{51}\text{Fe}+^{12}\text{C}$ for incident energies between 9 and 22 MeV and 32 and 48 MeV, respectively. The data were deduced from angular distributions of four pure electric quadrupole transitions in ^{67}Ga . For the heavy-ion induced reaction a slight decrease of alignment with incident energy has been observed while there is a strong energy dependence of nuclear alignment for the α -induced reaction due to the feeding mechanism. The attenuation coefficients are consistent with the Gaussian magnet substate population hypothesis except where direct and cascade feeding compete with comparable intensities. (10 refs.)

60130 Neutron and proton matrix elements for low-lying 2^+ transitions and the probe dependence of the nuclear deformation parameter. A.M.Bernstein, V.R.Brown, V.A.Madsen.

Comments Nucl. & Part. Phys. (GB), vol.11, no.5, p.203-15 (1983). It is shown that the ratio of multiple matrix elements M_n and M_p of neutrons and protons in the nucleus is not simply proportional to N/Z as in the homogeneous collective model but depends on the shell structure of the nucleus. Correspondingly, the deformation parameter for nuclear neutrons is in general different from that of protons. This difference results in a dependence of the measured deformation parameter δ for a given transition on the external field which produces it. The systematics of M_n/M_p for single-closed shell and the external field dependence of δ is demonstrated for the low-lying collective 2^+ transitions. (19 refs.)

60131 The decay of Ag-105g. Jasbir Singh, M.L.Garg, Ravinder Kaur, S.S.Sooch, Nirmal Singh, P.N.Trehan (Dept. of Phys., Panjab Univ., Chandigarh, India).

IEEE Trans. Nucl. Sci. (USA), vol.ns-30, no.2, p.1143-5 (April 1983). (1982 IEEE Conference on the Application of Accelerators in Research and Industry, Denton, TX, USA, 8-10 Nov. 1982).

The level structure of Pd-105 has been studied from the decay of Ag-105g. The energies and intensities of 50 gamma rays have been precisely measured using a 64.1 CC Ge(Li) detector (FWHM=2.1 keV at 1.33 MeV). The gamma ray singles spectrum measurements confirm the existence of the 158.93, 167.5, 202.17, 216.11, 382.5, 486.65, 576.64, 583.01, 844.34, 860.20, 921.23, 929.01 and 1124.90 keV gamma rays in the decay of Ag-105g. However, the 270.5, 564.39, 580.13, 610.0, 640.5, 709.8, 768.9 and 796.25 keV weak transitions reported by earlier workers could not be observed in the present investigations. Also the γ - γ directional correlation coefficients for 7 cascades in Pd-105 have been measured. Out of these, the 361-(447)-280 and 807-280 keV cascades have been attempted for the first time. From these correlation measurements spin value of $1/2^+$ has been confirmed for the 673.03 keV level. Also these measurements have been used to deduce the multipole mixing ratios of seven transitions in Pd-105. (12 refs.)

60132 Absolute strength determinations of dipole transitions and unique spin-parity assignments in ^{52}Cr and ^{56}Fe . P.B.Smith, W.Segeth (Lab. voor Algemene Natuurkunde, Univ. of Groningen, Groningen, Netherlands).

Nucl. Phys. A (Netherlands), vol.A398, no.3, p.397-407 (2 May 1983). Two strong levels at 9.14 MeV in ^{52}Cr and ^{56}Fe have been excited by resonance fluorescence with linearly polarized mono-energetic gamma rays. Both decay to the ground state with essentially 100% probability. The azimuthal and polar asymmetry of the resonance-scattered radiation lead to unique spin-parity assignments of $J^\pi=1^+$ and $J^\pi=1^-$ for the ^{52}Cr and ^{56}Fe levels, respectively. Resonance absorption measurements lead to absolute determination of the ground-state transition strengths. (9 refs.)

60133 Search for M1 strength in ^{51}V and the difference in $^{51}\text{V}(e,e')$ and $^{51}\text{V}(p,p')$ spectra. D.Bender, G.Eulenberg, A.Richter, E.Spamer (Inst. fur Kernphys., Tech. Hochschule Darmstadt, Darmstadt, Germany), B.C.Metsch, W.Knupper.

Nucl. Phys. A (Netherlands), vol.A398, no.3, p.408-14 (2 May 1983). Following the studies of the distribution of M1 strength in the even-even $N=28$ isotones ^{48}Ca , ^{50}Ti , ^{52}Cr and ^{54}Fe by inelastic electron scattering, the result of a search for M1 transitions in the odd-even $N=28$ nucleus ^{51}V is reported. No strong M1 excitation has been detected, in contrast to a recent (p,p') experiment. There is no immediate explanation for this discrepancy. Shell-model calculations indicate that a part of it might be accounted for by an interference between the spin and orbital terms of the electromagnetic transition operator in the (e,e') experiment. (9 refs.)

60134 A study of the $^{84}\text{Kr}(a,2n)^{86}\text{Sr}$ reaction. C.A.Fields, F.W.N.De Boer (Dept. of Phys., Univ. of Colorado, Boulder, CO, USA), J.Sau.

Nucl. Phys. A (Netherlands), vol.A398, no.3, p.512-24 (2 May 1983). Decay properties of levels of ^{86}Sr populated by the $^{28}\text{MeV } ^{84}\text{Kr}(a,2n\gamma)$ reaction have been studied by in-beam γ -ray spectroscopy. The observation of several new levels with $J^\pi \geq 6$ allows a detailed comparison of the $2p$ - $2n$ structures of ^{86}Sr with those of neighboring $N=48$ nuclei. The results are discussed in terms of the weak-coupling model. (20 refs.)

60135 The theorem of Ehrenfest in the theory of direct radiative transitions between unbound states. V.A.Pluyko, V.A.Poyarkov (Kiev State Univ., Kiev, USSR).

Phys. Lett. B (Netherlands), vol.123B, no.6, p.373-4 (14 April 1983). The validity of Ehrenfest's theorem in the theory of radiative transitions between unbound states is proved in the calculation of probability amplitudes. (6 refs.)

60136 Transition densities for charge-exchange components of giant isovector resonances and the proton-neutron density distributions in nuclei. N.Auerbach (Los Alamos Nat. Lab., Los Alamos, NM, USA), A.Klein.

Phys. Rev. C (USA), vol.27, no.4, p.1818-21 (April 1983). Sum rules that hold in the case of a self-consistent charge-exchange random-phase approximation theory are used here to derive transition densities for the charge-exchange components of isovector giant resonances. The derived transition densities are then employed in a calculation of (π^+, π^0) cross sections. (15 refs.)

60137 Level structure of ^{109}Ag from studies of the decay of ^{109}Pd . C.Dednam, D.W.Mingay (Phys. Div., Nuclear Dev. Corp. of South Africa, Pretoria, S Africa).

S. Afr. J. Phys. (S. Africa), vol.5, no.4, p.100-10 (1982). The energy levels of ^{109}Ag , populated in the decay of ^{109}Pd ($T_{1/2}=13.45$ h), have been studied by means of high-resolution Ge(Li) detectors using both time-dependent singles and coincidence gamma-ray detection techniques. Generally good agreement with previous measurements was obtained in terms of the energy levels and decay scheme of ^{109}Ag , with the exception of the 697- and 811-keV levels originally proposed by El Bedewi et al. (1975). These are shown to have arisen as a result of the misidentification of transitions. The resultant energy level diagram and branching ratios deduced are presented. The half-life of ^{109}Pd was measured as 13.45 ± 0.02 h. (27 refs.)

Selective population of high-j states via heavy-ion induced transfer reactions ... See Entry 60095

On the pairing field in nuclei See Entry 60100

An approximate calculation of the energy spectrum for particular angular momentum states See Entry 60103

Level structure of the doubly odd nucleus ^{112}In from the (p,n γ) reaction See Entry 60107

Excited states of ^{96}Ru See Entry 60110

V1343 Aquilae See Entry 64492

23.20C Lifetimes and transition probabilities

Reduction of the neutron-induced background using a pulse-type beam chopper in an ISOL experiment See Entry 60504

23.40 BETA DECAY; ELECTRON AND MUON CAPTURE

60138 Calorimetric redetermination of the half-life of ^{90}Sr . H.Ramthun (Phys.-Tech. Bundesanstalt, Braunschweig, Germany).

Nucl. Instrum. & Methods Phys. Res. (Netherlands), vol.207, no.3, p.445-8 (1 April 1983). Measurements of the heat power of a sealed $^{90}\text{Sr}+^{90}\text{Y}$ source carried out over a period of 19 years yielded a half-life $T_{1/2}=28.99 \pm 0.25$ a. A description is given of the source, the calorimeter and the evaluation method used. (11 refs.)

60139 Final state branching ratio in the ^7Be decay. D.P.Balamuth, L.Brown, T.E.Chapuran, J.Klein, R.Middleton, R.W.Zurmuhle (Dept. of Phys., Univ. of Pennsylvania, Philadelphia, PA, USA).

Phys. Rev. C (USA), vol.27, no.4, p.1724-7 (April 1983). The fractional decay branch in the EC decay of ^7Be leading to the first excited state of ^7Li has been measured. ^7Be ions from a beam produced by a tandem Van de Graaff accelerator were implanted into a surface-barrier detector; the decay γ -rays were then counted using a well-shielded Ge(Li) detector of known absolute efficiency. The resulting decay branch, $(10.10 \pm 0.45)\%$, is in good agreement with previously published values and in strong disagreement with a recent measurement. (14 refs.)

60140 ^7Be decay scheme and the solar neutrino problem. E.B.Norman, T.E.Chupp, K.T.Lesko, J.L.Osborne (Nuclear Phys. Lab., Univ. of Washington, Seattle, WA, USA), P.J.Grant, G.L.Woodruff.

Phys. Rev. C (USA), vol.27, no.4, p.1728-31 (April 1983). The decay scheme of ^7Be has been reinvestigated. Known numbers of ^7Be nuclei were produced in targets via the $^7\text{Li}(p,n)$ reaction. Following activation, the yields of 478-keV γ -rays from the targets were measured. From three such measurements, performed at different bombarding energies, the ^7Be decay branching ratio to the first excited state of ^7Li has been determined to be $10.8 \pm 0.4\%$. The implications of this result for the solar neutrino problem are discussed. (26 refs.)

60141 $1/2^+ \rightarrow 1/2^+$ beta decay with neutrino mass effects in the elementary particle treatment of weak interactions. Chong-en Wu (Guangxi Univ., Nanning, China), W.W.Repko.

Phys. Rev. C (USA), vol.27, no.4, p.1754-60 (April 1983). The authors compute the effect of a nonvanishing neutrino mass on the electron spectrum of tritium beta decay using the elementary particle treatment of weak interactions. Coulomb corrections are taken into account in this formalism, as are the effects of weak magnetism and nuclear recoil. The effect of a mixture of excited atomic final states is also discussed. These corrections combine to make small changes in the shape of the end point, which could be important in determinations of the neutrino mass. (9 refs.)

60142 Atomic final-state interactions in tritium decay. R.D.Williams, S.E.Koonin (W.K. Kellogg Radiation Lab., California Inst. of Technol., Pasadena, CA, USA).

Phys. Rev. C (USA), vol.27, no.4, p.1815-17 (April 1983). The authors calculate the effect of the Coulomb interaction of the ejected β ray with the bound atomic electron in the β decay of a tritium atom. The excited state probabilities of the residual helium ion are changed by at most 0.17% from the usual sudden approximation. (8 refs.)

60143 Emission of heavy neutrinos in muon capture. J.P.Deutsch, M.Lebrun, R.Prieels (Inst. de Phys., Univ. Catholique de Louvain, Louvain-la-Neuve, Belgium).

Phys. Rev. D (USA), vol.27, no.7, p.1644-7 (1 April 1983). The possible use of various muon-capture observables is assessed in the search for heavy neutrinos mixed in the dominant variety. Existing data on the triton recoil spectrum measured in the reaction $\mu^- + ^3\text{He} \rightarrow ^3\text{H} + \nu$ readily allow the exclusion of the emission of heavy neutrinos of mass m_{ν_j} between 60 and 72 MeV/ c^2 with probability higher than $|U_{\mu j}|^2 \approx 0.01$. This complements limits on $|U_{\mu j}|^2$ obtained from the reactions $\pi^- \rightarrow \mu^- \nu_\mu$ and $K^- \rightarrow \mu^- \nu_\mu$. (19 refs.)

60144 Neutrinoless double- β decay with quasi-Dirac neutrinos. J.W.F.Valle (Dept. of Phys., Syracuse Univ., Syracuse, NY, USA).

Phys. Rev. D (USA), vol.27, no.7, p.1672-4 (1 April 1983). A mechanism to generate the neutrinoless double- β decay process with quasi-Dirac neutrinos and no right-handed currents is described. Relatively heavy neutrinos can easily be made consistent with the constraints on the $(\beta\beta)_0$ rate. The proposed scheme for the violation of lepton number can in principle be distinguished from a Majorana mass in $\Delta L=2$ oscillation phenomena. (12 refs.)

Beta decay opens the way to weak interactions See Entry 59577

Levels in ^{148}Ce from the decay of mass separated ^{148}La See Entry 60111

Beta-decay energies and masses of $^{103-105}\text{In}$ See Entry 60112

The decay of Ag-105g See Entry 60131

Level structure of ^{109}Ag from studies of the decay of ^{109}Pd .. See Entry 60137

Gamow-Teller strength in the $^{18}\text{O}(p,n)^{18}\text{F}$ reaction at 135 MeV See Entry 60179

The production of neutron-rich nuclides in the heavy-element region via ^3He induced reactions See Entry 60186

23.60 ALPHA DECAY

60145 A search on the parity-forbidden alpha width of the $E_{\alpha}=4.753$ MeV ($J^{\pi}, T=0^{+}, 1$) level of ^{18}F . F.Lecchia, P.Hubert, P.Mennrath (Inst. Nat. de Phys. Nucleaire et de Phys. des Particules, Gradignan, France), A.Morales, J.Morales, R.Nunez-Lagos, M.Plo.
Nuovo Cimento A (Italy), vol.74A, ser.2, no.1, p.28-36 (1 March 1983).
Results on the parity-nonconserving alpha width $\Gamma_{\alpha}^{\text{PNC}}$ of the ($J^{\pi}, T=0^{+}, 1$) $E_{\alpha}=4.753$ MeV level of ^{18}F are reported. This level is tentatively fed by the $^{18}\text{N}(\alpha,\gamma)^{18}\text{F}$ reaction and the absence of de-excitation γ -ray allows the authors to set an upper limit of $\Gamma_{\alpha}^{\text{PNC}}\leq 1.2\times 10^{-3}$ eV. (30 refs.)

24.00 NUCLEAR REACTIONS AND SCATTERING: GENERAL

24.10 NUCLEAR REACTION AND SCATTERING MODELS AND METHODS

60146 Atomic electrons in nuclear processes: attractive nuisance or useful telltale?. E.Merzbacher, J.M.Feagin.
Comments Nucl. & Part. Phys. (GB), vol.11, no.4, p.139-47 (1983).
In low-energy nuclear reactions, atomic electrons which are initially bound to one of the collision partners are not always inert bystanders. Atomic transitions carry information on reaction widths; conversely, nuclear excitation functions may show evidence of atomic satellites. Experimental and theoretical work is reviewed. (14 refs.)

60147 Comments on recent progress in few particle physics. I.Slaus ('Ruder Boskovic' Inst., Zagreb, Yugoslavia).
IEEE Trans. Nucl. Sci. (USA), vol.ns-30, no.2, p.1128-31 (April 1983).
(1982 IEEE Conference on the Application of Accelerators in Research and Industry, Denton, TX, USA, 8-10 Nov. 1982).
Status of the present understanding of multiparticle reaction mechanism is summarized. The studies of the reaction $\text{D}(p,2p)n$ show that the mechanism can be very important even if not easily noticeable in a particular representation, e.g. even a deep minimum is understood as a destructive interference between neutron-proton and proton-proton quasifree scattering. Information about nuclear interaction derived from few particle studies is discussed. The correct neutron-neutron effective range parameters are those extracted from the $\text{D}(\pi^{-},\gamma)2n$ reaction. Values extracted from the $\text{D}(n,p)2n$ reaction are influenced by the three body force. Evidences for the three body force are summarized. (20 refs.)

60148 A finite algorithm for the R-matrix description of nuclear resonances. G.Pisent (Istituto di Fisica, Univ. di Padova, Padova, Italy).
Leit. Nuovo Cimento (Italy), vol.36, ser.2, no.14, p.461-6 (2 April 1983).
A central point in the R-matrix theory is to transform the problem of inverting a fundamental channel matrix into that of inverting a level matrix (whose dimensions were assumed to be smaller). A similar case has been treated recently by the author (see *ibid.*, vol.72, p.303, 1982) where the transformation was from a channel space to a smaller space spanned by the rank index of a separable nuclear potential. In that paper the suitable algebra was found, able to draw explicit matrix inversion, in a very general and convenient way. The present paper deals with application of that inversion technique to the R-matrix theory. (3 refs.)

60149 Time compound nucleus for high energy nuclear reactions. K.Izumo, H.Araseki (Dept. of Phys., Coll. of Sci. & Technol., Nihon Univ., Tokyo, Japan).
Prog. Theor. Phys. (Japan), vol.69, no.1, p.158-70 (Jan. 1983).
A new compound nucleus, which the authors call a time compound nucleus, is introduced to analyze general features of high energy nuclear reactions. The compound nucleus resonates in a Lorentzian form as a function of time delay of reaction. Two time compound states characterized by time widths $\tau_1=9.6\times 10^{-24}$ sec and $\tau_2=2.0\times 10^{-23}$ sec are identified by the comparison with experimental angular-energy spectra of fragments of nuclear reactions. They estimate that the compound states consist of about 20 baryons. (14 refs.)

60150 Supermultiplet symmetry in nuclear reactions: application to $^3\text{He}(p,H)2p$ and $^6\text{He}(^3\text{H},^6\text{He})^6\text{Li}^*$. C.Wertz (Catholic Univ. of America, Washington, DC, USA).
Phys. Rev. C (USA), vol.27, no.4, p.1375-86 (April 1983).
A detailed analysis of the extension of the Barshay-Temmer theorem to reaction product pairs that are members of the same SU(4) multiplet (Wigner supermultiplet) is presented. Nonzero values of the total orbital angular momentum within fragments in the presence of residual spin orbit splitting is shown to destroy symmetry of the reaction products around 90° except in a sum rule sense. Departures from reaction symmetry are related to the SU(4) breaking parameter in the effective nucleon-nucleon potential and it is shown that the asymmetry should decrease with increasing A. A comparison of the $^3\text{He}(p,H)2p$ and $^6\text{Be}(^3\text{H},^6\text{He})^6\text{Li}$ angular distributions illustrates this point. Finally, a prediction is made for the ratio of analyzing powers for the $^6\text{He}+^6\text{Li}$ and $^6\text{He}+^6\text{Li}^*(3,56)$ final states. (18 refs.)

60151 Comparison of the Chandler-Gibson and the Baer, Kouri, Levin, and Tobocman many-body scattering formalisms. W.Tobocman (Phys. Dept., Case Western Res. Univ., Cleveland, OH, USA).
Phys. Rev. C (USA), vol.27, no.4, p.1405-14 (April 1983).
The Chandler-Gibson N-body scattering formalism is shown to be related to the one of Baer, Kouri, Levin, and Tobocman in that both are the result of selecting a set of Lippmann-Schwinger equations to serve as a set of simultaneous coupled integral equations for all the elements in a row or column of the transition operator matrix. The Baer, Kouri, Levin, and Tobocman choice has the advantage that the equations decouple on iteration to give a set of uncoupled connected kernel equations whereas the Chandler-Gibson choice has the advantage of coupling the partitions in a symmetrical manner. This might cause the Chandler-Gibson formalism to be less sensitive than the Baer, Kouri, Levin, and Tobocman formalism to truncations on the spectrum of allowed intermediate virtual states. The Chandler-Gibson formalism is shown to be consistent with unitarity provided the coupling scheme includes all open channels. An alternative method for introducing projectors into the Chandler-Gibson formalism is suggested as a method for generating connected

kernel equations. The Chandler-Gibson wave function equations are derived and compared with the coupled reaction channels equations. Finally, we show that like the Baer, Kouri, Levin, and Tobocman equations, the Chandler-Gibson equations decouple and, in fact, reduce to a single wave operator equation of particularly simple form. (18 refs.)

60152 Lee model field theory of three-nucleon system. M.Sawicki (Inst. of Theoretical Phys., Warsaw Univ., Warsaw, Poland).
Phys. Rev. C (USA), vol.27, no.4, p.1415-30 (April 1983).
The VNN sector of the nonstatic Lee model is investigated as a prototype of the three-nucleon pnn system, leading to an effective three-body Hamiltonian with a new kind of disconnected three-body force. The solution of the disconnectedness problem is presented in terms of modified Faddeev equations. The state vectors of the deuteron and triton are constructed and scattering amplitudes for reactions $n+p\rightarrow n+p$, $n+p\rightarrow n+n+\pi^{+}$, and $n+d\rightarrow n+d$ are derived. All effects of off-shell renormalization are included in a complete and consistent way. (25 refs.)

60153 Chew-Low model and the potential description of the πN interaction. M.G.Fuda (Dept. of Phys. & Astron., State Univ. of New York, Amherst, NY, USA).
Phys. Rev. C (USA), vol.27, no.4, p.1693-6 (April 1983).
The inverse scattering problem for the Chew-Low model is solved and the solution is used to construct three different forms for the off-shell πN T matrix. The three forms differ in their treatment of the nucleon pole and the crossing cut. One of the forms is shown to be equivalent to a separable potential model with an energy dependent strength. The analysis gives some insight into the question of the range of the πN interaction. (21 refs.)

60154 Nuclear structure effects in high momentum transfer reactions. F.Cannata (Istituto di Fisica, Univ. di Bologna, Bologna, Italy), J.-P.Dedonder, S.A.Gurvitz.
Phys. Rev. C (USA), vol.27, no.4, p.1697-709 (April 1983).
It is shown that, at large momentum transfers, one can extract nuclear structure information from the response (function) of the nucleus to an external scalar probe by factorizing the on-shell form factor associated to the struck nucleon. This result, derived both for elastic and inelastic scattering, arises from compensations between off-shell effects and exchange current effects generated by the (local) nucleon-nucleon interaction. The corrections to this on-shell factorization are in general found to be small at large momentum transfers. The role of the final state interaction in the nuclear transition form factor is then investigated and it is shown how one can, for instance, correct the orthogonality defect introduced by using a plane wave approximation for the struck nucleon. (19 refs.)

60155 Separable expansions for virtual states and resonances. S.K.Adhikari, A.C.Fonseca, L.Tomio (Dept. de Fisica, Univ. Federal de Pernambuco, Pe, Brazil).
Phys. Rev. C (USA), vol.27, no.4, p.1826-9 (April 1983).
Finite rank expansions for two- and three-body T matrices are analytically continued to the unphysical sheet of the complex energy plane associated with the lowest two-body scattering threshold in order to obtain the position and residue of the virtual state and resonance poles. The present method is applied to study the 1S_0 virtual state of two nucleons, the Efimov virtual states of three identical bosons, and the doublet virtual state of three nucleons. (11 refs.)

60156 Comment on 'scattering with absorptive interactions'. S.Joffily (Groupe de Phys. Nucleaire Theorique, Univ. Louis Pasteur, Strasbourg, France).
Phys. Rev. C (USA), vol.27, no.4, p.1830-1 (April 1983).
In a recently published paper, Cassing and collaborators (*ibid.*, vol.26, p.22, 1982) discussed the general tendencies of the motion of the complex poles of the S matrix of a complex potential with increasing absorption. In this comment it is pointed out that their conclusions are, in fact, model dependent and therefore are not valid for as wide a class of complex potentials as is suggested. Because of the model dependence of these conclusions, questions about the generalised Levinson's theorem proposed by these authors for complex interactions are raised. (6 refs.)

Weak nuclear interactions in a hybrid baryon-quark model: p-p asymmetry	See Entry 60004
Energy levels of the odd manganese nuclei from the ($d, ^3\text{He}$) reaction	See Entry 60104
A study of the $^{86}\text{Sr}(^3\text{He},t)^{86}\text{Y}$ reaction	See Entry 60106
Nuclear structure of even lead isotopes by the (p,t) reaction	See Entry 60109
The composite particle representation theory. II. The composite particle approximation	See Entry 60118
Resonant-state perturbation formalisms	See Entry 60160
The possibility of measuring the nuclear correlation width via atomic electron spectroscopy	See Entry 60161
Firestreak model	See Entry 60162
Pion-exchange contributions to the Lobashov experiment	See Entry 60166
Scaling in quasi-elastic electron scattering on nuclei	See Entry 60171
Effects of final state interactions in disintegration of three-nucleon nuclei	See Entry 60172
Special features of the alpha induced deuteron breakup	See Entry 60182
Bare potential DWBA for (d, p) reactions	See Entry 60184
Quasifree scattering at low energies in $^6\text{Li}(\alpha,2\alpha)^2\text{H}$	See Entry 60188
Role of the ^3He optical model potential ambiguity in the distorted-wave Born approximation description of the $^{58}\text{Ni}(^3\text{He},d)^{59}\text{Cu}$ reaction at 130 MeV incident energy	See Entry 60189
Microscopic study on di-nucleus states of $^{16}\text{O}+^{40}\text{Ca}$ and $^{40}\text{Ca}+^{40}\text{Ca}$. I	See Entry 60191
Liquid-gas phase instabilities in nuclear systems	See Entry 60193
Elastic breakup of 70 MeV ^7Li ions on lead	See Entry 60194
Giant resonance excitation in the $^{27}\text{Al}(^6\text{Li},^6\text{He})^{27}\text{Si}$ reaction at 93 MeV	See Entry 60196
Stretched excitations and the spin-dependent part of the pion-nucleon interaction	See Entry 60209
Reaction $\pi^{+}+d\rightarrow p+p$ at 65 to 140 MeV	See Entry 60213
Role of accelerators in uniform identification of thermal neutrons	See Entry 60214

24.10H Optical and diffraction models

- 60157 Energy dependence versus angular momentum dependence of optical potentials. W.Bauhoff (Theoretische Kernphys., Univ. Hamburg, Hamburg, Germany). *Phys. Rev. C (USA)*, vol.27, no.4, p.1822-5 (April 1983).
An optical potential depending linearly on the energy is transformed into a phase-equivalent energy-independent potential which depends on the angular momentum via $l(l+1)$. The transformation is exact and can be performed explicitly for an arbitrary shape of the potential. It is illustrated for the case of a Woods-Saxon potential. (7 refs.)
- The density dependence and the range of effective projectile-nucleon interaction from optical model analysis See Entry 60115
- Extended folding potential model for Λ -deuteron system with hard core potential See Entry 60128
- Deformation effects in aligned ^6Li scattering See Entry 60167
- Bare potential DWBA for (d, p) reactions See Entry 60184
- Role of the ^3He optical model potential ambiguity in the distorted-wave Born approximation description of the $^{58}\text{Ni}(^3\text{He}, d)^{59}\text{Cu}$ reaction at 130 MeV incident energy See Entry 60189
- A modified Glauber approximation and the formation of shock waves in high-energy heavy ion collisions See Entry 60192
- Quadrupole effects in ^7Li scattering at 88 MeV See Entry 60197
- Fusion cross sections for $^9\text{Be} + ^{40}\text{Ca}$ See Entry 60200
- Single and double scattering contributions to K^+ -deuteron vector analyzing power at 1.5 GeV/c See Entry 60205
- Diffraction theory and the double-charge-exchange reaction $^{18}\text{O}(\pi^+, \pi^-)^{18}\text{Ne}$ See Entry 60207
- Bound states in the pion-nucleus velocity-dependent potential See Entry 60210
- Pion single and double charge exchange in the resonance region: dynamical corrections See Entry 60211

24.30 RESONANCE REACTIONS AND SCATTERING

- 60158 On the normal modes of vibration in light deformed nuclei. F.Arickx, J.Broeckhove (Dienst Theoretische en Wiskundige Natuurkunde, Rijksuniv. Centrum, Antwerpen, Belgium), E.Caurier, E.Deumens, P.Van Leuven. *Nucl. Phys. A (Netherlands)*, vol.A398, no.3, p.467-75 (2 May 1983).
An analysis of generator coordinate method calculations on density vibrations in axially deformed light nuclei, demonstrates that the normal modes are harmonic vibrations parallel and orthogonal to the symmetry axis. (8 refs.)
- 60159 Investigation of isobaric analog resonances in ^{53}Mn . P.Kleinwächter, H.U.Gersch, H.Schobert (Zentralinst. für Kernforschung Rossendorf, Dresden, Germany). *Nucl. Phys. A (Netherlands)*, vol.A398, no.3, p.476-92 (2 May 1983).
The isobaric analog resonances in ^{53}Mn with different spins and parities are investigated by means of the $^{52}\text{Cr}(p, p')$, (p, p') , (p, p'') and (p, γ) reactions. Spectroscopic factors are derived and the experimental (p, γ) strengths are compared with theoretical single-particle estimations. (27 refs.)
- 60160 Resonant-state perturbation formalisms. W.J.Romo (Dept. of Phys., Carleton Univ., Ottawa, Canada). *Nucl. Phys. A (Netherlands)*, vol.A398, no.3, p.525-43 (2 May 1983).
Three different formalisms for determining bound-state, virtual-state, and resonant-state energies of a perturbed system are developed. Two of the formalisms are based on expansions of the unperturbed Green function in terms of bound-state, resonant-state and deformed-continuum-state contributions of the form developed by T. Berggren (1968). The third formalism is based on a Mittag-Leffler expansion of the unperturbed Green function. The three formalisms are compared and the relative merits of calculation schemes based on them are examined. (28 refs.)
- 60161 The possibility of measuring the nuclear correlation width via atomic electron spectroscopy. W.Koenig, K.W.McVoy, H.A.Weidenmüller (Max-Planck-Inst. für Kernphys., Heidelberg, Germany), P.Kienle. *Phys. Lett. B (Netherlands)*, vol.123B, no.5, p.279-83 (7 April 1983).
The correlation width Γ of the autocorrelation function of the nuclear scattering matrix, usually determined through the analysis of Ericson fluctuations of nuclear cross sections, manifests itself also in the spectra of atomic electrons ejected coherently prior to and after nuclear scattering. The authors propose to determine Γ from a coincidence measurement between nuclear reaction products and atomic electrons, a method which does not require a good energy resolution of the incident beam, and which would make it possible to measure Γ in a range of values not accessible before. (8 refs.)
- Transition densities for charge-exchange components of giant isovector resonances and the proton-neutron density distributions in nuclei See Entry 60136
- A finite algorithm for the R -matrix description of nuclear resonances See Entry 60148
- Time compound nucleus for high energy nuclear reactions See Entry 60149
- Separable expansions for virtual states and resonances See Entry 60155
- The photodisintegration of ^{40}Ar See Entry 60170
- High resolution proton resonance measurements See Entry 60174
- Excited-state giant dipole resonances in (p, γ) : a new probe of single-particle strengths See Entry 60178
- Radiation proton trapping by ^{51}V , ^{59}Co , $^{63,65}\text{Cu}$ Nuclei See Entry 60181
- Heavy ion resonances in the s -d shell See Entry 60190
- Giant resonance excitation in the $^{27}\text{Al}(^6\text{Li}, ^6\text{He})^{27}\text{Si}$ reaction at 93 MeV See Entry 60196
- Search for resonant behaviour in $^{16}\text{O} + ^{24}\text{Mg}$ inelastic scattering See Entry 60201
- Observation of analog and nonanalog transitions in the reaction $^{56}\text{Fe}(\pi^+, \pi^-)^{56}\text{Ni}$ See Entry 60202
- Observation of the nuclear isovector monopole resonance See Entry 60204
- Diffraction theory and the double-charge-exchange reaction $^{18}\text{O}(\pi^+, \pi^-)^{18}\text{Ne}$ See Entry 60207
- Pion single and double charge exchange in the resonance region: dynamical corrections See Entry 60211
- Effects of a nuclear scattering resonance on bremsstrahlung production and K -shell ionization See Entry 60953
- Charged particle reaction cross sections and nucleosynthesis See Entry 64460

24.50 DIRECT REACTIONS

- Energy levels of the odd manganese nuclei from the $(d, ^3\text{He})$ reaction See Entry 60104
- Special features of the alpha induced deuteron breakup See Entry 60182
- Bremsstrahlung in the ^3He - ^2H interaction near the deuteron break-up threshold See Entry 60183

24.60 STATISTICAL THEORY AND FLUCTUATIONS

- 60162 Firestreak model. N.Mobed, S.Das Gupta (Phys. Dept., McGill Univ., Montreal, Quebec, Canada), B.K.Jennings. *Phys. Rev. C (USA)*, vol.27, no.4, p.1526-31 (April 1983).
Comparison with a recent experiment suggests that the yield functions of the firestreak model be redefined. The modified yield functions give better fits to inclusive cross section data. (13 refs.)
- Level density and shell structure: Rosenzweig model revisited See Entry 60108
- $^{113}\text{In}(\gamma, n)$ reaction isomeric and ground-state cross-sections See Entry 60169
- Comparison of the (p, xn) cross sections from ^{238}U , ^{235}U and ^{232}Th targets irradiated with 200 MeV protons See Entry 60176
- Radiation proton trapping by ^{51}V , ^{59}Co , $^{63,65}\text{Cu}$ Nuclei See Entry 60181
- Liquid-gas phase instabilities in nuclear systems See Entry 60193
- Charged particle reaction cross sections and nucleosynthesis See Entry 64460

24.70 POLARIZATION IN REACTIONS AND SCATTERING

- 60163 Observation of parity nonconservation in the integrated γ spectrum from (n, γ) reactions in Cl, Br, Cd, Sn, and La nuclei. V.A.Vesna, E.A.Kolomenskii, V.M.Lobashov, V.A.Nazarenko, A.N.Pirozhkov, L.M.Smotritskii, Yu.V.Sobolev, N.A.Titov (B.P. Konstantinov Inst. of Nuclear Phys., Acad. of Sci., USSR). *JETP Lett. (USA)*, vol.36, no.5, p.209-12 (5 Sept. 1982). Translation of: *Pis'ma v Zh. Eksp. & Teor. Fiz. (USSR)*, vol.36, no.5, p.169-72 (5 Sept. 1982). [received: April 1983]
A P -odd asymmetry has been observed in the emission of γ rays upon the capture of polarized thermal neutrons by Cl, Br, and La nuclei. A circular polarization of the γ rays has been observed during the capture of unpolarized neutrons by Cl, Br, Sn, and La nuclei. (9 refs.)
- 60164 Proton polarization in the photodisintegration of the deuteron at γ energies in the range 700-1100 MeV. A.S.Bratshevskii, A.A.Zybalov, S.P.Karasev, O.G.Konovalov, P.V.Sorokin, Yu.O.Storozhenko, A.E.Tenishev (Physicotech. Inst., Acad. of Sci., Ukrainian SSR). *JETP Lett. (USA)*, vol.36, no.5, p.216-18 (5 Sept. 1982). Translation of: *Pis'ma v Zh. Eksp. & Teor. Fiz. (USSR)*, vol.36, no.5, p.174-6 (5 Sept. 1982). [received: April 1983]
The polarization of protons in the reaction $\gamma + d \rightarrow p + n$ has been measured for γ energies over the range 700-1100 MeV. The protons are observed to have a large polarization over this entire γ energy range. (6 refs.)
- 60165 Investigation of the three-nucleon system by pd elastic scattering with polarized protons and deuterons. W.Gruebler, V.König, P.A.Schmelzbach, F.Sperisen, B.Jenny, R.E.White (Lab. für Kernphys., ETH, Zurich, Switzerland), F.Seiler, H.W.Roser. *Nucl. Phys. A (Netherlands)*, vol.A398, no.3, p.445-66 (2 May 1983).
Angular distributions of cross section and analyzing power A_y of protons scattered on deuterium were measured between 8.5 and 22.7 MeV. For the corresponding energy of incident deuterons scattered from hydrogen, angular distributions of the deuteron vector and tensor analyzing powers A_y^d , A_{yy} and A_{xx} were measured at 6 energies between 17 and 45.4 MeV. The proton and deuteron data together with corresponding data at lower energies are analyzed in terms of Legendre polynomials. The energy dependence of the resulting coefficients are discussed. (18 refs.)
- 60166 Pion-exchange contributions to the Lobashov experiment. J.L.Friar (Theoretical Div., Los Alamos Nat. Lab., Los Alamos, NM, USA), B.H.J.McKellar. *Phys. Lett. B (Netherlands)*, vol.123B, no.5, p.284-8 (7 April 1983).
The one-pion-exchange contributions to the Lobashov experiment (1972) are carefully calculated and are shown to be relativistic corrections. Their contribution to the circular polarization, P_n , is 1.1×10^{-9} A, where A measures the strength of the parity violating $\text{NN}\pi$ coupling. For $A=1$ this is approximately 10% of the usual nonrelativistic arising from heavy meson exchange. (12 refs.)
- 60167 Deformation effects in aligned ^6Li scattering. H.Nishioka, J.A.Tostevin, R.C.Johnson (Dept. of Phys., Univ. of Surrey, Guildford, England). *Phys. Lett. B (Netherlands)*, vol.124B, no.1-2, p.17-20 (21 April 1983).
A second rank tensor potential for ^6Li scattering is obtained within the framework of a single folding model by assuming an $\alpha+d$ cluster structure for ^6Li . The intercluster wavefunction contains D-state and S-state components with amplitudes chosen to reproduce the experimental value of the ^6Li Q -moment. Calculations are made for $^6\text{Li} + ^{58}\text{Ni}$ elastic scattering at $E_{\text{cm}} = 18.1$ MeV. The puzzling behaviour of the measured tensor analysing power (T_{20}) is reproduced. (16 refs.)
- Energy and projectile dependence of nuclear alignment in fusion-evaporation reactions See Entry 60129
- Absolute strength determinations of dipole transitions and unique spin-parity assignments in ^{52}Cr and ^{56}Fe See Entry 60132
- Simultaneous measurements of analyzing powers and differential cross sections for $n + ^{28}\text{Si}$ See Entry 60175
- Special features of the alpha induced deuteron breakup See Entry 60182
- Single and double scattering contributions to K^+ -deuteron vector analyzing power at 1.5 GeV/c See Entry 60205

24.75 GENERAL PROPERTIES OF FISSION

60168 Calculation of the nuclear fission by numerical solution of F-P equation. Wu Xi-zhen, Zhuo Yi-zhong, Chang Xi-zhen, Yang Ying-hui, Ma Zhong-yu, Feng Ren-fa (Inst. of Atomic Energy, Acad. Sinica, Beijing, China). *Commun. Theor. Phys. (China)*, vol.1, no.6, p.769-78 (1982). The two-dimensional Fokker-Planck Equation is exactly solved by means of the numerical method. The velocity distribution at the saddle point, the second moments of the coordinate and velocity, and the time development of the nuclear fission rate are studied. The maximum fission rate at a certain viscosity is exhibited by studying the dependence of the fission rate on the nuclear viscosity. (5 refs.)

25.00 NUCLEAR REACTIONS AND SCATTERING: SPECIFIC REACTIONS

25.10 NUCLEAR REACTIONS AND SCATTERING INVOLVING FEW-NUCLEON SYSTEMS

Comments on recent progress in few particle physics See Entry 60147
 Supermultiplet symmetry in nuclear reactions: application to $^3\text{He}, ^2\text{H}$ and $^9\text{Be}, ^3\text{H}, ^4\text{He}, ^6\text{Li}^*$ See Entry 60150
 Lee model field theory of three-nucleon system See Entry 60152
 Investigation of the three-nucleon system by pd elastic scattering with polarized protons and deuterons See Entry 60165
 Special features of the alpha induced deuteron breakup See Entry 60182
 Bremsstrahlung in the $^3\text{He}-^2\text{H}$ interaction near the deuteron break-up threshold See Entry 60183
 Nuclear reactions among the hydrogen isotopes at low energies See Entry 60215

25.20 PHOTONUCLEAR REACTIONS AND PHOTON SCATTERING

60169 $^{113}\text{In}(\gamma, n)$ reaction isomeric and ground-state cross-sections. S.A.S.Vitiello, I.D.Goldman (Inst. de Fisica, Univ. de Sao Paulo, Sao Paulo, Brazil). *Nuovo Cimento A (Italy)*, vol.74A, ser.2, no.1, p.17-27 (1 March 1983). The $^{113}\text{In}(\gamma, n)^{112}\text{In}^{\text{m}}$ reaction cross-sections were measured between 10 and 25 MeV. The measurements have been made by residual activity. A Lorentz line shape was fitted to the (γ, n) cross-section with $E_0 = (16.8 \pm 0.2)$ MeV, $\Gamma = (8.2 \pm 0.6)$ MeV and $\sigma_0 = (324 \pm 17)$ mb. The isomeric to ground-state ratio is approximately constant at a value of 2.5 with variations that do not exceed 10%. Theoretical calculations using the statistical model are consistent with the experimental data. (19 refs.)
60170 The photodisintegration of ^{40}Ar . R.A.Sutton, P.D.Allen, M.N.Thompson, E.G.Muirhead (School of Phys., Univ. of Melbourne, Parkville, Victoria, Australia). *Nucl. Phys. A (Netherlands)*, vol.A398, no.3, p.415-33 (2 May 1983). High resolution measurements of the (γ, n) , $(\gamma, 2n)$, (γ, p) , (γ, np) and $(\gamma, 2p)$ cross sections of ^{40}Ar over a photon energy range of 10 to 28 MeV are reported. From this data, the total photon absorption cross section integrated to 26 MeV is found to be 434 ± 40 MeV.mb. The results of a dynamic collective model (DCM) calculation compare favourably with the photoabsorption cross section, supporting the use of the DCM in this mass region. It is confirmed that isospin plays an important role in the decay of the ^{40}Ar giant dipole resonance. (53 refs.)
 Absolute strength determinations of dipole transitions and unique spin-parity assignments in ^{52}Cr and ^{56}Fe See Entry 60132
 Proton polarization in the photodisintegration of the deuteron at γ energies in the range 700-1100 MeV See Entry 60164
 Measurement of activity yields for $^{12}\text{C}(\gamma, n)^{11}\text{C}$, $^{14}\text{N}(\gamma, n)^{13}\text{N}$, and $^{16}\text{O}(\gamma, n)^{15}\text{O}$ reactions as a function of electron beam energy and angle from the electron beam using thick target produced bremsstrahlung See Entry 63963

25.30 LEPTON-INDUCED REACTIONS AND SCATTERING

60171 Scaling in quasi-elastic electron scattering on nuclei. P.Christillin (CERN, Geneva, Switzerland). *Phys. Lett. B (Netherlands)*, vol.124B, no.1-2, p.14-16 (21 April 1983). The properties of quasi-elastic electron scattering with respect to the scaling variable $y = \omega/q - q/2M$ are examined. It is shown that different sets of scattering experiments can indeed be related through the scaling variable. (8 refs.)
60172 Effects of final state interactions in disintegration of three-nucleon nuclei. E.M.Malyarzh, I.V.Kozlovskii, V.K.Tartakovskii. *Ukr. Fiz. Zh. (USSR)*, vol.28, no.3, p.326-31 (March 1983). In Russian. An interpolation model is applied to calculate angular distributions and energy spectra of products of ^3He nucleus two-particle electrodisintegration for three various cases with detecting: a) electron-proton coincidences; b) electron-deuteron coincidences; c) deuteron only. Final state interactions are shown to be significant in all the cases under consideration. (14 refs.)
 Comment on the problem of the off-shell γNN vertex function in ed elastic scattering See Entry 60051
 Off-shell γNN vertex function in ed elastic scattering See Entry 60052
 Search for M1 strength in ^{51}V and the difference in $^{51}\text{V}(e, e')$ and $^{51}\text{V}(p, p')$ spectra See Entry 60133
 Emission of heavy neutrinos in muon capture See Entry 60143

25.40 NUCLEON-INDUCED REACTIONS AND SCATTERING

(see also 28.20 Neutron physics)

60173 Nucleon-induced pion production on nucleons and nuclei. G.E.Walker. *Comments Nucl. & Part. Phys. (GB)*, vol.11, no.4, p.155-70 (1983). The current status of experiment and theory for the (p, π) reaction is discussed. (32 refs.)
60174 High resolution proton resonance measurements. G.E.Mitchell (North Carolina State Univ., Raleigh, NC, USA). *IEEE Trans. Nucl. Sci. (USA)*, vol.ns-30, no.2, p.1115-18 (April 1983). (1982 IEEE Conference on the Application of Accelerators in Research and Industry, Denton, TX, USA, 8-10 Nov. 1982). With present technology, nuclear densities restrict charged particle resonance studies to below mass $A=70$. Many of the most interesting materials engineering and solid state applications, as well as astrophysical questions, involve light nuclei. Good experimental resolution is crucial; for solid targets the author obtains an overall resolution of 300 eV. The author observes two main types of results. One is characteristic of the FP shell, with many small levels very close together. A contrasting pattern is usually observed in the sd shell, where the level density is much lower, and very broad states coexist with very narrow states. Just in this narrow energy region resonances with angular momentum and parity of $1/2^+$, $1/2^-$, $3/2^-$, $3/2^+$, $5/2^+$, $5/2^-$ and $7/2^-$ are observed, with widths ranging from 10 eV to 30000 eV. (20 refs.)
60175 Simultaneous measurements of analyzing powers and differential cross sections for $n+^{28}\text{Si}$. C.R.Howell, R.L.Walter (Dept. of Phys., Duke Univ., Durham, NC, USA). *IEEE Trans. Nucl. Sci. (USA)*, vol.ns-30, no.2, p.1132-5 (April 1983). (1982 IEEE Conference on the Application of Accelerators in Research and Industry, Denton, TX, USA, 8-10 Nov. 1982). Scattering experiments conducted with beams of polarized neutrons give special information about the spin sensitive part of the neutron-nucleus interaction. Carefully controlled measurements of the analyzing power $A(\theta)$ for the scattering of polarized neutron beams can also give accurate values for the more conventional observable, the differential cross section $\sigma(\theta)$. The paper focuses on an attempt to obtain $\sigma(\theta)$ values for $^{28}\text{Si}(n, p)$ from an experiment originally intended to determine only the function $A(\theta)$. As a test the data are compared to cross sections measured in a conventional neutron scattering experiment. (6 refs.)
60176 Comparison of the (p, xn) cross sections from ^{238}U , ^{235}U and ^{232}Th targets irradiated with 200 MeV protons. Y.Y.Chu, M.L.Zhou (Dept. of Chem., Brookhaven Nat. Lab., Upton, NY, USA). *IEEE Trans. Nucl. Sci. (USA)*, vol.ns-30, no.2, p.1153-5 (April 1983). (1982 IEEE Conference on the Application of Accelerators in Research and Industry, Denton, TX, USA, 8-10 Nov. 1982). The authors have measured absolute cross sections for (p, xn) reactions (x ranges from 0 to 8) from ^{238}U , ^{235}U , and ^{232}Th targets irradiated with 200 MeV protons at the Brookhaven AGS Linac injector. Chemical yields were determined by using ^{239}Np and ^{233}Pa as tracers. Yield patterns obtained in this work can be compared to the experimental results and theoretical calculations from earlier work and they are consistent within the framework of intranuclear cascade followed by neutron evaporation and fission competition. (20 refs.)
60177 Cyclotron production of ^{67}Ga . Cross sections and thick-target yields for the $^{67}\text{Zn}(p, n)$ and $^{68}\text{Zn}(p, 2n)$ reactions. F.E.Little, M.C.Lagunas-Solar (Crocketer Nuclear Lab., Univ. of California, Davis, CA, USA). *Int. J. Appl. Radiat. & Isot. (GB)*, vol.34, no.3, p.631-7 (March 1983). Natural zinc foils were irradiated with ≥ 35 -MeV protons and cross sections were measured for the reactions $^{67}\text{Zn}(p, n)^{67}\text{Ga}$, $^{67}\text{Zn}(p, 2n)^{66}\text{Ga}$, $^{68}\text{Zn}(p, 2n)^{67}\text{Ga}$ and $^{68}\text{Zn}(p, 3n)^{66}\text{Ga}$. Thick-target yields as well as radiocontaminant ratios were calculated from the cross-section data. Targets were also irradiated under near production conditions and the yields were compared with calculated values. An alternative production method based upon the $^{67}\text{Zn}(p, n)^{67}\text{Ga}$ reaction was found to provide equivalent yields to those obtained from the $^{68}\text{Zn}(p, 2n)^{67}\text{Ga}$ reaction. The possibility of using double targets is also discussed. (16 refs.)
60178 Excited-state giant dipole resonances in (p, γ) : a new probe of single-particle strengths. D.H.Dowell, G.Feldman, K.A.Snover (Dept. of Phys., Univ. of Washington, Seattle, WA, USA), A.M.Sandorfi, M.T.Collins. *Phys. Rev. Lett. (USA)*, vol.50, no.16, p.1191-4 (18 April 1983). The (p, γ) reaction populating highly excited states in ^{28}Si is shown to be dominated by giant dipole resonances built upon one-particle, one-hole states. Each giant resonance is centered at $E_x \approx 20$ MeV, with a width which increases with the energy of the one-particle, one-hole state, and with a strength that is simply related to the proton stripping strength to the same final state. (13 refs.)
60179 Gamow-Teller strength in the $^{18}\text{O}(p, n)^{18}\text{F}$ reaction at 135 MeV. B.D.Anderson, A.Fazely, R.J.McCarthy, P.C.Tandy, J.W.Watson, R.Madey (Dept. of Phys., Kent State Univ., Kent, OH, USA), W.Bertozzi, T.N.Buti, J.M.Finn, J.Kelly, M.A.Kovash, B.Pugh, B.H.Wildenthal, C.C.Foster. *Phys. Rev. C (USA)*, vol.27, no.4, p.1387-93 (April 1983). The distribution of Gamow-Teller strength in the $^{18}\text{O}(p, n)^{18}\text{F}$ reaction was studied at a bombarding energy of 135 MeV. Five 1^+ , $T=0$ states are identified below $E_x=7$ MeV and a concentration of 1^+ states of presumed $T=1$ character is observed between $E_x=9.5$ and 12 MeV. Approximately 82% of the 1^+ strength is concentrated into the ground-state transition and only 5.5% is seen in the $T=1$ component. Normalization of the ground-state transition to the known Gamow-Teller matrix element from the analogous beta decay of ^{18}Ne allows the (p, n) cross sections to be related to the Gamow-Teller strength. The resulting total Gamow-Teller strength observed in the (p, n) reaction is about two-thirds of the minimum value required by the sum rule for a $T=1$ nucleus. This result is in reasonable agreement with the total Gamow-Teller strength predicted from a shell-model calculation which uses empirically renormalized single-particle Gamow-Teller matrix elements. The concentration of the $T=0$ strength predominantly into the ground state and the observed ratio of $T=1$ to $T=0$ strength also are consistent with these calculations. (24 refs.)
60180 Cross section calculations for nucleon- ^{40}Ca and α - ^{40}Ca elastic scattering from microscopic nonlocal optical potentials. H.Dermawan, F.Osterfeld (Inst. fur Kernphys., KFA Juelich, Juelich, Germany), V.A.Madsen. *Phys. Rev. C (USA)*, vol.27, no.4, p.1474-82 (April 1983). Microscopic calculations of the second-order optical potential are made for $^{40}\text{Ca}(n, n)$, $^{40}\text{Ca}(p, p)$, and $^{40}\text{Ca}(\alpha, \alpha)$ at various incident energies using random phase approximation transition densities for intermediate excited states. Elastic scattering cross sections are calculated from the microscopic nonlocal potentials and are compared with cross sections which have

been calculated from the equivalent local potentials. The validity of the local approximation to the nonlocal potentials is discussed. (29 refs.)

60181 Radiation proton trapping by ^{51}V , ^{59}Co , $^{63,65}\text{Cu}$ Nuclei. B.A.Nemashkalo, V.V.Voronov, V.E.Storizhko. *Ukr. Fiz. Zh. (USSR)*, vol.28, no.3, p.332-8 (March 1983). In Russian. Radiation proton trapping by ^{51}V , ^{59}Co , $^{63,65}\text{Cu}$ nuclei at energies below 3.0 MeV was studied by the method of averaged resonances. The analysis was performed in terms of a statistical theory. (24 refs.)

Search for the second excited $11/2^-$ state and weak-coupling scheme in ^{117}Sn See Entry 60096

Excitation of the 6^- particle-hole state with the $^{40}\text{Ca}(p,n)^{40}\text{Sc}$ reaction at 133.5 MeV See Entry 60099

Level structure of the doubly odd nucleus ^{112}In from the (p,γ) reaction See Entry 60107

Nuclear structure of even lead isotopes by the (p,t) reaction See Entry 60109

The density dependence and the range of effective projectile-nucleon interaction from optical model analysis See Entry 60115

Search for M1 strength in ^{51}V and the difference in $^{51}\text{V}(e,e')$ and $^{51}\text{V}(p,p')$ spectra See Entry 60133

Comments on recent progress in few particle physics See Entry 60147

Supermultiplet symmetry in nuclear reactions: application to $^3\text{He}(p,^3\text{H})2p$ and $^6\text{Be}(^3\text{H},^6\text{He})^6\text{Li}^*$ See Entry 60150

Investigation of isobaric analog resonances in ^{53}Mn See Entry 60159

Observation of parity nonconservation in the integrated γ spectrum from (n,γ) reactions in Cl, Br, Cd, Sn, and La nuclei See Entry 60163

Investigation of the three-nucleon system by pd elastic scattering with polarized protons and deuterons See Entry 60165

Pion-exchange contributions to the Lobashov experiment See Entry 60166

Role of accelerators in uniform identification of thermal neutrons See Entry 60214

Effects of a nuclear scattering resonance on bremsstrahlung production and K-shell ionization See Entry 60953

Charged particle reaction cross sections and nucleosynthesis See Entry 64460

25.50 ^2H - AND ^3H -INDUCED REACTIONS AND SCATTERING

60182 Special features of the alpha induced deuteron breakup. J.M.Lambert, P.A.Treado (Dept. of Phys., Georgetown Univ., Washington, DC, USA), I.Slaus, Y.Koike, F.D.Corrall, R.E.Brown, R.A.Hardekopf, N.Jarmie. *IEEE Trans. Nucl. Sci. (USA)*, vol.30, no.2, p.1146-8 (April 1983). (1982 IEEE Conference on the Application of Accelerators in Research and Industry, Denton, TX, USA, 8-10 Nov. 1982).

The alpha induced deuteron breakup reactions have been of interest since the nucleon induced deuteron breakup problem was addressed with tractable and predictive models based on the Faddeev formalism and with appropriate nucleon-nucleon forces. The authors discuss a few special features of the alpha induced deuteron breakup reactions. Specifically, they point out the importance of the n-p tensor force in the predictions of the three-body model that fit the tensor analyzing powers better and the concomitant deterioration of the fit to the vector analyzing power caused by the inclusion of the tensor force. They suggest that there exists evidence for the 1S_0 n-p interaction, which is isospin forbidden, in both the cross section and spin observables data. Finally, they discuss certain characteristics of the p- α quasifree-scattering and n- α final-state-interaction processes. (10 refs.)

60183 Bremsstrahlung in the ^3He - ^2H interaction near the deuteron break-up threshold. P.Bricault, R.J.Slobodrian, C.Rioux, L.Potvin, R.Roy, R.Larue (Dept. de Phys., Univ. Laval, Quebec, Canada), B.Frois. *J. Phys. (France)*, vol.44, no.4, p.461-5 (April 1983).

The nuclear bremsstrahlung cross-section in the ^3He - ^2H interaction in the neighbourhood of the deuteron break-up threshold has been measured for the first time at seven energies, via detection in the final state of the charged particles ^3He and ^2H at the correlation angles 33° - 24° . A comparison with theoretical calculations shows a systematic deviation, but statistics of the very small cross-sections are not sufficient to claim unambiguously a threshold effect. (9 refs.)

60184 Bare potential DWBA for (d, p) reactions. M.Ichimura (Inst. of Phys., Univ. of Tokyo, Tokyo, Japan), M.Kawai. *Prog. Theor. Phys. (Japan)*, vol.69, no.1, p.128-41 (Jan. 1983).

Applicability of 'bare potential DWBA' (BPDWBA) to light ion induced transfer reactions is investigated. The reaction $^{16}\text{O}(d, p)^{17}\text{O}$ and $^{40}\text{Ca}(d, p)^{41}\text{Ca}$ at $E_d=10.5$ MeV are studied, for which coupled channel (CC) calculations exist. Search is made of the 'optical' potential which fit the CC results of (d, d) and (p, p) scatterings. The 'optical' potentials and/or the bare potentials (the distorting potentials in the CC equations) are used in DWBA calculations of (d, p) cross sections. Results of the various types of DWBA distinguished by the choice of the distorting potentials are compared with the CC results. It is found that none of such DWBAs reproduces the CC cross sections. Physical implications of these types of DWBA are discussed in detail. (18 refs.)

60185 Structure of ^{209}Bi deduced from the $^{208}\text{Pb}(t,2n\gamma)$ reaction. K.H.Maier (Hahn-Meitner Inst., Berlin, Germany), T.Nail, R.K.Sheline, W.Stoffl, J.A.Becker, J.B.Carson, R.G.Lanier, L.G.Mann, G.L.Struble, J.A.Cizewski, B.H.Erkila. *Phys. Rev. C (USA)*, vol.27, no.4, p.1431-53 (April 1983).

States in ^{209}Bi were populated with the $^{208}\text{Pb}(t,2n)$ reaction. Incident triton energies between 11 and 16 MeV were used. Gamma-ray excitation functions, angular distributions, and γ - γ -time coincidence spectra were measured. Approximately 50 newly-observed γ rays have been assigned to transitions in ^{209}Bi . Previously-unresolved doublets at $E_\gamma=2600$, 3135, and 3154 keV have been identified. A new level at 3270 keV is reported, and the 3197-keV level is verified. ^{209}Bi level energies are reported with an accuracy of 600 eV or less. A level scheme for $E_\gamma<4.14$ MeV is presented, including spin-parity assignments. A new M1 transition between the $5/2^+$ and $3/2^+$ members of the $\pi h_{9/2}\otimes 3^-$ septuplet is reported. The 19 levels belonging to the $\nu g_{7/2}p_{1/2}^{-1}$, $h_{9/2}$ are identified. (26 refs.)

Search for the second excited $11/2^-$ state and weak-coupling scheme in ^{117}Sn See Entry 60096

Energy levels of the odd manganese nuclei from the $(d, ^3\text{He})$ reaction See Entry 60104

The density dependence and the range of effective projectile-nucleon interaction from optical model analysis See Entry 60115

Supermultiplet symmetry in nuclear reactions: application to $^3\text{He}(p,^3\text{H})2p$ and $^6\text{Be}(^3\text{H},^6\text{He})^6\text{Li}^*$ See Entry 60150

Investigation of the three-nucleon system by pd elastic scattering with polarized protons and deuterons See Entry 60165

Nuclear reactions among the hydrogen isotopes at low energies See Entry 60215

25.60 ^3He - AND ^4He -INDUCED REACTIONS AND SCATTERING

60186 The production of neutron-rich nuclides in the heavy-element region via ^3He induced reactions. Y.Y.Chu, M.L.Zhou (Dept. of Chem., Brookhaven Nat. Lab., Upton, NY, USA).

IEEE Trans. Nucl. Sci. (USA), vol.ns-30, no.2, p.1149-52 (April 1983). (1982 IEEE Conference on the Application of Accelerators in Research and Industry, Denton, TX, USA, 8-10 Nov. 1982).

The authors have measured the production cross sections for ^{233}Th and ^{231}Th from the bombardment of ^{238}U with ^3He ions at 46-, 53-, and 60-MeV at the Brookhaven 60-in. isochronous cyclotron. They have also attempted to observe the decay of ^{233}Ac produced via $^{238}\text{U}(^3\text{He}, ^8\text{B})$ or equivalent reactions using 61 MeV ^3He ions by first separating thorium from actinium and then performing chemical purifications on the second thorium sample into which the actinium has decayed. In the four experiments they performed, three gave results consistent with the β half-life of ^{233}Ac somewhat longer than 120 s and the production cross section from this target-projectile combination in the order of 1-2 μb . (19 refs.)

60187 Continuous spectra of deuterons from $^3\text{He}+^{12}\text{C}$ at low energy. G.Calvi, M.Lattuada, C.Spitalen (Istituti di Fisica, Univ. di Catania, Italy), F.Riggi, D.Vinciguena, C.M.Sutera, A.Panteleo.

Lett. Nuovo Cimento (Italy), vol.36, ser.2, no.14, p.475-80 (2 April 1983).

The simple spectator model for this reaction assumes that the detected particle is spectator of the process, thus retaining the velocity it had before the interaction. For instance a peak around $2/3 E_0$ is expected in the deuteron spectra, while the corresponding proton carries out the energy $1/3 E_0 - |B|$, $B=-5.5$ MeV being the binding energy of the proton in ^3He . This feature is commonly observed at incident energies much higher than the binding energy. However, when the ^3He incident energy is less than 16.5 MeV the proton cannot carry away the energy $1/3 E_0 - |B|$, so that the break-up process could show uninvestigated features in the continuous deuteron spectra. In order to study the importance of this mechanism a systematic study of the inclusive spectra of the reaction products from the interaction of ^3He ions with different target nuclei was undertaken. The authors report preliminary data about the contribution of the process on the ^{12}C nucleus. (9 refs.)

60188 Quasifree scattering at low energies in $^6\text{Li}(\alpha,2\alpha)^2\text{H}$. D.Gola, W.Bretfeld, W.Burgmer, H.Eichner, Ch.Heinrich, H.J.Helten, H.Kretzer, K.Prescher, H.Oswald, W.Schnorrenberg, H.Paetz gen. Schick (Inst. fur Kernphys., Univ. of Koln, Koln, Germany).

Phys. Rev. C (USA), vol.27, no.4, p.1394-400 (April 1983).

α - α quasifree scattering was investigated in the reaction $^6\text{Li}(\alpha,2\alpha)^2\text{H}$ as a function of energy of the incident α particles. In the energy range $E_\alpha=6.6$ to 13.0 MeV 51 spectra under kinematically complete conditions were obtained at symmetrical angles such that the spectator momentum $p_{\text{S1}}=0$. The widths and magnitudes of the spectator momentum distributions are strongly energy dependent. This dependence can be reproduced by a plane wave impulse approximation modified by a reflection coefficient calculated semiclassically in WKB approximation. (13 refs.)

60189 Role of the ^3He optical model potential ambiguity in the distorted-wave Born approximation description of the $^{58}\text{Ni}(^3\text{He},d)^{59}\text{Cu}$ reaction at 130 MeV incident energy. A.Djaloeis, C.Alderliesten, J.Bojowald, C.Mayer-Borikce, W.Oelert, P.Turek (Inst. fur Kernphys., KFA Julich, Julich, Germany).

Phys. Rev. C (USA), vol.27, no.4, p.1483-8 (April 1983).

Angular distributions of $^{58}\text{Ni}(^3\text{He},d)^{59}\text{Cu}$ transitions leading to the $(0.0 \text{ MeV}, 3/2^-)$, $(0.91 \text{ MeV}, 5/2^-)$, and $(3.04 \text{ MeV}, 7/2^+)$ states in ^{59}Cu have been measured at an incident energy of 130 MeV. The experimental data have been used to study mainly the role of the ^3He optical model potential ambiguity in the distorted-wave Born approximation description of the reaction. Satisfactory fits to the data are obtained using a deep helion potential in standard local zero-range calculations. For a shallow ^3He potential a comparable description can be achieved if the depth of the real part of the deuteron optical potential is reduced considerably, and nonlocality as well as finite-range corrections are taken into account. Under these conditions, the use of a ^3He potential constructed according to the Johnson-Soper prescription yields similar results. (25 refs.)

Search for the second excited $11/2^-$ state and weak-coupling scheme in ^{117}Sn See Entry 60096

The density dependence and the range of effective projectile-nucleon interaction from optical model analysis See Entry 60115

Energy and projectile dependence of nuclear alignment in fusion-evaporation reactions See Entry 60129

A study of the $^{84}\text{Kr}(\alpha,2n\gamma)^{86}\text{Sr}$ reaction See Entry 60134

A search on the parity-forbidden alpha width of the $E_\alpha=4.753$ MeV ($J^\pi=7^-, 1$) level of ^{20}F See Entry 60145

Cross section calculations for nucleon- ^{40}Ca and α - ^{40}Ca elastic scattering from microscopic nonlocal optical potentials See Entry 60180

Charged particle reaction cross sections and nucleosynthesis See Entry 64460

25.70 HEAVY ION INDUCED REACTIONS AND SCATTERING

60190 Heavy ion resonances in the s-d shell. G.Vourvopoulos (NRC Demokritos, Athens, Greece).

IEEE Trans. Nucl. Sci. (USA), vol.ns-30, no.2, p.1119-23 (April 1983). (1982 IEEE Conference on the Application of Accelerators in Research and Industry, Denton, TX, USA, 8-10 Nov. 1982).

In spite of the wealth of experimental information that exists on heavy ion resonances the theoretical interpretations proposed have been proven inadequate. One of the early arguments given for the observation of resonances in systems such as $^{12}\text{C}+^{12}\text{C}$ and $^{12}\text{C}+^{16}\text{O}$ has been the low level density of these systems. On the contrary, systems such as $^{16}\text{O}+^{16}\text{O}$ are characterized by a much higher level density and do not exhibit any structure. In this context, systems such as $^9\text{Be}+^{12}\text{C}$ and $^9\text{Be}+^{13}\text{C}$, having a level density comparable to that of $^{12}\text{C}+^{12}\text{C}$ should also exhibit resonant behavior. Two points are addressed: (a) the level density argument and (b) the α -like structure argument. The experimental investigation of the systems $^9\text{Be}+^{12}\text{C}$, $^9\text{Be}+^{13}\text{C}$,

$^{12}\text{C}+^{18}\text{O}$ and $^{16}\text{O}+^{14}\text{C}$ are presented leading to the discussion of the above arguments. Finally the correlation of the heavy ion resonances and those seen in light ion experiments is shown. (20 refs.)

60191 Microscopic study on di-nuclear states of $^{16}\text{O}+^{40}\text{Ca}$ and $^{40}\text{Ca}+^{40}\text{Ca}$. I. A. Tohsaki-Suzuki (Faculty of Textile Sci. & Technol., Shinshu Univ., Ueda, Japan), K. Ikeda. *Prog. Theor. Phys. (Japan)*, vol.69, no.1, p.113-27 (Jan. 1983). The di-nuclear states of $^{16}\text{O}+^{40}\text{Ca}$ and $^{40}\text{Ca}+^{40}\text{Ca}$ are studied from a microscopic point of view within a framework of the generator coordinate method (GCM). The GCM energy kernels including the Coulomb one are exactly treated up to high angular momenta. The states with di-nuclear configuration for the two systems are calculated under a bound state approximation. The following properties of the rotational bands are studied quantitatively: the number of possible bands, their band head energies and moments of inertia. The remarkable shell effects are found in the rotational spectra at high angular momentum nearly equal to that of the state forbidden by a shell model. The potential barriers are also evaluated. (8 refs.)

60192 A modified Glauber approximation and the formation of shock waves in high-energy heavy ion collisions. M. Iwasaki (Dept. of Phys., Kochi Univ., Kochi, Japan), S. Takagi. *Prog. Theor. Phys. (Japan)*, vol.69, no.1, p.142-57 (Jan. 1983). Coherent features in high energy heavy ion collisions are investigated from a microscopic viewpoint. A modified Glauber approximation which enables one to include the slowing down of the relative motion between the centers of masses of both nuclei is presented. The generation of the shock wave is shown to be suppressed by this slowing down effect. As an application, inclusive nucleon spectra and the two-particle correlation are calculated in the case of $\text{Ne}+\text{U}$ collision at 400 MeV/A. (8 refs.)

60193 Liquid-gas phase instabilities in nuclear systems. M.W. Curtin, H. Toki, D.K. Scott (Nat. Superconducting Cyclotron Lab., Michigan State Univ., East Lansing, MI, USA). *Phys. Lett. B (Netherlands)*, vol.123B, no.5, p.289-92 (7 April 1983). The conventional approach to composite fragment production in heavy ion collisions from a single gaseous phase may require modification at temperatures below 20 MeV due to the onset of a liquid-gas phase instability. Clusters heavier than the α -particle are necessary for an unambiguous experimental signature. (14 refs.)

60194 Elastic breakup of 70 MeV ^7Li ions on lead. I.J. Thompson (Dept. of Theoretical Phys., Manchester Univ., Manchester, England), M.A. Nagarajan. *Phys. Lett. B (Netherlands)*, vol.123B, no.6, p.379-82 (14 April 1983). The breakup cross section, in the reaction of 70 MeV ^7Li ions on ^{208}Pb leaving the lead target in its ground state, is calculated in various approximations. It is shown that the prior form of DWBA as well as the high energy adiabatic approximation to the breakup amplitude yield cross sections which are much larger than the experimentally observed cross section. It is suggested that it is necessary to include non-adiabatic corrections, and that a more realistic approach to the Coulomb distortion of the projectile by the target nucleus is necessary. (10 refs.)

60195 Anomalous reaction mean free paths of nuclear projectile fragments from heavy ion collisions at 2A GeV. E.M. Friedlander, R.W. Gimpel, H.H. Heckman, Y.J. Karant (Lawrence Berkeley Lab., Univ. of California, CA, USA), B. Judek, E. Ganssauge. *Phys. Rev. C (USA)*, vol.27, no.4, p.1489-520 (April 1983). The authors present in detail the description and the analysis of two independent experiments using beams of ^{16}O and ^{36}Fe . From their results it is concluded that the reaction mean free paths of relativistic projectile fragments, $3 \leq Z \leq 26$, are shorter for a few centimeters after emission than at large distances, where they are compatible with values predicted from experiments on beam nuclei. The probability that this effect is due to a statistical fluctuation is $<10^{-3}$. The effect is enhanced in later generations of fragments, the correlation between successive generations suggesting a kind of 'memory' for the anomaly. Various systematic and spurious effects as well as conventional explanations are discussed, mainly on the basis of direct experimental observations internal to our data, and found not to explain our results. The data can be interpreted by the relatively rare occurrence of anomalous fragments that interact with an unexpectedly large cross section. The statistical methods used in the analysis of the observations are fully described. (30 refs.)

60196 Giant resonance excitation in the $^{27}\text{Al}(^6\text{Li},^4\text{He})^{27}\text{Si}$ reaction at 93 MeV. A. Guterman, G. Ciangaru, C.C. Chang, J.D. Siik (Dept. of Phys. & Astron., Univ. of Maryland, College Park, MD, USA), D.L. Hendrie, T.J.M. Symons, J. Mahoney. *Phys. Rev. C (USA)*, vol.27, no.4, p.1521-5 (April 1983). A giant resonance in ^{27}Si is observed in the excitation energy region of 10-18 MeV in the spin-isospin flip $^{27}\text{Al}(^6\text{Li},^4\text{He})^{27}\text{Si}$ reaction. A microscopic distorted-wave Born approximation analysis using a G-matrix nucleon-nucleon force and a local energy approximation knockout exchange correction indicates multipolarities between $\lambda=3$ and $\lambda=5$ for the giant resonance. (15 refs.)

60197 Quadrupole effects in ^7Li scattering at 88 MeV. J. Cook, M.F. Vineyard, K.W. Kemper (Dept. of Phys., Florida State Univ., Tallahassee, FL, USA), V. Hnizdo. *Phys. Rev. C (USA)*, vol.27, no.4, p.1536-9 (April 1983). Calculations for ^7Li elastic scattering at 88 MeV have been made explicitly including a quadrupole term in the optical potential resulting from folding of an effective nucleon-nucleon interaction with the quadrupole deformation of ^7Li . Data for ^{40}Ca could be fitted without a renormalization of the folded potential, but this was not possible for lighter targets which required a renormalization of about 0.6 even when the quadrupole potential was included. (18 refs.)

60198 $^{12}\text{C}(^{16}\text{O},\alpha)^{24}\text{Mg}^*$ reaction in the energy region $E_{\text{cm}}=26.6$ to 42.9 MeV. M.J. Bechara, A.J. Lazzarini, R.J. Ledoux, E.R. Cosman (Dept. of Phys., MIT, Cambridge, MA, USA). *Phys. Rev. C (USA)*, vol.27, no.4, p.1540-9 (April 1983). The $^{12}\text{C}+^{16}\text{O}$ resonance structure in the ^{28}Si nucleus is examined by means of the $^{12}\text{C}(^{16}\text{O},\alpha)^{24}\text{Mg}$ reaction excitation functions in the energy range $E_{\text{cm}}=26.6$ to 42.9 MeV in 430 keV steps at $\theta_{\text{lab}}=7.5^\circ$. The authors could identify 64 discrete states in ^{24}Mg up to 31.7 MeV of excitation energy. The excitation functions show abundant structure over the entire energy range. The summed excitation functions, which tend to average out statistical fluctuations, show pronounced intermediate structure enhancement in the cross section at $E_{\text{cm}} \approx 29.5, 32.2$, and 35 MeV and indicate the presence of a smaller peak at 37.3 MeV. The widths of these structures are about 1 MeV, which is intermediate between the value expected from ion-ion potential resonances and statistical fluctuations. The nonstatistical character of these structures is reinforced by some statistical tests and by the correlations in energy and width found in several exit channels. The data also suggest a possible

structural relationship between the ^{28}Si resonances and certain ^{24}Mg final states. (27 refs.)

60199 Structure in the $^{12}\text{C}+^{12}\text{C}$ and $^8\text{Be}+^{16}\text{O}$ fission width distribution of ^{24}Mg observed via the reaction $^{12}\text{C}(^{16}\text{O},\alpha)^{24}\text{Mg} \rightarrow X+Y$. A.J. Lazzarini, S.G. Steadman, R.J. Ledoux, A. Sperduto, G.R. Young, K. Van Bibber, E.R. Cosman (Dept. of Phys., MIT, Cambridge, MA, USA). *Phys. Rev. C (USA)*, vol.27, no.4, p.1550-60 (April 1983). Prominent gross and intermediate width structures are observed in the $^{12}\text{C}+^{12}\text{C}$, $^{12}\text{C}+^{12}\text{C}^*(2^+)$, $^{12}\text{C}^*(2^+)+^{12}\text{C}^*(2^+)$, $^8\text{Be}+^{16}\text{O}$, and $^8\text{Be}+^{16}\text{O}^*$ ($3^-, 0^+$) decay channels following $^{24}\text{Mg}^*$ population via the $^{12}\text{C}(^{16}\text{O},\alpha)^{24}\text{Mg}$ reaction at $E_{\text{cm}}=33$ MeV. Evidence that the $^{12}\text{C}(^{16}\text{O},\alpha)^{24}\text{Mg}$ reaction populates states in ^{24}Mg which are associated with $^{12}\text{C}+^{12}\text{C}$ resonances is presented in the form of correlation analyses between the $\alpha+^{12}\text{C}+^{12}\text{C}$ three-body spectra and previously measured $^{12}\text{C}+^{12}\text{C}$ elastic and inelastic excitation functions. Direct determination of $^{12}\text{C}+^{12}\text{C}$ widths from these measurements is obscured by a background of other strong transitions which appear to be present in the $^{12}\text{C}(^{16}\text{O},\alpha)^{24}\text{Mg}$ singles spectrum. (30 refs.)

60200 Fusion cross sections for $^9\text{Be}+^{40}\text{Ca}$. J.S. Eck, A.R. Omar (Dept. of Phys., Kansas State Univ., Manhattan, KS, USA), J.R. Leigh, T.R. Ophel. *Phys. Rev. C (USA)*, vol.27, no.4, p.1807-10 (April 1983). The total fusion cross sections for $^9\text{Be}+^{40}\text{Ca}$ were measured in the ^9Be bombarding energy range 35-60 MeV in 5 MeV steps by detecting the evaporation residues with a gas ionisation $E-\Delta E$ detector. The measured fusion cross sections are significantly smaller than the total reaction cross sections calculated using optical model parameters obtained from fitting the elastic scattering cross sections in the same energy range. Similar results were obtained earlier for the case of $^9\text{Be}+^{28}\text{Si}$ fusion. The fact that ^9Be is weakly bound and is easily dissociated in the Coulomb and nuclear fields of either the ^{40}Ca or ^{28}Si nucleus is believed to have a strong influence on the observed fusion and elastic scattering cross sections. Sources of possible discrepancy between fusion cross sections measured by determining the yield of heavy evaporation residues and those by summing the cross sections for the emission of light particles such as protons, neutrons, and alpha particles from the compound system are discussed. (10 refs.)

60201 Search for resonant behaviour in $^{16}\text{O}+^{24}\text{Mg}$ inelastic scattering. B.R. Fulton, J.S. Lilley (Daresbury Lab., Sci. & Engng. Res. Council, Warrington, England), T.M. Cormier, P.M. Stwertka. *Phys. Rev. C (USA)*, vol.27, no.4, p.1811-14 (April 1983). A search has been made for indications of resonant behaviour in forward angle ($20^\circ < \theta_{\text{lab}} < 40^\circ$) $^{16}\text{O}+^{24}\text{Mg}$ inelastic scattering. No evidence of resonant structure has been observed over the bombarding energy range 25 MeV $< E_{\text{cm}} < 39$ MeV. An upper limit for the reduced partial width in the $^{24}\text{Mg}(2^+, \pi^+)+^{16}\text{O}$ channel is deduced. (11 refs.)

Energy densities, initial conditions and hydrodynamic equations for ultra-relativistic nucleus-nucleus collisions See Entry 60025

Selective population of high- j states via heavy-ion induced transfer reactions See Entry 60095

Nuclear g factors of the $^{17}/_2^-$ and $^{21}/_2^+$ isomeric states of ^{91}Mo See Entry 60101

Level density and shell structure: Rosenzweig model revisited .. See Entry 60108

Excited states of ^{96}Ru See Entry 60110

Energy and projectile dependence of nuclear alignment in fusion-evaporation reactions See Entry 60129

Time compound nucleus for high energy nuclear reactions See Entry 60149

Deformation effects in aligned ^6Li scattering See Entry 60167

Quantized ATDHF calculations for subbarrier fusion of heavy ions See Entry 60216

Radioactive ion beams for studying astrophysical nuclear reactions See Entry 60510

25.80 MESON- AND HYPERON-INDUCED REACTIONS AND SCATTERING

60202 Observation of analog and nonanalog transitions in the reaction $^{56}\text{Fe}(\pi^+, \pi^-)^{56}\text{Ni}$. P.A. Seidl, R.R. Kiziah, M.K. Brown, C.F. Moore (Univ. of Texas, Austin, TX, USA), C.L. Morris, H. Baer, S.J. Greene, G.R. Burleson, W.B. Cottingham, L.C. Bland, R. Gilman, H.T. Fortune. *Phys. Rev. Lett. (USA)*, vol.50, no.15, p.1106-9 (11 April 1983). An excitation function for the reaction $^{56}\text{Fe}(\pi^+, \pi^-)^{56}\text{Ni}$ has been measured at $\theta_{\text{lab}}=5^\circ$ for incident pion energies of 140-290 MeV. The transition to the lowest-lying $T=0$ state is similar to previous observations, but that to the lowest-lying $T=2$ state is not, except in the high-energy range. (15 refs.)

60203 Observation of a quasideuteron component in the reaction $^{12}\text{C}(\pi^+, 2p)$. A. Altman, E. Pisetzky, J. Lichtenstadt, A.Y. Yavin (Dept. of Phys., Tel Aviv Univ., Tel Aviv, Israel), D. Ashery, R.J. Powers, W. Bertl, L. Felawka, H.K. Walter, R.G. Winter, J. van der Pluym. *Phys. Rev. Lett. (USA)*, vol.50, no.16, p.1187-90 (18 April 1983). The reaction $^{12}\text{C}(\pi^+, 2p)$ was studied at 165 and 245 MeV over a broad kinematic range by coincidence measurement of the outgoing protons. The p - p angular correlations and proton energy spectra allow an identification of the 'quasideuteron' component of the reaction. The angular distribution of this component has a shape similar to that of the $\pi^+d \rightarrow pp$ reaction. It is found that one-step quasideuteron absorption accounts for at most 25% of the total absorption cross section. (14 refs.)

60204 Observation of the nuclear isovector monopole resonance. J.D. Bowman, H.W. Baer, R. Bolton, M.D. Cooper, F.H. Cverna, N.S.P. King, M. Leitch, H.S. Matis (Los Alamos Nat. Lab., Los Alamos, NM, USA), A. Erell, J. Alster, A. Doron, M.A. Moinester, E. Blackmore, E.R. Siciliano. *Phys. Rev. Lett. (USA)*, vol.50, no.16, p.1195-8 (18 April 1983). Observation of the $T=1$ component of the isovector monopole and the giant dipole resonances in the reactions ^{90}Zr and $^{120}\text{Sn}(\pi^-, \pi^0)$ at $T_{\pi^-}=165$ MeV is reported. The isobaric analog state and $T=1$ component of the giant dipole resonance in the reaction $^{120}\text{Sn}(\pi^+, \pi^0)$ were also observed. Excitation energies and widths of the monopole are given. (12 refs.)

60205 Single and double scattering contributions to K^+ -deuteron vector analyzing power at 1.5 GeV/c. K. Hashimoto (Dept. of Phys., Virginia Polytech. Inst. & State Univ., Blacksburg, VA, USA). *Phys. Rev. C (USA)*, vol.27, no.4, p.1572-7 (April 1983). The vector analyzing power for $\text{K}^+ ^2\text{H}$ elastic scattering at 1.5 GeV/c is predicted based on the Glauber model. The calculation, including the single and double KN scattering processes, uses the KN amplitudes obtained by an original phase-shift analysis. Results are also compared with those calculated by another KN analysis. It is shown that the deuteron analyzing power is sensitive to the structure of the KN amplitudes and is strongly affected by the KN polarization. (22 refs.)

60206 Quasielastic scattering of pions from ^{16}O at energies around the $\Delta(1232)$ resonance. C.H.Q. Ingram (Schweizerisches Inst. für Nuklearforschung, Villigen, Switzerland), P.A.M. Gram, J. Jansen, R.E. Mischke, J. Zichy, J. Bolger, E.T. Boschitz, G. Probst, J. Arvieux. *Phys. Rev. C (USA)*, vol.27, no.4, p.1578-601 (April 1983). Inelastic pion scattering from ^{16}O has been studied by measuring the spectrum of pions down to 40 MeV at five angles between 30° and 134° for three incident pion energies: 114, 163, and 240 MeV. The spectra are dominated by a broad peak due to quasielastic scattering from a single nucleon in the nucleus. The systematics of the spectra are discussed with emphasis on the pion-nucleus interaction dynamics including the effect of absorption. The partial $\pi^+{}^{16}\text{O}$ cross sections for all nonradiative channels are estimated. (36 refs.)

60207 Diffraction theory and the double-charge-exchange reaction $^{18}\text{O}(\pi^+, \pi^-)^{18}\text{Ne}$. L.C. Liu (Los Alamos Nat. Lab., Los Alamos, NM, USA). *Phys. Rev. C (USA)*, vol.27, no.4, p.1611-20 (April 1983). The angular distribution and the excitation function of the reaction $^{18}\text{O}(\pi^+, \pi^-)^{18}\text{Ne}$ (double isobaric analog state) can be well understood in the framework of a coupled-channel diffractive scattering theory provided higher-order processes are included. Use of a scaling theory allows an essentially parameter-free calculation of these processes and makes possible the study of effects arising from finer aspects of nuclear structure such as the core excitation of ^{18}O . (22 refs.)

60208 Spin flip transitions in ^{13}C and ^{19}F probed with the (π^-, γ) reaction. C.J. Martoff, J.A. Bistirlich, C.W. Clawson, K.M. Crowe, M. Koike, J.P. Miller, S.S. Rosenblum, W.A. Zajc (Lawrence Berkeley Lab., Univ. of California, Berkeley, CA, USA), H.W. Baer, A.H. Wapstra, G. Strassner, P. Truol. *Phys. Rev. C (USA)*, vol.27, no.4, p.1621-35 (April 1983).

Photon spectra from radiative capture of stopped negative pions captured by ^{13}C and ^{19}F nuclei have been measured with a high resolution pair spectrometer. In the bound region transitions have been observed to $^{13}\text{B}(\text{g.s.})$, $^{13}\text{C}(3.5 \text{ MeV})$, $^{19}\text{O}(\text{g.s.})$, $^{19}\text{O}(4.9 \text{ MeV})$, and $^{19}\text{O}(6.3 \text{ MeV})$. In addition, strong transitions to narrow states above the neutron separation threshold were observed in both cases. The results for ^{13}C are in agreement with detailed shell model calculations of this process. Major strength is observed for states formed by coupling extra nucleons or holes to the spin-quadrupole $d_{5/2}$ and $d_{3/2}$, $J^\pi = 2^-$ states in ^{16}O . The $^{13}\text{C}(\pi^-, \gamma)^{13}\text{B}_{\text{g.s.}}$ branching ratio is shown to be consistent with beta decay and electroexcitation data, through a combined phenomenological analysis. The observed transition strengths are accounted for by matrix elements of the spin-density operators $[\sigma \times Y_0]_1^{1+}$ and $[\sigma \times Y_1]_1^{1+}$. (42 refs.)

60209 Stretched excitations and the spin-dependent part of the pion-nucleon interaction. J.A. Carr, F. Petrovich, D. Halderon (Dept. of Phys., Florida State Univ., Tallahassee, FL, USA), D.B. Holtkamp, W.B. Cottingham. *Phys. Rev. C (USA)*, vol.27, no.4, p.1636-41 (April 1983).

The p -wave form of the spin-orbit operator provides the basis for a single scattering model for the excitation of unnatural parity levels in pion-nucleon scattering in the region of the Δ resonance. The model is found to give a reasonable description of the π^+ and π^- experimental cross sections for the excitation of stretched 4^- and 6^- states in ^{16}O and ^{28}Si . In the calculations the interaction strength was fixed from the free pion-nucleon data and the spin transition densities were determined from recent (e, e') and (p, p') data. A schematic discussion of possible corrections to the model is also presented. (36 refs.)

60210 Bound states in the pion-nucleus velocity-dependent potential. J.F. Carinena, J. Sesma (Dept. de Física Teórica, Facultad de Ciencias, Zaragoza, Spain).

Phys. Rev. C (USA), vol.27, no.4, p.1642-6 (April 1983). The possibility of bound states in a velocity-dependent potential of the Kisslinger type, such as that used to describe the low-energy pion-nucleus interaction, is discussed. It is shown in a specific example that, for a real potential, the number of bound states is finite and their binding energies are real, in contradiction with general results claimed by other authors. (12 refs.)

60211 Pion single and double charge exchange in the resonance region: dynamical corrections. M.B. Johnson (Los Alamos Nat. Lab., Los Alamos, NM, USA), E.R. Siciliano.

Phys. Rev. C (USA), vol.27, no.4, p.1647-68 (April 1983). The authors consider pion-nucleus elastic scattering and single- and double-charge-exchange scattering to isobaric analog states near the $(3,3)$ resonance within an isospin invariant framework. They extend previous theories by introducing terms into the optical potential U that are quadratic in density and consistent with isospin invariance of the strong interaction. They study the sensitivity of single and double charge exchange angular distributions to parameters of the second-order potential both numerically, by integrating the Klein-Gordon equation, and analytically, by using semiclassical approximations that explicate the dependence of the exact numerical results to the parameters of U . The magnitude and shape of double charge exchange angular distributions are more sensitive to the isosensor term in U than has been hitherto appreciated. An examination of recent experimental data shows that puzzles in the shape of the $^{18}\text{O}(\pi^+, \pi^-)^{18}\text{Ne}$ angular distribution at 164 MeV and in the A dependence of the forward double charge exchange scattering on ^{18}O , ^{26}Mg , ^{42}Ca , and ^{48}Ca at the same energy may be resolved by adding an isosensor term in U . (38 refs.)

60212 Q -value systematics applied to the absorption of mesons on complex nuclei. H. Oeschler, Y. Cassagnou, R. Fonte, R. Legrain (Dept. de Phys. Nucleaire, CENS, Gif-sur-Yvette, France).

Phys. Rev. C (USA), vol.27, no.4, p.1677-84 (April 1983). The isotopic yields both from deep inelastic collisions between heavy ions and from fragmentation processes have been successfully described by Q -value systematics. In order to test their range of validity and to investigate correlations with specific reaction mechanisms, the Q -value systematics have been applied to the multinucleon-removal spectra following pion and kaon absorption on complex nuclei. Indeed, the isotopic distribution derived from these spectra shows the following feature: most of the yields are not strongly influenced by the charge of the pion and can be explained by nuclear evaporation following pion absorption. In contrast, the yields of elements far removed from the target show a better agreement with a Q_{res} law under the assumption that the pion is implanted in the target. The influence of the pion charge upon the yield distribution is thus evidenced even after the removal of 10-14 nucleons from the target. As a dominant evaporation process would not reproduce this effect, this indicates the importance of direct reaction mechanisms associated with pion absorption. This could support the hypothesis of an absorption on a complex cluster or a very strong final-state interaction. The parameter T extracted from the Q -value systematics appears proportional to the total energy brought by the meson into the system. (22 refs.)

60213 Reaction $\pi^+ + d \rightarrow p + p$ at 65 to 140 MeV. B.G. Ritchie, G.S. Blaupied, R.S. Moore, B.M. Preadom (Univ. of South Carolina, Columbia, SC, USA), K. Goto, R.C. Minehart, J. Boswell, G. Das, H.J. Ziock, N.S. Chant, P.G. Roos, W.J. Burger, S. Gilad, R.P. Redwine. *Phys. Rev. C (USA)*, vol.27, no.4, p.1685-92 (April 1983).

Differential cross sections for the reaction $\pi^+ + d \rightarrow p + p$ were measured for pion laboratory energies of 65, 72.5, 80, 95, 110, 125, and 140 MeV. The integrated cross sections for these energies were found to be 7.51 ± 0.19 , 7.91 ± 0.16 , 8.64 ± 0.15 , 9.61 ± 0.15 , 11.3 ± 0.2 , 11.7 ± 0.3 , and 11.3 ± 0.3 mb, respectively. These values indicate that the centroid and width of the energy dependence for the resonance in this reaction is lower and greater, respectively, than predicted by most theoretical models of the process. Comparisons made with predictions by Blankleider and Afnan show a qualitative difference between experimental measurements and calculations of the $P_2(\cos\theta)$ term in the polynomial expansion of the differential cross section. This may indicate a more important role for p -like exchange in the reaction mechanism than that included by the calculations. (14 refs.)

Quark contributions to the $pp \rightarrow d\pi^+$ reaction See Entry 60005

Extended folding potential model for Δ -deuteron system with hard core potential See Entry 60128

Transition densities for charge-exchange components of giant isovector resonances and the proton-neutron density distributions in nuclei .. See Entry 60136

Comments on recent progress in few particle physics See Entry 60147

Chew-Low model and the potential description of the πN interaction See Entry 60153

25.85 FISSION REACTIONS

60214 Role of accelerators in uniform identification of thermal neutrons. K. Denno (Dept. Electrical Engng., N.J. Inst. of Technol., Newark, NJ, USA).

IEEE Trans. Nucl. Sci. (USA), vol.ns-30, no.2, p.1173-4 (April 1983). (1982 IEEE Conference on the Application of Accelerators in Research and Industry, Denton, TX, USA, 8-10 Nov. 1982).

Control of nuclear reactors power output is centrally dependent on the level response of thermal neutrons flux as well as on their dynamic and kinetic spectra. The paper presents a set of uniform parametric properties for delayed neutrons based on accelerator experiments. Calculations have established several patterns linking energies of accelerated incident neutrons with respect to continuous spectra of delayed neutrons, mean yield of neutrons per fission, time response of neutron lethargy and energy spectra and delayed neutrons. Also mathematical models are developed for neutrons yield and spectra in the time domain with respect to ^{235}U and Pu^{239} material targets. Results obtained are important in accelerator selectivity application as well as in the planned control of nuclear thermal reactors, for ensuring adequate compatibility between power level and reactor reactivity trajectories. (5 refs.)

25.88 FUSION REACTIONS

60215 Nuclear reactions among the hydrogen isotopes at low energies. R.E. Brown, N. Jarmie, R.A. Hardekopf (Los Alamos Nat. Lab., Los Alamos, NM, USA).

IEEE Trans. Nucl. Sci. (USA), vol.ns-30, no.2, p.1164-8 (April 1983). (1982 IEEE Conference on the Application of Accelerators in Research and Industry, Denton, TX, USA, 8-10 Nov. 1982).

The low-energy fusion cross-section (LEFCS) apparatus installed at the Los Alamos Van de Graaff facility has been used to measure the cross sections for the important fusion-energy reaction $\text{D}(t, \alpha)n$ over the triton bombarding energy range of 12.5 to 117 keV. This corresponds to an equivalent deuteron bombarding energy range of 8.3 to 78.1 keV and to a $\text{D}+\text{T}$ plasma temperature (kT) range of 0.7 to 18.8 keV. Over most of the energy range the cross sections are accurate to 1.4%, with the error rising to 4.8% at the lowest energy. A data base was constructed for deuteron bombarding energies up to about 250 keV that included the authors' data and four other data sets. This data base can be fitted quite well with a single-level $(3/2^+)$ resonance formula in the R-matrix formalism. (17 refs.)

60216 Quantized ATDHF calculations for subbarrier fusion of heavy ions. K. Goeke, F. Grummer (Inst. für Kernphys., KFA, Jülich, Jülich, Germany), P.-G. Reinhard.

Phys. Lett. B (Netherlands), vol.124B, no.1-2, p.21-5 (21 April 1983). The quantized adiabatic time-dependent Hartree-Fock theory (quantized ATDHF) is applied to the subbarrier fusion process of $^{16}\text{O} + ^{16}\text{O} \rightarrow ^{32}\text{S}$. The corresponding optimal, i.e. maximally decoupled collective path is evaluated by means of three-dimensional coordinate and momentum space grid techniques using the Bonche-Koonin-Negele interaction completed by the Coulomb force. Collective mass parameters, potentials, quantum corrections and rotational moments of inertia are evaluated in dependence of the distance between the ions. The results are compared to experimental fusion data and to the outcome of Hartree-Fock with quadrupole constraint. (23 refs.)

Energy and projectile dependence of nuclear alignment in fusion-evaporation reactions See Entry 60129

Fusion cross sections for $^9\text{Be} + ^{40}\text{Ca}$ See Entry 60200

Charged particle reaction cross sections and nucleosynthesis ... See Entry 64460

25.90 OTHER TOPICS IN NUCLEAR REACTIONS AND SCATTERING: SPECIFIC REACTIONS

Charged particle reaction cross sections and nucleosynthesis ... See Entry 64460

27.00 PROPERTIES OF SPECIFIC NUCLEI LISTED BY MASS RANGES

27.10 $A \leq 5$

Quark contributions to the $pp \rightarrow d\pi^+$ reaction See Entry 60005

Comment on the problem of the off-shell γNN vertex function in ed elastic scattering See Entry 60051

Off-shell γNN vertex function in ed elastic scattering See Entry 60052

Shell model calculations using modified Sussex matrix elements for $A \leq 4$ See Entry 60102

Extended folding potential model for Λ -deuteron system with hard core potential	See Entry 60128
$1/2^+ \rightarrow 1/2^+$ beta decay with neutrino mass effects in the elementary particle treatment of weak interactions	See Entry 60141
Atomic final-state interactions in tritium decay	See Entry 60142
Emission of heavy neutrinos in muon capture	See Entry 60143
Comments on recent progress in few particle physics	See Entry 60147
Supermultiplet symmetry in nuclear reactions: application to $^3\text{He}(p,^2\text{H})2p$ and $^7\text{Be}(^3\text{H},^6\text{He})^6\text{Li}^*$	See Entry 60150
Proton polarization in the photodisintegration of the deuteron at γ energies in the range 700-1100 MeV	See Entry 60164
Investigation of the three-nucleon system by pd elastic scattering with polarized protons and deuterons	See Entry 60165
Pion-exchange contributions to the Lobashov experiment	See Entry 60166
Effects of final state interactions in disintegration of three-nucleon nuclei	See Entry 60172
Special features of the alpha induced deuteron breakup	See Entry 60182
Bremsstrahlung in the $^3\text{He}\text{-}^2\text{H}$ interaction near the deuteron break-up threshold	See Entry 60183
Single and double scattering contributions to K^+ -deuteron vector analyzing power at 1.5 GeV/c	See Entry 60205
Reaction $\pi^+ + d \rightarrow p + p$ at 65 to 140 MeV	See Entry 60213
Nuclear reactions among the hydrogen isotopes at low energies	See Entry 60215
Radioactive ion beams for studying astrophysical nuclear reactions	See Entry 60510

27.20 6 ≤ A ≤ 19

Final state branching ratio in the ^7Be decay	See Entry 60139
^7Be decay scheme and the solar neutrino problem	See Entry 60140
A search on the parity-forbidden alpha width of the $E_x=4.753$ MeV ($J^\pi, T=0^+, 1$) level of ^{19}F	See Entry 60145
Supermultiplet symmetry in nuclear reactions: application to $^3\text{He}(p,^2\text{H})2p$ and $^7\text{Be}(^3\text{H},^6\text{He})^6\text{Li}^*$	See Entry 60150
On the normal modes of vibration in light deformed nuclei	See Entry 60158
Gamow-Teller strength in the $^{18}\text{O}(p,n)^{18}\text{F}$ reaction at 135 MeV	See Entry 60179
Bare potential DWBA for (d, p) reactions	See Entry 60184
Continuous spectra of deuterons from $^3\text{He} + ^{12}\text{C}$ at low energy	See Entry 60187
Quasifree scattering at low energies in $^6\text{Li}(\alpha, 2\alpha)^2\text{H}$	See Entry 60188
Heavy ion resonances in the s-d shell	See Entry 60190
Anomalous reaction mean free paths of nuclear projectile fragments from heavy ion collisions at 2A GeV	See Entry 60195
$^{12}\text{C}(^{16}\text{O}, \alpha)^{24}\text{Mg}^*$ reaction in the energy region $E_{\text{c.m.}}=26.6$ to 42.9 MeV	See Entry 60198
Structure in the $^{12}\text{C} + ^{12}\text{C}$ and $^8\text{Be} + ^{16}\text{O}$ fission width distribution of ^{24}Mg observed via the reaction $^{12}\text{C}(^{16}\text{O}, \alpha)^{24}\text{Mg} \rightarrow X + Y$	See Entry 60199
Observation of a quasideuteron component in the reaction $^{12}\text{C}(\pi^+, 2p)$	See Entry 60203
Quasielastic scattering of pions from ^{16}O at energies around the $\Delta(1232)$ resonance	See Entry 60206
Diffraction theory and the double-charge-exchange reaction $^{18}\text{O}(\pi^+ \pi^-)^{18}\text{Ne}$	See Entry 60207
Spin flip transitions in ^{13}C and ^{19}F probed with the (π^-, γ) reaction	See Entry 60208
Stretched excitations and the spin-dependent part of the pion-nucleon interaction	See Entry 60209
Quantized ATDHF calculations for subbarrier fusion of heavy ions	See Entry 60216
Effects of a nuclear scattering resonance on bremsstrahlung production and K-shell ionization	See Entry 60953
Measurement of activity yields for $^{12}\text{C}(\gamma, n)^{11}\text{C}$, $^{14}\text{N}(\gamma, n)^{13}\text{N}$, and $^{16}\text{O}(\gamma, n)^{15}\text{O}$ reactions as a function of electron beam energy and angle from the electron beam using thick target produced bremsstrahlung	See Entry 63963

27.30 20 ≤ A ≤ 38

An approximate calculation of the energy spectrum for particular angular momentum states	See Entry 60103
On the normal modes of vibration in light deformed nuclei	See Entry 60158
High resolution proton resonance measurements	See Entry 60174
Simultaneous measurements of analyzing powers and differential cross sections for $n + ^{28}\text{Si}$	See Entry 60175
Excited-state giant dipole resonances in (p, γ) : a new probe of single-particle strengths	See Entry 60178
Radiation proton trapping by ^{51}V , ^{59}Co , $^{63,65}\text{Cu}$ Nuclei	See Entry 60181
Giant resonance excitation in the $^{27}\text{Al}(^6\text{Li}, ^4\text{He})^{27}\text{Si}$ reaction at 93 MeV	See Entry 60196
Quadrupole effects in ^7Li scattering at 88 MeV	See Entry 60197
$^{12}\text{C}(^{16}\text{O}, \alpha)^{24}\text{Mg}^*$ reaction in the energy region $E_{\text{c.m.}}=26.6$ to 42.9 MeV	See Entry 60198
Structure in the $^{12}\text{C} + ^{12}\text{C}$ and $^8\text{Be} + ^{16}\text{O}$ fission width distribution of ^{24}Mg observed via the reaction $^{12}\text{C}(^{16}\text{O}, \alpha)^{24}\text{Mg} \rightarrow X + Y$	See Entry 60199
Search for resonant behaviour in $^{16}\text{O} + ^{24}\text{Mg}$ inelastic scattering	See Entry 60201
Stretched excitations and the spin-dependent part of the pion-nucleon interaction	See Entry 60209
V1343 Aquilae	See Entry 64492

27.40 39 ≤ A ≤ 58

Excitation of the 6^- particle-hole state with the $^{40}\text{Ca}(p, n)^{40}\text{Sc}$ reaction at 133.5 MeV	See Entry 60099
Energy levels of the odd manganese nuclei from the $(d, ^3\text{He})$ reaction	See Entry 60104
Energy and projectile dependence of nuclear alignment in fusion-evaporation reactions	See Entry 60129
Absolute strength determinations of dipole transitions and unique spin-parity assignments in ^{52}Cr and ^{56}Fe	See Entry 60132
Search for M1 strength in ^{51}V and the difference in $^{51}\text{V}(e, e')$ and $^{51}\text{V}(p, p')$ spectra	See Entry 60133
Transition densities for charge-exchange components of giant isovector resonances and the proton-neutron density distributions in nuclei ..	See Entry 60136
Investigation of isobaric analog resonances in ^{53}Mn	See Entry 60159
Deformation effects in aligned ^6Li scattering	See Entry 60167
The photodisintegration of ^{40}Ar	See Entry 60170
High resolution proton resonance measurements	See Entry 60174
Cross section calculations for nucleon- ^{40}Ca and α - ^{40}Ca elastic scattering from microscopic nonlocal optical potentials	See Entry 60180
Radiation proton trapping by ^{51}V , ^{59}Co , $^{63,65}\text{Cu}$ Nuclei	See Entry 60181
Bare potential DWBA for (d, p) reactions	See Entry 60184
Role of the ^3He optical model potential ambiguity in the distorted-wave Born approximation description of the $^{58}\text{Ni}(^3\text{He}, d)^{59}\text{Cu}$ reaction at 130 MeV incident energy	See Entry 60189
Microscopic study on di-nucleus states of $^{16}\text{O} + ^{40}\text{Ca}$ and $^{40}\text{Ca} + ^{40}\text{Ca}$ I	See Entry 60191
Anomalous reaction mean free paths of nuclear projectile fragments from heavy ion collisions at 2A GeV	See Entry 60195
Quadrupole effects in ^7Li scattering at 88 MeV	See Entry 60197
Fusion cross sections for $^9\text{Be} + ^{40}\text{Ca}$	See Entry 60200
Observation of analog and nonanalog transitions in the reaction $^{56}\text{Fe}(\pi^-, \pi^-)^{56}\text{Ni}$	See Entry 60202

27.50 59 ≤ A ≤ 89

Nuclear g factors of the $17/2^-$ and $21/2^+$ isomeric states of ^{91}Mo	See Entry 60101
A study of the $^{86}\text{Sr}(^3\text{He}, t)^{86}\text{Y}$ reaction	See Entry 60106
Cluster (quadrupole-octupole) phonon model: application to ^{89}Y	See Entry 60113
Energy and projectile dependence of nuclear alignment in fusion-evaporation reactions	See Entry 60129
A study of the $^{84}\text{Kr}(\alpha, 2n\gamma)^{86}\text{Sr}$ reaction	See Entry 60134
Cyclotron production of ^{67}Ga . Cross sections and thick-target yields for the $^{67}\text{Zn}(p, n)$ and $^{68}\text{Zn}(p, 2n)$ reactions	See Entry 60177
Role of the ^3He optical model potential ambiguity in the distorted-wave Born approximation description of the $^{58}\text{Ni}(^3\text{He}, d)^{59}\text{Cu}$ reaction at 130 MeV incident energy	See Entry 60189
Q-value systematics applied to the absorption of mesons on complex nuclei	See Entry 60212
Reduction of the neutron-induced background using a pulse-type beam chopper in an ISOL experiment	See Entry 60504
Regularities of the dose field formation in placing ^{252}Cf and ^{60}Co sources on the same plane	See Entry 63967

27.60 90 ≤ A ≤ 149

Selective population of high-j states via heavy-ion induced transfer reactions ...	See Entry 60095
Search for the second excited $11/2^-$ state and weak-coupling scheme in ^{117}Sn	See Entry 60096
Nuclear g factors of the $17/2^-$ and $21/2^+$ isomeric states of ^{91}Mo	See Entry 60101
Level structure of the doubly odd nucleus ^{112}In from the $(p, n\gamma)$ reaction	See Entry 60107
Excited states of ^{96}Ru	See Entry 60110
Levels in ^{148}Ce from the decay of mass separated ^{148}La	See Entry 60111
Beta-decay energies and masses of $^{103-105}\text{In}$	See Entry 60112
The decay of Ag-105g	See Entry 60131
Level structure of ^{109}Ag from studies of the decay of ^{109}Pd ..	See Entry 60137
Calorimetric redetermination of the half-life of ^{90}Sr	See Entry 60138
$^{113}\text{In}(\gamma, n)$ reaction isomeric and ground-state cross-sections	See Entry 60169
Observation of the nuclear isovector monopole resonance	See Entry 60204
Determination of the specific activity of fission-based ^{99}Mo using differential pulse polarography	See Entry 60556

27.70 150 ≤ A ≤ 189

Muonic X-ray measurement of the monopole and quadrupole charge parameters of $^{154-158, 160}\text{Gd}$	See Entry 60105
---	-----------------

27.80 190 ≤ A ≤ 219

Nuclear structure of even lead isotopes by the (p, t) reaction	See Entry 60109
Structure of ^{209}Bi deduced from the $^{208}\text{Pb}(t, 2n\gamma)$ reaction	See Entry 60185
Elastic breakup of 70 MeV ^7Li ions on lead	See Entry 60194

27.90 220 ≤ A

Comparison of the (p, xn) cross sections from ^{238}U , ^{235}U and ^{232}Th targets irradiated with 200 MeV protons	See Entry 60176
The production of neutron-rich nuclides in the heavy-element region via ^3He induced reactions	See Entry 60186

- A modified Glauber approximation and the formation of shock waves in high-energy heavy ion collisions See Entry 60192
- Role of accelerators in uniform identification of thermal neutrons See Entry 60214
- Ion extraction in the laser process of uranium enrichment by selective ionization of atomic vapour See Entry 61005
- Regularities of the dose field formation in placing ^{252}Cf and ^{60}Co sources on the same plane See Entry 63967

28.00 NUCLEAR ENGINEERING AND NUCLEAR POWER STUDIES

(see also 86.10 Energy resources and their utilisation)

28.20 NEUTRON PHYSICS

(see also 25.40 Nucleon-induced reactions and scattering)

- 60217 Measured neutron leakage spectra from ferrous spheres. M. Holman. *Jad. Energ. (Czechoslovakia)*, vol.29, no.3, p.92-7 (March 1983). In Czech. The absolute leakage flux spectra of neutrons from ferrous spheres were measured in the energy range of 10 keV-10 MeV using a stilbene neutron spectrometer and proportional counters. (8 refs.)
- A finite element solution to the group diffusion problems with albedo-type boundary conditions See Entry 60221

28.41 FISSION REACTOR THEORY AND DESIGN

- 60218 Pressure testing the THTR-300 reactor pressure vessel. F. Bremer, J. Schoning (Krupp GmbH, Essen, Germany). *Atomwirtsch.-Atomtech. (Germany)*, vol.28, no.4, p.189-92 (April 1983). In German.

The pressure and leak test successfully passed by the reactor pressure vessel of the THTR-300 high temperature reactor in the last week in September of 1982 has been a decisive step towards commissioning this prototype nuclear power plant, which is being built by the consortium of Brown, Boveri & Cie. AG (BBC), Hochttemperatur-Reaktorbau GmbH (HRB), and Nukem GmbH on behalf of Hochttemperatur-Kernkraftwerk GmbH (HKG). The fuels to be used in the reactor are uranium and thorium. The prestressed concrete vessel of the THTR-300 is shaped like an upright cylinder of 28 m height and 25 m diameter. The thickness of the walls and the bottom is approx. 5 m. The vessel concept is based on the experience of twenty years of international development; it represents a mature design. Problem-free construction and flexible design principles make for short construction times. The computer programs and confirmed materials data employed in the THTR vessel constitute a sufficiently sound basis for dimensioning prestressed concrete pressure vessels of different geometries for power plants up to the largest unit power sizes. (no refs.)

- 60219 Computer codes for system reliability engineering. P. Skvarka (Vyskumny ustav Energeticky, Pobocka, Bratislava, Czechoslovakia). *Jad. Energ. (Czechoslovakia)*, vol.29, no.3, p.103-5 (March 1983). In Czech. Present day state of computer programs for system reliability engineering in the world and codes used in design and research in nuclear engineering in Czechoslovakia are reviewed as well as the classification of computer codes by their purpose. (43 refs.)

- 60220 Generation and benchmark test of 26-group constant set for fast reactor calculations. Jung-Do Kim, Jong Tai Lee (Korea Advanced Energy Res. Inst., Seoul, Korea). *J. Korean Nucl. Soc.*, vol.14, no.4, p.163-71 (Dec. 1982). [received: April 1983]

An ABBN-type 26-group constant set, KAERI=26G, which can be reliably applied to fast reactor calculations has been generated using the nuclear data of ENDF/B-IV or ENDF-78 and a processing code ETOX-K4. The KAERI-26G set was evaluated by analysing measured integral quantities such as the effective multiplication factor, central reaction-rate ratio, and central reactivity coefficient for a variety of critical assemblies, and these calculated quantities were compared with results from other workers using similar type sets. (20 refs.)

- 60221 A finite element solution to the group diffusion problems with albedo-type boundary conditions. Kun Joong Yoo (Korea Advanced Energy Res. Inst., Seoul, Korea), Chang Hyo Kim, Chang Hyun Chung. *J. Korean Nucl. Soc.*, vol.14, no.4, p.178-85 (Dec. 1982). [received: April 1983]

An albedo-type boundary condition is incorporated into the finite element formulation of the cubic Hermite polynomials for the two-dimensional solution of the two-group diffusion problem. Two modifications are introduced with respect to the conventional expression for the weak form of the group diffusion equation with the zero flux of zero current boundary condition and the cubic element functions over the boundary nodes. The finite element formulations obtained from those modifications are tested with the two-dimensional ZION problem. The numerical effectiveness of the modifications is examined. (4 refs.)

- 60222 Review and application of the TRAC-PD2 computer code. R.K.-C. Chan, P.J. Masiello. *Report EPRI-NP-2826*, Electr. Power Res. Inst., Palo Alto, CA, USA (Jan. 1983). 128 pp.

Available from Res. Rep. Center, Box 50490, Palo Alto, CA 94303, USA. A review is presented of the theoretical modeling and numerical methods and solution techniques used in the TRAC-PIA and TRAC-PD2 computer codes. Results that correspond primarily with TRAC-PD2 are reported: (1) an analysis of the numerical selection techniques used in the codes, (2) a review of the constitutive relations used in thermal-hydraulic models and (3) a comparison of code results with experimental data from various reflood and small-break tests.

- 60223 Feasibility study: A new cable tray hanger connector for nuclear power plants. M.W. Dixon, B.K. Pearce, J.E. Jackson, F.R. Bourne. *Report EPRI-NP-2910*, Electr. Power Res. Inst., Palo Alto, CA, USA (March 1983). 120 pp.
- Available from Res. Rep. Center, Box 50490, Palo Alto, CA 94303, USA. Describes a feasibility study on the potential use of flexible connectors to reduce seismically induced loads in nuclear power plants. Finite element, classical analytic, and experimental examinations are detailed. Although it was concluded that a flexible connector system can provide a better dynamic

response than the conventional-type system using rigid connectors, additional work is required before this concept can be validated in actual plant designs.

- 60224 Comparison of COMETHE-IIIJ and FCODE-BETA fission gas release predictions with measurements. S. Lee, L. Rayces, E. Rumble, D. Wheeler, A. Woods. *Report EPRI-NP-2903*, Electr. Power Res. Inst., Palo Alto, CA, USA (March 1983). 72 pp.
- Available from Res. Rep. Center, Box 50490, Palo Alto, CA 94303, USA. Compares the fission product gas release (FGR) predictability of two LWR fuel rod modeling codes: COMETHE-IIIJ and FCODE-BETA. The comparison is made using 124 all-characterized fuel rods with FGR measurements in the EPRI fuel performance data base.

- Design study of a spent fuel shipping cask for Korea Nuclear Unit-1 See Entry 60242

- Reactor physics constants for the medium enriched-uranium core of Kyoto University Critical Assembly See Entry 60336

- Prospekt-1 program for recovering the neutron spectra of nuclear reactors See Entry 60337

- BWR refill-reflood program constitutive correlations for shear and heat transfer for the BWR version of TRAC See Entry 60338

- NATBWR: A steady-state model for natural circulation in boiling water reactors See Entry 60339

- Thermal-hydraulic code qualification: ATHOS2 and data from Bugey 4 and Tricastin I See Entry 60342

- Study on the steam line break accident for Kori Unit-1 See Entry 60352

- Analysis and synthesis of the theoretical studies performed on the control and safety of LWR's burning plutonium fuel See Entry 60358

- Safety aspects in the development and construction of fast neutron reactors cooled by sodium See Entry 60386

28.42 FISSION REACTOR MATERIALS

- 60225 Experience with LOMI agents in cleaning cooling systems. H. Cole (AERE, Harwell, England). *Atomwirtsch.-Atomtech. (Germany)*, vol.28, no.1, p.26-8 (Jan. 1983). In German.

Research has revealed the corrosion products most frequently encountered in contaminated cooling water to be oxide compounds. It has been the practice for many years, both in nuclear and nonnuclear facilities, to remove oxide deposits by flushing with concentrated oxidants and chelating agents followed by citrates. Though very effective, these methods suffer from the drawback, especially in nuclear plants, of requiring huge amounts of flushing water, thus producing enormous volumes of liquid radioactive effluents. Ideally, decontaminants should have low agent concentrations and dissolve oxides fast in order for their presence not to cause further corrosion. Studies of the problems associated with the decontamination of reactor cooling water in Britain focused on improvements of the rate of dissolution, with the conclusion that the simplest way to achieve this would be by modifying the chemical structure of the oxide. (no refs.)

- 60226 Measures for increasing IAEA safeguards effectiveness. C.R. Hatcher (Los Alamos Nat. Lab., Los Alamos, NM, USA). *J. Inst. Nucl. Mater. Manage. (USA)*, vol.11, no.4, p.22-8 (Winter 1982).

The effectiveness of International Atomic Energy Agency (IAEA) safeguards depends not only on the quality of IAEA inspection and independent verification of declared nuclear material and facility use, but also on the perception of and reaction to IAEA safeguards by the nations who make up the international community. Because perceptions and reactions often involve nontechnical as well as technical factors, it has proven difficult to describe IAEA safeguards effectiveness in quantitative technical terms. This study uses a flow diagram to examine how IAEA inspections and the resulting verification statements lead to the main political objectives of IAEA safeguards, assurance and deterrence. Based on this approach, a figure of merit called the IAEA safeguards effectiveness ratio is defined, and measures for increasing IAEA safeguards effectiveness are identified and discussed. (14 refs.)

- 60227 Anticipated amounts of nuclear materials under IAEA safeguards (1981-1990). A. Bilyk (International Atomic Energy Agency, Vienna, Austria). *J. Inst. Nucl. Mater. Manage. (USA)*, vol.11, no.4, p.29-33 (Winter 1982).

To assess the scope of nuclear activities subject to safeguards in the future, the System Studies Section of the Department of Safeguards of the IAEA maintains a computerized data base file where data on nuclear fuel cycle facilities under operation, under construction, and planned, collected from open publications, are stored and updated. A set of computerized programmes has been worked out to forecast both the number of nuclear facilities of different types and the amounts of nuclear materials that may come under safeguards in the future. Simplified models simulating the flows of nuclear materials associated with the operation of power reactors have been adopted for the forecasting of the amounts of nuclear materials. The calculation has dealt only with those types of power reactors for which the operational experience exists and for which a model approach based on that experience could be reasonably applied (PWRs, BWRs, PHWRs and GCRs). (no refs.)

- 60228 Attributes model sampling schemes for international material accountability verification. J.B. Sanborn (Brookhaven Nat. Lab., Upton, NY, USA). *J. Inst. Nucl. Mater. Manage. (USA)*, vol.11, no.4, p.34-41 (Winter 1982).

Addresses the question of detecting falsifications in material balance accountability reporting by comparing independently measured values to the declared values of a randomly selected sample of items in the material balance. A two-level strategy is considered, consisting of a relatively large number of measurements made at low accuracy, and a smaller number of measurements made at high accuracy. Sampling schemes for both types of measurements are derived, and rigorous proofs supplied that guarantee desired detection probabilities. Sample sizes derived using these methods are sometimes considerably smaller than those calculated previously. (3 refs.)

- 60229 Development of an improved monitor for portal detection of the unauthorized removal of special nuclear material. L.W. Kruse, B. Dominguez (Sandia Nat. Labs., Albuquerque, NM, USA). *J. Inst. Nucl. Mater. Manage. (USA)*, vol.11, no.4, p.42-7 (Winter 1982).

A study was made of alternative designs for the portal detection of special nuclear material. Changes in the detector, signal-processing, and alarm logic components improved detection sensitivity and make the system less prone to false alarms. The resulting performance complies with the criteria for allowable frequency of false alarms specified by the Nuclear Regulatory Commission. (7 refs.)

60230 A statistic sensitive to deviations from the zero-loss condition in a sequence of material balances. D.Sellenschegg (Kernforschungszentrum Karlsruhe, Karlsruhe, Germany).

J. Inst. Nucl. Mater. Manage. (USA), vol.11, no.4, p.48-59 (Winter 1982). The CUMUFR (cumulative sum of standardized MUF-residuals) statistic is proposed to examine materials balance data for deviations from the zero-loss condition. The time series of MUF-residuals is shown to be a linear transformation of the MUF-time series. The MUF-residuals can directly be obtained by applying the transformation or they can be obtained, approximately, by the application of a Kalman filter to estimate the true state of MUF. A modified sequential test with power one is formulated for testing the CUMUFR statistic. The detection capability of the proposed examination procedure is demonstrated by an example, based on Monte Carlo simulations, where the materials balance of the chemical separation process in a reference reprocessing facility is considered. It is shown that abrupt as well as protracted loss patterns are detected with rather high probability when they occur after a zero-loss period. (16 refs.)

60231 A review of the regulations in various countries with regard to nuclear waste disposal. N.Pelzer (Univ. Göttingen, Göttingen, Germany), P.-G.Gutermuth.

Energiewirtschaft. Tagesfragen (Germany), vol.33, no.3, p.144-8 (March 1983). In German.

An attempt is made to define 'nuclear waste' and 'disposal', both being interpreted somewhat differently in different countries. The German and Swiss legislation regarding waste disposal is similar. A survey of legislation and methods of waste disposal in other countries is made. In some European countries the disposal is carried out by private contractors but in every case the government has the overall control and responsibility. Little is known about legislation and methods of disposal in the USSR and Japan, the latter because of lack of a reliable translation of the relevant Japanese documents. (62 refs.) G.R.S.

60232 Nuclear and materials studies with ion beams. T.W.Conlon (AERE Harwell Lab., Harwell, England).

IEEE Trans. Nucl. Sci. (USA), vol.ns-30, no.2, p.1209-13 (April 1983). (1982 IEEE Conference on the Application of Accelerators in Research and Industry, Denton, TX, USA, 8-10 Nov. 1982).

The main role of the Harwell Laboratory is to develop technology for nuclear power. Broadly this means the elucidation of the nuclear physics underlying fission and fusion concepts and the study and development of suitable materials for all aspects of the fuel cycle. An important and growing part of the Nuclear Physics Division's (NPD) work is the development of programmes spanning both roles. This synergy is clearly apparent in the ion beam work based on the Harwell suite of charged particle accelerators. This report covers aspects of nuclear studies on the accelerators (viz. heavy ion reaction mechanisms; heavy ion range, energy loss and straggling) the associated development of techniques for materials analysis (viz. thin layer activation, microbeam analysis, multielement profiling, etc.) and the commercial exploitation of accelerators and techniques. (5 refs.)

60233 Microbeam analysis of a Commercial Advanced Gas Cooled Reactor material. S.O.Olabanji, J.M.Calvert (Dept. of Phys., Schuster Lab., Univ. of Manchester, Manchester, England).

IEEE Trans. Nucl. Sci. (USA), vol.ns-30, no.2, p.1246-8 (April 1983). (1982 IEEE Conference on the Application of Accelerators in Research and Industry, Denton, TX, USA, 8-10 Nov. 1982).

The role of silicon as a corrosion inhibitor was investigated by determining the concentration profiles of silicon and the other associated elements in the Commercial Advanced Gas Cooled Reactor (CAGR) material. The microbeam scanning method was employed. Three different alloys namely Fe-9Cr, Fe-9Cr-0.3%Si and Fe-9Cr-0.6%Si were studied by this structure. This, together with the microbeam analysis established the presence of silicon at the metal-oxide interface either alone as silica or coupled with the local chromium to form a chromium-silicon rich barrier layer which influenced the overall oxidation kinetics. (10 refs.)

60234 Evaluation of fuel performance in reactor (PWR). IV. Transient behavior after happening of cladding defect. T.Aoki (Kansai Electric Power Co., Mihama, Japan).

J. At. Energy Soc. Jpn. (Japan), vol.25, no.1, p.29 (Jan. 1983). In Japanese.

For Pt.III see *ibid.*, vol.24, no.12, p.944-62 (1982). Transient phenomena of iodine concentrations in primary coolant which appear after sudden opening of hair crack on fuel cladding under constant power state are analyzed. From these analyses it is understood that the information on every state of cladding defect are given by the observed ^{131}I and ^{133}I concentrations. The direct ejection of uranium fuel by fission fragments and knock-out phenomena to primary coolant which may occur under the most unfavorable condition, are excluded from the paper. Observations of iodine concentrations in primary coolant in every 12 h or 24 h, or even every 48 h under power state are very convenient to get information of cladding defects. (5 refs.)

60235 Proton irradiation damage in cyclically stressed aluminum. W.F.Sommer (Los Alamos Nat. Lab., Los Alamos, NM, USA), D.S.Phillips, W.V.Green, L.W.Hobbs, C.A.Wert.

J. Nucl. Mater. (Netherlands), vol.114, no.2-3, p.267-76 (Feb. 1983).

High purity aluminum specimens have been irradiated at 50°C with 800 MeV protons using the Los Alamos Meson Physics Facility (LAMPF). Specimens cyclically stressed during irradiation produced only a third as many voids as unstressed control specimens. This is consistent with a model of Green and Weertman which predicts that moving dislocations should be better vacancy sinks than stationary ones. The reduced swelling was observed under the severe conditions of peak swelling temperature and simultaneous He implantation by transmutation. The detailed mode of dislocation motion responsible for the reduction is still under investigation. (28 refs.)

60236 Evaluation of the resistance of irradiated zirconium-liner cladding to iodine-induced stress corrosion cracking. S.Shimada, M.Nagai (Nippon Nuclear Fuel Dev. Co. Ltd., Ibaraki, Japan).

J. Nucl. Mater. (Netherlands), vol.114, no.2-3, p.305-11 (Feb. 1983).

An evaluation was made of irradiated zirconium-liner cladding for its resistance to iodine-induced stress corrosion cracking (SCC). Emphasis was put on irradiation-induced hardening in zirconium and SCC resistance in zirconium-liner cladding as compared with Zircaloy-2 cladding. The Vickers microhardness test revealed that crystal bar zirconium experienced less hardening than Zircaloy-2 during neutron exposure. The SCC resistance of zirconium-liner cladding was evaluated for failure strains under the tube pressurization SCC test, and compared with the results of Zircaloy-2 cladding. The failure strains of zirconium-liner cladding were significantly larger than those of Zircaloy-2 cladding over all neutron fluence ranges examined, e.g. more than ten times at $1.0 \times 10^{21} \text{ n/cm}^2$ ($E > 1 \text{ MeV}$). Judging from the results on the Vickers microhardness and SCC tests, good SCC resistance of zirconium-liner cladding could be expected even at high fluences. (12 refs.)

60237 Testing and performance of electrolytic oxygen meters for use in liquid sodium. R.G.Taylor, R.Thompson (UKAEA, Chem. Technol. Div., AERE, Harwell, England).

J. Nucl. Mater. (Netherlands), vol.115, no.1, p.25-38 (March 1983).

The performance of yttria-doped thorita ceramic electrochemical oxygen meters in liquid sodium is described. Tests were carried out using laboratory loops. Temperature coefficients of the oxygen meters have been measured between 380°C and 480°C, and the response to changes in oxygen level using cold-trap temperatures from 125°C to 250°C was determined. The ceramic has been shown to give good performance over lifetimes exceeding 400 days in some cases. The temperature coefficients and response to oxygen level changes are in good agreement with thermodynamic predictions. The effect of running the meters in high-oxygen sodium has been studied and a general mode of failure has been shown to be grain-boundary attack by oxygen/sodium solutions. The effect of γ -radiation on the meters has been studied. The meters with a metal/metal oxide reference electrode were unaffected by dose rates up to 52860 mGy h⁻¹. Meters with an air reference electrode do show an effect as a voltage reduction at levels down to 2420 mGy h⁻¹. This effect was temperature-dependent and was insignificant at 500°C. (13 refs.)

60238 Performance of coated UO₂ particles gettered with ZrC. R.E.Bullock, J.L.Kaas (General Atomic Co., San Diego, CA, USA).

J. Nucl. Mater. (Netherlands), vol.115, no.1, p.69-83 (March 1983).

In irradiation tests kernel migration in coated UO₂ fuel was eliminated through the use of a ZrC oxygen getter in two types of particles: one in which a solid layer of ZrC was deposited over the kernel, and another in which ZrC was dispersed throughout the pyrocarbon buffer layer surrounding the kernel. Postirradiation annealing tests on these TRISO-coated particles revealed an additional advantage for the particle having the solid ZrC overcoat in that no fission products were released during testing for 36 Ms (10000 h) at 1500°C. The other ZrC-gettered particle, as well as UO₂, UC₂, and mixed UO₂-UC₂ fuels that were included for comparison, released significant amounts of silver and europium through intact coatings in much shorter periods of time under the same conditions. (62 refs.)

60239 Oxygen potentials of (U,Gd)O_{2+x} solid solutions in the temperature range 1000-1500°C. K.Une, M.Oguma (Nippon Nuclear Fuel Dev. Co. Ltd., Ibaraki, Japan).

J. Nucl. Mater. (Netherlands), vol.115, no.1, p.84-90 (March 1983).

Oxygen potentials of U_{0.86}Gd_{0.14}O_{2+x} and U_{0.73}Gd_{0.27}O_{2+x} solid solutions, together with UO_{2+x}, have been measured at 1000, 1300, and 1500°C by using a thermogravimetric technique. The results at 1000°C show good agreement with the results of a previous solid electrolyte galvanic cell measurement. The oxygen potentials for the solid solutions increase positively with increasing Gd content. Stable hypostoichiometric phases are seen at the oxygen potentials below -65 and -50 kcal/mol between 1000 and 1500°C for U_{0.86}Gd_{0.14}O₂ and U_{0.73}Gd_{0.27}O₂, respectively. From the oxygen partial pressure dependence of x , models for the defect structure in hyper- and hypostoichiometric solid solutions are suggested. (23 refs.)

60240 Titanium-sponge bed to scavenge tritium from inert gases. M.Nishikawa, H.Kido, K.Kotoh, M.Sugisaki (Dept. of Nuclear Engng., Kyushu Univ., Fukuoka, Japan).

J. Nucl. Mater. (Netherlands), vol.115, no.1, p.101-9 (March 1983).

Chemical getters can be used to scavenge hydrogen isotopes from inert gases in HTGRs or fusion reactors. It is necessary that getter materials have a large gas-solid mass transfer capacity coefficient for scavenging hydrogen isotopes from inert gases. Absorption and desorption characteristics of hydrogen isotopes in a titanium sponge bed is examined. Discussions are mainly based on data obtained from breakthrough curves. Experimental results show that the titanium-sponge bed is a good candidate material for scavenging and fixation of tritium from inert gases. (23 refs.)

60241 Treatment of radioactive wastes by calcination. I. J.Napravnik, L.Neumann, P.Ditl (CVUT, Fakulta Strojní, Praha, Czechoslovakia).

Jad. Energ. (Czechoslovakia), vol.29, no.3, p.86-92 (March 1983). In Czech.

The present paper summarizes recently obtained results in research of radioactive wastes treatment reached in cooperation of Nuclear Research Institute and Prague Technical University. On the basis of gained results and experiences the advantages, disadvantages and trends of the technologies investigated were compared. Main attention was devoted to the research of calcination and denitration. (13 refs.)

60242 Design study of a spent fuel shipping cask for Korea Nuclear Unit-1. Moo Han Kim, Chang Sun Kang (Seoul Nat. Univ., Seoul, Korea).

J. Korean Nucl. Soc., vol.14, no.4, p.196-203 (Dec. 1982). [received: April 1983]

To transport the spent fuel assemblies of Korea Nuclear Unit 1, which is a Westinghouse type two loop pressurized water reactor, it has been found that steel is the most appropriate material for the design of a shipping cask in comparison with lead and depleted uranium. The proposed shipping cask will transport nine fuel assemblies at the same time and is well within the weight limit of transportation by unrestricted rail car. As a safety analysis, the fuel cladding and centerline temperatures were calculated under the accident condition of complete loss of water coolant, and it was found that the temperature was much lower than the limit of the melting point. k_{eff} was calculated with fresh fuel assemblies, and found to be well below 0.95. For shielding computation, the multipurpose Monte Carlo code MORSE-CG and one dimensional discrete ordinates transport code ANISN were used, and the Monte Carlo codes KENO and MORSE-CG were used for criticality calculations. The radiation source terms were calculated using ORIGEN-79. (18 refs.)

60243 The planar track model and the prediction of alpha-recoil aging in radwaste materials. J.Borg, J.C.Dran, Y.Langevin, M.Maurette, J.C.Petit, B.Vassent (Lab. Rene Bernas, Orsay, France).

Radiat. Eff. (GB), vol.65, no.1-4, p.173-81 (1982). (Proceedings of the First International Conference on 'Radiation Effects in Insulators', Arco, Largo di Garda, Italy, 1981).

The authors consider the effects of heavy ion irradiation on the chemical reactivity of radioactive waste materials. They present experimental techniques using Pb ions and report new results on the ion-induced etchability of muscovite mica and soda-lime glass which are conveniently described by a refined version of the planar track model. (10 refs.)

60244 Etude theorique des caracteristiques physiques d'un moniteur de reference de mesure de dechets solides contamines au Pu par neutrons passifs en vue de son optimisation (Theoretical study of the physics characteristics of a reference monitor to measure Pu contaminated solid waste by passive neutrons). C.Souga.

Univ. Lyon, France thesis, 10 June 1982. Lyon, France: Univ. Lyon (1982), 114 pp. In French.

A three energy group theory is established to study physical characteristics of plutonium contaminated solid waste reference monitor for passive neutrons measurements. Spontaneous fission neutrons interaction with waste stream

material and neutron leakage interaction with detector assembly are evaluated as a function of a set of physical and geometrical parameters (mass removal coefficient ρR_s (g/cm²); thickness of polyethylene moderator d (cm) and energy E (eV)) using 1D ANISN-W transport code in S_8P_3 and 100 groups approximations. Moreover this study allowed the author to show the 'cross-over' value of ρR_s in proximity of which the dispersion around the mean effective escape probability ^{235}Pu is minimal and to evaluate the 'albedo effect' which represents interaction between sample and detector assembly. The detection probability was evaluated as a function of different geometrical configurations of the detector in order to optimize its construction. Effective neutron escape probabilities calculated for three reference materials (polyethylene, iron and graphite) are in accordance with those given by experimental measurement. (16 refs.)

60245 *Modeles d'interpretation des mesures des actinides par spectrometrie gamma choix d'un moniteur de reference (Model interpretation of actinide measurement by gamma spectrometry using a reference monitor).* J.L.Barou. Univ. Lyon, France thesis, 24 June 1982. Lyon, France: Univ. Lyon (1982), 97 pp. In French.

Passive gamma assay is based on spectrum analysis of the radiation leaked out from the Pu contaminated wastes. Three models for the response of the assay system are developed: point detector, 4π scanning and segmented gamma scanning. The distance between the source and the point detector should be high; the count rate is so low that the source calculated is bad. If source and attenuation inhomogeneity are properly controlled, the 4π detector gives a good accuracy. Inhomogeneity is better treated with segmented gamma scanning employing individual transmission and sample activity measurements for each segment. (25 refs.)

60246 *Criticality safety hazards arising from the transport of fissile materials.* K.M.Leigh, D.J.Mather, P.M.Shaw, K.C.Rushton, P.Hague. Report EUR 8345 EN, Comm. European Communities, Luxembourg (1983), 86 pp. Contract XVII/322/80.5.

A study has been made of hypothetical accidents to a particular design of transport flask, although some of the considerations would apply more generally. Two accidents are considered—one involving the sudden displacement of an element; the other the movement of fragmented fuel from damaged pins. In both cases in order to make the system critical, it has been necessary to arbitrarily alter the calculated values of the effective multiplication factor. Two computer programs are used for the study. The first calculates the initial power pulse and its corresponding energy input to the flask. The second program calculates the longer term diffusion of heat from the fuel through the clad and into the water. Since the study is hypothetical it has been possible to arbitrarily alter the peak values of the effective multiplication factor and determine how this affects the energy release. It is shown how the latter may be dependent also on the boundary conditions to fuel movement, as well as the Doppler effect due to fuel temperature rise and to the reactivity change from density reduction. (5 refs.)

60247 *Catalogue of facilities in Member States of the European Communities for testing the packaging of radioactive materials.* A.Marchal, G.E.Swindell.

Report EUR 8254 EN, Comm. European Communities, Luxembourg (1983), 104 pp.

A group of experts convened by the Commission of the European Communities in Brussels on 2 July 1980 to suggest possible actions in connection with the safe transport of radioactive materials recommended, among other things, that the Commission should collect and distribute information on packaging test facilities in Member States. In response to that recommendation a letter of enquiry was sent informally, on behalf of the Commission, to the competent authorities of the Member States. The purpose of the enquiry is to assist in the effective implementation of the internationally accepted Regulations for the Safe Transport of Radioactive Materials through the dissemination of information on test facilities and on the terms and conditions under which the services of these facilities could be made available for the testing of packaging designed in other countries. As an aid to the presentation of the material in a harmonised format, it was suggested that the information provided should cover relevant topics. The information received by the Commission has been assembled for each installation according to this format.

60248 *General and localized corrosion of carbon and low-alloy steels in oxygenated high-temperature water.* D.D.Macdonald, S.Smalowska, S.Pednekar, T.Mizuno, H.J.Choi.

Report EPRI-NP-2853, Electr. Power Res. Inst., Palo Alto, CA, USA (Feb. 1983), 80 pp.

Available from Res. Rep. Center, Box 50490, Palo Alto, CA 94303, USA. The susceptibilities to stress corrosion cracking of two carbon steels (SA106-grB and SA333-gr6) and a low-alloy pressure vessel steel (A508-C12) are studied in high-purity water as a function of oxygen concentration (0.16 to 8 ppm) and high temperature (50 to 288°C). The fracture surfaces of the test specimens are also examined using scanning electron microscopy to determine the mode of failure. The results show that the steels studied are susceptible to stress corrosion cracking in high-temperature oxygenated water under monotonically-rising loads.

60249 *Results of EDF/Framatome underclad crack detection methods.*

P.Sermadiras, J.P.Launay. Report EPRI-NP-2841, Electr. Power Res. Inst., Palo Alto, CA, USA (Jan. 1983), 118 pp.

Available from Res. Rep. Center, Box 50490, Palo Alto, CA 94303, USA. Describes the development of detection techniques for cracks under the clad of reactor pressure vessel nozzles and steam generator tubesheets. A description of the origin of the underclad cracking problem, the techniques developed to detect the cracks, and the verification of the methods is given.

60250 *Need for geological characterization of low-level nuclear waste disposal sites.* W.B.Caswell (Wright-Pierce Inc., Topsham, ME, USA).

Proceedings of the Symposium on Low-Level Waste Disposal. Site Characterization and Monitoring (NUREG/CP-0028), Arlington, VA, USA, 16-17 June 1982 (Oak Ridge, TN, USA: Oak Ridge Nat. Lab. 1982), p.7-31. Shallow burial of low-level nuclear wastes should facilitate (1) absorption of radiation, (2) long detention time allowing for radioactive decay, and (3) slow release and recycling of the waste products into the environment. Subsurface disposal sites are typically dominated by water that occurs either as soil moisture in the unsaturated zone or as groundwater in the underlying saturated zone. Migration from the burial site is inevitably along hydraulic gradients by soil moisture and ground water. Even under the most simple of geologic situations, the measurement, calculation and use of hydraulic conductivity values and other important factors needed to assess groundwater impacts requires the use of simplifying assumptions. The fact that geologic complexities exist makes it imperative that they be fully characterized such that the simplifying assumptions necessary for hydraulic analysis can be made and the reasonableness of their application verified. (no refs.)

60251 *Geological and geophysical techniques for development of siting and design parameters.* A.W.Hatheway (Dept. of Geological Engng., Univ. of Missouri, Rolla, MO, USA).

Proceedings of the Symposium on Low-Level Waste Disposal. Site Characterization and Monitoring (NUREG/CP-0028), Arlington, VA, USA, 16-17 June 1982 (Oak Ridge, TN, USA: Oak Ridge Nat. Lab. 1982), p.33-50. The licensability and functionality of each low-level radioactive waste disposal facility will be determined by the geologic environment in which it is to be placed, and by the expertise and goodwill of the scientists and engineers involved in its design and licensing. Geologic site characterization is the first and most basic step in that process. The geological and geophysical means by which this characterization is accomplished must be chosen and employed in the full mutuality of the fact that geology governs geophysical response and that geophysical interpretation is absolutely essential in characterizing the length, breadth, and depth of each site. Each step in the employment of geological and geophysical techniques must be made with total incorporation of related data and findings. Severe introspection and questioning must be accomplished immediately on the development of each line of evidence, and the results must be applied directly and immediately to each remaining activity. (3 refs.)

60252 *A geological case history: lessons learned at Sheffield, Illinois.* K.Kartwright (Illinois State Geological Survey, Champaign, IL, USA).

Proceedings of the Symposium on Low-Level Waste Disposal. Site Characterization and Monitoring (NUREG/CP-0028), Arlington, VA, USA, 16-17 June 1982 (Oak Ridge, TN, USA: Oak Ridge Nat. Lab. 1982), p.67-80. The Sheffield Low-Level Radioactive Waste Disposal Facility was established in 1968 following a two-year site evaluation process. The site exploration program was considered at the time to be extensive and quite complete. However, in current practice, a site exploration program of the type conducted in 1967-1968 is only considered a preliminary program to determine if a detailed investigation of the site is warranted. Subsequent investigations at Sheffield have disclosed hydrogeologic conditions much more complex than indicated by initial exploration program. But the question still remains regarding the degree of site exploration necessary to adequately characterize a potential disposal site. Both excessive and inadequate exploration programs are to be avoided. Given the present state of knowledge of the stratigraphy and hydrogeology of the site, the question remains whether the site would be licensable in 1982. (4 refs.)

60253 *Geotechnical and geomechanical parameters required for characterization of sites.* D.E.Daniel (Univ. of Texas, Austin, TX, USA).

Proceedings of the Symposium on Low-Level Waste Disposal. Site Characterization and Monitoring (NUREG/CP-0028), Arlington, VA, USA, 16-17 June 1982 (Oak Ridge, TN, USA: Oak Ridge Nat. Lab. 1982), p.93-115. Characterization of disposal sites will involve geotechnical investigations and measurement of dozens of geomechanical parameters. The required investigations may be performed in stages, beginning with a preliminary study, or in a single evaluation. The geotechnical investigation will deal with the actual disposal site and the immediate area surrounding the site, and may include more detailed evaluation of the waste, disposal pits, and waste handling or processing structures. With respect to the actual site, the investigation is likely to focus on evaluating: (1) the types of subsurface soils or rocks present; (2) stability of the site; (3) potential for erosion; (4) groundwater conditions; and (5) sources for construction materials. A variety of tests, some routine and some requiring state-of-the-art techniques, would be needed to measure parameters related to strength, compressibility, and permeability. The important mechanical properties of the waste (average density, compressibility, and potential for generation of gas) may be measured or, in some cases, estimated from experience. (3 refs.)

60254 *Variations of geomechanical properties.* P.A.Hustad, J.A.Ruf (Burns & McDonnell Engng. Co., Kansas City, MO, USA).

Proceedings of the Symposium on Low-Level Waste Disposal. Site Characterization and Monitoring (NUREG/CP-0028), Arlington, VA, USA, 16-17 June 1982 (Oak Ridge, TN, USA: Oak Ridge Nat. Lab. 1982), p.117-49. Discusses the role of the geotechnical engineer in acquiring the subsurface data necessary for the design and analysis of low-level radioactive waste disposal facilities. First, it should be recognized that the design and analysis of these environmentally complex facilities encompass a large number of technical disciplines. In regard to subsurface characterization of disposal sites the disciplines of geology, ground-water hydrology, environmental/civil engineering, and geotechnical engineering must work hand in hand. This close working relationship is necessary because each specialist is dependent upon the other for input that is required for adequate characterization of the site in regard to the proposed disposal facilities. (15 refs.)

60255 *Geotechnical measurements at the Maxey Flats, Kentucky low-level radioactive waste disposal site—lessons learned.* J.L.Grant (Law Engng. Testing Co., Englewood, CO, USA).

Proceedings of the Symposium on Low-Level Waste Disposal. Site Characterization and Monitoring (NUREG/CP-0028), Arlington, VA, USA, 16-17 June 1982 (Oak Ridge, TN, USA: Oak Ridge Nat. Lab. 1982), p.151-63. The Maxey Flats site was opened in 1963 and used for the disposal of low-level radioactive waste until site closure in July, 1978. Prior to opening, studies were conducted to assess suitability of the site for the disposal of low-level radioactive waste. The scope of these studies was consistent with that of similar studies at the time, but was less detailed than similar studies today. A significant quantity of radioactive materials has been disposed at the site without apparent damage to the surrounding environment, indicating a reasonably successful site design. However, several operational problems were encountered. The author reviews major operational problems at the site, and to assess the knowledge from the experience gained at the Maxey Flats site which can be related to geotechnical investigations at similar sites. (6 refs.)

60256 *Hydrologic characterization of sites for shallow disposal of low-level radioactive wastes.* S.N.Davis (Dept. of Hydrology & Water Resources, Univ. of Arizona, Tucson, AZ, USA).

Proceedings of the Symposium on Low-Level Waste Disposal. Site Characterization and Monitoring (NUREG/CP-0028), Arlington, VA, USA, 16-17 June 1982 (Oak Ridge, TN, USA: Oak Ridge Nat. Lab. 1982), p.177-94. For site characterization of low-level disposal sites, point measurements of hydraulic head, hydraulic conductivity, sorptive characteristics of the solid materials, and water chemistry (including stable and unstable nuclides) must be numerous enough to define local paths and rates of potential contaminant movement. Special attention must be given to local zones of high conductivity which are commonly fractures in clay-rich materials but may also be small lenses of coarse silt, sand, and gravel within non-indurated sediments. For shallow hydrogeologic systems, the presence of anthropogenic materials in subsurface gas and water provides the best information on existing rates and directions of fluid movement. Of the numerous materials which can be detected, tritium and chlorofluoromethanes have proved most useful. Chlorine-36 from thermocuclear testing can be used to pinpoint 1954-1964

water. If analytical methods could be simplified, helium-3 and krypton-85 would be also highly useful. (10 refs.)

60257 Techniques of groundwater investigation at proposed low-level nuclear waste disposal sites. C.W.Fetter, Jr. (Law Engng. Testing Co., Marietta, GA, USA).

Proceedings of the Symposium on Low-Level Waste Disposal. Site Characterization and Monitoring (NUREG/CP-0028), Arlington, VA, USA, 16-17 June 1982 (Oak Ridge, TN, USA: Oak Ridge Nat. Lab. 1982), p.195-216. The proposed rule 10CFR Part 61 for licensing of LLW near surface disposal sites states that 'the groundwater pathway will generally be the most significant in terms of releases of radioactivity'. The various techniques for investigating the properties of groundwater at a proposed disposal site are described. (17 refs.)

60258 Ground-water monitoring techniques for low-level radioactive disposal sites. S.D.Johannsen, D.G.Nichols (Residuals Management Technol. Inc., Madison, WI, USA).

Proceedings of the Symposium on Low-Level Waste Disposal. Site Characterization and Monitoring (NUREG/CP-0028), Arlington, VA, USA, 16-17 June 1982 (Oak Ridge, TN, USA: Oak Ridge Nat. Lab. 1982), p.217-36. Ground-water quality monitoring at low-level radioactive waste land disposal sites will provide needed data for evaluating whether these sites are meeting the performance objectives specified in the Nuclear Regulatory Commission's licence requirements. The authors summarize the techniques available for collection and analysis of ground-water samples, particularly for radiological parameters. Quality control and quality assurance are emphasized in all monitoring methods presented. Each aspect of monitoring, from system design to sample collection and laboratory analysis, must follow prescribed methods in order to yield data which are representative of actual ground-water quality. Routine evaluation of the data is also discussed in relation to both quality control analysis and determination of low-level facility performance. (10 refs.)

60259 Lessons learned in a hydrogeological case at Sheffield, Illinois. J.B.Foster (US Geological Survey, Urbana, IL, USA).

Proceedings of the Symposium on Low-Level Waste Disposal. Site Characterization and Monitoring (NUREG/CP-0028), Arlington, VA, USA, 16-17 June 1982 (Oak Ridge, TN, USA: Oak Ridge Nat. Lab. 1982), p.237-44. The US Geological Survey began a study of the hydrogeology of the low-level radioactive-waste disposal site near Sheffield, Illinois, in 1976. The purpose of the study was to determine how the glacial sediments were functioning as a containment for radionuclides. The scope of the study was to define geologic, hydrologic, and geochemical elements necessary to describe the hydrogeologic system. The geologic elements to be described were the stratigraphy, lithology, and mineralogy. The hydrologic elements included the hydraulic properties of the sediments and the rate and direction of water movement through both unsaturated and saturated zones within the glacial deposits. Geochemical elements included cation exchange capacity, soluble mineral chemistry, and ground-water quality. Hydrogeologic information from Sheffield and other radioactive-waste sites will be used to define the essential hydrogeologic factors necessary to quantitatively predict the concentration of radionuclides migrating in ground water from future burial sites. (2 refs.)

60260 Surface water considerations for low-level radioactive waste site. Y.C.Chang (Environmental Engng. Div., Stone & Webster Engng. Corp., Boston, MA, USA).

Proceedings of the Symposium on Low-Level Waste Disposal. Site Characterization and Monitoring (NUREG/CP-0028), Arlington, VA, USA, 16-17 June 1982 (Oak Ridge, TN, USA: Oak Ridge Nat. Lab. 1982), p.263-71. To ensure that the objective of isolation of low-level radioactive wastes and stability of the disposal site after closure can be achieved, the surface hydrology of the potential site must be carefully characterized prior to engineering and operation. At a site the most important considerations with regard to flooding, infiltration, erosion, and pathway of radionuclides are addressed as they relate to streams, ponds, hydraulic structures, and surface water users. To satisfactorily characterize the site, the type and amount of data and analyses needed for licence applications and the environmental report are discussed. The discussion also includes potential sources of available data, the field data collection program that may be necessary, and methodologies that can be used for analysis. (23 refs.)

60261 Hydrologic and hydrodynamic aspects of low-level radioactive waste disposal to streams. P.H.Carrigan, Jr. (US Geological Survey, Reston, VA, USA).

Proceedings of the Symposium on Low-Level Waste Disposal. Site Characterization and Monitoring (NUREG/CP-0028), Arlington, VA, USA, 16-17 June 1982 (Oak Ridge, TN, USA: Oak Ridge Nat. Lab. 1982), p.273-94. Characterization and monitoring of disposal sites require unique approaches in gathering information on hydrologic and hydrodynamic aspects of low-level radioactive waste disposal to streams. Continuous monitoring of a receiving stream is needed to detect the onset of contamination and to determine the subsequent contaminant loading. With expected low radionuclide levels, the monitoring will involve regular withdrawal, concentration, and analysis of samples. Therefore the monitoring system includes streamflow measuring stations as well as sample-collection systems. Depending on flow measuring conditions, the sampling may be continuous and in proportion to the flow, automated, or done manually. (41 refs.)

60262 Effect of releases from near-surface low-level waste sites on surface water quality. F.L.Parker (Vanderbilt Univ., Nashville, TN, USA).

Proceedings of the Symposium on Low-Level Waste Disposal. Site Characterization and Monitoring (NUREG/CP-0028), Arlington, VA, USA, 16-17 June 1982 (Oak Ridge, TN, USA: Oak Ridge Nat. Lab. 1982), p.295-327. Discusses the effects and detection of radioactive releases from near-surface LLW sites in streams. The surface water quality is also discussed. (67 refs.)

60263 Environmental information needed to license a low-level waste disposal facility. C.A.Little, L.D.Voorhees, R.M.Reed (Oak Ridge Nat. Lab., Oak Ridge, TN, USA).

Proceedings of the Symposium on Low-Level Waste Disposal. Site Characterization and Monitoring (NUREG/CP-0028), Arlington, VA, USA, 16-17 June 1982 (Oak Ridge, TN, USA: Oak Ridge Nat. Lab. 1982), p.341-75. Proposed Nuclear Regulatory Commission Rules 10 CFR Part 61 and 51 describe licensing requirements for land disposal of low-level radioactive waste. Necessary site-specific information required to estimate public health impacts include, but are not limited to, descriptions of facility design, radiologic inventory, demography, soils, topography, surface and subsurface hydrology, meteorology, ecology, and land use practices in the vicinity of the site. Low-level waste disposal actions may also be constrained by potentially significant environmental issues such as impacts to endangered species, removal of prime and unique farmland, effects on cultural resources and location on floodplains or wetlands. A thorough review of both radiological and nonradiological issues conducted early in the development of a project will facilitate compliance with environmental legislation so that unnecessary project delays may be avoided. (17 refs.)

60264 Some interactive factors affecting trench cover integrity on low-level waste sites. T.E.Hakanson, L.J.Lane, J.G.Steger, G.L.DePoorter (Los Alamos Nat. Lab., Los Alamos, NM, USA).

Proceedings of the Symposium on Low-Level Waste Disposal. Site Characterization and Monitoring (NUREG/CP-0028), Arlington, VA, USA, 16-17 June 1982 (Oak Ridge, TN, USA: Oak Ridge Nat. Lab. 1982), p.377-93. Identifies and discusses trench cover related processes by which radionuclides from low-level waste disposal sites may enter biological pathways, based on a review of past performance of commercial and Department of Energy sites, and on an analysis of the interdependence of those processes using a state-of-the-art water balance model. From that analysis, information needs for site characterization and monitoring are identified to assist in designing effective trench cover systems and to monitor site performance. (42 refs.)

60265 Air quality measurements for site characterization. M.W.Carter, W.C.Conklin (School of Nuclear Engng. & Health Phys., Georgia Inst. of Technol., Atlanta, GA, USA).

Proceedings of the Symposium on Low-Level Waste Disposal. Site Characterization and Monitoring (NUREG/CP-0028), Arlington, VA, USA, 16-17 June 1982 (Oak Ridge, TN, USA: Oak Ridge Nat. Lab. 1982), p.401-22. Effective and timely site characterization is an important part of selecting a site for low-level waste disposal. Parameters measured can be compared with pertinent regulatory requirements, used for a reference base, helpful in evaluating environmental impacts, utilized in documenting changes in control programs, of value in modeling studies and other data uses, and beneficial in providing relevant sampling and methodology training. The authors focus on specific air quality measurements which should be an inherent part of the site characterization program. The program is designed to measure, quantify, and identify contributions from site uses (operational procedures), atmospheric fallout, natural radioactivity, and vicinity and regional applications of radionuclides. The recommended air quality measurements program will be described in association with a reference site developed by the US Nuclear Regulatory Commission. (19 refs.)

60266 Radiochemical measurements for evaluating air quality in the vicinity of low-level waste burial sites—the West Valley experience. J.M.Matuszek (Center for Labs. & Res., New York State Dept. of Health, Albany, NY, USA).

Proceedings of the Symposium on Low-Level Waste Disposal. Site Characterization and Monitoring (NUREG/CP-0028), Arlington, VA, USA, 16-17 June 1982 (Oak Ridge, TN, USA: Oak Ridge Nat. Lab. 1982), p.423-42. The waste buried at the West Valley site, New York, consists mainly of low density, low specific activity substances which decomposed in the wet surroundings giving rise to various radioactive gases. Radiochemical measurements for evaluating the air quality in the vicinity of the site are described. (32 refs.)

60267 Meteorology and climatology as parameters on low level waste disposal monitoring. W.M.Culkowski (Atmospheric Turbulence & Diffusion Lab., NOAA, Oak Ridge, TN, USA).

Proceedings of the Symposium on Low-Level Waste Disposal. Site Characterization and Monitoring (NUREG/CP-0028), Arlington, VA, USA, 16-17 June 1982 (Oak Ridge, TN, USA: Oak Ridge Nat. Lab. 1982), p.449-54. Once a site has been chosen for the burial of low level wastes, meteorological input is required in two forms, as climatology and as an estimator of airborne concentrations. The climatological data are fundamental to assessing hydrologic flow which may transport waste material from the original site. Airborne nuclear activity may occur by accidental release of material during the active burial phase or may result from gas formation in the trenches over a period of years. (18 refs.)

60268 On-site meteorological measurements for low-level radioactive waste disposal. T.J.Lockhart (Meteorology Res. Inc., Altadena, CA, USA).

Proceedings of the Symposium on Low-Level Waste Disposal. Site Characterization and Monitoring (NUREG/CP-0028), Arlington, VA, USA, 16-17 June 1982 (Oak Ridge, TN, USA: Oak Ridge Nat. Lab. 1982), p.455-61. The technical position paper (April 1, 1982) of the Low-Level Waste Licensing Branch of the US Nuclear Regulatory Commission suggests the variables to be measured, the time period for measurement and the application for which the measurements are required. The author discusses hardware and software considerations for the meteorological monitoring system in terms of accuracy requirements by variable, system quality control, data validation, and representativeness by variable. A cost estimate of this effort is also discussed. (7 refs.)

60269 Characterization of mechanical properties of nuclear waste glasses. H.Richter (Fraunhofer-Inst. fur Werkstoffmechanik, Freiburg, Germany), P.Offermann.

Scientific Basis for Nuclear Waste Management V. Proceedings of the Materials Research Society Fifth International Symposium on the Scientific Basis for Nuclear Waste, Berlin, Germany, 7-10 June 1982 (New York, USA: North-Holland 1982), p.229-38.

Glass and glass ceramics are regarded as suitable nuclear waste solidification products; mechanical stability is one of the important properties of the material. Such mechanical stability is necessary on the one hand for the safe handling and transportation of nuclear waste glass, and on the other for its relevance to leaching processes. Leaching by water or by aqueous solutions must be regarded as the most dangerous process by which radioactive materials can be set free from the glass. Because the leaching rate is proportional to the total surface area of the materials exposed to the liquid, it is of utmost importance to keep this area as small as possible and to prevent any enlargement by cracking processes which can arise due to mechanically or thermally induced stresses. (8 refs.)

60270 Fracture appraisal of large scale glass blocks under realistic thermal conditions. F.Laude, E.Vernaz, M.Saint-Gaudens (Dept. de Genie Radioactif, CEA, Valrhon, France).

Scientific Basis for Nuclear Waste Management V. Proceedings of the Materials Research Society Fifth International Symposium on the Scientific Basis for Nuclear Waste, Berlin, Germany, 7-10 June 1982 (New York, USA: North-Holland 1982), p.239-47.

The compositions of borosilicate glasses used to solidify fission product solutions are selected for their low leach rates. Fracturing of the glass blocks, caused primarily by thermal and residual stresses during cooling, increases the potential leaching surface area and the number of small particles, both of which are undesirable since long term container failure must be considered. It is therefore important to know the state of fracture of the glass occurring at different stages of its thermal history. A theoretical appraisal of the fracture state of the glass is presented, complemented by an experimental study using industrial scale glass blocks under realistic thermal conditions. (5 refs.)

- 60271 An attempt to assess the long-term crystallization rate of nuclear waste glasses.** N.Jacquet-Francillon, F.Pacaud, P.Queille (Dept. de Genie Radioactif, CEA, Valrho, France). Scientific Basis for Nuclear Waste Management V. Proceedings of the Materials Research Society Fifth International Symposium on the Scientific Basis for Nuclear Waste, Berlin, Germany, 7-10 June 1982 (New York, USA: North-Holland 1982), p.249-59. The crystallization of fission product glasses is generally caused by maintaining these glasses at high temperatures (600° to 900°C) for several days or weeks in order to evaluate the effects of crystallization on leach resistance and mechanical properties. At the CEA Marcoule, isothermal calorimetry has been used to measure the thermal release which accompanies crystallization in order to attempt to quantify the devitrification capacity of the different glasses tested and to establish the time-temperature relationships. Such data could allow for long-term, low temperature extrapolation of the behaviour of the glass during geological storage. The present work describes the results obtained using three non-radioactive glasses of increasing chemical complexity. (16 refs.)
- 60272 Quantitative determination of crystalline phases in nuclear waste glasses.** R.H.Feld, M.Stammler (Battelle-Inst. eV, Frankfurt/Main, Germany). Scientific Basis for Nuclear Waste Management V. Proceedings of the Materials Research Society Fifth International Symposium on the Scientific Basis for Nuclear Waste, Berlin, Germany, 7-10 June 1982 (New York, USA: North-Holland 1982), p.261-71. In order to assess the longterm chemical and physical stability of high level waste glasses it is important to know the amounts of crystalline phases present. To test the merits of the quantitative X-ray powder diffraction analysis for the characterization of nuclear waste glasses, measurements were carried out to determine relatively small weight fractions of crystalline phases next to high concentrations of amorphous materials, test whether components remain stable in their crystalline state, yield new crystalline compounds or dissolve in the glass matrix, and determine the total crystallinity of nuclear waste products. The 'matrix flushing' method was chosen since it was considered to be accurate, fast, and relatively easy to apply. (8 refs.)
- 60273 Effect of Fe₂O₃/ZnO on two glass compositions for solidification of Swedish nuclear wastes.** J.L.Nogues (Lab. des Verres, Univ. des Sci. et Tech. du Languedoc, Montpellier, France). Scientific Basis for Nuclear Waste Management V. Proceedings of the Materials Research Society Fifth International Symposium on the Scientific Basis for Nuclear Waste, Berlin, Germany, 7-10 June 1982 (New York, USA: North-Holland 1982), p.273-8. A recent study concluded that addition of Fe₂O₃ to a soda borosilicate nuclear waste glass may significantly reduce damage by water attack due to formation of a Fe-rich film on the glass surface. However, differences in SiO₂, B₂O₃, CaO and concentration of fission products in previous glass compositions make it impossible to ascribe the improved leach resistance solely to Fe₂O₃ content. In the present work, leaching behavior of two glasses are compared which differ only by the substitution of Fe₂O₃ for some of the ZnO in the glass. Both glass compositions are compatible with the French AVM process and contain 9% (by weight) of simulated waste products characteristic of the Swedish nuclear waste program. (6 refs.)
- 60274 Investigation on the oxidation state and the behaviour of molybdenum in silicate glass.** A.Horneber (Inst. für Werkstoffwissenschaften III, Univ. Erlangen-Nürnberg, Erlangen, Germany). Scientific Basis for Nuclear Waste Management V. Proceedings of the Materials Research Society Fifth International Symposium on the Scientific Basis for Nuclear Waste, Berlin, Germany, 7-10 June 1982 (New York, USA: North-Holland 1982), p.279-88. Knowledge about the oxidation state of molybdenum in glasses and glass ceramics which contain nuclear waste is important because of the danger of formation of water-soluble Cs-molybdate with Cs-137. The authors deal with the following aspects: (1) oxidation state of Mo when organic reducing agents, i.e. formic acid, formaldehyde, tannic acid, are added to the batch; (2) dependence of Mo 'solubility' on the melting atmosphere; (3) behaviour of the different oxidation states of Mo depending on the temperature and the basicity of the glass; and (4) redox interaction of Mo with Fe, Cr and Ti. (14 refs.)
- 60275 The materials balance—scientific fundamentals for the quality assurance of vitrified waste.** E.Schiewer, H.Rabe, S.Weisenburger (Hahn-Meitner-Inst. für Kernforschung Berlin GmbH, Berlin, Germany). Scientific Basis for Nuclear Waste Management V. Proceedings of the Materials Research Society Fifth International Symposium on the Scientific Basis for Nuclear Waste, Berlin, Germany, 7-10 June 1982 (New York, USA: North-Holland 1982), p.289-97. In the vitrification of HLW the aim is to create a product, the stability (thermal, mechanical) of which is, to the greatest possible degree, independent of fluctuations in its composition. Process control during vitrification of HLW is necessary in order to assure the quality of the final glass product. The chemical processes are controlled by quantitative analysis of all material streams entering and leaving the melting device. There are six material streams to consider: frit input, waste input, corrosion products (generated by the vitrification process), off-gas, recycled off-gas, glass output. Additionally, the capacity of the glass for buffering short-term fluctuations in the incoming streams must be known. Sufficient sampling during non-radioactive vitrification in addition to materials tests can provide the necessary data basis. The results are combined in a materials balance, which might provide a scientific basis for reliable quality assurance when sampling is limited. (2 refs.)
- 60276 Incorporation of high-level wastes in Synroc: results from recent process engineering studies at Lawrence Livermore National Laboratory.** J.H.Campbell, C.L.Hoenig, F.J.Ackerman, P.E.Peters, J.Z.Grens (Lawrence Livermore Nat. Lab., Livermore, CA, USA). Scientific Basis for Nuclear Waste Management V. Proceedings of the Materials Research Society Fifth International Symposium on the Scientific Basis for Nuclear Waste, Berlin, Germany, 7-10 June 1982 (New York, USA: North-Holland 1982), p.299-308. In October 1981 Synroc-D was selected as the reference alternate waste form for borosilicate glass for immobilisation of defence waste. A total of eight candidate waste forms competed in this selection process and the decision of which alternate waste form to choose was based primarily on performance properties. The authors summarise highlights from recent engineering research and development, in particular, results from fluidised bed calcination studies of Synroc slurry. (13 refs.)

- 60277 The microstructure of Synroc.** D.R.Cousens, S.Myhra, J.Penrose, R.L.Segall, R.St.C.Smart, P.S.Turner (School of Sci., Griffith Univ., Nathan, Queensland, Australia). Scientific Basis for Nuclear Waste Management V. Proceedings of the Materials Research Society Fifth International Symposium on the Scientific Basis for Nuclear Waste, Berlin, Germany, 7-10 June 1982 (New York, USA: North-Holland 1982), p.309-18. The Synroc concept was introduced by Ringwood in 1978 and, as is well known, the material now proposed for the disposal of high-level civilian nuclear waste consists primarily of hollandite (BaAl₂Ti₂O₁₀), perovskite (CaTiO₃) and zirconolite (CaZrTi₂O₇). Microstructural information for Synroc B and Synroc C are given. (13 refs.)
- 60278 SIMS depth profiling studies of sphene-based ceramics and glass ceramics leached in synthetic groundwater.** P.J.Hayward, W.H.Hocking, F.E.Doern, E.V.Cecchetto (Whiteshell Nuclear Res. Estab., Atomic Energy of Canada Ltd., Pinawa, Manitoba, Canada). Scientific Basis for Nuclear Waste Management V. Proceedings of the Materials Research Society Fifth International Symposium on the Scientific Basis for Nuclear Waste, Berlin, Germany, 7-10 June 1982 (New York, USA: North-Holland 1982), p.319-28. Glass ceramics and ceramics based on the mineral sphene (CaTiSiO₆) are being developed to host the wastes arising from possible future CANDU fuel reprocessing. Results from leaching tests in deionised water and in synthetic groundwater indicate that these materials are highly durable. Secondary ion mass spectrometry (SIMS) depth profiling of leached specimens suggests that leaching in the glass ceramics is predominantly confined to the glass phase. The high ionic strength and composition of the groundwater have a significant passivating effect on leaching and surface alteration phenomena, and encourage the precipitation of new phases on the ceramic surface. Leaching results, scanning electron microscope observations and SIMS depth profile measurements are compared and discussed. (11 refs.)
- 60279 Leaching of natural and synthetic sphene and perovskite.** J.B.Metson, G.M.Bancroft, S.M.Kanetkar, H.W.Nesbitt, W.S.Eyre (Dept. of Geology, Univ. of Western Ontario, London, Ontario, Canada), P.J.Hayward. Scientific Basis for Nuclear Waste Management V. Proceedings of the Materials Research Society Fifth International Symposium on the Scientific Basis for Nuclear Waste, Berlin, Germany, 7-10 June 1982 (New York, USA: North-Holland 1982), p.329-38. Atomic Energy of Canada Limited (AECL) is currently investigating the use of sphene-based glass ceramics to host the wastes produced from possible reprocessing of irradiated CANDU fuels. The authors report on the leaching behaviour of natural and synthetic sphenes and a CaTiSiO₆ glass, in deionised water, with varying pH and with Ca²⁺ and silica additions to the leachant. Leaching studies on natural and synthetic perovskite in deionised water are also reported. (11 refs.)
- 60280 Effects of radiation damage and radiolysis on the leaching of vitrified waste.** W.G.Burns, A.E.Hughes, J.A.C.Marples, R.S.Nelson, A.M.Stoneham (AERE, Harwell, England). Scientific Basis for Nuclear Waste Management V. Proceedings of the Materials Research Society Fifth International Symposium on the Scientific Basis for Nuclear Waste, Berlin, Germany, 7-10 June 1982 (New York, USA: North-Holland 1982), p.339-48. Attack on the glass by leaching in water is the only probable process by which the long-lived radioactive isotopes incorporated in vitrified waste might be returned to the environment after future disposal. Radiation from the incorporated waste could increase the leach rate either by damaging the structure of the glass or by radiolysing the water near the glass surface to produce ionic species that attack the glass more readily. (25 refs.)
- 60281 Structural effects of radiation damage in silica based glasses.** A.Manara, P.N.Gibson (Joint Res. Centre, Ispra, Italy), M.Antonini. Scientific Basis for Nuclear Waste Management V. Proceedings of the Materials Research Society Fifth International Symposium on the Scientific Basis for Nuclear Waste, Berlin, Germany, 7-10 June 1982 (New York, USA: North-Holland 1982), p.349-56. The results of recent measurements of optical absorption, etching rate and transmission electron microscopy in pure silica and borosilicate glasses are reported and discussed. At dose saturation conditions, the dependence of the optical density associated with the production of single atomic defects from the mass of the impinging particle shows a marked saturation at masses ≥ 20 amu. The corresponding etching rates increase by about 4 times with respect to unirradiated samples. In borosilicate glasses, the temperature dependence of the threshold dose rate of electrons to initiate the nucleation of bubbles shows a marked increase from about 300 to 600K. (9 refs.)
- 60282 Near-surface leaching studies of Pb-implanted Savannah River waste glass.** G.W.Arnold, C.J.M.Northrup (Sandia Nat. Labs., Albuquerque, NM, USA), N.E.Bibler. Scientific Basis for Nuclear Waste Management V. Proceedings of the Materials Research Society Fifth International Symposium on the Scientific Basis for Nuclear Waste, Berlin, Germany, 7-10 June 1982 (New York, USA: North-Holland 1982), p.357-68. The present experiments with SRP simulated nuclear waste glass implanted with Pb ions (see the Experimental Section), used RBS and ERD to follow in detail the changes in composition which occur in the near-surface region upon leaching in deionised water at 90°C. Analyses of the leach solutions were made in an attempt to correlate the actual leach rate with the observed near-surface compositional changes. These experiments show that radiation damage can cause changes in the composition of the near-surface of the leached glass. The authors also find that a critical fluence is reached where abrupt changes of the surface elemental composition occur as a result of leaching. The analyses which were made indicate that the amount of material actually leaving the glass is not significantly increased as a result of the radiation damage. (18 refs.)
- 60283 A study of radiation effects in curium-doped Gd₂Ti₂O₇ (pyrochlore) and CaZrTi₂O₇ (zirconolite).** J.W.Wald (Pacific Northwest Lab., Richland, WA, USA), P.Offermann. Scientific Basis for Nuclear Waste Management V. Proceedings of the Materials Research Society Fifth International Symposium on the Scientific Basis for Nuclear Waste, Berlin, Germany, 7-10 June 1982 (New York, USA: North-Holland 1982), p.369-78. The experimental results presented describe alpha decay self-damage studies in ²⁴⁴Cm-doped Gd₂Ti₂O₇ and CaZrTi₂O₇ single-phase, polycrystalline materials. Property behaviour was monitored at ambient temperature by X-ray diffraction and apparent density measurements during the initial damage ingrowth period (approximately 2-year time span). Microstructural examination was conducted by optical metallographic techniques after an X-ray amorphous state was reached. Results are compared with those of others on the ingrowth of damage effects in natural and synthetic zirconolites. (21 refs.)

60284 Dose-dependence of Pb-ion implantation damage in zirconolite, hollandite, and zircon. T.J.Headley, G.W.Arnold, C.J.M.Northrup (Sandia Nat. Labs., Albuquerque, NM, USA).

Scientific Basis for Nuclear Waste Management V. Proceedings of the Materials Research Society Fifth International Symposium on the Scientific Basis for Nuclear Waste, Berlin, Germany, 7-10 June 1982 (New York, USA: North-Holland 1982), p.379-88.

An accelerated ageing test which reliably simulates the α -recoil damage accumulated during thousands of years of waste storage is desirable. One recent approach to this simulation is to implant the waste form with heavy Pb-ions. If the validity of this approach is to be fully assessed, two important questions which have not yet been investigated must be answered. (1) Is the structural damage, including cumulative effects, similar for irradiation by Pb-ions and α -recoil nuclei in a given material? (2) Is the dose-dependence of the accumulated damage similar? The purpose of this investigation was to assess the extent of these similarities in selected materials. The authors utilised transmission electron microscopy (TEM) to characterise the radiation damage and measure its dose-dependence. Synthetic crystalline zirconolite and (Ba,Ti)-hollandite, and natural crystalline zircon were implanted with Pb-ions over a wide range of equivalent α -doses and then characterised by TEM. (20 refs.)

60285 Leachability of zircon as a function of alpha dose. R.C.Ewing, R.F.Haaker, W.Lutze (Dept. of Geology, Univ. of New Mexico, Albuquerque, NM, USA).

Scientific Basis for Nuclear Waste Management V. Proceedings of the Materials Research Society Fifth International Symposium on the Scientific Basis for Nuclear Waste, Berlin, Germany, 7-10 June 1982 (New York, USA: North-Holland 1982), p.389-97.

The variation in the leachability of naturally occurring zircons ($ZrSiO_4$) as a function of total alpha dose has been measured at 87°C. For calculated doses in the range of 10^{16} to 10^{18} alphas/gm there is an increase of one order of magnitude in the weight percent of zircon that is dissolved and an increase in the leach rate of the zircon 2.9×10^{-8} to 2.3×10^{-7} gm/cm² day. Totally metamict specimens (dose $\geq 10^{19}$ alphas/gm) have leach rates as high as 1.8×10^{-6} gm/cm² day. (29 refs.)

60286 Isotopic fractionation of thorium and uranium upon leaching of monazite: alpha-recoil damage effects. Y.Eyal (Dept. of Nuclear Engng., Technion-Israel Inst. of Technol., Haifa, Israel).

Scientific Basis for Nuclear Waste Management V. Proceedings of the Materials Research Society Fifth International Symposium on the Scientific Basis for Nuclear Waste, Berlin, Germany, 7-10 June 1982 (New York, USA: North-Holland 1982), p.399-408.

Studies a monazite sample from New Mexico, USA and presents data on the leaching behaviour up to dissolution of ~1.8% of the total ²³²Th radioactivity. These studies are of use in the field of nuclear waste disposal. (4 refs.)

60287 Investigation of titanium in metamict Nb-Ta-Ti oxides using the extended X-ray absorption fine structure technique. R.B.Greger, F.W.Lytle (Boeing Co., Seattle, WA, USA), R.C.Ewing, R.F.Haaker.

Scientific Basis for Nuclear Waste Management V. Proceedings of the Materials Research Society Fifth International Symposium on the Scientific Basis for Nuclear Waste, Berlin, Germany, 7-10 June 1982 (New York, USA: North-Holland 1982), p.409-18.

An important approach in the evaluation of crystalline waveforms is to study the long term stabilities of closely related mineral species which have become metamict (radiation damaged) and have been exposed to weathering processes for geologic periods of time. The documented metamictisation and alteration effects can then be used as 'benchmarks' for comparison with the results of short term laboratory leaching and irradiation experiments which have been designed to simulate long term effects. The Nb-Ta-Ti complex oxide minerals, containing appreciable rare earth elements (REE), U, and Th, are natural analogues for phases in proposed titanate radioactive wasteforms. Because of the geochemical similarities among Ti, Nb and Ta, a study of the metamict state and alteration effects in complex Nb-Ta-Ti oxides may yield data that is important in evaluating the long term stability of radioactive wasteforms. The investigation reported here is concerned with the application of the extended X-ray absorption fine structure and X-ray absorption near edge structure spectroscopy to the study of the structure of the metamict state. (18 refs.)

60288 The isolation capability of a salt dome utilised for high-level waste disposal. J.Hamstra (Netherlands Energy Res. Found., Petten, Netherlands).

Scientific Basis for Nuclear Waste Management V. Proceedings of the Materials Research Society Fifth International Symposium on the Scientific Basis for Nuclear Waste, Berlin, Germany, 7-10 June 1982 (New York, USA: North-Holland 1982), p.419-28.

Rock salt can, because of its plastic properties, be utilised as a potential host rock in such a way that its function as a natural barrier becomes dominant in the overall disposal concept. It is this rock salt and more in particular this salt dome specific potential that is discussed. (4 refs.)

60289 Dissolution rate of salt domes on the basis of interpretation of measured salinity profiles. K.E.Lindstrom Jensen (Elsam, Fredericia, Denmark).

Scientific Basis for Nuclear Waste Management V. Proceedings of the Materials Research Society Fifth International Symposium on the Scientific Basis for Nuclear Waste, Berlin, Germany, 7-10 June 1982 (New York, USA: North-Holland 1982), p.429-38.

When radioactive waste is disposed in a salt dome, it is important to evaluate the hydrologic stability of the dome. It depends on the dissolution rate of the dome, which again is determined by the transport and dispersion properties of the cap rock and the other formations surrounding the dome. The same properties are also required in safety assessment work for calculation of migration of radionuclides, which might be released from the dome to the surrounding strata. Analytical solutions are described for calculation of salt concentrations in ground water corresponding to a certain dissolution rate of the dome. Using these solutions a method is described, which makes it possible to determine rate of dissolution, ground water velocity, and dispersivity in the strata just above cap rock on basis of measured salinity profiles above the dome. (3 refs.)

60290 Dissolution of evaporites and its possible impact on the integrity of the Waste Isolation Pilot Plant (WIPP) New Mexico, USA. M.Zand (New Mexico Health & Environment Dept., Santa Fe, NM, USA).

Scientific Basis for Nuclear Waste Management V. Proceedings of the Materials Research Society Fifth International Symposium on the Scientific Basis for Nuclear Waste, Berlin, Germany, 7-10 June 1982 (New York, USA: North-Holland 1982), p.439-48.

Discusses the manifestation of dissolution processes (such as land subsidence and method of formation of breccia pipes and brine reservoirs) in the bedded salt of southeastern New Mexico in the vicinity of the WIPP site. The author postulates conditions under which breaches of the repository might occur, discusses radiological consequences of such breaches, and identifies areas that need further investigation. (15 refs.)

60291 Deformation-dissolution potential of bedded salt, Waste Isolation Pilot Plant site, Delaware Basin, New Mexico. R.Y.Anderson (Dept. of Geology, Univ. of New Mexico, Albuquerque, NM, USA).

Scientific Basis for Nuclear Waste Management V. Proceedings of the Materials Research Society Fifth International Symposium on the Scientific Basis for Nuclear Waste, Berlin, Germany, 7-10 June 1982 (New York, USA: North-Holland 1982), p.449-58.

Deep-seated collapse and brecciation is a feature common to bedded salt in a number of evaporite basins. The origin of these features is poorly understood. The relatively young geologic age of uplift and exposure of evaporites in the Delaware Basin, and a still-active hydrologic system, provides a unique opportunity to examine the pathways of water movement related to collapse features and salt dissolution. In addition, salt deformation structures are closely associated with brine, dissolution, and collapse. The author briefly discusses evidence for deep-seated dissolution, considers the relationship between deformation, dissolution, and brine, and examines the potential for dissolution at the WIPP (Waste Isolation Pilot Plant) site with respect to stages in the deformation-dissolution process. (15 refs.)

60292 Mineralogical and geochemical factors influencing the final disposal of HLW in the Stassfurt Halite. H.Gies (Gesellschaft für Strahlen- und Umweltforschung mbH München, Inst. für Tief Lagerung, Braunschweig, Germany).

Scientific Basis for Nuclear Waste Management V. Proceedings of the Materials Research Society Fifth International Symposium on the Scientific Basis for Nuclear Waste, Berlin, Germany, 7-10 June 1982 (New York, USA: North-Holland 1982), p.459-65.

As the thickest and primarily monomineralic saline horizon in the Federal Republic of Germany, investigation of the Zechstein-2-series, Stassfurt-Halite (Na₂) is being emphasized for the final disposal of HLW. This horizon is of particular importance, especially since it is the base of the whole saline formation in northern Germany. Mineralogical and geochemical factors are discussed. (8 refs.)

60293 Gas production and liberation from rock salt samples and potential consequences on the disposal of high-level radioactive waste in salt domes. N.Jockwer (Gesellschaft für Strahlen- und Umweltforschung mbH, Inst. für Tief Lagerung, Braunschweig, Germany).

Scientific Basis for Nuclear Waste Management V. Proceedings of the Materials Research Society Fifth International Symposium on the Scientific Basis for Nuclear Waste, Berlin, Germany, 7-10 June 1982 (New York, USA: North-Holland 1982), p.467-75.

Rock salt from the north German salt domes which are to be used for disposing high level radioactive waste consist, along with the major mineral halite, the minor minerals anhydrite, polyhalite and kieserite and of some trace minerals such as carbonates, clay, bitumen components. In the surroundings of an emplacement borehole with high level radioactive waste the rock salt will be heated to about 200°C and the water of the hydrated minerals as well as the water and gas adsorbed on the crystal boundaries and present as inclusions will be liberated into the intergranular spaces. At the elevated temperature carbon dioxide, different hydrocarbons, hydrochloric acid and sulphur dioxide may be generated by thermal decomposition of the carbonates, clay, bitumen and other trace minerals. As a result of γ -radiation gases such as hydrogen, oxygen, hydrochloric acid and carbon dioxide will be generated by radiolysis. (3 refs.)

60294 Thermomechanical in-situ experiments and finite element computations. A.Pudewils, R.Müller, E.Korthaus, R.Koster (Inst. für Nukleare Entsorgungstechnik, Kernforschungszentrum Karlsruhe, Karlsruhe, Germany).

Scientific Basis for Nuclear Waste Management V. Proceedings of the Materials Research Society Fifth International Symposium on the Scientific Basis for Nuclear Waste, Berlin, Germany, 7-10 June 1982 (New York, USA: North-Holland 1982), p.477-86.

In the ultimate storage of high level wastes in rock salt thermomechanical phenomena caused by the temperature rises play an important role for elaborating the storage concept. Important factors are both large space effects concerning the repository and the geological formation and small space phenomena influencing to a considerable extent the interaction between waste blocks and the host rock. While the large space aspects are largely inaccessible to an experimental investigation, the small space effects, especially the convergence behavior of individual heated bore-holes, are eligible for a systematic experimental and computational study allowing verification of available computational methods and thermomechanical material laws for rock salt. Three in-situ experiments were performed in ASSE, using a convergence measuring probe specifically developed for such investigations, and evaluated with the help of thermomechanical model computations. (3 refs.)

60295 Investigations of the solution behaviour of NaCl in the quinary system NaCl-KCl-MgCl₂-MgSO₄-H₂O at different temperatures. R.Conradi, H.Engelke, A.Kaiser (Fraunhofer-Inst. für Silicatsforschung, Würzburg, Germany).

Scientific Basis for Nuclear Waste Management V. Proceedings of the Materials Research Society Fifth International Symposium on the Scientific Basis for Nuclear Waste, Berlin, Germany, 7-10 June 1982 (New York, USA: North-Holland 1982), p.487-90.

The German concept of high level waste final storage by the aid of waste glasses is based on rock salt formations as deposits. Investigations consider the accidental case of water entrance into the deposit where the waste forms then are exposed to highly concentrated salt brines at elevated temperatures and pressures. In order to achieve standard corrosion conditions for the investigations of waste forms, a set of salt brines of definite composition has been generally accepted as possible corroding agents. The agreement is based on a model for the process of a hypothetical water entrance saying that in the initial period the entering water approaches a solution equilibrium at lower temperatures with the solid phases containing sodium, potassium and magnesium sulfates and chlorides. In the rock salt environment of the deposit higher temperatures will occur due to the radioactivity of the waste forms. That is why an additional uptake of NaCl by the 'standard brines' has to be taken into account. The intent of the investigations was to determine the additional amount of NaCl which can be dissolved at higher temperatures in a so-called Q-solution. (2 refs.)

60296 Investigation of diffusion of UO₂Cl₂ in saturated NaCl solutions. H.Murso, B.Plewinsky, D.Leopold, G.Marx (Inst. of Inorganic & Analytical Chem., Free Univ. of Berlin, Berlin, Germany).

Scientific Basis for Nuclear Waste Management V. Proceedings of the Materials Research Society Fifth International Symposium on the Scientific Basis for Nuclear Waste, Berlin, Germany, 7-10 June 1982 (New York, USA: North-Holland 1982), p.491-6.

Even in the early 1960s it had already been decided to place high-level radioactive waste in the salt formations of the Federal Republic of Germany. However a major concern is the formation of highly corrosive brines in the event of water filling the repositories. In order to estimate the risks of waste storage in salt repositories it is necessary to investigate the physico-chemical

properties of the waste materials and of those radionuclides extracted into brine. The extraction of radionuclides from borosilicate glasses or spent fuel elements has been previously discussed, taking into consideration the two transport mechanisms: diffusion and convection. Diffusion measurements of actinides in saturated NaCl solutions have been made in order to determine which mechanism is rate determining. The diffusion coefficients of UO_2Cl_2 in saturated NaCl solutions were measured by use of an ultracentrifuge at 25, 40 and 50°C. The results are compared with those determined for the binary system $\text{UO}_2\text{Cl}_2\text{-H}_2\text{O}$. Measurements of viscosity and molar mass were made in order to elucidate the difference in diffusion velocities in the systems studied. (12 refs.)

60297 The importance of near-field phenomena for nuclide release from a flooded salt dome repository. R.Storck (Tech. Univ. Berlin, Berlin, Germany).

Scientific Basis for Nuclear Waste Management V. Proceedings of the Materials Research Society Fifth International Symposium on the Scientific Basis for Nuclear Waste, Berlin, Germany, 7-10 June 1982 (New York, USA: North-Holland 1982), p.497-507

Deals with the first step in identification of relevant near field phenomena for the scenario 'penetration of brine into a backfilled HLW-repository, directly after its closure'. By use of parameter variation, the relevant phenomena for the release of Tc-99 from the salt dome are identified. (9 refs.)

60298 Diffusion in crystalline rocks. K.Skagius, I.Neretnieks (Dept. of Chem. Engng., Royal Inst. of Technol., Stockholm, Sweden).

Scientific Basis for Nuclear Waste Management V. Proceedings of the Materials Research Society Fifth International Symposium on the Scientific Basis for Nuclear Waste, Berlin, Germany, 7-10 June 1982 (New York, USA: North-Holland 1982), p.509-18

Laboratory experiments to determine the sorption and the rate of diffusion of cesium and strontium in pieces of granite have been performed. The effective diffusivity, D_{p-p} was found to be $1.2 \times 10^{-12} \text{ m}^2/\text{s}$ for both cesium and strontium. The diffusion of nonsorbing species in granites and other rock materials have been studied in laboratory scale. The non-sorbing species were iodide, tritiated water, Cr-EDTA and Uranine. In granites the effective diffusivities were determined to be $0.7\text{-}1.3 \times 10^{-13} \text{ m}^2/\text{s}$ for iodide and $1.3\text{-}1.8 \times 10^{-13} \text{ m}^2/\text{s}$ for tritiated water. Electrical resistivity measurements in salt water saturated rock cores have been performed. The resistivity is measured in the saturated core and in the salt solution with which the core has been saturated. The ratio between these two resistivities has a direct relation to the ratio of the effective diffusivity for a component in the rock material and the diffusivity in free water for the same component. (8 refs.)

60299 Diffusion in the matrix of granitic rock. Field test in the Stripa mine. L.Birgersson, I.Neretnieks (Dept. of Chem. Engng., Royal Inst. of Technol., Stockholm, Sweden).

Scientific Basis for Nuclear Waste Management V. Proceedings of the Materials Research Society Fifth International Symposium on the Scientific Basis for Nuclear Waste, Berlin, Germany, 7-10 June 1982 (New York, USA: North-Holland 1982), p.519-28

A migration experiment with the objective to investigate the existence of a connected pore system in 'undisturbed' rock has been performed in the Stripa mine at the 360 m-level. Since all three tracers (Cr-EDTA, I^- and Uranine) that were used in the experiment migrated at least 11 cm into the rock under a three month period, this experiment indicates the existence of a connected pore system in 'undisturbed' rock. (9 refs.)

60300 Migration in a single fracture. H.Abelin, J.Gidlund, I.Neretnieks (Dept. of Chem. Engng., Royal Inst. of Technol., Stockholm, Sweden).

Scientific Basis for Nuclear Waste Management V. Proceedings of the Materials Research Society Fifth International Symposium on the Scientific Basis for Nuclear Waste, Berlin, Germany, 7-10 June 1982 (New York, USA: North-Holland 1982), p.529-38

It has been decided to investigate flow and sorption in a readily identifiable fracture which can be excavated for a detailed examination of flow path and sorption sites. The investigation is performed in the Stripa mine, 360 m below ground, where there is a natural flow towards the drift. The bedrock is granite. A method of tracer injection into a fracture, either as a step or a pulse, and of collection of water samples under anoxic atmosphere has been suggested and tested in a preparatory investigation. The introduction of tracers can be done either under natural pressure or by injection with over pressure. An injection of Rhodamine-WT, Na-iodide and Na-fluorescein with cover pressure has been performed. It has been found that Rhodamine-WT is influenced in some way along the flow path. (5 refs.)

60301 Model for near field migration. G.Andersson, A.Rasmuson, I.Neretnieks (Dept. of Chem. Engng., Royal Inst. of Technol., Stockholm, Sweden).

Scientific Basis for Nuclear Waste Management V. Proceedings of the Materials Research Society Fifth International Symposium on the Scientific Basis for Nuclear Waste, Berlin, Germany, 7-10 June 1982 (New York, USA: North-Holland 1982), p.539-48

A model is proposed which describes the transport to and from a waste canister in a repository. The model includes flow and diffusion in the fractures in the bedrock as well as diffusion in the backfill. Calculations have been made on the inward transport of corrosive agents to a buried canister from the surrounding bedrock. The oxidants are transported from the flowing groundwater through the backfill to the surface of the canister, were they are assumed to react instantaneously with the canister material. The rock is modeled as a discrete fracture system. The fractures are assumed to be evenly spaced and the groundwater movement is described by potential flow. The model is three dimensional. (9 refs.)

60302 Model for far field migration. A.Rasmuson, I.Neretnieks (Dept. of Chem. Engng., Royal Inst. of Technol., Stockholm, Sweden).

Scientific Basis for Nuclear Waste Management V. Proceedings of the Materials Research Society Fifth International Symposium on the Scientific Basis for Nuclear Waste, Berlin, Germany, 7-10 June 1982 (New York, USA: North-Holland 1982), p.549-58

A transport model of radionuclide migration in fissured rock is presented. It includes advection and hydrodynamic dispersion in the fissures and diffusion and sorption in the rock blocks. 1 and 2D analytical and 3D numerical solutions of the model have been developed. A large number of calculations for the approximate range of variation of the input parameters have been performed. A large impact of hydrodynamic dispersion and micropore diffusion on the amount of radioactive material reaching the biosphere is found. (17 refs.)

60303 Leach rates of high level waste and spent fuel: limiting rates as determined by backfill and bedrock conditions. I.Neretnieks (Dept. of Chem. Engng., Royal Inst. of Technol., Stockholm, Sweden).

Scientific Basis for Nuclear Waste Management V. Proceedings of the Materials Research Society Fifth International Symposium on the Scientific Basis for Nuclear Waste, Berlin, Germany, 7-10 June 1982 (New York, USA: North-Holland 1982), p.559-68

The release rate of radionuclides from a degraded canister containing radioactive waste is controlled by diffusion through the backfill and by diffusion into the water flowing past the canister. In low porosity low permeability bedrock like the Swedish granites the amount of water which can be contaminated may be very small. Two sample cases are calculated. One uses the conditions for a repository for vitrified high level waste, the other applied to a repository for spent fuel. The small amount of water which can carry the waste in combination with the low solubilities for the major longlived actinides limit the release rate from the repositories to very small values. (12 refs.)

60304 Aqueous phase diffusion in crystalline rock. M.H.Bradbury, D.Lever, D.Kinsey (Harwell Labs, Harwell, England).

Scientific Basis for Nuclear Waste Management V. Proceedings of the Materials Research Society Fifth International Symposium on the Scientific Basis for Nuclear Waste, Berlin, Germany, 7-10 June 1982 (New York, USA: North-Holland 1982), p.569-78

One of the options being considered for the disposal of radioactive waste is deep burial in crystalline rocks such as granite. Recent theoretical studies have indicated the importance of diffusion into pores and micro-fissures in the rock matrix as an additional retardation and dispersion mechanism, particularly for species only weakly sorbed. This would delay the migration of radionuclides moving with the groundwater along major fissures or fractures. Because of the potential importance of this mechanism in radionuclide migration, a programme was started to measure diffusion coefficients of soluble species in water through rock. Diffusion coefficients have been measured in a number of granites, as a typical rock, using the very weakly sorbed iodide ion as tracer. In addition, measurements on weakly sorbed nuclides have yielded values of the sorption coefficient where other techniques are inadequate. (9 refs.)

60305 Permeability monitoring technique of the near-field and far-field interface of underground openings. A.T.Jakubick, V.De Korompay (Ontario Hydro, Toronto, Ontario, Canada).

Scientific Basis for Nuclear Waste Management V. Proceedings of the Materials Research Society Fifth International Symposium on the Scientific Basis for Nuclear Waste, Berlin, Germany, 7-10 June 1982 (New York, USA: North-Holland 1982), p.579-86

In July/August 1981 and February/March 1982 the authors sampled water for isotope analysis from water-bearing fractures of two mines in Elliot Lake. Permission for sampling was given to Ontario Hydro by Denison Mines Ltd. and Rio Algom Ltd., Quirke Mine in conjunction with the CANMET mine safety tests. The purpose of the investigation was to find out whether there is a relationship between the water present in some fractures in a deep mine and the shallow groundwater in the far-field of the mine. ^{18}O and ^2H contents are analysed. (11 refs.)

60306 Hydrothermal conditions around a radioactive waste repository. R.Thunvik, C.Braester (Royal Inst. of Technol., Stockholm, Sweden).

Scientific Basis for Nuclear Waste Management V. Proceedings of the Materials Research Society Fifth International Symposium on the Scientific Basis for Nuclear Waste, Berlin, Germany, 7-10 June 1982 (New York, USA: North-Holland 1982), p.587-95

The possibility of permanent burial of radioactive waste from nuclear power plants, is studied in Sweden at the KBS (Nuclear Fuel Safety)—project. Definite repository sites have not yet been selected, but the general principles of construction regarding the layout have been devised. The feasibility of a prospective site for radioactive waste disposal is highly dependent on the geohydrological conditions. Heat emitted by the decaying waste will increase the temperature of the rock, changing groundwater density gradients and creating convective currents. Under certain conditions water particles passing through the repository may reach the ground surface. It is therefore of significant interest in the safety analysis to predict pathlines and travel times of water particles, should any of the waste canisters be breached and the groundwater be contaminated. The solutions presented illustrate the effect of heat released from a hypothetical repository on the groundwater movements around the repository. (6 refs.)

60307 Modeling approach to determine short- and long-term thermal and thermomechanical effects of waste emplacement in a repository in basalt. T.F.Lehnhoff (Univ. of Missouri-Rolla, Rolla, MO, USA), K.Thirumalai, A.D.Krug.

Scientific Basis for Nuclear Waste Management V. Proceedings of the Materials Research Society Fifth International Symposium on the Scientific Basis for Nuclear Waste, Berlin, Germany, 7-10 June 1982 (New York, USA: North-Holland 1982), p.597-609

The Columbia River basalts, which underlie a large portion of the Pacific Northwest of the United States of America, are being investigated as one of the candidate media for a nuclear waste repository. The Basalt Waste Isolation Project of Rockwell Hanford Operations (Rockwell) is conducting these investigations for the US Department of Energy. Since the inception of the program in 1976, a number of studies have led to the selection of a reference repository location and the start of construction of an exploratory shaft. Near- and far-field effects are discussed here for thermal and thermomechanical properties in a basalt repository. (3 refs.)

60308 A combined analytical model for performance assessment of the waste package/geologic medium systems. A.K.Rays (Dept. of Chem. Engng., Univ. of Kentucky, Lexington, KY, USA), S.Nair, H.E.Nuttall.

Scientific Basis for Nuclear Waste Management V. Proceedings of the Materials Research Society Fifth International Symposium on the Scientific Basis for Nuclear Waste, Berlin, Germany, 7-10 June 1982 (New York, USA: North-Holland 1982), p.611-18

The authors have developed a three dimensional model which incorporates the sequence of events preceding migration of nuclides to biosphere. (7 refs.)

60309 Engineered components for spent fuel radioactive waste isolation. H.C.Burkholder (Battelle Memorial Inst., Office of Nuclear Waste Isolation, Columbus, OH, USA).

Scientific Basis for Nuclear Waste Management V. Proceedings of the Materials Research Society Fifth International Symposium on the Scientific Basis for Nuclear Waste, Berlin, Germany, 7-10 June 1982 (New York, USA: North-Holland 1982), p.619-30

In response to draft radioactive waste disposal standards, R&D programs have been initiated in the United States which are aimed at developing and ultimately using radionuclide transport-delaying (e.g., long-lived waste containers) and radionuclide transport-controlling (e.g., very low release rate waste forms) engineered components as part of the isolation system. Before these programs proceed significantly, it seems prudent to evaluate the techni-

cal justification for development and use of sophisticated engineered components in radioactive waste isolation. (27 refs.)

60310 Recent advances in repository seal materials. D.M.Roy (Materials Res. Lab., Pennsylvania State Univ., University Park, PA, USA), F.L.Burns. Scientific Basis for Nuclear Waste Management V. Proceedings of the Materials Research Society Fifth International Symposium on the Scientific Basis for Nuclear Waste, Berlin, Germany, 7-10 June 1982 (New York, USA: North-Holland 1982), p.631-9

One long-term solution proposed for isolating radioactive waste from the biosphere is containment in underground geologic repositories. A requirement for this procedure is that most penetrations into the repository region be sealed following emplacement of the waste. The general requirements of repository seal materials and the seal system are that these potential pathways to the biosphere be sealed adequately to prevent (a) excess fluid flow into the repository and (b) radionuclides in the waste from reaching the biosphere in quantities in excess of acceptable levels. Here the authors report mostly on cementitious seal materials, with some studies of clays and zeolites. (18 refs.)

60311 Development of a backfill for containment of high-level nuclear waste. F.N.Hodges, J.H.Westik, Jr., L.A.Bray (Pacific Northwest Lab., Richland, WA, USA).

Scientific Basis for Nuclear Waste Management V. Proceedings of the Materials Research Society Fifth International Symposium on the Scientific Basis for Nuclear Waste, Berlin, Germany, 7-10 June 1982 (New York, USA: North-Holland 1982), p.641-8

Sodium and calcium bentonites, pressed to densities between 1.9 and 2.2 g/cm³, have hydraulic conductivities in the range of 10⁻¹¹ to 10⁻¹³ cm/s. Batch sorption distribution ratios (R_d) indicate that Sr, Cs, and Am are strongly sorbed on bentonites and zeolites, that Np and U are moderately sorbed on bentonites and zeolites, and that Am, Np, U, I, and Tc are strongly sorbed on charcoal. Sorption results with basalt and tuff ground waters are similar; however, iodine in tuff ground water sorbs more strongly on bentonites. Thermal diffusivity measurements for dry, compacted ($\rho \sim 2.1$ g/cm³) sodium bentonite indicate that the thermal conductivity of a high density bentonite backfill should be roughly similar to that of silicate host rocks (basalt, granite, tuff). These results indicate that a bentonite backfill can significantly delay the first release of many radionuclides into the host rock and that by forming a diffusion barrier a bentonite backfill can significantly decrease the long-term release rate of radionuclides from the waste package. (10 refs.)

60312 Ion water migration phenomena in dense bentonites. R.Pusch (Div. of Soil Mech., Univ. of Lulea, Lulea, Sweden), T.Eriksen, A.Jacobsson. Scientific Basis for Nuclear Waste Management V. Proceedings of the Materials Research Society Fifth International Symposium on the Scientific Basis for Nuclear Waste, Berlin, Germany, 7-10 June 1982 (New York, USA: North-Holland 1982), p.649-58

The development of a suitable technique for isolating unprocessed nuclear reactor wastes from the biosphere has led to the Swedish multibarrier concept KBS 2 with two engineered components, a thick-walled copper canister and a clay body which confines the canister. The clay consists of well fitting blocks of highly compacted Na bentonite made by 'isostatic' compression of bentonite powder. They are not water saturated when placed in the deposition holes but take up water from the surrounding rock, swell and ultimately form a tight contact with the rock and the canisters. When the bentonite is in physical equilibrium with the surroundings it from a medium with a number of valuable properties, such as self-healing and ion exchange capacities. The healing means that initial joints between blocks and voids, or local passages in the clay caused by slight rock or canister displacements, will be sealed by the swelling potential of the clay. The high ion exchange capacity retards the migration of radionuclides through the clay barrier after corrosion of the canisters. The most important feature is, however, the very low hydraulic conductivity and the low ion diffusivity. (6 refs.)

60313 Transport of actinides through a bentonite backfill. B.Torstenfelt, H.Kipatsi, K.Andersson, B.Allard, U.Olofsson (Dept. of Nuclear Chem., Chalmers Univ. of Technol., Goteborg, Sweden).

Scientific Basis for Nuclear Waste Management V. Proceedings of the Materials Research Society Fifth International Symposium on the Scientific Basis for Nuclear Waste, Berlin, Germany, 7-10 June 1982 (New York, USA: North-Holland 1982), p.659-68

Compacted bentonite has been proposed as a suitable backfill material in the Swedish concept for underground storage of high-level waste. The backfill barrier will serve both as a physical barrier, preventing convective water flow and allowing radionuclide penetration only by diffusion, and as a chemical barrier capable of chemically interacting with the radionuclides. The authors present measurements of the diffusion and sorption of actinides in bentonite and the technique used for these studies. (14 refs.)

60314 Evaluation of solubility and speciation of actinides in natural groundwaters. M.R.Schweingruber (Swiss Federal Inst. for Reactor Res., Wurenlingen, Switzerland).

Scientific Basis for Nuclear Waste Management V. Proceedings of the Materials Research Society Fifth International Symposium on the Scientific Basis for Nuclear Waste, Berlin, Germany, 7-10 June 1982 (New York, USA: North-Holland 1982), p.679-88

Summarizes first modeling efforts undertaken to evaluate the speciation and solubility of U, Th, Np and Pu in two selected Swiss groundwaters. Starting from a rather general box model, two simple case studies will be defined. The first could be visualized as pertaining to the far-field, the second to the near-field of a repository. For both cases the required model parameters are specified. Some emphasis is laid upon the effect of kinetically hindered solid phase precipitation. (17 refs.)

60315 Study of radionuclide migration from deep-lying repository sites with overlying sedimentary layers. J.Hadernann, F.Roesel (Swiss Federal Inst. for Reactor Res., Wurenlingen, Switzerland).

Scientific Basis for Nuclear Waste Management V. Proceedings of the Materials Research Society Fifth International Symposium on the Scientific Basis for Nuclear Waste, Berlin, Germany, 7-10 June 1982 (New York, USA: North-Holland 1982), p.689-96

In Switzerland the host rock formations currently considered for disposal of high-level wastes lie in the northern part of the country. They form the crystalline basement and are covered by substantial layers of sedimentary rocks. First predictions of regional groundwater flow fields for this hydrologic system have become available recently. These define preferential migration paths to the biosphere and groundwater velocities to be used as input to radionuclide transport model calculations. The authors consider a one-dimensional transport along these preferential paths from a source described by a leaching model. The source is located at notional repository depths of 1500 and 2400 meters, respectively. In each case the depth in granitic rock is 1000 meters. As a source inventory they have chosen the ²⁴³Cm chain because it includes the nuclide ²³⁷Np which appears to be crucial in long-term

safety analyses. As far as possible field and laboratory data are used in the calculations. (7 refs.)

60316 A comparison of in-situ radionuclide migration studies in the Studsvik area and laboratory measurements. O.Landstrom (Studsvik Energiteknik, Nykoping, Sweden), C.E.Klockars, O.Persson, K.Andersson, B.Torstenfelt, B.Allard, S.A.Larsson, E.L.Tullborg.

Scientific Basis for Nuclear Waste Management V. Proceedings of the Materials Research Society Fifth International Symposium on the Scientific Basis for Nuclear Waste, Berlin, Germany, 7-10 June 1982 (New York, USA: North-Holland 1982), p.697-706

A series of in-situ radionuclide migration tests are in progress in the Studsvik area on the Swedish east coast. Three well defined flowpaths have been located and characterized using non-sorbing tracers (I-131 and H-3), and one of these pathways has been used for a study of the migration of sorbing elements (Sr-85). Laboratory sorption studies with Sr-85 have been performed on materials (rock-water) from the same location as the field tests and with variation of parameters not easily varied in-situ (e.g. pH and nuclide concentration). A fairly good correlation was obtained between retention in natural fractures (field experiment) and laboratory column studies, although the latter were formed on crushed samples of whole rock (retention factors 15-30). (14 refs.)

60317 Radionuclide retardation and release rates for oceanic sediments and clay. F.Schreiner, S.Fried, A.Friedman (Chem. Div., Argonne Nat. Lab., Argonne, IL, USA).

Scientific Basis for Nuclear Waste Management V. Proceedings of the Materials Research Society Fifth International Symposium on the Scientific Basis for Nuclear Waste, Berlin, Germany, 7-10 June 1982 (New York, USA: North-Holland 1982), p.707-14

The concept of emplacing nuclear waste in the argillaceous sediments covering extensive regions of the ocean floor is being given serious consideration by a group of interested nations. For such a subseabed repository to be acceptable the effectiveness in isolating the radioactive material must be demonstrated. Since the waste form cannot be relied upon to retain its integrity in the suboceanic environment, the subseabed repository relies principally on the containment qualities of the sediment that forms the geologic barrier impeding the spread of radionuclides. For the past several years the authors' laboratory has been engaged in the measurement of the parameters that characterize the mobility of actinide element ions and other radioactive species in marine sediments and in terrestrial clay. As a result of this work the authors are able to present convincing evidence showing the sediment to represent an adequate barrier for the isolation of nuclear wastes. (5 refs.)

60318 Liquid chromatography in migration studies. L.Carlsen, W.Batsberg (Chem. Dept., Riso Nat. Lab., Roskilde, Denmark).

Scientific Basis for Nuclear Waste Management V. Proceedings of the Materials Research Society Fifth International Symposium on the Scientific Basis for Nuclear Waste, Berlin, Germany, 7-10 June 1982 (New York, USA: North-Holland 1982), p.715-23

A detailed knowledge of the geochemical environment of a site for the disposal of radioactive waste is of fundamental importance. To evaluate the migration behaviour of radionuclides in geological media a series of data are needed, amongst others a number of physico-chemical properties of the media, such as permeability, porosity, dispersion, diffusion, and sorption characteristics. In this connection liquid chromatography appears to be advantageous as a facile experimental technique to obtain relevant data for these physico-chemical properties. The capabilities of the liquid chromatography technique in connection with migration studies are illustrated by examples from recent studies on the cretaceous formation overlying the Erslev salt dome (North Jutland, Denmark). (11 refs.)

60319 Studies of the mobilization of thorium from the Morro do Ferro. M.Eisenbud, W.Lei, R.Ballad (New York Univ. Medical Center, New York, NY, USA), E.Penna Franca, N.Mickeyley, T.Cullen, K.Krauskopf.

Scientific Basis for Nuclear Waste Management V. Proceedings of the Materials Research Society Fifth International Symposium on the Scientific Basis for Nuclear Waste, Berlin, Germany, 7-10 June 1982 (New York, USA: North-Holland 1982), p.735-44

The studies have three objectives: (1) to predict by analogy with the thorium deposit, the environmental implications of an ancient residue of plutonium in a nuclear waste repository that has been eroded to the surface or has been subject to groundwater intrusion; (2) to develop models for transport of Th, U, Ra-226, Ra-228, rare earths, and possibly other elements; and (3) to evaluate the dosimetric implications to human living near the site. This is a progress report that will be limited to the findings with respect to the first objective, the use of this plutonium analogue to predict the environmental implications of a nuclear waste repository that has been breached. (13 refs.)

60320 Properties and mobilities of actinide colloids in geologic systems. U.Olofsson, B.Allard, B.Torstenfelt, K.Andersson (Dept. of Nuclear Chem., Chalmers Univ. of Technol., Goteborg, Sweden).

Scientific Basis for Nuclear Waste Management V. Proceedings of the Materials Research Society Fifth International Symposium on the Scientific Basis for Nuclear Waste, Berlin, Germany, 7-10 June 1982 (New York, USA: North-Holland 1982), p.755-64

The interaction between radionuclides in solution and exposed geologic media, e.g. in connection with underground storage of radioactive waste, is largely determined by the chemical properties of the system. The mobility of radionuclides in contact with low-capacity minerals would depend on the chemical state of the element (e.g. degree of hydrolysis, formation of organic and inorganic complexes, etc.). Particularly for the actinides in their lower oxidation states (III, IV), however, would a formation of colloid particles be feasible in the groundwater environment. These colloids could be either true radiocolloids, i.e. aggregates of the radionuclide itself, or pseudocolloids, i.e. colloid material already present in the groundwater, onto which the radionuclide has sorbed. These colloidal particles may be very poorly sorbed on water exposed geologic media in comparison with radionuclides in true solution. Studies on the formation and properties of some actinide colloids (Am, Np, Pu) are discussed. (8 refs.)

60321 The migration of radionuclides with ground water. A discussion of the relevance of the input parameters used in model calculations. B.S.Jensen (Dept. of Chem., Riso Nat. Lab., Roskilde, Denmark).

Scientific Basis for Nuclear Waste Management V. Proceedings of the Materials Research Society Fifth International Symposium on the Scientific Basis for Nuclear Waste, Berlin, Germany, 7-10 June 1982 (New York, USA: North-Holland 1982), p.765-74

The plans for the disposal of radioactive waste leave very little time for testing long term performance of a repository so the evaluation of the hazards involved in the operation relies heavily on model calculations. It is therefore of utmost importance that these model calculations take all important parameters into account and are based on a thorough understanding of the possible physical and chemical processes in which the migrating species take

part. The author discusses many of the geophysical and geochemical processes in which migrating species can take part. (6 refs.)

60322 Sorption of actinides in well-defined oxidation states on geologic media. B. Allard, U. Olofsson, B. Torstenfeld, H. Kipatsi, K. Andersson (Dept. of Nuclear Chem., Chalmers Univ. of Technol., Göteborg, Sweden).

Scientific Basis for Nuclear Waste Management V. Proceedings of the Materials Research Society Fifth International Symposium on the Scientific Basis for Nuclear Waste, Berlin, Germany, 7-10 June 1982 (New York, USA: North-Holland 1982), p.775-82

The purpose of the present study is to get information on the mechanisms of actinide sorption on geologic material under well-defined conditions and using actinides in discrete oxidation states. For americium, the only oxidation state, that would be obtained under oxic conditions and in the absence of strong complexing agents, would be the trivalent state. For thorium, only the tetravalent state would exist in aqueous solution. Under oxic conditions and in the pH-range of environmental interest neptunium and uranium would exist entirely as penta- and hexavalent species, respectively, in solution. By performing experiments under oxic conditions Am(III), Th(IV), Np(V) and U(VI) would be obtained purely in one single oxidation state without any rigorous control of the redox potential. Thus, they may serve as reference systems. Hereby, it is possible to illustrate the importance of characterizing the redox properties of e.g. a potential geologic repository site and the effect of a sudden change of the pH or redox potential on the retention of a specific actinide. (9 refs.)

60323 Laboratory tests on the migration behavior of selected fission products in aquifer materials from a potential disposal site in northern Germany. H. Behrens, D. Klotz, H. Lang, H. Moser (Inst. für Radiohydrometrie, Gesellschaft für Strahlen- und Umweltforschung mbH München, Neuherberg, Germany), G. Barke, H. Bruhl, S. Gehler, U. Mühlenweg.

Scientific Basis for Nuclear Waste Management V. Proceedings of the Materials Research Society Fifth International Symposium on the Scientific Basis for Nuclear Waste, Berlin, Germany, 7-10 June 1982 (New York, USA: North-Holland 1982), p.783-90

The migration behaviour with respect to retardation by sorption of radioactive Ce, Cs, I, Nb, Ru, Sm, Sr, Te and Zr in fluvialite and aeolian sand aquifers has been examined in laboratory tests. In these tests it was attempted to simulate the natural conditions of the field. The tests were performed as batch and column experiments. The results of both types of experimental procedures agree within the error limits and show small sorption for I^- and TeO_4^{2-} ; medium sorption for Sr^{2+} , and high sorption for Cs^+ , Ce^{3+} , Sm^{3+} , Ru^{4+} , Zr^{4+} and Nb^{5+} . The investigations will be continued with other geologic materials from the same site. (5 refs.)

60324 Modelling of the migration of lanthanoids and actinoids in ground water; the medium dependence of equilibrium constants. G. Biedermann, J. Gruno, D. Ferri, I. Grenthe, F. Salvatore, K. Spahiu (Dept. of Inorganic Chem., Royal Inst. of Technol., Stockholm, Sweden).

Scientific Basis for Nuclear Waste Management V. Proceedings of the Materials Research Society Fifth International Symposium on the Scientific Basis for Nuclear Waste, Berlin, Germany, 7-10 June 1982 (New York, USA: North-Holland 1982), p.791-800 (14 refs.)

60325 Evaluation of radionuclide transport: effect of radionuclide sorption and solubility. P.F. Salter, G.K. Jacobs (Basalt Waste Isolation Project, Rockwell Hanford Operations, Richland, WA, USA).

Scientific Basis for Nuclear Waste Management V. Proceedings of the Materials Research Society Fifth International Symposium on the Scientific Basis for Nuclear Waste, Berlin, Germany, 7-10 June 1982 (New York, USA: North-Holland 1982), p.801-10

The sorption and solubility behavior of several potentially hazardous (key) radionuclides in the Columbia River Basalt geohydrologic system is discussed. Utilizing the transport characteristics of the site and the available sorption and solubility data, a preliminary site performance analysis is performed through comparison of the resultant predicted radionuclide transport behaviour with proposed US environmental regulations. (18 refs.)

60326 Radionuclide retardation during transport through fractured granite. I.G. McKinley, J.M. West (Inst. of Geological Sci., AERE Harwell, Didcot, England).

Scientific Basis for Nuclear Waste Management V. Proceedings of the Materials Research Society Fifth International Symposium on the Scientific Basis for Nuclear Waste, Berlin, Germany, 7-10 June 1982 (New York, USA: North-Holland 1982), p.811-20

The results of laboratory sorption studies of particular radionuclides (isotopes of Cs, Sr, Co and Ce) onto naturally weathered granite fracture infill are reported. Complementary mechanistic studies investigating the effect of reaction direction, temperature and competing ions on sorption isotherms are also briefly summarised. By use of simple computer models of groundwater flow, the consequences of observed 'isotherm non-linearity' on resultant nuclide migration are illustrative and compared with retardation calculated assuming 'matrix-diffusion' effects. (7 refs.)

60327 A comparative analysis of fractured and porous medium radionuclide transport. B.J. Travis (Earth & Space Sci. Div., Los Alamos Nat. Lab., Los Alamos, NM, USA), H.E. Nuttall.

Scientific Basis for Nuclear Waste Management V. Proceedings of the Materials Research Society Fifth International Symposium on the Scientific Basis for Nuclear Waste, Berlin, Germany, 7-10 June 1982 (New York, USA: North-Holland 1982), p.821-30

Provides a comparative study of porous and fractured medium nuclide transport by modeling the far field (1 km) problem for three different types of geomedia, i.e. a homogeneous porous medium, a single fracture in the porous medium, and a multi-fracture medium. Analytical models were used to study the homogeneous and single fracture geometries while an advanced numerical code was used to model the multi-fractured medium. (7 refs.)

60328 The effect of microbial activity on the containment of radioactive waste in a deep geological repository. J.M. West, I.G. McKinley, N.A. Chapman (Inst. of Geological Sci., Harwell Lab., Didcot, England).

Scientific Basis for Nuclear Waste Management V. Proceedings of the Materials Research Society Fifth International Symposium on the Scientific Basis for Nuclear Waste, Berlin, Germany, 7-10 June 1982 (New York, USA: North-Holland 1982), p.831-8

Describes preliminary experiments designed to study the effect of ambient microbial populations on radionuclide migration. (5 refs.)

Plutonium recycling scenario in light water reactors. Assessment of the environmental impact in the European Community See Entry 59523

Proceedings of the Symposium on Low-Level Waste Disposal. Site Characterization and Monitoring (NUREG/CP-0028) See Entry 59537

Research and development on radioactive waste management and storage. First annual progress report of the European Community programme 1980-1984 See Entry 59548

Pressure testing the THTR-300 reactor pressure vessel See Entry 60218

Comparison of COMETHE-III and FCODE-BETA fission gas release predictions with measurements See Entry 60224

After Creys-Malville: the prospects for the integrated site See Entry 60331

Reactor physics constants for the medium enriched-uranium core of Kyoto University Critical Assembly See Entry 60336

Eddy-current NDE for intergranular attack See Entry 60341

Analysis and synthesis of the theoretical studies performed on the control and safety of LWR's burning plutonium fuel See Entry 60358

Full-scale turbine missile concrete impact experiments See Entry 60363

Waterside corrosion of zircaloy fuel rods See Entry 60389

Effects of quenching and fission damage on the low temperature electrical resistivity of single crystal UO₂ See Entry 61981

Precipitation and void-swelling in nickel-manganese austenitic stainless steels See Entry 61986

On the critical dose for blistering in helium irradiated zirconium and Zr-Nb See Entry 61987

Thermal stability of cesium monouranate See Entry 62128

Diffusion and permeation of hydrogen in sodium [liquid] See Entry 62144

⁵¹Cr diffusion in Zr-Sn alloys See Entry 62165

Tritium permeability and pressure dependence of 304L stainless steel in the temperature range 723 to 1023K See Entry 62169

Thermal conductivity of stoichiometric (Pu, Nd)₂O₃ and (Pu, Y)₂O₃ solid solutions See Entry 62188

Thermal conductivity of near-stoichiometric (U,Nd)₂O₃, (U,Sm)₂O₃ and (U,Eu)₂O₃ solid solutions See Entry 62189

Thermal conductivity of (Pu_{1-x}Nd_x)₂O_{3-y} and (Pu_{1-x}Y_x)₂O_{3-y} solid solutions See Entry 62190

Sintering of SYNROC: case history for phase formation and densification of complex oxide systems See Entry 63233

Comments on the manuscript entitled: On the existence of a two-phase field in the uranium-oxygen system within the composition range 2.65<O/U<2.67 below 1273K [A. Caneiro, J.P. Abriata and J. Garces, J. Nucl. Mater. 113 (1983) 260-262] [and reply] See Entry 63275

Temperature and rate conditions for development of superplasticity in Zr-2.5% Nb alloy See Entry 63360

Comparison of the impact strength of 10GN2MFA and 15Kh2NMFA steels with the similarity of local failure taken into account See Entry 63381

Crack arrest in thick section steel plate See Entry 63385

Analysis of the corrosion products formed on Ti and a Ti-Pd alloy during exposure in hot water See Entry 63471

The radiation chemistry of nuclear reactor decontaminating reagents See Entry 63571

Hydrocarbon chemistry in irradiated CO₂/CO/CH₄/H₂O/H₂ mixtures. I. A survey of the initial reactions See Entry 63579

Some aspects of the influence of surface and ground water chemistry on the mobility of thorium in the 'Morro do Ferro' environment See Entry 63751

Potential for the rapid transport of plutonium in groundwater as demonstrated by core column studies See Entry 63752

28.42H Fuel preparation and reprocessing (inc. isotope separation and enrichment)

60329 Fuel cycle costs for molten-salt reactors. K. Nagashima (Sumitomo Atomic Energy Industries Ltd., Osaka, Japan).

J. At. Energy Soc. Jpn. (Japan), vol.25, no.1, p.49-57 (Jan. 1983). In Japanese.

The report describes FCC (fuel cycle cost) estimates for MSCR (molten-salt converter reactor) and MSBR (molten-salt breeder reactor) compared with those for LWRs (PWR and BWR). The calculation is based on the present worth technique with a given discount rate for each item, which enables one to make comparison between FCCs for MSCR, MSBR and LWRs. It is shown that the FCCs for MSCR and MSBR are 70~60% lower than the values for LWRs. And it could be said that the FCC for MSCR (Pu-converter) is about 10% lower than that for MSBR, because of the smaller amount of fissile inventory of MSCR than the inventory of MSBR. (10 refs.)

60330 Canadian accelerator breeder system development. S.O. Schriber. Report AECL-7840, Atomic Energy Canada Ltd., Chalk River, Ont. (Nov. 1982), 25 pp.

A shortage of fissile material at a reasonable price is expected to occur in the early part of the twenty-first century. Converting fertile material to fissile material by electronuclear methods is an option that can extend the world's resources of fissionable material, supplying fuel for nuclear power stations. This paper presents the rationale for electronuclear breeders and describes the Canadian development program for an accelerator breeder facility that could produce 1 Mg of fissile material per year. (7 refs.)

60331 After Creys-Malville: the prospects for the integrated site. C. Aycober, J. Leclercq (COGEMA, Cherbourg, France).

Proceedings of the L.M.F.B.R. Safety Topical Meeting, Lyon-Ecully, France, 19-23 July 1982 (Paris, France: Societe Francaise d'Energie Nucleaire 1982), p.155-73 In French.

The integrated site concept is defined as the juxtaposition of fuel element manufacture and reprocess plant with the nuclear reactor and turbo-generator halls, which is considered to be particularly advantageous following the development of fast reactors. A description is given of the project 'RAPIDE 1500 MW'. A 3600 MW (thermal) unit caters for the movement of 470 elements per year to and from a parallelepiped-shaped common vault. Details are given of the fuel fabrication process, which includes the stages of plutonium and uranium oxide grinding, mixing and calcining. Other plant items on the same site are the fuel and liquid waste reprocessing units. The reprocessing is divided into spent fuel treatment cycles for plutonium oxide, uranium nitrate, liquified waste and vitrified solid waste. (no refs.) G.C.

Plutonium recycling scenario in light water reactors. Assessment of the environmental impact in the European Community See Entry 59523

A statistic sensitive to deviations from the zero-loss condition in a sequence of material balances See Entry 60230

A high-purity inert atmosphere cell suite for research purposes—design and operating experience See Entry 60479

States of Am in aqueous solution See Entry 60582
Ion extraction in the laser process of uranium enrichment by selective ionization of atomic vapour See Entry 61005

28.43 FISSION REACTOR OPERATION

60332 Automatic time differential boiler leak location system. J.C.P. Garrett, G.D. Hall (Sci. Services Dept., CEGB, Manchester, England). *CEGB Tech. Disclosure Bull. (GB)*, no. 380, 4 pp. (Jan. 1983). A time differential technique is described for boiler leak location for gas cooled nuclear reactors. The principle of operation is based on common-mode rejection utilising commercial moisture measuring equipment, gas sampling valves and a microprocessor. The technique can be applied in principle to other online processes. (no refs.)

60333 A study of reactor internal dynamics by reactor noise analysis. Hee-Young Chun, Byoung-Joon Koh, Kyun-Kook Shin (Korean Inst. Electrical Engrs., Seoul, Korea). *Trans. Korean Inst. Electr. Eng.*, vol. 31, no. 10, p. 109-15 (1982). In Korean. At the TRIGA MARK II reactor whose rated power is 250 kW thermal, the power spectral densities of the noise were measured by a stochastic method with high resolution digital filters and fast Fourier transforms. The transfer function of the reactor at zero power was identical to the theoretical characteristics. When the power was increased above 1 kW, it showed power resonances at 3 Hz and 10 Hz generated by heat transfer and coolant flow effects and by nuclear reaction effects, respectively. (14 refs.)

60334 Recovery of hydrogen isotopes using a uranium bed. T. Tanabe, T. Yamamoto, S. Imoto (Dept. of Nuclear Engng., Osaka Univ., Osaka, Japan).

J. Less-Common Met. (Switzerland), vol. 89, no. 2, p. 393-8 (Feb. 1983). (International Symposium on the Properties and Applications of Metal Hydrides, Toba, Japan, 30 May-4 June 1982). A breakthrough experiment was used to investigate the recovery of hydrogen isotopes from contaminated inert gases by using a reactive uranium powder bed column under various conditions. Before the break point, the partial pressure of hydrogen in the outlet gas is almost equal to the plateau pressure of UH_3 at the column temperature. The breakthrough curve can be described by Meinschein's gas phase mass-transfer-limited model. The column is still effective at 273K where the partial pressure of hydrogen at the outlet is 10^{-5} Pa. (9 refs.)

60335 Filter for the selective removal of tritium from the coolant gas of a high temperature nuclear reactor. N. Iniotakis, W. Frohling, C.B. von der Decken (KFA Jülich, Jülich, Germany). *J. Less-Common Met. (Switzerland)*, vol. 89, no. 2, p. 465-74 (Feb. 1983). (International Symposium on the Properties and Applications of Metal Hydrides, Toba, Japan, 30 May-4 June 1982). A filter for the selective and continuous removal of tritium or deuterium from an inert gas stream is proposed. It is based on the permeation of hydrogen and its isotopes through a highly permeable wall and the removal of for example tritium on the secondary side. The necessary concentration drop to the secondary side is effected by isotope exchange of the tritium atoms on the secondary side with water. The filter concept and the mathematical model, investigations of the influence of various parameters and the selection of the wall material are reported. (2 refs.)

60336 Reactor physics constants for the medium enriched-uranium core of Kyoto University Critical Assembly. S. Wakamatsu, K. Nishina (Dept. of Nuclear Engng., Nagoya Univ., Nagoya, Japan). *Mem. Fac. Eng. Nagoya Univ. (Japan)*, vol. 34, no. 1, p. 125-38 (May 1982). In English. [received: March 1983]

Two energy-group eleven-region constants are determined for the single cylindrical core of the Kyoto University Critical Assembly (KUCA) loaded with uranium fuel of forty-five per cent enrichment. The procedure is based on the twenty-six group microscopic cross section libraries MGCL26GR and SMF26GR as its starting point, and on flux calculations by the one-dimensional transport theory code ANISN-JR. Cross sections are averaged with these fluxes as weighting functions. Although the constants do not produce complete agreement with experiment when used for criticality calculations, they are given as a form of an interim report. For the various analyses of the experiment being conducted at KUCA, only a relatively simple form of the constants is needed. Because of its complicated fuel-region geometry however, repeated spectrum calculations are required. (23 refs.)

60337 Prospekt-1 program for recovering the neutron spectra of nuclear reactors. V.M. Bukhshtaber, E.I. Grigor'ev, V.G. Markin, G.V. Tarnovskii, V.P. Yaryna.

Meas. Tech. (USA), vol. 25, no. 7, p. 624-5 (July 1982). Translation of: *Izmer. Tekh. (USSR)*, vol. 25, no. 7, p. 62-3 (July 1982). [received: Feb. 1983] The Prospekt-1 method is the first stage in the creation of an up-to-date program for recovering the spectra of nuclear reactors over a wide energy range. It provides a very detailed characterization of the neutron distribution, viz. the differential neutron flux density $\phi(E)$ as a function of the energy E (neutron spectrum) in the range 0.5 eV-18 MeV. The Prospekt-1 program has been realized with the ES computers. The minimum configuration is a central processor with not less than 256 bytes of executive memory, the OS ES operating system, and three ES-5052 disk stores, including those necessary for operation of the OS ES system. The program has been written in PL/I. The run time with an ES 1033 is 6-12 min in accordance with the composition of the initial data. (8 refs.)

60338 BWR refill-reflood program constitutive correlations for shear and heat transfer for the BWR version of TRAC. J.G.M. Andersen, K.H. Chu. *Report EPRI-NP-1582*, Electr. Power Res. Inst., Palo Alto, CA, USA (Jan. 1983). 100 pp. Contract NUREG/CR-2134 GEAP-24940. Available from Res. Rep. Center, Box 50490, Palo Alto, CA 94303, USA. Describes the constitutive correlations for shear and heat transfer in the BWR version of the transient reactor analysis code which is a computer code for best-estimate analysis of the thermal-hydraulic conditions in a reactor system. Basic equations are presented as well as a discussion of interfacial shear and wall friction.

60339 NATBWR: A steady-state model for natural circulation in boiling water reactors. J.M. Heazler, D. Abdollahian. *Report EPRI-NP-2856-CCM*, Electr. Power Res. Inst., Palo Alto, CA, USA (Feb. 1983). 168 pp. Available from Res. Rep. Center, Box 50490, Palo Alto, CA 94303, USA. Documents the NATBWR steady-state BWR natural circulation model and data gathered to predict and benchmark the natural circulation operation of the BWR. The NATBWR model is described, together with its applications to available BWR natural circulation data; user and programming information about the model is also provided. The available natural circulation data of five different operating BWRs are compared to model predictions, and the behavior of the BWR system at reduced inventory is analyzed.

60340 Cleaning steam generators off-line (soaking) with chelants. R.G. Charles, J.G. Cleary. *Report EPRI-NP-2815*, Electr. Power Res. Inst., Palo Alto, CA, USA (Feb. 1983). 236 pp. Available from Res. Rep. Center, Box 50490, Palo Alto, CA 94303, USA. Provides a detailed description of laboratory testing conducted to determine the feasibility of using organic chelating agents in an off-line soak mode of application to arrest denting corrosion in steam generators. Several unique laboratory techniques for determining chelant thermal stability, chelant reaction rates with magnetite, and chelant corrosivity toward carbon steel structural materials are also discussed.

60341 Eddy-current NDE for intergranular attack. *Report EPRI-NP-2862*, Electr. Power Res. Inst., Palo Alto, CA, USA (Feb. 1983). 118 pp. Available from Res. Rep. Center, Box 50490, Palo Alto, CA 94303, USA. Details one of a series of projects to develop nondestructive examination methods, focusing on improved eddy-current inspection methods for detecting and characterizing intergranular attack in steam generator tubing. Metallographic and eddy-current data on 30 removed tubes from three operating plants are reviewed, and laboratory analysis of the eddy-current data is discussed to define the capabilities of various techniques used in the field inspection.

60342 Thermal-hydraulic code qualification: ATHOS2 and data from Bugey 4 and Tricastin 1. P.J. Masiello. *Report EPRI-NP-2872*, Electr. Power Res. Inst., Palo Alto, CA, USA (Feb. 1983). 124 pp. Available from Res. Rep. Center, Box 50490, Palo Alto, CA 94303, USA.

Describes the use of measured data from steam generators at Bugey 4 and Tricastin 1 nuclear power plants in the qualification of the ATHOS2 computer code, a three-dimensional, two-phase thermal-hydraulic code for the steady-state and transient analysis of recirculating-type steam generators. Comparison cases, including steady-state-conditions at various power levels, are presented, and the study parameters of circulation ratio and temperature distribution across the tubesheet are discussed.

60343 Dual-process. A highly reliable process control system. L. Burger, A. Gossanyi, T. Parkanyi, G. Szabo, E. Vegh. *Report KFKI-1983-08*, Hungarian Acad. Sci., Budapest (1983). 34 pp.

A multiprocessor process control system is described. During its development the reliability was the most important aspect because it is used in the computerized control of a 5 MW research reactor. DUAL-PROCESS is fully compatible with the earlier single processor control system PROCESS-24K. The paper deals in detail with the communication, synchronisation, error detection and error recovery problems of the operating system. (5 refs.)

60344 Fast breeder nuclear boiler with heat carrying liquid metal. Preliminary study of the abolition of the secondary sodium circuit. P. Petraud, J.L. Quinot, A. Villemeur (Res. & Dev. Div., Electricite de France, Chateau, France).

Proceedings of the L.M.F.B.R. Safety Topical Meeting, Lyon-Ecully, France, 19-23 July 1982 (Paris, France: Societe Francaise d'Energie Nucleaire 1982), p. 201-11 vol. 3. Reports a preliminary study of double wall tube steam generators, which do away with the need for an intermediate cooling system in FBRs. This type of steam generator is described briefly and two safety requirements are examined in detail. These are the probability of a major water leak and the impact of a sodium-water reaction following a leak. Preliminary results, which require a more thorough confirmation, show a good safety margin. (5 refs.)

60345 A synthesis of ten years' tests on scale models of LMFBR steam generators at the CGVS facility. J.P. Fontaine, J.L. Quinot (Direction des Etudes et Recherches, Electricite de France, Chateau, France). Proceedings of the L.M.F.B.R. Safety Topical Meeting, Lyon-Ecully, France, 19-23 July 1982 (Paris, France: Societe Francaise d'Energie Nucleaire 1982), p. 213-21 vol. 3.

Discusses experiments on a high power sodium heated SG facility (CGVS), capable of reproducing all possible operating conditions, to study the behaviour of scale-models of industrial apparatus. Four 45 MW test-SG were studied. The main findings of these experiments were as follows: heat exchange surfaces remained perfectly leakproof; hydrogen detection in the sodium and argon constitute additional systems for monitoring the impermeability to leaks of a SG with a free sodium surface; extrapolation of the findings to the SUPER PHENIX SG shows that water leaking at a rate of 100 mg/s would induce in ten minutes a 50% rise of the signal produced by the hydrogen monitoring device in the sodium; acoustic method can detect leaks of the order of one g/s in a 45 MW SG sited in an industrial environment. (5 refs.)

60346 Evaluation of angle transducers for a high performance manipulator. R.C. Holt (Marchwood Engng. Labs., CEGB, Marchwood, England). Colloquium on 'Axes Measurement Systems for Robots, Manipulators and other NC Devices', London, England, 2 March 1983 (London, England: IEE 1983). 3 pp.

Future repair tasks inside CEGB reactors will almost certainly involve welding and an advanced manipulator is being developed for this purpose. In order to weld successfully a manipulator must control its 'end effector' to within about 0.5 mm. One restriction which prohibits the use of commercial welding robots is that access to a reactor is through a 200 mm diameter hole. When evaluating angle transducers it is important to distinguish between resolution, accuracy and repeatability. (no refs.)

A finite element solution to the group diffusion problems with albedo-type boundary conditions See Entry 60221

Experience with LOMI agents in cleaning cooling systems See Entry 60225

Results of EDF/Framatome underclad crack detection methods See Entry 60249

The hydrogen problem See Entry 60349

LOBI program—results of the first test phase (loss-of-coolant accidents) See Entry 60350

Study on the steam line break accident for Kori Unit-1 See Entry 60352

Description and discussion of the current state of the knowledge about the Leidenfrost phenomenon See Entry 60353

An analysis of the hydrogen bubble concerns in the Three-Mile Island Unit-2 Reactor vessel See Entry 60355

Radiolysis of iodine compounds in model systems of PWR See Entry 60356

Valve inlet fluid conditions for pressurizer safety and relief valves in Westinghouse-designed plants See Entry 60357

Analysis and synthesis of the theoretical studies performed on the control and safety of LWR's burning plutonium fuel See Entry 60358

Monitoring system for determining air leakage and oxygen concentrations in the secondary cycle of pressurized water reactor plants See Entry 60362

- New insights in sodium water reactions and their effects on steam generators .
See Entry 60381
- Study of the effects of major water leakage in a sodium-heated steam generator
See Entry 60385
- Hydrocarbon chemistry in irradiated $\text{CO}_2/\text{CO}/\text{CH}_4/\text{H}_2\text{O}/\text{H}_2$ mixtures. I. A survey of the initial reactions
See Entry 63579
- The effect of radiation on the release of corrosion products from 304 stainless steel in high temperature water-II effects of flow rate and duration of corrosion experiment
See Entry 63595

28.44 FISSION REACTOR PROTECTION SYSTEMS, SAFETY AND ACCIDENTS

- 60347 Method of developing reliable software for computer-assisted safety systems.** H.Trauboth, U.Voges (Kernforschungszentrum Karlsruhe GmbH, Karlsruhe, Germany). *Atomwirtsch.-Atomtech. (Germany)*, vol.28, no.1, p.43-8 (Jan. 1983). In German.
- A reactor protection system as part of the safety system is functionally separated from the control system and is intended, in dangerous situations, to transfer the reactor into a safe state as quickly as possible and without causing any damage to persons or the plant. Until now, this scram has been initiated abruptly, shutting the reactor down completely. Since any scram and subsequent restarting subjects the reactor to major stresses the number of such 'hard' scrams should be minimized. For this purpose, the short-term protection system should be added to an early warning and fault diagnosing system. This improved transparency of the operating processes allows the plant personnel to initiate specific corrections and, for instance, run the plant at a reduced power level or shut it down 'softly', i.e. in steps. This intelligent mode of control needs more capable software, the development and structure of which is outlined in this article. (16 refs.)
- 60348 Assessing the availability of nuclear power plants.** U.Hansen (Univ. Essen-GHS, Essen, Germany). *Atomwirtsch.-Atomtech. (Germany)*, vol.28, no.4, p.184-5 (April 1983). In German.
- Outages of nuclear power plants are due to many causes. However, frequently the origins are minor, harmless events which would have permitted conventional power plants to go on, whereas nuclear power plants are required to cease operation until another absolutely reliable proof of safety has been produced. This also reflects in the statistics of plant availability. Differences in the availabilities of competing systems also affect their relative economics. Power plants suffering from occasional outages need standby capacity to be maintained, and potential effects on the overall system must be taken into account in investment decisions. An approach is outlined in this article in which differences in availability are considered as internal costs of the respective types of power plants. (6 refs.)
- 60349 The hydrogen problem.** H.Karwat (Tech. Univ., Munchen, Garching, Germany). *Atomwirtsch.-Atomtech. (Germany)*, vol.28, no.4, p.186-8 (April 1983). In German.
- The possibility of larger quantities of hydrogen being generated from the metal-water vapor reaction at the elevated temperatures which can be expected to exist in water cooled reactors in the course of loss-of-coolant accidents was recognized already in the early technical development of nuclear power plants. Very early, reference was also made to the resultant consequences with respect to the maintenance of containment integrity. The criteria drafted for assessing the effectiveness of the emergency core cooling systems installed in all light water reactors centered around the fundamental idea of effectively excluding the onset of the strongly exothermic zircaloy-water vapor reaction as an additional heat source in the process of core heating. The whole complex of problems was regarded as solved—till the accident in the American TMI-2 nuclear power plant. After that accident, new countermeasures to control hydrogen in accidents were demanded especially in the United States. In the Federal Republic of Germany and in France the American approach has not been followed so far. Instead, it is to be proved that the existing emergency cooling systems will ensure with sufficient reliability that hydrogen will not occur on the scale discussed. Avoiding the formation of hydrogen, and proving it, will help safety more than controlling the consequences of hydrogen generation by dubious means. (13 refs.)
- 60350 LOBI program—results of the first test phase (loss-of-coolant accidents).** W.L.Riebold, P.Mork-Morkenstein, L.Piplies, H.Stadtke (Kommission der Europäischen Gemeinschaften, Ispra/Varese, Italy). *Atomwirtsch.-Atomtech. (Germany)*, vol.28, no.4, p.196-202 (April 1983). In German.
- The LOBI Project is a large scale project in the field of reactor safety research currently implemented at the Euratom Joint Nuclear Research Establishment of Ispra, Italy, in a joint international effort by the Federal Ministry for Research and Technology (Federal Republic of Germany) and the Commission of the European Communities. It is concerned with investigations of assumed loss-of-coolant accidents in pressurized water reactors. For this purpose, the LOBI test facility was built, at present the only high pressure integral systems test facility in Europe. The experiments run in the A1 program phase on large breaks cover a wide spectrum of test parameters, e.g. break size (25 to 200%), break location (cold leg, hot leg, pump bend), and the type of emergency cooling water feed (cold leg, cold and hot legs combined, no feed). The sequence of accident events observed in the blowdown (high pressure) phase of the experiment was correctly described in advance calculations, both qualitatively and in most cases also quantitatively, when existing blowdown computer programs were applied correctly. The importance of the competence of the users of such computer programs is apparent from the large deviations in the computed results encountered in the LOBI PREX standard problem. (12 refs.)
- 60351 Safeguards and nuclear safety: a personal perspective.** L.M.Muntzing (American Nuclear Soc., La Grange Park, IL, USA). *Int. At. Energy Agency Bull. (Austria)*, vol.24, no.4, p.7-10 (Dec. 1982).
- Reviews the accomplishments, appraises the present status and sets out the imperatives for the future activities of the IAEA on its twenty-fifth anniversary. (no refs.)
- 60352 Study on the steam line break accident for Kori Unit-1.** Tae Woon Kim, Jung In Choi, Un Chul Lee (Seoul Nat. Univ., Seoul, Korea), Ki In Han. *J. Korean Nucl. Soc.*, vol.14, no.4, p.186-95 (Dec. 1982). [received: April 1983]
- A steam line break accident in Kori Unit 1 is analyzed by the SYSRAN code which calculates the nuclear power and heat flux using the point kinetics equation and the lumped-parameter model, and the system transients using the mass and energy balance equation with the assumption of uniform reactor

coolant system pressure. The accident is analyzed at the EOL (End of Life) hot shutdown condition in which case it would be severe. The steam discharge rate is assumed to follow the Moody critical flow model. The results reveal a peak heat flux of 38% of nominal full power value at 60 seconds after the accident initiates. A sensitivity study shows that this accident is very sensitive to the moderator density coefficient and the lower plenum mixing factor. The point kinetics equation, the lumped-parameter model and the system transient model are verified as effective to follow the system transient phenomena of nuclear power plants. (11 refs.)

60353 Description and discussion of the current state of the knowledge about the Leidenfrost phenomenon. Moon Ki Chung, Young Whan Lee (Korea Advanced Energy Res. Inst., Seoul, Korea). *J. Korean Nucl. Soc.*, vol.14, no.4, p.204-18 (Dec. 1982). [received: April 1983]

The authors describe and discuss the current state of the knowledge about the Leidenfrost phenomenon which is a heavily studied subject in the field of boiling heat transfer. The strong interest is due to reactor safety considerations since it is desirable to obtain a better understanding of the physical mechanisms involved in the rewetting of high temperature surface after a low coolant accident. A brief survey of theoretical and experimental results indicates that considerable discrepancy exists in the prediction of the Leidenfrost temperature at elevated pressures and more investigations are needed in this area. (40 refs.)

60354 How Inpo is helping to improve safety and reliability. R.L.Haueter, R.L.Simard, S.L.Rosen (Inpo, Atlanta, GA, USA). *Nucl. Eng. Int. (GB)*, vol.28, no.339, p.30-4 (April 1983).

About three-quarters of the world's operating reactors are now tied into data base programmes of the Institute of Nuclear Power Operations (Inpo) in the United States. The use and effectiveness of the programmes, which cover reliability data on systems and equipment, analysis of event reports and a computer conferencing system, are continuing to expand. (no refs.)

60355 An analysis of the hydrogen bubble concerns in the Three-Mile Island Unit-2 Reactor vessel. S.Gordon, K.H.Schmidt, J.R.Honekamp (Chem. Div., Argonne Nat. Lab., Argonne, IL, USA). *Radiat. Phys. & Chem. (GB)*, vol.21, no.3, p.247-58 (1983).

On 30 March 1979, two days after the accident at the Three-Mile Island Reactor near Harrisburg, Pennsylvania, press reports appeared about a non-condensable bubble in the reactor vessel. This bubble was said to consist mainly of hydrogen, and to grow rapidly, possibly due to the development of oxygen. Danger of explosion was reported to be imminent. The authors analyzed all possible sources of noncondensable gases, including radiolysis, and determined that a continuing growth of the bubble during several days after the accident was not possible. Their main conclusions were the following: (1) Most of the initial hydrogen in the bubble was produced by the reaction of the Zircalloy cladding with the super-heated water. (2) During the first 16 hr after shutdown, when boiling of the primary coolant water took place, in the worst case stoichiometric amounts of hydrogen and oxygen could have been produced by radiolysis, leading to a maximum amount of oxygen in the bubble, of 0.7% of the hydrogen, which is well below the explosion limit. (3) After this 16 hr period, when boiling had totally ceased, no further oxygen could have been produced by radiolysis of the primary cooling water. On the contrary, oxygen was recombined with hydrogen due to radiolysis at such a rate that the oxygen in the water was completely removed in less than five minutes. The subsequent rate of removal of oxygen from the bubble by dissolution and radiolysis depended essentially on the rate of dissolution. (23 refs.)

60356 Radiolysis of iodine compounds in model systems of PWR. A.Habersbergerova, B.Bartonicek (Nuclear Res. Inst., Rez, Czechoslovakia). *Radiat. Phys. & Chem. (GB)*, vol.21, no.3, p.289-93 (1983).

The paper gives a survey of experimental results concerning the chemical behaviour and radiation chemical reactions of inorganic iodine compounds in a model WWER coolant, the reactions of iodine with methane taking place in the gas phase on irradiation and the radiolysis of inorganic iodine compounds as well as of CH_3I in the spray solutions. (22 refs.)

60357 Valve inlet fluid conditions for pressurizer safety and relief valves in Westinghouse-designed plants. A.Meliksetian, A.M.Sklencar. *Report EPRI-NP-2296*, Electr. Power Res. Inst., Palo Alto, CA, USA (Dec. 1982), 60 pp.

Available from Res. Rep. Center, Box 50490, Palo Alto, CA 94303, USA. The expected range of fluid inlet conditions is presented for pressurizer safety and relief valves utilized in Westinghouse-designed PWR units. The conditions are determined based on consideration of FSAR, extended high-pressure liquid injection, and cold overpressurization events. The Westinghouse PWR units are grouped by design and layout; a reference plant is chosen for each group; and valve fluid inlet conditions, resulting from limited FSAR events, are determined for each reference plant.

60358 Analysis and synthesis of the theoretical studies performed on the control and safety of LWR's burning plutonium fuel. J.Basselier, A.Remard, R.Holzer, K.Hnilica, A.Charlier, C.Vandenberg, W.Fehrenbach.

Report EUR 8118 EN, Comm. European Communities, Luxembourg (1982), vi+338 pp. Contract 049-79 RPU-B 050-79 RPU-D.

The purpose of the work is to analyse and synthesise the theoretical studies performed on the control and the safety of LWR's burning plutonium fuel. These studies cover the following areas: the comparative investigations of parameters for plutonium fuelled power stations (PWR and BWR) under steady state and dynamic conditions for typical accidents. In each study, the same reactor fuelled only with uranium is taken as the standard reference; the handling and the storage of plutonium fuel assemblies.

60359 Scale modeling of turbine missile impact into concrete. S.McHugh, L.Seaman, Y.Gupta.

Report EPRI-NP-2746, Electr. Power Res. Inst., Palo Alto, CA, USA (Feb. 1983), 160 pp.

Available from Res. Rep. Center, Box 50490, Palo Alto, CA 94303, USA. Results are presented of scale model turbine missile impact tests conducted as part of a program to provide data on the impact resistance of structures that protect safety-related equipment in nuclear power plants. The 1/11-scale-model experiments are studied, and the results are compared with two previously conducted full-scale tests. Details are also provided of the experimental method and components, symmetric missile tests, and finite difference computations of a missile impact.

60360 Postaccident decontamination of reactor primary systems and test loops. C.J.Card.

Report EPRI-NP-2842, Electr. Power Res. Inst., Palo Alto, CA, USA (Jan. 1983), 114 pp.

Available from Res. Rep. Center, Box 50490, Palo Alto, CA 94303, USA. Documents past decontamination efforts on reactor systems and test loops and relates this information to the decontamination of LWRs particularly that at Three Mile Island Unit-2. Emphasizing postaccident situations involving both

fission products and fuel debris, this report details decontamination experiences on four experimental reactors and eight test loops. Studies of the 12 chemical solutions used in the experiments are included.

60361 Scale model turbine missile casing impact tests. C.M.Romander, A.L.Florence.

Report EPRI-NP-2742, Electr. Power Res. Inst., Palo Alto, CA, USA (Jan. 1983), 112 pp.

Available from Res. Rep. Center, Box 50490, Palo Alto, CA 94303, USA. Describes three 1/5-scale model turbine missile impact experiments performed to provide benchmark data for assessing turbine missile effects in nuclear plant design. The development of an explosive launcher to accelerate the 1/5-scale models of a turbine missile to the desired impact velocities is described. Comparison of results with those of full-scale experiments demonstrates scalability.

60362 Monitoring system for determining air leakage and oxygen concentrations in the secondary cycle of pressurized water reactor plants. D.T.Snyder, J.Blok.

Report EPRI-NP-2865, Electr. Power Res. Inst., Palo Alto, CA, USA (Feb. 1983), 120 pp.

Available from Res. Rep. Center, Box 50490, Palo Alto, CA 94303, USA. Details are provided on a dissolved gas analysis system developed for accurately determining the concentration of dissolved gases in condensate and feedwater process streams of PWRs in order to obtain improved diagnostic information on corrosion and corrosion-related phenomena in piping and system components. The design, calibration, and laboratory testing of the prototype dissolved-gas analyzer is documented, a series of gas and liquid measurements in an operating PWR is described, and detailed installation and operating instructions for the prototype instrument are included.

60363 Full-scale turbine missile concrete impact experiments. R.L.Woodfin.

Report EPRI-NP-2745, Electr. Power Res. Inst., Palo Alto, CA, USA (Feb. 1983), 174 pp.

Available from Res. Rep. Center, Box 50490, Palo Alto, CA 94303, USA. Describes four full-scale rocket sled experiments conducted to provide data on the response of reinforced concrete containment walls to impact and penetration by turbine missiles. Variations in the missiles' mass, velocity, and attitude and the steel liner thickness are discussed, and the measures of damage are detailed, including penetration depth, crater volume, and rear face cracking. Test results are compared with existing empirical penetration formulas.

60364 Fire tests in ventilated rooms. Detection of cable tray and exposure fires. J.S.Newman.

Report EPRI-NP-2751, Electr. Power Res. Inst., Palo Alto, CA, USA (Feb. 1983), 102 pp.

Available from Res. Rep. Center, Box 50490, Palo Alto, CA 94303, USA. Examines work to assess the response of typical commercial smoke detectors (ionisation and photoelectric types) to fires in ventilated rooms representative of utility environments. Detector response relationships are developed as a function of smoke transit time, detection time factor, detector sensitivity factor, ventilation factor, and nondimensional detector spacing. An example of detector spacing requirements is given based on results of cable tray fire tests in a ventilated environment.

60365 Assessment of chemical processes for the postaccident decontamination of reactor coolant systems. L.F.Munson, C.J.Card, J.R.Divine.

Report EPRI-NP-2866, Electr. Power Res. Inst., Palo Alto, CA, USA (Feb. 1983), 270 pp.

Available from Res. Rep. Center, Box 50490, Palo Alto, CA 94303, USA. The following topics were dealt with: the examination of previously used chemical decontamination processes and potentially useful new decontamination processes is discussed. Both generic fuel damage accidents and the accident at TMI-2 are considered, and a total of 14 processes are evaluated. Process evaluation includes data in the following categories: technical description of the process, recorded past usage, effectiveness, process limitation, safety consideration, and waste management.

60366 The role of carbon dioxide in the combustion of sodium in air. R.N.Newman (CEGB, Berkeley Nuclear Labs., Berkeley, England).

Proceedings of the L.M.F.B.R. Safety Topical Meeting, Lyon-Ecully, France, 19-23 July 1982 (Paris, France: Societe Francaise d'Energie Nucleaire 1982), p.3-11 vol.3

The nature of the sodium surface during sodium pool fires has been observed at varying temperatures. At temperatures below $\sim 600^\circ\text{C}$ the fuel is fed to small flame zones through wicks of sodium oxides. Above 600°C the oxides, which are more dense than sodium sink into the pool. The surface layer that supports these oxide wicks has been isolated, analyzed and found to contain carbon derived from reaction between the sodium and CO_2 . A sodium oxide catalysed oxidation of this carbon layer is suggested to explain its destruction. The influence of CO_2 was further investigated by studying the burning of sodium in CO_2 enriched atmospheres. The results are used to explain the effect of carbon containing extinguishants and ignition delays of split sodium. (7 refs.)

60367 Experimental studies on sodium columnar fire and pool fire. T.Sano, Y.Abe (Mitsubishi Heavy Industries Ltd., Takasago Tech. Inst., Hyogo, Japan), T.Kiyokawa.

Proceedings of the L.M.F.B.R. Safety Topical Meeting, Lyon-Ecully, France, 19-23 July 1982 (Paris, France: Societe Francaise d'Energie Nucleaire 1982), p.13-22 vol.3

Sodium columnar and pool fire tests were performed to ensure the integrity of a container cell and to examine quantitative aspects of sodium fire. Tests were carried out in an enclosed steel-lined concrete cell of 21 m^3 , which was filled with air or nitrogen gas, and into which 1 m^3 max. and 530°C max. sodium was spilled. To predict fire characteristics, a computer code for columnar and pool fire was developed and the calculations were compared with the experimental results. Many sodium fire tests demonstrated that the cell maintained its integrity. The computer code gave good agreement with most of the experimental data, except for the tests in which many fire spots existed on the surface of pool. (1 ref.)

60368 Sodium-water reaction in a non-confined medium. M.Amblard, G.Berthoud, A.Pion (CEN Grenoble, Grenoble, France), V.Lyaly, R.Sesny.

Proceedings of the L.M.F.B.R. Safety Topical Meeting, Lyon-Ecully, France, 19-23 July 1982 (Paris, France: Societe Francaise d'Energie Nucleaire 1982), p.23-31 vol.3

The sodium-liquid water reaction is studied experimentally in small-scale tests with the substances brought into contact in different modes, some fundamental, others more realistic, reproducing an accident scenario. The experiments are analysed by means of a thermohydraulic model taking hydrodynamic instabilities into account. (no refs.)

60369 The Brasimone sodium-water reaction test facility—test BA 12—pressure wave effects and steam generator tube bundle deformations following 'guillotine failure' of a tube. J.Biscarel, M.Hugla, C.Lorin, J.Raffailhac, M.Moronesi, M.Pacifico, G.Pasquale, M.Pigeon, J.Raffailhac (CEA Cadarache, Saint Paul les Durance, France).

Proceedings of the L.M.F.B.R. Safety Topical Meeting, Lyon-Ecully, France, 19-23 July 1982 (Paris, France: Societe Francaise d'Energie Nucleaire 1982), p.33-44 vol.3

The water-sodium reaction test has been carried out under geometrical conditions selected to permit extrapolation to Superphenix 1 steam generators. The authors discuss the comparison of calculated and experimental results concerning the pressure waves arising from injection of a high-volume water flow into a sodium mass, together with nondestructive examination and metallurgical analysis conducted on the bundle after the test. The eddy current method has a good detection limit for the type of defect being observed. (1 ref.)

60370 LMFBFR plant design features for sodium spill and fire protection. R.E.Palm (Burns & Roe Inc., Oradell, NJ, USA).

Proceedings of the L.M.F.B.R. Safety Topical Meeting, Lyon-Ecully, France, 19-23 July 1982 (Paris, France: Societe Francaise d'Energie Nucleaire 1982), p.45-53 vol.3

Design features have been developed for an LMFBFR plant to protect the concrete structures from potential liquid sodium spills and fires and prevent sodium-concrete reactions. The inclusion of these features in the plant design reduces the severity of design basis accident conditions imposed on containment and other critical plant structures. Steel liners are provided in cells containing radioactive sodium systems, and catch pans are located in non-radioactive sodium system cells. The design requirements and descriptions of each of these protective features are presented. The loading conditions, analytical approach and numerical results are also included. Design of concrete cell structures that are subject to high temperature effects from sodium spills is discussed. The structural design considers the influence of high temperature on design properties of concrete and carbon steel materials based on results of a comprehensive test program. The development of these design features and high temperature design considerations for the Clinch River Breeder Reactor Plant are presented. (no refs.)

60371 Experimental and analytical studies of sodium interactions with various concretes. A.Suo-Anttila, J.E.Smaardyk (Sandia Nat. Labs., Albuquerque, NM, USA).

Proceedings of the L.M.F.B.R. Safety Topical Meeting, Lyon-Ecully, France, 19-23 July 1982 (Paris, France: Societe Francaise d'Energie Nucleaire 1982), p.55-63 vol.3

Mechanistic models of sodium/concrete interactions are described. The SCAM model of interactions with basaltic concrete is being verified by experiments. Modelling of sodium interactions with limestone concrete is still at a preliminary stage but shows promise of being able to quantitatively predict the experimental results. Comparisons with experiment are presented. (3 refs.)

60372 Experiments and analyses of sodium spray combustion. R.Kawabe, A.Suzuoki (Energy Res. Lab., Hitachi Ltd., Hitachi-shi, Japan), N.Sagawa.

Proceedings of the L.M.F.B.R. Safety Topical Meeting, Lyon-Ecully, France, 19-23 July 1982 (Paris, France: Societe Francaise d'Energie Nucleaire 1982), p.65-70 vol.3

Combustion experiments for sodium spray were made in a closed vessel of 2 m^3 , containing nitrogen and 0-21 vol% oxygen. About 400 g sodium were injected into the vessel through a spray nozzle at the bottom. The results revealed that oxygen consumption observed in the experiment was not more than 80% of that expected for complete combustion of sodium and the temperature in the spray outer region was higher than that of inner region, analogous to a candle flame. A computer program SOFIA-II was developed to analyze the experiments. In the code, the combustion of single droplets is calculated from an analytical model based on heat and mass balance at the flame. Using the calculated single droplet combustion rate, SOFIA-II also calculates the pressure and temperature transients in the vessel. The calculated transient of pressure was generally in agreement with the observed value. (no refs.)

60373 Physical and chemical characterisation of sodium fire aerosols. W.Cherdron, S.Jordan (Lab. fur Aerosolphys. und Filtertech., KFK, Karlsruhe, Germany).

Proceedings of the L.M.F.B.R. Safety Topical Meeting, Lyon-Ecully, France, 19-23 July 1982 (Paris, France: Societe Francaise d'Energie Nucleaire 1982), p.71-9 vol.3

The characterisation of nuclear aerosols is of fundamental importance for the calculation of the radiological consequences of reactor accidents. In LMFBFR accidents one of the main sources of aerosols is burning sodium. To investigate the release and behavior of sodium fire aerosols large pool fire (up to 500 kg sodium) and spray fire (up to 40 kg/sec) experiments have been performed in the FAUNA-facility. In this experiment the physical properties of sodium fire particles as well as chemical reactions has been studied. (5 refs.)

60374 Accommodation of sodium spills with a cell drainage system in an LMFBFR. G.Garabedian, H.R.Michael, J.M.Oddo (Stone & Webster Engng. Corp., Boston, MA, USA).

Proceedings of the L.M.F.B.R. Safety Topical Meeting, Lyon-Ecully, France, 19-23 July 1982 (Paris, France: Societe Francaise d'Energie Nucleaire 1982), p.81-9 vol.3

As part of a series of feasibility studies a primary heat transport system cell's ability to accommodate potential large sodium spills was evaluated. In previous cell designs, the cell liner had to contain the spill indefinitely. In a new concept, sodium resulting from a large spill flows, by gravity, to a drain tank located below the cell floor. In this design, the cell liner no longer must be a high integrity sodium-leak tight liner. The authors describe this concept. They also discuss an analytical evaluation of the cell's ability to accommodate a large sodium spill; this evaluation was conducted using the CACECO and SPRAY computer codes. (no refs.)

60375 A chemical study of the sodium-concrete reaction. M.G.Barker, P.G.Gadd (Dept. of Chem., Univ. of Nottingham, Nottingham, England).

Proceedings of the L.M.F.B.R. Safety Topical Meeting, Lyon-Ecully, France, 19-23 July 1982 (Paris, France: Societe Francaise d'Energie Nucleaire 1982), p.91-107 vol.3

A differential thermal analysis apparatus has been used to determine the heats of reaction and reaction temperatures of commercial concretes and their individual components with liquid sodium at temperatures up to 600°C . For reproducible results to be obtained the sodium had to be stirred during the determinations. X-ray powder diffraction was used to identify reaction products. The heats of reaction of aggregate materials were found to vary widely with values ranging from 200 J g^{-1} to 2172 J g^{-1} whilst SiO_2 gave a value of 1607 J g^{-1} . Reasons for this wide range of values have been proposed. (3 refs.)

60376 Sodium concrete interaction. J.Dufresne, J.Fermandjian (Dept. de Surete Nucleaire, CEA, Fontenay Aux Roses, France), C.Casselmann, J.C.Malet, M.Bolvin, Herber.

Proceedings of the L.M.F.B.R. Safety Topical Meeting, Lyon-Ecully, France, 19-23 July 1982 (Paris, France: Societe Francaise d'Energie Nucleaire 1982), p.109-19 vol.3

Computer codes have been developed in order to study the response of the containment building of a liquid metal fast breeder reactor to a sodium pool fire with sodium-concrete interaction: the NABE 1 code for safety analysis and the SORBET code for project calculations. The authors describe the computer codes, in particular the physical phenomena considered and the input and output data. They also present examples of comparison cases between experimental and calculated results with NABE 1 code. (2 refs.)

60377 Sodium oxide aerosol behavior in a containment vessel. Experimental tests and computer models. J.Fermandjian, C.Hervouet, D.Boulard (CEA/IPSN, Fontenay-aux-Roses, France), A.L'Homme, G.Lhiaubet, S.Goldstein, J.P.Magnaud, A.Meiane, J.C.Malet, C.Casselmann, V.Prodi.

Proceedings of the L.M.F.B.R. Safety Topical Meeting, Lyon-Ecully, France, 19-23 July 1982 (Paris, France: Societe Francaise d'Energie Nucleaire 1982), p.121-32 vol.3

Describes experiments to validate computer models that predict aerosol behaviour during LMFBR accidents. The authors discuss the aerosol source term using containment vessel tests, compare instruments that measure aerosol size distribution, and describe both theory and experiment concerning natural convection and aerosol deposition. (no refs.)

60378 Large leak sodium-water reaction code SWACS and its validation. O.Miyake, Y.Shindo, H.Hiroi, H.Tanabe, M.Sato (Power Reactor & Nuclear Fuel Dev. Corp., Tokyo, Japan).

Proceedings of the L.M.F.B.R. Safety Topical Meeting, Lyon-Ecully, France, 19-23 July 1982 (Paris, France: Societe Francaise d'Energie Nucleaire 1982), p.133-42 vol.3

A computer code SWACS for analyzing the large leak accident of an LMFBR steam generator has been developed and validated. Five tests data obtained by SWAT-3 test facility were compared with code results. In each of SWAT-3 tests, a double-ended guillotine rupture of one tube was simulated in a helical coil steam generator model with 1/2.5 scaled test vessel to the prototype SG. The analytical results, including an initial pressure spike, a propagated pressure in a secondary system, and a quasisteady pressure, indicate that the overall large-leak event could be predicted in reasonably good agreement. (4 refs.)

60379 Sodium-concrete reaction model development. D.H.Nguyen, L.D.Muhlestein, A.K.Postma (Hanford Engng. Dev. Lab., Richland, WA, USA).

Proceedings of the L.M.F.B.R. Safety Topical Meeting, Lyon-Ecully, France, 19-23 July 1982 (Paris, France: Societe Francaise d'Energie Nucleaire 1982), p.143-52 vol.3

Major observations are formulated after reviewing test results for over 100 sodium-concrete reaction tests. The observations form the basis for developing a mechanistic model to predict the transient behavior of sodium-concrete reactions. The major observations are listed. Mechanisms associated with sodium and water transport to the reaction zone are identified, and represented by appropriate mathematical expressions. The model attempts to explain large-scale, long-term (100 hr) test results where sodium-concrete reactions terminated even in the presence of unreacted sodium and concrete. (1 ref.)

60380 Air cleaning devices for vented filtered LMFBR containment. L.D.Muhlestein, R.K.Hilliard (Hanford Engng. Dev. Lab., Richland, WA, USA).

Proceedings of the L.M.F.B.R. Safety Topical Meeting, Lyon-Ecully, France, 19-23 July 1982 (Paris, France: Societe Francaise d'Energie Nucleaire 1982), p.153-9 vol.3

An effort lasting several years is summarized. The effort evaluated, developed and tested air cleaning devices for potential use in breeder reactor containment venting applications. State-of-technology evaluations were completed for both a hypothetical head release accident and a primary vessel melt-through accident. Commercially available systems or components were tested which included HEPA filters, sand and gravel beds, and aqueous scrubbers. Large-scale demonstration tests were completed and results are presented for two- and three-stage conventional aqueous scrubber systems; and for a newly developed passive, submerged gravel scrubber. (3 refs.)

60381 New insights in sodium water reactions and their effects on steam generators. J.K.van Westenbrugge, P.H.L.Groenenboom, J.J.de Jong, J.Joziasse, B.V.Neratoom.

Proceedings of the L.M.F.B.R. Safety Topical Meeting, Lyon-Ecully, France, 19-23 July 1982 (Paris, France: Societe Francaise d'Energie Nucleaire 1982), p.161-70 vol.3

Discusses the effects of sodium water reactions on steam generator internals. Mention can be made of the resonance effects of pressure waves on helical bundles. Also computer codes for 3D-pressure waves are being developed. On the experimental side tests have been performed comparing the behaviour of different holes, in 12 Cr-steel and in stabilized 2 1/4 Cr 1 Mo-steel, during water injections in to sodium. (6 refs.)

60382 The Esmeralda project for studying extensive sodium fire. Y.Sophy, M.Loubriat, A.Bentz, A.Gerosa, H.Freslon, U.Piatti (Nuclear Safety Dept., CEN Cadarache, Saint Paul les Durance, France).

Proceedings of the L.M.F.B.R. Safety Topical Meeting, Lyon-Ecully, France, 19-23 July 1982 (Paris, France: Societe Francaise d'Energie Nucleaire 1982), p.171-81 vol.3

Describes the Esmeralda Project for studying extensive fires involving up to 70 metric tons of sodium. The decision to create this research facility was related to construction of the Super-Phenix breeder reactor and to the scale effect problems posed by the use of very large quantities of sodium. Information is given on the dimensions of the installation, the objectives of the project, the means to be employed, the timetable to be followed, and the organization which was created for this project within the context of Franco-Italian cooperation. (no refs.)

60383 Sodium fires in SUPER-PHENIX. F.Hedin, A.Bentz, A.Gadola (NERSA, Lyon, France), A.Herauld, J.C.Malet.

Proceedings of the L.M.F.B.R. Safety Topical Meeting, Lyon-Ecully, France, 19-23 July 1982 (Paris, France: Societe Francaise d'Energie Nucleaire 1982), p.183-200 vol.3

Presents the features adopted in SUPER-PHENIX to take into account the risk connected with sodium-air reaction. The discussion covers the main options of design, prevention, detection, lay-out, venting, means of fighting against a hypothetical sodium fire, accidental and functional analysis. (no refs.)

60384 Aerosol leakage through containment walls. J.F.van de Vate, W.F.van Leeuwen, H.C.D.Smit (Netherlands Energy Res. Found., Petten, Netherlands).

Proceedings of the L.M.F.B.R. Safety Topical Meeting, Lyon-Ecully, France, 19-23 July 1982 (Paris, France: Societe Francaise d'Energie Nucleaire 1982), p.223-32 vol.3

Experimental results are presented on aerosol penetration through artificial cracks, simulating leaks in concrete walls of safety containments, and through model leaks of glass bead columns. The results on aerosol removal from a leak flow through leak paths compare fairly well with model calculations assuming turbulent inertial deposition in a high flow rate regime and sedimentation in a low flow rate regime. Other aerosol removal mechanisms are dealt with too. Briefly, results are reported on aerodynamics of sodium oxide particles. For the application of the results of this study to a nuclear safety analysis knowledge on leaks through containment walls and on aerosol particle size under severe accident conditions is lacking. (16 refs.)

60385 Study of the effects of major water leakage in a sodium-heated steam generator. J.Biscarel (CEA/DRNR/STRS, Saint Paul les Durance, France), M.Hugla, P.Peturaud.

Proceedings of the L.M.F.B.R. Safety Topical Meeting, Lyon-Ecully, France, 19-23 July 1982 (Paris, France: Societe Francaise d'Energie Nucleaire 1982), p.233-41 vol.3

Presents the assumptions and computer codes used by the CEA and EDF to simulate the consequences of a major water leak in a sodium-heated steam generator. The following subjects are covered in turn: determining the leakage flow rate; developing a physicochemical model of the resulting sodium-water reaction; hydrodynamic calculations of the effects on the structural components. The results of an experiment are also presented together with a numerical interpretation. (7 refs.)

60386 Safety aspects in the development and construction of fast neutron reactors cooled by sodium. B.Saitcevsy (NERSA, Lyon, France).

Proceedings of the L.M.F.B.R. Safety Topical Meeting, Lyon-Ecully, France, 19-23 July 1982 (Paris, France: Societe Francaise d'Energie Nucleaire 1982), p.123-38 In French.

Safety criteria relating to fast neutron, sodium cooled reactors were published for Super-Phenix in 1973. The major accident conditions examined have been summarised as main energy release, earthquake behaviour, thermo-hydraulics, handling of liquid sodium and activity releases requiring in-service inspection. Detailed discussion relates to Creys-Malville (1200 MWe, Rhone Valley), for which an outline vertical cross-section diagram is included, showing primary and secondary containment systems, nitrogen and argon circuits and filtration units. Under the thermo-hydraulic heading, mention is made of double wall vessels for separation into two redans, conical and toroidal. Additional details are given for safety aspects of the steam generator, shut-down plant, sodium fire detection, the sodium-water reaction and the monitoring of personnel irradiation doses. (no refs.) G.C.

60387 Safety methods and their application at the PHENIX nuclear power station. F.Conte.

Proceedings of the L.M.F.B.R. Safety Topical Meeting, Lyon-Ecully, France, 19-23 July 1982 (Paris, France: Societe Francaise d'Energie Nucleaire 1982), p.247-55 In French.

The operational performance of the Phenix research reactor (9 years critical, 8 years operational) is detailed by monthly power histograms since 1974. Some personnel irradiation dose values are quoted. Safety stops have numbered about 100, causes being listed, the most frequent being 28 stops due to the sodium pump controls. A number of operating experiences are discussed. On the whole, most plant items worked without trouble. In 1982, there was a sodium-water reactor which lead to a shut-down and the replacement of certain items. Many details are given of the man/machine interface liaison, and techniques for improvement, which include the binocular viewing of vernier scales, and 27 closed circuit television cameras, linked to 7 receivers. (no refs.) G.C.

60388 Regulations, options and safety criteria. M.Laverie (SCSIN, Paris, France).

Proceedings of the L.M.F.B.R. Safety Topical Meeting, Lyon-Ecully, France, 19-23 July 1982 (Paris, France: Societe Francaise d'Energie Nucleaire 1982), p.345-61 In French.

The French nuclear safety service was initiated on 13th March, 1973, with two permanent groups of experts, one concerned with nuclear reactors and one with other nuclear plant. The functions of the organisation are to set up an authorisation procedure, to survey the installation and to interpret control regulations. The departmental organisation is described, showing the breakdown of responsibilities from the Minister for Research and Industry to 17 industrial departments and 3 special groups (pressure vessels, nuclear reactors, laboratories and factories). Also detailed are the reporting procedures to be followed for authorisation of construction and commissioning. A separate section is included relevant to Creys-Malville for which 29 inspections have been carried out during the last six months. (no refs.) G.C.

Measures for increasing IAEA safeguards effectiveness See Entry 60226

Anticipated amounts of nuclear materials under IAEA safeguards (1981-1990) See Entry 60227

Attributes mode sampling schemes for international material accountability verification See Entry 60228

Development of an improved monitor for portal detection of the unauthorized removal of special nuclear material See Entry 60229

A statistic sensitive to deviations from the zero-loss condition in a sequence of material balances See Entry 60230

After Creys-Malville: the prospects for the integrated site See Entry 60331

Automatic time differential boiler leak location system See Entry 60332

Filter for the selective removal of tritium from the coolant gas of a high temperature nuclear reactor See Entry 60335

Fast breeder nuclear boiler with heat carrying liquid metal. Preliminary study of the abolition of the secondary sodium circuit See Entry 60344

A synthesis of ten years' tests on scale models of LMFBR steam generators at the CGVS facility See Entry 60345

Evaluation of angle transducers for a high performance manipulator See Entry 60346

Steam explosion experiments with single drops of iron oxide melted with a CO₂ laser See Entry 62077

Biological effects of neutron radiation and their implications for the nuclear power industry See Entry 63890

28.50 FISSION REACTOR TYPES AND APPLICATIONS

60389 Waterside corrosion of zircaloy fuel rods. F.Garzaroli, W.Jung, H.Schoenfeld, A.M.Garde, G.W.Parry, P.G.Smerd. Report EPRI-NP-2789, Electr. Power Res. Inst., Palo Alto, CA, USA (Dec. 1982), 192 pp.

Available from Res. Rep. Center, Box 50490, Palo Alto, CA 94303, USA.

This two-part report presents the results of a comprehensive investigation of Zircaloy cladding corrosion in PWRs. Part 1 discusses the oxide thickness measurements and the effect of various design and reactor operating parameters on Zircaloy corrosion. Oxide film characterization data, thermal-hydraulic analyses, and statistical analyses of the data are also presented. Part 2, on microfiche, provides the oxide thickness data obtained from individual fuel rods.

Plutonium recycling scenario in light water reactors. Assessment of the environmental impact in the European Community See Entry 59523

Energy reviews. Nuclear power systems. Vol.1 See Entry 59549

Generation and benchmark test of 26-group constant set for fast reactor calculations See Entry 60220

A finite element solution to the group diffusion problems with albedo-type boundary conditions See Entry 60221

Comparison of COMETHE-IIIJ and FCODE-BETA fission gas release predictions with measurements See Entry 60224

Microbeam analysis of a Commercial Advanced Gas Cooled Reactor material See Entry 60233

Evaluation of fuel performance in reactor (PWR). IV. Transient behavior after happening of cladding defect See Entry 60234

Titanium-sponge bed to scavenge tritium from inert gases See Entry 60240

Design study of a spent fuel shipping cask for Korea Nuclear Unit-1 See Entry 60242

General and localized corrosion of carbon and low-alloy steels in oxygenated high-temperature water See Entry 60248

Fuel cycle costs for molten-salt reactors See Entry 60329

After Creys-Malville: the prospects for the integrated site See Entry 60331

Automatic time differential boiler leak location system See Entry 60332

A study of reactor internal dynamics by reactor noise analysis See Entry 60333

Dual-process. A highly reliable process control system See Entry 60343

Fast breeder nuclear boiler with heat carrying liquid metal. Preliminary study of the abolition of the secondary sodium circuit See Entry 60344

Study on the steam line break accident for Kori Unit-1 See Entry 60352

Valve inlet fluid conditions for pressurizer safety and relief valves in Westinghouse-designed plants See Entry 60357

Analysis and synthesis of the theoretical studies performed on the control and safety of LWR's burning plutonium fuel See Entry 60358

Monitoring system for determining air leakage and oxygen concentrations in the secondary cycle of pressurized water reactor plants See Entry 60362

The role of carbon dioxide in the combustion of sodium in air See Entry 60366

Experimental studies on sodium columnar fire and pool fire See Entry 60367

Sodium-water reaction in a non-confined medium See Entry 60368

The Brasimone sodium-water reaction test facility—test BA 12—pressure wave effects and steam generator tube bundle deformations following 'guillotine failure' of a tube See Entry 60369

LMFBR plant design features for sodium spill and fire protection See Entry 60370

Experimental and analytical studies of sodium interactions with various concretes See Entry 60371

Experiments and analyses of sodium spray combustion See Entry 60372

Physical and chemical characterisation of sodium fire aerosols See Entry 60373

Accommodation of sodium spills with a cell drainage system in an LMFBR See Entry 60374

A chemical study of the sodium-concrete reaction See Entry 60375

Sodium concrete interaction See Entry 60376

Sodium oxide aerosol behavior in a containment vessel. Experimental tests and computer models See Entry 60377

Large leak sodium-water reaction code SWACS and its validation See Entry 60378

Sodium-concrete reaction model development See Entry 60379

Air cleaning devices for vented filtered LMFBR containment See Entry 60380

New insights in sodium water reactions and their effects on steam generators See Entry 60381

Sodium fires in SUPER-PHENIX See Entry 60383

Aerosol leakage through containment walls See Entry 60384

Study of the effects of major water leakage in a sodium-heated steam generator See Entry 60385

Safety aspects in the development and construction of fast neutron reactors cooled by sodium See Entry 60386

Safety methods and their application at the PHENIX nuclear power station See Entry 60387

Regulations, options and safety criteria See Entry 60388

The effect of radiation on the release of corrosion products from 304 stainless steel in high temperature water-II effects of flow rate and duration of corrosion experiment See Entry 63595

The place for fast breeders in the French energy situation See Entry 63653

28.52 FUSION REACTORS

(for confinement, see 52.55)

60390 Trapping and surface recombination of deuterium in fusion reactor metals. S.M.Myers (Ion Solid Interactions Div., Sandia Nat. Lab., Albuquerque, NM, USA).

IEEE Trans. Nucl. Sci. (USA), vol.ns-30, no.2, p.1175-8 (April 1983). (1982 IEEE Conference on the Application of Accelerators in Research and Industry, Denton, TX, USA, 8-10 Nov. 1982).

Ion implantation and ion beam analysis were used to examine bulk trapping and surface recombination for deuterium in Fe, Ni, and austenitic stainless steel. Irradiation-defect traps were characterized in the three metals, and substantially stronger traps were shown to be associated with small He bubbles. The rate of deuterium release at stainless steel and Fe surfaces was measured as a function of temperature and solution concentration. Trapping and surface recombination parameters were extracted by applying established theory for solute diffusion within a field of traps. (12 refs.)

60391 MeV light atom beams for heating and/or diagnostics of Tokamak plasmas. L.R.Grisham, D.E.Post, D.R.Mikkelsen (Plasma Phys. Lab., Princeton Univ., Princeton, NJ, USA).

IEEE Trans. Nucl. Sci. (USA), vol.ns-30, no.2, p.1179-82 (April 1983). (1982 IEEE Conference on the Application of Accelerators in Research and Industry, Denton, TX, USA, 8-10 Nov. 1982).

The authors have studied the possible usefulness and feasibility of multi-MeV beams of light atoms ($4 \leq A \leq 30$) for applications in magnetically confined plasmas heating or current drive, and as a diagnostic to probe the velocity distribution function of the confined energetic alpha particles which result from fusion reactions between deuterium and tritium. The combined current and energy requirements for these applications appear to preclude the use of electrostatic acceleration. However, electric-quadrupole-focused RF linear accelerators such as the radio frequency quadrupole (being developed at LASL) or the MEQUALAC (at BNL) appear to be promising technologies. (14 refs.)

60392 An application of SIMS to fusion energy research determination of ion impact desorption cross sections. R.Bastasz (Sandia Nat. Labs., Livermore, CA, USA).

IEEE Trans. Nucl. Sci. (USA), vol.ns-30, no.2, p.1183-6 (April 1983). (1982 IEEE Conference on the Application of Accelerators in Research and Industry, Denton, TX, USA, 8-10 Nov. 1982).

Measurements of plasma effects on materials are required in the design and evaluation of fusion reactor components. One of the more prevalent effects is ion impact desorption (IID) of surface impurities, which may influence plasma temperatures and fuel recycling rates. This paper describes the application of secondary ion mass spectrometry (SIMS) to measure IID processes. (10 refs.)

60393 Multi-megawatt neutral beams for MFTF-B. R.G.Kerr (Lawrence Livermore Nat. Lab., Univ. of California, Livermore, CA, USA).

IEEE Trans. Nucl. Sci. (USA), vol.ns-30, no.2, p.1197-200 (April 1983). (1982 IEEE Conference on the Application of Accelerators in Research and Industry, Denton, TX, USA, 8-10 Nov. 1982).

The Mirror Fusion Test Facility (MFTF-B) at Lawrence Livermore National Laboratory is a reactor-scale tandem-mirror experiment that will provide physics and technology bases for a D-T burning, tandem-mirror facility in the 1990s. Neutral beams of deuterium are injected into the vessel at various places and for different purposes. Plasma streaming guns located on the vessel end domes will provide a 30-cm radius, $2 \times 10^{12} \text{ cm}^{-3}$ density to act as a target. Ten 20-kV, 100-A sources will fire into the anchor region for 10 ms and sixteen 80-kV, 80-A, 0.5-s sources will fire into various regions to raise the plasma density to 4.8×10^{13} in the solenoidal central-cell region. (7 refs.)

60394 A design study of a palladium diffuser for a D-T fusion reactor fuel clean-up system. S.Konishi, H.Yoshida, Y.Naruse (Tokai Res. Establ., JAERI, Ibaraki, Japan).

J. Less-Common Met. (Switzerland), vol.89, no.2, p.457-64 (Feb. 1983). (International Symposium on the Properties and Applications of Metal Hydrides, Toba, Japan, 30 May-4 June 1982).

In a recent study a palladium diffuser was shown to be feasible for a fusion fuel purification process which removes various impurities from plasma exhaust gases. In this study a mathematical model was developed to analyse the separation characteristics for a tubular palladium diffuser. Experiments with H₂-He mixtures were carried out to determine some parameters for an actual diffuser. The hydrogen recovery ratio is defined as a function of the tube dimensions and operating conditions for a diffuser with a high recovery ratio are estimated. A fuel clean-up system for a fusion reactor equipped with the diffuser was also designed. (7 refs.)

60395 Experimental studies on biconical, explosion-driven thermonuclear-fusion system. H.Derentowicz, L.Grygoruk, K.Jach, J.Wrobel, Z.Ziolkowski (S. Kaliski Inst. of Plasma Phys. & Laser Microfusion, Warsaw, Poland).

J. Tech. Phys. (Poland), vol.22, no.4, p.371-8 (1981).

In the authors' studies on biconical explosion-driven systems, the thermonuclear-fusion reaction was obtained as a result of compressing small-size cylindrical UD₃ and UD₃T targets. The fusion neutron-emission was registered at the level of $N \approx 10^4 \div 10^5$ neutrons per shot for UD₃ and 10^7 for UD₃T. The ad hoc developed measuring- and registering setup employed enables measurements to be performed of short nano-second neutron pulses from the level already of $N \approx 10^3$ neutrons per shot. The ad hoc developed biconical system, in view of its constructional features and of the small mass of explosive, constitutes a convenient device for basic studies of the physical phenomena in the field of thermonuclear microfusion. (9 refs.)

60396 Generation of pulses of intense magnetic field with up to 350 Tesla induction by the method of explosion-produced compression. A.Farynski, L.Karpinski, A.Nowak (Skaliski Inst. of Plasma Phys. & Laser Microfusion, Warsaw, Poland).

J. Tech. Phys. (Poland), vol.22, no.4, p.379-90 (1981).

A system has been developed that permits the induction $B_{\text{max}} \leq 350 \text{ T}$ to be obtained by the cumulation method, within a volume of $0.25\text{-}0.5 \text{ cm}^3$. For that purpose a bank of capacitors is needed of an energy of about 100 kJ, and the necessary amount of explosive is about 2 kg. The average frequency of experiments along with the production cycle was one shot per 1-2 weeks. In the last series in all the shots $B_{\text{max}} > 100 \text{ T}$ was measured. Discrepancy of results in the series in which identical systems were operated is to be accounted for chiefly by the stochastic nature of the development of Rayleigh-Taylor instabilities that destroy the measuring probes at various instants of the final stage of the field compression by the conducting liner. (11 refs.)

60397 A simple ablative implosion model—shell dynamics. F.J.Mayer, J.T.Larsen, J.W.Steele (KMS Fusion Inc., Ann Arbor, MI, USA).

Phys. Fluids (USA), vol.26, no.3, p.830-4 (March 1983).

A simple model, derived from Newton's Second Law, for the ablative implosion of a thin spherical shell is presented. The scaling dependence of the implosion time, shell velocity, and mass loss on shell dimensions and the critical physical parameter, the ablation pressure, is derived. Finally, the model is used to examine implosion energy efficiency and to describe an interesting application, wall-recoil heating of a contained fuel gas. (10 refs.)

60398 Implosion symmetry of laser irradiated fusion pellet. T.Mochizuki, S.Sakabe, H.Shiraga, K.Okada, T.Yabe, C.Yamanaka (Inst. of Laser Engng., Osaka Univ., Osaka, Japan).

Phys. Scr. (Sweden), vol.T2, no.2, p.479-85 (1982). [received: April 1983] (1982 International Conference on Plasma Physics, Goteborg, Sweden, 9-15 June 1982).

Implosion processes of 1.053 μm laser irradiated (1) thin solid density Be coated plastic microballoons and (2) thick low Z from coated glass microballoons have been diagnosed by an X-ray flash radiography method to investigate implosion symmetry of the pellet shell. Asymmetric implosion of Be coated pellet is due to a strong inhibition of lateral energy transport by a self-generated magnetic field. In the foam coated pellet significant improvement of the symmetry has been achieved. (14 refs.)

60399 Inertial confinement fusion. C.Yamanaka (Inst. of Laser Engng., Osaka Univ., Osaka, Japan).

Phys. Scr. (Sweden), vol.T2, no.2, p.486-9 (1982). [received: April 1983] (1982 International Conference on Plasma Physics, Goteborg, Sweden, 9-15 June 1982).

Implosion process has been investigated by using blue, green, red and far infrared lasers. Various types of target are compared to improve the implosion properties. A 'cannon ball' target is proposed and tested to show the high efficiency in implosion. (5 refs.)

60400 On the ignition conditions for turbulent plasmas. V.N.Tsytochik (Lebedev Inst. of Phys., Moscow, USSR).

Phys. Scr. (Sweden), vol.T2, no.2, p.588-9 (1982). [received: April 1983] (1982 International Conference on Plasma Physics, Goteborg, Sweden, 9-15 June 1982).

Possible change of ignition condition by plasma turbulence is discussed. (2 refs.)

60401 Physics of neutronless fusion reacting plasmas. B.Coppi (MIT, Cambridge, MA, USA).

Phys. Scr. (Sweden), vol.T2, no.2, p.590-5 (1982). [received: April 1983] (1982 International Conference on Plasma Physics, Goteborg, Sweden, 9-15 June 1982).

On the basis of present day knowledge of plasma physics and available technologies it is shown that experiments to test the thermonuclear burn conditions of plasmas with fusion reactions that do not produce neutrons can be undertaken. (30 refs.)

60402 A historic achievement: controlled nuclear fusion. J.Buj.

Rev. Esp. Electron. (Spain), vol.30, no.339, p.10-13 (Feb. 1983). In Spanish. The background to the achievement of a controlled nuclear fusion is outlined. The simultaneous conditions necessary for a controlled nuclear fusion are described. Slow and rapid fusion are discussed and the stages leading up to the achievement are described. (no refs.) S.M.H.

60403 Nuclear fusion and the outlook for commercial fusion reactors. J.R.O'Mahony.

Trans. S. Afr. Inst. Electr. Eng. (S. Africa), vol.74, pt.1, p.3-6 (Jan. 1983). Nuclear fusion must rank as one of the most promising long term solutions to the energy problems facing the industrialised world. The fusion principle is described together with its possible advantages and disadvantages. (7 refs.)

60404 Nuclear fusion research at Pelindaba. F.J.Retief, J.R.O'Mahony (Dept. of Electrical Engng., Univ. of Pretoria, S. Africa).

Trans. S. Afr. Inst. Electr. Eng. (S. Africa), vol.74, pt.1, p.7-12 (Jan. 1983). Describes 'Tokoloshe', a medium-sized Tokamak type high temperature plasma physics experiment which was designed and built by the Atomic Energy Board. The electrical engineering aspects of the project are emphasized. (no refs.)

60405 A comparison of helium bubble behaviour in an austenitic and a ferritic steel. T.R.Armstrong, Z.H.Luklinska, S.K.Tyler, P.J.Goodhew (Dept. of Metall. & Materials Technol., Univ. of Surrey, Guildford, England).

Fusion Technology 1982. Proceedings of the Twelfth Symposium, Julich, Germany, 13-17 Sept. 1982 (Oxford, England: Pergamon 1983), p.743-8 vol.2 Helium bubble populations have been created in a 316 stainless steel and an FI ferritic/martensitic steel by ion implantation and isothermal annealing. The bubble growth kinetics have been studied by electron microscopy: the bubbles grow by Brownian migration and coalescence and in the temperature range 600-700°C the dominant mechanism appears to be volume diffusion. However, in the ferritic material the shape of the faceted bubbles leads to the nucleation of steps on bubble faces becoming rate-limiting and this restricts the growth of the cuboidal bubbles. In comparison, for the many-sided bubbles in the austenitic material ledge nucleation does not become the rate-limiting step. (12 refs.)

60406 FATMAC. A machine for the fatigue testing of CT type samples in the HFR, Petten, Holland. P.Blanchard, P.May, H.Scheurer (Joint Res. Centre, Comm. of the European Communities, Petten, Netherlands).

Fusion Technology 1982. Proceedings of the Twelfth Symposium, Julich, Germany, 13-17 Sept. 1982 (Oxford, England: Pergamon 1983), p.749-52 vol.2

FATMAC is a new type of in-pile crack testing facility, for conducting tests on CT type samples of any metal. FATMAC offers a continuous testing capability for a number of samples, even up to 20, with a comprehensive spectrum of specifications and instrumentation. In short, FATMAC is a flexible experimental approach to cater for an expanding need for an efficient, professional, in-pile material testing facility, such as is required in the growing field of fusion reactor materials research. (no refs.)

60407 The Technology Development Facility (TDF). J.N.Doggett (Lawrence Livermore Nat. Lab., Univ. of California, Livermore, CA, USA).

Fusion Technology 1982. Proceedings of the Twelfth Symposium, Julich, Germany, 13-17 Sept. 1982 (Oxford, England: Pergamon 1983), p.753-7 vol.2 The author has been studying small, driven, magnetic-mirror-based fusion reactors for the Technology Development Facility (TDF), that will test fusion reactor materials, components, and subsystems. Magnetic mirror systems are particularly interesting for this application because of their inherent steady-state operation, potentially high neutron wall loading, and relatively small size. The design is a tandem mirror device first described by Fowler and Logan (1981) based on the physics of the TMX experiments at Lawrence Livermore National Laboratory (LLNL). The device produces 20 MW of fusion power with a first-wall, uncollided 14-MeV neutron flux of 1.4 MW/m² on an area of approximately 8 m², while consuming approximately

250 MW of electrical power. The work was done by a combined industrial-laboratory-university group. (3 refs.)

60408 Spontaneous and continuous structure and surface transformations of refractory transition metals by hydrogen. H.Meusemann, L.V.Erichsen, H.Haverkamp, F.Luckner, A.Maas (Inst. fur Phys. Chem., Univ. Bonn, Bonn, Germany).

Fusion Technology 1982. Proceedings of the Twelfth Symposium, Julich, Germany, 13-17 Sept. 1982 (Oxford, England: Pergamon 1983), p.759-65 vol.2

A survey is given on the behaviour of some refractory transition metals under pure molecular hydrogen. During many repeated cycles with alternating increase and decrease of temperature and gas pressure, the samples are observed in a Sieverts type device. In addition, a new SEM method has been developed allowing a continuous observation of the metal-hydrogen reaction in-situ. Thus the effects of surface morphological alterations can be photographically recorded. Results are presented for the metals vanadium, niobium, tantalum, yttrium and titanium. Beyond material failure due to phase transformations, unexpected interface phenomena like reduction of surface layers, erosion by chemical sputtering, especially at grain boundaries, whisker growth and high temperature hydrogen embrittlement have been found. (8 refs.)

60409 Structural and mechanical anisotropy of a nuclear grade AISI 316 stainless steel. M.M.Farag, R.Matera, T.Sasaki, E.Ruedl (Joint Res. Centre, Comm. of the European Communities, Ispra, Italy).

Fusion Technology 1982. Proceedings of the Twelfth Symposium, Julich, Germany, 13-17 Sept. 1982 (Oxford, England: Pergamon 1983), p.767-72 vol.2

The effects of thermomechanical treatments on the grain size, precipitate phases and mechanical properties have been investigated on a nuclear grade type AISI 316 stainless steel. The aim of this study was to characterize small thickness samples prior to the light ion irradiation experiments foreseen for this steel. A noticeable effect of grain size inhomogeneity was observed on the precipitation kinetic and on the mechanical properties. (13 refs.)

60410 Helium bubbles at grain boundaries in an austenitic steel. P.L.Lane, P.J.Goodhew (Dept. of Metall. & Materials Technol., Univ. of Surrey, Guildford, England).

Fusion Technology 1982. Proceedings of the Twelfth Symposium, Julich, Germany, 13-17 Sept. 1982 (Oxford, England: Pergamon 1983), p.773-8 vol.2 Helium bubbles are expected to contribute to both swelling and embrittlement in fusion reactor first wall materials. In particular, the nucleation and growth of helium bubbles at grain boundaries is likely to determine the extent of embrittlement. The authors report the results of a study of gas bubble nucleation at various interfaces in an austenitic alloy after helium implantation at 600°C. The results show that the total cavity volume is significantly enhanced at grain boundaries. Bubble nucleation has been related to the boundary structure; bubbles are aligned along dislocations only when the Burgers vector is large. (9 refs.)

60411 Irradiation creep in first wall model alloys. P.Jung (Inst. fur Festkörperforschung, KFA Julich GmbH, Julich, Germany).

Fusion Technology 1982. Proceedings of the Twelfth Symposium, Julich, Germany, 13-17 Sept. 1982 (Oxford, England: Pergamon 1983), p.779-82 vol.2

Creep enhancement by 7 MeV proton irradiation has been investigated in 20% cold worked specimens of Ni, Ni-3.4 w/o W, FeCrNi, FeCrNiMo and type 316 stainless steel. Dependence of irradiation creep on stress, temperature and dose rate were studied, as well as transient effects arising from changing these parameters. (8 refs.)

60412 Tritium in vanadium. R.Lasser, H.Wenzl (Inst. fur Festkörperforschung, KFA Julich, Julich, Germany).

Fusion Technology 1982. Proceedings of the Twelfth Symposium, Julich, Germany, 13-17 Sept. 1982 (Oxford, England: Pergamon 1983), p.783-8 vol.2 All-metal tritium facilities have been built for handling about 1000 Curie T₂, preparation of concentrated metal tritides MT_x, measurements of phase diagrams, etc. Properties of tritium in VT_x have been determined: out-gassing rates, lattice parameter changes, diffusion coefficient, structure and phase diagram. (9 refs.)

60413 Plastic flow and fracture of Ti-modified 316 austenitic stainless steel after high temperature aging in hydrogen. M.Mark-Markowitch, Y.Rosenthal, A.Stern (Nuclear Res. Centre, Beer Sheva, Israel).

Fusion Technology 1982. Proceedings of the Twelfth Symposium, Julich, Germany, 13-17 Sept. 1982 (Oxford, England: Pergamon 1983), p.789-95 vol.2

300-400 at. ppm of hydrogen introduced by thermal aging at 780°C induces noticeable changes in mechanical properties and microstructure of 316-Ti ASS, in the annealed and 22% cold-worked condition, respectively. Hydrogen-softening and ductilizing effects were observed, also effects on fracture morphology. H trapping at interfaces of secondary phases is believed to be responsible for the various effects. (10 refs.)

60414 Thermal fatigue test facilities for simulating the first wall and limiter operating conditions. R.Matera (Joint Res. Centre, Comm. of the European Communities, Ispra, Italy), A.Perfumo.

Fusion Technology 1982. Proceedings of the Twelfth Symposium, Julich, Germany, 13-17 Sept. 1982 (Oxford, England: Pergamon 1983), p.797-801 vol.2

A number of facilities are in operation or under study at the JRC Ispra in order to test the behaviour of FW and limiter structural component under thermal fatigue. They range from laboratory scale experiment to full scale facility suited to perform thermo-mechanical tests on a real size FW module. The characteristics of the experimental facilities and an outline of the relative test programme is given in this paper. (7 refs.)

60415 A programme for the study of fatigue of fusion reactor structural materials. F.Moons, M.Snykers, W.Vandermeulen (Nuclear Res. Centre, Mol, Belgium).

Fusion Technology 1982. Proceedings of the Twelfth Symposium, Julich, Germany, 13-17 Sept. 1982 (Oxford, England: Pergamon 1983), p.803-7 vol.2 Fatigue of fusion reactor first wall structural materials is considered as an important life limiting factor. The first wall is subjected to an intense irradiation of neutrons which cause atomic displacements and a relatively high production of helium. This production of helium is higher as compared with fast fission reactors because of the strong increase of the cross section of (n, α) reactions for energies higher than 5 MeV. The aims of a collaborative programme between US, Japan and CEG are: study of the influence of different He to dpa ratios. For this purpose post-irradiation fatigue tests will be performed on specimens irradiated in the Belgian BR2 reactor and in HFIR; comparison of post and in-pile fatigue. Similar specimens will be tested in-pile and after irradiation. For this purpose a miniature fatigue testing module is being designed which will allow in-pile fatigue loading of a small hourglass specimen. Two to four of such modules will be placed in one irradiation rig.

Possible factors, which might contribute to a different in-pile and post irradiation behaviour, are discussed. (no refs.)

60416 Prospects for low activity aluminum structures. J.R.Powell, J.A.Fillo (Dept. of Nuclear Energy, Brookhaven Nat. Lab., Upton, NY, USA).

Fusion Technology 1982. Proceedings of the Twelfth Symposium, Julich, Germany, 13-17 Sept. 1982 (Oxford, England: Pergamon 1983), p.809-14 vol.2

High-purity, low-activity powder metallurgy Al alloys can be developed for use in a fusion reactor at 300° to 400°C using He as a heat transfer medium. Hot water as a coolant may limit Al to 200°C. Based on the dual- or two-temperature design approach, commercial fusion reactor blanket designs are feasible. Aluminum appears well suited for experimental fusion reactors operating at wall temperatures below 200°C. (3 refs.)

60417 Helium ion damage in an amorphous Fe-Ni-Mo-B alloy. H.Van Swijgenhoven, L.M.Stals, G.Knuyt (Limburgs Univ. Centrum, Diepenbeek, Belgium).

Fusion Technology 1982. Proceedings of the Twelfth Symposium, Julich, Germany, 13-17 Sept. 1982 (Oxford, England: Pergamon 1983), p.823-8 vol.2 Data are presented on helium gas bubble and helium blister formation for Metglas 2826MB during 5 keV He⁺-implantation in the temperature range 200K-600K and dose range 5.10²⁴-10²² He⁺/m². It is concluded that amorphous alloys are less radiation resistant as has been taught earlier. (37 refs.)

60418 The surface topography of Inconel, stainless steel and copper after argon ion bombardment. K.Vogelbruch, E.Vietzke (Inst. fur Chem., KFA Julich GmbH, Julich, Germany).

Fusion Technology 1982. Proceedings of the Twelfth Symposium, Julich, Germany, 13-17 Sept. 1982 (Oxford, England: Pergamon 1983), p.829-33 vol.2

Energetic particle bombardment of metals is known to change the surface topography. To simulate the behaviour of the first wall of a fusion device under real plasma conditions, the authors have investigated the surface topography of rotating targets after 30 keV argon ion bombardment at 70° incident angle by electron scanning micrographs. Under these conditions Inconel 600, 601, 625, stainless steel, and copper showed no cones, pyramids or cliffs, but only etching figures and at higher ion doses relatively flat hills. Thus it can be concluded that the influence of energetic particles on the first wall of fusion reactor is smaller than expected from the results of such sputtering experiments, which have dealt with the formation of surface structures under ion bombardment at constant incident direction. (5 refs.)

60419 Evaluation of the energy required for constructing and operating a fusion power plant. R.Bunde (Max-Planck-Inst. fur Plasmaphys., Garching, Germany).

Fusion Technology 1982. Proceedings of the Twelfth Symposium, Julich, Germany, 13-17 Sept. 1982 (Oxford, England: Pergamon 1983), p.837-44 vol.2

The energy required for constructing and operating a Tokamak fusion power plant is appraised with respect to the energy output during the lifetime of the plant. A harvesting factor is deduced as a relevant figure of energetic merit and is used for a comparison between fusion, fission and coal-fired power plants. Because fusion power plants involve considerable uncertainties the comparison is supplemented by a sensitivity analysis. In comparison with Light Water Reactor plants fusion power plants appear to be rather favourable in this respect. The energy required for providing the fuel is relatively low for fusion plants, thus overcompensating the considerably higher amount of energy necessary for constructing the fusion power plant. (5 refs.)

60420 The design of a 316 stainless steel first wall for a pulsed fusion reactor with wall loading greater than 10 MWm⁻². A.Caie (Associated Nuclear Services, Epsom, England), G.J.Butterworth.

Fusion Technology 1982. Proceedings of the Twelfth Symposium, Julich, Germany, 13-17 Sept. 1982 (Oxford, England: Pergamon 1983), p.845-50 vol.2

A preliminary design study has been made of a 316 stainless steel first wall for a fusion reactor operating at a neutron wall loading of about 10 MWm⁻² and a burn cycle of about 1000 seconds. The study highlights the conflicting requirements of providing sacrificial material to withstand erosion whilst limiting the cyclic thermal stresses to give adequate fatigue life. The analysis is based on the ASME boiler and pressure vessel code Section III, particularly the high temperature case N47. The merits of helium and water cooling are compared and it is found that the high cyclic wall loading strongly favours water cooling. The maximum life of the first wall is governed by the erosion rate of the front surface and the fatigue characteristics of the material. The 20% cold-worked form of the material is found to be advantageous in resisting ratcheting under cyclic thermal stresses. The first wall geometry analysed consisted of parallel plain tubes arranged in an overlapping array. The relative disadvantages of other cross-sectional forms and of membrane wall layouts are discussed. It is suggested that the problems of accommodating irradiation-induced swelling strains will determine the layout and mode of support of the tubes but have only a minor influence on the choice of cross-sectional form. (6 refs.)

60421 Tokamak and reversed field pinch reactor cost scaling. P.I.H.Cooke (Culham Lab., UKAEA, Abingdon, England).

Fusion Technology 1982. Proceedings of the Twelfth Symposium, Julich, Germany, 13-17 Sept. 1982 (Oxford, England: Pergamon 1983), p.851-6 vol.2 The interactions between the basic parameters of a Tokamak or reversed field pinch reactor have been modelled to show their relative influences on the reactor capital cost. The model shows that at a given power output, β -value and toroidal magnetic field at the coil, there is a maximum wall loading which can be attained for the Tokamak. If blanket costs scale approximately linearly with wall loading high wall loadings are not economically favoured, particularly for the reversed field pinch. (5 refs.)

60422 Lifetime considerations for the first wall of a DEMO reactor. W.Daenner (Max-Planck-Inst. fur Plasmaphys., Garching, Germany).

Fusion Technology 1982. Proceedings of the Twelfth Symposium, Julich, Germany, 13-17 Sept. 1982 (Oxford, England: Pergamon 1983), p.857-62 vol.2

For a DEMO reactor operating at a neutron wall loading of 2 MW/m², a first wall lifetime of about 10 to 15 MW-yr/m² is desired. The consequences with respect to swelling and irradiation creep deformation as well as to the permissible erosion rates are discussed. It is concluded that the envisaged fluence goal can only be met if deformations in excess of 10% can be tolerated restricting at the same time erosion to about 0.1 to 0.2 cm/yr. Under more conservative assumptions a value of about 6 MW-yr/m² turns out to be a realistic goal. All investigations are based on a modular first-wall concept assuming helium as the coolant and 20% cold worked 316 SS as the first-wall material. For the lifetime estimates made by means of the FWLTB computer program the best current guesses about the irradiation behaviour of 316 SS in a fusion reactor environment were used. (6 refs.)

60423 Mechanical stress analysis for the twisted coils of the advanced stellarator WENDELSTEIN VII-AS. U.Brossmann, S.B.Mukherjee, J.Sapper (Max-Planck-Inst. fur Plasmaphys., Garching, Germany).

Fusion Technology 1982. Proceedings of the Twelfth Symposium, Julich, Germany, 13-17 Sept. 1982 (Oxford, England: Pergamon 1983), p.991-6 vol.2 The standard confinement field of the advanced stellarator WENDELSTEIN VII-AS is exclusively generated by a modularly designed coil set. Forty-five twisted coils produced a toroidal field of 3 T during a pulse time of 5 sec. Water cooled copper wires carry a winding current of 40 kA at 3.3 kV. Force components in the radial, poloidal and toroidal directions are calculated for the individual coils using EFFI-code (Sackett, 1978). On the basis of an optimized support concept a stress analysis for the coils was carried out using SAP V (2). (7 refs.)

60424 Development of material for the JET mechanical structure. G.Celentano, M.Huguet, E.Salpietro (JET Joint Undertaking, Culham, England), K.Feuring, F.Reimann.

Fusion Technology 1982. Proceedings of the Twelfth Symposium, Julich, Germany, 13-17 Sept. 1982 (Oxford, England: Pergamon 1983), p.997-1004 vol.2

The mechanical structure of JET device, shaped like a large spherical shell is made up of 64 castings with weights varying between 5 to 10 tonnes each. These castings have to withstand the very large forces arising from the toroidal and poloidal magnetic field of the JET machine. An extensive study was carried out to select a suitable material to produce such big castings and to set up a reliable industrial production method to suit the design requirements. The assessment led to the selection of an austenitic nodular cast iron. A review of the static and dynamic mechanical tests, fracture mechanic tests and functional tests carried out throughout all stages during the development and production is presented. (6 refs.)

60425 Mechanical analysis of TORE SUPRA superconducting toroidal field coils. J.J.Cordier, P.Libeyre, D.Lionnet, A.Torossian (Dept. de Recherches sur la Fusion Controlée, CEN, Fontenay-aux-Roses, France).

Fusion Technology 1982. Proceedings of the Twelfth Symposium, Julich, Germany, 13-17 Sept. 1982 (Oxford, England: Pergamon 1983), p.1005-10 vol.2

The detailed mechanical analysis of the TORE SUPRA toroidal magnet, has been achieved by using the finite element method, with the CASTEM system developed by CEA at Saclay. The strong anisotropy of the winding has been taken into account with orthotropic elements. Two steps characterise the study: a refined analysis of the most stressed area under toroidal field using bidimensional calculation led to an improvement of the design of the structure; a three dimensional analysis with rougher mesh but allowing, however, enough accuracy in the results was then undertaken to check average values. Only preliminary results for this last part are presented. (2 refs.)

60426 Poloidal field coils for the international Tokamak reactor study 'INTOR'. H.G.Dittrich, U.Jeske (Kernforschungszentrum Karlsruhe, Inst. fur Tech. Phys., Karlsruhe, Germany).

Fusion Technology 1982. Proceedings of the Twelfth Symposium, Julich, Germany, 13-17 Sept. 1982 (Oxford, England: Pergamon 1983), p.1011-13 vol.2

The poloidal field (PF) coil system consists of 21 solenoids. All these solenoids are superconducting and they are positioned outside the toroidal field coils. Thirteen of the PF coils are positioned inside the inner vault of the torus and have an outer diameter of 1.7 m. Seven of these 13 coils are provided for the ohmic heating of the plasma. The distribution of the rest of the PF coils is highly unsymmetric with big divertor coils at the bottom of the reactor in order to provide a single null poloidal divertor configuration. The outer diameter of the largest coil is 12.6 m. (no refs.)

60427 Mechanical tests on components used in the TORE SUPRA superconducting coils. D.Duthoo, J.Hamelin, P.Libeyre, A.Torossian (Dept. de Recherches sur la Fusion Controlée, CEN, Fontenay-aux-Roses, France).

Fusion Technology 1982. Proceedings of the Twelfth Symposium, Julich, Germany, 13-17 Sept. 1982 (Oxford, England: Pergamon 1983), p.1015-20 vol.2

Reports the test results on glass-epoxy composites and on stainless steel which are extensively used for the coil, and for the casing respectively. In the case of glass-epoxy, industrial products have provided satisfactory results under static and dynamic loads. Two welding processes of stainless steel have been tested and it is shown that the joints fit the high requested characteristics. Tests performed on small mockups of the winding have permitted the determination of its Young's and Coulomb's moduli. (3 refs.)

60428 Toroidal field coils for INTOR. H.-G.Dittrich, J.Erb, R.Flukiger (Kernforschungszentrum Karlsruhe, Inst. fur Tech. Phys., Karlsruhe, Germany), M.Hilal, U.Jeske, A.Nyilas, G.Ries.

Fusion Technology 1982. Proceedings of the Twelfth Symposium, Julich, Germany, 13-17 Sept. 1982 (Oxford, England: Pergamon 1983), p.1021-6 vol.2

The toroidal field (TF) coil for INTOR consists of two subcoils, a NbTi coil with a maximum induction of 7.6T and 10.9 kA conductor current and a Nb₃Sn coil with 11 T maximum induction and 20 kA conductor current. The overall coil dimensions are 8.56 m x 11.06 m. The TF coil is centered by a double vault. Each supports individually the centering forces of each subcoil. The vault dimensions are designed to maintain a mechanical stress below 400 MPa. All TF coils are embedded in an overturning force support structure. (2 refs.)

60429 Employment of the Large Coil Test Facility in toroidal field coil development. P.N.Haubenreich, R.E.Bohanan, J.N.Luton, J.R.May, H.E.Miller, T.L.Ryan (Oak Ridge Nat. Lab., Oak Ridge, TN, USA).

Fusion Technology 1982. Proceedings of the Twelfth Symposium, Julich, Germany, 13-17 Sept. 1982 (Oxford, England: Pergamon 1983), p.1027-32 vol.2

The international large coil task (LCT), involving EURATOM, Japan, Switzerland, and the United States, is developing competing concepts of superconducting toroidal field coils. Six different coils will be tested together in the Large Coil Test Facility (LCTF). All participants are collaborating in planning and will share all test data. (6 refs.)

60430 Numerical calculations of an effective elasticity tensor and peak stresses for the large fusion magnets. T.Iwanicki (Brown, Boveri & Cie, Mannheim, Germany), W.Maurer, W.Heinz.

Fusion Technology 1982. Proceedings of the Twelfth Symposium, Julich, Germany, 13-17 Sept. 1982 (Oxford, England: Pergamon 1983), p.1033-8 vol.2

For the calculation of mechanical properties of large magnet systems in 3-dimensional space, a very fine subdivision of the magnet structure is necessary. In the finite element programs, this will lead to unacceptable long computing times and to the limits of computer-storage capacity. The problem can be solved by the numerical method, called 'numerical simulation', by which an effective elasticity tensor is obtained for a composite material. It is possible to calculate the average stress using the effective elasticity tensor and

the peak stresses in each point of the structure using the surface displacement interpolation. A good agreement is found between the experimental and theoretical moduli of elasticity. All the calculations are performed by the finite element computer code ASKA for one of the toroidal magnet coils from LCT. (5 refs.)

60431 The toroidal field magnet concept of ASDEX Upgrade. O.Jandl, H.Kolotzek, E.Springmann, B.Streibl (Max-Planck-Inst. fur Plasmaphys., Garching, Germany).

Fusion Technology 1982. Proceedings of the Twelfth Symposium, Julich, Germany, 13-17 Sept. 1982 (Oxford, England: Pergamon 1983), p.1039-44 vol.2

ASDEX Upgrade (UG), a divertor Tokamak with a minor plasma radius of $a=0.5$ m and a plasma current of 1.2 to 1.5 MA, is intended to succeed ASDEX. A major target of this experiment is to investigate a reactor-compatible plasma boundary. This requires a toroidal field (B_0) at the plasma centre normalized to the aspect ratio (A) of $B_0/A \approx 1.2$. The toroidal field (TF) magnet designed to meet these requirements is presented. Its turnover structure aspects, such as force transfer, coil housing and access to the plasma vessel are described. The coil concept developed in collaboration with industry is also presented. Results of the cooling and stress analysis are summarized. (1 ref.)

60432 On strength of welded joints in high strength, large scale copper coils for nuclear fusion equipment. H.Kimoto, H.Kojima, S.Hioki, T.Takizawa, T.Watanabe, K.Imai, T.Uehara (Mech. Engng. Res. Lab., Hitachi Ltd., Ibaraki-ken, Japan).

Fusion Technology 1982. Proceedings of the Twelfth Symposium, Julich, Germany, 13-17 Sept. 1982 (Oxford, England: Pergamon 1983), p.1045-50 vol.2

Experimental studies were done to improve and evaluate the strength for heavy copper welded joints of coils using special welding techniques. The cold press-working process is used for the improvement of softened and weakened parts of welded joints of copper. To evaluate the strength of copper welded joints, static and fatigue tests are carried out. The results of tests demonstrate that the strength of improved welded joints of copper satisfies the severe design specifications. The fatigue life of welded defects is estimated with a high degree of confidence with fracture mechanics. (6 refs.)

60433 Vacuum magnetic fields and modular coil system of the advanced stellarator Wendelstein VII-AS. J.Kisslinger, F.Rau, H.Wobig (Max-Planck-Inst. fur Plasmaphys., Garching, Germany).

Fusion Technology 1982. Proceedings of the Twelfth Symposium, Julich, Germany, 13-17 Sept. 1982 (Oxford, England: Pergamon 1983), p.1051-7 vol.2

The vacuum field and the modular coils of the advanced stellarator WENDELSTEIN VII-AS are described. Each of the five field periods contains 9 different twisted coils, one of them with increased dimensions and current to provide sufficient access for neutral beam injection. The standard configuration ($B=3$ T, rotational transform $t=0.39$, aspect ratio ≈ 10 , low shear, and magnetic well) can be varied by toroidal and vertical fields, or by changing independently the current in the special coils. From a study of magnetic field perturbations some estimates are given for the admissible coil tolerances. (17 refs.)

60434 Strength analysis of cooling pipe joints for poloidal field coil for nuclear fusion equipment. H.Kojima, H.Kimoto, S.Hioki, T.Takizawa, M.Furuyama (Mech. Engng. Res. Lab., Hitachi Ltd., Ibaraki-ken, Japan).

Fusion Technology 1982. Proceedings of the Twelfth Symposium, Julich, Germany, 13-17 Sept. 1982 (Oxford, England: Pergamon 1983), p.1059-66 vol.2

It is necessary to confirm the reliability of a poloidal field coil (PFC) under operating loads during the design process. One of the most important points in this confirmation is the evaluation of PFC fatigue strength, because coils are used under conditions where the applied stress may be close to the elastic proportional limit of copper. Since a PFC is welded or brazed structure in which each turn consists of several copper conductor segments, the cooling pipe laid in the conductor also has pipe joints. These pipe joints determine PFC strength. A stress analysis is carried out to determine a reasonable structure for cooling pipe joints, given the limited space available for the joints. Experimental studies are also performed to evaluate the fatigue strength of pipe joints. As a result of these strength analyses, a bellow structure was selected as the most appropriate PFC cooling pipe joint. It was confirmed that such joints are strong enough to be used in PFCs. (8 refs.)

60435 The technical concept of the ASDEX UG poloidal field coils. H.Kolotzek, M.Pillsticker, F.Werner (Max-Planck-Inst. fur Plasmaphys., Garching, Germany).

Fusion Technology 1982. Proceedings of the Twelfth Symposium, Julich, Germany, 13-17 Sept. 1982 (Oxford, England: Pergamon 1983), p.1067-71 vol.2

The ASDEX UG Tokamak poloidal field coil system will comprise three ohmic heating coils and three vertical field coils. The ohmic heating coils consist of a highly excited coil in the central bore of the toroidal field magnet and coils outside the toroidal magnet arranged in pairs symmetric to the torus midplane. This coil arrangement is expected to generate a magnetic flux swing of about 9.5 Vs for a total discharge time of the plasma of 10 s. The vertical field coils can be arranged (a) all outside the toroidal magnet system, and (b) partially between the toroidal magnet system and the vacuum vessel, likewise in pairs symmetric to the torus midplane. (2 refs.)

60436 Electromagnetic systems for high-field Tokamaks. Yu.Alekseev, V.Demichev, M.Safonova, V.Chuyanov (I.V. Kurchatov Inst. of Atomic Energy, Moscow, USSR).

Fusion Technology 1982. Proceedings of the Twelfth Symposium, Julich, Germany, 13-17 Sept. 1982 (Oxford, England: Pergamon 1983), p.1073-9 vol.2

The concept and principal parameters of a toroidal magnetic system for a high-field Tokamak are discussed. The temperatures, suitable for the reactor, and the confinement parameter can be reached with high plasma density, high magnetic fields and with adiabatic compression of the plasma column as the main technique of heating (not due to large dimensions of the Tokamak). The use of high fields is aimed at decreasing the dimensions and cost of an installation. The optimization of the field strength with different restrictions to a material of the coil has been done. The rated field on the plasma column axis is ~ 130 kOe, that on the conductor surface is ~ 200 kOe, the field-flat-top-duration is 200 ms. The possibility of designing a toroidal magnetic system is discussed. Each section of this system is a massive turn bandaged with a high-strength steel. Thermal regimes of the magnet are calculated. (7 refs.)

60437 Manufacturing of the European LCT-coil for the large coil task. H.Krauth, A.Nyilas, A.Ulbricht (Inst. fur Tech. Phys., Kernforschungszentrum Karlsruhe, Karlsruhe, Germany), C.Albrecht, H.Salzburger.

Fusion Technology 1982. Proceedings of the Twelfth Symposium, Julich, Germany, 13-17 Sept. 1982 (Oxford, England: Pergamon 1983), p.1095-100 vol.2

The major manufacturing steps of the European LCT-coil are described. About 7 km of forced flow cooled superconductor were fabricated in the required unit lengths of 500 m. Each two lengths are wound by hand into a double pancake. A total of 7 double pancakes are stacked in a segmented mould for vacuum-pressure impregnation with epoxy resin. The impregnated winding pack will be inserted and force locked in the prefabricated coil case made from a 316 LN type stainless steel. Extensive instrumentation is applied to the coil for diagnostic purposes during the testing period. (9 refs.)

60438 Numerical analysis of the metal forming process during the winding procedure of the European LCT coil. G.Messemer, H.Zehlein (Kernforschungszentrum Karlsruhe GmbH, Karlsruhe, Germany).

Fusion Technology 1982. Proceedings of the Twelfth Symposium, Julich, Germany, 13-17 Sept. 1982 (Oxford, England: Pergamon 1983), p.1101-6 vol.2

Presents a numerical study of the mechanical behaviour of the superconductor cable for the European LCT coil during the winding procedure. A simplified discrete elastic model was applied to describe the sharply rising bending moment near the touching point on the bobbin under different tension forces. A bilinear elasto-plastic bending moment-curvature relationship as derived from bending experiments was used. The circumferential distributions of the relevant process variables over the D-shaped coil contour show a pronounced influence of the tension force and the local coil curvature. (11 refs.)

60439 A procedure for the computation of magnetic field, temperature and force distributions in the design of Tokamak toroidal coils. P.Molfino, G.Molinari (Inst. di Elettrotecnica, Univ. di Genova, Genova, Italy), F.Rosatelli, A.Viviani.

Fusion Technology 1982. Proceedings of the Twelfth Symposium, Julich, Germany, 13-17 Sept. 1982 (Oxford, England: Pergamon 1983), p.1107-13 vol.2

Presents a formulation of the problem of coupled electric, magnetic and thermal fields in Tokamak toroidal coil, oriented to give satisfactory results with reduced computer resources. This goal is achieved by the introduction of an equivalent two-dimensional coil, whose solution is related to the solution of the original three-dimensional problem. A package allowing the solution of the resulting set of partial differential equations is also presented, its features are described and some results are displayed are discussed. (3 refs.)

60440 The design bending stress criterion for JT-60 coil. M.Ohkubo (JAERI, Ibaraki-ken, Japan).

Fusion Technology 1982. Proceedings of the Twelfth Symposium, Julich, Germany, 13-17 Sept. 1982 (Oxford, England: Pergamon 1983), p.1115-20 vol.2

The design bending stress criterion of the JT-60 coil conductor are described. JT-60 coil conductors are made of 0.2% silver bearing oxygen free copper (0.2%Ag-OFC) hardened by cold-rolling. They are connected by welding or brazing to make full turn. The relationship between load and deformations for a conductor subjected to an axial and a lateral loads is taken into consideration in the stress analysis and the collapse load and true strain are calculated by the derived equations. It is clear from the analysis results that the materials with yield-tensile ratio more than 0.5 have a safety factor of 3 and those with yield-tensile ratio less than 0.5 have a higher safety factor more than 3 when the coils are designed in accordance with ASME section III. In the JT-60 coil, the design value has sufficient factor higher than 3, which may guarantee the reliability of the coil. The present analysis may be applicable not only to the copper conductors but also to the other materials such as steel. (3 refs.)

60441 Toroidal field magnet for FT-U device. A.Pizzuto (Centro Ricerche Energia Frascati, EURATOM-ENEA sulla Fusione, Rome, Italy).

Fusion Technology 1982. Proceedings of the Twelfth Symposium, Julich, Germany, 13-17 Sept. 1982 (Oxford, England: Pergamon 1983), p.1121-6 vol.2

The FT-upgrade Tokamak in order to accomplish its aims has to operate its magnet under very high stress for a large number of shots. In order to assess the feasibility to a magnet capable of this performance, an extensive three dimensional finite element stress analysis and an extensive material cryogenic test program has been developed. The main results obtained are illustrated. (4 refs.)

60442 Manufacture, assembly and testing of the inner poloidal coil stacks of JET and TFTR. J.C.Rauch, Th.Roman, F.Konig (BBC Brown Boveri & Co. Ltd., Zurich, Switzerland).

Fusion Technology 1982. Proceedings of the Twelfth Symposium, Julich, Germany, 13-17 Sept. 1982 (Oxford, England: Pergamon 1983), p.1127-32 vol.2

The insulation of both JET and TFTR inner poloidal coils is based on the Oriltherm resin system. JET and TFTR have a comparable test voltage level. Nevertheless, insulation thickness and build-up are different. Results of electrical sample testing of the two insulations are presented. Some special design features of JET and TFTR coils are shown in various manufacturing steps. The presentation of the coil stack assembly procedure of JET and TFTR reflects the two concepts of the toroidal coil load bracing. (3 refs.)

60443 Manufacture and test of the TEXTOR BT-coils. U.Schwarz (Inst. fur Plasmaphys., KFA, Julich GmbH, Germany), P.J.Ferry.

Fusion Technology 1982. Proceedings of the Twelfth Symposium, Julich, Germany, 13-17 Sept. 1982 (Oxford, England: Pergamon 1983), p.1133-8 vol.2

The TEXTOR TF-magnet consists of 16 circular coils. Each coil consists of two essential parts—the copper winding and the amagnetic steel frame. The paper describes the manufacturing of these different pieces and the tests applied on quality assurance. (4 refs.)

60444 Finite-element stress analysis and its impact on the design of the Swiss LCT coil. A.Segessenmann, Th.Hilpert, J.C.Rauch, R.K.Maix (BBC Brown Boveri & Co., Zurich, Switzerland).

Fusion Technology 1982. Proceedings of the Twelfth Symposium, Julich, Germany, 13-17 Sept. 1982 (Oxford, England: Pergamon 1983), p.1139-44 vol.2

The design of the Swiss LCT coil is based on a cabled and soldered forced-flow cooled conductor, out of which the coil is wound in 11 double pancakes and impregnated with epoxy resin. The coil is embedded in a stainless steel case, the subassemblies of which are bolted together. In order to prove this concept a three-dimensional finite-element analysis was carried out to obtain stress distributions in the coil and the case. Based on this, two-dimensional detailed calculations were made for highly stressed areas of the coil and the case. The impact of these investigations on the design is shown. (6 refs.)

60445 The toroidal field coil support structure for the Culham MKIIC Tokamak reactor. W.R. Spears (Culham Lab., UKAEA, Abingdon, England), S.F. Calvert, D.H. Prothero.

Fusion Technology 1982. Proceedings of the Twelfth Symposium, Julich, Germany, 13-17 Sept. 1982 (Oxford, England: Pergamon 1983), p.1145-50 vol.2

Describes the first stage of a study into the design of a support structure for the toroidal magnetic field coil system of the Culham MKIIC Tokamak Reactor. A structure is developed which will permit blanket removal and maintenance without breaking the toroidal field coil cryostat. The study includes consideration of fault conditions and the significance of cyclic stresses, and indicates problem areas which are now being considered in greater detail. (8 refs.)

60446 Electrical insulation system fit for cyclic high strain (development of insulation of JT-60 poloidal field coil). T. Watanabe, H. Kamiya, F. Aki (Hitachi Works, Hitachi Ltd., Ibaraki-ken, Japan), M. Nagai, K. Kadotani, M. Ohkubo, T. Ando, M. Masuda.

Fusion Technology 1982. Proceedings of the Twelfth Symposium, Julich, Germany, 13-17 Sept. 1982 (Oxford, England: Pergamon 1983), p.1151-6 vol.2

For cyclic high strain requirement of JT-60 poloidal field coil the authors have developed a new insulation system. They have manufactured some bar coil specimens whose cross section size is the same as the JT-60 PFC. They have loaded these specimens with 4 points bending moment, and confirmed that the new insulation system is fit for a cyclic strain of $0.27\% \sim 5 \times 10^4$ cycles. (4 refs.)

60447 Design-relevant local mechanical effects under fault conditions of the European LCT coil. H. Zehlein, G. Messemer (KFA Karlsruhe GmbH, Karlsruhe, Germany).

Fusion Technology 1982. Proceedings of the Twelfth Symposium, Julich, Germany, 13-17 Sept. 1982 (Oxford, England: Pergamon 1983), p.1157-62 vol.2

The paper presents simplified descriptions of two types of local mechanical effects: support load diffusion effects under asymmetric loading due to a faulty neighbouring coil and containment of quench pressure inside a faulty superconductor cable within the winding pack. The design-relevance in terms of model simplification as well as safety margins is discussed for the European LCT coil. (8 refs.)

60448 The TORE SUPRA poloidal field system. M.d'Alencón, B. Barety, H. Cortial, C. Leloup, G. Rey, E. Rijnoudt, G. Schenk, B. Taquet (Dept. de Recherches sur la Fusion Contrôlée, CEN, Fontenay-Aux-Roses, France).

Fusion Technology 1982. Proceedings of the Twelfth Symposium, Julich, Germany, 13-17 Sept. 1982 (Oxford, England: Pergamon 1983), p.1165-71 vol.2

The aims of the TORE SUPRA poloidal field system are to induce, provide equilibrium for and maintain during half a minute, a plasma current of 1.7 MA with poloidal β values up to 3.5. The main objects of the TORE SUPRA Poloidal field system are: a saturated iron core transformer—a single poloidal field coil system, all coils located outside the toroidal field coils, connected in parallel with differential voltage control—the use of a 1.1 GVA thyristor DC breaker—a direct supply from the 400 kV network. (4 refs.)

60449 Efficiency of passive circuits for vertical stability in INTOR reactor. S. Bobbio, E. Coccorese, G. Fabricatore, R. Martone, G. Rubinacci (Inst. di Elettr., Univ. di Napoli, Napoli, Italy).

Fusion Technology 1982. Proceedings of the Twelfth Symposium, Julich, Germany, 13-17 Sept. 1982 (Oxford, England: Pergamon 1983), p.1173-8 vol.2

Passive stabilization, usually performed by the vacuum vessel, is scarcely effective in INTOR because of its distance from the plasma. Therefore a stabilization system made of a set of split conductors vertically connected at the ends of each blanket module is studied. This work aims to develop calculation tools, able to optimize the design of the stabilizing passive conductors (SPC) and to carry out a sensitivity analysis with respect to their main parameters. A new circuit form of the energy principle is used for the position optimization (model NRD) and a modal-analysis technique for the evaluation of the growth rate (model PCRD). The possibility of putting conductors either on the first wall or between blanket and shield is studied: optimal position and information on the dimensions of the conductors are shown. (7 refs.)

60450 Measurement and dynamic control of plasma position in TEXTOR Tokamak. W.A. Broeke, G. Waidmann (Zentrallab. für Elektronik, KFA Jülich GmbH, Jülich, Germany).

Fusion Technology 1982. Proceedings of the Twelfth Symposium, Julich, Germany, 13-17 Sept. 1982 (Oxford, England: Pergamon 1983), p.1179-84 vol.2

A control system for TEXTOR Tokamak has been designed using a detailed model including important eddy currents in machine components. Plasma displacements and current are controlled by 4 different coil currents. Realistic power supply models were provided. Actual values of controlled variables were evaluated by analogue computation from the tangential and normal component of the poloidal magnetic field. Magnetic sensors for these field components were developed from heat resistant steel cable. The feedback loops were optimized to stabilize the system against recurrent step function disturbances. Classical system design and decoupling allow the loops to be operated one by one. (7 refs.)

60451 The FTU poloidal field system. M. Gasparotto, L. Lovisetto, G.B. Righetti (Centro Ricerche Energia Frascati, EURATOM-ENEA sulla Fusione, Rome, Italy).

Fusion Technology 1982. Proceedings of the Twelfth Symposium, Julich, Germany, 13-17 Sept. 1982 (Oxford, England: Pergamon 1983), p.1215-20 vol.2

The poloidal field system of the FTU machine is subdivided in three sets of windings, transformer (TR), vertical field (VF) and feedback (F) to reach the following objectives: (a) to preprogram the plasma current time dependence using the transformer; (b) to maintain circular plasma in an equilibrium position irrespective of the poloidal β variations, using the VF windings, without affecting the plasma current; (c) to keep the plasma displacements from the equilibrium position within reasonable limits using the feedback windings again without interfering with the plasma current. The decoupling of the different effects is obtained using a decoupling transformer external to the machine. Many of the techniques employed are based on the experience gained on the FT Tokamak. (5 refs.)

60452 Time evolution of the coil currents shaping and centering a D-shaped reactor plasma. A. Nicolai (KFA Jülich GmbH, Jülich, Germany).

Fusion Technology 1982. Proceedings of the Twelfth Symposium, Julich, Germany, 13-17 Sept. 1982 (Oxford, England: Pergamon 1983), p.1221-6 vol.2

The currents in the poloidal field coils surrounding a D-shaped reactor plasma can in a good approximation be computed from the current density in a dense

coil fence, if the coil number is sufficiently high. The current density in the fence is calculated from the equilibrium parameters which emanate from the plasma current, the plasma shape, the pressure and the q-profile. During the ignition phase the coil current at the inner side must be decreased by 30% and the outer side increased by 40% if the temperature during the burn phase is 15 keV. (9 refs.)

60453 A 100 kV, 80 A, 10 sec power supply for neutral beam injector. M. Matsuoaka, O. Higa, M. Kawai, Y. Oguchi, Y. Ohara, T. Ohga, H. Ohtsuki, S. Matsuda, T. Shibata, K. Yoshida (JAERI, Ibaraki, Japan).

Fusion Technology 1982. Proceedings of the Twelfth Symposium, Julich, Germany, 13-17 Sept. 1982 (Oxford, England: Pergamon 1983), p.1361-6 vol.2

Prototype injector unit for JT-60 has been operating since last November. The authors describe the design of power supplies for the ion sources and their operating performances. Most of the efforts have been devoted to the system reliability, in particular, the control system and grounding system. Transient voltage analysis in case of breakdown was made by numerical calculation and was confirmed by the use of pulse generator in an actual set up. (5 refs.)

60454 Compact launching structures for lower hybrid waves. T.K. Nguyen, D. Moreau (Dept. de Recherches sur la Fusion Contrôlée, CEA, Grenoble, France).

Fusion Technology 1982. Proceedings of the Twelfth Symposium, Julich, Germany, 13-17 Sept. 1982 (Oxford, England: Pergamon 1983), p.1381-6 vol.2

Compact Lower Hybrid launching structures are described using a waveguide array in tandem with an E plane junction, phase shifters or passive waveguides. It can be shown that coupling between the waveguide apertures and the E junction plane does not perturb the N_1 wavenumber spectrum (parallel to the toroidal magnetic field) required for the slow wave penetration into the plasma provided that the electric length between these discontinuities is sufficient for the evanescence of upper parasitic modes. Numerical results are given for the alternate active and passive waveguide array first proposed by Motley and Hooke and for a new compact heating and current drive LH antenna. (6 refs.)

60455 Improved performance of the ASDEX neutral beam injectors. O. Vollmer, D. Cooper, J.H. Feist, R.C. Kunze, H. Lohner, W. Melkus, E. Speth, A. Stabler (Max-Planck-Inst. für Plasmaphys., Garching, Germany), Z.Yu.

Fusion Technology 1982. Proceedings of the Twelfth Symposium, Julich, Germany, 13-17 Sept. 1982 (Oxford, England: Pergamon 1983), p.1387-91 vol.2

In January 1982 the second beamline of the ASDEX neutral beam injection system was commissioned. Within a few weeks of operation the design value of 2.5 MW total neutral beam power into the torus was obtained with sufficient reliability. Already during the experimental period lasting to the end of July, the injected power could be increased up to about 3.3 MW, mostly based on improvements of the power supplies. A further improvement could be achieved by additional gas feed to the neutralizers. To eliminate the effects of the ASDEX magnetic stray field on the ion sources, a compensation system has been tested. Finally first experiments with respect to an increased power or pulse length of the ion sources are reported. (3 refs.)

60456 Design of a 3 MW ICRH system for ASDEX and W VII. F. Braun, R. Fritsch, F. Hofmeister, E. van Mark, S. Puri, M. Soll, F. Wesner, H. Wedler (Max-Planck-Inst. für Plasmaphys., Garching, Germany).

Fusion Technology 1982. Proceedings of the Twelfth Symposium, Julich, Germany, 13-17 Sept. 1982 (Oxford, England: Pergamon 1983), p.1393-8 vol.2

Additional RF heating in the ion cyclotron range of frequencies is planned to be applied to the ASDEX Tokamak and to the W VII-A and AS stellarators. To meet the physics requirements of these experiments, an RF power of 3 MW for 10 s is necessary at frequencies between 30 and 115 MHz. This power will be produced by one common generator system and transported to the experiments by long coaxial transmission lines. The ICRH system is described including the antenna design for ASDEX and W VII-A, the RF generator, the transmission lines and the tuning systems. Based on antenna calculations and model measurements the layout of the antennas and of the tuning systems has been optimized in order to reduce the electrical stress at critical points and to provide a maximum of radiated power within given geometrical limitations. (4 refs.)

60457 An integrated system for data acquisition, archiving and analysis in ETA-BETA II. G. Flor, N. Guarino (CNR, Univ. di Padova, Padova, Italy).

Fusion Technology 1982. Proceedings of the Twelfth Symposium, Julich, Germany, 13-17 Sept. 1982 (Oxford, England: Pergamon 1983), p.1405-9 vol.2

Describes the conceptual design of a new system, built around the functional blocks of data acquisition and archiving. Various kinds of data are recognized, on which specific functions are to be performed: shot setting parameters, shot attributes, raw data, intermediate results and also software module names. In order to adequately describe an intrinsically dynamic experiment the concept of experiment model is introduced, with a hierarchical structure reflecting logical and physical relationships. The interactions between blocks and with the environment are standardized by the definition of interface data structures. An integrated archiving system for raw data, intermediate results and related computing procedures is described, whose main goal is to simplify and standardize data access and analysis. (13 refs.)

60458 Computer control and data acquisition for neutral beam injectors. A.S. Glad (General Atomic Co., San Diego, CA, USA).

Fusion Technology 1982. Proceedings of the Twelfth Symposium, Julich, Germany, 13-17 Sept. 1982 (Oxford, England: Pergamon 1983), p.1411-19 vol.2

Computer support of General Atomic's Doublet III neutral beam injectors provides: the capability of acquiring, processing and displaying all beam physics data. The real time periodic monitoring and control of all neutral beam subsystems. The sequencing of multiple ion sources asynchronously from the same computer system. The permanent archiving of all beam physics and diagnostic data. (5 refs.)

60459 Monitoring and control of the TEXTOR grounding system. P. Huttemann, F. Schöngen, U. Schwarz (Inst. für Plasmaphys., KFA, Jülich GmbH, Jülich, Germany).

Fusion Technology 1982. Proceedings of the Twelfth Symposium, Julich, Germany, 13-17 Sept. 1982 (Oxford, England: Pergamon 1983), p.1421-6 vol.2

The grounding system of the Tokamak experiment TEXTOR consists of 5 single parts. A main part is the load ground (BE). All major parts of the Tokamak itself are connected to BE via suitable ohmic resistances. Thus load potentials against ground are kept low and fault currents are limited. During commissioning of the Tokamak frequent, careful and complete checks of BE turned out to be important for a troublefree operation of the Tokamak. The

paper describes the additional equipment for monitoring the components of the load ground BE. (1 ref.)

60460 Computer control system development for large fusion experiments. M.J.Kear, D.Richardson, E.G.Murphy, T.Jackson, K.Colyer (Culham Lab., UKAEA, Abingdon, England). Fusion Technology 1982. Proceedings of the Twelfth Symposium, Julich, Germany, 13-17 Sept. 1982 (Oxford, England: Pergamon 1983), p.1431-6 vol.2

The design of computer based control systems for large fusion experiments requires a structured approach. This involves identifying the requirements and documenting the functional specification before the detailed design can be started. The authors discuss the procedures that were adopted in the early design stages of such a computer based control system and the way in which the detailed design evolved. Areas requiring particular attention such as the operator interface and inter-computer communication are discussed in detail. The design approach adopted is based on experience gained from designing, building, commissioning and successfully operating a prototype, distributed intelligence computer-control system. During this phase a great deal of experience was gained for future software handling techniques applicable to large experiments. The system is currently operating reliably and is to be submitted for safety approval in the near future. (5 refs.)

60461 System design of ZENKEI, the central control system of JT-60. I.Kondo, T.Kimura, N.Hosogane, T.Kawasaki, T.Kobayashi, R.Yoshino, K.Kurihara, Y.Suzuki, T.Nakayama, K.Moriyama (JAERI, Tokai, Japan). Fusion Technology 1982. Proceedings of the Twelfth Symposium, Julich, Germany, 13-17 Sept. 1982 (Oxford, England: Pergamon 1983), p.1437-42 vol.2

ZENKEI, the central control system of JT-60 is in the final design stage. The authors have been extending the system to make it possible to control the plasma parameters such as density and temperature. This paper gives a brief description of the most recent design, especially those of the modification of the discharge control system. An additional computer and dual port memory with D-port were adopted. For event-oriented control of plasma discharges, the timing system was improved. (1 ref.)

60462 The TEXTOR diagnostic data acquisition system development status and first experience. M.Korten (Inst. fuer Plasmaphys., KFA Julich GmbH, Julich, Germany). Fusion Technology 1982. Proceedings of the Twelfth Symposium, Julich, Germany, 13-17 Sept. 1982 (Oxford, England: Pergamon 1983), p.1443-7 vol.2

A computerized data acquisition system for the Tokamak experiment TEXTOR is under implementation and has been tested in the first experimental phase. The computer system consists of a VAX 11/780 processor as interface to the experimentalists and a PDP 11/44 as front-end computer interfaced to the diagnostic subsystems for TEXTOR. Connection between the data acquisition system and the various diagnostic subsystems is done by CAMAC instrumentation. The software system has been developed from the DIOS/GALE systems adopted from the IPP Garching, modified to enable decentralized operation of the participants. (7 refs.)

60463 Structure of the main control system for the FTU device. L.Panaccone (Centro Ricerche Energia Frascati, Rome, Italy). Fusion Technology 1982. Proceedings of the Twelfth Symposium, Julich, Germany, 13-17 Sept. 1982 (Oxford, England: Pergamon 1983), p.1449-54 vol.2

The computer based control system for FTU (Fascati Tokamak Upgrade) machine is a distributed intelligence control system consisting of various subsystems, called 'specific units'. A specific unit can work as a stand-alone small system or as a part of more complex systems, together with other units, in any possible combination. In the case of combined units working mode, a dedicated specific unit performs supervisory functions. Communication between specific units is done on a dedicated bus-like network, in the form of temporary master-slave relationship. There are three groups of specific units: Plant Control Units, Supervisory Control Unit and Synoptic Handling Unit. Performances and structures of these specific units are described. In addition, a very simple hard-wired safety system works in parallel with the computer based control system, in order to save personnel and apparatus. (no refs.)

60464 Control and data acquisition system for the RF heating plant of the FT Tokamak. M.Panella (Centro Ricerche Energia Frascati, Rome, Italy). Fusion Technology 1982. Proceedings of the Twelfth Symposium, Julich, Germany, 13-17 Sept. 1982 (Oxford, England: Pergamon 1983), p.1455-9 vol.2

The control and data acquisition system of the additional RF heating plant has been implemented by means of two intelligent CAMAC crates. The crate controllers are based on the LSI11 Digital microcomputer in a stand-alone configuration. The system hardware consists both of standard CAMAC modules and 'ad hoc' constructed modules. Several operating phases are described and interesting parameters and characteristics of the system are briefly mentioned. (1 ref.)

60465 The data acquisition system for ASDEX. D.Zimmermann, N.Ruhs, H.Hohenocker (Max-Planck-Inst. fur Plasmaphys., Garching, Germany). Fusion Technology 1982. Proceedings of the Twelfth Symposium, Julich, Germany, 13-17 Sept. 1982 (Oxford, England: Pergamon 1983), p.1461-6 vol.2

The ASDEX Data Acquisition System is built as a distributed system to collect a large number of data from many diagnostics. The data acquisition system software GALE is adaptable to different experiments, flexible with respect to hardware configuration changes and simple to use for the experimentalist. A distributed system and a flexible acquisition software is the adequate response to fast growing demands for computer power of fusion experiments. (5 refs.)

60466 Experience with software-driven control and acquisition system. A.Simik (Ecole Polytech. Federale de Lausanne, Lausanne, Switzerland). Fusion Technology 1982. Proceedings of the Twelfth Symposium, Julich, Germany, 13-17 Sept. 1982 (Oxford, England: Pergamon 1983), p.1467-71 vol.2

The design of the TCA Tokamak control and data acquisition system was reported at the 11th SOFT Conference (1980). The major part of the apparatus was complete in 1980. During 1981 and 1982 the experiment has been continuously operated and the author has implemented some more units. The use of software-controlled devices instead of hard-wired units substantially simplified the construction and also considerably reduced the cost of the hardware. (10 refs.)

60467 The control and data acquisition system of SPICA II. C.A.J.van der Geer, W.Kooijman, A.A.M.Oomens, P.H.M.Smeets, F.T.M.Koenen, A.J.Putter, H.J.F.van Ramele (FOM-Inst. voor Plasmafysica, Nieuwegein, Netherlands). Fusion Technology 1982. Proceedings of the Twelfth Symposium, Julich, Germany, 13-17 Sept. 1982 (Oxford, England: Pergamon 1983), p.1473-9 vol.2

Describes the control and data acquisition system of SPICA II. Some recently developed hardware components are presented in detail. (4 refs.)

60468 PCM recorder for raw diagnostic data storage (Data Processing System for the JT-60). R.Toyokawa (JAERI, Ibaraki, Japan), A.Ogata, M.Shiho, H.Maeda, T.Kambe, S.Tahira, T.Kumahara, K.Tamamura, A.Fujioka, M.Fujita, O.Maeda, O.Mochizuki, N.Tahara. Fusion Technology 1982. Proceedings of the Twelfth Symposium, Julich, Germany, 13-17 Sept. 1982 (Oxford, England: Pergamon 1983), p.1481-6 vol.2

Studies in physics, especially those concerning unstable phenomena, require very frequent simultaneous samplings from many data channels related to various diagnostic devices. Moreover, it is often necessary to compare current data with previous data. Neither CAMAC memory modules nor computer peripherals fulfil these requirements. To cope with this problem, the large Tokamak JT-60 is equipped with PCM recorders, which serve as a mass data recording subsystem in the data processing system. This subsystem consists of diagnostic data formatting and transfer sections, PCM recorders, and a data base system based on an intershot processor. (6 refs.)

60469 A high speed transient recorder for fusion research applications. D.L.Trotman, P.R.Rhodes (Culham Lab., UKAEA, Abingdon, England), N.L.Bragg. Fusion Technology 1982. Proceedings of the Twelfth Symposium, Julich, Germany, 13-17 Sept. 1982 (Oxford, England: Pergamon 1983), p.1487-92 vol.2

Use of digital computers for the analysis of data from diagnostics of fusion experiments has resulted in a wide range of digital data recording systems of varying accuracies and speeds. The system described is capable of use in a wide range of applications, being able to convert samples of analogue signals into 10 bit digital codes at a minimum interval between samples of 100 ns. The relative timing between samples may be defined in a versatile sequence generator to be between 100 ns and approximately 30 years. Storage has been provided for a minimum of 4K samples, this number being extendable to a maximum of 64K samples. The transient recorder is formed by a series of CAMAC modules, permitting the extensive computer control of the recorder. Details of the system performance are also included. (2 refs.)

60470 Designing and development of the real-time control system for JT-60 plasma discharge. R.Yoshino, T.Kimura, N.Hosogane, K.Kurihara, I.Yonekawa, I.Kondo, Y.Suzuki (Tokai Res. Establ., JAERI, Ibaraki, Japan). Fusion Technology 1982. Proceedings of the Twelfth Symposium, Julich, Germany, 13-17 Sept. 1982 (Oxford, England: Pergamon 1983), p.1493-8 vol.2

Real-time plasma control is planned to be executed in JT-60 experiments. The object of which is to obtain the Q=1 plasma, protecting the JT-60 machine from the electromagnetic force, heat load, etc. The authors present the design of this control system. (1 ref.)

60471 D₂ pellet acceleration with a centrifuge. W.Amenda, R.S.Lang (Max-Planck-Inst. fur Plasmaphys., Garching, Germany). Fusion Technology 1982. Proceedings of the Twelfth Symposium, Julich, Germany, 13-17 Sept. 1982 (Oxford, England: Pergamon 1983), p.1501-5 vol.2

A promising candidate for quasi-continuous pellet injection is pellet acceleration with a centrifuge. The development of this mechanical acceleration method was first begun at ORNL and later at IPP Garching. This acceleration technique uses a guiding structure like a tube or a groove on a rotating disc or arm. With the exit tangential to the rotation circle the velocity of the accelerated pellet (neglecting friction) should be twice the peripheral speed of the centrifugal rotor. At IPP two possible techniques for feeding solid deuterium pellets into the entrance of the rotating guiding structure are envisaged. One is to cut a pellet from a prefabricated deuterium filament and throw it with high precision in time and position into the region of acceptance of the accelerating channel. The other is to insert the prefabricated deuterium filament directly during a rotation with a length required for the pellet and then let the pellet be cut by the entrance of the acceleration tube. At a convenient frequency of the centrifuge of up to 500 Hz and a maximum pellet length of 4 mm this calls for an insertion velocity of up to 2 m s⁻¹. This is a specification of the solid deuterium supply which cannot easily be accomplished. (8 refs.)

60472 Launching of D₂-pellets through guide tubes. K.Buchl, W.Sandmann (Max-Planck-Inst. fur Plasmaphys., Garching, Germany). Fusion Technology 1982. Proceedings of the Twelfth Symposium, Julich, Germany, 13-17 Sept. 1982 (Oxford, England: Pergamon 1983), p.1507-11 vol.2

Cylindrical D₂-pellets of different sizes (diameter and length respectively 0.6, 1.5 and 2.5 mm) were launched with velocities of 400 to 1000 m/s through straight and curved guide tubes at room temperature up to a length of 12 m. Velocity losses of 12%, mass losses of 10 to 30% and divergence angles of the pellet trajectory up to 2° were measured depending on tube diameter and length. No difference could be observed for straight and curved guide tubes of curvature radius larger than 1 m. (2 refs.)

60473 Pellet fuelling development at Oak Ridge National Laboratory. C.A.Foster, S.L.Milora, D.D.Schuresko, S.K.Combs, R.V.Lunsford (Oak Ridge, Nat. Lab., Oak Ridge, TN, USA). Fusion Technology 1982. Proceedings of the Twelfth Symposium, Julich, Germany, 13-17 Sept. 1982 (Oxford, England: Pergamon 1983), p.1513-18 vol.2

A pellet injector development program has been under way at the Oak Ridge National Laboratory (ORNL) since 1976 with the goals of developing D₂, T₂ pellet fuel injectors capable of reliable repetitive fuelling of reactors and of continued experimentation on contemporary plasma devices. The development has focused primarily on two types of injectors that show promise. One of these injectors is the centrifuge-type injector, which accelerates pellets in a high speed rotating track. The other is the gas or pneumatic gun, which accelerates pellets in a gun barrel using compressed helium or H₂ gas. (13 refs.)

60474 On the injection of deuterium pellets. H.Sorensen, P.Andersen, S.A.Andersen, V.Andersen, P.B.Jensen, H.E.Skovgard Jensen, A.Nordkov Nielsen, B.Sass, K.-V.Weisberg (Riso Nat. Lab., Roskilde, Denmark). Fusion Technology 1982. Proceedings of the Twelfth Symposium, Julich, Germany, 13-17 Sept. 1982 (Oxford, England: Pergamon 1983), p.1519-23 vol.2

Two pellet injector systems are described. One is used for injecting small D₂ pellets (5.10¹⁷ molecules and 150 m/s) into a small Tokamak, Dante, and one

is planned for injecting larger D_2 pellets (8.10^{18} molecules and 650 m/s) into the TFR Tokamak at CEN, Fontenay-aux-Roses, Paris. (5 refs.)

- Nuclear and materials studies with ion beams See Entry 60232
 Recovery of hydrogen isotopes using a uranium bed See Entry 60334
 The cyclotron facility for radiation damage experiments at the JRC-ISPRA See Entry 60498
 Pulsed ion source of B_2 -diode type with cryogenic anode See Entry 60526
 The Julich ion source design and related thermo-mechanical pre-testing See Entry 60527
 Development of an ion source for long-pulse (30-s) neutral beam injection See Entry 60528
 A proposed method of hydrogen isotope separation using palladium alloy membranes See Entry 61009
 Particle orbits and stochasticity See Entry 61605
 Recent results obtained by use of accelerators on plasma edge properties in controlled fusion devices and on properties of high power neutral beams See Entry 61658
 Sputtering of titanium and niobium hydrides See Entry 61660
 Vaporization mode and state of the ablatant of a deuterium pellet in Tokamak discharges See Entry 61668
 Towards upper bound levels: thermonuclear fusion See Entry 61670
 The computational model for the control of plasma position in TEXTOR See Entry 61686
 Equilibrium and stability of plasma motion in an iron-core Tokamak See Entry 61687
 Experience with feedback and feedforward for plasma control in ASDEX See Entry 61688
 Applicability verification of Tokamak plasma equilibrium control models See Entry 61689
 Magnetic fusion energy and computers See Entry 61695
 Experiments in Belfast relevant to fusion diagnostics See Entry 61699
 Applications of recent measurements of low energy charged particles induced nuclear reactions on light nuclei See Entry 61700
 Experience of T-7 operation in plasma experiments See Entry 61708
 Control system of plasma position and current in a Tokamak with strong magnetic field See Entry 61709
 Plasma parameter control experiments on 'Tuman-3' See Entry 61710
 T-15 poloidal field control system See Entry 61711
 Low temperature neutron and gamma irradiation of glass fiber reinforced epoxies See Entry 61980
 An investigation into the potential importance of helium trapping during the nucleation of radiation-induced voids See Entry 61985
 Precipitation and void-swelling in nickel-manganese austenitic stainless steels See Entry 61986
 Effects of impurities on hydrogen permeability through palladium alloy membranes at comparatively high pressures and temperatures See Entry 62164
 Methane formation during deuteron bombardment of carbon in the energy range of 100 to 1500 eV See Entry 63575

28.58 INTEGRATED REACTOR SYSTEMS

- Canadian accelerator breeder system development See Entry 60330

28.70 NUCLEAR EXPLOSIONS

(see also 47.40 Shock and detonation phenomena)

- Reevaluations of Dosimetric Factors, Hiroshima and Nagasaki. Proceedings of a Symposium See Entry 59542
 The road to Los Alamos See Entry 59578

28.80 RADIATION TECHNOLOGY, INCLUDING SHIELDING

(see also 87.60 Medical and biomedical uses of fields, radiations and radioactivity)

- 60475 A low energy X-ray fluorescence method for high dose measurements on double emulsion photographic films. J.Swahn, G.Roubaud, J.W.N.Tuyn (Health & Safety Dept., CERN, Geneva, Switzerland). *Radiat. Prot. Dosim. (GB)*, vol.3, no.4, p.219-21 (1982).
 The exposures of Kodak Personal Monitoring Type 2 films were evaluated using X-ray fluorescence of the low-energy silver $L\alpha$ X-rays excited by a ^{109}Cd source. This method allows the separate reading of both the fast and the slow emulsion without the need to strip the films. Exposures of up to 250 rad of γ -radiation can be evaluated. The method is useful in evaluating accidental exposures. (5 refs.)
 60476 A simple modification to improve the energy dependence of ion chamber survey meters. A.Kannan, V.W.Naik, P.N.M.R.Vijayam (Radiological Standards Lab., Bhabha Atomic Res. Centre, Bombay, India). *Radiat. Prot. Dosim. (GB)*, vol.3, no.4, p.223-5 (1982).
 The use of high Z materials like phosphor bronze to ensure good electrical contacts inside the ionisation chambers of some survey meters increases their energy dependence at photon energies below 600 keV. A simple modification to reduce such enhanced energy dependence is described. (3 refs.)
 60477 Influence of light transmission on the response of LiF thermoluminescence detectors to thermal neutrons. M.Buxerolle (Nuclear Res. Centre, Cadarache, Saint-Paul-lez-Durance, France), F.Spurny. *Radiat. Prot. Dosim. (GB)*, vol.3, no.4, p.233-5 (1982).
 The influence of light transmission on the response of opaque LiF thermoluminescence detectors to thermal neutrons has been studied. It was found that this can be significant. TL signals read from the surface of ^6LiF detectors irradiated in a directional beam of thermal neutrons differ by up to 80%. A quantitative parameter characterising this effect using one-side alpha particle irradiation has been established. The parameter allowed the influence of opacity on TL reading after thermal neutron irradiation to be calculated. Good agreement was found between calculated and experimental results. Some implications of the effect studied on thermal neutron detection with LiF are discussed. (4 refs.)

- 60478 A polystyrene-water calorimeter. S.R.Domen (Center for Radiation Res., NBS, Washington, DC, USA). *Int. J. Appl. Radiat. & Isot. (GB)*, vol.34, no.3, p.643-4 (March 1983).
 A new type of calorimeter consisting of polystyrene discs in water is described for the measurement of absorbed dose in polystyrene, which is reported (for some irradiation conditions) to have a heat defect of $<1\%$. This calorimeter provides another investigative tool for comparison with absorbed dose measurements in water, which is the standard reference material. Measurements using ^{60}Co γ -radiation showed that converting the results to water agreed within 1% with similarly determined results when using a graphite calorimeter. These results are $\sim 3\%$ lower than those determined with a water calorimeter, suggesting a negative heat defect in water $\sim 3\%$ —when measuring an absorbed dose rate ~ 1 Gy/min that produced an accumulated dose up to 150 Gy. (9 refs.)
 60479 A high-purity inert atmosphere cell suite for research purposes—design and operating experience. J.T.Demant (AERE, Harwell, England). *Nucl. Energy (GB)*, vol.22, no.2, p.95-9 (April 1983).
 A small specialized hot-cell suite has been developed for the handling, examination and storage of irradiated nuclear fuel samples containing alkali metal and other oxygen- and moisture-sensitive materials. High atmospheric integrity is the prime consideration and the facility achieves a nitrogen atmosphere with oxygen and moisture levels each below 50 vpm. Provided certain precautions are taken, metallographic mounting, preparation, microscope examination and sample transfer to remote analytical instruments can be carried out under adequate α -containment and $\beta\gamma$ -shielding without significant decomposition of the materials of interest. (no refs.)
 60480 Measurement of iodine-129 at the femtogram level by negative surface ionization mass spectrometry. J.J.Stoffels (Pacific Northwest Lab., Richland, WA, USA). *Radiochem. & Radioanal. Lett. (Switzerland)*, vol.55, no.2, p.99-105 (23 Dec. 1982).
 A mass spectrometer method is developed for measurement of environmental iodine-129. Negative surface ionization of iodine on a lanthanum hexaboride-coated rhenium filament is used to produce I^- ions with higher efficiency. A three-stage mass spectrometer provides high abundance sensitivity for measurement of the large $^{127}\text{I}/^{129}\text{I}$ isotope ratios encountered in environmental samples. The ability to measure 10^7 atoms (2×10^{-13} g) of iodine-129 in a pure sample of sodium iodide which has a $^{127}\text{I}/^{129}\text{I}$ isotope ratio of 0.5×10^8 has been demonstrated. (12 refs.)
 Plutonium recycling scenario in light water reactors. Assessment of the environmental impact in the European Community See Entry 59523
 The importance of near-field phenomena for nuclide release from a flooded salt dome repository See Entry 60297
 Filter for the selective removal of tritium from the coolant gas of a high temperature nuclear reactor See Entry 60335
 Postaccident decontamination of reactor primary systems and test loops See Entry 60360
 Air cleaning devices for vented filtered LMFR containment See Entry 60380
 Saturation curves of parallel-plate ionization chambers See Entry 60545
 Biological effects of neutron radiation and their implications for the nuclear power industry See Entry 63890
 Calculation of low-energy neutron dose indices and depth doses in the ICRU tissue sphere See Entry 63982
 Classification of radionuclides See Entry 63984

28.90 OTHER TOPICS IN NUCLEAR ENGINEERING AND NUCLEAR POWER STUDIES

- Postaccident decontamination of reactor primary systems and test loops See Entry 60360
 Assessment of chemical processes for the postaccident decontamination of reactor coolant systems See Entry 60365

29.00 EXPERIMENTAL METHODS AND INSTRUMENTATION FOR ELEMENTARY-PARTICLE AND NUCLEAR PHYSICS

29.15 ELECTROSTATIC AND LINEAR PARTICLE ACCELERATORS

- 60481 Superconducting linear accelerators for heavy ions. P.Paul, G.D.Sproule. *Comments Nucl. & Part. Phys. (GB)*, vol.11, no.5, p.217-29 (1983).
 A survey is given on recent advances in the application of RF superconductivity to heavy ion linear accelerators. Specific aspects of the ATLAS project at Argonne National Laboratory and the superconducting LINAC at Stony Brook are discussed as examples. (10 refs.)
 60482 High-speed, high-voltage pulse generator [electron accelerator application]. Yu.A.Kotov, V.P.Kuznetsov (Tomsk Polytech. Inst., Tomsk, USSR). *Instrum. & Exp. Tech. (USA)*, vol.25, no.4, pt.1, p.889-92 (July-Aug. 1982).
 Translation of: *Prib. & Tekh. Eksp. (USSR)*, vol.25, no.4, p.101-3 (July-Aug. 1982). [received: April 1983]
 A six-stage pulse generator for triggering an oil trigatron in an electron acceleration was developed. The generator features the following parameters: capacitance at moment of discharge, 1 nF; voltage amplitude, 180 kV; voltage rise time 6 nsec. The dischargers of the second and third stages are triggered by a pulse formed by the discharge of an additional capacitor across the first discharger. This permits shortening the response time of the generator to 30 ± 2 nsec. (5 refs.)
 60483 Observations of ion acceleration by a relativistic electron beam. G.S.Kerslick, A.K.L.Dymoke-Bradshaw, A.E.Dangor (Blackett Lab., Imperial Coll. of Sci. & Technol., London, England). *J. Phys. D (GB)*, vol.16, no.4, p.613-19 (14 April 1983).
 Experimental evidence is presented for the collective acceleration of ions by a 350 keV, 50 kA, 100 ns electron beam. Accelerated ions are observed for

vacuum injection, and at hydrogen fill-pressures below 50 m Torr. Measurements with different anode foils indicate that thicker foils reduce the number of ions accelerated. An applied magnetic field is found to increase the energy spread of the ions while leaving the total number accelerated unchanged. The total number of ions accelerated is $\sim 10^{12}$, with peak currents of 7 A. (17 refs.)

60484 Experimental investigation of the process of ion accumulation in electron rings. V.P.Sarantsev, V.D.Inkin, A.A.Mozelev. *Sov. Phys.-Tech. Phys. (USA)*, vol.27, no.9, p.1107-9 (Sept. 1982). Translation of: *Zh. Tekh. Fiz. (USSR)*, vol.52, no.9, p.1806-9 (Sept. 1982). [received: April 1983]

The process of ion accumulation in electron rings has been investigated experimentally. Relations have been found for the dependence of the ion storage on the pressure in the buncher chamber and on the intensity of the electron component of the rings. The experimental relations are in agreement with the calculated relations. (12 refs.)

60485 Theory of the transverse instability of an electron beam. N.I.Aizatskii (Physicotech. Inst., Acad. of Sci., Khar'kov, Ukrainian SSR). *Sov. Phys.-Tech. Phys. (USA)*, vol.27, no.9, p.1113-15 (Sept. 1982). Translation of: *Zh. Tekh. Fiz. (USSR)*, vol.52, no.9, p.1815-19 (Sept. 1982). [received: April 1983]

The author describes the results of theoretical studies of the development of a transverse instability in a single accelerating section, taking account of the dynamics of the interaction of beam particles with a finite number of eigenmodes of the resonator. The dependence of the critical current on the parameters of the section is calculated. It is shown that the calculated characteristics are in good agreement with experimental data. (10 refs.)

60486 Transverse electron motion and emittance development in the injector of an electron linear accelerator. I.N.Mondrus (Physicotech. Inst., Acad. of Sci., Khar'kov, Ukrainian SSR). *Sov. Phys.-Tech. Phys. (USA)*, vol.27, no.9, p.1116-18 (Sept. 1982). Translation of: *Zh. Tekh. Fiz. (USSR)*, vol.52, no.9, p.1820 (Sept. 1982). [received: April 1983]

Approximate asymptotic solutions of the equations of transverse motion in the injector of an electron linear accelerator are obtained for the case of a large, longitudinal, magnetic focusing field. These solutions are used to study the development of the transverse phase volume in injection systems where the cathode is shielded from the magnetic field and where the cathode is located in the magnetic field. (4 refs.)

1982 IEEE Conference on the Application of Accelerators in Research and Industry See Entry 59528

Early history of physics with accelerators See Entry 59569

Three-dimensional profiling with the Sandia nuclear microprobe See Entry 59882

Nuclear and materials studies with ion beams See Entry 60232

MeV light atom beams for heating and/or diagnostics of Tokamak plasmas See Entry 60391

A high-power current pulse generator See Entry 60493

Space-charge conditions in an intense relativistic particle beam See Entry 61064

Repair of the energy slit on an AECL Therac-20 accelerator . See Entry 63950

Comments on 'Radiation leakage from electron applicator assembly on a linear accelerator' [and reply] See Entry 63951

29.20 CYCLIC ACCELERATORS AND STORAGE FACILITIES

(for plasma accelerators, see 52.75)

60487 Linear optics design of the superconducting low- β insertion in the intersecting storage rings at CERN. A.Verdier (CERN, Geneva, Switzerland). *Nucl. Instrum. & Methods Phys. Res. (Netherlands)*, vol.207, no.3, p.301-7 (1 April 1983).

A superconducting insertion has been installed in the ISR at CERN and has made it possible to obtain a luminosity in excess of $10^{32} \text{ cm}^{-2} \text{ s}^{-1}$. The different steps of the optics design of this insertion are described. The method used for the final design is based on the exact calculation of the width of the gradient stopband associated with any focusing perturbation in a circular machine. Some consequences of operating a storage ring with a large gradient stopband are analysed. (15 refs.)

60488 Transverse mode coupling in a bunched beam. K.Satoh, Y.Chin (Nat. Lab. for High Energy Phys., Ibaraki, Japan). *Nucl. Instrum. & Methods Phys. Res. (Netherlands)*, vol.207, no.3, p.309-20 (1 April 1983).

A fast transverse single bunch instability has been observed and has restricted the stored currents in several storage rings, e.g. PEP and PETRA. The paper describes a method, which is the generalization of Sacherer's theory without mode couplings, to analyse the fast transverse instability in a Gaussian bunch. This method includes the radial modes and requires negative azimuthal modes. It makes clear that the fast instability in PEP and PETRA is caused by the mode coupling between the azimuthal modes $m=0$ and $m=-1$, and that its growth rate rises very rapidly above the threshold. The method also predicts that the threshold current could not be improved by a large factor even if the bunch length is increased to several centimeters. The TRISTAN threshold current estimated by scaling from the PEP experimental data is about 3.5 mA per bunch for the worst case. (21 refs.)

60489 The mechanism of integer resonance crossing and the prospects for higher energies in cyclotrons. L.A.Sarkisyan (Inst. of Nuclear Phys., Moscow State Univ., Moscow, USSR). *Nucl. Instrum. & Methods Phys. Res. (Netherlands)*, vol.207, no.3, p.325-9 (1 April 1983).

The problems arising in studying the mechanism of dynamic integer resonance crossing of free radial oscillations Q_r in an isochronous cyclotron are discussed. Numerical simulation of the motion on the basis of complete equations is used to find and study the slow crossing of the most hazardous integer resonance $Q_r=2$ (energy $\sim E_0$) with subsequent acceleration to $\sim 1200 \text{ MeV}$ where $Q_r \approx 2.3$. The results of the calculations for resonance crossing in linear and nonlinear systems are compared; the role of linear and nonlinear effects is demonstrated. The mechanism of integer resonance crossing in the cyclotron is accounted for in the case of slow energy gain per turn. Successful integer resonance crossing permits cyclotron acceleration of protons and ions in the 1-10 GeV/nucleon range. The projects of such cyclotrons have been published in several countries. The prospects for and trends in cyclotron acceleration of particles up to high energies are discussed. (12 refs.)

60490 Bunched beam instability associated with cavity impedance.

H.Nishimura (Dept. of Phys., Univ. of Tokyo, Tokyo, Japan).

Jpn. J. Appl. Phys. Part 1 (Japan), vol.22, no.3, p.518-21 (March 1983).

Investigation is made on the longitudinal single bunch instability of the electron beam in a high energy storage ring. It is shown that the Robinson instability of a parasitic mode is caused by the interaction between a high order synchrotron oscillation and a higher order resonant mode of an RF cavity. Two damping mechanisms, the Landau damping and the radiation damping, are investigated and the stability criteria are obtained. (11 refs.)

60491 The University of Illinois nuclear physics laboratory, 1982. P.Axel, L.S.Cardman, R.A.Daniel, A.O.Hanson, R.A.Hoffswell, R.M.Laszewski, W.C.Selvey, N.Towne, A.M.Vetter (Dept. of Phys., Univ. of Illinois, Urbana, IL, USA).

IEEE Trans. Nucl. Sci. (USA), vol.ns-30, no.2, p.1112-14 (April 1983). (1982 IEEE Conference on the Application of Accelerators in Research and Industry, Denton, TX, USA, 8-10 Nov. 1982).

A six-traversal microtron using a superconducting linac, MUSL-2, provides 100% duty factor electron beams with energies between 2 and 80 MeV. Five major experimental facilities have been developed to exploit the high duty cycle, including both low and high energy bremsstrahlung facilities, two photon tagging systems, and an electron scattering coincidence facility. The properties of the accelerator and the work in progress to improve its performance are outlined. The capabilities of each experimental area are discussed with examples from recent research projects. Finally, the authors' plans to construct a 750 MeV, 100 μA cascade microtron using room-temperature linacs are presented. (27 refs.)

60492 Stabilization of longitudinal instabilities in heavy-ion storage rings.

P.R.Zenkevich, D.G.Koshkarev.

Instrum. & Exp. Tech. (USA), vol.25, no.4, pt.1, p.817-21 (July-Aug. 1982). Translation of: *Prib. & Tekh. Eksp. (USSR)*, vol.25, no.4, p.36-9 (July-Aug. 1982). [received: April 1983]

Considers the instability of longitudinal coherent oscillations in heavy-ion storage rings. It is shown that dissipative coherent instabilities in such rings can be stabilized by selecting a special momentum distribution function of the particles. (5 refs.)

60493 A high-power current pulse generator. V.I.Amelichkin, B.G.Kudasov, Yu.P.Kuropatkin.

Instrum. & Exp. Tech. (USA), vol.25, no.4, pt.1, p.884-6 (July-Aug. 1982). Translation of: *Prib. & Tekh. Eksp. (USSR)*, vol.25, no.4, p.97-8 (July-Aug. 1982). [received: April 1983]

The circuits and operating principles are described, and the fundamental characteristics of the generator for supplying a low-inductance ($\sim 100 \mu\text{H}$) accelerator electro-magnet with sinusoidal current pulses 20 kA in amplitude, $\sim 650 \mu\text{s}$ in length, and with a repetition frequency of 3 Hz are presented. The basic features of the generator are the fact that it employs a solid-state switch and the energy-storage effects. (3 refs.)

60494 Orbital stability of the high-current betatron. G.Barak, N.Rostoker

(Dept. of Phys., Univ. of California, Irvine, CA, USA).

Phys. Fluids (USA), vol.26, no.3, p.856-66 (March 1983).

Orbital stability of the high-current betatron is analyzed. In this modified betatron a toroidal magnetic field is added to the conventional betatron magnetic field. This increases substantially the space charge limit during injection. It gives rise, however, to new problems during acceleration, such as ring stability, Fermi drift, and orbital resonances. A detailed analysis is presented showing that two serious problems may arise: (i) The beam becomes highly unstable when the net focusing force on it becomes zero. The dominant instability in this region is the Fermi drift. This may, however, be utilized in extracting the beam. (ii) Errors in the vertical (betatron) magnetic field result in driven resonances that must be crossed during acceleration. The amplitude growth of the transverse betatron oscillations due to these resonances is negligible up to very high γ (low n resonances). In practice, it may become very difficult to cross the $n=1$ resonance. Thus, extracting the beam again making use of the Fermi drift while $n>1$ is preferable. (16 refs.)

60495 Limiting electron beam current for cyclic induction acceleration in a constant guide field. V.N.Kannikov.

Sov. Phys.-Tech. Phys. (USA), vol.27, no.9, p.1118-22 (Sept. 1982). Translation of: *Zh. Tekh. Fiz. (USSR)*, vol.52, no.9, p.1825-31 (Sept. 1982). [received: April 1983]

Theoretical relations are derived for the limiting beam current in a cyclic induction accelerator (CIA) with a constant guide field. The calculations are in agreement with the available experimental data. It is shown that the limiting average beam current in a CIA is of the order of 100 microamperes, i.e. the level attained in microtrons and linear accelerators. The CIA may find industrial applications. (11 refs.)

60496 Experimental study of stochastic cooling in the NAP-M proton

accelerator. E.N.Dement'ev, N.I.Zinevich, A.S.Medvedko, V.V.Parkhomchuk,

D.V.Pestrikov (Inst. of Nuclear Phys., Acad. of Sci., Novosibirsk, USSR).

Sov. Phys.-Tech. Phys. (USA), vol.27, no.10, p.1225-30 (Oct. 1982). Translation of: *Zh. Tekh. Fiz. (USSR)*, vol.52, no.10, p.1993-2001 (Oct. 1982). [received: April 1983]

Experimental results are reported for stochastic cooling of the energy spread in a proton beam. The behavior of the damping rates is studied as a function of the beam phase density, number of working harmonics, and feedback circuit gain. The steady-state energy spread in the beam was determined by the noise in the electronic equipment. Coherent beam instability was found to be associated with movement of the beam in the pickup electrode. The limitations of the experimental method due to noise from the electronic equipment and collective effects in intense beams are discussed. (8 refs.)

60497 Status of the superconducting cyclotron project in Milan.

E.Acerbi, F.Aghion, F.Alessandria, G.Baccagioni, G.Bellomo, C.Birattari,

J.Camon, C.De Martinis, E.Fabrics, C.Pagani, F.Resmini, L.Rossi, A.Salome,

L.Serafini, G.Varisco, V.Venturini.

Report INFN/TC-82/12, Ist. Naz. Fis. Nucl., Milan, Italy (18 Aug. 1982), 25 pp.

The authors give a comprehensive status report on the Superconducting Cyclotron now under construction at the University of Milan. Since the project was extensively reviewed at the time of the International Conference on Cyclotrons held in Caen in September 1981, the emphasis will be on the progress made since then and on the few design changes which have taken place meanwhile. (11 refs.)

60498 The cyclotron facility for radiation damage experiments at the

JRC-ISPR. G.Riccobono, M.Castiglioni, A.E.Merlini (Joint Res. Centre,

Comm. of the European Communities, Ispra, Italy).

Fusion Technology 1982. Proceedings of the Twelfth Symposium, Julich, Germany, 13-17 Sept. 1982 (Oxford, England: Pergamon 1983), p.815-21

vol.2

The light particles variable energy cyclotron installed at the Physics Division of the JRC, Ispra, accelerates protons and α -particle in the energy range from

9 MeV to 38 MeV, and deuterons from 5 MeV to 18 MeV. The maximum current for protons and deuterons is 65 μ A in the entire energy range and 30 μ A for α -particles. A switching magnet equipped with seven exit ports steers the beam to three radiation cells. The cyclotron was installed to simulate the radiation damage of 14 MeV neutrons in structural materials of interest to fusion reactors. A brief description of the experimental facilities in preparation is given. (5 refs.)

1982 IEEE Conference on the Application of Accelerators in Research and Industry See Entry 59528

Early history of physics with accelerators See Entry 59569

High-speed, high-voltage pulse generator [electron accelerator application] See Entry 60482

The state and prospects in the development of the medical proton tract on the synchrocyclotron in Gatchina See Entry 60499

Bunch length measurements in CESR using an X-ray sensitive photoconducting detector See Entry 60500

Effects of nonresonance harmonics on slow extraction from synchrotrons See Entry 60505

Improved system for energy-dispersive X-ray diffraction with synchrotron radiation See Entry 61731

Analytical description of dose fields from accelerated electrons See Entry 63969

29.25 PARTICLE SOURCES AND TARGETS, PREPARATION AND TECHNOLOGY

(see also 07.77 Particle production and handling; targets)

60499 The state and prospects in the development of the medical proton tract on the synchrocyclotron in Gatchina. D.L.Karlin, B.A.Konov, V.B.Nizkovols, N.K.Abrsimov, A.A.Vorob'ev, A.V.Kulikov, G.A.Ryabov. *Med. Radiol. (USSR)*, vol.28, no.3, p.28-32 (March 1983). In Russian.

The medical proton beam on the synchrocyclotron in Gatchina, modernized in 1980, is characterized by a simplicity of the beam adjustment that amounts to standard operations, the time of adjustment being reduced considerably. The optical scheme ensures a good reproducibility of all the beam parameters from session to session. A large zone of convergence makes it possible to select a necessary irradiation field size with the diameter from 3 to 10 mm. A new medical complex with a 2-room premises for irradiation is envisaged on the basis of a second beam to expand the medical program. The piercing technique of moving field irradiation with proton at an energy of 1 Gy and the utilization of the convergent beam ensure the ratio of the focal dose to the surface dose 200:1. (6 refs.)

60500 Bunch length measurements in CESR using an X-ray sensitive photoconducting detector. E.B.Blum, R.H.Siemann (Lab. of Nuclear Studies, Cornell Univ., Ithaca, NY, USA), D.H.Auston, R.R.Freeman, P.Smith, D.M.Mills. *Nucl. Instrum. & Methods Phys. Res. (Netherlands)*, vol.207, no.3, p.321-4 (1 April 1983).

A novel photoconducting detector has been used for bunch length measurements in CESR. The detector and measurements are described in detail. At 5.17 GeV beam energy no bunch lengthening was observed for beam currents up to 26.0 mA (4.2×10^{11} electrons) in a single bunch. These results agree well with bunch lengthening calculations. (6 refs.)

60501 An energy calibration of the TUNL dual-90° magnet analyzing system. J.F.Wilkerson, T.B.Clegg, E.J.Ludwig (Dept. of Phys. & Astron., Univ. of North Carolina, Chapel Hill, NC, USA).

Nucl. Instrum. & Methods Phys. Res. (Netherlands), vol.207, no.3, p.331-8 (1 April 1983).

An energy calibration of the dual-90° magnet momentum analyzing system has been completed for proton beams spanning the energy range of 1.9 to 14.2 MeV. The absolute calibration points used resulted from measurements of both (p,n) thresholds and narrow (p,p) resonances. The calibration measurements were made during several separate experimental runs over a time period of approximately $11/2$ y. Through careful monitoring of the system parameters and by using consistent magnet recycling procedures, the calibration allows accurate measurements of beam energies to within ± 2 keV. The dual-90° magnet system was determined to have a non-constant energy-to-frequency relationship for low magnetic fields. (14 refs.)

60502 Characteristics of α -transitions in an atomic-beam polarized deuteron source. H.Hasuyama, Y.Kanda (Dept. of Energy Conversion Engng., Kyushu Univ., Kasuga, Japan), A.Katase, Y.Wakuta.

Nucl. Instrum. & Methods Phys. Res. (Netherlands), vol.207, no.3, p.475-85 (1 April 1983).

Quantum mechanical calculations of the degree of polarization after inducing α -transitions in an atomic-beam polarized deuteron source have been done. Four parameters are found to be important for characterizing the performance of RF transitions. These are the strength of the RF oscillating magnetic field, the field gradient of the static magnetic field, the separation efficiency of atomic states and the temperature of atomic gas. It is shown that the degree of polarization can conveniently be evaluated by an 'adiabatic field factor' which is defined by the first two of these four parameters irrespective of the kind of α -transition. Some applications of the present results are also discussed. (17 refs.)

60503 High efficiency ionization of low-density elements in beam-plasma type ion sources. J.Ishikawa, A.Motamed Ekessabi, T.Takagi (Dept. of Electronics, Kyoto Univ., Kyoto, Japan).

Nucl. Instrum. & Methods Phys. Res. (Netherlands), vol.207, no.3, p.487-92 (1 April 1983).

An experimental approach is made to the problems of the gas efficiency of a beam-plasma type ion source under simple and well defined conditions. Two distinct modes of ion source operation, i.e. the 'monoenergetic electron impact ionization' and the 'beam-plasma discharge' are compared with respect to the gas efficiency. The gas efficiency for argon is about 25% under the beam-plasma discharge conditions. The authors also propose a method for high efficiency ionization of low-density elements which can not satisfy the threshold gas pressure conditions for commencement of the discharge, by making use of a ballast gas. Utilization of the ballast gas increases the gas efficiency of the low density elements by about 40 times. Finally, experimental results are given on high efficiency multiply charged ion beam ($Ar^{2+}/Ar^{1+} > 2$) extraction from the ion source when the beam-plasma discharge is initiated in helium. (21 refs.)

60504 Reduction of the neutron-induced background using a pulse-type beam chopper in an ISOL experiment. E.Tanaka (Dept. of Phys., Tohoku Univ., Sendai, Japan), T.Shinozuka, M.Fujioka, Y.Arai, H.Miyatake, M.Yoshii, H.Hama, T.Ishimatsu.

Jpn. J. Appl. Phys. Part 1 (Japan), vol.22, no.3, p.547 (March 1983).

When the nuclear decay of short-lived isotopes is studied with an ISOL (isotope separator on-line), the reduction of backgrounds for β - and γ -ray measurements becomes especially important because of the low yield of activities collected by the isotope separator. Recently, the authors have succeeded in reducing the neutron-induced background with the use of a 'pulse type' beam chopper (hereafter denoted as P-chopper). As an example they measured the decay of ^{59}Zn ($T_{1/2}=182$ ms) produced by the $^{58}Ni(^{4}He,2n)^{59}Zn$ reaction and mass-separated by the Tohoku ISOL facility. In accordance with the timing of the P-chopper, a microcomputer controlled the electrostatic deflection of the mass-separated beam, the motion of collection tape and the data-taking. (3 refs.)

60505 Effects of nonresonance harmonics on slow extraction from synchrotrons. Chen Limin, Fang Shouxian, Huang Nan (Inst. of High Energy Phys., Acad. Sinica, Beijing, China).

Commun. Theor. Phys. (China), vol.2, no.1, p.899-906 (1983).

The average effect of nonresonance harmonics on slow extraction from synchrotrons does not vanish in a long period, and in some cases becomes so important that it cannot be neglected. A method based on the theory of averages is employed to study the problem. The asymmetric shape of the separatrices in the phase-plane of the third-order resonance extraction is explained, and the effect of sextupole fields on the half-integer resonance extraction is analyzed in detail. It is shown that the extraction efficiency would be improved if some sextupoles are introduced properly into the half-integer resonance extraction system. (4 refs.)

60506 An experimental apparatus for low energy high charge heavy ions to study collisions on atomic hydrogen. C.Can, T.J.Gray, J.M.Hall, L.N.Tunnell (Phys. Dept., Kansas State Univ., Manhattan, KS, USA), S.L.Varghese.

IEEE Trans. Nucl. Sci. (USA), vol.ns-30, no.2, p.943-5 (April 1983).

(1982 IEEE Conference on the Application of Accelerators in Research and Industry, Denton, TX, USA, 8-10 Nov. 1982).

The design and performance of a recoil ion source system which includes a recoil ion source, atomic hydrogen thermal oven target and an electrostatic analysis system are discussed. The recoil ion source produces low velocity highly charged ions via collisions between heavy fast pump beams from the EN tandem accelerator and target gases. Time-of-flight techniques provide initial recoil charge state separation. Collisions of the recoils with atomic hydrogen are being studied. The atomic hydrogen is provided by a thermal oven which features long life time operation and low input power requirements. Dissociation fractions of 80% are achieved for 300 watts of input power. A hemispherical electrostatic analyzer allows the final charge states of the recoil ions to be determined thereby allowing the measurement of charge exchange processes for an energy range of 100 eV/q to 5000 eV/q for the incident recoil ions. (13 refs.)

60507 Atomic collision experiments utilizing low-velocity, highly-charged ion beams. B.M.Johnson, K.W.Jones, M.Meron (Brookhaven Nat. Lab., Upton, NY, USA).

IEEE Trans. Nucl. Sci. (USA), vol.ns-30, no.2, p.946-9 (April 1983).

(1982 IEEE Conference on the Application of Accelerators in Research and Industry, Denton, TX, USA, 8-10 Nov. 1982).

Intense beams of highly-stripped ions are now routinely produced at low velocities using the Brookhaven dual MP-tandem in a unique four-stage accel/decel model. This mode of operation combines three stages of acceleration, stripping at high energy, and one stage of deceleration to near-zero velocity. To date, experiments have used 10-100 nA beams of bare and few-electron heavy ions at energies as low as 0.2 MeV/amu, and upgrades of the facility should push the lower limit below 0.1 MeV/amu. Recent experiments, such as measurements of charge transfer and X-ray production for S^{16+} on He and Ar at 6-20 MeV and P(b) measurements for MO X-rays produced in $Cl^{16+} + Ar$ collisions at 20, 10 and 5 MeV have demonstrated the usefulness of highly-stripped, a low-velocity projectiles. These experiments and a few possibilities for future experiments are discussed. (27 refs.)

60508 Studies of fast beam produced recoil ions in a Penning trap. W.S.Burns, D.A.Church, R.A.Kenefick (Texas A&M Univ., College Station, TX, USA), S.B.Elston, R.Holmes, D.Taylor, J.-P.Rozet, S.Berry, I.A.Sellin.

IEEE Trans. Nucl. Sci. (USA), vol.ns-30, no.2, p.977-80 (April 1983).

(1982 IEEE Conference on the Application of Accelerators in Research and Industry, Denton, TX, USA, 8-10 Nov. 1982).

Low energy recoil ions (He^{+4} , $1 \leq q \leq 8$) have been produced and contained in a Penning-type ion trap by means of a stripped 35 MeV Cl^{+3} beam from the Oak Ridge National Laboratory EN Tandem Van de Graaff. Initial investigation of the axial energy distribution of the stored recoil ions indicates that mean energies are less than 2q eV. The rate constants for several electron transfer processes were determined by the direct measurement of stored ion population decay as a function of pressure. (16 refs.)

60509 An overview of research at NBS using synchrotron radiation at SURF-II. D.L.Ederer, R.P.Madden, A.C.Parr, G.Rakowsky, E.B.Saloman (Center for Radiation Res., NBS, Washington, DC, USA), J.Cooper, R.Stockbauer, T.E.Madey, J.L.Dehmer.

IEEE Trans. Nucl. Sci. (USA), vol.ns-30, no.2, p.1020-5 (April 1983).

(1982 IEEE Conference on the Application of Accelerators in Research and Industry, Denton, TX, USA, 8-10 Nov. 1982).

The National Bureau of Standards (NBS) Synchrotron Ultraviolet Radiation Facility (SURF-II) is used in conjunction with several high throughput monochromators to study the interaction of vacuum ultraviolet photons with solids and gases. Recent work has been concerned with the photon stimulated desorption of atomic and molecular ions from surfaces, with the effect of electric fields on molecular photoabsorption and with the study of molecular photoionization by angle resolved photoelectron spectroscopy. These research programs yield new information about molecular bonding at surfaces, molecular dynamics near ionization thresholds, and the coupling of the electronic and nuclear motion near resonances in molecules. In addition to these programs in basic research SURF-II is used for the calibration of transfer standard detectors over a photon energy range 20-250 eV. Calibration of monochromator systems is achieved over the photon energy range 5.250 eV by using the now calculable spectral intensity radiated by the electrons, which are confined in a nearly circular orbit. (22 refs.)

60510 Radioactive ion beams for studying astrophysical nuclear reactions. R.C.Haight, G.J.Mathews, R.M.White, L.A.Aviles, S.E.Woodard (Lawrence Livermore Nat. Lab., Univ. of California, Livermore, CA, USA).

IEEE Trans. Nucl. Sci. (USA), vol.ns-30, no.2, p.1160-3 (April 1983).

(1982 IEEE Conference on the Application of Accelerators in Research and Industry, Denton, TX, USA, 8-10 Nov. 1982).

Beams of radioactive ions can be produced as secondary beams following the interaction of conventional accelerator beams with suitable targets. For exam-

ple the authors have used beams of ^7Li and ^{12}C from an EN Tandem Van de Graaff accelerator to produce beams of ^7Be and ^{13}N via the (p,n) and (d,n) reactions respectively. These beams are focused by a system of magnetic quadrupole lenses to a secondary target. Reactions of such nuclides, especially proton capture and (p, α) reactions, are of interest in solar physics and in the CNO multi-cycle in massive stars. Progress toward the measurement of these reactions is discussed. (8 refs.)

60511 Tritium target performance at RTNS-II. D.W.Heikinen, C.M.Logan (Lawrence Livermore Nat. Lab., Livermore, CA, USA). *IEEE Trans. Nucl. Sci. (USA)*, vol.30, no.2, p.1193-6 (April 1983). (1982 IEEE Conference on the Application of Accelerators in Research and Industry, Denton, TX, USA, 8-10 Nov. 1982).

The Rotating Target Neutron Source (RTNS-II) uses a 360-keV deuteron beam and the $^2\text{H}(d,n)^3\text{He}$ reaction to generate 14-MeV neutrons. The neutrons are used for fusion materials damage studies. The tritium target consists of a band of titanium tritide on copper alloy substrates of 23- or 50-cm diameter. During operation, the substrates are internally cooled and rotated at ~ 4000 rpm to withstand beam intensities in excess of 100 mA. Neutron production data have been accumulated for fifty-eight 23-cm and five 50-cm targets. From these data, using a nonlinear least-squares fitting procedure, target performance parameters have been obtained which permit a quantitative comparison of individual targets. Average parameters are obtained for the 23- and 50-cm targets. (8 refs.)

60512 Porous tungsten relativistic electron beam cathodes compared with carbon cathodes. H.Matsuzawa, H.Kanai (Faculty of Engng., Yamanashi Univ., Kofu, Japan).

Rev. Sci. Instrum. (USA), vol.54, no.4, p.508-9 (April 1983). Porous tungsten cathodes have electron emission characteristics similar to those of plain carbon cathodes, and carbon cathodes with many grooves on the front surface and with silicon resin coating on the lateral surface are superior in emission current to plain carbon cathodes by a factor of 50%. (2 refs.)

60513 Joule-Thomson effect in a Pierce electron gun. V.A.Batalin. *Sov. Phys.-Tech. Phys. (USA)*, vol.27, no.9, p.1110-12 (Sept. 1982). Translation of: *Zh. Tekh. Fiz. (USSR)*, vol.52, no.9, p.1810-14 (Sept. 1982). [received: April 1983]

A thermodynamic approach to the problem of propagation of an electron beam enables the emittance of the beam to be determined. It is shown that the growth of the emittance of an electron beam in a Pierce gun is similar to the Joule-Thomson effect for gases. The effect grows as the initial temperature of the beam is lowered. When the transverse temperature of the beam is of the order of 0.1 eV or lower the increase in the emittance may become significant even in perfect (aberration-free) Pierce optics. (11 refs.)

60514 Fiber-optic data transmission lines in charged-particle accelerator automatic control systems. P.G.Vanichkin, V.M.Batutin, A.I.Vagin, M.D.Kontorov, Yu.I.Monin, A.A.Nikolayev. *Telecommun. & Radio Eng. Part 2 (USA)*, vol.37, no.4, p.64-9 (April 1982). Translation of: *Radioelektronika, Moskva (USSR)*, vol.37, no.4, p.30-4 (April 1982). [received: April 1983]

The use of optical information transmission lines in the automatic control systems [ACS] of accelerator facilities is examined. Specific developments are described and their characteristics are given. Fiber-optic communication lines can be used at all levels of the ACS of modern accelerator facilities. Ambient effects on the line characteristics are reduced significantly. The results of studies of the characteristics of fiber and combined optical communication lines, as well as their practical realization, show that the use of such lines in the ACS of accelerator facilities is highly effective. (10 refs.)

60515 Radioisotope neutron sources. G.F.Knoll (Univ. of Michigan, Ann Arbor, MI, USA).

In book: *Neutron sources. For basic physics and applications*, p.7-18. Oxford, England: Pergamon (1983), xx+349 pp. [0 08 029351 4]

Neutron sources that are based on the use of radioactive materials have been widely utilized in radiation laboratories for many years. These sources share a number of relative advantages compared with other sources of neutrons. They are of small size and therefore quite portable, relatively low in cost, and are characterized by a very reliable neutron yield of predictable intensity. Their 100% duty cycle and complete freedom from maintenance considerations are in marked contrast with accelerator-based neutron sources. These sources also have a number of significant limitations. In order to produce useful yields, relatively large activities of the various isotopes are required, necessitating careful fabrication techniques and attention to radiological safety precautions in their use. Even with relatively active sources, however, the neutron yield is often limited to several orders of magnitude below that obtainable with competing techniques. The neutrons that are produced have a fixed energy spectrum that is often quite broad. While many of the radioisotopes used have half-lives that are very long, some short-lived isotopes require frequent replenishment or reactivation. Also, some of these neutron sources may also produce gamma rays that can interfere with some applications and, in extreme cases, may require special handling techniques.

60516 Sources of monoenergetic neutrons. C.A.Uttley (AERE, Harwell, England).

In book: *Neutron sources. For basic physics and applications*, p.19-55. Oxford, England: Pergamon (1983), xx+349 pp. [0 08 029351 4]

Monoenergetic neutron beams within the range from a few keV to 20 MeV are produced by electrostatic generators or cyclotrons and are in routine use in many laboratories. This energy range covers many of the neutron nuclear data requirements for both fission reactor (<10 MeV) and fusion (<15 MeV) applications, some of which can most precisely be satisfied using continuous or pulsed monoenergetic neutron beams. Nuclear data measured at fixed neutron energies in the MeV region can also usefully supplement data more commonly produced with pulsed white spectrum neutron sources from electron linear accelerators or cyclotrons, since problems with background neutrons are often less severe. The production of monoenergetic neutron beams is discussed followed by a description of the main properties and limitations of the more important source reactions. Electronic collimation of neutrons is considered in some detail because it provides accurately calibrated beams with a small energy spread which are used both for the measurement of absolute neutron cross sections and neutron detector efficiencies.

60517 14 MeV D-T sources. H.H.Barschall (Univ. of Wisconsin, Madison, WI, USA).

In book: *Neutron sources. For basic physics and applications*, p.57-80. Oxford, England: Pergamon (1983), xx+349 pp. [0 08 029351 4]

Among the neutron producing reactions the reaction of ^2H with ^3H , the D-T reaction, has by far the largest cross section. It reaches 5 b at a deuteron bombarding energy of 105 keV. This large cross section at a low bombarding energy has made the D-T reaction the most widely used reaction for applications in which a compact intense neutron source is needed. Usually deuterons of energy between 100 and 400 keV are stopped in a metallic target in which tritium has been absorbed. Much effort has gone into the design of targets

that will provide a strong neutron source over a long time. Target performance is also strongly influenced by the energy, composition, and spatial current distribution of the bombarding deuteron beam.

60518 Accelerator-based pulsed white neutron sources. S.Cierjacks (Kernforschungszentrum Karlsruhe, Karlsruhe, Germany).

In book: *Neutron sources. For basic physics and applications*, p.81-132. Oxford, England: Pergamon (1983), xx+349 pp. [0 08 029351 4]

Accelerator-based pulsed white (PW) neutron sources are presently the most efficient neutron sources for high-resolution measurements of microscopic neutron cross sections. Moreover, these sources are the only ones which can continuously cover the whole range from thermal energies (~ 25 meV) up to several tens of MeV. Their common characteristic is that short bursts of neutrons with a broad continuous energy spectrum are produced by nuclear reactions of energetic photons or charged particles. From the optical analogy such sources are described as 'white' or more precisely 'white spectrum' neutron sources.

60519 Intense deuteron and proton induced (CW)-neutron sources. M.A.Lone, C.B.Bigham (AECL, Chalk River, Ontario, Canada).

In book: *Neutron sources. For basic physics and applications*, p.133-55. Oxford, England: Pergamon (1983), xx+349 pp. [0 08 029351 4]

High energy neutron sources based on high current continuous wave (CW) deuteron or proton accelerators and thick targets of light nuclei provide intensities that at present cannot be generated by other methods. This makes these sources attractive for neutron radiotherapy and for the materials irradiation facilities required in fusion-power technology. Because of the broad energy distribution and lack of suitable pulsing, CW sources are generally not adaptable to high-resolution nuclear data measurements. However, the higher intensities are useful for integral measurements of low cross sections and of isotope yields and for simulation of the neutronics in future fusion-power reactor blankets. The authors describe the characteristics of broad-spectrum, high intensity CW sources of neutrons with average energy above 10 MeV. These sources are based on deuteron or proton reactions at projectile energies below about 50 MeV. Some technical features of thick targets and of high current CW accelerators used in neutron sources of this type are also discussed.

60520 Pulsed reactor sources. W.L.Whittemore, G.B.West (General Atomic Co., San Diego, CA, USA).

In book: *Neutron sources. For basic physics and applications*, p.157-75. Oxford, England: Pergamon (1983), xx+349 pp. [0 08 029351 4]

With the development of pulsed reactors, both fast and thermal, has come a wide variety of applications. While the primary interest is on neutron sources for neutron and nuclear research, the authors briefly cover a much broader range of applications. The singly pulsed reactors have provided also neutron sources for studying transient radiation effects in electronic circuits and components. They have been used extensively for evaluating the safety aspects of transient operation. A fast burst reactor with neutron moderator has been used to perform measurements of fission product nuclide yields. Thermal pulsed reactors in particular have been used for a variety of radiochemistry research efforts, and for neutron radiography. Both thermal and fast pulsed reactors have been used for nuclear pumped laser investigations. The underground single pulsed assemblies (nuclear explosion devices) have been used with long flight paths to measure neutron cross sections where advantage is taken of excellent signal-to-background conditions over a wide range of neutron energies.

60521 Filtered neutron beams. R.C.Block (Rensselaer Polytech. Inst., Troy, NY, USA), R.M.Brugger.

In book: *Neutron sources. For basic physics and applications*, p.177-96. Oxford, England: Pergamon (1983), xx+349 pp. [0 08 029351 4]

In the past 15 years a need has developed for strong quasi-monochromatic neutron sources for applications to neutron physics, health physics, radiobiology, and dosimetry. Although only modest neutron resolution is required for these applications, it is important that these sources have a low background contamination from other energy neutrons and gamma rays. Simpson and Miller (1968) achieved these criteria at the Materials Testing Reactor (MTR) in Idaho by transmitting a beam of radiation from a reactor through a thick sample of Sc metal. The resulting neutron beam (800 eV wide at full-width-half-maximum (FWHM)) was centred about the 2-keV minimum in the Sc neutron total cross section. This technique was further developed at the MTR by Simpson and co-workers to produce an improved 2-keV filtered beam with Sc. In addition, beams centred at 24 keV with Fe and at 144 keV with Si filters were also produced. Filtered-beam facilities have since been set up at several reactors in the United States, Canada, Germany, Russia and India, and bands of neutrons near 186 eV, 2 keV, 24 keV, 55 keV, 144 keV and 2.35 MeV are now obtained with ^{238}U , Sc, Fe, Si, and O_2 filters respectively. Research has been reported in the areas of neutron cross section measurements, capture gamma-ray studies, and dosimetry studies.

60522 Pulsed neutron beams from steady state reactors. R.E.Chrien (Brookhaven Nat. Lab., Upton, NY, USA).

In book: *Neutron sources. For basic physics and applications*, p.197-216. Oxford, England: Pergamon (1983), xx+349 pp. [0 08 029351 4]

The techniques of neutron energy measurements by time-of-flight were originally developed for pulsed cyclotron neutron sources in the late 1930s and early 1940s. In the postwar period, the high flux research reactors came into operation, and these techniques were adapted to reactor sources. In this discussion, a distinction is to be made between mechanical velocity 'selectors' and 'choppers'. The former instrument can be traced back to Dunning (1935), who used a pair of rotating wheels to demonstrate the Maxwellian nature of the energy distribution of neutrons in equilibrium with a system of moderator atoms at some temperature. The essence of the selector is its ability to transmit a narrow range of neutron energies by virtue of their motion through a suitably shaped slit, or set of displaced slits. A chopper, on the other hand, is capable of passing a broad range of energies, i.e. a 'white spectrum', through a rotating slit to form bursts of neutrons in space and time. These bursts are subsequently allowed to travel a flight path and their time of arrival is recorded by a detector, relative to a fiducial time signal derived from the chopper.

60523 Spallation neutron sources. J.S.Fraser, G.A.Bartholomew (AECL, Chalk River, Ontario, Canada).

In book: *Neutron sources. For basic physics and applications*, p.217-35. Oxford, England: Pergamon (1983), xx+349 pp. [0 08 029351 4]

Spallation neutron sources consist basically of an accelerator providing a beam of high-energy (≥ 1 GeV) protons or possibly heavier ions and a suitable target of heavy-element material. The physics and computational modelling of the primary target and descriptions of the essential components of representative types of target assembly for basic research and for energy applications are given. The types of accelerators used, and the performance and layout of the end-use components, i.e. moderators and beam tubes for research devices and blanket systems for energy applications, are discussed peripherally.

60524 Plasma neutron sources. H.Conrads (KFA Julich, Julich, Germany).

In book: *Neutron sources. For basic physics and applications*, p.237-58. Oxford, England: Pergamon (1983), xx+349 pp. [0 08 029351 4]. One of the main tasks in plasma physics and thermonuclear fusion research for developing a new energy source is the production of large quantities of neutrons, whose accumulated energies far exceed the energy needed for their production. If this goal can be achieved, plasmas will be one of the most intense neutron sources.

60525 Sources of polarized neutrons. L.Walter (Duke Univ., Durham, NC, USA).

In book: *Neutron sources. For basic physics and applications*, p.259-83. Oxford, England: Pergamon (1983), xx+349 pp. [0 08 029351 4]. The authors surveys only one small aspect of the published reports on neutron polarization studies, and that is the modes of generating beams of polarized fast neutrons to be used successfully in scattering or reaction experiments.

60526 Pulsed ion source of B-diode type with cryogenic anode. K.Kasuya, K.Horioka, T.Takahashi, A.Urai, H.Yoneda (Dept. of Energy Sci., Tokyo Inst. of Technol., Yokohama, Japan). Fusion Technology 1982. Proceedings of the Twelfth Symposium, Julich, Germany, 13-17 Sept. 1982 (Oxford, England: Pergamon 1983), p.1081-6 vol.2

An applied-B, magnetically insulated diode (MID) with cryogenically refrigerated anode is proposed as a new type of ion source. With this ion source, proton beams of about 22 A/cm² and deuteron beams of about 15 A/cm², with their energy of 150 keV have been produced from the refrigerated anode with good reproducibility. These values are twice the Child-Langmuir prediction and not at all inferior to those extracted from conventional anodes. (5 refs.)

60527 The Julich ion source design and related thermo-mechanical pre-testing. P.Kupschus, J.Hemmerich, E.Deksnis, H.Fraenkle, C.Meixner, H.Reimer (KFA Julich, Julich, Germany). Fusion Technology 1982. Proceedings of the Twelfth Symposium, Julich, Germany, 13-17 Sept. 1982 (Oxford, England: Pergamon 1983), p.1367-73 vol.2

Neutral injection for TEXTOR and other present and future fusion devices require pulse time capabilities in the multi-second range for their beam generators. The design principles and features of a multi-aperture ion source basically capable of an ion current of 100 A from a total area of about 20X50 cm² for a pulse length unlimited by the thermal loading of ion source components by plasma or beam are described. To confirm, in particular, construction principles and critical parameters of the design—which is presently under construction—certain models have been built and been subjected to thermo-mechanical testing; two of the more important ones are dealt with in more detail and results are given. (5 refs.)

60528 Development of an ion source for long-pulse (30-s) neutral beam injection. M.M.Menon, G.C.Barber, W.K.Blue, W.K.Dagenhart, W.L.Gardner, H.H.Haselton, J.A.Moeller, N.S.Ponte, P.M.Ryan, D.E.Schechter, W.L.Stirling, C.C.Tsai, J.H.Wheaton, R.E.Wright (Oak Ridge Nat. Lab., Oak Ridge, TN, USA). Fusion Technology 1982. Proceedings of the Twelfth Symposium, Julich, Germany, 13-17 Sept. 1982 (Oxford, England: Pergamon 1983), p.1375-9 vol.2

Describes the development of a long-pulse positive ion source that has been designed to provide high brightness deuterium beams (divergence $\approx 0.25^\circ$ r.m.s., current density ≈ 0.15 A/cm²) of 40-5 A, at a beam energy of 80 keV, for pulse lengths up to 30 s. The design and construction of the ion source components are described with particular emphasis placed on the long-pulse cathode assembly and ion accelerator. (9 refs.)

60529 An electronic energy measuring system for pulsed neutral beam calorimeters. D.Cooper, A.Stabler, O.Vollmer (Max-Planck-Inst. fur Plasma-phys., Garching, Germany), Z.Yu. Fusion Technology 1982. Proceedings of the Twelfth Symposium, Julich, Germany, 13-17 Sept. 1982 (Oxford, England: Pergamon 1983), p.1401-4 vol.2

Describes an electronic system for measuring and displaying signals from a 'neutral beamline' calorimeter. The system is modular and has been designed with simplicity and ease of use as the primary goal while maintaining reasonable accuracy. This system uses an LSI 11 microcomputer to measure temperature distributions over the calorimeter, and hardware logic for control and some processing. The hardware is integrated into the beamline control system and provides interlock information to the control system. The system provides time averaged as well as short term measurements of water flow rate and temperature, also total energy removed from the calorimeter in a predetermined time. Some modules can function independently therefore enhancing overall system reliability. Also particular attention was given to noise immunity in view of the Tokamak's hostile electrical environment. (1 ref.)

Neutron sources. For basic physics and applications See Entry 59546

Beam-plasma type metal ion source See Entry 59877

Nonlinear multichannel pulse-sharpening line containing ferrite rings with non-rectangular hysteresis loop See Entry 59878

Utilization of MeV Van de Graaff electrons to produce characteristic X-rays for precision measurements See Entry 59899

Calorimetric redetermination of the half-life of ⁹⁰Sr See Entry 60138

Superconducting linear accelerators for heavy ions See Entry 60481

Observations of ion acceleration by a relativistic electron beam See Entry 60483

Transverse electron motion and emittance development in the injector of an electron linear accelerator See Entry 60486

Linear optics design of the superconducting low- β insertion in the intersecting storage rings at CERN See Entry 60487

Transverse mode coupling in a bunched beam See Entry 60488

The mechanism of integer resonance crossing and the prospects for higher energies in cyclotrons See Entry 60489

Bunched beam instability associated with cavity impedance See Entry 60490

Stabilization of longitudinal instabilities in heavy-ion storage rings See Entry 60492

Orbital stability of the high-current betatron See Entry 60494

Experimental study of stochastic cooling in the NAP-M proton accelerator See Entry 60496

Two-coordinate scintillation hodoscope on the basis of hodoscope photomultipliers See Entry 60541

Improved system for energy-dispersive X-ray diffraction with synchrotron radiation See Entry 61731

An ¹⁸O₂-target for the high yield production of ¹⁸F-fluoride See Entry 63962

Dose distributions of fast electrons with an energy of 7-24 MeV in the electromagnetic formation of a beam See Entry 63965

The operation and life of the Zetatron neutron tube in a borehole logging application See Entry 64257

29.30 RADIATION SPECTROMETERS AND SPECTROSCOPIC TECHNIQUES

60530 A semiconductor beta ray spectrometer. V.R.Bom (Phys. Dept., Delft Univ. of Technol., Delft, Netherlands).

Nucl. Instrum. & Methods Phys. Res. (Netherlands), vol.207, no.3, p.395-402 (1 April 1983).

The design and construction of a beta spectrometer which uses a hyper-pure germanium crystal for energy determination is described. Due to the good energy resolution, end points of continuous beta spectra can be measured accurately, even if the nuclides have short half-lives. The spectrometer is therefore especially suited for atomic mass determination in on-line mass separator experiments. A simple wire chamber is used to discriminate beta particles from gamma radiation. Disadvantages arise from the large amounts of scattered beta particles, deforming the continua; a method is described to minimize this scattering. (14 refs.)

60531 System of moving the source in a nuclear gamma resonance spectrometer. A.V.Golubev, V.M.Erkin, G.I.Kileinikov, V.D.Chervenko (Ogarev State Univ., Saransk, USSR).

Ind. Lab. (USSR), vol.48, no.6, p.574-7 (June 1982). Translation of: *Zavod. Lab. (USSR)*, vol.48, no.6, p.39-41 (June 1982). [received: March 1983]

The present work presents a description of a simple, highly stable system of controlling the motion of the stem of an electromechanical vibrator based on an operational amplifier with low input current. It consists of two functionally complete and self-contained units: the unit of the driving sawtooth voltage based on amplifiers, and a unit consisting of the error-signal amplifier based on another amplifier, and the power amplifier based on transistors. (5 refs.)

60532 Progress report on heavy ion identification by Bragg Curve Spectroscopy at the Legnaro XTU Tandem Laboratory. G.D'Erasmio, D.Fabris, F.Gramegna, I.Iori, A.Moroni, G.Nebbia, A.Pantaleo, G.Prete, R.A.Ricci, G.Viesti, Li Zu Yu.

Report INFN/BE-82/4, Ist. Naz. Fis. Nucl., Legnaro, Italy (1 Dec. 1982), 13 pp.

The experimental work on heavy ion identification by Bragg Curve Spectroscopy at the XTU Tandem Laboratory is summarized. The problems in using BCS detectors and the lines of future work are discussed. (11 refs.)

A microprocessor controlled spectrometer for thermal scan Mossbauer spectroscopy See Entry 59897

Utilization of MeV Van de Graaff electrons to produce characteristic X-rays for precision measurements See Entry 59899

29.40 RADIATION DETECTORS

(for mass spectrometers, see 07.75)

60533 Use of a large multicell ionization detector—the external particle identifier—in experiments with the BEBC hydrogen bubble chamber. V.Baruzzi (CERN, Geneva, Switzerland), R.Carosio, F.Crijns, L.Gerdyukov, Y.Goldschmidt-Clermont, A.Grant, D.Johnson, F.Kroner, I.Lehraus, R.Matthewson, C.Milstone, V.Nikolaenko, Y.Oren, Y.Petrovikh, R.T.Ross, P.Sixel, M.Spyropoulou-Stassinaki, A.Stergiou, W.Tejesy, P.Theocharopoulos, G.Vassiliadis, P.R.S.Wright, J.Zoll.

Nucl. Instrum. & Methods Phys. Res. (Netherlands), vol.207, no.3, p.339-56 (1 April 1983).

Fast secondary particles from interactions of K⁺ at 70 GeV/c and K⁻ at 110 GeV/c in the BEBC hydrogen bubble chamber are identified by use of the relativistic rise of ionization in argon. The ionization is measured in a large multicell ionization counter system, the external particle identifier (EPI). The operation of this hybrid system, the calibration and the procedures of off-line analysis leading to particle identification are described. For a sample of 9283 secondary particles collected in the K⁺ p experiment the authors present the measurements of ionization, and the determination of acceptance and identification efficiencies. The momentum-dependent populations of pions, kaons and protons have been obtained. Track by track identification procedures yielding samples of pions and kaons with a contamination $\leq 12\%$ are discussed. A study of the resolution of the EPI in these experimental conditions shows average values in a range of 7.6% of 11% depending on the number of ionization samples remaining after removal of background. These values extrapolate to a value consistent with the 6.6% FWHM measured over the whole device for single particles during calibration with a 50 GeV/c π^- beam. (13 refs.)

60534 Small high-precision wire chambers for the measurement of pp elastic scattering at the CERN collider. J.Buskens, B.Koene, L.Linssen, P.Rewiersma, H.Schuijlenburg, R.van Swol, J.Timmermans (NIKHEF-H, Amsterdam, Netherlands), M.Hagenauer, G.Roiron, J.Velasco.

Nucl. Instrum. & Methods Phys. Res. (Netherlands), vol.207, no.3, p.365-78 (1 April 1983).

The authors describe the construction and performance of a set of small wire chambers for the detection of elastically scattered particles at the CERN pp collider. A chamber contains four drift planes followed by a multiwire proportional plane with charge division readout. The chamber wall facing the beam axis of the collider consists of a thin plate with field restoring strips that keep the resolution and efficiency of the chamber nearly unchanged to within one millimeter from the wall. The intrinsic resolution of the drift planes is ~ 80 μ m per wire while after track reconstruction an accuracy per wire of ~ 100 μ m is obtained. The accuracy of the charge division is ~ 0.4 mm over a wire length of 64 mm. This number includes uncertainties in the calibration of the readout electronics. (13 refs.)

60535 Spatial resolution of induction chambers. A.E.Bondar, A.P.Onuchin, V.S.Panin, V.I.Telov (Inst. of Nuclear Phys., Novosibirsk, USSR).

Nucl. Instrum. & Methods Phys. Res. (Netherlands), vol.207, no.3, p.379-88 (1 April 1983).

The spatial resolution of proportional chambers with the delay line connected to the cathode plane has been studied. A coaxial cable was used as a delay line. For the relativistic electrons a spatial resolution of 25 μ m (RMS) for normal incidence and 120 μ m for an angle of inclination of 35° has been obtained. For protons with an energy of 65 MeV a spatial resolution of 15 μ m has been achieved for normal incidence. The factors that limit the accuracy of the method are discussed. (26 refs.)

60536 A variable geometry high-purity germanium detector telescope system for use with intermediate energy charged particles. D.L.Friesel, B.S.Flanders (Indiana Univ., Bloomington, IN, USA), R.H.Pehl. *Nucl. Instrum. & Methods Phys. Res. (Netherlands)*, vol.207, no.3, p.403-15 (1 April 1983).

A versatile variable geometry detector telescope system consisting of silicon surface barrier and high-purity germanium planar detectors has been developed and used at intermediate light ion energies at IUCF for several years. Detailed descriptions of the telescope system and its operational properties are given. The practical experiences of using detectors fabricated from both n- and p-type high-purity germanium for a variety of particles and energies are described along with details of the effects of long-term storage, radiation damage, and radiation damage annealing procedures on detector properties. Diffusion of the Li^+ contact after many radiation damage and anneal cycles is also discussed. (25 refs.)

60537 A large-area xenon gas scintillation proportional counter (GSPC) with timing information for the detection of low energy X-rays. H.P.von Arb, J.Bocklin, R.Dittus, R.Ferreira Marques, H.Hofer, F.Kotmann, R.Schaeren, D.Taqui, M.Walchli (Lab. für Hochenergiephys., ETH-Zürich, Villigen, Switzerland).

Nucl. Instrum. & Methods Phys. Res. (Netherlands), vol.207, no.3, p.429-35 (1 April 1983).

A large area xenon gas scintillation proportional counter has been developed for the study of low energy X-rays. A time resolution of 40 ns (FWHM) at 5.5 keV was obtained by producing secondary scintillation light in the drift space. A simple model of the processes leading to secondary light production describes the measured time distributions and their energy dependence. The energy resolution at 5.9 keV was 8.8% (FWHM) for collimated X-rays. For a uniform irradiation over the sensitive area of 314 cm², a resolution of 9.5% is obtained after correcting for the pulse height dependence on the position of X-ray absorption. The reduction of pulse height due to small H₂O and O₂ contaminations was measured. (10 refs.)

60538 A technique for constructing scintillation panels with very large areas using granulated NaI(Tl). H.Griffiths (H.H. Wills Phys. Lab., Univ. of Bristol, Bristol, England).

Nucl. Instrum. & Methods Phys. Res. (Netherlands), vol.207, no.3, p.449-54 (1 April 1983).

A method has been developed for constructing scintillation panels with very large areas at low cost using granulated NaI(Tl). The panels are equivalent to slabs of sodium iodide, 0.35 mm in thickness giving a quantum efficiency greater than 10% up to a photon energy of 130 keV. Under diffusing lightbox conditions the panels give an output of light 2.5 times greater than that from a single crystal of NaI(Tl). (3 refs.)

60539 Composite neutron recording systems. I.M.Kozlov, O.P.Nikotin, A.S.Chekrenev (Leningrad Technol. Inst., Leningrad, USSR).

Instrum. & Exp. Tech. (USA), vol.25, no.4, pt.1, p.821-4 (July-Aug. 1982). Translation of: *Prib. & Tekh. Eksp. (USSR)*, vol.25, no.4, p.39-42 (July-Aug. 1982). [received: April 1983]

Describes the design of a neutron recording system built from a large number of ³He-filled proportional counters of thermal neutrons. A particular logic switching unit is suggested for performing a series of experiments and for adjusting and monitoring the counting characteristic of the system. (4 refs.)

60540 Single-coordinate position-sensitive neutron detector with digital processor. V.I.Gordeli, Yu.B.Zasadych, M.Z.Ishmukhametov, V.I.Lazin, V.E.Novozhilov.

Instrum. & Exp. Tech. (USA), vol.25, no.4, pt.1, p.825-8 (July-Aug. 1982). Translation of: *Prib. & Tekh. Eksp. (USSR)*, vol.25, no.4, p.42-5 (July-Aug. 1982). [received: April 1983]

Describes a cylindrical ³He-filled position-sensitive proportional neutron detector with a high-resistance wire as anode electrode. The coordinates at which a neutron is recorded by the detector are determined with the aid of two analog-digital converters analyzing the amplitude of pulses obtained from both ends of the anode electrode and with the aid of a special unit including a divider circuit of integers. (6 refs.)

60541 Two-coordinate scintillation hodoscope on the basis of hodoscope photomultipliers. N.K.Vishnevskii, A.I.Ronzhin, V.K.Semenov, B.A.Khachaturov (Inst. of High-Energy Phys., Serpukhov, USSR).

Instrum. & Exp. Tech. (USA), vol.25, no.4, pt.1, p.833-6 (July-Aug. 1982). Translation of: *Prib. & Tekh. Eksp. (USSR)*, vol.25, no.4, p.49-52 (July-Aug. 1982). [received: April 1983]

Describes the results of research on a scintillation hodoscope based on hodoscope photomultipliers; the instrument allows the simultaneous measurement of two particle coordinates (X and Y). Owing to its small size and mobility, the two-coordinate photomultiplier hodoscope is used for the operational position guidance of the beam onto the target and the monitoring of beam position, beam shape and beam dimensions in the very region of the polarised target. (6 refs.)

60542 Using scintillation hodoscopes with hodoscope photomultipliers in particle-momentum measurements and in fast sampling. A.N.Vasil'ev, N.K.Vishnevskii, Yu.A.Matulenko, E.A.Monich, S.B.Nurushev, A.I.Ronzhin, V.I.Rykalin, V.K.Semenov, B.A.Khachaturov (Inst. of High-Energy Phys., Serpukhov, USSR).

Instrum. & Exp. Tech. (USA), vol.25, no.4, pt.1, p.836-41 (July-Aug. 1982). Translation of: *Prib. & Tekh. Eksp. (USSR)*, vol.25, no.4, p.52-6 (July-Aug. 1982). [received: April 1983]

Presents the results obtained in the use of scintillation hodoscopes with hodoscope photomultipliers in measurements of particle momenta. A setup facilitating particle-momentum sampling on an analog level during a time of about 500 nsec is described. The setup was tested with the electron and pion beams of the synchrotron of the Institute of High-Energy Physics (Serpukhov). (11 refs.)

60543 Matching the spectral characteristics of scintillators and photo-diodes. V.D.Ryzhikov, P.E.Stadnik, Yu.A.Yakovlev.

Instrum. & Exp. Tech. (USA), vol.25, no.4, pt.1, p.842-5 (July-Aug. 1982). Translation of: *Prib. & Tekh. Eksp. (USSR)*, vol.25, no.4, p.57-60 (July-Aug. 1982). [received: April 1983]

The matching of the spectral characteristics is assessed from the radiation spectra of scintillators and the photosensitivity spectra of photodetectors. It is shown that semiconductor scintillators on the basis of A^{III}B^{VI} compounds (CdS, ZnS and ZnSe) match photodiodes in a better way than CsI(TZ) scintillators which are usually employed in scintillator-photodiode systems. (8 refs.)

60544 A nitrogen-filled ionization chamber. K.M.Avakyan, G.V.Azizbekyan, P.S.Mnatsakanyan.

Instrum. & Exp. Tech. (USA), vol.25, no.4, pt.1, p.846-9 (July-Aug. 1982). Translation of: *Prib. & Tekh. Eksp. (USSR)*, vol.25, no.4, p.60-2 (July-Aug. 1982). [received: April 1983]

The operation of a nitrogen-filled ionization chamber at various pressures and degrees of gas purity was investigated. Comparative amplitude characteristics of nitrogen- and argon-filled chambers are considered. It is shown that it is possible to use nitrogen in larger ionization chambers. (10 refs.)

60545 Saturation curves of parallel-plate ionization chambers. B.G.Fallone, E.B.Podgorsak (Dept. of Radiation Oncology, McGill Univ., Montreal, Quebec, Canada).

Med. Phys. (USA), vol.10, no.2, p.191-6 (March-April 1983).

A new analytical expression is presented to describe the full saturation curve of parallel-plate ionization chambers. In contrast to the presently known expressions, which hold only for the near saturation region, this empirically determined expression is in excellent agreement with measurements in the whole collection efficiency range from 0 to 1 for X-ray sources with effective energies from 20 to 150 keV and cobalt-60 gamma rays. The dependence of the ion collection efficiency and the extrapolated electric field, which is a parameter in the new saturation curve expression, on electric field, dose, dose rate, beam quality, and chamber volume, is discussed. The effect of photoemission from the chamber polarizing electrode for low-energy X-ray beams on the saturation current is demonstrated. A universal ionization chamber constant is derived experimentally. It is shown that all parameters of the saturation curve equation and thus the saturation curve itself, can be calculated from one single measurement of ionization current at a given electric field and air gap thickness. (17 refs.)

60546 Multi-needle counter with cathode focusing used to detect the thermo-stimulated exoelectron emission (TSEE). G.Comby, J.Quidot, J.F.Chalot, G.Valladas, A.Zadra, M.Petel, J.Barthe (CENS, Gif-sur-Yvette, France).

Rev. Phys. Appl. (France), vol.18, no.4, p.263-70 (April 1983). In French.

The multi-needle detectors with cathode focusing, developed to detect and to localize single photo electrons are specially adapted to reveal events with a very poor number of primary electrons. In exo-emission phenomena each event appears like an emission of 1 to some electrons with a weak energy (~1 eV). This work describes the performances of the multi-needle counters when they are used to detect thermo-stimulated exoelectrons. (13 refs.)

60547 Theoretical analysis of photon drag detectors. J.G.Edwards, A.R.Roddie.

Report NPL-DES-76, Nat. Phys. Lab., Teddington, England (March 1983), 44 pp.

A theoretical analysis of the spatial response characteristics of photon drag detectors used for the measurement of high power pulses from CO₂ lasers is presented. Details of the model and the numerical methods employed are described and the results obtained for several electrode configurations together with a comparison of experimental values obtained for a typical commercial device are given. (10 refs.)

60548 CEDAR counters for particle identification in the SPS secondary beams: A description and an operation manual. C.Bovet, R.Maleyrans, L.Piomontese, A.Placci, M.Placidi.

Report CERN-82-13, CERN, Geneva, Switzerland (23 Dec. 1982), vi+37 pp.

The Cerenkov differential counter with achromatic ring focus (CEDAR) has been designed and a number built at CERN for the identification (and selection) of particles in the secondary beams of a high-energy accelerator. CEDAR-N can separate kaons from pions up to 300 GeV/c but can detect protons only down to 60 GeV/c; CEDAR-W can flag protons of 12 GeV/c and separate kaons from pions up to 150 GeV/c. After a brief account of the relevant physics of the Cerenkov effect, this report describes CEDARs with emphasis on those characteristics and construction features that are of interest to the user. Details are given of the high-precision optical system, the mechanical construction to achieve uniform temperature (0.1K) and rigidity, and the gas handling and measurement. The layout of the CEDARs in the secondary beams of the CERN Super Proton Synchrotron is described. The signals provided to the user are listed and explained, together with the programs for on-line control of the counters. Details are given of the performances attained, together with various hints and suggestions on the procedure to follow in order to set-up, tune, and operate a CEDAR. The dependence of the performance on beam optics is stressed. (10 refs.)

Development of the cosmic ray techniques See Entry 59568

Early cloud chamber experiments at the Pic-du-Midi See Entry 59571

Cosmic rays and particle physics at Berkeley See Entry 59572

Modeles d'interpretation des mesures des actinides par spectrometrie gamma

choix d'un moniteur de reference (Model interpretation of actinide measurement by gamma spectrometry using a reference monitor) See Entry 60245

A simple modification to improve the energy dependence of ion chamber survey

meters See Entry 60476

A semiconductor beta ray spectrometer See Entry 60530

Progress report on heavy ion identification by Bragg Curve Spectroscopy at the

Legnaro XTU Tandem Laboratory See Entry 60532

Controllable scanner for an automatic nuclear photoemulsion analyzer See Entry 60550

Particle identification by means of fine sampling dE/dX measurements See Entry 60553

Flight-time system with automatic adjustment and logic sampling of information for the Nataliya-2 telescope See Entry 64385

Flight-time system with automatic adjustment and logic sampling of information for the Nataliya-2 telescope See Entry 64385

Flight-time system with automatic adjustment and logic sampling of information for the Nataliya-2 telescope See Entry 64385

Flight-time system with automatic adjustment and logic sampling of information for the Nataliya-2 telescope See Entry 64385

Flight-time system with automatic adjustment and logic sampling of information for the Nataliya-2 telescope See Entry 64385

Flight-time system with automatic adjustment and logic sampling of information for the Nataliya-2 telescope See Entry 64385

Flight-time system with automatic adjustment and logic sampling of information for the Nataliya-2 telescope See Entry 64385

Flight-time system with automatic adjustment and logic sampling of information for the Nataliya-2 telescope See Entry 64385

Flight-time system with automatic adjustment and logic sampling of information for the Nataliya-2 telescope See Entry 64385

Flight-time system with automatic adjustment and logic sampling of information for the Nataliya-2 telescope See Entry 64385

Flight-time system with automatic adjustment and logic sampling of information for the Nataliya-2 telescope See Entry 64385

Flight-time system with automatic adjustment and logic sampling of information for the Nataliya-2 telescope See Entry 64385

Flight-time system with automatic adjustment and logic sampling of information for the Nataliya-2 telescope See Entry 64385

Flight-time system with automatic adjustment and logic sampling of information for the Nataliya-2 telescope See Entry 64385

Flight-time system with automatic adjustment and logic sampling of information for the Nataliya-2 telescope See Entry 64385

Flight-time system with automatic adjustment and logic sampling of information for the Nataliya-2 telescope See Entry 64385

Flight-time system with automatic adjustment and logic sampling of information for the Nataliya-2 telescope See Entry 64385

Flight-time system with automatic adjustment and logic sampling of information for the Nataliya-2 telescope See Entry 64385

Flight-time system with automatic adjustment and logic sampling of information for the Nataliya-2 telescope See Entry 64385

Flight-time system with automatic adjustment and logic sampling of information for the Nataliya-2 telescope See Entry 64385

Flight-time system with automatic adjustment and logic sampling of information for the Nataliya-2 telescope See Entry 64385

Flight-time system with automatic adjustment and logic sampling of information for the Nataliya-2 telescope See Entry 64385

Flight-time system with automatic adjustment and logic sampling of information for the Nataliya-2 telescope See Entry 64385

Flight-time system with automatic adjustment and logic sampling of information for the Nataliya-2 telescope See Entry 64385

Flight-time system with automatic adjustment and logic sampling of information for the Nataliya-2 telescope See Entry 64385

Flight-time system with automatic adjustment and logic sampling of information for the Nataliya-2 telescope See Entry 64385

Flight-time system with automatic adjustment and logic sampling of information for the Nataliya-2 telescope See Entry 64385

Flight-time system with automatic adjustment and logic sampling of information for the Nataliya-2 telescope See Entry 64385

60550 Controllable scanner for an automatic nuclear photoemulsion analyzer. V.A.Grashilin, Yu.Ya.Karlyshev (Inst. for Nuclear Studies, Acad. of Sci., Kiev, Ukrainian SSR).

Instrum. & Exp. Tech. (USA), vol.25, no.4, pt.1, p.874-6 (July-Aug. 1982). Translation of: *Prib. & Tekh. Eksp. (USSR)*, vol.25, no.4, p.87-9 (July-Aug. 1982). [received: April 1983]

A controllable scanner is described for use in an automatic device for counting grains on nuclear photoemulsions. The scanner is designed from digital-to-analog converters and can count a 512×512 frame in ~ 2.6 sec. The controllable sweep generator load consists of the beam-deflecting system of an OS-110LA oscilloscope and has conversion accuracy $\pm 1/2$ the lowest significant bit of the digital-to-analog converter. (8 refs.)

60551 Simple circuit for dynamically displaying digital data from one or several counters. S.U.Klimovich, Yu.P.Surkov.

Instrum. & Exp. Tech. (USA), vol.25, no.4, pt.1, p.877-9 (July-Aug. 1982). Translation of: *Prib. & Tekh. Eksp. (USSR)*, vol.25, no.4, p.90-2 (July-Aug. 1982). [received: April 1983]

A dynamic digital display is described which does not use synchronizing circuits. The display unit consists of four electronic switches (series 155 microcircuits), a 4-way pulse distributor, and four 514ID2 decoders. It is shown that it is possible to employ just one 514ID2 decoder. The data inputs of the counters whose states are displayed are functionally independent of the display conditions. Data from each counter are displayed decade-by-decade 50 times per second using a pulse distributor. The display device can record data decade-by-decade by connecting a code converter to the outputs of the electronic switches and by disabling the pulse distributor during the time needed to print out the data stored in a counter decoder. (1 ref.)

60552 Doppio discriminatore leading edge (Double leading edge discriminators). M.Castoldi.

Report INFN/TC-82/13, Ist. Naz. Fis. Nucl., Genoa, Italy (13 Oct. 1982), 5 pp. In Italian.

A double leading-edge discriminator for general use in particle counting is described which, though not of high precision or extremely accurate timing, can be used in the 'updating' and 'burst guard' modes, and can be easily and economically manufactured, being made up of standard ECL series 10000 components and includes power supplies.

Composite neutron recording systems See Entry 60539

Single-coordinate position-sensitive neutron detector with digital processor See Entry 60540

29.70 RADIATION MEASUREMENT, DETECTION AND COUNTING

(see also 29.30 Radiation spectrometers and spectroscopy, 29.40 Radiation detectors; for dosimetry, see 87.60M)

60553 Particle identification by means of fine sampling dE/dX measurements. A.Imanishi, T.Ishii, T.Onshima, H.Okuno, K.Shiino (Inst. for Nuclear Study, Univ. of Tokyo, Tokyo, Japan), F.Naito, T.Matsuda.

Nucl. Instrum. & Methods Phys. Res. (Netherlands), vol.207, no.3, p.357-64 (1 April 1983).

Identification of relativistic charged particles by means of fine sampling dE/dX measurements with a longitudinal drift chamber has been studied. Using a fast-sampling ADC (25 MHz), dE/dX was measured in a 1.4 mm gas thickness over an electron drift space of 51 mm. For the simulated 1 m long tracks of pions and electrons of 500 MeV/c, a particle separation of 10σ - 12σ has been obtained, where σ is the RMS resolution of the dE/dX measurement. This result with fine sampling is better by a factor of 1.7 compared to the dE/dX measurement with 21 mm sampling thickness. Further improvement achievable by reducing the correlation between neighbouring samples and simplification of electronics by use of the δ -ray clipping method are also discussed. (9 refs.)

60554 Deposited energy density for 100 MeV protons in lithium. K.B.Winterbon (Chalk River Nuclear Labs., Chalk River, Ontario, Canada).

Nucl. Instrum. & Methods Phys. Res. (Netherlands), vol.207, no.3, p.469-73 (1 April 1983).

The density of energy (LET) deposited in a lithium target by 100 MeV protons is estimated by two methods. The protons are slowed down by electronic stopping alone, nuclear stopping being negligible. Multiple scattering and transport of energy by recoil electrons (delta rays) are shown to be negligible. The continuous-slowing-down expression for the range straggling is used in a convolution with the no-straggling distribution in one method; in the other the appropriate transport integral equation is solved to first order in the straggling. The corresponding solution for the range distribution is also given. The results are nearly identical, numerically. The peak energy density is about 4.8 times the mean, and the FWHM is about 5.4% of the mean range. In the corresponding problem for 200 MeV protons on lead, the numbers are 4.4 and 6.3%, respectively. Simple scaling relations for peak and FWHM are given in terms of a straggling parameter. (8 refs.)

60555 The influence from low energy X-rays and Auger electrons on $4\pi\beta\gamma$ coincidence measurements of electron-capture-decaying nuclides. E.Funck, A.Nylandstedt Larsen (Phys.-Tech. Bundesanstalt, Braunschweig, Germany).

Int. J. Appl. Radiat. & Isot. (GB), vol.34, no.3, p.565-9 (March 1983). The influence of low energy X-rays and Auger electrons emitted by electron capture nuclides on $4\pi\beta\gamma$ coincidence measurements is investigated. Under the assumption that these radiations are not detected, correction terms are developed for a number of nuclides that are in common use. (13 refs.)

60556 Determination of the specific activity of fission-based ^{99}Mo using differential pulse polarography. R.K.Barnes, E.L.R.Hetherington (Australian Atomic Energy Comm., Res. Estab., Lucas Heights Res. Labs., Sutherland, NSW, Australia), M.Ohkuho.

Int. J. Appl. Radiat. & Isot. (GB), vol.34, no.3, p.603-6 (March 1983). The specific activity of fission-based ^{99}Mo is significantly lower than the theoretical 'carrier-free' value because of the contribution from a number of stable molybdenum isotopes which are formed concurrently during irradiation of the uranium target. A rapid analytical technique employing differential pulse polarography was devised to measure the concentrations of molybdenum, and hence the specific activity of ^{99}Mo , in small volumes of radioactive sample. Submicrogram quantities of the analyte can be measured by using the catalytic reduction wave of molybdenum in a nitric acid-ammonium nitrate based supporting electrolyte. Measured specific activities range from 3.1×10^6 to 5.4×10^6 Ci g $^{-1}$; these values were in close agreement with the theoretically computed values. (12 refs.)

60557 Standard radiometer for long-lived radionuclide aerosols. S.K.Belkina, Yu.E.Zalmanzon, V.D.Kamyshchenko, Yu.V.Kuznetsov, D.E.Fertman.

Meas. Tech. (USA), vol.25, no.7, p.626-7 (July 1982). Translation of: *Izmer. Tekh. (USSR)*, vol.25, no.7, p.63-4 (July 1982). [received: Feb. 1983] A standard radiometer is shown which can be used in checking, calibrating, and certifying working means of monitoring the bulk activities of aerosols for long-lived radionuclides. In particular, it has been used in calibrating and certifying units for detecting β -active aerosols having a measurement range of $3.7 \cdot 3.7 \times 10^4$ Bq/m 3 . The approach used in creating the standard radiometer enables one with relatively little effort to design a standard radiometer for the vapor of molecular iodine-131 using the new BDAG-01R detection unit. (5 refs.)

60558 Observation of large deviations from the Bethe-Bloch formula for relativistic uranium ions. S.P.Ahlen, G.Tarle (Dept. of Phys., Univ. of California, Berkeley, CA, USA).

Phys. Rev. Lett. (USA), vol.50, no.15, p.1110-13 (11 April 1983). By measuring the range deficit of 955-MeV/u ^{238}U ions in copper, the authors have identified very large deviations of the stopping power from the standard Bethe-Bloch formula. They show that this discrepancy can be accounted for by higher-order terms in the Mott cross section and by the relativistic Bloch correction. The significance of this result with regard to two high-energy astrophysics experiments is discussed. (22 refs.)

Development of the cosmic ray techniques See Entry 59568

The stability of cesium iodide X-ray photocathodes See Entry 59898

Intrinsic limits for acoustic detection of magnetic monopoles See Entry 60094

Development of an improved monitor for portal detection of the unauthorized removal of special nuclear material See Entry 60229

Bunch length measurements in CESR using an X-ray sensitive photoconductive detector See Entry 60500

Reduction of the neutron-induced background using a pulse-type beam chopper in an ISOL experiment See Entry 60504

A semiconductor beta ray spectrometer See Entry 60530

Progress report on heavy ion identification by Bragg Curve Spectroscopy at the Legnaro XTU Tandem Laboratory See Entry 60532

Use of a large multicell ionization detector—the external particle identifier—in experiments with the BEBC hydrogen bubble chamber See Entry 60533

Composite neutron recording systems See Entry 60539

Two-coordinate scintillation hodoscope on the basis of hodoscope photomultipliers See Entry 60541

Using scintillation hodoscopes with hodoscope photomultipliers in particle-momentum measurements and in fast sampling See Entry 60542

Flight-time system with automatic adjustment and logic sampling of information for the Nataliya-2 telescope See Entry 64385

29.90 OTHER TOPICS IN HIGH-ENERGY AND NUCLEAR EXPERIMENTAL METHODS AND INSTRUMENTATION

60559 Survey measurements of the magnetic field of the University of Manitoba spiral ridge cyclotron. J.Bruckshaw, V.Derenchuk, I.Gusdal, J.Lancaster, A.McLwain, S.Oh, S.Pogson, J.S.C.McKee (Cyclotron Lab., Univ. of Manitoba, Winnipeg, Manitoba, Canada).

Nucl. Instrum. & Methods Phys. Res. (Netherlands), vol.207, no.3, p.493-5 (1 April 1983).

A magnetic field mapping system having 52 flipping coils has been developed at the University of Manitoba. Measurements were made in vacuo with an estimated relative error of $\pm 0.04\%$. (12 refs.)

60560 Standard interfaces for program-modular multiprocessor systems (review) [nuclear physics application]. E.V.Chernykh (Joint Inst. for Nuclear Res., Dubna, USSR).

Instrum. & Exp. Tech. (USA), vol.25, no.4, pt.1, p.783-816 (July-Aug. 1982). Translation of: *Prib. & Tekh. Eksp. (USSR)*, vol.25, no.4, p.5-35 (July-Aug. 1982). [received: April 1983]

Interfaces for multiprocessor systems used in nuclear physics experiments are dealt with. The CAMAC system crate has found application in major physics laboratories in the world. Drafts of the interface standards for COMPLEX, E3S, and FASTBUS have been written under the aegis of the EOSNE and NIM committees. The common structural characteristics of multi-processor-system interfaces are identified and the various interfaces are composed on the basis of their throughput and relative cost. (50 refs.)

30.00 ATOMIC AND MOLECULAR PHYSICS

(for physical chemistry, see 82.)

31.00 THEORY OF ATOMS AND MOLECULES

(see also 71. Electron states in condensed matter)

31.10 GENERAL THEORY OF STRUCTURE, TRANSITIONS AND CHEMICAL BINDING

60561 Momentum space properties of atoms. A.Harmalkar, A.M.Simas, V.H.Smith, Jr., W.M.Westgate (Dept. of Chem., Queen's Univ., Kingston, Ontario, Canada).

Int. J. Quantum Chem. (USA), vol.23, no.3, p.811-20 (March 1983). (Proceedings of the Fourth International Congress in Quantum Chemistry, Uppsala, Sweden, 13-20 June 1982).

A systematic investigation of momentum densities $\bar{n}(p)$, Compton profiles $J(q)$, and internally folded densities $B(r)$ has been made for the ground states of the atoms from H to Kr. The data are presented in reduced form by means of the characteristic momentum $p^* = q^*$ and length $r^* = 1/p^*$, where $p^* = [J(0)/2\pi I(0)]^{1/2}$. The results indicate that p^* and $J(0)$ contain the gross

qualitative behavior of the atomic properties in momentum space. They also show that subtle effects over and above the gross scale and size are mostly periodic. (10 refs.)

Comparison of quantal, classical, and semiclassical behavior at an isolated avoided crossing See Entry 60848

Magnetism or bonding: a nearly periodic table of transition elements See Entry 61851

31.15 GENERAL MATHEMATICAL AND COMPUTATIONAL DEVELOPMENTS

60562 Recent advances in simple valence-bond theory and the theory of hybrid bond orbitals. Z.S.Herman (Linus Pauling Inst. of Sci. & Medicine, Palo Alto, CA, USA).

Int. J. Quantum Chem. (USA), vol.23, no.3, p.921-43 (March 1983). (Proceedings of the Fourth International Congress in Quantum Chemistry, Uppsala, Sweden, 13-20 June 1982).

The history of important developments in the theory of hybrid bond orbitals and its application in valence-bond theory is reviewed. One of the salient points, the bond strength of a hybrid orbital, is defined as the value of the angular part of the orbital along the bond direction. Characteristic bond angles corresponding to maxima in the bond strength are presented for various basis sets. In order to alleviate computational difficulties in determining the bond strength for complex systems, an approximation to it, the pair-defect-sum approximation, is described. The results of an exhaustive test of the validity of this approximation are presented. Applications of these ideas to coordinate chemistry are provided. Finally, the case is made for the continued viability of valence-bond theory in this age of omnipresent computer terminals. (97 refs.)

Effective handling of a large configuration state function expansion for an MCSCF state and improved efficiency for two-electron integral transformations in MCSCF See Entry 60570

Computer-generated formulas for some three-center molecular integrals over Slater-type orbitals See Entry 60574

31.20 SPECIFIC CALCULATIONS AND RESULTS

60563 Two-dimensional fully numerical solutions of molecular Hartree-Fock equations: LiH and BH. L.Laaksonen, P.Pyykko, D.Sundholm (Dept. of Phys. Chem., Abo Akad., Abo, Finland).

Chem. Phys. Lett. (Netherlands), vol.96, no.1, p.1-3 (25 March 1983).

A fully numerical Hartree-Fock approach is developed for diatomic molecules. The exchange potential is solved relaxing a local, Poisson-like equation. Improved Hartree-Fock limits are reported for LiH and BH. (12 refs.)

60564 The self-interaction-correlated local spin density approximation. A case of too much correlation?. J.G.Harrison (Dept. of Phys., North Dakota State Univ., Fargo, ND, USA).

Chem. Phys. Lett. (Netherlands), vol.96, no.2, p.181-2 (1 April 1983).

The author carried out total-energy calculations for atoms from H to Ar using the exchange-only (XO) version of Perdew's (1979) orbital self-interaction-correction functional. The author finds that for atoms beyond oxygen, this functional yields better total energies than the full exchange-correlation version. (8 refs.)

60565 Dynamic model and tunneling splittings in LMH₄ non-rigid hydrides. L.Ya.Baranov, A.I.Boldyrev (Inst. of new Chem. Problems, Acad. of Sci., Chernogolovka, USSR).

Chem. Phys. Lett. (Netherlands), vol.96, no.2, p.218-22 (1 April 1983).

A non-rigid model for the molecules LiBH₄, NaBH₄, LiCH₃⁺ is suggested on the basis of ab initio data. The model is used in numerical calculations of the levels of large-amplitude deformation-migration motion of the cation in these molecules. It is shown that the lowest states can be regarded as highly anharmonic bending vibrations, while levels above the barrier should be considered as hindered rotation of the MH₄ group. T_d symmetry is used to classify the states. Tunneling splittings of the vibrational states are 0.01-1 cm⁻¹. (7 refs.)

60566 Channel coupling theory of molecular structure: explanation and elimination of unphysical results. W.K.Ford (Xerox Webster Res. Center, Rochester, NY, USA), J.Sherzer, F.S.Levin.

Chem. Phys. Lett. (Netherlands), vol.96, no.2, p.223-7 (1 April 1983).

Earlier (LCAO) structure calculations for H₂⁺ ungerade and H₂ triplet states based on the channel coupling array (CCA) theory of many-particle collisions have yielded unphysical potential energy curves. It is shown for H₂⁺ that this is a result of not requiring the CCA wavefunction components to obey a certain boundary condition. A simple ansatz obeying this condition is constructed and shown to yield a physically correct, approximate ungerade potential energy. (17 refs.)

60567 Unusual low-energy isomers for simple radical cations. M.J.Frisch, K.Raghavachari (Dept. of Chem., Carnegie-Mellon Univ., Pittsburgh, PA, USA), J.A.Pople, W.J.Bouma, L.Radom.

Chem. Phys. (Netherlands), vol.75, no.3, p.323-9 (15 March 1983).

The radical cations of formalimine, methylamine, formaldehyde, methanol, diazene, hydrazine, nitroxyl, hydroxylamine and hydrogen peroxide, and of isomers derived formally from these systems by means of a 1,2-hydrogen shift have been studied using ab initio molecular orbital theory, including electron correlation. For the ions of formalimine, methylamine and methanol, evidence is presented that the 1,2-hydrogen-shifted species lie lower in energy than the conventional isomers. (30 refs.)

60568 A combination of pseudopotentials and density functionals: results for Li^{m+}, Na^{m+} and K^{m+} clusters (n≤4; m=0.1). J.Flad, G.Igel, M.Dolg, H.Stoll, H.Preuss (Inst. für Theoretische Chem., Univ. Stuttgart, Stuttgart, Germany).

Chem. Phys. (Netherlands), vol.75, no.3, p.331-45 (15 March 1983).

Semi-empirical pseudopotentials, corrected for core polarization, and local density functionals, corrected for self-interaction, are used in valence-only SCF calculations for neutral and singly ionized Li, Na and K clusters with up to four atoms. Results are given for structures, binding and ionization energies. Trends are discussed with special emphasis on the role of core-valence correlation. Comparison is made with accurate ab initio CI calculations where possible. (46 refs.)

60569 Cluster expansion of the wavefunction. Valence and Rydberg excitations, ionizations, and inner-valence ionizations of the CO₂ and N₂O studied by the SAC and SAC CI theories. H.Nakatsuji (Dept. of Hydrocarbon Chem., Kyoto Univ., Kyoto, Japan).

Chem. Phys. (Netherlands), vol.75, no.3, p.425-41 (15 March 1983).

Valence and Rydberg excitations, ionizations, and inner-valence ionizations of CO₂ and N₂O, which are isoelectronic, are studied by the SAC and SAC CI theories. The author has given a systematic assignment of the electronic spec-

tra of these molecules, though there were some controversial situations in the assignment of the spectra. The broad and overlapping features of the spectra of the inner-valence ionizations are due to the existence of a large number of ionization-excitation states mixing with the singly ionized states. The theoretical origins of the similarities and differences in the photoelectron spectra of CO₂ and N₂O are clarified. (48 refs.)

60570 Effective handling of a large configuration state function expansion for an MCSCF state and improved efficiency for two-electron integral transformations in MCSCF. J.Olsen, D.L.Yeager (Dept. of Chem., Texas A & M Univ., College Station, TX, USA).

Int. J. Quantum Chem. (USA), vol.23, no.3, p.789-809 (March 1983).

(Proceedings of the Fourth International Congress in Quantum Chemistry, Uppsala, Sweden, 13-20 June 1982).

Effective solutions for two difficulties which may be present in MCSCF calculation are discussed: (i) The authors show how the large configuration state function state expansion case may be handled simply and effectively without the introduction of extraneous projection operators or Lagrange multipliers; (ii) they present a simplified two-electron integral transformation procedure which significantly reduces the operation count (and hence computational efficiency is increased) for second order and particularly for third order MCSCF procedures. The procedures they introduce use some freedom available in the orthogonal complement CI space and the virtual orbital space to simplify MCSCF calculations. (31 refs.)

60571 Improved SCF interaction energy decomposition scheme corrected for basis set superposition effect. W.A.Sokalski, S.Roszak, P.C.Hariharan, J.J.Kaufman (Dept. of Chem., Johns Hopkins Univ., Baltimore, MD, USA).

Int. J. Quantum Chem. (USA), vol.23, no.3, p.847-54 (March 1983).

(Proceedings of the Fourth International Congress in Quantum Chemistry, Uppsala, Sweden, 13-20 June 1982).

A modified scheme for SCF interaction energy decomposition has been proposed where the nonphysical basis set superposition error (BSSE) has been corrected by means of the counterpoise method. A new procedure to separate the exchange and induction energy terms of nonphysical BSSE has been tested in the case of the H₂O dimer. The first order BSSE appears to be nonnegligible for strong hydrogen bonded complexes. In addition the scheme allows separation of the long-controversial charge-transfer contribution within the induction term, which has been considerably overestimated in previous studies. (26 refs.)

60572 Ordinary field-theoretic methods for self-consistent wave functions which describe bond formation and dissociation. II. Commutative coupling case. W.B.England (Dept. of Chem., Univ. of Wisconsin, Milwaukee, WI, USA).

Int. J. Quantum Chem. (USA), vol.23, no.3, p.905-14 (March 1983).

(Proceedings of the Fourth International Congress in Quantum Chemistry, Uppsala, Sweden, 13-20 June 1982).

For pt.1, see J. Phys. Chem., vol.86, p.1204, (1981). Hartree-Bogoliubov-Valatin (HBV) theory may be implemented with Lipkin Hamiltonians to obtain self-consistent BCS wave functions which describe bond formation and dissociation. These wave functions are in turn vacua for Nambu's representation of Feynman-Dyson-Goldstone diagrammatic perturbation theory, and hence provide suitable references for the many-body treatment of correlation. Exact SCF solutions of the HBV equations are equivalent to special even-replacement MC-SCF solutions. The latter are similar to generalized valence bond theory, and require one Fock operator for each one-particle shell. The commutative coupling case of HBV theory is realized when the number-conserving renormalized one-body and number-nonconserving pairing operators commute. In this case, a set of orbital equations which involves a single Fock operator may be solved. Since this could prove to be a significant simplification for large systems, the commutative coupling and exact solutions are compared here for the fragmentation of H₂ and F₂. Results suggest that commutative coupling orbitals will be useful for the aforementioned many-body theory. (42 refs.)

60573 Ab initio MO investigation of the ethanolamine-formic acid complex. T.Solmajer, M.Hodoseck, D.Hadzi (LEK, Chem. & Pharmaceutical Works, Ljubljana, Yugoslavia).

Int. J. Quantum Chem. (USA), vol.23, no.3, p.945-52 (March 1983).

(Proceedings of the Fourth International Congress in Quantum Chemistry, Uppsala, Sweden, 13-20 June 1982).

The title complex is considered a model for the interaction of catecholamine-type ligands with anionic sites of receptors. It is usually assumed that the ligands interact in the protonated form, but there is no direct evidence of this. Model computations of proton transfer processes should contribute to the elucidation of this important problem. As a first step in this direction the authors have made computations in the STO-4G base of the interaction energies, molecular electrostatic potentials, the potential curves, and the Mulliken population for three different arrangements of the acid and base molecules. Proton potential functions have also been computed for the complexes with two water molecules attached to the acid. The deeper potential well is nearer to the carboxylic oxygen in all cases examined. (27 refs.)

60574 Computer-generated formulas for some three-center molecular integrals over Slater-type orbitals. H.W.Jones (Dept. of Phys., Florida A & M Univ., Tallahassee, FL, USA).

Int. J. Quantum Chem. (USA), vol.23, no.3, p.953-7 (March 1983).

(Proceedings of the Fourth International Congress in Quantum Chemistry, Uppsala, Sweden, 13-20 June 1982).

Exact computer-generated formulas can be produced for each term of an infinite series that gives the value of three-center Coulomb integrals over Slater-type orbitals of the s-type with equal screening constants. As a specific example, the Coulomb energy of an equilateral triangular arrangement of all 1s orbitals is calculated using seven terms of an infinite expansion to obtain an answer comparable to earlier work in elliptic coordinates. Generalization to all three-center cases of this implementation of the Lowden α -function method is straightforward. (8 refs.)

60575 Multiconfigurational Hartree-Fock response functions. P.Jorgensen, P.Swanstrom (Dept. of Chem., Aarhus Univ., Aarhus, Denmark), D.L.Yeager, J.Olsen.

Int. J. Quantum Chem. (USA), vol.23, no.3, p.859-71 (March 1983).

(Proceedings of the Fourth International Congress in Quantum Chemistry, Uppsala, Sweden, 13-20 June 1982).

The linear, quadratic, and cubic response of a multiconfigurational Hartree-Fock state to a time independent one-electron perturbation has been derived. A comparison between the exact response functions as obtained from Rayleigh-Schrodinger perturbation theory and the multiconfigurational Hartree-Fock response functions allows an identification of matrix elements of the perturbation operator between the ground and excited states and between excited states. The authors discuss some ambiguities which result from such an identification. (18 refs.)

60576 Scaling in pseudopotential theory. R.Gaspar (Inst. fur Phys. Chem., Univ. Göttingen, Göttingen, Germany). *Int. J. Quantum Chem. (USA)*, vol.23, no.3, p.1017-24 (March 1983). (Proceedings of the Fourth International Congress in Quantum Chemistry, Uppsala, Sweden, 13-20 June 1982). Simple Gaussian nonlocal pseudopotentials are determined for K shells. Extrapolation formulas are derived for the parameters as functions of the reduced atomic number. Small hybrids are used for the basis function analysis. Comparison is made with the set of molecules in the book by Snyder and Basch (1972) and detailed results are presented for the molecules BH_3 , CH_4 , NH_3 , H_2O , HF , N_2 , CO , BF , CH_3F , C_2H_2 , HCN , CHONH_2 , and CHOOH . Results on energy levels, total energy, total valence energy and dipole moment and in a few cases some geometry predictions are made. (8 refs.)

60577 Molecular orbital study of the homocyclopropenyl cation. R.C.Haddon, K.Raghavachari (Bell Labs., Murray Hills, NJ, USA). *J. Am. Chem. Soc. (USA)*, vol.105, no.1, p.118-20 (12 Jan. 1983). The homocyclopropenyl cation is the simplest homoconjugated system and the first species for which homoaromatic character was involved. The authors hypothesize that at high alkane concentration H abstraction by free and π -complexed chlorine atoms occurs. (19 refs.)

60578 Restatement of conventional electronic wave function determination as a density functional procedure. M.R.Nyden, R.G.Parr (Dept. of Chem., Univ. of North Carolina, Chapel Hill, NC, USA). *J. Chem. Phys. (USA)*, vol.78, no.6, pt.2, p.4044-7 (15 March 1983). It is shown how any conventional ground-state electronic wave function determination starting from a basis set of orthonormal spatial orbitals f_k may be restated as a density functional procedure. Write $f_k = (\rho/N)^{1/2} \exp(i\theta_k)$, with ρ the total electron density, N the number of electrons, and θ_k a function which may have complex as well as real parts. All matrix elements are then expressible as functionals of ρ and the θ_k . Orthonormalization gives $[\rho \exp(-i(\theta_k - \theta_l))] dr = N\delta_{kl}$. With these conditions imposed as constraints, the variational process for determining the energy is equivalent to a procedure for starting from a guessed ρ , determining the θ_k , determining ρ again, and iterating, with the energy decreasing at each stage. The equations are given and discussed in detail for the four-electron Hartree-Fock problem for which the two orbitals are $\phi_1 = (\rho/4)^{1/2} \exp(i\theta)$ and $\phi_2 = (\rho/4)^{1/2} \exp(-i\theta)$, with θ real. A graph of θ is given for the atom Be. (12 refs.)

60579 An orthogonality constrained generalization of the Weizsacker density functional model. M.R.Nyden (Dept. of Chem., Univ. of North Carolina, Chapel Hill, NC, USA). *J. Chem. Phys. (USA)*, vol.78, no.6, pt.2, p.4048-51 (15 March 1983). An exact density functional theory for two orbital systems (such as Hartree-Fock beryllium) is extended to give a density functional model for first-row atoms. The new model is related to the Weizsacker model but it includes additional terms which arise from orthogonality constraints. Two approximate methods based on this model are tested numerically. (5 refs.)

60580 Hydrogen bonds between first-row hydrides and acetylene. M.J.Frisch, J.A.Pople (Dept. of Chem., Carnegie-Mellon Univ., Pittsburgh, PA USA), J.E.Del Bene. *J. Chem. Phys. (USA)*, vol.78, no.6, pt.2, p.4063-5 (15 March 1983). The structures and association energies of the complexes of NH_3 , H_2O and HF with acetylene have been determined using Hartree-Fock and Møller-Plesset theories. HF is found to act as a proton donor to acetylene, while H_2O and NH_3 act as proton acceptors. (13 refs.)

60581 Natural bond orbital analysis of near-Hartree-Fock water dimer. A.E.Reed, F.Weinhold (Dept. of Chem., Univ. of Wisconsin, Madison, WI, USA). *J. Chem. Phys. (USA)*, vol.78, no.6, pt.2, p.4066-73 (15 March 1983). The authors have carried out a natural bond orbital analysis of hydrogen bonding in the water dimer for the near-Hartree-Fock wave function of Pople, Kistenmacher, and Clementi (1973), extending previous studies based on smaller basis sets and less realistic geometry. They find that interactions which may properly be described as 'charge transfer' (particularly the $n \rightarrow \sigma^*_{\text{OH}}$ interaction along the H-bond axis) play a critical role in the formation of the hydrogen bond, and without these interactions the water dimer would be 3-5 kcal/mol repulsive at the observed equilibrium distance. They discuss this result in relationship to Klemperer's general picture of the bonding in van der Waals molecules, and to previous theoretical analyses of hydrogen bonding by the method of Kitauro and Morokuma (1976). (32 refs.)

60582 States of Am in aqueous solution. Won Mok Jae (Hanyang Univ., Seoul, Korea). *J. Korean Nucl. Soc.*, vol.14, no.4, p.172-7 (Dec. 1982). [received: April 1983]

The states of Am in a 10^{-5} M solution has been studied in the pH range of 5 to 10 by filtration and centrifugation methods. Hence the author estimates the possible Am hydrolysis products and solubility constants. If the solubility of $\text{Am}(\text{OH})_3$ estimated by Bacs and Mesmer (1976) is increased about a factor of 10, the calculated curve of Am concentration versus pH is found to agree completely with experimental values. (8 refs.)

60583 Calculation of the polarizability of the sodium atom from the Sturm virtual orbitals of the self-consistent-field method. P.F.Gruzdev, G.S.Soloveva, A.I.Sherstyuk.

Opt. & Spectrosc. (USA), vol.53, no.1, p.1-2 (July 1982). Translation of: *Opt. & Spektrosk. (USSR)*, vol.53, no.1, p.3-5 (July 1982). [received: April 1983] A method for constructing a complete system of basis functions of a purely discrete spectrum was proposed previously (see Opt. Spektrosk., vol.42, p.1198, 1977; Opt. Spectrosc., vol.42, p.690, 1977) for the problem of the perturbation of the stationary states of atoms described in the Hartree-Fock approximation. The present authors report the first numerical implementation of this method. An algorithm has been developed and a program written for solving the system of integro-differential equations of the Hartree-Fock method to find the Hartree-Fock eigenvalues and eigenfunctions and also to determine the eigenvalues and virtual orbitals of the Sturm-Liouville problem. For the particular case of the sodium atom, the possibilities for obtaining purely discrete virtual orbitals is demonstrated. (9 refs.)

60584 Theoretical study of the lowest $^2\Sigma^+$ doubly excited state of H_2 . A.U.Hazi (Lawrence Livermore Nat. Lab., Univ. of California, Livermore, CA, USA), C.Derkits, J.N.Bardsley. *Phys. Rev. A (USA)*, vol.27, no.4, p.1751-9 (April 1983). The energy and width of the $1\sigma_g^2\Sigma^+$ state of H_2 are calculated using Feshbach projection operators and the Stieltjes moment method. The results are compared with an analysis of the double minima in the potential-energy curves of the $^2\Sigma_g^+$ Rydberg states. The doubly excited $1\sigma_g^2$ configuration is unstable with respect to autoionization for $R < 2.65a_0$, and the autoionization rate is sensitive to both the value of the internuclear separation and the energy of the emitted electron. (25 refs.)

On the global variance in the 1-reduced local energy matrix for closed shell fermion systems See Entry 59674

Momentum space properties of atoms See Entry 60561

Recent advances in simple valence-bond theory and the theory of hybrid bond orbitals See Entry 60562

All-electron relativistic calculations on AgH. An investigation of the Cowan-Griffin operator in a molecular species See Entry 60614

Comments on fine-structure intervals of the $1s^2 2s^2 2p^5 \ ^2P$ state in fluorine isoelectronic sequence See Entry 60616

Molecular structure and photoelectron spectra of H_2S , H_2Se and H_2Te . Effective core potential calculations on ground and valence ionic states See Entry 60629

Calculation of X-ray line energies of molybdenum in the transient state by Slater's method See Entry 60640

Calculation of photoionization cross sections for lithium isoelectronic series ions by the Dirac-Fock method See Entry 60672

Derivation of the Hamiltonian of a linear molecule See Entry 60696

Raman spectra, ab initio molecular orbital calculations, vibrational analysis, and thermodynamic functions for NH_3AlX_3 ($\text{X} = \text{F}, \text{Cl}, \text{Br}$) See Entry 60725

A simple treatment of intermolecular interactions: synthesis of ab initio calculations and combination rules See Entry 60884

A semiclassical inversion procedure for the dipole-moment function for diatomic molecules See Entry 60886

An improved self-interaction-corrected local spin density functional for atoms See Entry 60889

A quantum-mechanical explanation of vibronic phenomena in atom-molecule collisions See Entry 60897

Electronegativity equalization and electron transfer in molecules See Entry 60975

Monte Carlo solutions of Schrodinger's equation for H_2^+ ion in strong magnetic fields. II See Entry 61015

Ab initio CI investigation of hydrogen atom adsorption on Li clusters: embedded cluster model See Entry 62254

Localised MO analysis of the 1,2-hydrogen shift mechanism .. See Entry 63511

Ab initio study of electronic coupling in the aqueous Fe^{2+} - Fe^{3+} electron exchange process See Entry 63530

31.20E Ab initio LCAO and GO SCF calculations

60585 Potassium fluoride and phosphorus acid: ab initio calculations and spectroscopic investigations. J.Emsley, J.Lucas, R.J.Parker (Dept. of Chem., King's Coll., London, England), R.E.Overill. *Polyhedron (GB)*, vol.2, no.1, p.19-24 (1983).

Ab initio calculations including the effects of solvation on the hydrogen bonding interactions between F^- and phosphorus acid, HPO_3H_2 , have been performed, resulting in a value of 61 kJ mol^{-1} for the hydrogen bond energy of $[\text{HPO}_3\text{H}_2\text{F}]^-$. Attempts to show that this species exists in aqueous solution have been made using ^{17}O , ^{19}F and ^{31}P NMR spectroscopy and pH and conductance studies, but these indicate that the principal reaction is an acid-base neutralization. Crystals of $\text{KF.HPO}_3\text{H}_2$ grow from aqueous solution but these are not the same as those from methanol solution which are known to be strongly hydrogen bonded. (30 refs.)

60586 Broken symmetry far from equilibrium in molecules within HF formalism. T.Ficker (J. Heyrovsky Inst. of Phys. Chem. & Electrochem., Czechoslovak Acad. of Sci., Prague, Czechoslovakia). *J. Chem. Phys. (USA)*, vol.78, no.6, pt.1, p.3339-41 (15 March 1983).

Considerable interest is currently devoted to the possibility of including relaxation and correlation corrections to the HF solution by lowering the symmetry constraints. The author considers the effects of broken symmetry in HF calculations on valence molecular ions with several symmetry equivalent sites. Ab initio LCAO MO SCF calculations were carried out for the ground, cone, and inner valence hole states of the N_2 molecule. (9 refs.)

60587 Use of the state-averaged MCSCF procedure: application to radiative transitions in MgO . R.N.Diffenderfer, D.R.Yarkony (Dept. of Chem., Johns Hopkins Univ., Baltimore, MD, USA). *J. Phys. Chem. (USA)*, vol.86, no.26, p.5098-105 (23 Dec. 1982).

A state-averaged multiconfiguration self-consistent-field (SA-MCSCF) procedure based on density matrix driven MCSCF algorithm is presented and discussed in terms of its use at the MCSCF/configuration interaction (CI) level. The results will be used to estimate line strengths for specific vibrational levels of the $2^1\Sigma^+$ state. Also presented is a study of the convergence properties of two possible implementations of the SA-MCSCF procedure. It was found that, for a general averaging of several eigenstates, a procedure which includes second derivatives with respect to both orbital and configuration state function parameters is required. (36 refs.)

60588 Molecular and electronic structure of carbonyls of the VIIIth periodic system group. P.Dobryszewski, J.Leszczynski, W.Wojciechowski (Inst. of Inorganic Chem. & Metall. of Rare Elements, Tech. Univ. of Wrocław, Wrocław, Poland).

Mater. Sci. (Poland), vol.7, no.4, p.399-418 (1981). The results of theoretical investigations concerning the molecular and electronic structure of the VIIIth group transition metal carbonyls are reviewed and compared with the experimental data. The properties of the carbonyls of all elements from iron to platinum are discussed as general attributes of the entire group. Special attention is paid to the theoretical quantum mechanical models. (66 refs.)

31.20G Other accurate, or nearly ab initio calculations (DIM method, SAMO method, etc.)

60589 $X\alpha$, Cr_2 , and the symmetry dilemma. B.I.Dunlap (Naval Res. Lab., Washington, DC, USA).

Phys. Rev. A (USA), vol.27, no.4, p.2217-19 (April 1983). $X\alpha$ calculations (with exchange parameter $\alpha=0.7$) are presented for Cr_2 in which the constraint of inversion symmetry on the one-electron orbitals is avoided. The ground state is antiferromagnetic, $^3\Sigma^+$, with equilibrium separation 2.75 Å, vibrational frequency 110 cm^{-1} , and dissociation energy 1.0 eV. This is in qualitative agreement with the generalized-valence-bond calculation of Goodgame and Goddard (1982). (24 refs.)

60590 Electronic structure of radical ions of polycyclic hydrocarbons. M.M.Mestechkin, V.N.Poltavets (Inst. of Phys. Organic Chem. & Coal Tar Chem., Acad. of Sci., Donetsk, Ukrainian SSR). *Theor. & Exp. Chem. (USA)*, vol.18, no.2, p.178-81 (March-April 1982). Translation of: *Teor. & Eksp. Khim. (USSR)*, vol.18, no.2, p.207-11 (March-April 1982). [received: Feb. 1983]
The ionization potentials of a number of conjugated hydrocarbons, as well as the spin densities in the corresponding radical ions, were calculated in the π -electronic approximation and are compared with the constants of hyperfine splitting on the protons. The method of direct calculation of electronic distribution within the framework of the restricted Hartree-Fock method is used in the calculations. (20 refs.)

Approximate relativistic calculations within the one-center approximation for the series CH_4 to PbH_4 See Entry 60611

Mossbauer studies of FeSn molecules isolated in rare-gas solids and SCF-X α -scattered-wave molecular-orbital analyses of Sn_2 and FeSn diatomic molecules See Entry 60774

Electronic structure and low-energy photoelectron spectra of 4,4'-disubstituted 2,2'-bipyridines See Entry 60840

SCF discrete-variational X α calculations of the NH_4Cl Auger spectrum See Entry 60845

31.20N Semi-empirical NDO calculations (CNDO, INDO, MINDO, PCICO methods, etc.)

60591 Quantum study of the ground state of a series of unsaturated boron-nitrogen compounds by the MNDO method. I. Geometries and stabilities. B.Maouche, J.Gayoso (Inst. de Chimie, Univ. des Sci. et de la Technol. Houari Boumediene, Dar-El-Beida, Algeria). *Int. J. Quantum Chem. (USA)*, vol.23, no.3, p.891-904 (March 1983). (Proceedings of the Fourth International Congress in Quantum Chemistry, Uppsala, Sweden, 13-20 June 1982).

A MNDO study of molecular geometries, enthalpies, formation, atomization, bond separation, and hydrogenation of a series of unsaturated boron-nitrogen compounds, linear with two and three members and cyclic with three, four, five, and six members are presented. For all these molecules, MNDO calculations are in excellent agreement with available ab initio calculations or experimental data. The high rotational barrier in aminoborane H_2BNH_2 , 30.6 kcal/mol, and the length of bond in iminoborane HBNH , 1.183 Å, imply strong double and triple BN bond character in these two molecules. In the odd membered heterocycles, examination of the molecular geometries and energies of equilibrium states shows that in all cases, the stability of the compounds grows with the number of boron atoms and decreases with that of the nitrogen atoms. Moreover, compared study of the two BN-fulvenes with their homologous hydrocarbon shows that only BN (BB)-fulvene has a polyenic structure to that of fulvene. (43 refs.)

60592 Transmission mechanisms of spin-spin coupling constants within the CHF approximation: their study using inner projections of the polarization propagator. A.R.Engelmann, R.H.Contreras (Dept. de Fisica, Univ. de Buenos Aires, Buenos Aires, Argentina). *Int. J. Quantum Chem. (USA)*, vol.23, no.3, p.1033-45 (March 1983). (Proceedings of the Fourth International Congress in Quantum Chemistry, Uppsala, Sweden, 13-20 June 1982).

A new method for separating differently transmitted components of spin-spin coupling constants is introduced which is suitable when couplings are calculated using the coupled Hartree-Fock (CHF) approximation via the polarization propagator. Contribution transmitted through different electronic subsystems are found choosing different subsets of orbitals with their corresponding virtual spaces for their description. Examples for two different channels of transmission are given, which are very well known among NMR spectroscopists, namely, components transmitted via π -electron systems, and 'through-space' interactions. In the first case a set of canonical orbitals is chosen, while in the latter noncanonical ones are used. For both cases, numerical results are given within the INDO approximation. These results are compared with others obtained previously by means of the partially restricted molecular orbital approach. The possibility of using this method of inner projections of the polarization propagator in decomposing other second order properties is suggested. (37 refs.)

60593 : A quantum mechanical investigation of clathrate compounds with He and Ne. A.B.Bolotin, V.A.Bolotin, M.-L.Z.Balyavichus, B.F.Gantmakher, E.P.Stumbris, V.M.Tatevskii, E.I.Shapiro, S.S.Yarovoii (Vilnius State Univ., Vilnius, Lithuanian SSR). *Theor. & Exp. Chem. (USA)*, vol.18, no.2, p.182-5 (March-April 1982). Translation of: *Teor. & Eksp. Khim. (USSR)*, vol.18, no.2, p.212-15 (March-April 1982). [received: Feb. 1983]

One of the problems of the present work was to determine the parameters of the semiempirical method on the basis of a comparison of the results of nonempirical calculations on the HeH^+ and NeH^+ molecular ions with calculations carried out in the CNDO/2 approximation. In the study of clathrate compounds, the elucidation of the pathways and the conditions for the insertion of the inert gases He and Ne, which possess the smallest volume in comparison with the other atoms of this group, into a convenient cage, the cubane molecule (C_8H_8), is a natural step. Hence, the second task consisted of studying the stability of the clathrates formed between cubane and He or Ne. (8 refs.)

Electron spin resonance investigation of sulphur-33 and nitrogen-15 substituted dithiazol-2-yl and dithiazolidin-2-yl free radicals See Entry 60765

ESR spectra and spin densities of the radical anions of magnesium and zinc azaporphyrates See Entry 60767

Calculation of the electrooptical parameters and the absolute intensities of the IR bands of the water molecule and its isotopically substituted derivatives See Entry 60777

A CNDO/2 study of the growth of model lithium clusters See Entry 61039

Single versus double insertion in a simple intermolecular carbene reaction See Entry 63517

31.20P Other semi-empirical calculations (Hückel, generalized Hückel, PPP methods, etc.)

60594 Application of the many-body perturbation theory by using localized orbitals. E.Kapuy, Z.Csepes, C.Kozmutza (Phys. Inst., Tech. Univ. Budapest, Budapest, Hungary). *Int. J. Quantum Chem. (USA)*, vol.23, no.3, p.981-90 (March 1983).

(Proceedings of the Fourth International Congress in Quantum Chemistry, Uppsala, Sweden, 13-20 June 1982).
Diagrammatic formulation of the many-body perturbation theory is investigated when both the occupied orbitals and the virtual ones are localized, i.e., they are unitary transforms of the canonical Hartree-Fock orbitals. All diagrams representing ground state correlation energy can be generated through fifth order. For cyclic polyenes C_6H_6 and $\text{C}_{10}\text{H}_{10}$ as model systems, the energy corrections are calculated in the Pariser-Parr-Pople approximation for a wide range of the coupling constant β^{-1} , through fourth order including some fifth order terms. The results are compared to those obtained by other methods: perturbation theory by using canonical orbitals and full CI. The effect of neglecting contributions from orbitals localized into neighbouring sites is also studied. (28 refs.)

60595 Excited states of linear polyenes in the SCF-RPA method. M.Baldo, R.Pucci, P.Tomasello (Istituto di Fisica, Univ. di Catania, Catania, Italy). *Int. J. Quantum Chem. (USA)*, vol.23, no.3, p.1111-19 (March 1983).

(Proceedings of the Fourth International Congress in Quantum Chemistry, Uppsala, Sweden, 13-20 June 1982).

In the framework of the PPP Hamiltonian, the authors have studied the low-lying spectra of all trans linear polyenes with the dielectric function method. It is shown that higher order processes, not included in the RPA scheme as local field correction (LFC) and self-energy (SE) effects can be introduced in a effective way by a suitable parametrization of the residual coulomb interaction. This parametrization is fixed along the polyene series both for singlet and triplet states, at variance with previous RPA calculations. Comparison with the most refined CI calculations as well as with the experimental findings shows very good agreement. Furthermore, chain length and geometry dependence of the electron-electron correlation is briefly discussed. (21 refs.)

60596 Theory of electronic structures and lattice distortions in polyacetylene and itinerant Peierls systems. II. Coulomb interaction dependences of the HF ground state, lattice dimerization and ^1Bu excited state in regular trans-polyacetylene. H.Fukutome, M.Sasai (Dept. of Phys., Kyoto Univ., Kyoto, Japan). *Prog. Theor. Phys. (Japan)*, vol.69, no.1, p.1-19 (Jan. 1983).

For pt.I see *ibid.*, vol.67, no.1, p.41-67 (1982). The authors study the Coulomb interaction dependences of the HF ground state, lattice dimerization and ^1Bu excited state in regular trans-polyacetylene using the PPP Hamiltonian model. The nature of the HF ground state is determined by the relative magnitudes of the on site and nearest neighbour parts and the screening of the longer range part of the effective Coulomb potential. The SSH model has implicitly taken into account the nearest neighbour exchange interaction. The Franck-Condon band gap is mostly determined by the nearest neighbour exchange interaction. The ^1Bu excited state is excitonic. The exciton binding energy is estimated for the effective Coulomb potential with the screened long range part. To explain the observed ^1Bu excitation energy, the short range part of the effective Coulomb potential must be screened by about half compared to the one in small conjugate molecules. The condition for splitting of the exciton into a zwitter ionic pair of charged solitons is discussed. (12 refs.)

60597 Quantum chemical investigations on colour and stereodynamics of acyclic azines. X. Potential parametrization in the framework of the QCFF-PI method for complete geometry optimisation of acyclic azines. S.Vettermann, K.Gustav (Sektion Chemie, Friedrich Schiller Univ., Jena, Germany). *Wiss. Z. Friedrich-Schiller-Univ. Jena, Math. Naturwiss. Reihe (Germany)*, vol.31, no.6, p.1107-12 (1982). In German. (16 refs.)

ESR spectra and spin densities of the radical anions of magnesium and zinc azaporphyrates See Entry 60767

Studies of some iron dithiolate complexes by the ESCA, Mossbauer and extended Hückel methods See Entry 60978

31.20T Electron correlation and CI calculations

60598 Broken-symmetry Hartree-Fock description of deep core and outer valence hole states: the $3d_{\sigma}$ and $4d_{\sigma}$ hole states of Ag_2^+ . M.Benard (Lab. de Chimie Quantique, Univ. Louis Pasteur, Strasbourg, France). *Chem. Phys. Lett. (Netherlands)*, vol.96, no.2, p.183-91 (1 April 1983).

Symmetry-adapted and broken-symmetry Hartree-Fock and CI calculations have been carried out on the $3d_{\sigma}$ and $4d_{\sigma}$ hole states of Ag_2^+ at various distances. The Cizek-Paldus (1967) doublet stability problem is investigated. Calculations confirm the reliability of broken-symmetry solutions for core hole states, but show that valence hole states are better described by a CI expansion restricted to single excitations with respect to the zeroth-order description of the ion. (25 refs.)

60599 Optical oscillator strengths of $3p^63d^2 \rightarrow 3p^53d^2 2^{\circ}p^{\circ}$, $2^{\circ}p^{\circ}$ transitions in Co^{8+} , Cu^{10+} and Zn^{11+} ions. S.N.Tiwary (Dept. of Appl. Math. & Theoretical Phys., Queen's Univ. of Belfast, Belfast, N Ireland).

Chem. Phys. Lett. (Netherlands), vol.96, no.3, p.333-6 (8 April 1983).
The author has calculated the excitation thresholds and optical oscillator strengths (OOS) for $3p^63d^2 \rightarrow 3p^53d^2 2^{\circ}p^{\circ}$, $2^{\circ}p^{\circ}$ and $2^{\circ}f^{\circ}$ transitions in Co^{8+} , Cu^{10+} and Zn^{11+} ions of the potassium isoelectronic sequence using Hartree-Fock (HF) and configuration interaction (CI) wavefunctions for both initial and final states. The CI values of the length and velocity form of OOS are in good agreement with each other. The trends in the oscillator strengths for the potassium isoelectronic sequences are plotted. (9 refs.)

60600 Cumulative B_k approximation as a method to select configurations for CI calculations of transition energies. M.A.C.Nascimento (Dept. de Fisico-Quimica, Univ. Federal do Rio de Janeiro, Rio de Janeiro, Brazil). *Int. J. Quantum Chem. (USA)*, vol.23, no.3, p.1011-16 (March 1983).

(Proceedings of the Fourth International Congress in Quantum Chemistry, Uppsala, Sweden, 13-20 June 1982).

A cumulative B_k approximation is examined as a method to select configurations for CI calculations of transition energies where all the matrix elements are computed (full CI). The results obtained by this approach indicate that the transition energies are comparable to the ones obtained at the full CI level. Even for truncation errors of 1 mhartree, the transition energies differ from the full CI ones by less than 0.1 eV. (20 refs.)

60601 On the nature of the bonding in Cu_2 —a comment. L. Pauling

(Linus Pauling Inst. of Sci. & Medicine, Palo Alto, CA, USA).
J. Chem. Phys. (USA), vol.78, no.6, pt.1, p.3346 (15 March 1983).
For original paper see C.W. Bauschlicher et al., *ibid.*, vol.76, p.6015 (1982). Bauschlicher, Walch, and Siegbahn have reported the results of their theoretical treatment of the structure of the Cu_2 molecule by an SCF-MCSCF-CI treatment. They concluded that the ground state involves a 4s-4s single bond, arising from the $^2\text{S}(3d^{10}4s^1)$ level of each of the two atoms. The author feels that they are good semiempirical arguments to support the thesis that the bond in this molecule is not a single bond, but is instead a triple bond based on the configuration $3d^9 4s^1$ for each of the two atoms. (8 refs.)

60602 On the nature of the bonding in Cu_2 —an ab initio viewpoint.

C.W. Bauschlicher, Jr. (NASA Ames Res. Center, Moffett Field, CA, USA), S.P. Walch, P.E.M. Siegbahn.
J. Chem. Phys. (USA), vol.78, no.6, pt.1, p.3347-8 (15 March 1983).
The authors have performed additional calculations on Cu_2 using the basis with f functions derived previously (*ibid.*, vol.76, p.6015 (1982)). In these calculations, a CASSCF calculation is performed, where the two 4s electrons are distributed in all possible ways among the 4s and 4p orbitals. This is followed by a 22 electron singles and doubles CI from the four most important references in the basis of natural orbitals of the CASSCF. (5 refs.)

60603 The nature of hydrogen bonding in the NN-HF, OC-HF, and HCN-HF complexes. M.A. Benz, C.E. Dykstra (Dept. of Chem., Univ. of Illinois, Urbana, IL, USA).

J. Chem. Phys. (USA), vol.78, no.6, pt.2, p.4052-62 (15 March 1983).
The nature of hydrogen bonding in the complexes NN-HF and OC-HF, as revealed from detailed ab initio electronic structure calculations, is unlike the bonding in the isoelectronic HCN-HF complex. The strong dipole-dipole attraction in HCN-HF is absent in the other two complexes. Competing effects that are possible in all hydrogen bonds are unmasked in NN-HF and OC-HF. Calculations have been performed with a number of large basis sets, extensive treatment of electron correlation, energetic partitioning, and evolution of molecular properties. The potential energy surfaces that were generated demonstrate the linearity of the equilibrium structures, and show roughly comparable flexibility for bending, thus refining somewhat the experimentally inferred picture. In NN-HF and OC-HF, less than one-half of the hydrogen bond strength of each is due to just the interaction of the unrelaxed charge distributions of the monomers; while polarization of monomer electron distributions accounts for most of the remaining attraction. There is consequently a substantial electric dipole moment enhancement. The total correlation effect is responsible for about one-third of the well depth in NN-HF and OC-HF. Charge transfer is unimportant in all three complexes. (98 refs.)

60604 The low-lying $2\Sigma^-$ states of OH. E.F. van Dishoeck (Sterrewacht-Huygens Lab., Leiden, Netherlands), S.R. Langhoff, A. Dalgarno.

J. Chem. Phys. (USA), vol.78, no.7, p.4552-61 (1 April 1983).
Potential energy curves for the two lowest $2\Sigma^-$ states of OH are computed at the configuration-interaction level using four different basis sets. Electronic transition dipole moments connecting the excited $1^2\Sigma^-$ and $2(D)^2\Sigma^-$ states with each other and with the ground $X^2\Pi$ state are presented as functions of internuclear distance. The theoretical absorption oscillator strengths for the $D^2\Sigma^-$ ($v''=0$)— $X^2\Pi(v''=0)$ transition are in good agreement with the empirical value derived from astronomical measurements. The photodissociation cross sections for absorption from the $v''=0$, 1, and 2 levels of the ground state into the continuum of the $1^2\Sigma^-$ state are calculated, and the interstellar and cometary photodissociation rates are derived. (17 refs.)

60605 A theoretical investigation of the bond length of dichromium. R.A. Kok, M.B. Hall (Dept. of Chem., Texas A&M Univ., College Station, TX, USA).

J. Phys. Chem. (USA), vol.87, no.5, p.715-17 (3 March 1983).
Generalized molecular orbital (GMO) and configuration interaction (CI) calculations of dichromium predict a bond length of 1.73 Å. This is in close agreement with recent resonant two-photon ionization spectroscopy results which yielded a bond length of 1.68 Å. (20 refs.)

60606 Theoretical calculation of the lowest electronic excited states of BO_2 . V. Sarawathy, J.J. Diamond, G.A. Segal (Dept. of Chem., Univ. of Southern California, Los Angeles, CA, USA).

J. Phys. Chem. (USA), vol.87, no.5, p.718-19 (3 March 1983).
Extensive configuration interaction calculations are reported for the first three doublet states of BO_2 . Agreement with available experimental data is excellent and the position of the $\text{C}^2\Sigma_g^+$ state is predicted. (9 refs.)

60607 Comparison of local density functional Hartree-Fock and configuration interaction in the STO-3G orbital basis for some first-row diatomics. T.B. Grimley, V.C. Jyothi Bhasu (Donnan Labs., Univ. of Liverpool, Liverpool, England).

J. Phys. B (GB), vol.16, no.7, p.1125-31 (14 April 1983).
The local density functional (LDF) scheme has been implemented in Gaussian orbital basis sets by modifying GAUSSIAN70. Calculations for H_2 , Li_2 , N_2 and F_2 with the STO-3G basis set show that the LDF scheme is generally better than Hartree-Fock in reproducing bond lengths and vibration frequencies, and is comparable with configuration interaction (CI) in the same basis. Energy changes in the valence electrons are, however, better described with LDF than with CI. STO-3G results for fourteen closed-shell atoms and ions in the LDF scheme are also given. (14 refs.)

60608 The direct CI method. A detailed analysis. V.R. Saunders (Daresbury Lab., SERC, Warrington, England), J.H. van Lenthe.

Mol. Phys. (GB), vol.48, no.5, p.923-54 (10 April 1983).
A thorough analysis of the direct CI method as applied to the case of a general set of reference configurations coupled to all single and double substitutions is presented. It is pointed out that there is no single strategy which proves optimal under all circumstances. A variety of procedures are therefore presented together with rules to enable the selection of the most favourable under a given circumstance. Much emphasis has been placed on organizing the calculations via a series of matrix multiplications, which enables a vector or array processing computer to be used to best effect. Some consideration is given to using an atomic integral (rather than molecular integral) driven scheme for some interactions, thus removing the necessity for a complete transformation of the molecular integrals to a molecular orbital basis, and the advantages and disadvantages of so doing are discussed. Improved procedures for carrying out both full and partial transformations of the molecular integrals are described. A number of test case calculations involving configuration lists of the order of 10^4 have been analysed in detail, to give a clear picture of the cost of the various interaction types which arise, and indicating that integrals carrying two external molecular orbital indices account for approximately 60 per cent of the cost in typical cases. Typically, a calculation involving 10^5 configurations requires approximately two minutes of CRAY-1 computer time, allowing for ten iterations of the diagonalization procedure. The cost of the calculations is found, somewhat surprisingly, to be approxi-

mately linear in the dimension of the configuration space, indicating that calculations involving 10^6 configurations are now quite feasible. (37 refs.)

60609 Resonance scattering theory: application to the broad $\text{He}^- 1s2s2p^2P^0$ resonance. Y. Komminos, G. Aspromalis, C.A. Nicolaides (Theoretical & Physical Chem. Inst., Res. Found., Athens, Greece).
Phys. Rev. A (USA), vol.27, no.4, p.1865-70 (April 1983).

A resonance scattering theory for many-electron resonances is applied to the analysis of the $\text{He}^- 1s2s2p^2P^0$ resonance. The authors have found that multi-configurational Hartree-Fock theory is applicable even in such cases and predicts the Feshbach nature of the state. Furthermore, by including electron correlation and off-energy-shell pseudostates, they demonstrate the strong energy dependence of the width of this resonance. They suggest that this is the reason for the discrepancy of recent theoretical results with experimental ones, the theoretically predicted cross section is asymmetric, whereas the recent experimental one is symmetric but non-Lorentzian. Defining the position and width of the resonance at maximum and half-maximum values of the cross section correspondingly, they find $E_R=20.26$ eV and $\Gamma_R=600$ meV, compared with the experimental values of $E_R=20.27$ eV and $\Gamma_R=780$ meV. (22 refs.)

Cluster expansion of the wavefunction. Valence and Rydberg excitations, ionizations, and inner-valence ionizations of the CO_2 and N_2O studied by the SAC and SAC CI theories See Entry 60569

A theoretical study on the mechanism of electronic to vibrational energy transfer in $\text{Hg}(\text{P})+\text{CO}$ collisions See Entry 60926

Nonadjustable exchange-correlation model for electron scattering from closed-shell atoms and molecules See Entry 60987

Molecular clustering about a positive ion. Structures, energetics, and vibrational frequencies of the protonated hydrogen clusters H_3^+ , H_5^+ , H_7^+ , and H_9^+ See Entry 61044

C_{2v} insertion pathway for BeH_2 : a test problem for the coupled-cluster single and double excitation model See Entry 63515

Contracted CI calculations of models for catalytic reactions involving transition metals See Entry 63516

Single versus double insertion in a simple intermolecular carbene reaction See Entry 63517

31.30 CORRECTIONS TO ELECTRONIC STRUCTURE

60610 Jahn-Teller-like progressions in the absence and presence of Jahn-Teller distortions. B. Scharf (Dept. of Chem., Ben-Gurion Univ. of the Negev, Beer Sheva, Israel).

Chem. Phys. Lett. (Netherlands), vol.96, no.1, p.89-92 (25 March 1983).
Prominent progressions of non-totally symmetric modes may ensue in non-linear molecules in electronic transitions involving degenerate states in the absence of Jahn-Teller distortions. In the presence of Jahn-Teller interactions prominent non-Jahn-Teller progressions may result. (46 refs.)

60611 Approximate relativistic calculations within the one-center approximation for the series CH_4 to PbH_4 . A. Aguilar-Ancoño, J.L. Gázquez, J. Keller (Facultad de Química, Univ. Nacional Autónoma de México, México City, México).

Chem. Phys. Lett. (Netherlands), vol.96, no.2, p.200-3 (1 April 1983).
Using a one-component relativistic theory combined with an $X\alpha\beta$ local exchange, the authors carried out calculations for the series CH_4 to PbH_4 within the spherically symmetric one-center expansion approximation. Bond lengths, breathing force constants, ionization potentials and spin-orbit splitting of the filled valence p shell thus obtained, are found to be in excellent agreement with Dirac-Hartree-Fock results. (20 refs.)

60612 Atomic inner-shell transitions—theory and the need for experiments. B. Crasemann (Chem. Phys. Inst., Univ. of Oregon, Eugene, OR, USA).

IEEE Trans. Nucl. Sci. (USA), vol.ns-30, no.2, p.887-90 (April 1983). (1982 IEEE Conference on the Application of Accelerators in Research and Industry, Denton, TX, USA, 8-10 Nov. 1982).

The physics of the innermost shells of atoms is qualitatively different in several respects from that of outer electrons. For single deep holes, correlation effects are slight, while the effects of relativity are pronounced and quantum-electrodynamic shifts can be substantial. These relativistic and QED effects can be explored with high precision because many-body aspects are limited and self-consistent-field approaches can be relied upon. Problems of particular current interest concern the screening of the self energy and the effect of the Breit interaction on multiplet splitting and on X-ray hyperfine shifts. Experimental studies as well as calculations of the properties of few-hole and few-electron atomic systems can lead to significant tests of current theory. (27 refs.)

60613 General variation method for the relativistic calculations of atoms and molecules. T. Kagawa (Dept. of Phys., Nara Women's Univ., Nara, Japan).

Int. J. Quantum Chem. (USA), vol.23, no.3, p.973-9 (March 1983). (Proceedings of the Fourth International Congress in Quantum Chemistry, Uppsala, Sweden, 13-20 June 1982).

Use of the general variation method of Weinstein and MacDonald for the relativistic calculation of atoms and molecules is proposed. It is shown from the numerical calculations for hydrogenlike atomic systems that this method is useful in judging an accuracy of energies and wave functions obtained with a relativistic Hamiltonian whose spectra are not bounded. It is also shown that this method can be used to find spurious solutions such as $1p_{1/2}$ or $2d_{3/2}$ appearing in atomic systems. Problems in extending the method to many-electron atoms and molecules are discussed. (12 refs.)

60614 All-electron relativistic calculations on AgH. An investigation of the Cowan-Griffin operator in a molecular species. R.L. Martin (Theoretical Div., Los Alamos Nat. Lab., Los Alamos, NM, USA).

J. Phys. Chem. (USA), vol.87, no.5, p.750-4 (3 March 1983).
The Cowan-Griffin relativistic operator, which retains only the mass-velocity and one-electron Darwin terms of the Breit-Pauli Hamiltonian, has been shown to provide a remarkably good approximation to the more sophisticated Dirac-Hartree-Fock (DHF) approach for many atomic systems. The result of applying the Cowan-Griffin operator in first order to a nonrelativistic self-consistent-field (SCF) wave function expanded in a basis of Gaussian functions is reported for Ag and AgH. Comparisons are made with previously reported numerical wave functions for Ag and with the recent Slater-type-orbital expansion of the DHF wave function for AgH reported by Lee and McLean (1982). (15 refs.)

60615 1/Z expansion calculation of the Bethe logarithm for the ground state Lamb shift of two-electron ions. S.P.Goldman (Dept. of Phys., Univ. of Western Ontario, London, Ontario, Canada), G.W.F.Drake. *J. Phys. B (GB)*, vol.16, no.7, p.L183-7 (14 April 1983).

The leading two terms in the 1/Z expansion of the two-electron Bethe logarithm are calculated by the application of a few finite basis set method. The results can be expressed in the form $\ln(1s^2 S) = \ln[19.77(Z - 0.0063)^2]$. The high-Z behaviour appears to differ from that of a previous variational calculation by Ashamar and Austvik (1976). (18 refs.)

60616 Comments on fine-structure intervals of the $1s^2 2s^2 2p^5$ 2P state in fluorine isoelectronic sequence. J.Hata, I.P.Grant (Theoretical Chem. Dept., Univ. of Oxford, Oxford, England), B.P.Das. *J. Phys. B (GB)*, vol.16, no.7, p.L189-92 (14 April 1983).

The MCDF-EAL method is used to calculate fine-structure intervals of the $1s^2 2s^2 2p^5$ 2P state in the fluorine isoelectronic sequence, and compared with experiment and MCDF-OL results by Kim and Huang (1982). No systematic discrepancies between the theory and experiment are found. (9 refs.)

60617 Sum rules including first order quantum corrections for neutron scattering experiments on isotopic mixtures of monatomic fluids. H.Fredrikze (Interuniv. Reactor Inst., Delft, Netherlands). *Mol. Phys. (GB)*, vol.48, no.5, p.903-22 (10 April 1983).

The sum rules for neutron scattering experiments on monatomic isotopic mixtures are studied. The scattering is separated into a selfpart and a distinct part rather than into an incoherent part and a coherent part. Exact expressions for the moments are derived in terms of polynomials in \hbar^2 . The coefficients in these polynomials are sums of averages of hermitean operators that have a classical analogue. For the interpretation, the coefficients are approximated including first order quantum corrections. It is argued that the separation into coherent and incoherent scattering is not justified in the presence of 'isotopic incoherence'. Approximate expressions for the sum rules are proposed, in which combined averages (over the isotopic composition) appear of the scattering amplitudes and masses of the scattering atoms. These expressions, including first order quantum corrections to the sum rules, are not available in the literature. The importance of correct averaging over the isotopic composition of expressions that involve scattering amplitudes and masses is discussed for the case of a maximum incoherent mixture of ^{36}Ar and ^{40}Ar . (11 refs.)

60618 Relativistic corrections in atomic calculations. I.J.Ketley (Dept. of Maths., Univ. of Southampton, Southampton, England), R.E.Moss. *Mol. Phys. (GB)*, vol.48, no.5, p.1131-3 (10 April 1983).

Despite advances in fully relativistic calculations on atoms and molecules a number of problems remain and such calculations are not yet routine. The estimation of relativistic corrections and effects will continue to be made using non-relativistic wavefunctions and perturbation theory. This note is confined to the one electron problem for which Titchmarsh (1962) has shown that, for certain cases including the hydrogen atom, the relativistic problem may in principle be treated as a perturbed Schrodinger equation and the eigenvalues and eigenvectors expanded as power series in α the fine structure constant. However, when attempts are made to do this in practice, problems are encountered for relativistic corrections of order $mc^2 \alpha^6$ and higher, where mc^2 is the electron rest energy. This is because the Coulomb potential due to a nucleus is singular, so that divergent energy contributions appear and, in addition, delta function contributions arise. If these problems are not recognized, unreliable results may be obtained in numerical calculations, since the cancellation of very large numbers may occur, and also some contributions may be missed. (7 refs.)

Atomic electrons in nuclear processes: attractive nuisance or useful telltale? See Entry 60146

Use of the state-averaged MCSCF procedure: application to radiative transitions in MgO See Entry 60587

Technique for Lamb-shift measurements on high-Z ions produced by a hot plasma See Entry 60656

The rotational spectrum and molecular properties of the hydrogen cyanide hydrogen bromide complex See Entry 60701

^{83}Kr nuclear quadrupole coupling, microwave spectrum, and structure of KrHCN See Entry 60704

The rotational spectrum and molecular structure of the benzene-hydrogen chloride complex See Entry 60705

The structure and molecular properties of the acetylene-HCN complex as determined from the rotational spectra See Entry 60706

The relativistic theory of the chemical shift See Entry 60746

Measurement of the ^{14}N nuclear quadrupole couplings in the lowest ($n\pi^*$) excited triplet state of pyrazine by ODMR See Entry 60748

ESR of pseudorotating $^6\text{Li}_3$ and $^7\text{Li}_3$ See Entry 60763

High-resolution gas phase emission and laser induced fluorescence excitation spectra of $1,3,5\text{-C}_6\text{F}_3\text{H}_3^+$ and $1,3,5\text{-C}_6\text{F}_3\text{D}_3^+$: critical bands in the Jahn-Teller effect analysis See Entry 60805

The unimolecular decomposition rates of energy selected methylnitrite and deuterated methylnitrite ions See Entry 63526

31.50 EXCITED STATES

60619 Electronic excited state transport among molecules distributed randomly in a finite volume. M.D.Ediger, M.D.Fayer (Dept. of Chem., Stanford Univ., Stanford, CA, USA).

J. Chem. Phys. (USA), vol.78, no.5, p.2518-24 (1 March 1983). A theoretical study of electronic excited state transport among molecules randomly distributed in a finite volume is carried out. Two special cases of the general transport and trapping problem are treated. A truncated series expansion in powers in the chromophore density is used as an approximation for one component systems (i.e. donor-donor transport only). In two component systems of donors and traps, the Forster limit, in which transfer can occur only from donors to trap due to low donor concentrations, is solved exactly for a finite spherical volume. In both cases, the results presented demonstrate that time-dependent observables can be significantly altered in finite volume systems relative to infinite volume systems. These calculations have implications for the interpretation of experiments performed on real finite volume systems, e.g. energy transport among the chromophores of an isolated polymer chain. (15 refs.)

60620 Evidence that the excited-state geometry of diphenylbutadiene is nearly planar. W.A.Yee, J.S.Horwitz, R.A.Goldbeck, C.M.Einterz, D.S.Kliker (Div. of Natural Sci., Univ. of California, Santa Cruz, CA, USA). *J. Phys. Chem. (USA)*, vol.87, no.3, p.380-2 (3 Feb. 1983).

A structural analogue of diphenylbutadiene (DPB), 1,5-diphenyl-2,3,4,6,7,8-hexahydronaphthalene (HHN), was synthesized and its spectral properties

were studied. Absorption and fluorescence spectra indicate that HHN has a ground-state geometry in which the phenyl rings are twisted relative to the polyene unit and a nearly planar lowest excited B_u state geometry. The $S_0 \rightarrow S_1$ spectra of DPB and HHN are similar as are the $T_0 \rightarrow T_1$ spectra. DPB and HHN show temperature dependences of fluorescence lifetimes with similar Arrhenius activation energies and similar radiative decay constants. It is concluded that relaxation of excited DPB occurs from an excited state in which the polyene moiety is nearly planar. (23 refs.)

60621 Dispersion coefficients for atoms in different states. B.Silvi (Lab. de Spectrochimie Moléculaire, Univ. Pierre et Marie Curie, Paris, France), V.Chandrasekharan.

Mol. Phys. (GB), vol.48, no.5, p.1053-66 (10 April 1983). A formalism allowing the calculation of dispersion coefficients between atoms in different excited states is presented. The validity of the integral transformation involving dynamical polarizabilities of each atom at imaginary frequencies is discussed and for this case a partition of the second order energy which allows a partial separation into single centre contributions is proposed. With respect to the interaction of ground state atoms a new contribution, the dynamic induction due to the allowed downward transitions, appears. The C_6 coefficients of $\text{H}_1 + \text{H}_{2s}$, $\text{H}_1 + \text{H}_{2p}$ and $\text{H}_{2s} + \text{H}_{2s}$ are calculated exactly. Approximate formulae are proposed and discussed. Upper and lower bounds are calculated by the method of Pade approximant for the interaction of excited hydrogen with ground state gas atoms. (47 refs.)

60622 Population of the three major exit channels in the $3d$ resonance region of atomic gallium. M.O.Krause (Oak Ridge Nat. Lab., Oak Ridge, TN, USA), F.Cerrina, A.Fahlman.

Phys. Rev. Lett. (USA), vol.50, no.15, p.1118-21 (11 April 1983). The exit channels in the region of the $3d \rightarrow 4p$ resonance of atomic gallium were determined in a photoemission experiment. The population of the three major channels involving $4p$ and $4s$ electrons was measured by the constant-ionization-state method for twenty resonant states between 18.8 and 21.7 eV, and the angular distribution of the emitted electrons was obtained. As a result, an autoionization case in which many resonances and many continua are coupled has been characterized in the most comprehensive experiment to date. (15 refs.)

60623 Hyperfine structure and three-channel quantum-defect theory of $6snd^1D_2$ Rydberg states of Ba. H.Rinneberg, J.Neukammer (Inst. für Atom- und Festkörperphys., Freie Univ. Berlin, Berlin, Germany). *Phys. Rev. A (USA)*, vol.27, no.4, p.1779-89 (April 1983).

The hyperfine structure of $6snd^1D_2$ Rydberg states of $^{135,137}\text{Ba}$ is reported for principal quantum numbers ranging between $n=10$ and $n=50$. From the authors' data, singlet-triplet mixing coefficients have been deduced. A three-channel quantum-defect model has been used to analyze the resonance in singlet-triplet mixing of $6snd^1D_2$ and 3D_2 Rydberg states in the vicinity of the $5d^1D_2$ perturber. For the determination of the scattering matrix, hyperfine-structure data were found to be essential. Good agreement has been achieved between calculated and experimental singlet-triplet mixing coefficients. (21 refs.)

60624 Application of the Faddeev-Watson expansion to thermal collisions of Rydberg atoms with neutral particles. E.de Prunelle (Service de Phys. des Atomes et des Surfaces, CENS, Gif-sur-Yvette, France).

Phys. Rev. A (USA), vol.27, no.4, p.1831-43 (April 1983). The Faddeev-Watson expansion (FWE) for the T operator is applied to the study of thermal collisions between Rydberg atom and neutral atom. These collisions are considered as a three-body problem (the perturber, the Rydberg electron, and its parent core) and it is assumed, as already done in most theoretical works dealing with Rydberg-atom-atom collisions, that the core-perturber interaction can be neglected. Then the evaluation of the FWE first- and second-order terms is made tractable by using an appropriate separable potential for the Rydberg-electron-perturber interaction. The evaluation of the second-order term allows the authors to estimate the importance of taking into account explicitly the Rydberg-electron-core interaction in the expression of the (three-body) T operator for the thermal collisions considered. Detailed calculations for the process $\text{Rb}(n,l=0) + \text{He} \rightarrow \text{Rb}(n',l') + \text{He}$ are presented and discussed. The FWE second-order term has been evaluated for the first time by taking the (two-body) t operator associated with the Rydberg atom (valence electron plus parent core) as the Coulomb potential. The contribution of the FWE second-order term to the scattering amplitude decreases as n increases and is found especially significant when both the momentum transfers involved in the collision are large and the values of l and l' are small. (19 refs.)

60625 Radiative lifetimes of excited states of atoms. Ya.F.Verolain, A.Ya.Nikolaich (A.A. Zhdanov Leningrad State Univ., Leningrad, USSR). *Sov. Phys.-Usp. (USA)*, vol.25, no.6, p.431-47 (June 1982). Translation of: *Usp. Fiz. Nauk (USSR)*, vol.137, no.2, p.305-38 (June 1982). [received: April 1983].

A review of experimental and theoretical studies of radiative lifetimes of excited states of the hydrogen atom, of atoms of alkali metals, and atoms of the copper subgroup is presented. A complete compilation of all published values of radiative lifetimes of all excited states with a critical analysis for every atom is given. The regularities in the variation of radiative lifetimes in spectral series of excited states are brought out and constants of the power-law dependences on the effective principal quantum number are determined. A correlation between the behavior of lifetimes and the effective orbital parameter is established and it is proposed to use this correlation for the determination of the application limits of the power-law constants for evaluation of lifetimes of uninvestigated states. On the basis of a critical analysis of published sources, of the regularities in the variation of lifetimes and of a statistical treatment of values available in the literature, a table of recommended values of radiative lifetimes of excited states of all atoms of the first group is compiled. (175 refs.)

Atomic final-state interactions in tritium decay See Entry 60142

Channel coupling theory of molecular structure: explanation and elimination of unphysical results See Entry 60566

Multiconfigurational Hartree-Fock response functions See Entry 60575

Excited states of linear polyenes in the SCF-RPA method See Entry 60595

Theoretical calculation of the lowest electronic excited states of BO_2 See Entry 60606

Molecular structure and photoelectron spectra of H_2S , H_2Se and H_2Te . Effective core potential calculations on ground and valence ionic states See Entry 60629

Two-step optogalvanic spectroscopy of neutral barium: observation and interpretation of the even levels above the $6s$ ionization limit between 5.2 and 7 eV See Entry 60634

Z dependence of the probabilities for 3-3 and 2-2 transitions for excited states in the isoelectronic sequence of Ne See Entry 60651

- Regularities in the radiative lifetimes of excited states of the hydrogen atom ... See Entry 60653
- Interaction between two Rydberg series of autoionizing levels in barium See Entry 60667
- Theoretical cross sections for nonresonant five-photon ionisation of sodium See Entry 60669
- Microwave ionization of Na Rydberg levels See Entry 60673
- $\lambda^2\Pi - \lambda^2\Sigma^+$ infrared electronic transition of C_2H^+ See Entry 60719
- Supersonic expansion cooling of electronically excited OH radicals See Entry 60739
- Rydberg series converging to the \tilde{C} state of $C_6F_6^+$ in threshold photoelectron and VUV absorption spectra of hexafluorobenzene See Entry 60743
- Measurement of the ^{14}N nuclear quadrupole couplings in the lowest ($n\pi^*$) excited triplet state of pyrazine by ODMR See Entry 60748
- Rydberg-Rydberg transitions of NO using an optical-optical double resonance multiphoton ionization technique See Entry 60768
- Rydberg states of 7Li_2 by pulsed optical-optical double resonance spectroscopy: molecular constants of $^7Li_2^+$ See Entry 60769
- Sublevel decay kinetics of the triplet state of bacteriochlorophyll a and b in methyltetrahydrofuran at 1.2K See Entry 60771
- Singlet excited-state 'energy hopping' in alkylbenzenes See Entry 60784
- Effects of aggregation on the phosphorescence of phenyl alkyl ketones in 77K rigid glass solutions See Entry 60790
- Solvent effect on 1O_2 yield and the mechanism of polycyclic hydrocarbon triplet-state quenching by oxygen See Entry 60791
- Nickel porphyrin photophysics and photochemistry. A picosecond investigation of ligand binding and release in the excited state See Entry 60792
- Intracoil triplet-triplet annihilation in poly(2-vinylnaphthalene) in benzene solution See Entry 60818
- Temperature dependence of the nonradiative relaxation process of the lowest excited singlet states of meso-substituted bromoanthracenes See Entry 60820
- SCF discrete-variational $X\alpha$ calculations of the NH_4Cl Auger spectrum See Entry 60845
- Subpicosecond time resolved multiphoton ionization: excited state dynamics of cis-stilbene under collision free conditions See Entry 60851
- Interactions between neutral dissociation and ionization continua in N_2O See Entry 60852
- Photodissociation of CO_3^- : evidence for a long-lived excited state See Entry 60859
- Rotational predissociation of the Ar.HCl van der Waals complex: close-coupled scattering calculations See Entry 60865
- Population of the 3s state in hydrogen due to H^+ , H_2^+ and H_3^+ impact on ethylene, 1-butene and cis-2-butene See Entry 60950
- Determination of the Penning excitation cross sections of Mg atoms by He, Ne and Ar metastable atoms See Entry 60955
- Experimental investigation of Hornbeck-Molnar ionisation in collisions between excited $He(5^3P)$ and He atoms See Entry 60956
- A new diabatic molecular representation for triplet-triplet transitions in $He^+ - He^+$ collisions See Entry 60959
- Charge transfer to helium ions from metastable helium See Entry 60960
- Luminescent charge transfer of ground-state and metastable B^+ ions See Entry 60961
- Production of 3s state hydrogen by H_2^+ impact on noble gases See Entry 60969
- Charge exchange of C^{+6} and O^{+8} ions with hydrogen atoms: Strong coupling calculation See Entry 60977
- The electron excitation of Si^+ See Entry 60991
- Effective cross sections for electron-impact excitation of barium atoms from the 5^3D_2 metastable state See Entry 60995
- Direct-excitation cross sections for Cd II low-lying excited states by single-electron impact on Cd atoms See Entry 60997
- Non-dipole excitation of core holes by electron impact. Multiplet splitting in CO and N_2 See Entry 60999
- Rydberg-atom masers. I. A theoretical and experimental study of super-radiant systems in the millimeter-wave domain See Entry 61121
- Quasi-CW lasing due to transitions from the resonance 1P_1 to the metastable 3D_2 level of the calcium atom See Entry 61139
- Resonant transfer and excitation (RTE) in ion-atom collisions and dielectronic recombination in plasmas See Entry 61608
- Unimolecular and bimolecular reactions in the $C_2H_6^+$ system: experiment and theory See Entry 63525

31.70 EFFECTS OF MOLECULAR INTERACTIONS ON ELECTRONIC STRUCTURE

(see also 34. Atomic and molecular collision processes and interactions)

- 60626 Satellite structure in the $2p\sigma$ molecular orbital transitions in slow heavy ion collisions. M.P.Stockli (James R. Macdonald Lab., Kansas State Univ., Manhattan, KS, USA). *IEEE Trans. Nucl. Sci. (USA)*, vol.ns-30, no.2, p.916-18 (April 1983). (1982 IEEE Conference on the Application of Accelerators in Research and Industry, Denton, TX, USA, 8-10 Nov. 1982).
- The binding energy of the $2p\sigma$ molecular orbital formed transiently in a slow heavy ion collisions shows a flat minimum at a large internuclear distance. Electronic transitions in this minimum provide a satellite structure in the $2p\sigma$ X-ray continuum. Measurements show that the satellite is only evident at very small collision velocities, since the collision broadening is much larger for asymmetric collision systems than the theory predicts. The present theory of collision broadening takes into account only the linear term of the change in transition energy dE/dR which may not be appropriate in cases where the second term d^2E/dR^2 is likely to be dominant. (12 refs.)

31.70D Environmental and solvent effects

- 60627 Monte Carlo simulation of solvent effects on vibrational and electronic spectra. M.F.Herman (Dept. of Chem., Tulane Univ., New Orleans, LA, USA), B.J.Berne. *J. Chem. Phys. (USA)*, vol.78, no.6, pt.2, p.4103-17 (15 March 1983).
- Solvent effects on vibrational states are treated in the Born-Oppenheimer approximation. A Monte Carlo procedure is devised for simulating a system in which the vibrations are treated as quantum degrees of freedom and all other degrees of freedom are treated classically. The key to this method is the use of a restructured perturbation theory for solving the vibrational Schrödinger equation at each of the solvent configurations sampled. This method also is used to compute Franck-Condon factors. The methods developed are applied to two different problems. First, solvent effects on vibrational transitions in the ground electronic state are considered. It is found that the frequency shift from the gas phase frequency is to the red at low solvent densities, but to blue at high solvent densities. Secondly, the heterogeneous electronic absorption and emission line shapes are simulated in a variety of model solute-solvent systems and the results are discussed in terms of a simple theoretical model. (31 refs.)
- 60628 Quantum theory of solvent effects on electronic spectra: Predictions of the exact solution of the mean spherical model. K.S.Schweizer, D.Chandler (School of Chem. Sci., Univ. of Illinois, Urbana, IL, USA). *J. Chem. Phys. (USA)*, vol.78, no.6, pt.2, p.4118-25 (15 March 1983).
- A microscopic quantum statistical mechanical theory for the solvent modification of the electronic spectra of nonpolar solutes is developed. Attention is focused on the solute frequency shift as a function of molecular parameters, solvent dielectric constant, and density. Comparison of the predictions of the quantum theory and dielectric continuum models (Onsager-Botcher and Wertheim) based on the macroscopic reaction field picture are made. Significant differences are found which indicate the importance of solvent structure and nonzero frequency effects absent in the dielectric models. The theory is also applied to several aromatic hydrocarbon molecules in dilute solution with emphasis on the isothermal density dependence of the electronic frequency shift. Generalization of the quantum theory to treat polar solutes is briefly outlined. (30 refs.)
- Effects of excited-state prototropic equilibria on the fluorescence energies of benzimidazole and thiabenzimidazole homologues See Entry 60814
- Excitation-frequency dependence of the efficiency of directed nonradiative energy transfer in two-component solid solutions of organic compounds See Entry 60825
- Role of energy migration between monomeric molecules of rhodamine dyes in the concentration quenching of the luminescence of the solutions See Entry 60826
- Spectral-luminescent properties of phthalimides in aqueous-miscellar solutions of sodium dodecyl sulfate See Entry 60827

31.70F Potential-energy surfaces for collisions

(see also 82.20K in chemical kinetics, 34.20 Intermolecular forces, 34.50L in beam studies)

- 60629 Molecular structure and photoelectron spectra of H_2S , H_2Se and H_2Te . Effective core potential calculations on ground and valence ionic states. J.Muller, L.J.Saethre, O.Gropen (Inst. of Math. & Phys. Sci., Univ. of Tromsø, Tromsø, Norway). *Chem. Phys. (Netherlands)*, vol.75, no.3, p.395-404 (15 March 1983).
- Hartree-Fock effective core potential calculations have been performed for the neutral ground state (1A_1) and the first three low-lying ionic states (2B_1 , 2A_1 and 2B_2) of H_2S , H_2Se and H_2Te . The computational method enabled the authors to use the same, relatively large, basis for all three molecules. The calculations include potential energy curves for the three ionic states, equilibrium geometries, vibrational frequencies, Franck-Condon factors, and ionization potentials. The results show satisfactory agreement between calculated and experimental values when comparison is possible, and indicate that molecules and ions containing heavy elements may be studied at a satisfactory level with the effective core potential method. (42 refs.)
- 60630 Semiclassical determination of adiabatic barriers on a three-dimensional potential energy surface. E.Pollak (Chem. Phys. Dept., Weizmann Inst. of Sci., Rehovot, Israel), R.E.Wyatt. *J. Chem. Phys. (USA)*, vol.78, no.7, p.4464-76 (1 April 1983).
- A recently proposed method, based on periodic orbits, for finding vibrationally adiabatic barriers and wells in collinear collisions is generalized to the full three-dimensional case. The main idea is a consistent use of the adiabatic approximation—one first solves for the fast vibrational motion to obtain an effective Hamiltonian for the slower bend motion which in turn is solved to obtain an effective Hamiltonian for the overall rotation. The method is applied to the hydrogen exchange reaction. The authors find the bend-vibration adiabatic barrier levels for the $H_2(v=1)$ state. The zero point motion in the bend degree of freedom is found to be substantial (0.1 eV) and is a source for nonnegligible discrepancies between approximate theories such as the infinite order sudden and quasiclassical trajectory approach and exact quantal scattering computations. Having found the barrier levels they are able to evaluate the collision cross section. Their analysis points out that differences between experimental cross sections and theoretical predictions may be due to inaccuracy in the potential energy surfaces. The available surfaces probably overestimate the adiabatic barrier height. (67 refs.)
- Topography of potential energy surfaces: DIM surface for $H+F_2$ See Entry 60901
- State resolved rotational excitation in $HD+D_2$ collisions. II. Angular dependence of 0-2 transitions See Entry 60922
- Rotational rainbow scattering in collisions of Ar with Cl_2 See Entry 60958
- Adiabatic T matrix theory for three dimensional reactive scattering: application to the (H,H_2) system See Entry 63534

31.70H Time-dependent phenomena: excitation and relaxation processes, and reaction rates

(see also 34. Atomic and molecular collisions)

- Gauge invariant derivation of the AC Stark shift See Entry 60645
- Time-resolved study of the laser optogalvanic effect in I_2 See Entry 60775
- Reactive and non-reactive quenching of $O(^1D_2)$ by COF_2 See Entry 60785
- Measurement of sub-nanosecond single-rovibronic fluorescence with a pulsed dye laser See Entry 60794

- Laser vaporization of tin: spectra and ground state molecular parameters of Sn_2 See Entry 60801
 Picosecond studies of energy transfer of donor and acceptor dye molecules in solution. II. A concentration dependence See Entry 60828
 Collisional depopulation of Na ns states by H_2 and CO See Entry 60929

31.70K Molecular solids

- Hindered internal rotations in Van der Waals molecules and molecular crystals See Entry 60885
 Vibrational spectroscopy of solid state molecular dimers See Entry 62954

31.90 OTHER TOPICS IN THE THEORY OF ATOMS AND MOLECULES

(inc. properties other than energy)

- 60631 Application of AGP wave functions to the ground states of Li_2 and CH^+ . N.Elander, E.Sangfelt, H.Kurtz, O.Goscinski (Quantum Chem. Group., Univ. of Uppsala, Uppsala, Sweden). *Int. J. Quantum Chem. (USA)*, vol.23, no.3, p.1047-56 (March 1983). (Proceedings of the Fourth International Congress in Quantum Chemistry, Uppsala, Sweden, 13-20 June 1982).
 The AGP wave function is used to describe the ground state potential energy curves of Li_2 and CH^+ . Moderate size basis sets are used. The computational aspects of the AGP optimization are discussed and the nature of the AGP wave function versus internuclear separation is examined. (22 refs.)
 60632 The ground state of an atom moving in a medium. P.P.Meyer (Obs. de Meudon, Meudon, France). *Phys. Lett. A (Netherlands)*, vol.94A, no.6-7, p.290-2 (21 March 1983).
 The author studies the relaxation, towards its ground state, of a moving two-level atom interacting with a field in a medium and he finds that a shift occurs when the atom velocity is above the phase velocity of the field. (1 ref.)
 Channel coupling theory of molecular structure: explanation and elimination of unphysical results See Entry 60566
 Ordinary field-theoretic methods for self-consistent wave functions which describe bond formation and dissociation. II. Commutative coupling case See Entry 60572
 Ab initio MO investigation of the ethanolamine-formic acid complex See Entry 60573
 The nature of hydrogen bonding in the NN-HF, OC-HF, and HCN-HF complexes See Entry 60603
 Spectroscopic evidence in σXYZ molecules for the three groups X, Y, Z acting as a whole, whatever the symmetry may be, in their long range interactions with the chromophore See Entry 60698
 Predissociation of HD-Ar van der Waals molecules by internal rotation See Entry 60866
 A simple analytical approximation for the potential energy of diatomics See Entry 60882
 Improvement for the RKR procedure obtained by semiclassical calculations See Entry 60883

32.00 ATOMIC SPECTRA AND INTERACTIONS WITH PHOTONS

32.20 ATOMIC SPECTRA GROUPED BY WAVELENGTH RANGES

- 60633 Self-broadening of the sodium resonance lines and excitation transfer between the $3P_{3/2}$ and $3P_{1/2}$ levels. J.Huennkens, A.Gallagher (Joint Inst. for Lab. Astrophys., Univ. of Colorado, Boulder, CO, USA). *Phys. Rev. A (USA)*, vol.27, no.4, p.1851-64 (April 1983).
 Sodium vapor, in the density range 10^{13} to $5 \times 10^{14} \text{ cm}^{-3}$, was excited by a CW dye laser, tuned 20-150 GHz from either the D_1 or D_2 resonance line. The authors observed a three-peak scattered spectrum, consisting of the Rayleigh component at the laser frequency, and the two fluorescence components (direct and sensitized) at the atomic resonance-line frequencies. Corrections to the Rayleigh signals for anisotropy and polarization effects, and to the fluorescence signals for radiation trapping, were made in order to obtain the ratio of the sum of the total intensities of the two fluorescence components to that of the Rayleigh component. This ratio combined with a measurement of the line-wing absorption coefficient yields the sodium density and the D-line self-broadening rate coefficients [$k_{\text{bb}} = 4.67 \times 10^{-7} \text{ cm}^3 \text{ s}^{-1}$ ($\pm 15\%$) for the D_2 line and $k_{\text{bb}} = 3.07 \times 10^{-7} \text{ cm}^3 \text{ s}^{-1}$ ($\pm 15\%$) for the D_1 line]. Asymmetry in the self-broadened line wings due to fine-structure recoupling was observed. The measured intensity ratio of the D lines, combined with pulsed measurements of the effective radiative decay rates in the presence of radiation trapping, yields the fine-structure collisional-mixing cross section [$\sigma(3P_{3/2} \rightarrow 3P_{1/2}) = 172 \text{ \AA}^2$ ($\pm 18\%$)] at $T \approx 300^\circ\text{C}$. Their results are compared to other experiments and to theory. (51 refs.)
 60634 Two-step optogalvanic spectroscopy of neutral barium: observation and interpretation of the even levels above the 6s ionization limit between 5.2 and 7 eV. P.Camus, M.Dieulin, A.El.Himdy, M.Aymar (Lab. Aime Cotton, CNRS, Orsay, France). *Phys. Scr. (Sweden)*, vol.27, no.2, p.125-59 (Feb. 1983).
 Even parity levels of neutral barium above the 6s ionization limit have been investigated by using a two-step pulsed laser excitation with optogalvanic detection. From the metastable states, $5d6s$, populated by a DC discharge in a heat-pipe vapour, one reaches the $5dnl$ even Rydberg series with J values ranging from 0 to 5, the $6p^2 \text{ } ^1S_0$ state and the low-lying members ($n=7$ and 8) of the $6pnp$ series above the $5d$ limits. The $5dnd$ configurations (18 levels for each n member) are observed from $n=8$ up to $n=45$ using optogalvanic spectra recorded from five intermediate $5d6p$ levels: $^3P_{1,2}$, $^3F_{3,4}$ and 1P_1 . These eighteen series are observed for the first time. Fine structure is resolved up to $n=25$ and has been analyzed using Slater-Condon parametric calculations. In addition, the $5d_{3/2}nJ=1$ and $5d_{5/2}nJ=3$ series are observed up to $n=38$ and 42 respectively, as well as sharp resonances interpreted as $5d_{3/2}nJ=2$ and $5d_{5/2}nJ=1,2$ series up to $n=27$ and $n=28$ respectively. In conclusion, the energies of 636 new levels between 6s and $5d$ limits are

given with their term and configuration identifications. Above the $5d_{3/2}$ limit, broad resonances observed from the $5d6p \text{ } ^1P_1$, $6s7p \text{ } ^1P_1$ and $^3P_{0,1,2}$ intermediate levels have been identified with levels of the $6p7p$ and $6p8p$ configurations using parametric calculations based on the Slater-Condon theory. (15 refs.)

- Optical oscillator strengths of $3p^3d^2D \rightarrow 3p^3d^2 \text{ } ^2P^o$, $^2D^o$, $^2F^o$ transitions in Co^{8+} , Cu^{10+} and Zn^{11+} ions See Entry 60599
 Analytic expression for bound-bound and bound-free dipole transition matrix elements of atomic inner shells See Entry 60893
 Collision-induced absorption in Ne+Ar See Entry 60896
 Oscillator strengths and Ne abundance in B stars See Entry 64468

32.20B Radiofrequency, microwave, and infrared spectra

(inc. magnetic resonance spectra)

- Characteristics of σ -transitions in an atomic-beam polarized deuteron source See Entry 60502
 Intense emission from an Ar:Xe mixture pumped by a microsecond electron beam See Entry 60644
 Specific mass shift in the $1s2s^3S$ and $1s5p^3P$ states of helium See Entry 60657
 The Breit interaction in external magnetic fields See Entry 60747
 Experimental observation of the intercollisional interference effect on the S_1 pure rotation line of the collision induced spectra of the H_2 -He mixture See Entry 60932

32.20J Visible and ultraviolet spectra

(for fluorescence and phosphorescence spectra, see 32.50)

- 60635 Mn VI spectrum at 140-220 Å. A.N.Ryabiev. *Opt. & Spectrosc. (USA)*, vol.53, no.1, p.13-15 (July 1982). Translation of: *Opt. & Spektrosk. (USSR)*, vol.53, no.1, p.23-6 (July 1982). [received: April 1983]
 The Mn VI spectrum excited in a three-electrode vacuum spark has been studied with a grazing-incidence vacuum spectrograph with a grating 3 m in radius (3600 lines/mm). The results are used to classify 151 lines corresponding to transitions from the $3dnf$ ($n=4-8$), $3d5p$, and $3p^33d^2$ configurations to the $3d^2$ configuration. The Mn VI ionization potential has been determined from the $3dnf$ ($n=6-8$) series to be $772.250 \pm 150 \text{ cm}^{-1}$. (9 refs.)
 60636 Beam-foil study of the $2s^22p^5 \text{ } ^3P$ and $2s2p^6 \text{ } ^3P$ configurations of Ar IX. M.C.Buchet-Poulizac, J.P.Buchet (Lab. de Spectrometrie Ionique et Moleculaire, Univ. Lyon I, Villeurbanne, France). *Phys. Scr. (Sweden)*, vol.27, no.2, p.99-102 (Feb. 1983).
 The spectrum of Ar IX has been observed in the 450-900 Å wavelength range. A total of 36 lines has been measured. Thirty of them have been classified as transitions between the $2s^22p^5 \text{ } ^3S$, 3P and $3d$ configurations and six other lines have been ascribed to the $2s2p^6 \text{ } ^3P$ configurations. Energy levels of the $2s^22p^5 \text{ } ^3P$ configurations have been deduced. These identifications have been supported by an isoelectronic comparison. Three main lines have been measured. (19 refs.)
 Arc measurements of Fe II transition probabilities See Entry 60648
 Low pressure shift of the $2p^33p\text{-}2p^55s$ spectral lines of neon perturbed by neon and helium See Entry 60658
 Electron-impact excitation of vanadium atoms See Entry 60994
 Spectra of highly ionized atoms in hot plasmas: conditions for production and observation See Entry 61704
 Atomic calculations for Ca XVII; UV and X-ray lines See Entry 64365
 Investigation of damping constant for the neutral iron line profiles in undisturbed solar photosphere See Entry 64442

32.20R X-ray spectra

- 60637 Atomic calculations for the Fe XX X-ray lines. H.E.Mason, A.K.Bhatia (Lab. for Astron. & Solar Phys., NASA, Goddard Space Flight Center, Greenbelt, MD, USA). *Astron. & Astrophys. Suppl. Ser. (France)*, vol.52, no.1, p.181-92 (April 1983).
 Atomic data are tabulated for the transitions between levels in the $2s^22p^3$ and $2s^22p^23s$, $2s^22p^23d$ configurations of Fe^{19} . The electron collision strengths are calculated using the 'distorted wave' approximation. Theoretical intensity ratios are tabulated for the X-ray lines. New identifications of spectral lines from a solar flare are presented. (15 refs.)
 60638 Widths, shapes and asymmetries of the Mo $K\alpha_1$ and Ag $K\alpha_1$ X-ray lines. J.S.Thomsen (Dept. of Phys., Johns Hopkins Univ., Baltimore, MD, USA). *J. Phys. B (GB)*, vol.16, no.7, p.1171-89 (14 April 1983).
 Analyses the shapes, possible asymmetries and widths of the Mo $K\alpha_1$ and Ag $K\alpha_1$ X-ray lines. The width determination utilises a novel approach, which should be useful in similar experiments. This simple technique is applicable to measurements in the $(1, \pm n)$ positions of the double-crystal (two-crystal) spectrometer with $n > 1$. Under suitable restrictions, subtraction of the experimentally measured widths in the two positions leads to the desired linewidth, with instrumental correction eliminated to first order. It also yields a 'crystal correction term'; for comparison, the value of this term is obtained in terms of the Darwin solution. The effects of the vertical divergence window on width and asymmetry are also considered. Results are applied to the Mo $K\alpha_1$ and Ag $K\alpha_1$ data of Bearden; the respective widths are found as $6.28 \pm 0.07 \text{ eV}$ and $8.97 \pm 0.08 \text{ eV}$, in good agreement with theory. Both lines are found to follow closely the Lorentzian form, with RMS deviations probably within 0.3%. Both lines show small asymmetries of the order of ~ 0.003 , the minus sign indicating greater width on the short-wavelength side. The method of linewidth computation is also applied to the data of Bearden and Shaw for elements 25 Mn through 32 Ge. (35 refs.)
 60639 Origin of the so called spin doublets in X-ray satellite spectra. B.G.Gokhale, U.D.Misra (Phys. Dept., Lucknow Univ., Lucknow, India). *J. Phys. B (GB)*, vol.16, no.7, p.1191-8 (14 April 1983).
 It is pointed out that one should not expect to find spin doublets in X-ray satellites since the level system of two-hole atoms should consist of singlets and triplets. The energies of the two-hole multiplets L_2M_1 and L_2M_2 ($i=1$ to 5) have been calculated for $Z=35$ to 50 using the Auger electron energy values tabulated recently by Larkins (1977). It is found that whatever may be the spectator vacancy, the satellite pair formed as a result of the transitions

L_2M_1 , $L_2 \rightarrow Y$ and L_3M_1 , $L_3 \rightarrow Y$ where Y is a lower common level, will follow the characteristics of spin doublets in X-ray diagram lines. It is concluded that the occurrence of the so called spin doublets in X-ray satellites is a direct consequence of the fact that the parental one-hole doublet behavior persists even in atoms which have two holes in their inner shells. (9 refs.)

60640 Calculation of X-ray line energies of molybdenum in the transient state by Slater's method. S.G.Gagarin, I.G.Falkov. *Opt. & Spectrosc. (USA)*, vol.53, no.1, p.94-5 (July 1982). Translation of: *Opt. & Spektrosk. (USSR)*, vol.53, no.1, p.160-2 (July 1982). [Received: April 1983]

It is shown that the transient state principle introduced by Slater may be applied to calculation of X-ray transition energies in the framework of the Hartree-Fock-Dirac-Slater (HFDS) method. In the case of molybdenum, the error in the description of the L lines is 2%, and of the K lines 0.2%. For calculation of the latter with $z \geq 40$ it is necessary to take into account relativistic corrections to the exchange part of the potential. (17 refs.)

Effect of collisional mixing of lower levels of Li-like ions on the intensity of the resonance line satellite structures of He-like ions See Entry 60909

Projectile-charge dependence of quasi-free-electron bremsstrahlung See Entry 60910

Deuteron and alpha-induced K-shell ionization cross section ratios in the $Z=12-17$ region See Entry 60939

Proton-induced K-vacancy production cross sections for Sc, Ti, V, Cr, Co, Ni, Cu, and Zn See Entry 60940

Recent results on K-shell ionization by ion collisions See Entry 60941

L-subshell X-ray production cross sections of Ba, La and Ce for proton energies from 0.25 to 2.00 MeV See Entry 60942

Proton induced L-subshell ionization on silver and iodine See Entry 60943

L-shell ionization of gold by nitrogen ion impact See Entry 60944

Vacancy-transfer cross sections and L-vacancy lifetimes for low-energy collisions of Ar^{2+} with Mg, Al, and Si See Entry 60947

A study of transfer excitation in $F^{8+} + He$, Ne and Ar collisions See Entry 60948

Effects of neutrino recoil on the X-ray emission of bound electron capture atoms See Entry 60973

Atomic calculations for Ca XVII; UV and X-ray lines See Entry 64365

32.50 FLUORESCENCE, PHOSPHORESCENCE

(inc. quenching)

60641 Intensity correlations in resonance fluorescence from coupled two-level atoms. M.Wiegand (Theoretische Festkörperphys., Tech. Hochschule Darmstadt, Darmstadt, Germany). *J. Phys. B (GB)*, vol.16, no.7, p.1133-58 (14 April 1983).

The normalised intensity correlation function of resonance fluorescence radiation from two-level atoms is studied in various respects. In the first part of the paper the author discusses only interference effects for several uncoupled, linearly arranged, atoms. It is shown that, depending on the distance between the atoms, the direction of observation and the strength of the driving field, an antibunching effect as well as a very big bunching effect may be observed. In the second part of the paper he studies for the case of two atoms and weak external fields the influence of the interaction between the atoms by means of a perturbation theory. It is shown that the coupling between the atoms strongly modifies the normalised intensity correlation function in comparison with the case of uncoupled atoms. He takes as the driving field a coherent external field as well as laser light and thermal light. (34 refs.)

60642 Delay in the spontaneous decay of excited atoms in a resonator. I.V.Sokolov. *Opt. & Spectrosc. (USA)*, vol.53, no.1, p.5-6 (July 1982). Translation of: *Opt. & Spektrosk. (USSR)*, vol.53, no.1, p.9-11 (July 1982). [received: April 1983]

The possibility is pointed out of controlling the rate of spontaneous emission in an interferometer with closely spaced plane-parallel mirrors (a Fabry-Perot interferometer). From the results it can be seen that scanning the thickness of the interferometer around the value $l=\lambda/2$ will change the average radiation constant by a factor of 3 and lead to a complete arrest of the decay for certain sublevels. For an experimental demonstration of this arrest of spontaneous decay, it is important to note that the resonator discussed requires collimation of the atomic beam along only a single coordinate. In contrast with a tubular waveguide, the thickness of the gap in this case can be scanned around the critical value to distinguish the delay in the spontaneous decay from other effects (e.g. the quenching of atoms at the walls). (4 refs.)

60643 Measurement system for temporal response of atomic and molecular systems using the correlation method with pseudorandomly modulated laser light. H.Baba, K.Sakurai (Dept. of Pure & Appl. Sci., Univ. of Tokyo, Tokyo, Japan), F.Shimizu. *Rev. Sci. Instrum. (USA)*, vol.54, no.4, p.454-7 (April 1983).

A system to measure the temporal behavior of atomic or molecular fluorescence, which is disturbed by large noise background, has been developed. This system uses the pseudorandom modulation technique of length up to 1023, temporal resolution of approximately 83 ns, and a photon counting capacity of 10^7 counts/s. Data processing by a minicomputer and a hardware demodulation circuit enable quick analysis of a large volume of data. The signal-to-noise ratio of this measurement system is discussed with some experimental comparisons. The system is tested in the decay time measurement of I_2 fluorescence. (10 refs.)

60644 Intense emission from an Ar:Xe mixture pumped by a microsecond electron beam. Yu.I.Bychkov, V.F.Losev, V.F.Tarasenko, E.N.Tel'minov (Inst. of High-Current Electronics, Acad. of Sci., Tomsk, USSR). *Sov. Tech. Phys. Lett. (USA)*, vol.8, no.7, p.361-3 (July 1982). Translation of: *Pisma v Zh. Tekh. Fiz. (USSR)*, vol.8, no.13-14, p.837-40 (July 1982). [received: April 1983]

The authors have achieved efficient emission in the near-IR part of the spectrum from atomic transitions of xenon by pumping an Ar:Xe mixture with a microsecond electron beam. The specific output energy was 2.3 J/liter; the efficiency was $\sim 1\%$ in terms of the energy pumped in by the electron beam; and the total output energy was 7 J. (4 refs.)

Atomic inner-shell transitions—theory and the need for experiments See Entry 60612

Self-broadening of the sodium resonance lines and excitation transfer between the $3P_{3/2}$ and $3P_{1/2}$ levels See Entry 60633

Investigation of atomic relaxation by the three-level echoes See Entry 60681

Collisional depopulation of Na ns states by H_2 and CO See Entry 60929

Luminescent charge transfer of ground-state and metastable B^+ ions See Entry 60961

Autoionisation versus radiative decay of resonances in electron impact excitation cross sections See Entry 60992

Direct-excitation cross sections for Cd II low-lying excited states by single-electron impact on Cd atoms See Entry 60997

Kinetics of the Cl-H₂ system. II. Abstraction vs exchange in D+HCl See Entry 63522

Atomic nitrogen emissions from photodissociation of N₂ See Entry 64236

32.60 ZEEMAN AND STARK EFFECTS

60645 Gauge invariant derivation of the AC Stark shift. D.H.Kobe (Dept. of Phys., North Texas State Univ., Denton, TX, USA). *J. Phys. B (GB)*, vol.16, no.7, p.1159-69 (14 April 1983).

The time-dependent AC Stark shift for an atom in a classical electromagnetic field is derived in a manifestly gauge invariant way. In the electric dipole approximation (EDA) the time-dependent AC Stark shift is obtained in second order both from the gauge invariant formula and from the conventional approach. The conventional approach uses the unperturbed Hamiltonian H_0 with an interaction $A \cdot p$ plus A^2 (constants omitted). In the EDA the gauge invariant approach simplifies in a gauge in which the energy operator reduces to H_0 and the interaction is proportional to $E \cdot r$. The time-dependent AC Stark shifts calculated by the two methods are different. In the static limit the gauge invariant energy gives the correct shift, while the energy calculated from the conventional interaction does not. When the energies are averaged over all times the same average AC Stark shifts are obtained. (39 refs.)

60646 Fine-structure parameters of the helium 1s3d configuration from the experimental crossing positions of Zeeman sublevels. G.P.Anisimova, R.I.Semenov. *Opt. & Spectrosc. (USA)*, vol.53, no.1, p.10-13 (July 1982). Translation of: *Opt. & Spektrosk. (USSR)*, vol.53, no.1, p.17-22 (July 1982). [received: April 1983]

Experimental data on the crossing fields are used to calculate the fine-structure energy intervals in a zero magnetic field, the parameters of the fine structure, the gyromagnetic ratios, and the singlet-triplet mixing ratio for the 1s3d He I configuration in the single-configuration approximation. The magnetic-field intervals for all other crossings of magnetic sublevels in the 0-300-Oe interval that have not yet been observed experimentally are calculated; the errors in the measurements of the crossing fields and the parameter of the electrostatic exchange interaction are taken into account. If the parameters are to be refined and these intervals narrowed, it will be necessary to carry out more accurate measurements of the parameter of the electrostatic exchange interaction. (11 refs.)

60647 Magnetic-sublevel shifts of potassium atoms in a constant magnetic field and in the electric fields of laser beams of various polarizations. T.Ya.Karagodova, A.I.Karagodov. *Opt. & Spectrosc. (USA)*, vol.53, no.2, p.123-5 (Aug. 1982). Translation of: *Opt. & Spektrosk. (USSR)*, vol.53, no.2, p.206-10 (Aug. 1982). [received: April 1983]

The shifts of the magnetic sublevels of potassium atoms that result from the interaction of these atoms with a constant magnetic field and with the electric field of a laser beam are calculated for an arbitrary relationship between the fine-structure interval and the Zeeman and Stark shifts. The cases of linear and circular polarization of the laser beam are considered. The results are compared with the experimental data available. (3 refs.)

Inhomogeneous light shift in alkali-metal atoms See Entry 60655

Microwave ionization of Na Rydberg levels See Entry 60673

Zeeman transitions in collisions of Na with Xe See Entry 60898

Resonance line at the $M = +1 - M = 0$ transition in 1^3S_1 positronium See Entry 61024

Hyperfine structure of positronium energy levels in a crystal field See Entry 61025

Stabilisation of carbon dioxide lasers using the Stark effect ... See Entry 61126

32.70 SPECTRAL LINE SHAPES AND INTENSITIES

60648 Arc measurements of Fe II transition probabilities. J.Moity (Obs. de Meudon, Meudon, France). *Astron. & Astrophys. Suppl. Ser. (France)*, vol.52, no.1, p.37-62 (April 1983).

Relative oscillator strengths for 494 Fe II lines in the wavelength range 2550-5300 Å were experimentally determined by use of a wall-stabilized arc operated in argon with a small admixture of iron carbonyl. Plasma temperature and electron density were about 9000K and $4.75 \times 10^{15} \text{ cm}^{-3}$ respectively. The relative gf-values are brought onto an absolute scale by use of the Saha equation and by comparing the intensity of a given Fe II line with those of neighbouring Fe I lines that are known rather precisely (Fuhr et al., 1981). The results are compared with available literature data. All other previous experiments and calculations show scale shifts. After corrections of these shifts the scatters are generally low, except with the semi-empirical calculations of Kurucz and Peytremann (1975). From those literature data the authors derive additional Fe II gf-values that are adjusted onto their scale, thus extending the wavelength range on both sides to 2030-7700 Å. (53 refs.)

60649 Lifetime ratios for Ar I 4p levels. K.Musiol, D.W.Jones, W.L.Wiese (Atomic & Plasma Radiation Div., NBS, Washington, DC, USA).

J. Quant. Spectrosc. & Radiat. Transfer (GB), vol.29, no.4, p.321-7 (April 1983).

Relative transition probabilities of 13 transitions between the $3p^4s$ and $3p^4p$ configurations in Ar I have been measured in emission with a wall-stabilized arc. These data have been combined to yield relative lifetimes which are compared with recent direct lifetime measurements. An important consideration in the authors' experiment was to minimize effects of radiation imprisonment since this effect may have played an important role in lifetime measurements by other methods. Their results agree well with most previously published lifetime data and emission measurements. (16 refs.)

60650 Transition probabilities for Ne I lines. A.Magazzu, V.Pirronello, G.Strazzulla (Osservatorio Astrofisico, Catania, Italy).

J. Quant. Spectrosc. & Radiat. Transfer (GB), vol.29, no.4, p.375-8 (April 1983).

Calculated transition probabilities for about 140 lines of Ne I are presented. The general agreement the authors have found with other existing data, for those values for which comparisons were carried out, verifies the reliability of their calculations and gives them confidence in these values for applications in astrophysics and plasma physics. (13 refs.)

60651 Z dependence of the probabilities for 3-3 and 2-2 transitions for excited states in the isoelectronic sequence of Ne. A.K.Pokleba, U.I.Safro-nova.

Opt. & Spectrosc. (USA), vol.53, no.1, p.7-9 (July 1982). Translation of: *Opt. & Spektrosk. (USSR)*, vol.53, no.1, p.12-16 (July 1982). [received: April 1983]

The Z dependence of the probabilities for 2-2 transitions ($2s2p^63l-2s^22p^53l$) and 3-3 transitions ($2s2p^63d-2s2p^63p-2s2p^63s$, $2s^22p^63d-2s^22p^63p-2s^22p^63s$) has been studied. Calculations were carried out in an intermediate coupling model on the basis of a perturbation theory using $1/Z$ as a small parameter. (16 refs.)

60652 Properties of nonlinear three-level resonances with arbitrary ratio between homogeneous and inhomogeneous transition widths. O.G.Bykova, V.V.Lebedeva, N.G.Bykova, A.V.Petukhov.

Opt. & Spectrosc. (USA), vol.53, no.1, p.101-3 (July 1982). Translation of: *Opt. & Spektrosk. (USSR)*, vol.53, no.1, p.171-4 (July 1982). [received: April 1983]

The physical bases of structure formation in the Doppler-broadened contour of a transition in the presence of a strong monochromatic field in an adjacent transition are in their general features well known. However, a detailed analysis of the structure has been conducted only in the approximation $kV \gg \Gamma$ (the Doppler limit). In this approximation in the limiting cases of strong and weak saturation, analytical expressions for the form of the spectrum have been obtained. The authors present a correct account of the influence of the Doppler width of a transition on the character of nonlinear resonances. A three-level scheme of the bent type serves as the object of investigation. However, the regularities peculiar to it also occur for other three-level schemes. (7 refs.)

60653 Regularities in the radiative lifetimes of excited states of the hydrogen atom. Ya.F.Verolainen.

Opt. & Spectrosc. (USA), vol.53, no.2, p.200-2 (Aug. 1982). Translation of: *Opt. & Spektrosk. (USSR)*, vol.53, no.2, p.342-5 (Aug. 1982). [received: April 1983]

Using all the data on the experimental and theoretical determination of radiative lifetimes of the excited states for the hydrogen atom that are found in the literature, the author has constructed graphical dependences of the lifetimes on the principal quantum number for all series and analyzed their behavior by a least-squares method with the aim of determining the constant of the exponential dependence. (17 refs.)

60654 Lifetimes of $ns(3/2)$ ($n=6, 7, 8, 9$) levels and transition probabilities of $4p$ - ns lines of Ar I. M.J.G.Borge, J.Campos (Catedra de Fisica Atomica Experimental, Facultad de Ciencias Fisicas, Madrid, Spain).

Phys. Rev. A (USA), vol.27, no.4, p.1910-13 (April 1983).

Forty-eight transition probabilities for lines belonging to the $4p$ - ns ($n=6, 7, 8, 9$) transition arrays of Ar I have been determined by means of emission-line-intensity measurements. The single-photon delayed-coincidence method has been used to obtain the lifetime values of the $ns(3/2)$ ($n=6, 7, 8, 9$) levels. With the taking into account of these lifetimes together with theoretical calculation in jK coupling for the lines beyond the experimental range, the relative transition probabilities were put on an absolute scale. The lifetime values obtained in the present work are original in the literature excepting the $7s(3/2)$ -level lifetime. Four transition probabilities are also the first values found in the literature. (14 refs.)

60655 Inhomogeneous light shift in alkali-metal atoms. J.C.Camparo, R.P.Frueholz, C.H.Volk (Chem. & Phys. Lab., Aerospace Corp., Los Angeles, CA, USA).

Phys. Rev. A (USA), vol.27, no.4, p.1914-24 (April 1983).

The dynamic Stark shift of an inhomogeneously broadened spectral transition has been studied. The authors' measurements show a shift in the observed ^{87}Rb ground-state hyperfine transition which has a nonlinear dependence on light intensity when the conditions for inhomogeneous broadening are met. The nonlinearity is the result of light-intensity gradients in the signal volume, which produce an inhomogeneously broadened asymmetric microwave transition. They show that their measurements are in full agreement with the second-order perturbation-theory treatment of light-induced energy-level shifts, when the effects of inhomogeneities are properly taken into consideration. The effects of inhomogeneous broadening must be carefully considered when extracting oscillator strengths from light-shift data, or when performing high-precision laser spectroscopy. (21 refs.)

60656 Technique for Lamb-shift measurements on high-Z ions produced by a hot plasma. R.J.Knize (Plasma Phys. Lab., Princeton Univ., Princeton, NJ, USA).

Phys. Rev. A (USA), vol.27, no.4, p.2258-60 (April 1983).

A new technique is proposed for the measurement of high-Z Lamb shifts using ions created by a hot Tokamak plasma. By using the laser resonance technique to measure the $2S_{1/2}-2P_{1/2}$ or $3/2$ energy splittings, it is possible to obtain a fractional accuracy of 10^{-10} . This would be a considerable improvement on existing measurements and would allow a clear test of current calculations. (16 refs.)

60657 Specific mass shift in the $1s2s^3S$ and $1s5p^3P$ states of helium. L.A.Bloomfield, H.Gerhardt, T.W.Hansch (Dept. of Phys., Stanford Univ., Stanford, CA, USA).

Phys. Rev. A (USA), vol.27, no.4, p.2261-4 (April 1983).

The authors report the first measurement of the specific mass shift of the 5^3P level between ^4He and ^3He . A value $\Delta\mu_s = -113.1 \pm 5.0$ MHz, twenty times more accurate than the best known theoretical value, was obtained by ultraviolet-infrared double-resonance laser spectroscopy of the $2^3S-5^3P-13^1S$ Δ transition. (13 refs.)

60658 Low pressure shift of the $2p^3p^2-2p^25s$ spectral lines of neon perturbed by neon and helium. A.Bielski, R.Bobkowski, R.Dygda, J.Wawrzynski (Inst. of Phys., Nicholas Copernicus Univ., Torun, Poland).

Physica B & C (Netherlands), vol.115 B+C, no.2, p.261-5 (Jan. 1983).

The shift of five spectral lines arising from the $2p^3p^2-2p^25s$ transitions of neon and emitted from a low-pressure glow discharge in pure neon and neon-helium mixture have been measured. The values of the pressure shift coefficients were determined. The results are interpreted in terms of the impact theory assuming a Lennard-Jones potential. Results obtained in this work indicate that the Lennard-Jones potential cannot describe adequately the shift of most spectral lines corresponding to the $2p^3p^2-2p^25s$ transitions. (14 refs.)

60659 Determination of the absolute intensity of the afterglow in flash photolysis of tellurium vapor. A.P.Ubelis, A.E.Lezdin' (P. Stuchka State Univ., Riga, Latvian SSR).

Sov. J. Quantum Electron. (USA), vol.12, no.10, p.1364-5 (Oct. 1982). Translation of: *Kvantovaya Elektron., Moskva (USSR)*, vol.9, no.10, p.2097-9 (Oct. 1982). [received: April 1983]

An investigation was made of the spectral distribution of the absolute intensity of the afterglow of tellurium vapor. Measurements were made using a

high-temperature flash photolysis system at a tellurium vapor pressure of 0.23 Torr, a xenon pressure of 20 Torr, and a cell temperature of 950K. The afterglow was attributed to the photorecombination of tellurium atoms in the ground state $^3P_{0,1,2}$. An estimate was obtained of the lower limit of the photorecombination coefficient which was found to be $2.65 \times 10^{-16} \text{ cm}^3 \cdot \text{molecule}^{-1} \cdot \text{sec}^{-1}$. (7 refs.)

Optical oscillator strengths of $3p^63d^2D-3p^53d^2^2P^0$, $^2D^0$, $^2F^0$ transitions in Co^{2+} , Cu^{1+} and Zn^{1+} ions See Entry 60599

$1/Z$ expansion calculation of the Bethe logarithm for the ground state Lamb shift of two-electron ions See Entry 60615

Radiative lifetimes of excited states of atoms See Entry 60625

Self-broadening of the sodium resonance lines and excitation transfer between the $3P_{3/2}$ and $3P_{1/2}$ levels See Entry 60633

Widths, shapes and asymmetries of the Mo $K\alpha_1$ and Ag $K\alpha_1$ X-ray lines See Entry 60638

Gauge invariant derivation of the AC Stark shift See Entry 60645

Fine-structure parameters of the helium $1s3d$ configuration from the experimental crossing positions of Zeeman sublevels See Entry 60646

^{235}U isotope enrichment in the metastable levels of U I See Entry 60663

Kinetics of the plasma decay in lithium vapor; population inversion for the $3p$ - $3s$ transition See Entry 60664

Recent developments in accelerator based atomic physics See Entry 60933

Autoionisation versus radiative decay of resonances in electron impact excitation cross sections See Entry 60992

Efficient parametric sum-frequency generation by noncoherent two-photon pumping of metal vapors See Entry 61235

Atomic calculations for Ca XVII; UV and X-ray lines See Entry 64365

Investigation of damping constant for the neutral iron line profiles in undisturbed solar photosphere See Entry 64442

Oscillator strengths and Ne abundance in B stars See Entry 64468

32.80 PHOTON INTERACTIONS WITH ATOMS

60660 Resonance light pressure in the field of partially coherent laser radiation. V.G.Minogin.

Opt. & Spectrosc. (USA), vol.53, no.1, p.73-6 (July 1982). Translation of: *Opt. & Spektrosk. (USSR)*, vol.53, no.1, p.125-9 (July 1982). [received: April 1983]

A kinetic Fokker-Planck-type equation is derived for the distribution function of atoms moving in a resonance light field with a fluctuating frequency. It is shown that the stochastic nature of the light field leads to a simplification of the light-pressure force and of the momentum diffusion tensor. (12 refs.)

60661 Local velocity distribution of atoms in a light wave in resonance with an atomic transition. V.G.Minogin.

Sov. Phys.-Tech. Phys. (USA), vol.27, no.10, p.1173-5 (Oct. 1982). Translation of: *Zh. Tekh. Fiz. (USSR)*, vol.52, no.10, p.1905-9 (Oct. 1982). [received: April 1983]

The velocity distribution of atoms moving in a plane light wave in resonance with an optical atomic transition is determined. The Fokker-Planck equation for the atomic distribution function is written out to third-order terms, inclusive. It is shown by analyzing the functional form of the equation that in the spatially uniform case, the asymptotic atomic velocity distribution is determined by terms through order two in the Fokker-Planck equation; the terms of order three and higher give small corrections to the macroscopic moments and to the velocity distribution. It is concluded that only terms up to second order need to be considered for accurate calculation of the local atomic velocity distribution using the infinite system of Fokker-Planck equations. (8 refs.)

Analytic expression for bound-bound and bound-free dipole transition matrix elements of atomic inner shells See Entry 60893

Atomic structure contribution to high-energy electron-photon atomic scattering: results for all momentum transfers See Entry 60990

32.80B Level crossing and optical pumping

60662 Optical pumping of stripped relativistic ions. G.C.Baldwin, N.J.DiGiacomo (Los Alamos Nat. Lab., Los Alamos, NM, USA).

IEEE Trans. Nucl. Sci. (USA), vol.ns-30, no.2, p.981-6 (April 1983). (1982 IEEE Conference on the Application of Accelerators in Research and Industry, Denton, TX, USA, 8-10 Nov. 1982).

Selected states of ions in the sodium-like isoelectronic sequence (P through Ca) in a beam accelerated to relativistic energies can be excited by a beam of optical laser radiation that intersects their trajectory at an appropriate angle. Pumping rates can be estimated, assuming the line broadening mechanism to be Doppler and available laser intensities. The authors find that it is possible to generate population inversions between the $3^2D_{3/2}$ states and the $3^2P_{3/2}$ states of those ions by selectively exciting the $4^2P_{1/2}$ state. To a fixed observer, the radiation from transitions between those states will be Doppler-upshifted into the X-ray region and will be tunable. Moreover, given sufficiently high ion density and a low beam emittance, and assuming that backward emission can be suppressed by means of a traveling-wave pumping system, moderate gain by stimulated emission along the ion column may be achieved. (5 refs.)

60663 ^{235}U isotope enrichment in the metastable levels of U I. J.M.Gagne, Y.Demers, C.Dreze, P.Pianarosa (Dept. de Genie Phys., Ecole Polytech., Montreal, Canada).

J. Opt. Soc. Am. (USA), vol.73, no.4, p.498-9 (April 1983).

The authors have used optical pumping to produce a substantial ^{235}U enrichment in the metastable levels of U I in the discharge afterglow of a hollow-cathode vapor generator. The measured isotope-enrichment factor for the level at 3800 cm^{-1} is approximately 20. (7 refs.)

60664 Kinetics of the plasma decay in lithium vapor; population inversion for the $3p$ - $3s$ transition. L.V.Voronyuk, V.A.Kvitsinskii, V.I.Lukashenko, G.V.Pitatev.

Opt. & Spectrosc. (USA), vol.53, no.1, p.18-22 (July 1982). Translation of: *Opt. & Spektrosk. (USSR)*, vol.53, no.1, p.33-9 (July 1982). [received: April 1983]

The kinetics of the plasma decay and the formation of a population inversion between the $3p$ and $3s$ levels have been studied in a lithium-helium mixture at a helium pressure of 40 Torr and at a lithium vapor density of $7 \times 10^{13} \text{ cm}^{-3}$. Regardless of the discharge conditions, an inversion occurs if the density of the cooled electrons is below $2 \times 10^{12} \text{ cm}^{-3}$ because of the different radiative lifetimes of the $3p$ and $3s$ levels. The cross section for electron-

impact $3p\text{-}3s$ deexcitation transitions has been determined. The gain at the $2.69\text{-}\mu\text{m}$ wavelength is estimated. (16 refs.)

60665 Nuclear polarisation of helium 3 by a colour centre laser. M.Leduc (Lab. de Spectroscopie Herzienne, ENS, Paris, France). *Rev. Cethedec (France)*, vol.19, no.NS82-2, p.3-14 (1982). In French. A colour centre laser using $(F_2)^+$ centres in NaF was developed for the near infrared. The long time stability of the laser crystals was improved and good conditions for the single frequency operation of this laser were found. Such an apparatus allowed large nuclear polarisation of a ^3He vapour by optical pumping. (20 refs.)

60666 Dependence of the total concentration of optically oriented atoms on the radius of the pump beam. M.B.Gornyi, B.G.Matsov (M.I. Kalinin Polytech. Inst., Leningrad, USSR). *Sov. Tech. Phys. Lett. (USA)*, vol.8, no.7, p.372-3 (July 1982). Translation of: *Pis'ma v Zh. Tekh. Fiz. (USSR)*, vol.8, no.13-14, p.859-62 (July 1982). [received: April 1983]

The spatial distribution of the optically oriented atoms in the gas-filled cells in various quantum-electronics devices is described by the optical-pumping equation. The authors use an analytical solution of this equation to predict a possible substantial increase in the total number of oriented atoms in the cell, achieved by decreasing (to an optimum value) the radius B of the pump beam in comparison with the cell radius A . The idea is to reduce the effect of relaxation at the wall as a result of the appearance of a diffusion layer around the light beam. (3 refs.)

Fine-structure parameters of the helium $1s3d$ configuration from the experimental crossing positions of Zeeman sublevels See Entry 60646
Efficient parametric sum-frequency generation by noncoherent two-photon pumping of metal vapors See Entry 61235

32.80D Autoionization

60667 Interaction between two Rydberg series of autoionizing levels in barium. F.Gounand, T.F.Gallagher, W.Sandner, K.A.Safina, R.Kachru (Molecular Phys. Lab., SRI Internat., Menlo Park, CA, USA). *Phys. Rev. A (USA)*, vol.27, no.4, p.1925-38 (April 1983).

Using a three-step laser excitation approach, the authors have studied the autoionizing $(6p_{1/2})_{1-3}$ states of neutral barium. The $6p_{1/2}$ series is essentially unperturbed and exhibits a constant quantum defect and autoionization widths which scale as v^{-3} , where v is the effective quantum number. The $6p_{1/2}$ states are narrower than the $6p_{3/2}$ states and are perturbed by their interaction with the $6p_{3/2}$ states. The perturbation leads to variations in the quantum defects of the $6p_{1/2}$ states and departures from the v^{-3} scaling of the widths. The interaction is most apparent in the excitation of the $6p_{1/2}10d$ state which is degenerate with the $6p_{1/2}$ states for $n=20$. The observed excitation spectrum clearly shows the influence of the degenerate $6p_{1/2}nd$ states and is shown to represent the spectral density of the $6p_{3/2}10d$ state. This spectrum as well as all the above-mentioned observations may be connected by a quantum-defect treatment. (22 refs.)

60668 Photoexcitation of an autoionizing resonance in the presence of off-diagonal relaxation. K.Rzazewski, J.H.Eberly (Dept. of Phys. & Astron., Univ. of Rochester, Rochester, NY, USA). *Phys. Rev. A (USA)*, vol.27, no.4, p.2026-42 (April 1983). The authors discuss the theory of photoexcitation of an autoionizing resonance. They solve a set of coupled stochastic integrodifferential equations which are based on the Fano model for autoionization, but which include the effects of weak elastic collisions, weak or strong laser excitation, and finite laser bandwidth. They determine the exact photoelectron spectrum and give formulas for spectral peak positions and widths. Redistributive scattering is evident, as are various effects normally associated only with transitions between discrete levels. Under certain conditions symmetries and fixed points of the electron spectrum can be predicted. (24 refs.)

Population of the three major exit channels in the $3d$ resonance region of atomic gallium See Entry 60622

Autoionisation versus radiative decay of resonances in electron impact excitation cross sections See Entry 60992

32.80F Photoionization and photodetachment

60669 Theoretical cross sections for nonresonant five-photon ionisation of sodium. S.N.Dixit (Corporate Res. Sci. Labs., Exxon Res. & Engng. Co., Linden, NJ, USA). *J. Phys. B (GB)*, vol.16, no.7, p.1205-9 (14 April 1983).

Truncated summation results for the differential cross sections for nonresonant five-photon ionisation of sodium are presented. The agreement between the recently measured total cross section and calculated one is fair while the photoelectron angular distributions differ considerably in the two cases. (10 refs.)

60670 Molecular beam study of photoionization of uranium and uranium oxide. R.Talukdar, A.Tripathy, P.N.Bajaj, P.K.Chakraborti, G.D.Saksena (Spectroscopy Group, Bhabha Atomic Res. Centre, Trombay, Bombay, India). *Opt. Commun. (Netherlands)*, vol.45, no.3, p.179-82 (1 April 1983). Crossed laser molecular beam configuration was used to study the photoionization of U and UO by the UV-lines of an argon ion laser. Photoionization efficiencies of both U and UO were found to be line sensitive. Photoionization by the 3638 Å line was observed for the first time. Uranium atom ionization efficiency being higher for the 3345 Å and 3511 Å groups of lines, while UO ionization efficiency being maximum for the 3638 Å line. Dependence of photoion signal on laser power and relative photoionization efficiencies of the two isotopic species of uranium are also investigated. (12 refs.)

60671 Effect of atomic polarization on two-photon electron detachment from the corresponding negative ions. P.A.Golovinskiy, B.A.Zon. *Opt. & Spectrosc. (USA)*, vol.53, no.2, p.125-8 (Aug. 1982). Translation of: *Opt. & Spektrosk. (USSR)*, vol.53, no.2, p.211-16 (Aug. 1982). [received: April 1983]

The polarization of the atoms is incorporated in an analysis of the two-photon detachment of electrons from negative ions. The probabilities for electron detachment from negative ions of alkali elements by linearly and circularly polarized light are calculated. (9 refs.)

60672 Calculation of photoionization cross sections for lithium isoelectronic series ions by the Dirac-Fock method. V.A.Zilitis. *Opt. & Spectrosc. (USA)*, vol.53, no.2, p.204-5 (Aug. 1982). Translation of: *Opt. & Spektrosk. (USSR)*, vol.53, no.2, p.348-51 (Aug. 1982). [received: April 1983]

Studies the photoionization of lithium-like ions from S^{13+} to Yb^{67+} on the basis of the relativistic self-consistent-field method with a correct account of exchange. (13 refs.)

60673 Microwave ionization of Na Rydberg levels. P.Pillet, W.W.Smith, R.Kachru, N.H.Tran, T.F.Gallagher (Molecular Phys. Lab., SRI Internat., Menlo Park, CA, USA).

Phys. Rev. Lett. (USA), vol.50, no.14, p.1042-5 (4 April 1983). The authors have observed the ionization of Na Rydberg states by strong microwave fields and have found that the field required for ionization is $1/(3.7n^2)$ (in atomic units) for $n=20\text{-}37$. This field is close to the field $1/(3n^2)$ at which the Stark manifolds of principal quantum numbers n and $n+1$ intersect. The ionization can be shown to arise from transitions occurring near these intersections. (14 refs.)

60674 Angular distribution of Xe $5s\text{-}4p$ photoelectrons: disagreement between experiment and theory. A.Fahlan, T.A.Carlson, M.O.Krause (Oak Ridge Nat. Lab., Oak Ridge, TN, USA). *Phys. Rev. Lett. (USA)*, vol.50, no.15, p.1114-17 (11 April 1983).

The angular asymmetry parameter β for the Xe $5s\text{-}4p$ photoelectrons has been studied with use of synchrotron radiation ($h\nu=28\text{-}65\text{ eV}$). The present results show that the relativistic random-phase approximation theory does not satisfactorily describe the Xe $5s$ photoionization process close to the Cooper minimum and thus require a renewed theoretical approach. The $5s$ partial photoionization cross section was obtained over the same photon region and the results agree with experimental values found in the literature. (19 refs.)

60675 Photoionization cross section of neutral calcium including double electron resonances. Z.Altun, S.L.Carter, H.P.Kelly (Dept. of Phys., Univ. of Virginia, Charlottesville, VA, USA). *Phys. Rev. A (USA)*, vol.27, no.4, p.1943-57 (April 1983).

Many-body perturbation theory has been used to calculate the photoionization cross section of neutral calcium from threshold at 6.11 to 70 eV . Near-threshold resonance structure due to double electron excitation has been included and is compared with the results of several experiments. At higher energy, resonance structure due to $3p$ excitations to bound states with $l=0$ and 2 has also been calculated and compared with a measurement by Mansfield and Newsom (1977). The $3p^24s^23d^1P$ resonance is found to be particularly prominent, in agreement with experiment. The authors' results are also compared with a recent calculation using the relativistic random-phase approximation. (45 refs.)

60676 Photoelectron spectrum from laser-induced autoionization in the presence of spontaneous emission and off-diagonal relaxation. G.S.Agarwal (School of Phys., Univ. of Hyderabad, Hyderabad, India), D.Agassi. *Phys. Rev. A (USA)*, vol.27, no.4, p.2254-7 (April 1983).

The exact solution of the Fano model, including both radiative recombination to the initial state (recycling) and off-diagonal phase-jitter relaxation, is obtained by two different methods. The authors derive a simple substitution rule stating that, by replacing $\pm i\omega_l \rightarrow \pm i\omega_l + \gamma_l$, the phase-jitter effects are included. The time dependence of the solution has a convolution form. The results for the electron spectrum exhibit an increasing elastic-peak line narrowing the faster the spontaneous decay becomes. For very fast spontaneous decay, the elastic linewidth saturates to γ_l . The relevant thresholds are discussed and demonstrated. (10 refs.)

60677 Multiple photoionization of isotropic atoms. T.Arisawa, Y.Maru-yama, Y.Suzuki, K.Shiba (JAERI, Naka-gun, Ibaraki-ken, Japan). *Physica B & C (Netherlands)*, vol.115 B+C, no.2, p.266-70 (Jan. 1983).

Three-photon ionization spectroscopy was applied in the visible wavelength region using a Nd:YAG laser-pumped dye laser having a line width of 1.1 GHz . It is observed that the ionization peaks are broadened and the isotopic peaks cannot be resolved in the higher power density region. (14 refs.)

60678 Direct measurement of K-shell photoionization cross sections by means of the coincidence method. C.Ranganathaiah, B.Sanjeeviah (Dept. of Phys., Univ. of Mysore, Mysore, India).

Physica B & C (Netherlands), vol.115 B+C, no.3, p.411-14 (March 1983). The coincidence method developed by authors for the measurement of K-shell photoionization cross sections for photon energies above 500 keV (see C. Ranganath et al., *Nucl. Instrum. and Methods*, vol.154, p.331, 1978) has been used at a lower photon energy to check the accuracy of the method in comparison with the other methods described in the literature. K-shell photoionization cross sections in tin, gold, lead and thorium targets for ^{51}Cr gamma rays have been measured. The results are compared with other measurements and with theoretical data. Good agreement is observed between the theoretical cross sections and the present experimental ones. (15 refs.)

60679 Spatial diagnostics of a gallium atomic beam by the method of two-stage laser photoionization. A.T.Tursunov, N.B.Eshkabilov (Alisher Navoi State Univ., Samarkand, USSR).

Sov. J. Quantum Electron. (USA), vol.12, no.10, p.1363-4 (Oct. 1982). Translation of: *Kvantovaya Elektron., Moskva (USSR)*, vol.9, no.10, p.2096-7 (Oct. 1982). [received: April 1983]

An experimental investigation was made of the spatial structure of a gallium atomic beam of the method of two-stage laser photoionization. The width of an atomic beam at various distances from the source was determined. (4 refs.)

Population of the three major exit channels in the $3d$ resonance region of atomic gallium See Entry 60622

Photoexcitation of an autoionizing resonance in the presence of off-diagonal relaxation See Entry 60668

Real-time multiphoton ionization detection of iodine atoms produced by infrared multiphoton dissociation of perfluoroalkyl iodides See Entry 60680

The threshold laws for electron-atom and positron-atom impact ionization See Entry 60989

32.80K Multiphoton processes

60680 Real-time multiphoton ionization detection of iodine atoms produced by infrared multiphoton dissociation of perfluoroalkyl iodides. P.A.Hackett, P.John, M.Mayhew, D.M.Rayner (Div. of Chem., Nat. Res. Council, Ottawa, Ontario, Canada).

Chem. Phys. Lett. (Netherlands), vol.96, no.2, p.139-42 (1 April 1983). The authors report the direct detection of iodine atoms following infrared multiphoton dissociation of perfluoroalkyl iodides. The technique, three-photon resonant two-photon ionization, shows great promise as an actinometer for primary dissociation yield in IRMPD. (18 refs.)

60681 Investigation of atomic relaxation by the three-level echoes. A.I.Alekseev, A.M.Basharov (Engng. Phys. Inst., Moscow, USSR). *Opt. Commun. (Netherlands)*, vol.45, no.3, p.171-8 (1 April 1983).

A method for identification of two-photon (optically forbidden) transitions and determination of all their relaxation parameters due to depolarizing atomic collisions was developed on the basis of studying polarization properties and decay laws of the three-level echoes. (13 refs.)

60682 Multiphoton interactions. G.R.Bennett.

Univ. Wales, Swansea thesis, Sept. 1982

This dissertation presents an account of some of the many types of interaction which take place in gases and metal vapours and at solid surfaces illuminated by very powerful flashes of laser radiation. Typically the laser beam intensities are $\geq 10^{11}$ W cm⁻² and at such high values the interactions involve the 'simultaneous' absorption of several photons. This is in contrast to the usual single photon interactions such as photoionisation and photoelectric emission which occur commonly in electrical discharges in gases. The processes of multiphoton absorption and ionisation are examined theoretically and experimental results for a wide range of photon energies and fluxes illuminating a wide variety of gases, metal vapours and solids are presented. A new simple analytical procedure is developed which enables the multiphoton ionisation rate for hydrogen to be computed. This gives results which are in agreement with those obtained from a more complicated quantum mechanical treatment. Applications of multiphoton absorption processes in spectroscopy, detection of trace quantities (single atom) and isotope separation are described.

Theoretical cross sections for nonresonant five-photon ionisation of sodium See Entry 60669

Effect of atomic polarization on two-photon electron detachment from the corresponding negative ions See Entry 60671

Multiple photoionization of isotropic atoms See Entry 60677

32.90 OTHER TOPICS IN ATOMIC SPECTRA AND INTERACTIONS WITH PHOTONS

60683 Spontaneous emission without field quantization. R.J.Cook (Dept. of Phys., Air Force Inst. of Technol., Wright Patterson Air Force Base, Dayton, OH, USA). *Phys. Rev. A (USA)*, vol.27, no.4, p.2265-7 (April 1983).

A theory of spontaneous emission is presented which does not quantize the radiation field. By allowing the atomic electron's radiation-reaction field to act in the equation of motion for the atomic density operator, the theory accounts for spontaneous emission without leaving the Hilbert space of the atom. The theory is quite simple and leads to exactly the same relaxation terms in the density-operator equation of motion as those predicted by the quantum theory of radiation. (11 refs.)

Beam-foil study of the $2s^2 2p^5$ 3/ and $2s 2p^6$ 3/ configurations of Ar IX See Entry 60636

Photoelectron spectrum from laser-induced autoionization in the presence of spontaneous emission and off-diagonal relaxation See Entry 60676

Rydberg-atom masers. I. A theoretical and experimental study of super-radiant systems in the millimeter-wave domain See Entry 61121

33.00 MOLECULAR SPECTRA AND INTERACTIONS WITH PHOTONS

33.10 CALCULATION OF MOLECULAR SPECTRA

60684 Infrared dephasing of degenerate fundamentals: the ν_6 mode of liquid CD₃I. W.G.Rothschild, J.Sousen-Jacob, J.Vincent-Geisse (Lab. de Recherches Phys., Univ. Pierre et Marie Curie, Paris, France). *Chem. Phys. Lett. (Netherlands)*, vol.96, no.1, p.43-6 (25 March 1983).

A model of vibrational dephasing with motional narrowing by the librational motions of the molecules in their cages is tested on the example of the ν_6 degenerate infrared fundamental of liquid CD₃I at room temperature. (14 refs.)

60685 A model for the pseudorotation of cycloheptane. V.Elsner (Lawrence Berkeley Lab., Univ. of California, Berkeley, CA, USA), H.L.Strauss. *Chem. Phys. Lett. (Netherlands)*, vol.96, no.3, p.276-8 (8 April 1983).

A very simple model for a seven-membered ring having fixed bond lengths and fixed ring bond angles is presented. The model pseudorotates in both the twist-chair/chair and the twist-boat/boat conformations and gives reasonably accurate detailed geometries. (4 refs.)

60686 Chaotic motions in vibrating molecules: the generalized Henon-Heiles model. R.Ramaswamy (Tata Inst. of Fundamental Res., Bombay, India). *Chem. Phys. (Netherlands)*, vol.76, no.1, p.15-24 (1 April 1983).

The method of avoided crossings is applied to a simple molecular model, the generalized Henon-Heiles system of coupled oscillators. The aim is to determine the onset of widespread chaotic motions. The method is used to locate, in a simple manner, the resonances that lead to chaotic motions for different choices of parameters, wherein the frequencies of the unperturbed oscillators are in the ratio 3:4 and 7:13. The accuracy of the prediction is verified against numerical calculations of classical trajectories. (36 refs.)

60687 Spectroscopic properties and relaxation processes of impurity molecules in solids. I. Rotational spectra. H.Kono, S.H.Lin (Dept. of Chem., Arizona State Univ., Tempe, AZ, USA).

The spectroscopic properties and relaxation processes of impurity diatomic molecules are studied theoretically. In order to treat the eigenvalue problem and the relaxation process consistently, the authors propose a unified theory based on the adiabatic approximation for the system of a diatomic molecule in monoatomic crystal. The adiabatic approximation is used to separate the total number of degrees of freedom of the system into the intramolecular vibrational, rotational, and lattice vibrational degrees of freedom. In this paper, the authors report the calculation of the rotational level shifts for HCl in rare gas matrices, using the M5 potential proposed by Hutson and Howard (1982). The effect of lattice vibration is appropriately taken into consideration by means of the Green's function method for point defects developed by Maradudin et al. (1971). The agreement between the theory and experimental results is good. It is shown that the coupling between the molecular rotation and lattice vibration is important, which improves the idea of the cell model in which the effect of host atoms is completely neglected. (38 refs.)

60688 Classical and quantum dynamics of long lived doubly excited vibrational states of triatomic molecules. R.M.Hedges, Jr., W.P.Reinhardt (Dept. of Chem., Univ. of Colorado, Boulder, CO, USA).

J. Chem. Phys. (USA), vol.78, no.6, pt.2, p.3964-75 (15 March 1983).

Local mode A-B-A triatomic molecules are modeled as coupled Morse oscillators using classical and quantum techniques. Classical studies indicate large volumes of nondissociating classical phase space, even well above the dissociation threshold. The trapped classical motion corresponds to excitation in both bond modes of the system. Quantum studies have been performed as a function of coupling constant (mass ratio) and of dissociation energy. Quantum doubly excited vibrational resonances are found with lifetimes of up to 10^6 vibrational periods. The lifetimes of the states, as \hbar (or dissociation energy) is varied, are in accordance with the correspondence principle. Substantial deviation from the predictions of statistical theories is noted in the distributions of lifetimes, as well as in the fact that all of the resonances are only weakly coupled 'direct' dissociation channels. (52 refs.)

60689 On the onset of strong mode coupling in small polyatomic molecules. R.S.Berry (Dept. of Chem., Univ. of Chicago, Chicago, IL, USA).

J. Chem. Phys. (USA), vol.78, no.6, pt.2, p.3976-80 (15 March 1983).

The number of vibrational states corresponding to separable, quasiperiodic motion of low dimensionality is estimated by a generalization of the analysis of the quantum-mechanical Henon-Heiles problem by Hose and Taylor (1982). The number of nonseparable states with strongly coupled modes appears to overwhelm the number of separable 'quasiperiodic' states whenever the molecule in question contains five or more vibrational quanta, and may dominate for states with four or even three vibrational quanta. Some comments are made to try to clarify the concepts of separability and quasiperiodicity. (15 refs.)

60690 Local modes and cross-correlation functions. J.T.Muckerman (Chem. Dept., Brookhaven Nat. Lab., Upton, NY, USA), D.W.Noid, M.S.Child.

J. Chem. Phys. (USA), vol.78, no.6, pt.2, p.3981-9 (15 March 1983).

It is shown how the use of cross-correlation functions and their Fourier transform provides a convenient probe of the division of the classical phase space for stretching vibrations of H₂O into local, normal, stochastic fractions. Resulting classical estimates for the numbers of total and local states, $N(E)$ and $N_l(E)$, respectively, as functions of energy are in excellent agreement with previous quantal and semiclassical results. The classical estimate of the number of stochastic states $N_s(E)$ as a function of energy is a new result. The present method is readily generalizable to polyatomic molecules with many vibrational degrees of freedom. (19 refs.)

60691 Local modes: their relaxation, polarization, and stereoselective excitation by lasers. J.W.Perry, A.H.Zewail (Arthur Amos Noyes Lab. of Chem. Phys., California Inst. of Technol., Pasadena, CA, USA).

J. Phys. Chem. (USA), vol.86, no.26, p.5197-205 (23 Dec. 1982).

Results are presented concerning the nature and relaxation of methyl and aromatic CH stretching overtones of low-temperature crystalline durene (1,2,4,5-tetramethylbenzene). The experimental polarization ratios of the bands are used to compare three limiting models (local modes, independent methyl modes, and fully delocalized modes) in the light of new information on the conformation of durene obtained by low-temperature X-ray diffraction. A picture is provided for the origin of the splittings observed for the $\Delta\nu_{CH}=5$ spectra at 1.7K and the nature of the vibrational energy distribution of the single-photon excited states of the methyl and aromatic subsets. (39 refs.)

60692 High-lying levels of ozone via an algebraic approach. I.Benjamin, R.D.Levine, J.L.Kinsey (Fritz Haber Molecular Dynamics Res. Center, Hebrew Univ., Jerusalem Israel).

J. Phys. Chem. (USA), vol.87, no.5, p.727-9 (3 March 1983).

An algebraic Hamiltonian for the vibrational motion in ozone, including a Darling-Dennison type coupling term, used to fit the recently observed high overtones. The good quality of the fit is due to the coupling of anharmonic normal modes by quartic order (Darling-Dennison type) coupling term. The algebraic Hamiltonian contains six parameters and these suffice to provide a better fit than the six-parameter spectroscopic term formula which uses a Darling-Dennison type coupling among harmonic modes. The present results provide a hitherto unexplored quantitative application of the algebraic approach to perturbed high lying states of triatomics. (13 refs.)

60693 Vibrational state of chemisorbed molecule on metal surface. H.Ueba (Dept. of Electronics, Toyama Univ., Toyama, Japan).

J. Electron Spectrosc. & Relat. Phenom. (Netherlands), vol.29, p.157-62 (15 Jan. 1983). (Proceedings of the Third International Conference on 'Vibrations at Surfaces', Asilomar, CA, USA, 1-4 Sept. 1982).

The vibrational state of a chemisorbed molecule on a metal surface is studied by focusing attention on the role of electron-hole pair excitations of the coupled molecule-metal system. The vibrational line shapes thus calculated are characterized by both large red shift in the frequency and broad width (short lifetime) compared with those of free molecules. (9 refs.)

60694 Allowance for the dependence of the repulsion branch of the potential of intermolecular interactions on the vibrational coordinates in the description of the displacements of the vibrational frequencies of molecules in a vapor-liquid transition. S.I.Lukyanov, S.Kh.Akopyan.

Opt. & Spectrosc. (USA), vol.53, no.1, p.34-8 (July 1982). Translation of:

Opt. & Spektrosk. (USSR), vol.53, no.1, p.60-6 (July 1982). [received: April 1983]

A method has been proposed for describing the dependence of the repulsion potential on the vibrational coordinates, based on the use of a dumbbell model. The displacement of the principal vibrational band of the nitrogen molecule in the vapor-liquid phase transformation has been calculated with allowance for the difference in the relative changes in the forces of repulsion and attraction on optical excitation of the molecule. (43 refs.)

60695 Theory of absorption and emission of light by molecular systems with multiwell potentials. B.D.Fainberg.

Opt. & Spectrosc. (USA), vol.53, no.1, p.105-7 (July 1982). Translation of:

Opt. & Spektrosk. (USSR), vol.53, no.1, p.176-80 (July 1982). [received: April 1983]

When considering processes of absorption and emission of light by complex molecules experiencing nuclear regrouping by impurity centers in crystals, and by excitons with charge transfer, etc., a situation very often occurs in which the optical transition takes place between states whose adiabatic potentials have two or more minima. The author uses functional integration to develop a method for calculating the Lax moments and the semiclassical electronic-vibrational spectra of systems in which both the ground state a and the excited state b are characterized by multiwell potentials. The effects of other vibrations (multidimensionality of the adiabatic potential) are also taken into account. (10 refs.)

60696 Derivation of the Hamiltonian of a linear molecule. A.Ya.Tsaune. *Opt. & Spectrosc. (USA)*, vol.53, no.2, p.134-7 (Aug. 1982). Translation of: *Opt. & Spektrosk. (USSR)*, vol.53, no.2, p.228-34 (Aug. 1982). [received: April 1983]

Fundamental questions concerning the derivation of a Hamiltonian are considered. The meaning of the Wilson-Howard conditions is explained, a nonholonomic condition, supplementing the definition of the behavior of a moving system in a linear molecule is introduced, and expressions are obtained for the angular momenta satisfying the usual commutation conditions and the Wilson-Howard conditions. The procedure for constructing a Hamiltonian is demonstrated both in the Wilson-Howard scheme, as well as for direct transition to molecular coordinates and the final expression for the Hamiltonian is given. (17 refs.)

60697 Study of molecules in a rotation-vibration level excited along a supersonic free jet. D.Boscher, D.Goffe, M.Huetz-Aubert, J.P.Martin (Groupe de Recherches Thermiques, CNRS, Chateaufort-Malabry, France), R.Campargue, M.A.Gaveau, J.Rousseau. *Rev. Cehedec (France)*, vol.19, no.NS82-2, p.81-95 (1982). In French. The ro-vibrational populations of CO are measured along supersonic free jets. When the jet is produced by a high enthalpy generator ($P_0=30$ bar, $T_0=1800$ K), the vibrational and rotational degrees of freedom are in Boltzmann equilibrium even if $T_v \gg T_r$. But, when $P_0=50$ torr, the rotation is no more in internal equilibrium and the high J levels are overpopulated. (19 refs.)

60698 Spectroscopic evidence in ϕ CXYZ molecules for the three groups X, Y, Z acting as a whole, whatever the symmetry may be, in their long range interactions with the chromophore. D.Courtois, B.Vidal (Lab. de Spectroscopie de la Reactivite Chimique, Univ. des Sci. et Tech. de Lille, Villeneuve d'Ascq, France). *Spectrosc. Lett. (USA)*, vol.15, no.12, p.983-90 (1982).

Long range interactions, in structures whose type is ϕ CH₂X, between the aromatic chromophore and an auxochrome X, involve a σ, π coupling through the methylene C_α-H bonds. That hyperconjugative effect encountered with the hydrogen atoms linked to C_α and the modulation of their effect by the auxochrome, allow one to understand the spectroscopic behaviour of the secondary transition in many molecular systems. The authors present some spectroscopic results showing that other bonds than C-H on C_α can also transmit interactions with a great efficiency. The experimental work enables one to determine to what extent σ, π coupling is still possible when none of the symmetry conditions, which however seem to be required from the substituent for the coupling, is satisfied. (14 refs.)

60699 On the application of the method of moments to the investigation of molecular structureless electronic spectra. S.Rashev (Inst. of Solid State Phys., Sofia, Bulgaria). *Spectrosc. Lett. (USA)*, vol.15, no.12, p.1009-16 (1982).

The author outlines a procedure which makes possible the determination of the shift of the optically active vibration in the electronic transition from structurally unresolved absorption or emission spectra, which are typical for polyatomic molecules. (10 refs.)

60700 Heterogeneous relaxation of a vibration-excited molecular gas. E.Ya.Kogan, V.N.Malnev. *Ukr. Fiz. Zh. (USSR)*, vol.28, no.3, p.374-81 (March 1983). In Russian.

A quantum theory is developed for transitions in the vibrational spectrum of a diatomic symmetric molecule in the process of its interaction with a solid surface. Transition probabilities in vibrational spectra of the molecule and surface are estimated on the basis of model interaction potential. Analysis of experimental data was performed for a symmetric molecule vibration relaxation on a solid surface and comparison was made with predictions. (5 refs.)

Dynamic model and tunneling splittings in LMH₄ non-rigid hydrides See Entry 60565

Comparison of local density functional Hartree-Fock and configuration interaction in the STO-3G orbital basis for some first-row diatomics See Entry 60607

Approximate relativistic calculations within the one-center approximation for the series CH₄ to PbH₄ See Entry 60611

The rotational spectrum and molecular properties of the hydrogen cyanide hydrogen bromide complex See Entry 60701

Wavelength dependence of the strengths of the electronic transitions of diatomic molecules See Entry 60703

The rotational spectrum and molecular structure of the benzene-hydrogen chloride complex See Entry 60705

The structure and molecular properties of the acetylene-HCN complex as determined from the rotational spectra See Entry 60706

The rotational spectrum and molecular structure of the furan-HCl complex See Entry 60708

Beam maser spectroscopy on CD₃CN See Entry 60710

On the 1 μ m system of iron hydride See Entry 60714

The infrared absorption spectra of (HCCH)₂ and (DCCD)₂ See Entry 60718

$\lambda^2\Pi-\tilde{\lambda}^2\Sigma^+$ infrared electronic transition of C₂H⁺ See Entry 60719

Detection of the free rotation of NH₃ molecules in polymers from the far IR spectra See Entry 60722

Intramolecular-vibration spectra of D₂O in H₂O ice matrices. Calculation and interpretation of the contours of the IR absorption and Raman scattering See Entry 60723

Raman spectra, ab initio molecular orbital calculations, vibrational analysis, and thermodynamic functions for NH₃:AlX₃ (X=F, Cl, Br) See Entry 60725

Tricopper. A fluxional molecule See Entry 60728

Homogeneous and inhomogeneous vibrational dephasing processes in aqueous thiocyanate solutions See Entry 60729

The high-resolution visible overtone spectrum of acetylene See Entry 60734

High-resolution study of InCl spectra See Entry 60736

The rotational and hyperfine spectrum and structure of H₂CO-HF See Entry 60750

Electric dipole moment of the diatomic TlF in its higher vibrational states See Entry 60779

Electric dipole moments of excited vibrational levels in the $\tilde{X}1A_1$ state of formaldehyde by stimulated emission spectroscopy See Entry 60780

Some theoretical considerations for magnetic vibrational circular dichroism spectra See Entry 60781

Measurement of sub-nanosecond single-rovibronic fluorescence with a pulsed dye laser See Entry 60794

Observation of the asymmetric O-U-O stretch in the vibronic absorption spectrum of uranyl formate monohydrate See Entry 60798

Laser vaporization of tin: spectra and ground state molecular parameters of Sn₂ See Entry 60801

High-resolution gas phase emission and laser induced fluorescence excitation spectra of 1,3,5-C₆F₃H₃⁺ and 1,3,5-C₆F₃D₃⁺: critical bands in the Jahn-Teller effect analysis See Entry 60805

Rotational effects in the intermediate-case radiationless decay of pyrimidine See Entry 60813

Rotational relaxation in ground-state p-difluorobenzene: State selection by stimulated emission pumping See Entry 60815

Vibrational relaxation within mixed electronic states See Entry 60816

Vibrationally resolved photoelectron angular distributions for H₂ See Entry 60832

Precision measurements of hyperfine predissociation in I₂ vapor using a two-photon resonant scattering technique See Entry 60856

Vibronic interactions in s-triazine spectra See Entry 60875

Systematics in two-photon rovibrational contours of 14₀¹ (¹B_{2u}-¹A_{1g}) in benzene derivatives See Entry 60878

Comparison of the Floquet and rotating-wave methods for multiphoton excitation of SF₆ See Entry 60879

Experimental observation of the intercollisional interference effect on the S₁ pure rotation line of the collision induced spectra of the H₂-He mixture See Entry 60932

Molecular clustering about a positive ion. Structures, energetics, and vibrational frequencies of the protonated hydrogen clusters H₃⁺, H₅⁺, H₇⁺, and H₉⁺ See Entry 61044

Study of the infrared absorption of carbon tetrafluoride at 9 μ m See Entry 61134

Rovibrational excitation within the infinite conical well: desorption of diatomic molecules See Entry 62268

Vibrational analysis of the products from thermal decomposition of OCS and CO₂ See Entry 63507

Production of vibrationally excited OH in chemiluminescent reactions of ozone with monoterpenes See Entry 63509

33.20 MOLECULAR SPECTRA GROUPED BY WAVELENGTH RANGES

(for magneto-optical and electro-optical spectra, see 33.45; for fluorescence and phosphorescence spectra, see 33.50; for photoelectron spectra, see 33.65)

60701 The rotational spectrum and molecular properties of the hydrogen cyanide hydrogen bromide complex. E.J.Campbell, A.C.Legon, W.H.Flygare (Noyes Chem. Lab., Univ. of Illinois, Urbana, IL, USA).

J. Chem. Phys. (USA), vol.78, no.6, pt.2, p.3494-500 (15 March 1983). Rotational spectra have been assigned for four isotopic species of a linear hydrogen-bonded complex formed between hydrogen cyanide and hydrogen bromide. The vibrational ground state spectroscopic constants are HC¹³N, H⁷⁹Br: B₀=1396.59577(60) MHz, D₁=1.892(27) kHz, x_{aa}^{Br}=426.4164(103) MHz, x_{aa}^N=-4.026(11) MHz. HC¹⁴N, H⁸¹Br: B₀=1388.05125(45) MHz, D₁=1.877(19) kHz, x_{aa}^{Br}=356.2316(85) MHz, x_{aa}^N=-4.016(9) MHz. HC¹⁵N, H⁷⁹Br: B₀=1372.50545(25) MHz, x_{aa}^N=1.865(6) kHz, x_{aa}^{Br}=426.6234(61) MHz, C_B=2.51(39) kHz. HC¹⁵N, H⁸¹Br: B₀=1363.88746(30) MHz, D₁=1.840(8) kHz, x_{aa}^{Br}=356.4074(65) MHz, C_B=2.48(44) kHz. The order of the atoms is HCNHBr with an N-Br separation of 3.61 Å. (33 refs.)

60702 Multidimensional spectroscopy. I. Perturbation theory. B.Blumich, D.Ziessow (Iwan N. Stranski-Inst., Tech. Univ. Berlin, Berlin, Germany). *Mol. Phys. (GB)*, vol.48, no.5, p.955-68 (10 April 1983).

The quantum states produced by non-linear interaction of a coherent uniform radiation field with dipolar matter are evaluated by a time-dependent perturbation expansion of the density matrix. The non-linear terms of the expansion are Fourier transformed to yield multi-dimensional spectra which indicate the connectivities in the underlying energy level diagrams. The spectra can be measured in experiments with multiple resonance, multiple pulse or stochastic excitation. Although the theory presented is of general validity in coherent spectroscopy, emphasis is placed on its application in non-linear NMR spectroscopy. It illustrates particularly well the common basis of double, 2D correlated and multi-dimensional stochastic magnetic resonance. (21 refs.)

60703 Wavelength dependence of the strengths of the electronic transitions of diatomic molecules. N.E.Kuzmenko, L.A.Kuznetsova, V.K.Mateev. *Opt. & Spectrosc. (USA)*, vol.53, no.2, p.137-9 (Aug. 1982). Translation of: *Opt. & Spektrosk. (USSR)*, vol.53, no.2, p.235-8 (Aug. 1982). [received: April 1983]

Analytical expressions have been obtained describing the wavelength dependence of the strengths of the electronic transitions for thirty-five electronic systems of diatomic molecules. The recommended S₀^{int}(λ) relationship is particularly convenient for carrying out technical calculations of radiative processes in strongly heated gases and in a low-temperature plasma. (5 refs.)

Jahn-Teller-like progressions in the absence and presence of Jahn-Teller distortions See Entry 60610

Monte Carlo simulation of solvent effects on vibrational and electronic spectra See Entry 60627

Quantum theory of solvent effects on electronic spectra: Predictions of the exact solution of the mean spherical model See Entry 60628

Theory of absorption and emission of light by molecular systems with multiwell potentials See Entry 60695

On the application of the Rydberg-Kratzer potential to some diatomic molecules See Entry 60890

Spectral evidence of line collisional interference in NH₃ inversion spectrum See Entry 60908

33.20B Radiofrequency and microwave spectra

(for NMR spectra, see 33.25; for EPR spectra, see 33.30)

60704 ^{83}Kr nuclear quadrupole coupling, microwave spectrum, and structure of KrHCN . E.J.Campbell, L.W.Buxton, A.C.Legon (Noyes Chem. Lab., Univ. of Illinois, Urbana, IL, USA). *J. Chem. Phys. (USA)*, vol.78, no.6, pt.2, p.3483-93 (15 March 1983). Rotational spectra have been observed for ten isotopic species of KrHCN using the pulsed Fabry-Perot Fourier transform technique. The ^{83}Kr nuclear quadrupole coupling constant has been measured in $^{83}\text{KrHC}^{14}\text{N}$, $^{83}\text{KrHC}^{15}\text{N}$, and $^{83}\text{KrDC}^{14}\text{N}$. Values of the rotational constants B_0 , centrifugal distortion constants D_1 and H_1 , ^{14}N and ^{15}N nuclear quadrupole coupling constants are: $^{83}\text{KrHC}^{14}\text{N}$: $B_0 = 1188.50879(211)$ MHz, $D_1 = 47.889(245)$ kHz, $H_1 = 72.1(75)$ Hz, $\chi_{\text{Kr}} = -3.2719(103)$, $^{83}\text{KrHC}^{15}\text{N}$: $B_0 = 1184.9826$ MHz, $\chi_{\text{Kr}} = -3.2630(60)$, $\chi_{\text{N}} = 7.457(50)$, $^{84}\text{KrHC}^{14}\text{N}$: $B_0 = 1181.55187(38)$ MHz, $D_1 = 46.913(26)$ kHz, $H_1 = 66.6(5)$ Hz, $\chi_{\text{Kr}} = -3.2780(16)$, $^{86}\text{KrHC}^{14}\text{N}$: $B_0 = 1174.91501(51)$ MHz, $D_1 = 46.071(63)$ kHz, $H_1 = 62.9(5)$ Hz, $\chi_{\text{Kr}} = -3.2712(52)$, $^{82}\text{KrHC}^{15}\text{N}$: $B_0 = 1144.01609(45)$, $D_1 = 40.772(31)$ kHz, $H_1 = 56.0(6)$ Hz, $^{83}\text{KrHC}^{15}\text{N}$: $B_0 = 1140.53244$ MHz, $\chi_{\text{Kr}} = 7.540(50)$, $^{84}\text{KrHC}^{15}\text{N}$: $B_0 = 1137.14193(72)$, $D_1 = 39.928(35)$ kHz, $H_1 = 52.5(5)$ Hz, $^{86}\text{KrHC}^{15}\text{N}$: $B_0 = 1130.58509(43)$ MHz, $D_1 = 39.307(30)$ kHz, $H_1 = 52.9(6)$ Hz, $^{83}\text{KrDC}^{14}\text{N}$: $B_0 = 1162.05255$ MHz, $\chi_{\text{Kr}} = -3.4739(139)$, $\chi_{\text{N}} = 8.034(45)$, $^{84}\text{KrDC}^{14}\text{N}$: $B_0 = 1158.64567(82)$ MHz, $D_1 = 26.973(48)$ kHz, $H_1 = 27.2(8)$ Hz, $\chi_{\text{Kr}} = -3.4937(80)$. (a) Calculated using $D_1 = 47.401$ kHz, $H_1 = 69.4$ Hz. (b) Calculated using $D_1 = 40.350$ kHz, $H_1 = 54.3$ Hz. (c) Calculated using $D_1 = 26.973$ kHz, $H_1 = 27.2$ Hz. These constants are consistent with a linear or near-linear configuration, with a Kr-HCN center-of-mass separation of 4.54 Å, and the Kr atom located 27° off the HCN figure axis on average, where the vertex of this angle is placed on the HCN center-of-mass. KrHCN exhibits unusually large centrifugal distortion in comparison with previously studied Kr-hydrogen halide systems. The authors find that the measured ^{83}Kr nuclear quadrupole coupling constants in $^{83}\text{KrHC}^{14}\text{N}$ and $^{83}\text{KrDC}^{14}\text{N}$ are consistent with a long range polarization model previously used to explain values of χ_{Kr} in KrH(D)Cl and KrH(D)F . (39 refs.)

60705 The rotational spectrum and molecular structure of the benzene-hydrogen chloride complex. W.G.Read, E.J.Campbell, G.Henderson (Noyes Chem. Lab., Univ. of Illinois, Urbana, IL, USA). *J. Chem. Phys. (USA)*, vol.78, no.6, pt.2, p.3501-8 (15 March 1983). The microwave spectrum of the weakly bound complex benzene-HCl was studied in the gas phase using Fourier transform microwave spectroscopy carried out in a Fabry-Perot cavity with a pulsed supersonic nozzle as the molecular source. Several R-branch α -dipole transitions have been observed for benzene- ^2H ^{35}Cl , benzene- ^2H ^{37}Cl , and benzene- (d_6) - ^2H ^{35}Cl . The spectrum was characteristic of a symmetric top, indicating that the time averaged displacement of the H and Cl atoms from the benzene C_6 axis is zero. Deuterium substitution of HCl demonstrated that the acidic proton lies between the Cl atom and the benzene ring. The chlorine nuclear quadrupole coupling constant χ_{Cl} was measured for all four isotopic species and is interpreted in terms of a projection of the chlorine quadrupole coupling constant in free HCl, averaged over two degenerate vibrational ground state bending modes involving the angles between the benzene C_6 axis and the HCl bond axis. The spectroscopic constants for benzene-HCl are: Benzene- ^2H ^{35}Cl : $B_0 = 1237.6835(5)$ MHz, $D_1 = 1.22(1)$ kHz, $D_{JK} = 13.35(2)$ kHz, $\chi_{\text{Cl}} = 52.19(2)$ MHz, Benzene- ^2H ^{37}Cl : $B_0 = 1201.925(2)$ MHz, $D_1 = 1.16(4)$, $D_{JK} = 13.4(8)$ kHz, $\chi_{\text{Cl}} = -41.2(3)$ MHz, Benzene- (d_6) ^{35}Cl : $B_0 = 1228.2440(6)$ MHz, $D_1 = 1.19(2)$, $D_{JK} = 14.57(3)$, $\chi_{\text{Cl}} = -54.70(2)$ MHz, Benzene- (d_6) ^{37}Cl : $B_0 = 1165.1542(6)$ MHz, $D_1 = 1.08(1)$, $D_{JK} = 10.93(4)$ kHz, $\chi_{\text{Cl}} = -52.25(2)$ MHz. Numbers in parentheses represent one standard deviation in the fit. (36 refs.)

60706 The structure and molecular properties of the acetylene-HCN complex as determined from the rotational spectra. P.D.Aldrich, S.G.Kukulich, E.J.Campbell (Noyes Chem. Lab., Univ. of Illinois, Urbana, IL, USA). *J. Chem. Phys. (USA)*, vol.78, no.6, pt.2, p.3521-30 (15 March 1983). The microwave spectra for four isotopic species of a complex formed between acetylene and HCN have been obtained using the pulsed, Fourier-transform method with gas pulsed into an evacuated Fabry-Perot cavity. The spectra indicate the complex to be a T-shaped near-prolate asymmetric rotor ($\kappa = -0.993$) in its ground vibrational state in which HCN lies on the C_2 symmetry axis with the hydrogen atom of HCN pointing to the middle of the triple bond of acetylene. The carbon atom of HCN is situated 3.656 Å from the acetylene center of mass. Nuclear quadrupole coupling constants for N are obtained for all four isotopes and deuterium quadrupole coupling constants are obtained for two isotopes. Various contributions to the electric field gradients at quadrupolar nuclei are discussed. (35 refs.)

60707 Centrifugal distortion and internal rotation analysis of the microwave spectrum of ethyl fluoride. E.Fliege, H.Dreizler (Abteilung Chem. Phys., Inst. für Phys. Chem., Univ. Kiel, Kiel, Germany), J.Demaion, D.Boucher, J.Burie, A.Dubrule. *J. Chem. Phys. (USA)*, vol.78, no.6, pt.2, p.3541-4 (15 March 1983). The internal rotation fine structure of the microwave spectrum of ethyl fluoride $\text{CH}_3\text{CH}_2\text{F}$ was resolved and analyzed in the ground state. The assignment of the high J lines was checked by a centrifugal distortion analysis. The barrier height V_3 determined from the ground state is 3349 ± 4 cal/mol. (18 refs.)

60708 The rotational spectrum and molecular structure of the furan-HCl complex. J.A.Shea, S.G.Kukulich (Noyes Chem. Lab., Univ. of Illinois, Urbana, IL, USA). *J. Chem. Phys. (USA)*, vol.78, no.6, pt.2, p.3545-51 (15 March 1983). The microwave spectrum of the furan-HCl complex in the ground vibrational state has been measured and assigned using a Fourier-transform microwave spectrometer employing a Fabry-Perot cavity and a pulsed supersonic nozzle as a molecular source. Furan-HCl is planar, with the axis of the HCl subunit oriented along the a axis of furan, bisecting the oxygen-carbon angle. A hydrogen bond is formed between the HCl proton and the lone electron pair of oxygen. The spectroscopic constants for furan- ^{35}Cl in MHz are: $A'' = 9421.3(39)$, $B'' = 1004.2001(27)$, $C'' = 904.5526(26)$, $\tau_1 = -0.9392(12)$, $\tau_2 = -0.0751(2)$, $\tau_{\text{bbbb}} = -0.004$ 01(19), $\tau_{\text{cccc}} = -0.002$ 17(17), $\chi_{\text{aa}} = -52.803(17)$, $\chi_{\text{bb}} = 25.626(54)$, and $\chi_{\text{cc}} = 27.177(54)$. Rotational transitions for the isotopic species furan- ^{37}Cl and furan- ^2H ^{35}Cl were also measured and assigned. The oxygen-chlorine distance is 3.26(1) Å. The binding of the HCl to oxygen, rather than to the π bonds between the β carbon atoms, was confirmed by measurements on the 2-D furan- ^{35}Cl complex. (18 refs.)

60709 Microwave spectrum, structure, and quadrupole coupling for the ethylene-hydrogen cyanide complex. S.G.Kukulich, W.G.Read, P.D.Aldrich (Noyes Chem. Lab., Univ. of Illinois, Urbana, IL, USA). *J. Chem. Phys. (USA)*, vol.78, no.6, pt.2, p.3552-6 (15 March 1983). Microwave spectra for the complexes ethylene-HCN and ethylene-DCN were observed with the pulsed beam, Fourier transform spectrometer. The complexes are T shaped with the HCN hydrogen atom adjacent to the C-C double bond of ethylene. The HCN molecule lies on a line perpendicular to the plane of ethylene and passing through the ethylene center of mass. The HCN carbon atom is 3.702(10) Å above the ethylene plane. The nitrogen quadrupole coupling strength is $eQq_{\text{aa}}(\text{N}) = -4.363(2)$ MHz for ethylene-HCN and $eQq_{\text{aa}}(\text{N}) = -4.396(3)$ MHz for ethylene-DCN. The deuterium quadrupole coupling strength is $eQq_{\text{aa}}(\text{D}) = 0.178(7)$ MHz for ethylene-DCN. The anisotropy in the nitrogen quadrupole coupling $eQ(q_{\text{bb}} - q_{\text{cc}})(\text{N})$ is 0.013(3) MHz for ethylene-HCN and 0.047(12) MHz for ethylene-DCN. The rotational constants are: for ethylene-HCN, $A = 25496(689)$, $B = 1906.581(5)$, $C = 1808.878(5)$ and for ethylene-DCN, $A = 24960(1101)$, $B = 1904.739(6)$, $C = 1807.344(6)$. Centrifugal distortion constants D_J and D_{JK} were obtained. (13 refs.)

60710 Beam maser spectroscopy on CD_3CN . A.M.Murray, S.G.Kukulich (Dept. of Chem., Univ. of Arizona, Tucson, AZ, USA). *J. Chem. Phys. (USA)*, vol.78, no.6, pt.2, p.3557-9 (15 March 1983). The $J=1-0$ rotational transitions of CD_3CN were measured using a two-cavity molecular beam maser spectrometer. This spectrometer employs the Ramsey method of separated oscillating fields to obtain very high resolutions and allows precise measurements of the hyperfine structure splittings. The nitrogen quadrupole coupling constant is $eQq_{\text{aa}}(\text{N}) = -4229.2 \pm 0.6$ kHz and the deuterium quadrupole constant is $eQq_{\text{aa}}(\text{D}) = -55.1 \pm 0.4$ kHz. Assuming cylindrical symmetry about the C-D bond axis the authors obtain the C-D bond-axis deuterium quadrupole coupling strength of $eQq_{\text{aa}}(\text{D}) = 169.6 \pm 4.5$ kHz. The b-axis rotational constant, and nitrogen and deuterium spin-rotation interaction strengths are also reported. (9 refs.)

60711 Microwave spectral study of bicyclo[2.2.2]octene and bicyclo[2.2.2]octadiene. R.N.Nandi, M.D.Harmony (Dept. of Chem., Univ. of Kansas, Lawrence, KS, USA), A.E.Howard, S.W.Staley. *J. Chem. Phys. (USA)*, vol.78, no.6, pt.2, p.3560-1 (15 March 1983). Microwave spectral studies of bicyclo[2.2.2]octene (C_8H_{12}) and bicyclo[2.2.2]octadiene (C_8H_{10}) have led to the following rotational constants in MHz: for C_8H_{12} , $A = 2576.721 \pm 0.002$, $B = 2508.998 \pm 0.002$, $C = 2462.272 \pm 0.009$; and for C_8H_{10} , $A = 2730.116 \pm 0.002$, $B = 2650.520 \pm 0.002$, $C = 2631.710 \pm 0.002$. The dipole moments of the C_8 molecules have also been obtained, the values along the symmetry axis being $\mu_a = 0.253 \pm 0.001$ D for C_8H_{12} and $\mu_c = 0.432 \pm 0.002$ D for C_8H_{10} . (11 refs.)

60712 Microwave spectrum, dipole moment, barrier to internal rotation of 1,1-dimethylborane. C.W.Chui, A.B.Burg, R.A.Baudet (Dept. of Chem., Univ. of Southern California, Los Angeles, CA, USA). *J. Chem. Phys. (USA)*, vol.78, no.6, pt.2, p.3562-6 (15 March 1983). The microwave spectra of four isotopic species of 1,1-dimethylborane have been investigated in the region between 18.0 and 40.0 GHz. The observed rotational constants (MHz) for the normal species are $A = 7070.68(7)$, $B = 6606.57(3)$, $C = 3660.33(1)$; for $^{10}\text{B}_2$ species, $A = 7069.87(15)$, $B = 6605.79(5)$, $C = 3659.88(3)$; and for $^{10}\text{B}_2$ species, $A = 7070.63(27)$, $B = 6889.89(10)$, $C = 3745.92(6)$. The B-B distance determined by the Kraitchman method is 1.76(2) Å. The carbon-boron structure could be fitted to the moments of inertia by assuming reasonable values for the other structural parameters: $r(\text{B}-\text{C}) = 1.59$ Å and $\angle \text{CBC} = 121.2^\circ$. From the Stark effect measurements, the dipole moment is measured to be 0.87(3) D. Assuming no coupling between the rotors, the barrier height to internal rotation is 1.39(16) kcal/mol. (15 refs.)

Electric dipole moment of the diatomic TIF in its higher vibrational states See Entry 60779

33.20E Infrared spectra

60713 FTIR spectra of $(\text{HF})_3$ species in solid argon at 12K. L.Andrews, G.L.Johnson (Dept. of Chem., Univ. of Virginia, Charlottesville, VA, USA). *Chem. Phys. Lett. (Netherlands)*, vol.96, no.2, p.133-8 (1 April 1983). Condensation of argon/HF mixtures at 12K revealed sharp new 3825.5 and 3702.0 cm^{-1} absorptions which exhibited different growth behaviour on sample warming. Mixed HF/DF samples revealed a single mixed isotopic satellite near the DF counterpart of the former band assigned to $(\text{HF})_2$ and a group of satellites for the latter band assigned to $(\text{HF})_3$. (20 refs.)

60714 On the 1 μm system of iron hydride. W.J.Balfour, B.Lindgren (Inst. of Phys., Univ. of Stockholm, Stockholm, Sweden), S.O'Connor. *Chem. Phys. Lett. (Netherlands)*, vol.96, no.2, p.251-2 (1 April 1983). The 987.7 nm system of FeD has been shown by rotational analysis of the (1,0) and (0,0) bands to be due to a $^4\Delta-^4\text{F}$ electronic transition. The bond lengths in the $v=0$ levels of the upper and lower states are $r'_0 = 0.1705$ nm and $r''_0 = 0.1589$ nm, respectively, and the $(v'=1)-(v'=0)$ vibrational interval of the upper state is ≈ 1035 cm^{-1} . (7 refs.)

60715 The infrared absorption spectrum of a supersonic expansion of methyl chloride. D.L.Snively, D.L.Wiberg, S.D.Colson (Sterling Chem. Lab., Yale Univ., New Haven, CT, USA). *Chem. Phys. Lett. (Netherlands)*, vol.96, no.3, p.319-23 (8 April 1983). The infrared absorption spectrum of a rotationally cooled supersonic jet of neat methyl chloride is reported. The rotational constants of ν_3 , ν_2 and ν_1 are determined. Using a 0.05 mm nozzle diameter and a 2 atm stagnation pressure, a Boltzmann population distribution is found with a characteristic rotational temperature of 120K. (14 refs.)

60716 Distribution of gauche bonds in crystalline $n\text{-C}_{21}\text{H}_{44}$ in phase II. R.G.Snyder, M.Marocelli, H.L.Strauss (Dept. of Chem., Univ. of California, Berkeley, CA, USA), C.A.Elliger, D.G.Cameron, H.L.Casal, H.H.Mantsch. *J. Am. Chem. Soc. (USA)*, vol.105, no.1, p.133-4 (12 Jan 1983). Significant conformational alteration has been shown to exist in crystalline n-alkanes in phase II, the 'hexagonal' or 'rotator' phase as it is sometimes called. This disorder, which is manifest as a low concentration of gauche bonds in otherwise trans-planar chains, makes phase II n-alkanes a particularly suitable model system for the study of more complex assemblies of hydrocarbon chains such as lipid bilayers. The distribution of defects along the chain still remains in question. The authors report the results of an infrared study in which the concentration of gauche bonds located at four sites in the n-alkane $n\text{-C}_{21}$ in phase II was determined directly. In summary they have found that conformational disorder may occur anywhere along the chain although it tends to be greatest nearest the chain ends. (13 refs.)

60717 Photochemical formation and dissociation of molybdenum-dinitrogen complexes in krypton matrices. T.Foosnaes, M.J.Pellin, D.M.Gruen (Chem. Div., Argonne Nat. Lab., Argonne, IL, USA). *J. Chem. Phys. (USA)*, vol.78, no.6, pt.1, p.2889-98 (15 March 1983). Three molybdenum-dinitrogen complexes $[\text{MoN}_2]$, $[\text{Mo}_2(\text{N}_2)_2]$ and $[\text{Mo}(\text{N}_2)_3]$ have been synthesized in Kr matrices and characterized by means of the effects of isotopic substitution on the dinitrogen stretching frequencies. The Mo-N force constants calculated from these spectra are found to be 17.21 ± 0.02 mdyn/Å for MoN_2 and $f_r = 18.72$ mdyn/Å and $f_{rr} = 0.36$ mdyn/Å for $\text{Mo}(\text{N}_2)_3$. The Mo complexes appear to be unique in that rapid formation during co-deposition with N_2 occurs only upon photoexcitation of the Mo $^5s^2\text{P}$ atomic resonance transition situated at 355 nm in Kr matrices. Although minor amounts of the dinitrogen complexes are formed during deposition in the absence of radiation, their concentration is not increased by thermal annealing. Each of the complexes gives rise to its own electronic absorption spectrum. Irradiation into the electronic absorption bands of individual complexes induced selective photodissociation. Photoinduced growth and decomposition studies allowed correlations to be made between the vibrational and corresponding electronic spectra. (31 refs.)

60718 The infrared absorption spectra of $(\text{HCCCH})_2$ and $(\text{DCCD})_2$. R.D.Pendley, G.E.Ewing (Dept. of Chem., Indiana Univ., Bloomington, IN, USA). *J. Chem. Phys. (USA)*, vol.78, no.6, pt.2, p.3531-40 (15 March 1983). The infrared absorption bands of acetylene dimers have been investigated with long path low temperature Fourier transform infrared spectroscopy. Five bands were found, three of $(\text{HCCCH})_2$ and two of $(\text{DCCD})_2$. Four of these bands can be assigned as coupled monomer modes. Normal mode analysis based on a theoretical intermolecular potential confirms these assignments. One band shows evidence of fast vibrational predissociation, and a symmetry based argument is made to support the claim that the predissociation fragments are rotationally excited. (29 refs.)

60719 $^2\text{I}^+ \text{I}^- \text{X}^{2+}$ infrared electronic transition of C_2H^+ . P.G.Carrick, A.J.Merer, R.F.Curl, Jr. (Chem. Dept., Rice Univ., Houston, TX, USA). *J. Chem. Phys. (USA)*, vol.78, no.6, pt.2, p.3652-8 (15 March 1983). Five bands of the $^2\text{I}^+ \text{I}^- \text{X}^{2+}$ lowest electronic transition of C_2H^+ have been observed in the region 3600-4200 cm^{-1} in an argon discharge over polycetylene using color center laser spectroscopy with magnetic rotation sensitivity enhancement. The band origins are approximately 3692, 3773, 3785, 4011, and 4106 cm^{-1} . Rotational assignments and preliminary fittings of all five bands have been made. Four of the bands have a $^2\Sigma^+$ lower vibronic state which is undoubtedly the ground vibronic state of the molecule, and different $^2\text{I}^+$ upper vibronic states which correspond to mixtures of the lowest vibronic state of the A electronic state and three different vibrationally excited levels of the X electronic state with an odd number of quanta in the bending mode and overall $^2\text{I}^+$ symmetry. These three ground state vibrational levels have been tentatively assigned as (1,1,0), (0,1,2), and (0,5,1). The four $^2\text{I}^+$ vibronic levels are mixed by vibronic coupling between the X and A electronic states thereby providing electronic oscillator strength for the vibrational transitions. The fifth band is a $^2\Sigma^+ \text{I}^+ \text{I}^-$ hot band with the lower state the first excited bending level (0,1,0) of the ground electronic state and upper state the $^2\Sigma^+$ component of the (0,1,0) excited bending level of the excited electronic state. From these observations a value of 1.30 Å for the CC bond length in the excited electronic state and a value of ~ 375 cm^{-1} for the bending frequency of the X ground electronic state are obtained. (24 refs.)

60720 Difference frequency laser spectroscopy of the ν_1 band of the HO_2 radical. C.Yamada, Y.Endo, E.Hirota (Inst. for Molecular Sci., Okazaki, Japan).

J. Chem. Phys. (USA), vol.78, no.7, p.4379-84 (1 April 1983). The ν_1 (O-H stretching) band of the HO_2 radical was observed in absorption by using a difference frequency output obtained from an Ar ion laser and a CW dye laser as a source, combined with a multiple-reflection discharge cell. Zeeman modulation was employed to improve the sensitivity. The HO_2 radical was generated directly in the cell by a DC discharge in a mixture of allyl alcohol and oxygen. About 280 lines were observed and analyzed to precisely determine the rotational constants, centrifugal distortion constants, and spin-rotation interaction constants in the $\nu_1 = 1$ state. The band origin was determined to be 3436.1951(4) cm^{-1} , which is 22 cm^{-1} higher than the value previously obtained by a matrix isolation study. (29 refs.)

60721 Infrared matrix isolation spectrum of the Si_2C molecule. Z.H.Kafafi, R.H.Hauge, L.Fredin, J.L.Margrave (Dept. of Chem., Rice Univ., Houston, TX, USA). *J. Phys. Chem. (USA)*, vol.87, no.5, p.797-800 (3 March 1983). Infrared spectra of Si_2^{12}C and Si_2^{29}C isolated in solid argon in 15K have been reported in the 400-4000- cm^{-1} region. Two absorptions at 1188.9 and 658.2 cm^{-1} that exhibit carbon-13 shifts of 35.2 and 14.9 cm^{-1} , respectively, have been detected. Based on the measured IR data, the authors conclude that the molecule has C_{2v} symmetry with a lower limit of 110° for the SiCSi bond angle. (21 refs.)

60722 Detection of the free rotation of NH_3 molecules in polymers from the far IR spectra. N.M.Grigorovich, M.V.Tonkov. *Opt. & Spectrosc. (USA)*, vol.53, no.2, p.116-17 (Aug. 1982). Translation of: *Opt. & Spektrosk. (USSR)*, vol.53, no.2, p.194-6 (Aug. 1982). [received: April 1983]

The authors obtained the IR absorption spectrum of ammonia dissolved in the polymeric material poly-4-methylpent-1-ene, which indicates that the free rotation of the NH_3 molecules is preserved on going from the gaseous phase to the polymer matrix. The results also indicate that it is possible to determine the concentration of ammonia and to study its properties in polymeric matrices from far IR absorption data. (2 refs.)

60723 Intramolecular-vibration spectra of D_2O in H_2O ice matrices. Calculation and interpretation of the contours of the IR absorption and Raman scattering. Yu.Ya.Efimov, Yu.I.Naberukhin. *Opt. & Spectrosc. (USA)*, vol.53, no.2, p.157-62 (Aug. 1982). Translation of: *Opt. & Spektrosk. (USSR)*, vol.53, no.2, p.270-7 (Aug. 1982). [received: April 1983]

On the basis of a theoretical calculation, the form of the bands of the recently recorded IR spectra has been reconstructed, and the form of the Raman spectra is predicted for molecules of heavy water in matrices of cubic and amorphous ice H_2O , and the results have been interpreted. The values of the intramolecular parameters of the D_2O molecules in the above mixed ice specimens have been established. A simple method for calculating the spectral frequencies and intensities for an ensemble of molecules of the water type, perturbed in nonequivalent fashion by the medium, has been demonstrated. In the particular case of the interaction of infinitely narrow and broad distributions of the vibrational frequencies, an analytical expression for the envelope of the spectral contour has been given. The anomalous broadening of the intramolecular spectra is explained quantitatively by fluctuations in the parameters of the hydrogen bonds in the specimen. The important role of

Fermi resonance in the production of the ice spectra has been demonstrated. (21 refs.)

Electroreflectance vibrational spectroscopy: a new surface analysis technique using diode lasers See Entry 59860

Infrared dephasing of degenerate fundamentals: the ν_6 mode of liquid CD_3I See Entry 60684

Raman spectra, ab initio molecular orbital calculations, vibrational analysis, and thermodynamic functions for NH_3AlX_3 ($\text{X} = \text{F}, \text{Cl}, \text{Br}$) See Entry 60725

Calculation of the electrooptical parameters and the absolute intensities of the IR bands of the water molecule and its isotopically substituted derivatives See Entry 60777

Effect of foreign gases on IR absorption bands of polyatomic molecules See Entry 60844

The line shape of a zero-field level-crossing effect in methyl fluoride See Entry 60847

Experimental observation of the intercollisional interference effect on the S_1 pure rotation line of the collision induced spectra of the $\text{H}_2\text{-He}$ mixture See Entry 60932

Electronic structure of molecules and infrared continua caused by intramolecular hydrogen bonds with great proton polarizability See Entry 61017

Study of the infrared absorption of carbon tetrafluoride at 9 μm See Entry 61134

High resolution infrared study of hydrogen chemisorbed on Si (100) See Entry 62252

The reflection-absorption infrared spectrum of the dioxygen species adsorbed on platinum recorded by FT-IR spectroscopy See Entry 62965

Infrared emission spectroscopy of CO on Ni See Entry 62966

Infrared spectroscopy of adsorbates on low-area surfaces; the advantages of a photons-in photons-out technique See Entry 62978

The application of reflection infrared and surface enhanced Raman spectroscopy to the characterization of chemisorbed organic disulfides on Au See Entry 62979

Infrared specular reflection and SERS spectra of molecules adsorbed on smooth surfaces See Entry 62980

Infrared spectroscopic investigation of the adsorption of fluoromethane on sodium chloride surfaces under ultra high vacuum See Entry 62983

Infrared spectra of CO adsorbed at low temperatures on Ni See Entry 62984

EMIRS study of adsorbate bonding in the electrode solution interfacial region See Entry 62986

Study of adsorption at the electrode/solution interphase by in-situ infrared reflectance spectroscopy—adsorption of methanol on a platinum electrode See Entry 62989

The oxidation of methanol on Cu(100) studied by infrared spectroscopy See Entry 63540

Infrared study of three butanediols adsorbed on silica immersed in carbon tetrachloride See Entry 63593

Far-infrared rotational transition lines of the interstellar water vapor See Entry 64535

33.20F Raman and Rayleigh spectra (inc. scattering)

60724 Resonance Rayleigh light scattering of some porphyrins in solution: intensities and depolarization ratios. J.Anglistter, I.Z.Steinberg (Dept. of Chem. Phys., Weizmann Inst. of Sci., Rehovot, Israel). *Chem. Phys. (Netherlands)*, vol.75, no.3, p.443-52 (15 March 1983).

Resonance Rayleigh light scattering was measured at the Soret absorption band of meso-tetraphenyl porphine (in the free-base form), chlorophyll a, and meso-tetra(4-pyridyl) porphine (in the fully protonated form). The last compound showed unexpected fluorescence on the red side of, but close to, its Soret absorption band, and scattering experiments were not possible in the spectral range where fluorescence was detectable. The depolarization ratios measured for the Rayleigh scattered light of all three compounds were close to the value 1/8 expected for a planar oscillator, in line with previous conclusions that even when the in-plane degeneracy is lifted, the splitting of the in-plane bands at the Soret frequencies is small and the two transitions overlap considerably. The observed discrepancy between the experimentally determined intensities and those calculated from the absorption spectra may be due to momentary heterogeneity in the absorption coefficients, ϵ , in the population of absorbing molecules, the absorption and scattering depending each on different averages of ϵ . This heterogeneity is accentuated in the red part of the bands, where transitions from thermally excited molecules are more pronounced than in other parts of the absorption bands. (22 refs.)

60725 Raman spectra, ab initio molecular orbital calculations, vibrational analysis, and thermodynamic functions for NH_3AlX_3 ($\text{X} = \text{F}, \text{Cl}, \text{Br}$). G.N.Papatheodorou, L.A.Curtiss, V.A.Maroni (Argonne Nat. Lab., Argonne, IL, USA).

J. Chem. Phys. (USA), vol.78, no.6, pt.1, p.3303-15 (15 March 1983). Raman spectra of gaseous NH_3AlCl_3 and NH_3AlBr_3 were recorded at 400°C . The observed Raman frequencies for combination with reported infrared frequencies for NH_3AlCl_3 and ab initio molecular orbital calculations on NH_3AlCl_3 and NH_3AlF_3 were used to derive force constants for all three NH_3AlX_3 complexes ($\text{X} = \text{F}, \text{Cl}, \text{Br}$) based on an adjusted valence force field (AVFF) concept. The resulting force constant calculations produced complete sets of A_1 and E mode frequencies for each complex. Statistical mechanical analyses were then performed using the A_1 and E mode frequencies together with estimated values for the torsional mode of each complex and published enthalpy data. From these analyses, the relative thermodynamic stability of each complex was determined. At 700 and 1000K, NH_3AlCl_3 was found to be more stable than NH_3AlBr_3 . It was further predicted that the reaction of gaseous NH_3 with solid AlF_3 to form NH_3AlF_3 is not favored in this temperature range, which provides an explanation for the lack of success in prior efforts to produce NH_3AlF_3 . (37 refs.)

60726 Reorientation of small molecules and anions in solution studied by resonance enhanced dynamic Rayleigh scattering. S.G.Stanton, R.Pecora (Dept. of Chem., Stanford Univ., Stanford, CA, USA), B.S.Hudson. *J. Chem. Phys. (USA)*, vol.78, no.6, pt.2, p.3363-71 (15 March 1983). Resonance enhanced dynamic depolarized Rayleigh scattering is used to measure reorientation times of two nitrophenolate anions in millimolar aqueous and ethanolic solutions. Reorientation times of the corresponding neutral molecules in 0.01 to 0.1 M solutions are also reported. The reorientation time of 3,4-dinitrophenolate anion has a linear viscosity dependence when the viscosity is varied by varying temperature. The ratio of reorientation time

to viscosity C is the same for neutral 3,4-dinitrophenol and its anion in water to within experimental error. In ethanol the C values for both neutral molecule and anion are much larger than the corresponding water values and the anion C value depends upon counterion. This final observation suggests ion pairing occurs in these solutions. The spectra of picrate salts in ethanol clearly show the presence of a second species (ion pair). The picrate anion C value in ethanol determined from the broad component of a two Lorentzian fit is slightly larger than the corresponding water value. The results from the work are compared with reorientation times of small anions reported in the literature, most of which were obtained using picosecond absorption and fluorescence techniques. Ion pairing has not been properly accounted for in many of these experiments, preventing further conclusions concerning solute-solvent interactions. Some suggestions for further experiments are given. (38 refs.)

60727 Vibrational phase relaxation in ethane at moderate densities, including the critical region. K.A.Wood, H.L.Strauss (Dept. of Chem., Univ. of California, Berkeley, CA, USA).

J. Chem. Phys. (USA), vol.78, no.6, pt.2, p.3455-61 (15 March 1983). The bandwidth of the isotropic component and the frequency of the ν_3 (C-C stretch) Raman band of ethane have been measured for a range of densities at constant temperature, and for a range of temperatures at the critical density. No critical anomaly is observed. The rotation-vibration coupling contribution to the bandwidth is calculated. The remaining contribution to the bandwidth increases with increasing density in a manner consistent with current theories that take into account both the repulsive and attractive intermolecular forces. However, the attractive force contribution cannot be related in a simple fashion to the macroscopic compressibility. Data taken over a wider range of density and temperature will be required to quantitatively determine the separate repulsive and attractive contributions to the width. (35 refs.)

60728 Tricopper. A fluxional molecule. D.P.DiLella, K.V.Taylor, M.Moskovits (Dept. of Chem., Univ. of Toronto, Toronto, Ontario, Canada).

J. Phys. Chem. (USA), vol.87, no.3, p.524-7 (3 Feb. 1983). The resonance Raman spectrum of matrix-isolated Cu_3 is reported. On the basis of the irregularity of the observed progression and the unusual isotopic structure shown by the vibrational spectral components, Cu_3 is proposed to be a fluxional Jahn-Teller molecule. A symmetric stretching frequency of 354 cm^{-1} is found for the molecule. (8 refs.)

60729 Homogeneous and inhomogeneous vibrational dephasing processes in aqueous thiocyanate solutions. T.Kato (Seibo Women's Jr. Coll., Kyoto, Japan).

Mol. Phys. (GB), vol.48, no.5, p.1119-29 (10 April 1983). The vibrational correlation functions are calculated from the isotropic Raman spectra for the CN stretching mode of SCN^- anions in aqueous LiSCN, NaSCN and KSCN solutions, at concentrations 1-10 M and at temperatures 30, 55 and 80°C . These correlation functions are analysed on the basis of a model of simultaneous homogeneous and inhomogeneous vibrational dephasing, and both the homogeneous and inhomogeneous broadening contributions are extracted. The CN mode in aqueous thiocyanate solutions is found to be inhomogeneously broadened to various degrees depending on cation species, concentration and temperature. The homogeneous contribution increases and the inhomogeneous contribution decreases with increasing temperature because of increased molecular motion. Increase of salt concentration is found to develop inhomogeneity, probably because the strong interaction in concentrated solutions results in long lived local structures. An increase of inhomogeneous and a decrease of homogeneous broadening contributions with increasing salt concentration compensate in KSCN solutions. However, in LiSCN and NaSCN solutions, the increase of inhomogeneous contribution dominates the homogeneous contribution, which leads to concentration broadening. The band in 10 M LiSCN solution at 30°C , which is the broadest of all the CN bands investigated here, is found to be broadened only by the inhomogeneous process. (4 refs.)

60730 Picosecond CARS study of the ν_2 -band of liquid benzene. G.Barowsky (Abteilung Laserphys., Max-Planck-Inst. für Biophys., Göttingen, Germany), P.Anliker, Q.Munir.

Opt. Commun. (Netherlands), vol.45, no.3, p.183-6 (1 April 1983). A picosecond CARS-study, using mode-locked CW-lasers has been performed to record the spectrum of the CH-stretching mode (ν_2 -band) of liquid benzene. From the shape of the spectrum centered at 3061.9 cm^{-1} a dephasing time $\tau_{\text{ph}} = 0.7 \text{ ps}$ has been derived together with a nonresonant background contribution to $\chi^{(2)}$ of 14% at resonance. (13 refs.)

60731 Measurement of relative effective Raman scattering cross sections for hydrogen, oxygen, and water molecules under ultraviolet excitation. A.A.Eliseev, T.N.Popova, O.V.Ravodina, V.V.Stenina.

Opt. & Spectrosc. (USA), vol.53, no.2, p.190-2 (Aug. 1982). Translation of: *Opt. & Spektrosk. (USSR)*, vol.53, no.2, p.328-31 (Aug. 1982). [received: April 1983] Presents the results of measurements of the relative (with respect to the cross section of the Q branch of the Raman vibration band for N_2) effective cross sections of vibrational Raman scattering by H_2O , H_2 , and O_2 molecules. The effective Raman cross section for an O_2 molecule was measured to check the validity of the experimental methods, because this cross section has been reliably determined for the visible and UV spectral regions. As a source of excitation an LGI-21 pulsed molecular-nitrogen laser with $\lambda = 337.1 \text{ nm}$ and an average power of $\approx 3 \text{ mW}$ was used. (13 refs.)

60732 Wavelength dependence of Raman scattering cross sections from 200-600 nm. W.K.Bischel, G.Black (Molecular Phys. Lab., SRI Internat., Menlo Park, CA, USA).

Topical Meeting on Excimer Lasers, Incline Village, NV, USA, 10-12 Jan. 1983 (Washington, DC, USA: Opt. Soc. America 1983), p.TuB4/1-4 The authors have used a combination of ArF, KrF, and Nd:YAG lasers to experimentally determine the wavelength dependence of the absolute vibrational Raman scattering cross section for H_2 , D_2 , CH_4 , N_2 , and O_2 for laser wavelengths spanning the range of 200-600 nm. (6 refs.)

60733 Temperature dependence of the Raman linewidth in H_2^+ . W.K.Bischel, M.J.Dyer (Molecular Phys. Lab., SRI Internat., Menlo Park, CA, USA).

Topical Meeting on Excimer Lasers, Incline Village, NV, USA, 10-12 Jan. 1983 (Washington, DC, USA: Opt. Soc. America 1983), p.TuB4/1-4 Using CW stimulated Raman gain spectroscopy (SRGS), the authors have measured the temperature dependence of the Raman linewidth in H_2 from 223 to 433 K . For a constant density of 10 amagat , the authors observe an increase in the linewidth of approximately 0.4% per K . (4 refs.)

Spectroscopic properties and relaxation processes of impurity molecules in solids. I. Rotational spectra See Entry 60687

Intramolecular-vibration spectra of D_2O in H_2O ice matrices. Calculation and interpretation of the contours of the IR absorption and Raman scattering See Entry 60723

C-H stretching modes and the structure of n -alkyl chains. I. Long, disordered chains See Entry 61018

Using surface enhanced Raman scattering to study vibrations of adsorbates on thin metallic overlayers on silver See Entry 62266

Acetylene adsorption on silver films: a Raman vibrational study See Entry 62267

Rayleigh-Brillouin scattering of transverse and longitudinal acoustic waves in a supercooled viscoelastic liquid See Entry 62928

Raman scattering from $\text{Pt}(\text{CN})_2^{2-}$ adsorbed on Pt colloids See Entry 62955

Theory of surface enhanced Raman scattering See Entry 62959

On the contribution of charge transfer excitations to SERS See Entry 62967

Multichannel Raman spectroscopy of unroughened noble metal and nonnoble metal films and tunnel junctions See Entry 62968

Orientation dependence of surface enhanced Raman intensities: results from ab initio calculations See Entry 62969

Surface enhanced Raman scattering (SERS) from silver, copper, and gold films in UHV: excitation spectra See Entry 62970

A comparison of Raman scattering, resonance Raman scattering, and fluorescence from molecules adsorbed on silver island films See Entry 62971

Influence of foreign metal atoms deposited at electrodes on local and nonlocal processes in surface enhanced Raman scattering See Entry 62972

Surface Raman spectroscopy without enhancement: pyridine on Ag (111) See Entry 62973

Raman spectra of pyridine adsorbed on Ni (111) See Entry 62974

Surface enhanced Raman spectroscopy of palladium See Entry 62975

The SERS phenomenon in light of recent excitation profile measurements See Entry 62976

The application of reflection infrared and surface enhanced Raman spectroscopy to the characterization of chemisorbed organic disulfides on Au See Entry 62979

Infrared specular reflection and SERS spectra of molecules adsorbed on smooth surfaces See Entry 62980

Enhanced adsorbate Raman scattering and surface plasmon radiation See Entry 62981

Surface enhanced Raman scattering of water on an Ag electrode See Entry 62985

Spectral properties of pyrazine adsorbed on silver electrodes and cold silver films from surface enhanced Raman scattering (SERS) See Entry 62987

SERS study of pyridine vapor exposed to silver substrates electrochemically prepared See Entry 62988

Intensity enhancement and spectral change in Raman scattering of mercaptobenzothiazole adsorbed on silver electrode See Entry 62990

Raman spectrum of n -propylamine in cyclohexane See Entry 63000

Induced isotropic scattering from liquid carbon dioxide See Entry 63007

33.20K Visible spectra

60734 The high-resolution visible overtone spectrum of acetylene. G.J.Scherer, K.K.Lehmann, W.Klemperer (Dept. of Chem., Harvard Univ., Cambridge, MA, USA).

J. Chem. Phys. (USA), vol.78, no.6, pt.1, p.2817-32 (15 March 1983). Direct, gas-phase overtone spectra of states corresponding to five and six quanta of C-H stretch have been obtained for the four isotopically substituted acetylenes in the region 14900 - 18500 cm^{-1} . Peak positions of individual rotation-vibration lines were determined to a precision of about 0.003 cm^{-1} . A total of 39 bands are analyzed: 16 for $^{12}\text{C}_2$; 14 for $^{13}\text{C}_2\text{H}_2$; five for $^{12}\text{C}^{13}\text{CH}_2$; and four for $^{12}\text{C}_2\text{HD}$. The rotational structure of the bands is fit to a semirigid rotor Hamiltonian. However, the band suffer from severe rotational perturbations, with typical matrix elements being on the order of 0.3 cm^{-1} or less. The error in the determined band origins varies between 0.001 and 0.1 cm^{-1} , depending on the degree of perturbation. Precision rotational constants are also determined for the observed bands. The vibrational term values cannot be adequately explained in terms of the usual slightly anharmonic normal mode expansion. Even though acetylene represents in an intermediate case between the local mode and normal mode limits, the simple local mode theory described by Child and Lawton [M.S. Child and R.T. Lawton, Faraday Discuss., vol.71, p.273 (1981)] can be used to rationalize many aspects of the spectrum—e.g., the splitting of the states $[005^0 0 1]$ and $[005^0 0 1']$ is found to be only 0.44 cm^{-1} . The intermediate character of acetylene is seen upon single deuterium substitution. The state corresponding to five quanta of ^{12}C -H stretch shifts about 100 cm^{-1} to the blue, a result which is certainly anomalous from the point of view of intuitive local mode theory. The band origins for the observed Σ - Σ transitions for all four acetylenes studied are found to be in good agreement with the results of a recent variational calculation [L. Halonen, M.S. Child, and S. Carter, Mol. Phys., vol.47, p.1097 (1982)]. It is also observed that the anharmonic shifts of the sequence band transitions are quite large—for the $\nu=5$ overtone band, the sequence bands are shifted 74 cm^{-1} for the I_g bend and 39 cm^{-1} for the I_u bend. (43 refs.)

60735 Electronic spectra and intramolecular proton transfer in Mannich bases in liquid and solid vitreous solutions. M.Rospenk, I.G.Rumynskaya, V.M.Shraber.

J. Appl. Spectrosc. (USA), vol.36, no.5, p.526-30 (May 1982). Translation of: *Zh. Prikl. Spektrosk. (USSR)*, vol.36, no.5, p.756-61 (May 1982). [received: Feb. 1983]

The authors set out to ascertain, first, whether proton transfer and the establishment of equilibrium in nonpolar and slightly polar solvents, as well as in systems in which the equilibrium is not observed and in polar solvents can be recorded spectroscopically at lower temperatures secondly, to measure the equilibrium constants and determine the thermodynamic characteristics of proton transfer; and finally, to investigate the behaviour of the equilibrium as the solvent is converted from liquid to the rigid vitreous state. (14 refs.)

60736 High-resolution study of InCl spectra. J.Borkowska-Brunecka, W.Zyrynicky (Inst. of Inorganic Chem. & Metall. of Rare Elements, Tech. Univ. Wrocław, Wrocław, Poland).

Physica B & C (Netherlands), vol.115 B+C, no.3, p.415-18 (March 1983). The rotational structure of the $^1\text{X}^1\Sigma^+ 0-0$ and $0-1$ bands and the $^3\text{X}^1\Sigma^+ 0-0$ subbands have been reanalyzed at high resolution. Rotational constants of the upper states have been corrected and improved. (15 refs.)

60737 New results on EDA-iodine complexes. F.Lux, R.Pactzold (Sektion Chemie, Friedrich Schiller Univ., Jena, Germany). *Wiss. Z. Friedrich-Schiller-Universität Jena, Math. Naturwiss. Reihe (Germany)*, vol.31, no.6, p.1125-9 (1982). In German.
The ionisation energies of R'R'SO donors are related to both the thermodynamic stability and the blue-shift of the visible iodine band of R'R'SO-I₂ complexes. For decreasing ionisation energies an increase of $-\Delta H$, $-\Delta G$ and $\Delta\lambda_{1/2}$ is observed. A comparison of these results with the corresponding data of R'R'R'PO-I₂ complexes shows that the correlation for both oxodonor series are different. For EDA complexes between iodine and ethyl- and ethoxysubstituted R'R'R'PS donors a linear dependence of the position of the CT band on the donor ionisation energy is found. (8 refs.)

60738 The triatomic rare gas halide excimers. D.L.Huestis (Molecular Phys. Lab., SRI Internat., Menlo Park, CA, USA), G.Marowsky, F.K.Tittel. *Physical Meeting on Excimer Lasers*, Incline Village, NV, USA, 10-12 Jan. 1983 (Washington, DC, USA: Opt. Soc. America 1983), p.TuC4/1.
Summary form only given as follows. Reviews the spectroscopy and kinetics of broad-band triatomic excimers. Laser considerations such as gain and absorption are also discussed, with emphasis on Xe₂Cl. (no refs.)

Evidence that the excited-state geometry of diphenylbutadiene is nearly planar See Entry 60620

Photochemical formation and dissociation of molybdenum-dinitrogen complexes in krypton matrices See Entry 60717

State-selective spectroscopy in a molecular nitrogen discharge by use of optical-galvanic double-resonance spectroscopy See Entry 60770

Solvent effect on ¹⁸O₂ yield and the mechanism of polycyclic hydrocarbon triplet-state quenching by oxygen See Entry 60791

Observation of the asymmetric O-U-O stretch in the vibronic absorption spectrum of uranyl formate monohydrate See Entry 60798

Luminescence of the excited mercury diethylamine complex. Attachment by ligand exchange See Entry 60806

Participation of molecular singlet oxygen in process of accelerated fading of dye mixtures See Entry 60824

Influence of hydrogen bonds on electronic spectral shifts of some 9-amino acridines See Entry 61016

33.20L Ultraviolet spectra

60739 Supersonic expansion cooling of electronically excited OH radicals. A.T.Droege, P.C.Engelking (Dept. of Chem., Univ. of Oregon, Eugene, OR, USA). *Chem. Phys. Lett. (Netherlands)*, vol.96, no.3, p.316-18 (8 April 1983).

Supersonic nozzle cooling of excited-state molecular radicals produced in a corona discharge is demonstrated and investigated using hydroxyl radicals. Rotational temperatures of 11 ± 2 K and vibrational temperatures of 3400 ± 300 K are typically observed in the OH A²Σ⁺ state. (10 refs.)

60740 A model for the interpretation of the electronic spectra of the complex ions M(bpy)₃²⁺ (M=Fe, Ru, Os) in D₃ and C₂ sites. J.Ferguson, F.Herren (Res. School of Chem., Australian Nat. Univ., Canberra, Australia). *Chem. Phys. (Netherlands)*, vol.76, no.1, p.45-59 (1 April 1983).

A theoretical model of the electronic structure of the metal-to-ligand charge-transfer states of the complex ions M(bpy)₃²⁺ (M=Fe, Ru, Os) is described. It is applied to new spectroscopic data obtained for these ions in two host crystals. In one host the site symmetry of the guest is close to D₃, while in the other it is C₂. The model has four parameters, the spin-orbit coupling constant of M²⁺, the trigonal field splitting of the metal-ion d orbitals, the trigonal field splitting of the ligand orbitals and an exchange integral between the metal-ion d electrons and the ligand π electrons. Analyses of the absorption spectra are consistent with the energy order $\epsilon < a_1$ for the metal-ion d orbitals. The major source of the charge-transfer intensity comes from the transfer term. A detailed analysis of the luminescence from Ru(bpy)₃²⁺ in both crystal hosts shows that three E states are involved and the model accounts for all of the essential features of the luminescence. (27 refs.)

60741 The vapour-phase ultraviolet spectra of metallo-organic precursors to III-V compounds. J.Haigh (British Telecom Res. Labs., Ipswich, England). *J. Mater. Sci. (GB)*, vol.18, no.4, p.1072-6 (April 1983).

Vapour-phase UV (ultraviolet) spectra are reported for the trimethyls and triethyls of gallium and indium, aluminium triethyl and indium cyclopentadienyl. Strong absorptions are observed between 200 and 300 nm; these are adequate for efficient energy coupling in photolysis. (8 refs.)

60742 High resolution absorption cross section measurements and band oscillator strengths of the (1,0)-(12,0) Schumann-Runge bands of O₂. K.Yoshino, D.E.Freeman, J.R.Esmond, W.H.Parkinson (Harvard-Smithsonian Center for Astrophysics, Cambridge, MA, USA). *Planet. & Space Sci. (GB)*, vol.31, no.3, p.339-53 (March 1983).

Cross sections of O₂ at 300K have been obtained from photoabsorption measurements at various pressures throughout the wavelength region 179.3-201.5 nm with a 6.65 m photoelectric scanning spectrometer equipped with a 2400 lines mm⁻¹ grating and having an instrumental width (FWHM) of 0.0013 nm. The measured absorption cross sections of the Schumann-Runge bands (12,0) through (1,0) in this wavelength region are absolute i.e. independent of the instrumental width, a result not achieved previously. The measured cross sections are presented graphically and are available at wavelength intervals of ~ 0.1 cm⁻¹ as numerical complications stored on magnetic tape from the National Space Science Data Center, NASA/Goddard Space Flight Center, Greenbelt, MD 20771, USA. Band oscillator strengths of the (12,0) through (1,0) bands have been determined by direct numerical integration of the measured cross sections. (45 refs.)

Evidence that the excited-state geometry of diphenylbutadiene is nearly planar See Entry 60620

Photochemical formation and dissociation of molybdenum-dinitrogen complexes in krypton matrices See Entry 60717

Excited states of mixed-ligand chelate complexes of ruthenium(II). A re-examination of the evidence for strong interligand coupling See Entry 60756

pH correlation of the absorption, fluorescence and polarization spectra of fluorescein isothiocyanate See Entry 60783

Observation of the asymmetric O-U-O stretch in the vibronic absorption spectrum of uranyl formate monohydrate See Entry 60798

Two-photon excitation of the D¹Δ-X¹Σ⁺ transition in carbon monoxide See Entry 60804

Laser spectroscopy on ion beams: application to the polyatomic ion N₂O⁺ See Entry 60871

Atomic nitrogen emissions from photodissociation of N₂ See Entry 64236

Electron-impact excitation of the Cameron system (a³π-X¹Σ⁺) of CO See Entry 64369

33.20N Vacuum ultraviolet spectra

60743 Rydberg series converging to the \tilde{C} state of C₆F₆⁺ in threshold photoelectron and VUV absorption spectra of hexafluorobenzene. G.Dujardin, S.Leach (Univ. Paris-Sud, Orsay, France). *Chem. Phys. Lett. (Netherlands)*, vol.96, no.3, p.337-42 (8 April 1983).

A series of peaks in the threshold photoelectron spectrum (TPES) of hexafluorobenzene in the 13 eV region are found to have the same energies as Rydberg bands in the VUV absorption spectrum. The TPES and VUV absorption features are interpreted as an nd Rydberg series, with a quantum defect $\delta = -0.02$, converging to the C electronic state of C₆F₆⁺ at 13.88 eV. The ion \tilde{C} state is shown to have ²B_{2u} electronic symmetry. (11 refs.)

33.20R X-ray spectra

60744 X-ray absorption spectra of nitrogen and oxygen in the series of N₂, NO, and O₂ molecules. V.N.Akimov, A.S.Vinogradov, T.M.Zimkina. *Opt. & Spectrosc. (USA)*, vol.53, no.1, p.63-6 (July 1982). Translation of: *Opt. & Spektrosk. (USSR)*, vol.53, no.1, p.109-13 (July 1982). [received: April 1983]

The K absorption spectra of nitrogen and oxygen atoms in N₂, NO, and O₂ molecules, obtained with the aid of a common experimental method, are considered jointly. The correlation between the resonancelike characteristics manifested in the absorption spectra of these molecules is traced, and their nature is evaluated in terms of resonance scattering of the photoelectron by the anisotropic potential of the molecule. It is hypothesized that with a movement along the molecular series N₂-NO-O₂ there is a shift in the shape resonance from the continuous to the discrete region of the spectrum, which is one of the possible causes of the qualitative difference observed in the near-threshold structure of the absorption spectrum of the O₂ molecule and the absorption spectra of the N₂ and NO molecules. (18 refs.)

60745 X-ray absorption spectra of tetrahedral molecules. Characteristic features of the symmetry of the wave function of the photoelectrons. M.Ya.Amusa, A.A.Pavlychev, A.S.Vinogradov, D.E.Onopko, S.A.Titov. *Opt. & Spectrosc. (USA)*, vol.53, no.1, p.91-3 (July 1982). Translation of: *Opt. & Spektrosk. (USSR)*, vol.53, no.1, p.157-60 (July 1982). [received: April 1983]

Examines changes in the symmetry of the photoelectron wave under the influence of the molecular field. For this purpose the authors carried out calculations of the spectral behavior of the absorption cross section of the SiL₂₃(11)2p subshell of the SiF₄ molecule and the CK(1s)-level of CF₄ in the region of the near fine structure (NFS) and (0 < ε < 2.5 Ry). The wave function (WF) of the final state of the photo-electron χ(ε,r) was determined from the condition of regularity close to the nuclei of the atoms and asymptotic behavior as r → ∞. (7 refs.)

Satellite structure in the 2pσ molecular orbital transitions in slow heavy ion collisions See Entry 60626

33.25 NUCLEAR MAGNETIC RESONANCE AND RELAXATION; NUCLEAR QUADRUPOLE RESONANCE (NQR)

60746 The relativistic theory of the chemical shift. N.C.Pyper (Dept. of Theoretical Chem., Univ. of Cambridge, Cambridge, England). *Chem. Phys. Lett. (Netherlands)*, vol.96, no.2, p.204-10 (1 April 1983).

A relativistic theory of the NMR chemical shift for a closed-shell system is presented. The final expression for the shielding, derived by applying two Gordon decompositions to the Dirac current operator, closely parallels the Ramsey nonrelativistic result. (26 refs.)

60747 The Breit interaction in external magnetic fields. N.C.Pyper (Dept. of Theoretical Chem., Univ. of Cambridge, Cambridge, England). *Chem. Phys. Lett. (Netherlands)*, vol.96, no.2, p.211-17 (1 April 1983).

The Breit energy of a system, which is shown to depend on the external magnetic vector potential, is exactly transformed, by applying Gordon decompositions, to a form explicitly exhibiting some of the field dependence. The result is used to derive the leading Breit contributions to NMR chemical shifts and atomic g factors. (12 refs.)

60748 Measurement of the ¹⁴N nuclear quadrupole couplings in the lowest (ππ*) excited triplet state of pyrazine by ODMR. W.Frohling, W.J.Winsom, K.Mobius (Inst. für Molekularphys., Freie Univ. Berlin, Berlin, Germany). *Chem. Phys. (Netherlands)*, vol.75, no.3, p.389-94 (15 March 1983).

High-resolution optically detected magnetic resonance (ODMR) and optically detected electron-electron double resonance (ODEEOR) have been performed on the lowest excited triplet states of pyrazine-h₄ and pyrazine-d₄, as dilute guests in polycrystalline benzene and cyclohexane host matrices. Computer simulated spectra have been fitted to those experimentally observed, using a spin Hamiltonian which takes into account the ¹⁴N and ¹H (or ²D) nuclei of the pyrazine guest molecule. Good agreement is obtained when one ¹⁴N nuclear quadrupole energy difference, |e_NN₁-e_NN₂| ≤ 1.3 MHz, and the remaining component, |e_NN₁| = 0.6 ± 0.2 MHz for pyrazine-d₄ in benzene-d₆. (25 refs.)

60749 NMR study of intramolecular processes in EDTA metal complexes. M.C.Gennaro, P.Mirti, C.Casolino (Istituto di Chimica Analitica, Univ. di Torino, Torino, Italy). *Polyhedron (GB)*, vol.2, no.1, p.13-18 (1983).

The kinetics of the intramolecular acetate scramblings occurring in thirteen ethylenediaminetetraacetate (EDTA) complexes have been studied by analyzing the modification observed in the NMR spectra of their D₂O solutions, when temperature is changed. The experimental results indicate that the Δ, Δ conversion is a fast process on the NMR time scale for each of the complexes considered, whereas the nitrogen inversion occurs at an observable rate in the case of the Cd(II), In(III), Sc(III), Y(III) and Lu(III) chelates and is too rapid in the other complexes. Computer analysis of the experimental NMR spectra has been performed in order to obtain enthalpy, entropy and free energy of activation concerning the N inversion of the cited chelates. Twist and bond breaking mechanisms are discussed with reference to both scrambling processes. (34 refs.)

60750 The rotational and hyperfine spectrum and structure of $\text{H}_2\text{CO}\cdot\text{HF}$. F.A. Baiocchi, W. Klemperer (Dept. of Chem., Harvard Univ., Cambridge, MA, USA).

J. Chem. Phys. (USA), vol. 78, no. 6, pt. 2, p.3509-20 (15 March 1983).

The rotational spectrum of the hydrogen bonded complex formed between hydrogen fluoride and formaldehyde has been obtained from 3 to 35000 MHz using molecular beam electric resonance spectroscopy. The molecule is found to be a prolate slightly asymmetric rotor with $\kappa = -0.98$ and an inertial defect of $\Delta = 0.62 \text{ amu } \text{\AA}^2$. The rotational constants determine that the average geometry of the three heavy atoms is bent with an O-F distance of 2.66 Å and a C-O-F angle of 109.5°. The large value of μ_a shows that HF is hydrogen bonded to the oxygen. The average orientation of the HF axis with respect to the inertial axes is obtained from the two components (S_a and S_b) of the direct nuclear spin-spin hyperfine coupling tensor. Both the hyperfine data and the value of μ_b indicate a nonlinear hydrogen bond in this species. Finally, the observation of hyperfine splittings in the spectrum attributable to the presence of the triplet spin state of formaldehyde provides experimental information regarding the tunneling of the formaldehyde protons. The spectra are consistent with a rigid planar structure. Some of the spectroscopic and average structural constants are summarized: $A - \Delta = 50543.205(23) \text{ MHz}$; $B = 4832.232(33) \text{ MHz}$; $C = 4386.621(33) \text{ MHz}$; $\mu_a = 3.7535(2) \text{ D}$; $\mu_b = 1.399(1) \text{ D}$; $S_a^{\text{HF}} = 93.6(8) \text{ kHz}$; $S_b^{\text{HF}} = -31.7(11) \text{ kHz}$; $r_{\text{O-F}} = 1.794 \text{ Å}$; $r_{\text{O-C}} = 2.659 \text{ Å}$; $\angle \text{C-O-F} = 109.5^\circ$; $\angle \text{C-O-H} = 115^\circ$. (33 refs.)

60751 Possible P, T-odd effects in NMR spectroscopy of molecules. V.L. Varentsov, V.G. Gorshkov, V.F. Ezhov, M.G. Kozlov, L.N. Labzovskii, V.N. Migichev (B.P. Konstantinov Inst. of Nuclear Phys., Acad. of Sci., USSR).

JETP Lett. (USA), vol. 36, no. 5, p.175-8 (5 Sept. 1982). Translation of: *Pisma v Zh. Eksp. i Teor. Fiz. (USSR)*, vol. 36, no. 5, p.141-4 (5 Sept. 1982). [received: April 1983]

The methods of NMR spectroscopy might be useful for an experimental search of P- and T-odd effects in molecules. The accuracy of such measurements is estimated. The existing upper limit on the electric dipole moment of the proton might be reduced by two orders of magnitude by taking this approach. (4 refs.)

60752 NMR spin-echo spectra of molecules containing four spin-1/2 nuclei with an AA'BB' symmetry in liquid-crystalline samples. A.G. Avent, J.W. Emsley, D.L. Turner (Dept. of Chem., Univ. of Southampton, Southampton, England).

J. Magn. Resonance (USA), vol. 52, no. 1, p.57-70 (March 1983).

A series of model compounds in which an AA'BB' system is coupled to increasingly complex groups of heteronuclei is used to demonstrate that accurate values for homonuclear dipolar coupling constants may easily be extracted from their spin-echo spectra. This is an important step in the analysis of complex spectra from solutes in liquid-crystalline solvents and provides an alternative to spin decoupling in studies of partially deuterated liquid crystals. (11 refs.)

60753 Reexamination of a sequence designed to cancel ^{13}C signals of protonated carbons. M.R. Bendall, D.T. Pegg (School of Sci., Griffith Univ., Nathan, Queensland, Australia).

J. Magn. Resonance (USA), vol. 52, no. 1, p.136-8 (March 1983).

Recently, Rutar (ibid., vol. 48, p.155, 1982) described a two-step spin-echo pulse sequence, sequence [A], which was designed to eliminate efficiently the ^{13}C signals of all protonated carbons: $\tau_{1/2}[\text{C}] - 1/4\pi[\text{H}] - 1/4\pi[\text{decouple for } 1/2\tau_{1/2}] - \pi[\text{C}] - 1/2\tau_{1/2}$ acquire ^{13}C , decouple ^1H . [A]. This sequence combined the simple one-step proton flip and gated decoupler methods. Consequently, it was expected to be more accurate than the one-step methods in canceling protonated carbon signals when the single-bond $^{13}\text{C}\cdot^1\text{H}$ J values diverge from the values used in setting the sequence delay times, because both steps were expected to reduce these signals. This expectation was supported by experimental evidence using a sample of *s*-butyl benzene. The mechanism of this sequence, and indeed any spin-echo sequence, is examined experimentally and theoretically by removing the π refocusing pulses. (10 refs.)

60754 Bismuth NMR spectroscopy: ^{209}Bi and ^{19}F high-resolution NMR spectra of the hexafluorobismuthate(V) ion. K. Morgan, B.G. Sayer, J. Schrobilgen (Dept. of Chem., McMaster Univ., Hamilton, Ontario, Canada).

J. Magn. Resonance (USA), vol. 52, no. 1, p.139-42 (March 1983).

Bismuth-209 (natural abundance, 100%) is among the more sensitive NMR nuclei, possessing a sensitivity relative to the proton of 0.136, but due to quadrupolar relaxation effects the only solution studies of a ^{209}Bi resonance have been of aqueous solutions of $\text{Bi}(\text{NO}_3)_3$ which gave broad resonances ($\Delta\nu = 3200 \text{ Hz}$). There also have been a number of solid-state ^{209}Bi NMR studies concerned with measuring Knight shifts. Only in the case of polycrystalline KBiF_6 have the effects of spin-spin coupling been observed. Spin-spin coupling between ^{209}Bi and ^{19}F , which was masked by magnetic dipole-dipole interactions, was derived from a lineshape analysis of the ^{19}F NMR spectrum which yielded $|J_{209\text{Bi}-19\text{F}}| = 2700 \pm 300 \text{ Hz}$. The authors present a high-resolution solution study of ^{209}Bi in BiF_6^- . The latter, like its group V congeners PF_6^- , AsF_6^- , and SbF_6^- , is octahedral. Although ^{209}Bi possesses a considerable quadrupole moment ($Q = 0.4 \times 10^{-28} \text{ m}^2$), the effect of quadrupole line broadening is diminished by the large size of the spin for ^{209}Bi ($I = 9/2$) and octahedral symmetry. (12 refs.)

60755 Spin trapping of $\cdot\text{NO}_2$ radicals produced by UV photolysis of RDX, HMX and nitroguanidine. M.D. Pace, B.S. Holmes (Naval Res. Lab., Washington, DC, USA).

J. Magn. Resonance (USA), vol. 52, no. 1, p.143-6 (March 1983).

In a recent study, evidence was reported of $\cdot\text{NO}_2$ free-radical formation in single crystals of RDX (Pace et al. 1982). The $\cdot\text{NO}_2$ free radicals were produced in the RDX single crystals by UV photolysis at 77K, but the EPR signal decayed when the single crystals were warmed to room temperature. Similar observations have been reported for $\cdot\text{NO}_2$ free radicals which are trapped in a frozen matrix. Such evidence suggests that UV photolysis of the nitramines nitroguanidine [NQ : $(\text{H}_2\text{N})_2\text{C}(\text{NO}_2)_2$], RDX [$\text{C}_3\text{H}_6\text{N}_6\text{O}_6$], and HMX [$\text{C}_4\text{H}_8\text{N}_8\text{O}_8$] can produce free radicals which rapidly decay before being detected by CW EPR spectroscopy. The authors have employed the spin-trapping capacity of DMSO and DMSO- d_6 to indirect $\cdot\text{NO}_2$ free radicals which are generated from MQ, RDX, and HMX by UV radiation at room temperature. (7 refs.)

60756 Excited states of mixed-ligand chelate complexes of ruthenium(II). A re-examination of the evidence for strong interligand coupling. J.E. Baggott, G.K. Gregory, M.J. Pilling, S. Anderson, K.R. Seddon, J.E. Turp (Oxford Univ., Oxford, England).

J. Chem. Soc. Faraday Trans. II (GB), vol. 79, pt. 2, p.195-210 (Feb. 1983).

It has been shown that the evidence produced by G.A. Crosby and W.M. Elfring (1976) to argue for the presence of strong interligand coupling is ambiguous, and that there is an alternative interpretation of their data. In contrast with their observations, the present authors find that the low-field ^1H NMR spectra of $[\text{Ru}(\text{bipy})_2(\text{phen})]^{2+}$ and $[\text{Ru}(\text{bipy})(\text{phen})_2]^{2+}$ reveal no significant correlation between chemical shift and ligand composition, and thus

provide no evidence for strong interligand interactions. The development of a kinetic model for the coupling between electronic states has led to the demonstration that the excited state decay characteristics of mixed-ligand complexes of ruthenium(II) are consistent with strong kinetic coupling and that such behaviour can be obtained when measurable spectroscopic shifts are absent. Finally, the electronic absorption spectra provide some evidence for localised $\pi \rightarrow \pi^*$ excited states. (30 refs.)

60757 Multi-dimensional spectroscopy. II. Analysis of 3D lineshapes obtained from stochastic NMR of two level systems. B. Blumich (Iwan N. Stranski Inst., Tech. Univ. Berlin, Berlin, Germany).

Mol. Phys. (GB), vol. 48, no. 5, p.969-80 (10 April 1983).

For pt. I see ibid., vol. 48, no. 5, p.955-68 (1983). Three-dimensional lineshapes which are observed in non-linear stochastic NMR spectroscopy are analysed in terms of 1D and 2D cross-sections. Two important results are obtained: (1) A 1D sub-diagonal cross-section, which is similar to a conventional CW or FT NMR spectrum, can exhibit a narrower line-shape than obtained in 1D FT-spectroscopy. (2) The relaxation times T_1 and T_2 can be determined from the lineshapes of selected cross-sections, independent of magnetic field inhomogeneity. (11 refs.)

60758 On the twist-boat conformation of the tetrahydropyran cycle in the trioxa-bis-spiroketal series. M.F. Grenier-Loustalot, F. Métras (Lab. de Chimie Organique Phys., Inst. Univ. de Recherche Sci., Pau, France), L. Cottier, G. Descotes.

Spectrosc. Lett. (USA), vol. 15, no. 12, p.963-7 (1982).

The authors studied the molecules by PMR and ^{13}C NMR at 500 MHz. Coupling constants are analysed and the twist-boat conformation confirmed. (4 refs.)

60759 Effects of electron transfer on the chemical polarization of nuclei in the recombination of radical-ion pair in strong magnetic fields. K.M. Salikhov, F.S. Sarvarov (Inst. of Chem. Kinetics & Combustion, Acad. of Sci., Novosibirsk, USSR).

Theor. & Exp. Chem. (USA), vol. 18, no. 2, p.124-32 (March-April 1982). Translation of: *Teor. & Eksp. Khim. (USSR)*, vol. 18, no. 2, p.146-55 (March-April 1982). [received: Feb. 1983]

The authors show how electron transfer substantially alters the CNP effect (chemical nuclear polarization) for all nuclei in the radical anions and cations. The effects of electron transfer on CNP can be interpreted as due to reduction in the role of hyperfine interactions in the radical anion in the singlet-triplet evolution of the radical-ion pairs. (8 refs.)

60760 Structure of the binuclear 3,7-dimethylene-bicyclo[3.3.1]nonane-silver nitrate-Eu(fod)₃ complex by PMR spectroscopy. P.A. Krasutskii, A.G. Yurchenko, M. Jones, M.Yu. Kornilov, L.S. Degtyarev, V.I. Zamkovo (Kiev Polytech. Inst., Kiev State Univ., Kiev, Ukrainian SSR).

Theor. & Exp. Chem. (USA), vol. 18, no. 2, p.162-5 (March-April 1982). Translation of: *Teor. & Eksp. Khim. (USSR)*, vol. 18, no. 2, p.189-93 (March-April 1982). [received: Feb. 1983] (13 refs.)

60761 Use of luminescence spectra of adducts of europium β -diketonates with methyl-substituted pyridines in interpreting NMR data obtained by the use of lanthanide shift reagents. V.F. Zolin, L.G. Koreneva, A.E. Obukhov, V.P. Zvolinskii, I.R. Kordova (Inst. of Radio Engng. & Electronics, Acad. of Sci., USSR).

Theor. & Exp. Chem. (USA), vol. 18, no. 2, p.166-72 (March-April 1982). Translation of: *Teor. & Eksp. Khim. (USSR)*, vol. 18, no. 2, p.193-200 (March-April 1982). [received: Feb. 1983] (28 refs.)

Practice of multidimensional stochastic NMR spectroscopy. The derivation of 1D, 2D, and 3D spectra See Entry 59810

Elimination of solvent signals in carbon magnetic resonance spectroscopy See Entry 59813

Correlation of isotropic shifts and chemical shift anisotropies by two-dimensional Fourier-Transform magic-angle hopping NMR spectroscopy See Entry 59814

NMR broadband decoupling with low radiofrequency power See Entry 59816

Potassium fluoride and phosphorous acid: ab initio calculations and spectroscopic investigations See Entry 60585

Transmission mechanisms of spin-spin coupling constants within the CHF approximation: their study using inner projections of the polarization propagator See Entry 60592

Multidimensional spectroscopy. I. Perturbation theory See Entry 60702

^{83}Kr nuclear quadrupole coupling, microwave spectrum, and structure of KrHCN See Entry 60704

Microwave spectrum, structure, and quadrupole coupling for the ethylene-hydrogen cyanide complex See Entry 60709

Beam maser spectroscopy on CD_3CN See Entry 60710

Electronic structure of molecules and infrared continua caused by intramolecular hydrogen bonds with great proton polarizability See Entry 61017

Optical multiple pulse sequences for multiphoton selective excitation and enhancement of forbidden transitions See Entry 61245

Selective scattering of electromagnetic radiation in radio-frequency resonance conditions See Entry 62867

Radiofrequency labelling of molecules in chemical reactions See Entry 63506

Water proton spin-lattice relaxation behaviour in heterogeneous biological systems See Entry 63786

Two-dimensional deuterium NMR of lipid membranes See Entry 63798

33.30 ELECTRON PARAMAGNETIC RESONANCE AND RELAXATION

60762 Electron spin resonance spectroscopic evidence for steric enhancement of resonance. K. Ganapathy, T. Balasubramanian, K. Pandiarajan (Dept. of Chem., Annamalai Univ., Annamalaiagar, India).

Curr. Sci. (India), vol. 51, no. 23, p.1114-15 (5 Dec. 1982).

ESR spectral data on radical anions obtained by the electrolytic reduction of the aromatic nitro compounds in acetonitrile are used to substantiate the phenomenon of steric enhancement observed previously (V. Baliah and M. Uma, 1960). (11 refs.)

60763 ESR of pseudorotating ^6Li and ^7Li . D.A. Garland, D.M. Lindsay (Dept. of Chem., City Univ. of New York, New York, NY, USA).

J. Chem. Phys. (USA), vol. 78, no. 6, pt. 1, p.2813-16 (15 March 1983).

ESR spectra assigned to pseudorotating ^6Li and ^7Li molecules have been produced by arc lamp photolysis of argon matrices doped with isotopically enriched ^6Li or ^7Li . The spectrum of ^6Li consists of seven equally spaced first derivative transitions with relative intensities in good agreement with the expected values for three equivalent $I = 1$ nuclei. The measured HF constant

and g value are $\bar{A}=12.2(1)$ G and $g_0=2.00282(1)$. The absence of a stationary trimer spectrum suggests that the ground vibronic state of Li_3 is relatively nonlocalized. The average isotropic spin population of trimer $\bar{p}=0.225$ is in excellent agreement with the predictions of ab initio calculations. The total isotropic spin population $3\bar{p}\approx 0.68$ suggests an approximately 30% p -character for the unpaired electro wave function. A comparison of the orbital composition of M , M_2 , M_3 , M_∞ ($\text{M}=\text{Li}$, Na , K) shows (i) a diminishing s -character with increasing cluster size, (ii) a remarkable similarity between Na and K for all cluster sizes, and (iii) a smaller s -character (greater hybridization) for Li clusters. (25 refs.)

60764 High-spin molecules: electron spin resonance of manganese halides and sulfide at 4 K. C.A.Baumann, R.J.van Zee, W.Weltner, Jr. (Dept. of Chem., Univ. of Florida, Gainesville, FL, USA). *J. Phys. Chem. (USA)*, vol.86, no.26, p.5084-93 (23 Dec. 1982).

The zero-field splittings (D), ^{55}Mn hyperfine (h) interaction constants, and g values have been measured, where possible, for the MnCl_2 , MnBr_2 , MnI_2 , and MnS molecules having ^6S ground states and for the $^7\Sigma$ molecules MnCl , MnBr , and MnI . Among the heavier dihalides, $|D|$ increases from 0.44 to >2 cm^{-1} down the series, the ^{55}Mn and halogen h s are within the line widths (<50 G), agreeing with the decreasing ionicity. Among the heavier monohalides, $|D|$ increases from 0.07 to >0.5 cm^{-1} down the series, but observed ^{55}Mn h s, unexpectedly, do not show a monotonic variation from MnF to MnI . MnS has $|D|>2$ cm^{-1} , but much smaller ^{55}Mn h s than MnO , indicating considerably more covalency in the heavier molecule. (55 refs.)

60765 Electron spin resonance investigation of sulphur-33 and nitrogen-15 substituted dithiazol-2-yl and dithiazolidin-2-yl free radicals. S.A.Fairhurst, R.S.Pilkington, L.H.Sutcliffe (Donnan Chem. Labs., Univ. of Liverpool, Liverpool, England).

J. Chem. Soc. Faraday Trans. 1 (GB), vol.79, pt.4, p.925-40 (April 1983). Thermal cyclo-addition reactions of tetrasulphur dinitride with certain alkenes generate a new series of stable free radicals possessing the 1,3,2-dithiazolyl ring. The radicals have simple ESR spectra and are potentially useful spin probes or labels. The sharpness of the spectral lines has enabled the authors to observe natural abundance lines from nitrogen-15, sulphur-33 and carbon-13. The presence of two equivalent sulphur atoms in the heterocyclic ring has been demonstrated by isotopic double labelling with nitrogen-15 and sulphur-33. An isotopic triple labelling experiment with the latter two isotopes and with deuterium was carried out with the related 1,3,2-dithiazolidinyl radicals. Temperature coefficients of coupling constants were measured for both classes of radicals and INDO calculations showed that nitrogen out-of-plane wagging is responsible for all the temperature coefficients. Molecular orbital calculations were performed for the 1,3,2-dithiazolyl and 1,3,2-dithiazolidinyl structures using semi-empirical INDO and ab initio Gaussian 76 computer programs: the optimised structural parameters from both calculations are in good agreement. The INDO calculations gave signs and magnitudes of isotropic coupling constants in overall agreement with those observed experimentally. (35 refs.)

60766 Electron spin resonance spectra and structure of the α,α -difluoroethyl radical. A.Hasegawa, T.Wakabayashi, M.Hayashi (Dept. of Chem., Hiroshima Univ., Hiroshima, Japan), M.C.R.Symons.

J. Chem. Soc. Faraday Trans. 1 (GB), vol.79, pt.4, p.941-51 (April 1983). Exposure of solid $\text{CH}_3\text{CF}_2\text{Cl}$ and solid solutions of $\text{CH}_3\text{CF}_2\text{Cl}$ in some organic solvents to ^{60}Co γ -rays at 77K gives anisotropic ESR spectra of CH_3CF_2 radicals. Using the spectra it has been shown that the internal rotation of the CH_3 group is greatly hindered at 77K and that the hyperfine splitting of only one of the hydrogens in the CH_3 group is observed, reflecting a dihedral angle of 0° between the C-H bond and the half-filled orbital at the C_α atom. The anisotropic spectra are in excellent agreement with a simulation spectrum which was made for a pyramidal structure very similar to that optimized by INDO calculations. On annealing of the irradiated solid $\text{CH}_3\text{CF}_2\text{Cl}$ the spectrum of the CH_3CF_2 radical changed irreversibly at ca. 100K, indicating the presence of a high-temperature form of the CH_3CF_2 radical. The ESR spectrum for the high-temperature species has been satisfactorily interpreted on the assumption that the radical is undergoing libration about the axis passing through the mid-point of the two F atoms and that of the two C atoms of the pyramidal CH_3CF_2 radical. (15 refs.)

60767 ESR spectra and spin densities of the radical anions of magnesium and zinc azaporphyrates. K.Dzilin'ski, G.N.Sinyakov (Inst. of Phys., Acad. of Sci., Minsk, Belorussian SSR). *Theor. & Exp. Chem. (USA)*, vol.18, no.2, p.196-201 (March-April 1982). Translation of: *Teor. & Ekspr. Khim. (USSR)*, vol.18, no.2, p.227-33 (March-April 1982). [received: Feb. 1983]

The authors give the results of quantum-chemistry calculations of the distribution of spin density in the radical anions of the zinc and magnesium complexes of monoazetioporphyrin II, of monoazetioporphyrin IV, and of diazetioporphyrin II. On the basis of the results of the calculation the complex partially resolved ESR spectra of these compounds are modeled. (28 refs.)

Electron spin resonance spectra of tetrafluoroethylene radical cation See Entry 63568

33.35 DOUBLE RESONANCES AND OTHER MULTIPLE RESONANCES

60768 Rydberg-Rydberg transitions of NO using an optical-optical double resonance multiphoton ionization technique. Wan Yee Cheung, W.A.Chupka, S.D.Colson, D.Gauyacq (Sterling Chem. Lab., Yale Univ., New Haven, CT, USA), P.Avoiris, J.J.Wynne.

J. Chem. Phys. (USA), vol.78, no.6, pt.2, p.3625-34 (15 March 1983). New Rydberg-Rydberg transitions of $^{14}\text{N}^{16}\text{O}$ have been observed by the technique of optical-optical double resonance multiphoton ionization (OODR-MPI). The analysis of $S^2\Sigma^+ \leftarrow A^2\Sigma^+$ (0, 0), (1, 1) and $4f \leftarrow A^2\Sigma^+$ (1, 1) bands are reported. Molecular constants of the $S^2\Sigma^+ \nu=0$, 1 levels are in good agreement with those derived from absorption data. The structure of the $4f(\nu=1)$ level of the $^{14}\text{N}^{16}\text{O}$ isotope can be fully investigated for the first time since the OODR-MPI spectrum is free from any overlap, in contrast to the corresponding absorption spectral region. No detectable spectral perturbation was observed for levels up to $N=10$, although the non-Rydberg $G^2\Sigma^+$ ($\nu=8$) level lies at the same energy as the $4f(\nu=1)$ level. The $4f(\nu=1)$ rotational levels are described by an intermediate case (b)/case (d) coupling scheme and present a similar pattern to that of the $4f(\nu=0)$ rotational levels previously studied from absorption data. Rotational constants $B_1=1.968$ cm^{-1} and $\alpha_1=0.020$ cm^{-1} have been derived from the analysis and the B_0 value already known from absorption work. The constant k , which is related to the quadrupole moment of the vibrating molecular core, has also been derived for the $4f(\nu=1)$ level. The authors' observations suggest the presence of a 'significant' amount of $l=2$ character in the lowest member of the ns series ($3\sigma\sigma$)

$A^2\Sigma^+$ state, and confirm the pure $l=3$ character of the $4f$ Rydberg level. (21 refs.)

60769 Rydberg states of $^7\text{Li}_2$ by pulsed optical-optical double resonance spectroscopy: molecular constants of $^7\text{Li}_2^+$. R.A.Bernheim, L.P.Gold, T.Tipton (Dept. of Chem., Pennsylvania State Univ., University Park, PA, USA). *J. Chem. Phys. (USA)*, vol.78, no.6, pt.2, p.3635-46 (15 March 1983).

Three Rydberg series of electronic states of $^7\text{Li}_2$ have been characterized by pulsed optical-optical double resonance spectroscopy. The observed Rydberg states, which include the previously reported $E^2\Sigma_g^+$ and $G^2\Pi_u$ states, have been identified as $3-10\sigma^+ \Sigma_g^+$, $3-10\sigma^+ \Sigma_g^+$, and $3-15\sigma^+ \Pi_g$. The molecular constants for several of the upper members of each of the above series have been used to deduce the ionization potential of $^7\text{Li}_2$ and molecular constants for the $X^2\Sigma_g^+$ state of $^7\text{Li}_2^+$. The former was determined to be $T_0(\infty)=41496 \pm 4$ cm^{-1} . The latter were found to be in good agreement with recent ab initio calculations. (36 refs.)

60770 State-selective spectroscopy in a molecular nitrogen discharge by use of optogalvanic double-resonance spectroscopy. K.Miyazaki, H.Schein-graber, C.R.Vidal (Max-Planck-Inst. fur Extraterrestrische Phys., Garching, München, Germany). *Phys. Rev. Lett. (USA)*, vol.50, no.14, p.1046-9 (4 April 1983).

Transitions between excited states of molecular nitrogen, which are generated in a hollow-cathode discharge, have been studied by use of optogalvanic double-resonance spectroscopy as a state-selective method. By pumping of the known (0,0) band of the $c_4^+ \Pi_u \leftarrow a_1^+ \Sigma_g^+$ system in N_2 , the (16,0) and (17,0) bands of the $b_1^+ \Sigma_g^+ \leftarrow a_1^+ \Sigma_g^+$ system have been identified for the first time, and the recent assignment for the (0,0) band of the $c_5^+ \Sigma_u^+ \leftarrow a_1^+ \Sigma_g^+$ system has been verified. (7 refs.)

ORAND—a new NMR double resonance technique for obtaining symmetrically intensive multiplets by off-resonance experiments See Entry 59806

ENDOR study of bis(acetylacetonato)copper(II) in solid solution See Entry 62834

33.35H MODR and PMDR (microwave optical double resonance and phosphorescence microwave double resonance)

60771 Sublevel decay kinetics of the triplet state of bacteriochlorophyll a and b in methyltetrahydrofuran at 1.2K. H.J.Den Blanken, A.J.Hoff (Bio-phys. Dept., Huygens Lab., State Univ. Leyden, Leyden, Netherlands). *Chem. Phys. Lett. (Netherlands)*, vol.96, no.3, p.343-17 (8 April 1983).

The decay rates of the triplet sublevels of monomeric BChl a and b have been reexamined with pulsed microwave excitation. The values of k_2 and k_3 are significantly higher than published values. The new results are discussed in relation to the exciton model of the special pair making up the primary electron donor in photosynthetic purple bacteria. (25 refs.)

60772 Microwave studies of collision-induced transitions between rotational levels. VIII. Collisions between NH_3 and polar molecules. A.R.Fabris, T.Oka (Herzberg Inst. of Astrophys., Nat. Res. Council of Canada, Ottawa, Ontario, Canada).

J. Chem. Phys. (USA), vol.78, no.6, pt.2, p.3462-6 (15 March 1983). The technique of four-level microwave double resonance has been applied to the study of rotation-inversion transitions of NH_3 induced by collisions with various polar molecules. H_2O , D_2O , CH_3OH , CH_3X and CH_3X_2 ($\text{X}=\text{F}$, Cl , Br , I), NO , CO , and OCS were used as collision partners. The values of $\nu=\Delta I/I$ observed for many four-level systems which are connected by dipole-type transitions ($\Delta J=\pm 1$, $\Delta K=0$, parity $+$ or $-$) are given and qualitatively explained taking into account the long-range dipole-dipole interaction and the pattern of rotational energy levels of the collision partners. (26 refs.)

60773 A microwave double resonance study of collision-induced transitions between the M components of a rotational transition of OCS . H.Bomdsdorf, H.Mader (Abteilung Chem. Phys., Inst. fur Phys. Chem., Univ. Kiel, Kiel, Germany).

J. Chem. Phys. (USA), vol.78, no.6, pt.2, p.3467-75 (15 March 1983). Four-level MW-MW double resonance experiments on the rotational Stark levels $M=0$ and $M=\pm 1$ of the $\text{OCS } J=1-2$ transition have been performed to investigate collision-induced population transfer due to OCS self-collisions. A MW bridge has been used as a filter in order to discriminate between the pump and signal radiation and the relative change of signal line intensity η has been determined for both M components by means of a double modulation technique. A two-level Bloch-type description of the signal transition is given to estimate additional effects of the off-resonant pump radiation in the absence of collisions. (20 refs.)

33.40 MÖSSBAUER SPECTRA

60774 Mossbauer studies of FeSn molecules isolated in rare-gas solids and SCF-X α -scattered-wave molecular-orbital analyses of Sn_2 and FeSn diatomic molecules. H.M.Nagarathna, P.A.Montano (Dept. of Phys., West Virginia Univ., Morgantown, WV, USA).

J. Chem. Soc. Faraday Trans. II (GB), vol.79, pt.2, p.271-82 (Feb. 1983). Iron-tin molecules were isolated in rare-gas solids and studied using both ^{57}Fe and ^{119}Sn Mossbauer isotopes. Experiments at very dilute concentrations were performed to detect FeSn diatomic molecules. Larger clusters were identified by concentration dependence studies and Monte Carlo calculations. The ^{57}Fe and ^{119}Sn isomer shifts (IS) for FeSn diatomic molecules suggest a covalent bonding between Fe and Sn atoms. Similar behaviour was observed for large iron-tin clusters (Fe_xSn_y , $x,y\geq 3$). SCF-X α -SW calculations were performed for Sn_2 and FeSn diatomic molecules. Sn_2 shows a $^3\Sigma_g$ ground state and gives a quadrupole splitting consistent with the experimentally measured value at an equilibrium distance of 2.75 Å. (23 refs.)

Studies of some iron dithiolate complexes by the ESCA, Mossbauer and extended Huckel methods See Entry 60978

Protein dynamics from Mossbauer spectra. The temperature dependence See Entry 63770

33.45 MAGNETO-OPTICAL AND ELECTRO-OPTICAL SPECTRA; DICHROISM

60775 Time-resolved study of the laser optogalvanic effect in I_2 . D.A.Haner (Chem. Dept., California Polytech. State Univ., Pomona, CA, USA), C.R.Webster, P.H.Flamant, I.S.McDermid.

Chem. Phys. Lett. (Netherlands), vol.96, no.3, p.302-6 (8 April 1983). A time-resolved study of the optogalvanic effect in a pure iodine discharge is reported for pulsed dye laser irradiation at 585 nm. By varying both the spatial location and pulse energy of the laser probe, several contributions to

the time evolution of the optogalvanic signal are identified and their origin discussed. (21 refs.)

60776 The study of enantioselectivity in copper complexes with some 1,3-dicarbonyl ligands by circular dichroism spectroscopy. A.A.Kurganov, L.Ya.Zhuchkova, V.A.Davankov (Nesmeyanov Inst. of Organo-Element Compounds, Acad. of Sci., Moscow, USSR). *Polyhedron (GB)*, vol.2, no.1, p.37-41 (1983). The circular dichroism spectra of copper(II) complexes with hydroxymethylene camphor, hydroxymethylene menthone, and trifluoroacetyl camphor as well as of mixed-ligand complexes with acetylacetone have been studied in different solvents at different temperatures. The changes observed in the spectra are attributed to a strong coordination of the solvent molecules in axial positions of square-planar complexes. It has been shown that the contributions of two ligands to the net spectrum of circular dichroism are additive and that the absorption spectra of the complexes do not depend on the optical configuration of the ligands. The conclusion has been drawn that no noticeable inter-ligand interactions exist in the complexes and no enantioselective effects are exhibited. (14 refs.)

60777 Calculation of the electrooptical parameters and the absolute intensities of the IR bands of the water molecule and its isotopically substituted derivatives. S.P.Gavva, E.N.Bolitina, L.M.Sverdlov, M.D.Elkin. *Opt. & Spectrosc. (USA)*, vol.53, no.1, p.29-31 (July 1982). Translation of: *Opt. & Spektrosk. (USSR)*, vol.53, no.1, p.31-4 (July 1982). [received: April 1983]

The electrooptical parameters of water, $\partial\mu_{OH}/\partial q_1$, $\partial\mu_{OH}/\partial q_2$, and $\partial\mu_{OH}/\partial \gamma$, have been determined from the experimental values of the absolute intensities of the IR bands of the H₂O molecule within the framework of valence-optical theory. These parameters have been used to calculate the derivatives of the dipole moment with respect to the normal coordinates, and the absolute intensities of the molecules D₂O, T₂O, HOD, HOT, and DOT. The signs of $\partial P_{\alpha}/\partial Q_i$ were selected using the results of a quantum-mechanical calculation. The quantum-mechanical calculation of the dipole moment P of the H₂O molecule and the derivatives of the dipole moment with respect to the normal coordinates were carried out by the CNDO/2 method. The results of the calculations show satisfactory agreement with experiment. (15 refs.)

60778 Temperature-dependent electrooptical Kerr effect in spherical-top molecules. I.Ya.Ogurtsov, V.L.Ostrovskii, I.B.Bersuker. *Opt. & Spectrosc. (USA)*, vol.53, no.2, p.210-11 (Aug. 1982). Translation of: *Opt. & Spektrosk. (USSR)*, vol.53, no.2, p.356-8 (Aug. 1982). [received: April 1983]

It is shown that in the case of molecules with T_d or O_h symmetry, the electronic state of which is degenerate, there is a significant temperature-dependent contribution to the electrooptical Kerr constant that is analogous to the contribution due to the Langevin mechanism for anisotropic molecules. The Kerr effect can serve as a means of investigating the anisotropic polarizability of spherical tops in orbitally degenerate states. Consideration of the Jahn-Teller effect, which is significant when there is electron degeneracy, leads to a complication of the temperature dependence of the Kerr constant but does not change its order of magnitude. (8 refs.)

33.45B Zeeman and Stark effects

60779 Electric dipole moment of the diatomic TlF in its higher vibrational states. K.P.R.Nair, J.Hoef (Inst. für Molekülphys., Freie Univ. Berlin, Berlin, Germany).

Chem. Phys. Lett. (Netherlands), vol.96, no.3, p.348-51 (8 April 1983). The electric dipole moment of $^{205}\text{Tl}^{19}\text{F}$ has been measured in its higher vibrational states up to $v=7$ by studying the Stark effect in the $J=0 \rightarrow 1$ rotational transitions. The variation of the electric dipole moment with vibrational states is discussed. The electric dipole moment can be written as $|\mu_v| = 4.1941(15) + 0.0681(12)(v + 1/2)\text{D}$. (8 refs.)

60780 Electric dipole moments of excited vibrational levels in the $\tilde{X}1_A$ state of formaldehyde by stimulated emission spectroscopy. P.H.Vaccaro, J.L.Kinsey, R.W.Field, Hai-Lung Dai (Dept. of Chem., MIT, Cambridge, MA, USA).

J. Chem. Phys. (USA), vol.78, no.6, pt.2, p.3659-64 (15 March 1983). The electric dipole moments of the 4_4 ($E_{44} = 4628.4\text{ cm}^{-1}$), 2_4 , $2_{4,2}$ ($E_{2,2} = 5770\text{ cm}^{-1}$), and $2_{4,4}$ ($E_{2,2} = 6347\text{ cm}^{-1}$) levels of H₂CO are measured as 2.2723(86), 2.3222(47), and 2.2825(33) D, respectively. This first combination of stimulated emission pumping (SEP) with a static electric field demonstrates the possibility of systematically measuring dipole moments for highly excited vibrational levels of polyatomic molecules in their electronic ground states. The present dipole moment measurements and all previous ones involving overtones and combinations of the C-O stretch (ν_2) and out-of-plane bend (ν_4) are reduced to two types of expansions. The dipole moment μ is expressed both as an expansion in the normal coordinate displacements and as an expansion through squared terms in the ν_2 and ν_4 vibrational quantum numbers. (21 refs.)

Microwave spectrum, dipole moment, barrier to internal rotation of 1,1-dimethyldiborane See Entry 60712

Difference frequency laser spectroscopy of the ν_1 band of the HO₂ radical See Entry 60720

A microwave double resonance study of collision-induced transitions between the M components of a rotational transition of OCS See Entry 60773

The line shape of a zero-field level-crossing effect in methyl fluoride See Entry 60847

33.45C Magnetic circular dichroism

60781 Some theoretical considerations for magnetic vibrational circular dichroism spectra. L.Laux, V.Pultz, C.Marcotti, J.Overend, A.Moscowitz (Dept. of Chem., Univ. of Minnesota, Minneapolis, MN, USA).

J. Chem. Phys. (USA), vol.78, no.6, pt.2, p.4096-102 (15 March 1983). Expressions are derived for the A terms, B terms, and associated partial anisotropy factors relevant for the magnetic vibrational circular dichroism (MVCD) spectra of molecules with nondegenerated ground states. These expressions are derived subject to the approximations of the harmonic fixed partial charge model and the condition of magnetic coupling among only the ground electronic state vibrational levels. Numerical values for partial anisotropy factors calculated from these expressions, when taken in conjunction with the recent MVCD data of Keiderling (1981), suggest the importance of magnetic coupling of the ground electronic state with higher electronic states in the case of B terms. Symmetry constraints on the nonvanishing of such coupling terms also suggest the possible utility of MVCD data for processing spectroscopic and molecular structural information. (11 refs.)

33.50 FLUORESCENCE, PHOSPHORESCENCE; RADIATIONLESS TRANSITIONS (INTERSYSTEM CROSSING, INTERNAL CONVERSION)

60782 Laser-saturated fluorescence measurements of OH concentration in flames. R.P.Lucht, D.W.Sweeney, N.M.Laurendeau (Flame Res. Lab., School of Mech. Engrg., Purdue Univ., West Lafayette, IN, USA).

Combust. & Flame (USA), vol.50, no.2, p.189-205 (March 1983). A laser-saturated fluorescence technique which can be used to measure accurate OH radical concentrations over wide ranges of flame pressure, composition, and temperature has been developed. The balanced cross-rate model is used to analyze the fluorescence data. The basic premise of the model is that the population of the upper and lower rotational levels which are coupled by the laser is approximately constant during the laser pulse. Using the balanced cross-rate model to calculate concentrations, OH number densities calculated from saturated fluorescence agree to within 20% with number densities calculated from independent absorption measurements over a wide range of flame conditions. In addition, the ratio of number densities calculated from saturated fluorescence and absorption is constant over an order of magnitude range of flame pressure, demonstrating the insensitivity of the saturated fluorescence signal to collisional quenching rates. The estimated OH detection limit of the fluorescence system is 10^{12} - 10^{13} molecules/cm³. (47 refs.)

60783 pH correlation of the absorption, fluorescence and polarization spectra of fluorescein isothiocyanate. D.P.Dimitrov (Res. Lab., Bulgarian Acad. of Sci., Sofia, Bulgaria).

C.R. Acad. Bulg. Sci. (Bulgaria), vol.35, no.11, p.1467-70 (1982). In the present study the influence of H⁺ concentration on the absorption, fluorescence and polarization spectra of free and protein-bound FITC was investigated. The results will help in the interpretation of the induced structural transition in proteins using the fluorescence probe method. A stock solution of fluorescein isothiocyanate was prepared in acetone and diluted till the necessary concentration in the phosphate buffer. The absorption and fluorescence spectra was measured by Perkin Elmer 450 UV spectrophotometer with fluorescence attachment. The investigations of fluorescence polarization were carried out with spectropolarimeter constructed according to Weber's scheme. (12 refs.)

60784 Singlet excited-state 'energy hopping' in alkylbenzenes. H.Morrison, G.Pandey (Dept. of Chem., Purdue Univ., West Lafayette, IN, USA).

Chem. Phys. Lett. (Netherlands), vol.96, no.1, p.126-8 (25 March 1983). The quenching of toluene fluorescence by cis-6-phenyl-2-hexene has been studied to determine the rate of single 'energy hopping' in dilute solutions of alkylbenzenes. The singlet lifetime data have been analyzed by the Stern-Volmer method to give the quasi-isoenergetic rate, k_{10} , as $1.2 \times 10^{10}\text{ M}^{-1}\text{ s}^{-1}$. This result is consistent with an excimer formation-dissociation mechanism for alkylaromatic singlet energy transfer in dilute solution. (12 refs.)

60785 Reactive and non-reactive quenching of O(¹D₂) by COF₂. P.H.Wine, A.R.Ravishankara (Engrg. Experiment Station, Georgia Inst. of Technol., Atlanta, GA, USA).

Chem. Phys. Lett. (Netherlands), vol.96, no.1, p.129-31 (25 March 1983). Quenching of O(¹D₂) by COF₂ has been investigated by time-resolved resonance fluorescence monitoring of the product O(³P₂) following 248 nm pulsed laser photolysis of O₃. The rate constant for total removal of O(¹D₂) by COF₂ is $(7.4 \pm 1.2) \times 10^{-11}\text{ cm}^3\text{ molecule}^{-1}\text{ s}^{-1}$, $71 \pm 7\%$ of the quenching interactions result in formation of O(³P₂). (8 refs.)

60786 Effect of anion coordination upon radiationless transitions of the uranyl ion. G.C.Joshi, G.C.Dangwal (Dept. of Phys., Garhwal Univ., Srinagar, India), D.D.Pant, H.B.Tripathi.

Chem. Phys. Lett. (Netherlands), vol.96, no.2, p.167-70 (1 April 1983). At 80K, where the deactivation processes in uranyl luminescence in solutions are temperature independent, the radiationless transition rate depends upon the presence of H₂O in the first coordination sphere of the uranyl ion, UO₂²⁺. It is found that such radiationless transitions are due to a photophysical intramolecular process. (12 refs.)

60787 Excited-state relaxation in 1-amino-8-naphthalene sulphonate. J.Drew, P.Thistlethwaite, G.Woolfe (Phys. Chem. Dept., Melbourne Univ., Parkville, Victoria, Australia).

Chem. Phys. Lett. (Netherlands), vol.96, no.3, p.296-301 (8 April 1983). Fluorescence quantum yields and lifetimes have been measured for the isomeric species, 1-amino-8-naphthalene sulphonate and 2-amino-1-naphthalene sulphonate, in a range of solvents. The former shows a change in both radiative and nonradiative rate with solvent, while in the latter, the radiative rate is constant. The results suggest that, for 1-amino-naphthalene sulphonate, relaxation from the Franck-Condon state involves an increase in charge-transfer character. (15 refs.)

60788 Lifetimes in the B²Π_{1/2} state and the heat of formation of NCO. B.J.Sullivan, G.P.Smith, D.R.Crosley (Molecular Phys. Lab., SRI Internat., Menlo Park, CA, USA).

Chem. Phys. Lett. (Netherlands), vol.96, no.3, p.307-10 (8 April 1983). Using laser-induced fluorescence in a low-pressure flow system, the lifetimes of the 00⁰ and 10⁰ vibrational levels of the B²Π_{1/2} state of NCO have been measured. The results, 63 and $\leq 10\text{ ns}$ respectively, indicate that the dissociation limit to N(²D) + CO lies between these levels. This corresponds to a dissociation energy $D_0^{\circ} \geq 1.68\text{ eV}$ and an enthalpy of formation $\Delta H_{298}^{\circ} \geq 48\text{ kcal/mole}$ for NCO, and $\Delta H_{298}^{\circ}(\text{HNC}) \geq -14\text{ kcal/mole}$. (15 refs.)

60789 Laser spectroscopic investigation of the X²Σ_{1/2} state of the van der Waals molecule NaAr. G.Aepfelbach, A.Nunemann, D.Zimmermann (Inst. für Strahlungs- und Kernphys., Tech. Univ. Berlin, Berlin, Germany).

Chem. Phys. Lett. (Netherlands), vol.96, no.3, p.311-15 (8 April 1983). The laser-excitation spectrum of the transition X²Σ⁺ ← A²Π of NaAr has been investigated using a supersonic expansion of a mixture of sodium vapor and argon gas for production of the molecules. In comparison to previous investigations the rotational constants of the vibrational levels $v''=2$, 3 and 4 of the X²Σ⁺ state could in addition be determined. From the results the authors deduce a value of $R_e = 5.008(5) \times 10^{-10}\text{ m}$ for the equilibrium internuclear distance and of $D_e = 41.7(8)\text{ cm}^{-1}$ for the well depth of the X²Σ⁺ state. (24 refs.)

60790 Effects of aggregation on the phosphorescence of phenyl alkyl ketones in 77K rigid glass solutions. T.Wismontski-Knitel, T.Kilp (Radiation Lab., Univ. of Notre Dame, Notre Dame, IN, USA).

Chem. Phys. Lett. (Netherlands), vol.96, no.3, p.352-6 (8 April 1983). The concentration dependence of the 77K phosphorescence of propiophenone and acetophenone in methylcyclohexane and isopentane glasses implies extensive solute aggregation, arising from partial phase separation. Rationales for the observation of multiple emissions that are based on matrix rigidity dependent rates of conformational relaxation of the triplet state should be viewed with a great deal of caution when aliphatic hydrocarbon glasses are used. (17 refs.)

60791 Solvent effect on 1O_2 yield and the mechanism of polycyclic hydrocarbon triplet-state quenching by oxygen. A.P.Darmanyan (Inst. of Chem. Phys., Acad. of Sci., Moscow, USSR).

Chem. Phys. Lett. (Netherlands), vol.96, no.3, p.383-9 (8 April 1983). The yield of singlet oxygen (1O_2) in quenching of the triplets of 1,2,5,6-dibenzanthracene, 1,2-benzanthracene, anthracene, pyranthrene and duroquinone by oxygen has been studied using the laser photolysis technique. It was found that in toluene $\Phi(^1O_2) = 1.0 \pm 0.1$ and the quenching occurs via the energy transfer mechanism on account of an exchange interaction in the encounter complex. In benzonitrile the charge transfer contributes to a significant extent, leading to a considerable decrease in $\Phi(^1O_2)$. (26 refs.)

60792 Nickel porphyrin photophysics and photochemistry. A picosecond investigation of ligand binding and release in the excited state. D.Kim, C.Kirmaier, D.Holten (Dept. of Chem., Washington Univ., St. Louis, MO, USA).

Chem. Phys. (Netherlands), vol.75, no.3, p.305-22 (15 March 1983). The photophysical behaviour and some photochemical processes for nickel (II) porphyrins have been examined with picosecond transient absorption techniques. Detailed results are reported for Ni-octaethylporphyrin (NiOEP) and Ni-protoporphyrin IX dimethyl ether (NiPPDME) in toluene, pyridine and piperidine. Excitation flashes at six wavelengths between 355 and 532 nm have been employed. In toluene, rapid (≤ 15 ps) radiationless decay occurs via several pathways to the low-lying $^3B_{1g}$ excited state. In the basic solvents pyridine and piperidine, excited states with nickel $^1A_{1g}$ (d_2) character have a tendency to release ligands bound to the metal. Excited states with nickel $^3B_{1g}$ ($d(z^2)$, $d(x^2-y^2)$) character on the other hand, have an affinity for basic ligands, which rapidly bind to the metal. The competition between radiationless decay, ligand binding, and ligand release depends on the nickel porphyrin, solvent, and excitation wavelength. A set of 'rules' has been developed that gives a consistent view of all our results and those of previous investigators. These results may be helpful in understanding photoprocesses in other transition-metal porphyrins, including hemes, which have particular biological significance. (33 refs.)

60793 Fluorescence quenching of tertiary amines by halocarbons. P.C.Alford, C.G.Cureton, R.A.Lampert, D.Phillips (Davy-Faraday Lab., Royal Instn., London, England).

Chem. Phys. (Netherlands), vol.76, no.1, p.103-9 (1 April 1983). The quenching of fluorescence of a variety of tertiary amines by halocarbons has been investigated in both vapour and solution phases. In the vapour phase, quenching cross sections do not correlate well with a parameter based upon well-depth for collision complexes, but reasonable correlation between rate constant and free energy change for charge-transfer complex formation is obtained. The quenching by halocarbons is very efficient. In solution phase, evidence of static quenching is presented. (30 refs.)

60794 Measurement of sub-nanosecond single-rovibronic fluorescence with a pulsed dye laser. T.Suzuki, K.Yamada, T.Kasuya (Inst. of Phys. & Chem. Res., Saitama, Japan).

Jpn. J. Appl. Phys. Part 1 (Japan), vol.22, no.3, p.522-6 (March 1983). A method of fluorescence-decay measurement of sub-nanosecond time-resolution is presented which employs a narrow band pulsed dye laser for molecular excitation and a computer-controlled waveform digitizer for decay-data recording. The kinematical parameters of single rovibronic molecular relaxation are thereby deduced routinely from the observed time-evolution of fluorescence decay through a curve-fitting procedure of convolution-integral treatment. A specimen observation of fluorescing dye solution demonstrates the capability of determining fluorescence decay time as short as 0.2 ns with a precision of better than ± 0.05 ns. The method was applied to a systematic single rovibronic observation of fluorescence from the predisociative state of an interhalogen molecule.

60795 Circular polarization in the fluorescence of β,γ -enones: distortion in the $^1n\pi^*$ state. P.H.Schippers, J.P.M.van der Ploeg, H.P.J.M.Dekkers (Dept. of Theoretical Organic Chem., Univ. of Leiden, Leiden, Netherlands).

J. Am. Chem. Soc. (USA), vol.105, no.1, p.84-9 (12 Jan. 1983). The circular dichroism (CD) and the circular polarization of the luminescence (CPL) in the $n\pi^*$ transition were measured for a series of five rigid β,γ -unsaturated ketones: (1S,3R)-4-methyleneadamantan-2-one (1), (1S,3R)-4-adamantylidenediamantan-2-one (1a), (1R,4R)-bicyclo[2.2.1]hept-5-en-2-one (2), (1R)-7-methylenebicyclo[2.2.1]heptan-2-one (3), and (1S)-2-methylenebicyclo[2.2.1]heptan-7-one (4). All compounds exhibit marked differences between the degree of circular polarization in absorption and in fluorescence, giving evidence of important changes in molecular geometry upon excitation. The nature of these distortions is tentatively analyzed by using the previously found quantitative chirality rule for β,γ -enones (preceding paper in this issue). In the $n\pi^*$ state of β,γ -enones, the carbonyl group no longer is planar but is pyramidal due to an out-of-plane displacement of the oxygen atom (local symmetry C_1 instead of C_{2v}). The out-of-plane angle is large, and its direction is such that the oxygen approaches the double bond, pointing to a bonding interaction in the excited state, which is briefly discussed. (47 refs.)

60796 Circular polarization of luminescence as a probe for intramolecular $n\pi^*$ energy transfer in meso-diketones. P.H.Schippers, H.P.J.M.Dekkers (Gorlaeus Labs., Univ. of Leiden, Leiden, Netherlands).

J. Am. Chem. Soc. (USA), vol.105, no.1, p.145-6 (12 Jan. 1983). When a racemic mixture is excited with circularly polarized light, the degree of circular polarization in the luminescence (CPL) provides information on the rate of racemization in the excited state. It appears, however, that the CPL technique can also be used to study intramolecular excitation energy transfer. The authors report measurements on aliphatic diketones that contain two remove carbonyl chromophores of opposite chirality and thus are, in the ground state, meso structures (RS). In the $n\pi^*$ state they may occur in two enantiomeric forms, R^*S and RS^* , provided the excitation energy remains localized at a carbonyl group. (18 refs.)

60797 Radiative decay rates from deperturbed $V=0-7$ vibrational levels of CO A $^1\Pi$ measured using synchrotron radiation. R.W.Field, O.B.d'Azy, M.Lavollee, R.L.Delgado, A.Trainer (LURE, Univ. Paris-Sud, Orsay, France).

J. Chem. Phys. (USA), vol.78, no.6, pt.1, p.2838-46 (15 March 1983). Fluorescence decay times from single vibronic levels and from restricted groups of rotational levels are measured for CO A $^1\Pi$ under selective excitation by synchrotron radiation. The largest cause of variation of decay curves with v' and J' quantum numbers is singlet-triplet perturbations. These perturbations cause measured, rotationally averaged decay rates to differ from the deperturbed, pure A $^1\Pi$ decay rate by up to 20%. Failure to take perturbation effects into account could systematically affect transition moment functions derived from radiative lifetimes, but not those from absorption oscillator strengths or fluorescence branching ratios. The dependence of the CO A $^1\Pi-X^1\Sigma^+$ transition moment on internuclear distance is evaluated from deperturbed lifetimes of A $^1\Pi$ $v=0-7$ vibrational levels and found, assuming linear R_e vs \bar{r} variation within the region $1.0 \leq \bar{r}_{v,v'} \leq 1.6$ Å, to be

$R_e(\bar{r}_{v,v'}) = [7.48_{-0.34}^{+0.34}] [1 - (0.683_{-0.008}^{+0.006}) \bar{r}_{v,v'}] D$, where $R_e(\bar{r}_{v,v'})$ is the r centroid and the correlated uncertainties cited correspond to three standard deviations. However, the occurrence of strong A-X fluorescence bands with r centroids near 1.46 Å implies a decidedly nonlinear form for $R_e(\bar{r})$. Since the $v=0-7$ A $^1\Pi$ lifetimes sample $R_e(\bar{r})$ very weakly at $\bar{r} > 1.3$ Å, the transition moment function derived here is valid only for $1.0 \leq \bar{r} \leq 1.3$ Å. The $R_e(\bar{r})$ function determined here is nearly identical to that derived by Mumma et al. [ibid., vol.54, p.2627 (1971)] from the radiative lifetimes measured by Hesser [ibid., vol.48, p.2518 (1968)]. This is a coincidence, not evidence that perturbation effects are inconsequential. (28 refs.)

60798 Observation of the asymmetric O-U-O stretch in the vibronic absorption spectrum of uranyl formate monohydrate. W.P.West, C.H.Muller, III, J.T.Porter, II (GA Technol. Inc., San Diego, CA, USA), M.M.Malley.

J. Chem. Phys. (USA), vol.78, no.6, pt.1, p.3338-9 (15 March 1983). The visible and near UV absorption spectra of uranyl compounds at cryogenic temperatures are characterized by regular progressions of narrow lines. The vibronic structure is built principally on the symmetric stretching mode of the uranyl ion. The authors report the first observation of unusual vibronic absorption in isotopically labeled uranyl formate monohydrate, $UO_2(HCOO)_2 \cdot H_2O$ at 4.2 K. They have established that the asymmetric O-U-O mode is vibronically active in this compound and further that its frequency is lower than that of the symmetric mode, i.e. the order is reversed from that previously observed and expected assuming a simple valence bond model. By adding a bond interaction term to the usual valence bond model the authors are able to fit the stretch frequencies and find excellent agreement between the observed and predicted uranium and oxygen isotope shifts. (4 refs.)

60799 The effect of solvent environment on molecular electronic transition moment directions: symmetry lowering in pyrene. F.W.Langkilde, E.W.Thulstrup, J.Michi (Dept. of Chem., Aarhus Univ., Aarhus, Denmark).

J. Chem. Phys. (USA), vol.78, no.6, pt.2, p.3372-81 (15 March 1983). Measurements of polarized fluorescence and phosphorescence of pyrene, 2-fluoropyrene, and 2-methylpyrene in 3-methylpentane glass at 77 K reveal significant differences among the three molecules. These are interpreted in terms of solvent-induced mixing of the L_a and L_b states. It is proposed that such symmetry-lowering effects of the solvent environment may well be important contributors to the often observed discrepancies between the theoretical limiting values of polarization ratios and the values actually observed. (41 refs.)

60800 Spectroscopy of large molecular complexes in supersonic jets. U.Even, J.Jortner (Dept. of Chem., Tel Aviv Univ., Tel Aviv, Israel).

J. Chem. Phys. (USA), vol.78, no.6, pt.2, p.3445-54 (15 March 1983). In the paper the authors report the results of an experimental study of laser-induced fluorescence spectroscopy of MX_n van der Waals complexes, consisting of medium-sized molecules (X =methane, carbon tetrachloride, ammonia, water, methanol, acetonitrile, benzene, and toluene) bound to a large aromatic molecule (M =tetracene and fluorene). These large complexes were synthesized in pulsed supersonic jets of He seeded with M and X . The spectral features assigned to $S_0 \rightarrow S_1$ electronic-vibrational excitations of these large MX_n complexes, which are characterized by narrow linewidths (FWHM) of $2-4$ cm^{-1} , were attributed to three distinct categories: (i) A vibrationless excitation of MX_n , (ii) vibrational excitations of M in MX_n , and (iii) excitations of the vibrations involving relative motion of M and X in the MX_n complex. (20 refs.)

60801 Laser vaporization of jets: spectra and ground state molecular parameters of Sn_2 . V.E.Bondybe, M.Heaven, T.A.Miller (Bell Labs., Murray Hill, NJ, USA).

J. Chem. Phys. (USA), vol.78, no.6, pt.2, p.3593-8 (15 March 1983). Sn_2 molecules are produced by YAG laser vaporization of tin metal in a stream of cold helium gas and studied by time resolved induced fluorescence. Several vibronic bands of an electronic transition with origin near 18200 cm^{-1} are analyzed and the ground state vibrational frequency and equilibrium molecular constants are determined. The electronic structure of Sn_2 is discussed and an assignment of the observed transition proposed. (28 refs.)

60802 First observation of bound-continuum transitions in the laser-induced $X^1\Sigma^+ \rightarrow X^1\Sigma_g^+$ fluorescence of Na_2 . K.K.Verma, J.T.Bahns, A.R.Rajaei-Rizi, W.C.Stwalley (Dept. of Chem. & Phys., Univ. of Iowa, Iowa City, IA, USA), W.T.Zemke.

J. Chem. Phys. (USA), vol.78, no.6, pt.2, p.3599-613 (15 March 1983). The authors report an interesting spectrum of Na_2 excited by a Kr^+ (5682 Å) laser which shows a long series of R-P doublets in the region 5600-8000 Å and a continuum with three very broad maxima beyond 8000 Å. The spectral analysis reveals that the laser populates the $v'=34$, $J'=50$ level in the $A^1\Sigma^+$ state from where Na_2 molecules fluoresce not only to the bound vibrational levels of the entire ground state potential well ($3 \leq v'' \leq 56$) but also to the continuum levels above the well. The authors have made an independent theoretical quantitative prediction of the continuous emission and the agreement between experiment and theory is found to be excellent. Almost the entire (99.6%) ground state RKR potential is constructed using the bound state experimental data which leads to a more accurate value of the dissociation energy ($D_0'' = 6024 \pm 6$ cm^{-1}). The feasibility of a continuously tunable near infrared Na_2 laser based upon this radiative dissociation process is discussed. Finally, they present a comprehensive bibliography for the Na_2 molecule similar to that given by Hessel and Vidal for Li_2 [ibid., vol.70, p.4439 (1979)]. (329 refs.)

60803 Observation of levels near dissociation in the $X^1\Sigma^+$ state of 7Li_2 . K.K.Verma, M.E.Koch, W.C.Stwalley (Depts. of Chem. & Phys., Univ. of Iowa, Iowa City, IA, USA).

J. Chem. Phys. (USA), vol.78, no.6, pt.2, p.3614-22 (15 March 1983). The fluorescence spectrum of 7Li_2 excited by a Kr^+ (5682 Å) laser has been observed and analyzed. The laser simultaneously excites the $A^1\Sigma^+$ and the $B^1\Pi_u$ states of the 7Li_2 molecule. The analysis reveals two very interesting things: (a) the A-X spectrum consists of the transitions involving v' levels of the entire ground state potential well ($5 \leq v'' \leq 36$) and thus the authors have made the very first observation of the levels near the dissociation limit in the ground state of 7Li_2 , which suggests that $D_0'' = 8521.5 \pm 4$ cm^{-1} ; and (b) the B-X spectrum is actually enhanced by the fluorescence from the A state which is an interesting single frequency analog of 'modulated population spectroscopy' or 'optical-optical double resonance' which the authors call 'coupled laser induced fluorescence series' (CLIFS). (17 refs.)

60804 Two-photon excitation of the $D^1\Delta-X^1\Sigma^+$ transition in carbon monoxide. C.Kittrell, S.Cameron, L.Butler, R.W.Field (Dept. of Chem., MIT, Cambridge, MA, USA), R.F.Barrow.

J. Chem. Phys. (USA), vol.78, no.6, pt.2, p.3623-5 (15 March 1983). A frequency doubled pulsed dye laser is used to promote two-photon excitation of the $D^1\Delta-X^1\Sigma^+$ transition in carbon monoxide. Collisional transfer to $A^1\Pi$ leads to ultraviolet fluorescence which is detected with a solar blind photomultiplier. Rotationally resolved structure belonging to bands of three isotopically substituted molecules has been measured relative to the visible

spectrum of iodine. Preliminary values of molecular constants are given. (13 refs.)

60805 High-resolution gas phase emission and laser induced fluorescence excitation spectra of $1,3,5\text{-C}_6\text{F}_3\text{H}_3^+$ and $1,3,5\text{-C}_6\text{F}_3\text{D}_3^+$: critical bands in the Jahn-Teller effect analysis. C.Cossart-Magos, D.Cossart, S.Leach (Lab. de Photophys. Moléculaire du CNRS, Univ. Paris-Sud, Orsay, France), J.P.Maier, L.Misev.

J. Chem. Phys. (USA), vol.78, no.6, pt.2, p.3673-87 (15 March 1983). Cooled gas phase laser induced fluorescence excitation (LIFEX) spectra of $1,3,5\text{-C}_6\text{F}_3\text{H}_3^+$ (h_3^+) and $1,3,5\text{-C}_6\text{F}_3\text{D}_3^+$ (d_3^+) ions were obtained between 4600 and 4110 Å at a resolution of 1 cm^{-1} . Band intensities were corrected for laser power variations. Gas phase discharge emission spectra of the same ions were photographed at a resolution of 0.25 cm^{-1} from 4450 to 4800 Å and at 0.1 cm^{-1} between 4500 and 4700 Å. In emission, only the spectra region $\lambda < 4580\text{ Å}$, corresponding to the O_0^+ band and bands to lower wavelengths, is reported here. Particular regions of the LIFEX spectra were also recorded at a resolution of 0.25 cm^{-1} . Vibronic analysis of the $B^2A_2^- \rightarrow X^2E^+$ transition is made on the basis of five (seven) e' , three a_1' , and one a_2' excited state fundamental frequencies which were assigned in the h_3^+ (d_3^+) ions. A few low-lying ground state levels, among which the first $j=3/2$ (A_1, A_2) levels of mode 6 (e'), the most active Jahn-Teller (JT) mode, are particularly critical. Some discrepancies in band relative intensities and absolute wave numbers are found between the h_3^+ LIFEX spectrum obtained here and that previously published by Bondybey et al. (1979). Nevertheless, interpretation of the authors h_3^+ and d_3^+ spectra is more consistent with the high values of JT parameters derived by Bondybey, et al. (1980), rather than the low values obtained in earlier work by Cossart-Magos and Leach (1980). Some differences between observed and calculated JT features are rationalized in terms of model inadequacies. (28 refs.)

60806 Luminescence of the excited mercury diethylamine complex. Attachment by ligand exchange. A.B.Calleary, C.P.Devonport (Phys. Chem. Dept., Univ. of Cambridge, Cambridge, England).

J. Chem. Phys. (USA), vol.78, no.6, pt.2, p.3738-46 (15 March 1983). The possibility of molecular attachment to excited atoms in gases by ligand exchange has been examined. It was first confirmed that mixtures of mercury vapor and diethylamine Et_2NH give negligible luminescence when subject to irradiation with the 2537 Å mercury resonance line. The emission was then examined from mercury vapor with added amine up to 100 Torr, in the presence of an excess NH_3 . With NH_3 alone, a strong emission was observed due to HgNH_3^+ , a complex of $\text{Hg}(\text{P}_0)$ and NH_3 , with $\lambda_{\text{max}} \sim 3500\text{ Å}$. The addition of Et_2NH gave rise to a second band to the long wavelength, extending throughout the visible region, with $\lambda_{\text{max}} \sim 5140\text{ Å}$; the ratio of the intensity of the long wavelength member to the residual emission in the 3500 Å region was found to be proportional to the amine pressure. For various $[\text{Et}_2\text{NH}]$ and fixed $[\text{NH}_3]$, the set of normalized spectral profiles are isosbestic, corresponding to the superposition of just two basic functions. From the cw experiments, it was added that the addition of quite small pressures of Et_2NH , $\sim 1\text{ Torr}$, to NH_3 at 1 atm pressure effectively extinguishes the HgNH_3^+ luminescence by a fast ligand exchange reaction $\text{HgNH}_3^+ + \text{Et}_2\text{NH} \rightarrow \text{Hg}(\text{Et}_2\text{NH})^+ + \text{NH}_3$. The two basic functions which comprise the spectra are due to $\text{Hg}(\text{Et}_2\text{NH})^+$ and the dimer $\text{Hg}(\text{Et}_2\text{NH})_2^+$, which is the carrier of the long wavelength component. This scheme was confirmed using the resonance flash technique to time resolve the exchange of ligands; the rate coefficient is $\sim 2 \times 10^{-10}\text{ cm}^3\text{ molecule}^{-1}\text{ s}^{-1}$ for the above reaction. The radiative lifetime of the $\text{Hg}(\text{Et}_2\text{NH})^+$ monomer is $1.15\text{ }\mu\text{s}$. The large red shift and broadening associated with attachment of the second ligand arises because the emission is from an upper state which belongs to the $\text{Hg}(\text{P}_1)$ asymptote, and which is more strongly bound than the state which correlates with $\text{Hg}(\text{P}_0)$. (16 refs.)

60807 IR laser induced loss of fluorescence in $\text{UO}_2(\text{hfacac})_2\text{TMP}$. I. Real time detection of multiple photon excitation of the ground electronic state. R.B.Hall (Corporate Res. Sci. Lab., Exxon Res. & Engng. Co., Linden, NJ, USA).

J. Chem. Phys. (USA), vol.78, no.6, pt.2, p.3792-805 (15 March 1983). The infrared multiple photon excitation and unimolecular reaction of $\text{UO}_2(\text{hfacac})_2\text{TMP}$ is monitored in real time by the loss of dye laser induced fluorescence (LIF) intensity. The loss of fluorescence results from a change in the chemical structure and not from a change in the vibrational state population of the ground or excited electronic state. Absorption into the emitting states also becomes forbidden following IR excitation. The observed rates of fluorescence depletion are greater than 10^6 s^{-1} with excitation the rate limiting step over the range of laser intensities studied. At low extents of depletion the observed rate follows the single photon absorption rate. At higher yields, the observed rate is within a factor of 2 of the rate derived from the measured dependence of the yield on laser power using the analysis given by Quack (1980). Such an analysis can provide a reasonable estimate of the reaction rate when no rate measurements can be made. The ensemble dynamics contribute significantly to the observed kinetics. The excitation and reaction behavior is characteristic of molecules in the quasicontinuum excitation regime from the absorption of the first photon. No fluence or power threshold for reaction is observed. At a fixed fluence, the yield remains constant over a change in the peak power of more than an order of magnitude and thus appears to be independent of the rate at which the photons are absorbed. In addition, the absorption profile is homogeneous with respect to reaction; the yield remains proportional to the product of fluence times the small signal absorption cross section for any laser transition within the $\nu=0$ to $\nu=1$ absorption profile of any of the accessible vibrational modes. Collision cross sections for fluorescence quenching by $\text{UO}_2(\text{hfacac})_2\text{TMP}$ and by the products of the multiple photon excitation $\text{UO}_2(\text{hfacac})$ and TMP are also obtained. (31 refs.)

60808 Vibrational relaxation of HCN(002). P.W.Hastings, M.K.Osborn, C.M.Sadowski, I.W.M.Smith (Dept. of Phys. Chem., Univ. Chem. Labs., Cambridge, England).

J. Chem. Phys. (USA), vol.78, no.6, pt.2, p.3893-8 (15 March 1983). Tuned output from an optical parametric oscillator has been used to excite HCN to its (002) level for measurements of vibrational energy transfer. By observing time-resolved (002,001) fluorescence in the presence of different collision partners, the following rate constants ($k_{002}/\text{cm}^3\text{ molecule}^{-1}\text{ s}^{-1}$) was obtained for relaxation of HCN(002) at $298 \pm 4\text{ K}$: $k(\text{HCN}) = (6.8 \pm 0.4) \times 10^{-12}$, $k(\text{He}) = (5.6 \pm 0.25) \times 10^{-13}$, $k(\text{Ne}) = (3.8 \pm 0.16) \times 10^{-15}$, $k(\text{Ar}) = (3.0 \pm 0.4) \times 10^{-15}$, $k(\text{O}_2) = (1.39 \pm 0.08) \times 10^{-14}$, $k(\text{N}_2) = (2.6 \pm 0.15) \times 10^{-14}$, $k(\text{CO}) = (6.8 \pm 0.4) \times 10^{-14}$. These results are compared with the rate constants (k_{001}) obtained for relaxation of HCN(001) and the mechanisms for relaxation are discussed. With noble gases as collision partners, the ratios (k_{002}/k_{001}) are less than one. Comparison of these ratios with predictions of the 'breathing sphere' theory indicates that relaxation HCN(00₂) \rightarrow 1,2 occurs via transfer to HCN ($12^0_{12} \nu_3 - 1$), the lower rate for $\nu_3 = 2$ being due to the increased energy gap between initial and final states. (28 refs.)

60809 Intramolecular vibrational relaxation from C-H stretch fundamentals. G.M.Stewart, J.D.McDonald (School of Chem. Sci., Univ. of Illinois, Urbana, IL, USA).

J. Chem. Phys. (USA), vol.78, no.6, pt.2, p.3907-15 (15 March 1983). Infrared fluorescence measurements have been used to determine the presence or absence of intramolecular vibrational relaxation (or more precisely state mixing) from an excited C-H stretch in 23 representative molecules varying in size from methane to nonbornene. Included are aliphatic hydrocarbons, aromatic molecules, ethers, and ketones, including a cyclic molecule. The rate of resonance fluorescence, calculated relative to a nonrelaxing molecule, was used as the criterion of relaxation. Small rates imply state mixing and hence in the large molecule limit, relaxation. The primary correlation with the presence of mixing is with state density; about ten states per wave number (cm^{-1}) are needed to insure mixing. The spread in threshold densities reflects variations in anharmonicity. For some molecules true relaxed (non C-H stretch) fluorescence is observed. These experiments were done in a molecular beam, using a pulsed optical parametric oscillator for excitation and a circular variable filter for spectral resolution. (52 refs.)

60810 The collisional flow of vibrational energy into surrounding vibrational fields within S_1 benzene. K.Y.Tang (SRI Internat., Menlo Park, CA, USA), C.S.Parmenter.

J. Chem. Phys. (USA), vol.78, no.6, pt.2, p.3922-34 (15 March 1983). Vapor phase fluorescence spectra are used to determine the absolute rate constants for the collisional transfer of vibrational energy from initial single vibronic levels of S_1 benzene into the surrounding S_1 vibronic field. 11 initial levels are probed with vibrational energies ranging to 2368 cm^{-1} where the level density is about 10 per cm^{-1} . CO, isopentane, and S_0 benzene are the collision partners. Benzene rate constants are three to four times gas kinetic for all levels, and electronic energy switching between the initial S_1 molecule and the S_0 collision partner probably makes important contributions. Isopentane efficiencies range from one to two times gas kinetic. Most of the transfer from low S_1 levels occurs within excitation of vibrational energy within isopentane. These V-V contributions decline to only about 10% for the high transfer. CO-induced transfer by V-T,R processes for all levels. The CO efficiency rises from about 0.1 for low regions to about unity for levels above 1500 cm^{-1} . The CO efficiencies retain significant sensitivity to initial level identity even in the higher regions. Propensity rules derived from collisional mode-to-mode transfer among lower levels of S_1 benzene are used to calculate the relative CO efficiencies. The calculated efficiencies agree well enough with the data to suggest that it may be meaningful to model vibrational equilibration with the use of propensity rules. The rules suggest that only a small number of levels among the thousands surrounding a high initial level contribute significantly to the total relaxation cross section and that this number is rather independent of the level density. While CO and isopentane have comparable efficiencies for relaxation of a high S_1 level, CO is much less efficient for inducing full thermal equilibration. CO, which uses V-T,R processes only, becomes a relatively poor transfer partner once low levels are reached during the equilibration, whereas V-V transfer sustains isopentane's large efficiency for all levels. (22 refs.)

60811 Laser induced fluorescence excitation spectrum of jet-cooled benzoic acid dimers. D.E.Poelzl, J.K.McVey (Dept. of Chem., Princeton Univ., NJ, USA).

J. Chem. Phys. (USA), vol.78, no.7, p.4349-55 (1 April 1983). Inter-molecular hydrogen bonding in gas phase dimers of benzoic acid is investigated following preparation in a pulsed free-jet expansion. Laser induced fluorescence excitation spectra are analyzed to provide information regarding the vibrational assignments of the 1^1L_b excited state. In agreement with studies in low temperature mixed crystals, the electronic excitation is essentially localized on one monomer unit in the dimer. A 58 cm^{-1} band is associated with the ν_3 hydrogen bonding stretch+bend mode and is prominent in combination bands involving internal motion in the carboxyl groups. The free jet technique has been shown to be particularly advantageous in studies of inter-molecular hydrogen bonding. (13 refs.)

60812 Fluctuations of cross sections in chemical processes: infrared photoquenching of fluorescent states in thiophosgene. J.R.Grover, D.M.Brenner (Dept. of Chem., Brookhaven Nat. Lab., Upton, NY, USA).

J. Chem. Phys. (USA), vol.78, no.7, p.4385-99 (1 April 1983). Pronounced fluctuations have been observed in the cross section for the quenching of the fluorescence of the different members of the vibrational manifold belonging to the 4^1A_2 state of thiophosgene. This phenomenon is reminiscent of fluctuations that occur for nuclear reactions in regions of high level density, and that can be interpreted in terms of reduced transition amplitudes that are approximately normally distributed. The analysis of the fluctuations gives an effective number of independent reaction channels; in general, the greater the number of channels, the narrower is the range of the fluctuations. A knowledge of the number of independently contributing channels can be useful in the interpretation of experimental results, and sometimes lends important insight into reaction processes. The quenching cross sections for thiophosgene were therefore examined to see whether an analysis of their fluctuations would be useful. It was found necessary to develop a form of analysis that circumvents a serious obstacle in the chemical data, namely, the existence of significant correlations among the cross sections. The resulting formalism is quite simple to apply however, and, after suitable generalization, should be widely applicable to chemical experiments in which resolved cross sections that exhibit fluctuations are measured. Application of this formalism to the thiophosgene quenching cross sections shows that two hypotheses of the quenching mechanism must be rejected, but provides no reason to reject a third, that quenching is via absorption by states in a 'bottleneck' region that is reached by rapid photon transitions from the fluorescent target states, which transitions cannot be statistically distributed. The analysis also reveals the existence of an important, experimentally determined constraint that must still be accounted for by any successful hypothesis, viz. the number of channels increases approximately as the square root of the peak power of the quenching infrared radiation. (15 refs.)

60813 Rotational effects in the intermediate-case radiationless decay of pyrimidine. D.M.Bartels, K.G.Spears (Dept. of Chem., Northwestern Univ., Evanston, IL, USA).

J. Phys. Chem. (USA), vol.86, no.26, p.5180-91 (23 Dec. 1982). The rotational contour dependence of pyrimidine fluorescence decay has been investigated under collision-free conditions in a supersonic nozzle expansion. Lifetimes for the long component of the intermediate-case biexponential decay were measured with a pulsed dye laser of 0.6-cm^{-1} resolution and a boxcar integrator detection method. Measurements were obtained at 0.25-cm^{-1} intervals across the 0-0 and $6b_2$ vibronic band contours at a number of different rotational temperatures. The data have both an excitation frequency and a temperature dependence. (45 refs.)

60814 Effects of excited-state prototropic equilibria on the fluorescence energies of benzimidazole and thiazobenzimidazole homologues. P.C.Tway, L.J.Cline Love (Dept. of Chem., Seton Hall Univ., South Orange, NJ, USA).

J. Phys. Chem. (USA), vol.86, no.26, p.5227-30 (23 Dec. 1982).
Excited-state prototropic equilibria are proposed to explain the appearance of new charge transfer bands in the fluorescence spectra of certain benzimidazole and thiazobenzimidazole homologues. The effects of pH on fluorescence energies and intensities, proton NMR data, low-temperature luminescence studies, and pK_a values are used to support the postulated mechanisms. The 5-amino derivatives are believed to undergo excited-state deprotonation, while the 5-hydroxy derivative forms an excited-state zwitterion. (12 refs.)

60815 Rotational relaxation in ground-state *p*-difluorobenzene: State selection by stimulated emission pumping. W.D.Lawrence, A.E.W.Knight (School of Sci., Griffith Univ., Nathan, Brisbane, Queensland, Australia).

J. Phys. Chem. (USA), vol.87, no.3, p.389-91 (3 Feb. 1983).
An estimate is obtained for the cross section for rotational relaxation from a small subset of $|J,K\rangle$ states in the S_0 vibrational level of S_0 *p*-difluorobenzene. The method of stimulated emission pumping (SEP) is used to prepare the initial $|J,K\rangle$ population. Collisional relaxation induced by the bath of *p*-difluorobenzene molecules in Boltzmann equilibrium is monitored from the intensity of wavelength-resolved single vibronic level fluorescence generated via selective excitation from the SEP-prepared levels. The average efficiency for rotational relaxation σ/σ_{HS} , relative to the hard-sphere cross section σ_{HS} , is found to be 5 ± 2 for ground-state *p*-difluorobenzene. This study demonstrates that rotational relaxation in a nonpolar polyatomic molecule in its S_0 state is as efficient as that found for similar polyatomics in their S_1 electronic states. (9 refs.)

60816 Vibrational relaxation within mixed electronic states. A.E.W.Knight (School of Sci., Griffith Univ., Nathan, Brisbane, Queensland, Australia), C.S.Parmeter.

J. Phys. Chem. (USA), vol.87, no.3, p.417-24 (3 Feb. 1983).
The efficiency of collisional vibrational relaxation within a fluorescing state of a polyatomic molecule is discussed for cases where the fluorescing state is of mixed electronic character involving both a radiative and nonradiative state. It is shown that the efficiency of vibrational relaxation should be changed from that within the pure radiative state by the factor A_1^2 , where A_1 is the fraction of radiative state character in the mixed electronic state. Severe reductions in vibrational relaxation efficiencies are predicted, and they are likely to occur in polyatomic whose fluorescence decay is consistent with the strong coupling, intermediate case of radiationless transition theory. Pyrimidine and pyrazine are proposed as examples. Analysis of pyrimidine data in particular shows that S_1 vibrational relaxation efficiencies are reduced by at least two orders of magnitude from those commonly found for relaxation within pure S_1 states. Such a reduction is consistent with the theory when the (known) mixed singlet-triplet character of the pyrimidine fluorescing state is considered. (20 refs.)

60817 Effect of polar solvents on amine quenching for *p*-fluorotoluene fluorescence. K.E.Al-Ani, M.Al-Sabti (Dept. of Chem., Coll. of Education, Univ. of Baghdad, Baghdad, Iraq).

J. Phys. Chem. (USA), vol.87, no.3, p.446-9 (3 Feb. 1983).
An increase in solvent polarity was found to cause a blue shift in the absorption spectrum of *p*-fluorotoluene. The Stern-Volmer constants for quenching of *p*-fluorotoluene fluorescence by primary, secondary, and tertiary aliphatic amines have been measured in 2-propanol, ethanol, and acetonitrile solvents. A strong correlation between the vertical ionization potential of the quenchers and $\log k_Q$ was observed. As the vertical ionization potential increases, the quenching rate constant decreases. In acetonitrile, secondary amines were shown to have a higher quenching ability than primary and tertiary amines. This may be due to the interaction of solvent with the formed encounter complex which enhances the formation of radical anions and cations, a full discussion of which is made. (17 refs.)

60818 Intracoll triplet-triplet annihilation in poly(2-vinylnaphthalene) in benzene solution. J.F.Pratt, S.E.Webber (Dept. of Chem., Univ. of Texas, Austin, TX, USA).

J. Phys. Chem. (USA), vol.87, no.3, p.449-54 (3 Feb. 1983).
The triplet state of poly(2-vinylnaphthalene) (P2VN) in benzene solution has been sensitized by the benzophenone triplet state and a naphthalenic excimer delayed fluorescence (DF) has been observed. Kinetic models have been tested against the experimental data, including the effect of the molecular weight on the time dependence of the DF. It has been concluded that a homogeneous, intracoll mechanism best fits the trend of the data. This implies that triplet migration along the P2VN chain is occurring in the solution phase. (15 refs.)

60819 Exciplex photophysics. VII. Steric effects in exciplex photophysics. S.T.Cheung, W.R.Ware (Dept. of Chem., Univ. of Western Ontario, London, Ontario, Canada).

J. Phys. Chem. (USA), vol.87, no.3, p.466-73 (3 Feb. 1983).
For pt.VI see *J. Am. Chem. Soc.*, vol.101, p.121 (1979). The influence of steric interference with sandwich-type exciplex formation has been investigated by using mono- and di-tert-butyl substitution of *N,N'*-dimethylaniline (DMA). Pyrene was the electron acceptor and studies were carried out with both steady-state and fluorescence lifetime technique in hexane and tetrahydrofuran (THF). All the rate constants of the classical exciplex mechanism were determined along with temperature coefficients. It was found that the most significant effect of tert-butyl substitution was a substantial decrease in the process $(AQ)^+ \rightarrow A^+ + Q$. Solvent effects, exciplex thermodynamics and activation parameters are discussed for the unsubstituted and tert-butyl-substituted systems. (41 refs.)

60820 Temperature dependence of the nonradiative relaxation process of the lowest excited singlet states of meso-substituted bromoanthracenes. M.Tanaka, I.Tanaka (Dept. of Chem., Tokyo Inst. of Technol., Tokyo, Japan), S.Tai, K.Hamanoue, M.Sumitani, K.Yoshihara.

J. Phys. Chem. (USA), vol.87, no.5, p.813-16 (3 March 1983).
Direct measurements of the temperature dependence of the fluorescence lifetimes of 9-bromoanthracene (BA) and 9,10-dibromoanthracene (DBA) have allowed the determination of the rate constant for intersystem crossing (isc) in the form $k_{isc} = A_{isc} \exp(-\Delta E/kT)$. This isc is attributed to that from the lowest excited singlet state S_1 to an adjacent higher excited triplet state T_1 . The values of ΔE , i.e. 600-710 cm^{-1} for BA and 1100 cm^{-1} for DBA, are about 300 cm^{-1} larger than those deduced from the $T_1 \rightarrow T_2$ fluorescence (TTF) measurement by Gillispie and Lim (Chem. Phys. Lett., vol.63, p.355, 1979). The values of the S_1 decay constants consistent with those of the buildup times for triplet-triplet absorptions lead to the suggestion that the T_1 lifetimes are tens of picoseconds, and this estimate gives good agreement between calculated and experimental Φ_{TTF} of DBA. (24 refs.)

60821 Fluorescence branching ratios from the $A^{2+}(\nu'=0)$ state of NO. T.J.McGee, G.E.Miller (NASA, Goddard Space Flight Center, Greenbelt, MD, USA), J.Burris, Jr., T.J.McIlraith.

J. Quant. Spectrosc. & Radiat. Transfer (GB), vol.29, no.4, p.333-8 (April 1983).

The emission spectrum of NO from several rotational levels in the first excited state has been recorded. Branching ratios have been measured and Franck-Condon factors calculated from the experimental data. Lifetimes of the lines used have been measured and Einstein A-values calculated. (9 refs.)

60822 Electronic quenching of pyrene $^1B_{1u}$ by olefins in the vapour phase. A.Davis, M.J.Pilling (Phys. Chem. Lab., Univ. of Oxford, Oxford, England).

J. Chem. Soc. Faraday Trans. 1 (GB), vol.79, no.1, p.235-44 (Jan. 1983).
The rate of quenching of electronically excited singlet pyrene by olefins has been investigated in the vapour phase over the temperature range 420-570K. Rate constants and activation energies have been determined and correlations with ionization potentials of the quenchers suggest an exciplex intermediate. A model previously proposed for concentration quenching of pyrene has been applied to investigate the temperature and pressure dependence of the rate constant and of the Arrhenius pre-exponential factor. (24 refs.)

60823 Annihilation-delayed fluorescence of eosin and rhodamine 6G and polyvinyl alcohol films. N.Kh.Ibraev, G.A.Ketsle, L.V.Levshin, Yu.A.Soinikov, V.I.Yuzhakov.

J. Appl. Spectrosc. (USA), vol.36, no.5, p.521-5 (May 1982). Translation of: *Zh. Prikl. Spektrosk. (USSR)*, vol.36, no.5, p.750-5 (May 1982). [received: Feb. 1983]

Presents the results of a study of energy transfer in polymer films of polyvinyl alcohol (PVA), not containing aromatic nuclei. Eosin and rhodamine 6G molecules were used as energy acceptors. Since double bonds are absent in PVA macromolecules, it should be expected that the polymer will absorb radiation in the UV region ($\lambda \leq 190 \text{ nm}$) of the spectrum. At the same time, it is unlikely that with photoexcitation of PVA in the absorption band it will reveal luminescence. However, the investigations showed that with pulsed irradiation of a polymer film through a UFS-2 light filter ($\lambda_{\text{max}} = 335 \text{ nm}$) in the region $\lambda_{\text{max}} = 460 \text{ nm}$, there arises a wide structureless span of long-lived luminescence, which could be associated with its phosphorescence. This conclusion is based on the results of investigations of energy transfer between polymers and dye molecules. When the temperature of the PVA film is decreased to 77K, the intensity of its phosphorescence increases on the average by a factor of 2, while the rate constant for quenching luminescence decreases from 4.6×10^4 to $1.8 \times 10^4 \text{ sec}^{-1}$. It is interesting that the intensity of the luminescence of the film also depends on its thickness. (11 refs.)

60824 Participation of molecular singlet oxygen in process of accelerated fading of dye mixtures. I.M.Byetev, O.L.Golomb, G.P.Gurinovich, V.V.Karpov.

J. Appl. Spectrosc. (USA), vol.36, no.5, p.540-5 (May 1982). Translation of: *Zh. Prikl. Spektrosk. (USSR)*, vol.36, no.5, p.770-6 (May 1982). [received: Feb. 1983]

It has been established that accelerated fading is more severe when oxygen is present, and research on the kinetics of the processes in solutions with quenching agents indicates that single-excited molecular oxygen $O_2(^1\Delta_g)$ takes part in these processes. Singlet oxygen can be detected in solutions by sensitized luminescence in the 1.27 μm region, corresponding to the $\Delta_g \rightarrow ^3\Sigma_g^-$ transition in the O_2 molecule. The authors report an investigation of the O_2 luminescence sensitization capability of dyes that take part in accelerated fading, this work being further directed toward elucidation of the mechanism of this phenomenon. (17 refs.)

60825 Excitation-frequency dependence of the efficiency of directed nonradiative energy transfer in two-component solid solutions of organic compounds. N.A.Nemkovich, I.M.Gulis, V.I.Tomin.

Opt. & Spectrosc. (USA), vol.53, no.2, p.140-3 (Aug. 1982). Translation of: *Opt. & Spektrosk. (USSR)*, vol.53, no.2, p.239-44 (Aug. 1982). [received: April 1983]

The influence of the excitation frequency on the kinetics of the luminescence spectra and the spectra of the afterglow of solid concentrated polar solutions of phthalimide derivatives has been studied experimentally and theoretically. It has been found that the low-frequency excitation of the systems studied leads to the disappearance of the displacement of the luminescence spectrum with time and the dependence of the duration of the afterglow on the frequency of recording, related to the directed nonradiative transfer of energy through monomeric molecules with nonuniformly broadened electronic levels. It has been shown that the observed regular features are determined by the specific characteristics of the migration of energy in solutions with nonuniformly broadened electronic spectra and are due to the decrease in the efficiency of the directed transfer of energy through the monomeric molecules with decrease in the frequency of the excitation. (14 refs.)

60826 Role of energy migration between monomeric molecules of rhodamine dyes in the concentration quenching of the luminescence of the solutions. S.V.Zhuravlev, L.V.Levshin, A.M.Saetskii, V.I.Yuzhakov.

Opt. & Spectrosc. (USA), vol.53, no.2, p.143-7 (Aug. 1982). Translation of: *Opt. & Spektrosk. (USSR)*, vol.53, no.2, p.245-51 (Aug. 1982). [received: April 1983]

The concentration dependence of the relative yields, durations, and anisotropy of the luminescence of rhodamine dyes in different solvents with different degrees of association has been studied. With allowance for the influence of the diffusion of the molecules on the concentration quenching of the luminescence, it has been shown that for the systems studied, the migration of the excitation energy between monomeric molecules does not lead to quenching of the luminescence. (22 refs.)

60827 Spectral-luminescent properties of phthalimides in aqueous-miscellar solutions of sodium dodecyl sulfate. E.N.Viktorova, T.V.Veselova, M.I.Snegov, A.S.Cherkasov.

Opt. & Spectrosc. (USA), vol.53, no.2, p.148-51 (Aug. 1982). Translation of: *Opt. & Spektrosk. (USSR)*, vol.53, no.2, p.252-7 (Aug. 1982). [received: April 1983]

The absorption-luminescence properties of a series of phthalimides in water and heavy water with the addition of a detergent (sodium dodecyl sulfate) have been studied, and the differences in properties for phthalimides with different structures have been explained. Questions related to the solubilization of the phthalimides in the detergent micelles and the influence of the basic solvent on the luminescence properties of the solubilized molecules have been discussed. (8 refs.)

60828 Picosecond studies of energy transfer of donor and acceptor dye molecules in solution. II. A concentration dependence. P.Y.Lu, Z.X.Yu, R.R.Alfano, J.I.Gersten (Phys. Dept., City Coll. of New York, New York, NY, USA).

Phys. Rev. A (USA), vol.27, no.4, p.2100-9 (April 1983).
For pt.I see *ibid.*, vol.26, p.3610 (1982). The energy transfer between donor and acceptor molecules has been studied by steady-state and picosecond time-resolved spectroscopies in solutions with a given concentration of donor

molecules and different concentrations of acceptor molecules. The rise and decay times of the fluorescence from donor and acceptor molecules were measured. The decrease of the decay times of the donors and the rise time of the acceptors with an increase of the concentration of acceptors observed in the mixed solution indicates a faster energy-transfer rate between the donors and acceptors. Theoretically calculated fluorescence profiles and efficiencies of energy transfer are in agreement with the experimental results. (2 refs.)

60829 Cyclization dynamics of polymers. VII. Applications of the pyrene excimer technique to the internal dynamics of poly(dimethylsiloxane) chains. P.Svirskaya, J.Danheka, A.E.C.Redpath, M.A.Winnik (Dept. of Chem., Univ. of Toronto, Toronto, Ontario, Canada). *Polymer (GB)*, vol.24, no.3, p.319-22 (March 1983). Poly(dimethylsiloxane) (PDMS) polymers end-capped on both ends with pyrene chromophores have been synthesized. Rate constants for end-to-end cyclization (k_1) have been determined for dilute solutions of these polymers in toluene solution using a combination of fluorescence decay and steady-state fluorescence measurements. While precise values of the critical exponent for the chain length (N) dependence of (k_1) are not yet available, these results are consistent with the $N^{-3/2}$ dependence predicted by Wilemski-Fixman theory. PDMS chains cyclize somewhat more than two times faster than polystyrene chains of the same length in solvents of similar solvating power and viscosity. These results provide strong support for similar predictions made several years ago by Perico and Cuniberti (1977) who used intrinsic viscosity data to parametrize the Rouse-Zimm model for analysis of polymer cyclization dynamics. (15 refs.)

60830 Laser induced fluorescence studies of XeF(B-X). H.Helm, D.L.Huestis, D.C.Lorents (Molecular Phys. Lab., SRI Internat., Menlo Park, CA, USA).

Topical Meeting on Excimer Lasers, Incline Village, NV, USA, 10-12 Jan. 1983 (Washington, DC, USA: Opt. Soc. America 1983), p.TuC2/1-3. Describes a method for producing and observing the time dependent decay of specific vibrational levels of the XeF(B1/2) state in order to measure the level dependent radiative lifetimes, B-C mixing rates, vibrational relaxation rates and quenching rates. (2 refs.)

60831 Quenching and formation processes of XeF and Xe₂F excimers. R.Sauerbrey, F.K.Tittel, W.Walter, W.L.Wilson, Jr. (Electrical Engng. Dept., Rice Univ., Houston, TX, USA).

Topical Meeting on Excimer Lasers, Incline Village, NV, USA, 10-12 Jan. 1983 (Washington, DC, USA: Opt. Soc. America 1983), p.TuC5/1-4. Presents details of two- and three-body quenching and formation constant measurements made for electron-beam excited XeF(B,C) and Xe₂F. XeF(C) is identified as the precursor of Xe₂F. (8 refs.)

Evidence that the excited-state geometry of diphenylbutadiene is nearly planar See Entry 60620

Measurement system for temporal response of atomic and molecular systems using the correlation method with pseudorandomly modulated laser light See Entry 60643

Excited states of mixed-ligand chelate complexes of ruthenium(II). A re-examination of the evidence for strong interligand coupling See Entry 60756

Use of luminescence spectra of adducts of europium β -diketonates with methyl-substituted pyridines in interpreting NMR data obtained by the use of lanthanide shift reagents See Entry 60761

Interactions between neutral dissociation and ionization continua in N₂O See Entry 60852

Rate equations analysis of vibrational quenching in IR multiphoton dissociation of pure SF₆ See Entry 60858

The unimolecular reaction of (CH₃)₂CNO following $n \rightarrow \pi^*$ excitation with a tunable dye laser See Entry 60863

Influence of temperature on the photodecomposition of various molecules with the formation of electronically excited fragments See Entry 60868

Vibronic interactions in s-triazine spectra See Entry 60875

Resonance transformation by molecules of polychromatic radiation in the form of a periodic pulse train. Spectral and spectral-time characteristics of secondary radiation See Entry 60880

A complete energy transfer map for COF₂ See Entry 60902

Intramolecular vibrational relaxation: effects on electronic nonradiative relaxation rates See Entry 60915

Laser-induced fluorescence studies of vibrational and rotational relaxation in a supersonic molecular beam of bromine monochloride See Entry 60928

Study of rotational transfer by collision in diatomic molecules See Entry 60930

Influence of hydrogen bonds on electronic spectral shifts of some 9-amino acidines See Entry 61016

A comparison of Raman scattering, resonance Raman scattering, and fluorescence from molecules adsorbed on silver island films See Entry 62971

Radiationless transitions in *p*-terphenyl crystals doped with anthracene, tetracene and pentacene See Entry 63041

Laser photolysis/laser-induced fluorescence study of the reaction of hydroxyl radical with ethylene See Entry 63508

Reactive and inelastic processes involving I₂(D'² Σ^+) with the collision partners CH₄, CH₃Cl, CF₃Cl, and CF₄ See Entry 63524

Solvatochromism of ketocyanines: binary complexes See Entry 63558

Electron-impact excitation of the Cameron system ($a^2\Pi-X^1\Sigma$) of CO See Entry 64369

33.65 PHOTOELECTRON SPECTRA

60832 Vibrationally resolved photoelectron angular distributions for H₂. E.D.Poliakoff, J.L.Dehermer, P.M.Dehermer (Argonne Nat. Lab., Argonne, IL, USA), A.C.Parr.

Chem. Phys. Lett. (Netherlands), vol.96, no.1, p.52-6 (25 March 1983). The photoelectron asymmetry parameter, β , is reported for individual vibrational levels of H₂⁺ ($X^2\Sigma^+$) formed by photoionization of H₂($X^1\Sigma^+$) at wavelengths of 736, 584, 461 and 304 Å. At 584 Å, β exhibits a monotonic increase with vibrational quantum number (decreasing photoelectron kinetic energy) confirming the trend predicted by Itikawa (1979). (47 refs.)

60833 Kinetic energy release distributions in the fragmentation of energy-selected iodopropane ions. W.A.Brand, T.Baer (Dept. of Chem., Univ. of North Carolina, Chapel Hill, NC, USA), C.E.Klots. *Chem. Phys. (Netherlands)*, vol.76, no.1, p.111-20 (1 April 1983). The technique of threshold photoelectron-photoion coincidence (PEPICO) has been employed to determine the average kinetic energy release and the kinetic energy release distribution (KERD) for the iodine loss from 1- and 2-

iodopropane ions as a function of the ion internal energy. The KERDs at all precursor-ion energies investigated (0-3 eV excess energy) have the shape of statistically expected distributions, 1-iodopropane ions which dissociate with an apparent 0.16 eV reverse activation barrier, are shown to isomerize at low energies prior to dissociation, to produce subsequently the 2-propyl C₃H₇⁺ structure. At high energies they may form a different C₃H₇⁺ isomer. The experimentally observed average kinetic energy releases are approximately a factor of 2 greater than expected statistically suggesting that not all vibrational modes participate in the energy disposal. The secondary dissociation of the C₃H₇⁺ isomers to C₃H₃ which is inhibited by a reverse activation barrier of ≈ 0.4 eV indicates that the 1- and 2-iodopropane ions dissociate 75% and 60%, respectively, to form the excited I(²P_{1/2}) atoms. (30 refs.)

60834 UV photoelectron spectra of some transition metal(II) acetylacetonates. S.Kitagawa (Dept. of Chem., Kinki Univ., Higashi-Osaka, Japan), I.Morishima, K.Yoshikawa.

Polyhedron (GB), vol.2, no.1, p.43-6 (1983). The He(I) photoelectron spectra of acetylacetonate (HAA) and its metal complexes, M(II)(AA)₂ (M(II)=Mn, Co, Ni, Cu and Zn), have been measured. These spectra show characteristic metal-dependence, from which the assignment is made. The order of the orbital energy level, $d\pi_2 > n_2 > n_1$, holds for all the complexes reported here. The splitting of these orbitals is found to depend on the central metal ion specifically. (12 refs.)

60835 Use of effective core potentials in perturbation corrections to the Koopmans theorem: vertical ionization potentials of Cl₂, ClN₃, and CINCO. S.R.Langhoff, R.L.Jaffe (NASA Ames Res. Center, Moffett Field, CA, USA), D.P.Chong.

Int. J. Quantum Chem. (USA), vol.23, no.3, p.875-86 (March 1983). (Proceedings of the Fourth International Congress in Quantum Chemistry, Uppsala, Sweden, 13-20 June 1982).

The valence-shell vertical ionization potentials of Cl₂ were calculated by perturbation corrections to the Koopmans theorem using a traditional effective core potential based on a Phillips-Kleinman derivation and an improved effective core potential obtained by Christiansen, Lee, and Pitzer (1979). Comparison of the results with an all-electron calculation demonstrated the reliability of the Christiansen-Lee-Pitzer effective core potential, which was then used to compute the vertical ionization potentials of ClN₃ and CINCO. The results shed new light in the interpretation of the photoelectron spectra of these molecules. (24 refs.)

60836 Benzaldehyde photochemistry studied with laser ionization mass and photoelectron spectroscopy. S.R.Long, J.T.Meek, P.J.Harrington, J.P.Reilly (Dept. of Chem., Indiana Univ., Bloomington, IN, USA).

J. Chem. Phys. (USA), vol.78, no.6, pt.1, p.3341-3 (15 March 1983). Multiphoton ionization has been successfully employed for several years as a molecular spectroscopic tool. In two-step ionization, a molecule is first promoted to an excited electronic state from which it is subsequently ionized. If it dissociates or rearranges following the first step but before the second, the observed mass and photoelectron spectra can be affected. In the course of ionizing benzaldehyde unanticipated spectra are generated, and their description and interpretation provide the subject of this correspondence. (18 refs.)

60837 X-ray photoelectron spectroscopy of cadmium arachidate monolayers on various metal surfaces. F.C.Burns, J.D.Swalen (IBM Res. Lab., San Jose, CA, USA).

J. Phys. Chem. (USA), vol.86, no.26, p.5123-7 (23 Dec. 1982). X-ray photoelectron spectra were measured for a single cadmium arachidate (cadmium eicosonate) monolayer bonded via the carboxylate group to various metal and metal oxide surfaces. Two well-defined peaks were observed in the C 1s spectra of these systems: an intense peak due to ionizations from the CH₂ and CH₃ carbons and a less intense peak due to ionizations from CO₂ carbon. Differences between the binding energies of these two carbon peaks were found to vary with the surface to which arachidate was bonded and these differences are interpreted as arising from differences in the charge transfer between the various surfaces and the arachidate. (15 refs.)

60838 The valence-shell electronic structure and UV photoelectron spectra of the tetrahaloethylenes. A.W.Potts, I.Novak, M.L.Lyus (Dept. of Phys., King's Coll., London, England).

J. Electron Spectrosc. & Relat. Phenom. (Netherlands), vol.31, no.1, p.57-62 (April 1983).

Calculations have been presented recently on the valence-shell electronic structures of C₂Cl₄ and C₂I₄, and by reference to the photoelectron spectra of these molecules valence-shell electronic configurations have been proposed. Using these results and the He(I)/II spectra of C₂Br₄ recorded by Lyus previously (1980), it is possible to test the consistency of the C₂Cl₄ and C₂I₄ assignments by drawing a correlation of photoelectron features for the group C₂Cl₄, C₂Br₄ and C₂I₄ and in this way also to establish assignments for tetrabromoethylene. (10 refs.)

60839 Core electron ionization energies and electronic structure of Ti(NO₃)₄ and Cu(NO₃)₂. P.C.Ford, A.A.MacDowell, I.H.Hillier, C.D.Garner (Dept. of Chem., Univ. of Manchester, Manchester, England).

J. Electron Spectrosc. & Relat. Phenom. (Netherlands), vol.31, no.1, p.75-80 (April 1983).

Gas phase X-ray photoelectron spectra of Ti(NO₃)₄ and Cu(NO₃)₂ are reported and discussed in terms of the molecular charge distributions. No measurable splitting is observed between the 1s ionization energies of the chemically distinct oxygen atoms in either molecule. Ab initio calculations for Cu(NO₃)₂ suggest that this is due in large measure to differential orbital relaxation occurring upon core electron ionization. (20 refs.)

60840 Electronic structure and low-energy photoelectron spectra of 4,4'-disubstituted 2,2'-bipyridines. B.Dobson, I.H.Hillier, J.A.Connor, D.Moncrieff, M.J.Scanlan, C.D.Garner (Chem. Dept., Univ. of Manchester, Manchester, England).

J. Chem. Soc. Faraday Trans. II (GB), vol.79, pt.2, p.295-301 (Feb. 1983). The He I photoelectron spectra of 4,4'-(di-X)-2,2'-bipyridines [X=H, Cl, CH₃, N(CH₃)₂] are reported. The low-energy regions of the spectra arising from orbitals which correlate with the $a_2(\pi)$, $a_1(n_N)$ and $b_1(\pi)$ orbitals of pyridine are assigned using the results of ab initio calculations on pyridine and 2,2'-bipyridine, together with spectra of the 4-substituted pyridines. (9 refs.)

Proceedings of the Third International Conference on 'Vibrations at Surfaces' See Entry 59532

Rydberg series converging to the \bar{C} state of C₆F₆⁺ in threshold photoelectron and VUV absorption spectra of hexafluorobenzene See Entry 60743

X-ray absorption spectra of tetrahedral molecules. Characteristic features of the symmetry of the wave function of the photoelectrons See Entry 60745

Interactions between neutral dissociation and ionization continua in N₂O See Entry 60852

- Rotational intensities in photodetachment and photoionization See Entry 60855
- Resonant multiphoton ionization of H_2 via the $B^2\Sigma_u^+$, $v=7$, $J=2$ and 4 levels with photoelectron energy analysis See Entry 60877
- Photoabsorption and electron yields of La and Gd in the vicinity of the 3d thresholds See Entry 60980
- Effect of the group IV elements on the II anion and cation states of thiophene and furan determined by means of ETS and UPS See Entry 60981

33.70 INTENSITIES AND SHAPES OF MOLECULAR SPECTRAL LINES AND BANDS

- 60841 Band absorption by the spectral lines with a super-Lorentz line shape. M.Hirono, T.Suda (Faculty of Engng., Niigata Univ., Niigata, Japan). *J. Phys. Soc. Jpn. (Japan)*, vol.52, no.4, p.1157-63 (April 1983). The equivalent width of a single line with a super-Lorentz line shape has been expressed in terms of a function $L(x, \eta)$ which reduces to the Ladenburg-Reiche function for the special case of $\eta=2$. Some values of the function $L(x, \eta)$ have been tabulated. Band absorption by the spectral lines with a super-Lorentz line shape has also been calculated from the random model with a constant distribution of line intensities. (10 refs.)
- 60842 Radiative lifetimes and transition moments in MgO . R.N.Differderfer, D.R.Yarkony, P.J.Dagdigan (Dept. of Chem., Johns Hopkins Univ., Baltimore, MD, USA). *J. Quant. Spectrosc. & Radiat. Transfer (GB)*, vol.29, no.4, p.329-31 (April 1983). An experimental and theoretical study of several transitions in the MgO molecule is reported. The radiative lifetime of the MgO $B^1\Sigma^+ v=0$ level is measured to be 32.7 ± 1.7 nsec, while that of the electronic state(s) excited by 372 nm radiation ($d^2\Delta$ and/or $f^2\Pi$) is 11.8 ± 0.5 nsec. The $B-X$ and $A-X$ transition moments are calculated using state averaged multiconfiguration self-consistent field and configuration interaction methods. With an estimate of the $B-A$ transition moment derived from an earlier calculation, the radiative lifetime of the $B^1\Sigma^+ v=0$ level is computed to be 24 nsec. A value of 0.23 msc is calculated for the lifetime of $A^1\Pi v=0$. (23 refs.)
- 60843 Measurement of the pressure broadening and shift of the $asR(0,0)$ line of the $^{15}NH_3$ ammonia v_2 band. M.O.Bulanin, Yu.M.Ladvischenko, E.B.Khodov. *Opt. & Spectrosc. (USA)*, vol.53, no.2, p.119-20 (Aug. 1982). Translation of: *Opt. & Spektrosk. (USSR)*, vol.53, no.2, p.198-201 (Aug. 1982). [received: April 1983] One of the methods for studying the effect of pressure on the parameters of vibration-rotation line contours of molecular gases is the measurement of the absorption by the gas of laser radiation of a frequency ν_l that is close to the frequency ν_0 of the maximum of the line of interest. If the pressures are such that one can ignore Doppler broadening and does not have to consider contributions to the absorption from neighbouring lines, the parameters of the contour can be determined by approximating the dependence of the absorption coefficient $\chi(\text{cm}^{-1})$ on the gas pressure P by some model function. Utilizing the unique example of a simultaneous quasi-coincidence of the frequencies for two gas laser lines they have isolated the vibration-rotation line as $R(0,0)$ of the fundamental band of the $^{15}NH_3$ molecule's v_2 vibration. (12 refs.)
- 60844 Effect of foreign gases on IR absorption bands of polyatomic molecules. N.A.Borisevich, G.A.Zalesskaya, V.A.Lastochkina, T.Shukurov (Inst. of Phys., Acad. of Sci., Minsk, USSR). *Spectrosc. Lett. (USA)*, vol.15, no.12, p.991-1008 (1982). The effect of foreign gases (He, Ar, N_2 and CO_2) on IR vapour absorption bands corresponding to vibrations of different symmetry is studied for some symmetric- and asymmetric-top molecules (chloroform, bromoform, trichloroethylene, chlorobenzene, naphthalene). It is shown that rotational P-, Q- and R-branches collapse and a single structureless bandshape appears when foreign gases are added at no more than 75 atm pressure of CO_2 or 175 atm of N_2 . A conclusion is made that the contour variations in high pressure gas mixtures are satisfactorily interpreted by the J-diffusion model. (24 refs.)
- Theory of electronic structures and lattice distortions in polyacetylene and itinerant Peierls systems. II. Coulomb interaction dependences of the HF ground state, lattice dimerization and 1Bu excited state in regular trans-polyacetylene See Entry 60596
- The low-lying $^2\Sigma$ states of OH See Entry 60604
- Evidence that the excited-state geometry of diphenylbutadiene is nearly planar See Entry 60620
- Satellite structure in the $2p\sigma$ molecular orbital transitions in slow heavy ion collisions See Entry 60626
- Monte Carlo simulation of solvent effects on vibrational and electronic spectra See Entry 60627
- Quantum theory of solvent effects on electronic spectra: Predictions of the exact solution of the mean spherical model See Entry 60628
- Molecular structure and photoelectron spectra of H_2S , H_2Se and H_2Te . Effective core potential calculations on ground and valence ionic states See Entry 60629
- Spectroscopic properties and relaxation processes of impurity molecules in solids. I. Rotational spectra See Entry 60687
- Vibrational state of chemisorbed molecule on metal surface See Entry 60693
- Heterogeneous relaxation of a vibration-excited molecular gas See Entry 60700
- Wavelength dependence of the strengths of the electronic transitions of diatomic molecules See Entry 60703
- $\tilde{A}^1\Pi - \tilde{X}^2\Sigma^+$ infrared electronic transition of C_2H^+ See Entry 60719
- Infrared matrix isolation spectrum of the Si_2C molecule See Entry 60721
- Resonance Rayleigh light scattering of some porphyrins in solution: intensities and depolarization ratios See Entry 60724
- Homogeneous and inhomogeneous vibrational dephasing processes in aqueous thiocyanate solutions See Entry 60729
- Picosecond CARS study of the ν_2 -band of liquid benzene See Entry 60730
- Temperature dependence of the Raman linewidth in H_2^+ See Entry 60733
- The high-resolution visible overtone spectrum of acetylene See Entry 60734
- High resolution absorption cross section measurements and band oscillator strengths of the $(1,0)-(12,0)$ Schumann-Runge bands of O_2 See Entry 60742
- Excited states of mixed-ligand chelate complexes of ruthenium(II). A re-examination of the evidence for strong interligand coupling See Entry 60756

- Multi-dimensional spectroscopy. II. Analysis of 3D lineshapes obtained from stochastic NMR of two level systems See Entry 60757
- Calculation of the electropotential parameters and the absolute intensities of the IR bands of the water molecule and its isotopically substituted derivatives See Entry 60777
- Singlet excited-state 'energy hopping' in alkylbenzenes See Entry 60784
- Excited-state relaxation in 1-amino-8-naphthalene sulphonate See Entry 60787
- Lifetimes in the $B^2\Pi$ state and the heat of formation of NCO See Entry 60788
- Radiative decay rates from deperturbed $V=0-7$ vibrational levels of CO $A^1\Pi$ measured using synchrotron radiation See Entry 60797
- Observation of the asymmetric O-U-O stretch in the vibronic absorption spectrum of uranyl formate monohydrate See Entry 60798
- The effect of solvent environment on molecular electronic transition moment directions: symmetry lowering in pyrene See Entry 60799
- Spectroscopy of large molecular complexes in supersonic jets See Entry 60800
- Luminescence of the excited mercury diethylamine complex. Attachment by ligand exchange See Entry 60806
- Temperature dependence of the nonradiative relaxation process of the lowest excited singlet states of meso-substituted bromoanthracenes See Entry 60820
- Fluorescence branching ratios from the $A^2\Sigma^+(v=0)$ state of NO See Entry 60821
- Laser induced fluorescence studies of $XeF(B-X)$ See Entry 60830
- The line shape of a zero-field level-crossing effect in methyl fluoride See Entry 60847
- Interaction between high-intensity arbitrarily polarized radiation and molecules under collisional relaxation conditions See Entry 60850
- Auger spectra of tetrahedral halides and hydrides See Entry 60853
- Rotational intensities in photodetachment and photoionization See Entry 60855
- Precision measurements of hyperfine predissociation in I_2 vapor using a two-photon resonant scattering technique See Entry 60856
- Photodissociation of CO_3 : evidence for a long-lived excited state See Entry 60859
- Multiphoton dissociation of $OCCl_2$ at 193 nm: formation of electronically excited Cl_2 See Entry 60862
- Systematics in two-photon rovibrational contours of $14_0^1(B_{2u}-A_{1g})$ in benzene derivatives See Entry 60878
- Comparison of the Floquet and rotating-wave methods for multiphoton excitation of SF_6 See Entry 60879
- A complete energy transfer map for COF_2 See Entry 60902
- Spectral evidence of line collisional interference in NH_3 inversion spectrum See Entry 60908
- Collision dynamical information from pressure broadening measurements: Application to carbon monoxide See Entry 60921
- Influence of hydrogen bonds on electronic spectral shifts of some 9-amino acridines See Entry 61016
- Induced isotropic scattering from liquid carbon dioxide See Entry 63007

33.80 PHOTON INTERACTIONS WITH MOLECULES

- 60845 SCF discrete-variational $X\alpha$ calculations of the NH_4Cl Auger spectrum. G.M.Mikhailov, G.L.Gutsev, Ju.G.Borod'ko (Inst. of Chem. Phys., Acad. of Sci., Chernogolovka, USSR). *Chem. Phys. Lett. (Netherlands)*, vol.96, no.1, p.70-5 (25 March 1983). Formalism for calculations of the singlet and triplet Auger energies within the $X\alpha$ model is presented. Using this method the KVV Auger spectrum of NH_4Cl is calculated and the theoretical intensities are determined within a one-center approximation. The calculated spectrum reproduces quite well all the main features observed for solid NH_4Cl . A new interpretation of the spectrum is suggested. (24 refs.)
- Time-resolved study of the laser optogalvanic effect in I_2 See Entry 60775
- Light-induced collisions involving molecules without change in the chemical bonds See Entry 60907
- Non-dipole excitation of core holes by electron impact. Multiplet splitting in CO and N_2 See Entry 60999
- System for identification of individual components in mixtures on the basis of Shpol'skii spectra See Entry 63623

33.80B Level crossing and optical pumping

- 60846 On the statistics of an ensemble of oscillators under excitation. IV. Evaluation of the time for kinetic excitation into the quasicontinuum based on Kramers' theory. V.N.Sazonov, I.E.Khromov (Dept. of Theoretical Phys., P.N. Lebedev Phys. Inst., Moscow, USSR). *Chem. Phys. (Netherlands)*, vol.76, no.1, p.25-9 (1 April 1983). For pt.III see ibid., vol.69, no.3, p.459 (1982). The authors consider the model with kinetic excitation into the quasicontinuum (KEQ) for resonant polyatomic molecules which absorb laser radiation and are surrounded by buffer molecules. KEQ takes place when the resonant molecules in the lower part of the energy spectrum interact weakly with the laser radiation, but the molecules in the quasicontinuum are rapidly excited to still higher energy and dissociate. Under these conditions the collisions of the resonant and buffer molecules lead to excitation of resonant molecules into the quasicontinuum because the population of the quasicontinuum is much less than its thermodynamical equilibrium value. The smaller the V-T relaxation time τ_{VT} , the larger the rate of KEQ and the dissociation rate (if only τ_{VT} is not too small). Thus, if they change the experimental conditions and decrease τ_{VT} (for instance, by passing from the heavy buffer gas Xe to the light buffer gas He), for some resonant molecules they may observe that the probability of dissociation increases. (20 refs.)
- 60847 The line shape of a zero-field level-crossing effect in methyl fluoride. S.T.Sandholm, R.H.Schwendeman (Dept. of Chem., Michigan State Univ., East Lansing, MI, USA). *J. Chem. Phys. (USA)*, vol.78, no.6, pt.2, p.3476-82 (15 March 1983). The line shape of the zero-field level-crossing effect that occurs when $^{13}CH_3F$ is irradiated by the 9P(32) CO_2 laser has been recorded by an infrared laser

Stark spectrometer operating under computer control. The level-crossing effect, which occurs as a narrow decrease in the absorption due to superposition of the m components of the Doppler-broadened $R(4,3)$ transition in the n_2 band, has been recorded at several pressures. Comparison of the experimental line shapes with theoretically calculated curves leads to a value of 13.9 ± 0.9 MHz/Torr for the pressure broadening parameter for this transition. An algebraic solution is given for the linear system that occurs in the density matrix treatment of the steady state line shape of a level crossing or level anticrossing effect. The modifications of the solution required to treat three-level double resonance or two-photon effects are also given. (32 refs.)

60848 Comparison of quantal, classical, and semiclassical behavior at an isolated avoided crossing. D.W.Noid (Oak Ridge Nat. Lab., Oak Ridge, TN, USA), M.L.Koszykowski, R.A.Marcus.

J. Chem. Phys. (USA), vol.78, no.6, pt.2, p.4018-24 (15 March 1983). The quantal and classical/semiclassical behavior at an isolated avoided crossing are compared. While the quantum mechanical eigenvalue perturbation parameter plots exhibit the avoided crossing, the corresponding primitive semiclassical eigenvalue plots pass through the intersection. Otherwise, the eigenvalues agree well with the quantum mechanical values. The semiclassical splitting at the intersection is calculated from an appropriate Fourier transform. In this quasiperiodic regime, a quantum state near an avoided crossing is seen to exhibit typically more delocalization than the classical state. However, trajectories near the 'separatrix' display a quasiperiodic 'transition' between two zeroth order classical states. (20 refs.)

60849 Stimulated emission from the $A^1\Sigma_u^+$ band of sodium dimer. H.Itoh (Dept. of Phys., Kagawa Univ., Takamatsu, Japan), Y.Fukuda, H.Uchiki, K.Yamada, M.Matsuoka.

J. Phys. Soc. Jpn. (Japan), vol.52, no.4, p.1148-56 (April 1983). Intense stimulated emission from sodium vapor is observed at around 800 nm when it is pumped by a pulsed dye laser around 600 nm. The spectral lines are localized around 800 nm. To investigate the origin of this emission, the authors try to assign the stimulated lines excited by a dye laser at 632.8 nm (the wavelength of the He-Ne laser) and by a ruby laser at 694.3 nm. Moreover, the $A^1\Sigma_u^+$ transitions at 595.728 and 594.664 nm of a Na_2 which are newly assigned by using polarization labelling spectroscopy are excited by the output from a CW-dye-laser amplified with N_2 laser-pumped dye amplifier, and some of the stimulated lines are assigned. It is then concluded that the origin of these stimulated emission lines is the $A^1\Sigma_u^+$ transition. Also it can be explained that these stimulated lines come from around the band edge of the $A^1\Sigma_u^+$ transition.

60850 Interaction between high-intensity arbitrarily polarized radiation and molecules under collisional relaxation conditions. K.A.Nasyrov, A.M.Shalagin (Inst. of Automation & Electrometry, Acad. of Sci., Novosibirsk, USSR). *Sov. J. Quantum Electron. (USA)*, vol.12, no.10, p.1298-303 (Oct. 1982). Translation of: *Kvantovaya Elektron., Moskva (USSR)*, vol.9, no.10, p.1997-2007 (Oct. 1982). [received: April 1983]

Rate equations for the density matrix are used to describe classically the orientational states of the angular momenta of levels and are solved for arbitrary intensities and polarizations. Allowances are made for collisions which alter the velocity, orientation, and magnitude of the angular momentum, and also the quantum number of a molecular vibrational state. Expressions are derived for the polarization of the medium in the case of homogeneously and inhomogeneously broadened lines. An analysis is made of the polarization dynamics of high-intensity radiation (deformation and rotation of the polarization ellipse) during its propagation in amplifying (absorbing) media. (6 refs.)

Electric dipole moments of excited vibrational levels in the $\tilde{X}1A_1$ state of formaldehyde by stimulated emission spectroscopy See Entry 60780

Rotational relaxation in ground-state p -difluorobenzene: State selection by stimulated emission pumping See Entry 60815

Multiphoton dissociation of a rotating molecule See Entry 60857

Optical multiple pulse sequences for multiphoton selective excitation and enhancement of forbidden transitions See Entry 61245

Reactive and inelastic processes involving $I_2(D^1\Sigma_u^+)$ with the collision partners CH_4 , CH_3Cl , CF_3Cl , and CF_4 See Entry 63524

33.80E Autoionization, photoionization, and photodetachment

60851 Subpicosecond time resolved multiphoton ionization: excited state dynamics of cis-stilbene under collision free conditions. B.I.Greene, R.C.Farrow (Bell Lab., Murray Hill, NJ, USA).

J. Chem. Phys. (USA), vol.78, no.6, pt.1, p.3336-8 (15 March 1983). The authors report the result of a novel subpicosecond measurement performed on cis-stilbene in the vapor phase. They have extended a well-known pulsed laser technique into the 10^{-13} s time regime, and choose to focus renewed scientific attention on the dynamics of stilbene photoisomerization. They believe this measurement will establish the technique of gas phase multiphoton ionization as a viable and potentially powerful subpicosecond probe of intramolecular dynamics. An intense visible subpicosecond laser pulse is utilized to probe, via multiphoton ionization, a population of excited state cis-stilbene molecules. (15 refs.)

60852 Interactions between neutral dissociation and ionization continua in N_2O . P.M.Guyon, T.Baer, I.Nenner (LURE, Lab. CNRS, Univ. Paris-Sud, Orsay, France).

J. Chem. Phys. (USA), vol.78, no.6, pt.2, p.3665-72 (15 March 1983). Autoionized Rydberg states converging to the $A^2\Sigma^+$ and $B^2\Pi$ states of N_2O^+ are shown to be predissociated into neutral fragments. The decay to excited neutral fragments is observed by their fluorescence in the visible and ultraviolet regions of the spectrum. These decay channels are in competition with autoionization, which was shown in a previous study to yield unexpectedly large numbers of low energy electrons. On the basis of the striking similarity between the fluorescence excitation and the threshold photoelectron spectra, models are presented which connect dissociative channels to the production of threshold electrons. Ionization of dissociating neutral states and Rydberg states converging to the ground electronic state of $N_2O^+(X^2\Pi)$ are suggested as being responsible for the production of low energy electrons. The distribution of photoelectron energies resulting from such autoionization channels are calculated. (35 refs.)

60853 Auger spectra of tetrahedral halides and hydrides. R.R.Rye, J.E.Houston (Sandia Nat. Labs., Albuquerque, NM, USA).

J. Chem. Phys. (USA), vol.78, no.7, p.4321-30 (1 April 1983). Auger electron spectra are presented for the gas-phase molecular species CF_4 , SiF_4 , CCl_4 , and $SiCl_4$ and discussed in terms of the effect of the interaction of the two final-state holes on the spectral line shapes. The highly polar character of the bonding for this series leads to systematic behavior with respect to this hole-hole interaction, showing rare gas-like localized halide

spectra for SiF_4 and a delocalized component of increasing intensity as the authors proceed through the series to $SiCl_4$, CF_4 , and CCl_4 . The central atom spectra show a composite line shape resulting from the sum of two versions of the same one-electron final states but with different values of U (the hole-hole interaction energy). The Auger process occurs as a result of the electron density available at the central atom site but, since the one-electron orbitals are highly polarized towards the halide, the two holes principally appear around the halide sites. With both holes on the same halide site a rather large U results, but with the two holes on separate halide sites one obtains a reduced value of U . The relative intensity of the smaller U component appears to increase as we proceed through the series SiF_4 , $SiCl_4$, CF_4 , and CCl_4 . This tendency in both the halide spectra and in the central atom spectra depends on the strength of the intersite interaction. The molecular parameter which seems most reasonable to predict this division between localized and delocalized behavior is the ratio of the halide-halide distance to the halide radius. In addition, the authors demonstrate that for a rather extended series of molecular species the trends in the value of U can be predicted surprisingly well on the basis of an experimental value of U for Ne and the known atomic and molecular dimensions. The implications of this simple predictive capability to other molecular systems is discussed. (40 refs.)

60854 Stepwise photoionization of anthracene in the gas phase by ultraviolet laser pulses. G.A.Abakumov, B.I.Polyakov, A.P.Simonov, L.S.Chuiko, V.T.Yaroslavtsev.

Opt. & Spectrosc. (USA), vol.53, no.2, p.151-3 (Aug. 1982). Translation of: *Opt. & Spektrosk. (USSR)*, vol.53, no.2, p.258-62 (Aug. 1982). [received: April 1983]

A quantitative study of two-photon stepwise ionization of anthracene in the gas phase is reported. The cross sections for the ionization of the excited singlet and triplet anthracene molecules were measured at various wavelengths of the exciting and ionizing beams. The results show that these cross sections depend on the amount of vibrational energy in the excited molecules for a given value of the total energy imparted to the molecules in the course of the two-step ionization. (6 refs.)

60855 Rotational intensities in photodetachment and photoionization. P.A.Schulz, R.D.Meard, W.C.Lineberger (Dept. of Chem., Univ. of Colorado, Boulder, CO, USA).

Phys. Rev. A (USA), vol.27, no.4, p.2229-32 (April 1983).

The authors extend the work on the frame-transformation method to give an analytic form for the relative intensities of rotational transitions in photodetachment and photoionization. The specific case of photoabsorption by a Σ species, resulting in a $^1\Pi$ species and an s electron, is treated analytically. The results are in good agreement with both threshold photodetachment cross sections and photoelectron spectra. (16 refs.)

Theoretical study of the lowest $^1\Sigma_g^+$ doubly excited state of H_2 See Entry 60584

Molecular beam study of photoionization of uranium and uranium oxide See Entry 60670

Real-time multiphoton ionization detection of iodine atoms produced by infrared multiphoton dissociation of perfluoroalkyl iodides See Entry 60680

Rydberg-Rydberg transitions of NO using an optical-optical double resonance multiphoton ionization technique See Entry 60768

Kinetic energy release distributions in the fragmentation of energy-selected iodopropane ions See Entry 60833

Benzaldehyde photochemistry studied with laser ionization mass and photoelectron spectroscopy See Entry 60836

Site-specific fragmentation of small molecules following soft-X-ray excitation See Entry 60870

Vibronic interactions in s-triazine spectra See Entry 60875

Two-photon ionization. Capability of lasers for trace analysis See Entry 60876

Resonant multiphoton ionization of H_2 via the $B^1\Sigma_u^+$, $v=7$, $J=2$ and 4 levels with photoelectron energy analysis See Entry 60877

Systematics in two-photon rovibrational contours of 14_0 ($^1B_{2u}$ - $^1A_{1g}$) in benzene derivatives See Entry 60878

Supersonic copper clusters See Entry 61043

33.80G Diffuse spectra; predissociation, photodissociation

60856 Precision measurements of hyperfine predissociation in I_2 vapor using a two-photon resonant scattering technique. R.E.Tench, S.Ezekiel (Res. Lab. of Electronics, MIT, Cambridge, MA, USA).

Chem. Phys. Lett. (Netherlands), vol.96, no.2, p.253-8 (1 April 1983).

A two-photon resonant scattering technique is used to measure natural line-widths of individual hyperfine components of the $v'=43$, $J'=12$ and 16 rovibrational levels in the I_2 B state ($^3\Pi_{0g^+}$). Differences in the linewidths due to hyperfine predissociation are precisely determined. The predissociation constants and the radiative linewidth for $v'=43$ are found to be $|d_v|^2 = 3.36 \pm 0.09$ kHz, $|c_v|^2 = 4.67 \pm 0.51$ Hz and $\Gamma_r = 51 \pm 4$ kHz, respectively. (17 refs.)

60857 Multiphoton dissociation of a rotating molecule. C.Bottcher (Phys. Div., Oak Ridge Nat. Lab., Oak Ridge, TN, USA), C.Feillade.

Chem. Phys. Lett. (Netherlands), vol.96, no.3, p.279-83 (8 April 1983). A formalism is outlined for multiphoton pumping and dissociation within a molecular rotational-vibrational ladder. The density matrix is expanded in spherical tensors, leading to a set of Bloch equations which take full account of the rotational degeneracy of the levels. Time-dependent solutions of these 'ladder' equations are analyzed in terms of normal modes, providing fresh insight into the mechanism of dissociation. (12 refs.)

60858 Rate equations analysis of vibrational quenching in IR multiphoton dissociation of pure SF_6 . Hai-Lung Dai (Dept. of Chem., Univ. of California, Berkeley, CA, USA).

Chem. Phys. Lett. (Netherlands), vol.96, no.3, p.324-7 (8 April 1983).

A rate equations model was used to calculate the pressure dependence of SF_6 multiphoton dissociation yields caused by vibrational self-quenching. Between 1000 and 3000 cm^{-1} of energy is removed from SF_6 excited to ≥ 60 kcal/mole by collision with a cold SF_6 molecule at gas kinetic rate. Calculations have shown that the fluence dependence of dissociation varies strongly with pressure, and the decrease of dissociation at higher pressures can be approximated exponentially only for narrow pressure ranges. (18 refs.)

- 60859 Photodissociation of CO_2^- : evidence for a long-lived excited state.** D.E.Huntton, M.Hofmann, T.G.Lindeman, A.W.Castleman, Jr. (Dept. of Chem., Pennsylvania State Univ., University Park, PA, USA). *Chem. Phys. Lett. (Netherlands)*, vol.96, no.3, p.328-32 (8 April 1983). Energy analysis of the photofragment O^- ions produced in the photodissociation reaction $\text{CO}_2^- + h\nu \rightarrow \text{O}^- + \text{CO}_2$ identifies two distinct O^- production mechanisms: a two-photon absorption via an intermediate bound electronic state, and a collision-assisted single-photon process via a long-lived excited state. This species has a radiative lifetime exceeding one microsecond, and a collisional dissociation cross section measurably higher than that of the ground state. (19 refs.)
- 60860 The state distribution of OH radicals photodissociated from H_2O_2 at 193 and 248 nm.** G.Ondrey, N.van Veen, R.Bersohn (Dept. of Chem., Columbia Univ., New York, NY, USA). *J. Chem. Phys. (USA)*, vol.78, no.6, pt.2, p.3732-7 (15 March 1983). Photodissociation of H_2O_2 at 248 and 193 nm yields largely vibrationless OH radicals in their ground electronic state. At 248 nm, on the average about 64 and 3 kcal/mol of energy are released as translational and rotational energy, respectively. At 193 nm the corresponding quantities are 92 and 8 kcal/mol. The distribution of the OH radicals over K'' peaks near $K''=5$ when dissociated at 248 nm and near $K''=6$ at 193 nm but the latter distribution is somewhat broader. Doppler width anisotropy data imply that at 248 nm a single upper state is reached but that at 193 nm several upper surfaces may be responsible for the absorption. It is concluded that the upper state potential functions(s) may be represented by the sum of a large repulsive term depending only upon the distance between centers of mass of the OH radicals and a small angularly dependent term which generates the rotational excitation. (25 refs.)
- 60861 Infrared photodissociation of sulfur dioxide ions in a fast ion beam.** H.Stein, M.Erben-Russ, K.L.Kompa (Max-Planck-Inst. für Quantenoptik, Garching, Germany). *J. Chem. Phys. (USA)*, vol.78, no.6, pt.2, p.3774-8 (15 March 1983). A laser-ion beam apparatus for studying laser-induced photodissociation and fragmentation of fast molecular ions in both coaxial and crossed beams configurations has been constructed. IR photodissociation of highly internally excited SO_2^+ ions is reported using a low power cw CO_2 laser. The fragmentation of SO_2^+ into $\text{SO}^+ + \text{O}$ and $\text{S}^+ + \text{O}_2$ has been observed and the relative dissociation yields as function of laser frequency and power dependence of the two dissociation channels have been measured. No IR photodissociation could be observed for SO^+ and SO_3^+ at 934.9 cm^{-1} . (24 refs.)
- 60862 Multiphoton dissociation of OCCl_2 at 193 nm: formation of electronically excited Cl_2 .** M.W.Wilson, M.Rothschild, C.K.Rhodes (Dept. of Phys., Univ. of Illinois, Chicago, IL, USA). *J. Chem. Phys. (USA)*, vol.78, no.6, pt.2, p.3779-84 (15 March 1983). Two-quantum excitation of OCCl_2 with 193 nm radiation, although corresponding to an energy above the ionization limit, is observed to produce a yield upon dissociation into excited neutral fragments; namely, CO in the $\nu=7$ of its $X^1\Sigma^+$ state and Cl_2 in the first electronically excited Cl_2^* and Cl_2^+ states of ionic character. Strong emissions originating from Cl_2^* were observed at 199 and 258 nm together with a weaker band at 244 nm. The radiative lifetime τ_r of the $\text{Cl}_2^*(\text{Cl}_2^*)$ state was determined to be $\tau_r=23\pm 2$ ns. Quenching rate constants of the $\text{Cl}_2^*(\text{Cl}_2^*)$ level by rare gases were also measured. Strong enhancement of the 258 nm radiation was observed in the presence of He and Ne, while intense emissions from KrCl^* and XeCl^* indicate the role of atomic displacement reactions of the type $\text{Cl}_2^* + (\text{Kr/Xe}) \rightarrow (\text{Kr/Xe})\text{Cl}^* + \text{Cl}$. (30 refs.)
- 60863 The unimolecular reaction of $(\text{CH}_3)_2\text{CNO}$ following $n-\pi^*$ excitation with a tunable dye laser.** H.Reisler, F.B.T.Pessine, Y.Haas, C.Wittig (Univ. of Southern California, Los Angeles, CA, USA). *J. Chem. Phys. (USA)*, vol.78, no.6, pt.2, p.3785-91 (15 March 1983). The predissociation of $(\text{CH}_3)_2\text{CNO}$ following the 570-710 nm laser excitation of the $n-\pi^*$ transition is reported. The small fluorescence quantum yield and its short lifetime (<20 ns) indicate efficient radiationless processes prior to dissociation. NO is the major dissociation product and its concentration was monitored in real time by using the two-photon laser excited fluorescence technique. The NO yield as a function of wavelength followed very closely the absorption contours of $(\text{CH}_3)_2\text{CNO}$. The NO production rate was $>10^6 \text{ s}^{-1}$ at all wavelengths studied and this rate is too fast to be consistent with a mechanism involving a radiationless transition to the ground electronic state followed by energy randomization and dissociation. Alternative predissociation mechanisms are considered. (37 refs.)
- 60864 Competing dissociation channels in the infrared multiphoton decomposition of ethyl vinyl ether.** F.Huisken, D.Krajnovich, Z.Zhang, Y.R.Shen, Y.T.Lee (Materials & Molecular Res. Div., Lawrence Berkeley Lab., Berkeley, CA, USA). *J. Chem. Phys. (USA)*, vol.78, no.6, pt.2, p.3806-15 (15 March 1983). Infrared multiphoton decomposition of ethyl vinyl ether (EVE) has been investigated by the crossed laser-molecular beam technique. Competition is observed between the two lowest-energy dissociation channels: (1) $\text{EVE} \rightarrow \text{CH}_3\text{CHO} + \text{C}_2\text{H}_4$, and (2) $\text{EVE} \rightarrow \text{CH}_2\text{CHO} + \text{C}_2\text{H}_5$. Center-of-mass product translational energy distributions were obtained for both dissociation channels. The products of reactions (1) and (2) are formed with mean translational energies of 31 and 5 kcal/mol, respectively. The branching ratio shifts dramatically in favor of the higher energy radical producing channel as the laser intensity and energy fluence are increased, in agreement with the qualitative predictions of statistical unimolecular rate theory. (24 refs.)
- 60865 Rotational predissociation of the Ar.HCl van der Waals complex: close-coupled scattering calculations.** C.J.Ashton, M.S.Child (Theoretical Chem. Dept., Oxford Univ., Oxford, England), J.M.Hutson. *J. Chem. Phys. (USA)*, vol.78, no.6, pt.2, p.4025-39 (15 March 1983). The authors report an extensive computational study of rotationally predissociating metastable states of the Ar.HCl van der Waals complex, using a highly realistic empirical intermolecular potential recently proposed by Hutson and Howard (1982). The states are characterized by fully converged, close-coupled, scattering calculations. Resonance energies, widths, and partial widths are extracted by fitting the energy dependence of S matrices. Total angular momenta of 0 and 1 are studied, and the calculations span an energy range from 0 to 1400 cm^{-1} . The resonance widths vary from $<10^{-4}$ to $>5 \text{ cm}^{-1}$, and it is shown that the isolated narrow resonance approximation calculations enables assignment of approximate quantum numbers to the metastable states. Physical explanations are suggested for the strong trends in resonance parameters as a function of the intermolecular stretching, diatom rotation, and molecule-fixed angular momentum projection quantum numbers. A changeover from a near-molecular-fixed to a near-space-fixed coupling scheme, as angular momentum is increased, is clearly demonstrated. The results are of considerable relevance to the design of experiments and the development of approximate computational methods in this area. (50 refs.)
- 60866 Predissociation of HD-Ar van der Waals molecules by internal rotation.** J.M.Hutson, R.J.Le Roy (Guelph-Waterloo Centre for Graduate Work in Chem., Univ. of Waterloo, Waterloo, Ontario, Canada). *J. Chem. Phys. (USA)*, vol.78, no.6, pt.2, p.4040-3 (15 March 1983). Accurate close-coupling calculations of level energies and widths of predissociating levels of HD-Ar have been carried out using the Le Roy-Carley BC_3 potential (1980) for H_2 -Ar. The calculated widths agree well with the experimental data of McKellar (1982). The principal product from predissociation of $\text{HD}(\nu=1, j=2) \rightarrow \text{R}$ is HD in its $\nu=1, j=1$ state. This channel is symmetry forbidden for $\text{H}_2(1,2)$ -Ar, and its presence accounts for the much larger spectroscopic linewidths found for HD-Ar. (14 refs.)
- 60867 Photodissociation of NH_3 at 106-200 nm.** M.Suto, L.C.Lee (Dept. of Electrical & Computer Engng., San Diego State Univ., San Diego, CA, USA). *J. Chem. Phys. (USA)*, vol.78, no.7, p.4515-22 (1 April 1983). Cross sections and quantum yields of emissions from the photofragments of NH_3 were measured in the 106-200 nm region using synchrotron radiation as a light source. The emission systems of NH_2 ($A^2A_1 \rightarrow X^2B_1$), $\text{NH}(c^1\Pi \rightarrow a^1\Sigma^+)$, and $\text{NH}(b^1\Sigma^+ \rightarrow X^2\Sigma^+)$ were observed from the NH_3 photodissociation. The dependences of emission intensities on the NH_3 and/or He (buffer gas) pressures were studied. The $\text{NH}(c \rightarrow a)$ and $\text{NH}(b \rightarrow X)$ emissions were observed when the $\text{NH}_2(A^2A_1)$ species was quenched by 10 Torr of He. The $\text{NH}(b \rightarrow X)$ and $\text{NH}(c \rightarrow a)$ emissions start to appear at 182.3 ± 1.5 and 127.9 ± 0.9 nm, respectively. From these emission thresholds the threshold energy for photodissociation of NH_3 into $\text{NH}(X^2\Sigma^+) + \text{H}_2(X^1\Sigma^+)$ is determined to be 4.17 ± 0.06 eV, and the upper limit for the heat of formation of NH is 3.81 ± 0.06 eV. For excitation wavelengths longer than 128 nm the $\text{NH}(b^1\Sigma^+)$ species is produced by a primary photodissociation process, and at shorter excitation wavelengths the $\text{NH}(b^1\Sigma^+)$ may be partly produced by a cascading process following the $\text{NH}(c \rightarrow b)$ transition. Contrary to previous theoretical interpretations, all the vibronic levels of the NH_3 (B and C) states produce the $\text{NH}_2(A \rightarrow X)$ emission. The quantum yield for the C state is lower than that of the B state. The vibronic levels of the C state are renumbered in accordance with their quantum yields. (38 refs.)
- 60868 Influence of temperature on the photodecomposition of various molecules with the formation of electronically excited fragments.** I.P.Vinogradov, V.V.Firsov. *Opt. & Spectrosc. (USA)*, vol.53, no.1, p.26-8 (July 1982). Translation of: *Opt. & Spektrosk. (USSR)*, vol.53, no.1, p.46-50 (July 1982). [received: April 1983]. The photolysis of NH_3 I and N_2H_4 II molecules at room temperature and at elevated temperatures has been studied. The absolute cross sections of the decomposition of I and II into electronically excited fragments in the range from the threshold to 90 nm have been determined at these temperatures. It has been established that there is a marked increase in the cross section of formation of $\text{NH}(A^2\Pi)$ and $\text{NH}_2(A^2A_1)$ in the photolysis of II with increase in temperature. Possible mechanisms of this phenomenon have been discussed. (9 refs.)
- 60869 Saturation laser photodissociation of a gas of diatomic molecules.** M.A.Vaksman. *Opt. & Spectrosc. (USA)*, vol.53, no.2, p.154-7 (Aug. 1982). Translation of: *Opt. & Spektrosk. (USSR)*, vol.53, no.2, p.263-9 (Aug. 1982). [received: April 1983]. Saturation photodissociation is analyzed theoretically. The heat of reaction and the scale time for the relaxation to a steady-state distribution are calculated. An equation relating the local densities of atoms and molecules during the dissociation is found. A method is proposed for finding the steady-state spatial distribution of atoms in the absence of diffusion, for slow diffusion, and also for very rapid diffusion. A solution is derived for an arbitrary diffusion coefficient in a particular case. The stability of the steady-state distribution is analyzed. (12 refs.)
- 60870 Site-specific fragmentation of small molecules following soft-X-ray excitation.** W.Eberhardt (Dept. of Phys., Brookhaven Nat. Lab., Upton, NY, USA), T.K.Sham, R.Carr, S.Krummacher, M.Strongin, S.L.Weng, D.Wesner. *Phys. Rev. Lett. (USA)*, vol.50, no.14, p.1038-41 (4 April 1983). Soft-X-ray excitation involving C 1s electrons in CO and acetone, $(\text{CH}_3)_2\text{CO}$, is found to result in ionic fragmentation of the original molecule. The fragmentation pattern changes whether the C 1s electron gets ionized or excited into a Rydberg-line orbital or into an antibonding π^* molecular orbital. Moreover, the fragmentation occurs specifically around the site of the carbon atom where the optical excitation takes place. Based on these observations one might consider the use of tunable soft X-rays to stimulate chemical reactions or to selectively break large organic molecules. (15 refs.)
- 60871 Laser spectroscopy on ion beams: application to the polyatomic ion N_2O^+ .** M.Dufay (Lab. de Spectrometrie Ionique et Moleculaire, Univ. Lyon-I, Lyon, France). *Rev. Cethedec (France)*, vol.19, no.NS82-2, p.97-111 (1982). In French. Presents a photodissociation study of a highly accelerated molecular ion beam by interaction with collinear laser radiation. The development of a high resolution spectroscopy method using nonoptical detection is described. The hyperfine structure of N_2O^+ is studied in its $A^2\Sigma^+$ state. (11 refs.)
- 60872 Analysis of multistage dissociation of polyatomic molecules.** V.M.Akulov, N.V.Karlov, A.M.Prokhorov (P.N. Lebedev Phys. Inst., Acad. of Sci., Moscow, USSR). *Sov. J. Quantum Electron. (USA)*, vol.12, no.10, p.1274-6 (Oct. 1982). Translation of: *Kvantovaya Elektron., Moskva (USSR)*, vol.9, no.10, p.1955-9 (Oct. 1982). [received: April 1983]. Simple models are used to investigate the laws governing the behavior of molecules near the dissociation limit on exposure to high-power laser radiation. It is shown that anomalous dependences of the dissociation probability on the laser radiation intensity may be observed for some molecules. (2 refs.)
- 60873 Photodissociation of Xe_2^+ and Kr_2^+ in the ultraviolet.** A.W.McCown, M.N.Ediger, S.M.Stazak, J.G.Eden (Univ. of Illinois, Urbana, IL, USA). *Topical Meeting on Excimer Lasers, Incline Village, NV, USA, 10-12 Jan. 1983* (Washington, DC, USA: Opt. Soc. America 1983), p.TuC3/1-4. Describes an optical method which has been developed for detecting Xe_2^+ and Kr_2^+ in real-time by photodissociating these ions in the ultraviolet with a UV (XeF or N_2) laser. (2 refs.)
- 60874 Multiphoton dissociation of phosgene (OCCl_2) at 193 nm: formation of electronically excited Cl_2^* .** M.W.Wilson, M.Rothschild, C.K.Rhodes (Dept. of Phys., Univ. of Illinois, Chicago, IL, USA). *Topical Meeting on Excimer Lasers, Incline Village, NV, USA, 10-12 Jan. 1983* (Washington, DC, USA: Opt. Soc. America 1983), p.WB4/1-8. Reports the observation of electronically excited Cl_2 upon dissociation of phosgene. Evidence for the formation of neutral fragments arising from states embedded in the ionization continuum is also discussed. (17 refs.)

- Photochemical formation and dissociation of molybdenum-dinitrogen complexes in krypton matrices See Entry 60717
- The infrared absorption spectra of $(\text{HCCH})_2$ and $(\text{DCCD})_2$ See Entry 60718
- Observation of levels near dissociation in the $X^1\Sigma_g^+$ state of $^7\text{Li}_2$ See Entry 60803
- IR laser induced loss of fluorescence in $\text{UO}_2(\text{hfacac})_2\text{TMP}$. I. Real time detection of multiple photon excitation of the ground electronic state See Entry 60807
- Interactions between neutral dissociation and ionization continua in N_2O See Entry 60852
- Vibrational predissociation and intramolecular vibrational relaxation in electronically excited s-tetrazine-argon van der Waals complex See Entry 60914
- Photofragmentation of CH_3I , CD_3I and CF_3I . Formation of $\text{I}(^2P_{1/2})$ as a function of wavelength See Entry 63576
- Atomic nitrogen emissions from photodissociation of N_2 See Entry 64236

33.80K Multiphoton processes

- 60875 Vibronic interactions in s-triazine spectra. G.Fischer, B.Katz (Dept. of Chem., Ben Gurion Univ. of the Negev, Beer-Sheva, Israel). *Chem. Phys. Lett. (Netherlands)*, vol.96, no.1, p.47-51 (25 March 1983). The two-photon absorption spectrum of s-triazine has been measured using multiphoton ionization. A vibronic coupling scheme, comprising the first excited 'E' state coupled by the $\nu_6(e')$ vibration to the ' A_2 ' and ' A_1 ' states, successfully reproduces the essential features of the absorption, fluorescence and two-photon absorption spectra. (11 refs.)
- 60876 Two-photon ionization. Capability of lasers for trace analysis. L.Woste (Inst. de Phys. Experimentale, Ecole Polytech. Federale de Lausanne, Lausanne, Switzerland). *Laser & Optoelektron. (Germany)*, vol.15, no.1, p.9-15 (March 1983). In German. The method of two-photon ionization (TPI) has been used to study metal complexes under molecular beam conditions. The molecules were electronically excited using a tunable laser, and then ionized by a second laser, in order to be detected by means of mass spectrometry. The spectra obtained show clearly the vibrational and rotational structure of the molecules investigated. Particle mixtures and subsequent fragmentation processes are well separated by the mass spectrometer. A careful analysis of the power dependencies allowed the determination of the optimum operation parameters for the laser system. In this way, detection efficiencies close to 'single molecule detection' were obtained. Since the method exhibits an extreme selectivity, it seems to be well suited for the analysis of trace amounts. (16 refs.)
- 60877 Resonant multiphoton ionization of H_2 via the $B^1\Sigma_u^+$, $v=7$, $J=2$ and 4 levels with photoelectron energy analysis. S.T.Pratt, P.M.Dehmer, J.L.Dehmer (Argonne Nat. Lab., Argonne, IL, USA). *J. Chem. Phys. (USA)*, vol.78, no.7, p.4315-20 (1 April 1983). The authors report measurements of photoelectron spectra of an electronically excited state of $\text{H}_2(B^1\Sigma_u^+)$ in selected vibrational and rotational levels. The excited state was prepared by resonant three photon excitation of $\text{H}_2 X^1\Sigma_g^+$, $v=0$, $J=3$ and subsequently, was ionized by a single additional photon. Partially resolved rotational structure is observed in the photoelectron spectra and is discussed in terms of the selection rules for direct photoionization and the partial wave composition of the ejected photoelectrons. An additional peak is observed in the spectra, which is tentatively interpreted as arising from photoionization of $\text{H}^+(n=2)$ formed by photodissociation of H_2 in the $B^1\Sigma_u^+$ state. (24 refs.)
- 60878 Systematics in two-photon rovibrational contours of 14_0^1 ($B_{2u}^1-A_{1g}^1$) in benzene derivatives. A.N.Thakur, L.Goodman (Dept. of Chem., Rutgers Univ., New Brunswick, NJ, USA). *J. Chem. Phys. (USA)*, vol.78, no.7, p.4356-62 (1 April 1983). Two-photon rotational contours of the principal vibronic band (14_0^1) in the $B_{2u}^1-A_{1g}^1$ transition in benzene and its $s\text{-C}_6\text{H}_5\text{D}$, $o\text{-C}_6\text{H}_4\text{D}_2$, $\text{C}_6\text{H}_5\text{F}$, $p\text{-C}_6\text{H}_4\text{F}_2$, $o\text{-C}_6\text{H}_4\text{F}_2$ derivatives have been recorded by multiphoton ionization at room temperature with a laser excitation bandwidth of 0.1 cm^{-1} . The main peaks in the rotational contour are shown to result from multiple coincidences of rovibronic transitions due to 'oblate rotorlike' and 'prolate rotorlike' behaviour of the asymmetric rotor molecules. The observed separations between these features agree very well with the predicted ones obtained from simple formulas. These systematics in the two-photon rotational contours are found to hold over a range of the asymmetry parameter from the least $\kappa=1$ to $\kappa=-0.9$. The theory is used to obtain the rotationless origin for each of the molecules studied. (33 refs.)
- 60879 Comparison of the Floquet and rotating-wave methods for multiphoton excitation of SF_6 . D.C.Clary (Dept. of Chem., Univ. of Manchester Inst. of Sci. & Technol., Manchester, England). *J. Phys. Chem. (USA)*, vol.87, no.5, p.735-9 (3 March 1983). The Floquet method of calculating exact molecular multiphoton transition probabilities for a given Hamiltonian is compared to the rotating-wave approximation (RWA). The two methods are used in calculations on the multiphoton excitation of the ν_3 vibrational mode of SF_6 . An accurate, three-dimensional molecular Hamiltonian is employed. The rotating-wave and Floquet results are in excellent agreement. (13 refs.)
- Real-time multiphoton ionization detection of iodine atoms produced by infrared multiphoton dissociation of perfluoroalkyl iodides See Entry 60680
- Multiphoton interactions See Entry 60682
- Rydberg-Rydberg transitions of NO using an optical-optical double resonance multiphoton ionization technique See Entry 60768
- Two-photon excitation of the $D^1\Delta-X^1\Sigma^+$ transition in carbon monoxide See Entry 60804
- IR laser induced loss of fluorescence in $\text{UO}_2(\text{hfacac})_2\text{TMP}$. I. Real time detection of multiple photon excitation of the ground electronic state See Entry 60807
- Benzaldehyde photochemistry studied with laser ionization mass and photoelectron spectroscopy See Entry 60836
- Subpicosecond time resolved multiphoton ionization: excited state dynamics of cis-stilbene under collision free conditions See Entry 60851
- Stepwise photoionization of anthracene in the gas phase by ultraviolet laser pulses See Entry 60854
- Precision measurements of hyperfine predissociation in I_2 vapor using a two-photon resonant scattering technique See Entry 60856
- Multiphoton dissociation of a rotating molecule See Entry 60857
- Rate equations analysis of vibrational quenching in IR multiphoton dissociation of pure SF_6 See Entry 60858

- Photodissociation of CO_3^- : evidence for a long-lived excited state See Entry 60859
- Multiphoton dissociation of OCCl_2 at 193 nm: formation of electronically excited Cl_2 See Entry 60862
- Competing dissociation channels in the infrared multiphoton decomposition of ethyl vinyl ether See Entry 60864
- Multiphoton dissociation of phosgene (OCCl_2) at 193 nm: formation of electronically excited Cl_2^* See Entry 60874
- Investigation of the rotation of a wave front in a molecular multipass amplifier See Entry 61220
- Polarization four-photon spectroscopy within the absorption line: role of coherent Rayleigh scattering and of the multilevel nature of molecules See Entry 61234
- Optical multiple pulse sequences for multiphoton selective excitation and enhancement of forbidden transitions See Entry 61245

33.90 OTHER TOPICS IN MOLECULAR SPECTRA AND INTERACTIONS WITH PHOTONS

- 60880 Resonance transformation by molecules of polychromatic radiation in the form of a periodic pulse train. Spectral and spectral-time characteristics of secondary radiation. V.A.Morozov, P.P.Shorygin. *Opt. & Spectrosc. (USA)*, vol.53, no.1, p.69-73 (July 1982). Translation of: *Opt. & Spektrosk. (USSR)*, vol.53, no.1, p.118-24 (July 1982). [received: April 1983] The spectral-time characteristics of secondary radiation are given in the scope of a classical theory of light transformation by a harmonic oscillator associated with a nonstationary regime of illumination, and a comparison with these characteristics is performed in the semiclassical and quantum theories. Properties of secondary radiation are discussed during transformation of bichromatic and trichromatic radiation by the molecules. (6 refs.)
- Dynamic model and tunneling splittings in LMH_4 non-rigid hydrides See Entry 60565
- Experimental study of relative intensities in inelastic electron tunneling spectroscopy (IETS) See Entry 62236
- Conference overview: experimental [surface vibrations] See Entry 62238
- Tunneling spectroscopy as a probe of adsorbate-surface interactions See Entry 62270
- The interaction of ions and easily ionized species with oxide surfaces as studied by tunneling spectroscopy See Entry 62271

34.00 ATOMIC AND MOLECULAR COLLISION PROCESSES AND INTERACTIONS

34.10 GENERAL THEORIES AND MODELS

(inc. statistical theories, transition state, stochastic and trajectory models, etc; see also 82.20)

- Sum rules including first order quantum corrections for neutron scattering experiments on isotopic mixtures of monatomic fluids See Entry 60617
- Diffusion description of vibrational relaxation in a binary mixture of diatomic molecules (Harmonic oscillators) See Entry 60931

34.20 INTERATOMIC AND INTERMOLECULAR POTENTIALS AND FORCES

(for molecular solids, see 31.70K)

- 60881 Corrected formula for first quantum corrections to second virial coefficients for nonspherical molecules. R.T.Pack (Theoretical Div., Los Alamos Nat. Lab., Los Alamos, NM, USA). *Chem. Phys. Lett. (Netherlands)*, vol.96, no.2, p.171-4 (1 April 1983). The formulas of Wang Chang (1944), commonly used to calculate quantum corrections to the second virial coefficient for anisotropic interactions, are found to contain an error. A simple, correct formula, valid for any like or unlike combination of atoms and molecules of complexity up to and including symmetric tops, are given. (11 refs.)
- 60882 A simple analytical approximation for the potential energy of diatomics. I.K.Dmitrieva, V.A.Zenevich (Lukov Heat & Mass Transfer Inst., Acad. of Sci., Minsk, Belorussian SSR). *Chem. Phys. Lett. (Netherlands)*, vol.96, no.2, p.228-31 (1 April 1983). A correlation between the Dunham expansion coefficients, $a_2 \approx 0.64a_1^2$, is found which holds for diatomics of different types. Based on this correlation, a four-parameter power approximation using ω_e , B_e , α_e and D_e is suggested which reproduces the ground-state potential curves for diatomics within 2%. (9 refs.)
- 60883 Improvement for the RKR procedure obtained by semiclassical calculations. G.Gouedard, J.Vigue (Lab. de Spectroscopie Hertzienne, ENS, Paris, France). *Chem. Phys. Lett. (Netherlands)*, vol.96, no.3, p.293-5 (8 April 1983). The authors present a new technique to improve RKR molecular potential curve calculations. The potential curve obtained gives calculated $G(v)$ and $B(v)$ values extremely close to the measured ones. The aim of these calculations is the same as that of the inverted perturbation approach of Vidal and Sheingraber (1977), but the potential-well corrections are calculated by using Watson's (1979) semiclassical inversion procedure. (6 refs.)
- 60884 A simple treatment of intermolecular interactions: synthesis of ab initio calculations and combination rules. J.Hoinkis, R.Ahlrichs, H.-J.Bohm (Inst. für Phys. Chemie und Elektrochem., Univ. Karlsruhe, Karlsruhe, Germany). *Int. J. Quantum Chem. (USA)*, vol.23, no.3, p.821-34 (March 1983). (Proceedings of the Fourth International Congress in Quantum Chemistry, Uppsala, Sweden, 13-20 June 1982). A new technique for a simple and efficient treatment of intermolecular interactions is proposed and tested. The method is based on an approximation of the first order SCF term $E_{\text{SCF}}^{(1)}$ which is the most structured contribution to the total interaction. $E_{\text{SCF}}^{(1)}$ is represented by a site-site potential V of (exp,

1/R)-type, which accounts for the exchange plus penetration and the long range Coulomb forces (by means of a point charge model). The individual contributions to V are obtained by means of combination rules from corresponding site parameters of interacting molecules. The site parameters are consequently molecular and not intermolecular properties and can conveniently be determined by probing a molecule with appropriate test particles. Site parameters are reported for He, Ne, Ar, N_2 , CO , CO_2 , CS_2 , and HCl. Comparisons show close agreement of V with E_{SCF} which in turn is close to ΔE_{SCF} if polarization and charge transfer effects are small. (40 refs.)

60885 Hindered internal rotations in Van der Waals molecules and molecular crystals. W.J.Briels, J.Tennyson, M.Claessens, T.Van der Lee, A.Van der Avoird (Inst. of Theoretical Chem., Univ. of Nijmegen, Nijmegen, Netherlands).

Int. J. Quantum Chem. (USA), vol.23, no.3, p.1091-100 (March 1983). (Proceedings of the Fourth International Congress in Quantum Chemistry, Uppsala, Sweden, 13-20 June 1982).

The quantum dynamical behavior of the Van der Waals molecule $(N_2)_2$ and that of the ordered α and γ phases of solid N_2 have recently been calculated, starting from the same ab initio N_2-N_2 potential. By interpreting the results of these calculations the authors try to improve their understanding of the libration/internal rotation motions of the N_2 monomers and the orientational order-disorder (α - β) phase transition. Some new results are presented and further (mean-field and libron-model) calculations are proposed which assess explicitly the intermolecular pair correlation effects caused by anisotropic interaction potential. (28 refs.)

60886 A semiclassical inversion procedure for the dipole-moment function for diatomic molecules. J.R.Stine (Los Alamos Nat. Lab., Los Alamos, NM, USA), D.W.Noid.

J. Chem. Phys. (USA), vol.78, no.6, pt.2, p.3647-51 (15 March 1983).

A simple formalism is presented to deduce the dipole moment as a function of internuclear distance from experimental vibrational intensity data. This method, like the RKR method for obtaining the potential-energy function, is based on the semiclassical WKB formalism and no particular functional form need be assumed for the dipole moment. The method is applied to the experimental data of Sileo and Cool (1976) for HF. (29 refs.)

60887 Matrix elements for Morse oscillators. V.S.Vasan, R.J.Cross (Dept. of Chem., Yale Univ., New Haven, CT, USA).

J. Chem. Phys. (USA), vol.78, no.6, pt.2, p.3869-71 (15 March 1983).

The authors have derived exact analytic expressions for the following matrix elements for a Morse oscillator: $\langle m | \exp[\gamma(r-r_0)] | n \rangle$, $\langle m | (r-r_0) \exp[-a(r-r_0)] | n \rangle$, and $\langle m | (r-r_0) \exp[-2a(r-r_0)] | n \rangle$, where a is the Morse range parameter and γ is an arbitrary constant. They have found that several of the commonly used expressions for various diagonal matrix elements of the Morse oscillator involve considerable roundoff error. Due to near cancellation of terms the result may be many orders of magnitude lower than any of the terms. They obtain simple yet accurate asymptotic approximations for the diagonal elements which avoid these problems. These approximations are obtained for $\langle m | (r-r_0) | m \rangle$, $\langle m | (r-r_0)^2 | m \rangle$, and the cases mentioned above. (12 refs.)

60888 The dissociation energies of the diatomic alkali hydrides. S.C.Yang, D.D.Nelson, Jr. (Dept. of Chem., Univ. of Rhode Island, Kingston, RI, USA), W.C.Stwalley.

J. Chem. Phys. (USA), vol.78, no.7, p.4541-3 (1 April 1983).

A new method for estimating the dissociation energies for the alkali hydride molecules is reported. It involves extrapolating the known Rydberg-Klein-Rees potential curve of the $A^1\Sigma^+$ state to the ionic-covalent avoided crossing point. The estimated dissociation energies $D_e(X)$ are $16000 \pm 400 \text{ cm}^{-1}$ for NaH, $15020 \pm 400 \text{ cm}^{-1}$ for KH, and $14580 \pm 600 \text{ cm}^{-1}$ for RbH. (31 refs.)

60889 An improved self-interaction-corrected local spin density functional for atoms. J.G.Harrison (Dept. of Phys., North Dakota State Univ., Fargo, ND, USA).

J. Chem. Phys. (USA), vol.78, no.7, p.4562-6 (1 April 1983).

The application of the self-interaction-corrected local spin density approximation (SIC-LSDA) to atoms is reexamined. It is shown that a more careful application of the central-field approximation results in a modified functional which yields accurate total energies, correlation energies, and, in the 'exchange-only' (X-O) version, exchange energies in good agreement with Hartree-Fock (HF) values. It is also shown that the X-O version of the earlier SIC-LSDA functional yields total energies in close agreement with experiment for second-row atoms. The proposed modification removes this tendency of the X-O functional to mimic a correlated functional. (25 refs.)

60890 On the application of the Rydberg-Kratzer potential to some diatomic molecules. K.Ramani, A.M.Ghodgaonkar (Western Regional Instrumentation Centre, Univ. of Bombay, Bombay, India).

J. Quant. Spectrosc. & Radiat. Transfer (GB), vol.29, no.4, p.379-80 (April 1983).

The spectroscopic constants α_e and $\omega_e X_e$ for some diatomic molecules have been calculated using a combination of the Rydberg and Kratzer potentials. The dissociation energies D_e for these molecules were calculated previously by others using RKR potential energy curves. Agreement of the authors' spectroscopic constants with experimental data is satisfactory. (9 refs.)

60891 Ground-state diatomic potentials. P.Huxley, J.N.Murrell (School of Chem. & Molecular Sci., Univ. of Sussex, Brighton, England).

J. Chem. Soc. Faraday Trans. II (GB), vol.79, pt.2, p.323-8 (Feb. 1983).

Extended-Rydberg potentials have been derived for the ground states of all diatomic molecules obtained from atoms in the periodic list Li to Cl for which accurate spectroscopic data are available. From a comparison with RKR data where these are known the authors conclude that this simple function is an excellent representation of the potential in the valence region. (14 refs.)

60892 Study of ion-molecule and ion-ion interactions in nitromethane medium by means of infrared absorption spectroscopy. L.S.Perelygin, M.A.Klimchuk.

J. Appl. Spectrosc. (USA), vol.36, no.5, p.531-5 (May 1982). Translation of: *Zh. Prikl. Spektrosk. (USSR)*, vol.36, no.5, p.761-6 (May 1982). [received: Feb. 1983]

Presents results obtained in an IR spectroscopic study of ion-molecule and ion-ion interactions that are realized in solutions of $LiClO_4$, $Mg(ClO_4)_2$, and LiNCS in nitromethane. These salts have relatively high solubilities in nitromethane, and hence the authors were able to determine the influence of the counter-ion type on the interactions under investigation and to follow the concentration dependence of the observed effects. Spectra over a range of $400-4000 \text{ cm}^{-1}$ were obtained in a UR-20 infrared spectrophotometer equipped with a two-beam thermostated cuvette for temperature studies and the band positions were determined to within $\pm 1-2 \text{ cm}^{-1}$. (16 refs.)

60893 Analytic expression for bound-bound and bound-free dipole transition matrix elements of atomic inner shells. M.S.Wang, R.H.Pratt (Dept. of Phys. & Astron., Univ. of Pittsburgh, Pittsburgh, PA, USA).

Phys. Rev. A (USA), vol.27, no.4, p.1939-42 (April 1983).

Analytic expressions are obtained which well represent the nonrelativistic single-electron ($nl, n'l'$) dipole transition rates in screened central potentials, not only when both states are inner shell in character, as had been previously achieved, but also when only one of the states has an inner-shell character. The key idea is to expand one of the screened bound-state wave functions (outer shell) in terms of an unbound negative-energy Coulomb wave function with the same energy shift as the screening shift of the inner-shell bound state. The expressions obtained are an analytic continuation (in photon energy) of corresponding bound-free matrix elements. (15 refs.)

60894 Long-range forces between a charged and neutral system. G.Feinberg (Dept. of Phys., Columbia Univ., New York, NY, USA), J.Sucher.

Phys. Rev. A (USA), vol.27, no.4, p.1958-67 (April 1983).

Dispersion-theory techniques, previously used to calculate the two-photon exchange potential $V_{2\gamma}(R)$ between two neutral systems, are used to study $V_{2\gamma}(R)$ acting between a neutral system A and a charged system B . For the case when A is an atom and B an electron, general results are given for all corrections of order λ_e/R or of order $(a_0/R)^2$ relative to the leading R^{-4} term. (13 refs.)

60895 Determination of interatomic potentials via the single scattering function on a surface. Nguyen Nam Anh, R.G.Barantsev, V.L.Sergeev.

Vestn. Leningr. Univ. Ser. Mat. Mekh. & Astron. (USSR), no.1, p.120-2 (Jan. 1983). In Russian.

The inverse scattering problem is solved for a finite mass ratio and oblique incidence. For steep potentials some asymptotic formulas are given. (4 refs.)

Scattering in view of the Titchmarsh-Weyl theory See Entry 56065

Improved SCF interaction energy decomposition scheme corrected for basis set superposition effect See Entry 60571

Ab initio MO investigation of the ethanolamine-formic acid complex See Entry 60573

The low-lying $2\Sigma^-$ states of OH See Entry 60604

Low pressure shift of the $2p^5 3p-2p^5 5s$ spectral lines of neon perturbed by neon and helium See Entry 60658

Spectroscopic properties and relaxation processes of impurity molecules in solids. I. Rotational spectra See Entry 60687

Allowance for the dependence of the repulsion branch of the potential of intermolecular interactions on the vibrational coordinates in the description of the displacements of the vibrational frequencies of molecules in a vapor-liquid transition See Entry 60694

Theory of absorption and emission of light by molecular systems with multiwell potentials See Entry 60695

The infrared absorption spectra of $(HCCl)_2$ and $(DCCl)_2$ See Entry 60718

Vibrational phase relaxation in ethane at moderate densities, including the critical region See Entry 60727

Spectroscopy of large molecular complexes in supersonic jets See Entry 60800

First observation of bound-continuum transitions in the laser-induced $A^1\Sigma_g^+ \rightarrow X^1\Sigma_g^+$ fluorescence of Na_2 See Entry 60802

Observation of levels near dissociation in the $X^1\Sigma_g^+$ state of $^{13}Li_2$ See Entry 60803

Rotational predissociation of the Ar.HCl van der Waals complex: close-coupled scattering calculations See Entry 60865

Zeeman transitions in collisions of Na with Xe See Entry 60898

Vibrational predissociation and intramolecular vibrational relaxation in electronically excited s-tetrazine-argon van der Waals complex See Entry 60914

The use of static potentials in atomic collisions. Application to the excitation of hydrogen atoms by helium ions at intermediate energies See Entry 60974

Nonadjustable exchange-correlation model for electron scattering from closed-shell atoms and molecules See Entry 60987

On the origin of the occurrence of 'magic numbers' in cluster size distributions of xenon in the compressed gas phase See Entry 61041

van der Waals forces in solutions See Entry 61744

FTIR studies of polymer blends containing the poly(hydroxy ether of bisphenol A) and poly(ϵ -caprolactone) See Entry 62999

34.40 ELASTIC SCATTERING OF ATOMS AND MOLECULES

Calculation of higher-order semiclassical scattering phase shifts: the effect of a barrier maximum See Entry 60904

Imbedded matrix Green's functions in atomic and molecular scattering theory See Entry 60905

A new diabatic molecular representation for triplet-triplet transitions in He^+-He^+ collisions See Entry 60959

34.50 INELASTIC SCATTERING OF ATOMS AND MOLECULES

60896 Collision-induced absorption in $Ne+Ar$. A.Raczynski (Inst. of Phys., Nicholas Copernicus Univ., Torun, Poland).

Chem. Phys. Lett. (Netherlands), vol.96, no.1, p.9-13 (25 March 1983).

Accurate quantum-mechanical values of the collision-induced absorption coefficient are reported for a Ne-Ar mixture in the binary-collision approximation. Two of the known expressions for the induced dipole moment are tested and two others are proposed to obtain good agreement with experiment. (9 refs.)

60897 A quantum-mechanical explanation of vibronic phenomena in atom-molecule collisions. M.R.Spallburg, J.Los (FOM Inst. for Atomic & Molecular Phys., Amsterdam, Netherlands), Sidis V.

Chem. Phys. Lett. (Netherlands), vol.96, no.1, p.14-19 (25 March 1983).

The quantum-mechanical equivalent of a classically vibrating molecular ion during an ion-pair formation collision is presented. The classical vibration in the quantal representation is explained as an interference between partial waves which evolve along neighbouring vibronic states during the collision. (14 refs.)

- 60898 Zeeman transitions in collisions of Na with Xe.** T.F. George (Dept. of Chem., Univ. of Rochester, Rochester, NY, USA), P.L. Devries. *Chem. Phys. Lett. (Netherlands)*, vol.96, no.1, p.99-102 (25 March 1983). Transitions between the Zeeman states of a sodium atom induced by collision with a ground-state xenon atom have been investigated by quantum-mechanical methods. The calculations were carried out using the pseudo-potentials of Czuchaj and Sienkiewicz (1979), and results pertinent to crossed atomic beam experiments are reported. Comparison with previous theoretical work indicates that thermally averaged cross section (relevant to cell-type experiment) would be in excellent agreement with recent experimental results. (20 refs.)
- 60899 Observation of two components in molecular cusp spectra for \sim MeV/u H^+ , He^{+2} projectiles on $m \geq 4$ hydrocarbon molecules.** G. Bissinger, J. Gaiser, J.M. Joyce (East Carolina Univ., Greenville, NC, USA). *IEEE Trans. Nucl. Sci. (USA)*, vol.ns-30, no.2, p.1015-17 (April 1983). (1982 IEEE Conference on the Application of Accelerators in Research and Industry, Denton, TX, USA, 8-10 Nov. 1982). The authors report the results of an investigation of the cusp shapes obtained for varying size hydrocarbon molecule targets bombarded with \sim MeV/u H^+ , He^{+2} projectiles. The results also indicate the presence of multiple contributions to the overall cusp shape for the larger molecules. (7 refs.)
- 60900 Anisotropies of the Na₂-rare gas interaction potentials from angularly resolved inelastic scattering.** P.L. Jones, E. Gottwald, U. Heftner, K. Bergmann (Fachbereich Phys., Univ. Kaiserslautern, Kaiserslautern, Germany). *J. Chem. Phys. (USA)*, vol.78, no.6, pt.2, p.3838-41 (15 March 1983). Rotational rainbow angular positions in the inelastic differential scattering cross sections of argon, krypton, and xenon from Na₂ are reported. The observed transitions for small rotational quantum number change ($\Delta j \leq 16$) are analyzed in terms of the classical model of hard ellipsoid scattering which relates the rainbow angle to the anisotropy ϵ of the potential, where ϵ is the difference in length of the long and short axes. The analysis yields $\epsilon = 0.67 \pm 0.05$, 0.79 ± 0.09 , and 0.66 ± 0.05 Å for the systems Na₂-Ar, Kr, and Xe, respectively. From earlier work, the anisotropies for Na₂-He and Na₂-Ne are known to be $\epsilon = 0.70$ (calculated) and 0.72 ± 0.05 Å. The data demonstrate the similarity within this model for the anisotropies of all the Na₂-rare gas interaction potentials for low effective collision energies. (21 refs.)
- 60901 Topography of potential energy surfaces: DIM surface for $H+F_2$.** J.J. Duggan, R. Grice (Chem. Dept., Univ. of Manchester, Manchester, England). *J. Chem. Phys. (USA)*, vol.78, no.6, pt.2, p.3842-9 (15 March 1983). Potential energy surfaces have been calculated over the full range of nuclear configurations for the $H+F_2$ reaction using the DIM method with the 14 polyatomic basis functions arising from the atomic states $H(2S)$, $F(2P_x)$, $H^+(1S)$ and $F^-(1S)$. The lowest potential energy surface agrees with the LEPS surface only in the collinear configuration. Qualitatively different forms are observed in strongly bent configurations which are determined by configuration interaction with low-lying surfaces corresponding to electronically excited states which are inadequately treated in the LEPS formulation. Trajectory calculations using the LEPS surface at higher collision energy or for vibrationally excited F_2 are likely to give erroneous results when broadside configurations contribute to the scattering. (22 refs.)
- 60902 A complete energy transfer map for COF_2 .** J.L. Ahl, R.K. Bohn, K.H. Casleton, Y.V.C. Rao, G.W. Flynn (Dept. of Chem., Columbia Univ., New York, NY, USA). *J. Chem. Phys. (USA)*, vol.78, no.6, pt.2, p.3899-906 (15 March 1983). Fluorescence from the v_1 , v_4 , v_6 , and v_3/v_2 states has been observed following Q-switched CO_2 laser excitation of the v_2 C-F stretch mode of COF_2 . A kinetic model is presented which is consistent with the observed fluorescence lifetimes. Following excitation of the v_2 mode, $2v_2$ is rapidly pumped by ladder climbing collisions. The $2v_2$ states are collisionlessly coupled to the v_1 mode by Fermi resonance leading to the creation of a steady state between the v_1 and v_2 manifolds with 30 gas kinetic collisions. Subsequently, the v_2 state decays to the v_6 mode in 800 collisions, and also fills the v_4 mode in 2000 gas kinetic collisions. The v_4 level rapidly equilibrates with the near resonant states $2v_3$, $2v_5$, and v_3+v_5 after about 25 collisions, and these states rapidly decay to the v_3 and v_6 fundamentals in less than or about 100 collisions. The v_6 state relaxes to the v_3/v_2 states, in approximately 190 collisions, while vibration-translation/rotation relaxation of v_3 and v_2 to the ground state occurs on a time scale of 1200 collisions. (30 refs.)
- 60903 Complex coordinate calculations of Feshbach resonance energies and widths for a collinear triatomic system.** K.M. Christoffel, J.M. Bowman (Dept. of Chem., Illinois Inst. of Technol., Chicago, IL, USA). *J. Chem. Phys. (USA)*, vol.78, no.6, pt.2, p.3952-8 (15 March 1983). Complex resonance energies are calculated for a model triatomic system studied previously by Eastes and Marcus [W. Eastes and R.A. Marcus, *J. Chem. Phys.*, 59, 4757 (1973)]. The complex coordinate method is employed to obtain resonance positions and widths for six states. The positions are all in excellent agreement with previous scattering and stabilization results and there is also good agreement with the one width obtained previously from scattering calculations. The additional widths obtained are given for the first time. Some speculations about possible laser induced absorption and emission among these resonances and true bound states are made. (41 refs.)
- 60904 Calculation of higher-order semiclassical scattering phase shifts: the effect of a barrier maximum.** J. Luppi, P. Pajunen (Dept. of Phys. Chem., Univ. of Helsinki, Helsinki, Finland). *J. Chem. Phys. (USA)*, vol.78, no.7, p.4451-5 (1 April 1983). Evaluation of high-order semiclassical scattering phase shifts is extended to situations involving a potential barrier. Calculations by using appropriate semiclassical phase shift formulas yield accurate results for energies above and below as well as in the immediate neighbourhood of the barrier maximum. (14 refs.)
- 60905 Imbedded matrix Green's functions in atomic and molecular scattering theory.** J.V. Lill (Dept. of Chem., Univ. of Chicago, Chicago, IL, USA), T.G. Schmalz, J.C. Light. *J. Chem. Phys. (USA)*, vol.78, no.7, p.4456-63 (1 April 1983). The paper presents a general, simple, and unified treatment of Green's function approaches to the solution of the sets of coupled second order differential equations encountered in the theory of inelastic and reactive scattering. The standard scalar theory of Sturm-Liouville problems is extended to systems of equations without recourse to spectral resolutions of the Green's operator. A nonstandard approach to invariant imbedding is then developed to yield the most general kind of recursion relation for Wigner R matrices possible; the R-matrix propagation of Light and Walker (1976) and the variable interval-variable step algorithm of Parker, Schmalz, and Light (1980) are shown to be particularly simple examples of this more general scheme. Extensions and simplifications are offered. Also recurrence relations, stabilization of solutions, adiabatic and diabatic representations, and the use of nonorthogonal bases are all treated in a transparent manner. (33 refs.)
- 60906 Exact scattering solutions in an energy sudden (ES) representation.** B. Chang, L. Eno, H. Rabitz (Dept. of Chem., Princeton Univ., Princeton, NJ, USA). *J. Chem. Phys. (USA)*, vol.78, no.7, p.4477-85 (1 April 1983). In the paper, the authors lay down the theoretical foundations for computing exact scattering wave functions in a reference frame which moves in unison with the system internal coordinates. In this frame the (internal) coordinates appear to be fixed and its adoption leads very naturally (in zeroth order) to the energy sudden (ES) approximation [and the related infinite order sudden (IOS) method]. For this reason they call the new representation for describing the exact dynamics of a many channel scattering problem, the ES representation. Exact scattering solutions are derived in both time dependent and time independent frameworks for the representation and many interesting results in these frames are established. It is shown, for example, that in a time dependent frame the usual Schrodinger propagator factorizes into internal Hamiltonian, ES, and energy correcting propagators. They also show that in a time independent frame the full Green's functions can be similarly factorized. Another important feature of the new representation is that it forms a firm foundation for seeking corrections to the ES approximation. Thus, for example, the singularity which arises in conventional perturbative expansions of the full Green's functions (with the ES Green's function as the zeroth order solution) is avoided in the ES representation. Finally, a number of both time independent and time dependent ES correction schemes are suggested. (27 refs.)
- 60907 Light-induced collisions involving molecules without change in the chemical bonds.** V.S. Dubov. *Opt. & Spectrosc. (USA)*, vol.53, no.1, p.22-6 (July 1982). Translation of: *Opt. & Spektrosk. (USSR)*, vol.53, no.1, p.40-5 (July 1982). [received: April 1983]. The simplest case of light-induced collisions with the participation of molecules, involving an atom A and a diatomic molecule BC in a weak electromagnetic field, has been examined. The conditions for the applicability of the approximations previously used in the study of light-induced collisions of atoms have been studied. In particular, the correctness of the two-state approximation has been discussed. In a weak field, it is applicable if the intermolecular interaction is weak and adiabatic. The overlap of the lines of light-induced collisions leads to the formation of an unresolved band, which can be constructed by summation of the lines. The analytical equations obtained have been used to estimate the parameters of the absorption band of the light-induced collision $Cs(6^2S_{1/2}) + CO(\nu''=0) + h\nu \rightarrow Cs(7^2S_{1/2}) + CO(\nu'=1)$. It has been shown that the reduced absorption coefficient for this reaction reaches 10^{-41} cm². The possibility of carrying out the experiment has been discussed. (24 refs.)
- 60908 Spectral evidence of line collisional interference in NH_3 inversion spectrum.** A.I. Petrova. *Opt. & Spectrosc. (USA)*, vol.53, no.1, p.31-3 (July 1982). Translation of: *Opt. & Spektrosk. (USSR)*, vol.53, no.1, p.55-9 (July 1982). [received: April 1983]. In this work an analysis, based on collision theory and taking into account exchange between inversion emission and absorption lines, of the anomaly in the information of the form of the inversion spectrum of NH_3 is presented. In the range of pressures where the collision approximation is applicable an analysis of absorption for such microsystems as NH_3-N_2 , NH_3-CO_2 , NH_3-NH_3 is given; and a comparison of contours computed in the approximation of isolated lines with the shape of an inversion spectrum, taking account of spectral exchange between inversion lines, is presented. With the help of the computed parameter α describing the quadratic dependence of frequency shift on pressure, one can determine at which inversion frequency for given pressure maximum absorption will be observed. (9 refs.)
- 60909 Effect of collisional mixing of lower levels of Li-like ions on the intensity of the resonance line satellite structures of He-like ions.** S.A. Pikuz, I.Yu. Skobelev, A.N. Tkachev, A.Ya. Faenov. *Opt. & Spectrosc. (USA)*, vol.53, no.2, p.194-5 (Aug. 1982). Translation of: *Opt. & Spektrosk. (USSR)*, vol.53, no.2, p.333-6 (Aug. 1982). [received: April 1983]. Presents an analysis of the effect of collisional transitions between the $1s^2 2s^2 S_{1/2}$, $1s^2 2p^2 P_{1/2}$, and $1s^2 2p^2 P_{3/2}$ levels of Li-like ions on the relative intensities of the resonance-line satellite structures of He-like ions. (10 refs.)
- 60910 Projectile-charge dependence of quasi-free-electron bremsstrahlung.** K. Ishii, K. Sera (Cyclotron & Radioisotope Center, Tohoku Univ., Sendai, Japan), H. Arai, S. Morita, K. Tokuda. *Phys. Rev. A (USA)*, vol.27, no.4, p.2225-8 (April 1983). Continuum X-rays induced by bombardments of a Be target with 20.14-MeV/amu protons and $^3He^{2+}$ ions have been measured with a Si(Li) detector in the direction of 90° with respect to the incident beam. Differences in the X-ray-production cross sections multiplied by the X-ray energy $\hbar\omega/\hbar\omega_0(\hbar\omega)/[4-\sigma_p(\hbar\omega)]$, and ratio of the cross sections $R(\hbar\omega) \equiv [\sigma_{He}(\hbar\omega)/4\sigma_p(\hbar\omega)]$ for the proton and $^3He^{2+}$ -ion impact, where $\sigma_p(\hbar\omega)$ and $\sigma_{He}(\hbar\omega)$ are the X-ray-production cross sections for proton and $^3He^{2+}$ -ion impact, respectively, were obtained as a function of the X-ray energy. Both the difference and the ratio show peaks in the region where the X-ray energy is equal to the relative kinetic energy between the projectile and the inner-shell electron to be scattered by the projectile. From the comparison with a theory of quasi-free-electron bremsstrahlung based on the impulse approximation it is found that this peak corresponds to the maximum of the velocity-distribution function of the inner-shell electron. Furthermore, the contribution of the radiative electron-capture process in the case of proton and $^3He^{2+}$ impact is clearly found. (5 refs.)
- Dispersion coefficients for atoms in different states See Entry 60621
- Application of the Faddeev-Watson expansion to thermal collisions of Rydberg atoms with neutral particles See Entry 60624
- Satellite structure in the $2p\sigma$ molecular orbital transitions in slow heavy ion collisions See Entry 60626
- Two-photon excitation of the $D^1\Delta-X^1\Sigma^+$ transition in carbon monoxide See Entry 60804
- Electronic quenching of pyrene 1B_u by olefins in the vapour phase See Entry 60822
- Rate equations analysis of vibrational quenching in IR multiphoton dissociation of pure SF_6 See Entry 60858
- Classical S-matrix theory of viscomagnetic production cross section See Entry 61587
- Reactive and inelastic processes involving $I_2(D^1\Sigma_u^+)$ with the collision partners CH_4 , CH_3Cl , CF_3Cl , and CF_4 See Entry 63524

34.50E Rotational and vibrational energy transfer

60911 Experimental and theoretical study of the vibrational relaxation of $\text{CO}(\nu=1)$ and $\text{N}_2(\nu=1)$: V-T relaxation by the isotopes of helium. M.M. Maricq, E.A. Gregory, C.T. Wickham-Jones, D.J. Cartwright, C.J.S.M. Simpson (Phys. Chem. Lab., Oxford Univ., Oxford, England). *Chem. Phys. (Netherlands)*, vol.75, no.3, p.347-70 (15 March 1983).

Experimental results are reported for the rate constants for the vibrational relaxation of $\text{CO}(\nu=1)$, $^{14}\text{N}_2(\nu=1)$ and $^{15}\text{N}_2(\nu=1)$ by ^3He and ^4He in the temperature range from 300-80K. These are compared to rate constants determined from the numerical solution of the quantum scattering equations. The infinite-order sudden approximation can be used to reduce the number of coupled channels to those required for the vibrational levels. The calculations are applied to ab initio potentials and a model based on the anisotropic Morse potential. The major features which govern the rate of vibrational deactivation are shown to be the energy of the vibrational quantum, the mass of the collision partner and the steepness of the repulsive part of the intermolecular potential. Including an attractive well in the potential preferentially increases the relaxation rate constants at low temperatures. The roles of the attractive terms and the anisotropy of the potential in the deviations of the experimental data from the Landau-Teller predictions are discussed. (45 refs.)

60912 Intramolecular vibrational relaxation in the dual-channel 5-methyl-3-hexyl radical system excited by different activation pathways. S.P. Wrigley, K.W. Smith, B.S. Rabinovitch (Dept. of Chem., Univ. of Washington, Seattle, WA, USA).

Chem. Phys. (Netherlands), vol.75, no.3, p.453-62 (15 March 1983).

The study of the rate of vibrational energy relaxation in chemically activated systems has been extended to the competitive channel decomposition of 5-methyl-3-hexyl radicals activated to the average level of $\approx 44 \text{ kcal mol}^{-1}$ over the range of H_2 bath gas pressures from 1 to 46500 Torr at 298K. Two activation pathways were used. One is addition of H atoms to cis-5-methyl-2-hexene. Preferential decomposition of the initially formed, internally nonrandomized 5-methyl-3-hexyl radical occurs on a picosecond time scale to produce 4-methyl-1-pentene product. Formation of 1-butene product by the second decomposition channel has its onset only after internal randomization of the energy which was initially deposited by the activation reaction has occurred. By contrast, activation of 5-methyl-3-hexyl by addition of H atoms to trans-2-methyl-3-hexene should not, and does not give rise to initial formation of 4-methyl-1-pentene at short times. Instead, 1-butene is formed preferentially, as is expected for this mode of production of the initially nonrandomized state. From the pressure dependence of the product ratios, relaxation times in the range 0.1-0.6 ps are obtained, given plausible extremes of alternative assumptions about the size of the initially excited subset of vibrations. The percentage of mode-specified chemistry (nonrandom decomposition) is $10^{-4}\%$ in these systems in contrast to some of the author's earlier work where this percentage reached 2-10%. (24 refs.)

60913 Ground state vibrational randomization in alkylbenzenes. J.B. Hopkins, P.R.R. Langridge-Smith, R.E. Smalley (Dept. of Chem., Rice Univ., Houston, TX, USA).

J. Chem. Phys. (USA), vol.78, no.6, pt.2, p.3410-14 (15 March 1983).

Measurements of intramolecular vibrational randomization (IVR) previously carried out on the S_1 excited state of a series of jet-cooled alkylbenzenes have been extended to the ground electronic state. The ground state ring modes $6b_1$, 1, and 12 were conveniently activated by pulsed laser excitation of the 0_0^0 vibronic band of the $S_1 \leftarrow S_0$ ultraviolet absorption system, followed by fluorescence. The onset of IVR was then probed by resonant two-photon ionization (R2PI) of these vibrationally activated ground state alkylbenzenes. When the alkyl chain exceeded three carbon atoms in length, the hot band 12_1^0 ($E_v \approx 1010 \text{ cm}^{-1}$) was found to be absent from the R2PI-probed spectrum, while the $6b_1^0$ hot band ($E_v \approx 625 \text{ cm}^{-1}$) remained easily observable through n-pentylbenzene. This overall pattern of IVR is essentially the same as that observed previously in the S_1 excited state. In both electronic states, the only effective barrier to vibrational energy decay from the ring to the chain appears to be an inadequate density of states. Above the critical state density, IVR appears to be complete, and this critical state density appears to be about the same in both the ground and excited electronic states. (18 refs.)

60914 Vibrational predissociation and intramolecular vibrational relaxation in electronically excited s-tetrazine-argon van der Waals complex. D.V. Brumbaugh, J.E. Kenny, D.H. Levy (Dept. of Chem., Univ. of Chicago, Chicago, IL, USA).

J. Chem. Phys. (USA), vol.78, no.6, pt.2, p.3415-34 (15 March 1983).

The van der Waals complex tetrazine-argon formed in a supersonic expansion has been investigated by means of laser-induced excitation and fluorescence spectroscopy. Excitation spectra reveal the band shift $D_0^0 - D_0^0 = -23 \text{ cm}^{-1}$, the tetrazine-argon stretch frequency $\nu_{\text{as}} = 44 \text{ cm}^{-1}$, and a lower limit to the dissociation energy $D_0^0 > 254 \text{ cm}^{-1}$. The band shift is vibrationally dependent in the case of two low frequency out-of-plane modes of tetrazine. The absence of additional broadening of the excitation linewidths due to the presence of argon shows that the dynamical processes in the complex are slower than the photodissociation of tetrazine itself (0.5-1.4 ns) which serves as an internal timing mechanism. At five single vibronic levels of tetrazine-argon above the S_1 zero-point level, the rates of vibrational predissociation and intramolecular vibrational relaxation are $\sim 10^8 \text{ s}^{-1}$. The V-V propensities in dissociation and relaxation are selective and different from collision-induced propensities. Among the V-V channels in dissociation, the authors find the lowest upper limit to D_0^0 is 381 cm^{-1} . Considerable rotational excitation of the tetrazine fragment is observed following dissociation which may reduce the estimate of D_0^0 to as low as 306 cm^{-1} . Although redistribution of vibrational energy during dissociation is selective, no mode selective effects could be attributed to the initial level of excitation, despite variations in the energy gap, number of quanta, total energy, or the dynamics of the vibrational motion. The van der Waals potential is virtually identical in the two electronic states. (42 refs.)

60915 Intramolecular vibrational relaxation: effects on electronic nonradiative relaxation rates. M.D. Morse, A.C. Pui, R.E. Smalley (Dept. of Chem., Rice Univ., Houston, TX, USA).

J. Chem. Phys. (USA), vol.78, no.6, pt.2, p.3435-44 (15 March 1983).

The effects of intramolecular vibrational relaxation (IVR) on radiationless transition rates are investigated. IVR has previously been suggested as an explanation of the observed saturation of the decay rate in tetrazene $S_1 \leftarrow S_0$ internal conversion and in toluene $T_1 \leftarrow S_0$ intersystem crossing at high vibrational energies. Explicit calculations for transition rates under weak coupling in the statistical limit are presented which demonstrate that when IVR is operative a slow exponential increase of the nonradiative decay rate with vibrational energy is expected, in contrast to the experimentally observed rapid increase followed by saturation at higher vibrational energies. Speculations of alternative decay mechanisms are presented, and new, simple approximate formulas are derived for the relative nonradiative decay rates of single vibronic levels. (43 refs.)

60916 Transfer of state multipoles in open shell molecule-open shell molecule scattering. B.J. Whitaker, A.J. McCaffery (School of Chem. & Molecular Sci., Univ. of Sussex, Brighton, England).

J. Chem. Phys. (USA), vol.78, no.6, pt.2, p.3857-68 (15 March 1983).

General expressions are derived for the transfer of state multipoles in open shell polyatomic-open shell polyatomic rotationally inelastic collisions. These are then used to write expressions for the circular polarizations of spin and rotationally resolved spectral emission lines. Using the distorted wave Born approximation (DWBA), circular polarization ratios are calculated for the specific case of inelastic $\text{H} + \text{NH}_2$ collisions. The potential is decomposed into a spin-dependent term and an exchange term using tensor methods to facilitate the calculation. Alternatively, the scattering may be considered to take place on singlet or triplet surfaces. An interesting feature of the results is that rotation appears to be faster on the triplet surface than on the singlet. (25 refs.)

60917 Vibrational relaxation of gaseous $\text{CO}(\nu=1)$ and $\text{N}_2(\nu=1)$ from 300K to liquid temperatures: a comparison with liquid state relaxation. E.A. Gregory, M. Maricq, R.M. Siddles, C.T. Wickham-Jones, C.J.S.M. Simpson (Phys. Chem. Lab., Univ. of Oxford, Oxford, England).

J. Chem. Phys. (USA), vol.78, no.6, pt.2, p.3881-92 (15 March 1983).

The V-V energy transfer rate constants are reported for the deactivation of both $\text{CO}(\nu=1)$ and $\text{N}_2(\nu=1)$ by O_2 and CH_4 in the temperature range 300 to 80K. The results are obtained by an infrared fluorescence technique. In order to study the relaxation of $\text{N}_2(\nu=1)$, a small amount of CO is added to the gas mixture to function both as a pump and a probe. The probability vs. temperature curves are approximately parallel for the deactivation of $\text{CO}(\nu=1)$ as compared to the $\text{N}_2(\nu=1)$. This temperature dependence is found to resemble that for the V-T deactivation of CO at low temperatures. This is due to the large mismatch for these V-V energy transfer processes. The rate constants at liquid N_2 temperatures are compared with rate constants measured by other researchers for relaxation of the same systems in the liquid phase. The results show that the relaxation rate constants, expressed in terms of $\text{cm}^3 \text{ s}^{-1} \text{ molecule}^{-1}$, are approximately equal in the two phases. The implications of this result with respect to the cell and statistical models of vibrational relaxation in liquids is discussed. (56 refs.)

60918 Fast and exceptionally slow vibrational energy transfer in acetylene and phenylacetylene in solution. W. Zinth, C. Kolmeder, B. Benna, A. Irgens-Defregger, S.F. Fischer, W. Kaiser (Phys. Dept., Tech. Univ. Munchen, Munchen, Germany).

J. Chem. Phys. (USA), vol.78, no.6, pt.2, p.3916-21 (15 March 1983).

The excitation of the CH-stretching mode (ν_3) of C_2H_2 in CCl_4 leads to fast population ($< 2 \text{ ps}$) and very slow depopulation (240 ps) of the symmetric CC-stretching mode (ν_2). The long lifetime of ν_2 is due to the absence of anharmonic interaction to neighboring states (symmetry forbidden). The corresponding CC-stretching mode of $\text{C}_6\text{H}_5\text{-C}_2\text{H}$ has a lifetime of 15 ps. The phenyl group relaxes the symmetry restrictions and introduces new decay channels. (9 refs.)

60919 Very low energy collision induced vibrational relaxation of $^1\text{A}_g$ glyoxal. C. Jouve, M. Sulkes, S.A. Rice (Dept. of Chem. & James Franck Inst., Univ. of Chicago, Chicago, IL, USA).

J. Chem. Phys. (USA), vol.78, no.6, pt.2, p.3935-41 (15 March 1983).

The authors report the results of a study of very low energy collision induced vibrational relaxation of $^1\text{A}_g$ glyoxal. The effective collision energy is found to be different from different initial vibronic states, and the final states populated are drawn from a small subset of all available final states. The observed pathways of relaxation are interpreted using a previously proposed orbiting resonance model for the He: glyoxal collisions. It is inferred that (i) single collision-single quantum transfers dominate the relaxation process, and (ii) when there are near degeneracies in the vibrational manifold the lowering of symmetry in the orbiting resonance can permit mode mixing that is prohibited in the isolated molecule. (12 refs.)

60920 Vibrational energy transfer in atom-polyatomic collisions: the role of intramolecular dynamics in Li^+/CO_2 and $\text{Li}^+/\text{N}_2\text{O}$. E. Viallonga, D.A. Micha (Dept. of Chem. & Phys., Univ. of Florida, Gainesville, FL, USA).

J. Chem. Phys. (USA), vol.78, no.6, pt.2, p.3942-51 (15 March 1983).

Using a quantum many-body theory of hyperthermal atom-polyatomic collisions, the authors present a detailed study of the role of intramolecular dynamics in vibrational energy transfer. In this approach, differential vibrational cross sections are given by time-correlation functions (TCFs) of the motions of the target atoms. Slow rotations of polyatomic molecules are decoupled from vibrations, and the authors concentrate on vibrational energy transfer. The dependence of the TCFs on collision energy, scattering angle, and changes in vibrational quantum numbers is examined in detail for a general polyatomic, and it is shown how each target atom contributes to vibrational energy transfer. For the systems Li^+/CO_2 and $\text{Li}^+/\text{N}_2\text{O}$, they present vibrational differential cross sections calculated with new multicenter short-range potentials obtained from the uniform electron-gas model. Comparison of theoretical results with experimental measurements of the Li^+/CO_2 system shows good agreement for several collision energies and scattering angles. Furthermore, they show how the structure of the vibrational cross section is related to the atomic parameters of the target and to the relative sizes of the repulsive cores of the intermolecular potential. (33 refs.)

60921 Collision dynamical information from pressure broadening measurements: Application to carbon monoxide. J.J. Del Bruno (Dept. of Chem., Princeton Univ., Princeton, NJ, USA), J. Gelfand, H. Rabitz.

J. Chem. Phys. (USA), vol.78, no.6, pt.2, p.3990-8 (15 March 1983).

Self- and helium-broadened carbon monoxide linewidths have been inverted to obtain state-to-state rate constants using the energy corrected sudden scaling formalism. Selected rotation-rotation and rotation-translation rate constants are discussed as a function of vibrational and rotational levels for the CO-CO and He-CO systems. The authors find that there is no dependence of the collision dynamics upon the vibrational state of the collision partners up to $v=3$. In addition, relaxation in both these systems is found to be dominated by rotation-translation collisions. However they are qualitatively different in their dynamical characteristics and result in significantly varied state-to-state rate constants. An analysis of the effect of collision partners in the CO-X ($\text{X} = \text{CO}, \text{He}, \text{Ne}, \text{Ar}, \text{Xe}, \text{H}_2$) system is presented. Comparisons are made with the available data in the literature. (26 refs.)

60922 State resolved rotational excitation in HD+D₂ collisions. II. Angular dependence of 0-2 transitions. U. Buck, F. Huisken, G. Maneke (Max-Planck-Inst. fur Stromungsforschung, Gottingen, Germany), J. Schaefer.

J. Chem. Phys. (USA), vol.78, no.7, p.4430-8 (1 April 1983).

For pt.1 see ibid., vol.74, no.1, p.535, 1981. Time-of-flight spectra for the scattering of HD molecules from D₂ molecules have been measured at a collision energy of $E = 70.3 \text{ meV}$ over a range of center-of-mass scattering angles from 45° to 158° . The spectra reveal clearly resolved transitions at the energy loss $\Delta E = 33 \text{ meV}$ which corresponds to 0-2 transitions of HD and the double transition 0-1 of HD and 0-2 of D₂. The differential cross

sections derived from these spectra increase with increasing scattering angle from 1.7% to 34.7% of the elastic cross section. The pure 0-2 transition of D_2 which only needs 22 meV to be induced could not be detected within the experimental sensitivity of $0.02 \text{ \AA}^2/\text{sr}$. Closed coupled calculations based on the ab initio potential surface of Meyer and Schaefer show that this result can be explained by the different coupling terms which are responsible for these transitions. In contrast to the 0-1 transition the 0-2 transition of HD proved to be sensitive to the anisotropic part of the interaction potential for the homonuclear system. The comparison of experimental and calculated cross sections for the ab initio potential of Meyer and Schaefer reveals discrepancies for the 0-1 transition of HD, but shows agreement for the 0-2 transition of HD at intermediate angles. (28 refs.)

60923 State resolved rotational excitation in D_2+H_2 collisions. U.Buck, F.Huisken, A.Kohlhase, D.Otten (Max-Planck-Inst. für Stromungsforschung, Göttingen, Germany), J.Schaefer.

J. Chem. Phys. (USA), vol.78, no.7, p.4439-50 (1 April 1983). In a crossed molecular beam experiment time-of-flight distributions of ortho D_2 molecules scattered from normal H_2 (nH_2) and para H_2 (pH_2) have been measured in a center-of-mass angular range of 75° to 180° . The collision energies were 84.1 and 87.2 meV, respectively. In all spectra the rotational excitation of D_2 from $j=0$ to $j=2$ has been resolved. With pH_2 as secondary beam the same transition could also be observed for H_2 . The measurements show that the probability for rotational excitation of D_2 depends on whether the scattering partner H_2 is rotating (nH_2) or not (pH_2). In the first case the cross sections are larger by a factor of approximately 2. The reason for this behaviour is the presence of an additional interaction term which is at long range distances, identical to the quadrupole-quadrupole interaction and which is absent if H_2 is in the $j=0$ state. The experimentally derived differential cross sections for the rotational excitation of D_2 and H_2 are compared with theoretical results obtained by close coupling calculations based on the ab initio potential surface of Meyer and Schaefer. The comparison shows a remarkable agreement. However, small deviations in the positions of the diffraction oscillations of the elastic differential cross section curve suggest that the isotropic potential term has to be shifted to smaller distances. In order to maintain the relative position of the inelastic differential cross section curves which are well predicted by the ab initio potential the same shift has to be applied to the anisotropic potential terms. (39 refs.)

60924 Rotational relaxation of HF in a free-jet expansion of dilute HF-He mixtures: information content on state-to-state rate constants. T.E.Gough (Univ. of Waterloo, Waterloo, Ontario, Canada), R.E.Miller.

J. Chem. Phys. (USA), vol.78, no.7, p.4486-93 (1 April 1983). An F-center laser-molecular beam spectroscopy has been used to provide detailed information concerning the translational and rotational relaxation resulting from the free-jet expansion of dilute mixtures of hydrogen fluoride in helium. The observed non-Boltzmann rotational state distributions are modeled using an empirical kinetic approach and are shown to contain information concerning the individual state-to-state rate constants for HF-He. (22 refs.)

60925 Quantum theory of vibrational, rotational, and translational energy exchange in collisions of polyatomic molecules. Application to methyl halides. A.Miklavc (Boris Kidric Inst. of Chem., Ljubljana, Yugoslavia).

J. Chem. Phys. (USA), vol.78, no.7, p.4502-14 (1 April 1983). The author derives a quantum theory of inter- and intramolecular transfer of vibrational, rotational, and translational energy in collisions of polyatomic molecules, in the case that short range forces between the collision partners are of prevailing importance. For this purpose, he first transforms the Hamiltonian into the form which enables him to eliminate the coordinates which are cyclic in the limit of zero range forces and can thus be expected to be approximately ignorable when forces are of short, but finite, range. Instead of six rotational and three translational coordinates one is then left with one single relevant generalized coordinate. The corresponding mass can easily be calculated; it depends on the usual reduced mass of the colliding molecules, on their moments of inertia, and on the geometry of the potential surface. The motion of the only relevant generalized coordinate is then quantized. To calculate the probabilities for the collision induced vibrational-rotational transitions, one can make use of any of a large number of the approximation schemes which have been developed in scattering theory. In the present work, the author uses the distorted wave expansion, for its simplicity and also because it leads, in the corresponding limit, directly to the results obtained recently by the semiclassical theory. As an application, he studies vibrational deactivation probabilities of methyl halides colliding with inert gases: He, Ne, Ar, Kr, and Xe. Calculations are performed for two intermolecular potentials: exponential repulsive and Morse potential. The results obtained by the two potentials are very similar and agree well with the measured vibrational transition probabilities. (33 refs.)

60926 A theoretical study on the mechanism of electronic to vibrational energy transfer in $Hg(^3P)+CO$ collisions. S.Kato (Inst. for Molecular Sci., Okazaki, Japan), R.L.Jaffe, A.Komornicki, K.Morokuma.

J. Chem. Phys. (USA), vol.78, no.7, p.4567-80 (1 April 1983). The mechanism of electronic-to-vibrational ($E-V$) energy transfer in $Hg(^3P)+CO$ collisions has been studied theoretically. The configuration interaction (CI) method was employed to calculate potential energy surfaces of the collision system. A simplified theoretical model, based on the reaction coordinate concept and the calculated potential energy characteristics, was used to discuss the mechanism of the singlet-triplet transition and the energy disposal in the collision. The results obtained were that: (a) the quenching process proceeds via a collision complex mechanism; and that (b) the triplet-singlet transition occurs near the collinear geometry. A model classical trajectory calculation gives a product CO vibrational distribution in good agreement with the experimental result. (31 refs.)

60927 Ion energy-loss spectroscopy for the collisions of $Kr^+(^2P_{1/2})$ with N_2 , CO, NO and O_2 . Y.Itoh, T.Nakamura, N.Kobayashi, Y.Kaneko (Dept. of Phys., Tokyo Metropolitan Univ., Tokyo, Japan).

J. Phys. Soc. Jpn. (Japan), vol.52, no.4, p.1091-4 (April 1983). Ion energy-loss spectra for 1308 eV $Kr^+(^2P_{1/2})$ incident on N_2 , CO, NO and O_2 were measured. For all molecules, fine-structure transitions between different J states of the projectile and vibrational excitations of the molecules were observed. In the case of N_2 and NO, the spectra were relatively simple and only the excitations of fundamental vibrations were found. For CO and O_2 , the excitations of the harmonics, $v=0-2$, were also observed. In addition to these, for CO, the peak due to the process, $Kr^+(^2P_{1/2})+CO(\Sigma, v=0) \rightarrow Kr^+(^2P_{3/2})+CO(\Sigma, v=1)$, was found. For O_2 , the peak due to the electronic excitation in the target, $^3\Sigma \rightarrow ^1\Delta$, was observed as well as the prominent peak corresponding to the process, $Kr^+(^2P_{1/2})+O_2(\Sigma, v=0) \rightarrow Kr^+(^2P_{3/2})+O_2(\Delta, v=0)$.

60928 Laser-induced fluorescence studies of vibrational and rotational relaxation in a supersonic molecular beam of bromine monochloride. J.W.Farthing, I.W.Fletcher, J.C.Whitehead (Dept. of Chem., Univ. of Manchester, Manchester, England).

Mol. Phys. (GB), vol.48, no.5, p.1067-73 (10 April 1983). Using time-of-flight and laser-induced fluorescence methods, the efficiencies of rotational and vibrational relaxation of BrCl by Cl_2 have been studied by measuring the final translational, rotational and vibrational temperatures of a supersonic beam of BrCl seeded in Cl_2 . Collision numbers, $Z_R \sim 1$ and $Z_V \sim 28$, have been obtained. Rotational relaxation is found to occur at a rate close to gas kinetic. Vibrational relaxation appears to be very efficient at the low temperatures of the beam and this is attributed to additional relaxation being achieved due to the formation of metastable orbiting complexes. (26 refs.)

60929 Collisional depopulation of Na ns states by H_2 and CO. T.F.Gallagher, K.A.Safinya, G.A.Ruff (Molecular Phys. Lab., SRI Internat., Menlo Park, CA, USA).

Phys. Rev. A (USA), vol.27, no.4, p.2222-4 (April 1983). The authors report the measurement of the depopulation cross sections of the Na ns states from $n=5$ to 11 by H_2 and CO, using a time- and wavelength-resolved fluorescence approach. The cross sections rise to a plateau value of 60 and 160 \AA for H_2 and CO, respectively. The increased size of the cross sections relative to those for the rare gases is attributed to energy transfer to molecular vibration. (11 refs.)

60930 Study of rotational transfer by collision in diatomic molecules. J.Derouard, J.Dufayard (Lab. de Spectrometrie Phys., Univ. Sci. et Medicales de Grenoble, Grenoble, France), O.Nedelec, N.Sadeghi.

Rev. Cethedec (France), vol.19, no.NS82-2, p.113-41 (1982). In French. The laser induced fluorescence technique has been used for studying angular momentum transfer in diatomic molecules upon collisions with various partners. Two types of molecules have been studied, which provide complementary information concerning the different aspects of the process: first diatomic hydrides $BH^+(A \text{ } ^1\Pi)$ and $COH^+(A \text{ } ^2\Pi_{1/2})$ colliding with He, Ar and H_2 , then iodine molecule $I_2^+(B_0, ^+)$ colliding with He, Ne, Ar, and I_2 . In the first case it has been found that the rotational transfer rates depend strongly on the symmetry of the levels involved; this is explained within the first Born approximation as resulting from the symmetry of the electronic state of the hydride considered. In the case of I_2 , a large number of transfer rates have been measured in order to determine whether ECS scaling laws (Brunner et al., 1981) are justified. In fact, the I_2+He transfer rates show an exponentially declining behaviour as a function of the exchanged angular momentum; on the contrary in the other cases, I_2+Ne , Ar or I_2 , one observes the usual inverse power scaling law in Δj . Three parameters are sufficient in each case to reproduce all the measured rotational transfer rates. Also collisional de-excitation rates have been determined. (31 refs.)

60931 Diffusion description of vibrational relaxation in a binary mixture of diatomic molecules (Harmonic oscillators). V.M.Volokhov, O.V.Skrebkov (Inst. of Chem. Phys., Acad. of Sci., Moscow, USSR).

Theor. & Exp. Chem. (USA), vol.18, no.2, p.111-17 (March-April 1982). Translation of: *Teor. & Eksp. Khim. (USSR)*, vol.18, no.2, p.131-8 (March-April 1982). [received: Feb. 1983]. The authors show how one can apply the formalism of classical diffusion theory to the vibrational relaxation of diatomic molecules in order to use models for harmonic and quasiharmonic oscillators (anharmonic one-mode oscillators) to allow for the effects of multiquantum transitions. (6 refs.)

Vibrational phase relaxation in ethane at moderate densities, including the critical region See Entry 60727

Microwave studies of collision-induced transitions between rotational levels. VIII. Collisions between NH_3 and polar molecules See Entry 60772

A microwave double resonance study of collision-induced transitions between the M components of a rotational transition of OCS See Entry 60773

Vibrational relaxation of HCN(002) See Entry 60808

Intramolecular vibrational relaxation from C-H stretch fundamentals See Entry 60809

The collisional flow of vibrational energy into surrounding vibrational fields within S_1 benzene See Entry 60810

Rotational relaxation in ground-state p-difluorobenzene: State selection by stimulated emission pumping See Entry 60815

Vibrational relaxation within mixed electronic states See Entry 60816

Laser induced fluorescence studies of XeF(B-X) See Entry 60830

Effect of foreign gases on IR absorption bands of polyatomic molecules See Entry 60844

On the statistics of an ensemble of oscillators under excitation. IV. Evaluation of the time for kinetic excitation into the quasicontinuum based on Kramers' theory See Entry 60846

A complete energy transfer map for COF_2 See Entry 60902

Double infrared-third-harmonic-generation resonance as a method for investigating vibrational energy exchange See Entry 61021

Time scale considerations on the relaxation of electronic and vibrational energy distributions in a nitrogen afterglow See Entry 61716

Rovibrational excitation within the infinite conical well: desorption of diatomic molecules See Entry 62268

Internal state distributions of molecules scattering and desorbing from surfaces See Entry 63120

Measurements of collisional energy transfer in unimolecular processes See Entry 63501

Vibrational energy disposal in reactions of fluorine atoms with hydrides of groups III, IV and V See Entry 63514

Selective vibrational excitation of the ethylene-fluorine reaction in a nitrogen matrix. I See Entry 63521

Vibrational energy transfer efficiency in a three-channel thermal unimolecular system. Temperature dependence See Entry 63529

Adiabatic T matrix theory for three dimensional reactive scattering: application to the (H, H_2) system See Entry 63534

34.50H Electronic excitation and ionization (inc. beam-foil excitation and ionization)

60932 Experimental observation of the intercollisional interference effect on the S_1 pure rotation line of the collision induced spectra of the H_2 -He mixture. G.Bachet (Lab. des Interactions Atomiques et Moléculaires, Marseille, France).

C.R. Seances Acad. Sci. Ser. II (France), vol.296, no.5, p.325-8 (7 Feb. 1983). In French.

The absorption coefficients of the collision induced spectrum of the interaction H_2 -He at 300K between 200 and 700 cm^{-1} are presented. A lack of absorption (dip) due to the intercollisional interference effect is clearly seen at the frequency of the pure rotation line S_1 of the free molecule of H_2 . (15 refs.)

60933 Recent developments in accelerator based atomic physics. S.Datz (Oak Ridge Nat. Lab., Oak Ridge, TN, USA).

IEEE Trans. Nucl. Sci. (USA), vol.ns-30, no.2, p.881-6 (April 1983). (1982 IEEE Conference on the Application of Accelerators in Research and Industry, Denton, TX, USA, 8-10 Nov. 1982).

Much progress toward a detailed understanding of atomic collision phenomena and atomic structure has recently been made with the aid of accelerated ion beams. Beams foil Lamb shift measurements and the possible observation of spontaneously created positrons from quasi-superheavy atoms give promise for critical tests of QED. The mechanisms of inner-shell ionization and charge transfer in ion atom collisions have been intensively investigated and the results have brought together the various approaches—Coulomb excitation and MO treatments for these processes. That violent collisions at high energies can cause multiple ionization of the target atom has been known for some time. However, only recently have theoretical treatments been able to predict, e.g. the degree of L shell ionization accompanying K shell ionization. The highly charged ions formed in these collisions have themselves come under intensive investigation and are used for the study of the structure and collision physics of multiply charged species. Electro-Ion collision studies have also been started and initial results on dielectronic recombination are reported. (27 refs.)

60934 Simultaneous electron capture and excitation in ion-atom collisions. J.A.Tanis, E.M.Bernstein (Western Michigan Univ., Kalamazoo, MI, USA), W.G.Graham, M.Clark, S.M.Shafroth, B.M.Johnson, K.Jones, M.Meron.

IEEE Trans. Nucl. Sci. (USA), vol.ns-30, no.2, p.898-901 (April 1983). (1982 IEEE Conference on the Application of Accelerators in Research and Industry, Denton, TX, USA, 8-10 Nov. 1982).

A review of recent efforts to observe simultaneous electron capture-and-K-shell excitation in ion-atom collisions is presented. This process which has been referred to as resonant-transfer-and-excitation (RTE), is qualitatively analogous to dielectronic recombination (inverse Auger transition) in free-electron-ion collisions, and hence, is expected to be resonant. Experimentally, events having the correct signature for simultaneous capture-and-excitation are isolated by detecting projectile K X-rays in coincidence with ions which capture a single electron. In a recent experiment involving 70-160 MeV S^{3+} ions incident on Ar, a maximum was observed in the yield of projectile K X-rays associated with electron capture. This maximum is attributed to simultaneous capture- and excitation. The position (120 MeV) and width (60 MeV) of the observed maximum are in good agreement with theoretical calculations. The data indicate that RTE is an important mechanism for inner-shell vacancy production in the energy range studied. (10 refs.)

60935 Electron capture in M-shell X-ray production from heavy elements by 25- and 35-MeV fluorine ions. R.Mehta, J.L.Duggan, F.D.McDaniel, M.C.Andrews (Dept. of Phys., North Texas State Univ., Denton, TX, USA), G.Lapicki, P.D.Miller, L.A.Rayburn, A.R.Zander.

IEEE Trans. Nucl. Sci. (USA), vol.ns-30, no.2, p.906-8 (April 1983). (1982 IEEE Conference on the Application of Accelerators in Research and Industry, Denton, TX, USA, 8-10 Nov. 1982).

M-shell X-ray production cross sections have been measured for thin solid targets ($\sim 2 \mu g/cm^2$) of Au, Pb, Bi, and U for 25 and 35 MeV incident F^{9+} ions ($q=4, 5, 6, 8, 9$). The target M-shell X-ray production cross sections by projectiles with one or two K-shell vacancies are found to be enhanced over those by projectiles without K-shell vacancies. The cross sections averaged over target thickness were measured as a function of target thicknesses. Electron capture (EC) to the L-, M-, ... shells and EC to the K-shell of the projectile, have been extracted from the data. (11 refs.)

60936 Mechanisms for rapid electron transfer in ionic solids following multiple ionization by heavy-ion impact. R.L.Watson, O.Benka, K.Parthasaradhi, R.A.Kenefick, R.J.Maurer, J.M.Sanders, B.Bandong, T.Ritter (Cyclotron Inst., Texas A&M Univ., College Station, TX, USA).

IEEE Trans. Nucl. Sci. (USA), vol.ns-30, no.2, p.919-22 (April 1983). (1982 IEEE Conference on the Application of Accelerators in Research and Industry, Denton, TX, USA, 8-10 Nov. 1982).

Systematic measurements of the spectra of fluorine K α X-rays produced by the bombardment of alkali and alkaline earth fluorides with 2-MeV/amu ions ranging from He to Ar have given new information on the mechanisms for rapid electron transfer within the K-hole lifetime ($\sim 10^{-13}$ sec.). Spectra obtained with He ions provide clear evidence of the occurrence of resonant electron transfer (RET) following $1s_{2p}$ ionization of F^- in the compounds KF and SrF $_2$. Calculations employing a point-charge model support the conclusion that the anomalously low KL X-ray satellite intensities observed for these two compounds are the result of a resonant exchange of an electron between the outermost p level of the metal ion and the 2p level of the fluorine ion. (10 refs.)

60937 Multiple ionization of atomic targets by proton impact. L.H.Toburen, R.D.DuBois (Pacific Northwest Lab., Richland, WA, USA), S.T.Manson.

IEEE Trans. Nucl. Sci. (USA), vol.ns-30, no.2, p.923-7 (April 1983). (1982 IEEE Conference on the Application of Accelerators in Research and Industry, Denton, TX, USA, 8-10 Nov. 1982).

The authors have combined experimental measurements of multiply charged ion production, doubly differential electron emission cross sections and Auger electron spectra produced in fast-proton noble-gas collisions with theoretical inner and outer shell ionization cross sections in an effort to provide a unified description of the ionization process. A detailed analysis is provided for 1.4 MeV proton ionization of krypton. They measured relative yields of Kr^{+2} and Kr^{+3} ions are in approximate agreement with the photoionization results of Krause and Carlson (1966). If one assumes nearly half of the 3d vacancies created in Kr are filled through multiple (3dNNN) Auger transitions, the M-subshell ionization cross sections that they derive from their Auger electron spectra are in good agreement with theoretical calculations. The measured absolute yields of Kr^{+2} and Kr^{+3} are, however, a factor of 2 smaller than those derived from the decay of inner shell vacancies. This discrepancy leads

the authors to believe that multiple ionization in the initial interaction is a significant contribution to the observed yields. (8 refs.)

60938 M-shell X-ray production cross sections for 19 elements in the range $Z=54-92$ by H^+ and He^{+2} ions from 300 keV to 40 MeV. R.Mehta, J.L.Duggan, F.D.McDaniel, P.M.Kocur, J.L.Price (Dept. of Phys., North Texas State Univ., Denton, TX, USA).

IEEE Trans. Nucl. Sci. (USA), vol.ns-30, no.2, p.950-3 (April 1983). (1982 IEEE Conference on the Application of Accelerators in Research and Industry, Denton, TX, USA, 8-10 Nov. 1982).

Measurements performed over the last three decades at various laboratories are surveyed. The elements studied were Xe, Pr, Nd, Sm, Eu, Gd, Tb, Dy, Ho, Yb, Hf, Ta, W, Pt, Au, Hg, Pb, Bi, and U. The projectile energies investigated range from 300 keV to 40 MeV for the protons and 250 keV to 2.5 MeV for He^+ ions. Also reported are the M-shell X-ray production cross sections of some rare-earth elements recently measured at NTSU. For these measurements the energy of incident H^+ and He^+ ions ranged from 0.25 to 2.5 MeV. The experimental data are compared to the M-shell ionization cross section predictions of first Born approximation. Comparison is also made with the theory by Brandt and Lapicki that goes beyond the first Born approximation. (24 refs.)

60939 Deuteron and alpha-induced K-shell ionization cross section ratios in the $Z=12-17$ region. J.S.Lopes (Dept. de Fisica, Faculdade de Ciencias, Univ. de Lisboa, Lisboa, Portugal), A.P.Jesus, M.F.da Silva.

IEEE Trans. Nucl. Sci. (USA), vol.ns-30, no.2, p.954-6 (April 1983). (1982 IEEE Conference on the Application of Accelerators in Research and Industry, Denton, TX, USA, 8-10 Nov. 1982).

Experimental deuteron- and alpha-induced K-shell ionization cross section ratios are presented for elements ranging from Mg to Cl ($Z=12-17$) in the incident energy range 0.2 to 0.45 MeV/u. The experimental ratios $R=\sigma_{\alpha}/\sigma_d$ are generally close but slightly higher than the theoretical ratios calculated according to the procedure of Brandt and Lapicki (1979); the largest differences occur for Al and Si where the experimental values are 15-20% too high. The experimental ratios show roughly the same dependence on reduced projectile velocity, $\xi=(v_1/v_K)(2/\eta_K)$, as the theoretical ones in the reduced incident velocity range used in the present work, $\xi=0.45$ to $\xi=1$. This is in opposition to the results previously obtained in the velocity range $\xi=0.25$ to $\xi=0.55$ for elements ranging from Ca to Cu ($Z=20-29$), where the observed ratios are rather independent of the reduced velocity. (10 refs.)

60940 Proton-induced K-vacancy production cross sections for Sc, Ti, V, Cr, Co, Ni, Cu, and Zn. M.D.Brown, D.G.Simons, D.J.Land, J.G.Brennan (Naval Surface Weapons Center, Silver Spring, MD, USA).

IEEE Trans. Nucl. Sci. (USA), vol.ns-30, no.2, p.957-60 (April 1983). (1982 IEEE Conference on the Application of Accelerators in Research and Industry, Denton, TX, USA, 8-10 Nov. 1982).

Absolute K-shell X-ray-production cross sections have been measured for thin-foil targets of Sc, Ti, V, Cr, Co, Ni, Cu; and Zn for incident protons with energies from 500 to 2200 keV. In order to determine the X-ray production cross sections with high precision ($\approx 5\%$), particular care was necessary in the control of experimental conditions. The overall agreement of the proton-induced cross sections with recent data obtained by other workers generally is to within 10% and frequently is to within the 5% accuracy of the results. (7 refs.)

60941 Recent results on K-shell ionization by ion collisions. L.Avaldi, M.Milazzo, G.Trivisa (Istituto di Fisica Generale Applicata, Milano, Italy), I.V.Mitchell.

IEEE Trans. Nucl. Sci. (USA), vol.ns-30, no.2, p.961-3 (April 1983). (1982 IEEE Conference on the Application of Accelerators in Research and Industry, Denton, TX, USA, 8-10 Nov. 1982).

The experimental K-shell ionization cross sections of Cd, Sn, Te, I and Ba for alpha particles, between 2.2 MeV and 2.8 MeV, and of Te for protons, between 1.6 and 3 MeV, are presented. The justification for making these measurements comes, on the one hand, in filling a region where, at present, data are sparse (for example, Te ionization cross sections by alpha particles have never been reported before), and, on the other hand, checking between previously reported and diverging sets of experimental results. (10 refs.)

60942 L-subshell X-ray production cross sections of Ba, La and Ce for proton energies from 0.25 to 2.00 MeV. L.A.Rayburn (Dept. of Phys., Univ. of Texas, Arlington, TX, USA).

IEEE Trans. Nucl. Sci. (USA), vol.ns-30, no.2, p.964-6 (April 1983). (1982 IEEE Conference on the Application of Accelerators in Research and Industry, Denton, TX, USA, 8-10 Nov. 1982).

Protons from the University of Texas at Arlington's 2 MV Van de Graaff accelerator were used to produce characteristic L X-rays from thin targets of Ba, La and Ce. The incident proton energy was varied from 0.25 to 2.00 MeV. The X-rays were detected by a detector mounted at 90° to the incident beam direction. Measured X-ray production cross sections were converted to ionization cross sections by the use of subshell fluorescence yields and Coster-Kronig transition probabilities taken from Bambynek (1972). Inflection points are found in the L_1 -subshell ionization cross section for all three elements. (14 refs.)

60943 Proton induced L-subshell ionization on silver and iodine. E.Rosato, P.Cuzzocrea, N.De Cesare, E.Perillo, G.Spadacini (Istituto di Fisica Sperimentale, Univ. di Napoli, Napoli, Italy).

IEEE Trans. Nucl. Sci. (USA), vol.ns-30, no.2, p.967-9 (April 1983). (1982 IEEE Conference on the Application of Accelerators in Research and Industry, Denton, TX, USA, 8-10 Nov. 1982).

L-X-ray production cross sections were measured in the proton energy range 0.3-5.0 MeV for Ag and I. Subshell ionization cross sections were extracted and compared with predictions of the perturbed stationary state theory, the binary encounter approximation and the semiclassical approximation with binding, polarization, relativistic, energy loss and Coulomb deflection corrections included (ECPSSR, BEABC, SCABCR). The agreement is quite good especially for the shape and the magnitude of the kink in the L_1 subshell cross section due to the node of the $2s$ wavefunction. (22 refs.)

60944 L-shell ionization of gold by nitrogen ion impact. J.Palinkas, L.Sarkadi, B.Schlenk, I.Torok, Gy.Kalman (Inst. of Nuclear Res., Hungarian Acad. of Sci., Debrecen, Hungary), C.Bauer, K.Brakoff, D.Bramble, C.Heiser, W.Rudolph, H.J.Thomas.

IEEE Trans. Nucl. Sci. (USA), vol.ns-30, no.2, p.970-2 (April 1983). (1982 IEEE Conference on the Application of Accelerators in Research and Industry, Denton, TX, USA, 8-10 Nov. 1982).

Measuring the angular distributions and the absolute intensities of the L X-ray lines of gold at 2.4-18.2 MeV nitrogen ion impact, the absolute sub-shell ionization cross-sections and the alignment parameter of the L_2 -subshell have been determined and compared to the theoretical results. (14 refs.)

60945 Single and double ionization of He by fast light ions. L.H. Andersen (Univ. of Tennessee, Knoxville, TN, USA).

IEEE Trans. Nucl. Sci. (USA), vol.ns-30, no.2, p.973-6 (April 1983). (1982 IEEE Conference on the Application of Accelerators in Research and Industry, Denton, TX, USA, 8-10 Nov. 1982).

The cross sections for single and double ionization of He by H, He, Li, B, C and O ions were measured. The ion velocity ranged from $\sim 2 v_0$ to $\sim 10 v_0$. The Bethe-Born results of Gillespie and Inokuti are found to be in good agreement with the data for single ionization at low projectile charges. The breakdown of the perturbation region is discussed and in the strong interaction region the experimental single ionization data are compared with results of Bohr and Janev. The double ionization data are presented and a theoretical estimate based on an independent electron model is discussed. (13 refs.)

60946 Recent progress in fast ion beam spectroscopy. E.J.Knystautas (Dept. de Phys., Univ. Laval, Quebec, Canada).

IEEE Trans. Nucl. Sci. (USA), vol.ns-30, no.2, p.987-90 (April 1983). (1982 IEEE Conference on the Application of Accelerators in Research and Industry, Denton, TX, USA, 8-10 Nov. 1982).

Considerable improvements in technique have recently led to greatly increased accuracy in the measurements of transition energies and lifetimes for excited states of highly stripped ions by beam-foil and beam-foil-laser spectroscopy. Such measurements for two-electron ions of high Z can now be used to determine relativistic and QED corrections for such systems to a few parts per thousand. The ion-foil interaction is now much better understood as a result of experiments which study the polarisation of the light emitted by the foil-excited beam. These and other developments in the field are discussed, including laser excitation, electron emission from the target, recoil ion spectroscopy in gases, and ion collisions with surfaces at glancing angles. (11 refs.)

60947 Vacancy-transfer cross sections and Li-vacancy lifetimes for low-energy collisions of Ar^{2+} with Mg, Al, and Si. S.J.Cipolla, M.Mildebrath (Phys. Dept., Creighton Univ., Omaha, NE, USA).

IEEE Trans. Nucl. Sci. (USA), vol.ns-30, no.2, p.999-1001 (April 1983). (1982 IEEE Conference on the Application of Accelerators in Research and Industry, Denton, TX, USA, 8-10 Nov. 1982).

Electron promotion via rotational coupling of the $2p\pi=2p\sigma$ molecular orbitals in the quasimolecule formed during a near-symmetric collision between a heavy ion and a lighter target atom has successfully explained the K X-ray emission from the target atom. For atoms in a solid target, the target density fosters a double-collision mechanism whereby a fraction of the ion beam brings an L-shell vacancy into a subsequent collision with a target atom so that K-electron transfer from the target to the projectile can occur. On this basis the authors have performed a thick-target K-shell ionization analysis on target X-ray yields for 160-380 keV Ar^{2+} impinging on Mg, Al, and Si. The measurements yield the equilibrium L-vacancy fraction and the L-vacancy lifetime for the Ar^{2+} beam moving through these targets. (16 refs.)

60948 A study of transfer excitation in $\text{F}^{8+}+\text{He}$, Ne and Ar collisions. P.L.Pepmiller, P.Richard, J.Newcomb, R.Dillingham, J.M.Hall, T.J.Gray, M.Stockli (Dept. of Phys., Kansas State Univ., Manhattan, KS, USA).

IEEE Trans. Nucl. Sci. (USA), vol.ns-30, no.2, p.1002-4 (April 1983). (1982 IEEE Conference on the Application of Accelerators in Research and Industry, Denton, TX, USA, 8-10 Nov. 1982).

High resolution X-ray spectroscopy has been used to measure F K X-rays resulting from the decay of doubly excited two electron states formed during $\text{F}^{8+}+\text{He}$, Ne, or Ar collisions. The energy range spanned by the spectrometer includes the $2s2p(^3\text{P})-1s2s(^3\text{S})$, $2s2p(^1\text{P})-1s2s(^1\text{S})$, $2p^2(^3\text{D})-1s2p(^3\text{P})$, $2p^2(^1\text{D})-1s2p(^1\text{P})$ and the $2p^2(^3\text{S})-1s2p(^3\text{P})$ transitions. These states may be formed by nonresonant transfer excitation, in which electron excitation is coupled with electron capture to an excited state, or by resonant transfer excitation, a process related to dielectronic recombination, in which the capture of a loosely bound target electron results in projectile electron excitation. Calculations have been performed to estimate the contribution of each process to the total measured cross section. (9 refs.)

60949 Transfer ionization in slow multiply charged ion-atom collisions. A.S.Schlachter, W.Groh, A.Müller, E.Salzborn (Lawrence Berkeley Lab., Univ. of California, Berkeley, CA, USA).

IEEE Trans. Nucl. Sci. (USA), vol.ns-30, no.2, p.1008-11 (April 1983). (1982 IEEE Conference on the Application of Accelerators in Research and Industry, Denton, TX, USA, 8-10 Nov. 1982).

Transfer ionization, or exothermic capture ionization, is found to be an important reaction mechanism in slow multiply charged ion-atom collisions: more electrons are released from the target in creating a recoil ion than are found to be captured by the projectile when viewed long after the collision. These collisions generally depend upon the internal potential energy of the collision system rather than on the projectile kinetic energy. (18 refs.)

60950 Population of the 3s state in hydrogen due to H^+ , H_2^+ and H_3^+ impact on ethylene, 1-butene and cis-2-butene. D.H.Lloyd, H.R.Dawson (Dept. of Phys., Angelo State Univ., San Angelo, TX, USA).

IEEE Trans. Nucl. Sci. (USA), vol.ns-30, no.2, p.1012-14 (April 1983). (1982 IEEE Conference on the Application of Accelerators in Research and Industry, Denton, TX, USA, 8-10 Nov. 1982).

Absolute cross sections were measured for capture or dissociation into the 3s state of atomic hydrogen due to impact of 14-28 keV H^+ , H_2^+ and H_3^+ ions on ethylene, 1-butene and cis-2-butene. The cross sections obtained for the butene targets were almost identical and support the additive rule for cross sections. Ethylene cross sections were 21% lower than the values predicted by the additive rule, which agrees well with the observed trend toward reduction in total electron capture cross sections for protons on these gases at much higher energies. (27 refs.)

60951 Coherent K-ionization using a H_2^+ beam. Cheng-Ming Fou (Dept. of Phys., Univ. of Delaware, Newark, DE, USA), T.S.Fou.

IEEE Trans. Nucl. Sci. (USA), vol.ns-30, no.2, p.1018-19 (April 1983). (1982 IEEE Conference on the Application of Accelerators in Research and Industry, Denton, TX, USA, 8-10 Nov. 1982).

A 1.0 MeV H_2^+ beam from the University of Delaware Van de Graaff accelerator was used to bombard a thin nickel target. Characteristic K X-ray from Ni was measured with a thin NaI(Tl) detector in coincidence with protons scattered into 90° and 165° lab angles. The energy of the protons detected in those angles corresponds to the elastic scattering of 0.5 MeV incident H^+ beam because of the negligible (2.65 eV) bound energy between H and proton in H_2^+ . However, the ionization probabilities measured in the 1 MeV H_2^+ beam case differ from that measured with a 0.5 MeV proton beam. While the ionization probability for the 165° scattering is increased with the H_2^+ beam, the reverse is true for the 90° scattering. Possible coherent effect is being considered. (4 refs.)

60952 Effects of a polarized wave function in calculations of inner-shell ionization probability. D.J.Land, G.Basbas, M.D.Brown, D.G.Simons (Naval Surface Weapons Center, Silver Spring, MD, USA).

IEEE Trans. Nucl. Sci. (USA), vol.ns-30, no.2, p.1103-5 (April 1983). (1982 IEEE Conference on the Application of Accelerators in Research and Industry, Denton, TX, USA, 8-10 Nov. 1982).

Theoretical calculations for the proton-induced K-shell ionization probability in which the ground-state electron wave function is allowed to be polarized under the influence of the incident projectile are described. These calculations extend the results of a previous theoretical model in which the wave function is allowed only a spherically symmetric distortion. The model is based upon lowest-order perturbed-stationary-state theory. Comparisons between calculations performed with different wave functions as well as between calculations performed with the polarized wave function and experimental data are shown for 0.3 to 2.4 MeV protons in titanium. (10 refs.)

60953 Effects of a nuclear scattering resonance on bremsstrahlung production and K-shell ionization. C.C.Trail, P.M.S.Lesser, M.K.Liou (Brooklyn Coll., City Univ. of New York, New York, NY, USA).

IEEE Trans. Nucl. Sci. (USA), vol.ns-30, no.2, p.1124-7 (April 1983). (1982 IEEE Conference on the Application of Accelerators in Research and Industry, Denton, TX, USA, 8-10 Nov. 1982).

While the effects of nuclear resonances on nuclear bremsstrahlung emission have been the focus of current bremsstrahlung studies in nuclear physics, such effects on atomic K-shell ionization have attracted much attention recently. The authors review the recent developments of these two topics with the emphasis upon their common features. Special attention is given to the effect of the nuclear resonance near 461 keV in p^{12}C where experimental results are available for bremsstrahlung production and K-shell ionization. (17 refs.)

60954 Effective ionic radii of NO_2^- and SCN^- estimated in terms of the Botcher equation and the Lorentz-Lorenz equation. Y.Iwade, K.Kawamura (Res. Lab. for Nuclear Reactors, Tokyo Inst. of Technol., Tokyo, Japan), K.Igarashi, J.Mochinaga.

J. Phys. Chem. (USA), vol.86, no.26, p.5205-8 (23 Dec. 1982).

The electronic polarizabilities of NO_2^- and SCN^- ions have been estimated from the refractive index data by use of the Lorentz-Lorenz equation and the Botcher equation. The effective ionic radii of NO_2^- and SCN^- have been evaluated from the obtained electronic polarizabilities to be 1.77-1.81 Å (320°C) and 2.15-2.20 Å (300°C), respectively, by using the correlation between the third power of the ionic radius and the electronic polarizability of an ion and also taking into account the structure of the ion. It has been concluded that the Botcher equation does not hold good for molten ionic liquids such as NaNO_2 and LiSCN in the optical frequency region. (27 refs.)

60955 Determination of the Penning excitation cross sections of Mg atoms by He, Ne and Ar metastable atoms. S.Inaba (Dept. of Electrical Engng., Gifu Tech. Coll., Gifu, Japan), T.Goto, S.Hattori.

J. Phys. Soc. Jpn. (Japan), vol.52, no.4, p.1164-7 (April 1983).

The relative Penning excitation rates for the individual Mg(II) states by He(2S) atoms, by He(2S) atoms and by Ne(3P) atoms have been measured separately using Penning electron spectroscopy. The absolute values of the Penning excitation cross sections have been estimated by comparing the Penning electron energy spectrum for the Mg(II) ground state with that for the Zn(II) ground state. Using the same method, the Penning excitation cross section of Mg atoms by Ar(4P) atoms has been also estimated. (13 refs.)

60956 Experimental investigation of Hornbeck-Molnar ionisation in collisions between excited He(5P) and He atoms. A.Pesnelle, S.Runge, M.Perdrix, D.Sevin, G.Watel (Service de Phys. des Atomes et des Surfaces, CENS, Gif-sur-Yvette, France).

J. Phys. B (GB), vol.16, no.7, p.L193-9 (14 April 1983).

The dependence of the Hornbeck-Molnar ionisation cross section on the relative kinetic energy of the colliding partners $\text{He(5P)}_2 + \text{He}$ has been measured for the first time over the 0.015-0.40 eV range (1200-6000 m s^{-1}) in a crossed-beam experiment using a time-of-flight technique. The 5^1P level is obtained by optical excitation of the 2^3S metastable level at 294 nm; the CW radiation is generated by intracavity frequency doubling in a ring laser. The most striking feature of this cross section is a pronounced maximum which corroborates Cohen's approach for this type of ionisation in He^* ($n=3$ and 4) + He systems. (18 refs.)

60957 Formation of molecular ions in binary collisions of excited inert-gas atoms. A.Z.Devdariani, V.I.Demidov, N.B.Kolokolov, V.I.Rubtsov (A.A. Zhdanov State Univ., Leningrad, USSR).

Sov. Tech. Phys. Lett. (USA), vol.8, no.7, p.334-5 (July 1982). Translation of: *Pisma v Zh. Tekh. Fiz. (USSR)*, vol.8, no.13-14, p.772-5 (July 1982).

Binary collisions of excited atoms at thermal energies lead to the formation of both atomic ions (through Penning ionization) and molecular ions (through associative ionization). Extremely little information on the ratio Q_m of the rate constant for associative ionization to the total ionization constant has been obtained by the mass-spectroscopy method, and the results which have been obtained for a common subject of these studies, the reaction $\text{He(2S)}_2 + \text{He(2S)}$, differ by more than an order of magnitude. The new method of plasma electron spectroscopy which combines the possibility of arranging a high density of excited atoms in afterglow experiments with the possibilities of Penning electron spectroscopy, has been used to determine Q_m from experimental spectra for the reactions $\text{He(2S)}_2 + \text{He(2S)}$ and $\text{He(2S)}_2 + \text{He(2S)}$. (6 refs.)

Atomic collision experiments utilizing low-velocity, highly-charged ion beams See Entry 60507

Electronic excited state transport among molecules distributed randomly in a finite volume See Entry 60619

Beam-foil study of the $2s^2 2p^5 \ 3/2$ and $2s^2 2p^5 \ 3/2$ configurations of Ar IX See Entry 60636

Rotational rainbow scattering in collisions of Ar with Cl_2 See Entry 60958

Electron capture to the continuum at asymptotically high velocities See Entry 60965

Additivity failure in electron capture from C-bearing molecules to continuum states of $\sim \text{MeV/u H}^+$, H^{2+} projectiles See Entry 60966

Electron capture from C-bearing molecules to bound states of 0.8-3.0 MeV H^+ : additivity corrections using electron loss cross sections See Entry 60967

Quasi-resonant K-K charge exchange in F-Ne collisions See Entry 60968

Production of 3s state hydrogen by H_2^+ impact on noble gases See Entry 60969

The use of static potentials in atomic collisions. Application to the excitation of hydrogen atoms by helium ions at intermediate energies See Entry 60974

Resonant transfer and excitation (RTE) in ion-atom collisions and dielectronic recombination in plasmas See Entry 61608

34.50L Chemical reactions, energy disposal, and angular distribution, as studied by atomic and molecular beams

(see also 31.70F and 82.20K Potential-energy surfaces, 82.40D Beam reactions)

60958 Rotational rainbow scattering in collisions of Ar with Cl_2 . M.A.Hoffbauer, S.Burdenski, C.F.Giese, W.R.Gentry (Chem. Dynamics Lab., Univ. of Minnesota, Minneapolis, MN, USA). *J. Chem. Phys. (USA)*, vol.78, no.6, pt.2, p.3832-7 (15 March 1983). The pulsed molecular beam technique has been used to measure speed and angle-resolved differential cross sections for scattering of Ar by Cl_2 , over the range of initial relative kinetic energies from 0.09 to 0.16 eV. Angular rainbows are observed at small scattering angles. At large scattering angles, the product speed distributions at constant center-of-mass scattering angles display rotational rainbow structure which corresponds to a large fraction of the initial relative kinetic energy appearing as rotational energy in the Cl_2 product. The large-angle data may be interpreted in terms of the classical rigid-ellipsoid model, which expresses the anisotropy of the potential energy surface with a single parameter. (21 refs.)

Competing dissociation channels in the infrared multiphoton decomposition of ethyl vinyl ether See Entry 60864

The reaction $\text{Hg} + \text{I}_2 \rightarrow \text{HgI} + \text{I}$ revisited See Entry 63527

34.70 CHARGE TRANSFER

(see also 82.30 Charge transfer reactions)

60959 A new diabatic molecular representation for triplet-triplet transitions in $\text{He}^+ - \text{He}^*$ collisions. T.K.Rai Dasidhar (Dept. of Chem., Univ. of Southern California, Los Angeles, CA, USA), K.Rai Dasidhar, R.Sen Gupta. *Chem. Phys. Lett. (Netherlands)*, vol.96, no.1, p.85-8 (25 March 1983). A 'frozen-orbital' diabatic basis has been constructed for an impact parameter treatment of collisions of He^+ with metastable $\text{He}(2^3\text{S})$ at 1000 eV laboratory ion energy. Except for the two highest states used, the diabatic states correlate very well with the separated-atom energies, and the $\Sigma - \Pi$ rotational couplings deviate little from the proper asymptotic behaviour ($\approx R^{-2}$). Cross sections and transition probabilities are presented for some elastic and inelastic channels. (10 refs.)

60960 Charge transfer to helium ions from metastable helium. P.Gangopadhyay, J.N.Bardsley (Dept. of Phys. & Astron., Univ. of Pittsburgh, Pittsburgh, PA, USA). *Chem. Phys. Lett. (Netherlands)*, vol.96, no.3, p.379-82 (8 April 1983). The cross section for charge transfer in $\text{He}^+ - \text{He}(2^3\text{S})$ collisions is calculated using the asymptotic theory of ion-atom interactions, including the effects of polarization and momentum transfer. The results agree well with recent measurements by the merged beam technique. (10 refs.)

60961 Luminescent charge transfer of ground-state and metastable B^+ ions. C.Ottinger, J.Reichmuth, M.Yang (Max-Planck-Inst. für Stromungsforschung Göttingen, Göttingen, Germany). *Chem. Phys. (Netherlands)*, vol.76, no.1, p.61-9 (1 April 1983). Endothermic charge-transfer reactions between $\text{B}^+(^1\text{S}$ and $^3\text{P})$ ions and several simple gases have been observed in a beam experiment at moderate and low energies. The products $\text{b}^+(\text{S}$ and $^2\text{D})$ were observed by means of their UV emission. Absolute cross sections for the four reaction channels were measured, ranging from 10^{-21} to 10^{-18} cm^2 . The relative cross sections depend markedly on the collision partner, and are discussed in terms of system symmetry and schematic energy diagrams. (12 refs.)

60962 Density functional estimates of charge transfer and chemical potentials in hydrogen halides and mixed halides. J.A.Alonso, N.H.March (Theoretical Chem. Dept., Univ. of Oxford, Oxford, England). *Chem. Phys. (Netherlands)*, vol.76, no.1, p.121-4 (1 April 1983). A simple model, based on the principle of constant chemical potential, is used to calculate the charge transfer in hydrogen halides and mixed halide molecules. (22 refs.)

60963 Angular-dependent electron-capture probabilities. E.Horsdal-Pedersen, J.L.Rasmussen (Inst. of Phys., Univ. of Aarhus, Aarhus, Denmark). *IEEE Trans. Nucl. Sci. (USA)*, vol.ns-30, no.2, p.891-4 (April 1983). (1982 IEEE Conference on the Application of Accelerators in Research and Industry, Denton, TX, USA, 8-10 Nov. 1982). The angular dependence of the electron capture probability for monoenergetic protons scattered off Ne atoms in fast binary encounters has been studied experimentally. A qualitative discussion of the physics of the angular dependence is presented and a simple model is developed which fits the experimental angular dependences well. (15 refs.)

60964 Electron capture cross sections for low velocity Ne^{q+} ($q=2, 3, 4, 5$, and 6) incident upon atomic hydrogen. T.J.Gray, C.Can, J.M.Hall, L.Tunnell (Kansas State Univ., Manhattan, KS, USA), Varghese, S.L. *IEEE Trans. Nucl. Sci. (USA)*, vol.ns-30, no.2, p.895-7 (April 1983). (1982 IEEE Conference on the Application of Accelerators in Research and Industry, Denton, TX, USA, 8-10 Nov. 1982). Measurements of electron capture cross sections for low velocity Ne^{q+} ions ($q=2, 3, 4, 5$ and 6) in collisions with atomic hydrogen are discussed. The Ne ions are obtained from a recoil ion source using a F^{4+} pump beam from the EN tandem accelerator. Time-of-flight techniques and post interaction electrostatic analysis provide for the experimental determination of the electron capture cross sections. Comparisons to the theories of Olson and Salop (1976) and Ryufuku et al. (1980) presented. (12 refs.)

60965 Electron capture to the continuum at asymptotically high velocities. S.D.Berry, I.A.Sellin, K.-O.Groeneveld, D.Hofmann, L.H.Andersen, M.Breinig, S.B.Elston, M.M.Schauer (Univ. of Tennessee, Knoxville, TN, USA), N.Stolterfoht, H.Schmidt-Bocking, G.Nolte, G.Schwiertz. *IEEE Trans. Nucl. Sci. (USA)*, vol.ns-30, no.2, p.902-5 (April 1983). (1982 IEEE Conference on the Application of Accelerators in Research and Industry, Denton, TX, USA, 8-10 Nov. 1982). The velocity distributions of electrons ejected from gaseous He targets into the forward direction by 15-18 au velocity bare O, Ne and Ar nuclei are measured. The shape of the resulting ECC (electron capture to be continuum) cusps is studied in detail by three fitting methods and compared to theory. The results favor theoretical treatments which include higher-order ejected electron partial waves to describe the observed asymmetry. (14 refs.)

60966 Additivity failure in electron capture from C-bearing molecules to continuum states of $\sim \text{MeV/u } \text{H}^+, \text{H}^{++}$ projectiles. J.Gaiser, J.M.Joyce, G.Bissinger (East Carolina Univ., Greenville, NC, USA). *IEEE Trans. Nucl. Sci. (USA)*, vol.ns-30, no.2, p.909-10 (April 1983). (1982 IEEE Conference on the Application of Accelerators in Research and Industry, Denton, TX, USA, 8-10 Nov. 1982). The failure of additivity in electron capture from molecules to bound states (ECB) of projectiles has been measured sporadically for more than twenty years. However until now there has been no report of similar additivity measurements for electron capture to continuum states (ECC). The measurements reported here show that additivity of 'atomic' cross sections fails in ECC processes also. (5 refs.)

60967 Electron capture from C-bearing molecules to bound states of 0.8-3.0 MeV H^+ : additivity corrections using electron loss cross sections. J.M.Joyce, G.Bissinger (East Carolina Univ., Greenville, NC, USA). *IEEE Trans. Nucl. Sci. (USA)*, vol.ns-30, no.2, p.911-12 (April 1983). (1982 IEEE Conference on the Application of Accelerators in Research and Industry, Denton, TX, USA, 8-10 Nov. 1982). Estimates of electron capture-to-bound-states (ECB) cross sections for molecular targets are normally made by assuming additivity of 'atomic' cross sections. This assumption leads to a familiar problem—it doesn't work. The authors have recently estimated the magnitude of ECB additivity failure observed in H^+ bombardment of hydrocarbon gases by assuming that additivity failure arises from intramolecular electron loss collisions that succeed the capture collision. Using capture-loss calculations adapted to molecules, additivity failure could be quite well accounted for in these terms. Here they apply the same basic approach but estimate additivity failure in a hard sphere geometric scattering model (GSM) that removes some of the inherent difficulties in capture-loss calculations pertaining to areal densities and molecular orientations. (5 refs.)

60968 Quasi-resonant K-K charge exchange in F-Ne collisions. S.Hagmann (Dept. of Phys., Kansas State Univ., Manhattan, KS, USA). *IEEE Trans. Nucl. Sci. (USA)*, vol.ns-30, no.2, p.928-30 (April 1983). (1982 IEEE Conference on the Application of Accelerators in Research and Industry, Denton, TX, USA, 8-10 Nov. 1982). K-K charge transfer has been identified as a major K-vacancy creating mechanism in near symmetric collisions systems by measuring either the projectile charge dependence of the target K-vacancy production or by high resolution study of the deexcitation processes after inner-shell vacancy production. The complexity of the simultaneous outershell excitation during a collision which creates a K vacancy requires that for a more systematic study a system be chosen which allows a more or less straightforward derivation of the K-vacancy probabilities from the observed decay of the excited state. An immediate candidate is the $\text{F}^{9+} - \text{Ne}$ system, which had been studied spectroscopically very extensively by Kauffman (1975) and Woods (1975) and who suggested that the K-vacancy production cross section could be extracted directly from the K-Auger cross sections because the fluorescence yield to be applied in the ionized case still is very small. (8 refs.)

60969 Production of 3s state hydrogen by H_2^+ impact on noble gases. M.L.Jones, B.M.Doughty (East Texas State Univ., Commerce, TX, USA). *IEEE Trans. Nucl. Sci. (USA)*, vol.ns-30, no.2, p.996-8 (April 1983). (1982 IEEE Conference on the Application of Accelerators in Research and Industry, Denton, TX, USA, 8-10 Nov. 1982). Absolute cross sections are reported for the production of 3s atomic hydrogen by 20-150 keV H_2^+ ions incident on He, Kr, and Xe. These measurements were made with an established technique used previously at East Texas State University for proton charge transfer cross sections. This basic technique has also been used by laboratories at Georgia Tech. and the University of Arkansas to make additional H_2^+ measurements. Results from these three laboratories are in good agreement and when combined provide a relatively consistent set of 3s cross sections for the five rare gases from 20-700 keV. Excited hydrogen atoms may be formed through several reaction channels; this experimental technique does not identify the relative contributions of these channels to the total 3s production. The multiple features of these cross section curves indicate that the internal structure of the targets plays an important role in the dissociation mechanism and that detailed theoretical descriptions will be quite involved. (17 refs.)

60970 The strong potential approximation with non-orthogonality terms. J.H.McGuire (Dept. of Phys., Kansas State Univ., Manhattan, KS, USA). *IEEE Trans. Nucl. Sci. (USA)*, vol.ns-30, no.2, p.1100-2 (April 1983). (1982 IEEE Conference on the Application of Accelerators in Research and Industry, Denton, TX, USA, 8-10 Nov. 1982). Non-orthogonality contributions are included in the strong potential approximation (SPA) for electron capture. These non-orthogonality contributions occur because the off-energy-shell Coulomb wave functions, representing the intermediate states of the collision, are not orthogonal to the initial bound state wave functions. As a result of this non-orthogonality an extra term arises in the matrix element between initial and intermediate states. This term may be written as an addition to the interaction potential which is treated in first order perturbation theory in the SPA method. It is shown that this nonorthogonality contribution is zero in the SPA when peaking approximations are applied. (6 refs.)

60971 Positive charge transfer in mixed alkane glasses. J.Cyglar, G.G.Teather, N.V.Klassen (Div. of Phys., Nat. Res. Council of Canada, Ottawa, Canada). *J. Phys. Chem. (USA)*, vol.87, no.3, p.455-60 (3 Feb. 1983). Positive charge transfer between the initial cation and the solute has been reexamined in detail at 6 and 72K for 3-methylcyclohexane (3MO) glasses containing squalene (SQ). A good fit to the observed decay of the 3-methylcyclohexane cation (3MO^+) was obtained by using the tunneling expression. The binding energy calculated, $B=0.33 \text{ eV}$, does not agree with the electron tunneling model. The results are discussed in terms of alternate tunneling mechanisms. The positive charge transfer $3\text{MO}^+ + \text{SQ} \rightarrow 3\text{MO} + \text{SQ}^+$ was separated kinetically from all other reactions, and the ratio $\epsilon_{\text{max}}(\text{SQ}^+)/\epsilon_{\text{max}}(3\text{MO}^+)=1.6$ was calculated, in good agreement with an independent determination made by using pyrene (Py) as a cation scavenger. Positive charge transfer was also examined in several other mixed alkane systems. (30 refs.)

60972 Electron capture by multiple charged low energy ions in charge exchange collisions with atomic targets. S.Bluman, S.Dousson, B.Jacquot, D.Van Houtte (CENG, Grenoble, France). *J. Phys. (France)*, vol.44, no.4, p.467-72 (April 1983). Single and double electron capture cross sections for low velocity Ar^{q+} ions with initial charges $2 \leq q \leq 12$ colliding with gaseous targets (Kr and Xe) have been measured. In the considered energy range ($2 \text{ q-}10 \text{ keV}$) it is confirmed that the cross section of single electron capture is quasi energy independent. Comparisons of the actual results are made to theoretically calculated and to previously measured cross-sections. It is shown from the results that an experimental tendency is observed for $\sigma_{q,q-1}/\sigma_{q,q-2} \approx C/q/[IP]^2$ where q is the incident ion charge, IP the target ionization potential. (38 refs.)

60973 Effects of neutrino recoil on the X-ray emission of bound electron capture atoms. G.Brunner (Zentralinst. für Isotopen- und Strahlenforschung, Akad. der Wissenschaften, Leipzig, Germany). *J. Phys. B (GB)*, vol.16, no.7, p.1199-204 (14 April 1983). Due to neutrino emission during the capture process, the nucleus experiences a recoiling motion. If one assumes that those valence charge fractions which are localised, but also bound to ligands, cannot follow the nuclear and core motion immediately, a certain electron cloud deformation takes place besides the 'normal' static chemical polarisation. This gives rise to additional X-ray transitions from the valence band to 1s for K-electron capture. For intensity reasons in connection with radioactive sources the energy dispersive version of X-ray spectrometry is mostly applied and, therefore, a $K_{\beta\gamma}$ -type emission cannot be resolved, but it increases the relative (to K_{α}) K_{β} intensity and enhances the chemical sensitivity of the K_{β}/K_{α} ratio. Numerical estimates for the ^{51}Cr decay give up to 5% effects for the limiting case of absolutely fixed valence charge fractions. 'Kinetic polarisation' is proposed to explain some experimentally observable and analytically applicable aspects of the K_{β}/K_{α} ratio of electron capture (EC) nuclides. (14 refs.)

60974 The use of static potentials in atomic collisions. Application to the excitation of hydrogen atoms by helium ions at intermediate energies. J.M.Maidagan, R.D.Rivarola (Inst. de Física Rosario, Rosario, Argentina). *J. Phys. B (GB)*, vol.16, no.7, p.1211-23 (14 April 1983). A model based on the independent-electron approximation and the impact parameter formalism has been developed, in order to take into account the influence of passive electrons in collisions between multielectron ion(atom) projectiles and mono-electron ion (atom) targets, and where only the electron in the target is active. Differential cross sections for excitation to the $n=2$ states of hydrogen by He^+ impact, in the intermediate energy region, are calculated as an application of this model. A reasonable agreement with recent experimental data is obtained using a two-state atomic expansion. The negligible influence of the $\text{He}(1s, 2p_{\pm 1})$ capture state on the excitation processes has been determined. (13 refs.)

60975 Electronegativity equalization and electron transfer in molecules. L.C.Balbas, J.A.Alonso, E.Las Heras (Univ. de Valladolid, Valladolid, Spain). *Mol. Phys. (GB)*, vol.48, no.5, p.981-8 (10 April 1983). A simple model for the electron transfer in an XY molecule is considered in which the amount of charge transfer Q is determined by the condition of equality of the electronegativities of the components, that is $\phi_X(Q) = \phi_Y(-Q)$. To calculate Q , $\phi_i(Q)$ ($i=X, Y$) is expanded in powers of Q about $Q=0$. The coefficients of the powers of Q in this expansion have been calculated by a density functional pseudopotential method. (17 refs.)

60976 Ion-atom differential cross sections at intermediate energies. R.E.Olson (Phys. Dept., Univ. of Missouri, Rolla, MO, USA). *Phys. Rev. A (USA)*, vol.27, no.4, p.1871-8 (April 1983). The classical-trajectory Monte Carlo method has been used to calculate $\text{H}^+ + \text{H}(1s)$ electron-capture and ionization differential cross sections in the range 25-200 keV. The results indicate the importance of including excited product states to describe the small-angle electron-capture scattering. Angular scattering of the electron removed by the ionization process has been studied as a function of ejected-electron velocity v_e . The classical calculations are in reasonable agreement with coupled-channel results of Shakeshaft [Phys. Rev. A 18, 1930 (1978)] as to the 'electron capture to the continuum' (ECC) component of the ionization process where this term is defined as the ejected electron being more closely centered to the projectile than the target nucleus after the collision. The ECC cross section σ_{ECC} was studied as a function of collision energy (50-500 keV/amu) and projectile charge state ($q=1-10$). At high energies, σ_{ECC} scales as $q^{2.5}/E^{2.5}$. The maximum value for σ_{ECC} was determined to be an energy $E_{\text{max}} \approx (56 \text{ keV/amu})^{0.4}$. Restricting the ECC component to small electron-scattering angles, $\theta_{\text{lab}} \leq 5^\circ$, and electron-ejection velocities $v_e = v_p(1.0 \pm 0.1)$, where v_p is the projectile velocity, indicates this process is a minor component of the total ionization cross section at intermediate energies. (27 refs.)

60977 Charge exchange of C^{+6} and O^{+8} ions with hydrogen atoms: Strong coupling calculation. A.K.Kazanskii, I.V.Komarov. *Sov. Phys.-Tech. Phys. (USA)*, vol.27, no.9, p.1064-8 (Sept. 1982). Translation of: *Zh. Tekh. Fiz. (USSR)*, vol.52, no.9, p.1734-40 (Sept. 1982). [received: April 1983] A strong coupling method with an adiabatic assumption is used for calculating charge exchange of the C^{+6} and O^{+8} ions on $\text{H}(1s)$ hydrogen atoms for velocities in the interval $v=0.1-0.4$ a.u. The basis includes radial and rotational coupling of five states for C^{+6} and six states for O^{+8} . The total cross sections and the distributions of excited states over the principal quantum number in the C^{+5} and O^{+7} ion states are computed. (14 refs.)

Atomic collision experiments utilizing low-velocity, highly-charged ion beams .. See Entry 60507

Effects of electron transfer on the chemical polarization of nuclei in the recombination of radical-ion pair in strong magnetic fields .. See Entry 60759

Projectile-charge dependence of quasi-free-electron bremsstrahlung .. See Entry 60910

Recent developments in accelerator based atomic physics .. See Entry 60933

Simultaneous electron capture and excitation in ion-atom collisions .. See Entry 60934

Electron capture in M-shell X-ray production from heavy elements by 25- and 35-MeV fluorine ions .. See Entry 60935

Mechanisms for rapid electron transfer in ionic solids following multiple ionization by heavy-ion impact .. See Entry 60936

M-shell X-ray production cross sections for 19 elements in the range $Z=54-92$ by H^+ and He^{+2+} ions from 300 keV to 40 MeV .. See Entry 60938

A study of transfer excitation in $\text{F}^{8+} + \text{He}$, Ne and Ar collisions .. See Entry 60948

Transfer ionization in slow multiply charged ion-atom collisions .. See Entry 60949

Population of the 3s state in hydrogen due to H^+ , H_2^+ and H_3^+ impact on ethylene, 1-butene and cis-2-butene .. See Entry 60950

Application of the retarded potential method in mass spectrometry for the investigation of mechanisms of field ion formation .. See Entry 61022

A mechanism for producing inversion in gas lasers .. See Entry 61135

Resonant transfer and excitation (RTE) in ion-atom collisions and dielectronic recombination in plasmas .. See Entry 61608

Electron capture and loss processes in heavy ion and molecular ion collisions with solids .. See Entry 63113

A quantitative interpretation of the magnetic field effect on hyperfine-coupling-induced triplet formation from radical ion pairs .. See Entry 63504

34.80 ELECTRON SCATTERING

60978 Studies of some iron dithiolate complexes by the ESCA, Mossbauer and extended Huckel methods. J.Blomquist, U.Helgeson (Inst. of Phys., Univ. of Stockholm, Stockholm, Sweden), B.Folkesson, R.Larsson. *Chem. Phys. (Netherlands)*, vol.76, no.1, p.71-8 (1 April 1983). Iron dithiolate complexes have been studied by Mossbauer and ESCA spectroscopy. Atomic charges and iron atom populations have been evaluated. Molecular orbital calculations have been made using the iterative extended Huckel method. The theoretical results are compared with the experimentally obtained charge distributions. (19 refs.)

60979 Scavenging probability of a geminate pair in the presence of an external electric field. Application of the method of matched perturbation solutions. H.Sano (Inst. of Phys., Univ. of Tokyo, Tokyo, Japan). *J. Chem. Phys. (USA)*, vol.78, no.7, p.4423-9 (1 April 1983). An analytical expression for the scavenging probability of a geminate pair interacting with a general potential in the presence of an external electric field is derived for both small scavenger concentrations and small field strengths. The derivation is based on the method of matched perturbation solutions of the differential equation satisfied by the recombination probability. The expression includes as an integral part the rate constant observed for reaction of the geminate partners in the bulk. Agreement of the expression with the exact ones is found when it is applied to ion recombination and recombination of the electron photodetached from an anion. (35 refs.)

60980 Photoabsorption and electron yields of La and Gd in the vicinity of the 3d thresholds. J.M.Esteve (Univ. Paris-Sud, Orsay, France), R.C.Karnatak, J.P.Connerade. *J. Electron Spectrosc. & Relat. Phenom. (Netherlands)*, vol.31, no.1, p.1-12 (April 1983).

A comparative study of the 3d photoabsorption and electron-yield spectra of La and Gd using synchrotron radiation emitted by the Orsay storage ring (ACO) is presented. The effects of sample thickness on each kind of spectrum are discussed. The mean sampling depths for La and Gd are determined from the variations in intensity of the main excitation lines as a function of film thickness in the yield spectra. The advantages and potential of the yield technique for the study of lanthanide spectra are pointed out. (29 refs.)

60981 Effect of the group IV elements on the Π anion and cation states of thiophene and furan determined by means of ETS and UPS. A.Modelli (Istituto Chimico G. Ciamician, Univ. di Bologna, Bologna, Italy), G.Distefano, D.Jones, G.Seconi.

J. Electron Spectrosc. & Relat. Phenom. (Netherlands), vol.31, no.1, p.63-73 (April 1983).

The electron-transmission and He(I) photoelectron spectra of $-\text{Si}(\text{CH}_3)_3$, $-\text{Sn}(\text{CH}_3)_3$ and $-\text{CH}_2\text{Si}(\text{CH}_3)_3$ derivatives of thiophene and furan have been recorded. The first two substituents perturb the energies of the outer filled π orbitals and of the empty π^* orbitals in opposite directions, causing a reduction of the HOMO/LUMO energy separation. The stabilization experienced by the π^* MO's depends on their wavefunction coefficients at the site of substitution, and is attributed to interaction with low-lying empty orbitals of the substituent groups. The relatively small size (~ 0.4 eV) of this effect on the unoccupied ring MOs suggests that it should not appreciably affect the energy of the filled MOs. The strong conjugation between the π^* unoccupied orbital of the nitro group and those of thiophene has also been investigated. (19 refs.)

The possibility of measuring the nuclear correlation width via atomic electron spectroscopy .. See Entry 60161

Anomalous electron attachment properties of perfluoropropylene ($1-\text{C}_3\text{F}_6$) and their effect on the breakdown strength of this gas .. See Entry 61713

Vibrations spectra of oxygen chemisorbed on nickel (110) surfaces .. See Entry 62253

Attachment of low-energy electrons to O_2 molecules in some gases and liquids: an instrument for measuring concentrations of electronegative impurities in gases .. See Entry 63628

34.80B Elastic scattering of electrons by atoms and molecules

60982 Monte Carlo simulation of electron-ion recombination at high pressure. W.L.Morgan (Lawrence Livermore Nat. Lab., Univ. of California, Livermore, CA, USA), J.N.Bardsley.

Chem. Phys. Lett. (Netherlands), vol.96, no.1, p.93-8 (25 March 1983). The Monte Carlo method is applied to the study of electron-ion recombination in CO_2 , CH_4 and NH_3 over a wide range of pressures. Dissociative recombination is enhanced by energy transfer to the ambient gas molecules and the recombination rates peak at 11, 2 and $9 \times 10^5 \text{ cm}^3 \text{ s}^{-1}$, respectively. At very high pressures, the rate approaches the Langevin limit. (23 refs.)

60983 Positron-gas scattering measurements. W.E.Kaupilla, T.S.Stein (Dept. of Phys. & Astron., Wayne State Univ., Detroit, MI, USA). *IEEE Trans. Nucl. Sci. (USA)*, vol.30, no.2, p.1156-9 (April 1983). 1982 IEEE Conference on the Application of Accelerators in Research and Industry, Denton, TX, USA, 8-10 Nov. 1982).

A 4.75 MeV proton beam from a Van de Graaff accelerator is used to generate an ^{11}C positron source by making use of the $^{11}\text{B}(p,n)^{11}\text{C}$ reaction. Moderated, low energy positrons emerging from the boron target are then electrostatically focused into a beam which is used in positron-gas scattering experiments. Total scattering cross sections have been measured for 0.3 to 800 eV positrons scattering from several atoms and molecules. Comparisons of these measurements with the corresponding electron total scattering cross section measurements (made with the same apparatus and technique) reveal many interesting similarities and differences. Positronium formation has been found to play an important role in positron scattering from the gases that have been studied. (27 refs.)

60984 Coupled-channels optical theory for e-H scattering. I.E.McCarthy, A.T.Stelbovics (Inst. for Atomic Studies, Flinders Univ. of South Australia, Bedford Park, Australia).

J. Phys. B (GB), vol.16, no.7, p.1233-45 (14 April 1983). Cross sections and angular correlation parameters for scattering within the 1s, 2s, 2p channel space in the electron-hydrogen problem are calculated at 50, 54.4, 100 and 200 eV. The integral equations for the momentum-space formulation of the problem are solved with a numerical accuracy of approximately 1%. Discrete and continuum channels outside the reaction space are explicitly taken into account by computing the corresponding optical potentials and adding them to the coupling potential. Exchange terms are calculated at all stages. Relative elastic cross sections, absolute inelastic cross sections, total reaction cross sections, and angular correlation parameters up to 60° agree with experiment. (26 refs.)

60985 Resonances in the scattering of ultraslow electrons at alkali atoms.

I.I.Fabrikant. *Opt. & Spectrosc. (USA)*, vol.53, no.2, p.131-3 (Aug. 1982). Translation of: *Opt. & Spektrosk. (USSR)*, vol.53, no.2, p.223-7 (Aug. 1982). [received: April 1983]

A theory for the effective radius for scattering at strongly polarized atoms is constructed that permits the author to extrapolate the results of calculations for the scattering phases for energies $E \geq 0.1$ eV to a region of lower energies. The proposed theory in contrast with that used earlier does not put a requirement on the smallness of αE , where α is the polarizability of the atom, and, therefore, is valid in a broader region. The theory is used for the parameterization of 3P resonances in the scattering of electrons at alkali atoms and for finding the binding energies. It is shown that extrapolation of the phases known up to the present of the scattering of electrons at Cs atoms leads to the existence of a bound 3P state of Cs instead of a 1P resonance. One possible cause of such a result involves the use of atomic wave functions, which overestimate the polarizability of the Cs atom. (22 refs.)

60986 Multichannel resonances in electron-hydrogen scattering. Y.K.Ho, J.Callaway (Dept. of Phys. & Astron., Louisiana State Univ., Baton Rouge, LA, USA).

Phys. Rev. A (USA), vol.27, no.4, p.1887-92 (April 1983).

Some lower-lying doubly excited resonances in electron-hydrogen scattering converging on the $N=3, 4$, and 5 hydrogenic thresholds, as well as some lower-lying P -wave resonances associated with the $N=6$ threshold, have been calculated by a method of complex-coordinate rotation. Hylleraas-type wave functions are used for $L=0$ and $L=1$ resonances, and products of Slater orbitals for states with $L \geq 2$. Results are compared with recent calculations. Furthermore, in addition to the usual resonances of parities $(-1)^L$, resonant states with parities $(-1)^{L+1}$ are also calculated. Results are used to construct the 'super-multiplet' structures of the doubly excited resonances of two-electron atoms. (16 refs.)

60987 Nonadjustable exchange-correlation model for electron scattering from closed-shell atoms and molecules. J.K.O'Connell, N.F.Lane (Phys. Dept., Rice Univ., Houston, TX, USA).

Phys. Rev. A (USA), vol.27, no.4, p.1893-903 (April 1983).

A nonadjustable-model potential is proposed for electron scattering that includes both electron exchange and correlation effects in a hybridization of local electron-gas theory and the long-range polarization. The model potential energy function consists of the sum of the energy-dependent electron-gas exchange potential (Hara version) and the energy-independent electron-gas correlation potential smoothly joined onto the long-range polarization interaction. Illustrative calculations of elastic scattering phase shifts and cross sections are described for the rare-gas atoms, where reasonable agreement with accurate calculations suggests usefulness of the model for more complex systems. (46 refs.)

60988 Electron-atom scattering: the state of the experiments. F.H.Read (Dept. of Phys., Univ. of Manchester, Manchester, England).

Phys. Scr. (Sweden), vol.27, no.2, p.103-16 (Feb. 1983).

The state of the experiments in low-energy electron-atom scattering is reviewed as part of the proceedings of the second George J. Schulz Symposium. Particular emphasis is placed on those experimental investigations that require a high electron energy resolution, such as studies of narrow resonances and threshold excitation and ionization processes. (123 refs.)

Atomic structure contribution to high-energy electron-photon atomic scattering: results for all momentum transfers See Entry 60990

Generalised quantum defect theory for electron scattering by polar molecules See Entry 61002

34.80D Atomic excitation and ionization by electron impact**60989 The threshold laws for electron-atom and positron-atom impact ionization.** A.Temkin (Lab. for Astron. & Solar Phys., NASA/Goddard Space Flight Center, Greenbelt, MD, USA).

IEEE Trans. Nucl. Sci. (USA), vol.ns-30, no.2, p.1106-11 (April 1983). (1982 IEEE Conference on the Application of Accelerators in Research and Industry, Denton, TX, USA, 8-10 Nov. 1982).

Reviews only the most salient aspects of the electron-atom impact ionisation, which has recently culminated with the derivation of the correct threshold law. The author emphasises that because the problem deals with three separating charged particles at the lowest energy at which they can escape from one another, this is the most basic three-body problem in the continuum involving Coulomb forces. At the same time it also involves quantum mechanics in very fundamental way. The author discusses the Coulomb-dipole theory, the positron-atom impact ionisation and two-electron photodetachment of H^- . (18 refs.)

60990 Atomic structure contribution to high-energy electron-photon atomic scattering: results for all momentum transfers. A.Lami, N.K.Rahman (Istituto di Chimica Quantistica ed Energetica Molecolare, CNR, Pisa, Italy).

J. Phys. B (GB), vol.16, no.7, p.L207-10 (14 April 1983).

Previous results for obtaining the atomic contribution, which are valid only for low momentum transfer, are extended to all values of the momentum transfer for an electron-photon system which is scattered from a hydrogen atom, using second-order perturbation theory. The effect of the virtual transition is obtained by means of the Coulombic Green's function. At large frequencies, the atomic structure (virtual transitions) plays a predominant role. (15 refs.)

60991 The electron excitation of Si^+ . A.E.Kingston, A.Thompson, K.A.Berrington (Dept. of Appl. Maths. & Theoretical Phys., Queen's Univ. of Belfast, Belfast, N Ireland), P.L.Dufton.

J. Phys. B (GB), vol.16, no.7, p.L207-10 (14 April 1983).

The R -matrix method has been used to calculate the collision strengths for the electron excitation of the spin-forbidden transitions $3s^2 3p^2 \ ^3P^o \rightarrow 3s3p^2 \ ^4P$ and $3s3p^2 \ ^4P \rightarrow 3s3p^2 \ ^2D$ in Si^+ . Eight target states were used in the calculations. There are significant resonance series converging to the higher excitation thresholds. Effective collision strengths are given for temperatures from 1×10^3 to 1×10^5 K. (9 refs.)

60992 Autoionisation versus radiative decay of resonances in electron impact excitation cross sections. E.Treffitz (Max-Planck-Inst. fur Phys. und Astrophys., Inst. fur Astrophys., Garching, München, Germany).

J. Phys. B (GB), vol.16, no.7, p.1247-51 (14 April 1983).

As shown by Pradhan (1981) the contribution of resonances to electron impact excitation cross sections may be reduced drastically by radiative decay of the resonance. It is shown here that this effect is important only in certain cases of which highly charged helium-like ions are the most prominent. In other ions, where the most important resonance series converge to target

states which do not differ from the ground state in principal quantum number, radiative decay is much less important. (5 refs.)

60993 Determination of electron-xenon total excitation cross-sections, from threshold to 100 eV, from experimental values of Townsend's α . M.Hayashi (Nagoya Inst. of Technol., Nagoya, Japan).

J. Phys. D (GB), vol.16, no.4, p.581-9 (14 April 1983).

Recommended values are presented for q_m , q_i and Q_T (momentum transfer cross-sections for elastic collisions, total cross-sections for elastic collisions and total collision cross-sections, respectively) of electrons in xenon for electron energies from 0 to 10⁵ eV. Recommended values of ionisation cross-sections q_i are also presented. Using these values of q_m together with values of q_i and Townsend ionisation coefficients α , recommended values of total excitation cross-sections q_e are determined. The values of q_m for electron energies from 5 to 20 eV are smaller than those of Frost and Phelps (1964) by a considerable amount. The values of q_e for energies from about 20 to 100 eV are much larger than those of de Heer et al. (1979). (47 refs.)

60994 Electron-impact excitation of vanadium atoms. V.V.Melnikov, Yu.M.Smirnov.

Opt. & Spectrosc. (USA), vol.53, no.1, p.15-18 (July 1982). Translation of: *Opt. & Spektrosk. (USSR)*, vol.53, no.1, p.27-32 (July 1982). [received: April 1983]

The cross sections for electron-impact excitation of the spectral lines of the vanadium atom have been measured for the first time by an intersecting-beam method. The measurements were carried out over the 300-600-nm spectral interval at incident-electron energies of 0-250 eV. The cross sections and excitation functions were measured for more than fifty spectral lines corresponding to transitions between quartet and sextet terms. The resonance transition $4^4F-x^4G^o$ has the largest excitation cross section, 1.3×10^{-15} cm² at the maximum. There are some differences between the excitation of the vanadium and that of other elements for which the d shell is being filled. (6 refs.)

60995 Effective cross sections for electron-impact excitation of barium atoms from the 5^1D_2 metastable state. I.S.Aleksakhin, S.B.Zagrebina, D.A.Ozolishin, A.V.Samson, I.I.Shafranosh, T.A.Shishova.

Opt. & Spectrosc. (USA), vol.53, no.2, p.222-4 (Aug. 1982). Translation of: *Opt. & Spektrosk. (USSR)*, vol.53, no.2, p.375-8 (Aug. 1982). [received: April 1983]

The process of excitation of the spectral lines of barium from the 5^1D_2 singlet metastable state was investigated for the first time. An effusion beam of normal barium atoms passed through a discharge chamber, in which atoms were converted to the 5^1D_2 and $5^3D_{1,2,3}$ metastable states. At 15 mm from the discharge chamber the atomic beam was intersected by the beam of a tunable dye laser tuned to the 582.6-nm wavelength, which corresponds to the $6s5d^1D_2-5d6p^1P_1$ transition. From the upper level of this transition the atoms, as a result of spontaneous emission (the 350.1-nm line), effectively transitioned to the ground state. The laser radiation was modulated. During this the population of the 5^1D_2 level also turned out to be modulated with the same frequency. If this level is connected with other levels by any processes, the populations of the latter will also change. (4 refs.)

60996 Quantum-defect and distorted-wave theory applied to the resonance contribution of inelastic electron scattering. R.E.H.Clark, A.L.Merts, J.B.Mann, L.A.Collins (Los Alamos Nat. Lab., Los Alamos, NM, USA).

Phys. Rev. A (USA), vol.27, no.2, p.1812-20 (April 1983).

The importance of the resonance contributions to inelastic scattering of electrons from atoms and ions has been appreciated for quite some time. The authors have used an approximate method to compute the resonance contributions to selected inelastic transitions in O VI and S IV and compare our results with other theoretical calculations. They find that their total resonance-enhanced collision strengths are in very good agreement with other calculations. They also can accurately compute the positions of individual resonances but can sometimes be in error by a factor of 2 on individual resonance widths. (20 refs.)

60997 Direct-excitation cross sections for Cd II low-lying excited states by single-electron impact on Cd atoms. T.Goto, K.Hane, M.Okuda, S.Hattori (Dept. of Electronics, Nagoya Univ., Nagoya, Japan).

Phys. Rev. A (USA), vol.27, no.4, p.1844-50 (April 1983).

Emission cross sections for ten spectral lines transiting from Cd II low-lying excited states formed by single-electron impact on Cd atoms have been measured with a photon-counting technique. Polarizations of these lines have also been examined. By the use of these results and removing the influence of cascade transitions, direct-excitation cross sections for seven low-lying states ($5^2P^o_{1/2,3/2}$, $5s^2D_{3/2,5/2}$, $6s^2S_{1/2}$, $5d^2D_{3/2,5/2}$) have been determined as a function of electron energy. They are found to be of the order of 10^{-17} cm² for the $5p$ and $5s^2$ states and of 10^{-18} cm² for the $6s$ and $5d$ states at their maxima. (12 refs.)

60998 Positronium formation in positron-hydrogen scattering. P.Khan (Muralidhar Girl's School, Calcutta, India), A.S.Ghosh.

Phys. Rev. A (USA), vol.27, no.4, p.1904-9 (April 1983).

The positronium-formation cross section in positron-hydrogen scattering has been calculated by using the distorted-wave approximation in which the total incident wave function is obtained by the method of polarized orbitals. The two variants of the polarized-orbital method, one due to Temkin and Lamkin (1961) and the other due to Callaway et al. (1968), have been employed to estimate their relative importance. The present results have been compared with those obtained by elaborate variational methods. The results obtained by using the potential of Temkin and Lamkin have been found to be encouraging. (13 refs.)

Atomic final-state interactions in tritium decay See Entry 60142

Atomic calculations for the Fe XX X-ray lines See Entry 60637

Kinetics of the plasma decay in lithium vapor; population inversion for the $3p-3s$ transition See Entry 60664

Long-range forces between a charged and neutral system See Entry 60894

Recent developments in accelerator based atomic physics See Entry 60933

Effective ionic radii of NO_2^- and SCN^- estimated in terms of the Botcher equation and the Lorentz-Lorenz equation See Entry 60954

Monte Carlo simulation of electron-ion recombination at high pressure See Entry 60982

Positron-gas scattering measurements See Entry 60983

Coupled-channels optical theory for e-H scattering See Entry 60984

Electron-atom scattering: the state of the experiments See Entry 60988

Quasi-CW lasing due to transitions from the resonance 1P_1 to the metastable 1D_2 level of the calcium atom See Entry 61139

34.80G Molecular excitation, ionization, and dissociation by electron impact

60999 Non-dipole excitation of core holes by electron impact. Multiplet splitting in CO and N₂. L.Ungier, T.D.Thomas (Dept. of Chem., Oregon State Univ., Corvallis, OR, USA).

Chem. Phys. Lett. (Netherlands), vol.96, no.2, p.247-50 (1 April 1983). Low-energy electron impact leads to non-dipole excitation of core electrons to triplet states. The multiplet splitting in CO is in agreement with theory and shows that the 2 π orbital is localized predominantly on the carbon. The splitting affects both energy-loss and Auger spectra of CO and N₂. (11 refs.)

61000 Internal energy dependence of the autodetachment and dissociation times of the SF₆⁻ ion. J.P.Astruc, R.Barbe, A.Lagrez, J.P.Schermann (Lab. de Phys. des Lasers, Univ. Paris Nord, Villetaneuse, France).

Chem. Phys. (Netherlands), vol.75, no.3, p.405-16 (15 March 1983). The dependence of the autodetachment and dissociation times of the SF₆⁻ molecular ion on the temperature of its SF₆ parent molecule has been studied in a crossed-beam experiment. The use of atoms in highly excited states (Rydberg atoms) provides a source of a well-defined nearly zero-energy electrons. By means of an inverse Laplace transform of the negative ion numbers, the authors have determined the dependence of these autodetachment and dissociation times upon the internal energy of the negative ion. The presence of a positive ionic core during the creation of the negative molecular ion is taken into account by considering a collisional stabilization process. These measurements agree with previous experiments using free electrons but cannot be reconciled with the existing statistical theory. (23 refs.)

61001 Molecular orbital electron momentum distributions and separation energies of CH₃CN. A.Minchinton, C.E.Brion, J.P.D.Cook, E.Weigold (School of Phys. Sci., Flinders Univ. of South Australia, Bedford Park, SA, Australia).

Chem. Phys. (Netherlands), vol.76, no.1, p.89-101 (1 April 1983). Acetonitrile (CH₃CN) has been studied by binary (e, 2e) spectroscopy at a total energy of 1200 eV in the symmetric non-coplanar geometry. The separation energy spectrum was determined at azimuthal angles of 0° and 8° in the energy range up to 40 eV. Above 23 eV the energy spectra show considerable intensity in addition to the two peaks expected from simple MO theory for ionization of the 5a₁ and 4a₁ orbitals. These findings are in qualitative agreement with recent theoretical predictions using the Green's function method. Electron momentum distributions have been measured for each of the valence orbitals and the results compared with two SCF wavefunction calculations using Gaussian basis sets. Position (charge) and momentum density maps were also calculated for each orbital. These maps are used to compare and contrast the electronic structure and bonding properties of CH₃CN in position and momentum space. (42 refs.)

61002 Generalised quantum defect theory for electron scattering by polar molecules. I.I.Fabrikant (Inst. of Phys., Acad. of Sci., Riga, Latvian SSR).

J. Phys. B (GB), vol.16, no.7, p.1253-67 (14 April 1983). By the use of effective-range theory electron scattering by polar molecules in the fixed-nuclei approximation is considered. The relationship between the scattering data and the electron affinity of the polar molecule is obtained. It is shown that three $2\Sigma^+$ states of the ions LiF⁺ and BeO⁺ exist. Differential and integrated cross sections for electron scattering by LiF and BeO are calculated. The relationship between the data for scattering by HCN and the electron affinity of HCN is considered. The electron affinities of HF and H₂O, calculated in the fixed-nuclei approximation, are used to obtain the scattering cross sections. (42 refs.)

61003 Frame transformation effective-range theory: application to interaction of polar molecules with electrons. I.I.Fabrikant (Inst. of Phys., Acad. of Sci., Riga, Latvian SSR).

J. Phys. B (GB), vol.16, no.7, p.1269-82 (14 April 1983). The scattering of electrons by polar molecules for energies of the order of, and less than the rotational constant B_r is considered. The formalism of the Chang and Fano (1972) frame transformation theory is used. The effective-range theory for the determination of the wavefunctions in the molecular frame is applied. The method for the calculation of the electron affinity of polar molecules is developed with rotation being taken into account. The result is applied to the calculation of eigenphases for scattering by LiF and HF molecules and to the investigation of the threshold behaviour of vibrational excitation cross sections. It is found that the ion LiF⁺ has two excited $2\Sigma^+$ states with binding energies of 0.49×10^{-2} and 0.23×10^{-2} eV. Long-range dipole forces lead to the appearance of resonances in the S, P and D waves. These resonances are too narrow (with widths of the order of 0.1 B_r) to be observed in vibrational excitation cross sections. However, they can be observed in photodetachment cross sections if the corresponding anion exists. (33 refs.)

61004 Ionisation and appearance potentials of CH₄ by electron impact. P.Plessis, P.Marmet, R.Dutil (Dept. de Phys., Univ. Laval, Laval, Quebec, Canada).

J. Phys. B (GB), vol.16, no.7, p.1283-94 (14 April 1983). The CH₄⁺ electroionisation efficiency curve and the CH₃⁺, CH₂⁺ and C⁺ appearance potential curves are presented. The data were obtained by an apparatus of very high sensitivity with an improved electron monochromator. The CH₄⁺ ionisation potential is measured to be 12.63 ± 0.02 eV. The results show that some previously reported appearance potential values should be corrected, in some cases by several electron volts. This is attributed to superior apparatus sensitivity. Ion-pair formation is clearly observed for the CH₃⁺ and CH₂⁺ fragments. The CH₃⁺ and C⁺ appearance potentials have been detected down to adiabatic threshold. The stable fragment CH₂²⁺, is also observed. (37 refs.)

Positron-gas scattering measurements See Entry 60983

Electron-impact excitation of the Cameron system ($\pi^3\pi^-\rightarrow X^1\Sigma$) of CO See Entry 64369

35.00 PROPERTIES OF ATOMS AND MOLECULES; INSTRUMENTS AND TECHNIQUES

35.10 ATOMS

35.10B Atomic masses, mass spectra, abundances, and isotopes

(inc. isotope separation; for mass spectrometry, see also 07.75; for radioisotope separation see 28.42H or 82.55)

61005 Ion extraction in the laser process of uranium enrichment by selective ionization of atomic vapour. C.Jacquot, J.Soubbaramayer (CENS, Gif-sur-Yvette, France).

C.R. Seances Acad. Sci. Ser. II (France), vol.296, no.3, p.181-4 (24 Jan. 1983). In French.

A method, taking advantage of the ambipolar diffusion is developed for the extraction of ions in the laser process of isotope separation with atomic vapour. The component of extraction is a system of electrostatic lenses, located at the periphery of the plasma generated by the laser. The method has the advantage of not accelerating the electrons and transporting the product without risk of pollution. (4 refs.)

61006 Variational transition state theory and tunneling for a heavy-light-heavy reaction using an ab initio potential energy surface. ³⁵Cl+H(D)³⁵Cl-H(D)³⁵Cl+³⁵Cl. B.C.Garrett (Chem. Dynamics Corp., Columbus, OH, USA), D.G.Truhlar, A.F.Wagner, T.H.Dunning, Jr.

J. Chem. Phys. (USA), vol.78, no.7, p.4400-13 (1 April 1983). Ab initio POL-Cl calculations, augmented by a dispersion term, are used to predict the potential energy surface for the reaction Cl+HCl. The saddle point is found to be nonlinear. The surface is represented by a rotated-Morse-oscillator spline fit for collinear geometries plus an analytic bend potential. Variational transition state theory calculations, based on a linear reference path, are carried out, and they yield much smaller rate constants than conventional transition state theory, confirming that earlier similar results for this heavy-light-heavy mass combination were consequences of the small skew angle and were not artifacts of the more approximate potential energy surfaces used in those studies. Transmission coefficients are calculated using approximations valid for large-reaction-path curvature and the potential along the reference path is scaled so that the calculated rate constant agrees with experiment. The resulting surface is used to compute the H/D kinetic isotope effect which is in qualitative agreement with experiment. (51 refs.)

61007 Hydrogen isotope exchange and separation in gas-solid phase systems. G.Sicking, P.Albers, E.Magomedbekov (Univ. of Munster, Munster, Germany).

J. Less-Common Met. (Switzerland), vol.89, no.2, p.373-91 (Feb. 1983). (International Symposium on the Properties and Applications of Metal Hydrides, Toba, Japan, 30 May-4 June 1982).

Systems of two or more hydrogen-containing phases in solution equilibrium with hydrogen may not be in isotopic equilibrium. The resulting exchange of hydrogen isotopes between the phases is discussed with respect to both the kinetic behaviour and the final equilibrium state. The advantages of tracer experiments using tritium are discussed in terms of the experimental arrangement and the information attainable. It is shown that the equilibrium separation factor reflects the state of the dissolved hydrogen in different sorption states and that the exchange kinetics are affected by the state of the interphase. The effect of the total hydrogen pressure on the tracer exchange with tritium is discussed. The relationships developed are applied to the metal-hydrogen systems PdH_x and Ti_{0.6}Mn_{0.6}H_x. The results are supplemented by pressure-composition isotherms, neutron vibrational spectra, scanning electron micrographs, Auger electron spectra and Auger electron spectroscopy depth profiles obtained using argon ions. (36 refs.)

61008 Cascades for hydrogen isotope separation using metal hydrides. F.B.Hill, V.Grzetic (Brookhaven Nat. Lab., Upton, NY, USA).

J. Less-Common Met. (Switzerland), vol.89, no.2, p.399-405 (Feb. 1983). (International Symposium on the Properties and Applications of Metal Hydrides, Toba, Japan, 30 May-4 June 1982).

Designs are presented for continuous countercurrent hydrogen isotope separation cascades based on the use of metal hydrides. The cascades are made up of pressure swing adsorption (PSA) or temperature swing adsorption (TSA) stages. The designs were evolved from consideration of previously conducted studies of the separation performance of four types of PSA and TSA processes. (7 refs.)

61009 A proposed method of hydrogen isotope separation using palladium alloy membranes. J.Evans, I.R.Harris (Dept. of Metall. & Materials, Univ. of Birmingham, Birmingham, England), D.K.Ross.

J. Less-Common Met. (Switzerland), vol.89, no.2, p.407-14 (Feb. 1983). (International Symposium on the Properties and Applications of Metal Hydrides, Toba, Japan, 30 May-4 June 1982).

The viability of using palladium alloy membranes in cascade to separate the hydrogen, deuterium and tritium produced in a fusion reactor is discussed. Values of the permeation separation factor are estimated for Pd-20%Ag from available data and corresponding estimates for the necessary number of stages and the total membrane area are given for the required isotopic purification. The results demonstrate the advantage of minimizing the operating temperatures and pressures and indicate that the method is perfectly feasible. The use of Pd-8%Y will probably even further improve the performance. (17 refs.)

61010 Characteristics of the permeation of hydrogen-inert gas mixtures through a palladium alloy tube wall. N.Mitsubishi, T.Yuki, I.Ichihara (Dept. of Nuclear Engng., Kyushu Univ., Fukuoka, Japan).

J. Less-Common Met. (Switzerland), vol.89, no.2, p.415-22 (Feb. 1983). (International Symposium on the Properties and Applications of Metal Hydrides, Toba, Japan, 30 May-4 June 1982).

A hydrogen window for the selective separation of hydrogen and deuterium in a gas stream permeating a palladium alloy tube wall was investigated. The palladium alloy used was Pd-20%Ag-5%Au and the tube was 100 mm long with an internal diameter of 1.44 mm. Permeabilities of hydrogen and deuterium were measured at 400°C and atmospheric pressure using H₂-Ar and D₂-Ar mixtures. A similar permeation experiment was performed using an H₂-D₂-Ar mixture. The permeation data for the mixture agreed with the theoretical predictions made using the permeability values obtained from the H₂-Ar and D₂-Ar experiments. Hence it was established that the permeation rates of hydrogen isotope mixtures through a hydrogen window can be estimated by the authors' equations. (9 refs.)

- 61011** Tritium isotope separation using resonance radiation. P.C.Stangeby.
Report OUEL-1429/82, Univ. Oxford, England (Aug. 1981), 41 pp.
 The isotope separation technique proposed involves exposure of a hydrogen isotopic mixture to resonance radiation from a light source (a gas discharge) containing just one isotope. Since the resonance lines are generally well separated for the hydrogen isotopes only the matching isotope in the mixture will be excited. It is envisaged that the excited atom is then ionised with the ion attracted to and trapped on an appropriate solid present within the reaction zone. (27 refs.)
Recovery of hydrogen isotopes using a uranium bed See Entry 60334
²³⁵U isotope enrichment in the metastable levels of U I See Entry 60663

35.10D Electric and magnetic moments, polarizability

- 61012** Estimation of some matrix elements of the dynamical dipolar polarizability of iodine atom from long-range dispersion energy terms for molecular iodine. J.Vigue (Lab. de Spectroscopie Hertziennne, Ecole Normale Supérieure, Paris, France), M.Saute, M.Aubert-Frecon.
J. Chem. Phys. (USA), vol.78, no.7, p.4544-6 (1 April 1983).
 The reduced matrix elements of the dynamical dipolar polarizability $\epsilon(k,k')$ of the iodine atom are derived from the dispersion energy matrix for I_2 . The preponderance of the $\epsilon(0,0)$ term, proportional to the mean value C_6 of the corresponding coefficients of all the different molecular states of I_2 , is strongly related to the quasi-isotropic feature of the C_6 coefficient. The authors' value for the static dipolar polarizability α is coherent with other determinations. (7 refs.)
61013 Use of reflection symmetry in calculating atomic polarizabilities. P.P.Vaiteckunas, A.Yu.Savukinas.
Opt. & Spectrosc. (USA), vol.53, no.2, p.120-2 (Aug. 1982). Translation of: *Opt. & Spektrosk. (USSR)*, vol.53, no.2, p.202-5 (Aug. 1982). [received: April 1983]
 By making use of reflection symmetry in calculations of the electric polarizabilities and magnetic susceptibilities of atoms, one can derive certain expressions from the others by making the substitution $J \rightarrow -J-1$ involving the angular momentum quantum numbers. (8 refs.)
Calculation of the polarizability of the sodium atom from the Sturm virtual orbitals of the self-consistent-field method See Entry 60583
Effect of atomic polarization on two-photon electron detachment from the corresponding negative ions See Entry 60671
The Breit interaction in external magnetic fields See Entry 60747
Fine-structure parameters of the $np^2n'p$ configurations of several inert gases and alkali metal ions See Entry 61014

35.10F Relativistic corrections, fine- and hyperfine-structure constants

- 61014** Fine-structure parameters of the $np^2n'p$ configurations of several inert gases and alkali metal ions. G.P.Anisimova, R.I.Semenov.
Opt. & Spectrosc. (USA), vol.53, no.2, p.128-31 (Aug. 1982). Translation of: *Opt. & Spektrosk. (USSR)*, vol.53, no.2, p.217-22 (Aug. 1982). [received: April 1983]
 A semiempirical method is used in the single-configuration approximation to calculate the fine-structure parameters, the gyromagnetic ratios, and the coupling coefficients for the $3p^25p$ and $3p^6p$ configurations of Ar I, the $4p^25p$ and $4p^6p$ configurations of Kr I, the $3p^24p$ configuration of K II, the $4p^25p$ configuration of Rb II, and the $5p^6p$ configuration of Cs II. Experimental values of the fine-structure energy intervals and the gyromagnetic ratios are used. It is shown by the examples of the $2p^33p$ and $4p$ configurations of Ne I and the $3p^6p$ configuration of Ar I that it is possible to carry out these calculations without appealing to experimental values of the gyromagnetic ratios. The results are compared with the data available in the literature. (12 refs.)
Characteristics of σ -transitions in an atomic-beam polarized deuteron source See Entry 60502
Comments on fine-structure intervals of the $1s^22s^22p^5$ 2P state in fluorine isoelectronic sequence See Entry 60616
Relativistic corrections in atomic calculations See Entry 60618
Hyperfine structure and three-channel quantum-defect theory of $6snd^2D_2$ Rydberg states of Ba See Entry 60623
Two-step opticalgalyvanic spectroscopy of neutral barium: observation and interpretation of the even levels above the $6s$ ionization limit between 5.2 and 7 eV See Entry 60634
Fine-structure parameters of the helium $1s3d$ configuration from the experimental crossing positions of Zeeman sublevels See Entry 60646
Magnetic-sublevel shifts of potassium atoms in a constant magnetic field and in the electric fields of laser beams of various polarizations See Entry 60647
Inhomogeneous light shift in alkali-metal atoms See Entry 60655
Zeeman transitions in collisions of Na with Xe See Entry 60898
Resonance line at the $M=\pm 1 \rightarrow M=0$ transition in 1^3S_1 positronium See Entry 61024

35.10H Ionization potentials, electron affinities

- Mn VI spectrum at 140-220 Å** See Entry 60635

35.20 MOLECULES

(see also 61.55, 61.60, and 61.65 Specific structures of metals and alloys, of other inorganic materials, and of organic materials, respectively)

35.20B General molecular conformation and symmetry; stereochemistry

- Hydrogen bonds between first-row hydrides and acetylene** See Entry 60580
Molecular and electronic structure of carbonyls of the VIIIth periodic system group See Entry 60588
Quantum study of the ground state of a series of unsaturated boron-nitrogen compounds by the MNDO method. I. Geometries and stabilities See Entry 60591

- Quantum chemical investigations on colour and stereodynamics of acyclic azines. X. Potential parametrisation in the framework of the QCFF-PI method for complete geometry optimisation of acyclic azines** See Entry 60597
Evidence that the excited-state geometry of diphenylbutadiene is nearly planar See Entry 60620
A model for the pseudorotation of cycloheptane See Entry 60685
⁸³Kr nuclear quadrupole coupling, microwave spectrum, and structure of KrHCN See Entry 60704
The rotational spectrum and molecular structure of the benzene-hydrogen chloride complex See Entry 60705
The structure and molecular properties of the acetylene-HCN complex as determined from the rotational spectra See Entry 60706
The rotational spectrum and molecular structure of the furan-HCl complex See Entry 60708
Microwave spectrum, structure, and quadrupole coupling for the ethylene-hydrogen cyanide complex See Entry 60709
The rotational and hyperfine spectrum and structure of H_2CO-HF See Entry 60750
On the twist-boat conformation of the tetrahydropyran cycle in the trioxabis-spiroketal series See Entry 60758
Structure of the binuclear 3,7-dimethylene-bicyclo[3.3.1]nonane-silver nitrate-Eu(fod)₃ complex by PMR spectroscopy See Entry 60760
Electron spin resonance spectra and structure of the α,α -difluoroethyl radical See Entry 60766
Molecular clustering about a positive ion. Structures, energetics, and vibrational frequencies of the protonated hydrogen clusters H_3^+ , H_5^+ , H_7^+ , and H_9^+ See Entry 61044
Crystal and molecular structure of tetrachlorophosphorus (V) hexachlorouranate (V) See Entry 61899
Crystal and molecular structures of two 15-membered crown ether triones: 1,4,7,10,13-pentaoxacyclopentadecane-3,11,15-trione and 4,7,10,13-tetraoxa-1-thiacyclopentadecane-3,11,15-trione See Entry 61903

35.20D Interatomic distances and angles

- 61015** Monte Carlo solutions of Schrodinger's equation for H_2^+ ion in strong magnetic fields. II. J.Ozaki, Y.Tomishima (Dept. of Phys., Okayama Univ., Okayama, Japan).
J. Phys. Soc. Jpn. (Japan), vol.52, no.4, p.1142-7 (April 1983).
 For pt.1 see *ibid.*, vol.49, p.1497 (1980). Corrected results are shown for the energies and the equilibrium nuclear separations for π_g state of H_2^+ ion in magnetic field, which are reported incorrectly in the previous paper. The critical field strength for which the antibonding π_g state changes to the bonding is between 0.1 and 1.0 in units of 2.35×10^{10} G. Similar calculations are also carried out for π_u state. Numerical results obtained are in good agreement with those of others. (9 refs.)
Quantum study of the ground state of a series of unsaturated boron-nitrogen compounds by the MNDO method. I. Geometries and stabilities See Entry 60591
On the nature of the bonding in Cu_2 —a comment See Entry 60601
On the nature of the bonding in Cu_2 —an ab initio viewpoint See Entry 60602
A theoretical investigation of the bond length of dichromium See Entry 60605
Microwave spectrum, dipole moment, barrier to internal rotation of 1,1-dimethyldiborane See Entry 60712
On the 1 μ m system of iron hydride See Entry 60714
 $\tilde{A}^1\Pi \rightarrow \tilde{X}^2\Sigma^+$ infrared electronic transition of C_2H^+ See Entry 60719
Laser spectroscopic investigation of the $X^2\Sigma_{1/2}$ state of the van der Waals molecule NaAr See Entry 60789

35.20G Bond strengths, dissociation energies, hydrogen bonding, etc

- 61016** Influence of hydrogen bonds on electronic spectral shifts of some 9-amino acridines. A.Marty, P.Viallet (Univ. de Perpignan, Perpignan, France).
C.R. Seances Acad. Sci. Ser. II (France), vol.296, no.5, p.343-6 (7 Feb. 1983). In French.
 The formation of hydrogen bonds which occur on amino groups and on the pyridine nitrogen atom of some 9-amino acridines is shown by the study of solvent effects on absorption and fluorescence spectra. The use of π^* , α and β parameters of Kamlet allows the relative importance of the two types of hydrogen bonds on spectral shifts to be quantified. (10 refs.)
61017 Electronic structure of molecules and infrared continua caused by intramolecular hydrogen bonds with great proton polarizability. B.Brzezinski (Inst. of Chem., A. Mickiewicz Univ., Poznan, Poland), G.Zundel.
J. Phys. Chem. (USA), vol.86, no.26, p.5133-5 (23 Dec. 1982).
 2-Quinclidene-carboxylic acid *N*-oxide (compound 1) and 3-methyl-2-pyridinecarboxylic acid *N*-oxide (compound 2) were studied by IR and NMR spectroscopy. With both compounds, strong, short intramolecular hydrogen bonds were formed. Both proton-limiting structures $OH \cdots ON \rightleftharpoons O \cdots H^+ \cdots ON$ had noticeable weight. Only with compound 1, but not with compound 2, was an intense IR continuum observed. Thus, only if the hydrogen-bond donor and acceptor groupings are not electronically conjugated do IR continua occur, since, when they are conjugated, the charge fluctuation connected with the proton fluctuation is compensated by an electron flux in the opposite direction within the molecule. (28 refs.)
61018 C-H stretching modes and the structure of *n*-alkyl chains. I. Long, disordered chains. R.G.Snyder, H.L.Strauss (Dept. of Chem., Univ. of California, Berkeley, CA, USA), C.A.Elliger.
J. Phys. Chem. (USA), vol.86, no.26, p.5145-50 (23 Dec. 1982).
 The C-H stretching modes of the conformationally disordered polymethylene chain were analyzed. Fermi resonance interaction involving HCH bending overtones was dominant in determining the shape of the Raman C-H stretching spectrum. In addition, however, it was found that the C-H stretching frequencies were significantly affected by the conformation of adjoining C-C bonds. (32 refs.)
Improved SCF interaction energy decomposition scheme corrected for basis set superposition effect See Entry 60571
Hydrogen bonds between first-row hydrides and acetylene See Entry 60580
Natural bond orbital analysis of near-Hartree-Fock water dimer See Entry 60581

- Potassium fluoride and phosphorous acid: ab initio calculations and spectroscopic investigations See Entry 60585
- $X\alpha$, Cr_2 , and the symmetry dilemma See Entry 60589
- On the nature of the bonding in Cu_2 —a comment See Entry 60601
- On the nature of the bonding in Cu_2 —an ab initio viewpoint See Entry 60602
- The nature of hydrogen bonding in the NN-HF, OC-HF, and HCN-HF complexes See Entry 60603
- The rotational spectrum and molecular structure of the furan-HCl complex See Entry 60708
- Distribution of Gauche bonds in crystalline $n-C_{21}H_{44}$ in phase II See Entry 60716
- Difference frequency laser spectroscopy of the ν_1 band of the HO_2 radical See Entry 60720
- New results on EDA-iodine complexes See Entry 60737
- The rotational and hyperfine spectrum and structure of H_2CO-HF See Entry 60750
- Electron spin resonance spectra and structure of the α,α -difluoroethyl radical See Entry 60766
- Rydberg states of 7Li , by pulsed optical-optical double resonance spectroscopy: molecular constants of $^7Li_2^+$ See Entry 60769
- Lifetimes in the $B^1\Pi$ state and the heat of formation of NCO See Entry 60788
- First observation of bound-continuum transitions in the laser-induced $A^1\Sigma_g^+ - X^1\Sigma_g^+$ fluorescence of Na_2 See Entry 60802
- Laser induced fluorescence excitation spectrum of jet-cooled benzoic acid dimers See Entry 60811
- Auger spectra of tetrahedral halides and hydrides See Entry 60853
- The dissociation energies of the diatomic alkali hydrides See Entry 60888
- Monte Carlo solutions of Schrodinger's equation for H_2^+ ion in strong magnetic fields. II See Entry 61015
- A CNDO/2 study of the growth of model lithium clusters See Entry 61039
- Molecular clustering about a positive ion. Structures, energetics, and vibrational frequencies of the protonated hydrogen clusters H_3^+ , H_5^+ , H_7^+ , and H_9^+ See Entry 61044

35.20J Barrier heights (internal rotation, inversion); rotational isomerism, conformational dynamics

- Dynamic model and tunneling splittings in LMH₄ non-rigid hydrides See Entry 60565
- A model for the pseudorotation of cycloheptane See Entry 60685
- Centrifugal distortion and internal rotation analysis of the microwave spectrum of ethyl fluoride See Entry 60707
- Microwave spectrum, dipole moment, barrier to internal rotation of 1,1-dimethyldiborane See Entry 60712
- NMR study of intramolecular processes in EDTA metal complexes See Entry 60749
- The study of enantioselectivity in copper complexes with some 1,3-dicarbonyl ligands by circular dichroism spectroscopy See Entry 60776
- Predissociation of HD-Ar van der Waals molecules by internal rotation See Entry 60866
- Hindered internal rotations in Van der Waals molecules and molecular crystals See Entry 60885
- Selective vibrational excitation of the ethylene-fluorine reaction in a nitrogen matrix. I See Entry 63521

35.20M Electric and magnetic moments (and derivatives), polarizability, and magnetic susceptibility

- Scaling in pseudopotential theory See Entry 60576
- The nature of hydrogen bonding in the NN-HF, OC-HF, and HCN-HF complexes See Entry 60603
- Microwave spectral study of bicyclo[2.2.2]octene and bicyclo[2.2.2]octadiene See Entry 60711
- Microwave spectrum, dipole moment, barrier to internal rotation of 1,1-dimethyldiborane See Entry 60712
- The Breit interaction in external magnetic fields See Entry 60747
- ESR of pseudorotating 6Li_3 and 7Li_3 See Entry 60763
- Calculation of the electrooptical parameters and the absolute intensities of the IR bands of the water molecule and its isotopically substituted derivatives See Entry 60777
- Electric dipole moment of the diatomic TiF in its higher vibrational states See Entry 60779
- Electric dipole moments of excited vibrational levels in the $\tilde{X}1A_1$ state of formaldehyde by stimulated emission spectroscopy See Entry 60780
- A semiclassical inversion procedure for the dipole-moment function for diatomic molecules See Entry 60886

35.20P Rotation, vibration, and vibration-rotation constants

- Intracavity dye-laser photothermal deflection spectroscopy See Entry 59861
- Infrared dephasing of degenerate fundamentals: the ν_6 mode of liquid CD_3I See Entry 60684
- Local modes: their relaxation, polarization, and stereoselective excitation by lasers See Entry 60691
- Centrifugal distortion and internal rotation analysis of the microwave spectrum of ethyl fluoride See Entry 60707
- The rotational spectrum and molecular structure of the furan-HCl complex See Entry 60708
- Beam maser spectroscopy on CD_3CN See Entry 60710
- Microwave spectral study of bicyclo[2.2.2]octene and bicyclo[2.2.2]octadiene See Entry 60711
- Microwave spectrum, dipole moment, barrier to internal rotation of 1,1-dimethyldiborane See Entry 60712

- The infrared absorption spectrum of a supersonic expansion of methyl chloride See Entry 60715
- Photochemical formation and dissociation of molybdenum-dinitrogen complexes in krypton matrices See Entry 60717
- Difference frequency laser spectroscopy of the ν_1 band of the HO_2 radical See Entry 60720
- Raman spectra, ab initio molecular orbital calculations, vibrational analysis, and thermodynamic functions for $NH_3:AlX_3$ ($X=F, Cl, Br$) See Entry 60725
- Wavelength dependence of Raman scattering cross sections from 200-600 nm See Entry 60732
- The high-resolution visible overtone spectrum of acetylene See Entry 60734
- High-resolution study of InCl spectra See Entry 60736
- Electron spin resonance spectra and structure of the α,α -difluoroethyl radical See Entry 60766
- Rydberg-Rydberg transitions of NO using an optical-optical double resonance multiphoton ionization technique See Entry 60768
- Rydberg states of 7Li , by pulsed optical-optical double resonance spectroscopy: molecular constants of $^7Li_2^+$ See Entry 60769
- Laser spectroscopic investigation of the $X^2\Sigma_{1/2}$ state of the van der Waals molecule NaAr See Entry 60789
- Laser vaporization of tin: spectra and ground state molecular parameters of Sn_2 See Entry 60801
- Two-photon excitation of the $D^1\Delta - X^1\Sigma^+$ transition in carbon monoxide See Entry 60804
- Laser induced fluorescence excitation spectrum of jet-cooled benzoic acid dimers See Entry 60811
- Rotational effects in the intermediate-case radiationless decay of pyrimidine See Entry 60813
- Rotational relaxation in ground-state *p*-difluorobenzene: State selection by stimulated emission pumping See Entry 60815
- Laser induced fluorescence studies of XeF(B-X) See Entry 60830
- Vibrationally resolved photoelectron angular distributions for H_2 See Entry 60832
- Measurement of the pressure broadening and shift of the $asR(0,0)$ line of the $^{15}NH_3$ ammonia ν_2 band See Entry 60843
- The state distribution of OH radicals photodissociated from H_2O_2 at 193 and 248 nm See Entry 60860
- Two-photon ionization. Capability of lasers for trace analysis See Entry 60876
- Resonant multiphoton ionization of H_2 via the $B^1\Sigma_g^+$, $v=7$, $J=2$ and 4 levels with photoelectron energy analysis See Entry 60877
- Systematics in two-photon rovibrational contours of 14_0^1 ($^1B_{2g} - ^1A_{1g}$) in benzene derivatives See Entry 60878
- C-H stretching modes and the structure of *n*-alkyl chains. I. Long, disordered chains See Entry 61018
- Infrared emission spectroscopy of CO on Ni See Entry 62966
- Production of vibrationally excited OH in chemiluminescent reactions of ozone with monoterpenes See Entry 63509
- Far-infrared rotational transition lines of the interstellar water vapor See Entry 64535

35.20S Hyperfine and fine-structure constants

- Centrifugal distortion and internal rotation analysis of the microwave spectrum of ethyl fluoride See Entry 60707
- Beam maser spectroscopy on CD_3CN See Entry 60710
- X-ray absorption spectra of nitrogen and oxygen in the series of N_2 , NO, and O_2 molecules See Entry 60744
- The rotational and hyperfine spectrum and structure of H_2CO-HF See Entry 60750
- ESR of pseudorotating 6Li_3 and 7Li_3 See Entry 60763
- High-spin molecules: electron spin resonance of manganese halides and sulfide at 4 K See Entry 60764
- Precision measurements of hyperfine predissociation in I_2 vapor using a two-photon resonant scattering technique See Entry 60856
- Laser spectroscopy on ion beams: application to the polyatomic ion N_2O^+ See Entry 60871

35.20V Ionization potentials, electron affinities, molecular core binding energy

- Hydrogen bonds between first-row hydrides and acetylene See Entry 60580
- Electronic structure of radical ions of polycyclic hydrocarbons See Entry 60590
- A quantum mechanical investigation of clathrate compounds with He and Ne See Entry 60593
- Approximate relativistic calculations within the one-center approximation for the series CH_4 to PhH_4 See Entry 60611
- General variation method for the relativistic calculations of atoms and molecules See Entry 60613
- Molecular structure and photoelectron spectra of H_2S , H_2Se and H_2Te . Effective core potential calculations on ground and valence ionic states See Entry 60629
- New results on EDA-iodine complexes See Entry 60737
- Rydberg states of 7Li , by pulsed optical-optical double resonance spectroscopy: molecular constants of $^7Li_2^+$ See Entry 60769
- UV photoelectron spectra of some transition metal(II) acetylacetonates See Entry 60834
- Use of effective core potentials in perturbation corrections to the Koopmans theorem: vertical ionization potentials of Cl_2 , ClN_3 , and $CINCO$ See Entry 60835
- Generalised quantum defect theory for electron scattering by polar molecules See Entry 61002
- Frame transformation effective-range theory: application to interaction of polar molecules with electrons See Entry 61003

- Ionisation and appearance potentials of CH₄ by electron impact See Entry 61004
 Supersonic copper clusters See Entry 61043

35.20X Mass spectra

- 61019 Molecular species in the As-O system. R.D.Brittain, K.H.Lau, D.L.Hildenbrand (SRI Internat., Menlo Park, CA, USA). *J. Phys. Chem. (USA)*, vol.86, no.26, p.5072-5 (23 Dec. 1982). Mass spectrometric analyses of saturated and unsaturated vapors over arsenolite, As₂O₃(s), and over an As₂O₃-CaO mixture have identified a surprisingly large number of thermodynamically stable As-O molecular species. These species, which include As₄O₆, As₄O₅, As₄O₄, As₂O₃, As₂O₂, AsO, and perhaps As₂O₄, were identified primarily from threshold appearance potential measurements. Considerable care was required, since some ions are produced both by fragmentation and by simple ionization. There may be several fragmentation pathways yielding As₃O₄⁺, but the evidence regarding this ion is complex and a clear decision cannot yet be made. The possible effects of temperature on the mass spectra of As₄O₆ and other complex As-O species are discussed, but the evidence to date appears inconclusive. (15 refs.)
 Benzaldehyde photochemistry studied with laser ionization mass and photoelectron spectroscopy See Entry 60836
 Supersonic copper clusters See Entry 61043
 The unimolecular decomposition rates of energy selected methylnitrite and deuterated methylnitrite ions See Entry 63526

35.80 ATOMIC AND MOLECULAR MEASUREMENTS AND TECHNIQUES

- 61020 Non-equilibrium behavior on pulsed laser evaporated surfaces. L.Lynds, B.A.Woody (United Technol. Res. Center, East Hartford, CT, USA). *J. Electron Spectrosc. & Relat. Phenom. (Netherlands)*, vol.29, p.147-53 (15 Jan. 1983). (Proceedings of the Third International Conference on 'Vibrations at Surfaces', Asilomar, CA, USA, 1-4 Sept. 1982). Absorption of intense pulsed laser optical fields by metallic surfaces generates dense neutral atomic beams with high average translational energies. Mechanisms explaining this behavior are based on an equilibrium model invoking high temperatures and pressures. The authors have made experimental observations on yttrium and uranium atomic beams produced from laser evaporated targets which suggest an alternative mechanism involving a non-equilibrium process. (15 refs.)
 61021 Double infrared-third-harmonic-generation resonance as a method for investigating vibrational energy exchange. V.N.Varakin, V.M.Gordienko (M.V. Lomonosov State Univ., Moscow, USSR). *Sov. J. Quantum Electron. (USA)*, vol.12, no.10, p.1265-6 (Oct. 1982). Translation of: *Kvantovaya Elektron., Moskva (USSR)*, vol.9, no.10, p.1941-2 (Oct. 1982). [received: April 1983]
 A diagnostic method is proposed for the study of kinetic processes. This method is based on the relationship between the power of the third harmonic of a probe beam and the populations of resonant vibrational levels. The results are reported of experiments involving a determination of the rate of the intermolecular V-V' relaxation in CF₃I-CD₄ gas mixtures. It is reported that the rate of relaxation increases on increase in the degree of vibrational excitation of the molecules. The advances of the double infrared-third-harmonic-generation resonance method are considered. (3 refs.)
 61022 Application of the retarded potential method in mass spectrometry for the investigation of mechanisms of field ion formation. B.G.Mischanchuk, V.A.Pokrovskii, V.P.Shabel'nikov, E.N.Korol' (L.V. Pissarshevskii Inst. of Phys. Chem., Acad. of Sci., Kiev, Ukrainian SSR). *Theor. & Exp. Chem. (USA)*, vol.18, no.2, p.172-7 (March-April 1982). Translation of: *Teor. & Eksp. Khim. (USSR)*, vol.18, no.2 (March-April 1982). [received: Feb. 1983]
 The authors first examine the energy balance in a very simple case, that of formation of molecular ions. They then carry out an experimental investigation of the influence of external factors on the formation energy of associative ions of water and ammonia. These results have been interpreted on the basis of the energy balance considerations. (9 refs.)
 CAMAC controller for a conventional and pseudorandom time-of-flight system See Entry 59768
 Matrix isolation spectroscopy. A method for investigation of chemisorption on model systems of metal catalysts. (Construction, building and testing of an apparatus for producing matrix isolated metal atom clusters) See Entry 59854
 Intracavity dye-laser photothermal deflection spectroscopy See Entry 59861
 Delay in the spontaneous decay of excited atoms in a resonator See Entry 60642
 Measurement system for temporal response of atomic and molecular systems using the correlation method with pseudorandomly modulated laser light See Entry 60643
 Nuclear polarisation of helium 3 by a colour centre laser See Entry 60665
 Direct measurement of K-shell photoionization cross sections by means of the coincidence method See Entry 60678
 Spatial diagnostics of a gallium atomic beam by the method of two-stage laser photoionization See Entry 60679
 Beam maser spectroscopy on CD₃CN See Entry 60710
 Possible P, T-odd effects in NMR spectroscopy of molecules See Entry 60751
 Use of luminescence spectra of adducts of europium β-diketonates with methyl-substituted pyridines in interpreting NMR data obtained by the use of lanthanide shift reagents See Entry 60761
 State-selective spectroscopy in a molecular nitrogen discharge by use of optical-galvanic double-resonance spectroscopy See Entry 60770
 pH correlation of the absorption, fluorescence and polarization spectra of fluorescein isothiocyanate See Entry 60783
 Measurement of sub-nanosecond single-rovibronic fluorescence with a pulsed dye laser See Entry 60794
 Laser spectroscopy on ion beams: application to the polyatomic ion N₂O⁺ See Entry 60871
 Two-photon ionization. Capability of lasers for trace analysis See Entry 60876
 State resolved rotational excitation in HD+D₂ collisions. II. Angular dependence of 0-2 transitions See Entry 60922
 State resolved rotational excitation in D₂+H₂ collisions See Entry 60923

- Laser-induced fluorescence studies of vibrational and rotational relaxation in a supersonic molecular beam of bromine monochloride See Entry 60928
 Attachment of low-energy electrons to O₂ molecules in some gases and liquids: an instrument for measuring concentrations of electronegative impurities in gases See Entry 63628

36.00 STUDIES OF SPECIAL ATOMS AND MOLECULES

36.10 EXOTIC ATOMS AND MOLECULES (CONTAINING MESONS, MUONS, AND OTHER ABNORMAL PARTICLES)

- 61023 Application to $\mu^+e^-e^+$ and $p\mu^-e^-$ of a new method for taking into account the finite nuclear mass in the determination of the absence of bound states. E.A.G.Armour (Math. Dept., Univ. of Nottingham, Nottingham, England). *J. Phys. B (GB)*, vol.16, no.7, p.1295-302 (14 April 1983).
 A recently published new method by Armour (1982) for taking into account finite nuclear mass in the determination of the absence of bound states is applied to a system made up of muonium (μ^+e^-) and a positron (e^+) and also to one made up of a mesic atom ($p\mu^-$) and a positron. It is shown that neither system has a bound state below the continuum. Some aspects of the method, which have only been briefly referred to hitherto, are discussed in detail. (14 refs.)
 61024 Resonance line at the $M=\pm 1 \rightarrow M=0$ transition in 1^3S_1 positronium. A.Z.Varisov. *Opt. & Spectrosc. (USA)*, vol.53, no.1, p.90-1 (July 1982). Translation of: *Opt. & Spektrosk. (USSR)*, vol.53, no.1, p.155-6 (July 1982). [received: April 1983]
 The measurement of the resonance variation of the coincidence counting rate of γ rays associated with 2γ annihilation caused by magnetic dipole transitions $M=\pm 1 \rightarrow M=0$ in 1^3S_1 positronium, induced by an alternating magnetic field $H_1 \cos \omega t$ perpendicular to a steady magnetic field H , detected the dependence of the size of the hyperfine splitting ΔE of the $1S$ state of positronium in gases on the gas pressure p : $\Delta E = \Delta E_0(1 + ap)$, where the constant $|a| \sim 10^{-5} - 10^{-4} \text{ atm}^{-1}$. In metal oxide powders (MgO, Al₂O₃, SiO₂) ΔE proved to be less than ΔE_0 by an amount of the order of $10^{-2} \Delta E_0$. The resonance signal was not observed in single-crystal silicon and fused quartz. An explanation is given of the foregoing facts. (9 refs.)
 61025 Hyperfine structure of positronium energy levels in a crystal field. A.Z.Varisov. *Opt. & Spectrosc. (USA)*, vol.53, no.2, p.162-5 (Aug. 1982). Translation of: *Opt. & Spektrosk. (USSR)*, vol.53, no.2, p.278-83 (Aug. 1982). [received: April 1983]
 An analysis has been carried out of the behavior of energy levels of the hyperfine structure of the positronium atom in a crystal field in the presence of an external magnetic field. For isotropic positronium, if the effective masses of the positron and electron are not identical, along with the splitting related to the square of the magnetic field there is also a linear Zeeman effect (for the levels of orthopositronium with $m=\pm 1$). For anisotropic positronium in an axial crystal field the character of the splitting depends on the mutual orientation of the magnetic field and the axis of symmetry of the crystal field. The special features of the hyperfine structure of the positronium atom in a crystal field can manifest themselves in experiments that observe the precession of the polarization vector of the positronium in the magnetic field and should lead to an anisotropy in the magnetic quenching of positronium in oriented crystals. (14 refs.)
 61026 Application of modified adiabatic approximation to $pp\mu$, $dd\mu$, and $tt\mu$ mesomolecules. M.N.Adamov, A.V.Filinskii. *Opt. & Spectrosc. (USA)*, vol.53, no.2, p.206-7 (Aug. 1982). Translation of: *Opt. & Spektrosk. (USSR)*, vol.53, no.2, p.351-4 (Aug. 1982). [received: April 1983]
 It is shown that the application to homonuclear mesomolecules of the modified adiabatic approximation (MAA) with the coefficient of adiabaticity independent of the slow subsystem coordinates yields results that are considerably more accurate than those obtained when the ordinary adiabatic approximation (OAA) is used. One can, therefore, attempt to use the MAA for calculation by expanding the desired wave function on the basis of modified two-center functions. (11 refs.)
 61027 Limit on exotic two-body decays of orthopositronium. G.Carboni (CERN, Geneva, Switzerland), W.Dahme. *Phys. Lett. B (Netherlands)*, vol.123B, no.5, p.349-52 (7 April 1983).
 The authors have searched for the exotic annihilation of orthopositronium, $e^+e^-(^3S_1) \rightarrow a^0\gamma$, where a^0 denotes a neutral particle of mass $m_a < 2m_e$. The negative results of this search allow them to derive an upper limit on the coupling constant $\tilde{\alpha}$ of the hypothetical a^0 in the mass range $150 < m_a < 900 \text{ keV}$. The bound is about 10 times lower than the one derived from the $(g-2)$ measurements. (7 refs.)
 61028 Diabatic-state treatment of negative-meson moderation and capture. II. Mixtures of hydrogen and helium. J.S.Cohen, R.L.Martin, W.R.Wadt (Los Alamos Nat. Lab., Univ. of California, Los Alamos, NM, USA). *Phys. Rev. A (USA)*, vol.27, no.4, p.1821-30 (April 1983).
 For p see *ibid.*, vol.24, no.1, p.33, 1981. Slowing-down and capture cross sections have been consistently calculated for μ^- , π^- , K^- , and p in collisions with hydrogen and helium atoms and isotopic variants. Capture-energy distributions are determined using the differential-energy-loss cross sections in the laboratory frame. Capture is found to occur predominantly at energies near or below the ionization potential of the target. Ratios of capture on different species are given as a function of the mole fraction of each species present in mixtures. For π^- in a He-H mixture the reduced capture ratio obtained is ~ 0.73 , slightly less than the experimental value of 0.92 for the He-H₂ mixture. In contrast with another recent theoretical calculation and in agreement with experimental analysis, it is found that atomic capture of pions in the helium-hydrogen mixture is only slightly nonlinear. It is pointed out that some prior theoretical treatments are in error because of inconsistent calculation of the slowing-down and capture processes and/or subsequent approximate treatment of the energy transport. Use of capture and transfer rates in muon kinetics, e.g. muon-catalyzed fusion, is discussed. (29 refs.)
 Monopole atoms and monopole catalysis of proton decay See Entry 59967
 Positronium formation in positron-hydrogen scattering See Entry 60998
 Induced decay of positronium and grassers See Entry 61123

36.20 MACROMOLECULES AND POLYMER MOLECULES

[for biological macromolecules, see also 87.15; for polymer reactions and polymerization, see 82.35]

61029 Systematic blobbing procedure for the calculation of universal polymer properties. G.F.AI-Noaimi (Dept. of Phys., Univ. of Qatar, Doha, Qatar), G.C.Martinez-Mekler, R.M.Velasco B. *J. Chem. Phys. (USA)*, vol.78, no.6, pt.1, p.3316-24 (15 March 1983).

A systematic renormalization group transformation along the chemical sequence of a polymer chain, systematic blobbing procedure (SBP), is introduced for the calculation of universal configurational properties. The method, which does not rely on the field theoretic analogy, gives to first order in ϵ ($\epsilon=4-d$, d =space dimension) a firm basis to the decimation procedure suggested by de Gennes (1977) and put into practice by Gabay and Garel (GG (1979)). The renormalization transformation acts on a 'Hamiltonian' of the system and produces Wilson-type approximate recursion relations for the coupling parameters. The SBP is used to calculate the exponent ν for a polymer chain in the good solvent region to first order in ϵ . The method can in principle be extended to higher orders in ϵ . By means of the SBP it is shown that the static universal properties of a polymer chain are not modified by the presence of a Gaussian random potential. The validity of the GG method is further strengthened by showing the equivalence, in the determination of ν , of their method and a Fixman perturbation matching procedure. The exponent ν is subsequently obtained to second order in ϵ . All the results agree with the 'corresponding' field theoretic calculations. (25 refs.)

61030 Dipolar rotational spin-echo ^{13}C NMR of polymers. J.Schaefer, R.A.McKay, E.O.Stejskal (Phys. Sci. Center, Monsanto, St. Louis, MO, USA), W.T.Dixon. *J. Magn. Resonance (USA)*, vol.52, no.1, p.123-9 (March 1983).

The strength of a static dipolar interaction between an isolated ^{13}C and ^1H spin pair is known if the internuclear distance is known. This is the usual situation for a directly bonded CH fragment in a solid polymer. The reduction in the strength of the CH dipolar interaction by molecular motion (of frequency comparable to or greater than the dipolar interaction itself) thus becomes a measure of the amplitude of the motion. In performing such a measurement on a real system, the condition that the ^{13}C - ^1H spin pair be isolated from many-body proton dipolar coupling is achieved by phase-shifted multiple-pulse (WAHUHA) ^1H - ^1H decoupling. The time evolution of the cross-polarization carbon magnetization is then detected under the influence of ^1H - ^{13}C coupling along. The resulting carbon signal can be observed with magic-angle spinning for high resolution. The pulse sequence for this experiment is shown. The evolution of the carbon magnetization due to chemical shift effects is refocused after two rotor periods by a carbon 180° pulse applied after the first rotor period. The ^1H - ^{13}C dipolar modulation is followed by varying the number of WAHUHA pulse sequences during a time t_1 . The spinning speed is chosen so that an integral number of WAHUHA cycles exactly fits into one rotor period. (24 refs.)

61031 Suppression of the solvent resonance in 2D NMR spectra of proteins in H_2O solution. G.Wider, R.V.Hosur, K.Wuthrich (Inst. für Molekularbiologie und Biophys., Eidgenössische Tech. Hochschule, Zurich, Switzerland).

J. Magn. Resonance (USA), vol.52, no.1, p.130-5 (March 1983). The abundance of publications on techniques for recording one-dimensional high-resolution ^1H NMR spectra of biological macromolecules in aqueous solution clearly indicates that the importance of such experiments for biological applications of ^1H NMR has long been recognized. Specifically for ^1H NMR studies of peptides and proteins, fundamental considerations show that the amide protons play a pivotal role for both the resonance assignments and the determination of the spatial structure. While in favorable cases certain amide protons in proteins exchange sufficiently slowly with the solvent to be studied in D_2O solution, investigations extending over the entire polypeptide chain will in all cases have to depend on data recorded in H_2O . Therefore, once the important advantages of two-dimensional (2D) NMR over conventional NMR experiments for studies of proteins were demonstrated with experiments in D_2O , it was of utmost importance to devise experimental schemes by which 2D NMR data sets could be recorded for proteins were demonstrated with experiments in D_2O , it was of utmost importance to devise experimental schemes by which 2D NMR data sets could be recorded for protein solutions in H_2O . The note reports on the authors' experience with the use of different solvent suppression schemes for such experiments. (21 refs.)

61032 Studies of cyclic and linear poly(dimethyl siloxanes). X. Calculations of radii of gyration. C.J.C.Edwards, D.Rigby, R.F.T.Stepto (Dept. of Polymer Sci. & Technol., Univ. of Manchester Inst. of Sci. & Technol., Manchester, England), K.Dodgson, J.A.Semlyen. *Polymer (GB)*, vol.24, no.4, p.391-4 (April 1983).

For pt.IX see *ibid.*, vol.23, p.873 (1982). A Monte Carlo method has been devised for calculating the conformation-dependent properties of cyclic poly(dimethyl siloxanes), using P.J. Flory, V. Crescenzi and J. Mark's rotational isomeric state model (1964). Calculated values of the mean-square radii of gyration ($\langle s^2 \rangle$) of ring molecules unperturbed by excluded volume effects and containing 8-100 skeletal atoms are compared with the (s^2) values for the corresponding unperturbed chain molecules. Exact enumeration methods were also employed for rings $[(\text{CH}_3)_2\text{SiO}]_{w/2}$ with $w \leq 24$ and the results found to be in close agreement with those obtained by the Monte Carlo method. The ratio $\langle s^2 \rangle / \langle s^2 \rangle_0$ was found to attain limiting values close to 2.0 for $w > 30$, in agreement with theoretical predictions. (53 refs.)

61033 Studies of cyclic and linear poly(dimethyl siloxanes). XI. Shapes of ring and chain molecules. C.J.C.Edwards, D.Rigby, R.F.T.Stepto (Dept. of Polymer Sci. & Technol., Univ. of Manchester Inst. of Sci. & Technol., Manchester, England), J.A.Semlyen. *Polymer (GB)*, vol.24, no.4, p.395-9 (April 1983).

For pt.X see *ibid.*, vol.24, p.391-4 (1983). The equilibrium shapes of cyclic and linear poly(dimethyl siloxane) (PDMS) molecules have been investigated using P.T. Flory, V. Crescenzi and J. Mark's rotational isomeric state model (1964), together with a Monte Carlo method. The principal axes of the equivalent ellipsoids have been computed and the major change on ring formation was found to be a reduction in the longest axis of the ellipsoid. The shapes of the cyclics $[(\text{CH}_3)_2\text{SiO}]_{w/2}$ in the region $w=20$ are disc-like and this observation is related to the different bond angles at silicon and oxygen atoms. Bulk densities and refractive indices of PDMS rings are discussed in relation to the calculated molecular shapes. (14 refs.)

61034 The effect of disorder in stereo-irregular polymer chains. R.Riklund, S.Stafstrom (Dept. of Phys. & Measurement Technol., Univ. of Linköping, Linköping, Sweden). *Philos. Mag. B (GB)*, vol.47, no.3, p.247-57 (March 1983).

The intricate interplay between electron-electron interactions and structural disorder is studied for a model polymeric stereo irregular chain of hydrogen

atoms, treating the constant bond length as a varying parameter. Eigenstates and densities of states are calculated using a modified spin-polarized Hartree-Fock scheme. The electronic structure is also compared with that of a regular chain. Based on the result from the numerical solution, a model Hamiltonian suitable for analytical treatment of this system is also proposed. (15 refs.)

61035 Calculation of the characteristics of the conduction band for excess electrons in proteins. S.L.Mironov (A.A. Bogomolet Inst. of Physiology, Acad. of Sci., Kiev, Ukrainian SSR).

Theor. & Exp. Chem. (USA), vol.18, no.2, p.132-6 (March-April 1982). Translation of: *Teor. & Eksp. Khim. (USSR)*, vol.18, no.2, p.155-61 (March-April 1982). [received: Feb. 1983]

The author has calculated the electron affinity of a peptide group and determined the characteristics of the conduction band for excess electrons in the energy spectrum of proteins for their α -helical and β -forms. (16 refs.)

61036 On diffusional mobility of chain molecules. V.P.Budtov.

Vysokomol. Soedin. Ser. A (USSR), vol.25, no.3, p.477-85 (March 1983). In Russian. English translation in: *Polym. Sci. USSR (GB)*

The various molecular models of diffusional motion of macromolecules in viscous and viscoelastic media are described. The main type of motion in a viscoelastic medium is the one-dimensional motion of short fragments of the chain: 'slip' and cooperative motion models. The concept of the diffusional segment of the chain b is introduced characterizing the distance between disturbance of the structure moving along the chain. For $L < b$ (L is the length of the chain) $D \sim M^{-1}$, while for $L > b$ $D \sim M^{-2}$. The contribution of end fragments of macromolecules into diffusional mobility is discussed. The results are compared with the data of computer simulation and NMR and 'labeled' atoms methods. The good coincidence of theoretical and experimental results is shown for polydimethylsiloxane permitting one to determine the main molecular parameters. The effect of MM of the matrix is also shown. For PE, PEO, polypropylene and butyl-styrene rubber the main parameters of diffusion of macromolecules in the melt are found. (17 refs.)

61037 Simulation of the structure of polyunsaturated macromolecules.

A.L.Rabinovich, V.G.Dashevskii.

Vysokomol. Soedin. Ser. A (USSR), vol.25, no.3, p.537-43 (March 1983). In Russian. English translation in: *Polym. Sci. USSR (GB)*

To study properties of nonbranched molecules of polyunsaturated hydrocarbons and methyl esters of fatty acids with methylene-discontinuous double bonds 20 fragments containing five-seven atoms in the main chain are chosen, and the maps of their conformational energy are drawn. The calculations are performed for the model of atom-atom potential functions (taking into account the nonvalent interactions, torsion and electrostatic terms). The analysis of conformational maps and experimental data permits one to conclude the expediency of the account of the continuous spectrum of conformations during the simulation of conformational properties of molecules of given class. (33 refs.)

61038 Conformational analysis of polyunsaturated macromolecules in solution continuum model. V.G.Dashevskii, A.L.Rabinovich.

Vysokomol. Soedin. Ser. A (USSR), vol.25, no.3, p.544-50 (March 1983). In Russian. English translation in: *Polym. Sci. USSR (GB)*

The method of the study of conformational properties of polyunsaturated molecules of hydrocarbons and methyl esters of fatty acids is proposed basing on the model of atom-atom potential functions. The algorithm of the generation of chains by the Monte Carlo method for the model with the continuous spectrum of conformations is derived taking into account the details of the stereochemical structure, correlation and retardation of internal rotations and excluded volume. (13 refs.)

Renormalization group description of polymer excluded volume See Entry 59698

Monte Carlo renormalization group calculations for polymers See Entry 59700

Equilibrium folding pathways for model proteins See Entry 59707

Intracoil triplet-triplet annihilation in poly(2-vinyl naphthalene) in benzene solution See Entry 60818

Cyclization dynamics of polymers. VII. Applications of the pyrene excimer technique to the internal dynamics of poly(dimethylsiloxane) chains See Entry 60829

C-H stretching modes and the structure of n -alkyl chains. I. Long, disordered chains See Entry 61018

Molecular mechanism of shrinkage of polyethylene terephthalate See Entry 61831

Variation with temperature of the thickness of an adsorbed polymer layer in the collapsed state See Entry 62249

Protein dynamics from Mossbauer spectra. The temperature dependence See Entry 63770

Soliton excitations in deoxyribonucleic acid (DNA) double helices See Entry 63772

A stochastic model for reversible pressure denaturation of chymotrypsinogen See Entry 63776

Protein folding as a stochastic process See Entry 63778

Transmission of conformational change in insulin See Entry 63779

Facile transition of poly[d(TG).d(CA)] into a left-handed helix in physiological conditions See Entry 63781

Secondary structures of proteins and peptides in amphiphilic environments (a review) See Entry 63781

DNA-divalent metal cation interactions measured by electrophoretic light scattering See Entry 63788

36.40 ATOMIC AND MOLECULAR CLUSTERS

61039 A CNDO/2 study of the growth of model lithium clusters. S.P.Delneshev (Inst. of Generale Inorganic Chem., Bulgarian Acad. of Sci., Sofia, Bulgaria).

C.R. Acad. Bulg. Sci. (Bulgaria), vol.35, no.11, p.1511-13 (1982). The energetically most favourable growth of a model lithium cluster is studied. The binding energy (BE) of the cluster is calculated by the Complete Neglect of Differential Overlap (CNDO/2) method. The geometry of the most stable cluster for each number of atoms is expected to be closer to the real geometry than that found by the HMO method. The expectations were based on the literature reporting satisfactory results obtained by the CNDO/2 method on stereochemical constants in certain molecules. The BE values for each cluster were used only as a measure in arranging, according to their stability, clusters having the same number of atoms in different positions. In

addition it is supposed that the CNDO/2 approximation leads to no qualitative changes in the clusters arrangement according to their stability. (11 refs.)

61040 A correlation between structure and reactivity in ion clusters. A.J.Stace, C.Moore (Dept. of Chem., Univ. of Southampton, Southampton, England). *Chem. Phys. Lett. (Netherlands)*, vol.96, no.1, p.80-4 (25 March 1983). Observations on metastable peaks resulting from the unimolecular decomposition of clusters show that intensity variations as a function of cluster size can reveal the presence of stable cluster configurations. This technique has been used to conform that $(\text{H}_2\text{O})_{21}\text{H}^+$ and $(\text{D}_2\text{O})_{21}\text{D}^+$ are stable ion clusters, and the method also provides evidence to suggest that Ar_{19}^+ is a particularly stable species. (23 refs.)

61041 On the origin of the occurrence of 'magic numbers' in cluster size distributions of xenon in the compressed gas phase. E.E.Polymeropoulos, J.Brickmann (Inst. für Phys. Chem., Tech. Hochschule Darmstadt, Darmstadt, Germany). *Chem. Phys. Lett. (Netherlands)*, vol.96, no.3, p.273-5 (8 April 1983). The formation of clusters in compressed argon and xenon gases is studied with the molecular dynamics simulation technique using two-body Lennard-Jones and three-body Axilrod-Teller potentials. It is suggested that the occurrence of clusters corresponding to the 'magic number' $n=13$ for xenon and the absence of such stable clusters for argons is due to the dispersion forces that result from triple-dipole interactions. (17 refs.)

61042 Binary compound clusters formed by free jet expansion. Y.Saito (Technol. Dev. Centre, Toyohashi Univ. of Technol., Toyohashi, Japan), K.Mihama, T.Noda. *Jpn. J. Appl. Phys. Part 2 (Japan)*, vol.22, no.3, p.179-81 (March 1983). Atom-clusters of NaCl, KCl, PbS and PbSe have been produced by adiabatic expansion of the vapour through a small nozzle. These clusters have been ionised by electron bombardment and analysed by time-of-flight mass spectrometry. Formation of compound clusters from MX to $(\text{MX})_n$ has been observed for all the samples, where M represents a cation and X an anion. Alkali halide clusters are considered to keep their stoichiometry. On the other hand, for lead chalcogenides, clusters having non-stoichiometric compositions as well as those having stoichiometric compositions are formed, though the former clusters are less abundant than the latter. (8 refs.)

61043 Supersonic copper clusters. D.E.Powers, S.G.Hansen, M.E.Geusic, D.L.Michalopoulos, R.E.Smalley (Dept. of Chem., Rice Univ., Houston, TX, USA). *J. Chem. Phys. (USA)*, vol.78, no.6, pt.1, p.2866-81 (15 March 1983). Copper clusters ranging in size from 1 to 29 atoms have been prepared in a supersonic beam by laser vaporization of a rotating copper target rod within the throat of a pulsed supersonic nozzle using helium for the carrier gas. The clusters were cooled extensively in the supersonic expansion [$T(\text{translational})$ 1 to 4 K, $T(\text{rotational})=4\text{K}$, $T(\text{vibrational})=20$ to 70K]. These clusters were detected in the supersonic beam by laser photoionization with time-of-flight mass analysis. Using a number of fixed frequency outputs of an exciplex laser, the threshold behavior of the photoionization cross section was monitored as a function of cluster size. The 7.9 eV photon energy of the F_2 excimer laser was found to be above the ionization potential of all clusters, and the photon mass spectrum thus produced showed the copper cluster concentration in the beam to follow a monotonically decreasing function of cluster size. The 6.4 eV ArF exciplex laser photon energy was found to be above the photoionization threshold of clusters with three or more atoms in the case of odd-numbered clusters, but only for clusters with eight or more atoms for even-numbered clusters. Extending out to clusters as large as 29 atoms, laser photoionization at 6.4 eV produced a time-of-flight mass distribution with a pronounced even/odd alternation in cluster photoion intensity. This alternation in ionization threshold behaviour was attributed to an even/odd alternation in the electronic structure of the copper clusters with the highest occupied molecular orbital (HOMO) of the even clusters being considerably more strongly bonding than it is in the clusters with an odd number of copper atoms. The 4.98 eV photon energy of the KrF exciplex laser was found to lie below the ionization threshold of all clusters in the 1 to 29 atom range. An extensive survey of the ultraviolet absorption spectrum of the copper dimer was also performed with this supersonic beam source. Resonance two-photon ionization (R2PI) with mass selective detection allowed the detection of five new electronic band systems in the region between 2690 and 3200 Å, for each of the three naturally occurring isotopic forms of Cu_2 . In the process of scanning the R2PI spectrum of these new electronic states, the ionization potential of the copper dimer was determined to be 7.894 ± 0.015 eV. (32 refs.)

61044 Molecular clustering about a positive ion. Structures, energetics, and vibrational frequencies of the protonated hydrogen clusters H_3^+ , H_5^+ , H_7^+ , and H_9^+ . Y.Yamaguchi, J.F.Gaw, H.F.Schaefer,III (Dept. of Chem., Univ. of California, Berkeley, CA, USA). *J. Chem. Phys. (USA)*, vol.78, no.6, pt.2, p.4074-85 (15 March 1983). The positive hydrogen clusters $\text{H}^+(\text{H}_2)_n$, for $n=1,2,3,4$ have been studied via nonempirical molecular electronic structure theory. Using double zeta (DZ) and double zeta plus polarization (DZ+P) basis sets, wave functions are reported at both the self-consistent field (SCF) and configuration interaction including all single and double excitations (CISD) levels of theory. In each case analytic gradient techniques have been used to locate stationary point geometries and to predict harmonic vibrational frequencies. The effects of electron correlation are shown to be greater for these loose molecular complexes than for ordinary molecules. Although H_3^+ in its lowest energy conformation is not qualitatively described as H_3^+ , H_5^+ , the larger molecular ions do fit the qualitative picture $\text{H}_3^+(\text{H}_2)_n$ with H_3^+ as a nucleating center. Of special interest here are the 'new' normal modes of these clusters, i.e., those modes having no counterpart in the isolated H_3^+ or H_2 species. There are 15 such vibrational degrees of freedom for H_9^+ , and the resulting harmonic vibrational frequencies range from 775 cm^{-1} all the way down to 63 cm^{-1} . Dissociation energies as a function of cluster size follow the pattern established experimentally by Hiraoka and Kebalre (1975). (47 refs.)

A combination of pseudopotentials and density functionals: results for Li_n^{m+} , Na_n^{m+} and K_n^{m+} clusters ($n \leq 4$; $m=0,1$)See Entry 60568

ESR of pseudorotating $^6\text{Li}_3$ and $^7\text{Li}_3$ See Entry 60763

Mossbauer studies of FeSn molecules isolated in rare-gas solids and SCF-X α -scattered-wave molecular-orbital analyses of Sn_2 and FeSn diatomic moleculesSee Entry 60774

Electron structure of stoichiometric and nonstoichiometric tungsten oxidesSee Entry 62338

40.00 CLASSICAL AREAS OF PHENOMENOLOGY

(inc. applications)

41.00 ELECTRICITY AND MAGNETISM; FIELDS AND CHARGED PARTICLES

(see also 03.50 Maxwell theory: general mathematical aspects)

41.10 CLASSICAL ELECTROMAGNETISM

Cartesian polytensorsSee Entry 59584

41.10D Electrostatics, magnetostatics

61045 Dual finite-element calculations for static electric and magnetic fields. P.Hammond (Dept. of Electrical Engng., Univ. of Southampton, Southampton, England), T.D.Tsiboukis. *IEE Proc. A (GB)*, vol.130, no.3, p.105-11 (May 1983).

The finite-element method is widely used for the solution of field problems but the method, as generally applied, suffers from the fact that it is not known how close the solution is to the actual value. This uncertainty can be reduced by providing a dual finite-element method which is so arranged that both methods together provide upper and lower bounds to the correct solution. It is found that the double approach also promises economies in the computation. The authors examine the physical basis of the dual method and apply it to Laplacian and Poissonian problems. (7 refs.)

61046 Creation and measurement of magnetic fields nearly dipolar. M.Bernheim (ENSIMAG, Grenoble, France). *Onde Electr. (France)*, vol.63, no.3, p.47-50 (March 1983). In French. An expression of a limited expansion in Cartesian coordinates of the static magnetic field produced by a cylindrical coil, is given. One of the first uses of the formula is to demonstrate how magnetic fields approaching complete dipolarity can be obtained. (2 refs.)

Design of electrostatic lenses with a concave cathodeSee Entry 61066

Quadrupole condensing lenses with a highly linear electric field distributionSee Entry 61068

41.10F Steady-state electromagnetic fields; electromagnetic induction

61047 An admittance solution for electromagnetic coupling through a small aperture. J.R.Mautz, R.F.Harrington (Dept. of Electrical & Computer Engng., Syracuse Univ., Syracuse, NY, USA). *Appl. Sci. Res. (Netherlands)*, vol.40, no.1, p.39-69 (1983).

An admittance solution for electromagnetic coupling through a small aperture in a conducting screen is obtained by the method of moments. This solution gives the equivalent magnetic current in the aperture as a linear combination of the three quasi-static magnetic currents responsible for the three dipole fields seen in the far zone. Because only the dipole effects of the quasi-static currents are known, the elements of the excitation vector and the admittance matrix cannot be evaluated directly. Reciprocity is used to express the elements of the excitation vector in terms of the short-circuit incident fields. The imaginary parts of the elements of the admittance matrix are evaluated by forcing the moment solution to be equal to the solution predicted by conventional small aperture theory. The real parts of the elements of the admittance matrix are extracted from the quadratic expression for the power radiated by the magnetic current. The solution is applied to three examples—an aperture in a conducting plane, an aperture in a transverse wall between two rectangular waveguides, and an aperture in a lateral wall of a rectangular waveguide coupling to a half-space. (8 refs.)

61048 Induced eddy current calculation in high permeability bodies using method of differences. M.Albach, L.Hannakam (Tech. Univ. Berlin, Berlin, Germany).

Arch. Elektrotech. (Germany), vol.66, no.2, p.67-74 (1983). In German. Shows that a conducting high permeability body brought into a magnetic field could be, in effect, studied through the introduction of a new boundary condition of the third kind, that stipulates the proportionality of the resultant vector-potential in air, defined on the surface of the body, to the normal differential of the same. As a result, the method of differences requires only this new boundary condition and the Laplace-equation for the surrounding medium. This procedure is applied to a rectangular body with special emphasis on the edges of the body. The induced surface eddy-current proportional to the vector-potential in the surrounding medium is calculated and compared with analytical solutions of the boundary value problem in the case of stationary skin-effect. (2 refs.)

61049 Skin effect and eddy currents in a thin tape. M.Krakowski, H.Morawski (Tech. Univ. of Lodz, Lodz, Poland). *Arch. Elektrotech. (Germany)*, vol.66, no.2, p.95-8 (1983).

The skin effect due to the a.c. flowing through a thin metallic tape is examined. The formulae for the resistance and internal inductance of the tape are derived. The eddy-current distribution and the eddy-current losses in the tape situated in a homogeneous TM field are analysed. (8 refs.)

61050 Eddy currents in circular, square and rectangular rods. B.Beland (Dept. of Electrical Engng., Univ. of Sherbrooke, Sherbrooke, Quebec, Canada). *IEE Proc. A (GB)*, vol.130, no.3, p.112-21 (May 1983).

Eddy-current losses due to sinusoidal magnetomotive force are computed for square, circular, and rectangular rods using a rectangular B/H curve. For all sections, it is assumed that the induced currents flow on a path parallel to the sides. The results are normalised and given in a table from which many computation steps can be saved. The saturating induction is chosen as the value of B which corresponds to a quarter of the applied magnetic field on the magnetisation curve. The validity of the hypothesis is confirmed by measurements made on 15 rings, constructed from mild steel, cast iron and special magnetic alloys. The power factor and losses are usually predicted within 10% for a field ranging from 200 to 70000 A/m. (6 refs.)

61051 Proximity effect between a wire carrying current and a rotating cylindrical conductor. I.R.Ciric (Dept. of Electrical Engng., Univ. of Manitoba, Winnipeg, Manitoba, Canada). *IEEE Proc. A (GB)*, vol.130, no.3, p.122-8 (May 1983).

The general expressions of the quasistationary electromagnetic field quantities, as well as the power loss, forces and torque, for a rotating cylindrical conductor in the proximity of a parallel straight wire carrying AC or DC, have been obtained by means of the magnetic vector potential, assuming a two-dimensional field. Specific motional field effects are shown explicitly in the DC case, when proximity factors and practical formulas of the losses, forces and torque are derived for values of motional depth of penetration large or small compared with the cylinder radius. (9 refs.)

61052 Symmetries in coherent and partially coherent fields. A.W.Lohmann, J.Ojeda-Castaneda, N.Streibl (Phys. Inst. Univ. Erlangen, Erlangen, Germany).

Opt. Acta (GB), vol.30, no.4, p.399-402 (April 1983).

The operator form of the solution for the wave equation is employed to indicate the symmetry properties of the diffracted field under coherent and partially coherent illumination. Such symmetries are of interest in holography, phase conjugation, and for automatic focusing. (9 refs.)

Dynamics of DC-magnets and their application in the instrument manufacture

..... See Entry 59801

On the motion of an ion near a conducting wall: correlation effects

..... See Entry 61059

41.10H Electromagnetic waves: theory

61053 Diffraction by a perfectly conducting elliptic cone. E.Vafiadis, J.N.Sahalos (Univ. of Thrace, Xanthi, Greece).

Arch. Elektrotech. (Germany), vol.66, no.2, p.117-24 (1983).

The exact solution for the electromagnetic field diffracted by a perfectly conducting elliptic cone is determined. The solution is presented in the form of a dyadic Green's function which is the most general form of solution. It uses the spheroidal coordinate system where the elliptic cone is one of the coordinate surfaces. Results are shown for the first main contributed eigenvalues and eigenfunctions and for the far zone field in some special cases. (7 refs.)

61054 Boundary diffraction of an inhomogeneous wave. P.-A.Belanger (Dept. de Phys., Univ. Laval, Quebec, Canada), M.Couture. *J. Opt. Soc. Am. (USA)*, vol.73, no.4, p.446-50 (April 1983).

An exact decomposition of the diffracted field into a direct wave and a boundary diffraction wave is obtained for an incident inhomogeneous wave, namely, the complex-source-point spherical wave. The authors' result, in the paraxial approximation, is consistent with already published results on the diffraction of a Gaussian beam. (15 refs.)

61055 Directional diagrams of coherent volume radiators and diffraction by 3-D periodic structures. Yu.V.Aristov, V.M.Rysakov.

Opt. & Spectrosc. (USA), vol.53, no.2, p.182-5 (Aug. 1982). Translation of: *Opt. & Spektrosk. (USSR)*, vol.53, no.2, p.313-19 (Aug. 1982). [received: April 1983]

It is shown that an expansion in a 3-D spatial spectrum of the envelope of an amplitude distribution of sources that varies slowly in space is an effective method of analyzing directional diagrams. With its help some general properties of the radiators are established. The treatment is illustrated with the example of a radiator in the form of a Gaussian ellipsoid of revolution. (8 refs.)

61056 Surface electromagnetic fields. P.J.Feibelman (Sandia Nat. Labs., Albuquerque, NM, USA).

Prog. Surf. Sci. (GB), vol.12, no.4, p.287-407 (1982).

Recent progress in the theory of surface electromagnetic fields is reviewed. Difficulties are noted in applying the textbook theory of refraction to fields within Å of a surface. These difficulties have been overcome with the development of a nonlocal description of surface optics, that has largely been applied to free-electron metal surfaces. Various model versions of non-local surface optics are described and quantitatively compared. Opportunities for, and actual contact between the theory of surface electromagnetic fields and experiments are described. Directions for future research in the area are discussed. (125 refs.)

61057 The wave vector component parallel to the magnetic field of the reflected cyclotron harmonic wave. T.Utsunomiya (Dept. of Electrical Engng., Nat. Defense Acad., Yokosuka, Japan).

Trans. Inst. Electron. & Commun. Eng. Jpn. Part B (Japan), vol.J66B, no.1, p.153-4 (Jan. 1983). In Japanese.

Shows that the magnitude of wave vector component parallel to the magnetic field of the reflected cyclotron harmonic wave is more limited by a frequency condition for propagation than the Landau damping condition alone. The condition is revealed with a numerical example for the permitted parallel component. (3 refs.)

61058 Diffraction of cylindrical wave by smooth and polygonal cylinders. H.Shirai, K.Hongo (Faculty of Engng., Shizuoka Univ., Hamamatsu, Japan), H.Kobayashi.

Trans. Inst. Electron. & Commun. Eng. Jpn. Sect. E (Japan), vol.E66, no.2, p.116-23 (Feb. 1983).

Expressions are derived for estimating the scattered and diffracted field in the presence of the polygonal cylinder using high frequency technique which is closely related with equivalent current or equivalent moment method. As a first step, the authors verify the method by applying it to various kinds of polygonal cylinders. The numerical results for radiation patterns are compared with those obtained by other methods. The agreement between them is fairly good and difference between them is not recognised except in a small region near a shadow boundary of the polygonal cylinder. Next, the authors study the estimation of the diffracted field of smooth convex cylinder by approximating it with corresponding polygonal cylinder. As an illustration they consider radiation of electric and magnetic line source in the presence of conducting circular cylinder since the exact solution of the problem is readily obtained. (9 refs.)

Parametric conversion of electromagnetic waves in a relativistic electron beam moving in a cylindrical waveguide

..... See Entry 61061

Bistatic low-frequency inverse scattering

..... See Entry 61324

41.70 PARTICLES IN ELECTROMAGNETIC FIELDS: CLASSICAL ASPECTS

(inc. synchrotron radiation)

61059 On the motion of an ion near a conducting wall: correlation effects. R.M.Mazo.

J. Chem. Phys. (USA), vol.78, no.5, p.2635-41 (1 March 1983).

When a charged particle moves near a conducting wall, the induced current exerts a retarding force on the particle. The magnitude of this retarding force for a single ion has previously been computed. Here, the effects of ionic spatial correlations in an electrolyte solution are examined. The author finds that, at large distances from the wall, there is partial screening of the retarding force. At small distances, where the entire effect is largest, the previously considered single ion contribution is dominant. (8 refs.)

61060 Motion and emission of a classical relativistic particle in a nonuniform laser wave. O.N.Metelitsa, A.A.Sokol'ski (State Univ., Minsk, Belorussian SSR).

Sov. Phys.-Tech. Phys. (USA), vol.27, no.9, p.1062-4 (Sept. 1982). Translation of: *Zh. Tekh. Fiz. (USSR)*, vol.52, no.9, p.1731-3 (Sept. 1982).

[received: April 1983]

In connection with an idea advanced by Baryshevskii (see Dokl. Akad. Nauk BSSR, vol.5, p.232, 1979) that high energy particles can channel through a nonuniform laser wave, a theoretical analysis of their motion and emission is carried out within the framework of classical theory. The effective potential, the Lindhard angle, and the minimum turning radius are obtained for a relativistic particle in an 'optical channel'. It is shown that the particle radiation is concentrated in two frequency regions. The higher-frequency component can exceed the frequency of the laser wave by a factor of $(E/mc^2)^2$. It is also shown that for a particle moving in a field produced by superposition of a circularly polarized laser wave and a time-independent nonuniform magnetic field it is possible to achieve a growth of the depth of the potential well with increasing particle energy. (3 refs.)

61061 Parametric conversion of electromagnetic waves in a relativistic electron beam moving in a cylindrical waveguide. N.Ya.Kotsarenko, A.A.Silivra.

Sov. Phys.-Tech. Phys. (USA), vol.27, no.10, p.1178-81 (Oct. 1982). Translation of: *Zh. Tekh. Fiz. (USSR)*, vol.52, no.10, p.1915-21 (Oct. 1982).

[received: April 1983]

Parametric interaction of two electromagnetic waves with a space charge wave in an electron beam is considered. The space charge wave frequency is equal to the difference in the frequencies of the two electromagnetic waves, and the electron beam travels in a round cylindrical waveguide. The relativistic electron beam is assumed to be monoenergetic and charge- and current-neutralized, and to uniformly fill the interior of the waveguide. It is shown that the finiteness of the beam and interaction region transverse to the beam results in generation of a whole spectrum of waves excited by the initial pumping wave. The nature of the resulting instability and the spectral distribution of the gain are determined. Numerical estimates are given for specific examples. (8 refs.)

61062 Undulator radiation of charged particles moving above a domain structure. V.L.Bratan, G.M.Genkin, V.V.Zil'berberg (Inst. of Appl. Phys., Acad. of Sci., Gorki, USSR).

Sov. Tech. Phys. Lett. (USA), vol.8, no.8, p.419-20 (Aug. 1982). Translation of: *Pis'ma v Zh. Tekh. Fiz. (USSR)*, vol.8, no.15-16, p.970-3 (Aug. 1982).

[received: April 1983]

The undulator radiation of high-energy particles in spatially periodic fields is a universal source of electromagnetic waves from the microwave range to the X-ray range. The undulators which are ordinarily used are macroscopic magnet systems with periods ranging from tens of centimeters to a few millimeters or the internal atomic fields of crystals. Periodic domain structures which occupy an intermediate position between these two types of undulators may also be of definite interest. The periods of these structures are several orders of magnitude smaller than those of macroscopic systems, and the fields are so strong that they can impart oscillatory velocities to the particles which are much higher than those in atomic undulators. Furthermore, in contrast with atomic undulators, short-wavelength radiation can be excited as the particles move in the fringing fields near the surface of a ferromagnet with an unclosed magnetic flux. This makes it possible in principle to use arbitrarily dense particle beams. (7 refs.)

Enhanced stopping of relativistic electron beams using applied magnetic fields

..... See Entry 61063

Space-charge conditions in an intense relativistic particle beam

..... See Entry 61064

Steady states of thin high-current relativistic electron beams in magnetic fields

..... See Entry 61067

Efficiency of free-electron lasers with a scattered electron beam

..... See Entry 61164

Intense free electron laser harmonic generation in a longitudinal magnetic wiggler

..... See Entry 61165

Nonlinear analysis of free-electron-laser amplifiers with axial fields

..... See Entry 61167

Nonlinear traveling-wave equilibria for free-electron-laser applications

..... See Entry 61168

Effects of electron energy spread on self-excitation of free-electron lasers

..... See Entry 61171

41.80 PARTICLE BEAMS AND PARTICLE OPTICS

(see also 07.80 Electron and ion microscopy, 07.77 Beam handling equipment)

Electrostatic charged particle analyzer with three coaxial cylindrical electrodes. II. Construction of a three-stage system with a central electrode of finite thickness and axis-axis focusing

..... See Entry 59890

41.80D Electron beams and electron optics

61063 Enhanced stopping of relativistic electron beams using applied magnetic fields. Y.Marou, A.E.Blaugrund (Weizmann Inst. of Sci., Rehovot, Israel).

J. Appl. Phys. (USA), vol.54, no.4, p.1666-9 (April 1983).

A high-current-density relativistic electron beam is extracted through a thin anode window from the pinch region of a diode. An externally applied azimuthal magnetic field forces the electrons to make multiple passes through the

anode window or through adjacent metal or insulator foils, thus causing enhanced energy deposition and X-ray emission. Enhancement factors of 2 to 4 have been observed. (13 refs.)

61064 Space-charge conditions in an intense relativistic particle beam. V.L.Aleynikov, Yu.A.Pirogov (Lomonosov State Univ., Moscow, USSR). *Sov. Phys.-Tech. Phys. (USA)*, vol.27, no.9, p.1123-6 (Sept. 1982). Translation of: *Zh. Tekh. Fiz. (USSR)*, vol.52, no.9, p.1832-7 (Sept. 1982). [received: April 1983]

A study is made of the passage of a unipolar flow through a diode gap with arbitrary potentials, including relativistic ones (generalized diode). Conditions are defined for space-charge limitation for relativistic fluxes, and deviations are demonstrated from the Child-Langmuir nonrelativistic relations from the exact relativistic formulas in the one-dimensional approximation. (11 refs.)

61065 Electrostatic single astigmatic cylindrical lenses. L.G.Glikman, Z.D.Iskakova (Inst. of Nuclear Phys., Acad. of Sci., Alma-Ata, Kazakh SSR).

Sov. Phys.-Tech. Phys. (USA), vol.27, no.9, p.1150-2 (Sept. 1982). Translation of: *Zh. Tekh. Fiz. (USSR)*, vol.52, no.9, p.1874-7 (Sept. 1982). [received: April 1983]

The authors have studied the electron-optical properties of three-electrode single astigmatic cylindrical lenses with identical electrode diameters. In the calculations it is assumed that the gaps between the electrodes are infinitesimal and the lines separating them form part of the line of intersection of two cylinders of identical radius. The authors have found the parameters characterizing the paraxial properties of the lenses and their coefficients of spherical aberration with the object at infinity for various values of the ratios of electrode potentials and the distances between slits. The three-electrode single lens collects beams of charged particles in one plane and scatters in another plane over an entire selected range of values of potential ratios. It is shown that in single lenses the coefficients of spherical aberration are of different signs and one of the coefficients passes through zero. (7 refs.)

61066 Design of electrostatic lenses with a concave cathode. N.K.Zolina, Yu.A.Flegontov.

Sov. Phys.-Tech. Phys. (USA), vol.27, no.10, p.1190-5 (Oct. 1982). Translation of: *Zh. Tekh. Fiz. (USSR)*, vol.52, no.10, p.1938-45 (Oct. 1982). [received: April 1983]

Analytic expressions are derived which describe quite accurately the imaging characteristics of a cathode lens with a concave cathode in terms of the field parameters (more precisely, in terms of the derivatives of the field at the cathode). These equations generalize those previously published for lenses with a flat cathode. The accuracy of the equations is illustrated by numerical examples in which the results are compared with other methods of calculation. Recommendations are given for approximating the field so as to maximize the accuracy of the derived equations. As an example, the field and electrode dimensions are calculated for a lens producing images with small distortion and meridional curvature error. (7 refs.)

61067 Steady states of thin high-current relativistic electron beams in magnetic fields. N.F.Kovalev, M.I.Fuks (Inst. of Appl. Phys., Acad. of Sci., Gorkii, USSR).

Sov. Phys.-Tech. Phys. (USA), vol.27, no.10, p.1230-4 (Oct. 1982). Translation of: *Zh. Tekh. Fiz. (USSR)*, vol.52, no.10, p.2002-8 (Oct. 1982). [received: April 1983]

A method is proposed for calculating the parameters of an electron beam from the injection plane to the collector in an irregular vacuum channel with an arbitrarily changing cross section. Beam formation and transport are considered by reducing the problem to a study of the solutions of a second-order ordinary differential equation. A qualitative steady-state theory is developed. (7 refs.)

61068 Quadrupole condensing lenses with a highly linear electric field distribution. A.B.Novgorodtsev (M.I. Kalinin Polytech. Inst., Leningrad, USSR).

Sov. Phys.-Tech. Phys. (USA), vol.27, no.10, p.1257-60 (Oct. 1982). Translation of: *Zh. Tekh. Fiz. (USSR)*, vol.52, no.10, p.2047-53 (Oct. 1982). [received: April 1983]

The electric field strength distribution is considered in quadrupole condensing lenses with polygonal electrodes, which are easier to fabricate than hyperbolic electrodes and give a strictly linear field distribution. The electrode profile is chosen to cancel the terms in the power series expansion of the complex field potential near the center of the system. Electrode configurations are determined which cancel the first, second, and third terms in the series expansion. The distribution of the field intensity gradient nonuniformities is investigated in the polygonal systems as well as in quadrupole condensing lenses having simpler electrodes (plates, angles, cylindrical surfaces). Recommendations are given for choosing the shapes of the electrodes to achieve a given degree of field gradient uniformity. (7 refs.)

An intense electron beam source See Entry 59879

A new electrostatic phase-shifting effect See Entry 59894

Joule-Thomson effect in a Pierce electron gun See Entry 60513

Parametric conversion of electromagnetic waves in a relativistic electron beam moving in a cylindrical waveguide See Entry 61061

41.80G Ion beams and ion optics

61069 Properties of ion beams formed from a nonstationary plasma. T.A.Basova, Yu.K.Altudov, Yu.A.Bykovskii, Yu.N.Kolosov, V.N.Nevolin (Engng. Phys. Inst., Moscow, USSR).

Sov. Phys.-Tech. Phys. (USA), vol.27, no.9, p.1088-90 (Sept. 1982). Translation of: *Zh. Tekh. Fiz. (USSR)*, vol.52, no.9, p.1773-7 (Sept. 1982). [received: April 1983]

The phase volume of ion beams is investigated and the beam emittance for three different beam-extraction systems is determined. Calculation of the brightness of the source showed that it was higher than that of any other known ion source. A plasma ion source employing monochromatic emission has been used for implanting ions into different materials. (7 refs.)

61070 Dynamics of pulsed ion beam production by a plasma lens. I.S.Gasanov, I.M.Protchenko (Inst. of Phys., Acad. of Sci., Kiev, Ukrainian SSR).

Sov. Phys.-Tech. Phys. (USA), vol.27, no.9, p.1094-5 (Sept. 1982). Translation of: *Zh. Tekh. Fiz. (USSR)*, vol.52, no.9, p.1783-6 (Sept. 1982). [received: April 1983]

The results of experiments in which a pulsed beam of helium ions with energy up to 35 keV and current up to 50 mA is focused by a plasma lens are given. Information is given about the processes that determine the dynamics of formation and attenuation of electric fields in the lens. The focusing of the ion flux passing through the system occurs in the time required for considerable accumulation of electrons ejected from the walls of the cold compensator. At high residual-gas pressures the duration of effective operation of the

lens is limited by the time of accumulation of slow ions formed by ionization. (7 refs.)

Criterion for optimizing ion sources produced by electron impact ionization See Entry 59876

42.00 OPTICS

(for properties of gases and of liquids and solids, see 51.70 and 78. respectively; for atmospheric optics, see 92.65; for physiology of the eye, see 87.32)

42.10 PROPAGATION AND TRANSMISSION IN HOMOGENEOUS MEDIA

61071 Mach fringes as a physical phenomenon. H.Nieck (Sektion Phys., Martin-Luther Univ., Halle, Germany).

Exp. Tech. Phys. (Germany), vol.31, no.1, p.53-7 (1983). In German. Mach fringes can also be measured by physical radiation receptors, showing that they are a physical effect. From instantaneous photos it is shown that every moving diffusely reflecting bright face forms a dark fringe outside and a bright fringe inside at its limit with a dark face. Therefore a moving oblique face produces Mach fringes. Mach fringes at the limits of half-shade from an extended light source are interpreted by diffraction at a half-plane. (5 refs.)

61072 Rigorous coupled-wave analysis of grating diffraction—E-mode polarization and losses. M.G.Moharam, T.K.Gaylord (School of Electrical Engng., Georgia Inst. of Technol., Atlanta, GA, USA).

J. Opt. Soc. Am. (USA), vol.73, no.4, p.451-5 (April 1983). Rigorous coupled-wave theory of diffraction by dielectric gratings is extended to cover E-mode polarization and losses. Unlike in the H-mode-polarization case, it is shown that, in the E-mode case, direct coupling exists between all diffracted orders rather than just between adjacent orders. (6 refs.)

61073 Generalized curvilinear diffraction gratings. III. Euclidian diffraction gratings. R.A.Lee (Div. of Appl. Organic Chem., CSIRO, Melbourne, Victoria, Australia).

Opt. Acta (GB), vol.30, no.4, p.431-9 (April 1983). For p.II see *ibid.*, vol.30, no.3, p.291 (1983). Studies classes of plane uncrossed diffraction gratings which have the common property that their Fourier transform patterns consist of sharp-line caustics. These types of generalized gratings are referred to as 'Euclidian diffraction gratings', because the condition for the formation of line caustics is equivalent to the global vanishing of the Gaussian curvature of the grating line pattern function. The analysis is applied to the laser material processing system discussed in the last paper. (1 ref.)

61074 Generalized curvilinear diffraction gratings. IV. Plane singular crossed gratings. R.A.Lee (Div. of Appl. Organic Chem., CSIRO, Melbourne, Victoria, Australia).

Opt. Acta (GB), vol.30, no.4, p.441-7 (April 1983). For p.III see *ibid.*, vol.30, no.4, p.431 (1983). Discusses the Fraunhofer diffraction properties of plane crossed-line gratings which consist of a product of two uncrossed-line gratings. In particular, the author establishes a set of conditions which the grating functions must satisfy for the diffraction pattern to consist of a purely singular line pattern. For these singular gratings, the author shows that the diffraction pattern consists of a product of the orders of each uncrossed-line grating plus additional orders due to couplings between the separate gratings. (2 refs.)

61075 Generalized curvilinear diffraction gratings. V. Diffraction catastrophes. R.A.Lee (Div. of Appl. Organic Chem., CSIRO, Melbourne, Victoria, Australia).

Opt. Acta (GB), vol.30, no.4, p.449-64 (April 1983). The author shows how the bifurcation properties of two-dimensional potential functions may be studied via a diffraction grating representation. In particular, the author derives the grating functions appropriate to Thom's seven elementary catastrophes. The author then presents a detailed study of the cusp grating and discusses the behaviour of its point source image diffraction pattern (IDP) in the context of catastrophe theory. In this way, the author shows how catastrophe theory allows for a simple geometric interpretation of discontinuous type image diffraction patterns. (9 refs.)

61076 Spatial periodicities in partially coherent fields. A.W.Lohmann, J.Ojeda-Castaneda (Phys. Inst. Univ. Erlangen, Erlangen, Germany).

Opt. Acta (GB), vol.30, no.4, p.475-9 (April 1983). If the mutual intensity of partially coherent illumination is periodic in the lateral direction then it is also periodic in the longitudinal direction. This statement is proved for quasi-monochromatic light and for a cosine periodicity. Next an experimental set-up for the production of periodic mutual intensities is proposed. Finally, the theoretical result is generalized to other than cosine-shaped periodicities. (9 refs.)

61077 Fresnel diffraction of a Gaussian beam by one-dimensional opaque objects. C.Ozkul (Faculte des Sci. et des Tech., Univ. de Rouen, Mont-Saint-Aignan, France).

Opt. Acta (GB), vol.30, no.4, p.505-10 (April 1983). Fresnel diffraction fields of one-dimensional opaque objects under collimated Gaussian beam illumination are described. The irradiance distribution function is derived and the resultant formulae are compared with the case of uniform beam illumination. Experimental observation of irradiance as a function of position is in good agreement with numerically calculated results. (14 refs.)

61078 Modification of Fresnel diffraction by a straight edge object with acoustically coherence-controllable illumination. Y.Ohtsuka (Dept. of Engng. Sci., Hokkaido Univ. Hokkaido, Japan).

Opt. Acta (GB), vol.30, no.4, p.545-55 (April 1983). An attempt to modify a ringing fringe pattern of Fresnel diffraction is described. Fringe formation is heavily dependent on the illumination condition of partial coherence controlled by a progressive acoustic wave. Periodic envelope modification results in a fringe pattern due to periodicity of the acoustic wave. The ringing is appreciably suppressed near the geometrical shadow edge of the object. Successive maxima and minima of the fringe pattern are reversed if the acoustic power crosses over a critical level. (13 refs.)

61079 Diffraction efficiency of photochromic absorption gratings. T.Jaaskelainen (Dept. of Phys., Univ. of Kuopio, Kuopio, Finland). *Opt. Commun. (Netherlands)*, vol.45, no.3, p.145-8 (1 April 1983). Efficiencies of thick photochromic absorption gratings are theoretically investigated. The treatment is based on a realistic photochromic grating model,

which includes both spatial and temporal variations of the absorption coefficient. Simple analytic solutions for dynamic diffraction characteristics are derived. This nonlinear model shows that the maximum diffraction efficiency of photochromic absorption gratings may exceed 10%. (6 refs.)

61080 Reflection of a plane monochromatic wave from a medium with spatial dispersion. V.V.Yatsyshen.

Opt. & Spectrosc. (USA), vol.53, no.2, p.172-5 (Aug. 1982). Translation of: *Opt. & Spektrosk. (USSR)*, vol.53, no.2, p.296-300 (Aug. 1982). [received: April 1983]

The problem of the reflection of an electromagnetic wave from a medium close to exciton resonance is investigated in the paper for the general case of oblique incidence. The question of whether the law of conservation of energy is satisfied in the case when an additional wave with spatial dispersion arises in the medium is considered. Since the distribution of energy between the reflected and refracted waves is regulated by the system of boundary conditions, limitations on the form of the additional condition and the remaining boundary conditions are found for which the law of conservation of energy is satisfied. It is shown that the system of inhomogeneous boundary conditions, including the inhomogeneous additional boundary condition and the condition of discontinuity of magnetic field at the boundary, is internally consistent for a specific relationship between the inhomogeneous terms of both conditions. (9 refs.)

61081 Orientation of an arbitrary ray, passing through a two-wedge compensator. G.A.Guzenko.

Sov. J. Opt. Technol. (USA), vol.49, no.7, p.433-5 (July 1982). Translation of: *Opt.-Mekh. Prom.-st. (USSR)*, vol.49, no.7, p.30-2 (July 1982). [received: April 1983]

Universal mathematical expressions are obtained for the vertical and horizontal orientation angles of a ray, passing through a two-wedge compensator, for arbitrary direction of the incident ray and compensator position. (3 refs.)

61082 Retrieval and synthesis problems in optics—an overview. H.P.Baltes (Landis & Gyr Zug AG, Zug, Switzerland).

Topical Meeting on Signal Recovery and Synthesis with Incomplete Information and Partial Constraints, Incline Village, NV, USA, 12-14 Jan. 1983 (Washington, DC, USA: Opt. Soc. America 1983), p.WA1/1-4

Presents a synopsis of the large variety of inverse problems in optical physics with emphasis on the underlying questions of uniqueness, stability and prior knowledge. Two specific examples are discussed. One is a deterministic problem on the level of electromagnetic inverse scattering, namely the design of grating profiles tailored to yield certain desired diffraction efficiencies. The other is a problem of statistical optics, namely the question of how a phase grating hidden behind a diffuser can be retrieved by observing the degree of coherence of scattered light. (4 refs.)

Ring polarization interferometer. Measurement of the flow rates of transparent media See Entry 59837

Surface electromagnetic fields See Entry 61056

Condition for the limiting resolution of optical systems for partially coherent illumination See Entry 61098

On obtaining a specified light-field distribution See Entry 61112

A tunable 90° rotator using a total reflection by a monodomain cholesteric liquid crystal cell See Entry 61258

Waveguide loss evaluation by the ray-optics method See Entry 61269

Single-mode anisotropic cylindrical dielectric waveguides See Entry 61271

Mode coupling in a specifically tapered Bragg grating coupler See Entry 61272

Gaussian approximation of the waveguide EH₁₁ mode pattern in the far field See Entry 61273

Inverse-square wavelength dependence of attenuation in infrared polycrystalline fibers See Entry 61293

Design of a new thin-film electro-optic switch See Entry 61304

Corrections to Maxwell boundary conditions in gyrotropic crystals See Entry 62921

Selective light scattering by disperse birefringent media with an isotropic point See Entry 62923

42.20 PROPAGATION AND TRANSMISSION IN INHOMOGENEOUS MEDIA

61083 Light scattering by bubbles in liquids: comments and application of results to circularly polarized incident light. P.L.Marston (Dept. of Phys., Washington State Univ., Pullman, WA, USA).

Appl. Sci. Res. (Netherlands), vol.40, no.1, p.3-5 (1983). Recently published Mie theoretic computations of the scattering of linearly polarized light from a bubble in water also apply, in certain cases, to the scattering of circularly polarized incident light. A correction to the labeling of one of the figures in the paper by Marston et al. (1982) is noted. (4 refs.)

61084 Second-order Rytov approximation. H.T.Yura (Aerospace Corp., Los Angeles, CA, USA), C.C.Sung, S.F.Clifford, R.J.Hill.

J. Opt. Soc. Am. (USA), vol.73, no.4, p.500-2 (April 1983). The authors obtain an explicit and useful formulation of the solution for the second-order Rytov approximation for an arbitrary source geometry. From this solution a condition of validity for the Rytov solution is obtained. The authors conclude that both the Born and the Rytov approximations have the same domain of validity. (10 refs.)

61085 Surface waves in backscattering and the localization principle. J.R.Probert-Jones (Dept. of Phys., Imperial Coll., London, England).

J. Opt. Soc. Am. (USA), vol.73, no.4, p.503 (April 1983). It is shown that use of the localization principle indicates that the spikes observed in the backscattering from large dielectric spheres cannot be due to surface waves. (8 refs.)

61086 Modification of the Rayleigh-Debye approximation. K.Shimizu (Res. Inst. of Appl. Electricity, Hokkaido Univ., Sapporo, Japan).

J. Opt. Soc. Am. (USA), vol.73, no.4, p.504-7 (April 1983). A modification of the Rayleigh-Debye approximation is given in two ways so that it includes the information of the refractive index of scatterers in the calculation of scattering patterns. The improvement that is due to the modification is demonstrated by comparing the approximation with the exact Mie calculation. (9 refs.)

61087 Measurements of Gaussian speckle statistics using both direct and heterodyne detection of CO₂ laser radiation. D.L.Jordan, R.C.Hollins (Royal Signals & Radar Estab., Malvern, England).

Opt. Acta (GB), vol.30, no.4, p.417-23 (April 1983). The characteristics of speckle patterns produced using scattered 10.6 μ m CO₂ laser radiation are described. At this wavelength, heterodyne detection offers

significant experimental advantages over direct detection of sensitivity and reduced contrast. As a simple illustration of heterodyne speckle techniques the heterodyne signals received from radiation scattered from a deep random phase screen are confirmed experimentally to follow a Rayleigh distribution. (9 refs.)

61088 Speckle intensity mean value dependence on the number of scatterers. B.Grzegorzewski, J.Mallek (Inst. of Math. & Phys., Acad. of Technol. & Agriculture, Bydgoszcz, Poland).

Opt. Commun. (Netherlands), vol.45, no.3, p.160-4 (1 April 1983). The number of scatterers contributing to the speckle amplitude can be determined by the spot size of the incident light or by the amplitude point spread function of the optical system. The speckle intensity mean value measurement results with two methods of choosing the number of scatterers applied are presented. The values of the RMS phase deviation and correlation length obtained from two methods agree well. The properties of both methods are discussed. The possibilities for the roughness measurement are suggested. (13 refs.)

61089 Parameters of the 'speckled pattern' formed when coherent radiation passes through opal glasses. N.A.Voishvillo, N.I.Sherbakova.

Sov. J. Opt. Technol. (USA), vol.49, no.7, p.413-15 (July 1982). Translation of: *Opt.-Mekh. Prom.-st. (USSR)*, vol.49, no.7, p.12-15 (July 1982). [received: April 1983]

The dependence of the measured parameters of the 'speckled pattern' on the dimensions and shape of the aperture diaphragm of the receiver, the laser operating conditions, the diameter of the illuminating beam and the radiation scattering direction has been investigated. (9 refs.)

61090 Effects of the director of light scattered from an object on speckle interference patterns. L.Marti-Lopez (A.F. Ioffe Physicotech. Inst., Acad. of Sci., Leningrad, USSR).

Sov. Phys.-Tech. Phys. (USA), vol.27, no.10, p.1248-50 (Oct. 1982). Translation of: *Zh. Tekh. Fiz. (USSR)*, vol.52, no.10, p.2032-5 (Oct. 1982). [received: April 1983]

The influence of the scattered light director on the form of the diffraction halo is considered. The interference patterns are interpreted using the Young fringes in doubly exposed speckle photographs. It is shown that the form of the diffraction halo is determined by the output aperture of the optical system only when the aperture is completely and uniformly filled by light scattered by each point on the surface of the object. If this condition does not hold, the diffraction halo (and hence the transverse resolution achievable using speckle interference patterns) is determined by how the scattered light from point of the object passes through the aperture, as well as by the aperture diameter. (7 refs.)

61091 Experimental investigations of fluctuations of optical signals and disturbances in the atmosphere. E.R.Milyutin, Yu.I.Yaremenko (M.A. Bonch-Bruvich Electrical Engng. Inst. of Communications, Leningrad, USSR).

Sov. J. Quantum Electron. (USA), vol.12, no.10, p.1357-8 (Oct. 1982). Translation of: *Kvantovaya Elektron., Moskva (USSR)*, vol.9, no.10, p.2088-90 (Oct. 1982). [received: April 1983]

An investigation was made of the statistical characteristics of signals and noise at the output of an optical detector placed at the end of a 500-m slightly inclined path. The probabilistic distribution law of the envelope of the background noise was determined for a single detector (receiver) aperture. A study was made of the distribution of the total signal in the case of coherent (linear) addition during direct tripled spatially separated detection for different degrees of atmospheric turbulence. An analysis was made of the experimental data. (1 ref.)

Low-cost microprocessor-based photon correlator See Entry 59826

Analysis of the shift-and-add method for imaging through turbulent media See Entry 61093

Periodic structures and the visual representation of phase objects in free space See Entry 61097

Laser microspeckle technique in displacement measurement near a crack tip See Entry 61462

Experimental study of volume scattering function of particles suspended in water See Entry 64148

Scattering matrix of nonspherical particles See Entry 64233

On isoplanatism by the arrival angles for light rays in telescopes See Entry 64234

42.30 OPTICAL INFORMATION, IMAGE FORMATION AND ANALYSIS

61092 Plasma polymerized films for optical recording. Y.Asano, H.Yamazaki, A.Morinaka (Ibaraki Electrical Communication Lab., Nippon Telegraph & Telephone Public Corp., Ibaraki, Japan).

Jpn. J. Appl. Phys. Part 1 (Japan), vol.22, no.3, p.480-4 (March 1983).

Metals containing plasma polymerized films have been investigated as media for laser thermal recording. The Te containing plasma polymerized carbon disulfide films (CS₂-Te) and Bi containing plasma polymerized carbon disulfide films (CS₂-Bi) are suitable for recording with respect to melting and vaporization, because they have low vaporizing temperature and low heat conductivity. In particular, the CS₂-Te unprotected antireflection structure showed the highest sensitivity. On the other hand, the CS₂-Te protective antireflection structure showed a lower sensitivity than the unprotected structure, but is preferable from the viewpoint of its high stability. The Te containing plasma polymerized styrene film is suitable for recording with respect to crystallization, because it shows a large optical change due to crystallization.

61093 Analysis of the shift-and-add method for imaging through turbulent media. B.R.Hunt (Dept. of Electrical Engng., Univ. of Arizona, Tucson, AZ, USA), W.R.Fright, R.H.T.Bates.

J. Opt. Soc. Am. (USA), vol.73, no.4, p.456-65 (April 1983).

The authors examine the statistical basis of the shift-and-add technique, by which true images of objects (viewed through fluctuating, distorting media) are formed by a particular kind of averaging of speckle images. The authors' theory agrees with experimental results for objects consisting of isolated unresolvable points. The authors develop a preliminary analysis for extended objects (i.e. objects having continuous, resolvable brightness distributions). (14 refs.)

61094 Effect of sample displacement in time-sequential sampling of spatiotemporal signals. J.P.Alebach (Dept. of Electrical Engng., Univ. of Delaware, Newark, DE, USA).

J. Opt. Soc. Am. (USA), vol.73, no.4, p.466-72 (April 1983).

Algorithms for digitally processing sampled spatiotemporal signals typically ignore the fact that those samples were obtained time-sequentially, rather

than instantaneously, at the beginning of each frame period. The effect of displacing time-sequentially obtained samples to a non-time-sequential lattice is analyzed for both deterministic and nondeterministic signals. Sample displacement is shown to cause unavoidable frequency-domain aliasing. The resulting artifacts are compared in test signals that have been sampled with a lexicographic and bit-reversed ordering of the sample points. (8 refs.)

61095 Extraction of difference using a polarization-shifted periodic carrier. A.Ghosh, A.K.Chakraborty (Dept. of Appl. Phys., Calcutta Univ., Calcutta, India).

Opt. Acta (GB), vol.30, no.4, p.425-30 (April 1983).

A method is proposed for subtracting two images using a polarization-shifted periodic carrier. The method has been successfully used to find the intensity gradient of a test object in the form of a transparency. Some experimental results are presented. (6 refs.)

61096 A comparison study of some computational methods for locating the zeros of entire functions. J.W.Wood, T.J.Hall, M.A.Fiddy (Dept. of Phys., Queen Elizabeth Coll., London, England).

Opt. Acta (GB), vol.30, no.4, p.511-27 (April 1983).

The zero description of entire functions of exponential type is reviewed. Serial and parallel methods of zero location from sampled data are introduced, and the results of applying these methods to simulated data are given. One method is also suitable for locating the zeros of finite-degree polynomials, and is thus particularly useful for use with the z transform of an input sequence. The relationship between the algorithms is discussed, and a recommendation of the most reliable method is given. (18 refs.)

61097 Periodic structures and the visual representation of phase objects in free space. V.A.Zverev, T.P.Kosobud, F.A.Markus.

Opt. & Spectrosc. (USA), vol.53, no.2, p.221-2 (Aug. 1982). Translation of: *Opt. & Spektrosk. (USSR)*, vol.53, no.2, p.373-5 (Aug. 1982). [received: April 1983]

It is shown that periodic phase inhomogeneities can also be presented visually in free space by using gratings to introduce an additional modulation of the field. This method is similar to the method of defocused diaphragms but does not require the presence of lenses in the design of the apparatus for its implementation. By selecting the grating period one can make it more compact than in the method of defocused diaphragms. Still another advantage of visual representation in free space becomes apparent when investigating self-luminous inhomogeneities. In this method of visual representation the illumination is uniform over the whole plane of observation and introduces a smaller error. (5 refs.)

61098 Condition for the limiting resolution of optical systems for partially coherent illumination. A.D.Stolyarov.

Opt. & Spectrosc. (USA), vol.53, no.2, p.224-5 (Aug. 1982). Translation of: *Opt. & Spektrosk. (USSR)*, vol.53, no.2, p.378-80 (Aug. 1982). [received: April 1983]

It is shown that to calculate the least resolvable distance between points it is sufficient to know the degree of coherence of the illumination and the transmission function of the optical system or the pupil function of the optical system. (3 refs.)

61099 A two-dimensional diffraction pattern sampling system for determining the optimum parameters of a matched spatial filter. S.Jutamulia, H.Fujii, T.Asakura (Res. Inst. of Appl. Electricity, Hokkaido Univ., Hokkaido, Japan).

Opt. & Laser Technol. (GB), vol.15, no.2, p.101-4 (April 1983).

The synthesis of a matched spatial filter based on holographic methods requires that the spatial frequency band in which the holographic fringe pattern with the best modulation is formed be tuned to the appropriate weighting at the Fourier transform plane of the spatial frequencies of the input object to be studied. For this purpose both the spectral intensity distribution of an input object at the Fourier transform plane and the intensity distribution of a reference beam at that plane must be accurately known beforehand. A two-dimensional diffraction pattern sampling system has been constructed which enables the Fourier spectral intensity distribution of the input object and the reference beam intensity distribution to be faithfully recorded. A preliminary experimental study shows the usefulness of this system. (8 refs.)

61100 Reconstruction of objects from coded images by simulated annealing. W.E.Smith, H.H.Barrett, R.G.Paxman (Optical Sci. Center, Univ. of Arizona, Tucson, AZ, USA).

Opt. Lett. (USA), vol.8, no.4, p.199-201 (April 1983).

A new Monte Carlo reconstruction procedure is presented for retrieval of objects from their coded images. The reconstruction process is modeled as an optimization problem whose cost function is related to how well the coded-image constraints are satisfied. Reduction of the cost function is achieved by an annealing process analogous to the cooling of a melt to produce an ordered crystal. The method is demonstrated by reconstructing two two-dimensional objects from their one-dimensional coded images. (10 refs.)

61101 Modulation transfer functions of a lens-array photographic system. B.K.Rozhkov.

Sov. J. Opt. Technol. (USA), vol.49, no.7, p.451-2 (July 1982). Translation of: *Opt.-Mekh. Prom-st. (USSR)*, vol.49, no.7, p.48-9 (July 1982). [received: April 1983]

It is shown that a lens-array photographic system is capable of forming a three-dimensional integral image having a modulation transfer coefficient that meets the requirements of practical photography. (11 refs.)

61102 Extraction of surface gradient from shading images. H.Kitagawa (Faculty of Sci. & Technol., Keio Univ., Yokohama, Japan), M.Suzuki, H.Fujita.

Trans. Inst. Electron. & Commun. Eng. Jpn. Part D (Japan), vol.166D, no.1, p.65-72 (Jan. 1983). In Japanese.

A method for extracting the surface gradient of bodies was developed by using shading images. The object is irradiated by a light source and observed by a camera. The light source moves around the optical axis of the camera, so that the irradiance at each image point varies sinusoidally. From this varying irradiance, one can obtain a particular surface gradient. The shape was measured with an experiment of a polyhedral object. In this case, one could also obtain the edge information. With the knowledge obtained from gradient and edge informations, a polyhedral object was reconstructed accurately. (10 refs.)

Computerized evaluation of schlieren images [temperature field reconstruction] See Entry 59775

Spectroscopy and integral image quality See Entry 59870

Generalized curvilinear diffraction gratings. III. Euclidian diffraction gratings See Entry 61073

Influence of partial coherence and misalignments on holographic methods (single and double exposure) of adding or subtracting pictures See Entry 61104

Method of analyzing wave aberration of a two-component holographic objective See Entry 61107

Self-consistent choice of code and phase mask for improving uniformity of Fourier hologram interference patterns See Entry 61113

Holographic intensity correlator with a laser electron beam tube for inputting images for processing See Entry 61114

Effect of conicoid asphericity on the Tscherning ellipses of ophthalmic spectacle lenses See Entry 61252

Real-time Fourier transformation in dispersive optical fibers See Entry 61295

Photoinduced spectral change in the rotation of the plane of polarization of light in FeBO₃ See Entry 62951

A regularized iterative algorithm for limited-angle inverse Radon transform See Entry 63952

On isoplanatism by the arrival angles for light rays in telescopes See Entry 64234

How to achieve diffraction limited resolution with large space telescopes See Entry 64379

A posteriori spatial filtering of a short-exposure image distorted by the atmosphere See Entry 64398

42.40 HOLOGRAPHY

(for acoustic holography, see 43.63)

61103 Conditions of stigmatism of holographic concave gratings used in normal incidence. M.Pouey (Univ. Paris-XI, Orsay, France).

C.R. Seances Acad. Sci. Ser. II (France), vol.296, no.4, p.225-7 (31 Jan. 1983). In French.

Actual design rules for holographic concave grating devices are derived from peculiar solutions of the tangential focus equation. However, for normal incidence devices, by satisfying the Fermat principle independently in the object and the image space, a new focusing condition for the location of the stigmatic coma-free points could be derived. This condition is obtained by considering first the conditions for which the third order aberration terms vanish. The object may be located anywhere on the spherical holographic grating's normal (radius of curvature R), the locus of the diffracted images being a circle, whose radius is proportional to R and the grooves density, and passing through the summit and the curvature centre of the grating. (6 refs.)

61104 Influence of partial coherence and misalignments on holographic methods (single and double exposure) of adding or subtracting pictures. R.Hild, S.Kessler (Sektion Phys., Friedrich-Schiller Univ., Jena, Germany).

Exp. Tech. Phys. (Germany), vol.31, no.1, p.1-9 (1983). In German.

General results are given for the influence of coherence and misalignments on the complex amplitude addition and subtraction by two holographic methods. One method is holographic Fourier transformation and the other is subtraction via processing simultaneously recorded holographic images. (6 refs.)

61105 Cascaded phase Fourier holograms. J.Slaby, T.Szoplik, K.Chalasinska-Macukow (Warsaw Univ., Warsaw, Poland).

Opt. Acta (GB), vol.30, no.4, p.529-43 (April 1983).

A stacked system of phase Fourier holograms on which binary information is recorded has been built and its performance studied. The properties of the zero-order beam propagating through the stack have been investigated. The results show how the energy and intensity distributions of the read-out beam change as the beam propagates through the system, and the values of the imaging efficiency η_n of successive holograms and the signal-to-noise ratio (S/N) are measured in successive reconstructed images. The evolution of the zero-order beam is described mathematically. (17 refs.)

61106 Fresnel detour-phase circular computer generated holograms. H.Y.Wu, P.Chavel, D.Joyeux, J.Brunol (Inst. d'Optique, Univ. de Paris-Sud, Orsay, France).

Opt. Commun. (Netherlands), vol.45, no.3, p.155-9 (1 April 1983).

When a circularly symmetric wavefront has to be encoded onto a computer generated hologram, it is highly desirable to preserve the symmetry. The coding scheme must therefore be circularly symmetric itself. This paper introduces a particular kind of computer generated hologram which extends circular symmetry to the detour phase technique; this is obtained by working in Fresnel diffraction. The wavefront should be sampled using a circular sampling theorem such as the one derived from the Dini-Bessel expansion. The hologram then consists of weighted unit masses distributed on a set of circles, which in practice are replaced by annuli of suitable inner and outer radii. The approximations due to the detour phase method and to the annuli widths are discussed and an experimental example is shown. (13 refs.)

61107 Method of analyzing wave aberration of a two-component holographic objective. V.G.Shitov, G.I.Greiskuh, V.A.Vanin, M.M.Butusov.

Opt. & Spectrosc. (USA), vol.53, no.1, p.76-8 (July 1982). Translation of: *Opt. & Spektrosk. (USSR)*, vol.53, no.1, p.130-4 (July 1982). [received: April 1983]

A method is given for calculating the monochromatic wave aberration of a diffraction objective consisting of two closely placed holographic lenses. The method is based on an analysis of the phase of the wave front reconstructed by the objective and expressed in radicals. (6 refs.)

61108 Use of a holographic diffraction grating for deflecting a laser beam. N.G.Kiselev.

Opt. & Spectrosc. (USA), vol.53, no.1, p.79-82 (July 1982). Translation of: *Opt. & Spektrosk. (USSR)*, vol.53, no.1, p.135-40 (July 1982). [received: April 1983]

The properties of a holographic diffraction grating as an element for deflecting a laser beam are considered. It is shown that by comparison with traditional deflecting elements, such as a mirror and a glass prism, the holographic diffraction grating possesses wider functional possibilities. An analysis is made of a deflecting device based on a holographic diffraction grating whose plane is orthogonal to the axis of rotation. It is shown that on the basis of such a scheme it is possible to construct a deflecting device that is satisfactory for many practical applications regarding both the linearity of deflection as well as the curvature of the lines formed. Compared with a known deflecting device, such as a mirror drum, the proposed device is much less massive and has a low sensitivity to angular displacements (shaking) of the axis of rotation. (7 refs.)

61109 Infrared-spectrophotometric investigation of the recording of an optical image on dichromated gelatin. A.L.Kartuzhanskii, V.M.Kalyuzhnyi, A.A.Krut, V.A.Tsendrovskii.

Opt. & Spectrosc. (USA), vol.53, no.2, p.225-6 (Aug. 1982). Translation of: *Opt. & Spektrosk. (USSR)*, vol.53, no.2, p.380-2 (Aug. 1982). [received: April 1983]

The experience acquired by the authors in a previous IR spectrophotometric study enables them to apply the same approach to studying the processes in dichromated gelatin and to understand why different specimens of gelatin possess different phototanning abilities and the effect of the different diffraction efficiency on the holographic gratings recorded on them. The photo-

graphic process in dichromated gelatin, from the point of view of its structural changes, can be interpreted as follows. Chromating intensifies the bands connected with vibrations in the amine and hydroxyl groups of the gelatin macromolecule. The bands shorter than 1000 cm^{-1} that appear belong to vibrations of the groups of the chromium complex bound to water. Illumination partially destroys and disorders the complexes, blurring and reducing the intensity of all the bands characteristic of them. Simultaneously, the intensity of the vibrational bands of the hydroxyl groups, bound to the gelatin macromolecule is increased. Development practically destroys all the chromium complexes and their bonds with the water molecules, returning the degree of hydration of the macromolecule to its initial state. A layer of dichromated gelatin on a base of strongly hydrated gelatin with a large number of carboxyl groups in the side chains should have the highest light sensitivity and diffraction efficiency. (5 refs.)

61110 HS-1 holocamera. Z.Jankiewicz, W.Nowakowski, W.Bobak. *Pol. Tech. Rev. (Poland)*, no.5-6, p.10-12 (1982).

The HS-1 holographic camera is designed for investigating the deformation of objects using double-pulse holographic interferometry methods. This unique measuring system has been built for fundamental research laboratories, but its mobile structure makes it also suitable for performing measurements in industrial conditions. A diagram of the optical-mechanical assembly mounted on a platform resting on a TV tripod is shown and its technical data given. (1 ref.)

61111 Real-time holographic interferometry of moving objects in oppositely directed beams. N.V.Morozov, Yu.I.Ostrovskii, L.M.Boeva (A.F. Ioffe Physico-techn. Inst., Acad. of Sci., Leningrad, USSR). *Sov. Phys.-Tech. Phys. (USA)*, vol.27, no.9, p.1137-9 (Sept. 1982). Translation of: *Zh. Tekh. Fiz. (USSR)*, vol.52, no.9, p.1854-8 (Sept. 1982). [received: April 1983]

The distinctive features of holographic interferograms obtained in real time are investigated for the case in which a reflection hologram of the initial state of the object is recorded in oppositely directed beams. It is shown that the deformation of objects moving translationally can be studied by real-time holographic interferometry when the hologram is rigidly fixed relative to the object and moves together with it. An analysis yields the admissible values of the translational and angular displacements of the object-hologram system in real-time observation. The optimal conditions for recording the hologram and interference fringes are also discussed. (5 refs.)

61112 On obtaining a specified light-field distribution. T.D.Ebralidze (Inst. of Cybernetics, Acad. of Sci., Tbilisi, Georgian SSR). *Sov. Phys.-Tech. Phys. (USA)*, vol.27, no.9, p.1144-6 (Sept. 1982). Translation of: *Zh. Tekh. Fiz. (USSR)*, vol.52, no.9, p.1865-8 (Sept. 1982). [received: April 1983]

The holographic recording and reconstruction of a light wave having some original direction of polarization is investigated. It is shown that to reconstruct from a hologram the object and reference waves with the original directions of polarization it is sufficient to reproduce, at every point in the hologram, linearly polarized light having a certain amplitude and the direction of the polarization vector. (7 refs.)

61113 Self-consistent choice of code and phase mask for improving uniformity of Fourier hologram interference patterns. V.S.Vorozheikin, S.A.Shoidin. *Sov. Phys.-Tech. Phys. (USA)*, vol.27, no.10, p.1242-5 (Oct. 1982). Translation of: *Zh. Tekh. Fiz. (USSR)*, vol.52, no.10, p.2022-6 (Oct. 1982). [received: April 1983]

The structure of the phase mask is matched with the data word length and selected according to code combinations in order to improve uniformity in Fourier hologram interference patterns. It is then possible to reduce the probability that all or most of the open cells in the transparency lie on regions of the phase mask with identical phase [for a given code, such a pattern corresponds to recording an unlikely (in practice, extremely unlikely) message]. The probability of phase-coincident cells decreases with increasing word length, and the structure of the phase mask is also simplified. (5 refs.)

61114 Holographic intensity correlator with a laser electron beam tube for inputting images for processing. V.I.Kozlovskii, A.S.Nasibov, O.I.Potaturnik, P.V.Reznikov, Ya.K.Skasyrskii, B.I.Spektol (P.N. Lebedev Phys. Inst., Acad. of Sci., Moscow, USSR). *Sov. Phys.-Tech. Phys. (USA)*, vol.27, no.10, p.1245-7 (Oct. 1982). Translation of: *Zh. Tekh. Fiz. (USSR)*, vol.52, no.10, p.2027-31 (Oct. 1982). [received: April 1983]

Optical processing of images (including real-time images) input as electrical signals is considered. The use of a laser electron beam tube is proposed to input the images into an optical processor and an optical system consisting of a holographic intensity correlator. The incoherence of the laser light then permits linear image processing (in terms of intensity). Experimental results are reported. (7 refs.)

61115 Contributions of amplitude and phase modulation to diffraction efficiency in three-dimensional reflective holograms. A.V.Alekseev-Popov, S.A.Gevelyuk (I.I. Mechnikov Sci. Res. Inst. of Phys., Odessa State Univ., Odessa, USSR).

Sov. Phys.-Tech. Phys. (USA), vol.27, no.10, p.1289-91 (Oct. 1982). Translation of: *Zh. Tekh. Fiz. (USSR)*, vol.52, no.10, p.2100-2 (Oct. 1982). [received: April 1983]

It is demonstrated that concurrent phase and amplitude modulation alters the qualitative form of the angular selectivity curves in three-dimensional reflecting holograms. It is possible and indeed desirable to use the algorithm to calculate the amplitude and phase modulation coefficients when analyzing reflecting holograms. (5 refs.)

61116 Light refraction in crystals with bipolar photoconductivity. S.I.Stepanov (A.F. Ioffe Physico-techn. Inst., Acad. of Sci., Leningrad, USSR). *Sov. Phys.-Tech. Phys. (USA)*, vol.27, no.10, p.1300-1 (Oct. 1982). Translation of: *Zh. Tekh. Fiz. (USSR)*, vol.52, no.10, p.2114-16 (Oct. 1982). [received: April 1983]

Analyzes theoretically the main features of holographic recording. It is shown that bipolar photoconductivity in a light-refracting crystal has an appreciable effect on the steady-state hologram grating amplitude when the hologram is recorded in the absence of an external electric field. (9 refs.)

61117 Data storage in a holographic archive with the aid of an optically controlled transparency. T.A.Belozherova, A.A.Komlev, N.F.Kovtonyuk, S.S.Kuz'min, A.L.Mikaelyan. *Sov. J. Quantum Electron. (USA)*, vol.12, no.10, p.1368-70 (Oct. 1982). Translation of: *Kvantovaya Elektron. Moskva (USSR)*, vol.9, no.10, p.2102-4 (Oct. 1982). [received: April 1983]

Data were stored in a holographic archive memory using an optically controlled transparency. The requirements which the transparency should satisfy for the use as an input original were determined. A liquid-crystal transparency used is described. A report is given of the characteristics of an image obtained using such a transparency and also of an image reconstructed from a

hologram recorded with the aid of the transparency. Ways of improving the image quality are indicated. (4 refs.)

61118 Synthesis of optical elements giving a focal line of arbitrary shape. V.A.Danilov, V.V.Popov, A.M.Prokhorov, D.M.Sagatelyan, I.N.Sisakyan, V.A.Solifer (P.N. Lebedev Phys. Inst., Acad. of Sci., Moscow, USSR). *Sov. Tech. Phys. Lett. (USA)*, vol.8, no.7, p.351-3 (July 1982). Translation of: *Pis'ma v Zh. Tekh. Fiz. (USSR)*, vol.8, no.13-14, p.810-15 (July 1982). [received: April 1983]

The authors are interested in the synthesis of optical elements which can produce a planar focal line of arbitrary shape. These elements have an important property, which may be called 'modularity': Parts of one element can, independently, produce different curves, so that quite complicated figures can be produced. Optical elements of this type may be of interest in various fields of science, engineering, and technology. The procedure for synthesizing a focuser (computer-synthesized kineform elements) consists of the following independent steps: 1) The construction of a mathematical model and the derivation of equations for the phase function of the focuser; 2) computer calculation of the phase function of the focuser; 3) creation of the calculated phase function on a physical carrier. (7 refs.)

61119 Time-varying light amplification by dynamic holograms in spatially nonuniform light beams. A.M.Dukhovnyi, D.I.Stasel'ko. *Sov. Tech. Phys. Lett. (USA)*, vol.8, no.8, p.436-7 (Aug. 1982). Translation of: *Pis'ma v Zh. Tekh. Fiz. (USSR)*, vol.8, no.15-16, p.1009-14 (Aug. 1982). [received: April 1983]

Reports a study of the time-varying-intensification of weak beams by dynamic holograms in media having an inertial local response ('unbiased' dynamic holograms) in the case in which the intense beam has an amplitude-phase distribution with a small-scale nonuniformity. (11 refs.)

The possibilities of applying holographic interferometry in temperature measurement See Entry 59784

A two-dimensional diffraction pattern sampling system for determining the optimum parameters of a matched spatial filter See Entry 61099

High power TEA CO₂ laser tuned by a holographic grating See Entry 61181

Simplified method for calculating the parameters of a symmetric monochromator with a concave holographic diffraction grating See Entry 61263

Secondary structures formed during the inscribing of diffractive three-dimensional phase gratings See Entry 61264

Investigation of the possibility of using an optical matching filter to test the geometry of parts in precision instrument manufacturing See Entry 61310

Study of deformed samples using an interferometer attached to the sample See Entry 61469

42.50 QUANTUM OPTICS

61120 Gain dynamics for a degenerate three-level system excited by a square pulse of a pumping signal. V.A.Efremov. *Ukr. Fiz. Zh. (USSR)*, vol.28, no.3, p.365-71 (March 1983). In Russian. Dynamics of a degenerate three-level system is considered for the case of its excitation by a square pulse of a pumping signal. The life-time of transition processes and the delay time of the system gain are strongly dependent on the gas medium and interacting field parameters. (5 refs.)

On Pearson's random walk and some statistical properties of a quasiperiodic observable in a simple quantum model See Entry 59701

Reconstruction of field statistics from the photocount statistics of an inertial detector See Entry 59846

Resonance light pressure in the field of partially coherent laser radiation See Entry 60660

Local velocity distribution of atoms in a light wave in resonance with an atomic transition See Entry 60661

Einstein relations for gain-guided semiconductor lasers See Entry 61151

Optical bistability in multimode systems with second- and third-order dispersive nonlinearity See Entry 61221

42.52 MASERS

61121 Rydberg-atom masers. I. A theoretical and experimental study of super-radiant systems in the millimeter-wave domain. L.Moi, P.Goy, M.Gross, J.M.Raimond, C.Fabre, S.Haroche (Lab. de Phys., Ecole Normale Supérieure, Paris, France). *Phys. Rev. A (USA)*, vol.27, no.4, p.2043-64 (April 1983).

The operation of maser devices using highly excited Rydberg atoms as active medium is investigated. These systems, working in a transient regime, reminiscent of super-radiance generate few-hundred-ns-long bursts of mm-wave radiation. They are characterized by extremely low inversion density thresholds ($N_0 \sim 10^4$ atoms typically) and very small peak power outputs (in the 10^{-11} to 10^{-33} watt range). This study is interesting in the context of new tests of super-radiance and electrodynamics theory. It also opens new possibilities in the important domain of mm-wave amplification and detection. In this paper, the authors present a simple semiclassical theory of transient Rydberg maser operation and they report the experimental observation of a large number of maser emission lines on Na atoms, spanning a wide frequency interval ($60 < \nu < 950$ GHz). The technique used to monitor the emission is the indirect field ionization procedure which reveals fast radiative transfers occurring between Rydberg levels. Another method involving the direct detection of the maser radiation by a heterodyne receiver is described in a subsequent paper, along with a report on the investigation of various effects related to the triggering of the transient maser emission by external radiation. (23 refs.)

61122 Rydberg-atom masers. II. Triggering by external radiation and application to millimeter-wave detectors. P.Goy, L.Moi, M.Gross, J.M.Raimond, C.Fabre, S.Haroche (Lab. de Phys., Ecole Normale Supérieure, Paris, France).

Phys. Rev. A (USA), vol.27, no.4, p.2065-81 (April 1983). For pt.I see *ibid.*, vol.27, no.4, p.2043 (1983). The 'triggering' of transient maser systems using excited Rydberg atoms as active medium is investigated theoretically and experimentally. The authors show how the maser pulse characteristics are modified by the interaction of the active medium with small amounts of resonant mm-wave radiation. The phase, polarization, and emission delay of the radiated field are modified by this triggering: this can be used to detect very small powers of mm- or sub-mm-wave radiation. A complete discussion of the quantum and thermal noise of these detectors is presented. A demonstration of the feasibility of this technique is reported. Triggering signals corresponding to a detectivity of $3 \times 10^{-17} \text{ W/Hz}^{1/2}$ at 108 GHz ($\lambda = 2.8 \text{ mm}$) have been measured at room temperature. The quantum-

noise limit—corresponding to 6×10^{-19} W/Hz^{1/2}—should be reached with liquid-helium-temperature-cooled detectors. (14 refs.)

42.55 LASING PROCESSES

61123 Induced decay of positronium and grasers. D.M.Heffernan, R.L.Liboff (Dept. of Phys., Cornell Univ., Ithaca, NY, USA). *Int. J. Theor. Phys. (USA)*, vol.22, no.2, p.193-206 (Feb. 1983). The differential cross section and the total cross section for the stimulated decay of positronium by an incident photon of frequency ω is calculated as a function of the dimensionless variable $\xi = \hbar\omega/mc^2$. For $\xi \gg 1$ the total cross section is found to decrease as ξ^{-2} . The authors also look at the particular case of positronium in a black-body radiation field. Expressions for the number of induced annihilations per second as functions of the dimensionless ratio mc^2/kT and the number of positronium atoms are obtained. It is found that this rate is proportional to (kT/mc^2) for $kT \leq mc^2$ and to $(kT/mc^2) \ln(kT/mc^2)$ for $kT \gg mc^2$. The possibility of utilizing induced two-photon decay of positronium as a γ -ray laser at the wavelength $\lambda_c/2$ is examined, where λ_c is the Compton wavelength. (13 refs.)

Asymmetry in the coupling coefficients of oppositely traveling waves in a ring laser See Entry 61173

42.55B General theory of lasing action

61124 Wave propagation in media with focused gain. B.N.Perry, P.Rabinowitz, M.Newstein (Corporate Res. Sci. Lab., Exxon Res. & Engng. Co., Linden, NJ, USA). *Phys. Rev. A (USA)*, vol.27, no.4, p.1989-2002 (April 1983). A solution of the scalar wave equation in a rotationally symmetric focused Gaussian amplifying medium is constructed from coupled Gaussian-Laguerre solutions of the free-space wave equation and is formally exact. The solution allows for the construction of the characteristic eigenmodes of the system and has direct application to Raman lasers, dye lasers, and the free-electron laser. The eigenvalues corresponding to the eigenmodes are directly related to mode growth rates and phase velocities. Numerical results for single- and multiple-pass growth are evaluated and exhibit an unpredicted gain enhancement that can be related to the phenomenon of 'gain focusing' first described for uniform parabolic gain distributions. The solution for a focused parabolic gain distribution is also presented. Output intensity distributions are found for initial conditions corresponding to spontaneous emission and to a specified initial field. The same method of solution can be applied to a medium with a focused Gaussian refractive index. (20 refs.)

Gain dynamics for a degenerate three-level system excited by a square pulse of a pumping signal See Entry 61120
Einstein relations for gain-guided semiconductor lasers See Entry 61151
Static model of DH laser See Entry 61154

42.55D CO₂ lasers

61125 Pressure wave attenuation due to anode mufflers in pulsed lasers. B.N.Srivastava (Avco Everett Res. Lab. Inc., Everett, MA, USA). *AIAA J. (USA)*, vol.21, no.3, p.381-9 (March 1983). The paper addresses some new technical aspects of acoustic suppression in an open cycle pulsed laser device. An open cycle pulsed CO₂ laser system has been studied in order to predict the effect of various acoustic design parameters on the cavity clearing process. More specifically, the effect of an anode muffler (commonly used for transverse wave attenuation), in combination with a downstream acoustic horn, on the cavity-generated longitudinal waves is discussed by developing numerical solutions of the flow conservation equations. The results presented suggest that anode mufflers can provide an effective means of achieving rapid acoustic clearing in the laser cavity. (13 refs.)

61126 Stabilisation of carbon dioxide lasers using the Stark effect. S.A.Rackley, R.J.Butcher (Cavendish Lab., Univ. of Cambridge, Cambridge, England). *J. Phys. D (GB)*, vol.16, no.4, p.505-16 (14 April 1983). A large number of Stark-tuned molecular absorptions have been investigated as possible references for Stark stabilisation of waveguide CO₂ lasers. A set of potentially useful absorptions have been selected and transition tuning rates, absorption coefficients, and electrical breakdown characteristics have been measured for a number of these. A discussion of the optimisation of a Stark stabilisation system is given. Predictions of absorptions that will be useful in stabilising isotopic lasers are also reported. (17 refs.)

61127 LIMP in continuously coupled unstable resonators. E.K.Gorton, P.J.Gorton, E.W.Parcell (Royal Signals & Radar Estab., Great Malvern, England). *J. Phys. D (GB)*, vol.16, no.4, p.517-24 (14 April 1983). The Laser Induced Medium Perturbation (LIMP) effect is shown to be a volumetric effect which plays a significant role in the beam quality obtainable from a CO₂ laser employing a continuously coupled unstable resonator. (10 refs.)

Helical-flow CO₂ laser See Entry 61178
High power TEA CO₂ laser tuned by a holographic grating See Entry 61181
Effect of outgassing on the performance of a TE CO₂ laser sealed in an acrylic chamber See Entry 61188
Operating characteristics of a transverse-excited 16 μ m CO₂ laser with profile electrodes and UV-pre-ionization See Entry 61190
Electric-discharge CW industrial CO₂ laser See Entry 61191
Pulse evolution and mode selection characteristics in a TEA-CO₂ laser perturbed by injection of external radiation See Entry 61206
Multiple beams from Rogowski-profile solid electrode TEA CO₂ lasers See Entry 61208
Investigation of the rotation of a wave front in a molecular multipass amplifier See Entry 61220

42.55F Inert gas lasers

61128 Pumping of gas lasers by runaway-electron beams. P.A.Bokhan, A.R.Sorokin (Inst. of Thermal Phys., Acad. of Sci., Novosibirsk, USSR). *Sov. Tech. Phys. Lett. (USA)*, vol.8, no.8, p.411-12 (Aug. 1982). Translation of: *Pis'ma v Zh. Tekh. Fiz. (USSR)*, vol.8, no.15-16, p.947-50 (Aug. 1982). [received: April 1983]
Shows that pumping by runaway electron beams can be used to arrange lasing in a variety of working media. The lasers were pumped in a cell 1 cm in diameter and 10 cm long with an accelerator gap of 0.7 mm. There was a

transverse injection of electrons through a grid with a geometric transparency of 50%. Results are presented by a He-Hg laser with an output wavelength of 615 nm. Measurements of output energy, output pulse length, and delay in the onset of lasing with respect to the maximum of the beam current are reported. Applications to a He-Xe laser are also briefly discussed. (5 refs.)

A low-power He-Ne laser head See Entry 61186
Temperature control of an acousto-optic modulator in an Argon ion laser using an R.F. servo loop See Entry 61202
Influence of linear phase anisotropy induced in the active medium on the characteristics of gas-laser radiation See Entry 61204
Frequency reproducibility of ring He-He/CH₄ lasers See Entry 61212

42.55H Lasing action in other gas lasers

61129 Temporal measurement of the gain of a CuCl laser. K.Kuroda, M.Takeda, M.Chihara, I.Ogura (Inst. of Industrial Sci., Univ. of Tokyo, Tokyo, Japan). *J. Appl. Phys. (USA)*, vol.54, no.4, p.1670-4 (April 1983). The temporal behaviour of the population inversion density of a CuCl laser was investigated using the gain method. The amplifier model which included the effect of the pumping during the amplification was discussed and used to analyze the experimental data. The populations of the laser transition levels were inverted during about 50 ns in the laser. The mechanism of the construction and destruction of the population inversion was discussed using the numerical model of a CuCl laser, and the variation of the electron temperature would be the main cause of the behavior of the population inversion density. (14 refs.)

61130 High repetition rate operation of a N₂ waveguide laser. R.Buffa (Istituto de Elettronica Quantistica del Consiglio Nazionale delle Ricerche, Firenze, Italy). *J. Phys. D (GB)*, vol.16, no.4, p.167-9 (14 April 1983). The high repetition rate operation of a capacitively-coupled-discharge, low-dielectric waveguide laser is reported. By using superfluorescent nitrogen as the active medium, a laser pulse output of energy 2.5 μ J and duration 2 ns has been achieved. A pulse repetition rate as high as 100 p.p.s. has been obtained without gas flow but with cooling of the gas by heating transfer to the cell walls after every discharge pulse. (7 refs.)

61131 Effect of capture on the beat contour of oppositely traveling waves in a ring gas laser. Yu.M.Golubev, V.P.Gryaznevich. *Opt. & Spectrosc. (USA)*, vol.53, no.2, p.202-3 (Aug. 1982). Translation of: *Opt. & Spektrosk. (USSR)*, vol.53, no.2, p.346-8 (Aug. 1982). [received: April 1983]
In the widely used He-Ne laser operating at a wavelength of 0.63 μ m, the spontaneous emission from the upper working level is effectively captured. Capture may, however, have a nontrivial effect in that when the population of the upper level is being formed it interferes with the lasing. Hence, in addition to the separate action of capture and emission, the results of which are quite obvious one would expect there to be a more complex effect, which the authors analyze. The authors carry out a theoretical analysis in the framework of quantum electrodynamics using the kinetic-equation method for the density matrix of the emission field. (4 refs.)

61132 Noise measurement in a He-Zn hollow cathode laser tube. T.Iijima (Coll. of Technol., Seikei Univ., Tokyo, Japan). *Physica B & C (Netherlands)*, vol.115 B+C, no.2, p.257-60 (Jan. 1983). The noise in a He-Zn hollow cathode laser tube with long life and stable operation was measured. The fluctuation of laser power at 758 Å in Zn II for a short period of time was compared with those of He I, Zn I and Zn II spectral line intensities. In the laser noise spectrum, the apparent peaks and periodic oscillation have not been observed in the range of 0-10 MHz. The laser light noise measured under the optimum operating conditions was 0.3% (RMS). By the addition of a small amount of neon, the laser light noise was somewhat suppressed. (9 refs.)

61133 New supersonic lasers at very low temperature and high density. B.Fontaine, B.Forestier (Inst. de Mecanique des Fluides de Marseille, Univ. d'Aix-Marseille-II, Marseille, France). *Rev. Cethedec (France)*, vol.19, no.NS82-2, p.55-80 (1982). In French. Data obtained for ultraviolet and visible high energy lasers with supersonic flow and excitation either by an electron beam or by a discharge assisted or stabilised by e-beam or X-rays are presented. The positive effects of an important temperature decrease are underlined. Moreover the effects of a supersonic flow on the optical properties of the active medium are discussed. The prospects of high energy short wavelength are envisaged. (21 refs.)

61134 Study of the infrared absorption of carbon tetrafluoride at 9 μ m. J.Dupre, C.Meyer, G.Poussigue, G.Tarrago (Travaile Realise au Lab. d'Infrarouge, Univ. de Paris-Sud, Orsay, France). *Rev. Cethedec (France)*, vol.19, no.NS82-2, p.143-54 (1982). In French. The CF₄ molecule can be pumped by a CO₂ laser to give a vibrational laser emitting at 16 μ m. In order to get a better understanding of the functioning of this laser, the authors have analysed the infrared absorption of the $\nu_3 + \nu_4$ CF₄ band at 9 μ m. This analysis, extended to J=40, leads to the identification of 2300 rovibrational transitions which could be reproduced by the model with a standard deviation of 0.003 cm⁻¹. From this study, a complete list of CF₄ transitions has been tabulated located within ± 0.050 cm⁻¹ of any line of ¹²C¹⁶O₂ and ¹²C¹⁸O₂ lasers. (5 refs.)

61135 A mechanism for producing inversion in gas lasers. B.I.Grinenko (Inst. of High Temperatures, Acad. of Sci., Moscow, USSR). *Sov. Phys.-Tech. Phys. (USA)*, vol.27, no.9, p.1163-4 (Sept. 1982). Translation of: *Zh. Tekh. Fiz. (USSR)*, vol.52, no.9, p.1892-4 (Sept. 1982). [received: April 1983]
A new approach to the kinetics of the formation of inversion in certain types of gas lasers by means of charge transfer reactions of singly and doubly charged ions with excited atoms. Although this reaction, according to calculations, plays an important role in the kinetics of a large group of lasers including metal vapor lasers, the active media are discussed in great detail and the existing interpretations of the basic processes of formation that have been advanced are, for a number of reasons, insufficiently persuasive. (15 refs.)

61136 Pumping of pulsed gas lasers by bulk and sliding spark discharges. E.P.Bel'kov, P.N.Dashuk, G.L.Spichkin (M.I. Kalinin Polytech. Inst., Leningrad, USSR). *Sov. Phys.-Tech. Phys. (USA)*, vol.27, no.10, p.1216-18 (Oct. 1982). Translation of: *Zh. Tekh. Fiz. (USSR)*, vol.52, no.10, p.1979-82 (Oct. 1982). [received: April 1983]
Results are reported from an experimental study of bulk discharge formation in inert gas mixtures containing an electronegative gas when a bulk discharge is produced using a sliding spark along the surface of a titanium-containing ceramic. A capacitor (dielectric ceramic plate) was repeatedly charged during

the time the slipping discharge developed along the surface of the ceramic, and the capacitor discharged into the primary winding of a pulse transformer. The secondary winding of the transformer was powered by a voltage pulse ≤ 120 kV of duration ~ 100 ns which was used to ignite the bulk discharge. The power characteristics of the bulk discharge are reported. (3 refs.)

61137 Efficiency of a stimulated Raman scattering laser using a medium with population inversion. A.S.Eremenko, S.N.Karpukhin, A.I.Stepanov. *Sov. Phys.-Tech. Phys. (USA)*, vol.27, no.10, p.1240-2 (Oct. 1982). Translation of: *Zh. Tekh. Fiz. (USSR)*, vol.52, no.10, p.2018-21 (Oct. 1982). [received: April 1983]

A simplified method is proposed for solving the equations describing a stimulated Raman scattering laser using a medium with population inversion. The output signal and efficiency of a stimulated Raman scattering laser are calculated as a function of the duration of a coherent pumping square-wave pulse for the example of photodissociation of CF_3 and $\text{C}_3\text{F}_7\text{I}$. Methods are given for optimizing laser operation to increase the efficiency. (6 refs.)

61138 Thermal physics of transverse-discharge copper vapor lasers. B.L.Borovich, R.A.Grigoryan, G.P.Kazeko, G.N.Nikolaev, V.M.Smirnov. *Sov. J. Quantum Electron. (USA)*, vol.12, no.10, p.1289-95 (Oct. 1982). Translation of: *Kvantovaya Elektron., Moskva (USSR)*, vol.9, no.10, p.1983-92 (Oct. 1982). [received: April 1983]

One of the factors determining the ultimate characteristics of copper vapor lasers is the heating of the active medium by the pulse-periodic discharge providing the excitation. The gas temperature was measured on the axis of the discharge gap of a transversely excited copper vapor laser. Two methods were used: a spectroscopic method (based on the Doppler width of an emission line on the neon buffer gas) and an interferometric method (based on the fringe shift in a Mach-Zehnder interferometer at the instants when the discharge was switched abruptly on and off). Both methods yielded values close 2200K. The temperature distribution in the active zone with a rectangular cross section was computed numerically. The results of a theoretical calculation were used to estimate the efficiency of conversion of the discharge energy into heat, which was around 40%. (14 refs.)

61139 Quasi-CW lasing due to transitions from the resonance 1P_1 to the metastable 3D_2 level of the calcium atom. V.M.Batenin, S.V.Kalinin, I.I.Klimovskii (Inst. of High Temperatures, Acad. of Sci., Moscow, USSR). *Sov. J. Quantum Electron. (USA)*, vol.12, no.10, p.1345-7 (Oct. 1982). Translation of: *Kvantovaya Elektron., Moskva (USSR)*, vol.9, no.10, p.2075-7 (Oct. 1982). [received: April 1983]

A description is given of the method and the results are reported of an experiment in which quasi-CW lasing was obtained as a result of transitions from a resonance to a metastable level of the calcium atom without the use of any special impurities to quench the lower metastable state. Under these experimental conditions the metastable level was depopulated not as a result of collisions of the second kind or as a result of a chemical reaction, but because of the ionization, electron-impact excitation, and diffusion of metastable atoms to the discharge tube wall. (12 refs.)

61140 Excimer lasers using fission-reactor ionization. G.A.Batyrbekov, S.A.Kostritsa, Yu.E.Kuz'min, A.B.Teluzhanov, M.U.Khasenov (Inst. of Nuclear Phys., Acad. of Sci., Alma-Ata, Kazakh SSR). *Sov. Tech. Phys. Lett. (USA)*, vol.8, no.7, p.341-2 (July 1982). Translation of: *Pis'ma v Zh. Tekh. Fiz. (USSR)*, vol.8, no.13-14, p.789-91 (July 1982). [received: April 1983]

Considerable interest has recently been attracted to the development of excimer lasers with working volumes of tens of liters and pulse repetition frequencies of tens of kilohertz. The neutron flux of a steady-state nuclear reactor makes it possible to uniformly ionize a gas volume of tens of liters, and the electrical energy required to pump the excimer laser can be generated at the same reactor. The authors report a diagnostic study of the plasma produced in the radiation field of a steady-state nuclear reactor in the active mixtures $^3\text{He} + \text{Xe} + \text{NF}_3$ and $^4\text{He} + \text{Xe} + \text{CCl}_4$. The charge-carrier density was determined from the voltage-current characteristics of the steady-state, externally sustained discharge. (8 refs.)

61141 Influence of characteristics of the spark gap on the output energy in a Blumlein type nitrogen laser. A.Nomura, N.Takagishi, Y.Saito, T.Kano (Faculty of Engng., Shinshu Univ., Nagano, Japan). *Trans. Inst. Electron. & Commun. Eng. Jpn. Part C (Japan)*, vol.166C, no.1, p.102-3 (Jan. 1983). In Japanese.

In the Blumlein type nitrogen laser, the residual inductance and resistance of the spark gap circuit were measured under a variety of conditions of pressure and electrode distance of the spark gap. The influences of these circuit parameters on the laser output energy were examined. (2 refs.)

Kinetics of the plasma decay in lithium vapor; population inversion for the 3p-3s transition See Entry 60664

The triatomic rare gas halide excimers See Entry 60738

Laser induced fluorescence studies of XeF(B-X) See Entry 60830

Pumping of gas lasers by runaway-electron beams See Entry 61128

Stabilization of the light output delay of a pulsed nitrogen laser See Entry 61172

Inexpensive low temporal jitter laser triggering circuit See Entry 61175

Tunable sealed-off CW CO laser at room temperature See Entry 61182

High-power-density electron-beam-sustained laser See Entry 61187

High-pressure $\text{NH}_3\text{-N}_2$ laser See Entry 61192

Aperture combined Raman laser See Entry 61195

Resonances of the polarization of gas laser radiation under mode self-locking conditions See Entry 61213

Anti-Stokes Raman scattering of excimer and tunable UV lasers in chemically pumped CO See Entry 61217

Possibility of using certain transitions of He-Ne and He-Xe lasers for the analysis of nitric oxide, sulfur dioxide, and higher hydrocarbons See Entry 63762

42.55K Chemical lasers

(see also 82.40T Chemiluminescence and chemical laser kinetics)

61142 Theoretical simulation of a pulsed HF optical resonance transfer laser. S.Yamaguchi, K.Kumamoto, F.Kannari, M.Obara, T.Fujioka (Dept. of Electrical Engng., Keio Univ., Yokohama-shi, Japan). *J. Appl. Phys. (USA)*, vol.54, no.4, p.1675-85 (April 1983).

The high-efficiency pulsed HF Optical Resonance Transfer Laser (ORTL) is described in this paper. The multiline laser output, pulse shape, pulse width, and efficiency were all calculated by using the HF computer codes which have been developed in the authors' laboratory. Parametric studies were also done to optimize system efficiency and, as a result, the ratio of laser output

energy to pumping energy was as large as 56%. The lasing lines of the ORTL covered the wavelength region between 3.0 and 3.8 μm . Comparison of the results of this simulation with the experiments of CW-ORTL shows that the pulsed ORTL could be more efficient operation. (14 refs.)

61143 Flashlamp-pumped iodine monobromide laser characteristics. L.E.Zapata (Miami Univ., Oxford, OH, USA), R.J.De Young. *J. Appl. Phys. (USA)*, vol.54, no.4, p.1686-92 (April 1983).

The operating characteristics of a flashlamp-pumped IBr laser were investigated to evaluate its suitability for solar-pumped laser applications. A peak power of 350 W/cm² at 2.7 μm was achieved at 12-Torr IBr pressure. At 500-J flashlamp energy, the IBr output saturated; a gain of 0.17% cm⁻¹ was measured for IBr. Neon was found to be effective for enhancing the recombination of the photodissociation products. With neon as a buffer gas, the laser pulse length was extended to 53 μsec . The termination of the laser pulse, within the flashlamp pulse, is thought to be due to the temperature rise in the gas. Increasing the IBr initial temperature decreased the lasing output. At 300°C, output dropped to approximately one-half the room temperature value. The dominant quencher is thought to be atomic iodine. IBr was found to couple better to the flashlamp energy than $\text{C}_3\text{F}_7\text{I}$. (12 refs.)

61144 Localization of a light beam in a narrow inverted zone formed as a result of chemical processes in parallel streams of reagents. V.A.Kochelap, L.Yu.Mel'nikov (Inst. of Semiconductors, Acad. of Sci., Kiev, Ukrainian SSR).

Sov. J. Quantum Electron. (USA), vol.12, no.10, p.1352-4 (Oct. 1982). Translation of: *Kvantovaya Elektron., Moskva (USSR)*, vol.9, no.10, p.2083-5 (Oct. 1982). [received: April 1983]

It is shown theoretically that injection of an optically dense jet between two parallel planar streams establishes a dielectric gas waveguide which localizes light in a narrow reaction zone. It then becomes possible to use narrow inversion zones (with a thickness of the order of 10^{-2} cm) in CW chemical lasers without suffering the diffraction losses of light. This waveguide effect should make it possible to use gas streams at pressures ≥ 1 atm in chemical lasers. A fast chemical reaction, $\text{Ba} + \text{S}_2\text{Cl}_2 \rightarrow \text{S}_2(\text{B}) + \text{BaCl}_2$, resulting in the emission of visible light is considered by way of example. (13 refs.)

Photodissociation CW laser using condensation and evaporation for a closed cycle See Entry 61194

Production of a bulk discharge in an electronegative gas mixture See Entry 61722

42.55M Lasing action in liquids and organic dyes

Intracavity dye-laser photothermal deflection spectroscopy See Entry 59861

Tunable picosecond pulses around 1.3 μm generated by a synchronously pumped infrared dye laser See Entry 61174

Simultaneous two-wavelength tunable dye laser with no mode competition and with a wavelength separation of more than 200 nm See Entry 61180

Laser oscillator using resonator with self-pumped phase-conjugate mirror See Entry 61183

42.55P Lasing action in semiconductors with junctions

61145 Intrinsic pulsation induced by lateral carrier waveguiding in stripe geometry DH semiconductor lasers. Guo Changzhi, Wang Kaige (Dept. of Phys., Peking Univ., Peking, China).

Chin. J. Semicond. (China), vol.4, no.2, p.161-70 (March 1983). In Chinese. Effects of lateral optical and carrier distributions and their interaction on dynamic processes in stripe geometry DH semiconductor lasers are analyzed theoretically. The rate and field equations are simultaneously solved in rather strict manner for numerical transient solutions. The results calculated show that when the index waveguiding of the carrier distribution and the carrier diffusion become pronounced, 'intrinsic' pulsation characterized by the lateral optical beam width with continuous and significant oscillation during pulsation may occur in the laser output in a certain range of injected current. (21 refs.)

61146 An investigation on visible-infrared GaAlAs lasers. Zheng Guangfu, Liao Xianbing, Zheng Xianming, Hu Enzhi (Inst. of Semiconductor Optoelectronics, Yongchuan Sichuan, China).

Chin. J. Semicond. (China), vol.4, no.2, p.200-5 (March 1983). In Chinese. Visible GaAlAs lasers with CW operation at room temperature and lasing wavelength of ~ 7600 Å, have been achieved. Their electrical and optical parameters are similar to those of infrared GaAlAs lasers. The lasing wavelength of infrared GaAlAs lasers is ~ 8800 Å, at room temperature the CW life is of the order of magnitude of 10^4 hours, and the highest CW operating ambient temperature can be as high as 150°C. (3 refs.)

61147 Stress tests on 1.3 μm buried-heterostructure laser diode. T.Ikigami, K.Takaei, M.Fukuda, K.Kuroiwa (Musashino Electrical Communication Lab., Nippon Telegraph & Telephone Public Corp., Tokyo, Japan).

Electron. Lett. (GB), vol.19, no.8, p.282-3 (14 April 1983). Preliminary results of the accelerated aging test under stresses of temperature and current are presented. The degradation modes are found to be divided into two patterns which can be mapped in co-ordinates of these stresses. (2 refs.)

61148 Comparison of noise characteristics of Fabry-Perot-type and travelling-wave-type semiconductor laser amplifiers. J.C.Simon, J.L.Favennec (CNET, Lannion, France), J.Chariel.

Electron. Lett. (GB), vol.19, no.8, p.288-90 (14 April 1983). The authors report results of comparative noise measurements on AlGaAs semiconductor laser amplifiers of the Fabry-Perot and travelling-wave types. They show that, for the same net gain, the electrical baseband signal/noise ratio of a photodetector placed at the amplifier output (after an optical filter) is higher for a travelling-wave-type amplifier, especially at high-gain values where the Fabry-Perot amplifier is operated at oscillation threshold. For a net gain of 20.5 dB, the signal/noise ratio of the travelling-wave-type amplifier is 4-5 dB better. (12 refs.)

61149 Tuning characteristics of optical amplification in 1.5 μm InGaAsP/InP lasers. H.Kuwahara, T.Chikama, T.Nakagami (Fujitsu Labs. Ltd., Kawasaki, Japan).

Electron. Lett. (GB), vol.19, no.8, p.295-7 (14 April 1983). The bias current dependence of tuning wavelength in an optical amplifier is investigated in detail. Tuning wavelength decreases below threshold at the rate of -0.36 Å/mA, mainly due to the change of carrier density, and increases at the rate of 0.11 Å/mA above threshold due to the thermal effect. (4 refs.)

61150 Suppression of intensity fluctuation of a longitudinal mode in directly modulated GaInAsP/InP dynamic single-mode laser. F.Koyama, T.Tanbun-et, S.Arai, S.Wang, Y.Suematsu, K.Furuya (Dept. of Phys. Electronics, Tokyo, Inst. of Technol., Tokyo, Japan). *Electron. Lett. (GB)*, vol.19, no.9, p.325-7 (28 April 1983). The intensity fluctuation of a longitudinal mode in a modulated dynamic single-mode laser consisting of a 1.6 μm GaInAsP/InP buried-heterostructure laser with butt-jointed built-in distributed-Bragg-reflector (BH-BJB-DBR) was suppressed to 30 dB less than that of a conventional laser. The possibility of wideband single-mode-fibre communications in the 1.5-1.6 μm wavelength region without degradation of the bandwidth caused by mode partition noise is suggested. (10 refs.)

61151 Einstein relations for gain-guided semiconductor lasers. W.Elsaber, E.O.Gobel (Max-Planck-Inst. für Festkörperforschung, Stuttgart, Germany). *Electron. Lett. (GB)*, vol.19, no.9, p.335-6 (28 April 1983). The Einstein equations which relate the transition rates for stimulated emission, spontaneous emission and stimulated absorption in a laser active medium are re-examined for the special case of a semiconductor laser with complex wave guiding. It is shown that, owing to the nonorthogonality of the gain-guided laser modes, the Einstein relations have to be modified. In particular, the spontaneous emission rate per laser mode no longer equals the stimulated emission rate per laser photon. (8 refs.)

61152 Very low threshold GaInAsP/InP double-heterostructure lasers grown by LP MOCVD. R.Blondau, B.de Cremoux, J.P.Duchemin, M.Razeghi, S.Hersec, P.Hirtz (Thomson-CSF., Lab. Centrale Recherches, Orsay, France). *Electron. Lett. (GB)*, vol.19, no.9, p.336-7 (28 April 1983).

Room-temperature GaInAsP/InP DH lasers emitting at 1.3 μm and having very low threshold current densities have been grown by LP MOCVD. Thresholds were lower than the best values reported for comparable devices grown by LPE, the lowest threshold being 430 A/cm² for a cavity length of 950 μm (width 150 μm) with an active-layer thickness of $d=2200$ Å. (7 refs.)

61153 New mechanism for bistable operation of closely coupled twin stripe lasers. I.H.White, J.E.Carroll (Engng. Dept., Univ. of Cambridge, Cambridge, England).

Electron. Lett. (GB), vol.19, no.9, p.337-9 (28 April 1983). Evidence for a novel mechanism causing bistable operation of closely coupled GaAlAs twin stripe lasers is reported. Current switched bistable operation has been demonstrated stably at room temperature, through the light beam being switched from a central mode to one where the optical filament crosses diagonally from under one laser stripe to the other. (7 refs.)

61154 Static model of DH laser. J.Machac (Inst. of Radio Engng. & Electronics, Czechoslovak Acad. of Sci., Prague, Czechoslovakia). *IEEE Proc. I (GB)*, vol.130, no.2, p.61-6 (April 1983).

A method of complex analysis of the double-heterostructure stripe-geometry laser, based on a new static model, is presented. The optical field distribution in the active region of the laser is described by the wave equation. The interaction between the optical field and free-charge carriers is expressed by the set of rate equations describing also the carrier-concentration profile. Owing to the interaction, it is necessary to solve these equations by a self-consistent procedure. The results of the analysis are light-current characteristics, current dependences of a modal gain, spectra and a near-field pattern. These characteristics are demonstrated in an example. (19 refs.)

61155 Ultrashort pulses from semiconductor diode lasers. B.K.Garside, R.E.Park (Opto-Electronics Ltd., Oakville, Ontario, Canada). *Opt. & Laser Technol. (GB)*, vol.15, no.2, p.91-4 (April 1983).

Careful design of mounting structures and drive-circuit parameters is essential to obtain very short pulse-lengths with high peak powers from semiconductor diode lasers. The authors have developed a diode laser model using a coupled rate equation approach to predict operating regimes producing ultrashort output pulses. The model has been refined through comparison with experiment, and a 10 ps source, designed on the basis of this model, has been implemented. (5 refs.)

61156 Bistable operation of a semiconductor laser. S.A.Gurevich, E.L.Portnoi, M.E.Raikh, B.S.Rykin, F.N.Timofeev, K.Fronts (A.F. Ioffe Physicotech. Inst., Acad. of Sci., Leningrad, USSR). *Sov. Tech. Phys. Lett. (USA)*, vol.8, no.7, p.381-4 (July 1982). Translation of: *Pis'ma v Zh. Tekh. Fiz. (USSR)*, vol.8, no.13-14, p.879-83 (July 1982). [received: April 1983]

The authors consider the existence of a type of bistability in a laser with a saturable absorber. In this case, both of the stable states are present in the output. To a large extent, the implementation of this idea rests upon using as the saturable absorber a semiconductor whose band gap is larger than that of the active medium. They have observed bistability in the output of GaAs-GaAlAs injection heterojunction lasers made from LOC structures in which the band gap of the material of one of the emitters, serving as the saturable absorber, is just slightly greater than the band gap of the material making up the active layer. (7 refs.)

61157 Limiting capabilities of the optimum injection-laser radiation modulation conditions. A.S.Logginov, Yu.F.Yul'berdin.

Telecommun. & Radio Eng. Part 2 (USA), vol.37, no.4, p.56-60 (April 1982). Translation of: *Radiotekhnika, Moskva (USSR)*, vol.37, no.4, p.21-5 (April 1982). [received: April 1983]

Relationships are established between the value of the prepumping current, the injection-laser parameters, and the parameters of the modulating current pulses that result in the optimum pulse-code modulation mode for the radiation with maximum speed of response. (11 refs.)

GaAs/GaAlAs active-passive-interference laser See Entry 61177

Injection laser diodes See Entry 61179

Distributed-feedback heterojunction laser fabricated by interference laser annealing See Entry 61193

CW operation of an injection ring laser See Entry 61197

Total radiant power measurement of laser diode by a calorimetric method See Entry 61203

Joining a semiconductor laser to a planar optical waveguide ... See Entry 61305

Curvature radius and layer stresses for thermal strain in semiconductor multi-layer structures See Entry 62311

Simple method of calculating phonon-assisted Auger recombination rate in direct-gap semiconductors See Entry 62423

Cathodoluminescence of some semiconductors and development of lasers with electron-beam excitation See Entry 63059

42.55R Lasing action in other solids

(inc. solid Raman lasers)

61158 Vibronic solid state lasers: the transition metal ion laser. U.Durr (Phys. Inst., Univ. Stuttgart, Stuttgart, Germany).

Laser & Optoelektron. (Germany), vol.15, no.1, p.31-9 (March 1983). In German.

Vibronic lasers are tunable powerful infrared solid state lasers based on insulating crystals doped with transition metal ions. Up to now the tuning range of pulsed systems extends between 0.7 μm -0.8 μm and 1.1 μm -2.3 μm . CW operation is possible between 1.1 μm -2.1 μm . An overview is given about the properties and recent developments of these lasers. Future possible tendencies are discussed. (18 refs.)

61159 Colour centre lasers using alkaline earth fluorides. J.Margerie (Lab. de Phys. Cristalline, Univ. Paris-sud, Orsay, France).

Rev. Cethedec (France), vol.19, no.NS82-2, p.15-31 (1982). In French.

The author's final aim is to build a tunable c.w. laser using colour centres in CaF₂:Na⁺ and SrF₂:Na⁺; for instance F_{2A}-centres with which Arkhangel'skaya et al. (1978, 1979) realised a pulsed laser. To obtain the required samples, a Bridgman crystal-growth technique was developed. The chief difficulty in achieving c.w. laser action is the bleaching of F_{2A}-centres under strong illumination. In order to circumvent it, various possible schemes are discussed, using either F_{2A} or other centres in CaF₂:Na⁺. Experimental results are described concerning the spectroscopy of colour centres in CaF₂:Na⁺, both in its static and dynamic aspects. (26 refs.)

61160 Auger recombination in GaSb and its effects on laser characteristics. I.V.Kryukova, V.I.Leskovich, E.V.Matveenko (All-Union Sci. Res. Inst. for Physicooptical Measurements, Moscow, USSR).

Sov. Phys.-Tech. Phys. (USA), vol.27, no.10, p.1285-7 (Oct. 1982). Translation of: *Zh. Tekh. Fiz. (USSR)*, vol.52, no.10, p.2095-7 (Oct. 1982). [received: April 1983]

It was previously discovered (see Sov. J. Quantum Electron, vol.6, p.1199, 1976) that heating to 300K seriously degrades the performance of GaSb lasers, a finding which is at variance with similar studies using closely related semiconductors such as GaAs. The present authors show that this difference is due to the high probability of radiationless Auger recombination in GaSb, which reduces the internal photon yield β . The experimental values for the interband Auger transition coefficients C_{ZZ} at 80 and 300K are in agreement with theoretical predictions according to which the probability of Auger recombination in p-type semiconductors such as GaSb and InAs is increased owing to special features of the band structure. Calculation of the temperature dependence of the threshold current density using measured values for C_{ZZ} is in satisfactory agreement with experimental data. GaSb crystals doped with tellurium (n-type) or zinc (p-type) and epitaxial p-type films with residual acceptor densities $p \approx 0.6 \cdot 10^{17} \text{ cm}^{-3}$ which were deliberately not doped were tested. Emission was stimulated by a 50-keV electron beam with pulse duration 100 ns and repetition frequency 50 Hz. (8 refs.)

61161 Laser gain and excitation threshold in semiconductors with transitions between localized states. I.V.Kryukova, S.P.Prokof'eva (All-Union Sci. Res. Inst. for Physicooptical Measurements, Moscow, USSR).

Sov. Phys.-Tech. Phys. (USA), vol.27, no.10, p.1287-9 (Oct. 1982). Translation of: *Zh. Tekh. Fiz. (USSR)*, vol.52, no.10, p.2097-9 (Oct. 1982). [received: April 1983]

Experiments in recent years have demonstrated that the efficiency of semiconductor lasers pumped by electron beams can be increased by using doped crystals as the active medium material [e.g. GaAs, GaSb and certain other compounds GaInAsP, CdS, in which shallow discrete acceptor levels participate in radiative recombination]. The authors propose a method for calculating gains and threshold excitations n- and p-type materials and report some calculated values. The transitions are assumed to be from the conduction band to shallow discrete acceptor levels. Values are compared with experimental data and calculations also given for undoped crystals. The quantum mechanical theory describing absorption and emission of light in straight-band semiconductors is used. It is found that the energy arrangement of the electron states is most favorable in n-type material which is heavily doped (degenerate) and contains shallow acceptor levels. The threshold density of nonequilibrium carriers is then much less than in undoped samples and the laser efficiency is maximal (~30%). On the other hand, because of the high density of equilibrium and nonequilibrium holes, particularly at 300K, absorption of emitted light by free holes is a fundamental limitation on laser efficiency when undoped or p-type crystals are used. (11 refs.)

61162 Excitation of active impurities in laser crystals under electric discharge conditions. V.M.Mikhitarian, V.R.Nikogosyan, Kh.V.Partamyan (Inst. of Phys. Res., Acad. of Sci., Erevan, Armenian SSR).

Sov. J. Quantum Electron. (USA), vol.12, no.10, p.1350-1 (Oct. 1982). Translation of: *Kvantovaya Elektron., Moskva (USSR)*, vol.9, no.10, p.2081-2 (Oct. 1982). [received: April 1983]

A study was made of the excitation of active impurities in laser crystals by an electric discharge. The spectral kinetics of the luminescence indicated that the excitation was by direct electron impact. (5 refs.)

61163 Improvement of the characteristics of ZnSe single-crystal semiconductor lasers pumped longitudinally by an electron beam. I.V.Akimov, A.V.Dudenkova, V.I.Kozlovskii, Yu.V.Korostelin, A.S.Nasibov, P.V.Reznikov, E.M.Tishina, P.V.Shapkin (P.N. Lebedev Phys. Inst., Acad. of Sci., Moscow, USSR).

Sov. J. Quantum Electron. (USA), vol.12, no.10, p.1366-8 (Oct. 1982). Translation of: *Kvantovaya Elektron., Moskva (USSR)*, vol.9, no.10, p.2099-102 (Oct. 1982). [received: April 1983]

The cathodoluminescence spectrum of ZnSe single crystals grown from the vapor and liquid phases was investigated in the range 400-800 nm and the internal quantum efficiency η was measured at $T=77\text{K}$. A correlation was found between η and the free-electron line intensity, but there was no correlation between η and other luminescence lines. A comparison of the photoluminescence spectra recorded at 4.2K for zinc selenide samples annealed in zinc and selenium with the spectra of the original samples indicated that the saturation with zinc during annealing increased η and improved the laser characteristics. (7 refs.)

Intracavity laser spectrometer with a dispersive resonator using F₂⁻ color centers in an LiF crystal See Entry 59863

Nuclear polarisation of helium 3 by a colour centre laser See Entry 60665

A continuous-wave laser See Entry 61184

YAG 50B pulsed laser See Entry 61185

Solid-state laser having a reflector that transmits IR and UV radiation See Entry 61189

Continuous-wave YAG:Nd³⁺ laser with mode locking and intracavity frequency doubling See Entry 61200

- Use of passive switches in the generation of a train of nanosecond pulses by a neodymium glass laser See Entry 61201
- Stimulated Raman scattering in optical fibers See Entry 61237
- Towards upper bound levels: thermonuclear fusion See Entry 61670
- Cathodoluminescence of some semiconductors and development of lasers with electron-beam excitation See Entry 63059

42.55T Free electron lasers

- 61164 Efficiency of free-electron lasers with a scattered electron beam.** T.J.T.Kwan, C.M.Snell (Advanced Concepts & Plasma Phys. Group, Los Alamos Nat. Lab., Los Alamos, NM, USA).

Phys. Fluids (USA), vol.26, no.3, p.835-9 (March 1983).

The quality of the relativistic electron beam in a free-electron laser is an important factor in determining its efficiency of radiation production. In this work, the problem of beam quality is addressed by considering an electron beam that has a scattered velocity distribution but is otherwise monoenergetic. A newly developed particle-in-cell plasma simulation code is used to study the nonlinear stage of the free-electron laser; in particular, the efficiency of energy extraction is determined as a function of the amount of beam scattering. It is found that the mean scattering angle of the electron beam of a free-electron laser in the Raman regime is a much more sensitive parameter than expected. The efficiency of radiation production decreases rapidly for electron beams with finite scattering angles. (10 refs.)

- 61165 Intense free electron laser harmonic generation in a longitudinal magnetic wiggler.** R.C.Davidson (Plasma Res. Inst., Sci. Applications Inc., Boulder, CO, USA), W.A.McMullen.

Phys. Fluids (USA), vol.26, no.3, p.840-7 (March 1983).

The free electron laser instability is investigated theoretically for a tenuous relativistic electron beam propagating parallel to a longitudinal wiggler field ($B_0 + \delta B \sin k_0 z$) \hat{e}_z . The stability analysis is based on the linearized Vlasov-Maxwell equations for perturbations about the beam equilibrium $f_0 = (n_b/2\pi p_1) \delta(p_1 - \gamma_b m V)$ $\delta(p_2 - \gamma_b m V_b)$. For $(\omega_{cb}/k_0 V_b)(\delta B/B_0)$ of order unity or larger, it is found that the transverse electron orbits experience a strong temporal modulation at harmonics of $k_0 v_b \approx k_0 V_b$. In the stability analysis, this orbit modulation is manifest by radiation amplification occurring near the simultaneous zeroes of $\omega = kc$ and $\omega - k V_b - \omega_{cb} = nk_0 V_b$ for the general harmonic number n , which corresponds to an upshifted (for $n \geq 1$) wavenumber $k_n = (1 - V_b/c)^{-1}(\omega_{cb}/c + nk_0 V_b/c)$. For $(\omega_{cb}/k_0 V_b)(\delta B/B_0) > 1$, the instability is typically broadband with several harmonics excited. Moreover, depending on beam and field parameters, the characteristic maximum growth rate can be substantial with $\text{Im} \omega / c k_0 = (\sqrt{3}/2) \times \{ (V_{\perp}^2/4c^2)(\omega_{pb}^2/c^2 k_0^2) n J_n^2(\omega_{cb} \delta B / k_0 V_b B_0) \}^{1/3}$. (19 refs.)

- 61166 Multimode theory of free-electron laser oscillators.** W.B.Colson (Dept. of Phys., Univ. of California, Santa Barbara, CA, USA), J.L.Richardson.

Phys. Rev. Lett. (USA), vol.50, no.14, p.1050-3 (4 April 1983).

The nonlinear self-consistent theory of short-pulse free-electron laser oscillators can now be extended to include transverse diffraction within the optical resonator mode. The theory provides efficient solutions to the three-dimensional parabolic-wave equation coupled to the Lorentz force equation. The method is general enough to include arbitrary magnet designs, optical mirror arrangements, and driving currents. New mode structures are predicted which should be observed in future experiments at Stanford University. (19 refs.)

- 61167 Nonlinear analysis of free-electron-laser amplifiers with axial fields.** H.P.Freund (Naval Res. Lab., Washington, DC, USA).

Phys. Rev. A (USA), vol.27, no.4, p.1977-88 (April 1983).

The nonlinear evolution of free-electron lasers in the presence of an axial guide field is investigated numerically. A set of coupled nonlinear differential equations is derived which governs the self-consistent evolution of the wave fields and particle trajectories in an amplifier configuration. The nonlinear currents which mediate the interaction are computed by means of an average over particle phases, and the inclusion of fluctuating space-charge fields in the formulation permits the investigation of both the stimulated Raman and Compton scattering regimes. The initial conditions are chosen to describe the injection of a cold, axially propagating electron beam into the interaction region which consists of a uniform axial guide field and a helical wiggler field which increases to a constant level adiabatically over a distance of ten wiggler periods. After an initial transient phase, the results show a region of exponential growth of the radiation field which is in excellent agreement with linear theory. Saturation occurs by means of particle trapping. The efficiency of the interaction has been studied for a wide range of axial guide fields, and substantial enhancements have been found relative to the zero-guide-field limit. (14 refs.)

- 61168 Nonlinear traveling-wave equilibria for free-electron-laser applications.** B.Lane, R.C.Davidson (Plasma Fusion Center, MIT, Cambridge, MA, USA).

Phys. Rev. A (USA), vol.27, no.4, p.2008-25 (April 1983).

The class of large-amplitude traveling-wave solutions to the nonlinear Vlasov-Maxwell equations is investigated in which the wave pattern is stationary in a frame of reference moving with the ponderomotive phase velocity $v_p = \omega/(k + k_0)$. Here, $\lambda_0 = 2\pi/k_0$ is the wavelength of the transverse helical wiggler field, and (ω, k) are, respectively, the frequency and wave number of the saturated radiation field which is assumed to be monochromatic and circularly polarized. The conservation of (average) density, momentum, and energy are imposed as additional exact constraint equations that connect the final (saturated) and initial states of the combined electron-beam/radiation-field/wiggler-field system. These constraint equations reduce the generality of the nonlinear equilibrium Bernstein-Greene-Kruskal solutions and allow estimates to be made of the saturated field amplitude in terms of initial properties of beam-wiggler system. As a simple example that is analytically tractable, the authors consider the case where the initial distribution $F_0(\gamma)$ and the saturated untrapped distribution $F_s(\gamma')$ are prescribed by rectangular distribution functions centered around axial velocity $v_z = \sigma/(k + k_0)$, assuming a moderate field amplitude with $b_1 = eB_1/mc^2 k < 1$ and small fractional energy spread in the beam electrons. For a tenuous beam with $\omega \approx kc$ and $k \approx (1 + v_p/c)\gamma_z^2 k_0$, where $\gamma_z = (1 - v_p^2/c^2)^{-1/2}$, it is found that the saturated amplitude of the radiation field is given approximately by $\delta B_1 = \Delta_1 \omega_p^2 / 10(1 + b_w^2)^{1/2} c^2 k_0^2 [1 + v_p/c] \bar{B}_w$, where $b_w = eB_w/mc^2 k_0$, $\Delta_1 m^2$ is the characteristic half-width energy spread in the laboratory frame, and $\omega_p^2 = 4\pi n_b e^2/m$ is the nonrelativistic plasma frequency squared. (16 refs.)

- 61169 Laser and noise-driven operation in swept-gain lasers.** F.A.Hopf (Optical Sci. Center, Univ. of Arizona, Tucson, AZ, USA).

Phys. Rev. A (USA), vol.27, no.4, p.2268-71 (April 1983).

The influence of noise on laser operation is considered for swept-gain lasers and laser amplifiers in which the velocity of the gain medium must be decreased relative to the velocity of light in order to achieve lasing action.

The noise is introduced through the tipping-angle approximation, which leads to a simple, if perhaps unrealistic, formulation of the problem. Such a laser is tuned by desynchronizing the gain medium with the optical pulse, which is the procedure used in the Stanford free-electron laser (FEL). In so doing, the FEL tunes over regions of the true lasing (gain > loss), and over regions where the output is sustained by amplified spontaneous emission (noise driven). The power in the noise-driven regime is not necessarily small compared to the power in the lasing regime. These regimes are identified, the fluctuations are computed, and the connection with the FEL is discussed. (24 refs.)

- 61170 The role of plasma turbulence for wave excitation in a free-electron-laser combined with a molecular and plasma medium.** L.Stenflo (Inst. of Phys., Umea Univ., Umea, Sweden), V.N.Tsytoich, H.Wilhelmsson.

Phys. Scr. (Sweden), vol.T2, no.2, p.538-40 (1982). [received: April 1983]

(1982 International Conference on Plasma Physics, Goteborg, Sweden, 9-15 June 1982).

The effects of plasma turbulence on the generation of radiation in a system of a free-electron-laser and a molecular and plasma medium are investigated by means of a kinetic description. The results are that low frequency waves become damped due to the presence of turbulence, whereas for sufficiently high frequencies ($\omega > \omega_{pe}$, the plasma frequency times the relativistic factor) the turbulence, also in the presence of a molecular medium ($\omega > \omega_r$, the molecular resonance frequency), may lead to amplification of the radiation. (7 refs.)

- 61171 Effects of electron energy spread on self-excitation of free-electron lasers.** L.V.Rodygin, A.V.Smorgonskii (Inst. of Appl. Phys., Acad. of Sci., Gor'kii, USSR).

Sov. Phys.-Tech. Phys. (USA), vol.27, no.10, p.1237-9 (Oct. 1982).

Translation of: *Zh. Tekh. Fiz. (USSR)*, vol.52, no.10, p.2013-17 (Oct. 1982).

[received: April 1983]

As in other electronic devices, in free-electron lasers, electrons interact most efficiently with waves when the spread in the particle parameters is small and hydrodynamic conditions exist (i.e. in laser terminology, line broadening is uniform). However, it is difficult and by no means always possible to achieve hydrodynamic conditions. It is therefore important to know the performance parameters of free-electron lasers when the particle parameters differ widely and there is a kinetic stage of interaction (nonuniform line broadening). (4 refs.)

42.60 LASER SYSTEMS AND LASER BEAM APPLICATIONS

- 61172 Stabilization of the light output delay of a pulsed nitrogen laser.** Cl.Alaimé, J.Bertrand, L.Bonnet, Y.El Masri, L.Palfy, P.Pellegrin, R.Prieels (Inst. de Phys. Corpusculaire, Louvain-la-Neuve, Belgium).

Nucl. Instrum. & Methods Phys. Res. (Netherlands), vol.207, no.3, p.423-7 (1 April 1983).

The authors describe a new type of phaser and demonstrate its efficiency in stabilizing the delay of the light output of a pulsed nitrogen laser with respect to the beam bursts delivered by a cyclotron. (4 refs.)

- 61173 Asymmetry in the coupling coefficients of oppositely traveling waves in a ring laser.** A.Ya.Birman, A.F.Savushkin, V.A.Solomatina.

Opt. & Spectrosc. (USA), vol.53, no.1, p.103-4 (July 1982).

Translation of: *Opt. & Spektrosk. (USSR)*, vol.53, no.1, p.174-6 (July 1982). [received: April 1983]

The coupling coefficients S_a and S_b between the oppositely traveling waves obey the symmetry relation $S_a = S_b$ in scattering at the rough surface of the perfectly conducting reflector of a ring laser. This relation is valid for any realization of a random surface satisfying the condition $\sigma \ll \lambda$, where σ is the RMS height of the unevenness, λ is the wavelength of the radiation. The conclusion on the symmetry of the coupling coefficients for scattering by a perfectly conducting rough surface, however, is not accurate and is valid only on account of the approximations assumed in analyzing the coupling coefficients. The authors give the results of a more detailed analysis of the symmetry properties of the coupling coefficients for scattering at a perfectly conducting rough surface employing the Kirchhoff method. (5 refs.)

- 61174 Tunable picosecond pulses around 1.3 μ m generated by a synchronously pumped infrared dye laser.** A.Seilmeier, W.Kaiser (Phys. Dept., Tech. Univ. Munchen, Munchen, Germany), B.Sens, K.H.Drexhage.

Opt. Lett. (USA), vol.8, no.4, p.205-7 (April 1983).

An infrared dye laser is synchronously pumped by a CW mode-locked Nd:YAG system at 1.06 μ m. The tuning range extends from 1.20 to 1.32 μ m. A pulse duration of 3 psec was measured at 1.25 μ m. The high photostability of the laser dye makes the laser system a practical device. (8 refs.)

- 61175 Inexpensive low temporal jitter laser triggering circuit.** F.A.M.Leal, A.S.L.Gomes, J.R.R.Leite, C.B.de Araujo (Dept. de Fisica, Univ. Federal de Pernambuco, Recife, Brasil).

Rev. Sci. Instrum. (USA), vol.54, no.4, p.501-2 (April 1983).

The authors present a simple and inexpensive triggering circuit which provides a laser pulse jitter of 0.5 ns. (3 refs.)

- 61176 Measurement of ultrafast phenomena in the femtosecond time domain.** C.V.Shank (Quantum Phys. & Electronics Dept., Bell Labs., Holmdel, NJ, USA).

Science (USA), vol.219, no.4588, p.1027-31 (4 March 1983).

Considerable progress has taken place in the generation and application of ultrashort optical pulses. The methods and techniques for extending time-resolved measurements into the femtosecond (10^{-15} second) time domain are described, and applications and fertile areas for investigation with femtosecond pulses are discussed. (32 refs.)

42.60B Design of specific laser systems

- 61177 GaAs/GaAlAs active-passive-interference laser.** H.K.Choi, S.Wang (Dept. of Electrical Engng. & Computer Sci., Univ. of California, Berkeley, CA, USA).

Electron. Lett. (GB), vol.19, no.8, p.302-3 (14 April 1983).

A GaAs/GaAlAs interference laser with an active and a passive section is reported. A very clean single longitudinal mode is obtained and maintained without mode hopping over about 10°C, which results from the combined effect of interference and real index waveguiding in the lateral direction. (6 refs.)

- 61178 Helical-flow CO₂ laser.** M.Yessik (Photon Sources Inc., Ann Arbor, MI, USA).

J. Appl. Phys. (USA), vol.54, no.4, p.1693-8 (April 1983).

A CO₂ laser based on a helical gas-flow design has been developed. The major features of this device are as follows: (1) an integral heat exchanger plasmabute with much lower gas flow rates than other convection-cooled lasers, (2) a multiply segmented plasmabute for high-voltage standoff (3)

coaxial beam and electric discharge with small diameter-to-length ratio resulting in high beam quality and high discharge stability, and, (4) a magnetically stabilized discharge position. Gain profile measurements show that the gain distribution highly favors low-order modes, as desired. Temperature profile measurements of the gas in the plasm tube verify the efficiency of the integral heat exchange concept. Specific laser configurations based on this design concept, intended for industrial material-processing applications, and with output powers of 400-500 W/m, are described. (11 refs.)

61179 Injection laser diodes. B.Dance.

New Electron. (GB), vol.16, no.6, p.76-8 (22 March 1983).

Discusses semiconductor laser diodes which are far smaller, more efficient and need less operating power than conventional gas and solid-state lasers. Although the mean output power from semiconductor lasers tends to be more limited than that from the other types, they have the advantage that their output can easily be modulated with signals which may have a very high frequency. Device structures and typical drive circuits are described. (no refs.)

61180 Simultaneous two-wavelength tunable dye laser with no mode competition and a wavelength separation of more than 200 nm. S.W.Williams, D.W.O.Hedde (Dept. of Phys., Royal Holloway Coll., Egham, England).

Opt. Commun. (Netherlands), vol.45, no.2, p.112-14 (15 March 1983).

A versatile simultaneous two-wavelength tunable dye laser is described. The two wavelengths are generated by means of a novel pumping arrangement which is suitable for operating with a linewidth between 0.001 nm and the broadband regime. There is no mode competition between the two wavelengths and the power ratio is continuously variable. If required, separate dyes can be used to generate the two wavelengths so facilitating a broad range of wavelength separations. Each wavelength is independently tunable but only one dispersive element is required in the cavity. (12 refs.)

61181 High power TEA CO₂ laser tuned by a holographic grating. K.P.Francke, G.Korn, H.Albrecht, S.Polze (Akad. der Wissenschaften, Zentralinst. fur Optik und Spektroskopie, Berlin, Germany).

Opt. Commun. (Netherlands), vol.45, no.2, p.115-16 (15 March 1983).

Wavelength tuning of a TEA CO₂ laser by means of a holographic grating with sinusoidal profile is reported for the first time. The grating with 136 lines/mm had an optimized efficiency according to the gain of the laser. The laser beam was coupled out through the zeroth grating order. (5 refs.)

61182 Tunable sealed-off CW CO laser at room temperature. P.J.M.Peters, W.J.Witte, Z.Krzyzanowski (Dept. of Appl. Phys., Twente Univ. of Technol., Enschede, Netherlands).

Opt. Commun. (Netherlands), vol.45, no.3, p.193-5 (1 April 1983).

Starting from a sealed-off CO laser with a long-life output of 29 W/m in multiline operation, the authors developed a tunable version of this device. The system described has a discharge length of 97 cm. It was made transition-selective by using a three-mirror configuration. In this way the authors were able to tune the laser to more than 70 oscillating vibrational-rotational transitions of the CO molecule. (4 refs.)

61183 Laser oscillator using resonator with self-pumped phase-conjugate mirror. R.A.McFarlane, D.G.Steel (Hughes Res. Labs., Malibu, CA, USA).

Opt. Lett. (USA), vol.8, no.4, p.208-10 (April 1983).

A laser oscillator has been operated in which one reflector is a self-pumped phase-conjugate mirror. The laser is tunable and employs rhodamine 6G as a broadband gain medium. The oscillating linewidth was measured to be 2 GHz at half-power points. (7 refs.)

61184 A continuous-wave laser. Z.Jankiewicz, M.Mindak, W.Pichola, J.Szydlak.

Pol. Tech. Rev. (Poland), no.5-6, p.4-5 (1982).

The LCB-6B continuous-wave laser developed and built at the Institute of Optoelectronics of the Military Technical Academy, Warsaw, generates a beam of monochromatic infrared radiation ($\lambda=1.06 \mu\text{m}$) with power of 50 W, and finds application for cutting semi-conductor structures, in scientific research and for didactic purposes. It comprises: a laser head assembly, a power supply circuit and a cooling system. The active material of this laser is a YAG:Na³⁺ crystal measuring 5 mm diameter \times 80 mm. Its faces are coated with antireflection layers. The laser rod made of the active material and an exciting linear krypton tube are placed at the two foci of an elliptical reflector. The reflecting surfaces of the reflector (side and face surfaces) are gold-coated. (no refs.)

61185 YAG 50B pulsed laser. Z.Jankiewicz, W.Pichola, M.Skorczakowski, J.Szydlak.

Pol. Tech. Rev. (Poland), no.5-6, p.6-7 (1982).

The laser head incorporates a YAG:Na³⁺ rod diameter 3 mm \times 55 mm, a gas discharge lamp 3F 2K, in an elliptical reflector and two front reflectors. (no refs.)

61186 A low-power He-Ne laser head. M.Gebczak, J.Tuszynski.

Pol. Tech. Rev. (Poland), no.5-6, p.8 (1982).

Describes the series of LM-type He-Ne laser heads, LM-200, LM-300, LM-500, designed for use in laser geodetic instruments developed at the Institute of Optoelectronics of the Military Technical Academy, Warsaw. The LM-type He-Ne laser heads feature good mechanical, thermal and power stability characteristics. The concentric discharge tube is closed by Brewster windows which ensures linear polarization of the laser beam. An aluminium cold cathode is used. The laser heads incorporate a hemispherical resonator, ensuring the TM_{00q} mode operation. (no refs.)

61187 High-power-density electron-beam-sustained laser. M.Casey, P.W.Smith, M.H.R.Hutchinson (Blackett Lab., Imperial Coll., London, England).

Rev. Sci. Instrum. (USA), vol.54, no.4, p.458-62 (April 1983).

A high optical power-density excimer laser pumped by an electron-beam-sustained discharge has been developed. The electron-beam generator comprised a 200-kV pulse transformer-driven power supply and an electrostatically focused electron-beam diode. The careful design and optimization of this generator has allowed very reliable, reproducible operation of the complete laser system with a high enhancement ratio of 4.8. An average output power density of 0.63 MW cm⁻² in a 250-nm (FWHM) pulse has been obtained from an e-beam-sustained discharge XeCl* laser with an extraction efficiency of 1.5%. (7 refs.)

61188 Effect of outgassing on the performance of a TE CO₂ laser sealed in an acrylic chamber. D.J.Biswas, A.K.Nath, U.K.Chatterjee (Laser Section, Bhabha Atomic Res. Centre, Bombay, India).

Rev. Sci. Instrum. (USA), vol.54, no.4, p.473-5 (April 1983).

Outgassing of contamination in large quantity was observed in a helical TE CO₂ laser housed in an acrylic (Perspex) chamber. This considerably reduced the sealed operational life of the device. In a helium-free mixture the laser energy initially improved and then reduced with time, while in the mixtures with helium it reduced monotonically. Water vapor seemed to be the main constituent in the contamination. By circulating the contaminated gas through

a trap at dry-ice temperature, the water vapor was condensed, enhancing the sealed-off life of the device. (10 refs.)

61189 Solid-state laser having a reflector that transmits IR and UV radiation. I.F.Balashov, B.G.Berezin, B.P.Kryzhanovskii, M.I.Polyakov, S.I.Khanikov, G.A.Nikitina.

Sov. J. Opt. Technol. (USA), vol.49, no.8, p.500-1 (Aug. 1982). Translation of: *Opt.-Mekh. Prom.-st. (USSR)*, vol.49, no.8, p.28-9 (Aug. 1982). [received: April 1983]

The possibility of short-term stabilization of the energy parameters of a laser, cooled by natural radiant heat removal through the use of a reflector having a selective coating that transmits IR and UV radiation, is investigated. (5 refs.)

61190 Operating characteristics of a transverse-excited 16 μm CO₂ laser with profile electrodes and UV-preionization. K.-J.Schmatjko, H.-J.Cirkel (Kraftwerk Union AG, Erlangen, Germany).

Siemens Forsch. & Entwicklungsber. (Germany), vol.12, no.2, p.135-9 (1983).

The maximum attainable inversion density for the 16 μm laser transition of a direct-discharge CO₂ laser is limited by fast collisional deactivation processes. The optical volume can, however, be extended significantly by a transverse homogeneous volume discharge. Effective UV preionization and a well-damped fast discharge circuit are essential to this purpose. Electrical energy density for optimized excitation is limited only by the allowable heating of the laser gas under these conditions. (24 refs.)

61191 Electric-discharge CW industrial CO₂ laser. V.P.Garashchuk, P.A.Vasilets, V.I.Kirsej, I.A.Porazhinskii, A.A.Svirgun (E.O. Paton Inst. of Electric Welding, Acad. of Sci., Kiev, Ukrainian SSR).

Sov. J. Quantum Electron. (USA), vol.12, no.10, p.1316-20 (Oct. 1982). Translation of: *Kvantovaya Elektron., Moskva (USSR)*, vol.9, no.10, p.2028-35 (Oct. 1982). [received: April 1983]

An experimental CO₂ laser is described, having an output power of 1.5 kW. The use of an electric-discharge unit containing a plane anode and nickel rod cathodes made it possible to couple 150 W into the active medium per cathode (input energy per unit mass 200 J/g, input power per unit volume 5.5 W/cm³, maximum electrooptic efficiency 24%). The service life of the cathodes exceeded 400 h. The relative stability of the output power, without recourse to stabilization, was 2-3% for continuous operation (without switching off) over a period of 8 h. The laser could be operated for 8 h without replenishing the active mixture and a helium-free CO₂-N₂-H₂O mixture could be used. (24 refs.)

61192 High-pressure NH₃-N₂ laser. M.Akhrarov, B.I.Vasil'ev, A.Z.Gras-yuk, A.B.Yastrebov (P.N. Lebedev Phys. Inst., Acad. of Sci., Moscow, USSR).

Sov. J. Quantum Electron. (USA), vol.12, no.10, p.1326-9 (Oct. 1982). Translation of: *Kvantovaya Elektron., Moskva (USSR)*, vol.9, no.10, p.2044-9 (Oct. 1982). [received: April 1983]

A pulsed high-pressure-(up to 3 atm) NH₃-N₂ laser is described, having an output power of 10 kW at a frequency of 868 cm⁻¹ and optically pumped by radiation from a TEA CO₂ laser. It was established that when the parameters of the NH₃-N₂ laser resonator and the pump intensity were fixed one could achieve an increase in the operating pressure of the active medium on using a depleted NH₃-N₂ mixture having an increased partial pressure of ammonia. (10 refs.)

61193 Distributed-feedback heterojunction laser fabricated by interference laser annealing. Zh.I.Alferov, K.G.Kalandarishvili, Yu.V.Koval'chuk, E.L.Portnoi, V.B.Smirtinskii (A.F. Ioffe Physicotech. Inst., Acad. of Sci., Leningrad, USSR).

Sov. Tech. Phys. Lett. (USA), vol.8, no.7, p.333-4 (July 1982). Translation of: *Pis'ma v Zh. Tekh. Fiz. (USSR)*, vol.8, no.13-14, p.769-72 (July 1982). [received: April 1983]

Reports the experimental fabrication of distributed-feedback heterojunction lasers by an interference laser annealing of epitaxial films of InGaAsP/InP heterostructures. The gap width of the quaternary compound was chosen smaller than the photon energy corresponding to the fundamental frequency of a neodymium laser ($\lambda=1.06 \mu\text{m}$): $E_g=1.08 \text{ eV}$. (4 refs.)

61194 Photodissociation CW laser using condensation and evaporation for a closed cycle. V.O.Zaleskii, A.M.Kokushkin, S.S.Polikarpov.

Sov. Tech. Phys. Lett. (USA), vol.8, no.8, p.393-5 (Aug. 1982). Translation of: *Pis'ma v Zh. Tekh. Fiz. (USSR)*, vol.8, no.15-16, p.907-11 (Aug. 1982). [received: April 1983]

In an effort to overcome difficulties associated with the output power and duration of operation of the I laser, the authors used a condensation-evaporation apparatus, consisting of two communicating vessels, to move and purify the gas. As the working gas leaves the laser tube it is liquefied in one of the vessels (the condenser); the liquid passes through a column containing an adsorbent (activated charcoal) and enters the other vessel (the evaporator). The evaporating medium enters the laser tube. The pressure head required to overcome the drag of the transport system is balanced by a difference between the levels of the liquid phase in the communicating vessels. (4 refs.)

61195 Aperture combined Raman laser. C.Woods, K.Tang, C.Hownton, D.Muller, R.O.Hunter, Jr. (Western Res. Corp., San Diego, CA, USA).

Topical Meeting on Excimer Lasers, Incline Village, NV, USA, 10-12 Jan. 1983 (Washington, DC, USA: Opt. Soc. America 1983), p.TuB6/1-3

Discusses the use of an injection-locked KrF laser to excite a Raman laser using the Stokes shift in hydrogen gas with off-axis pumping. (4 refs.)

Nuclear polarisation of helium 3 by a colour centre laserSee Entry 60665

New supersonic lasers at very low temperature and high densitySee Entry 61133

Flashlamp-pumped iodine monobromide laser characteristics ...See Entry 61143

Very low threshold GaInAsP/InP double-heterostructure lasers grown by LP MOCVDSee Entry 61152

New mechanism for bistable operation of closely coupled twin stripe lasersSee Entry 61153

CW operation of an injection ring laserSee Entry 61197

Performance of a laser beam wave-front sensorSee Entry 61210

Towards upper bound levels: thermonuclear fusionSee Entry 61670

Curvature radius and layer stresses for thermal strain in semiconductor multi-layer structuresSee Entry 62311

42.60D Laser resonators and cavities

61196 Influence of a nonlinear active medium on the structure of natural oscillation modes of a Fabry-Perot interferometer. A.V. Butkovskii. *Sov. J. Quantum Electron. (USA)*, vol.12, no.10, p.1286-9 (Oct. 1982). Translation of: *Kvantovaya Elektron., Moskva (USSR)*, vol.9, no.10, p.1977-83 (Oct. 1982). [received: April 1983]

The results are given of a parametric calculation of the mode structure of a circular Fabry-Perot resonator of a solid-state laser. It is shown that an increase in the equivalent Fresnel number of the resonator (when its value is sufficiently large) alters the mode field distribution in some cases so that it resembles the modes of increasing order occupying the main part of the resonator, whereas in other cases the mode field is concentrated in a decreasing region near the resonator axis. The existence of several different solutions for the same mode is demonstrated. In the case of resonators with an equivalent Fresnel number much greater than unity the distributions of the intensity are close to geometric in the main volume of the resonator and estimates are given of the angular divergence of the output radiation. (10 refs.)

61197 CW operation of an injection ring laser. A.P. Bogatov, P.G. Eliseev, O.G. Okhotnikov, G.T. Pak, M.P. Rakhval'skii, K.A. Khairetdinov (P.N. Lebedev Phys. Inst., Acad. of Sci., Moscow, USSR). *Sov. Tech. Phys. Lett. (USA)*, vol.8, no.7, p.346-7 (July 1982). Translation of: *Pis'ma v Zh. Tekh. Fiz. (USSR)*, vol.8, no.13-14, p.799-803 (July 1982). [received: April 1983]

The authors have, for the first time, demonstrated CW single frequency operation of an AlGaAs heterojunction semiconductor laser with a ring resonator. The arrangement proposed makes it possible to minimise the coupling between the oppositely charged waves. At a light density of 2.10^5 W/cm², one observes an approximate travelling wave operation. (2 refs.)

Intracavity dye-laser photothermal deflection spectroscopy See Entry 59861

Intracavity laser spectrometer with a dispersive resonator using F_2 color centers in an LiF crystal See Entry 59863

LIMP in continuously coupled unstable resonators See Entry 61127

Effect of capture on the beat contour of oppositely traveling waves in a ring gas laser See Entry 61131

Multimode theory of free-electron laser oscillators See Entry 61166

Simultaneous two-wavelength tunable dye laser with no mode competition and with a wavelength separation of more than 200 nm See Entry 61180

Laser oscillator using resonator with self-pumped phase-conjugate mirror See Entry 61183

A low-power He-Ne laser head See Entry 61186

High-pressure NH₃-N₂ laser See Entry 61192

A miniature modulator See Entry 61198

Continuous-wave YAG:Nd³⁺ laser with mode locking and intracavity frequency doubling See Entry 61200

Stabilizing a gas discharge laser with an external absorption cell under modulated operation See Entry 61205

Pulse evolution and mode selection characteristics in a TEA-CO₂ laser perturbed by injection of external radiation See Entry 61206

Frequency reproducibility of ring He-He/CH₄ lasers See Entry 61212

Resonances of the polarization of gas laser radiation under mode self-locking conditions See Entry 61213

Atmospheric laser spectrometer with an external cavity mirror See Entry 64267

42.60F Laser beam modulation

61198 A miniature modulator. W. Aleksinski, K. Rozanski. *Pol. Tech. Rev. (Poland)*, no.5-6, p.9-10 (1982).

Discusses the MMP-2 laser beam modulator for the generation of high power, short pulses 10 to 50 ns, achieved by the Q-switching of the laser resonator. The MMP2-modulator can be used for Q-switching of ruby lasers and neodymium lasers, and for modulating laser light beam. This modulator consists of two assemblies: a pockels cell, and a power supply and control circuit. A KDP crystal is used as active material in the Pockels cell. (no refs.)

61199 Generation of femtosecond intense optical pulses and applications to time resolved spectroscopy. A. Antonetti, R. Astier (Lab. d'Optique Appliquee, ENSTA, Ecole Polytech., Palaiseau, France), D. Hulin, J.L. Martin, A. Migus, A. Orszag.

Rev. Cethedec (France), vol.19, no.NS82-2, p.155-74 (1982). In French. New techniques have been developed for producing GW peak power optical pulses, in the femtosecond regime with a new capability of wavelength tunability. Such an experimental advance has made possible the theoretical understanding of some ultrafast phenomena in solid-state physics or in biology: (1) formation of a superdense electron-hole plasma in CuCl, whose emission corresponds to a band gap renormalisation effect; (2) existence of a very short lived excited state (250-300 fs) in the photodissociation of CO or O₂ hemoprotein; (3) explanation of the low quantum yield of dissociation of MbO₂ by relaxation of excited states and geminate recombination. (22 refs.)

61200 Continuous-wave YAG:Nd³⁺ laser with mode locking and intracavity frequency doubling. Yu.D. Golyaev, S.A. Grodskii, V.G. Dmitriev, P.G. Konvisar, S.V. Lantratov, V.Yu. Mikhailov, S.R. Rustamov. *Sov. J. Quantum Electron. (USA)*, vol.12, no.10, p.1360-2 (Oct. 1982). Translation of: *Kvantovaya Elektron., Moskva (USSR)*, vol.9, no.10, p.2093-5 (Oct. 1982). [received: April 1983]

An investigation was made of acoustooptic mode locking in a YAG:Nd³⁺ laser with intracavity frequency doubling in a lithium iodate crystal. The energy, noise, and 'mismatch' characteristics of the laser were investigated. It was found that the mode locking zone increase in size to several millimeters, compared with the regime in the absence of frequency doubling. The maximum power of the second harmonic observed in the mode-locked regime was 5 W, which was approximately three times higher than in the pure CW regime. (9 refs.)

61201 Use of passive switches in the generation of a train of nanosecond pulses by a neodymium glass laser. V.A. Rusov, A.I. Stepanov, A.A. Tarasov. *Sov. J. Quantum Electron. (USA)*, vol.12, no.10, p.1371-3 (Oct. 1982). Translation of: *Kvantovaya Elektron., Moskva (USSR)*, vol.9, no.10, p.2106-8 (Oct. 1982). [received: April 1983]

A train of nanosecond pulses was generated by a neodymium glass laser when a passive laser switch based on a LiF crystal with F_2 color centers was used to control the Q factor. The total radiation energy in a train reached 100 J, the number of pulses in a train exceeded 50, and the instability of the power and repetition frequency of the pulses was within 20-30%. It was found

that, when used in the selected operating regime, switches of this kind were superior to passive switches composed of organic dye solutions. (7 refs.)

61202 Temperature control of an acousto-optic modulator in an Argon ion laser using an R.F. servo loop. J.G. Edwards, D. Henderson. *Report NPL-DES-78*, Nat. Phys. Lab., Teddington, England (Feb. 1983), 20 pp.

A servo system is described to control the temperature of the modulator prism for a mode locked argon ion laser. The loop uses the phase of the reflected RF power to sense the temperature of the glass prism and controls this temperature via the RF, hence maintaining resonance and allowing full use of the available RF power. A second loop using a thermistor and DC heaters defends the first against room temperature fluctuations.

Suppression of intensity fluctuation of a longitudinal mode in directly modulated GaInAsP/InP dynamic single-mode laser See Entry 61150

Ultrashort pulses from semiconductor diode lasers See Entry 61155

Limiting capabilities of the optimum injection-laser radiation modulation conditions See Entry 61157

Stabilizing a gas discharge laser with an external absorption cell under modulated operation See Entry 61205

Thin-film Ge-As₂S₃ waveguide with diffractive input coupling of a CO₂ laser beam See Entry 61279

42.60H Optical problems related to properties and interactions of laser beams

61203 Total radiant power measurement of laser diode by a calorimetric method. T. Inoue, K. Yamamura (Electrotech. Lab., Ibaraki, Japan). *Electron. Lett. (GB)*, vol.19, no.9, p.320-1 (28 April 1983).

A calorimetric measurement method for the absolute value of total radiant power from a laser diode is described. The radiant power is measured from the difference between input DC power to the laser diode and its heat loss by a calorimeter. The method is also useful for an ordinary semiconductor light source. (1 ref.)

61204 Influence of linear phase anisotropy induced in the active medium on the characteristics of gas-laser radiation. A.P. Voitevich, V.S. Kalinov, A.Ya. Smirnov, L.L. Teplyashin. *J. Appl. Spectrosc. (USA)*, vol.36, no.5, p.489-93 (May 1982). Translation of: *Zh. Prikl. Spektrosk. (USSR)*, vol.36, no.5, p.717-22 (May 1982). [received: Feb. 1983]

The possibility of using the linear phase anisotropy induced in the active medium of a laser to control the spectrum of the generated laser radiation is known. Experimentally, considerable constriction to the center of the amplification contour of the generation spectrum has been obtained in a helium-neon laser with a radiation wavelength of 0.63 μ , inducing anisotropy by means of a transverse magnetic field. However, the potential for the use of linear phase anisotropy to control the spectrum of the generated radiation is not exhausted by constriction of the generation region. It is of interest to obtain frequency retuning of the generation region and to study the possibility of transverse-mode discrimination. The authors examine the influence of phase anisotropy and the transverse magnetic field in general on the generation power, with different mutual orientations of the magnetic field strength and the principal directions of the polarizer. (6 refs.)

61205 Stabilizing a gas discharge laser with an external absorption cell under modulated operation. A.V. Mironov, V.E. Privalov.

J. Appl. Spectrosc. (USA), vol.36, no.5, p.494-8 (May 1982). Translation of: *Zh. Prikl. Spektrosk. (USSR)*, vol.36, no.5, p.722-7 (May 1982). [received: Feb. 1983]

Considers some properties of the operation of stabilized lasers with linear and ring cavities utilizing gain modulation. It is assumed that the automatic frequency tuning system has sufficient gain in the feedback circuit that the frequency instability in the laser emission is determined by the error signal. (8 refs.)

61206 Pulse evolution and mode selection characteristics in a TEA-CO₂ laser perturbed by injection of external radiation. P.H. Flamant, R.T. Menzies, M.J. Kavaya, U.P. Oppenheim (Jet Propulsion Lab., California Inst. of Technol., Pasadena, CA, USA).

Opt. Commun. (Netherlands), vol.45, no.2, p.105-11 (15 March 1983).

A grating-tunable TEA-CO₂ laser with an unstable resonator cavity, modified to allow injection of CW CO₂ laser radiation at the resonant transition line by means of an intracavity NaCl window, has been used to study the coupling requirements for generation of single frequency pulses. The width and shape of the mode selection region, and the dependence of the gain-switched spike buildup time and the pulse shapes on the intensity and detuning frequency of the injected radiation are reported. Comparisons of the experimental results with previously reported mode selection behavior are discussed. (10 refs.)

61207 Laser heating: an analytical approach to the theory. D.J. Gibbons (Central Res. Labs., Thorn EMI plc, Hayes, England).

Opt. & Laser Technol. (GB), vol.15, no.2, p.95-9 (April 1983).

The theory of pulsed and scanned laser beams is developed and the results are shown to agree with similar analyses by other authors. A new expression, however, for the temperature rise caused by a very small laser spot agrees well with recent experiments. (9 refs.)

61208 Multiple beams from Rogowski-profile solid electrode TEA CO₂ lasers. S.A. Hamadto (Dept. of Phys., King Saud Univ., Riyadh, Saudi Arabia).

Opt. & Laser Technol. (GB), vol.15, no.2, p.105-7 (April 1983).

Three and five beams were observed to emerge with angular symmetry from Rogowski-profile solid electrode TEA CO₂ lasers. A simple geometrical optics theory of the external reflection guided-modes within the rectangular cavity formed by the laser mirrors and electrodes has successfully accounted for the number and angular separation of these multiple beams, and has established criteria for their elimination. (5 refs.)

61209 Laser-power fluctuations: an analog signal-correction technique. D. Kumar, R.V. Nauman, R. Mohanty, S.P. McGlynn (Dept. of Chem., Louisiana State Univ., Baton Rouge, LA, USA), G.L. Findley. *Rev. Sci. Instrum. (USA)*, vol.54, no.4, p.463-8 (April 1983).

A simple and inexpensive analog technique which corrects spectroscopic signals for pulse-to-pulse fluctuations in the output power of an excitation laser is described. The technique is applicable to both linear and nonlinear spectroscopy and, in the latter case, requires no fast electronic function generator. This design yields an improved time-constant characteristic which parallels the approach of the effective time constant toward RC. Furthermore, since this improvement does not require any preintegration, pulse shape information is preserved. A description of a photoacoustic (PA) spectrometer which incorporates the signal-correction device and which relies on the photogalvanic effect for wavelength calibration is presented as an example. Finally, signal-

corrected PA spectra of the $S_1 \leftarrow S_0$ transition in azulene are presented. (20 refs.)

61210 Performance of a laser beam wave-front sensor. C.P.Wang (Aero-phys. Lab., Aerospace Corp., Los Angeles, CA, USA). *Rev. Sci. Instrum. (USA)*, vol.54, no.4, p.469-72 (April 1983). Laser beam wave-front measurement is important for laser beam quality evaluation and beam control. In this paper the author reports on a laser beam wave-front sensor consisting of a phase detector and a scanner. With the use of this sensor, the wave-front phase profile across a hydrogen fluoride (HF) laser beam has been obtained. The major advantages of this technique are that it is fast, sensitive, and compact. Other features are electric scanning, self-alignment, noise cancellation, and no drift. Wave-front sensor operational principles, features, and experimental results are presented. The sensitivity of the sensor was 5° . This sensitivity corresponds to the change of beam quality parameter, the Strehl ratio, by 1%. Hence it is a sensitive beam quality measurement technique. (14 refs.)

61211 Problem of accurate intensity measurements in focused laser beams. Yu.K.Daniileiko, T.P.Lebedev, V.N.Nikolaev, A.V.Sidorin (P.N. Lebedev Phys. Inst., Acad. of Sci., Moscow, USSR). *Sov. J. Quantum Electron. (USA)*, vol.12, no.10, p.1295-7 (Oct. 1982). Translation of: *Kvantovaya Elektron., Moskva (USSR)*, vol.9, no.10, p.1992-7 (Oct. 1982). [received: April 1983] The problem of intensity measurements in sharply focused Gaussian laser beams is discussed. It is shown that existing methods have many disadvantages, particularly for small caustics. A new method is proposed for measuring the aberrations of focusing lens systems and determining the maximum intensity in a caustic. (3 refs.)

61212 Frequency reproducibility of ring He-He/CH₄ lasers. M.V.Daniileiko, A.M.Fal', V.P.Fedin, M.T.Shpak, L.P.Yatsenko (Inst. of Phys., Acad. of Sci., Kiev, Ukrainian SSR). *Sov. J. Quantum Electron. (USA)*, vol.12, no.10, p.1307-16 (Oct. 1982). Translation of: *Kvantovaya Elektron., Moskva (USSR)*, vol.9, no.10, p.2013-27 (Oct. 1982). [received: April 1983] An investigation was made of the factors governing the frequency reproducibility of ring gas lasers stabilized using resonances of nonlinear absorption in methane. The laser was of monolithic construction convenient in many practical applications. Frequency stabilization by competitive and phase resonances of nonlinear absorption ensured a frequency reproducibility of 5×10^{-13} and 4×10^{-12} , respectively, and this reproducibility was governed mainly by the inaccuracy of the establishment of the necessary pressure in the amplifying medium. A theory of nonlinear resonances in ring gas lasers was developed for an arbitrary degree of saturation of the absorption and this theory could be compared directly with the experimental results. (26 refs.)

61213 Resonances of the polarization of gas laser radiation under mode self-locking conditions. G.I.Kozin, I.P.Kononov, V.N.Petrovskii, E.D.Prosenko, A.N.Rurukin (Engng. Phys. Inst., Moscow, USSR). *Sov. J. Quantum Electron. (USA)*, vol.12, no.10, p.1321-6 (Oct. 1982). Translation of: *Kvantovaya Elektron., Moskva (USSR)*, vol.9, no.10, p.2035-44 (Oct. 1982). [received: April 1983] A theoretical analysis is made of a gas laser with an internal absorption cell operating in the regime of self-locking of two orthogonally polarized modes with a finite spatial shift along the resonator axis. It is shown that the radiation emitted by such a laser exhibits polarization resonances. Potential applications of these resonances in ultrahigh-sensitivity spectroscopy are considered. (9 refs.)

61214 Use of high-frequency laser-intensity fluctuations for optical measurements. A.B.Bukhman, E.M.Dianov, A.Ya.Karasik, V.A.Kozlov, A.M.Prokhorov, A.K.Senatorov (P.N. Lebedev Phys. Inst., Acad. of Sci., Moscow, USSR). *Sov. Tech. Phys. Lett. (USA)*, vol.8, no.8, p.389-90 (Aug. 1982). Translation of: *Pis'ma v Zh. Tekh. Fiz. (USSR)*, vol.8, no.15-16, p.897-900 (Aug. 1982). [received: April 1983] Proposes the exploitation for optical measurements of laser intensity fluctuations in the frequency range from tens of kilohertz to hundreds of megahertz. The intensity fluctuations are similar to a white noise and correlate with the laser output intensity, so that useful information about an optical signal can be extracted from the level of this noise. The authors selected three types of CW lasers: an LG-52-1 commercial He-Ne laser operating in a single transverse mode ($\lambda = 0.63 \mu\text{m}$), an injection semiconductor laser ($\lambda = 0.85 \mu\text{m}$), and a neodymium garnet laser ($\lambda = 1.064 \mu\text{m}$). The solid-state lasers operated in several transverse modes. (6 refs.)

61215 Thermo-optic-conversion method for detecting the spatial mode structure of a TEA CO₂ laser beam. E.A.Chernov (Lenin Komsomol State Univ., Voronezh, USSR). *Sov. Tech. Phys. Lett. (USA)*, vol.8, no.8, p.429-30 (Aug. 1982). Translation of: *Pis'ma v Zh. Tekh. Fiz. (USSR)*, vol.8, no.15-16, p.992-5 (Aug. 1982). [received: April 1983] Proposes a simple and convenient method, usable in any laser laboratory, which makes use of a thermo-optic converter, which has been used previously to measure the spatial structure of the beams from CW CO₂ lasers. The converter is a thin film of CdS deposited in vacuum on a piece of Muskovite television mica $60 \times 60 \text{ mm}^2$ in size. (9 refs.)

61216 Beam-profile measurement of laser pulses using a spatial filter to sample the hermite modes for a string of pulses. E.G.Johnson, Jr.. Report NBS-TN-1057, Nat. Bur. Stand., Washington, DC, USA (Sept. 1982), iii+39 pp. As a first step in the development of a beam-profile measuring instrument for laser sources that is capable of determining the distribution of low-order (less than 25) Hermitean modes in a series of laser pulses, the author has designed and evaluated the three key parts of such an instrument. First, there is the telescope system which allows the incident laser beam to be phase, beam-width, and beam center matched to the optical spatial filter. Second, there is a brief error analysis of the structure of the mismatch function between the beam out of the telescope and that expected by the filter. Finally, there is the detailed analysis and design of the computer-generated spatial filter that will cause the incident-laser beam to be cross correlated with the low-order Hermite modes and will create an array of light spots in the detector (Fourier transform) plane each of which can be uniquely related to a particular Hermite mode of the original laser pulse. The principal conclusion is that the Hermite mode analysis can be done with better than 99 percent separation between modes, provided the phase between modes is uncorrelated from pulse to pulse when the filter has been fabricated with a two-level, gray-scale structure which samples the profile with either 0 percent, or 100 percent transmission. (8 refs.)

61217 Anti-Stokes Raman scattering of excimer and tunable UV lasers in chemically pumped CO. J.C.White (Bell Telephone Labs., Holmdel, NJ, USA), T.A.Miller, M.Heaven. Topical Meeting on Excimer Lasers, Incline Village, NV, USA, 10-12 Jan. 1983 (Washington, DC, USA: Opt. Soc. America 1983), p.TuB5/1-3

Presents experiments in which chemically pumped CO has been studied as a storage medium for anti Stokes Raman lasers (ASRL) operating in the VUV. Excited CO is particularly attractive as a medium for ASRL action due to the ease with which it can be prepared, the large energy shift (e.g. 3-4 eV), and the position and strength of the various electronic transitions. Initial experiments aimed at constructing an ASRL tunable from 140 nm to 170 nm with mJ output energy have been conducted, and the authors report spectroscopic studies in which excimer and tunable laser sources have been used to pump the CO inversion in a small scale device. Although ASRL action is yet to be achieved, these studies indicate that such a device is indeed feasible as an excimer laser up-converter. (3 refs.)

Use of a holographic diffraction grating for deflecting a laser beam See Entry 61108

Laser alignment techniques See Entry 61218

Thermal model for interference laser annealing See Entry 61964

42.60K Optical problems related to applications of laser beams

61218 Laser alignment techniques. D.C.Williams (NPL, Teddington, England). *Phys. Technol. (GB)*, vol.14, no.2, p.61-7 (March 1983).

Describes the relevant properties of a laser beam and the techniques and instruments which are available for alignment work. Amongst the techniques discussed are three-point systems and various commercial levelling systems. The effect of ambient air and accessories used in laser alignment work, particularly the pentagonal prism, are dealt with. (9 refs.)

61219 A study of laser Doppler anemometer based on colliding beams. V.M.Zemlyanskii, N.P.Divnich, A.M.Demeschik. *Ukr. Fiz. Zh. (USSR)*, vol.28, no.3, p.357-61 (March 1983). In Russian.

A laser Doppler anemometer based on colliding beams is analyzed using the vector theory of light scattering. Doppler signal calculation results are presented for conditions of scattering by spheres of polystyrene (dia=1.5 μm) and water (dia=1.98 μm) for various states of illuminating beam polarization. (5 refs.)

Automatic magnetic dichrometer for the $\lambda = 10.6 \mu\text{m}$ range [for free carrier concentration determination] See Entry 59820

Laser scanning microscope with automatic focusing See Entry 59840

Intracavity dye-laser photothermal deflection spectroscopy See Entry 59861

Deep UV lithography by using excimer lasers. (Photo-etching characteristics and development of uniform intensity irradiation system) See Entry 59874

Rotational effects in the intermediate-case radiationless decay of pyrimidine See Entry 60813

Measurements of Gaussian speckle statistics using both direct and heterodyne detection of CO₂ laser radiation See Entry 61087

Holographic intensity correlator with a laser electron beam tube for inputting images for processing See Entry 61114

A low-power He-Ne laser head See Entry 61186

Laser-power fluctuations: an analog signal-correction technique See Entry 61209

Use of high-frequency laser-intensity fluctuations for optical measurements See Entry 61214

Laser microspeckle technique in displacement measurement near a crack tip See Entry 61462

A comparison of experimental and numerical results obtained for the secondary flow in a large turbine cascade See Entry 61576

Apparatus for examining the sedimentation stability of a filled polymer [using laser radiation] See Entry 63601

Methods of spectral analysis with laser selection of the sample and its vaporization in arc discharges See Entry 63622

High-sensitivity atmospheric gas analysis based on intracavity laser detection of scattered radiation See Entry 63763

Laser measurements of the stratospheric ozone layer See Entry 64243

Atmospheric laser spectrometer with an external cavity mirror See Entry 64267

Application of excimer lasers for remote sensing See Entry 64276

The automatic photoelectric device with a laser interferometer for measuring photographs of limbs in meridian instruments See Entry 64388

42.65 NONLINEAR OPTICS

61220 Investigation of the rotation of a wave front in a molecular multipass amplifier. N.E.Aver'yanov, Yu.A.Baloshin, A.I.Dernyatn, I.V.Pavlishin. *J. Appl. Spectrosc. (USA)*, vol.36, no.5, p.502-4 (May 1982). Translation of: *Zh. Prikl. Spektrosk. (USSR)*, vol.36, no.5, p.730-3 (May 1982). [received: Feb. 1983]

Presents the results of a numerical computer investigation into the phenomenon of rotation of a wave front (RWF) with four-photon mixing (FPM) in the medium of a nonlinear (with partial saturation) molecular multipass TEA-amplifier based on CO₂. The authors investigated RWF with FPM in an amplifier with $\tau_p \leq 10^{-7}$ sec. (5 refs.)

61221 Optical bistability in multimode systems with second- and third-order dispersive nonlinearity. F.-J.Schutte, K.Germey, R.Tiebel, K.Worlitzer (Pädagogische Hochschule 'Karl Liebknecht', Potsdam, Germany). *Opt. Acta (GB)*, vol.30, no.4, p.465-74 (April 1983).

Mutual optical bistability is found for several modes in open cavities containing second- or third-order nonlinear materials. The quantum-statistical treatment yields the Fokker-Planck equation for any system of damped boson modes. Under certain conditions it is possible to state the extrema of the steady solution of the Fokker-Planck equation. They are compared with the steady states resulting from the classical deterministic treatment. In some cases both statements coincide. (12 refs.)

61222 Excitation of surface polaritons by nondegenerate four-wave mixing of evanescent waves. S.T.Hendow, K.Ujihara (Dept. of Phys. & Astron., Univ. of New Mexico, Albuquerque, NM, USA). *Opt. Commun. (Netherlands)*, vol.45, no.2, p.138-42 (15 March 1983). Proposes a method for exciting a surface polariton wave by nonlinear mixing of three evanescent waves. The nonlinear polarization and phase matching conditions are analysed for diatomic cubic crystals and a numerical example is given for GaP showing that this scheme is possible. Furthermore, by consideration of the energy balance in the crystal, the gain coefficient for the surface wave and the intensity of the wave coupled to the vacuum are also calculated. (18 refs.)

On the interaction operator in the optical spectroscopies See Entry 59849

Nonlinear effects in TIPE-LiNbO₃ waveguides for optical communications See Entry 61267

Nonlinear absorption of light in glassy arsenic sulfide fibers in the energy range $h\nu < E_g$ See Entry 61297

High-speed signal processing with nonlinear integrated optics See Entry 61303

The polariton in CdSe: measurement of time of flight and nonlinear transmission See Entry 62347

Determination of cubic optical susceptibilities of liquid crystals by coherent four-photon spectroscopy See Entry 62914

42.65B General theory

Time-varying light amplification by dynamic holograms in spatially nonuniform light beams See Entry 61119

42.65C Stimulated Raman, Brillouin and Rayleigh scattering; parametric oscillations and harmonic generation

61223 Difference-frequency as a tunable source for detection of free radicals. P.-V.Nickles, T.Lungershausen, G.Fritsch (Akad. der Wissenschaften, Zentralinst. fuer Optik & Spektroskopie, Berlin, Germany). *Exp. Tech. Phys. (Germany)*, vol.31, no.1, p.65-73 (1983). In German. The radiation of a dye-laser and the SHG of a YAG-laser are frequency-mixed in LiIO₃ as the nonlinear crystal. The so formed difference-radiation is tunable in the IR-region 2.8...5.6 μ m with pulsepower of some watts. This system is suitable for linear absorption measurements. The system parameters are discussed for the detection of free CH₃-radicals in the IR-region. (11 refs.)

61224 Spectroscopic and line-narrowing properties of resonant sum and difference frequency generation. B.Dick, R.M.Hochstrasser (Dept. of Chem., Univ. of Pennsylvania, Philadelphia, PA, USA). *J. Chem. Phys. (USA)*, vol.78, no.6, pt.2, p.3398-409 (15 March 1983). Three wave mixing is investigated with respect to its spectroscopic applications under fully resonant conditions. A theoretical study of the appropriate second order susceptibility $\chi^{(2)}$ reveals interesting features both for sum and difference frequency generation. For difference frequency generation two different mechanisms are possible, one of which allows the observation of resonances between excited states and the study of dephasing induced coherent emission. The coherence decay rate between the two excited states may be measured and also its pure dephasing rate. The line-narrowing characteristics of the fully resonant $\chi^{(2)}$ are studied with respect to correlation between the inhomogeneous distribution for different levels. The line-narrowing capabilities are found to be partly complementary for the sum- and the two difference frequency resonance configurations. This leads to the suggestion of new line-narrowing techniques which could provide information about type and amount of correlation in inhomogeneously broadened systems. (35 refs.)

61225 Nonlinear optical phenomena in a multiple interferometer. V.N.Lugovoi (P.N. Lebedev Phys. Inst., Acad. of Sci., Moscow, USSR). *J. Opt. Soc. Am. (USA)*, vol.73, no.4, p.473-8 (April 1983). A multiple interferometer is proposed and stimulated Raman radiation, stimulated Mandel'stam-Brillouin radiation, and Cerenkov-type optical parametric oscillation are considered in this interferometer, which is excited by an external light beam. An extremely low threshold intensity of the exciting beam is noted. Optical bistability and hysteresis, self-pulsing of the radiation intensities, amplification of amplitude-phase deviations in the incident pumping beam, limitation of the intensity of the beam transmitted by the interferometer, and nonlinear reflection of the beam from the multiple interferometer are predicted and discussed. It is also noted that the threshold for generation of the second Stokes component of stimulated Raman radiation and stimulated Mandel'stam-Brillouin radiation under the conditions discussed is usually not achieved, even for high excess of the exciting beam intensity over the threshold for generation of the first Stokes component. (25 refs.)

61226 Nonlinear interferometry in Langmuir-Blodgett multilayers of polydiacetylene. F.Kajzar, J.Messier (CEA-CENS, Gif-sur-Yvette, France), J.Zyss, I.Ledoux. *Opt. Commun. (Netherlands)*, vol.45, no.2, p.133-7 (15 March 1983). A new technique of nonlinear spectroscopy in highly absorbing media is demonstrated for polydiacetylenes. Third harmonic of a Nd:YAG laser is generated and measured by interference between two Langmuir-Blodgett multilayers of polymer. The intensity recorded after two 2700 Å thick multilayers is comparable to that obtained from a CaCO₃ 1.91 mm thick phase matched crystal. (13 refs.)

61227 Shift of stimulated Brillouin scattering component in certain liquid mixtures. N.F.Andreev. *Opt. & Spectrosc. (USSR)*, vol.53, no.1, p.4-5 (July 1982). Translation of: *Opt. & Spektrosk. (USSR)*, vol.53, no.1, p.7-9 (July 1982). [received: April 1983] It is shown that during stimulated Brillouin scattering the frequency shift of the stimulated Brillouin scattering component is again a nonmonotonic function of the solution concentration. Consequently, there may be significantly expanded opportunities for tuning the frequency of high-power laser beams in optical experiments. For the present experiments binary mixtures of organic liquids: ethanol (C₂H₅OH) and carbon tetrachloride (CCl₄); acetone (C₃H₆O) and carbon tetrachloride; benzene (C₆H₆) and carbon tetrachloride; and acetone and benzene were used. The nonmonotonic dependence of the shift of the stimulated Brillouin component (or of the hypersonic frequency) on the solution concentration may be evidence of the presence of complexes and associations in the solution, and it may yield information on the composition and structure of these formations. (8 refs.)

61228 Observation of resonantly enhanced sum-frequency generation involving sodium Rydberg states. D.J.Gauthier, J.Krasinski, R.W.Boyd (Inst. of Optics, Univ. of Rochester, Rochester, NY, USA). *Opt. Lett. (USA)*, vol.8, no.4, p.211-13 (April 1983). A large, DC-electric-field-induced nonlinear optical susceptibility is exploited to produce ultraviolet radiation in the range 2453-2476 Å by the process of sum-frequency generation in sodium. The interaction is resonantly enhanced at the first intermediate level by the ³P_{3/2} state and at the second intermediate level by a Rydberg state. Conversion efficiencies of 10⁻³ have been obtained; improvement of this value by a factor of 10³ should be possible. (10 refs.)

61229 Generation of 35.5-nm coherent radiation. J.Bokor (Bell Labs., Holmdel, NJ, USA), P.H.Bucksbaum, R.R.Freeman. *Opt. Lett. (USA)*, vol.8, no.4, p.217-19 (April 1983). Tunable coherent radiation was produced at 35.5 nm by seventh-harmonic conversion of 248-nm radiation from a krypton fluoride excimer laser. The nonlinear interaction took place at the intersection of the laser focus and a pulsed, supersonic helium gas jet. Third- and fifth-harmonic generation produced coherent outputs at 83 and 50 nm in both helium and xenon gas jets. (15 refs.)

61230 Effect of laser fluctuations on squeezed states in a degenerate parametric amplifier. K.Wodkiewicz, M.S.Zubairy (Max-Planck-Inst. fur Quantenoptik, Garching, München, Germany). *Phys. Rev. A (USA)*, vol.27, no.4, p.2003-7 (April 1983). The effect of phase and amplitude fluctuations of the pump mode on the quantum-statistical properties of the signal mode is considered. It is shown that these fluctuations in the laser field tend to decrease the squeezing of the signal field. (15 refs.)

61231 Self-compensating optical frequency conversion. R.B.Weisman (Dept. of Chem., Rice Univ., Houston, TX, USA). *Rev. Sci. Instrum. (USA)*, vol.54, no.4, p.502-3 (April 1983). A novel optical configuration is described for use with angle-tuned nonlinear frequency conversion crystals. By double passing the beams through the crystal, the new method suppresses wavelength-dependent beam displacements more thoroughly and conveniently than previous approaches. This configuration is useful in automatic phase-matching systems and experiments requiring overlapped beams. (5 refs.)

61232 Present prospects for continuous coherent ultraviolet sources. B.Couillaud, A.Ducasse (Centre de Phys. Moléculaire Optique et Hertzienne, Univ. de Bordeaux-I, Talence, France). *Rev. Cethedex (France)*, vol.19, no.NS82-2, p.33-55 (1982). In French. Presents a brief and incomplete review of the progress that has been made in the generation of highly monochromatic ultraviolet radiation, as well as a review of the different experiments that have been performed in this frequency domain. The methods of frequency doubling or mixing using nonlinear crystals located inside the laser cavity or inside an external enhancement cavity are compared and the results that have been obtained are given. Finally a new method that the authors have recently proposed, in which the crystal is located inside an injected CW laser, is described. Preliminary results are included. (30 refs.)

61233 Stimulated scattering of electromagnetic waves by a magnetized relativistic beam of oscillators. S.N.Belov, N.I.Karbushev, A.A.Rukhadze (P.N. Lebedev Phys. Inst., Acad. of Sci., Moscow, USSR). *Sov. Phys.-Tech. Phys. (USA)*, vol.27, no.9, p.1068-72 (Sept. 1982). Translation of: *Zh. Tekh. Fiz. (USSR)*, vol.52, no.9, p.1741-7 (Sept. 1982). [received: April 1983]

A theory is derived for the stimulated scattering of electromagnetic waves by a relativistic beam of oscillators. A general dispersion relation is derived and analyzed in detail for the case with cyclotron resonances. The enhancement of the scattered radiation and the starting currents for stimulated Raman and Compton scattering are derived for spatially bounded systems. The efficiency of the stimulated scattering of electromagnetic radiation under cyclotron-resonance conditions is derived from the condition for electron trapping in the field of the scattered wave and for complete modulation of the beam of oscillators. (11 refs.)

61234 Polarization four-photon spectroscopy within the absorption line: role of coherent Rayleigh scattering and of the multilevel nature of molecules. N.I.Koroteev, M.F.Ternovskaya (M.F. Lomonosov State Univ., Moscow, USSR).

Sov. J. Quantum Electron. (USA), vol.12, no.10, p.1281-6 (Oct. 1982). Translation of: *Kvantovaya Elektron. Moskva (USSR)*, vol.9, no.10, p.1967-77 (Oct. 1982). [received: April 1983]

It is shown that in order to obtain a correct interpretation of experiments on four-photon nonlinear spectroscopy within the absorption line, it is necessary to allow not only for a coherent four-photon process due to a resonant electronic nonlinearity but also for a similar process involving generation of optically induced diffraction gratings followed by the diffraction of one of the probe beams from these gratings. It is also necessary to allow for the contribution of highly excited molecular states to the resonant electronic nonlinearity. General expressions are derived and investigated for the cubic susceptibility in an isotropic medium. It is found that all nonzero components of this tensor may be expressed in terms of a single scalar function of the interacting wave frequencies. The explicit form of this function is determined in the lowest order of perturbation theory. (23 refs.)

61235 Efficient parametric sum-frequency generation by noncoherent two-photon pumping of metal vapors. A.V.Aleksandrov, S.A.Pleshanov, V.S.Solomatina (M.V. Lomonosov State Univ., Moscow, USSR). *Sov. J. Quantum Electron. (USA)*, vol.12, no.10, p.1337-9 (Oct. 1982). Translation of: *Kvantovaya Elektron. Moskva (USSR)*, vol.9, no.10, p.2060-5 (Oct. 1982). [received: April 1983]

Four-photon parametric sum-frequency generation in a randomly modulated (noncoherent) pump field was investigated, and an expression obtained for the quantum conversion efficiency. It was found experimentally that on broadening the pump line by a factor of 20-30 (lowering the spectral density by a factor of 10-20) the quantum conversion efficiency for 9.27 μ radiation in sodium vapor reached 35%, exceeding that for the case of quasimonochromatic pumping. (14 refs.)

61236 Interaction in frequency doubling of ultrashort laser pulses. L.S.Telegin, A.S.Chirkin (M.V. Lomonosov State Univ., Acad. of Sci., Moscow, USSR).

Sov. J. Quantum Electron. (USA), vol.12, no.10, p.1354-6 (Oct. 1982). Translation of: *Kvantovaya Elektron. Moskva (USSR)*, vol.9, no.10, p.2086-8 (Oct. 1982). [received: April 1983]

A study of the multiplication of the frequency of picosecond pulses revealed a shift of the central frequency of the second harmonic spectrum dependent on the intensity of the fundamental-frequency radiation. It was found that the effect was associated with the cubic nonlinearity of the medium. A theory of

second harmonic generation was developed in the constant intensity approximation allowing for the quadratic and cubic nonlinearities. (11 refs.)

61237 Stimulated Raman scattering in optical fibers. Y.Ohmori, Y.Sasaki, T.Edahiro (Ibaraki Electrical Communication Lab., NTT, Ibaraki, Japan).

Trans. Inst. Electron. & Commun. Eng. Jpn. Sect. E (Japan), vol.E66, no.2, p.146-52 (Feb. 1983).

Stimulated Raman scattering is investigated in optical fibers, pumped by a mode-locked and Q-switched Nd:YAG laser or a CW Nd:YAG laser. The critical powers for the first five Stokes, at which each Stokes begins to build up, decreased with an increase in the length of fiber and became constant values above 200 meter long in the case of a mode-locked and Q-switched pump. The first and the second Stokes were observed with 0.6 W and 2.1 W of CW pump power input, respectively, in a 35 km single-span fiber. Experiments showed that the pulse wave separation effect played an important role in stimulated Raman scattering characteristics of optical fibers. (13 refs.)

A tunable, single frequency UV source for high resolution spectroscopy in the 293-330 nm range See Entry 59855

Measurement of relative effective Raman scattering cross sections for hydrogen, oxygen, and water molecules under ultraviolet excitation See Entry 60731

Wavelength dependence of Raman scattering cross sections from 200-600 nm See Entry 60732

Temperature dependence of the Raman linewidth in H₂* See Entry 60733

Double infrared-third-harmonic-generation resonance as a method for investigating vibrational energy exchange See Entry 61021

Parametric conversion of electromagnetic waves in a relativistic electron beam moving in a cylindrical waveguide See Entry 61061

Efficiency of a stimulated Raman scattering laser using a medium with population inversion See Entry 61137

Intense free electron laser harmonic generation in a longitudinal magnetic wiggler See Entry 61165

Nonlinear analysis of free-electron-laser amplifiers with axial fields See Entry 61167

Aperture combined Raman laser See Entry 61195

Continuous-wave YAG:Nd³⁺ laser with mode locking and intracavity frequency doubling See Entry 61200

Anti-Stokes Raman scattering of excimer and tunable UV lasers in chemically pumped CO See Entry 61217

Four wave mixing due to the optical Kerr effect and Rayleigh-wing scattering See Entry 61239

Effect of the laser breakdown of a glass stimulated-Brillouin-scattering mirror on its phase-conjugation properties See Entry 61244

Designing optical fibers for frequency conversion and optical amplification by stimulated Raman scattering and phase-matched four-photon mixing See Entry 61283

Stimulated Brillouin scattering in a monomode optical fiber See Entry 61284

Fluctuations anisotropy arising from velocity or temperature gradients See Entry 61569

42.65F Phase conjugation

61238 Efficient phase conjugation by Brillouin enhanced four wave mixing. A.M.Scott (Royal Signals & Radar Estab., Great Malvern, England).

Opt. Commun. (Netherlands), vol.45, no.2, p.127-32 (15 March 1983). It is shown that frequency detuning and phase mismatch effects can strongly affect the reflection coefficient of Brillouin enhanced four-wave mixing. Extremely large reflectivities ($R > 10^6$) can be obtained if the intensities and frequency of the pump beams and the length of the interaction region all take on certain critical values. This theory accounts for the high reflectivity which has been reported by another author. (7 refs.)

61239 Four wave mixing due to the optical Kerr effect and Rayleigh-wing scattering. A.M.Scott (Royal Signals & Radar Estab., Malvern, England).

Opt. Commun. (Netherlands), vol.45, no.3, p.207-11 (1 April 1983). The nearly degenerate four-wave mixing process is considered when the interaction arises through the Kerr nonlinearity and Rayleigh-wing scattering. It is found that the reflection coefficient depends on the product of the pump field strengths, and that it progressively becomes smaller as the signal beam is detuned from the pump beam. This is in contrast with the electrostrictive case (i.e. the Brillouin type of interaction) where the reflectivity may become large at certain frequency detunings, and may depend on the ratio of the two pump fields, and the phase mismatch. (9 refs.)

61240 Phase conjugation with phenomenological pump depletion. N.C.Kothari, M.Yoshizawa, T.Kobayashi (Dept. of Phys., Univ. of Tokyo, Tokyo, Japan).

Opt. Commun. (Netherlands), vol.45, no.3, p.211-14 (1 April 1983). The authors introduce phenomenological depletion terms of the pump beams in the phase conjugate coupled equations of Yariv and Pepper (see Optics Lett., vol.1, p.16, 1977), and obtain the modified expressions for conjugate reflectivity and probe transmissivity. The results are compared with the experiments of Bloom et al. and it is shown that under their experimental conditions the authors' theoretical expressions give reasonably good matching. (12 refs.)

61241 Improvement of phase-conjugate beam fidelity in degenerate four-wave mixing by focused probe fields. E.Bochove (Telecommunicacoes Brasileiras S/A, Campinas, Sao Paulo, Brazil).

Opt. Lett. (USA), vol.8, no.4, p.202-4 (April 1983). It is shown that signal-beam fidelity in degenerate four-wave mixing, which is affected by the finite beam widths of the pump beams, may be largely restored over a wide range of spatial frequencies. The technique consists of focusing the probe beam into the mixing cell. This permits restoration of up to about 90% of the principal distortion effect. (6 refs.)

61242 Forced Rayleigh scattering: thermal and acoustic effects in phase-conjugate wave-front generation. R.C.Desai, M.D.Levenson, J.A.Barker (IBM Res. Labs., San Jose, CA, USA).

Phys. Rev. A (USA), vol.27, no.4, p.1968-76 (April 1983). The authors present and discuss a theory for hydrodynamic effects in forced-Rayleigh-scattering experiments. The efficiency of phase-conjugate wave-front generation by forced Rayleigh scattering varies significantly with the nature of the solvent and the scattering angle. Acoustic effects become important for small scattering angles and times shorter than 0.5 ns under which conditions the simple thermal-diffusion theory fails. The phase-conjugate reflection efficiency predicted by the authors' theory at short times

is much smaller than that predicted by the thermal-diffusion theory, and thus need not obscure other quantum electronic processes. (18 refs.)

61243 Four-wave interaction of low-power CO₂ laser radiation in SF₆. N.K.Berger, I.A.Deryugin, V.V.Novokhatskii (Polytech. Inst., Khabarovsk, USSR).

Sov. J. Quantum Electron. (USA), vol.12, no.10, p.1359-60 (Oct. 1982). Translation of: *Kvantovaya Elektron., Moskva (USSR)*, vol.9, no.10, p.2091-2 (Oct. 1982). [received: April 1983]

A four-wave interaction of CO₂ laser radiation was studied. The pump wave power was 3-5 W and the signal wave power was 0.5-0.8 W. The nonlinear medium was gaseous SF₆. The pressure dependence of the reflection coefficient was determined (a maximum was of the order of 0.1%). The influence of heating of SF₆ by CO₂ laser radiation was considered. (7 refs.)

61244 Effect of the laser breakdown of a glass stimulated-Brillouin-scattering mirror on its phase-conjugation properties. P.I.Bal'kyavichyus, A.S.Dement'ev, I.P.Lukoshyus, E.K.Malutis, V.P.Tarulis (Inst. of Phys., Acad. of Sci., Vilnius, Lithuanian SSR).

Sov. Tech. Phys. Lett. (USA), vol.8, no.7, p.353-4 (July 1982). Translation of: *Pis'ma v Zh. Tekh. Fiz. (USSR)*, vol.8, no.13-14, p.816-19 (July 1982). [received: April 1983]

Most experimental studies of phase conjugation (or 'wavefront inversion') during stimulated Brillouin scattering use lightguides filled with liquids (usually carbon disulfide) or compressed gases. For several applications, however, there is interest in the phase conjugation which occurs in the stimulated Brillouin scattering of focused beams in solid media, of which the most important for laser systems are optical glasses. Because of the high threshold intensities for stimulated Brillouin scattering of focused beams, the phase conjugation is frequently accompanied by simultaneous self-focusing and laser breakdown of the medium. It is thus important to study the efficiency and quality of the phase conjugation under various focusing conditions and at various pump intensities, close to the threshold intensities for the breakdown of solids. In the present experiments the authors studied the effect of damage in K-8 glass and in KSG quartz glass on the efficiency of subsequent stimulated Brillouin scattering and phase conjugation. They used the second harmonic ($\lambda = 0.53 \mu\text{m}$) of a neodymium-glass laser. (10 refs.)

A Fabry-Perot etalon with one phase-conjugate mirror See Entry 59835

Laser oscillator using resonator with self-pumped phase-conjugate mirror See Entry 61183

42.65G Photon echoes, self-induced transparency, optical saturation and related effects

61245 Optical multiple pulse sequences for multiphoton selective excitation and enhancement of forbidden transitions. W.S.Warren (Dept. of Chem., Princeton Univ., Princeton, NJ, USA), A.H.Zewail.

J. Chem. Phys. (USA), vol.78, no.6, pt.2, p.3583-92 (15 March 1983).

In this paper the authors present novel and simple pulse sequences for enhancing the intensity of forbidden or highly nonresonant optical transitions. These sequences provide a straightforward approach to circumventing the most serious limitation of optical coherent transient spectroscopy. Available laser intensities are often insufficient to excite a significant fraction of the ground state population into desired excited states, either because of large inhomogeneous broadening or, in the case of multiphoton absorption, large anharmonicities. Optical phase modulation (which can be produced by an acousto-optic modulator) or amplitude modulation (which can be produced by an interferometer) with carefully chosen pulse flip angles and delays can effectively remove even very large energy mismatches, thus permitting essentially complete population inversions arbitrarily far from resonance. Coherent averaging theory and computer calculations are used to derive particularly valuable sequences. Pumping enhancement of 10^3 - 10^5 (depending on individual molecular parameters) for these modulated pulse sequences are predicted. Specific applications to multiphoton pumping of local vibrational modes are discussed. (30 refs.)

61246 Narrow optical hole burning and related effects in ruby. T.Endo, T.Muramoto, T.Hashi (Dept. of Phys., Kyoto Univ., Kyoto, Japan).

Opt. Commun. (Netherlands), vol.45, no.2, p.122-6 (15 March 1983).

The authors observed a narrow optical hole burning in ruby whose width (FWHM = 107 kHz) is the narrowest of those reported so far in solids. The steady state, 'transient hole' was used as the basis for theoretical analysis of the hole burning, and the first observation of optical wiggles and the detection of superhyperfine structures near zero frequency are reported as two new effects related to the narrow optical hole burning. (8 refs.)

Nonlinear analysis of free-electron-laser amplifiers with axial fields See Entry 61167

Frequency reproducibility of ring He-He/CH₄ lasers See Entry 61212

42.65J Beam trapping, self focusing, thermal blooming, and related effects

61247 Thermal defocusing and transformation of the statistics of a spatially noncoherent light beam. V.A.Aleshkevich, S.S.Lebedev, A.N.Matveev (M.V. Lomonosov State Univ., Moscow, USSR).

Sov. J. Quantum Electron. (USA), vol.12, no.10, p.1340-2 (Oct. 1982). Translation of: *Kvantovaya Elektron., Moskva (USSR)*, vol.9, no.10, p.2066-70 (Oct. 1982). [received: April 1983]

The Monte Carlo method is used to consider the problem of thermal self-interaction of a multimode light beam. A study is made of the transformation of the statistics of the distributions of the intensity and phase of the radiation, and also of the behavior of the average width and of the spatial coherence radius. It is shown that at distances of the order of the nonlinear thermal self-interaction length of coherent radiation a multimode beam splits into filaments and this results in deterioration of its spatial coherent and in a considerable change in the statistics of the radiation. (7 refs.)

Four wave mixing due to the optical Kerr effect and Rayleigh-wing scattering See Entry 61239

Faraday and Cotton-Mouton effects in gases in the presence of a strong light field See Entry 61602

42.70 OPTICAL MATERIALS

Measurement of weak laser light absorption in materials transparent to infrared radiation See Entry 59862

Plasma polymerized films for optical recording See Entry 61092

Hydration and dehydration of the surface of fused silica See Entry 62275

- Internal stresses in thin Ge, ZnS, and ZnSe films See Entry 62303
 Transparent conductors—a status review See Entry 63078
 Increased-strength black chromium coatings See Entry 63183
 Composition, optical properties and degradation modes of Cu/(graded metal-carbon) solar selective surfaces See Entry 63728
 Optimization and microstructural analysis of cobalt-sulfide-pigmented aluminum oxide See Entry 63729

42.70C Glass

- 61248 Optical homogeneity of oxygen-free chalcogenide glasses. V.I.Voskresenskaya, V.S.Mozhaiskaya, G.V.Shkal'kova. *Sov. J. Opt. Technol. (USA)*, vol.49, no.8, p.502-5 (Aug. 1982). Translation of: *Opt.-Mekh. Prom.-st. (USSR)*, vol.49, no.8, p.30-2 (Aug. 1982). [received: April 1983]
 The results of an analysis of the physical inhomogeneities in commercially manufactured 50-80-mm diameter chalcogenide glasses are presented. The effect of the annealing parameters on optical homogeneity is examined. (5 refs.)
 61249 Bending strength of F102 and NS9 optical glasses. A.V.Matveev, V.A.Karpov. *Sov. J. Opt. Technol. (USA)*, vol.49, no.8, p.532-4 (Aug. 1982). Translation of: *Opt.-Mekh. Prom.-st. (USSR)*, vol.49, no.8, p.60-2 (Aug. 1982). [received: April 1983]
 The results of tests on the strength of F102 and NS9 optical glasses by the central symmetrical bending method are presented. (4 refs.)
 The sol-gel method for optical fiber fabrication See Entry 61307
 Formation and relaxation kinetics of mechanical stress in a glass surface layer during ion bombardment See Entry 62000
 Investigation of the influence of water on the surface conductivity of optical glass See Entry 62479
 IR reflection investigation of corrosion of optical glasses See Entry 63005

42.70G Light-sensitive materials

- 61250 Evaluation of mechanical and physical properties of films under dynamical loading. S.G.Mestkovsky. *Tekh. Kino & Telev. (USSR)*, no.3, p.12-15 (March 1983). In Russian. Describes a technique and a stand for determining the mechanical and physical properties of motion picture films. The elastic modulus values of films characterising resistance of the material under dynamic loads are specified. (9 refs.)

42.72 OPTICAL SOURCES AND STANDARDS

(for spectroscopic light sources, see also 07.65)

- 61251 Emission of high-current tubular xenon flashlamps in the ultraviolet. V.E.Gavrilov, O.B.Danilov, A.P.Zhevlakov, S.A.Tul'skii. *Sov. J. Opt. Technol. (USA)*, vol.49, no.7, p.403-6 (July 1982). Translation of: *Opt.-Mekh. Prom.-st. (USSR)*, vol.49, no.7, p.3-6 (July 1982). [received: April 1983]
 The luminance and emission efficiency in the 250-290 nm spectral region and the load characteristics of high-current xenon flashlamps for a discharge duration of less than 50 μ m sec are investigated. It is shown that the luminance temperature is 17000-25000K in this spectral interval, and the emission efficiency amounts to 5-11%. (13 refs.)
 A tunable, single frequency UV source for high resolution spectroscopy in the 293-330 nm range See Entry 59855
 Electronic photo-flash with photoelectric release See Entry 59868
 Generation of femtosecond intense optical pulses and applications to time resolved spectroscopy See Entry 61199
 Present prospects for continuous coherent ultraviolet sources See Entry 61232
 Illuminator for IAB-451 schlieren instrument to implement the four-slit color method See Entry 61261

42.78 OPTICAL LENS AND MIRROR SYSTEMS

(for microscopes, see 07.60P; for photographic instruments, see 07.68; for astronomical telescopes, see 95.55)

- 61252 Effect of conicoid asphericity on the Tscherning ellipses of ophthalmic spectacle lenses. G.Smith, D.A.Aitchison (Dept. of Optometry, Univ. of Melbourne, Parkville, Victoria, Australia). *J. Opt. Soc. Am. (USA)*, vol.73, no.4, p.441-5 (April 1983).
 One of the criteria in ophthalmic spectacle lens design is the elimination of oblique astigmatism. For a range of equivalent powers, Seidel (primary or third-order) astigmatism can be eliminated, and the solutions of back- (or front-) surface power are commonly displayed graphically in the form of ellipses (Tscherning ellipses). The Tscherning ellipses apply only to lenses constructed from spherical surfaces. If one or both surfaces are made aspheric, the solutions for zero astigmatism are no longer in the form of ellipses. If one surface, usually the front surface, is made as a conicoid aspheric, the solutions for zero astigmatism can be presented graphically similarly to the Tscherning ellipses. For any given equivalent power, there are two or no solutions for spherical lenses. However, there is always one and up to three solutions for conicoid aspheric lenses. (12 refs.)
 61253 Luneburg lens: unitary invariance and point characteristic. H.A.Buchdahl (Dept. of Theoretical Phys., Faculty of Sci., Australian Nat. Univ., Canberra, Australia). *J. Opt. Soc. Am. (USA)*, vol.73, no.4, p.490-4 (April 1983).
 The Hamiltonian of the Luneburg lens K is invariant not merely under rotations but under a wider group of unitary transformations. This has two immediate consequences: First, by inspection one can write down ray integrals sufficient in number to describe fully the shapes and deposition of rays; second, K is one of the rare, nontrivial systems for which the point characteristic can be exhibited in closed, nonparametric form. This paper sets out in detail what has just been described in outline. (9 refs.)
 61254 Second-stage concentrators—a new formalism. E.M.Kritchman (Dept. of Phys., Univ. of Chicago, Chicago, IL, USA). *J. Opt. Soc. Am. (USA)*, vol.73, no.4, p.508-11 (April 1983).
 The concept of second-stage nonimaging concentrators is redefined. A model of an incoherent source of limited emitting angle serves to simulate the input rays to these elements. Hence the second stages may be classified as a sub-

group of ideal concentrators that collect all the radiation emitted by such sources and concentrate it up to the maximum achievable limit. As a consequence of this discussion, it becomes obvious that, for any given plane behind a primary, an ideal second stage can be designed with its entrance aperture located on that plane. Implications for the design of ideal reflectors with shielding windows are discussed. (18 refs.)

- 61255 Rectangular Luneburg-type lenses for integrated optics. E.Van Wood, J.R.Busch (Columbus Labs., Battelle Memorial Inst., Columbus, OH, USA), D.T.Moore, C.B.Wooley, W.H.Southwell. *Opt. Lett. (USA)*, vol.8, no.4, p.226-8 (April 1983).
 Compact Luneburg-type lenses of rectangular outline as viewed from above have been made by thermal evaporation of As_2S_3 glass onto single-mode $LiNbO_3:Ti$ waveguides through suitably shaped masks and subsequent exposure of the glass to ultraviolet light. The best lenses had speeds of $f/5.5$ at an aperture of 10 mm and focal spots at reduced aperture about 1.2 times the diffraction-limited size. These lenses have a field of view of at least 25° inside the waveguide. (5 refs.)
 61256 General principles for compiling computer archives of optical systems to be used as reference designs. I.M.Mal'tsev. *Sov. J. Opt. Technol. (USA)*, vol.49, no.7, p.431-3 (July 1982). Translation of: *Opt.-Mekh. Prom.-st. (USSR)*, vol.49, no.7, p.28-30 (July 1982). [received: April 1983]
 A general approach to the development of a computer archive of optical systems to be used as reference designs, which is included in a dialog system based on the BESM-6 computer, is described. The classification of the archive optical systems in terms of their functional purpose and special attributes is presented as a special case of possible classifications. An example of the interaction procedure between optical designer and computer archive is discussed. (4 refs.)
 Absolute spectral reflectance of mirrors See Entry 59829
 A Fabry-Perot etalon with one phase-conjugate mirror See Entry 59835
 Modulation transfer functions of a lens-array photographic system See Entry 61101
 Method of analyzing wave aberration of a two-component holographic objective See Entry 61107
 Synthesis of optical elements giving a focal line of arbitrary shape See Entry 61118
 Effect of the laser breakdown of a glass stimulated-Brillouin-scattering mirror on its phase-conjugation properties See Entry 61244
 On centering of lenses during cementing See Entry 61309
 Micro Fresnel lenses blazed by electron beam lithography See Entry 61315
 Method for focusing and clamping objective lens See Entry 61317
 Planar solar reflectors See Entry 63726
 Construction, specification, and mathematical description of aspheric surfaces See Entry 63917

42.78H Coatings

- 61257 Metallic multilayers: new possibilities in X-UV optics. P.Dhez (LURE, Univ. Paris Sud, Orsay, France). *Adv. Space Res. (GB)*, vol.2, no.4, p.199-206 (1982). (Proceedings of Symposium 4 of the COSPAR Twenty-Fourth Plenary Meeting, Ottawa, Canada, 16 May-2 June 1982).
 Reflectivities measured on metallic multilayers obtained by evaporation methods have demonstrated the validity of theoretical predictions. Experimental tests using wavelengths from 1.54 Å to several hundred of angstroms give a firm basis for proposed new designs for X-UV optics. This new kind of Bragg reflector can be tailored for any wavelength and any incidence angle, because the period of evaporation of the layered synthetic medium can be freely chosen. Such artificial Bragg reflectors are more efficient than natural, organic or molecular crystals which have been employed until now in the X-UV, and can overcome the weak luminosity and astigmatism problems encountered in grazing incidence optics. The possibility of evaporating multilayers on shaped substrates will lead to optics with focusing and selectivity functions given by a single reflection. (29 refs.)
 Analysis of operation of double-beam photometer for monitoring the thickness of thin films See Entry 59827
 Solid-state laser having a reflector that transmits IR and UV radiation See Entry 61189
 Recent developments in ultraviolet filters and coatings See Entry 61262

42.80 OPTICAL DEVICES, TECHNIQUES AND APPLICATIONS

(for optical instruments and techniques, see 07.60; for optical spectroscopy, see 07.65; for photography, see 07.68; for holography, see 42.40; for lasers, see 42.55 and 42.60; for masers, see 42.52)

- 61258 A tunable 90° rotator using a total reflection by a monodomain cholesteric liquid crystal cell. H.Takezoe, Y.Ouchi, M.Hara, A.Fukuda, E.Kuze (Dept. of Textile & Polymeric Materials, Tokyo Inst. of Technol., Tokyo, Japan). *Jpn. J. Appl. Phys. Part 2 (Japan)*, vol.22, no.3, p.L185-7 (March 1983).
 A tunable 90° rotator using a cholesteric liquid crystal cell is presented. The idea is based on a unique optical feature of cholesterics, a total reflection. In the total reflection region, linearly polarised incident light is totally reflected and the incident polarisation is rotated by about 70° . In other words, 80% of the incident light intensity can be converted to the perpendicular component to the incident polarisation over a relatively wide spectral range, 485 nm-670 nm. The cell of another tuning range is also easily obtained by choosing the helical pitch of cholesterics. (4 refs.)
 61259 Analysis of effect of fabrication errors of a scanning four-component prism on the ray paths in it. Yu.A.Gogolev, I.I.Druz'. *Sov. J. Opt. Technol. (USA)*, vol.49, no.7, p.428-30 (July 1982). Translation of: *Opt.-Mekh. Prom.-st. (USSR)*, vol.49, no.7, p.26-8 (July 1982). [received: April 1983]
 The allowable fabrication errors of a scanning four-component prism are analyzed. Special selection of the right-angle prisms, comprising the four-component prism, is proposed in order to broaden the tolerances on its fabrication. (4 refs.)

- 61260 Increased-accuracy triaxial autocollimator.** I.A.Konyakin, E.D.Pankov.
Sov. J. Opt. Technol. (USA), vol.49, no.8, p.514-15 (Aug. 1982). Translation of: *Opt.-Mekh. Prom.-st. (USSR)*, vol.49, no.8, p.41-3 (Aug. 1982). [received: April 1983]
The operating principle and metrological capabilities of triaxial autocollimator, built on the basis of the AK-0.25 instrument, are examined. (5 refs.)
- 61261 Illuminator for IAB-451 schlieren instrument to implement the four-slit color method.** T.N.Besmenova, V.Ya.Bruckman, V.B.Dmitrieva, V.A.Novikov, V.A.Yakovlev.
Sov. J. Opt. Technol. (USA), vol.49, no.8, p.531-2 (Aug. 1982). Translation of: *Opt.-Mekh. Prom.-st. (USSR)*, vol.49, no.8, p.59-60 (Aug. 1982). [received: April 1983]
An attachment to the IAB-451 schlieren instrument has been developed in which one light source and lightguides are used to illuminate the four slits of the illuminator diaphragm. (2 refs.)
- Computerized evaluation of schlieren images [temperature field reconstruction]** See Entry 59775
- Measuring thin film parameters by inputting light through a prism** See Entry 59821
- Temperature control of an acousto-optic modulator in an Argon ion laser using an R.F. servo loop** See Entry 61202
- Thermooptic-conversion method for detecting the spatial mode structure of a TEA CO₂ laser beam** See Entry 61215
- Laser alignment techniques** See Entry 61218
- Design of a new thin-film electro-optic switch** See Entry 61304

42.80B Spatial filters, zone plates

- A two-dimensional diffraction pattern sampling system for determining the optimum parameters of a matched spatial filter** See Entry 61099
- Beam-profile measurement of laser pulses using a spatial filter to sample the hermite modes for a string of pulses** See Entry 61216
- A posteriori spatial filtering of a short-exposure image distorted by the atmosphere** See Entry 64398

42.80C Spectral and other filters

- 61262 Recent developments in ultraviolet filters and coatings.** B.K.Flnt (Acton Res. Corp., Acton, MA, USA).
Adv. Space Res. (GB), vol.2, no.4, p.135-42 (1982). (Proceedings of Symposium 4 of the COSPAR Twenty-Fourth Plenary Meeting, Ottawa, Canada, 16 May-2 June 1982).
A number of new high efficiency optical coatings have recently been developed at wavelengths in the ultraviolet and vacuum ultraviolet for use in space science experiments. The development of these coatings has resulted in the design and manufacture of wavelength selective filters used in reflectance at near normal incidence that have high VUV reflectance with little near-UV and visible reflectance. Material limitations, more severe than those in the visible, place certain restrictions on the size, wavelength, and degree of selectivity that is achievable with present technology. A summary of the current commercial technology along with the material limitations is presented. (6 refs.)
- Investigation of the possibility of using an optical matching filter to test the geometry of parts in precision instrument manufacturing** See Entry 61310
- Photinduced spectral change in the rotation of the plane of polarization of light in FeBO₃** See Entry 62951
- Measurement of factors affecting VDU readability** See Entry 63855

42.80D Monochromators

- 61263 Simplified method for calculating the parameters of a symmetric monochromator with a concave holographic diffraction grating.** I.V.Peiskhson, N.G.Romanova, N.Yu.Chernyak.
Opt. & Spectrosc. (USA), vol.53, no.2, p.219-20 (Aug. 1982). Translation of: *Opt. & Spektrosk. (USSR)*, vol.53, no.2, p.369-73 (Aug. 1982). [received: April 1983]
A method is proposed that can be used to calculate the parameters of the optical scheme of a symmetric monochromator with a concave spherical holographic grating and the recording conditions that ensure minimal defocusing when scanning the spectrum, with a simultaneous correction of astigmatism and coma for the mean wavelength of the operating range. The calculations involved in this method do not require complicated calculations and can be carried out with the help of desk-type minicomputers (a DZ-28 type, for example). (3 refs.)

42.80E Shutters, windows, diaphragms, deflectors, choppers

- Orientation of an arbitrary ray, passing through a two-wedge compensator** See Entry 61081
- Use of a holographic diffraction grating for deflecting a laser beam** See Entry 61108

42.80F Gratings, echelles

- 61264 Secondary structures formed during the inscribing of diffractive three-dimensional phase gratings.** V.B.Konstantinov, Yu.F.Romanov, A.F.Rykhlov, A.Yu.Tropechenko (A.F. Ioffe Physicotech. Inst., Acad. of Sci., Leningrad, USSR).
Sov. Phys.-Tech. Phys. (USA), vol.27, no.9, p.1134-6 (Sept. 1982). Translation of: *Zh. Tekh. Fiz. (USSR)*, vol.52, no.9, p.1849-53 (Sept. 1982). [received: April 1983]
The secondary structures which arise during the holographic inscribing of three-dimensional phase gratings are examined. These structures result from the reflection of light from the boundaries of the photographic plate. Their relation to the secondary diffracted waves observed during reconstruction is discussed. It is found that the experimental ratio of the diffraction efficiencies of the secondary structures agrees with the theoretical predictions. (5 refs.)

- Possibilities of increasing the resolution of diffraction spectrographs** See Entry 59857
- Rigorous coupled-wave analysis of grating diffraction—E-mode polarization and losses** See Entry 61072
- Generalized curvilinear diffraction gratings. III. Euclidian diffraction gratings** See Entry 61073
- Generalized curvilinear diffraction gratings. IV. Plane singular crossed gratings** See Entry 61074
- Generalized curvilinear diffraction gratings. V. Diffraction catastrophes** See Entry 61075
- Diffraction efficiency of photochromic absorption gratings** See Entry 61079
- Periodic structures and the visual representation of phase objects in free space** See Entry 61097
- Conditions of stigmatism of holographic concave gratings used in normal incidence** See Entry 61103
- Method of analyzing wave aberration of a two-component holographic objective** See Entry 61107
- Use of a holographic diffraction grating for deflecting a laser beam** See Entry 61108
- Infrared-spectrophotometric investigation of the recording of an optical image on dichromated gelatin** See Entry 61109
- Light refraction in crystals with bipolar photoconductivity** See Entry 61116
- High power TEA CO₂ laser tuned by a holographic grating** See Entry 61181
- Simplified method for calculating the parameters of a symmetric monochromator with a concave holographic diffraction grating** See Entry 61263
- Mode coupling in a specifically tapered Bragg grating coupler** See Entry 61272
- Exact calculations of scattering and enhanced fields of electromagnetic waves on grating surfaces** See Entry 62977

42.80K Optical beam modulators

- 61265 Technological problems in the manufacture of acousto-optical TeO₂ modulators.** L.Jakab, T.Behringer, L.Kocsanyi.
Finomtech.-Mikrotech. (Hungary), vol.22, no.2, p.47-50 (Feb. 1983). In Hungarian.
Deals with the production of a small series of acousto-optical TeO₂ modulators. The technology assures a 60% productivity with the advantage of using domestic raw materials. The devices may be applied to light-modulation purposes and their parameters are such as to allow exports to foreign countries as well. (6 refs.)
- 61266 Use of ferrite-garnet films as magneto-optic modulators.** I.L.Berezin, Yu.M.Golubovskii, V.L.Ivashintsova, L.N.Pivovarova.
Sov. J. Opt. Technol. (USA), vol.49, no.7, p.448-50 (July 1982). Translation of: *Opt.-Mekh. Prom.-st. (USSR)*, vol.49, no.7, p.45-7 (July 1982). [received: April 1983]
This paper presents the results of a test of ferrite-garnet film modulators that are capable of oscillating the polarization plane of the transmitted radiation. The possibility of building a small modulator having a power consumption of less than 1 VA is shown. (3 refs.)
- Contributions of amplitude and phase modulation to diffraction efficiency in three-dimensional reflective holograms** See Entry 61115
- A miniature modulator** See Entry 61198
- Temperature control of an acousto-optic modulator in an Argon ion laser using an R.F. servo loop** See Entry 61202
- Mode coupling in a specifically tapered Bragg grating coupler** See Entry 61272
- Thin-film Ge-As₂S₃ waveguide with diffractive input coupling of a CO₂ laser beam** See Entry 61279

42.80L Optical waveguides

(for fibre optical waveguides, see 42.80M)

- 61267 Nonlinear effects in TIPE-LiNbO₃ waveguides for optical communications.** M.De Micheli (Univ. de Nice, Nice, France).
J. Opt. Commun. (Germany), vol.4, no.1, p.25-31 (March 1983).
A new fabrication process of waveguides in LiNbO₃, Titanium Indiffusion Proton Exchange (TIPE) is reported, and the waveguides are characterized. Their nonlinear possibilities are studied and compared to existing systems, and some prospective applications are given. (12 refs.)
- 61268 Loss reduction in curved dielectric optical slab waveguide.** M.Geshire, S.Sawa (Dept. Electronics Engng., Ehime Univ., Ehime, Japan).
Electron. Lett. (GB), vol.19, no.9, p.321-3 (28 April 1983).
Formulas of the pure bending loss and the transition loss valid for TM modes in dielectric optical slab waveguides are presented. The characteristic of the total transmission loss of a step-index slab waveguide containing a circular bend having an asymmetric waveguide structure are analysed numerically by applying derived loss formulas. It is found that the features of the total transmission loss of TM modes are closely analogous to those of TE modes except for small discrepancies in the numerical values. (3 refs.)
- 61269 Waveguide loss evaluation by the ray-optics method.** M.Miyagi, S.Kawakami (Res. Inst. of Electrical Communication, Tohoku Univ., Sendai, Japan).
J. Opt. Soc. Am. (USA), vol.73, no.4, p.486-9 (April 1983).
Attenuation constants of bound or leaky modes in a general class of straight planar waveguides evaluated by the ray-optics method are analytically shown to be identical in the first-order of approximation with those obtained from the characteristic equation when one takes the Goos-Hanchen shift into account. It is also pointed out that significant errors will result if the Goos-Hanchen shift is ignored. (6 refs.)
- 61270 Optical mode conversions in Nd substituted iron garnet films.** N.Koshizuka, T.Okuda, Y.Yokoyama, K.Ando (Electrotech. Lab., Ibaraki, Japan).
J. Magn. & Magn. Mater. (Netherlands), vol.35, no.1-3, p.167-9 (March 1983). (Proceedings of the 10th International Colloquium on Magnetic Films and Surfaces, Yokohama, Japan, 13-16 Sept. 1982).
Magneto-optical TE-TM mode conversion was studied in LPE grown (YNd)₃Fe₅O₁₂ films as functions of growth temperature and film thickness. High conversion efficiency (~80%) was found for the film in the in-plane field higher than 3 Oe. The phase matching was explained by the small stress induced birefringence (1×10⁻³). (8 refs.)

61271 Single-mode anisotropic cylindrical dielectric waveguides. R.F.Alvarez-Estrada, M.L.Calvo (Facultad de Ciencias Fisicas, Univ. Complutense, Madrid, Spain).

Opt. Acta (GB), vol.30, no.4, p.481-503 (April 1983).

The authors study anisotropic cylindrical dielectric waveguides under the following conditions: (1) their cross section Ω has arbitrary shape; (2) the dielectric permittivity tensor ϵ has discontinuities at the boundaries, as well as a graded spatial variation; (3) Ω is small, and ϵ minus the unit 3×3 matrix (I) is small and smooth, so that only one pair of propagation modes is allowed. A general and exact dispersion relation for the propagation modes is derived, using integral equation techniques and the long wavelength singularity of the free-space Green's function in two dimensions. The authors present approximate explicit solutions of the dispersion relation to first order in $(\epsilon-I)$, which exhibit a logarithmic dependence and birefringence in general. Some numerical estimates are also given. Approximate dispersion relations up to and including second order in $(\epsilon-I)$ are also discussed. The scattering problem is treated briefly. (17 refs.)

61272 Mode coupling in a specifically tapered Bragg grating coupler. M.Hofman, J.Nezval (Inst. of Radio Engng. & Electronics, Czechoslovak Acad. of Sci., Praha, Czechoslovakia).

Opt. Commun. (Netherlands), vol.45, no.3, p.143-4 (1 April 1983).

Analytic expressions of the coupling process between a guided surface wave and a backward travelling diffraction order are derived by means of coupled wave theory for specifically tapered Bragg grating couplers. Numerical results are presented for a linear taper. (7 refs.)

61273 Gaussian approximation of the waveguide EH_{11} mode pattern in the far field. P.Belland, J.P.Crenn (Dept. de Recherches sur la Fusion Controlee, CEN, Fontenay-aux-Roses, France).

Opt. Commun. (Netherlands), vol.45, no.3, p.165-70 (1 April 1983).

The calculation of the far-field intensity pattern of the EH_{11} mode launched from a hollow dielectric circular waveguide is carried out as a particular case of the Gaussian beam diffraction by a circular aperture. The result derived by using a Gaussian approximation agrees very well with that computed from Fresnel diffraction theory and with experimental values obtained from the study of the beam launched from EH_{11} single mode waveguide lasers. (22 refs.)

61274 Coupling of optical fibres: a simple but precise technique.

Rev. Polytech. (Switzerland), no.12, p.1603 (Dec. 1982). In French. Describes a plug-and-socket method of joining optical fibres developed by Philips. The connection is thus simply made and with minimum loss. The connector is manufactured using a small optically-controlled turret concentric to the core of the fibre. (no refs.) L.A.F.

61275 Extending the working temperature range of high-aperture light guides. I.V.Aleksandrov, S.Ya.Fel'd, O.E.Shushpanov (Inst. of Radio Engng. & Electronics, Acad. of Sci., Moscow, USSR).

Sov. Phys.-Tech. Phys. (USA), vol.27, no.9, p.1140-3 (Sept. 1982). Translation of: *Zh. Tekh. Fiz. (USSR)*, vol.52, no.9, p.1859-64 (Sept. 1982). [received: April 1983]

It is shown on the basis of existing experimental data that the increase in the refractive index of the light-reflecting cladding of a light guide of the glass-polymer type upon cooling is due to an increase in the density of the polymer. The range of working temperatures of the light guide can be widened by introducing an additional outside covering to decrease the change in the density of the light-reflecting polymer cladding by restricting its deformation. The deformation of the light-reflecting cladding can be effectively limited if its thickness is properly chosen. Approximate formulas are given for designing such a light guide for a specified range of working temperatures. The validity of these formulas is checked by comparison with the results of exact calculations. The results of a numerical experiment are presented, which show that by choosing the design in accordance with these formulas, one can achieve the specified working range even when a relatively soft polymer is used for the outer coating, and even at small thicknesses. The requirements on the construction of a light guide having the minimum diameter for a given range of working temperatures are formulated. Such an optimization permits the diameter of the light guide to be substantially decreased, resulting in increased flexibility and service life. (9 refs.)

61276 Extraction of radiation from a planar optical waveguide by diffraction in noncollinear mode interaction with the lattice. S.S.Dremov, V.E.Strigalev, Yu.P.Udoev (Kalinin Polytech. Inst., Leningrad, USSR).

Sov. Phys.-Tech. Phys. (USA), vol.27, no.9, p.1170-2 (Sept. 1982). Translation of: *Zh. Tekh. Fiz. (USSR)*, vol.52, no.9, p.1902-4 (Sept. 1982). [received: April 1983]

Measurements were made for waveguide layers and additionally for a $Ti:LiNbO_3$ diffusion waveguide. Corrugation was produced by ion etching with a URM-3-279-036 apparatus through photoresist masks previously prepared on the waveguide by holographic means with a diffraction method of checking the etching depth of the photoresist directly during chemical etching of the exposed layer. The results indicate that the corrugation method has a marked effect on the characteristics of a noncollinear integrated-optics communication element. The data can be used in rough estimates of the necessary corrugation depth and interaction length in developing such communication elements for waveguide structured close to those examined. (3 refs.)

61277 Time-dependent theory of resonant tunnel coupling in optical waveguides. V.V.Malov, D.A.Pavlovskii, L.V.Iogansen (All-Union Correspondence Inst. for Textile & Consumer Industry, Moscow, USSR).

Sov. Phys.-Tech. Phys. (USA), vol.27, no.10, p.1182-4 (Oct. 1982). Translation of: *Zh. Tekh. Fiz. (USSR)*, vol.52, no.10, p.1922-6 (Oct. 1982). [received: April 1983]

The time-dependent theory of coupled waves is considered. Conditions are found under which the nonstationary wave-coupling theory must be used and the equations are solved explicitly for the case of two coupled waves. The time evolution of a rectangular input pulse is examined in detail. (8 refs.)

61278 Optical waveguides from epitaxial lithium niobate films. A.P.Vorono, M.B.Kosmyrna, A.P.Ostroumenko, V.P.Prudkii, E.F.Chaikovskii, A.V.Shmalko.

Sov. Tech. Phys. Lett. (USA), vol.8, no.7, p.349-50 (July 1982). Translation of: *Pis'ma v Zh. Tekh. Fiz. (USSR)*, vol.8, no.13-14, p.806-10 (July 1982). [received: April 1983]

Reports a study of planar optical waveguides made from epitaxial lithium niobate single-crystal films grown by liquid-phase epitaxy from a $Li_2O-Nb_2O_5-V_2O_5$ molten solution on lithium tantalate substrates. The waveguides have an essentially uniform index distribution. (12 refs.)

61279 Thin-film Ge-As₂S₃ waveguide with diffraction input coupling of a CO₂ laser beam. M.A.Vasil'eva, L.E.Vorobn'ev, S.N.Danilov, V.I.Stafeev, D.A.Firsov.

Sov. Tech. Phys. Lett. (USA), vol.8, no.8, p.438-9 (Aug. 1982). Translation of: *Pis'ma v Zh. Tekh. Fiz. (USSR)*, vol.8, no.15-16, p.1014-17 (Aug. 1982). [received: April 1983]

Reports a study of the waveguide properties of the modulators and the efficiency at which the beam from a CO₂ laser can be coupled in for a particular Ge-As₂S₃ structure. This structure may serve as the starting point for the development of a thin-film IR modulator made from p-Ge or from n-InSb, which has similar optical properties, but it is necessary to adhere strictly to the optimum conditions in order to maximize the efficiency. This may be achieved by coupling the light in and out through the substrate: $p_m/(p_m + p_m) = 1$. In this case an efficiency of the order of 50% can be achieved. A second approach to increasing the efficiency might be to metalize the waveguide under the gratings. It might also be possible to arrange single-mode input, which would increase η . (6 refs.)

61280 Production of 'Gradan'-type lightguide blanks on automated equipment (model UIZS-1). V.V.Grigor'yants, M.E.Zhabotinskii, G.A.Ivanov, V.N.Isakov, N.A.Koreneva, A.G.Novikov, V.V.Petyukevich, V.V.Storozhev.

Telecommun. & Radio Eng. Part 2 (USA), vol.37, no.3, p.123-6 (March 1982). Translation of: *Radiotekhnika, Moskva (USSR)*, vol.37, no.3, p.70-5 (March 1982). [received: April 1983]

Automated equipment is described for fabricating lightguide blanks by the chemical vapor-phase precipitation method. The parameters of the fiber lightguides, obtained from the blanks, are given. (8 refs.)

61281 Large-aperture lightguides with a hard outside coating. I.V.Aleksandrov, S.Ya.Fel'd, O.E.Shushpanov.

Telecommun. & Radio Eng. Part 2 (USA), vol.37, no.3, p.126-31 (March 1982). Translation of: *Radiotekhnika, Moskva (USSR)*, vol.37, no.3, p.75-80 (March 1982). [received: April 1983]

The glass-polymer type of lightguide with a hard external coating applied to the cladding is examined. It is shown that this approach can increase significantly the numerical aperture and range of operating temperatures of the lightguide. (11 refs.)

61282 The effect of the quartz support tubes on the amount of light attenuation in fiber lightguides. V.V.Grigor'yants, A.V.Zigunskeya, G.A.Ivanov, N.A.Koreneva, Yu.K.Chamorovskii, V.V.Shemet.

Telecommun. & Radio Eng. Part 2 (USA), vol.37, no.4, p.60-4 (April 1982). Translation of: *Radiotekhnika, Moskva (USSR)*, vol.37, no.4, p.25-30 (April 1982). [received: April 1983]

The effect of the quartz support tubes on the amount of light attenuation in multimode fiber lightguides is investigated. It is shown that this effect is caused by contamination of the light-conducting layers with impurities contained in the support tube and by imperfections in the fiber lightguides associated with defects of the quartz support tube. (14 refs.)

OFC '83. Sixth Topical Meeting on Optical Fiber Communication (papers in summary form only received) See Entry 59536

A fiber-optic rotation transducer See Entry 59839

Localization of a light beam in a narrow inverted zone formed as a result of chemical processes in parallel streams of reagents See Entry 61144

Joining a semiconductor laser to a planar optical waveguide See Entry 61305

LPE growth of YNd-iron garnet films for magnetooptical waveguides See Entry 63182

42.80M Fibre optics

61283 Designing optical fibers for frequency conversion and optical amplification by stimulated Raman scattering and phase-matched four-photon mixing. C.Lin (Bell Labs., Holmdel, NJ, USA).

J. Opt. Commun. (Germany), vol.4, no.1, p.2-9 (March 1983).

Discusses fiber design considerations for frequency conversion and optical amplification applications in the visible and the near infrared. Both the material parameters (Raman spectra, absorption spectra, refractive-index dispersion, etc.), and the fiber parameters (transmission loss, core diameter, dispersion properties, etc.) need to be considered for efficient conversion by stimulated Raman scattering and phase-matched stimulated four-photon mixing. The use of birefringence and schemes of group velocity matching are also discussed. (28 refs.)

61284 Stimulated Brillouin scattering in a monomode optical fiber. D.Cotter (British Telecom Res. Labs., Ipswich, England).

J. Opt. Commun. (Germany), vol.4, no.1, p.10-19 (March 1983).

Stimulated Brillouin scattering (SBS) has recently been observed in low-loss monomode fibers at power levels of only a few milliwatts. This article reviews the increasingly important influence which SBS will have on the design and operating range of future optical communications systems which employ low-loss fiber and narrowband laser transmitters. The important dependence of the SBS gain and threshold on the spectrum and modulation parameters of the optical transmitter is described. Possible techniques for suppressing SBS in optical communications systems are discussed. (38 refs.)

61285 Optical fibres: a solution looking for a problem? S.Hannington.

Electr. Times (GB), no.4693, p.8, 9, 11 (11 March 1983). Looks at the development of optical fibres during the past six years. The initial prophecy of a 'great industrial future' was followed by a market slump. However, a new range of equipment from several manufacturers has revitalised interest in optical fibre products. Available equipment is reviewed. (no refs.)

61286 Spontaneous Brillouin noise in long-distance high-bandwidth optical-fibre transmission. J.Stone, A.R.Chraplyvy (Crawford Hill Lab., Bell Labs., Holmdel, NJ, USA).

Electron. Lett. (GB), vol.19, no.8, p.275-7 (14 April 1983).

The light propagating in a single-mode optical fibre is found to be converted gradually into forward-scattered spontaneous Rayleigh-Brillouin power. The Brillouin component has a linewidth of ~500 MHz and constitutes ~1/200 of the propagating power at 1.3 μ m wavelength after 600 km. The measured backscatter-Brillouin shift coefficient is ~0.15 GHz/wt.% GeO₂. (10 refs.)

61287 Single-mode-fibre cutoff measurements using offset splice technique: excess loss effects. J.E.Chapman, D.Wu (Valtec, A. Philips-M/A-COM Venture, West Boylston, MA, USA).

Electron. Lett. (GB), vol.19, no.8, p.290-1 (14 April 1983).

The effect of excess loss mechanisms on the measurement of the LP₁₁ mode cutoff wavelength using the offset splice technique is investigated. The authors show that the measured cutoff wavelength will shift towards shorter wavelengths only if excess attenuation is present in both the emitting and receiving fibres. The shift is not observed if the excess loss is only present in one of the two fibres. (6 refs.)

- 61288 Characterisation of single-mode fibres by near-field measurement.** G. Coppa, P. Di Vita, U. Rossi (CSEL, Torino, Italy). *Electron. Lett. (GB)*, vol.19, no.8, p.293-4 (14 April 1983). A new technique for the determination of the refractive-index profile of single-mode optical fibres from a simple near-field measurement is proposed. This permits one to deduce accurately all the important parameters of the fibre. (6 refs.)
- 61289 Derivation of fundamental-mode electric field and modal properties of single-mode fibres from variable-aperture launch method.** F. Alard, P. Sansonetti (CNET LAB/MER/FOG, Lannion, France). *Electron. Lett. (GB)*, vol.19, no.9, p.313-14 (28 April 1983). Reports a simple derivation of the electric field and modal properties of the fundamental mode of single-mode optical fibres only from the results of the variable-aperture launch method performed on the fibre. (6 refs.)
- 61290 Segmented-core single-mode fibres with low loss and low dispersion.** V.A. Bhagavatula, M.S. Spatz, W.F. Love, D.B. Keck (Corning Glass Works, Res. & Dev. Div., Corning, NY, USA). *Electron. Lett. (GB)*, vol.19, no.9, p.317-18 (28 April 1983). Single-mode-fibre designs with segmented core for achieving simultaneously low loss and dispersion are described. Results showing dispersion flattening of ± 1.5 ps/km nm over a 280 nm range are presented. Such dispersion flattening is achieved while maintaining spot sizes of 4-5 μ m, which compare favourably with those for earlier designs without dispersion flattening. (11 refs.)
- 61291 Simple power spectrum of microbendings in single-mode fibres.** P. Danielson (Electromagnetics Inst., Tech. Univ. of Denmark, Lyngby, Denmark). *Electron. Lett. (GB)*, vol.19, no.9, p.318-20 (28 April 1983). A simple model is set up yielding the power spectrum of the microbendings in single-mode optical fibres. The model rests on an assumption of random short curvatures of the fibre axis. Employing the effective spot size instead of the RMS spot size the author achieved good agreement with experimental data. (4 refs.)
- 61292 Radiation from graded-index single-mode fibres.** C.D. Hussey (School of Electronic Engng., Nat. Inst. for Higher Education, Dublin, Ireland). *IEE Proc. H (GB)*, vol.130, no.3, p.225-9 (April 1983). Radiation from the fundamental mode due to sources in graded-index single-mode optical fibres can be examined by determining the effect of the presence of the perturbing core on the free-space (i.e. uniform cladding) radiation field. The author looks at this effect for fibres with power-law-profile cores. Using these examples he discusses the following two approximation schemes: (i) a new equivalent step approximation where the step has the same 'degree of guidance' as the graded core, and (ii) a previously proposed WKB asymptotic approximation. (9 refs.)
- 61293 Inverse-square wavelength dependence of attenuation in infrared polycrystalline fibers.** J.A. Harrington (Hughes Res. Labs., Malibu, CA, USA), M. Sparks. *Opt. Lett. (USA)*, vol.8, no.4, p.223-5 (April 1983). The total-attenuation coefficient α_T in polycrystalline thallium bromiodide fibers varies as λ^{-2} , in sharp contrast to the Rayleigh λ^{-4} dependence in silica fibers. The authors developed a model showing that this λ^{-2} attenuation results from the combination of bulk scattering from large-scale, optically thin imperfections and surface scattering and absorption. The model also explains the authors' scattering sphere result that the attenuation coefficient that is due to scattering, α_s , at 10.6 μ m increases linearly with fiber length, in contrast to the situation in glass fibers in which α_s is constant along the fiber. (8 refs.)
- 61294 Laser phase noise effects in fiber-optic signal processors with recirculating loops.** M. Tur, B. Moslehi (Stanford Univ., Stanford, CA, USA). *Opt. Lett. (USA)*, vol.8, no.4, p.229-32 (April 1983). The power spectrum of the optical intensity at the output of a single-mode-fiber recirculating delay line driven by a multimode semiconductor laser is shown to exhibit a spectral structure with notches at zero frequency as well as at other multiples of 1/(loop delay). A theoretical model based on laser phase noise is suggested to explain the experimental data. (10 refs.)
- 61295 Real-time Fourier transformation in dispersive optical fibers.** T. Jansson (Res. Div., Nat. Tech. Systems Inc., Los Angeles, CA, USA). *Opt. Lett. (USA)*, vol.8, no.4, p.232-4 (April 1983). The general concept of temporal Fourier transformation in dispersive media is analyzed. The real-time optical Fourier transformer is shown to be realizable by using dispersive single-mode fibers and chirping lasers. (15 refs.)
- 61296 Beam-oscillation suppressor for multimode gradient-index fibers.** W.K. Kahn, Shuwen Yang (Dept. of Electrical Engng., George Washington Univ., Washington, DC, USA). *Opt. Lett. (USA)*, vol.8, no.4, p.238-40 (April 1983). The oscillations about the fiber axis that generally accompany a beam injected eccentrically into a gradient-index fiber can be substantially suppressed. It is shown how the constraint of Liouville's theorem, which was thought to preclude this effect, is satisfied in a system of two coupled fibers. The length of the coupled-fiber section required for operation is found. (9 refs.)
- 61297 Nonlinear absorption of light in glassy arsenic sulfide fibers in the energy range $h\nu < E_g$.** V.G. Abashkin, A.M. Andriesh, V.V. Ponomarev (Inst. of Appl. Phys., Acad. of Sci., Kishinev, Moldavian SSR). *Sov. J. Quantum Electron. (USA)*, vol.12, no.10, p.1343-5 (Oct. 1982). Translation of *Kvantovaya Elektron., Moskva (USSR)*, vol.9, no.10, p.2070-4 (Oct. 1982). [received: April 1983] Nonlinear absorption of light was discovered in waveguides made of glassy arsenic sulfide at $h\nu < E_g$. The transmission of the fibers at $\lambda = 0.63 \mu$ m varied several fold as a function of the intensity of the radiation, and of the time for which it acted, for intensities exceeding 1 W/cm^2 . The recovery of the transmission coefficient also depended on the exposure conditions. The results obtained were interpreted on the basis of a two-step transition model. (6 refs.)
- 61298 Determination of the amplitude-frequency characteristics of W-type fiber waveguides.** I.V. Golubenko, V.V. Savvin, D.K. Sattarov. *Sov. J. Quantum Electron. (USA)*, vol.12, no.10, p.1347-9 (Oct. 1982). Translation of *Kvantovaya Elektron., Moskva (USSR)*, vol.9, no.10, p.2078-80 (Oct. 1982). [received: April 1983] The results are given of theoretical and experimental investigations of the amplitude-frequency characteristics of fiber waveguides obtained using continuous optical radiation modulated by a microwave signal. A simple analytic expression is derived for the transfer function of an ideal fiber waveguide when a Gaussian light beam is coupled in and the numerical aperture of the fiber is considerably less than unity. The results are given of experimental determinations of the amplitude-frequency characteristics of quartz multimode fiber waveguides with a W-like profile of the refractive index, obtained in the

modulation frequency range 800-1250 MHz. The amplitude-frequency characteristics determined in this way are compared with calculated results. (4 refs.)

- 61299 Development of radiation resistant optical glass fiber.** K. Yagi, K. Shibuya, T. Iwamoto, K. Adachi, N. Sugiyama. *Showa Wire & Cable Rev. (Japan)*, vol.32, no.2, p.67-76 (1982). In Japanese. A study on the material, structure, characteristics and other factors of an optical fiber which is usable under a radiological environment has revealed the fact that pure silica core fiber is most excellent in resisting radiation. The study was also conducted in detail on the dose rate, temperature and effects that are imposed by OH contained in the fiber core on the transmission loss in actual applications. As a result, new knowledge had been gained on the basic transmission and mechanical characteristics of this fiber. It has been revealed that, when an optical glass fiber is irradiated with gamma rays, its transmission loss increases not with the increasing total dose but with the increasing dose rate, decreases with rising temperature and decreases with increasing OH concentration. As far as structure is concerned a fiber 50/125 μ m in diameter is recommendable as the pure silica glass core should be of the step index type. (12 refs.)
- 61300 Fiber optics takes its place in the subscriber loop.** G.W. Shaffer (Ohio Region of Mid-Continent Telephone Service Corp., Hudson, OH, USA). *Telephony (USA)*, vol.204, no.5, p.24-6 (31 Jan. 1983). Discusses Western Reserve Tel decision to choose a fiber optics system for its subscriber loop in order to reduce potential electrical interference from a nearby nuclear plant. The system includes six-fiber lightwave cable and a Timespan 128 pulse code modulation (PCM) pair gain system, both supplied by Anaconda-Eucsson Inc. The digital switching system includes a Litespan optical span card, which converts electrical signals to optical signals. (no refs.)
- Acoustic sensitivity of a fiber-optic interferometer See Entry 59836
- Stimulated Raman scattering in optical fibers See Entry 61237
- Statistical connector loss estimation in optical fiber transmission line including a number of connectors See Entry 61302
- The sol-gel method for optical fiber fabrication See Entry 61307
- Monitoring method for axis alignment of single-mode optical fiber and splice-loss estimation See Entry 61308
- Radiation induced effects and annealing methods in fiber optics and glasses See Entry 61966
- Enhancement of contrast in living and fixed specimens by the use of fiber optics See Entry 64012
- ## 42.80Q Image detectors, convertors, and intensifiers
- Measurement of the minimum resolvable temperature difference for thermal viewers See Entry 59776
- ## 42.80S Optical communications devices
- 61301 Relevance of optics in electronic instrumentation for communication systems.** V.V. Rampal (Defence Electronics Appl. Lab., Dehradun, India). *CSIO Commun. (India)*, vol.9, no.1, p.18-21 (Jan.-March 1982). [received: March 1983] The increasing relevance of the optical band and the importance of optical feedback devices for providing optical analogues to electronic devices in communication systems is discussed with a view to project the futuristic trends. (5 refs.)
- 61302 Statistical connector loss estimation in optical fiber transmission line including a number of connectors.** Y. Koyamada (Ibaraki Electrical Communication Lab., NTT, Ibaraki, Japan), Y. Tamura, A. Sakamoto. *Trans. Inst. Electron. & Commun. Eng. Jpn. Part B (Japan)*, vol.166B, no.1, p.63-70 (Jan. 1983). In Japanese. Statistical connector loss estimation is presented. Connector losses due to offset, tilt and mismatch of fiber parameters were estimated considering the distribution of connector plug dimensions and fiber parameters. The change of mode power distribution with the location of connectors along transmission lines were taken into account for the connector loss estimation. As an example, connectors used at the field trial of the intra-office optical transmission systems were examined. Good agreement was seen between estimated and measured connector losses. (7 refs.)
- OFC '83. Sixth Topical Meeting on Optical Fiber Communication (papers in summary form only received) See Entry 59536
- Suppression of intensity fluctuation of a longitudinal mode in directly modulated GaInAsP/InP dynamic single-mode laser See Entry 61150
- Nonlinear effects in TIPE-LiNbO₃ waveguides for optical communications See Entry 61267
- Two-channel integrated-optics multiplexer in a redundancy system See Entry 61306
- ## 42.82 INTEGRATED OPTICS
- (for optical waveguides see also 42.80L)
- 61303 High-speed signal processing with nonlinear integrated optics.** G.I. Stegeman (Optical Sci. Center, Univ. of Arizona, Tucson, AZ, USA). *J. Opt. Commun. (Germany)*, vol.4, no.1, p.20-4 (March 1983). The application of a combination of nonlinear and integrated optics to obtain high-speed, real-time signal processing is demonstrated. Both second- and third-order nonlinearities are considered, and interaction geometries are given for real-time convolution, pulse compression and expansion, and time inversion. (10 refs.)
- 61304 Design of a new thin-film electro-optic switch.** P.S. Chung, K.S. Chiang (School of Electrical Engng. & Computer Sci., Univ. of New South Wales, Kensington, NSW, Australia). *Opt. & Laser Technol. (GB)*, vol.15, no.2, p.83-90 (April 1983). A new thin-film electro-optic switch employing two stable states of polarization is proposed and investigated. The design can be further employed to realize a TE-TM polarization converter by constructing a Mach-Zehnder type interferometer integrated optical switch. The limitations and design procedures for electro-optic devices are also discussed. (19 refs.)

61305 Joining a semiconductor laser to a planar optical waveguide. V.L.Aksenov, A.V.Kukharev, A.A.Lipovskii, A.V.Pavlenko, V.Yu.Petrunkin (M.I. Kalinin Polytech. Inst., Leningrad, USSR). *Sov. Tech. Phys. Lett. (USA)*, vol.8, no.7, p.358-9 (July 1982). Translation of: *Pis'ma v Zh. Tekh. Fiz. (USSR)*, vol.8, no.13-14, p.828-31 (July 1982). [received: April 1983]

The effective exploitation of optical methods for information processing and transmission requires an extensive use of integrated-optics elements and devices. The authors have studied the possibility of joining an ILPN-102 standard CW semiconductor laser with a planar optical waveguide, using the end of the waveguide. (6 refs.)

61306 Two-channel integrated-optics multiplexer in a redundancy system. V.L.Maslennikov, Yu.A.Sarkisov, V.A.Sychugov, A.V.Tishchenko, Yu.F.Fedorov (P.N. Lebedev Phys. Inst., Acad. of Sci., Moscow, USSR). *Sov. Tech. Phys. Lett. (USA)*, vol.8, no.7, p.373-5 (July 1982). Translation of: *Pis'ma v Zh. Tekh. Fiz. (USSR)*, vol.8, no.13-14, p.862-6 (July 1982). [received: April 1983]

The authors have developed a two-channel integrated-optics multiplexer which operates in a redundancy mode. The device consists basically of stripe waveguides in glass. There are two symmetric inputs, which are brought together to form a single output channel, and there is also a control channel, used in operation in the redundancy mode. The inputs and outputs are terminated with parabolic flare sections, which allow the system to be coupled to production-model semiconductor lasers. All the inputs and outputs are spatially separated; this is a very important consideration for the development of practical devices. (2 refs.)

Rectangular Luneburg-type lenses for integrated optics See Entry 61255

Optical mode conversions in Nd substituted iron garnet films See Entry 61270

Extraction of radiation from a planar optical waveguide by diffraction in non-collinear mode interaction with the lattice See Entry 61276

Time-dependent theory of resonant tunnel coupling in optical waveguides See Entry 61277

42.85 OPTICAL TESTING AND WORKSHOP TECHNIQUES

61307 The sol-gel method for optical fiber fabrication. A.L.Harmer, R.Puyane, C.Gonzalez-Oliver (Battelle Res. Inst., Geneva, Switzerland). *IFOC Int. Fiber Opt. & Commun. (USA)*, vol.3, no.6, p.40-4 (Nov.-Dec. 1982).

The sol-gel method is a general technique for the preparation of glasses starting with inorganic salts or organometallic solutions. These solutions are transformed by polycondensation to a gel: a jelly-like solid which is highly porous. The next stage is to remove the rest of the solution from the pores by drying and then to sinter the gel, at relatively moderate temperatures, to a solid glass. Thus, optical fiber preforms may be produced from pure liquid starting materials and then pulled into fibers by conventional drawing techniques. The technique, which holds promise for mass production of optical fibers is described in detail. (no refs.)

61308 Monitoring method for axis alignment of single-mode optical fiber and splice-loss estimation. T.Hiabara, M.Matsumoto, T.Tanifuji, M.Tokuda (Nippon Telegraph & Telephone Public Corp., Tokai, Ibaraki-ken, Japan). *Opt. Lett. (USA)*, vol.8, no.4, p.235-7 (April 1983).

A new method for core-axis alignment and precise splice-loss estimation for single-mode optical fibers is presented. By using a differential interference contrast microscope one can achieve core-axis alignment with an offset below 0.3 μm , which results in a butt-joint loss increase of 0.04 dB compared with that obtained by alignment using a conventional optical monitoring method. Furthermore, splice-loss estimation with a precision of 0.05 dB is attained for a low-loss region without using an index-matching liquid. (5 refs.)

61309 On centering of lenses during cementing. V.M.Mudholkar, G.K.Sharma (Instruments Res. & Dev. Establ., Dehra Dun, India). *Rev. Sci. Instrum. (USA)*, vol.54, no.4, p.507-8 (April 1983).

An apparatus has been designed for direct viewing of centering errors in cemented doublets. The centering errors can be corrected in situ during cementing. This enables easy rectification and is applicable both to thermoplastic and thermosetting cemented lens systems. Multiple lenses can also be easily centered and cemented using this apparatus. (2 refs.)

61310 Investigation of the possibility of using an optical matching filter to test the geometry of parts in precision instrument manufacturing. V.I.Shanin. *Sov. J. Opt. Technol. (USA)*, vol.49, no.7, p.416-18 (July 1982). Translation of: *Opt.-Mekh. Prom.-st. (USSR)*, vol.49, no.7, p.15-17 (July 1982). [received: April 1983]

The metrological possibilities of optical matched filtering in problems of checking the geometry of parts in precision instrument manufacturing are analyzed theoretically. A method is proposed for reducing the absolute testing error, and the requirements are established for positioning the parts at the input to the test system. (7 refs.)

61311 General-purpose UELI-1M electron-beam evaporator. L.Yu.Vol'fon, A.N.Kabanov, B.N.Vasichev, A.P.Bdulenko, V.V.Polivanov, A.G.Klyukov, V.I.Solomentsev. *Sov. J. Opt. Technol. (USA)*, vol.49, no.7, p.440-1 (July 1982). Translation of: *Opt.-Mekh. Prom.-st. (USSR)*, vol.49, no.7, p.36-7 (July 1982). [received: April 1983]

A 6-kW general-purpose electron-beam evaporator, which has been developed and placed into batch production, is described. This equipment is designed for use in the optical industry. (1 ref.)

61312 Investigation of sintering activator distribution in refractory materials by means of an X-ray microanalyzer. E.E.Khrishch, V.K.Pavlovskii. *Sov. J. Opt. Technol. (USA)*, vol.49, no.7, p.442-4 (July 1982). Translation of: *Opt.-Mekh. Prom.-st. (USSR)*, vol.49, no.7, p.38-40 (July 1982). [received: April 1983]

A method has been developed that uses the MAR-2 X-ray spectral microanalyzer to evaluate the distribution uniformity of sintering activators throughout the volume of a refractory for optical glass making and to determine the dimensions of regions having an elevated concentration of the introduced ingredients. (5 refs.)

61313 Optimizing the technology of fabricating low-stiffness optical plates. B.E.Shilshvskii, G.V.Maslakov, Z.A.Migus'kina, Z.E.Alekseeva. *Sov. J. Opt. Technol. (USA)*, vol.49, no.7, p.444-5 (July 1982). Translation of: *Opt.-Mekh. Prom.-st. (USSR)*, vol.49, no.7, p.40-2 (July 1982). [received: April 1983]

The technology of grinding and polishing extremely low-stiffness 16×20×0.2 and 40×40×0.5 mm optical plates by employing differentiation of the operations, the use of high-stiffness tools, selective combining and special methods of blocking is examined. This technology makes it possible to increase the

labor productivity by ten times, stabilize the quality of the parts and mechanize the heavy manual labor. (2 refs.)

61314 Methods of in-shop testing of microscope optical-system centering. V.B.Rabinovich. *Sov. J. Opt. Technol. (USA)*, vol.49, no.7, p.446-8 (July 1982). Translation of: *Opt.-Mekh. Prom.-st. (USSR)*, vol.49, no.7, p.42-5 (July 1982). [received: April 1983]

Two methods are examined for checking the centering of a microscope optical system: by using an autocollimation Gaussian eyepiece and telescope objective, and by using a centered objective heating an index mark. The errors that arise during testing by these methods are analyzed. (2 refs.)

61315 Micro Fresnel lenses blazed by electron beam lithography. T.Fujita, H.Nishihara, J.Koyama (Faculty of Engng., Osaka Univ., Suita, Japan).

Trans. Inst. Electron. & Commun. Eng. Jpn. Part C (Japan), vol.66C, no.1, p.85-91 (Jan. 1983). In Japanese.

The authors have examined a blazing technique using electron beam lithography in order to increase efficiency of micro Fresnel lenses. First, with respect to uniform-period linear gratings, the variation of diffraction efficiency as a function of deviation from an ideal sawtooth relief profile was calculated. Then, on the basis of the measured exposure-sensitivity characteristics of a PMMA resist, blazed gratings have been formed in the resist and an efficiency of more than 60% was achieved at 0.633 μm wavelength. By a similar method, blazed-type micro Fresnel lenses of 5 mm focal length and 1 mm diameter have been fabricated and a performance of 50% efficiency and nearly diffraction-limited focusing was confirmed. (12 refs.)

Analysis of operation of double-beam photometer for monitoring the thickness of thin films See Entry 59827

Absolute spectral reflectance of mirrors See Entry 59829

Analysis of effect of fabrication errors of a scanning four-component prism on the ray paths in it See Entry 61259

Nonlinear effects in TIPE-LiNbO₃ waveguides for optical communications See Entry 61267

Increased-strength black chromium coatings See Entry 63183

Optical surface testing with diffused light See Entry 63474

42.90 OTHER TOPICS IN OPTICS

61316 Improved helmet for supporting optical instruments. S.I.Kruglov, A.K.Khannolainen. *Sov. J. Opt. Technol. (USA)*, vol.49, no.7, p.462-3 (July 1982). Translation of: *Opt.-Mekh. Prom.-st. (USSR)*, vol.49, no.7, p.58-9 (July 1982). [received: April 1983]

A helmet construction is described that provides for improved clamping stability of optical instruments relative to the operator's head. (3 refs.)

61317 Mechanism for focusing and clamping objective lens. A.G.Prikhod'ko, E.A.Snisarenko. *Sov. J. Opt. Technol. (USA)*, vol.49, no.7, p.467 (July 1982). Translation of: *Opt.-Mekh. Prom.-st. (USSR)*, vol.49, no.7, p.62 (July 1982). [received: April 1983]

The construction of a mechanism for focusing and clamping an objective lens is described. In order to eliminate residual stresses the objective lens is freed of clamping forces; to do this the amount has slots into which appropriate threaded ring inserts are placed and are held by set screws. (6 refs.)

43.00 ACOUSTICS

(for audition, see 87.34; for speech, see 87.36; for sound effects on living matter, see 87.50C)

43.20 GENERAL LINEAR ACOUSTICS

(see also 03.40K Mathematical problems in waves and wave propagation)

61318 Propagation of spherical waves above ground. R.Seznec, M.Berengier, V.Legeay (Lab. Central des Ponts et Chaussées, Bouguenais, France). *Appl. Acoust. (GB)*, vol.16, no.3, p.163-8 (1983).

A new methodology is developed for the problem of sound propagation above ground. The respective advantages of pure tones generated by a pressure driver with a $\lambda/4$ tube and impulsive noises issued from an 8 mm alarm pistol with a double cavity absorbing silencer, are analysed. Use is made of minimum phase linear systems for which the modulus and phase of the transfer function are related by a Hilbert transform. Finally, the different parameters of a locally reacting model are calculated using a nonlinear fitting procedure and the specific impedance values of the tested ground are estimated from the attenuations experimentally measured under grazing or oblique incidence. (4 refs.)

61319 Scattering of SH waves by spherical elastic layers. A.Gerard (Lab. de Mecanique Theorique, Univ. Pierre et Marie Curie, Paris, France). *Rev. Acoust. (France)*, vol.15, no.63, p.250-2 (1982). In French.

Determines the exact solution of SH wave propagation in a pattern of an infinite space containing a source point outside a finite number of concentric spheres without using Cramer's technique. The series solution obtained is interpreted in terms of multiple reflections and refractions and the assumption of the infinite interactions which accompanies the method proposed in Int. J. Engng. Sc. vol.18, p.583-595, (1980) is wholly justified. (8 refs.)

61320 Acoustic waves in a Rijke tube with radiation impedance. A.Trad (Lab. d'Etudes Aerodynamiques et Thermiques, Poitiers, France). *C.R. Seances Acad. Sci. Ser. II (France)*, vol.296, no.3, p.177-80 (24 Jan. 1983). In French.

Considers a Rijke tube as a limit of a hot porous tube. An asymptotic theory is developed, to study acoustic waves in that tube, when the impedance of radiation at the ends of the tube has been taken into account. (3 refs.)

61321 Sound attenuation in lined rectangular ducts in the presence of fluid motion. Zhao Song-ling, Wu Mei-qin (Tongji Univ., Shanghai, China). *Acta Acust. (China)*, vol.7, no.6, p.380-6 (Nov. 1982). In Chinese.

The theory dealing with sound attenuation in lined rectangular ducts in the presence of fluid motion is discussed. The following improvements are made: 1. The figures representing the relation between the acoustic impedance on the boundary surface and the sound propagation parameter in narrow rectangular ducts in the static case are re-plotted and improved. 2. By introducing

certain equivalent parameters, a normal rectangular duct may be transformed into an equivalent narrow one. 3. In the presence of fluid motion the sound propagation parameter may be approached systematically by means of solutions obtained in the static case. (5 refs.)

61322 The finite element formula of sound field by the weighted residual method. Qin You-guo (Dept. of Architecture, Qinghua Univ., China). *Acta Acust. (China)*, vol.7, no.6, p.387-91 (Nov. 1982). In Chinese. The finite element formula of a sound field, in which there are sound sources of which the boundary is non-rigid and absorbent, can be worked out by the weighted residual method. The formulae of the characteristic value problem of a sound field, which has been deduced using a variational method, may be taken as a particular case. (4 refs.)

61323 Experimental investigation of the scattering effects of a sphere in a cylindrical resonant chamber. M.Barmatz, J.L.Allen, M.Gaspar (Jet Propulsion Lab., California Inst. of Technol., Pasadena, CA, USA). *J. Acoust. Soc. Am. (USA)*, vol.73, no.3, p.725-32 (March 1983). The resonance frequency, acoustic pressure, and quality factor for various longitudinal and transverse modes of a cylindrical chamber were measured as a function of sphere position along the chamber axis. In the limit of small spherical blockages, the shift in the plane-wave resonance frequency is proportional to the ratio of sample-to-chamber volumes, v_s/v , as predicted by analytical models. The frequency shift measurements are compared to a phenomenological model based on the ratio of sample-to-chamber cross-sectional areas, a_s/a , and sample diameter to chamber length, d_s/l . The frequency shift, $\Delta f/f_0$, for plane waves is proportional to a_s/a , d_s/l , and v_s/v for ratios less than about 0.2, 0.1, and 0.013, respectively. Measurements for large values of these ratios for spherical and cylindrical blockages are in good agreement with the three-dimensional Green's function theory of El-Raheb and Wagner [J. Acoust. Soc. Am. 72, 1046 (1982)]. An approximate analytical frequency shift expression is derived for the intermediate ratio region. The frequency shift measurements for modes containing a transverse propagation component were smaller in magnitude and different in shape than those of the plane-wave modes. (8 refs.)

61324 Bistatic low-frequency inverse scattering. N.N.Bojarski. *J. Acoust. Soc. Am. (USA)*, vol.73, no.3, p.733-5 (March 1983). The monostatic acoustic and electromagnetic low-frequency inverse scattering solutions of this author [Office of Naval Research Contract N00014-76-C-0082 Report (25 July 1982); IEEE Trans. Antennas Propag. AP-30 (4), 775-778 (July 1982)] are generalized to the bistatic case. Specifically, derived are bistatic acoustic and electromagnetic low-frequency direct scattering approximations in terms of the characteristic function of a scatterer. These bistatic approximations satisfy the principle of reciprocity, and consist of a generalization of the monostatic-bistatic equivalence theorem, valid for wide bistatic angles. Unlike the monostatic case, for which the acoustic and electromagnetic low-frequency direct scattering approximations are identical, and for which the electromagnetic low-frequency direct scattering approximation fails to yield depolarization information, the bistatic acoustic and electromagnetic low-frequency direct scattering approximations are different, and the electromagnetic bistatic low-frequency direct scattering approximation does yield depolarization information. An inverse scattering solution for the complete set of moments tensors of this characteristic function is obtained. It is shown that this bistatic inverse scattering solution is a bistatic generalization of Rayleigh's monostatic volume law, yielding the Rayleigh volume of the scatterer for the moments tensor of rank zero. The moments tensors of rank one and two are shown to be the spatial position centroid and the principal dimensions (and their spatial orientation) of the scatterer, respectively. It is shown that the inverse scattering solution can be implemented with one transmitting and one receiving location, and a modest spatial spread in one, the other, or both locations. (8 refs.)

61325 Acoustic scattering by elastic solid cylinders and spheres in viscous fluids. W.H.Lin, A.C.Raptis (Components Technol. Div., Argonne Nat. Lab., Argonne, IL, USA). *J. Acoust. Soc. Am. (USA)*, vol.73, no.3, p.736-48 (March 1983). This paper deals with analytic studies and numerical results of the scattering of plane sound waves from an elastic circular cylinder and from an elastic sphere in a viscous fluid. The elastic properties of the cylinder and the sphere and the viscosity of the surrounding fluid are taken into account in the solution of the acoustic-scattering problems. The associated acoustic quantities, such as the acoustic-scattering patterns, the acoustic-radiation forces, and the acoustic attenuation, are first derived in closed forms and then evaluated numerically for a given set of material properties. Numerical results show that increasing fluid viscosity tends to increase the directionality of the angular distribution of the scattering patterns, especially in the forward direction. The acoustic-radiation force on the cylinder or on the sphere is in the direction of the incident wave and increases as the viscosity of the fluid increases. The plots of the acoustic-attenuation coefficients versus the dimensionless wavenumber of the incident sound wave reveal oscillatory phenomena, which are caused by the resonant vibrations of the cylinder or the sphere. (40 refs.)

61326 Horizontal covariance of surface reverberation: Comparison of a point-scatterer model to experiment. C.R.Wilson, M.E.Frazer (Appl. Res. Labs., Univ. of Texas, Austin, TX, USA). *J. Acoust. Soc. Am. (USA)*, vol.73, no.3, p.749-60 (March 1983). A theoretical model of reverberation developed by D. Middleton was implemented to predict the spatial-temporal covariance of surface reverberation. The implementation assumed narrow-band transmissions and point scatterers treated as perfect point reflectors distributed uniformly over the plane of the mean surface level. The implementation of the model under these assumptions is presented, and the results are compared to experimental measurements of the covariance of surface reverberation measured by a horizontal array of receivers. The dependence of the covariance on spatial separation of the receivers, time, and time difference was modeled. The modeled results were found to agree well with the experimental measurements. The effects of off-axis scattering due to the azimuthal directivity of the projector and the bandwidth of the projector and receivers were shown to be significant and were also shown to be properly taken into account by the model. (25 refs.)

61327 Acoustical characteristics of rigid fibrous absorbents and granular materials. K.Attanborough (Engng. Mech. Discipline, Faculty of Technol., Open Univ., Milton Keynes, England). *J. Acoust. Soc. Am. (USA)*, vol.73, no.3, p.785-99 (March 1983). A model is developed that predicts the acoustical characteristics of rigid fibrous absorbents soils and sands from five parameters. These parameters are porosity, flow resistivity, tortuosity, steady flow shape factor, and dynamic shape factor. Tortuosity is shown to be related simply to porosity and a simple relationship between the shape factors is postulated. In practice, therefore, only two measurable parameters (porosity and flow resistivity) are required together with a third shape factor parameter, appropriate values of which are deduced for the media of interest by comparison with appropriate

measurements. The model is shown to give superior predictions to those of empirical formulae that use flow resistivity only, particularly when applied to high flow resistivity soils and sands at low frequencies such that the stated range of validity of the empirical formulae is exceeded. (28 refs.)

61328 Diffraction of spherical wave at a slit and an aperture in a plane screen. M.Yuzawa (Tohoku Inst. of Technol., Sendai, Japan). *J. Acoust. Soc. Jpn. (Japan)*, vol.38, no.12, p.755-63 (Dec. 1982). In Japanese.

A method of predicting the diffracted sound field behind the respective infinite plane screens with slits or a rectangular aperture is described. Macdonald's formula (1915) for a thin barrier and Pierce's formula (1974) for the double-edge diffraction by a thick three-sided barrier are used in this study, and this procedure for a rectangular aperture primarily follows Fresnel-Kirchhoff's diffraction theory. The calculated results for several kinds of small-scale model obtained by the present procedure, are compared with experimental results. (14 refs.)

61329 Finite-element analysis of topographic waveguides for acoustic surface waves using approximate analytical solutions for substrate region. M.Koshiba, M.Okada, M.Suzuki (Faculty of Engng., Hokkaido Univ., Sapporo, Japan). *Trans. Inst. Electron. & Commun. Eng. Jpn. Sect. E (Japan)*, vol.E66, no.2, p.75-81 (Feb. 1983).

An efficient finite-element program utilizing approximate analytical solutions is described for the analysis of topographic waveguides for acoustic surface waves. In this method, the only ridge region is divided into triangular elements, and therefore it is possible to use computer memory more economically. Calculations are made for the rectangular ridge waveguide, the dovetail ridge waveguide, the truncated knife edge waveguide and the wedge waveguide. The results obtained agree well with the earlier theoretical and experimental results. (18 refs.)

61330 The boundary value problem of the sound propagation in the rarefied gas. Yu.R.Romanovskii. *Vestn. Leningr. Univ. Ser. Mat. Mekh. & Astron. (USSR)*, no.1, p.80-4 (Jan. 1983). In Russian.

Considers the boundary value problem of sound generated at an oscillating wall propagating into a halfspace. An existence and uniqueness theorem for the solution of this problem is proved for the linear Boltzmann equation with a general cut-off intermolecular potential for all frequencies. (5 refs.)

Coupled mode solution for a cylindrically symmetric oceanic waveguide with a range and depth dependent refractive index and a time varying rough sea surface See Entry 61338

On the calculation of normal mode group velocity and attenuation See Entry 61342

Transmission of a pulsed acoustic signal at a two-fluid interface See Entry 61343

The tight-coupled monopole active attenuator in a duct See Entry 61349

43.25 NONLINEAR ACOUSTICS AND MACROSONICS

(see also 43.60 Acoustic signal processing; 43.88 Transduction; devices for generation and production of sound)

61331 Breadth effects on the penetration of an acoustic beam into a solid. P.Gatignon (Univ. de Technol. de Compiègne, Compiègne, France). *Rev. Acoust. (France)*, vol.15, no.63, p.246-9 (1982). In French.

Studies the refraction and the reflection of a bounded monochromatic acoustic beam at a liquid-solid interface. Using an analytical approach and a far-field approximation for the relevant Fourier integrals, it is shown that the highest pressure lines do not satisfy the usual Descartes laws. The corresponding angular shifts are computed for various values of the adimensional breadth k_a and of the incidence of the beam. Two different forms of incident beam are considered. (5 refs.)

61332 Propagation of finite-amplitude ultrasonic waves in air. I. Spherically diverging waves in the free field. J.A.Gallego-Juarez, L.Gaete-Garretón (Lab. de Ultrasonidos, Inst. de Acustica, Consejo Superior de Investigaciones Científicas, Madrid, Spain). *J. Acoust. Soc. Am. (USA)*, vol.73, no.3, p.761-7 (March 1983).

An investigation of the free-field propagation in air of sinusoidal spherical waves of finite amplitude is described. It includes experiments made at 20.4 kHz and a theoretical interpretation using weak shock theory. The acoustic source used was a new high-power and highly directional ultrasonic transducer which is able to generate a nearly pure sinusoidal wave at sound pressure levels over 160 dB. The experiments were done in an anechoic chamber, using a CW mode. They consisted essentially of measuring the amplitude of the fundamental component of the wave and its first three harmonics for different source levels and at various distances along the axis of the source. In addition, oscillograms and directivity patterns were recorded. In general, the experimental data confirm the predictions of the theoretical model. (10 refs.)

61333 Propagation of finite-amplitude ultrasonic waves in air. II. Plane waves in a tube. L.Gaete-Garretón, J.A.Gallego-Juarez (Lab. de Ultrasonidos, Inst. de Acustica, Consejo Superior de Investigaciones Científicas, Madrid, Spain). *J. Acoust. Soc. Am. (USA)*, vol.73, no.3, p.768-73 (March 1983).

For pt.1 see ibid., pt.73, no.3, p.761-67 (1983). This paper is concerned with an investigation of the nonlinear behavior of sinusoidal plane progressive acoustic waves of finite amplitude in air at a frequency of about 21 kHz. The various stages in the distortion of the wave have been experimentally studied and the results compared with theoretical models. The experiments were done in a tube 5.5 m long and 8-mm internal diameter with an absorbing termination. The acoustic source used was a prestressed piezoelectric sandwich transducer with a titanium stepped mechanical amplifier, the small end of which was the piston that produced the high-amplitude motion inside the tube. This source was capable of generating a nearly pure sinusoidal wave at sound pressure levels up to about 155 dB (re: 0.0002 μ bar). Interestingly, as compared to previous reports on this field, the use of a high frequency has allowed the study of all the propagation regions (including the old age region) of the wave using a short length tube. (11 refs.)

61334 Distortion of finite amplitude ultrasound in lossy media. M.E.Haran (Office of Radiological Health, Rockville, MD, USA), B.D.Cook. *J. Acoust. Soc. Am. (USA)*, vol.73, no.3, p.774-9 (March 1983).

A form of Burgers' equation is used to derive an algorithm for calculating harmonic generation by a continuous plane wave of ultrasound propagating in a nonlinear, lossy, nondispersive medium. The algorithm accounts for attenuation that is not quadratically related to the frequency of the wave. Attenuation strongly affects the rate of harmonic production. The effect of variations

of the relationship between attenuation and frequency is shown. Biological tissue is an example of a highly lossy medium where the attenuation does not increase with the square of the frequency. Calculations for several types of tissue and biological fluids are presented that show, for certain conditions, finite amplitude distortion is possible. (15 refs.)

Acoustic scattering by elastic solid cylinders and spheres in viscous fluids See Entry 61325

Improved technique for amplitude inversion of backscattering in the study of cavities and flat defects See Entry 61360

43.28 AEROACOUSTICS AND ATMOSPHERIC SOUND

(see also 92.60 Meteorology)

61335 The dependence of sound extinction on the parameters of thermal turbulence in the atmospheric boundary layer. L.G.Shamanaeva (Inst. of Atmospheric Optics, Acad. of Sci., Tomsk, USSR). *J. Acoust. Soc. Am. (USA)*, vol.73, no.3, p.780-4 (March 1983). Scattering coefficients and normalized scattering phase function were calculated using the Von Karman spectrum of temperature fluctuations in the atmospheric boundary layer which enabled one to take into account the outer scale of turbulence. It was shown that the scattering coefficient had a quadratic frequency dependence and 1.68-1.69 power dependence upon the outer scale of turbulence. At the same time, the scattering cross section was proportional to the cube root of the sound frequency which agreed with the previously obtained results. The normalized scattering phase function was calculated for small scattering angles. It was shown that in the presence of small scale inhomogeneities in the atmosphere the portion of power removed from the original beam increases because the lateral scattering becomes prevailing. The obtained results are in good agreement with the experimental data. (14 refs.)

61336 The use of quasi-random scanning for designing sound scattering surfaces. M.Yu.Laneh, S.A.Pavlov, G.D.Tolstyykh. *Tekh. Kino i Telev. (USSR)*, no.3, p.3-6 (March 1983). In Russian.

Considers a method for designing sound scattering surfaces based on surfaces synthesis with caissons of various depths. A spectral method of determining caisson depths and evaluating a sound scattering surface quality is described. An example of such a surface is given and the results of evaluating sound scattering properties of the model surface are presented. (5 refs.)

Propagation of finite-amplitude ultrasonic waves in air. I. Spherically diverging waves in the free field See Entry 61332

Propagation of finite-amplitude ultrasonic waves in air. II. Plane waves in a tube See Entry 61333

Airfoil noise analysis by nearfield and farfield microphone arrays See Entry 61348

A new measurement method for separating airborne and structureborne aircraft interior noise See Entry 61362

Acoustic wave radiated by head-on collision of two vortex rings See Entry 61517

43.30 UNDERWATER SOUND

(see also 92.10 Physics of the ocean)

61337 A corrected match for coherent part of time-variant channel. Xu Jun-hua, Chen-Geng (Inst. of Acoustics, Acad. Sinica, Peking, China). *Acta Acust. (China)*, vol.7, no.6, p.352-63 (Nov. 1982). In Chinese.

The detection performance of a matched filter with the transmitted signal as a reference signal will be degraded in an underwater acoustic channel due to the multipath effect and time variability. Two methods of channel match are presented in this paper: (1) Pulse-to-pulse correlation method for the channel match. (2) Deconvolution method. In the first method the received signal is used as a reference signal of the matched filter to improve the detection performance of the matched filter. In the second method a short pulse is used to excite the channel. To obtain the response function of the channel, the Wiener-Hopf equation in matrix form is used. The equation can be solved by several deconvolution methods. Then the solved response function of the channel is convoluted with the transmitted signal and the result of the convolution is used as a reference signal of the corrected matched filter. In this paper, with the aid of a computer the corrected match for several channel models and for the real underwater acoustic propagation channel is given and the comparison between the conventional and corrected matched filters is illustrated. (5 refs.)

61338 Coupled mode solution for a cylindrically symmetric oceanic waveguide with a range and depth dependent refractive index and a time varying rough sea surface. C.A.Boyles (Appl. Phys. Lab., Johns Hopkins Univ., Laurel, MD, USA).

J. Acoust. Soc. Am. (USA), vol.73, no.3, p.800-5 (March 1983). The paper uses the technique of coupled, local normal modes to obtain an exact numerical solution of the Helmholtz equation for the case of a two-dimensional, oceanic waveguide which can possess both horizontal and vertical sound-speed gradients as well as time varying rough sea surface. By a two-dimensional waveguide, the authors mean one that can be described by two coordinates; viz., a radial coordinate r to describe variations with horizontal range and a depth coordinate z to describe variations with depth below the sea surface. The speed of sound in the waveguide $c(r,z)$ can then be a function of both range and depth. (29 refs.)

61339 Geometric dispersion of acoustic signals propagated in a deep ocean channel. K.D.Flowers (Naval Res. Lab., Washington, DC, USA).

J. Acoust. Soc. Am. (USA), vol.73, no.3, p.806-9 (March 1983). In this paper the authors consider two sinusoidal signals generated in such a way as to have a constant frequency ratio. Then, except for dispersive effects of the propagation channel, the two signal frequencies should remain correspondingly related at a distant receiver. As a measure of this relationship a correlation function is defined for signals of different frequencies. The signals are assumed to have a frequency relationship $\omega_2 = q\omega_1$, where q is a real number. As an illustration of the use of this correlation function, model calculations are made of signals propagated over long ranges through the deep ocean. It is determined that geometric dispersion in a deep ocean channel degrades the correlation slightly but limits the precision to which q may be evaluated. The variations in q are directly proportional to q . It is found that the correlation function degrades with signal-to-noise ratio, q , and frequency. In general, it is concluded that the dispersive effects of the ocean channel at long range can be significant for broadband signals when signal coherence is an important consideration. (10 refs.)

61340 A cautionary note on the use of range-dependent propagation models in underwater acoustics. R.F.Henrick (Appl. Phys. Lab., Johns Hopkins Univ., Laurel, MD, USA).

J. Acoust. Soc. Am. (USA), vol.73, no.3, p.810-12 (March 1983). A caution is given to the users of range-dependent models that utilize single ocean sound-speed profiles for discrete range intervals. It is shown that, if new profiles are not input every few kilometers, the effect of the discontinuities in the ocean may produce erroneous results. An example illustrates potential errors of as much as 18 dB using the parabolic equation method (PE) to compute propagation through a Gulf Stream ring. It is argued that range interpolation routines should be used to produce closely spaced profiles as a standard part of applying these acoustic propagation codes. (8 refs.)

61341 Optimum frequency of propagation in shallow water environments. F.B.Jensen, W.A.Kuperman (SACLANT ASW Res. Centre, La Spezia, Italy).

J. Acoust. Soc. Am. (USA), vol.73, no.3, p.813-19 (March 1983). The optimum frequency of propagation in shallow-water environments is the result of competing propagation and attenuation mechanisms at high and low frequencies. It is shown that the optimum frequency is strongly dependent on water depth, that it has some dependence on the sound-speed profile, while it is only weakly dependent on the bottom type. A comparison between experimental data and normal-mode theory indicates the importance of shear waves in the bottom, both in determining the optimum frequency of propagation and in determining the actual propagation-loss levels at lower frequencies. (23 refs.)

61342 On the calculation of normal mode group velocity and attenuation. R.A.Koch, C.Penland, P.J.Vidmar, K.E.Hawker (Appl. Res. Labs., Univ. of Texas, Austin, TX, USA).

J. Acoust. Soc. Am. (USA), vol.73, no.3, p.820-5 (March 1983). The group velocity for a normal mode can be calculated without invoking a finite difference approximation requiring a second eigenmode calculation. The reciprocity relation is employed in a derivation of the normal mode group velocity and attenuation coefficient. The group velocity thus calculated is more accurate than a comparable finite difference approximation. Arbitrarily arranged layers of solid and fluid media are considered. (10 refs.)

61343 Transmission of a pulsed acoustic signal at a two-fluid interface. J.Naze Tjøtta, S.Tjøtta (Dept. of Math., Univ. of Bergen, Bergen, Norway).

J. Acoust. Soc. Am. (USA), vol.73, no.3, p.826-34 (March 1983). The transmission of an acoustic pulse with a plane front at a two-fluid interface is considered. An exact solution is obtained and several properties are derived. Numerical examples are given, showing patterns of the transmitted signal for different pulse shapes and incident angles. It appears that penetration at angles above the critical incidence (according to Snell's Law) is indeed possible, depending on how the incident pulse is shaped. This happens at the cost of a self-demodulation of the signal. (13 refs.)

61344 Response of underwater structures to convective component of flow noise. K.L.Chandiramani (Bolt Beranek & Newman Inc., Cambridge, MA, USA).

J. Acoust. Soc. Am. (USA), vol.73, no.3, p.835-9 (March 1983). Convective component of flow noise (for example, a turbulent boundary layer) is characterized by length scales of the order U/f , where U is the mean flow speed and f is the frequency. Nonresonant response of underwater structures to the convective component of flow noise is often of interest. An exact theory of transmission of sound across an isotropic flat plate, involving longitudinal and shear waves, is modified so as to apply at high, convective wavenumbers. Closed form results are presented. Such results can in turn be used as inputs to scattering analyses, and as a guide to treating more complicated problems involving multiple-layered structures. However, these later topics are not the subject of this paper. (5 refs.)

Horizontal covariance of surface reverberation: Comparison of a point-scatterer model to experiment See Entry 61326

43.35 ULTRASONICS, QUANTUM ACOUSTICS, AND PHYSICAL EFFECTS OF SOUND

(for phonons in crystal lattices, see 63.; for plasma acoustics, see 52.35; for low-temperature acoustics and sound in liquid helium, see 67.; for acoustic properties of liquids, see 62.60; for acoustical properties of solids, see 62.65; for ultrasonic relaxation, see 62.80; for acoustic properties of thin films, see 68.60; for surface waves in solids, see 68.25; for acoustoelectric effects and acoustic wave amplification, see 72.50; for magnetoacoustic effects, oscillations and resonance, see 72.55; for acousto-optical effects and acoustic holography, see 78.20H and 43.63; for sound effects on living matter, see 87.50)

Modification of Fresnel diffraction by a straight edge object with acoustically coherence-controllable illumination See Entry 61078

43.40 MECHANICAL VIBRATIONS AND SHOCK

(see also 46.30M Vibrations, aeroelasticity, hydroelasticity, mechanical waves and shocks)

61345 The input mobility of an infinite circular cylindrical elastic shell filled with fluid. C.R.Fuller (NASA Langley Res. Center, Hampton, VA, USA).

J. Sound & Vib. (GB), vol.87, no.3, p.409-27 (8 April 1983). The force input mobility of an infinite elastic circular cylindrical shell filled with fluid is derived by using the spectral equations of motion. Mobilities are evaluated and their physical interpretations are discussed for a steel shell of thickness $h/a=0.05$ filled with water and vibrating in the $n=0, 1$ and 2 circumferential modes. The results are subsequently used to analyze the related situations of wave transmission through a radial ring constraint and the far field vibrational energy distributions between the contained fluid and the shell wall for line and point driving forces. (12 refs.)

61346 Resonant oscillations of fluid-loaded struts. D.G.Crighton (Dept. of Appl. Math. Studies, Univ. of Leeds, Leeds, England).

J. Sound & Vib. (GB), vol.87, no.3, p.429-37 (8 April 1983). A simplified model is used to obtain a description of the way in which radiation damping limits the resonant oscillations of a cantilever or strut. It is shown that radiation damping is equivalent, in the low frequency limit, to a fictitious internal dissipation, with loss factor $\eta_m = (\pi/2)[m'/(m+m')](k_0 a)^2$, where $2a$ is the strut thickness, m its mass per unit length and m' the virtual fluid mass per unit length. Typical values of η_m appear to be slightly higher than internal loss factors, showing that the resonant amplitude is limited only

by radiation loss, even for thin struts for which $k_0a \ll 1$. When $k_0a \gg 1$ it is found that η_{rad} is much larger than any internal loss factor, and therefore that high frequency resonances are heavily damped, regardless of internal dissipation. The pressure field near the strut is also examined, and in the case $k_0a \ll 1$ is found at resonance to exceed the driving pressure field by the large factor $(k_0a)^{-2}$. The far field pressure at resonance may, under some conditions, also greatly exceed the off-resonance scattered field, and this great scattering efficiency of a thin strut at resonance is demonstrated by detailed examination of a particular case. (6 refs.)

Hearing the shape of an annular drum See Entry 61355
Sound power determination from surface intensity measurements on a vibrating cylinder See Entry 61363
Horizontally polarized waves in composites and bonds See Entry 61435

43.50 NOISE, ITS EFFECTS AND CONTROL

(see also 86.70J Environmental science)

61347 Effect of size on measurements of the sound reduction index of a window or a pane. N.Michelsen (Danish Acoustical Inst., Tech. Univ. of Denmark, Lyngby, Denmark).

Appl. Acoust. (GB), vol.16, no.3, p.215-34 (1983).

The variation in the sound reduction index as a function of the size of a test specimen was investigated. Five different sizes of one particular hinged window were tested. In addition, tests were carried out with a sound insulating double glazing and a laminated pane mounted in normal wooden frames. Some differences in the sound reduction index due to the different test specimen sizes were found. However, these differences were slight compared with the practical difficulties and costs which tests on several sizes would involve. One size of test specimen is therefore considered to be sufficient for sound reduction index measurements in windows with respect to labelling. This practice is currently in use in Denmark. (7 refs.)

61348 Airfoil noise analysis by nearfield and farfield microphone arrays. L.Gaudriot, A.Hellion, B.Beguet (Metravib, Ecully, France), H.Arbej. *Rev. Acoust. (France)*, vol.15, no.63, p.208-10 (1982). In French.

Airfoil noise radiated spectrum has two components: broadband noise and a set of pure tone peaks. A farfield array has enabled the authors to determine the pure tone source location. A nearfield array placed in the vicinity of the airfoil has given the directivity of both types of sources, even in the downstream direction, when the array is imbedded in the flow. (8 refs.)

61349 The tight-coupled monopole active attenuator in a duct. Kh.Eghtesadi (Dept. of Electrical Engng., Abadan Inst. of Technol., Abadan, Iran), W.K.W.Hong, H.G.Leventhal.

Noise Control Eng. J. (USA), vol.20, no.1, p.16-20 (Jan.-Feb. 1983).

Methods of active attenuation of noise, that is the cancelling of noise from a source by the addition of further noise, include both absorptive and non-absorptive systems. The paper reviews the theory of one-dimensional active attenuation for ductborne noise and follows with an overview of a monopole system used to realize attenuation. A number of configurations of active attenuators are possible. In these, one, two or three sources have been used to produce the secondary cancelling noise. The tight-coupled monopole attenuator uses a completely different approach to the question of acoustic feedback to other attenuation systems. Previous approaches have always been to isolate the attenuator microphone from acoustic feedback from the attenuator loudspeakers; most systems use an acoustic method of achieving this, while the chelsea monopole attenuator uses an electronic method. In the tight-coupled monopole attenuator the acoustic feedback can be used as an integral part of the system in order to provide automatic compensation. This leads to a simple attenuation system which can be constructed from standard equipment, without special electronic systems. The experimental results showed significant attenuation. (22 refs.)

61350 Barrier insertion loss versus Fresnel number and secondary parameters. Z.Hu, R.L.M.Wong (Inst. for Aerospace Studies, Univ. of Toronto, Downsview, Ontario, Canada).

Noise Control Eng. J. (USA), vol.20, no.1, p.31-6 (Jan.-Feb. 1983).

The authors provide a quick, but accurate, estimation of sound reduction by a semi-infinite barrier for a wide range of source/observer geometries. In addition to Fresnel number N (in a range down to 0.05), it brings out the influence of three secondary parameters; although often neglected, these can be significant. The insertion loss for a pure tone point source is computed via the exact solution given by both Carslaw (1899) and Macdonald (1915). The numerical results are approximated analytically by modifying the diffraction formulation of Keller (1962) and others. The approximate formulae are applied to several test cases and agree well with the exact theory and experimental measurements. (11 refs.)

Proceedings of the Third International Workshop on Railway and Tracked Transit System Noise See Entry 59530

A study of reactor internal dynamics by reactor noise analysis See Entry 60333

Response of underwater structures to convective component of flow noise See Entry 61344

A new measurement method for separating airborne and structureborne aircraft interior noise See Entry 61362

Sound power determination from surface intensity measurements on a vibrating cylinder See Entry 61363

An investigation into noise radiation from flow control valves with particular reference to flow rate measurement See Entry 61497

Using the NRR to estimate the real world performance of hearing protectors See Entry 63759

43.55 ARCHITECTURAL ACOUSTICS

The spark generator as an impulsive acoustic signal source See Entry 61356

43.60 ACOUSTIC SIGNAL PROCESSING

61351 Errors induced by analog to digital conversion over a wide dynamic range. C.Azais, J.P.Guilhot (LAMI Univ. Paul Sabatier, Toulouse, France).

Rev. Acoust. (France), vol.15, no.63, p.216-20 (1982). In French.

Digital analysis of an acoustical signal is based on analog to digital conversion over a wide dynamic range. The authors made a comparison between several types of converters, taking as a criteria the relative error on the estimate root mean square value of a signal of known probability density function. They propose a device making a floating point conversion over a 95 dB wide dynamic range with an error less than ± 0.2 dB. (no refs.)

The use of quasi-random scanning for designing sound scattering surfaces See Entry 61336

Study and synthesis of signal types with a view to the testing of L_{eq} meters See Entry 61358

An acoustical synthetic focus imaging with pseudo-random signal See Entry 61368

43.70 SPEECH COMMUNICATION

(inc. speech perception, speech intelligibility, and speech synthesis; see also 87.36 Speech)

61352 Selective linear prediction of speech using the generalized inverse of matrices. R.Mizoguchi, M.Yanagida, Y.Taniguchi, O.Kakusho (Inst. of Sci. & Industrial Res., Osaka Univ., Ibaraki, Japan).

Trans. Inst. Electron. & Commun. Eng. Jpn. Part A (Japan), vol.J66A, no.1, p.56-63 (Jan. 1983). In Japanese.

The authors present a new approach to LPC analysis based on selective use of speech data to reject the data disturbed by the excitation source. This is called the selective linear prediction method. First, the formulation of linear prediction is presented using the generalized inverse matrices. Then, a successive computation is described based on Givens' reduction. The selective computation, which plays an essential role in the method, owes its efficiency to Givens' reduction. Finally, the advantage of the proposed method is demonstrated by computer simulation using both synthetic and natural speech. (12 refs.)

61353 Isolated words recognition using DP-matching and Mahalanobis' distance. T.Takara, S.Imai (Res. Lab. of Precision Machinery & Electronics, Tokyo Inst. of Technol., Yokohama, Japan).

Trans. Inst. Electron. & Commun. Eng. Jpn. Part A (Japan), vol.J66A, no.1, p.64-70 (Jan. 1983). In Japanese.

The authors propose a new DP-matching method in which the covariance matrix for each frame absorbs the variation of phonemic characteristics among the speakers. The method maximizes a likelihood, and both the calculations and memory size necessary for the recognition can be kept as small as possible, since the conventional spectral representation is not needed for the feature parameter. Using the Fourier transform of Mel-Sone spectrum (3 dimensional vector) as the feature parameter, the ten Japanese digits spoken by 8 males were examined. The recognition scores of 95.4% and 98.8% were obtained in speaker and utterance open tests, respectively. (7 refs.)

43.75 MUSIC AND MUSICAL INSTRUMENTS

61354 Anomalies in the frequency-length functions in violin strings. N.C.Pickering (Norman Pickering Co., Southampton, NY, USA).

J. Audio Eng. Soc. (USA), vol.31, no.3, p.145-50 (March 1983).

A computer-controlled machine has been constructed which accurately stops the string of a violin at known positions. The string is excited electromagnetically at each position and the frequency measured. Correlation between body resonances and frequency perturbations is clearly demonstrated. Errors, often attributed to 'false' strings, are inherent, and of the order of 10-30 cents. Violins vary widely. (5 refs.)

61355 Hearing the shape of an annular drum. H.P.W.Gottlieb (School of Sci., Griffith Univ., Nathan, Queensland, Australia).

J. Aust. Math. Soc. Ser. B (Australia), vol.24, pt.4, p.435-8 (April 1983).

The asymptotic expansion for a spectral function of the Laplacian operator, involving geometrical properties of the domain, is demonstrated by direct calculation for a doubly-connected region in the form of a narrow annular membrane. From a known formula for the zeros of the eigenvalue equation containing Bessel functions the area total perimeter and connectivity are all extracted explicitly. (10 refs.)

43.85 ACOUSTICAL MEASUREMENTS AND INSTRUMENTATION

(for acoustic noise measurement, see also 43.50; for photoacoustic spectroscopy, see 07.65)

61356 The spark generator as an impulsive acoustic signal source. C.B.Chinoy (Univ. of Wales Inst. of Sci. & Technol., Cardiff, Wales).

Acoust. Lett. (GB), vol.6, no.4, p.44-51 (Oct. 1982). [received: March 1983]

The application of impulse analysis techniques to acoustical systems offers the acoustician both a powerful design and diagnostic method of investigating the characteristics of transmission channels. This paper considers one of the most suitable means of generating input signals for this application—the utilisation of a spark generator as an impulsive signal source. The main requirements of an impulsive signal to be used to investigate sound transmission characteristics through buildings are discussed and the theoretical background, design, construction and performance of a spark generator are described. (3 refs.)

61357 Errors combination in acoustical measurements. J.Guilhot, C.Legros, J.P.Flenner.

Rev. Acoust. (France), vol.15, no.63, p.221-3 (1982). In French.

The error on a measurement depends upon the precision of the device and the random properties of the phenomenon. In acoustical measurements, one knows the precision of the device only by partial tolerances. Furthermore, each physical phenomenon is a particular case. Collecting what is known in this domain, the authors tried to estimate the overall error on an acoustical measurement in some usual cases. (7 refs.)

61358 Study and synthesis of signal types with a view to the testing of L_{eq} meters. M.Labit, J.P.Grasmuck (LAMI, Univ. Paul Sabatier, Toulouse, France).

Rev. Acoust. (France), vol.15, no.63, p.224-9 (1982). In French.

Proposes a method for testing integrating sound level meters. After some generalizations about the errors due to the measurement, the authors discuss: (1) A method for typing different acoustic signals. Traffic noise has been especially studied. (2) A method of digital generation of random noise and the description of an automatic testing bench for integrating sound level meters. (9 refs.)

61359 Application of ultrasonic microscopy to the investigation of mechanical properties and defects in solids. J.Attal (CNRS, Univ. des Sci. et Tech. du Languedoc, Montpellier, France).

Rev. Acoust. (France), vol.15, no.63, p.231-3 (1982). In French.

A mechanical scanned acoustic microscope is described operating in the 0.6-1.2 GHz range specially devoted to the interior resolution of $5 \mu\text{m}$ and a depth penetration of several hundreds of microns, such a technique appears useful in various nondestructive tests, metallography and biological tissues. (3 refs.)

61360 Improved technique for amplitude inversion of backscattering in the study of cavities and flat defects. F.Cohen-Tenoudji (Ecole Normale Supérieure, Univ. Paris VII, France), B.R.Tittmann, G.Quentin. *Rev. Acoust. (France)*, vol.15, no.63, p.239-41 (1982). In French. A technique is proposed for the inversion of elastic scattering data in order to extract the geometrical properties of a scatterer embedded in a solid. The technique is partly based on the Kirchhoff approximation but goes much further by taking into account waves travelling on the scatterer in the shadow region. Results are presented for 'exact' theoretical and experimental data. (7 refs.)

61361 Technique for measurement of ultrasonic velocity with sing-around system. V.S.Soitkar, K.P.Sunnapwar, G.N.Navaneeth (Dept. of Phys., Nagpur Univ., Nagpur, India). *CSIO Commun. (India)*, vol.9, no.1, p.30-9 (Jan.-March 1982). [received: March 1983]

A solid state sing-around system developed by the authors has been successfully used to determine ultrasonic velocity in aqueous solutions of sulphuric acid of very weak concentrations. The authors present details of two mechanical assemblies used and of the time decay averaging method employed to increase the time resolution and, hence, the accuracy of the method. The results are compared with the data in the literature. An accuracy of 1 part in 10^4 has been obtained for determination of ultrasonic velocity from changes in delays. The system can be suitably employed to measure ultrasonic velocity in other liquids. (20 refs.)

61362 A new measurement method for separating airborne and structure-borne aircraft interior noise. M.C.McGary, W.H.Mayes (Noise Effects Branch, NASA Langley Res. Center, Hampton, VA, USA). *Noise Control Eng. J. (USA)*, vol.20, no.1, p.21-30 (Jan.-Feb. 1983).

Presents a new measurement method for separating airborne and structure-borne noise in propeller driven aircraft. The theory of the measurement method and the results of two experiments designed to validate the theory are presented. The method is based on the two-microphone cross spectral acoustic intensity measurement method and the theory of sound radiation of plate and thin shell structures. The measurements were performed on a plexiglass sheet mounted in the NASA Langley Research Center Noise Transmission Loss Facility and on a Beechcraft Baron fuselage. (23 refs.)

61363 Sound power determination from surface intensity measurements on a vibrating cylinder. N.Kaemmer, M.J.Crocker (Ray W. Herrick Labs., School of Mech. Engrg., Purdue Univ., West Lafayette, IN, USA). *J. Acoust. Soc. Am. (USA)*, vol.73, no.3, p.856-66 (March 1983).

The feasibility of using surface intensity measurements for the determination of sound power as a tool for noise source identification was studied with an experiment on a circular cylinder. This cylinder was an idealized model of a muffler shell of a heavy diesel truck. Two experiments were performed with the cylinder excited by an electromagnetic shaker. In the first one, the shaker was driven with a one-third octave band of white noise centered at 6300 Hz and in the second experiment it was driven with broadband white noise between 1000 and 5000 Hz. The sound power measurements were made in a reverberant room and the reverberant room method was used to provide a comparison with the sound power levels obtained from the surface intensity measurement. The acoustic surface intensity was computed from the cross-spectral density between the acoustic pressure and the normal surface velocity of the cylinder. An equation was developed to allow for inclusion of a correction for phase shifts that were caused by the instrumentation and by the finite distance between the microphone and the vibrating surface. The phase shift resulting from this distance was found to have a dominant effect in the higher frequency range and it was important to make these phase-shift corrections in order to obtain accurate measurements of sound power. After including these phase-shift corrections, reasonably good agreement was achieved between the sound power levels obtained from the surface intensity measurements and those from the reverberant room method. (21 refs.)

61364 Continuous-wave acoustic velocimeter with feedback. S.R.Stefanov, Yu.P.Chistoserdov. *Meas. Tech. (USA)*, vol.25, no.8, p.716-18 (Aug. 1982). Translation of: *Izmer. Tekh. (USSR)*, vol.25, no.8, p.70-1 (Aug. 1982). [received: April 1983]

The authors have developed an acoustic velocimeter in which the phase method with a frequency output is implemented in a simple form by means of an arrangement for the radiation and reception of acoustic waves with positive feedback. This arrangement has the same advantages for field experiments as the sing-around technique, but can provide significantly higher sensitivities. Further improvement can be achieved by means of an arrangement with two closed loops (two receivers). Theoretical and experimental investigations have indicated that the two-receiver configuration has a number of advantages over other acoustic velocimeters and can be operated in various liquid and gases. (3 refs.)

61365 Automatic echo selection logic for ultrasonic attenuation measurement system. L.Pathak, N.Murali, S.U.Rani (Reactor Res. Centre, Kalpakam, India). *Rev. Sci. Instrum. (USA)*, vol.54, no.4, p.482-5 (April 1983).

A simple low-cost circuit for automatic selection of two successive echoes during measurement of ultrasonic attenuation is described. When ultrasonic attenuation is measured as a function of a varying parameter like temperature, the transit time through the sample also changes, resulting in the shift of echo positions. This calls for manual adjustment of sample pulses used for sample and hold circuits. The present logic eliminates the need for manual adjustment. Details of the logic circuitry along with salient features of peak detectors and sample-and-hold circuits used are described. The results of performance tests are presented. (5 refs.)

61366 Acoustic polarizer using an electrically controlled piezoelectric element. E.K.Grishchenko (N.N. Andreev Acoustics Inst., Acad. of Sci., Moscow, USSR).

Sov. Tech. Phys. Lett. (USA), vol.8, no.7, p.340-1 (July 1982). Translation of: *Pis'ma v Zh. Tekh. Fiz. (USSR)*, vol.8, no.13-14, p.785-8 (July 1982). [received: April 1983]

Reports preliminary results of experiments on a controllable acoustic polarizer using an electrically controllable piezoelectric device. The rotation of the plane of polarization of the acoustic wave introduced by the electrically controllable piezoelectric device was measured on an apparatus designed for studying delay lines. (7 refs.)

61367 Surface-acoustic-wave diffraction grating from thin zinc oxide films. I.M.Grarkin, Yu.V.Nepochatkykh.

Sov. Tech. Phys. Lett. (USA), vol.8, no.8, p.424-5 (Aug. 1982). Translation of: *Pis'ma v Zh. Tekh. Fiz. (USSR)*, vol.8, no.15-16, p.981-4 (Aug. 1982). [received: April 1983]

Reports a study of a diffraction grating made from islands of a three-layer metal-zinc-oxide-metal film system on a fused quartz substrate. The experiments show that the necessary 180° phase shift between the oscillations in the SAW beams propagating along the free surface and along the surface covered

by the multilayer system can be achieved over the calculated path length, but the region of the transition from one oscillation phase to the other as the probe beam moves along the SAW front is $\approx 5\lambda$, where λ is the SAW wavelength. The period of the phase grating thus cannot be smaller than 10λ . (3 refs.)

61368 An acoustical synthetic focus imaging with pseudo-random signal. K.Nagai, S.Sano (Inst. of Appl. Phys., Univ. of Tsukuba, Ibaraki, Japan). *Trans. Inst. Electron. & Commun. Eng. Jpn. Part C (Japan)*, vol.J66C, no.1, p.108-9 (Jan. 1983). In Japanese.

A new synthetic focus digital acoustic imaging technique is described. The technique uses correlation of m -sequence signals to get prolonged impulse responses, by which digital images of objects are reconstructed. The result of the basic experiment is also presented to demonstrate the discussion. (5 refs.)

61369 Methods and feasibilities for the determination of the power radiated by an acoustic source. I. Survey about the traditional methods for estimating the sound power. I.Veit (Fraunhofer Inst. für Bauphys., Stuttgart, Germany).

Tech. Mess. tm (Germany), vol.50, no.3, p.87-92 (March 1983). In German. The sound power radiated by an acoustic source cannot be measured directly. Practical test conditions which have to be taken into account in estimating the radiated power from measurements of the sound pressure are discussed. Some new techniques for estimating the radiated power are discussed following a review of more traditional methods. One new technique that is becoming increasingly important utilizes the sound intensity and is based on measurement of the cross-spectral density function $K_{12}(\omega)$. The principle that underlies this approach is discussed. A novel sound power estimation procedure, the so-called phase gradient method, is also described. (19 refs.)

Acoustic sensitivity of a fiber-optic interferometer See Entry 59836

A study of reactor internal dynamics by reactor noise analysis See Entry 60333

Effect of size on measurements of the sound reduction index of a window or a pane See Entry 61347

The tight-coupled monopole active attenuator in a duct See Entry 61349

Wedge ultrasonic transducers having thickness extensional vibration See Entry 61371

Acoustic emission monitoring See Entry 63489

The significance of acoustic emission activity in stress-corrosion testing See Entry 63490

43.88 TRANSDUCTION; DEVICES FOR THE GENERATION AND REPRODUCTION OF SOUND

61370 Principle of piezoelectric frequency-tunable transducer. Wang Chen-hao, Zhao Zhe-ying (Inst. of Acoustics, Acad. Sinica, Peking, China).

Acta Acust. (China), vol.7, no.6, p.364-71 (Nov. 1982). In Chinese. Recently, the effect of electric load on the characteristics of a piezoelectric vibration system has been obtained. The resonant frequency of such a system changes continually with the changing of the electric load. In accordance with this effect, the authors made piezoelectric frequency-tunable transducers. In this paper, the principle of this frequency-tunable piezoelectric transducer is described. The authors theoretically analyse the piezoelectric frequency-tuning of the sandwich transducers and experimentally investigate a sandwich transducer of length-vibration bar with field parallel to length. The theoretical and experimental results show that such frequency-tuning is available at one and half octaves. For piezoelectric frequency-tunable transducer, the frequency tuning is convenient, continual and instantaneous. (4 refs.)

61371 Wedged ultrasonic transducers having thickness extensional vibration. T.Kobayashi (Coll. of Engrg., Nihon Univ., Koriyama, Japan). *J. Acoust. Soc. Jpn. (Japan)*, vol.38, no.12, p.748-54 (Dec. 1982). In Japanese.

Usually, ultrasonic transducers can only radiate ultrasonic waves of a narrow bandwidth, but it is possible to make a broad bandwidth by making a wedged type. The wedged transducers are made of PZT having thickness extensional vibration. The fundamental characteristics of them are investigated, and applications using them are attempted. First, the frequency characteristics of the free impedance and of the phase of the wedged transducers are measured. Also, the radiation patterns are observed using the schlieren method. Next, for the applications using those transducers, two experiments are attempted. One is the ultrasonic radiation of a broad bandwidth toward one direction using the semicylindrical wedged transducer. The other is the ultrasonic thickness measurement with resonance technique using the plate wedged and semicylindrical wedged transducer. (12 refs.)

61372 The effect of Fe-Ni films on the insertion loss of SAW. H.Yoshida, K.J.Sun, J.Schmidt, M.Levy (Phys. Dept., Univ. of Wisconsin, Milwaukee, WI, USA).

J. Magn. & Magn. Mater. (Netherlands), vol.35, no.1-3, p.178-80 (March 1983). (Proceedings of the 10th International Colloquium on Magnetic Films and Surfaces, Yokohama, Japan, 13-16 Sept. 1982).

The insertion loss of 618 MHz quartz SAW delay lines with nickel-rich Fe-Ni alloy films deposited between the interdigital electrodes exhibits as large a response to an applied magnetic field as that observed with pure nickel films. In addition, the alloys exhibit an enhanced domain wall motion effect. (5 refs.)

44.00 HEAT FLOW, THERMAL AND THERMODYNAMIC PROCESSES

44.10 HEAT CONDUCTION (MODELS, PHENOMENOLOGICAL DESCRIPTION)

61373 Insulating circular rugs. G.J.Weir (Appl. Math. Div., DSIR, Wellington, New Zealand).

J. Aust. Math. Soc. Ser. B (Australia), vol.24, pt.4, p.359-65 (April 1983). A thin, partially insulating circular rug is placed on a uniform half-space up through which a steady heat flow passes. The corresponding dual integral equations are solved using Tranter's method, finite Legendre transforms and Mellin-Barnes contour integrals. An untabulated Bessel (or Stieltjes) transform similar to the discontinuous Weber-Schafheitlin integral is evaluated, and a simple expression derived for the rug's surface temperature. (5 refs.)

61374 Investigation of transient temperature fields by electrical analogy. A. Faludi.

Meres & Autom. (Hungary), vol.31, no.2, p.68-71 (1983). In Hungarian. The author describes an electrical analog model constructed from active and passive electronic units which can be advantageously used for testing two-dimensional transient temperature fields. The electrical model consists of small uniform cubes with several kinds of functions. Thus, one can easily and quickly model cases of various geometry and different boundary conditions. Because of the rapid variational possibility and the stability of the solution the use of the electrical analogy can be put next to the numerical methods carried out by up-to-date computers. The practical application is briefly outlined through examples. (4 refs.)

On the problem of evolution criterion for thermodynamical waves See Entry 61396

A heat storage reactor for metal hydrides See Entry 63736

44.25 CONVECTIVE AND CONSTRAINED HEAT TRANSFER

(see also 47.25Q Convection and heat transfer)

61375 Heat transfer in subcooled liquid cryogenics. Yu.A.Kirichenko, K.V.Rusanov, E.G.Tyurina (Phys.-Tech. Inst. of Low Temperature, Acad. of Sci., Kharkov, Ukrainian SSR).

Cryogenics (GB), vol.23, no.4, p.209-11 (April 1983). An experimental study of heat transfer in helium, hydrogen and nitrogen has been carried out over a wide range of pressures and subcooling. Empirical correlations are obtained to calculate heat transfer coefficients at nucleate boiling, film boiling and single-phase convection. Conditions are determined for transitions from one heat transfer mode to another. (6 refs.)

61376 A solution for dispersed flow heat transfer using equilibrium fluid conditions. G.L.Yoder, Jr., W.M.Rohsenow (MIT, Cambridge, MA, USA).

Trans. ASME. J. Heat Transfer (USA), vol.105, no.1, p.10-17 (Feb. 1983). A method for predicting steady state dispersed vertical upflow film boiling heat transfer under constant heat flux conditions is presented. Differential transport equations and accepted heat transfer correlations are used to form a solution dependent upon knowledge of conditions at the dryout point only. Thermal nonequilibrium is included in the analysis and the actual flow quality is determined from local equilibrium conditions. A nondimensional grouping is derived which indicates the extent of nonequilibrium present in the flow. Results of this analysis are compared to data of three fluids in tube geometry: Freon 12, nitrogen, and steam. Predictions compare favorably with data from all three fluids. (22 refs.)

61377 Approximate phase change solutions for insulated buried cylinders. V.J.Lunardini (US Army Cold Regions Res. & Engng. Lab., Hanover, NH, USA).

Trans. ASME. J. Heat Transfer (USA), vol.105, no.1, p.25-32 (Feb. 1983). The conduction problem for cylinders embedded in a medium with variable thermal properties cannot be solved exactly if phase change occurs. New approximate solutions have been found using the quasi-steady method. These solutions consider heat flow from the entire pipe surface, rather than from a single point, as has been assumed in the past. The temperature field, phase change location, and pipe surface heat transfer can be evaluated using graphs presented for parametric ranges of temperature, thermal properties, burial depth, and insulation thickness. The theoretical results show good agreement with complete numerical solutions. The accuracy of the method increases as the Stefan number decreases and the results are of particular value for insulated hot pipes or refrigerated gas lines. (14 refs.)

61378 Radiation-natural convection interactions in two-dimensional complex enclosures. L.C.Chang, K.T.Yang, J.R.Lloyd (Dept. of Aerospace, Univ. of Notre Dame, Notre Dame, IN, USA).

Trans. ASME. J. Heat Transfer (USA), vol.105, no.1, p.89-95 (Feb. 1983). A numerical finite-difference study has been carried out for the two-dimensional radiation-natural convection interaction phenomena in square enclosures with equal vertical finite-thickness partitions located at the centers of the ceiling and floor. Both participating gases (CO_2 and NH_3) and nonparticipating gas (air) are considered. In the radiation calculations, the nongray exponential wide-band models for CO_2 and NH_3 are used, together with a radial flux method utilizing a more realistic polar description for the radiation exchange in the enclosure. Results on the effects of both surface and gas radiation on the velocity and temperature fields and the overall heat transfer rates as functions of the partition heights at two levels of the Grashof number are presented and discussed in terms of the physical phenomena. (13 refs.)

61379 An experimental study of free convection heat transfer from a horizontal cylinder in a vertical array set in free space between parallel walls. I.Tokura, H.Saito, K.Kishinami, K.Muramoto (Dept. Industrial Mech. Engng., Muroran Inst. of Technol., Muroran, Japan).

Trans. ASME. J. Heat Transfer (USA), vol.105, no.1, p.102-7 (Feb. 1983). Empirical formulas are proposed from experiments on free convective heat transfer from a cylinder array arranged in a vertical line. Subsequently, experiments were carried out to examine the effect of two parallel plates enclosing the array as a heat transfer promoter. Finally, through a discussion of the heat transfer from the entire cylinder systems, both in open and in restricted spaces, a recommendation is made for designing a heat exchanger of a single-line type of cylinder bank. (8 refs.)

61380 Natural convection heat transfer between eccentric horizontal cylinders. J.Prusa (Dept. of Mech. & Industrial Engng., Univ. of Illinois, Urbana, IL, USA), L.S.Yao.

Trans. ASME. J. Heat Transfer (USA), vol.105, no.1, p.108-16 (Feb. 1983). Laminar natural convection flow between vertically eccentric horizontal cylinders is studied numerically. The inner and outer cylinders are heated and cooled, respectively, to maintain constant surface temperatures. A physical model is introduced which accounts for the effects of fluid buoyancy as well as the eccentricity of the outer cylinder. A radial transformation is used to map the eccentric outer boundary into a concentric circle. Both field of a fluid between horizontal cylinders. The effect of buoyancy, which enhances average heat transfer, increases with the Grashof number. Eccentricity influences the flow in two ways. First, by decreasing the distance between the two cylinders over part of their surfaces, it increases the local heat transfer due to conduction. Secondly the eccentricity influences the convective mode of heat transfer. Results show that moderate positive values of eccentricity, enhance convective heat transfer. Results for a range of Grashof number are given, for varying eccentricity, for a radius ratio of 2.6 and a Prandtl number of 0.706. (24 refs.)

61381 Natural convection at the interface between a vertical porous layer and an open space. A.Bejan, R.Anderson (Dept. of Mech. Engng., Univ. of Colorado, Boulder, CO, USA).

Trans. ASME. J. Heat Transfer (USA), vol.105, no.1, p.124-9 (Feb. 1983). This paper examines the interaction by natural convection between a fluid-saturated porous medium and a fluid reservoir separated by a vertical impermeable partition. The two fluid systems are maintained at different temperatures. The analysis is simplified by assuming $\text{Pr} \gg 1$ in the fluid reservoir. It is shown analytically that the flow and temperature fields in the boundary layer regime consist of two fluid layers in counterflow. The interface temperatures is shown to increase monotonically with altitude. The important dimensionless group which governs the fluid mechanics is $B = (kR_{AK})^{1/2} / (k'R_A)^{1/4}$, where k, k', R_{AK} and R_A are, respectively, the porous medium conductivity, reservoir fluid conductivity, Darcy-modified Rayleigh number based on partition height, and the reservoir Rayleigh number based on partition height. The effect of parameter, B , on the flow, temperature, and heat transfer is documented in the range $0 < B < \infty$. (14 refs.)

61382 A correlation theory for steady natural convective heat transport in horizontal annuli. R.D.Boyd (Sandia Nat. Labs., Albuquerque, NM, USA).

Trans. ASME. J. Heat Transfer (USA), vol.105, no.1, p.144-50 (Feb. 1983). A correlation theory for two-dimensional natural convective heat transport data for horizontal annuli of arbitrary cross section has been developed and applied to two configurations: (i) concentric circular cylinders and (ii) annular formed by an inner hexagonal cylinder and an outer circular cylinder. Also embodied in the theory is the capability to predict local as well as mean heat transfer. Thermal boundary conditions of the form T^*x^m can be accommodated. Data for the Rayleigh number (R_{AK}) varied from 10 to 10^7 , Prandtl number (Pr) varied from 0.7 to 3100, and the aspect ratio (Δ/r), maximum annulus gap/minimum radius of inner annulus varied from 0.5 to 2.0. Even with these large variations, the present correlation theory collapses all the experimental data for the annular geometries to a single line. The physical problem appears to be completely specified by a single equation when the following is known: thermal boundary condition (i.e., m), the fluid (i.e., Pr), the aspect ratio, the Rayleigh number, and the geometry. This work demonstrates that the present theory is applicable to annuli of arbitrary cross section, and therefore the theory will be extended to include curvature effects and axisymmetric geometry. (16 refs.)

61383 Heat transfer from interrupted plates. R.L.Zelenka (Bur. of Reclamation, Denver, CO, USA), R.L.Loehrk.

Trans. ASME. J. Heat Transfer (USA), vol.105, no.1, p.172-7 (Feb. 1983). The forced convection heat transfer from two plates aligned with the flow direction in a wind tunnel was measured. The effects of leading edge bluntness, plate spacing distance, and Reynolds number on the leading and trailing plate average heat transfer rate were studied. The low Reynolds number steady laminar and transitional flow regimes investigated are typical for compact heat exchangers. The measured heat transfer rate from the leading plate agrees well with laminar theory for thin plates when the leading edge is rounded. The heat transfer rate from the leading plate with a blunt nose ranges from slightly below theoretical at a Reynolds number which gives a long, steady separation bubble to well above theoretical under conditions of laminar separation and turbulent reattachment. The heat transfer rate from the second plate is influenced by the leading edge configuration of the first plate only at small plate spacing distances and high Reynolds number. At large spacings the mixing provided by the unsteady wake of the first plate dominates that due to the turbulence formed by leading edge separation on the first plate. The leading edge configuration of the second plate is important only at large values of plate spacing. The heat transfer rate from the second plate is generally higher than that predicted by theory for laminar, steady flow over thin plates and may be higher than that on the leading plate. (18 refs.)

Particulate fouling on the gas-side of finned tube heat exchangers See Entry 59778

Evaluation of a method for heat transfer measurements and thermal visualization using a composite of a heater element and liquid crystals See Entry 59779

A semi-circle theorem in thermohaline convection with rotation and magnetic field See Entry 61500

Natural convection heat transfer of water within a horizontal cylindrical annulus with density inversion effects See Entry 61507

44.30 HEAT TRANSFER IN INHOMOGENEOUS MEDIA AND THROUGH INTERFACES

61384 Effective thermal conductivity of metal hydride beds. S.Suda, Y.Komazaki, N.Kobayashi (Dept. of Chem. Engng., Kogakuin Univ., Tokyo, Japan).

J. Less-Common Met. (Switzerland), vol.89, no.2, p.317-24 (Feb. 1983). (International Symposium on the Properties and Applications of Metal Hydrides, Tobu, Japan, 30 May-4 June 1982).

An experimental investigation aimed at improving the effective thermal conductivity of activated metal hydride is reported. Of the many material configurations which have been used to enhance heat transmission through metal hydride beds, a three-dimensional structure of a porous aluminium composite has shown the best results giving transmissions a factor of 9 or 10 greater than those of the unmodified hydride bed. The experimental results were used to derive equations for estimating the effective thermal conductivity as a function of the system pressure, the temperature, the hydride composition and the void fraction of the materials used. (3 refs.)

61385 Heat transmission analysis of metal hydride beds. S.Suda, N.Kobayashi, E.Morishita, N.Takemoto (Dept. of Chem. Engng., Kogakuin Univ., Tokyo, Japan).

J. Less-Common Met. (Switzerland), vol.89, no.2, p.325-32 (Feb. 1983). (International Symposium on the Properties and Applications of Metal Hydrides, Tobu, Japan, 30 May-4 June 1982).

Heat transmission studies were performed using a test unit designed to evaluate temperature profiles generated during hydriding and dehydriding reactions in a single metal hydride bed. By solving differential heat balance equations it is possible to predict temperature profiles, hydrogen gas transfer and temperature changes in heat transfer fluids. The computed results are in good agreement with the experimental data. The maximum error in the computed bed temperature was 4°C and the hydrogen flow rates were estimated with a maximum error of 15%. (3 refs.)

61386 An examination into the validity of various prediction methods for void fraction in boiling flow. S. Esaki, K. Sekoguchi, O. Tanaka. *Technol. Rep. Kyushu Univ. (Japan)*, vol.55, no.4, p.357-64 (Aug. 1982). In Japanese. [received: Feb. 1983]

A number of methods have been proposed for predicting the void fraction of boiling flow in the subcooled and saturated regions. The present study examines the validity of these methods by comparing the predicted void fractions with the experimental data available in the literature, including the authors' data. The data points used amount 1685 obtained from 162 test runs covering the experimental ranges: pressure of 1.0–140.6 atm, heat flux of $(1.6\text{--}326)\times 10^4$ kcal/m²h, and mass velocity of 310–5097 kg/m²s. Critical reviews are made as to the suitability and accuracy of individual methods. (21 refs.)

61387 Interaction of the nucleation phenomena at adjacent sites in nucleate boiling. M. Sultan (Westinghouse Canada Ltd., Hamilton, Ontario, Canada), R. L. Judd.

Trans. ASME. J. Heat Transfer (USA), vol.105, no.1, p.3-9 (Feb. 1983). The present investigation is an original study in nucleate pool boiling heat transfer combining theory and experiment in which water boiling at atmospheric pressure on a single copper surface at two different levels of heat and different levels of subcooling was studied. Cross spectral analysis of the signals generated by the emission of bubbles at adjacent nucleation sites was used to determine the relationship of the time elapsed between the start of bubble growth at the two neighbouring active sites with the distance separating them. The experimental results obtained indicated that for the lower level of heat flux at three different levels of subcooling, the elapsed time and distance were directly related. Theoretical predictions of a temperature disturbance propagating through the heating surface in the radial direction gave good agreement with the experimental findings, suggesting that this is the mechanism responsible for the activation of the surrounding nucleation sites. (13 refs.)

Effect of solar gain through walls and windows on annual building heat needs See Entry 63643

A technique for analyzing reversible metal hydride system performance See Entry 63735

A heat storage reactor for metal hydrides See Entry 63736

44.40 RADIATIVE HEAT TRANSFER

61388 Asymptotic analysis of radiative transfer problems. E. W. Larsen (Los Alamos Nat. Lab., Univ. of California, Los Alamos, NM, USA), G. C. Pomraning, V. C. Badham.

J. Quant. Spectrosc. & Radiat. Transfer (GB), vol.29, no.4, p.285-310 (April 1983).

The equations of radiative transfer are systematically analyzed by asymptotic methods. To lowest order, the classical equilibrium diffusion approximation is recovered. The next order analysis leads to the equilibrium diffusion differential equations and initial condition, but with a boundary condition containing a linear extrapolation distance α . This quantity is related to the solution of a canonical halfspace problem and is computed by deriving an appropriate variational principle. For the case of no scattering, an exact Wiener-Hopf solution is available. The F_N solution technique is also applied to the problem of obtaining α with good results. Higher order asymptotic radiative transfer descriptions are discussed and, while not immediately constituting practical calculational techniques, do have implications for computing the parameters in the multiband treatment of the frequency variable. (35 refs.)

61389 The nonequilibrium Marshak wave problem: a transport theory solution. B. D. Ganapol (Dept. of Nuclear & Energy Engng., Univ. of Arizona, Tucson, AZ, USA), G. C. Pomraning.

J. Quant. Spectrosc. & Radiat. Transfer (GB), vol.29, no.4, p.311-20 (April 1983).

An analytic solution to a particular Marshak problem is given. The radiative transfer model used is the one-group grey transport description coupled with the material energy balance. This solution provides a benchmark for validating time-dependent radiative transfer algorithms and constitutes a transport solution to the same problem previously solved using diffusion and low-order P_N approximations. Typical numerical results are given for surface and integral quantities and comparisons are made with the previously reported diffusion solution, as well as with a Monte Carlo result. (10 refs.)

61390 A multidimensional differential approximation for absorbing/emitting and anisotropically scattering media with collimated irradiation. M. F. Modest, S. Tabanfar (Dept. of Mech. Engng., Univ. of Southern California, Los Angeles, CA, USA).

J. Quant. Spectrosc. & Radiat. Transfer (GB), vol.29, no.4, p.339-51 (April 1983).

By considering the intensity within a medium to consist of a collimated and a fairly diffuse part, the overall problem of radiative transfer is reduced to two simpler ones: first the collimated intensity is obtained (equivalent in complexity to a nonscattering medium); for the evaluation of the diffuse part of the radiation (due to emission and scattering), a new differential approximation has been developed. To demonstrate the accuracy and simplicity of the present method, two sample cases are presented for which some exact solutions can be found in the literature: results are presented (i) for cosine-varying irradiation incident upon a two-dimensional, isotropically scattering slab and (ii) for irradiation with a Gaussian intensity distribution of a two-dimensional, anisotropically scattering semiinfinite cylindrical medium. (17 refs.)

61391 Radiative heat transfer in fibrous insulations. I. Analytical study. T. W. Tong (Dept. of Mech. Engng., Univ. of Kentucky, Lexington, KY, USA), C. L. Tien.

Trans. ASME. J. Heat Transfer (USA), vol.105, no.1, p.70-5 (Feb. 1983).

The purpose of this work is to develop models for predicting the radiant heat flux in lightweight fibrous insulations (LWFI). The radiative transport process is modeled by the two-flux solution and the linear anisotropic scattering solution of the equation of transfer. The radiative properties of LWFI consistent with these solutions have been determined based on extinction of electromagnetic radiation by the fibres. Their dependence on the physical characteristics of fibrous insulations has been investigated. It has been found that the radiant heat flux can be minimized by making the mean radius of the fibers close to that which yields the maximum extinction coefficient. The results obtained are useful to those concerned with the design and application of LWFI. (14 refs.)

61392 Radiative heat transfer in fibrous insulations. II. Experimental study. T. W. Tong (Dept. of Mech. Engng., Univ. of Kentucky, Lexington, KY, USA), Q. S. Yang, C. L. Tien.

Trans. ASME. J. Heat Transfer (USA), vol.105, no.1, p.76-81 (Feb. 1983).

For pt. I see *ibid.*, vol.105, p.76 (1983). Two experiments have been conducted to study radiative heat transfer in light-weight fibrous insulations (LWFI).

The spectral extinction coefficients for a commercial LWFI have been measured via transmission measurements, and a guarded hot plate apparatus has been used to measure the radiant heat flux as well as the total heat flux in the insulation. The experimental results are compared with the theoretical values calculated according to the analytical models presented in pt. I of this paper. The comparisons reveal that the analytical models are useful in giving representative values for the radiative properties of typical LWFI. However, only qualitative agreements have been obtained for the heat transfer results. (10 refs.)

61393 Radiation and smoke from the gas turbine combustor using heavy fuels. Y. S. H. Najjar (Mech. Engng. Dept., Yarmouk Univ., Irbid, Jordan), E. M. Goodger.

Trans. ASME. J. Heat Transfer (USA), vol.105, no.1, p.82-8 (Feb. 1983). Broadening of aviation fuel specifications has been simulated using blends of gas oil and residual fuel oil. Radiation, smoke, and temperature measurements in an experimental combustor at various air pressure, inlet temperature, and air/fuel ratios showed a diminishing rate of increase of radiation with soot concentration and reduced sensitivity of smoke to fuel hydrogen content at higher combustor pressures. (6 refs.)

Insulating circular rugs See Entry 61373

44.50 THERMAL PROPERTIES OF MATTER (PHENOMENOLOGY, EXPERIMENTAL TECHNIQUES)

(see also 07.20 Thermal instruments and techniques)

61394 The insulation effectiveness of a porous material as measured by the screening technique. C. R. Maiti (Cryogenic Engng. Centre, Indian Inst. of Technol., Kharagpur, India).

Cryogenics (GB), vol.23, no.4, p.207-8 (April 1983). The percentage transmittance of infrared radiant energy through porous material at room temperature has been reported. It can be utilised to compare the insulation effectiveness under high vacuum. (2 refs.)

61395 Thermal radiation effects in thermal conductivity measurements: analysis and remedies. M. Locatelli, J. Lopez, M. Nunez-Regueiro (Lab. de Cryophys., CENG, Grenoble, France).

J. Phys. D (GB), vol.16, no.4, p.479-87 (14 April 1983).

The authors have studied the effect of thermal radiation on measurements of the thermal conductivity of small samples below room temperature. By using the different thermal conductivity technique they were able to measure the importance of these effects for temperatures greater than about 100K and to determine the principal source of error of the double flux correction, i.e. the different heater temperature with each different heat flux. They thus propose a better configuration for performing such measurements. (2 refs.)

The effective conductivity of a periodic array of spheres See Entry 59750

Effective thermal conductivity of metal hydride beds See Entry 61384

Heat transmission analysis of metal hydride beds See Entry 61385

An ion-implanted resistor as thermal transient sensor for the determination of the thermal diffusivity in silicon See Entry 62194

A technique for analyzing reversible metal hydride system performance See Entry 63735

44.60 THERMODYNAMIC PROCESSES (PHENOMENOLOGY, EXPERIMENTAL TECHNIQUES)

(see also 05.70 Thermodynamics, 07.20 Thermal instruments and techniques)

61396 On the problem of evolution criterion for thermodynamical waves. D. K. Bhattacharya (Tech. Univ. of Budapest, Budapest, Hungary).

Acta Mech. (Austria), vol.47, no.1-2, p.87-94 (1983).

Irreversible systems in which both dissipative and relaxation phenomena are taking place can be appropriately described by the wave approach of Onsagerian thermodynamics proposed by Gyarmati. An important consequence of this theory is that it leads to hyperbolic transfer equations and these are referred to as thermodynamical waves. The author examines the possibility of existence of an evolution criterion for such thermodynamical waves. A monotonic transition of the thermodynamical waves from non-equilibrium states to stationary states is insured only when dissipative processes are dominant over relaxation phenomena. (22 refs.)

61397 A hybrid computer algorithm for temperature distribution analysis of irregular two dimensional shapes. P. Valisalo (Dept. of Industrial & Systems Engng., Univ. of Florida, Gainesville, FL, USA), D. Bergquist, V. McGrew.

10th IMACS World Congress on System Simulation and Scientific Computation, Montreal, Canada, 8-13 Aug. 1982 (New Brunswick, NJ, USA: IMACS 1982), p.17-19 vol.2

The principle of random walk was used to determine the temperature at a given point on a two dimensional plate, using a Monte Carlo method for solving linear partial differential equation. To determine the number of walks required the relationship between the grid size (i.e. the distance from one point to the next one) and the standard deviation of the random noise driving the x- and y-axis on an x-y plotter, a simple square plate was used. Three of the sides were subjected to a certain temperature on the contour line, C, and one to a different temperature. Because an analytical solution for this problem is readily available, this test was used for comparison purposes. A methodology was developed whereby a two dimensional plate of any shape subjected to a number of different temperatures along a contour line could be analysed. The methodology is described. A recommendation is made on how to expand this to three dimensions and how to improve it if more sophisticated equipment is available. (3 refs.)

A technique for analyzing reversible metal hydride system performance See Entry 63735

46.00 MECHANICS, ELASTICITY, RHEOLOGY

46.10 MECHANICS OF DISCRETE SYSTEMS

(see also 03.20 General mathematical aspects)

61398 Numerical analysis of flexural vibrations of rotors resting on elastic supports. Z.Dzygadło.

J. Tech. Phys. (Poland), vol.22, no.4, p.415-27 (1981).

The method of analysis of natural and forced flexural vibrations of rotors proposed enabled the author to determine the dynamic characteristics of rotors of various structures, the elastic and damping properties of the supports being taken into account. (9 refs.)

61399 Numerical determination of the dynamic stability parameter and of the periodic oscillations of planar mechanisms. Nguyen van Khang (Polytech. Hochschule Hanoi, Hanoi, Vietnam).

Rev. Roum. Sci. Tech. Ser. Mec. Appl. (Rumania), vol.27, no.4, p.495-507 (July-Aug. 1982). In German. [received: March 1983]

Relates to a mechanical system with many degrees of freedom. The solution of the equations is carried out with a computer. The linear differential equations with periodic parameters are treated with matrices, and indications are given for calculating the initial values using the FORTRAN programming language. The numerical solution is illustrated with an example of a crank and linkage coupled mechanism. (18 refs.) I.G.

61400 On nonlinear resonances in the problem of a body moving about its centre of mass under Lorentz forces. N.V.Chikova.

Vestn. Leningr. Univ. Ser. Mat. Mekh. & Astron. (USSR), no.1, p.85-91 (Jan. 1983). In Russian.

Considers the motion about its centre of mass of a gravity-gradient stabilized satellite with electrostatic protection implemented as a charged sphere for resonance cases. In the equations of motion terms up to the second order are retained. (3 refs.)

The unsymmetric gyroscope under the influence of a frictional and a magnetic torque See Entry 59772

46.20 CONTINUUM MECHANICS

(see also 03.40 General mathematical aspects)

61401 Numerical solution of two-dimensional static boundary problems for flexible conical shells. Ya.M.Grigorenko (Acad. of Sci., Ukrainian SSR), N.N.Kryukov, Kh.Saparov.

Dopov. Akad. Nauk UkrSR. Ser. A (USSR), no.2, p.28-31 (1983). In Ukrainian.

Presents an approach to a numerical solution of a two-dimensional nonlinear boundary problem concerning the geometrically nonlinear deformation of conical shells of variable thickness. The two-dimensional boundary problem is reduced to a one dimensional problem by means of a difference approximation along a circular coordinate. This latter problem is solved by the method of linearization. The calculation results illustrate the process of convergence. (9 refs.)

61402 Analysis of shells with Monge's middle surfaces by a semianalytical finite element method. Ya.G.Savula.

Dopov. Akad. Nauk UkrSR. Ser. A (USSR), no.2, p.37-40 (1983). In Ukrainian.

Presents an analysis of shells with Monge's middle surfaces. The analysis is carried out using a semianalytical finite element method. Numerical results are obtained for two classes of shells: curved tubes and zero Gauss curvature shells. The error bound for the semianalytical method is established. (8 refs.)

61403 On the Lagrangian formulation of continuum mechanics. A.Golebiewska-Herrmann (Div. of Appl. Mech., Stanford Univ., Stanford, CA, USA).

Physica A (Netherlands), vol.118A, no.1-3, p.300-14 (March 1983). (Proceedings of the Conference on Nonlinear Fluid Behavior, Boulder, CO, USA, 7-11 June 1982).

The aim of the paper is to show that a Lagrangian formulation of continuum mechanics (in the spirit of field theory) can deliver not only equations of motion but the conservation laws related to the material symmetries in the perfect continuum. Those conservation laws in the presence of defects lead to the path-independent integrals broadly used in fracture mechanics. They are basically related to the (material) forces on a defect in a continuum and can be interpreted as the equations of motion for a defect with respect to the material. The quantity playing the role of the stress tensor in this formulation is the material momentum tensor. A simple example of a material force in the form of a path-independent integral in the fluid is considered. (13 refs.)

A matrix method for the study of the stress and deformation of continuous beams, statically non-determined, subjected to bending See Entry 61422

Fast convergence modal analysis for continuous systems See Entry 61436

46.30 MECHANICS OF SOLIDS AND RHEOLOGY

(see also 62.20 Mechanical properties of solids, as related to microscopic structure)

46.30C Static elasticity

61404 A St. Venant principle for nonlinear elasticity. R.J.Knops (Heriot-Watt Univ., Edinburgh, Scotland), L.E.Payne.

Arch. Ration. Mech. & Anal. (Germany), vol.81, no.1, p.1-12 (1983).

The authors consider a semi-infinite cylinder made from homogeneous nonlinear elastic material and loaded on its base by a self-equilibrated distribution of forces. The lateral sides are stress-free, but it is not assumed a priori that the stresses and displacement vanish at infinity. They prescribe that their absolute values do not grow faster than a given exponential. Under certain constitutive hypotheses, it is then possible to prove that the L_2 -integral of the displacement taken over a cross-section of the cylinder either grows faster than some exponential or decays at least exponentially with distance from the base of the cylinder. A similar result is proved when the displacement is held fixed on the lateral sides, but then it is found that the force distribution over the base need not necessarily be self-equilibrated. (24 refs.)

61405 St. Venant formulae for generalized St. Venant problems. P.Podio-Guidugli (Univ. de Pisa, Pisa, Italy).

Arch. Ration. Mech. & Anal. (Germany), vol.81, no.1, p.13-20 (1983).

For an isotropic, linearly elastic cylinder subject to end tractions equipollent to a torque M , the 'twist' τ is defined in such a way that $M = (\mu R)\tau$, where

μR , the torsional rigidity of the cylinder, is resolved into the factors μ , the shear modulus, and R , a geometric quantity depending only on the cross-section. As remarked by Truesdell (*Appl. Mech. Reviews* vol.12, p.75 (1959)) and recalled by Day (*ibid.*, vol.76, p.283 (1981)), such a twist would generalize St. Venant's motion of twist so as to apply also to solutions of the torsion problem corresponding to distributions of end tractions different from one assumed by St. Venant. The author investigates whether, were Truesdell's problem rephrased in the obvious manner, Day's procedure would apply to further generalized St. Venant problems. (7 refs.)

61406 A coupled thermoelastic problem of an infinitely extended thin plate containing a circular hole with thermal relaxation. N.Bhatta, S.K.Roy Choudhuri (Dept. of Maths., Burdwan Univ., Burdwan, India).

Indian J. Pure & Appl. Math., vol.14, no.1, p.85-95 (Jan. 1983).

Generalised dynamical theories of thermoelasticity are employed to study a two dimensional thermoelastic problem of an infinitely extended thin plate containing a circular hole whose free inner boundary is subjected to a step rise in temperature. Short time-approximation for stresses are derived using the Laplace transform technique. (6 refs.)

61407 Influence of the coupling effect on a transient thermoelastic problem in a solid sphere. Y.Takeuti, Y.Tanigawa (Dept. of Mech. Engng., Univ. of Osaka Prefecture, Sakai, Japan).

J. Tech. Phys. (Poland), vol.22, no.4, p.463-75 (1981).

The authors consider the coupled problems of a spherical region. Using a new technique, they succeed in separating the analysis of the temperature field and the associated stress fields. For the illustrative purposes they have obtained the coupled solution for a solid sphere, due to axisymmetrical local heating, without any approximations, which is effective enough for the whole time range. They have also carried out numerical calculations using the most realistic value of the coupling parameter. From the numerical results it can be seen that the effect of the thermoelastic coupling term shows a clear lag in the temperature and the stress distributions in comparison with the uncoupled results. (1 ref.)

61408 Non-linear optimization of the material constants in Ogden's stress-deformation function for incompressible isotropic elastic materials. E.H.Twizell, R.W.Ogden (Dept. of Math., Brunel Univ., Uxbridge, England).

J. Aust. Math. Soc. Ser. B (Australia), vol.24, pt.4, p.424-34 (April 1983).

The present paper improves upon established correlation between theory and experiment by a systematic optimization procedure for calculating material constants. For purposes of illustration the Levenberg-Marquardt non-linear least squares optimization algorithm is adapted to determine the material constants in Ogden's three-term stress-deformation function. Calculations are carried out also in respect of a four-term stress-deformation function and further improvement in the fit is achieved over a large range of deformation. (10 refs.)

61409 Bending of a plate with a periodic system of cuts. V.A.Merkulov. *Mech. Solids (USA)*, vol.17, no.4, p.171-6 (1982). Translation of: *Izv. Akad. Nauk SSSR Mekh. Tverd. Tela*, vol.17, no.4, p.187-92 (1982).

On the basis of the method previously proposed for the two-dimensional problems, the author obtains the integral equations of the problem of elasticity for bending of a thin plate with a periodic system of through curvilinear cuts loaded by systems of forces and moments that are self-equilibrated on each cut. It is established that the equation is solvable, and that a solution of the initial boundary-value problem exists and is unique. The problem is solved in quadratures for cuts along one straight line. When only the principal vector is equal to zero on each cut, for cuts along one line, the problem can also be solved in quadrature by the method of linear conjunction of the boundary values. For the case of one cut in a period, the stress intensity coefficients are obtained upon bending of the plate by moments applied both to the edges of the cut and at infinity. (7 refs.)

61410 Finite anti-plane shear of a semi-infinite strip subject to a self-equilibrated end traction. C.O.Horgan, R.Abeyaratne (Michigan State Univ., East Lansing, MI, USA).

Q. Appl. Math. (USA), vol.40, no.4, p.407-17 (Jan. 1983).

In a recent paper (see C.O. Horgan, H.K. Knowles, *J. Elasticity*, vol.11, p.271-91, 1981), a version of Saint-Venant's principle was formulated and established for finite elastostatics. The present authors refer to the previous work and the references cited therein for a discussion of the issues underlying Saint-Venant's principle both for linear and nonlinear elasticity. The semi-infinite strip problem is considered for the special case of self-equilibrated applied end traction ($\tau=0$). An exponential decay inequality for the nonvanishing component of shear stress on the long sides of the strip is established. This result is qualitatively similar to that previously obtained but provides a sharper estimate. (7 refs.)

61411 Thermal stresses in anisotropic noncylindrical beams. S.Chirita (Univ. of Iasi, Iasi, Rumania).

Rev. Roum. Sci. Tech. Ser. Mec. Appl. (Rumania), vol.28, no.1, p.63-74 (Jan.-Feb. 1983).

The deformation of some noncylindrical beams under the action of a temperature variation, of polynomial form in the axial coordinate, is studied. The case of the almost cylindrical beams, the naturally twisted beams and the naturally slightly curved beams made of an anisotropic and inhomogeneous elastic material are considered. The thermoelastic coefficients are independent of the axial coordinate. (12 refs.)

61412 Large deflection finite element analysis of elastic beams under a follower force. N.Uda, K.Kunoo, H.Ohira.

Technol. Rep. Kyushu Univ. (Japan), vol.55, no.4, p.365-70 (Aug. 1982). In Japanese. [received: Feb. 1983]

Presents a nonlinear analysis of elastic beams subjected to a follower force by a finite element method. The special effect of follower forces which are dependent on displacement is formulated as a load stiffness matrix. The large deflection behavior of elastic systems under a follower force is analysed statically by the finite element method using the incremental technique. The critical load for divergence or flutter is obtained by applying the dynamic criterion at each step of the load increment. The use of the present method is demonstrated on several assemblies of the beam element. (9 refs.)

A decreasing property of solutions of parabolic equations with applications to thermoelasticity See Entry 59595

Coupled vibrations of beams—an exact dynamic element stiffness matrix See Entry 61432

Three-dimensional problem of diffraction of plane elastic waves by a wedge See Entry 61443

Excitation of waves by a vibrating elastic cylinder in a layer See Entry 61444

Lamb waves in a prestressed plate of isotropic nonlinear-elastic incompressible material See Entry 61445

Numerical ways of solving the problems of vibrations of thin plates subjected to impact loads See Entry 61449

Some remarks on elastic fracture mechanics See Entry 61451
 Nonsteady interaction between a die and an elastic medium See Entry 61458

46.30J Viscoelasticity, plasticity, viscoplasticity, creep, and stress relaxation (inc. rheology of solids)

61413 A theory of viscoelastic composites modeled as interpenetrating solid continua with memory. M.F.McCarthy (Nat. Univ. of Ireland, Galway, Ireland), H.F.Tiersten.

Arch. Ration. Mech. & Anal. (Germany), vol.81, no.1, p.21-51 (1983).
 An existing description of composite materials modeled as interpenetrating solid continua is extended to include constitutive response functionals over the histories of the constitutive variables of the n -consistent composite. As in the earlier work, the relative displacement of the individual constituents is required to be infinitesimal in order that the composite does not rupture even though the motion of the combined composite is finite. Conditions on the response functionals under the assumption of fading memory are obtained from the Clausius-Duhem inequality for the combined composite. Relaxation and cyclical processes are discussed and it is shown that the equilibrium response of the composite considered is the same as that of the elastic composites treated in the earlier work. Some detailed results are obtained for the case of two-constituents under the additional assumption of finite linear viscoelastic response. (36 refs.)

61414 Viscoplastic localization in simple shear: exact results in nonlinear theory. A.Molinari (Univ. de Metz, Metz, France).
C.R. Seances Acad. Sci. Ser. II (France), vol.296, no.1, p.1-4 (10 Jan. 1983). In French.

Examines the onset and evolution of shear bands occurring in a simple shear deformation initially quasi-homogeneous. The material is viscoplastic and thermomechanical coupling is accounted for. The problem is assumed quasi-static and adiabatic. The localization process is described for temperature and deformation with respect to different constitutive laws, specially for strain hardening materials and Arrhenius laws. (5 refs.)

61415 A generalization of plastic zone representations under antiplane strain of ideally elastic plastic solids with a pointed stress concentrator. V.A.Kriven'.

Dopov. Akad. Nauk UkrSR. Ser. A (USSR), no.2, p.31-4 (1983). In Ukrainian.

Deals with the solution of elasto-plastic problems of a longitudinal shear of nonhardenable solids with a wedge-like notch, using the supposition that the plastic zone is formed by a bunch of plastic stripes coming out from the corner point of the notch. It is shown that discontinuous solutions describing such plasticity zones under conditions of an infinite increase in stripe number turn into continuous solutions describing plastic strains distributed in a certain three-dimensional region. (6 refs.)

61416 Elasto-plastic analysis of anisotropic plates and shells by the semi-loof element. D.R.J.Owen (Dept. of Civil Engng., Univ. of Wales, Swansea, Wales), J.A.Figueiras.

Int. J. Numer. Methods Eng. (GB), vol.19, no.4, p.521-39 (April 1983).
 An elasto-plastic analysis of thin plates and shells by means of the finite element displacement method is considered for anisotropic materials, using the Semi-loof curved shell element. The elasto-plastic analysis is based on the Huber-Mises yield criterion extended by Hill for anisotropic materials. The yield function is generalized by introducing anisotropic parameters of plasticity which are updated during the material strain hardening history. Numerical examples are presented and compared with available solutions. The effects of anisotropy on these solutions are also discussed. The practical problem of an aerofoil blade is also considered and some results presented. (20 refs.)

61417 Anisotropic elasto-plastic finite element analysis of thick and thin plates and shells. D.R.J.Owen (Dept. of Civil Engng., Univ. of Wales, Swansea, Wales), J.A.Figueiras.

Int. J. Numer. Methods Eng. (GB), vol.19, no.4, p.541-66 (April 1983).
 An elasto-plastic analysis of anisotropic plates and shells is undertaken by means of the finite element displacement method. A thick shell formulation accounting for shear deformation is considered, which is based on a degenerate three-dimensional continuum element. The accommodation of variable material properties, not only along the surface of the structure but also through the thickness, is made possible by a discrete layered approach. Although isoparametric elements of the Serendipity family give satisfactory solutions for thick and moderately thin shells the results exhibit 'locking' for an increasing ratio of span to thickness. To develop a numerical model which is applicable to thick or thin plates and shells, the nine-node Lagrangian element and the Heterosis element are also introduced into the present model. Plastic yielding is based on the Huber-Mises yield surface extended by Hill for anisotropic materials. The yield function is generalized by introducing anisotropic parameters of plasticity which are updated during the material strain hardening history. (35 refs.)

61418 The elasto-plastic problem of a thin rotating disc with variable thickness. J.G.Chakravorty, P.K.Choudhuri (Dept. of Appl. Maths., Univ. Coll. of Sci. & Technol., Calcutta, India).

Indian J. Pure & Appl. Math., vol.14, no.1, p.70-8 (Jan. 1983).
 Investigates the problem of a thin rotating disc with a central circular hole and thickness varying with the radial distance. The problem has been solved in the elasto-plastic range assuming two arbitrary functions for the thickness of the disc. The angular velocity for which the disc becomes completely plastic has been computed numerically for both cases and has been compared with its value when the disc is uniform in thickness. (9 refs.)

61419 Creep of structural elements with random parameters. V.N.Ilin, V.V.Kashelkin, S.A.Shestarikov.

Mech. Solids (USA), vol.17, no.4, p.145-51 (1982). Translation of: *Izv. Akad. Nauk SSSR Mekh. Tverd. Tela*, vol.17, no.4, p.159-67 (1982).
 A probabilistic and statistical approach is proposed to creep calculations for mechanical elements of structures such as rods, plates, and shells. It is assumed that the mathematical model of deformation of the elements in question has been reduced to a Cauchy problem for ordinary differential equations containing a finite number of random parameters $a_j (j=1, \dots, k)$ with known joint probability distribution density $p_k(a_1, \dots, a_k)$. Under the assumption that the scatter $a_j (j=1, \dots, k)$ is statistically small, a solution of the fundamental problem of statistical structural dynamics is offered in relation to creep of these elements. The small-parameter method and approximate canonical expansions of the unknown random functions are employed.

61420 Bending of a plate containing coated pores. A.I.Plotnikov, Yu.A.Fedorov, A.M.Chernikov.

Mech. Solids (USA), vol.17, no.4, p.177-82 (1982). Translation of: *Izv. Akad. Nauk SSSR Mekh. Tverd. Tela*, vol.17, no.4, p.193-9 (1982).
 Porous materials exist in which a layer of material different from the matrix forms on the pore surface. This layer can create internal stresses, thus exerting considerable influence on the physical and mechanical properties of the material. If the coated pores are in a fairly thin plate, then the internal stresses may be the cause of bending of the plate. The authors calculate the bending of a circular plate resulting from stresses of this type. (5 refs.)

61421 When is a nonlinear viscoelastic material hyperelastic. D.W.Reynolds (Univ. Coll. Dublin, Dublin, Ireland).

Q. Appl. Math. (USA), vol.40, no.4, p.492-6 (Jan. 1983).
 Presents two different characterizations, in terms of work, of hyperelastic materials within the wider class of nonlinear viscoelastic ones. A viscoelastic material is regarded as one in which the stress depends continuously on strain history and has a mild form of fading memory. If the stress equals the gradient of potential evaluated at the present strain, the material is hyperelastic. In such a material, the stress depends on the strain history only through its present value. (8 refs.)

61422 A matrix method for the study of the stress and deformation of continuous beams, statically non-determined, subjected to bending. D.Voiculescu, D.Mateescu (Inst. Polytech., Bucharest, Rumania).

Rev. Roum. Sci. Tech. Ser. Mec. Appl. (Rumania), vol.27, no.5, p.629-50 (Sept.-Oct. 1982). In French. [received: March 1983]

Presents a study of continuous beams, statically non-determined, subjected to continuous or distributed loads and shows discontinuities in the shape or the displacement. A matrix method is described in order to determine the deformation-stress vector on a portion of the beam situated between two consecutive supports. The application of this method to a continuous beam on several supports leads to a system of equations on a Jacobi type of matrix, which is resolved by the decomposition of each matrix into a product of biological matrices. This method may be applied whatever the conditions at the extremities of the continuous beam. (6 refs.) H.C.B.

61423 Antiplane deformation of a body with a curved elastic sharp-ended inclusion. L.T.Berezhnitskii, P.S.Kachur, L.P.Mazurak, Ya.I.Khodan' (G.V. Karpenko Physicomech. Inst., Acad. of Sci., Lvov, Ukrainian SSR).

Sov. Mater. Sci. (USA), vol.18, no.3, p.245-50 (May-June 1982). Translation of: *Fiz.-Khim. Mekh. Mater. (USSR)*, vol.18, no.3, p.63-9 (May-June 1982). [received: Feb. 1983]

An algorithm is proposed for calculating the stress intensity factors close to the tip (the cusp on the contour) of a foreign inclusion in an isotropic body in antiplane deformation. On the basis of the method of 'disturbance of the form of the boundary' recurrent equations were obtained for the coefficients of expansion of the complex functions of stresses. A determination is given of the convergence of the stress intensity factors, and the relationship of these values to the configuration of the inclusion and to the difference between the elastic characteristics of the materials of the composite is investigated. (5 refs.)

61424 Numerical solutions for analyzing the nonaxisymmetric 2-dimensional deformation processes. S.Nishimura (Dept. of Precision Engng., Tohoku Univ., Sendai, Japan).

Technol. Rep. Tohoku Univ. (Japan), vol.47, no.2, p.189-201 (1982). In English.

A method for analyzing non-axisymmetric 2-dimensional deformation processes is presented. In the state of non-axisymmetric plane stress, incremental strains are not integrable with respect to time, since the principal axes of the incremental strains are rotated with respect to the material element. The fundamental equations are more complicated than those in the axisymmetric case because two position variables are necessary and one-to-one correspondence between differential representations of the displacements and strains is not satisfied due to shearing strains. In the present method, avoiding these difficulties, only stresses and displacements are used as dependent variables, so that the compatibility equations do not come into the analysis explicitly. The difference method may be, then, easily adopted for the numerical solutions. The present method is considered to be useful in the problems which are investigated by means of the flow theory for work-hardening materials. (6 refs.)

Bending of a plate with a periodic system of cuts See Entry 61409

Dynamic loading of nonlinearly flowing cylindrical and spherical shells See Entry 61430

Propagation of plastic waves in a bar of material exhibiting strain-rate effect (on the existence of strain plateau) See Entry 61440

Elasto-plastic wave propagation in a finite bar with consideration of temperature rise caused by plastic work See Entry 61441

Numerical ways of solving the problems of vibrations of thin plates subjected to impact loads See Entry 61449

On the measurement of visco-elastic properties of matters by the Mossbauer effect See Entry 61461

Viscoelastic thermal stress analysis See Entry 61463

Use of nonlinear viscoelastic materials in the polarization-optical method See Entry 61465

Experimental investigation of plastic strains of porous solids—a review See Entry 63190

46.30L Static buckling and instability

61425 Optimal laminated composite shells for buckling and vibration. Y.S.Nshanian (Ministry of Agriculture, Yerevan, USSR), M.Pappas.

AIAA J. (USA), vol.21, no.3, p.430-7 (March 1983).
 Methods are proposed for the determination of the optimal ply angle variation through the thickness of symmetric angle-ply shells of uniform thickness. These methods use continuous piecewise-linear segment approximations or discontinuous piecewise-constant segment approximations to the ply angle function. A mathematical programming (MP) problem is formulated using segment ply angles and thicknesses as design variables. A special MP algorithm, capable of treating multiple objective functions, combined with a critical mode search is used to solve this problem. The procedure is applied to the maximization of the minimum natural frequency or buckling load of a thin, simply supported, circular, cylindrical, angle-ply shell. Results show large performance gains result from the use of optimal variable ply angle configurations, compared to an optimal constant ply angle. The continuously variable ply angle approximation is particularly effective. (15 refs.)

61426 Dynamic stability boundaries for a sinusoidal shallow arch under pulse loads. M.T.Donaldson, R.H.Plaut (Virginia Polytech. Inst. & State Univ., Blacksburg, VA, USA).

AIAA J. (USA), vol.21, no.3, p.469-71 (March 1983).

The dynamic snap-through of shallow elastic arch subjected to triangular pulse loads is investigated. Concentrated loads with independent magnitudes are applied at the quarter points of the arch as a means of assessing the effects of load asymmetry. Critical load combinations are determined and the effects of the pulse duration and external damping on the interaction curves are examined. The behaviour is similar to that of some shallow shells under blast loads and demonstrates that asymmetric loading may have much lower critical values than symmetric loading. (10 refs.)

61427 Use of the Southwell method to predict buckling strengths of stringer stiffened cylindrical shells. C.G.Foster (Dept. of Civil & Mech. Engng., Univ. of Tasmania, Hobart, Tasmania, Australia), R.C.Tennyson. *Strain (GB)*, vol.19, no.2, p.63-7 (May 1983).

Presents the results of some tests that were conducted on stringer stiffened epoxy cylindrical shells. The object of the investigation was to determine if the Southwell technique for estimating buckling loads could reasonably be used for the nonlinear collapse of cylindrical shells. The results showed that the technique provides a useful estimate of the buckling load provided care is taken in interpreting the results. In some instances the estimate is likely to be greater than the actual load. Where two buckling modes are encountered at the same time the Southwell technique appears to predict the critical load associated with either mode depending on the deflection parameter being measured as well as on the interpretation of the results. (3 refs.)

61428 On lateral buckling—fracture stability of thin-sheet structural components with deep cracks. H.-P.Rossmann (Inst. für Mech., Tech. Univ. Wien, Wien, Austria).

Z. Flugwiss. & Weltraumforsch. (Germany), vol.7, no.1, p.29-33 (Jan.-Feb. 1983). In German.

Fracture mechanics and stability aspects of combined cracking, lateral buckling and small scale yielding phenomena are investigated for particular thin-walled structural components fabricated of brittle or semi-ductile materials. (8 refs.)

Speckle-interferometry, a simple method for deformation analysis

See Entry 61464

46.30M Vibrations, aeroelasticity, hydroelasticity, mechanical waves, and shocks

(see also 43.40 Mechanical vibrations and shock)

61429 On the Liapounov-Movchan stability of equilibrium of elastic orthotropic plates. J.L.Nowinski (Univ. of Delaware, Newark, DE, USA).

Acta Mech. (Austria), vol.47, no.1-2, p.27-38 (1983).

On the basis of the Liapounov definition of stability and the necessary and sufficient Liapounov-Movchan conditions for a continuous body to remain stable, an elastic orthotropic rectangular plate subject to a uniformly distributed inplane compression, is analyzed. Two types of loading are considered: a conservative dead load and a nonconservative follower load. Two metrics discussed involve the maximum and the mean-square values of the deflection. The secondary critical load is found to depend heavily on the kind of anisotropy. (18 refs.)

61430 Dynamic loading of nonlinearly flowing cylindrical and spherical shells. S.B.Maksimov, V.A.Lupin, L.V.Maksiova.

Combust. Explos. & Shock Waves (USA), vol.18, no.4, p.495-8 (July-Aug. 1982). Translation of: *Fiz. Goreniya & Vzryva (USSR)*, vol.18, no.4, p.120-3 (July-Aug. 1982). [received: March 1983]

The utilization of highly intensive dynamic loads in modern engineering, in the explosion of high explosives (HE), say, requires a study of dynamics of behavior of structures and the solution of strength problems. The substantial strain rates originating here often result in the appearance of nonlinearly flowing properties of materials. The inertial expansion of cylindrical and spherical shells in a resisting medium is examined. (10 refs.)

61431 A shell-type structure under the effect of an impulsive load. P.S.Lugovii, V.N.Chaban.

Dopov. Akad. Nauk UKRSR. Ser. A (USSR), no.2, p.34-7 (1983). In Ukrainian.

Studies the dynamics of an axisymmetrical composite shell under the effect of a radial uniformly distributed pulse. (2 refs.)

61432 Coupled vibrations of beams—an exact dynamic element stiffness matrix. P.O.Friberg (Div. of Solid Mech., Chalmers Univ. of Technol., Gothenburg, Sweden).

Int. J. Numer. Methods Eng. (GB), vol.19, no.4, p.479-93 (April 1983).

A uniform linearly elastic beam element with non-coinciding centres of geometry, shear and mass is studied under stationary harmonic end excitation. The Euler-Bernoulli-Saint Venant theory is applied. Thus the effect of warping is not taken into account. The frequency-dependent 12×12 element stiffness matrix is established by use of an exact method. The translational and rotational displacement functions are represented as sums (real) of complex exponential terms where the complex exponents are numerically found. Built-up structures containing beam elements of the described type can be analysed with ease and certainty using existing library subroutines. (39 refs.)

61433 Vibration of a plate of arbitrary shape with free and simply supported mixed edges. K.Nagaya (Dept. of Mech. Engng., Faculty of Engng., Gunma Univ., Gunma, Japan).

J. Acoust. Soc. Am. (USA), vol.73, no.3, p.844-50 (March 1983).

This paper is concerned with a method for solving vibration problems of a plate of arbitrary shape with free and simply supported mixed edges. In the analysis the exact solution of the equation of motion which includes terms representing the reaction forces of the simply supported edges is applied. The boundary conditions along the edges of arbitrary shape have been satisfied directly by making use of the Fourier expansion collocation method which has been developed by the author on vibration, dynamic response, and wave propagation problems of membranes, plates, and rods with arbitrarily shaped boundaries. The equation for finding the eigenfrequencies of plates of arbitrary shape with free and simply supported mixed edges has been obtained. As applications of the present result, numerical calculations have been carried out for polygonal plates, trapezoidal plates, truncated elliptical plates, and parabolic plates with the mixed edges. (15 refs.)

61434 Free vibration of cantilever quadrilateral plates. R.S.Srinivasan, B.J.Babu (Indian Inst. of Technol., Madras, India).

J. Acoust. Soc. Am. (USA), vol.73, no.3, p.851-5 (March 1983).

In this paper, a numerical method for the free vibration analysis of cantilever quadrilateral plates of general shape is presented. Using quadrilateral coordinates and integral equation of beams, the expressions for the strain energy and kinetic energy have been developed. The formulation and derivation of

equations are in the matrix form 'ab initio'. Then the eigenvalue problem is solved for frequencies and mode shapes. Numerical work has been done for particular cases and the results compared with those of other investigators. The effect of sweep back angle has also been studied. (15 refs.)

61435 Horizontally polarized waves in composites and bonds. A.H.Nayfeh (Coll. of Engng., Yarmouk Univ., Irbid, Jordan), E.Abel-Ati, M.Nassar.

J. Sound & Vib. (GB), vol.87, no.3, p.439-47 (8 April 1983).

A simple continuum model is developed in order to investigate the propagation of horizontally polarized waves in laminated composites with bonds. The geometric arrangement of the composite with the bond is treated as a special type of a trilaminated composite in which each of its major constituents is sandwiched between two bonding layers. In this model the details of the propagation process in the bonding material are ignored, but its effects manifest themselves as modifiers to the interface conditions. The exact dispersion relation for the bilaminated composite subjected to the modified interface conditions is also derived. Results of both models are compared with each other and also with the exact dispersion relation obtained for the trilaminated composite. (3 refs.)

61436 Fast convergence modal analysis for continuous systems. A.Y.T.Leung (Dept. of Civil Engng., Univ. of Hong Kong, Hong Kong).

J. Sound & Vib. (GB), vol.87, no.3, p.449-67 (8 April 1983).

A continuous system has an infinite number of degrees of freedom (n.d.o.f.) in a dynamic analysis. The dynamic stiffness method is able to produce an infinite number of natural modes with use of only a finite number of co-ordinates. The associated modal analysis is the only widely applicable approximate method for computing the response without discretizing the continuous system by methods such as the finite element method, in which the infinite n.d.o.f. is not retained. However, this modal analysis converges very slowly as the number of modes is increased if the loading distribution does not follow the patterns of the first few modes. A method is suggested in the paper to accelerate the convergence. A mixed mass matrix is introduced according to the reciprocal theorem to evaluate the initial transient while retaining the infinite n.d.o.f. with a finite number of co-ordinates. Explicit formulae are given for space frames. (6 refs.)

61437 A parametrically driven harmonic analysis of a non-linear stretched string with time-varying length. G.Tagata (Nippon Gakki Co. Ltd., Hamamatsu, Japan).

J. Sound & Vib. (GB), vol.87, no.3, p.493-511 (8 April 1983).

The paper is concerned with the first, second and third harmonic lateral vibrations of a string having a forced, periodic, small length variation. Account is taken of the non-linear term arising from the correction to the tension of the string due to local elongation. It is found that increasing the amplitude of the length variation of the string results in a narrowing of the frequency response range of each of the harmonic oscillation components. Both numerical and analytical calculations of the harmonic frequency responses have been carried out. The relationships for initial values between the original differential equation and the approximate differential equations for the harmonic responses are discussed in detail. (13 refs.)

61438 Comments on 'On the axial vibration of rotating bars'. D.H.Hodges (US Army Res. & Technol. Labs., Ames Res. Center, Moffett Field, CA, USA), C.Vankatesan, V.T.Nagaraj.

J. Sound & Vib. (GB), vol.87, no.3, p.513-18 (8 April 1983).

For original paper see C. Venkatesan and V.T. Nagaraj, *ibid.*, vol.74, p.143-7 (1981). Venkatesan and Nagaraj derived a non-linear equation that governs the axial vibration of a bar normal to and rotating about an inertially-fixed axis. A linearized perturbation solution for the fundamental frequency was obtained that is similar to the result of D.H. Hodges (1977). The authors consider three conclusions of Venkatesan and Nagaraj's paper: (1) that the analysis by Hodges contains an error; (2) that the fundamental frequency of vibration increases as rotor angular speed increases; and (3) that this change in frequency is negligible for typical helicopter blades. A reply by Venkatesan and Nagaraj is also included. (15 refs.)

61439 Natural frequencies of epicycloidal plates. T.Irie, G.Yamada, M.Sonoda (Dept. of Mech. Engng., Hokkaido Univ., Sapporo, Japan).

J. Sound & Vib. (GB), vol.87, no.3, p.519-23 (8 April 1983).

The natural frequencies (the eigenvalues of vibration) are presented for epicycloidal plates. The epicycloidal plates are transformed into circular regions of unit radius by a conformal mapping. Both clamped and simply supported plates are considered. (7 refs.)

61440 Propagation of plastic waves in a bar of material exhibiting strain-rate effect (on the existence of strain plateau). M.Naitoh, M.Daimaru (Muroran Inst. of Technol., Muroran, Japan), W.Kishimoto.

J. Soc. Mater. Sci. Jpn. (Japan), vol.31, no.350, p.1068-72 (Nov. 1982). In Japanese. [received: April 1983]

Deals with a problem of propagation of longitudinal plastic waves in a semi-infinite bar subjected to a constant impact velocity, according to Malvern's strain-rate dependent theory. The authors discuss whether or not Malvern's theory (1951) can account for the plateau of uniform plastic strain adjacent to the impact end of the bar, which is predicted by Karman's theory neglecting a strain-rate effect and is observed experimentally. Malvern could not explain the strain plateau in his own calculations. This is considered so far to be only a weak point in the strain-rate dependent theory, though it can account for the extensive phenomena of high-rate deformation and plastic wave propagation in a bar. The existence of the strain plateau can also be predicted by Malvern's theory. Its appearance requires a relaxation time which is governed by the strain-rate dependence of material and the impact velocity at the end of a bar. As the strain-rate dependence of material and the impact velocity increase, the relaxation time needed for the appearance of the strain plateau increases. (8 refs.)

61441 Elasto-plastic wave propagation in a finite bar with consideration of temperature rise caused by plastic work. H.Date (Faculty of Engng., Tohoku Gakuin Univ., Tagajo, Japan).

J. Soc. Mater. Sci. Jpn. (Japan), vol.31, no.350, p.1073-9 (Nov. 1982). In Japanese. [received: April 1983]

The simulation of an elasto-plastic wave propagation in a finite bar, which impinged on a flat rigid anvil, has been made with a computer by taking the temperature rise into account. A constitutive equation used in the analysis is rate-dependent. The temperature rise has an influence upon the static stress-strain relation without a delay time. The static stress is a linear function of absolute temperature. The problem was formulated and solved numerically by the method of characteristics with a supplemental rectangular net. The numerical results show that temperature rise has the influence upon the deformation resistance of the specimen and unloading wave from free end. Consequently, the specimen length, impact stress, material constant K defined plastic strain rate and initial temperature have considerable influence upon stress, strain and time of contact. (20 refs.)

61442 Exact solution to the formation and propagation problem of a non-stationary shock wave in bilinear media. E.Włodarczyk.
J. Tech. Phys. (Poland), vol.22, no.4, p.391-406 (1981).

An exact solution is presented to the formation and propagation problem of a nonstationary plane shock wave in the medium with a concave (rigid) characteristic $\sigma - \epsilon[\sigma](\epsilon) < 0$, approximated by the bilinear model. The form is explicitly defined of a shock wave in the loading and unloading zone. Exact formulae are derived for the parameters of state and motion of the medium behind the wave front. (24 refs.)

61443 Three-dimensional problem of diffraction of plane elastic waves by a wedge. S.Kh.Sharipova.
Mech. Solids (USA), vol.17, no.4, p.115-22 (1982). Translation of: *Izv. Akad. Nauk SSSR Mekh. Tverd. Tela*, vol.17, no.4, p.127-35 (1982).

Using the regular method that was previously developed for dynamic problems of elasticity theory, exact analytic solutions are obtained of three-dimensional nonstationary problems of diffraction of plane longitudinal and transverse waves by a smooth wedge. The author allows for the fact that the desired three-dimensional solutions of problems of plane wave diffraction are obtained from the solutions of the corresponding spherical-wave diffraction problems as the sources become infinitely distant. (13 refs.)

61444 Excitation of waves by a vibrating elastic cylinder in a layer. S.P.Pel'ts, V.L.Tsvetyanski.
Mech. Solids (USA), vol.17, no.4, p.128-32 (1982). Translation of: *Izv. Akad. Nauk SSSR Mekh. Tverd. Tela*, vol.17, no.4, p.141-5 (1982).

The axisymmetric problem of forced nonresonant harmonic oscillations of an elastic cylinder on an elastic layer is considered. A solution is constructed for the problem on the basis of the generalized orthogonality relations for the system of dynamic homogeneous solutions of the cylinder. The statement of the problem presupposes that there is a static load that presses the cylinder to the layer and inhibits the formation of separation zones. A solution of the dynamic component of the problem is offered. (11 refs.)

61445 Lamb waves in a prestressed plate of isotropic nonlinear-elastic incompressible material. M.G.Yakovenko.
Mech. Solids (USA), vol.17, no.4, p.133-7 (1982). Translation of: *Izv. Akad. Nauk SSSR Mekh. Tverd. Tela*, vol.17, no.4, p.146-50 (1982).

Investigates the effect of prestresses and of finite deformations on the phase velocity of Lamb wave propagation in a plate (layer) of arbitrary isotropic Cauchy-nonlinear-elastic incompressible material. The basic equations of a previous paper are employed, which dealt with the analogous problem for Rayleigh surface waves. Dispersion equations for antisymmetrical and symmetrical forms are obtained. These equations can be represented as explicit dependences of the initial stresses on the elongations, phase velocity, and wavelength, something that is extremely convenient for investigating the effect of the parameters of the initial stress-strain state on the phase velocity. The relationship to the solution of the problem of instability of such a plate is demonstrated. The author considers the case in which the principal stresses are equal; asymptotic formulas for very long waves are derived; and some numerical results are presented. (4 refs.)

61446 Effect of static stressed state on free vibrations of a shell. N.N.Rogacheva.
Mech. Solids (USA), vol.17, no.4, p.183-8 (1982). Translation of: *Izv. Akad. Nauk SSSR Mekh. Tverd. Tela*, vol.17, no.4, p.200-6 (1982).

The asymptotic method previously proposed is employed to qualitatively investigate the effect of a preliminary static stressed state on free vibrations of shells. The results make it possible, without solving the problem, to estimate the effect of a static load on free vibrations of an arbitrary shell. (6 refs.)

61447 An algorithm for kinetoelastodynamic analysis of rectilinear element plane mechanisms. M.Buculei, D.Marghitu (Univ. of Craiova, Craiova, Rumania).

Rev. Roum. Sci. Tech. Ser. Mec. Appl. (Rumania), vol.27, no.5, p.597-604 (Sept.-Oct. 1982). In French. [received: March 1983]

The algorithm of kinetoelastodynamic analysis is based on the method of successive approximations, having as a starting point the determination of limiting conditions attached to each of the kinematic elements. The integral transformations yield solutions of linear-elastic displacements for vibrations of the kinematic elements of the straight line type. (12 refs.) H.C.B.

61448 On the determination of the frequencies of the lateral vibration of a disc with concentrated masses. I. S.Nishimura (Dept. of Precision Engng., Tohoku Univ., Sendai, Japan).

Technol. Rep. Tohoku Univ. (Japan), vol.47, no.2, p.175-87 (1982). In English.

A method for obtaining the frequencies of lateral vibration of a disc is presented. The disc is of axisymmetrically variable thickness, has concentrated masses attached at arbitrary places and is clamped at the inner edge and free at the outer edge. It is quite troublesome to find frequencies of the vibration because the fundamental differential equation of vibration has singularities due to the concentrated masses. In this paper, an integral equation is derived by applying Green's formula to the fundamental equation for the Green function to avoid this difficulty. This method allows a larger part of the determination of the frequencies of the vibrations to be made through analytical treatments and thus is considered to be very useful in this kind of problem. (5 refs.)

61449 Numerical ways of solving the problems of vibrations of thin plates subjected to impact loads. Zh.N.Dmitrieva, E.V.Nikiforova, V.L.Fomin.
Vestn. Leningr. Univ. Ser. Mat. Mekh. & Astron. (USSR), no.1, p.111-14 (Jan. 1983). In Russian.

Non-linear vibrations of a thin circular plate under the action of impact normal loads are studied. Vibrations for large deflections of elastic plates and the bending vibrations of elastic-plastic plates are investigated. A numerical technique on the basis of the finite difference method is developed. (2 refs.)

Optically recording interferometer for velocity measurements with subnanosecond resolution See Entry 59832

The input mobility of an infinite circular cylindrical elastic shell filled with fluid See Entry 61345

Resonant oscillations of fluid-loaded struts See Entry 61346

Numerical analysis of flexural vibrations of rotors resting on elastic supports See Entry 61398

Optimal laminated composite shells for buckling and vibration See Entry 61425

Work of spalling fracture See Entry 61452

On the measurement of visco-elastic properties of matters by the Mossbauer effect See Entry 61461

Random walk of dislocations following a high-velocity impact See Entry 62027

Energy transport velocity of surface elastic waves See Entry 62223

46.30N Fracture mechanics, fatigue, and cracks

61450 Appearance aspects of isochromatic mode-I crack tip fringe loops. H.-P.Rossmann (Tech. Univ. Wien, Wien, Austria).

Acta Mech. (Austria), vol.47, no.1-2, p.53-64 (1983). A special perturbation method is employed to demonstrate how the non-singular stress fields associated with the Taylor-series expansions of a pair of Westergaard type stress functions $Z(z)$ and $Y(z)$ will influence the configuration of the isochromatic fringe loops in the vicinity of static crack tips. (9 refs.)

61451 Some remarks on elastic fracture mechanics. P.Destuynder (Dept. Mecanique et Modeles Numeriques, Electricite de France, Paris, France), M.Djaoua, S.Lescure.

Bull. Dir. Etud. & Rech. Ser. C (France), no.2, p.5-26 (1982). In French. A thermodynamical approach of propagation laws in elastic media is given. From a particular choice of an energy dissipation potential, the authors deduce some propagation laws corresponding to particular loading cases. Finally a new computational method of the energy release rate is suggested and discussed. (25 refs.)

61452 Work of spalling fracture. G.I.Kanel'.
Combust. Explos. & Shock Waves (USA), vol.18, no.4, p.461-4 (July-Aug. 1982). Translation of: *Fiz. Goreniya & Vzryva (USSR)*, vol.18, no.4, p.84-8 (July-Aug. 1982). [received: March 1983]

Methods of estimating the work of fracture by means of the results of two kinds of experiments are discussed. The authors consider the energy balance in a plate of thickness L after the insertion of one-dimensional compression wave in which the total energy increment per unit area is E_0 , while the momentum is P_0 . Because of multiple passages through the plate, the compression wave damps out therein, and its energy goes partially over into kinetic energy of the plate as a whole and partially is expended in dissipative processes, including fracture. (11 refs.)

61453 Interaction between the edges of a crack in a complexly loaded state. Yu.V.Zhitnikov, B.M.Tulinov.

Mech. Solids (USA), vol.17, no.4, p.152-6 (1982). Translation of: *Izv. Akad. Nauk SSSR Mekh. Tverd. Tela*, vol.17, no.4, p.168-72 (1982).

As a rule, in analyzing crack equilibrium, shear motion of the edges relative to one another over the entire length of the crack has been allowed. This assumption makes it possible to consider only a limited class of problems in which the loading process cannot simultaneously involve regions of relative movement of the edges and regions in which there is no such movement. The authors propose a way of distinguishing such regions in calculating limiting equilibrium of a rigid body with a crack, and also establish how the final stressed state depends on the loading trajectory. (7 refs.)

61454 Formation of fracture structures of weakly interacting cracks. R.V.Gol'dshteyn, A.V.Kapstov.

Mech. Solids (USA), vol.17, no.4, p.157-66 (1982). Translation of: *Izv. Akad. Nauk SSSR Mekh. Tverd. Tela*, vol.17, no.4, p.173-82 (1982).

Considers features of the formation of three-dimensional fracture structures, whose elements are plane cracks (separation or shear cracks) that arise at considerable distances from one another, so that their interaction may be regarded as weak and can be taken into account by summing the perturbations of the elastic field caused by individual cracks. The situation, frequently encountered in practice, in which the material, by virtue of its structure, texture, and so forth, possesses a certain geometry of weakened places is analysed. The authors distinguish the following forms of weakened zones: a system of parallel planes and parallel straight lines; crossed straight lines; and single straight line, which are characteristic of many natural and artificial materials. As an example, one can cite low- and medium-strength construction seals with pronounced 'striation' and some forms of laminar or fiber composite materials. Anisotropy of strength properties caused by structural features of the material frequently manifests itself more strongly than anisotropy of the deformation properties; this occurs, e.g., in striated steels. (16 refs.)

61455 Combined models of fracture and their use in predicting service life. V.V.Bolotin (A.A. Blagonravov Inst. of Mech. Engng., Acad. of Sci., Moscow, USSR).

Sov. Mater. Sci. (USA), vol.18, no.3, p.195-201 (May-June 1982). Translation of: *Fiz.-Khim. Mekh. Mater. (USSR)*, vol.18, no.3, p.3-12 (May-June 1982). [received: Feb. 1983]

Combined phenomenological and structural models of fracture are investigated in relation to the prediction of service life. The general approaches presented are applied to materials of different structures, and in particular to fibre reinforced composites. (15 refs.)

61456 Equivalence of the energy and force approaches in the theory of cracks in the general case of two-dimensional loading. N.B.Romal's (Lenin Komsomol Voronezh State Univ., USSR).

Sov. Mater. Sci. (USA), vol.18, no.3, p.202-4 (May-June 1982). Translation of: *Fiz.-Khim. Mekh. Mater. (USSR)*, vol.18, no.3, p.12-15 (May-June 1982). [received: Feb. 1983]

An analog of the Griffith-Irwin criterion of fracture is constructed for a crack of arbitrary form in the general case of a two-dimensional load. (8 refs.)

61457 Stressed state of a square sample for crack resistance tests of sheet materials. M.P.Savruk, S.Ya.Yarema, P.N.Osiv (G.V. Karpenko Physico-mech. Inst., Acad. of Sci., Lvov, Ukrainian SSR).

Sov. Mater. Sci. (USA), vol.18, no.3, p.240-4 (May-June 1982). Translation of: *Fiz.-Khim. Mekh. Mater. (USSR)*, vol.18, no.3, p.57-63 (May-June 1982). [received: Feb. 1983]

Investigation of the stressed state at the tip of a crack in design elements is the original stage in predicting their effectiveness and life. The accomplishment of such an investigation is eased to a significant degree as a result of development of the method of singular integral equations for the solution of plane problems of the theory of elasticity for multiply connected areas weakened by holes and cracks. This method was used for determining the stress intensity factors in a square plate in tension, which is proposed as an alternative to a disk sample for crack resistance testing of sheet materials. The sample was loaded the same way as a disk sample and was similarly by two forces applied to circular rigid inclusions. (7 refs.)

On the Lagrangian formulation of continuum mechanics See Entry 61403

Antiplane deformation of a body with a curved elastic sharp-ended inclusion See Entry 61423

On lateral buckling - fracture stability of thin-sheet structural components with deep cracks See Entry 61428

Laser microspeckle technique in displacement measurement near a crack tip See Entry 61462

Fatigue life estimation using simple fracture mechanics See Entry 62019

Evaluation of creep crack growth criteria for IN-100 at elevated temperature See Entry 63375

- Near-threshold growth of short fatigue cracks See Entry 63421
 Statistical rules of fatigue crack development See Entry 63422
 On the theory of stress-assisted diffusion. II See Entry 63437

46.30P Friction, wear, adherence, hardness, mechanical contacts

- 61458** Nonsteady interaction between a die and an elastic medium. V.A. Babeshko, Zh.F. Zinchenko, A.V. Smirnova. *Mech. Solids (USA)*, vol.17, no.4, p.123-7 (1982). Translation of: *Izv. Akad. Nauk SSSR Mekh. Tverd. Tela*, vol.17, no.4, p.136-40 (1982).
 Considers problems of interaction between an elastic laminar medium and a rigid die that occupies region Ω that is arbitrary in plan, under the assumption that the contact is frictionless and the die either moves in accordance with a specified law over time or has a nonsteady wave incident on it. The boundary-value problem is reduced to an integral equation of the first kind that depends on the parameter of the Laplace transformation, for which the authors establish uniqueness and solvability theorems and investigate the properties of the solution. To construct the solution, after analyzing the available approaches to numerical inversion of the Laplace transformation, the method of Tikhonov (1963) is employed, this method being the most efficient and convenient for the given class of problems. (9 refs.)
- 61459** Analysis of a free boundary problem in partial lubrication. G. Bayada (Inst. National. des Sci., Appliquées de Lyon, Villeurbanne, France), M. Chambaut. *Q. Appl. Math. (USA)*, vol.40, no.4, p.369-75 (Jan. 1983).
 Hydrodynamic lubrication is concerned with a particular form of creeping flow between surfaces in relative motion where cavitation takes place. The determination of the free boundary of the cavitation area is then of fundamental importance for the computation of the characteristics of the mechanisms. Different conditions at the free boundary have been introduced. The authors study two of them and compare corresponding solutions with respect to film extent and pressure repartition. (11 refs.)
- Analysis of the stressed state of the forward slip zone in the seat of deformation of a powder being rolled See Entry 63191
 Thermally stressed condition occurring in the surface layers of flat parts during friction hardening See Entry 63429

46.30R Measurement methods and techniques

(see also 07.10 Mechanical instruments and techniques, 81.70 Materials testing)

- 61460** Detection of deformations obtained by a moiré pattern corresponding to a specific grid. H. Annoni (Ecole Nat. Supérieure des Arts et Industries, Strasbourg, France). *C.R. Seances Acad. Sci. Ser. II (France)*, vol.296, no.1, p.39-41 (10 Jan. 1983). In French.
 A method is presented for testing the conformity of an object with a model by means of a projection of a grid (specially calculated from the shape of the model) on the object and observing a moiré pattern: the fringes are straight lines if the object has the right shape. (3 refs.)
- 61461** On the measurement of visco-elastic properties of matters by the Mossbauer effect. F.E. Fujita (Dept. of Material Phys., Osaka Univ., Toyonaka, Japan). *Jpn. J. Appl. Phys. Part I (Japan)*, vol.22, no.3, p.475-9 (March 1983).
 A technique to measure the visco-elastic properties of materials by using the Mossbauer effect is proposed. Assuming that a spring coil specimen is attached to the transducer of Mossbauer spectrometer, which gives a sinusoidal Doppler motion between the gamma ray source and the absorber, the visco-elastic vibration of the specimen is calculated and the mechanical resonance conditions are found. When the gamma ray source and absorber are connected to the visco-elastic system, the Mossbauer pattern will be subjected to a modulation, from which the elastic constant and the viscosity of the specimen can be measured, especially from the mechanical resonance condition. A variety of ways of connection between the mechanical and Mossbauer system are considered and applications of the technique are discussed. (15 refs.)
- 61462** Laser speckle technique in displacement measurement near a crack tip. Z.Q. Tan, K.C. Wu, C.H. Cheng, S.S. Chern, C.C. Hsiao (Dept. of Aerospace Engng. & Mech., Univ. of Minnesota, Minneapolis, MN, USA). *J. Appl. Phys. (USA)*, vol.54, no.4, p.1651-5 (April 1983).
 The laser speckle method has been found quite useful in obtaining in-plane displacement measurements. It is especially useful if the displacement field in a small region can be effectively determined. By obtaining directly the speckle patterns at higher magnifications, a better distinction of the displacements in the vicinity of a crack tip is possible. In this short report some results are obtained and compared with those calculated from linear fracture mechanics and the finite element method for an aluminum crack. (5 refs.)
- 61463** Viscoelastic thermal stress analysis. G.W. Scherer (Corning Glass Works, Corning, NY, USA). *J. Non-Cryst. Solids (Netherlands)*, vol.54, no.3, p.223-40 (March 1983).
 The viscoelastic/elastic analogy leads directly to the viscoelastic solution for thermal stresses in a variety of glass-to-metal seals. This paper examines the conditions which must be met for that approach to be applicable, and shows that it cannot be used in most bodies with spatially varying temperature or composition. A method is presented which leads easily to solutions for the stresses in tempered or ion-exchanged plates and in glass-to-glass sandwich seals. In the latter case, calculated stresses agree well with measured stresses reported in the literature. (18 refs.)
- 61464** Speckle-interferometry, a simple method for deformation analysis. H. Schwieger, R. Streubel. *Mater. Test. (Germany)*, vol.25, no.4, p.105-12 (April 1983). In German.
 Speckle-interferometry is a simple method for deformation-analysis of mechanically loaded structures or their models. This method can be applied to both static and dynamic deformation. This method is mainly suitable for the determination of components of the displacement-vector at the surface of a structure and of deflection-gradients of a bend plate. The theoretical fundamentals are presented and the applicability of this method is illustrated with simple test-examples. (40 refs.)
- 61465** Use of nonlinear viscoelastic materials in the polarization-optical method. G.Z. Sharafutdinov. *Mech. Solids (USA)*, vol.17, no.4, p.138-44 (1982). Translation of: *Izv. Akad. Nauk SSSR Mekh. Tverd. Tela*, vol.17, no.4, p.151-8 (1982).
 The basis for the application of the polarization-optical method to problems of nonlinear viscoelasticity, or of the method of nonlinear photoviscoelasticity,

is provided by fairly well-developed experimental techniques, the possibility of choosing modes of deformation or loading such that an optically sensitive material possesses nonlinear viscoelastic properties, and also the availability of physically nonlinear theories of viscoelasticity. The author investigates the optomechanical characteristics of optically sensitive materials, and determines their material functions, on the basis of the principal quasi-linear and principal cubic theories. One of the most important aspects of the method, namely modelling of deformation processes in the nonlinear region is also considered. Experiments were conducted using specimens of a material based on ED-6MA epoxy resin with the addition of 25% polyester, as well as polycarbonate specimens. These materials possess the set of properties required for use in photoviscoelasticity. (8 refs.)

- 61466** Passage of light through a general three dimensional model—equations linking characteristic parameters with system parameters. S.Y. Keshavan (Dept. of Mech. Engng., Univ. of the West Indies, St. Augustine, Trinidad). *Strain (GB)*, vol.19, no.2, p.59-62 (May 1983).
 The determination of the secondary principal stress difference and their orientations for a discrete slice of thickness dz along a particular light path in a three dimensional photoelastic model is discussed. These quantities are determined in terms of the characteristic parameters and their variations at discrete points distance x and z - rdz along the light path. The variations of the characteristic parameters are obtained by deriving the equations linking the characteristic parameters for the light path and the system parameters of the discrete element. The validity of the equations so derived has also been checked by applying these equations to the solution of the problem of a uniformly twisted prismatic bar. (4 refs.)
- 61467** Strain field analysis with the X-ray integration method. A. Peiter, W. Lode (Materialprüfamt des Saarlandes, Saarbrücken, Germany). *Strain (GB)*, vol.19, no.2, p.69-75 (May 1983).
 The so-called X-ray $\sin\psi$ method for measuring internal stresses is not always acceptable, because it postulates a constant orthogonal stress distribution in the layer passed by the beam. It is demonstrated that the often measured non-linear distribution of deformations is numerically connected with stress distributions, which are variable and inclined against the surface. The calculation of the internal stresses and their parameters is based on the solution of trigonometric polynomials of the variable ψ with integrals. The penetration depth of the X-ray beam must be known. For general numeric solutions a computer program can be given. Solutions step by step can be carried out with a programmable pocket calculator. The ' $\sin\psi$ method' is a special case of the integration method, which is still developing. (4 refs.)
- 61468** A simple technique for installing strain gauges on cylindrical surfaces. Sadhu Singh (Coll. of Technol., G.B. Pant Univ. of Agriculture & Technol., Pantnagar, India). *Strain (GB)*, vol.19, no.2, p.77-8 (May 1983).
 A simple technique for the installation of strain gauges on circular and conical cylindrical surfaces is described. The technique may be adopted in an experimental stress analysis laboratory where sophisticated equipment is not available. (3 refs.)
- 61469** Study of deformed samples using an interferometer attached to the sample. V.A. Zhilkin, S.I. Gerasimov (Inst. of Railroad Engrs., Novosibirsk, USSR). *Sov. Phys.-Tech. Phys. (USA)*, vol.27, no.10, p.1276-9 (Oct. 1982). Translation of: *Zh. Tekh. Fiz. (USSR)*, vol.52, no.10, p.2079-85 (Oct. 1982). [received: April 1983]
 It is suggested that holographic interference patterns recorded in oppositely directed beams as proposed by Yu.N. Denisyuk be used to study static problems in the mechanics of deformed samples. The photographic plates are attached to the surface of the sample on top of an intermediate optically transparent material. The effects of the rigidity of the photographic plate and optically transparent material on the measured deformations and the vibrational noise reaching the photographic plate are estimated. Equations are derived which relate the displacements of points on the deformed sample surface to the difference in path lengths of the interfering waves. The method is illustrated by considering the deformed state of a spherically stressed sample using a slit condenser. (11 refs.)
- An exact technique for mixing of immersion fluids [refractive index matching for photoelastic applications] See Entry 59830
 Optically recording interferometer for velocity measurements with subnanosecond resolution See Entry 59832
 Real-time holographic interferometry of moving objects in oppositely directed beams See Entry 61111
 Use of the Southwell method to predict buckling strengths of stringer stiffened cylindrical shells See Entry 61427
 Work of spalling fracture See Entry 61452
 Stressed state of a square sample for crack resistance tests of sheet materials See Entry 61457
 Microhardness of an implanted system See Entry 61944
 Resistance change of thin Permalloy films caused by applied stress and its application to strain measurements See Entry 62508
 Microdeformation machine for testing thin films with automatic tension-diagram recording See Entry 63482

46.60 RHEOLOGY OF FLUIDS AND PASTES

- 61470** Pulsating viscoelastic flows in non-rigid tube. R. Rakotomalala, D. Bellet, Dang Phuoc Ly (IMFTLA, CNRS, Toulouse, France). *C.R. Seances Acad. Sci. Ser. II (France)*, vol.296, no.2, p.131-4 (17 Jan. 1983). In French.
 Studies the pulsating flows of viscoelastic fluids in non-rigid tubes. The influence of the elasticity of the fluid upon the attenuation factor, the wave speed and the velocity profiles have been analysed. (4 refs.)
- 61471** Low frequency viscoelastic behavior at the sol-gel transition. B. Gauthier-Manuel (CENS, Gif-sur-Yvette, France), C. Allain, E. Guyon. *C.R. Seances Acad. Sci. Ser. II (France)*, vol.296, no.4, p.217-19 (31 Jan. 1983). In French.
 Viscoelastic behaviour is associated with the transition region from the viscous one in a sol phase to the elastic one in a gel phase. Using a sphere rheometer at finite frequency f it is shown that the apparent sol-gel transition point shifts with the value of f . (5 refs.)
- A kinetic theory for polymeric fluids See Entry 61769
 Plastic behavior and polymorphism of smectic liquid crystal See Entry 61783

47.00 FLUID DYNAMICS

(for fluid dynamics of quantum fluids, see 67.; for geophysical fluid dynamics, see 92.10; for astrophysical gas dynamics, see 95.30; for biological fluid dynamics, see 87.45)

47.10 GENERAL THEORY

(see also 03.40G Mathematical aspects)

61472 Steady state thermodynamics and spatial correlations. J. Keizer (Chem. Dept., Univ. of California, Davis, CA, USA). *Physica A (Netherlands)*, vol.118A, no.1-3, p.350-9 (March 1983). (Proceedings of the Conference on Nonlinear Fluid Behavior, Boulder, CO, USA, 7-11 June 1982).

The formulation of thermodynamic functions based on the statistical distribution of extensive variables at nonequilibrium steady states is reviewed. The case of Couette flow is considered, and the necessity of introducing functionally dependent state functions is discussed. Using these techniques the author gives a consistent derivation of the equations used by Hanley and Evans (1982) to analyze their computer dynamics calculations of homogeneous shear flow. Finally, the connection between thermodynamic state functions and spatial correlations is illustrated for a solution phase chemical reaction scheme. (18 refs.)

61473 Number of modes governing two-dimensional viscous, incompressible flows. C. Foias (Indiana Univ., Bloomington, IN, USA), O.P. Manley, R. Temam, Y.M. Treve. *Phys. Rev. Lett. (USA)*, vol.50, no.14, p.1031-4 (4 April 1983). Recent efforts to estimate the number of modes sufficient for the approximate solutions of Navier-Stokes equations in two dimensions are summarized. Several such estimates have been obtained, and their relations to one another are discussed. The physical significance of the results is noted and used to infer the possible nature of similar estimates in three dimensions. (13 refs.)

A solvable weak-potential model of a nonNewtonian fluid See Entry 61531

Some elementary exact channel flows See Entry 61553

47.15 LAMINAR FLOWS

61474 RTD for diffusion-free laminar flow of non-Newtonian fluids through coiled tubes. A.K. Saxena, K.M. Nigam, K.D.P. Nigam (Dept. of Chem. Engng., Indian Inst. of Technol., New Delhi, India). *Can. J. Chem. Eng. (Canada)*, vol.61, no.1, p.50-2 (Feb. 1983). The residence time distribution (RTD) for diffusion-free laminar helical flow of non-Newtonian fluids has been numerically computed for values of the power-law index from 0.2 to 2.0. Experimental verification is also provided. Excellent agreement is also shown with independently calculated RTDs appearing in the literature. (13 refs.)

61475 Laminar dispersion in helically coiled tubes of square cross-section. A.K. Saxena, K.D.P. Nigam (Dept. of Chem. Engng., Indian Inst. of Technol., New Delhi, India). *Can. J. Chem. Eng. (Canada)*, vol.61, no.1, p.53-7 (Feb. 1983). In coiled tubes of non-circular cross-section the orientation of the cross-sectional plane with respect to the direction of the centrifugal force has a significant effect on residence time distribution (RTD) which has been recognized for the first time. This aspect has been experimentally investigated in helically coiled tubes of square cross-section, under the conditions of negligible and significant molecular diffusion. (28 refs.)

61476 Computer 'experiment' for nonlinear thermodynamics of Couette flow. D.J. Evans (Res. School of Chem., Australian Nat. Univ., Canberra, Australia). *J. Chem. Phys. (USA)*, vol.78, no.6, pt.1, p.3297-302 (15 March 1983). Nonequilibrium computer simulations reveal that the equation of state of fluids undergoing shear flow varies with strain rate. This observation prompted the development of a nonlinear generalization of irreversible thermodynamics to describe steady planar Couette flow, very far from equilibrium. In this paper the author uses computer simulation to perform a quantitative test of a prediction of this thermodynamics. The prediction tested is: fluids which exhibit positive shear dilatancy for isothermal shear flow should also cool as the strain rate is increased while keeping the internal energy constant. To perform calculations of this effect a new nonequilibrium molecular dynamics algorithm was developed to simulate Couette flow at constant internal energy. (19 refs.)

Correlation of Preston tube data with laminar skin friction See Entry 61523

Comments on 'Stability of shear flow in a magnetized plasma' [and reply] See Entry 61624

47.15C Laminar boundary layers

61477 Plastic boundary layers induced by variable wall friction. D. Durban, M.R. Sitzer (Technion-Israel Inst. of Technol., Haifa, Israel). *Acta Mech. (Austria)*, vol.47, no.1-2, p.161-5 (1983). An introductory exposition of plastic boundary layers has been presented by the authors previously (see *ibid.*, vol.45, p.73-89, 1982), within the context of steady rectilinear flow, of rigid/linear-hardening solids. The main findings were that (a) sufficiently high wall friction induces a plastic boundary layer into the flowing material, and that (b) the extent of that layer increases in the direction of flow. In the present study the authors amplify these results via a more detailed analysis of plastic boundary layers induced by non-uniform wall friction. They focus attention on steady rectilinear flow through circular pipes and employ a suitable Fourier expansion of the resisting shear stress along the wall. A few representative examples are discussed and the corresponding growth of the plastic boundary layers is displayed in accompanying figures. (1 ref.)

61478 A method for an accurate determination of the wall pressure in fluid flows. C. Ducruet (IMFL, Lille, France). *C.R. Seances Acad. Sci. Ser. II (France)*, vol.296, no.5, p.309-12 (7 Feb. 1983). In French. The principle of the method of correction has been presented in a previous article. The formula of correction is completed in incompressible fluid by considering the influence of wall curvature. Then, its validity is checked in flows around a cylinder and an airfoil. (2 refs.)

61479 Boundary layers of a nematic liquid crystal in fine capillaries. A.N. Somov, N.V. Churaev (Inst. of Phys. Chem., Acad. of Sci., Moscow, USSR). *Colloid J. USSR (USA)*, vol.44, no.3, p.556-7 (May-June 1982). Translation of: *Kolloid. Zh. (USSR)*, vol.44, no.3, p.614-15 (May-June 1982). [received: Feb. 1983]

It has been observed that in capillaries with a radius $R \leq 7.4 \mu\text{m}$ molecules of a nematic liquid crystal, N-(p-methoxybenzylidene)-p-butylaniline (MBBA), have a planar orientation which becomes homeotropic in capillaries with a large radius. Flowing destroys the homeotropic orientation the more noticeably, the higher the flow velocity v and the larger the radius of the capillary. The thickness of the boundary layers in homeotropic orientation reaches several micrometers when $v = 10^{-2} \text{ cm/sec}$. (5 refs.)

61480 On the slipping boundary condition for low density gas flow. R. Peralta-Fabi (Dept. de Fisica, Univ. Autonoma Metropolitana, Mexico City, Mexico), R. Zwanig. *J. Chem. Phys. (USA)*, vol.78, no.5, p.2525-9 (1 March 1983).

The authors discuss the slipping boundary condition in fluid dynamics. They argue that when the boundary is a well defined and smooth surface, the slipping boundary condition is the correct choice. The Grad 13-moment equations are used to describe the hydrodynamic fields for the slow stationary flow of a viscous compressible and low density fluid. The authors study a planar Couette flow and flow around an arbitrary obstacle. The equations are solved for the flow past a sphere. The drag on the sphere is calculated to second order in the mean free path. (6 refs.)

61481 Anomalies of the laminar flow of a smectic A around a cylindrical obstacle. P. Oswald (Lab. de Phys. des Solides, Univ. Paris-Sud, Orsay, France).

J. Phys. Lett. (France), vol.44, no.8, p.L303-9 (15 April 1983). In French. When shearing a homeotropic sample of smectic A, a strong rigidification of the central part of the flow has been observed. This effect has probably to do with the presence of defects that are not visible under the microscope. It subsists when a cylindrical thread is glued on one side of the sample. Two static regions then spread out on both sides of this obstacle. They are connected to the central part of the flow through a thin layer of permeation. An estimate of the dissipation gives the author a rough value of the permeation length, first introduced by de Gennes: $\chi^{-1} = \sqrt{\eta\lambda}$. Lastly the author shows that a dilation under shear leads to a lattice of focal parabola, which is asymmetrical with respect to the obstacle. (9 refs.)

Thresholds for the onset of fluid and magnetofluid turbulence See Entry 61489

Buoyancy effects on a boundary layer along an infinite cylinder with a step change of surface temperature See Entry 61506

A stationary free boundary problem for a circular flow with or without surface tension See Entry 64374

47.15F Stability of laminar flows

61482 Low Reynolds number flow between interrupted flat plates. R.E. Roadman (Fabricating Technol. Div., Alcoa Labs., Alcoa Center, PA, USA), R.I. Lochrke.

Trans. ASME. J. Heat Transfer (USA), vol.105, no.1, p.166-71 (Feb. 1983). The flow between pairs of flat plates was studied experimentally to gain insight into the operation of compact heat exchangers with interrupted surfaces. The plates were tested at low Reynolds number in both water and air streams. The investigation focused on the region of transition from steady to unsteady laminar flow between plates. A critical velocity depends strongly on the thickness of the plates, t , plate length, L , and plate separation distance, $4 \leq L/t \leq 159$, are correlated using plate wake width as a single plate length scale. The downstream, plate was found to have a pronounced upstream influence may be lower than that required to produce detectable oscillations at the same point in the upstream plate wake in absence of the second plate. This feedback effect may be responsible for the relative insensitivity of the results to the turbulence level in the free stream. (14 refs.)

Intermittency associated with the breakdown of the chaos symmetry See Entry 59716

Navier-Stokes solution on the CYBER-203 by a pseudospectral technique See Entry 61519

Stability of a laminar flame front propagating within a tube .. See Entry 61566

47.20 HYDRODYNAMIC STABILITY

61483 Hydroelastic effects of separated flow. L.E. Ericsson (Lockheed Missiles & Space Co. Inc., Sunnyvale, CA, USA).

AIAA J. (USA), vol.21, no.3, p.452-8 (March 1983). In a previous publication it was shown that separated flow can cause catastrophic divergent oscillations of an underwater structure that has a low drag cross-sectional profile. In the present paper the analysis is extended to rectangular prismatic sections, and to consider both bending and torsional oscillations. It is shown that the adverse hydroelastic effects of separated flow can be very large, requiring that a fix of some kind is used. Various means by which the hydroelastic instability can be avoided are described. (17 refs.)

61484 Subharmonic oscillations of a mixing layer-wedge system associated with free surface effects. S. Ziada (Labs. for Vibrations & Acoustics, Sulzer Bros., Winterthur, Switzerland), D. Rockwell.

J. Sound & Vib. (GB), vol.87, no.3, p.483-91 (8 April 1983). An unstable mixing layer, in conjunction with free surface wave effects, can give rise to well-defined subharmonic oscillations of the vortex shedding frequency provided certain streamwise phase conditions are satisfied. Visualization of these oscillations, forces acting on the impingement edge, and streamwise evolution of velocity spectra are addressed. (5 refs.)

61485 Kinetics of fluctuations for systems undergoing phase transition—interfacial approach. K. Kawasaki, T. Ohta (Dept. of Phys., Kyushu Univ., Fukuoka, Japan). *Physica A (Netherlands)*, vol.118A, no.1-3, p.175-90 (March 1983). (Proceedings of the Conference on Nonlinear Fluid Behavior, Boulder, CO, USA, 7-11 June 1982).

Studies on kinetics of fluctuations in quenched fluid systems are reviewed on the basis of a new dynamical interfacial model. All the processes known to take place in critical fluid mixtures are identified for this model. The authors briefly discuss the Ostwald ripening and the interface stability with this model. An analogy with fully developed turbulence is noted and a possibility of intermittent states is indicated. (33 refs.)

61486 What causes noise in a convecting fluid? J.P.Gollub (Phys. Dept., Haverford Coll., Haverford, PA, USA). *Physica A (Netherlands)*, vol.118A, no.1-3, p.329-34 (March 1983). (Proceedings of the Conference on Nonlinear Fluid Behavior, Boulder, CO, USA, 7-11 June 1982).

Several different sources of hydrodynamic noise have been found in recent experiments on convecting fluids, including long-lived complicated transients associated with pattern evolution and noise due to secondary instabilities. In other circumstances strange attractors or stochastic models are required to explain the data. (12 refs.)

61487 Stratification instability of switching front in an active trigger diffusive medium. Yu.I.Balkarei, A.A.Zakharova (Inst. of Radio Engng. & Electronics, Acad. of Sci., Moscow, USSR). *Sov. Phys.-Tech. Phys. (USA)*, vol.27, no.9, p.1148-50 (Sept. 1982). Translation of: *Zh. Tekh. Fiz. (USSR)*, vol.52, no.9, p.1871-3 (Sept. 1982). [received: April 1983]

Considers a simple model of a diffusion active trigger medium, a model in which an exact expression can be obtained for the shape of a stationary switching front (domain wall) and a detailed study can be made of the spectrum and shape of linear fluctuations, leading to periodic stratification of the front. The mathematical model of an autowave medium, that is used, consists of the well known system of Fitz-Hugh-Nagumo equations, generalized by the introduction of anisotropic diffusion coefficients. (11 refs.)

Appearance aspects of isochromatic mode-I crack tip fringe loops See Entry 61450

Convective instabilities of binary mixtures with fast chemical reaction in a porous medium See Entry 63552

47.25 TURBULENT FLOWS, CONVECTION, AND HEAT TRANSFER

61488 Measurements of the coherence of the fluctuating pressure field on a square prism placed in a turbulent flow. J.-P.Huot, H.Arbej, C.Rey (Lab. de Mecanique des Fluides, Ecole Centrale de Lyon, Ecully, France). *C.R. Seances Acad. Sci. Ser. II (France)*, vol.296, no.5, p.305-8 (7 Feb. 1983). In French.

A study of the fluctuating pressure field on a square prism placed in a turbulent stream was undertaken. An experimental investigation including the measurements of the characteristics of the incident turbulent flow as well as those of the induced pressure field was realized. The various mechanisms which contribute to the generation of the unsteady pressure field are analysed. (4 refs.)

Number of modes governing two-dimensional viscous, incompressible flows See Entry 61473

On the propagation of non-linear pressure waves in pipes with turbulent non-zero mean flow See Entry 61551

Spectral behaviour of a concentration field in turbulence environment with rapid chemical reaction See Entry 61564

Premixed, turbulent combustion of a sudden-expansion flow ... See Entry 63550

47.25C Isotropic turbulence

61489 Thresholds for the onset of fluid and magnetofluid turbulence. D.Montgomery (Phys. Dept., Coll. of William & Mary, Williamsburg, VA, USA).

Phys. Scr. (Sweden), vol.T2, no.2, p.506-10 (1982). [received: April 1983] (1982 International Conference on Plasma Physics, Goteborg, Sweden, 9-15 June 1982).

Hydrodynamic stability theory has focused on a few simple test cases to obtain the sharpest possible confrontations between theory and experiment. Six of these are briefly reviewed: plane Poiseuille and Couette flow, pipe flow, rotating Couette flow, thermally-driven Bénard convection, and the Blasius laminar boundary layer. Linear perturbation theory seems inadequate in the first three cases, and satisfactory in the last three. Insufficient information, experimental or theoretical, exists in magnetohydrodynamics to make any comparably decisive tests. (33 refs.)

Kinetics of fluctuations for systems undergoing phase transitions—interfacial approach See Entry 61485

The generation of electric currents by the turbulent flow of dielectric liquids. II. Pipes of finite length See Entry 61561

47.25F Boundary layer and shear turbulence

61490 Turbulence measurements in wall jets along strongly concave surfaces. R.Kobayashi, N.Fujisawa (Tohoku Univ., Sendai, Japan). *Acta Mech. (Austria)*, vol.47, no.1-2, p.39-52 (1983).

The present experiment found that turbulence intensities in turbulent wall jets along a concave surface increase remarkably, when the radius of curvature becomes smaller beyond a certain condition. The critical condition is discussed in comparison with the Taylor-Görtler instability for turbulent wall jets. The measurements are also made for the mean velocity field, the Reynolds stress, the turbulence energy balance and the velocity correlations. (8 refs.)

61491 An unsteady interactive separation process. L.L.van Dommelen, S.F.Shen (Cornell Univ., Ithaca, NY, USA). *AIAA J. (USA)*, vol.21, no.3, p.358-62 (March 1983).

Recently, Sychev addressed the question of unsteady separation moving upstream along the wall. Here, by a least-square procedure, an interaction solution is shown to exist in which the boundary-layer approximation remains uniformly valid. No additional vortex layers are introduced in the interaction region, thus avoiding the difficulties inherent in Sychev's proposal. Remarkably, according to the solution, the principal mechanics of separation is a bifurcation-free divergence of streamlines. (13 refs.)

61492 Comment on 'Improved method for the measurement of turbulence quantities'. M.K.Swaminathan, G.W.Rankin, K.Sridhar (Univ. of Windsor, Windsor, Canada), S.Sampath, V.Ganesan, B.H.L.Gowda. *AIAA J. (USA)*, vol.21, no.3, p.476-7 (March 1983).

Swaminathan et al. comment on the work of Sampath et al., discussing a number of points which are likely to prove vital in improving the results of the present method and in ensuring that proper comparisons are made with results of others. Sampath et al. reply back to these comments highlighting the flaws present. (6 refs.)

61493 Spatial periodicity of the mean static pressure gradient in turbulent pulsating flow. S.Burnel, J.-M.Thomas (Univ. d'Orleans, Orleans, France). *C.R. Seances Acad. Sci. Ser. II (France)*, vol.296, no.3, p.165-8 (24 Jan. 1983). In French.

For an unsteady fully developed flow, the study of the mean values shows that the velocity profiles are independent of the pulsations; on the other hand, the amplitude of the static pressure gradient variations can reach $\pm 70\%$ of the steady pressure gradient value. The results indicate that the mean value of the friction factor is equal to that of the associated steady flow if the correlation which exists between the longitudinal gradient of the velocity modulation and that of the mean static pressure is taken into account. (3 refs.)

61494 The distortion of turbulence by a flat plate and its relevance to the pressure fluctuation on the obstacle. J.-P.Huot, H.Arbej, C.Rey (Ecole Centrale de Lyon, Ecully, France). *C.R. Seances Acad. Sci. Ser. II (France)*, vol.296, no.4, p.213-16 (31 Jan. 1983). In French.

A study of the distortion of turbulence upstream of a flat plate placed normal to the mean flow is undertaken in the case when the integral scale of turbulence is small with respect of the width of the obstacle. An experimental investigation is performed, including measurements of the evolution of turbulence intensities and longitudinal spectra for different locations along the stagnation streamline. A comparison between the experimental results and those inferred from theory is given. (8 refs.)

61495 Influence of free-stream turbulence on turbulent boundary layer heat transfer and mean profile development. I. Experimental data. M.F.Blair (Trans. ASME, J. Heat Transfer (USA), vol.105, no.1, p.33-40 (Feb. 1983).

An experimental research program was conducted to determine the influence of free-stream turbulence on zero pressure gradient, fully turbulent boundary layer flow. Convective heat transfer coefficients and boundary layer mean velocity and temperature profile data were obtained for a constant free-stream velocity of 30 m/s and free-stream turbulence intensities ranging from approximately 1/4 to 7 percent. Free-stream multicomponent turbulence intensity, longitudinal integral scale, and spectral distributions were obtained for the full range of turbulence levels. The test results with 1/4 percent free-stream turbulence indicate that these data were in excellent agreement with classic two-dimensional, low free-stream turbulence, turbulent boundary layer correlations. For fully turbulent boundary layer flow, both the skin friction and heat transfer were found to be substantially increased (up to ~ 20 percent) for the higher levels of free-stream turbulence. (35 refs.)

61496 Influence of free-stream turbulence on turbulent boundary layer heat transfer and mean profile development. II. Analysis of results. M.F.Blair (United Technol. Res. Center, East Hartford, CT, USA).

Trans. ASME, J. Heat Transfer (USA), vol.105, no.1, p.41-7 (Feb. 1983). For pt.I see *ibid.*, vol.105, p.33 (1983). An experimental research program was conducted to determine the influence of free-stream turbulence on zero pressure gradient fully turbulent boundary layer flow. In pt. I of this paper, convective heat transfer coefficients, boundary layer mean velocity and temperature profile data, as well as wall skin friction coefficient distribution data were presented for five flow conditions of constant free-stream velocity (30 m/s) and free-stream turbulence intensities ranging from approximately 1/4 to 7 percent. These data indicated that the turbulence and significant effects on both the turbulent boundary layer skin friction and heat transfer. In the current paper, these new data are compared to various independent experimental data and analytical correlations of free-stream turbulence effects. This analysis has shown that the effects documented in pt. I were a function of the free-stream turbulence intensity, the turbulence length scale, and the boundary layer momentum thickness Reynolds number. In addition, the Reynolds analogy factor ($2St/c_p$) was shown to increase by just over 1 percent for each 1 percent increase in free-stream turbulence level. New correlations for the influence of free-stream turbulence on skin friction, heat transfer, and the Reynolds analogy factor are presented. (20 refs.)

Response of underwater structures to convective component of flow noise See Entry 61344

Unsteady transonic flow over wings including inviscid/viscous interaction See Entry 61522

Correlation of Preston tube data with laminar skin friction ... See Entry 61523

Freestream turbulence and transonic flow over a 'bump' model See Entry 61524

Flow visualisation methods for separated three-dimensional shock wave/turbulent boundary-layer interactions See Entry 61526

Heat transfer and fluid flow experiments with a tube fed by a plenum having nonaligned inlet and exit See Entry 61554

Premixed combustion in a turbulent boundary layer with injection See Entry 61565

47.25J Turbulent diffusion

A study of the fluctuation concentration field in a turbulent jet. On the measurement of the concentration fluctuation intensity and the self-preservation See Entry 61538

47.25M Noise (turbulence generated)

61497 An investigation into noise radiation from flow control valves with particular reference to flow rate measurement. K.A.El-Shorbagy (Faculty of Engng., Alexandria Univ., Alexandria, Egypt). *Appl. Acoust. (GB)*, vol.16, no.3, p.169-81 (1983).

Flow control valve noise has been investigated, both analytically and experimentally, for two cases of variable orifice area and variable mass flow rate. The analysis is based on Lighthill's (1952, 1954) acoustic analogy, together with Curle's (1955) theory for noise generation from fluid-solid boundary interactions. Results indicate that monitoring sound levels of valve noise could be useful as a feasible means for flow rate measurements and online automatic flow control in pipes. (19 refs.)

61498 Emission and propagation of noise in moving air. R.Legendre (ONERA, Chatillon, France). *C.R. Seances Acad. Sci. Ser. II (France)*, vol.296, no.4, p.229-31 (31 Jan. 1983). In French.

A change in the definition of pseudosound brings more clearly to light the mechanisms by which noise is generated by turbulence and propagates. (no refs.)

61499 Spectrum of propeller cavitation noise. Tao Du-chum (Inst. of Acoustics, Acad. Sinica, Peking, China). *Acta Acust. (China)*, vol.7, no.6, p.344-51 (Nov. 1982). In Chinese.

The cause of propeller cavitation noise is described. Spectra of propeller cavitation noise are calculated. The resultant spectra are in good agreement with experimental results. The time-variant characteristics of propeller cavitation noise are explained in terms of a physical mechanism. The nonuniformity of modulation in the frequency domain is illustrated. (19 refs.)

Pressure wave attenuation due to anode mufflers in pulsed lasers See Entry 61125

Response of underwater structures to convective component of flow noise See Entry 61344

Airfoil noise analysis by nearfield and farfield microphone arrays See Entry 61348

What causes noise in a convecting fluid? See Entry 61486

Onset of turbulent convection in large cells See Entry 61501

Correlation of Preston tube data with laminar skin friction See Entry 61523

Conventional profile coaxial jet noise prediction See Entry 61534

47.25Q Convection and heat transfer

(see also 44.25 Convective and constrained heat transfer)

61500 A semi-circle theorem in thermohaline convection with rotation and magnetic field. J.R.Gupta, S.K.Sood, R.G.Shandil (Dept. of Maths., Himachal Pradesh Univ., Summer Hill, Simla, India). *Indian J. Pure & Appl. Math.*, vol.14, no.1, p.115-28 (Jan. 1983).

A mathematical analysis of the governing equations of thermohaline convection [Veronis' (1965) configuration] with a uniform vertical rotation and magnetic field for the case of rigid conducting boundaries shows that the complex growth rate p of an oscillatory perturbation, neutral or unstable with wave number $a^2 \geq 0/2\sigma$, must lie inside a semi-circle in the right half of the complex p -plane. A similar result holds good for Stern's (1960) configuration with a uniform vertical rotation and magnetic field. (5 refs.)

61501 Onset of turbulent convection in large cells. E.Siggia (Dept. of Phys., Cornell Univ., Ithaca, NY, USA). *Physica A (Netherlands)*, vol.118A, no.1-3, p.335 (March 1983). (Proceedings of the Conference on Nonlinear Fluid Behavior, Boulder, CO, USA, 7-11 June 1982).

Summary form only given, as follows. Convection experiments in small aspect ratio (=lateral size/depth) cells have shown many of the sharp changes in temporal properties that are characteristic of low order dissipative dynamical systems. In large cells there are generally no sharp transitions between regimes with different temporal signatures and broad band noise develops relatively smoothly from frequencies. One infers that the multiplicity of spatial patterns allowed in the larger cell is responsible for this difference. Because of the complexity of doing realistic calculations with the Boussinesq equations a number of effects which act together in a real experiment have been isolated for theoretical study. In a third class of problems one seeks to determine the effective long wavelength dynamics of a locally ordered convection pattern following much the same reasoning that takes one from microscopic physics to hydrodynamics. The first equations of this kind that get beyond the Ginzburg-Landau from (which obviously cannot describe persistent time dependent flow) were described by Siggia and Zippelius (1981). (5 refs.)

61502 Time dependence in Rayleigh-Benard convection with a variable cylindrical geometry. R.P.Behringer, H.Gao (Dept. of Phys., Duke Univ., Durham, NC, USA), J.N.Shaumeyer. *Phys. Rev. Lett. (USA)*, vol.50, no.16, p.1199-202 (18 April 1983).

Studies of the first time dependence in Rayleigh-Benard convection in ^4He are reported. The aspect ratio Γ could be varied continuously. Data at 31 Γ values with $4 < \Gamma < 13$ show that near onset the first time dependence is always periodic and associated with changes in the heat transport. The dominant periodicity has a nonzero amplitude, A , and vanishing frequency at onset. Changes in A with Γ show wave-number effects. Except for the time dependence, the transition is consistent with predictions for the skew-varicose instability. (12 refs.)

61503 Heat transfer in hydromagnetic flow near an oscillating porous flat plate. S.Narasimha Murthy, H.M.Thimmarayappa (Coll. of Basic Sci. & Humanities, Univ. of Agricultural Sci., Bangalore, India). *Rev. Roum. Sci. Tech. Ser. Mec. Appl. (Rumania)*, vol.28, no.1, p.33-7 (Jan.-Feb. 1983).

The temperature distribution for the problem of the motion of a viscous incompressible and electrically conducting fluid near an infinite porous flat plate in the presence of a transverse magnetic field fixed relative to the fluid is studied, taking the viscous dissipation into account. It is seen that, in a particular case, the heat flows from the liquid to the plate irrespective of the fact that the plate is maintained at a higher temperature than the ambient liquid. Further, it is observed that suction alone does not affect the conditions of heat transfer. Also, the two different physical mechanisms such as suction and magnetic field have the same effect in regard to the heat transfer. (3 refs.)

61504 Heat transfer coefficients and patterns of fluid flow for contacting spheres at various angles of attack. E.M.Sparrow, R.F.Prieto (Dept. of Mech. Engng., Univ. of Minnesota, Minneapolis, MN, USA). *Trans. ASME. J. Heat Transfer (USA)*, vol.105, no.1, p.48-55 (Feb. 1983).

Wind tunnel experiments were performed to determine heat transfer coefficients and fluid flow patterns for two contacting spheres. The experiments were carried out at three different angles of attack and for Reynolds numbers in the range from 4000 to 26000. Three heat transfer conditions were considered: (a) both spheres thermally active, (b) forwardmost sphere thermally active and rearmost sphere adiabatic, and (c) forwardmost sphere adiabatic and rearmost sphere thermally active. Complementary experiments for a single sphere, encompassing the same parameter ranges, yielded baseline information for comparison with the two-sphere results. It was found that the largest effects of the sphere-to-sphere interaction on the heat transfer occurred when the two spheres were in line. At this orientation and for higher Reynolds numbers in the investigated range, there was substantial enhancement of the heat transfer with respect to that for the single sphere. At the other angles of attack, there was lesser enhancement. The visualization studies revealed such key fluid flow features as the reattachment of the separated flow from the first sphere on the second, the presence of strong recirculations, and the delay of separation due to pressure-driven transverse flows. (8 refs.)

61505 Heat transfer from the heated convex wall of a return bend with rectangular cross section. N.Seki, S.Fukusako, M.Yoneta (Dept. of Mech. Engng., Hokkaido Univ., Sapporo, Japan). *Trans. ASME. J. Heat Transfer (USA)*, vol.105, no.1, p.64-9 (Feb. 1983).

An experimental investigation has been performed to clarify the turbulent heat transfer characteristics along the heated convex wall of a return bend which has a rectangular cross section with large aspect ratio for various heights of the duct. The experiments are carried out under the condition that the convex wall is heated at constant heat flux while the concave wall is insulated. Water is used as the working fluid with duct heights of 15, 40, 60 and 80 mm, Reynolds numbers of 8×10^3 to 8×10^4 , and Prandtl numbers ranging from 6.5 to 8.5. The mean and the local heat transfer coefficients are always smaller than those for the straight parallel plates and straight ducts. Both the local and the mean heat transfer coefficients decrease as the duct height increases. Near the outlet region of the return bend the local heat transfer coefficient increases in the flow direction as the height decreases. Behavior is just the opposite at the inlet. Correlation equations for the mean and the local Nusselt numbers are determined in the range of parameters covered. (11 refs.)

61506 Buoyancy effects on a boundary layer along an infinite cylinder with a step change of surface temperature. L.S.Yao (Dept. of Mech. & Aerospace Engng., Arizona State Univ., Tempe, AZ, USA). *Trans. ASME. J. Heat Transfer (USA)*, vol.105, no.1, p.96-101 (Feb. 1983).

The laminar boundary layer induced by a horizontal forced flow along an infinite vertical cylinder with a step change of surface temperature is studied by a finite-difference method. Close to the thermal leading edge, the buoyancy force induces a strong free-convection boundary layer. Slightly above the thermal leading edge, the boundary layer starts to separate at the rear stagnation line ($\phi = 180$ deg). The region of separated flow grows toward the forward stagnation line and becomes stationary at ≈ 104 deg as one moves upward. In other words, free convection dominates the heat transfer along the thermal leading edge. The importance of forced convection increases as one moves vertically from the thermal leading edge and eventually becomes the dominant mode. The numerical results show that the free-convection boundary layer is suppressed at the forward stagnation line and is carried toward the rear stagnation line by the forced convection. The phenomenon shares many similarities with a thermal plume affected by forced convection. (13 refs.)

61507 Natural convection heat transfer of water within a horizontal cylindrical annulus with density inversion effects. P.Vasseur, L.Robillard, B.Chandra Shekar (Dept. of Civil Engng. Ecole Polytech., Univ. de Montreal, Montreal, Quebec, Canada). *Trans. ASME. J. Heat Transfer (USA)*, vol.105, no.1, p.117-23 (Feb. 1983).

The effect of density inversion on steady natural convection heat transfer of cold water, between two horizontal concentric cylinders of gap width, L , is studied numerically. Water near its freezing point is characterized by a density maximum at 4°C . Numerical solutions are obtained for cylinders with nonlinear Rayleigh numbers RA ranging from 2×10^3 to 7.6×10^4 , a radius ratio $1.75 \leq r_a \leq 2.6$ and an inversion parameter γ , relating the temperature for maximum density with the cavity wall temperatures, between -2 and 2 . The results obtained are presented graphically in the form of streamline and isotherm contour plots. The heat transfer characteristics, velocity profiles, and local and overall Nusselt numbers are studied. The results of the present study were found qualitatively valid when compared with an experimental investigation carried out in the past. (28 refs.)

Performance of a compact cooling unit utilizing air-water mist flow See Entry 59777

Response of underwater structures to convective component of flow noise See Entry 61344

A solution for dispersed flow heat transfer using equilibrium fluid conditions See Entry 61376

Natural convection heat transfer between eccentric horizontal cylinders See Entry 61380

An examination into the validity of various prediction methods for void fraction in boiling flow See Entry 61386

Interaction of the nucleation phenomena at adjacent sites in nucleate boiling See Entry 61387

What causes noise in a convecting fluid? See Entry 61486

Influence of free-stream turbulence on turbulent boundary layer heat transfer and mean profile development. I. Experimental data See Entry 61495

Influence of free-stream turbulence on turbulent boundary layer heat transfer and mean profile development. II. Analysis of results See Entry 61496

Hypersonic slender-wedge analysis with gradual change in angle of attack See Entry 61525

An experimental investigation of heat transfer near the leading edge of an inclined flat plate in hypersonic flow See Entry 61528

Vapor flow through a porous membrane—a throttling process with condensation and evaporation See Entry 61546

Heat transfer and fluid flow experiments with a tube fed by a plenum having nonaligned inlet and exit See Entry 61554

Hydromagnetic flow and heat transfer between two horizontal plates, the lower plate being a stretching sheet See Entry 61563

Convective instabilities of binary mixtures with fast chemical reaction in a porous medium See Entry 63552

47.25R Wakes

Unsteady transonic flow over wings including inviscid/viscous interaction See Entry 61522

47.30 ROTATIONAL FLOW AND VORTICITY

61508 Self-excited wave oscillations in a water table. W.Calarese, W.L.Hankey (Air Force Wright Aeronautical Labs., Wright-Patterson AFB, OH, USA). *AIAA J. (USA)*, vol.21, no.3, p.372-8 (March 1983).

An experimental investigation has been performed on self-excited wave oscillations on cavity, spike-tipped, and inlet models in a water table. Buzzing was generated by positioning the models at a small angle of attack with respect to the freestream flow. The hydraulic analogy was used to compare the results obtained in water to results obtained in gas. High-speed and real-time photography were used in the experiment. The frequencies of oscillations in water and air were consistent with the hydraulic analogy. Numerical solutions of the phenomenon were also obtained. (10 refs.)

61509 Comment on 'Inviscid solution for the secondary flow in curved ducts'. N.H.Kemp (Phys. Sci. Inc., Andover, MA, USA). *AIAA J. (USA)*, vol.21, no.3, p.477-8 (March 1983).

The author comments on the equations solved by Abdallah and Hamed for inviscid, incompressible steady flow in curved ducts. It is pointed out that these equations are in fact the continuity equation and two components of the vector vorticity equation (the steady Helmholtz equations). The nature of these equations is briefly studied and the point is made that nothing new is presented. (3 refs.)

61510 On the use of the rotating disc electrode. J.-L.Bousgarbier, J.Pechoux (Lab. d'Etudes Aérodynamiques et Thermiques, Poitiers, France). *C.R. Seances Acad. Sci. Ser. II (France)*, vol.296, no.3, p.161-3 (24 Jan. 1983). In French.

The flow pattern currently used for predicting rotating disc electrode performances and the velocity field inside the experimental device are sometimes different. Using fluid mechanics results the estimation error caused by this difference is given. (8 refs.)

61511 Stabilisation of the solution for a system of rotating compressible fluid. P.K.Pal (Dept. of Differential Equations & Functional Analysis, Patrice Lumumba Univ., Moscow, USSR). *Indian J. Pure & Appl. Math.*, vol.14, no.1, p.108-14 (Jan. 1983).

The system of partial differential equations of motion of a rotating compressible ideal fluid is considered. Using the explicit form of the solution the behaviour as $t \rightarrow \infty$ of the solution is investigated. Stabilisation of the solution in the case of an external force, independent of time is established. (6 refs.)

61512 Experiments on the stable biased flow through a flat-plate row. M.Hayashi, A.Sakurai, Y.Ohya. *Technol. Rep. Kyushu Univ. (Japan)*, vol.55, no.4, p.399-406 (Aug. 1982). In Japanese. [received: Feb. 1983]

When a row of multiple flat plates is arranged side by side to the approaching flow, the flows passing through the slits (gap flows) are biased either upward or downward in a stable manner if the slit ratio (ratio of the slit width to the plate width) is small. What causes the biasing and how stable it are are investigated experimentally at both low and high Reynolds numbers ($Re=30-120$ and 10^4). When the slit ratio is very small, the gap flow acts like a simple bleed, and it seems to be biased owing to the Coanda effect between the gap flow and the outer shear layer. When the slit ratio is increased, the individual plate on the biased side makes distinct vortex shedding. In this case, the biased gap flow is strongly related to the vortex shedding of each plate and the stability of the biasing is due to the dominant vortex formation and shedding from the plate on the biased side. These vortices formed behind the biased side engulf the gap flow ceaselessly and prevent the plate on the unbiased side from making its own vortex formation. (8 refs.)

Subharmonic oscillations of a mixing layer-wedge system associated with free surface effects See Entry 61484

Thresholds for the onset of fluid and magnetofluid turbulence See Entry 61489

An unsteady interactive separation process See Entry 61491

Acoustic wave radiated by head-on collision of two vortex rings See Entry 61517

The rotary movements of compressible fluids. II See Entry 61518

Numerical solution of transonic stream function equation See Entry 61520

Inviscid axisymmetric jet impingement with recirculating stagnation regions See Entry 61535

Effect of Hall current on unsteady hydromagnetic boundary layers in rotating dust fluid See Entry 61560

47.35 WAVES

61513 Supplementary conservation laws and collisions in a theory of shallow water in cylindrical coordinates. L.Restuccia (Istituto Matematico, Univ. di Messina, Messina, Italy).

Atti Semin. Mat. & Fis. Univ. Modena (Italy), vol.30, no.2, p.345-54 (1981). The author points out several properties connected with the mathematical model describing the flow of nonlinear shallow water waves in cylindrical coordinates. Among other results she shows that the basic system of equations admits infinite supplementary conservation laws and determines the behaviour of the shock generating function. (11 refs.)

61514 Propagation of flexural gravitational waves in floating plate. V.V.Yakovlev. *Dopov. Akad. Nauk UkrSR. Ser. A (USSR)*, no.2, p.40-3 (1983). In Ukrainian.

Considers the generation and propagation of flexural gravity waves in a floating elastic plate. These waves are excited by a normal distributed load that moves with constant velocity and then is stopped. A numerical analysis is made of the dependence of the surface normal stress on the fluid depth, plate thickness and velocity of load movement. (7 refs.)

Subharmonic oscillations of a mixing layer-wedge system associated with free surface effects See Entry 61484

47.40 COMPRESSIBLE FLOWS; SHOCK AND DETONATION PHENOMENA

(see also 28.70 Nuclear explosions, 52.35T Plasma shock waves)

61515 Reparameterization of the Becker-Kistiakowsky-Wilson equation of state for water-gel explosives. V.K.Mohan (IDL Chem. Ltd., Hyderabad, India), J.E.Hay.

Combust. & Flame (USA), vol.50, no.2, p.207-18 (March 1983). Describes the results of the reparameterization studies on the Becker-Kistiakowsky-Wilson (BKW) equation of state (EQS) for water-gel explosives. The original set of BKW parameters ($\alpha=0.5$, $\beta=0.1$, $\kappa=11.85$, and $\theta=400$) predicts a higher detonation velocity and detonation pressure and a lower detonation temperature compared with the experimental values for these explosives. Among the several combinations of parameters examined, the following set— $\alpha=0.5$, $\beta=0.1$, $\kappa=8.85$, and $\theta=1850$ —is found to give realistic values for the various detonation properties. Moreover, the predicted and the experimental detonation velocities are seen to be in fair agreement. A comparison of the computed and the experimental (obtained from Crawshaw-Jones measurements) fume characteristics shows that (1) inclusion of the wrapper material in the explosive composition increases the concentration of fumes and gives correspondence between the two for products such as CO , H_2 , NH_3 , and CH_4 , (2) the measured NO_x concentration is difficult to get in these computations, and (3) calculations of the product compositions for the isentropic expansion of detonation products along the Chapman-Jouguet (C-J)

isentropic give freeze-out temperatures in the range of 1000-1800K. These computations were also performed for two ammonium nitrate-fuel oil mixtures and are found to be in good agreement with the experimental data. (27 refs.)

61516 Experimental study on cylindrical and spherical implosions. K.Terao (Dept. of Mech. Engng., Yokohama Nat. Univ., Yokohama, Japan). *Jpn. J. Appl. Phys. Part 1 (Japan)*, vol.22, no.3, p.446-53 (March 1983).

Cylindrically and spherically imploding detonation waves in a stoichiometric propane-oxygen mixture, produced in vessels of about 40 cm internal diameter having different convergent spaces, were experimentally investigated by applying a radially divergent detonation. The experimental results have shown that the ratio of the pressure P behind the imploding detonation waves to the initial mixture pressure P_0 is related to the radial distance r from the implosion center to the detonation front. The pressure increases with the propagation of the imploding detonation in every case higher than the theoretical one. (14 refs.)

61517 Acoustic wave radiated by head-on collision of two vortex rings. T.Kambe, T.Minota (Dept. of Appl. Sci., Kyushu Univ., Fukuoka, Japan). *Proc. R. Soc. London Ser. A (GB)*, vol.386, no.1791, p.277-308 (8 April 1983).

An attempt has been made to detect the acoustic wave radiated by the collision of two vortex rings and to compare it with predictions made by the theory of aerodynamic sound with and without fluid viscosity. It has been found that the detected acoustic pressure p obeys the scaling law $p \propto (\rho_0/c^2)U^4R/r$ predicted by the theory. Analysis of the observed signals shows that the acoustic pressure is composed of quadrupole and monopole radiation. Although the inviscid theory can account for the initial part of the detected signal quantitatively, it fails to predict the appearance of the monopole, and it is also not possible to give even a qualitative description of the quadrupole in the later stages. A viscous theory is presented to obtain an improved fit to the observed profile; the monopole radiation is related to the viscous decay of total kinetic energy, and the main quadrupole is affected by the decay of the vortex strength as a result of pair annihilation under the action of viscosity. Hence the initial inviscid phase is followed by phases dominated by the action of viscosity. (31 refs.)

61518 The rotary movements of compressible fluids. II. C.Jacob (Univ. de Bucharest, Bucharest, Rumania).

Rev. Roum. Sci. Tech. Ser. Mec. Appl. (Rumania), vol.27, no.4, p.437-52 (July-Aug. 1982). In French. [received: March 1983]

For pt.1 see *ibid.*, vol.26, no.3, p.357-69 (1981). Derives the basic equation of steady-state motion with variables referred to a moving coordinates system with a particular application to the plane-parallel case. This provides a definition of two families of curves forming the Mach lines which are real for speeds away from the critical level. The simplified assumptions allow the basic equation for velocities potential to be linearised and used for the theory of thin wings. (2 refs.) I.G.

61519 Navier-Stokes solution on the CYBER-203 by a pseudospectral technique. J.J.Lambiotte (Analysis & Computation Div., NASA Langley Res. Center, Hampton, VA, USA), M.Y.Hussaini, S.Bakhar, S.A.Orszag. 10th IMACS World Congress on System Simulation and Scientific Computation, Montreal, Canada, 8-13 Aug. 1982 (New Brunswick, NJ, USA: IMACS 1982), p.305-7 vol.1

Describes a three-level, time-split, mixed spectral/finite difference method for the numerical solution of the three-dimensional, compressible Navier-Stokes equations developed for and implemented on the Control Data Corporation CYBER-203. This method uses a spectral representation for the flow variables in the streamwise and spanwise coordinates, and central differences in the normal direction. The five dependent variables are interleaved one horizontal plane at a time and the array of their values at the grid points of each horizontal plane is a typical vector in our computation. The code is organized so as to require, per time step, a single forward-backward pass through the entire database. The one- and two-dimensional fast Fourier transforms are performed using software especially developed for the CYBER-203. (5 refs.)

On the slipping boundary condition for low density gas flow .. See Entry 61480

Stabilisation of the solution for a system of rotating compressible fluid See Entry 61511

Compression of a spherical gas bubble in ideal liquid by the finite pressure-pulse See Entry 61543

Behavior of a perturbed rarefaction wave See Entry 61573

47.40H Transonic flows

61520 Numerical solution of transonic stream function equation. M.Hafez, D.Lovell (George Washington Univ., NASA Langley Res. Centre, Hampton, VA, USA).

AIAA J. (USA), vol.21, no.3, p.327-35 (March 1983). The stream function equation, in conservation form, looks similar to the full potential equation and existing methods (e.g. artificial compressibility) can be readily applied. Rotational flows can be calculated once the vorticity (due to shocks or nonuniformity) is evaluated. There are, however, two main difficulties. The first is that the density is not uniquely determined in terms of the flux (there are two solutions: the subsonic and the supersonic branch with a square root singularity at the sonic point). Methods to overcome this difficulty are studied and results are presented with some remarks on inviscid separation and closed streamlines. The second difficulty, the need of two stream functions for three-dimensional calculations is briefly discussed. (26 refs.)

61521 A finite element formulation for steady transonic Euler equations. A.Eeer, H.U.Akay (Purdue Univ., Indianapolis, IN, USA).

AIAA J. (USA), vol.21, no.3, p.343-50 (March 1983). Solution of two-dimensional, steady, transonic Euler equations is considered. Based on a variational principle, the problem is formulated in terms of three new Clebsch-type variables (ϕ , α , β). After a finite element formulation, a set of nonlinear equations is obtained in terms of these variables. This new formulation allows the Euler equations to be expressed in a second-order form, eliminating the difficulties encountered in the solution of first-order equations. It also provides a unified procedure for isentropic (potential) and nonisentropic (Euler) equations. A relaxation technique is employed to obtain steady-state solutions. Numerical results for flows through a channel are presented to demonstrate the effectiveness and accuracy of the numerical scheme. (14 refs.)

61522 Unsteady transonic flow over wings including inviscid/viscous interaction. D.P.Rizzetta, C.J.Borland (Boeing Military Airplane Co., Seattle, WA, USA).

AIAA J. (USA), vol.21, no.3, p.363-71 (March 1983). A numerical procedure is presented for computing the unsteady transonic flowfield about swept wings undergoing time-dependent motions. The outer

inviscid portion of the flow is assumed to be governed by the modified unsteady transonic small disturbance potential equation which is integrated in the time domain by means of an alternating direction implicit algorithm. Dominant effects of the shock/boundary-layer interaction are accounted for by a simple empirically defined model. Viscous flow regions adjacent to the wing surface and in the trailing wake are described by a set of integral equations appropriate for compressible turbulent shear layers. The two-dimensional boundary-layer equations are applied quasistatically stripwise across the span. Coupling with the outer inviscid flow is implemented through use of the displacement thickness concept. Validity of the assumptions underlying the method is established by comparison with experimental data for the flow about a high aspect ratio transport wing having an advanced airfoil section. (30 refs.)

61523 Correlation of Preston tube data with laminar skin friction. T.D.Reed, A.Abu-Mostafa (Oklahoma State Univ., Stillwater, OK, USA), F.S.Steinle, Jr.

AIAA J. (USA), vol.21, no.3, p.379-80 (March 1983).

The work reported herein constitutes one step in the search for an improved procedure for calibrating the effects of noise on model tests in transonic wind tunnels. Earlier work by Treon et al. (1971) suggested that a sharp-nose 10-deg. cone could be useful in explaining differences between three transonic wind tunnel tests of the same C-5A aircraft model. Subsequently, a comprehensive series of tests were undertaken to measure free transition on a single cone in 23 wind tunnels and in flight. This cone was designated the AEDC Transition Cone and is a sharp-nose 10-deg. cone with a highly polished surface and a traversing mechanism to move a miniature (0.025 cm high) Pitot probe along the surface. The basic purpose of the traversing probe is to detect the location of boundary-layer transition. (9 refs.)

61524 Freestream turbulence and transonic flow over a 'bump' model. S.Raghunathan, R.J.W.McAdam (Queen's Univ. of Belfast, Belfast, N Ireland).

AIAA J. (USA), vol.21, no.3, p.467-9 (March 1983).

In transonic flow, predictions of free-flight conditions from wind tunnel tests need a close simulation of Reynolds number. However, Reynolds number simulation is not adequate, since results from wind tunnel tests are influenced by effects of tunnel environment, such as noise and turbulence levels. A recent paper by the authors (1982), showed a strong influence of turbulence on attached turbulent boundary layers at zero pressure gradient in the Mach number range of 0.8 and boundary-layer momentum thickness Reynolds number range of 3000-10⁴. This note presents the general characteristics of transonic flow over a 'bump' model at various freestream turbulence levels. (5 refs.)

47.40K Supersonic and hypersonic flows

61525 Hypersonic slender-wedge analysis with gradual change in angle of attack. R.N.Gupta (Nasa-Langley Res. Center, Hampton, VA, USA), S.P.Joshi, C.M.Rodkiewicz.

Acta Mech. (Austria), vol.47, no.1-2, p.107-15 (1983).

A slender two-dimensional wedge-wing moving at a high Mach number is subjected to an angle of attack changing exponentially with time. The obtained results give the time history of wall shear, heat transfer, displacement thickness, and viscous induced pressure. The unsteady character of the flow appears to be confined to the initial stages of the change in the angle of attack. (7 refs.)

61526 Flow visualisation methods for separated three-dimensional shock wave/turbulent boundary-layer interactions. G.S.Settles, Hsueh-Ying Teng (Princeton Univ., Princeton, NJ, USA).

AIAA J. (USA), vol.21, no.3, p.390-7 (March 1983).

A collection of techniques is presented for the visualisation of separated turbulent flows at high speeds. Some of these techniques—including a method of generating a localised vapour visualisation—have not been available previously. Others, such as the conical shadowgraph and stereoscopic schlieren methods, have been used before in other contexts. The authors apply all the available techniques to the study of three-dimensional supersonic flows generated by swept compression corners. The paper discusses the techniques and some of the fluid mechanical insights revealed by the visualisations, including the structure of the observed three-dimensional flow separations and associated shock wave systems. (34 refs.)

61527 Body resistance in a detonating gas flow. M.M.Gilinskii, T.S.Novikova.

Combust. Explos. & Shock Waves (USA), vol.18, no.4, p.489-92 (July-Aug. 1982). Translation of: *Fiz. Goreniya & Vzryva (USSR)*, vol.18, no.4, p.114-17 (July-Aug. 1982). [received: March 1983].

Analyses the effect of heat liberation on the value of braking pressure behind a detonation discontinuity. Using the Rankin-Hugoniot relationship on the detonation polarity and the formulas for isentropic compression behind the wave, the authors obtain the ratio of the braking pressure behind the detonation wave p_{01} to the conventional shock wave pressure p_0 . (8 refs.)

61528 An experimental investigation of heat transfer near the leading edge of an inclined flat plate in hypersonic flow. M.Iwasaki, M.Hashiguchi, T.Ueno, O.Kondo.

Technol. Rep. Kyushu Univ. (Japan), vol.55, no.4, p.371-7 (Aug. 1982). In Japanese. [received: Feb. 1983].

The heat transfer near the leading edge of a flat plate at various angles of attack immersed in hypersonic flow is experimentally investigated in a hypersonic shock tunnel with a conical nozzle. Steady heat transfer rates are measured by means of thin film heat transfer gauges at argon test flow Mach numbers around 12, free stream Reynolds numbers of about 0.7×10^6 and 1.5×10^6 per cm, and stagnation temperatures of about 2000°C and 10000°C where the test flow is weakly ionized. A modified Stollery's strong interaction theory which is made by including the source flow effects due to conical nozzle is proposed by applying Hall's small perturbation method. The results of the present approach and Stollery's theory are compared with those of the experiment. It is found that the present method provides the theoretical Stanton number in qualitatively good agreement with the experimental one for the un-ionized gas flow. (12 refs.)

61529 Asymptotic solution near the shock-layer separation point for a hypersonic flow past pointed bodies. V.G.Ignatenko.

Vestn. Leningr. Univ. Ser. Mat. Mekh. & Astron. (USSR), no.1, p.64-9 (Jan. 1983). In Russian.

A perfect gas hypersonic flow for small $\epsilon = (x-1)/(x+1)$ is considered near the shock-layer separation point. An explicit asymptotic solution is found for a large class of pointed bodies with a continuous curvature. (6 refs.)

Measurements of a supersonic velocity in a nitrogen flow using inverse Raman spectroscopy See Entry 61582

47.40N Shock-wave interactions

61530 Strong shock implosion approximate solution. Y.Fujimoto, E.A.Mishkin, C.Alejandro (Polytech. Inst. of New York, New York, NY, USA).

Physica B & C (Netherlands), vol.115 B+C, no.2, p.271-83 (Jan. 1983).

The self-similar, center-bound motion of a strong spherical, or cylindrical, shock wave moving through an ideal gas with a constant $\gamma = c_p/c_v$, is considered and a linearized, approximate solution is derived. An X, Y phase plane of the self-similar solution is defined and the representative curve of the system behind the shock front is replaced by a straight line connecting the mappings of the shock front with that of its tail. The reduced pressure $P(\xi)$, density $R(\xi)$ and velocity $U(\xi)$ are found in closed, quite accurate, form. Comparison with numerically obtained results, for $\gamma = 5/3$ and $\gamma = 7/5$, is shown. (21 refs.)

Flow visualisation methods for separated three-dimensional shock wave/turbulent boundary-layer interactions See Entry 61526

Asymptotic solution near the shock-layer separation point for a hypersonic flow past pointed bodies See Entry 61529

47.45 RAREFIED GAS DYNAMICS

(see also 07.30 Vacuum production and techniques)

On the slipping boundary condition for low density gas flow .. See Entry 61480

The pressure distribution on an arbitrary oriented plane impinged by a strongly underexpanded jet of rarefied gas See Entry 61539

Monte Carlo simulation of diffusion of gases in a porous solid: calculations for a new class of solids See Entry 61549

Behavior of a perturbed rarefaction wave See Entry 61573

Measurements of a supersonic velocity in a nitrogen flow using inverse Raman spectroscopy See Entry 61582

Direct measurements of aerosol diffusion constants in the intermediate Knudsen regime See Entry 61593

47.50 NON-NEWTONIAN DYNAMICS

61531 A solvable weak-potential model of a nonNewtonian fluid.

J.C.Rainwater (Nat. Engng. Lab., NBS, Boulder, CO, USA), S.Hess.

Physica A (Netherlands), vol.118A, no.1-3, p.371-82 (March 1983). (Proceedings of the Conference on Nonlinear Fluid Behavior, Boulder, CO, USA, 7-11 June 1982).

A theoretical model is developed for a nonNewtonian fluid of spherical molecules interacting with a weak potential. The Kirkwood-Smoluchowski equation for planar Couette flow reduces in leading order in potential strength to a shear-diffusion equation with an inhomogeneous source term. The pressure tensor elements are calculated and, for a Gaussian potential, reduce to one-dimensional integrals which are evaluated numerically. The model reproduces several qualitative features of nonNewtonian liquids and the computer simulations of Evans and Hanley (1980). These features include shear thinning, shear dilatancy, normal pressure differences and dependence on shear rate to a half-integer power. (20 refs.)

RTD for diffusion-free laminar flow of non-Newtonian fluids through coiled tubes See Entry 61474

Theoretical and experimental studies on the formation of an air core in a swirl spray pressure nozzle using a power law non-Newtonian liquid See Entry 61540

47.55 NONHOMOGENEOUS FLOWS

47.55B Cavitation

61532 Recombination mechanism for emission accompanying collapse of a cavitation bubble induced by a high-voltage electrical discharge. P.I.Golubnichii, V.M.Gromenko, A.D.Filonenko (Voroshilovgrad State Univ., Voroshilovgrad, USSR).

Sov. Phys.-Tech. Phys. (USA), vol.27, no.10, p.1208-11 (Oct. 1982). Translation of: *Zh. Tekh. Fiz. (USSR)*, vol.52, no.10, p.1966-71 (Oct. 1982). [received: April 1983].

A recombination mechanism for emission associated with collapse of a cavitation bubble induced by a high-voltage electrical discharge in liquid is found experimentally and confirmed by numerical estimates. The recombination mechanism is found to be predominant when bubbles are formed by relatively long (~ 0.1 of the collapse period) discharges in chlorine-containing liquids (carbon tetrachloride, chloroform). These liquids have a high saturated vapor pressure, so that the ratio of the maximum to the minimum bubble diameters is small. Elementary estimates of the duration of the light pulse and an examination of the form of the light pulse associated with plasma 'chilling' give results in good agreement with experiment. (9 refs.)

Analysis of a free boundary problem in partial lubrication See Entry 61459

47.55C Jets

61533 Investigation of water jet pulses generated by an impact piston device. G.Rehbinder (Swedish Rock Mech., Res. Foundation, Stockholm, Sweden).

Appl. Sci. Res. (Netherlands), vol.40, no.1, p.7-37 (1983).

High speed water pulses for destruction of rock, concrete etc. have been studied for more than a decade. The high speed pulses can be created in different ways and some investigations have been published about supersonic pulse generators. In this paper a device called impact pipe is studied theoretically as well as experimentally. In an impact pipe the impact velocity of a piston is transferred to pressure in a pressure chamber provided with a small nozzle through which a jet comes out. It is shown that theoretically the maximum pressure of 400 MPa is achieved if the length of the impacting piston is sufficiently long. Pressure measurements and high speed photography show that the water pulse coming out through the nozzle has violent radial bursts due to the pressure waves in the pressure chamber. (26 refs.)

61534 Conventional profile coaxial jet noise prediction. J.R.Stone, D.E.Groesbeck, C.L.Zola (NASA Lewis Res. Centre, Cleveland, OH, USA).

AIAA J. (USA), vol.21, no.3, p.336-42 (March 1983).

A semiempirical model for predicting the noise generated by conventional velocity-profile jets exhausting from coaxial nozzles is presented and compared with small-scale static data. The present method is an updated version

of that part of the original NASA Aircraft Noise Prediction Program (1974) relating to coaxial jet noise. The new procedure is more theoretically based and has also been improved by some empirical adjustments. (13 refs.)

61535 Inviscid axisymmetric jet impingement with recirculating stagnation regions. A.Rubel (Grumman Aerospace Corp., Bethpage, NY, USA). *AIAA J. (USA)*, vol.21, no.3, p.351-7 (March 1983).

Numerical solutions for the normal impingement of inviscid axisymmetric jets with energy deficient cores reveal three distinct classes of behaviour: (1) a small defect regime where the flow structure is unchanged from the zero defect case; (2) a moderate defect regime where stagnation bubbles first appear and grow with increased defect; and (3) a strong defect regime, where no solutions have been found. The recirculation zone model presumes that vorticity over radius is constant and continuous across the dividing stream surface. A local analytic solution to the governing partial differential equation for the stagnation bubble is consistent with the computational results. (14 refs.)

61536 Axially symmetric jet flows. H.W.Alt (Univ. of Heidelberg, Heidelberg, Germany), L.A.Caffarelli, A.Friedman. *Arch. Ration. Mech. & Anal. (Germany)*, vol.81, no.2, p.97-149 (1983).

The authors establish a general existence and uniqueness theorem for three dimensional axially symmetric jet flow. The results also apply (with trivial changes) to symmetric two dimensional jet flows and provide far reaching generalisations of the known existence theorems. (19 refs.)

61537 Joint probability density distribution in a radial axisymmetric plane wall jet. D.Codazzi, C.Kopp, R.Teitgen, H.Burnage (Univ. Louis-Pasteur de Strasbourg, Strasbourg, France). *C.R. Seances Acad. Sci. Ser. II (France)*, vol.296, no.1, p.15-17 (10 Jan. 1983). In French.

Joint probability density distributions computed in the outer self-preserved region of a turbulent plane radial axisymmetric wall jet are presented. This method shows that the fluctuating velocity vector has a preferred direction which appears to be different from its mean orientation. Hence, the most probable value (MPV) of the fluctuating velocity vector is not zero. The pattern of the MPV velocity vectors is given. Conditional sampling techniques lead to the following result: the MPV vector pattern which can be considered as MPV streamlines appears to be statistically stable. (5 refs.)

61538 A study of the fluctuation concentration field in a turbulent jet. On the measurement of the concentration fluctuation intensity and the self-preservation. I.Nakamura, Y.Sakai (Dept. of Mech. Engng., Nagoya Univ., Nagoya, Japan), M.Miyata.

Mem. Fac. Eng. Nagoya Univ. (Japan), vol.34, no.1, p.113-24 (May 1982). In English. [received: March 1983]

Experimental results on the diffusion process, in a circular jet of a dye solution issuing into a quiescent water are presented. Also a semi-empirical theory for the radial profile of the concentration field for a dye solution were performed by a light absorption method because of the simplicity of its measuring principle and movability of the probe. Experimental results showed that the radial profiles of the mean axial velocity and mean concentration respectively had well-known Gaussian distributions. A self-preserving form for the profiles of the concentration fluctuation intensity was observed in the downstream region, $x/d_0 \geq 100$. Using these experimental results and assumptions on the gradient type diffusion process, an analysis and calculations are presented on the self-preserving profile of the concentration fluctuation intensity. (14 refs.)

61539 The pressure distribution on an arbitrary oriented plane impinged by a strongly underexpanded jet of rarefied gas. B.F.Panov. *Vestn. Leningr. Univ. Ser. Mat. Mekh. & Astron. (USSR)*, no.1, p.74-80 (Jan. 1983). In Russian.

The results of experimental research into the pressure distribution of an arbitrary plane exposed to rarefied air jet from a sonic nozzle are presented. A method of calculating the pressure on a surface is proposed and empirical formulae are suggested. (12 refs.)

Turbulence measurements in wall jets along strongly concave surfaces See Entry 61490

Premixed, turbulent combustion of a sudden-expansion flow See Entry 63550

47.55E Nozzles

61540 Theoretical and experimental studies on the formation of an air core in a swirl spray pressure nozzle using a power law non-Newtonian liquid. S.K.Som (Dept. of Mech. Engng., Indian Inst. of Technol., Kharagpur, India). *Appl. Sci. Res. (Netherlands)*, vol.40, no.1, p.71-91 (1983).

An extension of the recent work (see Som and Mukherjee, 1980) has been made to evaluate the air core diameter both theoretically and experimentally in the case of a swirl nozzle using a time independent pure viscous power law non-Newtonian fluid. The theoretical predictions have been made through an approximated analytical solution of the hydrodynamics of flow inside the nozzle. A series of experiments has been carried out with solutions of CMC (carboxymethyl cellulose sodium salt) powder in water with different concentrations as the working fluids. The rheological properties of the working fluids were measured by a capillary tube viscometer. Finally it has been recognised from both the theory and experiment that, regarding the injection condition and the fluid properties, the generalised Reynolds number $Re_{G(0)}$ at the inlet to the nozzle and the flow behaviour index n of the fluid become the pertinent independent input parameters in non-dimensional forms. The air core diameter increased with $Re_{G(0)}$ and decreases with n . The effect of nozzle geometry on the air core diameter is similar to that in the case of Newtonian fluids. (19 refs.)

Conventional profile coaxial jet noise prediction See Entry 61534

The pressure distribution on an arbitrary oriented plane impinged by a strongly underexpanded jet of rarefied gas See Entry 61539

47.55H Stratified flows

61541 The effect of nonlinear density stratification on the stability of a vertical water layer in the conduction regime. A.H.Shaaban, M.N.Ozizik (Dept. of Mech. & Aerospace Engng., North Carolina state Univ., Raleigh, NC, USA).

Trans. ASME, J. Heat Transfer (USA), vol.105, no.1, p.130-7 (Feb. 1983). The thermal stability of a layer of water between two vertical parallel plates maintained at different temperatures, T_1 and T_2 , is investigated for the conduction regime. Three cases are considered include where: (a) the maximum density layer is within the water region; (b) is at the boundary; and (c) is outside the water region. Cubic polynomials are used to represent the density-temperature relation in the temperature range 0-55°C. The numerical results show that the critical states of stability do not depend on Prandtl

number but instead depends on the combinations of T_1 and T_2 . Of the three cases considered, the first case is the most unstable. In all three cases, the instabilities set in as a traveling wave, moving against gravity, for most T_1 and T_2 combinations. Stationary waves were also found for case (c). (19 refs.)

Stratification instability of switching front in an active trigger diffusive medium See Entry 61487

47.55K Multiphase flows

61542 Experimental determination of velocity statistical distributions in suspension flows. B.Oesterle (Univ. de Nancy-I, Nancy, Vandoeuvre, France).

C.R. Seances Acad. Sci. Ser. II (France), vol.296, no.1, p.9-14 (10 Jan. 1983). In French.

An experimental method for statistical study of particle velocities in a suspension flow is described. Velocities are measured by laser anemometry, a plot of velocity histogram being obtained by a microprocessor circuit. Care must be taken in the exploitation of these histograms, to derive the corresponding probability densities curves. Examples of results are given in the case of a gas-solid horizontal pipe flow. (8 refs.)

61543 Compression of a spherical gas bubble in ideal liquid by the finite pressure-pulse. W.Trzcinski, E.Wlodarczyk. *J. Tech. Phys. (Poland)*, vol.22, no.4, p.429-42 (1981).

A rigorous solution is given to the problem of compression of a gas bubble immersed in an incompressible ideal liquid subjected to external pressure varying in time. In particular, the case is analysed where the short-lived pressure-pulse in the liquid at infinity has the form of a rectangle. (9 refs.)

61544 Sheared colloidal suspensions. B.J.Ackerson (Dept. of Phys., Oklahoma State Univ., Stillwater, OK, USA), N.A.Clark. *Physica A (Netherlands)*, vol.118A, no.1-3, p.221-49 (March 1983). (Proceedings of the Conference on Nonlinear Fluid Behavior, Boulder, CO, USA, 7-11 June 1982).

The structure of aqueous suspensions of electrostatically interacting submicron polymer spheres is studied as a function of shear. These model colloidal suspensions exhibit a variety of equilibrium and nonequilibrium structures and phase transitions. Both shear induced melting of solid-like structures and shear induced distortion of liquid-like structures are observed. Several models are presented to explain the observed effects. The analogy between these colloidal suspensions and pure fluid systems is discussed. (70 refs.)

61545 Axisymmetric flow of a dusty gas between two contracting or distending discs. E.Chandrasekharan, G.Ramanaiah (Faculty of Sci., Madras Inst. of Technol., Madras, India).

Rev. Roum. Sci. Tech. Ser. Mec. Appl. (Rumania), vol.28, no.1, p.21-32 (Jan.-Feb. 1983).

The axisymmetric flow of an incompressible viscous dusty fluid between two parallel contracting/distending discs is investigated, when the dust particles are assumed to move with a small velocity as compared with that of the fluid. Using a similarity solution technique numerical solutions are obtained for the instantaneous velocities of the fluid and dust particles. Also the streamlines for the fluid and dust particles, the pressure distribution between the discs and the stress on the discs are determined and in each case the results are compared with those of the clean fluid. Further, it is found that along the axial direction the dust particles have a tendency to move towards the mid-region between the two discs. (10 refs.)

Inviscid axisymmetric jet impingement with recirculating stagnation regions See Entry 61535

Vapor flow through a porous membrane—a throttling process with condensation and evaporation See Entry 61546

Oxygen mass transfer in three-phase fluidized beds working at large flow rates See Entry 61547

Deformation of bubbles in an electric field See Entry 61556

Effect of Hall current on unsteady hydromagnetic boundary layers in rotating dust fluid See Entry 61560

Direct measurements of aerosol diffusion constants in the intermediate Knudsen regime See Entry 61593

Interface and transport phenomena under reduced gravity. II. Surface shapes and kinetics of wetting See Entry 62218

47.55M Flow through porous media

61546 Vapor flow through a porous membrane—a throttling process with condensation and evaporation. W.Schneider (Tech. Univ. Wien, Wien, Austria).

Acta Mech. (Austria), vol.47, no.1-2, p.15-25 (1983).

The one-dimensional flow of a vapor through a porous membrane is considered. Upstream the membrane the vapor is assumed to be in a state of saturation, downstream the membrane there may be superheated vapor, saturated vapor or a two-phase mixture. It is shown that heat conduction in flow direction is important if the Joule-Kelvin coefficient of the vapor is positive and the permeability of the membrane is sufficiently small. This results in condensation at the front surface of the membrane, liquid flow in the membrane or part of it, and re-evaporation at the rear surface or in an evaporation front in the interior of the membrane. If the permeability of the membrane is below a critical value that depends on thermodynamic quantities only, the energy balance requires the formation of a condensate film in front of the membrane. Four possible types of throttling processes are analyzed for small pressure variations and an equation for the mass flow rate in terms of the pressure difference across the membrane is given. The predicted mass flow rate of isobutane through a microporous polypropylene membrane compares favourably with measurements. (13 refs.)

61547 Oxygen mass transfer in three-phase fluidized beds working at large flow rates. M.Alvarez-Cuenca, C.G.J.Baker, M.A.Bergougnou, M.A.Nerenberg (Faculty of Engng. Sci., Univ. of Western Ontario, London, Ontario, Canada).

Can. J. Chem. Eng. (Canada), vol.61, no.1, p.58-63 (Feb. 1983). The published literature on gas mass transfer in three-phase fluidized beds indicates that most of the research done in the last two decades has been carried out at low superficial velocities and/or volumetric flow rates. These experimental limitations are reflected in the current understanding of these systems. In this investigation, performed at large gas and liquid velocities and flow rates, the behaviour of three-phase fluidized beds of 0.1, 0.3 and 0.5 cm diameter glass beads has been studied. Computer-made contour diagrams, obtained from the mapping of the oxygen concentration in the column have proven to be an effective probing technique. These diagrams permit the description of flow patterns and bed hydrodynamic properties otherwise not

observable with tracers. The use of concentration and pressure profiles complements the observations made with the contour diagrams. At low gas and liquid velocities the concentration profiles are S-shaped. As V_0 and V_1 increase the three absorption zones, observed in those S-shaped profiles, become two zone similar to those observed in bubble columns. The interface between the dense bed and dilute phase is characterized by an unusually high mass transfer activity. (18 refs.)

61548 Fluidized bed expansion as a result of biomass growth. S.-C.Wang, C.Tien (Dept. of Chem. Engng. & Materials Sci., Syracuse Univ., Syracuse, NY, USA).

Can. J. Chem. Eng. (Canada), vol.61, no.1, p.64-7 (Feb. 1983).

A relationship which is capable of predicting the height of a fluidized bed with the extent of the biomass growth at the surface of the fluidized particles is proposed. The application of this relationship for the determination of one of the biological parameters of waste water treatment is demonstrated. (8 refs.)

61549 Monte Carlo simulation of diffusion of gases in a porous solid: calculations for a new class of solids. Y.Nakano, J.W.Evans (Dept. of Materials Sci. & Mineral Engng., Univ. of California, Berkeley, CA, USA).

J. Chem. Phys. (USA), vol.78, no.5, p.2568-72 (1 March 1983).

In a previous paper, a Monte Carlo simulation of the Knudsen diffusion of a gas in a porous solid was carried out. The simulated porous solid had pore walls that were convex. In the present paper, the simulation is repeated using simulated solids whose pore walls are concave. It was found that the results of both studies could be correlated by a single equation. This equation enables the prediction of the Knudsen diffusivity from the porosity and mean pore size without resort to a tortuosity factor. (5 refs.)

61550 General problems of motion in a homogeneous porous medium exhibiting cavities. S.Gogonea.

Rev. Roum. Sci. Tech. Ser. Mec. Appl. (Romania), vol.27, no.4, p.467-86 (July-Aug. 1982). In French. [received: March 1983]

Mathematical analysis is applied to a porous environment with an arbitrary number of cavities and impermeable inclusions while the fluid is considered to be incompressible and ideal. The derived equations provide a unique solution and an example of the filtration process is provided. (5 refs.) I.G.

Heat transfer in hydromagnetic flow near an oscillating porous flat plate See Entry 61503

Premixed combustion in a turbulent boundary layer with injection See Entry 61565

Hydrogen separation from gas mixtures using LaNi₅ pellets ... See Entry 61567

General characteristics of flows formed during spinning of chemical fibres See Entry 63186

Convective instabilities of binary mixtures with fast chemical reaction in a porous medium See Entry 63552

47.60 FLOWS IN DUCTS, CHANNELS, AND CONDUITS

(for biological fluid dynamics, see 87.45)

61551 On the propagation of non-linear pressure waves in pipes with turbulent non-zero mean flow. A.Kluwick, N.Stross (Tech. Univ. Wien, Wien, Austria).

Acta Mech. (Austria), vol.47, no.1-2, p.73-86 (1983).

Deals with the propagation of small-amplitude finite-rate waves in gas filled pipes with non zero mean flow. Adopting the assumption of quasi-one-dimensional flow it is shown that the wave motion can be studied analytically provided the characteristic wave length is sufficiently small. The combined effects of stratification non-linearity and frictional attenuation are discussed in detail for left-running and right-running waves. (7 refs.)

61552 Approach flow direction effects on the cross-flow induced vibrations of a square array of tubes. D.S.Weaver (Dept. of Mech. Engng., McMaster Univ., Hamilton, Ontario, Canada), H.C.Yeung.

J. Sound & Vib. (GB), vol.87, no.3, p.469-82 (8 April 1983).

Water tunnel experiments were conducted on a square array of tubes with a pitch ratio of 1.5. The array could be rotated about an axis perpendicular to the direction of flow so that the effects of incident flow direction on cross-flow tube response could be studied. Constant Strouhal number vorticity response was observed over a range of orientations with some Strouhal number dependence on orientation angle. While incident flow direction was found to have some effect on the fluid-elastic stability threshold, no dramatic changes, such as occurred for triangular arrays, were found. Experiments were also conducted to determine the stability behaviour of a single flexible tube in otherwise rigid arrays. (24 refs.)

61553 Some elementary exact channel flows. N.De Mestre, T.Parkes (Dept. of Math., Royal Military Coll., Duntroon, Australia).

J. Aust. Math. Soc. Ser. B (Australia), vol.24, pt.4, p.484-91 (April 1983).

New polynomial solutions of the Navier-Stokes equations for steady unidirectional flow of a viscous incompressible fluid with a free surface, down inclined channels of specialized cross-section are considered. An inverse method is used to obtain the geometrical shape of the channel by equating the polynomial solution to zero (i.e. the no-slip condition) and thence determining the boundary shape. (2 refs.)

61554 Heat transfer and fluid flow experiments with a tube fed by a plenum having nonaligned inlet and exit. E.M.Sparrow, L.D.Bosmans (Dept. of Mech. Engng., Univ. of Minnesota, Minneapolis, MN, USA).

Trans. ASME, J. Heat Transfer (USA), vol.105, no.1, p.56-63 (Feb. 1983).

Local turbulent heat transfer coefficients for airflow were measured in a tube situated downstream of a cylindrical plenum chamber in which the inflow was radial and the outflow was axial. Pressure drop measurements and flow visualization were performed to supplement the heat transfer experiments. The plenum length and diameter were varied systematically during the experiments, and the Reynolds number ranged from 10000 to 60000. Substantially higher Nusselt numbers in the tube were encountered for the present nonaligned plenum inlet/exit configuration than for a plenum with axially aligned inlet and exit or for an upstream hydrodynamic development section. For a given Reynolds number, the Nusselt numbers corresponding to the present plenum configuration were quite insensitive to the investigated geometrical parameters. The thermal development length was found to be substantially elongated due to swirl carried into the tube from the plenum; the presence of the swirl was confirmed by flow visualization. The net pressure loss due to the presence of the plenum was about 1.75 velocity heads and was quite insensitive to the geometrical parameters and to the Reynolds number. (4 refs.)

Natural convection heat transfer between eccentric horizontal cylinders See Entry 61380

Pulsating viscoelastic flows in non-rigid tube See Entry 61470

RTD for diffusion-free laminar flow of non-Newtonian fluids through coiled tubes See Entry 61474

Laminar dispersion in helically coiled tubes of square cross-section See Entry 61475

Plastic boundary layers induced by variable wall friction See Entry 61477

Boundary layers of a nematic liquid crystal in fine capillaries See Entry 61479

Thresholds for the onset of fluid and magnetofluid turbulence See Entry 61489

An investigation into noise radiation from flow control valves with particular reference to flow rate measurement See Entry 61497

Heat transfer from the heated convex wall of a return bend with rectangular cross section See Entry 61505

Natural convection heat transfer of water within a horizontal cylindrical annulus with density inversion effects See Entry 61507

Self-excited wave oscillations in a water table See Entry 61508

Comment on 'Inviscid solution for the secondary flow in curved ducts' See Entry 61509

A finite element formulation for steady transonic Euler equations See Entry 61521

Correlation of Preston tube data with laminar skin friction See Entry 61523

Experimental determination of velocity statistical distributions in suspension flows See Entry 61542

Oxygen mass transfer in three-phase fluidized beds working at large flow rates See Entry 61547

The numerical and exact solutions of MHD flow through a pipe whose section is a sector See Entry 61559

The generation of electric currents by the turbulent flow of dielectric liquids. II. Pipes of finite length See Entry 61561

Measurement of instantaneous flow rate through estimation of velocity profiles See Entry 61574

A measurement method for the slippage of fluid flowing over the wall in a circular pipe See Entry 61583

Flame quenching by a cold wall See Entry 63551

47.65 MAGNETOHYDRODYNAMICS AND ELECTROHYDRODYNAMICS

(for MHD in plasma, see 52.30)

61555 Effects of the Hall current on the stationary hydromagnetic motions of a compressible, barotropic and viscous fluid. V.Salone (Univ. di Catania, Catania, Italy).

Atti Semin. Mat. & Fis. Univ. Modena (Italy), vol.30, no.2, p.213-38 (1981). In Italian.

The conditions which stationary hydromagnetic motions, in the presence of the Hall effect, must satisfy are determined on the hypothesis that the components of the magnetic and kinetic field depend on all three space coordinates, all the other elements depending on two co-ordinate planes. The hydromagnetic motions fall into three classes according to whether their existence is limited to the MHD with or without the Hall effect, or exist in any case. The conditions which stationary, Hall-free hydromagnetic motions must satisfy are derived. (23 refs.) J.S.

61556 Deformation of bubbles in an electric field. A.Beroual (Ecole Nat. Polytech., Algiers, Algeria).

C.R. Seances Acad. Sci. Ser. II (France), vol.296, no.3, p.169-72 (24 Jan. 1983). In French.

The shape of a bubble—gas or liquid—in suspension within liquid medium and subjected to an electric field between parallel plate electrodes is discussed. It is shown that the deformation of a bubble charged or situated near the electrode is not symmetric. This dissymmetry has been verified experimentally using a fast photo camera. (4 refs.)

61557 Electrohydrodynamic stability of an insulating liquid lying between two concentric spheres and subjected to a weak unipolar injection. S.Oliveri, P.Atten (Lab. d'Electrostatique, CNRS, Grenoble, France).

C.R. Seances Acad. Sci. Ser. II (France), vol.296, no.5, p.313-16 (7 Feb. 1983). In French.

An insulating incompressible liquid lying between two concentric conducting spheres is subjected to a unipolar injection by one or the other of the two spheres. In both cases, the critical conditions for hydrodynamic stability (linear theory) is determined for the asymptotic limit of very weak injections. (7 refs.)

61558 Unsteady hydromagnetic flow of fluid with microstructure between parallel plates. N.Venkata Narayana (Dept. of Appl. Maths., Andhra Univ., Waltair, India).

Indian J. Pure & Appl. Math., vol.14, no.1, p.129-45 (Jan. 1983).

Two types of unsteady hydromagnetic flow of the fluid have been considered. (i) Initially the fluid is at rest and the motion is caused by a sudden change of pressure gradient from zero to a constant value, (ii) One plate is fixed while the other is accelerated with a velocity $v = Ut^n$ (U and n being positive constants). The flow pattern is discussed in both cases in detail. (1 ref.)

61559 The numerical and exact solutions of MHD flow through a pipe whose section is a sector. Bani Singh (Dept. of Maths., Univ. of Roorkee, Roorkee, India), Jia Lal.

Indian J. Pure & Appl. Math., vol.14, no.1, p.146-58 (Jan. 1983).

The exact and numerical solutions have been found and the results compared. Since the exact solution is not suitable for computational purposes, a fast direct method based on Hockney's technique (1965) has been used to obtain the numerical results. For this, the section is first transformed into a rectangle for which a high accuracy nine-point formula is used. The results show very good agreement with those obtained from the exact solution. Tables, graphs and reliefs are given to show the variation of velocity, induced magnetic field and flux for various Hartmann numbers. (14 refs.)

61560 Effect of Hall current on unsteady hydromagnetic boundary layers in rotating dust fluid. R.Tiwari, Kamal Singh (Dept. of Maths., Banaras Hindu Univ., Varanasi, India).

Indian J. Pure & Appl. Math., vol.14, no.1, p.159-65 (Jan. 1983).

An asymptotic analysis of the unsteady hydromagnetic boundary layer flow generated impulsively in an incompressible viscous conducting fluid with uniform distribution of dust particles bounded by a semi-infinite plate is given. It

is shown that the initial motion for small times describes the general feature of the unsteady hydromagnetic boundary layer flow and consists of two distinct boundary layers which are unaffected by dusty parameters as well as rotation and magnetic terms. In subsequent large times, the effect of dusty parameter, magnetic parameter, Ekman parameter and Hall current parameter are reflected on the solution and associated boundary layer thickness increases with increase in dusty and Hall current parameter. While at large times the steady state is reached in the limit $t \rightarrow \infty$ with $\Omega \neq 0$, $\omega = 0$. (8 refs.)

61561 The generation of electric currents by the turbulent flow of dielectric liquids. II. Pipes of finite length. H.L.Walmsley (Shell Res. Ltd., Thornton Res. Centre, Chester, England).

J. Phys. D (GB), vol.16, no.4, p.553-72 (14 April 1983).

For pt.1 see *ibid.*, vol.15, p.1907-34 (1982). A recent theory for the generation of electric currents by hydrocarbon fuels in infinitely long pipes has been modified to describe the finite pipe lengths obtained in practice. The boundary conditions used in the original model only permitted ions to be adsorbed at the wall; the authors have now extended them to allow the desorption (injection) of ions as well. The extended model has been applied to both the generation and the relaxation of charge in pipes of finite length. (9 refs.)

61562 Smooth global solutions for the one-dimensional equations magnetohydrodynamics. S.Kawashima (Dept. of Math., Nara Women's Univ., Nara, Japan), M.Okada.

Proc. Jpn. Acad. Ser. A (Japan), vol.58, no.9, p.384-7 (Nov. 1982). [received: April 1983]

The authors seek smooth solutions to Lagrangian representation equations for the motion of electrically conducting fluids on one space coordinate. (5 refs.)

61563 Hydromagnetic flow and heat transfer between two horizontal plates, the lower plate being a stretching sheet. A.K.Borkakoti, A.Bharali (Dibrugarh Univ., Dibrugarh, India).

Q. Appl. Math. (USA), vol.40, no.4, p.461-7 (Jan. 1983).

Hydromagnetic flow and heat transfer between two horizontal parallel plates, where the lower one is a stretching sheet and the upper one is a porous solid plate are studied in the presence of a transverse magnetic field. Fluid velocities and temperature distributions are obtained and plotted graphically. (5 refs.)

Thresholds for the onset of fluid and magnetofluid turbulence See Entry 61489

A semi-circle theorem in thermohaline convection with rotation and magnetic field See Entry 61500

Heat transfer in hydromagnetic flow near an oscillating porous flat plate See Entry 61503

Recombination mechanism for emission accompanying collapse of a cavitation bubble induced by a high-voltage electrical discharge See Entry 61532

Idealised model for plasma acceleration in an MHD channel See Entry 61623

Variation in flatness in the successive transitions to turbulence of nematic liquid crystals See Entry 61775

47.70 REACTIVE, RADIATIVE, OR NONEQUILIBRIUM FLOWS

61564 Spectral behaviour of a concentration field in turbulence environment with rapid chemical reaction. A.Bennani, J.-N.Gence, J.Mathieu (Lab. de Mecanique des Fluides, Ecole Centrale de Lyon, Ecully, France).

C.R. Seances Acad. Sci. Ser. II (France), vol.296, no.1, p.5-8 (10 Jan. 1983). In French.

A second order reaction is used in order to identify the spectral behaviour of a concentration field in turbulence environment. The role played by the Damkohler number is emphasized but the spectral shape of concentration of one of the two species A has to be examined as a function of the downstream position with respect to the injection grid generating turbulence. (5 refs.)

61565 Premixed combustion in a turbulent boundary layer with injection. S.Meunier, M.Champion, J.C.Bellet (Lab. d'Energetique et de Detonique, ENSMA, Poitiers, France).

Combust. & Flame (USA), vol.50, no.2, p.231-8 (March 1983).

The reactive flow obtained by injecting a fresh mixture of propane and air into a stream of hot gas through a porous plate is studied both theoretically and experimentally. Using mass weighted Favre averages, the authors close the system of partial differential equations through a $k-\epsilon$ model of turbulence and a probability density function of the product mass fraction. The closed set of seven mean transport equations is solved for an injection rate varying between 0 and 2%. The numerical results are compared with measurements of mean velocity, streamwise rms velocity, and mean temperature, and good agreement is shown for injection rate values up to 1%. For larger rates of injection, factors such as the transverse pressure gradient and dissipation of the turbulent kinetic energy due to heat release, not taken into account by the $k-\epsilon$ model, become important and the extent of agreement is reduced. (4 refs.)

61566 Stability of a laminar flame front propagating within a tube. G.D.Salamandra, N.I.Maiorov.

Combust. Explos. & Shock Waves (USA), vol.18, no.4, p.439-42 (July-Aug. 1982). Translation of: *Fiz. Goreniya & Vzryva (USSR)*, vol.18, no.4, p.61-4 (July-Aug. 1982). [received: March 1983]

If a perturbation is created by some noncontact method on a small portion of the flame front, cine photography can be used to trace the change on flame front form under the action of the perturbation. The difficulties connected with the limited time available for development of these perturbations are not as great as would appear at first glance. The present study will examine the deformation of a flame propagating in a semi-closed horizontal tube under the action of perturbations artificially created on the flame surface by brief action of a transverse electrical field on the combustion zone. (9 refs.)

61567 Hydrogen separation from gas mixtures using LaNi₃ pellets. P.S.Rudman, G.D.Sandrock, P.D.Goodell (Inco Res. & Dev. Center Inc., Suffern, NY, USA).

J. Less-Common Met. (Switzerland), vol.89, no.2, p.437-46 (Feb. 1983). (International Symposium on the Properties and Applications of Metal Hydrides, Toba, Japan, 30 May-4 June 1982).

Porous pellets containing the hydride-former LaNi₃ for use in an absorption bed for extracting hydrogen from gas mixtures were prepared and tested. The unique aspect of these pellets is their incorporation of thermal ballast. By this means, the thermal effects of hydriding and dehydriding are reduced to controlled temperature swings, and adiabatic operation is possible. Pellet bonding has been accomplished by: (1) sintering of a nickel powder thermal ballast; (2) the addition of silicone rubber binder; and (3) the addition of a Teflon-polyethylene binder. A flow-through reactor was designed and employed to evaluate pellet behavior in nondilute gas mixtures. A model for hydrogen

absorption from gas mixtures was developed to resolve the absorption kinetics data into the following rate-limiting factors: (1) intrinsic rate; (2) intrinsic rate retardation; (3) microflow and (intrapellet gas transport); (4) macroflow (interpellet gas transport). Flow-through absorption kinetics data are presented for the pellets in H₂-NH₃ gas mixtures. (11 refs.)

61568 Hydrogen separation from mixed gas streams using reversible metal hydrides. J.J.Sheridan, III, F.G.Eisenberg, E.J.Greskovich (Air Products & Chem. Inc., Allentown, PA, USA), G.D.Sandrock, E.L.Huston.

J. Less-Common Met. (Switzerland), vol.89, no.2, p.447-55 (Feb. 1983). (International Symposium on the Properties and Applications of Metal Hydrides, Toba, Japan, 30 May-4 June 1982).

A novel hydrogen separation process utilizing the selective absorption properties of metal hydrides was developed. Performance and operational data generated during a 9 month pilot plant demonstration of the process are used to describe the important technical features of the process. When applied to the separation of the hydrogen from the argon vent stream of an ammonia synthesis loop, the process is capable of producing a final hydrogen product of minimum purity 99% at an overall recovery of 90%-93%. Unique features of the hydrogen absorbent and absorber performance are discussed. (5 refs.)

61569 Fluctuations anisotropy arising from velocity or temperature gradients. D.Beyens (Div. de la Phys., CEA, CENS, Gif-sur-Yvette, France).

Physica A (Netherlands), vol.118A, no.1-3, p.250-67 (March 1983). (Proceedings of the Conference on Nonlinear Fluid Behavior, Boulder, CO, USA, 7-11 June 1982).

Fluids out of equilibrium may exhibit unusual behaviour. Thus a thermal gradient can induce long-range correlations in the sound modes, whereas a shear flow is able to suppress the large correlations occurring near a critical point. Light scattering techniques allow these different behaviors to be detected. In the first case, an asymmetry in the Brillouin lines becomes visible; in the second case a strong anisotropy in the order parameter fluctuations appears, so that mean-field theory applies. This theory should be valid at equilibrium only in a space of dimensionality higher than 4. (24 refs.)

Steady state thermodynamics and spatial correlations See Entry 61472

Ignition of a gas by a hot horizontal cylinder See Entry 61595

Convective instabilities of binary mixtures with fast chemical reaction in a porous medium See Entry 63552

The calculation of a fire in a large building See Entry 63554

Soot volume fraction profiles in forced-combusting boundary layers See Entry 63555

47.75 RELATIVISTIC FLUID DYNAMICS

61570 Speed of propagation of infinitesimal disturbances in a relativistic gas. C.Cercignani (Dipartimento di Matematica, Politecnico di Milano, Milano, Italy).

Phys. Rev. Lett. (USA), vol.50, no.15, p.1122-4 (11 April 1983).

The phase speed of infinitesimal disturbances in a relativistic gas is shown to be less than the speed of light. The result is obtained by means of the kinetic theory of gases and is valid for any collision operator. The treatment applies, in particular, to the speeds of propagation of sound, shear, and heat waves. These waves are further shown to be damped. (31 refs.)

Maxwellian formalism of incompressible fluid mechanics See Entry 59643

47.80 INSTRUMENTATION FOR FLUID DYNAMICS

61571 Uncertainty in flow measurements using the bell prover of the Institute of Mechanics, Cagliari. R.Vallascas.

Autom. & Strum. (Italy), vol.31, no.2, p.112-15 (Feb. 1983). In Italian.

The procedures adopted to determine the degree of uncertainty associated with the calibration curves of flowmeters calibrated by means of the bell prover of the Institute of Mechanics, Cagliari are reported upon. The effect which certain parameters, which include the sensibility threshold on starting up, have on the quantitative and qualitative characterisation of the apparatus is also underlined. (7 refs.)

61572 A microprocessor-based pulse-height analyzer. R.Hariharan, V.D.Kulkarni (Indian Inst. of Sci., Bangalore, India).

IEEE Micro (USA), vol.2, no.3, p.86-91 (Aug. 1982). [received: March 1983]

Particle size is measured by an acoustic or optical technique; an acoustic wave or a beam of light is passed through a region and is reflected from the particles in that region. This reflected energy is converted into electrical pulses by appropriate instrumentation. The amplitude of the pulses are proportional to the sizes of the particles. In order to determine the distribution of particle sizes in flow over a period of time, the pulses must be grouped into various bands according to their amplitudes. This can be accomplished by means of a microprocessor-based pulse-height analyzer developed by the authors. This system is meant for cavitation applications in hydraulic systems, where pulse amplitudes in the range of 10 mV to 1.3 V (representing particle sizes in the range of 5 to 20 micrometers) are encountered. In such applications, the pulse width is on the order of 1 to 2 μ s and the pulse repetition frequency is about 20 KHz. The system divides the 10-mV to 1.3-V range into 12 bands, with the individual band levels fixed so as not to miss any pulse of interest. It is based on Intel's 8085 A-2 central processing unit. (2 refs.)

61573 Behavior of a perturbed rarefaction wave. B.A.Klopov, E.E.Meshkov.

Combust. Explos. & Shock Waves (USA), vol.18, no.4, p.472-5 (July-Aug. 1982). Translation of: *Fiz. Goreniya & Vzryva (USSR)*, vol.18, no.4, p.96-100 (July-Aug. 1982). [received: March 1983]

Results of an experimental investigation of the behavior of a plane centered rarefaction wave which has a perturbation of the front shape at the time of origination, are described. The experiments were conducted in a shock tube of rectangular 120x40 mm section. The measuring section of the shock tube from organic glass ST-1, consisted of separate weldable blocks 1-2 assembled in a common frame. Collected, the blocks formed a channel that was a continuation of the shock tube channel. (3 refs.)

61574 Measurement of instantaneous flow rate through estimation of velocity profiles. M.Uchiyama, K.Hakomori.

IEEE Trans. Autom. Control (USA), vol.AC-28, no.3, p.380-8 (March 1983).

It is very important, but difficult to measure instantaneous flow rate in the unsteady flow regime, since the variation of velocity profile limits the dynamic accuracy of flowmeters. Consideration of the velocity profile variation is crucial to improving their dynamic performance. The paper presents a new method of measuring the instantaneous flow rate of unsteady flow in a circular pipe by estimating the velocity profile of the flow. The estimation is formulated as a discrete Kalman filter problem where the dynamics of the

velocity profile, which is governed by a linear partial differential equation, is approximated using a finite-dimensional model. An instantaneous flowmeter consisting of a laser Doppler velocimeter (LDV) and an 8-bit microcomputer which implements the solution of the filter problem has been developed. Successful measurements of a pulsating flow and a stepwise changing flow by this flowmeter are presented. (8 refs.)

61575 Computation of electromagnetic flowmeter characteristics from magnetic field data. II. Errors. D.G.Wyatt (Nuffield Inst. for Medical Res., Univ. of Oxford, Oxford, England).

J. Phys. D (GB), vol.16, no.4, p.465-78 (14 April 1983).

For pt.I see M.K. Bevir et al., *ibid.*, vol.14, p.373-88 (1981). Examines the errors involved in evaluating the functions $\sum_{m=1,3,5}^{\infty} A(m,p) \int_0^{2\pi} B_m(\theta_0) \cos m\theta_0 d\theta_0$ and $\int_0^{\infty} T(\gamma,m,p) \int_0^{\infty} B_m(l) \cos \gamma l d\gamma$. $A(m,p)$ and $T(\gamma,m,p)$ tend to zero as m and γ respectively tend to ∞ . B_m is available only at specified sampling intervals in θ_0 and l . The summation in m and the integration with respect to γ are done before the integrations with respect to θ_0 and l . The functions are special examples, which are suitable for error analysis, of the expression for the axisymmetric weight function of an electromagnetic flowmeter when derived from magnetic field data (see pt.I). It is shown that the errors are generally smaller when the trapezoidal rule, rather than Simpson's rule, is used to perform the integrations with respect to θ_0 and l . It is also shown that m, γ should be limited to values related to the sampling intervals in θ_0, l respectively in order to avoid unnecessary error. B_m represents measured values of the magnetic field and the magnitude of the errors is explored for representative functions $B_m(\theta_0)$ and $B_m(l)$. The effect of the finite dimensions of the device used to measure B_m is also considered. An assessment is given of the error due to these effects in pt.I. (8 refs.)

61576 A comparison of experimental and numerical results obtained for the secondary flow in a large turbine cascade. W.N.Dawes, P.H.Richards (CEGB Marchwood Engng. Labs., Southampton, England).

J. Phys. D (GB), vol.16, no.4, p.539-51 (14 April 1983).

Laser Doppler anemometry has been used to measure the flowfield in a low-speed turbine cascade. The LDA technique successfully resolves the secondary velocity components associated with the formation of a strong passage vortex embedded in the blade suction-surface-endwall corner. The measured results are compared with numerical calculations made using a fully three-dimensional time-marching method which solves the inviscid equations of fluid motion. It is shown that good agreement could be achieved between the computations and the measurements, but only after ad hoc adjustment of the numerical viscosity terms. Nevertheless, it is suggested that until methods solving the viscous equations of motion are readily available, use of inviscid methods may provide a satisfactory approximation. (13 refs.)

61577 Viscosity measurement. II. P.J.Tily (Dept. of Industry, Warren Spring Lab., Stevenage, England).

Meas. & Control (GB), vol.16, no.4, p.137-9 (April 1983).

For pt.I see *ibid.*, vol.16, no.3, p.111 (1983). Looks at the types of process viscometers available and their applications, the importance of shear rate in viscosity measurement, and the process control application. (21 refs.)

61578 On-line analytical instrumentation in the water industry—problems and practical solutions. II. Potential solutions. R.Briggs.

Meas. & Control (GB), vol.16, no.4, p.151-5 (April 1983).

For pt.I see *ibid.*, vol.18, no.3, p.94-7 (1983). This part is concerned with relevant advances in some areas of sensor development, with organisational and logistical aspects, and with the consideration of 'new horizons' which may ultimately lead to significant and relevant advances in the required instrumentation. (20 refs.)

61579 Modern flow measurement. O.Fiedler (Sektion Tech. Elektronik, Wilhelm-Pieck-Univ., Rostock, Germany).

MSR (Mess. Steuern Regeln) (Germany), vol.26, no.3, p.122-8 (March 1983). In German.

Flow measurement transmitters are important for the simulation and automation of flow processes in gases and liquids. Besides hot-wire probes and actual pressure gauges, noncontacting methods and probes used more and more. Developments and applications of acoustical, optical and inductive flow meters are presented in connection with electronic measurement value acquisition, and explained by means of examples. (21 refs.)

61580 Pressure gauges and inclinometers listing magnetic liquids. O.Fiedler, R.Jaskulke (Sektion Tech. Elektronik, Wilhelm-Pieck-Univ., Rostock, Germany).

MSR (Mess. Steuern Regeln) (Germany), vol.26, no.3, p.129-31 (March 1983). In German.

The authors present solutions for the realization of measurement transmitters based upon the functions principle of simple U-pipe devices for pressure, flow and inclination angle measurement. The use of magnetic liquids as medium in such apparatus allows a simple change over to electrical measurement value acquisition. The measurement methods are characterized by simple construction, high sensitivity and linear measurement value conversion. (no refs.)

61581 LDA measurement equipment for serial multi-component measurement with microcomputer-coupled period meter. W.Kroger, H.E.Albrecht, W.Fuchs (Sektion Tech. Elektronik, Wilhelm Pieck Univ., Rostock, Germany).

MSR (Mess. Steuern Regeln) (Germany), vol.26, no.3, p.134-40 (March 1983). In German.

The authors describe a flow velocity measurement equipment for hydrodynamical measurement problems based on laser Doppler anemometry. They present the system component optics, signal detection and signal processing and give hints for dimensioning. As for the signal evaluation, a new developed period measurement method is used for in connection with a K1510 microcomputer. (16 refs.)

61582 Measurements of a supersonic velocity in a nitrogen flow using inverse Raman spectroscopy. G.C.Herring, S.A.Lee, C.Y.She (Dept. of Phys., Colorado State Univ., Fort Collins, CO, USA).

Opt. Lett. (USA), vol.8, no.4, p.214-16 (April 1983).

Results of supersonic molecular flow-velocity measurements using inverse Raman spectroscopy are reported for the first time to the authors' knowledge. Because of potential wind-tunnel applications, flowing N_2 molecules are probed directly, and their flow velocity, temperature, and density are measured. The uncertainties are less than 5% for the velocity measurements and about 10% for the temperature and density measurements. To achieve the quoted precision, I_2 fluorescence, I_2 saturated-absorption, and differential-detection techniques are used to stabilize the probe laser, provide an absolute-frequency reference and reduce detection noise, respectively. (6 refs.)

61583 A measurement method for the slippage of fluid flowing over the wall in a circular pipe. N.Kojima (Faculty of Engng., Meiji Univ., Kawasaki, Japan).

Trans. Soc. Instrum. & Control Eng. (Japan), vol.19, no.1, p.41-7 (Jan. 1983). In Japanese.

The author deals with a useful method for slippage measurement and the slippage effects on flow velocity distribution in a circular pipe. The main

merit of the method is to be able to obtain the amount of slippage from the pipe radius, the flow rate and the maximum flow velocity, independent of the pressure difference or the fluid viscosity. A slippage index number, which is obtained by the ratio of the slippage coefficient to the square of hydraulic mean depth, is proposed. When water flows in a circular pipe, the variation of the slippage coefficient is experimentally observed for changes of the pipe radii even if inside surface conditions of pipes are the same, but the slippage index number does not vary and remains constant. Therefore, the usage of the slippage index number is very convenient for obtaining generalized slippage. (3 refs.)

61584 Elektronische Einrichtungen als Teile von Messgeräten zur Mengemessung von Fluiden (Electronic systems as a part of a measurement device for flow measurement of fluids). D.Mencke.

Report PTB-Me-40, Phys.-Tech. Bundesanstalt, Braunschweig, Germany (Dec. 1982), 14 pp. In German.

The author explains that quantities of fluid can either be measured at rest in a container or while flowing through a pipe. By means of tables he details the various types of fluids which require to be metered, gives examples of the tests to which they are usually subjected, mentions the various principles of measurement used and indicates the data which require to be measured. The metered signals are then classified in six groups: quantities measured without any electronic equipment; electrical voltages, currents and resistances; frequencies; times and periods of time; numbers of pulses or other events; and, finally, integers. In the last five groups the signals to be measured can be classified as being measured by analogue, incremental and coded methods. The general requirements on the construction of calibrated electronic equipment are discussed in detail and include: the specifications for any transmission line; the error limits; the increments or decrements to be indicated for discontinuous displays; the pulse rate for flying start and stop tests; the effects of influential factors and of external interference; the necessary data that must be provided on any metering equipment; this last matter is treated under various categories. A table and its appendix explain clearly how the construction of the metering equipment must depend on the signal to be measured and the stage over which it has to be transmitted. (5 refs.) G.W.

A system for determining fluid properties up to 136 MPa and 473K See Entry 59794

Ring polarization interferometer. Measurement of the flow rates of transparent media See Entry 59837

A study of laser Doppler anemometer based on colliding beams See Entry 61219

Turbulence measurements in wall jets along strongly concave surfaces See Entry 61490

An investigation into noise radiation from flow control valves with particular reference to flow rate measurement See Entry 61497

Heat transfer and fluid flow experiments with a tube fed by a plenum having nonaligned inlet and exit See Entry 61554

Turbulent flow in chill block casting See Entry 63282

47.90 OTHER TOPICS IN FLUID DYNAMICS

Pulsating viscoelastic flows in non-rigid tube See Entry 61470

50.00 FLUIDS, PLASMAS AND ELECTRIC DISCHARGES

(for fluid dynamics, see 47.; for the physics of condensed matter, see 60. and 70.)

51.00 KINETIC AND TRANSPORT THEORY OF FLUIDS; PHYSICAL PROPERTIES OF GASES

51.10 KINETIC AND TRANSPORT THEORY

61585 Determination of refractivity virial coefficients of CH_4 at 25°C. G.Montixi, R.Coulon (Faculte des Sci. et Tech. de Saint-Jerome, Marseille, France).

C.R. Seances Acad. Sci. Ser. II (France), vol.296, no.2, p.135-8 (17 Jan. 1983). In French.

A method is presented of direct measurement of the absolute refractive index of a gas vs. pressure, and the calculation of the first three refractivity virial coefficients. (12 refs.)

61586 Gas-phase transient diffusion in droplet vaporization and combustion. M.Matalon (Dept. of Engng. Sci. & Appl. Math., Northwestern Univ., Evanston, IL, USA), C.K.Law.

Combust. & Flame (USA), vol.50, no.2, p.219-29 (March 1983).

By suppressing the relaxation process of fuel vapor accumulation through the use of d^2 -law results as the initial conditions, the present study isolates gas-phase transient diffusion as the only transient process during droplet vaporization and combustion, and thereby successfully identifies its influence on the bulk droplet gasification characteristics. The cases of pure vaporization and flame sheet combustion are analytically solved using perturbation methods and the matched asymptotic expansion technique in the limit of the small gas-to-liquid density ratio. Results demonstrate that transient diffusion enhances the vaporization and burning rates, reduces the flame front standoff ratio, and elevates the flame temperature. However, contrary to predictions of previous studies which have inadvertently included fuel vapor accumulation; these transient diffusion effects are very small so that gas-phase quasi steadiness is indeed an adequate and useful assumption for the modeling of subcritical droplet combustion. (12 refs.)

61587 Classical S-matrix theory of viscomagnetic production cross section. Wing-Ki Liu (Dept. of Phys., Univ. of Waterloo, Waterloo, Ontario, Canada).

Chem. Phys. Lett. (Netherlands), vol.96, no.2, p.175-80 (1 April 1983). The semiclassical theory of Marcus (1972) and Miller (1974) is applied to obtain an expression for the production cross section in the shear viscosity

Senftleben-Beenakker effect, whose exact expression has been recently obtained by Liu et al. (1979). The result involves a multi-dimensional integral over a function of their orientation angles between the initial orbital angular momentum and the final rotational angular momentum, and in principle can be evaluated by a Monte Carlo procedure through the computation of classical trajectories. (21 refs.)

61588 Kinetic and hydrodynamic theories of nonequilibrium fluctuations. M.C. Marchetti, J.W. Dufty (Dept. of Phys., Univ. of Florida, Gainesville, FL, USA).

Physica A (Netherlands), vol.118A, no.1-3, p.205-16 (March 1983). (Proceedings of the Conference on Nonlinear Fluid Behavior, Boulder, CO, USA, 7-11 June 1982).

A unified formulation of both transport and fluctuations in a low density nonequilibrium gas is described. The method is based on an analysis of a generating functional for fluctuations of the single particle phase space density. It is shown that the first functional derivative obeys an inhomogeneous nonlinear Boltzmann equation, from which the dynamics of multi-space and -time fluctuations may be obtained by suitable functional differentiation. In particular, the equations for two-time and equal time fluctuations are obtained to illustrate the method. In this way, the description of nonequilibrium fluctuations in a low density gas input on the same theoretical basis as the usual Boltzmann kinetic theory. A hydrodynamic theory of fluctuations also may be derived from the kinetic theory; the procedure and results are indicated. (11 refs.)

61589 Gas with a nonMaxwellian velocity distribution. R.McFee (Dept. of Electrical Engng., Syracuse Univ., Syracuse, NY, USA).

Phys. Rev. A (USA), vol.27, no.4, p.2233-6 (April 1983). The velocity distribution of a monatomic gas in a very strong magnetic field (e.g., 10^5 T) is computed two ways: with classical statistical mechanics and with rarefied-gas kinetic theory. The same nonMaxwellian distribution is found in both cases. This anomaly arises from the saturation of the electrical polarization of the atoms by the enormous electric fields which they see when moving. (7 refs.)

61590 Simplified kinetic models for relaxation of a gas with internal structure. G.V. Dubrovskii (A.A. Zhdanov State Univ., Leningrad, USSR).

Sov. Phys.-Tech. Phys. (USA), vol.27, no.10, p.1184-90 (Oct. 1982). Translation of: *Zh. Tekh. Fiz. (USSR)*, vol.52, no.10, p.1927-37 (Oct. 1982). [received: April 1983] Simplified models for the kinetic behavior of a gas consisting of particles with internal structure are considered in a general theoretical framework. Approximate relaxation equations are derived, the zeroth approximation for the distribution function in the Chapman-Enskog method is found, and the behavior of the dimensionless parameters and parameter ratios is analyzed. Approximate effective scattering T -operators are introduced which greatly simplify the calculation of inelastic cross sections in gases. Model treatments of the collision integrals are discussed. The diffusion approximation is derived for the relaxation equations for continuum scattering, generalizing previous results to the case when exchange is not assumed to involve equal numbers of photons and relaxation occurs over discrete levels (not treated in the standard diffusion model). The arguments used are important in constructing more specialized collision and relaxation models in molecular gas kinetic theory starting from the actual laws governing particle interactions. (17 refs.)

61591 Fluctuation-dissipation relations in the scattering problem and the method of fluctuations in the kinetic theory of gases. Yu.L. Klimontovich.

Sov. Tech. Phys. Lett. (USA), vol.8, no.8, p.434-5 (Aug. 1982). Translation of: *Pis'ma v Zh. Tekh. Fiz. (USSR)*, vol.8, no.15-16, p.1005-9 (Aug. 1982). [received: April 1983] The lack of a common method for simultaneously taking into account both the strong and the weak collective interactions of the particles complicates the solution of several fundamental problems of kinetic theory, e.g. that of constructing a kinetic theory of a partially ionized plasma. The solution of this problem requires deriving a fluctuational method for evaluating the Boltzmann collision integral in the kinetic theory of gases. This approach also generates some new fluctuation-dissipation relations (more general than those in the Callen-Welton theory), which are typical of the scattering problem. These new relations can in turn be derived from the most general fluctuation-dissipation relations for many-particle distribution functions. (6 refs.)

Speed of propagation of infinitesimal disturbances in a relativistic gas See Entry 61570

Asymptotic time behavior of the velocity autocorrelation function See Entry 61594

Thermal conductivity of polyatomic gases at low density See Entry 61596

Calculations of drift velocity of electrons in inert gases at low E/N See Entry 61599

51.20 VISCOSITY AND DIFFUSION: EXPERIMENTAL

61592 Capacity ratios and diffusion coefficients of low-volatile organic compounds in supercritical carbon dioxide from supercritical fluid chromatography (SFC). A. Wilsch, R. Feist, G.M. Schneider (Dept. of Chem., Univ. of Bochum, Bochum, Germany).

Fluid Phase Equilibria (Netherlands), vol.10, no.2-3, p.299-306 (March 1983). (Supercritical Fluids. Their Chemistry and Application, Cambridge, England, 13-15 Sept. 1982).

Capacity ratios k have been determined for phenyl myristate, phenyl palmitate and phenyl stearate from supercritical fluid chromatography (SFC) at 35 to 56°C and 85 to 190 bar using supercritical CO_2 as mobile phase and Perisorb A and Perisorb RP8 as stationary phases. For the esters used a rise in pressure from 90 to 190 bar produces a drop of k by about two orders of magnitude giving evidence of the rapidly increasing solvent power of supercritical CO_2 with increasing density. At a constant CO_2 density, k decreases with increasing temperature. The separation of the esters was found to be the better the lower the pressure was. An apparatus for the chromatographic determination of binary diffusion coefficients in supercritical gases is described. D_{12} values for some organic compounds in carbon dioxide at 40°C and in the pressure range from 80 to 160 bar are presented. With an improved electronic flow regulator an overall precision of the D_{12} values of $\pm 3\%$ is obtained. (11 refs.)

61593 Direct measurements of aerosol diffusion constants in the intermediate Knudsen regime. G.B. King, C.M. Sorensen, T.W. Lester, J.F. Merklin (Dept. of Nuclear Engng. & Phys., Kansas State Univ., Manhattan, KS, USA).

Phys. Rev. Lett. (USA), vol.50, no.15, p.1125-8 (11 April 1983). The authors have measured the diffusion constants of aerosols whose size compares to the mean free path of the gas in three different aerosols. The

experimental diffusion constants do not agree with the kinetic-theory calculations in this intermediate Knudsen regime. (17 refs.)

61594 Asymptotic time behavior of the velocity autocorrelation function. W. Schommers (Kernforschungszentrum Karlsruhe, Inst. für Angewandte Kernphys., Karlsruhe, Germany).

Phys. Rev. A (USA), vol.27, no.4, p.2241-4 (April 1983). The asymptotic time behavior of the velocity autocorrelation function has been investigated by means of molecular dynamics with and without the presence of three-body forces, respectively. It turned out that the long-time tail is strongly influenced by three-body forces. The famous $t^{-3/2}$ law has been observed in the calculation with the presence of three-body forces. (20 refs.)

A system for determining fluid properties up to 136 MPa and 473K See Entry 59794

Classical S-matrix theory of viscomagnetic production cross section See Entry 61587

51.30 THERMAL PROPERTIES OF GASES

61595 Ignition of a gas by a hot horizontal cylinder. E.P. Kostogorov, E.A. Shtessel.

Combust. Explos. & Shock Waves (USA), vol.18, no.4, p.392-6 (July-Aug. 1982). Translation of: *Fiz. Goreniya & Vzryva (USSR)*, vol.18, no.4, p.11-16 (July-Aug. 1982). [received: March 1983]

Discusses the joint solution of the equations describing the ignition process and the equations of motion. The authors consider the problem of the ignition of a chemically reacting gas by a cylindrical body in the presence of natural convection. (4 refs.)

61596 Thermal conductivity of polyatomic gases at low density. G.C. Maitland, M. Mustafa, W.A. Wakeham (Dept. of Chem. Engng. & Chem. Technol., Imperial Coll., London, England).

J. Chem. Soc. Faraday Trans. 1 (GB), vol.79, no.1, p.163-72 (Jan. 1983). The authors present a critical examination of the kinetic theory of dilute polyatomic gases using accurate data for their transport coefficients which have recently become available. Particular attention is concentrated upon the role of inelastic collision processes in the relationship between the thermal conductivity and viscosity of the polyatomic gases H_2 , D_2 , N_2 , CO , CO_2 , N_2O , CH_4 , C_2H_4 and C_2H_6 . The thermal conductivity coefficient calculated from the viscosity coefficient with the aid of the most sophisticated kinetic-theory formulae currently available deviates from the experimental data by as much as 15%. These deviations are principally attributed to the neglect of inelastic collision effects which implicitly enter the kinetic-theory formulation and which have traditionally been ignored. (28 refs.)

61597 Natural convection correlations for vertical surfaces including influences of variable properties. A.M. Clausing (Dept. of Mech. & Industrial Engng., Univ. of Illinois, Urbana, IL, USA).

Trans. ASME, J. Heat Transfer (USA), vol.105, no.1, p.138-43 (Feb. 1983). New correlations are presented for natural convective heat transfer from vertical isothermal surfaces in gases. The influences of variable properties are accounted for by using empirical equations which are of the general form $\text{Nu} = g(\text{Ra})f(\text{Ra}, T_w/T_\infty)$. The influence of the reference temperature at which the thermal properties are evaluated is also established. Comparisons with available data are made over a Rayleigh number range $10^4 < \text{Ra} < 10^{12}$ and a range in the surface-to-ambient temperature ratio of $1 < T_w/T_\infty < 2.6$. Five data sets, which represent over 200 test points, are examined. (14 refs.)

Supercritical Fluids. Their Chemistry and Application See Entry 59525

Raman spectra, ab initio molecular orbital calculations, vibrational analysis, and thermodynamic functions for NH_3AlX_3 ($\text{X} = \text{F}, \text{Cl}, \text{Br}$) See Entry 60725

Thermal physics of transverse-discharge copper vapor lasers See Entry 61138

Ionization-superheating mechanism in current channel formation in molecular gases See Entry 61600

Thermophysical properties of supercritical fluids with special consideration of aqueous systems See Entry 62073

Thermodynamics of supercritical steam+carbon dioxide mixtures See Entry 62074

Phase equilibria and critical phenomena in fluid (n-alkane+water) systems at high pressures and temperatures See Entry 62075

51.40 ACOUSTICAL PROPERTIES OF GASES; ULTRASONIC RELAXATION

(see also 43. Acoustics; for acoustic properties of liquids, see 62.60; for ultrasonic relaxation in liquids, see 62.80)

The boundary value problem of the sound propagation in the rarefied gas See Entry 61330

51.50 ELECTRICAL PHENOMENA IN GASES

(see also 52. Plasma and electric discharges)

61598 Electron drift velocities in gas mixtures of He, N_2 , and CO_2 . M.C. Cornell, I.M. Littlewood, H.L. Brooks, K.J. Nygaard (Dept. of Phys., Univ. of Missouri-Rolla, Rolla, MO, USA).

J. Appl. Phys. (USA), vol.54, no.4, p.1723-4 (April 1983). An electron swarm experiment has been used to obtain electron drift velocities in the $\text{He:CO}_2:\text{N}_2$ mixtures 0:1:1, 3:1:2, and 3:1:1. The E/N range of 3 to 57 Td was studied with total gas pressure varied from 50 to 200 Torr. These particular mixtures have not been previously studied experimentally. Good agreement is observed between theoretical calculations and experimental data. (4 refs.)

61599 Calculations of drift velocity of electrons in inert gases at low E/N . M. Hayashi (Nagoya Inst. of Technol., Nagoya, Japan), S. Ushiroda.

J. Chem. Phys. (USA), vol.78, no.5, p.2621-5 (1 March 1983). The zero field reduced mobilities of electrons μ_0 in helium, neon, argon, krypton, and xenon have been calculated as a function of gas temperatures T using the Boltzmann equation and compared with the values of the thermal electron mobilities of electrons μ_N obtained by Mozumder (ibid., vol.72, p.6289, 1980). Discussion has been made about the large discrepancies between the measured and calculated values of μ_N in neon which were pointed out by Mozumder. The calculated exact drift velocities W in helium as a function of E/N and T have been compared with the experimental results of W for wide E/N and T ranges. A summarized figure is shown for anomalous electron mobilities in helium as a function of N at low E/N . (16 refs.)

61600 Ionization-superheating mechanism in current channel formation in molecular gases. K.N.Ul'yanov, V.V.Chulkov (V.I. Lenin All-Union Electrotech. Inst., Moscow, USSR). *Sov. Phys.-Tech. Phys. (USA)*, vol.27, no.10, p.1200-3 (Oct. 1982). Translation of: *Zh. Tekh. Fiz. (USSR)*, vol.52, no.10, p.1953-8 (Oct. 1982). [received: April 1983]
Equations are derived for the rate of spreading of a conducting channel in an externally maintained glow discharge in an ambient gas with nonsteady temperature for fixed geometric channel dimensions. Two cases are considered corresponding to predominantly self-sustaining ionization and predominantly externally induced ionization in the region ahead of the channel. The calculated rate of channel spreading is in agreement with the experimentally measured rate. (10 refs.)

61601 Mass spectroscopic study of precursors in a nitrogen-filled electrical shock tube. Yu.I.Chutov, V.N.Podolskii, V.Yu.Palkin (T.G. Shevchenko State Univ., Kiev, Ukrainian SSR). *Sov. Phys.-Tech. Phys. (USA)*, vol.27, no.10, p.1212-15 (Oct. 1982). Translation of: *Zh. Tekh. Fiz. (USSR)*, vol.52, no.10, p.1972-8 (Oct. 1982). [received: April 1983]
A modified MKh-7301 mass spectrometer is used to study the ionic composition precursors in a small electric shock tube (diameter 1.7 cm and length $l \sim 50$ cm) filled with nitrogen at pressures 0.2-1.2 torr. The electron density and temperature in the foreshock were measured using a cylindrical tungsten probe. The ions N^+ , N_2^+ , and N_3^+ were detected and their relative densities determined. The precursor was found to propagate by diffusion. A simplified scheme is proposed for handling the main ionization processes occurring in the precursor, including light diffusion, formation of highly excited molecules, and subsequent ionization of the latter in collisions with neutral and excited molecules. (20 refs.)

Gas breakdown near metal surfaces caused by ultraviolet laser light See Entry 61603
Anomalous electron attachment properties of perfluoropropylene (C_3F_8) and their effect on the breakdown strength of this gas See Entry 61713
Calculation of swarm parameters in xenon at high E/N by a Monte Carlo simulation method See Entry 61714
Glow discharge in a transverse magnetic field See Entry 61719

51.60 MAGNETIC PHENOMENA IN GASES

(for liquids, see 75.)

Classical S-matrix theory of viscomagnetic production cross section See Entry 61587
Faraday and Cotton-Mouton effects in gases in the presence of a strong light field See Entry 61602

51.70 OPTICAL PHENOMENA IN GASES

(for liquids, see 78.)

61602 Faraday and Cotton-Mouton effects in gases in the presence of a strong light field. G.G.Adonts, S.G.Pilyan. *Opt. & Spectrosc. (USA)*, vol.53, no.1, p.67-9 (July 1982). Translation of: *Opt. & Spektrosk. (USSR)*, vol.53, no.1, p.114-17 (July 1982). [received: April 1983]
The change in polarization of a probe light signal propagating through a resonance medium in the presence of a constant magnetic field and a strong light field is investigated theoretically. Both the longitudinal as well as the transverse propagation of light relative to the direction of the magnetic field (nonlinear Faraday and Cotton-Mouton effects) are considered. Formulas for the refractive indices of the different polarization components of the probe light signal are found exactly in terms of the strong light field. It is shown that the presence of interference magnetic-light-induced rotation of the plane of polarization allows the local value of magnetic field, spatially inhomogeneous in magnitude, to be determined. This can be applied in plasma diagnostics and spectroscopic investigations. (6 refs.)

61603 Gas breakdown near metal surfaces caused by ultraviolet laser light. A.M.Popov (M.V. Lomonosov State Univ., Moscow, USSR). *Sov. Phys.-Tech. Phys. (USA)*, vol.27, no.10, p.1293-4 (Oct. 1982). Translation of: *Zh. Tekh. Fiz. (USSR)*, vol.52, no.10, p.2105-6 (Oct. 1982). [received: April 1983]
A possible mechanism is described for breakdown in metal vapor caused by UV light. It is shown that since the photon energy in excimer lasers is several electron volts, electron multiplication can occur via ionization of metal atoms from excited levels. (7 refs.)

Electric-field-induced differential rotational Raman scattering See Entry 59850
Luminescence of the excited mercury diethylamine complex. Attachment by ligand exchange See Entry 60806
Determination of refractivity virial coefficients of CH_4 at $25^\circ C$ See Entry 61585

52.00 THE PHYSICS OF PLASMAS AND ELECTRIC DISCHARGES

(for solid-state plasma, see 72.30)

52.20 ELEMENTARY PROCESSES IN PLASMA

61604 Effective potential description and long wavelength structure of three-point correlations in strongly coupled plasmas. K.I.Golden (Dept. of Phys., Nanjing Univ., Nanjing, China). *Commun. Theor. Phys. (China)*, vol.1, no.6, p.793-6 (1982).
Analyzes the effective potential of a strongly coupled one-component plasma and shows that beyond a critical value $\gamma_c \sim 10$ of the plasma parameter, the liquid state is characterized by the predominance of attraction between like charges as mediated by the medium. A new exact long wavelength expression is derived for the three-point structure function. (8 refs.)

61605 Particle orbits and stochasticity. A.H.Boozer (Princeton Univ., Princeton Univ., Princeton, NJ, USA).
10th IMACS World Congress on System Simulation and Scientific Computation, Montreal, Canada, 8-13 Aug. 1982 (New Brunswick, NJ, USA: IMACS 1982), p.197-vol.4
A method of evaluating particle trajectories in the complex magnetic field of a fusion reactor is given. In this method, the particle motion is fundamentally determined by two scalar functions. One is the field strength. The other characterizes the stochasticity of the magnetic field. (3 refs.)

Collisional coupling of fluctuations in plasmas See Entry 61610
Influence of collisions and incoherence on ion-cyclotron transport in mirror plasmas See Entry 61617
X-ray generation from laser-produced plasmas and its atomic-number dependence See Entry 61620
Oblique collision of cylindrical outgoing ion-acoustic solitons See Entry 61629
Resonant absorption in a self-consistent density profile at moderate intensities See Entry 61653

52.20F Electron collisions

61606 Second-order collisions between slow electrons and metastable krypton atoms in the 3P_2 state. G.A.Agaonova, N.B.Kolokolov, O.G.Toronov. *Opt. & Spectrosc. (USA)*, vol.53, no.2, p.117-18 (Aug. 1982). Translation of: *Opt. & Spektrosk. (USSR)*, vol.53, no.2, p.196-8 (Aug. 1982). [received: April 1983]

Measurement of the rapid part of the energy distribution function of electrons in the plasma of the afterglow of krypton was used to determine the absolute value of the rate constant β_2 for the reaction $Kr(^3P_2) + e \rightarrow Kr(^1S_0) + e$ in the range of electronic temperature $580 \leq T_e \leq 1200$ K. This process may play an important role in the disappearance of the metastable atoms and in the energy balance of the electrons. (11 refs.)

61607 Measurements of collisional excitation rate coefficients for Fe X ions in a plasma. Jieh-shan Wang, H.R.Griem (Lab. for Plasma & Fusion Energy Studies, Univ. of Maryland, College Park, MD, USA). *Phys. Rev. A (USA)*, vol.27, no.4, p.2249-53 (April 1983).
About 1% or more of iron was introduced into a hydrogen-filled theta pinch by a gun-injection method. The Fe X density in the plasma was determined from the measured intensity of the Fe X forbidden (coronal) line at 6374.5 Å. Electron collisional excitation rate coefficients for Fe X were obtained from measurements of Fe X vacuum-ultraviolet line intensities, electron density and temperature, and Fe X density. The experimental rate coefficients are compared with theoretical results. (13 refs.)

Kinetics of the plasma decay in lithium vapor; population inversion for the 3p-3s transition See Entry 60664
A classical path calculation of Stark broadening of isolated ion lines by plasmas See Entry 61609

Recent development in the statistical theory of high-density plasma See Entry 61612
Vaporization mode and state of the ablatant of a deuterium pellet in Tokamak discharges See Entry 61668
Monte Carlo calculation of the erosion rate and ion current at a vacuum arc cathode See Entry 61717
Effect of stepwise excitation processes on the electron velocity distribution function in argon See Entry 61721

52.20H Atomic, molecular, heavy-particle collisions

61608 Resonant transfer and excitation (RTE) in ion-atom collisions and dielectronic recombination in plasmas. D.Brandt (Dept. of Phys. & Astron. Univ. of North Carolina, Chapel Hill, NC, USA).
IEEE Trans. Nucl. Sci. (USA), vol.ns-30, no.2, p.1005-7 (April 1983). (1982 IEEE Conference on the Application of Accelerators in Research and Industry, Denton, TX, USA, 8-10 Nov. 1982).

In the resonant (charge) transfer and excitation (RTE) process, resonance states in the charge changed projectile are formed due to Coulomb-interaction with the target electrons. The calculated RTE cross section is proportional to the cross section for dielectronic recombination and its projectile energy dependence reflects the momentum distribution of the target electrons. Sample calculations for K X-ray production in S^{13+} and Ar collisions are discussed. An estimate of the experimental background indicates that RTE is more pronounced for heavy projectiles and light targets. (12 refs.)

61609 A classical path calculation of Stark broadening of isolated ion lines by plasmas. J.D.Hey, P.Breger (Dept. of Phys., Univ. of Cape Town, Rondebosch, S Africa).
S. Afr. J. Phys. (S. Africa), vol.5, no.4, p.111-22 (1982).

The impact approximation of Baranger (1958) is applied to the calculation of the widths of isolated ion lines broadened primarily by electron perturbers in the plasma. The electron perturbers are treated as classical particles moving along hyperbolic trajectories about the radiating ions, and a formula is derived for the monopole-dipole excitation cross-section which is a continuous function of perturber energy. Validity criteria for the application of the classical-path and impact approximations are discussed in detail, in order to justify the procedure. The excitation cross-section contains two important ingredients: the effective Gaunt factor and the line strength. An expression for the first of these which is compact and readily programmable, follows from the present treatment. The line strength contains the various radiator structural factors which can play a role in determining the Stark broadening of the observed spectrum. The formalism thus has two advantages: it enables reliable and rapid computations to be carried out of Stark widths of ion spectra for astrophysical purposes, and it readily lends itself to the study of radiator structural effects such as the breakdown of LS coupling and configuration interaction. (68 refs.)

Kinetics of the plasma decay in lithium vapor; population inversion for the 3p-3s transition See Entry 60664
Effect of collisional mixing of lower levels of Li-like ions on the intensity of the resonance line satellite structures of He-like ions See Entry 60909
Second-order collisions between slow electrons and metastable krypton atoms in the 3P_2 state See Entry 61606
Measurements of collisional excitation rate coefficients for Fe X ions in a plasma See Entry 61607
Monte Carlo calculation of the erosion rate and ion current at a vacuum arc cathode See Entry 61717
Effect of stepwise excitation processes on the electron velocity distribution function in argon See Entry 61721

52.25 PLASMA BASIC PROPERTIES

61610 Collisional coupling of fluctuations in plasmas. P.Uddholm (Dept. of Plasma Phys., Umea Univ., Umea, Sweden).

J. Phys. A (GB), vol.16, no.6, p.1315-30 (21 April 1983).

The transition probability function approach is extended to plasmas in which the fluctuations in the various particle species are coupled through the collisions. The collisions may be either particle conserving or particle non-conserving (chemical reactions). Particular attention is paid to the case of particle non-conserving collisions, because certain difficulties connected with the use of the fluctuation dissipation theorem then arise. This does not mean that the fluctuation dissipation theorem is erroneous, but only that the appropriate force-response pair is at best difficult to find. Such is the case for the density fluctuation spectrum. The transition probability function approach avoids this difficulty. (17 refs.)

61611 Vibrational population densities of the $A^3\Sigma_u^+$, $B^3\Pi_u$, $W^3\Delta_u$, $B^3\Sigma_u^-$, and $C^3\Pi_u$ states in nitrogen plasmas. A.Ali, P.K.Ghosh (Dept. of Chem., Indian Inst. of Technol., Kanpur, India).

J. Quant. Spectrosc. & Radiat. Transfer (GB), vol.29, no.4, p.353-67 (April 1983).

Population densities of vibrational levels of triplet excited states have been calculated using a collisional-radiative model applicable to nitrogen gas discharges with a Maxwellian electron energy distribution. Relative contributions of various electron impact and radiative processes, including intrasystem cascade, to the total cross sections of the triplet excited states are investigated. (41 refs.)

61612 Recent development in the statistical theory of high-density plasma. S.Ichamaru (Dept. of Phys., Univ. of Tokyo, Tokyo, Japan).

Phys. Scr. (Sweden), vol.T2, no.1, p.198-205 (1982). (1982 International Conference on Plasma Physics, Goteborg, Sweden, 9-15 June 1982).

Describes a density functional theory of dense plasmas leading to a systematic improvement over the hypernetted chain equations. The author then presents an analytic formula for the dielectric function of the degenerate electron liquids, which satisfies a number of self-consistency requirements and which accurately reproduces the recent Monte Carlo results as well as those of the microscopic calculations. Some problems associated with the electron-ion interactions are treated: The topics include corrections to the thermodynamic functions, the electric resistivity, the plasmon linewidth and the frequency shift. (36 refs.)

61613 Effect of trapped electrons on the wave-induced current. M.Taguchi.

Report IPPJ-620, Nagoya Univ., Japan (Jan. 1983), 22 pp.

The wave-induced current in a toroidal magnetic field is computed by use of the adjoint drift-kinetic equation for electrons. The inverse aspect ratio of a toroidal device is assumed to be small and the lowest-order terms of this ratio are retained. As the wave-absorption mechanism, the electron cyclotron damping and the electron Landau damping are considered. It is found that the induced current decreases considerably by the effect of the trapped electrons when the phase velocity of a plasma wave is low. (13 refs.)

61614 Measurement of small-scale density fluctuation in JIPP T-II plasma by millimeter and sub-millimeter wave scattering. T.Tetsuka, A.Nishizawa, T.Sakai, K.Kawahata, A.Mase, T.Tsukishima, J.Fujita.

Report IPPJ-619, Nagoya Univ., Japan (Dec. 1982), 30 pp.

The small-space density fluctuations have been studied by both millimeter (2 mm) and sub-millimeter (337 μ m) wave scattering techniques in JIPP T-II plasmas. Experiments were performed in two types of plasma: Tokamak and stellarator plasmas. In both plasmas, the density fluctuations are localised in outer region of the plasma column, and show the characteristics of the drift wave mode turbulence. The density fluctuation level is $\delta n/n_0 \approx 1-1.5\%$ around the plasma edge, and this value is inversely proportional to the mean electron density. Further, the dependence of the fluctuation level on the plasma parameters is studied and compared with the scaling law of the energy confinement time of the plasma. The diffusion coefficient estimated from the density fluctuation is about one third of the global diffusion coefficient. (22 refs.)

Gravitational radiation of plasma in a magnetic field See Entry 59644

Effective potential description and long wavelength structure of three-point correlations in strongly coupled plasmas See Entry 61604

Second-order collisions between slow electrons and metastable krypton atoms in the 2P_2 state See Entry 61606

Measurements of collisional excitation rate coefficients for Fe X ions in a plasma See Entry 61607

Dense and multicomponent plasmas See Entry 61618

Ion-ion two-stream instability in multispecies laser-produced plasma See Entry 61631

Thermal cavitons See Entry 61638

Nonlinear effects in a beam plasma system: second harmonic emission and density depression formation See Entry 61639

Comments on 'Gravitational instability of a rotating anisotropic plasma with Hall's effect' See Entry 61645

Theoretical determination of the electron distribution in the presence of an ion-acoustic turbulence See Entry 61646

Resonant absorption in a self-consistent density profile at moderate intensities See Entry 61653

Measurement of surface wave dispersion in nonuniform plasma waveguides See Entry 61657

Kinetic theory of phase space vortices and double layers See Entry 61662

Vaporization mode and state of the ablatant of a deuterium pellet in Tokamak discharges See Entry 61668

Theory of heating and compression of double-shell spherical targets exposed to a laser pulse See Entry 61672

Electron confinement studies on the EBT-S Bumpy Torus experiment using soft X-ray techniques See Entry 61678

Surface density profile of the one-component plasma See Entry 61690

Two pulse multiple position Thomson scattering system See Entry 61698

On the observability of forbidden lines See Entry 61701

Line radiation of highly ionised impurities in plasma produced in the plasma-focus device See Entry 61702

Axial and angular distribution of current density in a thermionic converter with nonisothermal electrodes See Entry 61707

Monte Carlo calculation of the erosion rate and ion current at a vacuum arc cathode See Entry 61717

52.25F Transport properties

61615 Influence of diffusion on the quasi-linear growth of magnetic islands. A.M.Hilsdorf-Marotta (Inst. de Fisica Gleb Wataghin, Univ. Estadual de Campinas, Sao Paulo, Brazil), R.M.O.Galvao.

Phys. Lett. A (Netherlands), vol.94A, no.6-7, p.295-7 (21 March 1983).

It is shown that the rate at which a magnetic island grows in the non-linear stage of a tearing mode is reduced by the equilibrium resistive flow. (13 refs.)

61616 Plasma convection and line-tying. S.Fornaca (Dept. of Phys., Univ. of California, Irvine, CA, USA).

Phys. Fluids (USA), vol.26, no.3, p.797-804 (March 1983).

The directed motion of a low- β plasma across a toroidal magnetic field is examined as the degree of electrical contact between the plasma and a conducting end wall (line-tying) is varied in a controlled manner. Experimentally, little difference is found between the motion of a completely isolated plasma and that of a plasma in contact with a wall that does not emit electrons. As the degree of line-tying is increased by making the end wall electron-emitting, the cross-field convection of the plasma is increasingly suppressed. Beyond a critical emission current density, no further suppression is observed. When the system is in the surface-line-tying configuration, the suppression of the directed cross-field motion is accompanied by a large increase in the radial transport of plasma. (18 refs.)

61617 Influence of collisions and incoherence on ion-cyclotron transport in mirror plasmas. B.I.Cohen, R.H.Cohen, B.D.Rognien (Lawrence Livermore Nat. Lab., Univ. of California, Livermore, CA, USA).

Phys. Fluids (USA), vol.26, no.3, p.808-19 (March 1983).

The effects of classical Coulomb collisions and wave incoherence on drift-cyclotron-loss-cone (drift-cone) mode anomalous transport are studied analytically and by simulation. Pitch-angle collisions have a cumulative effect on the gyrophase angle, and the spatially varying magnetic field in a mirror well contributes a large geometrical amplification of the gyrophase-angle diffusion. Analytical calculations of this effect for particles with arbitrary pitch angle are confirmed by Monte Carlo simulations. However, for the levels of drift-cone turbulence observed in the 2XIIIB magnetic mirror experiment and for its relative collisionality, the effect of pitch-angle collisions on anomalous transport is small. In particular, heating of ions to 40 keV energies cannot be explained by this mechanism. Wave incoherence also destroys superadiabaticity, leads to velocity transport, and provides an approximate model of the finite frequency bandwidth of drift-cone turbulence, e.g. due to bursting effects in 2XIIIB. Monte Carlo simulations corroborate the analytical transport theory presented. The simulations exhibit significantly enhanced velocity-space transport and heating of ions to nearly 40 keV energies due to wave incoherence for parameters at the limit of applicability to the 2XIIIB experiment. These same considerations of resonant wave-particle interactions are also directly relevant to electron and ion-cyclotron resonance heating and to velocity diffusion driven by unstable Alfvén-ion-cyclotron waves in other mirror experiments. (19 refs.)

61618 Dense and multicomponent plasmas. C.Deutsch (Lab. de Phys. des Plasmas, Univ. Paris XI, Orsay, France).

Phys. Scr. (Sweden), vol.T2, no.1, p.192-7 (1982). (1982 International Conference on Plasma Physics, Goteborg, Sweden, 9-15 June 1982).

Multicomponent systems of point charges with either sign are considered. Equilibrium and transport properties are investigated through temperature-dependent effective interactions taking into account the required amount of short-ranged and quantum effects (diffraction, symmetry, extended ion core). A particular emphasis is paid to the equation of state in the Sun interior, in connection with the neutrinos dilemma. The challenged Fe-H demixion is unlikely to occur. The author also considers quantum corrections to the particle diffusion in an electron-ion system, transversely to a very large and steady magnetic field ($q_2 \gg \omega_{pi}$). (20 refs.)

61619 Transport modelling in magnetic confinement experiments.

K.V.Roberts (Culham Lab., UKAEA, Abingdon, England).

10th IMACS World Congress on System Simulation and Scientific Computation, Montreal, Canada, 8-13 Aug. 1982 (New Brunswick, NJ, USA: IMACS 1982), p.194-vol.4

Transport calculations in Tokamak devices model the time evolution of an azimuthal structure of plasma and magnetic field through a sequence of quasiequilibrium states, taking into account a variety of plasma and energy production and loss processes together with the behaviour of neutrals and impurities. The calculations alternate a 2D elliptic computation of the adiabatic changes in flux surface geometry with a coupled set of 1D parabolic diffusion equations for the entropy-generating processes. (20 refs.)

Gravitational radiation of plasma in a magnetic field See Entry 59644

Recent development in the statistical theory of high-density plasma See Entry 61612

Experimental evidence of temperature gradient effects on the neutral gas penetration into a magnetized rotating plasma See Entry 61648

Hot-electron energy deposition in CO₂-laser-irradiated targets consistent with magnetic-field-induced surface transport See Entry 61669

Intense relativistic electron beam injector system for Tokamak current drive See Entry 61675

Diffusion losses of ions and electrons in the 'Jupiter-1A' electromagnetic trap See Entry 61683

Particle simulation of plasmas See Entry 61692

Monte Carlo calculation of the erosion rate and ion current at a vacuum arc cathode See Entry 61717

Numerical modeling of a laminar pulsed discharge including radiative transport See Entry 61718

Effect of stepwise excitation processes on the electron velocity distribution function in argon See Entry 61721

52.25P Emission, absorption, and scattering of radiation

61620 X-ray generation from laser-produced plasmas and its atomic-number dependence. N.Nakano, H.Kuroda (Inst. for Solid State Phys., Univ. of Tokyo, Tokyo, Japan).

Phys. Rev. A (USA), vol.27, no.4, p.2168-77 (April 1983).

Experimental studies of the X-ray generation from laser plasmas are performed by using a picosecond high-power laser. The intensity of emitted X-rays shows a periodic variation as a function of the atomic number of target materials. Calculations based on the transient collisional-radiative model rather than the conventional steady-state coronal model, are carried out. Experimental and computational results show good agreement with each

other, and indicate the importance of the transient nature of multiple-ionization processes. The dependence of hot-electron temperature on the atomic number is briefly discussed. (33 refs.)

61621 Transition radiation and transition scattering. V.L.Ginzburg (P.N. Lebedev Phys. Inst., Acad. of Sci., Moscow, USSR). *Phys. Scr. (Sweden)*, vol.T2, no.1, p.182-91 (1982). (1982 International Conference on Plasma Physics, Goteborg, Sweden, 9-15 June 1982).

Transition radiation is a process of a rather general character. It occurs when some source, which does not have a proper frequency (for example, a charge), moves at a constant velocity in an inhomogeneous and (or) nonstationary medium or near such a medium. The simplest type of transition radiation takes place when a charge crosses a boundary between two media (the role of one of the media may be played by vacuum). In the case of periodic variation of the medium, transition radiation processes some specific features (resonance transition radiation or transition scattering). Transition scattering occurs, in particular when a permittivity wave falls onto an nonmoving (fixed) charge. Transition scattering is closely connected with transition bremsstrahlung radiation. All these transition processes are essential for plasma physics. Transition radiation and transition scattering have analogues outside the framework of electrodynamics (like in the case of Vavilov-Cherenkov radiation). The corresponding range of phenomena is elucidated, as far as possible, in a generally physical aspect. (12 refs.)

61622 Characteristic features of transition radiation of charged particles in nonstationary magnetoactive plasma. L.I.Bondarenko, N.S.Erokhin. *Ukr. Fiz. Zh. (USSR)*, vol.28, no.3, p.401-6 (March 1983). In Russian.

Transition radiation and the linear transformation of charged particles are considered arising when the charge moves uniformly through a homogeneous non-stationary magnetized plasma. (5 refs.)

A classical path calculation of Stark broadening of isolated ion lines by plasmas See Entry 61609

Resonant absorption in a self-consistent density profile at moderate intensities See Entry 61653

Efficient way to prevent reflection from stimulated Brillouin backscattering See Entry 61654

Coherent electromagnetic radiation of an electron-ion beam See Entry 61666

Hot-electron energy deposition in CO₂-laser-irradiated targets consistent with magnetic-field-induced surface transport See Entry 61669

Synchrotron emission from a relativistic loss-cone distribution with application to the ELMO Bumpy-Torus experiment See Entry 61677

Line radiation of highly ionised impurities in plasma produced in the plasma-focus device See Entry 61702

52.30 PLASMA FLOW; MAGNETOHYDRODYNAMICS

(see also 47.65 Fluid dynamics)

61623 Idealised model for plasma acceleration in an MHD channel. K.Kuriki, Y.Kunii, Y.Shimizu (Inst. of Space and Astronautical Sci., Tokyo, Japan).

AIAA J. (USA), vol.21, no.3, p.322-6 (March 1983).

A quasi-one-dimensional plasma acceleration by a self-induced magnetic field was analysed in the magnetohydrodynamic framework. The magnetic Reynolds number was a similar parameter to describe the fields of flow and discharge current. The discharge current was found to be concentrated not only at the exit but also the entrance of the channel. By suitable electrode geometry, the current concentration was relaxed and the thrust efficiency was enhanced compared with the straight geometry. (7 refs.)

61624 Comments on 'Stability of shear flow in a magnetized plasma' [and reply]. B.K.Shivamoggi (Res. School of Phys. Sci., Australian Nat. Univ., Canberra, Australia), Y.Y.Lan, C.S.Liu. *Phys. Fluids (USA)*, vol.26, no.3, p.867-8 (March 1983).

For original paper see Y.Y. Lau and C.S. Liu, *ibid.*, vol.23, p.939 (1980). The initial value problem analysis of the hydromagnetic Couette flow by Lau and Liu shows that the disturbances undergo a transient growth and an ultimate decay. The author feels that while this trend is in accord with the results in the hydrodynamic case the results still need further explanation. Lau and Liu reply to these comments. (11 refs.)

61625 Numerical investigation of the interaction between a plasma stream and a transverse magnetic field. Yu.N.Makarov (Polytech. Inst., Leningrad, USSR).

Sov. Phys.-Tech. Phys. (USA), vol.27, no.9, p.1104-6 (Sept. 1982). Translation of: *Zh. Tekh. Fiz. (USSR)*, vol.52, no.9, p.1802-5 (Sept. 1982). [received: April 1983]

A shock-capturing technique is used to investigate the interaction of the flow behind a shock wave with a transverse magnetic field. The calculation is based on the three-fluid model of a nonequilibrium ionized gas. The applicability of the simpler two- and one-fluid models is discussed. The flow in a regime with an open longitudinal current is investigated in detail, and the features of the deceleration and heating of a plasma in a regime with a short-circuited longitudinal current are described. The calculation results are compared with experimental data. (8 refs.)

Tearing modes in a general cross-section force-free cylindrical Tokamak See Entry 61627

Magnetohydrodynamic stability of magnetic slabs See Entry 61628

Resistive MHD stability in Tokamaks See Entry 61643

Linear MHD stability calculations See Entry 61644

Characteristics of oblique shock waves produced in an expanding laser plasma See Entry 61651

Analysis of axial-outflow in cylindrical deuterium-plasma sample compressed radially by imploding liner See Entry 61674

Computational methods for 3D nonlinear magnetohydrodynamics See Entry 61685

3D nonlinear initial value calculations in resistive MHD See Entry 61693

Simulation of plasma formation and attainment of equilibrium See Entry 61694

Plasma parameter control experiments on 'Tuman-3' See Entry 61710

Numerical modeling of a laminar pulsed discharge including radiative transport See Entry 61718

52.35 WAVES, OSCILLATIONS, AND INSTABILITIES IN PLASMA

61626 Propagation of lower hybrid resonance cones in Tokamaks. P.M.Bellan (California Inst. of Technol. Pasadena, CA, USA).

Phys. Fluids (USA), vol.26, no.3, p.741-6 (March 1983).

The trajectory of the lower hybrid resonance cone surface is calculated for propagation in the helical magnetic field of a Tokamak. The surface is found to be a deformed cone, having symmetry axis following the magnetic field helicity. By superimposing cone fields excited by adjacent, poloidally separated point sources, the field excited by a source of finite poloidal extent is deduced. For sources having large poloidal extent, the superimposed cones destructively interfere everywhere except in a small region of constructive reinforcement which is located towards the plasma center; sources having small poloidal extent excite an individual resonance cone, which extends from near the plasma center all the way to the wall. Numerical calculations are presented for Verasator, Alcator-A and -C, JFT-2, and PLT Tokamak parameters. (21 refs.)

61627 Tearing modes in a general cross-section force-free cylindrical Tokamak. J.K.Lee, M.S.Chu, F.J.Helton (General Atomic Co., San Diego, CA, USA).

Phys. Fluids (USA), vol.26, no.3, p.766-74 (March 1983).

The stability of magnetohydrodynamic tearing modes for a large aspect ratio force-free Tokamak with general cross section is studied in terms of an energy principle. Determinations of the marginal stability boundary Δ' and island size using this general two-dimensional method give good agreement with those of known methods for circular equilibria. Results for noncircular equilibria are also presented. (19 refs.)

61628 Magnetohydrodynamic stability of magnetic slabs. A.Banos, Jr., E.A.Adler, B.D.Fried, J.Echart (Dept. of Phys., Univ. of California, Los Angeles, CA, USA).

Phys. Fluids (USA), vol.26, no.3, p.780-9 (March 1983).

A simplified procedure is developed for calculating the ideal magnetohydrodynamic stability of a 'magnetic slab' consisting of two planar rows of staggered parallel conductors carrying oppositely directed (equal or unequal) currents, a configuration which is the planar analog of the University of California, Los Angeles, Large Mirror Ratio Experiment (LAMEX). Instead of solving the Grad-Shafranov equation to find the magnetic field corresponding to magnetohydrodynamic equilibrium, use was made of conformal mapping techniques to obtain analytical expressions for the vector potential A for the sharp boundary case, and then the plasma was allowed to 'spill over' into the vacuum region with a permissible pressure profile $p(A)$. Using conventional magnetohydrodynamic analysis, based on the well-known energy principle, the maximum stable pressure gradient on each magnetic surface was determined and, from that, the optimum permissible pressure profile $p(A)$ as a function of the spacings (horizontal and vertical) between the conductors and the currents in the two rows was also determined. Significant reductions in maximum stable beta are found compared to the sharp boundary case. (5 refs.)

61629 Oblique collision of cylindrical outgoing ion-acoustic solitons. I.Tsukabayashi, Y.Nakamura, F.Kako, K.E.Longgren (Inst. of Space & Astronaut. Sci., Tokyo, Japan).

Phys. Fluids (USA), vol.26, no.3, p.790-4 (March 1983).

Two identical cylindrical outgoing ion-acoustic solitons are transmitted in a double-plasma device to observe an oblique collision. The colliding angle of the solitons is smaller than the resonance angle given by $2 \tan^{-1}[(\partial n/\partial n)^{1/2}]$, where $\partial n/\partial n$ is the normalized amplitude of the solitons. Two new waves are observed to form in the region of the interaction. The experimental results are compared with a numerical integration of a modified Boussinesq equation and with a theory of three-wave interaction. (25 refs.)

61630 Measurement of growth rate of plasma drift wave excited by slow electrons. P.J.Barrett (Plasma Phys. Res. Inst., Univ. of Natal, Durban, S Africa), G.R.Allen.

Phys. Fluids (USA), vol.26, no.3, p.795-6 (March 1983).

Measurements are presented on drift waves which are driven unstable by an annular beam of slow electrons. The growth rate of the most unstable mode varies linearly with the injection velocity of the beam, in accordance with fluid theory. (8 refs.)

61631 Ion-ion two-stream instability in multispecies laser-produced plasma. S.P.Sarraf, E.A.Williams (Lab. for Laser Energetics, Univ. of Rochester, Rochester, NY, USA), L.M.Goldman.

Phys. Rev. A (USA), vol.27, no.4, p.2110-13 (April 1983).

Experimental observations of the high-energy ions (>10 keV/Z), expanding from a laser-produced plasma, have shown strong evidence of coronal electrostatic fields. In this paper, it is shown by a linear analysis that a multispecies streaming plasma can be subject to a two-stream ion-ion instability leading to density modulations. The effect of the charge-to-mass ratio on growth rate for different species accelerated by the same background electric field has been investigated. The theoretical model is consistent with experimental observations. (9 refs.)

61632 Experimental studies of parametric interaction near quarter critical density. H.A.Baldis, C.J.Walsh (Div. of Phys., Nat. Res. Council of Canada, Ottawa, Ontario, Canada).

Phys. Scr. (Sweden), vol.T2, no.2, p.492-7 (1982). [received: April 1983]. (1982 International Conference on Plasma Physics, Goteborg, Sweden, 9-15 June 1982).

The authors present the results of a study, using Thomson scattering, of parametrically driven ion and electron plasma waves in a CO₂ laser-plasma interaction. The experiments were conducted in a pre-formed plasma at a density near the quarter critical density of the CO₂. Waves produced by two plasmon decay as well as the Raman and Brillouin scattering instabilities are observed. (22 refs.)

61633 Natural Poisson structures of nonlinear plasma dynamics. A.N.Kaufman (Lawrence Berkeley Lab., Univ. of California, Berkeley, CA, USA).

Phys. Scr. (Sweden), vol.T2, no.2, p.517-21 (1982). [received: April 1983]. (1982 International Conference on Plasma Physics, Goteborg, Sweden, 9-15 June 1982).

Hamiltonian field theories, for models of nonlinear plasma dynamics, require a Poisson bracket structure for functionals of the field variables. These are presented, applied, and derived for several sets of field variables: coherent waves, incoherent waves; particle distributions, and multifield electrodynamics. Parametric coupling of waves and plasma yields concise expressions for ponderomotive effects (in kinetic and fluid models) and for induced scattering. (20 refs.)

61634 Nonlinear drift waves. T.Taniuti (Dept. of Phys., Nagoya Univ., Nagoya, Japan), A.Hasegawa.

Phys. Scr. (Sweden), vol.T2, no.2, p.529-33 (1982). [received: April 1983] (1982 International Conference on Plasma Physics, Goteborg, Sweden, 9-15 June 1982).

Turbulence and solitary vortex structures of electrostatic drift waves are presented using a simple model equation based on two-dimensional cold ions and Boltzmann electrons. (12 refs.)

61635 Interaction of Langmuir solitons with resonant particles. K.Rypdal (Inst. for Math. & Phys. Sci., Univ. of Tromsø, Tromsø, Norway), J.P.Lynov, H.L.Pecseli, J.J.Rasmussen, K.Thomsen.

Phys. Scr. (Sweden), vol.T2, no.2, p.534-7 (1982). [received: April 1983] (1982 International Conference on Plasma Physics, Goteborg, Sweden, 9-15 June 1982).

The effects of resonant particles on the propagation of Langmuir solitons are studied. The main effects are a deceleration of the solitons, and for high-amplitude solitons, emission of ion-sound tails. Results from perturbation theory are compared with numerical solutions of the model equations. (12 refs.)

61636 Transient effects of nonlinear wave propagation in magnetized plasmas. H.L.Pecseli, K.Thomsen (Riso Nat. Lab., Roskilde, Denmark).

Phys. Scr. (Sweden), vol.T2, no.2, p.541-5 (1982). [received: April 1983] (1982 International Conference on Plasma Physics, Goteborg, Sweden, 9-15 June 1982).

The evolution of a steep wavefront propagating perpendicular to an externally applied homogeneous magnetic field is considered. The propagation is accompanied by the excitation of low-frequency waves. When the nonlinear interaction is taken into account the authors observe the evolution of a modulational instability trailing the wavefront. (18 refs.)

61637 On the transient effects of nonlinear wave propagation in magnetized plasmas. K.E.Lonngrén, H.L.Pecseli, J.J.Rasmussen, K.Thomsen (Riso Nat. Lab., Roskilde, Denmark).

Phys. Scr. (Sweden), vol.T2, no.2, p.546-7 (1982). [received: April 1983] (1982 International Conference on Plasma Physics, Goteborg, Sweden, 9-15 June 1982).

Approximate analytical solutions are obtained for the set of coupled nonlinear partial differential equations which govern the evolution of a steep wavefront propagating perpendicular to an externally applied homogeneous magnetic field. Several of the features noted in a numerical solution of these equations by Pecseli and Thomsen (ibid., vol.12, p.541, 1982) are predicted by these approximate solutions. (5 refs.)

61638 Thermal cavitons. K.B.Dysthe, E.Mjølhus, H.Pecseli, K.Rypdal (Inst. of Math. & Phys. Sci., Univ. of Tromsø, Tromsø, Norway).

Phys. Scr. (Sweden), vol.T2, no.2, p.548-59 (1982). [received: April 1983] (1982 International Conference on Plasma Physics, Goteborg, Sweden, 9-15 June 1982).

The formation of small scale striations observed in ionospheric heating experiments is explained in terms of electrostatic waves propagating across the magnetic field, generated by linear conversion on the local density gradient and trapped in the density depletions. Enhancement of the process is due to ohmic overheating of the depletions, resulting in decreased density there. The process is centered at the upper hybrid level. Further growth is predicted when the initial density depressions exceed a threshold which is calculated. Such a nonlinear threshold is associated with a certain hysteresis phenomenon which has been observed in experiments. (28 refs.)

61639 Nonlinear effects in a beam plasma system: second harmonic emission and density depletion formation. J.A.Michel, P.J.Paris, M.Schneider, M.W.Tran (Ecole Polytech. Federale de Lausanne, Lausanne, Switzerland).

Phys. Scr. (Sweden), vol.T2, no.2, p.571-5 (1982). [received: April 1983] (1982 International Conference on Plasma Physics, Goteborg, Sweden, 9-15 June 1982).

The nonlinear evolution of Langmuir waves excited by the beam-plasma instability is studied experimentally. The emission of electromagnetic waves at the second harmonic of the plasma frequency and the formation of a density depression have been observed. These phenomena are consistent with the predictions of the strong Langmuir turbulence theory. (27 refs.)

61640 Experimental study of the dissipative trapped ion instability. G.A.Navratil, A.K.Sen, J.Slough (Columbia Univ., New York, NY, USA).

Phys. Scr. (Sweden), vol.T2, no.2, p.585-7 (1982). [received: April 1983] (1982 International Conference on Plasma Physics, Goteborg, Sweden, 9-15 June 1982).

Experiments have been performed in a steady-state linear machine with a low temperature, low density plasma in the collisionality regime of the dissipative trapped ion instability. This instability was seen and identified through the observed dependence of wave amplitude on trapped fraction, axial and radial structure, and collisionality and through the scaling of the real frequency with trapped fraction. (5 refs.)

61641 Collisionless relaxation of phase oscillations of trapped particles in an accelerating amplitude-modulated wave. V.Ya.Davydovskii, Yu.S.Filippov (V.D. Kalmykov Radiotech. Inst., Tagerog, USSR).

Sov. Phys.-Tech. Phys. (USA), vol.27, no.10, p.1175-8 (Oct. 1982). Translation of: *Zh. Tekh. Fiz. (USSR)*, vol.52, no.10, p.1910-14 (Oct. 1982). [received: April 1983]

Relaxation of phase oscillations of particles in accelerating waves is studied for relativistic particles in amplitude-modulated waves with phase velocity greater than the speed of light. The analysis is based on averaged equations of motion and uses adiabatic invariants. The damping rate is determined in the linear approximation. (11 refs.)

61642 Discrimination effects in wave parametric interaction in a relativistic electron stream plasma. V.P.Zakharov, V.V.Kulish.

Ukr. Fiz. Zh. (USSR), vol.28, no.3, p.406-11 (March 1983). In Russian. The process of the parametric interaction of two randomly polarized electromagnetic waves with the space-charge wave of a high-current relativistic electron stream is investigated. The effects of phase and polarization discrimination consisting of the gain coefficient dependence on the initial phases of oscillations and polarizations of the interacting waves are shown to produce a significant influence on the process of the electromagnetic signal gain. (8 refs.)

61643 Resistive MHD stability in Tokamaks. J.Manicham, R.C.Grimm, R.L.Dewar (Plasma Phys. Lab., Princeton Univ., Princeton, NJ, USA).

10th IMACS World Congress on System Simulation and Scientific Computation, Montreal, Canada, 8-13 Aug. 1982 (New Brunswick, NJ, USA: IMACS 1982), p.175-6 vol.4

Reports on a program designed to study the linear stability of resistive modes in finite pressure, finite aspect ratio, and arbitrary cross-section Tokamaks using a boundary layer approach. (5 refs.)

61644 Linear MHD stability calculations. W.Kerner (Max-Planck-Inst. für Plasmaphys., Garching, Germany).

10th IMACS World Congress on System Simulation and Scientific Computation, Montreal, Canada, 8-13 Aug. 1982 (New Brunswick, NJ, USA: IMACS 1982), p.179-81 vol.4

The Galerkin method is applied to the linearized MHD equations. For ideal MHD this leads to a Hermitian matrix eigenvalue problem, where accurate and efficient methods are known. But for nonideal MHD with general matrices the application is more difficult. (21 refs.)

Efficiency of passive circuits for vertical stability in INTOR reactor See Entry 60449

Effect of trapped electrons on the wave-induced current See Entry 61613

Influence of diffusion on the quasi-linear growth of magnetic islands See Entry 61615

Influence of collisions and incoherence on ion-cyclotron transport in mirror plasmas See Entry 61617

Comments on 'Stability of shear flow in a magnetized plasma' [and reply] See Entry 61624

Comments on 'Gravitational instability of a rotating anisotropic plasma with Hall's effect' See Entry 61645

Resonant absorption in a self-consistent density profile at moderate intensities See Entry 61653

Efficient way to prevent reflection from stimulated Brillouin backscattering See Entry 61654

Measurement of surface wave dispersion in nonuniform plasma waveguides See Entry 61657

Cyclotron excitation of fast magnetosonic waves by circulating thermonuclear alpha particles in a Tokamak See Entry 61663

Nonlinear energy flow in a beam-plasma system See Entry 61664

Coherent electromagnetic radiation of an electron-ion beam See Entry 61666

Plasma behaviors in the open field region of reversed-field theta-pinch See Entry 61676

Self-excitation of periodic cyclotron instability regimes in a plasma magnetic trap See Entry 61680

Tokamak disruptions See Entry 61684

Computational methods for 3D nonlinear magnetohydrodynamics See Entry 61685

The computational model for the control of plasma position in TEXTOR See Entry 61686

Experience with feedback and feedforward for plasma control in ASDEX See Entry 61688

Plasma parameter control experiments on 'Tuman-3' See Entry 61710

T-15 poloidal field control system See Entry 61711

Nonlinear phenomena in laboratory and space plasmas See Entry 64301

52.35R Plasma turbulence

61645 Comments on 'Gravitational instability of a rotating anisotropic plasma with Hall's effect'. B.K.Shivamoggi (Res. School of Phys. Sci., Australian Nat. Univ., Canberra, Australia).

Phys. Fluids (USA), vol.26, no.3, p.867 (March 1983).

For original paper see P.D. Ariel, ibid., vol.13, p.1644 (1970). One of the effects of the Hall currents is the introduction of a cross flow so that the Hall effects dynamically lead, among other consequences, to those due to rotation. The author comments that it does not seem worthwhile to include the Hall effects in a dynamical analysis in which a rotation is already present. He is in agreement with Ariel who found the Hall effects lead to consequences that are identical to those due to rotation. (2 refs.)

61646 Theoretical determination of the electron distribution in the presence of an ion-acoustic turbulence. Tu Khiet (Lab. de Phys. des Gaz et des Plasmas, Univ. Paris-Sud, Orsay, France).

Phys. Rev. A (USA), vol.27, no.4, p.2237-40 (April 1983).

The author shows that, in the presence of an ion-acoustic turbulence, the electron velocity distribution function deforms irreversibly to a flat-topped shape in the central region and a nonthermal one in the tail region. The runaway part which behaves as v^{-m} , with $m=9/2$, is created with a completely specified production rate and is given by the turbulent collision frequency. (9 refs.)

61647 Topics in strong Langmuir turbulence. D.R.Nicholson (Dept. of Phys. & Astron., Univ. of Iowa, Iowa City, IA, USA).

Phys. Scr. (Sweden), vol.27, no.2, p.77-82 (Feb. 1983).

Progress in two approaches to the study of strong Langmuir turbulence is reported. In two spatial dimensions, numerical solution of the Zakharov equations yields a steady state involving linear growth, linear damping, and a collection of coherent, long-lived entities which might loosely be called solitons. In one spatial dimension, a statistical theory is applied to the cubically nonlinear Schrödinger equation and is solved analytically in a special case. (52 refs.)

61648 Experimental evidence of temperature gradient effects on the neutral gas penetration into a magnetized rotating plasma. M.Bures (Dept. of Plasma Phys. & Fusion Res., Royal Inst. of Technol., Stockholm, Sweden).

Phys. Scr. (Sweden), vol.27, no.2, p.83-90 (Feb. 1983).

The experimental evidence of temperature gradient effects on the neutral gas penetration into a plasma is presented. It is found that an increased temperature gradient reduces the neutral gas content in the partially ionized boundary layer of a cold gas blanket system. A strong modification of the rotating plasma equilibrium is then observed. Such an equilibrium is a sensitive function of the neutral gas concentration both in the plasma and its boundary layers. The moderate values of the centrifugal force which act both on the ions and neutrals do not appreciably influence the plasma permeability to neutral gas. It is further observed that an acceleration of neutrals takes place in a rotating plasma. (26 refs.)

61649 Nonlinear Landau damping phenomenon in a strongly turbulent plasma. N.L.Shatashvili (Dept. of Phys., Tbilisi State Univ., Tbilisi, USSR), N.L.Tsintsadze.

Phys. Scr. (Sweden), vol.T2, no.2, p.511-16 (1982). [received: April 1983] (1982 International Conference on Plasma Physics, Goteborg, Sweden, 9-15 June 1982).

The authors give the systematic theory of the derivation of the generalized set of Zakharov equations for a collisionless isotropic plasma taking into account the nonlinear Landau damping and relativistic effect. The conditions of deriving the nonlinear Schrödinger equation from the generalized system are

shown. The new branch for modulational instability is found. The wave-wave-particle interaction leads to the braking of the soliton. (15 refs.)

61650 Magnetized-plasma turbulence. Dter Haar (Magdalen Coll., Univ. of Oxford, Oxford, England).

Phys. Scr. (Sweden), vol.T2, no.2, p.522-4 (1982). [received: April 1983] (1982 International Conference on Plasma Physics, Goteborg, Sweden, 9-15 June 1982).

The author discusses the generalized Zakharov equations derived by Ovenden and Statham and given reasons for being sceptical about using the fluid approximation as is done in the derivation of these equations—except perhaps for those situations which involve weakly magnetized Langmuir plasmas and the author also compares them with equations suggested by other authors to describe strong turbulence in a magnetized plasma. (16 refs.)

On the ignition conditions for turbulent plasmas See Entry 60400

The role of plasma turbulence for wave excitation in a free-electron-laser combined with a molecular and plasma medium See Entry 61170

Nonlinear drift waves See Entry 61634

Nonlinear effects in a beam plasma system: second harmonic emission and density depression formation See Entry 61639

High-frequency Stark-effect measurements in emission spectroscopy See Entry 61703

52.35T Shock waves

61651 Characteristics of oblique shock waves produced in an expanding laser plasma. Tong-Nyong Lee (Optical Sci. Div., Naval Res. Lab., Washington, DC, USA).

Phys. Rev. A (USA), vol.27, no.4, p.2082-99 (April 1983).

Stationary oblique shock waves produced by a laser-produced plasma (carbon and lithium) expanding over a wedge and related phenomena have been investigated experimentally. Such a plasma is characterised as an ionization-frozen multicomponent flow which consists of a number of different charge-state groups with different flow velocities. Well-defined multiple shock fronts which are formed around a wedge are differentiated using a spectroheliographic method. Data obtained from an ion-charge collector and from spectroheliographs indicate that these shock fronts (with differential inclinations) result from different flow components. The plasma behind the shock is predominantly recombining rather than ionizing. In addition, the innermost shock is found to be more like a transverse shock where the flow particles are transported along the shock plane. This is also evidenced by a large charged-particle cumulation (and collimation) which occurs when two such oblique shock waves are brought to intersect each other. The measured shock inclinations as a function of wedge angle indicate a considerable departure from a simple gasdynamic flow model. It is believed that the self-generated (reversed) magnetic field associated with the laser-produced-plasma shock greatly influences the shock behaviour. (39 refs.)

Numerical investigation of the interaction between a plasma stream and a transverse magnetic field See Entry 61625

Assessment of shock-waves convergence-radius in spherical systems of explosion-induced plasma compression See Entry 61673

52.40 PLASMA INTERACTIONS

61652 Formation of electrostatic potential barrier between different plasmas. R.Hatakeyama, Y.Suzuki, N.Sato (Dept. of Electronic Engng., Tohoku Univ., Sendai, Japan).

Phys. Rev. Lett. (USA), vol.50, no.16, p.1203-6 (18 April 1983).

A potential depression is formed between two magnetized plasmas with different electron temperatures and ion species in the absence of electric current passing through them. The depression is deep enough to reflect both groups of electrons, reducing thermal contact between the plasmas. By addition of a magnetic bump to a uniform magnetic field, the potential dip is localized around the mirror point. A dependence of the phenomenon on neutral-gas pressure is also clarified. (12 refs.)

52.40D Electromagnetic wave propagation in plasma

61653 Resonant absorption in a self-consistent density profile at moderate intensities. F.David (Dept. de Phys. Theorique, CENS, Gif-sur-Yvette, France), P.Mora, R.Pellat.

Phys. Fluids (USA), vol.26, no.3, p.747-54 (March 1983).

A model for the nonlinear resonant absorption of an electromagnetic wave in an inhomogeneous collision-dominated plasma at moderate intensities is proposed. The wave propagation equations are numerically solved in the time-independent self-consistent density profile. A density step appears at the critical point, and a surface wave develops which tends to enhance the absorption. Extensions of the model to collisionless situations are given when the damping can be conveniently described by some phenomenological self-consistent collision frequency. Finally the effect of a plasma expansion across the critical density is briefly discussed. (20 refs.)

61654 Efficient way to prevent reflection from stimulated Brillouin backscattering. C.Montes (Centre Nat. de la Recherche Sci. Interaction Laser Matière, Lab. de Phys. de la Matière Condensée, Nice, France).

Phys. Rev. Lett. (USA), vol.50, no.15, p.1129-32 (11 April 1983).

The same physical mechanism which causes stimulated Brillouin backscattering of a laser pulse when interacting with the underdense plasma (in laser fusion systems) can be used to reverse the scattering direction in order to drastically reduce the reflectivity. Forced stimulated rescattering may be obtained by additional radiation pulses or by a multihumped spectrum with each peak down-shifted by twice the acoustic frequency. Analytical four-mode and numerical six-mode models show strong reduction of the reflectivity for the same input intensity. (18 refs.)

61655 Simultaneous Brillouin and Raman scattering in CO₂ laser-plasma interaction. A.A.Offenberger, R.Fedosejevs, W.Tighe, W.Rozmus (Dept. of Electrical Engng., Univ. of Alberta, Edmonton, Alberta, Canada).

Phys. Scr. (Sweden), vol.T2, no.2, p.498-505 (1982). [received: April 1983] (1982 International Conference on Plasma Physics, Goteborg, Sweden, 9-15 June 1982).

The authors report on experimental and theoretical studies of stimulated Brillouin and Raman scattering occurring simultaneously in moderate density, long scale length plasma irradiated by a moderate intensity CO₂ laser beam. Saturated Brillouin (20%) and Raman (0.7%) backscatter are observed, the former as a convective and the latter as an absolute instability. Importantly, it is found both experimentally and theoretically that the presence of ion fluctuations associated with the Brillouin process can profoundly affect the Raman instability. (29 refs.)

61656 Effect of radiating aperture characteristics on results of measurement of plasma pulsation distribution over the wave number spectrum. A.N.Serikov.

Ukr. Fiz. Zh. (USSR), vol.28, no.3, p.388-94 (March 1983). In Russian. Relations are derived for the phase invariant dispersion of a modulated electromagnetic beam that passed through a statistically inhomogeneous plasma and for the weight function of a 'radiating aperture-medium under study-point receiver' system. It is shown that the weight functions of a system with a finite-size radiating aperture can significantly differ from similar ones for waves with a boundless front. When this fact is not taken into account, the plasma pulsation distribution over the wave number spectrum may be measured with an unjustifiably large error. (6 refs.)

Efficiency of free-electron lasers with a scattered electron beam See Entry 61164

Measurement of small-scale density fluctuation in JIPP T-II plasma by millimeter and sub-millimeter wave scattering See Entry 61614

Experimental studies of parametric interaction near quarter critical density See Entry 61632

Discrimination effects in wave parametric interaction in a relativistic electron stream plasma See Entry 61642

Self-excitation of periodic cyclotron instability regimes in a plasma magnetic trap See Entry 61680

Nonlinear phenomena in laboratory and space plasmas See Entry 64301

52.40F Antennas in plasma; plasma-filled wave guides

61657 Measurement of surface wave dispersion in nonuniform plasma waveguides. V.M.Vorob'ev, A.N.Kondratenko, V.M.Kuklin (A.M. Gor'kii State Univ., Khar'kov, Ukrainian SSR).

Sov. Phys.-Tech. Phys. (USA), vol.27, no.10, p.1301-2 (Oct. 1982). Translation of: *Zh. Tekh. Fiz. (USSR)*, vol.52, no.10, p.2116-18 (Oct. 1982). [received: April 1983]

Considers how a nonuniform plasma density distribution affects surface wave dispersion for waves propagating in cylindrical and planar plasma waveguides. Quasielectrostatic nonsymmetric oscillations in a free radially nonuniform waveguide of radius R filled with cold plasma, and nonpotential RF waves in a semiinfinite nonuniform plasma are dealt with. Changes in the degree of plasma nonuniformity near the waveguide boundary greatly distort the dispersion characteristics of surface oscillations. (2 refs.)

52.40H Solid-plasma interactions

61658 Recent results obtained by use of accelerators on plasma edge properties in controlled fusion devices and on properties of high power neutral beams. R.A.Langley (Fusion Energy Div., Oak Ridge Nat. Lab., Oak Ridge, TN, USA).

IEEE Trans. Nucl. Sci. (USA), vol.ns-30, no.2, p.1187-92 (April 1983). (1982 IEEE Conference on the Application of Accelerators in Research and Industry, Denton, TX, USA, 8-10 Nov. 1982).

The study of plasma-wall interactions is of primary importance in present fusion devices. Measurements of incident fuel and impurity fluxes, retention and release of fuel atoms, and erosion of internal components are of particular interest. Accelerators in the megaelectronvolt range are being used both to measure the depth profile of fuel atoms implanted in samples placed in the plasma edge by use of nuclear reactions and to measure impurities and film thicknesses by use of elastic scattering reactions. Secondary ion mass spectrometry (SIMS) is used to determine flux and energy distributions of fuel atoms and to measure species composition and impurities in the beams of high power neutral beam injectors. Recent results obtained with these techniques are presented and areas of future study are discussed. (30 refs.)

61659 Retention and recycling of plasma edge hydrogen isotopes in C and TiC. D.K.Brice, B.L.Doyle, W.R.Wampler, S.T.Picraux (Sandia Nat. Labs., Albuquerque, NM, USA), L.G.Haggmark.

J. Nucl. Mater. (Netherlands), vol.114, no.2-3, p.277-91 (Feb. 1983).

The retention, release, and isotopic exchange of hydrogen, deuterium, and tritium incident on room temperature C and TiC with Maxwellian velocity and isotropic angular distributions have been calculated using the Local Mixing Model. The calculations are based on the hydrogen saturation concentration, range distributions and isotopic exchange behavior, all of which have been verified experimentally by monoenergetic implants. Particle fluences (10^{16} to $10^{20}/\text{cm}^2$) and characteristic Maxwellian energies (50 eV to 3200 eV) were chosen in the range of interest for Tokamak plasma edge conditions. The results of these calculations are used to estimate tritium inventory build-up and to predict tritium changeout rates by isotopic exchange in Tokamaks and other fusion devices. Tritium inventories in the TiC components (which comprise $\geq 20\%$ of the TFTR first-wall surface) are anticipated to remain at reasonable levels in TFTR, and isotopic exchange is shown to be a feasible method to reduce these tritium inventories. (16 refs.)

61660 Sputtering of titanium and niobium hydrides. Y.Hirooka (Graphite Res. Lab., JAERI, Ibaraki, Japan), H.Shinmura, T.Sano.

J. Nucl. Mater. (Netherlands), vol.114, no.2-3, p.341-3 (Feb. 1983).

Since titanium has recently been proposed as an impurity gettering film to be deposited on vacuum walls because of its high absorptivity to gases, and over the last several years niobium has also been considered to be one of the candidate structural materials for fusion reactors, the authors considered it to be of interest from a fusion technology viewpoint to investigate sputtering behavior of these metals with certain hydrogen contents. Specimens used were cold rolled titanium and niobium sheets having the respective hydrogen concentration ranges of 0.0 to 1.0 and 0.0 to 0.7 in terms of the atomic ratio H/M. (20 refs.)

Plasma convection and line-tying See Entry 61616

Experimental evidence of temperature gradient effects on the neutral gas penetration into a magnetized rotating plasma See Entry 61648

Surface density profile of the one-component plasma See Entry 61690

52.40K Sheaths

61661 Numerical double layer solutions with ionisation. D.Andersson (Dept. of Plasma Phys., Royal Inst. of Technol., Stockholm, Sweden), J.Sorensen.

J. Phys. D (GB), vol.16, no.4, p.601-11 (14 April 1983).

Maxwell's equation $\text{div } D = \rho$ in one dimension is solved numerically, taking ionisation into account. Time independent anode sheath and double-layer solutions are obtained. By varying voltage, neutral gas pressure, temperature of the trapped ions on the cathode side and density and temperature of the

trapped electrons on the anode side, diagrams are constructed that show permissible combinations of these parameters. Results from a recent experiment form a subset. Distribution functions, the Langmuir condition, some scaling laws and a possible application to the lower ionosphere are discussed. (12 refs.)

61662 Kinetic theory of phase space vortices and double layers. H.Schamel (Inst. für Theoretische Phys., Ruhr-Univ. Bochum, Bochum, Germany).

Phys. Scr. (Sweden), vol.T2, no.1, p.228-37 (1982). (1982 International Conference on Plasma Physics, Göteborg, Sweden, 9-15 June 1982).

The time-stationary theory of phase space holes and double layers is reviewed. Smooth solutions of the Vlasov-Poisson-system for electron and ion-holes, and two kinds of double layers are presented and discussed. Both types of holes are shown to be nonlinear extensions of slow acoustic modes. They appear due to a distortion of the relevant distribution in the resonant region, thereby forming a vortex structure in phase space. The holes are found to be unstable with respect to transverse perturbations. In contrast to electron holes which can acquire any strength, the electrostatic energy associated with ion holes is limited by the electron thermal energy. In addition, a finite temperature ratio ($T_e/T_i \geq 3$) is required for ion holes to exist. An interpretation of ion acoustic double layers which are observed in current-driven simulations in terms of asymmetric ion holes is given. The solution for the monotonic double layer, which is found experimentally in beam or voltage-driven plasmas, proves the necessity of four kinds of beam-type distributions for free and trapped electrons and ions, respectively. The 'Bohm criterion' is justified from the kinetic point of view, and the 'Langmuir condition' is shown to be preferred by stability arguments. The scaling law for the width of strong double layers is confirmed analytically. Finally, a scenario of double layer formation suggested by recent particle simulations is sketched, in which electron reflection and current reduction play a dominant role. (77 refs.)

A review of double layer simulations See Entry 64373

52.40M Beam interactions in plasma

61663 Cyclotron excitation of fast magnetosonic waves by circulating thermonuclear alpha particles in a Tokamak. T.D.Kaladze, A.B.Mikhailovsky (I.N. Vekua Inst. of Appl. Math., Tbilisi State Univ., Tbilisi, USSR).

Phys. Lett. A (Netherlands), vol.94A, no.6-7, p.293-4 (21 March 1983). Resonant interaction of fast magnetosonic waves with circulating thermonuclear α -particles in a Tokamak reactor is theoretically investigated. It is shown that such an interaction causes an instability whose growth rate is higher than those of the instabilities considered so far. (8 refs.)

61664 Nonlinear energy flow in a beam-plasma system. D.A.Wheeler, R.L.Stenzel (Dept. of Phys., Univ. of California, Los Angeles, CA, USA).

Phys. Rev. Lett. (USA), vol.50, no.15, p.1133-6 (11 April 1983). The three-dimensional character of the beam-plasma instability is investigated. The true beam-electron distribution function is resolved with a novel directional energy analyzer. The electron plasma waves ($\omega \approx \omega_{pe} \gg \omega_{pi}$) are observed to develop a large spread in perpendicular wave numbers ($k_{\perp} \approx k_{\parallel}$) and damp in a relatively short distance producing an energetic electron tail on the background distribution. The damping is believed to be due to strong ion fluctuations which produce an anomalous resistivity. (13 refs.)

61665 Computer simulation on the scattering of electron beams in a plasma. H.Amamiya (Plasma Phys. Lab., Inst. Phys. & Chem. Res., Saitama, Japan).

Sci. Pap. Inst. Phys. & Chem. Res. (Japan), vol.76, no.4, p.83-95 (Dec. 1982).

Computer simulation on a one dimensional beam-plasma interaction is done in order to understand the nonlinear behavior of the primary electrons in low pressure discharge plasmas, where the beam is neither small in density nor cold. The particle-in-cell model is used with the electron represented as a charged rod with a length of one Debye length and a uniform charge, to see only the effect of collective modes. The dispersion of the excited wave agrees qualitatively well with the linear theory. The temporal behavior of the wave and the spatial variations of beam velocity and electric field are compared with the trapping theory, and some different features from those of the single wave theory for a small and cold beam are shown. The time-average beam velocity distribution function exhibits a splitting structure superimposed on a stochastic broadening. (37 refs.)

61666 Coherent electromagnetic radiation of an electron-ion beam. I.V.Bachin, V.V.Krasovitskii.

Ukr. Fiz. Zh. (USSR), vol.28, no.3, p.371-4 (March 1983). In Russian. Nonlinear electromagnetic oscillations are considered which arise due to electron-ion beam interaction with the field of a slow electromagnetic wave. It is shown that the polarization field due to nonlinear collective inhibition of an electron beam relative to an ion one exerts a significant effect on the process of instability development under conditions of an anomalous Doppler effect at low density of the background plasma. As a result the energy density for a coherent electron-ion beam radiation may be considerably higher than the analogous value for an electron beam. (4 refs.)

Gravitational radiation of plasma in a magnetic field See Entry 59644

High efficiency ionization of low-density elements in beam-plasma type ion sources See Entry 60503

Dynamics of pulsed ion beam production by a plasma lens See Entry 61070

Efficiency of free-electron lasers with a scattered electron beam See Entry 61164

Measurement of growth rate of plasma drift wave excited by slow electrons See Entry 61630

Nonlinear effects in a beam plasma system: second harmonic emission and density depression formation See Entry 61639

Intense relativistic electron beam injector system for Tokamak current drive See Entry 61675

52.50 PLASMA PRODUCTION AND HEATING

61667 An analysis of the induction plasma heating in the microwave frequency range. E.Reszke (Inst. of Telecommunication & Acoustics, Tech. Univ. of Wrocław, Wrocław, Poland).

Mater. Sci. (Poland), vol.7, no.4, p.453-61 (1981).

The simple theoretical model of the high pressure H-type microwave discharge and some exemplary results of calculations for nonflowing atmospheric pressure oxygen plasma are presented. In the analysis the existence of the LTE state in plasma has been assumed and only one component of the HF magnetic field parallel to the axis of the cylindrical plasma column has been considered. Using a numerical procedure the self-consistent system of differential equations has been solved giving typical distributions of electromagnetic

and temperature fields. The boundary conditions for heat transfer from plasma to the quartz tube surrounding the discharge were introduced analytically in order to find the real plot of the axial plasma temperature versus the density of the microwave energy absorbed. The results turn out to be useful for the future development of the new kind of microwave plasmatrons with the H-type discharges. (7 refs.)

61668 Vaporization mode and state of the ablatant of a deuterium pellet in Tokamak discharges. C.T.Chang (Riso Nat. Lab., Roskilde, Denmark).

Phys. Fluids (USA), vol.26, no.3, p.805-7 (March 1983).

The ablation of a deuterium pellet under prevailing Tokamak discharge conditions is shown to be a dynamic phase transition process. An alternative boundary condition at the pellet surface is formulated. Computational results based on the new boundary condition showed that the state of the ablatant in the subsonic region depends on the boundary condition used but is hardly affected in the supersonic region. The scaling law of the pellet ablation rate, therefore, is insensitive to the boundary condition imposed. (6 refs.)

A simple ablative implosion model—shell dynamics See Entry 60397

The technical concept of the ASDEX UG poloidal field coils See Entry 60435

Time evolution of the coil currents shaping and centering a D-shaped reactor plasma See Entry 60452

Influence of collisions and incoherence on ion-cyclotron transport in mirror plasmas See Entry 61617

Thermal cavitons See Entry 61638

Theory of heating and compression of double-shell spherical targets exposed to a laser pulse See Entry 61672

Electron confinement studies on the EBT-S Bumpy Torus experiment using soft X-ray techniques See Entry 61678

Control system of plasma position and current in a Tokamak with strong magnetic field See Entry 61709

Plasma parameter control experiments on 'Tuman-3' See Entry 61710

52.50J Plasma production and heating by laser beams

61669 Hot-electron energy deposition in CO₂-laser-irradiated targets consistent with magnetic-field-induced surface transport. J.C.Kieffer, H.Pépin, M.Piche, J.P.Matte, T.W.Johnston, P.Lavigne, F.Martin (Inst. Nat. de la Recherche Sci.-Energie, Univ. du Québec, Varennes, Québec, Canada), R.Decoste.

Phys. Rev. Lett. (USA), vol.50, no.14, p.1054-7 (4 April 1983).

Hard-X-ray continuum spectra from high-Z tracers are used to obtain lateral and axial energy-deposition profiles by hot electrons in CO₂-laser-irradiated slab targets. The interpretation of the results emphasizes a local direction of incidence of the hot electrons on the target and an energy-deposition pattern which are consistent with self-generated magnetic fields. (17 refs.)

61670 Towards upper bound levels: thermonuclear fusion. J.Vedel (Centre d'Etudes de Limeil, Villeneuve-Saint-Georges, France).

Rev. Gen. Electr. (France), no.2, p.89-95 (Feb. 1983). In French.

Introduces the use of power lasers to achieve controlled thermonuclear fusion. After describing thermonuclear fusion and the conditions of temperature density and duration, required to bring it into being, the author shows how the laser enables such conditions to be created. In order to illustrate the importance of a laser which will be used for studying the production of fusion reactions, he describes the neodymium-doped glass laser NOVA that is being installed at the Livermore Laboratory in the USA; at the time of its completion in 1984, this laser will be the most powerful in the world. In comparison the OCTAL laser in operation at the Limeil establishment Centre d'Etudes de Commissariat Français à l'Energie Atomique is more modest; it is also presented. To conclude the author presents a project for a thermal power station with a fusion reactor as heat source. Energy from fusion is recovered by liquid lithium which regenerates the consumed tritium through a nuclear reaction with emitted neutrons. (5 refs.)

61671 Plasma production during vaporization of materials by the radiation from a CO₂ TEA laser. S.V.Gaponov, M.D.Strikovskii (Inst. of Appl. Phys., Acad. of Sci., Gorki, USSR).

Sov. Phys.-Tech. Phys. (USA), vol.27, no.9, p.1127-30 (Sept. 1982). Translation of: *Zh. Tekh. Fiz. (USSR)*, vol.52, no.9, p.1838-42 (Sept. 1982).

[received: April 1983]

The energy and space and time dependence are investigated for a laser flare. Two qualitatively different regimes are discovered for the ejection of the plasma, where the transition between them has a threshold character (in the radiation flux density). The measured dependence of the threshold on the atomic number of the target element has a form which is indicative of a connection between the dynamics of the flare formation and the electronic structure of the atom. A model is proposed for interpreting this effect. (10 refs.)

61672 Theory of heating and compression of double-shell spherical targets exposed to a laser pulse. N.G.Basov, E.G.Gamali, S.Yu.Gus'kov, V.B.Rozanov (P.N. Lebedev Phys. Inst., Acad. of Sci., Moscow, USSR).

Sov. J. Quantum Electron. (USA), vol.12, no.10, p.1268-73 (Oct. 1982). Translation of: *Kvantovaya Elektron. Moskva (USSR)*, vol.9, no.10, p.1945-54 (Oct. 1982). [received: April 1983]

A theory is proposed for the acceleration, heating and compression of a double-shell target exposed to a laser pulse. It is shown that in the hydrodynamic regime the inner shell may be accelerated to velocities of ~ 200 km/sec, the energy density in the central stage may be increased whilst maintaining a high plasma density, and ultimately an inhomogeneous laser plasma configuration may be achieved, this being required for the evolution of a self-sustaining wave of fusion reactions. Depending on the aim of the experimental investigations (achieving a high plasma density of temperature), various systems for matching the parameters of a double-shell target with the characteristics of the laser pulse are proposed. (17 refs.)

X-ray generation from laser-produced plasmas and its atomic-number dependence See Entry 61620

Ion-ion two-stream instability in multispecies laser-produced plasma See Entry 61631

Characteristics of oblique shock waves produced in an expanding laser plasma See Entry 61651

Spectra of highly ionized atoms in hot plasmas: conditions for production and observation See Entry 61704

Processes occurring in an erosion plasma during laser vacuum deposition of films. III. Condensation in gas flows during laser vaporization of materials See Entry 63161

52.50L Plasma production and heating by shock wave and wire explosion

61673 Assessment of shock-waves convergence-radius in spherical systems of explosion-induced plasma compression. K.Jach (S. Kaliski Inst. of Plasma Phys. and Laser Microfusion, Warsaw, Poland).

J. Tech. Phys. (Poland), vol.22, no.4, p.407-13 (1981).

In order to effect real quantitative assessments of e.g. the neutron yield in microfusion systems, it is necessary to define a radius referred to as the convergence radius, for which the self-similar solution maintains its validity. It is shown that, in spherical symmetry, the radiation-induced limitation is stronger than the conduction-induced one. In cylindrical symmetry, the two dissipative effects are found to be competitive. (10 refs.)

61674 Analysis of axial-outflow in cylindrical deuterium-plasma sample compressed radially by imploding liner. A.Galkowski, R.Swierczynski, E.Wlodarczyk.

J. Tech. Phys. (Poland), vol.22, no.4, p.443-53 (1981).

The explosion-driven cylindrical layered system is considered. The problems of hydrodynamic outflow and of defining the zone of one-dimensional motion of plasma are analysed. (9 refs.)

Experimental studies on biconical, explosion-driven thermonuclear-fusion system See Entry 60395

Generation of pulses of intense magnetic field with up to 350 Tesla induction by the method of explosion-produced compression See Entry 60396

52.55 PLASMA EQUILIBRIUM AND CONFINEMENT

61675 Intense relativistic electron beam injector system for Tokamak current drive. V.L.Bailey, J.M.Creedon, B.M.Ecker, H.I.Helava (Phys., Internat. Co., San Leandro, CA, USA).

J. Appl. Phys. (USA), vol.54, no.4, p.1656-65 (April 1983).

The authors report experimental and theoretical studies of an intense relativistic electron beam (REB) injection system designed for Tokamak current drive experiments. The injection system uses a standard high-voltage pulsed REB generator and a magnetically insulated transmission line (MITL) to drive an REB-accelerating diode in plasma. A series of preliminary experiments has been carried out to test the system by injecting REBs into a test chamber with preformed plasma and applied magnetic field. REBs were accelerated from two types of diodes: a conventional vacuum diode with foil anode, and a plasma diode, i.e. an REB cathode immersed in the plasma. REB current was in the range of 50 to 100 kA and REB particle energy ranged from 0.1 to 1.0 MeV. MITL power density exceeded 10 GW/cm². Performance of the injection system and REB transport properties is documented for plasma densities from 5×10^{12} to 2×10^{14} cm⁻³. Injection system data are compared with numerical calculations of the performance of the coupled system consisting of the generator, MITL, and diode. (42 refs.)

61676 Plasma behaviors in the open field region of reversed-field theta-pinch. Y.Aso, K.I.Hirano (Inst. of Plasma Phys., Nagoya Univ., Nagoya, Japan).

J. Phys. Soc. Jpn. (Japan), vol.52, no.4, p.1095-7 (April 1983).

A characteristic behavior of the plasma in an open field region of reversed field theta pinch has been studied with the guide field (GF) which extends the field line along the axial direction. The experimental result suggests that the rotational instability may be induced after the plasma touches the wall at the ends of the open field. (3 refs.)

61677 Synchrotron emission from a relativistic loss-cone distribution with application to the ELMO Bumpy-Torus experiment. D.Winske, D.A.Boyd (Lab. for Plasma, Univ. of Maryland, College Park, MD, USA).

Phys. Fluids (USA), vol.26, no.3, p.755-65 (March 1983).

Analytic expressions for the power emitted per unit volume per solid angle per unit frequency at perpendicular propagation as synchrotron radiation from a relativistic loss-cone distribution of electrons are derived and compared with exact numerical results. These expressions are useful for understanding how the radiation scales and for inferring properties of the plasma from measurements of the radiation. As an example, it is shown that the temperature and loss-cone angle of the electron distribution in the ELMO Bumpy Torus (EBT) ring can be determined in a straightforward fashion from the ratio of radiation in the two polarizations at two frequencies. Also, it is demonstrated that the loss-cone angle can be determined from the frequency at which this emission ratio is a minimum, even if the emission ratio itself cannot be measured very accurately. (23 refs.)

61678 Electron confinement studies on the EBT-S Bumpy Torus experiment using soft X-ray techniques. D.L.Hillis, G.R.Haste, L.A.Berry (Oak Ridge Nat. Lab., Oak Ridge, TN, USA).

Phys. Fluids (USA), vol.26, no.3, p.820-9 (March 1983).

Soft X-ray bremsstrahlung measurements have been performed on the ELMO Bumpy Torus (EBT-S) plasma to determine the electron temperature T_e and electron density n_e using a calibrated Si(Li) detector over a wide range of operating conditions. The purpose of this paper is to outline the necessary assumptions and essential X-ray techniques that are inherent in soft X-ray measurements in order to investigate the electron heating and confinement properties of EBT-S. In addition, by utilizing the electron density as determined by the soft X-ray measurements, the previous EBT-S confinement analyses have been extended. The steady-state plasma of EBT-S is heated by microwaves using a continuous wave (CW) gyrotron that can operate up to power levels of 200 kW. From the soft X-ray measurements, both the electron temperature and density are found to increase at higher microwave power levels. For operation at microwave power levels of 200 kW, T_e approaches 1 keV while n_e approaches 1.2×10^{12} cm⁻³. In general, confinement properties are found to improve with increased microwave power. The data are compared with neoclassical transport scaling and the electron transport is found to be collisionless ($\nu/\Omega < 1$) as well as neoclassical. (26 refs.)

61679 Forced magnetic reconnection. R.M.Kulsrud, T.S.Hahm (Plasma Phys. Lab., Princeton Univ., Princeton, NJ, USA).

Phys. Scr. (Sweden), vol.T2, no.2, p.525-8 (1982). [received: April 1983]

(1982 International Conference on Plasma Physics, Goteborg, Sweden, 9-15 June 1982).

It has been generally accepted that a toroidal magnetostatic equilibrium can be specified by giving its boundary, the general topology of the magnetic field, and the distribution of mass. For example, if it is assumed that the magnetic field lies on nested toroidal magnetic surfaces and the pressure is given on each surface, then a unique equilibrium with these properties exists. In actual fact this need not be the case. If such an equilibrium exists, then by changing the state of the boundary in a manner that effectively resonates with the closed lines on one of the rational surfaces and demanding identical topology, a new equilibrium is produced that has surface currents on this

resonant surface. Equilibria which are exactly axisymmetric have nested toroidal surfaces. But it is obviously impossible to set up such exact surfaces so it is reasonable to expect that toroidal equilibria need not have nested magnetic surfaces, even of a nonsymmetric kind. Grad arrived at his conclusions from very general mathematical considerations and also from experience in numerical determination of equilibria such as in the Doublet. It was not possible for him to follow the evolution of equilibria in time because of the complexity of the general situation. Taylor suggested a much simpler model which brought out these problems in a much more explicit manner. The authors describe Taylor's model and then give the explicit evolution in time of the MHD system as it passes to a new equilibrium. (4 refs.)

61680 Self-excitation of periodic cyclotron instability regimes in a plasma magnetic trap. P.A.Bespalov (Inst. of Appl. Phys., Acad. of Sci., Gorky, USSR).

Phys. Scr. (Sweden), vol.T2, no.2, p.576-9 (1982). [received: April 1983]

(1982 International Conference on Plasma Physics, Goteborg, Sweden, 9-15 June 1982).

Steady-state cyclotron radiation of extraordinary electronic waves (whistlers) may be unstable in a plasma trap with magnetic mirrors. The periodic self-modulation of cyclotron instability takes place for a certain (sufficiently small) power of a particle source and a certain angular dependence of its parameters. This modulation is due to the change in the distribution function anisotropy. The change in anisotropy has an effect similar to that of an optic nonlinear filter. The characteristics of the spike-like periodic cyclotron instability regime are found. (12 refs.)

61681 Plasma stability in the axisymmetric open-ended systems.

V.V.Arsenin (I.V. Kurchatov Inst. of Atomic Energy, Moscow, USSR).

Phys. Scr. (Sweden), vol.T2, no.2, p.580-4 (1982). [received: April 1983]

(1982 International Conference on Plasma Physics, Goteborg, Sweden, 9-15 June 1982).

Different methods of plasma stabilization in axisymmetric mirrors are described. Some stabilizing mechanisms of MHD and kinetic nature are discussed for rather long systems. (21 refs.)

61682 Study of poloidal magnetic fields in the Tuman-3 Tokamak.

V.A.Belyakov, V.I.Vasil'ev, A.G.Kolchin, Yu.A.Kostov, R.N.Litunovskii, O.A.Minayev, M.P.Gryaznevich, N.V.Sakharov, A.N.Kozyrev, K.G.Shakhovets, A.A.Fedorov.

Sov. Phys.-Tech. Phys. (USA), vol.27, no.10, p.1196-9 (Oct. 1982).

Translation of: *Zh. Tekh. Fiz. (USSR)*, vol.52, no.10, p.1946-52 (Oct. 1982). [received: April 1983]

Results are reported from measurements of the poloidal magnetic fields in the Tuman-3 Tokamak. The iron core of the magnetic conductor inside the plasma-filled region (aspect ratio $R/a=2.3$) greatly influences the conditions needed to sustain an equilibrium plasma column. The experimental data are compared with calculations obtained by solving a magnetostatic problem in the axisymmetric approximation. The calculated results for the model magnetic conductor agree with the experimental data to within ~5%. For the configuration studied, the poloidal field sustained a stable equilibrium plasma column of large radius with small vertical instability; the cross section of the plasma column was nearly circular. Under the experimental conditions, the parameters of the poloidal magnetic field depend only weakly on the degree of saturation of the iron core. The measurements are used to design a system for controlling the position of the plasma column. (1 ref.)

61683 Diffusion losses of ions and electrons in the 'Jupiter-1A' electromagnetic trap. I.A.Stepanenko, A.D.Komarov.

Ukr. Fiz. Zh. (USSR), vol.28, no.3, p.395-400 (March 1983). In Russian.

Electron and ion diffusion currents out of an electromagnetic trap were investigated. Diffusion losses of electrons along the magnetic field amounted to 3÷30% of an integral electron losses and decreased exponentially with the cutoff voltage increase. The transverse diffusion of low-energy electrons trapped in the line cusp area is the main part of an electron loss. The characteristic frequency of this process is of the same order of magnitude as an electron-ion collision frequency. Ion losses through the line cusp are the main part of integral ion losses. Anomalous transverse diffusion losses were found in the near-axial area. The transverse ion losses accounted for a considerable part (25%) of the integral losses. (7 refs.)

61684 Tokamak disruptions. J.A.Wesson, A.Sykes, M.F.Turner.

Report CLM-R 233, UKAEA, Culham, Abingdon, Oxon., England (1982), 9 pp.

Available from HMSO, London, England.

An explanation is given for the occurrence of Tokamak disruptions. Under normal conditions the tearing instability is self-stabilising through its reduction of the destabilising current gradient and a saturated state can then exist. However, under certain conditions further growth of the instability is itself destabilising and a disruption results. The transition to disruption has the form of a catastrophe. (9 refs.)

61685 Computational methods for 3D nonlinear magnetohydrodynamics.

O.Betancourt (Courant Inst., New York Univ., New York, NY, USA).

10th IMACS World Congress on System Simulation and Scientific Computation, Montreal, Canada, 8-13 Aug. 1982 (New Brunswick, NJ, USA: IMACS 1982), p.177-8 vol.4

Computational methods are described to investigate the equilibrium and stability of a toroidal plasma in three dimensions, based upon the variational principle of magnetohydrodynamics. (9 refs.)

61686 The computational model for the control of plasma position in TEXTOR. A.Kalek (Inst. fur Plasmaphys., KFA, Julich GmbH, Julich, Germany).

Fusion Technology 1982. Proceedings of the Twelfth Symposium, Julich, Germany, 13-17 Sept. 1982 (Oxford, England: Pergamon 1983), p.1197-201 vol.2

Approximate equations describing the axisymmetric motion of the circular TEXTOR plasma without inertial terms are derived and discussed. Since TEXTOR has an iron-core transformer, the mutual inductances and their spatial derivatives had to be calculated by the POISSON code of Winslow (1966) which was improved by the ICCG method of DS Kershaw (1978). Also eddy currents in the vacuum vessel had to be calculated by a computer code. Positional stability and stabilization by eddy currents are considered, and the requirements on the feedback control system are ascertained. The equations resulting from this work have been the basis for the design of the feedback system of TEXTOR. (10 refs.)

61687 Equilibrium and stability of plasma motion in an iron-core Tokamak. A.V.Kuznetsov, R.N.Litunovskii, O.A.Minayev, P.P.Teplov (D.V. Efremov Sci. Res. Inst. of Electrophysics, Apparatus, Leningrad, USSR).

Fusion Technology 1982. Proceedings of the Twelfth Symposium, Julich, Germany, 13-17 Sept. 1982 (Oxford, England: Pergamon 1983), p.1203-7 vol.2

In developing and investigating the control system of the plasma position and current in a Tokamak, the main tasks are as follows: the main mode calculation

tion of the supply system of the poloidal field coils; the investigation of plasma motion stability. The first task can be solved by means of a magnetostatic code. It is preferable to use the dynamic mode calculation, which allows determination of the 'equilibrium' currents and voltages of the poloidal field coils. The calculation technique, applied to investigate the T-15 plasma position control system, is discussed. Similar calculations have been accomplished for the steep-type torus 'Tuman-3'. Results are compared with the experimental data, obtained for the ohmic heating Tokamak operation. In an iron-core Tokamak the effect of plasma attraction to the core changes greatly the horizontal motion picture. Results of the plasma motion stability in T-15 and 'Tuman-3' are presented. The operation conditions of 'Tuman-3' at the discharge start, when the inductor current is near zero and the magnetic flux is 'frozen' by the chamber current are discussed in detail. The experimental data of the plasma position control system for 'Tuman-3' are given. (3 refs.)

61688 Experience with feedback and feedforward for plasma control in ASDEX. F.Schneider (Max-Planck-Inst. für Plasmaphys., Garching, Germany).

Fusion Technology 1982. Proceedings of the Twelfth Symposium, Julich, Germany, 13-17 Sept. 1982 (Oxford, England: Pergamon 1983), p.1227-32 vol.2

Experimental results of vertical and radial position feedback are shown and discussed. In particular, stability problems of vertical position control are studied in detail. A feedforward procedure for the process computer is described and proved by measurements. (5 refs.)

61689 Applicability verification of Tokamak plasma equilibrium control models. K.Yoshioka, T.Kobayashi, M.Abe, S.Uchikawa, K.Takemaru (Energy Res. Lab., Hitachi Ltd., Hitachi, Japan).

Fusion Technology 1982. Proceedings of the Twelfth Symposium, Julich, Germany, 13-17 Sept. 1982 (Oxford, England: Pergamon 1983), p.1233-8 vol.2

The applicability of dynamic models used to evaluate the control performance of plasma equilibrium position is verified through the use of data obtained in experiments with the Hitachi Tokamak HT-1. The major radius of the plasma in the HT-1 is 0.35 m. Emphasis has been placed on the evaluation of the behavior of eddy currents on surrounding structures and on the evaluation of changes in the minor radius due to plasma displacement. A integral formulation of Maxwell equations has been solved numerically to evaluate eddy current behavior on the vacuum vessel and supporting disk. The calculated values obtained for the magnetic fields generated by the eddy currents agree with the measured values obtained for those fields with an error of about 10%. Feedback control gains of the HT-1 are adjusted on the basis of the results obtained from the models and phase margin criterion. The position of the plasma is regulated to within 5.0 mm of the desired position. (8 refs.)

Generation of pulses of intense magnetic field with up to 350 Tesla induction by the method of explosion-produced compression See Entry 60396

Inertial confinement fusion See Entry 60399

The TORE SUPRA poloidal field system See Entry 60448

Efficiency of passive circuits for vertical stability in INTOR reactor See Entry 60449

Measurement and dynamic control of plasma position in TEXTOR Tokamak See Entry 60450

The FTU poloidal field system See Entry 60451

Time evolution of the coil currents shaping and centering a D-shaped reactor plasma See Entry 60452

Particle orbits and stochasticity See Entry 61605

Measurements of collisional excitation rate coefficients for Fe X ions in a plasma See Entry 61607

Influence of collisions and incoherence on ion-cyclotron transport in mirror plasmas See Entry 61617

Transport modelling in magnetic confinement experiments See Entry 61619

Propagation of lower hybrid resonance cones in Tokamaks See Entry 61626

Tearing modes in a general cross-section force-free cylindrical Tokamak See Entry 61627

Magnetohydrodynamic stability of magnetic slabs See Entry 61628

Resistive MHD stability in Tokamaks See Entry 61643

Experimental evidence of temperature gradient effects on the neutral gas penetration into a magnetized rotating plasma See Entry 61648

Formation of electrostatic potential barrier between different plasmas See Entry 61652

Retention and recycling of plasma edge hydrogen isotopes in C and TiC See Entry 61659

Cyclotron excitation of fast magnetosonic waves by circulating thermonuclear alpha particles in a Tokamak See Entry 61663

Numerical simulation of slow spheromak formation: flux control by formation speed See Entry 61691

3D nonlinear initial value calculations in resistive MHD See Entry 61693

Simulation of plasma formation and attainment of equilibrium See Entry 61694

Magnetic fusion energy and computers See Entry 61695

Control system of plasma position and current in a Tokamak with strong magnetic field See Entry 61709

Plasma parameter control experiments on 'Tuman-3' See Entry 61710

T-15 poloidal field control system See Entry 61711

52.60 RELATIVISTIC PLASMA

Collisionless relaxation of phase oscillations of trapped particles in an accelerating amplitude-modulated wave See Entry 61641

Discrimination effects in wave parametric interaction in a relativistic electron stream plasma See Entry 61642

52.65 PLASMA SIMULATION

61690 Surface density profile of the one-component plasma. J.P.Badiali, M.L.Rosinberg (CNRS, Phys. des Liquides et Electrochimie, Univ. Pierre et Marie Curie, Paris, France), D.Levesque, J.J.Weis.

J. Phys. C (GB), vol.16, no.11, p.2183-95 (20 April 1983). Monte Carlo computations of the surface density profile and the surface energy of the classical one-component plasma have been made for different values of the plasma parameter Γ . Two different situations are considered: when the ions are in contact with an impenetrable wall and when they are

confined by the background itself. In the former case, comparison is made with the predictions of the integral equations based on the hypernetted chain and mean spherical approximations. The influence of the width of the background profile is also examined. (15 refs.)

61691 Numerical simulation of slow spheromak formation: flux control by formation speed. T.Sato (Inst. for Fusion Theory, Hiroshima Univ., Hiroshima, Japan), A.M.M.Todd, H.Okuda.

Phys. Fluids (USA), vol.26, no.3, p.775-9 (March 1983). Two-dimensional magnetohydrodynamic simulations of the Princeton S-1 Spheromak have been carried out for several formation speeds. It is found that the spheromak size and shape, and hence the confined poloidal and toroidal fluxes, are largely dependent upon the formation speed, provided this is moderately slow. Specifically, the total toroidal and poloidal fluxes in a spheromak increase as the formation speed is reduced. The role of externally driven reconnection as a cause for this dependence is discussed. (13 refs.)

61692 Particle simulation of plasmas. J.M.Dawson (Dept. of Phys., Univ. of California, Los Angeles, CA, USA).

Rev. Mod. Phys. (USA), vol.55, no.2, p.403-47 (April 1983). For plasma with a large number of degrees of freedom, particle simulation using high-speed computers can offer insights and information that supplement those gained by traditional experimental and theoretical approaches. The technique follows the motion of a large assembly of charged particles in their self-consistent electric and magnetic fields. With proper diagnostics, these numerical experiments reveal such details as distribution functions, linear and nonlinear behavior, stochastic and transport phenomena and approach to steady state. Such information can both guide and verify theoretical modeling of the physical processes underlying complex phenomena. It can also be used in the interpretation of experiments. (105 refs.)

61693 3D nonlinear initial value calculations in resistive MHD. J.A.Holmes, H.R.Hicks, B.A.Carreras, L.Garcia, V.E.Lynch, B.F.Masden (Computer Sci., Oak Ridge Nat. Lab., Oak Ridge, TN, USA).

10th IMACS World Congress on System Simulation and Scientific Computation, Montreal, Canada, 8-13 Aug. 1982 (New Brunswick, NJ, USA: IMACS 1982), p.183-4 vol.4

An approach to the simulation of the resistive MHD equations in toroidal geometry is described. The equations are solved as an initial value problem using a mixed finite difference-spectral technique in a coordinate system based on the equilibrium magnetic field. A partially implicit first order time integration techniques in order to minimize storage and computational work. (9 refs.)

61694 Simulation of plasma formation and attainment of equilibrium. C.K.Chu (Dept. of Appl. Phys. & Nuclear Engng., Columbia Univ., New York, NY, USA).

10th IMACS World Congress on System Simulation and Scientific Computation, Montreal, Canada, 8-13 Aug. 1982 (New Brunswick, NJ, USA: IMACS 1982), p.185-7 vol.4

Describes the main features and different applications of a two-dimensional magnetohydrodynamic code, that simulates plasma formation and the approach to equilibrium. The essential characteristics and most interesting results from each application are given, and a complete reference is appended for all the applications to date. Future developments and uses are discussed. (13 refs.)

61695 Magnetic fusion energy and computers. J.Killeen (Lawrence Livermore Nat. Lab., Univ. of California, Livermore, CA, USA).

10th IMACS World Congress on System Simulation and Scientific Computation, Montreal, Canada, 8-13 Aug. 1982 (New Brunswick, NJ, USA: IMACS 1982), p.188-90 vol.4

The application of computers to magnetic fusion energy research is essential. In the last several years the use of computers in the numerical modeling of fusion systems has increased substantially. There are several categories of computer models used to study the physics of magnetically confined plasmas. A comparable number of types of models for engineering studies are also in use. To meet the needs of the fusion program, the National Magnetic Fusion Energy Computer Center has been established at the Lawrence Livermore National Laboratory. A large central computing facility is linked to smaller computer centers at each of the major MFE laboratories by a communication network. In addition to providing cost effective computing services, the NMFEEC environment stimulates collaboration and the sharing of computer codes among the various fusion research groups. (2 refs.)

61696 Implicit methods in particle simulation. B.I.Cohen (Lawrence Livermore Nat. Lab., Univ. of California, Livermore, CA, USA).

10th IMACS World Congress on System Simulation and Scientific Computation, Montreal, Canada, 8-13 Aug. 1982 (New Brunswick, NJ, USA: IMACS 1982), p.191-3 vol.4

Surveys recent advances in the application of implicit integration schemes to particle simulation of plasmas. The use of implicit integration schemes is motivated by the goal of efficiently studying low-frequency plasma phenomena using a large timestep, while retaining accuracy and kinetics. Implicit schemes achieve numerical stability and provide selective damping of unwanted high-frequency waves. The author reviews the implicit moment and direct implicit methods. The merging of implicit methods with orbit averaging can result in additional computational savings. (18 refs.)

61697 Multi-dimensional hybrid simulation techniques in plasma physics. D.W.Hewett (Los Alamos Nat. Lab., Los Alamos, NM, USA).

10th IMACS World Congress on System Simulation and Scientific Computation, Montreal, Canada, 8-13 Aug. 1982 (New Brunswick, NJ, USA: IMACS 1982), p.198-200 vol.4

Multi-dimensional hybrid simulation models have been developed for use in studying plasma phenomena on extended time and distance scales. The models make fundamental use of the small Debye length or quasi-neutrality assumption. The ions are modeled by particle-in-cell (PIC) techniques while the electrons are considered a collision-dominated fluid. The fields are calculated in the nonradiative Darwin limit. Some electron inertial effects are retained in the finite electron mass model (FEM). (7 refs.)

The FTU poloidal field system See Entry 60451

Efficiency of free-electron lasers with a scattered electron beam See Entry 61164

Influence of collisions and incoherence on ion-cyclotron transport in mirror plasmas See Entry 61617

Kinetic theory of phase space vortices and double layers See Entry 61662

Computer simulation on the scattering of electron beams in a plasma See Entry 61665

Computational methods for 3D nonlinear magnetohydrodynamics See Entry 61685

A review of double layer simulations See Entry 64373

52.70 PLASMA DIAGNOSTIC TECHNIQUES AND INSTRUMENTATION

- 61698 Two pulse multiple position Thomson scattering system.** S.Sudo, K.Kondo, T.Mutoh, H.Zushi, A.Iiyoshi, K.Uo (Plasma Phys. Lab., Kyoto, Uji, Japan). *Jpn. J. Appl. Phys. Part 1 (Japan)*, vol.22, no.3, p.485-90 (March 1983).
A Thomson scattering system for simultaneous measurements of the electron temperature and density at ten different positions at two times during a single plasma shot has been developed for Heliotron E. The apparatus consists of two ruby lasers each delivering two pulses whose temporal separation is typically 100 ms; light collection optics including automatic positioning mechanisms; 80 detectors; and a data processing system. The author has obtained spatial profiles of T_e (0.05-1.3 keV) and n_e ($0.23\text{-}9.0 \times 10^{19} \text{ m}^{-3}$) in Heliotron E for each plasma shot.
- 61699 Experiments in Belfast relevant to fusion diagnostics.** H.B.Gilbody (Dept. of Pure & Appl. Phys., Queen's Univ. of Belfast, Belfast, N Ireland). *IEEE Trans. Nucl. Sci. (USA)*, vol.ns-30, no.2, p.1201-4 (April 1983). (1982 IEEE Conference on the Application of Accelerators in Research and Industry, Denton, TX, USA, 8-10 Nov. 1982).
A number of ion beam accelerators are being used in this laboratory to study charge transfer, ionization and excitation in ion-atom collision processes at energies ranging from ~ 100 eV to 2500 keV. Techniques include beam-static gas target, intersecting beam and both optical and energy loss/gain spectroscopy. Collisions involving hydrogen atoms are of particular interest. Some of the measurements are relevant to the diagnostics and modelling of high temperature plasmas in magnetic confinement devices and to schemes to promote inertial fusion by heavy ions. (37 refs.)
- 61700 Applications of recent measurements of low energy charged particles induced nuclear reactions on light nuclei.** F.E.Cecil (Dept. of Phys., Colorado School of Mines, Golden, CO, USA). *IEEE Trans. Nucl. Sci. (USA)*, vol.ns-30, no.2, p.1205-8 (April 1983). (1982 IEEE Conference on the Application of Accelerators in Research and Industry, Denton, TX, USA, 8-10 Nov. 1982).
The author discusses the applications of these reactions to the general problem of the diagnostics of charged and neutral particle beams and of high temperature deuterium and tritium plasmas. The motivation for these applications lies primarily in the crucial role which such beams and plasmas occupy in the contemporary CRT development effort. (4 refs.)
- 61701 On the observability of forbidden lines.** S.O.Kastner, A.K.Bhatia (NASA, Goddard Space Flight Center, Greenbelt, MD, USA). *J. Quant. Spectrosc. & Radiat. Transfer (GB)*, vol.29, no.4, p.369-74 (April 1983).
The disappearance of forbidden lines for O III at intermediate plasma densities may be due to background wing emission of the stronger allowed lines, rather than to Stark broadening of the forbidden lines as suggested recently. The general conclusion is supported that the classical explanation of quenching is erroneous, at least for O III. (6 refs.)
- 61702 Line radiation of highly ionised impurities in plasma produced in the plasma-focus device.** S.Czekaj, W.Kozarkiewicz, W.Skrzeczanski (S. Kaliski Inst. of Plasma Phys. and Laser Microfusion, Warsaw, Poland). *J. Tech. Phys. (Poland)*, vol.22, no.4, p.455-62 (1981).
The authors investigated the plasma spectrum within the X-ray range, and defined the plasma parameters, at the compression phase, on the grounds of an analysis of spectral lines of highly stripped neon, oxygen, nitrogen and carbon ions. The plasma was generated in the F-20 device of the plasma-focus type with bank of capacitors energy equal to 12.5 kJ, and 1.5 Tr pressure of the neon-admixed deuterium. (12 refs.)
- 61703 High-frequency Stark-effect measurements in emission spectroscopy.** N.J.Wiegart (Inst. für Experimentalphys., Ruhr-Univ., Bochum, Germany). *Phys. Rev. A (USA)*, vol.27, no.4, p.2114-19 (April 1983).
The applicability of the high-frequency Stark effect in the diagnostics of turbulent plasmas is demonstrated by measurements of He I line profiles (4^1D-2^1P) in a turbulent linear discharge. The existence of electron plasma waves with field strengths of 6-9 kV/cm is confirmed spectroscopically. Competing effects—e.g. the emission of molecular lines—are discussed in detail and are shown to be negligible under the experimental conditions. (25 refs.)
- 61704 Spectra of highly ionized atoms in hot plasmas: conditions for production and observation.** E.Ya.Kononov (Inst. for Spectroscopy, Acad. of Sci. Troitsk, USSR). *Phys. Scr. (Sweden)*, vol.27, no.2, p.117-24 (Feb. 1983).
Excitation conditions for spectra of highly ionized atoms in the low inductance vacuum spark and laser produced plasma are discussed in this review from the viewpoint of obtaining accurate numerical data on energy structure of electron shells. Some optimum observation conditions and data acquisition methods are suggested. (27 refs.)
- 61705 Space plasma diagnostics.** M.S.Agarwal (Dept. of Electrical Engng., Indian Inst. of Technol., Bombay, India). *Vac News (India)*, vol.13, no.3, p.13-17 (Sept. 1982). [received: March 1983]
The author describes some of the techniques employed for the identification of constituent elements and measurement of charged particle densities and energies, and the magnetic fields. The techniques discussed are electric and magnetic probes, spectral spectroscopy, RF interferometry and mass spectrometry. To test and calibrate the apparatus and devices used, many conditions of space plasma may very closely be simulated in laboratory through vacuum and low-pressure gaseous discharges. Some experimental results are presented and interpretations given. (8 refs.)
- Volume generation of H^- ions in plasmas** See Entry 59880
- The stability of cesium iodide X-ray photocathodes** See Entry 59898
- Implosion symmetry of laser irradiated fusion pellet** See Entry 60398
- Measurement and dynamic control of plasma position in TEXTOR Tokamak** See Entry 60450
- Technique for Lamb-shift measurements on high-Z ions produced by a hot plasma** See Entry 60656
- Kinetics of the plasma decay in lithium vapor; population inversion for the 3p-3s transition** See Entry 60664
- Excimer lasers using fission-reactor ionization** See Entry 61140
- Measurement of small-scale density fluctuation in JIPP T-II plasma by millimeter and sub-millimeter wave scattering** See Entry 61614
- X-ray generation from laser-produced plasmas and its atomic-number dependence** See Entry 61620
- Experimental studies of parametric interaction near quarter critical density** See Entry 61632
- Experimental study of the dissipative trapped ion instability** See Entry 61640

Characteristics of oblique shock waves produced in an expanding laser plasma

..... See Entry 61651

Effect of radiating aperture characteristics on results of measurement of plasma pulsation distribution over the wave number spectrum See Entry 61656

Recent results obtained by use of accelerators on plasma edge properties in controlled fusion devices and on properties of high power neutral beams See Entry 61658

Hot-electron energy deposition in CO_2 -laser-irradiated targets consistent with magnetic-field-induced surface transport See Entry 61669

Synchrotron emission from a relativistic loss-cone distribution with application to the ELMO Bumpy-Torus experiment See Entry 61677

Electron confinement studies on the EBT-S Bumpy Torus experiment using soft X-ray techniques See Entry 61678

Control system of plasma position and current in a Tokamak with strong magnetic field See Entry 61709

52.75 PLASMA DEVICES AND APPLICATIONS

(see also 28.52 Fusion reactors, 86.30L Electrodynamics and magnetohydrodynamic conversion; for ion sources, see 29.25 Particle sources and targets)

61706 The temperature distribution in a MHD plasma channel. I.Dogaru, Rev. Roum. Sci. Tech. Ser. Electrotech. & Energ. (Rumania), vol.28, no.1, p.85-8 (Jan.-March 1983). In French.

Calculates the temperature field distribution inside a metallic electrode (ceramic insertion) in the stationary state without heat sources. The finite difference method is used to integrate the heat conduction equation. As an example, an inoxidisable steel electrode in ZrO_2 , Al_2O_3 and CSI are considered for different geometries. The results are applicable to magnetohydrodynamic plasma channels. (4 refs.) L.A.F.

61707 Axial and angular distribution of current density in a thermionic converter with nonisothermal electrodes. A.D.Volkov, V.A.Ruzhnikov, P.P.Scherbinin.

Sov. Phys.-Tech. Phys. (USA), vol.27, no.9, p.1082-4 (Sept. 1982). Translation of: *Zh. Tekh. Fiz. (USSR)*, vol.52, no.9, p.1763-6 (Sept. 1982). [received: April 1983]

The results are presented of an experimental and theoretical study of the current-density distribution along an incandescent cylindrical emitter of a low-voltage arc discharge in cesium. It is shown that far from the minimum of the S-shaped curve describing the dependence of the emission current on the emitter temperature T_E , the current profile on its descending part coincides with the profile of the emitter temperature and varies inversely near the minimum of the S-shaped curve. An interpretation of this result is given. The azimuthal distribution of the current was measured with an anode made up of angular sections. The profile was found to be nonuniform; the character of the nonuniformity in the nonarcing regime changes during the transition from an undercompensated to an overcompensated discharge, which indicates that the emitter temperature is not uniform with respect to angle (the angular profile of T_E was not measured). The calculated profile of the current density along the emitter coincided with the experimental profile, which confirms the validity of the principle of additivity in the arc regime. (10 refs.)

61708 Experience of T-7 operation in plasma experiments. D.Ivanov, B.Staviskij (I.V. Kurchatov Inst. of Atomic Energy, Moscow, USSR).

Fusion Technology 1982. Proceedings of the Twelfth Symposium, Julich, Germany, 13-17 Sept. 1982 (Oxford, England: Pergamon 1983), p.1087-93 vol.2

On the ground of 3-year operation experience the analysis of serviceability of the basic constructive designs of superconducting magnetic system, vacuum chamber, cryostat and poloidal coils are carried out. The operating results of cryogenic system are discussed. Some specific peculiarities of plasma experiments in Tokamak with superconducting toroidal field coils are pointed out. (2 refs.)

61709 Control system of plasma position and current in a Tokamak with strong magnetic field. B.A.Alekseev, B.A.Belyakov, V.I.Vasil'ev, Yu.A.Kostov, I.V.Mozin, R.N.Litunovsky, V.N.Minyayev, V.L.Savikovsky, P.P.Teplov (D.V. Efremov Sci. Res. Inst. of Electrophys. Apparatus, Leningrad, USSR), Yu.Gribov, V.A.Chuyanov.

Fusion Technology 1982. Proceedings of the Twelfth Symposium, Julich, Germany, 13-17 Sept. 1982 (Oxford, England: Pergamon 1983), p.1185-9 vol.2

A high-magnetic field Tokamak is designed for plasma heating experiments by adiabatic compression of plasma over major and minor radii. Neutral beam injection heating is also used. The plasma position and current control system includes a diagnostic facilities with preliminary signal processing, an automatic control system, a computer with interface, power supplies and ohmic heating coil, compression coil, equilibrium coils for the first and second discharge stage, vertical and horizontal field correction coils. Combined adaptive program control and feedback loops are used. (no refs.)

61710 Plasma parameter control experiments on 'Tuman-3'. V.A.Belyakov, S.E.Bender, S.N.Vasil'ev, S.V.Gornostaev, N.M.Efremenko, A.G.Kolchin, Yu.A.Kostov, R.N.Litunovsky, O.A.Minyayev, P.P.Teplov (D.V. Efremov Sci. Res. Inst. of Electrophys. Apparatus, Leningrad, USSR), V.E.Golant, M.P.Gryaznevich, S.V.Lebede, N.V.Sakharov, K.G.Shakhovets, A.A.Fedorov.

Fusion Technology 1982. Proceedings of the Twelfth Symposium, Julich, Germany, 13-17 Sept. 1982 (Oxford, England: Pergamon 1983), p.1191-5 vol.2

The Tokamak 'Tuman-3' is designed for plasma compression experiments in a time-rising toroidal magnetic field. The Tokamak features are large aspect ratio ($R/a=2.3$), nearness of the iron core to the plasma region and low time constant of the vacuum chamber (0.15 ms). Feedback plasma position control improves essentially discharge repetition, makes easier to obtain operation conditions, allows to vary gas injection without breaking the equilibrium. The combined gas-discharge chamber cleaning, equilibrium control and programmed pulsed gas injection result in MHD-stable discharges with low safety factor (up to 2.2). The vertical plasma shift does not exceed 0.5 cm at the plasma current front and 0.2 cm at the stationary discharge stage. The horizontal plasma shift is within 0.2-0.5 cm. Further development of the control system includes the plasma current control system, density control and that of current profile and MHD-column activity level. Some experiments are conducted in 'Tuman-3' to study the effect of chamber cleaning, gas injection, additional heating etc. on discharge repetition and plasma parameters. (2 refs.)

61711 T-15 poloidal field control system. V.A.Belyakov, V.G.Ivkin, A.V.Kuznetsov, R.N.Litunovsky, I.V.Mozin, V.P.Smirnov, A.M.Stolov, P.P.Teplov (D.V. Efremov Sci. Res. Inst. of Electrophys. Apparatus, Leningrad, USSR).

Fusion Technology 1982. Proceedings of the Twelfth Symposium, Julich, Germany, 13-17 Sept. 1982 (Oxford, England: Pergamon 1983), p.1209-13 vol.2

The T-15 poloidal field control system is designed on the basis of experimental investigations, made on the Tokamak 'Tuman-3' and numerical modeling data. The purpose of the calculations is to investigate the plasma position and current control system, preparation of program motion correction algorithms for the mathematical model chosen, and determination of the requirements to the fast control loop. The control of horizontal plasma column position is constructed as a combination of an adaptive program feedforward and a fast feedback with controlled parameter. A counterturn scheme is used in the 'fast' coil and it is weakly coupled with other poloidal field coils. The poloidal field control system includes also the control of the plasma current and vertical position according to the given program. During the discharge continuous data acquisition on plasma parameters is made. During dwell time the information is processed in the TPA 1140 computer. On the basis of the data obtained, the power supply operation programs are corrected up to the moment of the next discharge. (no refs.)

Mechanical stress analysis for the twisted coils of the advanced stellarator WENDELSTEIN VII-AS See Entry 60423

Development of material for the JET mechanical structure See Entry 60424

Mechanical analysis of TORE SUPRA superconducting toroidal field coils See Entry 60425

Poloidal field coils for the international Tokamak reactor study 'INTOR' See Entry 60426

Mechanical tests on components used in the TORE SUPRA superconducting coils See Entry 60427

Toroidal field coils for INTOR See Entry 60428

Employment of the Large Coil Test Facility in toroidal field coil development See Entry 60429

The toroidal field magnet concept of ASDEX Upgrade See Entry 60431

On strength of welded joints in high strength, large scale copper coils for nuclear fusion equipment See Entry 60432

Vacuum magnetic fields and modular coil system of the advanced stellarator Wendelstein VII-AS See Entry 60433

Stength analysis of cooling pipe joints for poloidal field coil for nuclear fusion equipment See Entry 60434

The technical concept of the ASDEX UG poloidal field coils See Entry 60435

Electromagnetic systems for high-field Tokamaks See Entry 60436

Manufacturing of the European LCT-coil for the large coil task See Entry 60437

A procedure for the computation of magnetic field, temperature and force distributions in the design of Tokamak toroidal coils See Entry 60439

The design bending stress criterion for JT-60 coil See Entry 60440

Toroidal field magnet for FT-U device See Entry 60441

Manufacture, assembly and testing of the inner poloidal coil stacks of JET and TFTR See Entry 60442

Manufacture and test of the TEXTOR BT-coils See Entry 60443

The toroidal field coil support structure for the Culham MKIIC Tokamak reactor See Entry 60445

Electrical insulation system fit for cyclic high strain (development of insulation of JT-60 poloidal field coil) See Entry 60446

The TORE SUPRA poloidal field system See Entry 60448

Efficiency of passive circuits for vertical stability in INTOR reactor See Entry 60449

Measurement and dynamic control of plasma position in TEXTOR Tokamak See Entry 60450

The FTU poloidal field system See Entry 60451

Time evolution of the coil currents shaping and centering a D-shaped reactor plasma See Entry 60452

High efficiency ionization of low-density elements in beam-plasma type ion sources See Entry 60503

Properties of ion beams formed from a nonstationary plasma See Entry 61069

Dynamics of pulsed ion beam production by a plasma lens See Entry 61070

Oblique collision of cylindrical outgoing ion-acoustic solitons See Entry 61629

An analysis of the induction plasma heating in the microwave frequency range See Entry 61667

The computational model for the control of plasma position in TEXTOR See Entry 61686

Experience with feedback and feedforward for plasma control in ASDEX See Entry 61688

Applicability verification of Tokamak plasma equilibrium control models See Entry 61689

Line radiation of highly ionised impurities in plasma produced in the plasma-focus device See Entry 61702

52.80 ELECTRIC DISCHARGES

(see also 51.50 Electrical phenomena in gases)

61712 Lightning and switching impulse breakdown of rod/plane gaps in nitrogen and nitrogen/freon (CCl_2F_2) mixtures. T.V.Babu Rajendran, C.S.Lakshminarasimha, M.S.Naidu (Dept. of High Voltage Engng., Indian Inst. of Sci., Bangalore, India).

IEE Proc. A (GB), vol.130, no.3, p.134-9 (May 1983).

Lightning impulse (1.2/50 μs) and switching impulse (200/2000 μs) breakdown phenomena in nitrogen and nitrogen/freon mixtures have been investigated for rod/plane gaps at total pressures up to 5 bar and spacings up to 100 mm with freon concentrations varying from 1 to 20% in the mixture. Results of breakdown voltages show that, in general, substantial improvement in breakdown strength can be achieved, particularly for negative polarities with the addition of small percentages (\sim a few per cent) of CCl_2F_2 to N_2 . It is of interest to note that the characteristic 'pressure effect' in the positive point breakdown voltage against pressure curve observed in many strongly attaching gases is ill defined in these mixtures, and can be seen only over a limited range of experimental conditions. The corresponding effect for negative

point breakdown is observed in these mixtures at the relatively low pressures of 2 to 4 bar for long gaps (>40 mm). The breakdown voltages for a 100 mm gap with the switching impulse at pressures greater than 2 bar are generally 20% lower than the corresponding lightning impulse data. (19 refs.)

61713 Anomalous electron attachment properties of perfluoropropylene ($1-\text{C}_3\text{F}_6$) and their effect on the breakdown strength of this gas. S.R.Hunter, L.G.Christophorou, D.L.McCorkle, I.Sauers, H.W.Ellis, D.R.James (Health & Safety Res. Div., Oak Ridge Nat. Lab., Oak Ridge, TN, USA).

J. Phys. D (GB), vol.16, no.4, p.573-80 (14 April 1983).

Electron attachment to perfluoropropylene ($1-\text{C}_3\text{F}_6$) in $1-\text{C}_3\text{F}_6$ /buffer gas mixtures has been found to be anomalously dependent on both the $1-\text{C}_3\text{F}_6$ and buffer gas pressures, as well as on the gas temperature. The authors have found also that the uniform field breakdown strength of pure $1-\text{C}_3\text{F}_6$ is dependent on gas pressure but not on the gas temperature. A mass spectrometer study of the negative ions formed in a moderately high pressure corona discharge has been made, and the principal negative ions formed by electron attachment to $1-\text{C}_3\text{F}_6$ have been identified. Based on these studies, a reaction scheme for electron attachment to $1-\text{C}_3\text{F}_6$ is proposed which results in stable negative ion clusters but does not involve pre-existing dimers. Further, the authors propose that the observed pressure dependence in the breakdown strength of this gas is due to the large pressure dependence of the electron attachment process they observed. (29 refs.)

61714 Calculation of swarm parameters in xenon at high E/N by a Monte Carlo simulation method. M.Hayashi (Nagoya Inst. of Technol., Nagoya, Japan).

J. Phys. D (GB), vol.16, no.4, p.591-9 (14 April 1983).

Swarm parameters (electron drift velocities, ratios of electron radial diffusion coefficient to mobility, mean electron energies and electron energy distribution functions) have been calculated in xenon by a Monte Carlo simulation method. Values of these parameters have been obtained for ratios of the electric field to the gas number density E/N from 85 to 8500 Td ($E/p_0 = 30 \sim 3000$ V cm $^{-1}$ Torr $^{-1}$ at 0°C). Calculated results were compared with available experimental and other calculated data. Calculations relating to the non-equilibrium distance d_0 in front of the cathode and non-equilibrium distance near the anode were also carried out. For these calculations, elastic momentum transfer cross-sections and inelastic cross-sections up to 10^4 eV reported in the author's preceding paper (see *ibid.*, vol.16, p.581-9, 1983) were used. (19 refs.)

61715 Possible explanation of the mechanism of cathode spot motion. A.V.Zharinov, Yu.V.Sanochkin (V.I. Lenin All Union Electrical Engng. Inst., USSR).

JETP Lett. (USA), vol.36, no.5, p.182-5 (5 Sept. 1982). Translation of: *Pisma v Zh. Eksp. i Teor. Fiz. (USSR)*, vol.36, no.5, p.147-9 (5 Sept. 1982). [received: April 1983]

A thermal capillary mechanism for cathode spot motion is proposed. The velocity of the spot is determined and the convection pattern is examined. (3 refs.)

61716 Time scale considerations on the relaxation of electronic and vibrational energy distributions in a nitrogen afterglow. M.Capitelli, C.Gorse (Dipartimento di Chimica, CNR, Bari, Italy), A.Ricard.

J. Phys. Lett. (France), vol.44, no.7, p.L251-6 (1 April 1983).

The relaxation of the electron energy distribution function (edf) in vibrationally excited N_2 post discharges has been analysed by discussing the characteristic times necessary for 'edf' to achieve and maintain a quasistationary state and by comparing these times with other important times corresponding to electron losses by dissociative recombination and diffusion to the tube wall. The calculated results show that the vibrational collisions can create a quasistationary 'edf' in times of 10^{-7} - 10^{-6} s ($p = 5$ torr, $T = 500\text{K}$). This quasistationary state is characterised by a strong correlation between vibrational distribution and mean electron energy. It can last up to several 10^{-3} s till the electron density becomes too small as a result of recombination and diffusion. Comments of some earlier experimental results are given. (14 refs.)

61717 Monte Carlo calculation of the erosion rate and ion current at a vacuum arc cathode. V.A.Nemchinskii (All-Union Sci. Res. Inst. for Current Source Design & Technol., Leningrad, USSR).

Sov. Phys.-Tech. Phys. (USA), vol.27, no.9, p.1073-7 (Sept. 1982). Translation of: *Zh. Tekh. Fiz. (USSR)*, vol.52, no.9, p.1748-55 (Sept. 1982). [received: April 1983]

The Monte Carlo method is used to calculate the trajectories of particles vaporized from a vacuum arc cathode. Ionization and collisions between atoms, ions, and electrons are all treated. The atomic and ionic density, velocity, and temperature distributions are calculated along with the electric field in the plasma near the cathode. The number of vaporized particles subsequently returning to the cathode as neutrals or ions is determined. Electron-ion friction and electric field effects are shown to greatly increase the number of particles returning to the cathode. However, the returning particles are ionized only if the vaporized atoms can be ionized over distances a few times collision length in the plasma. If this condition is not satisfied, only neutral atoms return to the cathode and there is a large voltage drop in the quasineutral plasma comparable with the cathode drop. (2 refs.)

61718 Numerical modeling of a laminar pulsed discharge including radiative transport. G.S.Romanov, A.S.Smetannikov (Res. Inst. for Appl. Phys. Problems, State Univ., Minsk, Belorussian SSR).

Sov. Phys.-Tech. Phys. (USA), vol.27, no.9, p.1078-81 (Sept. 1982). Translation of: *Zh. Tekh. Fiz. (USSR)*, vol.52, no.9, p.1756-62 (Sept. 1982). [received: April 1983]

A system of MHD equations describing the dynamics of the evolution of a discharge having cylindrical symmetry was solved together with the radiation transport equations averaged over the spectrum in prescribed spectral intervals, in the 'forward reverse' approximation (along a normal to the symmetry axis). The calculations were performed for a cylindrical aluminum foil in air for two-sided (along the radius) and one-sided (towards the symmetry axis) expansion of the high-temperature vapor of the foil. The discharge energy per unit length was 8.5 kJ/cm, and the cylinder radius and wall thickness were 9 and 6 μm , respectively. The radiation-gasdynamic parameters of the discharge were determined; it was found that the energy radiated in the photon energy spectral interval 0.6-5 eV and in a time ~ 100 μs was $\sim 30\%$ in the first case and 40% in the second. Comparison of the calculation results with the published experimental data has shown them to be in fair agreement. (16 refs.)

61719 Glow discharge in a transverse magnetic field. V.N.Glazunov, V.G.Grechany, A.S.Metal' (V.I. Lenin All-Union Electrotech. Inst., USSR).

Sov. Phys.-Tech. Phys. (USA), vol.27, no.9, p.1084-7 (Sept. 1982). Translation of: *Zh. Tekh. Fiz. (USSR)*, vol.52, no.9, p.1767-72 (Sept. 1982). [received: April 1983]

The authors have determined the characteristics of a stationary rod-cathode glow discharge in helium and argon in the pressure range 10^{-2} - 10 torr in a magnetic field up to 16 kA/m and a current density at the cathode up to 10 mA/cm 2 . The authors have shown that in the range of parameters where the

length of the trajectory of oscillating primary electrons from the cathode to the first reversal point in the cathode fall region is less than half their ionization length—the part of the path along which the probability of their ionizing atoms of the working gas is different from zero—the properties of the discharge are similar to those of a hollow-cathode glow discharge. (9 refs.)

61720 Velocity of anode vapor in pulsed vacuum breakdown. R.B.Baksh, N.A.Ratakhin, N.A.Kablambayev (Inst. of High-Current Electronics, Acad. of Sci., Tomsk, USSR).

Sov. Phys.-Tech. Phys. (USA), vol.27, no.9, p.1091-3 (Sept. 1982). Translation of: *Zh. Tekh. Fiz. (USSR)*, vol.52, no.9, p.1778-82 (Sept. 1982). [received: April 1983]

The establishment of steady-state evaporation of the anode invacuum breakdown is discussed. It is shown that the vapor velocity is determined as the velocity with which a gaseous sphere with internal energy equal to $2 kT_{\text{sur}}$ expands into vacuum. The temperature T_{sur} is determined by the balance between the energy release of the electron beam in the anode material and the energy loss due to evaporation. Experimental and calculated data are compared. (10 refs.)

61721 Effect of stepwise excitation processes on the electron velocity distribution function in argon. I.Yu.Baranov, N.B.Kolokolov (A.A. Zhdanov State Univ., Leningrad, USSR).

Sov. Phys.-Tech. Phys. (USA), vol.27, no.9, p.1096-9 (Sept. 1982). Translation of: *Zh. Tekh. Fiz. (USSR)*, vol.52, no.9, p.1787-93 (Sept. 1982). [received: April 1983]

For the first time the distortion of the electron velocity distribution function by stepwise excitation processes has been observed experimentally. The measurements were performed in an argon plasma afterglow at pressures of 0.6 and 0.4 torr with current pulses of 7, 13, and 65 mA in a 30 mm diameter discharge tube. The experimental results were compared with the distribution function calculated in local and nonlocal approximations. A criterion is given for estimating the contribution of stepwise processes to the form of the distribution function. (8 refs.)

61722 Production of a bulk discharge in an electronegative gas mixture. E.P.Bel'kov, P.N.Dashchuk, Yu.I.Kozlov, A.K.Piskunov, Yu.V.Romanenko, G.L.Spichkin (Kalinin Polytech. Inst., Leningrad, USSR).

Sov. Phys.-Tech. Phys. (USA), vol.27, no.9, p.1100-3 (Sept. 1982). Translation of: *Zh. Tekh. Fiz. (USSR)*, vol.52, no.9, p.1794-801 (Sept. 1982). [received: April 1983]

Experimental results are presented on the conditions for production of a stable bulk discharge stabilized by dielectric barriers in mixtures of SF_6 and helium in the chamber with a working gap of 2-3 cm. The voltage-characteristics have been used to determine the specific energy deposition in the discharge. In mixtures at atmospheric pressure containing 1-8% SF_6 , the specific deposition was $5\text{--}10 \text{ mJ.cm}^{-2}$. The deposition depends strongly on the matching between the output parameters of the generator and the parameters of the discharge chamber. (3 refs.)

61723 The effect of the method of treatment of a molybdenum cathode on the normal cathode drop in a glow discharge. P.N.Chistyakov (Engng.-Phys. Inst., Moscow, USSR).

Sov. Phys.-Tech. Phys. (USA), vol.27, no.9, p.1160-1 (Sept. 1982). Translation of: *Zh. Tekh. Fiz. (USSR)*, vol.52, no.9, p.1888-90 (Sept. 1982). [received: April 1983]

The normal cathode potential drop U_n in a glow discharge is determined by the nature of the gas and the material of the cathode. To obtain values of U_n that are reproducible and stable with time in an inert gas requires that the surface of the cathode be atomically clean and the inert gas be highly purified. The object of this work was to obtain a reproducible and stable value of U_n for a molybdenum cathode in neon with the use only of electron and electrothermal treatment to provide just as clean experimental conditions as does ion treatment in an inert gas flow discharge. The results of using both kinds of treatment are compared and it is found that the effect of ion bombardment in an inert gas on the value of U_n is due to the embedding of neon ions into the crystal lattice of molybdenum. (3 refs.)

61724 Dynamics of the cathode layer in an externally maintained glow discharge. A.N.Lobanov, Ya.I.Londer, L.P.Menakhin, K.N.Ul'yanov (V.I. Lenin All-Union Electrotech. Inst., Moscow, USSR).

Sov. Phys.-Tech. Phys. (USA), vol.27, no.10, p.1204-8 (Oct. 1982). Translation of: *Zh. Tekh. Fiz. (USSR)*, vol.52, no.10, p.1959-65 (Oct. 1982). [received: April 1983]

The behavior of the cathode layer in an externally maintained glow discharge is examined by numerically solving a self-consistent system of nonstationary gas-dynamic equations together with the continuity equation for the current and the Poisson equation for the electric field. The time dependence of the cathode voltage drop has been measured and found to be in agreement with the calculated value. (14 refs.)

61725 Study of a high-power quasisteady discharge at megampere currents. B.P.Giterman, D.I.Zenkov, A.I.Pavlovskii, N.N.Petrov, E.N.Smirnov, G.M.Spirov.

Sov. Phys.-Tech. Phys. (USA), vol.27, no.10, p.1218-20 (Oct. 1982). Translation of: *Zh. Tekh. Fiz. (USSR)*, vol.52, no.10, p.1983-6 (Oct. 1982). [received: April 1983]

A discharge powered by a capacitor bank (stored energy 1.8 MJ) in an air-xenon mixture is studied experimentally. The maximum amplitude of the discharge current was 1.3 MA and the half-period of the discharge current was 250 μs . The brightness temperature was 26.10^3 K and the discharge was stable for $\sim 100 \mu\text{s}$. It is shown that even at MA currents the discharge converts electrical energy to light efficiently. (6 refs.)

61726 Several features of the free glow discharge. V.N.Melekhin, S.A.Mishin, N.Yu.Naumov (Inst. of Phys. Problems, Acad. of Sci., Moscow, USSR).

Sov. Tech. Phys. Lett. (USA), vol.8, no.8, p.400-1 (Aug. 1982). Translation of: *Pis'ma v Zh. Tekh. Fiz. (USSR)*, vol.8, no.15-16, p.923-6 (Aug. 1982). [received: April 1983]

The normal glow discharge in free space, not bounded by the walls of a discharge tube, has several interesting properties. These properties are conveniently observed for a cylindrical electrode geometry, with the discharge occurring between a round rod cathode 5-10 mm in diameter and a coaxial cylindrical anode a few centimeters in diameter. At an air pressure of 1-10 torr and at a discharge current of the order of a milliamper, the discharge is steady, with a cathode spot (the negative glow) having a characteristic saddle shape and drifting slowly along the cathode surface, undergoing a displacement in the azimuthal direction and also a displacement along the axis of the cathode, by 2-3 cm. (3 refs.)

61727 A study of underwater spark discharge characteristics under parametric variation of electric discharge circuits. A.I.Vorchenko.

Tekh. Elektrodin. (USSR), no.1, p.12-16 (Jan.-Feb. 1983). In Russian.

A mathematical model is proposed for calculating the characteristics of an underwater spark discharge. In contrast with existing models the proposed model takes into account the non-ideality of plasma in the determination of its electrical conductivity and ionization composition. Numerical methods are used to investigate the electrical and hydrodynamic characteristics of an electrical discharge in water and also the processes of emission of energy in the spark channel under a condition of parametric change in resistance, inductance and capacitance of the discharge circuit. It is shown that with the aid of the method examined it is possible to control the power characteristics of an underwater spark discharge, i.e. to shape pressure pulses of a complex predetermined form. (11 refs.) A.J.B.

Determination of the absolute intensity of the afterglow in flash photolysis of tellurium vapor See Entry 60659

State-selective spectroscopy in a molecular nitrogen discharge by use of optogalvanic double-resonance spectroscopy See Entry 60770

Determination of electron-xenon total excitation cross-sections, from threshold to 100 eV, from experimental values of Townsend's α See Entry 60993

Pumping of pulsed gas lasers by bulk and sliding spark discharges See Entry 61136

Electric-discharge CW industrial CO_2 laser See Entry 61191

Recombination mechanism for emission accompanying collapse of a cavitation bubble induced by a high-voltage electrical discharge See Entry 61532

Ionization-superheating mechanism in current channel formation in molecular gases See Entry 61600

Second-order collisions between slow electrons and metastable krypton atoms in the 3P_2 state See Entry 61606

An analysis of the induction plasma heating in the microwave frequency range See Entry 61667

Axial and angular distribution of current density in a thermionic converter with nonisothermal electrodes See Entry 61707

Methods of spectral analysis with laser selection of the sample and its vaporization in arc discharges See Entry 63622

Aerosol mode of ball lightning See Entry 64216

60.00 CONDENSED MATTER: STRUCTURE, THERMAL AND MECHANICAL PROPERTIES

Computer modelling of solids See Entry 59766

61.00 STRUCTURE OF LIQUIDS AND SOLIDS; CRYSTALLOGRAPHY

(see also 68.20 Solid surface structure, 71. Electron states)

61728 Use of extinctions in programs for indexing powder patterns. V.P.Serykh (Physicotech. Inst. of Acad. of Sci., Ukrainian SSR).

Sov. Phys.-Crystallogr. (USA), vol.27, no.5, p.596 (Sept.-Oct. 1982). Translation of: *Kristallografiya (USSR)*, vol.27, no.5, p.994 (Sept.-Oct. 1982). [received: April 1983]

Enlistment of the extinctions characteristic of the given crystal system enables one to make an additional selection of indices. Thus in the author's one of the calculated values Q_{101} and Q_{011} can be deflected owing to its failure to correspond to the extinctions of a face-centered monoclinic unit cell. The extinctions may conveniently be reduced to a two-dimensional array, the rows of which correspond to the diffraction groups, and the columns to be assigned number of the rule by which the generated indices are verified. Reliable operation of the algorithm should be ensured if the test is begun with groups with more complicated extinctions. (3 refs.)

61729 Graphical derivation of the several settings of an orthorhombic crystal. M.J.Buerger (MIT, Cambridge, MA, USA).

Z. Kristallogr. (Germany), vol.161, no.1-2, p.119-26 (1982).

A simple graphical method for deriving the various settings of an orthorhombic crystal from what has been called the 'standard' setting is briefly discussed. The 'standard' setting is not necessarily the most useful one to use when a crystal is to be oriented according to the relative dimensions of its three cell translations. (no refs.)

61.10 X-RAY DETERMINATION OF STRUCTURES

(see also 61.80 Radiation damage and other irradiation effects; for specific determinations, see 61.55 to 61.80)

61.10D Theories of diffraction and scattering

61730 The phase problem of X-ray crystallography from the viewpoint of signal recovery. G.Bricogne (Dept. of Biochem., Coll. of Physicians & Surgeons, Columbia Univ., New York, NY, USA).

Topical Meeting on Signal Recovery and Synthesis with Incomplete Information and Partial Constraints, Incline Village, NV, USA, 12-14 Jan. 1983 (Washington, DC, USA: Opt. Soc. America 1983), p.FA12/1-3

The statistical theory of the X-ray phase problem is reviewed, and recent work relating it to Jaynes's maximum-entropy formalism is presented. (4 refs.)

61.10F Experimental techniques

(inc. apparatus, techniques and calculation methods for analyzing experimental results; see also 07.85 X-ray, gamma-ray instruments and techniques)

61731 Improved system for energy-dispersive X-ray diffraction with synchrotron radiation. E.F.Skelton, S.B.Qadri, A.W.Webb, C.W.Lee, J.P.Krikland (Stanford Synchrotron Radiation Lab., Stanford Univ., Stanford, CA, USA). *Rev. Sci. Instrum. (USA)*, vol.54, no.4, p.403-9 (April 1983). A number of improvements in a facility developed over the past three years at the Stanford Synchrotron Radiation Laboratory for the study of pressure and/or temperature effects on materials are described. These include improved beam collimation to both reduce background and eliminate gasket scatter, a remote, pneumatically operated pressurizer, and introduction of a variety of electronics hardware to allow both computer control of experiments and on-line data analyses. Considerations are given to the possible effects of heating of the pressure cavity by the incident beam and to possible fluctuations of the incident beam intensity/energy profile. In both cases, there was no evidence to indicate that these phenomena warranted any further consideration, i.e. they are not considered to be problems in terms of analyzing the data. Extended measurements of a well-defined diffraction peak indicated that a considerable improvement over the authors' earlier work has been realized in terms of the precision in the determination of the energy of the peak, viz. a precision of better than 0.04% for measurement periods as short as 10 s; the estimated precision in the net peak area is less than 3%. The system was used to examine the kinetics of the B1-to-B2 pressure-induced phase transition in KBr. The volume change in the two-phase region is measured to be $10.41\% \pm 0.10\%$, in excellent agreement with most of the previous measurements. A plot of the time dependence of the growth rate of the high-pressure phase indicates that the phase transformation can be described by the Avrami equation. Constants for the phase transition kinetics are given. (27 refs.)

61732 Reconstruction of the electron density of a partly determined structure. D.I.Kalinin (Inst. of Appl. Math., Acad. of Sci., USSR). *Sov. Phys.-Crystallogr. (USA)*, vol.27, no.5, p.521-6 (Sept.-Oct. 1982). Translation of: *Kristallografiya (USSR)*, vol.27, no.5, p.867-75 (Sept.-Oct. 1982). [received: April 1983]

The author investigates the form of the function $\rho_e(x)$, synthesized from Fourier coefficients, the moduli of which are the moduli of the Fourier coefficients of the true electron density of a crystal structure $\rho_c(x)$, while their phases are the phases of the Fourier coefficients of the density of a model, $\rho_m(x)$, imitating part of this structure, without the imposition of any limitations on the form of the functions $\rho_c(x)$ and $\rho_m(x)$. (6 refs.)

61733 Use of an iteration method to eliminate instrumental factors from experimental spectra obtained in diffractometers from weakly absorbing materials by the reflection method. V.F.Pleshakov (All-Union Sci.-Res. & Design-Technol. Inst. of Electrocarbon Products, USSR). *Sov. Phys.-Crystallogr. (USA)*, vol.27, no.5, p.527-9 (Sept.-Oct. 1982). Translation of: *Kristallografiya (USSR)*, vol.27, no.5, p.876-80 (Sept.-Oct. 1982). [received: April 1983]

The author solves the problem of finding the true spectrum from the integral equation by the method of iterations. The method is used to eliminate instrumental distortions from an experimental spectrum obtained from vitreous carbon treated at 2500°C. The method used to eliminate the instrumental factors is shown to be precise and efficient. Very weak reflections are clearly shown up in the intensity curves and interference function at $s=0.39, 0.735, 1.04, 1.085, 1.22, \text{ and } 1.27 \text{ \AA}^{-1}$. The results are compared with the solution of the integral convolution equation, in which the (004) reflection of graphite is used as the instrumental function. It is shown that the convolution equation is ineffective for eliminating instrumental distortions with the aim of showing up weak reflections and investigating the fine structure of carbon materials. (11 refs.)

61734 Polarization of X-rays in the region of the Bragg reflection curves of silicon crystals with dislocations. N.M.Olekhovich, V.L.Markovich, A.I.Olekhovich (Inst. of Solid State Phys. & Semiconductors, Acad. of Sci., Belorussian SSR).

Sov. Phys.-Crystallogr. (USA), vol.27, no.5, p.533-5 (Sept.-Oct. 1982). Translation of: *Kristallografiya (USSR)*, vol.27, no.5, p.886-90 (Sept.-Oct. 1982). [received: April 1983]

This article gives the results of investigations of the polarization factor P_R of X-rays of Bragg reflections from single crystals of silicon with various dislocation densities N_d . From the character of the angular dependence of P_R , the region of applicability of the mosaic model of the crystal is determined ($N_d \geq 10^4 \text{ mm}^{-2}$), and it is shown that scattering in mosaic crystals is governed by dynamic scattering in individual blocks and that secondary extinction does not take place. (15 refs.)

61735 Dynamic focusing of hard X-rays with transverse dispersion $D_s=0$. K.T.Gabrielyan, F.N.Chukhovskii (State Univ., Erevan, USSR). *Sov. Phys.-Tech. Phys. (USA)*, vol.27, no.10, p.1309-10 (Oct. 1982). Translation of: *Zh. Tekh. Fiz. (USSR)*, vol.52, no.10, p.2127-8 (Oct. 1982). [received: April 1983]

The authors' goal was to show that under certain conditions, when the transverse dispersion D_s of the diffracted X-rays is zero, chromatic aberration can be suppressed and dynamic X-ray focusing improved using elastically bent crystals. The findings are reported for the case of symmetric Laue diffraction of X-rays in a crystal bent without distortion of its cross section. (6 refs.)

Direct determination of the Au(110) reconstructed surface by X-ray diffraction See Entry 62221

X-ray diffraction intensity ratio method for the thickness measurement of ternary heterogeneous epitaxial layers on GaAs substrate See Entry 62281

Quantitative analysis of fiber texture in cubic films See Entry 62289

61.14 ELECTRON DETERMINATION OF STRUCTURES

(for specific determinations, see 61.55 to 61.80)

61.14D Theories of diffraction and scattering

61736 On the visibility of small metallic particles on crystalline substrates. M.Avalos-Borja (Dept. of Materials Sci. & Engng., Stanford Univ., Stanford, CA, USA), M.J.Yacaman.

Ultramicroscopy (Netherlands), vol.10, no.3, p.211-15 (1982). Dynamical diffraction theory was used to study the contrast of small metallic particles supported on crystalline substrates. The dependence of the particle visibility on the orientation and thickness is discussed. Experimental examples

of changes in particle visibility for Pt/alumina and Pt/sapphire are presented. (5 refs.)

61.14F Experimental diffraction and scattering

61737 Interpretation of the fading of diffraction patterns from organic substances irradiated with 100 keV electrons at 10-300K. L.Reimer, J.Spruth (Phys. Inst., Univ. Munster, Munster, Germany).

Ultramicroscopy (Netherlands), vol.10, no.3, p.199-210 (1982). The fading curves of Debye-Scherrer ring intensities have been recorded for evaporated films of some aliphatic and aromatic compounds at temperatures between $T_s=14-66\text{K}$ and room temperature. The lowest real specimen temperature T_s was calibrated by the condensation of different gas atoms and depends on the current density used, which has to be raised with increasing resistivity to radiation damage. The fading curves for the lowest specimen temperature were compared with a theory of Clark et al. (1980) modified by a multiple-hit model. By fitting the theory to experimental results, values of the cross-section σ for a single hit, the mean number m of hits necessary to destroy a sensitive unit and the ratio b of the damaged to the undamaged structure amplitude of a unit cell can be established. There are considerable differences in these quantities for different compounds. The temperature dependence of σ for tetracene and other compounds can be explained by an activation energy of the order of a few tens of one meV. (24 refs.)

61738 A comparison of techniques for obtaining convergent beam electron diffraction patterns with a JEOL 200CX. K.C.Lee (School of Appl. & Engng. Phys., Cornell Univ., Ithaca, NY, USA).

Ultramicroscopy (Netherlands), vol.10, no.3, p.217-22 (1982). Three different techniques for obtaining convergent beam electron diffraction (CBED) patterns using a JEOL 200CX transmission electron microscope are described and compared. The first technique, described by Goodman (1964), are shown to yield clear, undistorted patterns, but only with relatively large camera length, and a limited field of view. A second technique, which is a modification of Goodman's technique, is shown to yield CBED patterns of both large camera length and small camera length with a much larger angular coverage, but the magnitude of the beam convergence is limited by distortion in the pattern. A third technique is then presented which permits the formation of small camera length, relatively undistorted CBED patterns with large angular coverage and greatly increased beam convergence; high quality large camera length CBED patterns can also be obtained by simply increasing the strengths of the diffraction lenses. (7 refs.)

Determination of grain boundary rotation parameters from Kikuchi patterns. I. A simplified method for determining the accurate orientation relationship of two grains See Entry 61933

61.14H Low-energy electron diffraction (LEED) and reflection High-energy electron diffraction (RHEED)

61739 Model for intensity correction of high energy electron diffraction of small crystallites on solid surfaces. E.Muller (Sektion Chemie, Friedrich Schiller Univ., Jena, Germany).

Wiss. Z. Friedrich-Schiller-Univ. Jena, Math. Naturwiss. Reihe (Germany), vol.31, no.6, p.1073-83 (1982). In German.

Using the kinematical theory of diffraction a simple model was derived allowing one to correct the intensities of electron diffraction patterns of small crystallites on solid surfaces, observed on RHEED, as a function of the angle of inclination and diffraction, respectively. Other parameters are the mean radius of the particles, assumed as semispheres, their mean distance, the wavelength, the extinction coefficient, and a parameter of the diffraction spot halfwidth. This correction function by which the theoretical scattering factors have to be multiplied generally shows a non-monotonous behaviour. The influence of the various parameters on the intensity distribution is discussed. (4 refs.)

61.16 OTHER DETERMINATION OF STRUCTURES

(for specific determinations, see 61.55 to 61.80)

61.16D Electron microscopy determinations

61740 Visualization of Bloch waves of high energy electrons in high resolution electron microscopy. K.Kambe (Fritz-Haber-Inst., Max-Planck-Gesellschaft, Berlin, Germany).

Ultramicroscopy (Netherlands), vol.10, no.3, p.223-7 (1982). By applying the Bloch wave theory of electron diffraction to the problem of lattice images in high resolution electron microscopy, it is shown that those characteristic types of images as found for Ge(110) can be interpreted as images of individual Bloch waves formed by the incident electron inside the lattice. (3 refs.)

61741 Effect of the phase shift due to dynamical scattering on the contrast of crystal structure images. S.Horiuchi (Nat. Inst. for Res. in Inorganic Materials, Ibaraki, Japan).

Ultramicroscopy (Netherlands), vol.10, no.3, p.229-35 (1982). The contrast of through-focus images of a niobium tungsten bronze, $2\text{Nb}_2\text{O}_5 \cdot 7\text{WO}_3$, taken by a 1 MV high resolution electron microscope, is discussed in terms of the transfer function, in which, in addition to the conventional phase aberration, the phase shift due to the dynamical scattering is taken into account. It is found that the phase shift may be advantageous in the formation of structure images, as long as the crystal is very thin, i.e. a few nanometers in thickness. It is also made clear why the best defocus for optimum structure images differs from the Scherzer defocus, depending on the crystal thickness. An almost exact contrast reversal occurs at overfocus only in the images of extremely thin crystals, because the positive range of the transfer function is made narrower due to the above phase shift. The discussion is supported by computer simulation of the image contrast. (20 refs.)

61742 Direct interpretation of high resolution electron images of substitutional alloy systems with a column structure. D.Van Dyck, G.Van Tendeloo, S.Amelinckx (Univ. Antwerpen, Antwerpen, Belgium).

Ultramicroscopy (Netherlands), vol.10, no.3, p.263-80 (1982). It is shown that in substitutional alloy systems with a column structure, high resolution electron micrographs viewed along the columns may still show a one-to-one correspondence with the atomic configurations even for crystal thicknesses beyond the thin phase grating limit. For such cases the atomic positions can be determined unambiguously from the images, without any need for image simulation. The required experimental conditions and the nature of the contrast are discussed. (7 refs.)

- Trace structure analysis, ptychography, phase tomography See Entry 59892
- Secondary electron imaging as an aid to STEM microanalysis See Entry 59893
- Periodic images produced by random noise and a filter See Entry 59895
- Thickness dependence of the STEM ratio image See Entry 59896
- Interpretation of the fading of diffraction patterns from organic substances irradiated with 100 keV electrons at 10-300K See Entry 61737
- A comparison of techniques for obtaining convergent beam electron diffraction patterns with a JEOL 200CX See Entry 61738
- Improved technique for observation of dislocation structure of austenitic MnCrNi steels after small deformation See Entry 61920
- Weak beam images of dislocations triple ribbons See Entry 61921

61.20 CLASSICAL, SEMICLASSICAL, AND QUANTUM THEORIES OF LIQUID STRUCTURE

(for kinetic and transport theory, see 51.10; for electronic states, see 71.; for liquid helium, see 67.)

- 61743 A modified Wigner function set for the Smoluchowski operator representation in anisotropic liquids. G.Moro, P.L.Nordio (Inst. of Phys. Chem., Univ. of Padua, Padua, Italy). *Chem. Phys. Lett. (Netherlands)*, vol.96, no.2, p.192-9 (1 April 1983). The set of (non)orthogonal functions $D_{pq}^{(0)}(P)^{1/2}(\Omega)$, in which the Wigner rotation functions are multiplied by the equilibrium orientational distribution is shown to provide a convenient basis for the solution of the rotational diffusion problem in anisotropic liquids, in the entire range of orientational ordering. (17 refs.)

- 61744 van der Waals forces in solutions. V.V.Kuzii, V.I.Ryzhi. *Kolloid J. USSR (USA)*, vol.44, no.3, p.425-30 (May-June 1982). Translation of: *Kolloid. Zh. (USSR)*, vol.44, no.3, p.477-83 (May-June 1982). [received: Feb. 1983].

The densities of the van der Waals forces acting on dissolved substances, both in bulk solution and in a film of solution are obtained. They allow one to study the motion of dissolved substances in solutions. The density of van der Waals forces in the plane of a film of solution is used to calculate the energy of the van der Waals interaction of the atoms of a dissolved substance close to a bulk object. (5 refs.)

- 61745 On static dielectric function of simple ionic systems. M.F.Golovko, O.O.Pizio. *Dopov. Akad. Nauk UkrSR. Ser. A (USSR)*, no.2, p.47-9 (1983). In Ukrainian.

The static dielectric function is calculated for a model of charged hard spheres. It is shown to have the Debye asymptotics at large k in the entire thermodynamic parameter region. At small k in a certain region of thermodynamic parameters there is a branch of negative values which appeared due to changes of screening in the system. (10 refs.)

- 61746 On the use of the Ewald summation in computer simulation. D.J.Adams (Dept. of Chem., Univ. of Southampton, Southampton, England). *J. Chem. Phys. (USA)*, vol.78, no.5, p.2585-90 (1 March 1983). Monte Carlo calculations for the restricted primitive model at a point in the molten salt region have been made using a variety of summation methods. The empirical conclusion is that the Ewald summation is an excellent method for this work. It is shown that it does not produce significantly anisotropic pair distributions. It is shown that unlike some of the other methods considered it does not have a systematic bias towards lower energy for some configurations. It is argued that the shape of its effective pair potential does not lead to distortion of the melt structure. However, an approximate form of the Ewald summation is shown to produce significant distortions of the melt structure for the case examined. (25 refs.)

- 61747 Constant temperature molecular dynamics calculation on Lennard-Jones fluid and its application to water. H.Tanaka, K.Nakanishi, N.Watanabe (Dept. of Industrial Chem., Kyoto Univ., Kyoto, Japan). *J. Chem. Phys. (USA)*, vol.78, no.5, p.2626-34 (1 March 1983). Constant temperature molecular dynamics calculation has been carried out on Lennard-Jones liquid simulating argon. This method, proposed recently by Andersen (1980), intends to transform the system from microcanonical to canonical ensemble and to keep the temperature of the system a constant value by the generation of random velocities when molecules exchange their energies with heat reservoir with a certain probability. A simple scheme is given for the estimation of collision probability and the effect of introducing this probability on dynamic behavior is examined in detail for 108 argon atoms as a test simulation. It is established that a collision probability of 0.01 is sufficient to realize the constancy of temperature reasonably well with no appreciable disturbance in the dynamic behavior. A model of pure water with Matsuoaka-Clementi-Yoshimine (MCY) potential has also been simulated in the same manner. In the case of 216 MCY water at 298.15K, the temperature difference is only 0.73K with a collision probability of 0.005. Various static properties of MCY water have been calculated with reasonable agreement with those by previous Monte Carlo calculation, and moreover, the dynamic behavior calculated for MCY water gives a satisfactory picture on both translational and rotational motions in water, including reasonable agreement of diffusion coefficient with experimental datum. (21 refs.)

- 61748 A Monte Carlo study of semi-dilute hard sphere mixtures. P.H.Fries (Dept. de Recherche Fondamentale, CENG, Grenoble, France), J.-P.Hansen.

Mol. Phys. (GB), vol.48, no.5, p.891-901 (10 April 1983). The authors present Monte Carlo results for the high density equation of state and the partial pair distribution functions of semi-dilute solutions of large hard spheres in a solvent of smaller spheres. The simulation data for diameter ratios of 2:1 and 3:1 agree reasonably well with the predictions of Percus-Yevick theory and its semi-empirical modifications, except for the solute-solute pair distribution function. A free volume analysis of the equation of state data points to the existence of a well defined, concentration dependent, amorphous close packed density which is significantly higher than for a pure hard sphere fluid. (13 refs.)

- 61749 Virial-bias Monte Carlo methods. Efficient sampling in the (T, P, N) ensemble. M.Mezei (Dept. of Chem., City Univ. of New York, New York, NY, USA).

Mol. Phys. (GB), vol.48, no.5, p.1075-82 (10 April 1983). A new sampling technique is proposed for the isothermal-isobaric (T, P, N) ensemble Monte Carlo computer simulation. The new method selects the volume perturbations by using the partial derivative of the volume with respect to the internal energy. Test calculations on the Lennard-Jones fluid show significant improvements over the conventionally used method. (19 refs.)

- 61750 Information theory applied to time correlation functions in fluids.

J.G.Powles (Phys. Labs., Univ. of Kent, Canterbury, England). *Mol. Phys. (GB)*, vol.48, no.5, p.1083-92 (10 April 1983).

Information theory is used to predict the reorientational time correlation functions for a linear molecule in a fluid given only the moment of inertia and the mean squared torque. Comparison with 'exact' computer simulation results for a variety of fluids show that the method is remarkably successful—even when the torque is small. It is just as successful, for instance, as a much more elaborate memory-function perturbation theory which uses the same information. The method is quite general and can be usefully applied to any time correlation function. (19 refs.)

- 61751 Effective spherical potentials for molecular fluid thermodynamics.

M.S.Shaw, J.D.Johnson, B.L.Holian (Theoretical Div., Los Alamos Nat. Lab., Los Alamos, NM, USA).

Phys. Rev. Lett. (USA), vol.50, no.15, p.1141-4 (11 April 1983).

Through a thermodynamic perturbation expansion, a new sphericalization procedure has been obtained for anisotropic molecular potentials. For N_2 the resulting fluid pressures and internal energies for the effective spherical potential differ at high densities by at most 1.5% from exact molecular-dynamics calculations for the anisotropic N_2 potential. Results at lower densities are comparably good. Preliminary results for CO_2 , an even more anisotropic molecule, are also excellent. (13 refs.)

- 61752 Perturbation theory of structure factors of fluids away from their triple points. M.Itoh (School of Math. Phys., Univ. of East Anglia, Norwich, England).

Physica B & C (Netherlands), vol.115 B+C, no.2, p.240-6 (Jan. 1983).

A diagrammatic technique is applied to develop a perturbation theory of the structure factor of fluids. The authors analyse and improve the mean density approximation (MDA) by Henderson and Ashcroft (1976) which is known, within first order perturbation, to give correct small- q behaviour of the strong temperature dependence of the structure factor away from the triple point. The improved formula seems to work well for large q -values. (12 refs.)

- 61753 On the difference between the short-range order structures in a crystal and a liquid. V.P.Skripov, A.E.Galashev (Acad. of Sci., USSR).

Sov. Phys.-Crystallogr. (USA), vol.27, no.5, p.577-9 (Sept.-Oct. 1982). Translation of: *Kristallografiya (USSR)*, vol.27, no.5, p.961-5 (Sept.-Oct. 1982). [received: April 1983]

By means of a molecular-dynamic computer model, the authors obtain and compare the local structural characteristics of an FCC crystal and a liquid, for a substance of the argon type. In an analysis of the Voronogo polyhedra, together with timewise averaging, use is made of a statistical-geometrical approach. (8 refs.)

- 61754 On equilibrium properties of the multivalent ionic systems.

M.F.Golovko, O.A.Pizio, A.D.Trokhimchuk.

Ukr. Fiz. Zh. (USSR), vol.28, no.3, p.411-17 (March 1983). In Russian.

A system of charged hard spheres with arbitrary valency is considered. It simulates molten salts and an ionic subsystem of electrolyte solutions. Binary distribution functions, internal energy and the equation of state are calculated. Specific features of a short-range ionic ordering in the systems are investigated. The transition from the region of the Debye screening corresponds to the ionic gas-ionic liquid phase transition. Critical parameters are calculated at various valencies. (11 refs.)

- Comment on 'Exact statistical mechanical relations for the cell model of polyelectrolyte solutions' See Entry 61755

- Equilibrium properties of molecular fluids with charge distributions of quadrupolar symmetry See Entry 61758

- Kinetics of phase separation in binary fluids: nucleation near the critical point See Entry 62057

- Transport properties in the zero order Gaussian memory function approximation with phase integrals evaluated from Monte Carlo calculations See Entry 62148

- Smoluchowski-Vlasov theory of charge solvation dynamics See Entry 63531

61.25 STUDIES OF SPECIFIC LIQUID STRUCTURES

(see also 61.40 Amorphous and polymeric materials)

- 61755 Comment on 'Exact statistical mechanical relations for the cell model of polyelectrolyte solutions'. D.Brato (Dept. of Phys. Chem., Edvard Kardelj Univ., Ljubljana, Yugoslavia).

Chem. Phys. Lett. (Netherlands), vol.96, no.2, p.263-5 (1 April 1983).

For original paper see H. Wennesström (J. Chem. Phys., vol.76, p.4665, 1982). An extension of the recent derivation of the osmotic equation for highly symmetrical models of polyelectrolyte solutions by Wennesström et al. is proposed, leading to a generalized expression valid also for models of lower symmetry. (14 refs.)

- 61756 Sulphate-H₂O interactions in a concentrated aqueous H₂SO₄ solution. R.Caminiti (Istituto di Chimica Fisica e Industriale, Univ. di Cagliari, Cagliari, Italy).

Chem. Phys. Lett. (Netherlands), vol.96, no.3, p.390-4 (8 April 1983).

X-ray diffraction data from a H₂SO₄ solution were examined. Peaks in the range 3-5 Å in the correlation function reveal the presence of sulphate-H₂O interactions. Each sulphate ion interacts with eight water molecules. A model of hydration similar to that present in the crystal structure of H₂SO₄·4H₂O is shown to be consistent with these results. (27 refs.)

- 61757 Chemical effects in diffusion and structure of zinc chloride in aqueous solution. A.J.Eastale (Res. School of Phys. Sci., Australian Nat. Univ., Canberra, Australia), P.V.Giaquinta, N.H.March, M.P.Tosi.

Chem. Phys. (Netherlands), vol.76, no.1, p.125-8 (1 April 1983).

In the absence of neutron data, the authors have examined existing experimental data for X-ray, Raman scattering, EXAFS and thermodynamic activity studies in order to build up a consistent model of the structure of ZnCl₂ in aqueous solution in the range of molality from 2 up to saturation. The structure that emerges is that Zn is tetrahedrally coordinated and that in these coordination complexes the number of Cl ions per Zn ion increases with increasing molality, this implying the existence of extended Zn structures as the saturation concentration is approached. Relevant evidence in support of these structural models has been obtained by measuring the diffusion constants of Zn, Cl and H₂O when the stoichiometry of the solution is varied by replacing Zn by Li. This evidence strongly supports the model in which available Cl ions form complexes with Zn up to at least four Cl ions per Zn ion. (16 refs.)

- 61758 Equilibrium properties of molecular fluids with charge distributions of quadrupolar symmetry.** P.A.Monson, W.A.Steel (Dept. of Chem., Pennsylvania State Univ., University Park, PA, USA), W.B.Streett. *J. Chem. Phys. (USA)*, vol.78, no.6, pt.2, p.4126-32 (15 March 1983). Molecular dynamics simulations are reported for dense fluids of molecules with discrete charge distributions of quadrupolar symmetry. The nonelectrostatic parts of the intermolecular potentials were modeled by Lennard-Jones site-site interactions with the two sites in each molecule separated by 0.547 σ , where σ is the distance scaling parameter in the Lennard-Jones function. The charge distributions were comprised of a double negative charge at the molecular center. The magnitudes and separation distances of the charges were varied so that changes in the thermodynamic, quasithermodynamic (mean square force and torque), and structural properties of the fluid could be determined at a fixed quadrupole moment. At finite charge separation distances the multiple expansion yields ideal quadrupole-quadrupole plus higher order interactions. It is shown that the observed changes in thermodynamic properties can be accurately calculated by including the next highest multipole interaction terms in the series; namely, the ideal quadrupole-hexadecapole energies (plus a small contribution from the hexadecapole-hexadecapole terms at the largest charge separations). A low order perturbation theory calculation of the changes in structural properties is also presented; it is found not to give satisfactory values for the observed changes in radial distribution function with charge separation distance. (14 refs.)
- 61759 The interioric potential of mean force in a molecular polar solvent from an extended RISM equation.** F.Hirata, P.J.Rossky, B.M.Pettitt (Dept. of Chem., Univ. of Texas, Austin, TX, USA). *J. Chem. Phys. (USA)*, vol.78, no.6, pt.2, p.4133-44 (15 March 1983). The generalization of a recently proposed extension of the RISM integral equation to infinitely dilute isolated ions and ion pairs in polar, interaction site model, molecular solvents is outlined. An essential element of the development is the explicit separation of the contributions which yield a continuum dielectric solvent model from the remainder. Thus, it is only for this correction that one relies on the integral equation. Application is made to a system consisting of a diatomic polar solvent and atomic ions of varied charge and radius. The results of these calculations show that the present approach produces sensible qualitative features of ionic solvation including an appropriately varying degree of solvent orientational saturation with ionic charge and radius. Correspondingly, the calculated interioric potentials of mean force reproduce the same basic features manifest in already available studies of dipolar hard sphere solvents, including the positions of oscillatory features in the structure and the relatively short spatial range of the corrections to the continuum dielectric theory. A quantitative evaluation of the accuracy of the present predictions is not possible with presently available data. (33 refs.)
- 61760 Hydrogen bond dynamics in water studied by depolarized Rayleigh scattering.** O.Conde, J.Teixeira (Lab. de Phys. Thermique, Ecole de Phys. et Chimie, Paris, France). *J. Phys. (France)*, vol.44, no.4, p.525-9 (April 1983). The authors measured the depolarized Rayleigh light scattering by water from 80°C down to -17°C. The spectra obtained could be analysed into two lines, a broad and a sharp one. From the sharp line they deduced a relaxation time which can be interpreted as a reorientational time due to rotations. The broad line gives a relaxation time which is Arrhenius temperature dependent, with an activation energy $E=2.2$ kcal/mole. This shorter time can be associated with the mean lifetime of H-bonds in water and E is the activation energy of the formation and breaking of H-bonds process. This interpretation can be supported by recent measurements on quasi-elastic neutron scattering and by taking into account the librational frequencies from Raman spectroscopy. (18 refs.)
- 61761 The dynamics of water molecules in ionic solution.** N.A.Hewish (H.H. Wills Phys. Lab., Univ. of Bristol, Bristol, England), J.E.Enderby, W.S.Howells. *J. Phys. C (GB)*, vol.16, no.10, p.1777-91 (10 April 1983). High-resolution neutron quasi-elastic scattering has been applied to the problem of aqueous solutions. It is shown that for ions for which the primary hydration shell is in slow exchange with the remaining water, the frequently used two-state model is not appropriate. The experiments provide unambiguous evidence that the dynamics of water molecules other than those in the first shell are affected by the presence of ions. (25 refs.)
- 61762 Ionic dynamics in molten salts.** T.Gaskell, M.S.Woolfson (Dept. of Phys., Univ. of Sheffield, Sheffield, England). *J. Phys. C (GB)*, vol.16, no.10, p.1793-8 (10 April 1983). By means of a velocity field approach, expressions are derived for the velocity autocorrelation functions of the two ionic species in a molten salt. The theory is applied to NaCl, giving results which are in satisfactory agreement with computer simulation data. In addition to coupling to the momentum density fluctuations, the single-particle motion is also coupled to the charge density fluctuations, with a coupling constant which is proportional to the ionic mass difference. The latter effect is more significant for the lighter ion. (11 refs.)
- 61763 The study of liquid germanium structure.** M.Davidovic, M.Stojic, D.Jovic (Boris Kidrich Inst. of Nuclear Sci., Belgrade, Yugoslavia). *J. Phys. C (GB)*, vol.16, no.11, p.2053-8 (20 April 1983). The static structure factor $S(q)$ of liquid germanium is determined at 1123K by neutron diffraction techniques in the range from 0.4 to 8.5 Å⁻¹. The structure factor shows a clear low-lying shoulder on the high side of the scattering angle, near the first peak of $S(q)$. These two peaks indicate a dual structure of the germanium melt. The first one characterises the short-range order and the 'irregular' one is associated with a certain degeneracy of the atomic states of the liquid around the imperfections of the structure, which appear as single vacancies. (24 refs.)
- 61764 Scaling theory of polymer adsorption: proximal exponent.** P.G.de Gennes (Coll. de France, Paris, France), P.Pincus. *J. Phys. Lett. (France)*, vol.44, no.7, p.L241-6 (1 April 1983). The authors interpret some recent calculations of Eisenriegler, Kremer, and Binder (see *J. Chem. Phys.*, vol.77, p.6296, 1982), and related multi-critical results of Diehl and Dietrich (see *Phys. Rev. B*, vol.24, p.2878, 1981). They show that the monomer concentration profile $\phi(x)$ for isolated polymer chains in a good solvent and in close proximity to an adsorbing wall exhibits a singular behaviour; i.e. $\phi(x) \sim (a/x)^m$, where a is a monomer dimension and $m=1/3$. Taking into account the proximal exponent m , the authors correct earlier scaling results for the interfacial tension of semi-dilute polymer solutions in good solvents. They also find good agreement with a recent result by Ishinabe (1982) on the single chain energy. (13 refs.)
- 61765 Study of the short-range order of liquid polytetramethylene glycol.** V.V.Shilov, N.E.Kruglyak, Yu.S.Lipatov (Inst. of Macromolecular Chem., Acad. of Sci., Kiev, Ukrainian SSR). *J. Macromol. Sci. - Phys. (USA)*, vol.B22, no.1, p.79-109 (1983). X-ray investigations of polytetramethylene glycol oligomers with various molecular weights were carried out. Interatomic distance correlation curves were obtained using the Fourier transformation of the intensity curves. Theoretical curves of the correlation of the intramolecular interatomic distances were also calculated. The calculation of these curves has been done using the results of conformational analysis for different conformational states of the PTMG chain. Correlation curves for the intermolecular distances were then obtained by subtraction of the theoretical curves from the experimental ones. The results obtained are considered in the framework of the various models of the structural state of liquid polymers. The model of kink isomers shows the best fit with the authors' results. (46 refs.)
- 61766 Properties of polyamide gels with varying chain stiffness and length synthesized in the swollen state.** S.M.Aharoni, D.H.Wertz (Corporate Res. & Dev., Allied Corp., Morristown, NJ, USA). *J. Macromol. Sci. - Phys. (USA)*, vol.B22, no.1, p.129-57 (1983). Cross-linked networks of rigid, semirigid, and flexible polyamides were polymerized in solution. When transferred to DMAc the volume of the rigid and semirigid networks did not change significantly, but the flexible networks swelled several hundred percent. When gels previously equilibrated in DMAc were immersed in mixtures containing increasing amounts of nonsolvent, they shrank by an amount that depended on chain flexibility: the flexible and semirigid gels shrank to 30% to 40% of their as-synthesized volume, while the rigid gels shrank to only about 60% of their as-synthesized volume. Furthermore, the volume of the rigid gel decreased smoothly with the change in solvent composition. Unlike that of the rigid network, the volumes of the semirigid and flexible gels sharply decreased over a rather narrow range of solvent composition. Semirigid gels prepared at lower polymer concentration shrank over a narrower solvent composition than their counterparts prepared at higher polymer concentration. All gels changed from transparent through translucent to opaque as they shrank. The slope of the deswelling curves and the developing turbidity indicate that the collapse of the networks is not a first-order transition. (24 refs.)
- 61767 Neutron diffraction studies of water. III. Structural change as a function of temperature.** I.P.Gibson, J.C.Dore (Phys. Lab., Univ. of Kent, Canterbury, England). *Mol. Phys. (GB)*, vol.48, no.5, p.1019-30 (10 April 1983). For pt.II see *ibid.*, vol.34, p.21 (1977). Neutron diffraction measurements have been made for heavy water at five temperatures in the range 11-75°C using the diffractometers D2 and D4 at ILL. A first-order difference method has been used to determine the change in the intermolecular contributions to the observed cross-section. Fourier transformation techniques are used to give the changes in the real space distribution function. The results confirm the preliminary observations obtained in an earlier experiment and give a more precise indication of the structural variation. A detailed analysis shows that the intermolecular OD separation which corresponds to an effective hydrogen bond distance increases as the temperature rises. At larger distances there is a systematic but more complex variation which may be attributed to a change in the relative orientations of neighbouring molecules. (26 refs.)
- 61768 Neutron diffraction studies of water in meso- and micro-pores.** D.C.Steytler, J.C.Dore (Phys. Lab., Univ. of Kent, Canterbury, England), C.J.Wright. *Mol. Phys. (GB)*, vol.48, no.5, p.1031-51 (10 April 1983). Neutron diffraction studies have been made for D₂O water in two high surface area silica samples, Spherisorb and Gasil. The results show that the structural arrangement is similar to that of bulk water and that the modification due to the interface is restricted to a range of the order of 10 Å or less. Measurements also indicate that the dispersed water undergoes significant structural changes with temperature variation but the behaviour is similar to that of the bulk liquid. The differences observed in the diffraction patterns can be partially described in terms of diffraction broadening due to the small volume of the dispersed water, but there remains a significant variation which appears to be related to the hydrogen bonding interactions. (28 refs.)
- 61769 A kinetic theory for polymeric fluids.** C.F.Curtiss (Dept. of Chem., Univ. of Wisconsin, Madison, WI, USA), R.B.Bird. *Physica A (Netherlands)*, vol.118A, no.1-3, p.191-204 (March 1983). (Proceedings of the Conference on Nonlinear Fluid Behavior, Boulder, CO, USA, 7-11 June 1982). Molecular theories of polymeric fluids, both solutions and melts, have now been developed to a stage in which a broad class of nonlinear rheological phenomena may be described qualitatively and, in some cases, quantitatively. The theories contain several parameters, such as friction coefficients, chain length, and spring constants, that are determined by fitting data on rheological properties. The paper summarizes the development of these polymer kinetic theories, and particular attention is paid to the derivation of a rather general molecular theory expression for the stress tensor. The earlier dilute solution results of Kramers (1944), Risman and Kirkwood (1956), and Rouse, as well as the results of the reptation theory of Doi and Edwards (1978, 1979) for melts fit into this general development. (14 refs.)
- 61770 Dynamics of compatible polymer mixtures.** F.Brochard, P.G.de Gennes (Coll. de France, Paris, France). *Physica A (Netherlands)*, vol.118A, no.1-3, p.289-99 (March 1983). (Proceedings of the Conference on Nonlinear Fluid Behavior, Boulder, CO, USA, 7-11 June 1982). Discusses the mutual diffusion of a compatible molten mixture A+B, assuming that the chains are flexible and relatively short (non-entangled). In the macroscopic limit the mutual diffusion coefficient D_m is predicted to be extremely large (independent of the molecular weights). When one goes to shorter wave vectors q two cross-overs occur: a) when the frequency $D_m q^2$ becomes larger than the fundamental Rouse time τ_r of a single chain, the coefficient D_m becomes q dependent, $D_m \rightarrow D_m(q) \sim q^{-2}$; b) when the spatial scales become smaller than the coil size R_0 ($qR_0 > 1$) the width $D_m(q)q^2$ becomes independent of q , and is comparable to a local relaxation rate. These predictions could be tested by a combination of photon beat and neutron quasi elastic scattering. (22 refs.)
- On the use of the Ewald summation in computer simulation ...** See Entry 61746
- Constant temperature molecular dynamics calculation on Lennard-Jones fluid and its application to water ...** See Entry 61747
- Effective spherical potentials for molecular fluid thermodynamics ...** See Entry 61751
- On equilibrium properties of the multivalent ionic systems ...** See Entry 61754
- Lytropic polymeric liquid crystals ...** See Entry 61778
- Study of orientational properties of thermotropic liquid-crystalline polymer with side mesogenic groups by IR-spectroscopy method ...** See Entry 61798
- Generalized phase diagram polymer-solvent ...** See Entry 62063
- Viscosity of molten fluorozirconates ...** See Entry 62147
- Strongly entangled polymer chains in a melt. Description of NMR properties associated with a submolecule model ...** See Entry 62827
- Molecular rotation in ideal mixed systems: benzene-neopentane. I. Test of a hydrodynamic model of motion ...** See Entry 62828

- Dielectric properties and structure of *N*-methylpropionamide+methanol mixtures See Entry 62886
- The degree of order in liquid crystalline side chain polymers [from optical observations] See Entry 62922
- Interpretation of quasi-elastic light scattering data for flexible chains: model dependence See Entry 63011
- Infrared spectroscopic investigation of some carboxylic acids in nonpolar solvents See Entry 63545
- The influence of polymer concentration on the internal motion—intramolecular pyrene excimer formation—of a low molecular weight probe in solution See Entry 63577

61.25M Liquid metals

- 61771 X-ray investigation of the time dependence of liquid cast iron. B.A.Mel'nik. *Russ. Metall. (GB)*, no.6, p.49-51 (1981). Translation of: *Izv. Akad. Nauk. SSSR Met.*, no.6, p.52-4 (1981). The fine structure of the maxima of the intensities of molten commercial cast iron LK-3 (wt.%, 3.8 C, 2.67 Si, 0.64 Mn, 0.02 S, 0.1 P) was investigated as a function of the holding time (30 min, 1, 3 and 5 h) in the molten state. Diffraction patterns indicate the presence in the melt of micro-areas of cementite, graphite and austenite types. The most noticeable time-dependent changes in the structure occur during the first 15-30 min after melting, then (during 3-5 hr) the structure of the iron stabilizes to some extent. The presence of silicon in the melt causes some blurring of the diffraction effects, which are due to cementite type micro-areas, but these remain in the melt over a long period. (4 refs.)

61.30 LIQUID CRYSTALS

(see also 64.70M Transitions in liquid crystals)

- 61772 Light propagation in Williams domains as analyzed numerically by geometrical optics. K.Kondo (Dept. of Textile & Polymeric Materials, Tokyo Inst. of Technol., Tokyo, Japan), M.Arakawa, A.Fukuda, E.Kuze. *Jpn. J. Appl. Phys. Part 1 (Japan)*, vol.22, no.3, p.394-9 (March 1983). The authors have studied Williams Domain (WD) patterns in detail by observing tomograms with a polarizing optical microscope, confirming the following characteristic features: (1) there are two types of real images, upper and lower; (2) the spacings between the neighboring imaginary lines are not uniform; and (3) when the focussing plane of the objective is moved above the upper real image or under the imaginary image, the sharp image line splits into two. By taking into account the ray deflection from the wave front normal as well as the focussing effect, they have calculated numerically the characteristic distribution of phase (optical path length) as well as intensity. The results can reproduce the tomograms observed here and the photographs taken by Sato et al. (1979), holographically, showing directly the optical path length as the interference fringe patterns. (30 refs.)
- 61773 Flexoelectric constants of liquid crystals. Lin Lei (Inst. of Phys., Acad. Sinica, Beijing, China). *Commun. Theor. Phys. (China)*, vol.1, no.6, p.691-7 (1982). The elastic energy density of liquid crystal under the action of external electric field \vec{E} is given by $F = F(\vec{n}_i, n_{ij}, E_i, E_{ij}, \dots)$ where \vec{n} is the director and n_{ij} , E_{ij} the gradients. By a systematic expansion of F in polynomials and the use of material symmetries, the author obtains macroscopically for nematics and cholesterics all the possible external field effects. In addition to the well-known flexoelectric interaction $(\vec{E} \cdot \vec{n})^2$ and the flexoelectric effects of Meyer, $-e_1(\vec{E} \cdot \vec{n})(\nabla \cdot \vec{n}) - e_2(\vec{n} \cdot \nabla)\vec{n}$, the author finds a new term $e_0\vec{n} \cdot (\vec{n} \cdot \nabla)\vec{E}$ which corresponds to the flexoelectric effect related to electric quadrupoles introduced microscopically by Prost and Marcerou. This new term is not equivalent to the previous two terms of Meyer. An experiment to measure this new flexoelectric constant e_0 is proposed. Previous experiments measuring flexoelectric constants are compared and discussed in the light of the author's theory, which also applies to other cases of external vector fields. (13 refs.)
- 61774 On the possibility of microphase separation in liquid crystalline polymers. Yu.S.Lipatov, V.V.Tsukruk, V.V.Shilov (Inst. of Macromolecular Chem., Acad. of Sci., Kiev, Ukrainian SSR). *Polym. Commun. (GB)*, vol.24, no.3, p.75-7 (March 1983). The microphase structure of liquid crystalline polymers is considered in the framework of the thermodynamics of block copolymers. It is established that at a definite ratio of the flexible and rigid parts of mesogenic groups, phase separation takes place in liquid crystalline polymers. The polyesters of alkox-ybenzoic acids with 12-16 carbon atoms in the aliphatic chain end of the mesogenic groups are considered to be two-phase polymeric systems. (15 refs.)
- 61775 Variation in flatness in the successive transitions to turbulence of nematic liquid crystals. I.Matsuzaki, Y.Tsuchiya, T.Kawakubo (Dept. of Appl. Phys., Tokyo Inst. of Technol., Tokyo, Japan). *J. Phys. Soc. Jpn. (Japan)*, vol.52, no.4, p.1088-90 (April 1983). The authors have examined intermittent behavior in the successive electrohydrodynamic transitions to turbulence of nematic liquid crystals. The flatness which is a measure of the intermittency is found to enhance anomalously at the three transition points and decrease with increasing applied voltage in the turbulent region above the third enhancement point.
- 61776 Biaxial nematic phases in amphiphilic systems. A.Saupe, P.Boonbrahm, L.J.Yu (Dept. of Phys., Kent State Univ., Kent, OH, USA). *J. Chim. Phys. & Phys.-Chim. Biol. (France)*, vol.80, no.1, p.7-13 (Jan. 1983). The formation of biaxial nematic phases in mixtures of surfactants and water is discussed. Emphasis is given to experimental data that confirm the existence of a biaxial nematic phase. Some new microscopic observations and birefringence measurements are reported. Biaxial nematic phases were observed in two systems that have, in addition, two uniaxial nematic phases. The general features of the phase transitions involving these nematic phases are theoretically analyzed on the basis of a Landau expansion. Specific relations for the order parameters are derived that compare favorably with the experimental results. (21 refs.)
- 61777 Polymorphism of interfaces [Liquid crystalline phases of amphiphilic molecules]. J.Charvolin (Lab. de Phys. des Solides, Univ. Paris-Sud, Orsay, France). *J. Chim. Phys. & Phys.-Chim. Biol. (France)*, vol.80, no.1, p.15-23 (Jan. 1983). Liquid-crystalline phases are usually classified in two distinct groups: thermotropic and lyotropic. This terminology corresponds to the way they are obtained starting from the crystal of pure compound: by heating or by dilution with a solvent. Also it is generally considered that different molecular

species, called mesogenic or amphiphilic, are associated with each of these two classes. The author describes phases of classical amphiphilic molecules, mainly soaps, and consider in parallel smectic phases of various types formed by mesogenic molecules. Following this comparison the idea is proposed that a distinction between two classes of liquid-crystalline materials is arbitrary. It is suggested that the liquid-crystalline polymorphism in a general can be viewed in a more coherent fashion as a set of many variations about a unique theme, the division of space by an interface between two media, generated by a molecular structure, that is an assemblage of chemical group with different affinities and behaviors. (46 refs.)

- 61778 Lyotropic polymeric liquid crystals. E.T.Samulski (Dept. of Chem., Univ. of Connecticut, Storrs, CT, USA), D.B.Dupre. *J. Chim. Phys. & Phys.-Chim. Biol. (France)*, vol.80, no.1, p.25-30 (Jan. 1983). Experimental and theoretical developments in linear polymers that form liquid crystals in solution are reviewed. Emphasis is placed on results found in helical polypeptide liquid crystals. Advances in theoretical modeling of the order-disorder transition and the viscoelasticity of these phases are included together with a summary of recent experimental observations. (45 refs.)
- 61779 Polymorphism in polar mesogens. I. Physicochemistry and structure. F.Hardouin (Univ. Bordeaux, Talence, France), A.M.Levelut, M.F.Achard, G.Sigaud. *J. Chim. Phys. & Phys.-Chim. Biol. (France)*, vol.80, no.1, p.53-64 (Jan. 1983). In French. The authors present a synthesis of work about the physicochemistry of some fluid mesomorphic states; fluid means without tridimensional long range periodicities and with a liquid-like short range order. It embodies the updated thermodynamical and structural information describing the unexpected polymorphisms and phase transitions likely to occur from the various antiferroelectric arrangements of highly polar and polarizable molecules. In particular the uniqueness of the smectic A phase (or smectic C phase) is denied and two new bidimensional fluid mesophases have been discovered. (81 refs.)
- 61780 Polymorphism in polar mesogens. II. Theoretical aspects. J.Prost, P.Barois (Domaine Univ., Talence, France). *J. Chim. Phys. & Phys.-Chim. Biol. (France)*, vol.80, no.1, p.65-81 (Jan. 1983). For pt.I see *ibid.*, vol.80, p.53-64 (1983). A unique theoretical framework is shown to interpret not less than seven different smectic phases observed or expected in polar systems. A free energy with two coupled order parameters having a tendency to condense at two incommensurate wavevectors is used. The great number of smectic phases arises from the competition between these two incommensurate lengths: the impossibility to satisfy simultaneously contradictory tendencies is solved in many different ways, each of them corresponding to a distinct type of frustrated smectic. Several phase diagrams are presented. The stability and the expected electric properties of incommensurate phases are also discussed. (37 refs.)
- 61781 Polymorphism in polar mesogens. III. Molecular aspect. Nguyen Huu Tinh (Domaine Univ., Talence, France). *J. Chim. Phys. & Phys.-Chim. Biol. (France)*, vol.80, no.1, p.83-98 (Jan. 1983). In French. For pt.II see *ibid.*, vol.80, p.65-81 (1983). The rod-like molecules with a highly polar head exhibit an unexpected polymorphism often complex. The author proposes an analysis of the relationships between the molecular structure and the various phase sequences obtained so far. The influences of the polar end groups, of the length and the nature of the chain, of the sense of the dipole moments for the central groups, of the size and the hindrance of the core are taken in account with respect to the formation of the reentrant phases, of the different smectics A or smectics C and of the novel fluid bidimensional mesophases. The reentrant phenomenon, loses almost all its pathological character; on the other hand an increasing number of compounds owing very close molecular structures, seem likely to provide various phase transitions among phases with the same apparent symmetry. (55 refs.)
- 61782 Two dimensional ordering in liquid crystals: the SmF and SmI phases. J.J.Benattar (CENS, Gif-sur-Yvette, France), F.Moussa, M.Lambert. *J. Chim. Phys. & Phys.-Chim. Biol. (France)*, vol.80, no.1, p.99-110 (Jan. 1983). New smectic phases have been discovered: the SmF and SmI phases. They appear in some compounds when the length of the aliphatic chains reaches a sufficient value to minimize the interlayer coupling. They are characteristic of new stages between the three-dimensionally (3D) ordered SmB and SmG and the '2D liquid' SmC phase. These phases are made of stacked uncorrelated layers and exhibit either a topological 2D order in SmI or a short range order within a layer in SmF (hexatic phase). These main features are established from different experimental techniques: X-rays, neutrons, NMR and DTA. (37 refs.)
- 61783 Plastic behavior and polymorphism of smectic liquid crystal. G.Durand (Lab. de Phys. des Solides, Univ. de Paris-Sud, Orsay, France). *J. Chim. Phys. & Phys.-Chim. Biol. (France)*, vol.80, no.1, p.119-25 (Jan. 1983). Smectic systems are characterized by a lamellar ordering of more or less liquid layers. Mechanically, one expects the layers to present an elastic reaction to normal compression and a viscous reaction to a parallel shear. Rheological experiments are described in various smectic phases, which give the stress/strain relationship for small amplitude oscillations, in various geometries. Non-linear effects associated with texture instabilities are mechanically visible in the high frequency elastic regime. In smectic A, for layer compression at low frequency, a plastic relaxation probably due to the easy climb of edge dislocation, prevents the observation of the intrinsic viscoelastic relaxation associated with permeation. In smectic B, for shear parallel to the layers, above a low frequency Newtonian fluid-like behavior, one observes an elastic regime with a very low $C_{44} \sim 10^6$ cgs. This explains why the B phase appears practically as a lamellar phase, while presenting for X-rays a 3D positional ordering. (38 refs.)
- 61784 Twisted chiral mesophases. J.Billard (Lab. de Phys. de la Matière Condensée, Coll. de France, Paris, France). *J. Chim. Phys. & Phys.-Chim. Biol. (France)*, vol.80, no.1, p.127-35 (Jan. 1983). In French. The conditions for obtaining chiral mesophases with elongated molecules are studied. With the exception of the blue phases, all known chiral mesophases of these compounds are examined. Only one non-layered is twisted. The twist possibilities of the layered thermotropic mesophases are studied. Experimental data exists for five tilted smectics. The situation for four other tilted and for two normal smectics is examined. Peculiarities of the phase diagrams of two enantiomers are studied. Some physical properties of the twisted mesophases are reviewed: linear optical; surface, electric and magnetic fields alignments; textures; ferroelectricity; pyroelectricity and nonlinear optics. The methods to determine the twist sense are listed. Examples of the six known twisted mesophases are given. The most studied, the cholesteric, is emphasized. The most

useful applications of the liquid crystals, based on the particular properties of the twisted mesophases, are listed. (152 refs.)

61785 Disc-like molecules and mesogenic polymorphism. C.Destrade, H.Gasparoux, P.Foucher, Nguyen Huu Tinh (Domaine Univ., Talence, France), J.Malthete, J.Jacques.

J. Chim. Phys. & Phys.-Chim. Biol. (France), vol.80, no.1, p.137-48 (Jan. 1983). In French.

Among the various mesogenic polyaromatic cores, only benzene, triphenylene, truxene and anthraquinone hexasubstituted derivatives exhibit one or several D columnar phase and/or a N_D lenticular nematic phase. A simple answer is given for the nomenclature problem concerning the six different columnar phases: two structural parameters are sufficient for the differentiation of these phases: symmetry of the lattice, ordering or disordering in the columns. Several examples of disk-like compounds presenting these phases are described, with a discussion of the specificity of the corresponding optical textures. Then the complex polymorphism of these new mesogenic materials ('normal', 'inverse', reentrant columnar-nematic sequences) is reviewed. A simple classification of various lyotropic and thermotropic phases, based on the shape of structural element (finite or indefinite cylinder, disk, indefinite sheet, globule) is proposed. (90 refs.)

61786 Structures of mesophases formed by disc-like molecules. A.M.Lévil (Lab. de Phys. des Solides, Univ. Paris-Sud, Orsay, France).

J. Chem. Phys. & Phys.-Chim. Biol. (France), vol.80, no.1, p.149-61 (Jan. 1983). In French.

With disc-like molecules it is possible to obtain two classes of mesophases: In columnar (or canonic) mesophases, the molecules are stacked in parallel columns, these columns forming a periodic two-dimensional array. The nematic phase of disc-like molecules is similar to the ordinary nematic phase of rod-like molecules. Nevertheless a local order of columns still remains present in fluid mesophase. The author gives the limits for the disc-like phases assuming that a disc-like molecule must be (in the mesophase) made of a planar rigid core surrounded by a more or less planar ring of aliphatic chains. (40 refs.)

61787 Modulated crystal B phases and B-to-G phase transitions in two types of liquid crystalline compound. P.A.C.Gane, A.J.Leadbetter (Chem. Dept., Exeter Univ., Exeter, England).

J. Phys. C (GB), vol.16, no.11, p.2059-67 (20 April 1983).

X-ray diffraction measurements have been made of the wavevector and intensity of satellite diffraction spots as a function of temperature in two examples of crystal B phases. In N-(5-n butyloxybenzylidene)-4-n-heptylaniline (SO.7) a simple sinusoidal layer modulation of fixed wavelength grows in amplitude with decreasing temperature until the B-phase becomes unstable at the first-order B-to-G phase transition. In 4-n-pentyloxybenzenethio 4'-n-dodecyloxybenzoate (12S5) the layer modulation approximates to a ramp function which grows in wavelength at constant ramp angle with decreasing temperature until the G phase, having a very similar tilt angle is formed at a first-order transition. (9 refs.)

61788 Orientational effect of a surface light wave on liquid crystals. B.Ya.Zel'dovich, N.V.Tabiryann (Inst. of Problems in Mech., Acad. of Sci., Moscow, USSR).

JETP Lett. (USA), vol.36, no.5, p.179-82 (5 Sept. 1982). Translation of: *Pis'ma v Zh. Eksp. & Teor. Fiz. (USSR)*, vol.36, no.5, p.144-7 (5 Sept. 1982). [received: April 1983]

It is predicted that the nonpropagating light wave appearing with total internal reflection and localized near the interface has a strong effect on a nematic or cholesteric liquid crystal mesophase. The change in the Grandjean structure of the cholesteric liquid crystal is manifested as a change in pitch. On the other hand, the planar structure of the nematic liquid crystal becomes a critical structure under the action of the wave. (9 refs.)

61789 Bond orientational order in liquids and amorphous solids. D.R.Nelson (Dept. of Phys., Harvard Univ., Cambridge, MA, USA).

Physica A (Netherlands), vol.118A, no.1-3, p.315-16 (March 1983).

(Proceedings of the Conference on Nonlinear Fluid Behavior, Boulder, CO, USA, 7-11 June 1982).

Summary form only given, as follows. Recent theoretical work on the Kosterlitz-Thouless model of a dislocation-mediated melting in two dimensions suggests the existence of a new 'hexatic' phase of matter, intermediate between a solid and a liquid. Hexatic liquids display persistent correlations in the 'bonds' joining near neighbor atoms. Although computer simulations have produced conflicting evidence for an equilibrium hexatic phase, the discovery of a 'staked hexatic' phase in bulk smectic liquid crystals has been reported recently. It is interesting to consider bond orientational order in other contexts. Translational and orientational order can be studied, for example, in randomly packed planar array of hard spheres with two different sizes. For an appropriate size ratio, and a dilute concentration of large spheres, one finds a phase without translational order, but with very long range correlations in the orientations of local hexagonal axes. Bond orientational order can assume a variety of forms in bulk materials. Crystals disordered by an equilibrium concentration of unbound dislocation loops display bond orientational order with a cubic symmetry. Another possibility is orientational order with an 'icosahedral' symmetry. It is well known that an icosahedral clustering of twelve atoms about a central sphere is energetically preferable to crystalline packings for most simple pair potentials. (9 refs.)

61790 Microscopic derivation of nonlinear hydrodynamics in ordered systems with applications to nematic liquid crystals. Avraham Ben-Mizrachi, I.Procaccia (Chem. Phys. Dept., Weizmann Inst. of Sci., Rehovot, Israel).

Phys. Rev. A (USA), vol.27, no.4, p.2126-39 (April 1983).

A microscopic theory suitable for the derivation of nonlinear hydrodynamic equations in systems with a broken symmetry is presented. The theory is based on a recently introduced projection operator technique which yields results correct to any order in the deviation from equilibrium and rests on a gradient expansion around 'local-equilibrium' ensembles. The usefulness of the method is demonstrated by deriving nonlinear nematodynamics. The reversible as well as the dissipative nonlinearities are obtained in what seems to be a transparent fashion. Comparison with phenomenological derivations is presented. (20 refs.)

61791 Preliminary observations of defects in a polymeric nematic phase. M.Kleman, L.Liebert, L.Strzelecki (Lab. de Phys. des Solides, Univ. Paris-Sud, Orsay, France).

Polymer (GB), vol.24, no.3, p.295-9 (March 1983).

Some optical observations of defects (disclination lines) in a polyester nematic phase are presented. These observations clearly show the predominance of lines of half integer strength. This result, as well as other observations, seem to fit in with large values of the splay and bend constants K_1 and K_2 compared with the twist constant K_3 . However, K_1 seems to be much larger than K_3 . Interesting phenomena related to disclination core structure and to the surface lines, involving a particular molecular distribution in the surface, are described. (10 refs.)

61792 Use of molecular dynamics to investigate liquid-crystal systems consisting of disk-shaped molecules, and prediction of new mesophases in such systems. A.L.Tsykalo, A.D.Bagmet (Technol. Inst. of Refrigeration Industry, Odessa, USSR).

Sov. Phys.-Crystallogr. (USA), vol.27, no.5, p.565-9 (Sept.-Oct. 1982). Translation of: *Kristallografiya (USSR)*, vol.27, no.5, p.941-7 (Sept.-Oct. 1982). [received: April 1983]

The authors give a molecular-dynamic model of a liquid-crystal system of disk-shaped molecules. They determine the most important characteristics of the structure (orientational and translational distribution functions and order parameters). On the basis of these results they discuss the possibility of new liquid-crystal mesophases in such systems. (14 refs.)

61793 Physical properties of liquid crystals of 4-(4-alkylbicyclo[2,2,2]octyl)benzonitriles. P.Adomenas, D.Girdzhynaitis, V.A.Grozhiok, V.Sheskauskas (State Univ., Vilnius, Lithuanian SSR).

Sov. Phys.-Crystallogr. (USA), vol.27, no.5, p.607-8 (Sept.-Oct. 1982). Translation of: *Kristallografiya (USSR)*, vol.27, no.5, p.1012-13 (Sept.-Oct. 1982). [received: April 1983]

With the aim of assessing possible practical uses, the authors have synthesized several homologous 4-(4-alkylbicyclo[2,2,2]octyl)benzonitriles (1). They have studied the dielectric and optical properties and the kinematic viscosity of the compounds, including measurements of the dielectric constants and refractive indices. (8 refs.)

61794 Investigation of nematic liquid crystals by correlation spectroscopy. Determination of ratios of viscosity and elasticity constants. S.A.Ivanov, V.Yu.Vetrov (M.V. Lomonosov State Univ., Moscow, USSR).

Sov. Phys.-Crystallogr. (USA), vol.27, no.5, p.609-10 (Sept.-Oct. 1982). Translation of: *Kristallografiya (USSR)*, vol.27, no.5, p.1014-16 (Sept.-Oct. 1982). [received: April 1983]

Describes a light scattering method of determining the viscoelastic ratios of NLC, and gives the experimental geometries and results of determinations of these ratios in 4-methoxybenzylidene-4'-butylaniline (MBBA) and in a liquid-crystal mixture of p-butyl-p'-methoxyazoxybenzene (BMAOB) and p-butyl-p'-heptanoyloxyazoxybenzene (BHAOB) with marker ZhK-440. (5 refs.)

61795 An optical method of determining the elastic constant ratio K_{33}/K_{11} in nematic liquid crystals. S.A.Ivanov, V.Yu.Vetrov (M.V. Lomonosov State Univ., Moscow, USSR).

Sov. Phys.-Crystallogr. (USA), vol.27, no.5, p.611-12 (Sept.-Oct. 1982). Translation of: *Kristallografiya (USSR)*, vol.27, no.5, p.1017-18 (Sept.-Oct. 1982). [received: April 1983]

A proposed optical method of determining the elastic constant ratio K_{33}/K_{11} is based on the fact that for each oriented nematic there are two experimental geometries in which quasielastic scattering of light occurs in the B and S fluctuation modes, and that these geometries differ only in the position of the specimen. Experiments were performed with nematic liquid crystals of MBBA and ZhK-440 at temperature $t = 20^\circ\text{C}$. Planar orientation of the specimen was obtained by rubbing SnO₂-coated glass. The specimen thicknesses were 30 or 55 μ . The light source was a helium-neon laser, and the radiation receiver was an FEU-79 photomultiplier, from which the photocurrent was registered by a V2-22 digital voltmeter. The refractive indices n_o and n_e were taken from the literature: for MBBA, $n_o = 1.54$, $n_e = 1.75$; for ZhK-440, $n_o = 1.540$, $n_e = 1.784$. Starting from these values the authors calculated the laboratory scattering angles $\theta = 47^\circ$ for MBBA and $\theta = 51^\circ$ for ZhK-440. In calculating the elasticity constant ratio K_{33}/K_{11} , corrections were applied for the change in solid angle with scattering geometry, and also for one associated with the propagation of light in an anisotropic medium. (5 refs.)

61796 A new method for determining the elastic constant ratio K_{33}/K_{11} in nematic liquid crystals. G.A.Beresnev, V.G.Chigrinov, M.F.Grebenkin (Sci.-Res. Inst. of Organic Intermediate Products & Dyes, USSR).

Sov. Phys.-Crystallogr. (USA), vol.27, no.5, p.612-14 (Sept.-Oct. 1982). Translation of: *Kristallografiya (USSR)*, vol.27, no.5, p.1019-21 (Sept.-Oct. 1982). [received: April 1983]

The distinguishing feature of the authors' method is the use of a cell with so-called homeopolar orientation of the NLC (an ordinary cell of the sandwich type with transparent electrodes with the orientation of the NLC on one electrode planar, and on the other, homeotropic). The cell is placed between crossed polaroids and illuminated with light from a helium-neon laser (normally incident), and the transmission of the system is registered by a photoreceiver. If the dielectric anisotropy of the NLC is positive, then one applies to the cell a voltage sufficient to reorientate the NLC into a homeotropic structure, and, counting the number of maxima and minima of the transmission of the cell, one determines the phase lag. One does not need to know the exact dependence of the phase lag on the voltage. Using the experimental value of Δn_{hp} , K_{33}/K_{11} can be determined from computer calculations of the theoretical relationships between Δn_{hp} and K_{33}/K_{11} , in which the only other parameter is n_o/n_e . (5 refs.)

61797 Dominant role of 'weak' dispersion interactions in the formation of nematic order. V.K.Pershin, S.A.Skopinov (S.M. Kirov Ural Polytech. Inst., Sverdlovsk, USSR).

Sov. Phys.-Tech. Phys. (USA), vol.27, no.9, p.1165-6 (Sept. 1982). Translation of: *Zh. Tekh. Fiz. (USSR)*, vol.52, no.9, p.1894-6 (Sept. 1982). [received: April 1983]

It is shown that the concept of a cluster structure in NLC brings into quantitative agreement the theoretical and experimental results and explains qualitatively many of the observed phenomena. (8 refs.)

61798 Study of orientational properties of thermotropic liquid-crystalline polymer with side mesogenic groups by IR-spectroscopy method. V.L.Khodzaeva, M.V.Shishkina, V.S.Grebneva, I.I.Konstantinov.

Vysokomol. Soedin. Ser. A (USSR), vol.25, no.3, p.612-16 (March 1983). In Russian. English translation in: *Polym. Sci. USSR (GB)*

Orientational properties of thermotropic liquid-crystalline polymer with side mesogenic groups poly-p-n-butylloxyphenyl-p-metacryloyloxy-(11-undecanoyloxy)benzoate and of corresponding monomer have been comparatively studied by the IR-spectroscopy method. Both polymer and monomer were shown to form the homeotropically or homogeneously oriented liquid-crystalline films. The side mesogenic groups in these films are mutually ordered and oriented in the surface of a support normal to it, while the polymethylene spacer binding mesogenic groups with the main chain exists in the nonordered state. The degree of orientation of side mesogenic groups of a polymer corresponds of the degree of orientation of monomer molecules. Homogeneous orientation during cooling below the softening temperature is maintained which permits one to obtain oriented films of the glassy polymer. (3 refs.)

A tunable 90° rotator using a total reflection by a monodomain cholesteric liquid crystal cell See Entry 61258

Boundary layers of a nematic liquid crystal in fine capillaries See Entry 61479

- Anomalies of the laminar flow of a smectic A around a cylindrical obstacle See Entry 61481
- A modified Wigner function set for the Smoluchowski operator representation in anisotropic liquids See Entry 61743
- Phase-transition studies in polymeric compounds. I. Density studies in *N*-(*p*-*n*-hexyloxybenzylidene)-*p*-*n*-butylaniline See Entry 62097
- Microscopic and thermal phase studies on smectic and nematic liquid crystals at high pressures See Entry 62100
- Effect of the flexibility on the phase transition of polymeric liquid crystals See Entry 62101
- Electrohydrodynamic instability as a nonequilibrium phase transition See Entry 62102
- Phase transition from solid crystal to nematic liquid crystal and structural changes in an external electric field See Entry 62104
- Structure of reflection bands of Grandjean textures See Entry 62908
- Determination of cubic optical susceptibilities of liquid crystals by coherent four-photon spectroscopy See Entry 62914
- The degree of order in liquid crystalline side chain polymers [from optical observations] See Entry 62922
- Dynamics of ultrasound-induced diffraction effects in a nematic liquid crystal oriented with a magnetic field See Entry 62932

61.40 AMORPHOUS AND POLYMERIC MATERIALS

[see also 64.70P Glass transitions 81.20P to 81.20T, and 81.60 Materials science]

61799 Critical voltage effect in Ni₂Fe and FeCo ordering alloys. H.Matsuhata (Dept. of Materials Sci. & Technol., Kyushu Univ., Fukuoka, Japan), K.Kuroda, Y.Tomokiyu, T.Eguchi. *Jpn. J. Appl. Phys. Part 1 (Japan)*, vol.22, no.3, p.404-7 (March 1983). The critical voltages in ordered and disordered states of Ni₂Fe and FeCo alloys were measured for the systematic reflections without superlattice reflections. A small increase in the critical voltage was observed on ordering for the 111 systematic reflections of Li₁ type Ni₂Fe. The temperature factors and the Debye temperatures were evaluated from the measured critical voltages. The changes on ordering in the temperature factors and Debye temperatures were in reasonably good agreement with those derived by X-ray investigation and elastic constants. It is shown that the change in the critical voltage of Ni₂Fe is mainly due to the change in the thermal mean-square displacement of atoms. No obvious change in the critical voltage on ordering was detected for 110 systematic reflections of B₂ type FeCo. (19 refs.)

61800 About short-range order of amorphous i-B/N films investigated by energy loss spectroscopy. S.Klose, K.Breuer, B.Winde. *Exp. Tech. Phys. (Germany)*, vol.31, no.1, p.101-5 (1983). In German. Energy-loss-spectroscopy (ELS) is used for the investigation of ion-plated thin boron/nitrogen films. As stated in previous work, these films—when deposited adherently on various substrate materials—are hard and essentially amorphous. ELS yields information about short-range order. There is a remarkable part of material having a short-range order which corresponds to that of cubic boron nitride. (7 refs.)

61801 Transient gratings on a-GaAs under laser annealing conditions. W.Marine, J.Marfaing, F.Salvan (Dept. de Phys., Faculté des Sci. de Luminy, Marseille, France). *J. Phys. Lett. (France)*, vol.44, no.7, p.L271-8 (1 April 1983). Transient gratings are used to study the dynamical processes involved in a-GaAs crystallization on the nanosecond scale. When the irradiation power density is varied, two regimes are observed: $-3.5 \text{ MW/cm}^2 < W < 7.5 \text{ MW/cm}^2$: crystallization occurs without melting; $-7.5 \text{ MW/cm}^2 < W < 15 \text{ MW/cm}^2$: one observes a melted zone before crystallization. Free carrier diffusion is a very efficient mechanism in these laser annealing conditions. (31 refs.)

61802 Dual properties of conjugate disclination segment networks in amorphous materials. M.Kleman (Lab. de Phys. des Solides, Orsay, France). *J. Phys. Lett. (France)*, vol.44, no.8, p.L295-302 (15 April 1983). The author extends some recent results concerning the structural properties of amorphous materials deduced from a model in which the frustration effects leading to noncrystallographic short range order are described by curved spaces. It is proposed that the final structure obtained from the 'best' mapping from curved space consists in two conjugate irregular networks of straight segments, which are sources of distortions of opposite signs and of the elastic disclination type. Also, each network carries either spherical or hyperbolic curvature, in the sense that they correspond to different coordination numbers for the atoms. The typical size ξ of the network unit is estimated from a balance of (internal) elastic stresses and of core energies, at low temperature; at higher temperatures (above a typical T_0 temperature definitely smaller than T_m) the networks are mobile and their entropy must be taken into account, which leads to a dependence of ξ with temperature. Analogy and differences with a usual Vogel-Fulcher law are outlined, and the existence of some sort of long-range orientational order stressed. (14 refs.)

61803 Amorphization of crystalline diluted Ising ferromagnet. R.Honmura (Dept. de Física, Univ. Federal de Alagoas, Maceio, Brazil), I.P.Fittipaldi, E.F.Sarmiento, T.Kaneyoshi. *J. Magn. & Magn. Mater. (Netherlands)*, vol.31-34, pt.3, p.1485-6 (Feb. 1983). (Proceedings of the International Conference on Magnetism, Kyoto, Japan, 6-10 Sept. 1982).

The amorphization of a crystalline diluted Ising system is studied by using an effective-field theory. The exchange parameters are assumed to be distributed according to delta and Gaussian distributions. The authors have found that both the phase diagrams and the thermal behavior of the magnetization are strongly sensitive on the distribution assumed to the fluctuating exchange parameter. (4 refs.)

61804 Defect states in amorphous silicon. N.Ishii, M.Kumeda, T.Shimizu (Dept. of Electrical Engng. & Electronic Engng., Fukui Inst. of Technol., Fukui, Japan). *Phys. Status Solidi b (Germany)*, vol.116, no.1, p.91-100 (1 March 1983). The nature of defects in amorphous silicon is calculated by using several methods for clusters with varying size. The wave function of the dangling bond state has an approximately exponential decay with a decay length of about 0.2 nm. The correlation energy of electrons and the hyperfine structure constant with ²⁹Si for the dangling bond state are evaluated. The correlation energy and the *g*-values are calculated both for a weak bond and for a two-fold coordinated defect and are compared with experiments. (20 refs.)

61805 Effects of ionizing radiation on amorphous insulators. D.L.Griscom, E.J.Friebele (Naval Res. Lab., Washington, DC, USA).

Radiat. Eff. (GB), vol.65, no.1-4, p.63-72 (1982). (Proceedings of the First International Conference on 'Radiation Effects in Insulators', Arco, Largo di Garda, Italy, 1981).

Reviews the effects of ionizing radiation on amorphous insulators. The electronic and atomic structures of radiation-induced defect centers (trapped electrons or holes) are discussed primarily in terms of data deriving from the technique of electron spin resonance. Emphasis is placed on important fiber-optic materials (pure and doped fused silicas) and attention is directed to the problem of relating radiation-induced optical absorption bands to specific defect structures. (52 refs.)

The microstructure of Synroc See Entry 60277

Bond orientational order in liquids and amorphous solids See Entry 61789

Energy deposition effects on amorphous selenium, by low temperature neutron irradiation See Entry 61983

Annealing studies of irradiation effects in vitreous silica See Entry 61995

Photo-illumination effect on the glass transition of annealed amorphous selenium See Entry 62105

Structure of pyrolytic carbon in the process of its formation See Entry 62288

He⁺ backscattering study on Ar distribution in amorphous magnetic thin films See Entry 62293

Structure and magnetism of insoluble Pb-Fe alloy films See Entry 62294

In situ thin film differential thermal analysis of amorphous V₂O₅ thin films See Entry 62312

Magnetic properties, structure, and relaxation of amorphous Fe_{1-x}B_x films See Entry 62739

Magnetic properties of metastable crystalline and amorphous Fe alloys produced by RF sputtering See Entry 62741

Raman scattering studies on slow crystallization process from amorphous PbTiO₃ See Entry 62958

Structural interpretations for some Raman lines from vitreous silica See Entry 62963

Nonequilibrium crystallization and structural transitions during heating of microcircuit leads made of Fe-C and Fe-C-Si alloys See Entry 63285

61.40D Glasses

61806 X-ray diffraction methods to determine crystallinity and preferred orientation of lithium disilicate in Li-Zn-silicate glass-ceramic fibres. A.Benedetti, G.Cocco, G.Fagherazzi (Istituto di Chimica Fisica, Univ. Ca' Foscari, Venezia, Italy), B.Locardi, S.Meriani. *J. Mater. Sci. (GB)*, vol.18, no.4, p.1039-48 (April 1983).

Three X-ray diffraction methods for the evaluation of the microstructural features shown by glass-ceramic fibres obtained by various heat treatments have been developed and discussed. Fibres made of a Li-Zn-silicate glass of the following chemical composition were investigated (mol.%): SiO₂ 66.75, Li₂O 23.45, ZnO 8.00, K₂O 1.00, P₂O₅ 0.80. The first method is devoted to measure the preferred crystal orientation of lithium disilicate crystals which begin to grow starting from 580°C with the *c*-axis lying preferentially normal to the fibre external surface. This method has employed a four-circle diffractometer by means of which the intensity distribution of the equatorial 002 X-ray reflection could be evaluated. The other two methods regard the crystallinity content determination of lithium disilicate formed at 590°C as well as 620°C either after a nucleation step at 480°C or at 500°C, or without any nucleation treatment. The results obtained with both methods have been compared together and have been found in good agreement. (22 refs.)

61807 Mechanisms of nucleation and crystallization of lithium disilicate in Li-Zn-silicate glass-ceramic fibres. A.Benedetti, G.Cocco, G.Fagherazzi (Istituto di Chimica Fisica, Univ. Ca' Foscari, Venezia, Italy), S.Meriani, G.Scarinci. *J. Mater. Sci. (GB)*, vol.18, no.4, p.1049-58 (April 1983).

The preferred crystal orientation of Li₂Si₂O₇ crystallites has been evaluated in several partially crystallized glass fibres with the following chemical composition in mol.%: 66.75 SiO₂; 23.45 Li₂O; 8.00 ZnO; 1.00 K₂O and 0.80 P₂O₅. The crystallites were shown to be grown radially with the *c*-axis directed from the surface towards the core of the fibre. When glass fibres have been subjected to a nucleation treatment step, this preferred orientation slightly increases in the temperature range 590 to 620°C, by increasing the crystallinity content. A kinetic study on the crystalline volume coarsening, carried out according to the Johnson-Mehl-Avrami equations, showed a mechanism of linear growth for the lithium disilicate phase with the (001) growing planes moved inward from the surface to the core of the fibre. The small-angle X-ray scattering results were obtained by using a masking liquid with an electron density close to that of the glass fibres investigated, in order to eliminate the total external reflection and surface scattering. Results indicated that two distinct particle fractions are precipitated inside the fibres after glass-in-glass phase separation and nucleation at 500°C for various periods of time. The fraction of the largest particles, 13 to 20 nm in size, is probably constituted with vitreous SiO₂-rich droplets, whereas the smallest particles, 2.5 to 6.5 nm in size, are probably Li₂O-rich clusters containing P₂O₅. (38 refs.)

61808 Crystallization of amorphous Cu₆₀Zr₄₀ prepared by magnetron sputter deposition. R.G.Walmsley, A.F.Marshall, D.Bouchet, D.A.Stevenson (Center for Materials Res., Stanford Univ., Stanford, CA, USA). *J. Non-Cryst. Solids (Netherlands)*, vol.54, no.3, p.277-300 (March 1983).

The crystallization of amorphous Cu₆₀Zr₄₀ prepared by magnetron sputter deposition was studied by differential scanning calorimetry, X-ray diffraction and transmission electron microscopy. Calorimetric results were similar to those reported in the literature for liquid-quenched Cu₆₀Zr₄₀, including the manifestation of a glass transition. Crystallization above and below the glass transition temperature, *T*_g, occurred by nucleation and growth of the equilibrium phase, Cu₁₀Zr₇. This phase was characterized by convergent beam electron diffraction. With isothermal annealing below *T*_g, the time scale for crystallization indicated that the vapor-quenched alloy was kinetically more stable than the liquid-quenched alloy. This was interpreted as a difference in the quenched-in structures, produced by the different synthesis methods. During longer anneals, TEM analysis indicated that the structure was being contaminated by oxygen. (29 refs.)

61809 A study of primary crystallization in Fe₄₀Ni₃₀Mo₄B₁₈ glassy alloy by small angle X-ray scattering. G.Cocco, L.Schiffini (Istituto di Chimica Fisica Univ., Venezia, Venezia, Italy), L.Battezzati, A.Lucci. *J. Non-Cryst. Solids (Netherlands)*, vol.54, no.3, p.301-11 (March 1983).

The primary crystallization of the Fe₄₀Ni₃₀Mo₄B₁₈ glassy alloy was followed with a Kratky SAXS camera. By using SAXS conventional treatments of the experimental data, an interconnected structure was found distinctive of the

underlying texture in the early stage of the phase decomposition. At higher temperature treatments and well inside the DSC peak relevant to the solid solution appearance, the structural inhomogeneities reach a more defined morphology with a clear interphase boundary. Nevertheless, during this nucleation stage no distinctive crystalline states were detectable in the wide angle patterns. The particle size evolution points out that a coarsening mechanism starts with the achievement of the steady value of the SAXS integrated intensity and concurrently with the long range order establishment. (28 refs.)

61810 Characterization studies of $\text{AgI-Ag}_2\text{O-MoO}_3$ glasses. S.Hemlata, P.R.Sarode, K.J.Rao (Solid State & Structural Chem. Unit, Indian Inst. of Sci., Bangalore, India).

J. Non-Cryst. Solids (Netherlands), vol.54, no.3, p.313-21 (March 1983). Glass formation has been investigated in the system $\text{AgI-Ag}_2\text{O-MoO}_3$. X-ray absorption edge chemical shifts, infrared spectra and heat capacities of the various glass compositions have been measured. The probable anion structures in the oxygen excess and deficient regions have been discussed. (11 refs.)

61811 Structural relaxation in (Fe-Cr)-based glass. T.Katayama (Electrotech. Lab., Ibaraki, Japan), Y.Nishihara, M.Miyazaki, S.Ogawa.

J. Magn. & Magn. Mater. (Netherlands), vol.31-34, pt.3, p.1561-2 (Feb. 1983). (Proceedings of the International Conference on Magnetism, Kyoto, Japan, 6-10 Sept. 1982).

The Mossbauer effect of ^{57}Fe and Curie temperature in amorphous $\text{Fe}_{65}\text{Cr}_{20}\text{B}_{15}\text{Si}_2$ and $\text{Fe}_{64}\text{Ni}_{16}\text{B}_{14}\text{Si}_8$ were measured to investigate the microscopic mechanism of structural relaxation. Broadening of the Mossbauer spectra appears around 100 and 250°C of the annealing temperature in these alloys. Corresponding to the broadenings, T_c also changes after the annealing. (7 refs.)

61812 Structural relaxation and magnetism in amorphous alloys. T.Egami (Dept. of Materials Sci. & Engng., Univ. of Pennsylvania, Philadelphia, PA, USA).

J. Magn. & Magn. Mater. (Netherlands), vol.31-34, pt.3, p.1571-4 (Feb. 1983). (Proceedings of the International Conference on Magnetism, Kyoto, Japan, 6-10 Sept. 1982).

Structural relaxation phenomena in amorphous alloys caused by post-quenching heat treatments are discussed in relation to the magnetic properties. It is pointed out that both microscopically irreversible and reversible relaxation processes exist, and are related to the changes in the atomic level density fluctuation and shear fluctuation, respectively. The importance of the microscopic variables in determining the kinetics of the reversible relaxation process is emphasized. (30 refs.)

61813 Cristobalite-type cage structure models for alkali silicate glasses. A.Osaka, K.Takahashi (Dept. of Industrial Chem., Okayama Univ., Okayama, Japan).

Yogyo-Kyokai-Shi (Japan), vol.90, no.1048, p.703-9 (1982). Additivity for the molar volumes of alkali silicate glasses ($0 < R_2\text{O} < 33.3$ mol.%) was discussed in terms of two structural units, $\text{SiO}_{4/2}$ and $\text{ROSiO}_{3/2}$. The units were represented by the cristobalite-type cage skeletons composed of Si-O-Si and Si-OR-RO-Si bonds. The cages involved voids associated with the units and the glasses were regarded as the aggregates of those cage skeletons. The deviation from the linearity (additivity) of molar volumes against $R_2\text{O}$ molar fraction was excellently approximated by the random packing of two kinds of spheres which corresponded to the $\text{SiO}_{4/2}$ and $\text{ROSiO}_{3/2}$ units. Furthermore, based on the cage structure model, Si-Si distances at the bridging and non-bridging parts were evaluated. (14 refs.)

Quantitative determination of crystalline phases in nuclear waste glasses See Entry 60272

Structural effects of radiation damage in silica based glasses See Entry 60281

Helium ion damage in an amorphous Fe-Ni-Mo-B alloy See Entry 60417

Microstructural changes in irradiated silica based glasses See Entry 61975

Effect of prior large scale electron irradiation on crystallization in two Fe-Ni based metallic glasses See Entry 61976

Ion implantation effects in glasses See Entry 61992

Applications of thermoanalytical techniques to the study of crystallization kinetics in glass-forming liquids. I. Theory See Entry 62067

Electrical resistivity and thermoelectric power of glassy $\text{Fe}_{74}\text{Co}_{16}\text{B}_{10}$ and $\text{Fe}_{67}\text{Co}_{18}\text{B}_{15}\text{Si}_8$ alloys See Entry 62389

Crystallization and anisotropy in amorphous $\text{Fe}_{81}\text{B}_{13}\text{Si}_{3}\text{C}_2$ See Entry 62584

Magnetic hyperfine field distribution and structural relaxation of amorphous ($\text{Fe}_{81}\text{B}_{14}\text{Si}_4$) prepared with different quenching rates See Entry 62608

After-effect of permeability and magnetic loss of an amorphous $\text{Co}_{75}\text{Fe}_{20}\text{B}_5$ alloy See Entry 62722

Magnetic relaxation in amorphous ($\text{Fe}_{1-x}\text{Ni}_x$)/ $\text{Si}_{10}\text{B}_{13}$ alloys See Entry 62723

Dielectric characteristic in V_2O_5 crystal and crystallized glass $70 \text{ V}_2\text{O}_5 \cdot 30 \text{ P}_2\text{O}_5$ See Entry 62887

Raman and luminescence studies of alkali borate tungstate glasses See Entry 62962

Stability and crystallization of an amorphous nickel-based alloy See Entry 63266

The As_2S_3 -SnTe system See Entry 63268

61.40K Polymers, elastomers, and plastics

61814 Effect of molecular extension of a melt on the crystallinity of polyethylene, subjected to repeated crystallization. A.N.Melkumov, V.P.Prutkin, A.S.Bank, R.B.Gafurov, I.L.Gabaev.

Vysokomol. Soedin. Ser. B (USSR), vol.25, no.1, p.22 (1983). In Russian. The influence of prior molecular extension on the degree of crystallinity of recrystallized polyethylene was experimentally studied by applying different amounts of elongation to high-pressure polyethylene emerging from an extrusion die at 170°C, cooling the material to room temperature, remelting and re-extruding to thin films. Infra-red spectroscopic analysis of the films showed that, with increase in the amount of extension during the initial crystallization, the degree of crystallinity of the re-extruded polyethylene also increased, and was accompanied by a decrease in the proportion of gauche-isomers and an increase in that of trans-isomers. These results indicated that the structural elements produced under conditions of molecular extension did not disappear during subsequent melting and, during the second crystallization, served as centres for the growth of lamellae. (2 refs.) A.J.B.

61815 Structure of poly-n-phenylene-1,3,4-oxadiazole. N.I.Popik, M.V.Shabygin, L.V.Vilkov, A.S.Semenova, T.V.Kravchenko.

Vysokomol. Soedin. Ser. B (USSR), vol.25, no.1, p.38-40 (1983). In Russian. Experiments are described, aimed at elucidating the structural features of poly-n-phenylene-1,3,4-oxadiazole (POD) and based on the use of a model compound 2,5-diphenyl-1,3,4-oxadiazole (DOD). The structure of DOD was

investigated by the method of electron diffraction in the gaseous phase. The results of X-ray crystallographic analysis of crystalline DOD tended to confirm the validity of the suggested model of the structure of DOD. (17 refs.) A.J.B.

61816 Poly(ethylene sulfide): reevaluation of the electron diffraction structure analysis. B.Moss, D.L.Dorset (Electron Diffraction Dept., Medical Found. of Buffalo Inc., Buffalo, NY, USA).

J. Macromol. Sci. - Phys. (USA), vol.B22, no.1, p.69-77 (1983). The single-crystal electron diffraction data of poly(ethylene sulfide) reported by Hasegawa, Claffey, and Geil (see *ibid.*, vol.13, p.89, 1977) have been reinvestigated. Taking into account possible crystal bending effects and dynamical scattering leads to an improved structural model. The final agreement factor of $R=0.21$ is considerably better than that determined in the original analysis, $R=0.33$, attesting to the quality of the zonal electron diffraction data obtained by these investigators. (13 refs.)

61817 Radiation-induced crystallinity changes in pressure-crystallized ultrahigh molecular weight polyethylene. S.K.Bhateja (Dow Chem. Co., Midland, MI, USA).

J. Macromol. Sci. - Phys. (USA), vol.B22, no.1, p.159-68 (1983). Exposure to high-energy radiation has been known to induce structural changes in linear polyethylene (LPE). In the present work, it was decided to investigate the possibility of further enhancing, by irradiation and subsequent aging, the degree of crystallinity and melting temperature of pressure-crystallized ultrahigh molecular weight (UHMW) PE. (43 refs.)

61818 Observations of spherulitic structure by etched monolithic polypropylene samples by means of a scanning electron microscope. A.M.Atanasov, T.St.Gancheva (WMEI 'Lenin', katedra 'Chimia', Sofia, Bulgaria).

Polim. Tvorzywa Wielkocząsteczkowe (Poland), vol.27, no.8, p.303-5 (Aug. 1982). In Polish. [received: March 1983] The TEMSCANIEM 100C apparatus has been applied in the observation of spherulitic structure of bulk polypropylene samples (PD 161 grade of Hercules) etched with chromic mixture. The optimum composition of the etching solutions has been established and a high quality of patterns has been stated in recompense for the long duration of the process. (8 refs.)

61819 Structural order in alkali-degraded PAN as seen in studies of low-temperature thermal conductivity. N.S.Batty, A.J.Gradwell, J.T.Guthrie (Dept. of Color Chem. & Dyeing, Univ. of Leeds, Leeds, England), D.Greig, N.D.Hardy, R.Jakeways, M.Sahota.

Polymer (GB), vol.24, no.3, p.258-62 (March 1983). The thermal conductivity, κ , of polyacrylonitrile (PAN), subjected to varying degrees of degradation, has been measured in the temperature range 2-100K as a means of studying the structural order of the samples. Although, at higher temperatures, the variation in κ throughout the range of specimens is only ~30%, at 2K there is an order of magnitude increase in conductivity between the undegraded and most highly degraded samples. Such a change is indicative of a pronounced decrease in crystallinity, and this interpretation is supported by estimates of crystallinity as seen through X-ray analysis. (13 refs.)

61820 X-ray diffraction studies of some halatopolymers. T.A.Ibidapo, D.J.Johnson (Dept. of Textile Industries, Univ. of Leeds, Leeds, England).

Polymer (GB), vol.24, no.3, p.271-4 (March 1983). The crystal structure and degree of crystallinity of a number of melt-spinnable halatopolymers has been investigated. These materials can be characterized by a well defined 'ionic' peak at low diffraction angle. In general they have a tetragonal unit cell, although the more perfectly crystalline materials may well belong to a triclinic crystal system. Changes in crystallinity were investigated in terms of method and conditions of preparation, and of thermal treatment. Stannous dicarboxylates had the most widely variable crystallinity. (9 refs.)

61821 Small angle neutron scattering study of the structure of a triblock copolymer of styrene and isoprene during extension. R.W.Richards (Dept. of Pure & Appl. Chem., Univ. of Strathclyde, Glasgow, Scotland).

Polymer (GB), vol.24, no.3, p.275-8 (March 1983). A triblock copolymer with a styrene weight fraction of 0.41, has been examined at various extension ratios using small angle neutron scattering. The original 'polycrystalline' material with a face centred cubic arrangement of styrene domains acquires orientation as the extension ratio increases. Affine deformation is not obeyed at the supramolecular level and there is some evidence for nonuniform stress at this level. (16 refs.)

61822 The determination of molecular orientation in uniaxially compressed PMMA by X-ray scattering. G.R.Mitchell, A.H.Windle (Dept. of Metall. & Materials Sci., Univ. of Cambridge, Cambridge, England).

Polymer (GB), vol.24, no.3, p.285-90 (March 1983). A procedure is presented for obtaining full molecular orientation information from wide angle X-ray scattering patterns of deformed noncrystalline polymers. The method is based on the analysis of experimental and calculated scattering patterns into their spherical harmonics. The results obtained for PMMA are compared with values predicted by the pseudo affine and affine deformation schemes. (23 refs.)

61823 Crystal structure analysis of polyethylene with electron diffraction intensity data: deconvolution of multiple scattering effects. D.L.Dorset, B.Moss (Electron Diffraction Dept., Medical Foundation of Buffalo Inc., Buffalo, NY, USA).

Polymer (GB), vol.24, no.3, p.291-4 (March 1983). Recent determinations of n-paraffin and polyethylene crystal structures from electron diffraction data have claimed chain setting angles different from those reported for n-hexatriacontane. Re-evaluation of these data show that these determinations must be questioned because the intensities used were badly marred by multiple scattering. Due to the complexity of this phenomenon, efforts to deconvolute this error source are only partially successful. An independent structure determination for mostly unilamellar crystals of very low molecular weight polyethylene with data less affected by multiple scattering indicates that the atomic coordinates originally proposed for polyethylene in the earliest X-ray structure can still be justified. (27 refs.)

61824 Theoretical prediction of domain sizes in IPNs and related materials. J.K.Yeo, L.H.Sperling, D.A.Thomas (Materials Res. Center, Lehigh Univ., Bethlehem, PA, USA).

Polymer (GB), vol.24, no.3, p.307-13 (March 1983). A series of new theoretical equations for predicting the domain size in interpenetrating polymer networks, IPNs, and related materials was derived. The equations are based on a domain formation process comprising the crosslinking density of each polymer, mixing and demixing thermodynamics, network swelling and elastic deformation of each polymer network, and the interfacial tension between two polymers. The new equations are applicable to both crosslinked and linear materials. The experimental variables required to determine the domain size include the volume fraction and crosslink level of each polymer (or molecular weight, if linear), the interfacial tension, and the temperature. The theory was applied to poly(n-butyl acrylate)/polystyrene IPNs

and semi-IPNs. The results are also compared with the earlier theory of Donatielli et al. (1977). (32 refs.)

61825 Two-dimensional random coil chains on hexagonal lattices. V.Mom (Gorlaeus Labs, State Univ., Leiden, Netherlands). *Polymer (GB)*, vol.24, no.4, p.409-16 (April 1983). A method of formulating random coil chains that can be used as models of amorphous polymers is described. The method is based on an algorithm that finds self avoiding random chains on finite lattices. The lattice constant is chosen to be wide enough to avoid the substituents of the polymer interfering with one another. As an example, the construction of the two dimensional random coil packing structure of polyethylene is discussed. (4 refs.)

61826 Some electron microscopic observations of sulphonated EPDM polymers. P.K.Agarwal, E.B.Prestridge (Corporate Res.-Sci. Labs., Exxon Res. & Engng. Co., Linden, NJ, USA). *Polymer (GB)*, vol.24, no.4, p.487-90 (April 1983).

The electron microscopy observations have been conducted with films cast from dilute solution based on sulpho EPDMs derived from various cations. Some very interesting morphological features are observed. Aggregated regions of sizes in the range of 500 to 1000nm are found in the metal sulphonated polymers, while the absence of structure is observed in the base polymer and its acid derivative. This type of morphology has not been previously reported, and these aggregates appear about 100 times larger than typically expected for phase separated ionomers. Possible explanations of these morphologies are discussed. (23 refs.)

61827 Effect of poly(propylene oxide) segment size on structure-property relationships in elastomeric ionene. M.Watanabe, Y.Takizawa, I.Shinohara (Dept. of Polymer Chem., Waseda Univ., Tokyo, Japan). *Polymer (GB)*, vol.24, no.4, p.491-7 (April 1983).

The dynamic mechanical, thermal scanning, stress-strain and water sorption behaviours of the elastomeric ionene consisting of ionene and poly(propylene oxide) (PPO) segments are studied. The effect of PPO segment size on the microphase-separated structure in this material is described by the change of dynamic mechanical and thermal relaxation temperatures. The mixing of the PPO segment into the ionene segment domain increases with decrease of PPO segment size and reduces the crosslinking effect of the ionene segment domain, which leads to an increase in hysteresis of loading in this material. The number of equilibrium sorbed water molecules per ionene segment increases with increase in the purity of the ionene segment domain. (24 refs.)

61828 Investigation by the molecular-probe method of the changes in the packing density of filled epoxide compositions during hardening. G.Ya.Menzeres, A.N.Dyakova, M.S.Kligshstein, E.G.Moisya, F.G.Fabulyak (Inst. of Chem. of High-Molecular-Weight Compounds, Acad. of Sci., Kiev, Ukrainian SSR).

Theor. & Exp. Chem. (USA), vol.18, no.2, p.219-22 (March-April 1982). Translation of: *Teor. & Ekspr. Khim. (USSR)*, vol.18, no.2, p.253-6 (March-April 1982); [received: Feb. 1983]

The authors used the molecular probe method to investigate the dynamics of the change in the packing density during hardening of three-dimensional epoxide systems based on ED-20 and also evaluated the degree of heterogeneity of the resulting three-dimensional structures. (10 refs.)

61829 Effect of the filler on relaxational transitions in butadiene-methylstyrene copolymer. G.M.Bartenev, B.I.Revyakin, N.M.Lyalina, K.Boturov.

Vysokomol. Soedin. Ser. A (USSR), vol.25, no.3, p.511-16 (March 1983). In Russian. English translation in: *Polym. Sci. USSR (GB)*

In butadiene-methylstyrene copolymer being filled by carbon black ten relaxational transitions have been found above T_g : λ -transitions related with existence of macro-blocks of supersegmental and supermolecular structure of various nature, δ_1 and δ_2 -transitions related with the rearrangement and rupture of chemical S-S and C-C cross bonds, ϕ -transition related with the rearrangement of particles of the active filler. Introduction of the filler decreases the contribution of λ - and δ_2 -transitions. The correlation between temperatures of transitions calculated from the spectra of relaxation times (static method) and determined from the spectra of internal friction (dynamic method) is observed. (10 refs.)

61830 Structural features of smectic ordering in polymers with acrylate and methacrylate main chain. V.V.Tsukruk, V.V.Shilov, Yu.S.Lipatov, I.I.Konstantinov, Yu.B.Amerik.

Vysokomol. Soedin. Ser. A (USSR), vol.25, no.3, p.526-31 (March 1983). In Russian. English translation in: *Polym. Sci. USSR (GB)*

The structure of comb-like polymers with different main chains has been studied by small- and wide-angle X-ray scattering methods. The structural characteristics of polymers with various structure of side mesogenic groups were found (thickness of smectic layers, parameters of disordering of the layered packing, dimensions of layered stacks, fluctuations of electronic density). The layered structure in polymers with methacrylate main chains was shown to be essentially less perfect than in corresponding polymers with acrylate main chains. (16 refs.)

61831 Molecular mechanism of shrinkage of polyethylene terephthalate. P.M.Pakhomov, M.V.Shabilygin, B.A.Tsaplin, S.A.Baranova, Z.P.Vysotskaya. *Vysokomol. Soedin. Ser. A (USSR)*, vol.25, no.3, p.572-7 (March 1983). In Russian. English translation in: *Polym. Sci. USSR (GB)*

The molecular mechanism of shrinkage of amorphous oriented PETP has been studied by IR-spectroscopy method. The shrinkage phenomena in amorphous flexible polymers are shown to obey the rotational isomers mechanism related with the redistribution and change of the relative content of various conformers. The kinetic study of shrinkage shows that this process is related with cooperative conformational rearrangements in the field of molecular forces. (14 refs.)

61832 Morphology of polyallomers. V.P.Popov, Yu.K.Godovskii, Yu.M.Malinskii, N.M.Titova, V.A.Aulov, L.I.Bezruk, I.A.Litvinov.

Vysokomol. Soedin. Ser. A (USSR), vol.25, no.3, p.594-9 (March 1983). In Russian. English translation in: *Polym. Sci. USSR (GB)*

The morphology and some properties (density, crystallinity, T_m of both phases, temperatures of relaxational transitions) of polypropylene-polyethylene and polypropylene-polybutene-1 polyallomers have been studied by some physico-chemical and physical methods. The mutual influence of components on their crystallization was shown and the mechanism of this phenomenon was proposed. (15 refs.)

61833 Theoretical determination of crystalline structure of polyethylene. L.M.Borisanova, L.A.Zasurskaya, P.M.Zorkii.

Vysokomol. Soedin. Ser. A (USSR), vol.25, no.3, p.600-5 (March 1983). In Russian. English translation in: *Polym. Sci. USSR (GB)*

An approach to the theoretical prediction of crystalline structure of a polymer without use of experimental data about the packing of chains in a crystal has been worked out for PE. The theoretically possible packings of rhombic PE were obtained with the aid of the method of symmetry of potential functions of intermolecular interaction. The quantitative characteristics of these pack-

ings were determined by minimization of potential energy calculated in the atom-atom approximation. This approach permitted to choice of the limited number of variants including structures close to experimentally observed ones. (21 refs.)

The effect of disorder in stereo-irregular polymer chains See Entry 61034

On the work hardening rate of glassy polymers. I. Application to the physical ageing of atactic PMMA See Entry 62014

Interstitial polymers based on a polyurethane network. I. Melting points and fractional crystallinities See Entry 62068

Thermal and mechanical properties of tetramethyl-*p*-silphenylenesiloxane/dimethylsiloxane block copolymer See Entry 62069

Dependence of the glass transition temperature on relaxation times See Entry 62106

Distribution of double bonds in thermally degraded polyisobutylene. (PMR observations) See Entry 62820

Strongly entangled polymer chains in a melt. Description of NMR properties associated with a submolecule model See Entry 62827

The degree of order in liquid crystalline side chain polymers [from optical observations] See Entry 62922

Time dependent light scattering studies of phase separation in polymer blends See Entry 63008

Interpretation of quasi-elastic light scattering data for flexible chains: model dependence See Entry 63011

Orientation of polystyrene chains stretched above T_g as studied by fluorescence polarization See Entry 63048

Fluorescence probe for microenvironments: on the fluorescence properties of *p*-*N*,*N*-dialkylaminobenzylidenemalononitrile in polymer matrices See Entry 63049

Kinking in the drawing of linear polyethylene See Entry 63351

Structural-mechanical features of two-stage shear strain of oriented low density polyethylene See Entry 63372

The influence of polymer concentration on the internal motion—intramolecular pyrene excimer formation—of a low molecular weight probe in solution See Entry 63577

61.50 CRYSTALLINE STATE

(inc. molecular motions in solids; for magnetic structure and spin systems, see 75.25)

61834 Quantitative description of real close-packed structures and their analysis by diffraction effects. E.A.Pilyankevich, A.I.Ustinov, K.V.Chuistov (Inst. of Phys. of Metals, Acad. of Sci., Ukrainian SSR). *Sov. Phys.-Crystallogr. (USA)*, vol.27, no.5, p.530-2 (Sept.-Oct. 1982). Translation of: *Kristallografiya (USSR)*, vol.27, no.5, p.881-5 (Sept.-Oct. 1982). [received: April 1983]

In the framework of a unified description of one-dimensionally disordered structures, by the introduction of parameters characterizing the relative positions of packing displacements, the authors solve both the direct and the converse problems of diffraction, and are thus able to give a quantitative estimate of the degree of perfection of such a structure and to determine the short-range ideal lattice. (27 refs.)

Hindered internal rotations in Van der Waals molecules and molecular crystals See Entry 60885

On the difference between the short-range order structures in a crystal and a liquid See Entry 61753

Evidence of a 'glassy crystal' phase obtained by the quenching of the plastic phase of the cyanoadamantane See Entry 62107

Dielectric properties of 1-cyanoadamantane $C_{10}H_{15}CN$, in its plastic phase See Entry 62883

Tunnelling motion of dipolar impurities in alkali halides: the $KI:NO_2^-$ system [IR spectra] See Entry 63024

61.50C Physics of crystal growth

(for techniques of crystal growth and film deposition, see 81.10 and 81.15; for epitaxy, thin films, see 68.55; for whiskers, see 68.70)

61835 Kinetics of the collective crystallization of doped ZnS. F.K.Volynets, E.I.Gorokhova, A.D.Kashkai.

Inorg. Mater. (USA), vol.18, no.5, p.621-4 (May 1982). Translation of: *Izv. Akad. Nauk SSSR Neorg. Mater.*, vol.18, no.5, p.733-7 (May 1982). [received: Feb. 1983]

The effect of pressure on the mean grain size depends on the ratio of this pressure to the yield stress of the powder being pressed. If this ratio is less than one, then pressure promotes the preclusion of the inhibiting role of the pores and, thereby, promotes an increase in the mean grain size. When the ratio is greater than one, pressure is the cause of the plastic deformation of the grains and, consequently, of primary recrystallization coming into play. The mean grain size in the briquet which is obtained, as well as the energy of activation for the collective crystallization process, decrease. Readily fusible doping admixtures promote the compacting of the briquet and a growth in the mean grain size. It has been confirmed, using ZnS as the example, that collective recrystallization is dictated not by the grain size but by the extent, to which the angles at the triangular points deviate from 120° . (13 refs.)

61836 Determination of the Ising critical temperature of F slices with an application to garnet. J.J.M.Rijkema, H.J.F.Knops (Inst. of Theoretical Phys., Univ. of Nijmegen, Nijmegen, Netherlands), P.Bennema, J.P.van der Eerden.

J. Cryst. Growth (Netherlands), vol.61, no.2, p.295-306 (March 1983).

A general and simple method to calculate exactly the critical temperature for Ising nets on periodic structures is introduced. The method can be used to predict the morphological importance of F slices for realistic crystals. As an illustration it is applied to several types of garnet. The results are confronted with morphological data. (27 refs.)

61837 Growth kinetics of TGS. L.N.Rashkovich, V.T.Leshchenko, N.M.Sadykov (M.V. Lomonosov State Univ., Moscow, USSR).

Sov. Phys.-Crystallogr. (USA), vol.27, no.5, p.580-5 (Sept.-Oct. 1982). Translation of: *Kristallografiya (USSR)*, vol.27, no.5, p.966-74 (Sept.-Oct. 1982). [received: April 1983]

The authors describe an interference method of registration of the growth rates of large anisotropic crystals in a stirred solution. They show that for crystallization in constant conditions the RMS deviation σ of the growth rate of the (001) face about its mean is 5-10%, 2-3 times greater than the

experimental error. There are also rare but marked $\{3\text{-}4\sigma\}$ variations in the mean rate. In some intervals of time, the growth rate is independent of changes in the supersaturation of the solution. The authors suggest that the variations in rate are not governed by the structure of the surface. (14 refs.)

61838 Features of the growth of potassium pentaborate crystals. V.N.Voitsekhovskii, V.P.Nikolaeva, I.A.Velichko. *Sov. Phys.-Crystallogr. (USA)*, vol.27, no.5, p.585-7 (Sept.-Oct. 1982). Translation of: *Kristallografiya (USSR)*, vol.27, no.5, p.975-80 (Sept.-Oct. 1982). [received: April 1983]
Potassium pentaborate crystallizes from aqueous solutions in the form of twins with various habits, which are combinations of twinning on the planes $\{011\}$, $\{032\}$, and $\{001\}$. In twinning on $\{011\}$; the $\{111\}$ faces, which form the cap of the twinned concretion, have an enhanced growth rate owing to generation of growth layers at centers formed near the twin contact. Increase in the growth rate of individual faces of twinned concretions is a rather widespread phenomenon. (10 refs.)

61839 On the possibility of obtaining a uniform impurity distribution in growing crystals by the Bridgman-Stockbarger method. A.L.Mamyan, O.G.Nalbalyan (Sci.-Res. Inst. of Phys. of Condensed Media, State Univ., Erevan, USSR). *Sov. Phys.-Crystallogr. (USA)*, vol.27, no.5, p.622-3 (Sept.-Oct. 1982). Translation of: *Kristallografiya (USSR)*, vol.27, no.5, p.1034-5 (Sept.-Oct. 1982). [received: April 1983]
Steady growth is characterized by the presence of a definite excess of impurity ahead of the crystallization front. The total number n of growth-fusion cycles is determined by the thoroughness of purification of the initial section (of length x_0) from impurity. The occurrence of convection in the melt, when the boundary diffusion layer is shorter than x_0 , can have a marked influence on the effect in question. The authors conclude, following their theoretical discussion, that in the Bridgman-Stockbarger method, a uniform impurity distribution can be obtained only with small crucible diameters. (2 refs.)

61840 Influence of capsule diameter on the impurity distribution in a growing crystal. V.Krivandina (Inst. of Crystallography, Acad. of Sci., USSR). *Sov. Phys.-Crystallogr. (USA)*, vol.27, no.5, p.623-4 (Sept.-Oct. 1982). Translation of: *Kristallografiya (USSR)*, vol.27, no.5, p.1036-7 (Sept.-Oct. 1982). [received: April 1983]
To elucidate the influence of the container diameter on the impurity distribution along the crystal, the authors chose growth conditions in which marked macroperiodicity arises in dibenzyl crystals with tolan as impurity. Single crystals up to 135 mm long were obtained in a crystallization apparatus for growing crystals 10 mm in diameter. To avoid large changes in the design and operation mode of the apparatus, crystals of smaller diameter were grown in glass tubes with internal diameters of 6.8 and 3.7 mm, placed within the 10 mm tubes. The authors show that in vertical directed crystallization of a binary mixture of dibenzyl and tolan from a melt, as the container diameter is reduced, convective mass exchange becomes more difficult. These results lead them to the conclusions that the transition from a convective to a diffusional mechanism of transport depends not only on the crystallization conditions but also on the diameter of the container. (4 refs.)

61841 Initial growth forms of single crystals of chromium with copper on its surface. V.M.Gennad'ev, A.A.Nosov, N.P.Ovsyannikov (Radiotech. Inst., Ryazan', USSR). *Sov. Phys.-Crystallogr. (USA)*, vol.27, no.5, p.625-6 (Sept.-Oct. 1982). Translation of: *Kristallografiya (USSR)*, vol.27, no.5, p.1038-9 (Sept.-Oct. 1982). [received: April 1983]
The dynamics of formation of initial growth forms of chromium crystals were investigated by observing the crystal forms under the scanning electron microscope. The chromium crystals were formed by condensation of chromium from the vapor phase on a polycrystalline molybdenum substrate on which a layer of copper had been deposited. This was effected in a vacuum sputtering apparatus (residual gas pressure about 5×10^{-7} torr). The dynamics of formation of the relief of the chromium protuberances on the substrate surface was observed after stopping the deposition process at various stages. The results of X-ray microspectral analysis revealed that in this first stage the protuberances of chromium with hemispherical tops are covered by a film of copper. In the first stage of formation of the crystal, the presence of a layer of copper on the protuberances reduces the anisotropy of the growth rate and the surface energy. (6 refs.)

Morphology and crystal growth of structurally related A_2BX_4 and A_3BX_6 compounds See Entry 61896

Growth twins of biphenyl See Entry 61934

Shape of crystals at low temperatures: absence of quantum roughening See Entry 62207

Analysis of the process of deposition of solid solutions of composition $Ga_{1-x}In_xAs_{1-x}P_x$ form the gas phase using the method of particle pressure diagrams See Entry 63139

61.50E Crystal symmetry; models and space groups, and crystalline systems and classes

61842 Local symmetry points in crystal lattices. P.Kadura (Sektion Chemie, Friedrich Schiller Univ., Jena, Germany). *Wiss. Z. Friedrich-Schiller-Univ. Jena, Math. Naturwiss. Reihe (Germany)*, vol.31, no.6, p.963-73 (1982). In German.
The authors previously published a paper (see *ibid.*, vol.30, p.443, 1981) describing general methods how to find all local symmetry points of any crystal. The usefulness of these methods is demonstrated by applying it to actual lattices. (6 refs.)

New symmetry and structure for spinel See Entry 61885

61.50J Crystal morphology and orientation

61843 A method of calculating the rotation angle about a single rotation axis between any pair of measured crystallographic orientation relationships. K.Kobayashi (Dept. of Metal Sci. & Technol., Kyoto Univ., Kyoto, Japan), L.M.Hogan. *Met. Forum (Australia)*, vol.5, no.3, p.147-53 (Winter 1982).
A method of rotation is presented by which any departure from coincidence is expressed as a rotation angle. If the rotation angle is large, the two measured orientation relationships do not express the same relative orientation between the phases. The method is applicable to cubic crystals. (4 refs.)

61.50K Crystallographic aspects of polymorphic and order-disorder transformations

61844 Atomic ordering in solid solutions. V.V.Cherkashin, Yu.A.Vereshchagin, A.A.Kuranov, F.A.Sidorenko (S.M. Kirov Ural Polytech. Inst., Sverdlovsk, USSR). *Fiz. Met. & Metalloved. (USSR)*, vol.55, no.2, p.394-6 (Feb. 1983). In Russian. English translation in: *Phys. Met. & Metallogr. (GB)*
A study was made of the ranges of concentrations and temperatures in which superstructures were stable in $(Fe_{1-x}Mn_x)Pd$ solid solutions. The ranges of stability were deduced from X-ray diffraction data and from the temperature dependences of the paramagnetic susceptibility. It was found that a continuous series of solid solutions with the f.c.c. lattice was formed by the investigated system in the disordered state. Ordering took place below 935-890K giving rise to $L1_2$ superstructures in the range $0 \leq x \leq 0.45$ and to DO_{23} superstructures in the range $0.60 \leq x \leq 1.0$. (2 refs.) A.T.

61845 Study of $\alpha \rightleftharpoons \beta$ transition in americium. V.D.Shushakov, A.G.Seleznev, N.S.Kosulin, T.V.Shushakova. *Fiz. Met. & Metalloved. (USSR)*, vol.55, no.2, p.405-7 (Feb. 1983). In Russian. English translation in: *Phys. Met. & Metallogr. (GB)*
A detailed investigation was made of the transition occurring at $\sim 1044K$ in metallic americium: this transition transforms the double h.c.p. lattice into one with the f.c.c. structure. The study was carried out by the method of high-temperature X-ray diffraction. The rate of cooling or heating affected the transition temperature and so did an applied pressure. (5 refs.) A.T.

61846 Structural and thermal characterization of the γ'' polymorph of Bi_2MoO_6 . P.Gaucher, V.Ernst, P.Courtine (Dept. de Genie Chimique, Univ. de Technol. de Compiègne, Compiègne, France). *J. Solid State Chem. (USA)*, vol.47, no.1, p.47-52 (15 March 1983).
Among the different polymorphic phases of the Bi_2MoO_6 system, the intermediate γ'' compound has been characterized within a metastable state by high temperature X-ray diffraction and Raman spectroscopy. The transition $\gamma \rightleftharpoons \gamma''$ is found to be partially displacive and partially reconstructive. In the context of the ferroelectricity of γ , the nature of the paraelectric phase is discussed with the help of space group considerations and Buerger's theory of phase transitions. (8 refs.)

Structural transitions in superionic conductors See Entry 62090
Order-disorder transition in Fe_3Si alloy during mechanical crushing See Entry 63286

61.50L Crystal binding

61847 Fractionally charged ions in crystal lattices of organic ion-radical salts. L.Komorowski (Inst. of Organic & Phys. Chem., Tech. Univ. of Wrocław, Wrocław, Poland). *Chem. Phys. (Netherlands)*, vol.76, no.1, p.31-43 (1 April 1983).
The energy of an atom in a molecule is discussed on the basis of the definition of the chemical potential of electrons in a quantum system. An expression for the energy of the fractionally charged atom is proposed, and a master equation for the charge-dependent cohesive energy of a crystal is developed. Calculated net atomic charges in solid alkali halides are close to unity and their calculated cohesive energies indicate high percent of covalent bonding. The charge transfer at the energy minimum calculated for several organic, conducting ion-radical salts agree perfectly with the values determined experimentally. The lattice is stabilized by the charge transfer, although the ionic interactions reproduce only part of the crystal cohesive energy. (59 refs.)

61848 Monte Carlo simulations of solid nitrogen in the isothermal-isobaric ensemble with an ab initio SCF-CI potential. S.Romano, B.Jonsson, G.Karlstrom (Phys. Chem. 2, Chem. Centre, Lund, Sweden). *Int. J. Quantum Chem. (USA)*, vol.23, no.3, p.991-8 (March 1983). (Proceedings of the Fourth International Congress in Quantum Chemistry, Uppsala, Sweden, 13-20 June 1982).
Monte Carlo simulations in the isothermal-isobaric ensemble for the α phase of solid N_2 have been carried out with two different pair potentials obtained from ab initio quantum chemical calculations. Comparison is made with data obtained from empirical potentials as well as with experimental data, and in general, the agreement with experiment is found to be good. It is also found that the differences between experiment and theory can largely be attributed to correlation effects, not considered in the quantum mechanical calculations of the pair potential. (57 refs.)

61849 Nature of the chemical bond in titanium hydrocarbides. V.V.Nemoshkalenko, M.M.Kindrat, V.P.Krivitskii, B.P.Mamko, V.M.Prokopenko, A.I.Kharlamov (Inst. of Metallophys., Acad. of Sci., Ukrainian SSR). *Inorg. Mater. (USA)*, vol.18, no.5, p.669-72 (May 1982). Translation of: *Izv. Akad. Nauk SSSR Neorg. Mater.*, vol.18, no.5, p.795-9 (May 1982). [received: Feb. 1983]

In titanium hydrocarbides there is a hydrogen-carbon interaction. When hydrogen is absorbed by nonstoichiometric carbides, the hydrogen atoms occupy tetrahedral vacancies. The dissolution of hydrogen on nonstoichiometric titanium carbides does not lead to any change in the charge density in the spheres of the titanium and carbon atoms. (6 refs.)

61850 Basic-potential method for studying crystal potential. Y.Sakamoto, M.Miura, K.Hiraga, H.Murata (Hiroshima Univ., Hiroshima, Japan). *J. Sci. Hiroshima Univ. A (Japan)*, vol.46, no.2, p.267-336 (Jan. 1983).
The basic-potential (BP) method is reviewed, and is developed anew in many respects. It has a wide and neat applicability to a collective or accurate study of simple or complex crystals built by bond or antibond of various types: ionic, metallic, covalent, (electronutrally) molecular, and even pseudo-chemical types. Its comprehensiveness is supported from two sides. One is its cooperation with the lattice-complex method of describing the crystal structure. The other is its subsumptive unity in variety of potential peculiar to a bond type; thus Hund's and Jones's BP lump under Euler's BP, which then unites with Born's BP to form the Epstein zeta function. Euler's BP is raised to Birman's pair of BP's which can manage the source of force in an expanse-atom approximation. Two other kinds of standard potentials due to Naor and to Zucker are referred to. An effective coordination number is defined by reference to a crystal-potential factor. For the sake of the numerical application, basic formulas are arranged and available materials such as computer programs, tables, and graphs are listed. (124 refs.)

61851 Magnetism or bonding: a nearly periodic table of transition elements. J.L.Smith, E.A.Kmetko (Los Alamos Nat. Lab., Los Alamos, NM, USA). *J. Less-Common Met. (Switzerland)*, vol.90, no.1, p.83-8 (March 1983).
A table of the transition metal elements is constructed to show their dominant electronic features. The strictly periodic table of the elements is misleading

for the study of many useful metallic materials. The actinide series is central to this new view. (14 refs.)

- On basic thallium sulfates: structure of $\text{Ti}_2\text{TiOH}(\text{SO}_4)_2$ See Entry 61878
 The crystal structures of α - and β -forms of plutonium(IV) sulphate tetrahydrate See Entry 61894
 Crystal morphology of monoclinic potassium feldspars. A qualitative approach with special emphasis on the periodic bond chain theory of Hartman and Perdok See Entry 61895
 Effect of three-body forces on thermophysical and anharmonic properties of rare gas solid mixtures See Entry 62041
 Structural phase stability in third-period simple metals See Entry 62093
 Self-consistent semirelativistic pseudopotential calculation of the energy bands, cohesive energy, and bulk modulus of W See Entry 62329
 AES investigations of chemical composition of some alkali compounds See Entry 63630

61.55 SPECIFIC STRUCTURE OF ELEMENTS AND ALLOYS

61.55D Nonmetallic elements

- Solid and gaseous carbon allotropes in ultrahigh vacuum at 3K See Entry 64536

61.55F Metallic elements

- The projected atomic structure of a large angle $[001] \Sigma=5$ ($\theta=36.9^\circ$) twist boundary in gold: diffraction analysis and theoretical predictions See Entry 61930
 Self-consistent semirelativistic pseudopotential calculation of the energy bands, cohesive energy, and bulk modulus of W See Entry 62329
 Electron transfer of hydrogen in aluminum at 20 and 800°C See Entry 62372

61.55H Alloys

- 61852 The crystal structure of R_2GaCo_2 compounds ($\text{R}=\text{Y}, \text{Tb}, \text{Dy}, \text{Ho}, \text{Er}, \text{Tm}, \text{Lu}$). R.E. Gladshchevskii, Yu.M. Gryn', Ya.P. Yarmolyuk. *Dopov. Akad. Nauk UkrSR. Ser. A (USSR)*, no.2, p.67-70 (1983). In Ukrainian.

The crystal structure of the Ho_2GaCo_2 was investigated by examining a single crystal using an autodiffractometer: space group Immm , $a=0.9294$, $b=0.9370$, $c=0.9804$ nm, 8 Ho in 8(n): $x=0.2194$; $y=0.1836$; $z=0$; 8 Ho in 8(f): $0; 0.3029; 0.2668; 8 \text{ Ho in } 8(m): 0.1968; 0; 0.3210$; 2 Ga in 2(d): $0.5; 0; 0.5$; 2 Ga in 2(b): $0; 0.5; 0.5; 4 \text{ Co in } 4(h): 0; 0.134; 0.5; 4 \text{ Co in } 4(f): 0; 0; 0.116$. The final R-value is equal to 0.104 for 350 reflections. Coordination numbers for atoms of Ho are 13-15, Ga—12-14, Co—9-10. The structure is represented as a framework of Ho atoms, whose icosahedral and cuboctahedral vacancies are filled with Ga atoms and tetragonalantiprismatic vacancies—with Co atoms. Other methods of vacancy filling are represented in structures of As_2Co , Al_2W , $\text{P}_2\text{Fe}_2\text{La}$. Compounds isostructural to Ho_2GaCo_2 are found in the Y, Tb, Dy, Er, Tm and Lu systems. Their crystallographic characteristics are given. (5 refs.)

- 61853 Electron microscope studies on the Sm-Co and Sm-Ni intermetallic compounds. S. Takeda (Hiroshima Univ., Hiroshima, Japan). *J. Sci. Hiroshima Univ. A (Japan)*, vol.46, no.2, p.149-94 (Jan. 1983). Polytopy structures and lattice defects in the ferromagnetic Sm-Co and Sm-Ni intermetallic compounds are investigated by electron microscopy. In Sm_2Ti and Sm_2Ti_9 (T; Co or Ni) compounds several different crystallographic modifications (polytypes) are found besides the previously known 2H and 3R modifications. Crystal structures of the new polytypes are analysed by the electron diffraction method. The technique of high-resolution electron microscopy is applied to study the defect structures in the Sm_2Ti_9 compounds. One- or two-dimensional lattice images are obtained in Sm-Co or Sm-Ni compounds, respectively. Various kinds of the defects are observed and the atomic arrangements are analysed: (1) Stacking faults in Sm_2Ti_9 , (2) Intergrowth with the Sm_2Ti structure or unknown structures in the matrix of Sm_2Ti_9 , (3) Complicated defect structures which change the stacking sequence of Sm_2Ni_9 , and (4) Lattice defects observed in terminating region of the intergrowth. (46 refs.)

- 61854 $\text{CaMn}_x\text{Al}_{2-x}$ and CaMn_xAl_8 ternary representatives of MgNi_2 and ThMn_{12} structures, respectively. E. Czech, G. Cordier, H. Schafer (Eduard-Zintl-Inst., Tech. Hochschule, Darmstadt, Germany). *J. Less-Common Met. (Switzerland)*, vol.90, no.1, p.109-19 (March 1983). In German.

The new compound $\text{CaMn}_x\text{Al}_{2-x}$ (with $0.16 \leq x \leq 0.32$) crystallizes in the hexagonal system (space group, $P6_3/mmc$) in the MgNi_2 structure with lattice constants $a=572.3(3)$ pm, $c=1826.4(5)$ pm and $c/a=3.191$. The new compound CaMn_xAl_8 crystallizes in the tetragonal system (space group, $I4/mmm$) with constants $a=895.7(1)$ pm, $c=516.8(1)$ pm and $c/a=0.577$. The structure corresponds to a ternary variant of the ThMn_{12} structure. (23 refs.)

- 61855 A low temperature crystal modification of the rare earth ternary compounds RCuSi . A. Iandelli (Istituto di Chimica Fisica, Univ. di Genova, Genoa, Italy). *J. Less-Common Met. (Switzerland)*, vol.90, no.1, p.121-6 (March 1983). RCuSi compounds of the trivalent rare earths were prepared in a low temperature modification. Their structure corresponds to the Ni_2In -derived type with an ordered arrangement of copper and silicon atoms in flat hexagonal layers. It appears to satisfy a condition common to other isostructural compounds, i.e. a valence electron concentration of 8/3. (8 refs.)

- 61856 The crystal structure of UMn_2 . A.C. Lawson (Los Alamos Nat. Lab., Univ. of California, Los Alamos, NM, USA). *J. Less-Common Met. (Switzerland)*, vol.90, no.1, p.113-16 (March 1983). The author presents a re-analysis of the data of Marpo and Lander (1978), showing that at low temperatures UMn_2 has a more symmetric orthorhombic structure which is characterized by a single non-magnetic U-U nearest-neighbor distance. (2 refs.)

- 61857 Sr_2Pt_3 : an orthorhombic structure formed by Pt-centered trigonal prisms. M.L. Fornasini, A. Palenzona (Istituto di Chimica Fisica, Univ. di Genova, Genova, Italy). *J. Solid State Chem. (USA)*, vol.47, no.1, p.30-3 (15 March 1983). The phase Sr_2Pt_3 is orthorhombic with space group Pnma , and lattice constants $a=7.929(1)$, $b=24.326(6)$, $c=7.100(4)$ Å, $Z=4$. Direct methods were used for the structure resolution and anisotropic refinement led to an R value

of 0.065 for 535 reflections, collected on a four-circle diffractometer. The structure consists of trigonal prisms of Sr atoms centered by Pt and arranged in nets, analogous to those found in the Fe_2C and Mn_2C types. Differently from Fe_2C (isolated nets) and Mn_2C (double nets), the nets are here joined three by three through prism edges, forming slabs along the b axis. A description of the structure in terms of unit cell microtwinning is provided. (12 refs.)

- 61858 Magnetic and structural characteristics of $\text{Ho}_2\text{Fe}_{23}$ deuterides. A.T. Pedziwiatr, H.K. Smith, W.E. Wallace (Dept. of Chem., Univ. of Pittsburgh, Pittsburgh, PA, USA). *J. Solid State Chem. (USA)*, vol.47, no.1, p.41-6 (15 March 1983). The pressure-composition isotherm of the $\text{Ho}_2\text{Fe}_{23}\text{-D}_2$ system at 0°C was established, revealing the presence of two plateau regions. Using the isotherm, five compositions of the $\text{Ho}_2\text{Fe}_{23}\text{-D}_x$ system ($x=0, 1.5, 8.2, 12.1, 15.7$) were selected for investigation. These were examined by X-ray diffraction and magnetization measurements. The cubic lattice of the host metal is maintained to $x=8.2$. A tetragonal structure develops at $x=12.1$, but this reverts to cubic symmetry at the highest deuterium concentration studied. The observed structural changes are ascribed to preferential site occupancies by deuterium. Absorption of 15.7 deuterium atoms per formula unit in $\text{Ho}_2\text{Fe}_{23}$ caused a 10.2% increase of the unit cell volume. Increase in the deuterium content resulted in a striking increase in the Curie temperature T_c and in a linear decrease in compensation temperature T_{comp} . The saturation magnetization changed smoothly as the system changed from one structure type to another. There appears to be a significant increase in Fe magnetic moment upon deuterium absorption, which is ascribed to the removal of electrons from the 3d ion band by deuterium. (16 refs.)

- 61859 The crystal structure of La_3NiGe_2 and allied compounds. O.I. Bodak, V.A. Bruskov, V.K. Perchanskii (State Univ., Lvov, Ukrainian SSR). *Sov. Phys.-Crystallogr. (USA)*, vol.27, no.5, p.538-40 (Sept.-Oct. 1982). Translation of: *Kristallografiya (USSR)*, vol.27, no.5, p.896-9 (Sept.-Oct. 1982). [Received: April 1983]

The authors determine the crystal structure of the compound La_3NiGe_2 (space group Pnma), $a=12.041(5)$ Å, $b=4.358(2)$ Å, $c=11.871(6)$ Å, $Z=4$, which is of a new structural type. The atomic parameters are refined by the method of least squares in the isotropic ($R=0.068$) and anisotropic ($R=0.053$) approximations by means of 631 independent reflections ($I>1.96\sigma$) measured in a Syntex P2₁ automatic diffractometer. The compound La_3NiGe_2 belongs to a class of structures with trigonal-prismatic coordination of the smallest atoms (Ni and Ge) and is a filled-in analog of the previously known type Hf_3P_2 . The authors establish the existence of another ten previously unknown compounds R_3NiGe_2 of the structural type of La_3NiGe_2 ($\text{R}=\text{Y}, \text{Ce}, \text{Pr}, \text{Nd}, \text{Sm}, \text{Gd}, \text{Tb}, \text{Dy}, \text{Ho}, \text{Er}$). (10 refs.)

- 61860 The unit-cell dimensions of phases of Cu, Ag, or Au with the CsCl structure. E. Hellner (Inst. für Mineralogie, Petrologie & Kristallographie, Philipps-Univ., Marburg/Lahn, Germany), W.B. Pearson. *Z. Kristallogr. (Germany)*, vol.161, no.1-2, p.91-102 (1982). The unit-cell dimensions of phases with the CsCl structure that contain Cu, Ag or Au (A) are examined as a function of the diameters of the component atoms, D_A and D_B , and compared with those of phases of other A components. The cell dimensions of phases with upper composition of the B component limited by an electron concentration of 1.5 electrons per atom are controlled by the A-B contacts. The cell dimensions of phases containing the rare earths (B) controlled by the A-B and B-B contacts acting conjointly. The Li and Mg phases of Ag and Au have unusually small cell dimensions. Whereas the Ag and Au phases with composition limited by electron concentration 1.5 have the same cell sizes, the Li, Mg, Sc, Y and rare earth phases of Au have cell sizes on the average 0.051 Å smaller than the Ag phases. This is accounted for in terms of the electronegativity differences for this group of Au phases. The Au phases of the alkali metals are discussed; the size of the Au^- ion is deduced; the essential metallic nature of AuLi is demonstrated, and the nonexistence of AuNa and AuK is rationalized. The AgMg phase with a range of homogeneity, is considered in detail. (18 refs.)

- High-pressure phases in B group element alloys: a new sort of electronic phase See Entry 62096

- Quadrupolar coupling and structural instability in $\text{PrAg}_{1-x}\text{Cu}_x$ See Entry 62383

- Structure of bimetallic clusters. Extended X-ray absorption fine structure (EXAFS) studies of Ir-Rh clusters See Entry 63081

- The Th-Sn phase diagram See Entry 63260

- The structure of the modified 2H martensite in Cu-Zn-Al See Entry 63293

- Influence of residual gas pressure in annealing on the properties of niobium and its alloys See Entry 63333

- Examination of the effects of dimensional mismatch of the lattice parameters of the γ and γ' phases on the high-temperature strength of dispersion-hardened nickel alloys See Entry 63366

61.60 SPECIFIC STRUCTURE OF INORGANIC COMPOUNDS

- 61861 On a new series of cobalt+IV oxides. R. Salmon (Lab. de Chimie du Solide, CNRS, Talence, France), V. Linh. *C.R. Seances Acad. Sci. Ser. II (France)*, vol.296, no.1, p.53-5 (10 Jan. 1983). In French.

A new series of cobalt(+IV) compounds with general formula $\text{Ba}_4\text{Ln}_2\text{Co}_3\text{O}_{13}$ ($\text{Ln}=\text{Y}, \text{Nd-Yb}$) has been prepared and characterized. According to the X-ray diagram the unit cell is hexagonal. Magnetic susceptibility vs. temperature measurements give evidence of high spin Co^{4+} ions occupying tetrahedral sites. (3 refs.)

- 61862 Crystal structure of $\text{La}_2\text{Mn}_2\text{Ga}_2\text{Si}_4$. N. Rodier, M. Guittard, J. Flahaut (Lab. de Chimie Minérale, Chateaufort-Malabry, France). *C.R. Seances Acad. Sci. Ser. II (France)*, vol.296, no.1, p.65-70 (10 Jan. 1983). In French.

A hexagonal system, $\text{p}6_3$, $a=10.215(6)$ Å; $c=6.024(4)$ Å, $Z=1$. $R_w=0.039$ is found for 725 reflections ($I>2\sigma(I)$). All the metallic sites are fully occupied. The coordination polyhedra are: distorted dicapped trigonal prism for La, triangular antiprism for Mn (B site), tetrahedron for Ga (C site). The Mn atom is almost at the centre of the antiprism. This structure is the fundamental type for a large family of compounds having the formula $\text{R}_6[\text{B}_6]\text{C}_{12}\text{X}_{14}$ with $n=1/2, 2/3, 1$ or $4/3$; R-trivalent rare earth, B=3d, 1b, 11b or 111a... elements, C=111a, IV_A or V_A elements, X=S, Se. (16 refs.)

- 61863** Two new phases with tetragonal bronze-like structure in the diagram: $K_2O-CdO-Nb_2O_5$. J.Thoret (Lab. de Chimie Minérale, Univ. Pierre-et-Marie-Curie, Paris, France). *C.R. Seances Acad. Sci. Ser. II (France)*, vol.296, no.2, p.139-41 (17 Jan. 1983). In French.
- Some new 'tetragonal tungsten bronzes' phases have been obtained in the $K_2O-CdO-Nb_2O_5$ ternary diagram. Crystallographic, dielectric and nonlinear optical measurements have been performed. All these materials are piezoelectric at room temperature. Ferroelectric-paraelectric transitions appear at low temperature for some of them. (7 refs.)
- 61864** New cationic deficient phases $Bi_{12}[B_4]^{+V}[\square]_{1/5}O_{20}$ with sillenite structure. M.Devallet, G.Meunier, J.-P.Manaud, P.Hagenmuller (Univ. de Bordeaux I, Talence, France). *C.R. Seances Acad. Sci. Ser. II (France)*, vol.296, no.3, p.189-91 (24 Jan. 1983). In French.
- New cationic deficient phases $Bi_{12}[B_4]^{+V}[\square]_{1/5}O_{20}$ ($B^{+V}=P, As, V$) with sillenite structure have been obtained. At high temperature a reversible allotropic transformation may be detected. Transition temperatures and unit cell parameters have been determined. (8 refs.)
- 61865** The isostructural sulfides: Sr_2SnS_6 and Eu_2SnS_6 . M.Guittard, S.Jaulmes, M.Julien-Pouzol, E.Barthelemy, J.Flahaut (Lab. de Chimie Minérale Structurale, Paris, France). *C.R. Seances Acad. Sci. Ser. II (France)*, vol.296, no.4, p.249-51 (31 Jan. 1983). In French.
- Preparation and identification of two bimetallic sulfides, formed by tin IV with strontium or europium II and having, in addition to isolated S^{2-} anions, polysulphide chains formed by 3 sulphur atoms. Crystallographic and magnetic studies of Eu_2SnS_6 are also presented with the thermal decomposition of the two isomorphous compounds. (7 refs.)
- 61866** New complex antimonates and tellurates structurally related to lithium antimonate $LiSbO_3$. P.Tarte, M.Gabelica-Robert (Univ. de Liege, Liege, Belgium). *C.R. Seances Acad. Sci. Ser. II (France)*, vol.296, no.4, p.261-4 (31 Jan. 1983). In French.
- New antimonates and tellurates $LiM_2^{III}SbO_6$, $LiM^{III}M^{IV}SbO_6$ and $LiM^{III}M^{IV}TeO_6$ have been synthesized and investigated by X-ray diffraction and vibrational spectroscopy. All these compounds are orthorhombic and structurally related to $LiSbO_3$ but the cation distribution is ordered in antimonates $LiM_2^{III}SbO_6$ and tellurates, whereas it is very probably disordered in antimonates $LiM^{III}M^{IV}SbO_6$. (3 refs.)
- 61867** Structural approach of the Nd_3GaO_6 compounds. J.Coutures, J.Nicolas (CNRS, Lab. des Ultra-Refractaires Odeillo, Font, Romeu, France), E.Antic, G.Schiffmacher, J.-P.Coutures. *C.R. Seances Acad. Sci. Ser. II (France)*, vol.296, no.5, p.347-9 (7 Feb. 1983). In French.
- A structural study of the Nd_3GaO_6 compound by X-ray and electron diffraction shows that Nd_3GaO_6 is orthorhombic, space group $Pnna(D_{2h}^{16})$ with four units by cell. Optical absorption indicates that Nd^{3+} is on three sites with an average coordination number of 7. Nd_3GaO_6 is stable up to $1290^\circ C$. (3 refs.)
- 61868** First compounds containing only isolated Mo_9 clusters in Mo_9Se_{11} units: $Ag_4Mo_9Se_{11}(x=4)$ and $Ag_3Mo_9Se_{11}$. P.Gougeon, M.Potel, J.Padiou, M.Sergent (Lab. de Chimie Minérale B, Univ. de Rennes-Beaulieu, Rennes, France). *C.R. Seances Acad. Sci. Ser. II (France)*, vol.296, no.5, p.351-6 (7 Feb. 1983). In French.
- First compounds containing only isolated Mo_9 clusters in Mo_9Se_{11} units have been synthesized: $Ag_4Mo_9Se_{11}(x=4)$, $Ag_3Mo_9Se_{11}$. In these new phases, all silver atoms are delocalized in the channels around Mo_9Se_{11} units. (7 refs.)
- 61869** Structure of thorium sulphate octahydrate, $Th(SO_4)_3 \cdot 8H_2O$. J.Habash, A.J.Smith (Dept. of Chem., Univ. of Sheffield, Sheffield, England). *Acta Crystallogr. Sect. C (Denmark)*, vol.C39, pt.4, p.413-15 (15 April 1983). $M_r=568.3$, monoclinic, $P2_1/n$, $a=8.51$ Å, $b=11.86$ (2) Å, $c=13.46$ (2) Å, $\beta=92.65$ (1)°, $V=1357$ Å³, $Z=4$, $D_x=2.778$, $D_m=2.78$ g cm⁻³ (by flotation in iodobenzene/diiodomethane), $Mo\ K\alpha$, $\lambda=0.7107$ Å, $\mu=137.95$ cm⁻¹. Non-hydrogen atoms refined anisotropically to a final R of 0.1022. The thorium is ten-coordinate, both the sulphate groups being chelate, and six of the water oxygens being coordinated to thorium. The resulting complexes are linked together via hydrogen bonds. The thorium coordination polyhedron approximates closely to the bicapped square antiprism (1.4/4.1) of D_{4d} symmetry and with $\theta=63^\circ$. (12 refs.)
- 61870** $Mo_6Br_8S_8$: a new two-dimensional compound with octahedral Mo_6 clusters. C.Perrin, M.Potel, M.Sergent (Lab. de Chimie Minérale B, Univ. de Rennes, Rennes, France). *Acta Crystallogr. Sect. C (Denmark)*, vol.C39, pt.4, p.415-18 (15 April 1983). In French.
- $M_r=1151.3$, orthorhombic, $Cmcm$, $a=17.250$ (7), $b=6.600$ (4), $c=11.929$ (7) Å, $Z=4$, $V=1358$ Å³, $D_x=5.51$, $D_m=5.63$ Mg m⁻³, $\lambda(Mo\ K\alpha)=0.71069$ Å, $\mu(Mo\ K\alpha)=24.34$ mm⁻¹, $F(000)=2040$. The structure has been solved by direct methods and refined by least squares to $R=0.062$ ($R_w=0.052$) for 423 independent reflections. The structure can be described as a layer structure of $[Mo_6]_4$ units. Along c , these units are bonded by their apices to build up chains. Along b , these chains are linked by $Mo-S$ bonds. Along a , the cohesion is made only by contacts between Br atoms, leading to a two-dimensional character for this compound. (21 refs.)
- 61871** Structure of cadmium hydroxynitrate, $Cd(OH)(NO_3)$. A.-M.Rodriguez Roldan, M.Louer, J.-P.Auffredic, D.Louer (Lab. de Cristallographie, Univ. de Rennes, Rennes, France). *Acta Crystallogr. Sect. C (Denmark)*, vol.C39, pt.4, p.418-20 (15 April 1983). In French.
- $M_r=191.4$, orthorhombic, $P2_12_12_1$, $a=3.891$ (3), $b=7.407$ (4), $c=11.249$ (6) Å, $V=324.2$ (6) Å³, $Z=4$, $D_x=3.921$ Mg m⁻³, $F(000)=352$, $\lambda(Mo\ K\alpha)=0.71069$ Å. The structure has been solved from single-crystal data collected on a four-circle diffractometer by Patterson and Fourier syntheses. With anisotropic temperature factors, the final R value is 0.028 for 665 independent observed reflections. The NO_3 groups are symmetric bidentate and the Cd atoms are hexacoordinated by three $O(NO_3)$ and three OH groups, these polyhedra sharing corners in the [100] and [010] directions and edges in the [001] direction. (10 refs.)
- 61872** Structure refinement of mathiasite, $(K_{0.62}Na_{0.14}Ba_{0.16}Sr_{0.10}Th_{0.21}Ti_{12}Co_{10}Mg_1S_3Fe_{12}Zr_{0.6}Ca_{0.2}V_{0.1}Nb_{0.1}Al_{0.36}O_{38})$. B.M.Gatehouse (Dept. of Chem., Monash Univ., Clayton, Victoria, Australia), I.E.Grey, J.R.Smyth. *Acta Crystallogr. Sect. C (Denmark)*, vol.C39, pt.4, p.421-2 (15 April 1983). $M_r=1693.08$, rhombohedral, $R\bar{3}$, $a=9.119$ (3) Å, $a_c=69.24$ (2)°, $Z=1$, $D_x=4.39$ g cm⁻³, $\lambda(Mo\ K\alpha)=0.71069$ Å, $\mu=68.8$ cm⁻¹. Final $R=0.054$ for 892 observed independent diffractometer data. Mathiasite is isostructural with the crichtonite-group minerals, AM_2O_{38} , and is characterized by dominant potassium in the large-cation A site. Partial disorder in the M -cation sublattice is

interpreted as due to the partial occupation of a second anion site by large cations. (9 refs.)

- 61873** Tetradecapraseodymium hexanickel undecasilicide, $Pr_{12}Ni_6Si_{11}$, with centered trigonal rare-earth prisms. E.Hovestvedt, K.Klepp, E.Parthe (Lab. de Cristallographie aux Rayons X, Univ. de Geneve, Geneve, Switzerland). *Acta Crystallogr. Sect. C (Denmark)*, vol.C39, pt.4, p.422-5 (15 April 1983). $M_r=2634$, monoclinic, $C2/m$, $a=33.991$ (3), $b=4.2328$ (4), $c=21.330$ (3) Å, $\beta=113.72$ (1)°, $V=2809.7$ Å³, $Z=4$, $D_x=6.226$ Mg m⁻³, $Mo\ K\alpha$, $\lambda=0.71069$ Å, $\mu=27.99$ mm⁻¹, $F(000)=4592$, $T=293K$, $R=0.072$ for 2540 independent reflections. The structure consists of an arrangement of Ni- and Si-centered trigonal prisms of Pr atoms with two mutually perpendicular prism-axis directions. The Ni and Si atoms on the prism-center sites are ordered. A Ni atom has neither a Pr atom nor another Ni atom in prism-wise contact. The $Pr_{14}Ni_6Si_{11}$ structure is geometrically related to the $Ce_{14}(Ni, Si)_{17}$ structure. They can be considered as stacking variants of each other. (11 refs.)
- 61874** Neptunium tetrafluoride hydrate, $Np_2F_{12} \cdot H_2O$. A.Cousson, H.Abazli, M.Pages, M.Gasperin (Univ. Pierre et Marie Curie, Paris, France). *Acta Crystallogr. Sect. C (Denmark)*, vol.C39, pt.4, p.425-7 (15 April 1983). In French.
- $M_r=957$, triclinic, $P1$, $a=8.455$ (8), $b=8.858$ (9), $c=8.396$ (10) Å, $\alpha=113.83$, $\beta=116.64$, $\gamma=58.03^\circ$, $Z=2$, $V=465.2$ Å³, $D_x=6.83$ Mg m⁻³, $\lambda(Mo\ K\alpha)=0.71069$ Å, $F(000)=774$, $R(F)=0.079$, $R_w=0.104$ for 2848 independent reflections. Three kinds of F polyhedra surrounding Np are linked in a three-dimensional framework. Np-F distances vary between 2.18 (3) and 2.78 (4) Å; the shortest F-F is 2.44 (7) Å. Water molecules are located in the holes, respectively, at 2.54 (13) and 2.43 (10) Å from Np atoms. (2 refs.)
- 61875** Physicochemical properties of alloys of HgTe-MgTe system. V.M.Frasunyak, N.P.Galvalashko, I.A.Parenjuk (Chernovitsy State Univ., Chernovitsy, Ukrainian SSR). *Inorg. Mater. (USA)*, vol.18, no.6, p.882-4 (June 1982). Translation of: *Izv. Akad. Nauk SSSR Neorg. Mater.*, vol.18, no.6, p.1045-7 (June 1982). [received: Feb. 1983]
- Presents results from a physicochemical study of the HgTe-MgTe system (up to 20 mole% MgTe). The crystals were obtained by joint fusion of the original elements. The specimens were investigated by means of DTA and X-ray phase analysis; also, the hydrostatic density and microhardness were measured. In determining the elementary cell constants, the authors used precision photography with monochromatic Fe $K\alpha$ radiation. The X-ray parameters were used to calculate the density of the substance for a comparison with the density determined by hydrostatic weighing. (8 refs.)
- 61876** Cation distribution in the cupromanganese spinel $Cu_{0.5}Mn_{2.5}O_4$. S.E.Tsirkunova, Ya.O.Shint (Inst. of Phys., Acad. of Sci., Latvian SSR). *Inorg. Mater. (USA)*, vol.18, no.6, p.899-900 (June 1982). Translation of: *Izv. Akad. Nauk SSSR Neorg. Mater.*, vol.18, no.6, p.1060-1 (June 1982). [received: Feb. 1983]
- The spinel $Cu_{0.5}Mn_{2.5}O_4$ is tetragonal with the unit cell parameters $a=8.16$ Å, $c=8.95$ Å, and a Curie temperature below room temperature. For determining the crystal structure of this spinel the authors photographed its neutron diffraction pattern at room temperature. Analysis of the neutron diffraction pattern showed that the structure of this spinel has space group D_{4h}^{19} . (6 refs.)
- 61877** The crystal structure of Re_2Ge_7 . T.Siegrist, F.Hulliger (Lab. fur Festkörperphys., Eidgenössische Tech. Hochschule, Zurich, Switzerland), W.Petter. *J. Less-Common Met. (Switzerland)*, vol.90, no.1, p.143-51 (March 1983).
- The only normal pressure phase in the system Re-Ge was shown to possess the composition Re_2Ge_7 instead of $ReGe_2$ as reported in the literature. Re_2Ge_7 crystallizes in the space group $Cmcm$ with the orthorhombic cell lattice constants $a=3.227$ (1) Å, $b=9.045$ (1) Å, $c=21.956$ (2) Å, $Z=4$ and $d_x=11.06$ g cm⁻³. Its structure represents a new type which can be derived from a combination of the $PuBr_3$ type and the $OsGe_2$ type. (13 refs.)
- 61878** On basic thallium sulfates: structure of $Tl_2TiOH(SO_4)_2$. F.Abraham (Univ. de Valenciennes, Valenciennes, France), G.Nowogrocki, B.Jolibois, G.Laplace. *J. Solid State Chem. (USA)*, vol.47, no.1, p.1-5 (15 March 1983).
- The $Tl_2TiOH(SO_4)_2$ compound is monoclinic, $a=7.758$ (3), $b=17.587$ (9), $c=7.356$ (3) Å, $\beta=119.91$ (3)°, $SG\ C2$, $Z=4$. The structure was solved by full-matrix least square refinement to $R=0.033$ from 1242 single-crystal reflections collected on an automated diffractometer. Tl^{III} ions ensure bonding between $[Ti^{IV}OH(SO_4)_2]_{\infty}$ sheets. These sheets may be viewed as crisscrossing $Ti-SO_4$ chains. In the [101] direction, the linking of Tl^{III} is reinforced by bidentate OH groups, so the usual hexacoordination of trivalent thallium is preserved. A transition occurring at $104^\circ C$ is under investigation. (10 refs.)
- 61879** Structural chemistry of Magneli phases Ti_nO_{2n-1} ($4 \leq n \leq 9$). III. Valence ordering of titanium in Ti_5O_{11} at $130K$. Y.Le Page, P.Strobel (Nat. Res. Council of Canada, Ottawa, Ontario, Canada). *J. Solid State Chem. (USA)*, vol.47, no.1, p.6-15 (15 March 1983).
- For $Pt.II$ see *ibid.*, vol.44, no.2, p.273 (1982). The phase transition at $147K$ in Ti_5O_{11} corresponds to the occurrence of a superstructure with tripling of the cell volume on cooling. Its reduced cell parameters at $130 \pm 5K$ are $a=5.17$ (1), $b=11.98$ (2), $c=13.397$ (2) Å, $\alpha=88.29$ (1), $\beta=105.52$ (1), and $\gamma=107.79$ (1) degrees in space group $P1$ with $Z=6$. A systematic nomenclature adding one index to the substructure atom names permits calculation of the model's atomic coordinates in the asymmetric unit in terms of the rutile sub-substructure and keeps track of the structural changes. The superstructure was solved by direct methods and refined to $R_F=5.2\%$ on 3062 observed reflections assuming isotropic thermal motion. A complex pattern of Ti-O and Ti-Ti distance changes is observed. It is interpreted to correspond to valence ordering of the Ti atoms, probably complete in the shear-plane slab and partial in the rutile-like slab. The Ti-Ti distances, with one very short approach of 2.65 Å at a shared face, seem to be consistent with 'bipolarons' but can also be analyzed in terms of electrostatic repulsion which allows for the considerable lengthening of some distances as well. (11 refs.)
- 61880** Crystal structure and magnetic properties of a new form of NH_4MnFeF_6 . M.Lebanc, G.Ferey, Y.Calage, R.de Pape (Lab. des Fluorures et Oxyfluorures Ioniques, ERA, Le Mans, France). *J. Solid State Chem. (USA)*, vol.47, no.1, p.24-9 (15 March 1983).
- The hydrothermal synthesis at $380^\circ C$, 200 MPa of NH_4MnFeF_6 , NH_4MnCrF_6 , and $RbMnFeF_6$ leads to a new $AM^{II}M^{III}F_6$ structural type of orthorhombic symmetry with $Z=8$. The lattice constants are found to be, respectively, $a=7.844$ (4), $b=12.819$ (8), $c=10.582$ (6); $a=7.808$ (5), $b=12.755$ (9), $c=10.501$ (7); and $a=7.913$ (5), $b=12.858$ (9), $c=10.619$ (5). The structure was solved for NH_4MnFeF_6 from 755 X-ray reflections and refined to $R_w=0.029$ in the space group $Pb2n-C_6^2$. The network is built from edge-sharing $MnFeF_6$ bioctahedra connected to each other by their vertices.

RbMnFeF₆, upon heating, transforms irreversibly to the modified pyrochlore structure at 881 K. From magnetic and Mossbauer experiments, NH₄MnFeF₆ and NH₄MnCrF₆ are established to be antiferromagnetic with $T_N = 117.7 \pm 0.5$ K and < 6 K, respectively. (17 refs.)

61881 Electron microscopic study of barium hexaaluminates. N.Iyi, S. Takekawa, Y. Bando, S. Kimura (Nat. Inst. for Res. in Inorganic Materials, Ibaraki, Japan).

J. Solid State Chem. (USA), vol. 47, no. 1, p. 34-40 (15 March 1983). The crystallographic relation between phase I and phase II of barium hexaaluminates, which were conventionally considered as the single compound 'barium hexaaluminate (BaAl₂O₁₉)', was investigated using principally the electron diffraction method. Phase I (Ba_{0.79}Al_{10.9}O_{17.14}) was found to have a β -alumina type structure with space group $P6_3/mmc$. On the other hand, phase II (Ba_{2.34}Al_{21.0}O_{33.84}) exhibited an $a\sqrt{3} \times a\sqrt{3}$ superstructure, which is probably due to the ordering of excess Ba ions within Ba-O layers. Possible structure models of both phases are presented. (16 refs.)

61882 Hexagonal tungsten bronze-type Fe^{III} fluoride: (H₂O)_{0.33}FeF₃; crystal structure, magnetic properties, dehydration to a new form of iron trifluoride. M. Leblanc, G. Ferey, P. Chevallier, Y. Calage, R. de Pape (Lab. des Fluorures et Oxyfluorures Ioniques, ERA, Le Mans, France).

J. Solid State Chem. (USA), vol. 47, no. 1, p. 53-8 (15 March 1983). (H₂O)_{0.33}FeF₃, grown by hydrothermal synthesis, crystallizes in the orthorhombic system with cell dimensions $a = 7.423(3)$ Å, $b = 12.730(4)$ Å, $c = 7.526(3)$ Å, and space group $Cmcm$, $Z = 12$. The structure, derived from single crystal X-ray diffraction data (605 independent reflections) is refined to $R = 0.019$ ($R_w = 0.021$). The framework of the Fe^{III}Fe₆ octahedra is related to that of hexagonal tungsten bronze (HTB) Rb_{0.29}WO₃. At 122°C, a zeolitic water is evolved from hexagonal tunnels without any noticeable change of the fluorine skeleton. The related anhydrous compound represents a new form of iron trifluoride which is denoted HTB-FeF₃; at 525°C, it transforms into the cubic form of ReO₃-type. (H₂O)_{0.33}FeF₃ and HTB-FeF₃ are antiferromagnetic, with Neel temperatures of $T_N = 128.7 \pm 0.5$ K and $T_N = 97 \pm 2$ K, respectively. (13 refs.)

61883 Zirconium dodecarbides ZrB₁₂. Confirmation of the B₁₂ cubooctahedral unit. C.H.L. Kennard (Dept. of Chem., Univ. of Queensland, St. Lucia, Queensland, Australia), L. Davis.

J. Solid State Chem. (USA), vol. 47, no. 1, p. 103-6 (15 March 1983). Using powder, neutron diffraction and Rietveld's method of profile refinement, the structure of ZrB₁₂ was confirmed. (5 refs.)

61884 Crystal structure of a metallic two-dimensional conductor: the purple bronze of potassium and molybdenum, K_{0.9}Mo₆O₁₇. H. Vincent, M. Ghedira (Lab. de Cristallographie, CNRS, Grenoble, France), J. Marcus, J. Mercier, C. Schlenker.

J. Solid State Chem. (USA), vol. 47, no. 1, p. 113-21 (15 March 1983). In French.

Single crystals of the purple bronze K_{0.9}Mo₆O₁₇ have been grown by an electrolytic reduction technique. Measurements of the electrical resistivity show that this compound is a quasi two-dimensional metal. A crystal structure determination is used to explain the strongly anisotropic resistivity. K_{0.9}Mo₆O₁₇ is found to be trigonal with lattice parameters: $a = 5.538$ Å and $c = 13.656$ Å; $Z = 1$. The space group is $P3_1$. Zachariasen's (1978) bond length-bond strength relation has been applied to the Mo-O bonds. The computed effective mean Mo valences are +6 for Mo(1) on tetrahedral sites and about 5.1 and 5.8, respectively, for Mo(2) and Mo(3) on octahedral sites. The 4d electrons of Mo atoms are so located in the two-dimensional infinite slabs of octahedra. The 4d electrons of Mo atoms are so located in the two-dimensional infinite slabs of octahedra. The conduction band is expected to be an antibonding π^* band resulting from the hybridization of the Mo 4d t_{2g} and oxygen p_z states. The structural properties should lead to a very anisotropic Fermi surface and thus, to a quasi two-dimensional electrical conductivity. (15 refs.)

61885 New symmetry and structure for spinel. N.W. Grimes, P. Thompson (Dept. of Phys., Univ. of Aston, Birmingham, England), H.F. Kay.

Proc. R. Soc. London Ser. A (GB), vol. 386, no. 1791, p. 333-45 (8 April 1983). The crystal structure of magnesium aluminate is conventionally described within a symmetry corresponding to the centrosymmetrical space group Fd3m but this has created difficulties for the interpretation of many of its physical properties. Therefore, extensive X-ray diffraction intensity data have been collected from a small spherical synthetic single crystal and used for a structure parameter refinement assuming F43m symmetry as proposed by Grimes (1972), and also for refinement according to conventional symmetry. The F43m assumption yields the first direct measurement of the suspected deviations from the centrosymmetrical structure, and is found to provide a significantly superior fit to the experimental data, especially at high angles and with reflexions having structure factors less than 10.0. The weak reflexions include nine that are forbidden under Fd3m symmetry and it is shown that there is satisfactory agreement between observed and calculated structure factors in these cases. (48 refs.)

61886 X-ray study of niobium disulfide intercalated with copper. W. Thulke, R. Frahm, R. Haensel, P. Rabe.

Phys. Status Solidi A (Germany), vol. 75, no. 2, p. 501-9 (16 Feb. 1983). Bondlengths of nearest neighbours around the Cu and Nb atoms in a Cu_{0.5}NbS₂ single crystal are extracted from the extended X-ray absorption fine structure (EXAFS) and lattice parameters are measured by X-ray diffraction. It is found that the Cu atoms occupy tetrahedral sites in the Van der Waals gap. Upon intercalation the NbS₂ sandwiches are squeezed by 0.009 nm whereas the van der Waals gap expands by 0.067 nm. The Nb-Nb distance in the NbS₂ layers increases by 0.003 nm. The Nb-S bond length shortens by 0.001 nm. The positions of the K-edge energies indicate a charge transfer from the Cu atoms to the host sandwich layers. (24 refs.)

61887 Change in the valence of samarium ions in solid solutions based on isostructural SmB₆ phases. M.I. Aivazov, S.V. Aleksandrovich, B.A. Evseev, V.S. Mkrtchyan, V.N. Sorokin, O.M. Tsarev (Sci.-Industrial Assoc., 'Energiya', Moscow, USSR).

Sov. Phys.-Solid State (USA), vol. 24, no. 9, p. 1512-14 (Sept. 1982). Translation of: *Fiz. Tverd. Tela (USSR)*, vol. 24, no. 9, p. 2667-71 (Sept. 1982). [received: April 1983] Experimental values of lattice constants yielded the dependences $\epsilon(x)$ of the fraction of Sm^{2+} ions on the composition in the systems of solid solutions $\alpha\text{-SmB}_6\text{-Me}_x^{1+}\text{B}_6$ (Me = La, Ce, Pr, Nd) and $\beta\text{-SmB}_6\text{-Me}_x^{1+}\text{B}_6$ (Me = Nd, Gd). The change in valence for solid solutions based on $\alpha\text{-SmB}_6$ was appreciably greater than for those based on $\beta\text{-SmB}_6$. (12 refs.)

61888 Determination of crystal structure of triple magnesium calcium sodium orthophosphate Mg₂₁Ca₉Na₄(PO₄)₁₈. A.I. Domanskii, Yu.I. Smolin, Yu.F. Shepelev, J. Majling (Inst. of Silicate Chem., Acad. of Sci., USSR).

Sov. Phys.-Crystallogr. (USA), vol. 27, no. 5, p. 535-7 (Sept.-Oct. 1982). Translation of: *Kristallografiya (USSR)*, vol. 27, no. 5, p. 891-5 (Sept.-Oct. 1982). [received: April 1983]

The crystal structure of Mg₂₁Ca₉Na₄(PO₄)₁₈ ($a = 14.974(4)$ Å, $c = 42.74(1)$ Å, R_3 , $Z = 6$) is determined by direct methods and refined by the method of least squares in the anisotropic approximation to $R = 0.038$. A diffractometer is used to measure 3800 F(hkl). A crystal-chemical description of the structure is given. (10 refs.)

61889 The crystal structure of the deuteride ZrMoFeD_{2.6}. V.A. Yartys', V.V. Burnasheva, N.V. Fadeeva, S.P. Solov'ev, K.N. Semenenko (Inst. of New Chem. Problems, Acad. of Sci., USSR).

Sov. Phys.-Crystallogr. (USA), vol. 27, no. 5, p. 540-3 (Sept.-Oct. 1982). Translation of: *Kristallografiya (USSR)*, vol. 27, no. 5, p. 900-4 (Sept.-Oct. 1982). [received: April 1983]

Powder neutron diffraction is used to investigate the crystal structure of the deuteride ZrMoFeD_{2.6}, which is an interstitial derivative of the structural type of MgZn₂. It is found that the deuterium atoms in the structure of ZrMoFeD_{2.6} occupy tetrahedral gaps [GZr₂(MoO₅ + FeO₅)₂] of two types. (12 refs.)

61890 Crystal structure of Ge sodalite Na₈Al₆Si₆O₂₄(OH)₂. E.L. Belokoneva, L.N. Dem'yanets, T.G. Uvarova, N.V. Belov (Inst. of Crystallography, Acad. of Sci., USSR).

Sov. Phys.-Crystallogr. (USA), vol. 27, no. 5, p. 597-8 (Sept.-Oct. 1982). Translation of: *Kristallografiya (USSR)*, vol. 27, no. 5, p. 995-6 (Sept.-Oct. 1982). [received: April 1983]

The composition Na₈Al₆Si₆O₂₄(OH)₂·nH₂O corresponds to two natural minerals-natrodavnye and sodalite. With the aim of determining the influence of replacement of Si by Ge in sodalite, the authors synthesized single crystals of its germanium analog and investigated its structure. Crystals of the germanium analog of sodalite were obtained in hydrothermal conditions by means of a temperature difference. The parameter of the cubic primitive unit cell, $a = 9.029(5)$ Å, was determined on a spherical specimen on a PI Syntex automatic diffractometer. Three-dimensional data required for structural determination were obtained in the same diffractometer (Mo K α , $\sin \theta/\lambda \leq 1$ Å⁻¹, $2\theta/\theta$ method with variable scanning rate of 6-24 deg/min). Analysis of the systematic extinctions hkl indicated the space group P4₃n, characteristic of sodalite, and in this the authors interpreted the structure. (10 refs.)

61891 The crystal structure of α -NaTm(SO₄)₂. S.M. Chizhov, A.N. Pokrovskii, L.M. Kovba (M.V. Lomonosov State Univ., Moscow, USSR).

Sov. Phys.-Crystallogr. (USA), vol. 27, no. 5, p. 598-9 (Sept.-Oct. 1982). Translation of: *Kristallografiya (USSR)*, vol. 27, no. 5, p. 997-8 (Sept.-Oct. 1982). [received: April 1983]

By slow cooling of a melt containing 70 mole % Na₂SO₄ and 30 mole % Tm₂(SO₄)₃ from 880°C, the authors have obtained single crystals of the high-temperature modification of the double sulfate of sodium and thulium of the composition 1:1. An investigation of the crystal in a Hilger Y-290 diffractometer (Mo K α radiation, $\theta/2\theta$ scanning) revealed that the double sulfate is monoclinic (with space group P2₁/m, unit-cell parameters $a = 4.669(3)$, $b = 10.143(7)$, $c = 6.837(4)$ Å, $\gamma = 110.40(3)^\circ$, $Z = 2$, and isostructural with the double sulfate NaEr(SO₄)₂). Using the atomic coordinates for thulium and sulfur found from an analysis of the distribution of the interatomic Patterson function, the authors calculated a series of $\rho(x, y, z)$ syntheses which enabled us to determine the positions of all the atoms. Least-squares refinement led to a discrepancy index of 0.060. The coordinates of the basis atoms of the structure of the high-temperature double sulfate of sodium and thulium and the principal interatomic distances are listed. (1 ref.)

61892 Crystal chemistry of series of inhomogeneous linear structures. III. The crystal structures of Ce₂Ga₁₀Ni and La₂Ga₁₀Ni. Ya.P. Yarmolyuk, Yu.N. Grin', I.V. Rozhdvestvenskaya, O.A. Usov, A.M. Kuz'min, V.A. Bruskov, E.I. Gladyshevskii (State Univ., L'viv, Ukrainian SSR).

Sov. Phys.-Crystallogr. (USA), vol. 27, no. 5, p. 599-600 (Sept.-Oct. 1982). Translation of: *Kristallografiya (USSR)*, vol. 27, no. 5, p. 999-1001 (Sept.-Oct. 1982). [received: April 1983]

Investigates the crystal structures and structural relations of the compounds R₂Ga₁₀Ni (R = La, Ce), found in a study of the phase diagrams of the corresponding triple systems of rare-earth and transition metals with gallium, and belonging to the series of inhomogeneous linear structures. Laue photographs revealed tetragonal symmetry (4/mmm), and measurements of the unit-cell periods by means of rotation photographs (Cu K α) and in a Syntex P2₁ automatic diffractometer (Mo K α), gave the values $a = 4.262(3)$ Å, $c = 26.391(9)$ Å. As the array contained only reflections with $h+k+l=2n$, the possible space groups were 14/mmm, 14mm, 14m2, 142m, and 1422. A statistical test favored a centrosymmetric group. (4 refs.)

61893 Neutron diffraction study of the thermal and oxygen position parameters in rutile. W. Gonschorek (Dept. de Fisica, Univ. Coimbra, Coimbra, Portugal), R. Feld.

Z. Kristallogr. (Germany), vol. 161, no. 1-2, p. 1-5 (1982). Integrated neutron intensities for rutile (TiO₂) were measured up to $\sin \theta/\lambda = 0.94$ Å⁻¹ with two crystals of volumes 1.2 mm³ and 8.9×10^{-3} mm³. A statistical treatment showed the data not to be normally distributed. From the statistics of the symmetry-equivalent intensities there was no evidence of anisotropic extinction. Isotropic extinction parameters were refined for both crystals. There is no significant difference between the neutron and X-ray refined structure parameters. The thermal motion of titanium is larger than that of oxygen. (8 refs.)

61894 The crystal structures of α - and β -forms of plutonium(IV) sulphate tetrahydrate. N.C. Jayadevan, K.D. Singh Mudher, D.M. Chackraburty (Radiochem. Div., Bhabha Atomic Res. Centre, Bombay, India).

Z. Kristallogr. (Germany), vol. 161, no. 1-2, p. 7-13 (1982). Pu(SO₄)₂·4H₂O has been prepared in two polymorphic forms α - and β -.

The α -form crystals are orthorhombic, space group Fddd, with eight formula units in a cell of dimensions $a = 26.527(19)$, $b = 11.995(9)$ and $c = 5.687(4)$ Å. The β -form crystals are also orthorhombic, space group Pnma with four formula units in a cell of dimensions $a = 14.544(10)$, $b = 10.980(8)$ and $c = 5.667(3)$ Å. The structure of the β -form has been determined from three dimensional X-ray data obtained on Weissenberg films. A least-squares refinement has led to a value of the conventional R index of 0.089 for 476 observed reflections. The coordination geometry about the Pu(IV) ion is an archimedean square—an antiprism formed by oxygen atoms from four sulphate groups and four water molecules. Each sulphate group is shared by two Pu(IV) ions. Hydrogen bonds operate between the water molecules and sulphate oxygen atoms not bonded to plutonium. The structure of the α -form derived from powder data shows that it differs from the β -structure only in the functional nature of the hydrogen bonds. The α - to β -transformation can be achieved by slow heating up to 120°C. (8 refs.)

61895 Crystal morphology of monoclinic potassium feldspars. A qualitative approach with special emphasis on the periodic bond chain theory of Hartman and Perdok. C.F.Woensdrecht (Inst. voor Aardwetenschappen Utrecht, Utrecht, Netherlands).

Z. Kristallogr. (Germany), vol.161, no.1-2, p.15-33 (1982).

The influence of the crystal structure on the crystal morphology of monoclinic potassium feldspar has been investigated according to the theory of Hartman and Perdok (1955). There are a limited number of PBCs, i.e. uninterrupted chains of strong bonds, consisting exclusively of T(=Si,Al)-O bonds. These are parallel to $[001]$, $\langle 1/2/2 \rangle$, $[101]$, $[100]$, $\langle 1/2/2 \rangle$, $[010]$ and $[102]$. Many other PBCs are present having both T-O and K-O bonds as strong bonds, e.g. $\langle 1/2/2 \rangle$, $\langle 3/2/2 \rangle$, $[101]$, $\langle 1/2/2 \rangle$, $\langle 1/2/2 \rangle$, $[201]$ and $[111]$. The most important crystal faces can be classified as either F_1 faces parallel to at least two PBCs having only T-O, or as F_2 faces parallel to at least two PBCs, one of which contains in addition K-O bonds. The F_1 faces are $\{110\}$, $\{001\}$, $\{101\}$, $\{201\}$ and $\{111\}$. The F_2 faces are $\{130\}$, $\{021\}$, $\{221\}$, $\{112\}$, $\{100\}$ and $\{101\}$. The remaining faces parallel to the various PBCs are S faces. Crystals grown in nature display only F faces as the most important faces. The presence of S faces is induced by internal factors other than crystal structure or by external factors such as impurities and supersaturation. (25 refs.)

61896 Morphology and crystal growth of structurally related A_2BX_4 - and A_2BX_5 -compounds. H.Folner, H.Schwarz (Mineralogisch-Kristallographisches Inst., Tech. Univ. Clausthal, Clausthal-Zellerfeld, Germany).

Z. Kristallogr. (Germany), vol.161, no.1-2, p.35-43 (1982).

The morphological relationship of compounds of glaserite, Na_2SO_4 , low K_2SO_4 and olivine types is examined. The crystal structures can be retraced to a common basic structure. The morphological lattice is determined by a sign determination with the help of the Goldschmidt complication rule and with Fourier methods. The crystal growth of olivine, having a morphology similar to that of barite, deviates from the other compounds. The differences are indicated with the help of partitions of the three-dimensional space into Dirichlet domains of morphological points. The packing of space-filling polyhedra allow conclusions to be drawn on the growth mechanisms. (25 refs.)

61897 The crystal structure of $NaCrP_2O_7$. L.Bohaty, J.Liebertz (Inst. für Kristallographie, Univ. zu Köln, Köln, Germany), R.Frohlich.

Z. Kristallogr. (Germany), vol.161, no.1-2, p.53-9 (1982). In German.

The crystal structure of $NaCrP_2O_7$ has been determined by X-ray diffraction. The crystal data are: space group $P2_1/c$, $a=7.294(2)$, $b=7.838(2)$, $c=9.484(2)$ Å, $\beta=111.72(2)^\circ$, $V=503.8(4)$ Å³, $D_m=3.26$, $D_c=3.282$ Mg m⁻³, $Z=4$, $\mu(MoK\alpha)=2.89$ mm⁻¹. The structure was refined to $R=0.029$ for 2381 independent reflections ($|F_o| \geq 4\sigma(F_o)$). In addition, the lattice parameters of compounds isostructural with $NaCrP_2O_7$ were measured. (5 refs.)

61898 The crystal structure of antimony seleniodide, $SbSeI$. G.P.Voutsas, P.J.Rentzperis (Appl. Phys. Lab., Aristotle Univ. of Thessaloniki, Thessaloniki, Greece).

Z. Kristallogr. (Germany), vol.161, no.1-2, p.111-18 (1982).

The crystal structure of $SbSeI$ has been determined with the intensities of 821 independent reflections, measured on a computer-controlled Philips PW 1100 single-crystal diffractometer. The cell constants obtained by least-squares calculations from direct θ -value measurements on the diffractometer, are: $a=8.6862(9)$, $b=10.3927(9)$, $c=4.4152(3)$ Å, $Z=4$; space group $Pnam$. The positional and thermal parameters, with anisotropic temperature factors, were refined by full-matrix, least-squares calculations to a final $R=0.054$. (14 refs.)

X-ray diffraction methods to determine crystallinity and preferred orientation of lithium disilicate in Li-Zn-silicate glass-ceramic fibres See Entry 61806

Mechanisms of nucleation and crystallization of lithium disilicate in Li-Zn-silicate glass-ceramic fibres See Entry 61807

Structural and thermal characterization of the γ' polymorph of Bi_2MoO_6 See Entry 61846

Nature of the chemical bond in titanium hydrocarides See Entry 61849

Magnetic and structural characteristics of Ho_2Fe_{23} deuterides See Entry 61858

Evaluation of the valency of Fe, Cr, Cu, Sb doping ions in $Pb(Zr_{0.95}Ti_{0.05})O_3$ ceramics See Entry 61947

Radiation conversions in $MgCr_2O_4$ See Entry 61978

Solubility of hafnium dioxide in cerium dioxide See Entry 62108

Thermal expansion of barium orthovanadate See Entry 62133

Anomalous thermal expansion of europium vanadate See Entry 62134

Anomalous thermal expansion and character of layers of MV_2O_6 metavanadates ($M=Ca, Cd, Zn, Mg, Pb$) See Entry 62135

Mechanochemical effect in ZnTe powder associated with grinding See Entry 62444

Synthesis and magnetic properties of $(Mn_{1-x}Ta_x)_3B_4$ See Entry 62587

The thermal stability of calcium uranates in a hydrogen atmosphere See Entry 63539

61.65 SPECIFIC STRUCTURE OF ORGANIC COMPOUNDS

61899 Crystal and molecular structure of tetrachlorophosphorus (V) hexachlorouranate (V). J.C.Taylor, A.B.Waugh (Div. of Energy Chem., Lucas Heights Res. Labs., CSIRO, Sutherland, NSW, Australia).

Polyhedron (GB), vol.2, no.3, p.211-16 (1983).

The crystal structure of tetrachlorophosphorus (V) hexachlorouranate (V), $PCl_4^+UCl_6^-$, has been solved with 2492 independent F(hkl) collected by necessity from one component of a bocrystal: all crystals prepared were twinned. The structure is triclinic, space group $P1$, with $a=7.038(4)$, $b=7.373(4)$, $c=13.706(8)$ Å, $\alpha=89.38(3)^\circ$, $\beta=88.80(3)^\circ$, $\gamma=105.20(3)^\circ$, with $Z=2$. The two components of the bocrystal, in the volume ratio of 2.5 to 1, had their reciprocal lattice spots sufficiently separated to allow collection of the data set from component 1 with $AgK\alpha$ radiation ($\lambda=0.5608$ Å). A model was derived from the Patterson synthesis and refined by least squares to $R=\Sigma(|F_o|-|F_c|)/\Sigma|F_o|=0.146$. The structure was confirmed by a final ($\rho_r-\rho_c$) synthesis. The structure is an assembly of octahedral $U(1)Cl_6^-$, $U(2)Cl_6^-$ and tetrahedral PCl_4^+ groups. The chlorine atom array is hexagonal close-packed, while the polyhedra are regular within the experimental errors. The structure is isomorphous with the transition metal analogues PCl_5NbCl_5 and PCl_5TaCl_5 . (15 refs.)

61900 Crystal data for bis(η^5 -tert-butylcyclopentadienyl)hafnium(IV) dihydride dimer, $[(\eta^5-t-BuC_5H_7)_2HfH(\mu-H)]_2$. A.Laarif, F.Theobald (Faculte des Sci., Univ. de Besancon, Besancon, France); B.Gauthier, G.Tainturier.

J. Appl. Crystallogr. (Denmark), vol.16, pt.2, p.277 (1 April 1983).

Summary form only given, as follows. The air-sensitive title hydride $[(Hf(C_5H_7)_2)_2H_2]$ was prepared by hydrogenolysis of $(t-BuCp)_2HfMe_2$ (Conturier, 1980) and crystallized from a solution in heptane or toluene and hexane. The compound is triclinic with the following cell parameters: $a=7.22(3)$, $b=10.31(4)$, $c=12.47(6)$ Å, $\alpha=80.4(4)^\circ$, $\beta=74.6(4)^\circ$, $\gamma=72.1(3)^\circ$, $V=847$ Å³, $Z=1$, $D_x=1.67$ Mg m⁻³. Powder diffraction data were obtained from Debye-Scherrer photographs. The extended version of the paper examines several examples where Zr or Hf hydrides are monomers or dimers and shows that this structure is very similar to the related $[(MeCp)_2ZrH_2]$ compound (Jones & Petersen, 1981). This similarity and spectroscopic data show that the molecule probably has a center of symmetry situated between the two Hf atoms and the two bridging H atoms. The JCPDS Diffraction File No. for $[Hf(C_5H_7)_2)_2H_2]$ is 33-1996.

61901 Molecular and crystal structures of pregna-4, 16-dien-21-ol-3,20-dione acetate (16-dehydrocortexone) and pregna-1,4-dien-17 α ,21-diol-3,20-dione 21-acetate (dehydrocortexolone acetate). Z.I.Khazheeva, V.I.Simonov, A.V.Kamernitskii, N.S.Pavlova-Grishina, A.V.Skorova (Inst. of Crystallography, Acad. of Sci., USSR).

Sov. Phys.-Crystallogr. (USA), vol.27, no.5, p.543-6 (Sept.-Oct. 1982). Translation of: *Kristallografiya (USSR)*, vol.27, no.5, p.905-10 (Sept.-Oct. 1982). [received: April 1983]

Using diffractometric data and direct methods, the authors have determined and refined the structures of two steroid compounds: $C_{27}H_{30}O_4$ ($a=7.400$ Å, $b=12.926$ Å, $c=21.316$ Å, space group $P2_12_12_1$, $R=5.1\%$) and $C_{27}H_{30}O_5$ ($a=7.550$ Å, $b=11.805$ Å, $c=23.454$ Å, space group $P2_12_12_1$, $R=3.8\%$). The conformational parameters of the molecules of these biologically active compounds are established and analyzed. (7 refs.)

61902 Crystal structure of the π complex of cuprous chloride with acrylic acid. P.Yu.Zavaliy, V.S.Fundamenskii, M.G.Mys'kiv, E.I.Gladyshevskii (State Univ., L'vov, Ukrainian SSR).

Sov. Phys.-Crystallogr. (USA), vol.27, no.5, p.547-9 (Sept.-Oct. 1982). Translation of: *Kristallografiya (USSR)*, vol.27, no.5, p.911-15 (Sept.-Oct. 1982). [received: April 1983]

The authors make a complete X-ray structure analysis of the π complex of CuCl with acrylic acid, with the composition $CuCl.C_3H_5O_2$. The parameters of the orthorhombic unit cell are $a=8.153(2)$ Å, $b=6.2234(8)$ Å, $c=20.620(3)$ Å, space group $Pbca$, $Z=8$ (automatic diffractometer, Mo $K\alpha$ radiation, Patterson and Fourier syntheses, parameters of all atoms refined to $R=0.048$). The copper and chlorine atoms form layers of six-membered rings with the boat conformation. The Cu-Cl distances are 2.245, 2.256, and 3.104 Å. The acrylic acid molecules are bound into dimers by hydrogen bonds O-H...O 2.644 Å long. These centrosymmetric dimer molecules link the CuCl layers, coordinating the copper atoms from different layers by C=O bonds. The Cu...C distances are 2.040 and 2.043 Å. The length of the C=C bond in the acrylic acid in the complex is increased to 1.377 Å as against 1.30 Å in the free state. (4 refs.)

61903 Crystal and molecular structures of two 15-membered crown ether triones: 1,4,7,10,13-pentaaxycyclopentadecane-3,11,15-trione and 4,7,10,13-tetraoxa-1-thiacyclopentadecane-3,11,15-trione. Yu.G.Ganin, Yu.A.Simonov, N.G.Luk'yanenko, Yu.A.Popkov, A.V.Bogatskii (Inst. of Appl. Phys., Acad. of Sci., Moldavian SSR).

Sov. Phys.-Crystallogr. (USA), vol.27, no.5, p.550-3 (Sept.-Oct. 1982). Translation of: *Kristallografiya (USSR)*, vol.27, no.5, p.916-22 (Sept.-Oct. 1982). [received: April 1983]

The crystal structures of the compounds 1,4,7,10,13-pentaaxycyclopentadecane-3,11,15-trione (I) and 4,7,10,13-tetraoxa-1-thiacyclopentadecane-3,11,15-trione (II) are determined. The two 15-membered rings differ in the nature of the heteroatoms (O and S) in the first position. The conformations of the polyethylene and oxyacid parts are discussed. The authors advance the hypothesis that there is $\pi(p-d)$ interaction between the sulfur atom and the adjacent ether oxygens in II. Nonvalence 1,4-interactions, capable of stabilizing the conformations of the macrocyclic rings, are noted. (21 refs.)

61904 A new refinement of monoclinic tetracyanoethylene (TCNE) from X-ray and neutron data. U.Druck, H.Guth (Philipps-Univ., Marburg, Germany).

Z. Kristallogr. (Germany), vol.161, no.1-2, p.103-10 (1982).

The monoclinic phase of TCNE (C_6N_4) was submitted to a new X-ray and neutron diffraction analysis. Contrary to the results reported by Bekoe and Trueblood (1960) the authors found a slight disorder, such that 3.8-5% of the molecules are rotated about 90 degrees in the molecular plane around their center of gravity. The final R -values are 0.035 for the X-ray- and 0.033 for the neutron-data. The resulting X-N-map showed clearly resolved peaks, the heights of which correspond well with theoretical calculations. (13 refs.)

Structural states of MBBA during the transition from a frozen liquid-crystal state to a crystal See Entry 62095

Chlorine-35 nuclear quadrupole resonance of o-chloronitrobenzenes See Entry 62832

61.70 DEFECTS IN CRYSTALS

(see also 61.80 Radiation damage, 62. Mechanical and acoustic properties, 71.55 Impurity and defect levels, 76.30M EPR of colour centres and other defects, 78.50 Impurity and defect absorption in solids, 81.40 Treatment of materials)

61905 Observation of a new memory effect in a modulated structure. J.P.Jamet, P.Lederer (Lab. de Phys. des Solides, Univ. Paris-Sud, Orsay, France).

J. Phys. Lett. (France), vol.44, no.7, p.L257-64 (1 April 1983).

The authors report the first observation of a new memory effect in a modulated structure (deuterated thiourea). They present a qualitative explanation of this effect in terms of mobile defects, or impurities interacting with the modulation order parameter. The authors show that this effect can be used to obtain the lines of constant modulation wavevector in the E , T plane of the phase diagram, by thermodynamic methods. They suggest that a similar periodic modulation of defect concentration occurs in CDW systems like $NbSe_3$, and accounts for the non linearity induced by the electric field. (20 refs.)

61906 Oxygen defect profile in implanted garnet. P.Gerard, P.Martin, R.Danielou (LETI, CEA, Grenoble, France).

J. Magn. & Magn. Mater. (Netherlands), vol.35, no.1-3, p.303-6 (March 1983). (Proceedings of the 10th International Colloquium on Magnetic Films and Surfaces, Yokohama, Japan, 13-16 Sept. 1982).

For the first time direct measurements are presented for an oxygen defect profile, produced through implantation, in a bubble garnet material. An analysis of oxygen defects and of damage on heavy atoms profiles is given as a function of depth for the neon implantation at a dose of $2 \times 10^{14} \text{ cm}^{-2}$ by channeling experiments with nuclear reactions (NR) and Rutherford back-scattering (RBS). A good correlation is found between the present and the previous profiles obtained by using other experimental methods. (11 refs.)

61907 Comparison of different approaches to the study of local defects in crystals. I. Theoretical considerations and computational schemes. C.Pisani, R.Dovesi, P.Ugliengo (Inst. of Theoretical Chem., Univ. of Turin, Turin, Italy).

Phys. Status Solidi b (Germany), vol.116, no.1, p.249-59 (1 March 1983).

The standard way of treating local defects in crystals is to correct the Green function of the perfect periodic host system so as to account for the defect. This approach, which is termed here as 'perturbed crystal', is compared with a 'perturbed cluster' approach where instead the molecular solution for a cluster of atoms around and including the defect is corrected in order to account for the presence of the infinite surrounding medium. It is first shown that when a unique basis set is used to describe the crystal both before and after the defect is created, the perturbed crystal approach is essentially simpler. When however the defect is complicated and the use of different basis sets is practically compulsory, then the other approach is more natural and the corresponding computational scheme is more easily implementable. New explicit formulae for the perturbed cluster approach are derived which are more powerful and general than those used in previous works. (18 refs.)

61908 The mechanisms of the formation and growth of water bubbles and associated dislocation loops in synthetic quartz. A.C.McLaren, R.F.Cook, S.T.Hyde, R.C.Tobin (Dept. of Phys., Monash Univ., Clayton, Victoria, Australia).

Phys. & Chem. Miner. (Germany), vol.9, no.2, p.79-94 (1983).

The development of water bubbles in synthetic quartz has been monitored by measurements of (i) the intensity of the light scattered and (ii) the increase in volume of the crystal, both as a function of temperature and time. These macroscopic measurements have been complemented by observations of the resulting microstructures, using transmission electron microscopy (TEM). A mechanism is proposed on the assumption that hydrogen is incorporated in the quartz structure by means of $(4 \text{ H})_{\text{Si}}$ defects. On heating, these defects diffuse and clusters develop. A cluster of $n(4 \text{ H})_{\text{Si}}$ produces a water bubble of $(n-1)\text{H}_2\text{O}$, without any change of volume of the crystal. At any temperature T there is a critical bubble diameter above which the 'steam' pressure P exceeds the pressure p for a spherical bubble in mechanical equilibrium. If P becomes greater than p , then the bubble increases in volume until $P=p$, the increase in volume being achieved by the pipe diffusion, of Si and O away from the bubble site into a linked edge dislocation loop. This process produces the observed increase in volume of the crystal. The two diffusion processes take place virtually simultaneously and continue until all the $(4 \text{ H})_{\text{Si}}$ defects have been trapped in the bubbles. Values of the diffusion constant and the activation energy for the diffusion of the $(4 \text{ H})_{\text{Si}}$ defects are deduced. The relevance of these observations to the hydrolytic weakening of quartz is briefly discussed. (28 refs.)

Oxygen potentials of $(\text{U,Gd})\text{O}_{2+x}$ solid solutions in the temperature range 1000-1500°C See Entry 60239

An investigation into the potential importance of helium trapping during the nucleation of radiation-induced voids See Entry 61985

Precipitation and void-swelling in nickel-manganese austenitic stainless steels See Entry 61986

Small angle neutron scattering from oriented latent nuclear tracks See Entry 62005

Relationship between parameters of self-diffusion and of equilibrium defects and characteristics of monatomic crystals See Entry 62149

EuS ferromagnetic semiconductor films grown epitaxially on silicon See Entry 62296

Influence of defects on NQR relaxation processes in $\text{Bi}_{12}\text{GeO}_{20}$ and $\text{Bi}_{12}\text{SiO}_{20}$ See Entry 62831

Mossbauer spectroscopy in physical metallurgy See Entry 62840

Experimental investigation of the nature of infrared absorption by single crystals of $\alpha\text{-LiIO}_3$ See Entry 63003

Effect of sulfides and sulfide morphology on anisotropy of tensile ductility and toughness of hot-rolled C-Mn steels See Entry 63354

A technique for observing the cross sectional damage profiles in He-ion irradiated 316 stainless steel by transmission electron microscopy .. See Entry 63480

61.70B Interstitials and vacancies

(exc. colour centres)

61909 Effect of external stress on formation of vacancy loops in quenched aluminum. A.Sato, Y.Sugisaki, T.Mori (Dept. of Materials Sci. & Engng., Tokyo Inst. of Technol., Yokohama, Japan).

Acta Metall. (USA), vol.31, no.5, p.805-11 (May 1983).

Effects of tensile and compressive stresses on formation of vacancy loops in quenched 99.99% aluminum have been examined by using single crystals with the $\{110\}$ stress axis. Compressive stress acting on a $\{111\}$ plane promotes formation of faulted loops from vacancy clusters on this plane. Correspondingly, tensile stress retards formation of faulted loops on a $\{111\}$ plane, on which the stress acts. Based on a classical nucleation theory, a critical size for a vacancy disc to collapse into a faulted loop is estimated to be $\sim 3.0b$ in radius, containing ~ 37 lattice points on the fault plane, from the stress dependence of the nucleation rate of the loops. (17 refs.)

61910 An ephemeral Frenkel pair in iridium. M.-H.Gely, A.Dunlop, Y.Querre (CEN, Fontenay-aux-Rose, France).

C.R. Seances Acad. Sci. Ser. II (France), vol.296, no.1, p.23-8 (10 Jan. 1983). In French.

After activation by a neutron flux, iridium samples have been kept at low temperature (22K). The electrical resistivity decreases or increases according to whether the activation was moderate or high. A coherent interpretation is given implying the recoil-induced creation of a Frenkel pair during activation and its subsequent annihilation, with a probability ≈ 8 due to a second sub-threshold recoil. (11 refs.)

61911 Influence of ultrasound on the concentration of point defects in KBr crystals. Yu.A.Ivashkin, N.A.Tyapunina (M.V. Lomonosov State Univ., Moscow, USSR).

Sov. Phys.-Crystallogr. (USA), vol.27, no.5, p.604-5 (Sept.-Oct. 1982). Translation of: *Kristallografiya (USSR)*, vol.27, no.5, p.1007-9 (Sept.-Oct. 1982). [received: April 1983]

The authors have studied the process of PD formation in KBr crystals deformed by ultrasound. Point defects are formed in the process of plastic deformation as a result of the motion and interaction of dislocations. It had earlier been established that the excess PD concentration depends on the degree of plastic deformation and the stress in static conditions of loading. Two methods were used—flotation, based on precision measurements of the density of the specimens, and the method of control coloration. The flotation method gives an upper estimate of the change in vacancy concentration, since the change in density of the specimens is due not only to single vacancies but also to complexes of PD, pores, and microcracks. The control coloration method gives a lower estimate of the change in PD concentration, since it reflects only the change in concentration of F centers and their constituent anion vacancies. The functional dependences of the excess vacancy concentration on the stress, found by the two methods, are similar. It was of interest to use the control coloration method to investigate the concentration of anionic vacancies in crystals deformed by ultrasound. (20 refs.)

Proton irradiation damage in cyclically stressed aluminum See Entry 60235

The crystal structure of R_6GaCo_2 compounds ($\text{R}=\text{Y, Tb, Dy, Ho, Er, Tm, Lu}$) See Entry 61852

Changes in the concentration of 1.0 and 1.28 eV copper luminescence centers during annealing of electron-irradiated n -type GaAs See Entry 61948

On the interaction between a vacancy and an interstitial impurity atom in BCC transition metals See Entry 61953

Interaction of primary radiation defects with dislocations in indium antimonide See Entry 61955

Drift forces on vacancies and interstitials in alloys with radiation-induced segregation See Entry 61956

On the rate theory for pulsed irradiation See Entry 61957

Internal stress buildup in SiPA creep See Entry 61958

Point defect densities during the early transient stage of radiation-induced metal swelling See Entry 61960

Damage in the cation sublattice of $\alpha\text{-Al}_2\text{O}_3$ irradiated in an HVEM See Entry 61974

Vacancies and carbon impurities in α -iron: neutron irradiation See Entry 61979

Effects of quenching and fission damage on the low temperature electrical resistivity of single crystal UC See Entry 61981

Direct observation of the primary state of damage of ion-irradiated tungsten. II. Definitions, analyses and results See Entry 61989

Solvent diffusion in α -silver-tin alloys See Entry 62153

Recovery of quenched Cu-Ge alloys studied by positron annihilation See Entry 62156

Diffusion of rubidium ion in pure silver chloride crystals See Entry 62163

Influence of the internal electric field on the migration of substitutional impurities in diamond-structure semiconductors See Entry 62174

Some remarks on the carbon atoms pairs migrational relation in $\alpha\text{Fe-C}$ See Entry 62181

Quantum mechanical state of interstitial hydrogen in metals: energy and wavefunctions See Entry 62366

Oblique incidence effects in evaporated thin films See Entry 62752

X-ray photoelectron diffraction studies of zinc selenide See Entry 63137

A study of precipitation in interstitial alloys. II. A new metastable carbide phase in platinum See Entry 63296

A study of precipitation in interstitial alloys. III. Coherent and semicoherent growth mechanisms See Entry 63297

A study of precipitation in interstitial alloys. IV. The precipitation sequence in Pt-C See Entry 63298

Influence of residual gas pressure in annealing on the properties of niobium and its alloys See Entry 63333

Hydrogen-related internal friction peak in the A15 compound Nb_3Sn See Entry 63339

Influence of nitrogen on the penetration of hydrogen through constructional materials from nitrogen-hydrogen mixtures See Entry 63465

61.70D Colour centres

Colour centre lasers using alkaline earth fluorides See Entry 61159

Influence of ultrasound on the concentration of point defects in KBr crystals .. See Entry 61911

Comparison of heavy-ion, proton and electron irradiation effects in vitreous silica See Entry 61994

Annealing studies of irradiation effects in vitreous silica See Entry 61995

Divalent manganese in an axial symmetry site of additively coloured CaO single crystals See Entry 62802

On the role of Z centres in the supralinearity and sensitisation of LiF TLD phosphor See Entry 63062

61.70E Other point defects

Strain-ageing in silver chloride. I. The representative curve See Entry 62015

61.70G Dislocations: theory

61912 A model for the evolution of a twist dislocation network. F.A.McClintock, F.Prinz (Dept. of Mech. Engng., MIT, Cambridge, MA, USA).

Acta Metall. (USA), vol.31, no.5, p.827-32 (May 1983).

The transition from edge dislocation loops to a hexagonal grid of screw dislocations is followed for torsion of a single f.c.c. crystal with a $\{111\}$ cross section and $\{112\}$ faces, so that $\{110\}$ slip directions are parallel to the surface and in the plane of the cross section. Application of the results to stress-strain behavior, as well as computer modeling of the reactions, appears tractable. (12 refs.)

61913 Velocity of a finite dislocation. A.S.Mel'nichenko (Inst. of Steel & Alloys, Moscow, USSR).

Fiz. Met. & Metalloved. (USSR), vol.55, no.2, p.390-1 (Feb. 1983). In Russian. English translation in: *Phys. Met. & Metallogr. (GB)*. It is known that the velocity of a dislocation depends on its length if this length is less than a certain critical value. Calculations are compared with the experimental data for niobium and it is found that at 77K the critical length is considerably greater than the dimensions of moving dislocation segments. This conflict between the theory and experiment may be due to small amounts of impurities, which can reduce considerably the velocity of a kink without altering significantly the rate of formation of kinks. Another possibility is the presence, on moving dislocations, of steps separated by an average distance less than the critical value at 77K. (6 refs.) *A.T.*

61914 Structure of dislocation cores in the silicon crystal. S.L.Altmann (Dept. of Metall. & Sci. of Materials, Univ. of Oxford, Oxford, England), A.Lapicicella, K.W.Lodge.

Int. J. Quantum Chem. (USA), vol.23, no.3, p.1057-63 (March 1983). (Proceedings of the Fourth International Congress in Quantum Chemistry, Uppsala, Sweden, 13-20 June 1982).

The authors have recently produced a Lifson-Warshel force field for the silicon crystal. This field, that goes further than the harmonic approximation, is particularly adapted for the calculation of defect structures. It requires five free parameters, but one of them in the field already produced, the linear bending term, is significant for the perfect lattice structure only and should be eliminated in dealing with defect structures. Also, one of the fixed parameters can be adjusted to fit precisely the experimental value of the stacking fault energy. They show that an excellent fitting of the phonon dispersion curves, in the least squares sense, is obtained with the parameters thus changed. They illustrate the use of this field in discussing the problem of reconstruction of the 90° partial dislocation in silicon. (18 refs.)

61915 Core energies and core tensions of dissociated and partial dislocations in FCC and HCP metals. F.Prinz (Dept. of Mech. Engng., Carnegie-Mellon Univ., Pittsburgh, PA, USA), A.Korner, H.O.K.Kirchner. *Philos. Mag. A (GB)*, vol.47, no.3, p.441-52 (March 1983).

Using the anisotropic theory of elasticity and a semi-atomistic Peierls model, the core energies and core tensions of dislocations in FCC and HCP metals have been calculated. All the results were expressed in terms of Fourier expansions. A simple algorithm allowed the determination of the core energies and core tensions of individual Shockley partials which form the perfect dislocations in close-packed planes. (26 refs.)

61916 Dislocation clusters in elastic fields. V.I.Vladimirov, N.D.Priemskii (A.F. Ioffe Physicotech. Inst., Acad. of Sci., Leningrad, USSR).

Sov. Phys.-Tech. Phys. (USA), vol.27, no.9, p.1056-8 (Sept. 1982). Translation of: *Zh. Tekh. Fiz. (USSR)*, vol.52, no.9, p.1721-4 (Sept. 1982). [received: April 1983]

Results are reported from calculations of the parameters of dislocation clusters produced in elastic fields. A number of different approximate descriptions are used for the dislocations (continuum and several discrete models). It is shown that the distribution function for the dislocations in a cluster is very sensitive to the nature of the interactions among dislocations at small distances. Numerical calculations are used to demonstrate that the continuum approximation of dislocation clusters, previously suggested by the authors and is designed to find approximate solutions of kinetic and other nonlinear problems by discarding nonphysical terms from the cluster equilibrium equation, gives better results than the singular integral equation approach, which is best suited for problems admitting a solution in closed form. Frictional effects on the nature of the solution are investigated. (5 refs.)

Interactions between dislocations and grain boundaries in BCC metals See Entry 61954

Impurity-induced weakening of materials See Entry 62018

Random walk of dislocations following a high-velocity impact See Entry 62027

Kinetic enrichment of hydrogen at interfaces and voids by dislocation sweep-in of hydrogen See Entry 62168

A mathematical analysis of diffusion in dislocations. III. Diffusion in a dislocation array with diffusion zone overlap See Entry 62180

Electron structure of edge dislocations in metals See Entry 62371

Frustration of antiferromagnetic bonds around a screw dislocation See Entry 62555

Mechanism of influence of certain alloying elements on the hydrogen embrittlement of iron See Entry 63420

61.70J Etch pits, decoration, transmission electron-microscopy and other direct observations of dislocations

61917 Etching characterization of {001} semi-insulating GaAs wafers. Y.Okada (Electrotech. Lab., Ibaraki, Japan).

Jpn. J. Appl. Phys. Part I (Japan), vol.22, no.3, p.413-17 (March 1983). The characteristics of {001} semi-insulating GaAs wafers have been investigated by the etching/optical microscopy. New etch features such as groove have been revealed in only LEC crystals together with ridge features by an AB etch, but not in boat-grown crystals. The groove features are specifically revealed on gathering and twisting dislocations such as cell or lineage structures, and coincide with each dislocation lying near the surface. Small pits along the ridge features have been revealed in undoped LEC crystal, but not in undoped boat grown crystals. The distribution of the ridge features with the small pits correlates with that of 0.8 eV photoluminescence intensity in the wafer. (12 refs.)

61918 Dissolution kinetics and etch pit studies of potassium aluminium sulphate. B.van der Hoek, W.J.P.van Enckevort, W.H.van der Linden (RIM Lab. of Solid State Chem., Catholic Univ., Nijmegen, Netherlands).

J. Cryst. Growth (Netherlands), vol.61, no.2, p.181-93 (March 1983). The dissolution process of the {111} faces of potash alum is studied, both by microtopographic examinations of the etch pit patterns and by measurement of the dissolution kinetics in a rotating disc crystallizer. Both methods showed that the Cabrera-Levine dissolution theory holds for the two most common dislocation types ending on the {111} faces of potash alum. On the basis of the rotating disc experiments, the interfacial supersaturation of the etch pit experiments was roughly estimated. Using this, it was found that at interfacial supersaturations below -0.6% (dislocations with (110) Burgers vector) or below -0.85% (dislocations with (100) Burgers vector) numerous etch pits related to those dislocation types appeared. Below those undersaturations the dissolution process is mainly determined by volume diffusion. From the critical undersaturation, determined in the rotating disc crystallizer, the value of

the edge free energy of a step was found to be approximately 0.01 J/m². (31 refs.)

61919 Etch pits on single crystals and bicrystals of niobium. B.C.Cai, A.Dasgupta, Y.T.Chou (Dept. of Metall. & Materials Engng., Lehigh Univ., Bethlehem, PA, USA).

J. Less-Common Met. (Switzerland), vol.90, no.1, p.37-45 (March 1983). Three types of etch pit were observed on single crystals and bicrystals of niobium. The relationship between the shape of the pits and the orientation of the etching surface was established and discussed on the basis of the surface energy concept. It was demonstrated that misorientations of tilt boundaries can be determined in bicrystals using the etch pit technique. (9 refs.)

61920 Improved technique for observation of dislocation structure of austenitic MnCrNi steels after small deformation. A.Gemperle (Inst. of Phys., Czechoslovak Acad. of Sci., Praha, Czechoslovakia), I.Kasova, V.Cihal. *J. Microsc. & Spectrosc. Electron. (France)*, vol.7, no.6, p.559-74 (Dec. 1982).

Up to now, dislocation structures have been compared in statistically oriented grains in most papers dealing with plastic deformation of polycrystals. In these grains slip is accomplished on various slip systems with various intensities and only very distinct differences in dislocation arrangement in relation to e.p. stacking fault energy can be detected. In this paper an attempt is made to equalize the deformation conditions for the comparison of dislocation structures by a choice of grains having equal crystallographic orientation in respect to tensile axis. (6 refs.)

61921 Weak beam images of dislocations triple ribbons. G.Vanderschaeve (Univ. des Sci. et Tech. de Lille, Villeneuve d'Ascq, France). *J. Microsc. & Spectrosc. Electron. (France)*, vol.7, no.6, p.695-14 (Dec. 1982). In French.

Weak beam images of dislocations triple ribbons have been calculated, taking into account the overlap of the strain field due to each partial dislocation. It is shown that the separation of image peaks is very close to the actual separation between dislocations providing $|s|d > |g.b|$ for screw dislocations and $|s|e \geq 17|g.b|$ for edge dislocations, where d is the width of the narrower stacking fault ribbon. (18 refs.)

61922 Dissociation of dislocations in diamond. P.Pirouz, D.J.H.Cockayne (Dept. of Metall. & Sci. of Materials, Univ. of Oxford, Oxford, England), N.Sumida, P.Hirsch, A.R.Lang.

Proc. R. Soc. London Ser. A (GB), vol.386, no.1791, p.241-9 (8 April 1983).

Weak-beam electron microscopy has been applied to study the dissociation of dislocations in a type IIa diamond. Dislocations with Burgers vector $\frac{1}{2}[110]$ on (111) glide planes have been found to be dissociated into two Shockley partials, with separations between 2.5 and 4.3 nm, and extended nodes and dissociated dipoles have also been observed. The stacking fault energy has been determined, from the mean and distribution of the separations of the partials, to be 279 ± 41 mJ m⁻². The behaviour of dislocations in diamond appears to be similar to that of dislocations in Ge and Si. (36 refs.)

61923 Glide dislocations on cube planes in a low stacking-fault energy alloy. A.Korner, H.P.Karntaler (Inst. fur Festkörperphys., Univ. Wien, Wien, Austria).

Phys. Status Solidi a (Germany), vol.75, no.2, p.525-35 (16 Feb. 1983).

Single crystals of Cu-15 at.% Al strained into stage II are studied using electron microscopy methods. In spite of the very low stacking-fault energy total dislocations $\{a/2 [110] (001)\}$ are observed to bow out on the cube plane under the influence of the internal stresses. These dislocations can originate from the transformation of Lomer-Cottrell locks which can glide on (001) after being constructed. The shape of the half loops observed on (001) deviates strongly from the elliptical one and agrees well with the calculated shapes using anisotropic elasticity theory. From the curvature of the loops large stresses are deduced which are interpreted in terms of a dislocation locking stress caused by short-range-order effects pinning the dislocations. (25 refs.)

61924 Chemical etching of deformation sub-structures in quartz. M.W.Wegner, J.M.Christie (Dept. of Earth & Space Sci., Univ. of California, Los Angeles, CA, USA).

Phys. & Chem. Miner. (Germany), vol.9, no.2, p.67-78 (1983).

Chemical etching of dislocations has been studied in natural and synthetic quartz single crystals, is deformed synthetic quartz and in naturally and experimentally deformed quartzites. The ability of different etchants to produce polished or preferentially etched surfaces on quartz is described. Dislocation etching was achieved on all crystal planes examined by using a saturated solution of ammonium bifluoride as the etchant. Appropriate etching times were determined for etching quartzites for grain size, sub-grain boundaries, deformation lamellae, dislocations and twins. Growth and polished surfaces of synthetic single crystal quartz were similarly etched and dislocation etch pits, characteristic of various orientations were found. The use of ammonium bifluoride proved to be especially advantageous for the basal plane, producing a polished surface with etch pits, suitable for dislocation etch pit counting. 'Double' etch pits, have been found on Dauphine twin boundaries on the basal plane and the first order prism, using this etchant. Slip lines and deformation bands were suitably etched on deformed synthetic crystal surfaces for identification of the slip planes. Other acidic etchants have been explored and their application to the study of deformation structures in quartz crystals is discussed. (57 refs.)

61925 Effect of interaction of misfit dislocations in multilayer epitaxial films. A.I.Fedorenko, B.A.Savitskii, A.Yu.Sipatov, L.P.Shpakovskaya (Polytech. Inst., Khar'kov, Ukrainian SSR).

Sov. Phys.-Crystallogr. (USA), vol.27, no.5, p.569-74 (Sept.-Oct. 1982). Translation of: *Kristallografiya (USSR)*, vol.27, no.5, p.948-55 (Sept.-Oct. 1982). [received: April 1983]

Electron microscopy and electron diffraction are used to investigate the dislocation structures of three-layer epitaxial films, taking the chalcogenides of lead as an example. Systems of types *ABA* and *ABC* are considered, and are grown by successive deposition of chalcogenides *A*, *B*, and *C* (PbS, PbSe, PbTe). In both types of film, the preceding interphase surface is found to have a marked influence on the formation of a dislocation structure at the next interphase boundary. This is because of two effects: (i) interactions between the fields of elastic stresses of misfit dislocations at adjacent boundaries; (ii) inheritance of vertical 'tails' of misfit dislocations from the preceding interphase surface by the following epitaxial layer. (8 refs.)

61926 Observation of precipitates on 'growth' dislocations in GaAs single crystals with low impurity content. A.V.Markov, S.S.Shifrin, L.M.Morgulis (State Sci.-Res. & Design Inst. of Rare Metals Industry, USSR).

Sov. Phys.-Crystallogr. (USA), vol.27, no.5, p.620-2 (Sept.-Oct. 1982). Translation of: *Kristallografiya (USSR)*, vol.27, no.5, p.1031-3 (Sept.-Oct. 1982). [received: April 1983]

The authors have studied 'growth' dislocations in GaAs single crystals grown by the Czochralski method and also by horizontal directed crystallization, and doped with various impurities (Te, S, Sn, Si, Zn, Cr) over a wide range of

concentrations. The impurity concentrations were determined by means of electrophysical measurements; in the case of Cr-doped seminsulating GaAs, they were determined by means of chemiospectral analysis. The dislocations were revealed by means of Abrahams-Buiochi etching agent (AB), which gives high relief of the traces in the 'projection' etching pattern. After thinning in a polishing etchant of $H_2SO_4:H_2O_2:H_2O=3:1:1$ to about 40-50 μ , the specimens were finished off in AB etchant and dislocation traces led to a thin place which was transparent to electrons at an accelerating voltage of 100 kV. (8 refs.)

A comparison of helium bubble behaviour in an austenitic and a ferritic steel See Entry 60405

Polarization of X-rays in the region of the Bragg reflection curves of silicon crystals with dislocations See Entry 61734

The mechanisms of the formation and growth of water bubbles and associated dislocation loops in synthetic quartz See Entry 61908

Effect of external stress on formation of vacancy loops in quenched aluminum See Entry 61909

Irradiation damage of II-VI compounds in a high-voltage electron microscope See Entry 61972

Radiation damage in pure and helium-doped $\alpha-Al_2O_3$ in the HVEM. Qualitative aspects of void and aluminum colloid formation See Entry 61973

Damage in the cation sublattice of $\alpha-Al_2O_3$ irradiated in an HVEM See Entry 61974

Influence of doping with isovalent impurities on defect formation in homoepitaxial GaAs layers See Entry 62301

Crystal, impurity-related and growth defects in molecular beam epitaxial GaAs layers See Entry 62308

Direct observation of the interaction between magnetic domain walls and dislocations in iron See Entry 62682

Influence of Ni-additions on grain boundaries during sintering of Mo See Entry 63211

Microstructure of aluminium during creep at intermediate temperatures. III. The rate controlling process See Entry 63342

Characteristics of plastic deformation of silicon iron single crystals under hydrostatic pressures See Entry 63343

Variation of dislocation density during fatigue process of low carbon steel See Entry 63392

X-ray topographic investigations of solid state reactions. I. Changes in surface and bulk substructure during incipient thermal decomposition in sodium chlorate monocrystals See Entry 63542

61.70L Slip, creep, internal friction and other indirect evidence of dislocations

(see also 62.20H Creep, 62.40 Internal friction)

61927 The role of elastic interaction stresses on the onset of slip in polycrystalline alpha brass. I. Experimental determination of operating slip systems and qualitative analysis. K.Hashimoto, H.Margolin (Dept. of Phys. & Engng. Metall., Polytech. Inst. of New York, New York, NY, USA). *Acta Metall. (USA)*, vol.31, no.5, p.773-85 (May 1983).

Coarse grained α -brass specimens with grain sizes of 2.4 mm (as cast), 0.86 (wrought), 0.52 (as cast) and 0.19 (wrought) were compressed to the proportional limit. The orientation of a number of grains, including 67 which revealed cross slip, were determined by the back reflection Laue technique. Trace analysis of cross slipping systems permitted the determination of the operating slip systems. Of the 195 slip systems determined, 118 were primary or strongly operating. The remainder were either cross slip or secondary slip systems. Of the 118 primary slip systems only 30 had the highest Schmid Factor (S.F.) based on the applied stress. This indicated that internal stresses arising from the elastic interactions of neighboring grains, provided the necessary additional stress to permit the observed slip system to operate. A qualitative analysis, based on the elastic contribution of surrounding grains to slip in a given grain confirmed this inference. (16 refs.)

61928 Strains and internal stresses in silicon wafers. A.P.Oksanich. *Ind. Lab. (USA)*, vol.48, no.6, p.587-91 (June 1982). Translation of: *Zavod. Lab. (USSR)*, vol.48, no.6, p.52-5 (June 1982). [received: March 1983]

A study is made of complicated kinds of deformations in silicon wafers, and diagrams of macrostresses and dislocations in them are determined. A procedure and equipment are developed for checking complicated kinds of bends in which the degree of distortion is accounted for automatically as a function of crystallographic directions. (11 refs.)

61929 Comments on reported magneto-oscillations in dislocation drag at low temperatures. B.R.Watts (School of Math. & Phys., Univ. of East Anglia, Norwich, England). *Philos. Mag. B (GB)*, vol.47, no.3, p.L25-8 (March 1983).

The essential similarity between recently reported oscillations in the magnetic field dependence of dislocation drag and quantum oscillations of conduction electrons is pointed out. An explanation, in terms of magnetostriction, for the appearance of quantum oscillations in the dislocation drag experiments is given. A consequence is that the oscillatory, and possibly the non-oscillatory, magnetic field dependence is not associated with dislocation drag. (8 refs.)

Improved technique for observation of dislocation structure of austenitic MnCrNi steels after small deformation See Entry 61920

Chemical etching of deformation sub-structures in quartz See Entry 61924

Strain-ageing in silver chloride. I. The representative curve See Entry 62015

Orientation dependence of slip deformation of the conjugate system in Cu-6 at.% Al single crystals See Entry 62017

Hydrogen relaxation in lutetium See Entry 62026

Positron lifetime measurement of plastically deformed iron single crystals See Entry 63080

The effect of ITMT's and P/M processing on the microstructure and mechanical properties of the X7091 alloy See Entry 63319

The role of elastic interaction stresses on the onset of slip in polycrystalline alpha brass. II. Rationalization of slip behavior See Entry 63335

Internal friction study of AISI 410 stainless steel See Entry 63338

Microstructure of aluminium during creep at intermediate temperatures. III. The rate controlling process See Entry 63342

Characteristics of plastic deformation of silicon iron single crystals under hydrostatic pressures See Entry 63343

Microstructure and tensile ductility in a β heat treated titanium alloy See Entry 63400

61.70N Grain and twin boundaries

61930 The projected atomic structure of a large angle [001] $\Sigma=5$ ($\theta=36.9^\circ$) twist boundary in gold: diffraction analysis and theoretical predictions. J.Budai, P.D.Bristowe, S.L.Sass (Dept. of Materials Sci. & Engng., Cornell Univ., Ithaca, NY, USA).

Acta Metall. (USA), vol.31, no.5, p.699-712 (May 1983). The projected atomic structure of a large angle [001] $\Sigma=5$ ($\theta=36.9^\circ$) twist boundary in Au was determined using X-ray diffraction techniques. The extra reflections resulting from the periodic structure of the boundary were studied using synchrotron radiation. The observed structure factor rules are consistent with the boundary existing in the exact coincidence configuration. The projected structure was determined using a variable coordinate and reliability factor analysis which was simplified by the low value of Σ , the boundary symmetry and the assumption of a thin boundary region. The structure thus determined consists of groups of atoms which have undergone large rotations about '0'-elements in the planes immediately adjacent to the boundary. The structure is made up of separate patches of median f.c.c. structure in analogy with small angle boundaries. Various structures calculated by computer relaxation techniques using interatomic potentials are also presented and compared with the diffraction results. (34 refs.)

61931 Investigation of the structure of grain boundaries with special misorientations in tungsten. A.V.Volkov, L.K.Fionova (Inst. of Steel & Alloys, Moscow, USSR).

Fiz. Met. & Metalloved. (USSR), vol.55, no.2, p.402-5 (Feb. 1983). In Russian. English translation in: *Phys. Met. & Metallogr. (GB)*. A field-ion microscope was used to study the structure of grains with large values of the reciprocal of the density of common sites in the coincident-site lattice of tungsten of technical purity. It was found that a slight deviation of a tilt boundary from a plane of good matching resulted in the formation of microsteps, whereas the presence of a twist component was compensated by grain-boundary dislocations. (10 refs.) A.T.

61932 An investigation of the degree of randomness in the dispersion of point features (triple junctions) in a plane. S.R.Stock, J.E.Hilliard (Dept. of Materials Sci. & Engng., Northwestern Univ., Evanston, IL, USA).

J. Microsc. (GB), vol.130, pt.1, p.107-9 (April 1983).

The nearest-neighbour distance distribution was used as a criterion to investigate the dispersion of triple junctions. Comparison of the expected and measured distributions by the χ^2 -test indicated that the triple junctions were probably not randomly located, contrary to an earlier conclusion based on an areal probe of the same specimen. The present results suggest that areal probes are insensitive to large deviations from randomness in the location of points in a plane. (10 refs.)

61933 Determination of grain boundary rotation parameters from Kikuchi patterns. I. A simplified method for determining the accurate orientation relationship of two grains. H.O.Martikainen (Dept. of Mining & Metall., Helsinki Univ. of Technol., Espoo, Finland), M.A.Korhonen, V.K.Lindroos. *Phys. Status Solidi A (Germany)*, vol.75, no.2, p.559-66 (16 Feb. 1983).

A simplified method for analysing the crystallographic orientation relationship of two adjacent grains by using electron diffraction Kikuchi line patterns is described. The error estimates of rotation axis and angle determined by the method, are formulated. The present method appears to be particularly useful in fast and accurate orientation determinations. Furthermore, as the method of analysis is in a general form, it is not dependent on the crystal system in question. (14 refs.)

61934 Growth twins of biphenyl. O.G.Kozlova, E.D.Dukova, A.O.Orlova (Inst. of Crystallography, Acad. of Sci., USSR).

Sov. Phys.-Crystallogr. (USA), vol.27, no.5, p.574-6 (Sept.-Oct. 1982). Translation of: *Kristallografiya (USSR)*, vol.27, no.5, p.956-60 (Sept.-Oct. 1982). [received: April 1983]

The authors make goniometric measurements on macroscopic crystals of biphenyl and a twin of symmetry mm2. They find the conditions in which biphenyl forms twins when its crystals are grown from the vapor. Statistical data show that with $T=45^\circ\text{C}$ and $\Delta T=2-3^\circ$ composition of individual crystals into twins of symmetry mm2 occurs preferentially on the series of faces (101), (201), (301), belonging to the same crystallographic zone [010]. (7 refs.)

Features of the growth of potassium pentaborate crystals See Entry 61838

Crystal and molecular structure of tetrachlorophosphorus (V) hexachlorouranate (V) See Entry 61899

Etch pits on single crystals and bicrystals of niobium See Entry 61919

Chemical etching of deformation sub-structures in quartz See Entry 61924

Interactions between dislocations and grain boundaries in BCC metals See Entry 61954

Correlation between grain-boundary hardening and grain-boundary energy in niobium bicrystals See Entry 62020

Grain boundary diffusion in columnar structure polycrystalline materials See Entry 62177

Steady state and transient capacitance measurements of the energy levels of a low angle tilt boundary in a germanium bicrystal See Entry 62373

Characterization of grain boundaries in polycrystalline GaAs See Entry 62374

Electronic states associated with grain boundaries in silicon See Entry 62375

Grain boundary passivation in polycrystalline silicon: a DLTS study See Entry 62376

Electronic structure of grain boundaries and interfaces in polycrystalline zinc oxide See Entry 62377

The electronic properties of semiconductor grain boundaries See Entry 62409

Transport across silicon grain boundaries See Entry 62428

Electrical and structural properties of grain boundary in polycrystalline Si See Entry 62429

Relative influence of grain boundaries and intragrain defects on the photocurrents obtained with Bridgman polysilicon See Entry 62456

Light effects on grain boundary properties in silicon See Entry 62457

Dielectric characteristic in V_2O_5 crystal and crystallized glass 70 V_2O_5 .30 P_2O_5 See Entry 62887

Preparation of oriented GaAs bicrystal layers by vapor-phase epitaxy using lateral overgrowth See Entry 63172

Influence of Ni-additions on grain boundaries during sintering of Mo See Entry 63211

The grain growth in alumina derived from gels See Entry 63242

The effect of MgO on intragranular pore entrapment in sintered aluminium oxide See Entry 63244

- Grain boundaries in sintered carbides See Entry 63247
 Computer modelling of grain boundary segregation See Entry 63294
 Influence of texture on dislocation creep and grain boundary sliding in fine-grained cadmium See Entry 63341
 Structural mechanism of plastic deformation of Mn-Cu alloys in martensitic state See Entry 63345
 Microstructure and tensile ductility in a β heat treated titanium alloy See Entry 63400
 Intergranular zinc embrittlement and its inhibition by phosphorus in 55 pct Al-Zn-coated sheet steel See Entry 63453
 Grain boundary effects in polycrystalline silicon solar cells. I. Solution of the three-dimensional diffusion equation by the Green's function method See Entry 63666
 Grain boundary effects in polycrystalline silicon solar cells. II. Numerical calculation of the limiting parameters and maximum efficiency See Entry 63667

61.70P Stacking faults, stacking fault tetrahedra and other planar or extended defects

- Electron microscope studies on the Sm-Co and Sm-Ni intermetallic compounds See Entry 61853
 Improved technique for observation of dislocation structure of austenitic MnCrNi steels after small deformation See Entry 61920
 Dissociation of dislocations in diamond See Entry 61922
 Crystal, impurity-related and growth defects in molecular beam epitaxial GaAs layers See Entry 62308
 Some magnetological insights in the consolidation of metal powders See Entry 63208
 Influence of extended defects and of the porous texture in the reduction of chromium dioxide See Entry 63538

61.70R Crystal impurities: general

(see also 71.55 Impurity and defect levels; 81.10 Purification techniques)

- Random walk to and interaction with an impurity See Entry 59703
 Crystal, impurity-related and growth defects in molecular beam epitaxial GaAs layers See Entry 62308
 Semiempirical calculation of optical-ionization energy for the Tl^0 center in a KCl crystal See Entry 63026

61.70T Doping and implantation of impurities

- 61935 Kinetics of antimony doping in silicon molecular beam epitaxy. M.Tabe, K.Kajiyama (Musashino Electrical Communication Lab., Nippon Telegraph & Telephone Public Corp., Tokyo, Japan). *Jpn. J. Appl. Phys. Part 1 (Japan)*, vol.22, no.3, p.423-8 (March 1983).
 A new kinetic model for Sb doping into the Si MBE layer is proposed. In this model, Sb doping steps are assumed as follows: a fraction of impinging Sb₂ molecules adsorbs on the growing Si surface (adlayer) and monoatomic Sb desorbs from the adlayer into vapor; a fraction of monoatomic Sb in the adlayer is incorporated into the bulk, so that surface-concentration of Sb atoms may be in equilibrium with bulk-concentration of Sb. According to this model, calculated results successfully represent the present experimental data on relations between incident Sb₂ flux, Sb concentration in the adlayer and that in bulk. As a result, it is indicated that doping levels in MBE layers are uniquely determined by Sb concentration in the adlayer, and not by Sb₂ flux/Si flux ratio, when Si growth rate is lower than 1 Å/s.
 61936 A simple method to produce quasi-simultaneous multiple-energy helium implantation. F.Paszi, M.Fried, A.Manuaba, G.Mezei, E.Kotai, T.Lohner (Central Res. Inst. for Phys., Budapest, Hungary). *J. Nucl. Mater. (Netherlands)*, vol.114, no.2-3, p.330-3 (Feb. 1983).
 Demonstrates a simple and cheap method to produce a practically simultaneous multiple energy implantation where—in principle—no restrictions and limitations exist for obtaining different kinds of energy spectrum from a monoenergetic beam source. (11 refs.)
 61937 The post-hydrogenation of low-pressure chemical vapor deposited amorphous silicon. A.E.Widmer, R.Fehlmann, C.W.Magee (Lab. RCA Ltd., Zurich, Switzerland). *J. Non-Cryst. Solids (Netherlands)*, vol.54, no.3, p.199-205 (March 1983).
 Amorphous silicon films prepared by low pressure chemical vapor deposition were exposed to atomic hydrogen in an RF plasma. Concentrated hydrogen and 20% hydrogen in argon was used for the plasma. The hydrogen concentration as a function of depth was measured for various process parameters with secondary ion mass spectrometry (SIMS). Hydrogenation temperatures of 250 to 400°C and exposure times from 30-120 min were used. The hydrogen surface concentration varied between 4 and 10 at.%, whereby the higher values were obtained with plasma treatments in concentrated hydrogen. The fit of an error function diffusion profile to the experimentally measured SIMS concentration results in a diffusion coefficient at 400°C of $D=6 \times 10^{-14}$ cm² s⁻¹. (13 refs.)
 61938 High temperature and short time thermal annealing of ion-implanted silicon. S.Matsumoto, K.Kashiwabara, H.Maki (Dept. of Electrical Engng., Keio Univ., Kanagawa, Japan), T.Niimi. *J. Vac. Soc. Jpn. (Japan)*, vol.25, no.12, p.788-94 (1982). In Japanese.
 Arsenic and phosphorus-implanted silicon substrates have been annealed by a furnace with higher temperature and shorter time than those of the conventional furnace annealing. Carrier concentrations obtained by differential van der Pauw measurements lie on the as-implanted distribution, showing a complete electrical activation with negligible redistribution of dopants. The experimental values of Hall mobility coincide with those of the Irvin mobility, suggesting the regrowth of ion-implanted silicon. Diffusion profiles of dopants after the regrowth of ion-implanted silicon can be modelled by separating the regrowth and diffusion processes with an effective diffusion time. (20 refs.)
 61939 Changes induced by ion implantation in forsterite SiO₄ Mg₂. S.Massouh, C.Bovier, J.Serughetti (Dept. de Phys. des Materiaux, Univ. Claude Bernard, Villeurbanne, France). *Radiat. Eff. (GB)*, vol.65, no.1-4, p.73 (1982). (Proceedings of the First International Conference on 'Radiation Effects in Insulators', Arco, Largo di Garda, Italy, 1981).
 Summary form only given, as follows. The various methods of optical absorption spectroscopy, Rutherford back-scattering, transmission electron micro-

scopy and X-ray diffraction have been associated to study the high-dose ion implantation (150 keV, 10^{17} ions cm⁻²) phenomena in SiO₄Mg₂ single crystals. After thermal annealing at high temperature under vacuum or in atmosphere, different new phases appear: for an under vacuum anneal, the formation of solid solution is observed: SiO₄ (Mg, Fe)₂ by X-ray diffraction; for atmospheric anneal precipitates a spinelle phase of Fe₂O₄ or Mg Fe₂O₄. Preliminary results on the mechanical properties studied by creep technique will be discussed for these implanted and annealed crystals. (no refs.)

61940 Ion implantation and luminescence. F.J.Bryant (Dept. of Phys., Univ. of Hull, Hull, England). *Radiat. Eff. (GB)*, vol.65, no.1-4, p.81-93 (1982). (Proceedings of the First International Conference on 'Radiation Effects in Insulators', Arco, Largo di Garda, Italy, 1981).
 For insulators, the relationship between ion implantation and luminescence has been reviewed. Luminescence has been shown to be an important technique in the study of ion implanted layers and implantation mechanisms and the value of implantation doping in producing luminescence centres or devices has been discussed. Some particular topics have been chosen and considered to illustrate the useful relationship between luminescence and implantation. Cathodoluminescence studies have been used to investigate the importance of various implantation parameters in implantation doping. Identification of luminescence centres from post-implantation annealing treatments has led to an understanding of the lattice sites occupied by the implanted ions. The method of using optically-detected magnetic resonance (ODMR) to investigate implanted ions and the damage occurring during implantation has been illustrated by reference to phosphorus implantation in zinc selenide. The significance of depth-resolved cathodoluminescence in implantation studies has been briefly considered. Finally, the advantages of ion implantation in studying the role played by impurities in the radiation dosimeter material LiF are outlined. (33 refs.)

61941 Ion beam hydrogenation of polysilicon coated thermal oxide on silicon. J.Belson (Dept. of Electronic & Electrical Engng., Univ. of Surrey, Guildford, England). *Radiat. Eff. (GB)*, vol.65, no.1-4, p.95-9 (1982). (Proceedings of the First International Conference on 'Radiation Effects in Insulators', Arco, Largo di Garda, Italy, 1981).
 The annealing of bare thermal oxide on silicon at 400-500°C in a hydrogen bearing gas results in a reduced density of states N_{ss} at the substrate silicon/oxide interface. Treatments of this type have played a role in MOS processing schedules for several years. However, a similar approach applied to large areas (~cm²) of polysilicon coated oxide appears to be less effective in reducing N_{ss} . This may be due to the polysilicon acting as a partially impermeable barrier which tends to starve the substrate/oxide interface of hydrogen. In the present work hydrogenation of 2-inch diameter, polysilicon coated wafers has been accomplished by hydrogen ion implantation. H₂⁺ ions of 135 kV energy were implanted (to a dose of 10^{15} cm⁻²) through a 7000 Å polysilicon coating into an underlying 1400 Å SiO₂ layer. The polysilicon was removed after 30-min anneals carried out in pure N₂ at 300, 400 or 500°C. Aluminium dots, 1 mm in diameter were then deposited onto the oxide and high frequency (1 MHz) and quasistatic C-V curves recorded for determinations of N_{ss} . Control anneals on unimplanted material were carried out in pure N₂ and N₂-H₂ ambients. Control samples annealed in pure N₂ with their polysilicon coating intact had mid-gap N_{ss} values of not less than 4×10^{10} cm⁻² eV⁻¹. The corresponding value after N₂-H₂ anneals on polysilicon-free wafers was 3×10^{10} . H₂⁺ implanted samples annealed in pure N₂ with their hydrogenation may depend upon confinement of the associated displacement damage to the polysilicon. This allows the implanted hydrogen to be activated within the SiO₂ at temperatures similar to those employed for normal homogeneous gas annealing of the substrate silicon/oxide interface. (12 refs.)

61942 Chemical and catalytic effects of ion implantation. G.K.Wolf (Phys.-Chem. Inst., Heidelberg Univ., Heidelberg, Germany). *Radiat. Eff. (GB)*, vol.65, no.1-4, p.107-116 (1982). (Proceedings of the First International Conference on 'Radiation Effects in Insulators', Arco, Largo di Garda, Italy, 1981).
 Energetic particles are used for inducing chemical reactions as well as for modifying the properties of materials with regard to their bulk and surface chemical behavior. The effects are partly caused by radiation damage on phase intermixing, partly by the chemical properties of the individual bombarding particles. A survey of relevant applications of these techniques is presented which considers chemical reactions of implanted and recoil atoms and their use for syntheses, doping and labelling of compounds; the formation of thin films by decomposing chemical compounds with ion beams; catalytic effects on substrates treated by sputtering or ion implantation. Recent results with nonmetallic substrates are reviewed. Mainly hydrogenation reactions at a solid/gas interface or redox reactions at an electrified solid/liquid interface are mentioned. The present status and future prospects of these kinds of investigations will be discussed. (29 refs.)

61943 Implantation as a tool for performing selective materials (application to solar energy conversion). G.Chassagne, G.Abouchacra, J.Davenas, A.Delmas, C.Dupuy, J.Serughetti, M.Treilleux (Dept. de Phys. des Materiaux, Univ. Claude Bernard, Villeurbanne, France). *Radiat. Eff. (GB)*, vol.65, no.1-4, p.119-25 (1982). (Proceedings of the First International Conference on 'Radiation Effects in Insulators', Arco, Largo di Garda, Italy, 1981).
 A selective solar material must absorb most of the solar spectrum, principally the visible light, and reflect the IR light. Insulators are generally transparent in a wide part of the optical spectrum and the defects are revealed in these crystals by strong absorption bands. On the other hand, metals absorb much of the IR and near IR light and have a large reflection coefficient in the same region of the spectrum. In previous papers it has been shown that metallic colloids, formed by precipitation of impurities in insulators, are responsible for a strong absorption band. Such metallic inclusions may be easily produced in most insulators by implantation. According to the nature of the implanted metal a selective absorption can be obtained. So a composite material (cermet) may be performed combining a colloidal absorption in the visible and a metallic reflection. The authors discuss the different ways to achieve these properties using direct ion beam implantation. Various cermet (LiF:Na,Au; MgO:Na,Au) have been studied as function of energy (0.1-1 MeV) and dose (10^{16} - 10^{17} ions/cm²). Colloids are completely developed by consecutive annealing. The modelization of these cermet requires a careful characterization by optical methods (spectrophotometry) and microscopic investigation (TEM, SEM, RBS, SIMS). These techniques are used to determine the filling factor and the concentration profile of metal in the insulating matrix. With the help of the Maxwell-Garnett theory and using a single or multilayer model it is possible to suggest an interpretation of the optical properties. (9 refs.)

- 61944 Microhardness of an implanted system.** V.M.Gurov, A.I.Lyapin (Inst. of Mech. Engng., Mogilev, USSR). *Sov. Phys.-Tech. Phys. (USA)*, vol.27, no.10, p.1266-8 (Oct. 1982). Translation of: *Zh. Tekh. Fiz. (USSR)*, vol.52, no.10, p.2063-5 (Oct. 1982). [received: April 1983]
Results are reported from measurements of the microhardness of iron samples irradiated with W^{+} ions. It is shown that a PMT-3 microhardness gage can be used for such measurements. The data imply that solubility in the implanted layer can be assessed from the behavior of the microhardness as a function of the radiation dose. The properties of irradiated samples are found to vary when a DC current is passed through them. The radiation dose is the main factor determining whether the microhardness decreases or increases (i.e. the sign of the change). (1 ref.)
- Dose-dependence of Pb-ion implantation damage in zirconolite, hollandite, and zircon** See Entry 60284
- Sputtering of titanium and niobium hydrides** See Entry 61660
- Kinetics of the collective crystallization of doped ZnS** See Entry 61835
- Oxygen defect profile in implanted garnet** See Entry 61906
- Flash lamp annealing of ion-implanted polycrystalline silicon** .. See Entry 61959
- Microscopic processes in low-power annealing of ion-implanted Ge** See Entry 61961
- In-resonator laser annealing of semiconductors** See Entry 61963
- Semiconductor processing with excimer lasers** See Entry 61965
- The influence of helium implantation profile shapes on blister formation in metals** See Entry 61988
- Radiation damage, its recovery and platinum behavior and lattice location in ion bombarded MgO and Al_2O_3 as used for catalytic studies** .. See Entry 61990
- Optical, chemical and mechanical modifications induced by ion implantation on glass surfaces** See Entry 61993
- Ion beam induced composition changes during Auger sputter profiling of thin Al films on InP** See Entry 62001
- Growth of titanium silicide on ion-implanted silicon** See Entry 62182
- An ion-implanted resistor as thermal transient sensor for the determination of the thermal diffusivity in silicon** See Entry 62194
- Influence of doping with isovalent impurities on defect formation in homoepitaxial GaAs layers** See Entry 62301
- Investigations of implantation-induced changes in surface layers of epitaxial garnet thin films** See Entry 62755
- Large magnetic anisotropy change induced by hydrogen ion implantation in europium iron garnet LPE films** See Entry 62756
- Effects of high dose ion implantation on structure and magnetic properties of 3d-metal films** See Entry 62757
- Influences of ion implantation on charged wall properties in magnetic bubble devices** See Entry 62776
- Mossbauer spectroscopy of implanted sources** See Entry 62844
- Anodic dissolution behaviour of Si- and Ti-implanted iron** See Entry 63447
- Etude et réalisation de croissances épitaxiales de composés III-V par pyrolyse mixte d'organometalliques et d'hydrures sous pression réduite: Application à l'étude de structures de piles solaires (Study and realisation of epitaxial growth of III-V compounds by mixed pyrolysis of organometallics and hydrides under reduced pressure: Application to the study of solar cell structures)** See Entry 63678
- Antimony doping in vacuum deposited thin film silicon photovoltaic cells** See Entry 63698
- Silicon solar cells by ion implantation: E-beam and self annealing** See Entry 63704
- Implantation of boron and boron fluoride compounds into silicon for production of solar cells** See Entry 63708
- 61.70W Impurity concentration, distribution, and gradients**
(see also 66.30J Diffusion, migration and displacement of impurities)

61945 Optical absorption calibration curve for measurement of CR content in semi-insulating GaAs. Xu Zhenjia, Zhang Zehua, Sun Bokang (Inst. of Semiconductors, Acad. Sinica, Peking, China). *Chin. J. Semicond. (China)*, vol.4, no.2, p.194-6 (March 1983). In Chinese. A method using infrared absorption is described for measuring Cr content in semi-insulating GaAs, which is calibrated by neutron activation analysis. The applicability of the calibrated curve is also discussed. (7 refs.)

61946 Some mathematical results for impurity redistribution during the growth of a layer on a substrate. F.Bailly, M.Barbe, G.Cohen-Solal, D.Lincot (Lab. de Phys. des Solides, CNRS, Meudon, France). *J. Phys. (France)*, vol.44, no.4, p.489-95 (April 1983). Presents a series of results for the redistribution by diffusion of an impurity initially distributed homogeneously in a substrate during the growth of a layer on this substrate. It also gives results concerning the diffusion during the same growth process of an impurity coming from an exterior phase. In both cases the nature of the layer is different from that of the substrate. In addition to the obtained analytical results, the mathematical method used to obtain them is also of interest. (3 refs.)

61947 Evaluation of the valency of Fe, Cr, Cu, Sb doping ions in $Pb(Zr_{0.95}Ti_{0.05})O_3$ ceramics. P.Gonnard, M.Trocac (Lab. de Génie Electrique & Ferroelectricite, INSA, Villeurbanne, France). *J. Solid State Chem. (USA)*, vol.47, no.1, p.92-7 (15 March 1983). The valency of the ions Fe, Cr, Cu, Sb, incorporated in PZT 95/5 ceramics, is evaluated from the viewpoint of a correlation between the mean radius of the ions at the octahedral site and the following two parameters: the temperature of the antiferroelectric-ferroelectric phase transition, and the volume of the cubic unit cell. It is found that Fe and Cr enter as Fe^{2+} and Cr^{2+} at the B site. Experiments suggest that Cu is incorporated at the B site as Cu^{+} and Cu^{2+} and that Sb enters partly at the A site as Sb^{3+} and mainly at the B site as Sb^{5+} . (15 refs.)

61948 Changes in the concentration of 1.0 and 1.28 eV copper luminescence centers during annealing of electron-irradiated n-type GaAs. K.D.Glinchuk, N.S.Zayats, A.V.Prokhorovich (Inst. of Semiconductors, Acad. of Sci., Kiev, Ukrainian SSR).

Sov. Phys.-Semicond. (USA), vol.16, no.10, p.1189-90 (Oct. 1982). Translation of: *Fiz. & Tekh. Poluprovodn. (USSR)*, vol.16, no.10, p.1851-2 (Oct. 1982). [received: April 1983]

The authors have investigated the influence of electron irradiation and subsequent annealing on the luminescence of n-type GaAs and the efficient 'recombination' interaction between gallium vacancies V_{Ga} of radiation origin and interstitial Cu, copper impurity atoms (mutual annihilation of V_{Ga} and Cu, took place), which increased the concentration of 1.0 and 1.28 eV luminescence centers containing substitutional Cu_{Ga} copper atoms. (3 refs.)

61949 Post-deposition high temperature processing of silicon nitride. H.J.Stein, P.S.Peercey, R.J.Sokel (Sandia Nat. Labs., Albuquerque, NM, USA).

Thin Solid Films (Switzerland), vol.101, no.4, p.291-8 (25 March 1983).

Hydrogen, which is normally incorporated in silicon nitride in the form of Si-H and N-H bonds, is lost by trap-limited diffusion during high temperature post-deposition processing. Hydrogen loss occurs from films prepared by both atmospheric pressure chemical vapor deposition and low pressure chemical vapor deposition and such loss appears to be unimpeded by polycrystalline silicon gate layers. The authors have found that partial reloading of hydrogen-depleted films to reform N-H and Si-H bonds can be achieved by annealing in H_2 gas at 900°C. It is inferred, therefore, that silicon nitride does not reconstruct when hydrogen is lost during high temperature processing. Changes in the equilibrium positive charge parallel changes in the hydrogen concentration in silicon nitride, consistent with a previously reported parallel behavior between positive charge and Si-H bonds. (11 refs.)

61950 Impurity incorporation in RAO polysilicon layers and consequences on their electrical properties. G.Revel, N.Deschamps (Lab. Pierre Sue, CENS, Gif sur Yvette, France), J.P.Deville, C.Texier-Hervo, C.Belouet. Fourth E.C. Photovoltaic Solar Energy Conference. Proceedings of the International Conference, Stressa, Italy, 10-14 May 1982 (Dordrecht, Netherlands: Reidel 1982), p.970-5.

The growth of polysilicon layers by direct freezing of a film on a carbon ribbon by the RAD process goes along with a contamination of the silicon melt by carbon and its compositional impurities. The authors report on this contamination effect studied mainly by means of neutron activation analyses (NAA) and its consequences on the electrical properties of the layers. The purification of the carbon ribbons in chlorine at high temperatures results in low contamination levels of the melt; NAA evidenced a significant segregation at the growth front, the effective partition coefficients determined being in the 10^{-1} to 10^{-3} range. Even though impurities are shown to impair the device performances, it is concluded that they are not necessarily incorporated in an electrically active form. Finally, AM_1 conversion efficiencies of 12% are reported for RAD cells 4 cm² in size. (8 refs.)

On the possibility of obtaining a uniform impurity distribution in growing crystals by the Bridgman-Stockbarger method See Entry 61839

Influence of capsule diameter on the impurity distribution in a growing crystal See Entry 61840

Observation of precipitates on 'growth' dislocations in GaAs single crystals with low impurity content See Entry 61926

The post-hydrogenation of low-pressure chemical vapor deposited amorphous silicon See Entry 61937

High temperature and short time thermal annealing of ion-implanted silicon See Entry 61938

Vacancies and carbon impurities in α -iron: neutron irradiation See Entry 61979

On depth profiling an InGaAsP-InP heterojunction See Entry 62280

Hydrogen incorporation scheme in amorphous-microcrystalline mixed-phase Si:H films See Entry 62286

Dependence of the carbon density on an epitaxial GaAs film surface on the substrate orientation relative to the crystallographic plane See Entry 62298

Influence of doping with isovalent impurities on defect formation in homoepitaxial GaAs layers See Entry 62301

Influence of growth rate of epitaxial silicon layers on surface segregation of boron, phosphorus, and arsenic See Entry 62302

Preparation and study of the electrophysical properties of the copper chalcogenides and their solid solutions See Entry 62412

The depth dependence of the depth resolution in composition-depth profiling with Auger electron spectroscopy See Entry 63090

61.70Y Interaction between different crystal structure defects

61951 On the microhardness induced by impurity ions in the NaCl and KCl single crystals. S.R.Ghadekar, B.T.Deshmukh (Dept. of Phys., Nagpur Univ., Nagpur, India).

Curr. Sci. (India), vol.51, no.23, p.1109-11 (5 Dec. 1982).

The authors investigated the effect of dopant ions on dislocation density and microhardness of NaCl and KCl. It is found that the dopant ions with large ionic radii increase the microhardness by increasing the dislocation density due to lattice strains. Multivalent dopants create ion vacancies which provide obstacles to the dislocation motion thereby raising the microhardness of the crystals. (6 refs.)

61952 Interaction of lithium with multiply charged acceptors in germanium. G.M.Gavrilov, L.A.Goncharov, P.D.Kervashvili, N.V.Pan'kevich (50th Anniversary of the Great October Socialist Revolution Kiev Polytech. Inst., Kiev, Ukrainian SSR).

Inorg. Mater. (USA), vol.18, no.5, p.605-9 (May 1982). Translation of: *Izv. Akad. Nauk SSSR Neorg. Mater.*, vol.18, no.5, p.715-19 (May 1982). [received: Feb. 1983]

An analysis of the data obtained showed that when Li and a multiply charged impurity Ag, Fe, or Ni are introduced into germanium directly in the processes of crystallization, an interaction between them unquestionably occurs; moreover, the nature of this interaction varies. The main process of interaction of Li and Ag and of Li with Fe is electrical compression. The interaction of Li and Ni is of a more complex nature; in this case the possibility of formation of stable electrically active complexes should be taken into consideration. (7 refs.)

61953 On the interaction between a vacancy and an interstitial impurity atom in BCC transition metals. K.Masuda (Dept. of Materials Sci. & Engng., Tokyo Inst. of Technol., Tokyo, Japan). *Phys. Status Solidi b (Germany)*, vol.116, no.1, p.9-16 (1 March 1983). The binding energies are calculated between a vacancy and an interstitial impurity (like carbon) atom in BCC transition metals (α -Fe, Mo, and W). The changes in the total energy due to the introduction of lattice defects are calculated using a tight-binding type electronic theory and the Born-Mayer repulsive potential. A comparison is made with previous theoretical calculations as well as the recent experimental observations (positron annihilation experiments). In addition the detailed electronic structure is investigated of the impurity atom, assuming both, interstitial and substitutional occupations and using the recursion method by Haydock et al. (1972, 1975). It is shown that there are marked differences in the local p -orbital density of states between the octahedral and substitutional impurity (carbon) atoms. These calculations enable one to understand the stability of the vacancy-interstitial impurity pair in BCC transition metals. (20 refs.)

61954 Interactions between dislocations and grain boundaries in BCC metals. S.G.Zaychenko.

Russ. Metall. (GB), no.6, p.125-9 (1981). Translation of: *Izv. Akad. Nauk. SSSR Met.*, no.6, p.126-9 (1981).

On the example of α -Fe, computer calculations were made of the interactions between the dislocations in BCC metals and the boundary type (010), which separates a grain containing the dislocation from an adjacent one, displaced by the angle θ about [001]. The calculations were made within the framework of the anisotropic theory of elasticity. It is shown that the interaction consists of attraction for small disorientation angles, between 0 and 20°, and repulsion in the case of disorientations between 20 and 70°. Effect of the interaction: presence around the boundaries of areas free of dislocations, the dimensions of which are proportional to the interaction force between the dislocations and the boundary. (5 refs.)

61955 Interaction of primary radiation defects with dislocations in indium antimonide. F.A.Zaitov, O.V.Gorshkova, A.Ya.Polyakov.

Sov. Phys.-Semicond. (USA), vol.16, no.10, p.1198-9 (Oct. 1982). Translation of: *Fiz. & Tekh. Poluprovodn. (USSR)*, vol.16, no.10, p.1863-5 (Oct. 1982). [received: April 1983]

The interaction of neutron irradiation defects with dislocations is considered in InSb. The authors consider the dose dependence of the concentration of acceptors, donors and deep levels and the changes in the electron mobility. (19 refs.)

The mechanisms of the formation and growth of water bubbles and associated dislocation loops in synthetic quartz See Entry 61908

Velocity of a finite dislocation See Entry 61913

Observation of precipitates on 'growth' dislocations in GaAs single crystals with low impurity content See Entry 61926

Intrinsic defects in silicon and their interaction with boron impurities at low temperatures See Entry 61968

Strain-ageing in silver chloride. I. The representative curve See Entry 62015

The low-temperature flow stress of europium-doped sodium chloride See Entry 62016

Solvent diffusion in α -silver-tin alloys See Entry 62153

Diffusion of rubidium ion in pure silver chloride crystals See Entry 62163

Influence of the internal electric field on the migration of substitutional impurities in diamond-structure semiconductors See Entry 62174

61.80 RADIATION DAMAGE AND OTHER IRRADIATION EFFECTS

(for techniques of structure determination, see 61.10 to 61.16; for electron and ion impact phenomena, see 79.20)

61956 Drift forces on vacancies and interstitials in alloys with radiation-induced segregation. W.G.Wolfer (Nuclear Engng. Dept., Univ. of Wisconsin, Madison, WI, USA).

J. Nucl. Mater. (Netherlands), vol.114, no.2-3, p.292-304 (Feb. 1983).

Linear irreversible thermodynamics is employed to derive the total drift force on interstitials and vacancies in substitutional binary alloys. The obtained results are evaluated for binary Fe-Ni alloys. It is shown that radiation-induced segregation produces new drift forces which can be of the same order of magnitude as the stress-induced drift force produced by edge dislocations in an alloy with uniform composition. Hence, segregation results in a significant modification of the bias for void nucleation and swelling. The additional drift forces on interstitials and vacancies are due to the compositional dependence of the formation and migration energies; due to the dependence of the point defect strain energy on the local elastic properties; due to a coherency strain field caused by lattice parameter variations; and finally due to the Kirkendall force produced by the difference in tracer mobilities. Estimates of these forces given for Fe-Ni alloys indicate that the Kirkendall force is small compared to the other segregation-induced forces on interstitials. In contrast, the Kirkendall force seems to be the dominant one for vacancies. (29 refs.)

61957 On the rate theory for pulsed irradiation. H.Rauh, R.Bullough, M.H.Wood (Theoretical Phys. Div., AERE, Harwell, England).

J. Nucl. Mater. (Netherlands), vol.114, no.2-3, p.334-37 (Feb. 1983).

To date, no rigorous chemical rate theory framework has been established to allow for the pulsed mode of operation. Previous dynamical studies have only included the consequences of the transient damage rate in the concentration fluctuations and not in the sink strengths themselves, the adopted sink strength being those derived for a continuous damage rate. The authors have developed a more general dynamical rate theory and present first results for pulsed irradiation. (6 refs.)

61958 Internal stress buildup in SIPA creep. B.L.Adams (Dept. of Materials Sci. & Engng., Univ. of Florida, Gainesville, FL, USA).

J. Nucl. Mater. (Netherlands), vol.115, no.1, p.49-55 (March 1983).

A discrete simulation of internal stress effects, arising during stress-induced preferred-absorption (SIPA) irradiation creep, has been conducted for randomly oriented linear-elastic FCC polycrystals. Of particular interest are the intercrystalline incompatibility stresses arising during the development of faulted interstitial loops (Frank loops). These simulations suggest that a unique state of internal stress can develop at a sufficiently large loop volume-fraction. As this state is approached the deviatoric creep-rate reduces to zero. Extensive microstructural data suggest, that unfaulting processes limit loop volume-fractions to levels consistent with a maximum reduction in creep-rate of ~18%. A substantial coupling effect is predicted between faulted loop SIPA and other SIPA mechanisms, such as preferred absorption at perfect dislocations (SIPAD), and climb controlled glide (CCG). Faulted

loop SIPA coupled with CCG creep leads to an enhanced creep-rate. The opposite effect is predicted for the coupling with SIPAD creep. (31 refs.)

61959 Flash lamp annealing of ion-implanted polycrystalline silicon. K.B.Kadyrakunov, E.V.Nidaev, A.E.Plotnikov, L.S.Smirnov, I.G.Melnik, M.V.Makeev (Inst. of Semiconductor Phys., Acad. of Sci., Novosibirsk, USSR).

Phys. Status Solidi a (Germany), vol.75, no.2, p.483-8 (16 Feb. 1983). In German.

The behaviour of phosphorus implanted films of polycrystalline silicon deposited on SiO₂ is studied during the annealing with pulses of a xenon lamp of 10⁻² s duration. It is shown that the annealing with flash lamp pulses allows a complete activation of an implanted impurity during the annealing both in solid and in liquid phase. The melting of the film surface is accompanied by an increase of crystal sizes up to 5 μ m. The electron mobility in these layers reaches 250 cm²V⁻¹s⁻¹. The layers are stable to the subsequent heat treatments at temperatures up to 900K. (10 refs.)

61960 Point defect densities during the early transient stage of radiation-induced metal swelling. V.A.Pechenkin.

Sov. Phys.-Tech. Phys. (USA), vol.27, no.9, p.1051-6 (Sept. 1982). Translation of: *Zh. Tekh. Fiz. (USSR)*, vol.52, no.9, p.1712-20 (Sept. 1982). [received: April 1983]

The behavior of point defect densities during the initial period of irradiation is studied analytically and by solving the material balance equations numerically. Estimates are derived for the characteristic formation time of loops of interstitial atoms, the density and diameter of interstitial atoms, and the duration of the transient period. The influence of the transient density stage on radiation-induced porosity in metals is studied. (15 refs.)

Proceedings of the First International Conference on 'Radiation Effects in Insulators' See Entry 59534

Structural effects of radiation damage in silica based glasses See Entry 60281

Near-surface leaching studies of Pb-implanted Savannah River waste glass See Entry 60282

Effects of ionizing radiation on amorphous insulators See Entry 61805

Radiation-induced crystallinity changes in pressure-crystallized ultrahigh molecular weight polyethylene See Entry 61817

61.80B Laser beams

61961 Microscopic processes in low-power annealing of ion-implanted Ge. G.Vitali, M.Marinelli, U.Zammit (Istituto di Fisica, Facoltà di Ingegneria, Univ. of Rome, Rome, Italy), F.Scuderi.

Phys. Lett. A (Netherlands), vol.94A, no.6-7, p.320-4 (21 March 1983).

Recrystallization due to low-power ruby laser annealing of ion-implanted Ge is shown to be associated with small-scale migration of defects. In the present case no fusion processes can be invoked. The experimental analysis was performed with scanning (SEM) and transmission electron microscopy (TEM), and reflection high-energy electron diffraction (RHEED) techniques. (20 refs.)

61962 Spatial and size distributions of inhomogeneities initiating laser breakdown in alkali halide crystals at 10.6 μ m. A.V.Gorbanov (Inst. of Solid State Phys., Acad. of Sci., USSR).

Sov. Tech. Phys. Lett. (USA), vol.8, no.7, p.343-4 (July 1982). Translation of: *Pis'ma v Zh. Tekh. Fiz. (USSR)*, vol.8, no.13-14, p.792-5 (July 1982). [received: April 1983]

Reports a systematic study of the size effect in the breakdown of NaCl and KCl by pulses from a TEA CO₂ laser ($t_p=100$ ns), not only in the volume but also at the surface. The size dependence was studied in detail, and the author did not use randomly selected samples. Instead, samples were cleaved from various parts of large single-crystal bars grown from the melt by the Kyropoulos method with diameters and heights up to 200 mm. With some reservation it may thus be suggested that the nature of the breakdown centers did not change as their quantitative characteristics were varied. (12 refs.)

61963 In-resonator laser annealing of semiconductors. Yu.V.Koval'chuk, G.V.Ostrovskaya, V.B.Smirnitskii, O.V.Smol'skii, I.A.Sokolov (A.F. Ioffe Physicotechn. Inst., Acad. of Sci., Leningrad, USSR).

Sov. Tech. Phys. Lett. (USA), vol.8, no.8, p.398-9 (Aug. 1982). Translation of: *Pis'ma v Zh. Tekh. Fiz. (USSR)*, vol.8, no.15-16, p.917-20 (Aug. 1982). [received: April 1983]

Reports a study of the in-resonator laser annealing of GaP and GaAs wafers after ion implantation. The experiments show that it is necessary to control the orientation of the samples with respect to the laser beam during laser annealing in order to achieve reproducible results; alternatively, the laser oscillator must be optically decoupled from the laser amplifier stages. (3 refs.)

61964 Thermal model for interference laser annealing. V.N.Abakumov, Zh.I.Alferov, Yu.V.Koval'chuk, E.L.Portnoi.

Sov. Tech. Phys. Lett. (USA), vol.8, no.8, p.417-18 (Aug. 1982). Translation of: *Pis'ma v Zh. Tekh. Fiz. (USSR)*, vol.8, no.15-16, p.966-70 (Aug. 1982). [received: April 1983]

Analyzes interference laser annealing by studying the intensity distribution of the laser beam over the surface of the sample during the interference of two plane waves. There is a change in the absorption not only along the direction into the target (the y direction), which is the only direction in conventional laser annealing, but also along the surface (the x direction), perpendicular to the lines of the grating. For the analysis, the authors adopt a thermal model with melting and crystallization of a damaged surface layer. For a graphic description of the annealing they consider a simplified problem: the solid phase and the melt are isotropic, have a constant specific heat c , a thermal conductivity k , and the same density ρ . (3 refs.)

61965 Semiconductor processing with excimer lasers. R.T.Young (Helionetics Inc., San Diego, CA, USA).

Topical Meeting on Excimer Lasers, Incline Village, NV, USA, 10-12 Jan. 1983 (Washington, DC, USA: Opt. Soc. America 1983), p.WA2/1

Presents an evaluation of XeCl excimer laser suitability for laser processing of silicon. The results of extensive comparisons of the quality of annealing of ion implanted samples obtained with the XeCl and ruby lasers is also discussed. Simple p - n , shallow-junction solar cells with efficiencies over 15% AM1 have been fabricated from XeCl laser-annealed silicon single crystals. (no refs.)

Laser heating: an analytical approach to the theory See Entry 61207

Transient gratings on a -GaAs under laser annealing conditions See Entry 61801

Synthesis of Al₁₅Nb₃Ge by pulsed laser annealing See Entry 62282

Micro-probe reflection high-energy electron diffraction technique. III. Observation of polycrystalline silicon film on crystalline silicon substrate irradiated by continuous-wave Ar⁺-laser See Entry 62284

- Synthesis of AISb by laser and capacitive discharge annealing See Entry 62297
- Localized modification of magnetic anisotropy in LPE iron garnet films by laser annealing See Entry 62760
- Excitation of surface electromagnetic waves at a solid surface by an intense laser beam See Entry 63087
- Laser synthesis of V_2O_5 crystals with highly developed surfaces See Entry 63149
- Ultrafast solidification of ultrathin molten silicon films See Entry 63283
- Instability of surface combustion on exposure to laser radiation See Entry 63553
- Implantation of boron and boron fluoride compounds into silicon for production of solar cells See Entry 63708

61.80C X-rays

- Centres of slow recombination in cadmium bromide crystals See Entry 62427
- Thermoluminescence of low-temperature X-irradiated MgO and MgO:Li single crystals See Entry 63063

61.80E Gamma rays

- 61966** Radiation induced effects and annealing methods in fiberoptics and glasses. H.Bock, J.Siehs, N.Vana (Atominst. of the Austrian Univ., Wien, Austria). *Radiat. Eff. (GB)*, vol.65, no.1-4, p.75-8 (1982). (Proceedings of the First International Conference on 'Radiation Effects in Insulators', Arco, Largo di Garda, Italy, 1981).
- Radiation induced effects in glass-rods and fiberoptics have been studied to determine parameters affecting the application of these materials in nuclear technology, i.e. as fiberscopes for visual inspection in severe radiation environments. Different glass and fibertypes have been exposed to fission product gamma radiation. The radiation induced transmission loss was measured with a spectrophotometer and then different annealing methods were examined to improve the transmission properties again. Especially the changes in glass and fiber recovery vs. time as a function of radiation dose and annealing temperature were investigated. Annealing experiments were performed exposing the samples either to temperature treatment or to various light sources such as quartz lamp, arc lamp or UV-laser for optical annealing. The transmission recovery was then investigated either as a function of annealing temperature or of exposure time to the light sources. The results allow conclusions on the design and composition of optical fiber endoscopes to be used in severe radiation environment where image transmission is required in the presence of high level nuclear radiation. (2 refs.)
- 61967** Radiation-induced transmission loss in optical materials at infrared wavelengths. H.U.Fahrbach, A.Eberhagen (Max-Planck-Inst. für Plasma-phys., Garching, Germany). *Radiat. Eff. (GB)*, vol.65, no.1-4, p.127-30 (1982). (Proceedings of the First International Conference on 'Radiation Effects in Insulators', Arco, Largo di Garda, Italy, 1981).
- Information concerning the effect of irradiation on the optical properties of materials in the infrared, sub-mm- and mm-wavelength regions is of increasing importance in fusion plasma diagnostics. The radiation induced transmission loss of a number of materials has therefore been investigated at wavelengths in the ranges 200 nm to 40 μ m and 0.23 to 2.0 mm. The samples were irradiated with doses of up to 10^{10} rad in a nuclear reactor. While germanium shows considerable transmission loss at doses as low as 10^6 rad, and the transmission of TPX decreases at 10^9 rad, other materials, e.g. fused quartz and possibly ZnSe, exhibit sufficient radiation hardness for use in fusion plasma diagnostics. (10 refs.)
- 61968** Intrinsic defects in silicon and their interaction with boron impurities at low temperatures. V.V.Emtsev, T.V.Mashovets, E.Kh.Nazaryan (A.F. Ioffe Physicotech. Inst., Acad. of Sci., Leningrad, USSR). *Sov. Phys.-Semicond. (USA)*, vol.16, no.10, p.1225-7 (Oct. 1982). Translation of: *Fiz. i Tekh. Poluprovodn. (USSR)*, vol.16, no.10, p.1901-4 (Oct. 1982). [received: April 1983]
- Describes an investigation of the process of formation of defects in Si:B under conditions of low-temperature (4.2 and 78K) gamma irradiation. This was the first study of the effects of irradiation of p-type silicon with gamma rays at 4.2K. Moreover, the concentrations of group III acceptors and of compensating donors before and after low-temperature irradiations were determined separately for the first time. (21 refs.)
- 61969** Annealing of radiation defects in Ge-Si solid solutions. S.I.Shakhovtsova, I.N.Belokurova, I.S.Rogutskii, V.I.Shakhovtsov (Inst. of Phys., Acad. of Sci., Kiev, Ukrainian SSR). *Sov. Phys.-Semicond. (USA)*, vol.16, no.10, p.1230-1 (Oct. 1982). Translation of: *Fiz. i Tekh. Poluprovodn. (USSR)*, vol.16, no.10, p.1907-9 (Oct. 1982). [received: April 1983]
- The authors investigate the influence of radiation defects on electronic processes in n-type Ge-Si solid solutions. The Hall effect and the electrical resistivity were determined for antimony-doped Ge-Si single crystals at temperatures 10-300K. At room temperature the resistivity was 5 Ω cm and the difference between the donor and acceptor concentrations was 7×10^{14} cm $^{-3}$. The concentration of the second compound of the solid solutions was 0.01-1.5 at% Si. These crystals were irradiated with 2.5 MeV electrons and with ^{60}Co γ rays at room temperature. A study was made of the isochronous and isothermal annealing of defects. The annealing took place in the range 300-660K and measurements were made at 90K after the various annealing stages. In the isochronous annealing case the period at each temperature was 15 min. (10 refs.)
- Low temperature neutron and gamma irradiation of glass fiber reinforced epoxies See Entry 61980
- On mechanisms of thermostimulated luminescence excitation in γ -irradiated corundum See Entry 63064

61.80F Electrons and positrons

- 61970** Heating of a bilayered material bombarded by an electron beam. P.Montmitonnet, E.Dargue-Ceretti (Ecole des Mines de Paris, Valbonne, France). *J. Microsc. & Spectrosc. Electron. (France)*, vol.7, no.6, p.615-27 (Dec. 1982). In French.
- The temperature of a target bombarded by an electron beam is calculated analytically for a two-layered cylindrical material. No other geometric restriction is assumed. The model is compared with previous approximate calculations,

using more restrictive hypotheses. For very thin films, the present model confirms Roll's analysis. Furthermore, it allows precise calculation under quite general geometrical conditions. (8 refs.)

- 61971** Determination of electron depth-dose function for kilovolt electrons on GaAsP. G.Oelgart, H.Scholz (Sektion Phys., Humboldt-Univ. zu Berlin, Berlin, Germany). *Phys. Status Solidi a (Germany)*, vol.75, no.2, p.547-53 (16 Feb. 1983).
- A new technique to determine the depth-dose function is described using the measurement of the electron beam induced barrier current on bevelled homo p-n junction structures. A universal depth-dose function on GaAsP is found in the form $\Phi(z) = \Phi_0 \exp[-(z-a/z_0)^2]$ with $z_0 = 2.3a$ for $z \geq a$ and $1.3a$ for $0 \leq z < a$ in the investigated energy range from 10 to 45 keV. The distance of the maximum under the surface can be obtained by the relation $a = A_0 E_p^{0.65}$ with $A_0 = 2.95 \times 10^{-3}$ (E_p in keV, a in μ m). (8 refs.)
- 61972** Irradiation damage of II-VI compounds in a high-voltage electron microscope. T.Yoshiie, H.Iwanaga, N.Shibata (Faculty of Liberal Arts, Nagasaki Univ., Nagasaki, Japan), K.Suzuki, M.Ichihara, S.Takeuchi. *Philos. Mag. A (GB)*, vol.47, no.3, p.315-29 (March 1983).
- Dislocation loops produced by electron irradiation on a 1 MV electron microscope have been studied above room temperature for five II-VI compounds: CdS and ZnO, with the wurtzite structure, and CdTe, ZnSe and ZnS, with the zincblende structure. For all the crystals the density of loops decreased as the irradiation temperature increased, until no loops were produced above a certain temperature which varied from crystal to crystal. However, the loop density did not depend on the electron flux intensity, suggesting the heterogeneous nucleation at some impurity complex of equilibrium concentration. Diffraction contrast analyses showed that the loops are of interstitial type in each crystal, with Burgers vectors as follows: $1/2[0001]$ and $1/3[1120]$ for wurtzite crystals, the density ratio of the former type to the latter being increased with increasing temperature; mostly $1/3[111]$ and a few $1/2[110]$ for zincblende crystals, the latter type being presumably formed as a result of unfaulting in the former. An effect of crystal polarity on the shape of the loops in zincblende crystals has been observed. (21 refs.)
- 61973** Radiation damage in pure and helium-doped α - Al_2O_3 in the HVEM. Qualitative aspects of void and aluminium colloid formation. T.Shikama, G.Pells (Metall. Div., AERE, Harwell, England). *Philos. Mag. A (GB)*, vol.47, no.3, p.369-79 (March 1983).
- Thick foils of α - Al_2O_3 single crystals of both high purity and doped with 1000 at p.p.m. helium have been irradiated with 1 MV electrons at temperatures of 900-1130K in a high-voltage electron microscope (HVEM). Following irradiation the foils were thinned further and examined at room temperature in the HVEM by both bright-field and dark-field techniques. Both helium-doped and undoped samples exhibited three radiation damaged products which could be observed in bright field. These were dislocation tangles and small features which exhibited white or dark contrast. The white features showed the contrast behaviour of voids, whilst the dark features were best observed using diffraction contrast. Additional diffraction patterns were indexed as being from aluminium metal which, viewed in dark field, showed images corresponding to the dark features observed in bright field. Confirmation that the dark features were aluminium metal precipitates was obtained from loss of diffraction contrast when the specimen was heated above the melting point of aluminium. (10 refs.)
- 61974** Damage in the cation sublattice of α - Al_2O_3 irradiated in an HVEM. A.Y.Stathopoulos (Dept. of Metall. & Sci. of Materials, Univ. of Oxford, Oxford, England), G.P.Pells. *Philos. Mag. A (GB)*, vol.47, no.3, p.381-94 (March 1983).
- α - Al_2O_3 has been irradiated at high temperatures with 300 keV electrons at which energy only aluminium ions are displaced. Systematic examination in a 100 kV electron microscope revealed pure edge dislocations of interstitial character with $b = 1/3[0001]$ and $b = 1/3[1010]$ lying on basal and prismatic $\{1010\}$ planes respectively. The loops are stoichiometric but faulted on the aluminium sublattice. A model is proposed by which cation displacement at high temperatures results in aluminium interstitials precipitating between basal or $\{1010\}$ prismatic planes with simultaneous diffusion of oxygen ions between the aluminium layers producing the faulted loops. (14 refs.)
- 61975** Microstructural changes in irradiated silica based glasses. M.Antonini, A.Manara (Joint Res. Center, Ispra, Italy), S.Buckley. *Radiat. Eff. (GB)*, vol.65, no.1-4, p.55-61 (1982). (Proceedings of the First International Conference on 'Radiation Effects in Insulators', Arco, Largo di Garda, Italy, 1981).
- High voltage electron microscopy studies have been performed on irradiated pure silica and borosilicate glasses to check their long-term stability when these materials are employed near high energy radioactive sources, such as in fusion reactors and during the storage of nuclear waste. The intense energetic beam of electrons produced by the Harwell 1 MeV microscope, ranging from 10^{17} to 10^{20} e/cm 2 /s has been focused upon specimens of various composition and impurity content at different temperatures up to about 850°C. Pure silica samples have also been bombarded with 46.5 MeV Ni^{16+} ions at the Variable Energy Cyclotron. It is found that while no significant changes are detectable in pure irradiated silica, clear evidence is present in complex borosilicate glasses for the growing of large defect clusters (over 1000 Å, resembling gas bubbles) after electron doses of about 8.5×10^{19} e/cm 2 and dose rates exceeding 2×10^{18} e/cm 2 /sec. Moreover, small regions, about 100 Å wide, scattering electrons more than the matrix are also present. The nature of this fine microstructure has been established as a phase separation into crystalline tridymite. The observations are discussed in terms of their dependence on temperature, sample thickness, dose and dose rates. (18 refs.)
- 61976** Effect of prior large scale electron irradiation on crystallization in two Fe-Ni based metallic glasses. E.Schopf, M.von Heimendahl (Univ. Erlangen-Nürnberg, Erlangen, Germany). *Scr. Metall. (USA)*, vol.17, no.3, p.313-16 (March 1983).
- Amorphous metallic alloys Metglas 2826 and 2826A were subjected to a high energy electron irradiation of 1500 kV, 3.4×10^{18} e/cm 2 , at low temperature (about 100K) within an electron accelerator (Dynamitron). Afterwards, the specimens were heated in case of 2826A to 341°C or 381°C and in case of 2826 to 342°C or 386°C to produce crystallization. Whereas in 2826A nucleation of crystals was enhanced due to irradiation and growth was not influenced, in 2826 both nucleation and growth were unchanged. These results are in qualitative agreement with former in-situ HVEM experiments on the same alloys and are discussed in terms of incubation times, related to relaxation times. (14 refs.)
- 61977** The temperature dependence of the electron irradiation resistance of crystalline paraffin. R.H.Wade, J.Pelissier (CENG, Grenoble, France). *Ultramicroscopy (Netherlands)*, vol.10, no.3, p.285-90 (1982).
- Reports experimental data on the radiation resistance of crystalline paraffin for temperatures ranging upwards from helium temperature in the hope of throwing some light on the apparent incompatibility of previously published results. The method adopted was to follow the evolution of the electron diffraction pattern intensities as a function of the total electron dose. The latent

dose effect found by Siegel (1982) was confirmed by the low temperature results. (19 refs.)

- Interpretation of the fading of diffraction patterns from organic substances irradiated with 100 keV electrons at 10-300K See Entry 61737
- Changes in the concentration of 1.0 and 1.28 eV copper luminescence centers during annealing of electron-irradiated *n*-type GaAs See Entry 61948
- Annealing of radiation defects in Ge-Si solid solutions See Entry 61969
- Comparison of heavy-ion, proton and electron irradiation effects in vitreous silica See Entry 61994
- Annealing studies of irradiation effects in vitreous silica See Entry 61995
- Electron and ion beam effects in amorphous SiO₂ and Si₃N₄ films for electronic devices See Entry 61996
- Effect of electron bombardment on the phase transition in VO₂ films See Entry 62339
- 'Limiting' electrical properties of irradiated InP See Entry 62434
- Hot-carrier thermo-EMF created by a strong microwave electric field in Ge_{1-x}Si_x single crystals irradiated with fast electrons See Entry 62442
- Magnetization of electron-bombarded iron-cobalt films See Entry 62764
- Radiation-thermal sintering of europium oxide See Entry 63221
- Silicon solar cells by ion implantation: E-beam and self annealing See Entry 63704

61.80H Neutrons

- 61978 Radiation conversions in MgCr₂O₄. Yu.G.Chukalkin, V.V.Petrov, I.N.Dubrovina, B.N.Goshchitskii (Inst. of Metal Phys., Ural Sci. Center, Acad. of Sci., Sverdlovsk, USSR). *Inorg. Mater. (USA)*, vol.18, no.6, p.1055-7 (June 1982). Translation of: *Izv. Akad. Nauk SSSR Neorg. Mater.*, vol.18, no.6, p.894-6 (June 1982). [received: Feb. 1983]

The irradiation of compounds with a spinel structure with fast neutrons leads to a statistical redistribution of di- and trivalent cations over the tetrahedral (8a) and octahedral (16d) positions of the crystal lattice. Therefore, an attempt to fix Cr³⁺ ions in tetrahedral positions by irradiation was made. The object of investigation was magnesium chromite MgCr₂O₄. The samples were irradiated in a nuclear reactor at 343K with a flux of fast neutrons ($E_H \geq 1$ Mev) 2×10^{20} cm⁻². With the indicated flux, the sample should be entirely randomized. To investigate the structural changes the authors used a neutron diffraction method. The initial samples had a spinel structure (space group Fd3m), characterized by the lattice parameter $a = 8.33$ Å. Irradiation with fast neutrons radically changes the structure of the investigated compound. The diffraction picture of the irradiated sample corresponds to a structure of the NaCl type (space group Fm3m) with parameter of the unit cell equal to 4.18 Å. (3 refs.)

- 61979 Vacancies and carbon impurities in α -iron: neutron irradiation. P.Hautojarvi, L.Pollanen, A.Vehanen, J.Yli-Kauppi (Lab. of Phys., Helsinki Univ. of Technol., Espoo, Finland). *J. Nucl. Mater. (Netherlands)*, vol.114, no.2-3, p.250-9 (Feb. 1983).

Positron annihilation and resistivity measurements have been performed on neutron-irradiated pure Fe, Fe-50 at ppm C and Fe-750 at ppm C. Small vacancy clusters are observed already in the as-irradiated state at 77K. Vacancy migration is found to start at around 160K as correlated within the collision cascades. This results in additional vacancy agglomeration and carbon impurities have no effect on the phenomenon. At 350K carbon atoms segregate strongly around the existing vacancy clusters. All defects anneal out below 600K. (43 refs.)

- 61980 Low temperature neutron and gamma irradiation of glass fiber reinforced epoxies. H.W.Weber (Antoniustitut der Österreichischen Univ., Wien, Austria), E.Kubasta, W.Steiner, H.Benz, K.Nylund. *J. Nucl. Mater. (Netherlands)*, vol.115, no.1, p.11-15 (March 1983).

Measurements of the fracture strength of epoxies, which are reinforced with different types of fiber glass and used commercially for magnet insulation are described. The samples were exposed to reactor irradiation at 77K, and measurements of tensile strength in the direction of the fibers were taken at the same temperature without warm up. The results show moderate degradation of the fracture strengths up to a total dose of 7.4×10^5 Gy, a linear swelling by about 5% at the same dose and a total destruction of the composite after a dose of $\sim 1.5 \times 10^6$ Gy. (7 refs.)

- 61981 Effects of quenching and fission damage on the low temperature electrical resistivity of single crystal UO₂. H.Matsui, M.Horiki, N.Ohya, T.Kato, M.Osada (Dept. Nuclear Eng., Nagoya Univ., Nagoya, Japan). *J. Nucl. Mater. (Netherlands)*, vol.115, no.1, p.128-30 (March 1983).

The electrical resistivity of single crystal UO₂ at low temperatures was measured. Some specimens were investigated in aligned crystal directions [100] and [110]. Effects of crystal defects on the electrical resistivity were examined by an introduction of vacancies by quenching and of the Frenkel-type defects by neutron irradiation (fission damage). It was found that the temperature dependence of the resistivity could be divided into three regions for all samples investigated here, except the irradiated one. (9 refs.)

- 61982 The effects of ionizing radiation on HLW glasses. D.R.Cousens, S.Myhra (School of Sci., Griffith Univ., Nathan, Queensland, Australia). *J. Non-Cryst. Solids (Netherlands)*, vol.54, no.3, p.345-65 (March 1983).

The production of displacement damage in HLW glasses has been accelerated by a factor of 10³ by neutron-irradiation of a typical borosilicate glass which has been doped with up to 10% UO₂ so that (α, n) and (n, f) events are produced. The energetic products of these reactions constitute the primary knock-ons which initiate displacement cascades. A stored energy of ≈ 100 kJ/kg has been measured with differential scanning calorimetry. The effects of positive ion 'self-irradiation' on the chemical durability of the glass have been investigated by studying the leaching/dissolution of irradiated and control powder specimens in an aqueous solution. The initial leaching/dissolution rates for Li, Sr and Si are enhanced by a factor of 2-4 by irradiation while the longer term rates are typically increased by 50%. The effects of back-reactions and changing particle size distribution complicate the interpretation of the result. The release of some activation products and fission fragments have been monitored; most species are well retained, but Ru exhibits an anomalously high leaching rate. (17 refs.)

- 61983 Energy deposition effects on amorphous selenium, by low temperature neutron irradiation. E.Bonjour, R.Calemczuk (CENG, Grenoble, France). *Radiat. Eff. (GB)*, vol.65, no.1-4, p.79 (1982). (Proceedings of the First International Conference on 'Radiation Effects in Insulators', Arco, Largo di Garda, Italy, 1981).

Summary form only given, as follows. The authors have observed recently that neutron irradiation at low temperature can induce very strong changes in configurational disorder of glasses. This conclusion has been drawn from

enthalpy change diagrams performed near T_g by differential scanning calorimetry, on amorphous selenium. A progressive change was observed from a stabilized relaxation state to a highly quenched state as a function of the neutron dose. They explain these effects by a local heating process. The irradiation was done at low temperature (30K) and fission and capture effects were shielded by enclosing samples in NB cells. (no refs.)

- 61984 Friction and source hardening in irradiated mild steel. K.L.Murty, D.J.Oh (North Carolina State Univ., Raleigh, NC, USA). *Scr. Metall. (USA)*, vol.17, no.3, p.317-20 (March 1983).

The effect of neutron fluence on stress-strain behavior of mild steel at ambient temperature revealed that Luders strain increases with fluence, and at the highest fluence employed here, namely 1.4×10^{19} n/cm², fracture occurred during Luders propagation. The lower yield stress increased as cube root of fluence and friction stress increased as square root of fluence. The interstitial impurity atoms (C and N) combine with irradiation induced defects, thereby resulting in reduced net concentration of free C and N in solution, and thus the source pinning effect decreases in irradiated steels as observed here. The increase in Luders strain with the corresponding decrease in source hardening resulted in reduced work-hardening in irradiated steels as expected. (10 refs.)

- Evaluation of the resistance of irradiated zirconium-liner cladding to iodine-induced stress corrosion cracking See Entry 60236

- Performance of coated UO₂ particles gettered with ZrC See Entry 60238

- An ephemeral Frenkel pair in iridium See Entry 61910

- Interaction of primary radiation defects with dislocations in indium antimonide See Entry 61955

- Radiation-induced transmission loss in optical materials at infrared wavelengths See Entry 61967

- Crack arrest in thick section steel plate See Entry 63385

61.80J Ions

(for ion implantation, see 61.70T)

- 61985 An investigation into the potential importance of helium trapping during the nucleation of radiation-induced voids. M.P.Shaw, B.Ralph, W.M.Stobbs (Dept. of Metall. & Materials Sci., Univ. of Cambridge, Cambridge, England). *J. Nucl. Mater. (Netherlands)*, vol.115, no.1, p.1-10 (March 1983).

Transmission electron microscopy has been used to investigate the effect of small modifications in the concentration of γ -forming elements (Al, Ti and Si), in a model nickel-based superalloy, upon the formation of helium bubbles during post-implantation annealing. The results show that bubble formation and growth can be significantly influenced, and in some cases inhibited, depending upon specific combinations of elements that partition to γ . The results are discussed in relation to the possible mechanisms involved and their potential importance in minimizing void swelling in nuclear reactor constructional materials. (20 refs.)

- 61986 Precipitation and void-swelling in nickel-manganese austenitic stainless steels. R.M.Boothby, D.R.Harries, T.M.Williams (Metall. Div., AERE, Harwell, England). *J. Nucl. Mater. (Netherlands)*, vol.115, no.1, p.16-24 (March 1983).

The precipitation and void-swelling characteristics of austenitic stainless steels in which nickel is partially replaced by manganese have been investigated. Alloy compositions were chosen on the basis of manganese being half as effective as nickel in stabilizing austenite, and steels with 'nickel equivalent' contents of 25-37% were examined. The steels were irradiated with 46 MeV Ni⁶⁺ ions to 60 dpa at 625°C and also aged for 1000 h at 600°C. The high-Mn alloys (20-30% Mn) were very susceptible to the formation of inter-metallic phases during thermal ageing but less so in the shorter-duration irradiation experiment. Irradiation promoted the formation of Ni- and Si-rich phases—the silicide G phase (in which Mn can replace Ti) and in one instance M₆C. The Cr-rich carbide M₂₃C₆ formed in both the aged and irradiated steels. Among the high-Mn alloys, void-swelling decreased with increasing Ni and (Ni+Mn) contents, although a 25Ni-1Mn steel showed no swelling at 625°C. (30 refs.)

- 61987 On the critical dose for blistering in helium irradiated zirconium and Zr-Nb. R.H.Zee, J.F.Watters, O.M.Westcott (AECL, Chalk River, Nuclear Engng., Chalk River, Ontario, Canada). *J. Nucl. Mater. (Netherlands)*, vol.115, no.1, p.131-3 (March 1983).

A study was carried out in order to determine the critical dose for blister formation in pure Zr and Zr-Nb (0.25 wt.%) under helium ion irradiation. Specimens in the annealed and 40% cold-worked condition were used. It was found that alloying was more important than plastic deformation in reducing blister formation. (9 refs.)

- 61988 The influence of helium implantation profile shapes on blister formation in metals. I.M.Neklyudov, V.F.Rybalko, G.D.Tolstolutsaya (Inst. of Phys. & Technol., Acad. of Sci., Kharkov, Ukrainian SSR). *J. Nucl. Mater. (Netherlands)*, vol.115, no.1, p.134-6 (March 1983).

Experimental results revealing the influence of the helium implantation profiles on blister formation are presented. (10 refs.)

- 61989 Direct observation of the primary state of damage of ion-irradiated tungsten. II. Definitions, analyses and results. M.I.Current, C.-Y.Wei, D.N.Seidman (Dept. of Materials Sci. & Engng., Cornell Univ., Ithaca, NY, USA). *Philos. Mag. A (GB)*, vol.47, no.3, p.407-33 (March 1983).

For pt.I see *ibid.*, vol.44, p.459 (1981). In a previous paper (Wei, Current and Seidman, 1981) the results of an extensive field-ion microscope investigation of the vacancy portion of the primary state of damage of ion-irradiated tungsten specimens were presented. The vacancies were contained in depleted zones (DZs) which had been created, at ≤ 15 KeV, by a variety of single projectile ions with initial energies in the range 15 to 70 keV. In this paper the definitions of all the principal quantities used to characterize the three dimensional vacancy population with a DZ are presented; that is, the number of vacancies, the average diameter and orientation of a DZ with respect to the incident ion beam, the average vacancy concentration within a DZ, the radial distribution functions and the first-nearest-neighbour cluster functions. All the DZs are analysed in great detail, using these principal quantities, and the results are presented in graphical form. In addition, many other detailed physical properties of DZs are presented. (32 refs.)

61990 Radiation damage, its recovery and platinum behavior and lattice location in ion bombarded MgO and Al₂O₃ as used for catalytic studies. H.Matzke (European Inst. for Transuranium Elements, Karlsruhe, Germany), A.Turos, P.Rabette.

Radiat. Eff. (GB), vol.65, no.1-4, p.1-9 (1982). (Proceedings of the First International Conference on 'Radiation Effects in Insulators', Arco, Largo di Garda, Italy, 1981).

Channeling and back-scattering techniques were used to study single crystals of α -Al₂O₃ and MgO following bombardment with Pt- (or Xe-) ions of 30 keV energy and doses between 9×10^{15} and 8×10^{16} ions/cm², as used for catalytic investigations. The MgO crystals showed saturation damage after implantation with the lower dose. Damage recovery proceeded progressively with increasing temperature and was not complete before 1300°C was reached. The Pt formed coherent precipitates. In contrast, a quasi-amorphous zone was formed on ion bombarded Al₂O₃. Outdiffusion of the impurity and recovery of the bombardment damage started at ~650°C, the temperature of the phase change to the recrystallized state. At temperatures in excess of 900°C, the Pt precipitated into small single crystal grains of near spherical shape. The results can be used to interpret the catalytic behavior of the systems Pt/single crystalline support. (13 refs.)

61991 Nuclear and electronic energy loss of noble gas ions bombarding solid benzene and relative chemical effects. O.Puglisi, G.Marletta, A.Torrisi (Istituto Dipartimentale di Chimica e Chimica Industriale, Catania, Italy), G.Foti, L.Torrisi.

Radiat. Eff. (GB), vol.65, no.1-4, p.11-16 (1982). (Proceedings of the First International Conference on 'Radiation Effects in Insulators', Arco, Largo di Garda, Italy, 1981).

Solid benzene has been bombarded with several inert gas ions at various energies ranging between 15-100 keV. Under these conditions the energy deposition (η) which occurs via nuclear collisions ranged between $4 \times 10^{-3} \pm 1$ of total energy loss. After implantation many products have been found in the target, and good correlation between the C₁₃ product yield and η has been found. This correlation is explained in terms of different fragmentation events which occur after electronic nuclear energy deposition. (7 refs.)

61992 Ion implantation effects in glasses. G.W.Arnold (Sandia Nat. Labs., Albuquerque, NM, USA).

Radiat. Eff. (GB), vol.65, no.1-4, p.17-30 (1982). (Proceedings of the First International Conference on 'Radiation Effects in Insulators', Arco, Largo di Garda, Italy, 1981).

Ion implantation can be used to introduce network damage and to alter the chemical composition in glasses. Structural changes can be inferred from IR measurements near 1000 cm⁻¹ and by optical absorption near 2150 Å. Implantation-induced damage decreases the implanted volume in fused silica with consequent changes in the refractive index, the near-surface hardness, and the tensile surface stress. Prior work in these areas is reviewed. Implantation into alkali silicate glasses depletes the alkali content in the implanted region. These changes allow preferential surface crystallization in Li₂O-2SiO₂ glasses. Crystallization of amorphous SiO₂ can be induced by implantation of Li. Insight into the crystallization process is obtained by following the associated ion movement by elastic recoil detection (ERD) and optical techniques. Implantation of 20 keV H shows that saturation of implanted H-sites in fused silica occurs at about 2.2×10^{21} H/cm² in agreement with free volume estimates of the maximum number of available interstitial sites. Details of H and D interactions in fused silica were studied as a function of fluence and temperature. Results are of interest in studies of corrosion in glasses considered for nuclear waste encapsulation and for components in fusion reactors. (30 refs.)

61993 Optical, chemical and mechanical modifications induced by ion implantation on glass surfaces. V.Chinellato (Stazione Sperimentale del Vetro, Murano, Italy), V.Gottardi, S.Lo Russo, P.Mazzoldi, F.Nicoletti, P.Polato.

Radiat. Eff. (GB), vol.65, no.1-4, p.31-9 (1982). (Proceedings of the First International Conference on 'Radiation Effects in Insulators', Arco, Largo di Garda, Italy, 1981).

Soda-lime glasses have been implanted with 50 keV Ar ions. Modifications induced on the glass surface have been studied as a function of implanted dose, with particular regard to optical, chemical and mechanical properties. Optical measurements indicate a reduction of the refractive index, connected to the surface sodium content. The sodium profile has been measured using the Na²³(p,α)Ne²⁰ nuclear reaction. An improvement of the mechanical resistance has been observed at low implantation dose, together with a change of the chemical durability. An expansion of glass has been observed by SEM and interferometric microscopy for 80 keV implantation energy. (10 refs.)

61994 Comparison of heavy-ion, proton and electron irradiation effects in vitreous silica. M.Antonini (Univ., Modena, Modena, Italy), P.Camagni, P.N.Gibson, A.Manara.

Radiat. Eff. (GB), vol.65, no.1-4, p.41-8 (1982). (Proceedings of the First International Conference on 'Radiation Effects in Insulators', Arco, Largo di Garda, Italy, 1981).

Summarizes recent experiments at the JRC, aiming to determine the relative damage effects produced in a-SiO₂ by particles of different mass and energy, so as to correlate typical defects with specific production mechanisms. By systematic analysis of optical absorption spectra, the main colour centres that are currently associated with primary irradiation effects were characterized. Centres responsible for the B₂-band (5.04 eV) and E'-band (5.78 eV) were quantitatively investigated with respect to particle type, production yield and saturation behaviour. Arguments taken from energy loss and DPA seem to suggest that the E' centre is based on a stable structural substrate, which is not reconciled with simple ideas of a broken bond. The B₂ centre is confirmed to be associated with atomic defects produced by collisions. New determinations in the vacuum UV, performed on heavy-ion irradiated samples, seem to put this centre in quantitative relationship to a centre responsible for a 7.15 eV absorption. (20 refs.)

61995 Annealing studies of irradiation effects in vitreous silica. M.Antonini (Univ. Modena, Modena, Italy), P.Camagni, P.N.Gibson, A.Manara.

Radiat. Eff. (GB), vol.65, no.1-4, p.49-53 (1982). (Proceedings of the First International Conference on 'Radiation Effects in Insulators', Arco, Largo di Garda, Italy, 1981).

Describes a series of annealing experiments devoted to the study of the thermal behaviour of B₂ and E' centres produced by heavy-ion irradiations in v-SiO₂. Thermal bleaching of the B₂ component is shown to be complete and irreversible at relatively low temperatures ($\leq 500^\circ\text{C}$). On the other hand, bleaching of E' in the same range is reversible and the corresponding absorption band can be entirely recovered in subsequent electron irradiation, suggesting the existence of a stable precursor defect for this centre. By alternating isochronal annealing cycles with electron reirradiations, the annealing of such defects was investigated up to 1000°C, taking care to compare the behaviour of the heavy-ion damaged material with that of undamaged material. The results seem to suggest a structural difference between pre-existing E' precursors of normal SiO₂ and those produced in excess by dis-

placing radiation, the latter being characterized by a distinct process of destruction with an activation energy $Q \geq 0.6$ eV. (11 refs.)

61996 Electron and ion beam effects in amorphous SiO₂ and Si₃N₄ films for electronic devices. R.Hezel (Inst. für Werkstoffwissenschaften VI, Univ. Erlangen, Erlangen, Germany).

Radiat. Eff. (GB), vol.65, no.1-4, p.101-6 (1982). (Proceedings of the First International Conference on 'Radiation Effects in Insulators', Arco, Largo di Garda, Italy, 1981).

The effect of electron and ion beam irradiation on the Si₂₃ Auger spectra of SiO₂, Si₃N₄ and Si-oxy-nitride films was measured by the relative intensity of the 92 eV signal, characteristic for the formation of 'free' silicon during irradiation. While in Si-oxy-nitride (O/N=0.37) the beam effects were almost negligible, some damage was found in Si₃N₄, but SiO₂ appeared to be extremely sensitive for electron and ion beam irradiation. By low energy electron loss spectroscopy (ELS) of ion bombarded SiO₂ and Si₃N₄ films new electron states due to broken Si-O and Si-N bonds could be determined within the band energy gap of the insulators. The measured energy losses were interpreted by means of electron energy level schemes of the amorphous films. (13 refs.)

61997 On the registration of low energy (E~1 keV/amu) ion tracks in dielectric minerals. J.Borg, J.C.Dran, Y.Langevin, M.Maurette, J.C.Petit (Lab. Rene-Bernas, Orsay, France).

Radiat. Eff. (GB), vol.65, no.1-4, p.133-7 (1982). (Proceedings of the First International Conference on 'Radiation Effects in Insulators', Arco, Largo di Garda, Italy, 1981).

Deals with the interaction of low energy (~1 keV/amu), heavy (Z>10) ions with solid state track detectors. Such ions, losing their energy mainly by nuclear collisions, trigger the formation of very short latent tracks of damaged material showing an enhanced chemical reactivity. Indeed, shallow etch pits have been successfully revealed in muscovite mica etched in 40% hydrofluoric acid. The authors have investigated in detail the variations of these etch pit characteristics with various parameters (atomic number Z and energy E of the incident ions, thermal annealing temperature T). (4 refs.)

61998 Thermal stability and chemical reactivity of defects produced in silicates by high energy heavy ions. Y.Langevin (Lab. Rene-Bernas, Orsay, France), J.P.Duraud.

Radiat. Eff. (GB), vol.65, no.1-4, p.139-42 (1982). (Proceedings of the First International Conference on 'Radiation Effects in Insulators', Arco, Largo di Garda, Italy, 1981).

The authors study the heavy ion (Au and U) irradiation of labradorite and muscovite. The thermal behavior and chemical reactivity of these tracks show that the latent track is now a continuous cluster of defects, similar to an amorphous phase, along part of the range. From these results, they tentatively assess the relation between energy loss and defect production in silicates. (6 refs.)

61999 Preparation of superinsulating surfaces by the nuclear track technique. B.E.Fischer, D.Albrecht, R.Spöhr (GSI, Darmstadt, Germany).

Radiat. Eff. (GB), vol.65, no.1-4, p.143-4 (1982). (Proceedings of the First International Conference on 'Radiation Effects in Insulators', Arco, Largo di Garda, Italy, 1981).

The authors report on the preparation of superinsulated surfaces by heavy ion irradiation and etching. The dependence of the effect on a texture parameter called porosity (=track density \times cross section of an individual etched track channel) has been investigated in a preliminary experiment with 7.5 MeV/u xenon ions on a mica sample. To test the protection against conducting contaminants the resistance (R) of some irradiated and etched samples is compared with that (R₀) of an untreated sample after sputter-coating with 0.7 μm gold. (no refs.)

62000 Formation and relaxation kinetics of mechanical stress in a glass surface layer during ion bombardment. I.I.Daugela, L.I.Prankevicius (A. Snekhus Polytech. Inst., Kaunas, USSR).

Sov. Phys.-Tech. Phys. (USA), vol.27, no.10, p.1306-7 (Oct. 1982). Translation of: *Zh. Tekh. Fiz. (USSR)*, vol.52, no.10, p.2123-4 (Oct. 1982). [received: April 1983]

Studies mechanical stresses in K-8 optical glass caused by bombardment by He⁺ and Ar⁺ ions of energy 100 keV. The penetration depth of 100-keV He⁺ ions into the glass was 0.63 μm , considerably greater than the penetration depth 0.08 μm of Ar⁺ ions. The mechanical stresses in the layer are produced because the penetrating ions cause a large number of defects (dislocations, thermal peaks, etc.). Mobile defects may accumulate in the surface layer to form immobile continuous defects or extrude to the surface. The experimental findings indicate that when glass is irradiated with Ar⁺ ions, which give up most of their energy to the atomic nuclei (formation of defects), even small doses 2×10^{15} ion/cm² result in saturation and additional bombardment does not change the velocity of the surface acoustic waves. When bombardment is by light He⁺ ions, which lose much of their kinetic energy in the solid glass as a result of electron deceleration (excitation and ionization of atoms), saturation does not occur even at 10^{16} ion/cm² doses. (5 refs.)

62001 Ion beam induced composition changes during Auger sputter profiling of thin Al films on InP. D.K.Skinner (Allen Clark Res. Centre, Plessey Res. (Caswell), Caswell, Ltd., England), J.G.Swanson, C.V.Haynes.

Surf. & Interface Anal. (GB), vol.5, no.1, p.38-42 (Feb. 1983).

Auger sputter profiles of thin Al films on InP are presented and shown to be susceptible to an unusual type of ion beam induced interfacial distortion. It is found that recoil implantation and atomic mixing produce a differential broadening of the In and P at the interface which can seriously affect the integrity of the Auger profile. Energy shifts in the Al Auger peak indicate that this distortion is associated with AlP formation to a depth dictated by the ion beam energy and species. Experimental requirements for the reduction of interfacial distortion are discussed. The influence of the ion beam on the topography and morphology of the InP surface in relation to interfacial distortion is also considered. (17 refs.)

Proton irradiation damage in cyclically stressed aluminum See Entry 60235
The planar track model and the prediction of alpha-recoil aging in radwaste materials See Entry 60243

A study of radiation effects in curium-doped Gd₂Ti₂O₇ (pyrochlore) and CaZrTi₂O₇ (zirconolite) See Entry 60283

Dose-dependence of Pb-ion implantation damage in zirconolite, hollandite, and zircon See Entry 60284

Leachability of zircon as a function of alpha dose See Entry 60285

Isotopic fractionation of thorium and uranium upon leaching of monazite: alpha-recoil damage effects See Entry 60286

Investigation of titanium in metamict Nb-Ta-Ti oxides using the extended X-ray absorption fine structure technique See Entry 60287

Spontaneous and continuous structure and surface transformations of refractory transition metals by hydrogen See Entry 60408

- Structural and mechanical anisotropy of a nuclear grade AISI 316 stainless steel See Entry 60409
- Helium bubbles at grain boundaries in an austenitic steel See Entry 60410
- Irradiation creep in first wall model alloys See Entry 60411
- Helium ion damage in an amorphous Fe-Ni-Mo-B alloy See Entry 60417
- The surface topography of Inconel, stainless steel and copper after argon ion bombardment See Entry 60418
- The cyclotron facility for radiation damage experiments at the JRC-ISPRA See Entry 60498
- Sputtering of titanium and niobium hydrides See Entry 61660
- Oxygen defect profile in implanted garnet See Entry 61906
- Changes induced by ion implantation in forsterite $\text{SiO}_4 \text{ Mg}_2$ See Entry 61939
- Ion implantation and luminescence See Entry 61940
- Ion beam hydrogenation of polysilicon coated thermal oxide on silicon See Entry 61941
- Chemical and catalytic effects of ion implantation See Entry 61942
- Barrier height and surface states at cleaned InSb(110) surfaces See Entry 62470
- Work function measurements on ion bombardment damaged (111) surface of silver by photoelectric and CPD methods See Entry 62480
- The excitation of energetic atomic particles penetrating amorphous condensed matter See Entry 63060
- Molecular erosion of ice by keV ion bombardment See Entry 63126
- X-ray photoelectron diffraction studies of zinc selenide See Entry 63137
- A technique for observing the cross sectional damage profiles in He-ion irradiated 316 stainless steel by transmission electron microscopy See Entry 63480
- Electron microscopic observation of hard material using an ion sputtering technique See Entry 63495
- Silicon solar cells by ion implantation: E-beam and self annealing See Entry 63704

61.80M Channelling, blocking and energy loss of particles

(see also 29.70 Energy loss and range relations)

- 62002 A one dimensional microscopical model for the study of the coherence in the stopping power problem. III. P.Szilas, G.Sussmann (Theoretische Phys., Univ. Muenchen, Munich, Germany). *Z. Phys. B (Germany)*, vol.50, no.3, p.209-16 (1983). For pt.II see *ibid.*, vol.42, p.253 (1981). The authors consider the quantum mechanical problem of a particle being scattered inelastically by a chain of N infinitely heavy, equidistantly spaced two-level atoms. In a previous paper (Sussmann, G., Szilas, P.: *Z. Phys. B—Condensed Matter* 42, 253, 1981) the time dependent problem of a Gaussian wave packet impinging on the target atoms has been studied and an explicit asymptotic expression for the reduced density matrix ρ_R of the particle has been given. The authors now introduce the coarse grained density matrix $\bar{\rho}_R$. The incoherence $\beta = 1 - \text{Tr}(\bar{\rho}_R^2)$, i.e. the deviation of the state of the particle from a pure state, being small on certain conditions, they find a single particle wave function ψ with $\psi(x,t)\psi^*(x',t) \approx \langle x | \bar{\rho}_R | x' \rangle$ and a nonlinear Hermitean Hamiltonian $H_\psi = p^2/2m + W_\psi$ such that $i\hbar\psi(x,t) = H_\psi\psi(x,t)$ describes the time evolution. Finally the authors also consider W_ψ within the framework of the phenomenological theory of nonlinear frictional operators. (12 refs.)
- 62003 Crystallographic contrast due to primary ion channelling in the scanning ion microscope. P.H.La Marche, R.Levi-Setti, K.Lam (Dept. of Phys., Univ. of Chicago, Chicago, IL, USA). *IEEE Trans. Nucl. Sci. (USA)*, vol.ns-30, no.2, p.1240-2 (April 1983). (1982 IEEE Conference on the Application of Accelerators in Research and Industry, Denton, TX, USA, 8-10 Nov. 1982). The authors observe large crystallographic contrast, in scanning ion micrographs of recrystallized Cu and Si, made by collecting secondary ions or electrons. The contrast is attributed to primary ion-channelling effects. Observed relative secondary ion and electron yields are discussed in relation to the rate of energy loss, calculated for various crystallographic directions. (19 refs.)
- 62004 Nuclear tracks in solids. R.M.Walker (McDonnell Center, Washington Univ., St. Louis, MO, USA). *Radiat. Eff. (GB)*, vol.65, no.1-4, p.131-2 (1982). (Proceedings of the First International Conference on 'Radiation Effects in Insulators', Arco, Largo di Garda, Italy, 1981). A nuclear track is defined as a more or less contiguous set of radiation damage sites that form a linear array defining the trajectory of a charged particle. The author considers better methods to define the atomic nature of tracks prior to etching, a better understanding of the way in which energy transferred to the electronic system results in the displacement of nuclei and a clearer picture of annealing processes. (no refs.)
- 62005 Small angle neutron scattering from oriented latent nuclear tracks. D.Albrecht, P.Armbruster, R.Spohr (GSI, Darmstadt, Germany), M.Roth. *Radiat. Eff. (GB)*, vol.65, no.1-4, p.145-8 (1982). (Proceedings of the First International Conference on 'Radiation Effects in Insulators', Arco, Largo di Garda, Italy, 1981). Parallel arrays of long cylindrical objects with vanishing distance correlation and defined orientation, such as latent nuclear tracks, generated at the heavy ion accelerator facility GSI Darmstadt, represent an almost ideal case for a scattering experiment. A feasibility study has been conducted, using small angle neutron scattering, yielding the following results: 1) In contrast to transmission electron microscopy, the technique is virtually nondestructive and suitable also for low melting point organic materials. 2) Observation times between 0.1 and 1 h were sufficient at the neutron small-angle scattering apparatus D17 at ILL, Grenoble. Latent tracks at areal densities $< 3 \times 10^{11}$ ions per cm^2 could be observed safely below the track interference limit between neighbouring tracks. 3) Small-angle neutron scattering yields intense two-dimensional scattering distributions from which equivalent track radii can be determined. (3 refs.)
- 62006 Experimental determination of the limiting surface-channelling energy. L.L.Balashova, Sh.N.Garin, A.I.Dodonov, E.S.Mashkova, V.A.Molchanov, V.B.Flerov (M.V. Lomonosov State Univ., Moscow, USSR). *Sov. Tech. Phys. Lett. (USA)*, vol.8, no.7, p.363-4 (July 1982). Translation of: *Pisma v Zh. Tekh. Fiz. (USSR)*, vol.8, no.13-14, p.840-4 (July 1982). [received: April 1983] When accelerated particles interact with the surfaces of single crystals, one observes surface-channelling effects, analogous to the channelling effects which occur in the interior of the crystals. Surface-channelling effects can be

observed only if the energy of the transverse motion of the incident particles is not very low (so that the particles can cross the potential barrier created by the surface rows of the crystal). The authors report an experimental determination of this minimum energy. The target was the (100) face of a copper single crystal, on which the close-packed (110) atomic rows form deep semi-channels. The target was bombarded by 30-keV argon ions and 15-keV nitrogen ions. (6 refs.)

- Deposited energy density for 100 MeV protons in lithium See Entry 60554
- On the registration of low energy ($E \sim 1$ keV/amu) ion tracks in dielectric minerals See Entry 61997
- Thermal stability and chemical reactivity of defects produced in silicates by high energy heavy ions See Entry 61998

62.00 MECHANICAL AND ACOUSTIC PROPERTIES OF CONDENSED MATTER

(see also 46.30 Mechanics of solids and rheology, 61.70 Defects in crystals, 68.25 Surfaces and interfaces, 81. Materials science; for thermomechanical effects, see 65.70; for magnetomechanical effects, see 75.80; for piezoelectric effects, see 77.60; for elasto-optical effects, see 78.20H)

62.10 MECHANICAL PROPERTIES OF LIQUIDS

(for viscosity of liquids, see 66.20)

- 62007 Density and thermal expansion of liquid U-Nb alloys. W.D.Drotning (Sandia Nat. Labs., Albuquerque, NM, USA). *High Temp.-High Pressures (GB)*, vol.14, no.3, p.253-8 (1982). (10th Plansee Seminar on 'Trends in Refractory Metals, Hardmetals, and Special Materials, and their Technology', Reutte, Austria, 1-5 June 1981). The density and volumetric thermal expansion of U-Nb alloys were measured in the liquid phase by gamma densitometry. Compositions varied from 0 to 25 wt.% Nb, and data were obtained over a temperature range of 200-300K above the liquidus temperature for each of the six alloys. The density of each molten alloy was found to vary linearly with temperature. For pure uranium, the density in the liquid phase is given by $\rho/\text{g cm}^{-3} = 16.95 - 12.9 \times 10^{-7} [(T/\text{K}) - 1407]$. The liquid density at the liquidus temperature was found to vary smoothly with alloy composition. From the liquid density and thermal expansion data, the molar volume was calculated for each alloy. For intermediate compositions, the data indicate a volume expansion, typified by an excess molar volume of approximately 4% at 2000K for alloys near 40 at.% Nb. Experimental measurements at high temperature were also made of the solid phase linear thermal expansion for pure uranium and for the 10 and 15 wt.% Nb materials. (9 refs.)
- The effect of nonlinear density stratification on the stability of a vertical water layer in the conduction regime See Entry 61541
- Plastic behavior and polymorphism of smectic liquid crystal See Entry 61783
- Physical properties of liquid crystals of 4-(4-nalkylbicyclo[2,2,2]octyl)benzonitriles See Entry 61793
- Investigation of nematic liquid crystals by correlation spectroscopy. Determination of ratios of viscosity and elasticity constants See Entry 61794
- An optical method of determining the elastic constant ratio K_{33}/K_{11} in nematic liquid crystals See Entry 61795
- A new method for determining the elastic constant ratio K_{33}/K_{11} in nematic liquid crystals See Entry 61796
- Sound speeds and isotropic compressibilities of 1,1,2,2-tetrachloroethane with alcohols See Entry 62029
- Thermophysical properties of supercritical fluids with special consideration of aqueous systems See Entry 62073
- Phase-transition studies in polymeric compounds. I. Density studies in *N*-(*p*-hexyloxybenzylidene)-*p*-*n*-butylaniline See Entry 62097

62.20 MECHANICAL PROPERTIES OF SOLIDS (RELATED TO MICROSCOPIC STRUCTURE)

(see also 81.40 Treatment of materials and its effects on microstructures and properties, 81.70 Materials testing)

- Morphology of polyallomers See Entry 61832
- Determination of the optimum grain size in KhN67MVTy alloy taking account of the basic operational parameters See Entry 63303

62.20 Elastic constants

(see also 03.40D Mathematical theory of elasticity, 81.40J Elasticity and anelasticity)

- 62008 Computation of normal modes from identified complex modes. S.R.Ibrahim (Old Dominion Univ., Norfolk, VA, USA). *AIAA J. (USA)*, vol.21, no.3, p.446-51 (March 1983). A technique is presented to compute a set of normal modes from a set of measured (damped) complex modes. The number of elements in the modal vectors, which is equal to the number of measurements, can be larger than the number of modes under consideration. It is also shown in this paper that the practice of normal mode approximation to complex modes can lead to considerably large errors when the modes are too complex. A numerical example and a simulated experiment are presented to illustrate the concepts discussed and to support the theory presented. (18 refs.)
- 62009 Optimization of the computation of elastic constants from the measurements of ultrasonic velocities. B.Hosten, B.Castagnede (Lab. de Mecanique Phys., Univ. de Bordeaux-I, Talence, France). *C.R. Seances Acad. Sci. Ser. II (France)*, vol.296, no.5, p.297-300 (7 Feb. 1983). In French. An optimized process is proposed for the mechanical characterization of anisotropic materials by means of an ultrasonic method. Newton's method is adapted to a specific problem of optimization of the stiffness matrix coefficients. (4 refs.)

62010 Elastic properties of CsCN. A.Loidl (Inst. für Phys., Univ. Mainz, Mainz, Germany), S.Haussuhl, J.K.Kjems, *Z. Phys. B (Germany)*, vol.50, no.3, p.187-92 (1983).

The temperature dependence of the elastic constants of CsCN exhibiting the CsCl structure was measured with ultrasonic and neutron techniques. The room temperature values were found to be $c_{11}=18.8$, $c_{12}=10.7$ and $c_{44}=2.95 \times 10^{10}$ dyn/cm². The sound waves in T_{2g} and E_g symmetries exhibit anomalous temperature effects which are similar but definitively weaker than those in the NaCl type cyanides. In addition the authors measured the acoustic phonon dispersion along [100] and [110]. These results are compared with recent molecular dynamics calculations. (28 refs.)

62011 Elasticity moduli of TGS crystals for cylindrical samples. H.Wolniewicz (Inst. of Phys., Tech. Univ. of Wrocław, Wrocław, Poland). *Mater. Sci. (Poland)*, vol.7, no.4, p.475-9 (1981).

Elasticity moduli for triglycine sulphate (TGS) were determined by the electric resonance method. Resonance frequencies were estimated as a function of the sample diameters. Evaluation of the accuracy of results obtained indicates the most favourable diameters of the sample for which reasonable values of elasticity moduli are obtained. (8 refs.)

62012 On the elastic anisotropy of ferroelectric triglycine selenate. S.K.Khanna (Dept. of Phys., Indian Inst. of Technol., Madras, India). *Phys. Status Solidi b (Germany)*, vol.116, no.1, p.173-8 (1 March 1983).

The numerical values of the elastic constants C_{11} , C_{22} , C_{33} , C_{15} , C_{35} , C_{55} are determined experimentally by using an acousto-optical method. Results are reported of the anisotropy of the velocity of 10 MHz ultrasonic waves in the direct vicinity of the phase transition temperature. It is observed that in the ferroelectric phase the velocity rises with a rotation of the sound wave vector by 2 to 4° with respect to the z-axis in the Y-Z plane. On the other hand these critical anomalies of velocity are found to follow an identical logarithmic behaviour in the paraelectric phase. The results are discussed on the basis of Landau theory but at the same time taking into account the long range dipole-dipole interactions as well as the fluctuations of the order parameter. The correlation parameter is estimated from the temperature dependence of the elastic coefficient in the paraelectric phase ($\delta=0.2 \times 10^{-16}$ cm²). (12 refs.)

62013 Coincidence of bounds for some elastic moduli of polycrystals with [100] fibre texture. C.M.Sayers (Materials Phys. Div., AERE, Harwell, England). *Philos. Mag. A (GB)*, vol.47, no.3, p.L1-4 (March 1983).

Kroner and Wawra (1978) have demonstrated that the Voigt and Reuss bounds for the elastic constants C_{13} , C_{33} and C_{44} of a polycrystalline aggregate of cubic crystallites with [100] fibre texture coincide. In this paper it is shown in addition that the quantity $C_{11}+C_{12}$ has the same value in the Voigt and Reuss schemes, and that the difference in $C_{66}=(C_{11}-C_{12})/2$ varies with the square of the anisotropy factor $C=(C_{11}-C_{12}-2C_{44})$ of the crystallites from which the aggregate is composed for small anisotropy C . Expressions for the elastic stiffness and compliance constants in the Voigt and Reuss schemes are given which correct those recently given by Ledbetter (1982). (12 refs.)

The role of elastic interaction stresses on the onset of slip in polycrystalline alpha brass. I. Experimental determination of operating slip systems and qualitative analysis See Entry 61927

Brewster reflections of elastic waves in hexagonal crystals See Entry 62024

Effect of three-body forces on thermophysical and anharmonic properties of rare gas solid mixtures See Entry 62041

Lattice dynamics of α -quartz including the effect of the width of the atomic electron distribution See Entry 62045

Lattice dynamics of FCC Ca See Entry 62046

The relationship between the Gruneisen and other thermodynamic parameters and intermolecular forces in polymers See Entry 62130

Curvature radius and layer stresses for thermal strain in semiconductor multi-layer structures See Entry 62311

Self-consistent semirelativistic pseudopotential calculation of the energy bands, cohesive energy, and bulk modulus of W See Entry 62329

Characterization of the three dimensional properties of poled PZT 65/35 in the absence of losses See Entry 62894

Raman and luminescence studies of alkali borate tungstate glasses See Entry 62962

Single crystal growth and physical properties of cubic $Zn_4O(BO_3)_6$ See Entry 63151

Elastic behavior and phase stability of β_1 -AgCd alloy See Entry 63292

Effect of chromium and aluminum on the physical and mechanical properties of precipitation-hardening Fe-Mn Elinvar See Entry 63321

The role of elastic interaction stresses on the onset of slip in polycrystalline alpha brass. II. Rationalization of slip behavior See Entry 63335

Interrelationship of Poisson's ratio with other characteristics of pure metals See Entry 63340

Properties of polyethylene-propylene blends. III. Mechanical characterization of ultradown fibres See Entry 63348

Superplasticity in Al-Li based alloys See Entry 63369

Correlation of hardness and microstructure in unoriented lamellar polyethylene. II. Study of elastic modulus See Entry 63384

62.20F Deformation and plasticity

(inc. yield, ductility and superplasticity; see also 81.40L

Deformation, plasticity and creep)

62014 On the work hardening rate of glassy polymers. I. Application to the physical ageing of atactic PMMA. C.Bultel, J.M.Lefebvre, B.Escaig (Lab. des Structures et Propriétés de l'Etat Solide, Univ. des Sci. et Tech. de Lille, Villeneuve d'Ascq, France). *Polymer (GB)*, vol.24, no.4, p.476-80 (April 1983).

The authors introduce a new parameter to characterize the non-elastic behaviour of glassy polymers, namely the work hardening rate. The change in molecular microstructure induced by nonelastic deformation during the pre-yield stage is treated as a defect nucleation rate. Such defect nucleation is very sensitive to the past thermomechanical history of the material and therefore the parameter K , which characterizes the ability of the polymer to deform non-elastically, will be influenced by any structural variation. Application to physical ageing of atactic poly(methylmethacrylate) PMMA is presented. (13 refs.)

62015 Strain-ageing in silver chloride. I. The representative curve. H.Shalitt, M.T.Sprackling (Phys. Dept., Queen Elizabeth Coll., London, England). *Philos. Mag. A (GB)*, vol.47, no.3, p.331-42 (March 1983).

A study has been made of strain-ageing at room temperature in zone-refined silver chloride. It is found that if the yield stress after ageing is measured on a single specimen for a sequence of ever-increasing ageing times, the graph of change of flow stress against \ln (ageing time) is a reproducible curve that reflects the various mechanisms that operate during ageing, and has been called the representative curve. The representative curve for silver chloride at room temperature has four distinct regions which are interpreted in terms of the dislocation-point-defect interactions taking place in the material. (27 refs.)

62016 The low-temperature flow stress of europium-doped sodium chloride. B.Subramanian, J.J.Martin (Dept. of Phys., Oklahoma State Univ., Stillwater, OK, USA). *Philos. Mag. A (GB)*, vol.47, no.3, p.343-9 (March 1983).

The flow stress of single-crystal NaCl:Eu has been measured as a function of europium concentration and heat treatment at 80, 196, 273 and 300K. Samples that were fast-cooled from temperatures above 673K contain isolated Eu^{2+} -Na vacancy (IV) dipoles. These samples are considerably softer than samples which had been aged at 423K for 24 hours. The aged samples contain an aggregated phase. A linear dependence of flow stress on concentration was observed at all temperatures for the fast-cooled samples. At 80K the curve of the flow stress versus concentration had a line gradient approximately twice the value observed at the higher temperatures. If this linear dependence is caused by a Snoek-relaxation of the isolated IV dipoles, their relaxation time must be considerably modified by the presence of the moving dislocations. The aged samples showed a square-root dependence of flow stress on concentration for temperatures above 196K. (21 refs.)

62017 Orientation dependence of slip deformation of the conjugate system in Cu-6 at.% Al single crystals. T.Mori, H.Fujita (Dept. of Materials Sci. & Engng., Osaka Univ., Yamada-oka, Suita, Japan). *Philos. Mag. A (GB)*, vol.47, no.3, p.435-40 (March 1983).

The orientation dependence of slip deformation of the conjugate system has been examined in cylindrical Cu=6 at.% Al single crystals. The threshold stress of conjugate slip, which occurs abruptly in the later stages of deformation, is high when the crystal axis is near (111), but becomes lower as the axis approaches (100). Furthermore, as the initial axis is far away from the symmetry line of (100)-(111), the threshold stress becomes higher. This orientation dependence is just the reverse of that appropriate to twinning deformation. It is concluded that twinning and conjugate slip deformations are interdependent stress-relief mechanisms. (13 refs.)

62018 Impurity-induced weakening of materials. B.V.Petukhov (Inst. of Crystallography, Acad. of Sci., Moscow, USSR). *Sov. Tech. Phys. Lett. (USA)*, vol.8, no.7, p.360-1 (July 1982). Translation of: *Pis'ma v Zh. Tekh. Fiz. (USSR)*, vol.8, no.13-14, p.833-6 (July 1982).

[received: April 1983]
The authors derive a theory for the impurity induced weakening of materials. They consider the dislocation motion in plastic deformation and the effect of an impurity on the probability for thermally activated production of solitons. (8 refs.)

Thermal stresses in anisotropic noncylindrical beams See Entry 61411

Antiplane deformation of a body with a curved elastic sharp-ended inclusion See Entry 61423

Dynamic stability boundaries for a sinusoidal shallow arch under pulse loads See Entry 61426

Effect of molecular extension of a melt on the crystallinity of polyethylene, subjected to repeated crystallization See Entry 61814

Small angle neutron scattering study of the structure of a triblock copolymer of styrene and isoprene during extension See Entry 61821

Theoretical prediction of domain sizes in IPNs and related materials See Entry 61824

Effect of poly(propylene oxide) segment size on structure-property relationships in elastomeric ionene See Entry 61827

Kinetics of the collective crystallization of doped ZnS See Entry 61835

Influence of ultrasound on the concentration of point defects in KBr crystals See Entry 61911

A model for the evolution of a twist dislocation network See Entry 61912

Improved technique for observation of dislocation structure of austenitic MnCrNi steels after small deformation See Entry 61920

Chemical etching of deformation sub-structures in quartz See Entry 61924

The role of elastic interaction stresses on the onset of slip in polycrystalline alpha brass. I. Experimental determination of operating slip systems and qualitative analysis See Entry 61927

Changes induced by ion implantation in forsterite SiO_4 Mg₂ See Entry 61939

Friction and source hardening in irradiated mild steel See Entry 61984

On the critical dose for blistering in helium irradiated zirconium and Zr-Nb See Entry 61987

Wear resistance of friction elements working in oil See Entry 62021

Thermal and mechanical properties of tetramethyl-p-silphenylenesiloxane/dimethylsiloxane block copolymer See Entry 62069

Acoustically induced plastic deformation of conical microcrystals on copper surfaces See Entry 62227

Curvature radius and layer stresses for thermal strain in semiconductor multi-layer structures See Entry 62311

A theory of internal stress field and configuration of magnetic domain in amorphous ribbons See Entry 62688

Positron lifetime measurement of plastically deformed iron single crystals See Entry 63080

Experimental investigation of plastic strains of porous solids—a review See Entry 63190

Effect of thermal conditions of preparation of dispersion-strengthened nickel powders on the character of distribution of the strengthening phase See Entry 63205

Sintering of cast iron swarf powder and Fe-Si-C mixed powder See Entry 63213

Influence of alloying and preliminary deformation on phase composition and mechanical properties of Fe-Mn alloys See Entry 63291

Examination of applied stress and prestrain effects on recovery of work hardened Cu-SiO₂ See Entry 63306

The structural state and its association with low temperature work hardening of structural titanium alloys See Entry 63307

Influence of sulfur and nitrogen on the characteristics of texture formation as a result of deformation and annealing of Fe-3% Si single crystals See Entry 63309

Free-cutting stainless steel wire with high-strength See Entry 63315

Heat treatment of molybdenum, tungsten and their alloys up to 2100°C See Entry 63317

Thermomechanical treatments of a 1050 pearlite steel See Entry 63318

The effect of ITMT's and P/M processing on the microstructure and mechanical properties of the X7091 alloy See Entry 63319

Effect of chromium and aluminum on the physical and mechanical properties of precipitation-hardening Fe-Mn Elinvar See Entry 63321

Structure and properties of a maraging steel after thermomechanical and repeated heat treatment See Entry 63332

Influence of residual gas pressure in annealing on the properties of niobium and its alloys See Entry 63333

The role of elastic interaction stresses on the onset of slip in polycrystalline alpha brass. II. Rationalization of slip behavior See Entry 63335

The rheology of thin polystyrene films See Entry 63336

Influence of texture on dislocation creep and grain boundary sliding in fine-grained cadmium See Entry 63341

Microstructure of aluminium during creep at intermediate temperatures. III. The rate controlling process See Entry 63342

Characteristics of plastic deformation of silicon iron single crystals under hydrostatic pressures See Entry 63343

Influence of deformation and temperature on the structure and mechanical properties of high-cobalt alloy See Entry 63344

Structural mechanism of plastic deformation of Mn-Cu alloys in martensitic state See Entry 63345

Strengthening of cast low-pearlite steels by microalloying with vanadium See Entry 63346

On the origin of the first peak of acoustic emission in 7075 aluminium alloys .. See Entry 63347

Properties of polyethylene-propylene blends. III. Mechanical characterization of ultradown fibres See Entry 63348

Mechanochemical reaction of polyvinyl chloride at high pressures See Entry 63350

Kinking in the drawing of linear polyethylene See Entry 63351

Effects of complicated deformation history on inelastic deformation behaviour of metals See Entry 63352

On the Portevin-Le Chatelier effect due to Snoek strain aging in the niobium oxygen system See Entry 63353

Effect of sulfides and sulfide morphology on anisotropy of tensile ductility and toughness of hot-rolled C-Mn steels See Entry 63354

Alpha-beta interface sliding in Ti-Mn alloys See Entry 63355

Characteristics of structural transformations during deformation and heat treatment of Elinvar alloy 45 NKht See Entry 63356

Effect of heat treatment in magnetic field on the mechanical properties of carbon steels See Entry 63357

Ductility characteristics of thin sheet steel See Entry 63358

Effect of diffusion welding thermal cycle on the strength of alloy VT20 See Entry 63359

Temperature and rate conditions for development of superplasticity in Zr-2.5% Nb alloy See Entry 63360

Influence of melting method, modification, and cyclic temperature-force action on the ductility of IV7M6K12 steel See Entry 63361

Mechanical behaviour of isotactic polypropylene subjected to various strain histories in uniaxial extension See Entry 63363

Performance of the Ni-Ti alloy VTN-1 (54.5-55 wt. % Ni) in the case of shape restoration See Entry 63364

Influence of heat treatment on the mechanical properties of dispersion hardening Nb-Zr-N alloys See Entry 63365

Examination of the effects of dimensional mismatch of the lattice parameters of the γ and γ' phases on the high-temperature strength of dispersion-hardened nickel alloys See Entry 63366

Superplasticity in an austenitic stainless steel containing aluminium and manganese See Entry 63368

Superplasticity in Al-Li based alloys See Entry 63369

Anomalous dynamic superplasticity and quasiliquid condition of iron in the presence of hydrogen See Entry 63370

Stress-strain state in the rolling of blanks from granulated alloys See Entry 63371

Structural-mechanical features of two-stage shear strain of oriented low density polyethylene See Entry 63372

Effect of the annealing on the mechanism of plastic strain in oriented polypropylene See Entry 63373

The effects of molecular weight and cooling rate on fine structure, stress-strain behavior and wear of polytetrafluoroethylene See Entry 63374

Correlation of hardness and microstructure in unoriented lamellar polyethylene. II. Study of elastic modulus See Entry 63384

Notched unidirectional boron/aluminum: effect of matrix properties See Entry 63389

Mechanical properties and fatigue strength of steel protected from tuffriding by inorganic coating See Entry 63395

Effect of stress frequency on fatigue crack propagation rate in titanium See Entry 63399

Microstructure and tensile ductility in a β heat treated titanium alloy See Entry 63400

High temperature low cycle fatigue of IN 738 and application of strain range partitioning See Entry 63402

Improvement in lower temperature mechanical properties of 0.40 pct C-Nr-Cr-Mo ultrahigh strength steel with the second phase lower bainite See Entry 63403

Effect of cyclic plastic bending on the proneness of steel St3Sp to brittle fracture See Entry 63407

Tenacity, toughness, ductility of mild steel sheet in longitudinal and short transverse direction See Entry 63414

Mechanical properties of ageing of non-magnetic austenitic steels at low temperatures See Entry 63417

An analysis of the localization of deformation and weight loss during single-particle normal impact See Entry 63433

Changes in resistivity at low-temperature deformation and the subsequent recovery of the Ag-15 at.% Al alloy See Entry 63434

Heat treatment and magnetic properties of high-coercivity Fe-Co-Cr alloys with 3% Mo See Entry 63435

Microstructure and ductility of electroless copper deposits See Entry 63438

Effect of high-temperature vacuum annealing time on the structure and properties of titanium alloys See Entry 63457

Question of the safe boundaries of use of 12 MKh steel at increased temperatures and hydrogen pressures See Entry 63467

The use of time-of-flight neutron diffraction to study grain interaction stresses See Entry 63472

62.20H Creep

(see also 81.40L Deformation, plasticity and creep)

Irradiation creep in first wall model alloys See Entry 60411

Internal stress buildup in SIPA creep See Entry 61958

Influence of texture on dislocation creep and grain boundary sliding in fine-grained cadmium See Entry 63341

Microstructure of aluminium during creep at intermediate temperatures. III. The rate controlling process See Entry 63342

Effect of creep deformation on microstructural change in 12% Cr heat resisting steel See Entry 63349

Mechanical behaviour of isotactic polypropylene subjected to various strain histories in uniaxial extension See Entry 63363

Examination of the effects of dimensional mismatch of the lattice parameters of the γ and γ' phases on the high-temperature strength of dispersion-hardened nickel alloys See Entry 63366

Examination of the creep strength of single crystals of high-temperature nickel alloys See Entry 63367

Evaluation of creep crack growth criteria for IN-100 at elevated temperature .. See Entry 63375

62.20M Fatigue, brittleness, fracture, and cracks

(inc. hardness; see also 81.40N Fatigue, embrittlement and fracture)

62019 Fatigue life estimation using simple fracture mechanics. F.Sherratt (Univ. of Warwick, Warwick, England). *J. Soc. Environ. Eng. (GB)*, vol.22, no.1, iss.96, p.23-7, 35 (March 1983). Methods of using linear elastic fracture mechanics (LEFM) in static design are first dealt with. Various expressions for fatigue crack growth are presented and fracture mechanics in cumulative damage is then considered. (5 refs.)

62020 Correlation between grain-boundary hardening and grain-boundary energy in niobium bicrystals. Y.T.Chou, B.C.Cai, A.D.Romig, Jr., L.S.Lin (Dept. of Metall. & Materials Engng., Lehigh Univ., Bethlehem, PA, USA). *Philos. Mag. A (GB)*, vol.47, no.3, p.363-8 (March 1983). Grain-boundary hardening of oriented niobium bicrystals with symmetric tilt boundaries has been determined using microhardness measurements. The boundary hardening was found to be misorientation-dependent and related to the boundary energy. For bicrystals with low-angle boundaries, the hardening varies with misorientation with a linear relationship of the Read-Shockley type. For bicrystals with high-angle boundaries, hardening cusps (minima) were observed near the coincidence-site-lattice boundaries. (13 refs.)

Using an electron beam to study the surface microrelief of solids See Entry 59760

Evaluation of the resistance of irradiated zirconium-liner cladding to iodine-induced stress corrosion cracking See Entry 60236

On strength of welded joints in high strength, large scale copper coils for nuclear fusion equipment See Entry 60432

Bending strength of F102 and NS9 optical glasses See Entry 61249

Antiplane deformation of a body with a curved elastic sharp-ended inclusion See Entry 61423

Formation of fracture structures of weakly interacting cracks See Entry 61454

Combined models of fracture and their use in predicting service life See Entry 61455

Physicochemical properties of alloys of HgTe-MgTe system .. See Entry 61875

Microhardness of an implanted system See Entry 61944

On the microhardness induced by impurity ions in the NaCl and KCl single crystals See Entry 61951

Low temperature neutron and gamma irradiation of glass fiber reinforced epoxies See Entry 61980

Phase equilibria in systems of TiX with Cd(Zn)X (X=S, Se, Te) See Entry 62060

The $Tl_2Te + Ge \rightleftharpoons 2Ti + GeTe$ ternary interlinked system See Entry 62061

Chemical durability of ZrO_2 containing glasses See Entry 62159

Kinetic enrichment of hydrogen at interfaces and voids by dislocation sweep-in of hydrogen See Entry 62168

Emission of light from solids during crack formation See Entry 63055

Comparative studies of reactive sputtering, ion plating and CVD coating of TiN hard layers See Entry 63167

Effect of thermal conditions of preparation of dispersion-strengthened nickel powders on the character of distribution of the strengthening phase See Entry 63205

Repeated mechanical strengthening as a method of increasing the endurance of constructional steels See Entry 63314

Thermomechanical treatments of a 1050 pearlite steel See Entry 63318

The effect of ITMT's and P/M processing on the microstructure and mechanical properties of the X7091 alloy See Entry 63319

Effect of HTTT on the properties of alloy steel castings See Entry 63323

Structure and properties of low-pearlite steel with different titanium concentrations See Entry 63330

Influence of residual gas pressure in annealing on the properties of niobium and its alloys See Entry 63333

Kinking in the drawing of linear polyethylene See Entry 63351

Effect of sulfides and sulfide morphology on anisotropy of tensile ductility and toughness of hot-rolled C-Mn steels See Entry 63354

Effect of diffusion welding thermal cycle on the strength of alloy VT20 See Entry 63359

Mechanical behaviour of isotactic polypropylene subjected to various strain histories in uniaxial extension See Entry 63363

Evaluation of creep crack growth criteria for IN-100 at elevated temperature See Entry 63375

Fracture control and its application within the Agency's programmes [space vehicles] See Entry 63376

Influence of strain ageing of martensite by hydroextrusion on the fine structure and surface relief in ductile fracture of 30KhGSN2A steel See Entry 63377

Influence of high-temperature thermomechanical treatment on delayed fracture of hardened construction steel See Entry 63378

Investigation of the energy dissipated internally during fatigue of metals See Entry 63379

Indentation-induced cracks in hot-pressed Si_3N_4 See Entry 63380

Comparison of the impact strength of 10GN2MFA and 15Kh2NMFA steels with the similarity of local failure taken into account See Entry 63381

Dependence of critical temperatures of brittleness on the condition of operational fractures See Entry 63382

Parameter evaluations for polymer durabilities versus time See Entry 63383

Correlation of hardness and microstructure in unoriented lamellar polyethylene. II. Study of elastic modulus See Entry 63384

Crack arrest in thick section steel plate See Entry 63385

Indentation fracture transitions in polymethylmethacrylate See Entry 63386

A fracture criterion for edge-bonded bimaterial bodies See Entry 63387

Micromechanical predictions of crack initiation, propagation and crack growth resistance in boron/aluminum composites See Entry 63388

Notched unidirectional boron/aluminum: effect of matrix properties See Entry 63389

Energy absorption in composite tubes See Entry 63390

Tensile fracture of evaporated Au films. IV See Entry 63391

Variation of dislocation density during fatigue process of low carbon steel See Entry 63392

Fracture of alumina ceramics by application of internal pressure in thin-walled tube under hydrostatic pressure See Entry 63393

Fatigue strength under intermittent strain cycling at elevated temperatures (engineering life prediction) See Entry 63394

Mechanical properties and fatigue strength of steel protected from tuftiridizing by inorganic coating See Entry 63395

Influence of mean stress on coaxing effect of annealed 0.5% C steel under plane bending fatigue See Entry 63396

Fatigue of concrete under varying repeated load See Entry 63397

Effects of stress ratio and microstructure on near-threshold fatigue crack propagation in high-strength low alloy steel See Entry 63398

Effect of stress frequency on fatigue crack propagation rate in titanium See Entry 63399

Microstructure and tensile ductility in a β heat treated titanium alloy See Entry 63400

Roughness-induced crack closure: an explanation for microstructurally sensitive fatigue crack growth See Entry 63401

High temperature low cycle fatigue of IN 738 and application of strain range partitioning See Entry 63402

Improvement in lower temperature mechanical properties of 0.40 pct C-Nr-Cr-Mo ultrahigh strength steel with the second phase lower bainite See Entry 63403

Influence of annealing temperature on the character of fracture of 4KhMFSNB cast die steel See Entry 63404

Effect of heat treatment on the fatigue strength of steel 50KhFA and alloy 40KhNMVTYu See Entry 63405

Effect of structure on the ductile-brittle transition temperature of molybdenum alloy TsM-6 See Entry 63406

Effect of cyclic plastic bending on the proneness of steel St3Sp to brittle fracture See Entry 63407

Microhardness of nonmetallic inclusions at high temperature See Entry 63408

Effect of the test temperature on the microstructure of fractures in gray cast iron See Entry 63409

Effect of the temperature on crack nucleation in impurities upon deformation of steel 08T See Entry 63410

Failure mechanism for alloy KhN67VM under the action of a copper-silver solder See Entry 63411

Reasons for the reduction in the fracture toughness of alloy KhN77TYuR-VD at room temperature See Entry 63412

Development of knowledge about the embrittlement of steels by hydrogen. I. See Entry 63413

Tenacity, toughness, ductility of mild steel sheet in longitudinal and short transverse direction See Entry 63414

Influence of molecular weight on the fracture of poly(methyl methacrylate) (PMMA) See Entry 63415

Is it possible to avoid thermal embrittlement in ribbon-shaped glassy metals? See Entry 63416

Mechanical properties of ageing of non-magnetic austenitic steels at low temperatures See Entry 63417

Effect of retained austenite on the contact fatigue strength of steel in relation to the phase diagram See Entry 63418

Overload induced crack growth rate attenuation behavior in aluminum alloys See Entry 63419

Mechanism of influence of certain alloying elements on the hydrogen embrittlement of iron See Entry 63420

Near-threshold growth of short fatigue cracks See Entry 63421

Statistical rules of fatigue crack development See Entry 63422

Intergranular zinc embrittlement and its inhibition by phosphorus in 55 pct Al-Zn-coated sheet steel See Entry 63453

Effect of high-temperature vacuum annealing time on the structure and properties of titanium alloys See Entry 63457

Effect of annealing on the structure and properties of molybdenum coatings on steel Kh12M See Entry 63458

Effect of vibroabrasive treatment on the fatigue strength of high-alloy steels See Entry 63460

Fatigue strength of steel 45 with electrolytic iron coating, carbon nitrided with HF heating See Entry 63461

Fracture of metals under the action of hydrogen-containing media See Entry 63466

Question of the safe boundaries of use of 12 MKh steel at increased temperatures and hydrogen pressures See Entry 63467

Effect of specimen width on impact strength and location of brittleness temperature of St3ps steel See Entry 63475

62.20P Tribology

(see also 81.40P Friction, lubrication and wear)

62021 Wear resistance of friction elements working in oil. V.S.Fantalov, V.M.Zhuchkov, E.G.Yudin. *Izv. VUZ Mashinost.* (USSR), no.12, p.59-62 (1982). In Russian. The general form of the relationships between the wear of metal-ceramic discs, working in oil and paired with steel discs, is investigated as a function of parameters of the slipping process, using postulates from the molecular-mechanical theory of friction. Values of unknown coefficients, entering the equations derived, have been found using the results of experimental investigations, for a wide range of parameter changes in the disc slipping process. The dependence obtained can be applied to estimating the lifetime of units working in oil under friction. The metal-ceramic discs described are used in transmissions of transport machines. (2 refs.) Z.F.V.

62022 A new model for the erosion of metals at normal incidence. G.Sundararajan, P.G.Shewmon (Dept. of Metall. Engng., Ohio State Univ., Columbus, OH, USA). *Wear* (Switzerland), vol.84, no.2, p.237-58 (15 Jan. 1983). A new theoretical model is proposed for the erosion of metals by particles at normal incidence. The model employs a criterion of critical plastic strain to determine when the material will be removed. This critical plastic strain is defined as the strain at which the deformation in the target localizes and hence results in the lip formation. It is shown that, under typical erosion conditions, the 'localization' model is more appropriate than the 'fatigue' models. Finally, it is demonstrated that the new model predicts quite well all the essential features of the normal impact erosion process. (34 refs.)

Electrodeposition of tantalum carbide coatings from molten salts See Entry 62290

Analysis of the stressed state of the forward slip zone in the seat of deformation of a powder being rolled See Entry 63191

Some studies in the displacements of powder material during compaction See Entry 63203

Effect of HTTT on the properties of alloy steel castings See Entry 63323

The effects of molecular weight and cooling rate on fine structure, stress-strain behavior and wear of polytetrafluoroethylene See Entry 63374

Influence of ϵ -martensite on the friction and wear of high-manganese alloys See Entry 63423

Particle collisions in the vicinity of an eroding surface See Entry 63424

Optimizing the carbon and manganese concentrations in wear-resistant chromium cast irons See Entry 63425

Influence of structure on the wear resistance of alloys See Entry 63426

The determination of the coefficient of dynamic friction of organic powder compacts on steel See Entry 63427

Nitriding kinetics and wear resistance of titanium alloys See Entry 63428

Thermally stressed condition occurring in the surface layers of flat parts during friction hardening See Entry 63429

Influence of production media on the physicomechanical and electrochemical properties of steels See Entry 63430

Sliding friction behaviour of polymer-polymer material combinations See Entry 63431

Residual stresses and sliding wear See Entry 63432

An analysis of the localization of deformation and weight loss during single-particle normal impact See Entry 63433

Wear kinetics of a two-phase boride layer See Entry 63459

62.30 MECHANICAL AND ELASTIC WAVES

(see also 03.40K Mathematical aspects)

62023 Elastic wave propagation in solids in relation to acoustic emission. H.F.Pollard (School of Phys., Univ. of New South Wales, Kensington, NSW, Australia). *Met. Forum* (Australia), vol.5, no.3, p.158-66 (Winter 1982). Three-dimensional wave propagation in large solids, both isotropic and anisotropic, are discussed, together with the effects produced by surfaces and the formation of waveguide modes in finite solids. Some causes of wave energy loss are briefly treated, and a final section dealing with the problem of acoustic emission source identification is included. (12 refs.)

62024 Brewster reflections of elastic waves in hexagonal crystals. V.N.Lyubimov, V.I.Ai'shits (L.Ya. Karov Sci.-Res. Physicochem. Inst., Acad. of Sci., USSR). *Sov. Phys.-Crystallogr.* (USA), vol.27, no.5, p.512-16 (Sept.-Oct. 1982). Translation of: *Kristallografiya* (USSR), vol.27, no.5, p.851-8 (Sept.-Oct. 1982). [received: April 1983]

The authors describe two types of Brewster reflection of elastic waves in hexagonal crystals. They discuss the case in which the surface is parallel to the hexad symmetry axis and the plane of incidence is rotated through a small angle α relative to the plane of transverse isotropy. They establish the conditions which must be obeyed by the elastic constants if these reflections are to arise. The first type of Brewster reflections can arise if $\alpha=0$ (analogous reflections occur in isotropic bodies); when $\alpha=0$ there can be two such reflections, but when $\alpha \neq 0$ either both of them or only one of them (accord-

ing to the values of the elastic constants of the crystal) may split into two different Brewster reflections. The reflections existing when $\alpha=0$ may be isolated, but when $\alpha \neq 0$ they may be converted to leaky (or counter-leaky) waves. The second type of Brewster reflections arises from the transverse body wave which is propagated along the surface when $\alpha=0$, satisfying the boundary conditions. When $\alpha \neq 0$ this wave can give rise to two different Brewster reflections which have no analogue in an isotropic body. The maximum number of Brewster reflections of both types is six when $\alpha \neq 0$. A case is also possible in which there is no Brewster reflection either in the plane of transverse isotropy ($\alpha=0$) or in its vicinity ($\alpha \neq 0$). (13 refs.)

62025 Irreversible double refraction of elastic waves in crystals with magnetic structure and spatial dispersion. V.N.Belyi (Inst. of Phys., Acad. of Sci., Belorussian SSR).

Sov. Phys.-Crystallogr. (USA), vol.27, no.5, p.516-18 (Sept.-Oct. 1982). Translation of: *Kristallografiya (USSR)*, vol.27, no.5, p.859-62 (Sept.-Oct. 1982). [received: April 1983]

The author generalizes the coupling equation of the linear theory of elasticity for crystals with magnetic structure and spatial dispersion. He shows that in such media there is irreversible double refraction, consisting in a difference between the velocities of propagation of elastic waves for opposite wave-normal directions. He discusses the reflection of elastic shear waves from a plane-parallel layer. He shows that the polarization characteristics of the reflected wave depend on the Faraday rotation of the plane of polarization and the irreversibility parameter. (9 refs.)

Lattice dynamics of FCC Cu See Entry 62046

62.40 ANELASTICITY, INTERNAL FRICTION, AND DAMPING

(see also 81.40J Elasticity and anelasticity)

62026 Hydrogen relaxation in lutetium. P.Vajda, J.N.Daou (CNRS, Univ. de Paris-Sud, Orsay, France), P.Moser.

J. Phys. (France), vol.44, no.4, p.543-51 (April 1983).

The internal friction and the dynamic modulus have been measured between 4.2 and 470K in the system α -LuH(D)_x, with $x=0$ to 0.2. In well annealed specimens an (H)-peak is observed at 215-225K, which has a linearly x-dependent amplitude and exhibits an isotope effect on its activation energy and relaxation time. It is attributed to a Snoek-like relaxation of H-H pairs reorienting in the Lu-lattice. The isotope effect is interpreted in a model of tunnelling from different excited levels for LuH_x and LuD_x. Deformation introduces a (d-H)-peak at 250-260K in H(D)-containing samples only, also exhibiting an isotope effect; it is attributed to a Snoek-Koster type relaxation of H(D) trapped on dislocations. Two (d_{1,2})-peaks at 160 and 215K, which occur in the pure metal only, and a (d)-peak centred near 350K in all deformed specimens are ascribed to geometrical kink migration and to double-kink generation on a screw dislocation network, respectively. (45 refs.)

Use of nonlinear viscoelastic materials in the polarization-optical method See Entry 61465

Effect of the filler on relaxational transitions in butadiene-methylstyrene copolymer See Entry 61829

Friction and source hardening in irradiated mild steel See Entry 61984

The low-temperature flow stress of europium-doped sodium chloride See Entry 62016

Some remarks on the carbon atoms pairs migrational relation in α Fe-C See Entry 62181

Effects of mechanical drawing treatment on the characteristics of internal friction and thermally stimulated current on low density polyethylene See Entry 63308

The influence of fillers of different activity on the relaxation behaviour of elastomers See Entry 63337

Internal friction study of AISI 410 stainless steel See Entry 63338

Hydrogen-related internal friction peak in the A15 compound Nb₃Sn See Entry 63339

On the Portevin-Le Chatelier effect due to Snoek strain aging in the niobium oxygen system See Entry 63353

62.50 HIGH-PRESSURE AND SHOCK-WAVE EFFECTS IN SOLIDS

62027 Random walk of dislocations following a high-velocity impact. B.J.West, M.F.Shlesinger (Center for Studies of Nonlinear Dynamics, La Jolla Inst., La Jolla, CA, USA).

J. Stat. Phys. (USA), vol.30, no.2, p.527-35 (Feb. 1983). (Proceedings of a Symposium on Random Walks and Their Application to the Physical and Biological Sciences, Gaithersburg, MD, USA, 28 June-1 July 1982).

The permanent distortion of an elastic material due to a shock wave generated by a high-velocity impact is modeled by a random walk of dislocations. The dislocation movement is inhibited by a spatial and energetic distribution of activation barriers. The dislocations also experience a radially outward stress bias from the point of impact. The experimentally observed scaling of the total integrated momentum as well as the scaling with time of the penetration distance and strength of the shock wave are obtained in this model. (11 refs.)

62028 Effect of initial conditions on the evolution of a laser-generated shock wave. F.Cottet, J.P.Romain (Lab. d'Energetique et Detonique, ENSMA, Poitiers, France).

J. Phys. Lett. (France), vol.44, no.7, p.L235-40 (1 April 1983). In French. The evolution of a high amplitude laser-generated shock in a solid target is described by the use of a hydrodynamic model. In comparison with a previous model, this one takes into account the front face target propagation due to the ablation pressure effect. This model is also used to study the initial pressure profile effect on the shock wave decay. (10 refs.)

pVT data for liquid and solid hexamethyldisilane up to 3000 bar See Entry 62053

Effect of pressure on the thermal hysteresis of a first-order transition See Entry 62084

Structural transformations in solid nitrogen at high pressure See Entry 62092

Lithium, compression and high-pressure structure See Entry 62094

Electric resistance of Manganin to 2 GPa and 80K See Entry 62390

Metallization of mercury chalcogenides under ultrahigh pressures See Entry 62461

Effect of pressure on Raman spectra of solid bromine See Entry 62960

Phase equilibrium in the Ti-Se system at high pressures See Entry 63269

Characteristics of plastic deformation of silicon iron single crystals under hydrostatic pressures See Entry 63343

62.60 ACOUSTIC PROPERTIES OF LIQUIDS

(see also 62.80 Ultrasonic relaxation; for sound propagation, see 43.; for second sound in quantum fluids, see 67.40, 67.50 and 67.60)

62029 Sound speeds and isentropic compressibilities of 1,1,2,2-tetrachloroethane with alcohols. N.V.Choudary, J.C.Mouli, P.R.Naidu (Chem. Labs., Sri Venkateswara Univ., Tirupati, India).

Acoust. Lett. (GB), vol.6, no.4, p.56-61 (Oct. 1982). [received: March 1983]

New experimental data for sound velocity in binary mixtures of 1,1,2,2-tetrachloroethane with 1-propanol, 1-butanol, 1-pentanol, 1-hexanol, heptanol and 1-octanol were collected at 303.15K. The results have been analysed in terms of free-length theory and collision factor theory. The analyses showed that the former theory gives a better estimate of sound speed in the six mixtures than the latter. The sound speed data were also used to compute isentropic compressibilities. The deviation in isentropic compressibility suggests that the effects of interactions between like and unlike molecules balance each other to varying degrees in the mixtures. (17 refs.)

62030 Dynamic features of the aminopolycarboxylate complexes in aqueous solutions studied by the ultrasonic absorption method. Y.Funaki.

J. Sci. Hiroshima Univ. A (Japan), vol.46, no.2, p.253-66 (Jan. 1983).

Ultrasonic absorption was measured in aqueous solutions of ethylenediaminetetraacetate (EDTA) and trans-1,2-cyclohexanediaminetetraacetate (CyDTA) complexes of various divalent and trivalent metal ions. Relaxation absorption was observed only for the labile complexes, i.e. Ca, Sr, Ba, Co(II), Zn, Cd, La, Ce and Nd complexes. From the pH and concentration dependence of the relaxation parameters, the absorption was ascribed to the equilibrium of pentadentate form=hexadentate form of the coordinated ligand. It was clarified that the rate-determining step of the formation of the hexadentate form is the loss of water from the central metal ion. The rate and the stability constants and the volume change of the reaction were obtained. The effects of the structure of ligand and the charge of metal ion on the above equilibrium were studied by comparing the results of divalent metal-CyDTA and lanthanide-EDTA systems with those of divalent metal-EDTA systems. (23 refs.)

62031 Pressure effects and ultrasonic attenuation in the binary liquid mixture 3-methylpentane and nitroethane near the critical point. E.A.Clerke, J.V.Sengers, R.A.Ferrell, J.K.Bhattacharjee (Dept. of Phys. & Astron., Univ. of Maryland, College Park, MD, USA).

Phys. Rev. A (USA), vol.27, no.4, p.2140-51 (April 1983).

Experiments are reported in which a critical mixture of 3-methylpentane plus nitroethane has been subjected to varying pressures. By varying the static pressure the authors have determined the dependence of the critical temperature on pressure with considerable accuracy. By sudden depressurization they have cooled the sample adiabatically leading to phase separation via spinodal decomposition; from these experiments they have determined the adiabatic thermal pressure coefficient near the critical point. By combining the data with the experimental density data of Greer and Hocken (1973) the authors are able to determine the asymptotic critical behaviour of the thermal-expansion coefficient and of the specific heat, consistent with two-scale-factor universality. They also obtain a value for the adiabatic coupling constant which appears in the dynamic scaling theory for the frequency dependence of the critical sound attenuation. The thermodynamic data appear to be in good agreement with the critical ultrasonic attenuation data obtained by Ishida and Harada (1980) for 3-methylpentane plus nitroethane. (46 refs.)

Rayleigh-Briouin scattering of transverse and longitudinal acoustic waves in a supercooled viscoelastic liquid See Entry 62928

62.65 ACOUSTIC PROPERTIES OF SOLIDS

(see also 62.80 Ultrasonic relaxation; for sound propagation, see 43.; for lattice dynamics and phonons, see 63.; for magnetoacoustic effects, see 72.55; for acoustoelectric effects, see 72.50; for acousto-optical effects, see 78.20H)

62032 Wave propagation in a solid propellant. C.Dumont (Lab. de Mecanique des Solides, Ecole Polytech., Palaiseau, France).

Rev. Acoust. (France), vol.15, no.63, p.242-5 (1982). In French.

With a comparative method using an FFT (fast Fourier transform), the 1-dimensional propagation of short pulses in propellants is studied. Two experimental techniques for both emission and reception are used to scan two frequency bands. Phase velocity and attenuation curves are shown for low and high frequencies in various conditions of temperature and confining pressure. The technique using piezoelectric transducers is the most convenient one. (8 refs.)

62033 Effect of the Bragg and deformation-potential forces on ultrasonic propagation in metals. G.Feyder (Dept. of Phys., Purdue Univ., West Lafayette, IN, USA), E.Kartheuser, L.R.Ram Mohan, S.Rodriguez.

Phys. Rev. B (USA), vol.27, no.6, p.3213-20 (15 March 1983).

A study is given of the effect of the Bragg and deformation reaction forces on acoustic propagation in simple metals. The authors show that no significant alterations of the results obtained within the free-electron model are expected and that no change occurs in the position and strength of the helicon-phonon interaction. (11 refs.)

62034 Photoacoustic spectra of semiconductor compounds Dy₂S₃ and Nd₂S₃. G.A.Kurbatov, K.K.Sidorin, N.A.Chernukha.

Sov. Phys.-Semicond. (USA), vol.16, no.10, p.1221-2 (Oct. 1982). Translation of: *Fiz. & Tekh. Poluprovodn. (USSR)*, vol.16, no.10, p.1894-6 (Oct. 1982).

[received: April 1983] Reports the results of an investigation of the absorption and reflection spectra of Dy₂S₃ and Nd₂S₃ powders carried out at room temperature by the photoacoustic spectroscopy method. (8 refs.)

Influence of ultrasound on the concentration of point defects in KBr crystals See Entry 61911

Optimization of the computation of elastic constants from the measurements of ultrasonic velocities See Entry 62009

Elastic wave propagation in solids in relation to acoustic emission See Entry 62023

Sound emission by bubbles See Entry 62042

Phase diagram and transition properties of condensed ammonia to 10 kbar See Entry 62066

- Acoustically induced plastic deformation of conical microcrystals on copper surfaces See Entry 62227
- Energy and momentum accommodation coefficients on platinum and silver See Entry 62248
- Phase transition in $\text{AgPbSb}_3\text{S}_6$ crystals [superionic] See Entry 62462
- Generation of static dipole domains in dielectrics See Entry 62890

62.80 ULTRASONIC RELAXATION

(see also 74.30G Ultrasonic attenuation in superconductors, 43.35 Ultrasonics)

- Dynamic features of the aminopolycarboxylate complexes in aqueous solutions studied by the ultrasonic absorption method See Entry 62030

62.90 OTHER TOPICS IN MECHANICAL AND ACOUSTICAL PROPERTIES OF CONDENSED MATTER

- 62035 Topological limitations of effective-medium approximations in fluid-solid systems having two longitudinal-acoustic modes. P.N.Sea, D.L.Johnson (Schlumberger-Doll Res. Center, Ridgefield, CT, USA). *Phys. Rev. B (USA)*, vol.27, no.6, p.3133-7 (15 March 1983). Considers the acoustic properties of two-component composites. The authors show that in order for the system to have two distinct nondispersive longitudinal modes, one component must be a fluid, the other must be a solid, and each component must be part of an infinite, percolating cluster. Although the Biot theory is able to describe these modes, effective-medium theories, within the single-site approximation, cannot predict them precisely because some or all of the constituents are taken as unconnected inclusions. In the special case in which the solid constituent occurs as isolated particles within the fluid (a suspension) there is only one longitudinal mode and the Biot theory and the average- t -matrix approximation are in essential agreement with each other and with experiments in predicting its speed. (17 refs.)

63.00 LATTICE DYNAMICS AND CRYSTAL STATISTICS

(see also 05.50 Lattice theory, 65. Thermal properties, 66.70 Thermal conduction, 68.30 Dynamics of surface and interface vibrations, 78.30 Infrared and Raman spectra)

63.10 GENERAL THEORY

- 62036 Propagation of acoustic and optical solitons in nonlinear diatomic chains. St.Pnevmatikos, M.Refnissenet (Lab. d'Optique du Réseau Cristallin, Univ. de Dijon, Dijon, France), N.Flytzanis. *J. Phys. C (GB)*, vol.16, no.11, p.L305-10 (20 April 1983). The authors present an analytic and numerical study of a nonlinear diatomic chain with a quartic interaction potential between nearest neighbours. In the continuum approximation using scaling arguments and a decoupling ansatz for the motion of the two different masses they find 'acoustic' pulse type excitations which obey a modified Boussinesq equation and 'optical' envelope type solitary solutions of a nonlinear Schrödinger equation. Computer simulations on their propagation and interaction show these excitations to be long lived. (16 refs.)

63.20 PHONONS AND VIBRATIONS IN CRYSTAL LATTICES

- 62037 Comparative reinvestigation of the interaction of phonons with Wannier and Frenkel excitations in crystalline solids. J.Singh (Res. School of Chem., Australian Nat. Univ., Canberra, Australia). *Chem. Phys. (Netherlands)*, vol.75, no.3, p.371-7 (15 March 1983). The interaction of lattice vibrations with excitons in inorganic and organic semiconductors/insulators is reinvestigated. These results expose the comparative nature of exciton-phonon interaction in the two types of solids and produce two new coupling functions useful for Frenkel exciton-phonon interaction. (17 refs.)
- 62038 Lattice instability in one-dimensional molecular-type crystals. D.Feinberg, J.Ranninger (Groupe des Transitions de Phases, CNRS, Grenoble, France). *J. Phys. C (GB)*, vol.16, no.10, p.1875-85 (10 April 1983). The authors study crystalline systems which as far as the electrons are concerned behave like composites of diatomic molecules loosely coupled together. The electrons are in molecular states which weakly overlap between neighbouring molecular sites. They examine a linear chain of such molecules which are oriented orthogonally to the chain direction. They show that such a system is unstable under a deformation consisting in squeezing the diatomic molecules orthogonally to the chain direction in some periodic fashion along the chain direction. (10 refs.)
- 62039 Analysis of translation-rotation coupling in an orientationally disordered ionic crystal. R.M.Lynden-Bell (Dept. of Theoretical Chem., Univ. of Cambridge, Cambridge, England), I.R.McDonald, M.L.Klein. *Mol. Phys. (GB)*, vol.48, no.5, p.1093-117 (10 April 1983). Molecular dynamics calculations are used to study the coupling between translations and rotations in a model appropriate to solid sodium cyanide in its orientationally disordered high temperature cubic phase. Static properties are analysed via the formalism of Michel and Naudts (1978) through the introduction of a wavevector dependent parameter λ which measures the extent of translation-rotation coupling. The dynamics of the crystal are shown to be described accurately by a Mori-type theory, similar to that adopted by de Raedt and Michel (1980) in which collective time correlation functions are expressed in terms of λ and certain other static averages. The same approach is used to discuss the crystal dynamics in the region of long wavelength, where the molecular dynamics calculations yield no direct information. (35 refs.)

- 62040 Spin-phonon interactions in the Ising model with a transverse field. J.M.Wesselinowa (Dept. of Phys., Univ. of Sofia, Sofia, Bulgaria). *Phys. Status Solidi b (Germany)*, vol.116, no.1, p.71-82 (1 March 1983). A Green function technique is used to study the effects of spin-phonon interactions in the Ising model with a transverse field. The renormalized energy of the coupled mode, the damping of the spin waves, and the phonon damping are evaluated. The transverse dynamic structure factor exhibits three peaks due to the coupling of the transverse soft-mode and the acoustic phonon mode. The width of the central peak is proportional to the phonon damping. (30 refs.)
- 62041 Effect of three-body forces on thermophysical and anharmonic properties of rare gas solid mixtures. R.K.Singh, D.K.Neb, S.P.Sanyal (Dept. of Postgraduate Studies & Res. in Phys., Univ. of Jabalpur, Jabalpur, India). *Phys. Status Solidi b (Germany)*, vol.116, no.1, p.289-97 (1 March 1983). The effects of three-body forces on the thermophysical and anharmonic properties of rare gas solid (RGS) mixtures are investigated using the virtual crystal approximation and an interatomic potential consisting of the long-range van der Waals dipole dipole interaction and three-body forces, the short-range Born-Mayer type overlap repulsion, and the zero-point energy. The agreement between experimental and the authors' theoretical results of various properties of the host RGS is, generally, better than obtained by most earlier workers. The results on RGS mixtures follow systematic trends identical to those of diatomic solid mixtures but reliance in them will be deferred until the report of the corresponding measured data. (45 refs.)
- 62042 Sound emission by bubbles. A.V.Vershinin, A.L.Sukstanskii. *Ukr. Fiz. Zh. (USSR)*, vol.28, no.3, p.418-22 (March 1983). In Russian. A study has been made for interaction of a stationary-moving bubble with elastic lattice vibration (phonons). The latter are estimated for emission intensity and an extra slowing-down force acting upon the bubble and arising due to the interaction is discussed. The force is shown to be maximum at the bubble rate equal to the sound velocity. Sound emission by the bubble vibrating under the effect of an external magnetic field is considered. Sound intensity values are estimated for a case of solitary bubble vibrations and bubble lattice vibrations. A diagram of the generated sound directness is plotted for the case of lattice vibrations. (4 refs.)
- Tricopper. A fluxional molecule See Entry 60728
- Hindered internal rotations in Van der Waals molecules and molecular crystals See Entry 60885
- Spin-lattice relaxation of Cr^{+} in ZnS See Entry 62807
- Vibrational spectroscopy of solid state molecular dimers See Entry 62954
- Vibrational and electronic spectra of $\text{Na}[\text{UO}_2(\text{CH}_3\text{COO})_3]$ See Entry 62992
- Raman scattering in K_2SO_4 at high temperatures See Entry 62997
- Interference effects in resonant Raman scattering by S_2 molecules in crystalline KI See Entry 63001
- Exciton-phonon interaction in crystalline and vitreous SiO_2 See Entry 63019
- Tunnelling motion of dipolar impurities in alkali halides: the $\text{KI}:\text{NO}_2^-$ system [IR spectra] See Entry 63024
- Pure electronic, vibronic, and two-particle surface excitons on the anthracene crystal. I. General theoretical basis, experimental study, and analysis of the (0,0) region See Entry 63033

63.20D Phonon states and bands, normal modes, and phonon dispersion

- 62043 Phonon spectrum and Debye Waller-factors of niobium carbide (NbC). R.B.Yadav (Dept. of Phys., S.D.P.G. Coll., Muzaffarnagar, India). *Physica B & C (Netherlands)*, vol.115 B+C, no.2, p.233-6 (Jan. 1983). A consistent and comprehensive approach has been adopted to derive the framework of a deformation dipole model (DDM) which is capable of explaining successfully the lattice dynamics of ionic crystals. The application of this model to the case of niobium carbide crystal has reproduced fairly well the phonon dispersion and Debye-Waller factors. (9 refs.)
- 62044 Special features of vibrational properties of mixed crystals with TiSe structure. N.M.Gasany, A.S.Ragimov (Dept. of Phys., Azerbaijan State Univ., Baku, Azerbaijan SSR), A.F.Goncharov, N.N.Melnik, E.A.Vinogradov. *Physica B & C (Netherlands)*, vol.115 B+C, no.3, p.381-94 (March 1983). Polarized IR reflection and Raman scattering spectra have been studied in solid solutions based on TiSe structural type chain single crystals ($\text{TiS}_{1-x}\text{Se}_x$, $\text{TiGa}_{1-x}\text{Te}_x$ and $\text{TiIn}(\text{Se}_{1-x}\text{Te}_x)_2$). The results of processing the IR spectra of mixed crystals are analyzed from the standpoint of a random-element-isodisplacements (REI) model extended to the case of many oscillators. In the case of the formation of mixed cells in solid solutions, respective modes have been observed in IR reflection and Raman scattering spectra. (32 refs.)
- 62045 Lattice dynamics of α -quartz including the effect of the width of the atomic electron distribution. K.Iishi (Dept. of Mineralogical Sci. & Geology, Yamaguchi Univ., Yamaguchi, Japan), M.Miura, Y.Shiro, H.Murata. *Phys. & Chem. Miner. (Germany)*, vol.9, no.2, p.61-6 (1983). On the basis of the polarizable-ion model (PIM) the effect of the width of the atomic electron distribution on the lattice dynamics of α -quartz was taken into account using the Birman method. The frequencies of optical modes, elastic constants and piezoelectric constants were reproduced using the parameters of this model (an effective charge z , a width parameter w , an electronic polarizability α , and force constants). The width parameter of the oxygen atom was found to be about 0.59 Å, and the effective charge of the silicon atom 1.42 electron charges. (24 refs.)
- 62046 Lattice dynamics of FCC Ca. C.Stassis, J.Zaretsky, D.K.Misemer, H.L.Skriver, B.N.Harmon (Dept. of Phys., Iowa State Univ., Ames, IA, USA), R.M.Nicklow. *Phys. Rev. B (USA)*, vol.27, no.6, p.3303-7 (15 March 1983). A large single crystal of FCC Ca was grown and was used to study the lattice dynamics of this divalent metal by coherent inelastic neutron scattering. The phonon dispersion curves were measured, at room temperature, along the $\{000\}$, $\{\bar{1}\bar{1}0\}$, $\{\bar{1}\bar{1}\bar{1}\}$, and $\{0\bar{1}\bar{1}\}$ symmetry directions. The dispersion curves bear a striking resemblance to those of FCC Yb, which is also a divalent metal with an electronic band structure similar to that of Ca. In particular, the shear moduli c_{44} and $(c_{11}-c_{12})/2$ differ by a factor of 3.4, which implies that FCC Ca (like FCC Yb) is very anisotropic with regard to the propagation of elastic waves. The frequencies of the $T_1[\bar{1}\bar{1}0]$ branch for $\bar{1}$ between approximately 0.5 and 0.8 are slightly above the velocity-of-sound line determined from the low-frequency measurements. Since a similar effect has been observed in FCC Yb, it is natural to assume that the anomalous dispersion exhibited by the $T_1[\bar{1}\bar{1}0]$ branches of these metals is due to an electronic effect. To provide further support for this assumption the authors have performed a band theoretical calculation of the generalized susceptibility $\chi(\bar{q})$

of FCC Ca. The results suggest that, for ξ between approximately 0.6 and 0.8, there is a relative decrease in the electronic screening of the vibrational motion of the nuclei, which may account for the positive dispersion exhibited by the $T_1[\xi\theta]$ branch in this range of ξ values. The data were used to evaluate the elastic constants, the phonon density of states, and the lattice specific heat of FCC Ca. (22 refs.)

- Structure of dislocation cores in the silicon crystal See Entry 61914
Elastic properties of CsCN See Entry 62010
Quadrupolar coupling and structural instability in $\text{PrAg}_{1-x}\text{Cu}_x$ See Entry 62383
Refractive index in epitaxial $\text{Pb}_{1-x}\text{Sn}_x\text{Te}$ films See Entry 62919
Vibrational spectroscopy of solid state molecular dimers See Entry 62954

63.20K Phonon-electron interactions

- The electron-phonon interaction spectrum in beryllium See Entry 62349
Carrier capture by multiphonon emission at extrinsic deep centers induced by self-trapping in GaAs See Entry 62364
Thermo-EMF in bounded semiconductors under conditions of electron drag by phonons See Entry 62439
Resonance interband Raman scattering of light in semiconductors See Entry 63002
Pure electronic, vibronic, and two-particle surface excitons on the anthracene crystal. II. Experimental study and analysis of the (0,1) region See Entry 63012

63.20M Phonon-defect interactions

- The effect of phonon-grain boundary scattering, doping and alloying on the lattice thermal conductivity of lead telluride See Entry 62191
Thermal conductivity of germanium containing dislocations at low temperatures See Entry 62193

63.20P Localized modes

- 62047 Localized mode energies and hydrogen potential in refractory metals. D.Richter (Inst. fur Festkörperforschung, KFA Jülich, Jülich, Germany). *J. Less-Common Met. (Switzerland)*, vol.89, no.2, p.293-306 (Feb. 1983). (International Symposium on the Properties and Applications of Metal Hydrides, Toba, Japan, 30 May-4 June 1982). Recent experimental results on local vibrations of hydrogen atoms in niobium and tantalum are reviewed. First, high resolution measurements of pure Nb-H(D,T) and Ta-H(D) systems where well-defined second harmonics have been resolved are examined and interpreted in terms of a weakly anharmonic potential common to all hydrogen isotopes. Secondly, the first observations by spectroscopic methods of the trapping of hydrogen atoms in niobium are surveyed. The measurements revealed detailed microscopic information, e.g. on the symmetry of the trapping sites and their degree of disturbance. Interstitial oxygen and nitrogen impurities as well as substitutional titanium were found to be strong traps which suppressed the precipitation of hydride phases at low temperature, whereas in the case of vanadium the easily recognizable vibrational pattern of ordered hydride phases were observed. (27 refs.)
Local modes: their relaxation, polarization, and stereoselective excitation by lasers See Entry 60691
Interference effects in resonant Raman scattering by S_2^- molecules in crystalline KI See Entry 63001

63.70 STATISTICAL MECHANICS OF LATTICE VIBRATIONS

(see also 65. Thermal properties of condensed matter, 66.70 Thermal conduction)

- 62048 A quantitative systematization of hydrogen-induced changes in Debye temperatures of metals. I.Jacob (Dept. of Nuclear Engng., Ben Gurion Univ. of the Negev, Beer-Sheva, Israel). *J. Less-Common Met. (Switzerland)*, vol.89, no.2, p.309-16 (Feb. 1983). (International Symposium on the Properties and Applications of Metal Hydrides, Toba, Japan, 30 May-4 June 1982). Nuclear resonance scattering of γ -rays has recently been used to obtain information on the Debye temperatures θ_D of metal hydrides. In particular the contribution of nickel to the θ_D of Mg_2Ni , LaNi_2 and their hydrides was estimated. It was assumed that the different behaviour of θ_D for nickel in the two cases (i.e. an increase upon hydrogenation in Mg_2Ni and no change in LaNi_2) could be related to the different stabilities of the two hydrides. Consequently an empirical relationship connecting the Debye temperatures θ_M and θ_H of a metal and its hydride respectively with the heat ΔH_f of formation of the hydride was derived. It appeared, however, that two ambiguous calculating procedures were used to derive the θ_H values. One of these procedures was used consistently in the present work for all the metal-hydrogen systems and the original phenomenological rule was changed accordingly. The qualitative theoretical considerations preceding the derivation of the empirical relation are briefly presented. Some experimental data are discussed in terms of the proposed empirical rule. In particular, the obvious exceptions associated with the group IVa metal hydrides TiH_x and ZrH_x are attributed to the Jahn-Teller effect in these systems. (40 refs.)
62049 New model for thermal effects in photoelectron spectroscopy. H.Martensson (Dept. of Phys., Chalmers Univ. of Technol., Goteborg, Sweden). *Phys. Rev. B (USA)*, vol.27, no.7, p.4492-4 (1 April 1983). A new model is proposed to explain recently observed anomalous Debye-Waller factors in photoelectron spectra from Cu (110). The d -bands are described by a tight-binding formalism, and their response to thermal vibrations is found to be strongly dependent of k -space location. (6 refs.)
62050 The Debye-Waller factor in quasi-one-dimensional and quasi-two-dimensional crystals. M.A.Krivoglaz, A.V.Min'kov (Inst. of Metal Phys., Acad. of Sci., Ukrainian SSR). *Sov. Phys.-Crystallogr. (USA)*, vol.27, no.5, p.503-6 (Sept.-Oct. 1982). Translation of: *Kristallografiya (USSR)*, vol.27, no.5, p.837-42 (Sept.-Oct. 1982). [received: April 1983]
The authors make an analytical calculation of the Debye-Waller factor $\exp(-2M_2)$ in chain and layer crystals. They take account of the spatial dispersion, which influences the vibration spectra in these crystals. They investigate

the dependence of $2M_2$ and of the corresponding effective Debye temperatures θ on the temperature, the direction of the diffraction vector Q , and the parameters $\epsilon \ll 1$ characterizing the elastic anisotropy. They find that $2M_2$ depends markedly on the direction of Q . The linear temperature dependence of $2M_2$ extends into the region of low temperatures well below θ . At very low temperatures the effective Debye temperature strongly depends on T and becomes considerably higher than at high temperatures. (8 refs.)

- Critical voltage effect in Ni_3Fe and FeCo ordering alloys See Entry 61799
Effect of three-body forces on thermophysical and anharmonic properties of rare gas solid mixtures See Entry 62041
Phonon spectrum and Debye Waller-factors of niobium carbide (NbC) See Entry 62043
Lattice dynamics of α -quartz including the effect of the width of the atomic electron distribution See Entry 62045
The relationship between the Gruneisen and other thermodynamic parameters and intermolecular forces in polymers See Entry 62130
Thermal expansion coefficient of alkali metals See Entry 62136

63.75 STATISTICAL MECHANICS OF DISPLACIVE PHASE-TRANSITIONS

(for order-disorder and statistical mechanics of model systems, see 64.60; for crystallographic aspects of polymorphic and order-disorder transformations, see 61.50K)

- Spin-phonon interactions in the Ising model with a transverse field See Entry 62040

63.90 OTHER TOPICS IN LATTICE DYNAMICS AND CRYSTAL STATISTICS

- ^{87}Rb and ^{85}Rb NQR study of phase transitions in $\text{RbH}_2(\text{SeO}_3)_2$ See Entry 62829

64.00 EQUATIONS OF STATE, PHASE EQUILIBRIA, AND PHASE TRANSITIONS

(see also 82.60 Chemical thermodynamics)

64.10 GENERAL THEORY OF EQUATIONS OF STATE AND PHASE EQUILIBRIA

- 62051 Calculation and prediction of fluid phase equilibria from an equation of state. U.K.Deiters (Dept. of Chem., Univ. of Bochum, Bochum, Germany). *Fluid Phase Equilibria (Netherlands)*, vol.10, no.2-3, p.173-82 (March 1983). (Supercritical Fluids. Their Chemistry and Application, Cambridge, England, 13-15 Sept. 1982). Liquids or compressed gases consisting of light molecules show deviations from classical mechanics, which are caused by the discontinuity of energy levels. From the assumption that each molecule is confined to a cell with a size depending on the free volume, a quantum correction is derived which extends any van der Waals type equation of state to quantum gases. The correction is applied to a semiempirical equation of state developed by the author. The extended equation yields reasonable critical compressibility factors and gives a better representation of PVT data than the uncorrected equation. Furthermore high pressure phase equilibria in mixtures containing helium and hydrogen have been calculated. Again the agreement with experimental data is improved; the adjustable binary interaction parameters have values close to the Berthelot-Lorentz rules and are less temperature dependent. (11 refs.)
62052 Thermodynamic calculation of supercritical-fluid equilibria: New mixing rules for equations of state. K.W.Won (Process Methods & Data, Advanced Technol. Div., Fluor Engrs. Inc., Irvine, CA, USA). *Fluid Phase Equilibria (Netherlands)*, vol.10, no.2-3, p.191-210 (March 1983). (Supercritical Fluids. Their Chemistry and Application, Cambridge, England, 13-15 Sept. 1982). Simple cubic equations of state with conventional mixing rules have played an important role in the calculation of phase equilibria and other thermodynamic properties of non-polar fluid mixtures. In the application of supercritical fluids to separation processes, volumetric as well as phase equilibrium properties are very important for rational process design. Heyen (1980) proposed a cubic equation of state which shows better accuracy in the calculation of volumetric properties, compared to the Peng-Robinson equation of state. In order to apply his equation to polar mixtures, Heyen recently proposed a density-independent mixing rule, but this does not obey the universally-observed quadratic mixing rule of the second virial coefficient in the low-density limit. The paper proposes a new density-dependent mixing rule for the Heyen equation of state. The Heyen equation of state with the author's new mixing rule appears to calculate the phase equilibria and the volumetric properties of CO_2 -containing non-polar as well as polar mixtures with good accuracy. (23 refs.)
Effective spherical potentials for molecular fluid thermodynamics See Entry 61751
On equilibrium properties of the multivalent ionic systems See Entry 61754
Volume dependence of melting temperature at high pressure and its relation to a new dimensionless quantity See Entry 62064

64.30 EQUATIONS OF STATE OF SPECIFIC SUBSTANCES

(see also 65.70 Thermal expansion)

62053 *pvT* data for liquid and solid hexamethyldisilane up to 3000 bar. M.Briesse, A.Wurflinger (Inst. of Phys. Chem., Univ. of Bochum, Bochum, Germany).

High Temp.-High Pressures (GB), vol.14, no.3, p.323-6 (1982). (10th Plensee Seminar on 'Trends in Refractory Metals, Hardmetals, and Special Materials, and their Technology', Reutte, Austria, 1-5 June 1981).

pvT data have been determined for hexamethyldisilane in the temperature range 323-233K up to 3000 bar, including the volume changes accompanying the phase transitions. The volume changes allow the calculation of the corresponding enthalpy and entropy changes. The melting curve is described with the Simon equation. (17 refs.)

62054 Equation of state of polymer crystals: application to polyolefins. O.P.Pahuja, V.S.Nanda (Dept. of Phys. & Astrophys., Univ. of Delhi, Delhi, India).

J. Macromol. Sci. - Phys. (USA), vol.B22, no.1, p.43-51 (1983).

A quantum mechanical equation of state for anharmonic polymer crystals was developed and used earlier to explain the extensive P-V-T data for polyethylene. In this paper the authors have analyzed the corresponding data of polypropylene and poly(butene-1) in terms of the same theoretical expression. The trends shown by the various characteristic parameters for the three polyolefins are interpreted in terms of their structure. (13 refs.)

Reparameterization of the Becker-Kistiakowsky-Wilson equation of state for water-gel explosives See Entry 61515

Thermodynamics of supercritical steam+carbon dioxide mixtures See Entry 62074

Hydrogen at high pressures and temperatures See Entry 64363

64.60 GENERAL STUDIES OF PHASE TRANSITIONS

(for critical phenomena in quantum fluids, superconductors, magnetic materials and ferroelectrics, see 67., 74.40, 75.40 and 77.80 respectively)

62055 Kink and phase transition in three-dimensional system with double-well potential. Yang Zhen-qing, Chang Shu-ren (Dept. of Phys., Nan-kai Univ., Tientsin, China).

Commun. Theor. Phys. (China), vol.2, no.1, p.803-9 (1983).

The authors present a three-dimensional system in which kinks and phase transitions are treated at a unified level. As in the two-dimensional case, there are two sorts of kink which correspond to domain walls with 90° and 180° transition angles. But there are also two types of phase transition, one of which is displacive and the other is of order-disorder. (8 refs.)

62056 Microscopic surface tension and binary nucleation. C.Flageollet-Daniel, J.P.Garnier, P.Mirabel (Inst. de Chimie, Univ. Louis Pasteur, Strasbourg, France).

J. Chem. Phys. (USA), vol.78, no.5, p.2600-6 (1 March 1983).

Experimental results concerning the binary homogeneous nucleation from the vapor phase of water-alcohols mixtures are reexamined. It is shown that the large discrepancies between theory and experiment can be explained by the fact that, for those mixtures, the use of macroscopic surface tension values is not applicable to binary droplets. A lattice model is developed to describe a microscopic cluster. This allows the determination of the surface monolayer composition, and the calculation of the actual surface tension as a function of the cluster size. The introduction of this model in the classical theory of binary nucleation restores good agreement with the experimental results. (27 refs.)

62057 Kinetics of phase separation in binary fluids: nucleation near the critical point. J.S.Langer (Inst. for Theoretical Phys., Univ. of California, Santa Barbara, CA, USA).

Physica A (Netherlands), vol.118A, no.1-3, p.282 (March 1983). (Proceedings of the Conference on Nonlinear Fluid Behavior, Boulder, CO, USA, 7-11 June 1982).

Summary form only given, as follows. Recent interest in nucleation problem has been stimulated, at least in part, by a sharp disagreement between conventional droplet theories and observations of anomalously large supersaturations in binary fluids near their critical points. This problem apparently has been resolved by examining actual completion rates instead of focusing attention only on rates of droplet formation. Current calculations are in reasonable agreement with observed cloud points, but more detailed predictions of average sizes and numbers of droplets as functions of time after quench have not yet been checked by experiment. One outstanding theoretical problem is that of joining the early stage nucleation theory to the late stage theory of coarsening. An improved analysis of this transition will be necessary in order to make accurate predictions of the size distribution of droplets throughout the reaction. It will also be necessary to generalize the Lifshitz-Slyozov-Wagner theory of coarsening to account for finite volume fractions of the nucleating phase, especially if one wants to extend the theory to describe the relatively deep quenches achieved near the critical point. (10 refs.)

62058 Nucleation and growth of nonclassical droplets. D.W.Heermann, W.Klein (Dept. of Phys., Boston Univ., Boston, MA, USA).

Phys. Rev. Lett. (USA), vol.50, no.14, p.1062-5 (4 April 1983).

Nucleation and growth are studied in the metastable region of the Glauber-kinetic Ising model with medium-range interactions. Monte Carlo data indicate that the nucleating droplets are not in general compact but quickly become so during the initial phase of growth and then grow as compact droplets. This two-stage growth process is also predicted by a qualitative theory. (20 refs.)

62059 Effective field theory for interface delocalization transitions. R.Lipowsky, D.M.Kroll, R.K.P.Zia (Sektion Phys., Ludwig-Maximilians-Univ. Munchen, Munchen, Germany).

Phys. Rev. B (USA), vol.27, no.7, p.4499-502 (1 April 1983).

Semi-infinite systems are considered which give rise to a delocalization transition of the interface between two coexisting phases. Since the interface position becomes a zero mode at the transition, interface fluctuations invalidate mean-field theory for space dimension $d \leq 3$. An effective field-theoretic model for this zero mode is obtained via the collective-coordinate method. Results for a simplified version of this model in $d=2$ and in $d=3$ are reported. (23 refs.)

Critical point shifts in films See Entry 59749

Kinetics of bulk melting and overheating of metals See Entry 62065

Quantitative theory of solubility in supercritical fluids See Entry 62113

On the temperature derivative of the surface tension at a critical end point See Entry 62211

Chain fusion and orientational ordering in monomolecular layers of amphiphilic molecules See Entry 62216

Charge-density waves in a strong magnetic field. III. See Entry 62352

64.70 PHASE EQUILIBRIA, PHASE TRANSITIONS, AND CRITICAL POINTS

(see also 81.30 Phase diagrams and microstructures developed by solidification and solid-solid phase transformations)

62060 Phase equilibria in systems of TiX with Cd(Zn)X (X=S, Se, Te). F.Kh.Guseinov, M.B.Babanly, A.A.Kuliev (S.M. Kirov State Univ., Azer-baidzhan SSR).

Inorg. Mater. (USA), vol.18, no.5, p.642-5 (May 1982). Translation of: *Izv. Akad. Nauk SSSR Neorg. Mater.*, vol.18, no.5, p.759-63 (May 1982). [received: Feb. 1983]

The phase equilibria in TiX-Zn(Cd)X systems have been investigated by DTA, X-ray phase analysis, and measurement of the microhardness of the alloys. In these systems no TiZn(Cd)X₂ compounds are formed, the existence of which has been suggested previously in the literature. The TiSe-Zn(Cd)Se systems belong to the simple eutectic type and in the neighborhood of TiSe are characterized by a degenerate eutectic. A thermodynamic analysis has been made of the liquidus of the TiSe-CdSe and TiTe-Zn(Cd)Te systems in a regular-solution approximation with allowance for dissociation of the thallium chalcogenides in the liquid phase. (9 refs.)

62061 The Ti₂Te+Ge=2Ti+GeTe ternary interlinked system. N.A.Kulieva, M.B.Babanly, I.S.Sattar-zade (S.M. Kirov State Univ., Azer-baidzhan SSR).

Inorg. Mater. (USA), vol.18, no.5, p.646-9 (May 1982). Translation of: *Izv. Akad. Nauk SSSR Neorg. Mater.*, vol.18, no.5, p.764-8 (May 1982). [received: Feb. 1983]

The phase equilibria in the Ti₂Te+Ge=2Ti+GeTe system were investigated by differential thermal analysis and X-ray diffraction analysis and measurements of the EMF values and microhardnesses. It was established that the Ti₂Te-GeTe boundary system is quasi-binary and is characterized by the formation of Ti₃GeTe₂ and Ti₂GeTe₂ intermediate phases. The liquidus surface of the Ti₂Te+Ge=2Ti+GeTe system is primarily the region of primary crystallization of the solid solutions on the basis of Ge, which proceeds via a monotectic reaction over a significant range of concentrations. It is shown that Ti+Ge+Ti₂Te, Ti₂Te+Ti₃GeTe₂+Ge, Ti₂GeTe₂+GeTe+Ge three-phase regions that are bound by Ge-Ti₂Te (Ti₃GeTe₂, Ti₂GeTe₂) tie lines exist in this system below the solidus. (7 refs.)

62062 The establishment of equilibria in the Pd-H₂-D₂-H₂O-D₂O system. S.G.McKee, F.A.Lewis, J.P.Magennis, T.J.Kelly (Chem. Dept., Queen's Univ., Belfast, N Ireland).

J. Less-Common Met. (Switzerland), vol.89, no.2, p.475-80 (Feb. 1983). (International Symposium on the Properties and Applications of Metal Hydrides, Toba, Japan, 30 May-4 June 1982).

Palladium can absorb large volumes of the isotopes of hydrogen. Analysis of the ratios of isotopes in outgassed mixtures provides a means of determining electrolytic isotopic separation factors and also of determining ratios of isotopes absorbed within electrodes after equilibria have been established with respect to the hydrogen and deuterium dissolved in surrounding mixtures of H₂O and D₂O. Measurements were made at values of hydrogen (deuterium) contents corresponding to the α , α - β and β phase composition ranges in the Pd-H(D) system. (21 refs.)

62063 Generalized phase diagram polymer-solvent. V.P.Budtov. *Vysokomol. Soedin. Ser. A (USSR)*, vol.25, no.3, p.493-9 (March 1983). In Russian. English translation in: *Polym. Sci. USSR (GB)*

The analytical expressions for the spinodal and binodal on the phase diagram of a polymer solution are derived with and without taking into account the concentration dependence of the χ parameter. The method of drawing of the generalized phase diagram is proposed. Such a diagram in the proposed coordinates is general for a wide range of flexible polymers of various MM in different solvents. The calculated dependences are compared with experimental data for solutions of polystyrene, polyisobutylene and polyethylene in various solvents. The good coincidence of analytical expressions and experimental results is shown. (11 refs.)

Two new phases with tetragonal bronze-like structure in the diagram: K₂O-CdO-Nb₂O₅ See Entry 61863

Thermodynamics of the CaO-SiO₂ system See Entry 62109

Comparison of the fitting capabilities of several equations for the composition dependence of excess free enthalpy in binary alloys See Entry 62126

Phase equilibrium diagram for the vanadium-rhenium system See Entry 63259

The Th-Sn phase diagram See Entry 63260

Phase diagrams of binary rare earth metal-indium systems See Entry 63261

Solidus and liquidus temperatures in the Cs-Te system See Entry 63262

The magnetism corner of the Mg-Y-Ce system See Entry 63264

Phase equilibria in the Mg-Al-Sr system See Entry 63265

Stability and crystallization of an amorphous nickel-based alloy See Entry 63266

Coupled phase diagram and thermodynamic analysis of the 18 binary systems formed among Li₂CO₃, K₂CO₃, Na₂CO₃, LiOH, KOH, NaOH, Li₂SO₄, K₂SO₄, and Na₂SO₄ See Entry 63267

The Te-Ti-As₂Te₃-Te₂-Te₃ system See Entry 63270

The Ti-As-Te system See Entry 63271

Phase diagram of the Pb(PbO)₂-MoO₃ system See Entry 63272

Thermogravimetric study of the KNbO₃-KBO₃ system See Entry 63273

Multichemistry and microstructure of a multiphase aluminosilicate ceramic See Entry 63274

Comments on the manuscript entitled: On the existence of a two-phase field in the uranium-oxygen system within the composition range 2.65<O/U<2.67 below 1273K (A. Caneiro, J.P. Abriata and J. Garces, *J. Nucl. Mater.* 113 (1983) 260-262) [and reply] See Entry 63275

A study of precipitation in interstitial alloys. II. A new metastable carbide phase in platinum See Entry 63296

Physicochemical fundamentals of the development of heat-resistant niobium alloys See Entry 63305

- Heat treatment and magnetic properties of high-coercivity Fe-Co-Cr alloys with 3% Mo See Entry 63435
- Enthalpies of formation of liquid and solid binary alloys based on 3d metals. III. Alloys of iron See Entry 63581
- Quantitative X-ray phase analysis of R-Co alloys See Entry 63618

64.70D Solid-liquid transitions

(see also 81.30F Solidification)

62064 Volume dependence of melting temperature at high pressure and its relation to a new dimensionless quantity. U.Walzer (Akad. de Wissenschaften, Zentralinst. fuer Phys. der Erde, Jena, Germany). *Exp. Tech. Phys. (Germany)*, vol.31, no.1, p.33-51 (1983). In German. The dependence of melting temperature on the atomic volume is inferred in two separate ways from different assumptions. The first deduction is based on an interatomic pair potential and a dislocation model, while the second one is based on the equation of state by Ullmann and Pan'kov, on an expression for the dependence of the Grüneisen ratio on pressure and bulk modulus and on Lindemann's law. It is also possible to infer the equation of state from the lattice theory alone. From this, the exponents of the $T_m(v)$ equations are independently determined. They are found to be in agreement. Reversing the sequence of conclusions, one may, if one accepts the other aforementioned premises, infer Lindemann's law. However, this applies only for high coordination numbers and high pressures, respectively. If one might proceed from the assumption that, at an approximate pressure, but at an assumed zero temperature, the materials of the Earth's core would exist in the form of a close-packed structure, it is possible to determine the ratio of melting temperature to formula weight as a function of the pressure for the actual Earth's core. (52 refs.)

62065 Kinetics of bulk melting and overheating of metals. A.P.Baikov, V.I.Motorin, S.L.Musher, A.F.Shestak (Inst. of Automation & Electrometry, Acad. of Sci., Novosibirsk, USSR). *Fiz. Met. & Metallogr. (USSR)*, vol.55, no.2, p.323-30 (Feb. 1983). In Russian. English translation in: *Phys. Met. & Metallogr. (GB)*. A theory is developed of homogeneous nucleation in the course of bulk melting of metals. An expression is obtained for the overheating above the melting point $\Delta T = T - T_m$ (for typical metals $\Delta T = 100-200^\circ\text{C}$). The results are reported of an experimental study in which such values of ΔT were observed in the course of rapid Joule heating of copper samples. It is shown that the rate of growth of nuclei of the liquid phase is governed by the microscopic kinetics of melting and that the elastic forces have practically no influence on the dynamics of nucleation. The results are applicable also to other substances characterized by a low specific heat. (29 refs.) A.T.

62066 Phase diagram and transition properties of condensed ammonia to 10 kbar. R.L.Mills, D.H.Liebenberg, Ph.Pruzan (Los Alamos Nat. Lab., Univ. of California, Los Alamos, NM, USA). *J. Phys. Chem. (USA)*, vol.86, no.26, p.5219-22 (23 Dec. 1982). A piston-cylinder apparatus was used to measure the transition curves and corresponding volume changes in condensed NH_3 from 200 to 305K (0.9-10.5 kbar). The melting curve had two distinct branches: a lower one bounding solid I and an upper one bounding solid II. The two melting curves intersected at 217.34K (3.070 kbar), forming a solid I-solid II-liquid triple point. The solid I-solid II transition line was determined from the triple point up to 224K (8.0 kbar). From sound-velocity measurements, it appeared that ultrasonic signals were completely attenuated in both solids over wide P - T regions adjoining the melting curves. (17 refs.)

62067 Applications of thermoanalytical techniques to the study of crystallization kinetics in glass-forming liquids. I. Theory. H.Yinnon, D.R.Uhlmann (Dept. of Materials Sci. & Engng., MIT, Cambridge, MA, USA). *J. Non-Cryst. Solids (Netherlands)*, vol.54, no.3, p.253-75 (March 1983). A critical review is presented of mathematical method advanced over the last 20 years for the analysis of data obtained from non-isothermal thermoanalytical studies of crystallization of glass-forming liquids. The methods are based on the Avrami treatment of transformation kinetics and define an effective crystallization rate coefficient having an Arrhenian temperature dependence. Several different way of mathematically treating the data have been proposed. Most are shown to be based on an incorrect neglect of the temperature dependence of the rate coefficient. By taking proper account of the temperature dependence of the crystallization rate coefficient, the methods are shown to lead to similar conclusions. In detail, it is shown that the effective activation energy of the overall crystallization process can be calculated from the slope of the line obtained by plotting $\ln[Q/(T^2 - T_0)]$ versus $1/T^2$, where T^2 is the temperature of maximum crystallization rate, T_0 is an initial temperature and Q is the heating rate employed in the experiment. (38 refs.)

62068 Interstitial polymers based on a polyurethane network. I. Melting points and fractional crystallinities. I.Aladescu, N.B.Graham, R.W.Richards (Dept. of Pure & Appl. Chem., Univ. of Strathclyde, Glasgow, Scotland). *Polymer (GB)*, vol.24, no.3, p.279-84 (March 1983). The preparation of a series of interstitial polymers based on a polyurethane network is described, the 'guest' polymers being poly(methyl acrylate) and poly(methacrylic acid). Differential scanning calorimetry has been used to determine the melting points and heats of fusion of the interstitial polymers, and the latter data being used to calculate fractional crystallinity. Both melting point and crystallinity are reduced as the weight fraction of guest polymer increases, crystallinity disappearing entirely in the case of the poly(methacrylic acid) interstitial. For this latter material, there is evidence for the formation of a complex between the poly(methacrylic acid) and the network chains. (37 refs.)

62069 Thermal and mechanical properties of tetramethyl-p-silphenylenesiloxane/dimethylsiloxane block copolymer. Y.Nagase, T.Fukatsu, K.Ikeda, Y.Sekine (Dept. of Chem., Waseda Univ., Tokyo, Japan). *Polymer (GB)*, vol.24, no.4, p.463-8 (April 1983). Several kinds of tetramethyl-p-silphenylenesiloxane/dimethylsiloxane (TMPS/DMS) block copolymers having various compositions and segment lengths were synthesized. For these copolymers, differential scanning calorimetry was carried out to determine the melting temperatures, the heat of fusion and the crystallinities. The stress-strain behaviour and the dynamic mechanical behaviour were also investigated for these copolymers. The tensile strength was decreased and the percentage elongation was increased with increasing DMS content and segment length. In the case of the copolymers for which the DMS contents remained constant at 26 wt.%, two major transitions were observed at around -120° and -10°C for the copolymers having DMS block sizes of 300, 380 and 540. (13 refs.)

62070 Composition stabilization of a Ga-Al-Sb-As liquid phase (thermodynamic analysis). A.N.Baranov, Yu.P.Yakovlev (A.F. Ioffe Physicotech. Inst., Acad. of Sci., Leningrad, USSR). *Sov. Tech. Phys. Lett. (USA)*, vol.8, no.7, p.385-7 (July 1982). Translation of: *Pis'ma v Zh. Tekh. Fiz. (USSR)*, vol.8, no.13-14, p.888-92 (July 1982). [received: April 1983] The composition of a Ga-Al-Sb-As liquid phase in contact with a GaAs substrate can be stabilized. After the interaction with this substrate, the composition of the melt will be the same despite a variation of the original antimony concentration over a rather broad range. The authors offer a thermodynamic derivation of this effect; the composition stabilization of a liquid phase in contact with a certain substrate. (8 refs.)

- A new ultrasonic cell for measurement near melting point of metal See Entry 59786
- Radiation-induced crystallinity changes in pressure-crystallized ultrahigh molecular weight polyethylene See Entry 61817
- Flash lamp annealing of ion-implanted polycrystalline silicon See Entry 61959
- Thermal model for interference laser annealing See Entry 61964
- pvT data for liquid and solid hexamethyldisilane up to 3000 bar See Entry 62053
- Phase transition from solid crystal to nematic liquid crystal and structural changes in an external electric field See Entry 62104
- Shape of crystals at low temperatures: absence of quantum roughening See Entry 62207
- Measurements of the lamellar spacings of unidirectionally solidified Fe-FeS eutectic thin films See Entry 62285
- Change in the electrical resistivity of Al-3.5% Cu during thermal cycling in the solidus-liquidus range See Entry 63263
- The magnetism corner of the Mg-Y-Ce system See Entry 63264
- The As_2S_3 -SnTe system See Entry 63268
- Phase equilibrium in the Ti-Se system at high pressures See Entry 63269
- Discontinuity of temperature distribution due to phase transformations during the cooling of alloys See Entry 63276
- Solidification of copper and silver in near-zero-g experiments See Entry 63277
- Observations on the non-planar freezing of aqueous salt solutions See Entry 63278
- On the steady-state continuous casting Stefan problem with nonlinear cooling See Entry 63279
- Melting of peritectic intermediate phases in Cu-Zn and Cu-Ge systems See Entry 63280
- Analysis of the factors determining the yield of a peritectic reaction, important in choice of optimal heat-treatment conditions See Entry 63281
- Turbulent flow in chill block casting See Entry 63282
- Ultrafast solidification of ultrathin molten silicon films See Entry 63283

64.70F Liquid-vapour transitions

- 62071** Critical and supercritical fluids. J.S.Rowlinson (Phys. Chem. Lab., Oxford Univ., Oxford, England). *Fluid Phase Equilibria (Netherlands)*, vol.10, no.2-3, p.135-9 (March 1983). (Supercritical Fluids. Their Chemistry and Application, Cambridge, England, 13-15 Sept. 1982). The characteristic properties of fluids at the gas-liquid critical point and in the supercritical state are described briefly. (13 refs.)
- 62072** Mean-field lattice gas description of vapour-liquid and supercritical equilibria. L.A.Kleintjens (Res. & Patents, DSM, Geleen, Netherlands). *Fluid Phase Equilibria (Netherlands)*, vol.10, no.2-3, p.183-90 (March 1983). (Supercritical Fluids. Their Chemistry and Application, Cambridge, England, 13-15 Sept. 1982). Recently the authors improved the mean-field two-component lattice-gas model introducing interacting surface areas and an empirical entropy of mixing parameter. The treatment in its present form has proven to be well capable of describing almost quantitatively fluid-phase behaviour of non-polar and polar substances of low- and high molar mass and mixtures thereof in large temperature and pressure ranges. The model works particularly well in the critical fluid region which allows adjustment of the parameters to scarce experimental data with expressions for spinodal, critical condition and equation of state. (30 refs.)
- 62073** Thermophysical properties of supercritical fluids with special consideration of aqueous systems. E.U.Franck (Inst. fuer Phys. Chem., Univ. Karlsruhe, Karlsruhe, Germany). *Fluid Phase Equilibria (Netherlands)*, vol.10, no.2-3, p.211-22 (March 1983). (Supercritical Fluids. Their Chemistry and Application, Cambridge, England, 13-15 Sept. 1982). Selected thermophysical properties of polar, dense supercritical fluids are discussed. The static dielectric constant of water and the freon R22 (CHClF_2) is shown in some detail. Examples of critical curves for binary systems with water and methanol are given. New experimental data of excess volumes up to 400°C and 2000 bar are shown for water combined with H_2 , CH_4 and benzene. Excess Gibbs energies and activity coefficients for water-benzene are also shown. Results of the solubility of anthracene in ten different high pressure fluids, obtained by UV-spectroscopy, are presented. The PVT-data of concentrated supercritical aqueous NaCl-solutions and the ion product of pure water to 1000°C are discussed. (35 refs.)
- 62074** Thermodynamics of supercritical steam+carbon dioxide mixtures. C.J.Wormald, C.N.Colling, G.Smith (School of Chem., Bristol Univ., Bristol, England). *Fluid Phase Equilibria (Netherlands)*, vol.10, no.2-3, p.223-31 (March 1983). (Supercritical Fluids. Their Chemistry and Application, Cambridge, England, 13-15 Sept. 1982). Measurements of the excess enthalpy of steam+carbon dioxide have been made at temperatures from 363 to 698K at pressures up to 6 MPa. Analysis of the measurements at low pressures yields values of the cross term second virial coefficient B_{12} . Evidence for a specific interaction between water and carbon dioxide is found, the enthalpy of association is $\Delta H = -14 \pm 2 \text{ kJ mol}^{-1}$. The measurements at high pressures are fitted by the Peng-Robinson equation of state using values of the interaction parameter k_{ij} which are temperature dependent. (25 refs.)

62075 Phase equilibria and critical phenomena in fluid (n-alkane+water) systems at high pressures and temperatures. T.W.De Loos, J.H.Van Dorp, R.N.Lichtenthaler (Dept. of Chem., Delft Univ. of Technol., Delft, Netherlands).

Fluid Phase Equilibria (Netherlands), vol.10, no.2-3, p.279-87 (March 1983). (Supercritical Fluids. Their Chemistry and Application, Cambridge, England, 13-15 Sept. 1982).

In fluid (n-alkane+water) mixtures (gas+gas) equilibria of the second type are found. Phase equilibria in fluid (n-pentane+water) and (n-heptane+water) were measured in the temperature range 600 to 675K and at pressures from 15 to 170 MPa. The critical curve of these systems starts at the critical point of pure water and runs through a temperature minimum with increasing pressure. Experimental results are compared with previous studies and it is found that the data fit very well within the systematics of other (n-alkane+water) systems. (15 refs.)

62076 High-pressure phase studies on fluid mixtures of low-volatile organic substances with supercritical carbon dioxide. R.Konrad, I.Swaid, G.M.Schneider (Dept. of Chem., Univ. of Bochum, Bochum, Germany).

Fluid Phase Equilibria (Netherlands), vol.10, no.2-3, p.307-14 (March 1983). (Supercritical Fluids. Their Chemistry and Application, Cambridge, England, 13-15 Sept. 1982).

Two high-pressure phase equilibrium cells working according to the analytical method in the temperature range 300 to 450K and up to 200 MPa have been developed. In the first cell p,T,x,y equilibrium data can be determined by sampling and GC analysis. With this cell the gas-liquid phase behaviour of the ternary systems carbon dioxide+tridecane+hexadecane and carbon dioxide+tridecane+1-hexadecanol were determined at 423.4K and between 8 and 35 MPa. For the second apparatus a spectroscopic high-pressure cell fitted with two pairs of sapphire windows was developed. Molar absorptivities are obtained from calibration runs in the homogeneous region. Gas-liquid phase equilibria in the system decane+CO₂ were investigated from 342.8 to 400.2K and between 10 and 20 MPa; here absorption data were measured in the NIR region. (15 refs.)

62077 Steam explosion experiments with single drops of iron oxide melted with a CO₂ laser. L.S.Nelson, P.M.Duda (Sandia Nat. Labs., Albuquerque, NM, USA).

High Temp.-High Pressures (GB), vol.14, no.3, p.259-81 (1982). (10th Plansee Seminar on 'Trends in Refractory Metals, Hardmetals, and Special Materials, and their Technology', Reutte, Austria, 1-5 June 1981).

A carbon dioxide laser has been used to prepare single drops of molten iron oxide. Both spontaneous and triggered steam explosions can be produced when these drops fall into water. The techniques used permit quantitative examination of film boiling and the explosions via high-speed photography and pressure transducer traces. Permanent gas present in the boiling layer prevents spontaneous explosions of the drops. This gas is air entrained by the drops as they enter the water. There is a threshold region for triggering via an applied pressure transient between 0.2 and 0.4 MPa. Below this region there are no explosions; above, prompt explosions always occur. In the threshold region, the drops undulate violently and finally explode after delays as long as 100 ms. The steam explosion can involve multiple events where a steam bubble alternatively grows and collapses as the melt fragments. Significant pressures are generated by the collapse of these bubbles; these pressures are in the range 10-50 MPa near the drop. During the explosion, one molten iron oxide drop fragments into several million particles. Heat-to-work conversions of 2-3% have been estimated for single-drop experiments. (54 refs.)

Supercritical Fluids. Their Chemistry and Application See Entry 59525

Heat transfer in subcooled liquid cryogenes See Entry 61375

Interaction of the nucleation phenomena at adjacent sites in nucleate boiling See Entry 61387

Capacity ratios and diffusion coefficients of low-volatile organic compounds in supercritical carbon dioxide from supercritical fluid chromatography (SFC) See Entry 61592

On equilibrium properties of the multivalent ionic systems See Entry 61754

Thermodynamic calculation of supercritical-fluid equilibria: New mixing rules for equations of state See Entry 62052

Vaporization behaviour of the system AlF₃(s)-Al(l) See Entry 62079

Heat transfer to helium-I during different boiling regimes at high centrifugal accelerations See Entry 62198

Low temperature dielectric films from octavinylsilsequioxane See Entry 63163

Hydrogen at high pressures and temperatures See Entry 64363

64.70H Solid-vapour transitions

62078 Molecular composition of zinc-germanium diphosphide vapour. I.S.Gorban' (Acad. of Sci., Ukrainian SSR), G.Sh.Viksmán, S.B.Pyatakova, I.I.Tichina.

Dopov. Akad. Nauk UkrSR. Ser. A (USSR), no.2, p.70-2 (1983). In Ukrainian.

The evaporation mechanism and molecular composition of the ternary diamond-like semiconductor ZnGeP₂ vapour are determined by the mass-spectrometric method. The investigations show that evaporation of the ZnGeP₂ is dissociational. The ratio of the vapour compounds (Zn, P, P₂, P₃, Ge) is determined by the evaporation temperature. (6 refs.)

62079 Vaporization behaviour of the system AlF₃(s)-Al(l). H.Kvande (Inst. of Silicate & High-temperature Chem., Univ. of Trondheim, Trondheim, Norway).

High Temp.-High Pressures (GB), vol.14, no.3, p.245-52 (1982). (10th Plansee Seminar on 'Trends in Refractory Metals, Hardmetals, and Special Materials, and their Technology', Reutte, Austria, 1-5 June 1981).

Two methods, the boiling point method and the transpiration method, have been used to determine the partial pressures of AlF₃(g) and Al₂F₆(g) over solid aluminium trifluoride. These partial pressures are subtracted from the measured total pressure over AlF₃(s)+Al(l) to give the partial pressure of AlF(g), formed by the reaction $\frac{1}{3}\text{AlF}_3(\text{s}) + \frac{2}{3}\text{Al}(\text{l}) = \text{AlF}(\text{g})$. Thermodynamic values for these vaporization reactions are calculated and compared with literature data. (26 refs.)

62080 Thermodynamic functions for the congruent sublimation of cadmium telluride. B.de Lary, A.Finch, P.J.Gardner (Dept. of Chem., Royal Holloway Coll., Egham, England).

J. Cryst. Growth (Netherlands), vol.61, no.2, p.194-8 (March 1983).

Using a modified entrainment method the enthalpy and entropy changes for the reaction $\text{CdTe}(\text{c}) = \text{Cd}(\text{g}) + 0.5 \text{Te}_2(\text{g})$ at 298.15K were determined as 72.0±0.9 kcal mol⁻¹ and 51.0±0.8 cal K⁻¹, respectively, both values being significantly higher than previous estimates. (28 refs.)

62081 Study of the vaporization of solid AlAs. P.Imperatori, D.Ferro, V.Piacente (Istituto di Chimica Fisica, Univ. Degli Studi, Rome, Italy).

J. Less-Common Met. (Switzerland), vol.90, no.1, p.57-63 (March 1983).

The vaporization of solid AlAs was studied using the mass spectrometry and Knudsen effusion techniques. This compound vaporizes according to the reaction $\text{AlAs}(\text{s}) = \text{Al}(\text{s}) + \frac{1}{2}\text{As}_2(\text{g})$. The pressure of As₂(g) depends on the temperature according to the equation $\log P = (9.0 \pm 0.5) - (17.2 \pm 0.4) \times 10^3/T$, where P is in kilopascals. A value of $\Delta H_{298}^\circ = 163 \pm 7 \text{ kJ mol}^{-1}$ associated with the vaporization reaction was derived by second-law treatment of the pressure data. The free-energy function and the standard heat of formation ($\Delta H_{\text{form}}^\circ = 62 \pm 7 \text{ kJ mol}^{-1}$) of AlAs(s) were also calculated. (11 refs.)

64.70J Liquid-liquid transitions

Fast pressure quenches near the critical point of a binary liquid mixture See Entry 62119

64.70K Solid-solid transitions

(see also 61.50K Crystallographic aspects of polymorphic and order-disorder transformations, 81.30H, 81.30K, 81.30M
Microstructures developed by solid-solid phase transformations)

62082 Kinetics of the cubic-hexagonal transformation of cadmium sulfide. K.Matsumoto, K.Takagi (Res. Inst. of Electronics, Shizuoka Univ., Hamamatsu, Japan), S.Kaneko.

J. Electrochem. Soc. (USA), vol.130, no.2, p.423-6 (Feb. 1983).

The kinetics of cubic-hexagonal transformation of CdS conforms to a second-order rate equation with an activation energy of ca. 67 kcal/mol. The transformation is enhanced by the addition of NaCl of 0.001-0.1 weight ratio with little change of the activation energy. The role of the NaCl added is considered to reside, in that NaCl makes the movement and rearrangement of atoms in CdS easy as a flux, and that the contact points of CdS particles with NaCl provide the starting points of the further phase transformation. The mechanism of this transformation is presumed to be a linear growth process where the cubic-hexagonal interface moves progressively along the [111] direction of the cubic form. (21 refs.)

62083 Thin colloidal crystals: a series of structural transitions. B.Pansu, P.Pieranski, L.Strzelecki (Lab. de Phys. des Solides, Univ. de Paris-Sud, Orsay, France).

J. Phys. (France), vol.44, no.4, p.531-6 (April 1983).

The authors study thin layers of colloidal crystals made of polystyrene balls (1.1 µm diameter) in aqueous suspension. These thin layers are produced by confining colloidal crystals between two glass planes, which act as repulsive and perfectly smooth boundaries at colloidal scales. When the two planes form a wedge, a continuous passage from 2 to 3 dimensions is realized. Direct observation with an optical microscope reveals that this passage is characterized by a series of structural transitions consisting of changes in the number of layers and also in the structure of each layer. (9 refs.)

62084 Effect of pressure on the thermal hysteresis of a first-order transition. A.N.Das (Kandi Raj Coll., Kandi, Murshidabad, India), B.Ghosh.

J. Phys. C (GB), vol.16, no.10, p.1799-802 (10 April 1983).

The third- and fifth-order couplings between elastic strains and the order parameter of a first-order transition have been considered in the Landau free-energy expansion. The thermal hysteresis becomes pressure-dependent owing to the fifth-order coupling. The behaviour of the thermal hysteresis and the pressure hysteresis observed in some transitions of (NH₄)₂H(SO₄)₂ and (NH₄)HSO₄ crystals has been explained. (10 refs.)

62085 Effect of third- and fifth-order coupling terms on the spontaneous strain of a second-order structural phase transition. A.N.Das (Kandi Raj Coll., Kandi, Murshidabad, India), B.Ghosh.

J. Phys. C (GB), vol.16, no.10, p.1803-5 (10 April 1983).

The third- and fifth-order couplings between the order parameter and elastic strains for a second-order structural phase transition have been considered in the Landau phenomenological free-energy expansion and it is shown that the ratio of the contributions to the spontaneous strain due to the fifth-order coupling and the sum of third- and fifth-order coupling is directly related to the ratio of the temperature derivative of the order parameter and that of the spontaneous strain. (7 refs.)

62086 A theory of incommensurate phase transitions in anisotropically stressed BaMnF₄. J.Lorenc (Carnegie Lab. of Phys., Univ. of Dundee, Dundee, Scotland).

J. Phys. C (GB), vol.16, no.10, p.1807-26 (10 April 1983).

A simplified theory of incommensurate phase transitions in anisotropically stressed BaMnF₄ is proposed. The equilibrium properties and phase transitions induced by temperature and/or anisotropic stress are analysed in terms of the Landau-Ginzburg theory. A conjecture concerning the phase diagram is presented. The occurrence of critical end points or $n=2$ component 'renormalised' tricritical points is demonstrated within the renormalisation group approach. (31 refs.)

62087 Evidence for the incommensurate phase in AlPO₄ near α - β transition: a differential scanning calorimetry study. J.Durand, M.Lopez, L.Cot, O.Retout (Lab. de Chimie des Matériaux, Ecole Nat. Supérieure de Chimie, Montpellier, France), P.Saint-Gregoire.

J. Phys. C (GB), vol.16, no.11, p.1311-15 (20 April 1983).

Careful measurements of the specific heat of AlPO₄ near α - β phase transition are presented. They show that the intermediate phase is also realised in AlPO₄ in a temperature range of about 1°. The results are briefly discussed in comparison with those of quartz, in which an incommensurate intermediate phase has recently been discovered. (12 refs.)

62088 An X-ray diffraction study of the δ - α' transformation in a Pu-2 at.% Al alloy. E.G.Zukas, S.S.Hecker, R.A.Pereyra (Los Alamos Nat. Lab., Los Alamos, NM, USA).

J. Nucl. Mater. (Netherlands), vol.115, no.1, p.63-8 (March 1983).

The face-centered cubic (FCC) δ phase of plutonium is stable from 310° to 458°C. An addition of 2.0 at.% aluminium retains the δ phase metastably to room temperature. This δ phase transforms to α' during subzero thermal treatments. Under hydrostatic compression at room temperature, the δ transforms initially to β' , and this then transforms to α' at the higher pressures. During mechanical polishing, the δ phase transforms to α' . An X-ray diffraction study of this transformed zone by sequential removal of thin surface layers by electropolishing shows that this transformation is not directly from δ to α' , but from δ to γ with the γ phase then transforming to α' . There is no evidence for the presence of either the β or β' phases when the δ phase is transformed by mechanical polishing. (16 refs.)

62089 The secondary effect of the cooperative Jahn-Teller distortion in rare earth vanadates. H.Unoki (Electrotech. Lab., Ibaraki, Japan). *J. Magn. & Magn. Mater. (Netherlands)*, vol.31-34, pt.3, p.1063-4 (Feb. 1983). (Proceedings of the International Conference on Magnetism, Kyoto, Japan, 6-10 Sept. 1982).

A short range interaction between displacement of the rare-earth ion and the local deformation of its environment in rare earth vanadates is noticed. Anomalies in the dielectric constant as well as the specific heat are discussed based on this secondary effect accompanying the cooperative Jahn-Teller phase transition. (10 refs.)

62090 Structural transitions in superionic conductors. M.Parrinello, A.Rahman, P.Vashishta (Argonne Nat. Lab., Argonne, IL, USA). *Phys. Rev. Lett. (USA)*, vol.50, no.14, p.1083-6 (4 April 1983).

The $\alpha \rightarrow \beta$ phase transition in AgI is studied with use of the new molecular-dynamics technique which allows for a dynamical variation of the shape and size of the cell. In the present model, upon heating of β -AgI, the iodine ions undergo a HCP-BCC transformation and silver ions become mobile, whereas the reverse transformation is observed on cooling of α -AgI. The calculated $\alpha \rightarrow \beta$ transition temperature and structural and dynamical properties are in good agreement with experiments. (10 refs.)

62091 Two critical points on the γ - α phase boundary of cerium alloys. J.D.Thompson, Z.Fisk, J.M.Lawrence, J.L.Smith (Center for Materials Sci., Los Alamos Nat. Lab., Los Alamos, NM, USA), R.M.Martin. *Phys. Rev. Lett. (USA)*, vol.50, no.14, p.1081-4 (4 April 1983).

It is shown that the P - T diagram for the γ - α phase transition in $\text{Ce}_{0.9}\text{La}_{0.1}\text{Th}_{0.1}$ has two critical points with first-order transitions between them. This phase diagram follows from the Fermi-liquid properties of the $4f$ electronic system, the experimentally known volume dependence of $k_B T_{FL}$, and the dilution effect of alloying. (9 refs.)

62092 Structural transformations in solid nitrogen at high pressure. S.Nose, M.L.Klein (Chem. Div., Nat. Res. Council of Canada, Ottawa, Ontario, Canada).

Phys. Rev. Lett. (USA), vol.50, no.16, p.1207-10 (18 April 1983).

The Andersen-Parrinello-Rahman constant-pressure molecular-dynamics technique has been generalized to study molecular crystals. The method, which appears to have wide applicability, is used to study structural transformations in solid nitrogen at high pressures. (16 refs.)

62093 Structural phase stability in third-period simple metals. A.K.McMahan, J.A.Moriarty (Lawrence Livermore Nat. Lab., Univ. of California, Livermore, CA, USA). *Phys. Rev. B (USA)*, vol.27, no.6, p.3235-51 (15 March 1983).

Extensive phase-stability calculations for the FCC, HCP, and BCC structures of Na, Mg, Al, and Si are reported both near 1 atm and under high pressure, where Si becomes a natural member of this set of third-period simple metals. Calculations for each element have been carried out by two entirely different first-principles techniques: the generalized pseudopotential theory (GPT) and the linear-muffin-tin orbitals (LMTO) method. The two techniques give results in good qualitative agreement for Mg, Al, and Si and predict sequences of high-pressure structural phase transitions for these elements which arise from the lowering and partial filling of the initially empty $3d$ band under compression. Detailed analysis shows that major trends in the phase stability of the third-period metals are correlated with specific features both in the LMTO one-electron densities of states and in the GPT interatomic pair potentials. Quantitative comparisons between the two theoretical techniques, as well as with available experimental data and other recent calculations, are further used to assess the accuracy of the approximations employed by these methods in calculating structural energy differences. (39 refs.)

62094 Lithium, compression and high-pressure structure. B.Olinger, J.W.Shaner (Los Alamos Nat. Lab., Los Alamos, NM, USA). *Science (USA)*, vol.219, no.4588, p.1071-2 (4 March 1983).

Lithium is found to transform from a body-centered cubic (BCC) to a face-centered cubic (FCC) structure at 6.9 gigapascals (69 kilobars) and 296 kelvin. The relative volume of the BCC structured lithium at 6.9 gigapascals is 0.718, and the FCC structure is 0.25 percent denser. The bulk modulus and its pressure derivative for the BCC structure are 11.57 gigapascals and 3.4, and for the FCC structure are 13.1 gigapascals and 2.8. Extrapolation of the BCC-FCC phase boundary and the melting curve indicate a triple point around 15 gigapascals and 500 kelvin. (12 refs.)

62095 Structural states of MBBA during the transition from a frozen liquid-crystal state to a crystal. V.K.Dolganov, L.A.Novominskii, I.M.Shmyt'ko (Inst. of Solid-State Phys., Acad. of Sci., Chernogolovka, USSR).

Sov. Phys.-Solid State (USA), vol.24, no.9, p.1476-9 (Sept. 1982). Translation of: *Fiz. Tverd. Tela (USSR)*, vol.24, no.9, p.2605-9 (Sept. 1982). [received: April 1983]

The authors examine the structural changes in the solid state of the liquid crystal MBBA (4-methoxybenzylidene-4'-butylaniline). The warming of the frozen liquid-crystal samples is accompanied by the formation of a large number of metastable phases. The packing of the molecules in these phases is determined by the packing of the molecules in the original liquid-crystal structure. The equilibrium crystal structures which arise during the slow cooling of the nematic mesophase differ from the metastable phases in both their number and crystal structure. The crystal structure of the equilibrium phases is not related to the packing of the molecules in the original liquid-crystal state. The actual structure of the solid crystalline samples in the equilibrium phases obtained in the liquid-crystal-crystal transition 'inherits' the macroscopic packing of the molecules in the liquid-crystal state. (9 refs.)

62096 High-pressure phases in B group element alloys: a new sort of electronic phase. V.F.Degtyareva, E.G.Ponyatovskii (Inst. of Solid-State Phys., Acad. of Sci., Chernogolovka, USSR).

Sov. Phys.-Solid State (USA), vol.24, no.9, p.1514-19 (Sept. 1982). Translation of: *Fiz. Tverd. Tela (USSR)*, vol.24, no.9, p.2672-81 (Sept. 1982). [received: April 1983]

General relationships are discussed for phase formation in B group element alloys with increasing pressure. The main tendency is determined by the homology rule: the effect of pressure is to change the phase equilibria in the same way as when one component is replaced by a heavier element in the same group. The sequence of relative configurations of stability regions for intermediate phases in the phase diagrams depends on the electron density. As the mean number of electrons in the alloy increases, there is a sequence of phases, accompanied by a decrease in the coordination number and packing density of the structure. Phases with identical structures occur in various systems for similar values of the electron density per atomic volume. Isostructural phases in various systems with equal electron densities have similar values of the transition temperature to the superconducting state. These B-B phases, whose crystal structure and properties are governed by the electron density factor, form a new series of electronic phases of the Hume-Rothery type. (29 refs.)

Hindered internal rotations in Van der Waals molecules and molecular crystals See Entry 60885

Improved system for energy-dispersive X-ray diffraction with synchrotron radiation See Entry 61731

Atomic ordering in solid solutions See Entry 61844

Study of $\alpha \rightarrow \beta$ transition in americium See Entry 61845

Structural and thermal characterization of the γ'' polymorph of Bi_2MoO_6 See Entry 61846

New cationic deficient phases $\text{Bi}_{12}\text{B}_{4/5}^{+}\square_{1/5}\text{O}_{20}$ with sillenite structure See Entry 61864

Observation of a new memory effect in a modulated structure See Entry 61905

High temperature heat capacity of some Ag-Nd alloys See Entry 62124

Observation, close to roughening transition of critical-slowing-down See Entry 62206

Phase and bonding transitions in chemisorbed layers studied by vibrational frequency shifts See Entry 62251

Dependence of the band structure of $\text{Ge}_{2x}(\text{GaAs})_{1-x}$ solid solutions on the degree of order See Entry 62337

Electrical conduction properties of $\text{Mg}_{0.82}\text{Pt}(\text{C}_2\text{O}_4)_2 \cdot 6\text{H}_2\text{O}$ See Entry 62403

Preparation and study of the electrophysical properties of the copper chalcogenides and their solid solutions See Entry 62412

Ag_2Se thin film conductivity with a selenium excess See Entry 62513

Investigation of magnetic and martensitic phase transitions in Vicalloy-type alloys See Entry 62586

Magnetic behavior of SmCo_5 -hydrogen system See Entry 62718

^{87}Rb and ^{85}Rb NQR study of phase transitions in $\text{RbH}_3(\text{SeO}_3)_2$ See Entry 62829

^{14}N and ^{35}Cl double resonance study of the phase transition in the intercalated bilayer compound $\text{C}_{10}\text{H}_2\text{N}_3\text{Cl}$ See Entry 62836

Dielectric properties of $[\text{Ag}_{1-x}\text{K}_x]/\text{NbO}_3$ solid solutions See Entry 62872

Thermally stimulated surface currents in CH_3OH cryocondensates near the polymorphic phase transformation See Entry 62881

Raman scattering in K_2SO_4 at high temperatures See Entry 62997

Phase equilibrium in the Ti-Se system at high pressures See Entry 63269

Discontinuity of temperature distribution due to phase transformations during the cooling of alloys See Entry 63276

Formation and stability of reverted austenite in low-carbon nickel-molybdenum steels See Entry 63284

Nonequilibrium crystallization and structural transitions during heating of microcircuit leads made of Fe-C and Fe-C-Si alloys See Entry 63285

Order-disorder transition in Fe_3Si alloy during mechanical crushing See Entry 63286

Investigation of the phase composition, structure, and magnetic properties of alloy $\text{Sm}_2\text{Co}_{10}\text{Fe}_{3.2}\text{Cu}_{1.2}\text{Zr}_{0.4}$ See Entry 63287

Decomposition kinetics for supercooled austenite in steel 15KhM1F See Entry 63288

Carbon effect on ordering of γ - Ni_3Al in rapidly solidified $\text{Ni}_3\text{Al-C}$ alloys See Entry 63289

Ferrite growth during slow cooling from the intercritical annealing of a dual-phase steel See Entry 63290

Influence of alloying and preliminary deformation on phase composition and mechanical properties of Fe-Mn alloys See Entry 63291

Elastic behavior and phase stability of β_1 -AgCd alloy See Entry 63292

The structure of the modified 2H martensite in Cu-Zn-Al See Entry 63293

Characteristics of structural transformations during deformation and heat treatment of Elinvar alloy 45 NKHT See Entry 63356

Influence of ϵ -martensite on the friction and wear of high-manganese alloys See Entry 63423

Influence of nitrogen on the penetration of hydrogen through constructional materials from nitrogen-hydrogen mixtures See Entry 63465

Acoustic emission during phase transformations in alloys See Entry 63486

64.70M Transitions in liquid crystals

62097 Phase-transition studies in polymesomorphic compounds. I. Density studies in N -(p - n -hexyloxybenzylidene)- p - n -butylaniline. N.V.S.Rao, V.G.K.M.Pisipati (Faculty of Phys. Sci., Nagarjuna Univ., Nagar, India). *J. Phys. Chem. (USA)*, vol.87, no.5, p.899-902 (3 March 1983).

The density, ρ , of N -(p - n -hexyloxybenzylidene)- p - n -butylaniline (HBBA) is measured as a function of temperature from the isotropic liquid to the smectic-G phase. The compound is tetramorphic exhibiting three smectic phases S_G , S_B , S_A and a nematic phase. The changes in the density across the phase transformations, and the calculated thermal expansion coefficients, confirm the order of the transitions as first order. The particular importance of the smectic-A to nematic transformation, which is of first order, is apparent from the density jump across the transition. (36 refs.)

62098 The nematic to smectic-A transition: a theoretical overview. T.C.Lubensky (Group de Phys. des Solides, Ecole Normale Supérieure, Paris, France).

J. Chim. Phys. & Phys.-Chim. Biol. (France), vol.80, no.1, p.31-43 (Jan. 1983).

The de Gennes model is used as a basis for a discussion of the properties of the nematic and smectic-A phases and the transition between them. Order parameter and director correlation functions and the Landau-Peierls destruction of long range order in the smectic phases are reviewed. A gauge transformation that restores long range order to the smectic phase is introduced. Anisotropic scaling with correlation length exponents, ν_{\parallel} and ν_{\perp} is presented and shown to imply that the critical point in three dimensions with finite splay elastic constant must either be isotropic ($\nu_{\parallel} = \nu_{\perp}$) and in the same universality class as the superconducting transition or anisotropic with $\nu_{\parallel} = 2\nu_{\perp}$. Predictions for the behavior of physically measurable quantities for these two universality classes are presented and compared with experiment. Predictions for both classes are in agreement with some but not all experiments. (60 refs.)

62099 Multicritical phenomena in liquid crystals. D.L.Johnson (Phys. Dept., Kent State Univ., Kent, OH, USA). *J. Chem. Phys. & Phys.-Chim. Biol. (France)*, vol.80, no.1, p.45-51 (Jan. 1983).

A detailed review is given of the progress that has been made toward the understanding of the nematic-smectic A tricritical point and the nematic-smectic A-smectic C multicritical point. Other known or hypothetical liquid crystal multicritical points are reviewed briefly. (84 refs.)

62100 Microscopic and thermal phase studies on smectic and nematic liquid crystals at high pressures. J.Herrmann, H.D.Kleinhan, G.M.Schneider (Dept. of Chem., Univ. of Bochum, Bochum, Germany). *J. Chim. Phys. & Phys.-Chim. Biol. (France)*, vol.80, no.1, p.111-17 (Jan. 1983).

High pressure studies on the phase behaviour of liquid crystals were performed using a high pressure differential thermal analysis equipment and a diamond anvil cell. Results are presented and discussed on the polymorphism in the homologous series of the bis-(4,4'-n-alkoxybenzylidene)-1,4-phenylenediamines as well as to the reentrant nematic behaviour of 4-n-octyloxy-4'-cyanobiphenyl (80CB) and 4-cyanobenzylidene-4'-n-octyloxyaniline (CBOOA) and their mixtures and for pressures up to 3 kbar. (23 refs.)

62101 Effect of the flexibility on the phase transition of polymeric liquid crystals. A.Ten Bosch, P.Maissa, P.Sixou (Lab. de Physique de la Matière Condensée, CNRS, Nice, France). *Phys. Lett. A (Netherlands)*, vol.94A, no.6-7, p.298-300 (21 March 1983).

A mean-field theory of the nematic-isotropic transition in semi-flexible polymers is described. The effect of polymer-chain flexibility on the order parameter and phase-transition temperature is discussed. (12 refs.)

62102 Electrohydrodynamic instability as a nonequilibrium phase transition. S.V.Yablonskii, L.M.Blinov (Sci.-Res. Inst. of Organic Intermediate Products & Dyes, USSR). *Sov. Phys.-Crystallogr. (USA)*, vol.27, no.5, p.562-4 (Sept.-Oct. 1982). Translation of: *Kristallografiya (USSR)*, vol.27, no.5, p.936-40 (Sept.-Oct. 1982). [received: April 1983]

The authors have investigated electrohydrodynamic (EHD) instability in a nematic liquid crystal of MBBA near the threshold. From measurements of the diffraction efficiency of the phase lattice formed by the Kapustin-Williams domains together with measurements of the light transmission in the guest-host effect, they calculate the voltage dependence of the maximum angle of inclination of the director. The character of the dependence near the threshold is explained from the viewpoint of the theory of Landau phase transitions. (13 refs.)

62103 Thermodynamic characteristics of phase transitions in a binary smectic system. A.Boiy, P.Adomenas (State Univ., Vilnius, Lithuanian SSR). *Sov. Phys.-Crystallogr. (USA)*, vol.27, no.5, p.606-7 (Sept.-Oct. 1982). Translation of: *Kristallografiya (USSR)*, vol.27, no.5, p.1010-11 (Sept.-Oct. 1982). [received: April 1983]

The authors have used a Perkin-Elmer DSC-2 scanning calorimeter to study the binary mixture of 4-n-octyl-4'-cyanodiphenyl and 4-n-decyl-4'-cyanodiphenyl. The compounds were synthesized by an earlier method developed by the authors, and purified by distillation, chromatography, and crystallization. The phase diagram of the mixture is shown, and the enthalpies of the mixture phase transitions determined: smectic-isotropic, smectic-nematic, nematic-isotropic, and smectic-isotropic. (4 refs.)

62104 Phase transition from solid crystal to nematic liquid crystal and structural changes in an external electric field. S.I.Tatarinov, A.G.Finkel' (N.G. Chernyshevskii State Univ., Saratov, USSR). *Sov. Tech. Phys. Lett. (USA)*, vol.8, no.8, p.420-2 (Aug. 1982). Translation of: *Pis'ma v Zh. Tekh. Fiz. (USSR)*, vol.8, no.15-16, p.973-7 (Aug. 1982). [received: April 1983]

Reports the observation of a phase transition from a solid crystal to a nematic liquid crystal in an electric field. The authors have also studied the effect of an external electric field on the structure of the molecules and the solid crystal of 4-methoxy-4'-butylazobenzene (MBAOB) near the phase transition from the solid crystal to the liquid crystal (19°C). These experiments show that a study of the phase transition from a solid crystal to a liquid crystal in an electric field is a subtle method for studying the dynamics of the transition. The authors found from the IR spectra that the conformational changes which accompany the transition occur before the translational order is disrupted. (11 refs.)

Biaxial nematic phases in amphiphilic systems See Entry 61776

Lytotropic polymeric liquid crystals See Entry 61778

Polymorphism in polar mesogens. I. Physicochemistry and structure See Entry 61779

Polymorphism in polar mesogens. II. Theoretical aspects See Entry 61780

Polymorphism in polar mesogens. III. Molecular aspect See Entry 61781

Two dimensional ordering in liquid crystals: the SmF and SMI phases See Entry 61782

Modulated crystal B phases and B-to-G phase transitions in two types of liquid crystalline compound See Entry 61787

Orientational effect of a surface light wave on liquid crystals See Entry 61788

64.70P Glass transitions

62105 Photo-illumination effect on the glass transition of annealed amorphous selenium. H.Koseki, A.Oadajima (Dept. of Appl. Phys., Hokkaido Univ., Sapporo, Japan). *Jpn. J. Appl. Phys. Part 1 (Japan)*, vol.22, no.3, p.542 (March 1983).

It is well known that a glass after being cooled through the glass-transition temperature (T_g) relaxes towards a metastable state, for a sufficiently long stored time, corresponding to the equilibrium configuration of the supercooled liquid at the given temperature. Therefore, properties of a glass are dependent on its thermal history. In amorphous selenium (a-Se), the structural relaxation has often been investigated by means of thermal analyses such as DSC and DTA. The authors show that the illumination promotes the stabilization of the freshly evaporated film of a-Se, but it probes the reverse effect for the well-annealed films. (4 refs.)

62106 Dependence of the glass transition temperature on relaxation times. T.S.Chow (Xerox Webster Res. Center, Rochester, NY, USA). *Polym. Commun. (GB)*, vol.24, no.3, p.77-9 (March 1983).

A non-equilibrium criterion for the direct determination of kinetic effects on the glass transition temperature of amorphous polymers (T_g) is presented. Expressions for relaxation times are chosen which depend both on temperature and structure. Using the same non-equilibrium viewpoint, the effect of pressure on T_g is discussed. (9 refs.)

62107 Evidence of a 'glassy crystal' phase obtained by the quenching of the plastic phase of the cyanoadamantane. M.Foulon, J.P.Amoureux, J.L.Sauvajol, J.Lefebvre, M.Descamps (Lab. de Dynamique des Cristaux Moleculaires, Univ. de Lille I, Villeneuve d'Ascq, France). *J. Phys. C (GB)*, vol.16, no.10, p.L265-9 (10 April 1983).

The authors present experimental results which show the existence of a 'glassy crystal' phase obtained by the quenching of the 1-cyanoadamantane plastic phase. From the DSC data, the glass transition temperature has been obtained and the glassy crystalline 1-cyanoadamantane has been shown to relax during annealing at 160K. The 'glassy crystal' is cubic (FCC) and is characterised by the vanishing of some low-frequency Raman contributions of the plastic phase. (7 refs.)

Crystallization of amorphous $\text{Cu}_{60}\text{Zr}_{40}$ prepared by magnetron sputter deposition See Entry 61808

Characterization studies of $\text{AgI-Ag}_2\text{O-MoO}_3$ glasses See Entry 61810

Effect of poly(propylene oxide) segment size on structure-property relationships in elastomeric ionene See Entry 61827

64.75 SOLUBILITY, SEGREGATION, AND MIXING

62108 Solubility of hafnium dioxide in cerium dioxide. P.Malou, E.Debray (Univ. Paris Val-de-Marne, Creteil, France), B.Chappey, C.R. Seances Acad. Sci. Ser. II (France), vol.296, no.4, p.245-7 (31 Jan. 1983). In French.

The total electric conductivity and the lattice parameter evolution with hafnia content of $\text{CeO}_2\text{-HfO}_2$ solid solutions shows a remarkable point corresponding to a content adjoining 13 moles % associate to the limit solubility and to the probable formation of a chemically definite compound. (7 refs.)

62109 Thermodynamics of the CaO-SiO_2 system. Y.E.Lee (Technol. Center, Eltek Metals Co., Niagara Falls, NY, USA). *CALPHAD: Comput. Coupling Phase Diagrams & Thermochem. (GB)*, vol.6, no.4, p.283-91 (1982).

In order to maintain consistency, analytical expressions for the free energy of mixing of phases should reproduce not only the phase diagrams but also the experimentally determined activities. Information on the partial molar free energies and the phase boundaries, in turn, can be used to estimate the free energy of formation of compounds. An examination of thermochemical data in the CaO-SiO_2 system showed that ΔG° values for $\alpha\text{-Ca}_2\text{SiO}_4$, which are stable at temperatures above 1710K, are limited a maximum of 1800K. An analytical expression for the free energy of mixing of the liquid phase was obtained for the entire composition range in the CaO-SiO_2 system. Confidence in the estimated ΔG° for $\alpha\text{-Ca}_2\text{SiO}_4$ was demonstrated by good agreement of the calculated phase diagram and the experimentally determined activity of silica. (20 refs.)

62110 An empirical correlation between enthalpy and entropy interaction coefficients. A.Taskine, L.E.Holappa (Inst. of Process Metall., Helsinki Univ. of Technol., Espoo, Finland). *CALPHAD: Comput. Coupling Phase Diagrams & Thermochem. (GB)*, vol.6, no.4, p.293-6 (1982).

The solution thermodynamics of oxygen in dilute liquid metals have been under active study for the last decades. Considerable progress has been made in the determination of the first order interaction coefficients, ϵ_0 , using the solid electrolyte emf method. This can be expressed in terms of τ , which is considered as the apparent temperature at which the system would become ideal if the enthalpy and entropy interaction coefficients were independent of temperature. Therefore the questions: how universal is the constant τ and is it dependent mainly on the crystal structure of the solvent; and are there any correlations between τ and κ , cannot be answered now. In the future when more accurate values of the interaction energies between atoms in liquid metals become known. The physical explanations for τ and κ can be found. (33 refs.)

62111 Supercritical phase equilibria involving solids. R.Koningsveld, G.A.M.Diepen (Res. & Patents, DSM, Geleen, Netherlands). *Fluid Phase Equilibria (Netherlands)*, vol.10, no.2-3, p.159-72 (March 1983). (Supercritical Fluids, Their Chemistry and Application, Cambridge, England, 13-15 Sept. 1982).

The solubility of solids in supercritical solvents is reviewed in a phenomenological discussion of binary and ternary systems containing one highly volatile component. Solubility and selectivity are greatly determined by the course of the binary critical curves, the ternary critical end-point curves, and the locations of the triple points of the solids. The mean-field lattice-gas model is used to review some important molecular parameters. (7 refs.)

62112 Electron-microscopy study of the decomposition of a supersaturated solid solution in silicon. Yu.Yu.Loginov, V.M.Busygina (Krasnoyarsk State Univ., Krasnoyarsk, USSR). *Inorg. Mater. (USA)*, vol.18, no.5, p.601-5 (May 1982). Translation of: *Izv. Akad. Nauk SSSR Neorg. Mater.*, vol.18, no.5, p.709-14 (May 1982). [received: Feb. 1983]

The dependence of the character of precipitates in Si on the concentration of B and P and the conditions of heat treatment was demonstrated. The previously proposed mechanism of formation of precipitates from the basic admixture (B and P) was confirmed. The role of O and C in the precipitates was demonstrated. (28 refs.)

62113 Quantitative theory of solubility in supercritical fluids. M.Gitterman (Dept. of Phys., Bar-Ilan Univ., Ramat-Gan, Israel), I.Procaccia. *J. Chem. Phys. (USA)*, vol.78, no.5, p.2648-54 (1 March 1983).

The phenomenon of enhanced solubility of solids in supercritical fluids is analyzed. The entire region of pressures is considered on the basis of the thermodynamic approach, independently of specific models. General aspects of the phenomenon have been discovered by considering the slopes of solubility curves. These slopes are shown to diverge near the two existing critical points, namely the lower and upper critical end points. In the case of dilute solutions, a curve of the locus of maxima of slopes of solubility curves is found in the reduced pressure-reduced temperature plane. All available experimental data are unified under this approach and are found to agree with theoretical analysis. The results obtained can be used to optimize supercritical fluid extraction. (24 refs.)

62114 Irreversible effects in the FeTi-H system. J.J.Reilly, J.R.Johnson, J.F.Lynch, F.Reidinger (Dept. of Energy & Environment, Brookhaven Nat. Lab., Upton, NY, USA).

J. Less-Common Met. (Switzerland), vol.89, no.2, p.505-12 (Feb. 1983). (International Symposium on the Properties and Applications of Metal Hydrides, Toba, Japan, 30 May-4 June 1982).

The equilibrium hydrogen absorption isothermal using annealed strain-free FeTi exhibits only one plateau up to a composition of $\text{FeTiH}_{0.95}$. However, the desorption isotherm exhibits the usual two plateaux. X-ray diffraction

results of samples with compositions within the absorption plateau limits indicate the major phases present to be α and γ , although a small amount of β phase was always detected. Apparently the absorption isotherm represents the direct $\alpha \rightarrow \gamma$ conversion and β phase precipitation is almost completely suppressed. The results are attributed to the influence of lattice strain upon the behavior of the β_1 and β_2 phases. A practical consequence of the effect is the distortion of the pressure-composition isotherm in the β - γ region as a function of hydriding-dehydriding cycles. (10 refs.)

62115 Intermetallic compounds LnNi_5 , $\text{La}_{1-x}\text{Pr}_x\text{Ni}_5$ as sorbents and hydrogenation catalysts ($\text{Ln}=\text{La, Ce, Pr, Nd, Sm, Gd}$). E.M.Savitsky, E.I.Klabunovskii, I.R.Kononenko, N.I.Parfenova, V.P.Mordovin, T.P.Savostyanova, D.E.Bogatin (A.A. Baikov Inst. of Metall., Acad. of Sci., Moscow, USSR).

J. Less-Common Met. (Switzerland), vol.89, no.2, p.528 (Feb. 1983). (International Symposium on the Properties and Applications of Metal Hydrides, Toba, Japan, 30 May-4 June 1982).

Summary form only given, as follows. The sorption properties of the intermetallic compounds LnNi_5 ($\text{Ln}=\text{La, Ce, Pr, Nd, Sm, Gd}$) and $\text{La}_{1-x}\text{Pr}_x\text{Ni}_5$ ($0 \leq x \leq 1$) were studied in the pressure interval 1-60 atm and at a temperature of 20°C. The hydrogen sorption and desorption kinetics were also examined. It was shown that the sorption properties depend on the intermetallic matrix and on the nature of the rare earth metal contained in it. The effect of these intermetallic compounds and some of their hydrides on the hydrogenation of propene and the enantioselective hydrogenation of ethyl acetate on hydrides modified with $\text{RR}(+)\text{tartaric acid}$ was investigated. It was found that the sorption properties of the intermetallic compounds are connected with their catalytic activity in the hydrogenation reactions: the lower is the equilibrium pressure in the intermetallic compound-hydrogen system the higher is the catalytic activity. Some periodic changes in the sorption and catalytic properties of the LnNi_5 compounds was also found. (no refs.)

62116 Comments on 'Hysteresis in metal hydrides'. N.Shohji (Lab. Nacional de Engenharia e Tecnologia Industrial, Dept. de Metalurgia e Metalomecanica, Sacavem, Portugal).

J. Less-Common Met. (Switzerland), vol.90, no.1, p.15-6 (March 1983).

Flanagan and Clewley (1982) have recently developed an interesting approach to the problem of hysteresis in metal hydrides which appears to be qualitatively correct. Unfortunately the quantitative development of their argument does not appear to be very realistic and hence their results may be applicable only to a very limited number of M-H systems. In order to apply their theory to general M-H systems some modification of the equations may be necessary. Some doubtful assumptions in their paper are identified and possible modifications to their equations are proposed. (2 refs.)

62117 Enthalpies of mixing in some binary liquid alkali perchinate mixtures. W.Lukas, M.Gaune-Escard (Lab. de Dynamique et Thermophysique des Fluides, Univ. de Provence, Marseille, France).

J. Less-Common Met. (Switzerland), vol.90, no.1, p.17-18 (March 1983).

The authors aim was to determine the enthalpies of mixing for the liquid systems $\text{LiReO}_4\text{-CsReO}_4$, $\text{NaReO}_4\text{-CsReO}_4$, $\text{KReO}_4\text{-CsReO}_4$ and $\text{RbReO}_4\text{-CsReO}_4$. (11 refs.)

62118 Observation of the relaxation of composition fluctuations in a binary liquid mixture. N.Easwar, M.Joshua, J.V.Maher, W.I.Goldburg (Dept. of Phys. & Astron., Univ. of Pittsburgh, Pittsburgh, PA, USA).

Physica A (Netherlands), vol.118A, no.1-3, p.268-81 (March 1983). (Proceedings of the Conference on Nonlinear Fluid Behavior, Boulder, CO, USA, 7-11 June 1982).

Light scattering was used to study the decay of concentration fluctuations in a critical mixture is isobutyric acid and water. The aim of the experiment was to study the dynamic interaction between composition and velocity in the mixture. At large wavenumber, the structure factor $S(k,t)$ is observed to decay exponentially, with a relaxation rate somewhat smaller than the equilibrium value. At small k , however, there is a marked departure from the exponential relaxation one expects in the absence of coupling between composition and velocity. Also measured was the spinodal ring diameter, k_m , as a function of the total scattered intensity, $C_{\text{tot}}(t) = (2\pi)^{-2} \int S(k,t) k^2 dk$. A calculation of Ruiz, based on the above coupling effect, predicts a linear variation of $\ln k_m(t)$ with $C_{\text{tot}}(t)$ and such a linear variation is observed. (12 refs.)

62119 Fast pressure quenches near the critical point of a binary liquid mixture. E.A.Clerke, J.V.Sengers (Dept. of Phys. & Astron., Univ. of Maryland, College Park, MD, USA).

Physica A (Netherlands), vol.118A, no.1-3, p.350-70 (March 1983). (Proceedings of the Conference on Nonlinear Fluid Behavior, Boulder, CO, USA, 7-11 June 1982).

Spinoal decomposition can be induced in liquid mixtures near the critical point by application of a fast pressure quench. As a result of such a pressure quench 1) the relative temperature of the system with respect to the critical temperature changes because of the dependence of the critical temperature on pressure, and 2) the absolute temperature of the system changes because of the finite value of the adiabatic thermal pressure coefficient. Experiments show that the first effect is dominant in isobutyric acid+water studied by other investigators and the second effect is dominant in 3-methylpentane+nitroethane studied by the authors. It is demonstrated that the adiabatic thermal pressure coefficient undergoes a rapidly varying anomalous behavior at temperatures very close to the critical temperature. (30 refs.)

62120 Dynamics of phase separation in two-dimensional fluids: spinodal decomposition. S.W.Koch, R.C.Desai, F.F.Abraham (IBM Res. Lab., San Jose, CA, USA).

Phys. Rev. A (USA), vol.27, no.4, p.2152-67 (April 1983).

An extensive computer simulation investigation of the time dependence of spinodal decomposition in a two-dimensional, one-component fluid is reported. This investigation includes constant-temperature and constant-energy simulations, both of which are followed to very long times. The authors observe the detailed density morphology, finding different growth regions for the average size of the formed liquid clusters. The late-time growth law for the average cluster size is found to be $t^{1/2}$ for the isothermal and $t^{1/3}$ for the constant-energy simulation, respectively. The physical origin of these results is explained by asymptotic analysis of the governing equations of cluster growth. A linear hydrodynamic theory for the early stages of the separation process is also presented. (22 refs.)

62121 Dissolution kinetics of the compound ZrAl_3 in liquid aluminium. V.N.Eremenko, Ya.V.Natanzon, V.P.Titov.

Russ. Metall. (GB), no.6, p.204-8 (1981). Translation of: *Izv. Akad. Nauk. SSSR Met.*, no.6, p.211-15 (1981).

The method of successive saturation by means of a disc specimen revolving at rate of 16.67 rad/s for 6-15 h was used. During reaction of zirconium with liquid aluminium at 700°C ($\omega=16.67$ rad/s) the rate of formation of the ZrAl_3 phase is higher than the rate of dissolution of zirconium. Dissolution of ZrAl_3 in liquid aluminium at 750°C for the range of rotation speeds of the

disc specimen 6.61-36.80 rad/s is under diffusion conditions. The solubility, the rate constants of dissolution, and the coefficients of diffusion of zirconium in liquid aluminium were determined. (10 refs.)

States of Am in aqueous solution See Entry 60582

Capacity ratios and diffusion coefficients of low-volatile organic compounds in supercritical carbon dioxide from supercritical fluid chromatography (SFC) See Entry 61592

On the possibility of microphase separation in liquid crystalline polymers See Entry 61774

Nature of the chemical bond in titanium hydrocarbides See Entry 61849

Observation of precipitates on 'growth' dislocations in GaAs single crystals with low impurity content See Entry 61926

Changes induced by ion implantation in forsterite SiO_4Mg_2 See Entry 61939

Microhardness of an implanted system See Entry 61944

Impurity incorporation in RAO polysilicon layers and consequences on their electrical properties See Entry 61950

Radiation damage in pure and helium-doped $\alpha\text{-Al}_2\text{O}_3$ in the HVEM. Qualitative aspects of void and aluminium colloid formation See Entry 61973

Damage in the cation sublattice of $\alpha\text{-Al}_2\text{O}_3$ irradiated in an HVEM See Entry 61974

Microstructural changes in irradiated silica based glasses See Entry 61975

Precipitation and void-swelling in nickel-manganese austenitic stainless steels See Entry 61986

Radiation damage, its recovery and platinum behavior and lattice location in ion bombarded MgO and Al_2O_3 as used for catalytic studies See Entry 61990

Pressure effects and ultrasonic attenuation in the binary liquid mixture 3-methylpentane and nitroethane near the critical point See Entry 62031

Localized mode energies and hydrogen potential in refractory metals See Entry 62047

Thermodynamic calculation of supercritical-fluid equilibria: New mixing rules for equations of state See Entry 62052

The establishment of equilibria in the $\text{Pd-H}_2\text{-D}_2\text{-H}_2\text{O-D}_2\text{O}$ system See Entry 62062

A thermodynamic interpretation of the compatibility of chlorinated polyethylene with poly(methylmethacrylate) See Entry 62129

Recovery of quenched Cu-Ge alloys studied by positron annihilation See Entry 62156

Effect of pressure on the fast-ion conduction in $\text{AgI-Ag}_2\text{O-MoO}_3$ glasses See Entry 62161

Interfaces structure in relation with the mechanisms in the reaction copper-silicon See Entry 62279

Influence of growth rate of epitaxial silicon layers on surface segregation of boron, phosphorus, and arsenic See Entry 62302

Crystal, impurity-related and growth defects in molecular beam epitaxial GaAs layers See Entry 62308

Transport phenomena in $\text{TlIn}_x\text{Nd}_{1-x}\text{Se}_2$ solid solutions See Entry 62411

Shape anisotropy of ultrafine magnesium ferrite precipitates See Entry 62720

Time dependent light scattering studies of phase separation in polymer blends See Entry 63008

Interfacial segregation and enhanced sintering processes See Entry 63200

Microstructural changes at grain boundaries during sintering of doped BaTiO_3 ceramics with small additions of TiO_2 See Entry 63248

Interaction of hydrogen with traps and its solubility in maraging steel See Entry 63256

An investigation of the process of decomposition of the supersaturated solid solution of nitrogen in a niobium alloy See Entry 63258

Phase equilibrium diagram for the vanadium-rhenium system See Entry 63259

The magnetism corner of the Mg-Y-Ce system See Entry 63264

Investigation of the phase composition, structure, and magnetic properties of alloy $\text{Sm}_2\text{Co}_{10}\text{Fe}_{3.2}\text{Cu}_{1.2}\text{Zr}_{0.4}$ See Entry 63287

Decomposition kinetics for supercooled austenite in steel 15Kh1M1F See Entry 63288

Computer modelling of grain boundary segregation See Entry 63294

On the coarsening of γ' in Alloy 800 See Entry 63295

A study of precipitation in interstitial alloys. II. A new metastable carbide phase in platinum See Entry 63296

A study of precipitation in interstitial alloys. III. Coherent and semicoherent growth mechanisms See Entry 63297

A study of precipitation in interstitial alloys. IV. The precipitation sequence in Pt-C See Entry 63298

Resolution of Cu atoms in a GP[1] zone in Al-Cu by FIM and determination of the GP[1] structure See Entry 63299

Crystallographic aspects of precipitation of supersaturated aluminum-base solid solutions See Entry 63300

The effect of the nitrogen potential on the coarsening kinetics of VN precipitates See Entry 63301

Influence of sulfur and nitrogen on the characteristics of texture formation as a result of deformation and annealing of Fe+3% Si single crystals See Entry 63309

Structure and properties of low-pearlite steel with different titanium concentrations See Entry 63330

Effect of structure on the ductile-brittle transition temperature of molybdenum alloy TsM-6 See Entry 63406

Failure mechanism for alloy KhN67VM under the action of a copper-silver solder See Entry 63411

Intergranular zinc embrittlement and its inhibition by phosphorus in 55 pct Al-Zn-coated sheet steel See Entry 63453

Comments on 'Kinetics and mechanism of the U-H reaction' See Entry 63536

Anodic polarization behaviour of hydride-deuteride electrodes See Entry 63561

Enthalpies of formation of liquid and solid binary alloys based on 3d metals. III. Alloys of iron See Entry 63581

Hydrogen storage in thin film metal hydrides See Entry 63738

- Life properties of Ti-Mn alloy hydrides and their hydrogen purification effect See Entry 63739
 Hydrogen absorption in $\text{La}_3\text{Ni}_3\text{B}_2$ See Entry 63746

64.80 OTHER PHASE PROPERTIES OF SYSTEMS

- Physicochemical properties of alloys of HgTe-MgTe system .. See Entry 61875
 EuS ferromagnetic semiconductor films grown epitaxially on silicon See Entry 62296
 Phase equilibrium in the Ti-Se system at high pressures See Entry 63269
 The $\text{Te-Tl}_5\text{As}_2\text{Te}_3\text{-Tl}_5\text{Te}_3$ system See Entry 63270
 Investigation of the phase composition, structure, and magnetic properties of alloy $\text{Sm}_2\text{Co}_{10}\text{Fe}_{3.2}\text{Cu}_{1.2}\text{Zr}_{0.4}$ See Entry 63287
 Structure and properties of low-pearlite steel with different titanium concentrations See Entry 63330

65.00 THERMAL PROPERTIES OF CONDENSED MATTER

(see also 05.70 Thermodynamics, 63. Lattice dynamics; for thermal conduction in nonmetallic liquids, see 66.60; for thermal conduction in nonmetallic solids, see 66.70; for electronic thermal conduction, see 72.15, 72.20 and 74.30E; for thermodynamic properties of quantum fluids, see 67.40, 67.50, and 67.60; for thermal properties of solid helium, see 67.80)

65.20 HEAT CAPACITIES OF LIQUIDS

- Pressure effects and ultrasonic attenuation in the binary liquid mixture 3-methylpentane and nitroethane near the critical point See Entry 62031

65.40 HEAT CAPACITIES OF SOLIDS

(for specific heat of superconductors, see 74.30E; for specific heat of magnetic systems, see 75.40)

- 62122 Thermodynamic properties of Si_2ON_2 . V.I.Koshchenko, Ya.Kh.Grinberg (D.I. Mendeleev Moscow Chem. Technol. Inst., Moscow, USSR). *Inorg. Mater. (USA)*, vol.18, no.6, p.884-6 (June 1982). Translation of: *Izv. Akad. Nauk SSSR Neorg. Mater.*, vol.18, no.6, p.1047-9 (June 1982). [received: Feb. 1983]
 Measures the heat capacity of Si_2ON_2 in the range of 5-100K with a vacuum adiabatic calorimeter with automatic control of the adiabatic conditions. Liquid helium and nitrogen were used as the cooling agents. The relative error in the determination of C_p was 0.9 and 0.3% for temperature ranges of 5-25 and 25-100K, respectively. Benzoic acid was used as the standard for determination of the error. (5 refs.)

- 62123 Low temperature thermodynamics of asymmetric Anderson model. N.Kawakami, A.Okiji (Dept. of Appl. Phys., Osaka Univ., Osaka, Japan). *J. Phys. Soc. Jpn. (Japan)*, vol.52, no.4, p.1119-21 (April 1983).
 With the use of the exact solution, the coefficient of the electronic specific heat (γ) for the asymmetric Anderson model is calculated in the presence of an arbitrary magnetic field. It is also shown that the relation $\gamma = 1/2(\chi_m + \chi_c)$ holds exactly, where χ_m and χ_c are the magnetic and charge susceptibilities at finite magnetic fields. (6 refs.)

- 62124 High temperature heat capacity of some Ag-Nd alloys. A.M.Mulokozi, I.Stapf, H.Jehn (Max-Planck-Inst. für Metallforschung, Inst. für Werkstoffwissenschaften, Stuttgart, Germany). *J. Less-Common Met. (Switzerland)*, vol.90, no.1, p.75-82 (March 1983).
 The heat capacity of Ag-Nd alloys containing 30-45 at.% Nd was investigated in the temperature range 770-950K. The heat of transformation of the Ag_2Nd compound was determined as $122 \text{ J (g atom)}^{-1}$ at 893K. The stress effects on the thermodynamic properties as a result of the orthorhombic-hexagonal phase transformation of Ag_2Nd are discussed. The results confirm the need to complement differential thermal analysis studies with independent observations in order to obtain reliable information on the phase diagrams of silver alloys with light rare earth metals. (7 refs.)

- 62125 Low-temperature specific heats for amorphous Fe-B and Co-B alloys. M.Matsuura (Miyagi Tech. Coll., Miyagi, Japan), U.Mizutani. *J. Magn. & Magn. Mater. (Netherlands)*, vol.31-34, pt.3, p.1481-2 (Feb. 1983). (Proceedings of the International Conference on Magnetism, Kyoto, Japan, 6-10 Sept. 1982).

The low-temperature specific heats for amorphous Fe-B and Co-B alloys have been measured over the temperature range 1.5-6K. Like other physical properties for both amorphous alloys, the specific heats show marked contrast with each other. (10 refs.)

- Characterization studies of $\text{AgI-Ag}_2\text{O-MoO}_3$ glasses See Entry 61810
 Lattice dynamics of FCC Ca See Entry 62046
 Evidence for the incommensurate phase in AlPO_4 near α - β transition: a differential scanning calorimetry study See Entry 62087
 Thermodynamic properties of Si_3N_4 See Entry 62127
 The relationship between the Gruneisen and other thermodynamic parameters and intermolecular forces in polymers See Entry 62130
 Temperature-induced local moments in MnSi and FeSi See Entry 62549

65.50 THERMODYNAMIC PROPERTIES AND ENTROPY

- 62126 Comparison of the fitting capabilities of several equations for the composition dependence of excess free enthalpy in binary alloys. J.Vrestal, J.Velisek (Inst. of Phys. Metall., Czechoslovak Acad. of Sci., Brno, Czechoslovakia). *CALPHAD: Comput. Coupling Phase Diagrams & Thermochem. (GB)*, vol.6, no.4, p.297-305 (1982).
 One of the main tasks of thermodynamics in physical metallurgy is the determination of the stability of complex metallic systems. With the development of the basis of single-phase thermodynamic data, an experimental determina-

tion of equilibrium diagrams is frequently complemented by their calculation using thermodynamic methods. For the reasons of calculation it is important to express the dependence of the experimental thermodynamic data (i.e. integral and/or partial excess free enthalpy) on the molar fraction of components. Various functions have been developed to express this dependence and the fitting capabilities of several of these equations are compared with respect to the experimental data for binary metallic systems. (9 refs.)

- 62127 Thermodynamic properties of Si_3N_4 . V.I.Koshchenko, Ya.Kh.Grinberg (D.I. Mendeleev Chem. Technol. Inst., Moscow, USSR). *Inorg. Mater. (USA)*, vol.18, no.6, p.903-5 (June 1982). Translation of: *Izv. Akad. Nauk SSSR Neorg. Mater.*, vol.18, no.6, p.1064-6 (June 1982). [received: Feb. 1983]
 Trisilicon tetranitride was obtained by nitriding elementary silicon at 1723K. To measure the heat capacity over the range 5-100K, use was made of a vacuum adiabatic calorimetric apparatus with automatic regulation of the adiabatic conditions. Liquid nitrogen and liquid helium were used as refrigerants. From the value of the ordinates of the $C_p(T)$ and $C_p(\ln T)$ curves, determinations were made, by numerical integration of the values of the enthalpy, $H^0 - H^0_0$, and the entropy, $S^0 - S^0_0$, from which the values of the Gibbs energy function, $(G^0 - H^0_0)/T$, were found. (6 refs.)

- 62128 Thermal stability of cesium monouranate. Shyamala Bharadwaj, S.R.Dharwadkar, G.Chattopadhyay, M.S.Chandrasekhariah (Bhabha Atomic Res. Centre, Bombay, India). *J. Nucl. Mater. (Netherlands)*, vol.114, no.2-3, p.344-6 (Feb. 1983).
 A recent assessment by Sturcken (J. Nucl. Mater., vol.50, p.69, 1974) has shown considerable inconsistency in the thermal stability of Cs_2UO_4 . The authors were prompted to reinvestigate this material. A careful thermogravimetric study with a microbalance in a controlled gaseous environment showed that traces of moisture have considerable influence on the decomposition temperature of this phase. (11 refs.)

- 62129 A thermodynamic interpretation of the compatibility of chlorinated polyethylene with poly(methylmethacrylate). Chai Zhikuan, Sun Rouna (Inst. of Chem., Acad. Sinica, Beijing, China), D.J.Walsh, J.S.Higgins. *Polymer (GB)*, vol.24, no.3, p.263-70 (March 1983).
 The compatibility of chlorinated polyethylene with poly(methylmethacrylate) and the oligomer analogue chlorinated octadecane with oligomeric PMMA are interpreted using the equation of state theory. It is found that the interaction energy parameter χ_{12} and the interaction entropy parameter χ_{12} , obtained from the heat of mixing and the phase boundary of oligomeric mixtures, can be used to generate the phase boundary of the polymer mixture. The spinodals of different molecular weights so generated have less molecular weight dependence than might be expected, in agreement with experimental results. A negative χ_{12} indicates that some ordering may exist in the mixture due to specific interactions. (16 refs.)

- 62130 The relationship between the Gruneisen and other thermodynamic parameters and intermolecular forces in polymers. B.K.Sharma (Dept. of Phys., Regional Coll. of Education, Bhubaneswar, India). *Polymer (GB)*, vol.24, no.3, p.314-18 (March 1983).

A simple relationship between the Gruneisen parameter and Beyer's non-linearity parameter in the case of polymers has been obtained in terms of Mie potential parameters from the pressure dependence of bulk modulus. Using this simple model, it is shown that Beyer's parameter of nonlinearity, Carnevale and Litovitz's acoustical parameter, Moelwyn-Hughes parameter and the Gruneisen parameter are all related to each other and express the same physical quantity for polymers. The contribution of interchain vibrations to the total specific heat and the specific heat ratio has been found from the Gruneisen parameter in case of twelve polymers. It is proposed that the dependence of the isobaric specific heat of polymeric materials on the interchain forces is stronger than of the isochoric specific heat. (52 refs.)

- 62131 Shift of the electron chemical potential in relation to particle size in highly dispersed systems. N.S.Lidorenko, S.P.Chizhik, N.T.Gladikh, L.K.Grigor'yeva, R.N.Kuklin, R.G.Melkadze. *Russ. Metall. (GB)*, no.6, p.883-93 (1981). Translation of: *Izv. Akad. Nauk SSSR Met.*, no.6, p.91-5 (1981).

Due to the dimensional vacancy effect in high-dispersion systems, the chemical electron potential is lower than in the massive material. The dimensional shift of the electron potential leads to a decrease in the electron heat capacity, the magnetic susceptibility, the speed of sound in the small particle, and to an increase in compressibility, the speed of sound in the small particle, and to an increase in compressibility, and this explains the decrease in the cohesion energy and the ability of disperse particles to coagulate. The estimated decrease of the melting point of small particles based on the dimensional shift in the chemical potential of the electron is in agreement with experimental results. (15 refs.)

- 62132 Thermodynamics of nitrogen solutions in alloyed austenite. L.A.Bol'shov. *Russ. Metall. (GB)*, no.6, p.112-18 (1981). Translation of: *Izv. Akad. Nauk SSSR Met.*, no.6, p.115-19 (1981).

A statistical theory is proposed for the thermodynamic activity of nitrogen dissolved in austenite that contains considerable concentrations of alloying transition metals. In the general case it is not possible to describe this quantity for the entire range of possible compositions by means of generalised reaction parameters, because the series are divergent. Use of first- and second-order interaction parameters does not give good agreement with experimental values of the constants of the Sieverts law for nitrogen in the austenitic phase for the stainless 18/5 chromium-nickel steel at 1050°C. Calculation by means of a formula shows good agreement with experimental data. (21 refs.)

- A note on the use of different representations of excess-energies in ternary systems See Entry 59748

- Theoretical prediction of domain sizes in IPNs and related materials See Entry 61824

- pVT data for liquid and solid hexamethyldisilane up to 3000 bar See Entry 62053

- Phase equilibria in systems of TIX with Cd(Zn)X ($X = \text{S, Se, Te}$) See Entry 62060

- Thermophysical properties of supercritical fluids with special consideration of aqueous systems See Entry 62073

- Thermodynamic functions for the congruent sublimation of cadmium telluride .. See Entry 62080

- Thermodynamics of the CaO-SiO_2 system See Entry 62109

- An empirical correlation between enthalpy and entropy interaction coefficients See Entry 62110

- Comments on 'Hysteresis in metal hydrides' See Entry 62116

- Relationship between parameters of self-diffusion and of equilibrium defects and characteristics of monatomic crystals See Entry 62149

- Thermal effects accompanying the heating of metallized powders See Entry 63251
- Coupled phase diagram and thermodynamic analysis of the 18 binary systems formed among Li_2CO_3 , K_2CO_3 , Na_2CO_3 , LiOH , KOH , NaOH , Li_2SO_4 , K_2SO_4 and Na_2SO_4 See Entry 63267
- Thermodynamics of homogeneous formation of cementite in austenite during case hardening of steel See Entry 63462
- Enthalpies of formation of liquid and solid binary alloys based on 3d metals. III. Alloys of iron See Entry 63581

65.70 THERMAL EXPANSION AND THERMOMECHANICAL EFFECTS

(see also 64.30 Equations of state; for electronic thermal conduction, see 72.15 and 72.20; for thermal conductivity of superconductors, see 74.30E; for pyroelectric and electrocaloric effects, see 77.70)

- 62133 Thermal expansion of barium orthovanadate. T.I.Krasnenko, O.N.Syrneva, A.A.Fotiev (Inst. of Chem., Ural Sci., Center, Acad. of Sci., Sverdlovsk, USSR). *Inorg. Mater. (USA)*, vol.18, no.6, p.890-1 (June 1982). Translation of: *Izv. Akad. Nauk SSSR Neorg. Mater.*, vol.18, no.6, p.1052-3 (June 1982). [received: Feb. 1983]
- Uses $\text{Ba}_3(\text{VO}_4)_2$, the single-phase character of which was confirmed by X-ray diffraction. The X-ray and thermal studies were made with powdered $\text{Ba}_3(\text{VO}_4)_2$ and pellets were prepared for the measurements. Graphs of the dependence of the unit cell parameters and the coefficient of volume expansion of $\text{Ba}_3(\text{VO}_4)_2$ on the temperature are presented. It was established that the character of the α and $c(T)$ curves changes over the 1070-1200K range. The parameters of the samples hardened from 1270K in air and slowly cooled from the same temperature agree with the parameters of the starting sample within the limits of the experimental error. (2 refs.)
- 62134 Anomalous thermal expansion of europium vanadate. N.R.S.Reddy, K.S.Murthy (Dept. of Phys., Univ. Coll. of Sci., Osmania Univ., Hyderabad, India). *J. Less-Common Met. (Switzerland)*, vol.90, no.1, p.L7-8 (March 1983).
- The rare earth vanadates RVO_4 (R=trivalent rare earth ion) crystallize in the tetragonal zircon structure (space group, $I4_1/amd$). As part of a general programme of X-ray investigations of zircon-type compounds, the authors investigated the thermal expansion of europium vanadate at high temperatures. Accurate lattice parameters and the coefficients of thermal expansion at various high temperatures are presented. (3 refs.)
- 62135 Anomalous thermal expansion and character of layers of MV_2O_6 metavanadates ($M=\text{Ca}$, Cd , Zn , Mg , Pb). P.Garnier, D.Weigel (Ecole Centrale des Arts et Manufactures, Chateauf-Malabry, France). *J. Solid State Chem. (USA)*, vol.47, no.1, p.16-23 (15 March 1983). In French.
- The variations of cell parameters and thermal expansion tensors of metavanadates MV_2O_6 have been measured in the range 77-295K. The thermal expansion anisotropy is characteristic of layer structures especially for brannerite-type structures ($M=\text{Cd}$, Zn , Mg); this anisotropy is explained by the presence of $[\text{VO}_5]$ polyhedra, such as occur in the V_2O_5 layer structure. For CaV_2O_6 the variation of thermal expansion as a function of temperature is abnormal; peaks, typical of a diffuse transition, are observed at 260K for $\alpha_1(T)$ and $\alpha_2(T)$ curves. The temperature anomaly is reduced when cadmium is substituted for calcium. (19 refs.)
- 62136 Thermal expansion coefficient of alkali metals. T.Soma, H.-M.Kagaya, Y.Kimura (Dept. of Appl. Phys. & Maths., Mining College, Akita Univ., Akita, Japan). *Phys. Status Solidi b (Germany)*, vol.116, no.1, p.57-61 (1 March 1983).
- The thermal expansion of alkali metals is investigated using a local Heine-Abarankov model potential in the perturbational method. The mode Grüneisen parameters and the temperature-dependence of both the mean Grüneisen constant and the thermal expansion coefficient are calculated, and the obtained results are quantitatively in good agreement with the experimental data. (31 refs.)
- Density and thermal expansion of liquid U-Nb alloys See Entry 62007
- Pressure effects and ultrasonic attenuation in the binary liquid mixture 3-methylpentane and nitroethane near the critical point See Entry 62031
- Effect of three-body forces on thermophysical and anharmonic properties of rare gas solid mixtures See Entry 62041
- Phase-transition studies in polymesomorphic compounds. I. Density studies in *N*-(*p*-*n*-hexyloxybenzylidene)-*p*-*n*-butylaniline See Entry 62097
- Magnetoelastic phase transition in KMnF_3 See Entry 62592
- Single crystal growth and physical properties of cubic $\text{Zn}_3\text{O}(\text{BO}_2)_6$ See Entry 63151

65.90 OTHER TOPICS IN THERMAL PROPERTIES OF CONDENSED MATTER

- 62137 Experimental and theoretical studies of the influence of surface conditions on radiative properties of opaque materials. P.Demont, M.Huetz-Aubert, H.Tran N'Guyen (Groupe de Recherches Thermiques Ecole Centrale des Arts et Manufactures, Chateauf-Malabry, France). *Int. J. Thermophys. (USA)*, vol.3, no.4, p.335-64 (Dec. 1982). [received: April 1983]
- Radiative properties of opaque materials strongly depend on their surface condition. The fabrication of superficial cavities of various forms and dimensions modifies the directional spectral emissivities or absorptivities. They are usually increased compared to those of optically smooth material; the gain depends on the material, the type of cavities, as well as the wavelength λ and the direction Δ of the emitted or incident radiation. When grooves of dimensions larger than λ are fabricated in a sample, the models, taking into account the successive reflections on their inner sides, give a good agreement with experimental data. But a similar theory does not explain the substantial increase of the infrared emissivity of ballblasted samples. (22 refs.)
- Thermal model for interference laser annealing See Entry 61964
- Effect of solar gain through walls and windows on annual building heat needs See Entry 63643

66.00 TRANSPORT PROPERTIES OF CONDENSED MATTER (NONELECTRONIC)

66.10 DIFFUSION AND IONIC CONDUCTION IN LIQUIDS

- 62138 Predict liquid-phase diffusion coefficients. J.H.Weber (Univ. of Nebraska, Lincoln, NE, USA). *Chem. Eng. (USA)*, vol.90, no.5, p.161-3 (7 March 1983).
- Presents a program for the Texas Instruments TI-59 calculator to determine diffusion coefficients in dilute two-component solutions. The Wilke-Chang (1955), Scheibel (1954) and Reddy-Doraiswamy (1971) correlations are programmed, together with methods for finding liquid volume and viscosity. The program is listed in full. (7 refs.)
- 62139 Transport number of charge-transfer complexes in solution. V.P.Shedibalkar, S.N.Bhat (Chem. Dept., North-Eastern Hill Univ., Shillong, India). *Electrochim. Acta (GB)*, vol.28, no.3, p.359-61 (March 1983).
- Iodine, which is generally a nonconductor in nonpolar solvents, conducts electricity in methanol, ethanol and water. The majority of the charge carriers in the solutions of charge-transfer complexes of methanol-iodine and ethanol-iodine are anion constituents ($i_{-25^\circ\text{C}}$ are 0.739, 0.728 for 0.1N solution of iodine in methanol and ethanol respectively) and for water-iodine it is cation constituent ($i_{+25^\circ\text{C}}$ is 0.905 for 0.0024N iodine). The transport number of anion decreases with the increase in temperature whereas it increases with the increase in concentration at 25°C. (12 refs.)
- 62140 Pressure dependence of conductance of the lithium and cesium ions in cooled and supercooled water. N.Takizawa, J.Osugi, M.Nakahara (Dept. of Chem., Kyoto Univ., Kyoto, Japan). *J. Chem. Phys. (USA)*, vol.78, no.5, p.2591-7 (1 March 1983).
- Limiting molar conductances (λ^0) of the Li^+ and Cs^+ ions in water have been determined at 0, -5, and -10°C as a function of pressure up to 2 kbar. In the studied ranges of pressure and temperature, $\lambda^0(\text{Li}^+)$ increases monotonically with increasing pressure and $\lambda^0(\text{Cs}^+)$ has a maximum against pressure. The low-temperature conductances fit well an empirical equation of the critical law form over the pressure range studied; $\lambda^0=A(T/T_c-1)^{-1}$. The parameter T_c decreases with a rise in pressure below 1.5 kbar, but above that T_c is almost constant. The Hubbard-Onsager (HO) dielectric friction theory has been critically tested against the experimental results obtained under the extreme conditions after λ^0 are transformed into the drag coefficient ($\Delta\zeta$) subtracted by that due to Stokes' law for perfect slip ($4\pi\eta R$). The observed pressure coefficient $d\Delta\zeta/dP$ is negative for the small ion Li^+ even in cooled or supercooled water as predicted by the HO theory but positive for the large ion Cs^+ in contrast to the theoretical prediction. The following three kinds of anomalies in $\Delta\zeta(\text{Cs}^+)$ are revealed: $\Delta\zeta<0$, $d\Delta\zeta/dP>0$, and $d\Delta\zeta/dT>0$. The PTC mechanism proposed for explaining the large anomalies has been supported by model calculations; it turns out that the potential for the PTC process can be flat with a reasonable size of cavities. (30 refs.)
- 62141 Theory of conductance and related isothermal transport coefficients in electrolytes. A.R.Altenberger, H.L.Friedman (Chem. Dept., State Univ. of New York, Stony Brook, NY, USA). *J. Chem. Phys. (USA)*, vol.78, no.6, pt.2, p.4162-73 (15 March 1983).
- The transport coefficients are calculated from consideration of the fluctuations in local ion concentrations in view of a recent advance in the theory of inhomogeneous systems at equilibrium. The theory is applicable to mixed electrolytes of arbitrary charge type and to frequency dependent phenomena, although the example worked out here is for the zero frequency coefficients for a binary electrolyte. (43 refs.)
- 62142 Diffusivity in zinc chloride-potassium chloride electrolyte. D.Lof-tus, J.Roberts, R.Weaver, S.Leach, L.Nanis (SRI Internat., Menlo Park, CA, USA). *J. Electrochem. Soc. (USA)*, vol.130, no.2, p.332-4 (Feb. 1983).
- Integral and differential salt diffusivities have been measured by the capillary method for electrolytes of interest to mass transfer of zinc in the zinc-chlorine hydrate battery. No dependence of diffusivity on the concentration of ZnCl_2 was found over the range 0.4-1.6M ZnCl_2 in 3.5M KCl. The average diffusivity was $0.88\times 10^{-5}\text{ cm}^2\text{ sec}^{-1}$ at 26.5°C and $1.49\times 10^{-5}\text{ cm}^2\text{ sec}^{-1}$ at 47.5°C. (9 refs.)
- 62143 Chronopotentiometry of one- and two-ion transport at immiscible liquid interfaces: tests of theory. O.R.Melroy, W.E.Bronner, R.P.Buck (Dept. of Chem., Univ. of North Carolina, Chapel Hill, NC, USA). *J. Electrochem. Soc. (USA)*, vol.130, no.2, p.373-80 (Feb. 1983).
- Experimental verification for theoretical behavior of ion crossings at a water/nitrobenzene interface is given. This includes study of migration-dependent single ion transport, as well as diffusion-controlled simultaneous and successive two-ion transport. Chronopotentiograms have been obtained for tetra-n-alkylammonium salts from methyl through heptyl and for tetrabutylammonium ion in supporting electrolytes CsCl through LiCl . These are discussed in terms of partitioning effects, interfering ions, limited potential windows, and free energies of ion transfer. Problems in obtaining 'true' transition times and associated transfer coefficients for various ammonium ions are also discussed. (38 refs.)
- 62144 Diffusion and permeation of hydrogen in sodium [liquid]. J.Trouve, G.Laplanche (Dept. des Reacteurs a Neutrons Rapides, CEN, Saint Paul Lez Durance, France). *J. Nucl. Mater. (Netherlands)*, vol.115, no.1, p.56-62 (March 1983). In French.
- Knowledge about the behaviour of hydrogen impurity in liquid sodium is essential for the design of steam generators in fast reactors. This provides the motivation for the authors' study, in which the behaviour of a thin nickel sheet, serving to measure hydrogen content, was analysed and the diffusion coefficient of hydrogen in sodium was estimated. The aim was to determine an order of magnitude for this coefficient, and its variation as a function of temperature. (6 refs.)
- 62145 Diffusion of oxygen in molten iron. D.Ya.Povolotskiy, O.K.Tokoyov, A.P.Fedulov. *Russ. Metall. (GB)*, no.6, p.52-8 (1981). Translation of: *Izv. Akad. Nauk SSSR Met.*, no.6, p.55-60 (1981).
- A non-steady-state electrochemical method was used to measure the diffusion coefficient of oxygen in liquid iron in the temperature range 1550-1650°C and the activity coefficient of oxygen in iron with initial oxygen contents of 0.0030-0.950%. The temperature dependence of the diffusion coefficient of oxygen in liquid iron was determined. It was found that the content in liquid iron influences only slightly its diffusion coefficient. (16 refs.)

- Investigation of diffusion of UO_2Cl_2 in saturated NaCl solutions See Entry 60296
- On diffusional mobility of chain molecules See Entry 61036
- A modified Wigner function set for the Smoluchowski operator representation in anisotropic liquids See Entry 61743
- Chemical effects in diffusion and structure of zinc chloride in aqueous solution See Entry 61757
- Dynamics of compatible polymer mixtures See Entry 61770
- Dissolution kinetics of the compound ZrAl_3 in liquid aluminium See Entry 62121
- Transport properties in the zero order Gaussian memory function approximation with phase integrals evaluated from Monte Carlo calculations See Entry 62148
- Diffusion controlled processes among stationary reactive sinks: effective medium approach See Entry 63520

66.20 DIFFUSIVE MOMENTUM TRANSPORT

(inc. viscosity of liquids)

- 62146 An optimal equation for the temperature dependence of the relative viscosity of water in the range of 0...100°C. J.Einfeldt, M.Grigo, N.Schmelzer (Sektion Phys., Pieck Univ. Rostock, Rostock, Germany). *Exp. Tech. Phys. (Germany)*, vol.31, no.1, p.11-20 (1983). In German. Based on the most accurate experimental results of the viscosity of water and their recalculation by Kestin et al. (1973) the present authors have found an optimal temperature-viscosity relation in the range of 0...100°C with the 68.3%-confidential range of 0.01%. This equation reproduces all experimental data within experimental accuracy of 0.1%. With a given temperature-density equation it is also possible to calculate the temperature dependence of the kinematic viscosity of water. The given sets of data and equations can be proposed as a standard for the calibration of viscosimeters. (11 refs.)
- 62147 Viscosity of molten fluorozirconates. Hefang Hu, J.D.Mackenzie (Materials Sci. & Engng. Dept., Univ. of California, Los Angeles, CA, USA). *Non-Cryst. Solids (Netherlands)*, vol.54, no.3, p.241-51 (March 1983). The viscosity of a series of molten fluorozirconates with chemical composition of $30\text{BaF}_2\cdot 60\text{ZrF}_4\cdot 10\text{RF}_n$ (mol.%), where R represents Li, Na, K, Ca, Ba, Zn, Pb, Al, Y, La and Th, has been measured as a function of temperature in a nitrogen atmosphere from 550 to 950°C. Their viscous behavior is characterized by a low viscosity relative to normal glass-forming systems and a rapidly increasing activation energy for viscous flow with decreasing temperature. The melts probably consist of short chains or small rings of Zr_2F_9 anions linked together by cations through non-bridging fluorines. Similar to associated liquids, the degree of association increases with decreasing temperature. (24 refs.)
- 62148 Transport properties in the zero order Gaussian memory function approximation with phase integrals evaluated from Monte Carlo calculations. M.Luckas, K.Lucas (Fachgebiet Thermodynamik, Univ. Duisburg, Duisburg, Germany). *Mol. Phys. (GB)*, vol.48, no.5, p.989-1002 (10 April 1983). A Gaussian approximation to the zero order memory function is used to predict diffusion coefficient, viscosity and thermal conductivity of a pure Lennard-Jones fluid over a large region of states. Equilibrium integrals over the pair and triplet correlation functions are evaluated by Monte Carlo simulations. The results are qualitatively reasonable, but differ in detail from computer experiments and argon data. Various other approximations are also discussed. (17 refs.)
- A system for determining fluid properties up to 136 MPa and 473K See Entry 59794
- Physical properties of liquid crystals of 4-(4-nalkylbicyclo[2,2,2]octyl)benzonitriles See Entry 61793
- Investigation of nematic liquid crystals by correlation spectroscopy. Determination of ratios of viscosity and elasticity constants See Entry 61794

66.30 DIFFUSION IN SOLIDS

- Monte Carlo simulation of diffusion of gases in a porous solid: calculations for a new class of solids See Entry 61549
- On the rate theory for pulsed irradiation See Entry 61957
- Interfacial segregation and enhanced sintering processes See Entry 63200

66.30D Theory of diffusion and ionic conduction in solids

- 62149 Relationship between parameters of self-diffusion and of equilibrium defects and characteristics of monatomic crystals. S.M.Klotsman (Inst. of Metal Phys., Acad. of Sci., Sverdlovsk, USSR). *Fiz. Met. & Metalloved. (USSR)*, vol.55, no.2, p.297-309 (Feb. 1983). In Russian. English translation in: *Phys. Met. & Metallogr. (GB)*. It is demonstrated that a universal relationship between the self-diffusion parameters and the usually employed thermodynamic characteristics can be established for all monatomic crystals. An analysis of the results obtained only for crystals with monotypic binding forces based on two characteristics (melting point and Debye temperature) reflecting different properties of the interaction potential can yield the dependences of the parameters of self-diffusion and equilibrium defects on these characteristics. These dependences are at least as accurate as the results of experimental determinations of the enthalpy of activation of formation of equilibrium defects and of self-diffusion. (23 refs.) A.T.
- 62150 Motion mechanisms in framework solid electrolytes: correlated hopping and liquidlike diffusion. S.H.Jacobson (Xerox Corp., Rochester, NJ, USA), M.A.Ratner, A.Nitzan. *J. Chem. Phys. (USA)*, vol.78, no.6, pt.2, p.4154-61 (15 March 1983). Motion mechanisms for ions in framework solid electrolytes are investigated. The results are obtained from numerical studies on a one-dimensional model system, utilizing the method of stochastic Langevin dynamics. The authors find that, for commensurate systems (for which one mobile ion occurs exactly every l lattice sites), the mechanism always involves correlated hops, and the ion-ion repulsion decreases (always) the total conductivity. For incommensurate systems, the conductivity changes from hopping to liquidlike as the interaction forces are increased to dominate the potential due to the framework lattice. Different assumed ion-ion potentials produce different correlations, both local and overall; the nearest-neighbor harmonic forces, such as are

assumed in the Frenkel-Kontorova model, will generally produce substantially different correlation effects from the Coulomb repulsion. The frequency-dependent conductivity at low frequency is shown to be proportional to the square of the frequency; the proportionality coefficient is positive for correlated hopping mechanisms. A double-peaked structure in the frequency-dependent conductivity, due to local oscillation and to long-time, long-range diffusive behavior, is observed when particle-particle interactions are absent and damping is weak. (31 refs.)

- 62151 Modeling of high field ionic conduction in anodic oxide films. L.Young, D.J.Smith (Electrical Engng. Dept., Univ. of British Columbia, Vancouver, BC, Canada). *J. Electrochem. Soc. (USA)*, vol.130, no.2, p.408-12 (Feb. 1983). Experimental data for the stepped current and open-circuit transient methods were fitted to one form of the modeling equations given by Dignam (1965). A good representation of the data was obtained except that extreme linearity was found for $\log J_2$ vs. E data for the peak field in stepped current experiments where some degree of nonlinearity was expected. Another question involves the role of electrolyte incorporation in causing the observed curvature of steady-state $\log J$ vs. E plots. It is shown that if a model is preferred in which the history effects are due to structural changes in the glassy oxide rather than to the special current-driven polarization model of Dignam, then one can obtain equations equivalent to Dinam's by writing the activation energy for ionic transport as a function of a parameter describing the structural condition of oxide, except that some relations between parameters which follow naturally from Dignam's model do not then appear. (20 refs.)
- 62152 Random walk properties of lattices and correlation factors for diffusion via the vacancy mechanism in crystals. M.Koiwa, S.Ishioaka (Res. Inst. for Iron, Steel & Other Metals, Tohoku Univ., Sendai, Japan). *J. Stat. Phys. (USA)*, vol.30, no.2, p.477-85 (Feb. 1983). (Proceedings of a Symposium on Random Walks and Their Application to the Physical and Biological Sciences, Gaithersburg, MD, USA, 28 June-1 July 1982). Random walk properties and correlation factors for diffusion via the vacancy mechanism are calculated and compared for various three-dimensional lattices. By applying the theory of random walks on an imperfect lattice, the correlation factor for impurity diffusion is calculated rigorously for the 'five jump frequency model' in the FCC lattice. (16 refs.)

- Application of the method of time-lag analysis to the study of diffusion in solids of nonhomogeneous macroscopic structure See Entry 62183
- On the theory of stress-assisted diffusion. II See Entry 63437

66.30F Self-diffusion in metals, semimetals, and alloys

- 62153 Solvent diffusion in α -silver-tin alloys. T.Hehenkamp, F.Faupel (Inst. fur Metallphys., Univ. Gottingen, Gottingen/Clausthal, Germany). *Acta Metall. (USA)*, vol.31, no.5, p.691-7 (May 1983). Coefficients for diffusion of Ag 110 m in α -Ag-Sn alloys were measured as a function of temperature and concentration over the temperature range 950-1150K and 0 to 9 at.% tin. The latter involves less experimental effort and, as for relative measurements, even proved to be the more accurate. A strong non-linear increase in the solvent diffusion upon alloying was observed in agreement with results on similar alloys, such as Ag-Cd, Ag-In and Ag-Sb. The marked dependence of solvent diffusion on temperature and impurity concentration is discussed in terms of the complex model proposed by Hehenkamp, Schlett and Sander to describe the solvent and solute diffusion beyond the limit of infinite dilution. Changes in the solvent correlation factor upon alloying are taken into account by introducing effective jump frequencies. It is shown, how the experimentally observed proportionality of the normalized solvent diffusion coefficient to the normalized vacancy concentration serves to get useful information about the diffusion behaviour such as the linear enhancement factor, average effective jump frequencies, activation energies and free binding enthalpies of impurity-vacancy-associates. (21 refs.)
- Magnetic relaxation in amorphous $(\text{Fe}_{1-x}\text{Ni}_x)_2\text{SiO}_{13}$ alloys See Entry 62723
- Diffusion processes in sintering of multicomponent systems See Entry 63201

66.30H Self-diffusion and ionic conduction in nonmetals

- 62154 High field conduction in propylene carbonate. S.Theoleyre, R.Tobazeon (CNRS, Grenoble, France). *C.R. Seances Acad. Sci. Ser. II (France)*, vol.296, no.4, p.241-4 (31 Jan. 1983). In French. Measurements of transient currents and electric fields show that high field conduction in propylene carbonate between metallic electrodes is mainly due to negative ion injection at the metal-liquid interface. The variations of the current with the applied voltage and with the liquid gap are in accordance with the hypothesis that the ion creation is electrochemical in nature. (9 refs.)
- 62155 Influence of hafnia content on the electronic conductivity of binary oxides $\text{CeO}_2\text{-HfO}_2$. E.Debray, P.Malou, B.Chappey (Univ. Paris Val-de-Marne, Creteil, France). *C.R. Seances Acad. Sci. Ser. II (France)*, vol.296, no.5, p.337-42 (7 Feb. 1983). In French. In $\text{CeO}_2\text{-HfO}_2$ solid solutions, the formative energy of the electronic carriers lowers progressively with hafnia content so long as the latter does not reach the solubility limit; the solute reducing effect is then to a maximum. Beyond the limit the formative energy changes no more whereas the mobility energy is slightly increased. (4 refs.)
- 62156 Recovery of quenched Cu-Ge alloys studied by positron annihilation. I.Kanazawa, H.Murakami, T.Kurihara, Y.Sakurai (Dept. of Phys., Tokyo Gakuji Univ., Tokyo, Japan), M.Doyama. *Jpn. J. Appl. Phys. Part I (Japan)*, vol.22, no.3, p.408-12 (March 1983). The migration stages of single vacancies and vacancy-Ge atom pairs, and their clustering process are studied in quenched Cu-Ge alloys. The decrease in h parameter is observed from about -70°C to about 0°C in quenched Cu-1.0 at.% Ge alloy, and two mechanisms are proposed for this phenomenon. The increase of h parameter is observed by the aging from about 250°C to about 400°C . The stage can be deduced to be the growth of clusters of Ge atoms and vacancies, and gaseous bubbles. The presence of three dimensional small clusters of Ge atoms and vacancies, and stability of the clusters are discussed.

62157 Synthesis and study of electric conductivity of complex oxides in the $\text{Li}_2\text{O-ZnO-TiO}_2$ system. N.V.Porotnikov, N.G.Chaban, K.I.Petrov (M.V. Lomonosov Moscow Inst. of Fine Chem. Technol., Moscow, USSR). *Inorg. Mater. (USA)*, vol.18, no.6, p.906-7 (June 1982). Translation of: *Izv. Akad. Nauk SSSR Neorg. Mater.*, vol.18, no.6, p.1066-7 (June 1982). [received: Feb. 1983]
The authors synthesized several compositions of the $\text{Li}_2\text{O-ZnO-TiO}_2$ ternary system and studied their electric conductivity, which at room temperature does not exceed 10^{-8} S/cm. For $\text{Li}_2\text{ZnTiO}_8$ and $\text{Li}_2\text{Zn}_3\text{Ti}_4\text{O}_{12}$, the dependence of the electric conductivity on temperature is exponential in character. The relatively high value of the electric conductivity is due to the low mobility of lithium ions, which in these phases are located at tetrahedral positions. (9 refs.)

62158 Schottky diodes as a possible supplementary method for ionic transport investigations in semiconducting ionic solids—application to $n\text{-CdF}_2$. R.J.Iwanowski, A.Lemanska-Bajorek, J.M.Langer (Inst. of Phys., Polish Acad. of Sci., Warsaw, Poland). *J. Phys. (France)*, vol.44, no.4, p.553-8 (April 1983).
Transport measurements, including I - V and C - V characteristics, of the $\text{Au}/n\text{-CdF}_2$ (Y, Mn) diodes have been performed at room temperature. Time changes of the net donor concentration profiles, $N_D^{\text{eff}}(W/V)$, for the diodes biased with constant reverse voltage (V_r) as well as for $V_r=0$ are studied and interpreted using a model of the native point defect structure of the case of $n\text{-CdF}_2$. The results obtained show the possibility of observation of ionic transport in the depletion layer of MS junction for which the conditions of large barrier height and relatively small activation energy of the defect motion are fulfilled. (20 refs.)

62159 Chemical durability of ZrO_2 containing glasses. R.G.Simhan (Manville Service Corp., Denver, CO, USA). *J. Non-Cryst. Solids (Netherlands)*, vol.54, no.3, p.335-43 (March 1983).
Durability studies in water and Lawrence solution of two glasses containing 17% and 9% ZrO_2 are reported. The Na and Si leached from both glasses in water and Lawrence solution show the \sqrt{t} dependence confirming the process to be diffusion controlled. This is true even for longer times. In both solutions the glass with 17% ZrO_2 has the lower loss in sodium and silica. The tensile strength of this glass is also higher after immersion in Lawrence solution. Thus with higher amounts of ZrO_2 in the glass composition, the surface of the fibers is better protected. Possibly the formation of a hydrated layer of ZrO_2 on the surface gives protection at all pH values. (9 refs.)

62160 Effects of proton injection on the electrical properties of ice. V.F.Petrenko, R.W.Whitworth, J.W.Glen (Dept. of Phys., Univ. of Birmingham, Birmingham, England). *Philos. Mag. B (GB)*, vol.47, no.3, p.259-78 (March 1983).
Measurements have been made of the electrical properties of thin monocrystalline samples of ice with hydrogen-loaded palladium electrodes which permit the exchange of protons between the electrodes and the ice. At potential differences greater than 400 V, space-charge-limited currents are produced, and simultaneous measurements of the AC dispersion curves show changes due to the space charge. Experiments with blocking electrodes, and with one injecting and one blocking electrode are also described. A theory of the space-charge-limited properties is developed within the framework of the Jacard theory of the electrical properties of ice. This yields mobilities of H_3O^+ ions at -20°C of $\sim 10^{-6}\text{--}10^{-7}\text{ m}^2\text{V}^{-1}\text{ s}^{-1}$, but these values will be lower limits due to trapping. (8 refs.)

62161 Effect of pressure on the fast-ion conduction in $\text{AgI-Ag}_2\text{O-MoO}_3$ glasses. H.Senapati, G.Parthasarathy, S.T.Lakshmi Kumar, K.J.Rao (Solid State & Structural Chem. Unit, Indian Inst. of Sci., Bangalore, India). *Philos. Mag. B (GB)*, vol.47, no.3, p.291-7 (March 1983).
The effect of pressure (up to 80 kbars) on the electrical conductivity of a series of fast-ion conducting $\text{AgI-Ag}_2\text{O-MoO}_3$ glasses has been investigated. The results are consistent with a cluster model. (14 refs.)

62162 Electrical properties of thin solid films of the solid electrolyte $\text{AgI-W}_2\text{O}_8$. S.A.Suthanthiraraj, B.V.R.Chowdary, S.Radhakrishna (Dept. of Phys., Indian Inst. of Technol., Madras, India). *Thin Solid Films (Switzerland)*, vol.101, no.2, p.131-9 (11 March 1983).
A simple electrolytic method of preparing a solid electrolyte, $\text{Ag}_3\text{IW}_2\text{O}_8$, on a silver substrate is described. Films of different quality are formed when the electrolysis is carried out at different temperatures and current densities. X-ray diffraction studies were also carried out in order to confirm the formation of $\text{Ag}_3\text{IW}_2\text{O}_8$ films by calculating the d spacings corresponding to different reflections. The film deposited at 60°C has the best electrical properties, comparable with those of bulk $\text{Ag}_3\text{IW}_2\text{O}_8$, and these films show an electrical conductivity of $1.6 \times 10^{-5}\ \Omega^{-1}\text{ cm}^{-1}$ at 33°C . (7 refs.)

Structural transitions in superionic conductors See Entry 62090
Solubility of hafnium dioxide in cerium dioxide See Entry 62108
Phase transition in $\text{AgPbSb}_3\text{S}_6$ crystals [superionic] See Entry 62462
Vapour growth of argyrodite-type ionic conductors $\text{Cu}_6\text{PS}_4\text{Hal}$
..... See Entry 63171

66.30J Diffusion, migration, and displacement of Kf impurities

62163 Diffusion of rubidium ion in pure silver chloride crystals. P.A.Cardegna, A.L.Laskar (Dept. of Phys. & Astron., Clemson Univ., Clemson, SC, USA). *J. Phys. C (GB)*, vol.16, no.11, p.2075-86 (20 April 1983).
The diffusion of ^{86}Rb in AgCl has been measured in the temperature range 184–448 $^\circ\text{C}$ by a tracer-sectioning technique. The transport of Rb^+ is found to proceed by a vacancy mechanism. The temperature dependence of the diffusivity follows a linear Arrhenius law with parameters $D_0 = (1.10_{-0.37}^{+0.56}) \times 10^2\text{ cm}^2\text{ s}^{-1}$ and $H = 1.20 \pm 0.02\text{ eV}$. The data fail to exhibit the continuous positive curvature which is expected on the basis of a non-linear decrease in the Gibbs free energy for Frenkel defect formation with the increase of temperature. It is possible that a strain-induced and temperature-dependent binding energy between the oversized solute ion and a neighbouring vacancy washes out the expected curvature. When the diffusion results of other alkali ions are compared together with the diffusion of Rb^+ in AgCl , it seems likely that the temperature dependence of the motion energy is also to be considered along with those of the formation and solute-vacancy association. (42 refs.)

62164 Effects of impurities on hydrogen permeability through palladium alloy membranes at comparatively high pressures and temperatures. H.Yoshida, S.Konishi, Y.Naruse (Tokai Res. Estab., Japan Atomic Energy Res. Inst., Ibaraki-ken, Japan). *J. Less-Common Met. (Switzerland)*, vol.89, no.2, p.429-36 (Feb. 1983).
(International Symposium on the Properties and Applications of Metal Hydrides, Toba, Japan, 30 May–4 June 1982).
The palladium alloy membrane method has been proposed as a means of purifying fusion reactor fuel. The applicability of this method was studied by investigating the effects of impurities on the permeation characteristics of multicomponent palladium alloy membranes. The experiments were performed at comparatively high pressures and temperatures. The hydrogen permeability of commercial Pd-25wt.%(Ag-Au-Ru) was not affected by impurities such as NH_3 , CH_4 , CO , CO_2 and N_2 which are present in hydrogen at low concentrations (10–10000 ppm). However, the permeability deteriorated on contamination with oil vapour but could easily be recovered by baking in air followed by hydrogen reduction. Chemical reactions in the palladium diffuser and the effects of thermal cycling on permeability were also examined. (4 refs.)

62165 ^{51}Cr diffusion in Zr-Sn alloys. L.I.Nicolai, R.Migoni, R.H.de Tendler (Dept. de Materiales, CNEA, Buenos Aires, Argentina). *J. Nucl. Mater. (Netherlands)*, vol.115, no.1, p.39-48 (March 1983).
The volume diffusion of ^{51}Cr in Zr-Sn alloys was measured in coarse-grained polycrystals, using the 'thin film' method. The Sn content in the alloys ranged from 0.39 to 6.7 at.%. In the β -phase, diffusion temperatures were between 982 $^\circ\text{C}$ and 1240 $^\circ\text{C}$. Sn was found to reduce the ^{51}Cr diffusion in the β -phase, the effect being small but well defined. The linear dechancement coefficient b and its temperature dependence were calculated, assuming the formation of Sn-Cr dimers. For the more dilute alloys Q and D_0 were determined and upon application of the Zener theory for D_0 , a negative contribution to the activation entropy was found. In the α -phase where three experiments were done at different temperatures, ^{51}Cr was shown to be a very fast-diffusing solute. No definite correlation with the Sn content was found probably owing to the anisotropy of the α -phase. (27 refs.)

62166 Isotope effect in heat of transport of H, D and T in Nb. M.Sugisaki, S.Mukai, K.Idemitsu, H.Furuya (Dept. of Nuclear Engng., Kyushu Univ., Fukuoka, Japan). *J. Nucl. Mater. (Netherlands)*, vol.115, no.1, p.91-4 (March 1983).
The thermal diffusion of hydrogen isotopes, H and D, in Nb was studied at an average temperature of 168 $^\circ\text{C}$. By analyzing the redistribution of hydrogen in Nb on the basis of the irreversible thermodynamics, the heat of transport Q^* was determined for H and D as 9.5 kJ/mol and 16.0 kJ/mol, respectively. The large isotope dependence of Q^* was concluded by comparing these values with the value of 18.8 kJ/mol for T, which was previously reported by the present authors (1982). The coupling coefficients of H and D were also determined from the transient process of redistribution and found to be in good agreement with those based on the Gorsky effect. (10 refs.)

62167 Substitutional-interstitial diffusion with bulk vacancy generation in semiconductors. M.D.Zahari, B.Tuck (Dept. of Electrical & Electronic Engng., Univ. of Nottingham, Nottingham, England). *J. Phys. D (GB)*, vol.16, no.4, p.635-44 (14 April 1983).
A numerical technique is presented which gives a fairly complete description of the substitutional-interstitial diffusion mechanism. The mechanism is modelled directly on the computer without employing the differential equations which have been used by previous workers. Diffusion of the interstitial component of a diffusing impurity is taken into account together with self-diffusion by atoms of the host crystal and vacancy generation within the bulk of the crystal. The computed diffusion profiles compare well with experimental profiles found in certain semiconductor systems. The program is used to reproduce as closely as possible experimental diffusion profiles of silver in the III-V semiconductors GaAs and InP. The fitting parameters all represent physical quantities and the optimum values obtained are shown to be reasonable for the semiconductors concerned. (22 refs.)

62168 Kinetic enrichment of hydrogen at interfaces and voids by dislocation sweep-in of hydrogen. S.V.Nair, R.R.Jensen, J.K.Tien (Henry Krumb School of Mines, Columbia Univ., New York, NY, USA). *Metall. Trans. A (USA)*, vol.14A, no.3, p.385-93 (March 1983).
A rigorous treatment is presented to answer the question of whether the dislocation sweep-in of hydrogen can result in enrichment of hydrogen at voids and boundaries. It is concluded that significant enrichment can occur in both low and high hydrogen diffusivity situations whether the enrichment is contributed by a dislocation annihilation process or by stripping of hydrogen atoms from dislocations by the internal traps. The model presented is based on enrichment controlled by long-range diffusion. It calculates the diffusion leakage current for the case where unsaturated trap interfaces simultaneously fill and leak hydrogen atoms into the matrix by diffusion, and compares this amount with the arrival current of hydrogen to the traps by dislocation sweep-in. The relative magnitudes of the two currents are found to depend on appropriate, calculable time constant values. These values are evaluated for physical situations of interest. (30 refs.)

62169 Tritium permeability and pressure dependence of 304L stainless steel in the temperature range 723 to 1023K. M.Matsuyama (Tritium Res. Center, Toyama Univ., Toyama, Japan), J.D.Redman. *Metall. Trans. A (USA)*, vol.14A, no.3, p.498-500 (March 1983).
Tritium permeation through austenitic stainless steel was investigated. An Arrhenius-type plot for the tritium permeability is presented. The permeability constant, DK_0 , and activation energy for permeation of tritium were both higher than values measured by Bell et al. (1979) for other austenitic alloys. However, these results are consistent with the trend reported by Bell et al. in that both the permeability constant and the activation energy increase with decreasing nickel content of the austenitic alloys. (15 refs.)

62170 SIMS analysis of the impurity diffusion of In in Cu. W.Gust, C.Ostertag, B.Predel, U.Roll (Inst. fur Metallkunde, Max-Planck-Inst. fur Metallforschung, Stuttgart, Germany), A.Lodding, H.Odelius. *Philos. Mag. A (GB)*, vol.47, no.3, p.395-406 (March 1983).
Secondary-ion mass spectrometry (SIMS) has been used to study the bulk impurity diffusion of indium in monocrystalline copper. Sixteen samples were annealed at temperatures ranging from the vicinity of the melting point down to 602K, i.e. to regions relevant in grain-boundary diffusion. The diffusion coefficients D obtained extend over a very wide range: between 3.3×10^{-12} and $6.0 \times 10^{-21}\text{ m}^2\text{ s}^{-1}$. The results agree well with earlier data, obtained in a more restricted temperature range. Of several evaluations of the raw SIMS data, that based on the matrix-normalized $^{115}\text{In}^+$ signal is found to yield the most accurate Arrhenius parameters for the single-vacancy mechanism in the low-temperature region: $D_0^{\text{IV}} = 0.219(\pm 0.386, -0.140) \times 10^{-4}\text{ m}^2\text{ s}^{-1}$ and $Q^{\text{IV}} = 178.0 \pm 6.0\text{ kJ mol}^{-1}$. These results are compared with other values in the literature and discussed. (14 refs.)

62171 Hydrogen permeability of palladium-platinum alloys. Yu.N.Guk, G.E.Kagan, V.V.Lobanov, E.S.Levin, P.V.Gel'd. *Russ. Metall. (GB)*, no.6, p.187-9 (1981). Translation of: *Izv. Akad. Nauk. SSSR Met.*, no.6, p.191-4 (1981).

An important application of Pd-Pt alloys is in manufacturing thin membranes required in the production of extra-pure hydrogen. The coefficients of hydrogen penetration were examined for the temperature range 300-800°C in palladium alloys containing 4.0, 10.4, 25.7, 40.0, 50.2, 65.7 and 75.5 at.% Pt. The hydrogen permeability of Pd-Pt alloys with 4.0-7.5 at.% Pt decreases with increasing Pt concentration, and at 300-650°C the hydrogen permeability is considerably lower than it is for palladium. The hydrogen permeability in the range 700-800°C for Pd-Pt alloys with up to 40 at.% Pt is close to that of palladium. With increasing temperature of the Pd-Pt alloys the hydrogen permeability changes in a complex manner and above 500-700°C there is a deviation from the initial exponential dependence. (8 refs.)

62172 Interpretation of carbon diffusivity in Fe-Ni alloys. D.Farkas (Dept. of Materials Engrg., Virginia Polytech. Inst. & State Univ., Blacksburg, VA, USA).

Scr. Metall. (USA), vol.17, no.3, p.265-8 (March 1983). In the framework of the theory of absolute reaction rates a diffusion coefficient is obtained that is proportional to the product of activity coefficient and the square of the lattice parameter. This product can be calculated and it has maximum near 70% Ni, like the activities. The explanation of the observed behaviour of C diffusivities has to be found in the analysis of the activation energies and the activity of the activated complexes, as well as in the fraction of C that is trapped in low energy sites with more Fe atoms. (3 refs.)

62173 The influence of pressure on indium diffusion along single tin-germanium interphase boundaries. B.B.Straumal, L.M.Klinger, L.S.Shvindlerman (Inst. of Solid State Phys., Acad. of Sci., Chernogolovka, USSR).

Scr. Metall. (USA), vol.17, no.3, p.275-9 (March 1983). It is shown that the activation volume of diffusion along interphase boundaries is much higher than the activation volume typical of vacancy single diffusion mechanism. This effect is most pronounced for special boundaries, and with the increase in the interface perfection (with decreasing reciprocal density of coincidence sites Σ) the activation volume (and the activation energy) rises. (6 refs.)

62174 Influence of the internal electric field on the migration of substitutional impurities in diamond-structure semiconductors. M.I.Vasilevskii, V.A.Murav'ev, V.A.Pantelev (Physicotech. Res. Inst., N.I. Lobachevskii State Univ., Gorki, USSR).

Sov. Phys.-Solid State (USA), vol.24, no.9, p.1468-70 (Sept. 1982). Translation of: *Fiz. Tverd. Tela (USSR)*, vol.24, no.9, p.2589-94 (Sept. 1982). [received: April 1983]

The influence of an electric field on diffusion is studied by the method of many-particle correlation function chains. A vacancy mechanism of impurity diffusion is considered, which involves a series of successive events of impurity-vacancy complex formation, reorientation, and disintegration. The basic physical idea is that the field affects the frequencies of the elementary transitions of charged vacancies. By solving the transport equations for the many-particle correlation functions of defects, an expression is derived for the mobility of an impurity ion in terms of these frequencies. It is shown that, owing to correlation effects, the relation between the mobility and the diffusion coefficient of an impurity ion differs from the customary Einstein relation: moreover, if the reorientation probability for impurity-vacancy complexes is large compared with the disintegration probability, the sign of the mobility is anomalous (opposite to that of the ion charge), so that the drift of impurity ions in the internal field does not accelerate, but retards, the diffusion. The redistribution of vacancies in the field is also discussed; it causes a concentration dependence of the impurity diffusion coefficient and mobility. (11 refs.)

62175 Review on lattice diffusion of substitutional impurities in iron. A summary report. H.Oikawa (Dept. of Materials Sci., Tohoku Univ., Sendai, Japan).

Technol. Rep. Tohoku Univ. (Japan), vol.47, no.2, p.215-24 (1982). In English.

Diffusion data in the α - δ and the γ phases of iron have been critically assessed and the diffusion parameters, D_0 and Q , were recalculated based on individual datum points for 25 substitutional impurities: Ag, Al, As, Au, Be, Co, Cr, Cu, Hf, Mn, Mo, Nb, Ni, P, Pd, Pt, S, Sb, Se, Si, Sn, Ti, V, W, and Zn. Regularities with respect to the atomic number of impurity, X , have been noted in the ratio, D_X/D_{Fe} , and the activation energy difference, $Q_X - Q_{Fe}$. (75 refs.)

62176 Impurity diffusion in amorphous silicon and its implications for solar cells. S.Kalbitzer, M.Reinelt, W.Stolz (Max-Planck-Inst. fur Kernphys., Heidelberg, Germany).

Fourth E.C. Photovoltaic Solar Energy Conference, Proceedings of the International Conference, Stresa, Italy, 10-14 May 1982 (Dordrecht, Netherlands: Reidel 1982), p.1059-62.

Diffusion coefficients of a variety of impurities from different columns of the atomic table have been measured by high resolution nuclear spectroscopy. The relevance of the resulting distribution lengths with respect to solar cell properties is discussed for short time deposition processes at elevated temperatures and long time operation at ambient temperatures. (10 refs.)

Characteristics of the permeation of hydrogen-inert gas mixtures through a palladium alloy tube wall See Entry 61010

The post-hydrogenation of low-pressure chemical vapor deposited amorphous silicon See Entry 61937

High temperature and short time thermal annealing of ion-implanted silicon See Entry 61938

Some mathematical results for impurity redistribution during the growth of a layer on a substrate See Entry 61946

Radiation damage, its recovery and platinum behavior and lattice location in ion bombarded MgO and Al₂O₃ as used for catalytic studies See Entry 61990

Random walk properties of lattices and correlation factors for diffusion via the vacancy mechanism in crystals See Entry 62152

Mossbauer spectroscopy in physical metallurgy See Entry 62840

Diffusion modeling of the carburization process in stainless steels See Entry 63464

The effect of the surface state on the hydrogen permeability and the catalytic activity of palladium alloy membranes See Entry 63583

66.30L Diffusion, migration, and displacement of other defects

62177 Grain boundary diffusion in columnar structure polycrystalline materials. H.F.Ragaie (Electronics & Computer Dept., Ain Shams Univ., Cairo, Egypt).

Electron. Lett. (GB), vol.19, no.8, p.294-5 (14 April 1983). A simple but rigorous solution for the problem of grain boundary diffusion in columnar structure semi-infinite polycrystalline materials is proposed. The method is advantageous over other known methods in that it can be easily extended to media of finite thickness. (4 refs.)

62178 Calculations of phenomenological coefficients for matter transport by the matrix method of random walk theory. Y.Okamura, A.R.Allnatt (Dept. of Chem., Univ. of Western Ontario, London, Ontario, Canada).

J. Phys. C (GB), vol.16, no.10, p.1841-62 (10 April 1983). Linear response formulae for the phenomenological coefficients L_{AA} , L_{AB} and L_{BB} for matter transport by single vacancies in a very dilute isotropic alloy of solute B in solvent A are studied by the matrix method of random walk theory familiar in the calculation of impurity correlation factors. A symmetry classification of vacancy jumps based on symmetry with respect to the diffusion axis is introduced and applied to the linear response formulae in order to reduce them to compact forms. For typical models these forms contain a small number of functions K_{ij} which are linear combinations of vacancy migration Green functions for paths between sites of symmetry types i and j that do not pass through the impurity. The K_{ij} are calculated by inversion of a certain matrix of jump probabilities. Detailed calculations are made for models with first- and second-nearest-neighbour vacancy-impurity interactions for BCC, FCC and diamond lattices. The calculations of L_{AB} and L_{AA} are seen to be straightforward extensions of those already familiar in the calculation of L_{BB} and the impurity correlation factor. This suggests that extensions to other crystal structures and migration mechanisms can be made. (23 refs.)

62179 An exact solution to diffusion via the vacancy mechanism. L.Gunther (Phys. Dept., Tufts Univ., Medford, MA, USA), B.Gralla.

J. Phys. C (GB), vol.16, no.10, p.1863-74 (10 April 1983).

The authors have obtained an exact solution to the problem of diffusion by the vacancy mechanism in the sudden jump approximation, using the set of rate equations developed by Dobar-Ure and Flinn (1973) for self-diffusion. They have extended the equations and solution to the case of impurity diffusion via vacancies. The solutions are valid for all times and also yield the Bardeen-Herring correlation factor f in terms of an integral. Although numerical solutions have been obtained only for the square lattice in two dimensions, the method is easily extendable to other two-dimensional lattices and lattices of higher or lower dimensionality. (38 refs.)

62180 A mathematical analysis of diffusion in dislocations. III. Diffusion in a dislocation array with diffusion zone overlap. A.D.Le Claire, A.Rabinovich (Materials Dev. Div., AERE, Harwell, England).

J. Phys. C (GB), vol.16, no.11, p.2087-104 (20 April 1983).

For $pt \ll$ see *ibid.*, vol.15, p.3445 (1982). The authors consider diffusion from a surface $y=0$ into a solid containing a regular array of d dislocations per unit area, all normal to the surface and each represented as a pipe of radius a within which the diffusion coefficient D' is very much greater than that, D , for diffusion in a regular crystal. They calculate the mean concentrations $\langle c(y) \rangle$ at depths y , as determined in conventional sectioning experiments, for both constant concentration and thin-finite-source conditions at $y=0$. $\langle c \rangle$ is evaluated as a function of $\eta = y/(Dt)^{1/2}$, $\alpha = a/(Dt)^{1/2}$, $\Delta = D'/D$, $\epsilon = \pi a^2 d$ and of ϵ/α , the ratio of the mean diffusion length, $(Dt)^{1/2}$, to the effective half-spacing between dislocations, $(\pi d)^{-1/2}$. Full account is taken, through an appropriate Wigner-Seitz-like boundary condition, of the effects of the mutual overlap of the diffusion zones around dislocations. For $\epsilon/\alpha \leq 1$, values of $\langle c \rangle$ do not differ by more than a few per cent from those previously calculated by the authors for well spaced non-interacting dislocations; for $\epsilon/\alpha \geq 0.4$ the two solutions are numerically identical. As ϵ/α increases above one the effects of overlap rapidly become increasingly important. They examine the nature of the penetration plots, $\log \langle c \rangle$ versus y^2 , and the effective diffusion coefficients, D_{eff} , deduced from them. The case $\epsilon/\alpha \leq 1$ was discussed previously by the authors. The plots show maximum curvature around $\epsilon/\alpha \approx 5$ but would be difficult experimentally to distinguish from linear when $\epsilon/\alpha \geq 10$. For this range D_{eff} is found to be closely represented by the Hart relation, $D_{eff} = D(1 + \pi a^2 d (\Delta - 1))$, the condition of validity of which can now be specified more precisely than heretofore. (12 refs.)

62181 Some remarks on the carbon atoms pairs migrational relation in α -Fe-C. G.Haneczok, R.Kuska, J.W.Moron, J.Rasek (Inst. of Phys. & Chem. of Metals, Silesian Univ., Katowice, Poland).

Scr. Metall. (USA), vol.17, no.3, p.303-8 (March 1983).

The problem of the existence of directionally ordering pairs of interstitial atoms in BCC metals is considered. Results obtained for α -Fe-C using magnetic permeability disaccommodation measurements (MPD) are reviewed. Arrhenius law parameters for the C-C pairs in α -Fe obtained by the MPD method are presented. Theoretical investigations on crystallographic configuration, binding energy and relaxational properties of interstitial atom pairs are discussed. (35 refs.)

The mechanisms of the formation and growth of water bubbles and associated dislocation loops in synthetic quartz See Entry 61908

66.30N Chemical interdiffusion

62182 Growth of titanium silicide on ion-implanted silicon. P.Revesz, J.Gyimesi, E.Zsoldos (Central Res. Inst. for Phys., Budapest, Hungary).

J. Appl. Phys. (USA), vol.54, no.4, p.1860-4 (April 1983).

Silicon samples implanted with high doses of ^{121}Sb , ^{75}As , ^{31}P , ^{16}O , and ^{40}Ar prior to Ti evaporation were studied to measure the growth of Ti-silicide layers. The annealing behavior of these samples was investigated by four-point probe measurement, Rutherford backscattering, and by X-ray diffraction. The samples implanted with Sb, As, and P atoms enabled the growth of TiSi₂ to be observed, though its final thickness was less than half when compared to that of the nonimplanted samples. Simultaneously with the diffusing-out atoms of Sb, during annealing, segregation of Sb atoms takes place at the TiSi₂/Ti interface and at the Ti surface. Using a simple model for the out-diffusion of Sb atoms, the activation energy of the diffusion coefficient of Sb in the Ti silicide was determined, giving a value of $E_a = 1.9$ eV. During out-diffusion, As atoms tend to be distributed homogeneously in the silicide layer. With Ar- and O-implanted samples, precipitation of Ti atoms can be observed at the implantation depth, and at higher annealing temperatures, the metal layer flakes off the sample. A simple model is given to explain this behavior. X-ray diffraction measurements of these samples showed the presence of the unstable TiSi phase, but no trace of the TiSi₂ phase was found after annealing at 700°C. (13 refs.)

62183 Application of the method of time-lag analysis to the study of diffusion in solids of nonhomogeneous macroscopic structure. C.Savvakis, J.H.Petropoulos (Phys. Chem. Lab., Demokritos Nuclear Res. Center, Aghia Paraskevi, Athens, Greece).

J. Phys. Chem. (USA), vol.86, no.26, p.5128-33 (23 Dec. 1982).

The study of the anomalous diffusion of N_2 in microporous graphite compacts is investigated by systematically varying the mode of compaction. It is shown that the results of the method of time-lag analysis, can be successfully correlated with the axial nonhomogeneity of the macroscopic structure of the compacts through a suitable physical model. Previous conclusions about the nature of 'non-Fickian' diffusion of gases in microporous compacts are confirmed and extended. (15 refs.)

62184 Solid state SiC/Ni alloy reaction. M.R.Jackson, R.L.Mehan, A.M.Davis, E.L.Hall (General Electric Corporate Res. & Dev., Schenectady, NY, USA).

Metall. Trans. A (USA), vol.14A, no.3, p.355-64 (March 1983).

The solid state reaction between silicon carbide and a model superalloy consisting of 70 at. pct Ni, 20 at. pct Cr, and 10 at. pct Al was studied between 700°C and 1150°C for times ranging from 10' hours to 330 hours. Reaction couples consisting of SiC/Ni, SiC/Cr, and SiC/NiCr were also studied. The reactions were carried out in air with the materials, in the shape of discs, maintained in contact under a pressure of 7 MPa. A reaction was detected with SiC and model alloy at all temperatures studied, and the reaction was diffusion controlled with an activation energy of 184 kJ/mole. In the ceramic the reaction was dominated by the diffusion of Ni into the ceramic forming a banded structure consisting of alternating layers of δ -Ni₃Si and a two phase mixture of graphite and δ . On the metal side, the reaction was very dependent on the presence of alloying elements, with pure Ni reacting to the greatest extent, followed by the binary NiCr alloy, and finally by NiCrAl. The growth and presence of the phases detected in these reactions is consistent with phase equilibria concepts. (22 refs.)

62185 Analysis of diffusion mechanisms in thin polycrystalline Au-Ag films using Auger electron spectroscopy. A.Bukaluk (Inst. Matematyki i Fizyki, Akad. Tech. Rolnicza w Bydgoszczy, Bydgoszcz, Poland).

Surf. & Interface Anal. (GB), vol.5, no.1, p.20-7 (Feb. 1983).

The diffusion process of silver through gold polycrystalline films 1000 Å thick for different heating times and different temperatures was studied. Auger electron spectroscopy (AES) with simultaneous argon ion sputtering was used to obtain the composition profiles of silver diffusing through gold thin films. The interdiffusion coefficients were extracted from the diffusion profiles using the rate of decrease of the concentration gradient at the Au-Ag film interface (the 'centre gradient' method) and the rate of rise of Ag concentration plateau in the Au film (the 'plateau rise' method). The grain boundary diffusion coefficients have been evaluated by means of the depth profile analysis, based on the Whipple model. The activation energies of each mechanism have been determined from the Arrhenius plots. (26 refs.)

62186 Reactivity of cobalt, chromium, indium, magnesium, manganese, antimony and samarium thin films in couples with other metal films at room temperature. Z.Marinovic, V.Simic (Inst. of Phys., Belgrade, Yugoslavia).

Thin Solid Films (Switzerland), vol.101, no.4, p.L37-40 (25 March 1983).

Studies the phenomenon of compound formation through the spontaneous reaction of two different thin metal films at room temperature. The thin film couples were prepared by vacuum evaporation, and X-ray diffraction was used to examine the samples for compound formation. It was found that most of the compounds were formed in couples consisting of a component of low melting point (below 450°C) and a component of high melting point (850-1100°C). The metals of medium melting point (600-700°C) very rarely formed compounds, with either metals of low melting point (below 450°C) or those of very high melting point (up to 1500°C). (14 refs.)

Interfaces structure in relation with the mechanisms in the reaction copper-silicon See Entry 62279

Diffusion and magnetic properties of compositionally modulated films See Entry 62728

Diffusion processes in sintering of multicomponent systems See Entry 63201

Grain growth in doped-undoped ceramic BaTiO₃ couples See Entry 63246

Influence of nitrogen on the penetration of hydrogen through constructional materials from nitrogen-hydrogen mixtures See Entry 63465

High-temperatures reactions of metals with gases. II. Kinetics of growth of multiphase chemical compound layers at a metal/gas interface See Entry 63468

66.60 THERMAL CONDUCTION IN NONMETALLIC LIQUIDS

(for thermal conduction in liquid metals, see 72.15C)

Transport properties in the zero order Gaussian memory function approximation with phase integrals evaluated from Monte Carlo calculations See Entry 62148

66.70 NONELECTRONIC THERMAL CONDUCTION AND HEAT-PULSE PROPAGATION IN NONMETALLIC SOLIDS

(for thermal conduction in solid metals, see 72.15C and 72.15E; for statistical mechanics of lattice vibrations, see 63.70)

62187 Thermal diffusivity of pyrotechnic mixtures of tungsten and potassium dichromate by thermal analysis. T.Boddington, P.G.Laye, J.Tipping (Dept. of Phys. Chem., Univ. of Leeds, Leeds, England).

Combust. & Flame (USA), vol.50, no.2, p.139-51 (March 1983).

Two techniques have been developed to measure the thermal diffusivity of powders pressed into the form of cylinders. Both techniques use a modified commercial differential thermal analysis apparatus to monitor the temperature gradient inside the cylinder when the ambient temperature is increased either linearly with time or suddenly from one constant value to another. The theory is elaborated and graphs are presented which allow the thermal diffusivity to be obtained for a variety of cylinder geometries. Both techniques have been used to measure the thermal diffusivity of pyrotechnic mixtures of tungsten and potassium dichromate. (4 refs.)

62188 Thermal conductivity of stoichiometric (Pu, Nd)O₂ and (Pu, Y)O₂ solid solutions. S.Fukushima, T.Ohmichi, A.Maeda, M.Handa (JAERI, Ibaraki, Japan).

J. Nucl. Mater. (Netherlands), vol.114, no.2-3, p.260-6 (Feb. 1983).

The thermal conductivities of stoichiometric (Pu, R)O₂ solid solutions containing RO_{1.5} (R = Nd and Y) up to 10 mol.% were determined by the laser flash

method in the temperature range 700-1400K. The thermal conductivities for all solid solutions satisfied the phonon conduction equation $K = (A + BT)^{-1}$ within $\pm 6\%$. The lattice defect thermal resistivities ($= A$) increased gradually with the neodymium or yttrium content, while the intrinsic lattice thermal resistivities ($= BT$) were nearly equal to that measured for PuO₂. The measured thermal conductivities were consistent with the results of the lattice defect model calculation in which Pu⁴⁺, Pu³⁺ and R³⁺ ions were considered as phonon scattering centers. The lattice strain parameters $\epsilon = 85$ and 93 were obtained for (Pu, Nd)O₂ and (Pu, Y)O₂ solid solutions, respectively. (14 refs.)

62189 Thermal conductivity of near-stoichiometric (U,Nd)O₂, (U,Sm)O₂ and (U,Eu)O₂ solid solutions. S.Fukushima, T.Ohmichi, A.Maeda, M.Handa (JAERI, Ibaraki, Japan).

J. Nucl. Mater. (Netherlands), vol.114, no.2-3, p.312-25 (Feb. 1983).

The thermal conductivities of near-stoichiometric (U,R)O₂ solid solutions (R = Nd, Sm and Eu) containing RO_{1.5} up to 15 mol.% were determined in the temperature range 700-2000K by the measurement of thermal diffusivity. The thermal conductivities satisfied the phonon conduction equation $K = (A + BT)^{-1}$ within $\pm 5\%$. The constant A corresponding to the lattice defect thermal resistivity increased linearly with the rare earth element content, while the temperature coefficient B was almost independent of it. The change in A with the rare earth element content increased in order of (U,Eu)O₂, (U,Sm)O₂ and (U,Nd)O₂ solid solutions. The increase of A was explained reasonably by the lattice defect model considering U⁴⁺, U³⁺ and R³⁺ ions in the solid solutions as phonon scattering centers, using a common value for the strain parameter ($\epsilon = 110$). For all solid solutions, the lattice strain effect on the lattice defect thermal resistivities was much larger than the mass effect. In addition, the effect of U³⁺ ions on the lattice defect thermal resistivity caused by the lattice strain effect was larger than that of R³⁺ ions. (20 refs.)

62190 Thermal conductivity of (Pu_{1-x}Nd_x)O_{2-y} and (Pu_{1-x}Y_x)O_{2-y} solid solutions. S.Fukushima, T.Ohmichi, A.Maeda, M.Handa (JAERI, Ibaraki, Japan).

J. Nucl. Mater. (Netherlands), vol.115, no.1, p.118-27 (March 1983).

The thermal conductivities of (Pu_{1-x}R_x)O_{2-y} solid solutions (R = Nd and Y) containing RO_{1.5} up to 10 mol.% were determined in the temperature range 700-1450K from thermal diffusivities measured by the laser flash method. The thermal conductivities satisfied the phonon conduction equation $K = (A + BT)^{-1}$ within $\pm 7\%$. The values of A, corresponding to the lattice defect thermal resistivity, increased linearly with the neodymium or yttrium content, while those of B were nearly constant. The increasing rate of A for (Pu, Nd)O_{2-y} solid solutions was slightly larger than that for (Pu, Y)O_{2-y}. These increases were reasonably explained by the lattice defect model in which Pu⁴⁺, R³⁺, O²⁻ ions and oxygen vacancy in the solid solutions were considered as phonon scattering centers. For both solid solutions, the lattice strain effects on the lattice defect thermal resistivities were in preference to the mass effects. In addition, the stoichiometry effects on the additional defect thermal resistivities were about 1.3 times larger than the cation effects. (29 refs.)

62191 The effect of phonon-grain boundary scattering, doping and alloying on the lattice thermal conductivity of lead telluride. C.M.Bhandari, D.M.Rowe (Dept. of Phys., Electronics & Electrical Engng., Univ. of Wales Inst. of Sci. & Technol., Cardiff, Wales).

J. Phys. D (GB), vol.16, no.4, p.L75-7 (14 April 1983).

The lattice thermal conductivity of lead telluride has been investigated theoretically as a function of grain size, level of doping and alloying. Although there is some difficulty in making predictions of the precise dependence of the lattice thermal conductivity on these parameters, it is possible to indicate the range over which the results may vary. It is concluded that for moderately doped material having a grain size of 1 μ m the reduction in lattice thermal conductivity would lie in the range 4-6% for unalloyed lead telluride and 11-13% for highly disordered alloys. (7 refs.)

62192 Soliton-phonon scattering in TMMC and DMMC. J.A.H.M.Buys, W.J.M.de Jonge (Dept. of Phys., Eindhoven Univ. of Technol., Eindhoven, Netherlands).

J. Magn. & Magn. Mater. (Netherlands), vol.31-34, pt.3, p.1209-10 (Feb. 1983). (Proceedings of the International Conference on Magnetism, Kyoto, Japan, 6-10 Sept. 1982).

The magnetic field dependence of the thermal conductivity of the quasi 1d Heisenberg antiferromagnets TMMC and DMMC is measured between 1.5 and 7K and in fields up to 90 kOe. In the paramagnetic phase the data can be interpreted very well by soliton-phonon scattering. (6 refs.)

62193 Thermal conductivity of germanium containing dislocations at low temperatures. M.A.Ansari, A.Kumar, B.K.Srivastava (Dept. of Phys., Indian Inst. of Technol., Kharagpur, India).

Phys. Status Solidi b (Germany), vol.116, no.1, p.163-7 (1 March 1983).

To study the frequency dependence of the phonon-dislocation scattering, the phonon conductivity of germanium with dislocations is analysed using Holland's model (1963) and Kumar and Sinha's relaxation time for the phonon-dislocation scattering processes. A reasonably good agreement is observed between present theory and experimental data of Sato and Sumino (1974). (14 refs.)

62194 An ion-implanted resistor as thermal transient sensor for the determination of the thermal diffusivity in silicon. P.Turkes (Inst. of Angewandte Phys., Univ. Erlangen-Nurnberg, Erlangen, Germany).

Phys. Status Solidi a (Germany), vol.75, no.2, p.519-23 (16 Feb. 1983).

A high accuracy thermal transient sensor for investigations of doping influences on the thermal diffusivity in silicon is developed. The sensor is tested in a low doped n-type sample and in an intermediate doped p-type sample. In measurements on the p-type sample, doping effects are observable. (14 refs.)

Effective thermal conductivity of metal hydride beds See Entry 61384

Structural order in alkali-degraded PAN as seen in studies of low-temperature thermal conductivity See Entry 61819

Isotope effect in heat of transport of H, D and T in Nb See Entry 62166

67.00 QUANTUM FLUIDS AND SOLIDS; LIQUID AND SOLID HELIUM

(see also 05.30 Quantum statistical mechanics)

67.40 BOSON DEGENERACY AND SUPERFLUIDITY OF HELIUM-4

62195 Comments on 'Coupling between pressure and temperature amplitude in waves of second sound in liquid helium' [by Hofmann, A., Keck, K., and Schubert, G.V., *Z. Phys.*, **231**, 177 (1970)]. S. Garrett (Dept. of Phys., Naval Postgraduate School, Monterey, CA, USA).

Z. Phys. B (Germany), vol.50, no.3, p.275-6 (1983).

In Section V of the article by Hofmann et al., the authors claim to have applied the reciprocity method to the calibration of thermal transducers in superfluid helium. The author here gives reasons for believing that the expressions for transducer sensitivity, M_2 , and source strength, S , have absolutely nothing to do with the use of acoustical reciprocity, and are the result of a misunderstanding of the foundations of the reciprocity method. (2 refs.)

62196 Calibration of second sound transducers. A response on the comments of S. Garrett. A. Hofmann (Inst. fur Tech. Phys., Kernforschungszentrum, Karlsruhe, Germany).

Z. Phys. B (Germany), vol.50, no.3, p.277-9 (1983).

The authors previously described (see *Z. Phys.*, vol.231, p.177, 1970) a method of calibrating second sound transducers operated in liquid helium. This method was derived in analogy to the reciprocity technique applied to first sound. S. Garrett, however (see *ibid.*, vol.50, p.275, 1983), asserts that this calibration method 'has absolutely nothing to do with the use of acoustical reciprocity'. Because of the orthogonality of the two views the author would like to describe in detail his derivation of the given formalism which he believes to be correct. (2 refs.)

62197 Heat transfer with He II noiseless film boiling. Ye.V. Ametistov (Moscow Power Engng. Inst., Moscow, USSR).

Cryogenics (GB), vol.23, no.4, p.179-84 (April 1983).

An analytical heat transfer process description of noiseless superfluid helium films boiling on heating surfaces of different geometries is presented. Final calculation relationships stipulate the knowledge of the heat flux density magnitude at the interface He II-vapour. An approach to the analytical calculation of the boundary thermal resistance value to heat transfer at the interface on the liquid side has been suggested, the latter permitting theoretical calculations of the heat flux density on this boundary in the long term. The comparison of recommended calculation relations on the transfer intensity with He II noiseless film boiling demonstrates their satisfactory agreement with all experimental results available in the literature. Criteria are given which determine the limits to which the obtained calculation relations can be applied. (16 refs.)

62198 Heat transfer to helium-I during different boiling regimes at high centrifugal accelerations. Yu.A. Kirichenko, S.M. Kozlov, N.M. Levchenko (Phys.-Tech. Inst. of Low Temperatures, Acad. of Sci., Kharkov, Ukrainian SSR).

Cryogenics (GB), vol.23, no.4, p.217-19 (April 1983).

Heat transfer during nucleate and film boiling of helium and also the boiling crises up to relative accelerations of $(1 \div 2) \times 10^3$ have been investigated. The heat transfer surface was a flat copper heater. The heat transfer during nucleate boiling proved to be independent of the relative accelerations. For film boiling, it was found that $\alpha \sim \eta^{1/3}$. The dependence of the peak nucleate boiling heat flux and the minimum film boiling flux on the relative acceleration is non-monotonic. (5 refs.)

62199 Influence of surface characteristics of solids on the Kapitza resistance. G. Dharmadurai (Reactor Res. Centre, Kalpakkam, Nadu, India).

Physica B & C (Netherlands), vol.115 B+C, no.2, p.229-32 (Jan. 1983).

The authors examine the predictions of the acoustic mismatch model for the Kapitza boundary thermal resistance between solids and liquid helium in the light of the observation that the characteristic surface vibration temperatures of solids are less than their bulk vibration temperatures. They find that the above observation, in addition to a larger effective area arising from the surface structure in the solids, leads to an order of magnitude decrease in the Kapitza resistance, which significantly reduces the prevailing discrepancy between theory and experiment. (12 refs.)

62200 Superflows and superfluidity. E.B. Sonin (A.F. Ioffe Physicotech. Inst., Acad. of Sci. of the USSR, Leningrad, USSR).

Sov. Phys.-Usp. (USA), vol.25, no.6, p.409-30 (June 1982). Translation of: *Usp. Fiz. Nauk (USSR)*, vol.137, no.2, p.267-304 (June 1982). [received: April 1983]

The basic concepts of the theory of mass superflows in a superfluid are presented. The stability of such flows with respect to the creation and growth of linear defects (superfluid vortices), the relationship between superflows and the existence of long-range order, and the possible occurrence of persistent flows in one- and two-dimensional systems are discussed. Some analogs of the mass superflows in a superfluid are also examined: spin superflows in magnetically ordered systems having an easy-plane anisotropy and the current states of a Bose condensate of electron-hole pairs. The physical meaning of such 'flows' is discussed, and a theory for their stability is derived from the calculated probability for the creation of the linear defects which are analogs of superfluid vortices. There is a discussion of the applicability of the theory of spin superflows to several experiments on the magnetic properties of the A phase of superfluid helium-3 and to a possibility which follows from this theory: that domain walls might be generated in the interior of a sample of an easy-plane magnetically ordered material and that the motion of these walls might be controlled by fields applied to the surface of the sample. (105 refs.)

The crucial role of the vapour for the speed and attenuation of isothermal third sound in unsaturated helium films See Entry 62205

67.50 FERMI FLUIDS; LIQUID HELIUM-3

62201 Cooling liquid ^3He to around 100 μK . A.M. Guenault, V. Keith, C.J. Kennedy, I.E. Miller, G.R. Pickett (Dept. of Phys., Univ. of Lancaster, Lancaster, England).

Nature (GB), vol.302, no.5910, p.695-6 (21 April 1983).

An immersed-refrigerant cooling method was used to cool a sample of moderately pure ^3He . In the preliminary experiment, an extremely low helium temperature was achieved, certainly below 120 μK , at which temperature the superfluid B phase is so far below its transition temperature that the vibrating wire viscometer is essentially unable to detect the presence of any normal fluid component. In this regime the authors hope to be able to investigate any

interaction between the wire and the stiffness of the superfluid texture. (5 refs.)

62202 Effect of gap distortion on the field splitting of collective modes in superfluid $^3\text{He-B}$. N. Schopohl (Inst. fur Festkörperforschung, KFA Jülich, Jülich, Germany), M. Warnke, L. Tewordt.

Phys. Rev. Lett. (USA), vol.50, no.14, p.1066-9 (4 April 1983).

The field splitting of the real squashing, $J=2$, mode in $^3\text{He-B}$ is shown to become highly nonlinear at large fields as a result of the ellipsoidal deformation of the energy gap. This leads to crossings of the $J_z = +1$ and $J_z = 0$ levels with the $J_z = +2$ level. The crossing points depend sensitively on the couplings between the $J=2$, 1, and 0 modes. The theory is in good agreement with the observed field evolution and level crossing as measured recently by Shivaram et al. (1983). (15 refs.)

62203 Nonlinear Zeeman shifts in the collective-mode spectrum of $^3\text{He-B}$. B.S. Shivaram, M.W. Meisel, B.K. Sarma, W.P. Halperin, J.B. Ketterson (Dept. of Phys. & Astron., Northwestern Univ., Evanston, IL, USA).

Phys. Rev. Lett. (USA), vol.50, no.14, p.1070-2 (4 April 1983).

Zeeman shifts in one of the $J=2$ order-parameter collective-mode multiplets in $^3\text{He-B}$ have been measured in magnetic fields up to 0.16 T. The observed shifts are extremely nonlinear at higher fields. The extent of nonlinearity decreases as $T/T_c \rightarrow 0$ and for a given T/T_c is more predominant at lower pressures and/or frequencies. The observed effects can be attributed to the distortion of the B-phase energy gap in the presence of a magnetic field as suggested by Schopohl, Warnke, and Tewordt (1983). (19 refs.)

Superflows and superfluidity See Entry 62200

67.60 MIXED SYSTEMS; LIQUID HELIUM 3-4 MIXTURES

62204 Thermal diffusion measurements near the liquid-vapor critical point. L.H. Cohen, M.L. Dings, H. Meyer (Dept. of Phys., Duke Univ., Durham, NC, USA).

Phys. Rev. Lett. (USA), vol.50, no.14, p.1058-61 (4 April 1983).

The authors report measurements of the density and temperature gradients in $^3\text{He-}^4\text{He}$ mixtures near their liquid-vapor critical point, as induced by a heat flux. From these they deduce the thermal diffusion ratio k_T and the conductivity κ . They find that κ_T and κ diverge with respective effective exponents $\phi \approx 1.2$ and $\psi \approx 0.6$. Both of these results are in contradiction with the asymptotic predictions for binary mixtures and are discussed in the light of the hydrodynamic transport equations. (20 refs.)

67.70 FILMS

(inc. physical adsorption)

62205 The crucial role of the vapour for the speed and attenuation of isothermal third sound in unsaturated helium films. G. Bannink, M.G.M. Brocken, I.van An del, H.van Beelen (Kamerlingh Onnes Lab., Rijksuniversiteit, Leiden, Leiden, Netherlands).

Physica B & C (Netherlands), vol.115 B+C, no.3, p.376-80 (March 1983).

A thin-film oscillator is used to study superfluidity of ^4He films (thickness range 1.4-5.0 nm). Data on isothermal Helmholtz oscillations and standing third-sound waves are compared with each other, using a two-fluid description. It is demonstrated how the exchange of mass between film and vapor reduces the isothermal speed of third sound in confined geometries considerably. Absolute values of the areal superfluid density ρ_{s2} have been obtained. (7 refs.)

Heat transfer with He II noiseless film boiling See Entry 62197

Heat transfer to helium-I during different boiling regimes at high centrifugal accelerations See Entry 62198

67.80 SOLID HELIUM AND RELATED QUANTUM CRYSTALS

62206 Observation, close to roughening transition of critical-slowing-down. L. Puech, D. Hebral, D. Thoulouze, B. Castaing (CNRS, Grenoble, France).

C.R. Seances Acad. Sci. Ser. II (France), vol.296, no.1, p.19-22 (10 Jan. 1983). In French.

The times necessary to recover the stable size of a facet of a ^4He crystal in a slow growing process, close to the roughening transition of the facet ($T_R \approx 215$ mK) have been measured. These times exhibit a critical slowing down from 2 min. far from this transition to 44 min. to within several millikelvins of the transition. (10 refs.)

62207 Shape of crystals at low temperatures: absence of quantum roughening. D.S. Fisher (Bell Labs, Murray Hill, NJ, USA), J.D. Weeks.

Phys. Rev. Lett. (USA), vol.50, no.14, p.1077-80 (4 April 1983).

It has been suggested that quantum fluctuations would cause the interface of quantum crystals such as ^4He to be rough even at $T=0$. It is shown quite generally that this is incorrect: All stable faces must have nonzero roughening temperatures. This implies that the equilibrium shape of all crystals (classical or quantum) is faceted at sufficiently low temperatures. A criterion for estimating the roughening temperature of various crystal faces is discussed. (13 refs.)

67.90 OTHER TOPICS IN QUANTUM FLUIDS AND SOLIDS (E.G. NEUTRON-STAR MATTER)

NMR-induced recombination of spin-polarized hydrogen See Entry 62819

68.00 SURFACES AND INTERFACES; THIN FILMS AND WHISKERS

(for impact phenomena, see 79.; for physics of crystal growth, see 61.50C; for corrosion, oxidation, and surface treatments, see 81.60)

68.10 FLUID SURFACES AND INTERFACES WITH FLUIDS

(inc. surface tension, capillarity, wetting and related phenomena)

62208 A new method for computing surface tension using a drop of liquid. J.G.Powles, R.F.Fowler, W.A.B.Evans (Phys. Labs., Univ. of Kent, Canterbury, England).

Chem. Phys. Lett. (Netherlands), vol.96, no.3, p.289-92 (8 April 1983).

In the simulation of a liquid drop it is expensive to calculate the excess pressure and obtain the surface tension by the Laplace formula. The authors use the Kelvin formula which only requires the vapour density, or at most the virial pressure. Some results are given for a Lennard-Jones 12-6 fluid. (19 refs.)

62209 Surface tension and thickness of argon liquid/vapor interface. V.G.Baidakov (Physicotech. Branch for Problems in Power Engng., Acad. of Sci., Sverdlovsk, USSR), V.P.Skripov.

Colloid J. USSR (USA), vol.44, no.3, p.370-6 (May-June 1982). Translation of: *Kolloidn. Zh. (USSR)*, vol.44, no.3, p.409-16 (May-June 1982). [received: Feb. 1983]

The capillary constant has been measured and the surface tension σ of argon has been calculated in the temperature interval 85-143K. The values obtained for the surface tension have been compared with values of σ calculated by the use of different statistical theories. On the basis of the experimental data on surface tension and the thermodynamic properties of argon in the metastable region, by the use of the theory of inhomogeneous systems of van der Waals (1927) and Cahn-Hilliard (1958) and calculations have been performed to determine the pressure tensor and the density profile in the transition layer, the effective thickness of the layer, and the distance between the tension surface and the equimolecular interface. (22 refs.)

62210 Changes in contact angle during the process of capillary rise. V.V.Berezkin, N.V.Churayev (Inst. of Phys. Chem., Acad. of Sci., USSR).

Colloid J. USSR (USA), vol.44, no.3, p.376-82 (May-June 1982). Translation of: *Kolloidn. Zh. (USSR)*, vol.44, no.3, p.417-23 (May-June 1982). [received: Feb. 1983]

From measurements of the height and rate of capillary rise of water in quartz capillaries with nascent surfaces, relationships between the contact angle θ and the rate of meniscus movement v have been obtained. The relationships $\theta(v)$ have the same qualitative form as the theoretical relationships for dynamic contact angles. However, the deviations of θ from the static values proceed at a much lower rate than would be predicted from hydrodynamic calculations. (31 refs.)

62211 On the temperature derivative of the surface tension at a critical end point. M.Robert, P.Tavan (Baker Lab., Cornell Univ., Ithaca, NY, USA).

J. Chem. Phys. (USA), vol.78, no.5, p.2557-60 (1 March 1983).

It is shown that, according to the van der Waals theory of fluid interfaces, the surface tension of the interface between a noncritical and a critical phase has a continuous temperature derivative. This result holds for any number of phases and independently varying densities and is not restricted to classical values of the critical exponents. (16 refs.)

62212 Surface tension of binary molten salt mixtures. J.D.Pandey, U.Gupta (Dept. of Chem., Univ. of Allahabad, Allahabad, India).

J. Phys. Chem. (USA), vol.86, no.26, p.5234-7 (23 Dec. 1982).

The surface tension of binary molten salt mixtures has been evaluated by utilizing the Flory theory, the Eberhart equation, and the Brock-Bird relationship as a function of composition. The agreement between the theoretical and experimental values was satisfactory. The Eberhart relation overestimates surface tension values, whereas the Flory theory, in most of the systems, underestimates it. The maximum deviations were observed in the case of the Brock-Bird relation. (32 refs.)

62213 Alternative boundary conditions for a drop hanging from a circular tube. M.A.Fortes, R.M.Miranda (Centro de Mecânica e Materiais, Univ. Técnica de Lisboa, Lisboa, Portugal).

J. Chem. Soc. Faraday Trans. 1 (GB), vol.79, no.1, p.81-92 (Jan. 1983).

The stability of pendent liquid drops with axial symmetry is usually discussed for a specific type of boundary condition, ignoring the possibility of transitions between one type and another. The alternative configurations are denoted by θ , r_i and r_o according to whether the drop contacts the base of the tube or its inner (r_i) or outer edge (r_o). Transitions between these configurations are predicted from the appropriate thermodynamic functions for both volume- and pressure-controlled drops. The main conclusion is that in volume-controlled drops the r configurations are unstable relative to the θ configuration when the actual contact angle is reached, but in pressure-controlled drops the reverse may be true. The limiting stable configurations of drops are discussed, taking into account the transitions between different boundary conditions. (15 refs.)

62214 Mechanical model for a spherical interface with low tension. D.G.Hall (Port Sunlight Lab., Unilever Res., Bebington, England), D.J.Mitchell.

J. Chem. Soc. Faraday Trans. II (GB), vol.79, pt.2, p.185-93 (Feb. 1983).

The conventional treatment of a spherical interface models the mechanical properties of the system by regarding it as two bulk phases of uniform pressure separated by an infinitely thin membrane of uniform tension σ . This membrane is located at the surface of tension which is positioned so that the resultant forces and their first moments about the centre of the sphere in the model system match those in the real system. The basic results of this treatment including the relationship between mechanical and thermodynamic viewpoints are rederived in a simple yet illuminating way and without recourse to the assumption that bulk properties must be established within the interior of the sphere. (28 refs.)

62215 Calculation of the contact angle of mercury on plane solid oxides. A.T.Yeates, G.D.Halsey (Dept. of Chem., Univ. of Washington, Seattle, WA, USA).

Powder Technol. (Switzerland), vol.34, no.1, p.69-73 (Jan.-Feb. 1983).

Aside from its intrinsic interest, the contact angle for mercury on solid oxides is required for the interpretation of the intrusion pressure for mercury into porous oxide structures. The calculation presented is based on the model structureless mercury liquid brought into contact with specific surfaces of an FCC lattice composed of oxide ions. The pairwise interaction energy is calculated with the Kirkwood-Muller equation, and the lattice sums are based on

the work of Steele (see *Surface Sci.*, vol.36, p.317, 1973) as developed for physical adsorption. The results are compared with established advancing contact angles used in mercury porosimetry. (13 refs.)

62216 Chain fusion and orientational ordering in monomolecular layers of amphiphilic molecules. G.Albinet (Dept. de Phys. des Liquides, Univ. de Provence, Marseille, France), A.-M.S.Tremblay.

Phys. Rev. A (USA), vol.27, no.4, p.2206-16 (April 1983).

A model which describes the competition between chain melting and orientational ordering in a monomolecular layer of long-chain amphiphilic molecules is studied. This model is analogous to the Berker-Cardy-Nelson-Scalapino model for phase transitions in films of ^3He - ^4He mixtures. Their Midgal-Kadanoff renormalization-group approach is applied to the present problem. It reveals two phase transitions. A first-order one, associated with the melting of hydrophobic chains and a Kosterlitz-Thouless-type transition linked to the existence of topological orientational order of the chains in the high-molecular-area region. Isotherms and coexistence curves in the region of the liquid-expanded liquid-condensed transition are calculated. The disagreement with experimental results suggests that the model does not adequately describe the phase transition. This is in contradiction with a previous suggestion based on mean-field considerations. (39 refs.)

62217 Optical test of the equation of state of an interfacial region. E.V.Veitsman.

Sov. Tech. Phys. Lett. (USA), vol.8, no.8, p.410-11 (Aug. 1982). Translation of: *Pis'ma v Zh. Tekh. Fiz. (USSR)*, vol.8, no.15-16, p.944-7 (Aug. 1982). [received: April 1983]

The thickness (ΔL) of the interfacial region at a phase boundary has been determined for the first time by an optical method. A satisfactory agreement between the thicknesses of the interfacial regions determined from the thermodynamic expression and by the optical method has been achieved for 14 liquids. (7 refs.)

62218 Interface and transport phenomena under reduced gravity. II. Surface shapes and kinetics of wetting. A.Bewersdorff (Inst. für Raumsmulation, DFVLR, Köln, Germany), G.Müller, H.Oertel, Jr., P.R.Sahm, P.-J.Sell, S.Siekman.

Z. Flugwiss. & Weltraumforsch. (Germany), vol.7, no.1, p.1-7 (Jan.-Feb. 1983). In German.

Liquids contained in propellant tanks under near zero-g conditions are subject to reduced gravity forces, surface forces and boundary adhesion. Based on the principle of the minimum of the total potential energy, the governing equations of capillary hydrostatics are derived. The equilibrium configurations of a liquid in a rotationally symmetric container can then be determined analytically or numerically. Tank geometries for technical purposes are of particular interest. Out gassing of molten matter is a basic requirement with respect to materials processing in space. The motion of bubbles in a liquid can be investigated in a terrestrial workshop in a simple and reliable manner using a Hele-Shaw cell. The test apparatus permits the study of bubble dynamics under simulated microgravity and the influence of a temperature gradient. The wetting kinetics of model tubes under the conditions of a low gravitational environment is also dealt with in some detail. (40 refs.)

A system for determining fluid properties up to 136 MPa and 473K See Entry 59794

Boundary layers of a nematic liquid crystal in fine capillaries See Entry 61479

Scaling theory of polymer adsorption: proximal exponent See Entry 61764

Microscopic surface tension and binary nucleation See Entry 62056

Effective field theory for interface delocalization transitions ... See Entry 62059

Regularities in formation of composite materials by impregnation of dispersive diamond structures with metal melts See Entry 63217

Surface energy of silicate melts and its importance in sintering processes See Entry 63226

68.15 LIQUID THIN FILMS

van der Waals forces in solutions See Entry 61744

Infrared spectrum of thawed water See Entry 62957

68.20 SOLID SURFACE STRUCTURE

62219 Electron diffraction from ZrO_2 on $\alpha\text{-Zr}(10\bar{1}0)$. R.A.Ploc (Chalk River Nuclear Labs., AECL, Chalk River, Ontario, Canada).

J. Nucl. Mater. (Netherlands), vol.115, no.1, p.10-17 (March 1983).

A transmission electron diffraction study was made of oxide films grown anodically and thermally (573K) on $\alpha\text{-Zr}(10\bar{1}0)$. Considerable differences were noted. Several oxide/metal orientational relationships were found. These are apparently determined by stress and zirconium ion matching across the oxidizing metal interface. (11 refs.)

62220 Surface characterization of substrate by ellipsometry. T.Wada, Y.Katsuyama (R/D Dept., Sumitomo Special Metals Co. Ltd., Osaka, Japan).

J. Magn. & Magn. Mater. (Netherlands), vol.35, no.1-3, p.343-6 (March 1983). (Proceedings of the 10th International Colloquium on Magnetic Films and Surfaces, Yokohama, Japan, 13-16 Sept. 1982).

The surfaces of several kinds of substrate materials were polished by various methods. The quality of these polished surfaces was evaluated by a stylus instrument and ellipsometry. The thickness of the surface Beilby layer and some of its effects on the magnetic properties are discussed. (5 refs.)

62221 Direct determination of the $\text{Au}(110)$ reconstructed surface by X-ray diffraction. I.K.Robinson (Bell Labs., Murray Hill, NJ, USA).

Phys. Rev. Lett. (USA), vol.50, no.15, p.1145-8 (11 April 1983).

The method of glancing-incidence X-ray diffraction has been applied to the $\text{Au}(110)$ reconstructed surface. The long-range structure is incommensurate with the bulk in one direction, comprising locally 2×1 regions separated by domain walls. The atomic positions in the 2×1 cell are determined independently of any models, and their alignment with respect to the bulk is deduced; the result is a missing-row structure with lateral pairing displacements in the second layer of $0.122\pm 0.017 \text{ \AA}$. (15 refs.)

62222 The surface structure of $\alpha\text{-Sn}(100)$. D.P.Woodruff, K.Horn (Fritz-Haber-Inst., Max-Planck-Gesellschaft, Berlin, Germany).

Philos. Mag. A (GB), vol.47, no.3, p.15-8 (March 1983).

Low-energy electron diffraction studies of the semiconducting $\alpha\text{-Sn}(100)$ surface have shown that this surface is reconstructed with a (2×1) mesh and that while the adsorption of atomic hydrogen on this surface leads to some structural rearrangement, the (2×1) mesh is retained. These results are compared with the properties of $\text{Si}(100)$ and $\text{Ge}(100)$ surfaces. In particular, it is

proposed that hydrogen adsorption on α -Sn leads to the formation of a mono-hydride phase. (14 refs.)

Using an electron beam to study the surface microrelief of solids See Entry 59760

Imaging XPS—a new technique. I. Principles See Entry 59891

Model for intensity correction of high energy electron diffraction of small crystallites on solid surfaces See Entry 61739

Initial growth forms of single crystals of chromium with copper on its surface See Entry 61841

The influence of helium implantation profile shapes on blister formation in metals See Entry 61988

Optical, chemical and mechanical modifications induced by ion implantation on glass surfaces See Entry 61993

Formation and relaxation kinetics of mechanical stress in a glass surface layer during ion bombardment See Entry 62000

Observation, close to roughening transition of critical-slowing-down See Entry 62206

Dependence of the carbon density on an epitaxial GaAs film surface on the substrate orientation relative to the crystallographic plane See Entry 62298

Excitation of surface electromagnetic waves at a solid surface by an intense laser beam See Entry 63087

Summary abstract: vibrational excitations of hydrogen and oxygen on Pd(100) See Entry 63095

The adsorption of NO on Ru(001) and its co-adsorption with oxygen studied by vibrational spectroscopy See Entry 63103

Crystallographic determination of metal surfaces with helium scattering See Entry 63122

X-ray photoelectron diffraction studies of zinc selenide See Entry 63137

The development of nitrogen concentration profiles on nitriding iron See Entry 63452

Effect of high-temperature vacuum annealing time on the structure and properties of titanium alloys See Entry 63457

Influence of nitrogen on the penetration of hydrogen through constructional materials from nitrogen-hydrogen mixtures See Entry 63465

The effect of the surface state on the hydrogen permeability and the catalytic activity of palladium alloy membranes See Entry 63583

68.25 MECHANICAL AND ACOUSTICAL PROPERTIES OF SOLID SURFACES AND INTERFACES

[for tribology, see 62.20P and 81.40P]

62223 Energy transport velocity of surface elastic waves. S.R.Seshadri (Dept. of Electrical & Computer Engng., Univ. of Wisconsin, Madison, WI, USA).

J. Appl. Phys. (USA), vol.54, no.4, p.1699-703 (April 1983).

For the Love wave and the Rayleigh wave the power flux and the energies are evaluated, and, therefore, the group velocity is determined by the dynamic method and is verified to be identical to that obtained by the kinematic method. A proof based on a variation theorem is also provided to show in a general way that the kinematic and the dynamic methods yield identical results for the group velocity of the surface elastic waves. (12 refs.)

62224 Surface photoacoustic spectroscopy—a new technique for the study of surface vibrations. F.Trager, T.J.Chuang, H.Coufal (IBM Res. Lab., San Jose, CA, USA).

J. Electron Spectrosc. & Relat. Phenom. (Netherlands), vol.30, p.19-24 (Feb. 1983). (Proceedings of the Third International Conference on 'Vibrations at Surfaces', Asilomar, CA, USA, 1-4 Sept. 1982).

Photoacoustic studies of SF_6 adsorbed on Ag surfaces have been performed with a CO_2 laser. Simultaneous XPS measurements clearly demonstrate monolayer surface sensitivity of photoacoustic spectroscopy under UHV conditions. The photoacoustic spectrum at 0.2 monolayer surface coverage shows a characteristic SF_6 vibrational band. Furthermore, XPS spectra exhibit fine structures indicating distinctive SF_6 -Ag interactions. (15 refs.)

62225 Roughness-trapped shear horizontal surface acoustic waves. O.H.Dupare (Lab. d'Etude de Surfaces et Interfaces, ISEN, Lille, France).

J. Electron Spectrosc. & Relat. Phenom. (Netherlands), vol.30, p.145-50 (Feb. 1983). (Proceedings of the Third International Conference on 'Vibrations at Surfaces', Asilomar, CA, USA, 1-4 Sept. 1982).

Shear horizontal surface acoustic waves do not exist on the flat surface of a semi-infinite elastic medium. It has been shown by several authors recently that such waves can exist on a periodically corrugated, planar surface. The authors show on the basis of the Rayleigh method that shear horizontal surface acoustic waves exist on a randomly rough planar surface of an isotropic elastic medium. These waves are only weakly localized to the surface and they have a lifetime that is long due to their roughness-induced scattering into other surface acoustic waves and into bulk waves. (6 refs.)

62226 Leaky surface-elastic-waves on flat and highly corrugated surfaces for isotropic non-dissipative media. N.E.Glass, A.A.Maradudin (Dept. of Phys., Univ. of California, Irvine, CA, USA).

J. Electron Spectrosc. & Relat. Phenom. (Netherlands), vol.30, p.151-6 (Feb. 1983). (Proceedings of the Third International Conference on 'Vibrations at Surfaces', Asilomar, CA, USA, 1-4 Sept. 1982).

The dispersion relation for Rayleigh waves on a grating-surface of a semi-infinite, isotropic, nondissipative, elastic medium is solved numerically, with complex wave vector k or complex frequency, in the radiative region (above the bulk transverse sound-line) and within the first frequency-gap on the Brillouin zone boundary created by the grating periodicity. The acoustic attenuation, found from the imaginary part of k , agrees well with experiment. A dispersive branch, with corresponding complex-solutions for the flat surface, between the bulk transverse and longitudinal sound-lines, representing a new leaky mode or surface resonance, accounts for the principal peak in the attenuation. (6 refs.)

62227 Acoustically induced plastic deformation of conical microcrystals on copper surfaces. I.H.Wilson, J.Belson (Dept. of Electronic & Electrical Engng., Univ. of Surrey, Guildford, England).

Philos. Mag. A (GB), vol.47, no.3, p.351-61 (March 1983).

Micron-size conical microcrystals have been cultured on a copper surface using the sputtering action of a 100 keV argon-ion beam. When subsequently exposed to an intense 25 kHz acoustic field the cones were found to bend. The bent forms were identical in appearance to the distorted forms reported from time to time for unvibrated cones. These observations lend support to

the authors' recent theory that spontaneous bending is due to slip driven by surface stress which is accommodated by a tendency towards adoption of a helicoidal minimal surface shape. (7 refs.)

62228 Electrodynamic study of the ellipticity of surface acoustic waves near the phase transition in Rochelle salt. V.S.Borshchan, M.V.Manuilov, A.A.Podgornov, O.Yu.Serdobolskaya, I.Yu.Solodov (M.V. Lomonosov State Univ., Moscow, USSR).

Sov. Phys.-Solid State (USA), vol.24, no.9, p.1460-2 (Sept. 1982). Translation of: *Fiz. Tverd. Tela (USSR)*, vol.24, no.9, p.2574-7 (Sept. 1982). [received: April 1983]

An experimental study was made of the change in structure of surface acoustic wave displacements near the phase transition in Rochelle salt. It was found that the ratio of the vertical and horizontal components of the wave displacement ellipse on the surface of the sample increases considerably as the transition is approached. The direction of motion of the particles in the wave is unchanged, being contrary in both the paraelectric and the ferroelectric phase. (6 refs.)

Breadth effects on the penetration of an acoustic beam into a solid See Entry 61331

Ion implantation effects in glasses See Entry 61992

Optical, chemical and mechanical modifications induced by ion implantation on glass surfaces See Entry 61993

Formation and relaxation kinetics of mechanical stress in a glass surface layer during ion bombardment See Entry 62000

Optimization of multilayer structure for electron-acoustic-surface-wave correlators See Entry 62502

Giant attenuation of surface acoustic waves by ferromagnetic films See Entry 62791

The spectroscopy of surface vibrations by atom scattering See Entry 63119

68.30 DYNAMICS OF SOLID SURFACES AND INTERFACE VIBRATIONS

62229 Lateral interactions and vibrational lifetimes. B.N.J.Persson (Inst. für Festkörperforschung, KFA Jülich, Jülich, Germany).

J. Electron Spectrosc. & Relat. Phenom. (Netherlands), vol.29, p.43-57 (15 Jan. 1983). (Proceedings of the Third International Conference on 'Vibrations at Surfaces', Asilomar, CA, USA, 1-4 Sept. 1982).

The author considers three related topics, namely (A) Lateral interactions between adsorbed molecules; (B) Optical properties of two-dimensional systems of small metallic particles (C) Damping of excitations at surfaces. None of these topics are treated in great detail but the author shows that topics (A)-(C) are closely related and that they constitute a unified body of knowledge, which should be useful in gaining insight into such diverse fields as the optical properties of solar energy absorbers, heterogeneous catalysis and photosynthesis. (24 refs.)

62230 Dipole-dipole coupling in adsorbate vibrational mode spectra. Z.Schlesinger (Bell Labs., Murray Hill, NJ, USA), A.J.Sievers.

J. Electron Spectrosc. & Relat. Phenom. (Netherlands), vol.29, p.67 (15 Jan. 1983). (Proceedings of the Third International Conference on 'Vibrations at Surfaces', Asilomar, CA, USA, 1-4 Sept. 1982).

Summary form only given as follows: Separating chemical effects from those due to long range dipole interactions is a recurring problem in the analysis of adsorbate vibrational mode spectra. For adsorbate systems containing only one site and one type of adsorbate (homogeneous systems), agreement between theory and experiment has been obtained. For systems containing inequivalent occupied sites or more than one adsorbate species (inhomogeneous systems), the analysis of effects due to dipole coupling can become complicated. The authors show that a simple effective medium model, similar to those used for thin film coatings, can be used to analyze such systems. The validity of this model is tested by comparing its results to those obtained by numerically solving the exact equations of motion for arrays of coupled point dipole oscillators. Dramatic line narrowing due to dipole coupling, as well as the more well known frequency and intensity shifts are exhibited in both models. Using a sample prescription to determine the effective thickness and density for the effective medium model, the authors obtain results which are both qualitatively and quantitatively equivalent to those of the much less tractable point dipole model. The authors conclude that, despite its extreme simplicity, an effective medium model can be used to accurately treat the effects of dipole coupling in inhomogeneous as well as homogeneous adsorbate systems. (5 refs.)

62231 Electronic damping of the motion of adsorbates on metal surfaces. M.Persson, B.Hellsing, B.J.Lundqvist (Inst. of Theoretical Phys., Chalmers Univ. of Technol., Göteborg, Sweden).

J. Electron Spectrosc. & Relat. Phenom. (Netherlands), vol.29, p.119-24 (15 Jan. 1983). (Proceedings of the Third International Conference on 'Vibrations at Surfaces', Asilomar, CA, USA, 1-4 Sept. 1982).

First principle calculations of the electronic mechanism for the energy exchange between H and H_2 and a jellium substrate are reported. The vibrational damping rate of H_2 is found to be enhanced, when the molecule induces a resonant electronic state near the Fermi level of the substrate. The results for the vibrational broadening of H compares favourably with experimental observations, and the energy of a slowly incoming atom is, according to a friction description, found to be effectively accommodated by this electronic mechanism. (18 refs.)

62232 Theoretical vibrational frequencies for NH_x and CH_x reactive intermediates on nickel(100) and nickel(111) surfaces. J.J.Low, V.I. W.A.Goddard, III (Arthur Amos Noyes Lab. of Chem. Phys., California Inst. of Technol., Pasadena, CA, USA).

J. Electron Spectrosc. & Relat. Phenom. (Netherlands), vol.30, p.27 (Feb. 1983). (Proceedings of the Third International Conference on 'Vibrations at Surfaces', Asilomar, CA, USA, 1-4 Sept. 1982).

Summary form only given, as follows. Theoretical studies have been performed on CH_x and NH_x species chemisorbed on threefold and fourfold sites of nickel clusters. From this work the authors have obtained geometries and vibrational frequencies that can be compared with experimental data concerning these species chemisorbed on Ni(100) and Ni(111) surfaces. These results can be used to help assign the observed losses in EELS spectra for CH on the Ni(111) surface. (no refs.)

62233 Surface phonons in superlattices. B.Djafari-Rouhani, L.Dobrzynski, O.H.Dupare (Lab. d'Etude des Surfaces et Interfaces, Lille, France).

J. Electron Spectrosc. & Relat. Phenom. (Netherlands), vol.30, p.119-24 (Feb. 1983). (Proceedings of the Third International Conference on 'Vibrations at Surfaces', Asilomar, CA, USA, 1-4 Sept. 1982).

Reports the existence of surface localized phonons for a superlattice consisting of alternating slabs (parallel to the surface) of two different crystals. The

superlattice has a larger periodicity in the direction perpendicular to the slabs and therefore many phonon branches in the folded Brillouin zone. In the gaps existing between these phonon branches appear the surface localized models. (7 refs.)

62234 Bound states of two surface phonons at a crystal surface with an adsorbed monolayer. A.G.Eguiluz, A.A.Maradudin (Dept. of Phys., Univ. of California, Irvine, CA, USA). *J. Electron Spectrosc. & Relat. Phenom. (Netherlands)*, vol.30, p.125-30 (Feb. 1983). (Proceedings of the Third International Conference on 'Vibrations at Surfaces', Asilomar, CA, USA, 1-4 Sept. 1982). The authors obtain the Bethe-Salpeter Equation for the Green's function describing the propagation of two surface phonons interacting via cubic and quartic anharmonicity. They solve that equation by keeping only the latter contribution to its kernel. The two-dimensional nature of the problem is reflected in the existence of a bound state of two high-frequency surface phonons associated with the presence of an overlayer of light atoms, for all values of the coupling strength. This is illustrated with the detailed solution of a simple model. (12 refs.)

62235 A search for high frequency vibrational modes at a stepped surface. G.J.Pinas, A.A.Maradudin (Dept. of Phys., Univ. of California, Irvine, CA, USA).

J. Electron Spectrosc. & Relat. Phenom. (Netherlands), vol.30, p.131-6 (Feb. 1983). (Proceedings of the Third International Conference on 'Vibrations at Surfaces', Asilomar, CA, USA, 1-4 Sept. 1982). Presents a theory of the vibrations of atoms in the vicinity of a stepped surface on a Bravais crystal. The static relaxations in the positions of the atoms in the crystal are determined, and the atomic force constants are then calculated in the relaxed atomic configuration. The general theory is applied to a simple stepped surface, and the local phonon density of states is carried out for atoms at several points on the stepped surface by the real space continued fraction recursion method. No evidence is found for high frequency surface phonons. (5 refs.)

62236 Experimental study of relative intensities in inelastic electron tunneling spectroscopy (IETS). S.Gauthier, J.Klein, A.Leger, S.de Cheveigne, C.Guinet (Groupe de Phys. des Solides, Ecole Normale Supérieure, Paris, France).

J. Electron Spectrosc. & Relat. Phenom. (Netherlands), vol.30, p.209-14 (Feb. 1983). (Proceedings of the Third International Conference on 'Vibrations at Surfaces', Asilomar, CA, USA, 1-4 Sept. 1982). Presents an experimental study of the relative intensities in inelastic tunneling spectra of formic and acetic acid chemisorbed on alumina. The theoretical framework is given by the simplest theory of tunneling intensities, the theory of Scalapino and Marcus (1967). The comparison between the experimental results and the predictions of this theory provides evidence for an important discrepancy in the relative intensities in the spectrum of a given molecule. This disagreement is only partially resolved by considering the influence of the counter-electrode of the junction on the tunneling intensities. So, on the basis of an alternative derivation of the results of the theory of Scalapino and Marcus, the authors discuss to what extent it can be applied to the interpretation of tunneling spectra. (12 refs.)

62237 Conference overview, directions and future work and critical issues: theory [surface vibrations]. T.B.Grimley (Donnan Labs., Univ. of Liverpool, Liverpool, England).

J. Electron Spectrosc. & Relat. Phenom. (Netherlands), vol.30, p.229-35 (Feb. 1983). (Proceedings of the Third International Conference on 'Vibrations at Surfaces', Asilomar, CA, USA, 1-4 Sept. 1982). Describes the goals of theoretical work on vibrations at surfaces, and comments on some of the contributions to VAS-82. Its main purpose however is to specify areas where theoretical work is urgently needed, and to identify some critical issues. Among the latter, the most important is the use of clusters to model atomic and molecular processes on solid surfaces. (2 refs.)

62238 Conference overview: experimental [surface vibrations]. H.Ibach (Inst. für Grenzflächenforschung und Vakuumphys., KFA Jülich, Jülich, Germany).

J. Electron Spectrosc. & Relat. Phenom. (Netherlands), vol.30, p.237-46 (Feb. 1983). (Proceedings of the Third International Conference on 'Vibrations at Surfaces', Asilomar, CA, USA, 1-4 Sept. 1982). Current status and future development of experimental techniques for surface vibration spectroscopy are reviewed. It is proposed that in addition to the vibration frequencies the intensities in the spectra should be measured more carefully and then used as a source information. The need for a fast and still sensitive spectroscopy is emphasized. (17 refs.)

62239 Reemitted-positron energy-loss spectroscopy: a novel probe of adsorbate vibrational levels. D.A.Fischer, K.G.Lynn, W.E.Frieze (Brookhaven Nat. Lab., Upton, NY, USA).

Phys. Rev. Lett. (USA), vol.50, no.15, p.1149-52 (11 April 1983). Vibrational excitations of carbon monoxide on Ni(100) have been observed for the first time in the energy-loss spectrum of reemitted positrons. For Ni(100)(c)(2x2)CO at room temperature, energy-loss peaks are found at ~57 and ~248 meV, corresponding to Ni-C and C-O stretching vibrations, respectively. These peak positions are in good agreement with previously reported results for electron energy-loss spectroscopy. Anticipated improvements in resolution promise to make reemitted-positron energy-loss spectroscopy competitive with high-resolution electron energy-loss spectroscopy. (14 refs.)

62240 Effect of surface parameter of interband surface mode frequencies of finite diatomic chain. H.Puszkarski (Phys. Inst. A. Mickiewicz Univ., Poznań, Poland).

Physica B & C (Netherlands), vol.115 B+C, no.3, p.367-75 (March 1983). The surface modes of a finite diatomic chain of alternating atoms ($M_1 \neq M_2$) are investigated. The surface force constants are assumed to differ from the bulk ones, with the resulting surface parameter a identical on both ends of the chain. The criteria governing the existence of interband surface (IBS) modes with frequencies lying in the forbidden gap between acoustical and optical bulk band for natural ($a=1$) as well as non-natural ($a \neq 1$) surfaced defects are analyzed by the difference equation method. It is found that the IBS modes localize, depending on the value of the surface parameter a , either at the surface of lighter atoms (if a is positive), or at that of heavier atoms (if a is negative). Two, one or no IBS mode is found to exist in the chain depending on the relation between the mass ratio and surface parameter—the quantities on which the surface localization increment t depends. If two modes (one acoustical and the other optical) are present, their frequencies are displaced symmetrically with respect to the middle of the forbidden gap if the surface defect is natural, and asymmetrically if it is other than natural. If the localization of the IBS mode exceeds a well-defined critical value t_c , the mode frequency becomes complex, indicating that the mode undergoes a damping. A comparison of the present results and those obtained by Wallis (1957) for the diatomic chain with a natural surface defect is also given. (8 refs.)

Proceedings of the Third International Conference on 'Vibrations at Surfaces'

Excitation of surface polaritons by nondegenerate four-wave mixing of evanescent waves

Influence of surface characteristics of solids on the Kapitza resistance

Surface photoacoustic spectroscopy—a new technique for the study of surface vibrations

Surface vibration correlation with d-electron (hole) per atom ratio (d-bandfilling) in CO chemisorption on supported transition metal particles: dominance of Hund's rule and d-electron degeneracy in real supported catalysts

Low frequency surface resonance modes in electron energy loss spectroscopy

Acetylene adsorption on silver films: a Raman vibrational study

Tunneling spectroscopy as a probe of adsorbate-surface interactions

The interaction of ions and easily ionized species with oxide surfaces as studied by tunneling spectroscopy

Inelastic neutron scattering study of hydrogen adsorbed on impure palladium black

Linear response of a semi-infinite substrate with a two-dimensional conductive surface layer in the plasma-pole approximation

The reflection-absorption infrared spectrum of the dioxygen species adsorbed on platinum recorded by FT-IR spectroscopy

Enhanced adsorbate Raman scattering and surface plasmon radiation

Applications of surface polaritons for detection and vibrational spectral analysis of thin films on metals and dielectrics

High resolution EELS studies of clean and oxide covered semiconductor surfaces

Summary abstract: vibrational excitations of hydrogen and oxygen on Pd(100)

High resolution electron energy loss spectroscopic study of the interaction of oxygen with magnesium single crystal surfaces

Identification of surface vibrations on clean and oxygen covered Pt(111) surfaces with high resolution electron energy loss spectroscopy (EELS)

Vibrational spectra of ethylene and acetylene on metal surfaces—an electron energy loss study of ethylene adsorbed on Ni (110) and its carbided surface, and the use of metal-cluster analogies

Relation between dynamical processes at surfaces and electron-energy-loss measurements

Energy dissipation at metal surfaces: electronic versus vibrational excitations

The spectroscopy of surface vibrations by atom scattering

Measurement of $Au(111)$ surface phonons by low energy helium scattering

Hot atoms and cold facts: mysteries and opportunities in vibration-assisted surface chemistry

The adsorption and dehydrogenation of cyclopentane on Ru (001)

68.40 SURFACE ENERGY OF SOLIDS; THERMODYNAMIC PROPERTIES

62241 Harmonic surface entropy of noble gas crystals: cell cluster method. R.H.Kincaid, D.A.Huckaby (Dept. of Chem., Texas Christian Univ., Fort Worth, TX, USA).

J. Chem. Phys. (USA), vol.78, no.5, p.2598-9 (1 March 1983). The harmonic surface entropy was calculated for FCC and HCP crystals with first-neighbor interactions. The crystals chosen had shapes of minimum lattice energy under first-neighbor interactions. Although the bulk harmonic entropy is higher for FCC than the HCP crystals, the surface harmonic entropy was found to be higher for HCP than for FCC crystals. In fact, the overall harmonic entropy was found to be higher for HCP than for FCC crystals having fewer than a few thousand atoms. (10 refs.)

Sliding friction behaviour of polymer-polymer material combinations

Polymer-aluminium adhesion. I. The surface energy of aluminium in relation to its surface treatment

Fracture of metals under the action of hydrogen-containing media

68.45 SOLID-FLUID INTERFACE PROCESSES

(see also 82.65 Sorption and accommodation coefficients)

62242 Tight-binding cluster Bethe lattice model studies of chemisorption. B.C.Khanra (Solid State & Molecular Phys. Div., Saha Inst. of Nuclear Phys., Calcutta, India).

Chem. Phys. Lett. (Netherlands), vol.96, no.1, p.76-9 (25 March 1983). The surface Green's function which is used in model calculations for chemisorption systems has been approximated by the tight-binding cluster Bethe lattice model (TBCBLM). It is shown that for chemisorption of a single-orbital atom on a simple cubic lattice this model yields results in good agreement with Einstein and Schrieffer's results (1973). The effects of cluster size on the chemisorption properties are explored. (6 refs.)

62243 The influence of preadsorbed hydrogen and CO and adsorption of ethylene on the Pd(111) surface. I.Ratajczykowa, I.Szymerska (Inst. of Phys. Chem., Polish Acad. of Sci., Warsaw, Poland).

Chem. Phys. Lett. (Netherlands), vol.96, no.2, p.243-6 (1 April 1983). The coadsorption of C_2H_4 with H_2 and CO on Pd(111) has been investigated at 300 and 330K. At 300K two forms of adsorbed ethylene coexist on the surface in the presence of ethylene gas: a molecular form desorbing as C_2H_4 at 330K and a dissociatively adsorbed form (giving only hydrogen in desorption spectra) which is stable both in vacuum and in hydrogen at 10^{-8} Torr. The molecular form seems to be a precursor state for hydrogenation and for dissociative adsorption. Both processes are controlled by the amount of coadsorbed hydrogen which in turn is controlled by CO coverage. (11 refs.)

- 62244** An EELS and TDS study of molecular oxygen desorption and decomposition on Pt(111). N.R.Avery (Univ. of Melbourne, Parkville, Victoria, Australia). *Chem. Phys. Lett. (Netherlands)*, vol.96, no.3, p.371-3 (8 April 1983). Correlation of EEL and TD spectra for the adsorption of O_2 on Pt(111) at $<100K$ has identified the respective roles of the two molecularly adsorbed states in the apparently competing processes of desorption and dissociation. (8 refs.)
- 62245** LEED/AES studies of the Ge on Si(111)7 \times 7 surface. K.Shoji, M.Hyodo, H.Ueba, C.Tatsuyama (Dept. of Electronics, Faculty of Engng., Toyama Univ., Toyama, Japan). *Jpn. J. Appl. Phys. Part 2 (Japan)*, vol.22, no.3, p.L200-2 (March 1983). Germanium was evaporated on the clean Si(111)7 \times 7 surface at room temperature. With increase in Ge coverage θ , the intensity of the Si(LVV) AES signal decreased in accordance with a 2-dimensional growth mode up to a few monolayers, and the LEED pattern gradually changed from the (7 \times 7) structure to a diffused (1 \times 1) one at $\theta < 2$ monolayers and to a nonstructural one at $\theta > 2$. The LEED pattern and the AES intensity drastically changed by annealing. The Si(111)7 \times 7 surface covered by 2 monolayers of Ge shows a (5 \times 5) structure by annealing at temperature between 380 and 720°C.
- 62246** Theoretical studies of molecular adsorption on metal surfaces. B.I.Lundqvist, B.Hellsing, S.Holmstrom, P.Nordstrom, M.Persson (Inst. of Theoretical Phys., Chalmers Univ. of Technol., Goteborg, Sweden), J.K.Nor-skov. *Int. J. Quantum Chem. (USA)*, vol.23, no.3, p.1083-90 (March 1983). (Proceedings of the Fourth International Congress in Quantum Chemistry, Uppsala, Sweden, 13-20 June 1982). A theoretical program in surface physics aiming at a description of different aspects of adsorption of atoms and molecules on metal surfaces is shortly reviewed. (18 refs.)
- 62247** The mode of the attack of oxygen atoms on the basal plane of graphite. Chor Wong, R.T.Yang (Dept. of Chem. Engng., State Univ. of New York, Amherst, NY, USA), B.L.Halpern. *J. Chem. Phys. (USA)*, vol.78, no.6, pt.1, p.3325-8 (15 March 1983). Gold decoration of the basal lattice plane of graphite etched by atomic oxygen has been made possible by first desorbing the surface oxide layer on the basal plane. The formation of monolayer pits, as revealed by gold decoration, shows that anisotropy does exist, i.e. carbon atoms are preferentially attacked by atomic oxygen in the direction of a axes, rather than the direction of c axis. The monolayer pits are initiated from lattice vacancies which are continually formed by atomic oxygen. The monolayer pits created by atomic oxygen are, unlike the pits by O_2 which are circular, hexagonal in shape, the sides of which are composed of {1011} lattice planes. (14 refs.)
- 62248** Energy and momentum accommodation coefficients on platinum and silver. F.D.Shields (Univ. of Mississippi, Univ., MS, USA). *J. Chem. Phys. (USA)*, vol.78, no.6, pt.1, p.3329-33 (15 March 1983). Acoustical measurements of energy (EAC) and tangential momentum accommodation coefficients (TMAC) indicate that stable and reproducible Pt and Ag surfaces are obtained by heating in a vacuum. EAC and TMAC values are given for He and Ne on the heat-cleaned Pt and Ag surfaces and for these gases on Pt and Ag surfaces after exposure to various adsorbent gases. AC values are also given for the various adsorbent gases on themselves on the heat-cleaned Pt and Ag surfaces. (11 refs.)
- 62249** Variation with temperature of the thickness of an adsorbed polymer layer in the collapsed state. P.Dejardin (CNRS, Centre de Recherches sur les Macromolécules, Strasbourg, France). *J. Phys. (France)*, vol.44, no.4, p.537-42 (April 1983). The behaviour of the hydrodynamic thickness L_H , below the θ -temperature for the system polystyrene/trans-decalin, is consistent with the presence of a collapsed adsorbed polymer layer. For three samples of polystyrene ($M_w \approx 10^5$, $M_w = 6 \times 10^5$, $M_w = 4 \times 10^5$), one observes a power law dependence $L_H \sim (\theta - T)^\alpha$ with values of α (-0.87; -0.83; -0.80) close to 1.0 rather than to 1/3. These results are consistent with an interdependent macromolecule model. Attempts to obtain a logarithmic factor $[\ln(T/\theta - T)]^\beta$ give values of β between -0.39 and -0.65, to be compared with the value -0.636 obtained theoretically by De Gennes (1979) for a chain surrounded by solvent near the θ -temperature. (35 refs.)
- 62250** The thermodynamics of the system CaNi $_2$ H $_2$ using differential heat conduction calorimetry. J.J.Murray, M.L.Post, J.B.Taylor (Div. of Chem., Nat. Res. Council of Canada, Ottawa, Ontario, Canada). *J. Less-Common Met. (Switzerland)*, vol.90, no.1, p.65-73 (March 1983). The pressure-composition isotherms and enthalpies of 313.6K are reported for hydrogen absorption and desorption in CaNi $_2$ H $_2$ with $0 < x < 2$. Enthalpy measurements were made using a Calvet-Prat differential heat conduction calorimeter. Partial relative enthalpies for the α solution and the β single-phase regions are reported together with the enthalpies of transition for the $\alpha \rightarrow \beta$ and $\beta \rightarrow \gamma$ reactions. The latter enthalpies (negative or exothermic for absorption and positive for desorption) are 43.4 ± 0.7 and 33.1 ± 0.5 kJ (mol H $_2$) $^{-1}$, the quoted errors being the total probable errors. (16 refs.)
- 62251** Phase and bonding transitions in chemisorbed layers studied by vibrational frequency shifts. D.A.King (Donnan Labs., Univ. of Liverpool, Liverpool, England). *J. Electron Spectrosc. & Relat. Phenom. (Netherlands)*, vol.29, p.11-24 (15 Jan. 1983). (Proceedings of the Third International Conference on 'Vibrations at Surfaces', Asilomar, CA, USA, 1-4 Sept. 1982). Coverage-dependent frequency shifts have been observed for a wide variety of adsorbates on metal single crystal surfaces. In some cases, these shifts are attributable to changes in bonding coordination to surface metal atoms, or to alterations in the geometry of the chemisorbed complex. The major part of this review is concerned with the information that can be obtained from shifts which have been observed, both upward and downward in frequency, when bonding coordination or geometric effects do not occur. It is shown that when the observation of frequency shifts is combined with the measurement of singlet frequencies using the dilution limit isotopic mixing method of Crossley and King (1980) (now applied to CO adsorption on a variety of metal single crystals), shifts due to dipole coupling in the overlayer can be deconvoluted from shifts due to chemical (bonding) effects. A review of recent data for CO adsorption on Pt(111), {100} and {110}, Cu(111), {100} and {110}, Pd(100) and Ru(100) is presented which illustrates the information available from such data concerning phase boundaries between lattice gas, island and condensed phases, and also subtle changes in adsorbate bonding. (34 refs.)
- 62252** High resolution infrared study of hydrogen chemisorbed on Si (100). Y.J.Chabal, E.E.Chaban, S.B.Christman (Bell Labs., Murray Hill, NJ, USA). *J. Electron Spectrosc. & Relat. Phenom. (Netherlands)*, vol.29, p.35-40 (15 Jan. 1983). (Proceedings of the Third International Conference on 'Vibrations at Surfaces', Asilomar, CA, USA, 1-4 Sept. 1982). The vibrational spectrum associated with hydrogen chemisorbed on Si (100) was studied for the first time by means of Fourier transform infrared spectroscopy. The low coverage phase (monohydride) is characterized at room temperature by a broad line ($\Delta \approx 17$ cm $^{-1}$) at 2095 cm $^{-1}$ which sharpens upon mild annealing, indicating an ordering of the hydrogen monolayer. The high coverage phase (dihydride) features symmetric [$\nu_1 = 2099$ cm $^{-1}$, $\Delta = 5$ cm $^{-1}$] and antisymmetric [$\nu_2 = 2087$ cm $^{-1}$, $\Delta = 5$ cm $^{-1}$] stretching modes with dynamic dipole moments perpendicular and parallel to the surface, respectively. The effective charge, $e^+|e| \approx 0.01$, is consistent with early theoretical predictions. The resulting dipolar interaction is too weak to account for the 12 cm $^{-1}$ splitting, suggesting a small chemical interaction. (26 refs.)
- 62253** Vibrations spectra of oxygen chemisorbed on nickel (110) surfaces. G.Allan (Lab. de Phys. des Solides, Inst. Supérieur d'Electronique du Nord, Lille, France), J.Lopez. *J. Electron Spectrosc. & Relat. Phenom. (Netherlands)*, vol.29, p.61-6 (15 Jan. 1983). (Proceedings of the Third International Conference on 'Vibrations at Surfaces', Asilomar, CA, USA, 1-4 Sept. 1982). Using a simple tight-binding scheme to describe the nickel d states and the oxygen p states, the authors calculate the positions and the vibration frequencies of chemisorbed oxygen atoms on nickel (110) surfaces. The comparison between the authors' results and the high resolution electron loss measurements suggests a long bridge chemisorption site at low and high oxygen coverages on the nickel surface. (20 refs.)
- 62254** Ab initio CI investigation of hydrogen atom adsorption on Li clusters: embedded cluster model. H.O.Beckmann (Dept. of Chem., State Univ. of New York, Stony Brook, NY, USA). *J. Electron Spectrosc. & Relat. Phenom. (Netherlands)*, vol.29, p.77-81 (15 Jan. 1983). (Proceedings of the Third International Conference on 'Vibrations at Surfaces', Asilomar, CA, USA, 1-4 Sept. 1982). The chemisorption of H on clusters representing the (100) surface of Li BCC lattice has been studied with ab initio SCF and CI methods and an embedding theory based on orbital localization (Whitten and Pakkanen, Phys. Rev. B21 (1980), p.4357). The results suggest that a convergence of the properties for adsorption on cluster models is almost reached when all metal atoms involved in the adsorption are surrounded by their neighbors. (4 refs.)
- 62255** Investigation of lateral interactions in chemisorption. I.P.Batra (IBM Res. Lab., San Jose, CA, USA). *J. Electron Spectrosc. & Relat. Phenom. (Netherlands)*, vol.29, p.83-90 (15 Jan. 1983). (Proceedings of the Third International Conference on 'Vibrations at Surfaces', Asilomar, CA, USA, 1-4 Sept. 1982). It is believed that lateral interactions play an important role in chemisorption site selection. With the advent of angular resolved and polarization dependent photoemission spectroscopies, one is able to compare computed band structure with angular resolved photoemission data. This advance coupled with theoretical calculations provides an excellent opportunity for investigating direct (adsorbate-adsorbate) and indirect (through-substrate) lateral interactions at surfaces. The author modelled the chemisorption of oxygen on Al (111) using direct lateral interactions only (isolated monolayer). The calculated results provide a good framework for interpreting the data. For O_2 monolayer the direct lateral interactions are also appreciable and lead to significant dispersion in the calculated energy bands. The author has also computed the electronic structure for two dimensional isolated layers of CO in ordered configurations observed on a Pd (100) surface. The shape and width of the 4 σ -derived band is satisfactorily accounted for by this direct lateral interaction only model. Having demonstrated that direct lateral interactions lead to observable band dispersions, it is suggested that they might influence normal vibrational frequencies and ought to be included. (25 refs.)
- 62256** Selective desorption from the binary coadsorbate C_2H_4 -CH $_3$ F-NaCl by resonant vibrational excitation with laser infrared radiation. J.Heidberg, I.Hussla (Inst. fur Phys. Chem. und Elektrochem., Univ. Hannover, Hannover, Germany). *J. Electron Spectrosc. & Relat. Phenom. (Netherlands)*, vol.29, p.105-10 (15 Jan. 1983). (Proceedings of the Third International Conference on 'Vibrations at Surfaces', Asilomar, CA, USA, 1-4 Sept. 1982). After measuring the linear infrared absorption spectrum of the coadsorbate, selective desorption of CH $_3$ F from the binary coadsorbate C_2H_4 -CH $_3$ F-NaCl under ultrahigh vacuum conditions at 120K stimulated by resonant CO $_2$ laser pulses of small fluence ~ 0.1 J.cm $^{-2}$ has been carried out. No desorption of ethane, which is slightly more volatile, but has no significant infrared absorption at the laser frequency, was observed. The primary activation step is the resonant multiphoton excitation of the most intense internal CH $_3$ F-NaCl adsorbate vibration, the C-F stretching mode ν_3 . The substance separation seems to indicate high localisation of the activation in this desorption and could be of interest for applications. (12 refs.)
- 62257** Laser-induced thermal desorption of CO from clean polycrystalline copper: time-of-flight and surface diffusion measurements. R.Viswanathan, D.R.Burgess, Jr., P.C.Stair, E.Weitz (Dept. of Chem., Northwestern Univ., Evanston, IL, USA). *J. Electron Spectrosc. & Relat. Phenom. (Netherlands)*, vol.29, p.111 (15 Jan. 1983). (Proceedings of the Third International Conference on 'Vibrations at Surfaces', Asilomar, CA, USA, 1-4 Sept. 1982). Summary form only given as follows. Pulsed laser-induced thermal desorption was utilized as a technique to study the dynamics of desorption and surface diffusion of CO on clean polycrystalline copper at 85K in UHV. Single pulses of a focused KrF excimer laser (248 nm, 15 ns FWHM) were used to desorb the CO molecules, which were subsequently detected by a quadrupole mass spectrometer (effective time constant ≈ 4.4 μ s). The time-of-flight (TOF) plus distribution was recorded using a fast transient recorder (Biomat 610B/8100). The surface diffusion measurements were made using a versatile technique. The TOF desorption spectra could be fit to Boltzmann distributions, and effective translational temperatures of the desorbed CO molecules were obtained from these fits. The desorption process was studied as a function of laser power density, and a desorption threshold corresponding to an absorbed power density of 10 MW cm $^{-2}$ was observed. Near threshold, both the desorption flux and velocity distribution varied rapidly with laser power density. At power densities much larger than the threshold (30-75 MW cm $^{-2}$), the peak desorption flux varied approximately linearly with power density. In the range of power densities studied, the most probable velocity of the CO molecules varied between 350 and 500 m s $^{-1}$, corresponding to Boltzmann temperatures between 200 and 400K. The applicability of the classical desorption rate equation for laser induced desorption on polycrystalline copper at 110K yielded a value for the diffusion coefficient $D = 5 \times 10^{-7}$ cm 2 s $^{-1}$ ($\pm 2 \times 10^{-7}$ cm 2 s $^{-1}$) (ref.1). The temperature dependence of the

diffusion coefficient is currently being investigated in detail in order to accurately determine the activation energy for the diffusion process. (1 ref.)

62258 Surface vibration correlation with d-electron (hole) per atom ratio (d-bandfilling) in CO chemisorption on supported transition metal particles: dominance of Hund's rule and d-electron degeneracy in real supported catalysts. E.Siegel.

J. Electron Spectrosc. & Relat. Phenom. (Netherlands), vol.29, p.155 (15 Jan. 1983). (Proceedings of the Third International Conference on 'Vibrations at Surfaces', Asilomar, CA, USA, 1-4 Sept. 1982).

Summary form only given as follows. The findings of Guerra and Schulman (1969) of a correlation between force constant of metal-CO chemisorbed species (ad molecules) with the number of d-holes per atom (1-number of d-electrons per atom, or d-bandfilling) of the transition metal particle (supported) surface is treated using the tenfold degenerate Hubbard (TDHM) and Anderson (TDAM) models developed for magnetic and Mott metal-insulator transition problems in transition metals, alloys and compounds. Their experimental finding that via infrared spectroscopy on the CO adsorbed species (ad molecule) bond, the infrared surface vibrational frequency, CO bond order and CO bond force constant were nearly linear versus the number of d-holes per transition metal surface atom is easily explained via the TDHM and TDAM via their inherent d-bandfilling dependent (alloy specific) Coulomb and exchange enhanced coupling strength between d-electrons or d-holes. Even the Fulde correction to the number of d-electrons (holes) per surface atom as a function of transition metal particle size does not change the excellent agreement, but merely renormalizes the measured functional properties versus d-hole per atom ratio for a suite of equally fine sized transition metal particles. So it seems that in ad molecule chemisorption (at least for CO) the degenerate electronic properties to the surface dominate the vibrational and bonding properties of the ad molecular species rather completely. (5 refs.)

62259 The chemisorption of nitrogen on the (001) surface of ruthenium. A.B.Anton, N.R.Avery, B.H.Toby, W.H.Weinberg (Div. of Chem. & Chem. Engng., California Inst. of Technol., Pasadena, CA, USA).

J. Electron Spectrosc. & Relat. Phenom. (Netherlands), vol.29, p.181-6 (15 Jan. 1983). (Proceedings of the Third International Conference on 'Vibrations at Surfaces', Asilomar, CA, USA, 1-4 Sept. 1982).

High resolution electron energy loss spectroscopy (EELS), thermal desorption mass spectrometry (TDMS) and low energy electron diffraction (LEED) have been used to investigate the molecular chemisorption of N_2 on Ru(001) at 75K and 95K. Adsorption at 95K produces a single chemisorbed state, and, at saturation, a $(\sqrt{3} \times \sqrt{3})R30^\circ$ LEED pattern is observed. Adsorption at 75K produces an additional chemisorbed state of lower binding energy, and the probability of adsorption increases by a factor of two from its zero coverage value when the second chemisorbed state begins to populate. EEL spectra recorded for all coverages at 75K show only two dipolar modes $\nu(Ru-N_2)$ at $280-300\text{ cm}^{-1}$ and $\nu(N-N)$ at $2200-2250\text{ cm}^{-1}$ —indicating adsorption at on-top sites with the axis of the molecular standing perpendicular to the surface. The intensities of these loss features increase and $\nu(N-N)$ decreases with increasing surface coverage of both chemisorbed states. (15 refs.)

62260 Adsorbate structure modeling based on electron energy loss spectroscopy and lattice dynamical calculations: application to O/Al(111). R.L.Strong, B.Firey, F.W.deWette, J.L.Erskine.

J. Electron Spectrosc. & Relat. Phenom. (Netherlands), vol.29, p.187-90 (15 Jan. 1983). (Proceedings of the Third International Conference on 'Vibrations at Surfaces', Asilomar, CA, USA, 1-4 Sept. 1982).

High-resolution electron energy loss spectroscopy (EELS) and lattice dynamical calculations based on pair interactions are used to investigate oxygen chemisorption on Al(111). The O/Al(111) system is complicated by the simultaneous formation of an oxygen overlayer and underlayer. Oxygen atoms at overlayer and underlayer sites near the Al(111) surface produce well-defined vibrational loss peaks in EELS spectra; however, dynamical coupling between the oxygen and with the host lattice cause vibrational energies to shift with overlayer and underlayer concentrations. These shifts as well as structural parameters of the O/Al(111) complex can be deduced from a slab model of the surface lattice dynamics. (5 refs.)

62261 Low frequency surface resonance modes in electron energy loss spectroscopy. T.S.Rahman (Dept. of Phys., Univ. of California, Irvine, CA, USA), D.L.Mills, J.E.Black.

J. Electron Spectrosc. & Relat. Phenom. (Netherlands), vol.29, p.199-212 (15 Jan. 1983). (Proceedings of the Third International Conference on 'Vibrations at Surfaces', Asilomar, CA, USA, 1-4 Sept. 1982).

Electron energy loss spectroscopy has proved a powerful probe of vibrational modes of a wide variety of adsorbed species. The primary focus has been on modes with frequency well above the maximum phonon frequency of the substrate. Examples are internal vibration modes of adsorbed molecules, possibly shifted significantly in frequency from their gas phase analogues, and high frequency vibrations of an adsorbed molecule or atom against the substrate. Recent experiments explore features in the energy loss spectrum with frequency below the maximum phonon frequency of the substrate, for ordered overlayers of atoms adsorbed on low index metal surfaces. The authors summarize their theoretical studies of such spectra for several adsorbate/substrate combinations, with emphasis on the physical origin of the features which appear in the calculations. They obtain a good account of the existing data, within the framework of a rather simple lattice dynamical model, and the calculations show that the features which appear are quite sensitive to the symmetry of the adsorption sites, and other details of the surface geometry. The authors illustrate this with several specific examples. (17 refs.)

62262 Theoretical calculation of vibrations of adsorbed species. P.S.Bagus, I.P.Batra, C.W.Bauschlicher,Jr., R.Broer (IBM Res. Lab., San Jose, CA, USA).

J. Electron Spectrosc. & Relat. Phenom. (Netherlands), vol.29, p.225-32 (15 Jan. 1983). (Proceedings of the Third International Conference on 'Vibrations at Surfaces', Asilomar, CA, USA, 1-4 Sept. 1982).

The chemisorption of oxygen on lithium, aluminum, nickel and copper surfaces has been investigated using the ab initio Hartree-Fock cluster model. These substrates have the possibility for different bonding in that Li is a simple s metal, Al an s, p and Ni(Cu) an s, p, d metal. In all cases the authors have calculated binding energy curves as a function of the oxygen-metal distance. Using these curves, they have derived oxygen-metal normal vibrational frequencies, and the equilibrium bond distance. They have compared the calculated vibrational energy with electron energy loss spectroscopic (EELS) data for Al and find a satisfactory agreement. They discuss O adsorbed on Ni(100) for which coverage dependent loss peaks have been reported but no generally acceptable interpretation exists to date. (19 refs.)

62263 Hydrogen chemisorption on Ni(110) by high-resolution electron energy loss spectroscopy. M.Nishijima, S.Masuda, M.Jo, M.Onchi (Dept. of Chem., Kyoto Univ., Kyoto, Japan).

J. Electron Spectrosc. & Relat. Phenom. (Netherlands), vol.29, p.273-8 (15 Jan. 1983). (Proceedings of the Third International Conference on 'Vibrations at Surfaces', Asilomar, CA, USA, 1-4 Sept. 1982).

High-resolution electron energy loss spectra of hydrogen-covered Ni(110) surfaces both at 100 and 300K are presented. The adsorbed sites of hydrogen atoms are discussed. (10 refs.)

62264 Vibrational spectroscopy using HREELS of benzene adsorbed on the Rh (111) crystal surface. B.E.Koel, G.A.Somorjai (Dept. of Chem., Univ. of California, Berkeley, CA, USA).

J. Electron Spectrosc. & Relat. Phenom. (Netherlands), vol.29, p.287-92 (15 Jan. 1983). (Proceedings of the Third International Conference on 'Vibrations at Surfaces', Asilomar, CA, USA, 1-4 Sept. 1982).

High resolution electron energy loss spectroscopy (HREELS) and low energy electron diffraction (LEED) have been used to study the structure of adsorbed benzene (C_6H_6 and C_6D_6) monolayers on the Rh(111) surface at 300K. A surface bonding geometry is proposed for benzene adsorbed to give a $c(2\sqrt{3} \times 4)$ rectangular structure, which involves very little perturbation of the molecular structure with the ring plane parallel to the surface. Only one chemical environment for adsorbed benzene is indicated by a single frequency shift of the symmetric C-H out-of-plane bending mode. The adsorption site is tentatively assigned to benzene centered over a single Rh atom. (8 refs.)

62265 HREELS study of formic acid adsorption on gold (110) and (111) surfaces. M.Chtaib, P.A.Thiry, J.P.Delrieu, J.J.Pireaux, R.Caudano (Lab. de Spectroscopie Electronique, IRIS, Namur, Belgium).

J. Electron Spectrosc. & Relat. Phenom. (Netherlands), vol.29, p.293-9 (15 Jan. 1983). (Proceedings of the Third International Conference on 'Vibrations at Surfaces', Asilomar, CA, USA, 1-4 Sept. 1982).

The adsorption at 100K and the temperature decomposition of formic acid were investigated on (110) and (111) gold single crystal surfaces by high resolution electron energy loss spectroscopy. A multilayer build-up of physisorbed HCOOH with intense hydrogen bondings was observed at increasing coverages for the two gold surface orientations. Above room temperature, formic acid decomposed and desorbed from the (110) crystal, whereas it evolved into an intermediate formic anhydride on the (111) face. Further heating produced on the surfaces species similar to those observed on oxygen treated metals. (18 refs.)

62266 Using surface enhanced Raman scattering to study vibrations of adsorbates on thin metallic overlayers on silver. C.A.Murray (Bell Labs., Murray Hill, NJ, USA).

J. Electron Spectrosc. & Relat. Phenom. (Netherlands), vol.29, p.371-82 (15 Jan. 1983). (Proceedings of the Third International Conference on 'Vibrations at Surfaces', Asilomar, CA, USA, 1-4 Sept. 1982).

The author has studied the surface enhanced Raman scattering from molecules adsorbed on thin gold overlayers on silver island films. The Raman scattering of gold cyanide species adsorbed on gold overlayers decreases in intensity with gold overlayer thickness between 0.5-10 Å. This intensity decrease is consistent with a simple model which takes into account the damping of the electromagnetic resonances of the silver islands by the absorbing gold overlayer. Implications of these findings for the enhancement of Raman scattering from adsorbates on other metals deposited as overlayers on silver will be discussed. (22 refs.)

62267 Acetylene adsorption on silver films: a Raman vibrational study. I.Pockrand, C.Pettenkofer, A.Otto (Phys. Inst. III, Univ. Dusseldorf, Dusseldorf, Germany).

J. Electron Spectrosc. & Relat. Phenom. (Netherlands), vol.29, p.409-12 (15 Jan. 1983). (Proceedings of the Third International Conference on 'Vibrations at Surfaces', Asilomar, CA, USA, 1-4 Sept. 1982).

'Coldly' evaporated silver films exposed to acetylene at 120K exhibit characteristic, enhanced Raman spectra. Peaks are identified by isotope line shifts. The results point to weak interaction of acetylene with silver. (17 refs.)

62268 Rovibrational excitation within the infinite conical well: desorption of diatomic molecules. J.W.Gadzuk (NBS, Washington, DC, USA), U.Landman, E.J.Kuster, C.L.Cleveland, R.N.Barnett.

J. Electron Spectrosc. & Relat. Phenom. (Netherlands), vol.30, p.103-10 (Feb. 1983). (Proceedings of the Third International Conference on 'Vibrations at Surfaces', Asilomar, CA, USA, 1-4 Sept. 1982).

An analytic model for the hindered rotational states of a diatomic molecule adsorbed upright on a solid surface is discussed. Various model dynamics situations, within the sudden approximation, designed to simulate desorption are presented and rotational state distributions are calculated including both rotational and translational degrees of freedom. Criteria are established for observing rotationally cool desorbed molecules. (11 refs.)

62269 X-ray and neutron diffraction measurements on physisorbed films on graphite. M.Nielsen, K.Kjaer, J.Bohr (Riso Nat. Lab., Roskilde, Denmark), J.P.McTague.

J. Electron Spectrosc. & Relat. Phenom. (Netherlands), vol.30, p.111-18 (Feb. 1983). (Proceedings of the Third International Conference on 'Vibrations at Surfaces', Asilomar, CA, USA, 1-4 Sept. 1982).

Physisorbed films of rare gas atoms and of simple molecules on graphite surfaces are studied with the main purpose of studying the nature of phase transitions in two dimensional systems. Much progress has been made recently both in substrate properties and in diffraction technique. Especially the application of synchrotron X-ray diffraction has been important and has increased the range over which correlations can be measured by almost an order of magnitude. The authors show examples of experimental results from X-ray and neutron diffraction studies of melting and commensurate-incommensurate transitions in adsorbed films. (24 refs.)

62270 Tunneling spectroscopy as a probe of adsorbate-surface interactions. P.K.Hansma (Dept. of Phys., Univ. of California, Santa Barbara, CA, USA).

J. Electron Spectrosc. & Relat. Phenom. (Netherlands), vol.30, p.163-74 (Feb. 1983). (Proceedings of the Third International Conference on 'Vibrations at Surfaces', Asilomar, CA, USA, 1-4 Sept. 1982).

Tunneling spectroscopy is a sensitive probe of two classes of adsorbate-surface interactions: interactions of the adsorbate with the substrate on which it is adsorbed and adsorbate interactions with the top metal electrode that is evaporated on top of it. The author focuses on the second class. In general, the interaction of the adsorbed molecules with the top metal electrode produces a down-shift in the vibrational mode position ranging in size from $\leq 0.1\%$ to $\leq 10\%$ depending on the dipole derivative of the mode and the type of top metal electrode. (14 refs.)

62271 The interaction of ions and easily ionized species with oxide surfaces as studied by tunneling spectroscopy. K.W.Hipps (Dept. of Chem., Washington State Univ., Pullman, WA, USA).

J. Electron Spectrosc. & Relat. Phenom. (Netherlands), vol.30, p.175-88 (Feb. 1983). (Proceedings of the Third International Conference on 'Vibrations at Surfaces', Asilomar, CA, USA, 1-4 Sept. 1982).

The thin film properties of alumina and magnesia, the substrates most frequently used in tunneling spectroscopy, are reviewed. The composite barriers, Al_2O_3/SiO_2 and Al_2O_3/Si , are also discussed. Tunneling studies provide information about adsorbate-surface interactions; weak counterion adsorption effects through very strong direct chemical modifications can be studied. Tunneling studies of anionic transition metal complexes adsorbed on alumina provide significantly more information about the nature of the surface species than corresponding IR studies. The adsorption of TCNE on alumina from solution is used to exemplify how tunneling spectroscopy may be integrated into a manifold of conventional techniques (IR, ESR, and elution studies in this case). (37 refs.)

62272 Inelastic neutron scattering study of hydrogen adsorbed on impure palladium black. J.J.Braid, J.Howard (Dept. of Chem., Univ. of Durham, Durham, England), J.Tomkinson.

J. Chem. Soc. Faraday Trans. II (GB), vol.79, pt.2, p.253-62 (Feb. 1983). The incoherent inelastic neutron scattering (INS) spectra of hydrogen strongly chemisorbed on Pd black have been obtained (77K) without interference from absorbed or type-C adsorbed hydrogen. The spectra were assigned by comparison with the vibrational spectra of transition-metal hydridecarbonyl compounds and from the change in intensity of the INS bands with surface coverage. Only coverages greater than one monolayer were studied. The data indicate the occupation by H of two-fold bridging and terminal sites, the relative population of the terminal sites increasing at higher hydrogen coverage. (19 refs.)

62273 Corrugation studies for $p(2 \times 2)$ and $c(2 \times 2)$ phases of oxygen on Ni(001) and Cu(001). J.A.Barker, I.P.Batra (IBM Res. Lab., San Jose, CA, USA).

Phys. Rev. B (USA), vol.27, no.6, p.3138-43 (15 March 1983). Chemisorption of oxygen on Ni(001) shows $p(2 \times 2)$ low-energy electron diffraction (LEED) patterns at low exposures changing to $c(2 \times 2)$ at higher exposures. A recent quantum-mechanical cluster calculation and a lattice-dynamical calculation have suggested different vertical heights for the two phases of oxygen. Another ab initio cluster calculation and extended X-ray absorption fine-structure data indicate a single vertical height, in agreement with earlier LEED studies. More recent LEED calculations, however, do not rule out a closer distance for the $c(2 \times 2)$ phase. A He-diffraction study has just been completed for the $c(2 \times 2)$ and $p(2 \times 2)$ phases. The authors compare their calculated corrugation with these data and conclude that in both phases oxygen is at a vertical distance of about 0.9 Å. They predict similar results for oxygen on Cu(001). (25 refs.)

62274 Structure of potassium films on the (1010) face of rhenium. Ya.B.Lozoviy (Ivan Franko State Univ., Lvov, Ukrainian SSR). *Sov. Phys.-Solid State (USA)*, vol.24, no.9, p.1505-6 (Sept. 1982). Translation of: *Fiz. Tverd. Tela (USSR)*, vol.24, no.9, p.2655-7 (Sept. 1982). [received: April 1983]

Low-energy electron diffraction and contact potential methods were used to study the structure, work function, and thermal stability of potassium films on the (1010) face of rhenium. Throughout the investigated range of first layer coverage $2.5 \times 10^{14} < n < 6.15 \times 10^{14} \text{ cm}^{-2}$, the films have a centered structure $c(2 \times 1)/\sqrt{3}$, where $\sqrt{3} = n/n_{\text{re}}$, n is the potassium atom concentration, and n_{re} the concentration of rhenium atoms on the (1010) face. The minimum work function corresponds to the $c(2 \times 2)$ structure. A monolayer of potassium has the structure $c(2 \times 4)/3$. The second layer grows on the first as islands of the centered structure $c(2 \times \sim 1.7)$. (11 refs.)

62275 Hydration and dehydration of the surface of fused silica. A.A.Kuznetsov, A.P.Kuleshov. *Sov. J. Opt. Technol. (USA)*, vol.49, no.7, p.463-4 (July 1982). Translation of: *Opt.-Mekh. Prom.-st. (USSR)*, vol.49, no.7, p.59-60 (July 1982). [received: April 1983]

It is shown that physical sorption and chemisorption proceed simultaneously on the surface of fused silica and that the thickness of the water layer on the surface fluctuates within the limits 14-86 Å, depending on the atmospheric humidity. (7 refs.)

62276 Observation of an orientational polarizability of dipolar molecules adsorbed in fine-pore membranes. V.A.Kravchenko, Yu.N.Petrov, V.I.Kuznetsov, R.Alexandrescu, N.Comanici, I.Mihaiulescu, I.Morjan. *Sov. Tech. Phys. Lett. (Fiz.) (USSR)*, vol.8, no.13-14, p.848-52 (July 1982). Translation of: *Pis'ma v Zh. Tekh. Fiz. (USSR)*, vol.8, no.13-14, p.848-52 (July 1982). [received: April 1983]

The fact that adsorbate molecules can be oriented during adsorption should cause the polarizability at IR frequencies of a porous sample having such an adsorbate to be significantly higher than that of a clean sample, because of the appearance of an orientational polarizability and thus an increase in the refractive index n at these frequencies. The authors have studied the sorption of molecules with various dipole moments (air, CO_2 , CCl_4 , H_2O , C_2H_6 , CH_3I , C_5H_5N , C_7H_6O , CH_3CN , $C_6H_5NO_2$) in fine-pore mica and in a fine-pore polymer film. The membranes were fabricated by bombarding mica and film samples with the nuclei of heavy elements and then subjecting the resulting defective structures to chemical etching. (2 refs.)

62277 IR spectroscopic and gravimetric investigation of adsorption of acetonitrile on a disperse model glass system. W.Oertel, U.Munch, R.Reppold, R.Strubl, S.Herzog, O.Vogel, I.Plötzki, H.Dunken, P.Fink (Sektion Chemie, Friedrich Schiller Univ., Jena, Germany). *Wiss. Z. Friedrich-Schiller-Universität Jena, Math. Naturwiss. Reihe (Germany)*, vol.31, no.6, p.1025-30 (1982). In German.

The adsorption of acetonitrile is investigated on disperse model-glasses (BaO/SiO_2 , B_2O_3/SiO_2 and $K_2O/B_2O_3/SiO_2$) by means of infrared spectroscopy and gravimetry. Samples with BaO and K_2O shows a higher capacity of adsorption than $B_2O_3-SiO_2$. The different strength of surface sites can be detected by means of acetonitrile-adsorption. (9 refs.)

62278 Identification of arsenic surface species on the Si(100) surface. S.C.Perino, C.R.Helms (Dept. of Electrical Engng., Stanford Univ., Stanford, CA, USA).

Grain Boundaries in Semiconductors. Proceedings of the Materials Research Society Annual Meeting, Boston, MA, USA, Nov. 1981 (New York, USA: North-Holland 1982), p.147-51

The molecular character of arsenic adsorbed on the Si (100) surface has been investigated using thermal desorption spectroscopy (TDS) and Auger electron spectroscopy (AES). A variety of arsenic surface species were deposited on the silicon surface by employing different evaporation sources, including metallic arsenic, arsine gas, and chips of GaAs crystals. The authors present coverage dependent spectra showing the desorption of As_4 tetramers at 350°C and As_2 dimers at 900°C. The loosely bound arsenic is adsorbed from the

solid evaporation sources only and resides on the surface as tetramers. The tightly bound arsenic does not form multiple layers and the high desorption temperatures suggests the adsorbed arsenic exists as monomers. (19 refs.)

Proceedings of the Third International Conference on 'Vibrations at Surfaces' See Entry 59532

Adsorption on metal surfaces. An integrated approach See Entry 59555

Fourier transform infrared reflection-absorption spectroscopy of surface species See Entry 59859

Electroreflectance vibrational spectroscopy: a new surface analysis technique using diode lasers See Entry 59860

Vibrational state of chemisorbed molecule on metal surface See Entry 60693

Heterogeneous relaxation of a vibration-excited molecular gas See Entry 60700

Cascades for hydrogen isotope separation using metal hydrides See Entry 61008

Scaling theory of polymer adsorption: proximal exponent See Entry 61764

Effect of poly(propylene oxide) segment size on structure-property relationships in elastomeric ionene See Entry 61827

Irreversible effects in the FeTi-H system See Entry 62114

Intermetallic compounds $LaNi_5$, $La_{1-x}Pr_xNi_5$ as sorbents and hydrogenation catalysts ($Ln=La, Ce, Pr, Nd, Sm, Gd$) See Entry 62115

Application of the method of time-lag analysis to the study of diffusion in solids of nonhomogeneous macroscopic structure See Entry 62183

Shape of crystals at low temperatures: absence of quantum roughening See Entry 62207

The surface structure of α -Sn (100) See Entry 62222

Surface photoacoustic spectroscopy—a new technique for the study of surface vibrations See Entry 62224

Lateral interactions and vibrational lifetimes See Entry 62229

Dipole-dipole coupling in adsorbate vibrational mode spectra See Entry 62230

Electronic damping of the motion of adsorbates on metal surfaces See Entry 62231

Theoretical vibrational frequencies for NH_x and CH_x reactive intermediates on nickel(100) and nickel(111) surfaces See Entry 62232

Experimental study of relative intensities in inelastic electron tunneling spectroscopy (IETS) See Entry 62236

Reemitted-positron energy-loss spectroscopy: a novel probe of adsorbate vibrational levels See Entry 62239

A study of the palladium-platinum-hydrogen system over a wide range of hydrogen pressures See Entry 62393

Electronic structure of hydrogen-bonded H_2O See Entry 62469

Electronic structure of the $Me_6S_n^{n+}$ cluster units in MoS_2 , M_2ReS_6 ($M=Na, K$) and $[Fe_6S_8]P(Et_3)_6[BPh_4]_2$ analogs to Mo/S , Re/S and Fe/S adsorbate structures See Entry 62471

How local is the bonding of adsorbed hydrogen to the host metal? An attempt at answering the problem in the framework of the SW- X_2 method for the α -Pd/H system See Entry 62473

Theoretical investigation of the multiple bond in complexes of the type $[Re_2Cl_6]^{2-}$ See Entry 62474

Quantum chemical investigation on the mutual exchange of the solid surface with an atom using the partitioning technique See Entry 62475

Charging characteristics of a gallium arsenide surface upon gas adsorption See Entry 62483

Quantum chemical modelling of optical properties of simple and oxide clusters See Entry 62920

Raman scattering from $Pt(CN)_4^{2-}$ adsorbed on Pt colloids See Entry 62955

Theory of surface enhanced Raman scattering See Entry 62959

The reflection-absorption infrared spectrum of the dioxygen species adsorbed on platinum recorded by FT-IR spectroscopy See Entry 62965

Infrared emission spectroscopy of CO on Ni See Entry 62966

On the contribution of charge transfer excitations to SERS See Entry 62967

Multichannel Raman spectroscopy of unroughened noble metal and nonnoble metal films and tunnel junctions See Entry 62968

Orientation dependence of surface enhanced Raman intensities: results from ab initio calculations See Entry 62969

Surface enhanced Raman scattering (SERS) from silver, copper, and gold films in UVH: excitation spectra See Entry 62970

A comparison of Raman scattering, resonance Raman scattering, and fluorescence from molecules adsorbed on silver island films See Entry 62971

Influence of foreign metal atoms deposited at electrodes on local and nonlocal processes in surface enhanced Raman scattering See Entry 62972

Surface Raman spectroscopy without enhancement: pyridine on Ag (111) See Entry 62973

Raman spectra of pyridine adsorbed on Ni (111) See Entry 62974

Surface enhanced Raman spectroscopy of palladium See Entry 62975

The SERS phenomenon in light of recent excitation profile measurements See Entry 62976

Infrared spectroscopy of adsorbates on low-area surfaces; the advantages of a photons-in photons-out technique See Entry 62978

The application of reflection infrared and surface enhanced Raman spectroscopy to the characterization of chemisorbed organic disulfides on Au See Entry 62979

Infrared specular reflection and SERS spectra of molecules adsorbed on smooth surfaces See Entry 62980

Enhanced adsorbate Raman scattering and surface plasmon radiation See Entry 62981

The adsorption of CO on Pt(111) studied by infrared-reflection-absorption spectroscopy See Entry 62982

Infrared spectroscopic investigation of the adsorption of fluoromethane on sodium chloride surfaces under ultra high vacuum See Entry 62983

Infrared spectra of CO adsorbed at low temperatures on Ni See Entry 62984

Surface enhanced Raman scattering of water on an Ag electrode See Entry 62985

EMIRS study of adsorbate bonding in the electrode solution interfacial region See Entry 62986

- Spectral properties of pyrazine adsorbed on silver electrodes and cold silver films from surface enhanced Raman scattering (SERS) See Entry 62987
- SERS study of pyridine vapor exposed to silver substrates electrochemically prepared See Entry 62988
- Study of adsorption at the electrode/solution interphase by in-situ infrared reflectance spectroscopy—adsorption of methanol on a platinum electrode See Entry 62989
- Intensity enhancement and spectral change in Raman scattering of mercapto-benzothiazole adsorbed on silver electrode See Entry 62990
- Time dependence of surface enhanced Raman scattering during and after oxidation-reduction cycles See Entry 62991
- Molecular orientation in thin monolayer films by infrared spectroscopy See Entry 63071
- Applications of surface polaritons for detection and vibrational spectral analysis of thin films on metals and dielectrics See Entry 63072
- High resolution electron energy loss studies of adsorbates utilizing impact and resonance scattering See Entry 63093
- Summary abstract: vibrational excitations of hydrogen and oxygen on Pd(100) See Entry 63095
- Oxygen adsorption on the kinked Pt(321) surface See Entry 63097
- Calculation of the EELS spectra of the Ni(001) surface with $p(2 \times 2)$ and $c(2 \times 2)$ overlayers of oxygen See Entry 63098
- Contrasting bonding configurations of acetone on Pt(111) and Ru(001) surfaces See Entry 63099
- The methoxy intermediate on Mo(100): effects of surface oxidation See Entry 63100
- HREELS studies of adsorbates on polar solids: water on $\text{SrTiO}_3(100)$ See Entry 63101
- A vibrational study of ammonia chemisorbed on Ni(110) and Ni(111): whether goes the metal-nitrogen stretching mode on FCC (111) surfaces? See Entry 63102
- The adsorption of NO on Ru(001) and its co-adsorption with oxygen studied by vibrational spectroscopy See Entry 63103
- The adsorption of ammonia on a Fe(110) single crystal surface studied by high resolution electron energy loss spectroscopy (EELS) See Entry 63104
- Spatial intensity distributions from electron impact scattering modes: $\text{W}(100)(1 \times 1)\text{H}$ See Entry 63105
- Identification of surface vibrations on clean and oxygen covered Pt(111) surfaces with high resolution electron energy loss spectroscopy (EELS) See Entry 63106
- Electronic transitions of Ar, Xe, N_2 , CO physisorbed on Ag (111) and Al (111) See Entry 63107
- Vibrational spectra of ethylene and acetylene on metal surfaces—an electron energy loss study of ethylene adsorbed on Ni (110) and its carbided surface, and the use of metal-cluster analogies See Entry 63108
- Azimuthal dependence of impact scattering in electron energy loss spectroscopy See Entry 63109
- Energy dissipation at metal surfaces: electronic versus vibrational excitations See Entry 63118
- Internal state distributions of molecules scattering and desorbing from surfaces See Entry 63120
- CO chemisorption on Fe(110) studied by angle-resolved photoemission See Entry 63136
- The oxidation of methanol on Cu(100) studied by infrared spectroscopy See Entry 63540
- The effect of the surface state on the hydrogen permeability and the catalytic activity of palladium alloy membranes See Entry 63583
- Effect of the hydrogen concentration on the adsorption and catalytic properties of a Pd-Ru alloy See Entry 63584
- Infrared laser stimulated surface processes See Entry 63587
- The adsorption and dehydrogenation of cyclopentane on Ru (001) See Entry 63588
- Thermal evolution of C_2H_2 and C_4H_2 on Pd (111) studied by high-resolution electron energy loss spectroscopy See Entry 63589
- Electron energy loss spectroscopy of the decomposition of formic acid on Ru (001) See Entry 63590
- Studies of the surface of titanium dioxide. V. Thermal desorption of hydrogen See Entry 63591
- Infrared study of three butanediols adsorbed on silica immersed in carbon tetrachloride See Entry 63593
- The Balloon effect. A quantum chemical model of elementary steps in heterogeneous chemical reactions between simple gases and solid surfaces See Entry 63596
- Complex analysis of experimental adsorption data using KRS 4200 and ES 1040 computers See Entry 63597
- Thermodynamic values evaluation from adsorption isotherms using KRS 4200 computer See Entry 63598
- Life properties of Ti-Mn alloy hydrides and their hydrogen purification effect See Entry 63739

68.48 SOLID-SOLID INTERFACES

(inc. bicrystals; for grain boundaries, see 61.70N)

- 62279 Interfaces structure in relation with the mechanisms in the reaction copper-silicon. G.Weber, B.Gillot, P.Barret (Lab. de Recherches sur la Reactivité des Solides, CNRS, Mirande, Dijon, France). *Phys. Status Solidi a (Germany)*, vol.75, no.2, p.567-76 (16 Feb. 1983). The formation of $\eta\text{-Cu}_3\text{Si}$ precipitates on (100) and (111) silicon surfaces by reaction between silicon and cuprous chloride is studied. The precipitates are found to be crystallized epitaxially onto the single crystal substrate and have a geometrical pyramidal structure with a square (on the (100)_{Si} surface) or triangular (on the (111)_{Si} surface) shape with a pyramidal basis plane. In both cases the main growth direction is (110). The good epitaxial growth of $\eta\text{-Cu}_3\text{Si}$ is explained by the easy extraction of silicon atoms by chlorine which facilitates the nucleation and growth at (111)_{Si}- Cu_3Si interface. (18 refs.)

- 62280 On depth profiling an InGaAsP-InP heterojunction. R.Landers, F.C.Prince, V.S.Sundaram, N.B.Patel (Inst. de Física 'Gleb Wataghin', Univ. Estadual de Campinas, Campinas, Brazil). *Surf. & Interface Anal. (GB)*, vol.5, no.1, p.2-3 (Feb. 1983). An $\text{In}_{0.71}\text{Ga}_{0.29}\text{As}_{0.63}\text{P}_{0.37}/\text{In}_{0.97}\text{Ga}_{0.03}\text{As}_{0.10}\text{P}_{0.90}$ liquid phase epitaxy (LPE) grown low lattice mismatch ($\Delta a/a \leq 0.03\%$) interface has been profiled using 1 keV argon ions incident at 50° to sample surface normal in a commercial Varian Auger system. It was found that an interface width of 160 Å from P (120 eV) Auger peak intensities. (5 refs.)
- X-ray photoelectron spectroscopy of cadmium arachidate monolayers on various metal surfaces See Entry 60837
- Crystal and molecular structure of tetrachlorophosphorus (V) hexachlorouranate (V) See Entry 61899
- Effect of interaction of misfit dislocations in multilayer epitaxial films See Entry 61925
- Ion beam induced composition changes during Auger sputter profiling of thin Al films on InP See Entry 62001
- Growth of titanium silicide on ion-implanted silicon See Entry 62182
- Solid state SiC/Ni alloy reaction See Entry 62184
- Analysis of diffusion mechanisms in thin polycrystalline Au-Ag films using Auger electron spectroscopy See Entry 62185
- Reactivity of cobalt, chromium, indium, magnesium, manganese, antimony and samarium thin films in couples with other metal films at room temperature See Entry 62186
- Electron diffraction from ZrO_2 on $\alpha\text{-Zr}(1010)$ See Entry 62219
- Interfacial segregation and enhanced sintering processes See Entry 63200
- Structure in carbon/carbon fibre composites as studied by microscopy and etching with chromic acid See Entry 63441

68.55 THIN FILM GROWTH, STRUCTURE, AND EPITAXY

(for techniques of crystal growth and film deposition, see 81.10 and 81.15)

- 62281 X-ray diffraction intensity ratio method for the thickness measurement of ternary heterogeneous epitaxial layers on GaAs substrate. Yang Chuanzheng (Shanghai Inst. of Metall., Acad. Sinica, Shanghai, China). *Chin. J. Semicond. (China)*, vol.4, no.2, p.154-60 (March 1983). In Chinese. On the basis of symmetric Bragg reflection and dynamic diffraction and kinematic absorption, equations of each layer's thickness connected with the intensity ratios of certain X-ray diffraction lines have been derived for system with multipatixial layers on GaAs substrate. The values of intensity ratio are measured experimentally by X-ray diffraction. Consequently, the thickness of various epitaxial layers can be determined. The measured results considered kinematic absorption and agree fairly well with the cleavage method. Finally, the effect of various factors on the measured results is discussed briefly. (11 refs.)
- 62282 Synthesis of $\text{Al}_5\text{Nb}_3\text{Ge}$ by pulsed laser annealing. H.Asano, K.Nakamura, A.Terada (Ibaraki Electrical Communication lab., Nippon Telegraph & Telephone Public Corp., Ibaraki, Japan). *Jpn. J. Appl. Phys. Part 1 (Japan)*, vol.22, no.3, p.429-36 (March 1983). Poly-crystalline $\text{Al}_5\text{Nb}_3\text{Ge}$ with an abnormally small lattice parameter of 5.115 Å has been synthesized by illuminating Q-switched ruby laser pulses onto sputter-deposited Nb_2Ge films. A new kind of Al5 phase growth was detected in the X-ray diffraction patterns for films having different structures (amorphous Nb_2Ge , a mixture of amorphous Nb_2Ge and $\text{Al}_5\text{Nb}_3\text{Ge}$, and a mixture of $\text{Al}_5\text{Nb}_3\text{Ge}$ and hexagonal Nb_2Ge_3). Volume increased in the new Al5 phase due to the repeated laser pulse illumination. Electron microscopic studies also confirmed the growth of the new Al5 phase. In addition, oxygen diffusion within a near-surface layer about 1000 Å thick was detected in films illuminated in air. The maximum of superconducting transition onset was 8.5K. These results are discussed in this paper from the standpoint of the surface melting model of the pulsed laser annealing.
- 62283 Liquid-phase epitaxial growth of ZnSe on ZrTe substrate. H.Nakamura, Liang Yan Sun, A.Asano, Y.Nakamura, M.Washiyama, M.Aoki (Dept. of Electronic Engng., Univ. of Tokyo, Tokyo, Japan). *Jpn. J. Appl. Phys. Part 1 (Japan)*, vol.22, no.3, p.499-503 (March 1983). Epitaxial layers of ZnSe were grown on ZrTe substrates using a liquid-phase epitaxial growth (LPE) method. A presynthesized Te-Se solution was used as a solvent for LPE. Growth was done in an evacuated quartz tube by a tipping method. The Zn-Se-Te ternary phase diagram was also determined in order to take the basic data of the LPE growth. The ZnSe/ZrTe heterostructure showed fairly good photovoltaic properties. The open-circuit voltage was 0.9 V and the ZnSe epilayer was effective as a window material of the solar cell. (8 refs.)
- 62284 Micro-probe reflection high-energy electron diffraction technique. III. Observation of polycrystalline silicon film on crystalline silicon substrate irradiated by continuous-wave Ar^+ -laser. M.Ichikawa, M.Ohkura, K.Hayakawa (Central Res. Lab., Hitachi Ltd., Tokyo, Japan). *Jpn. J. Appl. Phys. Part 1 (Japan)*, vol.22, no.3, p.527-33 (March 1983). For pt.II see *ibid.*, vol.21, p.154 (1982). A micro-probe reflection high-energy electron diffraction (micro-probe RHEED) technique has been used to observe polycrystalline Si film on crystalline Si substrate irradiated by continuous-wave Ar^+ -laser. Dependency of degree of crystallization on laser irradiation conditions has been examined in detail by making areas irradiated under various conditions on the same sample surface. Two kinds of crystalline states have been found on the irradiated areas. The degree of crystallization of one is nearly equal, and the other inferior, to that of crystalline Si substrate. As laser power decreases and laser scan speed increases, the latter kind of crystalline state becomes predominant in the irradiated areas. These results show that the micro-probe RHEED technique is useful in studying crystal growth of materials whose surfaces can not be physically cleaned in order to maintain the initial crystal state. (24 refs.)
- 62285 Measurements of the lamellar spacings of unidirectionally solidified Fe-FeS eutectic thin films. N.Asahi (Dept. of Phys., Sci. Univ. of Tokyo, Chiba, Japan). *Jpn. J. Appl. Phys. Part 1 (Japan)*, vol.22, no.3, p.543 (March 1983). Previously the authors (see *ibid.*, vol.21, p.L71, 1982) reported that, when hypoeutectic and hyper-eutectic Fe-FeSi thin films are unidirectionally solidified by controlling appropriately the solidification rates and temperature gradient in the melt at the liquid-solid interface, lamellar structures are observed on the specimen surface. It has been known that for many lamellar growth alloys the lamellar spacing, S , varies with the solidification rate, R , according to the equation $S=A/\sqrt{R}$, where A is a constant. However, no measurement of the lamellar spacings for eutectic thin films have been made yet. In the

present experiment, lamellar spacings in the films of Fe-FeSi eutectic alloys were examined as a function of the solidification rate. It was found that the above equation is applicable to Fe-FeSi eutectic thin films. (7 refs.)

62286 Hydrogen incorporation scheme in amorphous-microcrystalline mixed-phase Si-H films. M.Kumeda, Y.Yonezawa, K.Nakazawa, S.Ueda, T.Shimizu (Dept. of Electronics, Faculty of Technol., Kanazawa Univ., Kanazawa, Japan).

Jpn. J. Appl. Phys. Part 2 (Japan), vol.22, no.3, p.L194-6 (March 1983). Silicon-hydrogen alloy films containing both microcrystalline phase and amorphous phase (μ -Si:H) are prepared by sputtering, magnetron sputtering and glow discharge methods. Results of NMR measurements for hydrogen in μ -Si:H are qualitatively similar to those in amorphous silicon-hydrogen alloy films except that hydrogens are easy to move and exhibit the motional narrowing effect. There seems to be little possibility of presence of a large amount of nonbonded hydrogens such as hydrogen molecules or atomic hydrogens.

62287 Morphology and composition of films based on gold on the surface of gallium arsenide during vacuum annealing. T.A.Bryantseva, I.N.Sveshnikova, A.B.Ormont, S.A.Semiletov (Inst. of Radiotechnol. & Electronics, Acad. of Sci., USSR).

Inorg. Mater. (USA), vol.18, no.5, p.613-17 (May 1982). Translation of: *Izv. Akad. Nauk SSSR Neorg. Mater.*, vol.18, no.5, p.724-8 (May 1982). [received: Feb. 1983]

X-ray microprobe analysis and scanning electron microscopy as well as direct observation under the optical microscope have been used to study the changes in the morphology and composition of layers of gold on gallium arsenide during thermal annealing under vacuum. It has been found that the morphology of thin layers of gold of its alloys on gallium arsenide depend on the composition which changes significantly when the samples are heated in vacuum, due to interaction with GaAs and the evaporation of As and Ga from the surface of the specimens. Ruptures are formed in the film and droplets during annealing, followed by crystallization (formation of oriented islets) and the formation of a more or less coherent layer. This sequence can repeat itself with increasing temperature. At annealing temperatures of 690-800 and 848-70K, cathodoluminescence with a wavelength of 0.4 μ m has been observed, indicating the formation of β -Ga₂O₃. (12 refs.)

62288 Structure of pyrolytic carbon in the process of its formation.

Yu.N.Lebedev, E.S.Shmakova, V.N.Sushin. *Inorg. Mater. (USA)*, vol.18, no.5, p.666-8 (May 1982). Translation of: *Izv. Akad. Nauk SSSR Neorg. Mater.*, vol.18, no.5, p.792-4 (May 1982). [received: Feb. 1983]

The deposition of pyrolytic carbon during pyrolysis of methane and the structure of the pyrolytic carbon layer were studied on a high-temperature X-ray apparatus. During the study of the kinetics of the deposition process, it was found that the effective activation energy of the deposition of the pyrolytic carbon during the pyrolysis of methane in the temperature range of 1500-2300°C is 260 kJ/mole. When the pyrolytic carbon layer cools from the temperature of preparation to room temperature, the level of microstrains inside the crystallites decreases. (5 refs.)

62289 Quantitative analysis of fiber texture in cubic films. S.Rao, C.R.Houska (Dept. of Materials Engng., Virginia Polytech. Inst. & State Univ., Blacksburg, VA, USA).

J. Appl. Phys. (USA), vol.54, no.4, p.1872-82 (April 1983). The method of Roe and Krigbaum for determining fiber texture has been extended to thin film applications. It is often desirable to make in situ pole density measurements of a film on a thick substrate. This does not permit complete data to be collected by X-ray transmission techniques. If the data are restricted to the range $0 \leq \chi \leq 75^\circ$, obtained by reflection, incomplete pole density plots are obtained, and it is necessary to devise a self-consistent extrapolation technique that extends the pole density data to 90° . This requires least-squares fitting over the range from $\chi=0$ to 75° and an iterative procedure for extrapolating with functions consistent with a single orientation function. The example of a 1.14- μ Mo film on a (111) Si substrate requires an expansion of the symmetry relations to order 46. The procedure established herein is readily extended to include the effect of static displacements resulting from embedded gas atoms that are associated with sputtered films. (11 refs.)

62290 Electrodeposition of tantalum carbide coatings from molten salts. K.H.Stern, S.T.Gadomski (Chem. Div., Naval Res. Lab., Washington, DC, USA).

J. Electrochem. Soc. (USA), vol.130, no.2, p.300-5 (Feb. 1983). Adherent tantalum carbide coatings have been deposited on nickel substrates from a ternary (Li₂Na₂K)₂F eutectic containing a few percent each of K₂TaF₇ and K₂CO₃. Tantalum and carbon are deposited simultaneously on the nickel cathode where they react to form the carbide at 750°-800°. The coatings are highly resistant to abrasion and are thermally stable to ~600°. (11 refs.)

62291 Electrodeposition of nickel by an asymmetric periodically reversed step current. O.Teschke, D.Menez Soares (Inst. de Física, Lab. Hidrogenio, UNICAMP, Sao Paulo, Brazil).

J. Electrochem. Soc. (USA), vol.130, no.2, p.306-10 (Feb. 1983). The authors report the investigation of high current density (~ 0.15 A/cm²) nickel electrodeposition with a periodically reversed step current and the characterization of the surface morphology of the coatings thus produced. The deposits show micro-structure coherency, characteristics of columnar growth, diameter and shape of growth features, and porosity, which are current controlled. For the same total deposited mass, the deposit thickness is shown to be a function of periodically reversed step current parameters. The control of deposit layers allows the fabrication of nickel coatings with well-defined mechanical and electrocatalytic properties. (11 refs.)

62292 On the reaction mechanism of GaAs MOCVD. J.Nishizawa, T.Kurabayashi (Res. Inst. of Electrical Communication, Tohoku Univ., Sendai, Japan).

J. Electrochem. Soc. (USA), vol.130, no.2, p.413-17 (Feb. 1983). The reaction mechanisms of GaAs metalorganic chemical vapor deposition (MOCVD) have been investigated using infrared absorption spectroscopy. The growth of GaAs from Ga(CH₃)₃ and AsH₃ under H₂ gas atmosphere in a hot wall reactor was studied. The compositions of gases which are sampled through a quartz capillary are observed by infrared spectroscopy. Infrared spectra of (Ga(CH₃)₃+H₂), (AsH₃+H₂), and (Ga(CH₃)₃+AsH₃+H₂) systems were measured in the range from room temperature to 930°C. In the (Ga(CH₃)₃+AsH₃+H₂) system, a new absorption peak at 2080 cm⁻¹ which exists in neither the (Ga(CH₃)₃+H₂) nor the (AsH₃+H₂) system is observed. In the (AsH₃+H₂) system, when Ga(CH₃)₃ is added into the reacting gas, the concentration of AsH₃ decreases drastically. The decomposition of AsH₃ is affected strongly by the addition of Ga(CH₃)₃. (8 refs.)

62293 He⁺ backscattering study on Ar distribution in amorphous magnetic thin films. N.S.Kazama, H.Fujimori, S.Yamaguchi, Y.Fujino (Res. Inst. for Iron, Steel & Other Metals, Tohoku Univ., Sendai, Japan).

J. Magn. & Magn. Mater. (Netherlands), vol.35, no.1-3, p.214-16 (March 1983). (Proceedings of the 10th International Colloquium on Magnetic Films and Surfaces, Yokohama, Japan, 13-16 Sept. 1982). Ar concentration in thin films introduced through Ar sputtering is examined by means of He⁺ ion backscattering. A considerable amount of Ar is entrapped and distributed uniformly in amorphous Si and amorphous Fe-Co alloys with metalloids, while no trace of Ar can be detected in crystalline Fe. (2 refs.)

62294 Structure and magnetism of insoluble Pb-Fe alloy films. Y.Asada, H.Nose (Nat. Res. Inst. for Metals, Tokyo, Japan).

J. Magn. & Magn. Mater. (Netherlands), vol.35, no.1-3, p.229-31 (March 1983). (Proceedings of the 10th International Colloquium on Magnetic Films and Surfaces, Yokohama, Japan, 13-16 Sept. 1982). The amorphous mixture film of Pb and Fe is obtained for the first time by simultaneously depositing them on a substrate kept at liquid nitrogen temperature. Pb-rich agglomerates, however, have been observed in the film deposited at room temperature. Ferromagnetic resonances have been observed in both films. (2 refs.)

62295 Columnar growth in evaporated iron films. H.Fujiwara, K.Hara, M.Kamiya, T.Hashimoto, K.Okamoto (Dept. of Materials Sci., Hiroshima Univ., Hiroshima, Japan).

J. Magn. & Magn. Mater. (Netherlands), vol.35, no.1-3, p.296-8 (March 1983). (Proceedings of the 10th International Colloquium on Magnetic Films and Surfaces, Yokohama, Japan, 13-16 Sept. 1982). The columnar grain structure of iron-film evaporated in the pressure range between 10^{-2} and 10^{-8} Torr was investigated. From electron micrographs, measurements of extinction coefficient and deviation angle of easy axis from the film plane, it was found that the movement of adatoms plays an important role for the columnar formation. (9 refs.)

62296 EuS ferromagnetic semiconductor films grown epitaxially on silicon. W.Zinn, B.Saif, N.Rasula, M.Mirabal, J.Kohne (Inst. für Festkörperforschung, KFA Jülich, Jülich, Germany).

J. Magn. & Magn. Mater. (Netherlands), vol.35, no.1-3, p.329-35 (March 1983). (Proceedings of the 10th International Colloquium on Magnetic Films and Surfaces, Yokohama, Japan, 13-16 Sept. 1982). Results on EuS(111), (100), and (110) single crystal films, (EuS/SrS)(111) layered structures, Eu₂Sr_{1-x}S mixed crystal films, and EuS/Pb sandwiches grown by molecular beam epitaxy (MBE) on substrates of silicon crystals are reviewed. From electron diffraction and Rutherford backscattering studies their stoichiometry and crystal perfection are shown to be of good MBE quality. The magnetic properties reveal the expected magnetic anisotropy axes. The remagnetization and susceptibility behaviour of layered and mixed films are compared with typical single crystal film and bulk data. First results on coupled states of EuS/Pb sandwich films are reported. (23 refs.)

62297 Synthesis of AlSb by laser and capacitive discharge annealing. L.Baufay, R.Andrew, A.Pigeolet, L.D.Laude (Univ. de l'Etat, Mons, Belgium).

Rev. Phys. Appl. (France), vol.18, no.4, p.207-12 (April 1983). In French. The preparation of AlSb films by pulsed laser is compared with a capacity discharge annealing of Al/Sb sandwiches in order to shed light upon the nature of the transformation. Using 1000 Å thick multilayer films supported by glass substrates, the authors investigate the energy threshold for complete transformation as a function of (laser or capacity discharge) pulse duration from 10^{-7} to 10^{-1} s. They calculate the temperature raise directly induced by the energy pulse to be, in the two regimes, at least 900K, which is approximately the melting points of the metallic components. (11 refs.)

62298 Dependence of the carbon density on an epitaxial GaAs film surface on the substrate orientation relative to the crystallographic plane. N.N.Loiko, S.N.Maksimovskii, E.L.Nolle, I.A.Penin, A.E.Petrov, A.G.Tur'yanskii (P.N. Lebedev Phys. Inst., Acad. of Sci., Moscow, USSR).

Sov. Phys.-Solid State (USA), vol.24, no.9, p.1471-2 (Sept. 1982). Translation of: *Fiz. Tverd. Tela (USSR)*, vol.24, no.9, p.2595-8 (Sept. 1982). [received: April 1983] It is established that when a gallium arsenide film is simultaneously heated and exposed to light in its intrinsic absorption band, the carbon density on its surface is substantially lower than if heat treatment is used. It is shown further that the density of the carbon remaining on the film surface after the joint thermal and optical treatment depends on the misorientation angle of the substrate relative to the crystallographic plane, and decreases with decreasing misorientation angle. (9 refs.)

62299 The hydrides, nitrides, and carbides of nickel. R.V.Baranova, Yu.P.Khodyrev, S.A.Semiletov (Inst. of Crystallography, Acad. of Sci., USSR).

Sov. Phys.-Crystallogr. (USA), vol.27, no.5, p.554-6 (Sept.-Oct. 1982). Translation of: *Kristallografiya (USSR)*, vol.27, no.5, p.923-7 (Sept.-Oct. 1982). [received: April 1983]

In the authors' experiments, nickel films are reacted with ammonia and treated in a nitrogen discharge. It was observed that the nitrides Ni₃N (hexagonal, $a=4.59$ Å, $c=4.31$ Å) and Ni₂N (cubic, $a=3.64$ -3.74 Å) are formed; these had previously been obtained by treating nickel in a discharge of commercial hydrogen. The formation of a nitride with a small hexagonal unit cell ($a \sim 2.6$ Å, $c \sim 4.3$ Å) was not recorded. Analysis of the literature data revealed that it was probably a mistake to assign a hexagonal lattice with parameters $a \sim 2.6$, $c \sim 4.3$ Å to nickel carbide Ni₃C and other related interstitial phases. (20 refs.)

62300 Orientational relations in heteroepitaxial structures (001)W/(1012)Al₂O₃. B.A.Malyukov, M.V.Surovnikov, N.M.Balalaeva.

Sov. Phys.-Crystallogr. (USA), vol.27, no.5, p.614-15 (Sept.-Oct. 1982). Translation of: *Kristallografiya (USSR)*, vol.27, no.5, p.1022-4 (Sept.-Oct. 1982). [received: April 1983] In (001)W/(1012)Al₂O₃, the disorientation effect is particularly well marked—the disorientation angle δ is greater than 4°. Sapphire substrates were cut from single crystals grown by the Kyropoulos method. The authors prepared 18 sapphire plates with surfaces variously disoriented relative to the (1012)Al₂O₃ plane; in no case did the angle α exceed 3°. The azimuthal orientation of the specimens was determined by means of the X-ray reflection from the (2021)Al₂O₃ plane. For each substrate the components α_x , α_y of the vector α were found: $\alpha = N - n_{(1012)}$, where N is a unit normal to the surface of the sapphire substrate. It is seen that the angle α between the vectors N and $n_{(1012)}$ satisfies the condition $\alpha \approx |\alpha|$. (8 refs.)

62301 Influence of doping with isovalent impurities on defect formation in homoepitaxial GaAs layers. N.V.Ganina, M.G.Mil'vidskii, A.N.Sherashkov, T.G.Yugova (State Sci.-Res. & Design Inst. of Rare-Metals Industry, USSR).

Sov. Phys.-Crystallogr. (USA), vol.27, no.5, p.616-18 (Sept.-Oct. 1982). Translation of: *Kristallografiya (USSR)*, vol.27, no.5, p.1025-7 (Sept.-Oct. 1982). [received: April 1983]

Discusses the formation of defects in homoepitaxial layers of GaAs doped with In and Sb. The doped layers were obtained by liquid-phase epitaxy with forced cooling. Growth was effected in two regimes: with the temperature falling through 200-250°C (1) and with the temperature falling through 20°C (2). The temperature of onset of epitaxy ranged from 750 to 900°C. Layers were obtained on substrates of semiinsulating GaAs doped with Cr and In. The substrates were oriented in the (100) plane; their dislocation densities were about $2 \times 10^4 \text{ cm}^{-2}$. The In and Sb concentrations in the layers were determined by X-ray spectral microanalysis. Dislocations in the epitaxial structures were revealed by etching in fused KOH. The distribution of dislocations through the thickness of the films was monitored on oblique sections cut at 3° to the surface of the film. (7 refs.)

62302 Influence of growth rate of epitaxial silicon layers on surface segregation of boron, phosphorus, and arsenic. N.A.Alyabina, R.G.Loginova, M.I.Ovsyannikov (Res. Physicotech. Inst., Gor'kii, USSR).

Sov. Phys.-Crystallogr. (USA), vol.27, no.5, p.618-19 (Sept.-Oct. 1982). Translation of: *Kristallografiya (USSR)*, vol.27, no.5, p.1028-30 (Sept.-Oct. 1982). [received: April 1983]

Epitaxial layers of silicon were deposited by sublimations in a vacuum of about 10^{-7} torr. The chosen dopants were boron, phosphorus, and arsenic. The substrates were plates of silicon in the (111), (110), and (100) orientations, cut from strongly doped single crystals of the p and n conductivity types for deposition of p-type and n-type layers, respectively. The sources were cut from single crystals of silicon doped with the above impurities to a level of about 10^{19} cm^{-3} . The substrates and sources were subjected to standard mechanical and chemical treatment before being placed in the working chamber. The width of the transition regions was determined from the impurity profiles of the structures, which were recorded by means of the results of C-V measurements of the MOS structures with successive removal of layers by anodic oxidation. The impurity profiles were constructed with the C-V measurement results corrected for screening of the field by mobile carriers. (10 refs.)

62303 Internal stresses in thin Ge, ZnS, and ZnSe films. A.G.Gusev, E.A.Nesmelov, A.S.Nikitin, I.S.Gainutdinov.

Sov. J. Opt. Technol. (USA), vol.49, no.8, p.508-10 (Aug. 1982). Translation of: *Opt.-Mekh. Prom.-st. (USSR)*, vol.49, no.8, p.35-7 (Aug. 1982). [received: April 1983]

The effect of sputtering conditions—substrate temperature and action of high-density light—on the magnitude of the internal stresses in thin Ge, ZnS and ZnSe films has been investigated. It is shown that by varying these conditions one can obtain films having minimum internal stresses. (12 refs.)

62304 The role of Joule heating in liquid phase electroepitaxy. A.N.Barchuk, A.I.Ivashchenko (S. Lazo Polytech. Inst., Kishinev, USSR).

Sov. Phys.-Tech. Phys. (USA), vol.27, no.9, p.1153-6 (Sept. 1982). Translation of: *Zh. Tekh. Fiz. (USSR)*, vol.52, no.9, p.1878-82 (Sept. 1982). [received: April 1983]

The temperature distribution at the crystallization front has been analyzed for a cylindrical growth cell for conditions which accurately reproduce experimental conditions. It is shown that heating of the crystallization front caused by the evolution of Joule heat in liquid phase electroepitaxy is fundamentally nonuniform and the contribution of convection in the melt in the typical situation is insignificant. The effect of the cross section of the growth cell and the resistivity of the semiconductor substrate on the temperature of the melt-substrate contact is also discussed. The results of the analysis make it possible to account for a number of phenomena peculiar to electroepitaxy, namely, the 'edge' effect, the appreciable nonplanarity of the epitaxial films, and the connection between the limitations of the current density in electroepitaxy and the area of the melt-substrate contact. (15 refs.)

62305 Theory of current control of the distribution of the composition over thickness in $\text{AlGa}_{1-x}\text{As}$ epitaxial films. S.Yu.Karpov, M.G.Mil'vidskii, S.A.Nikishin (A.F. Ioffe Physicotech. Inst., Acad. of Sci., Leningrad, USSR).

Sov. Tech. Phys. Lett. (USA), vol.8, no.7, p.383-4 (July 1982). Translation of: *Pis'ma v Zh. Tekh. Fiz. (USSR)*, vol.8, no.13-14, p.883-7 (July 1982). [received: April 1983]

The authors derive a theoretical description of electroliquid epitaxy from a bounded volume of melt, taking into account the depletion of the liquid phase during the crystallization and the replenishment of the liquid phase through dissolution of the source. (7 refs.)

62306 X-ray diffraction analysis of SnO_2 films prepared by oxidation of tin films. N.P.Sinha, M.Misra (Dept. of Phys., Univ. of Gorakhpur, Gorakhpur, India).

Thin Solid Films (Switzerland), vol.101, no.2, p.L33-4 (11 March 1983).

Tin (99.99% pure) was evaporated onto thoroughly cleaned optically flat photographic glass plates in a vacuum of the order of 10^{-6} Torr. The thickness of the tin films was 20000 Å. These films were then heated in an oxygen atmosphere for about 90 min. Oxidation of the tin films was carried out at five different heating temperatures: 300, 350, 400, 450, and 500°C. X-ray diffraction analysis of these films was carried out on a GE-XRD-5 diffractometer. At lower oxidation temperatures (300°C) the film is amorphous. This may arise as complete oxidation does not take place and some part of the film remains as insulating SnO . However, at higher oxidation temperatures (350, 400 and 500°C) the films were found to be polycrystalline. In the X-ray spectra, the maximum intensity observed at different angles varies with the oxidation temperature. As the oxidation temperature is increased the intensity of the peaks in the diffraction pattern also increases indicating that at higher oxidation temperatures the films are more polycrystalline with larger grain sizes. It appears that oxidation proceeds well at higher temperatures and nearly stoichiometric films of SnO_2 are formed. (10 refs.)

62307 Layered Pb/Ag films. M.Jalochowski (Dept. of Experimental Phys., Univ. of Marie Curie-Skłodowska, Lublin, Poland).

Thin Solid Films (Switzerland), vol.101, no.4, p.285-9 (25 March 1983).

Thin layered structures were produced by sequential vacuum evaporation of lead and silver. The layered samples showed strong [111] texture. The X-ray diffraction plots contained a series of additional satellite peaks characteristic of a superlattice. The experimental X-ray diffraction data and results of calculations based on a simple model of a superlattice were compared. The influence of room temperature annealing on the crystal structure of the layered Pb/Ag samples was observed. (15 refs.)

62308 Crystal, impurity-related and growth defects in molecular beam epitaxial GaAs layers. M.Balleur, A.Munoz-Yague (Lab. d'Automatique et d'Analyse des Systemes, CNRS, Toulouse, France).

Thin Solid Films (Switzerland), vol.101, no.4, p.299-310 (25 March 1983).

Crystallographic defects in GaAs layers grown by molecular beam epitaxy were studied. The methods used were photochemical etching, developed previously, and also optical and scanning electron microscopy. Dislocation, stacking faults, impurity microprecipitates and impurity out-diffusion from the substrate were observed. Large growth defects, namely oval defects and whiskers, were also studied using selective etching, transmission electron microscopy and electron microprobe analysis. The roles of the substrate quality, handling, surface preparation and epitaxial growth conditions were considered in connection with the formation of the crystallographic defects. (19 refs.)

62309 LiInSe_2 thin epitaxial films on $\{111\}$ A-oriented GaAs. A.Tempel, B.Schumann, S.Mitaray, G.Kuhn (Sektion Chem., Karl-Marx-Universität, Leipzig, Germany).

Thin Solid Films (Switzerland), vol.101, no.4, p.339-44 (25 March 1983).

LiInSe_2 thin epitaxial layers were prepared by flash evaporation on $\{111\}$ A-oriented GaAs substrates and investigated by reflection high energy electron diffraction. The overgrowth is characterized by one-dimensional epitaxy with preferred azimuthal orientation. In general, the LiInSe_2 thin films crystallize in the $\beta\text{-NaFeO}_2$ structure. In the substrate temperature range from 620 to 670K a second phase with chalcopyrite structure was observed besides the $\beta\text{-NaFeO}_2$ structure. (10 refs.)

62310 Composition distribution in Co-Cr perpendicular magnetic films. R.Sugita (Materials Res. Lab., Matsushita Electric Industrial Co. Ltd., Moriyuchi, Japan).

Trans. Inst. Electron. & Commun. Eng. Jpn. Part C (Japan), vol.J66C, no.1, p.55-61 (Jan. 1983). In Japanese.

Composition distribution in Co-Cr perpendicular magnetic films has been analyzed, and the relation between the distribution and magnetic properties of the films has been considered. It was clarified that there was Cr segregation layer at the surface of the columns constructing the columnar structure of the film. The columns have single domain characteristics with the increase of the Cr segregation. The experimental result, that the perpendicular coercive force of the films increased steeply with elevating substrate temperatures at deposition while the films had nearly constant values of c-axis orientation $\Delta\theta_{50}$, could be explained by the Cr segregation. (11 refs.)

Optical mode conversions in Nd substituted iron garnet films . See Entry 61270
About short-range order of amorphous I-B/N films investigated by energy loss spectroscopy . See Entry 61800

Initial growth forms of single crystals of chromium with copper on its surface . See Entry 61841

Some mathematical results for impurity redistribution during the growth of a layer on a substrate . See Entry 61946

Post-deposition high temperature processing of silicon nitride . See Entry 61949

Ion beam induced composition changes during Auger sputter profiling of thin Al films on InP . See Entry 62001

Electrical properties of thin solid films of the solid electrolyte $\text{Ag}_2\text{W}_2\text{O}_8$. See Entry 62162

Structure of potassium films on the (1010) face of rhenium . See Entry 62274

In situ thin film differential thermal analysis of amorphous V_2O_5 thin films . See Entry 62312

Study of the structure and elastoresistance properties of thin films of bismuth . See Entry 62418

Electrical properties of 70 wt. % Cr-30 wt. % SiO_2 thin films . See Entry 62511

Ag_2Se thin film conductivity with a selenium excess . See Entry 62513

Magnetic property changes in epitaxial metal film sandwiches . See Entry 62730

Magnetic and optical properties of Co, Bi substituted garnet films prepared by the LPE method and its application to thermomagnetic recording . See Entry 62733

Magnetic properties, structure, and relaxation of amorphous $\text{Fe}_{1-x}\text{B}_x$ films . See Entry 62739

Magnetic properties of metastable crystalline and amorphous Fe alloys produced by RF sputtering . See Entry 62741

Magnetic properties and microstructure in Ho-Co alloy thin films fabricated by RF sputtering technique . See Entry 62743

Oblique incidence effects in evaporated thin films . See Entry 62752

Structure and magnetic properties of iron films deposited at oblique incidence . See Entry 62753

Magnetization reversal modes in thin films with columnar microstructure . See Entry 62754

Effects of high dose ion implantation on structure and magnetic properties of 3d-metal films . See Entry 62757

Structure and magnetic properties of C-axis well oriented Ba-ferrite films deposited by targets-facing type of sputtering . See Entry 62765

Perpendicular magnetic anisotropy and microstructure of sputter-deposited Co-Cr film . See Entry 62775

Structure and magnetic domain walls of Dy ion implanted Fe films . See Entry 62777

Conversion Mossbauer studies of epitaxially mixed ferrite-garnet films . See Entry 62870

Electrical and optical properties of a $\text{Si}_3\text{C}_{1-x}\text{H}_x$ film prepared by GD SiH_4 and C_2H_4 . See Entry 63065

Transparent conductors—a status review . See Entry 63078

X-ray photoelectron diffraction studies of zinc selenide . See Entry 63137

Ge-seeded crystallisation on SiO_2 by using a slider system with RF heated strip heater . See Entry 63154

High-energy particles in AlN film preparation by reactive sputtering technique . See Entry 63155

Ion beam sputter deposition of layered magnetic thin films . See Entry 63157

High-rate sputter technique . See Entry 63158

Formation of cubic boron nitride films by boron evaporation and nitrogen ion beam bombardment . See Entry 63159

Fabrication of $\text{In}_2\text{O}_3\text{:SnO}_2$ transparent conducting films by electron beam evaporation . See Entry 63160

Characterization of Al- AlO_2 and Sn- SnO_2 cermet films deposited by reactive evaporation . See Entry 63162

- Low temperature dielectric films from octavinylsilsesquioxane See Entry 63163
- Vapor phase epitaxy of indium phosphide See Entry 63165
- Organometallic vapor phase epitaxial growth of $\text{In}_{1-x}\text{Ga}_x\text{As}_y\text{P}_{1-y}$ on GaAs See Entry 63166
- Comparative studies of reactive sputtering, ion plating and CVD coating of TiN hard layers See Entry 63167
- CVD coating of hard metals, especially with regard to boron and boron-containing substances See Entry 63168
- Deposition of TiB_2 layers from the gas phase See Entry 63173
- Preparation of molybdenum silicide films by RF ion plating See Entry 63176
- LPE growth of uniform (Ga, Al)P alloy crystal See Entry 63178
- Thickness of GaP liquid phase epitaxial layers grown by step-cooling, equilibrium-cooling, and ramp-cooling methods See Entry 63179
- Reproducibility of low carrier concentration in LPE InP using batch melts See Entry 63180
- A solution growth technique for the preparation of copper(II) selenide thin films See Entry 63181
- LPE growth of YNd-iron garnet films for magneto-optical waveguides See Entry 63182
- Deposition of cadmium chalcogenide thin films by a solution growth technique using triethanolamine as a complexing agent See Entry 63184
- Microstructure and ductility of electroless copper deposits See Entry 63438
- Effect of film thickness on oxidation of vacuum-deposited films of iron See Entry 63451
- Cellules solaires au CdTe en couches minces polycristallines. Elaboration par pulvérisation triode et transport a courte distance (CdTe solar cells in polycrystalline thin films. Elaboration for triode sputtering and short distance transfers) See Entry 63675
- Etude et réalisation de croissances épitaxiales de composés III-V par pyrolyse mixte d'organométalliques et d'hydrures sous pression réduite: Application à l'étude de structures de piles solaires (Study and realization of epitaxial growth of III-V compounds by mixed pyrolysis of organometallics and hydrides under reduced pressure: Application to the study of solar cell structures) See Entry 63678

68.60 PHYSICAL PROPERTIES OF THIN FILMS, NONELECTRONIC

- 62311 Curvature radius and layer stresses for thermal strain in semiconductor multilayer structures. Feng Zhechuan, Liu Hongdu (Dept. of Phys., Peking Univ., Peking, China). *Chin. J. Semicond.* (China), vol.4, no.2, p.171-80 (March 1983). In Chinese. The generalized formula is deduced for the curvature radius and layer stresses for thermal strain in semiconductor multilayer structure with different elastic moduli and growth temperatures, including the case of a substrate with initial curved momentum. Various approximate expressions are given, especially the useful forms for the thick substrate. Using the formulae derived, the active layer stress and its dependence on layer thicknesses and Al fractions are calculated for conventional GaAs-GaAlAs DH lasers and visible buffered GaAlAs DH lasers, the analytical expressions for the vanishing of active layer stress are obtained, the thermal expansion coefficient and Young's modulus of native oxide Ga_2O_3 measured, and the active layer stress due to native oxide and metallic films for MSTO structures calculated. (13 refs.)
- 62312 In situ thin film differential thermal analysis of amorphous V_2O_5 thin films. J.P. Audiere, A. Madi (Lab. de Physicochimie Minérale, Univ. Paris Sud, Orsay, France). *Thin Solid Films* (Switzerland), vol.101, no.2, p.L29-31 (11 March 1983). In situ differential thermal analysis (DTA) experiments were performed on highly quenched amorphous V_2O_5 thin films directly evaporated onto a thin film differential thermocouple microprobe. Irreversible low temperature relaxations were thus evidenced, a result impossible to obtain with a classical DTA apparatus using microcrucibles such as Setaram or Mettler TA 2000 devices. (10 refs.)
- Internal stresses in thin Ge, ZnS, and ZnSe films See Entry 62303
- Diffusion and magnetic properties of compositionally modulated films See Entry 62728
- Determination of the optical constants and thickness of amorphous V_2O_5 thin films See Entry 62918
- Tensile fracture of evaporated Au films. IV See Entry 63391
- Composition, optical properties and degradation modes of Cu/(graded metal-carbon) solar selective surfaces See Entry 63728

68.70 WHISKERS AND DENDRITES: GROWTH, STRUCTURE, AND NONELECTRONIC PROPERTIES

- 62313 Whiskerisation of carbon beads by vapour phase growth of carbon fibres to obtain sea urchin-type particles. M. Egashira, H. Katsuki, Y. Ogawa, S. Kawasumi (Dept. of Materials Sci. & Engng., Nagasaki Univ., Nagasaki, Japan). *Carbon* (GB), vol.21, no.1, p.89-92 (1983). Whiskerisation of sulfur-containing hard carbon beads with carbon fibres has been examined to prepare sea urchin-type particles. Propylene was used as a source material for the fibre growth and decomposed at 1000°C for 2 hr. Sulfur-catalysed carbon fibres 4-6 μm in diameter and 90-120 μm long formed with a density of 400-550 μm per bead on the surfaces of carbon beads containing ≥ 2.5 wt% sulfur. These beads were prepared by carbonisation of styrene/divinylbenzene copolymers sulfonated with fuming sulfuric acid. Very few, if any, fibres grew on beads from copolymers sulfonated with chlorosulfuric acid, probably because of lower sulfur contents (< 2.5 wt%) and/or inhibition by residual chlorine. (18 refs.)
- Crystal, impurity-related and growth defects in molecular beam epitaxial GaAs layers See Entry 62308

70.00 CONDENSED MATTER: ELECTRONIC STRUCTURE, ELECTRICAL, MAGNETIC, AND OPTICAL PROPERTIES

(see also 81.40R Electrical and magnetic properties related to materials treatment, 81.40T Optical properties related to materials treatment)

71.00 ELECTRON STATES

(see also 63. Lattice dynamics, 73. Surfaces, interfaces, and thin films)

71.10 GENERAL THEORIES AND COMPUTATIONAL TECHNIQUES

- 62314 Generalized pseudopotential model of inhomogeneous systems and its application to a simple-metal surface. P. Streitenberger (Sektion Math. und Phys., Wissenschaftsbereich Tech. Phys., Tech. Hochschule Otto von Guericke, Magdeburg, Germany). *Phys. Status Solidi b* (Germany), vol.116, no.1, p.179-90 (1 March 1983). General expressions in real-space representation are derived for charge density, total energy, and Hellmann-Feynman forces on an ion. They represent a uniform and systematic extension of the pseudopotential or pair-potential model to highly inhomogeneous electron-ion systems. Modifications appear in form of non-central pair potentials and additional one-body potentials arising from the screening in the inhomogeneous electron gas. The corresponding self-consistent charge density results from the superposition of overlapping non-spherical pseudopotentials and an additional charge density that is mainly localized in the defect region. A first application to the simple-metal surface is given where some general results within the jellium model are obtained. (40 refs.)
- 62315 Energy states and Bloch states for an accelerated electron in a periodic lattice. J.N. Churchill, F.E. Holmstrom (General Products Div., IBM Corp., San Jose, CA, USA). *Phys. Scr. (Sweden)*, vol.27, no.2, p.91-8 (Feb. 1983). The Hamiltonian for an accelerated electron in a periodic one-dimensional lattice is written using normalized coordinates. By this means, the exact functional form for the position and energy dependences of the energy eigenstates is obtained without resorting to the usual approximation methods, such as power-series expansions, perturbation procedures or one-band models. Bloch-type wave functions that fully satisfy Schrödinger's time-dependent equation are obtained by superimposing energy eigenstates using the Stark ladder spacing concept. Such phenomena as Bloch oscillations and Stark ladder effects are then re-examined as a consequence of this new perspective. (43 refs.)

71.20 ELECTRONIC DENSITY OF STATES DETERMINATIONS

(inc. energy states of liquid semiconductors; see also 65.40 Lattice and electronic heat capacity)

- 62316 Experimental investigation of the density of states of a quasi-one-dimensional vibrational exciton in isotopically mixed KNO_3 crystals. M.V. Belousov, D.E. Pogarev (Inst. of Phys., A.A. Zhdanov State Univ., Leningrad, USSR). *JETP Lett.* (USA), vol.36, no.5, p.189-91 (5 Sept. 1982). Translation of: *Pis'ma v Zh. Eksp. & Teor. Fiz.* (USSR), vol.36, no.5, p.152-5 (5 Sept. 1982). [received: April 1983] The possibility of directly measuring the density of states of a disordered crystal from the spectrum of compound transitions is noted and studied experimentally for the first time. The unusual behavior of the spectrum studied as a function of concentration is explained by the quasi-one-dimensional nature of the band. (8 refs.)
- 62317 A computational method for the evaluation of highly resolved DOS functions from APS measurements. K.-T. Schleicher, S.W. Schulz, R. Gmeiner, H.-U. Chun (Inst. für Theoretische und Physikalische Chem., Univ. Frankfurt, Frankfurt/M., Germany). *J. Electron Spectrosc. & Relat. Phenom.* (Netherlands), vol.31, no.1, p.33-56 (April 1983). A new computational procedure for evaluation of the density of unoccupied states from appearance-potential spectra is described. The data treatment is based on least-squares methods using quadratic spline functions and on a rigorous consideration of the different contributions to the appearance-potential signal. Certain physical, experimental and computational requirements have to be met in order to obtain highly resolved and reliable results. The performance of the computational procedure is demonstrated by application to synthesized spectrum of iron and to a realistic appearance-potential spectrum of polycrystalline ferromagnetic cobalt. In particular, this method provides more detailed information concerning the unoccupied states than previous studies. The position of the unoccupied d -band maximum in cobalt at 0.55 ± 0.15 eV does not agree with any of the greatly differing theoretical calculations in the literature. (39 refs.)
- 62318 Valence-electron density in silicon under high pressure. M.T. Yin (Bell Labs., Murray Hill, NJ, USA), M.L. Cohen. *Phys. Rev. Lett.* (USA), vol.50, no.15, p.1172 (11 April 1983). In a recent Letter (see *ibid.*, vol.49, p.1438, 1982), Yoder-Short, Collella, and Weinstein reported an investigation of high-pressure effects on the valence-electron density in Si and InSb by X-ray diffraction, where the forbidden (222) integrated intensity was found to decrease sharply just before the structural transition in both Si and InSb. They pointed out that this could arise from either a smearing of the bonding charges or an enhancement of phonon anharmonicity and suggested that recent *ab initio* pseudopotential calculations (see *ibid.*, vol.45, p.1004, 1980) may be used to resolve this issue. The authors have performed *ab initio* pseudopotential calculations for various atomic volumes of Si. The calculated X-ray structure factor $F(222)$ of Si at zero temperature is, respectively, 0.3398, 0.3403, 0.3401, 0.3395, 0.3390, 0.3379, and 0.3355 in units of electron per primitive cell for the volume of 1.031, 1.000, 0.971, 0.942, 0.918, 0.889, and 0.840 normalized to the measured free volume, Ω_0 . (7 refs.)

- Ion beam hydrogenation of polysilicon coated thermal oxide on silicon See Entry 61941
- On the Brillouin zone integration See Entry 62321
- Stability of amorphous silicon solar cells with pin structure See Entry 63694

71.25 NONLOCALIZED SINGLE-PARTICLE ELECTRONIC STATES

62319 A method in the study of band structure for GAC. Ye Ling, Zhang Kaiming (Modern Phys. Inst., Fudan Univ., Shanghai, China). *Chin. J. Semicond. (China)*, vol.4, no.2, p.117-23 (March 1983). In Chinese. A simpler but self-consistent scheme is proposed for studying the electronic structure of graphite acceptor compounds (GAC). The basic concept of the computer renormalization group (CRG) is applied in simplifying the interactions between graphite and the intercalates, and a 'pseudo-atom' is used to simulate the intercalant molecule. This model enables the authors to study different IC₈ type GAC in the same program, the extended Huckel energy band calculation method is developed and the resulting band structures and Fermi surface properties of GAC (FeCl₃, AsF₅) thus obtained are discussed and compared with the present data. (10 refs.)

62320 Crystalline phase effects on ESCA valence bands of Zr(IV) and Ti(IV) acid phosphates. G.Marletta, O.Puglisi, S.Pignataro (Istituto Dipartimentale di Chimica, Univ. di Catania, Catania, Italy), G.Alberti, U.Costantino. *Polyhedron (GB)*, vol.2, no.3, p.157-62 (1983).

The valence bands (VB) of ESCA spectra of Zr(IV) and Ti(IV) acid phosphates in different crystalline phases are reported. The various bands are assigned by comparison with Li₃PO₄. Variations on changing the crystalline phase for compounds having the same M(IV) ion are found. Two types of molecular orbitals are mainly involved. One related to P-O bonds is affected by the crystalline phase. The other, related to M(IV)-O bonds are confined into the layers of the compounds, are less sensitive to crystalline environment. Variation in the symmetry of the tetrahedral type PO₄³⁻ anion are proposed to be mainly responsible of the observed effects. (38 refs.)

Crystal structure of a metallic two-dimensional conductor: the purple bronze of potassium and molybdenum, K_{0.9}Mo₆O₁₇ See Entry 61884

Exchange, correlation, and band gaps in conjugated linear chains See Entry 62355

71.25C Techniques of band-structure calculation (general theory, applications of group theory, analytic continuation, etc)

62321 On the Brillouin zone integration. B.I.Reser (Inst. of Metal Phys., Acad. of Sci., Sverdlovsk, USSR). *Phys. Status Solidi b (Germany)*, vol.116, no.1, p.31-40 (1 March 1983).

A brief and simple description is given of three new methods of integration in the Brillouin zone; direct, ray, and hybrid tetrahedron, proposed by Chen (1977), McDonald et al. (1979). These methods are analyzed in detail in application to the calculation of the density and number of states of SC, BCC, and FCC crystals using tight-binding and empty lattice models. It is shown that all the methods considered exhibit a high accuracy: several hundred initial *k* points in the irreducible part of the Brillouin zone with not very complicated dispersion relations make it possible to calculate such a quantity, as the density of states, with an average error of less than 1%. The hybrid tetrahedron method is proved to be simpler and many times more effective than the other two methods. Only with dispersion relations close to isotropic is the ray method preferable. (9 refs.)

62322 Analytic approximation for random muffin-tin alloys. R.Mills (Dept. of Phys., Ohio State Univ., Columbus, OH, USA), L.J.Gray, T.Kaplan. *Phys. Rev. B (USA)*, vol.27, no.6, p.3252-62 (15 March 1983).

The methods introduced in a previous paper under the name of 'traveling-cluster approximation' (TCA) are applied, in a multiple-scattering approach, to the case of a random muffin-tin substitutional alloy. This permits the iterative part of a self-consistent calculation to be carried out entirely in terms of the on-the-energy-shell scattering amplitudes. Offshell components of the mean resolvent, needed for the calculation of spectral functions, are obtained by standard methods involving single-site scattering wave functions. The single-site TCA is just the usual coherent-potential approximation, expressed in a form particularly suited for iteration. A fixed-point theorem is proved for the general *t*-matrix TCA, ensuring convergence upon iteration to a unique self-consistent solution with the physically essential Herglotz properties. (13 refs.)

Self-consistent semirelativistic pseudopotential calculation of the energy bands, cohesive energy, and bulk modulus of W See Entry 62329

Electron structure and X-ray emission spectra of ScRh See Entry 63085

71.25H Measurement of Fermi surface parameters (inc. dHvA, magnetoacoustic, position annihilation, and cyclotron resonance studies, etc.)

62323 Magnetic field dependence of electron density in bismuth. Chhi-Chong Wu (Dept. of Appl. Maths., Nat. Chiao Tung Univ., Hsinchu, Taiwan, China), Mao-Hsiung Chen, Chau-Jy Lin. *J. Phys. C (GB)*, vol.16, no.11, p.L317-21 (20 April 1983).

Using time-independent perturbation theory, the energy eigenvalue equation for a free-electron gas in bismuth with the McClure-Choi modified non-ellipsoidal non-parabolic (MNENP) model in the presence of a uniform DC magnetic field has been solved. The authors investigate the effect of the magnetic field on the electron density at very low temperatures and compare numerical results for this new band model with those for the Cohen NENP (1961), LAX ENP (1958) and EP models. Results show that quantum oscillations of the electron density for the MNENP model appear much more salient and considerable than those for other models. It seems that this MNENP model could be better for describing some physical phenomena of the magnetic field effect in bismuth for the very low-temperature limit. (18 refs.)

62324 Shubnikov-de Haas oscillations in Cd₃(As_{0.7}P_{0.3})₂. E.K.Arushanov, A.V.Lashkul, L.N.Luk'yanova, A.N.Nateprov, S.I.Radautsan, V.V.Sologub (Inst. of Appl. Phys., Acad. of Sci., Kishinev, Moldavian SSR). *Sov. Phys.-Semicond. (USA)*, vol.16, no.10, p.1216-17 (Oct. 1982). Translation of: *Fiz. & Tekh. Poluprovodn. (USSR)*, vol.16, no.10, p.1888-90 (Oct. 1982). [received: April 1983]

The authors studied for the first time the Shubnikov-de Haas (SdH) oscillations in Cd₃(As_{0.7}P_{0.3})₂, determined the topology of the electron Fermi surface, and found the cyclotron effective mass *m*_c of electrons. Single crystals of Cd₃(As_{1-x}P_x)₂ solid solutions were grown from the vapor phase throughout the full composition range. The measurements were carried out at 4.2 and 2.7K in static magnetic fields B up to 6 T. Oscillations of the Hall voltage U_H, longitudinal magnetoresistance Δρ_l/ρ₀(B|C₄), and transverse magnetoresistance Δρ_t/ρ₀(B⊥C₄) were observed at 4.2K, and it was found that the Hall coefficient was independent of the magnetic field to within 10%. The angular dependences of the SdH period P were determined for magnetic field orientations ranging from B₁C₄ to B₁C₄. It was established that the period P did not vary by more than 3%, which was within the limits of the experimental error. (11 refs.)

On the Brillouin zone integration See Entry 62321

Effect of varying the orientation of a quantizing magnetic field on the effective electron mass in degenerate tetragonal semiconductors See Entry 62326

Electronic properties of bulk copper-aluminum and copper-zinc alloys See Entry 62395

Shubnikov-de Haas oscillations in an organic conductor tetramethyltetraselenafulvalene-2,5-dimethyl-7,7', 8,8' tetracyanoquinodimethane (TMTSF-DMTCNQ) See Entry 62404

Stability of amorphous silicon solar cells with pin structure See Entry 63694

71.25J Effective mass and g-factors

62325 Altered results for orbital and spin susceptibilities by inclusion of the diamagnetic contribution of the valence electrons in the evaluation of an Einstein de Haas experiment. J.Benkowitz (Kernforschungszentrum Karlsruhe, Inst. für Angewandte Kernphys., Karlsruhe, Germany), H.Winter. *Z. Phys. B (Germany)*, vol.50, no.3, p.217-17 (1983).

The g-factor experiments of Huguenin et al. (see J. Phys. F, vol.1, p.281, 1971) help to separate the spin and orbital susceptibility contributions of paramagnetic transition metals. In the evaluation of the experimental data, these authors took account of the Langevin diamagnetism of the core electrons whereas the valence electrons should be equally recognised for their diamagnetism. The introduction of this valence electron diamagnetism, obtained from band structure data, introduces significant changes of the results, leading to better agreement with other experiments and with theoretical results in most cases. (26 refs.)

62326 Effect of varying the orientation of a quantizing magnetic field on the effective electron mass in degenerate tetragonal semiconductors. A.N.Chakravarti, K.P.Ghatak, K.K.Ghosh, H.M.Mukherjee (Inst. of Radio Phys. & Electronics, Univ. Coll. of Sci. & Technol., Calcutta, India). *Phys. Status Solidi b (Germany)*, vol.116, no.1, p.17-24 (1 March 1983). An attempt is made to investigate the effects of varying the orientation of a quantizing magnetic field on the effective mass in tetragonal semiconductors. It is found, taking n-Cd₃As₂ as an example, that the crystal-field splitting results in different effective masses at the Fermi level corresponding to different magnetic sub-bands. These effective masses are found to be significantly influenced by the orientation of the magnetic field with respect to the *c*-axis. This behaviour is further noted to be strongly dependent on the carrier concentration but is relatively much less sensitive to changes in the magnetic field strength. (21 refs.)

Shubnikov-de Haas oscillations in Cd₃(As_{0.7}P_{0.3})₂ See Entry 62324

Determination of band-gap parameters of Hg_{1-x}Cd_xTe based on high-temperature carrier concentration See Entry 62334

Electrophysical properties of nickel boride phases See Entry 62396

Shubnikov-de Haas oscillations in an organic conductor tetramethyltetraselenafulvalene-2,5-dimethyl-7,7', 8,8' tetracyanoquinodimethane (TMTSF-DMTCNQ) See Entry 62404

Refractive index in epitaxial Pb_{1-x}Sn_xTe films See Entry 62919

71.25M Electron energy states in amorphous and glassy solids

62327 Preliminary study on the electronic structure of hydrogenated and fluorinated amorphous silicon. Jiang Ping (Modern Phys. Inst., Fudan Univ., Shanghai, China).

Chin. J. Semicond. (China), vol.4, no.2, p.133-4 (March 1983). In Chinese. By using a cluster model, the extended Huckel method is used to calculate the electronic states of hydrogenated and fluorinated amorphous silicon. The results calculated show that both hydrogen and fluorine can be used to reduce the gap states associated with dangling bonds, and fluorine is more efficient. The results obtained are in qualitative agreement with experimental measurements. (15 refs.)

62328 Treatment of aperiodicity and correlation in polymers. J.J.Ladik (Dept. of Theoretical Chem., Friedrich-Alexander-Univ., Erlangen-Nurnberg, Germany).

Int. J. Quantum Chem. (USA), vol.23, no.3, p.1073-81 (March 1983). (Proceedings of the Fourth International Congress in Quantum Chemistry, Uppsala, Sweden, 13-20 June 1982).

The negative factor counting method (in its simple and matrix block form) for the determination of the density of states of disordered polymer chains and its applications to different aperiodic organic polymers are reviewed. The problems of the calculation of the correlation energy in large systems like polymers will be discussed. Different ways for the partitioning of an energy band into regions make it possible to perform Moller-Plesset perturbation theoretical calculations on polymers. Applications to hydrogen chains are presented. Finally, possible applications to disordered polymers are also discussed. (35 refs.)

Use of the state-averaged MCSCF procedure: application to radiative transitions in MgO See Entry 60587

NMR in metallic glasses See Entry 62817

71.25P Band structure of crystalline metals

62329 Self-consistent semirelativistic pseudopotential calculation of the energy bands, cohesive energy, and bulk modulus of W. D.M. Bylander, L. Kleinman (Dept. of Phys., Univ. of Texas, Austin, TX, USA). *Phys. Rev. B (USA)*, vol.27, no.6, p.3152-9 (15 March 1983). The energy bands, equilibrium lattice constant, cohesive energy, and bulk modulus of tungsten have been calculated using a new semirelativistic pseudopotential. The agreement with experiment is exceptionally good. This can be attributed to the pseudopotential containing all relativistic effects, except spin-orbit, to order α^2 , where α is the fine-structure constant, and by taking the exchange-correlation potential to be $V_{xc}^{\text{val}} = V_{xc}(\rho_{\text{total}}) - V_{xc}(\rho_{\text{core}})$ rather than $V_{xc}^{\text{val}} = V_{xc}(\rho_{\text{val}})$. (27 refs.)

62330 Self-consistent pseudopotential calculation of the electronic structure of PdH and Pd₂H. C.T. Chan, S.G. Louie (Dept. of Phys., Univ. of California, Berkeley, CA, USA). *Phys. Rev. B (USA)*, vol.27, no.6, p.3325-37 (15 March 1983). The electronic structure of PdH and Pd₂H is studied in detail with a fully self-consistent pseudopotential approach using a mixed basis set. The band structure, density of states, angular-momentum-decomposed density of states, and charge densities are analyzed for both systems. Particular attention has been paid to the nature of the Pd-H bonding state and the effect of changing the hydrogen concentration as one goes from PdH to Pd₂H. Agreements with experimental data and previous calculations on PdH are very good. The essential physical nature of the hydride system is summarized in a simple conceptual picture which should be applicable to substoichiometric PdH_x and other hydrides for the prediction of Fermi-surface properties. (33 refs.)

Lattice dynamics of FCC Cu See Entry 62046
New model for thermal effects in photoelectron spectroscopy See Entry 62049
Structural phase stability in third-period simple metals See Entry 62093
Electronic properties of bulk copper-aluminum and copper-zinc alloys See Entry 62395
Electrophysical properties of nickel boride phases See Entry 62396
Electron structure and X-ray emission spectra of ScRh See Entry 63085
Auger electron appearance potential spectrum of Ni See Entry 63088
Photoemission spectra and band structures of d-band metals. X. Relativistic momentum matrix elements See Entry 63132
Photoemission study of Au overlayers on Pd(111) and the formation of a Pd-Au(111) alloy surface See Entry 63135

71.25R Band structure of crystalline elemental semiconductors

62331 A localized orbital description of Ge and α -Sn. P.V. Smith (Phys. Dept., Univ. of Newcastle, Newcastle, Australia). *Phys. Status Solidi b (Germany)*, vol.116, no.1, p.101-9 (1 March 1983). In previous work an accurate description of the band structure and the valence electron pseudo-charge density of Si is given in terms of a small set of well localized basis functions comprising only ten states of s, p, d, and f symmetry per atomic site. Now this work is extended to the case of Ge and α -Sn and it is shown that this localized orbital approach also provides an excellent representation of the electronic structure of these other diamond elemental semiconductors. Moreover, the resulting basis functions are again very well localized about their respective lattice sites. The implications of this work in relation to semiconductor impurity problems are also briefly discussed. (13 refs.)

Structural phase stability in third-period simple metals See Entry 62093
Valence-electron density in silicon under high pressure See Entry 62318
Magnetic field dependence of electron density in bismuth See Entry 62323

71.25T Band structure of crystalline semiconductor compounds and insulators

62332 Tight binding calculations for band structures and other electronic properties of GaAs-GaP superlattices. Liu Wenming, Li Jia (Dept. of Semiconductors, Jilin Univ., Jilin, China). *Chin. J. Semicond.* (China), vol.4, no.2, p.124-32 (March 1983). In Chinese. The tight binding method is used to study the band structures and other related electronic properties of GaAs-GaP superlattices. Second nearest neighbor interactions are included in the elements of secular matrices. The bands of superlattice (GaAs)_m(GaP)_n along three main symmetry lines in the Brillouin zone are presented. The energy values at Γ , X and M points are calculated for superlattices (GaAs)_m(GaP)_n where $m+n \leq 10$. Discussions are given for the variations of energy gap as a function of periodic length under the condition $m=n$, for the effect of fraction on the gap with an unchanged periodic length, and for the distributions of electrons in several typical one-electron states. (15 refs.)

62333 A crystal orbital investigation on the one-dimensional bis(glyoximate)pyrazine-iron system. M.C. Bohm (Organisch-Chem. Inst., Univ. Heidelberg, Heidelberg, Germany). *Chem. Phys. (Netherlands)*, vol.76, no.1, p.1-14 (1 April 1983). The band structure of bis(glyoximate)pyrazine-iron (I) has been studied in the crystal orbital (CO) formalism as derived in the tight-binding approximation. The computational framework is a semi-empirical INDO model. Two polymer geometries have been studied; one with long (2.1 Å) Fe-pyrazine distances and one with short (1.8 Å) axial bonds. Both types of one-dimensional materials are insulators, the forbidden band gap exceeds 6.5 eV. The highest filled bands of the unoxidized polymers are glyoximate lone-pair and π functions; Fe 3d bands are predicted 1.5-2.0 eV below the valence band of the transition-metal stack. For partially oxidized modifications of I trapped valences and localized Fe³⁺ hole-states are expected. The INDO CO results are compared with available experimental data and with extended Huckel CO calculations on topologically related transition-metal polymers. (56 refs.)

62334 Determination of band-gap parameters of Hg_{1-x}Cd_xTe based on high-temperature carrier concentration. E. Finkman (Microelectronics Res. Center, Technion-Israel Inst. of Technol., Haifa, Israel). *J. Appl. Phys. (USA)*, vol.54, no.4, p.1883-6 (April 1983). The temperature dependence of the carrier concentration of Hg_{1-x}Cd_xTe at elevated temperatures is used to determine its band parameters near the band edge. The electron concentration is calculated by using the Kane model (k.p method), and is fit to observed values derived from measurements of the Hall coefficient in the near-intrinsic region. This procedure results in expressions for the following parameters: the band-gap E_g and its dependence on temperature and composition; Kane's interband-coupling matrix element and

the heavy-hole effective mass ratio. Modified values of the intrinsic carrier concentration are calculated using these parameters. (20 refs.)

62335 The spin polarisation of conduction electrons in a ferromagnetic semiconductor. D.M. Edwards (Dept. of Maths., Imperial Coll., London, England). *J. Phys. C (GB)*, vol.16, no.11, p.L327-30 (20 April 1983).

It is argued that the 'multiband' model of Nolting (1979, 1980) for the conduction band of a ferromagnetic semiconductor is unrealistic and cannot provide a correct explanation of the spin polarisation of field-emitted electrons from a W-EuS junction. A simple theory is given which shows that the polarisation should be approximately proportional to the magnetisation of the EuS, in reasonable agreement with experiment. (11 refs.)

62336 Bulk and surface electron states in WO₃ and tungsten bronzes. D.W. Bullett (Max-Planck-Institut für Festkörperforschung, Stuttgart, Germany). *J. Phys. C (GB)*, vol.16, no.11, p.2197-207 (20 April 1983).

Calculations of the electronic structure of WO₃ suggest that the detailed crystallographic arrangement determines rather sensitively the size of the semiconducting energy gap. This increases from 1.6 eV in the perovskite-like cubic approximation to the structure, as used in the only previous study, to 2.4 eV in the full monoclinic distorted structure. Valence-band widths and density-of-states peaks are consistent with experimental photoemission spectra. The extra electrons introduced by alkali-metal atoms in the bronzes Na_xWO₃ enter the conduction band of W_{1/2} states, behaving rather like a rigid-band model. Surface states are predicted to be absent from the semiconducting energy gap of the defect-free (001) surface of WO₃. (74 refs.)

62337 Dependence of the band structure of Ge₂(GaAs)_{1-x} solid solutions on the degree of order. A.I. Gubanov, A.M. Polubotko (A.F. Ioffe Physicotech. Inst., Acad. of Sci., Leningrad, USSR).

Sov. Phys.-Semicond. (USA), vol.16, no.10, p.1187-9 (Oct. 1982). Translation of: *Fiz. & Tekh. Poluprovodn. (USSR)*, vol.16, no.10, p.1848-51 (Oct. 1982). [received: April 1983]

The authors consider the dependence of the energy band structure of Ge₂(GaAs)_{1-x} solid solutions on the degree of disorder in the case when the Ga and As sublattices are retained. They consider the influence of a structural phase transition on the band structure using the variational LCAO method. (5 refs.)

62338 Electron structure of stoichiometric and nonstoichiometric tungsten oxides. A.L. Gubskii, A.P. Kovtun, V.P. Sachenko. *Ukr. Fiz. Zh. (USSR)*, vol.28, no.3, p.441-9 (March 1983). In Russian.

The SCF X_α-SW method was applied to calculate the electronic structures of several clusters WO₆⁶⁺, W₈O₁₂⁴⁺, W₆O₁₂⁴⁺, W₈O₁₈²⁰⁺ and M₂O₁₂³⁺ where M=Nb, Mo, Ta, Re. It is found that main qualitative electronic structure features in the clusters are similar to those in the crystals according to the Goodenough classification. The conclusion is made that there is a decisive influence of short-range order on the electronic integral characteristics visible in X-ray photoelectron spectra of the valence band. (18 refs.)

Thermoelectric properties of GeTe at high hydrostatic pressure up to 8.5 GPa and its valence-band structure See Entry 62438

Optical properties of CVD-coated TiN, ZrN and HfN See Entry 62917

Semiconducting properties of silver thiocyanate See Entry 62964

Study of electronic structure of reduced TiO₂ and V_xTi_{1-x}O₂ crystals by ESCA and optical absorption See Entry 63018

71.30 METAL-INSULATOR TRANSITIONS

62339 Effect of electron bombardment on the phase transition in VO₂ films. I.A. Abroyan, V.Ya. Velichko, O.A. Podsvirov, F.A. Chudnovskii. *Sov. Tech. Phys. Lett. (USA)*, vol.8, no.7, p.336-7 (July 1982). Translation of: *Pis'ma v Zh. Tekh. Fiz. (USSR)*, vol.8, no.13-14, p.775-8 (July 1982). [received: April 1983]

An effort has recently been undertaken to develop radiation methods for controlling the parameters of the metal-semiconductor phase transition in vanadium dioxide; in particular, the effect of ion bombardment on this phase transition is the subject of active research. There is also considerable interest in the effect of electron bombardment on this phase transition. The authors report a study of the dose dependence of such characteristics of the metal-semiconductor phase transition in VO₂ films as the transition temperature ΔT_1 , its width ΔT_1^0 , and the width of the thermal hysteresis loop ($j=320$ $\mu\text{A}/\text{cm}^2$) in a vacuum of 10^{-4} Pa. The phase-transition parameters were determined from the temperature dependence of the optical reflection coefficient R at the wavelength $\lambda=0.6$ μm over the temperature interval from 283 to 360K. (10 refs.)

Incommensurate-commensurate transition in TaS₂ See Entry 62405

Metallization of mercury chalcogenides under ultrahigh pressures See Entry 62461

Mossbauer studies of valence fluctuations See Entry 62845

Magnetic and electronic properties of microcrystals of Fe₃O₄ See Entry 62857

Study of electronic structure of reduced TiO₂ and V_xTi_{1-x}O₂ crystals by ESCA and optical absorption See Entry 63018

71.35 EXCITONS AND RELATED PHENOMENA

(inc. electron-hole drops)

62340 Charge and spin locations in linear stacks of TCNQ. L. Shields (School of Chem., Univ. of Bradford, Bradford, England).

J. Chem. Soc. Faraday Trans. II (GB), vol.79, pt.2, p.243-51 (Feb. 1983). Charge and spin locations in stacks of TCNQ molecular ions are assessed. The fine-structure parameters of localised triplet excitons extending over three and four molecules in the stack are calculated relative to the fine-structure splitting of the TCNQ₂²⁻ dimer: the absence of resolved fine-structure is shown to be insufficient evidence for the absence of localised exciton traps. Both the charge and spin locations are assumed to be especially sensitive to the relative values of the intermolecular charge interaction and electron resonance. Spin magnetic susceptibilities observed in pyridinium TCNQ salts, which may derive from spin traps, spin excitons and free-electrons separately or in combination, are differentiated into these three components. (14 refs.)

62341 Parameters of bound multiexciton complexes in direct polar semiconductors. A. Haufe (Sektion Phys., Karl-Marx-Univ. Leipzig, Leipzig, Germany), K. Henneberger, J. Rosler, H.-J. Wunsche. *Phys. Status Solidi b (Germany)*, vol.116, no.1, p.191-203 (1 March 1983). Using a generalized density-functional method, which takes electron-phonon interaction into account, the ground state energies of donor-BMEC's D^NX_m ($m=1, \dots, 20$) are calculated for the polar semiconductors ZnS, CdS, and CdSe. The highest stability is obtained for complexes possessing filled

electron shells ($m=1, 7, 19$), whereas gaps of instability are located between these complexes. The spectral locations of luminescence lines connected with the radiative decay of BMECs are predicted and found to be concentrated between the luminescence lines of the bound exciton and the free exciton. Furthermore, analytic approximate expressions for the electron and hole densities are obtained and their shapes are extensively discussed. (22 refs.)

62342 Exciton trapping and sensitized luminescence: a generalized theory for all trap concentrations. V.M.Kenkre, P.E.Parris (Dept. of Phys. & Astron., Univ. of Rochester, Rochester, NY, USA). *Phys. Rev. B (USA)*, vol.27, no.6, p.3221-34 (15 March 1983).

The generalized-master-equation theory of sensitized luminescence in molecular crystals is extended to cover arbitrary guest concentrations by making use of a recently introduced formalism. Central to the formalism is a quantity termed the ν function, which is an ensemble average of the sum of host propagators over guest-influenced host sites. A variety of experimentally relevant sensitized luminescence observables, such as the host (and guest) luminescence intensity, the quantum yields, and the energy-transfer rates are simply related to the ν function. It is shown how the latter can be calculated for exciton motion possessing an arbitrary degree of coherence, dimensionality, and other transport characteristics, and for guest-molecule placement represented by any given pair correlation function. Specific cases are treated and results, some exact and others approximate, are presented for experimental observables. (26 refs.)

62343 Energy levels of excitons in cubic crystals. S.M.Zubkova, K.B.Tolpygo, V.G.Filin (Inst. of Problems in Materials Sci., Acad. of Sci., Kiev, Ukrainian SSR).

Sov. Phys.-Solid State (USA), vol.24, no.9, p.1466-7 (Sept. 1982). Translation of: *Fiz. Tverd. Tela (USSR)*, vol.24, no.9, p.2585-8 (Sept. 1982). [received: April 1983]

A numerical solution is given for the problem of the lowest energy levels of direct and indirect excitons in crystals having a diamond or zinc blende structure, including the spin-orbit split-off valence band and the anisotropy and nonparabolicity of the conduction band. (11 refs.)

62344 Temperature and kinetics of the exciton and biexciton gas in cadmium sulfide and selenide crystals. G.V.Mikhailov, B.S.Razbirin, L.S.Yudenchik, M.Brousseau, J.Collet, A.Cornet (A.F. Ioffe Physicotech. Inst., Acad. of Sci., Leningrad, USSR).

Sov. Phys.-Solid State (USA), vol.24, no.9, p.1479-83 (Sept. 1982). Translation of: *Fiz. Tverd. Tela (USSR)*, vol.24, no.9, p.2610-17 (Sept. 1982). [received: April 1983]

The luminescence spectra of cadmium sulfide and selenide crystals were studied at low temperatures and high excitation intensities. The variation of the electron temperature in the picosecond range of excitation pulses was analyzed. The loss rate for the mean exciton kinetic energy in the selenide was measured. Kinetics studies yielded further support for the idea that the P line is biexcitonic. In order to analyze the spectral characteristics of excitonic and biexcitonic luminescence lines in the sulfide, some statistical properties of exciton and biexciton gases were examined. It is shown that under the experimental conditions used the exciton and biexciton temperatures are the same and do not fall below 6-8 K when $T_{\text{lat}}=2\text{K}$. (9 refs.)

62345 Exciton and soliton excitation in molecular chains. A.A.Eremko, A.I.Sergienko.

Ukr. Fiz. Zh. (USSR), vol.28, no.3, p.338-42 (March 1983). In Russian. Deals with soliton excitations of molecular chains where dipole moments of a molecule transition into an excited state can be both parallel and perpendicular to the chain axes. If the exciton maximal group velocity is less than that of sound waves, the kinetic mass of a soliton can be less than that of a free exciton. The soliton limiting velocity in this case will be the maximal group velocity of excitons. (9 refs.)

62346 On the theory of soliton annihilation by excitons. A.A.Vakhnenko, Yu.B.Gaididei.

Ukr. Fiz. Zh. (USSR), vol.28, no.3, p.342-8 (March 1983). In Russian. The processes of soliton annihilation by localized electronic excitations in molecular chains are investigated. Temperature and solitonization degree dependences of the annihilation rate are obtained, which indicates a possibility of observing solitons experimentally. (5 refs.)

Master equation techniques for exciton motion, relaxation, capture, and annihilation See Entry 59688

Single and multiple random walks on random lattices: excitation trapping and annihilation simulations See Entry 59691

Trapping of excitation in the average T -matrix approximation See Entry 59692

Effect on spin variables and exciton motion on ground-state properties of the 'trion' See Entry 59737

Reflection of a plane monochromatic wave from a medium with spatial dispersion See Entry 61080

Comparative reinvestigation of the interaction of phonons with Wannier and Frenkel excitations in crystalline solids See Entry 62037

Experimental investigation of the density of states of a quasi-one-dimensional vibrational exciton in isotopically mixed KNO_3 crystals See Entry 62316

One-electron broken-symmetry approach to the core-hole spectra of semiconductors See Entry 62361

New aspects of the oxygen donor in gallium phosphide See Entry 62365

Spin relaxation and polarization under interaction of photocarriers with charged paramagnetic centers in a semiconductor See Entry 62800

Magnetic resonance on localized excited triplet states in 1,4-dibromonaphthalene [one-dimensional conductor] See Entry 62838

On the theory of the nonlinear acousto-optical effect in semiconductors See Entry 62929

Magnetopolaritons in ZnTe See Entry 62940

Thermoreflectance study of polydiacetylene-bis (toluene sulphonate) single crystal (PDA-TS) See Entry 62953

Forbidden luminescence and resonance Raman scattering of bound exciton states in CdS See Entry 62998

Raman scattering of light in crystals in the presence of Bose-Einstein condensate excitons See Entry 63004

Pure electronic, vibronic, and two-particle surface excitons on the anthracene crystal. II. Experimental study and analysis of the (0,1) region See Entry 63012

Direct and indirect exciton transitions in $\text{InBr}_x\text{I}_{1-x}$ mixed crystals See Entry 63013

Effect of oxygen on exciton spectra of ZnS lower polytypes and samples with packing defects See Entry 63016

Electroreflection of ground-state excitons in $\text{Al}^{\text{III}}\text{B}^{\text{VI}}$ crystals ... See Entry 63017

Exciton-phonon interaction in crystalline and vitreous SiO_2 ... See Entry 63019

Submillimeter emission of CdS crystals pumped by intense light See Entry 63021

Uniaxial stress and temperature dependences of photoluminescence in $\text{GaAs}_{1-x}\text{P}_x$ See Entry 63029

Pure electronic, vibronic, and two-particle surface excitons on the anthracene crystal. I. General theoretical basis, experimental study, and analysis of the (0,0) region See Entry 63033

Anomalous temperature-dependent phosphorescence of Cu porphyrin in anthracene See Entry 63034

Low-temperature energy trapping and emission line profile of disordered solids See Entry 63035

Luminescence analysis of group III and V impurities in silicon See Entry 63042

71.36 POLARITONS

(inc. photon-phonon and photon-magnon interactions)

62347 The polariton in CdSe: measurement of time of flight and nonlinear transmission. P.Lavallard, Pham Hong Duong (Groupe de Phys. des Solides, Ecole Normale Supérieure, Paris, France).

Rev. Cethedec (France), vol.19, no.NS82-2, p.175-88 (1982). In French. Polariton time of flight has been measured in CdSe. The dispersion curve parameters are deduced from the experiment: $\Delta_{\text{LT}}=1\text{ meV}$; $m=0.45 m_0$. For a strong incident light intensity, the polariton transmission becomes nonlinear: the absorption increases to such a degree that a decrease of transmitted intensity is observed when one increases the incident intensity. A model taking into account the formation of scattering centers by the beam itself, explains quite well the observed phenomena. (7 refs.)

Excitation of surface polaritons by nondegenerate four-wave mixing of evanescent waves See Entry 61222

Magnetopolaritons in ZnTe See Entry 62940

Exact calculations of scattering and enhanced fields of electromagnetic waves on grating surfaces See Entry 62977

Raman scattering of light in crystals in the presence of Bose-Einstein condensate excitons See Entry 63004

Applications of surface polaritons for detection and vibrational spectral analysis of thin films on metals and dielectrics See Entry 63072

71.38 POLARONS AND ELECTRON-PHONON INTERACTIONS

(for electron-phonon interactions in lattices, see also 63.20K)

62348 Perturbation theory for continuum bound polaron state. S.Mukhopadhyay, T.K.Mitra (Dept. of Theoretical Phys., Indian Assoc. for Cultivation of Sci., Calcutta, India).

Phys. Lett. A (Netherlands), vol.94A, no.6-7, p.301-4 (21 March 1983). Perturbation of a continuum state of a Coulomb bound polaron is considered for the first time and it is shown that the Frohlich limit is obtainable only from this state and not from the ground state of the bound polaron as is commonly believed. (11 refs.)

62349 The electron-phonon interaction spectrum in beryllium. Yu.G.Naidyuk, O.I.Shklyarevskii (Physicotech. Inst. for Low Temperatures, Acad. of Sci., Kharkov, Ukrainian SSR).

Sov. Phys.-Solid State (USA), vol.24, no.9, p.1491-3 (Sept. 1982). Translation of: *Fiz. Tverd. Tela (USSR)*, vol.24, no.9, p.2631-5 (Sept. 1982). [received: April 1983]

The method of microcontact spectroscopy is used to study spectra of electron-phonon interaction in beryllium. A detailed comparison of microcontact spectra with known dependences of the density of phonon states in this metal is performed. It is shown that microcontact spectra may be used for defining the phonon spectrum of beryllium more precisely. The integral parameter, λ , of the electron-phonon interaction is determined within the free-electron model. (21 refs.)

62350 Large deviation asymptotics and the polaron. M.D.Donsker, S.R.S.Varadhan (Courant Inst. of Math. Sci., New York Univ., New York, NY, USA).

Stochastic Processes in Quantum Theory and Statistical Physics. Proceedings of the International Workshop, Marseille, France, 29 June-4 July 1981 (Berlin, Germany: Springer-Verlag 1982), p.111-18

Describes in outline form the latest extension of the large deviation theory and how in particular the resulting asymptotics provide a solution to the polaron problem. The detailed proofs can be found elsewhere. (5 refs.)

Exciton and soliton excitation in molecular chains See Entry 62345

On the theory of soliton annihilation by excitons See Entry 62346

Electronic correlations and midgap absorption in polyacetylene See Entry 62356

Carrier capture by multiphonon emission at extrinsic deep centers induced by self-trapping in GaAs See Entry 62364

Direct observation of impact ionisation and hot electron effects in GaAs See Entry 62420

71.45 COLLECTIVE EFFECTS

62351 Velocity autocorrelation function of a 2D classical electron liquid. G.K.Agarwal, K.N.Pathak (Dept. of Phys., Panjab Univ., Chandigarh, India).

J. Phys. C (GB), vol.16, no.10, p.1887-92 (10 April 1983). Expressions for the first six frequency moments of the self-correlation function have been obtained appropriate for a 2D classical electron liquid interacting with a $1/r$ potential. The results of the moments and the Mori-Zwanzig formalism have been used to analyse the recent molecular dynamics data for the velocity autocorrelation function. It is found that a phenomenological form of the relaxation kernel with two relaxation times provides a good agreement with the molecular dynamics data. (13 refs.)

62352 Charge-density waves in a strong magnetic field. III. B.G.S.Doman (Dept. of Appl. Maths. & Theoretical Phys., Univ. of Liverpool, Liverpool, England).

J. Phys. C (GB), vol.16, no.11, p.2069-74 (20 April 1983). For pt.II see *ibid.*, vol.14, p.3393 (1981). The theory developed by Mertsching and Fischbeck (1981) to describe the incommensurate charge-density waves is

extended to examine the situation in the presence of a magnetic field. Phase diagrams are drawn for three different sizes of magnetic field. (9 refs.)

62353 Local nature of charge-density-wave conduction noise in niobium triselenide. N.P.Ong, G.Verma (Dept. of Phys., Univ. of Southern California, Los Angeles, CA, USA).

Phys. Rev. B (USA), vol.27, no.7, p.4495-8 (1 April 1983).

In four-probe samples the authors show that the charge-density-wave noise spectrum fundamental in each of the three segments oscillates independently. Amplitude studies also show that the conduction noise originates at the contacts rather than in the bulk. (11 refs.)

62354 Image forces and the range of stability of a two-dimensional Wigner crystal. B.Abdullaev, Yu.E.Lozovik (Inst. of Spectroscopy, Acad. of Sci., Troitsk, USSR).

Sov. Phys.-Solid State (USA), vol.24, no.9, p.1510-11 (Sept. 1982). Translation of: *Fiz. Tverd. Tela (USSR)*, vol.24, no.9, p.2663-6 (Sept. 1982). [received: April 1983]

A generalized phenomenological Lindemann melting criterion, which states that the relative mean square displacement of two neighboring particles along the stability curve represents a constant fraction of the square of the lattice period, is used to study the effect of image forces and of a transverse magnetic field on the stability range of a two-dimensional electron crystal. The image forces cause cold melting at low electron densities (rather than at high densities, as predicted by theories neglecting the image forces). In a finite magnetic field $H \neq 0$, the electron gas crystallizes again in the low-density limit. The two ranges of existence of a crystal phase (two 'humps') merge on increase in H . The crystal phase is stable in a magnetic field even when the image forces destroy completely the crystal order at $H=0$. (7 refs.)

Superflows and superfluidity See Entry 62200

Charge and spin locations in linear stacks of TCNQ See Entry 62340

Quantized Hall effect in very strong magnetic field See Entry 62384

Incommensurate-commensurate transition in TaS₂ See Entry 62405

Ground state of two-dimensional electrons in strong magnetic fields and $1/3$ quantized Hall effect See Entry 62432

71.45G Exchange, correlation, dielectric and magnetic functions, plasmons

62355 Exchange, correlation, and band gaps in conjugated linear chains. J.M.Andre, J.L.Bredas, B.Themans (Lab. de Chimie Theorique Appliquee, Facultes Univ. Notre-Dame de la Paix, Namur, Belgium), L.Piela.

Int. J. Quantum Chem. (USA), vol.23, no.3, p.1065-72 (March 1983). (Proceedings of the Fourth International Congress in Quantum Chemistry, Uppsala, Sweden, 13-20 June 1982).

In the case of conjugated polyenic chains (polyacetylene), the relationship between the long- (or short-) range nature of the restricted Hartree-Fock exchange interaction, the role of correlation effects, and the size of energy gaps are illustrated. (16 refs.)

62356 Electronic correlations and midgap absorption in polyacetylene. Z.G.Soo, L.R.Ducasse (Dept. of Chem., Princeton Univ., Princeton, NJ, USA).

J. Chem. Phys. (USA), vol.78, no.6, pt.2, p.4092-5 (15 March 1983).

Electronic correlations are important when they lift degeneracies of Huckel models. Standard Pariser-Parr-Pople (PPP) parameters split the degenerate midgap absorption of neutral solitons in undoped trans polyacetylene (CH)_x. The dipole intensity goes entirely to the upper state close to the optical gap E_g . PPP correlations lower slightly the nondegenerate transition at $E_g/2$ of charged solitons, which consequently provide all the $E \sim E_g/2$ intensity. Exact symmetries of correlated states and finite-chain computations are exploited in associating the midgap absorption of neat and lightly doped (CH)_x entirely with charged solitons. (25 refs.)

62357 $2p_F$ and $4p_F$ instabilities in the one-dimensional electron gas. J.E.Hirsch (Inst. for Theoretical Phys., Univ. of California, Santa Barbara, CA, USA), D.J.Scalapino.

Phys. Rev. Lett. (USA), vol.50, no.15, p.1168-71 (11 April 1983).

Charge- and spin-density response functions in the one-dimensional $1/d$ -filled extended Hubbard model have been studied by use of a Monte Carlo technique. The results show that Coulomb interactions suppress the $2p_F$ charge-density singularity, while they enhance the $2p_F$ spin-density singularity. The $4p_F$ response is only appreciable if, in addition to on-site repulsion, longer-range interactions exist. The present results are compared with weak-coupling renormalization-group predictions. (7 refs.)

62358 Second-order perturbation treatment of correlations in transition metal alloys. V.Drchal, J.Kudrnovsky (Inst. of Phys., Czechoslovakian Acad. of Sci., Prague, Czechoslovakia).

Phys. Status Solidi b (Germany), vol.116, no.1, p.119-28 (1 March 1983).

Correlation effects in disordered transition metal alloys are studied within the degenerated Hubbard model using the perturbation theory limited to the second order in U/w (U Coulomb integral w bandwidth). The influence of disorder is included within the coherent potential approximation. The theory is illustrated on a simple model of the copper-nickel alloy. (10 refs.)

62359 Linear response of a semi-infinite substrate with a two-dimensional conductive surface layer in the plasma-pole approximation. F.J.Crowne (US Army Electronics Res. & Dev. Command, Harry Diamond Labs., Adelphi, MD, USA).

Phys. Rev. B (USA), vol.27, no.6, p.3201-12 (15 March 1983).

The current-current linear-response function for a semi-infinite compressible electron-gas substrate with a surface layer of zero thickness is evaluated by treating the substrate hydrodynamically. No assumptions are made regarding the current-current response of the surface layer, and retardation effects are fully included. Contact is made with Nakayama's paper (1974) on surface plasmons, and a discussion of the effects of a finite compressibility of the background electron gas on the surface modes is included. Angular distributions for Raman scattering by a simple type of surface plasmon are calculated as an application of these results. (13 refs.)

Treatment of aperiodicity and correlation in polymers See Entry 62328

Interaction of charges with metallic surfaces—invalidity of the surface plasmon model See Entry 62468

Exact calculations of scattering and enhanced fields of electromagnetic waves on grating surfaces See Entry 62977

Enhanced adsorbate Raman scattering and surface plasmon radiation See Entry 62981

Visible and near ultraviolet radiation from ultrathin silver films bombarded by low energy electrons See Entry 63057

Calculation of the EELS spectra of the Ni(001) surface with $p(2 \times 2)$ and $c(2 \times 2)$ overlayers of oxygen See Entry 63098

71.45N Calculations of total electronic binding energy (see also 61.50L Crystal binding)

Self-consistent semirelativistic pseudopotential calculation of the energy bands, cohesive energy, and bulk modulus of W See Entry 62329

Self-consistent pseudopotential calculation of the electronic structure of PdH and Pd₄H See Entry 62330

71.50 LOCALIZED SINGLE-PARTICLE ELECTRONIC STATES

(exc. impurities; for localisation in disordered structures, see 71.55J)

62360 Gauge transformation study of two-dimensional localisation in magnetic fields. H.Aoki (Cavendish Lab., Univ. of Cambridge, Cambridge, England).

J. Phys. C (GB), vol.16, no.10, p.1893-900 (10 April 1983).

The effect of gauge transformation on the two-dimensional system in a strong magnetic field is studied numerically to shed light on the localisation of states. The result for the gauge dependence of energy levels and wavefunctions for periodic boundary conditions shows that an extended eigenstate is sensitive to the gauge transformation while a localised eigenstate is essentially unchanged indicating an exponential localisation. (22 refs.)

62361 One-electron broken-symmetry approach to the core-hole spectra of semiconductors. A.Zunger (Solar Energy Res. Inst., Golden, CO, USA).

Phys. Rev. Lett. (USA), vol.50, no.16, p.1215-18 (18 April 1983).

It is shown that in contrast to band theory, a self-consistent one-electron model with broken symmetries (crystal orbitals are not constrained to be Bloch periodic) provides a physical description of core-ionization, core-exciton, and core-to-conduction-band transition energies in semiconductors. Application to GaP shows that a hitherto unrecognized factor—the screening of the core-hole self-energy by the electron orbit—can explain many of the outstanding puzzles in core hole spectra. (21 refs.)

Local modes: their relaxation, polarization, and stereoselective excitation by lasers See Entry 60691

71.55 IMPURITY AND DEFECT LEVELS

62362 Theory of the autoionized state of impurities in semiconductors. Gan Zizhao, Han Ruqi (Peking Univ., Peking, China).

Chin. J. Semicond. (China), vol.4, no.2, p.105-16 (March 1983). In Chinese.

A theory of the autoionized state of impurities in semiconductors is developed. It is analogous to the configuration interaction model for autoionized state of atoms. From this theory, the formal expression of the position, width and wave function of autoionized state of impurities is obtained, and an explanation of the autoionized level manifesting itself in continuous absorption spectra, as an asymmetric peak which is called Fano's line shape, is given. A concrete computing method for the autoionized state of impurities, known as the complex coordinate method is developed. As an example, the position and width of an autoionized state of acceptor in Si, which belongs to the Γ_7 symmetry, are computed. (29 refs.)

62363 Theoretical study on the nitrogen isoelectronic trap in GaAs_{1-x}P_x. Li Hanqiu, Lu Fen (Fudan Univ., Shanghai, China).

Chin. J. Semicond. (China), vol.4, no.2, p.187-90 (March 1983). In Chinese.

Using a cluster model, the EHT method is used to calculate the electronic binding energy of the N-isoelectronic trap in GaAs_{1-x}P_x. It is shown that in order to make some major improvements in the results, it is necessary to take the excited orbitals of atoms into consideration. (7 refs.)

62364 Carrier capture by multiphonon emission at extrinsic deep centers induced by self-trapping in GaAs. H.Goto, Y.Adachi, T.Ikoma (Inst. of Industrial Sci., Univ. of Tokyo, Tokyo, Japan).

J. Appl. Phys. (USA), vol.54, no.4, p.1909-23 (April 1983).

The extent of electron-lattice coupling at neutral, extrinsic self-trapping-induced deep centers in III-V compound semiconductors is estimated by assuming a deformation potential interaction in the framework of a continuum lattice model, and its delocalization around these deep centers is pointed out. A model potential which takes into account the delocalization of the coupling is proposed and a theoretical expression is derived for capture cross sections at these centers by combining the model potential with multiphonon emission carrier capture scheme. The theory successfully explained both temperature dependence and the magnitude of capture cross sections observed at three electron traps (deep centers) in GaAs. Although the magnitude of capture cross sections at two of these three electron traps seem to deviate from the predicted by Henry and Lang, the multiphonon emission carrier capture scheme is still applicable to such deep states by employing the authors' model potential. (32 refs.)

62365 New aspects of the oxygen donor in gallium phosphide. P.J.Dean, M.S.Skolnick (RSRE, Great Malvern, England), Ch.Uihlein, D.C.Herbert.

J. Phys. C (GB), vol.16, no.11, p.2017-51 (20 April 1983).

Newly discovered or reconsidered experimental properties of the centre are presented. Particular emphasis is given to the properties of the second electron state, O_p^- . The authors show that occurrence, Zeeman effect, and hole electronic excited states of an absorption transition near 1.738 eV are consistent with the D^0, X BE for the centred O_p^0 donor, and deduce $E_g^* = 41.7$ meV, $E_g = 570$ meV. Complex behaviours of this D^0, X BE absorption in the PLE spectrum of distant DAP luminescence are fully explained. The exciton localisation energies of this BE are those of eight other donors in GaP, some nearly effective-mass-like, follow a single power-law dependence on E_g . Electron capture by O_p^- appears to proceed via 42 meV deep excited state of centred O_p^- , with a further excited state 37.5 meV below the conduction band. Zeeman splittings and shifts, lifetime and phonon coupling of this transition, with no-phonon line at 528 meV, and their relation to the D^0, X BE absorption and first electron capture luminescence are discussed. Evidence is presented that the absence of luminescence from the D^0, X BE and the broadening of the electronic transitions results from the short lifetime of the metastable centred O_p^- state before relaxation to the strongly distorted rebounded ground state. Zeeman properties of the D^0, X BE absorption, the distant discrete DAP no-phonon luminescence and the electron capture luminescence at O_p^- are all strikingly inconsistent with a recent reassignment of the single-electron state of O_p^- to 4T_1 rather than 2A_1 . An alternative interpretation is advanced for the strong temperature dependence of the optical cross section σ_{pl}^0 at low T , one of the main motivations for the reassignment. The Zeeman effect of the 0.841 eV capture luminescence is quantitatively consistent with a spin doublet to spin doublet transition, rather than the transition between spin quartet states of the alternative model. (54 refs.)

62366 Quantum mechanical state of interstitial hydrogen in metals: energy and wavefunctions. H.Sugimoto, Y.Fukai (Dept. of Phys., Chuo Univ., Tokyo, Japan).

J. Less-Common Met. (Switzerland), vol.89, no.2, p.307 (Feb. 1983). (International Symposium on the Properties and Applications of Metal Hydrides, Toba, Japan, 30 May-4 June 1982).

Summary form only given, as follows. The energy and wavefunctions of hydrogen (deuterium) atoms self-trapped on interstitial sites in FCC and BCC metals were calculated. The Schrodinger equation for a hydrogen (deuterium) atom is solved in the interaction potential field with the surrounding metal atoms approximated by the sum of central pair potentials. Both the ground and excited states were studied and compared with the observed inelastic neutron scattering spectra in the optic mode. These calculations show that a consistent understanding of many properties of the excited states of a hydrogen atom on the tetrahedral site in BCC vanadium, niobium and tantalum, on the octahedral site in body-centred tetragonal β -VH₂ and on the octahedral site in FCC palladium can be obtained. The calculated wavefunctions were also compared with Fourier-reconstructed density maps from neutron diffraction experiments. (1 ref.)

62367 Properties of some defect complexes of gold in silicon. H.Lemke (Zentralinst. fur Elektronenphys., Akad. der Wissenschaften, Germany). *Phys. Status Solidi a (Germany)*, vol.75, no.2, p.473-82 (16 Feb. 1983). In German.

The properties of some ion pairs between donors or double donors of the 3d-group and the acceptor gold are investigated by DLTS- and TSCA-techniques. The pair (Fe^+Au^-) is an acceptor at $E_c-0.34$ eV with $r_p^n=3\times 10^{-8}$ cm² s⁻¹ ($T=160$ K) and the pair (Cr^+Au^-) a donor at $E_v+0.35$ eV with $r_p^p=1\times 10^{-8}$ cm² s⁻¹ ($T=170$ K). The ion pair of Au with the double donor, Mn has two levels: an acceptor at $E_c-0.24$ eV with $r_p^n=4\times 10^{-8}$ cm² s⁻¹ ($T=120$ K) and a donor at $E_v+0.57$ eV with $r_p^p=3\times 10^{-8}$ cm² s⁻¹ ($T=250$ K). The pair levels for V lie at $E_c-0.20$ eV with $r_p^n=6\times 10^{-9}$ cm² s⁻¹ ($T=115$ K) and at $E_v+0.42$ eV with $r_p^p=8\times 10^{-9}$ cm² s⁻¹ ($T=200$ K). From the measurements of mass-action constants binding energies of 0.9 (Fe), 0.9 (Mn), 1.1 (Cr), and 1.6 eV (V) are determined. (15 refs.)

62368 Long-range part of the interaction between two hydrogen impurities in jellium. P.Perrot (CEA, Villeneuve-Saint-Georges, France), M.Rasolt. *Phys. Rev. B (USA)*, vol.27, no.6, p.3273-8 (15 March 1983).

The interaction of two hydrogen impurities in jellium is calculated in the 'overlapping densities' approximation where the total displaced charge is the sum of two frozen single ion screening densities. Using the fourth-order gradient expansion of the kinetic-energy functional, the authors obtain the results at various densities, corresponding to Al, Mg, and Na. The results provide an extension for the full treatment of the short-range proton-proton interaction to the asymptotic region where such exact calculation are as yet not available. (20 refs.)

62369 Energy of two-electron impurity states of tin in $\text{Pb}_{1-x}\text{Sn}_x\text{Se}$ solid solutions with low values of x . S.V.Zarubo, Yu.A.Nikulin, E.A.Gurieva, L.V.Prokof'eva, Yu.I.Ravich, M.N.Vinogradova, T.B.Zhukova (A.F. Ioffe Physicotechn. Inst., Acad. of Sci., Leningrad, USSR).

Sov. Phys.-Semicond. (USA), vol.16, no.10, p.1219-21 (Oct. 1982). Translation of: *Fiz. i Tekh. Poluprovodn. (USSR)*, vol.16, no.10, p.1892-4 (Oct. 1982). [received: April 1983]

The authors have investigated the temperature dependence of the Hall effect in $\text{Pb}_{1-x}\text{Sn}_x\text{Se}$ solid solutions near $x=0$ as a function of the degree of doping with an acceptor impurity (Na) which made it possible to determine the depth of the localized Sn states and its temperature dependence. Lightly doped p-type samples with $x=0.02$ were prepared by allowing the composition to deviate from stoichiometry, whereas heavily doped samples were formed as a result of introduction of NaSe in amounts from 0.1 to 1.5 mol%. The authors used both polycrystalline and single-crystal samples. A study of the dependence of the Hall density on the Na content showed that in the range $N_{\text{Na}}\leq 0.3$ at.% every Na atom gave up one carrier and there was no increase in the carrier density on further increase in N_{Na} . The maximum density of holes in this solid solution was 4.0×10^{15} cm⁻³ at 4.2K. (5 refs.)

62370 Resonance level of tellurium associated with the L minima of the conduction band of gallium antimonide. A.S.Filipchenko, E.Litvin-Staszewska (A.F. Ioffe Physicotechn. Inst., Acad. of Sci., Leningrad, USSR). *Sov. Phys.-Semicond. (USA)*, vol.16, no.10, p.1229 (Oct. 1982). Translation of: *Fiz. i Tekh. Poluprovodn. (USSR)*, vol.16, no.10, p.1906 (Oct. 1982). [received: April 1983]

The parameters of the L minima of the conduction band of gallium antimonide were determined using tellurium crystals under hydrostatic pressure conditions. The crystals used in these investigations had high concentrations of tellurium and, therefore, it was assumed that a resonance level of tellurium associated with the L minima of the conduction band was degenerate with these minima. The experimental dependencies of the relative change in the Hall coefficient with the applied hydrostatic pressure (in the saturation region of the dependence) can be used, with the aid of familiar formulas, to determine the ionization energy of resonance levels of tellurium associated with the L minima of the conduction band of gallium antimonide. The ionization energy of the tellurium levels associated with the L minima of the conduction is thus found to be ~ 10 meV. (3 refs.)

62371 Electron structure of edge dislocations in metals. M.I.Molotskii, V.S.Rostovtsev (Lenin Komsomol State Univ., Voronezh, USSR). *Sov. Phys.-Solid State (USA)*, vol.24, no.9, p.1455-7 (Sept. 1982). Translation of: *Fiz. Tverd. Tela (USSR)*, vol.24, no.9, p.2564-8 (Sept. 1982). [received: April 1983]

The electron structure of the core of an edge dislocation in copper is studied on the basis of a model which assumes the existence of dangling d bonds. The linear dislocation charge is calculated and the density of quasilocal d states is determined. The excess charge is found to be close to the charge near the axis of a screw dislocation. The density of the d states has a maximum near the Fermi level. Such a maximum leads to a resonant scattering of conduction electrons from dangling bonds, which may explain the high electrical resistivity associated with edge dislocations. (14 refs.)

62372 Electron transfer of hydrogen in aluminum at 20 and 800°C. O.M.Byalik, N.P.Volkotrub, V.M.Pinchuk, L.V.Golub, G.E.Detyarenko, D.F.Ivanchuk (Kiev Polytech. Inst., Kiev, Ukrainian SSR). *Sov. Mater. Sci. (USA)*, vol.18, no.3, p.221-4 (May-June 1982). Translation of: *Fiz.-Khim. Mekh. Mater. (USSR)*, vol.18, no.3, p.34-8 (May-June 1982). [received: Feb. 1983]

The electron transfer of hydrogen was investigated in the field of the crystalline lattice of aluminum. The tests were made on a special unit with the use of the six-probe method of measuring specific electrical resistance. To reveal the mechanism of electron transfer of hydrogen in the field of the crystalline lattice of aluminum, a quantum-mechanical calculation of the interaction of the H^+ and H^- ion complexes with the aluminum atoms was made. (8 refs.)

62373 Steady state and transient capacitance measurements of the energy levels of a low angle tilt boundary in a germanium bicrystal. A.Broniatowski (CNRS, Villeneuve, France), J.C.Bourgoin.

Grain Boundaries in Semiconductors. Proceedings of the Materials Research Society Annual Meeting, Boston, MA, USA, Nov. 1981 (New York, USA: North-Holland 1982), p.119-24

Steady state and transient capacitance (DLTS) measurements have been performed on a low angle tilt boundary in a germanium bicrystal, in combination with an electron microscope study of the boundary dislocation structure. A characteristic level has been found at 0.42 eV below the bottom of the conduction band, with a density about 10^{19} cm⁻² and an electronic capture cross-section about 5×10^{-12} cm². (15 refs.)

62374 Characterization of grain boundaries in polycrystalline GaAs. M.G.Spencer (Dept. of Electrical Engng., Howard Univ., Washington, DC, USA), W.J.Schaff, D.K.Wagner.

Grain Boundaries in Semiconductors. Proceedings of the Materials Research Society Annual Meeting, Boston, MA, USA, Nov. 1981 (New York, USA: North-Holland 1982), p.125-9

Examination of capacitance transients arising from the emission or capture of electrons at a charged GaAs grain boundary reveal for the first time the existence of discrete interface levels. The position of these levels in the band-gap and their associated capture cross sections are determined from the transients. (6 refs.)

62375 Electronic states associated with grain boundaries in silicon. C.M.Shyu, L.J.Cheng (Jet Propulsion Lab., California Inst. of Technol., Pasadena, CA, USA).

Grain Boundaries in Semiconductors. Proceedings of the Materials Research Society Annual Meeting, Boston, MA, USA, Nov. 1981 (New York, USA: North-Holland 1982), p.131-6

The density of states at the grain boundary is found to be a complicated function of both the defect state property and the physical location of the defect at the boundary. A modified double-depletion-layer model concerning the nonuniform distribution of defects along the boundary is presented. A method is developed which can estimate the level location from the complex DLTS spectra. (8 refs.)

62376 Grain boundary passivation in polycrystalline silicon: a DLTS study. P.C.Srivastava, J.C.Bourgoin (Groupe de Phys. des Solides, Univ. Paris VII, Paris, France).

Grain Boundaries in Semiconductors. Proceedings of the Materials Research Society Annual Meeting, Boston, MA, USA, Nov. 1981 (New York, USA: North-Holland 1982), p.137-40

After treatment in a deuterium plasma, the DLTS spectrum associated with grain boundaries in p-type Si is found to reduce to a narrow band centered at 0.32 ± 0.02 eV with a total density of 5×10^{15} cm⁻². However, the capture cross-section, measured to be $\sim 2\times 10^{-20}$ cm², is 10 times larger than the apparent cross-section associated with the states present in unpassivated material. (10 refs.)

62377 Electronic structure of grain boundaries and interfaces in polycrystalline zinc oxide. M.H.Sukkar, H.L.Tuller, K.H.Johnson (Dept. of Materials Sci. & Engng., MIT, Cambridge, MA, USA).

Grain Boundaries in Semiconductors. Proceedings of the Materials Research Society Annual Meeting, Boston, MA, USA, Nov. 1981 (New York, USA: North-Holland 1982), p.141-6

Preliminary theoretical models for the electronic structure of grain boundaries and interfaces in polycrystalline ZnO have been constructed on the basis of self-consistent-field X-alpha scattered-wave (SCF-X-alpha-SW) cluster molecular-orbital calculations. The disposition and character of the interface states, relative to the valence and conduction bands of the otherwise perfect crystalline material, have been studied for clusters representing coordinatively unsaturated Zn surface sites and molecular O₂ chemisorption thereon. The possible effects of the resulting interface states on electron transport at grain boundaries in ZnO varistors have been addressed. (16 refs.)

Laser gain and excitation threshold in semiconductors with transitions between localized states See Entry 61161

Changes in the concentration of 1.0 and 1.28 eV copper luminescence centers during annealing of electron-irradiated n-type GaAs See Entry 61948

On the interaction between a vacancy and an interstitial impurity atom in BCC transition metals See Entry 61953

Interaction of primary radiation defects with dislocations in indium antimonide See Entry 61955

Electron and ion beam effects in amorphous SiO₂ and Si₃N₄ films for electronic devices See Entry 61996

Exciton trapping and sensitized luminescence: a generalized theory for all trap concentrations See Entry 62342

Transport across silicon grain boundaries See Entry 62428

'Limiting' electrical properties of irradiated InP See Entry 62434

Light effects on grain boundary properties in silicon See Entry 62457

Transport properties of tungsten bronzes doped with tantalum See Entry 62459

Electric field effect on the thermal emission rate of holes trapped at gold donor center in Si p-n junction See Entry 62484

Spin relaxation and polarization under interaction of photocarriers with charged paramagnetic centers in a semiconductor See Entry 62800

Nonlinear susceptibility of impurity centres in semiconductors See Entry 62933

Study of electronic structure of reduced TiO₂ and V₂Ti_{1-x}O₂ crystals by ESCA and optical absorption See Entry 63018

Influence of the resonance interaction between molecules of a crystal and impurities on the Rashba effect for several impurity centers in molecular crystals See Entry 63025

Electronic structure and luminescent properties of Cu⁺ and Ag⁺ impurity centers in NaCl See Entry 63032

Optical properties of copper-related centres in InP See Entry 63036

Luminescence decay time of the 1.945 eV centre in type Ib diamond See Entry 63038

Characterisation of Mn-doped and nominally pure LPE Ga_{0.95}In_{0.05}As_{1-y}P_{1-y} (y=2.1x) between y=0 and y=1 using photoluminescence and electrical measurements See Entry 63039

Photon transport of mobile nonequilibrium carriers in variable-gap semiconductors as a result of band-impurity level radiative recombination See Entry 63052

The influence of X-trap on spin-lattice relaxation in the impurity phosphorescent state of a naphthalene crystal See Entry 63054

- Thermoluminescence of low-temperature X-irradiated MgO and MgO:Li single crystals See Entry 63063
- Effects of mechanical drawing treatment on the characteristics of internal friction and thermally stimulated current on low density polyethylene See Entry 63308

71.55J Localization in disordered structures

- Effects of ionizing radiation on amorphous insulators See Entry 61805
- Electrical conduction phenomena and negative resistance in Al-Al₂O₃-Au structure See Entry 62503

71.70 LEVEL SPLITTING AND INTERACTIONS

(see also 75.10 - in magnetic phenomena, 75.30E Exchange and superexchange interactions, 73.20 Electronic surface states)

- Excited states of mixed-ligand chelate complexes of ruthenium(II). A re-examination of the evidence for strong interligand coupling See Entry 60756
- Effects of excited-state prototropic equilibria on the fluorescence energies of benzimidazole and thiabendazole homologues See Entry 60814
- Positive charge transfer in mixed alkane glasses See Entry 60971
- Change in the valence of samarium ions in solid solutions based on isostructural SmB₆ phases See Entry 61887
- Two critical points on the γ - α phase boundary of cerium alloys See Entry 62091
- Semiconducting properties of V₂O₅ gels See Entry 62416
- Magnetic properties of amorphous Fe-Nb and Fe-Zr See Entry 62607
- Magnetic inhomogeneity in amorphous Fe-Zr alloys See Entry 62701
- NMR in metallic glasses See Entry 62817
- Mossbauer studies of valence fluctuations See Entry 62845
- Mossbauer and X-ray diffraction studies of amorphous Fe-Ni alloy films deposited by DC sputtering See Entry 62862
- Effect of an electric field on the photochromic effect in Bi₁₂GeO₂₀:Mn crystals See Entry 62938
- Thermodynamic study of the valence state of ytterbium in YbAl₂ and YbAl₃ compounds See Entry 62580

71.70C Crystal and ligand fields

- 62378 Application of the unitary group approach to crystal field theory. Wen Zhenyi (Dept. of Phys. Chem., Univ. of Copenhagen, Copenhagen, Denmark). *Int. J. Quantum Chem. (USA)*, vol.23, no.3, p.999-1009 (March 1983). (Proceedings of the Fourth International Congress in Quantum Chemistry, Uppsala, Sweden, 13-20 June 1982).
- An analytical treatment for a strong crystal field in an octahedral symmetry by using the unitary group approach is given. It shows that the convenience of the unitary group approach is comparable with that of the Racah method. (11 refs.)

- 62379 Effect of covalency on Slater parameters and the correction crystal field in transient-metal compounds. M.V.Eremin, A.A.Kornienko. *Opt. & Spectrosc. (USA)*, vol.53, no.1, p.45-8 (July 1982). Translation of: *Opt. & Spektrosk. (USSR)*, vol.53, no.1, p.79-85 (July 1982). [received: April 1983]

Simple formulas are obtained to calculate the influence of charge-transfer processes from ligand to metal on the parameters for two and three-particle operators, of a crystal field. As examples the compounds of manganese and nickel are considered. The calculated decreases of the Slater parameters due to the covalency of metal-fluorine binding is found to be ~2-8% and in order of magnitude agrees with experimental data. It is demonstrated that the second-rank correlation crystal field because of covalency may become very significant. (14 refs.)

- 62380 A microscopic interpretation of the spin-lattice coupling coefficients for S-state 4fⁿ ions. W.Pastusiak (Solid State Div., Inst. of Phys., A. Mickiewicz Univ., Poznan, Poland). *Phys. Status Solidi b (Germany)*, vol.116, no.1, p.63-70 (1 March 1983).
- A previously reported model for spin-lattice coupling for 4fⁿ electrons, based on the assumption that intraionic interactions are perturbed by relativistic interaction with crystal lattice, is developed. Analytical formula for second- and fourth-order spin-lattice coefficients are derived. Using these formula and the concepts of the relativistic crystal field in the point charge approach the values of the spin-lattice coefficients for Gd³⁺ in CaF₂ are calculated. These values are in much better agreement with the experimental values than those calculated so far. To the best of the authors knowledge the fourth-order spin-lattice coefficients are calculated the first time and their values are about ten times smaller than the experimental ones. (15 refs.)

- 62381 Crystal field splittings of PrX₃ compounds (X=Pt, Rh, Ir, Ru, Ni) studied by inelastic neutron scattering. F.J.A.M.Greidanus, L.J.De Jongh, W.J.Huiskamp (Kamerlingh Onnes Lab. Rijksuniv., Leiden, Netherlands), A.Furrer, K.H.J.Buschow. *Physica B & C (Netherlands)*, vol.115 B+C, no.2, p.137-55 (Jan. 1983).
- Neutron inelastic scattering experiments have been performed on polycrystalline samples of the cubic Laves phase compounds PrX₃ (X=Pt, Rh, Ir, Ni). Measurements in the paramagnetic state yield LLW parameters 0.6 < x < 1 and W < 0. In this region various levels cross at an x value 0.86 and as a consequence the electronic ground state in the paramagnetic regime is either the singlet Γ_1 , or the non-magnetic doublet Γ_3 . Measurements in the ferromagnetic state support these conclusions. The crystal-field parameters obtained can be used in model calculations of some macroscopic quantities, in particular the specific heat and the spontaneous magnetization. The variation of the x values in the present series of Laves phase compounds evidences the presence of a contribution by conduction electrons to the crystal field. (49 refs.)

- 62382 Variational approach to the Jahn-Teller problem in cobaltocene. R.Rai (Nat. Phys. Lab., New Delhi, India). *Physica B & C (Netherlands)*, vol.115 B+C, no.2, p.247-53 (Jan. 1983).
- The Jahn-Teller problem of a system of an electronic doublet having spin-orbit splitting in first order and interacting with a doubly degenerate vibration is considered. A canonical transformation and variational approach is used to determine the ground vibronic Kramers' doublets. The variational wave functions are used to calculate the zero-field splitting and ESR g-values, which are compared with the experimental results on cobaltocene. (18 refs.)

- Tricopper. A fluxional molecule See Entry 60728
- The secondary effect of the cooperative Jahn-Teller distortion in rare earth vanadates See Entry 62089
- Effect of varying the orientation of a quantizing magnetic field on the effective electron mass in degenerate tetragonal semiconductors See Entry 62326
- Quadrupolar coupling and structural instability in PrAg_{1-x}Cu_x See Entry 62383

- Cooperative quadrupolar ordering of Yb³⁺ ions in the Γ_8 electronic state See Entry 62533

- The influence of nuclear quadrupole interactions upon electron spin-echo modulation induced by weak hyperfine interactions See Entry 62797
- Divalent manganese in an axial symmetry site of additively coloured CaO single crystals See Entry 62802

- Determination of the correlation between the crystal field axis system and the crystallographic axes in chromium-doped β -Ga₂O₃ by EPR See Entry 62805
- Enhanced NMR of ¹⁶⁹Tm in TmAsO₄ See Entry 62816

- Local lattice expansion of Cu arising from dilute interstitial impurities, β -emitting nuclei ¹²B and ¹²N See Entry 62818

- NMR study of deuterium molybdenum bronze See Entry 62822

- Determination of hyperfine interaction parameters from poorly resolved Mossbauer spectra with the transmission integral See Entry 62839

- Mossbauer studies of valence fluctuations See Entry 62845

- A Mossbauer spectroscopic study of the six-coordinate high-spin ferrous compound (meso-tetraphenylporphinato)bis(tetrahydrofuran) iron(II) See Entry 62852

- Mossbauer spectroscopic studies of magnesium nickel ferrites See Entry 62854

- Application of the depth-selective conversion electron Mossbauer spectroscopy to rare-earth iron garnet films See Entry 62863

- Depth-selective conversion electron Mossbauer spectroscopy of thin Fe films See Entry 62864

- Applied magnetic field Mossbauer studies of the quasi one-dimensional system AFeS₂:A=K, Rb, Cs See Entry 62865

- Quadrupole interactions at ¹¹¹Cd nuclei in light rare earths See Entry 62868

- One- and two-photon spectra of NaF:Cu²⁺: Jahn-Teller and vibronic coupling effects See Entry 63022

- Site-selection spectroscopy of Eu³⁺-doped germinate glass See Entry 63023

- Anomalous temperature-dependent phosphorescence of Cu porphrin in anthracene See Entry 63034

- Thin film absorption spectra of lower valent p block halides See Entry 63077

71.70E Spin-orbit coupling, Zeeman, Stark and strain splitting

- Energy states and Bloch states for an accelerated electron in a periodic lattice See Entry 62315

- New aspects of the oxygen donor in gallium phosphide See Entry 62365

- Magnetostription of iron, cobalt and nickel ternary amorphous ribbons See Entry 62787

- Spectroscopic and magneto-optical properties of quasi 1D antiferromagnets AVX₃ (A=Cs, Rb; X=Cl, Br, I) See Entry 62943

- Photoemission spectra and band structures of d-band metals. X. Relativistic momentum matrix elements See Entry 63132

71.70J Nuclear states and interactions

- 62383 Quadrupolar coupling and structural instability in PrAg_{1-x}Cu_x. J.A.Gotaas, J.S.Kouvel (Dept. of Phys., Univ. of Illinois, Chicago, IL, USA), T.O.Brun, J.W.Cable.

- J. Magn. & Magn. Mater. (Netherlands)*, vol.36, no.1-2, p.208-12 (1 April 1983).

Results are reported for magnetization and neutron diffraction studies of the pseudobinary compounds PrAg_{1-x}Cu_x. As x is raised from zero to 0.25, the structure remains cubic CsCl-type and the bilinear exchange is nearly unchanged, whereas the effective quadrupolar coupling deduced from the detailed magnetization-field behavior above the antiferromagnetic Neel point (~10K) increases three-fold in magnitude. The x=0.5 compound, when cooled below ~150K, transforms from CsCl-type to an orthorhombic FeB₂-type structure. Detailed comparison of these structures shows that the instability of the CsCl-type may derive from the softening of zone-boundary phonons. Such phonons, via the dynamic Jahn-Teller mechanism would account for the quadrupolar interactions of negative (antiferro) sign which grow with increasing x. (12 refs.)

- Defect states in amorphous silicon See Entry 61804

- Magnetic hyperfine field distribution and structural relaxation of amorphous (Fe₈₁B₁₄Si₄) prepared with different quenching rates See Entry 62608

- Magnetic short-range order and spin freezing in the quasi-2D system LuFeMgO₄ See Entry 62642

- NMR study of deuterium molybdenum bronze See Entry 62822

- ⁸⁷Rb and ⁸⁵Rb NQR study of phase transitions in RbH₃(SeO₃)₂ See Entry 62829

- Mossbauer spectroscopic studies of magnesium nickel ferrites See Entry 62854

- Application of the depth-selective conversion electron Mossbauer spectroscopy to rare-earth iron garnet films See Entry 62863

- Depth-selective conversion electron Mossbauer spectroscopy of thin Fe films See Entry 62864

- Applied magnetic field Mossbauer studies of the quasi one-dimensional system AFeS₂:A=K, Rb, Cs See Entry 62865

72.00 ELECTRONIC TRANSPORT IN CONDENSED MATTER

(for surfaces, interfaces, and thin films, see 73.)

72.10 THEORY OF ELECTRONIC TRANSPORT; SCATTERING MECHANISMS

62384 Quantized Hall effect in very strong magnetic field. Lai Wu-yan, Shen Jue-lian (Inst. of Phys., Acad. of Sinica, Beijing, China), Su Zhao-bin, Yu Lu.

Commun. Theor. Phys. (China), vol.2, no.1, p.929-33 (1983).
The experimentally observed quantized Hall plateau of $\rho_{xy} = 3h/e^2$ in a two-dimensional electron gas, when the lowest Landau level is $1/3$ filled, is discussed. The consistency of the extremal condition for the Hartree-Fock potential in the possible charge-density-wave state with an opening of the energy gap at the Fermi level is indicated. The exactness of such $1/3$ 'fractional' quantization might be justified by a modified version of Laughlin's argument (1981) based on gauge invariance. (14 refs.)

62385 Localisation and interaction in one dimension. W.Apel, T.M.Rice (Theoretische Phys., ETH-Honggerberg, Zurich, Switzerland).
J. Phys. C (GB), vol.16, no.10, p.L271-3 (10 April 1983).

As the temperature is lowered in a system of interacting fermions in one dimension with static impurities, the ratio of the elastic and inelastic scattering lengths depends crucially on the interaction coupling constants. In one range, transport in the system is classical and the resistance decreases with decreasing temperature. In the other range of coupling constants the transport has to be treated quantum mechanically and Anderson localisation results. (8 refs.)

62386 Eddy currents in media with anisotropic electrical conductivity. L.A.Bityutskaya, E.N.Bormontov, A.R.Regel', V.F.Synorov.

Sov. Tech. Phys. Lett. (USA), vol.8, no.7, p.377-9 (July 1982). Translation of: *Pisma v Zh. Tekh. Fiz. (USSR)*, vol.8, no.13-14, p.869-74 (July 1982). [received: April 1983]

The authors examine the general conditions required for the occurrence of eddy currents caused by an anisotropy of the electrical conductivity in an anisotropic medium. They study the nature of these closed currents in the regions for which the mathematical description is simplest. (5 refs.)

72.15 ELECTRONIC CONDUCTION IN METALS AND ALLOYS

72.15C Electrical and thermal conduction in amorphous and liquid metals and alloys

62387 Magnetoresistance investigation of amorphous $(\text{Fe}_{1-x}\text{Cr}_x)_{84}\text{B}_{16}$ alloys. Y.Z.Wang, F.M.Yang, Y.S.Wu, M.Y.Feng, W.S.Zhan (Inst. of Phys., Chinese Acad. of Sci., Beijing, China).

J. Magn. & Magn. Mater. (Netherlands), vol.31-34, pt.3, p.1473-4 (Feb. 1983). (Proceedings of the International Conference on Magnetism, Kyoto, Japan, 6-10 Sept. 1982).

Systematic investigation of transverse and longitudinal magnetoresistance of amorphous $(\text{Fe}_{1-x}\text{Cr}_x)_{84}\text{B}_{16}$ alloys were performed. The measurement results show that the magnetoresistances of this system are dependent strongly on the Cr content. The low temperature resistance anomaly is suppressed obviously with increasing magnetic fields up to 70 kOe. These results can be interpreted in the light of magnetic origin. (5 refs.)

62388 Electrical resistivity and Hall effect of amorphous $\text{TM}_{77}\text{Si}_{10}\text{B}_{13}$ ($\text{TM} = \text{Fe, Co, Ni}$) alloys. T.K.Kim, C.O.Kim, Y.E.Ihm, B.W.Lau (Coll. of Engng., Chungnam Univ., Daejeon, Korea).

J. Magn. & Magn. Mater. (Netherlands), vol.31-34, pt.3, p.1477-8 (Feb. 1983). (Proceedings of the International Conference on Magnetism, Kyoto, Japan, 6-10 Sept. 1982).

To investigate the electronic transport phenomena of amorphous $(\text{Fe}_{1-x}\text{Ni}_x)_{77}\text{Si}_{10}\text{B}_{13}$ and $\text{Co}_{77}\text{Si}_{10}\text{B}_{13}$, the electrical and Hall resistivity were measured. The resistivity shows anomalous behaviour at Ni-rich composition. Ordinary Hall resistivity R_H , and spontaneous Hall conductivity γ_{HS} , decrease linearly with Ni content and R_H changes from positive to negative around $x=0.8$. Spontaneous Hall resistivity, R_s , decreases with Ni content and reaches zero around $x=0.8$. (4 refs.)

62389 Electrical resistivity and thermoelectric power of glassy $\text{Fe}_{74}\text{Co}_{10}\text{B}_{16}$ and $\text{Fe}_{67}\text{Co}_{18}\text{B}_{15}\text{Si}_1$ alloys. B.B.Prasad, A.K.Bhatnagar (School of Phys., Univ. of Hyderabad, Hyderabad, India).

J. Magn. & Magn. Mater. (Netherlands), vol.31-34, pt.3, p.1479-80 (Feb. 1983). (Proceedings of the International Conference on Magnetism, Kyoto, Japan, 6-10 Sept. 1982).

Electrical resistivity and thermoelectric power measurements of $\text{Fe}_{74}\text{Co}_{10}\text{B}_{16}$ and $\text{Fe}_{67}\text{Co}_{18}\text{B}_{15}\text{Si}_1$ have been performed in the temperature range 77 to 900K. For both the samples the crystallization takes place in a two step process. Thermoelectric power $S(T)$ for both samples is found to be negative and at lower temperatures, a minima in $S(T)$ is observed which shows a Kondo type behaviour. (2 refs.)

Structure and magnetism of insoluble Pb-Fe alloy films See Entry 62294

Magnetoresistance and Hall effect in amorphous CoZr films ..See Entry 62507

Composition and temperature dependence of resistivity in amorphous Gd-Co films See Entry 62509

Bias voltage effect on electrical resistivity of GdCo amorphous sputtered films See Entry 62510

Magnetic and electrical properties of amorphous $\text{Fe}_{1-x}\text{B}_x$ films See Entry 62740

Change in the electrical resistivity of Al-3.5% Cu during thermal cycling in the solidus-liquidus range See Entry 63263

72.15E Electrical and thermal conduction in crystalline metals and alloys

62390 Electric resistance of Manganin to 2 GPa and 80K. S.Tamura (Nat. Inst. for Res. in Inorganic Materials, Ibaraki, Japan).

High Temp.-High Pressures (GB), vol.14, no.3, p.307-10 (1982). (10th Plansee Seminar on 'Trends in Refractory Metals, Hardmetals, and Special Materials, and their Technology', Reutte, Austria, 1-5 June 1981).

The electric resistance of Manganin at high pressures (0-2 GPa) and low temperatures (80-250K) has been measured by using a piston-cylinder apparatus. 1-pentene is found to be an excellent pressure-transmitting medium in this temperature and pressure region. The pressure coefficient of resistance of Manganin decreases with decreasing temperature. (6 refs.)

62391 Contribution of solute aluminium in tungsten to the electrical resistivity. L.Uray, P.Tekula-Buxbaum (Res. Inst. for Tech. Phys., Hungarian Acad. of Sci., Budapest, Hungary).

J. Less-Common Met. (Switzerland), vol.90, no.1, p.89-94 (March 1983).

The contribution of aluminium dissolved in tungsten to the electrical resistivity was determined for various dilute WAl alloys prepared by diffusion alloying. The excess resistivity increased linearly with the aluminium concentration above a critical threshold concentration ($c_0 \approx 27$ wt.ppm), and so the contribution of the dissolved aluminium to the specific resistivity could be obtained from the slope of the plot of excess resistivity versus concentration. Since aluminium is volatile in tungsten, there is a radial evaporation profile in the thin wires used. The extrapolation to homogeneous solute distribution was carried out by means of an appropriate electrofinishing technique and stepwise resistance measurements. The contribution of aluminium to the specific resistivity of a homogeneous WAl alloy is $8 \pm 3 \mu\Omega \text{ cm}(\text{at.}\%)^{-1}$ at 77K. This value must be multiplied by 0.6 at 4.2K and by 1.4 at 300K. (8 refs.)

62392 The electrical conductivity of some silver, aluminium and cobalt alloys. Ch.J.Raub, W.Wopersnow (Forschungsinst. für Edelmetalle und Metallchem., Gmund, Germany).

J. Less-Common Met. (Switzerland), vol.90, no.1, p.153-9 (March 1983). In German.

Alloys of silver, aluminium and cobalt with titanium and zirconium show a negative temperature coefficient of electric resistance, depending on their composition and structure. This is especially pronounced at lower temperatures. Apparently the behaviour is connected with the occurrence of the β phase of titanium and zirconium or of other metastable phases in these alloys. (5 refs.)

62393 A study of the palladium-platinum-hydrogen system over a wide range of hydrogen pressures. B.Baranowski (Inst. of Phys. Chem., Polish Acad. of Sci., Warsaw, Poland), F.A.Lewis, W.D.McFall, S.Filipek, T.C. Witherspoon.

Proc. R. Soc. London Ser. A (GB), vol.386, no.1791, p.309-32 (8 April 1983).

Measurements with an extensive series of palladium-platinum alloys, of changes in electrical resistivity due to direct absorption of hydrogen from hydrogen gas at pressures up to 30 kbar (3GPa) have been made at 25 and 75°C. Interrelations at 25°C between hydrogen content, electrical resistivity and hydrogen pressures of up to ca. 20 bar have also been derived, for the more palladium-rich alloys, from measurements of electrode potentials. Finally the authors consider alterations of thermodynamic parameters with increasing platinum content, and decreasing hysteretic differences between relations derived during increases and decreases of hydrogen pressure. Particular comparisons are made with behaviour in the palladium-rhodium-hydrogen and palladium-nickel-hydrogen systems. (87 refs.)

62394 Temperature dependence of electrical resistivity of Al-Zn alloys. G.Vigier, J.Merlin (Groupe d'Etudes de Metall. Phys. et de Phys. des Materi-iaux, INSA de Lyon, Villeurbanne, France).

Philos. Mag. B (GB), vol.47, no.3, p.299-306 (March 1983).

The electrical resistivity of Al-4.4 and 5.3 at.% Zn alloys has been determined at various ageing temperatures, for various ageing times. It was found that within the limits of experimental accuracy the resistivity variations are not dependent on the measuring temperature. In particular the ageing time for the peak resistivity and the peak height are independent of the measuring temperature. These results cannot be explained by models which try to describe the resistivity variations by GP zone formation. (17 refs.)

62395 Electronic properties of bulk copper-aluminum and copper-zinc alloys. K.R.Mountfield, J.A.Rayne (Dept. of Phys., Carnegie-Mellon Univ., Pittsburgh, PA, USA).

Phys. Rev. B (USA), vol.27, no.6, p.3263-72 (15 March 1983).

Magnetic-susceptibility, as well as resistivity, Hall-effect, transverse-magnetoresistance, and thermoelectric-power measurements have been made on a series of well-characterized bulk samples covering the entire copper-aluminum and copper-zinc phase diagrams. In both systems the resistivity of the γ phase exhibits a sharp minimum as a function of composition. This minimum correlates with anomalies observed in the other measured properties and supports the hypothesis that the behaviour is due to electronic effects associated with overlap between the Fermi surface and the Jones zone for this structure. Comparison of the properties of other phases in the two systems indicates similarities which can be also ascribed to band-structure effects. (31 refs.)

62396 Electrophysical properties of nickel boride phases. M.D.Smolín, V.G.Grebenskina, Yu.M.Goryachev, L.I.Panov, E.I.Shvartsman (Inst. of Materials Sci., Acad. of Sci., Ukrainian SSR).

Sov. Powder Metall. & Met. Ceram. (USA), vol.21, no.8, p.662-5 (Aug. 1982). Translation of: *Poroshk. Metall. (USSR)*, vol.21, no.8, p.73-6 (Aug. 1982). [received: Feb. 1983]

The nickel boride phases were prepared by direct synthesis from 99.8% pure electrolytic nickel and 99.5% pure boron. Sintering was performed for 1.5 h in a vacuum at 0.9T_m. All specimens were found to have single-phase structures. The amount of conduction electrons was found to grow with the rise in nickel concentration in the boride phases. The Fermi energy shifted toward larger values, and the contribution of the two electron bands to conduction increased. With a rise in temperature, for the NiB phase the overlapping of the zones and the effective carrier mass decreased but for Ni₂B and Ni₃B the latter increased. (3 refs.)

An ephemeral Frenkel pair in iridium See Entry 61910

Electron transfer of hydrogen in aluminum at 20 and 800°C ..See Entry 62372

T^{1/2} dependence of resistivity and anomalous magnetoresistance in granular bismuth See Entry 62399

Temperature dependence of the electrical resistivity due to dislocations in metals See Entry 62406

Change in the electrical resistivity of Al-3.5% Cu during thermal cycling in the solidus-liquidus range See Entry 63263

Changes in resistivity at low-temperature deformation and the subsequent recovery of the Ag-15 at.% Al alloy See Entry 63434

72.15G Galvanomagnetic and other magnetotransport effects

62397 Longitudinal magnetoresistance of dilute alloys with localized magnetic moments in a quantizing magnetic field. I.G.Kuleev (Inst. of Metal Phys., Acad. of Sci., Sverdlovsk, USSR). *Fiz. Met. & Metalloved. (USSR)*, vol.55, no.2, p.213-24 (Feb. 1983). In Russian. English translation in: *Phys. Met. & Metall. (GB)*

A calculation is made of the longitudinal magnetoresistance of a conductor with a low concentration of magnetic impurities in a quantizing magnetic field. The calculation is made in the third order of perturbation theory in respect of the interaction between electrons and magnetic impurities. An analysis is made of the dependences of the smoothly varying and oscillatory parts of the longitudinal resistance on the temperature of a sample and on the magnetic field applied to it. It is shown that anomalous behaviour of the quantum oscillations associated with the Kondo effect is possible in the case of dilute solutions of the CuMn, AuMn, and AuFe type at low temperatures. (13 refs.) A.T.

62398 Magnetoresistance of Pd-Fe and Pd-Ni-Fe alloys. Y.Hsu, J.E.Schmidt, M.Gupta, S.Jen, J.L.Berger (Phys. Dept., Carnegie-Mellon Univ., Pittsburgh, PA, USA).

J. Appl. Phys. (USA), vol.54, no.4, p.1887-91 (April 1983).

The electrical resistivity of Pd-Fe alloys has been measured in magnetic fields parallel and perpendicular to the current, for a wide range of alloy compositions. The influence of atomic ordering on the magnetoresistance has been investigated. The ferromagnetic anisotropy of resistance $\Delta\rho/\rho_0$ reaches a maximum value of +9% in the ordered state between 30 and 35 at.% Fe, and +6% in the disordered state between 40 and 60 at.% Fe, at 4.2K. At 295K, $\Delta\rho/\rho_0$ never exceeds +1%. Similar measurements have been done on $(\text{Pd}_{50}\text{Ni}_{50})_{100-x}\text{Fe}_x$ for $x \leq 30$ at.% Fe. The maximum $\Delta\rho/\rho_0$ value of +7% is obtained for 10 at.% Fe at 4.2K. (26 refs.)

62399 $T^{1/2}$ dependence of resistivity and anomalous magnetoresistance in granular bismuth. Y.Koike, M.Okamura, T.Fukase (Res. Inst. for Iron, Steel & Other Metals, Tohoku Univ., Sendai, Japan).

J. Phys. Soc. Jpn. (Japan), vol.52, no.4, p.1115-18 (April 1983).

In granular bismuth, electrical resistivity with $T^{1/2}$ dependence was observed in the low temperature range 0.5-4.2K, while anomalous positive magnetoresistance was found in this range. This anomalous magnetoresistance, which increases with decreasing temperature, is fairly well explained by the three-dimensional localization theory taking account of the effect of strong spin-orbit interaction. The spin-orbit scattering time τ_{so} is estimated as 4×10^{-13} sec, and the inelastic scattering time τ_i changes in proportion to $T^{-2.7}$. On the other hand, $T^{1/2}$ dependence of resistivity seems due to the interaction effect between electrons.

62400 Magnetic and galvanomagnetic properties of rare earth intermetallic compounds of $\text{RAg}_{1-x}\text{In}_x$ (R=Gd, Tb, and Dy). K.Yagasaki (Hiroshima Univ., Hiroshima, Japan).

J. Sci. Hiroshima Univ. A (Japan), vol.46, no.2, p.113-47 (Jan. 1983).

Magnetic, electric, and galvanomagnetic measurements have been performed on polycrystalline specimens of $\text{RAg}_{1-x}\text{In}_x$ (R=Gd, Tb, and Dy) with compositions of $0 \leq x \leq 0.5$. The compounds of the Tb and Dy systems are all antiferromagnetic. On the contrary, the indium rich compounds of the Gd system are ferromagnetic. The paramagnetic Curie temperature, however, behaves almost similarly for all the systems. The Hall effect and transverse magnetoresistance were measured at paramagnetic temperatures and they were discussed on the basis of the two-band model. The ratio of the mobility of s -electrons to that of d -holes is estimated from the ordinary Hall coefficient to be constant within the experimental temperature region. The extraordinary Hall coefficient can be explained very well by assuming the force acting on the carrier due to the magnetic moment is proportional to the Lorentz force. The transverse magnetoresistance depends on H^2 and is subdivided into the ordinary and the extraordinary effects. The concentrations of s -electrons and d -holes are estimated from both the ordinary coefficients of the Hall effect and magnetoresistance. The concentrations above estimate the electrical conductivity due to the s -electron band at only a few percent of the whole, and the magnetic properties of all these systems can be explained satisfactorily by the simple RKKY model. (36 refs.)

62401 High accuracy measurement of the Hall effect in magnetic materials with an AC lock-in technique. J.B.Sousa, J.M.Moreira (Centro di Fisica, Univ. do Porto, Porto, Portugal).

Port. Phys. (Portugal), vol.13, no.3-4, p.137-72 (1982).

A very sensitive AC method is described for measurement of the Hall effect in metals. It uses a high quality lock-in amplifier with the oscillator incorporated, an operational power supply, and a low noise step-up transformer to increase the signal level. Voltage resolutions down to 1 nV are currently achieved, enabling the Hall coefficient of most magnetic metals to be measured within 1 part in 10^4 . A summary on the general transport equations and the correct definitions regarding the Hall effect in magnetic systems is presented. High accuracy data are given on the temperature dependence of the Hall resistivity (ρ_H) in a single crystal of gadolinium, with the magnetic field in the basal plane. For the first time, experimental data have been obtained on the temperature derivative $d\rho_H/dT$. This coefficient reveals clearly the critical behaviour associated with the ferro-paramagnetic transition point in gadolinium. A preliminary analysis on the critical behaviour is given, with specific suggestions for further developments. (39 refs.)

Electrical resistivity and Hall effect of amorphous $\text{TM}_{70}\text{Si}_{10}\text{B}_{13}$ (TM=Fe, Co, Ni) alloys See Entry 62388

Electronic properties of bulk copper-aluminum and copper-zinc alloys See Entry 62395

Shubnikov-de Haas oscillations in an organic conductor tetramethyltetraselenafulvalene-2,5-dimethyl-7,7', 8,8' tetracyanoquinodimethane (TMTSF-DMTCNQ) See Entry 62404

Magnetoresistance and Hall effect in amorphous CoZr films See Entry 62507

Magnetoresistance near the Curie point of TbZn single crystals See Entry 62645

Preparation and properties of RE-TM amorphous films See Entry 62736

Anomalous hysteresis loops in single and double layer sputtered TbFe films See Entry 62748

A new method for analysis of magnetic anisotropy in films using the spontaneous Hall effect See Entry 62761

72.15J Thermoelectric effects

62402 Thermo-e.m.f. of island metal films. V.I.Andreev, A.A.Benditskii, A.B.Granovskii, G.I.Rukman, B.M.Stepanov (All-Union Sci.-Res. Inst. of Optophysics, Measurements, Moscow, USSR).

Fiz. Met. & Metalloved. (USSR), vol.55, no.2, p.407-9 (Feb. 1983). In Russian. English translation in: *Phys. Met. & Metall. (GB)*
A qualitative theoretical study is made of the mechanisms which govern the magnitude and sign of the absolute thermo-e.m.f. of island metal films defined as films in which islands of 50-5 nm diameter are separated by distances of 1-3 nm. It is shown that both the magnitude and sign of the thermo-e.m.f. may differ from a bulk pure sample of the same metal. (7 refs.) A.T.

Electrical resistivity and thermoelectric power of glassy $\text{Fe}_{74}\text{Co}_{10}\text{B}_{16}$ and $\text{Fe}_{67}\text{Co}_{18}\text{B}_{14}\text{Si}_1$ alloys See Entry 62389

Electronic properties of bulk copper-aluminum and copper-zinc alloys See Entry 62395

Electrophysical properties of nickel boride phases See Entry 62396

Transport properties of tungsten bronzes doped with tantalum See Entry 62459

72.15N Collective modes, e.g. in one-dimensional conductors

62403 Electrical conduction properties of $\text{Mg}_{0.82}[\text{Pt}(\text{C}_2\text{O}_4)_2]_2\text{L}_2\text{H}_2\text{O}$. M.Mizuno, A.E.Underhill (School of Phys. & Molecular Sci., Univ. Coll. of North Wales, Bangor, Wales), K.Carneiro.

J. Phys. C (GB), vol.16, no.11, p.2105-13 (20 April 1983).

A detailed electrical conduction study of the one-dimensional conductor $\text{Mg}_{0.82}[\text{Pt}(\text{C}_2\text{O}_4)_2]_2\text{L}_2\text{H}_2\text{O}$ over the temperature range 80-335K is described. An anomaly in the electrical conductivity has been observed to occur in the range 280-295K corresponding to a previously observed orthorhombic to monoclinic phase transition. The temperature dependence of the electrical conductivity is discussed in relation to the development of a superstructure, which is not of the usual Peierls type. The behaviour suggests that the compound is in a chaotic state as a result of competing incommensurate instabilities. (23 refs.)

62404 Shubnikov-de Haas oscillations in an organic conductor tetramethyltetraselenafulvalene-2,5-dimethyl-7,7', 8,8' tetracyanoquinodimethane (TMTSF-DMTCNQ). S.Bouffard (Section d'Etude des Solides Irradiés, CEN, Fontenay-aux-Roses, France), M.Ribault, D.Jerome, K.Bechgaard.

J. Phys. Lett. (France), vol.44, no.8, p.L285-93 (15 April 1983).

The observation of Shubnikov-de Haas (SdH) oscillations in the metallic, high pressure phase (Metal-II) of TMTSF-DMTCNQ ($P > 10$ kbar) demonstrates the 3-dimensional, closed nature of the Fermi surface at low temperature ($T < 2$ K). The authors observe very small Fermi surface cross-sections of $1.16 \times 10^{17} \text{ m}^{-2}$ and $2.6 \times 10^{17} \text{ m}^{-2}$ in the ab and ac planes respectively. From the field and temperature dependence of the SdH oscillations, the authors extract a cyclotron mass $m_c/m_0 \approx 0.56$ and a Dingle temperature $T_D = 0.8$ K. Finally they discuss the discrepancy between these results and the very high DC conductivity ($\sigma_{1,2K} \approx 3 \times 10^5 (\Omega \text{cm})^{-1}$). (28 refs.)

62405 Incommensurate-commensurate transition in TaS_3 . Z.Z.Wang, H.Salva, P.Monceau, M.Renard (Centre de Recherches sur les Tres Basses Températures, Grenoble, France), C.Roucau, R.Ayroles, F.Levy, L.Guemas, A.Meerschaut.

J. Phys. Lett. (France), vol.44, no.8, p.L311-19 (15 April 1983).

Careful electron diffraction measurements show that the Peierls distortion, which appears in TaS_3 with the orthorhombic structure at $T_0 = 215$ K, is weakly incommensurate with the underlying lattice. The periodicity of the distortion is temperature dependent and locks at $T_0 = 140$ K to a value equal to four times the lattice constant. This incommensurate-commensurate transition is observable in transport measurements and also in dynamical properties of the charge density wave. The authors explain this transition with a model where the charge density waves on two sets of chains are strongly coupled. (17 refs.)

Charge and spin locations in linear stacks of TCNQ See Entry 62340

Magnetic resonance on localized excited triplet states in 1,4-dibromonaphthalene [one-dimensional conductor] See Entry 62388

72.15Q Scattering mechanisms and Kondo effect

(see also 75.20H Local moments in dilute alloys)

62406 Temperature dependence of the electrical resistivity due to dislocations in metals. T.Endo (Hiroshima Denki Inst. of Technol., Hiroshima, Japan).

J. Sci. Hiroshima Univ. A (Japan), vol.46, no.2, p.195-216 (Jan. 1983).

The temperature dependence of the electrical resistivities due to dislocations $\rho_d(T)$ in Au-0.003 at.%Sn have been measured. As the temperature is raised, the dislocation resistivity $\rho_d(T)$ decreases gradually and increases rapidly, showing a resistivity minimum in $\rho_d(T)$. Two models for the rapid increase in $\rho_d(T)$ have been compared with the experimental results obtained by the present author and others. Furthermore, the resistivity minimum in $\rho_d(T)$ has been examined in detail for pure aluminum, a dilute aluminum-magnesium alloy and pure gold, and has been discussed by using the two-state tunneling model firstly developed for amorphous metals. In conclusion, an additional electron level localized around a dislocation plays an important role for the temperature dependence of the dislocation resistivity in metals. (33 refs.)

Electron structure of edge dislocations in metals See Entry 62371

Electrical resistivity and thermoelectric power of glassy $\text{Fe}_{74}\text{Co}_{10}\text{B}_{16}$ and $\text{Fe}_{67}\text{Co}_{18}\text{B}_{14}\text{Si}_1$ alloys See Entry 62389

Longitudinal magnetoresistance of dilute alloys with localized magnetic moments in a quantizing magnetic field See Entry 62397

Solution of the Kondo problem See Entry 62551

72.20 CONDUCTIVITY PHENOMENA IN SEMICONDUCTORS AND INSULATORS (for nonelectronic thermal conduction, see 66.70)

62407 Electrical resistivity of mixed-valence systems in a two-band model. H.V.Sharma, I.Singh (Dept. of Phys., Univ. of Roorkee, Roorkee, India).

J. Phys. C (GB), vol.16, no.10, p.L279-83 (10 April 1983).
The authors study here the variation of electrical resistivity with temperature of mixed-valence systems using a two-band model. They find various types of

behaviour (e.g. metallic and semiconducting) for a different set of parameters in the theory. Results are compared with recent experimental findings on various mixed-valence systems, e.g. SmS , SmB_6 , CePd_3 . (15 refs.)

72.20D General theory, scattering mechanisms

62408 Mechanism of electrical conduction in rare-earth ferrocyanides. K.Tennakone (Ruhuna Univ. Coll., Matara, Sri Lanka).

J. Chem. Phys. (USA), vol.78, no.6, pt.1, p.3343-4 (15 March 1983).

The author observed that the semiconduction in ferrocyanides depends on the presence of water molecules in the lattice. The rare earth ferrocyanides generally contain variable amounts of water of crystallization, depending on the degree of drying. The values of electron activation energies are independent of the impurity concentration of the water molecules. However, the values of ρ_0 are dependent upon the water content and the data presented corresponds to a water impurity concentration of approximately one molecule per 200 molecules of the compound. The ferrocyanides examined could contain a maximum of five molecules of bound water of crystallization. Rare earth ferrocyanides do not show any ionic conduction until the concentration of water is largely in excess of the above maximum of bound water molecules. Thermoelectric tests show that in all cases, the charge carriers are predominantly electrons. The author gives a simple theory that explains how water molecules as an impurity could excite electronic semiconduction in ferrocyanides. (8 refs.)

62409 The electronic properties of semiconductor grain boundaries. C.H.Scager (Sandia Nat. Labs., Albuquerque, NM, USA).

Grain Boundaries in Semiconductors. Proceedings of the Materials Research Society Annual Meeting, Boston, MA, USA, Nov. 1981 (New York, USA: North-Holland 1982), p.85-98

Grain boundaries play an important role in determining the operating characteristics of devices such as varistors and thin film solar cells and transistors. In the last several years detailed one-electron expressions have been developed for the transport coefficients of majority and minority carriers at grain boundaries. These theories have been successful in predicting the measured electrical properties of bicrystals in lightly doped silicon. The status of our understanding in this area will be reviewed in some detail. Recent extensions of these calculations which have been necessary to explain measurements on grain boundaries in degenerately doped GaAs will also be reviewed. (34 refs.)

Random walks on random lattices with traps See Entry 59695

72.20F Low-field transport and mobility; piezoresistance

62410 Analysis of disorder scattering in $\text{Ga}_{0.47}\text{In}_{0.53}\text{As}$ using Gaussian potential. K.Hiramatsu (Dept. of Electrical Engng. & Electronics, Nagoya Univ., Nagoya, Japan), T.Nishinaga.

Jpn. J. Appl. Phys. Part 1 (Japan), vol.22, no.3, p.504-7 (March 1983).

Disorder scattering mobility in $\text{Ga}_{0.47}\text{In}_{0.53}\text{As}$ is calculated by using a sum of two Gaussian potentials; one representing the difference of strong short range core potentials and the other representing the relatively long range potential, the existence of which has been suggested by the authors previously. Approximate calculations are made and a much steeper temperature dependency than the Brooks' disorder scattering mobility is predicted giving good agreement with the recent mobility measurements. (11 refs.)

62411 Transport phenomena in $\text{TlIn}_{1-x}\text{Sb}_x$ solid solutions. E.M.Godzhayev, Sh.M.Guseinova, A.B.Nagiev, F.M.Godzhayeva, T.N.Bakhshajiev (M. Azizebekov Inst. of Petroleum & Chem., USSR).

Inorg. Mater. (USA), vol.18, no.5, p.636-7 (May 1982). Translation of: *Izv. Akad. Nauk SSSR Neorg. Mater.*, vol.18, no.5, p.752-3 (May 1982).

[received: Feb. 1983]

It has been established, during a study of the temperature dependencies of the electrical conductivity and the Hall coefficient over a wide range of temperatures from 300 to 1100K, that a wide solubility region on the basis of TlInSe_2 (70 to 100 mole % TlInSe_2) is observed in the TlInSe_2 - TlInSb_2 system. The width of the forbidden zone of the solid solutions decreases as the amount of neodymium is increased in a linear manner. (4 refs.)

62412 Preparation and study of the electrophysical properties of the copper chalcogenides and their solid solutions. K.Dovletov, S.N.Krzhevitskaya, N.K.Samakhotina, K.Tashliev, Kh.Erniyazov (Physicotech. Inst., Acad. of Sci., Turkmen SSR).

Inorg. Mater. (USA), vol.18, no.5, p.638-41 (May 1982). Translation of: *Izv. Akad. Nauk SSSR Neorg. Mater.*, vol.18, no.5, p.745-8 (May 1982).

[received: Feb. 1983]

In studies of the electrical and thermoelectric properties of solid solutions in the systems $\text{Cu}_2\text{BVI-IVBVI}$ over a wide range of temperatures and concentrations it has been established that germanium and tin tellurides reduce the number of defects in Cu_2Te and the charge carrier concentration. The polymorphic transformations characteristic of copper chalcogenides are less clearly defined in the solid solutions with germanium and tin chalcogenides. (4 refs.)

62413 Resistance changes of $\text{Pb}_{0.8}\text{Sn}_{0.2}\text{Te}$ under dynamic loading in the 0-100 kbar range. Z.Rosenberg (ADA, Haifa, Israel), J.Genossar.

J. Phys. D (GB), vol.16, no.4, p.661-7 (14 April 1983).

Resistance changes of thin $\text{Pb}_{0.8}\text{Sn}_{0.2}\text{Te}$ films under dynamic pressures were measured using the planar impact configuration. The resulting resistance versus pressure curve, in the 0-100 kbar range, resembles similar static curves which were obtained for PbTe and $\text{Pb}_{1-x}\text{Sn}_x\text{Te}$ alloys. The pressure at the jump in resistance (48 kbar) which the authors obtained is very close to the phase transition pressure this compound is thought to have. Data from the release branch of the stress pulse are used, from which one can estimate the pressure hysteresis in the jump of the resistance curve. (11 refs.)

62414 Anomalous transient-time dispersion in amorphous solids: oxadiazole. N.Crisa (Dipartimento di Fisica, Univ. di Milano, Milano, Italy).

Phys. Status Solidi b (Germany), vol.116, no.1, p.269-74 (1 March 1983).

Hole transport in thin films of an organic disordered solid (oxadiazole) is studied by time-of-flight techniques as a function of sample thickness and applied field. The experimental data are analyzed in terms of the theory of stochastic non-Gaussian transport by Scher and Montroll (1975) showing the validity of this model. The last section is devoted to an evaluation of the hole drift mobility; its resulting values are extremely low ($<10^{-6} \text{ cm}^2/\text{Vs}$). (13 refs.)

62415 Dielectric properties and polaronic conductivity of WO_3 and $\text{W}_2\text{Mo}_{1-x}\text{O}_3$. R.Gehlig, E.Salje (Inst. fur Kristallographie und Petrographie, Univ. Hannover, Hannover, Germany).

Philos. Mag. B (GB), vol.47, no.3, p.229-45 (March 1983).

An investigation of the Debye relaxations in WO_3 and $\text{W}_2\text{Mo}_{1-x}\text{O}_3$ confirm the mechanism of polaronic conduction at low temperatures. The Mo positions act as trapping centres, and the relaxation times and activation energies

depend largely on the crystallinity of the samples. Polarons are spin-paired in the ground state (bipolarons), and can be separated by optical irradiation giving rise to 'inner' photoconductivity. The transport mechanism of the bipolarons is found to take place in three steps: dissociation into two single polarons, their transport and subsequent recombination. This model is energetically favoured over the transport of the bipolarons as a whole. (24 refs.)

62416 Semiconducting properties of V_2O_5 gels. C.Sanchez, F.Babonneau, R.Morineau, J.Livage (Spectrochimie du Solide, Univ. Pierre et Marie Curie, Paris, France), J.Bulot.

Philos. Mag. B (GB), vol.47, no.3, p.279-90 (March 1983).

Mixed-valence vanadium pentoxide gels have been obtained by polymerization of vanadic acid. They exhibit semiconducting properties which arise from electron hopping between V^{IV} and V^{V} ions. Such gels can easily be deposited onto a substrate, giving layers of high electrical conductivity ($\sigma=0.1 \Omega^{-1} \text{ cm}^{-1}$ at 300K). Their electrical properties can be described by the small-polaron model, and the main parameters have been determined by conductivity measurements, ESR and optical spectroscopy. The optical and thermal activation energies are found to be $E_{\text{opt}}=0.87 \text{ eV}$ and $E_{\text{th}}=0.17 \text{ eV}$. The transfer integral $J=0.05 \text{ eV}$ is quite small, and the electron-phonon coupling parameter $\gamma=14$ is rather high. The structural disorder of this amorphous semiconductor was estimated from electrical and ESR experiments. It leads to a localization of the charge carriers. (34 refs.)

62417 On the degree of dispersion to be expected for the mechanism of carrier hopping in spatially disordered systems. J.M.Marshall (Dept. of Phys., Dundee Coll. of Technol., Dundee, Scotland).

Philos. Mag. B (GB), vol.47, no.3, p.323-30 (March 1983).

Adler and Silver (1982) have recently presented the results of a Monte Carlo simulation study of transport by hopping between sites in a random spatial array. As a consequence of their modified simulation procedures, these authors obtain a higher degree of dispersion than that previously reported by Marshall (1978). On the basis of their data, Adler and Silver argue that the 'r-hopping' mechanism is capable of providing the highly dispersive transit pulses observed in time-of-flight studies of carrier mobility. The origins of the differing degrees of dispersion found in the two studies are re-examined. It is argued that Adler and Silver's technique, in which a composite transit pulse is produced by combining data obtained for a high degree of dispersion. This assertion is supported by the fact that Adler and Silver's study is performed for an array of such site density that anomalous dispersion would not be expected on theoretical grounds. On the basis of these simulation studies, it is argued that the highly dispersive transit pulses observed in many studies of carrier transport are not consistent with hopping in the presence of spatial disorder alone. (5 refs.)

62418 Study of the structure and elastoresistance properties of thin films of bismuth. C.Butto, J.Berty (Lab. de Microscopie et Structure des Matériaux, Univ. Paul Sabatier, Toulouse, France).

Thin Solid Films (Switzerland), vol.101, no.4, p.357-68 (25 March 1983).

The authors studied the influence of different conditions of preparation on the structure and elastoresistance properties of bismuth thin films. Bismuth films grow mainly with a [0001] fibre axis texture but in some cases randomly oriented bismuth grains were observed. A suitable thermal treatment appreciably improves the gauge coefficient of thin films. The condensation rate has no marked influence on the structure and elastoresistance properties of the deposits. (14 refs.)

62419 Influence of high pressure and shear strains on some electrophysical properties of polyphthalocyanines. V.A.Zhorin, S.I.Beshenko, L.I.Makarova, A.I.Sherie, Yu.A.Berlin, N.S.Enikolopyan.

Vysokomol. Soedin. Ser. A (USSR), vol.25, no.3, p.551-7 (March 1983). In Russian. English translation in: *Polym. Sci. USSR (GB)*

The influence of high pressure and shear strain on conductivity G and capacitance C of nonmetallic polyphthalocyanines, PPC with macromolecules of different length, ordering and degree of crosslinking has been studied. Both G and C of polymers under study were found to increase with their compression. The analogous phenomenon is observed at the simultaneous action of high pressure and shear strain. In the last case the change of G requires the lesser pressure, than at the single compression. The spectral studies show that the effect of pressure and strain of loaded samples on their electrophysical properties does not depend on the chemical structure of PPC, but is a result of the change of the average distance between regions of continuous conjugation. The dimensions of these regions can be increased by preliminary thermal treatment of PPC. (13 refs.)

Theory of hopping and multiple-trapping transport in disordered systems See Entry 59690

Automatic magnetic dichrometer for the $\lambda=10.6 \mu\text{m}$ range [for free carrier concentration determination] See Entry 59820

High temperature and short time thermal annealing of ion-implanted silicon See Entry 61938

Impurity incorporation in RAO polysilicon layers and consequences on their electrical properties See Entry 61950

Interaction of primary radiation defects with dislocations in indium antimonide See Entry 61955

Flash lamp annealing of ion-implanted polycrystalline silicon .. See Entry 61959

Annealing of radiation defects in Ge-Si solid solutions See Entry 61969

Effects of quenching and fission damage on the low temperature electrical resistivity of single crystal UC See Entry 61981

Preparation of superinsulating surfaces by the nuclear track technique See Entry 61999

Determination of band-gap parameters of $\text{Hg}_{1-x}\text{Cd}_x\text{Te}$ based on high-temperature carrier concentration See Entry 62334

Mechanism of electrical conduction in rare-earth ferrocyanides See Entry 62408

Magnetoresistance and conductivity in the binary system titanium-oxygen. II. Semiconducting titanium oxides See Entry 62433

Semiconductor-type temperature dependence of the resistivity of $\text{Bi}_{1-x}\text{Sb}_x$ ($0.07 \leq x \leq 0.22$) alloy filaments See Entry 62436

Thermoelectric properties of GeTe at high hydrostatic pressure up to 8.5 GPa and its valence-band structure See Entry 62438

Mechanochemical effect in ZnTe powder associated with grinding See Entry 62444

Transport properties of tungsten bronzes doped with tantalum See Entry 62459

Resistance change of thin Permalloy films caused by applied stress and its application to strain measurements See Entry 62508

Electrical properties of SnO_2 polycrystalline thin films and single crystals exposed to O_2 - and H_2 -gases See Entry 62514

- Magnetic and electrical properties of FeCr_2S_4 ($0 \leq x \leq 1$) See Entry 62695
- Continuous deposition of photovoltaic grade CdS sheet at the unit operations scale See Entry 63164
- Novel plasma chemical methods for doping α -Si:H See Entry 63177
- Sprayed zinc-cadmium sulfide films for backwall $\text{Cu}_2\text{S}/(\text{ZnCd})\text{S}$ cells See Entry 63692

72.20H High-field and nonlinear effects

- 62420 Direct observation of impact ionisation and hot electron effects in GaAs. T.Ohyama (Dept. of Phys., College of General Education, Osaka Univ., Toyonaka, Osaka, Japan). *Jpn. J. Appl. Phys. Part 2 (Japan)*, vol.22, no.3, p.1188-90 (March 1983). Measurements of the far-infrared cyclotron resonance of conduction electrons and the Zeeman absorption of donors in optically excited GaAs have been carried out in the presence of an electric field. The electric field dependence of the resonance intensity as well as the line shape can be explained in terms of the hot electron distribution and impact ionisation of the donor electrons. Furthermore, the polaron pinning effect accounts for the nonparabolicity of the conduction band.
- 62421 Diagonal and off-diagonal contributions to autocorrelation of velocity fluctuations in semiconductors. R.Brunetti, C.Jacoboni (Gruppo Nazionale di Struttura della Materia, Istituto di Fisica, Univ. Modena, Modena, Italy). *Phys. Rev. Lett. (USA)*, vol.50, no.15, p.1164-7 (11 April 1983). A theoretical analysis of velocity fluctuations in semiconductors is presented, and results obtained from a Monte Carlo procedure are shown for Si. It has been found in particular that (i) off-diagonal contributions to the velocity autocorrelation function must be taken into account; (ii) the convective contribution is positive; and (iii) a long tail in the autocorrelation function, due to intervalley fluctuations, may be present. (17 refs.)
- 62422 N-type negative resistance region under conditions of the magnetoconcentration effect and nonlinear recombination of carriers. K.Yu.Guga, Yu.M.Malozovski, V.K.Malyutenko (Inst. of Semiconductors, Acad. of Sci., Kiev, Ukrainian SSR). *Sov. Phys.-Semicond. (USA)*, vol.16, no.10, p.1194-6 (Oct. 1982). Translation of: *Fiz. i Tekh. Poluprovodn. (USSR)*, vol.16, no.10, p.1858-61 (Oct. 1982). [received: April 1983]
- The authors report the results of an analysis of the N-type negative resistance effect in the case of nonlinear carrier recombination in the bulk of a crystal. A qualitative analysis will be made for a homogeneous p-type semiconductor in the form of a plate occupying a region $-d \leq y \leq d$, but not bounded in the x and z directions, and subjected to fields E_x and H_z . (5 refs.)
- Hot-carrier thermo-EMF created by a strong microwave electric field in $\text{Ge}_{1-x}\text{Si}_x$ single crystals irradiated with fast electrons See Entry 62442
- Investigation of the relaxation of the electrical conductivity in crossed alternating electric and static magnetic fields See Entry 62443
- Frequency dependence of the noise in n-type Si subjected to strong electric fields See Entry 62464
- Electric field effect on the thermal emission rate of holes trapped at gold donor center in Si p-n junction See Entry 62484
- Negative differential resistance in multilayer metal-barrier-metal tunneling structures See Entry 62504
- Carrier conduction in α -Si:H solar cells See Entry 63695

72.20J Charge carriers: generation, recombination, lifetime, and trapping

- 62423 Simple method of calculating phonon-assisted Auger recombination rate in direct-gap semiconductors. M.Takeshima (Semiconductor Lab., Matsushita Electronics Corp., Osaka, Japan). *Jpn. J. Appl. Phys. Part 1 (Japan)*, vol.22, no.3, p.491-8 (March 1983). A simple but approximate method is developed for calculating the phonon-assisted Auger recombination rate in direct-gap semiconductors, whose analysis is rigorously based on the Green's function formalism. The method is especially useful for analyzing loss mechanisms in a semiconductor laser which is made of a nondoped or a moderately doped layer. The usefulness of the method is demonstrated through the rigorous and the approximate calculations for typical materials GaAs, InP, GaSb and InAs. The condition, under which the early theory based on the second-order perturbation treatment is useful, shows up through a characteristic function. A brief discussion is also given of experiments.
- 62424 Trapping center parameters in indium selenide single crystals by thermally stimulated current measurements. G.Micocci, A.Rizzo, A.Tepore (Dipartimento di Fisica, Univ. di Lecce, Lecce, Italy). *J. Appl. Phys. (USA)*, vol.54, no.4, p.1924-9 (April 1983). Systematic investigations of trapping center parameters have been carried out on InSe single crystals grown from nonstoichiometric melt, by using a thermally stimulated current (TSC) technique. TSC measurements have been performed between 50 and 300K, and the results have been analyzed according to different methods. The trap characteristics have been determined. In particular, two levels located at 60 and 160 meV below the conduction band have been investigated in detail. Their capture cross sections have been found to be 1.5×10^{-23} and 9.2×10^{-21} cm^2 , respectively, and their concentrations are 1.9×10^{17} and 2.3×10^{16} cm^{-3} , respectively. It is concluded that in these centers retrapping is negligible. One additional level has been found at 340 meV with concentration $N_T = 4.2 \times 10^{16}$ cm^{-3} and capture cross section $\sigma = 3.5 \times 10^{-19}$ cm^2 . (21 refs.)

- 62425 Impurity scattering time in n-type InSb measured by Faraday rotation at far-infrared frequency. D.M.Zengin (Dept. of Phys., Bedford Coll., Univ. of London, London, England). *J. Phys. D (GB)*, vol.16, no.4, p.653-60 (14 April 1983). Low-temperature electron-impurity scattering times have been measured in n-type InSb samples with different electron densities from Faraday rotation by using a pulsed 0.337 mm HCN laser. The electron-impurity scattering times obtained from the experimental results using a curve-fitting method yielded values of 3 to 4×10^{-12} s at liquid helium temperatures for three different samples. These scattering times were in sharp contrast to the field dependent DC scattering times calculated from DC mobility measurements at 4.2K in zero magnetic field. However, there was good agreement between the impurity scattering times observed from the Faraday rotation measurements and those derived from the cyclotron resonance linewidth measurements at 4.2K. Possible explanations of the experimental results were also considered. (22 refs.)

- 62426 Influence of charging of local centers on the electrical properties of inhomogeneous CdS photoconducting structures. E.F.Afon'ko, A.S.Tonkoshkur (Ukraine & Russia Reunion Tercentenary State Univ., Dnepropetrovsk, USSR). *Sov. Phys.-Semicond. (USA)*, vol.16, no.10, p.1224-5 (Oct. 1982). Translation of: *Fiz. i Tekh. Poluprovodn. (USSR)*, vol.16, no.10, p.1899-901 (Oct. 1982). [received: April 1983]
- The processes of charging of local centers in the vicinity of macroscopic potential barriers are responsible for such properties of inhomogeneous semiconductors as a hysteresis of the current-voltage characteristics, residual conductivity, low-frequency dielectric dispersion, considerable discharge and thermally stimulated depolarization currents, data on which are needed in the development of memory devices. The authors analyze these phenomena and propose a method for determining the parameters of traps participating in these phenomena in array-type inhomogeneous photoconducting structures each representing a dispersion of fine particles of photosensitive CdS in a silicon insulator. (8 refs.)
- 62427 Centres of slow recombination in cadmium bromide crystals. V.D.Bondar'v, A.B.Lyskovich, S.B.Kharambura. *Ukr. Fiz. Zh. (USSR)*, vol.28, no.3, p.427-9 (March 1983). In Russian. The influence of X-ray irradiation on sensitivity was studied for CdBr_2 crystals. It is shown that slow recombination centres are formed in the process of CdBr_2 irradiation. These centres cause X-ray sensitivity of the crystals at low temperatures. (8 refs.)
- 62428 Transport across silicon grain boundaries. J.Werner, W.Jantsch, K.H.Froehner, H.J.QUEISSER (Max-Planck-Inst. fur Festkörperforschung, Stuttgart, Germany). Grain Boundaries in Semiconductors: Proceedings of the Materials Research Society Annual Meeting, Boston, MA, USA, Nov. 1981 (New York, USA: North-Holland 1982), p.99-104. By comparison of the capacitance and the conductivity of p-type Si bicrystals, the authors show quantitatively that current transport occurs through thermionic emission of holes across the potential barrier, which is caused by charged donors in the grain boundary. Starting from this finding, they propose a simple model which allows for the first time a spectroscopic determination of the grain boundary density of states from photocapacitance data. Results indicate the presence of band tails and additional mid-gap states. (11 refs.)
- 62429 Electrical and structural properties of grain boundary in polycrystalline Si. R.T.Young, J.Narayan, Y.K.Chang (Solid State Div., Oak Ridge Nat. Lab., Oak Ridge, TN, USA). Grain Boundaries in Semiconductors: Proceedings of the Materials Research Society Annual Meeting, Boston, MA, USA, Nov. 1981 (New York, USA: North-Holland 1982), p.111-17. A special type of high angle grain boundary with mirror symmetry of the crystallographic orientation between the two grains is examined electrically and structurally. Transmission electron microscopy investigations show the nonuniform nature of the grain boundary. Both coherent and incoherent regions are observed along the boundary plane, and the types of dislocations and their densities vary from place to place. Electrical measurements of the boundary properties indicate no measurable barrier height. Heat treatment of the sample in an oxygen atmosphere at 950°C for 30 min did not change the boundary resistance. However, recombination effects are enhanced after boron diffusion. When pulsed laser radiation was used to process this material, it was found that the grain boundary structures were modified by laser-induced surface melting, i.e. incoherent boundaries were converted to coherent boundaries in the melted region. (6 refs.)
- Theory of hopping and multiple-trapping transport in disordered systems See Entry 59690
- Trapping of excitation in the average T-matrix approximation See Entry 59692
- On the cryostat for TSC measurements See Entry 59791
- Carrier capture by multiphonon emission at extrinsic deep centers induced by self-trapping in GaAs See Entry 62364
- Preparation and study of the electrophysical properties of the copper chalcogenides and their solid solutions See Entry 62412
- Investigation of the relaxation of the electrical conductivity in crossed alternating electric and static magnetic fields See Entry 62443
- Photochemical reactions in $\text{CdS}_x\text{Se}_{1-x}$ single crystals See Entry 62448
- Photoelectric phenomena accompanying diffraction of X-rays in semiconducting crystals See Entry 62455
- Light effects on grain boundary properties in silicon See Entry 62457
- Electric field effect on the thermal emission rate of holes trapped at gold donor center in Si p-n junction See Entry 62484
- Determination of the efficiency of electron capture center parameters in the MOS structure dielectric layer See Entry 62500
- Electrical properties of SnO_2 polycrystalline thin films and single crystals exposed to O_2 - and H_2 -gases See Entry 62514
- Electron trapping in thin films of thermal SiO_2 at temperatures between 30 and 300K See Entry 62519
- Effects of mechanical drawing treatment on the characteristics of internal friction and thermally stimulated current on low density polyethylene See Entry 63308
- Diffusion length determination in n^+p - p^+n structure based silicon solar cells from the intensity dependence of the short-circuit current for illumination from the p^+ side See Entry 63668
- Increase of minority carrier diffusion length under the effect of a large band gap gradient [in solar cells] See Entry 63679

72.20M Galvanomagnetic and other magnetotransport effects

- 62430 Negative magnetoresistance in semiconductors in the hopping conduction region. B.L.A.Ishluer, A.G.Aronov, D.E.Khmel'nitskii (L.D. Landau Inst. of Theoretical Phys., Acad. of Sci., Moscow, USSR). *JETP Lett. (USA)*, vol.36, no.5, p.195-8 (5 Sept. 1982). Translation of: *Pis'ma v Zh. Eksp. i Teor. Fiz. (USSR)*, vol.36, no.5, p.157-60 (5 Sept. 1982). [received: April 1983]
- It is shown that negative magnetoresistance in the hopping conduction regime with variable hopping length can be explained by including the displacement of the metal-insulator transition point in an external magnetic field. This explanation can be verified by studying the dependence of the magnitude of the magnetoresistance on the angle between the field and the crystal axes in strongly anisotropic conductors such as deformed Ge and Si. (12 refs.)

62431 Magnetoresistance and magnetization in $\text{Fe}_{80-x}\text{Ti}_{20}$ metallic glasses. R.Kern, M.Naka, U.Gonser, H.Fujimori, I.Okamoto (Fachbereich Angewandte Phys., Univ. des Saarlandes, Saarbrücken, Germany). *J. Magn. & Magn. Mater. (Netherlands)*, vol.31-34, pt.3, p.1471-2 (Feb. 1983). (Proceedings of the International Conference on Magnetism, Kyoto, Japan, 6-10 Sept. 1982).

The decrease of the magnetoresistance anisotropy $\Delta\rho/\rho = (\rho_{\parallel} - \rho_{\perp})/\rho$ against T for $\text{Fe}_{80-x}\text{Ti}_{20}$ glasses is more pronounced when T is substituted by nonmagnetic Ti, V, Cr and Mn than in the case of Co and Ni. These T -dependencies can be described by the relation $\Delta\rho/\rho = A m_i^m$ where A and m are temperature dependent parameters. $\text{Fe}_{20-x}\text{Co}_{20}$ alloys are exceptional. (5 refs.)

62432 Ground state of two-dimensional electrons in strong magnetic fields and $1/3$ quantized Hall effect. D.Yoshioka (Bell Labs., Murray Hill, NJ, USA), B.I.Halperin, P.A.Lee.

Phys. Rev. Lett. (USA), vol.50, no.16, p.1219-22 (18 April 1983). The authors have diagonalized numerically the Hamiltonian of a two-dimensional system of up to six interacting electrons, in the lowest Landau level, in a rectangular box with 'periodic' boundary conditions. They find that the ground state has a pair correlation function quite different from that of a Wigner crystal, and its energy is significantly lower. They also find some indications of a downward cusp in the energy at $1/3$ filling. (14 refs.)

62433 Magnetoresistance and conductivity in the binary system titanium-oxygen. II. Semiconductive titanium oxides. H.Gruber, E.Krautz (Inst. fur Festkörperphys., Tech. Univ. Graz, Graz, Austria).

Phys. Status Solidi a (Germany), vol.75, no.2, p.511-18 (16 Feb. 1983). For pt.1 see *ibid.*, vol.69, p.287 (1982). In continuation of the investigations of the electrical and thermal conductivity as well as the magnetoresistance in the binary system titanium-oxygen for TiO_x with metallic conductivity for $x < 1.49$ the corresponding properties for the semiconductive compounds with $1.49 < x < 2$ are measured at low temperatures and magnetic inductions up to 15 T, especially the corundum phase Ti_2O_3 , the Magneli phase Ti_4O_7 and the reduce rutile phase TiO_{2-x} in dependence on oxygen content and temperature. (28 refs.)

62434 'Limiting' electrical properties of irradiated InP. V.N.Brudnyi, V.A.Novikov (V.D. Kuznetsov Physicotech. Sci.-Res. Inst., State Univ., Tomsk, USSR).

Sov. Phys.-Semicond. (USA), vol.16, no.10, p.1211-12 (Oct. 1982). Translation of: *Fiz. & Tekh. Poluprovodn. (USSR)*, vol.16, no.10, p.1880-2 (Oct. 1982). [received: April 1983]

Investigations of radiation defects in InP and in solid solutions based on this compound are of considerable practical and scientific importance. The results report the results of a preliminary investigation of the electrical properties, particularly the 'limiting' properties of InP crystals irradiated with $E = 2.2-2.3$ MeV electrons at 300K in doses D from 5×10^{14} to 1×10^{19} cm $^{-2}$. Some of the authors samples had n -type conduction with $n_0 \approx 4 \times 10^{17}$ cm $^{-3}$ as these were grown by the Czochralski method. Samples of p -type InP with $p_0 = 1.5 \times 10^{16}$ and $p_0 \approx 1.4 \times 10^{17}$ cm $^{-3}$ were prepared by the diffusion of zinc into the originally n -type material at $\sim 850^\circ\text{C}$ under an excess phosphorus vapor pressure of $\sim 2.026 \times 10^5$ Pa. Semiinsulating InP ($R_H \approx 1 \times 10^7$ cm 2 A $^{-1}$.sec $^{-1}$) was obtained as a result of diffusion of copper into originally n -type InP crystals; the diffusion took place at 950°C under a phosphorus vapor pressure of $\sim 2.026 \times 10^5$ Pa. (4 refs.)

62435 Characteristics of the magnetoresistance and photothermoelectric effect in single-crystal $\text{Cd}_{1-x}\text{Hg}_x\text{Te}$ plates subjected to quantizing magnetic fields. D.A.Kichigin, I.M.Rarenko, E.B.Tal'yanskii, D.D.Khalameida (Sci.-Res. Inst. of Radiophys. & Electronics, Acad. of Sci., Kharkov, Ukrainian SSR).

Sov. Phys.-Semicond. (USA), vol.16, no.10, p.1212-13 (Oct. 1982). Translation of: *Fiz. & Tekh. Poluprovodn. (USSR)*, vol.16, no.10, p.1882-4 (Oct. 1982). [received: April 1983]

Surface phenomena in thin semiconductor layers and plates are of considerable interest because such phenomena become more important on reduction in the thickness of a sample and, in some cases, particularly in inversion layers, they give rise to certain features typical of two-dimensional systems. The authors investigated the magnetoresistance and photothermoelectric effect in single-crystal $\text{Cd}_{1-x}\text{Hg}_x\text{Te}$ plates of different compositions ($0.135 \leq x \leq 0.185$) subjected to quantizing magnetic fields. The galvanomagnetic measurements were carried out by the usual method. The photothermoelectric effect was investigated during exposure of a sample to millimeter-wave radiation. In both cases the useful signal was selected by phase detection. (6 refs.)

62436 Semiconductor-type temperature dependence of the resistivity of $\text{Bi}_{1-x}\text{Sb}_x$ ($0.07 \leq x \leq 0.22$) alloy filaments. V.A.Dolma, F.M.Muntyanu (Inst. of Appl. Phys., Acad. of Sci., Kishinev, Moldavian SSR).

Sov. Phys.-Semicond. (USA), vol.16, no.10, p.1233-4 (Oct. 1982). Translation of: *Fiz. & Tekh. Poluprovodn. (USSR)*, vol.16, no.10, p.1911-13 (Oct. 1982). [received: April 1983]

The existence of a range of concentrations with a narrow band gap ($0 \leq E_g \leq 25$ meV) exhibited by BiSb alloys as well as the unusual dependence of the energy spectrum of carriers on the composition provide unique opportunities for experimental investigations of several electronic phenomena (such as electronic phase transitions, etc.) which appear under the influence of external agencies. The authors investigate the transport phenomena in filamentary crystals of BiSb alloys characterized by a high degree of perfection. The absence of semiconducting properties in the case of these alloys would prevent their potential use in some branches of microelectronics. The authors investigated the resistivity of thin ($0.3 \leq d \leq 40$ μ) filaments of $\text{P}_{1-x}\text{Sb}_x$ ($0.07 \leq x \leq 0.22$) alloys in a wide range of temperatures (4.2-300K) when subjected to static magnetic fields up to 15 T. (8 refs.)

Annealing of radiation defects in Ge-Si solid solutions See Entry 61969

Shubnikov-de Haas oscillations in $\text{Cd}_3(\text{As}_{0.7}\text{P}_{0.3})_2$ See Entry 62324

Energy of two-electron impurity states of tin in $\text{Pb}_{1-x}\text{Sn}_x\text{Se}$ solid solutions with low values of x See Entry 62369

Resonance level of tellurium associated with the L minima of the conduction band of gallium antimonide See Entry 62370

Transport phenomena in $\text{TiIn}_x\text{Nd}_{1-x}\text{Se}_2$ solid solutions See Entry 62411

Thermomagnetic and magnetothermoelectric quality factor of $n\text{-Ag}_2\text{Te}$ See Entry 62437

Charging characteristics of a gallium arsenide surface upon gas adsorption See Entry 62483

Electrical properties of SnTe epitaxial films on mica substrate See Entry 62517

Characteristics of magneto-resistive films controlled by grating surface of substrate See Entry 62520

A solution growth technique for the preparation of copper(II) selenide thin films See Entry 63181

72.20N Thermomagnetic effects

62437 Thermomagnetic and magnetothermoelectric quality factor of $n\text{-Ag}_2\text{Te}$. S.A.Aliev, D.Sh.Abdinov, E.F.Agaev, D.G.Arasly (Inst. of Phys., Acad. of Sci., Azerbaizhdan SSR).

Inorg. Mater. (USA), vol.18, no.6, p.880-1 (June 1982). Translation of: *Izv. Akad. Nauk SSSR Neorg. Mater.*, vol.18, no.6, p.1044-5 (June 1982). [received: Feb. 1983]

The level of interest in thermomagnetic (TM) and magnetothermoelectric (MT) transducers has increased greatly in recent years. The basic quality characterizing such transducers is the quality factor. Large values of the quality factors z_{TM} and z_{MT} can be expected in thermoelectric materials in which large longitudinal and transverse thermomagnetic effects are observed. Silver telluride is among the narrow-band semiconductors with a high mobility of electrons and a low lattice thermal conductivity. Therefore, it was of interest to determine the values of z_{TM} and z_{MT} in this material and to define the region of its practical application. On two specimens of Ag_2Te with $n = 1.5 \times 10^{18}$ and 3.1×10^{18} cm $^{-3}$, the authors carried out a joint investigation of the kinetic coefficients of thermal conductivity, thermal EMF, resistance, and Nernst-Ettingshausen effect in magnetic fields as great as 1.6 T. Experimental data are shown on the temperature dependence of κ , α , and ρ with $B = 0$ and $B = 1.6$ T and in a dimensionless N-E field $e_0 = QB^{-1}/\kappa e^{-1}$ with $B = 1.6$ T. On the basis of these data, the authors calculated the quality factors z_{TM} and z_{MT} . (7 refs.)

Characteristics of the magnetoresistance and photothermoelectric effect in single-crystal $\text{Cd}_{1-x}\text{Hg}_x\text{Te}$ plates subjected to quantizing magnetic fields See Entry 62435

72.20P Thermoelectric effects

62438 Thermoelectric properties of GeTe at high hydrostatic pressure up to 8.5 GPa and its valence-band structure. L.G.Khvostantsev, V.A.Sidorov (Inst. of High Pressure Phys., Acad. of Sci., Troitsk, USSR).

Phys. Status Solidi b (Germany), vol.116, no.1, p.83-9 (1 March 1983).

The thermopower and the relative electrical resistance of rhombohedral $\alpha\text{-GeTe}$ and orthorhombic $\gamma\text{-GeTe}$ polycrystalline samples with hole density between 3.9×10^{20} and 2×10^{21} cm $^{-3}$ are measured under hydrostatic pressure up to 8.5 GPa at room temperature. The phase transition of $\alpha\text{-GeTe}$ to the cubic rocksalt structure ($\beta\text{-GeTe}$) reported earlier at 3.5 GPa under nonhydrostatic pressure is not observed up to 8.5 GPa. Orthorhombic $\gamma\text{-GeTe}$ also exhibits no phase transition. The pressure dependences of the thermopower provide support for the multiple valence-band model of GeTe. (28 refs.)

62439 Thermo-EMF in bounded semiconductors under conditions of electron drag by phonons. A.M.Konin (Inst. of Semiconductor Phys., Acad. of Sci., Vilnius, Lithuanian SSR).

Sov. Phys.-Semicond. (USA), vol.16, no.10, p.1209-10 (Oct. 1982). Translation of: *Fiz. & Tekh. Poluprovodn. (USSR)*, vol.16, no.10, p.1877-80 (Oct. 1982). [received: April 1983]

The author deals with the dependence of the thermo-EMF of bounded semiconductors on the drag of electrons by phonons subject to realistic boundary conditions. The case of a local equilibrium of the phonon system is considered (it is assumed that long- and short-wavelength phonons have a common temperature and directional momentum). (6 refs.)

Preparation and study of the electrophysical properties of the copper chalcogenides and their solid solutions See Entry 62412

Thermomagnetic and magnetothermoelectric quality factor of $n\text{-Ag}_2\text{Te}$ See Entry 62437

Hot-carrier thermo-EMF created by a strong microwave electric field in $\text{Ge}_{1-x}\text{Si}_x$ single crystals irradiated with fast electrons See Entry 62442

Photothermopower of $a\text{-As}_2\text{Te}_3$ sputtered films See Entry 62447

Transport properties of tungsten bronzes doped with tantalum See Entry 62459

Electric field effect on the thermal emission rate of holes trapped at gold donor center in Si $p\text{-n}$ junction See Entry 62484

Thermoelectric properties of thin polycrystalline films See Entry 62518

Novel plasma chemical methods for doping $a\text{-Si:H}$ See Entry 63177

72.30 HIGH-FREQUENCY EFFECTS; PLASMA EFFECTS

62440 Nonreciprocal HF signal transmission by surface helicon. G.Ruibys, R.Tolulis (Inst. of Semiconductor Phys., Acad. of Sci., Vilnius, Lithuanian SSR).

Electron. Lett. (GB), vol.19, no.8, p.273 (14 April 1983).

Nonreciprocity of surface helicon propagation, its typical property which may be useful in practice, is stated experimentally. For this purpose the surface helicon has been separated from the bulk wave. The technique of wave reflection from a groove of different depth cut on the semiconductor surface was used. Some other surface helicon characteristics are also discussed. (3 refs.)

62441 Possibility of amorphous glassy state in astrophysical dense plasmas. S.Ichamaru, H.Iyetomi (Dept. of Phys., Univ. of Tokyo, Tokyo, Japan).

Phys. Scr. (Sweden), vol.T2, no.2, p.560-1 (1982). [received: April 1983]

(1982 International Conference on Plasma Physics, Göteborg, Sweden, 9-15 June 1982). Microscopic analysis on the basis of the improved hypernetted chain equations shows that the plasma fluid may form a metastable glassy state in the supercooled domain over a wide range of plasma parameters. Transition time from the metastable state to the crystalline state is estimated to be sufficiently large so that the possibility of the glassy state has an astrophysical relevance. (10 refs.)

62442 Hot-carrier thermo-EMF created by a strong microwave electric field in $\text{Ge}_{1-x}\text{Si}_x$ single crystals irradiated with fast electrons. A.Sh.Abdinov, A.K.Abiev, M.Ya.Bakirov, Yu.G.Nurullaev (Acad. of Sci., Baku, Azerbaizhdan SSR).

Sov. Phys.-Semicond. (USA), vol.16, no.10, p.1173-4 (Oct. 1982). Translation of: *Fiz. & Tekh. Poluprovodn. (USSR)*, vol.16, no.10, p.1828-30 (Oct. 1982). [received: April 1983]

The hot-carrier thermo-EMF U_T was detected and investigated in fast-electron-irradiated n - and p -type $\text{Ge}_{1-x}\text{Si}_x$ single crystals at temperatures

77-2500K. The study was carried out on samples with $x=0.05$ and $x=0.15$. It was found that the dependence $U_T(E)$ obtained for the fast-electron-irradiated $\text{Ge}_{1-x}\text{Si}_x$ single crystals differed considerably from the corresponding dependence in the case of unirradiated samples. (6 refs.)

62443 Investigation of the relaxation of the electrical conductivity in crossed alternating electric and static magnetic fields. V.Denis, Z.Martunas, G.Tvardauskas (Inst. of Semiconductor Phys., Acad. of Sci., Vilnius, Lithuanian SSR).

Sov. Phys.-Semicond. (USA), vol.16, no.10, p.1193-4 (Oct. 1982). Translation of: *Fiz. & Tekh. Poluprovodn. (USSR)*, vol.16, no.10, p.1856-8 (Oct. 1982). [received: April 1983]

An important parameter of a hot semiconductor plasma is the energy relaxation time τ_e . Accurate results can be obtained by a method based on the determination of the frequency dependence of the effective nonlinear coefficient α^* . The authors use a phenomenological theory to consider how the inertia of this process is reflected in the frequency dependence of the coefficient α^* . They consider a nondegenerate semiconductor with a simple isotropic band structure. An experimental check of the theoretical predictions was made on samples of chromium-compensated n-type InSb. (5 refs.)

Influence of the absorption of light by free carriers on their ambipolar drift See Entry 62935

Calculation of the EELS spectra of the Ni(001) surface with $p(2 \times 2)$ and $c(2 \times 2)$ overlayers of oxygen See Entry 63098

72.40 PHOTOCONDUCTION AND PHOTOVOLTAIC EFFECTS; PHOTODIELECTRIC EFFECTS

62444 Mechanochemical effect in ZnTe powder associated with grinding. M.Takeuchi (Dept. of Electrical Engng., Ibaraki Univ., Hitachi, Japan).

Jpn. J. Appl. Phys. Part 1 (Japan), vol.22, no.3, p.460-3 (March 1983). Single crystalline ZnTe powder was mechanically ground in air using an agate mortar and pestle, and changes in the structural and photoconductive properties were studied. The mean particle size was reduced to about 5 μm in the early stage of grinding. In the X-ray diffraction patterns, Te and ZnO lines appeared as 5 h and 8 h grindings, respectively. However, all the diffraction lines disappeared after 50 h grinding. Dark current in the ground ZnTe powder becomes maximum around 8 h grinding. This can be explained by the separation of Te associated with grinding. The original ZnTe powder showed photoconductive sensitivity to visible light. The sensitivity increased slightly in the early stage of grinding and then decreased with further grinding. Temperature dependences of the dark currents were measured in the temperature range of 170-370K. (11 refs.)

62445 PbO/CdS, Se/Cu mixed photoconductor system for electrophotography. Navneet, P.K.C.Pillai (Dept. of Phys., Indian Inst. of Technol., New Delhi, India).

Jpn. J. Appl. Phys. Part 1 (Japan), vol.22, no.3, p.508-10 (March 1983). A mixed system, consisting of lead monoxide (PbO) and cadmium sulfide selenide Cd(S, Se):Cu in acrylonitrile-butadiene-styrene (ABS) binder resin has been investigated with respect to electrophotographic characteristics. PbO and Cd(S, Se):Cu in 80:20 composition (by weight), when dispersed in ABS binder, (30% by weight) give optimum values for various electrophotographic parameters. Charge acceptance, dark and photoinduced decay, contrast potential and spectroresponse were the important electrophotographic properties, studied. The acceptance potential of the charged layer was 1092 volts. The fractional dark decay (observed 60 seconds after the charging) and fractional photoinduced decay (observed 10 seconds after the start of illumination) were 35.5% and 79.4% respectively. The intensity of illumination was 4.5 mW/cm². The absorption spectrum of the material spreads over a wide range covering UV as well as visible region.

62446 Measurement of photoconductivity at HgI₂ single crystals doped with iodine. K.Muller (Sektion Phys., Tech. Univ. Dresden, Dresden, Germany), A.I.Schulz.

Exp. Tech. Phys. (Germany), vol.31, no.1, p.89-96 (1983). In German. Presents the measurement of photoconductivity of two HgI₂ single crystal samples doped with iodine in concentrations 0.3 and 1.2 wt.%. After measuring photocurrent the samples were cleft in detector slices. The photocurrent I_{ph} was investigated versus irradiation intensity I_L at constant wavelength ($\lambda=555\text{--}570\text{ nm}$) and is given by $I_{ph} \sim I_L^\gamma$. The I_{ph} - I_L curves were characterized by the slope, the γ -value. The slices of sample doped with an iodine concentration 0.3 wt.%, having exhibited a γ -value of 0.95, showed a nearly linear photoconductivity and better detection properties than slices of sample doped with iodine in concentration 1.2 wt.% at which lower γ -values have been measured. In this manner a relationship between photocurrent and detection properties could be pointed out. It can be assumed that determination of photocurrent and estimation of γ -value allow a prediction of detector properties. (22 refs.)

62447 Photothermopower of a-As₂Te₃ sputtered films. D.M.Chui (Dept. of Electrical Engng., Univ. of Edinburgh, Edinburgh, Scotland).

J. Phys. D (GB), vol.16, no.4, p.L81-3 (14 April 1983). Photothermopower measurements on a-As₂Te₃ sputtered films reveal that within the temperature range 320-200K, both ambipolar and unipolar conduction are responsible for the conduction mechanism, in contrast with the previous belief that only unipolar conduction governs the behaviour of such material. However, outside this temperature range a unipolar conduction mechanism (holes) is found to be predominant. (1 ref.)

62448 Photochemical reactions in CdS_{1-x}Se_x single crystals. D.Raja Reddy, B.K.Reddy, P.J.Reddy (Dept. of Phys., SV Univ. Coll., Tirupati, India).

J. Phys. D (GB), vol.16, no.4, p.645-52 (14 April 1983). Thermally stimulated current (TSC) measurements in the temperature range 90-400K were carried out on vapour-phase grown CdS_{1-x}Se_x single crystals over the full range of x (1.00, 0.90, 0.70, 0.50, 0.30, 0.10 and 0.00) by continuously exciting the crystals from different temperatures while cooling (TEWC) in the range 400-90K. Large changes in the peak currents were observed for different illumination conditions. The existing photochemical models are not able to explain the TSC dependence on TEWC observed in the crystals. A tentative photochemical model which takes into account the variation of photochemical reaction with composition has been proposed. (16 refs.)

62449 A physicochemical interpretation of the photoconductivity of a-Si:H. H.Hamdi, A.Deneuville, J.C.Bruyere (Groupe des Transitions de Phases, CNRS, Grenoble, France).

J. Phys. Lett. (France), vol.44, no.7, p.L265-9 (1 April 1983). Total hydrogen content and its distribution among SiH, SiH₂ and other H' sites of sputtered a-Si:H films vary after posthydrogenation but the dangling bond concentrations remain constant. This can be explained by preferential H

diffusion in the tissue zone where most of the hydrogen is located, while the residual dangling bonds are in the islands. The photoconductivity is controlled by spinless defects of the tissue zone originating from back defects of H on their various sites. It decreases as the relative SiH₂ content increases. (14 refs.)

62450 One- and two-photon excited picosecond conductivity in CdS. V.Bruckner, F.Kerstan (Friedrich-Schiller-Univ., Sektion Phys., Jena, Germany).

Opt. Commun. (Netherlands), vol.45, no.3, p.187-93 (1 April 1983). Fast optoelectronic switching in CdS was studied in the case of high intensity picosecond laser excitation. At both one- and two-photon excitation two different mechanisms of the carrier recombination are measured and studied: recombination at slow centers (300-500 ns) and fast recombination (~700 ps) at high excitation levels, which may be explained by stimulated processes. A wide dynamic range in the switching efficiency was measured and discussed. (18 refs.)

62451 Low-frequency oscillations of the photocurrent in trigonal selenium single crystals. G.S.Kavalyauskene, V.S.Rinkyavichyus (V. Kapsukas State Univ., Vilnius, Lithuanian SSR).

Sov. Phys.-Semicond. (USA), vol.16, no.10, p.1190-1 (Oct. 1982). Translation of: *Fiz. & Tekh. Poluprovodn. (USSR)*, vol.16, no.10, p.1853-5 (Oct. 1982). [received: April 1983]

Low-frequency oscillations of the photocurrent were observed only in those trigonal selenium single crystals which were characterized by a dark current-voltage characteristic with a saturation region of the kind reported earlier for ZnS:Mn single crystals. The minimum critical field necessary for the excitation of these oscillations were 5.10⁵ V/cm. The oscillations appeared on illumination with light of wavelengths from 0.56 to 0.62 μm , corresponding to the maximum of the sensitivity region. (12 refs.)

62452 Singularity of the photoconductivity spectrum of tellurium-doped germanium. N.B.Radchuk, A.Yu.Ushakov (M.I. Kalinin Polytech. Inst., Leningrad, USSR).

Sov. Phys.-Semicond. (USA), vol.16, no.10, p.1192 (Oct. 1982). Translation of: *Fiz. & Tekh. Poluprovodn. (USSR)*, vol.16, no.10, p.1855 (Oct. 1982). [received: April 1983]

The authors have studied the photoconductivity spectrum of partly compensated Ge:Te and found a sharp peak at a photon energy 375 meV with a half-width 5.5 meV measured at the 0.9 level of the maximum amplitude. The signal at the peak maximum was 1.5-5 times greater than the signal due to the neighboring parts of the spectrum. (3 refs.)

62453 Flash nature of the kinetics of growth of the photocurrent in glassy arsenic sulfide. N.G.D'yachenko, A.Yu.Popov, M.Yu.Trofimenko, A.V.Tyurin, A.S.Sheveleva (Sci.-Res. Inst. of Phys., I.I. Mechnikov State Univ., Odessa, USSR).

Sov. Phys.-Semicond. (USA), vol.16, no.10, p.1205-6 (Oct. 1982). Translation of: *Fiz. & Tekh. Poluprovodn. (USSR)*, vol.16, no.10, p.1872-4 (Oct. 1982). [received: April 1983]

The authors study the flash nature of the photocurrent growth kinetics in the As₂S₃ chalcogenide glass. Photoconductivity measurements were made using a plane parallel plate of thickness ~0.3 mm covered with Al electrodes. (10 refs.)

62454 Nature of the photoconductivity and mobility anisotropy of photoelectrons in LiNbO₃:Fe. A.R.Pogosyan, B.N.Popov, E.M.Uyukin (A.V. Shubnikov Inst. of Crystallography, Acad. of Sci., Moscow, USSR).

Sov. Phys.-Solid State (USA), vol.24, no.9, p.1448-51 (Sept. 1982). Translation of: *Fiz. Tverd. Tela (USSR)*, vol.24, no.9, p.2551-7 (Sept. 1982). [received: April 1983]

The photorefractive and bulk photovoltaic effects in an external magnetic field were studied for the first time. The photoconductivity of lithium niobate was found to be largely due to the presence of nonthermalized electrons in the conduction band. A strong anisotropy of the mobilities of photovoltaic electrons was revealed, as well as a transverse photomagnetoconductance, together with transverse and longitudinal photovoltaic magnetoconductance effects in LiNbO₃:Fe crystals. (9 refs.)

62455 Photoelectric phenomena accompanying diffraction of X-rays in semiconducting crystals. A.M.Afanasyev, E.A.Manykin, E.F.Lobanovich, M.V.Koval'chuk, R.M.Imamov (A.V. Shubnikov Inst. of Crystallography, Acad. of Sci., Moscow, USSR).

Sov. Phys.-Solid State (USA), vol.24, no.9, p.1473-6 (Sept. 1982). Translation of: *Fiz. Tverd. Tela (USSR)*, vol.24, no.9, p.2599-604 (Sept. 1982). [received: April 1983]

The formation of an EMF accompanying irradiation of a p - n junction by X-rays under diffusion conditions is examined theoretically. The influence function that describes the contribution of current carriers created at different depths from the surface to the induced photo-EMF is determined. It is shown that the asymmetry of the photo-EMF curve in the region of diffraction angles is related to a characteristic length, which in this case is the diffusion length of the minority carriers. The theoretical results are illustrated by experimental data obtained for silicon p - n junctions having different resistivities. (7 refs.)

62456 Relative influence of grain boundaries and intragrain defects on the photocurrents obtained with Bridgman polysilicon. H.Amzil, M.Zchaf, J.P.Crest, E.Psaila, S.Martinuzzi (Lab. de Photoelectricite des Semiconducteurs, Univ. d'Aix-Marseille III, Marseille, France), J.Oualid.

Sol. Cells (Switzerland), vol.8, no.3, p.269-81 (April 1983). Photocurrents in Bridgman polysilicon were studied globally on small mesa diodes which were revealed on n^+ - p photocells cut from different regions of ingots (top, middle or bottom or periphery or centre), and locally by means of light-beam-induced current mappings. Their dependence on the electronic properties (the diffusion lengths) and on the physical properties (the number of grains per diode, the dislocations, the doping level etc.) was analysed. It was shown that the weaker the intragrain defect density and the conductivity are, the greater is the influence of the grain size on the electrical properties. This was confirmed by light-induced currents. It was shown that the photocurrents are more dependent on the grain size than on the diffusion length. The defects (the grain boundaries or dislocations) also have a strong influence on the dark forward current-voltage characteristics $I_f=f(V_f)$ and on the capacitance-reverse voltage curves $C^{-2}=f(V_R)$. (10 refs.)

62457 Light effects on grain boundary properties in silicon. L.J.Cheng, C.M.Shyu (Jet Propulsion Lab., California Inst. of Technol., Pasadena, CA, USA).

Grain Boundaries in Semiconductors. Proceedings of the Materials Research Society Annual Meeting, Boston, MA, USA, Nov. 1981 (New York, USA: North-Holland 1982), p.105-10

The authors have studied the photoconductivity of grain boundaries in p -type silicon. The result demonstrates the applicability of the technique for the measurement of minority carrier recombination velocity at the grain boundary. The experimental data are consistent with the thought that the recom-

- bination velocity increases with the boundary state density and light intensity. (9 refs.)
- Light refraction in crystals with bipolar photoconductivity See Entry 61116
- Dielectric properties and polaronic conductivity of WO_3 and $\text{W}_x\text{Mo}_{1-x}\text{O}_3$ See Entry 62415
- Influence of charging of local centers on the electrical properties of inhomogeneous CdS photoconducting structures See Entry 62426
- Electric and photoelectric characteristics of CdTe p-n homojunctions See Entry 62490
- Surface states at the $\text{TiO}_2/\text{H}_2\text{O}$ interface under UV illumination See Entry 62491
- Electronic properties of doped amorphous SiO_2 See Entry 62521
- Possible ferroelectric orientational phase transition induced by an electromagnetic field See Entry 62903
- Optical and electrical properties of a- $\text{Si}_x\text{C}_{1-x}\text{H}$ films prepared by glow discharge from SiH_4 and C_2H_4 See Entry 63075
- Deposition of cadmium chalcogenide thin films by a solution growth technique using triethanolamine as a complexing agent See Entry 63184
- The photoelectrochemical etching of TiO_2 single crystals See Entry 63445
- Photoelectrochemical behavior of Co^{2+} doped-zinc oxide electrodes See Entry 63560
- Grain boundary effects in polycrystalline silicon solar cells. I. Solution of the three-dimensional diffusion equation by the Green's function method See Entry 63666
- Grain boundary effects in polycrystalline silicon solar cells. II. Numerical calculation of the limiting parameters and maximum efficiency .. See Entry 63667
- Charge collection in a-Si:H solar cells See Entry 63687
- Sprayed zinc-cadmium sulfide films for backwall $\text{Cu}_2\text{S}/(\text{ZnCd})\text{S}$ cells See Entry 63692
- Stability of amorphous silicon solar cells with pin structure See Entry 63694
- Photocathodic reactions at p-InP See Entry 63718

72.50 ACOUSTOELECTRIC EFFECTS

- 62458 Acoustoelectric wave in a piezoelectric semiconductor with a Schottky barrier. D.A.Letnik, V.V.Popov (State Univ., Omsk, USSR). *Sov. Phys.-Semicond. (USA)*, vol.16, no.10, p.1200-1 (Oct. 1982). Translation of: *Fiz. & Tekh. Poluprovodn. (USSR)*, vol.16, no.10, p.1865-7 (Oct. 1982). [received: April 1983]
- The authors consider an acoustoelectric instability which appears on application of a constant bias to a piezoelectric semiconductor with one ohmic contact and the other contact in the form of a Schottky barrier. An acoustoelectric wave modulates not only the carrier density near the barrier but also the barrier height, and this makes it possible to generate oscillations in a sample. (4 refs.)

72.60 MIXED CONDUCTIVITY AND CONDUCTIVITY TRANSITIONS

- 62459 Transport properties of tungsten bronzes doped with tantalum. P.P.Dordor, J.P.Doumerc, G.Villeneuve (Lab. de Chimie du Solide, Talence, France). *Philos. Mag. B (GB)*, vol.47, no.3, p.315-22 (March 1983). In French.
- The thermoelectric power of several $\text{Na}_x\text{Ta}_y\text{W}_{1-y}\text{O}_3$ bronzes have been measured between 4.2 and 900K. As the number of d electrons decreases, a metal-non-metal transition occurs, which is ascribed to Anderson localization. The transport properties of the non-metallic samples are described in terms of three different hopping mechanisms at the Fermi level. With rising temperature, first variable-range hopping, then Miller-Abrahams (1960) and finally Heikes hopping successively prevail. (9 refs.)
- 62460 Influence of hydrostatic pressure on the electrical properties of filamentary tellurium crystals. S.S.Varshava, L.N.Pelekh, B.I.Sydir (Lenin Komsomol Polytech. Inst., Lvov, Ukrainian SSR). *Sov. Phys.-Semicond. (USA)*, vol.16, no.10, p.1196-7 (Oct. 1982). Translation of: *Fiz. & Tekh. Poluprovodn. (USSR)*, vol.16, no.10, p.1861-3 (Oct. 1982). [received: April 1983]
- The authors report a study of the influence of hydrostatic pressures up to $5 \cdot 10^8$ Pa on the electrical properties of filamentary Te crystals of different shapes (acicular, tubular, platelet) and dimensions. At room temperature the investigated samples exhibited mixed conductivity values of 0.1-0.5 Ωcm . The pressure coefficients of the band gap were also determined. (8 refs.)
- 62461 Metallization of mercury chalcogenides under ultrahigh pressures. I.M.Tsidil'kovskii, V.V.Shchennikov, N.G.Gluzman (Inst. of Metal Phys., Acad. of Sci., Sverdlovsk, USSR). *Sov. Phys.-Solid State (USA)*, vol.24, no.9, p.1507-9 (Sept. 1982). Translation of: *Fiz. Tverd. Tela (USSR)*, vol.24, no.9, p.2658-62 (Sept. 1982). [received: April 1983]
- The electrical resistance of the mercury chalcogenides HgTe , HgSe , and $\alpha\text{-HgS}$ under pressures up to 400kbar at 293-400K was studied in metal and diamond high pressure chambers. It is shown that the resistance and the band gap of the hexagonal modifications of the chalcogenides with the cinnabar ($\alpha\text{-HgS}$) structure decrease rapidly with rising pressure. This narrowing of the gap corresponds to the high compressibility of the hexagonal phases in HgTe , HgSe , and $\alpha\text{-HgS}$. Phase transitions to the metallic state were found at 100 ± 10 kbar for HgTe , 210 ± 20 kbar for HgSe , and 300 ± 30 kbar for $\alpha\text{-HgS}$. The hexagonal phases are shown to be similar to the group VI semiconductors selenium and tellurium. It is conjectured that the crystal and band structures of the mercury chalcogenide metallic phases are similar to those of the high-pressure metallic phases of selenium and tellurium. (12 refs.)
- 62462 Phase transition in $\text{AgPbSb}_2\text{S}_6$ crystals [superionic]. V.F.Mikuchenis, V.I.Yu.Valyukenas, N.N.Mozgova, A.P.Kezhenis, V.I.Samulenis, V.I.Skritskii, A.S.Orlyukas (V. Kapsukas State Univ., Vilnius, Lithuanian SSR). *Sov. Tech. Phys. Lett. (USA)*, vol.8, no.8, p.425-6 (Aug. 1982). Translation of: *Pis'ma v Zh. Tekh. Fiz. (USSR)*, vol.8, no.15-16, p.984-8 (Aug. 1982). [received: April 1983]
- Reports a study of the electrical conductivity, the dielectric properties, and the acoustic properties of $\text{AgPbSb}_2\text{S}_6$ crystals over the temperature range 300-500K. Naturally occurring crystals were used. An X-ray microspectral analysis showed the chemical composition of the samples to be 11.03% Ag (percent by weight), 23.14% Pb, 43.92% Sb, and 22.23% S, with impurities amounting to less than 0.1%. (17 refs.)

- Effect of electron bombardment on the phase transition in VO_2 films See Entry 62339
- Incommensurate-commensurate transition in TaS_2 See Entry 62405
- Electrical resistivity of mixed-valence systems in a two-band model See Entry 62407
- Ag_2Se thin film conductivity with a selenium excess See Entry 62513
- Characterization of Al-AlO_2 and Sn-SnO_2 cermet films deposited by reactive evaporation See Entry 63162

72.70 NOISE PROCESSES AND PHENOMENA

- 62463 Fractal dimensions and $1/f$ noise. R.Benzi (Centro Sci. IBM, Roma, Italy), L.Peliti, A.Vulpiani. *Lett. Nuovo Cimento (Italy)*, vol.36, ser.2, no.14, p.471-4 (2 April 1983).
- Considers theoretically the noise spectrum in metal films and in carbon resistors which shows a power law behaviour as a function of frequency with an exponent near to -1 . The current circulating in the resistor is viewed as a charged, weakly compressible fluid, and magnetohydrodynamics equations are applied. Using this theory both the power law dependence and the role of the system dimensionality are explained. (14 refs.)
- 62464 Frequency dependence of the noise in n-type Si subjected to strong electric fields. V.Bareikis, V.Viktoravichyus, A.Gal'dikas (Inst. of Semiconductor Phys., Acad. of Sci., Vilnius, Lithuanian SSR). *Sov. Phys.-Semicond. (USA)*, vol.16, no.10, p.1202-3 (Oct. 1982). Translation of: *Fiz. & Tekh. Poluprovodn. (USSR)*, vol.16, no.10, p.1868-70 (Oct. 1982). [received: April 1983]
- The authors report the results of an investigation of noise in n-type Si along a strong electric field, carried out in the frequency range 80 MHz-10 GHz where dispersion of the intervalley noise should be manifested. (21 refs.)
- Local nature of charge-density-wave conduction noise in niobium triselenide See Entry 62353
- Diagonal and off-diagonal contributions to autocorrelation of velocity fluctuations in semiconductors See Entry 62421

72.80 CONDUCTIVITY OF SPECIFIC SEMICONDUCTORS AND INSULATORS

(see also 81.40R Electrical and magnetic properties related to materials treatment)

- Influence of high pressure and shear strains on some electrophysical properties of polyphthalocyanines See Entry 62419
- Centres of slow recombination in cadmium bromide crystals See Entry 62427
- Electron trapping in thin films of thermal SiO_2 at temperatures between 30 and 300K See Entry 62519
- Formation of cubic boron nitride films by boron evaporation and nitrogen ion beam bombardment See Entry 63159

72.80C Elemental semiconductors

- High temperature and short time thermal annealing of ion-implanted silicon See Entry 61938
- Impurity incorporation in RAO polysilicon layers and consequences on their electrical properties See Entry 61950
- Flash lamp annealing of ion-implanted polycrystalline silicon See Entry 61959
- The electronic properties of semiconductor grain boundaries See Entry 62409
- Study of the structure and elastoresistance properties of thin films of bismuth See Entry 62418
- Diagonal and off-diagonal contributions to autocorrelation of velocity fluctuations in semiconductors See Entry 62421
- Transport across silicon grain boundaries See Entry 62428
- Electrical and structural properties of grain boundary in polycrystalline Si See Entry 62429
- A physicochemical interpretation of the photoconductivity of a-Si:H See Entry 62449
- Low-frequency oscillations of the photocurrent in trigonal selenium single crystals See Entry 62451
- Singularity of the photoconductivity spectrum of tellurium-doped germanium See Entry 62452
- Relative influence of grain boundaries and intragrain defects on the photocurrents obtained with Bridgman polysilicon See Entry 62456
- Light effects on grain boundary properties in silicon See Entry 62457
- Influence of hydrostatic pressure on the electrical properties of filamentary tellurium crystals See Entry 62460
- Frequency dependence of the noise in n-type Si subjected to strong electric fields See Entry 62464
- Influence of structure defects on the characteristics of warm electrons and holes near the surface of silicon See Entry 62501
- Novel plasma chemical methods for doping a-Si:H See Entry 63177
- Carrier conduction in a-Si:H solar cells See Entry 63695

72.80E III-V and II-VI semiconductors

- Interaction of primary radiation defects with dislocations in indium antimonide See Entry 61955
- Determination of band-gap parameters of $\text{Hg}_{1-x}\text{Cd}_x\text{Te}$ based on high-temperature carrier concentration See Entry 62334
- Carrier capture by multiphonon emission at extrinsic deep centers induced by self-trapping in GaAs See Entry 62364
- Resonance level of tellurium associated with the L minima of the conduction band of gallium antimonide See Entry 62370
- The electronic properties of semiconductor grain boundaries See Entry 62409
- Analysis of disorder scattering in $\text{Ga}_{0.47}\text{In}_{0.53}\text{As}$ using Gaussian potential See Entry 62410
- Direct observation of impact ionisation and hot electron effects in GaAs See Entry 62420
- Impurity scattering time in n-type InSb measured by Faraday rotation at far-infrared frequency See Entry 62425

- Influence of charging of local centers on the electrical properties of inhomogeneous CdS photoconducting structures See Entry 62426
- 'Limiting' electrical properties of irradiated InP See Entry 62434
- Characteristics of the magnetoresistance and photothermoelectric effect in single-crystal $\text{Cd}_{1-x}\text{Hg}_x\text{Te}$ plates subjected to quantizing magnetic fields See Entry 62435
- Mechanochemical effect in ZnTe powder associated with grinding See Entry 62444
- Photochemical reactions in $\text{CdS}_{1-x}\text{Se}_x$ single crystals See Entry 62448
- One- and two-photon excited picosecond conductivity in CdS See Entry 62450
- Barrier height and surface states at cleaned InSb(110) surfaces See Entry 62470
- Charging characteristics of a gallium arsenide surface upon gas adsorption See Entry 62483
- Electric and photoelectric characteristics of CdTe p-n homojunctions See Entry 62490
- Influence of spontaneous polarization of TGS crystals on the electrical properties of ZnTe thin films See Entry 62516
- Characterization of Mn-doped and nominally pure LPE $\text{Ga}_{1-x}\text{In}_x\text{As}_{1-y}\text{P}_y$ ($y=2.1x$) between $y=0$ and $y=1$ using photoluminescence and electrical measurements See Entry 63039

72.80G Transition-metal compounds

- Dielectric properties and polaronic conductivity of WO_3 and $\text{W}_x\text{Mo}_{1-x}\text{O}_3$ See Entry 62415
- Semiconducting properties of V_2O_5 gels See Entry 62416
- Magnetoresistance and conductivity in the binary system titanium-oxygen. II. Semiconductive titanium oxides See Entry 62433
- Thermomagnetic and magnetothermoelectric quality factor of $n\text{-Ag}_2\text{Te}$ See Entry 62437
- Magnetic and electrical properties of $\text{FeCr}_{1-x}\text{In}_x\text{S}_4$ ($0 \leq x \leq 1$) See Entry 62695
- A solution growth technique for the preparation of copper(II) selenide thin films See Entry 63181

72.80J Other crystalline inorganic semiconductors

- Annealing of radiation defects in Ge-Si solid solutions See Entry 61969
- X-ray diffraction analysis of SnO_2 films prepared by oxidation of tin films See Entry 62306
- Shubnikov-de Haas oscillations in $\text{Cd}_3(\text{As}_{0.7}\text{P}_{0.3})_2$ See Entry 62324
- Energy of two-electron impurity states of tin in $\text{Pb}_{1-x}\text{Sn}_x\text{Se}$ solid solutions with low values of x See Entry 62369
- Mechanism of electrical conduction in rare-earth ferrocyanides See Entry 62408
- Transport phenomena in $\text{TlIn}_x\text{Nd}_{1-x}\text{Se}_2$ solid solutions See Entry 62411
- Preparation and study of the electrophysical properties of the copper chalcogenides and their solid solutions See Entry 62412
- Resistance changes of $\text{Pb}_{0.8}\text{Sn}_{0.2}\text{Te}$ under dynamic loading in the 0-100 kbar range See Entry 62413
- Trapping center parameters in indium selenide single crystals by thermally stimulated current measurements See Entry 62424
- Semiconductor-type temperature dependence of the resistivity of $\text{Bi}_{1-x}\text{Sb}_x$ ($0.07 \leq x \leq 0.22$) alloy filaments See Entry 62436
- Thermoelectric properties of GeTe at high hydrostatic pressure up to 8.5 GPa and its valence-band structure See Entry 62438
- Hot-carrier thermo-EMF created by a strong microwave electric field in $\text{Ge}_{1-x}\text{Si}_x$ single crystals irradiated with fast electrons See Entry 62442
- Measurement of photoconductivity at HgI_2 single crystals doped with iodine See Entry 62446
- Nature of the photoconductivity and mobility anisotropy of photoelectrons in $\text{LiNbO}_3\text{:Fe}$ See Entry 62454
- Transport properties of tungsten bronzes doped with tantalum See Entry 62459
- Ag_2Se thin film conductivity with a selenium excess See Entry 62513
- Electrical properties of SnO_2 polycrystalline thin films and single crystals exposed to O_2 - and H_2 -gases See Entry 62514
- Electrical properties of SnTe epitaxial films on mica substrate See Entry 62517

72.80L Organic semiconductors

- Anomalous transient-time dispersion in amorphous solids: oxadiazole See Entry 62414

72.80N Amorphous and glassy semiconductors

- X-ray diffraction analysis of SnO_2 films prepared by oxidation of tin films See Entry 62306
- Semiconducting properties of V_2O_5 gels See Entry 62416
- Photothermopower of a- As_2Te_3 sputtered films See Entry 62447
- A physicochemical interpretation of the photoconductivity of a-Si:H See Entry 62449
- Flash nature of the kinetics of growth of the photocurrent in glassy arsenic sulfide See Entry 62453
- Optical and electrical properties of a-Si $_x\text{C}_{1-x}\text{H}$ films prepared by glow discharge from SiH_4 and C_2H_4 See Entry 63075
- Novel plasma chemical methods for doping a-Si:H See Entry 63177
- Carrier conduction in a-Si:H solar cells See Entry 63695

72.90 OTHER TOPICS IN ELECTRONIC TRANSPORT IN CONDENSED MATTER

- 62465 Two-dimensional inhomogeneous systems in strong magnetic fields. IV. L.V.Gorodza, Yu.P.Emets (Inst. of Electrodynamics, Acad. of Sci., Kiev, Ukrainian SSR). *Sov. Phys.-Tech. Phys. (USA)*, vol.27, no.9, p.1047-51 (Sept. 1982). Translation of: *Zh. Tekh. Fiz. (USSR)*, vol.52, no.9, p.1705-11 (Sept. 1982). [received: April 1983]
- For pt.III see *ibid.*, vol.27, p.389 (1982). Electric fields are calculated analytically and the effective parameters of the medium are evaluated for a continuous medium containing inhomogeneities in the form of highly conductive ribbons distributed in a regular order. When the Hall effect appears in the medium, the effective conductivity tensor depends strongly on the orientation of the inclusions with respect to the directions of the external electric and magnetic fields. The systems examined in the present work have regularly distributed inhomogeneities directed across the external magnetic field. The components of the conductivity tensor are studied as functions of the density of inclusions and the strength of the magnetic field. (2 refs.)
- Characterization of Al-AlO_2 and Sn-SnO_2 cermet films deposited by reactive evaporation See Entry 63162

73.00 ELECTRONIC STRUCTURE AND ELECTRICAL PROPERTIES OF SURFACES, INTERFACES, AND THIN FILMS

73.20 ELECTRONIC SURFACE STATES

(for emission and impact phenomena, see 79.)

- 62466 Distance dependence of electronic energy transfer to semiconductor surfaces: $\pi\pi^*$ pyrazine/ $\text{GaAs}(110)$. P.M.Whitmore, A.P.Alivisatos, C.B.Harris (Dept. of Chem. & Materials & Molecular Res., Univ. of California, Berkeley, CA, USA). *Phys. Rev. Lett. (USA)*, vol.50, no.14, p.1092-4 (4 April 1983).
- Energy transfer from $\pi\pi^*$ pyrazine to $\text{GaAs}(110)$ has been studied. Within experimental error, a classical dielectric model quantitatively reproduces measurements of the distance-dependent lifetime for emitter-surface separations from 430 to 20 Å. Analysis of the energy transfer shows that the molecular electronic excitation is dissipated through the creation of electron-hole pairs in the solid by the high-wave-vector components of the dipole near field. (10 refs.)
- 62467 Wave functions for surface states of a distorted surface. J.Neuberger (Dept. of Phys., Queens Coll., City Univ. of New York, Flushing, NY, USA), C.L.Roy. *Physica B & C (Netherlands)*, vol.115 B+C, no.2, p.172-8 (Jan. 1983).
- The form of the wave function to be used in a one-dimensional disordered system for the purpose of obtaining surface states is investigated. Two cases are considered: one where the defect occurs to the left of the origin and the second where the first cell is distorted. It is demonstrated that the two cases which seemingly yield quite different forms are actually the same, aside from an obvious change in sign. A more fundamental question which raises some doubt about the validity of Kronig-Penney wave functions to cells which are not periodic is pointed out. (6 refs.)
- 62468 Interaction of charges with metallic surfaces—invalidity of the surface plasmon model. M.Babiker (Phys. Dept., Univ. of Essex, Colchester, England). *Physica B & C (Netherlands)*, vol.115 B+C, no.3, p.339-66 (March 1983).
- It is argued that the surface plasmon (SP) model, according to which metallic surfaces manifest their interaction with a charge e only through the surface excitations, is invalid. A careful enumeration of the modes of the electromagnetic field in the presence of a (spatially dispersionless) jellium half-space is presented together with explicit calculations for the Coulomb potential on a charge outside the jellium. This potential is shown to arise from both volume (α) modes and surface (β) modes whose contributions are then discussed separately in various limits. In particular it is shown that the potential due to the surface modes subject to the so-called quasistatic approximation $c \rightarrow \infty$, i.e. $\mu \rightarrow 0$ ($\mu = 2Z/\lambda_p \approx 2Z\omega_p/c$, where ω_p is the bulk plasma frequency and Z the distance of the particle from the surface), agrees in magnitude but not in sign with the result in this limit of the (SP) model, while the total potential for finite μ is drastically different from the predictions of the (SP) models, while the total potential for finite μ is drastically different from the predictions of the (SP) model. It is argued that, for finite ω_p , the limit $c \rightarrow \infty$ is incompatible with the jellium assumption $\mu \rightarrow \infty$ represents the small Z limit, and analogy with classical theory is therefore inappropriate. The limit $\mu \rightarrow \infty$ represents the true classical limit of the theory. Here, the total potential is shown to arise predominantly from the volume (α) modes and it has the correct classical behaviour $-\epsilon/4Z$. The total potential is presented as a function of μ both analytically and graphically and implications of its form for the detailed properties of the particle near the metallic surface are discussed. (23 refs.)

- 62469 Electronic structure of hydrogen-bonded H_2O . D.Schmeisser, F.J.Himpel, G.Hollinger, B.Reihl (IBM Thomas J. Watson Res. Center, Yorktown Heights, NY, USA), K.Jacobi. *Phys. Rev. B (USA)*, vol.27, no.6, p.3279-86 (15 March 1983).
- The authors have studied the electronic structure of H_2O adsorbed on different metal surfaces between 7 and 200K using photoelectron spectroscopy. From the valence-orbital spectra they are able to distinguish three different phases of adsorbed H_2O : (a) single-adsorbed H_2O molecules at temperatures close to the desorption point, (b) partially hydrogen-bonded H_2O clusters for coverages of a monolayer or less, and (c) fully hydrogen-bonded ice at low temperatures and several monolayers of coverage. For phase (a), they find valence molecular orbitals which are almost rigidly shifted upwards relative to the gas phase by a final-state relaxation shift of 1.3 eV. All orbitals are broadened by 1.0-1.5 eV relative to the gas phase. For phase (b), two inequivalent types of H_2O molecules whose orbital energies differ by 1.5-2 eV are identified. This splitting is identical to the electrostatic shift of molecular-orbital energies as calculated for the hydrogen-bonded H_2O dimer by Umeyama and Morokuma (1977). In this model the set of molecular orbitals with higher binding energy is assigned to the hydrogen-acceptor molecule and the set with lower binding energy to the hydrogen-donor molecule. At

monolayer coverage about twice as many donors as acceptors are found. (27 refs.)

62470 Barrier height and surface states at cleaned InSb(110) surfaces. E.W.Kreutz, E.Rickus, N.Sotnik (Inst. für Angewandte Phys., Tech. Hochschule Darmstadt, Darmstadt, Germany). *Thin Solid Films (Switzerland)*, vol.101, no.2, p.153-65 (11 March 1983). The electronic properties of p-InSb(110) surfaces which were cleaned by the ion bombardment annealing technique are investigated by measurements of the integral and differential field effects. The field-induced changes in surface conductivity imply inversion layers with electron conduction in the space charge layer. The analysis of the experimental results yields the barrier height at the surface and the term spectrum of surface states. The general shape of the surface state density per energy interval shows a disorder-dependent continuous distribution with a minimum about midgap and increasing tails towards the bulk band edges. Near the conduction band minimum a peaking distribution of donor-type surface states is superimposed on the continuous distribution depending on the ion bombardment annealing conditions. The nature of the spectrum of surface states is discussed on the basis of intrinsic and extrinsic states. (39 refs.)

62471 Electronic structure of the $\text{Me}_2\text{S}_8^{n+}$ cluster units in Mo_2S_8 , $\text{M}_2\text{Re}_2\text{S}_8$ (M=Na, K) and $[\text{Fe}_2\text{S}_8][\text{P}(\text{Et})_3]_n$ analogs to Mo_2S_8 , Re_2S_8 and Fe_2S_8 adsorbate structures. F.Dubler, H.Müller (Sektion Chemie, Friedrich-Schiller-Universität, Jena, Germany). *Wiss. Z. Friedrich-Schiller-Universität, Jena, Math. Naturwiss. Reihe (Germany)*, vol.31, no.6, p.907-17 (1982). In German. By means of the SW-Xa-method the valence electronic structures of the common $\text{Me}_2\text{S}_8^{n+}$ -unit of the 3 title compounds has been calculated. A comparison of the results with previously discussed bonding schemes for such octahedral cluster compounds has been made. The result is that these bonding schemes do not apply in general to the considered cluster compounds. Thermochemical, spectroscopic and structural features of this class of compounds show relationships to the corresponding adsorption of sulfur on Mo, Re and Fe surfaces. (42 refs.)

62472 SW-Xa investigation of the electronic structure of palladium clusters. H.-G.Fritsche (Sektion Chemie, Friedrich Schiller Univ., Jena, Germany). *Wiss. Z. Friedrich-Schiller-Universität, Jena, Math. Naturwiss. Reihe (Germany)*, vol.31, no.6, p.919-29 (1982). In German. The electronic structures of O_h -symmetrical clusters Pd_6 , Pd_{13} , Pd_{14} calculated by the SW-Xa-method are compared with the electronic structure of the periodic Pd-lattice obtained by an APW-calculation. The influences of electronic configurations and additional scattering centers on the valence-bands of clusters are investigated. It is shown that SCF-calculations can only give better results for nearly isolated structural units. The rapid convergence of cluster-properties obtained by SW-Xa-method to APW-bulk-properties is discussed as a consequence of muffin-tin-approximation. (22 refs.)

62473 How local is the bonding of absorbed hydrogen to the host metal? An attempt at answering the problem in the framework of the SW-X_a method for the α -Pd/H system. H.-G.Fritsche, H.Müller (Sektion Chemie, Friedrich Schiller Univ., Jena, Germany). *Wiss. Z. Friedrich-Schiller-Universität, Jena, Math. Naturwiss. Reihe (Germany)*, vol.31, no.6, p.931-42 (1982). In German. The absorption of small amounts of atomic hydrogen in palladium (α -phase) was investigated by SW-Xa-calculations considering two Pd-spheres. The installation of hydrogen causes an energetical change in the spectrum and a local modification of the electronic density. The region near to the proton accepts electrons donated by the spheres around the palladium-atoms of the second neighbourhood to the proton. The charge transfer into the hydrogen-sphere is an effect of strongly localized interactions between hydrogen and 6 neighbouring palladium atoms. The orbitals of the so-called rigid band play an important role in the more delocalized alterations of electronic density in regions between palladium-atoms of the first and second neighbourhood to hydrogen. (23 refs.)

62474 Theoretical investigation of the multiple bond in complexes of the type $[\text{Re}_2\text{Cl}_8]^{2-}$. C.Opitz, H.Müller, R.Kastner (Sektion Chemie, Friedrich Schiller Univ., Jena, Germany). *Wiss. Z. Friedrich-Schiller-Universität, Jena, Math. Naturwiss. Reihe (Germany)*, vol.31, no.6, p.943-8 (1982). In German. The energy of the metal-metal-bond of complexes of the type $[\text{Me}_2\text{X}_8]^{n-}$ (Me=Re, Mo, Te; X=Cl, Br) has been evaluated in the frame of a simple free electron model and compared with experimental data. Due to the analysis of the bonding orbitals quadruple or stronger Me-Me-bonds have been found, corresponding to $\sigma^* \pi^{*2}$ and $\sigma^* \pi^{*3}$ bonding configurations. The charge density distribution of the bonding orbitals has been drawn. (15 refs.)

62475 Quantum chemical investigation on the mutual exchange of the solid surface with an atom using the partitioning technique. L.D.Kunne, A.Horn-bogen (Sektion Chemie, Friedrich Schiller Univ., Jena, Germany). *Wiss. Z. Friedrich-Schiller-Universität, Jena, Math. Naturwiss. Reihe (Germany)*, vol.31, no.6, p.949-61 (1982). In German. The partitioning technique is a useful mathematical tool to solve the eigenvalue problem in quantum chemistry. The authors apply this technique to the case of chemisorption of one atom on a solid surface. Using the tight binding approximation they obtain a simple equation to determine the eigenvalues, and closed formulae for the LCAO coefficients and charge distribution. These formulae bring to light three different kinds of interaction between the chemisorbed atom and the individual molecular orbitals of the solid. The applicability of the formulae is demonstrated in the case of chemisorption of H on Ni (100) surface. (10 refs.)

Ion beam hydrogenation of polysilicon coated thermal oxide on silicon See Entry 61941

Electronic damping of the motion of adsorbates on metal surfaces See Entry 62231

Ab initio CI investigation of hydrogen atom adsorption on Li clusters: embedded cluster model See Entry 62254

Investigation of lateral interactions in chemisorption See Entry 62255

Generalized pseudopotential model of inhomogeneous systems and its application to a simple-metal surface See Entry 62314

Bulk and surface electron states in WO_3 and tungsten bronzes See Entry 62336

Image forces and the range of stability of a two-dimensional Wigner crystal See Entry 62354

Electronic structure of grain boundaries and interfaces in polycrystalline zinc oxide See Entry 62377

Mechanism for local charge transport on the surface of a transparent ferroelectric ceramic See Entry 62478

Surface states at the $\text{TiO}_2/\text{H}_2\text{O}$ interface under UV illumination See Entry 62491

Semiconductor electrodes. XLVII. AC impedance technique for evaluating surface state properties of n-MoTe₂ in acetonitrile solutions containing various redox couples See Entry 62493

Quantum chemical modelling of optical properties of simple and oxide clusters See Entry 62920

Enhanced adsorbate Raman scattering and surface plasmon radiation See Entry 62981

Relation between dynamical processes at surfaces and electron-energy-loss measurements See Entry 63111

Energy dissipation at metal surfaces: electronic versus vibrational excitations See Entry 63118

Surface-atom X-ray photoemission from clean metals: Cu, Ag, and Au See Entry 63133

Photoemission from surface-atom core levels, surface densities of states, and metal-atom clusters: a unified picture See Entry 63134

73.25 SURFACE CONDUCTIVITY

62476 Irregularity in the electrical conductivity of technical-grade pericase. M.A.Samokhvalov (V.V. Kuibyshev Tomsk State Univ., Tomsk, USSR).

Inorg. Mater. (USA), vol.18, no.6, p.889-90 (June 1982). Translation of: *Izv. Akad. Nauk SSSR Neorg. Mater.*, vol.18, no.6, p.1051-2 (June 1982). [received: Feb. 1983]

To study the irregularity in the electrical conductivity of pericase, the authors developed a method of dry decoration of the volume conducting channels. The pericase sample was prepared in the form of plane-parallel plates with linear dimensions much larger than the thickness. One surface of the plate was coated with metal, while the other was processed thoroughly to decrease the surface conductivity. Charge was applied uniformly to the processed surface. The sample was then placed in a furnace on a grounded plate and allowed to discharge for a period of time. At the end of the discharge period, the irregular distribution of the charge on the surface of the sample reflects the irregularity in its electrical conductivity. The charge distribution becomes visible after decoration of the surface of the sample with finely dispersed charged particles of chromium oxide or other material. The results of decoration are then studied by means of an optical microscope. (1 ref.)

62477 An experimental test of the scaling theory of conduction in two dimensions. R.A.Davies, M.Pepper, M.Kaveh (Cavendish Lab., Univ. of Cambridge, Cambridge, England).

J. Phys. C (GB), vol.16, no.10, p.L285-9 (10 April 1983). The scaling theory of conduction has created much interest in the problem of conduction in a disordered system. Basic to this theory is the assumption that a one-parameter scaling function exists. An experimental test of this is presented for two-dimensional transport in silicon inversion layers. The results are found to be inconsistent with such an assumption and the authors conclude that the function does not exist. (17 refs.)

62478 Mechanism for local charge transport on the surface of a transparent ferroelectric ceramic. A.E.Krumin', U.Yu.Ilin', V.I.Dimza (Petr Stuchka State Univ., Latvian SSR).

Sov. Phys.-Tech. Phys. (USA), vol.27, no.10, p.1294-5 (Oct. 1982). Translation of: *Zh. Tekh. Fiz. (USSR)*, vol.52, no.10, p.2107-9 (Oct. 1982). [received: April 1983]

The goal of the work was to study surface phenomena in transparent ferroelectric ceramics by using pointed metal electrodes to transport charge carriers to the surface levels of a ferroelectric ceramic in the external field produced by the trapped carriers. A characteristic property of ferroelectrics, including transparent ferroelectric ceramics, is that this field can be observed directly because of the electrooptical effect. A transparent ferroelectric ceramic of composition ZTLX-X (lead zirconate and titanate modified with lanthanum) was studied where $X=8, 9, 10$ is the density of lanthanum ions in at.%. For purposes of comparison BaTiO_3 , $\text{Pb}(\text{Mg}_{1/3}\text{Nb}_{2/3})\text{O}_3$, KNbO_3 , and $(\text{BaSr})\text{Nb}_2\text{O}_6$ single crystals were also investigated. It is believed that the main charge transport mechanism involves tunneling of charge carriers across the metal-air interface and trapping near the surface of transparent ferroelectric ceramics. Charge localization results from two interdependent processes occurring in the intense electric field E near the sharp points of the electrodes. (4 refs.)

62479 Investigation of the influence of water on the surface conductivity of optical glass. D.Lenke, C.Nitschke (Friedrich Schiller Univ., Jena, Germany).

Wiss. Z. Friedrich-Schiller-Universität, Jena, Math. Naturwiss. Reihe (Germany), vol.31, no.6, p.1039-43 (1982). In German. The influence of water on the behaviour of optical glasses was investigated by means of surface conductivity measurements. The applied measuring method permitted statements on the ion exchange processes of the surface area. Differences in the corrosion tendency are discussed in dependence on the volume content of glasses. (14 refs.)

Preparation of superinsulating surfaces by the nuclear track technique See Entry 61999

Nonreciprocal HF signal transmission by surface helicon See Entry 62440

Barrier height and surface states at cleaned InSb(110) surfaces See Entry 62470

Charging characteristics of a gallium arsenide surface upon gas adsorption See Entry 62483

Thermally stimulated surface currents in CH_3OH crycondensates near the polymorphic phase transformation See Entry 62881

73.30 SURFACE DOUBLE LAYERS, SCHOTTKY BARRIERS, AND WORK FUNCTIONS

62480 Work function measurements on ion bombardment damaged (111) surface of silver by photoelectric and CPD methods. M.Chelvyayohan (Dept. of Pure & Appl. Phys., Queen's Univ. of Belfast, Belfast, N Ireland).

J. Phys. C (GB), vol.16, no.11, p.L323-5 (20 April 1983). Silver (111) surfaces damaged by argon ion bombardment showed a photoelectric work function higher than that measured by the CPD method. This observation is explained as being due to the effect of the surface defects on the surface potential barrier and hence on the photothreshold. (4 refs.)

62481 Electrical properties of Mo-cadmium chalcogenide Schottky barrier diodes. V.B.Bikbaev (V. Kapsukas State Univ., Vilnius, USA), S.C.Karpinskys, J.J.Vaitkus.

Phys. Status Solidi a (Germany), vol.75, no.2, p.583-90 (16 Feb. 1983). The electrical properties of Mo-cadmium chalcogenide Schottky barrier diodes formed by deposition of a semiconductor on Mo substrate in the flow of H_2 are investigated. From analysis of I - U , C - U , and I - T curves the parameters of the diodes are determined. It is found that the dominant current mechanism both, in forward and reverse directions is tunneling. The experimental results are in a good qualitative agreement with theoretical calculations. An inhomogeneous contact model originating from the growth conditions of polycrystalline films is proposed for explaining the quantitative disagreement between theory and experiment. The influence of the inhomogeneous barrier height distribution on the area of the contact on the thermionic emission current is discussed. (14 refs.)

62482 A simple formula for the electron work function of metals. B.Ya.Moizhes, V.A.Nemchinskii (All-Union Sci. Res. Inst. of Current Source Technol. & Design, Leningrad, USSR).

Sov. Phys.-Tech. Phys. (USA), vol.27, no.10, p.1298-300 (Oct. 1982). Translation of: *Zh. Tekh. Fiz. (USSR)*, vol.52, no.10, p.2111-14 (Oct. 1982). [received: April 1983]

In 1956 Gordy and Thomas (see *J. Chem. Phys.*, vol.24, p.439, 1956) established the equation $x_p = 0.44\phi$ (eV) - 0.15 relating the work function ϕ and electronegativity x in metals (here 0.44 and 0.15 are correlation parameters). There are two basic electronegativity scales in use for the chemical elements: the Pauling electronegativity x_p which is calculated from molecular bond energy data, and the Milliken electronegativity $x_M = (I + E)/2$ where I is the ionization potential and E the electron affinity of a free atom. The authors try to account for the equation using the theory of quasifree electrons in a periodic crystal field (which has been used successfully to explain the shape of the Fermi surface). The Wigner-Seitz cell model gives especially simple expressions for the alkali metals. (19 refs.)

Schottky diodes as a possible supplementary method for ionic transport investigations in semiconducting ionic solids—application to n -CdF₂ See Entry 62158

Structure of potassium films on the (1010) face of rhenium See Entry 62274

Acoustoelectric wave in a piezoelectric semiconductor with a Schottky barrier See Entry 62458

73.40 INTERFACES

Charging characteristics of a gallium arsenide surface upon gas adsorption See Entry 62483

73.40B Static electrification

62483 Charging characteristics of a gallium arsenide surface upon gas adsorption. F.E.Shakalov, I.A.Kirovskaya.

Inorg. Mater. (USA), vol.18, no.5, p.609-12 (May 1982). Translation of: *Izv. Akad. Nauk SSSR Neorg. Mater.*, vol.18, no.5, p.720-3 (May 1982). [received: Feb. 1983]

Quantitative characteristics of a real, charged GaAs surface were found through a combination of measurements of surface conductivity, contact potential difference, Hall effect, and current-voltage plus capacitance-voltage characteristics. The results showed satisfactory correlation with the literature as to the original evacuated surface. A mechanism was presented for the surface produced by gas adsorption. (7 refs.)

Irregularity in the electrical conductivity of technical-grade pericase See Entry 62476

73.40L Semiconductor-to-semiconductor contacts, p-n junctions, and heterojunctions

62484 Electric field effect on the thermal emission rate of holes trapped at gold donor center in Si p-n junction. Chen Kaimao, Mao Jinchang (Dept. of Phys., Peking Univ., Peking, China).

Chin. J. Semicond. (China), vol.4, no.2, p.142-8 (March 1983). In Chinese. In the temperature range from 115.2 to 162.3K, the electric field effect on the thermal emission rate of holes trapped at gold donor center in silicon p-n junction has been studied using the capacitance transient technique. The results obtained show that the electric field in the junction has great influence on the thermal emission rate. This influence depends strongly on the temperature. This can be explained by the lowering of the polarization potential barrier caused by the strong electric field in the junction. The form of polarization barrier is $V(r) = -Ar^{-4}$. In the temperature range studied A is from 8.8×10^{-27} to 1.1×10^{-27} eV·cm⁴. The effect of the boundary layer of space charge region on the measured results of the field dependence on thermal emission rate has been considered for the first time and a revised method suggested. (12 refs.)

62485 Energy loss rate in silicon inversion layers. M.C.Payne, R.A.Davies, J.C.Inkson, M.Pepper (Cavendish Lab., Univ. of Cambridge, Cambridge, England).

J. Phys. C (GB), vol.16, no.10, p.L291-9 (10 April 1983). The authors report the results of measurements on the rate of heat loss from hot electrons in silicon inversion layers at low temperatures. The results are interpreted in terms of the generation of acoustic phonons and it is found that disorder has a significant effect on this mechanism. In the low-disorder, high-temperature limit the energy relaxation time τ_e varies with electron temperature T_e as T_e^{-4} . In the high-disorder, low-temperature limit τ_e varies as T_e^{-2} . The electron temperature is measured by the effect on the weak two-dimensional localisation which allows the experiment to be performed at low temperatures. (19 refs.)

62486 Current-carrier transport in semiconducting heterojunctions. II. Experimental data on Si-Zn₃As₂ heterojunction. B.Kochan, J.M.Pawlikowski (Inst. of Phys., Tech. Univ. of Wrocław, Wrocław, Poland).

Mater. Sci. (Poland), vol.7, no.4, p.419-26 (1981). For pt.1 see ibid., vol.6, no.4, p.141 (1980). An application of well-known transport mechanisms of current carriers in semiconductor heterojunctions is discussed for the case of the Si-Zn₃As₂ heterojunction. Experimental results of current-voltage characteristics are compared with the theoretical ones obtained on the basis of the current-transport models and for Si and Zn₃As₂ data, so far available. The best fit was obtained for the Riben-Feucht tunneling-recombination model. The fitting parameters and schematic band diagram of the Si-Zn₃As₂ heterojunction is discussed. (18 refs.)

62487 p-n junctions in GaAs-GaSb solid solutions. A.Ya.Vul', V.N.Karyayev, P.G.Petrosyan, T.A.Polyanskaya, I.I.Saidashev, Yu.V.Shmaritsev (A.F. Ioffe Physicotech. Inst. Acad. of Sci., Leningrad, USSR).

Sov. Phys.-Semicond. (USA), vol.16, no.10, p.1179-82 (Oct. 1982). Translation of: *Fiz. & Tekh. Poluprovodn. (USSR)*, vol.16, no.10, p.1838-42 (Oct. 1982). [received: April 1983]

An investigation was made of p-n junctions in GaAs_{1-x}Sb_x ($x < 0.2$) solid solutions and the influence of mismatch between the lattice parameters of the substrate and epitaxial film on the current-voltage characteristics was analyzed. It was found that the breakdown of p-n junctions was of the tunnel nature. (24 refs.)

62488 Heterojunction formed from gallium selenide and indium selenide by laser melting. V.I.Tagirov, V.M.Salmanov, A.Sh.Mekhtiev, Kh.A.Asadov (S.M. Kirov State Univ., Baku, Azerbaidzhan SSR).

Sov. Phys.-Semicond. (USA), vol.16, no.10, p.1214 (Oct. 1982). Translation of: *Fiz. & Tekh. Poluprovodn. (USSR)*, vol.16, no.10, p.1885-6 (Oct. 1982). [received: April 1983]

Pulsed lasers are now used extensively in heterostructure fabrication. The authors aim was to determine the possibility of fabrication of heterojunctions from layer semiconductors by melting together two plates using high-power laser radiation. Semiconductor plates were irradiated from the wide-gap semiconductor side with a ruby laser operating under free-running conditions. The duration of a pulse was 6 msec. A heterojunction was formed from layer single crystals of p-type GaSe and n-type InSe. (2 refs.)

62489 On the passivation of p-n junctions in silicon through anodic oxidation. G.Mende, K.D.Butter, B.Schmidt (Zentralinst. für Kernforschung, Dresden, Germany).

Thin Solid Films (Switzerland), vol.102, no.1, p.65-9 (8 April 1983). In German.

An application of anodic SiO₂ for the passivation of electronic devices is advantageous especially in cases where low temperature passivation is preferred, e.g. for passivation of p-n junctions. It was demonstrated that the lifetime of minority carriers in silicon did not change after passivation with anodic SiO₂. Only a low current flows through anodically passivated nuclear radiation detectors under reverse bias. Such detectors have many applications, e.g. in α -spectrometry. (10 refs.)

62490 Electric and photoelectric characteristics of CdTe p-n homojunctions. F.Therez, A.Chicouche.

In Cellules solaires constituées de couches minces de CdTe polycrystallines (Solar cells made from polycrystalline CdTe thin films), 11 pp. Report EUR 8154 EN-FR, Comm. European Communities, Luxembourg (1982), 75 pp. In French. Contract 206-76 ESF.

Gives some experimental results on batches of CdTe p-n diodes to determine the fundamental parameters in darkness. These experiments were split into two types. The first type was epitaxial coatings without arsenic additive. Numerous graphs of experimental results are given, together with tabular figures obtained for various features. The second type was epitaxial coatings in the presence of a supplementary source of arsenic atoms. Again, a number of graphical results are presented and also tabular figures for various factors. The final section deals with characteristics under illumination of CdTe p-n epitaxialised diodes. Further graphical results are given, together with a few figures. (no refs.) G.V.D.

Tight binding calculations for band structures and other electronic properties of GaAs-GaP superlattices See Entry 62332

Ground state of two-dimensional electrons in strong magnetic fields and $1/3$ quantized Hall effect See Entry 62432

Photoelectric phenomena accompanying diffraction of X-rays in semiconducting crystals See Entry 62455

An experimental test of the scaling theory of conduction in two dimensions See Entry 62477

Ion etching of InP-InGaAsP heterostructures See Entry 63444

Cellules solaires au CdTe en couches minces polycrystallines. Elaboration par pulvérisation triode et transport a courte distance (CdTe solar cells in polycrystalline thin films. Elaboration for triode sputtering and short distance transport) See Entry 63675

Photovoltaic performance of CdS heterojunctions on polycrystalline silicon See Entry 63699

73.40M Semiconductor-electrolyte contacts

62491 Surface states at the TiO₂/H₂O interface under UV illumination. K.Kobayashi, M.Takata, S.Okamoto (Technol. Univ. of Nagaoka, Nagaoka, Japan), Y.Aikawa, M.Sugigara.

Chem. Phys. Lett. (Netherlands), vol.96, no.3, p.366-70 (8 April 1983).

The donor-like surface states at the TiO₂/H₂O interface were detected by measuring the capacitance under UV illumination. The surface states were located 0.65 eV below the bottom of the conduction band of TiO₂. The density of surface states was increased by increasing the light intensity. The surface states were observed under UV illumination but disappeared in the dark. (20 refs.)

62492 Characterization of the interface energetics for N-type cadmium selenide/nonaqueous electrolyte junctions. A.Aruchamy, J.A.Bruce, S.Tanaka, M.S.Wrighton (Dept. of Chem., MIT, Cambridge, MA, USA).

J. Electrochem. Soc. (USA), vol.130, no.2, p.359-64 (Feb. 1983). Single crystal, n-type CdSe photoanodes have been studied in 0.1M [n-Bu₄N][ClO₄]/CH₃CN solutions containing low concentrations of fast, outer-sphere one electron redox reagents. A number of redox couples were studied spanning a wide range of redox potentials, E° . The authors find that reversible electrochemical response is seen at both dark and illuminated (632.8 nm light) n-CdSe for couples with E° more negative than -1.2 V vs. SCE, e.g. Ru(bpy)₃²⁺/Ru(bpy)₃³⁺. For couples with E° positive of -1.2 V vs. SCE the authors find that CdSe is blocking to the oxidation of the reduced form of the redox couple in the dark, but illumination results in its oxidation. The photoanodic current peak in a cyclic voltammogram occurs more negative than at a Pt electrode, the difference between these values is the photovoltage, E_{ph} , taken to approximate the barrier height, E_b . The effect of a number of different etches on the interface energetics of CdSe was investigated, since it was previously determined that an oxidizing or reducing etch would yield quite different results for n-CdTe. For CdSe, however, the different etches do not give significantly different results with respect to E_b vs. E° , despite large variation in surface composition deduced from Auger and XPS spectra. (19 refs.)

62493 Semiconductor electrodes. XLVII. AC impedance technique for evaluating surface state properties of n-MoTe₂ in acetonitrile solutions containing various redox couples. G.Nagasubramanian, B.L.Wheeler, G.A.Hope, A.J.Bard (Dept. of Chem., Univ. of Texas, Austin, TX, USA). *J. Electrochem. Soc. (USA)*, vol.130, no.2, p.385-91 (Feb. 1983). Measurement of the in-phase (0°) and quadrature (90°) components of a small (12 mV) AC signal at frequencies of 1-5000 Hz imposed on the DC potential allows the determination of the AC equivalent circuit. Study of the AC impedance as a function of potential and frequency permits the determination of the properties of the semiconductor/solution interface. Results of measurements on n-MoTe₂ in MeCN containing various redox couples spanning a wide range of redox potentials are reported. The advantages of the in-phase (0°) component for extracting properties of surface states are discussed. In the region 0.3-0.5 V negative of the valence bandedge, the total surface-state density is ca. 10¹⁵ cm⁻². The adsorption in the I⁻/I₃ system on the n-MoTe₂ surface in aqueous and acetonitrile solvents are compared. (32 refs.)

62494 Open-circuit photopotentials at doped α -Fe₂O₃ electrodes in aqueous solution. R.Shinar, J.H.Kennedy (Dept. of Chem., Univ. of California, Santa Barbara, CA, USA). *J. Electrochem. Soc. (USA)*, vol.130, no.2, p.392-6 (Feb. 1983). The influence of redox couples in aqueous solution on the interface energetics of chemically and thermally doped polycrystalline α -Fe₂O₃ photoanodes has been investigated. Experiments were carried out at several pH values. Results are compared to those obtained from a single crystal electrode. It is shown that the potential of the semiconductor under illumination shifts toward positive values when the energy level of the redox couple in solution is increased. The role that grain boundaries in the sintered electrodes may play, the effect of pH and the redox couple concentration are discussed. (16 refs.)

Microwave absorption studies of interface phenomena at ZnO electrodes See Entry 63582

Ceramic SrTiO₃ photoanodes: enhancement of photoactivity through donor doping See Entry 63717

73.40N Metal-nonmetal contacts

62495 Specific contact resistance of metal-semiconductor ohmic contact. Chen Cunli (Dept. of Phys., Nanjing Univ., China). *Chin. J. Semicond. (China)*, vol.4, no.2, p.191-3 (March 1983). In Chinese. The measurement of the specific contact resistance of M-S ohmic contact is presented using a four-point configuration circular transmission line model. This method eliminates the necessity for the mesa isolation of contact pattern, thus simplifying the sample preparation and calculation. The experimental result is in agreement with the in-line geometry transmission line model. (2 refs.)

62496 Ohmic contact properties of magnesium evaporated onto undoped and P-doped α -Si:H. H.Matsuura, T.Okuno, H.Okushi, S.Yamasaki, A.Matsuda, N.Hata, H.Oheda, K.Tanaka (Electrotech. Lab., Ibaraki, Japan). *Jpn. J. Appl. Phys. Part 2 (Japan)*, vol.22, no.3, p.L197-9 (March 1983). The authors have investigated the current-voltage characteristics of metal/undoped α -Si:H/ n^+ (or p^+) α -Si structures using Mg, Au, Pt, and Al. It has been indicated that the energy band of undoped α -Si:H shows a downward bending against Mg, being analogous to n^+ α -Si:H/undoped α -Si:H contact, while the band shows an upward bending against Au, Pt and Al. Mg/undoped α -Si:H contact is found to allow injection of electrons into the conduction band of α -Si:H, providing a good ohmic contact property. This contact does not exhibit the thermal-degradation at least up to 100°C. (9 refs.)

62497 Effect of heat treatment on the forward current-voltage characteristic of Au-nGaP surface-barrier structures. Yu.A.Gol'dberg, T.A.Laperashvili, G.A.Nakashidze, B.V.Tsarenkov (A.F. Ioffe Physicotech. Inst., Acad. of Sci., Leningrad, USSR). *Sov. Tech. Phys. Lett. (USA)*, vol.8, no.7, p.375-6 (July 1982). Translation of: *Pis'ma v Zh. Tekh. Fiz. (USSR)*, vol.8, no.13-14, p.866-9 (July 1982). [received: April 1983] The authors use results of a study of the effect of heat treatment on the forward current-voltage characteristic to propose a method for developing surface-barrier structures which do not contain an intermediate dielectric layer and which have a forward current-voltage characteristic which corresponds to the ideal Bethe model of thermionic emission. (6 refs.)

Schottky diodes as a possible supplementary method for ionic transport investigations in semiconducting ionic solids—application to n-CdF₂ See Entry 62158

Electrical properties of Mo-cadmium chalcogenide Schottky barrier diodes See Entry 62481

Electroluminescence from ZnS during deformation of a metal contact See Entry 63056

73.40Q Metal-insulator-semiconductor structures (inc. semiconductor-to-insulator)

62498 Interface states induced in silicon by tungsten as a result of reactive ion beam etching. G.Gildenblat, B.A.Heath, W.Katz (Corporate Res. & Dev., General Electric Co., Schenectady, NY, USA). *J. Appl. Phys. (USA)*, vol.54, no.4, p.1855-9 (April 1983). Interface states induced in silicon by reactive ion beam etching (RIBE) have been investigated using a metal oxide semiconductor capacitance-voltage (MOS-CV) technique, secondary ion mass spectrometry (SIMS), and Rutherford backscattering spectrometry (RBS). RIBE using an ion beam extracted from a C₂F₆ plasma was used to selectively remove a layer of SiO₂ from the surface of single crystal silicon. MOS capacitors formed after the regrowth of a thin SiO₂ layer on the silicon showed the presence of a substantial interface state density ($N_{\text{ss}} = 10^{12}$ - 10^{13} eV⁻¹ cm⁻²) near the middle of the energy gap of Si. RBS experiments on the Si surfaces exposed to the reactive ion beam showed the presence of tungsten (presumably from the tungsten filaments used to ignite the plasma and neutralize the ion beam). SIMS depth profiles of these samples after reoxidation to form capacitors showed tungsten contamination which was at a maximum at the SiO₂-Si interface. The interface state density determined from CV measurements scaled linearly with the tungsten concentration at the interface as determined by SIMS. Interface states were formed only in the case where the Si surface was exposed to the reactive ion beam. As little as 10 nm of SiO₂ remaining on the Si surface after RIBE was sufficient to prevent interface states formation. (16 refs.)

62499 A model of conduction in inhomogeneous degenerate semiconductors: Application to silicon-on-sapphire films. J.L.Robert, J.M.Dusseau, P.Girard, J.Sicart (Centre d'Etudes d'Electroniques des Solides, Univ. des Sci. et Tech. du Languedoc, Montpellier, France). *J. Appl. Phys. (USA)*, vol.54, no.4, p.1903-8 (April 1983).

The electrical properties of silicon-on-sapphire films were investigated between 4.2 and 300K. The experimental results can be explained by considering the conduction process exclusively in the transition layer of the Si-Al₂O₃ interface. The properties of silicon-on-sapphire are interpreted in this study by means of a model in which long range fluctuations in potential occur, caused by the existence of inhomogeneities or local defects in the films. (11 refs.)

62500 Determination of the efficiency of electron capture center parameters in the MOS structure dielectric layer. N.I.Gavrulin, G.N.Demidova, E.N.Zhuravlev.

Meas. Tech. (USA), vol.25, no.7, p.618-20 (July 1982). Translation of: *Izmer. Tekh. (USSR)*, vol.25, no.7, p.58-60 (July 1982). [received: Feb. 1983] Deep-seated electron capture centers in the dielectric layer of MOS (metal-oxide-semiconductor) structures of the Al-SiO₂-Si type contribute to the formation of a negative space charge on the oxide when electrons are injected. Such a charge impairs the stability of operating characteristics of MOS devices by changing their threshold voltage, varying the slope of the transfer characteristic of transistors, etc. The theoretical principles of determining the effective electron capture cross section in traps and the effective trap density which can be used for the evaluation of the parameters of charge-carrier capture centers are outlined and an experimental method which enables determination of these parameters is described. Some experimental results for p-type MOS structures are presented. (7 refs.)

62501 Influence of structure defects on the characteristics of warm electrons and holes near the surface of silicon. E.M.Lapidus, E.A.Vygovskaya, A.A.Galaev, P.T.Mustaev (Inst. of Steel & Alloys, Moscow, USSR). *Sov. Phys.-Semicond. (USA)*, vol.16, no.10, p.1232-3 (Oct. 1982). Translation of: *Fiz. & Tekh. Poluprovodn. (USSR)*, vol.16, no.10, p.1909-11 (Oct. 1982). [received: April 1983]

One of the electrophysical parameters most sensitive to the nature of the scattering mechanism predominating in a given semiconductor is the coefficient β in the dependence of the mobility of warm carriers $\mu = \mu_0(1 + \beta E^2)$ on the intensity of a longitudinal field E. In the surface layers of a semiconductor the relationship between the sign of β and the nature of the scattering process can change because of the two-dimensional nature of carrier transport in a narrow potential well. The authors carry out a comparative investigation of the characteristics of warm carriers in MIS structures made of silicon and characterized by different defect densities, and analyze the relationship between the sign of β and the nature of the scattering mechanism in the surface layers of silicon. (7 refs.)

62502 Optimization of multilayer structure for electron-acoustic-surface-wave correlators. V.G.Kadenskii, S.S.Karinskii, V.V.Kryachko. *Sov. Tech. Phys. Lett. (USA)*, vol.8, no.7, p.379-80 (July 1982). Translation of: *Pis'ma v Zh. Tekh. Fiz. (USSR)*, vol.8, no.13-14, p.874-8 (July 1982). [received: April 1983]

The authors derived expressions for the potentials of electron-acoustic surface waves at local points on the surface of a metal-insulator-semiconductor structure away from the interdigital transducers, and use the results to calculate the recording efficiency. (3 refs.)

Standardization of the ohm by means of the Hall effect in silicon metal-oxide semiconductor structures at 0.4-0.7K See Entry 59799

Ion beam hydrogenation of polysilicon coated thermal oxide on silicon See Entry 61941

Electron trapping in thin films of thermal SiO₂ at temperatures between 30 and 300K See Entry 62519

Optimisation of new types of MIS silicon solar cells See Entry 63681

73.40R Metal-insulator-metal structures

62503 Electrical conduction phenomena and negative resistance in Al-Al₂O₃-Au structure. Bong-Heup Kim, Chang-Hi Hong (Korean Inst. Electrical Engrs., Seoul, Korea). *Trans. Korean Inst. Electr. Eng.*, vol.31, no.10, p.101-8 (1982). In Korean.

It is possible to confirm the diffusion effect of Au⁺ ions from an Au anode to the bulk of the thin insulation layer by observing voltage vs current characteristics of the MIM device. The inherent nature of the forming process is not yet clearly disclosed though, at least, the process locally accompanies structural modification in the dielectric layer such as a strongly disordered porous region containing a large number of several kinds of defects. O₂ vacancies and Au⁺ impurities act as localised energy states inside the forbidden band of Al₂O₃. The observed easy conduction mechanism at low voltage may originate in tunneling or hopping of electrons through the series of such localised energy states of the insulator. (17 refs.)

62504 Negative differential resistance in multilayer metal-barrier-metal tunneling structures. E.M.Belenov, I.N.Kompanets, Yu.M.Popov, I.A.Poluektov, S.I.Sagitov, E.M.Soboleva, A.G.Sobolev, A.V.Uskov, V.G.Tsukanov (P.N. Lebedev Phys. Inst., Acad. of Sci., Moscow, USSR).

Sov. Tech. Phys. Lett. (USA), vol.8, no.8, p.422-3 (Aug. 1982). Translation of: *Pis'ma v Zh. Tekh. Fiz. (USSR)*, vol.8, no.15-16, p.978-81 (Aug. 1982). [received: April 1983]

Studies of a metal-barrier-semiconductor-barrier-semiconductor-barrier-metal structure (MBSBSBM). Since the effective mass of the electrons in the semiconductor used in this experiment (In_{0.5}O₃) is 10-20 times smaller than that in a metal, the size quantization of the energy in the conduction band of the semiconductor is seen more clearly than it would be in a metal film. Furthermore, it turns out to be possible to significantly reduce the thickness of the insulating layers (barriers) which separate the semiconducting films from each other. The effective barrier B has a complicated shape, so that a region with a negative differential resistance, small in magnitude, can be produced. It may thus be expected that the structure proposed will prove useful for developing sources and amplifiers of electromagnetic radiation with a continuously tunable frequency over the range 10¹²-10¹⁵ Hz. The small dimensions of these structures and their adaptability to mass production make them promising for use in integrated circuits. (5 refs.)

73.40S Metal-semiconductor-metal structures

Surface-acoustic-wave diffraction grating from thin zinc oxide films See Entry 61367

73.60 ELECTRONIC PROPERTIES OF THIN FILMS

73.60D Metallic thin films

62505 Resistivity and temperature coefficient of resistance of chromium-copper alloy films. A.R.Patel, G.K.Shivakumar (Dept. of Phys., Sardar Patel Univ., Gujarat, India), N.C.Pandya, N.C.Chourasia.

J. Mater. Sci. (GB), vol.18, no.4, p.1028-30 (April 1983). Measurements of electrical resistivity and the temperature coefficient of resistance of vacuum deposited chromium-copper alloy films are reported. The mean free path of the conduction electrons calculated from resistivity data and TCR data is 37.6 and 36.6 nm, respectively. The resistivity and TCR of an infinitely thin film have been computed to be $3.83 \mu\Omega\text{cm}$ and $2.886 \times 10^{-6} \text{ } ^\circ\text{C}^{-1}$, respectively. The experimental data can be satisfactorily explained on the basis of Fuchs-Sondheimer theory assuming a total diffuse scattering. (8 refs.)

62506 On the theory of the spontaneous Hall effect in ferromagnetic films. E.M.Kogan, V.V.Ustinov, E.A.Turov (Inst. of Metal Phys., Acad. of Sci., Sverdlovsk, USSR).

J. Magn. & Magn. Mater. (Netherlands), vol.31-34, pt.2, p.961-2 (Feb. 1983). (Proceedings of the International Conference on Magnetism, Kyoto, Japan, 6-10 Sept. 1982).

The spontaneous Hall coefficient (SHC) of metallic ferromagnetic film is calculated. It is shown that the difference between the SHC of film and that of bulk ferromagnetic is caused by the inhomogeneous distribution of the current across the film and the asymmetric scattering of the conduction electrons on the surface defects. (9 refs.)

62507 Magnetoresistance and Hall effect in amorphous CoZr films. T.Yamagata, S.Ito (Microelectronics Res. Labs., Nippon Electric Co. Ltd., Kawasaki, Japan).

J. Magn. & Magn. Mater. (Netherlands), vol.31-34, pt.3, p.1475-6 (Feb. 1983). (Proceedings of the International Conference on Magnetism, Kyoto, Japan, 6-10 Sept. 1982).

Transport properties for RF sputtered amorphous $\text{Co}_{1-x}\text{Zr}_x$ ($0.05 < x < 0.28$) films have been investigated. It was found that anisotropic magnetoresistance is negative above $x=0.13$, unlike in most 3d alloys. Spontaneous Hall coefficient increased linearly with Zr content and was dominated by the side-jump contribution. (5 refs.)

62508 Resistance change of thin Permalloy films caused by applied stress and its application to strain measurements. S.Shinzato (Faculty of Education, Ryukyuu Univ., Okinawa, Japan), K.Kuwahara.

J. Magn. & Magn. Mater. (Netherlands), vol.35, no.1-3, p.77-9 (March 1983). (Proceedings of the 10th International Colloquium on Magnetic Films and Surfaces, Yokohama, Japan, 13-16 Sept. 1982).

The strain sensitivity of resistance is studied for thin 76Ni-24Fe films having a magnetic uniaxial anisotropy. It is found that a higher strain sensitivity and lower thermal coefficient of resistance than those of the usual strain gauges can be obtained at strains below 2×10^{-4} . (5 refs.)

62509 Composition and temperature dependence of resistivity in amorphous Gd-Co films. H.Okuno, Y.Sakurai (Dept. of Control Engng., Osaka Univ., Osaka, Japan).

J. Magn. & Magn. Mater. (Netherlands), vol.35, no.1-3, p.80-2 (March 1983). (Proceedings of the 10th International Colloquium on Magnetic Films and Surfaces, Yokohama, Japan, 13-16 Sept. 1982).

The composition and temperature dependence of electrical resistivity were studied for a series of amorphous Gd-Co films prepared by an RF-sputtering method. With increasing Gd concentration the electrical resistivity at 4.2K increased from $180 \mu\Omega\text{cm}$ to $350 \mu\Omega\text{cm}$ and the temperature coefficient of resistivity at 288K decreased and became negative above $220 \mu\Omega\text{cm}$. (15 refs.)

62510 Bias voltage effect on electrical resistivity of GdCo amorphous sputtered films. S.Honda, M.Ohkoshi, T.Kusuda (Dept. of Electronics, Hiroshima Univ., Higashi-Hiroshima, Japan).

J. Magn. & Magn. Mater. (Netherlands), vol.35, no.1-3, p.238-40 (March 1983). (Proceedings of the 10th International Colloquium on Magnetic Films and Surfaces, Yokohama, Japan, 13-16 Sept. 1982).

The temperature dependence of electrical resistivity ρ and both the effects of annealing and oxidation on the ρ -values have been investigated in GdCo films sputtered under various substrate bias voltages. It has been found that the oxidized films or the high biased films are unstable crystallographically. (8 refs.)

62511 Electrical properties of 70 wt.%Cr-30 wt.%SiO thin films. M.Milosavljevic, T.M.Nenadovic, N.Bibic, T.Dimitrijevic (Boris Kidric Inst. of Nuclear Sci., Belgrade, Yugoslavia).

Thin Solid Films (Switzerland), vol.101, no.2, p.167-78 (11 March 1983). The electrical and structural properties of flash-evaporated 70 wt.%Cr-30 wt.%SiO cermet films were investigated. It was found that the electrical properties depend on the deposition conditions, thickness of the films, substrate roughness and post-deposition thermal treatment. Structural investigations were made in order to find the causes of variations in the electrical properties of films deposited and thermally treated in different conditions.

The films were produced in the dielectric structural regime, with concentrations of chromium equal to or less than 40 vol.%. The temperature coefficient of resistance varied from -30 to $-200 \text{ ppm } ^\circ\text{C}^{-1}$ and the sheet resistivity varied from 200 to $1400 \Omega/\square$. The concentration and distribution of chromium, which vary with the deposition conditions, have the strongest influence on the electrical properties of the thin films. (12 refs.)

62512 Electrical properties of island aluminium films evaporated onto an NaCl substrate. E.Dobierzewska-Mozrzycka, P.Bieganski, A.Radosz (Inst. Fizyki, Politech. Wroclawska, Wroclaw, Poland), A.Bochenek.

Thin Solid Films (Switzerland), vol.102, no.1, p.77-86 (8 April 1983). Aluminium films with an island structure were evaporated onto an NaCl substrate under conditions of ultrahigh vacuum (10^{-9} Torr) and their electrical properties were examined. The temperature dependence of the film resistance in the range 100-400 $^\circ\text{C}$ was measured in vacuum in situ. Ohmic characteristics of the films were plotted for selected temperatures. The microstructure and crystallographic orientation were determined. (24 refs.)

Thermo-e.m.f. of island metal films See Entry 62402

Insoluble binary system thin film See Entry 62726

Anomalous hysteresis loops in single and double layer sputtered TbFe films See Entry 62748

Oblique incidence effects in evaporated thin films See Entry 62752

A new method for analysis of magnetic anisotropy in films using the spontaneous Hall effect See Entry 62761

73.60F Semiconductor films

62513 Ag_2Se thin film conductivity with a selenium excess. J.-C.Bernede, B.El Bouchairi (Univ. de Nantes, Nantes, France).

C.R. Seances Acad. Sci. Ser. II (France), vol.296, no.3, p.173-6 (24 Jan. 1983). In French.

Experimental results have shown that an excess of selenium (1 to 5%) in Ag_2Se thin films changes the properties of the β low temperature phase. There is a new transition temperature: below this temperature the film is metallic-like, above this temperature the film behaves as a semiconductor. The new metallic-like behaviour is explained by the disorder tied to the mixing of two crystalline structures. The new transition occurs when these crystalline structures give one single new structure. (4 refs.)

62514 Electrical properties of SnO_2 polycrystalline thin films and single crystals exposed to O_2 - and H_2 -gases. T.Yamazaki, U.Mizutani, Y.Iwama (Dept. of Crystalline Materials Sci., Nagoya Univ., Nagoya, Japan).

Jpn. J. Appl. Phys. Part I (Japan), vol.22, no.3, p.454-9 (March 1983).

The electrical conductivity σ and carrier density n have been measured in the range 77-670K for the SnO_2 single crystal and thin films prepared by the vapour deposition technique. It is found that the SnO_2 thin film possesses a carrier density of 10^{19} cm^{-3} , three orders of magnitude larger than that in the as-grown SnO_2 single crystal, and exhibits electrical properties characteristic of a degenerate semiconductor. Both single crystals and thin films undergo irreversible changes in electrical properties upon heat treatment in vacuum or exposure to O_2 - or H_2 -gases. This occurs as a result of reduction and oxidation of SnO_2 . However, the oxidation and reduction proceed in thin films at much lower temperatures than in single crystals. The unique gas-sensing character of thin films was interpreted by assuming that the oxidation and reduction preferentially proceed along the grain boundaries in the thin film. (16 refs.)

62515 Effects of weak electron localization in thin GaAs films. A.K.Savchenko, V.N.Luts'kii, V.I.Sergeev (Inst. of Radio Electronics, Acad. of Sci., Moscow, USSR).

JETP Lett. (USA), vol.36, no.5, p.185-8 (5 Sept. 1982). Translation of: *Pis'ma v Zh. Eksp. & Teor. Fiz. (USSR)*, vol.36, no.5, p.150-2 (5 Sept. 1982). [received: April 1983]

Negative magnetoresistance of GaAs films, which is interpreted on the basis of the theory of localization, is observed. The temperature dependences of the resistance and magnetoresistance are measured; the values of parameters entering into the theory are determined. (5 refs.)

62516 Influence of spontaneous polarization of TGS crystals on the electrical properties of ZnTe thin films. E.Sniadek, W.Gordon (Inst. of Phys., Tech. Univ. of Poznan, Poznan, Poland).

Mater. Sci. (Poland), vol.7, no.4, p.447-51 (1981).

The field effect and electrical resistivity of zinc telluride (ZnTe) thin films evaporated on (010) ferroelectric crystal surface of triglycine sulphate (TGS) were investigated in the range 297-350K to determine the influence of the spontaneous polarization of TGS crystals on changes in electrical resistivity of ZnTe thin films. The relationship $\Delta R(2P)$ in the temperature range 297-315K was found to be linear showing that the change in electrical resistivity of ZnTe thin films in the temperature region investigated is due solely to the spontaneous polarization of TGS. (14 refs.)

62517 Electrical properties of SnTe epitaxial films on mica substrate. S.Santhanam, A.K.Chaudhuri (Dept. of Phys., Indian Inst. of Technol., Kharagpur, India).

Physica B & C (Netherlands), vol.115 B+C, no.2, p.156-60 (Jan. 1983).

Epitaxial films of SnTe were grown on heated mica substrates (448K) and their galvanomagnetic properties were studied between 160 and 300K. The carrier concentration and the mobility for different thicknesses of the films are explained by means of a two valence band model. The mobility values calculated for heavy holes agree well with the experimental values whereas the calculated mobility values of light holes show a peculiar behaviour which cannot be explained if the band is assumed to be parabolic. (27 refs.)

62518 Thermoelectric properties of thin polycrystalline films. B.Ya.Balagurov.

Sov. Phys.-Semicond. (USA), vol.16, no.10, p.1204-5 (Oct. 1982). Translation of: *Fiz. & Tekh. Poluprovodn. (USSR)*, vol.16, no.10, p.1870-2 (Oct. 1982). [received: April 1983]

The author considers the thermoelectric properties of thin polycrystalline films (two dimensional polycrystals) using the Dykne method (1971). (3 refs.)

X-ray diffraction analysis of SnO_2 films prepared by oxidation of tin films See Entry 62306

Anomalous transient-time dispersion in amorphous solids: oxadiazole See Entry 62414

Photothermopower of a- As_2Te_3 sputtered films See Entry 62447

A physicochemical interpretation of the photoconductivity of a-Si:H See Entry 62449

Refractive index in epitaxial $\text{Pb}_{1-x}\text{Sn}_x\text{Te}$ films See Entry 62919

Characterisation of Mn-doped and nominally pure LPE $\text{Ga}_{1-x}\text{Al}_x\text{As}_2\text{P}_{1-y}$ ($y=2.1x$) between $y=0$ and $y=1$ using photoluminescence and electrical measurements See Entry 63039

Optical and electrical properties of a-Si $_x\text{C}_{1-x}\text{H}$ films prepared by glow discharge from SiH_4 and C_2H_4 See Entry 63075

Novel plasma chemical methods for doping a-Si:H See Entry 63177

Reproducibility of low carrier concentration in LPE InP using batch melts See Entry 63180

A solution growth technique for the preparation of copper(II) selenide thin films See Entry 63181

Deposition of cadmium chalcogenide thin films by a solution growth technique using triethanolamine as a complexing agent See Entry 63184

Cellules solaires au CdTe en couches minces polycristallines. Elaboration par pulvérisation triode et transport a courte distance (CdTe solar cells in polycrystalline thin films. Elaboration for triode sputtering and short distance transport) See Entry 63675

Large area hydrogenated amorphous silicon for photovoltaic application See Entry 63697

73.60H Insulating thin films

62519 Electron trapping in thin films of thermal SiO₂ at temperatures between 30 and 300K. M.Itsumi (Musashino Electrical Communication Lab., Nippon Telegraph & Telephone Public Corp., Tokyo, Japan). *J. Appl. Phys. (USA)*, vol.54, no.4, p.1930-6 (April 1983). Temperature dependence of electron trapping in thermally grown SiO₂ has been studied using metal-silicon dioxide-silicon (MOS) structures. The MOS samples are charged using avalanche injection from the Si substrate at temperatures between 30 and 300K. It is found that the rate of electron trapping increases monotonically as temperature decreases from 300 to 30K for both oxides subjected to H₂/N₂ annealing and oxides subjected to no H₂/N₂ annealing. The majority of electrons trapped at 77K is thermally reemitted, as the samples are warmed to room temperature. Analyses of the experimental results indicate that neutral trap centers responsible for electron trapping are characterized by the two discrete energies of 23 and 4 meV below the conduction band edge of SiO₂. (30 refs.)

62520 Characteristics of magneto-resistive films controlled by grating surface of substrate. N.Nomura, N.Kaminaka (Materials Res. Lab., Matsushita Electric Co. Ltd., Osaka, Japan). *J. Magn. & Magn. Mater. (Netherlands)*, vol.35, no.1-3, p.83-5 (March 1983). (Proceedings of the 10th International Colloquium on Magnetic Films and Surfaces, Yokohama, Japan, 13-16 Sept. 1982). Uniaxial magnetic anisotropy of a vacuum deposited magneto-resistive (MR) Al₂O₃ element is found to be induced by ruled surface roughness of a grated substrate, and a magnetostatic interpretation for the anisotropy is given. The response of MR element biased by grating-induced anisotropy shows excellent linearity without hysteresis. (5 refs.)

62521 Electronic properties of doped amorphous SiO_x. E.Holzenkammer, J.Stuke, R.Fischer (Fachbereich Phys., Univ. Marburg, Marburg, Germany). Fourth E.C. Photovoltaic Solar Energy Conference. Proceedings of the International Conference, Stresa, Italy, 10-14 May 1982 (Dordrecht, Netherlands: Reidel 1982), p.778-82. Films of a-SiO_xH (0 ≤ x ≤ 1) were prepared in a glow discharge of SiH₄-N₂O-mixtures. It is found that the band gap widens at a rate dE_g/dx = 1 eV. For fixed oxygen content, the band gap shrinks upon doping. This effect sets in at about 10¹⁹ ppm B; on the P side this effect is much weaker. For x = 0.23, the maximum values for the dark conductivity are ≈ 3.10⁻⁵ Ω⁻¹ cm⁻¹ (B-doping) and ≈ 10⁻⁶ Ω⁻¹ cm⁻¹ (P-doping). (6 refs.)

Formation of cubic boron nitride films by boron evaporation and nitrogen ion beam bombardment See Entry 63159

73.60K Superconducting films

Observation of vortex structures near a resistive transition in granular aluminum films See Entry 62524

X-ray diffraction and EPR studies of NbGe high T_c films See Entry 62528

Fluctuation enhanced electrical conductivity of Ge-covered superconducting films of tin See Entry 62530

The longitudinal critical current of a thin film of type II superconductors See Entry 62532

Magnetic property changes in epitaxial metal film sandwiches See Entry 62730

74.00 SUPERCONDUCTIVITY

74.10 OCCURRENCE, CRITICAL TEMPERATURE

62522 Electron-phonon coupling constant and critical temperature of binary and ternary superconducting alloys of Mo, Nb, Ta and V. P.Chatterjee (Dept. of General Phys. & X-rays, Indian Association for the Cultivation of Sci., Jadavpur, Calcutta, India). *Indian J. Cryog.*, vol.7, no.3, p.130-4 (1982). The modified version of the theory of Gaspari and Gyorffy (1972) for calculating the electron-phonon coupling constants, λ, for binary substitutional alloys has been used together with Allen and Dynes' expression (1975) for the superconducting transition temperature, T_c, to obtain λ and T_c for the superconducting alloys: NbTa, NbV, VMo and TaMo. The theory has been further extended via the average t-matrix approximation (ATA) to calculate λ and T_c for the ternary alloy: NbTaMo, having the same BCC structure as its components. The results agree favourably with experiments for NbTa, NbV and VMo. For TaMo and NbTaMo, for which experiments on T_c are yet to be performed, the authors predict that these are fairly good superconductors. (7 refs.)

62523 Some observations on the superconductivity of TaS₂ intercalated by pyridine. K.A.Kini (Central Fuel Res. Inst., Dhanbad, India). *Indian J. Cryog.*, vol.7, no.3, p.153 (1982). Intercalation of compounds of the type NbS₂, TaSe₂, and PdTe₂, by nitrogenous bases such as pyridine, and consequent exhibition of elevation of critical temperature of superconductivity, is a well-known phenomenon. However, this phenomenon does not seem to have been explained satisfactorily. The author offers some brief observations in order to explain the increase in critical temperature of TaS₂ intercalated by pyridine. (2 refs.)

62524 Observation of vortex structures near a resistive transition in granular aluminum films. V.Yu.Tarenkov, A.I.D'yachenko, V.V.Stupakov (Physicotech. Inst., Acad. of Sci., Donetsk, Ukrainian SSR). *Sov. Phys.-Solid State (USA)*, vol.24, no.9, p.1458-60 (Sept. 1982). Translation of: *Fiz. Tverd. Tela (USSR)*, vol.24, no.9, p.2569-73 (Sept. 1982). [received: April 1983]

Thermally excited vortex structures near a superconducting transition in thin films of aluminum were discovered by the use of a superconducting DC transformer circuit. (10 refs.)

High-pressure phases in B group element alloys: a new sort of electronic phase See Entry 62096

Synthesis of Al₁₅Nb₃Ge by pulsed laser annealing See Entry 62282

74.20 THEORY

62525 On an approximate form of the coupled equations of the order parameter with the weak electromagnetic field for the ideal superconductor. Su Zhao-bin, Chou Kuang-chao (Inst. of Theoretical Phys., Acad. Sinica, Beijing, China).

Commun. Theor. Phys. (China), vol.1, no.6, p.669-79 (1982). A simplified derivation of the macroscopic electrodynamic equations of Umezawa, Mancini et al. (1974) for superconductors is given in the framework of the closed time path Green's functions (CTPGF) using generalized Ward-Takahashi identities. It is shown that the forms of the equations obtained are the same for both thermoequilibrium and nonequilibrium stationary states provided the electromagnetic field is weak and its effect on the modulus of the order parameter can be neglected. The statistical behavior of the states is completely specified in the equations by parameters which can be calculated by the method of CTPGF. (9 refs.)

62526 The London equations for superconductors in a gravitational field. D.K.Ross (Dept. of Phys., Iowa State Univ., Ames, IA, USA).

J. Phys. A (GB), vol.16, no.6, p.1331-5 (21 April 1983). The author derives the modified London equations for a superconductor in a gravitational field, writes these equations in an elegant covariant form, and shows that these equations are consistent with the modified fluxoid quantisation condition in a gravitational field found by DeWitt (1966). (12 refs.)

Electron-phonon coupling constant and critical temperature of binary and ternary superconducting alloys of Mo, Nb, Ta and V See Entry 62522

74.30 GENERAL PROPERTIES

74.30C Magnetization curves, Meissner effect, penetration depth

62527 Meissner effect and magnetic field dependence of Cu clad Nb in mK region. Y.Oda, A.Sumiyama, H.Nagano (Inst. for Solid State Phys., Univ. of Tokyo, Tokyo, Japan).

Jpn. J. Appl. Phys. Part 1 (Japan), vol.22, no.3, p.464-6 (March 1983). The Meissner region induced by the proximity effect in a thick Cu clad Nb wire is measured down to 4.5 mK. It is found that the thickness ρ of the Meissner region in Cu increases with decreasing temperature in proportion to T^{-1/2}. The magnetic field dependence of ρ is also studied in this temperature region. It is found that ρ decreases in proportion to ln H except for the very low field region, if ρ is sufficiently smaller than the thickness of Cu. An if ρ becomes comparable to the thickness of Cu, an anomalous behaviour is observed.

74.30G Response to electromagnetic fields, nuclear magnetic resonance, ultrasonic attenuation

62528 X-ray diffraction and EPR studies of NbGe high T_c films. S.N.Ekbote, S.K.Gupta, K.C.Nagpal, A.V.Narlikar (Nat. Phys. Lab., New Delhi, India).

Indian J. Cryog., vol.7, no.3, p.140-2 (1982). The EPR and X-ray diffraction studies were carried out on superconducting Nb₃Ge films. These films were prepared by DC sputtering in argon and oxygen atmospheres and their T_c ranges from 8K to 22.65K. The EPR spectra were systematically studied from ambient to liquid air temperature. However, this study failed to reveal any form of oxygen present in these films though some other EPR signals were recorded. The X-ray study could not detect the formation of any oxide phase. These results suggest that oxygen is mainly behaving as a stabilizer for forming the A-15 Nb₃Ge phase, in agreement with other workers. (5 refs.)

62529 Energy gap in superconducting lead by ultrasonic technique. S.Sathish (Regional Coll. of Education Mysore, Mysore, India), B.K.Basu.

Indian J. Cryog., vol.7, no.3, p.150-2 (1982). Describes an experimental arrangement for the measurement of the energy gap in superconducting lead by an ultrasonic technique. The ultrasonic attenuation is measured in the normal and superconducting states by the usual pulse echo technique. The temperatures below 4.2K were attained by pumping liquid helium and temperatures above 4.2K were attained by varying the amount of exchange gas in the experimental chamber. The temperature stability above 4.2K is discussed and a brief outline of the cryostat is given. Some preliminary results on the energy gap are presented. (3 refs.)

74.40 FLUCTUATIONS AND CRITICAL EFFECTS

62530 Fluctuation enhanced electrical conductivity of Ge-covered superconducting films of tin. P.N.Dheer, R.S.Parashar (Dept. of Phys. & Astrophys., Univ. of Delhi, Delhi, India).

Indian J. Cryog., vol.7, no.3, p.147-9 (1982). Measurements of the fluctuation induced excess electrical conductivity, σ_f, above the superconducting transition temperature T_c, of thin films of tin with a protective covering of Ge have been carried out to investigate the effect of the superconducting-semiconductor interface on the thermodynamic fluctuations of the superconducting order parameter. The pair-breaking parameter δ, for covered films is found to be greater than that for the uncovered films. The experimental results also suggest that δ increases exponentially with the normal state sheet resistance of Ge-covered films. (10 refs.)

74.50 PROXIMITY EFFECTS, TUNNELLING PHENOMENA, AND JOSEPHSON EFFECT

62531 Fabrication of the weak-link Josephson junction on a microstep. G.Uehara, M.Nakanishi, K.Hara (Dept. of Math. Engng. & Instrumentation Phys., Univ. of Tokyo, Tokyo, Japan).

Jpn. J. Appl. Phys. Part 1 (Japan), vol.22, no.3, p.544 (March 1983). Theoretically, a weak-link type junction gives an ideal Josephson effect when the dimension of the weak-link is comparable with the coherence length ξ. Some workers have tried to fabricate weak-links along this line have succeeded to an extent. But in each of the above cases, the fabrication process is rather complicated or submicrometer patterning was essential. The authors report a new fabrication process, which is simple and does not need submicrometer patterning technology. (8 refs.)

Thin-film fourteen-hole DC SQUID gradiometer See Entry 59800

Meissner effect and magnetic field dependence of Cu clad Nb in mK region See Entry 62527

74.60 TYPE-II SUPERCONDUCTIVITY

74.60E Mixed state, H_{c2} , surface sheath

- Superconductivity in ternary compounds. II. Superconductivity and magnetism See Entry 59553
 A temperature-variable sample rotating cryostat in high magnetic fields See Entry 59788
 The longitudinal critical current of a thin film of type II superconductors See Entry 62532

74.60G Flux pinning; fluxon-defect interactions

- Observation of vortex structures near a resistive transition in granular aluminum films See Entry 62524

74.60J Critical currents

- 62532 The longitudinal critical current of a thin film of type II superconductors. Wu Hang-sheng, Gu Yi-ming (Univ. of Sci. & Technol. of China, Hefei, China). *Commun. Theor. Phys. (China)*, vol.1, no.6, p.681-90 (1982).
 The structure of the mixed state of a current-carrying thin film of ideal type II superconductors in longitudinal magnetic field H_z is analysed. It is shown that the lossless current flow through the films in the mixed state is possible only if H_z is larger than $H_{c1}(d)$. The curves of longitudinal critical current obtained have complex structures and show the peak effect in general. The main features of the theoretical I_c - H_z curve of the films with thickness d larger than 5λ are identical with those observed by Heaton and Rose-Innes in $Nb_{55}Ta_{45}$ alloys. (16 refs.)
 Superconductivity in ternary compounds. II. Superconductivity and magnetism See Entry 59553

74.70 SUPERCONDUCTING MATERIALS

74.70D Material effects on T_c , K , critical currents

(see also 81.40R Electrical properties related to materials treatment)

- X-ray diffraction and EPR studies of NbGe high T_c films See Entry 62528
 Studies on fabrication of superconducting V_3Ga wires See Entry 63202

74.70G Type-I superconductors (non transition metals)

- Observation of vortex structures near a resistive transition in granular aluminum films See Entry 62524
 Energy gap in superconducting lead by ultrasonic technique See Entry 62529

74.70L Type-II superconductors (transition metals, alloys and compounds)

- Superconductivity in ternary compounds. II. Superconductivity and magnetism See Entry 59553
 A temperature-variable sample rotating cryostat in high magnetic fields See Entry 59788
 Synthesis of Al_5Nb_3Ge by pulsed laser annealing See Entry 62282
 Observation of vortex structures near a resistive transition in granular aluminum films See Entry 62524
 Meissner effect and magnetic field dependence of Cu clad Nb in mK region See Entry 62527
 X-ray diffraction and EPR studies of NbGe high T_c films See Entry 62528
 Magnetic property changes in epitaxial metal film sandwiches See Entry 62730
 Studies on fabrication of superconducting V_3Ga wires See Entry 63202

75.00 MAGNETIC PROPERTIES AND MATERIALS

(see also 81.40R Magnetic properties related to materials treatment; for galvanomagnetic effects, see 72.15G and 72.20M; for magneto-optical effects, see 78.20L)

75.10 GENERAL THEORY AND MODELS OF MAGNETIC ORDERING

(see also 05.50 Ising problems, 71.25 Nonlocalized single-particle electronic states, 71.70 Level splitting and interactions)

- Two-dimensional iterated mapping for the mean-field theory of the chiral Potts model See Entry 59729

75.10D Crystal-field theory and spin Hamiltonians

- 62533 Cooperative quadrupolar ordering of Yb^{3+} ions in the Γ_8 electronic state. F.Hartmann-Boutron (Spectrometrie Phys., Univ. Sci. et Médicale Grenoble, Grenoble, France). *J. Magn. & Magn. Mater. (Netherlands)*, vol.31-34, pt.3, p.1079-80 (Feb. 1983). (Proceedings of the International Conference on Magnetism, Kyoto, Japan, 6-10 Sept. 1982).
 In connection with experiments on $YbCo_2$ the authors investigate theoretically the quadrupolar ordering of Yb^{3+} ions whose lowest electronic state is a Γ_8 quadruplet. Previous studies (devoted to $S=3/2$ or to Γ) assumed that only one component of the quadrupole was nonzero, but allowed for magnetic ordering. The present work is limited to pure quadrupolar ordering but all five components of the quadrupole are assumed to be nonzero. The authors

find two infinite families of degenerate solutions; the physical implications of these degeneracies are examined. (6 refs.)

- 62534 A singlet-singlet model for amorphous alloys with praseodymium. A.K.Bhattacharjee, B.Coqblin (Lab. de Phys. des Solides, Univ. Paris-Sud, Orsay, France). *J. Magn. & Magn. Mater. (Netherlands)*, vol.31-34, pt.3, p.1575-6 (Feb. 1983). (Proceedings of the International Conference on Magnetism, Kyoto, Japan, 6-10 Sept. 1982).
 A singlet-singlet model for induced magnetism in amorphous systems is developed by assuming a random distribution of the energy splitting over the rare-earth sites and the induced ordering is computed for both the ferromagnetic and the antiferromagnetic cases. The results agree with experiments on amorphous $Pr_{x}La_{30-x}Au_{20}$ alloys. (5 refs.)
 The influence of nuclear quadrupole interactions upon electron spin-echo modulation induced by weak hyperfine interactions See Entry 62797

75.10H Ising and other classical spin models

- 62535 The condensation of spin-1/2 lattice bosons. P.Fazekas (Inst. für Theoretische Phys., Univ. zu Köln, Köln, Germany), P.Entel. *Z. Phys. B (Germany)*, vol.50, no.3, p.231-8 (1983).
 The authors study the effect of an antiferromagnetic, Ising-like boson-boson interaction on the formation and structure of the Bose-condensed phases of a spin-1/2 Bose lattice gas. Their model is similar to those used in the description of spin-aligned atomic hydrogen. A mean-field treatment gives two Bose-condensed phases: one without, and one with a transverse component of the magnetisation. For a range of interaction strength, the system condenses first into a symmetrical state and, at a lower temperature, the condensate breaks the symmetry of the interaction with the appearance of transverse magnetisation. (17 refs.)
 62536 Multi-soliton solutions for a classical ferromagnetic chain. Pu Fuchou, Zhou Xin, Li Bozang (Inst. of Phys., Acad. of Sinica, Beijing, China). *Commun. Theor. Phys. (China)*, vol.2, no.1, p.797-802 (1983).
 The authors report the multisoliton solutions of the Landau-Lifshitz equation for a classical ferromagnetic chain and their asymptotic behaviors as well as the formulae for the shifts at their phases and centers of mass. They include the single- and double-soliton solutions as particular cases. (9 refs.)
 62537 Degenerate helimagnetic states, lines of soft modes and absence of long-range order in three dimensions. E.Rastelli, L.Reatto, A.Tassi (Istituto di Fisica, Univ. di Parma, Parma, Italy). *J. Phys. C (GB)*, vol.16, no.11, p.L331-5 (20 April 1983).
 The triangular and hexagonal classical Heisenberg model with suitable competing intraplane interactions have infinitely many ground states having inequivalent helical order of different pitch Q . The spin wave energy vanishes along a line in k space, the locus of the Q vectors. Helimagnetic long-range order is destroyed at finite temperature also in three dimensions. The existence of a new phase is suggested: an isotropic helimagnet that leads to a characteristic ring scattering. The effect of quantum corrections and of easy plane anisotropy is also considered. (8 refs.)
 62538 Two-dimensionally modulated phase in Ising models. Y.Saito (Inst. für Festkörperforschung, KFA Jülich, Jülich, Germany). *J. Magn. & Magn. Mater. (Netherlands)*, vol.31-34, pt.3, p.1049-51 (Feb. 1983). (Proceedings of the International Conference on Magnetism, Kyoto, Japan, 6-10 Sept. 1982).
 The possibility of an incommensurate phase with two-dimensional modulation is studied for spin 1/2 Ising models on a triangular lattice with antiferromagnetic nearest and next nearest neighbor interactions. A three dimensional system consisting of stacked triangular layers is also studied. (11 refs.)
 62539 One-dimensional decorated lattice: the $\nu \rightarrow \infty$ limit. L.L.Goncalves (Dept. de Fisica, Univ. Fortaleza, Fortaleza, Brazil), J.R.L.de Almeida. *J. Magn. & Magn. Mater. (Netherlands)*, vol.31-34, pt.3, p.1218-20 (Feb. 1983). (Proceedings of the International Conference on Magnetism, Kyoto, Japan, 6-10 Sept. 1982).
 It is shown that a one-dimensional model composed of Ising ($s=1/2$) and classical (ν -components) spin in the limit $\nu \rightarrow \infty$ can be mapped into the spherical model provided the exchange constant is suitably renormalized. By introducing a new technique the n -spin correlation functions are obtained and it is shown that the procedure can be applied to the model in arbitrary d -dimensional lattices. (5 refs.)
 62540 Transverse spin correlation function of the one-dimensional spin-1/2 XY model in a longitudinal magnetic field. T.Tonegawa (Dept. of Phys., Kobe Univ., Kobe, Japan). *J. Magn. & Magn. Mater. (Netherlands)*, vol.31-34, pt.3, p.1223-4 (Feb. 1983). (Proceedings of the International Conference on Magnetism, Kyoto, Japan, 6-10 Sept. 1982).
 The transverse spin correlation function and the transverse inverse correlation length of the one-dimensional spin-1/2 XY model in a longitudinal magnetic field are calculated exactly. It is shown that the longitudinal magnetic field has a marked effect on the transverse inverse correlation length at low temperatures. (4 refs.)
 62541 Modulated phases in diluted ANNNI models. T.Kawasaki (Phys. Dept., Coll. of Liberal Arts, Kyoto Univ., Kyoto, Japan). *J. Magn. & Magn. Mater. (Netherlands)*, vol.31-34, pt.3, p.1469-70 (Feb. 1983). (Proceedings of the International Conference on Magnetism, Kyoto, Japan, 6-10 Sept. 1982).
 Persistence of the modulated phases in an anisotropic Ising model with nearest- and next-nearest-neighbor interactions is examined in the diluted system, by using the high-temperature series expansion. There appears to be no remarkable difference from the pure system in the wider range of concentration. (6 refs.)
 62542 Reply to 'Comment on "Canonical-ensemble results for the Ising model with random bonds in two dimensions"'. J.F.Fernandez (Centro de Fisica, Inst. Venezolano Investigaciones Cientificas, Caracas, Venezuela). *Phys. Rev. B (USA)*, vol.27, no.7, p.4486-7 (1 April 1983).
 For original paper see *ibid.*, vol.25, p.417 (1982). In the previous Comment (reference unobtainable), Binder and Morgenstern use their previous result, $\langle S_i S_j \rangle^2 = c \exp(-r_{ij}/\xi)$ for small systems, plus their hypothesis that ξ and c depend weakly on L , to produce results strongly similar to what the author has obtained previously. They thus suggest that his results, contrary to his own conclusion, do not indicate the existence of a critical point in the Edwards-Anderson model in two dimensions. The author shows here that their claim is not well founded. (3 refs.)
 Determination of the Ising critical temperature of F slices with an application to garnet See Entry 61836
 Cluster decimation derivation of exact percolation-thermal crossover exponent in dilute spin models See Entry 62543

- Surface effects in Ising ferromagnets with anisotropy See Entry 62649
 Phase transitions on fractals. I. Quasi-linear lattices See Entry 62650
 Modulated structures of an Ising spin system on a triangular lattice See Entry 62655

75.10J Heisenberg and other quantized localized spin models

- 62543 Cluster decimation derivation of exact percolation-thermal crossover exponent in dilute spin models. R.B.Stinchcombe (Dept. of Theoretical Phys., Oxford Univ., Oxford, England). *J. Phys. A (GB)*, vol.16, no.6, p.1289-306 (21 April 1983). It is shown that the decimation method of renormalisation group theory in a restricted parameter space, applied to any cluster, gives the exact unit value for the percolation-thermal crossover exponent for bond-diluted Ising, Potts and anisotropic Heisenberg models. (19 refs.)
 Degenerate helimagnetic states, lines of soft modes and absence of long-range order in three dimensions See Entry 62537
 On the two-dimensionality of $\text{Fe}(\text{HCOO})_2 \cdot 2\text{H}_2\text{O}$ See Entry 62670
 Nonlinear field theory of large-spin Heisenberg antiferromagnets: semiclassically quantized solitons of the one-dimensional easy-axis Neel state See Entry 62674
 The Heisenberg model: dynamical interactions including odd-boson terms See Entry 62677

75.10L Band and itinerant models

- The spin polarisation of conduction electrons in a ferromagnetic semiconductor See Entry 62335
 Charge and spin locations in linear stacks of TCNQ See Entry 62340
 Temperature-induced local moments in MnSi and FeSi See Entry 62549
 Magnetism of amorphous metal-metal alloys See Entry 62566
 X_α method for the magnetic transition state and exchange interactions in KNiF_3 See Entry 62579
 The effect of paramagnetic impurities on the wave-vector of the spin-density-wave of an itinerant electron antiferromagnet See Entry 62598

75.20 DIAMAGNETISM AND PARAMAGNETISM

- 62544 Effects of dimensionality and randomness on magnetism of Heisenberg parameters. K.Kawasaki, R.A.Tahir-Kheli (Phys. Dept., Nara Women's Univ., Nara, Japan). *J. Magn. & Magn. Mater. (Netherlands)*, vol.31-34, pt.3, p.1246-8 (Feb. 1983). (Proceedings of the International Conference on Magnetism, Kyoto, Japan, 6-10 Sept. 1982). Both the statics and the dynamics of a randomly diluted quasi-low dimensional Heisenberg paramagnet are analyzed in terms of high temperature series expansions. Despite the relative shortness of the series, some crossover effects arising from the interplay between changes in dimensionality and randomness are noticed. (5 refs.)
 Curie-Weiss behavior in ferrofluids See Entry 62716

75.20C Nonmetals

- 62545 Magnetochemical study of titanium dioxide doped with tantalum pentoxide. M.A.Kvantov, Yu.P.Kostikov, A.I.Leonov. *Inorg. Mater. (USA)*, vol.18, no.6, p.886-8 (June 1982). Translation of: *Izv. Akad. Nauk SSSR Neorg. Mater.*, vol.18, no.6, p.1049-51 (June 1982). [received: Feb. 1983]
 The semiconducting properties of doped titanium dioxide may be explained by the appearance of trivalent titanium ions. The authors attempt to determine the physicochemical processes responsible for the appearance and stabilization of trivalent titanium in titanium dioxide when it is doped. X-ray diffraction investigations were performed. The temperature dependence of the magnetic susceptibility was measured by the Faraday method in the range 3-300K. ESCA and X-ray spectral microanalysis were used. (7 refs.)
 62546 On magnetic properties of some molybdenum oxides. H.Gruber (Inst. fur Festkorperphys., Tech. Univ. Graz, Graz, Austria), H.Haselmair, H.P.Fritzer. *J. Solid State Chem. (USA)*, vol.47, no.1, p.84-91 (15 March 1983). The temperature dependence of the magnetic susceptibility for the microcrystalline compounds MoO_3 , $\eta\text{-Mo}_2\text{O}_{11}$, $\gamma\text{-Mo}_2\text{O}_{11}$, Mo_7O_{27} , Mo_8O_{23} , Mo_9O_{26} , and $\text{Mo}_{10}\text{O}_{32}$, respectively, has been investigated between 77 and 550K at various external fields. The susceptibility increases slightly with temperature for all solids. At low temperatures the changes are more pronounced for $\eta\text{-Mo}_2\text{O}_{11}$, $\gamma\text{-Mo}_2\text{O}_{11}$, Mo_7O_{27} , and $\text{Mo}_{10}\text{O}_{32}$. The deviations from stoichiometry and the related changes in the concentration of charge carriers have a large influence on the values of the susceptibility. Furthermore, some indications of anisotropy were found. (19 refs.)
 62547 Investigation of the magnetic behaviour of the copper ions in some borate oxide glasses. Gh.Ilonca, I.Ardelean (Faculty of Phys., 'Babes-Bolyai' Univ., Cluj-Napoca, Rumania). *J. Magn. & Magn. Mater. (Netherlands)*, vol.31-34, pt.3, p.1427-8 (Feb. 1983). (Proceedings of the International Conference on Magnetism, Kyoto, Japan, 6-10 Sept. 1982). Using X-ray analysis, electron microscope and magnetic susceptibility measurements some borate oxide glasses with different glass matrix modifiers (Pb, Li, K) have been studied together with various contents of CuO , prepared in the same conditions. The valence states and distribution mode of copper ions depend of the glass matrix modifiers. (5 refs.)
 The isostructural sulfides: Sr_2SnS_2 and Eu_2SnS_2 See Entry 61865
 Soliton-phonon scattering in TMMC and DMMC See Entry 62192
 Enhanced NMR of ^{169}Tm in TmAsO_4 See Entry 62816
 Mossbauer study of acicular iron-nitride particles See Entry 62858

75.20E Metals and alloys

- 62548 Longitudinal and transverse fluctuations of the spin density in alpha manganese. P.J.Brown, K.R.A.Ziebeck (Inst. Laue-Langevin, Grenoble, France), J.G.Booth, H.Capellmann. *Z. Phys. B (Germany)*, vol.50, no.3, p.223-30 (1983). Polarised neutrons and polarisation analysis have been used to investigate the paramagnetic scattering from a powder sample of alpha manganese. A significant level of paramagnetic scattering was observed at all wave vectors with two peaks located at 1.25 and 2.0 \AA^{-1} . The anti-ferromagnetic spatial correlations giving rise to the observed peaks were found to persist beyond 5 T_N . Between 100 and 300K (i.e. up to 3 T_N) the paramagnetic scattering was found to increase with temperature for all wave vectors thus indicating an increase in the amplitude of the spin density. Above 3 T_N the scattering was found to decrease with increasing temperature. It is concluded that both transverse (angular) and longitudinal (amplitude) fluctuations of the spin density are important in defining the paramagnetic properties of alpha manganese. (26 refs.)
 Structural relaxation in (Fe-Cr)-based glass See Entry 61811
 Atomic ordering in solid solutions See Entry 61844
 Crystal field splittings of PrX_2 compounds (X=Pt, Rh, Ir, Ru, Ni) studied by inelastic neutron scattering See Entry 62381
 Electronic properties of bulk copper-aluminum and copper-zinc alloys See Entry 62395
 Magnetic and galvanomagnetic properties of rare earth intermetallic compounds of $\text{RAg}_{1-x}\text{In}_x$ (R=Gd, Tb, and Dy) See Entry 62400
 The spontaneous magnetization of nickel See Entry 62693
 NMR in metallic glasses See Entry 62817

75.20H Local moment in dilute alloys; Kondo effect (see also 72.15Q Electronic conduction)

- 62549 Temperature-induced local moments in MnSi and FeSi. S.N.Evangelou, D.M.Edwards (Dept. of Maths., Imperial Coll., London, England). *J. Phys. C (GB)*, vol.16, no.11, p.2121-31 (20 April 1983). A unified theory is given of the magnetic and thermal properties of the itinerant-electron magnet MnSi and the non-magnetic semiconductor FeSi. The calculations are based on the spin-fluctuation theory of Hasegawa (1981) and employ a model density of states derived from an existing band calculation. The exchange parameter is determined to give the observed spontaneous moment in MnSi at $T=0$. The finite-temperature properties are then calculated without adjustable parameters and semi-quantitative agreement with experiment is obtained for the temperature dependence of the susceptibility of MnSi and for the unusual susceptibility and specific heat of FeSi. In both materials the root-mean-square atomic moment increases rapidly with increasing temperature to values of 1.0-1.5 μ_B . The associated fluctuating exchange fields destroy the band gap in FeSi which explains the similarity in the resistivity of FeSi and MnSi for $T>400\text{K}$. (33 refs.)
 62550 Thermodynamic properties of the Anderson model. A.Okiji, N.Kawakami (Dept. of Appl. Phys., Osaka Univ., Osaka, Japan). *Phys. Rev. Lett. (USA)*, vol.50, no.15, p.1157-9 (11 April 1983). The temperature dependence of the impurity susceptibility and specific heat for the Anderson model is investigated on the basis of the exact solution already obtained for this model. (16 refs.)
 62551 Solution of the Kondo problem. N.Andrei (Dept. of Phys. & Astron., Rutgers Univ., New Brunswick, NJ, USA), K.Furuya, J.H.Lowenstein. *Rev. Mod. Phys. (USA)*, vol.55, no.2, p.331-402 (April 1983). The review covers in great detail the Bethe-ansatz approach to the solution of various versions of the Kondo problem. (86 refs.)
 Two critical points on the γ - α phase boundary of cerium alloys See Entry 62091
 Longitudinal magnetoresistance of dilute alloys with localized magnetic moments in a quantizing magnetic field See Entry 62397

75.25 SPIN ARRANGEMENTS IN MAGNETICALLY ORDERED MATERIALS (NEUTRON STUDIES, ETC)

- 62552 Magnetic field-induced incommensurate magnetic phases in the singlet-ground state system CsFeCl_3 . W.Knop, M.Steiner, P.Day (Hahn-Meitner-Inst., Berlin, Germany). *J. Magn. & Magn. Mater. (Netherlands)*, vol.31-34, pt.3, p.1033-4 (Feb. 1983). (Proceedings of the International Conference on Magnetism, Kyoto, Japan, 6-10 Sept. 1982). By means of elastic neutron scattering the authors have studied CsFeCl_3 in an external magnetic field. While at low fields no magnetic scattering can be observed in accordance with the nonmagnetic singlet ground-state of the Fe^{2+} in this system, the authors observe magnetic Bragg-peaks at $H>38$ kG. At this field H_1 reflections of the type $(\frac{1}{3}-\delta, \frac{1}{3}-\delta, 0)$ and $(\frac{1}{3}-\delta, \frac{1}{3}+\delta, 0)$ appear. At $H_2 \approx 39$ kG H_1 , a reflection of the type $(\frac{1}{3}-\delta, \frac{1}{3}-\delta, 0)$ appears, while the former disappear. Finally at $H_3 \approx 45$ kG the structure becomes commensurate characterized by the reflection $(\frac{1}{3}, \frac{1}{3}, 0)$. (6 refs.)
 62553 Magnetic structures and interaction constants in the two-dimensional Ising antiferromagnets $\text{RE}_2\text{O}_3\text{SO}_4$ (RE=Dy, Ho, Tb). H.G.Kahle, A.Kasten (Phys. Inst., Univ. Karlsruhe, Karlsruhe, Germany). *J. Magn. & Magn. Mater. (Netherlands)*, vol.31-34, pt.3, p.1081-3 (Feb. 1983). (Proceedings of the International Conference on Magnetism, Kyoto, Japan, 6-10 Sept. 1982). The oxisulfates of Dy, Ho and Tb are nearly two-dimensional Ising antiferromagnets with the complexity of their magnetic structure increasing in this succession. By establishing the magnetic phase diagrams and by analyzing the spectroscopic data, the superexchange interaction to nearest, next and third nearest neighbours could be derived. (8 refs.)
 62554 Randomness in mixed antiferromagnets with competing spin anisotropies. J.M.Newsam, Y.Endoh, Y.Ishikawa (Dept. of Phys., Tohoku Univ., Sendai, Japan), H.Takei. *J. Magn. & Magn. Mater. (Netherlands)*, vol.31-34, pt.3, p.1463-4 (Feb. 1983). (Proceedings of the International Conference on Magnetism, Kyoto, Japan, 6-10 Sept. 1982). The authors have studied the effect of randomness on the long range order in a mixture with competing spin anisotropies. The neutron diffuse scattering and the peak profile of the antiferromagnetic Bragg reflection from

$\text{Fe}_{0.65}\text{Co}_{0.35}\text{TiO}_3$ show marked temperature variations even at low temperatures well below T_N . (7 refs.)

62555 Frustration of antiferromagnetic bonds around a screw dislocation. T.Nakamura, K.Kawamura (Dept. of Materials Sci., Hiroshima Univ., Hiroshima, Japan).

J. Magn. & Magn. Mater. (Netherlands), vol.31-34, pt.3, p.1483-4 (Feb. 1983). (Proceedings of the International Conference on Magnetism, Kyoto, Japan, 6-10 Sept. 1982).

In simple cubic antiferromagnets which include a screw dislocation, the directions of two neighboring spins are not antiparallel and the order parameter is destroyed around the dislocation by the frustration. The specific heat does not jump at the Neel temperature T_N although the order parameter vanishes ultimately at T_N . (5 refs.)

Crystal field splittings of PrX_2 compounds ($X=\text{Pt, Rh, Ir, Ru, Ni}$) studied by inelastic neutron scattering See Entry 62381

Magnetic excitations in CeAs, an effective $S=1/2$ FCC antiferromagnet See Entry 62573

The magnetic ordering in a hexagonal antiferromagnet See Entry 62591

Random fields and ordering in antiferromagnetic insulators See Entry 62603

Neutron depolarization in the unannealed amorphous ribbon Metglas 2826 See Entry 62689

Polarised neutron study of $\text{Mn}_{1/4}\text{TaS}_2$: observation of conduction electron spin polarisation See Entry 62698

Surface magnetic properties of fine particles See Entry 62717

Application of neutron diffraction to the study of interface magnetization on thin films with artificial superlattices See Entry 62729

Mossbauer spectroscopic studies on surfaces and thin films See Entry 62859

Spectroscopic and magneto-optical properties of quasi 1D antiferromagnets AVX_3 ($A=\text{Cs, Rb}$; $X=\text{Cl, Br, I}$) See Entry 62943

75.30 MAGNETICALLY ORDERED MATERIALS, OTHER INTRINSIC PROPERTIES

(for critical point effects, see 75.40)

Structural relaxation and magnetism in amorphous alloys See Entry 61812

75.30C Saturation moments and magnetic susceptibility

62556 The interpretation with the spin-wave theory of the variation of the magnetization of iron and nickel as a function of the temperature and of the magnetic field. R.Pauthenot (CNRS, Grenoble, France).

C.R. Seances Acad. Sci. Ser. II (France), vol.296, no.1, p.29-32 (10 Jan. 1983). In French.

The variation of the spontaneous magnetization of iron and nickel as a function of the temperature and the variation of the isothermal magnetization as a function of the magnetic field were interpreted using the spin-wave theory. (13 refs.)

62557 Magnetic behaviour of spin-mixed iron(III) porphyrins. S.Mitra, V.R.Marathe, R.Birdy (Tata Inst. of Fundamental Res., Bombay, India).

Chem. Phys. Lett. (Netherlands), vol.96, no.1, p.103-7 (25 March 1983).

Detailed average magnetic susceptibility (295-4.2K) and average magnetisation (20-2K, 50-10 kOe) are reported for two novel spin-mixed iron(III) porphyrins, namely $\text{Fe}(\text{TPP})\text{ClO}_4$ and $\text{Fe}(\text{OEP})\text{ClO}_4$. The results confirm an $S=3/2$ ground state substantially spin-mixed with a low-lying $S=5/2$ state, but do not agree in detail with the crystal-field model of Maltempo (1974). (26 refs.)

62558 Magnetic properties of $\text{Fe}_x\text{V}_{3-x}\text{S}_4$ ($0 \leq x \leq 2$). H.Noza, H.Wada (Nat. Inst. for Res. in Inorganic Materials, Ibaraki, Japan).

J. Solid State Chem. (USA), vol.47, no.1, p.69-80 (15 March 1983).

The magnetic susceptibility data of $\text{Fe}_x\text{V}_{3-x}\text{S}_4$ ($0 \leq x \leq 2$) are reported in the temperature range 4.2 to 1300K. The behaviour of the susceptibility at high temperatures changes significantly at the composition boundary $x=1.0$. The magnitude of the effective magnetic moment remains unchanged at $3.2 \mu_B$ in the composition range $x < 1.0$. It decreases with increasing iron content in the range $x > 1.0$, and rapidly decreases for x close to 2.0. The c lattice parameter varies in a manner analogous to the change in magnetic moment. These phenomena suggest that metallic bonding forms between metal layers and that it becomes stronger with increasing x . The susceptibility measurements at low temperatures show that $\text{Fe}_x\text{V}_{3-x}\text{S}_4$ is basically antiferromagnetic, although some of the $\text{Fe}_x\text{V}_{3-x}\text{S}_4$ compounds become weakly ferromagnetic after cooling in a magnetic field. The origin of the weak ferromagnetism is briefly discussed. (30 refs.)

62559 Spin wave theory of susceptibility of quadratic-layer antiferromagnet K_2MnF_4 . K.Tsuru, N.Uryu (Dept. of Appl. Sci., Kyushu Univ., Fukuoka, Japan).

J. Magn. & Magn. Mater. (Netherlands), vol.31-34, pt.3, p.1201-2 (Feb. 1983). (Proceedings of the International Conference on Magnetism, Kyoto, Japan, 6-10 Sept. 1982).

The parallel and perpendicular susceptibilities, χ_{\parallel} and χ_{\perp} , of K_2MnF_4 are analyzed by the use of a renormalized spin-wave (RSW) theory. Good agreements with the experiments are obtained for both χ_{\parallel} and χ_{\perp} . (5 refs.)

62560 Quasielastic neutron scattering from the 1-D ferromagnet CsNiF_3 with an applied transverse field. K.Kakurai, M.Steiner (Hahn-Meitner-Inst. für Kernforschung GmbH, Berlin, Germany).

J. Magn. & Magn. Mater. (Netherlands), vol.31-34, pt.3, p.1215-17 (Feb. 1983). (Proceedings of the International Conference on Magnetism, Kyoto, Japan, 6-10 Sept. 1982).

By means of quasielastic neutron scattering the authors studied the magnetic field induced crossover in CsNiF_3 in the transverse magnetic field. The susceptibility at $q=0$ shows a broad maximum in its temperature dependence, which is best described by the static properties of the classical sine-Gordon chain. (10 refs.)

62561 Effects of external field on χ -T curve on cluster-glasses. M.Shiga, Y.Nakamura (Dept. of Metal Sci. & Technol., Kyoto Univ., Kyoto, Japan).

J. Magn. & Magn. Mater. (Netherlands), vol.31-34, pt.3, p.1411-12 (Feb. 1983). (Proceedings of the International Conference on Magnetism, Kyoto, Japan, 6-10 Sept. 1982).

The temperature dependence of magnetic susceptibility of some cluster-glass alloys, $\text{Fe}_{0.5}(\text{Ni}_{0.7}\text{Mn}_{0.26})_{0.5}$, $\text{Fe}_{1-x}\text{Al}_x$ and $\text{Y}(\text{Mn}_{1-x}\text{Co}_x)_2$, have been measured in various external fields. In addition to the maximum point, T_m , in the χ -T curve, an inflection point, T_i , was observed below T_m . It has been shown that T_i decreases with increasing external field, H , following the empirical relation, $T_i(H) = T_i(0) - A\sqrt{H}$. (5 refs.)

62562 Frustration effects in the disordered system CsMnFeF_6 . L.Bevara, P.M.H.L.Tegelaar, A.J.van Duynveldt, M.Steiner (Studiecentrum voor Kernenergie, Mol, Belgium).

J. Magn. & Magn. Mater. (Netherlands), vol.31-34, pt.3, p.1447-8 (Feb. 1983). (Proceedings of the International Conference on Magnetism, Kyoto, Japan, 6-10 Sept. 1982).

The magnetic properties of the highly frustrated system CsMnFeF_6 have been studied. At $T=300\text{K}$ clusters of canted antiferromagnet spins exist. Their resultant moments grow for decreasing T , whereas for $T \lesssim 80\text{K}$ these remain constant. At $T=26.3\text{K}$ the clusters freeze in and form domains in which their moments order ferromagnetically. Applying a magnetic field causes a splitting of the domains into microdomains. (4 refs.)

62563 A magnetic quasi-ordered state in $\text{Cr}_{1-x}\text{Ti}_x\text{S}$. S.Anzai, M.Nakada, S.Ohta, K.Tominaga, A.Fujii (Faculty of Sci. & Technol., Keio Univ., Yokohama-shi, Japan).

J. Magn. & Magn. Mater. (Netherlands), vol.31-34, pt.3, p.1467-8 (Feb. 1983). (Proceedings of the International Conference on Magnetism, Kyoto, Japan, 6-10 Sept. 1982).

Magnetic susceptibilities of a solid solution $\text{Cr}_{1-x}\text{Ti}_x\text{S}$ ($0.10 \leq x \leq 0.60$) are investigated. The Neel temperature steeply decreases with increasing x and disappears at a low critical concentration ($0.20 < x < 0.25$). A spin glass-like phase exists beyond this concentration. The spin glass-paramagnetic transition temperature decreases with increasing x . (6 refs.)

62564 An AC magnetic susceptibility study of domain nucleation in an amorphous alloy. P.J.Back (Dept. of Phys., Univ. of New South Wales, Duntroon, Australia), S.J.Campbell.

J. Magn. & Magn. Mater. (Netherlands), vol.31-34, pt.3, p.1543-5 (Feb. 1983). (Proceedings of the International Conference on Magnetism, Kyoto, Japan, 6-10 Sept. 1982).

The thermal nucleation of domains around the ordering temperature $T_c = (232.8 \pm 1.0)\text{K}$ of $\text{Fe}_{0.7}\text{Ni}_{0.3}\text{Cr}_{0.4}\text{P}_{0.3}\text{B}_0$ has been monitored by a variable temperature study (80-300K) of the AC magnetic susceptibility and its transient enhancement. This has delineated the susceptibility region free of domain effects for critical exponent analysis. (9 refs.)

62565 Magnetic moment of Fe-Ga-B amorphous alloys. K.Fukamichi, T.Sato, T.Masumoto (Res. Inst. for Iron, Steel & Other Metals, Tohoku Univ., Sendai, Japan).

J. Magn. & Magn. Mater. (Netherlands), vol.31-34, pt.3, p.1589-90 (Feb. 1983). (Proceedings of the International Conference on Magnetism, Kyoto, Japan, 6-10 Sept. 1982).

FeGaB and FeGeB amorphous ribbons were prepared by melt quenching. The magnetic properties of these alloys are explained by assuming a band structure of weak ferromagnetism. The crystallization temperature increases with increasing Ga and Ge content. (13 refs.)

62566 Magnetism of amorphous metal-metal alloys. A.P.Malozemoff, A.R.Williams, K.Terakura, V.L.Moruzzi, K.Fukamichi (IBM, Thomas J. Watson Res. Center, Yorktown Heights, NY, USA).

J. Magn. & Magn. Mater. (Netherlands), vol.35, no.1-3, p.192-8 (March 1983). (Proceedings of the 10th International Colloquium on Magnetic Films and Surfaces, Yokohama, Japan, 13-16 Sept. 1982).

Reviews available experimental data on the magnetism of amorphous alloys of iron and cobalt with early transition metals $E=\text{La, Y, Hf, Zr, Ti, Ta, Nb, V, W}$ and Mo. Then the authors present parameter-free, self-consistent band calculations for related ordered compounds which elucidate the mechanism of moment formation and magnetic weakness. (67 refs.)

62567 Magnetic properties of the weak ferromagnet NH_4MnF_3 . J.Bartolome, R.Burriel, F.Palacio, D.Gonzalez (Departamento de Termologia, Univ. de Zaragoza, Zaragoza, Spain), R.Navarro, J.A.Rojo, L.J.De Jongh.

Physica B & C (Netherlands), vol.115 B+C, no.2, p.190-204 (Jan. 1983).

The magnetic properties of NH_4MnF_3 have been studied by means of heat capacity, AC susceptibility at zero field and at $H=10\text{ kOe}$ as a function of temperature, and at $T=4.2\text{K}$ as a function of field. Moreover, magnetization measurements were carried out at $T=4.2\text{K}$ as a function of field up to 20 kOe in a vibrating sample magnetometer and up to 400 kOe in a pulsed-field magnet. The compound has the simple cubic perovskite structure at room temperature. At $G_c=182.1 \pm 0.1\text{K}$ a structural transition to a pseudotetragonal symmetry occurs, which gives rise to a small change in the paramagnetic susceptibility. The onset of antiferromagnetic ordering takes place at $T_N=75.1 \pm 0.1\text{K}$ at zero field, and a spin-flip transition at $T=4.2\text{K}$ is detected at $H_{SF}=3.7 \pm 0.2\text{ kOe}$. Evidence for the presence of a small weak-ferromagnetic moment is found from an anomaly in χ and from the presence of magnetic absorption near T_N . From a comparison of the data to predictions for the SC Heisenberg antiferromagnetic model, a value of $J/k = -3.1\text{K}$ is obtained for the exchange interaction. (40 refs.)

62568 The spin-wave theory of the susceptibility of Heisenberg antiferromagnets: application to a quadratic layer antiferromagnet K_2MnF_4 and comparison with $(\text{C}_2\text{H}_5\text{NH}_3)_2\text{CuCl}_4$. K.Tsuru, N.Uryu (Dept. of Appl. Sci., Kyushu Univ., Fukuoka, Japan).

Physica B & C (Netherlands), vol.115 B+C, no.2, p.205-18 (Jan. 1983).

Low-temperature magnetic susceptibilities of the quasi-two-dimensional antiferromagnet K_2MnF_4 are reanalyzed by the use of renormalized spin-wave (RSW) theory. For the parallel susceptibility χ_{\parallel} , the formula is obtained as $\chi_{\parallel} \propto Q/(1+(1/2)dQ)$, where Q is a quantity which is essentially proportional to χ_{\parallel} given by the free spin-wave (FSW) approximation, and d and the anisotropy parameters. The second term in the denominator represents a contribution from the spin-wave interaction. A good agreement with the experimental data is obtained up to near T_N by using this formula. For the perpendicular susceptibility, the authors adopt the quadratic part with RSW energy $\epsilon_k(T)$ as unperturbed part of the Hamiltonian and the Zeeman term as the perturbation. The second order perturbation energy has been calculated using the canonical transformation which eliminates the terms of the first and third degree with respect to the Boson operators. Up to the terms of $O(1/S^2)$, the result agrees partially with that of Oguchi (1960). It is shown that the correction terms have a form of double summation with respect to wave numbers or fourfold integral and are not so small compared with the term of $O(1/S)$. Finally, the different situation of $(\text{C}_2\text{H}_5\text{NH}_3)_2\text{CuCl}_4$, a nearly two-dimensional ferromagnet with very weak interlayer antiferromagnetic coupling, is discussed in a comparative way with the case of K_2MnF_4 . (18 refs.)

On a new series of cobalt-IV oxides See Entry 61861

Crystal structure and magnetic properties of a new form of NH_4MnF_6 See Entry 61880

Hexagonal tungsten bronze-type Fe^{III} fluoride: $(\text{H}_2\text{O})_{0.33}\text{FeF}_6$; crystal structure, magnetic properties, dehydration to a new form of iron trifluoride See Entry 61882

EuS ferromagnetic semiconductor films grown epitaxially on silicon See Entry 62296

- A singlet-singlet model for amorphous alloys with praseodymium See Entry 62534
- Temperature-induced local moments in MnSi and FeSi See Entry 62549
- Static properties of classical ferromagnetic chains in a magnetic field: an interacting spin-wave theory See Entry 62569
- Experiments on randomly mixed magnets with competing interactions See Entry 62574
- Magnetocrystalline anisotropy of dysprosium and erbium ions in compounds of the RCO_5 type See Entry 62580
- Magnetoelastic phase transition in KMnF_3 See Entry 62592
- Magnetic order in the $(\text{TM}_x\text{Y}_{1-x})_2(\text{SO}_4)_3 \cdot 8\text{H}_2\text{O}$ system See Entry 62593
- Ferro and antiferromagnetic ordering in $\text{N}(\text{C}_2\text{H}_5)_4\text{FeCl}_4$ depending on the cooling rate See Entry 62594
- Spin flopping in MnTiO_3 See Entry 62596
- Field-induced increase of the Neel temperature in a two-dimensional system See Entry 62600
- Magnetic properties of the quasi-2d easy plane antiferromagnet $\text{BaNi}_2(\text{PO}_4)_2$ See Entry 62601
- High temperature series expansion of staggered susceptibility of the three-state antiferromagnetic Potts model on d-dimensional hypercubic lattices See Entry 62615
- Magnetic phase transitions in presence of bilinear and quadrupolar interactions in rare earth compounds See Entry 62622
- Spin glass like behaviour of the solid solution $\text{Mn}_{3-x}\text{Ga}_x\text{N}$ See Entry 62626
- Dynamics of disordered spin systems studied by zero- and longitudinal-field μSR . I. $(\text{FeTiO}_3)_{88}(\text{Fe}_2\text{O}_3)_{12}$ See Entry 62627
- Spin-glass compound $(\text{Ti}_{1-x}\text{V}_x)_2\text{O}_3$: relaxation time and its field dependence See Entry 62630
- Spin dynamics of an insulating spin-glass $\text{Rb}_2\text{Mn}_{1-x}\text{Cr}_x\text{Cl}_4$ at the microwave region See Entry 62631
- Spin glass behaviour in chromium spinels See Entry 62633
- Dynamics and stability of the Sherrington-Kirkpatrick model See Entry 62638
- Magnetic short-range order and spin freezing in the quasi-2D system LuFeMgO_4 See Entry 62642
- Solitons in quantum-spin systems See Entry 62646
- Calculated specific heat and susceptibility for the crossover of an $S=\infty$ Heisenberg antiferromagnet compared with data on $\text{Rb}_2\text{FeCl}_4 \cdot \text{H}_2\text{O}$ See Entry 62672
- Anomalous temperature dependence of magnetization in amorphous $(\text{Fe}_{0.1}\text{Ni}_{0.9})_{77}\text{Si}_{10}\text{B}_{13}$ alloy See Entry 62699
- Magnetic properties of amorphous powders of alloy Mn_3B_4 See Entry 62710
- Dynamical properties of small particles; comparison with spin glass behaviour See Entry 62719
- On the magnetic dipole fields at surface atoms See Entry 62731
- Magnetic and electrical properties of amorphous $\text{Fe}_{1-x}\text{B}_x$ films See Entry 62740
- Effects of high dose ion implantation on structure and magnetic properties of 3d-metal films See Entry 62757

75.30D Spin waves

(see also 76.50 Spin wave resonance)

- 62569 Static properties of classical ferromagnetic chains in a magnetic field: an interacting spin-wave theory. U. Balucani, M.G. Pini, V. Tognetti (Istituto de Elettronica Quantistica, CNR, Firenze, Italy), A. Rettori. *J. Magn. & Magn. Mater. (Netherlands)*, vol.31-34, pt.3, p.1229-30 (Feb. 1983). (Proceedings of the International Conference on Magnetism, Kyoto, Japan, 6-10 Sept. 1982).
- Longitudinal spin susceptibility, energy susceptibility and related properties of classical ferromagnetic chains in a field are calculated by means of an interacting spin-wave theory. The validity of the theory is checked by exact numerical calculations by the transfer matrix method and excellent agreement is found. (4 refs.)
- 62570 Effect of magnetic and nonmagnetic impurities on the soliton dynamics in $(\text{CD}_3)_4\text{NMnCl}_3$. H. Benner (Inst. fur Festkorperphys., Tech. Hochschule Darmstadt, Darmstadt, Germany), J.P. Boucher, J.P. Renard, H. Seitz. *J. Magn. & Magn. Mater. (Netherlands)*, vol.31-34, pt.3, p.1233-4 (Feb. 1983). (Proceedings of the International Conference on Magnetism, Kyoto, Japan, 6-10 Sept. 1982).
- From nuclear relaxation-time measurements, the authors obtain experimental evidence for magnetic solitons propagating diffusively along the chains of $(\text{CD}_3)_4\text{NMnCl}_3$ doped with copper or cadmium. The diffusion constant is hardly affected by impurity concentrations $0.2 \leq c \leq 0.8$ at.% but differs strongly for magnetic and nonmagnetic impurities. (5 refs.)
- 62571 Theoretical study of magnetic properties of pseudo-one-dimensional system RbFeCl_3 . N. Suzuki (Dept. of Material Phys., Osaka Univ., Toyonaka, Japan). *J. Magn. & Magn. Mater. (Netherlands)*, vol.31-34, pt.3, p.1235-6 (Feb. 1983). (Proceedings of the International Conference on Magnetism, Kyoto, Japan, 6-10 Sept. 1982).
- Magnetic properties of pseudo-one-dimensional singlet-ground-state system RbFeCl_3 are studied by taking into account interchain coupling. On the basis of the dynamical CEF approximation various magnetic properties are well explained quantitatively. The ratio of the interchain coupling to the intrachain coupling is estimated to be ~ 0.1 . (12 refs.)
- 62572 Dynamic formfactor of neutron scattering on solitons in quasi-one-dimensional magnetics. V.K. Fedyanin (Joint Inst. for Nuclear Res., Dubna, Moscow, USSR). *J. Magn. & Magn. Mater. (Netherlands)*, vol.31-34, pt.3, p.1237-8 (Feb. 1983). (Proceedings of the International Conference on Magnetism, Kyoto, Japan, 6-10 Sept. 1982).
- The general expression the author has found earlier for the dynamic formfactor $S(\mathbf{q}, \omega)$ (1982) was used to analyse experiments on the neutron scattering by the 'gas' of solitons in magnetics: in magnetics of the type of 'light axis', 'light plane', quasi-one-dimensional, isotropic, Heisenberg ferromagnets with magnon-phonon interaction. (14 refs.)

- 62573 Magnetic excitations in CeAs, an effective $S=1/2$ FCC antiferromagnet. B. Halg, A. Furrer (Inst. fur Reaktortech., Eidgenossische Tech. Hochschule Zurich, Wurenlingen, Switzerland), J.K. Kjems, O. Vogt. *Phys. Rev. Lett. (USA)*, vol.50, no.14, p.1085-8 (4 April 1983).
- The magnetic excitations in the well isolated ground-state double Γ_7 of CeAs have been studied by inelastic neutron scattering. The spin-wave excitation is split into two modes of transverse polarization as a result of exchange anisotropy. One of these modes exhibits nearly zero energy gap and quadratic dispersion which have not previously been observed in antiferromagnets. A random-phase-approximation calculation based on a single-q type-I antiferromagnetic structure is in good agreement with the observed spectrum. (8 refs.)
- Soliton-phonon scattering in TMMC and DMMC See Entry 62192
- The interpretation with the spin-wave theory of the variation of the magnetization of iron and nickel as a function of the temperature and of the magnetic field See Entry 62556
- Spin wave theory of susceptibility of quadratic-layer antiferromagnet K_2MnF_4 See Entry 62559
- The spin-wave theory of the susceptibility of Heisenberg antiferromagnetics: application to a quadratic layer antiferromagnet K_2MnF_4 and comparison with $(\text{C}_2\text{H}_5\text{NH}_3)_2\text{CuCl}_4$ See Entry 62568
- Theoretical study of the magnetic properties of an antiferromagnetic system with two kinds of inequivalent magnetic-ion sites See Entry 62619
- Ferromagnetic and spin glass behavior near the critical concentration in amorphous $(\text{Fe}_x\text{Ni}_{100-x})_{75}\text{G}_{125}$ See Entry 62635
- Magnetic relaxation in ferromagnets with competing interactions See Entry 62636
- Solitons in quantum-spin systems See Entry 62646
- Spin-flop-paramagnetic phase transition See Entry 62669
- A binary ferromagnetic alloy with magnetic moments dependent on local environment. I. The Jaccarino-Walker model in the effective field approximation See Entry 62676
- The Heisenberg model: dynamical interactions including odd-boson terms See Entry 62677
- Micromagnetics of zigzag head-on domain walls See Entry 62690
- A universal dispersion equation of magnetostatic surface wave (MSSW) in the layer structures See Entry 62732
- Two-dimensional soliton contribution to the ESR linewidth in layered antiferromagnets? See Entry 62798
- Two-magnon scattering in iron-rich metallic glasses See Entry 62809
- Evidence for magnetic soliton in CsNiF_3 : nuclear magnetic relaxation studies See Entry 62826
- Interface magnetism in Fe-Sb multilayer films from ^{121}Sb and ^{57}Fe Mossbauer spectroscopy See Entry 62861

75.30E Exchange and superexchange interactions

(see also 71.70 Level splitting and interactions)

- 62574 Experiments on randomly mixed magnets with competing interactions. K. Katsumata (Res. Inst. of Appl. Electricity, Hokkaido Univ., Sapporo, Japan). *J. Magn. & Magn. Mater. (Netherlands)*, vol.31-34, pt.3, p.1435-8 (Feb. 1983). (Proceedings of the International Conference on Magnetism, Kyoto, Japan, 6-10 Sept. 1982).
- After a brief review of the experimental and theoretical studies on randomly mixed magnets with competing interactions, the author reports an experimental study of two kinds of randomly mixed magnets: (i) random mixture of two antiferromagnets with competing spin anisotropies and (ii) random mixture of an insulating ferromagnet and an insulating antiferromagnet. (53 refs.)
- 62575 Spin orientation and exchange interactions in $(\text{Fe}, \text{Co})\text{Cl}_2$. M.C.K. Wiltshire, B.D. Howes, C.H. Burton (Dept. of Solid State Phys., Australian Nat. Univ., Canberra, Australia). *J. Magn. & Magn. Mater. (Netherlands)*, vol.31-34, pt.3, p.1465-6 (Feb. 1983). (Proceedings of the International Conference on Magnetism, Kyoto, Japan, 6-10 Sept. 1982).
- The far infrared spectrum of $\text{FeCl}_2 \cdot \text{Co}$ shows a localised mode from whose position a set of Fe-Co exchange parameters has been determined. Mossbauer spectra of the mixtures $\text{Fe}_{1-x}\text{Co}_x\text{Cl}_2$ have been measured and their analysis yields a variation of iron-spin orientation consistent with calculations using these parameters. (5 refs.)
- 62576 Measuring the exchange constant A_{ex} in metglas 2826. E. Lopez, C. Aroca (Dept. de Magnetismo, Univ. Complutense, Madrid, Spain), P. Sanchez. *J. Magn. & Magn. Mater. (Netherlands)*, vol.36, no.1-2, p.175-9 (1 April 1983).
- The authors have measured the energy of Bloch's walls in amorphous ferromagnetic ribbons using a method devised by R. Aleonard et al. for thin monocrystalline ferromagnetic films. To do this, they had to induce unidirectional anisotropy in the amorphous samples using stress. By measuring the movements of the walls for different current intensities, using the Bitter technique, they have obtained the wall energy value and thus the exchange constant A_{ex} . The results were of the order of 6×10^{-12} J/m which tallies with the results of other researchers who used different methods. (8 refs.)
- 62577 A model calculation of superexchange interaction and comparison among different methods. N. Fuchikami (Dept. of Phys., Tokyo Metropolitan Univ., Tokyo, Japan). *Physica B & C (Netherlands)*, vol.115 B+C, no.2, p.219-24 (Jan. 1983).
- A perturbational formalism developed previously is applied to a 3-center 4-electron model of superexchange interactions. Both Lowdin's orthogonalized basis and biorthogonal basis set constructed from nonorthogonal atomic orbitals are used to obtain the exchange parameter and results are compared with complete configuration interaction calculations. The model shows ferromagnetic coupling for bond angles around 90° and an antiferromagnetic one for large and small angles. This qualitative feature is independent of the type of calculation and coincides with the results obtained by Van Kalker et al. (1979) based on several other methods. Simplified revisions of the perturbational formula are examined. (14 refs.)
- 62578 Extended-path-model analysis of superexchange coupling in the Cr^{3+} -doped spinel ZnGa_2O_4 . H.G. Wai (Dept. of Phys., Univ. of Hong Kong, Hong Kong), D.J. Newman. *Phys. Rev. B (USA)*, vol.27, no.7, p.4483-5 (1 April 1983).
- Hennig's path-model description of the isotropic exchange coupling between Cr^{3+} pairs in spinel is extended to include looped paths and some of the exchange and overlap integrals involved have been calculated. It is shown

that, with these developments, the model is no longer consistent with the experimental data. (6 refs.)

62579 X_r method for the magnetic transition state and exchange interactions in KNiF_3 . A.I.Likhtenshtein, V.A.Gubanov (Inst. of Chem., Acad. of Sci., Sverdlovsk, USSR). *Sov. Phys.-Solid State (USA)*, vol.24, no.9, p.1445-8 (Sept. 1982). Translation of: *Fiz. Tverd. Tela (USSR)*, vol.24, no.9, p.2545-50 (Sept. 1982). [received: April 1983]

The energies of magnetic excitations corresponding to spin reversal of a localized moment of a $3d$ ion in an antiferromagnetic insulator KNiF_3 are calculated. The first-principle method of a magnetic transition state is used to calculate the excitation energies within the framework of the local spin density functional with various forms of the exchange correlation potential. The calculated superexchange interaction parameters and the calculated Neel temperature are in good agreement with the experimental results. The effect of the chemical bonding on the magnetic properties of transition metal compounds is discussed. (18 refs.)

Amorphization of crystalline diluted Ising ferromagnet See Entry 61803

Magnetic and galvanomagnetic properties of rare earth intermetallic compounds of $\text{RAl}_{1-x}\text{In}_x$ ($\text{R}=\text{Gd, Tb, and Dy}$) See Entry 62400

A singlet-singlet model for amorphous alloys with praseodymium See Entry 62534

Magnetic structures and interaction constants in the two-dimensional Ising antiferromagnets $\text{RE}_2\text{O}_3\text{SO}_4$ ($\text{RE}=\text{Dy, Ho, Tb}$) See Entry 62553

Magnetic properties of the weak ferromagnet NH_4MnF_3 See Entry 62567

Magnetic excitations in CeAs, an effective $S=1/2$ FCC antiferromagnet See Entry 62573

Magnetocrystalline anisotropy of dysprosium and erbium ions in compounds of the RCO_3 type See Entry 62580

Magnetic properties of La_2Ni_7 See Entry 62588

Spin flopping in MnTiO_3 See Entry 62596

Effects of hydrostatic pressure on phase transition of some low-dimensional systems See Entry 62599

Ordering of spin and orbital moments in a lattice of $3d$ ions coupled by superexchange See Entry 62617

Ordering in an orbital superexchange model See Entry 62618

Theoretical study of the magnetic properties of an antiferromagnetic system with two kinds of inequivalent magnetic-ion sites See Entry 62619

Theoretical study of magnetism of spin system with alternating strong and weak exchange coupling See Entry 62624

Intrinsic hardness and micromagnetism in selected $\text{RMn}_{1-x}\text{Ni}_x$ ($\text{R}=\text{rare earth}$) See Entry 62644

Surface effects in Ising ferromagnets with anisotropy See Entry 62649

Monte Carlo calculations of phase diagrams of Ising systems with competing interactions See Entry 62658

Calculated specific heat and susceptibility for the crossover of an $S=\infty$ Heisenberg antiferromagnet compared with data on $\text{Rb}_2\text{FeCl}_4\cdot\text{H}_2\text{O}$ See Entry 62672

Polarised neutron study of $\text{Mn}_{1/4}\text{TaS}_2$: observation of conduction electron spin polarisation See Entry 62698

Magnetic property changes in epitaxial metal film sandwiches See Entry 62730

Large magnetic anisotropy change induced by hydrogen ion implantation in europium iron garnet LPE films See Entry 62756

Influences of ion implantation on charged wall properties in magnetic bubble devices See Entry 62776

Comparison of the magnetic properties of one- and two-layer iron garnet films See Entry 62781

Magnetostriction of iron, cobalt and nickel ternary amorphous ribbons See Entry 62787

Mossbauer spectroscopic studies on surfaces and thin films See Entry 62859

75.30G Anisotropy

62580 Magnetocrystalline anisotropy of dysprosium and erbium ions in compounds of the RCO_3 type. A.S.Ermolenko, A.F.Rozhda (Inst. of Metal Phys., Acad. of Sci., Sverdlovsk, USSR).

Fiz. Met. & Metalloved. (USSR), vol.55, no.2, p.267-72 (Feb. 1983). In Russian. English translation in: *Phys. Met. & Metallogr. (GB)*

A study was made of the magnetic moments and orientation of the easy magnetization axes of single crystals of $\text{Dy}_x\text{Y}_{1-x}\text{Co}_{5+0.2x}$, $\text{Dy}_x\text{Sm}_{1-x}\text{Co}_{5+0.2x}$, and $\text{Er}_x\text{Y}_{1-x}\text{Co}_{5+0.2x}$. The magnetization curves were recorded at 4.2K along various crystallographic directions and were then used to find the anisotropy constants of the Dy and Er ions, as well as the molecular fields of the exchange interaction with the Co sublattice acting on these ions. (10 refs.) A.T.

62581 Magnetic anisotropy in dilute Fe-Cu single crystal. M.Takahashi, S.Ishio, Y.Sasaki (Dept. of Appl. Phys., Tohoku Univ., Sendai, Japan).

J. Magn. & Magn. Mater. (Netherlands), vol.31-34, pt.3, p.1409-10 (Feb. 1983). (Proceedings of the International Conference on Magnetism, Kyoto, Japan, 6-10 Sept. 1982).

The change in the magnetic anisotropy for solution-quenched 0.9% Fe-Cu single crystal was measured with subsequent annealing. The results are analyzed in connection with environmental changes around the Fe atom. (3 refs.)

62582 Induced anisotropy in amorphous Co-P alloys. J.M.Riveiro, G.Rivero, M.C.Sanchez (Facultad de Fisicas, Univ. Complutense, Madrid, Spain).

J. Magn. & Magn. Mater. (Netherlands), vol.31-34, pt.3, p.1551-2 (Feb. 1983). (Proceedings of the International Conference on Magnetism, Kyoto, Japan, 6-10 Sept. 1982).

Anisotropy induced by magnetic annealing has been measured in electrodeposited amorphous Co-P alloys with between 9 and 20 at.% P. The maximum induced anisotropy takes place at ~ 11 at.% P and cancels out at ~ 22 at.% P. This result is compatible with the binary dense random packed hard spheres (DRPHS) model if the P cannot occupy the tetrahedral holes. (6 refs.)

62583 Helical anisotropy induced by annealing in Metglas 2826. A.Hernando, V.Madurga, J.M.Gonzalez, F.Cebollada (Lab. Magnetism, Facultad de Fisicas, Univ. Complutense, Madrid, Spain).

J. Magn. & Magn. Mater. (Netherlands), vol.31-34, pt.3, p.1553-4 (Feb. 1983). (Proceedings of the International Conference on Magnetism, Kyoto, Japan, 6-10 Sept. 1982).

The magnetic anisotropy induced by constant torsional strain annealing of an amorphous alloy with nominal composition $\text{Fe}_{40}\text{Ni}_{40}\text{P}_{14}\text{B}_6$ has been studied. The influence of annealing conditions is reported and discussed. The experimental results indicate that magnetoelastic coupling is the main source of the induced anisotropy, the anelastic and plastic creep contributions being almost negligible. (5 refs.)

62584 Crystallization and anisotropy in amorphous $\text{Fe}_{81}\text{B}_{13}\text{Si}_3\text{C}_2$. N.Saegusa, A.H.Morrish (Dept. of Phys., Univ. of Manitoba, Winnipeg, Manitoba, Canada).

J. Magn. & Magn. Mater. (Netherlands), vol.31-34, pt.3, p.1555-6 (Feb. 1983). (Proceedings of the International Conference on Magnetism, Kyoto, Japan, 6-10 Sept. 1982).

Magnetic anisotropy in amorphous $\text{Fe}_{81}\text{B}_{13}\text{Si}_3\text{C}_2$ ribbons (Metglas 2605SC) that develops after thermal treatments is correlated with the crystallization at the surface layers and in the bulk. (3 refs.)

62585 Anisotropies and domain structures in metallic glasses. P.Salzmänn, W.Grimm, A.Hubert (Inst. für Werkstoffwissenschaften, Univ. Erlangen, Erlangen, Germany).

J. Magn. & Magn. Mater. (Netherlands), vol.31-34, pt.3, p.1599-600 (Feb. 1983). (Proceedings of the International Conference on Magnetism, Kyoto, Japan, 6-10 Sept. 1982).

Demonstrates that a metallic glass with a so-called stress-pattern magnetization configuration could be an almost ideal soft magnetic material. To optimize the material in this direction it is useful to find methods to characterize such stress patterns. The authors show it is possible to determine all relevant anisotropy parameters by application of tension and twist to the specimen and demonstrate the procedure for a number of examples. (5 refs.)

The spin-wave theory of the susceptibility of Heisenberg antiferromagnets: application to a quadratic layer antiferromagnet K_2MnF_4 and comparison with $(\text{C}_2\text{H}_5\text{NH}_3)_2\text{CuCl}_4$ See Entry 62568

Magnetic excitations in CeAs, an effective $S=1/2$ FCC antiferromagnet See Entry 62573

Experiments on randomly mixed magnets with competing interactions See Entry 62574

Magnetic properties of La_2Ni_7 See Entry 62588

Spin flopping in MnTiO_3 See Entry 62596

Effects of hydrostatic pressure on phase transition of some low-dimensional systems See Entry 62599

Phase diagram of random mixtures of antiferromagnets with competing anisotropy See Entry 62605

Anisotropy effects in the ferromagnetic quantum chain systems $(\text{C}_6\text{H}_{11}\text{NH}_3)\text{CuCl}_3$ (CHAC) and $(\text{C}_6\text{H}_{11}\text{NH}_3)\text{CuBr}_3$ (CHAB) See Entry 62625

Surface effects in Ising ferromagnets with anisotropy See Entry 62649

Heisenberg spin classes with uniaxial anisotropy See Entry 62673

A theory of internal stress field and configuration of magnetic domain in amorphous ribbons See Entry 62688

Low field properties of FeNiMnB amorphous alloy See Entry 62700

Time variation of coercivity in cobalt-contained iron oxides particles See Entry 62714

Surface magnetic properties of fine particles See Entry 62717

Shape anisotropy of ultrafine magnesium ferrite precipitates See Entry 62720

Magnetic relaxation in amorphous $(\text{Fe}_{1-x}\text{Ni}_x)_7\text{Si}_{10}\text{B}_{13}$ alloys See Entry 62723

FMR and magnetic studies in amorphous Co-Nb films See Entry 62727

On the magnetic dipole fields at surface atoms See Entry 62731

Magnetic and optical properties of Co, Bi substituted garnet films prepared by the LPE method and its application to thermomagnetic recording See Entry 62733

Magnetic properties, structure, and relaxation of amorphous $\text{Fe}_{1-x}\text{B}_x$ films See Entry 62739

Magnetic properties and microstructure in Ho-Co alloy thin films fabricated by RF sputtering technique See Entry 62743

Magnetostriction and internal stress in GdFe amorphous films with perpendicular anisotropy prepared by RF diode sputtering See Entry 62745

Pair ordering and perpendicular anisotropy in RE-TM amorphous thin films See Entry 62749

Perpendicular magnetic anisotropy and ferromagnetic resonance in amorphous Gd-Co and Gd-Fe films See Entry 62750

Perpendicular anisotropy in Co-Cr films See Entry 62751

Oblique incidence effects in evaporated thin films See Entry 62752

Magnetization reversal modes in thin films with columnar microstructure See Entry 62754

Investigations of implantation-induced changes in surface layers of epitaxial garnet thin films See Entry 62755

Magnetocrystalline anisotropy energy K_1 of Co^{2+} and Ru^{3+} substituted bubble garnet films See Entry 62758

Localized modification of magnetic anisotropy in LPE iron garnet films by laser annealing See Entry 62760

A new method for analysis of magnetic anisotropy in films using the spontaneous Hall effect See Entry 62761

Structure and magnetic properties of C-axis well oriented Ba-ferrite films deposited by targets-facing type of sputtering See Entry 62765

Perpendicular magnetic anisotropy and microstructure of sputter-deposited Co-Cr film See Entry 62775

Structure and magnetic domain walls of Dy ion implanted Fe films See Entry 62777

Comparison of the magnetic properties of one- and two-layer iron garnet films See Entry 62781

Single-ion anisotropy and magnetostriction of amorphous alloys See Entry 62785

Electron spin resonance study of a disordered Ni-Mn alloy See Entry 62803

EPR experiments on the two-dimensional Heisenberg ferromagnet K_2CuF_4 See Entry 62806

Mossbauer and X-ray diffraction studies of amorphous Fe-Ni alloy films deposited by DC sputtering See Entry 62862

Applied magnetic field Mossbauer studies of the quasi one-dimensional system $\text{AFES}_2\text{A}=\text{K, Rb, Cs}$ See Entry 62865

Absorption line of magnetically anisotropic particles See Entry 62941

75.30H Magnetic impurity interactions

Effect of magnetic and nonmagnetic impurities on the soliton dynamics in $(\text{CD}_3)_2\text{NMnCl}_3$ See Entry 62570

Magnetic order in the $(\text{TM}_{1-x}\text{Y}_x)_2(\text{SO}_4)_3 \cdot 8\text{H}_2\text{O}$ system See Entry 62593

The effect of paramagnetic impurities on the wave-vector of the spin-density-wave of an itinerant electron antiferromagnet See Entry 62598

75.30K Magnetic phase boundaries

(inc. magnetic transitions, metamagnetism, etc)

62586 Investigation of magnetic and martensitic phase transitions in Vicalloy-type alloys. I.Ya.Georgieva, L.A.Matyushenko (Inst. of Metallography & Phys. of Metals, Moscow, USSR).

Fiz. Met. & Metallogr. (USSR), vol.55, no.2, p.358-62 (Feb. 1983). In Russian. English translation in: *Phys. Met. & Metallogr. (GB)*

A study was made of austenitic alloys based on Fe-Co and close in composition to Vicalloys but containing nickel. The replacement of iron with nickel resulted in a magnetic transition from the paramagnetic to the ferromagnetic state. Dilatometric measurements yielded the composition dependences of the martensitic point M_s of the γ - α transition and of the Curie points θ_c of austenite of two series of alloys: K52F9+Ni and K52F11+Ni. The magnetic and martensitic phase transitions in this system were similar to those in Fe-Ni alloys. The characteristic features of martensitic reactions were attributed to the magnetic inhomogeneity of the γ solid solution. (8 refs.) A.T.

62587 Synthesis and magnetic properties of $(\text{Mn}_{1-x}\text{Ta}_x)_2\text{B}_4$. T.Ishii, M.Shimada, M.Koizumi (Inst. of Sci., Industrial Res., Osaka Univ., Osaka, Japan).

J. Chem. Phys. (USA), vol.78, no.6, pt.1, p.3294-6 (15 March 1983).

Solid solution of $(\text{Mn}_{1-x}\text{Ta}_x)_2\text{B}_4$ ($0 \leq x \leq 1$) with Ta_2B_4 -type structures were synthesized under high pressure-temperature conditions, and their crystallographic and magnetic properties were examined. From the results of magnetic measurements, the solid solutions were found to be ferromagnetic in the range of $0.1 \leq x \leq 0.4$ and its Curie temperature change from 530 to 780K. The Curie temperature of $(\text{Mn}_{1-x}\text{M}_x)_2\text{B}_4$ ($\text{M}=\text{Cr, Mo, Ta}$) changes linearly with unit cell volume. (8 refs.)

62588 Magnetic properties of La_2Ni_3 . F.T.Parker, H.Oesterreicher (Dept. of Chem., Univ. of California, San Diego, La Jolla, CA, USA).

J. Less-Common Met. (Switzerland), vol.90, no.1, p.127-36 (March 1983).

The magnetic properties of La_2Ni_3 are examined. Single-phase hexagonal La_2Ni_3 is found to order antiferromagnetically at $T_N=51\text{K}$. The Curie-Weiss temperature is positive ($\theta=70\text{K}$). Metamagnetic behavior is observed. The metamagnetic field at 4.2K, which is about 61 kOe, indicates a large sublattice anisotropy ($K_2 > 1.6 \times 10^6 \text{ erg cm}^{-3}$). The metamagnetic fields for other temperatures are proportional to the sublattice moment. Hexagonal La_2Ni_3 is shown to exhibit itinerant exchange coupling properties and is thus an itinerant antiferromagnet. The sign of exchange coupling is found to oscillate in the RNi_3 compound series as a function of the number of d electrons per transition metal. The data for rhombohedral La_2Ni_3 indicate that this compound is ferromagnetic. (27 refs.)

62589 A conical-point instability in triangular antiferromagnets caused by the dipole-dipole interaction. H.Shiba, N.Suzuki (Inst. for Solid State Phys., Univ. of Tokyo, Tokyo, Japan).

J. Magn. & Magn. Mater. (Netherlands), vol.31-34, pt.3, p.1035-6 (Feb. 1983). (Proceedings of the International Conference on Magnetism, Kyoto, Japan, 6-10 Sept. 1982).

In triangular XY-like antiferromagnets the dipole interaction can cause a new type of incommensurate state reflecting the conical-point property of the dipole interaction. A study is made on the phase transition and the effect of the in-plane field. The theory is applicable to AFCl_3 ($\text{A}=\text{Rb, Cs, Tl}$). (9 refs.)

62590 In plane competitive interactions in uniaxial metamagnets. E.Rastelli, A.Tassi (Istituto di Fisica, Univ. di Parma, Parma, Italy).

J. Magn. & Magn. Mater. (Netherlands), vol.31-34, pt.3, p.1041-2 (Feb. 1983). (Proceedings of the International Conference on Magnetism, Kyoto, Japan, 6-10 Sept. 1982).

A sketch of the ladder approximation for metamagnets with small interplane coupling and in plane nnn antiferromagnetic interaction is given. Unexpected striking effects of the nnn coupling are found. The results are applied to FeCl_2 and FeBr_2 to provide thermal renormalization and damping of the uniform mode. The fit with the existing experimental data is satisfactory. (9 refs.)

62591 The magnetic ordering in a hexagonal antiferromagnet. F.Matsubara (Dept. of Engng. Sci., Tohoku Univ., Sendai, Japan).

J. Magn. & Magn. Mater. (Netherlands), vol.31-34, pt.3, p.1045-6 (Feb. 1983). (Proceedings of the International Conference on Magnetism, Kyoto, Japan, 6-10 Sept. 1982).

The magnetic ordering in a hexagonal antiferromagnetic model of $S=1$ with anisotropy energies is studied by using the molecular field approximation. This model is shown to exhibit a variety of magnetic ordering processes as the temperature lowers. The author's results qualitatively explain the phase diagram of CsNiCl_3 . (6 refs.)

62592 Magnetoelastic phase transition in KMnF_3 . J.Bartolome (Dept. of Thermodynamics, Univ. of Zaragoza, Zaragoza, Spain), J.A.Rojo, R.Navarro, D.Gonzalez, M.R.Ibarra, A.Del Moral.

J. Magn. & Magn. Mater. (Netherlands), vol.31-34, pt.3, p.1052-4 (Feb. 1983). (Proceedings of the International Conference on Magnetism, Kyoto, Japan, 6-10 Sept. 1982).

Linear thermal expansion at zero magnetic field and at 12 kOe, as well as magnetic AC susceptibility at zero DC field, for a single crystal and powdered samples of KMnF_3 are reported. The magnetic phase transition at 81K, which originates weak ferromagnetism is of magnetoelastic origin. The magnetic properties are analyzed in terms of the D_{2h} space group. (10 refs.)

62593 Magnetic order in the $(\text{TM}_{1-x}\text{Y}_x)_2(\text{SO}_4)_3 \cdot 8\text{H}_2\text{O}$ system. S.Simizu, S.A.Friedberg (Phys. Dept., Carnegie-Mellon Univ., Pittsburgh, PA, USA).

J. Magn. & Magn. Mater. (Netherlands), vol.31-34, pt.3, p.1065-6 (Feb. 1983). (Proceedings of the International Conference on Magnetism, Kyoto, Japan, 6-10 Sept. 1982).

The effect of dilution on induced-moment ordering in the system $(\text{TM}_{1-x}\text{Y}_x)_2(\text{SO}_4)_3 \cdot 8\text{H}_2\text{O}$ with $0.5 \leq x \leq 1$ was studied by magnetic measure-

ments between 0.06 and 4.2K. T_c falls much more slowly with x than predicted by mean-field theory including hyperfine interactions. Dipolar interactions may produce an ordered phase resembling a spin glass for $x \leq 0.9$. (5 refs.)

62594 Ferro and antiferromagnetic ordering in $\text{N}(\text{C}_2\text{H}_5)_4\text{FeCl}_4$ depending on the cooling rate. J.A.Puertolas (Dept. of Phys., Univ. of Zaragoza, Zaragoza, Spain), R.Navarro, F.Palacio, D.Gonzalez, R.L.Carlin, A.J.van Duyneveldt.

J. Magn. & Magn. Mater. (Netherlands), vol.31-34, pt.3, p.1067-8 (Feb. 1983). (Proceedings of the International Conference on Magnetism, Kyoto, Japan, 6-10 Sept. 1982).

Magnetic AC susceptibility at zero DC field of a single crystal and of powdered samples of $\text{N}(\text{C}_2\text{H}_5)_4\text{FeCl}_4$ are reported. Upon slow cooling the authors get an antiferromagnetic ordering below $T_c=2.9\text{K}$, whereas in the case of a fast cooling a ferromagnetic arrangement below $T_c=1.8\text{K}$ is detected. Explanations for such behaviour are advanced and a tentative analysis of the antiferromagnetic case is done. (8 refs.)

62595 Effect of Cu and Co impurities on the phase diagram and the bicritical point of $\text{CsMnCl}_3 \cdot 2\text{H}_2\text{O}$. E.Velu, R.Megy, J.Seiden, J.P.Renard (Inst. d'Electronique Fondamentale, Univ. Paris Sud, Orsay, France).

J. Magn. & Magn. Mater. (Netherlands), vol.31-34, pt.3, p.1069-70 (Feb. 1983). (Proceedings of the International Conference on Magnetism, Kyoto, Japan, 6-10 Sept. 1982).

The authors have measured the reduction of the Neel temperature and the bicritical field due to Cu and Co impurities in $\text{CsMnCl}_3 \cdot 2\text{H}_2\text{O}$ (CMC). They have determined the phase diagram near the bicritical point for CMC: 0.7% Cu. The results are not in accordance with the bicritical random field behavior. (13 refs.)

62596 Spin flopping in MnTiO_3 . H.Yamauchi, H.Hiroyoshi, M.Yamada, H.Watanabe, H.Takei (Res. Inst. for Iron, Steel & Other Metals, Tohoku Univ., Sendai, Japan).

J. Magn. & Magn. Mater. (Netherlands), vol.31-34, pt.3, p.1071-2 (Feb. 1983). (Proceedings of the International Conference on Magnetism, Kyoto, Japan, 6-10 Sept. 1982).

Susceptibility and magnetization have been measured on a single crystal of MnTiO_3 . Spin-flopping is observed in the magnetization curve with the field along the hexagonal c-axis. The exchange parameter and the anisotropy constant are estimated from the experimental data, the latter being 2.3 times smaller than the calculated value for the dipole interactions. (5 refs.)

62597 A microscopic model describing the spin-flip processes at the first-order antiferromagnetic-to-ferromagnetic phase transition in $\text{Dy}_2\text{O}_3\text{SO}_4$. H.Hulsing, H.G.Kahle, A.Kasten (Phys. Inst., Univ. Karlsruhe, Karlsruhe, Germany).

J. Magn. & Magn. Mater. (Netherlands), vol.31-34, pt.3, p.1073-4 (Feb. 1983). (Proceedings of the International Conference on Magnetism, Kyoto, Japan, 6-10 Sept. 1982).

In applied magnetic fields, the antiferromagnet (af) $\text{Dy}_2\text{O}_3\text{SO}_4$ is transformed into the paramagnetic saturated state via an intermediate ferrimagnetic (fi) phase. The effects leading to a pronounced asymmetric hysteresis and large time constants at the af-fi transition are explained within a microscopic model discussing the possible sequences of single spin-flip processes. (6 refs.)

62598 The effect of paramagnetic impurities on the wave-vector of the spin-density-wave of an itinerant electron antiferromagnet. L.Gunther (Dept. of Phys., Tufts Univ., Medford, MA, USA), M.M.Antonoff.

J. Magn. & Magn. Mater. (Netherlands), vol.31-34, pt.3, p.1077-8 (Feb. 1983). (Proceedings of the International Conference on Magnetism, Kyoto, Japan, 6-10 Sept. 1982).

It is shown that magnetic impurities can produce a first order phase transition between the commensurate and incommensurate spin-density-wave phases of an itinerant electron antiferromagnet. The result is a consequence of the impurity-induced discontinuity in the wave-vector of the SDW at the phase boundary. (1 ref.)

62599 Effects of hydrostatic pressure on phase transition of some low-dimensional systems. K.Takeda, M.Wada, A.Ohtani, A.Onodera, T.Haseda (Faculty of Engng. Sci., Osaka Univ., Toyonaka, Japan).

J. Magn. & Magn. Mater. (Netherlands), vol.31-34, pt.3, p.1193-5 (Feb. 1983). (Proceedings of the International Conference on Magnetism, Kyoto, Japan, 6-10 Sept. 1982).

The possibility of controlling the dimensionality of magnetic interactions and spin symmetry has been undertaken by applying the hydrostatic pressure to magnetic compounds. The Neel temperature, magnetic phase diagram, exchange constant and anisotropy field have been obtained as a function of the applied hydrostatic pressure in $\text{CoCl}_2 \cdot 6\text{H}_2\text{O}$. (3 refs.)

62600 Field-induced increase of the Neel temperature in a two-dimensional system. K.Koyama, K.Amaya, K.Takeda (Faculty of Engng. Sci., Osaka Univ., Toyonaka, Japan).

J. Magn. & Magn. Mater. (Netherlands), vol.31-34, pt.3, p.1196-8 (Feb. 1983). (Proceedings of the International Conference on Magnetism, Kyoto, Japan, 6-10 Sept. 1982).

The fully mapped magnetic phase diagram of a quasi-two-dimensional (2d) antiferromagnetic $\text{Mn}(\text{HCOO})_2 \cdot 2\text{H}_2\text{O}$ has been determined by measurement of the magnetic heat capacity and susceptibility. An anomalous increase of the Neel temperature $T_N(H)$ has been found for the first time in this 2d compound. (6 refs.)

62601 Magnetic properties of the quasi-2d easy plane antiferromagnet $\text{BaNi}_2(\text{PO}_4)_2$. L.P.Rognault, J.Rossat-Mignod, J.Y.Henry, L.J.De Jongh (Dept. de Recherche Fondamentale, CENG, Grenoble, France).

J. Magn. & Magn. Mater. (Netherlands), vol.31-34, pt.3, p.1205-6 (Feb. 1983). (Proceedings of the International Conference on Magnetism, Kyoto, Japan, 6-10 Sept. 1982).

The magnetic properties of the layered compound $\text{BaNi}_2(\text{PO}_4)_2$ have been studied using susceptibility, elastic and inelastic neutron scattering measurements. Important effects have been observed when the temperature approaches T_N , which suggest the existence of a phase transition of the Kosterlitz-Thouless type in this system. (10 refs.)

62602 The H-T phase diagram for the spin-glass Ag:Mn. R.V.Chamberlain, M.Hardiman, L.A.Turkevich, R.Orbach (Dept. of Phys., Univ. of California, Los Angeles, CA, USA).

J. Magn. & Magn. Mater. (Netherlands), vol.31-34, pt.3, p.1423-4 (Feb. 1983). (Proceedings of the International Conference on Magnetism, Kyoto, Japan, 6-10 Sept. 1982).

The magnetic field-temperature spin glass transition line has been measured for the dilute magnetic alloy Ag:Mn, and the insulator $\text{Eu}_{0.4}\text{Sr}_{0.6}\text{S}$ (by Bon-temps et al. 1982). In both cases, the longitudinal magnetization is of the de Almeida-Thouless form $(\Delta H)^{2/3} = (1 - [T_G(H)/T_G])^{2/3}$, where A depends on the time scale of the experiment. (11 refs.)

- 62603 Random fields and ordering in antiferromagnetic insulators.** R.A.Cowley (Brookhaven Nat. Lab., Upton, NY, USA). *J. Magn. & Magn. Mater. (Netherlands)*, vol.31-34, pt.3, p.1439-41 (Feb. 1983). (Proceedings of the International Conference on Magnetism, Kyoto, Japan, 6-10 Sept. 1982).
- Neutron scattering measurements of the effect on the long-range order and phase transitions of random magnetic fields are reviewed. The results at low temperatures in $\text{Rb}_2\text{Co}_2\text{Mg}_{1-x}\text{F}_4$ and $\text{Co}_2\text{Zn}_{1-x}\text{F}_2$ show that the long-range order is not established when samples are cooled in a magnetic field, but they form a state with unusually long magnetic correlations. In $\text{Mn}_2\text{Zn}_{1-x}\text{F}_2$ a similar state is formed by only very close in temperature to T_N . (10 refs.)
- 62604 Environment effect in random mixtures with competing magnetic anisotropies.** H.Mano (Dept. of Phys., Gakushuin Univ., Tokyo, Japan). *J. Magn. & Magn. Mater. (Netherlands)*, vol.31-34, pt.3, p.1453-4 (Feb. 1983). (Proceedings of the International Conference on Magnetism, Kyoto, Japan, 6-10 Sept. 1982).
- The magnetic properties of a mixture of two kinds of antiferromagnets are investigated taking into account the dependence of the effective field acting on a spin on its neighboring atomic configuration. A broad orientation distribution of thermal averages of spins is obtained in the oblique antiferromagnetic phase. (2 refs.)
- 62605 Phase diagram of random mixtures of antiferromagnets with competing anisotropy.** H.Miwa (Faculty of Liberal Arts, Shinshu Univ., Matsumoto, Japan). *J. Magn. & Magn. Mater. (Netherlands)*, vol.31-34, pt.3, p.1455-6 (Feb. 1983). (Proceedings of the International Conference on Magnetism, Kyoto, Japan, 6-10 Sept. 1982).
- A generalized molecular-field theory which takes into account local atomic environment explicitly, is developed to study the phase diagram of random mixtures with competing magnetic anisotropy. The lower transition temperature is found to be very sensitive to the approximation employed. (4 refs.)
- 62606 NMR observation of oblique phase in mixed crystals $(\text{CH}_3\text{NH}_3)_2\text{Cu}(\text{Cl}_{1-x}\text{Br}_x)_4$ ($0.5 \leq x \leq 1$).** H.Kubo, Y.Suzuki, K.Kirakawa (Faculty of Engng., Kyushu Univ., Fukuoka, Japan). *J. Magn. & Magn. Mater. (Netherlands)*, vol.31-34, pt.3, p.1461-2 (Feb. 1983). (Proceedings of the International Conference on Magnetism, Kyoto, Japan, 6-10 Sept. 1982).
- It was recently reported by Kimishima (1980) that the transition from the ferromagnetic to the antiferromagnet occurs at $x \approx 0.9$ in a mixed compound of $(\text{CH}_3\text{NH}_3)_2\text{Cu}(\text{Cl}_{1-x}\text{Br}_x)_4$. By the Cl NMR, the authors show that in the concentration region of the oblique phase, the Br^- ions occupy a position on the c -axis, contrary to anticipation. (6 refs.)
- 62607 Magnetic properties of amorphous Fe-Nb and Fe-Zr.** K.M.Unruh, C.L.Chien (Dept. of Phys., Johns Hopkins Univ., Baltimore, MD, USA). *J. Magn. & Magn. Mater. (Netherlands)*, vol.31-34, pt.3, p.1587-8 (Feb. 1983). (Proceedings of the International Conference on Magnetism, Kyoto, Japan, 6-10 Sept. 1982).
- Magnetic ordering temperatures and values of the effective hyperfine field have been obtained for a number of amorphous $\text{Fe}_x\text{Nb}_{100-x}$ and $\text{Fe}_x\text{Zr}_{100-x}$ alloys for compositions at and above the threshold for magnetic ordering, found at $x=55$ and $x=45$, respectively. For both sets of samples the effective hyperfine field is found to rise linearly with composition. The magnetic ordering temperatures, while rising monotonically in $a\text{-Fe}_x\text{Nb}_{100-x}$, display a maximum at about $x=85$ in $a\text{-Fe}_x\text{Zr}_{100-x}$. (4 refs.)
- 62608 Magnetic hyperfine field distribution and structural relaxation of amorphous $(\text{Fe}_{81.5}\text{B}_{14.5}\text{Si}_4)$ prepared with different quenching rates.** G.Fratucello, F.Ronconi (Istituto di Fisica, Univ. di Ferrara, Ferrara, Italy), P.Allia, G.P.Sordo, F.Vinai. *J. Magn. & Magn. Mater. (Netherlands)*, vol.31-34, pt.3, p.1591-3 (Feb. 1983). (Proceedings of the International Conference on Magnetism, Kyoto, Japan, 6-10 Sept. 1982).
- The hyperfine field distributions of the amorphous $(\text{Fe}_{81.5}\text{B}_{14.5}\text{Si}_4)$ alloy are explained in terms of structural disorder. The increase in Curie temperature with isothermal relaxation may be attributed to the increase of mean number of nearest-neighbor iron atoms around Fe, and so to reduction of topological short-range disorder. (10 refs.)
- 62609 Magnetic properties of $\text{US}_{1-x}\text{Se}_x$ solid solution.** T.Palewski, Z.Bukowski (Inst. of Inorganic Chem. & Metall. of Rare Elements, Tech. Univ. of Wrocław, Wrocław, Poland). *Mater. Sci. (Poland)*, vol.7, no.4, p.463-6 (1981).
- The magnetic parameter of the polycrystalline samples of $\text{US}_{1-x}\text{Se}_x$ solid solutions have been investigated in the temperature range 78-300K. The dependence of the Curie temperature on the mole fraction of selenium (x) exhibits two flat maxima at $x=0.2-0.3$ and $x=0.7-0.8$, the lattice constants and paramagnetic moments showing negative deviations from linearity. The magnetic properties of $\text{US}_{1-x}\text{Se}_x$ alloys are compared with other solid solutions of the uranium monocompounds. (10 refs.)
- 62610 Spin orientations in halides of the rare-earth and actinide series after magnetic phase transitions.** P.Rudra, M.K.Sikdar (Dept. of Phys., Univ. of Kalyani, Kalyani, India). *Phys. Rev. B (USA)*, vol.27, no.7, p.4479-82 (1 April 1983).
- Halides of a rare-earth and actinide series show several magnetic phase transitions where the order of the transitions is not always definitely fixed. Group theoretical analysis shows that second-order phase transition from one magnetic phase to another can occur only for definite magnetic structures. The authors have found out the possible magnetic structures that can arise as a result of second-order phase transitions in these chemical structures. (18 refs.)
- Measurement of Curie temperature and magnetization of ferromagnetic materials employing an RF oscillator See Entry 59802
- A microprocessor controlled spectrometer for thermal scan Mossbauer spectroscopy See Entry 59897
- Amorphization of crystalline diluted Ising ferromagnet See Entry 61803
- Structural relaxation in (Fe-Cr)-based glass See Entry 61811
- Magnetic and structural characteristics of $\text{Ho}_6\text{Fe}_{23}$ deuterides See Entry 61858
- Crystal structure and magnetic properties of a new form of $\text{NH}_4\text{MnFeF}_6$ See Entry 61880
- Hexagonal tungsten bronze-type Fe^{III} fluoride: $(\text{H}_2\text{O})_{0.33}\text{FeF}_3$; crystal structure, magnetic properties, dehydration to a new form of iron trifluoride See Entry 61882
- High accuracy measurement of the Hall effect in magnetic materials with an AC lock-in technique See Entry 62401
- Cooperative quadrupolar ordering of Yb^{3+} ions in the Γ_8 electronic state See Entry 62533

- Magnetic field-induced incommensurable magnetic phases in the singlet-ground state system CsFeCl_3 See Entry 62552
- Magnetic structures and interaction constants in the two-dimensional Ising antiferromagnets $\text{RE}_2\text{O}_2\text{SO}_4$ ($\text{RE}=\text{Dy, Ho, Tb}$) See Entry 62553
- Frustration of antiferromagnetic bonds around a screw dislocation See Entry 62555
- A magnetic quasi-ordered state in $\text{Cr}_{1-x}\text{Ti}_x\text{S}$ See Entry 62563
- Magnetic moment of Fe-Ga-B amorphous alloys See Entry 62565
- Magnetic properties of the weak ferromagnet NH_4MnF_3 See Entry 62567
- Experiments on randomly mixed magnets with competing interactions See Entry 62574
- X_α method for the magnetic transition state and exchange interactions in KNiF_3 See Entry 62579
- Ordering of spin and orbital moments in a lattice of 3d ions coupled by superexchange See Entry 62617
- Theoretical study of the magnetic properties of an antiferromagnetic system with two kinds of inequivalent magnetic-ion sites See Entry 62619
- Specific heat study of the transition from ferromagnetism to antiferromagnetism in terbium See Entry 62621
- Magnetic phase transitions in presence of bilinear and quadrupolar interactions in rare earth compounds See Entry 62622
- Dynamics of magnetic response near T_c See Entry 62623
- Magnetic relaxation in the spin glass $\text{BaO}_2\text{TiO}_2\text{Fe}_2\text{O}_3$ See Entry 62629
- Spin dynamics and spin glass transition in the quasi-1D system FeMgBO_4 See Entry 62634
- Ferromagnetic and spin glass behavior near the critical concentration in amorphous $(\text{Fe}_x\text{Ni}_{100-x})_{75}\text{Ge}_{25}$ See Entry 62635
- Point contact spectroscopy of internal field distributions in spin glasses See Entry 62637
- Critical exponents and the size of the critical region in amorphous GdAl spin glass See Entry 62640
- Spin glass in the site-diluted antiferromagnetic FCC See Entry 62643
- Magnetoresistance near the Curie point of TbZn single crystals See Entry 62645
- Monte Carlo calculations of phase diagrams of Ising systems with competing interactions See Entry 62658
- Some rigorous results on the phase diagram of the dilute Ising model See Entry 62662
- Spin-flop-paramagnetic phase transition See Entry 62669
- A binary ferromagnetic alloy with magnetic moments dependent on local environment. I. The Jaccarino-Walker model in the effective field approximation See Entry 62676
- Magnetization process of GdNi single crystal in the high magnetic field near the Curie temperature See Entry 62697
- Magnetic inhomogeneity in amorphous Fe-Zr alloys See Entry 62701
- Effect of fabrication condition on the magnetic properties of Fe-Mn-B system amorphous alloys See Entry 62704
- Magnetic properties of amorphous powders of alloy Mn_3B_4 See Entry 62710
- Diffusion and magnetic properties of compositionally modulated films See Entry 62728
- Magnetic properties and magnetic Kerr rotation of amorphous TbFeCo and TbFeCr films See Entry 62737
- Magnetic and electrical properties of amorphous $\text{Fe}_{1-x}\text{B}_x$ films See Entry 62740
- Perpendicular anisotropy in Co-Cr films See Entry 62751
- Interference enhanced Kerr spectroscopy for very thin absorbing films—application to amorphous terbium ion See Entry 62759
- Domain structure in single crystal ferromagnetic oxide films near the phase transitions See Entry 62771
- Comparison of the magnetic properties of one- and two-layer iron garnet films See Entry 62781
- On the magnetostrictive phenomena in metamagnetism See Entry 62796
- Electron spin resonance study of a disordered Ni-Mn alloy See Entry 62803
- Surface magnetism of $\alpha\text{-Fe}_2\text{O}_3$ by Mossbauer spectroscopy See Entry 62860
- Nonstoichiometry and physical properties of hot-pressed manganese-zinc ferrites See Entry 63223
- ## 75.30S Magnetocaloric effect
- 62611 Mechanism of thermomagnetic recording in an MnBi film.** S.N.Marchenko (All-Union Sci.-Res. Inst. of Optophys. Measurements, Moscow, USSR). *Fiz. Met. & Metallogr. (USSR)*, vol.55, no.2, p.259-62 (Feb. 1983). In Russian. English translation in: *Phys. Met. & Metallogr. (GB)*
- An investigation was made of thermomagnetic recording in an MnBi film and of its working temperature range. A quantitative dependence of the film magnetization after recording on the exposure was obtained near the threshold. It was found that reversed domains formed as a result of thermomagnetic recording in MnBi near the Curie temperature 743K in a temperature interval of $\sim 4.5\text{K}$. Heating of the film with a flashlamp (144 pulses) reduced the threshold energy density for recording with the aid of laser radiation. (8 refs.) A.T.
- 62612 Analysis of thermomagnetic coding characteristics.** Yu.A.Pavlov. *Tekhn. Kino & Telev. (USSR)*, no.3, p.35-7 (March 1983). In Russian.
- The paper analyses frequency response and non-linear characteristics of the magnetic recording thermoduplication process. Recommendations for making mastertapes are given. (3 refs.)
- Dynamical properties of small particles; comparison with spin glass behaviour See Entry 62719
- Magnetic and optical properties of Co, Bi substituted garnet films prepared by the LPE method and its application to thermomagnetic recording See Entry 62733
- Amorphous TbFe ultra thin film with reflective Au layer See Entry 62734
- Garnet film with rectangular hysteresis loop and its application to thermomagnetic recording medium See Entry 62735
- Preparation and properties of RE-TM amorphous films See Entry 62736

The thermo-magnetic writing and erasing properties and Kerr rotation angle of amorphous RE-Fe thin films See Entry 62738

Static and dynamic properties of thermomagnetic writing in amorphous TbFe films See Entry 62770

75.40 CRITICAL-POINT EFFECTS, SPECIFIC HEATS, SHORT-RANGE ORDER

(inc. spin glasses)

62613 Frequency dependent magnetic susceptibility and spin glass freezing in PtMn alloys. G.V.Lecomte, H.von Lohneysen (Phys. Inst., Rheinisch-Westfälischen, Tech. Hochschule Aachen, Aachen, Germany), E.F.Wassermann. *Z. Phys. B (Germany)*, vol.50, no.3, p.239-45 (1983).

Reports measurements of the low-field complex magnetic susceptibility on $\text{Pt}_{1-x}\text{Mn}_x$ for $x=0.01, 0.025$ and 0.05 and for frequencies ν between 10 and 4000 Hz. A strong frequency dependence of the freezing temperature T_f is observed: $\Delta T_f/T_f \Delta \ln \nu = 0.025$ (decade ν)⁻¹ for all three alloys. These results as well as previous other measurements are interpreted in terms of a phenomenological model. (34 refs.)

62614 Many-soliton solutions of equations for a nonisotropic magnetic material. A.B.Borisov (Inst. of Metal Phys., Acad. of Sci., Sverdlovsk, USSR).

Fiz. Met. & Metalloved. (USSR), vol.55, no.2, p.230-4 (Feb. 1983). In Russian. English translation in: *Phys. Met. & Metallogr. (GB)*

A procedure is proposed for integrating an equation for a nonisotropic magnetic material on the basis of the matrix Riemann problem for doubly periodic functions. The general form of many-soliton solutions is found. (15 refs.) A.T.

62615 High temperature series expansion of staggered susceptibility of the three-state antiferromagnetic Potts model on d-dimensional hypercubic lattices. T.Oguchi, H.Yoshida (Dept. of Phys., Tokyo Inst. of Technol., Tokyo, Japan).

J. Phys. Soc. Jpn. (Japan), vol.52, no.4, p.1102-4 (April 1983).

The three-state antiferromagnetic Potts model on d-dimensional hypercubic lattices is studied, where d is 2, 3, 4, 5 and 6. The Hamiltonian is expressed by the spin Hamiltonian with spin 1. The staggered susceptibility is calculated by the high temperature series expansion. By use of the ratio method and the Padé approximation, the critical temperature and the critical exponent γ are obtained. It is concluded that the three-state antiferromagnetic Potts model exhibits a second-order transition when $d \geq 3$.

62616 Evidence for cooperativity in quadrupolar glass freezing from Monte Carlo simulations. M.Devoret, D.Esteve (CENS, Gif-sur-Yvette, France).

J. Phys. C (GB), vol.16, no.10, p.1827-40 (10 April 1983).

The authors present a Monte Carlo study of a dilute system of interacting classical quadrupoles on an HCP lattice for quadrupole concentrations $X=0.68$ and $X=0.53$. Within their computation time limits which were 4×10^5 MCS per quadrupole for a sample of 96 sites and 10^5 MCS per quadrupole for a sample of 216 sites, they find a progressive growth of the local quadrupolarisations. However, an analysis of the orientational fluctuations sets a lower bound of the order of 10% on the number of correlated quadrupoles responsible for this growth. (20 refs.)

62617 Ordering of spin and orbital moments in a lattice of 3d ions coupled by superexchange. B.Hoppe, L.L.Hirst (Inst. für Theoretische Phys., Univ. Frankfurt, Frankfurt, Main, Germany).

J. Phys. C (GB), vol.16, no.10, p.1919-32 (10 April 1983).

The authors consider the statistical mechanics of a lattice of orbitally degenerate magnetic ions coupled by superexchange. In such systems the ordering phenomena involve orbital as well as spin moments and may lead to various ordered phases and phase transitions. In particular, it is shown that the characteristic product form of the superexchange coupling leads, by a sign-reversal mechanism, to orbital phase transitions that occur at temperatures small compared with the Neel temperature for spin ordering. To treat such systems they develop an approximation scheme based on a 'factorisation approximation' which separates the total problem into spin and orbital subproblems. Detailed calculations are given for the specific case of 3d ions with triplet crystal-field orbital ground levels in perovskites. (11 refs.)

62618 Ordering in an orbital superexchange model. B.Hoppe, R.Liebmann, L.L.Hirst (Inst. für Theoretische Phys., Univ. Frankfurt, Frankfurt/Main, Germany).

J. Phys. C (GB), vol.16, no.10, p.1933-44 (10 April 1983).

The orbital superexchange model is a semiclassical model in which the ions of simple cubic lattice each have three purely orbital states apiece, each of which couples preferentially along a different cubic axis. The authors investigate the statistical mechanics of this model by means of exact results, analytical approximations and expansions, and Monte Carlo calculations. They find that for a negative coupling constant there is a strongly discontinuous phase transition to a phase with simple ferro ordering, and a ground state with infinite degeneracy but vanishing entropy density. For a positive coupling constant there is no phase transition and a large zero-point entropy, S_0 . They derive rigorous upper and lower bounds for S_0 and obtain a Pauling estimate that is in good agreement with the Monte Carlo value. The absence of ordering when the coupling constant is positive is due not to frustration but rather to an opposite effect which they call saturation. (16 refs.)

62619 Theoretical study of the magnetic properties of an antiferromagnetic system with two kinds of inequivalent magnetic-ion sites. N.Suzuki, K.Motizuki (Dept. of Material Phys., Osaka Univ., Toyonaka, Japan).

J. Phys. C (GB), vol.16, no.11, p.2133-43 (20 April 1983).

On the basis of the dynamical correlated effective-field approximation (DCEFA) the authors study the magnetic properties of an antiferromagnetic system with crystal structure of the hexagonal BaTiO_3 type which has two kinds of inequivalent magnetic-ion sites. They calculate the Neel temperature and the sublattice magnetisation for various sets of exchange parameters. The results of calculation are compared with those obtained by the simple molecular-field approximation and the pair and lone spin model. One of the advantages of the DCEFA is that it can treat moment reduction of both kinds of inequivalent spins. The spin wave dispersion is also calculated. (19 refs.)

62620 Fully anisotropic triangular lattice quenched bond-random Potts ferromagnet: almost exact critical frontier. C.Tsallis (Centro Brasileiro de Pesquisas Fisicas/CNPq, Rio de Janeiro, Brazil).

J. Magn. & Magn. Mater. (Netherlands), vol.31-34, pt.3, p.1047-8 (Feb. 1983). (Proceedings of the International Conference on Magnetism, Kyoto, Japan, 6-10 Sept. 1982).

Through convenient duality and star-triangle-type generalized transformations, the author obtains a (presumably excellent for $1 \leq q \leq 4$) approximate phase diagram for the fully anisotropic triangular lattice quenched bond-random

q-state Potts ferromagnet. Several exact particular results are obtained; a small error is, however, present in one of the limiting slopes. (7 refs.)

62621 Specific heat study of the transition from ferromagnetism to antiferromagnetism in terbium. K.D.Jayasuriya, S.J.Campbell, A.M.Stewart, E.S.R.Gopal (Res. School of Phys. Sci., Australian Nat. Univ., Canberra, Australia).

J. Magn. & Magn. Mater. (Netherlands), vol.31-34, pt.3, p.1055-6 (Feb. 1983). (Proceedings of the International Conference on Magnetism, Kyoto, Japan, 6-10 Sept. 1982).

The specific heat of single crystal terbium has been measured over the range 200-400K. A value for the latent heat of $(13.6 \pm 0.6) \text{ J mol}^{-1}$ is obtained at the first order antiferromagnetic to ferromagnetic transition temperature $T_N = (221.45 \pm 0.03) \text{ K}$. A temperature hysteresis of $(0.24 \pm 0.03) \text{ K}$ is observed in the transition. (7 refs.)

62622 Magnetic phase transitions in presence of bilinear and quadrupolar interactions in rare earth compounds. P.Morin, D.Schmitt (Lab. Louis Neel, CNRS, Grenoble, France).

J. Magn. & Magn. Mater. (Netherlands), vol.31-34, pt.3, p.1059-60 (Feb. 1983). (Proceedings of the International Conference on Magnetism, Kyoto, Japan, 6-10 Sept. 1982).

A Landau expansion of the free energy in the non-ordered phase of cubic rare earth intermetallics is obtained from an analytical susceptibilities formalism taking into account the exact crystalline electric field. The deduced magnetic dipolar and quadrupolar phase diagram closely agrees with experimental observations. (6 refs.)

62623 Dynamics of magnetic response near T_c . A.S.Arrott, B.Heinrich (Dept. of Phys., Simon Fraser Univ., Burnaby, BC, Canada).

J. Magn. & Magn. Mater. (Netherlands), vol.31-34, pt.3, p.1084-5 (Feb. 1983). (Proceedings of the International Conference on Magnetism, Kyoto, Japan, 6-10 Sept. 1982).

Linear response theory is applied to systems with many low lying excitations that influence relaxation rates. Formulation is holistic. The place for power laws is discussed. Applications are to spin glasses and to dynamic critical behavior in ferromagnetic iron whiskers. (5 refs.)

62624 Theoretical study of magnetism of spin system with alternating strong and weak exchange coupling. K.Motizuki, N.Suzuki (Dept. of Material Phys., Osaka Univ., Toyonaka, Japan).

J. Magn. & Magn. Mater. (Netherlands), vol.31-34, pt.3, p.1225-6 (Feb. 1983). (Proceedings of the International Conference on Magnetism, Kyoto, Japan, 6-10 Sept. 1982).

The magnetic properties of antiferromagnetic systems with alternating strong and weak exchange couplings are theoretically studied on the basis of the pair- and lone-spin model and the dynamical correlated-effective-field approximation. The results of the calculations are compared with those that follow from the conventional molecular-field approximation. (7 refs.)

62625 Anisotropy effects in the ferromagnetic quantum chain systems $(\text{C}_6\text{H}_{11}\text{NH}_3)_2\text{CuCl}_2$ (CHAC) and $(\text{C}_6\text{H}_{11}\text{NH}_3)_2\text{CuBr}_2$ (CHAB). K.Kopinga, H.Nishihara, W.J.M.de Jonge (Eindhoven Univ. of Technol., Eindhoven, Netherlands).

J. Magn. & Magn. Mater. (Netherlands), vol.31-34, pt.3, p.1241-2 (Feb. 1983). (Proceedings of the International Conference on Magnetism, Kyoto, Japan, 6-10 Sept. 1982).

Heat capacity and magnetization measurements on the title compounds revealed that they are very good approximations of a ferromagnetic $S=1/2$ Heisenberg chain system. The small anisotropy present in these compounds gives rise to very pronounced cross-over effects. In CHAC, the cross-over temperature is increased by a magnetic field parallel to the easy axis. (5 refs.)

62626 Spin glass like behaviour of the solid solution $\text{Mn}_{3/2}\text{Ga}_{0.5}\text{N}$. J.Garcia (Dept. de Termologia, Univ. de Zaragoza, Zaragoza, Spain), J.A.Rojas, R.Navarro, J.Bartolome, D.Gonzalez.

J. Magn. & Magn. Mater. (Netherlands), vol.31-34, pt.3, p.1401-3 (Feb. 1983). (Proceedings of the International Conference on Magnetism, Kyoto, Japan, 6-10 Sept. 1982).

Magnetic AC susceptibility and magnetization measurements on the solid solution $\text{Mn}_{3/2}\text{Ga}_{0.5}\text{N}$ were performed. Analysis of the data led the authors to propose, for $T < 160 \text{ K}$, a spin-glass like magnetic phase. (7 refs.)

62627 Dynamics of disordered spin systems studied by zero- and longitudinal μSR . I. (FeTiO₃)₈₈(Fe₂O₃)₁₂. Y.J.Uemura, K.Nishiyama, R.Kadono, J.Imazato, Y.Kuno, K.Nagamine, T.Yamazaki, Y.Ishikawa (Dept. of Phys., Univ. of Tokyo, Tokyo, Japan).

J. Magn. & Magn. Mater. (Netherlands), vol.31-34, pt.3, p.1379-80 (Feb. 1983). (Proceedings of the International Conference on Magnetism, Kyoto, Japan, 6-10 Sept. 1982).

Zero-field muon spin relaxation measurement in a spin glass (FeTiO₃)₈₈(Fe₂O₃)₁₂ exhibited a gradual slowing down of dynamical fluctuation of Fe moments between $170 \text{ K} > T > 50 \text{ K}$, while an onset of static random local fields starts around $T \sim 30 \text{ K}$. Different sharpness of the temperature dependence of muon relaxation in different spin glasses is also pointed out. (8 refs.)

62628 Spin glass properties and magnetic correlation in FeTiO₃-Fe₂O₃ system. Y.Ishikawa, M.Arai, N.Saito, M.Kohgi (Phys. Dept., Tohoku Univ., Sendai, Japan), H.Takei.

J. Magn. & Magn. Mater. (Netherlands), vol.31-34, pt.3, p.1381-3 (Feb. 1983). (Proceedings of the International Conference on Magnetism, Kyoto, Japan, 6-10 Sept. 1982).

The c axis component of spins in a randomly mixed system 0.88 FeTiO₃-0.12 Fe₂O₃ exhibits spin glass properties below 38K. The temperature evolution of the magnetic correlations of both the c axis and the perpendicular components, $\langle M_i(q)M_j(-q) \rangle$ and $\langle M_i(q)M_j(-q) \rangle$, have been determined by neutron small angle scattering using a single crystal. (5 refs.)

62629 Magnetic relaxation in the spin glass BaO₂TiO₃·2Fe₂O₃. K.Iwawuchi, Y.Ikeda, N.Koizumi, Y.Bando (Inst. for Chem. Res., Kyoto Univ., Kyoto, Japan).

J. Magn. & Magn. Mater. (Netherlands), vol.31-34, pt.3, p.1384-6 (Feb. 1983). (Proceedings of the International Conference on Magnetism, Kyoto, Japan, 6-10 Sept. 1982).

The property and structure of an insulating spin glass, BaO₂TiO₃·2Fe₂O₃ were investigated. Spin glass freezing temperature is about 165K. It seems that the blocking of magnetic clusters surrounded by Ti ions is responsible for the spin glass property. There is a magnetic relaxation at 70K. (5 refs.)

62630 Spin-glass compound ($Ti_{1-x}V_xO_2$: relaxation time and its field dependence. T.Saito, Y.Miyako (Dept. of Phys., Hokkaido Univ., Sapporo, Japan), C.J.Sandberg.

J. Magn. & Magn. Mater. (Netherlands), vol.31-34, pt.3, p.1387-8 (Feb. 1983). (Proceedings of the International Conference on Magnetism, Kyoto, Japan, 6-10 Sept. 1982).

AC-susceptibility $\chi_0(\omega)$ on powdered $(Ti_{0.9}V_{0.1})_2O_3$ was measured with and without the static magnetic field H . With increasing H , the steep slope of $\ln \chi_0(\omega)$ around T_g becomes gradual and the inflection point shifted to lower temperatures. (8 refs.)

62631 Spin dynamics of an insulating spin-glass $Rb_2Mn_{1-x}Cr_xCl_4$ at the microwave region. M.Tanimoto, K.Katsumata (Res. Inst. of Appl. Electricity, Hokkaido Univ., Sapporo, Japan).

J. Magn. & Magn. Mater. (Netherlands), vol.31-34, pt.3, p.1389-90 (Feb. 1983). (Proceedings of the International Conference on Magnetism, Kyoto, Japan, 6-10 Sept. 1982).

Temperature dependence of electron spin resonance (ESR) and the imaginary part of the susceptibility $\chi''(\omega)$ in zero magnetic field at 9.00 GHz have been studied in a new spin-glass, $Rb_2Mn_{1-x}Cr_xCl_4$. Two peaks in $\chi''(\omega)$, one at 11K and the other at 35K, have been observed in the $x=0.5$ sample at zero external field. The former corresponds to the zero field ESR. The latter seems to be explained by the dynamical susceptibility calculated by Kinzel and Fischer (1977) and by Ueno (1980). (13 refs.)

62632 Specific heat measurements in the highly frustrated $CsMnFeF_6$ and $CsNiFeF_6$ compounds. C.Pappa, J.Hammann (Service de Physique du Solide et de Resonance Magnetique, CENS, Gif-sur-Yvette, France), C.Jacoboni.

J. Magn. & Magn. Mater. (Netherlands), vol.31-34, pt.3, p.1391-2 (Feb. 1983). (Proceedings of the International Conference on Magnetism, Kyoto, Japan, 6-10 Sept. 1982).

The authors performed specific heat measurements on $CsMnFeF_6$ and $CsNiFeF_6$ in the temperature range where the magnetic ordering phenomena occur (27K and 4.7K respectively). The magnetic specific heat of $CsMnFeF_6$ shows a maximum around 27K. No maximum appears in $CsNiFeF_6$, only a sudden change of slope is observed at 6K. Both curves can be fitted to a T^α law at low temperatures ($\alpha=1.35$ and 1.6). (7 refs.)

62633 Spin glass behaviour in chromium spinels. D.Fiorani (ITSE, CNR, Roma, Italy), S.Viticoli, J.L.Dormann, M.Nogues, J.L.Tholence, J.Hammann, A.P.Nurani.

J. Magn. & Magn. Mater. (Netherlands), vol.31-34, pt.3, p.1393-4 (Feb. 1983). (Proceedings of the International Conference on Magnetism, Kyoto, Japan, 6-10 Sept. 1982).

Experimental evidence of spin glass behaviour ($T_g=2.50K$ at $\nu=17$ Hz) is given for $ZnCr_{1-x}Ga_xO_4$ spinel by low field DC and AC susceptibility measurements, as well as by neutron diffraction measurements and Mossbauer spectra. (5 refs.)

62634 Spin dynamics and spin glass transition in the quasi-1D system $FeMgBO_4$. A.Wiedenmann (Inst. Phys. Chem., Univ. of Hamburg, Hamburg, Germany), W.Gunsser, P.Burlet, F.Mezei.

J. Magn. & Magn. Mater. (Netherlands), vol.31-34, pt.3, p.1395-6 (Feb. 1983). (Proceedings of the International Conference on Magnetism, Kyoto, Japan, 6-10 Sept. 1982).

Inelastic neutron scattering experiments revealed a diffusive behaviour of the spin dynamics. A quadratic Q - and a linear T -dependence of the relaxation rate above 30K is ascribed to isotropic helical 1D-correlations. A drastic increase of τ_r reflects a rather sharp cross-over transition to a highly frustrated 3D spin glass state. (7 refs.)

62635 Ferromagnetic and spin glass behavior near the critical concentration in amorphous $(Fe_{0.9}Ni_{0.1-x}Gd_x)_2P_{16}Al_3$. J.W.Lynn, R.W.Erwin (Dept. of Phys., Univ. of Maryland, College Park, MD, USA), J.J.Rhyne, H.S.Chen.

J. Magn. & Magn. Mater. (Netherlands), vol.31-34, pt.3, p.1397-8 (Feb. 1983). (Proceedings of the International Conference on Magnetism, Kyoto, Japan, 6-10 Sept. 1982).

The magnetic properties of amorphous $(Fe_{0.9}Ni_{0.1-x}Gd_x)_2P_{16}Al_3$ have been investigated above the critical concentration ($x=17$) for long range order via neutron scattering. For $x=30$ the spin wave stiffness parameter D first increases with decreasing temperature, but then decreases at lower temperatures as the spin state is approached. Accompanied by the decrease in D is an increase in the spin wave linewidths. (6 refs.)

62636 Magnetic relaxation in ferromagnets with competing interactions. M.A.Continentino (Inst. de Fisica, Univ. Federal Fluminense, Niteroi, Brazil).

J. Magn. & Magn. Mater. (Netherlands), vol.31-34, pt.3, p.1413-14 (Feb. 1983). (Proceedings of the International Conference on Magnetism, Kyoto, Japan, 6-10 Sept. 1982).

The author extends the theory of Anderson, Halperin and Varma (AHV) for spin glasses to ferromagnets with competing interactions. The coupling between magnons and two level systems (TLS) leads to a ferromagnetic instability which he associates with the disappearance of long range magnetic order on cooling in reentrant ferromagnet. (7 refs.)

62637 Point contact spectroscopy of internal field distributions in spin glasses. N.d'Ambrumenil, A.M.Duif, A.G.M.Jansen, P.Wyder (Max-Planck-Inst. fur Festkorperforschung, Stuttgart, Germany).

J. Magn. & Magn. Mater. (Netherlands), vol.31-34, pt.3, p.1415-16 (Feb. 1983). (Proceedings of the International Conference on Magnetism, Kyoto, Japan, 6-10 Sept. 1982).

The authors report the point contact spectra of dilute AuMn and CuMn spin glass alloys measured as a function of temperature in the neighbourhood of the spin-glass transition. They relate their results to the temperature-dependent internal field distribution. (4 refs.)

62638 Dynamics and stability of the Sherrington-Kirkpatrick model. J.A.Hertz (Nordita, Copenhagen, Denmark).

J. Magn. & Magn. Mater. (Netherlands), vol.31-34, pt.3, p.1419-20 (Feb. 1983). (Proceedings of the International Conference on Magnetism, Kyoto, Japan, 6-10 Sept. 1982).

The dynamics of a large (but finite) SK model are studied, paying particular attention to the fluctuation-dissipation theorem and the role of a symmetry-breaking external field. The susceptibility exhibits a symmetric cusp for short times and gradually approaches the value $1/T_g$ as the system comes to equilibrium. (10 refs.)

62639 Cooperative phenomena in spin glasses. S.Shtrikman (Dept. of Electronics, Weizmann Inst., Rehovoth, Israel), E.P.Wohlfarth.

J. Magn. & Magn. Mater. (Netherlands), vol.31-34, pt.3, p.1421-2 (Feb. 1983). (Proceedings of the International Conference on Magnetism, Kyoto, Japan, 6-10 Sept. 1982).

The reasons for considering cooperative phenomena in the Neel model of spin glasses are considered and the Vogel-Fulcher law derived approximately on this basis. As an example, lines in the H - T plane are calculated for different Vogel-Fulcher temperature. (13 refs.)

62640 Critical exponents and the size of the critical region in amorphous GdAl spin glass. A.P.Malozemoff, Y.Imry (IBM Thomas J. Watson Res. Center, Yorktown Heights, NY, USA).

J. Magn. & Magn. Mater. (Netherlands), vol.31-34, pt.3, p.1425-6 (Feb. 1983). (Proceedings of the International Conference on Magnetism, Kyoto, Japan, 6-10 Sept. 1982).

A scaling for susceptibility below the transition temperature T_g of a spin glass is proposed. In a GdAl spin glass, it is found to hold at all temperatures below T_g and out to 5000 Oe in field. (7 refs.)

62641 Critical phenomena in systems with random anisotropies. A.Aharony (Dept. of Phys. & Astron., Tel Aviv Univ., Tel Aviv, Israel).

J. Magn. & Magn. Mater. (Netherlands), vol.31-34, pt.3, p.1432-4 (Feb. 1983). (Proceedings of the International Conference on Magnetism, Kyoto, Japan, 6-10 Sept. 1982).

Current theoretical understanding of the effects of random fields and random anisotropies is reviewed, with emphasis on open questions. (30 refs.)

62642 Magnetic short-range order and spin freezing in the quasi-2D system $LuFeMgO_4$. A.Wiedenmann, W.Gunsser, J.Rossat-Mignod, M.O.Evrad (Inst. fur Phys. Chem., Univ. Hamburg, Hamburg, Germany).

J. Magn. & Magn. Mater. (Netherlands), vol.31-34, pt.3, p.1442-4 (Feb. 1983). (Proceedings of the International Conference on Magnetism, Kyoto, Japan, 6-10 Sept. 1982).

Neutron diffraction performed on the insulating compound $LuFeMgO_4$ revealed a gradual onset of anisotropic short-range ordering of the moments inside the random diluted double layers. Spin freezing which was observed by a saturation of the static correlations, Mossbauer hyperfine splitting and by a susceptibility maximum is ascribed to the competition between several antiferromagnetic interactions. (4 refs.)

62643 Spin glass in the site-diluted antiferromagnetic FCC. S.Fujiki, T.Suenaga, S.Katsura (Dept. of Appl. Phys., Tohoku Univ., Sendai, Japan).

J. Magn. & Magn. Mater. (Netherlands), vol.31-34, pt.3, p.1457-8 (Feb. 1983). (Proceedings of the International Conference on Magnetism, Kyoto, Japan, 6-10 Sept. 1982).

The diluted spin glass on the frustrated face-centered cubic lattice with the first and second neighbour interactions are considered by the square cactus approximation. Phase boundaries between the paramagnetic and ordered (ferromagnetic, superantiferromagnetic and spin glass) are obtained. The results qualitatively explain the experiments on $Eu_2S_{1-x}P_x$ and $Mn_2Co_{1-x}Te$. (5 refs.)

62644 Intrinsic hardness and micromagnetism in selected $RMn_2Ni_{5-x}Sc_x$ ($R=rare\ earth$). F.T.Parker, H.Oesterreicher (Dept. of Chem., Univ. of California, San Diego, La Jolla, CA, USA).

J. Magn. & Magn. Mater. (Netherlands), vol.36, no.1-2, p.195-207 (1 April 1983).

Bulk magnetic properties of selected compounds in the series $RMn_2Ni_{5-x}Sc_x$ ($R=rare\ earth$) are studied. Micromagnetic properties are pronounced for nonmagnetic or weakly magnetic rare earth analogs, but typical ferromagnetic behavior is seen for Sm analogs. Intrinsic magnetic hardness fields in the latter are quite large relative to their corresponding anisotropy fields, as compared to other typical $CaCu_2$ analogs. Thus, the strong Mn exchange fluctuations enhance domain wall pinning. (34 refs.)

62645 Magnetoresistance near the Curie point of TbZn single crystals. P.P.Freitas, J.Bessa Sousa (Centro de Fisica, Univ. do Porto, Porto, Portugal), P.Morin.

Port. Phys. (Portugal), vol.13, no.3-4, p.185-92 (1982).

Magnetoresistance studies of the intermetallic ferromagnetic TbZn compound have been performed for the first time, with accurate measurements of $\Delta\rho$ (T,H) and $(d\rho/dT)$ coefficients. Analysis of the results supports the theoretical predictions based on renormalization group calculations. (4 refs.)

62646 Solitons in quantum-spin systems. S.T.Chui (Bartol Res. Found., Univ. of Delaware, Newark, DE, USA), K.B.Ma.

Phys. Rev. B (USA), vol.27, no.7, p.4515-17 (1 April 1983).

Numerical results such as the specific heat, magnetic susceptibility, ground-state energy, and the magnon gap obtained with computer renormalization-group techniques are presented for $CsNiF_3$. No soliton states of the type analogous to the sine-Gordon kink were found. This is supported by analytic calculations of the quantum fluctuations of a winding number operation. (20 refs.)

62647 Long-time behavior of spin-glasses at low temperatures. I.Morgenstern (Inst. fur Theoretische Phys., Univ. Heidelberg, Heidelberg, Germany).

Phys. Rev. B (USA), vol.27, no.7, p.4522-5 (1 April 1983).

The free-energy barrier heights between different 'ground-state valleys' in configuration space are calculated by a new numerical method. The resulting relaxation times are so long that a decay of the freezing temperature T_f to zero as predicted by static theories is not to be observed in experiments. The absence of a phase transition occurs therefore only in a mathematical sense. (12 refs.)

The secondary effect of the cooperative Jahn-Teller distortion in rare earth vanadates See Entry 62089

Superflows and superfluidity See Entry 62200

High accuracy measurement of the Hall effect in magnetic materials with an AC lock-in technique See Entry 62401

Temperature-induced local moments in MnSi and FeSi See Entry 62549

Thermodynamic properties of the Anderson model See Entry 62550

Randomness in mixed antiferromagnets with competing spin anisotropies See Entry 62554

Frustration of antiferromagnetic bonds around a screw dislocation See Entry 62555

Effects of external field on χ - T curve on cluster-glasses See Entry 62561

Frustration effects in the disordered system $CsMnFeF_6$ See Entry 62562

A magnetic quasi-ordered state in $Cr_{1-x}Ti_xS_2$ See Entry 62563

Magnetic properties of the weak ferromagnet NH_4MnF_3 See Entry 62567

Spin orientation and exchange interactions in $(Fe,Co)Cl_2$ See Entry 62575

A conical-point instability in triangular antiferromagnets caused by the dipole-dipole interaction See Entry 62589

The magnetic ordering in a hexagonal antiferromagnet See Entry 62591

Magnetic order in the $(Tm,Y_{1-x})_2(SO_4)_3 \cdot 8H_2O$ system See Entry 62593

Effect of Cu and Co impurities on the phase diagram and the bicritical point of $CsMnCl_3 \cdot 2H_2O$ See Entry 62595

Spin flopping in $MnTiO_3$ See Entry 62596

A microscopic model describing the spin-flip processes at the first-order antiferromagnetic-to-ferrimagnetic phase transition in $Dy_2O_2SO_4$ See Entry 62597

- The effect of paramagnetic impurities on the wave-vector of the spin-density-wave of an itinerant electron antiferromagnet See Entry 62598
- Effects of hydrostatic pressure on phase transition of some low-dimensional systems See Entry 62599
- Field-induced increase of the Neel temperature in a two-dimensional system See Entry 62600
- The H - T phase diagram for the spin-glass Ag:Mn See Entry 62602
- Environment effect in random mixtures with competing magnetic anisotropies See Entry 62604
- Phase diagram of random mixtures of antiferromagnets with competing anisotropy See Entry 62605
- Magnetization process of GdNi single crystal in the high magnetic field near the Curie temperature See Entry 62697
- Anomalous temperature dependence of magnetization in amorphous $(\text{Fe}_{0.1}\text{Ni}_{0.9})_{77}\text{Si}_{10}\text{B}_{13}$ alloy See Entry 62699
- Dynamical properties of small particles; comparison with spin glass behaviour See Entry 62719
- Electron spin resonance study of a disordered Ni-Mn alloy See Entry 62803
- Investigation of the NMR enhancement factor in CuMn spin glasses See Entry 62812
- Application of the depth-selective conversion electron Mossbauer spectroscopy to rare-earth iron garnet films See Entry 62863

75.40D Ising and other classical spin models

- 62648 Monte Carlo study of an Ising gauge system.** S.Wansleben, A.Weinkauff (Inst. fur Theoretische Phys., Univ. zu Köln, Köln, Germany). *Z. Phys. B (Germany)*, vol.50, no.3, p.255-61 (1983).
The phase diagram of the 3-d Ising gauge model with additional ferromagnetic nearest neighbour Ising coupling is explored by Monte Carlo simulations. (11 refs.)
- 62649 Surface effects in Ising ferromagnets with anisotropy.** I.Tamura (Dept. of Phys., Nagoya Univ., Nagoya, Japan). *J. Phys. Soc. Jpn. (Japan)*, vol.52, no.4, p.1105-7 (April 1983).
The author extends a previous model of a semi-infinite Ising ferromagnet with anisotropy so as to incorporate not only the surface effects on anisotropy, but also those on exchange couplings into the model. The phase diagrams and the ordering temperatures for the surface magnetism of this extended model are examined by a new effective-field theory. The previous result that the surface cannot order before the bulk does when the author takes no account of the surface effects on the exchange couplings can be seen more clearly in those diagrams. The results obtained by a usual molecular-field theory are also given to compare with those of the effective-field theory. (5 refs.)
- 62650 Phase transitions on fractals. I. Quasi-linear lattices.** Y.Gefen, A.Aharony (Dept. of Phys. & Astron., Tel-Aviv Univ., Tel-Aviv, Israel), B.B.Mandelbrot. *J. Phys. A (GB)*, vol.16, no.6, p.1267-78 (21 April 1983).
Magnetic spin models and resistor networks are studied on certain self-similar fractal lattices, which are described as 'quasi-linear', because they share a significant property of the line: finite portions can be isolated from the rest by removal of two points (sites). In all cases, there is no long-range order at finite temperature. The transition at zero temperature has a discontinuity in the magnetisation, and the associated magnetic exponent is equal to the fractal dimensionality, D . When the lattice reduces to a non-branching curve the thermal exponent $\nu^{-1} = \gamma$ is equal to D . When the lattice is a branching curve, γ is related, respectively, to the dimensionality of the single-channel segments of the curve (for the Ising model), or to the exponent describing the resistivity (for models with continuous spin symmetry). (30 refs.)
- 62651 Stability of Parisi's solution of a spin glass model.** A.V.Goltsev (A.F. Ioffe Phys.-Tech. Inst., Acad. of Sci., Leningrad, USSR). *J. Phys. A (GB)*, vol.16, no.6, p.1337-43 (21 April 1983).
The condition of stability of Parisi's solution of the infinite-range spin glass model is obtained and examined near the transition temperature. The matrix of second derivatives $\partial^2 F / \partial Q_{\alpha\beta} \partial Q_{\gamma\delta}$ has non-negative eigenvalues only. There are two continuous branches of the eigenvalues and zero is an accumulation point of the eigenvalues. (14 refs.)
- 62652 Existence of spin-glass phases for three- and four-dimensional Ising and Heisenberg models.** A.Benyoussef, N.Boccaro (Service de Phys. du Solide et de Résonance Magnétique, CENS, Gif-sur-Yvette, France). *J. Phys. C (GB)*, vol.16, no.10, p.1901-18 (10 April 1983).
Using Migdal's recursion relations the authors investigate the existence of spin-glass phases for bond-diluted Ising and Heisenberg models with randomly distributed nearest-neighbour ferro- and antiferromagnetic interactions. For three-dimensional systems a spin-glass phase can only exist at zero temperature, while four-dimensional systems exhibit spin-glass phases at finite temperature. They show that very general considerations imply strong restrictions on the form of 1D recursion relations. As a consequence, the qualitative properties of all the systems they considered are very close. (19 refs.)
- 62653 Critical behaviour of impure Ising-Mattis model.** A.K.Roy, S.K.Roy, B.K.Chakrabarti (Saha Inst. of Nuclear Phys., Calcutta, India). *J. Phys. C (GB)*, vol.16, no.11, p.2115-20 (20 April 1983).
The effects of compressibility (annealed impurity) and dilution (quenched impurity) on the critical behaviour of the Ising-Mattis (spin-glass) model are investigated. The quenched impurity is seen to determine the ultimate critical behaviour unless it so happens that the quenched disorder can be completely transformed away when, of course, the annealed impurity shows up its effects. (13 refs.)
- 62654 Phase diagram for the triangular Ising lattice.** M.Kaburagi, T.Tonegawa, J.Kanamori (Coll. of Liberal Arts, Kobe Univ., Kobe, Japan). *J. Magn. & Magn. Mater. (Netherlands)*, vol.31-34, pt.3, p.1037-8 (Feb. 1983). (Proceedings of the International Conference on Magnetism, Kyoto, Japan, 6-10 Sept. 1982).
A magnetic phase diagram for the triangular Ising lattice with nearest-neighbor and next-nearest-neighbor interactions, both being antiferromagnetic, is calculated within the molecular field approximation. It is shown that there appear several intermediate phases between low-temperature and paramagnetic phases for an appropriate range of external magnetic field. (3 refs.)
- 62655 Modulated structures of an Ising spin system on a triangular lattice.** K.Nakanishi (Inst. for Solid State Phys., Univ. of Tokyo, Tokyo, Japan). *J. Magn. & Magn. Mater. (Netherlands)*, vol.31-34, pt.3, p.1039-40 (Feb. 1983). (Proceedings of the International Conference on Magnetism, Kyoto, Japan, 6-10 Sept. 1982).
Mean field calculations are performed to study an Ising spin system on a triangular (hexagonal) lattice. An infinite number of long-period modulated structures are shown to be stable in a wide temperature region. The stabilization mechanism of the modulated structures is discussed in terms of domain boundaries. (4 refs.)
- 62656 Monte Carlo simulation of a triangular Ising lattice.** K.Wada, H.Takayama, T.Ishikawa (Dept. of Phys., Hokkaido Univ., Sapporo, Japan). *J. Magn. & Magn. Mater. (Netherlands)*, vol.31-34, pt.3, p.1043-4 (Feb. 1983). (Proceedings of the International Conference on Magnetism, Kyoto, Japan, 6-10 Sept. 1982).
A Monte Carlo study has been made on a triangular Ising lattice with antiferromagnetic nearest neighbor and ferromagnetic next nearest neighbor interactions. The authors data suggest that a new phase may exist in the system, which is a generalization of the partially disordered antiferromagnetism associated with the sublattice switching. (4 refs.)
- 62657 Longitudinal spectra of classical ferromagnetic chains in a magnetic field.** U.Balucani, V.Tognetti (Istituto di Elettronica Quantistica, CNR, Firenze, Italy), A.Rettori. *J. Magn. & Magn. Mater. (Netherlands)*, vol.31-34, pt.3, p.1231-2 (Feb. 1983). (Proceedings of the International Conference on Magnetism, Kyoto, Japan, 6-10 Sept. 1982).
Recent computer experiments in classical ferromagnetic chains in a field have indicated that entirely new structures appear in the longitudinal spectra at finite temperatures. The authors show that all these dynamical features reflect a tendency toward a quasi-isotropic behaviour determined by a thermally induced spin-energy coupling. (5 refs.)
- 62658 Monte Carlo calculations of phase diagrams of Ising systems with competing interactions.** K.Binder, W.Kinzel, W.Selke (Inst. für Festkörperforschung, KFA Jülich, Jülich, Germany). *J. Magn. & Magn. Mater. (Netherlands)*, vol.31-34, pt.3, p.1445-6 (Feb. 1983). (Proceedings of the International Conference on Magnetism, Kyoto, Japan, 6-10 Sept. 1982).
FCC antiferromagnets with nearest (J_{nn}) and next-nearest neighbour exchange (J_{nnn}) in a field H are studied by Monte Carlo methods. For $J_{nnn}=0$, $H=H_c=4|J_{nn}|$ the 'fully frustrated' system stays always disordered. In a centered rectangular lattice, layered structures (2×1), (3×1) and an incommensurate phase are found. (8 refs.)
- 62659 Existence or non-existence of the ferromagnetic phase in the random-bond Ising model with competing interactions.** T.Horiguchi, T.Morita (Dept. of Engng. Sci., Tohoku Univ., Sendai, Japan). *J. Magn. & Magn. Mater. (Netherlands)*, vol.31-34, pt.3, p.1449-50 (Feb. 1983). (Proceedings of the International Conference on Magnetism, Kyoto, Japan, 6-10 Sept. 1982).
For a $\pm J$ Ising spin glass model on a square lattice, the authors give a sufficient condition for existence or for non-existence of the ferromagnetic phase. An upper and a lower bound to the critical concentration are 0.974 and $1/\sqrt{2}$, respectively. They give a physical interpretation to the obtained lower bound. (7 refs.)
- 62660 A quenched bond-mixed Ising model: Ferromagnetic phase stability limit.** E.F.Sarmiento (Dept. de Física, Univ. Federal de Alagoas, Maceio, Brazil), C.Tsallis, I.P.Fittipaldi. *J. Magn. & Magn. Mater. (Netherlands)*, vol.31-34, pt.3, p.1451-2 (Feb. 1983). (Proceedings of the International Conference on Magnetism, Kyoto, Japan, 6-10 Sept. 1982).
Within the framework of an effective field theory the authors discuss the ferromagnetic phase stability limit of a quenched bond-mixed spin $1/2$ Ising model in a simple cubic lattice. Whenever comparison is possible a satisfactory qualitative and to a certain extent quantitative agreement is observed. (4 refs.)
- 62661 Random-bond Ising system in the external magnetic field.** N.Miyamoto, S.Katsura (Dept. of Appl. Phys., Tohoku Univ., Sendai, Japan). *J. Magn. & Magn. Mater. (Netherlands)*, vol.31-34, pt.3, p.1459-60 (Feb. 1983). (Proceedings of the International Conference on Magnetism, Kyoto, Japan, 6-10 Sept. 1982).
The magnetization process and the distribution of the internal fields of the $\pm J$ model are treated by the pair approximation. The magnetization curves are shown to have several steps. A spin glass parameter for the random system under the external field is proposed and calculated at absolute zero. (5 refs.)
- 62662 Some rigorous results on the phase diagram of the dilute Ising model.** E.Olivieri, J.F.Perez, S.Goulart Rosa, Jr. (Istituto Matematico, Univ. di Roma, Rome, Italy). *Phys. Lett. A (Netherlands)*, vol.94A, no.6-7, p.309-11 (21 March 1983).
The authors consider bond dilute ferromagnetic systems and by using extended versions of correlation inequalities they prove the existence of a phase (below the critical temperature of the regular model) with nonanalytic behaviour, but with exponential clustering and zero magnetization. (9 refs.)
- 62663 Hidden Mattis phase in annealed system.** Y.Kasai, A.Okiji (Dept. of Appl. Phys., Osaka Univ., Suita, Japan). *Prog. Theor. Phys. (Japan)*, vol.69, no.1, p.20-31 (Jan. 1983).
The annealed Ising-spin system with competing exchange interactions (J and $-af$) is considered to have a Mattis-type ordered phase. This ordered phase is expected to show the critical slowing down although the free energy has no singularity at T_c . So, the authors call it the hidden Mattis phase. Further, the phase diagram (concentration vs. temperature) in this system exhibits a resemblance to that obtained approximately in the quenched system with the spin glasslike phase. (31 refs.)
- 62664 Investigation of Oguchi's procedure applied to the Ising model.** J.R.Faleiro Ferreira, N.P.Silva (Dept. de Física, Univ. Federal de Minas Gerais, Belo Horizonte, Brazil). *Phys. Status Solidi b (Germany)*, vol.116, no.1, p.155-62 (1 March 1983).
Approximate critical temperature of the anisotropic ferromagnetic Ising model is calculated using the procedure proposed by Oguchi (see Progr. Theor. Phys., vol.56, p.1442, 1976), with better results than those obtained by the use of Bogolyubov's principle. The calculation is made with linear and double chain trial Hamiltonians. (3 refs.)
- 62665 Exact solution of a one-dimensional Ising model in a random magnetic field.** G.Grinstein (IBM Thomas J. Watson Res. Center, Yorktown Heights, NY, USA), D.Mukamel. *Phys. Rev. B (USA)*, vol.27, no.7, p.4503-6 (1 April 1983).
Analytic results for the free energy, magnetic structure factor, and Edwards-Anderson order parameter of a one-dimensional ferromagnetic Ising model in a random magnetic field are obtained. The structure factor consists of both Lorentzian and Lorentzian-squared terms at all temperatures (T) greater than zero; the Lorentzian-squared terms vanish at $T=0$. The calculated correlation length agrees with predictions of the Imry-Ma domain argument. (10 refs.)

- 62666** Equivalence of statistical-mechanical and dynamic descriptions of the infinite-range Ising spin-glass. C.Dasgupta (Lyman Lab. of Phys., Harvard Univ., Cambridge, MA, USA), H.Sompolinsky. *Phys. Rev. B (USA)*, vol.27, no.7, p.4511-14 (1 April 1983). The authors prove the equivalence between the dynamic mean-field theory of the Ising spin-glass and the statistical-mechanical theory of Thouless, Anderson, and Palmer (TAP). Individual low-free-energy TAP solutions describe short-time properties, whereas thermodynamic equilibrium corresponds to averaging over all such solutions. The square of the staggered magnetization associated with the largest eigenvalue of the interaction matrix scales as $N^{5/6}$ (N is the number of spins). Results are confirmed by Monte Carlo simulation and numerical solution of the TAP equations. (12 refs.)
- 62667** Critical singularities of the random two-dimensional Ising model. Giancarlo Jug (Dept. of Theoretical Phys., Univ. of Oxford, Oxford, England). *Phys. Rev. B (USA)*, vol.27, no.7, p.4518-21 (1 April 1983). The critical properties of random ferromagnets with pure specific-heat exponent $\alpha_s=0$ are analyzed using renormalization-group methods. The origin and form of the impurity-induced logarithmic corrections for the random two-dimensional Ising model are discussed. Corrections develop only for the specific heat, which presents a new singularity of the $|\ln|T-T_c||^{1-\mu}$ as well as a heat critical exponent μ . (9 refs.)
- 62668** High-temperature path method for a two-dimensional random Ising model. D.Merlini (Math. Inst., Ruhr-Univ. Bochum, Bochum, Germany). Stochastic Processes in Quantum Theory and Statistical Physics. Proceedings of the International Workshop, Marseille, France, 29 June-4 July 1981 (Berlin, Germany: Springer-Verlag 1982), p.274-80. Develops a rigorous compact formulation of the high-temperature cluster expansion for a two-dimensional random Ising model and investigates the critical temperature of the model by the simple ratio method frequently employed in non-random spin systems. For a special class of a spin glass, it is found that the critical temperature is a monotonic decreasing function of the parameter describing the rate of disorder which varies from T_c (the Ising critical temperature) to $T=0$ (symmetric case). (13 refs.)
- Amorphization of crystalline diluted Ising ferromagnet** See Entry 61803
- Degenerate helimagnetic states, lines of soft modes and absence of long-range order in three dimensions** See Entry 62537
- Two-dimensionally modulated phase in Ising models** See Entry 62538
- Modulated phases in diluted ANNNI models** See Entry 62541
- Magnetic structures and interaction constants in the two-dimensional Ising antiferromagnets $\text{RE}_2\text{O}_3\text{SO}_4$ (RE=Dy, Ho, Tb)** See Entry 62553
- Static properties of classical ferromagnetic chains in a magnetic field: an interacting spin-wave theory** See Entry 62569

75.40F Heisenberg and other quantized spin models

- 62669** Spin-flop-paramagnetic phase transition. K.Muramatsu (Dept. of Phys., Tokyo Inst. of Technol., Tokyo, Japan). *J. Magn. & Magn. Mater. (Netherlands)*, vol.31-34, pt.3, p.1075-6 (Feb. 1983). (Proceedings of the International Conference on Magnetism, Kyoto, Japan, 6-10 Sept. 1982). A spin wave theory predicts that the SF-P transition of the Heisenberg antiferromagnet is to be of first order. Even in the zero anisotropy limit a non-zero excitation gap in the SF phase is found. These are discussed in terms of the $1/S$ expansion. The movement of spins in the $k=0$ mode is also considered. (2 refs.)
- 62670** On the two-dimensionality of $\text{Fe}(\text{HCOO})_2 \cdot 2\text{H}_2\text{O}$. I.Kimura, T.Idogaki (Dept. of Phys., Fukuoka Univ. of Education, Fukuoka, Japan). *J. Magn. & Magn. Mater. (Netherlands)*, vol.31-34, pt.3, p.1199-200 (Feb. 1983). (Proceedings of the International Conference on Magnetism, Kyoto, Japan, 6-10 Sept. 1982). With the use of decoration iteration transformation method, the effective coupling J between the successive A-planes of $\text{Fe}(\text{HCOO})_2 \cdot 2\text{H}_2\text{O}$ is calculated. It is shown that J tends to zero as $T \rightarrow 0\text{K}$ and the two-dimensionality becomes more remarkable. (3 refs.)
- 62671** Energy fluctuations at a linear Heisenberg ferromagnet. V.Tognetti, U.Balucani (Istituto di Elettronica Quantistica, CNR, Firenze, Italy), A.Rettori, J.M.Loveluck, E.Balcar. *J. Magn. & Magn. Mater. (Netherlands)*, vol.31-34, pt.3, p.1227-8 (Feb. 1983). (Proceedings of the International Conference on Magnetism, Kyoto, Japan, 6-10 Sept. 1982). The exchange energy fluctuations of the classical Heisenberg chain with an applied field are theoretically studied by a nonperturbative interacting-boson theory. Computer simulations are also presented at different wavevectors and found in satisfactory agreement. (6 refs.)
- 62672** Calculated specific heat and susceptibility for the crossover of an $S=\infty$ Heisenberg antiferromagnet compared with data on $\text{Rb}_2\text{FeCl}_4 \cdot \text{H}_2\text{O}$. J.A.Puertolas, R.Navarro (Dept. of Phys., ETSII, Univ. of Zaragoza, Zaragoza, Spain), F.Palacio, J.Bartolome, D.Gonzalez, R.L.Carlin. *J. Magn. & Magn. Mater. (Netherlands)*, vol.31-34, pt.3, p.1243-5 (Feb. 1983). (Proceedings of the International Conference on Magnetism, Kyoto, Japan, 6-10 Sept. 1982). Predictions for the thermodynamic behaviour of the $S=\infty$ Heisenberg antiferromagnet with two exchange interactions, J_1 and J_2 , for the SC net are obtained from Padé approximant analysis of the high temperature series. The results have been used to fit the data of $\text{Rb}_2\text{FeCl}_4 \cdot \text{H}_2\text{O}$. (8 refs.)
- 62673** Heisenberg spin glasses with uniaxial anisotropy. D.Sherrington, D.M.Cragg, D.J.Elderfield (Phys. Dept., Imperial Coll., London, England). *J. Magn. & Magn. Mater. (Netherlands)*, vol.31-34, pt.3, p.1417-18 (Feb. 1983). (Proceedings of the International Conference on Magnetism, Kyoto, Japan, 6-10 Sept. 1982). It is shown that the addition of local uniaxial anisotropy and magnetic fields to an exchange-isotropic vector spin glass model yields a system with a phase space of great richness, offering potential for a much improved probing of the basic spin glass problem. (8 refs.)
- 62674** Nonlinear field theory of large-spin Heisenberg antiferromagnets: semiclassically quantized solitons of the one-dimensional easy-axis Neel state. F.D.M.Haldane (Dept. of Phys., Univ. of Southern California, Los Angeles, CA, USA). *Phys. Rev. Lett. (USA)*, vol.50, no.15, p.1153-6 (11 April 1983). The continuum field theory describing the low-energy dynamics of the large-spin one-dimensional Heisenberg antiferromagnet is found to be the $\text{O}(3)$ nonlinear sigma model. When weak easy-axis anisotropy is present, soliton solutions of the equations of motion are obtained and semiclassically quantized. Integer and half-integer spin systems are distinguished. (10 refs.)

- 62675** Reaction field approximation for inhomogeneous ferromagnets. L.Wojtczak, T.Balcerzak (Dept. of Solid State Phys., Univ. of Lodz, Lodz, Poland). *Phys. Status Solidi b (Germany)*, vol.116, no.1, p.217-25 (1 March 1983). The reaction field approximation method for inhomogeneous magnetic systems is extended. The Curie temperature of inhomogeneous samples is calculated on the basis of perturbation theory. As a result the shift of the Curie temperature is obtained with respect to the value of the Curie temperature for an effective crystalline structure. A comparison of the results with those following from other methods shows that the accuracy of the presented method is the same as the cluster method and is much better than the molecular field approximation. (15 refs.)
- 62676** A binary ferromagnetic alloy with magnetic moments dependent on local environment. I. The Jaccarino-Walker model in the effective field approximation. A.V.Zaborov (Dept. of Phys., Ural Polytech. Inst., Sverdlovsk, USSR), M.V.Medvedev. *Phys. Status Solidi b (Germany)*, vol.116, no.1, p.227-38 (1 March 1983). A binary ferromagnetic alloy, in which the magnetic moments depend on their local chemical environment in a step-like manner (the Jaccarino-Walker model), is considered. It is assumed that Heisenberg exchange interactions of the nearest neighbours are responsible for the ferromagnetic ordering of these magnetic moments. Both the Curie temperatures versus concentration and the percolation thresholds of the existence of the long-range magnetic order are investigated for different variants of dependences of both the magnetic components on their local environments. The spin-wave spectrum is analyzed as well. (17 refs.)
- 62677** The Heisenberg model: dynamical interactions including odd-boson terms. C.A.M.Mulder (Kamerlingh Onnes Lab., Rijksuniv. Leiden, Leiden, Netherlands), H.W.Capel. *Physica B & C (Netherlands)*, vol.115 B+C, no.3, p.310-38 (March 1983). A systematic treatment is given of a rather general spin-wave Hamiltonian containing up to four-boson terms. The linear boson terms of leading order in the $1/S$ expansion disappear, applying an appropriate boson shift of rotation in spin space prior to the Holstein-Primakoff transformation. The remaining one- and all three-boson terms are eliminated using a Frohlich transformation which yields an effective Hamiltonian consisting of two- and four-boson terms apart from a constant. The free energy corresponding to this Hamiltonian is obtained using a variational type of approach. (29 refs.)
- Degenerate helimagnetic states, lines of soft modes and absence of long-range order in three dimensions** See Entry 62537
- The spin-wave theory of the susceptibility of Heisenberg antiferromagnets: application to a quadratic layer antiferromagnet K_2MnF_4 and comparison with $\text{C}_2\text{H}_5\text{NH}_3\text{CuCl}_4$** See Entry 62568
- Dynamic formfactor of neutron scattering on solitons in quasi-one-dimensional magnets** See Entry 62572
- Existence of spin-glass phases for three- and four-dimensional Ising and Heisenberg models** See Entry 62652
- EPR experiments on the two-dimensional Heisenberg ferromagnet K_2CuF_4** See Entry 62806
- ## 75.50 STUDIES OF SPECIFIC MAGNETIC MATERIALS
- (see also 81.40R Magnetic properties related to materials treatment)
- Measurement of Curie temperature and magnetization of ferromagnetic materials employing an RF oscillator** See Entry 59802
- ## 75.50B Ferromagnetism of Fe and its alloys
- 62678** Relative linearisation of current-carrying ferrous media in orthogonal magnetic fields. V.N.Ostreiko, Yu.L.Chernikov. *Izv. VUZ Elektromekh. (USSR)*, no.1, p.36-43 (Jan. 1983). In Russian. An analysis shows that in a multilayer ferrous medium, whose intrinsic magnetic field is orthogonal to the lateral magnetic field, the permeabilities of the layers may be determined, over a large range of flux density variations, from the corresponding magnetic curves on the basis of the lateral field only. From tabulated results of numerical experiments it follows that, by employing relative linearisation of the current-carrying medium, the error of calculating the magnetic induction is 1.5-2 times greater than the errors of calculating the flux and the inductance. When changing from weak to strong fields, the error changes sign. (8 refs.) Z.F.V.
- 62679** Experimental study of losses in cold-rolled steel using unidirectional periodic magnetisation. V.V.Vorob'ev, A.N.Tkachev. *Izv. VUZ Elektromekh. (USSR)*, no.1, p.134-8 (Jan. 1983). In Russian. An account is given of an experimental investigation of the effects of direction and the temporal shape of the magnetic induction, on losses in cold-rolled steel, at the magnetisation frequency of 50Hz. Measurements were made in eight directions of magnetisation, from 0 to 90 degrees to the direction of the rolling. Data were obtained for the losses in the steel, induction and intensity maxima, the form factor for the induction derivative, the dynamic hysteresis loops, and oscillography were taken for the induction and intensity on the surface of the packet. It is shown that for an arbitrary unidirectional magnetisation, the losses can be described by three generalised characteristics of the material. (6 refs.) Z.F.V.
- 62680** Calculation of the electromagnetism field and surface loss in a ferromagnetic plate using the straight line method. I.I.Yurtin. *Tekh. Elektrodin. (USSR)*, no.1, p.96-100 (Jan.-Feb. 1983). In Russian. The straight line method is used to obtain an approximate solution of the problem of determination of the electromagnetism field and mean value of surface loss in a ferromagnetic plate situated in an external uniform magnetic field. (6 refs.) A.J.B.
- A microprocessor controlled spectrometer for thermal scan Mossbauer spectroscopy** See Entry 59897
- The effect of Fe-Ni films on the insertion loss of SAW** See Entry 61372
- Structural relaxation in (Fe-Cr)-based glass** See Entry 61811
- Magnetic and structural characteristics of $\text{Ho}_2\text{Fe}_{23}$ deuterides** See Entry 61858
- Some remarks on the carbon atoms pairs migrational relation in $\alpha\text{Fe-C}$** See Entry 62181
- Structure and magnetism of insoluble Pb-Fe alloy films** See Entry 62294
- Magnetoresistance of Pd-Fe and Pd-Ni-Fe alloys** See Entry 62398

Resistance change of thin Permalloy films caused by applied stress and its application to strain measurements See Entry 62508

The interpretation with the spin-wave theory of the variation of the magnetization of iron and nickel as a function of the temperature and of the magnetic field See Entry 62556

Effects of external field on χ -T curve on cluster-glasses See Entry 62561

An AC magnetic susceptibility study of domain nucleation in an amorphous alloy See Entry 62564

Magnetic moment of Fe-Ga-B amorphous alloys See Entry 62565

Measuring the exchange constant A_{ex} in metglas 2826 See Entry 62576

Helical anisotropy induced by annealing in Metglas 2826 See Entry 62583

Crystallization and anisotropy in amorphous $Fe_{81}B_{13.5}Si_{3.5}C_2$ See Entry 62584

Anisotropies and domain structures in metallic glasses See Entry 62585

Investigation of magnetic and martensitic phase transitions in Vic alloy-type alloys See Entry 62586

Magnetic properties of amorphous Fe-Nb and Fe-Zr See Entry 62607

Magnetic hyperfine field distribution and structural relaxation of amorphous ($Fe_{81.5}B_{14.5}Si_4$) prepared with different quenching rates See Entry 62608

Ferromagnetic and spin glass behavior near the critical concentration in amorphous ($Fe_xNi_{100-x}Cr_{125}$) See Entry 62635

Intrinsic hardness and micromagnetism in selected RMn_xNi_{1-x} (R=rare earth) See Entry 62644

Direct observation of the interaction between magnetic domain walls and dislocations in iron See Entry 62682

Magnetic domains in HCP and DHCP Co-Fe alloys studied by 1 MV Lorentz electron microscopy See Entry 62683

Neutron depolarization in the unannealed amorphous ribbon Metglas 2826 See Entry 62689

Mechanism of formation of magnetic properties of amorphous alloy $Fe_{70}Co_{15}Si_{15}B_{10}$ during annealing See Entry 62694

Reversible permeability for perpendicularly superposed induction for $Fe_{40}Ni_{60}P_{14}B_6$ amorphous ribbon and its magnetisation process See Entry 62696

Anomalous temperature dependence of magnetization in amorphous ($Fe_{0.9}Ni_{0.97}Si_{10}B_{13}$) alloy See Entry 62699

Magnetic inhomogeneity in amorphous Fe-Zr alloys See Entry 62701

Effect of fabrication condition on the magnetic properties of Fe-Mn-B system amorphous alloys See Entry 62704

Energy losses in electrical steel under rotational magnetic reversal See Entry 62705

Remagnetisation phenomena in multicomponent rare-earth-cobalt alloys with increased temperature stability See Entry 62707

Statistical evaluation of basic parameters of cast magnetically hard materials See Entry 62708

The orientation of magnetic particles for high density recording See Entry 62711

Effect of heat-treatment on magnetic properties and morphology of iron particles See Entry 62712

The shape anisotropy of metal powder on magnetism See Entry 62713

Dynamical properties of small particles; comparison with spin glass behaviour See Entry 62719

Factors affecting the disaccommodations of amorphous magnetic materials See Entry 62721

After-effect of permeability and magnetic loss of an amorphous $Co_{75}Fe_{20}B_{20}$ alloy See Entry 62722

Magnetic relaxation in amorphous ($Fe_{1-x}Ni_x$) $_{77}Si_{10}B_{13}$ alloys See Entry 62723

Effects of field annealing on the magnetic characteristics and magnetic losses of amorphous ribbons $Fe_{78}Si_{10}B_{12}$ See Entry 62724

Diffusion and magnetic properties of compositionally modulated films See Entry 62728

On the magnetic dipole fields at surface atoms See Entry 62731

Magnetic properties, structure, and relaxation of amorphous $Fe_{1-x}B_x$ films See Entry 62739

Magnetic and electrical properties of amorphous $Fe_{1-x}B_x$ films See Entry 62740

Magnetic properties of metastable crystalline and amorphous Fe alloys produced by RF sputtering See Entry 62741

Oblique incidence effects in evaporated thin films See Entry 62752

Structure and magnetic properties of iron films deposited at oblique incidence See Entry 62753

Effects of high dose ion implantation on structure and magnetic properties of 3d-metal films See Entry 62757

Interference enhanced Kerr spectroscopy for very thin absorbing films—application to amorphous terbium ion See Entry 62759

Analysis of type-II magnetic contrast from ferromagnetic thin films in the scanning electron microscopy See Entry 62762

Magnetization of electron-bombarded iron-cobalt films See Entry 62764

Motion of tops of domains in thin films with low-coercivity channels See Entry 62768

Structure and magnetic domain walls of Dy ion implanted Fe films See Entry 62777

Magnetoelastic damping and ΔE effect in amorphous alloys based on Fe-Ni See Entry 62782

Magnetostriction and related properties in amorphous Fe-Nb-Si-B alloys See Entry 62786

Magnetostriction of iron, cobalt and nickel ternary amorphous ribbons See Entry 62787

Magnetoelastic effects in amorphous metals due to surface crystallisation and oxidation See Entry 62790

Giant attenuation of surface acoustic waves by ferromagnetic films See Entry 62791

Study of magnetoelastic waves by optical observation on the surface of magnetic materials See Entry 62794

Two-magnon scattering in iron-rich metallic glasses See Entry 62809

NMR in metallic glasses See Entry 62817

Spin echo of ^{59}Co and ^{63}Cu impurity nuclei in single-crystal iron films in the case of coincidence of nuclear magnetic and ferromagnetic resonance frequencies See Entry 62833

Mossbauer effect study of the internal magnetic field in small iron particles See Entry 62855

Mossbauer spectroscopic studies on surfaces and thin films See Entry 62859

Interface magnetism in Fe-Sb multilayer films from ^{121}Sb and ^{57}Fe Mossbauer spectroscopy See Entry 62861

Mossbauer and X-ray diffraction studies of amorphous Fe-Ni alloy films deposited by DC sputtering See Entry 62862

Order-disorder transition in Fe_3Si alloy during mechanical crushing See Entry 63286

Investigation of the phase composition, structure, and magnetic properties of alloy $Sm_2Co_{10}Fe_{3.2}Cu_{1.2}Zr_{0.4}$ See Entry 63287

75.50C Ferromagnetism of other metals

Electron microscope studies on the Sm-Co and Sm-Ni intermetallic compounds See Entry 61853

Composition distribution in Co-Cr perpendicular magnetic films See Entry 62310

Crystal field splittings of PrX_2 compounds (X=Pt, Rh, Ir, Ru, Ni) studied by inelastic neutron scattering See Entry 62381

Magnetic and galvanomagnetic properties of rare earth intermetallic compounds of $RaG_{1-x}In_x$ (R=Gd, Tb, and Dy) See Entry 62400

High accuracy measurement of the Hall effect in magnetic materials with an AC lock-in technique See Entry 62401

A singlet-singlet model for amorphous alloys with praseodymium See Entry 62534

The interpretation with the spin-wave theory of the variation of the magnetization of iron and nickel as a function of the temperature and of the magnetic field See Entry 62556

Effects of external field on χ -T curve on cluster-glasses See Entry 62561

Magnetocrystalline anisotropy of dysprosium and erbium ions in compounds of the RCO_5 type See Entry 62580

Induced anisotropy in amorphous Co-P alloys See Entry 62582

Magnetic properties of La_2Ni_7 See Entry 62588

Mechanism of thermomagnetic recording in an MnBi film See Entry 62611

Specific heat study of the transition from ferromagnetism to antiferromagnetism in terbium See Entry 62621

Magnetoresistance near the Curie point of TbZn single crystals See Entry 62645

The spontaneous magnetization of nickel See Entry 62693

Magnetization process of GdNi single crystal in the high magnetic field near the Curie temperature See Entry 62697

Remagnetisation phenomena in multicomponent rare-earth-cobalt alloys with increased temperature stability See Entry 62707

Magnetic behavior of $SmCo_5$ -hydrogen system See Entry 62718

FMR and magnetic studies in amorphous Co-Nb films See Entry 62727

Anomalous magnetization-temperature characteristics in amorphous NiP alloys See Entry 62742

Magnetostriction of Co-based amorphous alloys See Entry 62784

Magnetostriction of Co base amorphous alloys See Entry 62789

Giant attenuation of surface acoustic waves by ferromagnetic films See Entry 62791

Electron spin resonance study of a disordered Ni-Mn alloy See Entry 62803

Effect of a semiconductor substrate on the ferromagnetic resonance in a thin cobalt film See Entry 62811

NMR in metallic glasses See Entry 62817

Some magnetological insights in the consolidation of metal powders See Entry 63208

Metallographic and structural investigations of levitation splat cooled cobalt base cobalt-refractory carbide alloys See Entry 63253

Investigation of the phase composition, structure, and magnetic properties of alloy $Sm_2Co_{10}Fe_{3.2}Cu_{1.2}Zr_{0.4}$ See Entry 63287

75.50D Ferromagnetism of nonmetals

Magnetic and structural characteristics of Ho_2Fe_{23} deuterides See Entry 61858

EuS ferromagnetic semiconductor films grown epitaxially on silicon See Entry 62296

The spin polarisation of conduction electrons in a ferromagnetic semiconductor See Entry 62335

Temperature-induced local moments in MnSi and FeSi See Entry 62549

Quasielastic neutron scattering at the 1-D ferromagnet $CsNiF_4$ with an applied transverse field See Entry 62560

Frustration effects in the disordered system $CsMnFeF_6$ See Entry 62562

The spin-wave theory of the susceptibility of Heisenberg antiferromagnetics: application to a quadratic layer antiferromagnet K_2MnF_4 and comparison with $(C_2H_5NH_3)_2CuCl_4$ See Entry 62568

Experiments on randomly mixed magnets with competing interactions See Entry 62574

Synthesis and magnetic properties of $(Mn_{1-x}Ta_x)_2B_4$ See Entry 62587

Ferro and antiferromagnetic ordering in $Ni(C_2H_5)_4FeCl_4$ depending on the cooling rate See Entry 62594

NMR observation of oblique phase in mixed crystals $(CH_3NH_3)_2Cu(Cl_{1-x}Br_x)_4$ ($0.5 \leq x \leq 1$) See Entry 62606

Magnetic properties of $US_{1-x}Se_x$ solid solution See Entry 62609

Anisotropy effects in the ferromagnetic quantum chain systems $(C_6H_5)_3NH_3CuCl_3$ (CHAC) and $(C_6H_5)_3NH_3CuBr_3$ (CHAB) See Entry 62625

Domain structure in single crystal ferromagnetic oxide films near the phase transitions See Entry 62771

Saturation magnetostriction of some (FeCo)-metalloid-compounds and -amorphous alloys See Entry 62788

- EPR experiments on the two-dimensional Heisenberg ferromagnet K_2CuF_4 See Entry 62806
 Mossbauer study of acicular iron-nitride particles See Entry 62858
 Applied magnetic field Mossbauer studies of the quasi one-dimensional system $AFeS_2$; $A = K, Rb, Cs$ See Entry 62865

75.50E Antiferromagnetics

- Structural relaxation in (Fe-Cr)-based glass See Entry 61811
 Crystal structure and magnetic properties of a new form of NH_4MnFeF_6 See Entry 61880
 Hexagonal tungsten bronze-type Fe^{III} fluoride: $(H_2O)_{0.33}FeF_3$; crystal structure, magnetic properties, dehydration to a new form of iron trifluoride See Entry 61882
 Soliton-phonon scattering in TMMC and DMMC See Entry 62192
 Quadrupolar coupling and structural instability in $PrAg_{1-x}Cu_x$ See Entry 62383
 Magnetic and galvanomagnetic properties of rare earth intermetallic compounds of $RAg_{1-x}In_x$ ($R = Gd, Tb, Dy$) See Entry 62400
 A singlet-singlet model for amorphous alloys with praseodymium See Entry 62534
 Magnetic structures and interaction constants in the two-dimensional Ising antiferromagnets $RE_2O_4SO_4$ ($RE = Dy, Ho, Tb$) See Entry 62553
 Randomness in mixed antiferromagnets with competing spin anisotropies See Entry 62554
 Magnetic properties of $Fe_3V_{3-x}S_4$ ($0 \leq x \leq 2$) See Entry 62558
 Spin wave theory of susceptibility of quadratic-layer antiferromagnet K_2MnF_4 See Entry 62559
 Frustration effects in the disordered system $CsMnFeF_6$ See Entry 62562
 A magnetic quasi-ordered state in $Cr_{1-x}Ti_xS$ See Entry 62563
 Magnetic properties of the weak ferromagnet NH_4MnF_3 See Entry 62567
 The spin-wave theory of the susceptibility of Heisenberg antiferromagnetics; application to a quadratic layer antiferromagnet K_2MnF_4 and comparison with $(C_2H_5NH_3)_2CuCl_4$ See Entry 62568
 Effect of magnetic and nonmagnetic impurities on the soliton dynamics in $(CD_3)_4N MnCl_3$ See Entry 62570
 Theoretical study of magnetic properties of pseudo-one-dimensional system $RbFeCl_3$ See Entry 62571
 Magnetic excitations in CeAs, an effective $S = 1/2$ FCC antiferromagnet See Entry 62573
 Experiments on randomly mixed magnets with competing interactions See Entry 62574
 Spin orientation and exchange interactions in $(Fe,Co)Cl_2$ See Entry 62575
 X_α method for the magnetic transition state and exchange interactions in $KNiF_3$ See Entry 62579
 Magnetic properties of La_2Ni_7 See Entry 62588
 The magnetic ordering in a hexagonal antiferromagnet See Entry 62591
 Magnetoelastic phase transition in $KMnF_3$ See Entry 62592
 Ferro and antiferromagnetic ordering in $N(C_2H_5)_4FeCl_4$ depending on the cooling rate See Entry 62594
 Effect of Cu and Co impurities on the phase diagram and the bicritical point of $CsMnCl_3 \cdot 2H_2O$ See Entry 62595
 Spin flopping in $MnTiO_3$ See Entry 62596
 A microscopic model describing the spin-flip processes at the first-order antiferromagnetic-to-ferrimagnetic phase transition in $Dy_2O_3SO_4$ See Entry 62597
 Field-induced increase of the Neel temperature in a two-dimensional system See Entry 62600
 Magnetic properties of the quasi-2d easy plane antiferromagnet $BaNi_2(PO_4)_2$ See Entry 62601
 Random fields and ordering in antiferromagnetic insulators See Entry 62603
 NMR observation of oblique phase in mixed crystals $(CH_3NH_3)_2Cu(Cl_{1-x}Br_x)_4$ ($0.5 \leq x \leq 1$) See Entry 62606
 Theoretical study of the magnetic properties of an antiferromagnetic system with two kinds of inequivalent magnetic-ion sites See Entry 62619
 Specific heat study of the transition from ferromagnetism to antiferromagnetism in terbium See Entry 62621
 Theoretical study of magnetism of spin system with alternating strong and weak exchange coupling See Entry 62624
 Magnetic short-range order and spin freezing in the quasi-2D system $LuFeMgO_4$ See Entry 62642
 Spin glass in the site-diluted antiferromagnetic FCC See Entry 62643
 On the two-dimensionality of $Fe(HCOO)_2 \cdot 2H_2O$ See Entry 62670
 Observation of the Villain model in $CsCoBr_3$ See Entry 62686
 Evidence for very-large-area magnetic domain walls in haematite ($\alpha-Fe_2O_3$) See Entry 62691
 Magnetic properties of amorphous powders of alloy Mn_3B_4 See Entry 62710
 On the magnetostrictive phenomena in metamagnetism See Entry 62796
 Two-dimensional soliton contribution to the ESR linewidth in layered antiferromagnets? See Entry 62798
 Surface magnetism of $\alpha-Fe_2O_3$ by Mossbauer spectroscopy See Entry 62860
 Applied magnetic field Mossbauer studies of the quasi one-dimensional system $AFeS_2$; $A = K, Rb, Cs$ See Entry 62865
 Spectroscopic and magneto-optical properties of quasi 1D antiferromagnets AVX_3 ($A = Cs, Rb$; $X = Cl, Br, I$) See Entry 62943
 The influence of crystal symmetry on magneto-optical effects in orthoferrites See Entry 62950

75.50G Ferrimagnetics

- Optical mode conversions in Nd substituted iron garnet films See Entry 61270
 Magnetic behaviour of spin-mixed iron(III) porphyrins See Entry 62557
 A microscopic model describing the spin-flip processes at the first-order antiferromagnetic-to-ferrimagnetic phase transition in $Dy_2O_3SO_4$ See Entry 62597

- A new method for the study of magnetic domains at low temperatures See Entry 62684
 Magnetic charge effects in ion implanted garnets See Entry 62685
 Magnetic and electrical properties of $FeCr_{2-x}In_xS_4$ ($0 \leq x \leq 1$) See Entry 62695
 Long relaxation times in ferromagnets and their possible applications See Entry 62706
 Shape anisotropy of ultrafine magnesium ferrite precipitates See Entry 62720
 Magnetic and optical properties of Co, Bi substituted garnet films prepared by the LPE method and its application to thermomagnetic recording See Entry 62733
 Amorphous TbFe ultra thin film with reflective Au layer See Entry 62734
 Garnet film with rectangular hysteresis loop and its application to thermomagnetic recording medium See Entry 62735
 Magnetic properties and magnetic Kerr rotation of amorphous TbFeCo and TbFeCr films See Entry 62737
 The thermo-magnetic writing and erasing properties and Kerr rotation angle of amorphous RE-Fe thin films See Entry 62738
 Investigations of implantation-induced changes in surface layers of epitaxial garnet thin films See Entry 62755
 Large magnetic anisotropy change induced by hydrogen ion implantation in europium iron garnet LPE films See Entry 62756
 Magnetocrystalline anisotropy energy K_1 of Co^{3+} and Ru^{3+} substituted bubble garnet films See Entry 62758
 Localized modification of magnetic anisotropy in LPE iron garnet films by laser annealing See Entry 62760
 Structure and magnetic properties of C-axis well oriented Ba-ferrite films deposited by targets-facing type of sputtering See Entry 62765
 Formation of nonthrough magnetic domains in the course of magnetization switching in amorphous Gd-Co films See Entry 62766
 Static and dynamic properties of thermomagnetic writing in amorphous TbFe films See Entry 62770
 Influence of cation distribution induced by thermal annealing on magnetic bubbles properties in Ga-substituted garnet films See Entry 62773
 Standing waves of wall vibration See Entry 62774
 Influences of ion implantation on charged wall properties in magnetic bubble devices See Entry 62776
 High-speed photographic study of the dynamic properties of ferrite-garnet films with domain diameters less than $0.5 \mu m$ See Entry 62779
 Domain-wall velocity in iron garnet films in strong pulsed fields See Entry 62780
 Comparison of the magnetic properties of one- and two-layer iron garnet films See Entry 62781
 FMR line intensity and width in garnet ferrite films See Entry 62810
 Mossbauer spectroscopic studies of magnesium nickel ferrites See Entry 62854
 Application of the depth-selective conversion electron Mossbauer spectroscopy to rare-earth iron garnet films See Entry 62863
 Conversion Mossbauer studies of epitaxially mixed ferrite-garnet films See Entry 62870
 An investigation of diffraction efficiency of magneto-optic deflection in garnet film See Entry 62944
 Magneto-optical spectra of RF-sputtered amorphous Gd-Co and Gd-Fe films See Entry 62945
 Magneto-optical effect spectra of rare-earth-transition-metal amorphous films See Entry 62946
 LPE growth of YNd-iron garnet films for magneto-optical waveguides See Entry 63182
 Effect of low-temperature ferritization on the properties of ferrite powders See Entry 63222
 Nonstoichiometry and physical properties of hot-pressed manganese-zinc ferrites See Entry 63223

75.50K Amorphous magnetic materials

- Structural relaxation in (Fe-Cr)-based glass See Entry 61811
 Structural relaxation and magnetism in amorphous alloys See Entry 61812
 He^+ backscattering study on Ar distribution in amorphous magnetic thin films See Entry 62293
 Structure and magnetism of insoluble Pb-Fe alloy films See Entry 62294
 Magnetoresistance and magnetization in $Fe_{80-x}T_2B_{20}$ metallic glasses See Entry 62431
 A singlet-singlet model for amorphous alloys with praseodymium See Entry 62534
 Frustration effects in the disordered system $CsMnFeF_6$ See Entry 62562
 An AC magnetic susceptibility study of domain nucleation in an amorphous alloy See Entry 62564
 Magnetic moment of Fe-Ga-B amorphous alloys See Entry 62565
 Magnetism of amorphous metal-metal alloys See Entry 62566
 Measuring the exchange constant A_{ex} in metglas 2826 See Entry 62576
 Induced anisotropy in amorphous Co-P alloys See Entry 62582
 Helical anisotropy induced by annealing in Metglas 2826 See Entry 62583
 Crystallization and anisotropy in amorphous $Fe_{81}B_{13.5}Si_{3.5}C_2$ See Entry 62584
 Anisotropies and domain structures in metallic glasses See Entry 62585
 Magnetic properties of amorphous Fe-Nb and Fe-Zr See Entry 62607
 Magnetic hyperfine field distribution and structural relaxation of amorphous $(Fe_{81.5}B_{14.5}Si_4)$ prepared with different quenching rates See Entry 62608
 Ferromagnetic and spin glass behavior near the critical concentration in amorphous $(Fe_{81}Ni_{100-x})_{75}Cr_{25}$ See Entry 62635
 Critical exponents and the size of the critical region in amorphous GdAl spin glass See Entry 62640
 Influence of the viscosity field on the power losses in amorphous magnetic alloys See Entry 62687
 A theory of internal stress field and configuration of magnetic domain in amorphous ribbons See Entry 62688

- Neutron depolarization in the unannealed amorphous ribbon Metglas 2826 See Entry 62689
- Mechanism of formation of magnetic properties of amorphous alloy $\text{Fe}_{50}\text{Co}_{70}\text{Si}_{15}\text{B}_{10}$ during annealing See Entry 62694
- Reversible permeability for perpendicularly superposed induction for $\text{Fe}_{40}\text{Ni}_{40}\text{P}_{14}\text{B}_6$ amorphous ribbon and its magnetisation process See Entry 62696
- Anomalous temperature dependence of magnetization in amorphous $(\text{Fe}_{0.1}\text{Ni}_{0.9})_{77}\text{Si}_{10}\text{B}_{13}$ alloy See Entry 62699
- Low field properties of FeNiMnB amorphous alloy See Entry 62700
- Magnetic inhomogeneity in amorphous Fe-Zr alloys See Entry 62701
- Effect of fabrication condition on the magnetic properties of Fe-Mn-B system amorphous alloys See Entry 62704
- Magnetic properties of amorphous powders of alloy Mn_3B_4 See Entry 62710
- Factors affecting the disaccommodations of amorphous magnetic materials See Entry 62721
- After-effect of permeability and magnetic loss of an amorphous $\text{Co}_{75}\text{Fe}_{20}\text{B}_{20}$ alloy See Entry 62722
- Magnetic relaxation in amorphous $(\text{Fe}_{1-x}\text{Ni}_x)_{77}\text{Si}_{10}\text{B}_{13}$ alloys See Entry 62723
- Effects of field annealing on the magnetic characteristics and magnetic losses of amorphous ribbons $\text{Fe}_{72}\text{Si}_{10}\text{B}_{12}$ See Entry 62724
- FMR and magnetic studies in amorphous Co-Nb films See Entry 62727
- Amorphous TbFe ultra thin film with reflective Au layer See Entry 62734
- Preparation and properties of RE-TM amorphous films See Entry 62736
- Magnetic properties and magnetic Kerr rotation of amorphous TbFeCo and TbFeCr films See Entry 62737
- The thermo-magnetic writing and erasing properties and Kerr rotation angle of amorphous RE-Fe thin films See Entry 62738
- Magnetic properties, structure, and relaxation of amorphous $\text{Fe}_{1-x}\text{B}_x$ films See Entry 62739
- Magnetic and electrical properties of amorphous $\text{Fe}_{1-x}\text{B}_x$ films See Entry 62740
- Magnetic properties of metastable crystalline and amorphous Fe alloys produced by RF sputtering See Entry 62741
- Anomalous magnetization-temperature characteristics in amorphous NiP alloys See Entry 62742
- Substrate bias voltage dependences of magnetic properties in amorphous Tb-Fe films See Entry 62744
- Magnetostriction and internal stress in GdFe amorphous films with perpendicular anisotropy prepared by RF diode sputtering See Entry 62745
- Domain observation of amorphous Fe-B and Co-Fe-B films See Entry 62746
- Anomalous hysteresis loops in single and double layer sputtered TbFe films See Entry 62748
- Pair ordering and perpendicular anisotropy in RE-TM amorphous thin films See Entry 62749
- Perpendicular magnetic anisotropy and ferromagnetic resonance in amorphous Gd-Co and Gd-Fe films See Entry 62750
- Interference enhanced Kerr spectroscopy for very thin absorbing films—application to amorphous terbium ion See Entry 62759
- Formation of nonthrough magnetic domains in the course of magnetization switching in amorphous Gd-Co films See Entry 62766
- Static and dynamic properties of thermomagnetic writing in amorphous TbFe films See Entry 62770
- Magnetoelastic damping and ΔE effect in amorphous alloys based on Fe-Ni See Entry 62782
- Magnetostriction of Co-based amorphous alloys See Entry 62784
- Single-ion anisotropy and magnetostriction of amorphous alloys See Entry 62785
- Magnetostriction and related properties in amorphous Fe-Nb-Si-B alloys See Entry 62786
- Magnetostriction of iron, cobalt and nickel ternary amorphous ribbons See Entry 62787
- Saturation magnetostriction of some (FeCo)-metalloid-compounds and -amorphous alloys See Entry 62788
- Magnetostriction of Co base amorphous alloys See Entry 62789
- Magnetoelastic effects in amorphous metals due to surface crystallisation and oxidation See Entry 62790
- Evaluation of magnetostriction constant in amorphous ribbons utilizing the velocity change of a magnetoelastic wave See Entry 62792
- Temperature and field dependence of magnetostriction in amorphous thin films See Entry 62793
- Study of magnetoelastic waves by optical observation on the surface of magnetic materials See Entry 62794
- Electron spin resonance study of a disordered Ni-Mn alloy See Entry 62803
- Two-magnon scattering in iron-rich metallic glasses See Entry 62809
- NMR in metallic glasses See Entry 62817
- Mossbauer and X-ray diffraction studies of amorphous Fe-Ni alloy films deposited by DC sputtering See Entry 62862
- Magneto-optical spectra of RF-sputtered amorphous Gd-Co and Gd-Fe films See Entry 62945
- Magneto-optical effect spectra of rare-earth—transition-metal amorphous films See Entry 62946

75.50M Magnetic liquids

- A theory of correlations in a magnetically aligned ferrofluid .. See Entry 62715
- Curie-Weiss behavior in ferrofluids See Entry 62716

75.60 DOMAIN EFFECTS, MAGNETIZATION CURVES, AND HYSTERESIS

- Structural relaxation and magnetism in amorphous alloys See Entry 61812

75.60C Domain walls and domain structure (for magnetic bubbles, see 75.70K)

- 62681 A new method of domain structure investigation at temperatures below 35K. A.Szewczyk, K.Piotrowski, R.Szymczak (Inst. of Phys., Polish Acad. of Sci., Warsaw, Poland). *J. Phys. D (GB)*, vol.16, no.4, p.687-96 (14 April 1983).
A new method of Bitter pattern formation in the temperature range from 5K to 35K has been developed. The domain walls have been made visible by fined solid oxygen particles produced in the process of gaseous oxygen cooling in a helium atmosphere. The presented method is particularly useful for low temperature investigations of bulk materials. Photographs of Bitter patterns obtained at 6K for a YFeO_3 orthoferrite plate and a $\text{BaFe}_{12}\text{O}_{19}$ bulk crystal are shown. (14 refs.)
- 62682 Direct observation of the interaction between magnetic domain walls and dislocations in iron. R.A.Taylor, J.P.Jakubovics (Dept. of Metall. & Sci. of Materials, Univ. of Oxford, Oxford, England), B.Astie, J.Degaque. *J. Magn. & Magn. Mater. (Netherlands)*, vol.31-34, pt.2, p.970-2 (Feb. 1983). (Proceedings of the International Conference on Magnetism, Kyoto, Japan, 6-10 Sept. 1982).
The influence of dislocations on magnetisation processes in iron has been investigated by high voltage Lorentz microscopy. The dominant interaction between magnetic domain walls and dislocations changes with increasing strain level. Thin foil coercivities vary from 0.5 to 3 Oe for strain levels 0.6 to 16.4% respectively. (5 refs.)
- 62683 Magnetic domains in HCP and DHCP Co-Fe alloys studied by 1 MV Lorentz electron microscopy. D.Watanabe, T.Sekiguchi (Dept. of Phys., Faculty of Sci., Tohoku Univ., Sendai, Japan), T.Tanaka, M.Takahashi, T.Wakiyama, M.Takahashi. *J. Magn. & Magn. Mater. (Netherlands)*, vol.31-34, pt.2, p.973-5 (Feb. 1983). (Proceedings of the International Conference on Magnetism, Kyoto, Japan, 6-10 Sept. 1982).
Domain structures in the Co-alloys with 0.8-1.2 at.% Fe were examined, and fine structure of the 180° wall in the dhcp phase and domain configuration at the interface between hcp and dhcp phases were revealed. The temperature dependence of the domain structure was also studied. (4 refs.)
- 62684 A new method for the study of magnetic domains at low temperatures. K.Piotrowski, A.Szewczyk, R.Szymczak (Inst. of Phys., Acad. of Sci., Warsaw, Poland). *J. Magn. & Magn. Mater. (Netherlands)*, vol.31-34, pt.2, p.979-80 (Feb. 1983). (Proceedings of the International Conference on Magnetism, Kyoto, Japan, 6-10 Sept. 1982).
In this paper a new method is presented for obtaining Bitter patterns in bulk materials. As magnetic particles, active in forming of the domain patterns, the authors have used solid oxygen in temperature range between 5 and 35K. The observations of domain structures have been performed in YFeO_3 thin plate and $\text{BaFe}_{12}\text{O}_{19}$ and $\text{PbFe}_{12}\text{O}_{19}$ bulk crystals. The Bitter patterns obtained are presented in the photographs. (6 refs.)
- 62685 Magnetic charge effects in ion implanted garnets. H.Jouve, P.Pouget (LETI, CEA, Grenoble, France). *J. Magn. & Magn. Mater. (Netherlands)*, vol.31-34, pt.2, p.981-3 (Feb. 1983). (Proceedings of the International Conference on Magnetism, Kyoto, Japan, 6-10 Sept. 1982).
This paper describes a careful characterization of the static and dynamic properties of bubbles along a border defined by ion implantation. The data are dependent on the direction and the magnitude of an in-plane magnetic field. The results are interpreted as being due to the existence of magnetic charges appearing along the border of the implanted zone. (4 refs.)
- 62686 Observation of the Villain mode in CsCoBr_3 . S.E.Nagler, W.J.L.Buyers, R.L.Armstrong (AECL, Chalk River Nuclear Labs., Chalk River, Ontario, Canada), B.Brait. *J. Magn. & Magn. Mater. (Netherlands)*, vol.31-34, pt.3, p.1213-14 (Feb. 1983). (Proceedings of the International Conference on Magnetism, Kyoto, Japan, 6-10 Sept. 1982).
Neutron scattering experiments in CsCoBr_3 have shown that domain walls propagate along Ising-like antiferromagnetic chains so as to give rise to a characteristic inelastic collective peak in the spin response. The dispersion of the peak frequency agrees with the predictions of Villain (1975). The line-shape of the peak is found to be a sensitive test of collisions between the walls. (6 refs.)
- 62687 Influence of the viscosity field on the power losses in amorphous magnetic alloys. M.Celasco, A.Masero, P.Mazzetti, A.Stepanescu (Istituto Elettrotecnico Nazionale Galileo Ferraris, Torino, Italy). *J. Magn. & Magn. Mater. (Netherlands)*, vol.31-34, pt.3, p.1407-8 (Feb. 1983). (Proceedings of the International Conference on Magnetism, Kyoto, Japan, 6-10 Sept. 1982).
Thermal annealing of an amorphous alloy showing large viscosity field effects, as Metglas 2826, produces a strong reduction of the dynamic loss, probably related to a corresponding reduction of the viscosity field. The effect is not related to changes in the magnetic domain structure due to the anisotropy induced when the material is annealed under magnetic field, but seems to be simply related to a stabilization of the amorphous atomic structure. (5 refs.)
- 62688 A theory of internal stress field and configuration of magnetic domain in amorphous ribbons. Zhao-hua Lin, Dao-sheng Dai (Dept. of Phys., Peking Univ., Beijing, China). *J. Magn. & Magn. Mater. (Netherlands)*, vol.31-34, pt.3, p.1540-2 (Feb. 1983). (Proceedings of the International Conference on Magnetism, Kyoto, Japan, 6-10 Sept. 1982).
The distribution of the internal stress fields of different regions in an amorphous ribbon are found, and the magnetic anisotropies in these regions are also calculated. On the basis of these results the authors could easily understand the various configurations of domain structure and some experimental phenomena of domain observation of the amorphous ribbons. (3 refs.)
- 62689 Neutron depolarization in the unannealed amorphous ribbon Metglas 2826. M.Th.Rekvelid, T.G.Spanjer (Interuniv. Reactor Inst., Delft, Netherlands). *J. Magn. & Magn. Mater. (Netherlands)*, vol.31-34, pt.3, p.1585-6 (Feb. 1983). (Proceedings of the International Conference on Magnetism, Kyoto, Japan, 6-10 Sept. 1982).
Three dimensional neutron depolarization experiments have been carried out on an amorphous unannealed ribbon Metglas 2826 of dimensions $(50 \times 12.8 \times 0.047)\text{mm}^3$ in the presence of a magnetic field and a mechanical tension along the ribbon direction. Using a magnetic model for the domain structure, four parameters characterizing this model can be determined from the depolarization experiments. From this analysis the internal stress has been determined as a function of the depth. (6 refs.)

62690 Micromagnetics of zigzag head-on domain walls. R.F.Soochoo (Dept. of Electrical & Computer Engng., Univ. of California, Davis, CA, USA).

J. Magn. & Magn. Mater. (Netherlands), vol.35, no.1-3, p.261-2 (March 1983). (Proceedings of the 10th International Colloquium on Magnetic Films and Surfaces, Yokohama, Japan, 13-16 Sept. 1982).

The boundary between two domains of head-on magnetization, as occurred in digital recording has been observed to be zigzag in shape and the transition region carries a net charge. A method has been developed to calculate, with no approximations, the complex magnetization distribution within this transition region. (8 refs.)

62691 Evidence for very-large-area magnetic domain walls in haematite (α -Fe₂O₃). G.F.Clark, P.A.Goddard, J.R.S.Nicholson, B.K.Tanner (Dept. of Phys., Durham Univ., Durham, England), B.M.Wanklyn.

Philos. Mag. B (GB), vol.47, no.3, p.307-13 (March 1983). Magnetic domain walls up to approximately 20 nm² in area have been identified in thin basal plane platelets of the weak ferromagnet α -Fe₂O₃ using synchrotron radiation X-ray topography. The behaviour of these basal plane wall under small magnetic fields was examined in real time using the Daresbury X-ray imaging system. Area contrast is exhibited by the walls in white radiation X-ray topographs. (13 refs.)

62692 Stability and spectrum of the domain strip-structure oscillation of ferromagnets. V.G.Baryakhtar, Yu.I.Gorobets, S.I.Denisov.

Ukr. Fiz. Zh. (USSR), vol.28, no.3, p.436-40 (March 1983). In Russian. The spectrum of the domain strip-structure oscillation has been studied in one-axis ferromagnets. It is shown that in the presence of a bias field the spectrum consists of two branches with a fissure between them. A criterion is obtained for the DSS stability relative to the long-wave deformation of the form of the domain borders which are homogeneous in the plate thickness. (10 refs.)

Undulator radiation of charged particles moving above a domain structure See Entry 61062

Frustration effects in the disordered system CsMnFeF₆ See Entry 62562

An AC magnetic susceptibility study of domain nucleation in an amorphous alloy See Entry 62564

Measuring the exchange constant A_{ex} in metglas 2826 See Entry 62576

Anisotropies and domain structures in metallic glasses See Entry 62585

Intrinsic hardness and micromagnetism in selected RMn₂Ni_{5-x} (R=rare earth) See Entry 62644

Modulated structures of an Ising spin system on a triangular lattice See Entry 62655

Mechanism of formation of magnetic properties of amorphous alloy Fe₇₀Co₇Si₁₅B₁₀ during annealing See Entry 62694

Low field properties of FeNiMnB amorphous alloy See Entry 62700

Quantitative determination of magnetisation distributions in domains and domain walls by scanning transmission electron microscopy See Entry 62702

Remagnetisation phenomena in multicomponent rare-earth-cobalt alloys with increased temperature stability See Entry 62707

After-effect of permeability and magnetic loss of an amorphous Co₇₅Fe₂₅B₉₀ alloy See Entry 62722

Analysis of type-II magnetic contrast from ferromagnetic thin films in the scanning electron microscopy See Entry 62762

Formation of nonthrough magnetic domains in the course of magnetization switching in amorphous Gd-Co films See Entry 62766

Motion of tops of domains in thin films with low-coercivity channels See Entry 62768

Magnetoelastic effects in amorphous metals due to surface crystallisation and oxidation See Entry 62790

75.60E Magnetization curves, hysteresis, Barkhausen and related effects

62693 The spontaneous magnetization of nickel. G.H.Czerlinski (Biochem. & Biophys. Programs, Northwestern Univ., Chicago, IL, USA).

J. Biol. Phys. (USA), vol.10, no.4, p.189-98 (1982).

The original data of Weiss and Forrer on nickel (Ann. Phys. Paris, vol.5, p.153-213, 1926) are reanalyzed with the aim to obtain a simple empirical relation between the spontaneous magnetization and the temperature both below and above the Curie temperature. A simple relation between the spontaneous magnetization and the temperature is needed to separate easily between the ferromagnetic and the paramagnetic region in the plane given by temperature and field strength, needed for a comprehensive treatment of the magnetocaloric effect (compare *ibid.*, vol.9, p.27, 1981). Various methods of extrapolating to zero magnetic field strength are discussed and used to obtain specified values for the spontaneous magnetization at various temperatures. Starting with a simple expression of cooperativity among elements it is shown that a sufficiently good fit of models to the given data is only obtained with the assumption of three types of cooperativity differing in the intensity of coupling. This intensity of coupling is signified by the magnitude of the exponent in the independent variable (temperature). (16 refs.)

62694 Mechanism of formation of magnetic properties of amorphous alloy Fe₂₀Co₇₀Si₁₀B₁₀ during annealing. I.B.Kekalo, V.L.Stolyarov, V.Yu.Tsvetkov (Inst. of Steel & Alloys, Moscow, USSR).

Fiz. Met. & Metalloved. (USSR), vol.55, no.2, p.235-42 (Feb. 1983). In Russian. English translation in: *Phys. Met. & Metallogr. (GB)*

A study was made of the influence of low-temperature annealing on the magnetic properties of amorphous Fe₂₀Co₇₀Si₁₀B₁₀ in two states: after quenching from the melt and after a preliminary annealing at 410°C. The influence of the rate of cooling after this low-temperature annealing on the magnetic properties and the temperature dependences of the magnetic properties recorded during heating and cooling indicated that two processes occurring during annealing determined the magnetic properties: stabilization of domain walls by an induced local anisotropy and irreversible structural relaxation. Conditions for achieving good magnetic properties of amorphous alloys of the investigated type were formulated and it was found that in the case of Fe₂₀Co₇₀Si₁₀B₁₀ the following properties were achieved without annealing in a magnetic field: $H_c = 4$ mOe, $\mu_i = 40000$, and $\mu_{max} = 1100000$. (14 refs.) A.T.

62695 Magnetic and electrical properties of FeCr_{2-x}In_xS₄ (0 ≤ x ≤ 1). R.Z.Sadykhov, L.M.Valiev, I.G.Kerimov, A.A.Abdurragimov, A.D.Namazov (Inst. of Phys., Acad. of Sci., Azerbaizhdzhan SSR).

Inorg. Mater. (USA), vol.18, no.5, p.628-30 (May 1982). Translation of: *Izv. Akad. Nauk SSSR Neorg. Mater.*, vol.18, no.5, p.742-4 (May 1982). [received: Feb. 1983]

It was found that solid solutions of FeCr_{2-x}In_xS₄ (0 ≤ x ≤ 1), like the initial compound FeCr₂S₄, exhibit ferrimagnetic properties and have semiconductor type conductivity. (5 refs.)

62696 Reversible permeability for perpendicularly superposed induction for Fe₉₀Ni₁₀P₁₄B₆ amorphous ribbon and its magnetisation process. M.Teodoro, B.Hernando (Dept. de Física, Facultad de Ciencias, Univ. de Oviedo, Oviedo, Spain).

J. Phys. D (GB), vol.16, no.4, p.L85-7 (14 April 1983).

Measurements of the reversible permeability for perpendicularly superposed induction have been made in tape-wound cores of Fe₉₀Ni₁₀P₁₄B₆ amorphous ribbons. The results obtained show an increase of the permeability followed by a decrease, that reveals important magnetisation rotation processes in these materials. (7 refs.)

62697 Magnetization process of GdNi single crystal in the high magnetic field near the Curie temperature. Y.Isikawa, K.Higashi, T.Miyazaki, K.Sato (Coll. Liberal Arts, Toyama Univ., Toyama, Japan).

J. Magn. & Magn. Mater. (Netherlands), vol.31-34, pt.3, p.1057-8 (Feb. 1983). (Proceedings of the International Conference on Magnetism, Kyoto, Japan, 6-10 Sept. 1982).

The magnetizations of the rare earth intermetallic compound GdNi single crystal were measured in pulsed high magnetic fields up to 160 kOe near the Curie temperature. The critical exponents of β and γ were estimated to be 1/3 and 2 on the bases of the Arrott plots, respectively. (4 refs.)

62698 Polarised neutron study of Mn_{1/4}Ta_{3/4}S₂: observation of conduction electron spin polarisation. S.S.Parkin, E.A.Marsaglia (Cavendish Lab., Univ. of Cambridge, Cambridge, England), P.J.Brown.

J. Magn. & Magn. Mater. (Netherlands), vol.31-34, pt.3, p.1207-8 (Feb. 1983). (Proceedings of the International Conference on Magnetism, Kyoto, Japan, 6-10 Sept. 1982).

A polarised neutron study to determine the magnetisation density distribution in the metallic layered compound Mn_{1/4}Ta_{3/4}S₂ has been made. Although the magnetisation is principally localised on the Mn sites a significant spin polarisation of the conduction electrons was measured, suggesting that the exchange interaction between the Mn moments is of the RKKY type. (6 refs.)

62699 Anomalous temperature dependence of magnetization in amorphous (Fe_{0.9}Ni_{0.97}Si_{0.03})₈₀B₂₀ alloy. M.Takahashi, I.Okamoto, T.Miyazaki (Dept. of Appl. Phys., Tohoku Univ., Sendai, Japan).

J. Magn. & Magn. Mater. (Netherlands), vol.31-34, pt.3, p.1399-400 (Feb. 1983). (Proceedings of the International Conference on Magnetism, Kyoto, Japan, 6-10 Sept. 1982).

The temperature and magnetic field dependence of DC magnetization σ and AC susceptibility χ_{AC} were investigated for an amorphous (Fe_{0.9}Ni_{0.97}Si_{0.03})₈₀B₂₀ alloy to clarify the origin of the inflection of χ_{AC} vs. T curves observed at low temperatures. The results are discussed based upon the magnetic cluster model. (8 refs.)

62700 Low field properties of FeNiMnB amorphous alloy. Bingrong Zhang (Dept. of Phys., Nanjing Univ., Nanjing, China), Hongru Zhai, Songyao Shi, Qingzheng Xu.

J. Magn. & Magn. Mater. (Netherlands), vol.31-34, pt.3, p.1565-6 (Feb. 1983). (Proceedings of the International Conference on Magnetism, Kyoto, Japan, 6-10 Sept. 1982).

Low field properties of FeNiMnB amorphous alloy with $\lambda = 10^{-5}$ have been studied. High temperature thermomagnetic treatment followed by transverse TMT was found to reduce both the stress anisotropy and the induced anisotropy and eliminate pinning defects efficiently, thus improving the low field properties. A value of $\mu_0 = 10^4$ has been obtained. (2 refs.)

62701 Magnetic inhomogeneity in amorphous Fe-Zr alloys. H.Yamamoto, H.Onodera, K.Hosoyama, T.Masumoto, H.Yamauchi (Res. Inst. for Iron, Steel & Other Metals, Tohoku Univ., Sendai, Japan).

J. Magn. & Magn. Mater. (Netherlands), vol.31-34, pt.3, p.1579-80 (Feb. 1983). (Proceedings of the International Conference on Magnetism, Kyoto, Japan, 6-10 Sept. 1982).

Magnetic properties of amorphous Fe₇₀Zr₃₀ and Fe₉₀Zr₁₀ alloys have been studied by ⁵⁷Fe Mossbauer and magnetization measurements. The magnetic hyperfine field distribution spreads over a wide range and the temperature dependence of the hyperfine fields shows magnetically heterogeneous behaviour. Superparamagnetic behavior was observed on the magnetization curves above T_c . (7 refs.)

62702 Quantitative determination of magnetisation distributions in domains and domain walls by scanning transmission electron microscopy. J.N.Chapman, G.R.Morrison (Dept. of Natural Philosophy, Univ. of Glasgow, Glasgow, Scotland).

J. Magn. & Magn. Mater. (Netherlands), vol.35, no.1-3, p.254-60 (March 1983). (Proceedings of the 10th International Colloquium on Magnetic Films and Surfaces, Yokohama, Japan, 13-16 Sept. 1982).

Most modes of Lorentz microscopy in the transmission electron microscope yield results which are difficult to interpret quantitatively. The authors describe a new technique, differential phase contrast electron microscopy, which is well suited to the determination of both the magnetisation direction within domains and the spatial variation of the magnetisation in domain walls, the latter being averaged through the foil thickness. The mode of image formation and interpretation of images are discussed together with details of instrumental requirements. Finally results from a few magnetic elements and alloys are presented. (14 refs.)

62703 Magnetic hysteresis and minor loops: models and experiments. J.A.Barker, D.Schreiber, B.G.Huth (IBM Res. Lab., San Jose, CA, USA), D.H.Everett.

Proc. R. Soc. London Ser. A (GB), vol.386, no.1791, p.251-61 (8 April 1983). The features of minor loop behaviour in magnetic hysteresis are examined by comparing some experimental data on a Mn-Al-Ge film with two phenomenological models. The 'independent particle' model of Preisach and Everett proves to describe qualitatively all the observed behaviour. This model is generalized slightly to allow for the interaction of the 'particle' through an average demagnetizing field, and a convenient method for calculating the consequences of the model is described. (18 refs.)

62704 Effect of fabrication condition on the magnetic properties of Fe-Mn-B system amorphous alloys. S.Arai, M.Nagakura.

Res. Rep. Fac. Eng. Meiji Univ. (Japan), no.43, p.13-17 (1982). In Japanese. The effect of fabrication condition on magnetic properties of Fe-Mn-B ternary amorphous alloys are studied. Amorphous ribbons are prepared by melt quenching onto the surface of a rotating steel or copper roller. It is found

that the samples made by steel roller possess higher saturation magnetization than those made copper roller. However, the crystallization temperature of the samples obtained by copper roller is higher than that of those made by steel roller. A difference in Curie temperature is not observed for samples prepared by either method. (8 refs.)

62705 Energy losses in electrical steel under rotational magnetic reversal. G.S.Korzunin, L.A.Inisheva. *Sov. Electr. Eng. (USA)*, vol.52, no.12, p.19-24 (1981). Translation of: *Elektrotehnika (USSR)*, vol.52, no.12, p.10-12 (1981). Results are reported for an experimental investigation into the way in which energy losses during rotational magnetic reversal of cold-rolled and hot-rolled electrical steels depends on magnetizing current at 10-70 Hz. It is shown that at 50 Hz cold-rolled steel of the best grade has higher losses under rotational magnetic reversal than under cyclic reversal. This is accounted for qualitatively by the higher losses to eddy currents under rotational magnetic reversal. (6 refs.)

62706 Long relaxation times in ferromagnets and their possible applications. B.M.Lebed', I.I.Marchik. *Sov. Tech. Phys. Lett. (USA)*, vol.8, no.8, p.390-1 (Aug. 1982). Translation of: *Pis'ma v Zh. Tekh. Fiz. (USSR)*, vol.8, no.15-16, p.901-3 (Aug. 1982). [received: April 1983] Reports an experimental test of the slow relaxation in ferromagnets employing the 'rejuvenation' effect in which the original magnetic state of the ferromagnet is restored by annealing it at a temperature above the magnetic phase transition temperature. Measurements of the time dependence of the initial magnetic permeability of ferrites are presented, and applications to magnetic bearing rock are briefly discussed. (5 refs.)

Measurement of Curie temperature and magnetization of ferromagnetic materials employing an RF oscillator See Entry 59802
Amorphization of crystalline diluted Ising ferromagnet See Entry 61803
Magnetic and structural characteristics of $\text{Ho}_2\text{Fe}_{23}$ deuterides See Entry 61858
Surface characterization of substrate by ellipsometry See Entry 62220
EuS ferromagnetic semiconductor films grown epitaxially on silicon See Entry 62296
Composition distribution in Co-Cr perpendicular magnetic films See Entry 62310

Quadrupolar coupling and structural instability in $\text{PrAg}_{1-x}\text{Cu}_x$ See Entry 62383
Magnetoresistance and magnetization in $\text{Fe}_{80-x}\text{Ti}_x\text{B}_{20}$ metallic glasses See Entry 62431

Magnetic behaviour of spin-mixed iron(III) porphyrins See Entry 62557
Effects of external field on χ -T curve on cluster-glasses See Entry 62561
Magnetic moment of Fe-Ga-B amorphous alloys See Entry 62565
Magnetism of amorphous metal-metal alloys See Entry 62566
Magnetic properties of the weak ferromagnet NH_4MnF_3 See Entry 62567
Magnetocrystalline anisotropy of dysprosium and erbium ions in compounds of the RCO_5 type See Entry 62580
Anisotropies and domain structures in metallic glasses See Entry 62585

A microscopic model describing the spin-flip processes at the first-order antiferromagnetic-to-ferromagnetic phase transition in $\text{Dy}_2\text{O}_3\text{SO}_4$ See Entry 62597

Magnetic properties of the quasi-2d easy plane antiferromagnet $\text{BaNi}_2(\text{PO}_4)_2$ See Entry 62601

The H - T phase diagram for the spin-glass Ag:Mn See Entry 62602
Theoretical study of the magnetic properties of an antiferromagnetic system with two kinds of inequivalent magnetic-ion sites See Entry 62619

Anisotropy effects in the ferromagnetic quantum chain systems $(\text{C}_6\text{H}_{11}\text{NH}_3)\text{CuCl}_3$ (CHAC) and $(\text{C}_6\text{H}_{11}\text{NH}_3)\text{CuBr}_3$ (CHAB) See Entry 62625
Spin glass like behaviour of the solid solution $\text{Mn}_{3-x}\text{Ga}_x\text{N}$ See Entry 62626

Magnetic relaxation in the spin glass $\text{BaO}_2\text{TiO}_2\cdot 2\text{Fe}_2\text{O}_3$ See Entry 62629
Random-bond Ising system in the external magnetic field See Entry 62661
Experimental study of losses in cold-rolled steel using unidirectional periodic magnetisation See Entry 62679

Micromagnetics of zigzag head-on domain walls See Entry 62690
Remagnetisation phenomena in multicomponent rare-earth-cobalt alloys with increased temperature stability See Entry 62707

Statistical evaluation of basic parameters of cast magnetically hard materials See Entry 62708
The inversion magnet: a new type of permanent magnet See Entry 62709

Dynamical properties of small particles; comparison with spin glass behaviour See Entry 62719
Factors affecting the disaccommodations of amorphous magnetic materials See Entry 62721

After-effect of permeability and magnetic loss of an amorphous $\text{Co}_{75}\text{Fe}_{25}$ alloy See Entry 62722
Magnetic relaxation in amorphous $(\text{Fe}_{1-x}\text{Ni}_x)_{77}\text{Si}_{10}\text{B}_{13}$ alloys See Entry 62723

Magnetic properties of granular films $\text{Fe-Al}_2\text{O}_3$ See Entry 62725
FMR and magnetic studies in amorphous Co-Nb films See Entry 62727
Diffusion and magnetic properties of compositionally modulated films See Entry 62728

Garnet film with rectangular hysteresis loop and its application to thermomagnetic recording medium See Entry 62735
Preparation and properties of RE-TM amorphous films See Entry 62736

Magnetic properties and magnetic Kerr rotation of amorphous TbFeCo and TbFeCr films See Entry 62737
Magnetic properties, structure, and relaxation of amorphous $\text{Fe}_{1-x}\text{B}_x$ films See Entry 62739

Magnetic and electrical properties of amorphous $\text{Fe}_{1-x}\text{B}_x$ films See Entry 62740
Magnetic properties of metastable crystalline and amorphous Fe alloys produced by RF sputtering See Entry 62741

Anomalous magnetization-temperature characteristics in amorphous NiP alloys See Entry 62742
Magnetic properties and microstructure in Ho-Co alloy thin films fabricated by RF sputtering technique See Entry 62743

Substrate bias voltage dependences of magnetic properties in amorphous Tb-Fe films See Entry 62744

Electron microscopy of CoCr sputtered films See Entry 62747

Anomalous hysteresis loops in single and double layer sputtered TbFe films See Entry 62748

Perpendicular anisotropy in Co-Cr films See Entry 62751

Oblique incidence effects in evaporated thin films See Entry 62752

Magnetization reversal modes in thin films with columnar microstructure See Entry 62754

Localized modification of magnetic anisotropy in LPE iron garnet films by laser annealing See Entry 62760

The correlation length in thin film and semi-infinite medium See Entry 62763

Magnetization of electron-bombarded iron-cobalt films See Entry 62764

Structure and magnetic properties of C-axis well oriented Ba-ferrite films deposited by targets-facing type of sputtering See Entry 62765

Formation of nonthrough magnetic domains in the course of magnetization switching in amorphous Gd-Co films See Entry 62766

Domain structure in single crystal ferromagnetic oxide films near the phase transitions See Entry 62771

Magnetostriction of Co-based amorphous alloys See Entry 62784

Magnetostriction and related properties in amorphous Fe-Nb-Si-B alloys See Entry 62786

Mossbauer effect study of the internal magnetic field in small iron particles See Entry 62855

Effect of low-temperature ferritization on the properties of ferrite powders See Entry 63222

Nonstoichiometry and physical properties of hot-pressed manganese-zinc ferrites See Entry 63223

Order-disorder transition in Fe_3Si alloy during mechanical crushing See Entry 63286

75.60G High coercivity materials

62707 Remagnetisation phenomena in multicomponent rare-earth-cobalt alloys with increased temperature stability. D.D.Mishin, A.A.Lukin, N.P.Suponev, A.G.Pasushenkov, V.V.Levandovsky, M.B.Lyakhova. *Russ. Metall. (GB)*, no.6, p.179-81 (1981). Translation of: *Izv. Akad. Nauk. SSSR Met.*, no.6, p.184-5 (1981).

Multicomponent alloys of type Sm-Zr-Co-Cu-Fe with partial substitution of samarium by heavy r.e.m. are suitable for cast and sintered permanent magnets with an enhanced temperature stability. The mechanism of the coercive force in the cast and in the sintered state is due to the braking of the displacement of the domain boundaries by lattice defects uniformly distributed throughout the volume. (5 refs.)

62708 Statistical evaluation of basic parameters of cast magnetically hard materials. V.B.Ivanov.

Sov. Electr. Eng. (USA), vol.52, no.10, p.79-84 (1981). Translation of: *Elektrotehnika (USSR)*, vol.52, no.10, p.37-9 (1981).

A method is presented and results reported of a statistical investigation aimed at determining several quality characteristics for fundamental magnetic parameters: limiting values, tolerance, coordinate of tolerance-field center, relative coefficient of asymmetry, etc. (12 refs.)

62709 The inversion magnet: a new type of permanent magnet. A.V.Deryagin, N.V.Kudrevatykh, E.N.Tarasov (A.M. Gorkii Ural State Univ., Sverdlovsk, USSR).

Sov. Tech. Phys. Lett. (USA), vol.8, no.7, p.370-1 (July 1982). Translation of: *Pis'ma v Zh. Tekh. Fiz. (USSR)*, vol.8, no.13-14, p.856-8 (July 1982).

[received: April 1983] In a search for materials with a high coercive field over a broad temperature range T_1 - T_2 and with a high negative magnetization, and in an effort to develop permanent inversion magnets from these materials, the authors have studied the magnetic properties of the intermetallic compounds of thulium with cobalt TmCo_5 and Tm_2Co_7 . The alloys were produced by zone charging in an induction furnace in an atmosphere of pure helium, followed by a homogenizing at 1000°C for 100 h. (1 ref.)

Magnetocrystalline anisotropy of dysprosium and erbium ions in compounds of the RCO_5 type See Entry 62580

The shape anisotropy of metal powder on magnetism See Entry 62713

Time variation of coercivity in cobalt-contained iron oxides particles See Entry 62714

Magnetic behavior of SmCo_5 -hydrogen system See Entry 62718

Insoluble binary system thin film See Entry 62726

Structure and magnetic properties of iron films deposited at oblique incidence See Entry 62753

Magnetization reversal modes in thin films with columnar microstructure See Entry 62754

Some magnetological insights in the consolidation of metal powders See Entry 63208

Metallographic and structural investigations of levitation splat cooled cobalt base cobalt-refractory carbide alloys See Entry 63253

Investigation of the phase composition, structure, and magnetic properties of alloy $\text{Sm}_2\text{Co}_{10}\text{Fe}_{3.2}\text{Cu}_{1.2}\text{Zr}_{0.4}$ See Entry 63287

Heat treatment and magnetic properties of high-coercivity Fe-Co-Cr alloys with 3% Mo See Entry 63435

75.60J Fine-particle systems

62710 Magnetic properties of amorphous powders of alloy Mn_3B_4 . V.I.Timoshchuk, K.B.Vlasov, A.E.Ermakov, V.A.Barinov (Inst. of Metal Phys., Acad. of Sci., Sverdlovsk, USSR).

Fiz. Met. & Metalloved. (USSR), vol.55, no.2, p.263-6 (Feb. 1983). In Russian. English translation in: *Phys. Met. & Metallogr. (GB)* A study was made of the effects of strong mechanical crushing on the magnetic properties of layer antiferromagnet Mn_3B_4 ($T_N=403\text{K}$). The long-range atomic order was destroyed by sufficiently long crushing and the alloy assumed an amorphous state characterized by a spontaneous magnetization σ_0 . The effective Curie temperature was now $T_C \approx 250\text{K}$. The phase transition at T_C was strongly broadened on the temperature scale. The value of σ_0 was much less than the magnetization of the original antiferromagnetic alloy in fields sufficient to cause collapse of the antiferromagnetic sublattices, which

was attributed to the presence of an asperomagnetic structure in the amorphous state. (9 refs.) A.T.

62711 The orientation of magnetic particles for high density recording. K.Sumiya, S.Watatsani, F.Hayama (Dept. of Tech. Res., Hitachi Maxell Ltd., Kyoto, Japan), K.Nakamae, T.Matsumoto. *J. Magn. & Magn. Mater. (Netherlands)*, vol.31-34, pt.2, p.937-8 (Feb. 1983). (Proceedings of the International Conference on Magnetism, Kyoto, Japan, 6-10 Sept. 1982). The behavior of magnetic orientation of acicular α -Fe particles in paints and coatings was investigated. The high orientation of particles can be achieved by a new process line including a magnet for orientation, a solenoid for holding the orientation, and a hot air line for drying immediately. (1 ref.)

62712 Effect of heat-treatment on magnetic properties and morphology of iron particles. T.Sueyoshi, K.Tashita, S.Hirai, Y.Hayashi, M.Amamiya (Hitachi Maxell Ltd., Kyoto, Japan). *J. Magn. & Magn. Mater. (Netherlands)*, vol.31-34, pt.2, p.939-30 (Feb. 1983). (Proceedings of the International Conference on Magnetism, Kyoto, Japan, 6-10 Sept. 1982). Marked inhibition effect of surface coated silica on the crystal growth of hematite particles in the process of heat-treatment of goethite particles was reduced by the addition of calcium hydroxide to the silica-coat on the surface of goethite particles. Coercivity of iron particles, prepared by reduction of the hematite particles, significantly decreased with increase in crystallite size of iron particles. (4 refs.)

62713 The shape anisotropy of metal powder on magnetism. S.Suzuki, H.Sakumoto, Y.Omote (Res. & Dev. Center, Kanto Denka Kogyo Co. Ltd., Gunma, Japan). *J. Magn. & Magn. Mater. (Netherlands)*, vol.31-34, pt.2, p.941-2 (Feb. 1983). (Proceedings of the International Conference on Magnetism, Kyoto, Japan, 6-10 Sept. 1982). The shape anisotropy effect on the magnetism of the acicular Fe-Co alloy powder has been investigated. The effect in the coercivity was nearly 10%. Therefore, the coercivity was affected mainly by the size of the single unit particles which composed the shape of the alloy powder. (3 refs.)

62714 Time variation of coercivity in cobalt-contained iron oxides particles. M.Kishimoto, S.Kitaoaka, H.Andoh, M.Amamiya (Hitachi Maxwell Ltd., Kyoto, Japan). *J. Magn. & Magn. Mater. (Netherlands)*, vol.31-34, pt.2, p.943-4 (Feb. 1983). (Proceedings of the International Conference on Magnetism, Kyoto, Japan, 6-10 Sept. 1982). A variation of coercivity in annealing was examined for two different types of cobalt-contained iron oxide particles. The increase of coercivity by annealing cobalt substituted iron oxides was caused by the induced magnetic anisotropy. The stable coercivity of cobalt-epitaxial iron oxides resulted from the long relaxation time of the cobalt-ferrite crystallized on the oxides. (5 refs.)

62715 A theory of correlations in a magnetically aligned ferrofluid. R.Pynn, J.B.Hayter (Inst. Laue-Langevin, Grenoble, France). *J. Magn. & Magn. Mater. (Netherlands)*, vol.31-34, pt.2, p.955-7 (Feb. 1983). (Proceedings of the International Conference on Magnetism, Kyoto, Japan, 6-10 Sept. 1982). The authors have obtained an analytic form for the structure factor of a colloidal ferrofluid in which the particle moments are completely aligned by an applied magnetic field. The results obtained show the particle chaining first proposed by de Gennes and Pincus (1970). (9 refs.)

62716 Curie-Weiss behavior in ferrofluids. K.O'Grady, A.Bradbury, S.W.Charles, S.Menear, J.Popplewell (Univ. Coll. of North Wales, Bangor, Wales), R.W.Chantrell. *J. Magn. & Magn. Mater. (Netherlands)*, vol.31-34, pt.2, p.958-60 (Feb. 1983). (Proceedings of the International Conference on Magnetism, Kyoto, Japan, 6-10 Sept. 1982). Curie-Weiss behavior has been shown for magnetic liquids containing cobalt particles diameter $D_{vm}=27$ Å (sample A) and $D_{vm}=96$ Å (sample B). Values for an internal field of 650 Oe and 100 Oe have been calculated for samples A and B respectively which is interpreted in terms of interparticle interactions Monte Carlo calculations give some justification for this approach. (5 refs.)

62717 Surface magnetic properties of fine particles. A.H.Morrish, K.Haneda (Dept. of Phys., Univ. of Manitoba, Winnipeg, Manitoba, Canada). *J. Magn. & Magn. Mater. (Netherlands)*, vol.35, no.1-3, p.105-13 (March 1983). (Proceedings of the 10th International Colloquium on Magnetic Films and Surfaces, Yokohama, Japan, 13-16 Sept. 1982). Fine particles offer an attractive avenue for the study of the magnetic properties of surfaces. The use of small particles instead of thin films has some advantages. Although several experimental techniques can be employed profitably, Mossbauer spectroscopy is emphasized. The application of large magnetic fields has established that a noncollinear magnetic structure occurs in the surface layers of γ -Fe₂O₃, NiFe₂O₄, and CrO₂; the morphology of the particles appears to be important. Particles doped with Mossbauer isotopes, both throughout the volume and preferentially on the surface, provide additional useful information. Interfacial interactions and surface anisotropy are discussed. Some applications are considered. (39 refs.)

62718 Magnetic behavior of SmCo₅-hydrogen system. M.Yamaguchi, T.Ohta (Faculty of Engng., Yokohama Nat. Univ., Yokohama, Japan), Y.Osumi. *J. Magn. & Magn. Mater. (Netherlands)*, vol.35, no.1-3, p.114-16 (March 1983). (Proceedings of the 10th International Colloquium on Magnetic Films and Surfaces, Yokohama, Japan, 13-16 Sept. 1982). The magnetization of the hydrides of activated SmCo₅ powder has been determined as a function of hydrogen pressure (less than 6 MPa) and composition, and temperature under the direct influence of hydrogen. The hydride phase transformation and the effect of hydrogen on the magnetic moment have been studied. (7 refs.)

62719 Dynamical properties of small particles; comparison with spin glass behaviour. J.L.Dormann (Lab. de Magnetisme, CNRS, Meudon-Bellevue, France), D.Fiorani, J.L.Tholence, C.Sella. *J. Magn. & Magn. Mater. (Netherlands)*, vol.35, no.1-3, p.117-20 (March 1983). (Proceedings of the 10th International Colloquium on Magnetic Films and Surfaces, Yokohama, Japan, 13-16 Sept. 1982). Finely dispersed small iron particles in an amorphous alumina matrix are studied. AC susceptibility (17 Hz $\leq \nu \leq 11$ kHz), Mossbauer spectroscopy, magnetization, TRM and IRM measurements are performed. The time dependent properties are similar to those of spin glasses and are explained with the small particle model taking into account the interaction between particles. (9 refs.)

62720 Shape anisotropy of ultrafine magnesium ferrite precipitates. R.S.de Basi, T.C.Devezas (Secao de Engenharia e Ciencia dos Materiais, Inst. Militar de Engenharia, Rio de Janeiro, Brazil). *J. Magn. & Magn. Mater. (Netherlands)*, vol.35, no.1-3, p.121-2 (March 1983). (Proceedings of the 10th International Colloquium on Magnetic Films and Surfaces, Yokohama, Japan, 13-16 Sept. 1982). The temperature dependence of the resonance anisotropy field for a coherent assembly of ultrafine magnesium ferrite precipitates was investigated in the range 100-400K. The results are interpreted in terms of the shape anisotropy of the precipitates. (6 refs.)

Magnetic short-range order and spin freezing in the quasi-2D system LuFeMgO₄ See Entry 62642
Magnetic inhomogeneity in amorphous Fe-Zr alloys See Entry 62701
On the magnetic dipole fields at surface atoms See Entry 62731
Mossbauer effect study of the internal magnetic field in small iron particles See Entry 62855
Magnetic excitations in small NiFe₂O₄ particles See Entry 62856
Magnetic and electronic properties of microcrystals of Fe₂O₄ See Entry 62857
Mossbauer study of acicular iron-nitride particles See Entry 62858
Surface magnetism of α -Fe₂O₃ by Mossbauer spectroscopy See Entry 62860
Absorption line of magnetically anisotropic particles See Entry 62941

75.60L Magnetic aftereffects

62721 Factors affecting the disaccommodations of amorphous magnetic materials. K.Shirai, M.Yamato (Faculty of Engng. Sci., Osaka Univ., Toyonaka, Japan). *J. Magn. & Magn. Mater. (Netherlands)*, vol.31-34, pt.3, p.1557-8 (Feb. 1983). (Proceedings of the International Conference on Magnetism, Kyoto, Japan, 6-10 Sept. 1982). Disaccommodations of amorphous FeSiB are studied. With increase of the exciting frequency, the disaccommodation crosses zero and changes its sign thereafter. Tensile stress increases the disaccommodation, while compressive stress decreases it. A low Curie temperature means a low value of the disaccommodation. (3 refs.)

62722 After-effect of permeability and magnetic loss of an amorphous Co₇₅Fe₂₅B₂₀ alloy. S.Hatta, T.Mizoguchi (Faculty of Sci., Gakushuin Univ., Tokyo, Japan). *J. Magn. & Magn. Mater. (Netherlands)*, vol.31-34, pt.3, p.1559-60 (Feb. 1983). (Proceedings of the International Conference on Magnetism, Kyoto, Japan, 6-10 Sept. 1982). Disaccommodation effects in the permeability μ and loss angle δ in an amorphous Co₇₅Fe₂₅B₂₀ alloy were measured simultaneously. Observed discontinuous drops in both μ and δ are supposed to result from wall motion pinning associated with the structural relaxation of defects in the amorphous phase. (5 refs.)

62723 Magnetic relaxation in amorphous (Fe_{1-x}Ni_x)₇₇Si₁₀B₁₃ alloys. T.Miyazaki, M.Takahashi (Faculty of Engng., Tohoku Univ., Sendai, Japan), K.Hisatake. *J. Magn. & Magn. Mater. (Netherlands)*, vol.31-34, pt.3, p.1583-4 (Feb. 1983). (Proceedings of the International Conference on Magnetism, Kyoto, Japan, 6-10 Sept. 1982). Disaccommodation and magnetic annealing effects for amorphous (Fe_{1-x}Ni_x)₇₇Si₁₀B₁₃, $0 \leq x \leq 0.8$, alloys were studied to investigate the mechanism of structural relaxation. The structural relaxation is divided into two stages. The first stage, below 200°C, is caused by a movement of metalloid atoms and the second one, above 200°C, by diffusion of the alloy constituents. (7 refs.)

75.60N Magnetic annealing and temperature-hysteresis effects

62724 Effects of field annealing on the magnetic characteristics and magnetic losses of amorphous ribbons Fe₇₈Si₁₀B₁₂. Y.C.Kuo, L.S.Zhang, R.W.Gao (Phys. Dept., Shandong Univ., Jinan, China). *J. Magn. & Magn. Mater. (Netherlands)*, vol.31-34, pt.3, p.1563-4 (Feb. 1983). (Proceedings of the International Conference on Magnetism, Kyoto, Japan, 6-10 Sept. 1982). The effects of magnetic annealing on the magnetic characteristics and magnetic losses of amorphous ribbons of Fe₇₈Si₁₀B₁₂ were studied. The annealing temperature was chosen at 400°C, this being lower than the Curie temperature, 440°C. A magnetic field of 30 Oe was applied during the heat treatment, in a direction at an angle θ to the length of the ribbon, with $\theta=0^\circ, 45^\circ, 60^\circ, 90^\circ$. The magnetic characteristics in AC fields were measured at frequencies from 50 Hz to 10 kHz. The total losses W were measured and resolved into the hysteresis loss W_h , the classical eddy current loss W_e , and the anomalous eddy current loss W_a . In general, at a given frequency and a given maximum induction, W_a decreases and W_e increases with the direction θ . So the optimum annealing conditions for lowest total loss are different for different frequency and maximum induction. (3 refs.)

Induced anisotropy in amorphous Co-P alloys See Entry 62582
Magnetic relaxation in amorphous (Fe_{1-x}Ni_x)₇₇Si₁₀B₁₃ alloys See Entry 62723

75.70 MAGNETIC FILMS AND PLATES

62725 Magnetic properties of granular films Fe-Al₂O₃. D.Fiorani (CNRS, Grenoble, France), J.L.Tholence, J.L.Dormann. *J. Magn. & Magn. Mater. (Netherlands)*, vol.31-34, pt.2, p.947-8 (Feb. 1983). (Proceedings of the International Conference on Magnetism, Kyoto, Japan, 6-10 Sept. 1982). The frequency dependence (17 Hz $\leq \nu \leq 2103$ Hz) of the blocking temperature T_B and the time and temperature evolution of the thermoremanent magnetization TRM of granular Fe-Al₂O₃ (46% Fe) films have been studied. These properties are characteristic of fine ferromagnetic grains. (3 refs.)

62726 Insoluble binary system thin film. M.Takao, H.Senno (Materials Res. Lab., Matsushita Electric Industrial Co. Ltd., Osaka, Japan). *J. Magn. & Magn. Mater. (Netherlands)*, vol.31-34, pt.2, p.949-50 (Feb. 1983). (Proceedings of the International Conference on Magnetism, Kyoto, Japan, 6-10 Sept. 1982). Insoluble binary amorphous Fe-Ag and FeCo-Ag or slightly soluble crystalline Fe-Cu films were co-deposited. It was established that they were crystallized or segregated after heat treatment. During the treatment, electrical resistivity

drastically decreased at 250°C and coercivity surprisingly increased up to 840 Oe as a result of the shape anisotropy. (7 refs.)

62727 FMR and magnetic studies in amorphous Co-Nb films. M.Tarhouni, R.Krishnan, M.Tessier, J.Sztern (Lab. de Magnetisme, CNRS, Meudon-Bellevue, France). *J. Magn. & Magn. Mater. (Netherlands)*, vol.31-34, pt.3, p.1581-2 (Feb. 1983). (Proceedings of the International Conference on Magnetism, Kyoto, Japan, 6-10 Sept. 1982). Amorphous $\text{Co}_{1-x}\text{Nb}_x$ films have been prepared by co-evaporation in ultra high vacuum. $4\pi M_s$ decreases with an increase in x in a way similar to the case of Zr in spite of the higher valency of Nb. Nb over-coated films show a perpendicular anisotropy. The origin of this anisotropy and the effects of annealing are discussed. (9 refs.)

62728 Diffusion and magnetic properties of compositionally modulated films. N.S.Kazama, H.Fujimori (Res. Inst. for Iron, Steel & Other Metals, Tohoku Univ., Sendai, Japan). *J. Magn. & Magn. Mater. (Netherlands)*, vol.35, no.1-3, p.86-8 (March 1983). (Proceedings of the 10th International Colloquium on Magnetic Films and Surfaces, Yokohama, Japan, 13-16 Sept. 1982). Magnetization and interdiffusion measurements have been carried out on the compositionally modulated films $\text{Fe}_{80}\text{Co}_{20}/\text{Si}$. The magnetization and the Curie temperature have been significantly enhanced by the diffusion of Fe from FeC to Si for the films with a shorter modulation wavelength. On the contrary, for the longer modulation wavelength film, the ferromagnetism has been eliminated through the diffusion of Fe from Si to FeC. (8 refs.)

62729 Application of neutron diffraction to the study of interface magnetization on thin films with artificial superlattices. Y.Endoh (Dept. of Phys., Tohoku Univ., Sendai, Japan), N.Hosoi, T.Shinjo. *J. Magn. & Magn. Mater. (Netherlands)*, vol.35, no.1-3, p.93-8 (March 1983). (Proceedings of the 10th International Colloquium on Magnetic Films and Surfaces, Yokohama, Japan, 13-16 Sept. 1982). Studies interface magnetization by applying the simple kinematical theory of neutron diffraction for the periodic stratified structure. In order to realize the principle, the authors made an artificial superstructure film consisting of bilayers of ferromagnetic versus nonmagnetic materials. They discuss the principle of the application of neutron diffraction, the experiments and the results. They also compare the results with the depth profile analysis of Mossbauer spectroscopy. (13 refs.)

62730 Magnetic property changes in epitaxial metal film sandwiches. M.B.Brodsky (Materials Sci. Div., Argonne Nat. Lab., Argonne, IL, USA). *J. Magn. & Magn. Mater. (Netherlands)*, vol.35, no.1-3, p.99-104 (March 1983). (Proceedings of the 10th International Colloquium on Magnetic Films and Surfaces, Yokohama, Japan, 13-16 Sept. 1982). Epitaxial metal film sandwiches (EMFS) containing Pd or Cr, have been prepared between single crystal Ag or Au. The modified Pd/Cr show major changes in physical properties. Pd has a stretched lattice parameter in Au-Pd-Au, which combines with a tetragonal distortion to cause exchange enhancements up to 28000 and spin fluctuation temperatures of 1-10K. In Au-Cr-Au, Cr takes up the FCC structure, leading to superconductivity due to a high $N(E_F)$. These results are contrasted to data for Ag-Pd-Ag and Ag-Cr-Ag EMFS. (30 refs.)

62731 On the magnetic dipole fields at surface atoms. P.H.Christensen, S.Morup (Lab. of Appl. Phys. II, Tech. Univ. of Denmark, Lyngby, Denmark). *J. Magn. & Magn. Mater. (Netherlands)*, vol.35, no.1-3, p.130-2 (March 1983). (Proceedings of the 10th International Colloquium on Magnetic Films and Surfaces, Yokohama, Japan, 13-16 Sept. 1982). The magnetic dipole fields at atoms in small particles and thin films of α -Fe have been calculated. Only the dipole fields in the first surface layer are significantly affected by the presence of the surface. It is shown that the shape anisotropy energy of microcrystals is influenced by these surface effects. (3 refs.)

62732 A universal dispersion equation of magnetostatic surface wave (MSSW) in the layer structures. Hu Wenzhong, Liu Farang (Southwest Inst. of Appl. Magnetics, Sichuan, China). *J. Magn. & Magn. Mater. (Netherlands)*, vol.35, no.1-3, p.153-4 (March 1983). (Proceedings of the 10th International Colloquium on Magnetic Films and Surfaces, Yokohama, Japan, 13-16 Sept. 1982). A dispersion equation of MSSW propagation in the layer structures was derived. Two significant results were discovered in the numerical calculation from the equation: (1) a dispersion variable delay line could be made; (2) the linear dispersion regions and the differential delay time increase with the increasing number of the layers. (6 refs.)

62733 Magnetic and optical properties of Co, Bi substituted garnet films prepared by the LPE method and its application to thermomagnetic recording. F.Inoue, H.Mutoh, A.Itoh, K.Kawanishi (Dept. of Electronic Engng., Coll. of Sci. & Technol., Nihon Univ., Funabashi, Japan). *J. Magn. & Magn. Mater. (Netherlands)*, vol.35, no.1-3, p.170-2 (March 1983). (Proceedings of the 10th International Colloquium on Magnetic Films and Surfaces, Yokohama, Japan, 13-16 Sept. 1982). Co, Bi doped garnet films have a large Faraday rotation angle θ_F in the visible region, and the uniaxial anisotropy K_u and absorption coefficient α increases with Co substitution. Thermomagnetic recording threshold power is 4 mW for $\lambda=514.5$ nm and irradiation time $t=10$ μs , and 7.4 mW by coating of the Cr layer for $\lambda=632.8$ nm and $t=2$ μs . (7 refs.)

62734 Amorphous TbFe ultra thin film with reflective Au layer. F.Tanaka, N.Imamura (KDD Res. & Dev. Labs., Tokyo, Japan). *J. Magn. & Magn. Mater. (Netherlands)*, vol.35, no.1-3, p.173-4 (March 1983). (Proceedings of the 10th International Colloquium on Magnetic Films and Surfaces, Yokohama, Japan, 13-16 Sept. 1982). The thermomagnetic writing and reading of TbFe thin films with reflective layers were studied. As a result, the authors found the suitable thicknesses of SiO_2 -buffer and TbFe layers for low writing laser power and large effective Kerr rotation angle. (8 refs.)

62735 Garnet film with rectangular hysteresis loop and its application to thermomagnetic recording medium. Y.Yokoyama, S.Tsukahara, T.Tanaka (Electrotech. Lab., Ibaraki-ken, Japan). *J. Magn. & Magn. Mater. (Netherlands)*, vol.35, no.1-3, p.175-7 (March 1983). (Proceedings of the 10th International Colloquium on Magnetic Films and Surfaces, Yokohama, Japan, 13-16 Sept. 1982). Direct stacking of amorphous Dy-Fe and magnetic garnet layers resulted in a good medium for a thermomagnetic recording system. The composite film showed ten times larger optical rotation than the Dy-Fe film at $\lambda=550$ nm. The minimum diameter of the transcribed domain from Dy-Fe layer into the garnet layer was 4 μm . (6 refs.)

62736 Preparation and properties of RE-TM amorphous films. Y.Sakurai, K.Onishi (Faculty of Engng. Sci., Osaka Univ., Osaka, Japan). *J. Magn. & Magn. Mater. (Netherlands)*, vol.35, no.1-3, p.183-91 (March 1983). (Proceedings of the 10th International Colloquium on Magnetic Films and Surfaces, Yokohama, Japan, 13-16 Sept. 1982).

Amorphous magnetic thin films with perpendicular magnetization (GdFe, GdCo, TbFe etc.) are successfully prepared by a sputtering or evaporation technique. The magnetic compensation temperature of these films, which is estimated from $M-H$ curves by Kerr or Hall effect and is a meaningful parameter to study the film properties and devices application, is investigated as a function of preparation condition, temperature and thermal treatment after deposition. Other studies are involved with electrical properties, magnetic wall microscopic observation and its dynamics. Magneto-optic applications utilizing temperature dependence of coercivity are proposed such as thermomagnetic writing in high density thin film memory. (10 refs.)

62737 Magnetic properties and magnetic Kerr rotation of amorphous TbFeCo and TbFeCr films. H.Tsujimoto, M.Shouji, A.Saito, S.Matsushita, Y.Sakurai (Faculty of Engng. Sci., Osaka Univ., Osaka, Japan). *J. Magn. & Magn. Mater. (Netherlands)*, vol.35, no.1-3, p.199-201 (March 1983). (Proceedings of the 10th International Colloquium on Magnetic Films and Surfaces, Yokohama, Japan, 13-16 Sept. 1982).

The Kerr rotation angle θ_K of $\text{Tb}_{21}(\text{Fe}_{100-x}\text{Co}_x)_{79}$ increases from 0.18° to 0.36° with increasing Co content x from 0 to 15. On the other hand, θ_K of $\text{Tb}_{21}(\text{Fe}_{79})_{100-x}\text{Cr}_x$ reduced with increasing x . The Curie temperature of $\text{Tb}_{21}(\text{Fe}_{100-x}\text{Co}_x)_{79}$ and $\text{Tb}_{21}(\text{Fe}_{79})_{100-x}\text{Cr}_x$ rose with increasing Co and Cr concentration. (9 refs.)

62738 The thermo-magnetic writing and erasing properties and Kerr rotation angle of amorphous RE-Fe thin films. S.Tanaka, N.Imamura (KDD Res. & Dev. Labs., Tokyo, Japan).

J. Magn. & Magn. Mater. (Netherlands), vol.35, no.1-3, p.205-7 (March 1983). (Proceedings of the 10th International Colloquium on Magnetic Films and Surfaces, Yokohama, Japan, 13-16 Sept. 1982).

The thermo-magnetic writing and erasing properties and magneto-optical read-out properties of amorphous rare earth-iron (RE-Fe) thin films are studied. As a result, it is found that both properties depend on RE composition and that RE-rich film is rather suitable for magneto-optical recording media. (4 refs.)

62739 Magnetic properties, structure, and relaxation of amorphous $\text{Fe}_{1-x}\text{B}_x$ films. H.Hoffmann, M.Takahashi, J.Zweck (Inst. für Angewandte Phys., Univ. Regensburg, Regensburg, Germany). *J. Magn. & Magn. Mater. (Netherlands)*, vol.35, no.1-3, p.211-13 (March 1983). (Proceedings of the 10th International Colloquium on Magnetic Films and Surfaces, Yokohama, Japan, 13-16 Sept. 1982). Systematic investigations of the dependence of the magnetic and structural properties on the composition of as-sputtered and annealed $\text{Fe}_{1-x}\text{B}_x$ amorphous films were carried out. Most of the films were subject to strong relaxation during annealing. In the final state after annealing strong differences of magnetic properties, which originally existed due to the conditions of the preparation, vanished. (2 refs.)

62740 Magnetic and electrical properties of amorphous $\text{Fe}_{1-x}\text{B}_x$ films. T.Stobiecki (Solid State Phys. Dept., Acad. of Mining & Metall., Krakow, Poland), F.Stobiecki.

J. Magn. & Magn. Mater. (Netherlands), vol.35, no.1-3, p.217-18 (March 1983). (Proceedings of the 10th International Colloquium on Magnetic Films and Surfaces, Yokohama, Japan, 13-16 Sept. 1982).

Thin $\text{Fe}_{1-x}\text{B}_x$ ($0 \leq x \leq 0.70$) films were prepared by means of RF sputtering. The authors found that magnetic moments (μ_F) for ribbons are higher than for films and the change of μ_F with x is larger for films than for ribbons. The percolation threshold ($x_c \approx 0.65$) of magnetic order occurs for a lower concentration of B than the value linearly extrapolated from the side of iron-rich concentration. The temperature coefficient of resistivity shows that boron contributes more electrons to the conduction process in amorphous films than in ribbons. (14 refs.)

62741 Magnetic properties of metastable crystalline and amorphous Fe alloys produced by RF sputtering. K.Sumiya, Y.Nakamura (Dept. of Metal Sci. & Technol., Kyoto Univ., Kyoto, Japan).

J. Magn. & Magn. Mater. (Netherlands), vol.35, no.1-3, p.219-20 (March 1983). (Proceedings of the 10th International Colloquium on Magnetic Films and Surfaces, Yokohama, Japan, 13-16 Sept. 1982).

X-ray diffraction, magnetization and Mossbauer effect were measured for Fe-Ti, Fe-Mn, Fe-Ni and Fe-Cu sputtered alloys. The single BCC phase region is extended to a large extent in all of these sputtered alloys. Amorphous Fe-Ti and FCC Fe-Cu alloys with high alloy concentrations are obtained in marked contrast to the equilibrium phase diagram. Both of these alloys are ferromagnetic at low temperatures. (10 refs.)

62742 Anomalous magnetization-temperature characteristics in amorphous NiP alloys. K.Iida (Fundamental School of Sci. & Technol., Keio Univ., Yokohama, Japan).

J. Magn. & Magn. Mater. (Netherlands), vol.35, no.1-3, p.226-8 (March 1983). (Proceedings of the 10th International Colloquium on Magnetic Films and Surfaces, Yokohama, Japan, 13-16 Sept. 1982).

Amorphous $\text{Ni}_{1-x}\text{P}_x$ alloy films ($0.15 < x < 0.27$) were prepared by the electroless deposition technique and the magnetization-temperature characteristics of those films were investigated. The results show anomalous characteristics of concave downwards in the temperature dependence of the magnetization. Such a unique phenomena occurred only in the Ni-metalloid alloys with a small saturation magnetization value. (8 refs.)

62743 Magnetic properties and microstructure in Ho-Co alloy thin films fabricated by RF sputtering technique. T.Suzuki (Dept. of Appl. Phys., Tohoku Univ., Sendai, Japan).

J. Magn. & Magn. Mater. (Netherlands), vol.35, no.1-3, p.232-4 (March 1983). (Proceedings of the 10th International Colloquium on Magnetic Films and Surfaces, Yokohama, Japan, 13-16 Sept. 1982).

Magnetic properties and microstructure of Ho-Co films are discussed. A columnar structure observed by transmission electron microscopy is suggested to be responsible for the perpendicular magnetic anisotropy. The compensation temperature increases with Ho concentration between 15 and 25 at.% for the amorphous phase. (9 refs.)

62744 Substrate bias voltage dependences of magnetic properties in amorphous Tb-Fe films. T.Katayama, M.Miyazaki, Y.Nishihara, T.Shibata (Electrotech. Lab., Ibaraki, Japan).

J. Magn. & Magn. Mater. (Netherlands), vol.35, no.1-3, p.235-7 (March 1983). (Proceedings of the 10th International Colloquium on Magnetic Films and Surfaces, Yokohama, Japan, 13-16 Sept. 1982).

Substrate bias voltage dependences of magnetic properties were measured in amorphous Tb-Fe films. The bias voltage dependence of K_u shows a minimum around $V_b = -60$ V. This is explained by effects of the preferential resputtering and oxidation of Tb atoms during deposition. (5 refs.)

- 62745 Magnetostriction and internal stress in GdFe amorphous films with perpendicular anisotropy prepared by RF diode sputtering.** A.Itoh, H.Uekusa, Y.Tarusawa, F.Inoue, K.Kawanishi (Dept. of Electronic Engng., Coll. of Sci. & Technol., Nihon Univ., Chiba, Japan). *J. Magn. & Magn. Mater. (Netherlands)*, vol.35, no.1-3, p.241-2 (March 1983). (Proceedings of the 10th International Colloquium on Magnetic Films and Surfaces, Yokohama, Japan, 13-16 Sept. 1982). The influence of the substrate bias voltage (V_b) on the saturation magnetostriiction (λ_s) and the internal stress (σ) were measured for RF sputter-deposited Gd-Fe films. The V_b dependence of the stress induced anisotropy K_2 ($= -3/2\lambda_s\sigma$) is similar to that of K_u in the lower V_b region. (5 refs.)
- 62746 Domain observation of amorphous Fe-B and Co-Fe-B films.** M.Jimbo, Y.Machata, S.Tsunashima, S.Uchiyama (Faculty of Engng., Nagoya Univ., Nagoya, Japan). *J. Magn. & Magn. Mater. (Netherlands)*, vol.35, no.1-3, p.263-5 (March 1983). (Proceedings of the 10th International Colloquium on Magnetic Films and Surfaces, Yokohama, Japan, 13-16 Sept. 1982). The domain structure is observed in amorphous Fe-B and Co-Fe-B films annealed in a static (DFA) or a rotating (RFA) magnetic field. Ripple-like subdomains are observed by Bitter technique in RFA films, which are from a large angular dispersion of the anisotropy axes. The magnitude dispersion of the anisotropy fields is also suggested to be large in RFA films. (5 refs.)
- 62747 Electron microscopy of CoCr sputtered films.** M.Ohkoshi, H.Toba, S.Honda, T.Kusuda (Dept. of Electronics, Hiroshima Univ., Higashi-Hiroshima, Japan). *J. Magn. & Magn. Mater. (Netherlands)*, vol.35, no.1-3, p.266-8 (March 1983). (Proceedings of the 10th International Colloquium on Magnetic Films and Surfaces, Yokohama, Japan, 13-16 Sept. 1982). The magnetization curling in the CoCr film is found by a high resolution Lorentz microscopy technique. Several grains assemble to form a column, and it is observed to behave as a magnetic cluster. The magnetization-reversal process is performed by the rotational switching in the magnetostatically coupled individual cluster. (6 refs.)
- 62748 Anomalous hysteresis loops in single and double layer sputtered TbFe films.** Tu Chen, R.Malmhall (Xerox Palo Alto Res. Centers, Palo Alto, CA, USA). *J. Magn. & Magn. Mater. (Netherlands)*, vol.35, no.1-3, p.269-71 (March 1983). (Proceedings of the 10th International Colloquium on Magnetic Films and Surfaces, Yokohama, Japan, 13-16 Sept. 1982). Hall and Kerr effect observations indicate that the anomalous loop of the single layer film is associated with the propagation of a compensation wall through the thickness which can occur only in conjunction with a gradual composition variation, whereas the loop in the double layer film is a simple addition of the loops of each layer. (6 refs.)
- 62749 Pair ordering and perpendicular anisotropy in RE-TM amorphous thin films.** L.J.Makymowicz, L.Dargel, M.Lubecka, M.Pyka (Dept. of Solid State Phys., Acad. of Mining & Metall., Cracow, Poland). *J. Magn. & Magn. Mater. (Netherlands)*, vol.35, no.1-3, p.281-5 (March 1983). (Proceedings of the 10th International Colloquium on Magnetic Films and Surfaces, Yokohama, Japan, 13-16 Sept. 1982). Atomic pair ordering may play an important role in determining the uniaxial anisotropy in thin amorphous rare earth-transition metal alloys. The authors present results for annealed Gd-Co RF sputtered films. After annealing at a temperature of at least 100°C alignment of the easy axis perpendicular to the film plane and an increase of Gd-Gd pairs occur. (5 refs.)
- 62750 Perpendicular magnetic anisotropy and ferromagnetic resonance in amorphous Gd-Co and Gd-Fe films.** Jin Han-Min (Dept. of Phys., Jilin Univ., Changchun, China). *J. Magn. & Magn. Mater. (Netherlands)*, vol.35, no.1-3, p.283-5 (March 1983). (Proceedings of the 10th International Colloquium on Magnetic Films and Surfaces, Yokohama, Japan, 13-16 Sept. 1982). On the basis of a columnar microstructure model, formulae for perpendicular magnetic anisotropy (PA) and ferromagnetic resonance are deduced. The mechanism seems to be predominant in amorphous Gd-Co-Mo-Ar alloy films. The multi-peak FMR spectra observed in amorphous Gd-Co and Gd-Fe films can also be explained on this model. (12 refs.)
- 62751 Perpendicular anisotropy in Co-Cr films.** M.Ishizuka, T.Komoda, S.Tsushima, M.Yoshikawa, S.Ishio, M.Takahashi (Central Res. Labs., Engng. Center, Sharp Corp., Nara, Japan). *J. Magn. & Magn. Mater. (Netherlands)*, vol.35, no.1-3, p.286-8 (March 1983). (Proceedings of the 10th International Colloquium on Magnetic Films and Surfaces, Yokohama, Japan, 13-16 Sept. 1982). The temperature dependence of saturation magnetization and perpendicular magnetic anisotropy for 16 and 18% Cr-Co sputtered films was studied. The following were found: (i) the Curie temperatures of films are higher than those of bulk alloys; (ii) the perpendicular anisotropy constant increases after being heated to 400°C; and (iii) it changes from positive to negative at about 640°C. (6 refs.)
- 62752 Oblique incidence effects in evaporated thin films.** K.Ozawa (R&D Div., Magnetic Products Group, Sony Corp., Myagi-ken, Japan), T.Yanada, H.Masuya, M.Sato, S.Ishio, M.Takahashi. *J. Magn. & Magn. Mater. (Netherlands)*, vol.35, no.1-3, p.289-92 (March 1983). (Proceedings of the 10th International Colloquium on Magnetic Films and Surfaces, Yokohama, Japan, 13-16 Sept. 1982). Magnetic properties, electrical resistance and microstructures of evaporated iron thin films deposited at an oblique angle of incidence have been investigated. The structure differs along the thickness direction and contains interstices. It is observed by the dark field image that the columns formed appear to be single-crystals at high incidence angles. (4 refs.)
- 62753 Structure and magnetic properties of iron films deposited at oblique incidence.** Y.Takeno, Y.Iwama (Dept. of Crystalline Materials Sci., Nagoya Univ., Nagoya, Japan). *J. Magn. & Magn. Mater. (Netherlands)*, vol.35, no.1-3, p.293-5 (March 1983). (Proceedings of the 10th International Colloquium on Magnetic Films and Surfaces, Yokohama, Japan, 13-16 Sept. 1982). The structure and the magnetic properties of iron films deposited at oblique incidence are investigated by means of Rutherford back scattering technique, electron microscopy and magnetic measurement. It is found that there is a fair amount of Fe_3O_4 in the film and it affects the magnetic properties of the film. (4 refs.)
- 62754 Magnetization reversal modes in thin films with columnar microstructure.** H.Danan (Lab. Pierre Weiss, Univ. Louis Pasteur, Strasbourg, France), W.Andra. *J. Magn. & Magn. Mater. (Netherlands)*, vol.35, no.1-3, p.299-302 (March 1983). (Proceedings of the 10th International Colloquium on Magnetic Films and Surfaces, Yokohama, Japan, 13-16 Sept. 1982). Coherent rotation as well as curling may occur as a magnetization reversal mode in columnar films. The reversal is generally influenced by the surface anisotropy and the coercivity H_c depends on the columnar diameter a . Typical curves of $H_c(a)$ are calculated for Co and $\text{Co}_{85}\text{Cr}_{15}$. (11 refs.)
- 62755 Investigations of implantation-induced changes in surface layers of epitaxial garnet thin films.** M.H.Kryder, X.Wang, C.S.Krafft, A.M.Guzman (Carnegie-Mellon Univ., Pittsburgh, PA, USA). *J. Magn. & Magn. Mater. (Netherlands)*, vol.35, no.1-3, p.307-10 (March 1983). (Proceedings of the 10th International Colloquium on Magnetic Films and Surfaces, Yokohama, Japan, 13-16 Sept. 1982). Using newly improved FMR characterization techniques, the authors have established that mechanisms other than the implantation-induced stress are responsible for uniaxial anisotropy field change. They have measured λ_{111}/M_s and the crystalline anisotropy field H_1 in the implanted layer. H_1 is shown to decrease after implantation. (13 refs.)
- 62756 Large magnetic anisotropy change induced by hydrogen ion implantation in europium iron garnet LPE films.** H.Makino, Y.Hidaka, H.Matsutera (Microelectronics Res. Labs., Nippon Electric Co. Ltd., Kawasaki, Japan). *J. Magn. & Magn. Mater. (Netherlands)*, vol.35, no.1-3, p.311-14 (March 1983). (Proceedings of the 10th International Colloquium on Magnetic Films and Surfaces, Yokohama, Japan, 13-16 Sept. 1982). H_2^+ ion implantation in $(111) \text{Eu}_2\text{Fe}_{10}\text{O}_{12}$ LPE films is found to induce an unusually large anisotropy field change of an order of 3000 Oe. By annealing at 300°C, the H_2^+ implantation induced anisotropy field decreases drastically, but lattice strain still remains at a high level. It is concluded that the contribution of hydrogen ions, which exist within the garnet film, should be intrinsic for the observed large anisotropy field change. (10 refs.)
- 62757 Effects of high dose ion implantation on structure and magnetic properties of 3d-metal films.** Y.Suezawa, Y.Gondo, T.Nakao, K.Kakuno (Faculty of Engng., Yokohama Nat. Univ., Yokohama, Japan). *J. Magn. & Magn. Mater. (Netherlands)*, vol.35, no.1-3, p.323-5 (March 1983). (Proceedings of the 10th International Colloquium on Magnetic Films and Surfaces, Yokohama, Japan, 13-16 Sept. 1982). The decrease of the magnetic moment was measured of Dy^{+} ion implanted Ni films. With some He^{+} backscattering observations, the observed decrease indicated that a paramagnetic Dy-Ni alloy layer was formed with the high dose implantation. (5 refs.)
- 62758 Magnetocrystalline anisotropy energy K_1 of Co^{2+} and Ru^{3+} substituted bubble garnet films.** J.Mada, K.Yamaguchi, H.Uchishiba (Fujitsu Labs. Ltd., Kawasaki, Japan). *J. Magn. & Magn. Mater. (Netherlands)*, vol.35, no.1-3, p.326-8 (March 1983). (Proceedings of the 10th International Colloquium on Magnetic Films and Surfaces, Yokohama, Japan, 13-16 Sept. 1982). The effect of Co and Ru substitution on magnetocrystalline anisotropy constant K_1 is studied using ferromagnetic resonance (at 9.4 GHz) for epitaxial YSmLuCaGe films grown on $[100]$ oriented $\text{Gd}_3\text{Ga}_2\text{O}_{12}$ substrates. K_1 increases in low Co substitution regions, but decreases in regions with higher substitution. For Ru, K_1 decreases monotonously with increasing substitution. (4 refs.)
- 62759 Interference enhanced Kerr spectroscopy for very thin absorbing films—application to amorphous terbium ion.** G.A.N.Connell, R.Allen, M.Mansuripur (Xerox Palo Alto Res. Center, Palo Alto, CA, USA). *J. Magn. & Magn. Mater. (Netherlands)*, vol.35, no.1-3, p.337-9 (March 1983). (Proceedings of the 10th International Colloquium on Magnetic Films and Surfaces, Yokohama, Japan, 13-16 Sept. 1982). A new method of obtaining polar Kerr spectra from very thin absorbing films is used to study the thickness dependence of the Curie temperature, compensation temperature and critical behavior of the Fe-subnetwork of amorphous Tb-Fe alloy films. Significant deviations from bulk behaviour begin to occur at thicknesses below about 20 nm. (5 refs.)
- 62760 Localized modification of magnetic anisotropy in LPE iron garnet films by laser annealing.** K.Ando, Y.Yokoyama, T.Okuda, N.Koshizuka (Electrotech. Lab., Ibaraki, Japan). *J. Magn. & Magn. Mater. (Netherlands)*, vol.35, no.1-3, p.350-2 (March 1983). (Proceedings of the 10th International Colloquium on Magnetic Films and Surfaces, Yokohama, Japan, 13-16 Sept. 1982). A method of obtaining localized modification of magnetic anisotropy in LPE garnet film is described. Localized annealing was done by heating the film with a CW argon laser beam in a high temperature furnace. The direction change of magnetization was observed at the irradiated area. (7 refs.)
- 62761 A new method for analysis of magnetic anisotropy in films using the spontaneous Hall effect.** K.Okamoto (Dept. of Technol., Kagawa Univ., Kagawa, Japan). *J. Magn. & Magn. Mater. (Netherlands)*, vol.35, no.1-3, p.353-5 (March 1983). (Proceedings of the 10th International Colloquium on Magnetic Films and Surfaces, Yokohama, Japan, 13-16 Sept. 1982). A new method to determine the easy axis of films with uniaxial magnetic anisotropy using the spontaneous Hall effect is presented. The principle of the method is explained and its validity is verified by the experiments. (2 refs.)
- 62762 Analysis of type-II magnetic contrast from ferromagnetic thin films in the scanning electron microscopy.** T.Ikuta (Dept. of Appl. Electronics Osaka Electro-Communication Univ., Osaka, Japan), R.Shimizu. *J. Magn. & Magn. Mater. (Netherlands)*, vol.35, no.1-3, p.356-8 (March 1983). (Proceedings of the 10th International Colloquium on Magnetic Films and Surfaces, Yokohama, Japan, 13-16 Sept. 1982). Type-II magnetic contrast in the scanning electron microscopy is a new observation technique for the magnetic domain in the ferromagnetic materials. The analysis of type-II magnetic contrast for magnetic thin films is achieved by using Monte Carlo simulation. The results show that transmitted (forward-scattered) electron image contains the magnetic contrast as well as the conventional backscattered electron image. (9 refs.)
- 62763 The correlation length in thin film and semi-infinite medium.** W.Korneta (Dept. of Phys., Tech. Univ., Radom, Poland), Z.Pytel. *Phys. Lett. A (Netherlands)*, vol.94A, no.6-7, p.305-8 (21 March 1983). Correlation lengths in directions parallel and perpendicular to a surface of a thin ferromagnetic film and a semi-infinite ferromagnet are calculated. Their dependences both on temperature and distance to a surface are discussed. (6 refs.)
- 62764 Magnetization of electron-bombarded iron-cobalt films.** L.A.Chebotaevich, V.G.Lifshits, V.A.Nachinov, Yu.D.Vorob'ev, V.V.Veter, U.A.Ulmanis (Far-East State Univ., Vladivostok, USSR). *Sov. Phys-Solid State (USA)*, vol.24, no.9, p.1494-6 (Sept. 1982). Translation of: *Fiz. Tverd. Tela (USSR)*, vol.24, no.9, p.2636-40 (Sept. 1982). [received: April 1983] Chromium-doped iron-cobalt films are bombarded by electrons with energies of 75 keV and 3.8 MeV. The dose and concentration dependence of the relative magnetization are investigated. Estimates are made for the contributions to the change in the magnetization and coercive field due to the following radiation effects: the change in the chemical composition, amorphization,

the change in the thickness, and the formation of radiation defects. It is shown that the addition of chromium to $\text{Fe}_{0.6}\text{Co}_{0.4}$ films leads to a stronger decrease in the magnetization. (12 refs.)

62765 Structure and magnetic properties of C-axis well oriented Ba-ferrite films deposited by targets-facing type of sputtering. Y.Hoshi, M.Matsuoka, M.Naoe, S.Yamanaka (Faculty of Engng., Tokyo Inst. of Technol., Tokyo, Japan).

Trans. Inst. Electron. & Commun. Eng. Jpn. Part C (Japan), vol.166C, no.1, p.9-16 (Jan. 1983). In Japanese.

Ba-ferrite (BaM) films have been prepared by means of targets-facing type of sputtering method and their structure and magnetic properties have been investigated in detail. The film properties strongly depend on the sputtering conditions such as argon pressure P_{Ar} , substrate temperature T_s , crystal structure of the substrate and plasma confinement field. C-axis well oriented BaM films with good surface smoothness are obtained under certain preparation conditions a substrate which has amorphous crystal structure. The films show perpendicular magnetization and have almost the same magnetic anisotropy and saturation magnetization as those of single crystal BaM. (11 refs.)

Optical mode conversions in Nd substituted iron garnet films. See Entry 61270

The effect of Fe-Ni films on the insertion loss of SAW. See Entry 61372

He^+ backscattering study on Ar distribution in amorphous magnetic thin films. See Entry 62293

Structure and magnetism of insoluble Pb-Fe alloy films. See Entry 62294

EuS ferromagnetic semiconductor films grown epitaxially on silicon. See Entry 62296

Composition distribution in Co-Cr perpendicular magnetic films. See Entry 62310

Resistance change of thin Permalloy films caused by applied stress and its application to strain measurements. See Entry 62508

Micromagnetics of zigzag head-on domain walls. See Entry 62690

Quantitative determination of magnetisation distributions in domains and domain walls by scanning transmission electron microscopy. See Entry 62702

Magnetic hysteresis and minor loops: models and experiments. See Entry 62703

Giant attenuation of surface acoustic waves by ferromagnetic films. See Entry 62791

Evaluation of magnetostriction constant in amorphous ribbons utilizing the velocity change of a magnetoelastic wave. See Entry 62792

Temperature and field dependence of magnetostriction in amorphous thin films. See Entry 62793

Study of magnetoelastic waves by optical observation on the surface of magnetic materials. See Entry 62794

Propagation properties of magnetoelastic waves in a magnetic slab. See Entry 62795

Effect of a semiconductor substrate on the ferromagnetic resonance in a thin cobalt film. See Entry 62811

Spin echo of ^{59}Co and ^{63}Cu impurity nuclei in single-crystal iron films in the case of coincidence of nuclear magnetic and ferromagnetic resonance frequencies. See Entry 62833

Mossbauer spectroscopic studies on surfaces and thin films. See Entry 62859

Interface magnetism in Fe-Sb multilayer films from ^{125}Sb and ^{57}Fe Mossbauer spectroscopy. See Entry 62861

Mossbauer and X-ray diffraction studies of amorphous Fe-Ni alloy films deposited by DC sputtering. See Entry 62862

Application of the depth-selective conversion electron Mossbauer spectroscopy to rare-earth iron garnet films. See Entry 62863

Conversion Mossbauer studies of epitaxially mixed ferrite-garnet films. See Entry 62870

An investigation of diffraction efficiency of magneto-optic deflection in garnet film. See Entry 62944

Magneto-optical spectra of RF-sputtered amorphous Gd-Co and Gd-Fe films. See Entry 62945

Magneto-optical effect spectra of rare-earth-transition-metal amorphous films. See Entry 62946

Ion beam sputter deposition of layered magnetic thin films. See Entry 63157

LPE growth of YNd-iron garnet films for magneto-optical waveguides. See Entry 63182

62766 Formation of nonthrough magnetic domains in the course of magnetization switching in amorphous Gd-Co films. G.S.Kandaurova, M.F.Karimov (A.M. Gorki Ural State Univ., Sverdlovsk, USSR).

Fiz. Met. & Metalloved. (USSR), vol.55, no.2, p.248-52 (Feb. 1983). In Russian. English translation in: *Phys. Met. & Metallogr. (GB)*

A comparison was made of the magneto-optic magnetization curves, hysteresis loops, and domain structure on both surfaces of inhomogeneous Gd-Co films. It was found that transitions from a through to a nonthrough domain structure were possible in a magnetic field and that a system of nonthrough bubble domains could form. (9 refs.) A.T.

62767 Charged wall of a bubble domain. G.E.Khodenkov (Inst. of Electronic Control Machines, Moscow, USSR).

Fiz. Met. & Metalloved. (USSR), vol.55, no.2, p.400-2 (Feb. 1983). In Russian. English translation in: *Phys. Met. & Metallogr. (GB)*

An analytic explanation is given of the charging of domain walls in films with a bending-induced transverse anisotropy across the film thickness. (3 refs.) A.T.

62768 Motion of tops of domains in thin films with low-coercivity channels. A.V.Gavriluk, V.P.Karabanova, V.N.Popov, V.P.Panaetov, B.V.Gavriluk (Pedagogical Inst., Irkutsk, USSR).

Fiz. Met. & Metalloved. (USSR), vol.55, no.2, p.413-6 (Feb. 1983). In Russian. English translation in: *Phys. Met. & Metallogr. (GB)*

An electron microscope was used to study the motion of domains in thin films of the 83% Ni-17% Fe composition. It was found that the structure of the tops of domains determined the field needed to set these domains in motion in low-coercivity channels. (7 refs.) A.T.

62769 Observation of magnetic domain structure in thin ferromagnetic films by electron holography. A.Tonomura (Central Res. Lab., Hitachi Ltd., Tokyo, Japan).

J. Magn. & Magn. Mater. (Netherlands), vol.31-34, pt.2, p.963-9 (Feb. 1983). (Proceedings of the International Conference on Magnetism, Kyoto, Japan, 6-10 Sept. 1982).

An overview is provided of a new method that has been developed for observing fine details of magnetic domain structures in thin specimens. In this method, in-plane magnetic lines of force inside a specimen are directly observed in the electron interference micrograph. Quantitative measurement is also possible, since two neighboring contour lines contain a constant magnetic flux of h/e . This method is also applicable to observation of microscopic distributions of magnetic fields. Several practical applications are presented using this technique. (17 refs.)

62770 Static and dynamic properties of thermomagnetic writing in amorphous TbFe films. S.Honda, J.Hirokane, M.Ohkoshi, T.Kusuda (Dept. of Electronics, Hiroshima Univ., Hiroshima, Japan).

J. Magn. & Magn. Mater. (Netherlands), vol.35, no.1-3, p.208-10 (March 1983). (Proceedings of the 10th International Colloquium on Magnetic Films and Surfaces, Yokohama, Japan, 13-16 Sept. 1982).

The domain structure in the bit written thermomagnetically is investigated in detail, and also the dynamic process of the flux reversal in the writing is studied experimentally and theoretically. The formation of the domain structure in a written bit is explained consistently. (8 refs.)

62771 Domain structure in single crystal ferromagnetic oxide films near the phase transitions. R.Szymczak (Inst. of Phys., Polish Acad. of Sci., Warsaw, Poland).

J. Magn. & Magn. Mater. (Netherlands), vol.35, no.1-3, p.243-8 (March 1983). (Proceedings of the 10th International Colloquium on Magnetic Films and Surfaces, Yokohama, Japan, 13-16 Sept. 1982).

The observations of domain structure in single crystal ferromagnetic oxide films near phase transitions induced by temperature and by magnetic field have been carried out. The domain structure has been observed by means of the Faraday effect and by light diffraction. The following phase transition points have been studied in details: paramagnet-ferromagnet transition. Morin transition, compensation point and continuous spin reorientation points. It has been shown that in all considered cases dipolar interactions have significant influence on phase transitions and, in particular, on the magnetization distribution near the phase transition points. (28 refs.)

62772 Domain wall phenomena in bubble propagation layers. A.Hubert (Inst. fur Werkstoffwissenschaften, Univ. Erlangen, Erlangen, Germany).

J. Magn. & Magn. Mater. (Netherlands), vol.35, no.1-3, p.249-53 (March 1983). (Proceedings of the 10th International Colloquium on Magnetic Films and Surfaces, Yokohama, Japan, 13-16 Sept. 1982).

The role of domain walls in bubble propagation layers is reviewed. Conventional permalloy overlay structures of typically 0.4-0.5 μm thickness show stray field free domain wall structures. These walls are very wide and mobile. It is concluded that wall pinning and irreversibilities are primarily connected with Bloch lines and other 'singularities' which cannot be stray field free. In ion-implanted bubble memories domain walls play a more important role. Generally one expects symmetric Neel walls. By a partial stress relaxation 'charged' walls are produced which are used for bubble transportation. The behaviour of these charged walls in connection with the details of the magnetoelastic interaction is investigated. (32 refs.)

62773 Influence of cation distribution induced by thermal annealing on magnetic bubbles properties in Ga-substituted garnet films. J.Gouzerh, H.Le Gall, J.M.Desvignes, R.Khalafouni, I.Puchalska (Lab. de Magnetisme et d'Optique des Solides, CNRS, Meudon Bellevue, France).

J. Magn. & Magn. Mater. (Netherlands), vol.35, no.1-3, p.272-4 (March 1983). (Proceedings of the 10th International Colloquium on Magnetic Films and Surfaces, Yokohama, Japan, 13-16 Sept. 1982).

After being annealed at different equilibrium temperatures $1125 \leq T_e \leq 1473\text{K}$, Ga-substituted YIG films were quenched and the change of the magnetic properties of the material ($4\pi M_s$, K_u) and the bubble parameters (field stability range, diameter, collapse field, characteristic length, wall energy) associated with the cation migration induced by the thermal treatment were determined. The results are discussed. (7 refs.)

62774 Standing waves of wall vibration. J.C.Slonczewski (IBM Thomas J. Watson Res. Center, Yorktown Heights, NY, USA).

J. Magn. & Magn. Mater. (Netherlands), vol.35, no.1-3, p.275-7 (March 1983). (Proceedings of the 10th International Colloquium on Magnetic Films and Surfaces, Yokohama, Japan, 13-16 Sept. 1982).

The forced vibrations of an infinite chain of coupled masses with long-range interactions is analyzed. Calculations explain the standing wave patterns observed by Spreen and Argyle (1982) in an array of plane parallel 180° domain walls pinned by a pair of cracks in a garnet film. (4 refs.)

62775 Perpendicular magnetic anisotropy and microstructure of sputter-deposited Co-Cr film. N.Honda, H.Awano, T.Samoto, J.Hokkyo (Sony Corp. Res. Center, Yokohama, Japan).

J. Magn. & Magn. Mater. (Netherlands), vol.35, no.1-3, p.278-80 (March 1983). (Proceedings of the 10th International Colloquium on Magnetic Films and Surfaces, Yokohama, Japan, 13-16 Sept. 1982).

The Ar pressure dependence of both the microstructure and the magnetic properties of sputter-deposited Co-Cr film is investigated. As the Ar pressure decreases, the structural binding between columns in the film becomes denser and stronger. The columnar structure has no relation to the crystal orientation. A domain structure change is suggested. (4 refs.)

62776 Influences of ion implantation on charged wall properties in magnetic bubble devices. Y.Hidaka, H.Matsutera (Microelectronics Res. Labs., Nippon Electric Co. Ltd., Kawasaki, Japan).

J. Magn. & Magn. Mater. (Netherlands), vol.35, no.1-3, p.315-18 (March 1983). (Proceedings of the 10th International Colloquium on Magnetic Films and Surfaces, Yokohama, Japan, 13-16 Sept. 1982).

Bubble propagation properties for H_2^+ implanted contiguous disk tracks are investigated. The in-plane anisotropy energy along the good tracks' direction in the region between the tracks is found to be important for bubble propagation, due to the lattice strain relaxation at the pattern edge. (5 refs.)

62777 Structure and magnetic domain walls of Dy ion implanted Fe films. S.Tsukahara, T.Kanayama, H.Tanoue (Electrotech. Lab., Ibaraki, Japan).

J. Magn. & Magn. Mater. (Netherlands), vol.35, no.1-3, p.319-22 (March 1983). (Proceedings of the 10th International Colloquium on Magnetic Films and Surfaces, Yokohama, Japan, 13-16 Sept. 1982).

400 keV Dy^+ ions implanted into iron films stay interstitial among expanded BCC lattices of iron up to about 8 at.%, while the domain structure is dominated by the cubic anisotropy. At a little higher concentration of dysprosium the Dy-Fe film is transformed into amorphous, which accompanies an isotropic domain configuration. (3 refs.)

75.70K Domain structure (magnetic bubbles)

62778 Dynamic conversion of a magnetic bubble in a rotating gradient experiment. J.A.Nyenhuys, B.J.Guo, F.J.Friedlaender (School of Electrical Engng., Purdue Univ., West Lafayette, IN, USA), H.Sato. *J. Magn. & Magn. Mater. (Netherlands)*, vol.36, no.1-2, p.187-94 (1 April 1983).

The rotating gradient experiment was used to dynamically convert an $S=1$, unichiral bubble into one with a more complex domain wall structure. At least five distinct wall states were generated and could be identified by determining the momentum and winding number from the velocity vs. radial drive relation. The data provides evidence for the dynamic generation of vertical Bloch lines, Bloch curves and Bloch points. The bubble returned to the $S=1$, unichiral state when motion ceased. (15 refs.)

62779 High-speed photographic study of the dynamic properties of ferrite-garnet films with domain diameters less than 0.5 μm . L.P.Ivanov, A.S.Logginov, G.A.Nepokoichitskii, Yu.V.Starostin (M.V. Lomonosov State Univ., Moscow, USSR).

Sov. Phys. Tech. Phys. (USA), vol.27, no.10, p.1303-4 (Oct. 1982). Translation of: *Zh. Tekh. Fiz. (USSR)*, vol.52, no.10, p.2118-20 (Oct. 1982). [received: April 1983]

Reports the first experimental results obtained by high-speed photography using single light flashes concerning the dynamics of bubble domains of diameter $d \approx 0.4 \mu\text{m}$. By using a wide-aperture system the authors were able to achieve a spatial resolution $\sim 0.3 \mu\text{m}$ when the wavelength of the illuminating flash was $\sim 0.58 \mu\text{m}$. The time resolution of the equipment was $\sim 8 \text{ ns}$. Ferrite-garnet films of composition $(\text{Pb, Bi, Sm, Lu, Gd})_3(\text{Al, Si, Fe})_2\text{O}_{12}$ grown on the (111) plane on $\text{Ga}_2\text{Ga}_2\text{O}_3$ substrates. (14 refs.)

62780 Domain-wall velocity in iron garnet films in strong pulsed fields. A.F.Martynov, V.V.Randoshkin, R.V.Telesnin (M.V. Lomonosov State Univ., Moscow, USSR).

Sov. Tech. Phys. Lett. (USA), vol.8, no.7, p.348-9 (July 1982). Translation of: *Pisma v Zh. Tekh. Fiz. (USSR)*, vol.8, no.13-14, p.803-6 (July 1982). [received: April 1983]

Iron garnet films are promising materials for applications in a variety of magnetooptic information-processing devices. The speed of these devices increases with increasing velocity (v) of the domain walls. In the present experiments the authors used high-speed photography to study the motion of domain walls in iron garnet films in pulsed fields up to 1 kOe. The film was initially magnetized to saturation by a bias field H_b applied perpendicular to the plane of the film. A pulsed field H_p was applied antiparallel to the bias field. As a result, reverse-magnetization domains were nucleated in the film and grew. The velocity v was determined from the slope of the linear part of the time dependence of the displacement of the wall of a reverse-magnetization domain, corresponding to steady-state motion, at a large distance from the domain wall to the nucleation center. (6 refs.)

62781 Comparison of the magnetic properties of one- and two-layer iron garnet films. A.M.Yuzin, V.V.Randoshkin, R.V.Telesnin, A.V.Antonov, M.Yu.Gusev, Yu.V.Starostin (M.V. Lomonosov State Univ., Moscow, USSR). *Sov. Tech. Phys. Lett. (USA)*, vol.8, no.7, p.365-6 (July 1982). Translation of: *Pisma v Zh. Tekh. Fiz. (USSR)*, vol.8, no.13-14, p.844-8 (July 1982). [received: April 1983]

The authors report a study of the special magnetic properties of two layer iron garnet films due to the interaction between layers. As layer 1 they used films of the composition $(\text{Pb, Bi, Sm, Tm})_3(\text{Fe, Ga})_2\text{O}_{12}$, while layer 2 consisted of films of the composition $(\text{Gd, Y, Tm})_3(\text{Fe, Ga})_2\text{O}_{12}$. The film thickness h was measured by an interference method; the width W of the stripe domains and the bubble collapse field H_0 were measured by diffraction or magnetooptic methods; and the effective uniaxial anisotropy field $H_K = 4\pi M$, the width of the ferromagnetic resonance line ΔH , and the g -factor were measured by a ferromagnetic-resonance method at 9.34 GHz. The exchange-interaction constant A was determined from the Neel temperature T_N . (6 refs.)

Oxygen defect profile in implanted garnetSee Entry 61906

Mechanism of thermomagnetic recording in an MnBi filmSee Entry 62611

Preparation and properties of RE-TM amorphous filmsSee Entry 62736

FMR line intensity and width in garnet ferrite filmsSee Entry 62810

75.80 MAGNETOMECHANICAL AND MAGNETOELECTRIC EFFECTS, MAGNETOSTRICTION

62782 Magnetoelastic damping and ΔE effect in amorphous alloys based on Fe-Ni. Yu.E.Kalinin, B.G.Sukhodolov, I.V.Zolotukhin, V.P.Alekhin (Polytech. Inst. Voronezh, USSR).

Fiz. Met. & Metalloved. (USSR), vol.55, no.2, p.243-7 (Feb. 1983). In Russian. English translation in: *Phys. Met. & Metallogr. (GB)*

An investigation was made of the magnetoelastic damping and of the ΔE effect (representing the relative reduction in the Young modulus) of amorphous $\text{Fe}_{40}\text{Ni}_{60}\text{P}_{14}\text{B}_{0.06}$ before and after magnetothermal treatment. The observed damping and ΔE effect were attributed to a magnetomechanical hysteresis. (12 refs.) A.T.

62783 An observation of magnetoelastic wave propagation in magnetic thin strips and films. K.Kakuno, D.Inami, K.Komatsu, Y.Suezawa, Y.Gondo (Dept. of Electrical Engng., Yokohama Nat. Univ., Yokohama, Japan).

J. Magn. & Magn. Mater. (Netherlands), vol.31-34, pt.2, p.935-6 (Feb. 1983). (Proceedings of the International Conference on Magnetism, Kyoto, Japan, 6-10 Sept. 1982).

By the use of a microstrip line as a generator, the propagation characteristics of magnetoelastic waves are studied over a wide frequency range. The well defined attenuation constant is obtained as a function of frequency. It is found that the attenuation constant is almost directly proportional to the frequency. (1 ref.)

62784 Magnetostriction of Co-based amorphous alloys. K.Aso, S.Uedaira, M.Hayakawa, K.Hotai, Y.Ochiai, K.Hayashi, Y.Makino (Sony Corp. Res. Center, Yokohama, Japan).

J. Magn. & Magn. Mater. (Netherlands), vol.31-34, pt.3, p.1546-8 (Feb. 1983). (Proceedings of the International Conference on Magnetism, Kyoto, Japan, 6-10 Sept. 1982).

The magnetostriction λ of Co-based amorphous alloys $\text{Fe}_x\text{Co}_{1-x}\text{Ni}_{1-x}\text{Si}_2\text{B}_8$, prepared by a rapid quenching technique, was obtained by measuring the tension dependence of the magnetic hysteresis loop at 8 Hz. A least squares fitting analysis leads to $\lambda(x,y,z,p,q) \times 10^6 = 0.714x - 0.0831y - 0.306z + 0.101p + 0.0955q$ in at.%. (14 refs.)

62785 Single-ion anisotropy and magnetostriction of amorphous alloys. Y.Suzuki, T.Egami (Dept. of Materials Sci. & Engng., Univ. of Pennsylvania, Philadelphia, PA, USA).

J. Magn. & Magn. Mater. (Netherlands), vol.31-34, pt.3, p.1549-50 (Feb. 1983). (Proceedings of the International Conference on Magnetism, Kyoto, Japan, 6-10 Sept. 1982).

Local magnetic anisotropy and magnetostriction of amorphous alloys were studied using the point charge model. A simple formula was observed to describe linear magnetostriction. It was found that the unscreened point charge model always leads to zero magnetostriction, while ordinary screening makes the magnetostriction positive and anti-screening results in negative magnetostriction. (6 refs.)

62786 Magnetostriction and related properties in amorphous Fe-Nb-Si-B alloys. K.Inomata (Toshiba Res. & Dev. Center, Kawasaki, Japan), T.Kobayashi, M.Hasegawa, T.Sawa.

J. Magn. & Magn. Mater. (Netherlands), vol.31-34, pt.3, p.1577-8 (Feb. 1983). (Proceedings of the International Conference on Magnetism, Kyoto, Japan, 6-10 Sept. 1982).

A study was carried out to obtain Fe-based amorphous alloys with low magnetostriction. The magnetostriction (λ_s) was measured as functions of Nb and Fe content in Fe-Nb-Si-B amorphous alloys. It was found that the presence of Nb decreases λ_s , particularly in Fe-rich region. (8 refs.)

62787 Magnetostriction of iron, cobalt and nickel ternary amorphous ribbons. N.Tsuya, K.I.Arai (Res. Inst. of Electrical Communication, Tohoku Univ., Sendai, Japan).

J. Magn. & Magn. Mater. (Netherlands), vol.31-34, pt.3, p.1594-6 (Feb. 1983). (Proceedings of the International Conference on Magnetism, Kyoto, Japan, 6-10 Sept. 1982).

The magnetostriction of iron, cobalt and nickel ternary amorphous alloy ribbons is studied theoretically. The role of many electronic excited states coupled by intra-exchange, as well as the spin self-orbit interaction to the ground state, seems to be essential in accounting for the magnetostriction in these alloys. (14 refs.)

62788 Saturation magnetostriction of some (FeCo)-metalloid-compounds and -amorphous alloys. M.Goto, H.Tange, T.Kamimori, K.Okuma (Faculty of Sci., Ehime Univ., Matsuyama, Japan).

J. Magn. & Magn. Mater. (Netherlands), vol.31-34, pt.3, p.1601-2 (Feb. 1983). (Proceedings of the International Conference on Magnetism, Kyoto, Japan, 6-10 Sept. 1982).

$[(\text{FeCo})_3\text{P}]$ and amorphous $(\text{FeCo})_{70}\text{Si}_{10}\text{B}_{13}$ alloy is measured. Addition of Co tends to make λ_s negative without any significant difference among these substances. The λ_s seems to be due to one ion character. (6 refs.)

62789 Magnetostriction of Co base amorphous alloys. H.Fujimori, N.S.Kazama, K.Hirose (Res. Inst. for Iron, Steel & Other Metals, Tohoku Univ., Sendai, Japan).

J. Magn. & Magn. Mater. (Netherlands), vol.31-34, pt.3, p.1603-4 (Feb. 1983). (Proceedings of the International Conference on Magnetism, Kyoto, Japan, 6-10 Sept. 1982).

It has been found experimentally that the negative magnetostriction of $\text{Co}_{95}\text{Nb}_5$ amorphous alloy changes to positive values as Co is replaced by Fe, Mn and Ti, while its negative value is enhanced by Ni. The concentration trends of Fe and Mn can be explained in terms of pseudo-dipole interactions of the magnetic atom pairs involved. (8 refs.)

62790 Magnetoelastic effects in amorphous metals due to surface crystallisation and oxidation. U.Gonser, M.Ackermann, H.-G.Wagner (Univ. des Saarlandes, Saarbrücken, Germany).

J. Magn. & Magn. Mater. (Netherlands), vol.31-34, pt.3, p.1605-7 (Feb. 1983). (Proceedings of the International Conference on Magnetism, Kyoto, Japan, 6-10 Sept. 1982).

In Mossbauer spectra of amorphous ribbons, variations in the relative line intensities indicate reorientations in the domain structure which have sometimes been interpreted as a sign of a bulk structural change. The authors present evidence that surface oxidation and crystallization are responsible for the observed anisotropies. These effects could be verified by simultaneous observation of the bulk by means of γ -absorption Mossbauer spectroscopy and of the surface by means of (emission) conversion Mossbauer spectroscopy (CEMS). (4 refs.)

62791 Giant attenuation of surface acoustic waves by ferromagnetic films. M.Levy, H.Yoshida (Phys. Dept., Univ. of Wisconsin-Milwaukee, Milwaukee, WI, USA).

J. Magn. & Magn. Mater. (Netherlands), vol.35, no.1-3, p.139-45 (March 1983). (Proceedings of the 10th International Colloquium on Magnetic Films and Surfaces, Yokohama, Japan, 13-16 Sept. 1982).

The attenuation of surface acoustic waves at 618 MHz propagating through a 200 Å nickel film may be changed by 40 dB/cm by changing an applied magnetic field by $\pm 90 \text{ Oe}$. This giant effect is strongly dependent on the thickness of the nickel film. It appears that magnetoelastic coupling yields the proper magnitude for the giant effect. The frequency, thickness and temperature dependence of the effect are presented. Results obtained with Ni rich Fe-Ni alloy films are also presented. (10 refs.)

62792 Evaluation of magnetostriction constant in amorphous ribbons utilizing the velocity change of a magnetoelastic wave. T.Miyama, T.Fuji, K.Kumozaki, M.Inoue, H.Takahashi (Dept. of Electrical Engng. & Electron., Toyohashi Univ. of Technol., Aichi, Japan).

J. Magn. & Magn. Mater. (Netherlands), vol.35, no.1-3, p.146-8 (March 1983). (Proceedings of the 10th International Colloquium on Magnetic Films and Surfaces, Yokohama, Japan, 13-16 Sept. 1982).

The magnetoelastic coupling constant B , or the saturation magnetostrictive constant λ_s in highly magnetostrictive amorphous ribbons was evaluated indirectly from the change of the sound velocity under application of external field or uniaxial tensile strain by comparing with the theory based upon the one-dimensional elastic beam model. (5 refs.)

62793 Temperature and field dependence of magnetostriction in amorphous thin films. H.Szymczak, R.Zuberek (Inst. of Phys., Polish Acad. of Sci., Warsaw, Poland).

J. Magn. & Magn. Mater. (Netherlands), vol.35, no.1-3, p.149-52 (March 1983). (Proceedings of the 10th International Colloquium on Magnetic Films and Surfaces, Yokohama, Japan, 13-16 Sept. 1982).

The theory of temperature and magnetic field dependence of magnetostriction in amorphous thin films has been developed for the following models: pair-ordering model, random anisotropy model and columnar structure model. Detailed calculations have been performed within the molecular field approximation and spin-wave approximation. (14 refs.)

62794 Study of magnetoelastic waves by optical observation on the surface of magnetic materials. K.Kakuno, D.Inami, Y.Suezawa, Y.Gondo (Dept. of Electrical Engng., Yokohama Nat. Univ., Yokohama, Japan). *J. Magn. & Magn. Mater. (Netherlands)*, vol.35, no.1-3, p.155-7 (March 1983). (Proceedings of the 10th International Colloquium on Magnetic Films and Surfaces, Yokohama, Japan, 13-16 Sept. 1982). The wide band optical observation system of ME waves is developed by the use of a Kerr apparatus as a ME wave detector and a wide band microstrip line as a ME wave exciter. By means of this observation system, the strongly attenuated traveling magnetic waves are observed. (2 refs.)

62795 Propagation properties of magnetoelastic waves in a magnetic slab. M.Inoue, T.Fujii, T.Miyama (Dept. of Electrical Engng. & Electronics, Toyohashi Univ. of Technol., Aichi, Japan). *J. Magn. & Magn. Mater. (Netherlands)*, vol.35, no.1-3, p.158-60 (March 1983). (Proceedings of the 10th International Colloquium on Magnetic Films and Surfaces, Yokohama, Japan, 13-16 Sept. 1982). The theory of a magnetoelastic wave propagating in a magnetic slab with a uniaxial in-plane anisotropy is developed in order to explore the possibility of RF-magnetoacoustic devices. This is regarded as an extension of the theory of the Lamb wave in an elastic slab. Analysis suggests that the magnetoelastic surface wave is advantageous for some applications. (5 refs.)

62796 On the magnetostrictive phenomena in metamagnetism. J.A.Tuszynski, H.Cofta (Dept. of Phys., Univ. of Calgary, Calgary, Canada). *Physica B & C (Netherlands)*, vol.115 B+C, no.2, p.161-71 (Jan. 1983). A semi-classical model of a metamagnet exhibiting nonlinear temperature expansion is presented and analyzed. A direct comparison with the Mn_2GaC compounds as an example displaying such a phenomenon is made. Earlier predictions about the mechanisms involved are generalized and refined. Two distinct cases of the feasible metamagnetic behaviour are found and investigated. Both cases are free of internal contradictions and paradoxes, in contrast to the previous models. The possibilities of applications of this model to other types of magnetic substances are outlined. (36 refs.)

The effect of Fe-Ni films on the insertion loss of SAW See Entry 61372
Comments on reported magneto-oscillations in dislocation drag at low temperatures See Entry 61929

Helical anisotropy induced by annealing in Metglas 2826 See Entry 62583
Magnetoelastic phase transition in $KMnF_3$ See Entry 62592
Magnetostriction and internal stress in GdFe amorphous films with perpendicular anisotropy prepared by RF diode sputtering See Entry 62745

75.90 OTHER TOPICS IN MAGNETIC PROPERTIES AND MATERIALS

Magnetism or bonding: a nearly periodic table of transition elements See Entry 61851

76.00 MAGNETIC RESONANCES AND RELAXATION IN CONDENSED MATTER; MÖSSBAUER EFFECT

(for measurement techniques, see 07.58)

76.30 ELECTRON PARAMAGNETIC RESONANCE AND RELAXATION

62797 The influence of nuclear quadrupole interactions upon electron spin-echo modulation induced by weak hyperfine interactions. A.A.Shubin (Inst. of Catalysis, Novosibirsk, USSR), S.A.Dikanov.

J. Magn. Resonance (USA), vol.52, no.1, p.1-12 (March 1983). The influence of nuclear quadrupole interactions on the electron spin-echo modulation induced by weak hyperfine interaction was analyzed theoretically in terms of the perturbation theory as related to the nuclear Zeeman interaction. The possibility of applying the results obtained to investigation of modulations from different nuclei was assessed. The quadrupole interaction effects in the modulation damping in disordered systems were estimated quantitatively. (16 refs.)

62798 Two-dimensional soliton contribution to the ESR linewidth in layered antiferromagnets? F.Waldner (Phys.-Inst., Univ. of Zurich, Zurich, Switzerland).

J. Magn. & Magn. Mater. (Netherlands), vol.31-34, pt.3, p.1203-4 (Feb. 1983). (Proceedings of the International Conference on Magnetism, Kyoto, Japan, 6-10 Sept. 1982).

In layered two-dimensional (2d) antiferromagnets, Mikeska's theory is applied as an alternate interpretation of the broadening of ESR linewidths ΔH_e above T_N . Although ΔH_e is well described by Mikeska's $\exp(+T_e/T)$, the values $E=kT_e/2$ are unreasonably high for thermal excitation. However, they would agree with the energy of two reversed neighboring spins or with classical dynamic excitations (moving 2d solitons). (10 refs.)

62799 Spin-lattice relaxation in excited triplet states of 4,4'-dichlorobenzophenone crystals in strong magnetic fields at 2K. A.A.Avdenko, S.N.Pakulov.

Opt. & Spectrosc. (USA), vol.53, no.2, p.217-18 (Aug. 1982). Translation of: *Opt. & Spektrosk. (USSR)*, vol.53, no.2, p.367-9 (Aug. 1982). [received: April 1983]

The effect of induction and orientation of an external magnetic field on the electron spin-lattice relaxation (SLR) rate is studied in excited triplet states of X traps of a 4,4'-dichlorobenzophenone (DCB) crystal [the depth of the traps relative to the bottom of the triplet exciton band is 63 cm^{-1} , the zero-phonon emission band is located at $\lambda_{00}=413.54\text{ nm}$]. In the scope of the Debye model of the lattice the cubic dependence of the SLR rates on the magnitude of the magnetic field as well as the anisotropy of these rates in the field are in favor of a direct spin-lattice process occurring with the emission of resonant acoustic phonons. (11 refs.)

A microscopic interpretation of the spin-lattice coupling coefficients for S-state $4f$ ions See Entry 62380

X-ray diffraction and EPR studies of NbGe high T_c films See Entry 62528

76.30D Ions and impurities: general

62800 Spin relaxation and polarization under interaction of photocarriers with charged paramagnetic centers in a semiconductor. V.S.Vikhlin.

Opt. & Spectrosc. (USA), vol.53, no.1, p.110-11 (July 1982). Translation of: *Opt. & Spektrosk. (USSR)*, vol.53, no.1, p.185-6 (July 1982). [received: April 1983]

Discusses the processes of spin polarization (SP) and spin relaxation which are associated with hydrogenlike intermediate states of large radius formed under interaction of photocarriers with charged paramagnetic centers—a charged paramagnetic center+electron (hole)—with significant exchange interaction between the electron (hole) on an orbit of large radius and the paramagnetic core. It is shown that spin-dependent captures into like compound states, and their subsequent decay determine the SP and spin relaxation on charged paramagnetic impurities. The investigation was carried out by a method of kinetic equations. The decay of the Wannier-Mott exciton with the creation of a carrier of opposite sign and the capture of carriers by band-resonant exchange multiplets of the compound state is considered as the mechanism of spin-dependent capture in the compound state along with the cascade mechanism. (5 refs.)

76.30F Iron group (3d) ions and impurities (Ti-Cu)

62801 Detection of a new trigonal bipyramidal copper species in Cu-CaX zeolite by electron spin resonance and electron spin echo modulation analysis. M.Narayana, L.Kevan (Dept. of Chem., Univ. of Houston, Houston, TX, USA).

J. Chem. Phys. (USA), vol.78, no.6, pt.2, p.3573-8 (15 March 1983).

Electron spin resonance and electron spin echo modulation analysis are used to identify the location and coordination of Cu^{2+} in hydrated and dehydrated CaX zeolite. A new, trigonal bipyramidally coordinated Cu^{2+} is found to be the dominant copper center in this zeolite. It is located in a six ring window (site S11) and coordinated to three six ring oxygens and two hydroxyls, one in the α cage and the other in the β cage of the zeolite. This $Cu(O_2)_3(OH)_2$ species is found to be stable for dehydration up to 180°C . At higher temperatures the Cu^{2+} species seems to be reduced irreversibly. However, a Cu^{+} species can be regenerated by oxidation and hydration but most of it is only trigonally coordinated. (37 refs.)

62802 Divalent manganese in an axial symmetry site of additively coloured CaO single crystals. H.S.Murrieta (Inst. de Fisica, Univ. Nacional Autonoma de Mexico, Mexico City, Mexico), J.O.Rubio, M.G.Aguilar, J.Garcia-Sole.

J. Phys. C (GB), vol.16, no.10, p.1945-53 (10 April 1983).

Electron paramagnetic resonance data dealing with the first observation of a Mn^{2+} axial center in CaO are reported. The tetragonal EPR spectrum was found in additively coloured crystals at 100K the best-fit parameters to the spin-Hamiltonian were found to be: $g_{||}=2.0015$ (5), $g_{\perp}=2.0020$ (5), $b_2=+132.6$ (4) $\times 10^{-4}\text{ cm}^{-1}$, $b_4=+3.5$ (3) $\times 10^{-4}\text{ cm}^{-1}$, $b_6=+11.7$ (8) $\times 10^{-4}\text{ cm}^{-1}$, and $A=-67.2$ (5) $\times 10^{-4}\text{ cm}^{-1}$. The hyperfine coupling constant is anomalously small and points towards a considerable covalent bonding. The analysis of the data presented in this paper strongly suggests that the axial spectrum is due to Mn^{2+} ions perturbed by an adjacent F centre. Assuming this model, the reduction in the value of the hyperfine interaction relative to that of the free ion was estimated in terms of the approach of Simanek and Sroubek which puts the main emphasis of such a reduction on the covalent effects of the 4s orbitals of the Mn^{2+} ion and the result compares reasonably well with the experimental determination. (23 refs.)

62803 Electron spin resonance study of a disordered Ni-Mn alloy. H.Hurdequint, J.S.Kouvel, P.Monod (Lab. de Phys. des Solides, Univ. Paris-Sud, Orsay, France).

J. Magn. & Magn. Mater. (Netherlands), vol.31-34, pt.3, p.1429-31 (Feb. 1983). (Proceedings of the International Conference on Magnetism, Kyoto, Japan, 6-10 Sept. 1982).

ESR spectra were obtained for disordered $Ni_{74}Mn_{26}$ cooled to $\approx 4\text{K}$ in zero field and 10 kOe. The resonance observed after field-cooling are asymmetric with the applied field direction up to $\approx 30\text{K}$ and continue to show a macroscopic anisotropic field up to $\approx 80\text{K}$, where a transition occurs from spin-glass to ferromagnetism. (6 refs.)

62804 Electron spin resonance in metallic spin-glasses above T_g . P.M.Levy, C.Morgan-Pond (Dept. of Phys., New York Univ., New York, NY, USA), R.Raghavan.

Phys. Rev. Lett. (USA), vol.50, no.15, p.1160-3 (11 April 1983).

Recent ESR measurements on the spin-glass Mn in the paramagnetic phase reveal an increase in the linewidth over the expected linear temperature dependence for $T/T_g \leq 3$. The Mori-Kawasaki formalism was used to calculate quantitatively the linewidth due to the broadening by the Dzyaloshinsky-Moriya anisotropy interaction of an exchange-narrowed line. With no adjustable parameters the authors explain the increase in linewidth, and they also relate the shift in the resonance to the imaginary part of the frequency-dependent self-energy. (11 refs.)

62805 Determination of the correlation between the crystal field axis system and the crystallographic axes in chromium-doped β -Ga $_2$ O $_3$ by EPR. W.Gunsser, K.Rohwer (Inst. für Phys. Chem., Univ. Hamburg, Hamburg, Germany).

Phys. Status Solidi b (Germany), vol.116, no.1, p.275-8 (1 March 1983).

The correct relationship is found between the crystal field axes and crystallographic axes in β -Ga $_2$ O $_3$ by application of a simplified orientation method. A computer program is set up, which is able to calculate and to plot the angular variation of the resonance field strengths and of the energy levels involved in EPR. In this way, the strange angular dependence of the EPR lines can be explained and the correctness of the stated correlation between the two axis systems can be verified. From the measured resonance fields a set of spin Hamiltonian parameters is calculated. (15 refs.)

62806 EPR experiments on the two-dimensional Heisenberg ferromagnet K_2CuF_6 . I.Yamada, I.Morishita, T.Tokuyama (Dept. of Phys., Chiba Univ., Yayoi-cho, Chiba, Japan).

Physica B & C (Netherlands), vol.115 B+C, no.2, p.179-89 (Jan. 1983).

EPR experiments have been made on the ideal two-dimensional Heisenberg ferromagnet K_2CuF_6 ($T_c=6.25\text{K}$) at 9.3 and 23.5 GHz over the temperature range of 4.2-300K. Below about 100K, where the ferromagnetic short range order grows, several features due to the high-temperature diffusion relaxation of the time correlation functions of spins are found to become more and more distinctive as the temperature decreases to T_c : (i) The linewidth ΔH increases rapidly keeping an $[a(3\cos^2\theta-1)^2+b]$ -like angular anisotropy (θ is the angle between the c axis and the external field); the anisotropy $\delta H(\theta=0^\circ)/\Delta H(\theta=90^\circ)$ increases and eventually it reaches the value 4, which is the ratio between the values of $(3\cos^2\theta-1)^2$ at $\theta=0^\circ$ and $\theta=90^\circ$. (ii) The

line shape at $\theta=0^\circ$ departs remarkably from Lorentzian. (iii) The first order satellite absorption line ($2\omega_0$ -line) increases its intensity. (iv) The second order satellite ($3\omega_0$ -line) becomes observable near T_c . These phenomena reflect the increasing importance of long-wavelength ferromagnetic fluctuations of spins with decreasing temperature. (34 refs.)

62807 Spin-lattice relaxation of Cr^{3+} in ZnS . V.Ya.Bratus', A.A.Bugai, M.F.Bulanyi, B.D.Shanina (Inst. of Semiconductors, Acad. of Sci., Kiev, Ukrainian SSR). *Sov. Phys.-Solid State (USA)*, vol.24, no.9, p.1501-4 (Sept. 1982). Translation of: *Fiz. Tverd. Tela (USSR)*, vol.24, no.9, p.2648-54 (Sept. 1982). [received: April 1983]

The spin-lattice relaxation of Cr^{3+} in single crystals of cubic ZnS containing packing defects is investigated at 9.3 GHz. The recovery of various ESR lines after inversion is studied in the range of direct relaxation processes. The ratio of the probabilities of spin-phonon transitions with selection rules $\Delta M_s = \pm 1$ and $\Delta M_s = \pm 2$ is determined; it agrees with the values of the static coefficients $G_{11} = -0.054 \text{ cm}^{-1}$ and $G_{44} = 0.21 \text{ cm}^{-1}$. This ratio is observed to be dependent on angle, due to anisotropy of the spin-phonon interaction. In the temperature range 1.55-300K the relaxation rate τ_1^{-1} may be described by the expression $\tau_1^{-1} \text{ sec}^{-1} = 2.17 + 1.8 \times 10^{-8} T^7 J_6 (\phi/T)$, where $\phi = 144\text{K}$ and corresponds to the first peak of the phonon density of the ZnS crystal, which is associated with transverse acoustic modes. It is shown that for $T > 7\text{K}$ the observed relaxation rates are due to an anharmonic Raman process. (18 refs.)

Variational approach to the Jahn-Teller problem in cobaltocene See Entry 62382

Semiconducting properties of V_2O_5 gels See Entry 62416

Experiments on randomly mixed magnets with competing interactions See Entry 62574

Spin dynamics of an insulating spin-glass $\text{Rb}_2\text{Mn}_{1-x}\text{Cr}_x\text{Cl}_4$ at the microwave region See Entry 62631

Study of electronic structure of reduced TiO_2 and $\text{V}_x\text{Ti}_{1-x}\text{O}_2$ crystals by ESCA and optical absorption See Entry 63018

Stereochemical rearrangements of complexes in liquid crystals See Entry 63544

Investigation of precipitated alumina structures by secondary-ion mass spectrometry and electron paramagnetic resonance spectrometry. III. Structure of an alumina coating precipitated on rutile titanium dioxide See Entry 63592

76.30K Rare-earth ions and impurities

62808 Theoretical analysis of ESR measurements in $(\text{Gd}_x\text{Y}_{1-x})\text{Cu}$. E.Zipser (Inst. of Phys., Silesian Univ., Katowice, Poland). *J. Magn. & Magn. Mater. (Netherlands)*, vol.36, no.1-2, p.165-70 (1 April 1983).

A theoretical analysis of ESR measurements in $(\text{Gd}_x\text{Y}_{1-x})\text{Cu}$ [$x \in (0,1)$] which explains consistently the observed positive g shifts in unbottlenecked region and negative g shifts in bottlenecked region is performed. The concentration dependent density of states and the coherent scattering of the electrons by the impurities are taken into account. The theoretical calculations are in good agreement with experimental data. (17 refs.)

76.30M Colour centres and other defects

Defect states in amorphous silicon See Entry 61804

Electrical and optical properties of $\text{a-Si}_x\text{C}_{1-x}\text{H}$ film prepared by GD SiH_4 and C_2H_4 See Entry 63065

76.30R Free radicals

Electron spin resonance spectra of tetrafluoroethylene radical cation See Entry 63568

76.40 DIAMAGNETIC AND CYCLOTRON RESONANCES

Direct observation of impact ionisation and hot electron effects in GaAs See Entry 62420

76.50 FERROMAGNETIC, ANTIFERROMAGNETIC, AND FERRIMAGNETIC RESONANCES; SPIN WAVE RESONANCE

(see also 75.30D Spin waves)

62809 Two-magnon scattering in iron-rich metallic glasses. B.Heinrich, K.Myrtle, J.M.Rudd, J.F.Cochran (Dept. of Phys., Simon Fraser Univ., Burnaby, BC, Canada), R.Hasegawa. *J. Magn. & Magn. Mater. (Netherlands)*, vol.31-34, pt.3, p.1597-8 (Feb. 1983). (Proceedings of the International Conference on Magnetism, Kyoto, Japan, 6-10 Sept. 1982).

The FMR absorption linewidth has been measured at 9, 24, 39 and 73 GHz in $\text{Fe}_{81}\text{B}_{13}\text{Si}_3\text{C}_2$ and $\text{Fe}_{80}\text{B}_{13}\text{Si}_3\text{C}_2$ for the temperature range 20 to 350°C. The results can be interpreted as a consequence of the combined contributions from Landau-Lifshitz intrinsic damping, two-magnon scattering and thermally activated surface recrystallization. (3 refs.)

62810 FMR line intensity and width in garnet ferrite films. A.M.Zyuzin, V.V.Randoshkin, R.V.Telesin (Lomonosov State Univ., Moscow, USSR). *Sov. Phys.-Tech. Phys. (USA)*, vol.27, no.9, p.1166-7 (Sept. 1982). Translation of: *Zh. Tekh. Fiz. (USSR)*, vol.52, no.9, p.1896-8 (Sept. 1982). [received: April 1983]

A method suitable for measurements in materials bearing submicron cylindrical magnetic domains (CMD) is that of ferromagnetic resonance (FMR). When this is used one is usually interested in the resonance relations and the width of the FMR line, which enables one to determine the value of $H_K 4\pi M_s$ (H_K is the uniaxial anisotropy field and $4\pi M_s$ is the saturation magnetization), the gyromagnetic ratio γ , and the damping parameter α . It is shown that additional information can be obtained by measuring the absorption-line intensity. (4 refs.)

62811 Effect of a semiconductor substrate on the ferromagnetic resonance in a thin cobalt film. M.V.Belous, M.G.Lysenko, Yu.N.Rudoi (Fiftieth Anniversary of Great October Socialist Revolution Polytech. Inst., Kiev, Ukrainian SSR).

Sov. Tech. Phys. Lett. (USA), vol.8, no.8, p.402-3 (Aug. 1982). Translation of: *Pis'ma v Zh. Tekh. Fiz. (USSR)*, vol.8, no.15-16, p.927-9 (Aug. 1982). [received: April 1983]

Studies the effect of Si on the ferromagnetic resonance of a thin Co film. As the diffusing electrons play an important role in the appearance of ferromagnetic order, the diffusion into the semiconductor changes the macroscopic characteristics of the ferromagnet near the interface, and this influences the FMR line shape. (3 refs.)

Structure and magnetism of insoluble Pb-Fe alloy films See Entry 62294

Spin orientation and exchange interactions in $(\text{Fe},\text{Co})\text{Cl}_2$ See Entry 62575

FMR and magnetic studies in amorphous Co-Nb films See Entry 62727

Perpendicular magnetic anisotropy and ferromagnetic resonance in amorphous Gd-Co and Gd-Fe films See Entry 62750

Investigations of implantation-induced changes in surface layers of epitaxial garnet thin films See Entry 62755

Comparison of the magnetic properties of one- and two-layer iron garnet films See Entry 62781

Spin echo of ^{59}Co and ^{63}Cu impurity nuclei in single-crystal iron films in the case of coincidence of nuclear magnetic and ferromagnetic resonance frequencies See Entry 62833

Ion beam sputter deposition of layered magnetic thin films See Entry 63157

76.60 NUCLEAR MAGNETIC RESONANCE AND RELAXATION

62812 Investigation of the NMR enhancement factor in CuMn spin glasses. Ch.Schlosser, H.Bromer (Inst. für Metallphys. und Nukleare Festkörperphys., Tech. Univ. Braunschweig, Braunschweig, Germany). *Z. Phys. B (Germany)*, vol.50, no.3, p.247-54 (1983).

The NMR enhancement factor of a frozen CuMn spin glass has been measured at a temperature $T \approx T_g/5$. The measurements were performed as function of static magnetic fields of different directions. A two component model of a spin glass has been outlined. One component being a 'system of single spins' and the other one being a 'subsystem of clusters'. Both components were attributed to different kinds of interaction being RKKY and dipole interaction respectively. The effective anisotropy field of the single spin system consists of two unidirectional contributions H_A^z and H_A^x , which have been measured for different conditions. A second anisotropy field H_d binds the cluster system to the system of single spins. All anisotropy fields depend on the annealing temperature of the alloys. (16 refs.)

62813 Phosphorus NMR study of solid amorphous calcium phosphate. J.Tropp (Dept. of Chem., MIT, Cambridge, MA, USA), N.C.Blumenthal, J.S.Waugh.

J. Am. Chem. Soc. (USA), vol.105, no.1, p.22-6 (12 Jan. 1983). The authors have characterized solid synthetic amorphous calcium phosphate (ACP) by ^{31}P NMR, using magnetic angle spinning, proton enhancement via cross polarization, and variable temperature. With π cross polarization, the spinning sidebands of ACP are stronger than those of unprotonated phosphate in hydroxylapatite, but weaker than those of dibasic calcium phosphates. Cross polarization over a wide range of mixing times causes no change in the appearance of ACP spectra from 25 to -120°C . In contrast, mixtures of hydroxylapatite with dibasic calcium phosphates, which, without cross polarization mimic the appearance of ACP spectra, show large differential enhancements of sideband intensities when cross polarized. Octacalcium phosphate behaves similarly to the mixtures. Vacuum drying of ACP at 450°C removes tightly bound water. The sidebands of dried ACP are undiminished, but no cross polarization signal can be obtained. Similar drying of hydroxylapatite effects neither the sideband intensities nor the cross polarization. They conclude that the strength of ACP sidebands is due to a characteristic structural distortion of unprotonated phosphate and not to a mixture of protonated and unprotonated phosphates. Structural models of ACP and the implications for ^{31}P NMR studies of bone mineral are briefly discussed. (18 refs.)

62814 Multiple-quantum NMR in solids. Yu-Sze Yen, A.Pines (Dept. of Chem., Univ. of California, Berkeley, CA, USA).

J. Chem. Phys. (USA), vol.78, no.6, pt.2, p.3579-82 (15 March 1983). Multiple-quantum NMR has typically been observed in small groups of spins in isolated molecules. Due to the profusion of spin transitions in a solid, individual lines are unresolved. Excitation of high quantum transitions by normal schemes is thus difficult. To ensure that overlapping lines add constructively and to enhance sensitivity, time-reversal pulse sequences are used to generate all lines in phase. Up to 22-quantum ^1H absorption in solid adamantane is observed. (14 refs.)

62815 Nuclear magnetic resonance of ^{89}Y in intermetallic compounds $\text{Y}(\text{Fe}_{1-x}\text{Mn}_x)_2$. H.Nagai, H.Yoshie, A.Tsujimura (Dept. of Phys., Shinshu Univ., Matsumoto, Japan).

J. Phys. Soc. Jpn. (Japan), vol.52, no.4, p.1122-3 (April 1983). The NMR spectra of ^{89}Y have been observed at 4.2K to investigate the magnetic properties of $\text{Y}(\text{Fe}_{1-x}\text{Mn}_x)_2$. There are two kinds of Mn moments in low Mn-concentrations; one is antiparallel to the Fe moment and estimated to be $0.5 \mu_B$ per Mn (low spin state), and the other is parallel to the Fe moment and has $2.7 \mu_B$ per Mn (high spin state). (9 refs.)

62816 Enhanced NMR of ^{169}Tm in TmAsO_4 . B.Bleaney, J.F.Gregg, M.J.M.Leask, M.R.Wells (Clarendon Lab., Univ. of Oxford, Oxford, England).

J. Magn. & Magn. Mater. (Netherlands), vol.31-34, pt.3, p.1061-2 (Feb. 1983). (Proceedings of the International Conference on Magnetism, Kyoto, Japan, 6-10 Sept. 1982).

TmAsO_4 has doublet ground state which is split by a co-operative Jahn-Teller distortion below $T_D = 6.13\text{K}$. Optical absorption spectroscopy, magnetic susceptibility and enhanced NMR of $^{169}\text{Tm}(I=1/2)$ have been used to measure precisely the parameters g , B_0 and Δ_0 ; overall the results agree well with the predictions of mean field theory. (8 refs.)

62817 NMR in metallic glasses. J.Durand, P.Panissod (LMSES, Strasbourg, France).

J. Magn. & Magn. Mater. (Netherlands), vol.31-34, pt.3, p.1567-70 (Feb. 1983). (Proceedings of the International Conference on Magnetism, Kyoto, Japan, 6-10 Sept. 1982).

NMR measurements can yield some insight into the electronic structure of metallic glasses through the Korringa ratio in nonmagnetic alloys and through the mean value of the hyperfine field in amorphous ferromagnets. Some information on the local symmetry around a given nuclear site is provided by

analysis of the quadrupolar NMR spectra. Spin echo NMR spectra in amorphous ferromagnet exhibit structures whose origin is discussed for each family of alloy. These structures originate either from quadrupolar interactions, or from different magnetic states of the resonant species, or from well-defined regions of different local environments with different domain wall regions. (40 refs.)

62818 Local lattice expansion of Cu arising from dilute interstitial impurities, β -emitting nuclei ^{12}B and ^{12}N . T.Minamisano, Y.Nojiri, K.Matsuda (Faculty of Sci., Osaka Univ., Osaka, Japan). *Phys. Lett. A (Netherlands)*, vol.94A, no.6-7, p.312-16 (21 March 1983). Lattice expansions of Cu in the nearest octahedral surroundings of interstitial ^{12}N were determined to be $\Delta r/r = 0.11 \pm 0.02$ and 0.13 ± 0.06 respectively using NMR detection. The results are informative to the study of the hyperfine interactions of the impurities in ferromagnetic Ni. (10 refs.)

62819 NMR-induced recombination of spin-polarized hydrogen. B.Yurke, J.S.Denker, B.R.Johnson, N.Bigelow, L.P.Levy, D.M.Lee, J.H.Freed (Lab. of Atomic & Solid State Phys., Cornell Univ., Ithaca, NY, USA). *Phys. Rev. Lett. (USA)*, vol.50, no.15, p.1137-40 (11 April 1983). The presence of an inverted population of H \uparrow with very high electronic and nuclear spin polarization is confirmed with a new barometric-NMR method and by free-induction decay. With this new technique, the temperature dependence for the ratio of the two state-dependent recombination rate constants is measured. The rate of spin relaxation in the gas agrees with the latest theory, but relaxation on the surface is much faster than predicted, and there is an important surface one-body relaxation process. (12 refs.)

62820 Distribution of double bonds in thermally degraded polyisobutylene. [PMR observations]. T.Kuroki, T.Sawaguchi, K.Suzuki, S.Ide, T.Ikemura (Dept. of Industrial Chem., Coll. of Sci. & Technol., Nihon Univ., Tokyo, Japan).

Polymer (GB), vol.24, no.4, p.428-32 (April 1983). The distribution of double bonds in thermally degraded polyisobutylene was determined quantitatively by using pulsed Fourier transform ^1H NMR, spectroscopic analysis. The double bonds in the degraded polymer did not exist in the interior but at the terminal positions of the polymer chain. These olefins were of the terminal trisubstituted and terminal vinylidene types. The content of the former was much greater than that of the latter. This shows that radical chain transfer predominantly occurs at the methylene hydrogen rather than at the methyl groups of the polymer chain. The average number of double bonds per molecule, f , was greater than 1 and tended to be near 2. (15 refs.)

62821 NMR of mixed crystals $(\text{CH}_3\text{NH}_3)_x\text{Cu}(\text{Cl}_{1-x}\text{Br}_x)_4$ ($0 \leq x \leq 1$). II. Distribution of Cl and Br. Y.Suzuki, H.Kubo, K.Hirakawa. *Technol. Rep. Kyushu Univ. (Japan)*, vol.55, no.4, p.351-6 (Aug. 1982). In Japanese. [received: Feb. 1983] NMR measurements of Cu and Cl nuclei are carried out in the magnetically ordered state on the single crystals grown slowly in aqueous solutions. NMR lines are distinguished by n of the complex $(\text{CuCl}_{4-n}\text{Br}_n)$ ($n=0,1,2,3,4$). By comparing the relative intensities of the lines, the rates of the complexes $(\text{CuCl}_{4-n}\text{Br}_n)$ with different n can be determined. The rate of CuCl_2Br_2 is very large. It is also clarified that the ratio of NMR intensities of Cl nuclei on the c -axis to the c -plane becomes small with the increase of x . It is concluded that the Br ions preferentially occupy the positions on the c -axis. (4 refs.)

Superconductivity in ternary compounds. II. Superconductivity and magnetism See Entry 59553

Random walk to and interaction with an impurity See Entry 59703

Proton chemical shifts in polycrystalline solids determined by off-resonance decoupling ^{13}C CP-MAS NMR See Entry 59809

Practice of multidimensional stochastic NMR spectroscopy. The derivation of 1D, 2D, and 3D spectra See Entry 59810

Potassium fluoride and phosphorous acid: ab initio calculations and spectroscopic investigations See Entry 60585

Electronic structure of molecules and infrared continua caused by intramolecular hydrogen bonds with great proton polarizability See Entry 61017

Hydrogen incorporation scheme in amorphous-microcrystalline mixed-phase Si:H films See Entry 62286

NMR observation of oblique phase in mixed crystals $(\text{CH}_3\text{NH}_3)_x\text{Cu}(\text{Cl}_{1-x}\text{Br}_x)_4$ ($0.5 \leq x \leq 1$) See Entry 62606

Selective scattering of electromagnetic radiation in radio-frequency resonance conditions See Entry 62867

Nature of the phase transition in $\text{K}_{1-x}\text{TaO}_3$ See Entry 62901

76.60C Chemical and Knight shifts

Excited states of mixed-ligand chelate complexes of ruthenium(II). A re-examination of the evidence for strong interligand coupling See Entry 60756

76.60E Relaxation effects

62822 NMR study of deuterium molybdenum bronze. C.Marinos, S.Plesko, J.Jonas (Materials Res. Lab., Univ. of Illinois, Urbana, IL, USA), D.Tinet, J.J.Fripiat. *Chem. Phys. Lett. (Netherlands)*, vol.96, no.3, p.357-60 (8 April 1983).

The deuterium NMR lineshape and spin-lattice relaxation time, T_1 , have been measured in deuterium molybdenum bronze, $\text{D}_{16}\text{MoO}_3$, over the temperature range 166-400K. The ^2D quadrupole coupling constant is 21 kHz at room temperature. The temperature dependence of the ^2D T_1 has been interpreted in terms of two independent motional processes for deuterium. The data suggest that one of the processes corresponds to diffusion of the ^2D nuclei whereas the other may arise from a 180° flipping of the OD_2 moieties. This specific interpretation agrees with the results obtained for proton T_1 and proton lineshape data reported earlier. (15 refs.)

62823 Spin-spin and spin-lattice contributions to the rotating frame relaxation of ^{13}C in L-alanine. K.Akasaka, S.Ganapathy, C.A.McDowell, A.Naito (Dept. of Chem., Univ. of British Columbia, Vancouver, British Columbia, Canada). *J. Chem. Phys. (USA)*, vol.78, no.6, pt.2, p.3567-72 (15 March 1983).

The spin-lattice relaxation times in both the Zeeman (T_1^Z) and rotating (T_1^R) frames were determined for three chemically distinct carbon atoms (^{13}C) in polycrystalline L-alanine by combining cross polarization and magic angle spinning techniques together with proton decoupling. The spin-lattice and spin-spin contributions to the experimentally measured T_1^R could be separated by an experiment in which the ^{13}C spin-locking field was varied. The spin-lattice contributions (T_1^R), which contain motional information, were determined to be 21.7, 23.4, and 138 ms for the C_α , CH_3 , and COO^-

carbons, respectively. The spin-spin contribution (T_{CH}^D) was found to be exponential, namely, $(T_{CH}^D)^{-1} \propto \exp(-2\pi\nu_{CH}^D)$ in the low ^{13}C spin-locking field. Therefore, the assumption of a Lorentzian correlation function for the proton dipolar fluctuations is adequate for L-alanine. Furthermore, the proton dipolar correlation times τ_D were found to be the same (31 ± 1 μs) for all three carbons in L-alanine. The spin-lattice relaxation times in the Zeeman frame T_1^Z were determined to be 4.0 s, 38 ms, and 13 s for the C_α , CH_3 , and COO^- carbons, respectively. The experimental values of T_1^R and T_1^Z can be explained quantitatively by considering the internal rotations of the methyl and amino groups. (25 refs.)

62824 Nuclear magnetic relaxation study of fully deuterated sulfolan. H.Peemoller, A.R.Sharp (Dept. of Phys., Univ. of New Brunswick, Fredericton, New Brunswick, Canada), A.Watson, D.W.Kydon. *J. Chem. Phys. (USA)*, vol.78, no.7, p.4337-9 (1 April 1983).

Molecular motions of the fully deuterated sulfolan molecule ($\text{C}_4\text{D}_8\text{O}_2\text{S}$) have been studied in the solid state by NMR measurements of the deuteron spin-lattice relaxation times in the laboratory (T_1) and rotating ($T_{1\rho}$) frame. In the crystalline phase, it has been found that the relaxation is determined by the ring puckering motion of the molecule. The plastic crystal phase is found to exhibit effects from both isotropic reorientation and translational diffusion. The modified nature of this phase and the plastic-crystalline transition of the deuterated as compared to the undeuterated solid is discussed in terms of the C-H-O hydrogen bonding between molecules. (14 refs.)

62825 Pressure dependence of ^{19}F spin relaxation in $(\text{NH}_4)_2\text{SiF}_6$. M.Mackowiak, R.J.C.Brown (Dept. of Chem., Queen's Univ., Kingston, Ontario, Canada).

J. Magn. Resonance (USA), vol.52, no.1, p.71-5 (March 1983). The ^{19}F NMR spin-lattice relaxation time in the rotating frame, $T_{1\rho}$, was measured as a function of pressure and temperature for polycrystalline cubic $(\text{NH}_4)_2\text{SiF}_6$ for pressures up to 230 MPa. The $T_{1\rho}$ data were analyzed in terms of the molecular reorientation of the SiF_6^{2-} ions. The reorientational activation volume was $(12.4 \pm 0.2) \text{ cm}^3 \text{ mol}^{-1}$, which is 13.9% of the molar volume. (11 refs.)

62826 Evidence for magnetic soliton in CsNiF_3 : nuclear magnetic relaxation studies. T.Goto (Coll. of Liberal Arts, Kyoto Univ., Kyoto, Japan), Y.Yamaguchi.

J. Magn. & Magn. Mater. (Netherlands), vol.31-34, pt.3, p.1211-12 (Feb. 1983). (Proceedings of the International Conference on Magnetism, Kyoto, Japan, 6-10 Sept. 1982).

The spin-lattice relaxation times of ^{133}Cs in CsNiF_3 were measured with moderate fields applied in the easy plane. The data at relatively low fields and high temperatures, which exhibited deviations from exact calculations for the three-magnon process, were in reasonable agreement with the predictions of the soliton model. (6 refs.)

62827 Strongly entangled polymer chains in a melt. Description of NMR properties associated with a submolecule model. J.P.Cohen-Addad, R.Dupeyre (Lab. de Spectrometrie Phys., Univ. Sci. et Medicale de Grenoble, Grenoble, France).

Polymer (GB), vol.24, no.4, p.400-8 (April 1983). A model is proposed to illustrate properties of the transverse magnetic relaxation function, $G(t)$, of proton pairs linked to strongly entangled polymer chains in a melt. According to this model, any polymer molecule is described as a freely jointed chain and it is divided into submolecules of equal contour length L_c . Every link is supposed to carry a proton pair; dipolar spin couplings between different proton pairs are neglected. The disentanglement relaxation time is supposed to be much longer than any characteristic time of the spin system; consequently, any submolecule observed on an NMR time scale is supposed to have fixed ends. It is considered that the residual spin-coupling energy resulting from such a constraint governs the magnetic relaxation process. The free induction decay is expressed as a contour length function. Theoretical results are compared with magnetic relaxation process. The free induction decay is expressed as a contour length function. Theoretical results are compared with magnetic relaxation properties observed on entangled real chains: polydimethylsiloxane and cis-1,4-polybutadiene. (34 refs.)

62828 Molecular rotation in ideal mixed systems: benzene-neopentane. I. Test of a hydrodynamic model of motion. K.-L.Oehme, G.Rudakoff (Sektion Chemie, Friedrich Schiller Univ., Jena, Germany). *Wiss. Z. Friedrich-Schiller-Universität Jena, Math. Naturwiss. Reihe (Germany)*, vol.31, no.6, p.1085-92 (1982). In German.

A nuclear relaxation study (^2D - T_1) of neopentane- d_{12} dissolved in benzene, tetramethylsilane, and tetramethyltin is presented. The data are given as a function of viscosity. They are interpreted with the framework of the hydrodynamic 'slip' model. The boundary conditions necessary for the solution of the Navier-Stokes equation are sensitivity to a change in the chemical surroundings. Both rotational and translational motion are described by the same hydrodynamic parameters. (21 refs.)

Effect of magnetic and nonmagnetic impurities on the soliton dynamics in $(\text{CD}_3)_4\text{NMnCl}_3$ See Entry 62570

Influence of defects on NQR relaxation processes in $\text{Bi}_{12}\text{GeO}_{20}$ and $\text{Bi}_{12}\text{SiO}_{20}$ See Entry 62831

76.60G Quadrupole resonance

62829 ^{87}Rb and ^{85}Rb NQR study of phase transitions in $\text{RbH}_2(\text{SeO}_3)_2$. J.Seliger, V.Zagar, R.Bline (J. Stefan Inst., E. Kardelj Univ. of Ljubljana, Ljubljana, Yugoslavia), L.A.Shuvalov. *J. Phys. (France)*, vol.44, no.4, p.521-4 (April 1983).

The temperature dependence of the nuclear quadrupole resonance spectra of ^{87}Rb and ^{85}Rb in $\text{RbH}_2(\text{SeO}_3)_2$ has been measured by a proton-Rb double resonance technique in the laboratory frame. The increase in the number of chemically non-equivalent sites from one to four and the observed temperature dependence of the quadrupole coupling constants and the asymmetry parameters on going into the ferroelectric phase agrees with the proposed soft mode motion involving rotations of one type of SeO_3 groups. The existence of an intermediate incommensurate phase between T_c and $T_c + 4\text{K}$ has been confirmed. (22 refs.)

62830 Theory of coherent quasi-steady states in NQR multipulse experiments. V.L.Ermakov, D.Ya.Osokin (Physico-Tech. Inst., Acad. of Sci., Kazan, USSR). *Phys. Status Solidi b (Germany)*, vol.116, no.1, p.239-48 (1 March 1983).

On the basis of the average Hamiltonian theory the influence of the pulse sequence $\omega_{(1)}^0 - (\tau - \tau_{(2)}^0) \omega_{(2)}^0 - 2\tau - \tau_{(2)}^0 - \tau_{(1)}^0$ on a system of two dipolar coupled equivalent spin-1/2 nuclei each subject to local electric field gradients is studied. Using a fictitious spin-1/2 formalism a general method is developed for solving the Liouville equation for such spin systems, leading to results which reproduce the experimentally observed quasi-steady state of magnetization in nitrogen-14 pulse experiments. Expressions for the density matrix of

the system in terms of the effective time $\pi 4\tau$ and the parameters characterizing the quadrupolar and dipolar interactions are obtained. (9 refs.)

62831 Influence of defects on NQR relaxation processes in Bi_2GeO_5 and $\text{Bi}_{12}\text{SiO}_{20}$. A.Yu.Kudzin, S.M.Ryabchenko, A.D.Skorbin (Inst. of Phys., Acad. of Sci., Kiev, Ukrainian SSR). *Sov. Phys.-Solid State (USA)*, vol.24, no.9, p.1483-7 (Sept. 1982). Translation of: *Fiz. Tverd. Tela (USSR)*, vol.24, no.9, p.2618-25 (Sept. 1982). [received: April 1983]

In order to explain the observed anomalies in the functions $T_1(T)$ and $T_2(T)$ in NQR in Bi_2GeO_5 and $\text{Bi}_{12}\text{SiO}_{20}$, a mechanism is proposed that averages the inhomogeneous contributions to the line broadening as a result of the motion of the defects causing this broadening. It is suggested that there are several mechanisms of inhomogeneous broadening, the principal one being static. Agreement between theory and experiment is achieved. (7 refs.)

62832 Chlorine-35 nuclear quadrupole resonance of o-chloronitrobenzenes. I.A.Kyuntsel', G.B.Soffer, M.O.Loizinski (Perm State Univ., Perm, USSR). *Theor. & Exp. Chem. (USA)*, vol.18, no.2, p.213-15 (March-April 1982). Translation of: *Teor. & Eksp. Khim. (USSR)*, vol.18, no.2, p.246-9 (March-April 1982). [received: Feb. 1983]

The authors used ^{35}Cl NQR to determine the position of the NO_2 group with respect to the aromatic ring in crystals of ortho-chloronitrobenzenes. (14 refs.)

^{14}N and ^{35}Cl double resonance study of the phase transition in the intercalated bilayer compound $\text{C}_{10}\text{H}_{21}\text{NH}_3\text{Cl}$ See Entry 62836

76.60L Spin echoes

62833 Spin echo of ^{59}Co and ^{63}Cu impurity nuclei in single-crystal iron films in the case of coincidence of nuclear magnetic and ferromagnetic resonance frequencies. E.S.Mushailov, N.V.Baksheev (L.V. Kirenski Inst. of Phys., Acad. of Sci., Krasnoyarsk, USSR).

Fiz. Met. & Metalloved. (USSR), vol.55, no.2, p.253-8 (Feb. 1983). In Russian. English translation in: *Phys. Met. & Metallogr. (GB)*

Characteristics of the formation of a spin echo in an electron-nuclear system containing ^{59}Co and ^{63}Cu impurity nuclei in a single-crystal iron matrix were investigated by the simultaneous excitation of NMR and FMR. It was found that the echo signal intensity was a function of the nature of the effective fields H_i at the nuclei. In the case of a strong ferromagnetic coupling between the impurity and the matrix, the electron spin system determined the amplification of the RF pulse and the enhancement of the response of the nuclear system under resonance excitation conditions. In the case of a weak coupling (Cu atoms in the iron matrix) the situation was typical of the mechanism of formation of an echo signal in paramagnets and diamagnets subjected to strong RF fields. (15 refs.) A.T.

76.70 MAGNETIC DOUBLE RESONANCES AND CROSS EFFECTS

76.70D Electron-nuclear double resonance (ENDOR)

62834 ENDOR study of bis(acetylacetonato)copper(II) in solid solution. B.Kirste, H.van Willigen (Dept. of Chem., Univ. of Massachusetts, Boston, MA, USA).

J. Phys. Chem. (USA), vol.87, no.5, p.781-8 (3 March 1983).

The bis(acetylacetonato)copper(II) ($\text{Cu}(\text{acac})_2$) complex and its adducts with methanol and pyridine in frozen solution have been studied by using ENDOR and electron-nuclear-nuclear triple resonance (TRIPLE). The ENDOR spectra yield the values of the principal components of the hyperfine tensors of the CH and CH_3 protons. Signs of the hyperfine components were determined with the aid of TRIPLE and computer simulations. Measurements of quadrupole splittings in ^2H ENDOR spectra of $\text{Cu}(\text{acac}-3-d)_2$ oriented in a frozen liquid crystal allowed the assignment of the in-plane CH couplings to specific molecular axes and also provided information on the alignment of the molecule in the nematic phase. (33 refs.)

76.70F Double nuclear magnetic resonance (DNMR)

62835 ^{13}C NMR investigations of the ferroelectric phase transition of tris-sarcosine calcium chloride. D.Michel, F.Engelke (Sektion Phys., Karl-Marx-Univ. Leipzig, Leipzig, Germany).

Chem. Phys. Lett. (Netherlands), vol.96, no.3, p.361-5 (8 April 1983).

^{13}C NMR spectra were measured for tris-sarcosine calcium chloride (TSSC) crystals in the paraelectric phase (at temperatures of ≈ 300 and 150K) and in the ferroelectric phase (at temperatures of 119K) by double-resonance techniques with proton decoupling. The ferroelastic single crystals were rotated around their three crystallographic axes to derive the tensors of magnetic shielding for the different carboxylic carbon atoms. There is no change of the eigenvalues and eigenvectors of the tensors at the phase transition. The results are consistent with the interpretation of former EPR data. (13 refs.)

62836 ^{14}N and ^{35}Cl double resonance study of the phase transition in the intercalated bilayer compound $\text{C}_{10}\text{H}_{21}\text{NH}_3\text{Cl}$. J.Seliger, V.Zagar, R.Blinc (J. Stefan Inst., E. Kardelj Univ. of Ljubljana, Ljubljana, Yugoslavia), H.Arend, G.Chapuis.

J. Chem. Phys. (USA), vol.78, no.5, p.2661-4 (1 March 1983).

The pure nuclear quadrupole (NQR) spectra of ^{14}N , ^{35}Cl , and ^{37}Cl have been measured in $\text{C}_{10}\text{H}_{21}\text{NH}_3\text{Cl}$ as a function of temperature. The chlorine NQR frequency $\nu_Q(\text{Cl}) = 1215\text{ kHz}$ at 47°C is determined by the N-H...Cl hydrogen bonds and is the lowest reported so far. The ^{14}N quadrupole coupling data $e^2qQ/h = 760\text{ kHz}$, $\eta = 0$ shows that the C-N-H-Cl backbone is practically rigid at this temperature. Above 53°C the effects of the phase transition from an intercalated to a nonintercalated structure show up in the N-H...Cl backbone as a sharp drop of the NQR frequencies to $\sim 60\%$ of their rigid lattice values. A model accounting for this effect has been proposed. (10 refs.)

ORAND—a new NMR double resonance technique for obtaining symmetrically intense multiplets by off-resonance experiments See Entry 59806

76.70H Optical double magnetic resonance (ODMR)

62837 Optically detected magnetic resonance in amorphous semiconductors. K.Morigaki (Inst. for Solid State Phys., Univ. of Tokyo, Tokyo, Japan).

Jpn. J. Appl. Phys. Part 1 (Japan), vol.22, no.3, p.375-88 (March 1983).

The principle of optically detected magnetic resonance (ODMR) is briefly described, bearing in mind its application to amorphous semiconductors. The

ODMR measurements including those which are time-resolved are reviewed on amorphous semiconductors, particularly on hydrogenated amorphous silicon (a-Si:H). The nature of the recombination centres in a-Si:H is also discussed.

62838 Magnetic resonance on localized excited triplet states in 1,4-dibromonaphthalene [one-dimensional conductor]. Ch.H.L.Weytens, J.M.J.Vankan, V.S.Veeman (Dept. of Phys. Chem., Univ. of Nijmegen, Nijmegen, Netherlands).

Spectrosc. Lett. (USA), vol.15, no.12, p.953-62 (1982).

Kinetic parameters of localized excited triplet states in 1,4-dibromonaphthalene have been determined from ODMR and MDP experiments. The results show that no Boltzmann equilibrium exists over the triplet exciton sublevels at the moment of trapping. These experiments are in agreement with previously reported findings, that in 1,4-dibromonaphthalene excitons exist with a very short lifetime. (10 refs.)

76.80 MÖSSBAUER EFFECT; OTHER GAMMA-RAY SPECTROSCOPY

62839 Determination of hyperfine interaction parameters from poorly resolved Mossbauer spectra with the transmission integral. D.Gryffroy, R.E.Vandenberghe (Lab. of Magnetism, Gent State Univ., Gent, Belgium). *Nucl. Instrum. & Methods Phys. Res. (Netherlands)*, vol.207, no.3, p.455-8 (1 April 1983).

For badly resolved Mossbauer spectra of ^{61}Ni and ^{121}Sb it is demonstrated that even for moderate thickness the analysis with a sum of Lorentzians instead of the complete transmission integral may introduce significant deviations in determining hyperfine interaction constants. Graphs with the relative deviations for purely magnetic and quadrupolar interactions are shown. From these plots it is indicated when the use of the complete transmission integral is recommended. (9 refs.)

62840 Mossbauer spectroscopy in physical metallurgy. U.Gonser (Angewandte Phys., Univ. des Saarlandes, Saarbrücken, Germany).

Hyperfine Interactions (Netherlands), vol.13, no.1-3, p.5-23 (Jan. 1983).

In this anniversary contribution the natural and intimate 'match making' which occurs between the two star performers— ^{57}Fe in Mossbauer spectroscopy and iron in physical metallurgy—is described by selecting typical examples reflecting the author's interest: phases, f.c.c. $\gamma\text{-Fe}$, defects, diffusion and amorphous metals. (38 refs.)

62841 Mossbauer spectroscopy and magnetism. J.Chappert (Dept. de Recherche Fondamentale, CENG, Grenoble, France).

Hyperfine Interactions (Netherlands), vol.13, no.1-3, p.25-43 (Jan. 1983).

A review of the impact of the Mossbauer effect on the field of magnetism during the last twenty-five years is presented. After a brief description of the magnetic hyperfine interaction and its relationship to the basic ingredients of magnetism, one examines how various external parameters can affect the shape of the Mossbauer spectra. These data provide original information on the magnetic properties. (67 refs.)

62842 The impact of Mossbauer spectroscopy on chemistry. T.C.Gibb (Dept. of Inorganic & Structural Chem., Univ. of Leeds, Leeds, England).

Hyperfine Interactions (Netherlands), vol.13, no.1-3, p.45-56 (Jan. 1983).

The historical development of Mossbauer spectroscopy is briefly described from a chemist's viewpoint, and a critical assessment is made of its role in modern chemistry. (37 refs.)

62843 The understanding of nuclear structure through Mossbauer experiments. L.Grodzins (MIT, Cambridge, MA, USA).

Hyperfine Interactions (Netherlands), vol.13, no.1-3, p.57-64 (Jan. 1983).

Mossbauer's discovery vitalized the study of hyperfine interactions on nuclear states. The technique has been used to measure the electromagnetic moments of scores of nuclear levels and the results, especially on rotational states, have been important to the understanding of nuclear structure. Equally significant for nuclear physics has been the deep insight which Mossbauer studies have given us of the hyperfine interaction itself; using that knowledge, and a variety of techniques, the measurements of nuclear magnetic moments are now reliable and routine. (20 refs.)

62844 Mossbauer spectroscopy of implanted sources. L.Niesen (Lab. voor Algemene Natuurkunde, Materials Sci. Centre, Groningen, Netherlands).

Hyperfine Interactions (Netherlands), vol.13, no.1-3, p.65-88 (Jan. 1983).

A review is given of the field of Mossbauer spectroscopy of ion-implanted sources. After an introduction to the various aspects of the ion-implantation method, the following topics are treated: final site selection of implanted impurities; trapping of defects at implanted ions, on-line implantation; implantation in metals, semiconductors and insulators. (93 refs.)

62845 Mossbauer studies of valence fluctuations. I.Nowik (Racah Inst. of Phys., Hebrew Univ., Jerusalem, Israel).

Hyperfine Interactions (Netherlands), vol.13, no.1-3, p.89-118 (Jan. 1983).

In the last ten years the Mossbauer technique has made a considerable contribution to the research of the phenomena of mixed valencies, valence instabilities, valence fluctuations and intermediate valencies of transition elements. The sensitivity of the hyperfine interaction parameters and in particular the isomer shift, to the valency of the Mossbauer ion, enabled the research of dynamics of valence fluctuations and the temperature, pressure and composition dependence of the ionic intermediate valence state. Studies of ^{149}Sm , ^{152}Sm and ^{153}Eu in $\text{Sm}_{1-x}\text{R}_x$ contributed to the understanding of the outstanding insulator-metal phase transition that occurs in these systems. (57 refs.)

62846 ^{67}Zn Mossbauer spectroscopy. T.Katila, K.Riski (Dept. of Tech. Phys., Helsinki Univ. of Technol., Espoo, Finland).

Hyperfine Interactions (Netherlands), vol.13, no.1-3, p.119-48 (Jan. 1983).

Investigations on ^{67}Zn Mossbauer spectroscopy are reviewed. In the theoretical part, mainly phenomena to be observed due to the long nuclear lifetime of the Mossbauer state are discussed. Such phenomena include e.g. transient effects due to the phase modulation, the exceptionally large relative contribution of the second order Doppler shift and the narrowest line width observable today. Finally, a historical review of the ^{67}Zn Mossbauer measurements is presented. Results of the experimental investigations of various research groups are given in chronological order. (59 refs.)

62847 Mossbauer spectroscopy with $^{191,193}\text{Ir}$. F.E.Wagner (Phys.-Dept., Tech. Univ. München, Garching, Germany).

Hyperfine Interactions (Netherlands), vol.13, no.1-3, p.149-73 (Jan. 1983).

The contributions made by Ir Mossbauer spectroscopy to the determination of nuclear parameters, as well as applications in solid state physics and chemistry, are reviewed. In addition, a brief description of experimental techniques and source preparation procedures is given. (141 refs.)

- 62848 Mossbauer spectroscopy with actinide elements.** W.Potzel, J.Moser, L.Asch, G.M.Kalvius (Phys. Dept., Tech. Univ. Munchen, Garching, Germany). *Hyperfine Interactions (Netherlands)*, vol.13, no.1-3, p.175-98 (Jan. 1983). Although formally equivalent to the lanthanide (4f) elements, the light actinides show a much more varied behaviour due to the larger spatial extent and ionizability of the 5f electrons. The application of Mossbauer spectroscopy for the determination of electronic properties of the actinides is outlined. Emphasis is put on high pressure Mossbauer experiments using the 60 keV transition in ^{237}Np to study questions of delocalization of 5f electrons. (58 refs.)
- 62849 Experimental techniques for conversion electron Mossbauer spectroscopy.** J.A.Sawicki (Inst. of Phys., Jagellonian Univ., Cracow, Poland), B.D.Sawicka. *Hyperfine Interactions (Netherlands)*, vol.13, no.1-3, p.199-219 (Jan. 1983). Conversion electron Mossbauer spectroscopy has grown during the last decade as a new tool of surface science. High sensitivity, depth selectivity and capabilities of the method in nondestructive backscattering analysis are essential features of CEMS. These virtues made the method advantageous in various applications and stimulated considerable progress in experimental techniques. The latter is the subject of the present paper. (83 refs.)
- 62850 Isomer shift reference scales.** J.G.Stevens (Mossbauer Effect Data Center, Univ. of North Carolina, Asheville, NC, USA). *Hyperfine Interactions (Netherlands)*, vol.13, no.1-3, p.221-36 (Jan. 1983). The relative isomer shift values of materials commonly used as source and absorber standards for 17 common Mossbauer transitions have been evaluated. This data allows the comparison of isomer shifts among various laboratories despite differences in standards used as zero velocity standards. (3 refs.)
- 62851 Mossbauer-spectroscopic study of solid solutions based on cementite and chromium carbides.** Yu.I.Archakov, L.N.Seregina (All-Union Sci.-Res. Inst. of Petrochem. Processes, USSR). *Inorg. Mater. (USA)*, vol.18, no.5, p.673-6 (May 1982). Translation of: *Izv. Akad. Nauk SSSR Neorg. Mater.*, vol.18, no.5, p.800-4 (May 1982). [received: Feb. 1983] Solid solutions based on Fe_3C and Fe-Cr carbides with limiting concentration of iron have been investigated by means of Mossbauer spectroscopy on the isotope ^{57}Fe . The Mossbauer spectrum of $(\text{Cr}_{0.7}\text{Fe}_{0.3})_{23}\text{C}_6$ is a broadened line, and that of $(\text{Cr}_{0.5}\text{Fe}_{0.5})_3\text{C}_3$ is a doublet. The parameters of these spectra change only very slightly with temperature. The fine structure of the spectra of $(\text{Fe}_{1-x}\text{Cr}_x)_3\text{C}$ depends on the temperature. (10 refs.)
- 62852 A Mossbauer spectroscopic study of the six-coordinate high-spin ferrous compound (meso-tetraphenylporphinato)bis(tetrahydrofuran) iron(II).** B.Boso, G.Lang (Dept. of Phys., Pennsylvania State Univ., University Park, PA, USA), C.A.Reed. *J. Chem. Phys. (USA)*, vol.78, no.5, p.2561-7 (1 March 1983). Mossbauer spectra of a polycrystalline form of the six-coordinate high-spin ferrous compound (meso-tetraphenylporphinato)bis(tetrahydrofuran) iron(II) have been recorded over a range of temperatures (4.2-195K) and magnetic fields (0-6.0 T). Analysis of the spectra using a phenomenological model of the internal magnetic field and using an $S=2$ spin Hamiltonian, where applicable, yield the sign of V_{zz} negative, $\eta=0.4$, $D=6.0\text{ cm}^{-1}$, $E/D=0.1$, and $A^*g^*\nu_B = (-7.2, -7.2, \text{ and } -24.3\text{ T})$. These results suggest that the iron experiences an octahedral crystal field trigonally distorted in the (1,1,1) direction, producing a prolate orbital d_{z^2} as the ground state. Crystal field calculations confirm this interpretation by reproducing the spin Hamiltonian parameters listed above. The calculation predicts an orbital doublet 1667 cm^{-1} above the ground state. Comparisons with deoxyheme proteins and their synthetic analogs suggest some common gross features of the orbital state and structure-related trends in the character of the ground quintet. (27 refs.)
- 62853 Mossbauer diffraction on a single rotating crystal.** E.V.Zolotobajko, E.M.Jolin, A.V.Murmov (Inst. of Phys., Acad. of Sci., Riga, Latvian SSR). *J. Phys. D (GB)*, vol.16, no.4, p.697-704 (14 April 1983). The problem of coherent scattering of Mossbauer radiation in the case of a single rotating crystal is considered. It is shown that the resulting additional Doppler shift leads to the frequency dependence of the purely elastic intensity I_{el} . Due to the small value of the Mossbauer line width the intensity I_{el} is sensitive to small deviations of the reciprocal lattice vector from the rotating axis. In order to check the theoretical considerations, the Mossbauer diffraction experiment was carried out on a single pyrolytic graphite crystal. The authors analysed the influence of the mosaic structure of the sample as well as the deflection by the atomic planes from the crystal surface on the obtained results. (12 refs.)
- 62854 Mossbauer spectroscopic studies of magnesium nickel ferrites.** K.Seshan, A.S.Bommannavar, D.K.Chakrabarty (Dept. of Chem., Indian Inst. of Technol., Bombay, India). *J. Solid State Chem. (USA)*, vol.47, no.1, p.107-12 (15 March 1983). Mossbauer spectra of magnesium nickel ferrites having a spinel structure with varying percentages of nickel were obtained at room temperature. The split extreme high-resonance line could be resolved into two Lorentzians from which the cation distribution was calculated. The calculated cation distributions match very well with those obtained from magnetization measurements as well as from ferromagnetic resonance studies on the same samples. The observed quadrupolarly split and the hyperfine field values can be rationalized, based on the obtained cation distributions. (9 refs.)
- 62855 Mossbauer effect study of the internal magnetic field in small iron particles.** I.Tamura, M.Hayashi (Phys. Dept., Toyama Medical & Pharmaceutical Univ., Toyama, Japan). *J. Magn. & Magn. Mater. (Netherlands)*, vol.31-34, pt.2, p.945-6 (Feb. 1983). (Proceedings of the International Conference on Magnetism, Kyoto, Japan, 6-10 Sept. 1982). A temperature and size dependent enhancement of the internal magnetic field was observed for small iron particles produced by the gas evaporation technique and was explained by the demagnetization field and the dipole interaction of the particles. Thermal fluctuation of the magnetization and fusion between the particles have important effects. (5 refs.)
- 62856 Magnetic excitations in small NiFe_2O_4 particles.** K.Haneda, H.Kojima (Res. Inst. for Sci. Measurements, Tohoku Univ., Sendai, Japan), A.H.Morrish. *J. Magn. & Magn. Mater. (Netherlands)*, vol.31-34, pt.2, p.951-2 (Feb. 1983). (Proceedings of the International Conference on Magnetism, Kyoto, Japan, 6-10 Sept. 1982). Mossbauer absorption spectra for small NiFe_2O_4 particles with and without applying a high magnetic field have been discussed in connection with the apparently anomalous ratios of the B to A-site pattern for a completely inverse spinel. Analyses indicate that the collective magnetic excitation mechanism is acting. (5 refs.)
- 62857 Magnetic and electronic properties of microcrystals of Fe_3O_4 .** S.Morup (Lab. of Applied Phys. II, Tech. Univ. of Denmark, Lyngby, Denmark), H.Topsøe. *J. Magn. & Magn. Mater. (Netherlands)*, vol.31-34, pt.2, p.953-4 (Feb. 1983). (Proceedings of the International Conference on Magnetism, Kyoto, Japan, 6-10 Sept. 1982). Mossbauer studies of 60 Å particles of Fe_3O_4 show the presence of a Verwey transition between 4.2K and 80K. The spectrum of superparamagnetic particles contains two lines with slightly smaller isomer shifts than those of the A and B sites in bulk. The B-site linewidth suggests a slower electron 'hopping' than in bulk. (12 refs.)
- 62858 Mossbauer study of acicular iron-nitride particles.** N.Sagusa, A.H.Morrish (Dept. of Phys., Univ. of Manitoba, Winnipeg, Manitoba, Canada), A.Tasaki, K.Tagawa, E.Kita. *J. Magn. & Magn. Mater. (Netherlands)*, vol.35, no.1-3, p.123-5 (March 1983). (Proceedings of the 10th International Colloquium on Magnetic Films and Surfaces, Yokohama, Japan, 13-16 Sept. 1982). Acicular iron-nitride particles approximately 500 nm in length and 50 nm in diameter were studied by ^{57}Fe Mossbauer spectroscopy. At room temperature a ferromagnetic phase, probably $\gamma\text{-Fe}_4\text{N}$, coexists with a paramagnetic phase. (6 refs.)
- 62859 Mossbauer spectroscopic studies on surfaces and thin films.** J.Tyson, A.Owens, J.C.Walker (Dept. of Phys., Johns Hopkins Univ., Baltimore, MD, USA). *J. Magn. & Magn. Mater. (Netherlands)*, vol.35, no.1-3, p.126-9 (March 1983). (Proceedings of the 10th International Colloquium on Magnetic Films and Surfaces, Yokohama, Japan, 13-16 Sept. 1982). Investigates the magnetic properties of surface layers of Fe films using Mossbauer spectroscopy. (110) epitaxial Fe films were made of ^{56}Fe with appropriate probe layers of ^{57}Fe in the surface region. In this way the authors were able to profile the magnetism at and near the surface of the films. Studies of the temperature dependence of layers at the surface indicate a quasilinear dependence of magnetization on temperature while the temperature dependence of layers further inside the material show the usual $T^{3/2}$ dependence. A region of surface thermal spin deviations larger than bulk values extends over 3 to 4 layers at the surfaces. These results are in qualitative agreement with a number of theoretical studies. The quasilinear temperature dependence of the surface layer implies a weakening of the surface exchange. In addition to the unusual temperature dependence of the surface magnetization, the authors have generally observed larger surface magnetic hyperfine fields near $T=0$. (18 refs.)
- 62860 Surface magnetism of $\alpha\text{-Fe}_2\text{O}_3$ by Mossbauer spectroscopy.** T.Shinjo, M.Kiyama, N.Sugita, K.Watanabe, T.Takada (Inst. for Chem. Res., Kyoto Univ., Uji, Kyoto-fu, Japan). *J. Magn. & Magn. Mater. (Netherlands)*, vol.35, no.1-3, p.133-5 (March 1983). (Proceedings of the 10th International Colloquium on Magnetic Films and Surfaces, Yokohama, Japan, 13-16 Sept. 1982). $\alpha\text{-Fe}_2\text{O}_3$ particles were prepared from pure ^{56}Fe and the surface was very thinly coated with ^{57}Fe . Mossbauer results elucidated that the surface hyperfine field rapidly decreased with increase of temperature but the Morin transition took place at the same transition temperature as the bulk crystal. (7 refs.)
- 62861 Interface magnetism in Fe-Sb multilayer films from ^{121}Sb and ^{57}Fe Mossbauer spectroscopy.** J.M.Friedt, N.Hosoi, K.Kawaguchi, T.Shinjo (Centre de Recherches Nucleaires, Strasbourg, France). *J. Magn. & Magn. Mater. (Netherlands)*, vol.35, no.1-3, p.136-8 (March 1983). (Proceedings of the 10th International Colloquium on Magnetic Films and Surfaces, Yokohama, Japan, 13-16 Sept. 1982). Intense electronic charge and spin density perturbations occur at Sb-Fe interfaces by reference to bulk materials. The authors report the observation of a large hyperfine field (i.e. spin density) being transferred from the magnetic layer (Fe) into the nonmagnetic one (Sb) at the Fe-Sb interface. (12 refs.)
- 62862 Mossbauer and X-ray diffraction studies of amorphous Fe-Ni alloy films deposited by DC sputtering.** J.Arai, S.Nagata, M.Shirasaki (Faculty of Sci. & Technol., Sci. Univ. of Tokyo, Chiba, Japan). *J. Magn. & Magn. Mater. (Netherlands)*, vol.35, no.1-3, p.221-2 (March 1983). (Proceedings of the 10th International Colloquium on Magnetic Films and Surfaces, Yokohama, Japan, 13-16 Sept. 1982). The analysis of the Mossbauer spectra reveals that the amorphous Fe-Ni alloy films without metalloid produced by DC sputtering have strong uniaxial magnetic anisotropy perpendicular to the film plane and the hyperfine field in the amorphous state is larger than that in the crystalline state in Invar composition. (3 refs.)
- 62863 Application of the depth-selective conversion electron Mossbauer spectroscopy to rare-earth iron garnet films.** J.Itoh, Y.Yonekura, K.Saneyoshi, T.Toriyama, K.Hisatake (Dept. of Appl. Phys., Tokyo Inst. of Technol., Tokyo, Japan). *J. Magn. & Magn. Mater. (Netherlands)*, vol.35, no.1-3, p.340-2 (March 1983). (Proceedings of the 10th International Colloquium on Magnetic Films and Surfaces, Yokohama, Japan, 13-16 Sept. 1982). Mossbauer spectra of RIG were measured with an electron spectrometer for energies of 7.3, 7.1 and 6.6 keV. The spectra for 0-100, 100-300 and 300-1500 Å were deduced. Spin-orientation, area ratio of d- to a-site and line widths are derived as a function of depth. (4 refs.)
- 62864 Depth-selective conversion electron Mossbauer spectroscopy of thin Fe films.** S.Staniek, T.Shigematsu, W.Keune, H.-D.Pfannes (Lab. für Angewandte Phys., Univ. Duisburg, Duisburg, Germany). *J. Magn. & Magn. Mater. (Netherlands)*, vol.35, no.1-3, p.347-9 (March 1983). (Proceedings of the 10th International Colloquium on Magnetic Films and Surfaces, Yokohama, Japan, 13-16 Sept. 1982). The depth-sensitivity of energy-differential conversion electron Mossbauer spectroscopy (DCEMS) was tested by using a 50 Å ^{57}Fe film evaporated onto 1320 Å natural Fe and coated by 0, 50 and 100 Å natural Fe. The average hyperfine field of 34 Å ^{57}Fe on 340 Å ^{56}Fe was found to be slightly smaller than ($\sim 326\text{ kOe}$) the bulk field. Surface effects were drastically enhanced if Auger electron Mossbauer spectroscopy (AEMS) at 600 eV was performed. (10 refs.)
- 62865 Applied magnetic field Mossbauer studies of the quasi one-dimensional system $\text{AFES}_2\text{A}=\text{K, Rb, Cs}$.** D.M.Cooper, D.P.E.Dickson (Dept. of Phys., Univ. of Liverpool, Liverpool, England), P.H.Domingues, G.P.Gupta, C.E.Johnson, M.F.Thomas, C.A.Taft, P.J.Walker. *J. Magn. & Magn. Mater. (Netherlands)*, vol.36, no.1-2, p.171-4 (1 April 1983). Mossbauer measurements of single crystal and quasi single crystal samples of AFES_2 compounds show no evidence for any variation of the hyperfine field with applied fields up to 10.0 T. This is consistent with what would be expected in a quasi one-dimensional system with relatively high anisotropy,

and does not preclude a contribution to the anomalously low value of the saturation hyperfine field from zero point spin reduction effects. (10 refs.)

62866 Mixed-valent iron in synthetic rasumite, KFe_2S_3 . G.Amthauer (Inst. for Mineralogie, Univ. Marburg, Marburg, Germany), K.Bente. *Naturwissenschaften (Germany)*, vol.70, no.3, p.146-7 (March 1983). The authors synthesize rasumite and obtain additional experimental information on the temperatures and pressures of its formation in nature. They also determine the valence state of iron by means of Mossbauer spectroscopy of ^{57}Fe . (7 refs.)

62867 Selective scattering of electromagnetic radiation in radio-frequency resonance conditions. A.V.Mitin. *Opt. & Spectrosc. (USA)*, vol.53, no.2, p.168-72 (Aug. 1982). Translation of: *Opt. & Spektrosk. (USSR)*, vol.53, no.2, p.288-95 (Aug. 1982). [received: April 1983]

A theory is developed for the selective scattering of radiation by a system with discrete energy levels under conditions of radio-frequency resonance. The problem is solved with the assumption of spontaneous reemission while the rotating RF field is considered. On the basis of simultaneous solution of the system of equations for the density-matrix elements the presence of beats is demonstrated for scattered-radiation intensity at a frequency that is a multiple of the RF field frequency. It was noticed that at large RF field intensities a significant role in scattering is played by interference induced by the latter. Scattered-radiation polarization is considered. Results are analyzed using the example of Mossbauer scattering on Fe^{2+} nuclei in iron. (21 refs.)

62868 Quadrupole interactions at ^{111}Cd nuclei in light rare earths. S.N.Mishra, R.G.Pillay, P.N.Tandon, H.G.Devare (Tata Inst. of Fundamental Res., Bombay, India).

Phys. Lett. A (Netherlands), vol.94A, no.6-7, p.317-19 (21 March 1983). Quadrupole interactions at ^{111}Cd nuclei introduced as dilute impurity in light rare-earth hosts have been studied using the TDPAC technique. The electronic enhancement of the electric field gradient is found to be almost independent of the rare earth in the first half of the series contrary to a steep decrease in the second half with a sharp change at Gd. (11 refs.)

62869 The Mossbauer effect on ^{57}Fe nuclei in magnesium, yttrium and beryllium matrices. R.B.Yadav (Phys. Dept., S.D.P.G. Coll., Muzaffarnagar, India).

Physica B & C (Netherlands), vol.115 B+C, no.2, p.237-9 (Jan. 1983). The probability of recoilless resonant absorption of 14.4 keV γ -rays by ^{57}Fe in matrices of magnesium, yttrium and beryllium has been calculated in the temperature range 42-929K, respectively. The calculated results show good agreement with the experimental data. (9 refs.)

62870 Conversion Mossbauer studies of epitaxially mixed ferrite-garnet films. Sh.Sh.Bashkurov, N.G.Ivovlov, E.S.Romanov, A.P.Kirmenskii (V.I. Ulyanov-Lenin State Univ., Kazan, USSR).

Sov. Phys.-Solid State (USA), vol.24, no.9, p.1497-500 (Sept. 1982). Translation of: *Fiz. Tverd. Tela (USSR)*, vol.24, no.9, p.2641-7 (Sept. 1982). [received: April 1983]

Mossbauer, X-ray diffraction, and magnetooptical measurements are used to investigate epitaxial films with composition $(\text{YEuTmCa})_x(\text{FeGe})_{1-x}\text{O}_{12}$ grown on (111) Gd_2GaO_7 substrates. The local magnetic fields $H_{\text{eff}}^{\text{Fe}}$ and $H_{\text{eff}}^{\text{Gd}}$ on the nuclei of Fe^{3+} ions in octahedral and tetrahedral sites are measured. The coefficient of magnetic misorientation is found in the case of misoriented (111) films in the GaGe system. The effectiveness of determining the degree of diamagnetic substitution x using the Mossbauer conversion spectroscopy method is demonstrated. The films, even grown from a single solution melt under identical conditions, show considerable scatter with respect to the quantity x . Starting from the dependences of the values of $4\pi M_s$ on x , it is concluded that the concentration of Ge^{4+} ions is different in the surface and lower-lying layers. (22 refs.)

Superconductivity in ternary compounds. II. Superconductivity and magnetism. See Entry 59553

A microprocessor controlled spectrometer for thermal scan Mossbauer spectroscopy See Entry 59897

Mossbauer studies of FeSn molecules isolated in rare-gas solids and SCF-Xa-scattered-wave molecular-orbital analyses of Sn_2 and FeSn diatomic molecules See Entry 60774

On the measurement of visco-elastic properties of matters by the Mossbauer effect See Entry 61461

Structural relaxation in (Fe-Cr)-based glass See Entry 61811

Crystal structure and magnetic properties of a new form of $\text{NH}_4\text{MnFeF}_6$ See Entry 61880

Hexagonal tungsten bronze-type Fe^{III} fluoride: $(\text{H}_2\text{O})_{0.33}\text{FeF}_3$; crystal structure, magnetic properties, dehydration to a new form of iron trifluoride See Entry 61882

Spin orientation and exchange interactions in $(\text{Fe},\text{Co})\text{Cl}_2$ See Entry 62575

Magnetic properties of amorphous Fe-Nb and Fe-Zr See Entry 62607

Magnetic hyperfine field distribution and structural relaxation of amorphous $(\text{Fe}_{81}\text{Si}_{14}\text{Si}_4)$ prepared with different quenching rates See Entry 62608

Spin glass behaviour in chromium spinels See Entry 62633

Magnetic short-range order and spin freezing in the quasi-2D system LuFeMgO_4 See Entry 62642

Magnetic inhomogeneity in amorphous Fe-Zr alloys See Entry 62701

Surface magnetic properties of fine particles See Entry 62717

Dynamical properties of small particles; comparison with spin glass behaviour See Entry 62719

Application of neutron diffraction to the study of interface magnetization on thin films with artificial superlattices See Entry 62729

On the magnetic dipole fields at surface atoms See Entry 62731

Magnetic properties of metastable crystalline and amorphous Fe alloys produced by RF sputtering See Entry 62741

Magnetoelastic effects in amorphous metals due to surface crystallisation and oxidation See Entry 62790

Order-disorder transition in Fe_3Si alloy during mechanical crushing See Entry 63286

Is it possible to avoid thermal embrittlement in ribbon-shaped glassy metals? See Entry 63416

Protein dynamics from Mossbauer spectra. The temperature dependence See Entry 63770

76.90 OTHER TOPICS IN MAGNETIC RESONANCES AND RELAXATION

(inc. muon probe studies)

62871 Some characteristics of muon states in silicon. C.Boekema (Los Alamos Nat. Lab., Los Alamos, NM, USA).

Philos. Mag. B (GB), vol.47, no.3, p.331-6 (March 1983). Recent results of muon spin rotation studies on silicon are discussed. Special attention is paid to the temperature and doping dependences of the formation probabilities and relaxation rates of the observed muon states. It is argued that normal muonium (Mu) and anomalous muonium (Mu^*) are two completely different states with respect to physical and chemical properties. Mu^* is a localized state, whereas evidence suggests that Mu diffuses through the silicon lattice. (16 refs.)

Random walk to and interaction with an impurity See Entry 59703

Dynamics of disordered spin systems studied by zero- and longitudinal-field μSR . I. $(\text{FeTiO}_3)_{1-x}(\text{Fe}_2\text{O}_3)_x$ See Entry 62627

77.00 DIELECTRIC PROPERTIES AND MATERIALS

(for conductivity phenomena, see 72.20 and 72.80)

77.20 PERMITTIVITY

62872 Dielectric properties of $\text{Ag}_{1-x}\text{K}_x/\text{NbO}_3$ solid solutions. M.Lukas-zewski (Inst. of Phys., Silesian Univ., Katowice, Poland).

Ferroelectr. Lett. Sect. (GB), vol.44, no.11, p.319-24 (1983). The possibility of the occurrence of a critical point in $(\text{Ag}_{1-x}\text{K}_x)\text{NbO}_3$ solid solutions is discussed. (7 refs.)

62873 Precise millimeter-wave measurements of complex refractive index, complex dielectric permittivity and loss tangent of GaAs, Si, SiO_2 , Al_2O_3 , BeO, Macor, and glass. M.N.Afsar, K.J.Button (MIT, Cambridge, MA, USA). *IEEE Trans. Microwave Theory & Tech. (USA)*, vol.MTT-31, no.2, p.217-23 (Feb. 1983).

Highly accurate continuous spectra of the complex refractive index and complex dielectric permittivity are given in the millimeter range for a variety of potentially useful materials. The absorption coefficient is found to increase monotonically with increasing frequencies. Small amounts of glassy inclusions or water were found to increase losses at all frequencies, but impurities and radiation damage (except in semiconductors) have not yet proved to be detrimental to performance. Materials have been found for which the millimeter-wave losses can be tolerated when used as dielectric waveguide, high-power windows, and other applications. Nominal consideration must be given, however, to the conditions of preparation and the nature of contaminants. The measurements were made in a modular, polarizing, dispersive Fourier-transform spectrometer. (9 refs.)

62874 Dielectric constant of both amorphous and crystalline PbTiO_3 at low temperatures. Y.Miura, M.Takashi, T.Nakamura (Inst. for Solid State Phys., Univ. of Tokyo, Tokyo, Japan), W.N.Lawless, M.Shinohara, T.Furubayashi, N.Nishida, Y.Takano, H.Ishimoto, K.Ohno. *J. Phys. Soc. Jpn. (Japan)*, vol.52, no.4, p.1127-30 (April 1983).

The dielectric constant of PbTiO_3 in both amorphous and crystalline states has been measured down to 18 mK at several frequencies in the range between 0.3 and 100 kHz. In each state, the dielectric constant around 100 mK has a frequency-dependent minimum, which is characteristic of a vitreous state.

62875 Dielectric dispersion in KH_2PO_4 below 10K. H.Motegi, K.Kuramoto, E.Nakamura (Faculty of Sci., Hiroshima Univ., Hiroshima, Japan). *J. Phys. Soc. Jpn. (Japan)*, vol.52, no.4, p.1131-3 (April 1983).

Complex dielectric constants of KH_2PO_4 along the c and a -axes have been measured in the frequency range from 10 Hz to 20 kHz. Dielectric dispersions of relaxation type with small loss peaks have been observed at temperatures below 10K in both directions. Arrhenius plots of the relaxation frequencies give extremely small values of activation energies, 0.014 eV for the c -axis and 0.004 eV for the a -axis, respectively. (6 refs.)

62876 Dielectric and piezoelectric properties of modified lead titanate zirconate ceramics from 4.2 to 300K. X.L.Zhang, Z.X.Chen, L.E.Cross, W.A.Schulze (Materials Res. Lab., Pennsylvania State Univ., University Park, PA, USA).

J. Mater. Sci. (GB), vol.18, no.4, p.968-72 (April 1983). The dielectric and piezoelectric properties (d-p properties) of four kinds of doped lead titanate zirconate piezoelectric ceramics (PZTs) have been measured from 4.2 to 300K. The d-p properties of the materials converge with decreasing temperature down to liquid helium temperature, even though the properties have large differences at room temperature. The values of mechanical and electrical quality factors, Q_m , Q_e , and of the frequency constant, N , of the materials increased at low temperature. It is evident from the freeze out in K' and the associate temperature-frequency-dependent maxima in $\tan \delta$ that the relaxation processes including ferroelectric domain wall motion and thermal defect motion contribute to the d-p properties. The Navy type-II composition has a minimum temperature coefficient of d-p parameters and it is evident that PZT ceramics modified with Fe_2O_3 can provide good stability and also give the strongest piezoelectric response at liquid helium temperature. (8 refs.)

62877 Growth and some dielectric properties of K_2ZnCl_4 and Rb_2ZnCl_4 crystals. O.E.Bochkov, Yu.D.Krokhmal', S.A.Flerova, A.Yu.Kudzin (State Univ., Dnepropetrovsk, USSR). *Sov. Phys.-Crystallogr. (USA)*, vol.27, no.5, p.603-4 (Sept.-Oct. 1982). Translation of: *Kristallografiya (USSR)*, vol.27, no.5, p.1005-6 (Sept.-Oct. 1982). [received: April 1983]

The authors give the results of an investigation of the technology for obtaining K_2ZnCl_4 and Rb_2ZnCl_4 crystals, both in the pure state and doped with copper and cobalt ions. The crystals were grown by two methods: (i) by isothermal evaporation from saturated aqueous solutions; (ii) by pulling from a melt by the Czochralski method. The starting materials were potassium, rubidium, and zinc chlorides of commercial very pure and analytical-reagent grades (os.ch. and ch.d.a.). They were grown from aqueous solution both by spontaneous crystallization and by a dynamic method with seed crystals. The authors also performed experiments on the growth of crystals from solutions containing excess zinc chloride. Combined dielectric measurements were made on the crystals. A comparative analysis enabled the authors to relate the

difference in the dielectric behaviour of the crystals to the growth conditions. (3 refs.)

62878 Grain orientation and dielectric properties of ferroelectric BaBi₂Ti₄O₁₅ ceramic thick film. Z.-T. Zhang, K. Koumoto, H. Yanagida (Dept. of Industrial Chem., Univ. of Tokyo, Tokyo, Japan). *Yogyo-Kyokai-Shi (Japan)*, vol.90, no.1048, p.709-14 (1982). The effect of grain orientation on dielectric properties of a ferroelectric BaBi₂Ti₄O₁₅ ceramic thick film fabricated by a modified doctor blade method was investigated. For evaluation of the grain orientation, the equation $f = P_0 / (W_{\text{hkl}} - 1) / (1 - P_0)$ proposed by Zhang was fully examined and the degree of orientation F was newly defined. The F value for each crystal plane was calculated from an X-ray diffraction pattern, which was further correlated with the measured permittivity and dielectric loss ($\tan \delta$). The diffraction intensity of the crystal planes perpendicular to c -axis such as (008) and (0010) was observed to be higher than that for a non-oriented sample and resulted in $F > 0$. The intensity of the crystal planes parallel to c -axis such as (020), on the other hand, was lower, resulting in $F < 0$. The permittivity of a film was smaller than that of a normally sintered specimen in the temperature range 15°~480°C. It was concluded that the permittivity along c -axis was smaller than that along a - or b -axis for BaBi₂Ti₄O₁₅. (13 refs.)

Physical properties of liquid crystals of 4-(4-nalkylbicyclo[2,2,2]octyl)benzonitriles See Entry 61793

Two new phases with tetragonal bronze-like structure in the diagram: K₂O-CdO-Nb₂O₅ See Entry 61863

Thermophysical properties of supercritical fluids with special consideration of aqueous systems See Entry 62073

The secondary effect of the cooperative Jahn-Teller distortion in rare earth vanadates See Entry 62089

Dielectric properties and polaronic conductivity of WO₃ and W₁₈Mo₁₂O₃₀ See Entry 62415

Phase transition in AgPbSb₃S₆ crystals [superionic] See Entry 62462

Dielectric properties and structure of *N*-methylpropionamide+methanol mixtures See Entry 62886

Dielectric characteristic in V₂O₅ crystal and crystallized glass 70 V₂O₅.30P₂O₅ See Entry 62887

Characterization of the three dimensional properties of poled PZT 65/35 in the absence of losses See Entry 62894

Dielectric dispersion of relaxor ferroelectrics (SBN 75 and PLZT 8/65/35) See Entry 62895

Ferroelectric properties of tungsten bronze lead barium niobate (PBN) single crystals See Entry 62897

Nature of the phase transition in K_{1-x}TaO₃ See Entry 62901

Structure of reflection bands of Grandjean textures See Entry 62908

Refractive index in epitaxial Pb_{1-x}Sn_xTe films See Entry 62919

Permittivity anisotropy of InAs and Cd_{0.25}Hg_{0.75}Te induced by electron drift. Contribution of quantum corrections See Entry 62934

Single crystal growth and physical properties of cubic Zn₃(BO₃)₂ See Entry 63151

77.30 POLARIZATION AND DEPOLARIZATION EFFECTS

62879 Spatially varying polarization in ice. D.W.R.Gruen, S.Marcelja (Dept. of Appl. Math., Australian Nat. Univ., Canberra, Australia). *J. Chem. Soc. Faraday Trans. II (GB)*, vol.79, pt.2, p.211-23 (Feb. 1983).

The authors calculate the response of an ice crystal to a spatially varying applied electric field. The dielectric polarization of the ice is not assumed to be proportional to the local macroscopic electric field. Instead, the authors formulate an expression for the free-energy density of an ice crystal with non-uniform polarization and derive the functional forms of the electric and polarization fields which minimize the free energy of the whole system. In general, the two fields have different spatial variation. Their behaviour is governed by two characteristic lengths: the Debye length and a polarization decay length, determined, respectively, by the concentration of ions and Bjerrum defects in bulk ice. The model is a generalized Poisson-Boltzmann theory which includes the effects of the microscopic structure of the medium in a description of electrostatic screening of external charges. (11 refs.)

62880 Spatially varying polarization in water. A model for the electric double layer and the hydration force. D.W.R.Gruen, S.Marcelja (Dept. of Appl. Math., Australian Nat. Univ., Canberra, Australia). *J. Chem. Soc. Faraday Trans. II (GB)*, vol.79, pt.2, p.225-42 (Feb. 1983).

The response of aqueous solutions to a spatially-varying applied electric field is modelled. This leads to a generalized theory of the electric double layer which explicitly takes into account the microscopic structure of the solvent. As the solvent polarization is allowed to vary depending on both the macroscopic electric field and the specific interactions at the surface, the result is more freedom in the structure of the electric double layer. Generalized expressions are considered for the double-layer free energy, as well as the interaction of two double layers which include specific surface polarization. Such interaction consists of both classical double-layer repulsion and the strong, short-range 'hydration force'. (23 refs.)

62881 Thermally stimulated surface currents in CH₃OH cryocondensates near the polymorphic phase transformation. J.Chrzanowski, B.Sujak (Inst. of Experimental Phys., Univ. of Wrocław, Wrocław, Poland). *Thin Solid Films (Switzerland)*, vol.101, no.2, p.123-30 (11 March 1983).

Thermally stimulated surface currents (TSSCs) were measured in thin methanol cryocondensates after deposition of the layer onto a substrate at a temperature of 80K from a molecular beam followed by heating at a constant rate. It was found that the TSSC curves exhibit some local maxima. One of these peaks was found near $T = 158K$, i.e. in the temperature range where solid methanol undergoes a polymorphic phase transformation. The current-voltage characteristics obtained for these layers suggest fundamental changes in the electrical properties of the condensate surface that take place near this transformation ($\alpha \rightarrow \beta$). The current-voltage curve obtained at $T = 158K$ for the solidified methanol layer studied shows a similar shape to that of the current-voltage curves observed in dielectric materials within the space-charge limited current range. (18 refs.)

Influence of spontaneous polarization of TGS crystals on the electrical properties of ZnTe thin films See Entry 62516

Growth and some dielectric properties of K₂ZnCl₄ and Rb₂ZnCl₄ crystals See Entry 62877

Pressure-dependent secondary relaxation in a series of vinyl chloride-vinyl acetate copolymers See Entry 62882

Laws governing dielectric relaxation See Entry 62884

A possible model of the process of repolarization of a ferroelectric in a weak electric field See Entry 62896

Ferroelectric properties of tungsten bronze lead barium niobate (PBN) single crystals See Entry 62897

Incommensurate phase and dielectric properties of crystals in the NaK-tartrate-NaNH₄-tartrate system See Entry 62902

Exoemission and the electret effect in lithium niobate crystals See Entry 63138

77.40 DIELECTRIC LOSS AND RELAXATION

62882 Pressure-dependent secondary relaxation in a series of vinyl chloride-vinyl acetate copolymers. J.Krishnan, N.Sharma, K.K.Jain (Nat. Phys. Lab., New Delhi, India).

High Temp.-High Pressures (GB), vol.14, no.3, p.293-306 (1982). (10th Plansee Seminar on 'Trends in Refractory Metals, Hardmetals, and Special Materials, and their Technology', Reutte, Austria, 1-5 June 1981).

Depolarisation behaviour of solution-grown vinyl chloride-vinyl acetate copolymer films having 3, 10, and 17 wt.% concentration of vinyl acetate (VAc) have been studied as a function of the externally applied hydrostatic pressure and the poling field. A relaxation peak in the temperature region of 340-360K at 1 bar is observed with activation enthalpies of 0.66-0.78 eV and relaxation times at 300K of $(6.06-22.7) \times 10^{-3}$ s respectively. The magnitude of the maximum current, and hence the charge associated with it, increases linearly with the poling field and is attributed to a local twisting of the main chain or side-group motion. At higher pressure two peaks at about 330 and 360K are observed and are attributed to localised molecular motion of the main chain in two regions of different activation volumes. The shift in the peak position towards lower temperature with increase in VAc concentration could imply that VAc acts as a plasticiser loosening the entangled main polymer chain and hence increasing the mobility of the molecular motion. The shift to the higher temperature is then mainly dominated by the decrease in the free volume by applied pressure which increases the relaxation time of the molecular motions. The principal characteristics of the polymer, including the activation volume, activation enthalpy, and relaxation time of the molecular motion, have been computed. (27 refs.)

62883 Dielectric properties of 1-cyanoadamantane C₁₀H₁₅CN, in its plastic phase. J.P.Amoureux, M.Castelain, M.D.Benadda, M.Bee, J.L.Sauvageol. *J. Phys. (France)*, vol.44, no.4, p.513-20 (April 1983).

Dielectric properties of 1-cyanoadamantane C₁₀H₁₅CN are analysed in a very wide frequency band (10^{-10} Hz) between 200K and 400K. Dynamical relaxation effects are studied in relation to the structure of the plastic phase. The temperature variations of both single and correlated molecular motions are investigated. The results the authors obtain for the single molecular motions agree exactly with the corresponding ones deduced from NMR. The experimental Kirkwood correlation g factor indicates an anti-parallel local order in all the plastic phase of cyanoadamantane. (26 refs.)

62884 Laws governing dielectric relaxation. J.H.Calderwood (Dept. of Electronic Engng., Univ. Coll., Galway, Ireland). *J. Phys. C (GB)*, vol.16, no.10, p.L301-3 (10 April 1983).

A notional experiment has previously been described concerning the current decay curves in two identical dielectric specimens, each previously subjected for a long period to a constant electric field, and short-circuited at different times, the specimen subjected to the higher field being short-circuited first. If the polarisation mechanism exhibits a distribution of relaxation times, the current decay curves may cross over each other; on the other hand the mechanism is such that the current decay obeys a $t^{-1/2}$ law, then the curves will certainly cross over. Such a cross-over gives rise to certain apparent conceptual difficulties which are easily dealt with if a distribution of relaxation times is postulated, but otherwise remain to be explained. (3 refs.)

62885 A transient-state theory of dielectric relaxation and the Curie-von Schweidler law. T.C.Guo, W.W.Guo (IIT Res.Inst., Annapolis, MD, USA). *J. Phys. C (GB)*, vol.16, no.10, p.1955-60 (10 April 1983).

A theory of dielectric response that accounts for the nonsteady-state nature of many-body interactions in transient processes is presented. It is shown that the theory leads to the observed dielectric properties. Comparisons are also made with existing theories as regards their predictions, consequences and shortcomings. (13 refs.)

62886 Dielectric properties and structure of *N*-methylpropionamide+methanol mixtures. H.P.Bennetto, G.F.Evans, R.J.Sheppard (Queen Elizabeth Coll., Univ. of London, London, England). *J. Chem. Soc. Faraday Trans. II (GB)*, vol.79, no.1, p.245-51 (Jan. 1983).

The dielectric properties of mixtures of methanol with *N*-methylpropionamide (NMP) at 20°C have been investigated over the range of frequency 1 MHz to 4 GHz. The dielectric relaxation is described by a simple Debye dispersion equation, in contrast with the behaviour for many non-aqueous mixtures. An exponential dependence of the relaxation frequency on mole fraction composition reveals two distinct regions of dielectric response, attributed to methanol-dominated and NMP-dominated liquid structures. Results are discussed in terms of the polarisation of a homogeneous liquid of uniformly hydrogen-bonded structure, which varies with solvent composition. (24 refs.)

62887 Dielectric characteristic in V₂O₅ crystal and crystallized glass 70 V₂O₅.30P₂O₅. Y.Hakamatsuka, T.Tsuchiya, N.Yoneda (Faculty of Sci. & Technol., Sei. Univ. of Tokyo, Noda, Japan).

Yogyo-Kyokai-Shi (Japan), vol.90, no.1048, p.691-7 (1982). A large dielectric relaxation was observed in the crystallized glass containing a large amount of V₂O₅. The main crystalline precipitate in the crystallized glass 70V₂O₅.30P₂O₅ was V₂O₅ crystal. To clarify the origin of the large dielectric relaxation, the dielectric properties of the crystallized glass were studied and compared with those of polycrystalline V₂O₅ obtained by two different methods. The ϵ' of crystallized glass 70V₂O₅.30P₂O₅ is two or three times larger than that of the glass for the same composition. The sintered and oriented V₂O₅ polycrystalline materials show a large dielectric relaxation; the value of the static dielectric constant in the specimen sintered at 620°C for 5 h is 1000. The ϵ' of polycrystalline V₂O₅ changed with the sintering temperature and with the direction of the crystal axis in the oriented specimen. The results obtained were analyzed on the basis of the equivalent circuit model for a double-layer dielectric. According to this model, the ϵ' and σ of the crystal (the direction of b -axis) of the specimen oriented perpendicular to the electric field were 63 and 7.06×10^{-4} (mho/cm), respectively. (12 refs.)

Dielectric properties and polaronic conductivity of WO₃ and W₁₈Mo₁₂O₃₀ See Entry 62415

Precise millimeter-wave measurements of complex refractive index, complex dielectric permittivity and loss tangent of GaAs, Si, SiO₂, Al₂O₃, BeO, Macor, and glass See Entry 62873

- Dielectric dispersion in KHzPO_4 below 10K See Entry 62875
- Dielectric and piezoelectric properties of modified lead titanate zirconate ceramics from 4.2 to 300K See Entry 62876
- Grain orientation and dielectric properties of ferroelectric $\text{BaBi}_2\text{Ti}_4\text{O}_{15}$ ceramic thick film See Entry 62878
- Dielectric dispersion of relaxor ferroelectrics (SBN 75 and PLZT 8/65/35) See Entry 62895

77.50 DIELECTRIC BREAKDOWN AND SPACE-CHARGE EFFECTS

62888 Theoretical basis for the statistics of dielectric breakdown. R.M.Hill, L.A.Dissado (Chelsea Coll., Univ. of London, London, England). *J. Phys. C (GB)*, vol.16, no.11, p.2145-56 (20 April 1983). The statistics of dielectric breakdown processes are presented and compared with those derived from consideration of the fluctuation components of the dielectric response. It is shown that the Weibull statistic parameters have a direct physical meaning and that breakdown processes can be considered as cooperative events. (23 refs.)

62889 DC breakdown phenomena of the silicone oil/polymer film composite dielectrics. N.Narasaki, K.Kudo, S.Nishiyama. *Res. Rep. Fac. Eng. Meiji Univ. (Japan)*, no.43, p.55-60 (1982). In Japanese. Describes the investigation of breakdown phenomena of the silicone oil/polymer film composite dielectrics in a point-plane electrode system. DC breakdown voltages are measured as a function of water content in silicone oil, oil gap length and thickness of a polymer film. Variation of water content in silicone oil much affects the DC breakdown voltage with positive polarity. From the breakdown voltages with both polarities, it is found that polarity effect of each composite dielectric is dependent on conductivity of films. From the dependence on gap length of DC breakdown voltages, in case of applied voltage with positive polarity, breakdown voltages of composite dielectrics with PP, PET, Teflon FEP, and PA are always higher than those of only silicone oil in gap length, namely, the positive effect of composites is observed. On the other hand, in case of applied voltage with negative polarity, the negative effect of composites is observed in composite dielectrics with negative polarity, the negative effect of composites is observed in composite dielectrics with Teflon FEP, PP, PET in large gap length. This is caused by the influence of the electrification on the liquid/solid interface. (10 refs.)

62890 Generation of static dipole domains in dielectrics. G.N.Protsyuk, V.L.Uvarov. *Sov. Tech. Phys. Lett. (USA)*, vol.8, no.7, p.344-5 (July 1982). Translation of: *Pis'ma v Zh. Tekh. Fiz. (USSR)*, vol.8, no.13-14, p.795-8 (July 1982). [received: April 1983]

Acoustic emission by electron avalanches generated in polymer dielectrics in a nonuniform injected-charge field was described previously (see *ibid.*, vol.7, p.226, 1981). A low-frequency modulation of the signal from the acoustic transducer was ascribed to the electric dipole field formed as a result of the stopping and localization of avalanche electrons. Borrowing terminology from semiconductor physics, the authors refer to this type of bipolar charge structure as a 'static dipole domain'. Here they report measurements of the domain parameters in polymethyl methacrylate near the emission threshold. The authors also analyze the nature of the phenomenon. (10 refs.)

Spatial and size distributions of inhomogeneities initiating laser breakdown in alkali halide crystals at 10.6 μm See Entry 61962

77.55 DIELECTRIC THIN FILMS

Thermally stimulated surface currents in CH_3OH cryocondensates near the polymorphic phase transformation See Entry 62881

Pressure-dependent secondary relaxation in a series of vinyl chloride-vinyl acetate copolymers See Entry 62882

DC breakdown phenomena of the silicone oil/polymer film composite dielectrics See Entry 62889

Low temperature dielectric films from octavinylsilsesquioxane See Entry 63163

77.60 PIEZOELECTRICITY AND ELECTROSTRICTION

(for piezo-optical effects, see 78.20H)

62891 Piezoelectric coefficients of AgGaSe_2 . H.Horinaka, H.Noouchi, H.Sonomura, T.Miyauchi (Dept. of Electrical Engng., Univ. of Osaka Prefecture, Osaka, Japan).

Jpn. J. Appl. Phys. Part 1 (Japan), vol.22, no.3, p.546 (March 1983).

The ternary compounds I-III-V₂ and II-IV-V₂ crystallizing in chalcopyrite structure belong to the crystal class 42 m and consequently the piezoelectric tensor has three nonvanishing elements d_{14} , d_{25} , d_{36} . In this investigation, the measurement of the piezoelectric coefficients was made by a self-resonance method. Two kinds of samples, yz-bar and xy-bar, were prepared to determine d_{14} and d_{36} , respectively, by using the length-extensional mode. The piezoelectric coefficient can be calculated from the electro-mechanical coupling factor, the elastic compliance and the dielectric constant at constant stress. (3 refs.)

Thermally induced electric oscillations: a novel method of detection of piezoelectricity See Entry 59797

Two new phases with tetragonal bronze-like structure in the diagram: $\text{K}_2\text{O}-\text{CdO}-\text{Nb}_2\text{O}_5$ See Entry 61863

Lattice dynamics of α -quartz including the effect of the width of the atomic electron distribution See Entry 62045

Dielectric and piezoelectric properties of modified lead titanate zirconate ceramics from 4.2 to 300K See Entry 62876

Ferroelectric properties of tungsten bronze lead barium niobate (PBN) single crystals See Entry 62897

Concentration dependences of the Curie-Weiss coefficients, dielectric nonlinearity and electrostriction in $(\text{Ba,Sr})\text{TiO}_3$ solid solutions See Entry 62898

Effect of an electric field on the photochromic effect in $\text{Bi}_2\text{GeO}_5\text{:Mn}$ crystals See Entry 62938

Optical anisotropy and electrostriction in the anodic oxide of molybdenum See Entry 63067

Optical anisotropy and electrostriction in the anodic oxide of niobium See Entry 63068

Single crystal growth and physical properties of cubic $\text{Zn}_4\text{O}(\text{BO}_3)_6$ See Entry 63151

77.70 PYROELECTRIC AND ELECTROCALORIC EFFECTS

62892 Ferrielectricity of monoclinic RbD_2PO_4 . T.Osaka (Dept. of Appl. Phys., Sci. Univ. of Tokyo, Tokyo, Japan), M.Sumita, Y.Makita.

J. Phys. Soc. Jpn. (Japan), vol.52, no.4, p.1124-6 (April 1983). The pyroelectric charge of monoclinic RbD_2PO_4 along the *b* axis was measured through the lower transition temperature at 44°C (T_H) and the *D-E* hysteresis curves were examined below T_H . The *D-E* triple hysteresis loops were observed below T_H , corresponding to the development of a small pyroelectric charge below T_H . It is clarified that the crystal is ferrielectric below T_H with a small net polarization, 0.02 $\mu\text{C}/\text{cm}^2$, compared with the spontaneous polarization of the sublattice, 1.8 $\mu\text{C}/\text{cm}^2$, at 30°C.

62893 Temperature dependence of the pyroelectric coefficient of polar dielectrics. V.K.Novik, B.G.Bochkov, N.D.Gavrilova, S.N.Drozhdin. *Sov. Tech. Phys. Lett. (USA)*, vol.8, no.8, p.427-8 (Aug. 1982). Translation of: *Pis'ma v Zh. Tekh. Fiz. (USSR)*, vol.8, no.15-16, p.988-92 (Aug. 1982). [received: April 1983]

The authors measured the pyroelectric coefficients of some classical pyroelectrics—tourmaline and some group A^{II}B^{VI} crystals (ZnO, CdS, and BeO)—by the static method. (9 refs.)

Temperature compensation of pyroelectric radiation detectors See Entry 59842

Ferroelectric properties of tungsten bronze lead barium niobate (PBN) single crystals See Entry 62897

Fluctuations of composition and phase transition in ferroelectric $\text{SbSe}_{0.40}\text{S}_{0.60}\text{P}_{0.90}$ See Entry 62900

Exoemission and the electret effect in lithium niobate crystals See Entry 63138

77.80 FERROELECTRICITY AND ANTIFERROELECTRICITY

62894 Characterization of the three dimensional properties of poled PZT 65/35 in the absence of losses. P.J.Chen (Sandia Nat. Lab., Albuquerque, NM, USA).

Acta Mech. (Austria), vol.47, no.1-2, p.95-106 (1983).

The author characterizes the isothermal three dimensional properties of a poled ferroelectric ceramic PZT 65/35 in the absence of losses. The resulting constitutive relations, in the absence of mechanical dissipation, domain switching, dipole dynamics and phase transformation, are the standard ones which appear in the literature. The characterization of the constitutive relations requires the determination of five elastic constants, three piezoelectric constants and two dielectric constants. The author identifies the experimental measurements which are sufficient to determine these constants and describes the data reduction procedures. His results differ relatively and absolutely from those given in the literature. (11 refs.)

62895 Dielectric dispersion of relaxor ferroelectrics (SBN 75 and PLZT 8/65/35). O.Kersten, A.Rost, G.Schmidt (Sektion Phys., Martin-Luther-Universität, Halle, Germany).

Phys. Status Solidi a (Germany), vol.75, no.2, p.495-500 (16 Feb. 1983).

The temperature dependence of the complex dielectric constant of $\text{Sr}_{0.75}\text{Ba}_{0.25}\text{Nb}_2\text{O}_6$ single crystals and of PLZT 8/65/35 ceramics is measured at frequencies between 10 and 10^{10} Hz. The results can be described by Cole-Cole circles. The distribution of relaxation times decreases with increasing temperature. The activation energies are 0.45 and 0.42 eV, respectively. These results corroborate the idea of two-level system-type disorder modes. (15 refs.)

62896 A possible model of the process of repolarization of a ferroelectric in a weak electric field. E.V.Burtsev, S.P.Chervonobrodov (State Univ., Rostov, USSR).

Sov. Phys.-Crystallogr. (USA), vol.27, no.5, p.507-11 (Sept.-Oct. 1982).

Translation of: *Kristallografiya (USSR)*, vol.27, no.5, p.843-50 (Sept.-Oct. 1982). [received: April 1983]

The authors discuss the thermooctivation motion of 180° domain walls in the relief of the periodic Peierls potential. On the basis of a variation procedure they calculate the critical nucleus configuration and energy. They analyze the field and temperature dependences of the activation field in various regimes of nucleation. They give numerical estimates and compare them with experiment. (18 refs.)

Elasticity moduli of TGS crystals for cylindrical samples See Entry 62011

Mechanism for local charge transport on the surface of a transparent ferroelectric ceramic See Entry 62478

Influence of spontaneous polarization of TGS crystals on the electrical properties of ZnTe thin films See Entry 62516

Dielectric constant of both amorphous and crystalline PbTiO_3 at low temperatures See Entry 62874

Dielectric dispersion in KHzPO_4 below 10K See Entry 62875

Growth and some dielectric properties of K_2ZnCl_4 and Rb_2ZnCl_4 crystals See Entry 62877

Grain orientation and dielectric properties of ferroelectric $\text{BaBi}_2\text{Ti}_4\text{O}_{15}$ ceramic thick film See Entry 62878

Raman scattering studies on slow crystallization process from amorphous PbTiO_3 See Entry 62958

Exoemission and the electret effect in lithium niobate crystals See Entry 63138

77.80B Transitions and Curie point

62897 Ferroelectric properties of tungsten bronze lead barium niobate (PBN) single crystals. T.R.Shrouf, L.E.Cross (Materials Res. Lab., Pennsylvania State Univ., University Park, PA, USA), D.A.Hukin.

Ferroelectr. Lett. Sect. (GB), vol.44, no.11, p.325-30 (1983).

A ferroelectric tungsten bronze single crystal of $\text{Pb}_{0.35}\text{Ba}_{0.75}\text{Nb}_2\text{O}_6$ was grown from a melt using the Czochralski technique. The crystal belongs to the tetragonal point group 4 mm with the spontaneous polarization parallel to the 'c' axis. The room temperature lattice parameters were $a=12.50$ Å and $c=3.995$ Å. The spontaneous polarization was found to be 0.40 C/m²°C. The

Curie transition was 350°C as determined from the temperature dependence of the dielectric constants. The pyroelectric properties were found to be typical of other tetragonal ferroelectric bronzes. Dielectric constant ϵ_{11} and piezoelectric constant d_{33} show a strong enhancement from the approach of the tetragonal:orthorhombic morphotropic phase boundary and it is clear that crystals with composition in the tetragonal phase field closer to this boundary will be of major interest for piezoelectric and electro-optic applications. (13 refs.)

62898 Concentration dependences of the Curie-Weiss coefficients, dielectric nonlinearity and electrostriction in (Ba,Sr)TiO₃ solid solutions. O.P.Zdebskii, O.U.Savchuk. *Dopov. Akad. Nauk UkrSR. Ser. A (USSR)*, no.2, p.50-2 (1983). In Ukrainian.

Analyses the distinction between the Devonshire-Ginsburg expansion coefficients, obtained experimentally and those resulting from the theory of the first-order phase transitions on the basis of the dependence of dielectric nonlinearity coefficients on a uniaxial mechanical pressure. (8 refs.)

62899 Optical method of determining the Curie point displacement in ferroelectric crystals under external effects. B.G.Mytsyk, N.A.Romanyuk (I. Franko State Univ., Lvov, Ukrainian SSR).

Ind. Lab. (USA), vol.48, no.6, p.581-3 (June 1982). Translation of: *Zavod. Lab. (USSR)*, vol.48, no.6, p.48-50 (June 1982). [received: March 1983] An optical method is proposed for determining the Curie point shift ΔT_c which is simpler in practical accomplishment as compared with electrical methods and is assured by a simple polarization-optics apparatus with photoelectrical recording of the optical radiation. (7 refs.)

62900 Fluctuations of composition and phase transition in ferroelectric SbSe_{0.40}Sn_{0.60}I. M.H.Amaral, M.R.Chaves (Lab. de Fisica, Univ. do Porto, Porto, Portugal), A.Levelut, S.Ziolkiewicz. *Port. Phys. (Portugal)*, vol.13, no.3-4, p.173-83 (1982).

The pyroelectric coefficient (λ) was investigated in crystals of SbSe_{0.40}Sn_{0.60}I and a notorious broadening of the transition when x increases is verified. Spontaneous polarization (P_s) for SbSe_{0.40}Sn_{0.60}I is deduced from λ and the broadening of the transition is analysed by assuming a non-homogeneous distribution of Se atoms through the sample. (9 refs.)

62901 Nature of the phase transition in K_{1-x}TaO₃. J.J.van der Klink, D.Rytz (Inst. of Experimental Phys., Swiss Federal, Inst. of Technol., Lausanne, Switzerland).

Phys. Rev. B (USA), vol.27, no.7, p.4471-4 (1 April 1983). The authors present dielectric, elastic, and NMR measurements that point at the special character of the phase transition in K_{1-x}Na_xTaO₃ mixed crystals. At the onset of birefringence, a critical behavior is observed in the dielectric constant and in the elastic compliance, whereas the NMR measurements do not reflect any criticality. It is suggested that, related to the transition, an off-center displacement of the sodium ions of less than 0.1 Å occurs. (19 refs.)

62902 Incommensurate phase and dielectric properties of crystals in the NaK-tartrate/NaNH₄-tartrate system. V.V.Gladkii, S.N.Kallaev, V.A.Kirikov, L.A.Shuvalov, N.M.Shechagina (A.V. Shubnikov Inst. of Crystallography, Acad. of Sci., Moscow, USSR).

Sov. Phys-Solid State (USA), vol.24, no.9, p.1488-90 (Sept. 1982). Translation of: *Fiz. Tverd. Tela (USSR)*, vol.24, no.9, p.2626-30 (Sept. 1982). [received: April 1983]

The results are given from a study of the dielectric properties arising from the dependence of the macroscopic quadrupole moment on the external mechanical stress and on the temperature of crystals of the NaK_{1-w}(NH₄)₂ tartrate system with $w=0.4$ and 0.85 (group III) or $w=0.94$ and 1 (group IV) near the ferroelectric phase transition. All the crystals examined had, at the transition, thermal anomalies in the spontaneous quadrupole moment measured in the absence of external mechanical stresses and in the quadrupole 'compliance', proportional to the ratio of the change in the quadrupole moment and the mechanical stress causing this change. It is shown that the nonlinear dependences of the quadrupole moment on the external stress, which are typical of incommensurate phases in ferroelectrics, exist only in the polar phases of group IV crystals. (12 refs.)

62903 Possible ferroelectric orientational phase transition induced by an electromagnetic field. V.I.Emel'yanov, Z.Zokhdi (M.V. Lomonosov State Univ., Moscow, USSR).

Sov. Phys-Tech. Phys. (USA), vol.27, no.9, p.1156-9 (Sept. 1982). Translation of: *Zh. Tekh. Fiz. (USSR)*, vol.52, no.9, p.1883-7 (Sept. 1982). [received: April 1983]

It is of interest to study the possibility of inducing orientational ferroelectric phase transitions with a light wave (the transitions would involve aligning the dipoles in a single direction). For such transitions to occur, it is necessary that there be positive feedback: The static field which arises as a result of the spontaneous ordering should induce additional ordering. The authors investigate two possible mechanisms for photoinduced feedback in systems having a dipole-dipole interaction. The dipole-dipole interaction, which reflects the cooperative character of the system, is taken into account phenomenologically by introducing an effective Lorentz field. The first (quasiresonance) mechanism is due to the fact that the frequency of an infrared molecular transition in quasiresonance with the frequency of the light wave is shifted when a static field arises in the medium (electrochromism). The more effective mechanism, however, is that due to the change in the dipole moment of an electronic transition of the molecules in the static field. (6 refs.)

Structural and thermal characterization of the γ' polymorph of Bi₂MoO₆.See Entry 61846

Two new phases with tetragonal bronze-like structure in the diagram: K₂O-CdO-Nb₂O₅.See Entry 61863

Evaluation of the valency of Fe, Cr, Cu, Sb doping ions in Pb(Zr_{0.95}Ti_{0.05})O₃ ceramicsSee Entry 61947

On the elastic anisotropy of ferroelectric triglycine selenateSee Entry 62012

Spin-phonon interactions in the Ising model with a transverse fieldSee Entry 62040

Electrodynamical study of the ellipticity of surface acoustic waves near the phase transition in Rochelle saltSee Entry 62228

⁸⁷Rb and ⁸⁵Rb NQR study of phase transitions in RbH₂(SeO₃)₂See Entry 62829

¹³C NMR investigations of the ferroelectric phase transition of tris-sarcosine calcium chlorideSee Entry 62835

Domain structure of ferroelectric crystals by electron microscope decoration techniqueSee Entry 62904

77.80D Domain structure and effects; hysteresis

62904 Domain structure of ferroelectric crystals by electron microscope decoration technique. B.Hilzer, C.Pawlaczyk, L.Szczepniak (Inst. of Molecular Phys., Acad. of Sci., Poznan, Poland), K.P.Meyer, R.Scholz. *Mater. Sci. (Poland)*, vol.7, no.4, p.427-39 (1981).

Electron microscope decoration studies of the domain structure of some ferroelectric crystals were performed. In TGS single crystals, the domain wall thickness as well changes in domain patterns during spontaneous ageing were studied. Moreover the domain structure of TGS crystals with lattice defects was investigated. For GASH single crystals the domain structure topography and the relationship between the domain structure and the switching and dielectric properties of the crystals were examined. (34 refs.)

Ferroelectricity of monoclinic RbD₂PO₄See Entry 62892

77.90 OTHER TOPICS IN DIELECTRIC PROPERTIES AND MATERIALS

62905 Dielectric friction on a moving ion. B.U.Felderhof (Inst. fur Theoretische Phys. A, RWTH, Aachen, Aachen, Germany).

Mol. Phys. (GB), vol.48, no.5, p.1003-18 (10 April 1983). The author considers the continuum model for dielectric friction on an ion moving in a fluid. The ion may have non-zero polarizability and the frequency dependent dielectric constant of the fluid may involve more than one relaxation time. The frequency dependent friction coefficient is calculated to second order in the change of the ion. The author shows that the Hubbard-Onsager theory of ionic mobility needs to be corrected. (16 refs.)

Influence of high pressure and shear strains on some electrophysical properties of polyphthalocyaninesSee Entry 62419

78.00 OPTICAL PROPERTIES AND CONDENSED MATTER SPECTROSCOPY AND OTHER INTERACTIONS OF MATTER WITH PARTICLES AND RADIATION

(for phonon spectra, see 63.)

78.20 OPTICAL PROPERTIES AND MATERIALS

(see also 81.40T Optical properties related to materials treatment; for masers, and lasers see 42.52 and 42.55 respectively)

62906 Light-induced degradation of semiconductor surfaces as studied by photoacoustic spectroscopy: photodarkening process of Zn_{0.5}Cd_{0.5}Ag_{0.5}Al_{0.5} phosphors. Y.Ohba, M.Mizuta, H.Kukimoto (Imaging Sci. & Engng. Lab., Tokyo Inst. of Technol., Yokohama, Japan).

Jpn. J. Appl. Phys. Part 2 (Japan), vol.22, no.3, p.L182-4 (March 1983). A photoacoustic technique has been applied for studying light-induced darkening of Zn_{0.5}Cd_{0.5}Ag_{0.5}Al_{0.5} phosphors in various gas ambients. The threshold energy and the rate for the light-induced darkening depend on the bandgap energy of the materials. The darkening process occurs effectively in the mixed ambient gases of N₂, CO₂ and H₂O which are the components of air. A bleaching process has also been observed in a mixture of O₂ and H₂O.

62907 To some phenomenological aspects of the optical dispersion in solids. P.Bussemer, U.Dietrich, B.Wilhelmi (Sektion Phys., Friedrich-Schiller Univ., Jena, Germany).

Exp. Tech. Phys. (Germany), vol.31, no.1, p.21-31 (1983). In German. The behaviour of the dispersion $n(\omega)$ for crystalline and amorphous materials is described by the one-oscillator model due to Wemple (1971). The predictions of this model for the $n-\nu$ diagram (ν -Abbe value) and the $\vartheta-\nu$ diagram (ϑ -relative partial dispersion) are proved. For a more exact discussion it is necessary to add a second oscillator, the location of which is correlated with that of the first oscillator. (11 refs.)

62908 Structure of reflection bands of Grandjean textures. A.Saape (Liquid Crystal Inst., Kent State Univ., Kent, OH, USA), G.Meier. *Phys. Rev. A (USA)*, vol.27, no.4, p.2196-200 (April 1983).

The characteristic exponents of the normal modes for light in the Grandjean texture of a cholesteric film were calculated with values for the dielectric constants that are typical for common cholesteric derivatives. The reflection properties are discussed in terms of the penetration depth given by the real part of the characteristic exponent. The results are presented in graphs which give the structure and the reflection coefficients as a function of wavelength and angle of incidence. It was found that there are unpolarized bands that are missing in a stability chart published earlier. (8 refs.)

62909 Photochromism and its origin of heat-treated Na₂O-BaO-Al₂O₃-TiO₂ glasses. T.Kokubo, T.Hirata (Inst. for Chem. Res., Kyoto Univ., Uji, Japan).

Yogyo-Kyokai-Shi (Japan), vol.90, no.1048, p.698-703 (1982). Glasses with various compositions in the systems (mNa₂O₅+mBaO)-AlO_{1.5}-SiO₂, where n/m is 1/0, 2/1, 1/1, 1/2 or 0/1, were heated to various temperatures from 650°C to 950°C at a rate of 5°C/min in a SiC furnace, and then cooled outside the furnace. All the glasses examined darkened on 60 min-irradiation of 365 nm light of 6 W ultraviolet lamp, after heating to certain temperatures depending on their compositions. On the surfaces of all the heat-treated specimens showing photochromism, an unknown crystalline phase, X, was detected. All the specimens containing the X phase, however, did not always show the photochromism. Consequently, the cause of the photochromism of the heat-treated glasses described above was attributed to defects, probably induced by impurities, in the X phase precipitated on the surfaces of the glasses. The X phase was observed on the surfaces of both the BaO-free glasses and Na₂O-free glasses. The fluorescence X-ray analysis of powders of a Na₂O₅-BaO-AlO_{1.5}-TiO₂ glass which had been heated to 700°C and immersed in a 2N NaOH solution at 95°C for 100 h showed that the X phase is deficient in Al and rich in Ti. (7 refs.)

Reflection of a plane monochromatic wave from a medium with spatial dispersionSee Entry 61080

Lateral interactions and vibrational lifetimesSee Entry 62229

78.20B General theory (for pure homogeneous materials)

- 62910** Diffusion of optical excitation at finite temperatures. D.L. Huber (Dept. of Phys., Univ. of Wisconsin, Madison, WI, USA). *J. Chem. Phys. (USA)*, vol.78, no.5, p.2530-2 (1 March 1983). The author studies diffusion of optical excitation as a function of the ratio of the temperature to the inhomogeneous linewidth Δ . When $T \ll \Delta$ the diffusion constant associated with one-phonon-assisted dipolar transfer over a Gaussian line is suppressed by the factor $\exp(-\Delta^2/T^2)$. The effect is attributed to a decrease in the effective density of ions participating in the transfer. (9 refs.)
- Absorption of light by a crystal in the presence of additional high-power laser illumination See Entry 62936

78.20D Optical constants and parameters

- 62911** Differential refractive indices of star-shaped and linear polystyrenes. Siao Fang Sun, D.Chao, S.Lin (Dept. of Chem., St. John's Univ., Jamaica, NY, USA). *Polym. Commun. (GB)*, vol.24, no.3, p.84-6 (March 1983). The differential refractive indices of star-shaped and linear polystyrenes have been studied in good solvents (benzene, dioxane) and poor solvents (cyclohexane, 71.4% dioxane-28.6% methanol, v/v) over the temperature range 25°-55°C. It was found that the change in differential refractive index with temperature gives a straight line in all the solvents for the linear polystyrene, but not for the star-shaped polystyrene. From the original data of the differential refractive index as a function of temperature, two parameters were evaluated for each polymeric system: the temperature coefficient and the activation energy. The results suggest that there is a difference in the polarizability of the two polymers under the same conditions. The polarizability of the linear polystyrene is constraint free, while that of the star-shaped polystyrene is constrained. (12 refs.)
- 62912** Optical activity of β,γ -enones: a quantitative chirality rule. P.H. Schippers, H.P.J.M. Dekkers (Dept. of Theoretical Organic Chem., Univ. of Leiden, Leiden, Netherlands). *J. Am. Chem. Soc. (USA)*, vol.105, no.1, p.79-84 (12 Jan. 1983). Generally the relation between molecular geometry and circular dichroism (CD) of an electronic transition is made via the rotational strength R , which contains the scalar product of the magnetic ($\vec{\mu}$) and electric (\vec{R}) dipole moment in that transition. It is assumed that with β,γ -enones the optical properties of the $n \rightarrow \pi^*$ transition derive from a perturbation of the local $n_{CO} \rightarrow \pi^*_{CO}$ transition in the carbonyl chromophore by the remaining part of the molecule. Since the $n_{CO} \rightarrow \pi^*_{CO}$ transition is strongly magnetic dipole allowed (along the C=O bond, z direction) but electric dipole forbidden, the rotational strength in β,γ -enones probes the z component of the admixed extraneous transition moment R , whose magnitude is measured by the square root of the dipole strength D . It appears advantageous to express the optical activity as $R/(\vec{\mu} \cdot D)^{1/2} = \cos \theta$ since then it no longer contains the magnitude of \vec{r} and is a direct measure of the angle θ between the C=O bond and the direction of the admixed electric dipole transition moment. For a series of rigid β,γ -enones, a surprisingly high correlation is found between $\cos \theta$ and the cosine of the angle ξ between the C=O bond and the $C_{\alpha} = C_{\beta}$ bond: to a good approximation, $n \rightarrow \pi^*$ optical activity and enone structure are quantitatively related by the equation $\cos \theta = -(\text{sign } xy) \cdot (\cos \xi)$, where x and y are the coordinates of the olefine C_{β} atom in the ketone reference frame and xy is positive in the upper-right quadrant. This transport relationship indicates that the unique radiative properties of the $n \rightarrow \pi^*$ state of β,γ -enones derive from a small ethylenic $\pi_{CC} \rightarrow \pi^*_{CC}$ contamination in the carbonyl $n_{CO} \rightarrow \pi^*_{CO}$ state, which might be electrostatically brought in. Within limits, the chirality rule offers a quantitative tool in the study of β,γ -enone stereochemistry, as is illustrated for some examples. (38 refs.)
- 62913** Near-infrared refractive index of bismuth germanium oxide ($\text{Bi}_{12}\text{GeO}_{20}$). E. Burattini (Istituto Nazionale di Fisica Nucleare, Frascati, Italy), G. Cappuccio, M. Grandolfo, P. Vecchia, Sh. M. Efendiev. *J. Opt. Soc. Am. (USA)*, vol.73, no.4, p.495-7 (April 1983). The dispersion of the refractive index of $\text{Bi}_{12}\text{GeO}_{20}$ in the range 1.2-5.0 μm at room temperature has been obtained. Data have been analyzed in terms of Ketteler, Sellmeier-Drude, Lorentz-Lorenz, and Herzberger dispersion formulas. It is found that a Herzberger formula completely describes data on $n(\lambda)$ up to the visible region. (13 refs.)
- 62914** Determination of cubic optical susceptibilities of liquid crystals by coherent four-photon spectroscopy. L.S. Aslanyan, N.N. Badalyan, A.A. Petrosyan, M.A. Khurshudyan, Yu.S. Chilingaryan. *Opt. & Spectrosc. (USA)*, vol.53, no.1, p.54-8 (July 1982). Translation of: *Opt. & Spektrosk. (USSR)*, vol.53, no.1, p.94-9 (July 1982). [received: April 1983]. The cubic optical susceptibility tensor of the nematic liquid crystal MBBA (*N*-p-methoxy-benzylidene-p-butylaniline) close to the Raman resonance with $\Delta\nu = 1164 \text{ cm}^{-1}$ has been investigated using the method of active Raman spectroscopy. The components of the tensor $\chi_{ijkl}^{(3)}$ were measured first for a homeotropic sample. The composite-sample method employed in the experiment made it possible to measure the absolute value of the resonance and nonresonance constituents of several components of the third-order nonlinear optical susceptibility for MBBA in the nematic phase. Almost a complete set of values was measured for the component of cubic susceptibility, and this is sufficient for determining parameters of the order of S_2 and S_4 . (15 refs.)
- 62915** Ellipsometric investigation of oxidation processes of tin in solid and liquid states. I.A. Shaikievich, P.I. Drozd, L.V. Poprenko, N.V. Sopinskii. *Opt. & Spectrosc. (USA)*, vol.53, no.1, p.84-7 (July 1982). Translation of: *Opt. & Spektrosk. (USSR)*, vol.53, no.1, p.145-9 (July 1982). [received: April 1983]. Measurements are carried out on the optical constants of tin in the liquid and solid states by the Beattie method with the oxide film formed on the surface taken into account. The growth kinetics of the oxide layer on liquid tin is studied with the use of a mechanical cleaning of the surface during the measurement. Ion bombardment was used for cleaning the oxide layer from the tin surface in the solid state. The thicknesses and refractive index of the oxide layer on the tin surface were calculated within the framework of transition-layer theory. (12 refs.)
- 62916** Determination of volume and surface optical properties of materials by internal-reflection spectra. G.M. Mansurov, N.N. Rozanov, V.M. Zolotarev, S.M. Sutovskii. *Opt. & Spectrosc. (USA)*, vol.53, no.2, p.175-8 (Aug. 1982). Translation of: *Opt. & Spektrosk. (USSR)*, vol.53, no.2, p.301-6 (Aug. 1982). [received: April 1983]. Within the framework of the frustrated total-internal-reflection (FTIR) effect in the first order of the theory of small perturbations with regard to the

deviation of the permittivity of the specimen from its bulk value, an analytical expression is obtained for the amplitude reflection coefficient of s- and p-polarized light and the general form of the permittivity profile in the surface layer. A method is proposed that permits excluding the effect of the surface layer in determining the optical characteristics of the materials in the volume from the internal-reflection spectra. It is demonstrated in the example of studying the KU-1 glass that by using FTIR spectra the method proposed permits realizing a transition from the averaged effective permittivity values that are observed with the traditional methods of processing the spectra (if the influence of the surface layer is not taken into account) to the actual parameters that characterize the properties of the substance in volume and in the surface layer. (11 refs.)

- 62917** Optical properties of CVD-coated TiN, ZrN and HfN. B. Karlsson, R.P. Shimshock, B.O. Seraphin (Optical Sci. Center, Univ. of Arizona, Tucson, AZ, USA), J.C. Haygarth. *Sol. Energy Mater. (Netherlands)*, vol.7, no.4, p.401-11 (Jan.-Feb. 1983). The reflectivities of TiN, ZrN and HfN have been measured in the spectral energy range 0.1 to 6.2 eV. The optical constants have been determined by means of a Kramers-Kronig analysis. A separation into interband transitions and free electron behaviour was carried out. The extended free electron region is explained and the interband transitions are compared with allowed transitions in the density of states distribution. The possibility of improving the optical selectivity by shifting E_F is discussed. (28 refs.)
- 62918** Determination of the optical constants and thickness of amorphous V_2O_5 thin films. L. Michailovits, I. Hevesi, Liem Phan, Z. Varga (Inst. of Experimental Phys., Attila Jozsef Univ., Szeged, Hungary). *Thin Solid Films (Switzerland)*, vol.102, no.1, p.71-6 (8 April 1983). Amorphous V_2O_5 films of various thicknesses were prepared on glass substrates by vacuum evaporation. The transmission of the V_2O_5 film/substrate system and that of the substrate were measured in the wavelength range 550-2500 nm. The optical constants and thickness of the films were determined by an improved optical interference method. (9 refs.)
- 62919** Refractive index in epitaxial $\text{Pb}_{1-x}\text{Sn}_x\text{Te}$ films. K.V. Kozhukh, T.A. Kudrykina, I.A. Samoilova, G.A. Fedorus. *Ukr. Fiz. Zh. (USSR)*, vol.28, no.3, p.362-5 (March 1983). In Russian. Transmission spectra of epitaxial $\text{Pb}_{0.83}\text{Sn}_{0.17}\text{Te}$ films of n- and p-type are measured at 100, 300 and 400K within 5-15 μm wave-lengths and carrier concentration ranges of $6 \cdot 10^{19}$ - $9 \cdot 10^{18} \text{ cm}^{-3}$. The following parameters are determined: wave length dependence of the refractive index, high-frequency dielectric constants, effective carrier masses at the Fermi level in specimens with different carrier concentration, longitudinal high-frequency phonon energy $\hbar\omega_{LO} = 16.6 \pm 0.8 \text{ meV}$. A linear decrease is shown for the refractive index linearly with growth in the current carrier concentration. (10 refs.)
- 62920** Quantum chemical modelling of optical properties of simple and oxide clusters. H. Dunker (Sektion Chemie, Friedrich Schuller Univ., Jena, Germany). *Wiss. Z. Friedrich-Schiller-Univ. Jena, Math. Naturwiss. Reihe (Germany)*, vol.31, no.6, p.975-86 (1982). In German. The electronic transition energy values and the oscillator strength of small and oxide-clusters are calculated by means of simple quantum chemical approximation-method (HMO). The theoretical values of the refractive index are in a good agreement with experimental data. The refractive index ($\lambda = \text{const}$) of oxide-clusters increases with the degree of aggregation and decreases with the bond strength and the differences of electronegativity of the M-O bond. (24 refs.)
- Determination of optical constants by photometry See Entry 59824
- Method of measuring the refractive indices of absorbing media See Entry 59831
- Measurement of weak laser light absorption in materials transparent to infrared radiation See Entry 59862
- Nonlinear absorption of light in glassy arsenic sulfide fibers in the energy range $\hbar\nu < E_g$ See Entry 61297
- Physical properties of liquid crystals of 4-(4-alkylbicyclo[2,2,2]octyl)benzonitriles See Entry 61793
- A new method for determining the elastic constant ratio K_{33}/K_{11} in nematic liquid crystals See Entry 61796
- Radiation induced effects and annealing methods in fiber optics and glasses See Entry 61966
- Radiation-induced transmission loss in optical materials at infrared wavelengths See Entry 61967
- Ion implantation effects in glasses See Entry 61992
- Optical, chemical and mechanical modifications induced by ion implantation on glass surfaces See Entry 61993
- Observation of an orientational polarizability of dipolar molecules adsorbed in fine-pore membranes See Entry 62276
- Effect of electron bombardment on the phase transition in VO_2 films See Entry 62339
- The polariton in CdSe: measurement of time of flight and nonlinear transmission See Entry 62347
- Precise millimeter-wave measurements of complex refractive index, complex dielectric permittivity and loss tangent of GaAs, Si, SiO_2 , Al_2O_3 , BeO, Macor, and glass See Entry 62873
- Nonlinear susceptibility of impurity centres in semiconductors See Entry 62933
- Permittivity anisotropy of InAs and $\text{Cd}_{0.25}\text{Hg}_{0.75}\text{Te}$ induced by electron drift. Contribution of quantum corrections See Entry 62934
- Raman and luminescence studies of alkali borate tungstate glasses See Entry 62962
- Kramers-Kronig analysis of the reflection spectra of $\text{Ba}_2\text{NaNb}_2\text{O}_{15}$ See Entry 63015
- Electroreflection of ground-state excitons in $\text{Al}^{\text{III}}\text{B}^{\text{VI}}$ crystals See Entry 63017
- Study of electronic structure of reduced TiO_2 and $\text{V}_2\text{Ti}_{1-x}\text{O}_2$ crystals by ESCA and optical absorption See Entry 63018
- Electrical and optical properties of a-Si $_x$ C $_{1-x}$:H film prepared by GD SiH_4 and C_2H_4 See Entry 63065
- Influence of Ag photodoping on photoinduced changes in As_2S_3 glass films See Entry 63066
- Optical anisotropy and electrostriction in the anodic oxide of molybdenum See Entry 63067
- Optical anisotropy and electrostriction in the anodic oxide of niobium See Entry 63068

A numerical method for determining the complex refractive index from reflectance and transmittance of supported thin films See Entry 63070

Single crystal growth and physical properties of cubic $\text{Zn}_2\text{O}(\text{BO}_2)_2$ See Entry 63151

Composition, optical properties and degradation modes of Cu/(graded metal-carbon) solar selective surfaces See Entry 63728

78.20E Optical rotatory power

62921 Corrections to Maxwell boundary conditions in gyrotropic crystals. E.L.Ivchenko, A.V.Selkin. *Opt. & Spectrosc. (USA)*, vol.53, no.1, p.58-63 (July 1982). Translation of: *Opt. & Spektrosk. (USSR)*, vol.53, no.1, p.100-8 (July 1982). [received: April 1983]

Within the framework of the theory of additional light waves the limiting transition is performed to the longwave spectral region relative to the exciton resonance. As a result a physical explanation is given of the corrections to the Maxwell boundary conditions within the nonresonance frequency region for crystals with spatial dispersion, in particular for gyrotropic crystals. These corrections are shown to appear after exclusion of strongly damped (supplementary) light waves from the Maxwell boundary conditions by means of supplementary boundary conditions. An analysis is performed of the supplementary boundary conditions within the resonance region of frequencies for gyrotropic crystals from the standpoint of the fulfilment of the energy conservation law and the principle of symmetry of kinetic coefficients. (11 refs.)

A tunable 90° rotator using a total reflection by a monodomain cholesteric liquid crystal cell See Entry 61258

Interference of light in birefringent plates with optical activity and absorption See Entry 62924

Induced gyrotropy, birefringence, and dichroism in semiconductors excited by picosecond light pulses See Entry 62925

Measuring the piezogyration constants of cubic crystals See Entry 62931

Electrogyration in cubic alkaline earth nitrates See Entry 62939

78.20F Birefringence

(inc. stress birefringence, flow birefringence, etc)

62922 The degree of order in liquid crystalline side chain polymers [from optical observations]. H.Finkelmann, H.Bentack, G.Rehage (Inst. für Phys. Chem., Tech. Univ. Clausthal, Clausthal-Zellerfeld, Germany). *J. Chim. Phys. & Phys.-Chim. Biol. (France)*, vol.80, no.1, p.163-71 (Jan. 1983).

The order parameter S of liquid crystalline (LC) side chain polymers is compared with the order parameter of corresponding low molar mass LCs by measurements of the birefringence and of the linear dichroism of dye probes. It has been shown that the temperature dependence of S is identical for monomers and for polymers. For the LC polymers, however, the magnitude of S is about 10% smaller than S of the LC monomers. If the mesogenic molecules are linked via different flexible spacers to the backbone no change of S is observed. The nematic and smectic polymers that have been investigated exhibit a glassy state at low temperatures. Below the glass transition S is frozen in and does no longer change with temperature. (31 refs.)

62923 Selective light scattering by disperse birefringent media with an isotropic point. A.Kh.Zilbershtein, L.E.Solovov. *Opt. & Spectrosc. (USA)*, vol.53, no.2, p.196-7 (Aug. 1982). Translation of: *Opt. & Spektrosk. (USSR)*, vol.53, no.2, p.336-9 (Aug. 1982). [received: April 1983]

Investigates the selective character of light scattering due to the existence of a point of inversion of birefringence. It has been well known for a long time that finely dispersed isotropic bodies immersed in a liquid with a near refractive index demonstrate minimal scattering in that region of the spectrum where intersection of the dispersion curves (IDC) takes place. The well-known Christiansen filters are based on this phenomenon. It has been shown that in solid state two-component systems the Christiansen phenomenon is observed so distinctly that it has been possible to make narrow band optical filters for the IR region with a high transmission coefficient. (12 refs.)

62924 Interference of light in birefringent plates with optical activity and absorption. A.F.Konstantinova, A.I.Okorochnik, E.M.Uyukin (Inst. of Crystallography, Acad. of Sci., USSR). *Sov. Phys.-Crystallogr. (USA)*, vol.27, no.5, p.601-3 (Sept.-Oct. 1982). Translation of: *Kristallografiya (USSR)*, vol.27, no.5, p.1002-4 (Sept.-Oct. 1982). [received: April 1983]

The authors discuss the question: do dichroism and optical activity affect the results of measurements of changes in birefringence in optically active absorbent crystals? They consider the problem of determining the intensity of light after passage through the system polarizer-optically active absorbent crystal-analyzer for any arbitrary orientation of the optic axis of the crystal relative to the wave normal of the incident light beam. The problem is solved for the case of normal incidence of light on the plate, without taking account of multiple reflections or of the phase change at the boundary of the absorbent crystal. (12 refs.)

62925 Induced gyrotropy, birefringence, and dichroism in semiconductors excited by picosecond light pulses. A.A.Polyakov, V.N.Trukhin, I.D.Yaroshetskii. *Sov. Tech. Phys. Lett. (USA)*, vol.8, no.8, p.439-40 (Aug. 1982). Translation of: *Pisma v Zh. Tekh. Fiz. (USSR)*, vol.8, no.15-16, p.1018-21 (Aug. 1982). [received: April 1983]

Reports the picosecond observation of optically induced gyrotropy, birefringence, and dichroism in semiconductors, specifically, silicon and gallium arsenide. To study these effects the authors used a picosecond test beam method, which consists of studying the change caused in the polarization of a test beam by the intense pump light pulse. The light source is a YAG:Nd³⁺ laser in mode-locked operation producing a train of picosecond pulses. (7 refs.)

Observation of a new memory effect in a modulated structure See Entry 61905

Optical method of determining the Curie point displacement in ferroelectric crystals under external effects See Entry 62899

78.20H Piezo-, elasto- and acousto-optical effects

62926 Elastooptic properties of InP. N.Suzuki, K.Tada (Dept. of Electronic Engng., Univ. of Tokyo, Tokyo, Japan). *Jpn. J. Appl. Phys. Part 1 (Japan)*, vol.22, no.3, p.441-5 (March 1983). All of the elastooptic coefficients p_{11} , p_{12} and p_{44} in InP have been measured in the wavelength region from 1.06 μm to 1.50 μm at room temperature. The measurement has been carried out by the Dixon-Cohen method, but correction of acoustic wave diffraction, which causes large error in a measurement especially under the Raman-Nath diffraction condition, is made using a simple approximation. InP has a large elastooptic figure of merit comparable to that of GaAs. Using the obtained elastooptic coefficients, dispersion of strain-optic coefficients has been derived. The deformation potentials estimated from this analysis are $a \approx -(11 \pm 3)$ eV, $b \approx -(1.5 \pm 1.5)$ eV and $d \approx -(2.8 \pm 1.2)$ eV. (21 refs.)

62927 Piezochroism of swelled polymer solutions. Y.Ogo, Y.Nishino, T.Sato (Dept. of Appl. Chem., Osaka City Univ., Osaka, Japan). *High Temp.-High Pressures (GB)*, vol.14, no.3, p.319-22 (1982). (10th Plansee Seminar on 'Trends in Refractory Metals, Hardmetals, and Special Materials, and their Technology', Reutte, Austria, 1-5 June 1981). Piezochroic shifts (pressure colour changes) were observed for swelled poly(*N*-methyl methacrylamide) in benzonitrile, methyl benzoate, chlorobenzene, benzonitrile-toluene mixture, and α -methylstyrene-toluene mixture. These phenomena are explained on the basis of light scattering by the difference in refractive index of the transparent heterogeneous phases, as in the Christiansen filter effect. (2 refs.)

62928 Rayleigh-Brillouin scattering of transverse and longitudinal acoustic waves in a supercooled viscoelastic liquid. C.H.Wang, Quan-L. Liu (Dept. of Chem., Univ. of Utah, Salt Lake City, UT, USA). *J. Chem. Phys. (USA)*, vol.78, no.7, p.4363-73 (1 April 1983). Rayleigh-Brillouin spectra of 3-phenyl propanol are studied over the temperature range from -119.5° to 98.1°C . The orientation relaxation time is obtained as a function of temperature. The depolarized spectra exhibit clear shear wave sidebands at temperatures below -29.5°C . The polarized spectra give peaks due to the longitudinal acoustic wave whose frequency displays kinks at the glass transition temperature and at 37°C (T_g). T_g is 55°C above the melting temperature (-18°C). The shear wave frequency decreases linearly with increasing temperature. The experimental results on the VH scattering spectra are analyzed according to viscoelastic theories based upon the Voigt and Maxwell models. Comparison of the theory with observed spectra shows that the Voigt model gives a better fit to the experimental data. Microscopic theory has also been developed to derive the Voigt and Maxwell models. Angular dependent studies are proposed to differentiate the various theories which give different predictions about the physical nature of the parameters. (35 refs.)

62929 On the theory of the nonlinear acousto-optical effect in semiconductors. Hoang Ngoc Cam, Nguyen Van Hieu, Ha Vinh Tan (Inst. of Phys., Nat. Center of Sci., Research of Vietnam, Hanoi, Vietnam). *Phys. Status Solidi b (Germany)*, vol.116, no.1, p.25-9 (1 March 1983). The modulation of the dielectric susceptibility of direct band gap semiconductors due to the interaction with sound wave is considered up to second order of the deformation tensor. The role of the Coulomb interaction between electrons and the holes, i.e. that of exciton states with discrete and continuous energies, is taken into account. (11 refs.)

62930 Modulation piezoeffectance of cubic polycrystals. L.Bocanek, J.Musilova (Dept. of Solid State Phys., J.E. Purkyne Univ., Brno, Czechoslovakia).

Phys. Status Solidi a (Germany), vol.75, no.2, p.555-8 (16 Feb. 1983). A method for evaluating the hydrostatic component of the piezoeffectance tensor by means of two measurements of the AC piezoeffectance spectra of polycrystalline germanium in polarized light is given. (6 refs.)

62931 Measuring the piezogyration constants of cubic crystals. G.A.Babonas, A.A.Reza (Inst. of Phys. of Semiconductors, Acad. of Sci., Lithuanian SSR).

Sov. Phys.-Crystallogr. (USA), vol.27, no.5, p.559-61 (Sept.-Oct. 1982). Translation of: *Kristallografiya (USSR)*, vol.27, no.5, p.932-5 (Sept.-Oct. 1982). [received: April 1983]

The authors propose a method of investigating the piezogyration effect in nonabsorbing cubic crystals; this represents the change in the components of the gyration tensor under external mechanical stresses, and is determined by an axial tensor of the fourth rank. The authors give the results of an experimental investigation of this effect for crystals of bismuth germanate. (18 refs.)

62932 Dynamics of ultrasound-induced diffraction effects in a nematic liquid crystal oriented with a magnetic field. A.I.Popov, S.V.Pasechnik, V.F.Nozdrev, V.A.Balandin.

Sov. Tech. Phys. Lett. (USA), vol.8, no.8, p.431-3 (Aug. 1982). Translation of: *Pisma v Zh. Tekh. Fiz. (USSR)*, vol.8, no.15-16, p.998-1002 (Aug. 1982). [received: April 1983]

Studies the effect of a longitudinal ultrasonic wave on a homeotropically oriented layer of methoxy benzylidene butylaniline (MBBA) between two transparent plates. The ultrasound wave vector is directed along the Z axis, normal to the unit vector (the director, \hat{n}_0) of the optic axis of the single-domain nematic liquid crystal when unperturbed by the acoustic field. The magnetic induction B is parallel to \hat{n}_0 . Changes in the orientational structure are detected with a light beam propagating normal to the surface of the plates. The sample can be scanned along the Z axis with a change in the thickness h of the liquid-crystal layer over the range 5×10^{-3} to 10^{-3} m. It was found that light diffraction occurs when the MBBA layer is subjected to ultrasound at 4 MHz at an intensity above a certain threshold, which is, for example, $0.37 \times 10^3 \text{ W/m}^2$ at $T = 22^\circ\text{C}$, $h = 5 \times 10^{-4}$ m, and $B = 0$. The intensity and sharpness of the diffraction peaks depend on Z . (5 refs.)

On the elastic anisotropy of ferroelectric triglycine selenate See Entry 62012
Single crystal growth and physical properties of cubic $\text{Zn}_2\text{O}(\text{BO}_2)_2$ See Entry 63151

78.20J Electro-optical effects

62933 Nonlinear susceptibility of impurity centres in semiconductors. Yu.P.Drozhev (Moscow State Univ., Moscow, USSR).

Phys. Status Solidi b (Germany), vol.116, no.1, p.111-18 (1 March 1983). The nonlinear susceptibility coefficient responsible for the rotation of the light polarization vector in electromodulation experiments, is shown to exhibit a certain structure at a frequency corresponding to the impurity ionization energy. The influence of a strong modulation field and a random field upon the phenomena considered is discussed. (10 refs.)

62934 Permittivity anisotropy of InAs and $\text{Cd}_{0.25}\text{Hg}_{0.75}\text{Te}$ induced by electron drift. Contribution of quantum corrections. L.E.Vorob'ev, V.I.Stafeev, A.Yu.Ushakov, D.A.Firsov (M.I. Kalinin Polytech. Inst., Leningrad, USSR). *Sov. Phys.-Semicond. (USA)*, vol.16, no.10, p.1175-6 (Oct. 1982). Translation of: *Fiz. & Tekh. Poluprovodn. (USSR)*, vol.16, no.10, p.1831-3 (Oct. 1982). [received: April 1983]

An investigation was made of the electric-field dependence of the difference between the refractive indices associated with the electron contribution in the case of light polarized parallel and perpendicular to the field. The investigation was carried out on n -type InAs at $T=80\text{K}$. An analysis of the results obtained for light of the wavelengths $\lambda=10.6$ and $3.39\text{ }\mu\text{m}$ and a comparison with theoretical calculations led to the conclusion that a considerable contribution to the refractive index anisotropy of quantum corrections was made by interband virtual transitions in the case when $\epsilon_0 \approx \hbar\omega$. A similar effect was observed for light of the wavelength $\lambda=10.6\text{ }\mu\text{m}$ at $T=80\text{K}$ or higher in the case of n -type $\text{Cd}_{0.25}\text{Hg}_{0.75}\text{Te}$ in which case the contribution of the quantum corrections was also important. The agreement between the theory and experiment was good. (7 refs.)

62935 Influence of the absorption of light by free carriers on their ambipolar drift. Z.S.Gribnikov (Inst. of Semiconductors, Acad. of Sci., Kiev, Ukrainian SSR). *Sov. Phys.-Semicond. (USA)*, vol.16, no.10, p.1183-5 (Oct. 1982). Translation of: *Fiz. & Tekh. Poluprovodn. (USSR)*, vol.16, no.10, p.1843-6 (Oct. 1982). [received: April 1983]

It is shown that a strong density modulation can be expected in the case of ambipolar drift of an electron-hole plasma heated weakly by periodically space-modulated radiation absorbed by free carriers. Calculations are carried out in the approximation of an electron-hole temperature. It is shown that for asymptotically large currents the contrast of a density 'grating' is greater than that of the original radiation 'grating'. For intermediate currents of the ambipolar drift a phase shift appears between the density and radiation gratings and this is necessary for the energy exchange between beams forming a radiation grating. (2 refs.)

62936 Absorption of light by a crystal in the presence of additional high-power laser illumination. V.A.Pazderskii (V.I. Lenin State Univ., Tashkent, USSR).

Sov. Phys.-Semicond. (USA), vol.16, no.10, p.1222-3 (Oct. 1982). Translation of: *Fiz. & Tekh. Poluprovodn. (USSR)*, vol.16, no.10, p.1896-9 (Oct. 1982). [received: April 1983]

The absorption of light by a crystal in the presence of an additional strong electromagnetic field has been investigated on many occasions. A strong electromagnetic field modifies the electron spectrum of a crystal, which gives rise to special features in the frequency dependence of the absorption coefficient of a weak electromagnetic field (wave). Recent experiments on the influence of a strong electromagnetic field on the energy spectrum of carriers have failed to confirm some of the theoretical predictions. The author therefore reviews the problem. (8 refs.)

62937 Electrochromic coloring of vanadium (V) oxide. V.I.Gavriluk, I.M.Chernenko (Russia-Ukraine-Union Tercentennial Anniversary State Univ., Dnepropetrovsk, USSR).

Sov. Phys.-Tech. Phys. (USA), vol.27, no.10, p.1308-9 (Oct. 1982). Translation of: *Zh. Tekh. Fiz. (USSR)*, vol.52, no.10, p.2125-6 (Oct. 1982). [received: April 1983]

New information is obtained concerning the physical processes which occur during electrochromism in V_2O_5 by studying colored V_2O_5 single crystals using X-ray diffraction (phase analysis), thermogravimetry, and differential thermal analysis. The decreased mass of colored V_2O_5 for $T=300\text{-}490\text{K}$ and the absorption of heat are due to dehydration of the sample. The irreversible exothermal process which occurs for $T=545\text{-}590\text{K}$ and is the same for oxidizing or neutral atmospheres is characterized by a constant sample mass and cannot be attributed to oxidation or reduction of the sample. This constant-mass exothermal phase is probably due to restructuring (ordering) of the colored region of the crystal. The increase in the mass of colored V_2O_5 for $T>640\text{K}$, which occurs only in an oxidizing environment, may be attributed to oxidation of the sample if it is assumed that the sample was electrochemically reduced during electrochromic coloration. (4 refs.)

62938 Effect of an electric field on the photochromic effect in $\text{Bi}_{12}\text{GeO}_{20}\text{:Mn}$ crystals. Ya.V.Burak, A.S.Sai, I.V.Slonskii.

Sov. Tech. Phys. Lett. (USA), vol.8, no.8, p.430-1 (Aug. 1982). Translation of: *Pisma v Zh. Tekh. Fiz. (USSR)*, vol.8, no.15-16, p.996-8 (Aug. 1982). [received: April 1983]

The influence of the electric field on the photochromic effect does not depend on the polarity of the field or on whether the transparent electrode is in contact with the surface of the sample. These observations imply a purely field mechanism for the effect of the electric field. The photochromic effect in $\text{Bi}_{12}\text{GeO}_{20}\text{:Mn}$ is evidently caused by charge-transfer transitions which change the valence of the manganese ions. Since the $\text{Bi}_{12}\text{GeO}_{20}$ crystal is a good piezoelectric, the application of an electric field causes a polarization and creates stresses in the sample by virtue of the piezoelectric effect. This evidently results in slight changes in the conditions under which the manganese ions responsible for the photochromic effect are found, and the photochromic effect is intensified. (1 ref.)

62939 Electrogyration in cubic alkaline earth nitrates. H.-J.Weber (Inst. fur Kristallographie, Univ. zu Koln, Koln, Germany).

Z. Kristallogr. (Germany), vol.161, no.1-2, p.145-53 (1982). The authors have measured the electrogyration effect in $\text{Sr}(\text{NO}_3)_2$, $\text{Ba}(\text{NO}_3)_2$, and $\text{Pb}(\text{NO}_3)_2$ as a function of temperature and wavelength. Only $\text{Pb}(\text{NO}_3)_2$ displays a slight temperature dependence. The optical transitions responsible for electrogyration are centred between the onset of absorption and the resonance determined by the dispersion of refractive indices. A latent chirality of O^{2-} arrangements as the main source of the effect is suggested. (16 refs.)

Electroreflectance vibrational spectroscopy: a new surface analysis technique using diode lasers See Entry 59860

A miniature modulator See Entry 61198

Mechanism for local charge transport on the surface of a transparent ferroelectric ceramic See Entry 62478

Possible ferroelectric orientational phase transition induced by an electromagnetic field See Entry 62903

Electroreflection of ground-state excitons in $\text{A}^{\text{II}}\text{B}^{\text{VI}}$ crystals See Entry 63017

Transparent conductors—a status review See Entry 63078

Single crystal growth and physical properties of cubic $\text{Zn}_3(\text{BO}_3)_2$ See Entry 63151

78.20L Magneto-optical effects

62940 Magnetopolaritons in ZnTe. W.Maier, G.Schmieder (Max-Planck-Inst. fur Festkörperforschung, Grenoble, France), C.Klingshörn.

Z. Phys. B (Germany), vol.50, no.3, p.193-208 (1983). From an invariant expansion, the authors construct the exciton Hamiltonian for the $\Gamma_6 \times \Gamma_8$ excitons in the T_6 -type material ZnTe represented by an 8×8 matrix including the influences of a finite wave vector and an external magnetic field. They diagonalise the Hamiltonian matrix to obtain the exciton states. Then the excitons are coupled to the electromagnetic radiation field thus giving the polariton states. The theoretical dispersion curves are fitted to the results of two-photon Raman scattering and reflection experiments in magnetic fields up to 22 T. From this fit the authors deduce precise values for the eigenenergies, exciton masses, g -factors, and diamagnetic shifts. (34 refs.)

62941 Absorption line of magnetically anisotropic particles. R.S.Gekht (L.V. Kirenski Inst. of Phys., Acad. of Sci., Krasnoyarsk, USSR).

Fiz. Met. & Metalloved. (USSR), vol.55, no.2, p.225-9 (Feb. 1983). In Russian. English translation in: *Phys. Met. & Metallogr. (GB)*. An analysis is made of the profile and intensity of an absorption line of magnetically anisotropic particles subjected to a static magnetic field and this is done for various values of the ratio of the temperature T to the volume V of a particle. It is shown that the range of low values of T/V the line profile is asymmetric and the line width in the strongest field H_0 is independent of the sign of the anisotropy constant K of the particles but is proportional to the ratio $|K|T/H_0 M^2 V$. In the range of weak magnetic fields the line width depends strongly on the sign of K : if $K>0$, it is proportional to T/MV , whereas for $K<0$, it is proportional to $(|K|T/M^2 V)^{1/2}$. (10 refs.) A.T.

62942 Magneto-optical TE-TM mode conversion in $(\text{YNd})_2\text{Fe}_2\text{O}_{12}$ films. T.Okuda, N.Koshizuka, K.Ando (Electrotech. Lab., Ibaraki, Japan).

J. Magn. & Magn. Mater. (Netherlands), vol.31-34, pt.2, p.933-4 (Feb. 1983). (Proceedings of the International Conference on Magnetism, Kyoto, Japan, 6-10 Sept. 1982).

$(\text{YNd})_2\text{Fe}_2\text{O}_{12}$ films with in-plane magnetization for magneto-optical use were successfully grown by liquid phase epitaxy. High power conversion ratios ($>80\%$) were found. The growth temperature dependence of the observed film birefringence is larger than that of the birefringence resulting from the stress induced by lattice mismatch. (8 refs.)

62943 Spectroscopic and magneto-optical properties of quasi 1D antiferromagnets AVX_3 ($\text{A}=\text{Cs, Rb}$; $\text{X}=\text{Cl, Br, I}$). A.Häuser, H.U.Gudel (Inst. for Anorganische Chem., Univ. Bern, Bern, Switzerland).

J. Magn. & Magn. Mater. (Netherlands), vol.31-34, pt.3, p.1239-40 (Feb. 1983). (Proceedings of the International Conference on Magnetism, Kyoto, Japan, 6-10 Sept. 1982).

Single crystal absorption and Zeeman experiments on the $^4\text{A}_{2g} \rightarrow ^2\text{T}_{2g}$ transitions in CsVBr_2 show evidence of both 1D and 3D magnetic ordering. (7 refs.)

62944 An investigation of diffraction efficiency of magneto-optic deflection in garnet film. G.Tielian, He Yuchuan (Southwest Inst. of Appl. Magnetics, Mianyang, Sichuan, China).

J. Magn. & Magn. Mater. (Netherlands), vol.35, no.1-3, p.161-3 (March 1983). (Proceedings of the 10th International Colloquium on Magnetic Films and Surfaces, Yokohama, Japan, 13-16 Sept. 1982). A more precise analytic expression for the diffraction efficiency of the parallel stripe-domain magneto-optic deflection based on the Faraday rotation is derived. The calculated values are compared with the measured data. A new method to enhance the diffraction efficiency is presented. The experiment shows that the efficiency is increased by about 35 times. (7 refs.)

62945 Magneto-optical spectra of RF-sputtered amorphous Gd-Co and Gd-Fe films. K.Sato, Y.Togami (Broadcasting Sci. Res. Labs. of Nippon Hoso Kyokai, Tokyo, Japan).

J. Magn. & Magn. Mater. (Netherlands), vol.35, no.1-3, p.181-2 (March 1983). (Proceedings of the 10th International Colloquium on Magnetic Films and Surfaces, Yokohama, Japan, 13-16 Sept. 1982).

Spectra of polar magneto-optical effects of Gd-Co and Gd-Fe have been studied; Kerr rotation increases gradually from the visible to the near IR region with a hump around 1 eV and Kerr ellipticity changes sign at a certain photon energy, which depends on sputtering conditions. (9 refs.)

62946 Magneto-optical effect spectra of rare-earth-transition-metal amorphous films. D.F.Shen, T.Numata, Y.Sakurai (Faculty of Engng. Sci., Osaka Univ., Osaka, Japan), K.Sato.

J. Magn. & Magn. Mater. (Netherlands), vol.35, no.1-3, p.202-4 (March 1983). (Proceedings of the 10th International Colloquium on Magnetic Films and Surfaces, Yokohama, Japan, 13-16 Sept. 1982).

Some results of the magneto-optical effect spectra of rare-earth-transition-metal amorphous films are presented. These results suggest that the polarity reversal of the Kerr hysteresis loops on the surface of the films after annealing with limited oxidation is sometimes not due to the magnetic origin but may be mainly due to the change of the optical properties of the oxide surface layer. (5 refs.)

62947 Maximum amplification of the polar Kerr effect by surface coatings. V.S.Merkulov.

Opt. & Spectrosc. (USA), vol.53, no.1, p.82-4 (July 1982). Translation of: *Opt. & Spektrosk. (USSR)*, vol.53, no.1, p.141-4 (July 1982). [received: April 1983]

An expression is obtained for the maximum amplification by surface coatings of the coefficient $|r_p|$ in the polar Kerr effect in the case of normal incidence. (5 refs.)

62948 Polarization of electromagnetic waves in absorbing magnetically ordered media of middle and higher categories. S.S.Girgel.

Opt. & Spectrosc. (USA), vol.53, no.2, p.213-14 (Aug. 1982). Translation of: *Opt. & Spektrosk. (USSR)*, vol.53, no.2, p.361-4 (Aug. 1982). [received: April 1983]

Absorbing media of middle and higher categories having magnetic structure are investigated. The optical properties of such substances in the optical range of frequencies are described by a single complex non-Hermitian tensor of the reciprocal permittivity ϵ^{-1} , assuming $\mu=1$. In magnetically ordered crystals with the spinel or garnet-type structure, with the aid of an external applied magnetic field, one can change the direction of the singular axes within broad limits, which will cause modulation in phase, intensity, and polarization of light transmitted or reflected from the platelet. For all magnetic crystals of the cubic system, which are compensated antiferromagnetics, and also in the five magnetic classes of textures ocoom , ocoom' , cocoml' , ocoo , ocool' , the permittivity ϵ is a scalar quantity, and birefringence is absent; therefore, with respect to optical properties they behave like isotropic media. (7 refs.)

62949 Nonlinear magneto-optical phenomena of the third harmonic in semiconductors. H.Stramska (Inst. of Phys., Warsaw Univ., Warsaw, Poland).

Phys. Status Solidi b (Germany), vol.116, no.1, p.129-35 (1 March 1983).

The calculations are carried out starting from the Boltzmann equation. The Faraday rotation and ellipticity of the third harmonic in the current density, are associated with the energy dependence of the momentum relaxation time for a parabolic band and with the nonparabolicity of the band for a constant relaxation time. The present results predict a large enhancement due to resonance at high magnetic fields. It is shown that the magneto-optical effects have an oscillatory region. (9 refs.)

62950 The influence of crystal symmetry on magnetooptical effects in orthoferrites. J.Fink-Finowicki (Inst. of Phys., Polish Acad. of Sci., Warsaw, Poland).

Physica B & C (Netherlands), vol.115 B+C, no.2, p.225-8 (Jan. 1983).

The relation between magnetic structure and magnetooptical properties of orthoferrites is calculated. By means of a comparison with experimental data it is demonstrated that the triclinic distortion of Fe-O₆ complexes in these materials plays a crucial role in the origin of anomalously strong magnetooptical effects and also in the origin of the anisotropy of these effects. (12 refs.)

62951 Photoinduced spectral change in the rotation of the plane of polarization of light in FeBO₃. A.A.Leksikov, Yu.M.Fedorov (L.V. Kirenski Inst. of Phys., Acad. of Sci., Krasnoyarsk, USSR).

Sov. Tech. Phys. Lett. (USA), vol.8, no.8, p.405-6 (Aug. 1982). Translation of: *Pis'ma v Zh. Tekh. Fiz. (USSR)*, vol.8, no.15-16, p.934-7 (Aug. 1982). [received: April 1983]

Iron borate exhibits a photomemory and the properties of an optically controllable filter. Recording and readout can be carried out with light beams differing in both intensity and wavelength. The modulating effects are the linear magnetic dichroism and the Cotton-Mouton effect, so that the readout can be performed through a modulation of the beam by the medium in terms of three parameters: the intensity, the azimuthal position of the plane of polarization, and the phase shift. The modulation depth can be controlled by both the direction of the magnetic field at the time of the recording and the duration of the recording light pulse. (7 refs.)

62952 The influence of the parallel magnetic field on the interband optical absorption in thin films. M.Zaluzny (Inst. of Phys., M. Curie-Sklodowska Univ., Lublin, Poland).

Thin Solid Films (Switzerland), vol.102, no.1, p.87-96 (8 April 1983).

The effect of a parallel magnetic field on the interband optical absorption in size-quantized semiconductor layers is discussed on the basis of the effective mass approximation. The case of the simple and degenerate (germanium-like) valence band is considered. (12 refs.)

Automatic magnetic dichromator for the $\lambda=10.6 \mu\text{m}$ range [for free carrier concentration determination] See Entry 59820

The study of enantioselectivity in copper complexes with some 1,3-dicarbonyl ligands by circular dichroism spectroscopy See Entry 60776

Use of ferrite-garnet films as magneto-optic modulators See Entry 61266

Optical mode conversions in Nd substituted iron garnet films See Entry 61270

New aspects of the oxygen donor in gallium phosphide See Entry 62365

Direct observation of impact ionisation and hot electron effects in GaAs See Entry 62420

Impurity scattering time in n-type InSb measured by Faraday rotation at far-infrared frequency See Entry 62425

Magnetic and optical properties of Co, Bi substituted garnet films prepared by the LPE method and its application to thermomagnetic recording See Entry 62733

Amorphous TbFe ultra thin film with reflective Au layer See Entry 62734

Garnet film with rectangular hysteresis loop and its application to thermomagnetic recording medium See Entry 62735

Preparation and properties of RE-TM amorphous films See Entry 62736

Magnetic properties and magnetic Kerr rotation of amorphous TbFeCo and TbFeCr films See Entry 62737

The thermomagnetic writing and erasing properties and Kerr rotation angle of amorphous RE-Fe thin films See Entry 62738

Anomalous hysteresis loops in single and double layer sputtered TbFe films See Entry 62748

Interference enhanced Kerr spectroscopy for very thin absorbing films—application to amorphous terbium ion See Entry 62759

Formation of nonthrough magnetic domains in the course of magnetization switching in amorphous Gd-Co films See Entry 62766

Domain structure in single crystal ferromagnetic oxide films near the phase transitions See Entry 62771

Study of magnetoelastic waves by optical observation on the surface of magnetic materials See Entry 62794

Conversion Mossbauer studies of epitaxially mixed ferrite-garnet films See Entry 62870

The influence of X-trap on spin-lattice relaxation in the impurity phosphorescent state of a naphthalene crystal See Entry 63054

LPE growth of YNd-iron garnet films for magnetooptical waveguides See Entry 63182

78.20N Thermo-optical effects

62953 Thermorefectance study of polydiacetylene-bis (toluene sulphonate) single crystal (PDA-TS). S.Stizza, I.Davoli, V.Prantera (Inst. di Fisica, Univ. di Camerino, Camerino, Italy), A.Bianconi, J.Glinski, J.Kalinowski.

J. Phys. C (GB), vol.16, no.11, p.2165-76 (20 April 1983). For the first time studies have been made of the polarised thermorefectance of an oriented PDA-TS single crystal. The spectra in the photon energy range 1.9-2.5 eV are taken at room and liquid nitrogen temperature. From the different sensitivities to temperature the structures at 2.00 eV and 2.44 eV are assigned to excitonic and interband transitions, respectively. The binding energies of the excitons at room temperature (0.44 eV) and those corresponding to the low-temperature split band gap have been estimated to be nearly identical: 0.43 eV and 0.44 eV. The main thermorefectance structures are assigned to a Frenkel exciton interacting with phonons. (35 refs.)

Thermooptic-conversion method for detecting the spatial mode structure of a TEA CO₂ laser beam See Entry 61215

78.30 INFRARED AND RAMAN SPECTRA AND SCATTERING

62954 Vibrational spectroscopy of solid state molecular dimers. T.J.Kosic, C.L.Schösser, D.D.Dlott (Dept. of Chem., Univ. of Illinois, Urbana, IL, USA).

Chem. Phys. Lett. (Netherlands), vol.96, no.1, p.57-64 (25 March 1983).

The IR and Raman spectra of α - and β -perylene crystal vibrations are investigated. β -perylene is monomeric and α -perylene has face-to-face dimers. Frequencies and forms of the lattice vibrations as well as vibron relaxation and localization are discussed. Polarization ratios in α crystals are perturbed by coupling to dimer vibrations. (16 refs.)

62955 Raman scattering from Pt(CN)₄²⁻ adsorbed on Pt colloids. R.E.Benner (Appl. Phys. Div., Sandia Nat. Labs., Livermore, CA, USA), K.U.von Raben, K.C.Lee, J.F.Owen, R.K.Chang, B.L.Laube.

Chem. Phys. Lett. (Netherlands), vol.96, no.1, p.65-9 (25 March 1983). Raman scattering from Pt(CN)₄²⁻ adsorbed on Pt colloids (average diameter of 16 Å) is compared with the Raman signal from the same amount of Pt(CN)₄²⁻ in solution. The wavelength dependence of the adsorbate Raman intensity is measured from 308 to 647 nm and compared with a Lorenz/Mie calculation of the enhancement factor for the electromagnetic field intensity on the surface of a Pt sphere as a function of sphere radius and incident wavelength. (24 refs.)

62956 Functional groups in carbon black by FTIR spectroscopy. J.M.O'Reilly, R.A.Mosher (Webster Res. Centre, Joseph C. Wilson Centre for Technol., Rochester, NY, USA).

Carbon (GB), vol.21, no.1, p.47-51 (1983). Results of the application of Fourier transform infrared (FTIR) spectroscopy to determine the type and amount of surface functional groups in carbon black are reported. Surface functional groups in carbon black have been identified and analysed using carbon black dispersions in KBr. At low dilutions, less than 0.10% (wt/wt), Beer's law is followed. Absorbance at 1720 cm⁻¹ can be assigned to carboxylic acid, while the assignment of the strong band at 1600 cm⁻¹ is uncertain. Semi-quantitative analysis of band shapes indicates that there is a distribution of electronic environments in the carbon blacks. The magnitude of the absorbances (0.02-0.10) correspond to carboxylic or quinone groups in the amount of ~0.1-1.8 meq/g. Further developments of the technique could lead to a quantitative method for the determination of functional groups in carbon black. (11 refs.)

62957 Infrared spectrum of thawed water. B.V.Zhadanov, I.A.Polyakova (All-Union Sci. Res. Inst. of Chem. Reagents & Ultrapure Substances, Moscow, USSR).

Colloid J. USSR (USA), vol.44, no.3, p.560-1 (May-June 1982). Translation of: *Kolloidn. Zh. (USSR)*, vol.44, no.3, p.618-19 (May-June 1982). [received: Feb. 1983]

The infrared spectra of thin films (10 μm) of thawed water and of redistilled water have been obtained. No significant differences between the spectra were obtained in the region 1100-3100 cm⁻¹. It is concluded therefore that the differential spectrum of thawed water against redistilled water could not have been obtained experimentally, in view of the fact that too great a thickness of the fluorite cells ($l=2$ cm, about 10000 times greater than the admissible) has been chosen. (4 refs.)

62958 Raman scattering studies on slow crystallization process from amorphous PbTiO₃. M.Takashige, T.Nakamura, Y.Aikawa (Inst. for Solid State Phys., Univ. of Tokyo, Tokyo, Japan).

Ferroelectr. Lett. Sect. (GB), vol.44, no.11, p.313-18 (1983). The effect of isothermal annealing of amorphous PbTiO₃ below the crystallization temperature, T_{cryst} , has been investigated by Raman scattering measurements. The occurrence of the crystallization has been confirmed by the appearance of the soft mode. In the crystallized sample, the possibility of the occurrence of a crystalline phase, which is different from the tetragonal PbTiO₃ of perovskite structure, has been pointed out. (4 refs.)

62959 Theory of surface enhanced Raman scattering. K.A.Arunkumar, E.B.Bradley (Dept. of Electrical Engng., Univ. of Kentucky, Lexington, KY, USA).

J. Chem. Phys. (USA), vol.78, no.6, pt.1, p.2882-8 (15 March 1983).

It is now generally accepted that more than one mechanism could be at work in enhancing the Raman signal from molecules adsorbed onto a rough surface. In this paper the authors present a simple surface coverage, surface roughness dependent model that accounts for one such mechanism. According to the model, each adsorbate is subjected to both polarizing and depolarizing fields from its oscillating neighbors. Competition between these two fields is shown to determine the magnitude of signal enhancement. (62 refs.)

62960 Effect of pressure on Raman spectra of solid bromine. P.-G.Johannsen, W.B.Holzappel (Experimentalphys., Univ. GH Paderborn, Paderborn, Germany).

J. Phys. C (GB), vol.16, no.10, p.1961-5 (10 April 1983).

The effect of pressure on Raman spectra of solid bromine has been measured up to 33 GPa using a diamond anvil cell. Four of six Raman-active modes could be observed in first-order Stokes and anti-Stokes spectra at room temperature. Overlap of the two intramolecular peaks takes place at 24 GPa. The relative scattering intensities of the two intermolecular modes vary with pressure, exceeding finally those of the intramolecular modes. (8 refs.)

62961 Some oxygen donor complexes of cyclopentadienylneptunium(IV) trichloride. K.W.Bagnall, M.J.Plews (Chem. Dept., Univ. of Manchester, Manchester, England), D.Brown.

J. Less-Common Met. (Switzerland), vol.90, no.1, p.29-35 (March 1983).

The oxygen donor complexes [NpCl₄(dmpva)₂](dmpva≡Me₂CCONMe₂), [Np(cp)Cl₃L₂](cp≡ η^5 -C₅H₅; L₂=tetrahydrofuran (thf), MeCONMe₂ (dma), dmpva, Ph₃PO (tppo), (Me₂N)₂PO (hmpa), 1/2(Ph₂P(O)CH₂CH₂P(O)Ph₂)(1/2dppoe) and [Np(η^5 -C₅Me₄Et)Cl₃(tppo)₂] were prepared. The cyclopentadienyl complexes with dma, dmpva and tppo, but not that with hmpa, disproportionate to a mixture of [Np(cp)Cl] and [NpCl₄L₂] when recrystallization from thf is attempted. IR and near-IR-visible absorption (solution) spectra are reported for these compounds. (15 refs.)

62962 Raman and luminescence studies of alkali borate tungstate glasses. D.Deal, M.Burd, R.Braunstein (Univ. of California, Los Angeles, CA, USA).

J. Non-Cryst. Solids (Netherlands), vol.54, no.3, p.207-21 (March 1983). Raman and luminescence spectroscopy were used to determine the structure of alkali borate tungstate glasses: M₂O(B₂O₃)₂xWO₃, M=Li or Na(0<x<1). Raman scattering results showed the dominant tungstate species in these photochromic glasses to be tetrahedral WO₄²⁻. At high concentrations of WO₃, WO₃H₂O, and W₂O₇ are also present. Luminescent measurements provided evidence for an octahedral WO₃ structure not identified by the Raman results. The results also revealed a possible change in the structure of the glasses similar to that observed in alkali borate glasses and associated with the 'borate anomaly'. In addition, preliminary measurements

are reported on the variation of the band gap, density, index of refraction, and the elastic coefficient C_{11} determined by Brillouin scattering with composition. (23 refs.)

62963 Structural interpretations for some Raman lines from vitreous silica. A.G.Revesz (COMSAT Lab., Clarksburg, MD, USA), G.E.Walrafen. *J. Non-Cryst. Solids (Netherlands)*, vol.54, no.3, p.323-33 (March 1983).

An interpretation based on non-random structural features is advanced for the 490 and 604 cm^{-1} Raman lines from vitreous silica. The sharp, polarized 490 cm^{-1} line is considered to arise from a small concentration of planar rings involving three $\text{SiO}_4/2$ tetrahedra. The somewhat broader line at 604 cm^{-1} is thought to be associated with rings of various sizes, both planar and puckered, that are connected to the rest of the structure by elongated Si-O bonds. Changes in the concentration and/or Raman scattering cross-section of these ring structures produced by changes in fictive temperature, neutron irradiation, high elastic tensile and compressive stresses, annealing, and by changes in the Si-OH content are thought to produce the intensity variations observed in these two Raman lines. (31 refs.)

62964 Semiconducting properties of silver thiocyanate. K.Tennakone (Dept. of Phys., Ruhuna Univ. Coll., Matara, Sri Lanka), R.H.Wijayanayake. *J. Phys. D (GB)*, vol.16, no.4, p.L79-80 (14 April 1983).

The authors report measurements of the band gap of AgCNS by the study of optical absorption. It is concluded that silver thiocyanate is a p-type semiconductor with band gap ≈ 3.4 eV. (12 refs.)

62965 The reflection-absorption infrared spectrum of the dioxygen species adsorbed on platinum recorded by FT-IR spectroscopy. N.D.S.Canning, M.A.Chesters (School of Chem. Sci., Univ. of East Anglia, Norwich, England).

J. Electron Spectrosc. & Relat. Phenom. (Netherlands), vol.29, p.69-76 (15 Jan. 1983). (Proceedings of the Third International Conference on 'Vibrations at Surfaces', Asilomar, CA, USA, 1-4 Sept. 1982).

The reflection-absorption infrared spectrum of oxygen adsorbed on a recrystallized Pt foil at 80K shows a single band at 875 cm^{-1} at saturation coverage. The spectrum produced by an equilibrated mixture of oxygen isotopes confirms that the adsorbate is molecular. The apparent effective charge, e^* , calculated from the RAIR spectrum is in good agreement with that calculated from the electron energy loss (EEL) spectrum reported previously. The coverage dependent frequency shift can be accounted for by dipole-dipole coupling. The large inherent bandwidth is probably due to enhanced vibrational relaxation via electron-hole pair formation. (17 refs.)

62966 Infrared emission spectroscopy of CO on Ni. S.Chiang, R.G.Tobin, P.L.Richards (Dept. of Phys., Univ. of California, Berkeley, CA, USA).

J. Electron Spectrosc. & Relat. Phenom. (Netherlands), vol.29, p.113-18 (15 Jan. 1983). (Proceedings of the Third International Conference on 'Vibrations at Surfaces', Asilomar, CA, USA, 1-4 Sept. 1982).

The authors report the first observation of thermally emitted infrared radiation from vibrational modes of molecules adsorbed on clean, single crystal metal surfaces. The observation of emission from CO adsorbed on Ni demonstrates the surface sensitivity of a novel apparatus for infrared vibrational spectroscopy, with a resolution of 1 to 15 cm^{-1} over the frequency range from 330 to 3000 cm^{-1} . A liquid helium cooled grating spectrometer measures the thermal radiation from a room temperature, single crystal sample, which is mounted in an ultrahigh vacuum system. Measurements of frequencies and linewidths of CO on a single crystal Ni sample, as a function of coverage, are discussed. (12 refs.)

62967 On the contribution of charge transfer excitations to SERS.

A.Otto (Phys. Inst. III, Univ. Dusseldorf, Dusseldorf, Germany).

J. Electron Spectrosc. & Relat. Phenom. (Netherlands), vol.29, p.329-42 (15 Jan. 1983). (Proceedings of the Third International Conference on 'Vibrations at Surfaces', Asilomar, CA, USA, 1-4 Sept. 1982).

Resonant Raman scattering due to dynamical charge transfer from the silver metal to the lowest unoccupied orbital of pyridine and other adsorbates contributes 1 to 2 orders of magnitude to SERS. Several experimental observations indicate, that this mechanism is particularly effective at sites of atomic scale roughness. (60 refs.)

62968 Multichannel Raman spectroscopy of unroughened noble metal and nonnoble metal films and tunnel junctions. J.C.Tsang, Ph.Avoris, J.R.Kirtley (IBM Thomas J. Watson Res. Center, Yorktown Heights, NY, USA).

J. Electron Spectrosc. & Relat. Phenom. (Netherlands), vol.29, p.343-8 (15 Jan. 1983). (Proceedings of the Third International Conference on 'Vibrations at Surfaces', Asilomar, CA, USA, 1-4 Sept. 1982).

The authors demonstrate that multichannel optical detectors provide the capability of observing Raman scattering from molecular monolayers in solid-air and solid-solid interfaces in the absence of the conditions considered essential for surface enhanced Raman scattering. They present spectra of adsorbates on smooth Ag films, air-oxidized smooth Al films and Al gratings. Finally, they demonstrate a new configuration for surface enhanced Raman scattering which need not involve noble metals. Raman scattering from a doped $\text{Al}/\text{AlOx}/\text{Sn}$ tunnel junction provides a specific example of such a configuration. (12 refs.)

62969 Orientation dependence of surface enhanced Raman intensities: results from ab initio calculations. P.K.K.Pandey, G.C.Schatz (Dept. of Chem., Northwestern Univ., Evanston, IL, USA).

J. Electron Spectrosc. & Relat. Phenom. (Netherlands), vol.29, p.351-5 (15 Jan. 1983). (Proceedings of the Third International Conference on 'Vibrations at Surfaces', Asilomar, CA, USA, 1-4 Sept. 1982).

Time dependent Hartree-Fock methods have been used to calculate Raman intensities for H_2 adsorbed onto a model lithium cluster as a function of the orientation of H_2 relative to the cluster surface. The intensity is found to be largest for perpendicular adsorption, dropping to a small value at an intermediate angle, and then rising to a second but smaller maximum for parallel adsorption. The results are interpreted using a model which correlates enhancement to lithium cluster orbital energy shifts induced by the static quadrupole field of H_2 . (9 refs.)

62970 Surface enhanced Raman scattering (SERS) from silver, copper, and gold films in UHV: excitation spectra. I.Pockrand (Phys. Inst. III, Univ. Dusseldorf, Dusseldorf, Germany).

J. Electron Spectrosc. & Relat. Phenom. (Netherlands), vol.29, p.357-62 (15 Jan. 1983). (Proceedings of the Third International Conference on 'Vibrations at Surfaces', Asilomar, CA, USA, 1-4 Sept. 1982).

SER excitation spectra of different vibrational lines of various molecules ($\text{C}_2\text{H}_2\text{N}$, C_2H_4 , O_2 , CO) adsorbed on Ag-, Cu-, and Au-films in UHV have been studied. The experimental results are explained by assuming an electromagnetic origin of the observed excitation profile resonances. Within this frame the authors estimate a size of ~ 1.2 nm of the 'SERS relevant' surface roughness (bumps) and consequently a short range 'classical' enhancement restricted to mainly the first layer of adsorbed molecules. (20 refs.)

62971 A comparison of Raman scattering, resonance Raman scattering, and fluorescence from molecules adsorbed on silver island films. D.A.Weitz (Exxon Res. & Engng. Co., Linden, NJ, USA), S.Garoff, J.I.Gersten, A.Nitzan.

J. Electron Spectrosc. & Relat. Phenom. (Netherlands), vol.29, p.363-70 (15 Jan. 1983). (Proceedings of the Third International Conference on 'Vibrations at Surfaces', Asilomar, CA, USA, 1-4 Sept. 1982).

The enhancement of Raman scattering (RS), resonance Raman scattering (RRS), and fluorescence from molecules adsorbed on silver-island films is reported. A hierarchy of enhancements is found: 10^3 for RS, 10^3 for RRS, and 0.1-10 for fluorescence, depending on the quantum yield of the free molecule. Using the framework of the electromagnetic theory of surface-enhanced Raman scattering, generalized to treat molecular resonance phenomena, the authors develop a unified picture of the role of the surface plasmon resonances, and the surface-induced damping, in the light scattering processes. The observed hierarchy of enhancements is shown to have important spectroscopic consequences. (11 refs.)

62972 Influence of foreign metal atoms deposited at electrodes on local and nonlocal processes in surface enhanced Raman scattering. B.Pettinger, L.Moeri (Fritz-Haber-Inst., Max-Planck-Gesellschaft, Berlin, Germany).

J. Electron Spectrosc. & Relat. Phenom. (Netherlands), vol.29, p.383-95 (15 Jan. 1983). (Proceedings of the Third International Conference on 'Vibrations at Surfaces', Asilomar, CA, USA, 1-4 Sept. 1982).

Surface enhanced Raman scattering (SERS) from electrodes exhibits a reversible potential dependence in a limited potential range. Cathodic of this range it is irreversibly quenched on Ag electrodes by more than one order of magnitude. This holds for adsorbed pyridine molecules, for chloride, bromide, iodide, cyanide or thiocyanate ions, and for water or deuterium oxide. Since the (sub)microscope roughness is not altered by this procedure, the quenching has to be explained by a vanishing of SERS active sites, an idea which is clearly confirmed in metal deposition experiments using SERS for pyridine as a probe. In some cases, the deposition of a fraction of a monolayer (θ ca. 0.01) of a foreign metal on Ag is sufficient to significantly modify the intensity, the Raman shift and the halfwidth of the SERS bands. For example, the almost total quenching of SERS on Ag electrodes at cathodic potentials of -1.7 V is prevented to a great extent by Cu coverages of $\theta=0.003$. This evidences a low density of active sites. In other cases the impurity metal affect mainly on the SERS intensity, obviously by damping the electromagnetic resonances. These effects clearly reveal the importance and cooperation of local and nonlocal enhancement processes. (30 refs.)

62973 Surface Raman spectroscopy without enhancement: pyridine on Ag (111). A.Campion (Dept. of Chem., Univ. of Texas, Austin, TX, USA).

J. Electron Spectrosc. & Relat. Phenom. (Netherlands), vol.29, p.397-400 (15 Jan. 1983). (Proceedings of the Third International Conference on 'Vibrations at Surfaces', Asilomar, CA, USA, 1-4 Sept. 1982).

The author has observed normal Raman scattering from a monolayer of pyridine adsorbed on a Ag (111) surface at 110K. Unlike many previous studies of this system, he finds no appreciable enhancement of the scattering cross section. The results suggest that the short range enhancements observed on other well-characterized silver surfaces may be due to chemisorption on sites that are not available on the (111) surface. (9 refs.)

62974 Raman spectra of pyridine adsorbed on Ni (111). Chih-Cong Chou, C.E.Red, J.C.Hemminger, S.Ushioda (School of Phys. Sci., Univ. of California, Irvine, CA, USA).

J. Electron Spectrosc. & Relat. Phenom. (Netherlands), vol.29, p.401-6 (15 Jan. 1983). (Proceedings of the Third International Conference on 'Vibrations at Surfaces', Asilomar, CA, USA, 1-4 Sept. 1982).

The authors have measured the intensities of the 992 cm^{-1} (ν_1) and 1032 cm^{-1} (ν_2) lines in the Raman spectra of pyridine multilayers adsorbed on a Ni (111) surface, as a function of multilayer thickness. These experiments have been carried out in a standard ultra high vacuum chamber with Auger electron spectroscopy and mass spectroscopy capabilities. They find that the intensity of the 992 cm^{-1} line decreases linearly with multilayer thickness down to ~ 5 layers. From these data and spectra of submonolayer quantities of nitrobenzene on Ni (111) they predict an observable intensity for unenhanced spectra for monolayer amounts of pyridine on Ni (111). Attempts at observation of monolayer pyridine on this surface have been unsuccessful. The authors conclude that the scattering intensity of chemisorbed pyridine on Ni (111) is not enhanced and is less likely than would be predicted from the gas phase cross section. (8 refs.)

62975 Surface enhanced Raman spectroscopy of palladium. B.H.Loo (Materials Res. Lab., SRI Internat., Menlo Park, CA, USA).

J. Electron Spectrosc. & Relat. Phenom. (Netherlands), vol.29, p.407 (15 Jan. 1983). (Proceedings of the Third International Conference on 'Vibrations at Surfaces', Asilomar, CA, USA, 1-4 Sept. 1982).

Summary form only given as follows. Large enhancements in the Raman scattering signals have been observed from molecules and ions adsorbed on a palladium surface. The largest enhancement factor is in the order of 10^3 . Results will be discussed in terms of theoretical models on the surface enhanced Raman scattering process. (no refs.)

62976 The SERS phenomenon in light of recent excitation profile measurements. H.Seki (IBM Res. Lab., San Jose, CA, USA).

J. Electron Spectrosc. & Relat. Phenom. (Netherlands), vol.29, p.413-20 (15 Jan. 1983). (Proceedings of the Third International Conference on 'Vibrations at Surfaces', Asilomar, CA, USA, 1-4 Sept. 1982).

The author has recently reported on the measurements of the ultra high vacuum (UHV) surface enhanced Raman scattering (SERS) excitation profile for pyridine and CO on two different kinds of silver surfaces prepared in situ. The curves all show a maximum and the peak position depend both on the adsorbed molecule and the preparation of the silver surface. The optical spectra of these systems have also been measured using an oscillating beam spectrometer which compares the difference in the reflected light at two adjacent areas with and without the adsorbed molecules. The SERS phenomenon investigated in UHV is viewed in light of these results. (48 refs.)

62977 Exact calculations of scattering and enhanced fields of electromagnetic waves on grating surfaces. N.Garcia (Dept. de Fisica Fundamental, Univ. Autonoma de Madrid, Madrid, Spain).

J. Electron Spectrosc. & Relat. Phenom. (Netherlands), vol.29, p.421-5 (15 Jan. 1983). (Proceedings of the Third International Conference on 'Vibrations at Surfaces', Asilomar, CA, USA, 1-4 Sept. 1982).

Presents scattered intensities and values of the electromagnetic field for p-polarized light on Ag grating surfaces using the theory of Toigo, Marvin, Celli and Hill (1977). The theory is based on the application of the extinction theorem to Green's theorem. The program for calculations is set for any shape of the grating profile. Calculations are performed when the incident light is in resonance with the surface plasmon polariton. The shape of the scattered intensities are calculated for different grating amplitudes and it is shown that, for example, the reflectivity can present a minimum or a maximum depending on the amplitude and shape of the grating. It is shown that

the enhanced field (the ratio between the modulus squared of the scattered field to the modulus squared of the incident field)(e) has a maximum when the reflectivity is a minimum as a function of the incident angle. The maximum of e is larger when the minimum in the reflectivity is smaller as a function of the grating amplitude. The value of e is calculated in a fine grid near to the grating and the values of the maxima are of the order of 250, then if the Raman cross-section is proportional to the fourth power of the field this could produce 10^4 to 10^5 in the cross-section and explain SERS. The width of the resonances as well as the plasmon dispersion relation will be also presented. (18 refs.)

62978 Infrared spectroscopy of adsorbates on low-area surfaces; the advantages of a photons-in photons-out technique. J.Overend (Dept. of Chem., Univ. of Minnesota, Minneapolis, MN, USA).

J. Electron Spectrosc. & Relat. Phenom. (Netherlands), vol.30, p.1-10 (Feb. 1983). (Proceedings of the Third International Conference on 'Vibrations at Surfaces', Asilomar, CA, USA, 1-4 Sept. 1982).

The technique of double modulation infrared spectroscopy permits the simultaneous measurement of $(I_p - I_s)$ and $(I_p + I_s)$ where I_p and I_s are the intensities of radiation polarized parallel and perpendicular to the plane of incidence at the sample. This particular technique allows the infrared spectrum of a surface adsorbate to be measured in the presence of substantial quantities of bulk-phase adsorbant. The author has used this technique to study the infrared spectra of NO and CO adsorbates on Pt surfaces and of CO adsorbates on a Pt electrode surface in the presence of 1 M H_2SO_4 . The results of these studies shed new light on the origin of the well established wavenumber shifts which are associated with structural changes in the adlayers formed from simple diatomic molecules. (21 refs.)

62979 The application of reflection infrared and surface enhanced Raman spectroscopy to the characterization of chemisorbed organic disulfides on Au. D.L.Allara, R.G.Nuzzo (Bell Labs, Murray Hill, NJ, USA).

J. Electron Spectrosc. & Relat. Phenom. (Netherlands), vol.30, p.11 (Feb. 1983). (Proceedings of the Third International Conference on 'Vibrations at Surfaces', Asilomar, CA, USA, 1-4 Sept. 1982).

Summary form only given. The authors have found that a variety of organic molecules containing the S-S linkage strongly adsorb on freshly evaporated or electrochemically cleaned gold surfaces. Adsorption stops at monolayer coverage and the packing density of the molecules can be close to the limit set by the size of the molecules. Reflection infrared spectra show that the films are strongly oriented and in the case of long alkyl-chain-substituted disulfides the films have structures similar to those of Langmuir-Blodgett type films. Most of the films were prepared by freshly evaporating gold onto polished single crystal silicon substrates. Immediately after the deposition the films were removed from the vacuum system (under N_2) and placed in solutions of the disulfides. Infrared spectra were obtained using a Digilab 15B Fourier transform infrared spectrometer with a high f/number optical system and small beam spot size for glancing reflection. Spectra were obtained between 800 and 3200 cm^{-1} using a mercury cadmium telluride detector. (no refs.)

62980 Infrared specular reflection and SERS spectra of molecules adsorbed on smooth surfaces. H.Yamada, N.Tani, Y.Yamamoto (Dept. of Chem., Kwansei Gakuin Univ., Nishinomiya, Japan).

J. Electron Spectrosc. & Relat. Phenom. (Netherlands), vol.30, p.13-18 (Feb. 1983). (Proceedings of the Third International Conference on 'Vibrations at Surfaces', Asilomar, CA, USA, 1-4 Sept. 1982).

Infrared specular reflection and SERS spectra were measured for chemisorbed species on Ag and Ni at room temperature. Infrared spectra of benzoic acid and p-nitrobenzoic acid showed ionized CO_2 groups on the metals and orientation of molecular axes perpendicular to the surface. Carbon monoxide chemisorbed on Ag appeared at 1940 cm^{-1} (infrared) and at 2112 cm^{-1} (SERS), indicating that the chemisorbed species do not always give SERS. SERS of pyridine adsorbed on TiO_2 and Ti were observed. The resonance Raman scattering via charge transfer excitation is most plausible to explain these SERS phenomena. (12 refs.)

62981 Enhanced adsorbate Raman scattering and surface plasmon radiation. G.L.Easley (Dept. of Phys., General Motors Res. Labs., Warren, MI, USA).

J. Electron Spectrosc. & Relat. Phenom. (Netherlands), vol.30, p.25 (Feb. 1983). (Proceedings of the Third International Conference on 'Vibrations at Surfaces', Asilomar, CA, USA, 1-4 Sept. 1982).

Summary form only given, as follows. Presents the first experimental results which demonstrate a quadratic relationship between the enhanced Raman scattering from molecules on Ag surfaces and roughness-coupled surface-plasmon radiation. These results are interpreted by a model which includes both roughness assisted surface-plasmon scattering and radiative coupling. (no refs.)

62982 The adsorption of CO on Pt(111) studied by infrared-reflection-absorption spectroscopy. B.E.Hayden, A.M.Bradshaw (Fritz-Haber-Inst., Max-Planck-Gesellschaft, Berlin, Germany).

J. Electron Spectrosc. & Relat. Phenom. (Netherlands), vol.30, p.51 (Feb. 1983). (Proceedings of the Third International Conference on 'Vibrations at Surfaces', Asilomar, CA, USA, 1-4 Sept. 1982).

Summary form only given, as follows. The adsorption of CO on Pt(111) between 85K and 300K has been studied by infrared-reflection-absorption spectroscopy together with TPD and LEED. The intensity of the absorption band due to the CO stretch of the linear species shows a maximum at the formation of the $(\sqrt{3}\times\sqrt{3})R30^\circ$ LEED pattern followed by a minimum at the $c(4\times 2)$ structure during the adsorption of CO at low temperatures ($\leq 150K$). The adsorption band due to the C-O stretch of the bridging species appears only after the formation of the $(\sqrt{3}\times\sqrt{3})R30^\circ$ pattern and reaches maximum intensity at the $c(4\times 2)$ structure. Adsorption of CO to higher coverages (corresponding to the compression structures) broadens and shifts this absorption band. At higher temperatures ($\geq 150K$) a third peak is observed at $\sim 40\text{ cm}^{-1}$ below the peak due to the bridging species and is attributed to adsorption in the three-fold sites. At 300K both peaks in this region are very broad. The intensity data differs from that measured with EELS and favors a 'faultline' structure of the type proposed by Avery (1981). Together with the additional information from bandwidths it is possible to distinguish between the various structural models. The results obtained here may also be important in explaining data from other systems such as CO/Cu. (2 refs.)

62983 Infrared spectroscopic investigation of the adsorption of fluoromethane on sodium chloride surfaces under ultra high vacuum. J.Heidberg, I.Hussia, Z.Szilagy (Inst. fur Phys. Chem. und Elektrochem., Univ. Hannover, Hannover, Germany).

J. Electron Spectrosc. & Relat. Phenom. (Netherlands), vol.30, p.53-8 (Feb. 1983). (Proceedings of the Third International Conference on 'Vibrations at Surfaces', Asilomar, CA, USA, 1-4 Sept. 1982).

The adsorption of CH_3F on NaCl between 77K and 250K was investigated using infrared spectroscopy under ultra high vacuum conditions. All internal normal modes of the adsorbate were observed and assigned. Three adsorption

phases were detected. The largest frequency shift with respect to the gas takes place for the most intense mode, the C-F stretch ν_3 , 102 cm^{-1} (10%) for $\alpha\text{-CH}_3F\text{-NaCl(film)}$ on NaCl(100), while the other modes were much less influenced. No splitting of the vibrations degenerate in the gas occurs. Adsorption isotherms and the isosteric heats of adsorption were determined. (11 refs.)

62984 Infrared spectra of CO adsorbed at low temperatures on Ni. H.J.Levinson, R.G.Tobin, P.L.Richards (Dept. of Phys., Univ. of California, Berkeley, CA, USA).

J. Electron Spectrosc. & Relat. Phenom. (Netherlands), vol.30, p.65-7 (Feb. 1983). (Proceedings of the Third International Conference on 'Vibrations at Surfaces', Asilomar, CA, USA, 1-4 Sept. 1982).

At low temperatures (1.5K-40K), CO has been found to chemisorb into terminal, bridge, and three-fold sites on evaporated Ni films. The chemisorption takes place directly, rather than through a precursor state. At least two distinct terminal sites are occupied at high coverages. After the sample is warmed from 1.5K to 40K the infrared spectra change dramatically, showing substantial surface diffusion even at these low temperatures. (7 refs.)

62985 Surface enhanced Raman scattering of water on an Ag electrode. J.F.Owen, T.T.Chen, R.K.Chang (Dept. of Appl. Phys., Yale Univ., New Haven, CN, USA), B.L.Laube.

J. Electron Spectrosc. & Relat. Phenom. (Netherlands), vol.30, p.189 (Feb. 1983). (Proceedings of the Third International Conference on 'Vibrations at Surfaces', Asilomar, CA, USA, 1-4 Sept. 1982).

Summary form only given. Surface enhanced Raman scattering of adsorbates on an Ag electrode in various electrolytes (e.g., 0.1-1.0 M KF, KCl, KBr, KI, K_3PO_4 , and NaN_3) has been investigated in an effort to elucidate the mechanism of the enhancement of water compared to that for other adsorbates. (It is well known, for example, that pyridine exhibits large enhancement in 0.1 M KCl while SERS from water is not detectable unless the salt concentration is raised to almost 1 M.) Use of an optical multichannel analyzer allowed rapid recording of Raman spectra, and SERS intensities of adsorbates could therefore be monitored simultaneously during a continuous oxidation-reduction cycle. Potential dependencies of SERS intensities when the electrode potential is cycled in a non-faradic potential range immediately following oxidation and reduction indicate that adatoms are partially responsible for the Raman enhancement. Furthermore, the anions in the electrolyte play an important role in stabilizing these 'active sites'. For this reason, the degree of enhancement is influenced by the solubility of the Ag compound formed during oxidation and the specific adsorption of the anions to the Ag surface. (no refs.)

62986 EMIRS study of adsorbate bonding in the electrode solution interfacial region. A.Bewick, C.Gibilaro, N.Razaq (Dept. of Chem., Southampton Univ., Southampton, England), J.W.Russell.

J. Electron Spectrosc. & Relat. Phenom. (Netherlands), vol.30, p.191-6 (Feb. 1983). (Proceedings of the Third International Conference on 'Vibrations at Surfaces', Asilomar, CA, USA, 1-4 Sept. 1982).

EMIRS spectra for ^{12}CO , ^{13}CO mixtures on platinum, HSO_4^- and acrylonitrile on gold and water on silver are discussed. These examples illustrate the adsorbate identification, bonding, and orientation information which EMIRS data offer to complement electrochemical Raman data and infrared reflection absorption and EELS results. The advantages of experimental fine control of the electronegativity of the metal are shown with application to studies of coupling mechanisms between adsorbed species. (10 refs.)

62987 Spectral properties of pyrazine adsorbed on silver electrodes and cold silver films from surface enhanced Raman scattering (SERS). R.Dornhaus (I. Phys. Inst., Rheinisch Westfaelische, Tech. Hochschule Aachen, Aachen, Germany).

J. Electron Spectrosc. & Relat. Phenom. (Netherlands), vol.30, p.197-202 (Feb. 1983). (Proceedings of the Third International Conference on 'Vibrations at Surfaces', Asilomar, CA, USA, 1-4 Sept. 1982).

Surface enhanced Raman spectra of molecules adsorbed on electrode surfaces, metal-island films, colloidal particles and UHV-evaporated low-temperature substrates often show considerable differences in mode strength and positions between each other and the bulk molecular spectrum. These differences and their possible origins are discussed for pyrazine adsorbed on silver electrodes and cold silver films. (15 refs.)

62988 SERS study of pyridine vapor exposed to silver substrates electrochemically prepared. A.Regis, P.Dumas, J.Corset (Lab. de Spectrochimie, CNRS, Thiais, France).

J. Electron Spectrosc. & Relat. Phenom. (Netherlands), vol.30, p.203-8 (Feb. 1983). (Proceedings of the Third International Conference on 'Vibrations at Surfaces', Asilomar, CA, USA, 1-4 Sept. 1982).

Silver electrodes, previously prepared in KCl, KBr and KNO_3 electrolyte solutions, are exposed to a saturated vapour of pyridine, at room temperature. Surface complexes involving a silver halide and pyridine are detected during the gas-solid interaction. A low frequency band was observed, without exposure to pyridine, when a large amount of silver halide deposited on the electrode, is irradiated with a laser blue line. Photoreduction of the silver halide into metal aggregates occurs during the exposure to the laser. Some hypothesis about the absorption of pyridine at room temperature are advanced from results obtained with a silver electrode prepared in a KNO_3 solution. (10 refs.)

62989 Study of adsorption at the electrode/solution interphase by in-situ infrared reflectance spectroscopy—adsorption of methanol on a platinum electrode. K.Kunimatsu (Res. Inst. for Catalysis, Hokkaido Univ., Sapporo, Japan).

J. Electron Spectrosc. & Relat. Phenom. (Netherlands), vol.30, p.215-20 (Feb. 1983). (Proceedings of the Third International Conference on 'Vibrations at Surfaces', Asilomar, CA, USA, 1-4 Sept. 1982).

A detailed study has been carried out on the electrode potential dependence of spectra of adsorbed CO molecules produced by chemisorption of methanol molecules on a platinum electrode between 0.05 and 0.8 V (NHE). It has been shown that, in addition to the effect of surface charge on the band position, there is a considerable effect of co-adsorbed hydrogen species on the spectra which gives rise to the broadening of the band and to the lowering of the wave number for the maximum absorption. (11 refs.)

62990 Intensity enhancement and spectral change in Raman scattering of mercaptobenzothiazole adsorbed on silver electrode. M.Ohsawa, W.Suetaka (Lab. of Interface Sci. of Metals, Tohoku Univ., Sendai, Japan).

J. Electron Spectrosc. & Relat. Phenom. (Netherlands), vol.30, p.221-6 (Feb. 1983). (Proceedings of the Third International Conference on 'Vibrations at Surfaces', Asilomar, CA, USA, 1-4 Sept. 1982).

Mercaptobenzothiazole is adsorbed on silver electrodes in the form of ionized-thiol. Sudden changes in Raman intensity were observed in changing the concentration at 1×10^{-8} and $1\times 10^{-6}\text{ mol/l}$. The former change may be ascribed to the change in orientation of adsorbed molecule and the latter to the formation of multilayered film. The largest enhancement in Raman intensity is obtained for the species adsorbed in normal orientation. The addition

of halide ion resulted in the conversion of the thiol species to the thione one. The conversion may be related to the effect of halide ion impeding anticorrosion action of mercaptobenzothiazole. (6 refs.)

62991 Time dependence of surface enhanced Raman scattering during and after oxidation-reduction cycles. M.R.Philpott (IBM Res. Lab., San Jose, CA, USA), F.Barz, J.G.Gordon, II, M.J.Weaver.

J. Electron Spectrosc. & Relat. Phenom. (Netherlands), vol.30, p.227 (Feb. 1983). (Proceedings of the Third International Conference on 'Vibrations at Surfaces', Asilomar, CA, USA, 1-4 Sept. 1982).

Summary form only given, as follows. The time-development of surface enhanced Raman scattering from silver electrodes immersed in simple electrolytes has been measured during and after oxidation-reduction cycles of the linear scan double step type. Raman spectra were recorded in times as short as 0.1 second, using a spectrograph equipped with an optical multichannel detector and analyzer. Correlations between Raman spectra and current or charge passed were found, and in mixed electrolytes the displacement of one anion by a more strongly adsorbing anion was observed. In addition, unexpectedly strong effects of laser irradiation and hydrogen evolution prior to the oxidation-reduction cycle have been observed in the intensity of SERS bands after the cycle. These last two effects are attributed to peculiar surface morphologies. (no refs.)

62992 Vibrational and electronic spectra of $\text{Na}[\text{UO}_2(\text{CH}_3\text{COO})_3]$. C.D.Flint, P.Sharma (Dept. of Chem., Birkbeck Coll., Univ. of London, London, England).

J. Chem. Soc. Faraday Trans. II (GB), vol.79, pt.2, p.317-21 (Feb. 1983).

Raman, infrared, electronic absorption and luminescence spectra of $\text{Na}[\text{UO}_2(\text{CH}_3\text{COO})_3]$ have been measured at temperatures down to 10K. Multiple structure in the region of the lowest-energy electronic origin is shown to be due to the presence of a substantial concentration of defect sites. In the luminescence spectra these defect sites are populated by energy transfer from the majority species. Most of the vibrational modes of the uranyl and acetate groups have been identified and their vibronic intensity mechanism in the electronic spectra discussed. (11 refs.)

62993 Special features of angular dependence of spontaneous Raman scattering in LiNbO_3 . A.E.Semenov, E.V.Cherkasov.

Opt. & Spectrosc. (USA), vol.53, no.1, p.107-8 (July 1982). Translation of: *Opt. & Spektrosk. (USSR)*, vol.53, no.1, p.180-2 (July 1982). [received: April 1983]

Presents experimental data concerning the peculiarities of the polarized Raman spectra in nominally pure and iron-doped LiNbO_3 single crystals (C_{3v} point group) within the temperature interval $T=20-600^\circ\text{C}$. (5 refs.)

62994 High-frequency edge of tetragonal barium titanate Raman spectra.

A.A.Kukharskii.

Opt. & Spectrosc. (USA), vol.53, no.1, p.109-10 (July 1982). Translation of: *Opt. & Spektrosk. (USSR)*, vol.53, no.1, p.182-4 (July 1982). [received: April 1983] (20 refs.)

62995 Raman scattering in Bi_2SiO_5 and Bi_2GeO_5 single crystals.

G.A.Babonas, Yu.G.Zaretskii, G.A.Kurbatov, Yu.I.Ukhanov, Yu.V.Shmartshev. *Opt. & Spectrosc. (USA)*, vol.53, no.2, p.211-12 (Aug. 1982). Translation of: *Opt. & Spektrosk. (USSR)*, vol.53, no.2, p.358-61 (Aug. 1982). [received: April 1983]

Results obtained on the frequencies of spectral lines in the present work and previously (see S. Venugopalan and A.K. Ramdas, *Phys. Rev. B*, vol.5, p.4065, 1972 and W. Wojdowski et al., *Phys. Status Solidi B* vol.94, p.649, 1979) are compared. The total number of lines obtained in the Raman spectra for BGO and BSO is practically the same. (The Raman spectra of BSO consist of 47 lines, and those of BGO, 46 lines.) This result is natural for substances of very similar structure and makes it possible to postulate that the Raman spectra of other sillenites, obtained by means of a tetravalent metal oxide (TiO_2 , SnO_2 , etc.), will contain the same number of lines. (7 refs.)

62996 Temperature dependence of the $\tilde{E}-2A$ far-infrared absorption line of excited chromium ions in ruby. H.Lengfeller, J.Hummel, H.Netter, K.F.Renk (Inst. für Angewandte Phys., Univ. Regensburg, Regensburg, Germany).

Opt. Lett. (USA), vol.8, no.4, p.220-2 (April 1983).

By using far-infrared laser spectroscopy the authors have studied the temperature dependence of the absorption that is due to transitions between the $\tilde{E}^2(E)$ and $2A^2(E)$ levels of excited Cr^{3+} ions in ruby. From the temperature dependence of the linewidth the authors determined the inhomogeneous and the homogeneous contributions to line broadening. From the homogeneous width the lifetime of the $2A$ level was obtained. The authors found that, for temperatures up to 70K, the lifetime is due mainly to one-phonon relaxation, whereas at higher temperatures another relaxation process, probably a two-phonon Raman process, becomes strong. (11 refs.)

62997 Raman scattering in K_2SO_4 at high temperatures. M.Ishigame, S.Yamashita (Res. Inst. for Sci. Measurements, Tohoku Univ., Sendai, Japan).

Phys. Status Solidi b (Germany), vol.116, no.1, p.49-56 (1 March 1983).

Temperature dependence of Raman spectra of K_2SO_4 is measured in the temperature region from 300 to 1173K. A remarkable change of the Raman frequencies is not observed through the phase transition temperature T_c . Most of the Raman spectra measured above T_c can be explained by the vibrational modes of the K_2SO_4 crystal with space group D_{6h} . From the spectra of internal modes, however, it is suggested that a correlation between directions of two SO_4^{2-} ions in unit cell will exist locally in K_2SO_4 crystal above T_c . (8 refs.)

62998 Forbidden luminescence and resonance Raman scattering of bound exciton states in CdS. R.Baumert, I.Brosier, J.Gutowski, A.Hoffmann (Inst. für Festkörperphys., Tech. Univ. Berlin, Berlin, Germany).

Phys. Status Solidi b (Germany), vol.116, no.1, p.261-7 (1 March 1983).

A series of six energy levels is found at energy distances 2.5, 3.8, 4.7, 6.1, 7.0, and 8.3 meV on the high energy side of the neutral-acceptor bound exciton I_1 in CdS. They appear in the emission and absorption spectra of some freshly grown virgin crystals and of some crystals damaged by laser-irradiation. Resonance Raman scattering (RRS) establishes the new levels as intermediate states in every high quality crystal. These levels are interpreted as excited states of the bound exciton I_1 . The direct radiative recombination is forbidden due to parity selection rules. These selection rules are removed in symmetry disturbed crystals, at high excitation intensities, or by recombination with phonon participation. In consequence they are detected as forbidden luminescence, as LO phonon replica, or as 1-LO- and 2-LO-Raman lines. The 2-LO scattering cross section of the energy region of bound excitons in CdS is determined. (23 refs.)

62999 FTIR studies of polymer blends containing the poly(hydroxy ether of bisphenol A) and poly(ϵ -caprolactone). M.M.Coleman, E.J.Moskala (Dept. of Materials Sci. & Engng., Pennsylvania State Univ., University Park, PA, USA).

Polymer (GB), vol.24, no.3, p.251-7 (March 1983).

Fourier transform infra-red (FTIR) studies of the polymer blend system poly(hydroxyl ether of bisphenol A) (phenoxy)-poly(ϵ -caprolactone) (PCL) are presented. These two polymers are miscible in the amorphous state and information concerning the presence and nature of intermolecular interactions between the two polymers has been gained. Specifically, direct evidence has been obtained for a hydrogen bonding interaction between the PCL carbonyl group and the phenoxy hydroxyl group. Significantly, the relative strength of this interaction is found to be weaker than the corresponding intermolecular hydrogen bonding interaction in pure phenoxy. In contrast, a cursory FTIR study of phenoxy-poly(ethylene oxide) blends reveals that the intermolecular interaction occurring between these two polymeric components is stronger than that occurring in pure phenoxy. In addition, PCL is a crystallizable polymer and studies performed on the PCL-phenoxy blends at room temperature have led to further information on the state of order of PCL in these blends. The ramifications of these results are discussed. (21 refs.)

63000 Raman spectrum of n-propylamine in cyclohexane. B.Ri.Friedman, M.Schwartz (Dept. of Chem., North Texas State Univ., Denton, TX, USA).

Spectrosc. Lett. (USA), vol.15, no.12, p.945-52 (1982).

Polarized (isotropic) Raman spectra of the N-H valence region of n-propylamine have been recorded as a function of concentration in cyclohexane. Statistical analysis of the data using non-linear least squares techniques revealed the presence of a fourth spectral band in this region, not observed in an earlier IR study. This latter peak has been assigned to vibrations of monomers in the liquid. The resolved spectral parameters are consistent with a picture of diminishing molecular association upon dilution of the amine in this non-polar solvent. (13 refs.)

63001 Interference effects in resonant Raman scattering by S_2^- molecules in crystalline KI. L.A.Rebane, A.A.Khaav (Phys. Inst., Acad. of Sci., Tartu, Estonian SSR).

Sov. Phys.-Solid State (USA), vol.24, no.9, p.1452-5 (Sept. 1982). Translation of: *Fiz. Tverd. Tela (USSR)*, vol.24, no.9, p.2558-63 (Sept. 1982). [received: April 1983]

The resonant Raman scattering cross section for S_2^- molecules in crystalline KI at 5K was studied as a function of excitation frequency. Minima were observed in the cross section when the excitation lay in the zero phonon line and in the phonon wing of the impurity absorption spectrum, and their theoretical explanation is given. (18 refs.)

63002 Resonance interband Raman scattering of light in semiconductors.

V.I.Belitskii, A.V.Gol'tsev (A.F. Ioffe Physicotech. Inst., Acad. of Sci., Leningrad, USSR).

Sov. Phys.-Solid State (USA), vol.24, no.9, p.1462-5 (Sept. 1982). Translation of: *Fiz. Tverd. Tela (USSR)*, vol.24, no.9, p.2578-84 (Sept. 1982). [received: April 1983]

It is shown that the profile of a resonance line in the spectrum of the interband electron Raman scattering is Lorentzian only for certain values of the parameter $t=\gamma_{\mu 1}/\gamma_{\mu 0}$, where $\gamma_0^{-1}(\gamma_1^{-1})$ is the lifetime of electrons in the upper (lower) conduction band; $\mu=m_e m_0/(m_c+m_0)$, and m_c and m_0 are, respectively, the effective masses of an electron in the i th conduction band and of a hole in the valence band. When the interaction of electrons with longitudinal optical phonons is considered, the spectrum of the interband Raman scattering of light is shown to contain not only the principal resonance line but also a series of phonon replica lines. An interpretation of the resulting expression for the cross section of the Raman scattering based on the concepts of resonance scattering and hot luminescence is discussed. (12 refs.)

63003 Experimental investigation of the nature of infrared absorption by single crystals of α -LiIO₃. V.I.Bredikhin, L.A.Dmitrenko, N.V.Kiseleva, V.V.Korolikhin, M.A.Kotova, M.A.Novikov, V.I.Rubakha (Inst. of Appl. Phys., Acad. of Sci., USSR).

Sov. Phys.-Crystallogr. (USA), vol.27, no.5, p.557-9 (Sept.-Oct. 1982). Translation of: *Kristallografiya (USSR)*, vol.27, no.5, p.928-31 (Sept.-Oct. 1982). [received: April 1983]

The absorption spectra of α -LiIO₃ crystals, grown from solutions with various degrees of acidity, are investigated at wavelengths of 2.5-5.5 μ . By means of a comparison with the adsorption spectra of crystals of α -HIO₃ and of a solution of LiIO₃ in H₂O, it is shown that the absorption band with a maximum at 2.9 μ is due to inclusions of mother liquor, and that at 3.5 μ to HIO₃ present in the crystal. (5 refs.)

63004 Raman scattering of light in crystals in the presence of Bose-Einstein condensate excitons. Yu.D.Zavorotnev, L.I.Stefanovich.

Ukr. Fiz. Zh. (USSR), vol.28, no.3, p.348-53 (March 1983). In Russian.

Treats the effect of Raman scattering whose elementary act is characterized by a polariton annihilation and generation of a polariton with a modified frequency and a condensate exciton. For certain frequencies of pumping in the direction of the primary radiation, extension in the Stokes region of the spectrum it is accompanied by an appearance of a 'needle-like' line which is more intense than the Raman scattering line in the absence of the condensate. A tensor of scattering is established which is in coincidence with the tensor of the common Raman scattering. An example is given for cubic and uniaxial crystals to demonstrate at which geometry of scattering the said effect can be observed. (12 refs.)

63005 IR reflection investigation of corrosion of optical glasses. R.Stephonowitz (Sektion Chemie, Friedrich Schiller Univ., Jena, Germany).

Wiss. Z. Friedrich-Schiller-Univ. Jena, Math. Naturwiss. Reihe (Germany), vol.31, no.6, p.1017-23 (1982). In German.

Infrared reflection spectroscopy was used for characterizing corrosion of glass surfaces. Different corrosion agents cause typical reflection spectra. A table of the most important reflection peaks is given. (12 refs.)

63006 Raman spectroscopic investigations of polymethine dyes. K.Kneipp, G.Hinzmann, D.Fassler (Sektion Chemie, Friedrich Schiller Univ., Jena, Germany).

Wiss. Z. Friedrich-Schiller-Univ. Jena, Math. Naturwiss. Reihe (Germany), vol.31, no.6, p.1119-23 (1982). In German.

Spontaneous resonance Raman spectroscopic investigations of some polymethine dyes are reported. The resonance excitation behaviour of one dye was investigated quantitatively. (8 refs.)

Proceedings of the Third International Conference on 'Vibrations at Surfaces' See Entry 59532

Fourier transform infrared reflection-absorption spectroscopy of surface species See Entry 59859

Electroreflectance vibrational spectroscopy: a new surface analysis technique using diode lasers See Entry 59860

- Measurement of weak laser light absorption in materials transparent to infrared radiation See Entry 59862
- Distribution of Gauche bonds in crystalline $n\text{-C}_{21}\text{H}_{44}$ in phase II See Entry 60716
- Tricopper. A fluxional molecule See Entry 60728
- Homogeneous and inhomogeneous vibrational dephasing processes in aqueous thiocyanate solutions See Entry 60729
- Electronic structure of molecules and infrared continua caused by intramolecular hydrogen bonds with great proton polarizability See Entry 61017
- C-H stretching modes and the structure of n -alkyl chains. I. Long, disordered chains See Entry 61018
- Study of orientational properties of thermotropic liquid-crystalline polymer with side mesogenic groups by IR-spectroscopy method See Entry 61798
- Characterization studies of AgI-Ag₂O-MoO₃ glasses See Entry 61810
- Effect of molecular extension of a melt on the crystallinity of polyethylene, subjected to repeated crystallization See Entry 61814
- Molecular mechanism of shrinkage of polyethylene terephthalate See Entry 61831
- Structural and thermal characterization of the γ'' polymorph of Bi₂MoO₆ See Entry 61846
- New complex antimonates and tellurates structurally related to lithium antimonate LiSbO₃ See Entry 61866
- Optical absorption calibration curve for measurement of CR content in semi-insulating GaAs See Entry 61945
- Ion implantation effects in glasses See Entry 61992
- Special features of vibrational properties of mixed crystals with TiSe structure See Entry 62044
- Conference overview: experimental [surface vibrations] See Entry 62238
- High resolution infrared study of hydrogen chemisorbed on Si (100) See Entry 62252
- Selective desorption from the binary coadsorbate C₂H₂-CH₃F-NaCl by resonant vibrational excitation with laser infrared radiation See Entry 62256
- Surface vibration correlation with d-electron (hole) per atom ratio (d-bandfilling) in CO chemisorption on supported transition metal particles: dominance of Hund's rule and d-electron degeneracy in real supported catalysts See Entry 62258
- Using surface enhanced Raman scattering to study vibrations of adsorbates on thin metallic overlayers on silver See Entry 62266
- Acetylene adsorption on silver films: a Raman vibrational study See Entry 62267
- Observation of an orientational polarizability of dipolar molecules adsorbed in fine-pore membranes See Entry 62276
- IR spectroscopic and gravimetric investigation of adsorption of acetonitrile on a disperse model glass system See Entry 62277
- On the reaction mechanism of GaAs MOCVD See Entry 62292
- Linear response of a semi-infinite substrate with a two-dimensional conductive surface layer in the plasma-pole approximation See Entry 62359
- Semiconducting properties of V₂O₅ gels See Entry 62416
- Spin orientation and exchange interactions in (Fe,Co)Cl₂ See Entry 62575
- Refractive index in epitaxial Pb_{1-x}Sn_xTe films See Entry 62919
- Magnetopolaritons in ZnTe See Entry 62940
- Magneto-optical spectra of RF-sputtered amorphous Gd-Co and Gd-Fe films See Entry 62945
- Kramers-Kronig analysis of the reflection spectra of Ba₂NaNb₂O₁₅ See Entry 63015
- Tunnelling motion of dipolar impurities in alkali halides: the K⁺:NO₂⁻ system [IR spectra] See Entry 63024
- Electrical and optical properties of a-Si_xC_{1-x}:H film prepared by GD SiH₄ and C₂H₄ See Entry 63065
- Molecular orientation in thin monolayer films by infrared spectroscopy See Entry 63071
- Applications of surface polaritons for detection and vibrational spectral analysis of thin films on metals and dielectrics See Entry 63072
- Optical and electrical properties of a-Si_xC_{1-x}:H films prepared by glow discharge from SiH₄ and C₂H₄ See Entry 63075
- Infrared spectroscopic investigation of some carboxylic acids in nonpolar solvents See Entry 63545
- Laser-induced decomposition of sodium azide See Entry 63557
- Infrared study of three butanediols adsorbed on silica immersed in carbon tetrachloride See Entry 63593
- IR spectroscopic investigation of carboxylic acid salts of alkalis and thallium in nonpolar solvents See Entry 63608

78.35 BRILLOUIN AND RAYLEIGH SCATTERING

- 63007 Induced isotropic scattering from liquid carbon dioxide. A.de Santis, M.Sampoli (Istituto di Fisica, Univ. di Venezia, Venice, Italy). *Chem. Phys. Lett. (Netherlands)*, vol.96, no.1, p.114-18 (25 March 1983). The lineshape of the isotropic induced scattering has been measured from polarized and depolarized Rayleigh bands of CO₂ fluid. A comparison with other 'collision-induced' spectra has been performed. It is argued that the scattering is dominated by two- and three-body interactions. (22 refs.)
- 63008 Time dependent light scattering studies of phase separation in polymer blends. H.L.Snyder, P.Meakin (Central Res. & Dev. Dept., E.I. du Pont de Nemours & Co., Wilmington, DE, USA), S.Reich. *J. Chem. Phys. (USA)*, vol.78, no.6, pt.1, p.3334-6 (15 March 1983). The authors used a light scattering technique to obtain experimental information related to the time development of structural dynamics resulting from a liquid-liquid phase separation process in high molecular weight polymer blends, and report $S(k)$ measurements on early stage phase separation processes in high molecular weight polymers. The blends studied were composed of polystyrene with a GPC M_w of 60000 and a polydispersity of four and poly(vinylmethyl ether) with a GPC M_w of 63000 and a polydispersity of approximately two. (11 refs.)

63009 Electrophoretic light scattering studies of poly(L-lysine) in the ordinary and extraordinary phase. Effects of salt, molecular weight, and polyanion concentration. J.P.Wilcoxon, J.M.Schurr (Dept. of Chem., Univ. of Washington, Seattle, WA, USA). *J. Chem. Phys. (USA)*, vol.78, no.6, pt.2, p.3354-64 (15 March 1983). Electrophoretic light scattering (ELS) is employed to determine the electrophoretic mobilities μ_E and apparent diffusion coefficients D_{ELS} obtained from ELS linewidths for three samples of poly(L-lysine)HBr (PLL) of degree of polymerization $n=406$, $n=946$ and $n=2273$ as a function of salt (C_s) and polyanion (C_p) concentration. Dynamic light scattering (DLS) is used to determine apparent diffusion coefficients D_{app} of these same PLL samples in the absence of the applied field. The polyelectrolyte system exhibits an ordinary to extraordinary phase transition at low salt concentrations that is manifested by a more than 50-fold decrease in D_{app} as well as a twofold decrease in scattered intensity. In the extraordinary phase, the D_{ELS} values are typically very small, though still somewhat (frequently twofold) larger than D_{app} . When the salt concentration is raised to enter the ordinary phase D_{ELS} remains small, less than one tenth of D_{app} in the low-salt end of the ordinary phase, but increases with increasing C_p to become comparable with, though still about twofold smaller than, D_{app} in 0.1 M NaBr. The fluctuations in polyanion density responsible for the observed ELS signal are evidently relaxed very slowly under low-salt conditions, regardless of which phase prevails. In the ordinary phase μ_E increases rapidly with decreasing C_s , but in the extraordinary phase μ_E either remains nearly constant for ($n=946$), or actually decreases (for $n=2273$), as C_s decreases further to 0. The present μ_E data disagree with a previous empirical prediction of Schurr (1980) and rule out the particular interpretation of the diffusion virial coefficient upon which that was based. The theory of Manning (1981) predicts a value of the tracer mobility μ_p that is quite close to the value of μ_E observed for (lys)₄₀₆ at $C_s=0.1$ M, but predicts much too large an increase in μ_p with decreasing C_s , and fails to predict the significant molecular weight dependence of μ_E observed in the intermediate C_s range near 0.02 M. It is pointed out that incorporation of electrolyte friction into Manning's theory could improve the agreement with experiment. (30 refs.)

63010 Geometrical dependence of Raman and Rayleigh scattering intensities in fluids. C.D.Churcher, G.E.Stedman (Dept. of Phys., Univ. of Canterbury, Christchurch, New Zealand).

J. Phys. B (GB), vol.16, no.7, p.1303-18 (14 April 1983).

Angular momentum coupling techniques are used to determine the geometrical dependence of two-photon scattering effects in orientationally averaged systems under quite general conditions including chiral and linear field-induced effects and M2 and E3 couplings. The geometrical dependence of the intensity is separated from the physical constants and is expressed in terms of scalar and vector products of the polarisation and external field vectors. Independent measurements are suggested which suffice to determine completely the scattering properties of any fluid under a variety of constraints (symmetry of a scatterer, photon multipole coupling, applied field). Associated symmetries of, or selection rules on, such intensity contributions are analysed in detail. In Rayleigh scattering, for example, linear effects from an electric field in E1 coupling are forbidden, intensity contributions are always symmetric in incoming and outgoing photon labels and are symmetric or antisymmetric under time inversion of these photons as the applied field is time-even or time-odd. Attention is also given to the effects caused by alignment or distortion of the scatterers by the external field. (19 refs.)

63011 Interpretation of quasi-elastic light scattering data for flexible chains: model dependence. D.E.Kranbuehl (Dept. of Chem., Coll. of William & Mary, Williamsburg, VA, USA), P.H.Verdier. *Polymer (GB)*, vol.24, no.4, p.383-6 (April 1983).

The autocorrelation functions and corresponding relaxation times obtained from the forward depolarized quasi-elastic light scattering experiment are exhibited for two quite similar models of flexible polymer chains in solution. A very small change in the chain dynamics is found to be sufficient to change the relaxation time from a relatively short time independent of chain length, with an autocorrelation function suggestive of an unweighted sum of contributions from all the relaxation times in the spectrum of chain motion, to a long time with an autocorrelation function identical with that for the end-to-end vector, strongly dependent upon chain length and dominated by the longest relaxation time in the spectrum. (21 refs.)

Reorientation of small molecules and anions in solution studied by resonance enhanced dynamic Rayleigh scattering See Entry 60726

Shift of stimulated Brillouin scattering component in certain liquid mixtures See Entry 61227

Forced Rayleigh scattering: thermal and acoustic effects in phase-conjugate wave-front generation See Entry 61242

Hydrogen bond dynamics in water studied by depolarized Rayleigh scattering See Entry 61760

Investigation of nematic liquid crystals by correlation spectroscopy. Determination of ratios of viscosity and elasticity constants See Entry 61794

An optical method of determining the elastic constant ratio K_{33}/K_{11} in nematic liquid crystals See Entry 61795

Rayleigh-Brillouin scattering of transverse and longitudinal acoustic waves in a supercooled viscoelastic liquid See Entry 62928

Raman and luminescence studies of alkali borate tungstate glasses See Entry 62962

78.40 VISIBLE AND ULTRAVIOLET SPECTRA

- 63012 Pure electronic, vibronic, and two-particle surface excitons on the anthracene crystal. II. Experimental study and analysis of the (0,1) region. J.Bernard, M.Orrit, J.M.Turlet, Ph.Kottis (Centre de Phys. Moléculaire Optique et Hertzienne, Univ. de Bordeaux I, Talence, France). *J. Chem. Phys. (USA)*, vol.78, no.6, pt.1, p.2857-65 (15 March 1983). For pt.1 see ibid., vol.78, no.6, p.2847 (1983). In this second part, the authors present the experimental and theoretical study concerning vibronic surface transitions for the vibration modes 390 and 1400 cm⁻¹. They begin by a theoretical discussion of the different limiting cases of exciton-vibration coupling. In the experimental part, evidence of the surface character for the observed structures in surface emission excitation spectra is provided by their shifts upon surface coating. A general similarity of the surface states with the previously described bulk states, including a translational equivalence ($\delta=206$ cm⁻¹), is established. The observed structure are assigned to interacting single particle (vibron) resonances and two-particle bands. However, some slight discrepancies between surface and bulk band structures lead them to question the complete validity of their translational equivalence. Finally, the authors' observations show that the surface two-particle excitation profile (peak shaped) is quite different from the surface two-particle absorption profile (stepwise threshold profile). They propose a model mechanism of the surface

excitations relaxation which accounts quantitatively for this specific surface excitation profile. (19 refs.)

63013 Direct and indirect exciton transitions in $\text{InBr}_3\text{I}_{1-x}$ mixed crystals. M.Yoshida, N.Ohno, K.Nakamura, Y.Nakai (Dept. of Phys., Kyoto Univ., Kyoto, Japan).

J. Phys. Soc. Jpn. (Japan), vol.52, no.4, p.1108-10 (April 1983).

Reflection and absorption spectra of $\text{InBr}_3\text{I}_{1-x}$ mixed crystals have been measured at 2K by using polarized light. The lowest reflection peak shifts continuously from InI to InBr indicating the intra-cationic nature of the first exciton transition. In the absorption spectra of the mixed crystals with low iodine concentration, zero-phonon indirect exciton transition is identified and concentration dependence of its threshold energy is investigated. It is confirmed that the indirect-direct crossover occurs at the composition $x \approx 0.5$.

63014 A study of optical absorption edges in copper-calcium phosphate glasses containing iodine. C.A.Hogarth, A.A.Novikov (Dept. of Phys., Brunel Univ., Uxbridge, England).

J. Phys. D (GB), vol.16, no.4, p.675-8 (14 April 1983).

A series of glass specimens was prepared from mixtures of CuO , CaO , P_2O_5 and CuI and their optical absorption coefficients were measured as functions of photon energy in the range 3.0 to 4.5 eV. From the results the values of the optical energy gap are calculated and found to depend quite sensitively on the added iodine. (9 refs.)

63015 Kramers-Kronig analysis of the reflection spectra of $\text{Ba}_2\text{NaNb}_2\text{O}_{15}$. A.M.Mamedov, V.I.Shilnikov, I.S.Ibragimova, K.M.Nurieva, I.M.Efendieva. *Opt. & Spectrosc. (USA)*, vol.53, no.1, p.2-3 (July 1982). Translation of: *Opt. & Spektrosk. (USSR)*, vol.53, no.1, p.5-7 (July 1982). [received: April 1983] Reports measurements of the normal reflection spectrum ($\theta \approx 12^\circ$) of $\text{Ba}_2\text{NaNb}_2\text{O}_{15}$ (BSN) single crystals over the 0.1-35.0-eV energy range and over the 10-500K temperature range. This is one of the oxygen-octahedron crystals that exhibit strong nonlinear optical properties. Two spectral instruments were used: (1) a McPherson 225 vacuum monochromator with a 1200-line/mm diffraction grating, (2) a Perkin-Elmer 301 spectrometer ($\hbar\omega = 0.1-3.5$ eV). The experimental data were subjected to a Kramers-Kronig analysis to calculate the real and imaginary parts of the dielectric function $\epsilon = \epsilon_1 - i\epsilon_2$ and the energy-loss function $-\text{Im}\epsilon^{-1} = -\epsilon_2/(\epsilon_1^2 + \epsilon_2^2)$, which is a measure of the collective oscillations of valence electrons. The spectrum of the optical conductivity, $\sigma = 2\pi\hbar\omega$ is also shown. Comparison of the α and σ spectra shows that the energy positions of the maxima of these optical functions are correlated well. The spectra of k and ϵ_2 in contrast are similar to the spectrum of R and reach maxima at $\hbar\omega = 5.0-10.0$ eV. The small values of ϵ_1 and ϵ_2 for these single crystals should be noted; these values imply that the bonding of BSN is very ionic. (7 refs.)

63016 Effect of oxygen on exciton spectra of ZnS lower polytypes and samples with packing defects. N.K.Morozova. *Opt. & Spectrosc. (USA)*, vol.53, no.1, p.98-9 (July 1982). Translation of: *Opt. & Spektrosk. (USSR)*, vol.53, no.1, p.166-9 (July 1982). [received: April 1983]

The author found that ZnS polytype forms having hexagonal structure dissolve oxygen readily without formation of packing defects, and this substantially influences the width of their forbidden zone. To exclude the influence of dissolved oxygen, investigations were undertaken of single crystals of the ZnS polytype forms 2H, 4H, 6H, 8H, 3C obtained in a circulating system from the gas phase in H_2S at 1300°C. Results of exciton spectra of reflection are presented and it is evident that exclusion of the influence of oxygen gives linear dependence of E_g or the A exciton on α . The sizes of the energy gaps E_{AB} and E_{AC} change nonlinearly, which corresponds to a nonlinear displacement of the bands of the B and C excitons in the spectra. (6 refs.)

63017 Electoreflexion of ground-state excitons in $\text{A}^{\text{IV}}\text{B}^{\text{VI}}$ crystals. V.E.Mashchenko, A.V.Khomich, A.I.Ziborov.

Opt. & Spectrosc. (USA), vol.53, no.2, p.166-8 (Aug. 1982). Translation of: *Opt. & Spektrosk. (USSR)*, vol.53, no.2, p.284-7 (Aug. 1982). [received: April 1983]

The increments in the electric field of the real ($\Delta\epsilon_1$) and imaginary ($\Delta\epsilon_2$) parts of the complex permittivity have been calculated for a transition to the exciton ground state in CdSe, CdS, and ZnSe crystals at 77K. The computations used high-resolution experimental electoreflexion spectra and calculated data for the spectra of the absorption coefficient and refractive index in the region of exciton resonance. It is shown that the invariant form of the electoreflexion (ER) extremes of ground-state excitons in fields of the order of 10^3 V/cm⁻¹ is determined by the fact that the dominant contributions in the ER spectrum are introduced by absorption processes. The computed $\Delta\epsilon_2$ spectra repeat the spectral curve of the ER extremes of the ground state and are described by the second derivative of the absorption contour with regard to the Lorentz energy. Such a shape for the ER extremes of ground-state excitons is attributable to broadening of the lines in the electric field. (16 refs.)

63018 Study of electronic structure of reduced TiO_2 and $\text{V}_x\text{Ti}_{1-x}\text{O}_2$ crystals by ESCA and optical absorption. K.Sakata (Nat. Res. Inst. for Metals, Tokyo, Japan).

Phys. Status Solidi b (Germany), vol.116, no.1, p.145-53 (1 March 1983).

An analysis is made of optical absorption spectra and electron spectroscopy for chemical analysis (ESCA) on pure TiO_2 , reduced TiO_2 , and $\text{V}_x\text{Ti}_{1-x}\text{O}_2$. It is found that in the reduced TiO_2 , the film takes the variable valence states, Ti^{4+} , Ti^{3+} , Ti^{2+} , and they form a broad donor band which overlaps with the conduction band originating from $\text{Ti}4s$ levels. 3d-4s mixing results in a large change of the conductivity of TiO_2 from insulator to metal depending upon the degree of reduction. In TiO_2 doped with V, which behaves like a free ion, the excess 3d electrons of the V ions form impurity level just above the $02p$ valence band. In the reduced $\text{V}_x\text{Ti}_{1-x}\text{O}_2$, four different valence states, Ti^{4+} , Ti^{3+} , Ti^{2+} , and V^{4+} , are found and this accounts for the narrow optical gap of this material. (24 refs.)

63019 Exciton-phonon interaction in crystalline and vitreous SiO_2 . I.T.Godmanis (Inst. of Solid State Phys., Latvian State Univ., Riga, Latvian, USSR), A.N.Trukhin, K.Hubner.

Phys. Status Solidi b (Germany), vol.116, no.1, p.279-87 (1 March 1983).

An investigation of the Urbach rule in crystalline SiO_2 (α -quartz), crystalline SiO_2 -Ge, and vitreous SiO_2 in the framework of the models of Dow and Redfield (1972) and of Toyozawa (1964) shows that the fundamental optical absorption edge of SiO_2 is determined by strong exciton-phonon interactions. In the crystalline and vitreous SiO_2 low-energy excitons with $E = 9.1$ eV (α -quartz) and $E = 8.7$ eV (glass) interact mainly with longitudinal optical phonons. In the crystalline SiO_2 -Ge alloy the interaction with phonons is realized by excitons localized on germanium impurities. The exciton-phonon interaction in SiO_2 -Ge and vitreous SiO_2 is stronger than in crystalline SiO_2 due to the higher degree of localization of low-energy excitons in these disturbed SiO_2 forms. The strong exciton-phonon interaction leads to a momentary self-trapping of the low-energy excitons in crystalline and non-crystalline SiO_2 , and to a corresponding relaxation of the SiO_2 -Ge excitons localized on Ge impurities. Numerical values of the fundamental exciton parameters are deduced and discussed. (39 refs.)

Excited states of mixed-ligand chelate complexes of ruthenium(II). A re-

examination of the evidence for strong interligand coupling See Entry 60756

Metallic multilayers: new possibilities in X-UV optics See Entry 61257

Structural approach of the Nd_2GaO_6 compounds See Entry 61867

Comparison of heavy-ion, proton and electron irradiation effects in vitreous silica See Entry 61994

Photoacoustic spectra of semiconductor compounds Dy_2S_3 and Nd_2S_3 See Entry 62034

Thermophysical properties of supercritical fluids with special consideration of aqueous systems See Entry 62073

New aspects of the oxygen donor in gallium phosphide See Entry 62365

Semiconducting properties of V_2O_5 gels See Entry 62416

Enhanced NMR of ^{169}Tm in TmAsO_4 See Entry 62816

Spectroscopic and magneto-optical properties of quasi 1D antiferromagnets AVX_3 ($\text{A} = \text{Cs, Rb}$; $\text{X} = \text{Cl, Br, I}$) See Entry 62943

Magneto-optical spectra of RF-sputtered amorphous Gd-Co and Gd-Fe films See Entry 62945

Magneto-optical effect spectra of rare-earth-transition-metal amorphous films See Entry 62946

Thermorefectance study of polydiacetylene-bis (toluene sulphonate) single crystal (PDA-TS) See Entry 62953

Some oxygen donor complexes of cyclopentadienylneptunium(IV) trichloride See Entry 62961

Vibrational and electronic spectra of $[\text{Na}[\text{UO}_2(\text{CH}_3\text{COO})_3]]$ See Entry 62992

Interference effects in resonant Raman scattering by S_2^- molecules in crystalline KI See Entry 63001

One- and two-photon spectra of $\text{NaF}:\text{Cu}^+$: Jahn-Teller and vibronic coupling effects See Entry 63022

Site-selection spectroscopy of Eu^{3+} -doped germinate glass See Entry 63023

Absorption, fluorescence, and excitation spectra of thallium-activated rubidium bromide See Entry 63046

Optical absorption in hydrogenated microcrystalline silicon See Entry 63069

Fundamental reflectivity spectra of Cd_3As_2 thin films See Entry 63076

Thin film absorption spectra of lower valent p block halides See Entry 63077

A solution growth technique for the preparation of copper(II) selenide thin films See Entry 63181

Laser-induced decomposition of sodium azide See Entry 63557

Composition, optical properties and degradation modes of Cu/poly(graded metal-carbon) solar selective surfaces See Entry 63728

78.45 STIMULATED EMISSION

(see also 42.65C in nonlinear optics)

63020 Peculiarity of the $3-\mu$ stimulated emission of Er^{3+} ions in disordered fluoride crystals. A.A.Kaminskii, K.B.Seiranyan, A.Z.Arakelyan (A.V. Shubnikov Inst. of Crystallography, Acad. of Sci., USSR).

Inorg. Mater. (USA), vol.18, no.6, p.901-3 (June 1982). Translation of: *Izv. Akad. Nauk SSSR Neorg. Mater.*, vol.18, no.6, p.1061-3 (June 1982). [received: Feb. 1983]

The authors observed the generation of 3μ stimulated emission (SE) of Er^{3+} ions in a new disordered cubic (space group $O_h^3\text{-Fm}3m$) crystal of a solid solution of the $\text{SrF}_2\text{-ErF}_3$ system and measured its principal parameters. In the case of a crystal of the solid solution of the $\text{SrF}_2\text{-ErF}_3$ system (~ 10 mole% ErF_3) with a length of ~ 30 mm and a diameter of 6 mm the SE was excited under pulse conditions at 300K at three wavelengths—2.7285, 2.7450, and 2.7930 μm —of the $^4I_{11/2} \rightarrow ^4I_{13/2}$ self-saturated laser channel of Er^{3+} ions with approximately the same threshold $E_{th} \approx 25$ J. (8 refs.)

63021 Submillimeter emission of CdS crystals pumped by intense light. A.A.Fomichev, M.A.Yakhshin (Moscow Physicotech. Inst., Moscow, USSR).

Sov. Tech. Phys. Lett. (USA), vol.8, no.3, p.392-3 (Aug. 1982). Translation of: *Pis'ma v Zh. Tekh. Fiz. (USSR)*, vol.8, no.15-16, p.903-7 (Aug. 1982). [received: April 1983]

Reports measurements of the power level of pulsed submillimeter emission from CdS under intense pumping at 77 and 300K. The experiments have made it possible to observe simultaneously this emission and pulses of stimulated green emission and to observe a synchronised fading of the signals at the two wavelengths at high pump power densities, corresponding to the excitation of the P line of exciton radiative recombination. (9 refs.)

Auger recombination in GaSb and its effects on laser characteristics See Entry 61160

Laser gain and excitation threshold in semiconductors with transitions between localized states See Entry 61161

Excitation of active impurities in laser crystals under electric discharge conditions See Entry 61162

Improvement of the characteristics of ZnSe single-crystal semiconductor lasers pumped longitudinally by an electron beam See Entry 61163

78.50 IMPURITY AND DEFECT ABSORPTION IN SOLIDS

63022 One- and two-photon spectra of $\text{NaF}:\text{Cu}^+$: Jahn-Teller and vibronic coupling effects. S.A.Payne, A.B.Goldberg, D.S.McClure (Dept. of Chem., Princeton Univ., Princeton, NJ, USA).

J. Chem. Phys. (USA), vol.78, no.6, pt.2, p.3688-97 (15 March 1983).

Notwithstanding the fact that CuF does not exist, the dilute solid solution $\text{NaF}:\text{CuF}$ is stable. One- and two-photon spectra of the cubic single crystals were obtained for the near ultraviolet $3d^{10} \rightarrow 3d^9 4s$ transitions of Cu^+ over a range of temperatures from 2 to 300K. The two-photon polarized spectra allowed the separation of the E_g from the T_{2g} spectra, and revealed the double humped band characteristic of the Jahn-Teller effect. Zero phonon lines were observed in the two-photon spectra, and a progression in a low frequency t_{1g} mode was observed with even quanta in the two-photon, odd quanta in the one-photon spectra. From the fine structure and from the temperature dependence of the broad bands, information about the potential function of the Cu^+ in NaF was derived for d_{1g} , e_g , and t_{1g} coordinates. The Cu^+ is on center in the ground and excited states. The value of E_{JT} is 2250 cm^{-1} and 10 Dq is 1800 cm^{-1} for the d^9 configuration. (26 refs.)

63023 Site-selection spectroscopy of Eu³⁺-doped germinate glass. Xu Gang, G.Boulon, R.C.Powell (Dept. of Phys., Oklahoma State Univ., Stillwater, OK, USA).

J. Chem. Phys. (USA), vol.78, no.7, p.4374-8 (1 April 1983). A tunable dye laser was used to selectively excite Eu³⁺ ions in nonequivalent types of crystal field sites in a germinate glass host. The results demonstrate the existence of three major types of sites in this host. In addition, time-resolved spectroscopy results show the presence of energy transfer between ions in these different types of sites. (12 refs.)

63024 Tunnelling motion of dipolar impurities in alkali halides: the KI:NO₂⁻ system [IR spectra]. S.S.Khatir, A.L.Verma (Dept. of Phys., North-Eastern Hill Univ., Shillong, India).

J. Phys. C (GB), vol.16, no.11, p.2157-64 (20 April 1983). Motional states of the NO₂⁻ ion doped in KI single crystals have been investigated using high-resolution infrared techniques. At very low concentrations of the impurity, the antisymmetric stretching vibration (ν_3) of the NO₂⁻ ion shows multiplet structure at 1.7K. This structure can be understood in terms of contributions of different types of tunnelling motions of the NO₂⁻ ion among the twelve equivalent potential wells in the KI lattice. An attempt has been made to give an estimate of the potential barrier hindering reorientation of the ion in the KI lattice. (14 refs.)

63025 Influence of the resonance interaction between molecules of a crystal and impurities on the Rashba effect for several impurity centers in molecular crystals. L.Valkunas, G.Vektaris.

Opt. & Spectrosc. (USA), vol.53, no.1, p.49-50 (July 1982). Translation of: *Opt. & Spektrosk. (USSR)*, vol.53, no.1, p.86-8 (July 1982). [received: April 1983]

A model of an impurity center is studied in which a level of localized excitons interacts resonantly with an impurity level. This interaction determines the optical properties of localized levels for crystals with a weak oscillator strength of the intramolecular transition in the case of a distribution of localized and impurity levels at a specific distance from the exciton band and close to one another. In the opposite case, when the localized level is located near the exciton band, the Rashba effect occurs. Numerical calculations are carried out for the naphthalene crystal. (6 refs.)

63026 Semiempirical calculation of optical-ionization energy for the Ti⁰ center in a KCl crystal. A.N.Ermoshkin, E.A.Kotomin, R.A.Evarestov, I.A.Tale.

Opt. & Spectrosc. (USA), vol.53, no.1, p.112-13 (July 1982). Translation of: *Opt. & Spektrosk. (USSR)*, vol.53, no.1, p.186-9 (July 1982). [received: April 1983]

Discusses a method and the results of a quantum-chemical semiempirical calculation of the energy of optical ionization of the Ti⁰ activator center in KCl crystal. The thallium atom impurity is located at a cation node of the lattice and is negatively charged relative to it. The authors used the semiempirical method of Mulliken-Rudenberg (self-consistent with respect to charge and configuration) within the framework of a model of a molecular cluster. (12 refs.)

63027 Mechanism for the annealing out of radiation-induced Eu²⁺ from barium orthophosphate. V.G.Krongauz, L.M.Kanskaya, I.Kh.Shaver.

Sov. Tech. Phys. Lett. (USA), vol.8, no.8, p.433-4 (Aug. 1982). Translation of: *Pisma v Zh. Tekh. Fiz. (USSR)*, vol.8, no.15-16, p.1003-5 (Aug. 1982). [received: April 1983]

The activator in the X-ray phosphor Ba₃(PO₄)₂:Eu is present in the form of both Eu²⁺ and Eu³⁺ ions. X-ray bombardment converts part of the Eu²⁺ into Eu³⁺. The thermal annealing out of the radiation-induced Eu²⁺ is completed at 550-600K. A hole mechanism is most probably responsible for this annealing out. After X-ray bombardment at 77K, a Ba_{2.98}Eu_{0.02}(PO₄)₂ sample was illuminated with an incandescent lamp. The illumination caused the amount of Eu²⁺ (monitored on the basis of the intensity of the emission upon intracenter excitation: an absorption band peaking near 4.0 eV) to increase beyond the amount caused by the X-radiation. Simultaneously, the number of electrons at nonactivator capture centers decreased. (4 refs.)

Structural effects of radiation damage in silica based glasses. See Entry 60281

Optical absorption calibration curve for measurement of CR content in semi-insulating GaAs. See Entry 61945

Theory of the autoionized state of impurities in semiconductors. See Entry 62362

New aspects of the oxygen donor in gallium phosphide. See Entry 62365

Vibrational and electronic spectra of Na[VO₂(CH₃COO)₃]. See Entry 62992

Interference effects in resonant Raman scattering by S₂⁻ molecules in crystalline KI. See Entry 63001

Effect of oxygen on exciton spectra of ZnS lower polytypes and samples with packing defects. See Entry 63016

Exciton-phonon interaction in crystalline and vitreous SiO₂. See Entry 63019

Optical spectra of impurity centers with double-well adiabatic potentials. See Entry 63044

Influence of Ag photodoping on photoinduced changes in As₂S₃ glass films. See Entry 63066

78.55 PHOTOLUMINESCENCE

63028 Quenching of the delayed fluorescence by charge carriers in crystals of anthracene-TCNB CT complex. J.Funfschilling, M.Samoc, D.F.Williams (Nat. Res. Council, Ottawa, Ontario, Canada).

Chem. Phys. Lett. (Netherlands), vol.96, no.2, p.157-60 (1 April 1983). The decrease in delayed fluorescence intensity in anthracene-tetracyanobenzene upon application of an electric field is investigated. It is shown, that photogenerated free carriers are responsible for the observed quenching, and that the entity quenched is an intermediate state between a triplet-pair state and a fluorescent singlet state. A model is presented that identifies this state as a separated charge pair. This model can explain the main feature of the observations, namely the large quenching cross section, which is of the order of cross sections typical of carrier-carrier interactions. (15 refs.)

63029 Uniaxial stress and temperature dependences of photoluminescence in GaAs_{1-x}P_x. S.Narita, T.Kubota, M.Kobayashi (Dept. of Material Phys., Osaka Univ., Osaka, Japan).

Jpn. J. Appl. Phys. Part I (Japan), vol.22, no.3, p.467-74 (March 1983). The uniaxial stress and temperature dependences of the photoluminescence in GaAs_{1-x}P_x (x=0.38) are studied and three kinds of photoluminescence are observed. One of them is attributed to the surface anomaly and the other two annihilation of the bound excitons and donor-acceptor pair recombination. By combining the results of the uniaxial stress effect and the temperature change of the photoluminescence, the transition mechanisms for the luminescence are discussed.

63030 Photoluminescence in amorphous C:H films prepared by glow discharge charge decomposition of CH₄ or C₂H₆. I.Watanabe, M.Inoue (Dept. of Electronics, Faculty of Technol., Kanazawa Univ., Kanazawa, Japan).

Jpn. J. Appl. Phys. Part 2 (Japan), vol.22, no.3, p.L176-8 (March 1983).

Hydrogenated amorphous carbon films have been prepared by glow discharge decomposition of CH₄ or C₂H₆ gas. The films exhibit white photoluminescence with high efficiency and weak temperature dependence which can be observed even at room temperature. The peak energy and intensity of the emission band vary depending on gas temperature during glow discharge. The high efficiency and weak temperature dependence are suggested to result from a strong Coulomb interaction in photoexcited electron-hole pairs.

63031 Effect of annealing on photo-energy transfer in poly(2,6-dimethyl-1,4-phenylene oxide), polystyrene and their blends. M.Kryszewski, B.Wandelt (Polymer Inst., Tech. Univ., Lodz, Poland), D.J.S.Birch, R.E.Imhof, A.M.North, R.A.Pethrick.

Polym. Commun. (GB), vol.24, no.3, p.73-5 (March 1983). Observations of fluorescence intensity and lifetime in polystyrene, poly(2,6-dimethyl-1,4-phenylene oxide) and a blend of these show that annealing and storage permit chain packing rearrangements which favour non-radiative energy conversion and transfer processes at the expense of direct chromophore emission. (12 refs.)

63032 Electronic structure and luminescent properties of Cu⁺ and Ag⁺ impurity centers in NaCl. C.Pedrin (CNRS, Univ. Lyon-1, Villeurbanne, France), H.Chermette.

Int. J. Quantum Chem. (USA), vol.23, no.3, p.1025-32 (March 1983). (Proceedings of the Fourth International Congress in Quantum Chemistry, Uppsala, Sweden, 13-20 June 1982).

Fluorescence studies of Cu⁺ and Ag⁺ impurity centers embedded in NaCl are reported. The multiple scattering X_α method is used to describe the electronic structure of these ions in NaCl matrix. It is shown that taking into account the external lattice potential is necessary to obtain good results which can be compared to experiment. This has been done through the computation of an embedded NaCl₆⁻ cluster potential. Moreover, in NaCl:Ag⁺, it is also necessary to include relativistic corrections in order to obtain a reliable energy diagram. This is easily done by use of the Wood Hamiltonian, which allows the self-consistent inclusion of Darwin and mass-velocity terms in MS X_α codes. A good quantitative agreement with experiment is finally obtained for the optical excitations and the emission mechanism of the luminescent centers. The metal-chlorine distance is predicted slightly larger than the NaCl bulk value and the harmonic force constant of the a_{1g} vibrational breathing deformation of the cluster is calculated and found in good agreement within experiment. For the first time the Stoke shift of such systems is evaluated. (12 refs.)

63033 Pure electronic, vibronic, and two-particle surface excitons on the anthracene crystal. I. General theoretical basis, experimental study, and analysis of the (0,0) region. M.Orrit, J.Bernard, J.M.Turlet, Ph.Kottis (Centre de Phys. Moléculaire Optique et Hertzienne, Univ. de Bordeaux I, Talence, France).

J. Chem. Phys. (USA), vol.78, no.6, pt.1, p.2847-56 (15 March 1983).

These two papers (papers I and II) present a complete study—theoretical and experimental—of the first singlet-singlet electronic and vibronic transitions of the anthracene crystal. The authors interpret the new observed structures in terms of pure electronic, vibronic, and two-particle site shift surface exciton states. The first paper (I) begins by a model description of the bulk and surface excitons in a rigid lattice. They then describe the experimental study of the anthracene crystal reflectivity and surface emission excitation at low temperatures with and without nitrogen coating of the crystal surface. For the first time, they clearly established the following results: (1) The existence and the accurate position of the upper a polarized Davydov component for the pure electronic surface exciton. (2) The equality within the experimental accuracy ($\approx 23 \text{ cm}^{-1}$), of the surface and bulk excitonic Davydov splitting ($\Delta = 223 \text{ cm}^{-1}$) and the translational equivalence ($\delta = 206 \text{ cm}^{-1}$) of the surface structures with their bulk counterparts; (3) A variation of the surface Davydov splitting when the crystal surface is coated with frozen nitrogen. (24 refs.)

63034 Anomalous temperature-dependent phosphorescence of Cu porphyrin in anthracene. J.Bohandy, B.F.Kim (Milton S. Eisenhower Res. Center, Johns Hopkins Univ., Laurel, MD, USA).

J. Chem. Phys. (USA), vol.78, no.7, p.4331-6 (1 April 1983).

The temperature dependence of the phosphorescence spectrum of copper porphyrin in anthracene has been studied from room temperature down to 8K and the 4.2K spectrum has been obtained. A 23.4 cm^{-1} crystal field splitting of the orbital components of the T₀ state was observed. The 0-0 transition appears abruptly at approximately 25K and increases rapidly in intensity as the temperature is lowered. A model involving energy transfer from the copper porphyrin to the triplet exciton band of anthracene gives a satisfactory explanation for the anomalous temperature dependence of the copper porphyrin phosphorescence intensity. (13 refs.)

63035 Low-temperature energy trapping and emission line profile of disordered solids. J.R.Morgan, M.A.El-Sayed (Dept. of Chem. & Biochem., Univ. of California, Los Angeles, CA, USA).

J. Phys. Chem. (USA), vol.87, no.3, p.383-5 (3 Feb. 1983).

In a disordered solid, where random excitation energy and donor-acceptor separation are expected, low-temperature energy transfer between a high-energy excited molecule to a lower-energy acceptor might not be complete. As a result, the emission profile of the solid at low temperature is determined by the energy distribution of the emission of the trapping sites. Predictions based on these ideas are used and a fit is made up to the 4.2K observed phosphorescence profile of 1-bromo-4-chloronaphthalene (BCN), an orientationally disordered molecular solid. The theoretical fit to the observed emission profile is discussed in terms of the possible energy transfer mechanism(s) in this solid. (12 refs.)

63036 Optical properties of copper-related centres in InP. M.S.Skolnick, P.J.Dean, A.D.Pitt, Ch.Uihlein, H.Krath, B.Deveaud, E.J.Foulkes (Royal Signals & Radar Estab., Great Malvern, England).

J. Phys. C (GB), vol.16, no.10, p.1967-85 (10 April 1983).

A new Cu-related photoluminescence band in InP is reported. It consists of a sharp zero-phonon line at 1.2889 eV with sharp LO and 'gap mode' local phonon replicas to lower energy superimposed on a broad vibronic background. Zeeman studies show that the recombination process arises from an exciton bound to a neutral isoelectronic centre. Electron and hole g-values of 1.27 and 2.12 respectively are deduced, with both electron and hole having spin 1/2. The very strong diamagnetic shift of the spectrum is found to be equal to that of a shallow donor electron in InP. This demonstrates clearly that the hole is tightly bound in the short-range potential of the centre with binding energy E_b^h = 127.5 meV and that the electron is then weakly bound in the Coulomb field of the hole (E_b^e = 7.3 meV), so that the overall behaviour is of an isoelectronic donor. The thermal activation energy of the vibronic

sideband of the luminescence is found to be 135 ± 10 meV, in good agreement with the spectroscopic value of the hole binding energy. (46 refs.)

63037 Long-term photoluminescence fatigue in $\text{Ge}_x\text{Se}_{1-y}$ glasses. J.M.Chamberlain, A.J.Moseley (Dept. of Phys., Univ. of Nottingham, Nottingham, England).

J. Phys. C (GB), vol.16, no.10, p.1987-98 (10 April 1983).

Photoluminescence fatigue (PLF) of $\alpha\text{-Ge}_x\text{Se}_{1-y}$ ($0.05 < y < 0.38$) is investigated at 4K for irradiation times of up to two hours. Previous analyses of PLF cross sections (F_f) are shown to be inappropriate. A model involving the fatiguing of an effective fraction of all PL centres is introduced. The spectral and compositional dependences of F_f are obtained with this new model, and the convergence of F_f and the cross section, F_{pa} , for photoinduced absorption (PA) is observed for $y=0.33$ material. An 'apparent' fatigue due to self-absorption at extrinsic centres created in the material after prolonged irradiation is shown to provide an important contribution to PLF for large integrated exposure. Previously reported discrepancies in F_f and F_{pa} at $y=0.33$ are attributed to neglect of this extrinsic centre PLF mechanism. Specific defect structures are suggested for this material using the tight-binding approach of Robertson (1980), and their radiative properties are discussed in terms of configuration coordinate models. The nonzero PL of $y=0$ material is accounted for without recourse to unknown impurities. Mechanisms for PA/PR and PLF are proposed and the convergence of F_{pa} and F_f is explained by $y=0.33$ in terms of the proposed defects. (14 refs.)

63038 Luminescence decay time of the 1.945 eV centre in type Ib diamond. A.T.Collins (Wheatstone Phys. Lab., King's Coll., London, England), M.F.Thomaz, M.I.B.Jorge.

J. Phys. C (GB), vol.16, no.11, p.2177-81 (20 April 1983).

The luminescence decay time of the 1.945 eV centre has been determined as 13 ± 0.5 ns for natural type Ib diamonds. For synthetic diamonds the value is slightly lower, probably because of competitive non-radiative recombination in these relatively impure crystals. The similarity of the decay time to that for the H3 centre further supports the model proposed for the vacancy-enhanced aggregation of nitrogen in diamond. No temperature dependence of the 1.945 eV decay time has been detected in the range 77-700K, and this result is not inconsistent with the energy level scheme used to interpret ESR data for the 1.945 eV centre. (13 refs.)

63039 Characterisation of Mn-doped and nominally pure LPE $\text{Ga}_{1-x}\text{In}_x\text{As}_y\text{P}_{1-y}$ ($y=2.1x$) between $y=0$ and $y=1$ using photoluminescence and electrical measurements. A.W.Smith (Dept. of Phys., Univ. of Nottingham, Nottingham, England), L.G.Shantharama, L.Eaves, P.D.Greene, J.R.Hayes, A.R.Adams.

J. Phys. D (GB), vol.16, no.4, p.679-86 (14 April 1983).

Photoluminescence (PL) and electrical measurements have been made on a series of p-type, Mn-doped layers of $\text{Ga}_{1-x}\text{In}_x\text{As}_y\text{P}_{1-y}$ ($y=2.1x$) grown by liquid phase epitaxy on InP substrates and of a similar series of nominally pure crystals used as control samples. For small y , the Mn-doped samples shown an intense Mn-related PL band with a zero-phonon structure at 1.185 eV (4K) for the $y=0$ (InP) sample. This locates the Mn-acceptor level at 230 meV above the valence band edge. The PL band can be followed up to $y=0.40$ and the Mn-acceptor energy E_A is estimated to vary as (230-185) meV. For larger y , a broad, though strong, PL is observed on the low energy side of the near-band-edge lines. At these higher y values, electrical measurements have been used to determine E_A , giving $E_A=49$ meV for $y=0.93$ and 0.10 eV for $y=0.70$, in fairly good agreement with linear extrapolation of the PL data. The low temperature PL of six undoped control samples ($0.5 < y < 1$) reveal two sharp PL lines at (1.02-0.33y) and (1.00-0.33y) eV of as yet unknown origin. (19 refs.)

63040 Magnetic-field-induced breakdown of correlation between spins and moments of photoexcited electrons in GaAs crystals. I.Ya.Karlik, D.N.Mirlin, L.P.Nikitin, D.G.Polyakov, V.F.Sapega (A.F. Ioffe Physicotech. Inst., Acad. of Sci., Moscow, USSR).

JETP Lett. (USA), vol.36, no.5, p.192-4 (5 Sept. 1982). Translation of: *Pis'ma v Zh. Eksp. i Teor. Fiz. (USSR)*, vol.36, no.5, p.155-7 (5 Sept. 1982). [received: April 1983]

The effect of a longitudinal magnetic field on the circular polarization of recombination photoluminescence of hot electrons is observed. This effect is related to the change in the mutual orientation of correlated momenta and spins of photoexcited electrons. (3 refs.)

63041 Radiationless transitions in p-terphenyl crystals doped with anthracene, tetracene and pentacene. J.O.Williams, A.C.Jones, M.J.Davies (Edward Davies Chem. Labs., Univ. Coll. of Wales, Aberystwyth, Wales).

J. Chem. Soc. Faraday Trans. II (GB), vol.79, pt.2, p.263-9 (Feb. 1983).

The fluorescence spectra and lifetimes of anthracene, tetracene and pentacene molecules in a host p-terphenyl single crystalline lattice have been measured over the temperature range 10-300K. At low temperatures the molecules occupy different sites in the host lattice. The high-temperature fluorescence spectra are dominated by particular sites and the temperature dependence of the fluorescence lifetime of these sites is recorded. Neither O_4/O_3 sites for anthracene nor A_3/A_4 sites for tetracene exhibit a marked temperature dependence whereas the lifetime of O_1/O_2 sites for pentacene decreases with increasing temperature with an activation energy of 60-90 cm^{-1} . This temperature dependence is associated with an increased probability for intersystem crossings from O_1/O_2 to a triplet level (T_2) of the pentacene molecule which is located at $16960 \pm 15 \text{ cm}^{-1}$. (21 refs.)

63042 Luminescence analysis of group III and V impurities in silicon. A.S.Kaminskii, L.I.Kolesnik, B.M.Leiferov, Ya.E.Pokrovskii.

J. Appl. Spectrosc. (USA), vol.36, no.5, p.516-20 (May 1982). Translation of: *Zh. Prikl. Spektrosk. (USSR)*, vol.36, no.5, p.745-50 (May 1982). [received: Feb. 1983]

Describes a method for carrying out a qualitative and quantitative analysis of group III and V impurities in silicon. The analysis of the content group III and V impurities is based on the characteristic emission, arising with recombination of multiparticle exciton-impurity complexes (MEIC) at low temperatures ($\sim 4\text{K}$). Recombination of such complexes can occur both without the participation of phonons and with the participation of TA, LO and TO phonons. The identification of the nature of an impurity is based on the fact that the luminescence spectra consist of a series of narrow lines, characteristic of each of the group III and V impurities in silicon. The systems looked at were: Si:P, Si:As, Si:Sb, Si:Bi, Si:Al and Si:Ga. (5 refs.)

63043 Spectral-kinetic study of the intrinsic-luminescence characteristics of a fluorite-type crystal. N.N.Ershov, N.G.Zakharov, P.A.Rodnyi.

Opt. & Spectrosc. (USA), vol.53, no.1, p.51-4 (July 1982). Translation of: *Opt. & Spektrosk. (USSR)*, vol.53, no.1, p.89-93 (July 1982). [received: April 1983]

A spectral-kinetic study has been conducted on the luminescent properties of CaF_2 , SrF_2 , and BaF_2 crystals under conditions of brief (10 or 20 nsec) X-ray excitation. The fundamental parameters of the short and long components of the intrinsic luminescence of the crystals have been determined in the temperature range from 77 to 400K. It was found that the characteristic

long-lived component of the luminescence is well described by a model of recombination of F and H pairs, while the short-lived component is of the $V_k + e^-$ exciton type. (23 refs.)

63044 Optical spectra of impurity centers with double-well adiabatic potentials. S.A.Kulagin, I.S.Osadko.

Opt. & Spectrosc. (USA), vol.53, no.1, p.100-1 (July 1982). Translation of: *Opt. & Spektrosk. (USSR)*, vol.53, no.1, p.169-71 (July 1982). [received: April 1983]

The optical spectra of polyatomic organic molecules dissolved in n paraffins frequently have a multiplet structure. Discussing the nature of the multiplet, Shpol'skii proposed that the multiplet lines correspond to spatially separated impurity centers. Later the existence of inverse variations in multiplet lines under the action of laser light was discovered which contradicted Shpol'skii's hypothesis. It was thus proposed that some lines in such multiplets could correspond to impurity centers with double-well adiabatic potentials. On the basis of numerical calculations the authors discuss the differences between doublet spectra of a two-well nature and doublets produced by spatially separated centers. (7 refs.)

63045 Luminescence flash photostimulation spectra of silver chloride.

A.N.Latyshchev, M.A.Kushnir, V.V.Bokarev.

Opt. & Spectrosc. (USA), vol.53, no.2, p.215-16 (Aug. 1982). Translation of: *Opt. & Spektrosk. (USSR)*, vol.53, no.2, p.364-6 (Aug. 1982). [received: April 1983]

The results obtained indicate primarily that the initial result of the action of light on AgCl crystals is an increase in the concentration of deep electron traps (with ionization energies above 1.3 eV), which have a large effective cross section of light absorption and a decrease in the concentration of comparatively shallow traps. Even more striking are the changes taking place in the effective cross section of the traps. In comparatively shallow traps (< 1.2 eV), the effective cross section decreases, and in deep ones it increases sharply (threefold for 1.77 eV). This indicates a qualitative difference and a great variety of electron localization centers. (8 refs.)

63046 Absorption, fluorescence, and excitation spectra of thallium-activated rubidium bromide. V.B.Sharan (Dept. of Appl. Sci. & Humanities, Technol. Faculty, Kaila Nehru Inst. of Sci. & Technol., Sultanpur, USSR).

Phys. Status Solidi b (Germany), vol.116, no.1, p.41-7 (1 March 1983).

Absorption, excitation, and fluorescence spectra of polycrystalline RbBr:TI phosphors are presented at various thallium concentrations. For very low thallium content two absorption bands are obtained peaking at 224 and 260 nm. Additional absorption bands appear around 230, 244, 267, and 278 nm with rise of thallium content. An asymmetric fluorescence band in the ultraviolet region is obtained at low thallium concentration which can be resolved into two Gaussian emission bands peaking at 317 and 365 nm. Two additional visible fluorescence bands appear at 440 and 535 nm with rise of thallium content. The excitation spectra for the ultraviolet and visible emission bands are found to be different. Accordingly the ultraviolet emission band is attributed to the characteristic a-emission in TI^+ monomer entering substitutionally and the visible bands are attributed to dimer centers having D_{4h} site symmetry. (23 refs.)

63047 Theory of intrinsic recombination at zero temperature in small gap semiconductors. Estimations for PbSe. M.Mocker, M.Beiler (Sektion Phys., Humboldt-Univ. zu Berlin, Berlin, Germany).

Phys. Status Solidi b (Germany), vol.116, no.1, p.205-15 (1 March 1983).

A theory of intrinsic recombination at zero temperature is developed. Numerical results in a wide range of excitation and doping concentrations are given for a model adapted to $\text{PbSe}_0\text{Se}_{0.9}$. In order that first-order Auger recombination is possible a minimum value of majority carrier concentration has to be reached. Consequently, a finite small signal lifetime only exists if doping concentration $N_D > N_{D\text{min}}$, where for $\text{PbSe}_0\text{Se}_{0.9}$ $N_{D\text{min}} \approx 4.5 \times 10^{18} \text{ cm}^{-3}$ in case of parabolic model and $N_{D\text{min}} \approx 9 \times 10^{19} \text{ cm}^{-3}$ in case of Kane model of band structure. Radiative recombination rate only depends on minority carrier concentration p. At strong excitation the radiative lifetime behaves like $p^{-2/3}$ in parabolic and like $p^{-1/3}$ in Kane band approximation. Quantum efficiency η of radiative processes in dependence on N_D decreases steeply near $N_D \approx N_{D\text{min}}$. (13 refs.)

63048 Orientation of polystyrene chains stretched above T_g as studied by fluorescence polarization. R.Fajolle, J.F.Tassin, P.Sergot, C.Pambrun, L.Monnerie (Lab. de Physicochimie Structurale et Macromoléculaire, Ecole Supérieure de Phys. et Chimie Industrielles de la Ville de Paris, Paris, France).

Polymer (GB), vol.24, no.4, p.379-82 (April 1983).

Fluorescence polarization has been used to measure the orientation of polystyrene chains labelled by an anthracene group covalently bound in the middle of the chains and dispersed in atactic uncrosslinked polystyrene. Stretching is performed at constant strain rate and various temperatures above T_g using equipment which is described. The influence of strain rate and temperature on chain orientation is reported and leads to the conclusion that the orientation of the central part of the labelled chains is not related to the complete stress but is governed by the rubbery deformation. The occurrence of relaxation phenomena during stretching is demonstrated. (11 refs.)

63049 Fluorescence probe for microenvironments: on the fluorescence properties of p-N,N-dialkylaminobenzylidenemalononitrile in polymer matrices. K.Y.Law (Xerox Webster Res. Center, Webster, NY, USA), R.O.Loutfy.

Polymer (GB), vol.24, no.4, p.439-42 (April 1983).

The effect of an alkyl group (R) in a series of poly(alkylmethacrylate) and poly(alkylacrylate) polymers on the fluorescence properties of p-N,N-dialkylaminobenzylidenemalononitrile derivative, 1, has been studied. The fluorescence emission maximum shifts to the blue and the fluorescence quantum yield decreases as the chain length of R increases. These results are interpreted in terms of a model which assumes that the location of 1 is dependent on R and the change in quantum yield reflects the difference in free volume of polymer chain flexibility in various locations in these polymers. (16 refs.)

63050 Inductive effect of substituents and their influence on the rate of temperature quenching of Eu^{3+} luminescence in mixed ligand europium β -diketonates. V.E.Karasyov, A.G.Mirochnick, R.N.Shchelokov (Inst. of Chem., Far East Sci. Centre, Acad. of Sci., Vladivostok, USSR).

Spectrosc. Lett. (USA), vol.15, no.12, p.931-43 (1982).

The authors' investigation deals with the effect of donor-acceptor activity of terminal groups of the organic ligand on radiationless dissipation of Eu^{3+} electronic excitation energy to the surrounding ligand. (16 refs.)

63051 Photoluminescence of epitaxial GaSb films and of GaInAsSb solid solutions. A.E.Bochkarev, L.I.Kolesnik, A.M.Loshinskii, M.G.Mil'vidskii (State Sci.-Res. & Design Inst. of Rare-Metal Industry, Moscow, USSR). *Sov. Phys.-Semicond. (USA)*, vol.16, no.10, p.1215-16 (Oct. 1982). Translation of: *Fiz. & Tekh. Poluprovodn. (USSR)*, vol.16, no.10, p.1886-8 (Oct. 1982). [received: April 1983]
Epitaxial films of GaInAsSb solid solutions are the most promising materials for optoelectronic devices operating in the spectral range 1.7-3.2 μ . However, there is no published information on the luminescence properties of these semiconductors, although such properties determine largely the parameters of optoelectronic devices in which they are used. Therefore, the authors recorded not only the photoluminescence spectra of these solid solutions but also the corresponding spectrum of epitaxial films of gallium antimonide. (7 refs.)

63052 Photon transport of mobile nonequilibrium carriers in variable-gap semiconductors as a result of band-impurity level radiative recombination. G.V.Tsarenkov (A.F. Ioffe Physicotech. Inst., Acad. of Sci., Leningrad, USSR). *Sov. Phys.-Semicond. (USA)*, vol.16, no.10, p.1218-19 (Oct. 1982). Translation of: *Fiz. & Tekh. Poluprovodn. (USSR)*, vol.16, no.10, p.1890-2 (Oct. 1982). [received: April 1983]
Considers theoretically photoluminescence in a variable gap semiconductor under band-impurity level radiative recombination conditions. (2 refs.)

63053 Edge photoluminescence of CdGa₂Se₄ single crystals. T.G.Kerimova, Sh.S.Mamedov, E.Yu.Salav (Inst. of Phys., Acad. of Sci., Baku, Azerbaijan SSR). *Sov. Phys.-Semicond. (USA)*, vol.16, no.10, p.1228 (Oct. 1982). Translation of: *Fiz. & Tekh. Poluprovodn. (USSR)*, vol.16, no.10, p.1904-5 (Oct. 1982). [received: April 1983]
The authors investigated the photoluminescence spectra of CdGa₂Se₄ at 77 and 300K. Single crystals were prepared by the method of gas-transport reactions. Crystalline iodine was used to provide the transport gas. Single crystals prepared in this way were trihedral prisms with the [112] face most highly developed. The tetragonal c axis was inclined relative to the [112] direction by 37°. The photoluminescence was excited by an LPM-11 He-Cd laser ($\lambda=4416$ Å) and detected using an SPM-2 monochromator with a polarizer in front of the entry slit. The photoluminescence was emitted by the [112] face. (5 refs.)

63054 The influence of X-trap on spin-lattice relaxation in the impurity phosphorescent state of a naphthalene crystal. V.P.Vorob'ev, V.I.Mel'nik, M.T.Shpak. *Ukr. Fiz. Zh. (USSR)*, vol.28, no.3, p.430-6 (March 1983). In Russian.
It is shown theoretically that a spin-lattice relaxation (SLR) process in the lowest triplet impurity state may be connected with a thermally activated electronic excitation energy exchange between the impurity and an X-trap accompanying it. On the basis of carried out experimental investigations concerned with the temperature and magnetic field effect on the impurity phosphorescence intensity it has been concluded that such SLR-process occurs in case of β -chloronaphthalene impurity in naphthalene-H₈ and deuterionaphthalenes 1DH₇, 2DH₇. (20 refs.)

Excited states of mixed-ligand chelate complexes of ruthenium(II). A re-examination of the evidence for strong interligand coupling See Entry 60756
Effect of anion coordination upon radiationless transitions of the uranyl ion See Entry 60786

Effects of aggregation on the phosphorescence of phenyl alkyl ketones in 77K rigid glass solutions See Entry 60790
Circular polarization in the fluorescence of β,γ -enones: distortion in the $\pi\pi^*$ state See Entry 60795
Effects of excited-state prototropic equilibria on the fluorescence energies of benzimidazole and thiabendazole homologues See Entry 60814
Effect of polar solvents on amine quenching for *p*-fluorotoluene fluorescence See Entry 60817

Intracoll triplet-triplet annihilation in poly(2-vinylnaphthalene) in benzene solution See Entry 60818

Role of energy migration between monomeric molecules of rhodamine dyes in the concentration quenching of the luminescence of the solutions See Entry 60826
Spectral-luminescent properties of phthalimides in aqueous-micellar solutions of sodium dodecyl sulfate See Entry 60827

Investigation by the molecular-probe method of the changes in the packing density of filled epoxide compositions during hardening See Entry 61828

Etching characterization of {001} semi-insulating GaAs wafers See Entry 61917

Changes in the concentration of 1.0 and 1.28 eV copper luminescence centers during annealing of electron-irradiated *n*-type GaAs See Entry 61948

Parameters of bound multiexciton complexes in direct polar semiconductors See Entry 62341

Exciton trapping and sensitized luminescence: a generalized theory for all trap concentrations See Entry 62342

Temperature and kinetics of the exciton and biexciton gas in cadmium sulfide and selenide crystals See Entry 62344

New aspects of the oxygen donor in gallium phosphide See Entry 62365

Distance dependence of electronic energy transfer to semiconductor surfaces: $\pi\pi^*$ pyrazine/GaAs(110) See Entry 62466

Raman and luminescence studies of alkali borate tungstate glasses See Entry 62962

A comparison of Raman scattering, resonance Raman scattering, and fluorescence from molecules adsorbed on silver island films See Entry 62971

Vibrational and electronic spectra of Na[UO₂(CH₃COO)₃] See Entry 62992

Forbidden luminescence and resonance Raman scattering of bound exciton states in CdS See Entry 62998

Site-selection spectroscopy of Eu³⁺-doped germinate glass See Entry 63023

Mechanism for the annealing out of radiation-induced Eu²⁺ from barium orthophosphate See Entry 63027

Continuous deposition of photovoltaic grade CdS sheet at the unit operations scale See Entry 63164

Organometallic vapor phase epitaxial growth of In_{1-x}Ga_xAs₂P_{1-y} on GaAs See Entry 63166

The influence of polymer concentration on the internal motion-intramolecular pyrene excimer formation—a low molecular weight probe in solution See Entry 63577

78.60 OTHER LUMINESCENCE SPECTRA AND RADIATIVE RECOMBINATION

(for photoconduction and photovoltaic effects, see 72.40; for photoluminescence, see 78.55)

63055 Emission of light from solids during crack formation. A.M.Avilov, V.D.Volovik, A.A.Evtukh, S.I.Ivanov (A.M. Gorkii State Univ., Khar'kov, Ukrainian SSR). *Sov. Phys.-Tech. Phys. (USA)*, vol.27, no.10, p.1271-2 (Oct. 1982). Translation of: *Zh. Tekh. Fiz. (USSR)*, vol.52, no.10, p.2071-3 (Oct. 1982). [received: April 1983]
Methods for recording weak light fluxes are used to study emission during cracking and destruction of glass, fused quartz, mica, and silicon and bismuth single crystals. Relative emission intensities are reported for various materials, in addition to the duration τ and intensity I of the light flashes during destruction of glass as functions of the diameter d of the rigid mounting (determining the sample bending) and the length l of the crack produced. Emission spectra were recorded at wavelengths 389-700 nm during destruction of photographic glass and mica. (9 refs.)

78.60F Electroluminescence

63056 Electroluminescence from ZnS during deformation of a metal contact. L.F.Gavrilov, F.F.Gavrilov (S.M. Kirov Ural Polytech. Inst., Sverdlovsk, USSR). *Sov. Phys.-Tech. Phys. (USA)*, vol.27, no.10, p.1284-5 (Oct. 1982). Translation of: *Zh. Tekh. Fiz. (USSR)*, vol.52, no.10, p.2093-4 (Oct. 1982). [received: April 1983]
Contact phenomena are important in understanding electroluminescence. It was shown by Lehmann (see J. Electrochem. Soc., vol.104, p.45, 1957) that many powdered phosphorescent crystals do not exhibit electroluminescence under ordinary conditions but do so when mechanically mixed with metal powders. The purpose of the present authors is to determine the electron-injecting properties of metal contacts. The sensitivity of a luminophor, activated by Ag and CuAl at four different concentrations, to deformations of the substrate in contact with the luminophor was tested. The luminophor was most sensitive to deformation at Cu and Al concentrations 6×10^{-2} and 9×10^{-2} wt.%. It is shown how the intensity of electroluminescence in the blue spectrum from a ZnS-CuAl luminophor behaves during deformation of zinc and copper contacts when a 10 kHz AC voltage of magnitude 150 V was applied to the capacitor plates. Aluminum and nickel contacts were also tested. The findings suggest the following interpretation of Lehmann's results on contact electroluminescence. Intense exoelectronic emission caused by large deformation of the particle faces may be responsible for the observed irregular emission from a mixture of luminophor and metal powder (particularly near the sharp faces of the metal particles). (6 refs.)

Excitation of active impurities in laser crystals under electric discharge conditions See Entry 61162

78.60H Cathodoluminescence, ionoluminescence

63057 Visible and near ultraviolet radiation from ultrathin silver films bombarded by low energy electrons. F.Miserey, A.Septier (Conservatoire Nat. des Arts et Metiers, Paris, France). *C.R. Seances Acad. Sci. Ser. II (France)*, vol.296, no.5, p.321-4 (7 Feb. 1983). In French.
Ultrathin Ag films (thickness: 0.8-5 nm) deposited on Al substrate have been studied. The reflectance decreases in the energy range of surface plasmon excitation due to surface roughness. Measurements of radiation spectra produced by 12 keV incident electrons indicate that Ag transition radiation does appear when a single Ag monolayer is present on the substrate. Roughness-coupled surface plasmon radiation is also observed. (14 refs.)

63058 The low-energy-electron (LEE) excitation of SnO₂/Eu powder phosphor; fundamental characteristics. T.Matsuoka, T.Tohda, T.Nitta (Material Res. Lab., Matsushita Electric Industrial Co. Ltd., Osaka, Japan). *J. Electrochem. Soc. (USA)*, vol.130, no.2, p.417-23 (Feb. 1983).
The physicochemical properties and fundamental luminescent characteristics of SnO₂/Eu powder were examined for use as low-energy-electron (LEE) excitation phosphor. Solubility limit of Eu into SnO₂ was 0.05-0.06 a/o and smaller mean diameter, higher resistivity (order of 10¹⁰ Ω cm), and more intensive diffused reflectance were observed with increased Eu addition. Although the same emission spectra by f-f transition of Eu(⁵D₀-⁷F₁ strongest peaks) were observed in u.v., high and low-energy-electron excitation, broad intrinsic emission from SnO₂ matrix, which coexist with the f-f transition emission, was different for each excitation method. In LEE excitation, the maximum intensity wavelength of the intrinsic emission was longer than in high-energy-electron excitation. The intrinsic emission was not observed at room temperature in u.v. excitation. Excitation spectrum with a peak at 300 nm was attributed to matrix excitation, i.e. electron hole generation. Optimal addition of 0.1 a/o Eu for brightness, 5.9 msec decay (1/10), and an efficiency of 2 lm/W at 9~10V were observed under LEE excitation. Efficiency increased with lower voltage and current excitation due to sublinearities of brightness-voltage and current dependences. (22 refs.)

63059 Cathodoluminescence of some semiconductors and development of lasers with electron-beam excitation. L.N.Kurbatov, A.I.Dirochka, G.S.Kozina. *J. Appl. Spectrosc. (USA)*, vol.36, no.5, p.509-15 (May 1982). Translation of: *Zh. Prikl. Spektrosk. (USSR)*, vol.36, no.5, p.738-45 (May 1982). [received: Feb. 1983]
With a view to creating a sealed universal source of laser radiation for metrological purposes, the authors first investigate the cathodoluminescence of many semiconductors, and in particular Pb_{1-x}Sn_xTe and GaSe₂Te_{1-x}, and then present the generation spectra of a whole range of materials that can be used for electron-pumped semiconducting lasers. The materials looked at cover the laser range from the UV through the near-IR. (22 refs.)

63060 The excitation of energetic atomic particles penetrating amorphous condensed matter. W.Dziurda, L.Gabla, M.Tuleta (Inst. of Phys., Jagellonian Univ., Cracow, Poland). *Physica B & C (Netherlands)*, vol.115 B+C, no.3, p.419-25 (March 1983).
The emission of light from both the surface and the interior of a glass target bombarded by Ar⁺ ions of energy 2.5-5 keV was observed. The analysis of both kinds of radiation shows that excited Na atoms penetrating the glass undergo radiative relaxation. The relative number of Na atoms radiation inside the glass increases with increasing energy of incident ions. It was stated that the radiation of Na atoms penetrating the condensed matter was found when the NaCl single crystal was bombarded by the same ion beam. (8 refs.)

- Auger recombination in GaSb and its effects on laser characteristics See Entry 61160
- Improvement of the characteristics of ZnSe single-crystal semiconductor lasers pumped longitudinally by an electron beam See Entry 61163
- Ion implantation and luminescence See Entry 61940
- Morphology and composition of films based on gold on the surface of gallium arsenide during vacuum annealing See Entry 62287

78.60K Thermoluminescence

- 63061 Thermoluminescence emission spectra of KCl-KBr mixed systems.** B.Subramanian, K.G.Bansigir (School of Studies in Phys., Jiwaji Univ., Gwalior, India). *J. Phys. C (GB)*, vol.16, no.10, p.1999-2003 (10 April 1983). Thermoluminescence (TL) emission spectra of gamma-irradiated KCl, KBr and KCl-KBr mixed crystals have been obtained at various glow peak temperatures. The variation of emission-band wavelength with composition at different glow peaks has been studied. It shows a minimum for the intermediate composition. Also, the addition of Br^- ions to the KCl lattice has more influence on the TL emission of a KCl-KBr mixed system than the addition of Cl^- ions to KBr. (11 refs.)
- 63062 On the role of Z centres in the supralinearity and sensitisation of LiF TLD phosphor.** V.K.Jain (Health Phys. Div., Bhabha Atomic Res. Centre, Bombay, India). *J. Phys. D (GB)*, vol.16, no.4, p.L89-91 (14 April 1983). A Z-centre model was proposed by Nink and Kos (1976) to explain the thermoluminescent response of LiF. That model has been criticised by several authors. A modified version of the Z-centre model has since been proposed. This letter points out that even the modified version does not stand scrutiny. (14 refs.)
- 63063 Thermoluminescence of low-temperature X-irradiated MgO and MgO:Li single crystals.** V.D.Rodriguez, V.M.Orea (Dept. de Fisica Fundamental, Univ. de Zaragoza, Zaragoza, Spain), Y.Chen, R.Alcala. *Phys. Status Solidi A (Germany)*, vol.75, no.2, p.577-82 (16 Feb. 1983). Thermoluminescence measurements of 80K X-irradiated MgO and MgO:Li single crystals are performed. In pure MgO four glow peaks, observed at 175, 220, 245, and 265K, are associated with the release of holes from different traps. All these glow peaks show two emission bands at 375 and 700 nm (the latter due to Cr^{3+} ions) while a band at 245 nm is found only in the 175K peak. In MgO:Li five glow peaks appear at 120, 135, 150, 165, and 220K, all of which are due to the recombination of holes with electron centers. The peak at 220K is correlated with the thermal destruction of $[\text{Li}]^{\circ}$ centers. Two emission bands, observed at 430 and 700 nm, are detected in all of the glow peaks. The activation energies for thermal ionization of the traps, which are related with the main glow peaks, are also given. (21 refs.)
- 63064 On mechanisms of thermostimulated luminescence excitation in γ -irradiated corundum.** A.L.Apanasenko, A.E.Ovechkin. *Ukr. Fiz. Zh. (USSR)*, vol.28, no.3, p.354-7 (March 1983). In Russian. Thermostimulated conductivity (TSC), thermostimulated luminescence (TSL) and optical absorption of γ -irradiated $\alpha\text{-Al}_2\text{O}_3$ single crystals were investigated to determine the ways of charge transfer in TSL processes. It is found out that emission in the 3.0 eV region does not result directly from the current appearance. TSL in the regions of 3.8 eV and 1.8-2 eV is accompanied by appearance of free carriers in the allowed band. It is concluded that TSL processes in 3.0 eV region are due to transition inside complex centres. (5 refs.)
- Mechanism for the annealing out of radiation-induced Eu^{2+} from barium orthophosphate** See Entry 63027

78.60P Chemiluminescence

(see also 82.40T Chemiluminescence and chemical laser kinetics)

- The exposure dependence and emission spectrum of chemiluminescence produced during the oxidation of Si (111) by O_2 See Entry 63556
- Laser-induced decomposition of sodium azide See Entry 63557

78.65 OPTICAL PROPERTIES OF THIN FILMS

- 63065 Electrical and optical properties of a-Si_{1-x}C_xH film prepared by GD SiH₄ and C₂H₄.** Chen Guanghua, Zhang Fangqing, Du Ning, Xu Xixiang, Huang Shisheng (Dept. of Phys., Lanzhou Univ., China), Liu Zhi. *Chin. J. Semicond.* (China), vol.4, no.2, p.149-53 (March 1983). In Chinese. Optical technology conditions, infrared absorption (IR) spectra, variation of optical gap (E_{opt}) with x, measurement results of ESCA and ESR of a-Si_{1-x}C_xH films prepared by glow-discharge decomposition of silane-ethane mixture have been studied. Preliminary discussions about these experimental results are presented. (8 refs.)
- 63066 Influence of Ag photodoping on photoinduced changes in As₂S₃ glass films.** T.Yaji, S.Kurita (Dept. of Electrical Engng., Keio Univ., Yokohama, Japan). *Jpn. J. Appl. Phys. Part 1 (Japan)*, vol.22, no.3, p.400-3 (March 1983). The transient photoinduced optical absorption change (TOC) and the photodarkening have been studied in Ag photodoped As₂S₃ glass films. They were observed in all of the sample films we prepared ($(\text{As}_{0.4}\text{S}_{0.6})_{100-x}\text{Ag}_x$; $0 \leq x \leq 24.4$ at.%). For the photodarkening, the degree of the change in optical-gap energy due to the light irradiation and the heat treatment decreases with the increasing of Ag content. This may be ascribed to the fact that the motion of S atoms is hindered by the Ag atoms, causing a decrease in spatial flexibility. For the TOC, the spectral distribution of the optical absorption change has a broad peak. The peak center shifts to a lower energy position with the increasing of Ag content. (17 refs.)
- 63067 Optical anisotropy and electrostriction in the anodic oxide of molybdenum.** D.J.DeSmet (Dept. of Phys. & Astron., Univ. of Alabama, University, AL, USA), J.L.Ord. *J. Electrochem. Soc. (USA)*, vol.130, no.2, p.280-4 (Feb. 1983). The anodic oxidation of molybdenum in acetic acid electrolyte is studied using a self-nulling ellipsometer to follow field-induced changes in the optical properties of the oxide film. When oxidized at constant field, the oxide exhibits the greatest optical anisotropy of any oxide studied thus far. When the field is removed, the oxide retains more than half of its original anisotropy. The oxide film thickness increases when the field is applied, and the dependence of strain on field is linear at low fields. There is a corresponding decrease in the dielectric constant of the film when the film thickness increases. The zero-field optical anisotropy is not removed by an electrochromic conversion cycle. (12 refs.)

- 63068 Optical anisotropy and electrostriction in the anodic oxide of niobium.** C.G.Matthews, J.L.Ord, W.P.Wang (Dept. of Phys., Univ. of Waterloo, Waterloo, Ontario, Canada). *J. Electrochem. Soc. (USA)*, vol.130, no.2, p.285-90 (Feb. 1983). The anodic oxidation of niobium in sulfuric acid electrolyte is studied using a self-nulling ellipsometer to follow the optical changes that occur when the field in the oxide film is switched. The oxide is optically anisotropic with the anodizing field applied, and the degree of anisotropy, the ratio between index changes parallel and transverse to the field, is found to equal 2.2 by a procedure that requires consistency from the analysis of field-switching transients for a wide range of oxide film thicknesses. The film thickness increases and its refractive index values decrease when the field is applied. The dependences are not the parabolic dependences predicted by the theory of electrostriction, and the significance of this finding is discussed. Although the galvanostatic charge-discharge transients that are used to study the changes in the low frequency dielectric constant exhibit significant hysteresis, they show that the decrease in dielectric constant with increasing field observed at optical frequencies occurs also at low frequencies. The results are compared with the dependence of dielectric constant on field deduced from open-circuit transient analysis, and the significance of the discrepancy is discussed. It is concluded that the possibility that the oxide film has a significantly polar structure remains an open question. (16 refs.)
- 63069 Optical absorption in hydrogenated microcrystalline silicon.** Z.Iqbal, F.-A.Sarott, S.Veprek (Inst. of Inorganic Chem., Univ. of Zurich, Zurich, Switzerland). *J. Phys. C (GB)*, vol.16, no.10, p.2005-15 (10 April 1983). Optical absorption measurements between 0.35 and 2.5 eV at 22°C on hydrogenated microcrystalline silicon films prepared in a DC discharge at deposition temperatures (T_{dep}) between 110 and 450°C, are presented and discussed. Anomalous high optical-absorption was observed for films prepared at a floating potential, which is a few orders of magnitude higher than of single-crystal Si for samples prepared at T_{dep} between 260 and 350°C and in the photon energy range up to 2.0 eV, is also higher than that of amorphous Si. Samples prepared at a floating potential at $T_{\text{dep}} \leq 180^\circ\text{C}$ and $\geq 400^\circ\text{C}$, and those prepared at a negative substrate bias, show a lower optical absorption, which for the latter films is similar to that of amorphous silicon. Annealing up to 800°C under ultra-high vacuum resulted in a small but reproducible increase in absorption independent of T_{dep} . Similar annealing experiments followed by absorption measurements in high vacuum indicated no measurable effect of the adsorbed oxygen on the optical absorption. The angular dependence of the forward light scattering from the films was measured at various wavelengths and found to diffuse scattering and absorption in the films. Furthermore, quantitative estimates of the surface roughness of the films from reflection data and scanning electron micrographs were made, and these results are discussed with respect to the enhanced absorption and scattering in the films. (23 refs.)
- 63070 A numerical method for determining the complex refractive index from reflectance and transmittance of supported thin films.** R.T.Phillips (Cavendish Lab., Univ. of Cambridge, Cambridge, England). *J. Phys. D (GB)*, vol.16, no.4, p.489-97 (14 April 1983). It is known that several widely used methods of analysing reflectance (R) and transmittance (T) for a supported thin film neglect the effect of the rear surface of the substrate. Equations are given which relate R and T to the complex refractive index ($n-ik$) and thickness of the thin film, and a method for their solution is described. This relies on Powell's technique, and permits changes to be made to the equations relating R , T to ($n-ik$). This flexibility has allowed the calculation of the effect of the neglect of the rear of the substrate. An example is given of the use of the method for the determination of ($n-ik$) for an amorphous film of selenium, measured at 100K over the range of photon energies from 1.5 to 3.25 eV. (9 refs.)
- 63071 Molecular orientation in thin monolayer films by infrared spectroscopy.** J.F.Rabolt, F.C.Burns, N.E.Schlottter, J.D.Swales (IBM Res. Lab., San Jose, CA, USA). *J. Electron Spectrosc. & Relat. Phenom. (Netherlands)*, vol.30, p.29-34 (Feb. 1983). (Proceedings of the Third International Conference on 'Vibrations at Surfaces', Asilomar, CA, USA, 1-4 Sept. 1982). Fourier transform infrared spectroscopic measurements have been made on monolayer samples of cadmium arachidate in order to determine orientation and molecular packing on the surface. This was accomplished by using both grazing angle reflection methods, where the polarization of the infrared radiation is very close to being perpendicular to the surface, and transmission methods, where the incident optical electric field is polarized parallel to the surface. Hence these two methods are sensitive to molecular vibrations whose change in dipole moment lies along different directions. The results showed that independent of the substrate, silver for the reflection experiments and silver bromide for the transmission experiments, the chains of the fatty acid salt (no evidence for any free acid was found) are oriented within a few degrees of the normal to the surface of the substrate. From a detailed analysis of the observed vibrational bands in the two orientations, combined with the known literature values and assignments, the authors were able to make a 'complete assignment' of the observed bands. (12 refs.)
- 63072 Applications of surface polaritons for detection and vibrational spectral analysis of thin films on metals and dielectrics.** G.N.Zhizhin, M.A.Moskalova, E.A.Vinogradov, A.A.Sigarev, V.A.Yakovlev (Inst. of Spectroscopy, Acad. of Sci., Troitzk, USSR). *J. Electron Spectrosc. & Relat. Phenom. (Netherlands)*, vol.30, p.35-40 (Feb. 1983). (Proceedings of the Third International Conference on 'Vibrations at Surfaces', Asilomar, CA, USA, 1-4 Sept. 1982). Phonon-polaritons interactions with molecular vibrations of thin films were used for the detection of film oscillator spectral positions. The gap in the polariton branch was proportional to \sqrt{l} being the thickness of the film on dielectric support. The ATR method in the Otto configuration was used for measurements as well as thermal stimulated emission. The vibrational spectra (infrared absorption) of monomolecular films were detected by surface electromagnetic waves (SEW)—surface plasmon-polaritons propagating along the metallic substrate. A comparison of the reflection-absorption method with the SEW broadband ($650\text{-}2500\text{ cm}^{-1}$) FT-IR method of thin films detection is made. The better sensitivity of the last one is shown. The prism, grating and edge methods of SEW excitations in IR are discussed. (37 refs.)
- 63073 Method of determining refractive-index dispersion of film coatings from transmission spectra.** G.V.Pantelev, M.G.Cherenkov, V.I.Yampolskii, V.N.Egorov. *Opt. & Spectrosc. (USA)*, vol.53, no.2, p.192-3 (Aug. 1982). Translation of: *Opt. & Spektrosk. (USSR)*, vol.53, no.2, p.331-3 (Aug. 1982). [received: April 1983] A number of methods exist for finding the refractive index of films from the level of the extrema of reflection and transmission curves. In some cases the magnitude of refractive-index dispersion can be calculated from the transmission spectra. The authors consider the effect of refractive-index dispersion

of a film on the position of extreme points of the transmission curve. (6 refs.)

63074 Optical properties of oxide supermultilayer films. V.A.Kamin, M.V.Shilova. *Opt. & Spectrosc. (USA)*, vol.53, no.2, p.198-200 (Aug. 1982). Translation of: *Opt. & Spektrosk. (USSR)*, vol.53, no.2, p.339-42 (Aug. 1982). [received: April 1983]

Presents results of investigations into the optical transmission of supermultilayer films consisting of ~ 2 -1000 alternating layers of the dielectrics SiO and GeO. Measurement of the optical transmission of the supermultilayer dielectric films (SDF) was performed on an SF-26 spectrometer in the 300-800-nm wavelength range. The calculated thickness of the layers in the various samples came to ~ 1 -100 nm. The total thickness of the films was within the ~ 0.1 -10- μ m limits. (11 refs.)

63075 Optical and electrical properties of a-Si₁C_{1-x}H films prepared by glow discharge from SiH₄ and C₂H₄. Chen Guang-hua, Zhang Fang-qing, Du Ning, Wang Hui-sheng (Dept. of Phys., Lanzhou Univ., Lanzhou, China). *Sol. Energy Mater. (Netherlands)*, vol.7, no.4, p.413-20 (Jan.-Feb. 1983). Optical technology conditions, infrared absorption spectra, variation of optical gap (E_{opt}) with x , measurement results of ESCA and ESR of a-Si₁C_{1-x}H films prepared by glow-discharge decomposition of silane-ethene mixtures have been studied. Preliminary discussions about these experimental results have been made. (8 refs.)

63076 Fundamental reflectivity spectra of Cd₃As₂ thin films. K.Karnicka-Moscicka, A.Kisiel (Inst. of Phys., Jagellonian Univ., Krakow, Poland), L.Zdanowicz.

Thin Solid Films (Switzerland), vol.101, no.2, p.115-21 (11 March 1983). Fundamental reflectivity spectra of thin polycrystalline and amorphous thin Cd₃As₂ films are reported. The results for polycrystalline samples can be quantitatively explained in terms of reflecting surface roughness only. For amorphous films the most probable explanation is provided by variations in the short- and medium-range order. (15 refs.)

63077 Thin film absorption spectra of lower valent p block halides. A.J.Bruce, J.A.Duffy (Dept. of Chem., Univ. of Aberdeen, Aberdeen, Scotland).

Thin Solid Films (Switzerland), vol.101, no.2, p.179-92 (11 March 1983). Thin film absorption spectra (mainly in the UV region) of the halides of In⁺, Tl⁺, Sn²⁺, Pb²⁺, Sb³⁺ and Bi³⁺ are considered in the light of spectral data for these ions diluted in alkali halide crystals and other halide media. Assignments to $S_{0-1}P_1$, $S_{0-1}P_2$ and $S_{0-1}P_3$ transitions are made on the basis of plotting photon energy against the orbital expansion parameter h for the set of halides for each metal ion. The plots are required (i) to be linear, (ii) to have a similar slope to the corresponding plot for the A, B and C bands of dilute systems and (iii) to extrapolate to the photon energy of the free metal ion for $h=0$. The justification for adopting this ligand field approach, as opposed to an energy band approach, is discussed and it is decided that the effect of energy band formation upon the s-p energy separation in the metal ion is quite small. In many instances the photon energy in the binary halide is similar to that for the metal ion when diluted in halide media, e.g. the $S_{0-1}P_1$ energy in PbBr₂ is 3.98 eV whereas for Pb²⁺ in KBr it is 4.16 eV, suggesting that the effect of energy bands is more or less compensated for by the reduced electron donation from the smaller number of halide ions in the binary metal halides compared with that in the diluted halide media. (51 refs.)

63078 Transparent conductors—a status review. K.L.Chopra, S.Major, D.K.Pandya (Dept. of Phys., Indian Inst. of Technol., New Delhi, India).

Thin Solid Films (Switzerland), vol.102, no.1, p.1-46 (8 April 1983). Non-stoichiometric and doped films of oxides of tin, indium, cadmium, zinc and their various alloys, deposited by numerous techniques, exhibit high transmittance in the visible spectral region, high reflectance in the IR region and nearly metallic conductivity. The electrical as well as the optical properties of these unusual materials can be tailored by controlling the deposition parameters. These transparent conductors have found major applications in a vast number of active and passive electronic and opto-electronic devices ranging from aircraft window heaters to charge-coupled imaging devices. In this status review the authors present a comprehensive and up-to-date description of the deposition techniques, electro-optical properties, solid state physics of the electron transport and optical effects and some applications of these transparent conductors. (293 refs.)

Measuring thin film parameters by inputting light through a prism See Entry 59821

Determination of optical constants by photometry See Entry 59824

Metallic multilayers: new possibilities in X-UV optics See Entry 61257

Optical mode conversions in Nd substituted iron garnet films See Entry 61270

Observation of an orientational polarizability of dipolar molecules adsorbed in fine-pore membranes See Entry 62276

On the reaction mechanism of GaAs MOCVD See Entry 62292

Effect of electron bombardment on the phase transition in VO₂ films See Entry 62339

Magnetic and optical properties of Co, Bi substituted garnet films prepared by the LPE method and its application to thermomagnetic recording See Entry 62733

Amorphous TbFe ultra thin film with reflective Au layer See Entry 62734

Garnet film with rectangular hysteresis loop and its application to thermomagnetic recording medium See Entry 62735

Preparation and properties of RE-TM amorphous films See Entry 62736

Magnetic properties and magnetic Kerr rotation of amorphous TbFeCo and TbFeCr films See Entry 62737

The thermo-magnetic writing and erasing properties and Kerr rotation angle of amorphous RE-Fe thin films See Entry 62738

Formation of nonthrough magnetic domains in the course of magnetization switching in amorphous Gd-Co films See Entry 62766

Conversion Mossbauer studies of epitaxially mixed ferrite-garnet films See Entry 62870

Determination of the optical constants and thickness of amorphous V₂O₅ thin films See Entry 62918

Refractive index in epitaxial Pb_{1-x}Sn_xTe films See Entry 62919

Magneto-optical spectra of RF-sputtered amorphous Gd-Co and Gd-Fe films See Entry 62945

Magneto-optical effect spectra of rare-earth—transition-metal amorphous films See Entry 62946

Maximum amplification of the polar Kerr effect by surface coatings See Entry 62947

The influence of the parallel magnetic field on the interband optical absorption in thin films See Entry 62952

Infrared spectrum of thawed water See Entry 62957

Photoluminescence in amorphous C:H films prepared by glow discharge decomposition of CH₄ or C₂H₆ See Entry 63030

Effect of annealing on photo-energy transfer in poly(2,6-dimethyl-1,4-phenylene oxide), polystyrene and their blends See Entry 63031

Characterisation of Mn-doped and nominally pure LPE Ga_{1-x}As_xP_{1-y} (y=2.1x) between y=0 and y=1 using photoluminescence and electrical measurements See Entry 63039

Photoluminescence of epitaxial GaSb films and of GaInAsSb solid solutions See Entry 63051

Visible and near ultraviolet radiation from ultrathin silver films bombarded by low energy electrons See Entry 63057

High-energy particles in AlN film preparation by reactive sputtering technique See Entry 63155

Organometallic vapor phase epitaxial growth of In_{1-x}Ga_xAs_{1-y}P_{1-y} on GaAs See Entry 63166

A solution growth technique for the preparation of copper(II) selenide thin films See Entry 63181

LPE growth of YNd-iron garnet films for magneto-optical waveguides See Entry 63182

Deposition of cadmium chalcogenide thin films by a solution growth technique using triethanolamine as a complexing agent See Entry 63184

Composition, optical properties and degradation modes of Cu/(graded metal-carbon) solar selective surfaces See Entry 63728

78.70 OTHER INTERACTIONS OF MATTER WITH PARTICLES AND RADIATION

63079 Coherent emission by relativistic particles interacting with atomic rows during reflection from a crystal surface. V.I.Vit'ko, A.V.Voitsenya, S.V.Dyul'dya, N.N.Nasonov, V.V.Rozhkov (Physicotech. Inst., Acad. of Sci., Kharkov, Ukrainian SSR).

Sov. Tech. Phys. Lett. (USA), vol.8, no.8, p.399-400 (Aug. 1982). Translation of: *Pisma v Zh. Tekh. Fiz. (USSR)*, vol.8, no.15-16, p.921-3 (Aug. 1982). [received: April 1983]

A new type of bremsstrahlung—an emission by relativistic positrons which are reflected at small angles from a solid surface (reflection radiation) has been predicted. The analysis used the approximation of a continuous distribution of the atoms on the reflecting surface, which was assumed to coincide with an atomic plane. The authors show that the coherent interaction of particles with atomic rows on the surface of a single crystal results in fundamental changes in the spectral and polarization properties of reflection radiation at high frequencies. (6 refs.)

X-ray backlighting measurements of plane Al target velocity in 0.35 μ m laser interaction experiments See Entry 63086

78.70B Positron annihilation

(see also 71.65 Positron states)

63080 Positron lifetime measurement of plastically deformed iron single crystals. F.Kuramoto, Y.Aono, M.Takenaka, K.Kitajima (Res. Inst. for Appl. Mech., Kyushu Univ., Fukuoka, Japan).

J. Phys. Soc. Jpn. (Japan), vol.52, no.4, p.1098-101 (April 1983).

Positron lifetime measurement and analysis were made for pure iron single crystals plastically deformed at room temperature and 77K. Both second component I_2 (175 psec, dislocations and jogs) and third component I_3 (about 350 psec, vacancy clusters) in the specimen deformed at 77K were larger than those in the specimen deformed at room temperature. It must be concluded that jogs in the low temperature deformed specimen play an important role in positron trapping and also in production of vacancies. However, the jog number density estimated from the experiment is too high, which suggests that some modification in the model of positron trapping by jogs may be required. (3 refs.)

Recovery of quenched Cu-Ge alloys studied by positron annihilation See Entry 62156

Is it possible to avoid thermal embrittlement in ribbon-shaped glassy metals? ... See Entry 63416

78.70D X-ray absorption and absorption edges

63081 Structure of bimetallic clusters. Extended X-ray absorption fine structure (EXAFS) studies of Ir-Rh clusters. G.Meitzner, G.H.Via, F.W.Lytle, J.H.Sinfelt (Corporate Res. Sci. Labs., Exxon Res. & Engng. Co., Linden, NJ, USA).

J. Chem. Phys. (USA), vol.78, no.5, p.2533-41 (1 March 1983).

The extended X-ray absorption fine structures (EXAFS) associated with the L_{III} absorption edge of iridium and the K absorption edge of rhodium were investigated for catalysts containing bimetallic clusters of these elements dispersed on silica or alumina. The catalysts contained 1 wt.% iridium and 0.5 wt.% rhodium, which corresponds to an Ir/Rh atomic ratio close to 1. From the EXAFS data, it is concluded that the rhodium concentration in the surface region of the iridium-rhodium clusters is greater than it is in the interior. The EXAFS data also indicate that the iridium-rhodium clusters are more highly dispersed on alumina than on silica. (24 refs.)

63082 Soft X-ray absorption spectroscopy by electric potential scanning application to carbon, nitrogen and oxygen K edges. T.Muranaka (Dept. of Appl. Phys., Tohoku Univ., Sendai, Japan).

J. Vac. Soc. Jpn. (Japan), vol.25, no.12, p.775-80 (1982). In Japanese.

Carbon, nitrogen and oxygen K-absorption spectroscopy by electric potential scanning has been demonstrated for polymer samples of collodion and formvar using a nickel X-ray target. Besides representing these obtained spectra, some experimental aspects including background features without sample films are described for technical convenience. In addition, a recently proposed numerical procedure is applied to some of the observed spectra to obtain characteristic absorption functions which are not influenced by the incident X-ray intensity distributions. (18 refs.)

63083 Extended X-ray absorption fine structure investigation of local symmetry changes in Co^{2+} - and Ni^{2+} -exchanged zirconium phosphates. L. Alagna, T. Prosperi, A.A.G. Tomlinson (Istituto di Teoria e Struttura Elettronica dei Composti di Coordinazione, Rome, Italy), C. Ferragina, A. La Ginester. *J. Chem. Soc. Faraday Trans. 1 (GB)*, vol.79, pt.4, p.1039-47 (April 1983). The EXAFS spectra of Co^{2+} - and Ni^{2+} -exchange zirconium phosphates (mainly the α -forms) have been measured using synchrotron radiation. The M-O bond distances obtained are correlated with geometries inferred from electronic spectra. It is confirmed that there are changes in site geometry with degree of loading and calcination temperature. There is also further support for the presence of distorted tetrahedral sites in the anhydrous layered α -forms. For all the materials, a second shell is visible between 2.4 and 2.87 Å (non-phase-shift corrected) depending on the particular material; these are ascribed to M...P distances. The gross changes in these second-shell distances, the M-O bond distances and the inter-layer distances are combined to suggest sites for the metal ions. As for the Cu^{2+} analogues, and the zirconium phosphate layers do not remain rigid after exchange and calcination, but side (and, perhaps, twist) to accommodate the Co^{2+} or Ni^{2+} . (28 refs.)

63084 X-ray studies of 3d-transition metals in compounds with chlorine and bromine. G.P. Polovina. *Ukr. Fiz. Zh. (USSR)*, vol.28, no.3, p.422-6 (March 1983). In Russian. K-absorption spectra of Ni and Cu have been studied in NiCl_2 , NiF_2 , NiBr_2 , CuBr_2 as well as K-absorption spectra of Br—in CuBr_2 , ZnBr_2 , NiBr_2 , $\text{CoBr}_2 \cdot 6\text{H}_2\text{O}$ and the L_{α} -band of Cu—in CuBr . K- and L-spectra of CuCl were matched in a single energy scale in order to determine the nature of the 'white' line in the K-edge of Cl in the compound. The investigation shows that there is a 'white' line in K-edges of Cl and Br which corresponds to free 3d-states of the metal. Degrees of 3d electrons participation in the chemical bond are different for various halogens. (13 refs.)

Investigation of titanium in metamict Nb-Ta-Ti oxides using the extended X-ray absorption fine structure technique See Entry 60287
Metallic multilayers: new possibilities in X-UV optics See Entry 61257
X-ray study of niobium disulfide intercalated with copper See Entry 61886
Mechanism for the annealing out of radiation-induced Eu^{2+} from barium orthophosphate See Entry 63027

78.70E X-ray emission threshold and fluorescence

63085 Electron structure and X-ray emission spectra of ScRh . V.V. Nemoshkalenko (Acad. of Sci., Ukrainian SSR), M.A. Plotnikov, V.N. Antonov. *Dopov. Akad. Nauk UkrSR. Ser. A (USSR)*, no.2, p.56-8 (1983). In Ukrainian.

The band structure and intensity distribution in X-ray emission spectra of ScRh intermetallic compound with CsCl structure were calculated by the linear APW method. The ScRh band structure is shown to be characterized by two groups of d-bands genetically originating from Sc and Rh d-levels and separated by the energy gap with low density of states. The states of s-symmetry are shown to make an essential contribution of Sc M_{11} -emission band. (4 refs.)

Auger electron appearance potential spectrum of Ni See Entry 63088

79.00 ELECTRON AND ION EMISSION BY LIQUIDS AND SOLIDS; IMPACT PHENOMENA

79.20 IMPACT PHENOMENA

(inc. electron spectra and sputtering)

79.20D Laser-light impact phenomena

63086 X-ray backlighting measurements of plane Al target velocity in 0.35 μm laser interaction experiments. G. Thiell, B. Meyer, P. Aussage, X. Fortin (Centre d'Etudes de Limeil, Villeneuve-Saint-Georges, France). *C.R. Seances Acad. Sci. Ser. II (France)*, vol.296, no.4, p.209-12 (31 Jan. 1983). In French.

Velocity measurements by means of time and space resolved X-ray shadowgraphy are performed on planar aluminium disk targets irradiated with 1 ns frequency-tripled Nd-laser pulses. Comparison with velocity measurements deduced from visible interferometry and streak shadowgraphy as well as with the data of numerical simulations from a hydrodynamic code yields negligible target preheat effects and shows the harmful influence of beam non-uniformities on laser driven targets. (8 refs.)

63087 Excitation of surface electromagnetic waves at a solid surface by an intense laser beam. A.M. Prokhorov, V.A. Sychugov, A.V. Tishchenko, A.A. Khakimov (P.N. Lebedev Phys. Inst., Acad. of Sci., Moscow, USSR). *Sov. Tech. Phys. Lett. (USA)*, vol.8, no.8, p.415-16 (Aug. 1982). Translation of: *Pis'ma v Zh. Tekh. Fiz. (USSR)*, vol.8, no.15-16, p.961-6 (Aug. 1982). [received: April 1983]

Several recent studies of laser annealing and of the interaction of laser beams with matter have revealed the appearance of periodic structures of polished surfaces of various materials when bombarded by intense laser beams. Possibly, the wave incident on the surface interferes with a surface electromagnetic wave, which it excites, giving rise to the periodic structure. In an effort to identify the actual role played by surface electromagnetic waves in this process, the authors have analyzed the propagation of surface electromagnetic waves along a rippled interface between two media. A study of the nature of the damage caused to surfaces of various materials when bombarded by intense laser beams opens up some new possibilities for research on the materials themselves as well as some new possibilities for the technology of grating fabrication. (7 refs.)

Non-equilibrium behavior on pulsed laser evaporated surfaces See Entry 61020

Gas breakdown near metal surfaces caused by ultraviolet laser light See Entry 61603

Plasma production during vaporization of materials by the radiation from a CO_2 TEA laser See Entry 61671

Spatial and size distributions of inhomogeneities initiating laser breakdown in alkali halide crystals at 10.6 μm See Entry 61962

Effect of initial conditions on the evolution of a laser-generated shock wave See Entry 62028

Laser-induced thermal desorption of CO from clean polycrystalline copper: time-of-flight and surface diffusion measurements See Entry 62257

Heterojunction formed from gallium selenide and indium selenide by laser melting See Entry 62488

Processes occurring in an erosion plasma during laser vacuum deposition of films. III. Condensation in gas flows during laser vaporization of materials See Entry 63161

Infrared laser stimulated surface processes See Entry 63587

79.20F Electron impact: Auger emission

63088 Auger electron appearance potential spectrum of Ni. D.L. Grolemond, D. Chopra (Dept. of Phys., East Texas State Univ., Commerce, TX, USA).

IEEE Trans. Nucl. Sci. (USA), vol.30, no.2, p.934-6 (April 1983). (1982 IEEE Conference on the Application of Accelerators in Research and Industry, Denton, TX, USA, 8-10 Nov. 1982).

Electrons are accelerated onto a solid polycrystalline Ni surface. These primary electrons interact with the surface to produce one of two phenomena: X-ray fluorescence, or Auger electron emission. Auger electron appearance potential spectroscopy (AEAPS) is a process by which the Auger component of the secondary electron flux is analysed to extract qualitative information about the electronic structure of the empty conduction band states. In AEAPS, the threshold behavior of the Auger transitions is examined by taking the first derivative of the secondary electron current with respect to the incident electron energy using the potential modulation technique. Width of the empty band, degree of localization of the conduction band wave functions, overlapping of the 3d band with the 4s, and satellite phenomena are among the important parameters ascertainable by AEAPS. The present AEAPS measurements of L_{32} levels of Ni are compared with the reported data from Soft X-ray Appearance Potential Spectroscopy (SXAPS) of Ni. (16 refs.)

63089 Autoionization emission from transition metals by electron impact. S.D. Bader, G. Zajac, J. Zak (Materials Sci. & Technol. Div., Argonne Nat. Lab., Argonne, IL, USA).

Phys. Rev. Lett. (USA), vol.50, no.16, p.1211-14 (18 April 1983).

Intense gain satellites associated with the $M_{23}VV$ Auger transition have been observed for representative 3d transition metals. The satellites have line shapes and intensities that resemble those of the M_{23} electron-energy-loss and resonant photon-excited spectra of these materials and are identified as being due to autoionization electron emission. This identification satisfies the expectation that the Fano effect should be manifest in both absorption and emission experiments, whether photon or electron excited. (18 refs.)

63090 The depth dependence of the depth resolution in composition-depth profiling with Auger electron spectroscopy. M.P. Seah, C.P. Hunt (Div. of Materials Applications, NPL, Teddington, England).

Surf. & Interface Anal. (GB), vol.5, no.1, p.33-7 (Feb. 1983).

The depth dependence of the depth resolution in composition-depth profiles using Auger electron spectroscopy is briefly appraised to emphasize some of the different mechanisms operating for different classes of material and to show how the use of a characterized Ta_2O_5 on Ta reference material can help to optimize the depth resolution. In addition it is shown that, even for flat uniformly-layered samples sputtered under ideal conditions where the ion beam crater is flat and impurities may be ignored, five factors still limit the depth resolution: information depth, statistical effects and cascade mixing, electron stimulated desorption and sample roughening. These may each be observed to dominate at the appropriate depth for amorphous materials but, for evaporated polycrystalline metal films, the last term dominates for depths greater than 10 nm. (42 refs.)

Ion beam induced composition changes during Auger sputter profiling of thin Al films on InP See Entry 62001

Analysis of diffusion mechanisms in thin polycrystalline Au-Ag films using Auger electron spectroscopy See Entry 62185

Identification of arsenic surface species on the Si(100) surface See Entry 62278

On depth profiling an InGaAsP-InP heterojunction See Entry 62280

Electronic transitions of Ar, Xe, N_2 , CO physisorbed on Ag (111) and Al (111) See Entry 63107

Photoemission study of Au overlayers on Pd(111) and the formation of a Pd-Au(111) alloy surface See Entry 63135

Composition, optical properties and degradation modes of Cu/graded metal-carbon solar selective surfaces See Entry 63728

79.20K Other electron impact phenomena

63091 Improvement of sensitivity of electron energy loss spectroscopy. A. Koma, K. Yoshimura (Inst. of Materials Sci., Univ. of Tsukuba, Ibaraki, Japan).

Jpn. J. Appl. Phys. Part 2 (Japan), vol.22, no.3, p.L173-5 (March 1983).

A new method has been developed to drastically increase the sensitivity of low-energy electron energy loss spectroscopy. This method uses a pulse counting technique to detect a small number of analysed electrons and a difference formula to obtain the second-derivative spectrum. A personal-computer-controlled system has been developed for this purpose and the usefulness of the present method is demonstrated. (2 refs.)

63092 Thermal scattering of slow electrons during elastic specular reflection from a Cu (001) surface. R.E. Dietz, E.G. McRae, D.A. Kapirow (Bell Labs., Murray Hill, NJ, USA).

J. Electron Spectrosc. & Relat. Phenom. (Netherlands), vol.29, p.41 (15 Jan. 1983). (Proceedings of the Third International Conference on 'Vibrations at Surfaces', Asilomar, CA, USA, 1-4 Sept. 1982).

Summary form only given as follows: The authors studied the effects of thermal scattering of slow electrons ($E < 20$ eV) specularly and elastically reflected from a Cu (001) surface at temperatures up to 1000K. These effects are important in surface spectroscopies that depend on conservation of momentum parallel to the surface. The structure in the reflected electron current as a function of electron energy near diffracted beam emergence thresholds are found to be sensitive to temperature. The overall specular current decreases sharply with increasing T, and the current in the peaks close to threshold diminishes relative to the current in the lowest energy peak with increasing T and with decreasing polar angle of incidence. The authors fitted the observed lineshapes in I vs. E plots with a calculation which takes

account of (a) multiple scattering between the substrate and the surface potential barrier (SPB) modelled by a saturated image potential; (b) thermal diffuse scattering (TDS) at the substrate; and (c) electron energy loss due to electron-electron interactions as represented by a short-range imaginary potential. The TDS is taken to zeroth order for direct (Bragg) reflection, and to second order in the transferred momentum for indirect reflection wherein the electron is momentarily trapped by the SPB. The mean-square amplitudes of vibration perpendicular and parallel to the surface are taken as parameters, and values slightly larger than bulk values are found to satisfy the data. (2 refs.)

63093 High resolution electron energy loss studies of adsorbates utilizing impact and resonance scattering. J.E.Demuth (IBM Thomas J. Watson Res. Center, Yorktown Heights, NY, USA), P.A. Vouris, D.Schmeisser.

J. Electron Spectrosc. & Relat. Phenom. (Netherlands), vol.29, p.163-74 (15 Jan. 1983). (Proceedings of the Third International Conference on 'Vibrations at Surfaces', Asilomar, CA, USA, 1-4 Sept. 1982).

The nonpolar electron scattering processes of impact and resonance scattering from adsorbed molecules are discussed. Examples of O_2 , H_2 , benzene, pyridine and cyclohexane adsorption on Ag(111) are presented to illustrate the potential of nonpolar scattering to provide new physical information regarding adsorption and surface reactions. (22 refs.)

63094 High resolution EELS studies of clean and oxide covered semiconductor surfaces. L.H.Dubois, G.P.Schwartz (Bell Labs., Murray Hill, NJ, USA).

J. Electron Spectrosc. & Relat. Phenom. (Netherlands), vol.29, p.175-80 (15 Jan. 1983). (Proceedings of the Third International Conference on 'Vibrations at Surfaces', Asilomar, CA, USA, 1-4 Sept. 1982).

High resolution electron energy loss spectroscopy was used to study surface optical phonons on sputter-annealed samples of GaAs, InP, GaP, and CdTe. The measured phonon frequencies were in excellent agreement with theoretical predictions and were independent of crystal orientation, bulk doping level or method of surface preparation. Coupled plasmon-phonon modes in degenerately doped samples were observed to be weak or totally suppressed, suggesting that surface carrier depletion has occurred. Vibrational spectra have also been obtained from thermally grown native oxides on InP and GaP which support the existence of the respective orthophosphates $InPO_4$ and $GaPO_4$. (16 refs.)

63095 Summary abstract: vibrational excitations of hydrogen and oxygen on Pd(100). C.Nyberg, C.G.Tengst (Dept. of Phys., Chalmers Univ. of Technol., Goteborg, Sweden).

J. Electron Spectrosc. & Relat. Phenom. (Netherlands), vol.29, p.191-2 (15 Jan. 1983). (Proceedings of the Third International Conference on 'Vibrations at Surfaces', Asilomar, CA, USA, 1-4 Sept. 1982).

Summary form only given. The adsorption and coadsorption of hydrogen and oxygen on the Pd(100) surface have been studied using angle resolved high resolution electron energy loss spectroscopy (EELS) and low energy electron diffraction (LEED). The coadsorption of hydrogen and oxygen can give important information relevant to the catalytic oxidation of hydrogen on Pd. The Pd(100)p(2×2)O surface does not adsorb hydrogen at 80K, while oxygen adsorbs both dissociatively and associatively on the Pd(100)c(2×2)H surface at 80K. To study the changes in the coadsorbed overlayer as the temperature is increased up to the point where the water reaction occurs, the sample was exposed to 0.5 L oxygen followed by 5 L hydrogen at 80K. No ordering could be observed with LEED. The EEL spectrum not only reveals losses characteristic of atomic oxygen and hydrogen adsorbed in the hollow site but also a loss at 37 meV. The nature of this loss is not yet fully understood. It may be due to the vibration of oxygen atoms adsorbed in the vicinity of hydrogen atoms. Another possibility is that hydroxyl is formed during the adsorption, the 37 meV loss being due to the Pd-OH stretch vibration or the Pd-OH bend vibration. This would, however, give rise to a loss corresponding to the O-H stretch vibration. No loss is found in this region of the spectrum. Heating the sample to 275K causes the 37 meV peak to disappear. The LEED pattern reveals a sharp p(2×2) structure. This means that the oxygen and hydrogen atoms have redistributed on the surface, without any apparent water formation taking place as observed with the mass spectrometer. Finally, when the sample is heated to 300K water is formed and desorbs from the surface. (3 refs.)

63096 High resolution electron energy loss spectroscopic study of the interaction of oxygen with magnesium single crystal surfaces. P.A.Thiry, J.Ghijssen, J.Pireaux, R.Caudano (Lab. de Spectroscopie Electronique, IRIS, FNDP, Namur, Belgium).

J. Electron Spectrosc. & Relat. Phenom. (Netherlands), vol.29, p.193-8 (15 Jan. 1983). (Proceedings of the Third International Conference on 'Vibrations at Surfaces', Asilomar, CA, USA, 1-4 Sept. 1982).

From the beginning of the interaction of oxygen with the clean Mg(0001) and Mg(1100) surfaces, two vibrational bands were measured by HREELS. The first one at 480 cm^{-1} is attributed to atomic oxygen adsorbed at the surface. The second band at 620 cm^{-1} is related to the stretching vibration of incorporated oxygen precursor to oxide formation. No specific difference was observed in the position and evolution of the two bands for both surfaces, but the electronic intensity reflected in the specular peak exhibited a totally different behaviour. The widths of the vibrational bands suggest a strong coupling with the continuum of electron-hole pairs of the metal. (9 refs.)

63097 Oxygen adsorption on the kinked Pt(321) surface. M.R.McClellan (Dept. of Chem., MIT, Cambridge, MA, USA), J.L.Gland, F.R.McFeely.

J. Electron Spectrosc. & Relat. Phenom. (Netherlands), vol.29, p.213-18 (15 Jan. 1983). (Proceedings of the Third International Conference on 'Vibrations at Surfaces', Asilomar, CA, USA, 1-4 Sept. 1982).

Oxygen adsorption and desorption were characterized on the kinked Pt(321) surface using high resolution electron energy loss spectroscopy and thermal desorption spectroscopy. Molecular oxygen adsorbs mainly as a peroxo-like species at 100K with a heat of desorption of about 22 kJ/mol . Some of the molecular oxygen also adsorbs dissociatively at 100K. Atomic oxygen is adsorbed in three states. One state is due to adsorption on the terraces and another state is due to adsorption along the rough step sites. The heat of desorption of both of these states is approximately equal and decreases from 290 kJ/mol to 195 kJ/mol with increasing coverage. Atomic oxygen is also observed to adsorb in another state which is interpreted as adsorption at an on-top site. (8 refs.)

63098 Calculation of the EELS spectra of the Ni(001) surface with p(2×2) and c(2×2) overlayers of oxygen. V.Bortolani (Istituto di Fisica, Univ. di Modena, Modena, Italy), A.Franchini, F.Nizzoli, G.Santoro.

J. Electron Spectrosc. & Relat. Phenom. (Netherlands), vol.29, p.219-24 (15 Jan. 1983). (Proceedings of the Third International Conference on 'Vibrations at Surfaces', Asilomar, CA, USA, 1-4 Sept. 1982).

The authors present a force constant slab calculation of the nickel (001) surface phonons with p(2×2) and c(2×2) oxygen overlayers. According to very recent experimental results they assume in both configurations an equal distance of 0.9 Å between the oxygen overlayer and the nickel surface. With

two adjustable parameters (the O-Ni force constants) they are able to reproduce with good accuracy the position and the lineshape of four peaks present in the experimental EELS spectra. The nature of these peaks is investigated in detail and the noticeable difference between the spectra of the two overlayers is explained. (15 refs.)

63099 Contrasting bonding configurations of acetone on Pt(111) and Ru(001) surfaces. N.R.Avery, A.B.Anton, B.H.Toby, W.H.Weinberg (CSIRO Div. of Materials Sci., Univ. of Melbourne, Parkville, Victoria, Australia).

J. Electron Spectrosc. & Relat. Phenom. (Netherlands), vol.29, p.233-7 (15 Jan. 1983). (Proceedings of the Third International Conference on 'Vibrations at Surfaces', Asilomar, CA, USA, 1-4 Sept. 1982).

The comparative chemistry of acetone adsorption on Pt(111) and Ru(001) has been studied by EELS. On the more easily oxidized Ru(001) surface, acetone bonded in a side-on, $\eta^2(\text{O,C})$ configuration, whereas on the well-defined, close-packed regions of the Pt(111) surface acetone adopted a weak adduct-like, end-on, $\eta^1(\text{O})$ configuration. On Pt(111), some $\eta^2(\text{O,C})$ was also observed and associated with adsorption at low coordination accidental step sites. (10 refs.)

63100 The methoxy intermediate on Mo(100): effects of surface oxidation. S.L.Miles (Dept. of Chem., Princeton Univ., Princeton, NJ, USA), S.L.Bernasek, J.L.Gland.

J. Electron Spectrosc. & Relat. Phenom. (Netherlands), vol.29, p.239-46 (15 Jan. 1983). (Proceedings of the Third International Conference on 'Vibrations at Surfaces', Asilomar, CA, USA, 1-4 Sept. 1982).

Methanol adsorption and decomposition were characterized on clean, partially oxidized, and completely oxidized molybdenum (100) surfaces using high resolution electron energy loss spectroscopy and temperature programmed reaction spectroscopy. A methoxy intermediate was found on both the clean and partially oxidized surfaces but not on the completely oxidized surface. The adsorbed methoxy was bound more stably to the clean surface than to the partially oxidized surface. Molecular methanol adsorption was dominant on the completely oxidized surface. Surface passivation correlated directly with the degree of surface oxidation for methanol decomposition on the Mo(100) surface. (22 refs.)

63101 HREELS studies of adsorbates on polar solids: water on SrTiO₃(100). P.A.Cox, R.G.Egdell, P.D.Naylor (Inorganic Chem. Lab., Univ. of Oxford, Oxford, England).

J. Electron Spectrosc. & Relat. Phenom. (Netherlands), vol.29, p.247-52 (15 Jan. 1983). (Proceedings of the Third International Conference on 'Vibrations at Surfaces', Asilomar, CA, USA, 1-4 Sept. 1982).

The adsorption of water on SrTiO₃(100) has been studied by HREELS. Exposure of the defect free surface to water at 100K leads initially to nondissociative adsorption on surface cation sites with development of losses due to O-H stretching and bending modes at frequencies similar to those of free H₂O. Further exposure results in progressive attenuation of the surface phonon losses of the substrate with development of a loss spectrum characteristic of an ice multilayer. Binding of water in oxygen vacancy sites generated by argon ion etching is much stronger than to the defect free surface. (11 refs.)

63102 A vibrational study of ammonia chemisorbed on Ni(110) and Ni(111): whether goes the metal-nitrogen stretching mode on FCC (111) surfaces? G.B.Fisher, G.E.Mitchell (Phys. Chem. Dept., General Motors Res. Labs., Warren, MI, USA).

J. Electron Spectrosc. & Relat. Phenom. (Netherlands), vol.29, p.253-9 (15 Jan. 1983). (Proceedings of the Third International Conference on 'Vibrations at Surfaces', Asilomar, CA, USA, 1-4 Sept. 1982).

The adsorption of ammonia on the Ni(110) and Ni(111) surfaces has been studied with high resolution ($\leq 65\text{ meV}$) electron energy loss spectroscopy (EELS) combined with thermal desorption spectroscopy. The EELS spectra of the initial chemisorbed layer of a state on each surface are very different. Ammonia chemisorbed on the Ni(110) surface exhibits a strong Ni-N stretching mode at 570 cm^{-1} which is absent on the Ni(111) surface. The ammonia adsorption site appears to be different on the Ni(110) and Ni(111) surfaces. The authors suggest that the absence of the M-N stretching mode on the Ni(111) surface is a general characteristic of the ammonia adsorption site on the (111) surfaces of FCC Group VIII metals. (20 refs.)

63103 The adsorption of NO on Ru(001) and its co-adsorption with oxygen studied by vibrational spectroscopy. W.Stenzel, H.Conrad, B.E.Hayden, K.Kretschmar, A.M.Bradshaw (Fritz-Haber-Inst., Max-Planck-Gesellschaft, Berlin, Germany).

J. Electron Spectrosc. & Relat. Phenom. (Netherlands), vol.29, p.261 (15 Jan. 1983). (Proceedings of the Third International Conference on 'Vibrations at Surfaces', Asilomar, CA, USA, 1-4 Sept. 1982).

The adsorption of NO on Ru(001), and its co-adsorption with oxygen, has been studied by LEED, TPD, EELS and IRAS (with particular emphasis on the vibrational spectroscopies) over a wide range of temperatures. The adsorption of NO on Ru(001) at room temperature is initially dissociative with molecular adsorption taking place only after a dissociative layer is formed. The authors study the effect of oxygen co-adsorption on the adsorption of NO under well defined conditions. The dissociation layer is characterized by a (2×2) LEED structure and is found to influence the subsequent molecular adsorption of NO in exactly the same way as a saturated, pre-chemisorbed layer of oxygen. One effect of oxygen co-adsorption is to suppress the ν_1 intensity in the desorption spectra (the ν_2 peak remains essentially unchanged), while simultaneously producing a new TPD peak of NO ($\nu_1(\text{O})$) with lower binding energy. In the corresponding EELS spectra these two species (ν_1 and $\nu_1(\text{O})$) are clearly distinguished. The adsorption of NO at low temperature ($\sim 95\text{ K}$) initially produces a species of NO with an N-O stretch frequency of 1400 cm^{-1} . This is the only species observed up to an exposure of 0.5 Langmuirs, and on warming to room temperature it dissociates completely to produce the (2×2) pattern described above. Pre-adsorption of oxygen prevents the formation of this species of NO. Only subsequent to the saturation of this species during adsorption at low temperature do two bands at $\sim 1490\text{ cm}^{-1}$ and $\sim 1810\text{ cm}^{-1}$, associated with the ν_1 and ν_2 molecular species, appear. The authors suggest that the low temperature, low coverage species is lying down, and the molecular species ν_1 and ν_2 are both adsorbed on 'on top' sites but corresponding to the bent and linear forms of the NO molecule, respectively. (2 refs.)

63104 The adsorption of ammonia on a Fe(110) single crystal surface studied by high resolution electron energy loss spectroscopy (EELS). W.Erley, H.Ibach (IGV/KFA Julich, Julich, Germany).

J. Electron Spectrosc. & Relat. Phenom. (Netherlands), vol.29, p.263 (15 Jan. 1983). (Proceedings of the Third International Conference on 'Vibrations at Surfaces', Asilomar, CA, USA, 1-4 Sept. 1982).

EELS spectra of ammonia adsorbed on a Fe(110) single crystal surface at 120K reveal four different molecular adsorption states: 1. At very low exposures (0.05 L) three vibrational losses at 345 cm^{-1} , 1170 cm^{-1} and 3310 cm^{-1} are observed which are attributed to the symmetric Fe-N stretching, N-H₂ deformation and N-H₂ stretching modes of chemisorbed molecular

ammonia, respectively. 2. Further exposures up to 0.5 L cause the appearance of additional losses at 1450 cm^{-1} , 1640 cm^{-1} and 3370 cm^{-1} . The latter two are interpreted as the degenerate NH_3 deformation and stretching modes of molecularly adsorbed NH_3 . The 1450 cm^{-1} loss is a combination of the losses at 345 cm^{-1} and 1105 cm^{-1} . 3. In the exposure range from 0.5 to 2 L adsorption of molecular ammonia in a second layer is observed. This phase is characterized by a symmetric deformation mode at 1190 cm^{-1} and by two additional very intense modes at 160 cm^{-1} and 350 cm^{-1} which are due to rotational and translational modes. 4. Exposures above 2 L cause multilayer condensation of ammonia characterized by translational and rotational bands at 190 cm^{-1} , 415 cm^{-1} and 520 cm^{-1} , and a symmetric deformation mode at 1090 cm^{-1} . A broad loss feature around 3300 cm^{-1} is attributed to hydrogen bonding in the condensed layer. Thermal processing of an Fe(110) surface ammonia covered at 120K leads to decomposition of the ammonia into hydrogen and nitrogen above 260K. No vibrational modes due to adsorbed NH or HN_2 species were detected. (no refs.)

63105 Spatial intensity distributions from electron impact scattering modes: $\text{W}(100)(1\times 1)\text{H}$. S.R. Bare, P. Hofmann, M. Surman, D.A. King (Donnan Labs., Univ. of Liverpool, Liverpool, England).

J. Electron Spectrosc. & Relat. Phenom. (Netherlands), vol.29, p.265-72 (15 Jan. 1983). (Proceedings of the Third International Conference on 'Vibrations at Surfaces', Asilomar, CA, USA, 1-4 Sept. 1982).

The detailed mechanism of electron energy loss vibrational spectroscopy has been examined by recording a large data base of spectra with the detector moved both in and out of the incidence plane, for saturation coverage of atomic H adsorbed on $\text{W}(100)$ at 300K. In agreement with earlier work the authors find only a single electron loss (130 meV) in the specular direction, while away from the specular direction additional losses at 80 meV and 160 meV appear. These losses correspond to the symmetric stretching, the wagging and the asymmetric stretching modes respectively of H atoms occupying a C_{2v} bridge site. Large intensity variations of all these modes are found in backscattering directions and out of the incidence plane, in general agreement with recent theoretical predictions. The usefulness of these spatial intensity variations in adsorbate structure determination is discussed. The signal enhancement with electron collection in the plane orthogonal to the incidence plane may allow the observation of otherwise weak impact modes. (6 refs.)

63106 Identification of surface vibrations on clean and oxygen covered Pt(111) surfaces with high resolution electron energy loss spectroscopy (EELS). J.A. Schaefer, W. Gopel (Phys. Dept., Montana State Univ., Bozeman, MT, USA).

J. Electron Spectrosc. & Relat. Phenom. (Netherlands), vol.29, p.279-85 (15 Jan. 1983). (Proceedings of the Third International Conference on 'Vibrations at Surfaces', Asilomar, CA, USA, 1-4 Sept. 1982).

Clean and oxygen covered (111) recrystallized Pt surfaces were studied by EELS after surface preparation at $150\leq T\leq 1650\text{K}$. The clean surface shows Stokes as well as antiStokes lines of surface phonons at $\pm 195^{-1}$. Adsorption of small amounts of ($<10^{-2}$ monolayers) of O_2 or H_2 leads to substrate-derived phonon losses at $\pm 380\text{ cm}^{-1}$. Oxygen exposure at different pressures, times and temperatures leads to atomic and/or molecular adsorption as well as oxide-related features which have been identified by EELS. (13 refs.)

63107 Electronic transitions of Ar, Xe, N_2 , CO physisorbed on Ag (111) and Al (111). D. Schmeisser (Fritz-Haber-Inst., Max-Planck-Gesellschaft, Berlin, Germany), J.E. Demuth.

J. Electron Spectrosc. & Relat. Phenom. (Netherlands), vol.29, p.313 (15 Jan. 1983). (Proceedings of the Third International Conference on 'Vibrations at Surfaces', Asilomar, CA, USA, 1-4 Sept. 1982).

High resolution electron energy loss spectroscopy has been extended to study also the excitonic (low lying electronic) transitions of physisorbed rare gas atoms (Ar, Xe) and diatomic molecules (N_2 , CO) on Ag (111) and Al (111) surfaces at $\sim 20\text{K}$. Electron loss spectra were performed using a pair of hemispherical analyzers mounted at a fixed scattering angle (90°). This spectrometer allowed high transmission in the range of 0-15 eV loss energies and incident beam energies up to 20 eV. AES, LEED and UV Photoemission (HeI) were also used in situ to characterize these surfaces and to identify the adsorbed gases and delineate their absolute coverage regimes. (2 refs.)

63108 Vibrational spectra of ethylene and acetylene on metal surfaces—an electron energy loss study of ethylene adsorbed on Ni (110) and its carbided surface, and the use of metal-cluster analogies. C.E. Anson, B.J. Bandy, M.A. Chesters, B. Keiller, I.A. Oxtan, N. Sheppard (School of Chem. Sci., Univ. of East Anglia, Norwich, England).

J. Electron Spectrosc. & Relat. Phenom. (Netherlands), vol.29, p.315-16 (15 Jan. 1983). (Proceedings of the Third International Conference on 'Vibrations at Surfaces', Asilomar, CA, USA, 1-4 Sept. 1982).

An analysis has been made of on- and off-specular electron energy loss spectra (EELS) from C_2H_4 and C_2D_4 adsorbed on a clean Ni (110) and also a carbided Ni (110) surface. The carbided surface was prepared by heating the clean Ni surface in ethylene to 573K or above. EELS spectra were obtained using a Leybold-Heraeus spectrometer at a beam energy of 3.0 eV and with a resolution of ca. 6.5 meV (ca. 50 cm^{-1}). (12 refs.)

63109 Azimuthal dependence of impact scattering in electron energy loss spectroscopy. B.M. Davies, J.L. Erskine (Dept. of Phys., Univ. of Texas, Austin, TX, USA).

J. Electron Spectrosc. & Relat. Phenom. (Netherlands), vol.29, p.323-8 (15 Jan. 1983). (Proceedings of the Third International Conference on 'Vibrations at Surfaces', Asilomar, CA, USA, 1-4 Sept. 1982).

The azimuthal dependence of electron energy loss spectroscopy (EELS) dipole and impact scattering intensity has been measured. Spectra for a saturation coverage of H adsorbed on $\text{W}(110)$ exhibit loss peaks due to impact scattering from adsorbate vibrational modes. The intensity of the 160 meV loss peak has been measured as a function of the azimuthal angle between the scattering plane and a mirror plane of the surface. The angular pattern has strong maxima oriented perpendicular to the (111) rows of atoms on the surface, and has the C_{2v} symmetry of the $\text{W}(110)$ surface. This azimuthal dependence is strikingly different from the nearly isotropic angular dependence of dipole scattering from Cl adsorbed on $\text{W}(110)$. Selection rules for impact scattering account for the general features of the angular pattern based on asymmetric stretch modes associated with bridge site H atoms. (9 refs.)

63110 Wavenumber-resolved energy-loss spectra of Co_2Sm . P. Schattschneider, J. Fidler, V. Chopov (Inst. of Appl. & Tech. Phys., Tech. Univ. of Vienna, Vienna, Austria).

J. Electron Spectrosc. & Relat. Phenom. (Netherlands), vol.31, no.1, p.25-32 (April 1983).

Wavenumber-resolved spectra of Co_2Sm have been obtained by electron energy-loss spectroscopy using 40 kV electrons in the diffraction mode. Four losses are found between 15 and 22 eV which are identified as a volume plasma loss of Co_2Sm (15.3 eV), plasma losses modified by carbon contamination (17.3 and 20 eV) and a plasma loss of Sm_2O_3 . The observed features are nondispersive within the surveyed q -space range ($0\leq q<0.5\text{ \AA}^{-1}$). An

interpretation in terms of a plasma loss hybridized by nonvertical interband transitions is proposed. (14 refs.)

63111 Relation between dynamical processes at surfaces and electron-energy-loss measurements. B.N.J. Persson (IBM Res. Center, Yorktown Heights, NY, USA).

Phys. Rev. Lett. (USA), vol.50, no.14, p.1089-91 (4 April 1983). The surface response function $d_1(\omega)$ (the frequency-dependent centroid of the induced charge density) determines the influence of a metal surface on all dynamical processes occurring well outside of it. It is shown that this function can be measured directly by use of electron-energy-loss spectroscopy. (11 refs.)

63112 Indirect determination of the single loss function from plural scattering data. M.E. Twigg (Dept. of Metall., Univ. of Illinois, Urbana, IL, USA).

Ultramicroscopy (Netherlands), vol.10, no.3, p.291-6 (1982).

Recent advances in electron energy loss spectroscopy (EELS) and scanning transmission electron microscopy (STEM) promise improved analysis of light elements. However, further efforts are limited by the fact that such low energy excitations as plasmons and interband transitions are influenced by complicated solid state effects rather than by the cores of isolated atoms. The author has investigated the role of plural scattering and has extracted the modified single loss function from empirical data using already established discrete Fourier transform techniques. In an alternate procedure, the author has constructed a plural loss function $\pi''(z)$ which lacks only the contribution of the single loss peak. This function was then subtracted from the plural loss spectrum in order to obtain the modified single loss function. Though slightly more involved than the earlier procedure, the indirect route leads to a significantly cleaner single loss function. (11 refs.)

About short-range order of amorphous i-B/N films investigated by energy loss spectroscopy See Entry 61800

Heating of a bilayered material bombarded by an electron beam See Entry 61970

Conference overview: experimental [surface vibrations] See Entry 62238

Reemitted-positron energy-loss spectroscopy: a novel probe of adsorbate vibrational levels See Entry 62239

An EELS and TDS study of molecular oxygen desorption and decomposition on Pt(111) See Entry 62244

The chemisorption of nitrogen on the (001) surface of ruthenium See Entry 62259

Adsorbate structure modeling based on electron energy loss spectroscopy and lattice dynamical calculations: application to O/Al(111) See Entry 62260

Hydrogen chemisorption on Ni(110) by high-resolution electron energy loss spectroscopy See Entry 62263

Vibrational spectroscopy using HREELS of benzene adsorbed on the Rh (111) crystal surface See Entry 62264

HREELS study of formic acid adsorption on gold (110) and (111) surfaces See Entry 62265

Coherent emission by relativistic particles interacting with atomic rows during reflection from a crystal surface See Entry 63079

The adsorption and dehydrogenation of cyclopentane on Ru (001) See Entry 63588

79.20N Atom, molecule, and ion impact

63113 Electron capture and loss processes in heavy ion and molecular ion collisions with solids. R. Latz, J. Schader, H.J. Frischkorn, P. Koschar, K.O. Groeneveld (Inst. für Kernphys., Univ. Frankfurt, Frankfurt, Germany). *IEEE Trans. Nucl. Sci. (USA)*, vol.ns-30, no.2, p.913-15 (April 1983). (1982 IEEE Conference on the Application of Accelerators in Research and Industry, Denton, TX, USA, 8-10 Nov. 1982).

Angular (θ) and velocity (v_0) distributions of convoy electrons have been measured with monoatomic and molecular projectile ions (H^+ , D^+ , H_3^+ , D_2^+ , H_3^+ , He^+ , He^{2+} at 1.7 MeV/U and U^{28+} , Ti^{14+} at 1.4 MeV/U) as a function of the projectile dwell time t_D in carbon foils (2 to $50\text{ }\mu\text{g}/\text{cm}^2$). The spectra with light projectiles from carbon foils are compared with those of gaseous CH_4 targets. For the light and molecular projectiles the shapes and yield of convoy electrons depend strongly on the dwell time. A narrow, strongly θ -dependent contribution at $v_e=v_0$ can be distinguished from a θ -independent part at $v_e<v_0$ indicating different production mechanisms. A relation is presented which connects the yield of loss electrons from projectiles with the transmission of projectiles and electrons through solids. The yield of electrons in the spectrum for H_3^+ at $v_e=v_0$ and under zero degrees is found to be more than about 20 times as large as is expected from the contribution of loss electrons in last layer collisions. (8 refs.)

63114 Total yield and escape depth of electrons from heavy ion solid interactions. H.J. Frischkorn, P. Koschar, R. Latz, J. Schader, M. Burkhard, D. Hofmann, K.O. Groeneveld (Inst. für Kernphys., Univ. Frankfurt, Frankfurt, Germany).

IEEE Trans. Nucl. Sci. (USA), vol.ns-30, no.2, p.931-3 (April 1983). (1982 IEEE Conference on the Application of Accelerators in Research and Industry, Denton, TX, USA, 8-10 Nov. 1982).

At high projectile energies ($\sim\text{MeV/U}$) several mechanisms for electron production are discussed as e.g. direct ionization collisions, recoil particle cascades, collective electron emission. Results are presented of total electron yield (γ) measurements over a wide projectile energy E_p range ($40\text{ keV/U}<E_p/M<12\text{ MeV/U}$) and a wide projectile Z_p range ($1<Z_p\leq 92$) of both monoatomic and molecular projectiles and of different target thicknesses. From the target thickness dependence of γ the mean free path λ of electrons in carbon can be calculated. The data are discussed in the frame of current theories. Significant deviations from calculated values and predicted dependencies are found, in particular for projectile velocities v_p close to the Fermi velocity v_F of target electrons and for molecular projectile ions. (16 refs.)

63115 A review of recoil ion physics. T.J. Gray, C.L. Cocke (Dept. of Phys., Kansas State Univ., Manhattan, KS, USA).

IEEE Trans. Nucl. Sci. (USA), vol.ns-30, no.2, p.937-42 (April 1983). (1982 IEEE Conference on the Application of Accelerators in Research and Industry, Denton, TX, USA, 8-10 Nov. 1982).

A review of recoil ion physics is presented. A brief history on the subject is introduced. The production of low velocity highly-charged recoil ions by fast heavy ion beams is discussed. Experiments which utilize the LEHQ beams to measure charge exchange cross sections and energy gain spectroscopy are discussed. (27 refs.)

63116 Scattering of neutral atoms by a periodic potential: the Morse corrugated potential. G.Armand (Service de Phys. des Atomes et des Surfaces, CENS, Gif-sur-Yvette, France), J.R.Manson. *J. Phys. (France)*, vol.44, no.4, p.473-87 (April 1983).

Within the two-potential formalism a general set of t matrix integral equations is obtained which describes the scattering of a neutral particle by a periodic potential. Furthermore a projection method is developed which allows one in the case of resonance to get a new set of equations in which the resonance singularities do not appear. This formalism is applied to the Morse corrugated potential. The integral equation set is solved by an interactive process and in this way an exact solution is obtained. The convergence of the iterative expansion is studied and an approximate convergence criterion is found. Results are compared with those given by an equivalent exponential corrugated potential which demonstrates the influence of the well and potential slope on the distribution of the intensities among the different diffracted beams. In order to have a precise determination of the corrugation function it is shown that it is necessary to use a realistic potential and also to avoid approximate methods for the calculation of intensities. (19 refs.)

63117 Z_1 dependence of equilibrium charge state distributions of MeV He ions emerging from solid. Y.Haruyama, Y.Kanamori, T.Kido, A.Itoh, F.Fukuzawa (Dept. of Nuclear Engng., Kyoto Univ., Kyoto, Japan). *J. Phys. B (GB)*, vol.16, no.7, p.1225-32 (14 April 1983).

The equilibrium charge state distributions of He ions emerging from various solid targets were measured in the energy range 0.6-2.4 MeV. Atomically clean target surfaces were prepared by continuous evaporation for Ga, Ge, Se and In, and by heating for Sc, Fe, Ta, W and Pt. The measured charge fractions F_i ($i=0, 1, 2$) were tabulated at 0.2 MeV intervals. In this energy range, the ratio F_1/F_2 is represented fairly well by the empirical formula $AE^{1/2}$, where E is the energy and A and B are target-dependent constants. The present data, together with the previous data, show clearly oscillatory behaviour of the equilibrium mean charge of He ions with target atomic number Z_1 . This oscillation is found to be attributed to the shell structure of the target atom. (19 refs.)

63118 Energy dissipation at metal surfaces: electronic versus vibrational excitations. K.Schonhammer (Inst. für Theoretische Phys., Univ. Hamburg, Hamburg, Germany), O.Gunnarsson.

J. Electron Spectrosc. & Relat. Phenom. (Netherlands), vol.29, p.91-103 (15 Jan. 1983). (Proceedings of the Third International Conference on 'Vibrations at Surfaces', Asilomar, CA, USA, 1-4 Sept. 1982).

A theoretical description of the energy transfer between a surface and an atom or molecule approaching a surface is presented. Usually the excitation of substrate phonons by the impinging adsorbate is the dominating process. In the case of metal substrates, however, it has been realized that the excitation of electron-hole (e-h) pairs can lead to sticking coefficients or vibrational damping at surfaces of the same order as found experimentally. The authors focus on the description of the electronic excitations and compare their results with a very simple model of the phonon mechanism. The electronic mechanism turns out to be rather unimportant for the inelastic scattering of rare-gas atoms but cannot be neglected for light chemically reactive adsorbates. (29 refs.)

63119 The spectroscopy of surface vibrations by atom scattering. G.Benedek (Istituto di Fisica, Univ. Milano, Milano, Italy).

J. Electron Spectrosc. & Relat. Phenom. (Netherlands), vol.30, p.71-86 (Feb. 1983). (Proceedings of the Third International Conference on 'Vibrations at Surfaces', Asilomar, CA, USA, 1-4 Sept. 1982).

The recent progress in the production of highly monochromatic atomic beams is opening new perspectives in surface physics, having paved the way for a full determination of the surface vibrational structure. After a discussion on the possible determination of Rayleigh wave dispersion curves from angular distributions exploiting the kinematical focusing effect, a short review is presented on the direct measurement of surface phonon dispersion curves, first achieved by Brusdeylins et al. (1981) in alkali halides, from time-of-flight (TOF) spectra of scattered He atoms. A comparison is made with the existing theories of surface phonons in ionic crystals. The state of the art in the theory of inelastic processes is briefly illustrated in order to discuss the theoretical interpretation of TOF spectra. The one-phonon energy loss spectra of He scattering from LiF(001) calculated for a hard corrugated surface model are found to be in general good agreement with the experimental TOF spectra. From such a comparison evidence is obtained that: i) one-phonon processes are predominant, and ii) in addition to Rayleigh waves important contributions to the inelastic scattering come from the surface-projected density of bulk phonons. Important effects due to inelastic resonances with surface bound states are put in evidence and explained by simple kinematical arguments. The possible observation of surface optical modes in NaF(001) is finally discussed. (54 refs.)

63120 Internal state distributions of molecules scattering and desorbing from surfaces. D.J.Auerbach (IBM Res. Lab., San Jose, CA, USA).

J. Electron Spectrosc. & Relat. Phenom. (Netherlands), vol.30, p.87-98 (Feb. 1983). (Proceedings of the Third International Conference on 'Vibrations at Surfaces', Asilomar, CA, USA, 1-4 Sept. 1982).

Some recent applications of state specific detection techniques to studies of molecules interacting with surfaces are reviewed. The author concentrates on the direct inelastic scattering of NO from Ag(111). Coupling of translational to rotational motion is found to be a dominant energy transfer channel while vibrational excitation has a very small probability. Measured rotational state distributions exhibit several interesting features including rotational rainbows and rotational alignment. Quantum mechanical calculations on a simple model of the scattering provide a semi-quantitative description of the results and allow information on the interaction potentials to be derived. State specific measurements of molecules thermally desorbing from surfaces are also briefly discussed. (29 refs.)

63121 Hydrogen interactions with Ag(111): bound state scattering resonances and interaction potential determination. Chien-fan Yu, C.S.Hogg, S.J.Sibener (Dept. of Chem., Univ. of Chicago, Chicago, IL, USA).

J. Electron Spectrosc. & Relat. Phenom. (Netherlands), vol.30, p.99-101 (Feb. 1983). (Proceedings of the Third International Conference on 'Vibrations at Surfaces', Asilomar, CA, USA, 1-4 Sept. 1982).

Summary form only given. The elastic and rotationally resolved inelastic scattering of H_2 , D_2 , and HD supersonic molecular beams from Ag(111) has been examined. These studies have been undertaken primarily for two reasons: to determine the laterally averaged isotropic and anisotropic components of the hydrogen/Ag(111) interaction potential, and to test the accuracy of different levels of quantum gas-surface scattering calculations. (6 refs.)

63122 Crystallographic determination of metal surfaces with helium scattering. N.Garcia (Dept. de Física Fundamental, Univ. Autónoma de Madrid, Madrid, Spain), A.Barker, I.P.Batra.

J. Electron Spectrosc. & Relat. Phenom. (Netherlands), vol.30, p.137-44 (Feb. 1983). (Proceedings of the Third International Conference on 'Vibrations at Surfaces', Asilomar, CA, USA, 1-4 Sept. 1982).

Helium-surface diffraction data has been used to construct the interaction potential between a helium atom and a metal surface. The constructed potential fits experimental data for all beam energies and angles of incidence and more importantly is independent of beam energy. Such a potential essentially consists of two parts: a short range repulsive corrugated potential due to electronic overlap, and a long range attractive potential due to dispersion forces. The authors have generated potentials for He scattering for Ni, Cu and Au and in all cases found excellent agreement with experiments. They also report that the repulsive part of the He scattering potential can be obtained rather simply from first principles without adjustable parameters. This suggests that one can determine surface crystallography from first principles without adjustable parameters. (14 refs.)

63123 Measurement of $Au(111)$ surface phonons by low energy helium scattering. M.Cates, D.R.Miller (Dept. of Appl. Mech. & Engng. Sci., Univ. of California, San Diego, La Jolla, CA, USA).

J. Electron Spectrosc. & Relat. Phenom. (Netherlands), vol.30, p.157-62 (Feb. 1983). (Proceedings of the Third International Conference on 'Vibrations at Surfaces', Asilomar, CA, USA, 1-4 Sept. 1982).

Inelastic scattering of low energy helium atoms has been used to probe the surface phonon dispersion relation for $Au(111)$ along the (112) direction. The dominant scattering peak appears to be due to the Rayleigh surface mode with a measured speed of sound at low Q of ~ 1300 m/sec, bending over near the zone edge with a maximum ω of $\sim 11 \times 10^{12}$ sec $^{-1}$. Phonon scattering probabilities are given as a function of ω and fall off rapidly with ω . (10 refs.)

63124 The Ti KLL spectra of TiO_2 and $TiH_{1.64}$ generated by bremsstrahlung-excited Auger spectroscopy. T.N.Wittberg (Univ. of Dayton Res. Inst., Dayton, OH, USA), P.S.Wang.

J. Electron Spectrosc. & Relat. Phenom. (Netherlands), vol.31, no.1, p.81-3 (April 1983).

Recent studies have shown that excitation of Auger processes can result from the bremsstrahlung radiation which accompanies the characteristic radiation from magnesium and aluminium anodes. This effect has proved useful in studying a range of Auger transitions which are inaccessible to excitation by Al $K\alpha$ or Mg $K\alpha$ radiation. Bremsstrahlung excitation was used to study the Ti KLL Auger spectra of TiO_2 and $TiH_{1.64}$. The spectra were recorded using a modified AEI ES-100 spectrometer. The TiO_2 spectrum was recorded from a 100 nm thick anodic film which had been grown on polycrystalline titanium foil in an aqueous saturated solution of ammonium tetraborate. (10 refs.)

63125 The influence of the surface barrier on the trajectory of sputtered particles. T.G.Abdel-Malik, A.A.Aly, A.M.Abden, H.A.Motaweh (Dept. of Phys., Univ. of Tanta, Tanta, Egypt).

Phys. Status Solidi b (Germany), vol.116, no.1, p.169-72 (1 March 1983).

The parameters of a spherical surface barrier with refraction for the particles sputtered from Cu single crystals are computer calculated. Use is made of the method of straightforward simulation of the surface atom ejection in the field of the near-surface block of atoms. The interactions of the atoms are described by a Morse potential. (5 refs.)

63126 Molecular erosion of ice by keV ion bombardment. G.Ciavola, G.Foti, L.Torrisi (Inst. di Struttura della Materia, Univ. di Catania, Catania, Italy), V.Pirronello, G.Strazzulla.

Radiat. Eff. (GB), vol.65, no.1-4, p.167-72 (1982). (Proceedings of the First International Conference on 'Radiation Effects in Insulators', Arco, Largo di Garda, Italy, 1981).

High erosion has been detected during the bombardment of ice (H_2O and D_2O) at LN $_2$ temperature by helium and argon beams. In the range 20-100 keV, the erosion yield increases with the energy and mass of the impinging ions. The eroded particles have been analyzed by a quadrupole mass spectrometer and the main component is formed by H_2 (or D_2) H_2O (or D_2O) and O_2 molecules. (11 refs.)

63127 Mechanisms for rapid electron transfer in ionic solids following multiple ionization by heavy-ion impact See Entry 60936

63128 Recent progress in fast ion beam spectroscopy See Entry 60946

63129 Ion beam induced composition changes during Auger sputter profiling of thin Al films on InP See Entry 62001

63130 SIMS analysis of the impurity diffusion of In in Cu See Entry 62170

63131 Analysis of diffusion mechanisms in thin polycrystalline Au-Ag films using Auger electron spectroscopy See Entry 62185

63132 He $^+$ backscattering study on Ar distribution in amorphous magnetic thin films See Entry 62293

63133 Work function measurements on ion bombardment damaged (111) surface of silver by photoelectric and CPD methods See Entry 62480

63134 Methane formation during deuteron bombardment of carbon in the energy range of 100 to 1500 eV See Entry 63575

79.20R Atomic and molecular beam interactions

79.20R.1 Hydrogen interactions with Ag(111): bound state scattering resonances and interaction potential determination See Entry 63121

79.60 PHOTOEMISSION AND PHOTOELECTRON SPECTRA

63127 Characteristics of electrons emitted from aluminium, carbon and Mylar slabs irradiated by photons. M.Malbert, M.Terrissol, J.-P.Pataut (Centre de Phys. Atomique, Univ. Paul Sabatier, Toulouse, France), M.Angles. *Radiat. Prot. Dosim. (GB)*, vol.3, no.4, p.211-17 (1982).

The forward and backscattered electron fluence emitted by a slab under photon irradiation have been calculated using Monte-Carlo techniques for aluminium, carbon and mylar. The simulation methods used and the techniques chosen to study the low energy (<30 keV) electron transport are presented. The agreement with experimental and other theoretical results is good. (24 refs.)

63128 Low-energy (≤ 2 eV) electron escape depths of tetracene films. V.V.Grechov (Inst. of Phys. & Energetics, Acad. of Sci., Riga, Latvian SSR). *Chem. Phys. Lett. (Netherlands)*, vol.96, no.2, p.237-42 (1 April 1983).

It has been shown that the real escape depth L of low-energy (≤ 2 eV) electrons determined in homogeneous tetracene films (obtained by vacuum evaporation on cooled substrate at 120K) does not exceed 6-10 Å. For much

small L values photoemission should be considered as essentially a surface phenomenon since the energy distribution of emitted photo-electrons substantially depends on energetic and structural peculiarities of the near-surface molecules of the crystal. (30 refs.)

63129 Ionization potentials and polarization energies of tetraselenafulvalene (TSF) derivatives determined from ultraviolet photoelectron spectroscopy. N.Sato, G.Saito, H.Inokuchi (Inst. for Molecular Sci., Okazaki, Japan). *Chem. Phys. (Netherlands)*, vol.76, no.1, p.79-88 (1 April 1983). Gaseous and solid-state ionization potentials of several derivatives of tetraselenafulvalene (TSF) and tetrathiafulvalene (TTF) have been determined from ultraviolet photoelectron spectroscopy. The first ionization potentials of the molecules in the gaseous state are appraised in terms of their molecular structures and the substitution effects. The characteristics in the electronic structure of these molecules as donors forming conductive salts with various acceptors are discussed. The polarization energies, obtained as the difference of the threshold ionization potentials for both states of these compounds, ≈ 1.4 eV, were a little smaller than the nearly constant value for polycyclic aromatic hydrocarbons, ≈ 1.7 eV. As the value of the polarization energy is determined mainly by the molecular polarizability and by the molecular packing density in the solid, the molecular polarizabilities of these compounds were estimated from the observed polarization energies, using a simplified relation. Such values are also useful in characterizing electronic states of the solids containing them. (34 refs.)

63130 3s multiplets in X-ray photoemission from layered magnetic intercalates. J.J.Barry, H.P.Hughes (Cavendish Lab., Univ. of Cambridge, Cambridge, England). *J. Phys. C (GB)*, vol.16, no.10, p.L275-8 (10 April 1983). The authors report X-ray photoemission measurements of the intercalant 3s core levels in the magnetic layer compounds $Mn_{1/3}NbS_2$ and $Fe_{1/3}NbS_2$. Multiplet splittings of 6.1 eV (Mn 3s) and 4.5 eV (Fe 3s) are observed, which suggest, in agreement with previous magnetic studies, that the intercalant ions adopt 2^+ ionisation states; there is some evidence for hybridisation of the intercalant 3d orbitals with orbitals on the surrounding atoms, particularly in $Fe_{1/3}NbS_2$. (16 refs.)

63131 Satellite structure of ZnO and Zn(II) halides studied by X-ray photoelectron spectroscopy. M.Scrocco (Lab. di Metodologie Avanzate Inorganiche, Univ. di Roma, Roma, Italy). *Phys. Status Solidi b (Germany)*, vol.116, no.1, p.137-44 (1 March 1983). The satellite structure in the X-ray photoelectron spectra of Zn(II) halides and ZnO is examined, particular attention being paid to the 3p, 3s metal subshells and the valence region. The nature of the phenomena giving rise to these satellites and their relative importance in each spectral region, is discussed with reference to known theoretical results. (21 refs.)

63132 Photoemission spectra and band structures of d-band metals. X. Relativistic momentum matrix elements. R.L.Benbow (Dept. of Phys., Northern Illinois Univ., DeKalb, IL, USA), N.V.Smith. *Phys. Rev. B (USA)*, vol.27, no.6, p.3144-51 (15 March 1983). For pt.IX see *ibid.*, vol.25, no.2, p.738 (1982). Band-structure calculations are performed to assess the magnitude of relativistic effects in angle-resolved photoemission. The specific case of normal emission from Ag(111) is considered using a combined interpolation scheme which incorporates spin-orbit coupling both within the d bands and between the plane waves of the basis set. Detailed numerical results are presented for the momentum matrix elements in the nonrelativistic and relativistic cases for all the initial-state bands in both parallel and perpendicular polarization. The observability of relativistic effects in available and future experimental data is discussed. (19 refs.)

63133 Surface-atom X-ray photoemission from clean metals: Cu, Ag, and Au. P.H.Citrin, G.K.Wertheim (Bell Labs., Murray Hill, NJ, USA), Y.Baer. *Phys. Rev. B (USA)*, vol.27, no.6, p.3160-75 (15 March 1983). Surface-atom core-level shifts from evaporated noble metals are reported using angle-dependent X-ray photoemission with monochromatized AlK α radiation. The absence of line broadening with increasing takeoff angle for the case of aluminum metal, where the surface shift is known to be small, confirms that the shifts observed in the noble metals are real surface phenomena. An analysis procedure is developed which establishes that the effect of the vacuum-solid interface in these systems is confined to the first atomic layer. The asymmetric (final-state-related) line shapes of the surface- and bulk-atom photopeaks are also shown to be identical within experimental error. The surface core-level shifts are 0.40 ± 0.02 eV for Au, -0.08 ± 0.03 eV for Ag, and -0.24 ± 0.02 eV for Cu, with the surface contributions occurring at lower electron binding energy. The analysis additionally yields electron mean free paths of 19 ± 3 Å at 1400 eV in Au and 14 ± 3 Å at 550 eV in Cu. Using the surface to bulk intensity ratios of the Au4f core levels, it was possible to isolate the contribution of the surface-atom valence electrons. The width of the surface density of states is narrowed ($\pm 2\%$) with respect to the bulk density of states and its center of gravity is shifted by 0.5 ± 0.1 eV. The analysis procedures and conclusions presented should be applicable to core and valence surface-atom photoemission from a wide variety of other systems. (29 refs.)

63134 Photoemission from surface-atom core levels, surface densities of states, and metal-atom clusters: a unified picture. P.H.Citrin, G.K.Wertheim (Bell-Labs., Murray Hill, NJ, USA). *Phys. Rev. B (USA)*, vol.27, no.6, p.3176-200 (15 March 1983). A model is presented which relates the observed narrowing and shifting of the surface density of states, reported in an earlier paper, with the sign and magnitude of the surface-atom core-level shift (SCS). This relationship, along with the identical line shapes observed for the bulk and surface-atom core-level photoemission peaks, is shown to provide strong support for a predominantly initial-state interpretation of the SCS. Inclusion of final-state screening energy differences between surface and bulk atoms is discussed within the framework of a more quantitative description of the SCS. General consideration of the effects responsible for the modified surface band structure, i.e. reduced coordination number and the resulting redistribution of charge between and within the s,p and d bands, allows the model to be extended to the transition metals and allows apparently different theoretical explanations of the SCS to be unified within a single picture. The special case of those rare-earth metals in which narrow corelevel f levels appear close to the Fermi energy is also discussed. Our previously described measurements and analytical procedures are compared with other recently reported surface atom core level studies, and all experimental results are compared with self-consistent and semiempirical thermodynamic calculations. Generally encouraging qualitative agreement is obtained, particularly the sign of the SCS which changes from element to element across the Periodic Table. Quantitative agreement is most lacking for the more-open single-crystal surfaces and for the metals near the ends of the transition series. Finally, the closely related photoemission experiments from small metal-atom clusters (akin to supported catalysts) have been reinterpreted. Consistency between these and the present results is obtained, provided that a proper reference level is employed. (103 refs.)

63135 Photoemission study of Au overlayers on Pd(111) and the formation of a Pd-Au(111) alloy surface. D.L.Weissman-Wenocur, P.M.Stefan, B.B.Pate, M.L.Sheik, I.Lindau, W.E.Spicer (Stanford Electronics Labs., Stanford Univ., Stanford, CA, USA). *Phys. Rev. B (USA)*, vol.27, no.6, p.3308-17 (15 March 1983). The techniques of photoemission spectroscopy (PES), Auger spectroscopy, and low-energy electron diffraction were used to examine the interaction of Au and Pd for the following: (1) overlayers of Au on Pd(111), ranging from 0.1 to 10 monolayers; (2) Au diffused into the Pd matrix; and (3) a stabilized Pd-Au alloy surface, formed by diffusing a thick Au layer into the Pd until the composition stabilized. An ordered Au(111) layer formed on the Pd. For the Au overlayers, three effects were seen by PES: (1) structures appeared which merged smoothly into the metallic Au structure; (2) structures at the energies of the clean Pd peaks were sharpened when submonolayers of Au were evaporated; and (3) a new structure appeared which could not be definitely attributed to Pd or Au. Au diffused into the Pd evidenced a more atomically structure than the overlayers. The stabilized alloy, which was determined to have 30 at.% Au in the surface region, evidenced PES structure strikingly similar to the 0.3 monolayer overlayer. Direct transition effects were seen for the alloy. The Au-derived structure was found to narrow and shift to slightly lower binding energy for the alloy as compared to the 0.3 monolayer overlayer. Comparison is made between the thin layers of Au on Pd and thin layers of Cu on Zn. Comparison is also made between the stabilized Pd-Au alloy and the Cu-Ni alloy system. Theoretical support for direct transitions in alloys is cited. (30 refs.)

63136 CO chemisorption on Fe(110) studied by angle-resolved photoemission. E.S.Jensen (Cornell Materials Sci. Center, Cornell Univ., Ithaca, NY, USA), T.N.Rhodin. *Phys. Rev. B (USA)*, vol.27, no.6, p.3338-50 (15 March 1983). An angle-resolved ultraviolet photoemission spectroscopy (UPS) investigation of CO chemisorbed on Fe(110) at 200K is presented. The binding energies at normal emission of the CO 3σ , 4σ , 5σ and 1π molecular orbitals are determined to be 27, 11.0, 8.3 and 6.8 eV, respectively, at saturation coverage. The 5σ binding energy is coverage dependent, decreasing to 7.6 eV at very low coverage. The identification of the 5σ and 1π peaks is made with the symmetry rules for normal-emission UPS. The variations of the 4σ , 5σ and 1π peak positions with the parallel component of electronic momentum are extensively investigated. The bandwidths observed are 0.3, 0.8, and <0.3 eV for the 4σ , 5σ , and 1π peaks, respectively, in the [001] mirror-plane direction. In the [110] direction, they are 0.2, 0.5, and <0.3 eV. Both the bandwidths and momentum dependences observed for the 4σ and 5σ peak positions are much more isotropic than can be accounted for by simple band dispersion for the highly anisotropic rectangle implied by the low-energy electron diffraction (LEED) pattern. Accordingly, a more isotropic geometry is proposed that can also be made consistent with the LEED pattern. (30 refs.)

63137 X-ray photoelectron diffraction studies of zinc selenide. E.S.Crawford, S.Evans, E.Raftery, M.D.Scott (Edward Davies Chem. Labs., Univ. Coll. of Wales, Aberystwyth, Wales). *Surf. & Interface Anal. (GB)*, vol.5, no.1, p.28-32 (Feb. 1983). Polar and azimuthal angle-resolved XPS studies of ZnSe layers grown epitaxially on {100} GaAs by H_2 transport of the elements are described. Comparison of the polar X-ray photoelectron diffraction (XPD) patterns obtained for rotation about [110] and [110] axes confirms the dominant influence of structural factors in determining the shape of the patterns. Azimuthal XPD patterns are shown to reflect symmetry properties directly related to the emitting sites, and their use to determine the symmetry of an exposed single-crystal surface is demonstrated. The outermost ~ 100 Å of all the 'as-grown' ZnSe layers were ~ 20 -35% Zn rich. Ar ion bombardment (800 eV, ~ 5 μ A) rapidly restored the surface stoichiometry to within 10% of 1:1. The disorder concurrently introduced resulted in XPS peak broadening without impairment of the polar XPD pattern. Annealing at 300°C in high vacuum removed the disorder without affecting either the stoichiometry or the XPD pattern. It is inferred that split-(100) interstitials are the preferred sites both for atoms displaced by ion bombardment and for the excess Zn initially present. (18 refs.)

X-ray photoelectron spectroscopy of cadmium arachidate monolayers on various metal surfaces See Entry 60837

New model for thermal effects in photoelectron spectroscopy See Entry 62049

Surface photoacoustic spectroscopy—a new technique for the study of surface vibrations See Entry 62224

Crystalline phase effects on ESCA valence bands of Zn(IV) and Ti(IV) acid phosphates See Entry 62320

Bulk and surface electron states in WO_3 and tungsten bronzes See Entry 62336

Electron structure of stoichiometric and nonstoichiometric tungsten oxides See Entry 62338

Electronic structure of hydrogen-bonded H_2O See Entry 62469

Work function measurements on ion bombardment damaged (111) surface of silver by photoelectric and CPD methods See Entry 62480

Study of electronic structure of reduced TiO_2 and $V_xTi_{1-x}O_2$ crystals by ESCA and optical absorption See Entry 63018

Electronic transitions of Ar, Xe, N_2 , CO physisorbed on Ag (111) and Al (111) See Entry 63107

The performance of mechanical scraping tools in ultrahigh vacuum: an XPS study See Entry 63443

Combined vibrational/temperature programmed reaction spectroscopy studies of reaction intermediates on metal surfaces See Entry 63586

AES investigations of chemical composition of some alkali compounds See Entry 63630

79.70 FIELD EMISSION AND FIELD IONIZATION

Electron gun with a field-emission cathode for use in electron-probe instruments See Entry 59889

The spin polarisation of conduction electrons in a ferromagnetic semiconductor See Entry 62335

79.75 EXOELECTRON EMISSION

63138 Exoemission and the electret effect in lithium niobate crystals. G.I.Rozenman, I.S.Rez, Yu.L.Chepelev, N.B.Angert, E.I.Boikova (Lenin Komsomol Ural Forest Technol. Inst., Sverdlovsk, USSR). *Sov. Phys.-Tech. Phys. (USA)*, vol.27, no.9, p.1162-3 (Sept. 1982). Translation of: *Zh. Tekh. Fiz. (USSR)*, vol.52, no.9, p.1890-2 (Sept. 1982). [received: April 1983]

Exoelectron emission is known to occur in ferroelectrics when the pyroelectric effect takes place. The emission is caused by a field whose source is excess pyroelectric charge. It is to be expected that the electret charge as well as the pyroelectric charge may be the cause of the exoemission. Lithium niobate crystals, both pure and doped with vanadium, iron, silicon, molybdenum, and fluorine were studied. The temperature dependence is shown of the intensity of exoelectron emission from the (00-1) and (001) surfaces of a single-domain LiNbO_3 single crystal corresponding to the C^+ and C^- cuts, respectively. From the C^+ cut there is no emission in the temperature ranges -150 to -100°C , $+45$ to $+55^\circ\text{C}$, and above 200°C . From the C^- cut two weak maxima are observed in the first two of those temperature ranges. It is possible that the anomalous behavior of the exoemission is related to an electric field E_1 whose direction is opposite to the pyroelectric field E_p and which is formed when the lithium niobate crystal is heated. The fall-off of the emission current at $+200^\circ\text{C}$ upon heating the C^+ cut is probably due to an increase in the conductivity of the crystal resulting in complete screening of the pyroelectric field. Doping of the samples did not result in any basic change in the nature of the emission current. (6 refs.)

Multi-needle counter with cathode focusing used to detect the thermo-simulated exoelectronic emission (TSEE) See Entry 60546

Electroluminescence from ZnS during deformation of a metal contact See Entry 63056

79.90 OTHER TOPICS IN EMISSION AND IMPACT PHENOMENA IN CONDENSED MATTER

Quantum chemical models of elementary steps concerning plasma etching in the F/Si system See Entry 63446

80.00 CROSS-DISCIPLINARY PHYSICS AND RELATED AREAS OF SCIENCE AND TECHNOLOGY

81.00 MATERIALS SCIENCE

81.10 METHODS OF CRYSTAL GROWTH AND PURIFICATION

(for physics of crystal growth, see 61.50C; for epitaxial growth methods, see 81.15)

81.10B Growth from vapour

63139 Analysis of the process of deposition of solid solutions of composition $\text{Ga}_{1-x}\text{In}_x\text{As}_{1-y}\text{P}_y$ form the gas phase using the method of particle pressure diagrams. S.M.Eskin, E.N.Vigdorovich, T.P.Shapovalova, A.S.Pashinkin. *Inorg. Mater. (USA)*, vol.18, no.5, p.617-20 (May 1982). Translation of: *Izv. Akad. Nauk SSSR Neorg. Mater.*, vol.18, no.5, p.729-32 (May 1982). [received: Feb. 1983]

Partial pressure diagrams have been plotted which describe the process of deposition of solid solutions of composition $\text{Ga}_{1-x}\text{In}_x\text{As}_{1-y}\text{P}_y$ ($0.2 \leq x \leq 1.0$; $0.1 \leq y \leq 0.9$) from the gas phase using hydrogen chloride technology at 1000°K . It is shown that the size of the region of crystallization of the solid solution varies monotonically depending of x , y , and p_{HCl} in the system. (10 refs.)

Initial growth forms of single crystals of chromium with copper on its surface See Entry 61841

81.10D Growth from solutions

63140 In situ observation of mono-molecular growth steps on crystals growing in aqueous solutions. I. K.Tsukamoto (Inst. of Mineralogy, Petrology & Economic Geology, Tohoku Univ., Sendai, Japan). *J. Cryst. Growth (Netherlands)*, vol.61, no.2, p.199-209 (March 1983).

It is demonstrated that by combining optical phase contrast microscopy with a conventional TV system, mono-molecular spiral growth steps on crystals can be observed during the growth in aqueous solution. The image of the mono-molecular growth steps is stored either in a video tape recorder or through an A/D converter into the floppy disk in a computer. The minimal step height on CdI_2 crystals measured by the in situ interferometry described in a forthcoming paper is about 1.4 nm , which satisfactorily agrees with the mono-molecular growth step height derived from the crystal structure. This observation method has a great advantage in understanding the growth mechanism of crystals in more direct way when the growth rate measurement is coupled. (36 refs.)

63141 An improved method for the measurement of the rates of growth and dissolution of crystals under isothermal conditions. M.Rubbo, J.N.Sherwood (Dept. of Pure & Appl. Chem., Univ. of Strathclyde, Glasgow, Scotland).

J. Cryst. Growth (Netherlands), vol.61, no.2, p.210-14 (March 1983). A volumetric method for the measurement of the isothermal growth and dissolution kinetics of crystals is described. It application to the particular case of the growth of crystals of n-eicosane ($\text{C}_{20}\text{H}_{42}$) from solution in n-dodecane ($\text{C}_{12}\text{H}_{26}$) is discussed and the errors involved in the measurement are defined. (10 refs.)

63142 Growth rate dispersion among ADP crystals formed by primary nucleation. J.Garside, R.I.Ristic (Dept. of Chem. & Biochem. Engng., Univ. Coll. London, London, England).

J. Cryst. Growth (Netherlands), vol.61, no.2, p.215-20 (March 1983). The growth rates of many small ($<0.3 \text{ mm}$) ADP crystals in the [010] and [001] directions have been measured. Significant variations in growth rate between different crystals were observed and this variation can be represented by both a log-normal and a gamma distribution. The magnitude of growth rate variations has been related to the Burton-Cabrera-Frank spiral growth theory. (15 refs.)

63143 A refractometric method for continuous investigation of stirred crystal growth organic solutions. M.Sigelle, J.Flicstein, R.Hierle, J.Badan (CNET PMS/PAB, Bagnaux, France).

J. Cryst. Growth (Netherlands), vol.61, no.2, p.229-34 (March 1983). A continuous refractometric method with a He-Ne laser at $\lambda=6328 \text{ \AA}$ for investigating stirred crystal growth solutions is described. A measurement setup reliable for any long time running experiment was designed, which allows in situ non-destructive characterization of a 60 cm^3 volume cell thermostated at $\pm 0.01^\circ\text{C}$. The theoretical refractive index resolution is $|\Delta n_{\text{min}}|_{\text{th}} = 3 \times 10^{-6}$ while the effects of room temperature, atmospheric pressure, and beam waist broadening due to stirring flow birefringence are negligible. Only long time reproducibility considerations lead to an actual resolution $|\Delta n|_{\text{min}} = 6 \times 10^{-6}$. The capabilities of the system were investigated using a well purified low saturated solution of 3-methyl 4-nitropyridine 1-oxide-acetonitrile at a concentration $C_0 = 2.37 \times 10^{-2}$ mole/mole which is cooled from 34 down to 20°C . It is found that the method can be employed to follow any temperature programming, providing that the elemental segment is not less than $|\Delta T|_{\text{min}} = 0.015^\circ\text{C}$, while concentration changes at constant temperature as low as $\Delta C_{\text{min}} = 0.03 \text{ g/l}$ can be detected. No discontinuity around the solubility point at 29.5°C was noticed. (19 refs.)

63144 Flux growth of SrGa_2O_9 single crystals. F.Haberey (Inst. für Werkstoffe der Elektrotech., Ruhr-Univ. Bochum, Bochum, Germany), R.Leckebusch, M.Rosenberg, K.Sahl.

J. Cryst. Growth (Netherlands), vol.61, no.2, p.284-8 (March 1983). Flux growth and some properties of SrGa_2O_9 single crystals are reported. Li_2MoO_4 , Na_2MoO_4 and Bi_2O_3 were tried as flux components using the slow cooling technique. Only Bi_2O_3 proved to be suitable. Systematic variation in the proportion of starting components (SrCO_3 , Ga_2O_3 , Bi_2O_3) revealed an optimal starting composition (17.5 mole% SrCO_3 , 52.5 mole% Ga_2O_3 and 30 mole% Bi_2O_3). Tabular SrGa_2O_9 crystals up to several mm in diameter were obtained. Chemical, optical and X-ray investigations showed them to be useful substrates of LPE of magnetic hexaferrite layers with magnetoplumbite or related lattice. (10 refs.)

Growth kinetics of TGS See Entry 61837

Features of the growth of potassium pentaborate crystals See Entry 61838

Growth and some dielectric properties of K_2ZnCl_4 and Rb_2ZnCl_4 crystals See Entry 62877

Factors affecting the efficiency of chemically deposited CdSe based photoelectrochemical cells See Entry 63719

81.10F Growth from melts

63145 Numerical simulation of heat and concentration fields when growing single crystals by the Czochralski method. L.G.Kirillova. *Elektron. Model. (USSR)*, no.2, p.92-5 (March-April 1983). In Russian.

A mathematical model and algorithms are developed which permit the calculation of certain process control parameters to produce single crystals with a preset diameter and definite composition. (6 refs.)

63146 Skull melter single crystal growth of magnetite (Fe_3O_4)-ulvospinel (Fe_2TiO_4) solid solution members. R.Aragon, H.R.Harrison, R.H.McCallister, C.J.Sandberg (Purdue Univ., West Lafayette, IN, USA).

J. Cryst. Growth (Netherlands), vol.61, no.2, p.221-8 (March 1983). A modified Bridgman technique by crucibleless skull melting has been applied to the growth of equiaxed, centimeter sized titanomagnetite $[(\text{Fe}_3\text{O}_4)_{1-x}(\text{Fe}_2\text{TiO}_4)_x]$ single crystals, in oxygen-buffered atmospheres. The relation between atmosphere and spinel phase compositions has been systematically investigated, through characterization by X-ray diffraction, polarized reflected light microscopy and electron microprobe analysis. Guidelines are discussed for generalization of the method to single crystal growth of ferrites of arbitrary composition. (20 refs.)

63147 An experimental model of the flow in Czochralski growth. A.D.W.Jones (School of Math., Univ. of Bristol, Bristol, England).

J. Cryst. Growth (Netherlands), vol.61, no.2, p.235-44 (March 1983). An experiment has been built to model the flow of the melt in Czochralski growth. Water and a mixture of water and glycerol are used as the working fluids and the rates of rotation, temperature differences and dimensions of the apparatus are scaled so that the effects of rotation and buoyancy forces are correctly represented. Observations of the velocity and temperature fields are divided into six flow regimes (I-VI). The investigation of the separate effects of crystal rotation (I), differential rotation (II) and heating (III) leads to a better understanding of the flow due to heating with crystal rotation (IV) and heating with differential rotation (V and VI). It is expected that regimes IV, V and VI will occur during crystal growth. (16 refs.)

63148 The thermal field in a furnace for growing crystals by the Verneuil method. A.P.Chirkin, A.I.Pustyl'nik, O.G.Kapachinskaya (Inst. of Crystallography, Acad. of Sci., USSR).

Sov. Phys.-Crystallogr. (USA), vol.27, no.5, p.592-5 (Sept.-Oct. 1982). Translation of: *Kristallografiya (USSR)*, vol.27, no.5, p.988-93 (Sept.-Oct. 1982). [received: April 1983]

The authors suggest a method of studying the thermal fields in Verneuil furnaces. They study the distribution of the particles of the charge in the flame of the oxyhydrogen burner when the flow rates of gases and charge are varied. They show that changes in the charge flow rate have a marked influence on the temperature fluctuations at the crystallization front. (8 refs.)

63149 Laser synthesis of V_2O_5 crystals with highly developed surfaces. V.A.Bobyrev, F.V.Bunkin, E.Deli, N.A.Kirichenko, B.S.Luk'yanchuk, L.Nanai, A.V.Simakin, I.Hevesi, G.A.Shafeyev (P.N. Lebedev Phys. Inst., Acad. of Sci., Moscow, USSR).

Sov. J. Quantum Electron. (USA), vol.12, no.10, p.1267-8 (Oct. 1982). Translation of: *Kvantovaya Elektron., Moskva (USSR)*, vol.9, no.10, p.1943-4 (Oct. 1982). [received: April 1983]

An investigation was made of the laser synthesis of V_2O_5 crystals with large surface areas (these crystals are used as a catalyst in chemical reactions). It was found that the effective surface area of these crystals could be increased by a factor of 10^3 - 10^4 , which should make the crystals highly useful in chemical engineering. (1 ref.)

63150 Boron-doped GaAs single crystal. A.Kawasaki, K.Tada, T.Kotani, R.Nakai, T.Takebe, S.Murai (Res. & Dev. Group, Sumitomo Electric Industries Ltd., Osaka, Japan), S.Akai, T.Yamaguchi. *Sumitomo Electr. Tech. Rev. (Japan)*, no.22, p.235-42 (Jan. 1983). Describes the LEC (Liquid Encapsulated Czochralski) technique. In this technique, GaAs melt is coated with a liquid encapsulant B_2O_3 (boron oxide), and the GaAs single crystal is pulled up under high pressure of 2-60 atm to constrain decomposition of GaAs. While the B_2O_3 liquid encapsulant is a transparent liquid with high viscosity, it provides a large adiabatic effect so that it is difficult to control the temperature near the solid-liquid interface. Further, the convection of high-pressure gas induced during crystal growth makes temperature control near the solid-liquid interface more difficult. The authors describe a successful attempt to produce GaAs crystal having low dislocation density employing the direct synthesis method of elemental Ga and As in which electrically neutral boron was doped. Since the bond energy between boron and arsenic is larger than that between gallium and arsenic, it is expected that the boron-doped GaAs crystal would have a low dislocation density. (14 refs.)

63151 Single crystal growth and physical properties of cubic $Zn_4O(BO_3)_6$. L.Bohaty, S.Hausuhl, J.Liebertz, S.Stahr (Univ. zu Köln, Köln, Germany). *Z. Kristallogr. (Germany)*, vol.161, no.1-2, p.157-8 (1982). Reports on the suitability of $Zn_4O(BO_3)_6$ for technical applications. Large single crystals were grown by the Czochralski method. The crystals obtained (about 18 mm in diameter and 20 mm long) were of optical quality. The crystals were chemically stable in normal air and quasi-soluble in water. As the electrooptical and piezoelectrical constants are only of the same order of magnitude as those of α -quartz, the crystals are not suited for use in electrooptical modulator devices. However, qualitative measurements of the photoelastic properties showed unexpected high effects which suggest an application for acoustooptical deflection devices. The high mechanical stability, small thermal expansion and small thermoelastic constants will favour such applications. (6 refs.)

63152 Fast silicon-sheet growth with the supported-web method. J.G.Grabmaier, H.Föll, B.Freinstein, K.Geim (Siemens AG, München, Germany).

Fourth E.C. Photovoltaic Solar Energy Conference. Proceedings of the International Conference, Stresa, Italy, 10-14 May 1982 (Dordrecht, Netherlands: Reidel 1982), p.976-9

Directly grown Si ribbons or sheets are attractive for the manufacture of low-cost Si solar cells. Intensive research efforts have led to the development of ribbon growth methods that yield products suitable for the manufacture of efficient solar cells. However, the areal growth rates of most methods are rather small and this constitutes a serious obstacle to their large-scale implementation. The newly developed supported-web (S-Web) technique attempts to overcome this problem. It envisions the use of a carbon-fibre net which is pulled through a melt of liquid Si at a high pulling speed. Liquid films or webs of Si are spread out within the meshes of the net and crystallize some time after leaving the melt. In this way the formation and the crystallization of the Si ribbon is decoupled and very large areal growth rates should be possible. First experiments demonstrated the feasibility of this concept and pulling speeds of ≈ 2 m/min have been achieved. Problems exist with respect to the crystalline quality and the topography of the specimens obtained. (7 refs.)

On the possibility of obtaining a uniform impurity distribution in growing crystals by the Bridgman-Stockbarger method See Entry 61839

Influence of capsule diameter on the impurity distribution in a growing crystal See Entry 61840

Impurity incorporation in RAO polysilicon layers and consequences on their electrical properties See Entry 61950

Growth and some dielectric properties of K_2ZnCl_4 and Rb_2ZnCl_4 crystals See Entry 62877

Dissociation of liquid arsenic selenoiodide See Entry 63518

Low-cost solar power is on the horizon See Entry 63662

81.10H Zone melting and zone refining

63153 Elimination of boron in silicon by zone melting under a high-frequency inductive plasma: role of reactive plasmas and of slag. Characterisation of photovoltaic silicon. D.Morvan, J.Amouroux, M.C.Charpin (Ecole Nat. Supérieure de Chimie de Paris, Paris, France), H.Lauray. *Rev. Phys. Appl. (France)*, vol.18, no.4, p.239-51 (April 1983). In French. Preparation of photovoltaic silicon requires that one analyses systematically the purity and physical properties of the material. Previous studies show the critical effect of a number of impurities affecting the efficiency of the photocell. Nevertheless there still exists a gap in the studies concerning the chemistry combination which can occur between the impurities appearing during all technic operations of the material. The photovoltaic properties of the same material seem to depend on the different steps of elaboration of a given crystallized structure. Indeed, impurities segregate in the liquid concentrate towards the grain boundaries or react with the protection slag of the crucible giving new chemical boundaries. Among preparation methods for photovoltaic silicon the authors develop the original method of purification of metallurgical grade silicon with a reactive plasma process. This process, which is a liquid-solid, liquid-liquid and liquid-gas extraction, enables one to obtain a polycrystalline silicon having a high purity with crystals measuring 1 mm or slightly more. (27 refs.)

Ge-seeded crystallisation on SiO_2 by using a slider system with RF heated strip heater See Entry 63154

81.10J Growth from solid phases

(inc. multiphase diffusion and recrystallisation)

Ge-seeded crystallisation on SiO_2 by using a slider system with RF heated strip heater See Entry 63154

81.15 METHODS OF THIN FILM DEPOSITION

(inc. epitaxial growth methods; see also 68.55 Thin film growth, structure, and epitaxy)

63154 Ge-seeded crystallisation on SiO_2 by using a slider system with RF heated strip heater. Y.Ohmachi, T.Nishioka, Y.Shinoda (Musashino Electrical Communication Lab., Nippon Telegraph & Telephone Public Corp., Tokyo, Japan).

Electron. Lett. (GB), vol.19, no.8, p.274-5 (14 April 1983).

A slider system has been developed for crystallisation of semiconductor films on SiO_2 . The system consists of a graphite support, graphite strip heater and movable quartz substrate holder. A two heater procedure can be achieved with an RF heating coil. Single-crystal Ge films have been successfully grown over SiO_2 on a Si substrate using a heterolateral epitaxy by seeded solidification technique. (10 refs.)

Synthesis of AlSb by laser and capacitive discharge annealing See Entry 62297

81.15C Deposition by cathodic sputtering

63155 High-energy particles in AlN film preparation by reactive sputtering technique. K.Tominaga, S.Iwamura, Y.Shintani, O.Tada (Faculty of Engng., Tokushima Univ., Tokushima, Japan).

Jpn. J. Appl. Phys. Part 1 (Japan), vol.22, no.3, p.418-22 (March 1983).

AlN films were prepared by reactive DC-planar magnetron sputtering in atmosphere of N_2 gas or mixed gas of N_2 and H_2 . High-energy neutral particles bombarding the AlN film were observed by using a time-of-flight particle analyzer. It is found that the high-energy particles such as NO and OH (or O) due to residual H_2O in the discharge chamber or oxides at the Al target surface induce the coloring of film, the decrease of optical transmittance at shorter wavelength, the decrease of the degree of c -axis orientation of the film, etc. For the sputtering in mixed gas of N_2 and H_2 , a number of energetic H atoms are bombarding the AlN film. The influence of these energetic H atoms on the film growth is also studied.

63156 Cathode sputtering. II. G.Peto.

Finomtech-Mikrotech. (Hungary), vol.22, no.2, p.51-9 (Feb. 1983). In Hungarian.

For pt.1 see *ibid.*, vol.22, no.1, p.29-32 (1983). Cathode sputtering is a rapidly developing method applied in thin film technology and characterized by an ionic process which is parallel with the layer deposition. This condition may induce particular properties in thin films, so that the use of cathode sputtering predetermines certain layer properties. Cathode sputtering may be described as a combination of three processes: material emission under the effect of ion bombardment, ion source, layer deposition parallel to the ion bombardment. Besides the usual vacuum-technological questions, some new problems emerge on the design of equipment. The cathode sputtering is preferred in microcircuit applications, but in processes requiring very high purity, the evaporation method dominates at present. (4 refs.)

63157 Ion beam sputter deposition of layered magnetic thin films.

J.W.Smits, H.A.Algra, U.Enz, R.P.van Staple (Philips Res. Labs., Eindhoven, Netherlands).

J. Magn. & Magn. Mater. (Netherlands), vol.35, no.1-3, p.89-92 (March 1983). (Proceedings of the 10th International Colloquium on Magnetic Films and Surfaces, Yokohama, Japan, 13-16 Sept. 1982).

Magnetic thin films of Ni_2Fe_{21} (Permalloy) alternated with Cu were prepared by ion beam sputtering. Electrostatic deflection of the Ar^+ beam between two targets yields a layered structure. This is evidenced from the X-ray diffractograms which show satellites at intervals corresponding to the superstructure wavelength. FMR measurements show a resonance corresponding to the expected uniform mode, as well as a weak complicated spectrum at higher fields. The latter is connected with an imperfect layer structure. (5 refs.)

63158 High-rate sputter technique. S.Schiller, U.Heisig, K.Goedicke (Forschungsinstitut Manfred von Ardenne, Dresden, Germany).

Vak.-Tech. (Germany), vol.32, no.2, p.35-47 (March 1983). In German.

For some years high-rate sputtering has gained a decisive role among the physical vapour deposition techniques. The state and recent results of this technique are reported. The high-rate sputter sources of today are the result of a stepwise consistent technical development. The present efforts on source development refer to the target shape, the improvement of the material utilization, the long-term stability, and to the adaptation to the special deposition problem. Besides the planar and cylindrical source types a new 'tube plasmatron' is presented. Process research on high-rate sputtering is concentrated on reactive d.c. sputtering. The plant engineering is determined by the tendency to extensive process control, e.g. with the aid of optical spectrometers, and to an in-situ measurement of the film thickness. The application possibilities of high-rate sputtering are demonstrated by examples for the metallization of semiconductors, the manufacturing of transparent conducting layers, the manufacturing of thin film resistances with a high stability, the large-area coating of glass panes with heat-reflecting film systems, and for the deposition of wear-resistant and hard layers. (55 refs.)

Hydrogen incorporation scheme in amorphous-microcrystalline mixed-phase $Si:H$ films See Entry 62286

Preparation and properties of RE-TM amorphous films See Entry 62736

Electron microscopy of CoCr sputtered films See Entry 62747

Anomalous hysteresis loops in single and double layer sputtered TbFe films See Entry 62748

Perpendicular anisotropy in Co-Cr films See Entry 62751

Perpendicular magnetic anisotropy and microstructure of sputter-deposited Co-Cr film See Entry 62775

Comparative studies of reactive sputtering, ion plating and CVD coating of TiN hard layers See Entry 63167

Reactive sputtered Ta_2O_5 antireflection coatings See Entry 63670

Cellules solaires au CdTe en couches minces polycristallines. Elaboration par pulvérisation triode et transport a courte distance (CdTe solar cells in polycrystalline thin films. Elaboration by triode sputtering and short distance transport) See Entry 63675

Thin film heterojunction CdS/Cu ternary alloys solar cells with minority carrier mirrors See Entry 63690

81.15G Vacuum deposition

63159 Formation of cubic boron nitride films by boron evaporation and nitrogen ion beam bombardment. M.Satou (Government Industrial Res. Inst., Osaka, Japan), F.Fujimoto.

Jpn. J. Appl. Phys. Part 2 (Japan), vol.22, no.3, p.L171-2 (March 1983). The resistivity and structure of films deposited on tantalum and rocksalt substrates by the electron beam evaporation of boron and the simultaneous bombardment of 30 keV N_2^+ ion beam were studied. From observation by transmission electron microscope, it was found that cubic boron nitride was produced in the case where the prepared composition rate of boron to nitrogen was 2.5. (5 refs.)

63160 Fabrication of $In_2O_3:SnO_2$ transparent conducting films by electron beam evaporation. R.Nakano, H.Kawasaki, J.Sato, T.Yabumoto. *Res. Rep. Fac. Eng. Meiji Univ. (Japan)*, no.43, p.49-53 (1982). In Japanese. Conductive and transparent thin films of In_2O_3 mixed with 5 wt.% SnO_2 have been prepared by electron beam evaporation using the vacuum system with a high pressure limitation of 1×10^{-4} Torr. The deposited films have a sheet resistance of 15 Ω /sq and transmittance exceeding 90% (550 nm) under preparing condition that O_2 pressure is 2×10^{-5} Torr, deposition rate, 1 Å/s and substrate temperature, 325°C. (5 refs.)

63161 Processes occurring in an erosion plasma during laser vacuum deposition of films. III. Condensation in gas flows during laser vaporization of materials. S.V.Gaponov, A.A.Gudkov, A.A.Fraerman (Inst. of Appl. Phys., Acad. of Sci., Gorki, USSR).

Sov. Phys.-Tech. Phys. (USA), vol.27, no.9, p.1130-3 (Sept. 1982). Translation of: *Zh. Tekh. Fiz. (USSR)*, vol.52, no.9, p.1843-8 (Sept. 1982). [received: April 1983]

For pt.II see *Zh. Tekh. Fiz.*, vol.52, no.8, p.1584 (1982). *Sov. Phys. Tech. Phys.*, vol.27, no.8, p.969-73 (1982). A theoretical and experimental study of the possibility of condensed droplets appearing in the erosional flow produced by irradiating targets with millisecond pulses from a neodymium laser is reported ($\lambda=1.06 \mu m$, $\tau_p=6 \times 10^{-4}$ s, $W_p=20$ J, $q_0=10^8$ W/cm 2). The necessary conditions for a condensation discontinuity to occur during the expansion of the high-pressure region into vacuum are formulated. It is revealed that the formation of condensed droplets near the surface of the target is inhibited by the vaporizing action of the radiation incident on and reflected from the target. It is established that a condensation discontinuity is possible in artificially created thermalized regions. The nature of the degradation of the film by the high-energy particles is determined. It is shown that undamaged films of semiconductors and metals can be obtained. (4 refs.)

63162 Characterization of Al-AlO $_3$ and Sn-SnO $_2$ cermet films deposited by reactive evaporation. H.Demiryont (Dept. of Phys., Istanbul Univ., Istanbul, Turkey), N.Tezey.

Thin Solid Films (Switzerland), vol.101, no.4, p.345-56 (25 March 1983).

A new preparation technique called 'reactive evaporation' is discussed with reference to the production of Al-AlO $_3$ and Sn-SnO $_2$ cermet films. Sample properties characterized by the metallic particle concentration within the cermet films were found to depend on the deposition rate, the pressure and the species of residual gas during deposition, the source-substrate distance and substrate temperature. Al-AlO $_3$ cermets exhibits three distinct types of current-voltage characteristic, which can be related to the particle concentration. Ohmic conductivity, switching and memory effect properties and non-linear current-voltage characteristics were observed with Al-AlO $_3$ cermet films independently of the electrode material (aluminum, gold) and the sample thickness (100-1000 Å) when the aluminum particle concentration was decreased. Some general properties of Sn-SnO $_2$ cermet films were studied in relation to the preparation conditions. Microstructure examination by transmission electron microscopy, resistance measurements on SnO $_2$ films prepared in strip and sandwich form and optical transmissivity studies were carried out as functions of time. The effects of moderate heat treatment on the sample properties were also examined. (26 refs.)

63163 Low temperature dielectric films from octavinylsiloxane. V.P.Korchok, T.N.Martynova, V.I.Belyi (Inst. of Inorganic Chem., Novosibirsk, USSR).

Thin Solid Films (Switzerland), vol.101, no.4, p.373-6 (25 March 1983).

The temperature dependence of the equilibrium vapour pressure of volatile organosiloxane octavinylsiloxane (vinyl-T $_8$) was studied by the Knudsen method. Nickel was found to be the best material for the evaporation cell as it does not catalyse polymerization of vinyl-T $_8$. It was found that thin solid films of vinyl-T $_8$ are readily converted into amorphous siloxane polymer dielectric films by argon or nitrogen plasma treatment. (8 refs.)

63164 Continuous deposition of photovoltaic grade CdS sheet at the unit operations scale. R.E.Rochelleau, P.J.Lutz, D.F.Brestovansky, B.N.Baron, T.W.F.Russell (Dept. of Chem. Engng., Univ. of Delaware, Newark, DE, USA).

Fourth E.C. Photovoltaic Solar Energy Conference. Proceedings of the International Conference, Siresa, Italy, 10-14 May 1982 (Dordrecht, Netherlands: Reidel 1982), p.798-803

Uniform photovoltaic grade CdS sheet has been reproducibly deposited on a continuously moving flexible substrate in a reel to reel vacuum coater. Materials characterization by scanning electron microscopy, photoluminescence, and resistivity revealed that continuously deposited CdS is essentially equivalent to material that was deposited for making high efficiency Cu_2S/CdS cells in the laboratory scale process. Cells made using continuously deposited CdS sheet had efficiencies as high as 7.85%. (7 refs.)

Analysis of operation of double-beam photometer for monitoring the thickness of thin films See Entry 59827

General-purpose UELI-1M electron-beam evaporator See Entry 61311

Internal stresses in thin Ge, ZnS, and ZnSe films See Entry 62303

Crystal, impurity-related and growth defects in molecular beam epitaxial GaAs layers See Entry 62308

LiInSe $_2$ thin epitaxial films on {111}A-oriented GaAs See Entry 62309

Preparation and properties of RE-TM amorphous films See Entry 62736

Effect of annealing on the structure and properties of molybdenum coatings on steel Kh12M See Entry 63458

Antimony doping in vacuum deposited thin film silicon photovoltaic cells See Entry 63698

81.15H Chemical vapour deposition

63165 Vapor phase epitaxy of indium phosphide. Huang Shanxiang (Nanjing Solid State Devices Res. Inst., China). *Chin. J. Semicond. (China)*, vol.4, no.2, p.197-9 (March 1983). In Chinese. (2 refs.)

63166 Organometallic vapor phase epitaxial growth of $In_{1-x}Ga_xAs_yP_{1-y}$ on GaAs. T.Iwamoto, K.Mori, M.Mizuta, H.Kukimoto (Imaging Sci. & Engng. Lab., Tokyo Inst. of Technol., Yokohama, Japan).

Jpn. J. Appl. Phys. Part 2 (Japan), vol.22, no.3, p.L191-3 (March 1983). $In_{1-x}Ga_xAs_yP_{1-y}$ ($0.5 \leq x \leq 0.9$, $0 \leq y \leq 0.55$) layers have been grown on GaAs substrates by low-pressure organometallic vapour phase epitaxy using triethylindium (TEIn), triethylgallium (TEGa), arsine (AsH $_3$) and phosphine (PH $_3$). The surface morphology of the layers is mirror-like and the photoluminescence intensity is comparable to that of InGaP grown on GaAs by the same technique. The relationship between the fraction of AsH $_3$ flow and the solid fraction of As, y, is also mentioned. (9 refs.)

63167 Comparative studies of reactive sputtering, ion plating and CVD coating of TiN hard layers. H.Freller, H.Hassler, H.Schreiner (Siemens AG, Erlangen, Germany).

High Temp.-High Pressures (GB), vol.14, no.3, p.335-40 (1982). (10th Plansee Seminar on 'Trends in Refractory Metals, Hardmetals, and Special Materials, and their Technology', Reutte, Austria, 1-5 June 1981).

CVD techniques have been successfully applied to the coating of tools and structural parts for some years now. For certain applications, however, coating temperatures of around 1000°C, typical of the CVD process, are too high. For this reason an attempt has been made to deposit titanium nitride hard coatings by PVD methods; ion plating and sputtering. Because of the appreciably lower deposition temperatures, 200-400 °C, and the different way the compound forms, the structure of such coatings differs from that of CVD coatings. These were investigated by optical microscopy, scanning electron microscopy, and Vickers hardness measurements. In addition, the influence of specimen geometry on film thickness and film quality is briefly discussed. (5 refs.)

63168 CVD coating of hard metals, especially with regard to boron and boron-containing substances. K.Voigt, H.Westphal (DDR/VEB Hartmetallwerk Immelborn, Immelborn/Thuringen, Germany).

High Temp.-High Pressures (GB), vol.14, no.3, p.357-62 (1982). (10th Plansee Seminar on 'Trends in Refractory Metals, Hardmetals, and Special Materials, and their Technology', Reutte, Austria, 1-5 June 1981).

The possibilities of depositing hard materials containing boron on hard metal parts by the CVD technique are examined. A process has been developed which combined deposition of boron-containing hard layers with hardening of the base material in the zone adjacent to the coating. A CVD plant with a cold-wall retort has been found suitable for carrying out the coating. (11 refs.)

63169 Analysis of silicon crystal growth using low pressure chemical vapour deposition. F.Hottier, R.Cadoret (Labs. d'Electronique et de Phys. Appliquee, Limeil-Brevannes, France).

J. Cryst. Growth (Netherlands), vol.61, no.2, p.245-58 (March 1983).

The growth kinetics of silicon films deposited under low pressure conditions (Si-SiH $_4$ system) have been investigated by using an experimental reactor. Depending on the growth conditions, polycrystalline or monocrystalline films were obtained with different deposition kinetics. With the help of an ultra high vacuum chamber—equipped with surface analysis facilities—which was directly connected to the reactor chamber, a detailed assessment of the growth interface has been made. As shown by in situ ellipsometry, heating the substrate at a temperature higher than 900°C under an hydrogen flow induced a thermal etching of silicon which could be counterbalanced by a low silicon partial pressure. The stable state of growth for polycrystalline or monocrystalline film was also assessed by ellipsometry and additional information concerning the crystallinity or the crystal surface coverage of adsorbed molecules (mainly hydrogen) was obtained by using RHEED and AES techniques. (27 refs.)

63170 Mechanisms of silicon monocrystalline growth from SiH $_4$ /H $_2$ at reduced pressures. R.Cadoret (Lab. de Cristallographie et Phys. des Milieux Condenses, UER Sci., Aubiere, France), F.Hottier.

J. Cryst. Growth (Netherlands), vol.61, no.2, p.259-74 (March 1983).

The kinetics of monocrystalline Si deposition on slightly misoriented {111} Si substrates from SiH $_4$ diluted in H $_2$ at reduced pressures is theoretically analysed in terms of a condensation process of Si atoms and SiH $_4$ molecules, taking surface diffusion into account. The possibility of a homogeneous nucleation is considered by applying the classical homogeneous nucleation theory to published experimental results. A growth mechanism limited by diffusion of SiH $_4$ molecules on a surface inhibited by H absorption is in agreement with the growth rates of monocrystalline Si observed at reduced pressures, when the heated substrate has a surface that is not too large. A condensation of SiH $_4$ molecules explains the homogeneous nucleation. (26 refs.)

63171 Vapour growth of argyrodite-type ionic conductors Cu_2PS_4Hal . S.Fiechter, J.Eckstein, R.Nitsche (Kristallographisches Inst., Univ. Freiburg, Freiburg, Germany).

J. Cryst. Growth (Netherlands), vol.61, no.2, p.275-83 (March 1983).

Cu_2PS_4Hal compounds (with Hal=Cl, Br or I) have been crystallized around 950K by CVT with P, S and Hal (and combinations thereof). Chemical insight into the transport processes was gained from dissociation pressure measurements and spectroscopic vapour analysis. Lacking thermochemical data of the compounds were obtained from C_p measurements. Models, derived for the CVT mechanisms, yield transport rates and directions which agree qualitatively with experiments. The main vapour species (for Hal=Cl) are $PSCl_3$, S_2 , PCL_3 , P_2S_3 and $(CuCl)_3$. With a surplus of CuHal, VLS growth via liquid CuHal/ Cu_2S phases was observed. (13 refs.)

63172 Preparation of oriented GaAs bicrystal layers by vapor-phase epitaxy using lateral overgrowth. J.P.Salerno, R.W.Clelland, P.Vohl, J.C.C.Fan, W.Macropoulos, C.O.Bozler (Lincoln Lab., MIT, Lexington, MA, USA), A.F.Witt.

Grain Boundaries in Semiconductors. Proceedings of the Materials Research Society Annual Meeting, Boston, MA, USA, Nov. 1981 (New York, USA: North-Holland 1982), p.77-82

Describes a novel technique that utilizes vapor-phase epitaxy to grow bicrystal semiconductor layers with predetermined rotation axis, misorientation angle, and grain boundary plane. The geometrical structure of the grain boundary in each layer is therefore completely specified. The technique has been demonstrated by using the AsCl $_3$ -GaAs-H $_2$ method to grow a series of GaAs bicrystals, each containing a [110] tilt boundary formed by a grain with a (111)B boundary plane and a grain rotated from (111)B by a selected misorientation angle. The results of initial electrical measurements indicate that the height

of the potential barrier associated with each grain boundary varies with the misorientation angle. (14 refs.)

Very low threshold GaInAsP/InP double-heterostructure lasers grown by LP MOCVD See Entry 61152

Rectangular Luneburg-type lenses for integrated optics See Entry 61255

Production of 'Gradan'-type lightguide blanks on automated equipment (model UIZS-1) See Entry 61280

Post-deposition high temperature processing of silicon nitride See Entry 61949

On the reaction mechanism of GaAs MOCVD See Entry 62292

Etude et réalisation de croissances épitaxiales de composés III-V par pyrolyse mixte d'organometalliques et d'hydrures sous pression réduite: Application à l'étude de structures de piles solaires (Study and realisation of epitaxial growth of III-V compounds by mixed pyrolysis of organometallicals and hydrides under reduced pressure: Application to the study of solar cell structures) See Entry 63678

81.15J Ion plating and other vapour deposition

63173 Deposition of TiB₂ layers from the gas phase. F.Zeman, J.Mayerhofer, A.Kulmburg (Vereinigte Edelstahlwerke AG, Kapfenberg, Austria). *High Temp.-High Pressures (GB)*, vol.14, no.3, p.341-50 (1982). In German. (10th Plansee Seminar on 'Trends in Refractory Metals, Hardmetals, and Special Materials, and their Technology', Reutte, Austria, 1-5 June 1981). The deposition of TiB₂ layers at various temperatures on uncoated and TiC-precoated cemented carbide was investigated. The deposition rate increases with increasing temperature. In a hot-wall reactor, which was used for the study, the concentration of components used in the reaction decreases, which causes a decrease of the deposition rate at temperatures above 800°C. Uncoated cemented carbide reacts with boron present in the vapour phase, with the formation of a ternary CoWB phase. In the presence of a TiC coating acting as a diffusion barrier this phase is not observed. The crystallographic orientation of the TiB₂ deposits depends on the deposition temperature. (8 refs.)

63174 In-situ monitor of ion beam film growth and etching. P.R.Brosious, D.M.DeCain, J.M.E.Harper, A.W.Kleinsasser (IBM Corp., Armonk, NY, USA).

IBM Tech. Disclosure Bull. (USA), vol.25, no.9, p.4625-6 (Feb. 1983). Describes how positioning a quartz crystal film thickness monitor in the ion beam path, identically with wafers to be processed, permits a dynamic monitoring of film thickness on the wafers as the film is grown and etched. (no refs.)

63175 Large diameter plasma for ion plating of large volume. J.Uramoto (Inst. of Plasma Phys., Nagoya Univ., Aichi, Japan).

J. Vac. Soc. Jpn. (Japan), vol.25, no.12, p.781-7 (1982). In Japanese. First, a large diameter plasma with a uniform density (above 10 cm¹⁸) is produced in a DC discharge by utilizing a magnetic field composed of a circular ferrite permanent magnet and usual magnetic coil, whose magnetic field guides the DC discharge through two intermediate electrodes from a cathode to a large cylindrical anode and is reduced abruptly in the anode region to guide the discharge quickly toward the radial direction. Next, in order to apply this plasma source for the ion plating of large spaces the large diameter plasma is focused in a short distance on a hearth by arranging another permanent magnet under the hearth, while the cylindrical large diameter anode is floated electrically and the DC discharge power is almost concentrated to the hearth. Thus, one can utilize a high density plasma region over a large space of ion plating in comparison with an ordinary method in which only a diffusional plasma region from a small plasma column is used. (8 refs.)

63176 Preparation of molybdenum silicide films by RF ion plating. I.Okada (Nippon Telegraph & Telephone Public Corp., Tokyo, Japan).

J. Vac. Soc. Jpn. (Japan), vol.25, no.12, p.795-801 (1982). In Japanese. Thin films of molybdenum silicide were deposited on oxidized silicon wafers by RF ion plating. Molybdenum and silicon were supplied by electron beam evaporation and SiH₄ gas, respectively. Argon gas was used for the stabilization of the glow discharge. The Si/Mo atomic ratio in the film was changed from 1.4 to 2 by controlling the Mo evaporation rate. The effects of deposition condition, substrate potential, on film properties were investigated by X-ray diffraction analysis, sheet resistance and stress measurements. It was found that the films deposited at -2 kV substrate potential are polycrystalline partly before annealing and change to be polycrystalline wholly after annealing for 5 min at 1000°C. The annealed films show good adhesion to oxidized silicon, low resistivity, and low film stress. (7 refs.)

63177 Novel plasma chemical methods for doping a-Si:H. G.H.Bauer, G.Bilger (Inst. fuer Phys. Elektronik, Univ. Stuttgart, Stuttgart, Germany). Fourth E.C. Photovoltaic Solar Energy Conference, Proceedings of the International Conference, Stresa, Italy, 10-14 May 1982 (Dordrecht, Netherlands: Reidel 1982), p.773-7

Hydrogenated amorphous silicon prepared by decomposition of silane in a DC-glow discharge or by RF-sputtering in Ar/H₂ mixtures has been doped by methods of dopants injection into the plasma which base on interactions of plasma or the neutral gas with surfaces at different temperatures and varying electric potentials (co-sputtering, DC-sputtering, thermally activated injection to the neutral gas, plasma assisted transport). By these techniques various kinds of dopants (In, B, P, Sb and N) have been injected into the plasma and by this means incorporated into the film partially acting as electronically active donors and acceptors respectively. Analyses of doping effects and efficiencies by evaluation of temperature dependent conductivity and thermoelectric power data yield increases in room temperature conductivity up to a factor 10⁸ (to ≈10⁻² (Ωcm)⁻¹) and decreases of activation energies for extended states conduction which indicate the position of the Fermi level to <0.2 eV. (12 refs.)

Hydrogen incorporation scheme in amorphous-microcrystalline mixed-phase Si:H films See Entry 62286

Electronic properties of doped amorphous SiO_x See Entry 62521

Photoluminescence in amorphous C:H films prepared by glow discharge decomposition of CH₄ or C₂H₆ See Entry 63030

Electrical and optical properties of a-Si_{1-x}C_x:H film prepared by GD SiH₄ and C₂H₆ See Entry 63065

Comparative studies of reactive sputtering, ion plating and CVD coating of TiN hard layers See Entry 63167

Anodic oxidation of GaAs in oxygen plasma and qualitative analysis of anodic oxide films by AES and XPS See Entry 63439

Large area hydrogenated amorphous silicon for photovoltaic application See Entry 63697

81.15L Deposition from liquid phases (melts and solutions)

63178 LPE growth of uniform (Ga, Al)P alloy crystal. T.Sugiura, A.Tanaka, H.Unno, T.Sukegawa (Res. Inst. of Electronics, Shizuoka Univ., Shizuoka, Japan).

Jpn. J. Appl. Phys. Part 1 (Japan), vol.22, no.3, p.541 (March 1983).

One of the difficulties in the solution growth of (Ga, Al)P alloy crystals is the control of uniformity of Al concentration in epitaxial layers. This is due to the high segregation coefficient of Al from Ga solution. In order to avoid this problem, an Al source which keeps the melt composition constant during growth is necessary. Although AIP is an ideal source of Al, the grade of commercially available AIP is low (3N). The authors describe an experimental study obtaining a uniform (Ga, Al)P epitaxial layer by a temperature difference method with AlAs (5N) and AlSb (6N) as Al source. (2 refs.)

63179 Thickness of GaP liquid phase epitaxial layers grown by step-cooling, equilibrium-cooling, and ramp-cooling methods. Y.C.Kao, O.Eknoyan (Electrical Engng. Dept., Texas A&M Univ., College Station, TX, USA).

J. Appl. Phys. (USA), vol.54, no.4, p.1865-7 (April 1983). Using three different cooling processes, a series of liquid phase epitaxial growth experiments for GaP are performed to determine layer thickness, Δ , as a function of growth time, t , and amount of supercooling temperature, Δ . Comparison is made with layer thickness predictions that are derived from a diffusion-controlled model. Good agreement is obtained for growth times, t , less than the diffusion time, τ , of solute in the melt. The results indicate that, in addition to GaAs and InP, the diffusion-controlled model generally provides good predictions for liquid phase-epitaxial grown GaP layers thickness as well. (10 refs.)

63180 Reproducibility of low carrier concentration in LPE InP using batch melts. S.Yamazaki, K.Nakajima, T.Takanohashi, Y.Kishi, K.Akita (Semiconductor Materials Lab., Fujitsu Labs. Ltd., Kawasaki, Japan).

J. Cryst. Growth (Netherlands), vol.61, no.2, p.289-94 (March 1983).

A useful and practical method for obtaining n-InP layers with low carrier concentrations by liquid phase epitaxy is presented. This method combines batch preparation of growth melts with compensation of residual donors by the p-type dopant Cd, and needs no long-term baking of the melts. The carrier concentrations could be easily controlled in the range of $n=1.0 \times 10^{13}$ - 1.0×10^{16} cm⁻³ by varying the amounts of Cd in the batch-prepared melts. Good reproducibility of $n=(4.5 \pm 1.3) \times 10^{15}$ cm⁻³ has been obtained for 13 growth runs using the same kind of melts. Good uniformity of the carrier concentrations in n-InP layers was found within a wafer and along the growth direction. (13 refs.)

63181 A solution growth technique for the preparation of copper(II) selenide thin films. A.Mondal, P.Pramanik (Dept. of Chem., Indian Inst. of Technol., Kharagpur, India).

J. Solid State Chem. (USA), vol.47, no.1, p.81-3 (15 March 1983).

A solution growth technique has been developed for the deposition of thin films of copper(II) selenide on glass substrates using a copper(II) salt solution, triethanolamine, ammonia, and sodium selenosulfate as the reacting agents. The materials have been characterized through X-ray powder photography, optical absorption, and Hall measurements at room temperature. The films are found to be degenerate and p type with a Moss-Burstein shifted direct band gap of 2.14 eV. (9 refs.)

63182 LPE growth of YNd-iron garnet films for magneto-optical waveguides. T.Okuda, N.Koshizuka, K.Ando (Electrotech. Lab., Ibaraki, Japan).

J. Magn. & Magn. Mater. (Netherlands), vol.35, no.1-3, p.164-6 (March 1983). (Proceedings of the 10th International Colloquium on Magnetic Films and Surfaces, Yokohama, Japan, 13-16 Sept. 1982).

(YNd)₃Fe₂O₁₂ films for magneto-optical waveguides were successfully grown by liquid phase epitaxy. Both a segregation coefficient of Nd and a growth temperature dependence of the film lattice expansion due to Pb incorporation were determined. The optical phase-matching could be achieved by the precise control of the growth temperature together with that of the thickness. (9 refs.)

63183 Increased-strength black chromium coatings. N.V.Andreeva, V.S.Filimonov.

Sov. J. Opt. Technol. (USA), vol.49, no.8, p.506-7 (Aug. 1982). Translation of: *Opt.-Mekh. Prom.-st. (USSR)*, vol.49, no.8, p.33-5 (Aug. 1982). [received: April 1983]

A method is proposed for the periodic layer-by-layer desorption of black chromium in an electrolytic bath having a moving anode. The developed procedures make it possible to improve significantly the physical and mechanical characteristics of the coating, and they can be recommended for producing increased-thickness decorative coatings. (9 refs.)

63184 Deposition of cadmium chalcogenide thin films by a solution growth technique using triethanolamine as a complexing agent. A.Mondal (Dept. of Chem., Indian Inst. of Technol., Kharagpur, India), T.K.Chaudhuri, P.Pramanik.

Sol. Energy Mater. (Netherlands), vol.7, no.4, p.431-8 (Jan.-Feb. 1983).

A method has been developed for the chemical deposition of thin films of CdS and CdSe on glass substrate. For CdS deposition, a triethanolamine complex of cadmium ions, ammonia and thiourea solutions were used, while for CdSe films, sodium selenosulfate solution replaced thiourea, other reagents remaining unchanged. Variation of thickness with different bath parameters have been studied to obtain thickest deposition possible. X-ray characterization optical absorption and photoconductivity measurements have been performed to confirm the deposition of CdS and CdSe. Triethanolamine has been found to be useful complexing agent for the deposition of chalcogenide thin films. (14 refs.)

63185 Epitaxial growth of ZnO layers—a new aspect in homojunction models of ZnO varistors. I.Baumgartner, R.Einzinger (Res. Labs., Siemens AG, Munich, Germany).

Sintering - Theory and Practice. Proceedings of the 5th International Round Table Conference on Sintering, Portoroz, Yugoslavia, 7-10 Sept. 1981 (Amsterdam, Netherlands: Elsevier 1982), p.367-71

A powder mixture of bismuth oxide and a zinc antimony spinel phase of formula Zn₇Sb₂O₁₂ was sandwiched between two polished pellets of ZnO ceramics, heated at 1000°C for one hour, and subsequently cooled. The experiment shows that during the cooling period an epitaxial layer of ZnO is formed on the surface of the pellet substrate. By doping the ceramics with cobalt oxide this ZnO layer can be distinguished by optical and X-ray investigations. Considering the defect equilibrium in ZnO the epitaxial layers should be less conductive than the sintered ceramics. This may play an important role in the establishment of potential barriers initiating the varistor effect. (6 refs.)

- Electrical properties of thin solid films of the solid electrolyte Ag_2IWO_4 See Entry 62162
- Liquid-phase epitaxial growth of ZnSe on ZrTe substrate See Entry 62283
- Electrodeposition of tantalum carbide coatings from molten salts See Entry 62290
- Electrodeposition of nickel by an asymmetric periodically reversed step current See Entry 62291
- The role of Joule heating in liquid phase electroepitaxy See Entry 62304
- Microstructure and ductility of electroless copper deposits See Entry 63438
- Use of photovoltage for electrodeposition on solar cells See Entry 63658
- Low-cost solar power is on the horizon See Entry 63662

81.20 OTHER METHODS OF PREPARATION OF MATERIALS

- 63186 General characteristics of flows formed during spinning of chemical fibres. W.Kalita, J.Lubinski, A.Szaniawski (Inst. Podstawowych Problemow Techniki, Acad. of Sci., Warszawa, Poland). *Polim. Tworzywa Wielkocząsteczkowe (Poland)*, vol.27, no.8, p.305-8 (Aug. 1982). In Polish. [received: March 1983]

The authors treat general characteristics of flows, independent of the structural details, in the bulk of bundles of formed chemical fibres. The bulk (interior) of the bundles has been treated as an anisotropic and deformable filtration medium. Some practical conclusions resulting from a global analysis of such streams have been presented. (11 refs.)

- 63187 Critical technology limits to silicon material and sheet production. M.H.Leipold (California Inst. of Technol., Jet Propulsion Lab., Pasadena, CA, USA).

Fourth E.C. Photovoltaic Solar Energy Conference. Proceedings of the International Conference, Stresa, Italy, 10-14 May 1982 (Dordrecht, Netherlands: Reidel 1982), p.985-9

The reduction in scope of the Flat-Plate Solar Array Project has resulted in sharply focusing the developments within the programs involving silicon material and silicon sheet production. This has been accomplished by limiting the research to those elements which have the most impact on the long-term potential of each process under development. Silicon material development efforts include two approaches. The first involves the production of high purity silane and conversion to silicon particles in a fluidized-bed reactor. Here the critical element is the performance of the fluidized-bed reactor, specifically minimizing fines production and wall deposits and demonstrating purity. In the second, the dichlorosilane process, wall deposits in the rod reactor are limiting the conversion of dichlorosilane to silicon. Sheet preparation efforts involving Czochralski growth and wafering have largely been eliminated accompanied by reduction in casting development. Within ribbon development, the most critical elements here are reduction of ribbon stress and maintenance of flatness during high speed growth. Secondary efforts in improving conversion efficiency continue. (9 refs.)

- Synthesis and study of electric conductivity of complex oxides in the $\text{Li}_2\text{O}-\text{ZnO}-\text{TiO}_2$ system See Entry 62157

81.20E Powder techniques, compaction and sintering

- 63188 Some physicochemical aspects of $\text{Pd}-\text{PdO}-\text{Ag}$ -glass mixture sintering. I.Barycka, A.Misiuk (Inst. of Electronic Technol., Tech. Univ. of Wrocław, Wrocław, Poland).

Mater. Sci. (Poland), vol.7, no.4, p.467-74 (1981).

Transformations in sequentially annealed $\text{Pd}-\text{PdO}-\text{Ag}$ -glass samples with closely adjoining crystalline particles were investigated. Solid state processes were described by a series of chemical reactions being strongly dependent on sample preparation method. Relative amounts of Pd , PdO and Ag as well as the composition of the $\text{Pd}-\text{Ag}$ solid solution are dependent on the temperature and time of heating. Main crystalline constituents of samples heated above 700K were $\text{Pd}-\text{Ag}$ solid solution and PdO . It was stated that considerable amounts of silver can pass to the amorphous phase. (5 refs.)

- 63189 Theoretical investigation of the transverse pressing of particulate materials. II. Pressure and density distribution in the seat of deformation in transverse pressing with axial prepressing. G.M.Zhdanovich, V.A.Sidorov, Ch.A.Yakubovskii (Polytech. Inst., Belorussian SSR).

Sov. Powder Metall. & Met. Ceram. (USA), vol.21, no.8, p.603-7 (Aug. 1982). Translation of: *Poroshk. Metall. (USSR)*, vol.21, no.8, p.6-10 (Aug. 1982). [received: Feb. 1983]

For pt.1 see *ibid.*, vol.27, no.7, p.8 (1982). The density and pressure distributions in the transverse pressing of powders with axial prepressing are considered. (2 refs.)

- 63190 Experimental investigation of plastic strains of porous solids—a review. V.Z.Midukov, V.D.Rud' (Tomsk Polytech. Inst., Tomsk, USSR). *Sov. Powder Metall. & Met. Ceram. (USA)*, vol.21, no.8, p.607-11 (Aug. 1982). Translation of: *Poroshk. Metall. (USSR)*, vol.21, no.8, p.10-16 (Aug. 1982). [received: Feb. 1983]

An examination was made of statistically isotropic and microhomogeneous specimens produced by hydrostatic pressing, and special attention given to processes giving rise to small elastic-plastic strains. To obtain valid data, it was necessary to employ methods of preparation of specimens ensuring an even distribution of porosity throughout their volume. A large series of experiments was conducted with the aim of examining the effect of method of preparation of specimens on the uniformity of porosity distribution throughout their volume. Uniformity of density distribution was determined indirectly, by assessing strains in various sections through specimens after repressing by hydrostatic pressure. (21 refs.)

- 63191 Analysis of the stressed state of the forward slip zone in the seat of deformation of a powder being rolled. E.B.Lozhechnikov (Polytech. Inst., Belorussian SSR).

Sov. Powder Metall. & Met. Ceram. (USA), vol.21, no.8, p.612-16 (Aug. 1982). Translation of: *Poroshk. Metall. (USSR)*, vol.21, no.8, p.16-21 (Aug. 1982). [received: Feb. 1983]

The problem is considered as a two-dimensional one. The arc of contact of the powder with the rolls is replaced with a chord whose angle of slope in the direction of rolling is $\gamma/2$ (γ is the neutral angle). The parameters of properties of the powder undergoing deformation in the forward slip zone—angle of interparticle friction ϕ , angle of sliding friction of the powder on the roll surfaces ϕ_r , and cohesion of the powder c —are assumed to be constant. (11 refs.)

- 63192 Contemporary development of the science of sintering. M.M.Ristic (Belgrade Univ., Belgrade, Yugoslavia).

Sintering - Theory and Practice. Proceedings of the 5th International Round Table Conference on Sintering, Portoroz, Yugoslavia, 7-10 Sept. 1981 (Amsterdam, Netherlands: Elsevier 1982), p.1-15

The author reviews various models and concludes that a thorough analysis both of the modern development and state of the science of sintering points to the fact that fundamental investigations are based on an atomistic view of structure. Numerous attempts to analyse the principal mechanism of sintering phenomena have been made, but on models, only. Therefore particular attention should be paid to those endeavours striving to solve the problem of simultaneous action of two or more mechanisms. (55 refs.)

- 63193 Recent developments in the theoretical analysis of solid state sintering. D.L.Johnson (Northwestern Univ., Evanston, IL, USA).

Sintering - Theory and Practice. Proceedings of the 5th International Round Table Conference on Sintering, Portoroz, Yugoslavia, 7-10 Sept. 1981 (Amsterdam, Netherlands: Elsevier 1982), p.17-26

Numerical approaches of previous authors are reviewed with particular reference to sintering diagrams and nonisothermal simulations. It is concluded that the sintering models do not adequately predict nor describe sintering. The simple sintering models and maps do not take enough account of multiple mechanisms. (44 refs.)

- 63194 Liquid phase and activated sintering. G.Petzow, W.A.Kaysser, M.Amtenbrink (Max-Planck-Inst. für Metall., Stuttgart, Germany).

Sintering - Theory and Practice. Proceedings of the 5th International Round Table Conference on Sintering, Portoroz, Yugoslavia, 7-10 Sept. 1981 (Amsterdam, Netherlands: Elsevier 1982), p.27-36

The present state of liquid phase and activated sintering is considered. It is shown that the present theory of liquid phase sintering and its quantitative treatment have to be modified considerably if recent observations of a number of elementary mechanisms, such as particle disintegration, Ostwald ripening with shape accommodation and directional grain growth are to be taken into account. For activated sintering, new experimental results on nickel doped molybdenum powder compacts indicate that dislocation networks and sub-boundaries are preserved during the process of heating to the sintering temperature, which are not observed in compacts without nickel. Features which are common to liquid phase and activated sintering are particle rearrangement and directional grain growth. The latter phenomenon is further discussed on the basis of ideas regarding solid-solid and solid-liquid interfaces. (33 refs.)

- 63195 Statistical theory of sintering and microstructure evolution. G.C.Kuczynski (Univ. of Notre Dame, Notre Dame, IN, USA).

Sintering - Theory and Practice. Proceedings of the 5th International Round Table Conference on Sintering, Portoroz, Yugoslavia, 7-10 Sept. 1981 (Amsterdam, Netherlands: Elsevier 1982), p.37-44

Using statistical methods, a set of relationships among the measurable parameters describing the microstructure in a porous body, is developed. It has been shown that these parameters are always proportional to the porosity raised to some function of a single parameter x which in turn is a function of pore size distribution. In some cases x is also a function of diffusion coefficients of the transport processes involved. (11 refs.)

- 63196 Percolation theory approach to sintering. J.Kertész (Inst. for Theoretical Phys., Univ. of Cologne, Köln, Germany), T.Vicsek.

Sintering - Theory and Practice. Proceedings of the 5th International Round Table Conference on Sintering, Portoroz, Yugoslavia, 7-10 Sept. 1981 (Amsterdam, Netherlands: Elsevier 1982), p.53-9

The importance of collective phenomena in sintering is pointed out. The percolation model is briefly reviewed and the problem of percolation on a lattice and off a lattice is discussed in the light of Monte Carlo calculations. The percolation model is suggested to describe: (i) the insulator-conductor transition of the powder, (ii) the powder-solid transition, (iii) the microcrack structure of compacted and sintered materials, (iv) the network of the voids through which the additives evaporate during sintering. Monte Carlo calculations were carried out on some two and three dimensional percolation models. The possible application of the directed percolation to the description of the rupture of compacts is studied. The critical volume fraction of voids remaining among the intersecting spheres, where an infinite connected path through voids appears was determined. The theory of gas-permeability is discussed and points of view are given for avoiding the swelling of rods during sintering. (20 refs.)

- 63197 High-sensitivity dilatometric setup for investigation of sintering of high-melting compounds in controlled atmospheres. V.N.Klimenko, E.M.Petrova, V.A.Masljuk (Inst. for Materials Sci., Problems Acad. of Sci., Kiev, Ukrainian SSR).

Sintering - Theory and Practice. Proceedings of the 5th International Round Table Conference on Sintering, Portoroz, Yugoslavia, 7-10 Sept. 1981 (Amsterdam, Netherlands: Elsevier 1982), p.127-32

The design of a setup for investigating with a high accuracy the process of an 'active' sintering of high-melting material powders is described. The setup allows investigations to be conducted under isothermal and non-isothermal conditions over a temperature range of 20 to 2500°C in vacuum or inert gas atmospheres at heating rates from 0.08 to 1 deg.s⁻¹. The accuracy of measuring the variations in specimen dimensions in sintering is within 0.5%. A high efficiency of the developed setup in investigating the 'superplasticity' of high-melting powder materials is shown by way of example of sintering tungsten-nickel powder specimens. (8 refs.)

- 63198 The use of solid solution additives in sintering. R.J.Brook, S.P.Howlett, Su Xing Wu (Dept. of Ceramics, Univ. of Leeds, Leeds, England).

Sintering - Theory and Practice. Proceedings of the 5th International Round Table Conference on Sintering, Portoroz, Yugoslavia, 7-10 Sept. 1981 (Amsterdam, Netherlands: Elsevier 1982), p.135-44

Additives have proved to be one of the most effective ways of achieving high density in the solid state sintering of ceramic powders. Although many mechanisms can be proposed for the function of additives, there are few examples where an unambiguous interpretation of a particular mechanism has been achieved. The mechanisms are briefly reviewed together with rules for additive selection; it is argued that, since the broad function of the additive is to increase the ratio of densification rate to grain growth rate, the influence on both terms should be considered. Data on ZrO_2 and CoO are presented in the discussion. (15 refs.)

- 63199 Reactive sintering. R.L.Coble (MIT, Cambridge, MA, USA).

Sintering - Theory and Practice. Proceedings of the 5th International Round Table Conference on Sintering, Portoroz, Yugoslavia, 7-10 Sept. 1981 (Amsterdam, Netherlands: Elsevier 1982), p.145-51

Concerns powder metallurgy and ceramic products in which a chemical reaction takes place during sintering. Sintering and reaction models are reviewed. (17 refs.)

- 63200 Interfacial segregation and enhanced sintering processes.** R.M.German (Materials Engng. Dept., Rensselaer Polytech. Inst., Troy, NY, USA). Sintering - Theory and Practice. Proceedings of the 5th International Round Table Conference on Sintering, Portoroz, Yugoslavia, 7-10 Sept. 1981 (Amsterdam, Netherlands: Elsevier 1982), p.177-83.
The sintering process during the intermediate stage is viewed as a competition between densification, grain growth and pore rounding events. From a practical viewpoint it is most desirable to enhance densification while suppressing pore rounding and grain growth. To examine this problem, a mathematical model is constructed with a view towards enhanced sintering. Specific attention is given to interfacial segregation effects on grain growth and sintering; segregated solutes change the boundary cohesive energy, diffusivity and mobility. Analysis is focused on solutes which segregate to boundaries, increase the cohesive energy, lower the boundary mobility while providing high diffusivity transport paths. It is shown that diffusivity to mobility ratios over approximately 2×10^9 N/m² leads to enhanced sintering densification. (30 refs.)
- 63201 Diffusion processes in sintering of multicomponent systems.** P.A.Vitiaz (Powder Metall. Assoc., Minsk, USSR). Sintering - Theory and Practice. Proceedings of the 5th International Round Table Conference on Sintering, Portoroz, Yugoslavia, 7-10 Sept. 1981 (Amsterdam, Netherlands: Elsevier 1982), p.263-8.
A method for model investigation of diffusion processes in sintering of highly dense materials obtained by mixing powders with different chemical content has been developed. The method gives a precise account of concentration relations of self-diffusion and interdiffusion coefficients and includes numerical solution algorithms for diffusion equations, structure models of sintered steels and computer programs with information output in the form of histograms of concentration distributions. The method allows determination of principle phenomena of homogenization kinetics of materials produced from powder mixtures of iron and nickel or steel with high chromium content. (6 refs.)
- Sintering - Theory and Practice. Proceedings of the 5th International Round Table Conference on Sintering** See Entry 59538
- Investigation of sintering activator distribution in refractory materials by means of an X-ray microanalyzer** See Entry 61312
- Kinetics of the collective crystallization of doped ZnS** See Entry 61835
- Electrophysical properties of nickel boride phases** See Entry 62396
- Epitaxial growth of ZnO layers—a new aspect in homojunction models of ZnO varistors** See Entry 63185
- Some studies in the displacements of powder material during compaction** See Entry 63203
- Sintered boron—production and properties. I. Investigation of the sintering of boron** See Entry 63204
- Effect of thermal conditions of preparation of dispersion-strengthened nickel powders on the character of distribution of the strengthening phase** See Entry 63205
- General aspects for the optimization of pressing and sintering conditions of copper compacts** See Entry 63206
- The influence of particle size on intermediate and final stages of molybdenum sintering** See Entry 63207
- Some magnetological insights in the consolidation of metal powders** See Entry 63208
- Geometric and structural aspects of sintering of model and real systems** See Entry 63209
- Observations on dimensional changes during sintering of Al-Cu-compacts** See Entry 63210
- Influence of Ni-additions on grain boundaries during sintering of Mo** See Entry 63211
- Effect of alloying additions on sintering of iron-phosphorous premixes** See Entry 63212
- Sintering of cast iron swarf powder and Fe-Si-C mixed powder** See Entry 63213
- Particle growth by coalescence during liquid phase sintering of Fe-Cu** See Entry 63214
- Structure formation in chromium carbide alloy of eutectic type during sintering** See Entry 63215
- Effect of the combined carbon of tungsten monocarbide on the reaction of diamond with a hard metal** See Entry 63216
- Grain growth of tungsten fibres in a W-Ni composite during solid and liquid phase sintering** See Entry 63218
- Microstructure formation in wurtzite BN (Geksanit-R) sinterings** See Entry 63220
- Radiation-thermal sintering of europium oxide** See Entry 63221
- Effect of low-temperature ferritization on the properties of ferrite powders** See Entry 63222
- Nonstoichiometry and physical properties of hot-pressed manganese-zinc ferrites** See Entry 63223
- Reaction of powdered superhard materials with gases during high-temperature shock compression** See Entry 63224
- Kinetics and mechanism of sintering of covalent-ionic compounds** See Entry 63225
- Surface energy of silicate melts and its importance in sintering processes** See Entry 63226
- Comparison between theory and experiment in the sintering of undoped MgO** See Entry 63227
- Sintering of magnesium-oxide obtained from sea water** See Entry 63228
- Sintering and devitrification of slip-cast fused silica** See Entry 63229
- Investigation of MgO doped γ -Al₂O₃ sintering** See Entry 63230
- Effects of magnesium compound additives on sintering of magnesia** See Entry 63231
- Sintering kinetics of Al₂O₃ doped with MgNb₂O₆** See Entry 63232
- Sintering of SYNROC: case history for phase formation and densification of complex oxide systems** See Entry 63233
- Reactive sintering in the BaO:ZrO₂ 1:1 system** See Entry 63234
- Shrinkage and initial grain growth in BaTiO₃ ceramics** See Entry 63235
- Sintering of multiphase ceramics** See Entry 63236
- Sintering of beta alumina powders obtained by sol-gel process. Preliminary studies** See Entry 63237

- Sintering of ZrO₂-CaO and ZrO₂-Y₂O₃ powders obtained by sol-gel process** See Entry 63238
- Reactions and sintering of ZrO₂-doped spinel** See Entry 63239
- The influence of the liquid phase amount on the densification of Si₃N₄-base ceramics** See Entry 63240
- Some aspects of transient liquid phase sintering** See Entry 63241
- The grain growth in alumina derived from gels** See Entry 63242
- Growth of isolated macropores in a silica ceramic** See Entry 63243
- The effect of MgO on intragranular pore entrapment in sintered aluminium oxide** See Entry 63244
- Development of the microstructure of semiconducting BaTiO₃ ceramics** See Entry 63245
- Grain growth in doped-undoped ceramic BaTiO₃ couples** See Entry 63246
- Grain boundaries in sintered carbides** See Entry 63247
- Microstructural changes at grain boundaries during sintering of doped BaTiO₃ ceramics with small additions of TiO₂** See Entry 63248
- Short-time sintering of hard metals** See Entry 63249
- Sintering in the nickel-alumina system** See Entry 63252
- Metallographic and structural investigations of levitation splat cooled cobalt base cobalt-refractory carbide alloys** See Entry 63253
- The effect of ITMT's and P/M processing on the microstructure and mechanical properties of the X7091 alloy** See Entry 63319
- Stress-strain state in the rolling of blanks from granulated alloys** See Entry 63371
- The determination of the coefficient of dynamic friction of organic powder compacts on steel** See Entry 63427
- Hydrogen storage properties of FeTi_{1+x} and FeTi_{1+x}O_y flakes produced by splat quenching** See Entry 63740

81.20G Specific metals and alloys (compacts, pseudoalloys)

- 63202 Studies on fabrication of superconducting V₃Ga wires.** S.B.Sastry, K.Subba Ramaiah (Dept. of Phys., Indian Inst. of Technol., Madras, India). *Indian J. Cryog.*, vol.7, no.3, p.135-9 (1982).
A review of methods of processing V₃Ga wires through the surface diffusion process (SDP) and composite processes are presented. V₃Ga tapes wound in the form of pancakes were tested in magnetic fields up to 18.0 T. The multifilamentary wires made by the composite process have been studied in external magnetic fields up to 20.8 T. Effects of addition of impurities like Si, Ge, Au, Bi, Mn, Zr etc. have also been studied and reported in literature. Attempts being made in the authors' laboratory to process V₃Ga wires through the surface diffusion process are presented. Further studies planned on these wires are indicated. (11 refs.)
- 63203 Some studies in the displacements of powder material during compaction.** J.Duszczyk (Inst. of Precision & Electronic Engng., Tech. Univ. of Warsaw, Warsaw, Poland). *Powder Technol. (Switzerland)*, vol.34, no.1, p.57-68 (Jan.-Feb. 1983).
On the basis of the results of tribological investigations during the compaction of iron powder type NC.100.24 and of the distribution of porosity in sintered compacts, the character of powder material displacements was described for the last stage of compaction, i.e. after establishment of a preset compacting pressure. In those investigations, the model used was of the compaction of a powder material in a rotary die. The choice of such a model results from the necessity of programming an experiment with a more complex state of stresses within the mixed powder being compacted than that in standard static compaction. Decisive conditions are determined for depth of penetration of shearing stresses in the compacted material, as well as conditions of change of the state of friction of the compact against the stationary mandrel surface from static to kinetic friction. (23 refs.)
- 63204 Sintered boron—production and properties. I. Investigation of the sintering of boron.** R.A.Andrievskii, I.A.Bairamashvili, Yu.I.Solev, V.V.Khromonozhkin. *Sov. Powder Metall. & Met. Ceram. (USA)*, vol.21, no.8, p.622-7 (Aug. 1982). Translation of: *Poroshk. Metall. (USSR)*, vol.21, no.8, p.27-32 (Aug. 1982). [received: Feb. 1983].
The starting boron (β -modification) powder used was produced by annealing [1970-1980°C, vacuum corresponding to $1.3 \times (10^{-2}-10^{-3})$ Pa] electrolytic amorphous boron. Commination of the annealed powder was effected by ultrasonic milling. X-ray phase analysis was performed, using a DRON-0.5 apparatus, at angles ranging from 8 to 26°, which enabled the greatest changes in reflections to be obtained. Mean particle sizes after milling were assessed by the usual gas-permeability method of specific surface measurement. (15 refs.)
- 63205 Effect of thermal conditions of preparation of dispersion-strengthened nickel powders on the character of distribution of the strengthening phase.** B.N.Babich, A.A.Fofanov. *Sov. Powder Metall. & Met. Ceram. (USA)*, vol.21, no.8, p.637-9 (Aug. 1982). Translation of: *Poroshk. Metall. (USSR)*, vol.21, no.8, p.43-6 (Aug. 1982). [received: Feb. 1983].
It was found that thermal conditions of treatment of oxide powders produced by chemical coprecipitation exert a pronounced influence on the mechanical properties of semifinished products of dispersion-strengthened nickel made from these powders. Raising the calcining temperature of such oxide powders activates particle redistribution processes and has an adverse effect on the uniformity of distribution of the strengthening phase, which leads to the formation of large particles in the subsequent stages of plastic working and heat treatment of the powders and a steady deterioration in the mechanical properties of semifinished products. (9 refs.)
- 63206 General aspects for the optimization of pressing and sintering conditions of copper compacts.** H.Schreiner, R.Tusche (Div. for Technol., Central Div., Siemens AG, Erlangen, Germany). Sintering - Theory and Practice. Proceedings of the 5th International Round Table Conference on Sintering, Portoroz, Yugoslavia, 7-10 Sept. 1981 (Amsterdam, Netherlands: Elsevier 1982), p.45-51.
Solid state sintering of compacts made from dendritic copper powder has been studied in dependence upon compacting pressure and sintering temperature by means of dilatometrical measurements. With regard to high density in the sintered state these parameters must be suitably chosen in order to avoid a decrease in density by an overlapping swelling effect. Within the range of the compacting pressure of P=500 MPa up to P=800 MPa and sintering temperatures of T_S>1010K a decrease in density was always observed even in the

case of stepwise sintering. With $P=400$ MPa and $T_S=1123$ K, however, a continuous increase in density of the compacts was obtained. The microstructure of high pressed copper compacts showed intensive power coalescence after sintering; at the lower compacting pressure rounded, single pores with considerably lower total volume are dominant. (6 refs.)

63207 The influence of particle size on intermediate and final stages of molybdenum sintering. D.Uskokovic, B.Novakovic, V.Petrovic, M.M.Ristic (Inst. of Tech. Sci., Serbian Acad. of Sci. & Arts, Beograd, Yugoslavia). Sintering - Theory and Practice. Proceedings of the 5th International Round Table Conference on Sintering, Portoroz, Yugoslavia, 7-10 Sept. 1981 (Amsterdam, Netherlands: Elsevier 1982), p.69-74.
The influence of initial particle size on kinetics of molybdenum sintering was investigated. Three fractions of monodispersed molybdenum powder (2, 5 and 10 μ m) were used as well as a polydispersed powder with mean particle size of 12 μ m. Decrease in particle size accelerates to a great extent densification and grain growth processes. During sintering of 10 μ m powder and to a smaller extent in the case of polydispersed powder, Zener's relation was confirmed. Quantitative equations for the intermediate sintering stages could not be fitted to the investigated particulate systems, even though the grain growth process could be described by cubic law and though the volume diffusion coefficient and the surface energy were known with great reliability. (8 refs.)

63208 Some magnetological insights in the consolidation of metal powders. D.Dzevic, A.Kirin, A.Bonefacic (Electrotech. Inst. Rade Koncar, Univ. of Zagreb, Zagreb, Yugoslavia). Sintering - Theory and Practice. Proceedings of the 5th International Round Table Conference on Sintering, Portoroz, Yugoslavia, 7-10 Sept. 1981 (Amsterdam, Netherlands: Elsevier 1982), p.85-90.
Coercivity, retentivity, conductivity and X-ray diffraction measurements were performed on cobalt green compacts in the pressure range 0-660 MPa. Well pronounced property and anisotropy, respectively directions parallel and normal to the pressing action direction, is discussed. Mean internal stresses in compacts, assessed from magnetometry data, reach 400 MPa at highest pressure applied and are in reasonable agreement with stress values computed by using X-ray diffraction data. Crystallite size data and stacking fault probabilities are also considered. (18 refs.)

63209 Geometric and structural aspects of sintering of model and real systems. P.Lanyi, W.Hermel (Zentralinst. fur Festkorperphys., und Werkstoffforschung, Akad. der Wissenschaften, Dresden, Germany). Sintering - Theory and Practice. Proceedings of the 5th International Round Table Conference on Sintering, Portoroz, Yugoslavia, 7-10 Sept. 1981 (Amsterdam, Netherlands: Elsevier 1982), p.91-9.
A theoretical concept discussing the sintering as a problem of geometric and structural changes and their interactions is demonstrated. On the base of this concept an idea of the solid-state sintering of metallic one-component systems is formed which enables the sintering behaviour to be interpreted from a uniform point of view. The considerations refer to the early stages of sintering. Diffusion-dependent transport mechanisms are assumed to prevail. (9 refs.)

63210 Observations on dimensional changes during sintering of Al-Cu compacts. W.Kehl, H.Fischmeister (Austrian School of Mines, Leoben, Austria). Sintering - Theory and Practice. Proceedings of the 5th International Round Table Conference on Sintering, Portoroz, Yugoslavia, 7-10 Sept. 1981 (Amsterdam, Netherlands: Elsevier 1982), p.269-74.
Dilatometric measurements of the swelling and shrinkage of Al-Cu compacts during sintering are combined with metallographic and fractographic observations in order to elucidate the processes responsible for the dimensional changes during liquid phase sintering. (2 refs.)

63211 Influence of Ni-additions on grain boundaries during sintering of Mo. W.A.Kayser, M.Amentbrink, G.Petzow (Max-Planck-Inst. fur Metall., Inst. fur Werkstoffwissenschaften, Stuttgart, Germany). Sintering - Theory and Practice. Proceedings of the 5th International Round Table Conference on Sintering, Portoroz, Yugoslavia, 7-10 Sept. 1981 (Amsterdam, Netherlands: Elsevier 1982), p.275-82.
The shrinkage and the formation of a solid solution of Ni in Ni-doped Mo compacts pressed at different pressures were determined after sintering by heating at different rates and immediately cooling and by sintering isothermally. The phenomena were correlated with each other and with observation by TEM of the dislocation structure of the compacts. The dislocations appear to accelerate both formation of solid solutions and shrinkage. (5 refs.)

63212 Effect of alloying additions on sintering of iron-phosphorous pre-mixes. G.S.Upadhyaya, M.Hamuddin (Dept. of Metall. Engng., Indian Inst. of Technol., Kanpur, India). Sintering - Theory and Practice. Proceedings of the 5th International Round Table Conference on Sintering, Portoroz, Yugoslavia, 7-10 Sept. 1981 (Amsterdam, Netherlands: Elsevier 1982), p.291-8.
A comparative study of the effect of copper, nickel, or molybdenum (0-4% each) on the sintering behaviour of iron containing phosphorous (0-0.6%) has been made. The sintering was done at 1200°C for 1 hr in dry hydrogen. It was observed that copper decreases shrinkage, while nickel or molybdenum addition increases. The results have been discussed on the basis of liquid phase sintering and the generalised electronic model proposed by Samsonov (1973). (15 refs.)

63213 Sintering of cast iron swarf powder and Fe-Si-C mixed powder. Z.Hara, K.Akechi, K.Hanawa (Inst. of Industrial Sci., Univ. of Tokyo, Tokyo, Japan). Sintering - Theory and Practice. Proceedings of the 5th International Round Table Conference on Sintering, Portoroz, Yugoslavia, 7-10 Sept. 1981 (Amsterdam, Netherlands: Elsevier 1982), p.299-304.
The variation of graphite morphology with C content and its effects on tensile strength by using Fe-Si-C mixed powders is investigated. The products containing about 1%C, sintered for a long time or powder forged, showed high tensile strength, because graphite was nodularised. The products containing more than 2%C, however, showed inferior tensile strength, because graphite reveals a powder particle boundary morphology. These results were explained in terms of the gas-bubble theory; C atoms supersaturating in γ phase precipitate as graphite into pores in the sintered products. Further experiments were carried out to confirm the gas-bubble theory. The pore-containing white cast iron was produced from cast iron powder compacts by rapid melting and solidifying using a resistance sintering machine. Nodular graphite was formed during annealing of the pore-containing white cast iron but not in the case of pore-free white cast iron. (6 refs.)

63214 Particle growth by coalescence during liquid phase sintering of Fe-Cu. W.A.Kayser, S.Takajo, G.Petzow (Max-Planck-Inst. fur Metall., Inst. fur Werkstoffwissenschaften, Stuttgart, Germany). Sintering - Theory and Practice. Proceedings of the 5th International Round Table Conference on Sintering, Portoroz, Yugoslavia, 7-10 Sept. 1981 (Amsterdam, Netherlands: Elsevier 1982), p.321-7.
The contribution of particle coalescence to the particle growth during liquid phase sintering of Fe-Cu was investigated. Particle contacts involving grain boundaries with low energy, i.e. with large dihedral angles, were frequently observed. By means of electron channelling pattern investigations on the analogous system Cu-Ag, such low energy grain boundaries were proved to be low-indexed coincidence boundaries. With the assumption that particle coalescence following the low energy boundary formation mainly contributes to particle growth, the growth behaviours were treated generally on a statistical basis and then correlated to the special case of Fe-Cu. Average particle sizes and particle size distributions were calculated and compared with experimental results. It was found that coalescence contributes significantly to particle growth. (10 refs.)

Effect of fabrication condition on the magnetic properties of Fe-Mn-B system amorphous alloys See Entry 62704

High-sensitivity dilatometric setup for investigation of sintering of high-melting compounds in controlled atmospheres See Entry 63197

Reactive sintering See Entry 63199

Structure formation in chromium carbide alloy of eutectic type during sintering See Entry 63215

Physicochemical fundamentals of the development of heat-resistant niobium alloys See Entry 63305

The effect of ITMT's and P/M processing on the microstructure and mechanical properties of the X7091 alloy See Entry 63319

Stress-strain state in the rolling of blanks from granulated alloys See Entry 63371

Hydrogen storage properties of FeTi_{1+x} and $\text{FeTi}_{1+x}\text{O}_y$ flakes produced by splat quenching See Entry 63740

Recent production of rare earth metals as hydriding materials See Entry 63743

81.20J Dispersion-, fibre-, and platelet-reinforced metal-based composites

63215 Structure formation in chromium carbide alloy of eutectic type during sintering. V.P.Chepeleva (Inst. of Superhard Materials, Acad. of Sci., Ukrainian SSR). *Sov. Powder Metall. & Met. Ceram. (USA)*, vol.21, no.8, p.647-50 (Aug. 1982). Translation of: *Poroshk. Metall. (USSR)*, vol.21, no.8, p.55-9 (Aug. 1982). [received: Feb. 1983]

Structure formation was studied in a typical chromium carbide alloy—a composite consisting of Kh18N15 (18% Cr-15% Ni) austenitic stainless steel and chromium carbide. Kh18N15 steel and chromium carbide (Cr_7C_3) powders of 1- to 10- μ m particle size were mixed together, pressed (porosity ~50%), and sintered for 0.5, 1.0, 1.25, 1.5, and 2.5 h in a vacuum furnace at 1280°C. Sintered specimens were examined metallographically and subjected to X-ray phase analysis and electron probe microanalyses. (7 refs.)

63216 Effect of the combined carbon of tungsten monocarbide on the reaction of diamond with a hard metal. D.Kh.Bronstein (Inst. of Superhard Materials, Acad. of Sci., Ukrainian SSR). *Sov. Powder Metall. & Met. Ceram. (USA)*, vol.21, no.8, p.650-4 (Aug. 1982). Translation of: *Poroshk. Metall. (USSR)*, vol.21, no.8, p.59-64 (Aug. 1982). [received: Feb. 1983]

It was found that to minimize the degree of reaction of diamonds with a hard metal during the production of diamond-containing composites and at the same time preserve a strong bond between the diamond grains and the matrix material, it is necessary to ensure that the deficiency of combined carbon in the tungsten monocarbide compared with the stoichiometric composition does not exceed 0.10-0.15 wt.%. In this way, on the one hand a strong adhesion bond is allowed to form at the diamond/matrix interfaces and, on the other, the 'expenditure' of diamond in the impregnation of the WC with carbon is reduced to a minimum. (16 refs.)

63217 Regularities in formation of composite materials by impregnation of dispersive diamond structures with metal melts. Yu.V.Naidich, G.P.Volk, I.A.Lavrienco (Inst. for Problems of Materials Sci., Kiev, Ukrainian SSR). Sintering - Theory and Practice. Proceedings of the 5th International Round Table Conference on Sintering, Portoroz, Yugoslavia, 7-10 Sept. 1981 (Amsterdam, Netherlands: Elsevier 1982), p.305-9.
Presents some investigations on the kinetics of metal melt impregnation of the layer of diamond particles and the process of wetting the diamond with metal liquid associated with it. The materials investigated were synthetic diamond powders of various grades and grain sizes and a copper-base nickel-manganese alloy with a melting point of $980 \pm 20^\circ\text{C}$. (5 refs.)

63218 Grain growth of tungsten fibres in a W-Ni composite during solid and liquid phase sintering. L.Kozma (Res. Inst. for Tech. Phys., Hungarian Acad. of Sci., Budapest, Hungary), E.Th.Henig. Sintering - Theory and Practice. Proceedings of the 5th International Round Table Conference on Sintering, Portoroz, Yugoslavia, 7-10 Sept. 1981 (Amsterdam, Netherlands: Elsevier 1982), p.313-20.
The influence of nickel on the microstructural changes of tungsten wire drawn to high strain has been studied during sintering in the range 1350 to 2200K. It was found that the deformed structure of the as-drawn wires can be easily penetrated by Ni. According to the annealing temperature, two different microstructural changes and mechanisms of material rearrangement have been observed. Solid phase sintering (<1730) can activate only the recrystallisation leading to equiaxial grain morphology (activated recrystallisation). At higher temperature the liquid Ni attacks the fibre boundaries resulting in disintegration of the wire into elementary particles, which is followed by a complete dissolution of the fibres and reprecipitation (liquid phase sintering). The metallographic sections of the annealed material show large spherical particles embedded in the matrix. (16 refs.)

81.20L Ceramics and refractories

63219 On reactions between silicon and nitrogen. I. Mechanisms. H.M.Jennings (Dept. of Metall. & Materials Sci., Imperial Coll. of Sci. & Technol., London, England). *J. Mater. Sci. (GB)*, vol.18, no.4, p.951-67 (April 1983).

An attempt is made to rationalize various reaction mechanisms for the formation of Si_3N_4 from gaseous nitrogen and solid silicon. It is suggested that a

fundamental difference between α - and β - Si_3N_4 is that the former results from silicon complexing with molecular nitrogen and the latter results from complexing with essentially atomic nitrogen. Well established mechanisms (as well as controversial ones) are analysed in the light of this difference and are shown to be operative under various reaction conditions. The influence of some common reaction variables are interpreted with respect to their influence on either silicon or nitrogen or both. (84 refs.)

63220 Microstructure formation in wurtzite BN (Geksanit-R) sinterings. S.S.Dzhamarov, A.V.Kurdyumov, G.S.Oleinik, N.F.Ostrovskaya, A.N.Pilyankevich, A.V.Bochko (Inst. of Materials Sci., Acad. of Sci., Ukrainian SSR). *Sov. Powder Metall. & Met. Ceram. (USA)*, vol.21, no.8, p.627-31 (Aug. 1982). Translation of: *Poroshk. Metall. (USSR)*, vol.21, no.8, p.32-7 (Aug. 1982). [received: Feb. 1983]

It is concluded that the loading of wurtzite boron nitride to high static pressures (55-100 kbar) under room temperature conditions is accompanied by the processes of comminution of polycrystalline powder particles and their monocrystalline grains. Comminution of wurtzite boron nitride particles and grains has been found to take place also during sintering at high pressures and temperatures. The intensity of particle and grain comminution during loading and compression grows with increasing size of the particles in the starting condition. The comminution of particles and grains has a marked effect on structure formation in polycrystalline Geksanit-R alloy sintering. (6 refs.)

63221 Radiation-thermal sintering of europium oxide. A.P.Voronin, V.A.Neronov, V.V.Boldyrev, T.F.Melekova, V.L.Auslender, V.V.Aleksandrov, N.Z.Lyakhov, V.A.Polyakov, M.A.Savinkina (Inst. of Solid State Chem. & Ore Processing, Acad. of Sci., USSR).

Sov. Powder Metall. & Met. Ceram. (USA), vol.21, no.8, p.632-6 (Aug. 1982). Translation of: *Poroshk. Metall. (USSR)*, vol.21, no.8, p.38-42 (Aug. 1982). [received: Feb. 1983]

Investigates whether the RT effect can occur in high-temperature mass transport involving no chemical stage. As an example of such a process a study was made of the RT sintering of europium oxide, Eu_2O_3 , at 1323-1773K. A powder grade Eu_2O_3 of the low-temperature modification, covering a range of particle sizes, was used. Sintering experiments were carried out on europium oxide with and without 0.1-1.0% TiO_2 doping additions. Titania was introduced by mechanical mixing in such a way that no further comminution occurred. (7 refs.)

63222 Effect of low-temperature ferritization on the properties of ferrite powders. A.I.Antoshchuk, I.N.Barkova, G.I.Kamornina, B.I.Morozov, G.S.Podval'nykh, V.I.Rogachev, V.A.Tkachenko (Ivano-Frankovsk Inst. of Petroleum & Gas, USSR).

Sov. Powder Metall. & Met. Ceram. (USA), vol.21, no.8, p.665-8 (Aug. 1982). Translation of: *Poroshk. Metall. (USSR)*, vol.21, no.8, p.76-80 (Aug. 1982). [received: Feb. 1983]

A description is given of a method of preparation of a ferrite charge in which vibratory milling is performed at 400-650°C in an oxidizing atmosphere. This enables the milling and diffusional annealing operations to be combined, which has a marked effect on the charge ferritization process. The charge temperature falls from 800-1000 to 400-650°C, and the process is therefore known as low-temperature ferritization (LTF). A mixture of starting components of composition (%) 85.4 Fe_2O_3 , 7.55 Li_2CO_3 , 5.25 MnCO_3 , and 1.8 MgO was subjected to thermal vibratory treatment at a frequency of 25 Hz in a specially constructed apparatus. The quality of heat treatment of powders was assessed by their specific saturation magnetization intensity, specific surface, and compressibility indicator. (5 refs.)

63223 Nonstoichiometry and physical properties of hot-pressed manganese-zinc ferrites. V.P.Pashchenko, Yu.A.Bykov, S.N.Mikharskii, E.I.Osyka, P.P.Kirichok, I.M.Marchenko, O.R.Yatsura, T.Ya.Galavura. *Sov. Powder Metall. & Met. Ceram. (USA)*, vol.21, no.8, p.669-3 (Aug. 1982). Translation of: *Poroshk. Metall. (USSR)*, vol.21, no.8, p.80-5 (Aug. 1982). [received: Feb. 1983]

It is concluded that changing the pressure in the hot pressing of manganese-zinc ferrites affects both the composition and state of the solid-phase system and the structural characteristics of specimens. With a rise in hot-pressing pressure, the Fe^{2+} concentration, density, Curie temperature, and degree of inversion increase; there is also a tendency for the initial magnetic permeability to fall and for the crystallite size to grow. An interrelationship is shown to exist between the Fe^{2+} content of manganese-zinc ferrite spinel and the degrees of nonstoichiometry and inversion. (14 refs.)

63224 Reaction of powdered superhard materials with gases during high-temperature shock compression. G.I.Savvak, B.V.Fenochka (Inst. of Materials Sci., Acad. of Sci., Ukrainian SSR).

Sov. Powder Metall. & Met. Ceram. (USA), vol.21, no.8, p.673-6 (Aug. 1982). Translation of: *Poroshk. Metall. (USSR)*, vol.21, no.8, p.85-9 (Aug. 1982). [received: Feb. 1983]

Investigates the reaction of gases with SHM powders crystallizing during high-temperature shock compression under various conditions, resulting in different degrees of deviation of the starting phase toward instability. A mass-spectrometric study was made of the products of reaction of diamond and diamondlike boron nitride phases with hydrogen and other reducing gases. The intense reaction of SHM powders with gases observed not only during the transformation of material by shock compression into a gaseous phase and plasma but also in the solid phase suggests that in principle it should be possible to employ high-temperature shock compression for assembling by chemical means SHMs with controlled amounts of alloying components. (12 refs.)

63225 Kinetics and mechanism of sintering of covalent-ionic compounds. P.S.Kisly, M.A.Kuzenkova (Inst. for Superhard Materials, Acad. of Sci., Kiev, Ukrainian SSR).

Sintering - Theory and Practice. Proceedings of the 5th International Round Table Conference on Sintering, Portoroz, Yugoslavia, 7-10 Sept. 1981 (Amsterdam, Netherlands: Elsevier 1982), p.61-8

The process of sintering of refractory nonmetallic compounds is not yet studied sufficiently. The experimental data show that mass transfer in RCI (refractory covalent-ionic) compounds is mainly determined by the processes of destruction at high temperatures. RCI compounds melting without marked decomposition, such as aluminium nitride and boron nitride, are sintered in the region of premelting temperatures, whose contraction is effectively activated by using dispersion powders and of nonstoichiometric composition. RCI compounds which intensively decompose on heating, such as nitrides of boron and silicon, are sintered at high premelting temperatures as well, although only under the pressure of nitrogen exceeding the pressure of dissociation. (8 refs.)

63226 Surface energy of silicate melts and its importance in sintering processes. L.Zagar, O.E.Klinger, W.Stumpe, K.Lower (Inst. fur Gesteinskundkunde, RWTH, Aachen, Germany).

Sintering - Theory and Practice. Proceedings of the 5th International Round Table Conference on Sintering, Portoroz, Yugoslavia, 7-10 Sept. 1981 (Amsterdam, Netherlands: Elsevier 1982), p.73-84

The significance of the surface energy in relation to the sintering process is considered. The viscous flow, volume diffusion, surface diffusion, evaporation, condensation and, shrinkage of an isolated pore are examined. The sessile drop method and bubble pressure method of measurement are explained. (7 refs.)

63227 Comparison between theory and experiment in the sintering of undoped MgO . G.Tomandl, A.Stiegelschmitt (Inst. fur Werkstoffwissenschaften, Erlangen, Germany).

Sintering - Theory and Practice. Proceedings of the 5th International Round Table Conference on Sintering, Portoroz, Yugoslavia, 7-10 Sept. 1981 (Amsterdam, Netherlands: Elsevier 1982), p.101-6

Undoped MgO was sintered at temperatures from 1500 to 1800°C and times from 8 to 960 minutes. Using semiautomatic image analysis, particle size distributions were determined. These distributions were compared with theoretical functions obtained by a numerical solution of the differential equations according to a theory by Oel (1969). Within the experimental errors, which are discussed in detail, a correspondence could be found. A simplified method is shown for the determination of the velocity constant. (2 refs.)

63228 Sintering of magnesium-oxide obtained from sea water. B.Petric, N.Petric, N.Bogdanic, M.Mirosevic-Anzulovic.

Sintering - Theory and Practice. Proceedings of the 5th International Round Table Conference on Sintering, Portoroz, Yugoslavia, 7-10 Sept. 1981 (Amsterdam, Netherlands: Elsevier 1982), p.107-19

Presents the results obtained from examination of sintering of magnesium oxide p.a. and magnesium oxide obtained from sea water by nonstoichiometric and over-stoichiometric precipitation with dolomite lime. The density and apparent porosity were examined in order to determine the structure of the sintered samples. The examinations have been carried out by optical microscopy and electron microscopy, i.e. scanning. (7 refs.)

63229 Sintering and devitrification of slip-cast fused silica. D.Kicevic, M.Gasic (Materials Sci. Dept., Boris Kidric Inst. for Nuclear Sci., Belgrade, Yugoslavia).

Sintering - Theory and Practice. Proceedings of the 5th International Round Table Conference on Sintering, Portoroz, Yugoslavia, 7-10 Sept. 1981 (Amsterdam, Netherlands: Elsevier 1982), p.121-6

Sintering and devitrification of slip-cast commercial fused silica during firing in air were followed by density, compressive strength and X-ray diffraction determination. The influence of both firing temperature and time upon the fired samples properties was investigated using factorial design of experiments. Other influencing parameters, such as particle size distribution, solid phase content in slip, pH, slip viscosity and slip-casting conditions, were kept constant. Empirical mathematical models of properties dependence on influencing factor were established and discussed in terms of simultaneous effect of influencing factors and optimal conditions of obtaining dense, strong and thermally stable samples. (9 refs.)

63230 Investigation of MgO doped $\gamma\text{-Al}_2\text{O}_3$ sintering. J.Katanic-Popovic, M.Gasic, D.Kicevic (Boris Kidric Inst. for Nuclear Sci., Belgrade, Yugoslavia).

Sintering - Theory and Practice. Proceedings of the 5th International Round Table Conference on Sintering, Portoroz, Yugoslavia, 7-10 Sept. 1981 (Amsterdam, Netherlands: Elsevier 1982), p.153-8

The properties of $\gamma\text{-Al}_2\text{O}_3$, $\gamma\text{-Al}_2\text{O}_3$ with 1.5% MgO and spinel formed in equimolar mixture of Al_2O_3 and MgO powders fired at 550°C, were analysed. The sintering of catalyst supports made from $\gamma\text{-Al}_2\text{O}_3$ and $\gamma\text{-Al}_2\text{O}_3$ with 1.5% MgO in the temperature interval from 600° to 800°C was followed by density, porosity and specific surface measurements and compressive strength as well as microstructure determination. The sintering process in the temperature interval 600°-800°C was manifested by specific surface area decrease (with activation energy of 2.5 10^4 Jmol⁻¹), and pore size distribution change. The increase of pore radii with sintering temperature is more intensive process in samples with 1.5% MgO addition. (5 refs.)

63231 Effects of magnesium compound additives on sintering of magnesia. K.Hamano, Z.Nakagawa, H.Watanabe (Res. Lab. of Engng. Materials, Tokyo Inst. of Technol., Yokohama, Japan).

Sintering - Theory and Practice. Proceedings of the 5th International Round Table Conference on Sintering, Portoroz, Yugoslavia, 7-10 Sept. 1981 (Amsterdam, Netherlands: Elsevier 1982), p.159-64

The authors have examined the effect of magnesium compounds on sintering of magnesia, that is, the cation of additives is the same as that of the host oxide. For the additives, seven magnesium compounds were selected, and mixed with magnesium hydroxide in the ratio of 4 and 5 wt.% calculated as MgO . The mixtures were calcined and from which specimens were prepared by isostatic compression with pressure of 1000 kg/cm², then fired at 1400°C for 0-4 h. Sintering behaviour and microstructure of the fired specimens were examined. From the results obtained, it was concluded that the addition of various magnesium compounds showed markedly different effects on sintering of magnesia, though they have the same cation, Mg. Particularly in the case of addition of magnesium chloride, uniform sized and well crystallized periclase grains were formed during the calcination. Therefore green density of their specimens became very high and then dense fired bodies were obtained. For example, body having 98% theoretical density was obtained by firing at temperature of as low as 1400°C. (2 refs.)

63232 Sintering kinetics of Al_2O_3 doped with MgNb_2O_6 . G.Wroblewska (Glass & Ceramics Inst., Warsaw, Poland).

Sintering - Theory and Practice. Proceedings of the 5th International Round Table Conference on Sintering, Portoroz, Yugoslavia, 7-10 Sept. 1981 (Amsterdam, Netherlands: Elsevier 1982), p.165-71

The sintering process of Al_2O_3 with 0.1-1.5 mol.% MgNb_2O_6 was investigated. It has been found that with MgNb_2O_6 content in an amount of 0.5 mol.%, a material featuring 0.96 of theoretical density can be obtained after sintering at 1500°C. The dependence of linear shrinkage on sintering temperature and dopant concentration was studied. MgNb_2O_6 was found to decompose in the process of sintering. This is accompanied by the formation of a new compound, AlNbO_4 , which occurs in the structure of material besides the Al_2O_3 crystallites. (7 refs.)

63233 Sintering of SYNROC: case history for phase formation and densification of complex oxide systems. H.Palmour, III, T.M.Hare (North Carolina State Univ., Raleigh, NC, USA).

Sintering - Theory and Practice. Proceedings of the 5th International Round Table Conference on Sintering, Portoroz, Yugoslavia, 7-10 Sept. 1981 (Amsterdam, Netherlands: Elsevier 1982), p.185-92

Addresses several closely interwoven topics relating to the sintering of SYNROC, a potential ceramic waste form for disposal of high level radioactive

waste (HLW). SYNROC is an acronym (SYNthetic ROCK) first used in 1978 by Ringwood to describe his then-emergent concept of very durable, and hence very disposable, man-made crystalline ceramic waste forms for stabilization of HLW. SYNROC compositions are based on naturally-occurring titanate/zirconate minerals which are known to accommodate within their crystal structures a variety of naturally occurring radioactive species and to have endured within the deep earth environment for geologically long times. It has been argued that by thus emulating nature and forming synthetic rocks from these same very stable mineral assemblages, man can reliably expect to convert man-made HLW to earth-stable ceramic forms and thereafter to store them indefinitely, deep (>2000 m) within suitable geologic formations (granite, basalt, etc.). Since its introduction, the SYNROC concept has attracted considerable research attention in a number of locales in Australia and the US, with both defense and power wastes being considered. (33 refs.)

63234 Reactive sintering in the BaO:ZrO₂ 1:1 system. J.Brzezinska, K.Haberko, R.Pampuch (Inst. of Materials Sci., AGH, Cracow, Poland). Sintering - Theory and Practice. Proceedings of the 5th International Round Table Conference on Sintering, Portoroz, Yugoslavia, 7-10 Sept. 1981 (Amsterdam, Netherlands: Elsevier 1982), p.193-202. Evolution of the pore system and of morphology on calcination and sintering of powders obtained by coprecipitation from chloride aqueous solutions. Water and ethanol as washing media give rise to two types of agglomerates which differ in morphology and phase composition that determine two types of behaviour observed. With alcohol-washed systems dense BaZrO₃ may be obtained at 1773K. (24 refs.)

63235 Shrinkage and initial grain growth in BaTiO₃ ceramics. H.Schmelz (Siemens Res. Labs., Munich, Germany). Sintering - Theory and Practice. Proceedings of the 5th International Round Table Conference on Sintering, Portoroz, Yugoslavia, 7-10 Sept. 1981 (Amsterdam, Netherlands: Elsevier 1982), p.203-7. In order to understand microstructure development in BaTiO₃, the beginning of sintering was investigated. The temperature of shrinkage onset was found to be more than 100K below the eutectic point as determined by DTA. Both points depend on the chemical composition. The magnitude of the temperature difference between these two points leads to the conclusion that initial grain growth and shrinkage are controlled by solid state diffusion. In BaTiO₃ with SiO₂ impurities, an additional shrinkage mechanism by a direct influence of liquid phases is assumed. (3 refs.)

63236 Sintering of multiphase ceramics. P.Reynen, A.C.Firatli (Inst. für Geisteswissenschaften, Aachen, Germany). Sintering - Theory and Practice. Proceedings of the 5th International Round Table Conference on Sintering, Portoroz, Yugoslavia, 7-10 Sept. 1981 (Amsterdam, Netherlands: Elsevier 1982), p.209-18. Two compositions in the ternary system MgO-Al₂O₃-ZrO₂ were used in sintering experiments. Investigation of polished sections by SEM revealed a very uniform distribution of phases. It was concluded that multiphase ceramics show good sintering behaviour because discontinuous grain growth is inhibited. Full density with small grains could not be realised however due to parasitic pore growth. (9 refs.)

63237 Sintering of beta alumina powders obtained by sol-gel process. Preliminary studies. A.Deptula (Inst. of Nuclear Res., Warsaw, Poland), C.Majani, A.di Bartolomeo, M.Carewska. Sintering - Theory and Practice. Proceedings of the 5th International Round Table Conference on Sintering, Portoroz, Yugoslavia, 7-10 Sept. 1981 (Amsterdam, Netherlands: Elsevier 1982), p.219-26. The Al₂O₃ powders of spherical shape doped with Na₂O, MgO and Li₂O were obtained by sol-gel process. The temperature of calcination (500°C to 750°C) of powders and the temperature of sintering (1300°C to 1560°C) of pellets were varied to determine the optimum conditions to obtain β' alumina. (17 refs.)

63238 Sintering of ZrO₂-CaO and ZrO₂-Y₂O₃ powders obtained by sol-gel process. C.Majani (Centro di Studi Nucleari della Casaccia, CNEN, Roma, Italy), A.Deptula, M.Carewska, A.di Bartolomeo, R.Przytycka. Sintering - Theory and Practice. Proceedings of the 5th International Round Table Conference on Sintering, Portoroz, Yugoslavia, 7-10 Sept. 1981 (Amsterdam, Netherlands: Elsevier 1982), p.227-37. ZrO₂-CaO and ZrO₂-Y₂O₃ powders were obtained by sol-gel process. The temperature of calcination (400-1000°C) of powders, the time (8 to 48 hr) and the temperature of pellets' sinterization were varied to determine the optimum conditions to achieve the solid-solutions ZrO₂-CaO and ZrO₂-Y₂O₃. (24 refs.)

63239 Reactions and sintering of ZrO₂-doped spinel. J.Wallace, T.Kosmac, N.Claussen (Max-Planck-Inst. für Metall., Stuttgart, Germany). Sintering - Theory and Practice. Proceedings of the 5th International Round Table Conference on Sintering, Portoroz, Yugoslavia, 7-10 Sept. 1981 (Amsterdam, Netherlands: Elsevier 1982), p.239-44. The effect of 1000 ppm ZrO₂ dopants on the reaction and sintering of three different spinel compositions, stoichiometric, Al₂O₃-rich and MgO-rich, was studied in a recording dilatometer using a constant heating rate. The small ZrO₂ additions dropped the initial reaction temperature of all mixtures approximately 75°C due to the formation of cation vacancies. The powder composition did not affect the initial reaction temperature. The stoichiometry of the powder mixtures greatly influenced the sintering rate of the resulting spinel mixtures and the degree of the effect of ZrO₂ on the sintering rate; samples with excess MgO sintered very rapidly compared to the stoichiometric and Al₂O₃-rich composition. The 1000 ppm ZrO₂ additions greatly hindered the sintering rate of the MgO-rich samples but had much less effect on the stoichiometric and Al₂O₃-rich bodies. (13 refs.)

63240 The influence of the liquid phase amount on the densification of Si₃N₄-base ceramics. S.Boskovic ('Boris Kidric' Inst. of Nuclear Sci., Belgrade, Yugoslavia). Sintering - Theory and Practice. Proceedings of the 5th International Round Table Conference on Sintering, Portoroz, Yugoslavia, 7-10 Sept. 1981 (Amsterdam, Netherlands: Elsevier 1982), p.245-50. Processes taking place during sintering of Si₃N₄-base ceramics were investigated in the system Si₃N₄-YAG-β 60. It was found out that reaction occurs at 1450°C giving sialon as a reaction product. The influence of liquid phase amount on the densification, reaction and microstructure was discussed. (5 refs.)

63241 Some aspects of transient liquid phase sintering. S.J.Kiss, D.Cerovic, E.Kostic (Boris Kidric Inst. of Nuclear Sci., Vinca, Yugoslavia). Sintering - Theory and Practice. Proceedings of the 5th International Round Table Conference on Sintering, Portoroz, Yugoslavia, 7-10 Sept. 1981 (Amsterdam, Netherlands: Elsevier 1982), p.251-6. Some aspects of reaction sintering of Al₂O₃-SiO₂ and Al₂O₃-MgO mixtures in the presence of forsterite-cordierite-protonstatite eutectic were investigated. It was found out that heating rate up to 1450°C influenced the sintered samples

properties, as a consequence of different physico-chemical characteristics of the systems developed during heating up period. (9 refs.)

63242 The grain growth in alumina derived from gels. Lj.M.Zivkovic, M.M.Ristic (Electronic Faculty, Univ. of Nis, Beograd, Yugoslavia). Sintering - Theory and Practice. Proceedings of the 5th International Round Table Conference on Sintering, Portoroz, Yugoslavia, 7-10 Sept. 1981 (Amsterdam, Netherlands: Elsevier 1982), p.257-62. The grain growth of a gel-alumina was investigated and the effects on grain growth and densification of small additions of silica-gel were studied. For comparison purposes the behaviour of pure alpha-alumina under same conditions was investigated. From the grain size measurements using the classical grain growth law the constant n of grain boundary migration was evaluated. (6 refs.)

63243 Growth of isolated macropores in a silica ceramic. D.D.Gramatikov, M.I.Milosevski, M.M.Ristic (Serbian Acad. of Sci. & Arts, Beograd, Yugoslavia). Sintering - Theory and Practice. Proceedings of the 5th International Round Table Conference on Sintering, Portoroz, Yugoslavia, 7-10 Sept. 1981 (Amsterdam, Netherlands: Elsevier 1982), p.329-34. The pores growing in a silica ceramic have been studied. The physical parameters which characterise this process have been determined. The process is carried out via two stages. The first stage is characterised as reaction sintering, but in the second stage a liquid phase appears. (3 refs.)

63244 The effect of MgO on intragranular pore entrapment in sintered aluminium oxide. J.E.Burke, S.Prochazka (General Electric Corporate Res. & Dev., Schenectady, NY, USA). Sintering - Theory and Practice. Proceedings of the 5th International Round Table Conference on Sintering, Portoroz, Yugoslavia, 7-10 Sept. 1981 (Amsterdam, Netherlands: Elsevier 1982), p.335-41. It has long been known that less than 0.05% MgO will prevent discontinuous grain growth and entrapment of pores inside grains of sintering aluminium oxide. An early thesis was that magnesium adsorbed at the grain boundaries reduced grain boundary mobility and prevented the breakaway from pores during grain growth that occurs in pure alumina. Workers using Auger spectroscopy have been unable to detect excess magnesium at grain boundaries of sintered alumina and this has led to the rejection of the adsorption hypothesis and the suggestion of competing models. It is demonstrated that the MgO addition does not increase pore mobility and does reduce grain boundary mobility which supports the original hypothesis. (15 refs.)

63245 Development of the microstructure of semiconducting BaTiO₃ ceramics. K.Lubitz (Res. Labs., Siemens AG, Munich, Germany). Sintering - Theory and Practice. Proceedings of the 5th International Round Table Conference on Sintering, Portoroz, Yugoslavia, 7-10 Sept. 1981 (Amsterdam, Netherlands: Elsevier 1982), p.343-8. The microstructure of semiconducting BaTiO₃ ceramics develops as the result of secondary recrystallisation. A small amount of reactive melt-eutectic BaTiO₃-Ba₂Ti₇O₄₀ with the eutectic temperature $\vartheta_E \approx 1320^\circ\text{C}$ —is present in the ceramic and makes a process of dissolution and recrystallization. The grain size of the fired ceramic is determined by the nucleation. The response of BaTiO₃ to firing is studied with reference to the system BaTi_{1-x}Nb_xO₃+yTiO₂ (x≤0.05; y≤0.5). The way in which nucleation is influenced by the excess TiO₂, the doping concentration and the heating rate during firing is discussed. The grain size is controlled within broad limits by varying the heating rate near the eutectic temperature ϑ_E . (11 refs.)

63246 Grain growth in doped-undoped ceramic BaTiO₃ couples. B.Hoffmann (Inst. für Technol. Elektrotech., Univ. Karlsruhe, Karlsruhe, Germany), D.Hennings, M.Klerk. Sintering - Theory and Practice. Proceedings of the 5th International Round Table Conference on Sintering, Portoroz, Yugoslavia, 7-10 Sept. 1981 (Amsterdam, Netherlands: Elsevier 1982), p.349-54. Diffusion couples of La doped BaTiO₃ and undoped BaTiO₃ were heated from 10 min to 56 h at 1400°C. The couples were investigated after heating by means of light microscopy and electron microprobe analysis. Depending on the Ti/Ba atomic ratio on each side of the couple, different regions of exaggerated grain growth were observed. The thickness, position and chemical composition of such regions were studied. (5 refs.)

63247 Grain boundaries in sintered carbides. R.A.Andrievsky (Moscow Inst. of Fine Chem. Technol., Moscow, USSR). Sintering - Theory and Practice. Proceedings of the 5th International Round Table Conference on Sintering, Portoroz, Yugoslavia, 7-10 Sept. 1981 (Amsterdam, Netherlands: Elsevier 1982), p.355-9. Grain boundaries in sintered and hot-pressed samples of zirconium and tungsten carbides were studied with aid of X-ray microanalysis and other physical methods. The localisation of silicon, cobalt, iron in the grain-boundary regions was found. (7 refs.)

63248 Microstructural changes at grain boundaries during sintering of doped BaTiO₃ ceramics with small additions of TiO₂. M.Drofenik, S.Pejovnik, L.Irmanecnik (I. Stefan Inst., Kardelj, Univ., Ljubljana, Yugoslavia), I.Mochnik, V.Krasevec. Sintering - Theory and Practice. Proceedings of the 5th International Round Table Conference on Sintering, Portoroz, Yugoslavia, 7-10 Sept. 1981 (Amsterdam, Netherlands: Elsevier 1982), p.361-6. Doped and undoped BaTiO₃+4 mol% TiO₂ ceramics have been investigated by SEM, TEM and TGA with respect to the duration time of sintering. It was found that rapid grain growth in an early stage of sintering is associated with the release of oxygen and the presence of a liquid phase. In the later stage of sintering the liquid phase runs out of the samples while precipitation of second phases decorates grain boundaries. (5 refs.)

Electrophysical properties of nickel boride phases See Entry 62396
Epitaxial growth of ZnO layers—a new aspect in homojunction models of ZnO varistors See Entry 63185
The use of solid solution additives in sintering See Entry 63198
Reactive sintering See Entry 63199
Thermal and mechanical properties of multilic substrates for low-cost solar cells obtained by dry-pressing See Entry 63661

81.20N Cermets, ceramic and refractory composites

63249 Short-time sintering of hard metals. W.Hermel, R.Krumphold, G.Leitner (Zentralinst. für Festkörperphys. und Werkstoffforschung, Akad. der Wissenschaften, Dresden, Germany), K.Voigt. *High Temp.-High Pressures (GB)*, vol.14, no.3, p.351-6 (1982). (10th Plansee Seminar on 'Trends in Refractory Metals, Hardmetals, and Special Materials, and their Technology', Reutte, Austria, 1-5 June 1981). Short-time sintering by induction heating leads in a number of cases to considerable economies of time and energy, and increased output. Results of

development work on the applicability of short-time induction sintering to hard metals are described. The investigations, which concentrated on the influence of sintering time and temperature, show that in the case of commercial WC-Co and WC-TiC-Co hard metals, sintering times of a few minutes only are sufficient to attain properties which are equivalent to or better than those produced by conventional sintering. A short-time sintering process which uses induction heating has been developed for the production of hard metals. (7 refs.)

63250 The effects of pressure on the carbonization of pitch and pitch/carbon fibre composites. M.A.Forrest, H.Marsh (Northern Carbon Res. Lab., Univ. of Newcastle upon Tyne, Newcastle upon Tyne, England). *J. Mater. Sci. (GB)*, vol.18, no.4, p.978-90 (April 1983).

Three pitches which give carbons of varying optical texture have been carbonized singly and with different carbon fibres at pressures in the range 0.1 to 200 MPa. The effect of pressure on the carbonization system is to retard growth and coalescence of the growth units of mesophase, thus reducing the size of the optical texture of the resultant carbon. With increasing pressure botryoidal (spherical) structures are formed. On co-carbonization of pitches with carbon fibres the alignment of the basal planes of the matrix carbon parallel to the fibre length at the fibre/matrix interface is improved within a given pressure range. This range is dependent upon the parent pitch used and is experimentally determined. This effect is seen for all fibre types. (9 refs.)

63251 Thermal effects accompanying the heating of metallized powders. S.R.Pustotina, N.N.Novikov, L.K.Glukhova (Odessa Food Industry Technol. Inst., USSR).

Sov. Powder Metall. & Met. Ceram. (USA), vol.21, no.8, p.657-61 (Aug. 1982). Translation of: *Poroshk. Metall. (USSR)*, vol.21, no.8, p.67-72 (Aug. 1982). [received: Feb. 1983]

Assesses the energetic potentialities of thermally reacting alumina, zirconia, and tungsten carbide powders composed of particles covered with aluminum or two-layer aluminum-nickel shells. Composites were prepared by vacuum aluminizing and chemical nickel plating. The thermodynamic characteristics of possible exothermic reactions in the systems under consideration are given. A comparative assessment of the magnitudes of exothermic effects was carried out using an apparatus for the thermographic analysis of powders. (8 refs.)

63252 Sintering in the nickel-alumina system. I.P.Arsentjeva, D.Stefanovic, V.Mikijelj, M.Pavicevic, M.M.Ristic (Centre of Multidisciplinary Study, Belgrade Univ., Belgrade, Yugoslavia).

Sintering - Theory and Practice. Proceedings of the 5th International Round Table Conference on Sintering, Portoroz, Yugoslavia, 7-10 Sept. 1981 (Amsterdam, Netherlands: Elsevier 1982), p.283-9

Describes an investigation of sintering of the Ni-Al₂O₃ system. In the material prepared by a powder metallurgy technique, the bond formed between nickel oxide and α -Al₂O₃ was investigated by means of microprobe analyses and a suggestion was made as to the mechanism of interfacial reactions with alumina. (7 refs.)

63253 Metallographic and structural investigations of levitation splat cooled cobalt base cobalt-refractory carbide alloys. D.Duzevic (Electrotech. Inst. Rade Koncar, Zagreb, Yugoslavia), A.M.Tonejc, V.Krasevec.

Sintering - Theory and Practice. Proceedings of the 5th International Round Table Conference on Sintering, Portoroz, Yugoslavia, 7-10 Sept. 1981 (Amsterdam, Netherlands: Elsevier 1982), p.373-8

Levitation splat cooled Co-10 wt.% TaC and Co-5 wt.% TiC alloys were investigated by metallography, X-ray powder photography and transmission electron microscopy. Considerable hardness and coercivity growth in splat cooled samples, as compared with respective sintered master alloys, have been measured. Different position-dependent stages of carbide precipitation have been observed. (7 refs.)

81.20P Glasses

The sol-gel method for optical fiber fabricationSee Entry 61307

Investigation of sintering activator distribution in refractory materials by means of an X-ray microanalyzerSee Entry 61312

Some physicochemical aspects of Pd-PdO-Ag-glass mixture sinteringSee Entry 63188

81.20Q Glass-based composites, vitroceraamics

63254 A lanthanum-tantalum (Al) oxide porous glass ceramic. R.W.White, M.A.Res, J.Bednarik (Nat. Phys. Res. Lab., CSIR, Pretoria, S Africa). *J. Mater. Sci. (GB)*, vol.18, no.4, p.1021-7 (April 1983).

The substitution of the end-member oxides in the ternary glass forming sodium borosilicate system was studied. The replacement of SiO₂ with combinations of La₂O₃ and Ta₂O₅ was found to produce glasses which, after heat treatment decomposed to form a leachable sodium borate phase and an insoluble ceramic phase. The mode of phase decomposition is sensitive to impurities: the importance of crucible selection, e.g. Al₂O₃ or Pt/Rh is demonstrated by resulting differences in pore size, surface area, chemical resistance and structure of the insoluble phase for a series of La₂O₃-Ta₂O₅ and La₂O₃-Ta₂O₅-Al₂O₃ glass ceramic. These new materials have a specific surface area of up to 145 m² g⁻¹ and average pore radii ranging between 0.7 and 28.6 nm and show a varying degree of chemical resistance. (14 refs.)

81.20S Polymers

63255 Extrusion and extruders. Historical outline, actual situation and future trends. R.Sikora (Politech. Lubelska, Lubel, Poland).

Polim. Tworzywa Wielkocząsteczkowe (Poland), vol.27, no.8, p.316-20 (Aug. 1982). In Polish. [received: March 1983]

The development of extrusion methods of plastics starting with the year 1879 has been outlined. The recent theories of the extrusion process and up-to-date constructions of extruders have been presented. (31 refs.)

The determination of the coefficient of dynamic friction of organic powder compacts on steelSee Entry 63427

81.20T Reinforced polymers and polymer-based composites

Investigation by the molecular-probe method of the changes in the packing density of filled epoxide compositions during hardeningSee Entry 61828

81.30 PHASE DIAGRAMS AND MICROSTRUCTURES DEVELOPED BY SOLIDIFICATION AND SOLID-SOLID PHASE TRANSFORMATIONS

(see also 61. Structure of liquids and solids 64.70 Phase equilibria, phase transitions, and critical points)

63256 Interaction of hydrogen with traps and its solubility in maraging steel. V.I.Sarrak, G.A.Filippov, G.G.Kush (Inst. of Metallography & Phys. of Metals, Moscow, USSR).

Fiz. Met. & Metalloved. (USSR), vol.55, no.2, p.310-15 (Feb. 1983). In Russian. English translation in: *Phys. Met. & Metallogr. (GB)*

An investigation was made of the influence of the ageing temperature on the solubility of hydrogen in maraging steel N18K9M5T. A maximum was found of the hydrogen solubility after ageing at 450°C. This solubility maximum was attributed to the formation of hydrogen traps, representing local microstresses that appeared during earlier stages of ageing of coherent intermetallic particles. An estimate was obtained of the energy of the interaction of hydrogen with coherent intermetallic particles (0.4 eV), which was higher than the energy of the interaction of hydrogen with dislocations and titanium atoms. (13 refs.) A.T.

63257 Orientation relationships between BCC Mo and FCC γ in a Ni-Al-Mo-W superalloy. D.M.Dimiduk (AFWAL Materials Lab., Wright-Patterson AFB, OH, USA).

Metal. Trans. A (USA), vol.14A, no.3, p.493-8 (March 1983).

Describes the observed orientation relationships between the alpha (α) phase (Mo+W) and the gamma (γ) matrix after isothermal aging at 930°C for times up to 2000 hours. The alloy used was an experimental P/M Ni-base superalloy prepared by a centrifugal-atomization, forced-convective-cooling technique. (4 refs.)

63258 An investigation of the process of decomposition of the supersaturated solid solution of nitrogen in a niobium alloy. E.V.Vasil'yeva, T.A.Vorobova.

Russ. Metall. (GB), no.6, p.119-24 (1981). Translation of: *Izv. Akad. Nauk. SSSR Met.*, no.6, p.120-5 (1981).

Metallographic, electron-microscope, resistivity and internal-friction investigations were used to examine the relationships governing the decomposition of the saturated solid solution of nitrogen in the niobium alloy MN-1 (wt.% Nb+10 Mo, 3 Ti, 1 Zr). Alloying with nitrogen refines the grain size after heat treatment. Quenching of the nitrated MN-1 alloy freezes the saturated solid solution of nitrogen in the complex-alloyed matrix. The specifics of ageing of this alloy with nitrogen is determined by the decrease in the solubility of nitrogen in the matrix and the presence of alloying elements (Ti, Zr), which have a higher chemical affinity for nitrogen than the base metal. Decomposition of the saturated solid solution during heating in the range 1100-1400°C starts with the separation of metastable-phase particles and formation of nuclei of the stable phase. The latter was experimentally observed at 1200°C and is accompanied by generation of elastic stress fields due to lattice distortion in the matrix surrounding the nitride particles. (9 refs.)

Solid state SiC/Ni alloy reactionSee Entry 62184

Thermodynamics of homogeneous formation of cementite in austenite during case hardening of steelSee Entry 63462

Structure of titanium alloys and methods used for its controlSee Entry 63485

81.30B Phase diagrams of metals and alloys

63259 Phase equilibrium diagram for the vanadium-rhenium system. V.N.Eremenko (Acad. of Sci., Ukrainian SSR), A.M.Kharkova, T.Ya.Velikanova.

Dopov. Akad. Nauk UkrSR. Ser. A (USSR), no.2, p.72-6 (1983). In Ukrainian.

Using methods of X-ray analysis, optical microscopy, determination of the phase microhardness, Pirani-Altherum initial melting point, differential thermal analysis, determination of the temperature for transition into superconducting state the authors studied the alloy structure of the vanadium-rhenium system and plotted a diagram of the phase equilibrium. σ phase is congruently melted at 2903K, but at 1723[±]25K it undergoes eutectoid decomposition, $\sigma \rightleftharpoons \alpha_1 + \alpha$. A-phase is formed in a solid state $\alpha + \sigma \rightleftharpoons \alpha$ at temperatures ranged between 2223-2473K, but at 1373K it is decomposed following the reaction of $\alpha \rightleftharpoons \alpha_1$. Eutectic equilibrium $L \rightleftharpoons \alpha + \sigma$ takes place at 2853K. At this temperature solubility of the rhenium in vanadium covers a range of 65-69 at.% Re. Solubility limit of vanadium in rhenium is between 86-91 at.% Re at a temperature of 2873K, i.e. the temperature of common phase crystallization of σ and α_1 . $L \rightleftharpoons \sigma + \alpha_1$. (7 refs.)

63260 The Th-Sn phase diagram. S.Cirafici, A.Palenzona, P.Manfrinetti (Istituto di Chimica Fisica, Univ. di Genova, Genoa, Italy).

J. Less-Common Met. (Switzerland), vol.90, no.1, p.49-56 (March 1983).

The Th-Sn system was investigated by means of differential thermal and X-ray analysis and micrograph. Two eutectics are formed at about 80.0 at.% Th and 1.0 at.% Th with characteristic temperatures of 1600°C and 220°C respectively. Four intermetallic compounds (Th₃Sn₂, Th₃Sn₄, ThSn₂, and ThSn₃) were found and the crystal structures of all except ThSn₂ were determined using single-crystal diffractometric data. Th₃Sn₂ melts congruently at 1800°C, whereas ThSn₂ and ThSn₃ decompose peritectically at 1410°C and 955°C respectively. It was impossible to determine the decomposition point of Th₃Sn₄ and the temperature reported in the diagram (1550°C) is an estimated value. No appreciable solid solubility of thorium in tin or of tin in thorium was observed; the four intermediate phases also appear to be line compounds. (13 refs.)

63261 Phase diagrams of binary rare earth metal-indium systems. S.P.Yatsenko, A.A.Semyannikov, H.O.Shakarov, E.G.Fedorova (Inst. of Chem., Acad. of Sci., Sverdlovsk, USSR).

J. Less-Common Met. (Switzerland), vol.90, no.1, p.95-108 (March 1983).

X-ray diffraction, metallography and differential thermal analysis were used to establish the phase diagrams of binary rare earth-indium systems which have not previously been investigated. Some general characteristics of the phase diagrams of these binary systems are reported. (29 refs.)

63262 Solidus and liquidus temperatures in the Cs-Te system. M.G.Adamson, J.E.Leighy (General Electric Co., Vallecitos Nuclear Center, Pleasanton, CA, USA).

J. Nucl. Mater. (Netherlands), vol.114, no.2-3, p.327-9 (Feb. 1983). Reports the results of liquidus and solidus temperature measurements over the composition range 9:1 \geq Cs:Te \geq 1:9 and, on this limited basis, present a tentative high temperature Cs-Te phase diagram. (13 refs.)

63263 Change in the electrical resistivity of Al-3.5% Cu during thermal cycling in the solidus-liquidus range. A.S.Bubenshchikov, Yu.S.Nechayev, L.N.Shekhter.

Met. Sci. & Heat Treat. (USA), vol.24, no.7-8, p.542-4 (July-Aug. 1982). Translation of: *Metalloved. & Term. Obrab. Met. (USSR)*, vol.24, no.8, p.28-30 (Aug. 1982). [received: March 1983]

From the rate of the change in the temperature coefficient of electrical resistivity of Al-3.5% Cu in the solid-liquid state in the temperature range of 590-615°C it was established that individual dislocations can serve as the centers of melting. The activation energy of copper diffusion in aluminum $E=144.4$ kJ/mole. (8 refs.)

63264 The magnetism corner of the Mg-Y-Ce system. M.E.Drits, E.M.Padezhnova, T.V.Dobatkina, E.V.Voyekhova, V.V.Kinzhbalov. *Russ. Metall. (GB)*, no.6, p.200-3 (1981). Translation of: *Izv. Akad. Nauk. SSSR Met.*, no.6, p.206-10 (1981).

The projection of the surfaces of crystallisation is plotted for the system Mg-Y-Ce. The isothermal sections for 500 and 300°C are plotted and the simultaneous solubility of yttrium and cerium in magnesium at these temperatures was determined. (3 refs.)

63265 Phase equilibria in the Mg-Al-Sr system. M.M.Makhmudov, O.I.Bodak, A.V.Vakhobov, T.D.Dzhurayev. *Russ. Metall. (GB)*, no.6, p.209-12 (1981). Translation of: *Izv. Akad. Nauk. SSSR Met.*, no.6, p.216 et. seq. (1981).

The isothermal section was plotted for the Mg-Al-Sr diagram at 673K and wide ranges of solid solutions based on the compounds of the following binary systems were established: Sr_2Mg_{17} , Sr_6Mg_{23} , $SrMg_2$, $SrAl_4$ and $SrAl_2$. (11 refs.)

63266 Stability and crystallization of an amorphous nickel-based alloy. W.Ozgowicz, J.Tyrlík-Held (Inst. de Metall. Phys. et Soudage, Ecole Polytech. Silesienne, Gliwice, Poland), G.Thomas, A.Zahra, J.Le Coze. *Ser. Metall. (USA)*, vol.17, no.3, p.295-8 (March 1983).

Ribbons of the amorphous Ni-base alloy $Ni_{82}Cr_7Fe_5Si_3B_3$ were produced by the chill-block melt spinning method. Differential scanning calorimetry in the temperature range 20-600°C and X-ray diffraction in the range 20-800°C were used to study the crystallisation stages. Stage I, 20°C < T < 450°C, was short range order rearrangement of the glass solution. Stage II, T ≥ 450°C, was crystallisation of the solid solution α from the glass β. The glass transition (T_g) occurs at ~450°C. Stage III, T ~ 550°C, was crystallisation of Ni_3B from β. Stage IV, 550°C < T < 800°C, was the appearance of new, not well defined, phases, Ni_3Si_2 , $Fe_4Si_{18}B_6$ and Fe_3SiB . (15 refs.)

An X-ray diffraction study of the δ-α' transformation in a Pu-2 at.% Al alloy See Entry 62088

Two critical points on the γ-α phase boundary of cerium alloys See Entry 62091

High-pressure phases in B group element alloys: a new sort of electronic phase See Entry 62096

Comparison of the fitting capabilities of several equations for the composition dependence of excess free enthalpy in binary alloys See Entry 62126

Melting of peritectic intermediate phases in Cu-Zn and Cu-Ge systems See Entry 63280

A study of precipitation in interstitial alloys. II. A new metastable carbide phase in platinum See Entry 63296

Physicochemical fundamentals of the development of heat-resistant niobium alloys See Entry 63305

Effect of retained austenite on the contact fatigue strength of steel in relation to the phase diagram See Entry 63418

Heat treatment and magnetic properties of high-coercivity Fe-Co-Cr alloys with 3% Mo See Entry 63435

Enthalpies of formation of liquid and solid binary alloys based on 3d metals. III. Alloys of iron See Entry 63581

Quantitative X-ray phase analysis of R-Co alloys See Entry 63618

81.30D Phase diagrams of other materials

63267 Coupled phase diagram and thermodynamic analysis of the 18 binary systems formed among Li_2CO_3 , K_2CO_3 , Na_2CO_3 , $LiOH$, KOH , $NaOH$, Li_2SO_4 , K_2SO_4 and Na_2SO_4 . C.W.Bale, A.D.Pelton (Dept. de Genie Metall., Ecole Polytech., Montreal, Quebec, Canada).

CALPHAD: Comput. Coupling Phase Diagrams & Thermochem. (GB), vol.6, no.4, p.255-78 (1982).

Available phase diagram and thermodynamic data on the eighteen binary systems containing Li^+ , Na^+ , K^+ , SO_4^{2-} , CO_3^{2-} , and OH^- have been collected and critically assessed. A set of self-consistent thermodynamic parameters describing the free energies of the compounds, solid solutions, and liquid solutions in the binary systems has been formulated. The phase diagrams have been calculated, and estimated error limits of all diagrams are given. (51 refs.)

63268 The As_2S_3 -SnTe system. B.B.Kuliev, A.P.Gurshumov, E.M.Kuliev, Kh.Ya.Khalilov (V.I. Lenin State Pedagogical Inst., Azerbaidzhan SSR). *Inorg. Mater. (USA)*, vol.18, no.5, p.625-8 (May 1982). Translation of: *Izv. Akad. Nauk SSSR Neorg. Mater.*, vol.18, no.5, p.738-41 (May 1982). [received: Feb. 1983]

Reaction has been studied in, and a phase diagram has been constructed for, the As_2S_3 -SnTe system; the system is of the eutectic type, with formation of the compound $SnAs_2S_3Te$, which melts incongruently at 335°C. The eutectic point, found by means of a Tamman triangle, corresponds to an alloy with 25 mole% As_2S_3 at 240°C. The extent of solid solutions based on SnTe is up to about 3 mole% SnTe at room temperature. With slow cooling, a region of vitrification based on As_2S_3 is maintained up to 15 mole% of SnTe. (6 refs.)

63269 Phase equilibrium in the Ti-Se system at high pressures. E.G.Ponyatovskii, B.I.Kazandzhan. *Inorg. Mater. (USA)*, vol.18, no.5, p.630-6 (May 1982). Translation of: *Izv. Akad. Nauk SSSR Neorg. Mater.*, vol.18, no.5, p.745-51 (May 1982). [received: Feb. 1983]

Investigates phase equilibria in the Ti-Se system at high pressures using the DTA method. The phase Ti_3Se begins to melt incongruently with an elevation in pressure. A polymorphic transformation γ - $Ti_3Se \rightarrow \delta$ - Ti_3Se was observed with a small heat of transition and volume change. The authors established the existence of the phase Ti_3Se with a broad region of homogeneity and a very high pressure sensitivity of the melting point (166 K/G Pa), having a polymorphic transformation ϵ - $Ti_3Se \rightarrow \eta$ - Ti_3Se , the temperature of which is sharply reduced with pressure (280 K/G Pa). With an increase in pressure, the evolution of the T-C diagram of the Ti-Se system is determined by the fast-growing dome of congruent melting of Ti_3Se . (10 refs.)

63270 The Te - $Tl_2As_2Te_3$ - Tl_2Te_3 system. V.M.Dmitriev, V.V.Kirilenko, R.N.Shchelokov, V.A.Samokhov, N.G.Velikova (N.S. Kurnakov Inst. of General & Inorganic Chem., Acad. of Sci., USSR).

Inorg. Mater. (USA), vol.18, no.5, p.650-7 (May 1982). Translation of: *Izv. Akad. Nauk SSSR Neorg. Mater.*, vol.18, no.5, p.769-80 (May 1982). [received: Feb. 1983]

The following eight polythermal sections were studied by differential thermal analysis, X-ray diffraction analysis, investigation of the microstructures, and measurements of the microhardnesses: $Tl_2As_2Te_3$ - $TlTe_3$, which is partially quasi-binary, $(Tl_2As_2Te_3)_{0.1}Te_{0.9}$ -($Tl_2As_2Te_3$)_{0.25}(Tl_2Te_3)_{0.75}, Tl_2Te_3 -($Tl_2As_2Te_3$)_{0.118} $Te_{0.882}$, $(Tl_2As_2Te_3)_{0.118}Te_{0.882}$ -($Tl_2As_2Te_3$)_{0.118} $Te_{0.882}$, $(Tl_2As_2Te_3)_{0.118}Te_{0.882}$ -($Tl_2As_2Te_3$)_{0.118} $Te_{0.882}$, Tl_2Te_3 -($Tl_2As_2Te_3$)_{0.57}($Tl_2As_2Te_3$)_{0.429}, and Tl_2Te_3 -($Tl_2As_2Te_3$)_{0.1} $Te_{0.9}$. The temperature and concentration boundaries of the regions of primary crystallization of Te and the α- and β'-solid solutions and the boundaries of the regions of simultaneous crystallization of the components were determined. The Te - $Tl_2As_2Te_3$ - Tl_2Te_3 partial system is characterized by the existence of mono-variant eutectic and peritectic equilibria. Isothermal cross sections of the Te - $Tl_2As_2Te_3$ - Tl_2Te_3 partial system were constructed. (17 refs.)

63271 The Ti - As - Te system. V.M.Dmitriev, V.V.Kirilenko, R.N.Shchelokov, V.A.Samokhov, N.G.Velikova (N.S. Kurnakov Inst. of General & Inorganic Chem., Acad. of Sci., USSR).

Inorg. Mater. (USA), vol.18, no.5, p.658-63 (May 1982). Translation of: *Izv. Akad. Nauk SSSR Neorg. Mater.*, vol.18, no.5, p.781-8 (May 1982). [received: Feb. 1983]

The Ti - As - Te system was analyzed on the basis of experimental data. Most of the errors in the interpretation of the phase diagram of the Ti - As - Te system are due to the incorrect assumption of the existence of the $TiAsTe_3$ ternary compound. One cannot draw conclusions regarding the structure of the phase diagram of the ternary system without a detailed study or at least without a study of all of the quasibinary sections. (19 refs.)

63272 Phase diagram of the $Pb(PO_3)_2$ - MoO_3 system. G.A.Bukhalova, I.V.Mardirosova, N.P.Ocheret (Inst. of Construction Engng., Rostov-on-Don, USSR).

Inorg. Mater. (USA), vol.18, no.6, p.896-8 (June 1982). Translation of: *Izv. Akad. Nauk SSSR Neorg. Mater.*, vol.18, no.6, p.1057-9 (June 1982). [received: Feb. 1983]

Presents the results of a study of the phase diagram of the binary $Pb(PO_3)_2$ - MoO_3 system. Lead metaphosphate was synthesized. The melting point of the material obtained was 937K. A cp grade of molybdenum trioxide was used, with $T_m=1069K$. The phase diagram of the $Pb(PO_3)_2$ - MoO_3 system was investigated by differential thermal analysis. The thermography was performed in a pyrometer by plotting the heating curves in states where the alloys had been either forcibly crystallized or had been annealed to reach equilibrium. (8 refs.)

63273 Thermogravimetric study of the $KNbO_3$ - KBO_2 system. L.M.Rudkovskaya, V.G.Smotrakov (Rostov-on-Don State Univ., Rostov-on-Don, USSR).

Inorg. Mater. (USA), vol.18, no.6, p.911-12 (June 1982). Translation of: *Izv. Akad. Nauk SSSR Neorg. Mater.*, vol.18, no.6, p.1070-1 (June 1982). [received: Feb. 1983]

A thermogravimetric study of the $KNbO_3$ - KBO_2 system was carried out on the Paulik system derivatograph, and its phase diagram was plotted. The studies were carried out at temperatures from room to 1100°C at a heating rate of 10°C/min. The system was studied over the whole concentrations range, and is eutectic. The eutectic contains 73 mole% of KBO_2 and melts at $(860 \pm 5)^\circ C$. (6 refs.)

63274 Multichemistry and microstructure of a multiphase aluminosilicate ceramic. S.H.Risbud (Dept. of Ceramic Engng., Univ. of Illinois, Urbana, IL, USA), A.Zangvil.

J. Mater. Sci. (GB), vol.18, no.4, p.990-1004 (April 1983).

The microstructure and microchemistry of a sintered ($\approx 1700^\circ C$) aluminosilicate ceramic (60 wt.% Al_2O_3 -40 wt.% SiO_2) was investigated by optical, scanning (SEM and EDAX), and analytical electron microscopy (TEM and STEM). The microstructural features of the fired ceramic consisted of unreacted Al_2O_3 glass, porosity, and equilibrium and metastable mullite phases. Residual Al_2O_3 agglomerates (≈ 15 to 30 μm in size) were surrounded by a ≈ 6 μm layer of equilibrium mullite (≈ 71.3 to 73.5 wt.% Al_2O_3). The unreacted Al_2O_3 -equilibrium mullite assembly formed islands embedded in a silica rich glass (≈ 4.5 to 14 wt.% Al_2O_3) which also contained 2 to 3 μm thick metastable mullite needles (≈ 70 to 77 wt.% Al_2O_3). Phase separation and alumina rich glass compositions (≈ 57 to 59 wt.% Al_2O_3) were also observed in some areas of the microstructure. (7 refs.)

63275 Comments on the manuscript entitled: On the existence of a two-phase field in the uranium-oxygen system within the composition range 2.65 < O/U < 2.67 below 1273K (A. Caneiro, J.P. Abriata and J. Garces, J. Nucl. Mater. 113 (1983) 260-262) [and reply]. M.S.Chandrasekharaiah (Chem. Div., BARC, Trombay, Bombay, India).

J. Nucl. Mater. (Netherlands), vol.114, no.2-3, p.326 (Feb. 1983). Chandrasekharaiah comments on a paper by Caneiro et al. in which they state that their observed two-phase field is only during reduction. He suggests that this apparent metastable state is the result of a diffusion-controlled oxidation reaction due to the large sample (1g) used. Caneiro et al. reply maintaining that all plotted data points on isotherm De correspond to well-defined metastable equilibrium states of the U-O system. (1 ref.)

Phase equilibria in systems of TiX with $Cd(Zn)X$ ($X=S, Se, Te$) See Entry 62060

The $Ti, Te+Ge=2Ti+GeTe$ ternary interlinked system See Entry 62061

Phase diagram and transition properties of condensed ammonia to 10 kbar See Entry 62066

Thermodynamics of the $CaO-SiO_2$ system See Entry 62109

Sintering of SYNROC: case history for phase formation and densification of complex oxide systems See Entry 63233

81.30F Solidification

(see also 64.70D Solid-liquid transitions)

63276 Discontinuity of temperature distribution due to phase transformations during the cooling of alloys. T.Sato, K.Ikawa (Dept. of Metal Processing, Tohoku Univ., Sendai, Japan).

Acta Metall. (USA), vol.31, no.5, p.731-41 (May 1983).

Cooling curves have long been used to study phase transformations. The discontinuity in the partial time derivative has been analysed for the case of various transitions. These include liquid-to-solid (passage of dendrite front), liquid- and solid-to-solid (passage of austenite front), and liquid-to-gas- and -solid (passage of a front of pore formation). Application of this theory to cooling curves recorded during the solidification of an Al-6 wt% Cu alloy

revealed the exact moment of passage of the dendrite front, and the temperature of the latter, as well as the rate of increase of the fraction of solid at the thermocouple location. (6 refs.)

63277 Solidification of copper and silver in near-zero-g experiments. V.S.Zemskov, I.N.Belokurova, A.A.Barareko, V.V.Savtychev, N.F.Bogdanova (Baikov Inst. of Metall., Acad. of Sci., Moscow, USSR). *Acta Astronaut.* (GB), vol.9, no.10, p.609-11 (Oct. 1982). [received: March 1983]

The investigation, by light and electron microscopy, as well as by X-ray methods, of the structure of copper and silver samples obtained by containerless solidification in microgravity conditions has revealed a texture of single-crystal type and a clearly pronounced structure. In copper samples, pores have been found whose occurrence could be due to the formation of shrinkage cavities or to the evolution of gases the starting samples contained. The high purity of the materials, lack of contact with container walls and lack of convection have caused the solidification to occur in the conditions of high supercooling with the formation of few dendrites. (4 refs.)

63278 Observations on the non-planar freezing of aqueous salt solutions. C.Korber, M.W.Scheiwe (Helmholtz-Inst. für Biomedizinische Tech., RWTH Aachen, Aachen, Germany).

J. Cryst. Growth (Netherlands), vol.61, no.2, p.307-16 (March 1983). A light microscope equipped with a special freezing stage and a spectrophotometer was employed to study the non-planar solidification of the binary model system H₂O-NaMnO₄. Instabilities of the initially planar solid-liquid interface were detected visually and could be related to the constitutional supercooling criterion. The redistribution of solute in the interstices between the dendrite arms was measured densitometrically. The concentration profiles scanned along the interdendritic midlines were generally about linear. This result is in agreement with Flemings' dendritic solidification model which assumes local equilibrium according to phase diagram relations in small volume elements. (32 refs.)

63279 On the steady-state continuous casting Stefan problem with non-linear cooling. M.Chipot (Univ. de Nancy, Nancy, France), J.-F.Rodrigues. *Q. Appl. Math.* (USA), vol.40, no.4, p.476-91 (Jan. 1983).

A steady-state one-phase Stefan problem corresponding to the solidification process of an ingot of pure metal by continuous casting with nonlinear lateral cooling is considered via the weak formulation introduced for the dam problem. Two existence results are obtained, for a general nonlinear flux and for a maximal monotone flux. Comparison results and the regularity of the free boundary are discussed. A uniqueness theorem is given for the monotone case. (16 refs.)

63280 Melting of peritectic intermediate phases in Cu-Zn and Cu-Ge systems. E.S.Kucherenko.

Russ. Metall. (GB), vol.40, no.6, p.192-5 (1981). Translation of: *Izv. Akad. Nauk. SSSR Met.*, no.6, p.197-200 (1981).

The melting of the intermediate phases with a wide range of concentrational homogeneity was examined: ϵ -phase in the system Cu-Zn and the ξ -phase in Cu-Ge. Various processes were identified which led to the formation of fusion spots inside the grains as well as to complete melting of the initial solid phase. The mechanism is governed by the initial phase composition of the alloys and the type of phase equilibria in the solid and liquid phases. (3 refs.)

63281 Analysis of the factors determining the yield of a peritectic reaction, important in choice of optimal heat-treatment conditions. I.M.Galushko.

Russ. Metall. (GB), no.6, p.196-200 (1981). Translation of: *Izv. Akad. Nauk. SSSR Met.*, no.6, p.201-5 (1981).

The influence was examined of the external factors (cooling conditions, alloy composition) and internal ones (features of the structure of the equilibrium diagram), separately and combined, on the peritectic reaction which is determined by the formula $\epsilon = 1 - \eta_1/\eta_2$. The value of ϵ depends on the temperature of the peritectic horizontal during solidification of melts of peritectic systems with the criterion of the peritectic reaction $K > 1$. The influence was examined of the form of growth and the structure of the surfaces of the primary and peritectic phase crystals on the mechanism of the peritectic reaction, and a scheme is proposed to illustrate the dependence of ϵ on the form of growth of the grains which participate in the reaction. It is shown, on the example of Cu-Cd and Cu-Sn systems, that an increase in the relative quantity of primary grains in the solidifying melts lowers the yield (efficiency) of the peritectic reaction. (10 refs.)

63282 Turbulent flow in chill block casting. P.G.Zielinski, D.G.Ast (Dept. of Material Sci. & Engng., Cornell Univ., Ithaca, NY, USA).

Ser. Metall. (USA), vol.17, no.3, p.291-4 (March 1983).

Molten Ni₂Si₂B₇ alloy was ribbon cast ejecting from a nozzle onto a rapidly rotating drum. In order to visualize the flow pattern, WC particles were added to the melt. Uniform ribbons were obtained when the melt puddle which forms on top of the moving substrate was stable. Microscopic examination of the frozen-in flow patterns (revealed by the WC particle distribution) showed a set of concentric elliptical lines, elongated in the direction of the flow. The overall appearance was very similar to the formation of turbulent spots in liquids due to boundary layer instability. The edge of the crucible nozzle can be considered as a large localized disturbance producing a turbulent spot. These instabilities in the melt should be taken into account for refined descriptions of heat transfer and solidification during chill block casting of metallic glasses and microcrystalline alloys. (11 refs.)

63283 Ultrafast solidification of ultrathin molten silicon films.

P.H.Bucksbaum, J.Bokor (Bell Telephone Labs., Holmdel, NJ, USA).

Topical Meeting on Excimer Lasers, Incline Village, NV, USA, 10-12 Jan. 1983 (Washington, DC, USA: Opt. Soc. America 1983), p.WA3/1-4

The authors have utilized melting pulses produced by a picosecond injection locked KrF* laser to observe melts with solid-liquid regrowth velocities considerably higher than 20 m/s for the first time. These measurements provide new tests of thermodynamic models of silicon amorphization from an undercooled melt. (6 refs.)

Effect of prior large scale electron irradiation on crystallization in two Fe-Ni based metallic glasses See Entry 61976

Measurements of the lamellar spacings of unidirectionally solidified Fe-FeS eutectic thin films See Entry 62285

The magnetism corner of the Mg-Y-Ce system See Entry 63264

81.30H Constant-composition solid-solid phase transformations: polymorphic, massive, and order-disorder

(see also 64.70K Solid-solid transitions)

63284 Formation and stability of reverted austenite in low-carbon nickel-molybdenum steels. V.M.Schastlivtsev, I.L.Barmina, I.L.Yakovleva, Yu.L.Legostaev, V.A.Malyshvskii (Inst. of Metal Phys., Acad. of Sci., Sverdlovsk, USSR).

Fiz. Met. & Metalloved. (USSR), vol.55, no.2, p.316-22 (Feb. 1983). In Russian. English translation in: *Phys. Met. & Metallogr.* (GB) Magnetothermal and electron-microscopic methods were used to study the phase composition in the case of austenitization in the intercritical temperature range and the stability of reverted austenite (i.e. of austenite formed during heating temperatures in the intercritical temperature and retained after cooling to room temperature, which should be distinguished from residual austenite remaining in steel after treatment) in low-carbon nickel-molybdenum steels of electroslag origin. The heat treatment conditions were found for ensuring the maximum amount of the reverted austenite and the highest stability of this austenite. It was found that the amount of the reverted austenite was inversely proportional to the rate of cooling from the intercritical temperature range. (6 refs.) A.T.

63285 Nonequilibrium crystallization and structural transitions during heating of microcircuit leads made of Fe-C and Fe-C-Si alloys. V.F.Bashev (Ukraine & Russia Reunion Tercentenary State Univ., Dnepropetrovsk, Ukraine SSR).

Fiz. Met. & Metalloved. (USSR), vol.55, no.2, p.331-6 (Feb. 1983). In Russian. English translation in: *Phys. Met. & Metallogr.* (GB)

X-ray structure analysis and measurements of the electrical resistivity during continuous heating were used to study the influence of the method of cooling on the tendency of formation of metastable crystalline and amorphous phases in microcircuit leads made of Fe-C and Fe-C-Si alloys. The sequence of appearance of metastable intermediate phases during formation of an equilibrium state was established and the appearance of a new silicon carbide was studied. (8 refs.) A.T.

63286 Order-disorder transition in Fe₃Si alloy during mechanical crushing. E.P.Elsukov, V.A.Barinov, V.R.Galakhov, E.E.Yurchikov, A.E.Ermakov (Inst. of Metal Phys., Acad. of Sci., Sverdlovsk, USSR).

Fiz. Met. & Metalloved. (USSR), vol.55, no.2, p.337-40 (Feb. 1983). In Russian. English translation in: *Phys. Met. & Metallogr.* (GB)

The methods of Mossbauer spectroscopy, X-ray diffraction, and magnetization measurements were used in a study of mechanical crushing of ordered Fe₃Si, which produced a disordered state of this alloy. The disordering resulted in an increase in the parameters of the b.c.c. lattice and in a reduction in the average magnetic moment per iron atom in the alloy. (11 refs.) A.T.

63287 Investigation of the phase composition, structure, and magnetic properties of alloy Sm₂Co₁₀Fe₃Cu₁₂Zr₁₀. E.I.Teitel', A.G.Popov, V.G.Maikov, L.M.Magat, N.N.Shecheleva, Ya.S.Shur (Inst. of Metal Phys., Acad. of Sci., Sverdlovsk, USSR).

Fiz. Met. & Metalloved. (USSR), vol.55, no.2, p.349-57 (Feb. 1983). In Russian. English translation in: *Phys. Met. & Metallogr.* (GB)

Electron microscopy was used to study the phase composition and structure of sintered magnets made of Sm₂Co₁₀Fe₃Cu₁₂Zr₁₀ and subjected to homogenization and annealing. Annealing resulted in precipitation of phases of the SmCo₅ type and of hexagonal Sm₂Co₇. Moreover, the phase based on SmCo₁₇ was transformed from the hexagonal to the rhombohedral modification and this was accompanied by the formation of structural domains with the 60° or 180° misorientation (about the [111]_R direction). Possible influence of these structural components on the magnetic properties of the alloy was analysed. (7 refs.) A.T.

63288 Decomposition kinetics for supercooled austenite in steel 15Kh1M1F. A.P.Smirnova, I.I.Mints, M.M.Shtenberg (UralVTI, Chelyabinsk, USSR).

Met. Sci. & Heat Treat. (USA), vol.24, no.7-8, p.572-4 (July-Aug. 1982). Translation of: *Metalloved. & Term. Obrab. Met.* (USSR), vol.24, no.8, p.52-3 (Aug. 1982). [received: March 1983]

A study was made by magnetometric, dilatometric, and metallographic methods of decomposition kinetics for austenite in hot-rolled steel 15Kh1M1F; with uninterrupted cooling for specimens of two melts with carbon contents at the lower and upper limits of the specified composition, and under isothermal conditions for one melt. The austenitization temperature (1050°C) and soaking time (30 min) were selected in accordance with factory procedure for heat treating pipes made of steel 15Kh1M1F. The amount of residual austenite in the steel was determined by an X-ray method. (5 refs.)

63289 Carbon effect on ordering of γ -Ni₃Al in rapidly solidified Ni₂Al-C alloys. K.H.Han, W.K.Choo (Dept. of Materials Sci. & Engng., Korea Advanced Inst. of Sci. & Technol., Seoul, Korea).

Ser. Metall. (USA), vol.17, no.3, p.281-4 (March 1983).

Only the ordered FCC Ni₃Al_x ($x=0-0.34$) single phase was formed in pseudo-binary Ni₂Al-C alloys by RSP. In other words, the maximum solubility of carbon in γ -Ni₃Al was extended to about 7.8 at.%. A strong preferred orientation of RSP samples along the (100) direction normal to the substrate surface was observed, and it became more pronounced with increasing carbon content. By the structure analysis using the integrated intensity ratio I_{200}/I_{100} of the fundamental to superlattice reflections, it was found that the ordering of γ -Ni₃Al can be further induced by carbon atoms probably through the cooperative ordering of substitutional atoms (nickel and aluminum) and carbon atoms to form the L₁2 type Ni₃Al_x perovskite structure. (5 refs.)

63290 Ferrite growth during slow cooling from the intercritical annealing of a dual-phase steel. J.J.Yi, I.S.Kim (Korea Advanced Inst. of Sci. & Technol., Seoul, Korea).

Ser. Metall. (USA), vol.17, no.3, p.299-302 (March 1983).

The microstructural observations of austenite transformation during cooling from the intercritical annealing shows that the 'transformed' ferrite does not grow epitaxially on the 'retained' ferrite, but nucleates on the interior austenite grain boundaries of the austenite pool and grows inside the austenite pool leaving the sandwiched austenite between the 'transformed' and the 'retained' ferrite. The old ferrite-austenite interfaces which formed at the intercritical annealing temperature are much less mobile than those formed on cooling between the 'transformed' ferrite and the untransformed austenite. The isolated retained austenite particles are the remainders of the shrinking sandwiched austenite particles which are aligned between the 'transformed' and the 'retained' ferrite. The strength of the 'transformed' ferrite is always higher than that of the 'retained' ferrite as long as the sandwiched austenite was preserved during cooling. (9 refs.)

- Two new phases with tetragonal bronze-like structure in the diagram: K_2O - CdO - Nb_2O_5 See Entry 61863
- New cationic deficient phases $Bi_{1-x}B_{4/5+x}V_{1-x}O_{20}$ with sillenite structure See Entry 61864
- An X-ray diffraction study of the $\delta \rightarrow \alpha'$ transformation in a Pu-2 at.% Al alloy See Entry 62088
- Two critical points on the γ - α phase boundary of cerium alloys See Entry 62091
- Phase equilibrium in the Ti-Se system at high pressures See Entry 63269
- Discontinuity of temperature distribution due to phase transformations during the cooling of alloys See Entry 63276
- Characteristics of structural transformations during deformation and heat treatment of Elinvar alloy 45 NKHT See Entry 63356
- Influence of nitrogen on the penetration of hydrogen through constructional materials from nitrogen-hydrogen mixtures See Entry 63465

81.30K Martensitic transformations

(see also 64.70K Solid-solid transitions)

- 63291 Influence of alloying and preliminary deformation on phase composition and mechanical properties of Fe-Mn alloys. L.S.Malinov, E.Ya.Kharlanova. *Russ. Metall. (GB)*, no.6, p.140-5 (1981). Translation of: *Izv. Akad. Nauk. SSSR Met.*, no.6, p.141-7 (1981).
- An increase in the manganese content and additional alloying of alloy G20 with copper and aluminium reduces the tendency to martensite formation and strain strengthening. A good combination of the strength and ductility characteristics is achieved with a preliminary hot deformation which ensures a certain intensity of martensite transformation during loading. Preliminary hot deformation and treatment, which includes preliminary cold deformation followed by annealing at 400°C, affect differently the (ν - ϵ) and (γ - α) transformations. (14 refs.)
- 63292 Elastic behavior and phase stability of β_1 -AgCd alloy. Y.Matsuo, T.Makita, A.Nagasawa (Dept. of Phys., Nara Women's Univ., Nara, Japan). *Scr. Metall. (USA)*, vol.17, no.3, p.285-9 (March 1983).
- The temperature dependence of elastic constants of β_1 -AgCd was measured from just above the martensitic transformation to just below the decomposition. The phase stability of the metastable β_1 -phase is discussed in relation to the experimental observations. (14 refs.)
- 63293 The structure of the modified 2H martensite in Cu-Zn-Al. M.Sade, E.C.Lovey (Centro Atomico Bariloche, Bariloche, Argentina). *Scr. Metall. (USA)*, vol.17, no.3, p.333-8 (March 1983).
- A program was started to determine in detail by X-rays and transmission electron microscopy (TEM) the structures of various martensitic phases in Cu-Zn and Cu-Zn-Al alloys. Some of the results concerning a hexagonal martensitic phase are reported. (14 refs.)
- Investigation of magnetic and martensitic phase transitions in Vicalloy-type alloys See Entry 62586
- Decomposition kinetics for supercooled austenite in steel 15Kh1MIF See Entry 63288
- Austenite grain refining with rapid heating of steel 40 Kh See Entry 63322
- Effect of rate of heating for hardening on the structure of alloys VT23 and VT6 See Entry 63324
- Performance of the Ni-Ti alloy VTN-1 (54.5-55 wt.% Ni) in the case of shape restoration See Entry 63364
- Influence of ϵ -martensite on the friction and wear of high-manganese alloys See Entry 63423
- Acoustic emission during phase transformations in alloys See Entry 63486

81.30M Precipitation

(inc. segregation; see also 64.75 Solubility, segregation and mixing)

- 63294 Computer modelling of grain boundary segregation. M.A.V.Chapman, R.G.Faulkner (Univ. of Technol., Loughborough, England). *Acta Metall. (USA)*, vol.31, no.5, p.677-89 (May 1983).
- A computer model has been developed to simulate grain boundary segregation during cooling from high temperatures. During this cooling possibilities exist for the occurrence of both equilibrium and non-equilibrium segregation. The model accounts for these processes simultaneously. The model predictions for boron in steel are compared with previous experimental estimates and with the results from this work of an Auger electron spectroscopy study of grain boundary segregation in a tempered ferritic-martensitic 12% Cr steel. (16 refs.)
- 63295 On the coarsening of γ' in Alloy 800. M.Vittori, G.Guidi (Div. Sci. dei Materiali, ENEA, Roma, Italy). *Acta Metall. (USA)*, vol.31, no.5, p.725-9 (May 1983).
- In a γ' hardened steel the authors have observed that the γ' average radius changes from grain to grain after a long term ageing at the temperature of 600°C. This effect has been explained on the basis of a simple model in which the precipitation of $M_{23}C_6$ Cr rich carbides on the grain boundaries is taken into account. The precipitation of the carbides causes a Cr depletion in the matrix; the amount of Cr depletion results to change from grain to grain since it depends on the single grain linear size. Since the Cr content affects the solubility of the γ' forming elements, a different coarsening rate constant for γ' particles growing in grains of different size is then expected on the basis of the Lifshitz, Sroloviz and Wagner theory of particle coarsening. The experimental investigations have been carried out on samples of four heats of Alloy 800 differing each other by small variations in the Ti and Al contents, and aged at 600°C for times ranging from 10^3 to 10^4 h. Transmission electron microscopy and WDS microprobe analyzer have been used. (19 refs.)
- 63296 A study of precipitation in interstitial alloys. II. A new metastable carbide phase in platinum. M.J.Witcomb, U.Dahmen, K.H.Westmacott (Lawrence Berkeley Lab., Univ. of California, Berkeley, CA, USA). *Acta Metall. (USA)*, vol.31, no.5, p.743-7 (May 1983).
- Contrast and convergent beam diffraction studies of precipitates in quenched, aged platinum containing about 800 atomic ppm carbon have identified a body-centered tetragonal structure with $a=0.39$ nm, $c=0.59$ nm, $c/a=1.5$. An investigation of the microstructure of similarly treated platinum of various purities and of platinum doped with carbon indicates the precipitates to be a metastable carbide of composition at or close to Pt_2C . (12 refs.)

- 63297 A study of precipitation in interstitial alloys. III. Coherent and semicoherent growth mechanisms. U.Dahmen, K.H.Westmacott, M.J.Witcomb (Lawrence Berkeley Lab., Univ. of California, Berkeley, CA, USA). *Acta Metall. (USA)*, vol.31, no.5, p.749-54 (May 1983).
- For pt.III see *ibid.*, vol.31, no.5, p.743 (1983). Frank and Shockley partial dislocations have been generalized using the coherency concept of Olson and Cohen to describe coherent and semi-coherent growth ledges on plate-shaped precipitates. Carbide platelet precipitate growth on {001} planes in platinum was quantified in these terms using displacement fringe and strain contrast analysis of dislocations surrounding the precipitates. The first two stages in the growth sequence proceeded solely by semi-coherent ledges associated with $1/4\{001\}$ (Frank-type) dislocations. These stages thus correspond to the co-precipitation of vacancies and carbon atoms. Coherent ledges were observed only occasionally during the third stage of growth, the ledges being bounded by $1/4\{201\}$ (Shockley-type) dislocations. The uniqueness of this result is interpreted in terms of the low solubility of carbon in platinum which results in similar concentrations of quenched-in vacancies and carbon atoms. (15 refs.)
- 63298 A study of precipitation in interstitial alloys. IV. The precipitation sequence in Pt-C. K.H.Westmacott, M.J.Witcomb, U.Dahmen (Lawrence Berkeley Lab., Univ. of California, Berkeley, CA, USA). *Acta Metall. (USA)*, vol.31, no.5, p.755-62 (May 1983).
- For pt.III see *ibid.*, vol.31, no.5, p.749 (1983). A systematic transmission electron microscopy study of the entire carbide precipitate nucleation and growth process in quenched, aged platinum has been made. Five distinct stages have been identified in the growth sequence, four coincide with changes in the Burgers and displacement vectors and the fifth in the configuration of the precipitates. Diffraction contrast analysis has shown that all the precipitate platelets lie in {001} matrix planes, are vacancy in character and are semi-coherent. Precipitates form initially by co-precipitation of vacancies and carbon atoms and the growth sequence follows a ripening type process. At intermediate aging temperatures voids become the preferred growth sites presumably acting as vacancy sources. Various aspects of the precipitation reaction have been explained from the standpoint of the role of vacancies (V), and the system can be treated either as a Pt-C binary or a Pt-C-V ternary alloy. (16 refs.)
- 63299 Resolution of Cu atoms in a GP[1] zone in Al-Cu by FIM and determination of the GP[1] structure. T.Mori, M.Wada, H.Kita, R.Uemori, S.Horie, A.Sato, O.Nishikawa (Dept. of Materials Sci. & Engng., Tokyo Inst. of Technol., Yokohama, Japan). *Jpn. J. Appl. Phys. Part 2 (Japan)*, vol.22, no.3, p.L203-5 (March 1983).
- By FIM the atomic arrangement of a GP[1] zone in an aged Al-Cu alloy is resolved into isolated spots on the {024} planes. These resolved spots are identified as the images produced by individual Cu atoms of the GP[1] zone protruding on the {024} surfaces. By observing the position and shape formed by the spots corresponding to the Cu atoms during the successive field evaporation, it is concluded that a GP[1] zone consists of a single layer of Cu atoms on the {002} planes.
- 63300 Crystallographic aspects of precipitation of supersaturated aluminium-base solid solutions. T.V.Shegegoleva (Inst. of Metal Phys., Acad. of Sci., Sverdlovsk, USSR). *Fiz. Met. & Metalloved. (USSR)*, vol.55, no.2, p.273-96 (Feb. 1983). In Russian. English translation in: *Phys. Met. & Metallogr. (GB)*
- A review is given of the papers reporting studies of the mechanisms of ageing of aluminium alloys. It is confirmed that the ageing mechanism is determined by the methods of modification of a 'perfect' crystal structure of the matrix into the lattices of stable precipitation phases. Metastable phases with crystal lattices, which can be defect-free or containing defects, are formed at intermediate stages. It is shown that the formation of the h.c.p. and b.c.c. lattices from the f.c.c. structure involves a premartensitic state with an incomplete hear. A new explanation is provided of the phenomenon of recovery and of the influence of double heat treatment on the structure of alloys containing metastable phases with defect lattices. (128 refs.) A.T.
- 63301 The effect of the nitrogen potential on the coarsening kinetics of VN precipitates. O.E.Atasoy (Metall. Engng. Dept., Middle East Tech. Univ., Ankara, Turkey). *Metall. Trans. A (USA)*, vol.14A, no.3, p.379-84 (March 1983).
- An Fe-1.06 pct V alloy was used to study the kinetics of coarsening of VN precipitates. Nitriding was carried out at 600°C in purified NH_3 gas. Nitrided specimens were then annealed at 820°C in furnace atmospheres of different NH_3/H_2 ratios. The transmission electron microscopy technique was used to measure the precipitate sizes. The data on the precipitate sizes indicate that the coarsening of the plate shaped VN precipitates seems to be diffusion controlled. The precipitate coarsening rate appears to be lowered by the increase in NH_3 content in the furnace atmosphere. The particle size distributions were found to be broader than the predictions of the LSW theory. (19 refs.)
- Drift forces on vacancies and interstitials in alloys with radiation-induced segregation See Entry 61956
- Precipitation and void-swelling in nickel-manganese austenitic stainless steels See Entry 61986
- Electron-microscopy study of the decomposition of a supersaturated solid solution in silicon See Entry 62112
- Interfacial segregation and enhanced sintering processes See Entry 63200
- Development of the microstructure of semiconducting $BaTiO_3$ ceramics See Entry 63245
- Microstructural changes at grain boundaries during sintering of doped $BaTiO_3$ ceramics with small additions of TiO_2 See Entry 63248
- Metallographic and structural investigations of levitation splat cooled cobalt base cobalt-refractory carbide alloys See Entry 63253
- Investigation of the phase composition, structure, and magnetic properties of alloy $Sm_2Co_{10}Fe_{32}Cu_{12}Zr_{0.4}$ See Entry 63287
- Decomposition kinetics for supercooled austenite in steel 15Kh1MIF See Entry 63288
- Influence of sulfur and nitrogen on the characteristics of texture formation as a result of deformation and annealing of Fe+3% Si single crystals See Entry 63309
- Influence of cyclic annealing on the hardness and structure of high-speed steels See Entry 63327
- Structure and properties of low-pearlite steel with different titanium concentrations See Entry 63330
- Effect of creep deformation on microstructural change in 12% Cr heat resisting steel See Entry 63349
- Heterogeneity of microstrains in alloy N45KHT specimens under tension See Entry 63362

- Effect of structure on the ductile-brittle transition temperature of molybdenum alloy TSM-6 See Entry 63406
- Failure mechanism for alloy KhN67VM under the action of a copper-silver solder See Entry 63411
- Intergranular zinc embrittlement and its inhibition by phosphorus in 55 pct Al-Zn-coated sheet steel See Entry 63453

81.40 TREATMENT OF MATERIALS AND ITS EFFECTS ON MICROSTRUCTURES AND PROPERTIES

63302 The evolution of the structure of a two-dimensional soap froth [theory of grain growth]. D.Weaire, J.P.Kermode (Dept. of Phys., Univ. of Coll., Dublin, Ireland). *Philos. Mag. B (GB)*, vol.47, no.3, p.L29-31 (March 1983). Soap froths are of interest because they are considered to evolve by a similar mechanism to that which governs grain growth in metals and sintered materials. The authors draw attention to the fact that the conclusions of Smith and others concerning the evolution of two-dimensional (2-D) soap froths, which are based on early experimental data, do not appear consistent with later data analysed by the Aboav (1980). This shows no stable limiting distribution of cell shapes within the range of the experimental samples. If this is accepted, the asymptotic evolution of the 2-D soap froth system (and any other physical system governed by analogous principles) must be radically different from what it is generally assumed to be. (6 refs.)

63303 Determination of the optimum grain size in KhN67MVTYa alloy taking account of the basic operational parameters. I.V.Doronin. *Russ. Metall. (GB)*, no.6, p.101-4 (1981). Translation of: *Izv. Akad. Nauk. SSSR Met.*, no.6, p.103-6 (1981).

An attempt is made to establish the dependence of the optimal grain size which ensures maximum high-temperature strength, on the require operating time and service life in the temperature range 600-900°C and failure times form 0.1 to 1000 hr. A similar relationship was obtained for the alloy KhN78T but for a narrower range of temperatures and times to failure. The applicability of the obtained formula is limited because it does not take into account the state of the grain boundaries, the distribution and degree of dispersion of the strengthening phase. (6 refs.)

Characterization of mechanical properties of nuclear waste glasses See Entry 60269

Orientiation relationships between BCC Mo and FCC γ in a Ni-Al-Mo-W superalloy See Entry 63257

Structure of titanium alloys and methods used for its control See Entry 63485

81.40C Solid solution hardening, precipitation hardening, dispersion hardening

63304 Use of the 'Tosol-K' quenching fluid for the bulk quenching of steels. V.I.Astashchenko, N.P.Ionkina, G.I.Yantsen, I.E.Sorokin, M.G.Gedberg.

Met. Sci. & Heat Treat. (USA), vol.24, no.5-6, p.377-80 (June 1982). Translation of: *Metallized. & Term. Obrab. Met. (USSR)*, vol.24, no.6, p.5-8 (June 1982). [received: Feb. 1983]

Investigates the possibility of using the 'Tosol-K' fluid for bulk quenching of steels. The 'Tosol-K' fluid (TU 6-02-3-144-78) is a 50% aqueous solution of oxyethylized alkylphenol containing antifoam and anticorrosion additives. It was concluded that 'Tosol-K' fluid is recommended for the bulk quenching of steel 45, 40Kh, 40KhN2MA, and 42KhMFA components. The high hardenability of the components in the absence of quenching cracks is ensured by selection of the concentration and temperature of the aqueous 'Tosol-K' solutions: a solution concentration of 0-30% for components of carbon steels, and 30-65% for components of the alloy steels. The temperature of a solution of any concentration should not exceed 40°C. Production testing of a 65% 'Tosol-K' solution for the quenching of steel 42 KhMFA crankshafts and a 50% solution for the quenching of steel 40Kh components indicated the high technological characteristics and effectiveness of the use of this polymer quenching medium. (4 refs.)

63305 Physicochemical fundamentals of the development of heat-resistant niobium alloys. V.G.Grogorovich, E.N.Sheftel.

Met. Sci. & Heat Treat. (USA), vol.24, no.7-8, p.472-8 (July-Aug. 1982). Translation of: *Metallized. & Term. Obrab. Met. (USSR)*, vol.24, no.7, p.23-9 (July 1982). [received: March 1983]

The principal methods of improving the heat resistance of niobium alloys are solid solution alloying and strengthening with dispersed particles of refractory phase. These methods are discussed with reference to equilibrium diagrams. (15 refs.)

Friction and source hardening in irradiated mild steel See Entry 61984

Effect of thermal conditions of preparation of dispersion-strengthened nickel powders on the character of distribution of the strengthening phase See Entry 63205

On the coarsening of γ' in Alloy 800 See Entry 63295

Examination of applied stress and prestrain effects on recovery of work hardened Cu-SiO₂ See Entry 63306

Influence of melting method, modification, and cyclic temperature-force action on the ductility of 1V7M6K12 steel See Entry 63361

Influence of heat treatment on the mechanical properties of dispersion hardening Nb-Zr-N alloys See Entry 63365

Examination of the effects of dimensional mismatch of the lattice parameters of the γ and γ' phases on the high-temperature strength of dispersion-hardened nickel alloys See Entry 63366

Effect of heat treatment on the fatigue strength of steel 50KhFA and alloy 40KKhNMVTYu See Entry 63405

Effect of structure on the ductile-brittle transition temperature of molybdenum alloy TSM-6 See Entry 63406

The development of nitrogen concentration profiles on nitriding iron See Entry 63452

Thermodynamics of homogeneous formation of cementite in austenite during case hardening of steel See Entry 63462

81.40E Cold working, work hardening; annealing, recovery and recrystallisation; textures

63306 Examination of applied stress and prestrain effects on recovery of work hardened Cu-SiO₂. N.Shigenaka, M.Okabe, T.Mori (Dept. of Materials Sci. & Engng., Tokyo Inst. of Technol., Yokohama, Japan). *Acta Metall. (USA)*, vol.31, no.5, p.801-4 (May 1983).

Effects on external stress and prestrain on recovery of work hardening have been studied in Cu-SiO₂ crystals. When the external stress is below a critical value, approximately equal to the yield stress, the softening on annealing is independent of the external stress. The softening decreases when the external stress exceeds the critical value. The temperature dependence of the softening rate is insensitive to the amount of the prestrain which has caused work hardening. It is concluded that the interaction between Orowan loops surrounding a SiO₂ particle is not so strong as to affect the climb rate of individual Orowan loops considerably. (12 refs.)

63307 The structural state and its association with low temperature work hardening of structural titanium alloys. B.I.Verkin, F.F.Lavrentev, Yu.A.Pokhil, P.P.Dudko (Phys.-Tech. Inst. of Low Temperatures, Acad. of Sci., Kharkov, Ukrainian SSR). *Cryogenics (GB)*, vol.23, no.4, p.203-6 (April 1983).

On the basis of transmission electron microscope investigations on the structural state of some structural titanium alloys strained at 4.2K, the nature of low temperature ductility work hardening and jumplike character of the stress-strain curve is analysed. (11 refs.)

63308 Effects of mechanical drawing treatment on the characteristics of internal friction and thermally stimulated current on low density polyethylene. Bong-Heup Kim, Do-Yul Kang, Jae-Hwan Kim (Korean Inst. Electrical Engrs., Seoul, Korea). *Trans. Korean Inst. Electr. Eng.*, vol.31, no.10, p.116-23 (1982). In Korean.

Investigates the relaxation of molecular chain segments on a low density polyethylene above room temperature. A peak observed about 40°C in internal friction and the main peak observed above 60°C in thermally stimulated current are related to the molecular chain relaxation process in the crystalline phase. Melt-recrystallisation occurs in the course of mechanical drawing to more than double length even at room temperature. For the origin of the trap of injected electrons in bulk, it is plausible to assume the distorted potential around the molecular chain due to micro-physical deformities existing already as incompleteness in the crystal as well as the interface between crystalline and amorphous regions of the real specimen. It is estimated that the activation energies of traps in the crystal phase and interface are 0.9 eV and 1.1 eV respectively; the height of potential barrier existing in the interface is about 0.3 eV. (14 refs.)

63309 Influence of sulfur and nitrogen on the characteristics of texture formation as a result of deformation and annealing of Fe+3% Si single crystals. R.L.Gershman, V.Ya.Goldshstein (Sci.-Res. Inst. of Metall., Chelyabinsk, USSR). *Fiz. Met. & Metalloved. (USSR)*, vol.55, no.2, p.396-400 (Feb. 1983). In Russian. English translation in: *Phys. Met. & Metallogr. (GB)*

A study was made of the influence of second-phase particles precipitated during various stages of the process of deformation and annealing, on the formation of a texture during annealing of silicon iron single crystals. The deformation by 70% involved cold rolling and various annealing treatments were applied. Precipitation of nitride and sulfide particles before cold rolling resulted in a scatter of the strain texture parameters. Precipitation of disperse phases during stages preceding recrystallization tended to improve the primary recrystallization texture and facilitated a second recrystallization during high-temperature annealing. (2 refs.) A.T.

63310 Effect of extinction of the texture coefficients of uranium. C.N.Rao, R.Krishnan (Metall. Div., Bhabha Atomic Res. Centre, Bombay, India). *J. Nucl. Mater. (Netherlands)*, vol.114, no.2-3, p.347-8 (Feb. 1983).

In calculating the texture parameters from measured X-ray intensities, extinction effects are generally neglected. However, this can lead to considerable uncertainty in representing the degree of texture. The influence of extinction on the intensities of Bragg reflections of uranium have therefore been discussed. (8 refs.)

63311 Effect of structure, substructure, and crystallographic texture on the mechanical properties of titanium alloys. A.I.Khorev, A.A.Babareko, A.I.Krasnozhan, S.Ya.Betsofen (All-Union Sci.-Res. Inst. of Aviation Materials, USSR). *Met. Sci. & Heat Treat. (USA)*, vol.24, no.7-8, p.463-7 (July-Aug. 1982).

Translation of: *Metallized. & Term. Obrab. Met. (USSR)*, vol.24, no.7, p.16-19 (July 1982). [received: March 1983]

The effectiveness of textural hardening under biaxial symmetric tension increased with increasing intensity of the (0001) base texture of the α -phase and decreased with increasing amount of β -phase in the alloys (from VT5-1 to VT14 and VT15). Experimental data agreed well with computed values. Use of specially controlled strain, heat-treatment, and thermomechanical-treatment conditions made it possible to vary directly the microstructure, substructure, and crystallographic texture of various classes of titanium alloys and to achieve a high level of strength in the plane and complex stressed states. (3 refs.)

63312 Recrystallisation of austenite in low-alloy steels (0.7% V, 0.04% Nb) with carbo-nitride hardening. Yu.I.Matrosov, V.N.Filimonov, M.L.Bernshteyn. *Russ. Metall. (GB)*, no.6, p.93-100 (1981). Translation of: *Izv. Akad. Nauk. SSSR Met.*, no.6, p.96-102 (1981).

Examination of the effect of the austenisation temperature has shown that for steel 09G2 (1.6% Mn, without V and Nb) an increase in the initial heating temperature from 950 to 1150°C slows down the softening during post-deformation holding; this is attributed to the decrease in the number of spots with germination of recrystallisation volumes, associated with the growth of the austenite grain and its increased homogeneity. In steel 09G2FB (1.55% Mn, 0.07% V, 0.04% Nb) an increase in the austenisation temperature above 1050°C slows down sharply static recrystallisation, and this is attributed to intensive dissolution of niobium carbonitride at this temperature and alloying of the austenite with the niobium. Provided that the micro-additions of niobium are first dissolved in the austenite, static recrystallisation after hot-deformation at 1100-1050°C is retarded; below 925°C the recovery and recrystallisation in niobium steel are virtually suppressed, mainly due to the separation of disperse Nb(C,N) particles on the substructure. Post-deformation holding at 750°C causes considerable softening for both the above steels, which is due to the deformation-initiated evolution of ferrite. (7 refs.)

63313 Preferred orientation in extruded aluminum alloy rod. D.N.Lee (Dept. of Metall. Engng., Seoul Nat. Univ., Seoul, Korea), Y.H.Chung, M.C.Shin.

Scr. Metall. (USA), vol.17, no.3, p.339-42 (March 1983).

Preferred orientation in extruded rod is better described by the axial and radial orientations except in the center fiber. The texture of the center is of the fiber type and can be described adequately by the axial orientation of strong {111} and weak {100}. The texture of the outer layer may be described by {110}(335) where {110} corresponds to the plane normal to the radial direction and {335} to the axial direction of the rod. This texture is comparable with the rolling texture of aluminum or its alloys, where the axial and radial directions correspond to the rolling direction and the direction normal to rolling plane, respectively. (10 refs.)

63314 Repeated mechanical strengthening as a method of increasing the endurance of constructional steels. A.V.Dobrik, V.F.Kucherenko, V.P.Latysh (M.I. Arsinichev Dneprodzerzhinsk Industrial Inst., USSR).

Sov. Mater. Sci. (USA), vol.18, no.3, p.283-5 (May-June 1982). Translation of: *Fiz.-Khim. Mekh. Mater. (USSR)*, vol.18, no.3, p.105-7 (May-June 1982). [received: Feb. 1983]

It is concluded that surface mechanical strengthening may be successfully used for increasing the life of parts formerly in service, including those with cracks. Cracks in the form of a network of thermal erosion appear particularly in hot-rolling rolls. Repeated surface plastic deformation may be an effective operation for restoring their life. A determination was made of the effectiveness of repeated surface work hardening to increase the life of certain constructional steels. The materials of the investigation were the widely used roll steels 45, 50KhN, and 60Kh2M in the normalized condition. The fatigue tests were made with circular bending on unnotched cylindrical samples after grinding (class seven surface finish). The cold work hardening was done by burnishing on a three-roller attachment with a clamping load of $P=1600$ N. (6 refs.)

63315 Free-cutting stainless steel wire with high-strength. H.Ogita (Res. & Dev. Group, Sumitomo Electric Industries Ltd., Osaka, Japan), S.Yamamoto, K.Sato.

Sumitomo Electr. Tech. Rev. (Japan), no.22, p.189-94 (Jan. 1983).

Cold-drawn and work-hardened SUS 304 stainless steel wire is often used as high strength stainless steel wires. While SUS 304 stainless steel is excellent in strength, ductility, corrosion resistance, high-temperature stability and other properties, as well as having a relatively low production cost, this material has certain limitations. Typically, when it is used for compression-coiled springs, antennas or shafts, it offers inferior grindability at the end surfaces or sides, and limited suitability for machining with cutting tools. Sulphur added SUS 303 stainless steel, which is frequently used as free-cutting stainless steel, has lower strengths and is also not suited for use in springs or antennas. In order to improve the machinability and grindability of SUS 304 stainless steel without reducing the strength, ductility or corrosion resistance additions of small amounts of sulphur, molybdenum and lead were made. The anticipated result was obtained, and a detailed description of the successful experiments is given. (no refs.)

Viscoplastic localization in simple shear: exact results in nonlinear theory See Entry 61444

Numerical solutions for analyzing the nonaxisymmetric 2-dimensional deformation processes See Entry 61424

X-ray diffraction methods to determine crystallinity and preferred orientation of lithium disilicate in Li-Zn-silicate glass-ceramic fibres See Entry 61806

A model for the evolution of a twist dislocation network See Entry 61912

Grain growth of tungsten fibres in a W-Ni composite during solid and liquid phase sintering See Entry 63218

Solidification of copper and silver in near-zero-g experiments See Entry 63277

Crystallographic aspects of precipitation of supersaturated aluminium-base solid solutions See Entry 63300

Recovery of properties and nature of ordering of steels during tempering under load See Entry 63316

Thermomechanical treatments of a 1050 pearlite steel See Entry 63318

The effect of ITMT's and P/M processing on the microstructure and mechanical properties of the X7091 alloy See Entry 63319

Effect of chromium and aluminum on the physical and mechanical properties of precipitation-hardening Fe-Mn Elinvar See Entry 63321

Recrystallization of deformed austenite in high-speed steel R6M5 See Entry 63325

Structure and properties of a maraging steel after thermomechanical and repeated heat treatment See Entry 63332

Influence of texture on dislocation creep and grain boundary sliding in fine-grained cadmium See Entry 63341

Influence of deformation and temperature on the structure and mechanical properties of high-cobalt alloy See Entry 63344

Effect of creep deformation on microstructural change in 12% Cr heat resisting steel See Entry 63349

Ductility characteristics of thin sheet steel See Entry 63358

Performance of the Ni-Ti alloy VTN-1 (54.5-55 wt.% Ni) in the case of shape restoration See Entry 63364

Superplasticity in an austenitic stainless steel containing aluminium and manganese See Entry 63368

Influence of high-temperature thermomechanical treatment on delayed fracture of hardened construction steel See Entry 63378

Notched unidirectional boron/aluminum: effect of matrix properties See Entry 63389

Influence of mean stress on coaxing effect of annealed 0.5% C steel under plane bending fatigue See Entry 63396

Thermally stressed condition occurring in the surface layers of flat parts during friction hardening See Entry 63429

Corrosion resistance of deep drawing sheet steel See Entry 63456

Effect of high-temperature vacuum annealing time on the structure and properties of titanium alloys See Entry 63457

Effect of annealing on the structure and properties of molybdenum coatings on steel Kh12M See Entry 63458

Effect of vibroabrasive treatment on the fatigue strength of high-alloy steels See Entry 63460

The use of time-of-flight neutron diffraction to study grain interaction stresses See Entry 63472

81.40G Other heat and thermomechanical treatments

63316 Recovery of properties and nature of ordering of steels during tempering under load. V.V.Zabil'skii, V.I.Sarrak (Inst. of Metal Phys., Acad. of Sci., Sverdlovsk, USSR).

Fiz. Met. & Metalloved. (USSR), vol.55, no.2, p.368-73 (Feb. 1983). In Russian. English translation in: *Phys. Met. & Metallog. (GB)*

An investigation was made of the influence of second heating of steels after tempering under load on the stability of the residual strain and on the improvement in the strength characteristics. It was found that second heating resulted in a partial reduction (recovery) of the residual strain, which was influenced by the processes occurring during tempering, such as precipitation of a solid solution of carbon in martensite and relaxation of the residual microstresses. Recovery of the residual strain was accompanied by softening. It was concluded that relaxation of the peak stresses was not the only reason for the increase of the strength as a result of tempering under load. This increase in the strength was largely due to the formation (as a result of tempering under load) of stresses with the opposite sign, which disappeared during second tempering. (4 refs.) A.7.

63317 Heat treatment of molybdenum, tungsten and their alloys up to 2100°C. R.Eck (Metallwerk Plansee GmbH, Reutte, Austria).

High Temp.-High Pressures (GB), vol.14, no.3, p.327-33 (1982). (10th Plansee Seminar on 'Trends in Refractory Metals, Hardmetals, and Special Materials, and their Technology', Reutte, Austria, 1-5 June 1981).

The heat treatment of powder metallurgical products of pure or alloyed molybdenum and tungsten has a determining influence on the properties of semifinished and final products. For metals that crystallize in a cubic body-centred lattice without a crystallographic transformation, the development of a controlled grain structure is essential. Problems of annealing in connection with recovery, recrystallization, and grain-growth, phenomena are discussed for selected examples which had been subjected to different degrees of deformation. The effects of heat treatment of molybdenum and TZM in hydrogen and vacuum at temperatures up to 2100°C on tensile properties of these materials are discussed. W5Re develops ductility maxima dependent on degree of deformation and annealing temperature. Problems of stress-relieving anneals are discussed with tungsten sheet used as an example. (7 refs.)

63318 Thermomechanical treatments of a 1050 pearlite steel. L.J.Chen, T.W.Wu, H.C.Cheng (Dept. of Materials Sci. & Engng., National Tsing Hua Univ., Hsinchu, Taiwan).

Metall. Trans. A (USA), vol.14A, no.3, p.365-78 (March 1983).

A study of the microstructures and mechanical properties of thermomechanically treated 1050 steel has been carried out. The materials were first transformed to fine and coarse lamellar pearlite structures. These samples were reduced 75 pct in thickness by cold rolling, then heat treated at 780°C (up-quenching) or 650°C (annealing) for different periods of time, followed by air-cooling. The mechanical properties were found to be vastly improved by suitable thermomechanical treatments. A significant improvement in yield strength was accompanied by moderate increase in ultimate tensile strength, and the elongations were maintained above 15 pct in 3 cm gage length. The optimal mechanical properties were developed between 30 and 120 seconds during 780°C up-quenching for coarse pearlite samples and 100 to 400 seconds for both annealed coarse and fine pearlite specimens. The improvement in mechanical properties was correlated with distinct microstructures in pearlite regions, which were fine subgrains (or grains) less than 1 μ m in size and dispersed globular carbide particles along the subgrain (or grain) boundaries. (13 refs.)

63319 The effect of ITMT's and P/M processing on the microstructure and mechanical properties of the X7091 alloy. V.W.C.Kuo, E.A.Starke, Jr. (Fracture & Fatigue Res. Lab., Georgia Inst. of Technol., Atlanta, GA, USA).

Metall. Trans. A (USA), vol.14A, no.3, p.435-47 (March 1983).

The influence of microstructure and texture on the monotonic and cyclic properties of X7091-T651 was investigated. The various structures were developed from conventional ingot metallurgy (I/M), powder metallurgy (P/M) and intermediate thermal mechanical treatments (ITMT). Powder metallurgy produced a finer grain structure and particle distribution than I/M. Intermediate thermomechanical treatment produced a recrystallized, coarse grain structure with a weak texture, compared to the unrecrystallized grain structure and sharp texture obtained with conventional processing (CP). All materials had comparable monotonic properties. The resistance to fatigue crack initiation (FCI) increased with both a reduction in grain size and a finer particle distribution. It appears that large grains allow more reversible slip and reduce the amount of accumulated plastic strain within the reverse plastic zone. It is also believed that a greater degree of fatigue crack closure, which may be associated with large grains and a rough FCP surface, results in a lower FCGR in the low ΔK region. The intermediate thermomechanical treatment of P/M X7091 produced the optimum microstructure giving the best combination of mechanical properties. (48 refs.)

63320 Influence of surface condition on the magnetic properties of Fe-3% Si alloy. R.B.Puzhevich, V.G.Borisenko, L.A.Shyartsman, V.I.Chistyakov, Z.P.Ventskovich (Ural Sci.-Res. Inst. for Ferrous Metals, USSR).

Met. Sci. & Heat Treat. (USA), vol.24, no.5-6, p.422-5 (June 1982). Translation of: *Metall. & Term. Obrab. Met. (USSR)*, vol.24, no.6, p.39-41 (June 1982). [received: Feb. 1983]

An investigation was made of the influence of the primer coat on the magnetic properties of Fe-Si alloy after high temperature annealing. With the use of hydrated magnesium oxide to obtain the magnesium coating on Fe-3% Si alloy the negative influence of the coating on the magnetic properties of this alloy related to the introduction of oxides into the surface of the metal exceeds the positive influence caused by the occurrence of tensile stresses. The magnetic properties of Fe-3% Si alloy given a high temperature anneal without coating are higher than of the alloy annealed with a coating formed from hydrated magnesium oxide. A decrease in the negative influence of the primer coat may be obtained by selection of an original material for the coating which provides preferential formation of primer coats at temperatures exceeding the temperature of secondary recrystallization of the metal. A decrease in the moisture content of the original material, magnesium oxide, causes an increase in the temperature of formation of the primer coat of magnesium silicate coatings. (9 refs.)

63321 Effect of chromium and aluminum on the physical and mechanical properties of precipitation-hardening Fe-Mn Elinvar. O.A.Khomenko, I.F.Khil'kevich (Ural Sci.-Res. Inst. of Ferrous Metall., USSR).

Met. Sci. & Heat Treat. (USA), vol.24, no.5-6, p.425-8 (June 1982). Translation of: *Metall. & Term. Obrab. Met. (USSR)*, vol.24, no.6, p.42-4 (June 1982). [received: Feb. 1983]

Concerns the physical and mechanical properties of precipitation-hardening Fe-Mn Elinvars additionally alloyed with aluminum and chromium to improve the corrosion resistance. The combination of physical and mechanical properties and corrosion resistance is optimal for precipitation-hardening Fe-Mn

Elinvar with 5-6% Cr. This alloy can be recommended for elastic elements operating under various conditions. To obtain high strength and elasticity in combination with satisfactory ductility, the authors recommend that Elinvars be strengthened by mechanothermal treatment: water quenching from 1150-1200°, cold deformation with $\epsilon=25\%$, aging at 500° for 6 h. (2 refs.)

63322 Austenite grain refining with rapid heating of steel 40 Kh. K.Z. Shepelevskii, L.A. Lisitskaya (Moscow Evening Metall. Inst., Moscow, USSR).

Met. Sci. & Heat Treat. (USA), vol.24, no.7-8, p.443-5 (July-Aug. 1982). Translation of: *Metalloved. & Term. Obrab. Met. (USSR)*, vol.24, no.7, p.2-3 (July 1982). [received: March 1983]

In the process of rapid heating ($v_h=14$ deg/sec) of annealed steel 40 Kh the original austenite grains (grade 9) are refined twice—at the end of the $\alpha\rightarrow\gamma$ transformation at 860° (to grade 10) and at 950° (to grade 13). On the basis of the data obtained, it is proposed that nucleation and growth of austenite grains may occur by means of the $\alpha\rightarrow\gamma$ transformation with formation of finer austenite grains than the original grains and additional refining at a higher temperature, evidently due to recrystallization. It is recommended that the data obtained on austenite grain refining as the result of accelerated heating be used in selecting induction hardening conditions for steel in the high-strength condition. (6 refs.)

63323 Effect of HTTT on the properties of alloy steel castings. M.Kh. Sharifov, R.I. Shukuyrov (Baku Polytech. Inst., Azerbaidzhan SSR).

Met. Sci. & Heat Treat. (USA), vol.24, no.7-8, p.451-4 (July-Aug. 1982). Translation of: *Metalloved. & Term. Obrab. Met. (USSR)*, vol.24, no.7, p.8-10 (July 1982). [received: March 1983]

HTTT (as compared with quenching and high-temperature tempering) was found to improve the strength, ductile characteristics, and fracture toughness of castings of steels 20KhGSL, 30KhNML, and 40KhL. Tests of oil field equipment after HTTT indicated that the combination of mechanical properties is 30-50% better and the wear resistance 20% better. The significant characteristic of strengthening in steels 20KhGSL, 30KhNML, and 40KhL by HTTT was the substantial improvement in the mechanical properties after small deformations. (3 refs.)

63324 Effect of rate of heating for hardening on the structure of alloys VT23 and VT6. O.M. Ivasishin, S.P. Oshkaderov (Inst. of Metal Phys., Ukrainian SSR).

Met. Sci. & Heat Treat. (USA), vol.24, no.7-8, p.459-62 (July-Aug. 1982). Translation of: *Metalloved. & Term. Obrab. Met. (USSR)*, vol.24, no.7, p.14-16 (July 1982). [received: March 1983]

The mechanical properties of titanium alloys of a heterophase ($\alpha+\beta$) structure are determined not only the size of the grain, but also by the intragrain structure. In this connection, the authors analyzed the effect of rapid heating on the formation of the grain and intragrain structure in titanium alloys with an initial fine-grain structure formed during pressure treatment in the ($\alpha+\beta$)-region. (2 refs.)

63325 Recrystallization of deformed austenite in high-speed steel R6M5. Yu.P. Egorov, I.O. Khazanov (Tomsk Polytech. Inst., Tomsk, USSR).

Met. Sci. & Heat Treat. (USA), vol.24, no.7-8, p.509-14 (July-Aug. 1982). Translation of: *Metalloved. & Term. Obrab. Met. (USSR)*, vol.24, no.8, p.2-6 (Aug. 1982). [received: March 1983]

The main processes determining the formation of the austenitic structure in deformed steel R6M5 during heating to quenching temperature and in the process of holding at this temperature are found to be polygonization and recrystallization. With deformation near the critical the recrystallization process proceeds by recrystallization in place, which leads to sudden austenite grain growth. The proposed recrystallization mechanism with near-critical deformation is based on the possibility of a section of high-angle boundary transforming to a section with a low-angle misorientation in the process of recrystallization in place and later avalanche-like combination of original austenite grains. (10 refs.)

63326 Austenite grains in tungsten-molybdenum high-speed steels after repeated quenching. A.N. Popandopulo, S.D. Popova, E.F. Sil'nikova (Leningrad Polytech. Inst., Leningrad, USSR).

Met. Sci. & Heat Treat. (USA), vol.24, no.7-8, p.515-18 (July-Aug. 1982). Translation of: *Metalloved. & Term. Obrab. Met. (USSR)*, vol.24, no.8, p.6-8 (Aug. 1982). [received: March 1983]

Tungsten-molybdenum high-speed steels are found to be susceptible to intercrystalline fracture. Spontaneous recrystallization of austenite and solution of carbides preceded sudden grain growth. The sudden grain growth occurred by the fusion mechanism. The fusion and growth of silky grains occurred within the limits of the original grains. (8 refs.)

63327 Influence of cyclic annealing on the hardness and structure of high-speed steels. E.A. Smol'nikov, L.M. Orestova (All-Union Sci.-Res. Tool Inst., USSR).

Met. Sci. & Heat Treat. (USA), vol.24, no.7-8, p.519-25 (July-Aug. 1982). Translation of: *Metalloved. & Term. Obrab. Met. (USSR)*, vol.24, no.8, p.9-14 (Aug. 1982). [received: March 1983]

In individual cases with the necessity of rapid annealing of high-speed steel together with stepless annealing at 885-675°C, which is done in a single salt bath, cyclic stepped annealing in two salt baths with temperatures of 850 and 700°C and holds in each of them at from 10 to 30 min may be used. It is more rational to use stepless cyclic annealing for small diam. (≤ 30 mm) solid and welded pieces while stepped cyclic annealing may be used for larger pieces. In comparison with isothermal annealing, cyclic annealing using the recommended cycles provides a decrease in the width of the ferrite zone of welded parts in the area of the joint. The structure, distribution, and chemical composition of the carbide phase after cyclic and after isothermal annealing differ very little, which is indicated by the results of hardness measurement. (4 refs.)

63328 Heat resistance of the substructure of hot worked austenite. M.L. Bernshtein, L.M. Kaputkina, N.A. Nikishov (Moscow Inst. of Steel & Alloys, Moscow, USSR).

Met. Sci. & Heat Treat. (USA), vol.24, no.7-8, p.537-42 (July-Aug. 1982). Translation of: *Metalloved. & Term. Obrab. Met. (USSR)*, vol.24, no.8, p.24-8 (Aug. 1982). [received: March 1983]

Varying the hot deformation conditions made it possible to obtain a broad variety of structural and substructural conditions of austenite. Reducing the rate and raising the temperature made it possible to obtain a polygonized substructure after hot deformation and retain it after cooling. A homogeneous polygonized isotropic substructure with a fairly low density of dislocations within subgrains slowed down the initial stages in the development of recrystallization under conditions of hot deformation and controlled postdeformation holding. This substructure can be obtained in the steady stage of hot deformation and also by the development of static polygonization processes during brief postdeformation holding. (6 refs.)

63329 Recrystallization of nickel alloy KhN62BMKTYu during hot deformation and quenching. N.N. Korneeva, A.B. Notkin, A.S. Kleshech (All-Union Inst. of Light Alloys, USSR).

Met. Sci. & Heat Treat. (USA), vol.24, no.7-8, p.578-80 (July-Aug. 1982). Translation of: *Metalloved. & Term. Obrab. Met. (USSR)*, vol.24, no.8, p.55-7 (Aug. 1982). [received: March 1983]

Structural diagrams of recrystallization plotted in coordinates of temperature and deformation indicate regions of unrecrystallized, mixed, and completely recrystallized structure after deformation and quenching of alloy KhN62BMKTYu. The structure is polygonal in unrecrystallized sections after quenching from 1050-1080°C. (4 refs.)

63330 Structure and properties of low-pearlite steel with different titanium concentrations. A.G. Nasibov, G.A. Sveshnikov, G.G. Gulei, R.K. Guseinov, V.G. Lamintsev (I.P. Bardin Central Sci.-Res. Inst. of Ferrous Metall., USSR).

Met. Sci. & Heat Treat. (USA), vol.24, no.7-8, p.581-2 (July-Aug. 1982). Translation of: *Metalloved. & Term. Obrab. Met. (USSR)*, vol.24, no.8, p.58-9 (Aug. 1982). [received: March 1983]

The authors investigated the effect of Ti content on the structure, fracture toughness and susceptibility to brittle fracture of commercial low-pearlite steel 10G27. Changing the Ti content from 0.015 to 0.045% was found to have practically no effect on the mechanical properties; the main difference is the tendency to austenite grain growth. (1 ref.)

63331 Effect of technological inheritance on the hardness of malleable iron after heat treatment. S.N. Biler-Sirotkina (V.Ya. Chubar' Zaporozh'e Machine Construction Inst., USSR).

Met. Sci. & Heat Treat. (USA), vol.24, no.7-8, p.583 (July-Aug. 1982). Translation of: *Metalloved. & Term. Obrab. Met. (USSR)*, vol.24, no.8, p.59-60 (Aug. 1982). [received: March 1983]

Ten serially-produced castings of rear brake drums made of pearlitic malleable iron KCh 50-5 (GOST 1215-79) were normalized at 860°C (2 h) in order to determine the effect of inheritance on the hardness of the castings after heat treatment. It is found that the hardness curve after normalization is similar to the original hardness curve except that the values are consistently higher. Thus, from the original hardness it is possible to predict the hardness of the casting after heat treatment. (no refs.)

63332 Structure and properties of a maraging steel after thermomechanical and repeated heat treatment. M.L. Bernshteyn, L.M. Kaputkina, V.G. Prokoshkina, V.A. Varganov, G.S. Krivonogov, A.S. Klyuch.

Russ. Metall. (GB), no.6, p.105-12 (1981). Translation of: *Izv. Akad. Nauk. SSSR Met.*, no.6, p.107-14 (1981).

To model the structure of austenite hot-deformed during high-temperature thermomechanical treatment, a steel was chosen with a composition close to that of the commercial steel 08Kh15N5D2T, the only difference being that it also had an austenitic structure at room temperature which was achieved by increasing the nickel content by an additional 8%. An optimal combination of the mechanical properties after quenching and ageing for maximum hardness was achieved by using high degrees of deformation during the thermomechanical treatment. After optimal high-temperature thermomechanical treatment in the aged state, some increase in strength was achieved with a considerable increase in the impact strength and this applies in particular in the presence of stress concentrators. The improved properties are due to the favourable combination of direct inheritance of the polygonized austenite structure in the martensite grains, with refining of the austenite grain by partial recrystallization, as well as a more uniform and disperse evolution of copper during ageing. (7 refs.)

63333 Influence of residual gas pressure in annealing on the properties of niobium and its alloys. G.G. Maksimovich, E.M. Lyutiy, M.I. Ignatov (G.V. Karpenko Physicochem. Inst., Acad. of Sci., Lvov, Ukrainian SSR).

Sov. Mater. Sci. (USA), vol.18, no.3, p.257-61 (May-June 1982). Translation of: *Fiz.-Khim. Mekh. Mater. (USSR)*, vol.18, no.3, p.78-84 (May-June 1982). [received: Feb. 1983]

The authors investigated the influence of impregnation with interstitial impurities in annealing in 0.1 and 10 mPa vacuums on the properties of niobium and its alloys. The tests were made on microsamples with a gauge length cross section of 1×3 mm. According to the data of an analysis of the oxygen and nitrogen content in the investigated materials after annealing, the quantity of interstitial impurities in the samples increases somewhat, although it does not exceed measuring error (0.005 wt.%). It is concluded that in impregnation of samples by interstitials under the given conditions the distribution of oxygen is uniform. The quantity of nitrogen decreases from the surface into the body of the material, which leads to a change in mechanical properties across the cross section. (22 refs.)

63334 Recrystallization processes in amorphous and polycrystalline silicon. G. Ottaviani.

Report EUR 8141 EN, Comm. European Communities, Luxembourg (1982), 11 pp. Contract 445-78-7 ESI.

Investigates the recrystallization process using nonconventional heating techniques obtained by shining the sample with high power laser or electron pulses. The interaction between an amorphous silicon film and a metal layer when the whole structure is submitted to heat treatment either at low temperature using a conventional furnace or with a pulsed energy source is also studied.

Plastic flow and fracture of Ti-modified 316 austenitic stainless steel after high temperature aging in hydrogen See Entry 60413

Effect of external stress on formation of vacancy loops in quenched aluminum See Entry 61909

Electron-microscopy study of the decomposition of a supersaturated solid solution in silicon See Entry 62112

Morphology and composition of films based on gold on the surface of gallium arsenide during vacuum annealing See Entry 62287

Temperature dependence of electrical resistivity of Al-Zn alloys See Entry 62394

Mechanism of formation of magnetic properties of amorphous alloy Fe₅Co₇Si₁₅B₁₀ during annealing See Entry 62694

Low field properties of FeNiMnB amorphous alloy See Entry 62700

Effect of fabrication condition on the magnetic properties of Fe-Mn-B system amorphous alloys See Entry 62704

Short-time sintering of hard metals See Entry 63249

Interaction of hydrogen with traps and its solubility in maraging steel See Entry 63256

An investigation of the process of decomposition of the supersaturated solid solution of nitrogen in a niobium alloy See Entry 63258

Change in the electrical resistivity of Al-3.5% Cu during thermal cycling in the solidus-liquidus range See Entry 63263

- Formation and stability of reverted austenite in low-carbon nickel-molybdenum steels See Entry 63284
- Investigation of the phase composition, structure, and magnetic properties of alloy $\text{Sm}_2\text{Co}_{10}\text{Fe}_{3.2}\text{Cu}_{1.2}\text{Zr}_{0.4}$ See Entry 63287
- Decomposition kinetics for supercooled austenite in steel 15Kh1M1F See Entry 63288
- Influence of alloying and preliminary deformation on phase composition and mechanical properties of Fe-Mn alloys See Entry 63291
- Crystallographic aspects of precipitation of supersaturated aluminium-base solid solutions See Entry 63300
- Effect of structure, substructure, and crystallographic texture on the mechanical properties of titanium alloys See Entry 63311
- Internal friction study of AISI 410 stainless steel See Entry 63338
- Influence of deformation and temperature on the structure and mechanical properties of high-cobalt alloy See Entry 63344
- On the Portevin-Le Chatelier effect due to Snoek strain aging in the niobium oxygen system See Entry 63353
- Characteristics of structural transformations during deformation and heat treatment of Elinvar alloy 45 NKht See Entry 63356
- Effect of heat treatment in magnetic field on the mechanical properties of carbon steels See Entry 63357
- Effect of diffusion welding thermal cycle on the strength of alloy VT20 See Entry 63359
- Influence of melting method, modification, and cyclic temperature-force action on the ductility of IV7M6K12 steel See Entry 63361
- Influence of heat treatment on the mechanical properties of dispersion hardening Nb-Zr-N alloys See Entry 63365
- Anomalous dynamic superplasticity and quasiliquid condition of iron in the presence of hydrogen See Entry 63370
- Effect of the annealing on the mechanism of plastic strain in oriented polypropylene See Entry 63373
- Influence of strain ageing of martensite by hydroextrusion on the fine structure and surface relief in ductile fracture of 30KhGSN2A steel See Entry 63377
- Influence of high-temperature thermomechanical treatment on delayed fracture of hardened construction steel See Entry 63378
- Indentation-induced cracks in hot-pressed Si_3N_4 See Entry 63380
- Microstructure and tensile ductility in a β heat treated titanium alloy See Entry 63400
- Influence of annealing temperature on the character of fracture of 4KhMFSNB cast die steel See Entry 63404
- Effect of structure on the ductile-brittle transition temperature of molybdenum alloy TsM-6 See Entry 63406
- Reasons for the reduction in the fracture toughness of alloy KhN77TYuR-VD at room temperature See Entry 63412
- Mechanical properties of ageing of non-magnetic austenitic steels at low temperatures See Entry 63417
- Heat treatment and magnetic properties of high-coercivity Fe-Co-Cr alloys with 3% Mo See Entry 63435
- Corrosion resistance of deep drawing sheet steel See Entry 63456
- Fatigue strength of steel 45 with electrolytic iron coating, carbon nitrided with HF heating See Entry 63461
- Metallographic signs of forging overheating in 11Kh4F3S2V2M die steel See Entry 63483

81.40J Elasticity and anelasticity

(see also 62.20D Elastic constants, 62.40 Anelasticity, internal friction, and mechanical resonances)

- 63335 The role of elastic interaction stresses on the onset of slip in polycrystalline alpha brass. II. Rationalization of slip behavior. K.Hashimoto, H.Margolin (Dept. of Phys. & Engng. Metall., Polytech. Inst. of New York, New York, NY, USA). *Acta Metall. (USA)*, vol.31, no.5, p.787-800 (May 1983). For pt.1, see ibid., vol.31, no.5, p.773 (1983). A finite element method analysis, extended to three dimensions, was used to calculate the stresses in 11 grains of an as-cast, 2.4 mm grain size α -brass specimen strained to the proportional limit. Resolved shear stresses (RSS) were not uniformly distributed. However, the predicted slip system based on highest total RSS was found to operate in 9 of the 11 grains. In the other two cases it was not possible to predict which of the two highest RSS slip systems would operate because the RSS were too close. RSS at which slip occurred were compatible with those found by other investigators and measured slip offsets were generally higher where the calculated stresses were higher. Second highest or lower RSS slip systems, which did not form strong obstacles with the primary slip systems, were found to operate. The range of stresses in a given grain, over which slip occurred increased with grain size. On the basis of available evidence, it must be considered that elastic interaction stresses play an important role in the yield process and may exercise influence for strains of at least several percent. (12 refs.)
- 63336 The rheology of thin polystyrene films. B.J.Briscoe, A.C.Smith (Dept. of Chem. Engng. & Chem. Technol., Imperial Coll., London, England). *J. Macromol. Sci. - Phys. (USA)*, vol.B22, no.1, p.53-68 (1983). The interfacial shear strength of a polymer may conveniently be measured by confining a thin film in a sliding elastically deforming contact. The shear strength, defined as the frictional force per unit sheared area, is a measure of the energy dissipation in the film although it implies no particular mechanism. In this paper the shear strength is investigated as a function of both contact pressure and temperature for atactic and isotactic polystyrenes. The thin films have been cast from various solvents accompanied by a range of heat treatments. The data indicate that the casting solvent and the thermal history have a greater influence on the interfacial shear strength than the molecular architecture. The use of friction measurements to probe polymer-solvent interactions is discussed. (31 refs.)
- 63337 The influence of fillers of different activity on the relaxation behaviour of elastomers. G.M.Bartenew, I.L.Gorolova. *Plaste & Kautsch. (Germany)*, vol.30, no.1, p.13-18 (Jan. 1983). In German. Elastomers are complex colloidal systems in which various relaxation phenomena take place. The relaxation of filled elastomers can be caused by heating and one such characteristic relaxation spectrum at 20°C is illustrated, but it can also be effected by mechanical, electrical and magnetic stimulation.

Relaxation changes caused by fillers of different activities of polyisoprene SKI-3 were observed in a series of tests and results are reported. The relaxation time depends on temperature and a formula for its calculation is given. In order to explain the mechanism of relaxation, knowledge of the kinetics of molecular movement is essential and an attempt to tackle this problem is described. Tests using fillers such as soot, graphite, chalk on the SKI-3 polymer are described and relaxation time spectra resulting from these tests are shown. Experimental results agreed reasonably well with theoretical calculations. (11 refs.) G.R.S.

63338 Internal friction study of AISI 410 stainless steel. A.Wolfenden (Dept. of Mech. Engng., Texas A&M Univ., College Station, TX, USA). *Scr. Metall. (USA)*, vol.17, no.3, p.321-5 (March 1983). The results of an internal friction study done at low stress (<37 MPa) on AISI 410 stainless steel in four different conditions of heat treatment are reported. Young's modulus values are given and the strain amplitude dependence of Q^{-1} is analyzed in terms of the Granato-Lücke theory of dislocation damping (1956) to provide an interpretation of the internal friction in terms of microstructural features. Finally, a comparison of the results of this interpretation with metallographic observations on similar turbine blade alloys is made. (12 refs.)

63339 Hydrogen-related internal friction peak in the A15 compound Nb_3Sn . B.S.Berry, W.C.Pritchett (IBM Thomas J. Watson Res. Center, Yorktown Heights, NY, USA), J.F.Bussiere. *Scr. Metall. (USA)*, vol.17, no.3, p.327-32 (March 1983). Some aspects of the hydrogen peak in polycrystalline Nb_3Sn are similar to the hydrogen peak in amorphous Nb_3Ge , which is believed to be of the Snoek type. The two peaks are found at similar temperatures, and are of a comparable magnitude. For both materials, the peaks can only be of a Snoek type if hydrogen atoms act as much stronger elastic dipoles than appears to be the case for BCC Nb. There are, however, important characteristics of the peak in Nb_3Sn that are hard to reconcile with a Snoek-type mechanism. The most troublesome of these are (a) the behavior of the modulus, and (b) the large dispersion associated with the peak, which is even greater than that for the hydrogen peak in glassy Nb_3Ge . From the presently available evidence, therefore, the authors conclude that the 260K peak in Nb_3Sn is probably not a hydrogen Snoek peak. (20 refs.)

63340 Interrelationship of Poisson's ratio with other characteristics of pure metals. S.I.Mikitishin (G.V. Karpenko Physicomech. Inst., Acad. of Sci., Lvov, Ukrainian SSR). *Sov. Mater. Sci. (USA)*, vol.18, no.3, p.262-5 (May-June 1982). Translation of: *Fiz.-Khim. Mekh. Mater. (USSR)*, vol.18, no.3, p.84-8 (May-June 1982). [received: Feb. 1983] Investigates the physical nature of Poisson's ratio and the interrelationship of it with other characteristics of metals, including the melting point, hardness of the metal, and the elastic constants and also of its relationship to the temperature, amount of deformation, and structural condition of the material. (14 refs.)

Use of nonlinear viscoelastic materials in the polarization-optical method See Entry 61465

Theoretical prediction of domain sizes in IPNs and related materials See Entry 61824

The role of elastic interaction stresses on the onset of slip in polycrystalline alpha brass. I. Experimental determination of operating slip systems and qualitative analysis See Entry 61927

Computation of normal modes from identified complex modes See Entry 62008

Hydrogen relaxation in lutetium See Entry 62026

Some remarks on the carbon atoms pairs migrational relation in $\alpha\text{Fe-C}$ See Entry 62181

Characterization of the three dimensional properties of poled PZT 65/35 in the absence of losses See Entry 62894

Elastic behavior and phase stability of $\beta_1\text{-AgCd}$ alloy See Entry 63292

Effects of mechanical drawing treatment on the characteristics of internal friction and thermally stimulated current on low density polyethylene See Entry 63308

Effect of chromium and aluminum on the physical and mechanical properties of precipitation-hardening Fe-Mn Elinvar See Entry 63321

Properties of polyethylene-propylene blends. III. Mechanical characterization of ultradrawn fibres See Entry 63348

On the Portevin-Le Chatelier effect due to Snoek strain aging in the niobium oxygen system See Entry 63353

Superplasticity in Al-Li based alloys See Entry 63369

Correlation of hardness and microstructure in unoriented lamellar polyethylene. II. Study of elastic modulus See Entry 63384

81.40L Deformation, plasticity and creep

(see also 62.20F Deformation and plasticity, 62.20H Creep)

63341 Influence of texture on dislocation creep and grain boundary sliding in fine-grained cadmium. Shu-En Hsu (Nat. Taiwan Univ., Taipei, Taiwan), G.R.Edwards, O.D.Sherby. *Acta Metall. (USA)*, vol.31, no.5, p.763-72 (May 1983).

The creep behavior of cadmium was studied over the temperature range 0°-260°C (0.46-0.9 T_m) and was found to depend on grain size and texture. Whereas the creep behavior of cast cadmium of moderate grain size (150 μm) is comparable to the creep of most pure polycrystalline metals, unusual creep behavior was observed for a fine-grained (9 μm), textured, powder metallurgy cadmium. The following characteristics were noted for the fine grained textured material. At high stresses and low temperatures, marked change of texture with creep deformation are observed, and the stress exponents and activation energies obtained are consistent with control of deformation by a short circuit diffusion dislocation mechanism. At low stresses and high temperatures, all observations imply that deformation occurred by grain boundary sliding accommodated by slip in the vicinity of the grain boundary. A stress exponent of two, an activation energy equal to that for grain boundary diffusion and no strain hardening characterize plastic flow in this region; furthermore, it was noted that the ease of grain boundary sliding was influenced by texture, an observation which suggests that crystallographic factors contribute to grain boundary sliding. (53 refs.)

- 63342 Microstructure of aluminium during creep at intermediate temperatures. III. The rate controlling process.** D.Caillard, J.L.Martin (Lab. d'Optique Electronique, CNRS, Toulouse, France). *Acta Metall. (USA)*, vol.31, no.5, p.813-25 (May 1983). For pt.II see ibid., vol.30, p.791 (1982). A microscopic picture of the second stage of creep of aluminium at intermediate temperatures has been worked out. The movement of individual dislocations responsible for the main part of deformation during in situ experiments in a high voltage electron microscope is presented. The mobile dislocations are emitted by sources situated inside a few subgrains. They have to cut through subboundaries and this appears to be the rate controlling process. This mechanism which is described as insertion followed by extraction, is studied in detail, as well as annihilation of mobile dislocations in other subboundaries. It is easier than the Orowan process, and it involves cross slip, but no climb. However, the stress necessary is higher than the applied stress, so that extraction requires high local forward internal stresses in subboundaries. The different type of recovery observed—static and dynamic—are discussed, and it is concluded that cross slip is the rate controlling mechanism of creep of aluminium at intermediate temperatures. (36 refs.)
- 63343 Characteristics of plastic deformation of silicon iron single crystals under hydrostatic pressures.** A.V.Dobromyslov, G.V.Dolgikh, N.I.Taluts, V.T.Shtmatov, B.I.Beresnev (Inst. of Metal Phys., Acad. of Sci., Sverdlovsk, USSR). *Fiz. Met. & Metalloved. (USSR)*, vol.55, no.2, p.374-8 (Feb. 1983). In Russian. English translation in: *Phys. Met. & Metallogr. (GB)*. A study was made of the influence of hydrostatic pressure on the orientational dependence of the active slip plane in Fe-2.9% Si single crystals. A study of the slip geometry on the stretched and compressed sides of single crystals deformed by bending was made by X-ray structure analysis, and by optical and scanning electron spectroscopy. It was established that the application (during plastic deformation) of a hydrostatic pressure of 550 MPa altered the active slip plane in a certain range of orientations. The changes observed during compression and stretching were attributed to the action of normal stresses and to the special structure of screw dislocations in b.c.c. metals. (11 refs.) *A.T.*
- 63344 Influence of deformation and temperature on the structure and mechanical properties of high-cobalt alloy.** R.N.Eshchenko, V.A.Teplov, G.A.Lyadskaya, B.I.Beresnev (Inst. of Metal Phys., Acad. of Sci., Sverdlovsk, USSR). *Fiz. Met. & Metalloved. (USSR)*, vol.55, no.2, p.379-84 (Feb. 1983). In Russian. English translation in: *Phys. Met. & Metallogr. (GB)*. An investigation was made of the phase composition, structure, and mechanical properties of a Co-Ni-Cr-Mo alloy with 50% Co as a function of the degree of deformation in the course of hydroextrusion, temperature of the subsequent heat treatment, and temperatures during mechanical tests. It was found that hydroextrusion could result in a considerable increase in the strength. Recrystallization of the hydroextruded material produced a fine-grain structure characterized by a high plasticity above the recrystallization temperature. Electron-microscopic and X-ray structure data were used to analyze the relationships between the phase composition, structure, and mechanical properties. (9 refs.) *A.T.*
- 63345 Structural mechanism of plastic deformation of Mn-Cu alloys in martensitic state.** S.A.Demin, A.I.Ustinov, K.V.Chuistov (Inst. of Metal Phys., Acad. of Sci., Kiev, Ukrainian SSR). *Fiz. Met. & Metalloved. (USSR)*, vol.55, no.2, p.385-9 (Feb. 1983). In Russian. English translation in: *Phys. Met. & Metallogr. (GB)*. The dependence of the nature of deformation of Mn-Cu in the martensitic state was determined as a function of the magnitude and direction of external stresses. An X-ray diffraction study of the structural state of the investigated alloys was made in the presence of external stresses. Superplasticity of the martensitic Mn-Cu alloys was attributed to a change in the ratio of the twinning components in the martensite crystals at low deformations and to reorientation of the martensite crystals at high deformations. (9 refs.) *A.T.*
- 63346 Strengthening of cast low-pearlite steels by microalloying with vanadium.** M.S.Mikhalev, E.A.Murav'ev, T.B.Munarova (All-Union Res. Inst. of Railroad Transport, Sverdlovsk, USSR). *Fiz. Met. & Metalloved. (USSR)*, vol.55, no.2, p.410-12 (Feb. 1983). In Russian. English translation in: *Phys. Met. & Metallogr. (GB)*. Mechanical properties of over 20 low-carbon steels with different chemical compositions were studied. The effects of adding 0.1% V on the yield stress indicated that the addition of vanadium to normalized cast low-pearlite low-carbon steels was undesirable. (2 refs.) *A.T.*
- 63347 On the origin of the first peak of acoustic emission in 7075 aluminium alloys.** R.Wells (Dept. of Mech. Engng., Univ. of California, Davis, CA, USA), M.A.Hamstad, A.K.Mukherjee. *J. Mater. Sci. (GB)*, vol.18, no.4, p.1015-20 (April 1983). The origin of acoustic emission (AE) in 7075 aluminium alloy was investigated in tension and compression tests. It is suggested that the first peak associated with the root-mean-square (RMS) AE plot against time (or strain) is due to the unpinning of dislocation segments from solute atom clusters and is not due to the fracture of particles. Alteration in the value of the AE first peak and also in electrical resistivity values due to heat treatment of this alloy support the proposed origin of the AE first peak near yield. (32 refs.)
- 63348 Properties of polyethylene-propylene blends. III. Mechanical characterization of ultradrawn fibres.** Ma Rong Tang, R.Greco, G.Ragosta, S.Cimmino (Istituto di Recherche su Tecnologia dei Polimeri e Reologia, CNR, Arco Felice, Italy). *J. Mater. Sci. (GB)*, vol.18, no.4, p.1031-8 (April 1983). For pt.II see ibid., vol.16, p.1001 (1981). High density polyethylene-isotactic polypropylene blends have been analysed using mechanical tensile tests at temperature (T) ranging from 25 up to 150°C and at crosshead speeds ranging from 0.01 to 500 mm min⁻¹. The data have been tentatively interpreted in terms of cold and hot drawing mechanisms, depending on the values of T and v . Such interpretation is quite different from that previously suggested in the literature. Using the results of this analysis it has been possible, by a suitable choice of the operating variables T and v , to yield ultradrawn blend fibres. Their mechanical properties, obtained at room temperature and at a cross-head speed of 10 mm min⁻¹, have been analyzed and discussed. (16 refs.)
- 63349 Effect of creep deformation on microstructural change in 12% Cr heat resisting steel.** T.Tschiyama, T.Fujita (Faculty of Engng., Univ. of Tokyo, Tokyo, Japan). *J. Soc. Mater. Sci. Jpn. (Japan)*, vol.31, no.350, p.1080-5 (Nov. 1982). In Japanese. [received: April 1983]. The effect of creep deformation on microstructural change in 12% Cr heat resisting steel was investigated by comparing the gauge and head regions of creep ruptured specimens. Such microstructural changes as recovery, precipitation rate and coarseness of precipitates were promoted by creep deformation. When the precipitation behavior of the gauge and head regions with the same hardness was compared, the precipitation behavior of the gauge region was smaller in amount, smaller in mean diameter of precipitates and shorter in interparticle spacing, than that of the head region. The promoting ratio of recovery increased with increasing the strain and with lowering the temperature. This result supports the idea that increase in diffusion coefficient by creep deformation promotes microstructural change. (14 refs.)
- 63350 Mechanochemical reaction of polyvinyl chloride at high pressures.** Y.Okuri, N.Dan, Y.Ogo (Faculty of Engng., Osaka City Univ., Osaka, Japan). *J. Soc. Mater. Sci. Jpn. (Japan)*, vol.31, no.350, p.1135-9 (Nov. 1982). In Japanese. [received: April 1983]. The mechanochemical reactions of polyvinyl chloride (PVC) were investigated at room temperature by using a self-made high pressure apparatus capable of simultaneous shear deformation. Static pressures applied were 5, 10, 15 kbar for hard PVC resin and less than 5 kbar for soft PVC resin. The shearing curves for hard PVC resin showed the decrease of shearing stress at the initial stage of shearing because of the occurrence of the major mechanochemical reaction at this stage. The mechanochemical reaction rate and the limiting molecular weight were evaluated by fitting the rate equation to the experimental data on molecular weight of hard PVC resin. All shearing curves for soft PVC resin did not show any definite yield point. Although the addition of plasticizer affected the shearing behavior, the shear-strength under pressure was not appreciably affected by adding over 50 wt.% to pure PVC. No general conclusion about the effect of plasticizer content on the molecular weight was obtained. (6 refs.)
- 63351 Kinking in the drawing of linear polyethylene.** V.A.Marichin, L.P.Mjasnikova (Ioffe Phys. Tech. Inst., Acad. of Sci., Leningrad, USSR), Z.Pelzbauer. *J. Macromol. Sci. - Phys. (USA)*, vol.B22, no.1, p.111-27 (1983). The structure of oriented films of linear polyethylene drawn to an extent such that whitening sets in has been investigated using scanning and transmission electron microscopy. The whitening of the samples was shown to be related to kink band formation. Problems involved in the formation and development of kinks during drawing and their relation to the supermolecular structure of oriented films are discussed. It was found that the process of kinking led to the occurrence of a large number of submicroscopic and microscopic cracks which cause breaking by the samples in the process of drawing. (15 refs.)
- 63352 Effects of complicated deformation history on inelastic deformation behaviour of metals.** Y.Ohashi (Dept. of Mech. Engng., Univ. of Nagoya, Nagoya, Japan). *Mem. Fac. Eng. Nagoya Univ. (Japan)*, vol.34, no.1, p.1-76 (May 1982). In English. [received: March 1983]. The authors have carried out investigations to establish the constitutive equation reflecting history effects from the theoretical viewpoint of continuum mechanics, and in accordance with the experimental results of plastic deformation behaviours of various metals under combined loadings or deformations obtained by using an automatic combined loading testing machine. (33 refs.)
- 63353 On the Portevin-Le Chatelier effect due to Snoek strain aging in the niobium oxygen system.** S.C.Park (Dept. of Materials Sci. & Engng., Univ. of Florida, Gainesville, FL, USA), L.P.Beckerman, R.E.Reed-Hill. *Mettall. Trans. A (USA)*, vol.14A, no.3, p.463-9 (March 1983). Dynamic strain aging in niobium containing between 0.01 and 0.95 at. pct oxygen was investigated between 77 and 971K using a nominal strain rate of $8.8 \times 10^{-3} \text{ s}^{-1}$. At higher oxygen concentrations both type A and type B serrations were observed between 355 and 422K. It is proposed that all of this serrated flow is due to Snoek dynamic strain aging. This is supported by the appearance of the serrations at much lower temperatures than those normally associated with Cottrell strain aging and the observation that the time between the type A serrations on a stress-strain curve equals the jump time of an oxygen atom. Strain rate sensitivity measurements were consistent with the generally accepted view that serrations occur only when the strain rate sensitivity becomes sufficiently negative. (30 refs.)
- 63354 Effect of sulfides and sulfide morphology on anisotropy of tensile ductility and toughness of hot-rolled C-Mn steels.** W.A.Spitzig (Res. Lab., US Steel Corp., Monroeville, PA, USA). *Mettall. Trans. A (USA)*, vol.14A, no.3, p.471-84 (March 1983). The effects of sulfur content (0.004 or about 0.013 pct) and sulfide morphology (stringer or globular) on anisotropy of tensile ductility and Charpy V-notch (CVN) shelf energy were investigated in a series of 0.1 and 0.2 pct carbon, 1.0 pct manganese steels. The effect of sulfide inclusions on fracture strain or CVN shelf energy correlated with a single parameter, P , regardless of inclusion shape, stringer or globular, or test direction, longitudinal, transverse, or through-thickness. The parameter P was defined as the total projected length of inclusions per unit area on a plane parallel to the fracture plane. The fracture strain and CVN shelf energy decreased with an increase in P . The magnitude of P was directly proportional to the volume fraction of inclusions and inversely proportional to the inclusion dimension perpendicular to the fracture plane. The lower ductility in the 0.2 as compared with the 0.1% C steel was a consequence of the greater pearlite in the former steel. It appears that the decrease in tensile ductility with increasing pearlite content is a result of enhanced localized shearing, which promotes the coalescence of voids nucleated at second phases. (20 refs.)
- 63355 Alpha-beta interface sliding in Ti-Mn alloys.** S.Ankem (RMI Co., Niles, OH, USA), H.Margolin. *Mettall. Trans. A (USA)*, vol.14A, no.3, p.500-3 (March 1983). Reports on a brief examination of the effect of volume fraction of α and β phases and their morphology on the unexpected interface sliding behaviour. (15 refs.)
- 63356 Characteristics of structural transformations during deformation and heat treatment of Elinvar alloy 45 NkHt.** V.A.Strizhak, V.V.Kiselev, S.I.Stepanov. *Met. Sci. & Heat Treat. (USA)*, vol.24, no.5-6, p.428-31 (June 1982). Translation of: *Metalloved. & Term. Obrab. Met. (USSR)*, vol.24, no.6, p.44-7 (June 1982). [received: Feb. 1983]. Investigates the fine structure of alloy 45NkHt in relation to various conditions of melting, deformation, and heat treatment, and determine its effect on the properties of the alloy. (4 refs.)
- 63357 Effect of heat treatment in magnetic field on the mechanical properties of carbon steels.** P.I.Rusin, V.N.Pustovit, S.A.Grishin (Rostov-on-Don Inst. of Farm Machine Construction, Rostov, USSR). *Met. Sci. & Heat Treat. (USA)*, vol.24, no.7-8, p.445-7 (July-Aug. 1982). Translation of: *Metalloved. & Term. Obrab. Met. (USSR)*, vol.24, no.7, p.4-5 (July 1982). [received: March 1983]. The authors investigated the changes in the mechanical properties of carbon steels after isothermal treatment in the temperature range of the pearlitic transformation under the influence of magnetic field. The experiments were made with samples of steels 45 and U10A from commercial heats. It was

found that the mechanical properties of carbon steels change under the influence of magnetic field, the character of the change depending on the carbon content. (3 refs.)

63358 Ductility characteristics of thin sheet steel. R.E.Gliner (Gorky Automobile Factory, Gorky, USSR). *Met. Sci. & Heat Treat. (USA)*, vol.24, no.7-8, p.485-7 (July-Aug. 1982). Translation of: *Metalloved. & Term. Obrab. Met. (USSR)*, vol.24, no.7, p.33-5 (July 1982). [received: March 1983]
A method is proposed for determining δ_5 (uniform elongation in tension) from known standard ductility characteristics. The method can be used for evaluating the ductility properties of steels intended for both sheet and bulk cold forming. (3 refs.)

63359 Effect of diffusion welding thermal cycle on the strength of alloy VT20. S.V.Ivanov, E.S.Karakozov, A.Z.Pimenova (Moscow Evening Metall. Inst., Moscow, USSR). *Met. Sci. & Heat Treat. (USA)*, vol.24, no.7-8, p.488-90 (July-Aug. 1982). Translation of: *Metalloved. & Term. Obrab. Met. (USSR)*, vol.24, no.7, p.35-7 (July 1982). [received: March 1983]
Strength properties of alloy VT20 subjected to annealing simulating diffusion welding in the $(\alpha+\beta)$ -region are found to be greater than in the β -region. In using alloy VT20 for structures with stress concentrators in the form of sharp notches under cyclic loading conditions it is recommended that diffusion welding is carried out in the $(\alpha+\beta)$ -region. For structures operating under static loading conditions it is possible to employ welding in the β -region. (3 refs.)

63360 Temperature and rate conditions for development of superplasticity in Zr-2.5% Nb alloy. N.A.Makhutov, L.P.Fedorovich, A.V.Chirkir, B.G.Parfenov, A.I.Tananov (States Sci.-Res. Inst. of Engng., USSR). *Met. Sci. & Heat Treat. (USA)*, vol.24, no.7-8, p.491-4 (July-Aug. 1982). Translation of: *Metalloved. & Term. Obrab. Met. (USSR)*, vol.24, no.7, p.37-40 (July 1982). [received: March 1983]
A study of the mechanical properties and structure of Zr-2.5% Nb alloy during tensile deformation at rates of $2.6 \cdot 10^{-2}$ to $1.05 \cdot 10^{-4}$ sec $^{-1}$ made it possible to establish that isothermal deformation of this alloy in the center of the $\alpha+\beta$ -region at 770°C at a rate of $\sim 10^{-4}$ sec $^{-1}$ proceeded under superplastic conditions. This is confirmed by high elongation (450%) with low values of flow stress, high sensitivity to strain rate ($m=0.7$), the type of true tensile diagram, and also retention of equiaxed grains during deformation. (4 refs.)

63361 Influence of melting method, modification, and cyclic temperature-force action on the ductility of 1V7M6K12 steel. Yu.M.Skrynnchenko, V.N.Terekhov (Sci.-Res. Inst. for Special Steel, Ukrainian SSR). *Met. Sci. & Heat Treat. (USA)*, vol.24, no.7-8, p.533-6 (July-Aug. 1982). Translation of: *Metalloved. & Term. Obrab. Met. (USSR)*, vol.24, no.8, p.20-3 (Aug. 1982). [received: March 1983]
Vacuum induction remelting and modification were found not to lead to an increase in ductile properties of 1V7M6K12 steel. The impact strength of steel produced by the powder metallurgy method was 1.5-2 times greater than that of normally melted steels but its absolute values were quite low. Cyclic temperature-force action provided a substantial increase in the mechanical properties of the investigated steels. (4 refs.)

63362 Heterogeneity of microstrains in alloy N45KhT specimens under tension. A.A.Vainstein, V.S.Borovikov, V.A.Strizhak, V.V.Kiselev (S.M. Kirov Inst., Ural Polytech., Sverdlovsk, USSR). *Met. Sci. & Heat Treat. (USA)*, vol.24, no.7-8, p.585-8 (July-Aug. 1982). Translation of: *Metalloved. & Term. Obrab. Met. (USSR)*, vol.24, no.8, p.61-3 (Aug. 1982). [received: March 1983]
The heterogeneity of the microstrain field on loading steels and alloys is governed to a significant degree by the heterogeneity of the microstructure. The authors investigated the statistical characteristics of the microstrain field in tensioning alloy N45KhT (EP218) specimens heat-treated in accordance with various regimes. (7 refs.)

63363 Mechanical behaviour of isotactic polypropylene subjected to various strain histories in uniaxial extension. J.M.Crissman, L.J.Zapas (Center for Materials Sci., NBS, Washington, DC, USA). *Polymer (GB)*, vol.24, no.3, p.351-8 (March 1983).
The mechanical behaviour of a slowly quenched isotactic polypropylene has been studied for various strain histories in extension. Creep, constant rate of strain, and constant rate of loading experiments were carried out at deformations up to and beyond the point where necking occurs. A creep diagram, which includes the failure envelope, is presented. From the available data the authors have also obtained an extrapolated surface of the single step stress-relaxation behaviour. From this surface they can calculate, using the Bernstein and Zapas theory on the instability of viscoelastic bars, the deformation at which necking occurs for various strain histories. (10 refs.)

63364 Performance of the Ni-Ti alloy VTN-1 (54.5-55 wt.% Ni) in the case of shape restoration. Yu.A.Granatkin, I.B.Kalachev, G.N.Mekhed. *Russ. Metall. (GB)*, no.6, p.135-9 (1981). Translation of: *Izv. Akad. Nauk. SSSR Met.*, no.6, p.135-40 (1981).
Optimum mechanical properties were achieved after stabilisation annealing in the range 450-500°C. The maximum reactive stress (63 kg/mm 2) was achieved for a predetermined plastic deformation equalling 2.0-2.5%. The optimum operating temperature of thermally sensitive elements made of this alloy, that ensures full restoration of shape with retention of the limit reaction stress, is 250-280°C. The experimental data were used to plot the restoration diagram and to determine the specific work capacity of the alloy within a wide range of predetermined stresses and strains and various rigidity coefficients. The obtained experimental relationships can be used for calculating and designing thermally sensitive elements from alloys with a shape conservation memory. (18 refs.)

63365 Influence of heat treatment on the mechanical properties of dispersion hardening Nb-Zr-N alloys. V.K.Grigorovich, E.N.Sheftel', G.Sh.Uzmanova, V.K.Sul'zhenko. *Russ. Metall. (GB)*, no.6, p.145-9 (1981). Translation of: *Izv. Akad. Nauk. SSSR Met.*, no.6, p.148-52 (1981).
The effect of heat treatment on the short-duration mechanical properties of Nb-Zr-N alloys under tensile stress in the temperature range 20-1200°C was examined. The maximum strength was achieved after quenching from 1600-1700°C (1 h holding) and ageing for 20 h at 1000°C. There was some decrease in ductility. The strength increases with increasing quantity of the strengthening phase. Additional alloying with molybdenum increases the strength and ductility at all the test temperatures. The conditions of heat treatment are given for which the investigated alloys have the maximum strength. (7 refs.)

63366 Examination of the effects of dimensional mismatch of the lattice parameters of the γ and γ' phases on the high-temperature strength of dispersion-hardened nickel alloys. N.V.Petrushin, I.A.Ignatova, A.V.Logunov, A.I.Samoylov, I.M.Razumovsky. *Russ. Metall. (GB)*, no.6, p.150-6 (1981). Translation of: *Izv. Akad. Nauk. SSSR Met.*, no.6, p.153-9 (1981).

The influence was examined of the following alloying elements, wt.%: 2 and 7 Cr; 7 and 11 Co, 0.5 and 1.2 Nb, 8 and 12 W, on the lattice parameters of the γ and γ' phases of the nickel alloys Ni-Cr-Co-W-Al-Ti-Nb-Hf and their dimensional mismatch at 293 and 1173K. An increase in the chromium and tungsten contents reduces the absolute value of the mismatch of the lattice parameters of the phases negatively ($a_{\gamma}-a_{\gamma'}<0$) and positively ($a_{\gamma}-a_{\gamma'}>0$). Cobalt and niobium had no appreciable effect on the dimensional mismatch. Reduced high-temperature strength and considerably differing coefficients of thermal expansion of the phases are achieved in the case of alloying for which the lattice parameter of the γ solid solution is lower than that of the γ' phase. To obtain a high high-temperature strength a certain positive dimensional mismatch (with a low temperature gradient) between the lattice parameters of the γ and γ' phases is necessary. (16 refs.)

63367 Examination of the creep strength of single crystals of high-temperature nickel alloys. V.G.Lyuttsau, E.P.Kostyukova, V.N.Toloraiya, I.V.Kostina. *Russ. Metall. (GB)*, no.6, p.157-61 (1981). Translation of: *Izv. Akad. Nauk. SSSR Met.*, no.6, p.160-4 (1981).

The creep strength of single crystals of the tested high-temperature nickel alloys is higher for single crystals with the orientation [111] than it is in the case of orientations [001] and [011]. During creep, block structures with block dimensions of 0.1-0.2 mm form in the crystals. The transition from the second to the third stage of creep is not accompanied by macro-discontinuities in specimens with a single-crystal structure. Cracks are formed primarily along the carbide segregations at the end of the third stage. (3 refs.)

63368 Superplasticity in an austenitic stainless steel containing aluminium and manganese. E.H.Toscano (Dept. de Materiales, CNEA, Buenos Aires, Argentina). *Ser. Metall. (USA)*, vol.17, no.3, p.309-12 (March 1983).

An Fe-based alloy containing Al and Mn with an austenitic structure at room temperature was tested in tension, in the cold worked state, up to 1073K. At 973K and above the alloy showed a superplastic behaviour due to the precipitation of a second phase which generated a fine grained structure. From the tensile properties at room temperature, it was inferred that the precipitated phase is harder than the matrix causing brittle fracture at room temperature and giving at high temperature a superplastic mode similar to that of a nonNewtonian fluid containing rigid particles. (15 refs.)

63369 Superplasticity in Al-Li based alloys. J.Wadsworth, I.G.Palmer, D.D.Crooks (Lockheed Palo Alto Res. Lab., Palo Alto, CA, USA). *Ser. Metall. (USA)*, vol.17, no.3, p.347-52 (March 1983).

Two Al-Li based alloys have been developed having similar superplastic properties to existing commercial superplastic aluminum alloys, but offering significant weight savings in structural applications, as a result of their higher elastic modulus and lower density. (32 refs.)

63370 Anomalous dynamic superplasticity and quasiliquid condition of iron in the presence of hydrogen. V.I.Shapovalov, V.Yu.Karpov (Dnepropetrovsk Metall. Inst., Dnepropetrovsk, Ukrainian SSR). *Sov. Mater. Sci. (USSR)*, vol.18, no.3, p.224-7 (May-June 1982). Translation of: *Fiz.-Khim. Mekh. Mater. (USSR)*, vol.18, no.3, p.38-42 (May-June 1982). [received: Feb. 1983]

A series of experiments was made on determining the influence of hydrogen on the character of appearance of the dynamic superplasticity of iron in its thermal cycling in the $\alpha\rightarrow\gamma$ transformation temperature range. The cycling temperature range was 1123-1223K, and the hydrogen pressure in the gaseous phase was varied from 0 to 100 MPa. The original materials were carbonyl iron containing less than 0.003% impurities and hydrogen with a dew point of 209K. Primarily cylindrical samples with a diameter of 2.5 mm and a length of 5-25 mm were tested. The bending loads were transmitted by their natural weight with single cantilever fastening in a special stainless steel holder. The stress range was 0.2-8 kPa. The tests showed that the presence of hydrogen in thermal cycling leads to an anomalous drop in the yield strength of iron. (14 refs.)

63371 Stress-strain state in the rolling of blanks from granulated alloys. Yu.A.Gorbusov, I.G.Rusov, S.B.Sidel'nikov (Krasnoyarsk Inst. of Nonferrous Metals, Krasnoyarsk, USSR).

Sov. Powder Metall. & Met. Ceram. (USA), vol.21, no.8, p.617-21 (Aug. 1982). Translation of: *Poroshk. Metall. (USSR)*, vol.21, no.8, p.21-6 (Aug. 1982). [received: Feb. 1983]

The stressed and strained state in rolling was studied by carrying out experiments on blanks from high-strength granulated alloys of the aluminum-zinc-magnesium-copper and aluminum-zinc-magnesium systems and from aluminum-transition metal alloys. Blanks were produced by compacting granules, which was followed by extrusion and rolling. To the joint or side surfaces of the composite specimens employed were applied coordinate grids with 2-mm-square cells. The coordinate grid cells were measured in the starting and deformed conditions under an MMI-2 microscope with an accuracy to 0.005 mm. (3 refs.)

63372 Structural-mechanical features of two-stage shear strain of oriented low density polyethylene. V.I.Gerasimov, V.D.Zanegin. *Vysokomol. Soedin. Ser. A (USSR)*, vol.25, no.3, p.532-6 (March 1983). In Russian. English translation in: *Polym. Sci. USSR (GB)*

The structural transitions and changes of mechanical properties during shear strain of oriented samples of LDPE with crystallites being skewed in the same direction have been studied. The data obtained permit one to evaluate quantitatively the fraction of amorphous-crystalline fibrils and amorphous layers between them. The interfibrillar regions have a complicated structure and various mechanical characteristics dependent on the direction of shear. The recrystallization begins at the attainment of a definite shape of crystallites independent of the initial shape and the value of plastic strain. (9 refs.)

63373 Effect of the annealing on the mechanism of plastic strain in oriented polypropylene. A.V.Efimov, V.P.Lapshin, V.I.Fartinun, P.V.Kozlov, N.F.Bakeev. *Vysokomol. Soedin. Ser. A (USSR)*, vol.25, no.3, p.588-93 (March 1983). In Russian. English translation in: *Polym. Sci. USSR (GB)*

The effect of annealing of oriented crystalline polypropylene on its mechanical properties and morphological features of plastic strain in conditions of stretching have been studied. The samples of oriented PP annealed at temperatures close to the melting point are deformed through the formation of specific crazes. For nonannealed samples of oriented polymer and samples being annealed at lower temperatures the plastic strain without the distortion of continuity of material predominates. The prevalence of one of two possible mechanisms of the strain depends on the supermolecular organization of crystalline oriented polymer being changed under annealing. (20 refs.)

- 63374 The effects of molecular weight and cooling rate on fine structure, stress-strain behavior and wear of polytetrafluoroethylene. Ting-Yung Hu, N.S.Eiss, Jr. (Dept. of Mech. Engng., Virginia Polytech. Inst. & State Univ., Blacksburg, VA, USA). *Wear (Switzerland)*, vol.84, no.2, p.203-15 (15 Jan. 1983). The effects of the molecular weight of polytetrafluoroethylene (PTFE) resin and the cooling rate during the processing of PTFE on its fine structure, stress-strain behavior and wear were investigated. The studies revealed a correlation between the crystallinity, the morphology and the dimensions of the fine structure of PTFE. It was also found that the ultimate strength, ultimate elongation and wear are affected by both molecular weight and crystallinity. An increase in the molecular weight or crystallinity could result in a decrease in wear. However, different effects of both factors on wear were observed when different rubbing conditions were used in wear tests. The different effects might be attributed to a crystalline transition of PTFE at about room temperature. (11 refs.)
- Irradiation creep in first wall model alloys See Entry 60411
- Numerical solutions for analyzing the nonaxisymmetric 2-dimensional deformation processes See Entry 61424
- Effect of molecular extension of a melt on the crystallinity of polyethylene, subjected to repeated crystallization See Entry 61814
- Small angle neutron scattering study of the structure of a triblock copolymer of styrene and isoprene during extension See Entry 61821
- Effect of poly(propylene oxide) segment size on structure-property relationships in elastomeric ionene See Entry 61827
- Kinetics of the collective crystallization of doped ZnS See Entry 61835
- A model for the evolution of a twist dislocation network See Entry 61912
- Improved technique for observation of dislocation structure of austenitic MnCrNi steels after small deformation See Entry 61920
- The role of elastic interaction stresses on the onset of slip in polycrystalline alpha brass. I. Experimental determination of operating slip systems and qualitative analysis See Entry 61927
- Strains and internal stresses in silicon wafers See Entry 61928
- Internal stress buildup in SIPA creep See Entry 61958
- Friction and source hardening in irradiated mild steel See Entry 61984
- On the critical dose for blistering in helium irradiated zirconium and Zr-Nb See Entry 61987
- On the work hardening rate of glassy polymers. I. Application to the physical ageing of atactic PMMA See Entry 62014
- Orientation dependence of slip deformation of the conjugate system in Cu-6 at. % Al single crystals See Entry 62017
- Thermal and mechanical properties of tetramethyl-*p*-silphenylenesiloxane/dimethylsiloxane block copolymer See Entry 62069
- Experimental investigation of plastic strains of porous solids—a review See Entry 63190
- Effect of thermal conditions of preparation of dispersion-strengthened nickel powders on the character of distribution of the strengthening phase See Entry 63205
- Sintering of cast iron swarf powder and Fe-Si-C mixed powder See Entry 63213
- Influence of alloying and preliminary deformation on phase composition and mechanical properties of Fe-Mn alloys See Entry 63291
- Examination of applied stress and prestrain effects on recovery of work hardened Cu-SiO₂ See Entry 63306
- The structural state and its association with low temperature work hardening of structural titanium alloys See Entry 63307
- Influence of sulfur and nitrogen on the characteristics of texture formation as a result of deformation and annealing of Fe+3% Si single crystals See Entry 63309
- Free-cutting stainless steel wire with high-strength See Entry 63315
- Recovery of properties and nature of ordering of steels during tempering under load See Entry 63316
- Heat treatment of molybdenum, tungsten and their alloys up to 2100°C See Entry 63317
- Thermomechanical treatments of a 1050 pearlite steel See Entry 63318
- The effect of ITMT's and P/M processing on the microstructure and mechanical properties of the X7091 alloy See Entry 63319
- Effect of chromium and aluminum on the physical and mechanical properties of precipitation-hardening Fe-Mn Elinvar See Entry 63321
- Effect of HTTT on the properties of alloy steel castings See Entry 63323
- Structure and properties of a maraging steel after thermomechanical and repeated heat treatment See Entry 63332
- Influence of residual gas pressure in annealing on the properties of niobium and its alloys See Entry 63333
- The role of elastic interaction stresses on the onset of slip in polycrystalline alpha brass. II. Rationalization of slip behavior See Entry 63335
- Correlation of hardness and microstructure in unoriented lamellar polyethylene. II. Study of elastic modulus See Entry 63384
- Notched unidirectional boron/aluminum: effect of matrix properties See Entry 63389
- Mechanical properties and fatigue strength of steel protected from tufftriding by inorganic coating See Entry 63395
- Effect of stress frequency on fatigue crack propagation rate in titanium See Entry 63399
- Microstructure and tensile ductility in a β heat treated titanium alloy See Entry 63400
- High temperature low cycle fatigue of IN 738 and application of strain range partitioning See Entry 63402
- Improvement in lower temperature mechanical properties of 0.40 pct C-Nr-Cr-Mo ultrahigh strength steel with the second phase lower bainite See Entry 63403
- Effect of cyclic plastic bending on the proneness of steel St3Sp to brittle fracture See Entry 63407
- Tenacity, toughness, ductility of mild steel sheet in longitudinal and short transverse direction See Entry 63414
- Mechanical properties of ageing of non-magnetic austenitic steels at low temperatures See Entry 63417
- Influence of production media on the physicomechanical and electrochemical properties of steels See Entry 63430
- An analysis of the localization of deformation and weight loss during single-particle normal impact See Entry 63433
- Changes in resistivity at low-temperature deformation and the subsequent recovery of the Ag-15 at. % Al alloy See Entry 63434
- Heat treatment and magnetic properties of high-coercivity Fe-Co-Cr alloys with 3% Mo See Entry 63435
- Microstructure and ductility of electroless copper deposits See Entry 63438
- Effect of high-temperature vacuum annealing time on the structure and properties of titanium alloys See Entry 63457
- Question of the safe boundaries of use of 12 MKh steel at increased temperatures and hydrogen pressures See Entry 63467
- The use of time-of-flight neutron diffraction to study grain interaction stresses See Entry 63472
- ## 81.40N Fatigue, embrittlement, and fracture
- (inc. hardness; see also 62.20M Fatigue, brittleness, fracture and cracks)
- 63375 Evaluation of creep crack growth criteria for IN-100 at elevated temperature. T.D.Hinnerichs (US Air Force Weapons Lab., Kirtland AFB, NM, USA); A.N.Palazotto, T.Nicholas. *AIAA J. (USA)*, vol.21, no.3, p.438-45 (March 1983). Seven crack growth rate criteria from numerical computations of simulated creep crack growth experiments are evaluated. A finite element computer program is utilized to calculate the various parameters. Both nearfield, or local, as well as far-field criteria are examined. The results indicate that environment plays a major role in crack growth in a nickel-base superalloy, IN-100, at 732°C and that time effects must be considered in modelling crack growth using local criteria. Stress intensity and net-section stress are found to be adequate as correlating parameters but are unable to model observed transient phenomena. (22 refs.)
- 63376 Fracture control and its application within the Agency's programmes (space vehicles). G.Reibaldi (ESA Tech. Directorate, ESTEC, Noordwijk, Netherlands). *ESA Bull. (France)*, no.33, p.62-6 (Feb. 1983). Manned space programmes, with all their associated safety issues, have boosted the role of fracture-control techniques for space applications. All payloads to be carried inside the cargo bay of the Shuttle, for example, are subject to stringent fracture-control requirements, to ensure the safety of the crew. It has long been accepted that there are always defects present in mechanical structures due to the rigours of manufacturing, transportation and testing. The science of fracture mechanics that enables one to live with such defects without there being catastrophic structural failures is discussed. (no refs.)
- 63377 Influence of strain ageing of martensite by hydroextrusion on the fine structure and surface relief in ductile fracture of 30KhGSN2A steel. M.N.Spaskiy, Ya.B.Gurevich, V.E.Vaganov, M.S.Astrakhansev (Inst. of Metallography & Phys. of Metals, Moscow, USSR). *Fiz. Met. & Metalloved. (USSR)*, vol.55, no.2, p.363-7 (Feb. 1983). In Russian. English translation in: *Phys. Met. & Metallogr. (GB)*. An investigation was made of the mechanical properties and fine structure of 30KhGSN2A steel hardened by a high-temperature thermomechanical treatment and then subjected to strain ageing of martensite involving hydroextrusion. After deformation by 5% at +20°C this process increased the yield and breaking strengths of the investigated steel, but had practically no effect on the plastic properties or on the energy of impact fracture at room temperature. (14 refs.) A.T.
- 63378 Influence of high-temperature thermomechanical treatment on delayed fracture of hardened construction steel. M.A.Smirnov, N.T.Kareva, S.I.Ilin (Lenin Komsomol Polytech. Inst., Chelyabinsk, USSR). *Fiz. Met. & Metalloved. (USSR)*, vol.55, no.2, p.392-4 (Feb. 1983). In Russian. English translation in: *Phys. Met. & Metallogr. (GB)*. Industrial 38KhS steel was subjected to rolling at 900°C and quenching in water. Mechanical tests were made on notched samples. The results indicated that the applied thermomechanical treatment suppressed intergranular fracture and not only effectively weakened embrittlement processes during tempering, but also reduced the embrittlement in the hardened state. (6 refs.) A.T.
- 63379 Investigation of the energy dissipated internally during fatigue of metals. R.M.Chatnyan, V.B.Puz'ko. *Izv. VUZ Mashinostr. (USSR)*, no.12, p.17-20 (1982). In Russian. Procedure is described and experimental results are presented of investigations of the total energy dissipated internally in the process of fatigue of metals, during cyclic extension and compression, with symmetric and unsymmetric stress amplitudes. It is shown that the method proposed can be used for the measurements of the energy dissipated, up to stresses corresponding to the fatigue limits of the materials. (3 refs.) Z.F.V.
- 63380 Indentation-induced cracks in hot-pressed Si₃N₄. D.Chakraborty, J.Mukerji (Central Glass & Ceramic Res. Inst., Calcutta, India). *Indian J. Technol.*, vol.20, no.9, p.361-5 (Sept. 1982). [received: March 1983] Good fitting of Vickers microhardness (VMH) at loads of 1000 g and 2000 g of hot-pressed Si₃N₄ in the Meyer equation indicated that VMH values were not affected by the emergence of cracks VMH measured in planes perpendicular and parallel to the hot-pressing direction of Si₃N₄ did not differ significantly. Length of crack around indentation was found to vary inversely with VMH of hot-pressed Si₃N₄. Fracture toughness of hot-pressed Si₃N₄ was found to vary directly with its VMH. This observation supported the equation derived by previous workers. (18 refs.)
- 63381 Comparison of the impact strength of 10GN2MFA and 15Kh2NMFA steels with the similarity of local failure taken into account. A.D.Zotov, K.L.Ilnitskii (Mfg. Assoc. Atomash, USSR). *Ind. Lab. (USA)*, vol.48, no.6, p.597-602 (June 1982). Translation of: *Zavod. Lab. (USSR)*, vol.48, no.6, p.65-9 (June 1982). [received: March 1983] The authors compared with impact strength of the structural steels, which are used in nuclear reactors, at room and low temperatures. A functional relationship was established between impact strength and critical crack length in fracture for both steels. The use of the similarity criterion of local fracture showed that 10GN2MFA steel had better strength properties. (11 refs.)

63382 Dependence of critical temperatures of brittleness on the condition of operational fractures. N.N. Georgiev, B.G. Kudin (All-Union Sci.-Res. Inst. of Railroad Transport, USSR).

Ind. Lab. (USA), vol.48, no.6, p.602-5 (June 1982). Translation of: *Zavod. Lab. (USSR)*, vol.48, no.6, p.69-71 (June 1982). [received: March 1983]
Using as the basis the analysis of operational failures of a number of parts broken in service in western Siberia, the authors make an attempt to find a scientific basis for the critical work of fracture determined in impact bending tests. The work involved 30 fractures of the parts for which the chemical analysis (steel grade), heat treatment method, and temperature at which the fracture occurred, could be established. In addition, transverse impact specimens with stress concentrators of type 1 (1-mm radius) and type 15 (fatigue crack) were made from the metal near the point of failure and tested at the actual failure temperature. The fractures were divided into three groups: brittle fractures, fatigue fractures with brittle final fracture, and fatigue fractures with tough final fracture. (1 ref.)

63383 Parameter evaluations for polymer durabilities versus time. M.N. Bokshitskii (Neftekhimavtomatika, Moscow, USSR).

Ind. Lab. (USA), vol.48, no.6, p.612-18 (June 1982). Translation of: *Zavod. Lab. (USSR)*, vol.48, no.6, p.76-80 (June 1982). [received: March 1983]
The author proposes a phenomenological classification of endurance curves for brittle failure and develops a procedure for determining the parameters of strength as a function of time. A method for evaluation of safe stress, without a laborious analysis of creep kinetics, is outlined. (11 refs.)

63384 Correlation of hardness and microstructure in unoriented lamellar polyethylene. II. Study of elastic modulus. J.M. Salazar, F.J.B. Calleja (Inst. de Estructura de la Materia, CSIC, Madrid, Spain).

J. Mater. Sci. (GB), vol.18, no.4, p.1077-82 (April 1983).
For part I see *ibid.*, vol.16, p.739 (1981). The stress-strain diagrams of a stress of melt-crystallized polyethylene samples with a varying number of chain defects have been investigated. The elastic modulus, E , and the surface hardness, MH , markedly decrease with increasing number of defects. The mechanical behaviour of the lamellar structure of PE modulated by a major exclusion of chain defects from the crystals is discussed in the light of Takayanagi's two-phase model. The data suggest that E is very sensitive to the fraction of tight crystalline bridges between lamellae. The correlation found between E and MH emphasizes, in addition, the different and complementary role played by the amorphous layer in each mechanical test. In the former case one measures the elastic deformation of the layer reinforced by tie molecules. In the latter test the plastic deformation under compression of the lamellae sandwiched between noncrystalline layers is contemplated. In both cases the influence of the number of defects drastically affects the nature of the crystalline lamellae and surface layer and consequently substantially modifies both types of properties. (10 refs.)

63385 Crack arrest in thick section steel plate. E. Smith (Metall. Dept., Univ. of Manchester, Inst. of Sci. & Technol., Manchester, England).

J. Nucl. Mater. (Netherlands), vol.115, no.1, p.95-100 (March 1983).
Crack arrest in thick section steel plate is considered in relation to the conditions for crack arrest in a nuclear reactor pressure vessel, when this is subjected to thermal stresses resulting from a hypothetical loss of coolant accident. The results of a theoretical analysis, based primarily on recent developments in quasi-static crack propagation theory, provide further support for the view that the arrest toughness K_{Ia} is essentially a material property. However, since the theoretical results also suggest that K_{Ia} is reduced by neutron irradiation and because there is, as yet, no conclusive experimental data on the effect of neutron irradiation on K_{Ia} , it is proposed that with highly irradiated steel, instead of using a K_{Ia} crack arrest criterion, it is better to use a more conservative criterion, based on the concept that arrest occurs within the vessel at a position where the temperature exceeds that temperature above which the cleavage fracture mode is unable to operate. (23 refs.)

63386 Indentation fracture transitions in polymethylmethacrylate. K.E. Puttick, R.H. Yousif (Phys. Dept., Univ. of Surrey, Guildford, England).

J. Phys. D (GB), vol.16, no.4, p.621-33 (14 April 1983).
The temperature transition associated with fracture initiation by ball indentation of polymethylmethacrylate (PMMA) has been studied, and the results compared with the predictions of an energy scaling analysis. It is found that in accordance with the theory (i) the transition temperature, though subject to statistical variability, is a strong function of the size of geometrically similar indentations, (ii) there are two transitions corresponding to (a) the radial fracture of deep plastic-elastic indentations and (b) ring cracking under the quasi-Hertzian stress fields of shallow indentations, (iii) the criterion for fracture is approximately $a_c = \alpha E \Gamma / Y^2$ where a_c is the critical indentation diameter, E is Young's modulus, Y is yield stress in uniaxial testing and Γ is the fracture surface work, α is about 50 for radial fracture and 140 for ring crack initiation. Certain anomalies in the temperature range -10°C to $+10^\circ\text{C}$ are attributed to variation in craze length. There are marked changes in the mode of indentation fracture at low temperatures, where the polymer behaves like an inorganic glass; the transition temperature is also affected by the condition of the specimen surface and the presence at the interface of water and graphite. (18 refs.)

63387 A fracture criterion for edge-bonded bimaterial bodies. P.A. Gradin (Linköping Inst. of Technol., Linköping, Sweden).

J. Compos. Mater. (USA), vol.16, no.6, p.448-56 (Nov. 1982). [received: April 1983]

A fracture criterion for the bond between two different linear elastic materials is proposed. This criterion is based on the singular behaviour of the normal and shear stress in the vicinity of the point of intersection between the bond line and the outer boundary. (4 refs.)

63388 Micromechanical predictions of crack initiation, propagation and crack growth resistance in boron/aluminum composites. J.M. Mahishi, D.F. Adams (Composite Materials Res. Group, Univ. of Wyoming, Laramie, WY, USA).

J. Compos. Mater. (USA), vol.16, no.6, p.457-69 (Nov. 1982). [received: April 1983]

An elastoplastic, axisymmetric finite element model has been used to predict the initiation and propagation of a crack in a composite model consisting of a single broken boron fiber embedded in an annular sheath of aluminum matrix. The accuracy of the axisymmetric finite element model for crack problems has been established by solving the classical problem of a penny-shaped crack in a thick cylindrical rod under axial tension. Also, the stress intensity factors predicted by the present numerical model are compared with continuum results. A constant displacement boundary condition applied during an increment of crack growth permits a substantial amount of stable crack growth in the matrix material. The concept of crack growth resistance curves (K_R -curves) has been used to determine the point of crack instability. (18 refs.)

63389 Notched unidirectional boron/aluminum: effect of matrix properties. E.D. Reedy, Jr. (Sandia Nat. Labs., Albuquerque, NM, USA).

J. Compos. Mater. (USA), vol.16, no.6, p.495-509 (Nov. 1982). [received: April 1983]

The manner in which matrix properties affect the notched behavior of unidirectional boron/aluminum is assessed. Data are presented for center-notched tensile specimens of as-fabricated boron reinforced 1100 and 6061 aluminum. Results are also given for a heat-treated B/6061. The notched response of these materials shows significant differences. A shear-lag analysis, formulated for finite-dimensional monolayers made from work-hardening constituents, is shown capable of explaining such effects. The calculated relation between load and notch opening displacement for a uniform traction boundary condition is indistinguishable from that for a displacement condition when the matrix yield strength is sufficiently high. For such cases, the predicted relation is in excellent agreement with experiment. Specimens with a relatively low matrix yield strength exhibit different behavior: the predicted relation between load and notch opening displacement depends strongly on the type of boundary condition applied. This is a consequence of widespread matrix yielding. (6 refs.)

63390 Energy absorption in composite tubes. P.H. Thornton, P.J. Edwards (Ford Motor Co., Dearborn, MI, USA).

J. Compos. Mater. (USA), vol.16, no.6, p.521-45 (Nov. 1982). [received: April 1983]

The collapse characteristics and energy absorption of a variety of tubes made in glass, graphite and Kevlar fiber composites have been examined. Tubes made from glass or graphite fibers collapsed by a fracture mode. There was a critical range of tube geometry over which stable collapse occurred with high energy absorption; thinner wall tubes tended to collapse in an unstable manner with lower energy absorption. Changes in the lay-up which increased the modulus increased the energy absorption of the tube. Tubes made from, or including Kevlar fiber, tended to collapse in an unstable mode by buckling rather than by fracture, which led to low values for specific energy absorption. (9 refs.)

63391 Tensile fracture of evaporated Au films. IV. T. Hosaka (Inst. of Technol., Kanto Gakuin Univ., Kanagawa, Japan).

J. Vac. Soc. Jpn. (Japan), vol.25, no.12, p.770-4 (1982). In Japanese.

The dynamic tensile fracture of vacuum-evaporated gold films was observed directly in a scanning electron microscope by sticking the film on a rubber substrate with Aron-alpha and then painting the edges with Dotite. Gold films from 2200 to 4000 Å in thickness were heated at different temperatures ranging from 100 to 700°C. The dynamic fracture strain was found to increase as the grain of films was increased approximately 0.5 μm in diameter. The electron microscope observations of the fractured films showed that the fracture propagation occurred along grain boundaries by plastic deformation within the grains. The fracture strain ratio (ϵ_d/ϵ_s) of dynamic and static fracture gold films thicker than about 3000 Å was usually of the order of 1.1 to 1.4. (7 refs.)

63392 Variation of dislocation density during fatigue process of low carbon steel. S. Hattori, T. Tanaka (Faculty of Sci. & Engng., Ritsumeikan Univ., Kyoto, Japan).

J. Soc. Mater. Sci. Jpn. (Japan), vol.31, no.350, p.1061-7 (Nov. 1982). In Japanese. [received: April 1983]

Variation of dislocation density during the fatigue process of 0.1% aluminum-killed carbon steel was explored by the aid of the transmission electron microscopy technique. The fatigue tests were conducted under a constant axial stress amplitude with zero mean stress at a frequency of 30 Hz. The results showed that the dislocation density of about $10^8/\text{cm}^2$ under the annealed state increased with cycles and reached a value of $5 \times 10^9/\text{cm}^2$ at ten percent of the total life. This trend of growth corresponded well to that of plastic strain amplitude. By the analysis of multiplication and annihilation processes of dislocations, the change of dislocation density with the number of stress cycles was expressed by an equation. It was demonstrated that this equation was applicable not only to the present low carbon steel, but also to pure iron, pure aluminum and prestrained S15C steel. (21 refs.)

63393 Fracture of alumina ceramics by application of internal pressure in thin-walled tube under hydrostatic pressure. K. Ikeda, H. Igaki, T. Murakami (Coll. of Engng., Univ. of Osaka Prefecture, Sakai, Japan, M. Hirabayashi).

J. Soc. Mater. Sci. Jpn. (Japan), vol.31, no.350, p.1086-92 (Nov. 1982). In Japanese. [received: April 1983]

The material was fractured by applying internal pressure to a thin-walled tubular specimen with open ends under hydrostatic pressure. The fracture criterion was reexamined by comparing the experimental results with the results obtained previously (see *ibid.*, vol.30, no.328, p.72-7, 1981). The fracture stress plotted in the principal stress space showed a similar tendency to the theoretical results for the fracture criterion obtained by taking account of small cracks in the material, in which the material constants had been decided so as to satisfy the experimental results in bending tests under hydrostatic pressures. Thus, the validity of the assumptions in deriving the theoretical results was confirmed. The experimentally obtained fracture stress was somewhat lower than the theoretical results. This may indicate that the theoretical results include the effect of surface cracks or nonuniform stress distribution. In the fracture criterion, the respective material constants of $\pi K_{Ic}^2/4a$ and K_{Ic}/K_{IIc} were corrected, where K_{Ic} and K_{IIc} are the respective fracture toughness values for mode I and mode II, and a is the radius of a penny-shaped crack. The corrected fracture criterion agreed quantitatively with that determined from the experimental results. (29 refs.)

63394 Fatigue strength under intermittent strain cycling at elevated temperatures (engineering life prediction). T. Okada, T. Horikawa, T. Tsunenari, H. Nakamura (Tech. Res. Lab., Kawasaki Heavy Industries Ltd., Akashi, Japan).

J. Soc. Mater. Sci. Jpn. (Japan), vol.31, no.350, p.1093-9 (Nov. 1982). In Japanese. [received: April 1983]

Fatigue tests have been made on a SUS 316 stainless steel at 550°C under stress patterns of intermittent strain wave form which is composed of cycling of a large pulsating strain and superposed small strain cycling. The method of life prediction for the strain cycling was examined on the basis of a linear cumulative damage concept. A linear rule based on the fatigue life curve under a constant strain amplitude gave a reasonable prediction in the case that the superposed small strain was a larger fraction of the basic large pulsating strain, although it gave a poor prediction in the case that the superposed small strain was a small fraction of the latter. (8 refs.)

63395 Mechanical properties and fatigue strength of steel protected from tuftfridding by inorganic coating. N. Egami (Faculty of Sci. & Technol., Meiji Univ., Nagoya, Japan, C. Kagaya, S. Ishizuka, K. Onishi, M. Kato).

J. Soc. Mater. Sci. Jpn. (Japan), vol.31, no.350, p.1100-6 (Nov. 1982). In Japanese. [received: April 1983]

The fatigue strength and mechanical properties of anti-tuftfridded steel were studied. The non-tuftfridded, tuftfridded and anti-tuftfridded specimens of SS 41 and SM 50 A were used and their hardness, tensile strength and fatigue limit

were measured. The relation between the tensile load on spot welded cross joints and the tufting time was investigated and the fracture surfaces were observed by scanning electron micrographs in order to study the effects of inorganic coating of the antituffrided specimens. Differences in microstructures, hardness, tensile strength and compressive residual stress were apparent between the tufted and antituffrided specimens. But the fatigue limits of both specimens were approximately the same. (19 refs.)

63396 Influence of mean stress on coaxing effect of annealed 0.5% C steel under plane bending fatigue. H.Niisani (Faculty of Engng., Kyushu Univ., Fukuoka, Japan), S.Tanaka.

J. Soc. Mater. Sci. Jpn. (Japan), vol.31, no.350, p.1107-13 (Nov. 1982). In Japanese. [received: April 1983]

The coaxing effect in plane bending fatigue was investigated on the plain specimens of annealed 0.5% C steel under zero and positive mean stresses. The mean stress has hardly any effect on crack initiation, but crack propagation is remarkably affected by the value of mean stress. The fatigue limit, in the case where the mean stress is positive, is controlled by the limiting condition for propagation of a micro-crack. This is closely related to the coaxing effect. The coaxing effect of a plain specimen, in the case where a nonpropagating micro-crack formed under the first stress level is short, is more remarkable than that in the case where the micro-crack is long. The coaxing effect of a plain specimen is bigger in the case of positive mean stress than in the case of zero mean stress. (14 refs.)

63397 Fatigue of concrete under varying repeated load. S.Nishibayashi (Faculty of Engng., Tottori Univ., Tottori, Japan), K.Sakata, S.Inoue.

J. Soc. Mater. Sci. Jpn. (Japan), vol.31, no.350, p.1114-20 (Nov. 1982). In Japanese. [received: April 1983]

In order to understand the effects of various factors on fatigue life of concrete under varying repeated load, two-stage and three-stage stress fatigue tests were performed. The fatigue test results were evaluated statistically. The sum of cycles ratio for the same test condition follows a logarithmic normal distribution. The estimation of fatigue life with Miner's rule predicts on the unsafety side when the initial stress level is higher than the following stress level. The Miner's rule however, may be applicable for the prediction of fatigue life of concrete under varying repeated load when the order of repeated load is uncertain. (7 refs.)

63398 Effects of stress ratio and microstructure on near-threshold fatigue crack propagation in high-strength low alloy steel. Y.Nakai (Dept. of Mech. Engng., Osaka Univ., Suita, Japan), K.Tanaka, M.Yamashita.

J. Soc. Mater. Sci. Jpn. (Japan), vol.31, no.350, p.1121-7 (Nov. 1982). In Japanese. [received: April 1983]

The effects of stress ratio and microstructure on the fatigue crack propagation near the threshold in a high-strength low alloy steel were analysed based on the crack closure measurement and the microscopic observation of fracture surfaces. The effects of microstructure and stress ratio on the relation between the crack propagation rate and the stress intensity range were large in region A near the threshold. The threshold stress intensity range increased linearly with the square root of the mean free path. Region A was dividable into regions A1 and A2 in the relation between the rate and the effective stress intensity range. In regions A2 and B, the rate was expressed in a unique power function of the effective range without respect to the microstructure and the stress ratio. In region A1, very close to the threshold, the rate depended on the microstructure but not on the stress ratio. The transition from region A to B can be caused by either the transition in crack closure behavior or the change in crack growth mechanism. (22 refs.)

63399 Effect of stress frequency on fatigue crack propagation rate in titanium. S.Takezono, M.Sato (Faculty of Engng., Kumamoto Univ., Kumamoto, Japan), K.Kumagai, T.Murakami.

J. Soc. Mater. Sci. Jpn. (Japan), vol.31, no.350, p.1128-34 (Nov. 1982). In Japanese. [received: April 1983]

The effect of stress frequency on fatigue crack propagation in 99.5% pure titanium which has remarkable strain rate dependency in the plastic region was studied. Fatigue crack propagation tests were carried out under three kinds of stress frequencies (0.02, 0.2, 20 Hz). FEM elastovisco-plastic analysis of fatigue crack propagation was performed, and comparison made between the dependency of crack propagation rate on stress frequency and the strain behavior at the crack tip. It was found that the crack propagation rate was approximately in inverse proportion of $f^{1/2}$ ($f > 0$), where f is the stress frequency. The parameter closely related to the fatigue crack growth rate is the strain range $\Delta\epsilon$, or visco-plastic strain range $\Delta\epsilon_p$ at the crack tip. The effect of stress frequency on fatigue crack propagation rate may be explained by the variation of $\Delta\epsilon$ or $\Delta\epsilon_p$ based on the strain rate dependency of material. (22 refs.)

63400 Microstructure and tensile ductility in a β heat treated titanium alloy. D.Banerjee, D.Mukherjee, R.L.Saha, K.Bose (Titanium Alloy Dev. Group of Defence Metall. Res. Lab., Hyderabad, India).

Metall. Trans. A (USA), vol.14A, no.3, p.413-20 (March 1983).

The nature of tensile failure in a β -treated titanium alloy, Ti-6Al-1.6Zr-3.3Mo-0.3Si, is demonstrated to be strongly dependent on cooling rate following β treatment. A characterization of microstructure, the fracture surface of tensile tested samples, and the associated slip behavior shows the fracture mode to be determined by the microstructure as well as composition of the α laths. A martensitic matrix with fine grain boundary α particles leads to intergranular failure. At slower cooling rates, α laths form as side plates from grain boundary allotriomorphs, and an FCC interface phase is present at the α lath/retained β interfaces. This microstructure results in transgranular fracture caused by ductile failure at the α lath/ β interfaces within the grains rather than at grain boundary α . If the composition is equilibrated across the α laths by a long-term anneal following β treatment, the slip mode becomes extremely planar leading to slip band related cracking across the grains. (11 refs.)

63401 Roughness-induced crack closure: an explanation for microstructurally sensitive fatigue crack growth. G.T.Gray, III, J.C.Williams, A.W.Thompson (Dept. of Metall. Engng. & Materials Sci., Carnegie-Mellon Univ., Pittsburgh, PA, USA).

Metall. Trans. A (USA), vol.14A, no.3, p.421-33 (March 1983).

The concept of roughness-induced crack closure is utilized to explain the role of prior austenite grain size and pearlite interlamellar spacing on near-threshold fatigue crack propagation in fully pearlitic eutectoid steel tested at low and high stress ratio in lab air and purified helium. It is shown that at low load ratios, near-threshold growth rates are significantly reduced for coarse-grained microstructures, compared to fine-grained at constant yield strength, due to roughness-induced crack closure. Using roughness-profile microscopy, it was found that fracture surface roughness near threshold scaled with grain size and inversely with yield strength, macroscopic roughness at threshold being considerably larger than the conventionally calculated cyclic crack tip opening displacement. Auger analysis of near-threshold corrosion products showed it to be iron oxide; the oxide thickness was seen to be decreased by increased stress ratio. The significance of this model to near-

threshold fatigue crack growth behavior, in terms of load ratio, microstructure, and environment is discussed. (107 refs.)

63402 High temperature low cycle fatigue of IN 738 and application of strain range partitioning. M.Y.Nazmy (Brown Boveri Res. Center, Baden, Switzerland).

Metall. Trans. A (USA), vol.14A, no.3, p.449-61 (March 1983).

Effects of strain rate and strain wave shape on high temperature low cycle fatigue life of cast IN 738 nickel-base superalloy were investigated at 1123K. Intergranular crack initiation and mixed crack propagation were observed mainly in slow-fast saw tooth wave, slow-slow triangular wave, and in truncated wave with hold time in tension and in both tension and compression tests. A reduction in the fatigue life of the specimens tested under these wave shapes, compared to those under fast-fast type of triangular wave shape, corresponded with a variation in the fracture mode. On the basis of a defined crack initiation criterion the test results were analyzed by the strain range partitioning method proposed by Manson, Halford and Hirschberg. The observation that the wave shape effect on life was very sensitive when examined from the elastic strain range viewpoint suggested that a life prediction method that involves stresses may also be worthy of consideration. (30 refs.)

63403 Improvement in lower temperature mechanical properties of 0.40 pct C-Nr-Cr-Mo ultrahigh strength steel with the second phase lower bainite. Y.Tomita, K.Okabayashi (Dept. of Metall. Engng., Univ. of Osaka Prefecture, Osaka, Japan).

Metall. Trans. A (USA), vol.14A, no.3, p.485-92 (March 1983).

A study has been made of the effect of the second phase lower bainite on lower temperature mechanical properties from ambient temperature (287K) to 123K of a commercial steel corresponding to AISI 4340. When 25 vol pct lower bainite, which appeared in acicular form so as to partition prior austenite grains, was associated with martensite at 473K, it provided a better combination of strength and ductility than that achieved using 1133K direct water quenching irrespective of the test temperature. With the lower bainite, notch tensile strength was dramatically improved over the temperature region studied about 2150 MPa even at 123K; whereas, in the case of 1133K direct water quenching, it remained at about 1700 MPa. Similar trends were observed in the relationship between the lower bainite and the Charpy V-notch impact energy at and above 238K. The lower bainite also produced superior fracture ductility and notch toughness results with decreased temperature of testing as compared to those obtained using a $\gamma \rightarrow \alpha$ repetitive heat treatment for the same steel. The above beneficial effects of the second phase lower bainite on lower temperature mechanical properties are briefly discussed in terms of metallographic examinations, the law of mixtures, and so on. (30 refs.)

63404 Influence of annealing temperature on the character of fracture of 4KhMFSNB cast die steel. D.I.Bron, I.V.Sharmazan, I.I.Levites, Yu.M.Ven'slav (Sci.-Res. Inst. for Automobile Industry Technol., USSR).

Met. Sci. & Heat Treat. (USA), vol.24, no.5-6, p.402-5 (June 1982). Translation of: *Metalloved. & Term. Obrab. Met. (USSR)*, vol.24, no.6, p.25-6 (June 1982). [received: Feb. 1983]

An investigation was made of the influence of annealing temperature on the impact strength and character of fracture after tests at different temperatures of samples of cast 4KhMFSNB steel. The annealing was done at 850-1200°C for 15-20 h. To accelerate pearlitic decomposition the samples were tempered at 700°C for 5 h before annealing. The primary qualitative index of the resistance of cast 4KhMFSNB die steel to fracture is the form and character of the fracture of samples. As the result of its low value the impact strength is practically insensitive to a change in heat treatment. The character of the micro- and macrofractures of samples of cast 4KhMFSNB steel is determined by the annealing cycle and test temperature. After annealing at 850°C in all cases fracture of the samples occurs in the interdendritic grain boundaries. An increase in annealing temperature to 1150-1200°C leads to an increase in the share of transgranular fracture. One of the means of increasing the resistance of cast 4KhMFSNB steel dies to brittle fracture is increasing the annealing temperature. (no refs.)

63405 Effect of heat treatment on the fatigue strength of steel 50KhFA and alloy 40KhNMVTYu. V.A.Chernikhin (Cherepovets Nitrogen-Fertilizer Plant, USSR).

Met. Sci. & Heat Treat. (USA), vol.24, no.5-6, p.437-8 (June 1982). Translation of: *Metalloved. & Term. Obrab. Met. (USSR)*, vol.24, no.6, p.53-4 (June 1982). [received: Feb. 1983]

The effect of the cooling medium was investigated during the quenching of steel 50KhFA (0.52% C, 0.28% Si, 0.45% Mn, 0.88% Cr, and 0.20% W) and alloy 40KhNMVTYu (0.05% C, 20% Ni, 2.2% Mn, 12.3% Cr, 2.0% Ti, 39% Co, 6.0% W, 4% Mo, and 2.0% Ti) on their mechanical properties and fatigue strength in air and a synthetic-gas medium. Steel 50KhFA specimens were quenched from various temperatures in water glass of different densities. An increase in the density of the water glass from 1.1·10³ to 1.25·10³ kg/m³ increased the fatigue strength of quenched and tempered steel 50KhFA. With a further increase in the density of the water glass, σ_{-1} of this steel decreased. Alloy 40KhNMVTYu was found to possess a high endurance limit in a medium of 80% H₂ + 20% N₂ (synthetic gas) at a temperature of 200°C and pressure of 14.72 MPa as compared with steel 50 KhFA quenched in oil from 850°C and tempered at 230°C. (2 refs.)

63406 Effect of structure on the ductile-brittle transition temperature of molybdenum alloy TsM-6. N.I.Kazakova, N.N.Morgunova, E.N.Ageeva, M.M.Kantor (I.P. Bardin Central Sci.-Res. Inst. of Ferrous Metall., USSR).

Met. Sci. & Heat Treat. (USA), vol.24, no.7-8, p.479-81 (July-Aug. 1982). Translation of: *Metalloved. & Term. Obrab. Met. (USSR)*, vol.24, no.7, p.29-30 (July 1982). [received: March 1983]

The authors' studies showed that the highest values of ductile-brittle transition temperatures for alloy TsM-6 in the recrystallized condition are due to intergranular weakening that results from the initial stage of ageing in boundary areas of the alloy. (5 refs.)

63407 Effect of cyclic plastic bending on the proneness of steel St3Sp to brittle fracture. M.S.Podgaikii, A.B.Maksimov, A.V.Belik (Donets Res. Inst. of Ferrous Metals, Donets, USSR).

Met. Sci. & Heat Treat. (USA), vol.24, no.7-8, p.498-500 (July-Aug. 1982). Translation of: *Metalloved. & Term. Obrab. Met. (USSR)*, vol.24, no.7, p.43-4 (July 1982). [received: March 1983]

The authors investigated the effect of cycle bending on the proneness of thick sheet of steel St3Sp to brittle fracture, which was evaluated by the change of the stress intensity coefficient, the nominal breaking stress, and also by the temperature of cold shortness. (6 refs.)

63408 Microhardness of nonmetallic inclusions at high temperature. S.I.Gubenko (Dnepropetrovsk Metall. Inst., Dnepropetrovsk, USSR).

Met. Sci. & Heat Treat. (USA), vol.24, no.7-8, p.501-3 (July-Aug. 1982). Translation of: *Metalloved. & Term. Obrab. Met. (USSR)*, vol.24, no.7, p.45-7 (July 1982). [received: March 1983]

The properties of nonmetallic inclusions in steels 08kp, 08Yu, 08T, 08YuT, ShKh15, E3, 08Kh, Kh8, Kh18N10T, and 25KhGSA were studied. Inclusion

microhardness was studied at 20-1200°C at intervals of 20-100°C in a vacuum in IMASH-9-66 equipment with indenter loads of 0.01-0.2 N. (4 refs.)

63409 Effect of the test temperature on the microstructure of fractures in gray cast iron. V.I.Koshelov, A.F.Martynenko, S.Z.Fedorenko, N.M.Gumen, I.F.Omel'yankenko (Kharkov State Univ., Kharkov, Ukrainian SSR). *Met. Sci. & Heat Treat. (USA)*, vol.24, no.7-8, p.557-9 (July-Aug. 1982). Translation of: *Metalloved. & Term. Obrab. Met. (USSR)*, vol.24, no.8, p.40-1 (Aug. 1982). [received: March 1983]

At all the investigated test temperatures (from room temperature to 950°C) the nature of fractured specimens of cast iron Sch21-40 is mixed: sections of intergranular as well as of intragranular failure are found. On the fractures of specimens tested at room temperature, at 550 and 600°C the so-called 'pearlitic' structure is found. Beginning at the test temperature of 550°C, pits—elements of ductile fracture—begin to appear on the fractures of specimens. When the test temperature is raised from 600 to 650°C, the area of ductile fractures and pits greatly increases. Intensive formation of shallow arrow-shaped pits is not accompanied by a substantial increase of ductility. (4 refs.)

63410 Effect of the temperature on crack nucleation in impurities upon deformation of steel 08T. S.I.Gubenko, Yu.V.Yatsenko (Dnepropetrovsk Metall. Inst., Dnepropetrovsk, USSR). *Met. Sci. & Heat Treat. (USA)*, vol.24, no.7-8, p.559-63 (July-Aug. 1982). Translation of: *Metalloved. & Term. Obrab. Met. (USSR)*, vol.24, no.8, p.41-4 (Aug. 1982). [received: March 1983]

Brittle nonmetallic impurities are a source of microcrack nucleation in steel at the early stages of deformation at all the investigated temperatures. The temperature and type of impurities determine their critical size, the critical degree of deformation at which cracks begin to nucleate in the impurities; they determine the interval of deformations in which impurities are the sole source of crack nucleation; the role of impurities in the development of fracture and the number of impurities in which cracks nucleate. The mechanism of the origin of microfracture (cavities or cracks) also affects the investigated parameters. (4 refs.)

63411 Failure mechanism for alloy KhN67VM under the action of a copper-silver solder. V.N.Semenov, L.E.Alekseeva, I.M.Khatsinskaya, E.N.Lubnin. *Met. Sci. & Heat Treat. (USA)*, vol.24, no.7-8, p.566-71 (July-Aug. 1982). Translation of: *Metalloved. & Term. Obrab. Met. (USSR)*, vol.24, no.8, p.47-51 (Aug. 1982). [received: March 1983]

A dispersion-hardened alloy based on Ni-Cr is found to be susceptible to a reduction in strength under the action of solder in the temperature range 850-920°C. Alloy failure under the action of solder is caused by the simultaneous effect of tensile stresses in the alloy and the presence of surface-active fuser solder. The main factor causing a reduction in the tendency of alloy kh67VM towards crack formation (or crazing) during soldering is stabilization of its structure (formation of γ' -phase agglomeration before soldering). (10 refs.)

63412 Reasons for the reduction in the fracture toughness of alloy KhN77TYu-VD at room temperature. M.A.Kotkis, G.P.Kudryavtseva, A.G.Zil'berman (Moscow State Univ., Moscow, USSR).

Met. Sci. & Heat Treat. (USA), vol.24, no.7-8, p.574-7 (July-Aug. 1982). Translation of: *Metalloved. & Term. Obrab. Met. (USSR)*, vol.24, no.8, p.53-5 (Aug. 1982). [received: March 1983]

Low values of the fracture toughness at room temperature are characteristic of alloy KhN77TYuR, which fractures in sections with a high concentration of intermetallic hexagonal phase Ni₃Ti. Hexagonal phase can form in alloy KhN77TYuR with increasing amounts of titanium (and iron) and decreasing amounts of aluminum in microvoids due to insufficient homogenization of the solid solution during solutioning. Precipitation of hexagonal phase during deformation is not excluded. (2 refs.)

63413 Development of knowledge about the embrittlement of steels by hydrogen. L. G.M.Pressouyre, J.Dollet (Centre de Recherches Creusot-Loire, Le Creusot, France), B.Vieillard-Baron.

Mem. & Etud. Sci. Rev. Metall. (France), vol.79, no.4, p.161-76 (April 1982). In French. [received: Feb. 1983]

Presents problems of hydrogen embrittlement of steels in production, working and use. The development of methods of study is discussed. Improvements on the present solutions are suggested. (no refs.)

63414 Tenacity, toughness, ductility of mild steel sheet in longitudinal and short transverse direction. H.Aubert, J.Laniese, C.Lelong, M.Pigoury (CENS, Gif-sur-Yvette, France).

Mem. & Etud. Sci. Rev. Metall. (France), vol.79, no.4, p.189-201 (April 1982). In French. [received: Feb. 1983]

Presents a study of the structure and mechanical properties, in the rolling direction and the short transverse direction, of three structural steel sheets with very different inclusion densities. The influence of the structure of ferrite-pearlite zones has been investigated. The difference in the fracture process between the two directions of measurement is discussed. (13 refs.)

63415 Influence of molecular weight on the fracture of poly(methyl methacrylate) (PMMA). P.Prentice (Dept. of Mech. Engrg., Imperial Coll. of Sci. & Technol., London, England).

Polymer (GB), vol.24, no.3, p.344-50 (March 1983).

A model is proposed to explain the dependence of fracture parameters on the molecular weight of glassy polymers. The model assumes that the fracture event occurs in two stages: the first involves the orientation of polymer chain segments between entanglement points and the second, the fracture itself. A value has been calculated, ($\sim 0.6 \text{ J m}^{-2}$), for the fracture surface energy corresponding to the lower critical molecular weight between entanglements, $M = M_e$. Allowing for the simplifying assumptions made in its derivation, this value is in good agreement with that found experimentally. It is proposed that, possible mechanisms are involved; chain 'pull-out' up to a maximum governed by the time scale of the local fracture event, or chain scission. Using the concept of a reptating chain it is proposed that above $M \sim 2M_e$ there is a relationship between the fracture energy (γ) and the molecular weight of the form $\gamma \propto M^2$ up to a critical value of M , above which γ is constant. It has been shown that there is some agreement with experimental relationships determined independently. (34 refs.)

63416 Is it possible to avoid thermal embrittlement in ribbon-shaped glassy metals? C.Janot, B.George, D.Tierlinck, G.Marchal, C.Tete, P.Delcroix (Lab. de Phys. du Solide, Univ. de Nancy I, Vandoeuvre les Nancy, France).

Philos. Mag. A (GB), vol.47, no.3, p.301-13 (March 1983). In French.

A variety of ribbon-shaped metallic glasses of general composition (FeCr)_{~80}(PCSi)_{~20} become brittle far below their crystallization temperature. Bending tests in conjunction with Mossbauer spectroscopy data and positron lifetime measurements show that embrittlement could be due to the onset of precrystalline or microcrystalline layers on each side of the ribbon. Incidental initial brittleness would have a similar origin. (19 refs.)

63417 Mechanical properties of ageing of non-magnetic austenitic steels at low temperatures. M.A.Kablukovskaya, V.M.Blinov, O.A.Bannykh.

Russ. Metall. (GB), no.6, p.130-4 (1981). Translation of: *Izv. Akad. Nauk. SSSR Met.*, no.6, p.130-4 (1981).

Optimal conditions of heat treatment were determined which ensure higher strength and toughness at room and cryogenic temperatures. Steel 40G20N13F (0.39 C, 20.64 Mn, 12.50 Ni, 0.91 V, 0.36 Si, 0.008 S, 0.006 P) exhibited the following properties at +20 and -196°C after quenching from 1100°C and ageing at 650°C for 10 h: $\sigma_{0.2} = 80-110 \text{ kg/mm}^2$, $\sigma_H = 10-12 \text{ kg/cm}^2$. The stainless steel 40Kh14G15N10F (0.34 C, 16.00 Mn, 9.6 Ni, 14.6 Cr, 1.00 V, 0.39 Si, 0.009 S, 0.011 P) exhibited the following properties after quenching from 1150°C and ageing for 10 h at 650°C: $\sigma_{0.2} = 65-120 \text{ kg/mm}^2$, $\delta, \psi < 30\%$; this steel is useful for nonmagnetic highly-stressed parts in cryogenic equipment. Due to the increased technological ductility at elevated temperatures, these steels can be used for manufacturing parts by forging, rolling or stamping. (5 refs.)

63418 Effect of retained austenite on the contact fatigue strength of steel in relation to the phase diagram. B.B.Vinokur.

Russ. Metall. (GB), no.6, p.162-8 (1981). Translation of: *Izv. Akad. Nauk. SSSR Met.*, no.6, p.165-71 (1981).

The influence of temperature and carbon concentration on the contact fatigue strength in steel KhGMF (1.31 Cr, 1.34 Mn, 0.80 Ni, 0.23 Mo, 0.16 V) was examined for two compositions: high-carbon, with a uniform carbon content throughout the volume, and case-hardened (0.19% C in the core with a high-carbon content in the surface layer equal to that of the corresponding high-carbon steels). Both variants were produced with carbon contents of 0.55, 0.70, 0.80 and 0.95%. In the high-carbon steels this was achieved by fractional casting, whilst in the case-hardened steel it was achieved by different conditions of case-hardening (1.8-2.0 mm layer depth). An increase of the carbon content in the high-carbon steel lowers the resistance to pitting formation, whilst an increase in carbon in the case-hardened layer increases the contact fatigue strength. (4 refs.)

63419 Overload induced crack growth rate attenuation behavior in aluminum alloys. R.S.Vecchio, R.W.Hertzberg (Dept. of Metall. & Materials Engrg., Lehigh Univ., Bethlehem, PA, USA), R.Jaccard.

Ser. Metall. (USA), vol.17, no.3, p.343-6 (March 1983).

The influence of baseline stress intensity level on crack growth delay resulting from overload cycles is plotted for two aluminum alloys, 2024-T3 and AC062. The data are described by a 'U-shaped' plot which reflects large amounts of decay at both high and low stress intensity levels, but little delay at intermediate values. Improved component life under variable amplitude loading conditions may be expected if the width of the U-shaped curve could be decreased. (14 refs.)

63420 Mechanism of influence of certain alloying elements on the hydrogen embrittlement of iron. I.I.Vasilenko, Yu.N.Khomitskii, V.P.Koval' (G.V. Karpenko Physicomech. Inst., Acad. of Sci., Lvov, Ukrainian SSR). *Sov. Mater. Sci. (USA)*, vol.18, no.3, p.205-9 (May-June 1982). Translation of: *Fiz.-Khim. Mekh. Mater. (USSR)*, vol.18, no.3, p.16-21 (May-June 1982). [received: Feb. 1983]

One of the hypotheses of hydrogen embrittlement explains it by the precipitation of hydrogen at dislocations and other defects. Hydrogen, concentrating at a dislocation, may in a significant manner retard its movement, causing embrittlement of the metal. The authors consider the energy of the interaction of a foreign substitutional atom with dislocation, and the field of stresses created around the dislocation. (16 refs.)

63421 Near-threshold growth of short fatigue cracks. O.N.Romaniv, V.N.Simin'kovich, A.N.Tkach (G.V. Karpenko Physicomech. Inst., Acad. of Sci., Lvov, Ukrainian SSR).

Sov. Mater. Sci. (USA), vol.18, no.3, p.234-9 (May-June 1982). Translation of: *Fiz.-Khim. Mekh. Mater. (USSR)*, vol.18, no.3, p.50-7 (May-June 1982). [received: Feb. 1983]

A study is presented of the features of the growth of short fatigue cracks and the establishment of the rules of formation of the threshold stress intensity factors for such cracks. The experiments were made with samples of technical grade iron, 20Kh13 steel in two structural conditions, after annealing and after oil hardening from 980°C, Yu3 austenitic steel, and AMG-61 wrought aluminum alloy. The tensile tests, determination of fracture toughness K_{IC} , and construction of kinetic fatigue failure curves were done in air at room temperature. (20 refs.)

63422 Statistical rules of fatigue crack development. M.N.Stepnov, N.A.Makhtov, A.S.Setegin, A.N.Lisin (K.E. Tsiolkovskii Moscow Aviation Technol. Inst., Moscow, USSR).

Sov. Mater. Sci. (USA), vol.18, no.3, p.250-4 (May-June 1982). Translation of: *Fiz.-Khim. Mekh. Mater. (USSR)*, vol.18, no.3, p.70-4 (May-June 1982). [received: Feb. 1983]

Presents the results of a study of the probability rules of failure of AK4-1 and D1 aluminum alloys. The AK4-1 alloy samples were tested in pure bending. The D1 alloy samples were tested in symmetric plane bending with rigid loading. During the tests the crack length, starting with 0.03 mm, was measured. An analysis of the crack growth curves showed that in different samples with the same load the cracks develop at different rates. By graphic differentiation the crack development rates (v , mm/cycle) were determined at the points of measurement of their lengths and the ranges ΔK of the stress intensity factors were calculated. (7 refs.)

Evaluation of the resistance of irradiated zirconium-liner cladding to iodine-induced stress corrosion cracking See Entry 60236

Fracture appraisal of large scale glass blocks under realistic thermal conditions See Entry 60270

On strength of welded joints in high strength, large scale copper coils for nuclear fusion equipment See Entry 60432

Bending strength of F102 and NS9 optical glasses See Entry 61249

Formation of fracture structures of weakly interacting cracks See Entry 61454

Combined models of fracture and their use in predicting service life See Entry 61455

Microhardness of an implanted system See Entry 61944

Low temperature neutron and gamma irradiation of glass fiber reinforced epoxies See Entry 61980

Fatigue life estimation using simple fracture mechanics See Entry 62019

Chemical durability of ZrO₂ containing glasses See Entry 62159

Kinetic enrichment of hydrogen at interfaces and voids by dislocation sweep-in of hydrogen See Entry 62168

Emission of light from solids during crack formation See Entry 63055

Comparative studies of reactive sputtering, ion plating and CVD coating of TiN hard layers See Entry 63167

- Effect of thermal conditions of preparation of dispersion-strengthened nickel powders on the character of distribution of the strengthening phase See Entry 63205
- Repeated mechanical strengthening as a method of increasing the endurance of constructional steels See Entry 63314
- Thermomechanical treatments of a 1050 pearlite steel See Entry 63318
- The effect of ITMT's and P/M processing on the microstructure and mechanical properties of the X7091 alloy See Entry 63319
- Effect of HTTT on the properties of alloy steel castings See Entry 63323
- Influence of cyclic annealing on the hardness and structure of high-speed steels See Entry 63327
- Structure and properties of low-pearlite steel with different titanium concentrations See Entry 63330
- Effect of technological inheritance on the hardness of malleable iron after heat treatment See Entry 63331
- Structure and properties of a maraging steel after thermomechanical and repeated heat treatment See Entry 63332
- Influence of residual gas pressure in annealing on the properties of niobium and its alloys See Entry 63333
- Kinking in the drawing of linear polyethylene See Entry 63351
- Effect of sulfides and sulfide morphology on anisotropy of tensile ductility and toughness of hot-rolled C-Mn steels See Entry 63354
- Effect of diffusion welding thermal cycle on the strength of alloy VT20 See Entry 63359
- Mechanical behaviour of isotactic polypropylene subjected to various strain histories in uniaxial extension See Entry 63363
- Intergranular zinc embrittlement and its inhibition by phosphorus in 55 pct Al-Zn-coated sheet steel See Entry 63353
- Effect of high-temperature vacuum annealing time on the structure and properties of titanium alloys See Entry 63457
- Effect of annealing on the structure and properties of molybdenum coatings on steel Kh12M See Entry 63458
- Effect of vibroabrasive treatment on the fatigue strength of high-alloy steels See Entry 63460
- Fatigue strength of steel 45 with electrolytic iron coating, carbon nitrided with HF heating See Entry 63461
- Fracture of metals under the action of hydrogen-containing media See Entry 63466
- Question of the safe boundaries of use of 12 Mkh steel at increased temperatures and hydrogen pressures See Entry 63467
- Effect of specimen width on impact strength and location of brittleness temperature of St3ps steel See Entry 63475
- Plated weld mechanical characteristics See Entry 63476

81.40P Friction, lubrication, and wear

(see also 62.20P Tribology)

- 63423 Influence of ϵ -martensite on the friction and wear of high-manganese alloys. L.G.Korshunov, V.V.Sagaradze, N.A.Tereshchenko, N.L.Chernenko (Inst. of Metal Phys. Acad. of Sci., Sverdlovsk, USSR). *Fiz. Met. & Metalloved. (USSR)*, vol.55, no.2, p.341-8 (Feb. 1983). In Russian. English translation in: *Phys. Met. & Metallogr. (GB)*
- An investigation was made of structural transitions in G21 and 20G18S2F1 alloys during friction. The presence in the structure of the G21 alloy of a considerable amount of ϵ -martensite ($\geq 30\%$) with the h.c.p. crystal structure ensured a low friction coefficient of the alloy ($K=0.27-0.40$) and an increase in the resistance to wear under conditions when the bulk temperature in the surface layer exceeded 100°C . The occurrence of the $\epsilon\rightarrow\gamma$ transition during friction under conditions of strong heating of the surface was responsible for the increase in the friction coefficient and a reduction in the wear resistance of the alloys G21 and 20G18S2F1. (12 refs.) A.T.
- 63424 Particle collisions in the vicinity of an eroding surface. D.R.Andrews, N.Horsfield (Cavendish Lab., Cambridge Univ., Cambridge, England). *J. Phys. D (GB)*, vol.16, no.4, p.525-38 (14 April 1983).
- In the vicinity of a surface which is being eroded there is a region where particles arriving at and departing from the surface can collide. The frequency of collisions and the resulting motion of spherical particles have been investigated theoretically and experimentally. An expression is derived for the flux of spheres necessary for a high frequency of collisions. The directions and velocities of particles after collision have also been calculated, assuming elastic collisions. In the low-flux limit collisions do not reduce the number of particles reaching the surface. Long-exposure (ca. 1 s) and high-speed (5000 frames s^{-1}) photography confirms these findings for the case of 0.6 ± 0.1 mm diameter glass spheres travelling at 13 ± 1 m s^{-1} . These conclusions conflict with the ideas of many authors who suggest that collisions help protect the eroded surface. The present paper shows that collisions degrade the incident beam of particles by increasing the angular divergence of the beam and creating a spectrum of velocities. Stray particles have also been observed entering the region of interest, increasing the frequency of collisions. Stray particles and changes in the incident beam are probably the causes of the observed reduction in erosion rate at high levels of flux. (25 refs.)
- 63425 Optimizing the carbon and manganese concentrations in wear-resistant chromium cast irons. E.V.Rozhkova, O.M.Romanov (All-Union Sci.-Res. & Design-Technol. Inst. of Coal Mining Machine Construction, USSR). *Met. Sci. & Heat Treat. (USA)*, vol.24, no.5-6, p.418-20 (June 1982). Translation of: *Metalloved. & Term. Obrab. Met. (USSR)*, vol.24, no.6, p.36-8 (June 1982). [received: Feb. 1983]
- Concerns the combined effect of manganese and carbon on the abrasive (microcutting) and impact-abrasive wear resistance of chromium cast irons. The composition of cast iron intended for operation under abrasive wear conditions must be selected with at least two parameters kept in mind. The carbon and manganese concentrations have different effects on the abrasive and impact-abrasive wear resistant of cast iron. The abrasive wear resistance of cast iron rises with increasing amounts of carbon and drops with increasing amounts of manganese. (2 refs.)

- 63426 Influence of structure on the wear resistance of alloys. A.I.Stepina, L.I.Sidorova, E.V.Tolstenko (All-Union Sci.-Res. for Mechanization in Ferrous Metall., USSR). *Met. Sci. & Heat Treat. (USA)*, vol.24, no.5-6, p.438-40 (June 1982). Translation of: *Metalloved. & Term. Obrab. Met. (USSR)*, vol.24, no.6, p.54-5 (June 1982). [received: Feb. 1983]
- An investigation was made of wear resistance of irons and steels with wear of the samples by a flow of abrasive particles moving at angles of 20° and 90° to their surface. The kinetic energy of an abrasive particle reaching the surface of the sample at angles of attack of 20° and 90° was 4446 and 13000×10^{-7} J, respectively. It was found that under conditions of gas-abrasive wear and wear resistance of alloys is determined by their structure and hardness. During abrasive wear the surface layers of the alloys were intensely work hardened. Failure of the surface layers during abrasive wear occur only after reaching a certain value of microhardness and physical width of the diffraction line. For austenite steel these are H450-500 and $\beta(311)=0.035-0.045$ rad and for ferrite $\beta(211)=0.015-0.023$ rad. (3 refs.)
- 63427 The determination of the coefficient of dynamic friction of organic powder compacts on steel. M.B.James, J.M.Newton (Pharmacy Dept., Univ. of London, London, England). *Powder Technol. (Switzerland)*, vol.34, no.1, p.29-37 (Jan.-Feb. 1983).
- A practical experimental model system has been successfully used to study the frictional response of organic powder compacts sliding across a polished steel plate, representative of the die bore of a production compaction system. This system offers a controlled approach to the study of frictional phenomena occurring during compaction and facilitates a more detailed investigation into the fundamental mechanisms of friction than a simple resolution of forces within a punch and die apparatus. For acetylsalicylic acid sliding on steel, the dynamic friction coefficient was found to be dependent on the displacement and, to a lesser extent, the initial normal load, whereas for PTFE on steel, the dynamic friction coefficient was independent of displacement and load and estimated at 0.09. Thus, soft organic materials exhibit very different frictional characteristics to those of brittle materials. These differences reflect the differing importance and magnitude of the three frictional components, adhesion, shear and ploughing. (22 refs.)
- 63428 Nitriding kinetics and wear resistance of titanium alloys. D.P.Shaskov, A.V.Vinogradov, V.N.Polokhov. *Russ. Metall. (GB)*, no.6, p.168-73 (1981). Translation of: *Izv. Akad. Nauk. SSSR Met.*, no.6, p.172-7 (1981).
- The materials investigated were pure titanium grade VT1-0, $\alpha+\beta$ titanium alloy VT22, and the compound NiTi containing 54% Ni and 46% Ti. With increasing temperature and nitriding time, the thickness of the diffusion layers increases; in the case of NiTi the nitrided layer consists basically of a very hard titanium nitride. Examinations of the depth-distribution of the microhardness of the nitrided layer shows that the greatest increase in surface hardness occurred in the NiTi, its nitriding temperature being much lower (500°C) than for titanium or for the alloy VT 22 ($900-1000^\circ\text{C}$). The wear resistance after nitriding was higher by several orders of magnitude for NiTi than for the titanium and the VT22 alloy. Therefore, the alloy NiTi is recommended for parts subjected to intensive wear in low-noise equipment where a high strength in the core of the material is not required. (4 refs.)
- 63429 Thermally stressed condition occurring in the surface layers of flat parts during friction hardening. Yu.I.Babei, R.I.Glek, M.D.Maksimishin, N.A.Zhuravleva (G.V. Karpenko Physicomech. Inst., Acad. of Sci., Lvov, Ukrainian SSR). *Sov. Mater. Sci. (USA)*, vol.18, no.3, p.254-7 (May-June 1982). Translation of: *Fiz.-Khim. Mekh. Mater. (USSR)*, vol.18, no.3, p.75-8 (May-June 1982). [received: Feb. 1983]
- A part being subjected to friction hardening is simulated by a half-space. Since the maximum contact tangential stresses, which are primarily responsible for heating of the zone of contact, occur at a certain distance from the surface, in this problem the case of subsurface location of the heat source is discussed. An elastic semiinfinite body is considered. The choice of the coordinate system is made in such a manner that the y and z axes lie on the faces of the body and the x axis is directed into the depth. (4 refs.)
- 63430 Influence of production media on the physicochemical and electrochemical properties of steels. V.E.Shestopalov (Lenin Komosomol Lvov Polytech. Inst., Lvov, Ukrainian SSR). *Sov. Mater. Sci. (USA)*, vol.18, no.3, p.285-7 (May-June 1982). Translation of: *Fiz.-Khim. Mekh. Mater. (USSR)*, vol.18, no.3, p.107-9 (May-June 1982). [received: Feb. 1983]
- The results are presented of an investigation of the influence of a new form of production medium, polymer-containing, on the physicochemical and electrochemical properties of constructional steels. The use of polymer-containing media as production media leads to the occurrence of a process of thermomechanicochemical working, the effectiveness of which is determined by the presence, concentration, and nature of interaction of the products of breakdown of the polymer components of the production medium with the fresh surface of the metal. Water emulsion lubricating and cooling liquids based on ET-2 self-emulsifying oil, industrial production lubricants, and types MKhO polymer-containing production media were used as the production media. (7 refs.)
- 63431 Sliding friction behaviour of polymer-polymer material combinations. G.Erhard (BASF AG, Ludwigshafen, Germany). *Wear (Switzerland)*, vol.84, no.2, p.167-81 (15 Jan. 1983).
- The intermolecular bonding energies of polymeric materials can be employed in the evaluation of sliding under conditions determined predominantly by adhesion. The effect at the interface of these energies can be evaluated by reference to the surface energy and to its polar and dispersion-related components. Wetting angle measurements were used to determine the work of adhesion for a group of polymer-polymer material combinations. An exponential relationship exists between the work of adhesion and the coefficients of friction of these combinations, these coefficients of friction being determined primarily by adhesion. (22 refs.)
- 63432 Residual stresses and sliding wear. J.W.Ho, C.Noyan, J.B.Cohen (Dept. of Materials Sci. & Engng., Northwestern Univ., Evanston, IL, USA), V.D.Khanna, Z.Elizeer. *Wear (Switzerland)*, vol.84, no.2, p.183-202 (15 Jan. 1983).
- The residual stresses that develop during the wear of AISI-SAE 1018 and 4340 steels have been examined. The entire three-dimensional stress tensor was obtained. A normal stress perpendicular to the surface, predicted by theory, has been found, but its magnitude is too small to affect the wear rate. There are also significant shear stresses. The wear process rapidly alters any initial stress distribution produced by heat treatment or peening to such a degree that the wear rate is not affected by these stresses, unless they are initially larger than those that can be produced by the wear parameters. (21 refs.)

- 63433 An analysis of the localization of deformation and weight loss during single-particle normal impact. G.Sundararajan (Dept. of Metall. Engng., Ohio State Univ., Columbus, OH, USA). *Wear (Switzerland)*, vol.84, no.2, p.217-35 (15 Jan. 1983).
Localized lip formation and subsequent lip fracture is the dominant mechanism by which material is removed during the normal incidence of single spherical particles on ductile targets. A theoretical model which predicts the extent of lip formation as well as the weight loss during these single impact experiments is presented. The model postulates that the lip formation is the result of localization of deformation in the near-surface regions of the target and that the lip is removed either by inertial-stress-induced tensile fracture or by separation across adiabatic shear bands formed at the base of the lip. The single-impact data for copper, brass, thorium dispersed (TD) nickel and nickel targets are shown to compare very well with the predictions of the model. (17 refs.)
- Wear resistance of friction elements working in oil See Entry 62021
- A new model for the erosion of metals at normal incidence See Entry 62022
- Analysis of the stressed state of the forward slip zone in the seat of deformation of a powder being rolled See Entry 63191
- Some studies in the displacements of powder material during compaction See Entry 63203
- Effect of HTTT on the properties of alloy steel castings See Entry 63323
- The effects of molecular weight and cooling rate on fine structure, stress-strain behavior and wear of polytetrafluoroethylene See Entry 63374
- Effect of annealing on the structure and properties of molybdenum coatings on steel Kh12M See Entry 63458
- Wear kinetics of a two-phase boride layer See Entry 63459

81.40R Electrical and magnetic properties (related to treatment conditions)

(see also 72.80 Conductivity of specific semiconductors and insulators, 74.70 Superconducting materials, 75.50 Studies of specific magnetic materials)

- 63434 Changes in resistivity at low-temperature deformation and the subsequent recovery of the Ag-15 at.% Al alloy. V.S.Zubchenko, P.V.Petrenko, O.O.Tatarov. *Dopov. Akad. Nauk UkrSR. Ser. A (USSR)*, no.2, p.76-8 (1983). In Ukrainian.
- It is shown that in low-temperature deformation and subsequent annealing of the Ag-15 at.% Al alloy changes in electroresistivity are due to the ordering processes. (6 refs.)
- 63435 Heat treatment and magnetic properties of high-coercivity Fe-Co-Cr alloys with 3% Mo. B.A.Samarin, V.S.Shubakov, L.B.Vul'f (Moscow Inst. of Steel & Alloys, Moscow, USSR). *Met. Sci. & Heat Treat. (USA)*, vol.24, no.5-6, p.431-4 (June 1982). Translation of: *Metall. & Term. Obrab. Met. (USSR)*, vol.24, no.6, p.47-50 (June 1982). [received: Feb. 1983]
- Concerns the effect of molybdenum on the phase composition and magnetic properties of Fe-Co-Cr alloys with 15% Co and 25-35% Cr after various heat treatments. Alloying with molybdenum makes it possible to lower the quenching temperature to α solid solution of Fe-15% Co + (20-35%) Cr alloys, although the hot plastic deformation temperature must be raised due to the broader range in which the σ phase exists. The addition of molybdenum lowers the initial temperature of high-coercivity decomposition and leads to $H_c = 60-48$ kA/m without reducing the level of magnetic energy. (4 refs.)
- 63436 Effect of antimony on the magnetic properties and grindability of alloy YuND4. A.A.Bezuglov, G.N.Buzuglova, N.I.Sannikov (Shakhty Technol. Inst. of High-Speed Servicing, USSR). *Met. Sci. & Heat Treat. (USA)*, vol.24, no.5-6, p.434-6 (June 1982). Translation of: *Metall. & Term. Obrab. Met. (USSR)*, vol.24, no.6, p.50-2 (June 1982). [received: Feb. 1983]
- The effect of antimony additives (up to 1% by weight) on the magnetic properties, structure, and grindability of alloy YuND4 (25% Ni, 14% Al, 4% Cu, and the remainder Fe) was investigated. It was found that alloying with 0.2% of Sb and less does not give rise to an increase in the magnetic properties of alloy YuND4, but, conversely, effects their reduction. Analysis of the results indicated that an additive of 0.25% of Sb is optimum, since alloy YuND4 with 0.25% of Sb exhibits the best combination of magnetic energy and residual induction at a rather high coercive-force level. (no refs.)
- Temperature dependence of electrical resistivity of Al-Zn alloys See Entry 62394
- Mechanism of formation of magnetic properties of amorphous alloy $\text{Fe}_{50}\text{Co}_{20}\text{Si}_{15}\text{B}_{10}$ during annealing See Entry 62694
- Effect of fabrication condition on the magnetic properties of Fe-Mn-B system amorphous alloys See Entry 62704
- Remagnetisation phenomena in multicomponent rare-earth-cobalt alloys with increased temperature stability See Entry 62707
- Ion beam sputter deposition of layered magnetic thin films See Entry 63157
- Effect of low-temperature ferritization on the properties of ferrite powders See Entry 63222
- Nonstoichiometry and physical properties of hot-pressed manganese-zinc ferrites See Entry 63223
- Investigation of the phase composition, structure, and magnetic properties of alloy $\text{Sm}_2\text{Co}_{10}\text{Fe}_{3.2}\text{Cu}_{1.2}\text{Zr}_{0.4}$ See Entry 63287
- Effects of mechanical drawing treatment on the characteristics of internal friction and thermally stimulated current on low density polyethylene See Entry 63308
- Influence of surface condition on the magnetic properties of Fe-3% Si alloy See Entry 63320
- Effect of chromium and aluminum on the physical and mechanical properties of precipitation-hardening Fe-Mn Elinvar See Entry 63321

81.40T Optical properties (related to treatment conditions)

(see also 78.20 Optical properties and materials)

- Optical homogeneity of oxygen-free chalcogenide glasses See Entry 61248
- Photochromism and its origin of heat-treated $\text{Na}_2\text{O}-\text{BaO}-\text{Al}_2\text{O}_3-\text{TiO}_2$ glasses See Entry 62909

81.60 CORROSION, OXIDATION AND SURFACE TREATMENTS

- 63437 On the theory of stress-assisted diffusion. II. D.J.Unger, E.C.Aifantis (Univ. of Minnesota, Minneapolis, MN, USA). *Acta Mech. (Austria)*, vol.47, no.1-2, p.117-51 (1983).
For pt.I see *ibid.*, vol.45, no.3-4, p.273 (1982). Similarity and general steady-state solutions of a recently developed stress-assisted diffusion theory are derived. General transient solutions are obtained analytically for certain classes of stress distributions. For general stress distributions a perturbation method is employed to produce transient solutions. Under appropriate conditions the derived solutions are reduced to previous formulae that have unsystematically appeared in the literature. Examples of interesting crack problems involving stress singularities as well as the elimination of singularities are considered. An equilibrium solution is utilized together with a straightforward physical argument to produce rationally two empirical formulae previously proposed in the literature to model embrittlement and stress corrosion cracking phenomena. This solution is further used to model embrittlement and stress corrosion cracking data more successfully than previous attempts. An appendix on certain preliminary elastodiffusive fracture criteria is given. (44 refs.)
- 63438 Microstructure and ductility of electroless copper deposits. S.Nakahara, Y.Okinaka (Bell Labs., Murray Hill, NJ, USA). *Acta Metall. (USA)*, vol.31, no.5, p.713-24 (May 1983).
Transmission and scanning electron microscopes were used to characterize the microstructures of electroless copper deposits plated on large-grained copper sheets, amorphous Pd-Cu-Si alloy, and SnCl_2 -PdCl₂ activated plastic substrates. Nucleation and growth patterns were found to depend markedly on the type of substrate. The presence of a large number of small gas bubbles containing hydrogen is characteristic of these deposits. The effect of these bubbles on film ductility is discussed and shown to cause hydrogen embrittlement in the copper films. (37 refs.)
- 63439 Anodic oxidation of GaAs in oxygen plasma and qualitative analysis of anodic oxide films by AES and XPS. Zhang Guansheng, Tang Houshun, Huang Dusen, Yu Xitong (Fudan Univ., Shanghai, China). *Chin. J. Semicond. (China)*, vol.4, no.2, p.181-6 (March 1983). In Chinese.
The anodic oxidation of GaAs is carried out in an oxygen plasma generation by RF glow discharge. The diameter of the wafer is 40 mm. The grown films are amorphous and uniform. The breakdown electric field of the oxide is $\approx 10^6$ V/cm⁻¹, their resistivity is 10^{15} Ω -cm and the refractive index is 1.83-1.85 ($\lambda = 6328$ Å). According to the analysis of the oxide films by AES-XPS the in-depth profiles for the as-grown anodic oxide display three distinct layers: the first is an arsenic-deficient layer near the surface with a thickness of ~ 100 Å; the second layer, a center region, has a nearly constant composition in depth, the concentration ratio of gallium and arsenic is 1.2-1.6; and the third layer comprises the transition region from the oxide GaAs. (8 refs.)
- 63440 Anisotropic etching of silicon: a model diffusion-controlled reaction. D.M.Allen, I.A.Routledge (Cranfield Inst. of Technol., Cranfield, England). *IEE Proc. I (GB)*, vol.130, no.2, p.49-56 (April 1983).
In conventional isotropic etching of metals, it has been found that narrower slot take longer to etch than wider ones. This has been attributed largely to the restricted access of fresh etchant to the metal surface. Spent etchant remains at the metal surface and forms a physical etch-retarding barrier. Anisotropic etching of single crystals differs from isotropic etching, in that it is orientation dependent, and different crystal planes are etching at different rates under identical conditions. This investigation examines anisotropic etching of (110) silicon for different slot widths and compares it with the already available information on isotropic etching of metals. (10 refs.)
- 63441 Structure in carbon/carbon fibre composites as studied by microscopy and etching with chromic acid. J.A.Forrest, H.Marsh (Northern Carbon Res. Labs., Univ. of Newcastle upon Tyne, Newcastle upon Tyne, England). *J. Mater. Sci. (GB)*, vol.18, no.4, p.973-7 (April 1983).
Structure of the matrix carbon in two industrially prepared carbon/carbon fibre composites and in four composites prepared in the laboratory was studied using optical microscopy and SEM examination of surface topography after oxidation in chromic acid solution. In the industrial composites and in the laboratory composites prepared with PAN fibres, the orientation of the basal planes of the matrix carbon is parallel to the fibre length within ~ 5 μ m of the fibre. The fibre-matrix interface is an area of weakness. Use of CVD coated carbon fibres, however, prevented this alignment; here the basal planes of the matrix carbon are randomly aligned relative to the surfaces of the fibres. (10 refs.)
- 63442 The environmental stress corrosion cracking of glass fibre-reinforced laminates and single E-glass filaments. F.R.Jones, J.W.Rock, J.E.Bailey (Dept. of Metall. & Materials Technol., Univ. of Surrey, Guildford, England). *J. Mater. Sci. (GB)*, vol.18, no.4, p.1059-71 (April 1983).
The environmental stress corrosion cracking of epoxy/glass fibre crossply, unidirectional coupons and single E-glass filaments have been compared. At initial applied strains $>0.15\%$ the resin does not protect the fibres as shown by their equivalent failure times. The failure occurs in the environment and planar fractures occur because of the localized stress in the load bearing plies adjacent to a transverse crack in the 90° ply of the 0°/90°/0° coupons. These transverse cracks result from stress corrosion on the glass/resin interface, which leads to a reduction of the transverse cracking strain. At applied strains $<0.15\%$ fracture occurs within the unexposed half of the coupons and is thought to be caused by rapid transport of glass corrosion products where they crystallize within the coupon. This phenomenon is also responsible for the progressive transverse cracking that occurs in both the 0° and 90° plies of the unimmersed half of the crossply coupon under zero load. (28 refs.)
- 63443 The performance of mechanical scraping tools in ultrahigh vacuum: an XPS study. M.S.Lazarus (Dept. of Chem., Herbert H. Lehman Coll., City Univ. of New York, New York, NY, USA), T.K.Sham. *J. Electron Spectrosc. & Relat. Phenom. (Netherlands)*, vol.31, no.1, p.91-6 (April 1983).
The authors examine some of the considerations to be borne in mind when cleaning a sample surface, with emphasis on the scraping technique. In particular, comparisons are made between mechanically scraped surfaces and Ar⁺-etched surfaces of two materials. The importance of choosing the best scraping device for a particular surface is discussed. In general, they conclude that it is better to scrape the surface than to Ar⁺-etch it. (3 refs.)

- 63444 Ion etching of InP-InGaAsP heterostructures.** M.N.Zargar'yants, V.V.Krapukhin, I.A.Krykanov, N.B.Kagan. *Sov. Phys. Tech. Phys. (USA)*, vol.27, no.10, p.1291-2 (Oct. 1982). Translation of: *Zh. Tekh. Fiz. (USSR)*, vol.52, no.10, p.2102-4 (Oct. 1982). [received: April 1983]
The authors' purpose is to see if ion etching can be used to monitor the layer thicknesses and geometry of heterojunction boundaries in multilayer heterostructures, and to select optimal conditions for ion etching InP-InGaAsP heterostructures. The well-established experimental dependence of the ion sputtering rate on the composition of the sputtered material makes it possible to identify the heterojunction boundaries in semiconductor heterostructures. The three-electrode gas discharge ion source with magnetic field was used in the etching experiments. The authors studied how the depth of the etching details produced on the heterojunction boundaries depended on the ion beam current and found that for argon ions of energy 5 keV, details large enough to be observed in the scanning electron microscope are produced at current densities $(2-3) \times 10^{15} \text{ cm}^{-2}$. For the current densities in the ion source used this dosage was reached after 8-80 s. (9 refs.)
- 63445 The photoelectrochemical etching of TiO_2 single crystals.** A.Praet, F.Vanden Kerchove, W.P.Gomes (Lab. voor Fysische Scheikunde, Rijksunivers. Gent, Gent, Belgium), F.Cardon. *Sol. Energy Mater. (Netherlands)*, vol.7, no.4, p.481-90 (Jan.-Feb. 1983).
The photoelectrochemical behaviour of mechanically polished TiO_2 (rutile) single crystal electrodes was followed as a function of time during photoelectrochemical etching of the surface in acid solutions. It was found that, as a consequence of this treatment, not only the shape of the photocurrent-voltage curve changed, but that also the limiting photocurrent increased over one to two orders of magnitude. The results, combined with analytical data on the corrosion rate, were interpreted quantitatively by a model in which it was assumed that a damaged surface layer, containing a large number of recombination centers as a consequence of the polishing treatment, is gradually removed by photoelectrochemical etching. The usefulness of this photoelectrochemical etching treatment in research on photoelectrochemical solar cells is discussed. (20 refs.)
- 63446 Quantum chemical models of elementary steps concerning plasma etching in the F/Si system.** D.K.Fricke, H.Müller (Sektion Chemie, Friedrich Schiller Univ., Jena, Germany). *Wiss. Z. Friedrich-Schiller-Universität Jena, Math. Naturwiss. Reihe (Germany)*, vol.31, no.6, p.895-905 (1982). In German.
The authors make calculations of the microscopic processes of plasma etching on an atomic level. They use the cluster model of solid and a semiempirical quantum chemical method (extended Hückel-MO) for the calculation. Using the extended Balloon-effect, a proposal is given of the mechanism of plasma etching of silicon with fluorine. (30 refs.)
- Characterization of mechanical properties of nuclear waste glasses See Entry 60269
- Fracture appraisal of large scale glass blocks under realistic thermal conditions See Entry 60270
- An attempt to assess the long-term crystallization rate of nuclear waste glasses See Entry 60271
- Effect of $\text{Fe}_2\text{O}_3/\text{ZnO}$ on two glass compositions for solidification of Swedish nuclear wastes See Entry 60273
- SIMS depth profiling studies of sphene-based ceramics and glass ceramics leached in synthetic groundwater See Entry 60278
- Leaching of natural and synthetic sphene and perovskite See Entry 60279
- Effects of radiation damage and radiolysis on the leaching of vitrified waste See Entry 60280
- Near-surface leaching studies of Pb-implanted Savannah River waste glass See Entry 60282
- Leachability of zircon as a function of alpha dose See Entry 60285
- Isotopic fractionation of thorium and uranium upon leaching of monazite: alpha-recoil damage effects See Entry 60286
- Investigations of the solution behaviour of NaCl in the quinary system NaCl-KCl-MgCl₂-MgSO₄-H₂O at different temperatures See Entry 60295
- Observations of spherulitic structure by etched monolithic polypropylene samples by means of a scanning electron microscope See Entry 61818
- The mode of the attack of oxygen atoms on the basal plane of graphite See Entry 62247
- Investigation of the influence of water on the surface conductivity of optical glass See Entry 62479
- On the passivation of p-n junctions in silicon through anodic oxidation See Entry 62489
- IR reflection investigation of corrosion of optical glasses See Entry 63005
- Laser synthesis of V_2O_5 crystals with highly developed surfaces See Entry 63149
- Increased-strength black chromium coatings See Entry 63183
- Recrystallization processes in amorphous and polycrystalline silicon See Entry 63334
- Electron microscopic observation of hard material using an ion sputtering technique See Entry 63495
- Investigation of precipitated alumina structures by secondary-ion mass spectrometry and electron paramagnetic resonance spectrometry. III. Structure of an alumina coating precipitated on rutile titanium dioxide See Entry 63592
- Adsorption and reactive changes of octadecylamine on iron oxide surfaces See Entry 63599
- The application of plasma mass spectroscopy to plasma etching See Entry 63632

81.60B Metals and alloys

(inc. stress corrosion cracking; anticorrosion)

- 63447 Anodic dissolution behaviour of Si- and Ti-implanted iron.** Y.Okabe (Dept. of Electronic Engng., Faculty of Engng., Saitama Inst. of Technol., Saitama, Japan), M.Iwaki, K.Takahashi, K.Yoshida. *Jpn. J. Appl. Phys. Part 2 (Japan)*, vol.22, no.3, p.L165-7 (March 1983).
Effects of silicon and titanium ion-implantations on anodic dissolution behaviour of iron have been investigated by multisweep cyclic voltammetry in acetate buffer solution (pH~5), secondary ion mass spectrometry and scanning electron microscopy. Ion-implantations have been carried out with a dose of $1 \times 10^{17} \text{ ions/cm}^2$ at an energy of 150 keV at room temperature. It is found that electrochemical properties of Si^{+} - and Ti^{+} -implanted irons are more inert than that of pure iron. Anodic dissolution phenomena of ion-implanted

irons are discussed in relation to the shape of an electrochemically corroded surface observed by SEM and to the concentration profiles of implanted atoms measured by SIMS. (10 refs.)

- 63448 Inhibition of corrosion of aluminium in nitric acid by some carbohydrates.** C.Chakrabarty, M.M.Singh, C.V.Kagarwal (Appl. Chem. Section, Inst. of Technol., Banaras Hindu Univ., Varanasi, India). *Indian J. Technol.*, vol.20, no.9, p.371-2 (Sept. 1982). [received: March 1983]
Inhibitive effect of fructose, sucrose, glucose and fructose on the corrosion of aluminium in 20% nitric acid has been evaluated at 35°C by weight loss and potentiostatic methods. All the additives used showed certain degree of inhibition at all the concentrations tested. Lactose is found to be the most efficient at almost all the concentrations, followed by fructose and glucose. Sucrose showed very poor inhibitive effect at lower concentrations. (11 refs.)
- 63449 A surface treatment for Ti-6Al-4V.** T.Smith (Rockwell Internat. Sci. Center, Thousand Oaks, CA, USA). *J. Adhes. (GB)*, vol.15, no.2, p.137-49 (1983).
A simple nonchromate surface treatment that was developed for aluminum alloys (STAB(3)) has been found to provide Ti-6Al-4V, bonded with epoxy adhesives, with good hydrothermal endurance. The simplest form of the treatment is to degrease, dip in caustic soda, hard (i.e. forceful) spray-rinse and dry. A steel wool scrub prior to the NaOH dip enhances durability. Surface property measurements following the surface treatment indicate that a porous oxide layer is formed on top of a 300 Å barrier layer. The durability of this treatment is attributed to mechanical interlocking between the adhesive and the porous oxide (hydroxide) and to the chemical stability of the oxide (hydroxide) under hydrothermal stress. (18 refs.)
- 63450 Polymer-aluminium adhesion. I. The surface energy of aluminium in relation to its surface treatment.** A.Carre (Centre de Recherches sur la Phys., Chimie des Surfaces Solides, CNRS, Mulhouse, France), J.Schultz. *J. Adhes. (GB)*, vol.15, no.2, p.151-61 (1983).
The influence of different surface treatments (degassing, phosphatization sealed and non-sealed anodization) on the surface energy of an aluminium substrate has been examined. The surface energy has been determined by wettability measurements using the two liquid phase method and taking into account the roughness and porosity of the treated substrate. The comparison of the interfacial interaction energies Al/polymer and Al/water shows that the treatment leading to the highest γ_{p} value and the lowest surface polarity, i.e. phosphatization, gives the highest adhesion strength and the best moisture resistance of the metal/polymer assembly. (22 refs.)
- 63451 Effect of film thickness on oxidation of vacuum-deposited films of iron.** K.Maki, T.Kurumi, K.Nishi, Y.Terawa (Dept. of Phys., Yokohama City Univ., Kanagawa, Japan). *J. Magn. & Magn. Mater. (Netherlands)*, vol.35, no.1-3, p.223-5 (March 1983). (Proceedings of the 10th International Colloquium on Magnetic Films and Surfaces, Yokohama, Japan, 13-16 Sept. 1982).
Iron films at thicknesses below 4 Å change in an oxidized phase immediately after exposure to air. Electron micrographs of such thin films show a uniform contrast. This suggests that the films are composed of fine particles with sizes smaller than a few ten Å. (4 refs.)
- 63452 The development of nitrogen concentration profiles on nitriding iron.** H.C.F.Rozendaal, E.J.Mittermeijer, P.F.Colin, P.J.Van Der Schaaf (Lab. of Metall., Delft Univ. of Technol., Delft, Netherlands). *Metall. Trans. A (USA)*, vol.14A, no.3, p.395-9 (March 1983).
On nitriding iron specimens nitrogen concentration profiles within the specimens are built up. A numerical method for the calculation of such concentration profiles was developed. The results calculated were compared with experimental data. It was found that during nitriding the nitrogen surface concentration approached relatively slowly the equilibrium value. This effect strongly influenced the development of nitrogen concentration profile. The model predicted correctly the incubation time for compound (i.e. iron nitride) layer formation at the surface. If the fatigue resistance is strongly dependent on the (compressive) residual surface stress, the present treatment allows calculation of an optimum nitriding time by determining when the maximum (compressive) residual surface stress occurs. (18 refs.)
- 63453 Intergranular zinc embrittlement and its inhibition by phosphorus in 55 pct Al-Zn-coated sheet steel.** L.Allegre, R.G.Hart, H.E.Townsend (Sheet Steels & Coated Products Div., Res. Dept., Bethlehem Steel Corp., Bethlehem, PA, USA). *Metall. Trans. A (USA)*, vol.14A, no.3, p.401-11 (March 1983).
Room-temperature tensile and bend tests and Auger electron spectroscopy (AES) were used to study embrittlement in sheet steels coated with a 55 pct Al-Zn alloy and then heated in the range 316 to 538°C for up to 5000 hours. The results of these studies show that embrittlement is caused by diffusion of Zn from the coating into the ferrite grain boundaries of the steel substrate, reducing intergranular cohesion. The activation energy for grain boundary diffusion of Zn in iron is estimated at 89 kJ/mole. When present in the steel in concentrations of at least 0.04 pct by weight, P is shown to prevent embrittlement by preemptively segregating to the ferrite grain boundaries where it blocks intergranular diffusion of Zn. (10 refs.)
- 63454 Characteristics of controlled atmospheres with 20% and 40% H_2 during carburizing and carbonitriding.** A.K.Tikhonov, B.E.Sheindlin, S.Z.Chaikovskii, M.A.Krishtal (Volgograd Truck Plant, Tol'yatti Polytech. Inst., USSR). *Met. Sci. & Heat Treat. (USA)*, vol.24, no.5-6, p.411-15 (June 1982). Translation of: *Metalloved. & Term. Obrab. Met. (USSR)*, vol.24, no.6, p.30-3 (June 1982). [received: Feb. 1983]
Concerns the possibility of using an exo-endothermic (20% H_2) and endothermic atmosphere (40% H_2) as a gas carried for chemothermal treatment. It was necessary to determine the effect of the hydrogen concentration in these atmospheres on the mechanical properties of steels and also on the saturation rate during carburizing and carbonitriding. Use of a controlled atmosphere with 40% H_2 for carburizing leads to some increase in the thickness of the layer as compared with that obtained in an atmosphere with 20% H_2 . However, the acceleration of the carburizing process in the atmosphere with 40% H_2 gives it a slight advantage under production conditions. The use of a controlled atmosphere with 40% H_2 in place of 20% H_2 for carbonitriding does not change the saturation rate. Thus, the productivity is practically identical in carburizing and carbonitriding in atmospheres with 20 and 40% H_2 . The mechanical properties of samples treated in an atmosphere with 20% H_2 are superior to those of samples treated in an atmosphere with 40% H_2 . (9 refs.)
- 63455 Improving the technique of boriding from pastes.** N.N.Mitrokhovich, V.P.Fetisov, N.N.Lipchin (Perm Polytech. Inst., USSR). *Met. Sci. & Heat Treat. (USA)*, vol.24, no.5-6, p.415-17 (June 1982). Translation of: *Metalloved. & Term. Obrab. Met. (USSR)*, vol.24, no.6, p.34-5 (June 1982). [received: Feb. 1983]
The possibility of increasing the rate of saturation with boron without changing the cryolite content of the paste was investigated. In view of the results

obtained the authors recommend a paste of composition 70% B₂C+26% Na₃AlF₆+4% NaF. (1 ref.)

63456 Corrosion resistance of deep drawing sheet steel. V.V. Ploshkin, P.G. Vaganov, A.M. Ryabyshv (Moscow Automobile Factory Tech. Coll., Moscow, USSR).

Met. Sci. & Heat Treat. (USA), vol.24, no.7-8, p.448-51 (July-Aug. 1982). Translation of: *Metalloved. & Term. Obrab. Met. (USSR)*, vol.24, no.7, p.5-8 (July 1982). [received: March 1983]

The authors investigated the effect of several structural factors in low-alloy cold-rolled steels 20YuT and 08GSYuT and hot rolled steel 08Yu, with high-strength characteristics, on their corrosion resistance in 3% NaCl solution. The effect was also investigated of the rate of plastic deformation during stamping on the corrosion resistance of VAZ-2101 fenders made of cold-rolled steel 08Yu. (10 refs.)

63457 Effect of high-temperature vacuum annealing time on the structure and properties of titanium alloys. G.G. Maksimovich, Ya.I. Spektor, V.N. Fedirko, A.T. Pichugin, V.N. Moiseev.

Met. Sci. & Heat Treat. (USA), vol.24, no.7-8, p.455-9 (July-Aug. 1982). Translation of: *Metalloved. & Term. Obrab. Met. (USSR)*, vol.24, no.7, p.11-14 (July 1982). [received: March 1983]

The microrelief and structure of the surface, the concentrations of alloying elements in the surface layer, its structure and microhardness, the hydrogen content in the bulk of the metal, and the strength and fatigue characteristics of the alloys, were investigated. (7 refs.)

63458 Effect of annealing on the structure and properties of molybdenum coatings on steel Kh12M. A.A. Andreev, L.V. Bulatova, G.N. Kartmazov, T.V. Kostritsa, A.A. Romanov.

Met. Sci. & Heat Treat. (USA), vol.24, no.7-8, p.481-4 (July-Aug. 1982). Translation of: *Metalloved. & Term. Obrab. Met. (USSR)*, vol.24, no.7, p.31-2 (July 1982). [received: March 1983]

Molybdenum coatings obtained by the method of CIB (condensation from plasma phase upon arc atomisation in vacuum under ion bombardment conditions) on steel Kh12M, during the process of high-temperature annealing, became saturated with the carbon of the base, and the solid phase Mo₂C formed. In consequence of the opposite diffusion of carbon and molybdenum, a zone of increased hardness formed in the surface layer of the steel. The thickness of this zone depended on the annealing temperature. (4 refs.)

63459 Wear kinetics of a two-phase boride layer. E.V. Shadrachev, S.I. Rumyantsev (Northwest Correspondence Polytech. Inst., Leningrad, USSR).

Met. Sci. & Heat Treat. (USA), vol.24, no.7-8, p.495-8 (July-Aug. 1982). Translation of: *Metalloved. & Term. Obrab. Met. (USSR)*, vol.24, no.7, p.40-2 (July 1982). [received: March 1983]

The minimum wear rate in an abrasive medium is found to be exhibited by a layer whose friction surface is a matrix of Fe₂B containing 10-30% of mono-boride FeB inclusions. For single-phase layers consisting of Fe₂B a higher (by a factor of 1.4 to 1.5) wear rate is typical. The wear rate of solid FeB layers is not less than the wear rate of Fe₂B layers although the hardness of Fe₂B is less than that of FeB. (10 refs.)

63460 Effect of vibroabrasive treatment on the fatigue strength of high-alloy steels. V.G. Osipenko, G.Ya. Shapovalova, P.P. Aulov (Voroshilovgrad Engng. Inst., Voroshilovgrad, USSR).

Met. Sci. & Heat Treat. (USA), vol.24, no.7-8, p.504-5 (July-Aug. 1982). Translation of: *Metalloved. & Term. Obrab. Met. (USSR)*, vol.24, no.7, p.47-8 (July 1982). [received: March 1983]

A study was made of changes in surface layer condition under the action of chemically active solutions influencing article fatigue strength. The study was carried out on specimens made of steels 18Kh2N4MA and 18Kh2N4VA. (3 refs.)

63461 Fatigue strength of steel 45 with electrolytic iron coating, carbon nitrided with HF heating. V.I. Dobrya, I.V. Dushevskii, A.I. Murav'ev (Kishinev Agricultural Inst., Kishinev, USSR).

Met. Sci. & Heat Treat. (USA), vol.24, no.7-8, p.563-6 (July-Aug. 1982). Translation of: *Metalloved. & Term. Obrab. Met. (USSR)*, vol.24, no.8, p.44-7 (Aug. 1982). [received: March 1983]

Carbon nitriding of electrolytic iron coating using heating by HF current increased the fatigue strength of restored parts made of steel 45 to 10-12%. The conditions of electrolytic deposition of iron coatings have a substantial effect on the productivity of the process and on the quality of the hardened layers. Electrolysis with AC with reverse pulse greatly increased the possibilities of using thermochemical treatment for restoring parts with iron coatings. The suggested method of hardening worn surfaces may be recommended for restoring to serviceability parts that in operation are subjected to cyclic loads. (7 refs.)

63462 Thermodynamics of homogeneous formation of cementite in austenite during case hardening of steel. V.M. Pereverzev, V.I. Kolmykov, I.N. Roslyakov.

Russ. Metall. (GB), no.6, p.59-62 (1981). Translation of: *Izv. Akad. Nauk. SSSR Met.*, no.6, p.61-4 (1981).

A thermodynamic analysis is given of the effects of manganese and chromium on the shape of the cementite which forms in the austenite matrix during case-hardening. Manganese does not intensify the thermodynamic stimulus to homogeneous formation of cementite in the carbon-saturated austenite, therefore it does not induce formation of granular cementite during case-hardening. Chromium (1.3 at.%) increases by several times the negative change in the free energy during homogeneous decomposition of the saturated austenite into an equilibrium austenite-cementite mixture, thus ensuring the possibility of formation of granular cementite in steel during case-hardening in the austenitic state. (7 refs.)

63463 Influence of silicon and boron on the high-temperature oxidation of nickel-chromium alloys. E.M. Lazarev, A.M. Samarin, N.A. Korotkov.

Russ. Metall. (GB), no.6, p.181-6 (1981). Translation of: *Izv. Akad. Nauk. SSSR Met.*, no.6, p.186-90 (1981).

Alloying with up to 2% Si increases appreciably the adhesion of the scale to the alloy but has little effect on its resistance to oxidation in air at 1000°C. A boron content above 0.2% induces increased crumbling of the scale and the scale resistance decreases sharply. The phase composition of the scale in the case of high boron contents is the same as for alloys without boron but the formation of an oxide with the boron, which evaporates easily at elevated temperatures, causes loosening (crumbling) of the scale and lowers its protective properties. (13 refs.)

63464 Diffusion modeling of the carburization process in stainless steels. D. Farkas (Dept. of Materials Engng., Virginia Polytech. Inst. & State Univ., Blacksburg, VA, USA).

Scr. Metall. (USA), vol.17, no.3, p.261-4 (March 1983). One of the features of the carburization process in stainless steels is that some of the alloying elements oxidize preferentially and depletion at the surface gives rise to a ternary cross diffusion effect that strongly changes the

shape of the carbon diffusion profile. Goldstein and Moren (see Met. Trans. A, vol.9, p.1515, 1978) developed a formalism to solve the ternary diffusion equation by the Crank-Nicholson finite difference method. The authors extend the solution to higher alloying element contents, in order to apply the results to carburization of stainless steels. (11 refs.)

63465 Influence of nitrogen on the penetration of hydrogen through constructional materials from nitrogen-hydrogen mixtures. V.I. Pokhmurskii, B.F. Kachmar, V.V. Fedorov (G.V. Karpenko Physicomech. Inst., Acad. of Sci., Lvov, Ukrainian SSR).

Sov. Mater. Sci. (USA), vol.18, no.3, p.209-12 (May-June 1982). Translation of: *Fiz.-Khim. Mekh. Mater. (USSR)*, vol.18, no.3, p.21-5 (May-June 1982). [received: Feb. 1983]

For the purpose of studying the features of combined interaction of hydrogen and nitrogen with constructional materials, investigations were made of the influence of additions of nitrogen on the hydrogen permeability (P) of EP-199 and VKh-4 and 12Kh18N10T steel. The investigation of the role of interstitial impurities in atomic ordering of the alloys showed that under the influence of hydrogen the critical temperatures of the phase transformations drop but in the presence of nitrogen they increase. The hydrogen penetrability of EP-199 and VKh-4 alloys and 12Kh18N10T steel decreases in nitrogen-hydrogen mixtures with an increase in nitrogen concentration, which is the result of the formation of nitride phases on the surface of the metal. (12 refs.)

63466 Fracture of metals under the action of hydrogen-containing media. A.L. Bichuya (G.V. Karpenko Physicomech. Inst., Acad. of Sci., Lvov, Ukrainian SSR).

Sov. Mater. Sci. (USA), vol.18, no.3, p.213-16 (May-June 1982). Translation of: *Fiz.-Khim. Mekh. Mater. (USSR)*, vol.18, no.3, p.26-30 (May-June 1982). [received: Feb. 1983]

The stress-rupture strength of BrKh-08 and EP-799 alloys and the short-time strength in vacuum, hydrogen, and ammonia of previously nitrated Armo iron were investigated to elucidate the mechanism of fracture of metals in hydrogen-containing media. It is noted that the appearance of the effect of hydrogen brittleness is in direct relationship to the catalytic activity of the metal. (21 refs.)

63467 Question of the safe boundaries of use of 12 MKh steel at increased temperatures and hydrogen pressures. Yu.I. Archakov, B.M. Teslya (All-Union Sci.-Res. Inst. for Petrochem. Processes, Leningrad, USSR).

Sov. Mater. Sci. (USA), vol.18, no.3, p.216-20 (May-June 1982). Translation of: *Fiz.-Khim. Mekh. Mater. (USSR)*, vol.18, no.3, p.30-4 (May-June 1982). [received: Feb. 1983]

A study is presented of the rules of the hydrogen corrosion process and establishment of the safe boundaries of use of 12MKh steel in hydrogen. The tests were made under the all-sided and, to determine stress rupture strength, the one-sided pressure of gaseous hydrogen. The investigations made it possible to establish the differences in the change in mechanical properties, carbon content, and microstructure of 12MKh steel under the action of hydrogen with pressures of 4-100 MPa and temperatures of 450-600°C. Relationships of the time until the start of intense reduction in the ductility of the steel at various temperatures and pressures were found. An equation was set up for calculating the time until the start of hydrogen corrosion of the steel in relation to temperature and hydrogen pressure. The safe boundaries of the applicability of 12MKh steel at various temperatures and hydrogen pressures were determined. (15 refs.)

63468 High-temperatures reactions of metals with gases. II. Kinetics of growth of multiphase chemical compound layers at a metal/gas interface. V.I. Dybkov (Inst. of Materials Sci., Acad. of Sci., Ukrainian SSR).

Sov. Powder Metall. & Met. Ceram. (USA), vol.21, no.8, p.640-6 (Aug. 1982). Translation of: *Poroshk. Metall. (USSR)*, vol.21, no.8, p.47-54 (Aug. 1982). [received: Feb. 1983]

For pt. I see ibid., vol.21, no.7, p.52 (1982). The author considers the growth of layers of the chemical compounds M₂G₃ and M₂G₅ at the interface between the metal M and gas G. (7 refs.)

63469 Structural and morphological investigation of the oxidation of titanium diboride in various environments. II. Oxidation of titanium diboride in a steam-water environment. A.N. Pilyankevich, S.V. Papyan (Inst. of Materials Sci., Acad. of Sci., Ukrainian SSR).

Sov. Powder Metall. & Met. Ceram. (USA), vol.21, no.8, p.655-7 (Aug. 1982). Translation of: *Poroshk. Metall. (USSR)*, vol.21, no.8, p.64-7 (Aug. 1982). [received: Feb. 1983]

It was observed that titanium diboride oxidizes in steam at temperatures not exceeding 100°C. Qualitatively, the degree of oxidation, which depends on its duration, can be determined only by electron microscopy and, less accurately, by the petrographic technique. Oxidation is more intense in boiling water than in steam. This may be a consequence of partial elution of the oxide film being formed and exposure of fresh surfaces to the oxidizing environment. Under these conditions, the oxidation reaction takes place at the titanium diboride oxidizing environment interface. (1 ref.)

63470 Nature of the carboxylate species incorporated in anodic alumina films formed in oxalic acid solution. Y. Yamamoto, N. Baba (Lab. of Electrochem. & Inorganic Chem., Tokyo Metropolitan Univ., Tokyo, Japan).

Thin Solid Films (Switzerland), vol.101, no.4, p.329-38 (25 March 1983). Electron spin resonance (ESR) and IR spectroscopy, combined with a chemical sectioning technique supported by transmission electron microscopy, were employed to study the nature of oxalate species incorporated into porous anodic films formed on aluminum in an aqueous solution of oxalic acid. ESR spectroscopy combined with chemical sectioning of the oxides indicated that spin centres, which are supposed to be due to the cleavage of the chemical bonds of oxalate species, are present predominantly in the outer region of the cell walls of the oxide. No spin centres, however, were detected in the inner region nearest to the cell boundary, although a small amount of carboxylate species was still detected in that region. In addition, IR spectroscopy of the oxide, chemically sectioned for various periods, showed that the incorporated species are present in the oxide as carboxylate ions but their structures showed marked variation as a function of depth from the surface of the cell wall of the oxide. These results suggest strongly that oxalate anions incorporated into a barrier layer of the oxide are unstable and undergo decomposition in the high electric field present within the layer during anodization. (28 refs.)

63471 Analysis of the corrosion products formed on Ti and a Ti-Pd alloy during exposure in hot water. I. Olefjord, H. Mattsson (Dept. of Engng. Metals, Chalmers Univ. of Technol., Goteborg, Sweden).

Scientific Basis for Nuclear Waste Management V. Proceedings of the Materials Research Society Fifth International Symposium on the Scientific Basis for Nuclear Waste, Berlin, Germany, 7-10 June 1982 (New York, USA: North-Holland 1982), p.669-78.

This is a preliminary report dealing with the surface analysis of reaction products formed on Ti and Ti-Pd alloy during their exposure in hot water. The compositions of the aqueous media were varied with respect to the dis-

solved oxygen and the content of chloride ions. The temperature was 60°C and the exposure times were 10 min and 6 months. Work is in progress in which samples are exposed at 80°C and 95°C in the aqueous solutions. Surface analysis was also performed on a sample which had been exposed in water-saturated bentonite. It appears from the ESCA spectra that the oxide products formed on the surface consist of TiO_2 . The results also indicate that the thickness of the film formed at 60°C in water is in the range 50 Å to 100 Å. This is somewhat more than that obtained after exposure in water at room temperature. Exposure for 6 months increases the thickness of the oxide two to three times compared to that obtained during the short exposure at 60°C. The analyses of the samples that had been embedded in bentonite indicate that the surface reaction products are thinner than those found on the surface after exposure in an open vessel. (9 refs.)

Microbeam analysis of a Commercial Advanced Gas Cooled Reactor material See Entry 60233

Evaluation of the resistance of irradiated zirconium-liner cladding to iodine-induced stress corrosion cracking See Entry 60236

General and localized corrosion of carbon and low-alloy steels in oxygenated high-temperature water See Entry 60248

Cleaning steam generators off-line (soaking) with chelants See Entry 60340

Monitoring system for determining air leakage and oxygen concentrations in the secondary cycle of pressurized water reactor plants See Entry 60362

Waterside corrosion of zircaloy fuel rods See Entry 60389

The effect of the method of treatment of a molybdenum cathode on the normal cathode drop in a glow discharge See Entry 61723

Electron diffraction from ZrO_2 on $\alpha\text{-Zr}(10\bar{1}0)$ See Entry 62219

X-ray diffraction analysis of SnO_2 films prepared by oxidation of tin films See Entry 62306

Magnetoelastic effects in amorphous metals due to surface crystallisation and oxidation See Entry 62790

Ellipsometric investigation of oxidation processes of tin in solid and liquid states See Entry 62915

Optical anisotropy and electrostriction in the anodic oxide of molybdenum See Entry 63067

Optical anisotropy and electrostriction in the anodic oxide of niobium See Entry 63068

The methoxy intermediate on $\text{Mo}(100)$: effects of surface oxidation See Entry 63100

Recrystallisation of austenite in low-alloy steels (0.7% V, 0.04% Nb) with carbide-nitride hardening See Entry 63312

Repeated mechanical strengthening as a method of increasing the endurance of constructional steels See Entry 63314

Free-cutting stainless steel wire with high-strength See Entry 63315

Influence of surface condition on the magnetic properties of Fe-3% Si alloy See Entry 63320

Nitriding kinetics and wear resistance of titanium alloys See Entry 63428

Thermally stressed condition occurring in the surface layers of flat parts during friction hardening See Entry 63429

Influence of production media on the physicochemical and electrochemical properties of steels See Entry 63430

Question of determining the electrochemical condition in a developing crack in investigating the crack resistance in a corrosive medium See Entry 63493

A method of predicting the life of protective coatings See Entry 63494

The γ irradiation-enhanced corrosion of stainless and mild steels by water in the presence of air, argon and hydrogen See Entry 63594

The effect of radiation on the release of corrosion products from 304 stainless steel in high temperature water-II effects of flow rate and duration of corrosion experiment See Entry 63595

81.70 MATERIALS TESTING

(inc. sample preparation for examination, metallographic techniques, ion and electron microprobe techniques, Auger and photoelectron techniques, defectscopy; for measurement in the mechanics of solids and rheology, see 46.30R)

63472 The use of time-of-flight neutron diffraction to study grain interaction stresses. S.R.MacEwen, J.Faber, Jr., A.P.L.Turner (Materials Sci. Div., Argonne Nat. Lab., Argonne, IL, USA).

Acta Metall. (USA), vol.31, no.5, p.657-76 (May 1983). Time-of-flight neutron diffraction, using the General Purpose Powder Diffractometer at the IPNS (Intense Pulsed Neutron Source) at the Argonne National Laboratory, has been used to measure residual stresses in deformed, polycrystalline Zircaloy-2. It was found that a plastic tensile strain of 3% caused the (1010) and (1120) prism lines in the diffraction pattern to shift to higher d -spacings, while the (0002) basal line was shifted to a lower interplanar spacing. Compressive deformation reversed the direction of the shifts, with the prism and basal planes being left in residual compression and tension respectively. For the specimen deformed to 424 MPa in tension, the principal residual stresses after unloading were -188 MPa in the (c) direction and 173 MPa in the direction normal to the prism planes. The result is in good agreement with an analysis of the problem that considers an idealized texture that is representative of that found in Zircaloy-2 rod. The experiments demonstrate that time-of-flight neutron diffraction can be a sensitive and powerful tool for measuring residual stresses in bulk materials, where conventional X-ray techniques would be inapplicable. (48 refs.)

63473 Home resources serving to develop Auger and SIMS spectrometers for thin-film and surface analytical tests. G.Gergely. *Finnomech.-Mikrotech.* (Hungary), vol.22, no.2, p.60-3 (Feb. 1983). In Hungarian.

One of the tasks of the technology of material tests in the metal industry is the determination of the chemical composition of the surface and of its contaminations, as well as the composition-depth profiling of thin-films. Methods of surface and thin-film analytics mostly applied are Auger spectrometry (AES) and SIMS. With the use of a Riber OPC 103 CMA spectrometer and a QML 51 quadrupole mass-spectrometer the MTA MFKI developed, mainly based on home resources, its surface-analytical facilities. The author describes the UHV system operating in the 10^{-8} Pa pressure range (vacuum system, measuring chamber, manipulators) which has been developed in collaboration with Tungsram Research Institute. The bibliography offers a survey of the most important results obtained and of the material tests carried out with the devices. (14 refs.)

63474 Optical surface testing with diffused light. G.Thurn (Tech. Univ. Berlin, Berlin, Germany), T.Gast.

Feinwerktech. & Messtech. (Germany), vol.91, no.1, p.15-18 (Feb. 1983). In German.

Describes an optical measuring method for the testing of surfaces. A sensor detects the backscatter from rough surfaces with vertical illumination in a predetermined angle range. From the diffused light distribution, characteristics are evaluated with a microcomputer; these are used for the assessment of the quality and structure of the surfaces. Application possibilities for metallic materials are discussed. (15 refs.)

63475 Effect of specimen width on impact strength and location of brittle-ness temperature of St3ps steel. G.S.Schedrin (Technol. Inst. of Refrigeration Industry, Leningrad, USSR).

Ind. Lab. (USA), vol.48, no.6, p.605-6 (June 1982). Translation of: *Zavod. Lab. (USSR)*, vol.48, no.6, p.71-2 (June 1982). [received: March 1983]

The authors checked the effect of the specimen width on impact strength and position of critical brittleness temperature. It is found the use of sharp-notched specimens with any other than 10 mm width can produce marked changes in the impact strength and critical embrittlement temperature. (3 refs.)

63476 Plated weld mechanical characteristics. N.A.Makhutov, S.A.Ivanova (Blagovarov State Sci.-Res. Inst. of Machine Sci., Acad. of Sci., USSR). *Ind. Lab. (USA)*, vol.48, no.6, p.607-10 (June 1982). Translation of: *Zavod. Lab. (USSR)*, vol.48, no.6, p.73-5 (June 1982). [received: March 1983]

The authors' investigation of the strength of welded joints plated by the explosion method involved the determination of the local mechanical characteristics, since the presence of plating layers and the nonuniform hardening by impact waves resulted in a nonuniformity of properties over the weld thickness because individual zones of the joint hardened in different ways. The investigation was concerned with butt joints consisting of 20-mm thick St3ps steel plates plated on both sides by a 4-mm thick layer of Kh18Ni10T austenitic stainless steel. (4 refs.)

63477 Reliability of inspection of rolled steel for impact strength. M.I.Artem'ev, L.E.Valyaeva, F.D.Kamardina, N.E.Pakhomova (Magnitogorsk Mining-Metall. Inst., USSR).

Ind. Lab. (USA), vol.48, no.6, p.610-12 (June 1982). Translation of: *Zavod. Lab. (USSR)*, vol.48, no.6, p.75-6 (June 1982). [received: March 1983] (5 refs.)

63478 Influence of the type of stress state on the nature of acoustic-emission signals. A.V.Skoblo, A.P.Zhigun, S.A.Kolesov, L.P.Dunina (Gorki Automobile Plant, Gorki, USSR).

Ind. Lab. (USA), vol.48, no.6, p.625-7 (June 1982). Translation of: *Zavod. Lab. (USSR)*, vol.48, no.6, p.91-2 (June 1982). [received: March 1983]

The authors present the results of an analysis of acoustic-emission signals produced in samples of steel 30KhGSA (quenched from 880°C in oil, tempered at 210 and 570°C) subjected to various types of loading. (4 refs.)

63479 Accelerated determination of the stress-rupture strength of low alloy tubing steel. A.D.Kovaleva, S.R.Kudashevich (Nikopol South Tube Plant, USSR).

Ind. Lab. (USA), vol.48, no.6, p.627-9 (June 1982). Translation of: *Zavod. Lab. (USSR)*, vol.48, no.6, p.93-4 (June 1982). [received: March 1983]

Samples from 273×32 mm 12Kh1MF steel tubing were tested. The base was the standard test method. The characteristics of high temperature strength were determined at operating temperatures of 813 and 843K and also at the higher temperatures of 873 and 903K. The tests were made at three stresses for each temperature. The values of stress-rupture strength were determined by constructing the appropriate log-log curve to log σ vs. log T coordinates and by the method of orthogonal regression or of average least squares, the basis of which is the equation of the stress-rupture strength curve. Also investigated was the method of accelerated testing proposed by V.I. Nikitin (1959) and based on the use of the Larsen-Miller parameter. (1 ref.)

63480 A technique for observing the cross sectional damage profiles in He-ion irradiated 316 stainless steel by transmission electron microscopy. S.Hamada, M.Tanaka, K.Shiraishi (Div. of Nuclear Fuel Res., JAERI, Ibaraki, Japan).

J. Nucl. Mater. (Netherlands), vol.114, no.2-3, p.338-40 (Feb. 1983).

The technique described is a modification of the technique to observe the depth distribution of damage produced in the stainless steel without heat treatment after ion irradiation. The depth distributions of defect clusters created by atomic displacement and injected helium were observed separately in a He-irradiated type 316 stainless steel specimen by using this technique. (13 refs.)

63481 The connection of hardness indentation processes with the flow curve of metallic material. R.Boklen.

Mater. Test. (Germany), vol.25, no.4, p.117-19 (April 1983). In German.

10 steels and 10 nonferrous metal test pieces were examined after indentation axially with three differently shaped indenters and with 100° diamond cone indenter. The latter was found particularly suitable. Deviations from Hooke's law became first apparent between 80 and 90 N. There was a connection between indentation and flow curve which allowed for the calculation of tensile strength for 24 nonferrous metals and 18 steels with a scatter of ± 0.025 . (14 refs.) /R.S.

63482 Microdeformation machine for testing thin films with automatic tension-diagram recording. M.E.Scherbina, V.N.Zaruba.

Meas. Tech. (USA), vol.25, no.8, p.676-7 (Aug. 1982). Translation of: *Izmer. Tekh. (USSR)*, vol.25, no.8, p.44-5 (Aug. 1982). [received: April 1983]

Describes a microdeformation machine for examining the mechanical properties of thin films with automatic recording of the strain curve by active strain and also by creep methods. The design eliminates the effects of outside forces on the strain. The machine consists of a massive baseplate, on which are mounted the strain device and the support with an immobile clamp. The strain device includes a stand forming the parallelogram along with a plate which bear the mobile jaw on wires. During the deformation, the film is acted on by the resultant force and also the bending force arising from the motion of the jaw around the circle. The strain is determined by means of photoelectric transducers and recorded automatically by a ODS-021 XY-recorder. (2 refs.)

63483 Metallographic signs of forging overheating in 11Kh4F3S2V2M die steel. A.S.Muzheva, N.A.Makalkova, T.E.Marder (Kamaz Truck Plant, USSR).

Met. Sci. & Heat Treat. (USA), vol.24, no.5-6, p.405-8 (June 1982). Translation of: *Metalloved. & Term. Obrab. Met. (USSR)*, vol.24, no.6, p.26-8 (June 1982). [received: Feb. 1983]

An investigation was made of the influence of the original condition on the macro- and microstructure and the structure of the fractures of 11Kh4F3S2V2M steel after heat treatment. Signs of forging overheating in 11Kh4F3S2V2M are revealed in three conditions: in the original in the form of a structure of oriented fine granular pearlite (actually no.7-9 austenitic

grain size); in the hardened in the form of variation in grain size after austenitizing at the optimum temperatures (from no.12 to no.8 austenitic grain size); after final tempering in the form of facets of naphthalenelike fracture on a general background of a fine-grained fracture. In the fractures of samples after final heat treatment, traces of forging overheating appear in the form of area of fracture along martensite plates. In 11Kh4F3S2V2M steel hardened from a reduced (1060°C) temperature traces of forging overheating are revealed only by electron fractography (the presence of areas of fracture in martensite). (4 refs.)

63484 Specimens and apparatus for the magnetoluminescent quality control of components. P.F.Gritskov (Kamaz Truck Plant, USSR). *Met. Sci. & Heat Treat. (USA)*, vol.24, no.5-6, p.409-10 (June 1982). Translation of: *Metalloved. & Term. Obrab. Met. (USSR)*, vol.24, no.6, p.29 (June 1982). [received: Feb. 1983]

In evaluating the qualitative characteristics of powders and suspensions, the resolving power of magnetic powders, and their photocolouristic properties, and the extent to which the suspensions are contaminated by luminescent particles and to determine the concentration of the magnetoluminescent powder, developed and built a model in the Nondestructive Control Methods Laboratory at the Kamaz Truck Plant. (no refs.)

63485 Structure of titanium alloys and methods used for its control. G.V.Shakhonova, M.Ya.Brun (All-Union Inst. of Light Alloys, USSR). *Met. Sci. & Heat Treat. (USA)*, vol.24, no.7-8, p.547-53 (July-Aug. 1982). Translation of: *Metalloved. & Term. Obrab. Met. (USSR)*, vol.24, no.7, p.19-22 (July 1982). [received: March 1983]

A method is proposed for point rating of the structure of titanium ($\alpha+\beta$) alloys which places no restrictions on the varieties of structure that can be monitored. The quantitative principle, on the basis of which the structure is divided into points, renders this method objective and well-defined. (2 refs.)

63486 Acoustic emission during phase transformations in alloys. B.I.Voronenko (Gor'kii Res. Physicotech. Inst., Gor'kii, USSR). *Met. Sci. & Heat Treat. (USA)*, vol.24, no.7-8, p.584 (July-Aug. 1982). Translation of: *Metalloved. & Term. Obrab. Met. (USSR)*, vol.24, no.8, p.30-6 (Aug. 1982). [received: March 1983]

The phenomenon of acoustic emission can be used in studying the characteristic features of the mechanism, kinetics, and energy parameters of the martensitic transformations: determination of the martensite points and the amount of martensite that is formed, measurement of the rate of initiation and growth of martensite crystals, investigation of preliminary processes, establishment of the incubation period and the early stages of the formation of martensite, determination of the type of kinetics, structural mechanism, and morphology of the martensite that is formed, and the formation and annihilation of transformation twins, and determination of the degree of cooperativeness of the transformation, the presence and degree of the autocatalysis effect, and the heterogeneity of the shear strain during the transformation. (94 refs.)

63487 Device for fashioning a U-shaped notch in impact specimens. A.K.Shubina, A.F.Kozyrev (Kama Truck Plant, USSR). *Met. Sci. & Heat Treat. (USA)*, vol.24, no.7-8, p.584 (July-Aug. 1982). Translation of: *Metalloved. & Term. Obrab. Met. (USSR)*, vol.24, no.8, p.60-1 (Aug. 1982). [received: March 1983]

A device for the simultaneous fabrication of three type-I specimens or six type-III specimens with an identical notch is proposed. The material used to fabricate the specimens is steel with a hardness to HRC 40. The device is a II-shaped frame, in the channel of which specimens are placed. In both walls of the frame, there is a through hole 2 mm in diameter of a depth of 9 mm, which makes it possible to notch all the specimens simultaneously. (no refs.)

63488 Fundamentals of the surface-analytical methods AES/SAM, ESCA (XPS), SIMS, and ISS in comparison with X-ray microanalysis and their application for material testing. H.Hantsche (Bundesanstalt für Materialprüfung, Berlin, Germany).

Microsc. Acta (Germany), vol.87, no.2, p.97-128 (March 1983). In German. After describing the fundamental physical principles of excitation and emission of particles in the atom, the main differences of the four methods and their information content are discussed. The experimental technique is explained and some applications for characterization of interesting technical materials are shown: a depth profile of a TiN-layer on steel; a SIMS-spectrum of a boron treated chromium steel; ISS-spectra of the first one to three atomic layers of glass; Auger elemental distribution images of some light elements (spot welding electrodes); XPS-spectra of chromium metal and chromium oxide Cr₂O₃; grain boundary segregations on a metallic fracture surface. (45 refs.)

63489 Acoustic emission monitoring. D.Jaffrey (Dept. of Metall. & Mining, Royal Melbourne Inst. of Technol., Melbourne, Victoria, Australia). *Met. Forum (Australia)*, vol.5, no.3, p.154-7 (Winter 1982). The history of acoustic emission is discussed in relation to its limitations and applications. The current research and laboratory work on detection of martensite plates, deformation twins, slip bands, hydrogen cracking, and SCC is considered in relation to metals, ceramics, refractories, glasses, composite materials and rocks. (9 refs.)

63490 The significance of acoustic emission activity in stress-corrosion testing. W.J.Pollock (Aeronautical Res. Labs., Dept. of Defence Support, Melbourne, Victoria, Australia), D.Hardie. *Met. Forum (Australia)*, vol.5, no.3, p.186-91 (Winter 1982). Acoustic emission activity is proposed as a basis for determining the suitability of acoustic emission for monitoring stress-corrosion cracking. The practical and mechanistic implications of this concept are discussed with particular reference to acoustic emission ring-down count and amplitude analysis techniques. (17 refs.)

63491 Tests on quality of adhesion of polymers to metal surfaces. I. Theoretical and experimental principles—state and limits of testing techniques. C.Bischof, A.Bauer, H.W.Leonhardt. *Plaste & Kautsch. (Germany)*, vol.30, no.1, p.1-5 (Jan. 1983). In German. The basic theories relating to adhesion of polymers to metal surfaces, i.e. polarisation, diffusion, electrostatic attraction, thermodynamic forces, etc. are mentioned and it is concluded that since adhesion is a very complex phenomenon, no satisfactory quantitative test for it is at present available. The factors which exert the main influence on adhesion are described. At present destructive tests are still predominant. A systematic test procedure is listed consisting mainly of physical tests such as torsion, compression, ultrasonic vibration, centrifuging, etc. and comments on these tests are given. So far no one reliable method is in existence allowing a quantitative assessment of adhesion of polymers to metal surfaces to be made. (72 refs.) G.R.S.

63492 A penetration test for granular materials using various tip angles and penetrometer shapes. M.Yamashiro, Y.Yuasa (Dept. of Planning Technol., Ashikaga Inst. of Technol., Ashikaga, Japan). *Powder Technol. (Switzerland)*, vol.34, no.1, p.99-103 (Jan.-Feb. 1983).

The relationships between the penetrated depth and the load are investigated with various conical vertex angles and diameters of the penetrating bar by using glass beads and Toporex (trade name of styrol resin). (4 refs.)

63493 Question of determining the electrochemical condition in a developing crack in investigating the crack resistance in a corrosive medium. V.V.Panasyuk, L.V.Ratysh, I.H.Dmytrakh (G.V. Karpenko Physicomech. Inst., Acad. of Sci., Lvov, Ukrainian SSR).

Sov. Mater. Sci. (USA), vol.18, no.3, p.228-33 (May-June 1982). Translation of: *Fiz.-Khim. Mekh. Mater. (USSR)*, vol.18, no.3, p.42-9 (May-June 1982). [received: Feb. 1983]

A new method is presented of determining the pH and the electrode potential ϕ at the tip of a developing crack during crack resistance tests in aqueous media with the use of which investigations were made of the rules of change in the electrochemical condition at the tip, and a study was made of its influence on fatigue crack growth rate in 40Kh13 steel in a working medium with a pH of. (16 refs.)

63494 A method of predicting the life of protective coatings. V.I.Nikitin (I.I. Polzunov Central Sci. Res. & Design Boiler & Turbine Inst., Leningrad, USSR).

Sov. Mater. Sci. (USA), vol.18, no.3, p.273-7 (May-June 1982). Translation of: *Fiz.-Khim. Mekh. Mater. (USSR)*, vol.18, no.3, p.95-9 (May-June 1982). [received: Feb. 1983]

A basic problem in investigating the properties of protective coatings is evaluating their life under service conditions. The author proposes, first, determination of the effectiveness of the protective influence of coatings in corrosion tests and, second, the development of a method of predicting the service life of coatings under the operating conditions of machine parts based on the results of comparative short-time experiments. A variation of solution of this problem applicable to high-temperature sulfide oxide corrosion of protective coatings of gas-turbine blades is presented for the life of Co-Cu-Fe-ZrO₂ coatings on Zh56K alloy. (10 refs.)

63495 Electron microscopic observation of hard material using an ion sputtering technique. A.Doï (Itami Res. & Dev. Dept., Sumitomo Electric Industries Ltd., Osaka, Japan), H.Shima, S.Harada, T.Nishikawa. *Sumitomo Electr. Tech. Rev. (Japan)*, no.22, p.203-12 (Jan. 1983).

Describes a technique which has been introduced to prepare thin foil specimens of hard material for TEM observation with the aid of ion beam sputtering in which the atoms in the surface of the specimen are sputtered by an illuminating beam to the ionized material. The authors introduce an ion sputtering technique to prepare thin foil specimens of various ceramics and cemented carbides, make TEM observations using specimens thus prepared, and conduct elementary analysis of extremely localized areas with an energy dispersive X-ray spectroscopy that was attached to the TEM. By means of selective etching by ion beam sputtering, observation of microstructures that are otherwise difficult by means of chemical etching or other processes becomes possible. Results of observations of sintered microstructure using this technique are also given. (4 refs.)

Results of EDF/Framatome underload crack detection methods See Entry 60249

Eddy-current NDE for intergranular attack See Entry 60341

FATMAC. A machine for the fatigue testing of CT type samples in the HFR, Petten, Holland See Entry 60406

Structural and mechanical anisotropy of a nuclear grade AISI 316 stainless steel See Entry 60409

Thermal fatigue test facilities for simulating the first wall and limiter operating conditions See Entry 60414

A programme for the study of fatigue of fusion reactor structural materials See Entry 60415

Development of material for the JET mechanical structure See Entry 60424

Mechanical tests on components used in the TORE SUPRA superconducting coils See Entry 60427

Toroidal field magnet for FT-U device See Entry 60441

The cyclotron facility for radiation damage experiments at the JRC-ISPR See Entry 60498

Application of ultrasonic microscopy to the investigation of mechanical properties and defects in solids See Entry 61359

Improved technique for amplitude inversion of backscattering in the study of cavities and flat defects See Entry 61360

Stressed state of a square sample for crack resistance tests of sheet materials See Entry 61457

Calculation of the contact angle of mercury on plane solid oxides See Entry 62215

Dependence of critical temperatures of brittleness on the condition of operational fractures See Entry 63382

Quantitative X-ray phase analysis of R-Co alloys See Entry 63618

81.90 OTHER TOPICS IN MATERIALS SCIENCE

63496 Ultimate tensile measurements of filled gelatin gels. S.B.Ross-Murphy, S.Todd (Colworth Lab., Unilever Res., Sharnbrook, England). *Polymer (GB)*, vol.24, no.4, p.481-6 (April 1983).

Ultimate tensile measurements were performed on the model system of glass filled gelatin gels. By using a range of sizes of glass ballotin, and also shape sorted fragments of fractured ballotin (denoted 'cubes') at varying phase volume of filler, the effect of size, shape and phase volume on the ultimate tensile properties of the filled gel samples was investigated. By constructing a force-extension failure envelope, a relationship was developed which enabled all the fracture data for the samples to be simply related, and this empirical relation was within experimental error identical to previously derived theoretical treatments of the dependence of small deformation modulus on phase volume. (17 refs.)

82.00 PHYSICAL CHEMISTRY

82.20 CHEMICAL KINETICS

63497 The reactive quantum Boltzmann equations: a derivation from an arrangement channel space representation and BBGKY hierarchy. J.W.Evans, D.K.Hoffman (Dept. of Chem., Iowa State Univ., Ames, IA, USA), D.J.Kouri.

J. Chem. Phys. (USA), vol.78, no.5, p.2665-81 (1 March 1983).

A rigorous derivation of the reactive quantum Boltzmann equations is presented for systems where breakup and combination are excluded. The use of an arrangement channel space representation allows an exact decomposition of the N particle density matrix into components for different chemical compositions and an exact definition of reduced species density matrices (as opposed, e.g. to standard projection operator techniques). This necessitates the use of the combinatorially complex arrangement channel BBGKY hierarchy which, however, avoids the need for the usual heuristic specification of collision terms. Another advantage is that scattering equations generated for the reactive and nonreactive many body T matrices appearing in the Boltzmann equations have 'well-behaved' kernels (unlike the corresponding Lippmann-Schwinger equations). From the derived equations the authors readily obtain, e.g. reaction-diffusion equations and nonequilibrium expressions for the chemical reaction rates. (64 refs.)

63498 Analysis of periodic perturbations of limit cycles. P.Rehms, J.Ross (Dept. of Chem., Stanford Univ., Stanford, CA, USA).

J. Chem. Phys. (USA), vol.78, no.6, pt.2, p.3747-55 (15 March 1983).

An algorithm due to Loud (1961) is used to find asymptotically convergent series solutions for limit cycles subjected to weak periodic perturbations. If an exact or approximate solution to the unperturbed limit cycle is available near or far from marginal stability, then accurate predictions can be made for entrainment bands and the phase relationships between the various oscillatory chemical species and the perturbation. The utility of this method is shown for several model systems. In an appendix, the appearance and character of critical slowing down at the edges of entrainment bands is demonstrated. (47 refs.)

63499 On the theory of kinetic isotope effects in proton transfer reactions. Influence of the anharmonicity of proton potentials. J.Suhnel, K.Gustav (Sektion Chemie, Friedrich Schiller Univ., Jena, Germany).

Wiss. Z. Friedrich-Schiller-Univ. Jena, Math. Naturwiss. Reihe (Germany), vol.31, no.6, p.113-18 (1982). In German.

The influence of the anharmonicity of the proton potential on the kinetic isotope effect (KIE) in proton-transfer reactions is investigated within the framework of the quantum-statistical mechanical theory of rate processes. The dependence of the KIE on the shape of the interaction potential between the reactants is analogous from a qualitative point of view both for harmonic and anharmonic proton potentials. For realistic interaction potentials an increase of the KIE up to 15% is found if anharmonicity is taken into account. (10 refs.)

Diffusion-controlled reactions among stationary sinks See Entry 59696

A microcomputer based system for stopped-flow kinetics See Entry 59848

Reactive and non-reactive quenching of $O(^1D_2)$ by COF_2 See Entry 60785

Chiral symmetry breaking in nonequilibrium systems See Entry 63500

Radiofrequency labelling of molecules in chemical reactions ... See Entry 63506

The H_2 elimination reactions of $\dot{A}^+B_3C_2H_4^+$ and $C_2D_4^+$ See Entry 63510

Localised MO analysis of the 1,2-hydrogen shift mechanism .. See Entry 63511

Quantum-mechanical differential reaction cross sections for the $F+H_2(\nu=0) \rightarrow FH(\nu=2,3)+H$ reaction See Entry 63512

Cerium-induced excitability and nonperiodic behaviour in closed Belousov-Zhabotinsky systems See Entry 63513

Contracted CI calculations of models for catalytic reactions involving transition metals See Entry 63516

Single versus double insertion in a simple intermolecular carbene reaction See Entry 63517

Kinetics of the $Cl-H_2$ system. II. Abstraction vs exchange in $D+HCl$ See Entry 63522

Reactive and inelastic processes involving $I_2(D^1\Sigma_g^+)$ with the collision partners CH_4 , CH_3Cl , CF_3Cl , and CF_4 See Entry 63524

Reaction of ketenes with atomic oxygen See Entry 63535

Comments on 'Kinetics and mechanism of the U-H reaction' .. See Entry 63536

A new formalism of chemical exchange near the region of intermediate rate See Entry 63537

Elementary reactions of the $NOCl$ radical. I. Rate constants for the reactions $NOCl+NO \rightarrow N_2+2Cl$ and $O+NOCl \rightarrow NO+Cl$ See Entry 63541

Kinetics of photoprolytic reaction in coumarin-dye solution .. See Entry 63569

..... See Entry 63569

..... See Entry 63569

..... See Entry 63569

..... See Entry 63569

..... See Entry 63569

..... See Entry 63569

..... See Entry 63569

..... See Entry 63569

..... See Entry 63569

..... See Entry 63569

..... See Entry 63569

..... See Entry 63569

..... See Entry 63569

..... See Entry 63569

..... See Entry 63569

..... See Entry 63569

..... See Entry 63569

..... See Entry 63569

..... See Entry 63569

..... See Entry 63569

..... See Entry 63569

..... See Entry 63569

..... See Entry 63569

..... See Entry 63569

..... See Entry 63569

..... See Entry 63569

..... See Entry 63569

..... See Entry 63569

..... See Entry 63569

..... See Entry 63569

..... See Entry 63569

..... See Entry 63569

82.20K Potential energy surfaces for chemical reactions

(see also 31.70F -in atomic and molecular physics, 34.20

Intermolecular forces, 34.50L Atomic and molecular beam studies)

On the theory of kinetic isotope effects in proton transfer reactions. Influence of the anharmonicity of proton potentials See Entry 63499

The reaction $Hg+I_2 \rightarrow HgI+I$ revisited See Entry 63527

82.20M Nonequilibrium kinetics

63500 Chiral symmetry breaking in nonequilibrium systems. D.Kondepudi, G.W.Nelson (Center for Studies in Statistical Mech., Univ. of Texas., Austin, TX, USA).

Phys. Rev. Lett. (USA), vol.50, no.14, p.1023-6 (4 April 1983).

Sensitivity of a nonequilibrium chemical system to small symmetry-breaking influences is analyzed in the context of chiral-symmetry breaking. For a hypothetical model system, with realistic kinetic constants, a reaction energy barrier difference of $\Delta E/kT=10^{-17}-10^{-15}$ is shown to be sufficient to have a strong chiral selectivity. This is in the range of the estimated energy differences between right- and left-handed molecules due to weak neutral currents. (19 refs.)

Cerium-induced excitability and nonperiodic behaviour in closed Belousov-Zhabotinsky systems See Entry 63513

Oscillating reactivity of collinear symmetric heavy+light-heavy atom reactions See Entry 63528

82.20R Energy distribution and transfer, relaxation

(see also 31.70H Time-dependent phenomena in atomic and molecular physics)

63501 Measurements of collisional energy transfer in unimolecular processes. R.G.Gilbert (Dept. of Theoretical Chem., Univ. of Sydney, Sydney, NSW, Australia).

Chem. Phys. Lett. (Netherlands), vol.96, no.2, p.259-62 (1 April 1983).

It is shown that the optimal means of tabulating collisional energy transfer parameters in gas-phase uni- and ter-molecular reactions is as the average downward energy transfer, rather than the total energy transferred or the collision efficiency. (10 refs.)

82.30 SPECIFIC CHEMICAL REACTIONS; REACTION MECHANISMS

63502 Alkali-halide association and dissociation rates in an ambient gas. D.R.Bates (Harvard-Smithsonian Center for Astrophys., Harvard Univ., Cambridge, MA, USA).

Chem. Phys. Lett. (Netherlands), vol.96, no.1, p.4-8 (25 March 1983).

Calculations are carried out on the rate coefficients for the association of alkali and halogen atoms in an ambient gas. Because of curve crossing the rate coefficients can be quite high. Curve crossing will facilitate other association processes. Reciprocal lifetime of alkali halides towards collisional dissociation into atoms and into ions are also evaluated. (16 refs.)

63503 A new method for the measurement of vibrational-state-selected ion-molecule reactions at thermal energies. D.van Pijkeren, J.van Eck, A.Niehaus (Fysisch Lab., Rijksuniv. Utrecht, Utrecht, Netherlands).

Chem. Phys. Lett. (Netherlands), vol.96, no.1, p.20-3 (25 March 1983).

A photoelectron-secondary-ion-coincidence method is described that allows the authors to determine the relative vibrational-energy-dependent cross sections for reactions of molecular ions with neutral atoms or molecules at thermal energies. Results for reactions of $H_2^+(\nu)$ in vibrational states $\nu=0-8$ with $H_2(H_3^+)$, $Ne(NeH^+)$ and $He(HeH^+)$ are reported. (8 refs.)

63504 A quantitative interpretation of the magnetic field effect on hyperfine-coupling-induced triplet formation from radical ion pairs. A.Weller, F.Nolling, H.Staerk (Abteilung Spektroskopie, Max-Planck-Inst. fur Biophys. Chem., Göttingen, Germany).

Chem. Phys. Lett. (Netherlands), vol.96, no.1, p.24-7 (25 March 1983).

Experimental determined $B_{1/2}$ values characterizing the magnetic field dependence of molecular triplet production from radical ion pairs originating from photoinduced electron transfer are compared with semi-empirical values obtained according to $B_{1/2}(hf)=2(B_1^2+B_2^2)/(B_1+B_2)$ from the root-mean-square values for the hyperfine coupling of the two radicals, B_1 and B_2 . The very good agreement is discussed. (8 refs.)

63505 The exciplexes of thiindigo with duren and hexamethylbenzene and their influence on photoisomerization. E.Birckner, R.Paetzold (Sektion Chem., Friedrich-Schiller Univ., Jena, Germany), M.V.Kozmenko, M.G.Kuz'min.

Chem. Phys. Lett. (Netherlands), vol.96, no.1, p.38-42 (25 March 1983).

The quenching of thiindigo fluorescence by hexamethylbenzene and duren in solvents of low polarity is accompanied by exciplex emission. The exciplex formation and dissociation rate constants and its photophysical properties are determined. Thiindigo photoisomerization can proceed via exciplex formation. (11 refs.)

63506 Radiofrequency labelling of molecules in chemical reactions. R.Z.Sagdeev, T.V.Leshina, N.E.Polyakov, V.I.Maryasova, A.Y.Yurkovskaya, A.A.Obnynochy (Inst. of Chem. Kinetics & Combustion, Acad. of Sci., Novosibirsk, USSR).

Chem. Phys. Lett. (Netherlands), vol.96, no.1, p.108-13 (25 March 1983).

A method of radiofrequency labelling of molecules in chemical reactions has been proposed. It is based on selective RF pumping of molecules and on tracing the transformation of this label in the reaction products by the NMR spectra. Applications of this method in studying one-way reaction mechanisms are illustrated by some experimental examples. (9 refs.)

63507 Vibrational analysis of the products from thermal decomposition of OCS and CO_2 . J.A.Chenery, A.Fakhr, M.I.Wood, C.J.S.M.Simpson (Phys. Chem. Lab., Univ. of Oxford, Oxford, England).

Chem. Phys. Lett. (Netherlands), vol.96, no.2, p.143-7 (1 April 1983).

The thermal decomposition of CO_2 and OCS has been studied using a shock tube and CW CO probe laser. The energies of activation are in good agreement with the values of other workers. It has been shown that the CO formed from OCS has an initial nonthermal vibrational distribution with a large excess in $\nu=0$. (14 refs.)

63508 Laser photolysis/laser-induced fluorescence study of the reaction of hydroxyl radical with ethylene. F.P.Tully (Sandia Nat. Labs., Livermore, CA, USA).

Chem. Phys. Lett. (Netherlands), vol.96, no.2, p.148-53 (1 April 1983).

A new, laser-based chemical kinetics technique has been demonstrated in studies of the reaction of OH with C_2H_4 . The reaction mechanism is dominated by electrophilic addition of OH to the double bond at low temperatures, and by increasingly rapid decomposition of the thermalized adduct HO_2H_4 back to reactants as the temperature is raised. (29 refs.)

63509 Production of vibrationally excited OH in chemiluminescent reactions of ozone with monoterpenes. P.K.Arora, K.G.Vohra (Air Monitoring Section, Bhabha Atomic Res. Centre, Bombay, India).

Chem. Phys. Lett. (Netherlands), vol.96, no.2, p.161-6 (1 April 1983).

Emission from vibrationally excited OH molecules (Meinel bands) has been observed in chemiluminescent gas-phase reactions of ozone with myrcene, α -phellandrene, α -pinene, limonene and linalol. In addition emission from $HCHO(A_2)$ and methylglyoxal (A_1) has also been identified in reactions with myrcene, α -pinene and α -phellandrene. (10 refs.)

63510 The H_2 elimination reactions of $\dot{A}^+B_3C_2H_4^+$ and $C_2D_4^+$. P.D.Lightfoot, C.J.Danby, I.Powis (Phys. Chem. Lab., Oxford Univ., Oxford, England).

Chem. Phys. Lett. (Netherlands), vol.96, no.2, p.232-6 (1 April 1983).

Kinetic energy releases from the unimolecular H_2 (D_2) elimination reactions of energy-selected $\dot{A}^+B_3C_2H_4^+$ ($C_2D_4^+$) have been obtained by a photoelectron-photoion coincidence technique. The energy releases suggest a 1,1 elimination and are compatible with the presence of a small reverse activation energy barrier of the order of 0.02 eV. Such a barrier was indicated by a

detailed ab initio study of this dissociation and the present results are discussed in the light of this theoretical treatment. (10 refs.)

63511 Localized MO analysis of the 1,2-hydrogen shift mechanism. Tae-Kyu Ha (Lab. of Phys. Chem., Swiss Federal Inst. of Technol., Zurich, Switzerland), Minh-Tho Nguyen, M.Hendrickx, L.G.Vanquickenborne. *Chem. Phys. Lett. (Netherlands)*, vol.96, no.3, p.267-72 (8 April 1983).

For the 1,2-hydrogen shift, a localized SCF MO analysis shows that two different electronic rearrangement mechanisms are possible. In the first case, the migrating hydrogen behaves as a hydride along the entire reaction path; in the other case, the migrating hydrogen behaves as a hydride, but in the second half of the reaction behaves as a naked proton. The difference between two mechanisms appears to be related to the spatial orientation of the lone-pair orbitals. (16 refs.)

63512 Quantum-mechanical differential reaction cross sections for the $F+H_2(\nu=0) \rightarrow FH(\nu=2,3)+H$ reaction. R.E.Wyatt (Dept. of Chem., Univ. of Texas, Austin, TX, USA), M.J.Redmon. *Chem. Phys. Lett. (Netherlands)*, vol.96, no.3, p.284-8 (8 April 1983).

Velocity-scattering angle intensity maps for the $F+H_2(\nu=0; j=0) \rightarrow FH(\nu=2,3; j') + H$ reaction are predicted from quantum-mechanical J_z -conserving calculations. The extent of the shift in the angular distribution from backscattering at 1.8 kcal/mole to sideways scattering (intensity peak at 100°) at 3.0 kcal/mole is in quantitative agreement with recent crossed molecular beam experiments. (20 refs.)

63513 Cerium-induced excitability and nonperiodic behaviour in closed Belousov-Zhabotinsky systems. P.Ruoff (Dept. of Chem., Univ. of Oslo, Oslo, Norway).

Chem. Phys. Lett. (Netherlands), vol.96, no.3, p.374-8 (8 April 1983). In closed stirred Belousov-Zhabotinsky reactions high initial Ce(IV) concentrations lead to an excitable steady state situated between two oscillating domains. At intermediate Ce(IV) concentrations irregular oscillations and bursts are observed. In unstirred excitable media Ce(IV) waves are observed. (23 refs.)

63514 Vibrational energy disposal in reactions of fluorine atoms with hydrides of groups III, IV and V. A.S.Manocha, D.W.Setser, M.A.Wickramaratne (Dept. of Chem., Kansas State Univ., Manhattan, KS, USA).

Chem. Phys. (Netherlands), vol.76, no.1, p.129-46 (1 April 1983). The HF infrared chemiluminescence from the reactions of F atoms with BH_3 , CH_4 , CH_3F , CH_2F_2 , CH_2Cl_2 , CH_3ONO , CH_3NO_2 , NH_3 (and ND_3), PH_3 and $HNCO$ has been observed from a 300K flowing-afterglow reactor. Experiments were done for a range of CH_4 and F atom concentrations to identify conditions which were free of vibrational relaxation and secondary reactions, and these conditions were used to assign initial $HF(\nu)$ vibrational distributions for each reaction. The emission intensity from each reaction also was compared to that from CH_4 in order to obtain the relative HF formation rate constants at 300K. Since the absolute rate constant for $F+CH_4$ is well established, the combination of all of these data provides absolute rate constants for $HF(\nu)$ formation at 300K. The ND_3 reaction was studied to obtain information on more vibrational levels in order to better estimate the $HF(\nu=0)$ and $DF(\nu=0)$ components of the ammonia distributions. With NH_3 and ND_3 there is no significant isotope effect on the energy disposal. Except for $NHCO$, for which an addition-elimination channel is possible, the $HF(\nu)$ distributions are inverted and $\langle f_{\nu} \rangle \approx 0.60$. Differences between the $HF(\nu)$ distributions reported here and some other reports in the literature are noted; the present data are discussed as representative of direct H atom abstraction for 300K Boltzmann conditions. The HCl infrared chemiluminescence from the $F+CHCl_2$ secondary reaction also was observed; the $HCl(\nu)$ distribution was $\nu_1, \nu_2, \nu_3, \nu_4, \nu_5 = 0.47:0.23:0.18:0.08:0.04$. (57 refs.)

63515 C_{2v} insertion pathway for BeH_2 : a test problem for the coupled-cluster single and double excitation model. G.D.Purvis (Dept. of Chem., Univ. of Florida, Gainesville, FL, USA), R.Shepard, F.B.Brown, R.J.Bartlett. *Int. J. Quantum Chem. (USA)*, vol.23, no.3, p.835-45 (March 1983).

(Proceedings of the Fourth International Congress in Quantum Chemistry, Uppsala, Sweden, 13-20 June 1982). The coupled-cluster single and double excitation model (CCSD) is applied to an energy path for the insertion of Be into H_2 and compared to the full configuration interaction (FCI) and full valence-multiconfiguration self-consistent field (FV-MCSCF) results. This model problem is a severe test of a single-reference-function correlated method since two configurations are heavily weighted in the FCI description. CCSD is demonstrated to describe the FCI results using a single reference function which, however, changes orbital characteristics along the sampling path. In this case CCSD gives excellent agreement with the FCI results. (34 refs.)

63516 Contracted CI calculations of models for catalytic reactions involving transition metals. M.Blomberg, U.Brandemark, L.Petterson, P.Siegbahn (Inst. of Theoretical Phys., Univ. of Stockholm, Stockholm, Sweden).

Int. J. Quantum Chem. (USA), vol.23, no.3, p.855-63 (March 1983). (Proceedings of the Fourth International Congress in Quantum Chemistry, Uppsala, Sweden, 13-20 June 1982). Theoretical models for reductive elimination from transition metal containing molecules have been studied using large scale contracted CI calculations. Four different models were treated, namely, NiH_2 , PdH_2 , $Ni(CH_3)_2$, and $Pd(H_2O)_2H_2$ in order to study the effects of adding ligands, exchanging hydrogens with methyl groups, and comparing nickel and palladium. The most interesting result already appeared for the simplest system NiH_2 . A closed-shell-type A_1 state with a small bond angle of only 57° is bound compared to Ni and H_2 with only a very small barrier for formation. The bond distance is short, shorter than in NiH , and the d orbitals are strongly involved in the binding. The hydrogen atoms bind both to nickel and to each other. With methyl groups rather than hydrogens, this double sided bonding situation is destroyed and $Ni(CH_3)_2$ has a negative binding energy with the carbon bonds pointing towards nickel. For PdH_2 only a weakly bound complex between an essentially unchanged H_2 and Pd was found. The bond distance is very long. Adding H_2O ligands to Pd shortens the bond distance and significantly opens up the bond angle. The methods used in the investigation and the chemical implications of the results are discussed. (21 refs.)

63517 Single versus double insertion in a simple intermolecular carbene reaction. K.Jug, P.C.Mishra (Theoretische Chemie, Univ. Hannover, Hannover, Germany).

Int. J. Quantum Chem. (USA), vol.23, no.3, p.887-90 (March 1983). (Proceedings of the Fourth International Congress in Quantum Chemistry, Uppsala, Sweden, 13-20 June 1982).

The carbene reaction $^1CH_2+C_2H_6$ was studied with the semiempirical method SINDO1. The pertinent transition states and products were obtained by geometry optimization on a CI surface. The authors find the insertion reaction forming C_3H_8 greatly favored compared to the double insertion leading to $CH_4+C_2H_4$. The result is qualitatively the same for the reaction of the two possible intermediate radicals CH_3 and C_2H_5 . The geometries and energies of all transition states are presented. (9 refs.)

63518 Dissociation of liquid arsenic selenoiodide. Le Kong Hoai, B.G.Bakhyshov, S.M.Gadzhiev, I.S.Sattar-zade (S.M. Kirov State Univ., Azerbaizhan SSR).

Inorg. Mater. (USA), vol.18, no.5, p.664-6 (May 1982). Translation of: *Izv. Akad. Nauk SSSR Neorg. Mater.*, vol.18, no.5, p.789-91 (May 1982). [received: Feb. 1983]

The thermal dissociation of liquid arsenic selenoiodide was studied, and the composition of the liquid phase and the constant and rate of dissociation of AsSel were calculated. The temperature region of stability of AsSel was determined. The dependence $\log K=f(1/T)$ of the dissociation of liquid arsenic selenoiodide was determined. ΔH_T and ΔS_T of the dissociation of AsSel in the liquid phase were calculated. (6 refs.)

63519 π complexing of chlorine atoms: is that all there is? P.S.Skell, H.N.Baxter, III, C.K.Taylor (Dept. of Chem., Pennsylvania State Univ., University Park, PA, USA).

J. Am. Chem. Soc. (USA), vol.105, no.1, p.120-1 (12 Jan. 1983).

With low concentration of substrates the H-abstracting species would live longer before encountering a substrate molecule. The π -complex rationalization would predict no change in selectivity with decreasing concentration of substrate, only, perhaps, a decrease in yield of chlorinated substrate. The authors report that a very marked increase of selectivity occurs with progressive diminution of the substrate concentration. (5 refs.)

63520 Diffusion controlled processes among stationary reactive sinks: effective medium approach. R.I.Cukier (Dept. of Chem., Michigan State Univ., East Lansing, MI, USA), K.F.Freed.

J. Chem. Phys. (USA), vol.78, no.5, p.2573-8 (1 March 1983).

Formulates an effective medium theory for diffusion controlled processes among randomly distributed, stationary, reactive sinks. An implicit expression for the exact 'self-energy' of the combined reactive density field and sinks is obtained in terms of the exact medium propagator. The lowest order truncation of this expression can be solved by numerical iteration for the self-energy. The rate and diffusion coefficients as a function of sink concentration extracted from this self-energy. The authors also consider the next order truncation which explicitly introduces the pair correlation function of the sinks. (9 refs.)

63521 Selective vibrational excitation of the ethylene-fluorine reaction in a nitrogen matrix. L.H.Frei, G.C.Pimental (Chem. Dept., Univ. of California, Berkeley, CA, USA).

J. Chem. Phys. (USA), vol.78, no.6, pt.2, p.3698-712 (15 March 1983).

Selective vibrational excitation of the cryogenic reactions between fluorine and C_2H_4 , CH_2CD_2 , trans-CHDCHD, and cis-CHDCHD have been studied in solid nitrogen at 12K. For the C_2H_4, F_2 reaction, quantum yields showed a general increase over five orders of magnitude as photon energy increased; ν (cm^{-1}), ϕ , 953, $<3 \times 10^{-8}$, 1896, 6.6×10^{-4} , 2989, 2.3×10^{-2} ; 3076, 7.0×10^{-2} , 3105, 4.3×10^{-2} , 4209, 3.1×10^{-1} . Deviations from this general trend give evidence of mode selectivity. Similar deviations indicative of mode selectivity are found for trans-CHDCHD. At comparable photon energy, the quantum yields of the diderethylenes decrease markedly in the sequence $\phi(r\text{-CHDCHD}) > \phi(c\text{-CHDCHD}) \approx \phi(CH_2CD_2)$. These differences are attributable to a g, u selection rule in the phonon-relaxation mechanism. All of the results are consistent with a competition between chemical reaction of the vibrationally excited ethylene and phonon-assisted relaxation. The resulting cascading process accounts for the general rise in ϕ as ν increases and deviations from this general rise are attributable, at least in part, to mode selectivity. (21 refs.)

63522 Kinetics of the Cl- H_2 system. II. Abstraction vs exchange in $D+HCl$. J.C.Miller, R.J.Gordon (Dept. of Chem., Univ. of Illinois, Chicago, IL, USA).

J. Chem. Phys. (USA), vol.78, no.6, pt.2, p.3713-20 (15 March 1983).

For pt.1 see *ibid.*, vol.75, no.11, p.5305-10 (1981). The gas phase reaction of D with HCl was studied at room temperature by the method of flash photolysis, with resonance fluorescence detection of D, H, and Cl atoms. The D and Cl atoms were observed to decay exponentially, whereas no H atom signal from the exchange reaction was detectable. From the calibrated sensitivity of the H atom detector, an upper limit of 0.002 was set for the ratio of rate constants for the exchange vs abstraction channels. (58 refs.)

63523 A shock tube study of DF dissociation. J.F.Bott, N.Cohen (Aerophys. Lab., Aerospace Corp., Los Angeles, CA, USA).

J. Chem. Phys. (USA), vol.78, no.6, pt.2, p.3721-6 (15 March 1983).

The dissociation rate for DF in argon has been studied with shock tube experiments at temperatures between 3600 and 7200K. The data were best fitted by the rate coefficient equation $k_1 = 2.7 \times 10^{22} T^{-2} \exp(-137130/RT)$ $cm^3/mol \cdot s$. A few experiments performed at $\sim 5000K$ indicated that DF dissociates more rapidly in a helium bath than in argon by a factor of 2.9-4.1. A comparison of recombination rate coefficients for several hydrogen halides at 4000K reveals only small deviations from a value of $10^{14.4} cm^3/mol \cdot s$. (19 refs.)

63524 Reactive and inelastic processes involving $I_2(D^1\Sigma_u^+)$ with the collision partners CH_4 , CH_3Cl , CF_3Cl , and CF_4 . R.J.Donovan, B.V.O'Grady, L.Lain, C.Fotakis (Dept. of Chem., Univ. of Edinburgh, Edinburgh, Scotland).

J. Chem. Phys. (USA), vol.78, no.6, pt.2, p.3727-31 (15 March 1983).

Fluorescence from the $D^1\Sigma_u^+$ state of I_2 , and from other ion-pair states populated as a result of inelastic collisions with the molecules CH_4 , CH_3Cl , CF_3Cl , and CF_4 , was studied throughout the 200-510 nm region. $I_2(D^1\Sigma_u^+)$ was optically pumped using an ArF laser ($\lambda = 193$ nm) and the above spectral region recorded with single laser shots by employing an optical multichannel analyzer. The physical quenching of $I_2(D^1\Sigma_u^+)$ was found to involve an electronic cascade, through intermediate states, terminating in the lowest ion-pair state $I_2(^1\Pi_{2g})$. The presence of reactive channels was identified by the reduction in I_2 fluorescence following successive laser shots. Fluorescence from $I_2(D^1\Sigma_u^+)$ was also studied following excitation with a CW mercury lamp ($\lambda = 185$ nm) and Stern-Volmer analysis of these data yielded total removal rate constants (reactive+inelastic channels), viz. $k(CH_4) = (7.9 \pm 0.3) \times 10^{-10}$, $k(CH_3Cl) = (21.0 \pm 1.0) \times 10^{-10}$, $k(CF_3Cl) = (7.1 \pm 0.4) \times 10^{-10}$, $k(CF_4) = (6.0 \pm 1.0) \times 10^{-10}$ [all in cm^3 molecule $^{-1}$ s $^{-1}$ units]. The presence of reactive channels was confirmed using end-product analysis techniques and it was shown that the lowest ion-pair state $I_2(^1\Pi_{2g})$ also reacts with CH_4 and possibly with CF_3Cl . (12 refs.)

63525 Unimolecular and bimolecular reactions in the $C_4H_6^+$ system: experiment and theory. M.F.Jarrold, L.M.Bass, P.R.Kemper, P.A.M.van Koppen, M.T.Bowers (Dept. of Chem., Univ. of California, Santa Barbara, CA, USA).

J. Chem. Phys. (USA), vol.78, no.6, pt.2, p.3756-66 (15 March 1983).

New experimental data on the metastable reactions of $C_4H_6^+$ are presented. The bimolecular reactions between $C_2H_2^+$ and C_2H_4 and between $C_2H_4^+$ and C_2H_2 have been reinvestigated using a tandem ICR. Total rate constants and branching ratios were measured and isotopic scrambling investigated using deuterium labeling. The experimental data reported here and the

PIPECO data of Werner and Baer [J. Chem. Phys. 62, 2900 (1975)] are compared with the predictions of the transition state switching model. Good agreement was found between the predictions of the model and the experimental data. The branching ratios were found to be strong functions of both energy and angular momentum. In the bimolecular reaction between C_2H_2 and C_2H_4 charge transfer appears to occur predominantly via a loosely bound intermediate which only samples a small volume of the available $C_2H_6^+$ phase space. (45 refs.)

63526 The unimolecular decomposition rates of energy selected methylnitrite and deuterated methylnitrite ions. J.P.Gilman, T.Hsieh, G.G.Meisels (Dept. of Chem., Univ. of Nebraska, Lincoln, NE, USA). *J. Chem. Phys. (USA)*, vol.78, no.6, pt.2, p.3767-73 (15 March 1983). The fragmentation of methylnitrite ion (CH_3ONO^+) involves dissociation from noninterconverting electronic states characterized by the formation of CH_3O^+ ($m/z=31$) and NO^+ ($m/z=30$) ions. The lifetimes of the precursors of these ions have been determined from ion time-of-flight curves obtained by threshold photoelectron-photoion coincidence (TPEPICO) mass spectrometry. The deuterated methylnitrite ion (CD_3ONO^+) was also studied to examine the kinetic isotope effects on ion lifetimes. The rate constants for the reactions leading to the formation of CH_3O^+ and CD_3O^+ were found to be independent of internal energy over ~ 0.2 and 0.9 eV, respectively. The isotope effect increases with increasing internal energy, contrary to that expected from the quasiequilibrium theory (QET) of mass spectra. The authors suggest that methylnitrite ion fragmenting to CH_3O^+ and NO^+ occurs from noncompeting noninterconverting electronic states involving a surface crossing. (36 refs.)

63527 The reaction $Hg + I_2 \rightarrow HgI + I$ revisited. M.M.Oprysko, F.J.Aoiz, M.A.McMahan, R.B.Bernstein (Dept. of Chem., Columbia Univ., New York, NY, USA). *J. Chem. Phys. (USA)*, vol.78, no.6, pt.2, p.3816-31 (15 March 1983). The crossed molecular beam study of Mayer et al. (1977) on the subject reaction is revisited. The present work employs a different beam configuration and thus kinematic framework, and a larger range of relative translational energies is covered (i.e. from the threshold of 1.15 to 3.75 eV). Measurements include in-plane angular distributions and relative values of integral reaction cross sections as a function of energy. At low energies, the results of the present experiments are in good agreement with the previous work. Starting at the threshold, the reaction proceeds through the formation of a long-lived complex, presumed to be $IHgI$. At higher energies, the c.m. angular distributions show a gradual increase of the so-called 'backscattered component'. This is interpreted as the opening of a new reaction path: the direct-mode abstraction of I via collinear approach of the Hg atom to the I_2 molecule. The overall dynamics of this reaction are interpreted in the context of the semiempirical potential energy surfaces and electronic state correlation diagrams of Muckerman et al. (1977). From the present experimental results, the height of the barrier in the exit channel for the collinear configuration can be estimated to be in the range 2.0-2.3 eV. The excitation function rises from threshold and reaches a maximum at collision energy of 2.6 eV, falling off monotonically thereafter. (58 refs.)

63528 Oscillating reactivity of collinear symmetric heavy+light-heavy atom reactions. C.Hiller, J.Maniz (Lehrstuhl für Theoretische Chem., Tech. Univ. München, Garching, Germany), W.H.Müller, J.Romelt. *J. Chem. Phys. (USA)*, vol.78, no.6, pt.2, p.3850-6 (15 March 1983). The oscillatory reaction probability (as a function of energy) of collinear heavy+light-heavy systems (e.g. $I+HI \rightarrow IH+I$) that has been seen in earlier quantum mechanical reactive scattering calculations is shown to be described quantitatively by a semiclassical WKB model. Because these reactions are highly vibrationally adiabatic they reduce to a two-state symmetric resonance system (analogous to symmetric charge transfer, e.g. $H^+ + H \rightarrow H + H^+$) that involves only the phase shifts of the one-dimensional g (symmetric) and u (antisymmetric) combinations of the two states. Comparisons of the semiclassical and quantum mechanical reaction probabilities over a wide range of energy for the cases $I+MuI \rightarrow IMu+I$ and $I+HI \rightarrow IH+I$ show almost perfect agreement. The vibrationally adiabatic symmetry exchange problem is also solved classically (analytically) and is seen to have an interesting relation to the quantum/semiclassical result. The classical reaction probability is also an oscillatory function of energy, although the structure of the oscillations is different from the quantum/semiclassical ones ('saw-tooth' rather than sinusoidal) and the phase of the classical oscillations is only approximately the same as that of the quantum/semiclassical case. (In the high energy limit, the phase of the oscillations increases roughly as the square root of collision energy.) Thus, though the classical (light atom hopping between two heavy atoms) and quantum mechanical (resonance interference of g and u collision channels) interpretations of the oscillatory reactivity seem at first to be quite different, they are seen in fact to be essentially the same. (40 refs.)

63529 Vibrational energy transfer efficiency in a three-channel thermal unimolecular system. Temperature dependence. V.V.Krongauz, B.S.Rabinovitch (Dept. of Chem., Univ. of Washington, Seattle, WA, USA). *J. Chem. Phys. (USA)*, vol.78, no.6, pt.2, p.3872-80 (15 March 1983). Thermal isomerization in the three-channel cyclopropane-1,1,2,2,2 system was studied at 823 and 973K in the presence of Kr and CO_2 bath gases. It was found that CO_2 is more efficient in energy transfer from the hot cyclopropane than Kr, which is more efficient than He. For the stepladder model of energy transfer, the average energy removed per collision from energized cyclopropane-1,1,2,2,2 by a bath gas (ΔE) for Kr is 780 ± 90 cm $^{-1}$ at 823K and 520 ± 70 cm $^{-1}$ at 933K; while for CO_2 it is 1220 ± 90 cm $^{-1}$ at 823K and 800 ± 70 cm $^{-1}$ at 973K. The relative collision efficiency of both bath gases β_{rel} also declines with temperature rise. For Kr, β_{rel} is 0.17 at 823K and 0.07 at 973K; for CO_2 , β_{rel} is 0.40 at 823K and 0.17 at 973K. Comparison is made with earlier results. A T^{-1} ($\gamma \sim 5.5$) temperature dependence fits the existing data for He/cyclopropane systems and is in accord with the computational deductions of Tardy and Rabinovitch (1977). For stronger colliders, e.g. Kr and CO_2 , the temperature dependence of β_{rel} should be less than He. A value of ≈ 1 kcal/mol for the activation energy difference for T and H migration during cyclopropane-1,1,2,2,2 isomerization was confirmed. (36 refs.)

63530 Ab initio study of electronic coupling in the aqueous Fe^{2+}/Fe^{3+} electron exchange process. J.Logan, M.D.Newton (Dept. of Chem., Brookhaven Nat. Lab., Upton, NY, USA). *J. Chem. Phys. (USA)*, vol.78, no.6, pt.2, p.4086-91 (15 March 1983). Electronic Hamiltonian matrix elements between initial and final zeroth order states associated with electron exchange in the hexa-aquo Fe^{2+}/Fe^{3+} redox system has been calculated in terms of self-consistent field (SCF) ab initio wave functions. The face-to-face and apex-to-apex approach geometries of the quasi-octahedral reactants have been modeled, respectively, by the $[Fe(H_2O)_6]^{2+}$ cluster (D_{3h} symmetry) and the $[Fe(H_2O)_6]^{3+}$ cluster (O_h symmetry). For the latter cluster, the Condon approximation has been tested and found to be accurate to within ~ 1 cm $^{-1}$ for the important range of inner-shell FeO distances. The calculations employ ab initio effective core potentials for inner-shell electrons and explicitly

include all metal and ligand valence electrons. Due to weak 3d-3d overlap, the energy-preferred SCF solutions are charge localized (i.e. symmetry broken: $S_g \rightarrow C_3$ and $D_{2h} \rightarrow C_{2v}$). The present results for the interpenetrating face-to-face approach geometry are quite similar to earlier results based on a crystal-field model, implying an electronic transmission factor (κ) of $\sim 1/5$ at the most probable reactive encounter separation (5.3 Å). The alternative apex-to-apex approach geometry is found to be less kinetically favorable. Attempts to fit calculated values of the electronic matrix elements to functions of the form $P_n(r) \exp(-ar)$ for the range $r \sim 5-8$ Å, where r is the Fe...Fe separation in Å and $P_n(r)$ is a polynomial, yield values of a ranging from 0.8 to 2.4 Å $^{-1}$, depending on the values of n and m , the orientation of reactants, and the model employed for the ligands. The calculated matrix elements are found to be rather insensitive with respect to variation of certain features of the SCF wave functions. (22 refs.)

63531 Smoluchowski-Vlasov theory of charge solvation dynamics. D.F.Calef, P.G.Wolynes (Dept. of Chem., Harvard Univ., Cambridge, MA, USA). *J. Chem. Phys. (USA)*, vol.78, no.6, pt.2, p.4145-53 (15 March 1983). The dynamics of polar solvent reorganization near an instantaneously created charge are investigated. A linear, Vlasov-type equation is derived, where the interactions between the polar molecules are treated using a mean field term containing the direct correlation function. For the diffusive limit, a Smoluchowski-Vlasov equation for reorientation is studied. The results, for model solvents, are compared to the results from continuum dielectric theories, to experimental results, and to results from recent computer simulations. (25 refs.)

63532 A quasiclassical trajectory study of the $F+HH \rightarrow FH+H$ reaction. S.Ron (Israel Atomic Energy Comm., Tel-Aviv, Israel), M.Baer, E.Pollak. *J. Chem. Phys. (USA)*, vol.78, no.7, p.4414-22 (1 April 1983). A detailed forward and reverse quasiclassical trajectory computation for the FHH reaction is presented. An adiabatic analysis of the results shows that to a large extent the differences between HF($v=3$) and HF($v=2$) product distributions are due to the existence of an exit channel adiabatic barrier for the $v=3$ state. A sideways peak in the angular distribution for HF($v=2, j$) is found in the reverse quasiclassical computation. Total cross sections computed from reverse quasiclassical trajectories are in good agreement with the quantum I_{01} reactive infinite order sudden approximation. The authors conclude that many of the discrepancies between forward quasiclassical results and quantum computations are not due to quantal resonances but rather to the large boxing of vibrational states. (29 refs.)

63533 Trajectory studies within the framework of the infinite order sudden approximation for the $F+H_2 \rightarrow HF+H$ reaction. J.Jellinek (Dept. of Chem. Phys., Weizmann Inst. of Sci., Rehovot, Israel), M.Baer. *J. Chem. Phys. (USA)*, vol.78, no.7, p.4494-501 (1 April 1983). A detailed classical mechanical study of the $F+H_2$ reaction within the framework of the infinite order sudden approximation (IOSA) is presented. The main object of this research was to study the sensitivity of the state-to-state and total opacity functions and cross sections with respect to a parameter B which determines the border between the reagents and products channels. It was found that the results tend to vary when the value of B is changed but, within a particular range of B values, the IOSA results fit the exact results very nicely. Results of an approach where B is eliminated are also presented and compared with those obtained with the other treatments. (15 refs.)

63534 Adiabatic T matrix theory for three dimensional reactive scattering: application to the (H_2H_2) system. J.C.Sun, B.H.Choi, R.T.Poe, K.T.Tang (Dept. of Phys., Univ. of California, Riverside, CA, USA). *J. Chem. Phys. (USA)*, vol.78, no.7, p.4523-32 (1 April 1983). The authors present an adiabatic transition matrix (T matrix) method of atom-molecule reactive scattering. In this method, the coupling between vibrational and rotational motions is taken into account for obtaining the adiabatic molecular wave functions. These wave functions are expanded in terms of the basis functions taken from the eigenfunctions of a double well potential. From the full potential surface in the linear configuration of three atoms, the double well potential is obtained. Convergence of the expansion is achieved for evaluating the adiabatic wave functions and two body atom-molecule interaction potential. Cross sections are computed with the T matrix method employing the converged adiabatic wave functions. Numerical results for the $H+H_2$ reactive cross section on an ab initio potential surface are presented. Results on $D+H_2$ reaction will be reported in a subsequent paper. The differential cross sections and final state distributions computed from the present adiabatic T matrix method are similar to ones obtained from the adiabatic distorted wave approximation which the authors published earlier. However, the absolute cross section from the present approach is considerably larger than the previous one. The present results on the reactive cross section are in very good agreement with those obtained from a close coupling calculation. The present cross sections are much bigger than the classical ones in the threshold region. Among the cross sections from various T matrix approaches, the present one is the largest and seems to be most accurate. (36 refs.)

63535 Reaction of ketenes with atomic oxygen. N.Washida, S.Hatakeyama, H.Takagi (Div. of Atmospheric Environment, Nat. Inst. for Environmental Studies, Ibaraki, Japan), T.Kyogoku, S.Sato. *J. Chem. Phys. (USA)*, vol.78, no.7, p.4533-40 (1 April 1983). Rate constants for the reaction of atomic oxygen with ketene, and methyl, ethyl, and dimethyl ketene were measured over a temperature range of 230-449K using the pulse radiolysis resonance absorption system. Over the temperature range of the experiments, the rate data could be fitted by Arrhenius expressions: $O+CH_3CO$, $(2.92 \pm 0.78) \times 10^{-12} \exp(-1349 \pm 154 \text{ cal mol}^{-1}/RT)$; $O+(CH_3)CHCO$, $(4.79 \pm 1.31) \times 10^{-12} \exp(494.9 \pm 163.2 \text{ cal mol}^{-1}/RT)$; $O+(C_2H_5)CHCO$, $(5.36 \pm 0.83) \times 10^{-12} \exp(444.6 \pm 94.0 \text{ cal mol}^{-1}/RT)$; $O+(CH_3)_2CCO$, $(5.92 \pm 0.94) \times 10^{-12} \exp(1131 \pm 85 \text{ cal mol}^{-1}/RT)$; in units of cm 3 molecule $^{-1}$ s $^{-1}$. The rate constants at room temperature were also determined using a discharge-flow system coupled to a photoionization mass spectrometer. Rate constants obtained are 0.043 ± 0.04 , 1.16 ± 0.13 , 1.36 ± 0.11 , and $6.04 \pm 0.64 \times 10^{-11}$ cm 3 molecule $^{-1}$ s $^{-1}$ for CH_3CO , $(CH_3)CHCO$, $(C_2H_5)CHCO$, and $(CH_3)_2CCO$, respectively. Several reaction products were analyzed by the photoionization mass spectrometer. (29 refs.)

63536 Comments on 'Kinetics and mechanism of the U-H reaction'. J.B.Condon (Nuclear Div., Union Carbide Corp., Oak Ridge, TN, USA). *J. Less-Common Met. (Switzerland)*, vol.90, no.1, p.19-11 (March 1983). The author presents arguments to alleviate any possible misunderstanding that might result from the paper by Block and Mintz (1981) in which the perfluoro precipitation model, which Condon (1975) and others have successfully applied to the U-H system, was given an abrupt dismissal. (13 refs.)

63537 A new formalism of chemical exchange near the region of intermediate rate. K. Kimura (Instrument Center, Inst. for Molecular Sci., Okazaki, Japan).

J. Magn. Resonance (USA), vol. 52, no. 1, p. 13-22 (March 1983).

The Bloch equation incorporating chemical exchange between two environments is solved and is expanded in a power series of the exchange lifetime τ . The expansion near the fast exchange region is given by a power series in τ of which the first term corresponds to the fast exchange limit. The second term together with the first term defines the 'boundary' intermediate exchange region. In the slow exchange region, the expansion in both exchange regions are examined and as a result the chemical exchange is divided into five regions: fast limit, fast intermediate, pure intermediate, slow intermediate, and slow limit. In the 'pure' intermediate region, a conventional simulation procedure is needed in order to determine the exchange rate. On the other hand, an analytical form is derived for the linewidth in the other regions. The linewidth as a function of exchange rate, transverse relaxation time, content of component species, and chemical shift difference between two environments is examined in the light of the proposed formula. (8 refs.)

63538 Influence of extended defects and of the porous texture in the reduction of chromium dioxide. R. Saez-Puche, M.A. Alario-Franco (Dept. de Quimica Inorganica, Univ. Complutense, Madrid, Spain).

J. Solid State Chem. (USA), vol. 47, no. 1, p. 59-68 (15 March 1983).

The hydrogen reduction of very small single crystalline particles of CrO_2 to orthorhombic CrOOH is impeded by the presence of extended defects, crystallographic shear planes, formed in the process of attaining the reduction temperature in vacuum. However, if CrO_2 is predecomposed to a large extent, a porous texture is formed that facilitates the reduction. These results are in full agreement with a previously proposed reaction mechanism based on unidimensional diffusion. (20 refs.)

63539 The thermal stability of calcium uranates in a hydrogen atmosphere. J. Holc, D. Kolar (E. Kardelj Univ., Ljubljana, Yugoslavia).

J. Solid State Chem. (USA), vol. 47, no. 1, p. 98-102 (15 March 1983).

The stability and decomposition of CaUO_4 , Ca_2UO_6 , and Ca_3UO_7 on heating over hydrogen were investigated by X-ray powder diffraction and thermogravimetry. Ca_2UO_6 decomposes at 450°C into $\text{Ca}_2\text{UO}_{4.5}$ with a triclinic unit cell. At 850°C , it changes to monoclinic $\text{Ca}_2(\text{Ca}_{0.67}\text{U}_{0.33})\text{UO}_6$ which loses some oxygen up to the composition $\text{Ca}_2(\text{Ca}_{0.67}\text{U}_{0.33})\text{UO}_{5.83}$. At 1100°C , it decomposes to a UO_2 solid solution with CaO . CaUO_4 decomposes at 900°C to $\text{Ca}_2(\text{Ca}_{0.67}\text{U}_{0.33})\text{UO}_{5.83}$ and CaU_2O_6 . The decomposition products of Ca_3UO_7 at 850°C are $\text{Ca}_2(\text{Ca}_{0.67}\text{U}_{0.33})\text{UO}_{5.83}$ and CaO . (11 refs.)

63540 The oxidation of methanol on Cu(100) studied by infrared spectroscopy. R. Ryberg (Phys. Dept., Chalmers Univ. of Technol., Goteborg, Sweden).

J. Electron Spectrosc. & Relat. Phenom. (Netherlands), vol. 29, p. 59-60 (15 Jan. 1983). (Proceedings of the Third International Conference on 'Vibrations at Surfaces', Asilomar, CA, USA, 1-4 Sept. 1982).

Summary form only given as follows: Infrared spectroscopy has been used to study the C-O stretch vibrational mode of different coverages of CH_3O adsorbed on a Cu(100) surface. The spectra is taken with a resolution of 4 cm^{-1} and a scan time of 20 minutes. There is a large coverage dependent shift of the vibration frequency, which is mainly caused by the dipole-dipole interaction between the adsorbed molecules. (no refs.)

63541 Elementary reactions of the NCl radical. I. Rate constants for the reactions $\text{NCl} + \text{NCl} \rightarrow \text{N}_2 + 2\text{Cl}$ and $\text{O} + \text{NCl} \rightarrow \text{NO} + \text{Cl}$. M.A.A. Clyne, A.J. MacRobert.

J. Chem. Soc. Faraday Trans. II (GB), vol. 79, pt. 2, p. 283-93 (Feb. 1983).

A kinetic study of the NCl radical at 295K has been carried out in a discharge-flow system using mass-spectrometric detection with molecular-beam sampling. NCl radicals were generated by the reaction of Cl atoms with N_2Cl : $\text{Cl} + \text{N}_2\text{Cl} \rightarrow \text{N}_2 + \text{Cl}_2$ and $\text{Cl} + \text{N}_2\text{Cl} \rightarrow \text{NCl}(\text{b}^2\Sigma^+)$, $(\text{a}^4\Delta)$, $(\text{X}^2\Sigma^-) + \text{N}_2$. Metastable excited-state $(\text{a}^4\Delta)$, $(\text{b}^2\Sigma^+)$ NCl radicals were shown to react with Cl_2 to produce NCl_2 radicals: $\text{NCl}^* + \text{Cl}_2 \rightarrow \text{NCl}_2 + \text{Cl}$. The rate constants (295K) for the following reactions of ground-state $(\text{X}^2\Sigma^-)$ NCl radicals have been measured: $\text{NCl} + \text{NCl} \rightarrow \text{N}_2 + 2\text{Cl}$ and $\text{O} + \text{NCl} \rightarrow \text{NO} + \text{Cl}$. (22 refs.)

63542 X-ray topographic investigations of solid state reactions. I. Changes in surface and bulk substructure during incipient thermal decomposition in sodium chlorate monocrystals. I.D. Begg, P.J. Halfpenny (Dept. of Electrical Engng., Univ. of Southampton, Southampton, England), R.M. Hooper, R.S. Narang, K.J. Roberts, J.N. Sherwood.

Proc. R. Soc. London Ser. A (GB), vol. 386, no. 1791, p. 431-42 (8 April 1983).

On heating, sodium chlorate monocrystals undergo a limited degree of thermal decomposition in the solid state (0.1-1% mass loss) between 450K and the melting point, ca. 535K . Examination of thermally treated pristine surfaces with a microscope reveals distributions of decomposition sites characteristic of the reaction initiating where emergent dislocations intersect the crystal surface. There is little correlation, however, between dislocation etch-pits and decomposition centres. X-ray topographic studies of changes in bulk substructure during thermal treatment confirm that 'grown in' dislocations play little or no part in the nucleation of the decomposition process in the bulk; they may, however, contribute to the surface reaction. In the bulk, the potential nuclei are strained regions in the lattice. From these, and possibly from decomposition, dislocation loops are punched out into the surrounding lattice along (100) and (110) directions. Similar defects are emitted from localized regions at the surface, which may give rise to the surface decomposition patterns. Impurity doped crystals show considerably enhanced decomposition. (31 refs.)

63543 State-to-state and state-to-all-states reactive scattering angular distributions: $\text{F} + \text{H}_2 \rightarrow \text{HF} + \text{H}$. R.W. Emmons, S.H. Suck (Dept. of Phys., Univ. of Missouri, Rolla, MO, USA).

Phys. Rev. A (USA), vol. 27, no. 4, p. 1803-11 (April 1983).

How each state-to-state reactive transition determines nonundulatory 'state-to-all-states' angular distribution has not yet been investigated. The authors present a complete exposure of state-to-state distorted-wave Born-approximation angular distributions in order to examine how the nonoscillatory and backward-peaked state-to-all-states reactive scattering angular distribution occurs. (16 refs.)

63544 Stereochemical rearrangements of complexes in liquid crystals. I.G. Bikhantaev, I.V. Ovchinnikov (Kazan' Inst. of Tech. Phys., Acad. of Sci., USSR).

Theor. & Exp. Chem. (USA), vol. 18, no. 2, p. 201-3 (March-April 1982). Translation of: *Teor. & Ekspr. Khim. (USSR)*, vol. 18, no. 2, p. 233-5 (March-April 1982). [received: Feb. 1983]

The authors show how the use of liquid crystals permits, in principle, a new approach to the solution of the problem of stereochemical rearrangements in solution. As an example illustrating the proposed method, the stereochemical rearrangement reactions in a solution of fluorine-substituted copper β -diketonate with collidine are considered. The complex is dissolved in a eutectic mixture of MBBA and EBBA and after rapid freezing of the matrix, the ESR signals are examined. (3 refs.)

63545 Infrared spectroscopic investigation of some carboxylic acids in non-polar solvents. D.D. Thuc, G. Rudakoff.

Wiss. Z. Friedrich-Schiller-Universität Jena, Math. Naturwiss. Reihe (Germany), vol. 31, no. 6, p. 1093-7 (1982). In German.

The association behaviour of some carboxylic acids in CCl_4 , benzene and hexane was studied by IR-spectroscopy. The thermodynamical data are given. (11 refs.)

Unusual low-energy isomers for simple radical cations See Entry 60567

Ordinary field-theoretic methods for self-consistent wave functions which describe bond formation and dissociation. II. Commutative coupling case See Entry 60572

Hydrogen bonds between first-row hydrides and acetylene See Entry 60580

States of Am in aqueous solution See Entry 60582

Real-time multiphoton ionization detection of iodine atoms produced by infrared multiphoton dissociation of perfluoroalkyl iodides See Entry 60680

Electronic spectra and intramolecular proton transfer in Mannich bases in liquid and solid vitreous solutions See Entry 60735

Effects of electron transfer on the chemical polarization of nuclei in the recombination of radical-ion pair in strong magnetic fields See Entry 60759

Reactive and non-reactive quenching of $\text{O}(\text{D}_2)$ by COF_2 See Entry 60785

Kinetic energy release distributions in the fragmentation of energy-selected iodopropane ions See Entry 60833

Experimental investigation of Hornbeck-Molnar ionisation in collisions between excited $\text{He}(5^3\text{P})$ and He atoms See Entry 60956

Formation of molecular ions in binary collisions of excited inert-gas atoms See Entry 60957

Charge exchange of C^{+6} and O^{+8} ions with hydrogen atoms: Strong coupling calculation See Entry 60977

Variational transition state theory and tunneling for a heavy-light-heavy reaction using an ab initio potential energy surface, $^{37}\text{Cl} + \text{H}(\text{D})^{35}\text{Cl} \rightarrow \text{H}(\text{D})^{37}\text{Cl} + ^{35}\text{Cl}$ See Entry 61006

A correlation between structure and reactivity in ion clusters See Entry 61040

The interionic potential of mean force in a molecular polar solvent from an extended RISM equation See Entry 61759

The isostructural sulfides: Sr_2SnS_2 and Eu_2SnS_2 See Entry 61865

Chemical and catalytic effects of ion implantation See Entry 61942

Vaporization behaviour of the system $\text{AlF}_3(\text{s})\text{-Al}(\text{l})$ See Entry 62079

Structure of pyrolytic carbon in the process of its formation See Entry 62288

Distribution of double bonds in thermally degraded polyisobutylene. [PMR observations] See Entry 62820

Reaction of powdered superhard materials with gases during high-temperature shock compression See Entry 63224

The $\text{As}_2\text{S}_3\text{-SnTe}$ system See Entry 63268

High-temperatures reactions of metals with gases. II. Kinetics of growth of multiphase chemical compound layers at a metal/gas interface See Entry 63468

The reactive quantum Boltzmann equations: a derivation from an arrangement channel space representation and BBGKY hierarchy See Entry 63497

On the theory of kinetic isotope effects in proton transfer reactions. Influence of the anharmonicity of proton potentials See Entry 63499

Measurements of collisional energy transfer in unimolecular processes See Entry 63501

Lifetime uncertainty broadening in photoinduced electron transfer See Entry 63565

Benzophenone photoreduction by heteroatom-containing donors See Entry 63566

Smog chamber studies of NO_x transformation rate and nitrate/precursor relationships See Entry 63754

82.35 POLYMER REACTIONS AND POLYMERIZATION

63546 Equilibrium polymerization in one dimension: exact solution by transfer matrix and renormalization group. P.M. Pfeuty (Lab. de Phys. des Solides, Univ. Paris-Sud, Orsay, France), J.C. Wheeler.

Phys. Rev. A (USA), vol. 27, no. 4, p. 2178-95 (April 1983).

Equilibrium polymerization is very different in one dimension than in higher dimensionality. The transition that occurs in the limit of vanishing initiation equilibrium constant (which is a critical point in higher dimensionality) becomes a first-order transition at nonvanishing temperature in one dimension. A simple model of equilibrium polymerization that has been discussed recently for higher dimensionality is solved exactly by the transfer-matrix method in one dimension. The equivalent $n=0$ vector model of magnetism is also solved exactly for all fields and temperatures by transfer-matrix methods and is analyzed by an exact renormalization-group transformation. The renormalization-group analysis contains several interesting features including the fact that the parameter space of the Hamiltonian must be enlarged to six dimensions, yet remains finite. The connection of the model and transition treated here with the Zimm-Bragg model of the helix-coil transition and with the one-dimensional Ising model of magnetism is discussed. (26 refs.)

63547 Thermooxidative stability of polypropylene under the simultaneous action of high pressure and shear strains. V.A. Zhorin, N.Ya. Rapoport, A.N. Kryuchkov, L.S. Shibrayeva, N.S. Enikolopyan.

Vysokomol. Soedin. Ser. A (USSR), vol. 25, no. 3, p. 578-81 (March 1983). In Russian. English translation in: *Polym. Sci. USSR (GB)*

Thermooxidative stability of polypropylene is increased after the simultaneous action of high pressure and shear strains. The more the pressure is, the more the effect is observed. Introduction of the reactive monomer results in an increase of the induction time and decrease of the rate of oxidation, while introduction of amorphous SiO_2 results in an increase of the induction time without the change of the rate of oxidation. (13 refs.)

63548 Vinyl polymerization initiated by reducing compounds of transition metals. I. The polymerizing initiating effect of chromium (II) and titanium (II) compounds. N. Moszner, M. Hartmann (Sektion Chemie, Friedrich Schiller Univ., Jena, Germany).

Wiss. Z. Friedrich-Schiller-Universität Jena, Math. Naturwiss. Reihe (Germany), vol. 31, no. 6, p. 1139-49 (1982). In German.

The polymerization initiating effect of reducing compounds of transition metals such as chromium (II) and titanium (III) in the presence of organic compounds is described. Thereby the selective graft copolymerization in the

presence of chromium (II) and compounds and titanium (II) chloride are discussed. (70 refs.)

63549 Synthesis and properties of poly(maleic anhydride). M.Hartmann, B.Schulz (Sektion Chemie, Friedrich Schiller Univ., Jena, Germany). *Wiss. Z. Friedrich-Schiller-Univ. Jena, Math. Naturwiss. Reihe (Germany)*, vol.31, no.6, p.1151-9 (1982). In German.

A review is given both of the knowledge of the mechanism of the homopolymerization of maleic anhydride (MA), and the structures, properties and uses of poly(maleic anhydride). During the free-radical polymerization of MA linear polymers with succinic anhydride structure units are formed through the usual vinyl polymerization. The mechanism of the anionic MA-polymerization depends on the base used, there is no general conformity concerning the anionic polymerization mechanism and the structures of polymers formed in this reaction. (53 refs.)

Investigation by the molecular-probe method of the changes in the packing density of filled epoxide compositions during hardening See Entry 61828

Distribution of double bonds in thermally degraded polyisobutylene. [PMR observations] See Entry 62820

Low temperature dielectric films from octavinylsilsequioxane See Entry 63163

The influence of polymer concentration on the internal motion—intramolecular pyrene excimer formation—a low molecular weight probe in solution See Entry 63577

82.40 CHEMICAL KINETICS AND REACTIONS: SPECIAL REGIMES

63550 Premixed, turbulent combustion of a sudden-expansion flow. Y.El Banhawy (Ain-Shams Univ., Cairo, Egypt), S.Sivasegaram, J.H.Whitelaw. *Combust. & Flame (USA)*, vol.50, no.2, p.153-65 (March 1983).

Measurement of mean values of velocity, temperature and concentrations of carbon monoxide, carbon dioxide, unburned hydrocarbon, and oxygen have been obtained in the two-dimensional flows downstream of two backward facing steps which stabilized premixed methane-air flames of equivalence ratios 0.77, 0.90 and 0.95. The maximum mean temperature increased from 1710 to 2000K with equivalence ratio, and the maximum intensity of the temperature fluctuations, like those of velocity fluctuations, was close to coincident with inflections in the mean profiles. The intensity of the temperature fluctuations achieved values in excess of unity and, at the locations of maximum mean temperature, in excess of 0.5. The larger step gave rise to a wider reaction region and to a slightly different trajectory. An increase in the flow rate of cooling water and therefore, a decrease of wall temperature resulted in increased concentrations of unburned hydrocarbon and carbon monoxide in the near-wall region. Discrete frequency fluctuations occurred at the natural frequency of the flow chamber: the magnitude of the energy of these fluctuations was small. (19 refs.)

63551 Flame quenching by a cold wall. J.Jarosinski (Inst. of Aeronautics, Warsaw, Poland).

Combust. & Flame (USA), vol.50, no.2, p.167-75 (March 1983).

Quenching of upward and downward propagating flames in narrow channels is studied. The speed and the instantaneous flame temperature were measured and Schlieren photography was used in experiments. The experiments were carried out in a vertical 50X50-mm² tube 1 m long, with channels. Flame characteristics of methane-air mixtures were determined over the entire burning range. The results of the experiments showed that the channel quenching distance is, over the entire burning range. The results of the experiments showed that the channel quenching distance is, over the entire range of mixture composition, twice as wide as the flame thickness. These conditions are equivalent to the Peclet number $Pe = uD/a = 39$, where u and D , determined empirically, are the burning velocity and the quenching distance, respectively, and a is the thermal diffusivity of the unburned mixture. The appropriate Peclet number determined earlier for tubes was $Pe = 46$ (Putnam and Jensen, Third Symposium on Combustion, 1949, p.89). (16 refs.)

63552 Convective instabilities of binary mixtures with fast chemical reaction in a porous medium. V.Steinberg, H.Brand (Univ. of California, Santa Barbara, CA, USA).

J. Chem. Phys. (USA), vol.78, no.5, p.2655-60 (1 March 1983).

The instabilities which can occur when a layer of a binary mixture with fast chemical reaction in a porous medium is heated from below or from above are investigated. The authors find that both a stationary instability or an oscillatory instability can occur as the first bifurcation depending on the sign and the magnitude of the heat of reaction. (12 refs.)

63553 Instability of surface combustion on exposure to laser radiation. F.V.Bunkin, N.A.Kirichenko, B.S.Luk'yanchuk (P.N. Lebedev Phys. Inst., Acad. of Sci., Moscow, USSR).

Sov. J. Quantum Electron. (USA), vol.12, no.10, p.1276-80 (Oct. 1982). Translation of: *Kvantovaya Elektron., Moskva (USSR)*, vol.9, no.10, p.1959-67 (Oct. 1982). [received: April 1983]

An analysis is made of laser heating of a material on the surface of which an exothermic reaction takes place (oxidation). It is shown that there are critical values of the radiation parameters (beam radius and intensity) above which the thermal field becomes unstable and a combustion wave propagates without restriction over the surface of the material. The characteristic instability evolution times are found. The theory developed in the present paper agrees with the results of experiments on laser combustion of metals. (9 refs.)

63554 The calculation of a fire in a large building. H.W.Emmons (Div. of Appl. Sci., Harvard Univ., Cambridge, MA, USA).

Trans. ASME. J. Heat Transfer (USA), vol.105, no.1, p.151-8 (Feb. 1983).

The complex picture presented by a fire growing in a large building can be understood by considering the process is made up of a large number of space, time, and phenomena zones each one of which is to some degree independent of all others. This approach is explained in detail, the appropriate equations now in use in the Computer Fire Code are listed and some results compared with full-scale experimental results. (15 refs.)

63555 Soot volume fraction profiles in forced-combusting boundary layers. R.A.Beier, P.J.Pagni (Dept. of Mech. Engng., Univ. of California, Berkeley, CA, USA).

Trans. ASME. J. Heat Transfer (USA), vol.105, no.1, p.159-65 (Feb. 1983).

A multiwavelength laser transmission technique is used to determine soot volume fraction fields and approximate particle size distributions in a forced flow combustor boundary layer. Measurements are made in diffusion flames of polymethylmethacrylate (PMMA) and five liquid hydrocarbon fuels (n-heptane, iso-octane, cyclohexane, cyclohexene, and toluene) with ambient oxygen mass fractions in the range of 0.235 $Y_{O_2} \leq 0.50$. Soot is observed in a region between the pyrolyzing fuel surface and the flame zone. Soot volume fraction increases monotonically with Y_{O_2} , e.g. n-heptane and PMMA are similar with soot volume fractions, f_v , ranging from $f_v \sim 5 \times 10^{-7}$ at

$Y_{O_2} = 0.23$ to $f_v \sim 5 \times 10^{-6}$ at $Y_{O_2} = 0.50$. For an oxygen mass fraction the same as air, $Y_{O_2} = 0.23$, soot volume fractions are approximately the same as values previously reported in pool fires and a free combustor boundary layer. However, the shape of the f_v profile changes with more soot near the flame in forced flow than in free flow due to the different y-velocity fields in these two systems. For all fuels tested, a most probable particle radius is between 20 nm and 80 nm, and does not appear to change substantially with location, fuel, or oxygen mass fraction. (33 refs.)

A microcomputer based system for stopped-flow kinetics See Entry 59848

Laser-saturated fluorescence measurements of OH concentration in flames See Entry 60782

Reparameterization of the Becker-Kistiakowsky-Wilson equation of state for water-gel explosives See Entry 61515

Spectral behaviour of a concentration field in turbulence environment with rapid chemical reaction See Entry 61564

Premixed combustion in a turbulent boundary layer with injection See Entry 61565

Gas-phase transient diffusion in droplet vaporization and combustion See Entry 61586

Chemiluminescent SiCl₄+O₂+Ar(He) reactions See Entry 63559

82.40T Chemiluminescence and chemical laser kinetics (see also 42.55K Chemical lasers, 78.60P Chemiluminescence)

63556 The exposure dependence and emission spectrum of chemiluminescence produced during the oxidation of Si (111) by O₂. G.D.Kubiak, G.Sitz, J.E.Hurst, Jr., R.N.Zare (Dept. of Chem., Stanford Univ., Stanford, CA, USA).

J. Electron Spectrosc. & Relat. Phenom. (Netherlands), vol.29, p.139 (15 Jan. 1983). (Proceedings of the Third International Conference on 'Vibrations at Surfaces', Asilomar, CA, USA, 1-4 Sept. 1982).

Summary form only given as follows. Chemiluminescence produced during the low pressure oxidation of a Si(111) surface by O₂ has been investigated. Carefully cleaned and annealed samples yield chemiluminescence at pressures as low as 6×10^{-7} torr, corresponding to a peak chemiluminescence yield of 2.2×10^{-7} photons per incident molecule and comparing favorably with the value of 1×10^{-7} measured by Bruce and Comas (1971). The evolution of the emission shows a hyperbolic decrease in time at pressures above 1×10^{-4} torr but becomes more complex at the lowest exposures studied. The spectrally broad chemiluminescence was dispersed at medium resolution and recorded with an Optical Multichannel Analyzer in an attempt to identify and characterize the energy content of the emitting species. (1 ref.)

63557 Laser-induced decomposition of sodium azide. H.Y.Chiu, R.C.Benson (Appl. Phys. Lab., Johns Hopkins Univ., Laurel, MD, USA).

J. Electron Spectrosc. & Relat. Phenom. (Netherlands), vol.29, p.141-6 (15 Jan. 1983). (Proceedings of the Third International Conference on 'Vibrations at Surfaces', Asilomar, CA, USA, 1-4 Sept. 1982).

The decomposition of sodium azide, NaN₃, has been studied using a pulsed carbon dioxide laser. Chemiluminescence associated with the decomposition has been measured with and without the azide surface in the detector field of view. Near the decomposition threshold, emission has been observed in the wings of the Na 3p—3s transition at 589 nm that has not been observed in previous azide decomposition experiments. This emission may be a result of surface reactions. Raman and visible absorption spectra have been obtained for the irradiated material; a new, as yet unidentified, band was observed in the Raman spectrum. (7 refs.)

63558 Solvatochromism of ketocyanines: binary complexes. V.V.Danilov, G.G.Dyadyusha, A.A.Rykov.

Opt. & Spectrosc. (USA), vol.53, no.1, p.38-41 (July 1982). Translation of: *Opt. & Spektrosk. (USSR)*, vol.53, no.1, p.67-72 (July 1982). [received: April 1983]

Results are presented for studies of the spectral and luminescence characteristics of ketocyanines in two-component solvents. It is shown that the addition of small amounts of a proton donor to solutions of ketocyanines in inert solvents results in the formation of a ketocyanine-proton donor complex having a 1:1 composition. The solvatochromism of the complex itself is investigated. (7 refs.)

63559 Chemiluminescent SiCl₄+O₂+Ar(He) reactions. B.Kulakowska, W.Zyrnicki (Inst. of Inorganic Chem. & Metall. of Rare Elements, Tech. Univ. of Wrocław, Wrocław, Poland).

Spectrosc. Lett. (USA), vol.15, no.12, p.969-81 (1982).

A chemiluminescent flame was formed in the reaction between SiCl₄ and oxygen in an atmosphere of argon or helium. Internal state distributions of some reaction products were studied. Inverted vibrational populations in the A¹π and F²π_g states of SiO were observed. The relative electronic populations of atomic silicon and relative rotational populations in the SiO A¹π state corresponded to temperatures of about 3400K and 400K, respectively. (17 refs.)

Production of vibrationally excited OH in chemiluminescent reactions of ozone with monoterpenes See Entry 63509

Atomic nitrogen emissions from photodissociation of N₂ See Entry 64236

82.45 ELECTROCHEMISTRY AND ELECTROPHORESIS

(see also 66.10 Ionic conduction in liquids; for electro-osmosis, see 82.65)

63560 Photoelectrochemical behavior of Co²⁺ doped-zinc oxide electrodes. M.Jakani, G.Campet, B.Tanouti, R.Salmon, J.-C.Launay (Univ. de Bordeaux-I, Talence, France), J.Kossanyi, J.Clavierie.

C.R. Seances Acad. Sci. Ser. II (France), vol.296, no.5, p.357-60 (7 Feb. 1983). In French.

Zn_{0.99}Co_{0.01}O single crystal photoanodes show a large visible photocurrent down to 750 nm. Mechanisms responsible for this photoresponse are discussed. (8 refs.)

63561 Anodic polarization behaviour of hydride-deuteride electrodes. S.Wakao, Y.Yonemura (Tokai Univ., Kanagawa, Japan).

J. Less-Common Met. (Switzerland), vol.89, no.2, p.481-8 (Feb. 1983). (International Symposium on the Properties and Applications of Metal Hydrides, Tobu, Japan, 30 May-4 June 1982).

The results of electrochemical measurements performed on hydrogen-absorbing metal electrodes such as LaNi_{5-x}Al_x (x=0-1.0), MnNi₄Al (Mn=misch metal), LaNi₄Cu and TiNi_{0.6} are reported. The equilibrium hydrogen pressure; partial molar enthalpy ΔH and partial molar entropy ΔS

of hydride (or deuteride) formation were calculated on the basis of their electrode potentials. The values determined electrochemically agreed very closely with those obtained from the solid-gas equilibrium. The current is strongly governed by the diffusion process at a large anodic polarization of the hydride-deuteride electrodes. The experimental current-overpotential curves are discussed on the basis of electrode and diffusion theory. In the case of hydride electrodes with a small value of $-\Delta H$ the diffusion species are mainly the OH^- (or OD^-) ions in the electrolyte solution. As the value of $-\Delta H$ increases, the activation energy of diffusion becomes larger and the diffusion species become the hydrogen (or deuterium) atoms in the metal. (7 refs.)

63562 Hydrogen evolution at LaNi₅-type alloy electrodes. H.Tamura, C.Iwakura, T.Kitamura (Dept. of Appl. Chem., Osaka Univ., Osaka, Japan), *J. Less-Common Met. (Switzerland)*, vol.89, no.2, p.567-74 (Feb. 1983). (International Symposium on the Properties and Applications of Metal Hydrides, Toba, Japan, 30 May-4 June 1982). Several LaNi₅-type alloy electrodes were prepared and their cathodic polarization characteristics in alkaline solutions were investigated. As a result, they were found to have a high electrocatalytic activity for the hydrogen evolution reaction compared with the constituent metals, and their activities were almost comparable with those of platinum and palladium electrodes. Such a synergism was attributed to the large heat of formation of these alloys. The surface damage of these alloy electrodes was also found to be prevented by controlling the temperature and current density. (12 refs.)

63563 On the electrokinetic energy conversion in liquid mixtures. R.Hidalgo-Alvarez, F.Gonzalez-Caballero, G.Pardo (Dept. of Phys., Faculty of Sci., Univ. of Granada, Granada, Spain), *Phys. Lett. A (Netherlands)*, vol.94A, no.6-7, p.325-8 (21 March 1983). The dependence of the maximum efficiency of the electrokinetic energy conversion (η_{max}) on the composition of the liquid mixtures can be correlated to changes of the absolute viscosity, the dielectric constant and the specific electric conductance of these mixtures. (12 refs.)

63564 Maximum rate of the cathodic reaction in electroless copper deposition. D.Vitkavage, M.Paunovic (PCK Technol. Div., Kollmorgen Corp., Melville, NY, USA), *Plat. & Surf. Finish. (USA)*, vol.70, no.4, p.48-50 (April 1983).

Conventional electroless solutions deposit copper at the rate of 1 to 5 $\mu\text{m/hr}$ (0.04 to 0.20 mil/hr). But there is a growing interest in high-speed systems with deposition rates above 10 $\mu\text{m/hr}$. The practical limit for the deposition rate of high-speed electroless copper is presently unknown. This paper analyses factors that determine this limit. The approach to this problem is based on the mixed-potential theory of electroless metal deposition. (23 refs.)

Proceedings of the Third International Conference on 'Vibrations at Surfaces' See Entry 59532

Chronopotentiometry of one- and two-ion transport at immiscible liquid interfaces: tests of theory See Entry 62143

Characterization of the interface energetics for N-type cadmium selenide/nonaqueous electrolyte junctions See Entry 62492

Semiconductor electrodes. XLVII. AC impedance technique for evaluating surface state properties of n-MoTe₂ in acetonitrile solutions containing various redox couples See Entry 62493

Open-circuit photopotentials at doped $\alpha\text{-Fe}_2\text{O}_3$ electrodes in aqueous solution See Entry 62494

Spatially varying polarization in water. A model for the electric double layer and the hydration force See Entry 62880

Surface enhanced Raman scattering of water on an Ag electrode See Entry 62985

EMIRS study of adsorbate bonding in the electrode solution interfacial region See Entry 62986

SERS study of pyridine vapor exposed to silver substrates electrochemically prepared See Entry 62988

Study of adsorption at the electrode/solution interphase by in-situ infrared reflectance spectroscopy—adsorption of methanol on a platinum electrode See Entry 62989

Intensity enhancement and spectral change in Raman scattering of mercaptobenzothiazole adsorbed on silver electrode See Entry 62990

Time dependence of surface enhanced Raman scattering during and after oxidation-reduction cycles See Entry 62991

Influence of production media on the physicochemical and electrochemical properties of steels See Entry 63430

Anodic dissolution behaviour of Si- and Ti-implanted iron See Entry 63447

Question of determining the electrochemical condition in a developing crack in investigating the crack resistance in a corrosive medium See Entry 63493

Microwave absorption studies of interface phenomena at ZnO electrodes See Entry 63582

Electrode material for high-temperature oxygen partial pressure electrochemical sensors: strontium-doped lanthanum chromite See Entry 63626

Photocathodic reactions at p-InP See Entry 63718

Light-induced generation of hydrogen at CdS-monograin membranes See Entry 63734

82.50 PHOTOCHEMISTRY AND RADIATION CHEMISTRY

(see also 33.50 Fluorescence, phosphorescence; radiationless transitions)

63565 Lifetime uncertainty broadening in photoinduced electron transfer. H.Staerk, R.Treichel, A.Weller (Abteilung Spektroskopie, Max-Planck-Inst. fur Biophys., Gottingen, Germany), *Chem. Phys. Lett. (Netherlands)*, vol.96, no.1, p.28-30 (25 March 1983).

Two types of energy-level broadening, one caused by electron exchange between radicals and ground-state molecules, the other by selective sampling at short times, are investigated. Both lead, in accordance with the uncertainty principle, to an increase in the $B_{1/2}$ value. (11 refs.)

63566 Benzophenone photoreduction by heteroatom-containing donors. J.C.Ronfard-Haret, R.V.Bensasson (Lab. de Biophys., INSERM, Paris, France), *J.C.Gramain*, *Chem. Phys. Lett. (Netherlands)*, vol.96, no.1, p.31-3 (25 March 1983).

Nanosecond flash photolysis has been carried out on benzophenone solutions in benzene and acetonitrile in presence of oxygen- and sulfur-containing reductants such as anisole, thioanisole, dibutyl sulfide and methyl 2-octyl ether. The quantum yield of ketyl formation is compared to previous results on the

quantum yields of the final benzophenone disappearance. This comparison is also related to previous data on benzophenone reduction by nitrogen-containing reductants such as amines and amides and suggests a general mechanism for benzophenone photoreduction by heteroatom-containing donors. (12 refs.)

63567 Reactions induced by ion bombardment of solid cyclohexane at 77K. O.Puglisi, G.Marletta, S.Pignataro (Istituto Dipartimentale di Chimica e Chimica Industriale, Catania, Italy), G.Foti, *Chem. Phys. (Netherlands)*, vol.75, no.3, p.417-23 (15 March 1983). Cyclohexane at 77K has been bombarded with He^+ and Ar^+ at several keV energies. The main chemical products obtained have been identified by GC/MS. The results were compared with those obtained on benzene implantation. The product formations were interpreted in terms of a previously proposed model involving electronic and nuclear stopping mechanisms of the bombarding particles. Some important physicochemical reaction pathways are proposed and discussed. (21 refs.)

63568 Electron spin resonance spectra of tetrafluoroethylene radical cation. A.Hasegawa, M.C.R.Symons (Dept. of Chem., Univ. of Leicester, Leicester, England), *J. Chem. Soc. Faraday Trans. 1 (GB)*, vol.79, no.1, p.93-7 (Jan. 1983).

Exposure of a solid solution of FCCl_3 containing C_2F_4 to γ -rays at 77K gave a species whose ESR spectrum comprised an anisotropic quintet attributed to hyperfine coupling to the four equivalent fluorines of the C_2F_4 radical cation. An extra, small doublet splitting is assigned tentatively to the fluorine of a matrix molecule interacting with the radical cation. INDO calculations show that the radical cation has a planar structure with the unpaired electron in the bonding π orbital, the estimated ^{19}F coupling constants being in good agreement with the experimental data. (13 refs.)

63569 Kinetics of photoprotolytic reaction in coumarin-dye solution. L.D.Derkacheva, A.I.Krymova, V.A.Petukhov, N.S.Platonov, *Opt. & Spectrosc. (USA)*, vol.53, no.1, p.42-4 (July 1982). Translation of: *Opt. & Spektrosk. (USSR)*, vol.53, no.1, p.73-8 (July 1982). [received: April 1983]

The kinetics of the radiation from different ionic forms of esculin dye in ethanol with addition of acid is investigated using a high-speed image-converter tube. Radiation intensity scans with subnanosecond resolution are obtained. It is shown that the reaction of joining the proton from the solution can be described by a simple single-step scheme. The photoprotolytic reaction rate constants are calculated from the measured time dependence of the radiation intensity. (6 refs.)

63570 Vacuum ultraviolet as a source for producing intermediates in solid organic matrices. E.Hankiewicz, J.Kroh (Inst. of Appl. Radiation Chem., Tech. Univ., Lodz, Poland), *Radiochem. & Radioanal. Lett. (Switzerland)*, vol.55, no.2, p.87-97 (23 Dec. 1982).

The application of vacuum ultraviolet (VUV) lamps to study the intermediates in polycrystalline (n-hexane and acetone) and glassy (methylcyclohexane and aliphatic alcohols) matrices at 77K is described. The measurements were performed using EPR and radiothermoluminescence techniques. In glassy, VUV irradiated alcohols alkoxy radicals together with hydroxylalkyl radicals were formed. Methanol and ethanol were not ionized with VUV quanta of 10.195 eV energy, but in n-propanol and n-butanol ionic intermediates were observed. The decrease of ionization potential for pure glassy alcohols as compared with gaseous phase has been estimated as at least 0.3 eV. Similar value has been also found for polycrystalline n-hexane. (16 refs.)

63571 The radiation chemistry of nuclear reactor decontaminating reagents. R.M.Sellers (Berkeley Nuclear Labs., CEGB, Berkeley, England), *Radiat. Phys. & Chem. (GB)*, vol.21, no.3, p.295-305 (1983).

Processes involved in the radiation chemistry of some typical nuclear reactor decontaminating reagents including complexing, reducing and oxidising agents are described. It is concluded that radiation-induced decomposition is only likely to be a problem with dilute formulations, and/or with minor additives such as corrosion inhibitors which are not protected from attack by the other constituents. Addition of a 'sacrificial' compound may be necessary to overcome this. The importance of considering loss of function, rather than the decomposition rate of the starting material, is emphasised. Reagents based on low oxidation state metal ions (LOMI) can be regenerated by the radiation field in the presence of formate ion. (31 refs.)

63572 Chemical effects of fission recoils. IV. Temperature distribution in the tracks. J.A.LaVerne, G.G.Meisels (Dept. of Chem., Univ. of Nebraska, Lincoln, NE, USA), *Radiat. Phys. & Chem. (GB)*, vol.21, no.3, p.329-39 (1983).

The temperature in the track of a ^{235}U fission recoil is probed by utilizing the difference in the heats of formation of the isopropyl and normal propyl radicals (3.6 kcal/mol). End products of the reactions of the isomeric propyl radicals are analyzed in the radiolysis of gaseous propane and a mixture of methane, ammonia and propane with γ rays or fission recoils at the same density. The product distribution is independent of density in the γ radiolysis while it varies in the fission recoil radiolysis in a manner suggesting an increase in temperature with density. Kinetic analysis leads to an 'effective' temperature, which is a time average of a localized temperature from the time of particle passage until end product formation. The 'effective temperature' varies approximately linearly with density from ambient at 5 g/L to 40°C above ambient at 100 g/L. This is much lower than the rise calculated by assuming that the track region is heated adiabatically by the entire energy lost by the fission recoil. This is ascribed to diffusive migration of the initially produced species during the physico-chemical stage for a finite relaxation interval. This model suggests a relaxation interval of 2×10^{-10} sec. (44 refs.)

63573 Thermal action of laser radiation on imidization. N.V.Karlov, E.K.Karlova, N.A.Kirichenko, B.S.Luk'yanchuk, O.V.Neklyudova, I.Ya.Ravich, A.N.Sapetskii, T.N.Toroptseva (P.N. Lebedev Phys. Inst., Acad. of Sci., Moscow, USSR), *Sov. J. Quantum Electron. (USA)*, vol.12, no.10, p.1330-3 (Oct. 1982). Translation of: *Kvantovaya Elektron., Moskva (USSR)*, vol.9, no.10, p.2049-55 (Oct. 1982). [received: April 1983]

Results are presented of experimental and theoretical investigations of an imidization process on exposure to CW CO₂ radiation. It is shown that as a result of the establishment of strong disequilibrium in the system during laser heating, it is possible to achieve higher degrees of imidization than under isothermal conditions and in the presence of infrared photochemical action. (6 refs.)

63574 Spectral dependences of the quantum yields of $I(^2P_{1/2})$ and $I(^2P_{3/2})$ from photolysis of C_3H_7I and CH_3CHICH_3 by vacuum ultraviolet radiation. A.M.Pravilov, S.E.Ryabov (Sci.-Res. Inst. of Phys., A.A. Zhdanov State Univ., Leningrad, USSR).

Sov. J. Quantum Electron. (USA), vol.12, no.10, p.1334-6 (Oct. 1982). Translation of *Kvantovaya Elektron., Moskva (USSR)*, vol.9, no.10, p.2056-60 (Oct. 1982). [received: April 1983]

A method was developed for the determination of the spectral dependences of the quantum yields of photoprocesses resulting from irradiation of the investigated compounds with nonmonochromatic radiation. The spectral dependences of the absolute quantum yields of the formation of $I(^2P_{1/2})$ and $I(^2P_{3/2})$ atoms by photolysis of C_3H_7I and CH_3CHICH_3 were determined in the range 210-155 nm. It was found that practically throughout the investigated range the atoms of iodine were formed mainly in the excited $^2P_{1/2}$ state. (13 refs.)

63575 Methane formation during deuteron bombardment of carbon in the energy range of 100 to 1500 eV. K.Sone. Report CLM-R 236, UKAEA, Culham, Abingdon, Oxon., England (1982), 15 pp.

Available from HMSO, London, England.

Methane (CD_4) formation rates during deuteron bombardment of carbon (Papayex) have been measured in the energy range of 100 to 1500 eV. The temperature dependence of the methane formation rate is well explained by the model proposed by Erents et al. (1978) in the temperature range of 600 to 1150K. The model, however, does not explain the dependence of the methane formation rate on the flux of incident deuterons at a certain temperature near T_m at which the formation rate has a maximum value. An alternative model is proposed in which the methane formation rate is assumed to be proportional to the product of the following three parameters: the surface concentration of deuterium atoms, the chemical reaction rate for the formation of methane, and the rate of production of vacancies on the surface by the deuteron bombardment. This model predicts an energy dependence of methane formation which has a maximum around 900 eV even at different deuteron fluxes, when the calculated result by Weissman and Sigmund (1973) is used for the surface deposited energy responsible for the production of vacancies. (25 refs.)

Effects of radiation damage and radiolysis on the leaching of vitrified waste ... See Entry 60280

Determination of the absolute intensity of the afterglow in flash photolysis of tellurium vapor ... See Entry 60659

Photochemical formation and dissociation of molybdenum-dinitrogen complexes in krypton matrices ... See Entry 60717

Spin trapping of $\cdot NO_2$ radicals produced by UV photolysis of RDX, HMX and nitroguanidine ... See Entry 60755

Effects of excited-state prototropic equilibria on the fluorescence energies of benzimidazole and thiabenzimidazole homologues ... See Entry 60814

Benzaldehyde photochemistry studied with laser ionization mass and photoelectron spectroscopy ... See Entry 60836

Photodissociation of CO_3 : evidence for a long-lived excited state ... See Entry 60859

The state distribution of OH radicals photodissociated from H_2O_2 at 193 and 248 nm ... See Entry 60860

Infrared photodissociation of sulfur dioxide ions in a fast ion beam ... See Entry 60861

Multiphoton dissociation of $OCCl_2$ at 193 nm: formation of electronically excited Cl_2 ... See Entry 60862

The unimolecular reaction of $(CH_3)_3CNO$ following $n-\pi^*$ excitation with a tunable dye laser ... See Entry 60863

Competing dissociation channels in the infrared multiphoton decomposition of ethyl vinyl ether ... See Entry 60864

Saturation laser photodissociation of a gas of diatomic molecules ... See Entry 60869

Site-specific fragmentation of small molecules following soft-X-ray excitation ... See Entry 60870

Analysis of multistage dissociation of polyatomic molecules ... See Entry 60872

Ion extraction in the laser process of uranium enrichment by selective ionization of atomic vapour ... See Entry 61005

Photochemical reactions in $CdS_{1-x}Se_x$ single crystals ... See Entry 62448

SERS study of pyridine vapor exposed to silver substrates electrochemically prepared ... See Entry 62988

Radiation-thermal sintering of europium oxide ... See Entry 63221

The exciplexes of thioindigo with durenene and hexamethylbenzene and their influence on photoisomerization ... See Entry 63505

Laser photolysis/laser-induced fluorescence study of the reaction of hydroxyl radical with ethylene ... See Entry 63508

Kinetics of the $Cl-H_2$ system. II. Abstraction vs exchange in $D+HCl$... See Entry 63522

Photoelectrochemical behavior of Co^{2+} doped-zinc oxide electrodes ... See Entry 63560

Photofragmentation of CH_3I , CD_3I and CF_3I . Formation of $I(^2P_{1/2})$ as a function of wavelength ... See Entry 63576

Microwave absorption studies of interface phenomena at ZnO electrodes ... See Entry 63582

Infrared laser stimulated surface processes ... See Entry 63587

The γ irradiation-enhanced corrosion of stainless and mild steels by water in the presence of air, argon and hydrogen ... See Entry 63594

The effect of radiation on the release of corrosion products from 304 stainless steel in high temperature water-II effects of flow rate and duration of corrosion experiment ... See Entry 63595

Photocathodic reactions at p-InP ... See Entry 63718

Light-induced generation of hydrogen at CdS-monograin membranes ... See Entry 63734

82.50E. Photodissociation, photoionization as studied by luminescence and radiationless transitions

63576 Photofragmentation of CH_3I , CD_3I and CF_3I . Formation of $I(^2P_{1/2})$ as a function of wavelength. T.F.Hunter, S.Lunt (School of Chem. Sci., Univ. of East Anglia, Norwich, England), K.S.Kristjansson. *J. Chem. Soc. Faraday Trans. II (GB)*, vol.79, pt.2, p.303-16 (Feb. 1983). Using several excitation wavelengths in the region from 247.5 to 312.5 nm, the branching ratio $^2P_{1/2}/^2P_{3/2}$ has been established for the iodine atom pro-

duced in the photolysis of CH_3I , CD_3I and CF_3I . An optoacoustic system is used and details of technique and analysis are given. For each molecule three transitions are observed in the $\sigma^* \leftarrow n$ continuum and the position, intensity and bandwidth of each are given. The extent of curve-crossing following the $A_1^* \leftarrow A_1$ transition appears to be approximately the same for all three molecules. (44 refs.)

63577 The influence of polymer concentration on the internal motion—intramolecular pyrene excimer formation—of a low molecular weight probe in solution. M.A.Winnik, A.E.C.Redpath, P.Svirskaya, A.Mar (Dept. of Chem., Univ. of Toronto, Toronto, Ontario, Canada). *Polymer (GB)*, vol.24, no.4, p.473-5 (April 1983).

Fluorescence decay measurements were used to study the kinetics of end-to-end cyclization of the molecule $Py-(CH_2)_5Si(Me_2)OSi(Me_2)(CH_2)_5-Py$ (1), where $Py=1$ -pyrenyl. Experiments were carried out in toluene at 22°C and in cyclohexane at 35°C, in the absence and in the presence of added polystyrene (PS). Addition of even small amounts (0.01 g/ml) of PS caused the cyclization rate of probe molecule 1 to decrease substantially in cyclohexane, whereas in toluene, a much milder retardation of cyclization rate with increasing PS was observed. These effects are interpreted in terms of a coupling between the chain dynamics and that of the probe molecule 1, mediated by the solvent. These hydrodynamic screening interactions depend sensitively upon whether the polymer is in a good or a poor solvent. (11 refs.)

Influence of temperature on the photodecomposition of various molecules with the formation of electronically excited fragments ... See Entry 60868

Atomic nitrogen emissions from photodissociation of N_2 ... See Entry 64236

82.55 RADIOCHEMISTRY

63578 Formation of simple ^{14}C -labelled molecules by the nuclear reaction $^{14}N(p,\alpha)^{11}C$ in nitrogen containing solids. K.Rossler, M.Vogt, H.Lattke (KFA, Jülich GmbH, Jülich, Germany). *Radiat. Eff. (GB)*, vol.65, no.1-4, p.117-0 (1982). (Proceedings of the First International Conference on 'Radiation Effects in Insulators', Arco, Largo di Garda, Italy, 1981).

Summary form only given, as follows. Simple ^{14}C -labelled molecules which are formed by hot processes following the $^{14}N(p,\alpha)^{11}C$ nuclear reactions with 13 MeV protons in cyclotron targets are of interest as precursors for the synthesis of ^{14}C -radiopharmaceuticals. Solid targets show the advantage of greater stability against radiolysis and heat and a greater variability of chemical reactions. Frozen ammonia NH_3 , ammonium halides NH_4X ($X=F, Cl, Br, I$), and complex salts such as $Co(NH_3)_6Cl_3$ have been studied as matrices. The interaction of recoil carbon atoms with the lattice constituents leads to a very differentiated spectrum of ^{14}C containing compounds. Analysis of the system is performed by gas chromatography or high performance liquid chromatography. In contrast to the situation in alkali halides, the carbon atoms react to organic compounds such as $^{14}C(NH_2)$ -cyanamide, $^{14}CH_3NH_3^+$ -methylammonium, $^{14}CH(NH_2)_2^+$ -formamidine and $^{14}C(NH_2)_3^+$ -guanidine with radiochemical yields of 40%, 80%, 30% and 65%, respectively. Even at 5K, carbon stabilizes via H-abstraction to CN -radicals and insertion into N-H bonds. The amount of ammonium ions interacting with the carbon depends strongly on the lattice arrangement. This could be shown by experiments in different lattice structures, using low temperature cryostats. The above mentioned products can be transferred to ^{14}C labelled compounds such as pyrimidine-derivatives and barbiturates suited for nuclear medical applications. Moreover, the behaviour of carbon impurities in ionic crystals may serve as a model for the formation of organic compounds in inorganic matter. (no refs.)

63579 Hydrocarbon chemistry in irradiated $CO_2/CO/CH_4/H_2O/H_2$ mixtures. I. A survey of the initial reactions. D.J.Norfolk, R.F.Skinner, W.J.Williams (Berkeley Nuclear Labs., CEBG, Berkeley, England). *Radiat. Phys. & Chem. (GB)*, vol.21, no.3, p.307-19 (1983).

A survey is made of the reactions through which low levels of hydrocarbons are radiolysed in $CO_2/CO/CH_4/H_2O/H_2$ mixtures under conditions typical of a gas-cooled nuclear reactor. Species which react with hydrocarbons include clustered positive and possibly negative ions, together at high temperatures with O and H atoms and OH radicals. If all these species are effective the maximum initial rate of attack is $G(-hydrocarbon) \sim 16$. Some of the initial products contain oxygen but alkyl radicals are probably the most important class. (66 refs.)

The possibility of measuring the nuclear correlation width via atomic electron spectroscopy ... See Entry 60161

Radiochemical measurements for evaluating air quality in the vicinity of low-level waste burial sites—the West Valley experience ... See Entry 60266

Chemical effects of fission recoils. IV. Temperature distribution in the tracks ... See Entry 63572

82.60 CHEMICAL THERMODYNAMICS

(see also 05.70 Thermodynamics)

63580 Thermodynamic study of the valence state of ytterbium in $YbAl_2$ and $YbAl_3$ compounds. A.Pasturel, C.Chatillon-Colinet (Lab. de Thermodynamique et Physicochimie Metall., Ecole Nat. Supérieure d'Electrochimie et d'Electrometall., de Grenoble, Saint Martin d'Heres, France), A.Percheron-Guegan, J.C.Achard. *J. Less-Common Met. (Switzerland)*, vol.90, no.1, p.21-7 (March 1983).

The heats of dissolution of rare earth metals in liquid aluminium and the enthalpies of formation of $YbAl_2$ and $YbAl_3$ were measured by a calorimetric method. In the metallic state ytterbium is divalent, whereas in alloys it can become trivalent like the majority of the rare earth metals. The results of this experimental study show that the energy difference between divalent and trivalent ytterbium is 7 kcal (g atom) $^{-1}$. The enthalpies of formation of $YbAl_2$ and $YbAl_3$ are -26.1 kcal mol $^{-1}$ and -31.1 kcal mol $^{-1}$ respectively. The valence of ytterbium in these compounds was studied using Miedema's model (1977). (16 refs.)

63581 Enthalpies of formation of liquid and solid binary alloys based on 3d metals. III. Alloys of iron. R.Boom (Res. Labs., Hoogovens IJmuiden, IJmuiden, Netherlands), F.R.de Boer, A.K.Niessen, A.R.Miedema. *Physica B & C (Netherlands)*, vol.115 B+C, no.3, p.285-309 (March 1983). For pt.II see ibid., vol.113B, p.18 (1982). Model predictions are presented for heats of formation of intermetallic compounds of iron with arbitrary metal partners. For the corresponding liquid alloy systems heats of mixing and solution are predicted. Calculation enthalpies are compared with experimental data as well as with the qualitative information that can be derived from phase diagrams. The available binary iron-based phase diagrams are presented in schematic form. A general discussion of the alloying behaviour of iron is given and practical applications of the generated enthalpy data are indicated. (186 refs.)

- States of Am in aqueous solution See Entry 60582
 Lifetimes in the $B^1\Pi$ state and the heat of formation of NCO See Entry 60788
 Effects of excited-state prototropic equilibria on the fluorescence energies of benzimidazole and thiabendazole homologues See Entry 60814
 Vaporization behaviour of the system $AlF_3(s)-Al(l)$ See Entry 62079
 Study of the vaporization of solid AlAs See Entry 62081
 Thermodynamics of the $CaO-SiO_2$ system See Entry 62109
 High temperature heat capacity of some Ag-Nd alloys See Entry 62124
 The thermodynamics of the system $CaNi_2-H_2$ using differential heat conduction calorimetry See Entry 62250
 Thermal effects accompanying the heating of metallized powders See Entry 63251
 Dissociation of liquid arsenic selenoiodide See Entry 63518
 X-ray topographic investigations of solid state reactions. I. Changes in surface and bulk substructure during incipient thermal decomposition in sodium chlorate monocrystals See Entry 63542
 Equilibrium polymerization in one dimension: exact solution by transfer matrix and renormalization group See Entry 63546

82.65 SURFACE PROCESSES

- 63582** Microwave absorption studies of interface phenomena at ZnO electrodes. R.A.Bogomolnii, H.Tributsch, G.Petermann, M.P.Klein (Lawrence Berkeley Lab., Univ. of California, Berkeley, CA, USA). *J. Chem. Phys. (USA)*, vol.78, no.5, p.2579-84 (1 March 1983).
 In order to explore the feasibility of microwave absorption techniques as a tool for the study of interfaces and electrode reactions, the authors have measured the electrochemical and photochemical properties of ZnO in contact with an aqueous electrolyte by conventional electrochemical procedures and simultaneously by electrodeless detection of microwave absorption at 9.5 GHz in a resonant cavity. Pronounced potential dependent microwave absorption signals were found which proved to be influenced by illumination and electrochemical surface reactions. The comparison of microwave absorption with the electrochemically measured electrode behavior indicates that microwave absorption data can provide interesting complementary information on the nature and reactivity of charge carriers and dipoles in the electrode/electrolyte interface. The proposed method is so sensitive that signals arising from fractions of monolayers will be detectable. A comprehensive interpretation of the results is not yet attempted. Further experimental studies on simple electrode systems are needed to clarify the mechanism. Because of its nondestructive nature, the microwave method could develop into a valuable new technique in surface chemistry. (8 refs.)
- 63583** The effect of the surface state on the hydrogen permeability and the catalytic activity of palladium alloy membranes. N.R.Roshan, A.P.Mishchenko, V.P.Polyakova, N.I.Parenova, E.M.Savitsky, E.A.Voitikhova, V.M.Gryaznov, M.E.Sarylova (A.A. Baikov Inst. of Metall., Acad. of Sci., Moscow, USSR). *J. Less-Common Met. (Switzerland)*, vol.89, no.2, p.423-8 (Feb. 1983). (International Symposium on the Properties and Applications of Metal Hydrides, Tobu, Japan, 30 May-4 June 1982).
 The surface state of an active membrane has a marked effect on its hydrogen permeability and catalytic activity in reactions involving the addition or subtraction of hydrogen. Interactions of organic compounds, oxygen and hydrogen on membrane catalysts produce changes in their surface composition and structure such that the rates of catalytic reactions and hydrogen transfer are altered and carbon migrates into the membrane bulk. Polishing and chemical cleaning of the membrane surface increases the rate of hydrogen transfer through the membrane. Membranes with a porous surface display catalytic activity and hydrogen permeability which are an order of magnitude higher than those of the initial foils. (8 refs.)
- 63584** Effect of the hydrogen concentration on the adsorption and catalytic properties of a Pd-Ru alloy. V.G.Dobrokhotoy, V.M.Gryaznov (A.V. Topchiev Inst. of Petrochem. Synthesis, Moscow, USSR), L.F.Pavlova. *J. Less-Common Met. (Switzerland)*, vol.89, no.2, p.585-6 (Feb. 1983). (International Symposium on the Properties and Applications of Metal Hydrides, Tobu, Japan, 30 May-4 June 1982).
 An increase in the hydrogen concentration in the Pd-Ru alloy increases the adsorption of cyclohexane on the hydrogen-poor α phase and decreases it on the hydrogen-rich β phase. The kinetics of the hydrogenation of benzene to cyclohexane on the α and β phases are different. These phenomena indicate that the adsorbed hydrogen interacts with the hydrocarbon species. (no refs.)
- 63585** Hot atoms and cold facts: mysteries and opportunities in vibration-assisted surface chemistry. C.B.Duke (Xerox Webster Res. Center, Rochester, NY, USA). *J. Electron Spectrosc. & Relat. Phenom. (Netherlands)*, vol.29, p.1-9 (15 Jan. 1983). (Proceedings of the Third International Conference on 'Vibrations at Surfaces', Asilomar, CA, USA, 1-4 Sept. 1982).
 This paper is a synopsis of the keynote lecture at the Third International Conference on Vibrations at Surfaces. The science of hot atoms at surfaces is divided into three broad areas: spectroscopy, theory, and process dynamics. A brief overview of each area is given in which the main advances and mysteries which have emerged during the past few years are noted. The resolution of such mysteries provides the traditional type of opportunity for scientific discovery. Most of the currently visible frontiers lie in the development of applications of the techniques of vibrational spectroscopy, however, so that these scientific opportunities tend to be different in kind than they were a decade ago. Another type of opportunity is the development of hot-atom process technologies. Inspection of current activity reveals that a gap exists between the development of the techniques of vibrational spectroscopy as applied to well-defined model systems and the systematic application of these techniques to examine and extend process technologies based on surface chemistry. Radiation-induced surface chemistry is an example of an area which affords a unique opportunity for surface vibrational spectroscopy and theoretical chemistry to play a significant role in the development of fabrication technologies for electronic devices. This type of opportunity is shown to be particularly important for the future of surface vibrational spectroscopy in the current economic climate for research and development. (86 refs.)
- 63586** Combined vibrational/temperature programmed reaction spectroscopy studies of reaction intermediates on metal surfaces. R.J.Madix (Dept. of Chem. Engng., Stanford Univ., Stanford, CA, USA). *J. Electron Spectrosc. & Relat. Phenom. (Netherlands)*, vol.29, p.25-34 (15 Jan. 1983). (Proceedings of the Third International Conference on 'Vibrations at Surfaces', Asilomar, CA, USA, 1-4 Sept. 1982).
 In many cases temperature programmed reaction spectroscopy (TPRS) and surface vibrational spectroscopy can be effectively combined to yield the

details about the mechanism of surface reactions. When reaction products are evolved from the surface in reaction-limited steps, TPRS is often sufficient to identify the stable reaction intermediates. On the other hand, if product evolution is desorption-limited, vibrational spectroscopy, as well as XPS or UPS, is indispensable for identification of reaction intermediates. In some cases, the two methods complement one another, and both the identity of the intermediate and its orientation can be defined. Examples of the combined use of these techniques are given. Reactions of formic acid and methanol on metal surfaces are discussed. The dehydrogenation of formic acid on Ni (110) forms coadsorbed CO and formate intermediates, leading to abnormal decomposition kinetics of the formate due to lateral interactions. (29 refs.)

63587 Infrared laser stimulated surface processes. T.J.Chuang (IBM Res. Lab., San Jose, CA, USA). *J. Electron Spectrosc. & Relat. Phenom. (Netherlands)*, vol.29, p.125-38 (15 Jan. 1983). (Proceedings of the Third International Conference on 'Vibrations at Surfaces', Asilomar, CA, USA, 1-4 Sept. 1982).
 Gas-surface interactions including the process of chemisorption, the reaction involving the adsorbate and the adsorbent, the formation of reaction products and the desorption of adsorbed species enhanced by infrared laser radiation have been investigated. Specifically, SF_6 and SiF_4 interactions with silicon affected by CO₂ laser pulses, and the infrared photon stimulated desorption of C_2H_5N and C_2D_5N molecules from KCl, Ag (110) and Ag island films have been studied to illustrate the many facets of the vibrationally activated surface processes. Aspects related to surface reaction dynamics and molecular selectivity in photodesorption are discussed. (64 refs.)

63588 The adsorption and dehydrogenation of cyclopentane on Ru (001). F.M.Hoffmann (Exxon Corporate Res., Linden, NJ, USA), E.V.O'Brien, J.Hrbek, R.A.De Paola. *J. Electron Spectrosc. & Relat. Phenom. (Netherlands)*, vol.29, p.301-5 (15 Jan. 1983). (Proceedings of the Third International Conference on 'Vibrations at Surfaces', Asilomar, CA, USA, 1-4 Sept. 1982).
 The adsorption of cyclopentane on Ru (001) has been studied using electron energy loss spectroscopy (EELS) and thermal desorption mass spectroscopy (TDMS). Thermal desorption shows with increasing coverage a chemisorbed first layer desorbing at 180 K with subsequent multilayer formation. The vibrational spectrum of the first chemisorbed layer is characterized by a C-H soft mode at 2610 cm^{-1} . This mode is ascribed to a C-H-metal interaction, which is also responsible for the dehydrogenation to cyclopentene upon annealing to 200 K. It appears that a close geometrical fit between the entire molecule and the metal substrate is not necessary for this type of interaction. Coadsorbed oxygen suppresses the C-H-metal interaction. This is believed to be due to site-blocking or ligand effects of oxygen on the three-fold hollow sites of Ru (001). (10 refs.)

63589 Thermal evolution of C_2H_2 and C_2H_4 on Pd (111) studied by high-resolution electron energy loss spectroscopy. L.L.Kesmodel, J.A.Gates (Phys. Dept., Indiana Univ., Bloomington, IN, USA). *J. Electron Spectrosc. & Relat. Phenom. (Netherlands)*, vol.29, p.307-12 (15 Jan. 1983). (Proceedings of the Third International Conference on 'Vibrations at Surfaces', Asilomar, CA, USA, 1-4 Sept. 1982).
 The thermal evolution of acetylene and ethylene on a palladium (111) surface has been studied by high-resolution electron energy loss spectroscopy in the temperature range 150K-500K. Formation of ethylidyne ($\equiv C-CH_3$) near room temperature is important for both molecules, whereas CH is the major surface hydrocarbon species formed at high temperatures. (12 refs.)

63590 Electron energy loss spectroscopy of the decomposition of formic acid on Ru (001). B.H.Toby (Div. of Chem. & Chem. Engng., California Inst. of Technol., Pasadena, CA, USA), N.R.Avery, A.B.Anton, W.H.Weinberg. *J. Electron Spectrosc. & Relat. Phenom. (Netherlands)*, vol.29, p.317-21 (15 Jan. 1983). (Proceedings of the Third International Conference on 'Vibrations at Surfaces', Asilomar, CA, USA, 1-4 Sept. 1982).
 Electron energy loss spectroscopy has demonstrated the existence of both a monodentate and a symmetric bidentate bridging formate as stable intermediates in the decomposition of formic acid on the Ru (001) surface. The monodentate formate converts upon heating to the bidentate formate which decomposes via two pathways: C-H bond cleavage to yield CO₂ and adsorbed hydrogen; and C-O bond cleavage to yield adsorbed hydrogen, oxygen and CO. Thermal desorption spectra demonstrate the evolution of H₂, H₂O, CO and CO₂ as gaseous products of the decomposition reaction. The observation of this product distribution from Ru (100), Ni (100) and Ni (110) had prompted the proposal of a formic anhydride intermediate, the existence of which is rendered questionable by the spectroscopic results reported. (16 refs.)

63591 Studies of the surface of titanium dioxide. V. Thermal desorption of hydrogen. T.Iwaki (Faculty of Sci., Hiroshima Univ., Hiroshima, Japan). *J. Chem. Soc. Faraday Trans. 1 (GB)*, vol.79, no.1, p.137-46 (Jan. 1983).
 The thermal desorption of hydrogen adsorbed on titanium dioxide has been studied at temperatures between 298 and 1073K by two techniques: (i) temperature-programmed desorption (TPD), and (ii) measuring the hydrogen content. Chemisorption of hydrogen on titanium dioxide took place only when hydrogen was introduced above 623K. The onset of hydrogen desorption occurred at 523K on anatase and 573K on rutile. Anatase gave two H₂ desorption peaks while rutile gave a single broad peak. The hydrogen content on anatase was much larger than that on rutile. On the basis of these results the interaction of hydrogen with titanium dioxide is discussed in connection with the formation of surface hydroxy groups. (28 refs.)

63592 Investigation of precipitated alumina structures by secondary-ion mass spectrometry and electron paramagnetic resonance spectroscopy. III. Structure of an alumina coating precipitated on rutile titanium dioxide. A.S.Hare, J.C.Vickerman (Dept. of Chem., Univ. of Manchester Inst. of Sci. & Technol., Manchester, England). *J. Chem. Soc. Faraday Trans. 1 (GB)*, vol.79, no.1, p.185-93 (Jan. 1983).
 For Pt.II see ibid., vol.77, p.1113 (1981). Deposition of an alumina or alumina-silica coating upon a rutile substrate was achieved satisfactorily in an aqueous precipitation system, which may contain paramagnetic ions coprecipitated at trace levels. Secondary-ion mass spectra of powders extracted during the process are consistent with an independent coating mechanism, i.e. nucleation and growth of the coating occurred at the surface of the rutile particles. The depth distribution of alumina, estimated from secondary-ion mass spectroscopy and etching measurements in the ultimate product, has been confirmed by transmission electron microscopy. Chromium(3+) tracer electron paramagnetic resonance spectra suggest that pseudo-boehmitic sheet growth is well developed in the alumina coating component, even without ageing. (12 refs.)

63593 Infrared study of three butanediols adsorbed on silica immersed in carbon tetrachloride. W. Neagle, C.H. Rochester (Chem. Dept., Univ. of Dundee, Dundee, Scotland).

J. Chem. Soc. Faraday Trans. 1 (GB), vol.79, no.1, p.263-8 (Jan. 1983). Infrared spectra are reported of silica immersed in solutions of butan-2,3-diol, butan-1,3-diol and butan-1,4-diol in carbon tetrachloride. Associative adsorption involved the formation of hydrogen bonds between isolated surface silanol groups and either one or both hydroxy groups in each adsorbed molecule. Increasing the separation of the two hydroxy groups in the series of three diols enhanced the proportion of adsorbed molecules for which both groups interacted with the surface. Multilayer adsorption occurred at high concentrations of the diols in solution. (12 refs.)

63594 The γ irradiation-enhanced corrosion of stainless and mild steels by water in the presence of air, argon and hydrogen. W.G. Burns, W.R. Marsh, W.S. Walters (Chem. Div., AERE, Harwell, England).

Radiat. Phys. & Chem. (GB), vol.21, no.3, p.259-79 (1983). When air-saturated pure water was γ -irradiated in the presence of air to high doses (10^2 - 10^3 Mrad) in sealed stainless steel containers hydrogen and oxygen were formed. The amounts were less than one tenth of the maximum possible for continuous aqueous radiolysis but the increase in oxygen appearing as gas was less than that equivalent to the hydrogen formed from the water present, indicating that metallic corrosion had occurred. In the absence of radiation no change in gas composition was observed. When the air in solution and in the gas space was replaced by argon or by hydrogen, radiolysis and corrosion were virtually suppressed. When the container was made of mild steel or strips of mild steel were initially introduced into a sealed stainless steel container containing air and water, oxygen was consumed on irradiation, and hydrogen was formed, together with a suspended brown oxide. In the absence of radiation oxygen was consumed and hydrogen was formed but both at a lower rate than in the presence of radiation. In this case, unlike the case of stainless steel, the formation of hydrogen was not prevented by replacing the air present with argon. The rate of product formation from either system in the presence of air was found to be proportional to dose-rate, in the range 0.2 - 2 Mrad h^{-1} and mass changes of the solids, when measurable, corresponded to the oxygen deficit in the gas phase if the oxide was taken to be Fe_2O_3 . The effects are greater than hitherto reported. These results are interpreted on the basis of the surface reactions of transient radiolytic products, and product formation is analysed mathematically in terms of a multispecies reaction scheme (33 reactions) involving diffusion to the surface. (22 refs.)

63595 The effect of radiation on the release of corrosion products from 304 stainless steel in high temperature water-II effects of flow rate and duration of corrosion experiment. K. Ishiguro, H. Ikuse, K. Oshima (Dept. of Nuclear Engng., Univ. of Tokyo, Tokyo, Japan), N. Fujita, S. Ono.

Radiat. Phys. & Chem. (GB), vol.21, no.3, p.281-7 (1983).

The effect of γ -radiation on the release of corrosion products from 304 stainless steel was investigated using a small circulation loop at high temperature. It was found the flow rate has a significant effect on the release rate and the release behavior is quite different after long duration of the corrosion experiments from that at early stage. (9 refs.)

63596 The Balloon effect. A quantum chemical model of elementary steps in heterogeneous chemical reactions between simple gases and solid surfaces. H. Muller, C. Opitz (Sektion Chemie, Friedrich-Schiller Univ., Jena, Germany).

Wiss. Z. Friedrich-Schiller-Univ. Jena, Math. Naturwiss. Reihe (Germany), vol.31, no.6, p.885-93 (1982). In German.

Due to lack of knowledge of microscopic reaction steps for many solid reactions the authors describe the chemical attack of simple molecules (A) on single crystal surfaces (FKO) of different solids and discuss, in particular, the activation of the solid caused by the chemisorbed particle (A_{ads}), which results in formation of a surface complex (P_{ads}) by weakening all bonds between the attacked lattice point and the crystal whereby desorption (demetalization) of P_{ads} easily becomes possible ($\rightarrow P_{\text{gas}}$). This mechanism is called the Balloon effect. A number of applications are discussed and a more sophisticated version of this Balloon effect is presented. (9 refs.)

63597 Complex analysis of experimental adsorption data using KRS 4200 and ES 1040 computers. P. Brauer, K.-H. Henneberg, P. Hofer (Friedrich Schiller Univ., Jena, Germany).

Wiss. Z. Friedrich-Schiller-Univ. Jena, Math. Naturwiss. Reihe (Germany), vol.31, no.6, p.1001-5 (1982). In German.

The topics of computer programmes for analysis of adsorption isotherms are described. The programmes allow the phenomenological treatment of isotherms, the evaluation of surface and solid structure parameters and the calculation of adsorption energy distribution functions. (17 refs.)

63598 Thermodynamic values evaluation from adsorption isotherms using KRS 4200 computer. P. Brauer (Sektion Chemie, Friedrich Schiller Univ., Jena, Germany).

Wiss. Z. Friedrich-Schiller-Univ. Jena, Math. Naturwiss. Reihe (Germany), vol.31, no.6, p.1007-16 (1982). In German.

The equations to calculate thermodynamical values of adsorption of gases and vapours on solid surfaces are derived using the usual thermodynamical approach. To evaluate these adsorption values from adsorption isotherms a programme for the computer KRS 4200 is developed and described. This programme is tested by means of a model adsorption system. (13 refs.)

63599 Adsorption and reactive changes of octadecylamine on iron oxide surfaces. H. Hobert, K. Klostermann, H. Wachtel, I. Weber (Friedrich Schiller Univ., Jena, Germany).

Wiss. Z. Friedrich-Schiller-Univ. Jena, Math. Naturwiss. Reihe (Germany), vol.31, no.6, p.1059-63 (1982). In German.

The adsorption of octadecylamine from an aqueous-acetic acid solution gives a saturation concentration on the oxides, which corresponds to two monolayers in the case of Fe_2O_3 but to only one monolayer in the case of Fe_3O_4 . The interaction between octadecylamine and the iron oxides is connected with deamination and oxidation reactions. These reactions give di- and tri-octadecylamine and amid-like oxidation products. (7 refs.)

Proceedings of the Third International Conference on 'Vibrations at Surfaces'

..... See Entry 59532

Kinetics of adsorption on stepped surfaces and the determination of surface diffusion constants See Entry 59706

Matrix isolation spectroscopy. A method for investigation of chemisorption on model systems of metal catalysts. (Construction, building and testing of an apparatus for producing matrix isolated metal atom clusters) See Entry 59854

Vibrational state of chemisorbed molecule on metal surface See Entry 60693

X-ray photoelectron spectroscopy of cadmium arachidate monolayers on various metal surfaces See Entry 60837

A proposed method of hydrogen isotope separation using palladium alloy membranes See Entry 61009

Characteristics of the permeation of hydrogen-inert gas mixtures through a palladium alloy tube wall See Entry 61010

Hydrogen separation from gas mixtures using LaNi_5 pellets See Entry 61567

Hydrogen separation from mixed gas streams using reversible metal hydrides See Entry 61568

Chemical and catalytic effects of ion implantation See Entry 61942

Intermetallic compounds LaNi_5 , $\text{La}_{1-x}\text{Pr}_x\text{Ni}_5$ as sorbents and hydrogenation catalysts ($\text{La} \equiv \text{La, Ce, Pr, Nd, Sm, Gd}$) See Entry 62115

Effects of impurities on hydrogen permeability through palladium alloy membranes at comparatively high pressures and temperatures See Entry 62164

Application of the method of time-lag analysis to the study of diffusion in solids of nonhomogeneous macroscopic structure See Entry 62183

Theoretical vibrational frequencies for NH_x and CH_x reactive intermediates on nickel(100) and nickel(111) surfaces See Entry 62232

An EELS and TDS study of molecular oxygen desorption and decomposition on Pt(111) See Entry 62244

The thermodynamics of the system $\text{CaNi}_2\text{-H}_2$ using differential heat conduction calorimetry See Entry 62250

Phase and bonding transitions in chemisorbed layers studied by vibrational frequency shifts See Entry 62251

High resolution infrared study of hydrogen chemisorbed on Si(100) See Entry 62252

Vibrations spectra of oxygen chemisorbed on nickel (110) surfaces See Entry 62253

Investigation of lateral interactions in chemisorption See Entry 62255

Laser-induced thermal desorption of CO from clean polycrystalline copper: time-of-flight and surface diffusion measurements See Entry 62257

Surface vibration correlation with d-electron (hole) per atom ratio (d-bandfilling) in CO chemisorption on supported transition metal particles: dominance of Hund's rule and d-electron degeneracy in real supported catalysts See Entry 62258

The chemisorption of nitrogen on the (001) surface of ruthenium See Entry 62259

Adsorbate structure modeling based on electron energy loss spectroscopy and lattice dynamical calculations: application to $\text{O}/\text{Al}(111)$ See Entry 62260

Theoretical calculation of vibrations of adsorbed species See Entry 62262

HREELS study of formic acid adsorption on gold (110) and (111) surfaces See Entry 62265

IR spectroscopic and gravimetric investigation of adsorption of acetonitrile on a disperse model glass system See Entry 62277

The application of reflection infrared and surface enhanced Raman spectroscopy to the characterization of chemisorbed organic disulfides on Au See Entry 62979

Infrared spectroscopic investigation of the adsorption of fluoromethane on sodium chloride surfaces under ultra high vacuum See Entry 62983

Surface enhanced Raman scattering of water on an Ag electrode See Entry 62985

EMIRS study of adsorbate bonding in the electrode solution interfacial region See Entry 62986

Spectral properties of pyrazine adsorbed on silver electrodes and cold silver films from surface enhanced Raman scattering (SERS) See Entry 62987

SERS study of pyridine vapor exposed to silver substrates electrochemically prepared See Entry 62988

Study of adsorption at the electrode/solution interphase by in-situ infrared reflectance spectroscopy—adsorption of methanol on a platinum electrode See Entry 62989

Intensity enhancement and spectral change in Raman scattering of mercaptobenzothiazole adsorbed on silver electrode See Entry 62990

High resolution electron energy loss spectroscopic study of the interaction of oxygen with magnesium single crystal surfaces See Entry 63096

Influence of production media on the physicochemical and electrochemical properties of steels See Entry 63430

High-temperatures reactions of metals with gases. II. Kinetics of growth of multiphase chemical compound layers at a metal/gas interface See Entry 63468

Contracted CI calculations of models for catalytic reactions involving transition metals See Entry 63516

The oxidation of methanol on $\text{Cu}(100)$ studied by infrared spectroscopy See Entry 63540

The exposure dependence and emission spectrum of chemiluminescence produced during the oxidation of Si(111) by O_2 See Entry 63556

Laser-induced decomposition of sodium azide See Entry 63557

Hydrogen evolution at LaNi_5 -type alloy electrodes See Entry 63562

Methane formation during deuteron bombardment of carbon in the energy range of 100 to 1500 eV See Entry 63575

Adsorption on heterogeneous surfaces. IX. Evaluation of adsorption energy distribution functions from nitrogen adsorption isotherms on modified aerosols using different numerical methods See Entry 63604

The interaction of acetone and acetonitrile with surface centres of disperse silica See Entry 63605

Investigations of the adsorption behaviour of aliphatic amines on a silica gel surface See Entry 63606

IR spectroscopic investigations on the adsorption of propionic acid and N,N-dimethylformamide on SiO_2 and Al_2O_3 from the liquid phase See Entry 63607

Light-induced generation of hydrogen at CdS -monograin membranes See Entry 63734

82.70 DISPERSE SYSTEMS

(for flow behaviour, see 47.55K)

63600 Structure of a microemulsion in the critical region: neutron small-angle scattering results. J. Tabony, M. Drifford, A. de Geyer (Dept. de Phys.-Chimie, CENS, Gif-sur-Yvette, France).

Chem. Phys. Lett. (Netherlands), vol.96, no.1, p.119-25 (25 March 1983). Neutron small-angle scattering has been used to study the structure of an oil in water microemulsion in the critical region. The structure, one of small 'swollen' micelles, is independent of the critical fluctuations. This together

with other evidence strongly suggests that the latter are clusters of swollen micelles. (15 refs.)

63601 Apparatus for examining the sedimentation stability of a filled polymer [using laser radiation]. N.I.Duvankov, A.V.Vasin, M.A.Fioshina (Mendeleev Inst. of Chem. Technol., Moscow, USSR). *Ind. Lab. (USA)*, vol.48, no.6, p.594-6 (June 1982). Translation of: *Zavod. Lab. (USSR)*, vol.48, no.6, p.58-9 (June 1982). [received: March 1983]
The authors describe an apparatus for examining the stability of filled polymer compositions. The principle is automatic recording of the intensity of the radiation from a laser passing through the specimen in different layers during the mass-transport process. The beam is moved over the specimen in the cell by the reciprocating motion of a refracting prism. The apparatus enables one to measure the characteristics of filled polymers over wide ranges in temperature and degree of filling (0-80% by volume). (13 refs.)

63602 The multistate kinetics of nucleation in the presence of an aerosol. R.McGraw, W.H.Marlow (Dept. of Energy & Environment, Brookhaven Nat. Lab., Upton, NY, USA). *J. Chem. Phys. (USA)*, vol.78, no.5, p.2542-8 (1 March 1983).
The classical Becker-Döring homogeneous nucleation theory is rigorously extended to include monomer and cluster removal mechanisms capable of coupling to the usual Becker-Döring equations for evaporation and growth. Exact expressions are obtained in a compact continued fraction form for the steady state cluster distribution and nucleation rate in the presence of an aerosol. The unmodified classical theory is recovered in the limit of a particle free vapor. Recently proposed models for new particle formation in the presence of an aerosol and nucleation in a nonuniform vapor are shown to be contained within the present formulation. Condensation curves are calculated for a series of model condensable vapor species covering a wide volatility range in the presence of an aerosol. For those vapors having low equilibrium vapor pressures (less than 10^{-5} Torr at the highest aerosol concentrations considered) significant departures from predictions based on the unmodified classical theory are found. (15 refs.)

63603 Segmental motion of alkyl chains grafted on silica gel, studied by neutron scattering. J.P.Beaufils (Inst. Laue-Langevin, Grenoble, France), M.C.Hennion, R.Rosset. *J. Phys. (France)*, vol.44, no.4, p.497-503 (April 1983).
The quasielastic neutron scattering spectra of $C_{12}H_{25}$ grafted on silica are obtained for $n=4, 8, 12, 16, 18, 22$. The well known difficulty in determining the mass in the beam is overcome by using (as a reference) the integrated elastic and quasielastic scattering function, extrapolated to $q=0$. A correction for the coherent scattering contribution is applied. It is thus possible to determine the molar scattering functions of the chains $S_q(q, \omega)$. Assuming that in all chains there is a constant number n_c of end atoms contributing S_m to S_q , the authors obtain $S_m = S_c + (n - n_c) S_m$. This relationship is verified for the elastic incoherent structure factor and used to calculate S_m . The $n=22$ case is left apart, its anomalous behaviour is explained by interaction between neighbouring chains. The data agree with a 3-bonds jump model with a time between jumps equal to 1.9×10^{-11} s at room temperature. (10 refs.)

63604 Adsorption on heterogeneous surfaces. IX. Evaluation of adsorption energy distribution functions from nitrogen adsorption isotherms on modified aerosols using different numerical methods. P.Brauer, W.A.House, M.Jaronec (Friedrich Schiller Univ., Jena, Germany). *Wiss. Z. Friedrich-Schiller-Univ. Jena, Math. Naturwiss. Reihe (Germany)*, vol.31, no.6, p.987-100 (1982). In German.
The adsorption energy distribution functions have been evaluated from nitrogen adsorption data measured on four chemically modified aerosols at 78K. A comparison is made of the distribution functions derived using four different approximate methods and three different exact methods. Although the distributions differ in particular details, the main surface features for a given adsorption system are clearly evident. The more exact distribution functions are found with the HILDA algorithm. A chemical interpretation of the peaks in the HILDA adsorption energy distributions is suggested. (46 refs.)

63605 The interaction of acetone and acetonitrile with surface centres of disperse silica. P.Fink, I.Plötzki, P.Brauer (Sektion Chemie, Friedrich Schiller Univ., Jena, Germany). *Wiss. Z. Friedrich-Schiller-Univ. Jena, Math. Naturwiss. Reihe (Germany)*, vol.31, no.6, p.1031-8 (1982). In German.
The adsorption of acetonitrile and acetone on aerosol samples with different concentration and arrangement of OH groups and modified with trimethylsilyl, BOH and POH groups was investigated by infrared spectroscopy. With the help of acetone and acetonitrile as indicator molecules it is possible to distinguish clearly between the different surface centres. Acetone were able to form 1:2 complexes, acetonitrile only 1:1 complexes with OH groups. A specific interaction was observed between trimethylsilyl groups and acetone and acetonitrile respectively. The adsorption is in a small extent irreversible in the case of acetonitrile on aerosil and of acetone on boric acid modified aerosil. (7 refs.)

63606 Investigations of the adsorption behaviour of aliphatic amines on a silica gel surface. R.Toepel, W.Vogelsberger, G.Rudakoff (Sektion Chemie, Friedrich Schiller Univ., Jena, Germany). *Wiss. Z. Friedrich-Schiller-Univ. Jena, Math. Naturwiss. Reihe (Germany)*, vol.31, no.6, p.1045-52 (1982). In German.
Results about the adsorption of n-propylamine, n-butylamine and triethylamine on both hydrated and dehydrated silica gel surfaces are presented. An interaction between the amine and the free surface hydroxyl groups is found by IR-spectroscopy. This hydrogen bond complex is destroyed in vacuum. Only in the case of n-propylamine the formation of an ionic structure $R-NH_3^+$ on the surface is observed. The formation of the adsorbate complexes depends on the heat treatment of the silica gel, but also on the chain length and the structure of the organic residues present in the amines. (14 refs.)

63607 IR spectroscopic investigations on the adsorption of propionic acid and N,N-dimethylformamide on SiO_2 and Al_2O_3 from the liquid phase. M.Meyer (Sektion Chemie, Friedrich Schiller Univ., Jena, Germany). *Wiss. Z. Friedrich-Schiller-Univ. Jena, Math. Naturwiss. Reihe (Germany)*, vol.31, no.6, p.1053-8 (1982). In German.
The adsorption of propionic acid and N,N-dimethylformamide on SiO_2 and Al_2O_3 from CCl_4 -solution was investigated in situ in a new developed IR cell. During the absorption on SiO_2 the interaction mainly took place about the formation of hydrogen bonds between surface silanol groups and the adsorptives. Propionic acid was chemisorbed on Al_2O_3 as carboxylate which is stable on the surface at 673K. The adsorption of N,N-dimethylformamide on Al_2O_3 led like on SiO_2 to an interaction about hydrogen bonds. After heat treatment at 673K on the Al_2O_3 -surface very stable formate ($HCOO^-$) structures were formed. (5 refs.)

63608 IR spectroscopic investigation of carboxylic acid salts of alkalis and thallium in nonpolar solvents. D.D.Thuc, G.Rudakoff. *Wiss. Z. Friedrich-Schiller-Univ. Jena, Math. Naturwiss. Reihe (Germany)*, vol.31, no.6, p.1099-106 (1982). In German.
Solutions of salts of higher fatty acids in nonpolar solvents have been investigated by IR-spectroscopy. Depending on temperature, the solutions contain micelles, double molecules and ions. Addition of free fatty acids leads to a decay of micelles. During warm-up, the solvents used become air-oxidized. In the reaction soaps act as catalysts. (8 refs.)

Standard radiometer for long-lived radionuclide aerosols See Entry 60557
Low frequency viscoelastic behavior at the sol-gel transition See Entry 61471
Reparameterization of the Becker-Kistiakowsky-Wilson equation of state for water-gel explosives See Entry 61515
Experimental determination of velocity statistical distributions in suspension flows See Entry 61542
Sheared colloidal suspensions See Entry 61544
Direct measurements of aerosol diffusion constants in the intermediate Knudsen regime See Entry 61593
Biaxial nematic phases in amphiphilic systems See Entry 61776
Polymorphism of interfaces [Liquid crystalline phases of amphiphilic molecules] See Entry 61777

Thin colloidal crystals: a series of structural transitions See Entry 62083
IR spectroscopic and gravimetric investigation of adsorption of acetonitrile on a disperse model glass system See Entry 62277
Raman scattering from $Pt(CN)_4^{2-}$ adsorbed on Pt colloids See Entry 62955
Ultimate tensile measurements of filled gelatin gels See Entry 63496

82.80 CHEMICAL ANALYSIS AND RELATED PHYSICAL METHODS OF ANALYSIS

63609 LAMMA—a new approach for the application of lasers in the analysis of bulk material. H.Vogt, H.-J.Heinen, S.Meier (Leybold-Heraeus GmbH, Köln, Germany). *Laser & Optoelektron. (Germany)*, vol.15, no.1, p.23-9 (March 1983). In German.

The analytical potential of mass spectrometry is largely widened if microscopically small areas of a solid sample can selectively be analyzed. Lasers are very advantageous for ion generation from micro areas of the sample. Some basic aspects for the technical realization of a laser microprobe are discussed. The fields of application are demonstrated with a few selected examples. (5 refs.)

63610 Computerised spectrochemical analysis. E.Jagannatham (Mafatal Engineering Industries Ltd., Thane, India). *Electr. India*, vol.22, no.21, p.23-8 (15 Nov. 1982). [received: March 1983]
High speed computerised accuracy in the determination of elemental composition of metals and alloys is a requirement in steel mills, ferrous and non-ferrous foundries and quality control laboratories of metal users and transportation centres. Computerisation of spectrochemical analysis has become necessary and offers abundant facilities to the user. Here emphasis is laid on computerisation without going into the details of the spectrometer itself. However, principles of optical emission spectrometry are dealt with in order to understand the steps of computer operation during analysis. (no refs.)

63611 Elemental analysis performed with the Karlsruhe nuclear microprobe. D.Heck, E.Rokita (Kernforschungszentrum Karlsruhe GmbH, Inst. für Anewandte Kernphys., Karlsruhe, Germany). *IEEE Trans. Nucl. Sci. (USA)*, vol.ns-30, no.2, p.1220-3 (April 1983). (1982 IEEE Conference on the Application of Accelerators in Research and Industry, Denton, TX, USA, 8-10 Nov. 1982).
Proton induced X-rays have been used in the Karlsruhe nuclear microprobe to determine the content of some trace elements in normal and cancerously degenerated human stomach mucosa tissue. A 3 MeV proton beam produced in a single stage Van de Graaff accelerator is focussed down to 3 μm at 600 pA and swept across the specimens in a meandrous pattern. The local mass density of the specimens is determined by the yield of elastically scattered protons, which are registered in a surface barrier detector. Erythrocytes served as test objects to demonstrate the feasibility of the procedure. Specimens of stomach mucosa were prepared by two different methods of fixation. After irradiation the specimens were stained to identify the histological structure. All specimens show rather low structure in elemental concentrations except for iron. No significant shifts in the trace element contents between normal and cancerous stomach mucosa could be observed. (13 refs.)

63612 Chemical history with a nuclear microprobe. C.J.Maggiore, T.M.Benjamin, P.J.Hyde, P.S.Z.Rogers, S.Srinivasan, J.Tesmer (Los Alamos Nat. Lab., Los Alamos, NM, USA), D.S.Woolum, D.S.Burnett. *IEEE Trans. Nucl. Sci. (USA)*, vol.ns-30, no.2, p.1224-7 (April 1983). (1982 IEEE Conference on the Application of Accelerators in Research and Industry, Denton, TX, USA, 8-10 Nov. 1982).
A nuclear microprobe cannot give direct information on the chemical state of an element, but the spatial distribution of elements in a specimen is often determined by the chemical history of the sample. Fuel cells and minerals are examples of complex systems whose elemental distributions are determined by past chemical history. The distribution of catalyst in used fuel cell electrodes provides direct information on the chemical stability of dispersed catalysts under operating conditions. The authors have used spatially resolved Rutherford backscattering to measure the migration of platinum and vanadium from intermetallic catalysts and to determine their suitability for use under the extreme operating conditions found in phosphoric acid fuel cells. Geologic materials are complex, heterogeneous samples with small mineral grains. The trace element distribution within the individual mineral grains and between different mineral phases is sensitive to the details of the mineral formation and history. The spatial resolution and sub-100-ppm sensitivity available with a nuclear microprobe open up several new classes of experiments to the geochemist. Geochemistry and electrochemistry are two areas proving particularly fruitful for application of the nuclear microprobe. (1 ref.)

63613 Helium microprobe analysis of semiconductor materials. J.C.McCallum, C.D.McKenzie (School of Phys., Univ. of Melbourne, Parkville, Victoria, Australia). *IEEE Trans. Nucl. Sci. (USA)*, vol.ns-30, no.2, p.1228-31 (April 1983). (1982 IEEE Conference on the Application of Accelerators in Research and Industry, Denton, TX, USA, 8-10 Nov. 1982).
The Melbourne University nuclear microprobe is described. Recent improvements have enabled beam spot sizes of 1 μm to be obtained. Some applications of the probe to the analysis of semiconductor materials are discussed, in particular the use and map display of channelling over microscopic areas. (14 refs.)

63614 The analysis of fly ash particles with a proton microbeam. R.D.Vis, A.J.J.Bos, V.Valkovic, H.Verheul (Free Univ., Amsterdam, Netherlands).

IEEE Trans. Nucl. Sci. (USA), vol.ns-30, no.2, p.1236-9 (April 1983). (1982 IEEE Conference on the Application of Accelerators in Research and Industry, Denton, TX, USA, 8-10 Nov. 1982).

The use of a proton microbeam for the study of concentration profiles for different elements in single ash particles is reported. (18 refs.)

63615 Trace element mapping of biological tissues using PIXE and XRF. M.Prins, J.A. Van der Hiede (Eindhoven Univ. of Technol., Eindhoven, Netherlands), A.J.Bos, K.Bowen, S.Davies.

IEEE Trans. Nucl. Sci. (USA), vol.ns-30, no.2, p.1243-5 (April 1983). (1982 IEEE Conference on the Application of Accelerators in Research and Industry, Denton, TX, USA, 8-10 Nov. 1982).

For the measurement of the distributions of trace elements concentrations in biological samples the PIXE technique as well as the fluorescence of synchrotron radiation can be applied. At the Eindhoven University of Technology and the Free University of Amsterdam a PIXE microbeam facility has been used for analysis in a scanning mode of biological tissues. At the Synchrotron Radiation Source in Daresbury UK an XRF station for several mm beam sizes, equipped with a graphite mosaic crystal as a monochromator has been built. An X-ray microbeam facility with a silicon concave mirror as a focussing device is in Daresbury under construction. Due to the specific machine features synchrotron radiation is favourite for the analysis of lighter elements with atom number $9 < Z < 25$, while PIXE is more useful for the $K\alpha$ radiation of heavier elements. (6 refs.)

63616 Measurements of trace element concentration profiles across the diameter of human hair with micro-PIXE. A.J.J.Bos, C.C.A.H.Stap, W.J.M.Lenglet, R.D.Vis, V.Valkovic (Natuurkundig Lab., Vrije Univ., Amsterdam, Netherlands).

IEEE Trans. Nucl. Sci. (USA), vol.ns-30, no.2, p.1249-51 (April 1983). (1982 IEEE Conference on the Application of Accelerators in Research and Industry, Denton, TX, USA, 8-10 Nov. 1982).

Trace element distributions across single human hairs using a proton microbeam has been measured to study the origin of these elements in hair. A new way of concentration assignment for micro PIXE making use of both the Proton Induced characteristic X-rays and the Rutherford Backscattered protons is reported. (8 refs.)

63617 Surface spectroscopy using high energy heavy ions. B.L.Doyle, P.S.Peeray (Sandia Nat. Labs., Albuquerque, NM, USA), T.J.Gray, C.L.Cooke, E.Justiniano.

IEEE Trans. Nucl. Sci. (USA), vol.ns-30, no.2, p.1252-4 (April 1983). (1982 IEEE Conference on the Application of Accelerators in Research and Industry, Denton, TX, USA, 8-10 Nov. 1982).

Surface atoms ionized by high energy heavy ions have been detected by time-of-flight and quadrupole mass spectroscopic techniques. The experimental arrangements are described and potential applications are suggested. Both techniques are demonstrated to produce significant improvements in the detection of atomic hydrogen, with the TOF method producing a nine order of magnitude increase in the sensitivity of atomic hydrogen compared to standard nuclear analysis methods. (14 refs.)

63618 Quantitative X-ray phase analysis of R-Co alloys. V.A.Lyubushkin, L.M.Lyubushkina, I.D.Vetoshkin (Irkutsk State Teacher Training Inst., USSR).

Ind. Lab. (USSR), vol.48, no.6, p.578-80 (June 1982). Translation of: *Zavod. Lab. (USSR)*, vol.48, no.6, p.46-8 (June 1982). [received: March 1983]

The authors test the method of quantitative X-ray phase analysis of R-Co alloys using two-phase ($\text{RCO}_2\text{-R}_2\text{Co}_{17}$) alloys of Sm-Co and Pr-Co with known compositions and concentrations. The results are found to be in good agreement with metallographic and magnetic analyses. (3 refs.)

63619 Statistical analysis of the error of concentration measurements using an electron-probe microanalyzer. L.I.Erokhin, B.K.Akimov (Tula Polytech. Inst., Tula, USSR).

Ind. Lab. (USSR), vol.48, no.6, p.584-6 (June 1982). Translation of: *Zavod. Lab. (USSR)*, vol.48, no.6, p.50-2 (June 1982). [received: March 1983] (5 refs.)

63620 Installation for preparing samples for radioisotope-excited X-ray fluorescence analysis. V.A.Belyakov, V.I.Luk'yanova, G.A.Ivanyukovich (Sadon Lead-Zinc Combine, USSR).

Ind. Lab. (USSR), vol.48, no.6, p.623-5 (June 1982). Translation of: *Zavod. Lab. (USSR)*, vol.48, no.6, p.90-1 (June 1982). [received: March 1983]

The authors devised an installation for preparing samples incorporating vacuum filtering which is used in a system of radioisotope-excited X-ray fluorescence analysis in the inspection of the composition of ore concentrates, classifier discharge, and tailings. The installation is a rotating drum in which three vacuum filters are mounted; these are at the same time cassettes for samples. The installation has the following additional equipment: electric motor, sample cutoff with slurry conduit, funnel for washing off filter cake, settling tank connected to the vacuum system of the plant, and protective jacket. (1 ref.)

63621 Determining the saturated-vapor pressure of lead by the total-absorption method. V.G.Muradov, Yu.N.Kudryavtsev, O.N.Muradova.

J. Appl. Spectrosc. (USSR), vol.36, no.5, p.481-4 (May 1982). Translation of: *Zh. Prikl. Spektrosk. (USSR)*, vol.36, no.5, p.709-12 (May 1982). [received: Feb. 1983]

Using the basic resonance line PbI 283.3 nm the authors present the results of determining the partial pressure of lead atoms (p_{Pb}) by the total-absorption method. (7 refs.)

63622 Methods of spectral analysis with laser selection of the sample and its vaporization in arc discharges. M.L.Petukh, V.D.Satsunkevich, A.A.Yankovskii.

J. Appl. Spectrosc. (USSR), vol.36, no.5, p.485-8 (May 1982). Translation of: *Zh. Prikl. Spektrosk. (USSR)*, vol.36, no.5, p.712-17 (May 1982). [received: Feb. 1983]

Laser spectral analysis is often undertaken with devices in which the analytical sample is simultaneously acted upon by both laser radiation and electrical discharges. When focused laser radiation acts on the sample, scattering of the sample occurs, with the formation of a plasma cloud. In an electrical discharge induced by a laser plasma, additional vaporization of the sample occurs, together with the excitation of its spectrum. In the Korall-1 device used by the authors and intended for spectral analysis with laser selection of the sample, no synchronization of the laser and electrical pulses is required. In consequence, the analysis may be performed by methods of simultaneous, sequential, and separate selection and vaporization of the sample. The authors investigate and describe these methods. (9 refs.)

63623 System for identification of individual components in mixtures on the basis of Shpol'skii spectra. M.M.Pugovkin, G.A.Oik'khovik, O.N.Vylegzhanin.

J. Appl. Spectrosc. (USSR), vol.36, no.5, p.536-9 (May 1982). Translation of: *Zh. Prikl. Spektrosk. (USSR)*, vol.36, no.5, p.766-70 (May 1982). [received: Feb. 1983]

Describes a program system for working up quasi-line spectra of complex mixtures with the aim of identifying individual compounds in the mixtures. The system consists of a bank of spectra of 100 aromatic and heterocyclic compounds that are given in the atlas, plus a search and identification program. The bank of reference spectra is organized in the form of a sequential-access file on a magnetic disk. The record corresponding to one particular reference spectrum contains codes of the following data: index number of the document, index number of the substance in the catalog, empirical formula and name of compound, type of spectrum fluorescence or phosphorescence, excitation wavelength, type of instrument, and type of solvent. All these codes can serve as keywords, and the search program with respect to the proposed question selects the spectra in the catalog on the basis of any of these keys and also on the basis of any combination of keys. The file of reference spectra consists of 975 recordings of variable length, and it contains the complete set of radiation lines of the spectra without any accounting for their intensities. (7 refs.)

63624 X-ray microanalysis of nitrogen in presence of titanium with an automated electron microprobe. A.Armigliato, L.Dori, A.Garulli, P.Venturi (Istituto Lamel, CNR, Bologna, Italy).

J. Microsc. & Spectrosc. Electron. (France), vol.7, no.6, p.593-603 (Dec. 1982).

The X-ray analysis of nitrogen is particularly difficult when titanium is also present in the specimen to be analyzed; due to the well known interference between the $\text{N}K\alpha$ and the $\text{Ti}L$ lines. A few methods of subtraction of the $\text{N}K\alpha$ line from the experimental peak are discussed which can be used on the computer of an automated electron microprobe. As an example, the application of these methods to the analysis of TiN_xO_y films on silicon is reported. (14 refs.)

63625 Isotopic analysis of nanomole gas samples by means of dynamic flow mass spectrometry. S.Halas (Inst. of Phys., Marie Curie-Skłodowska Univ., Lublin, Poland), H.R.Krouse.

Rev. Sci. Instrum. (USA), vol.54, no.4, p.437-43 (April 1983).

The sample size for conventional double collector isotope mass spectrometry has been reduced more than three orders of magnitude by using a 'pushing' gas for precise stabilization of sample pressure. The sample is stored in a long microcontainer (50 cm, 0.5 mm i.d.) to moderate the effect of diffusive mixing of sample with the pushing gas. If the analysis is sufficiently rapid (e.g. a run of 1 min for the unknown sample between two runs on the standard), then almost total sample consumption is possible. This method retains the high precision and simplicity of dynamic flow, yet possesses the high sensitivity of static mass spectrometry. (16 refs.)

63626 Electrode material for high-temperature oxygen partial pressure electrochemical sensors: strontium-doped lanthanum chromite. G.B.Barbi (Comm. of the European Communities, Joint Res. Centre, Ispra, Italy), A.Casiraghi, C.M.Mari.

Rev. Sci. Instrum. (USA), vol.54, no.4, p.486-92 (April 1983).

The electrochemical behavior of 20% strontium-doped lanthanum chromite (SDLC), deposited onto an 8% yttria-stabilized zirconia (YSZ) solid electrolyte, has been investigated. The electromotive force developed across the interface SDLC/YSZ and a Pt/YSZ reference at 0.21 atm (air) corresponds to the Nernst theoretical relationship. This behavior has been tested between 700° and 1000°C in the range 10^{-5} and 10^{-13} - 10^{-20} atm of oxygen, the lower pressures by the equilibrium of carefully calibrated steam and hydrogen mixtures. Although not demonstrated, it is probable that the oxygen pressure range of applicability of this mixed oxide electrode covers the entire field of pure ionic conductivity of any zirconia-base electrolyte. The fair agreement between the measured values and the theoretical EMF values, the resistance of the electrode layer to scaling, as well as its good thermodynamic stability, suggest SDLC as a possible alternative to platinum in high-temperature oxygen pressure sensors. (24 refs.)

63627 Particle induced X-ray emission (PIXE) analysis using RIKEN heavy ion linac. K.Maeda, Y.Sasa, S.Nakamura, M.Uda (Inst. of Phys. & Chem. Res., Saitama, Japan).

Rep. Inst. Phys. & Chem. Res. (Japan), vol.58, no.6, p.117-21 (1982). In Japanese.

Preliminary experiments for particle induced X-ray emission (PIXE) analysis using heavy ions accelerated by RILAC (RIKEN heavy ion linac) were carried out. The experiments proved that the RILAC can be used for RIXE analysis. (6 refs.)

63628 Attachment of low-energy electrons to O_2 molecules in some gases and liquids: an instrument for measuring concentrations of electronegative impurities in gases. A.S.Barabash, A.A.Golubev, O.V.Kazachenko, B.M.Ovchinnikov (Inst. of Nuclear Res., Acad. of Sci., Moscow, USSR).

Sov. Phys.-Tech. Phys. (USSR), vol.27, no.10, p.1261-6 (Oct. 1982). Translation of: *Zh. Tekh. Fiz. (USSR)*, vol.52, no.10, p.2054-62 (Oct. 1982). [received: April 1983]

The attachment coefficients of electrons to O_2 molecules are measured in the following gases: Ar, CH_4 , 90% Ar+10% CH_4 , 50% Ar+50% CH_4 , and 95% Ar+5% NH_3 for pressures 3-12 kg/cm² and $E/P \leq 0.5$, and in liquid argon for $E=0.2-2$ kV/cm. An electron trap detector is described which produces a nearly spherical electric field and has an oxygen sensitivity in gaseous argon equal to 5×10^{-8} (by volume). It is shown that the sensitivity of electron trap detectors can be significantly increased by adding gases such as CH_4 , NH_3 , C_2H_6 , etc., to the sample. (26 refs.)

63629 Electroanalytical glucose sensor. U.Gebhardt, G.Luft, K.Mund, W.Preidel, G.J.Richter (Siemens AG, Erlangen, Germany).

Siemens Forsch. & Entwicklungsber. (Germany), vol.12, no.2, p.91-5 (1983). An artificial pancreas consists of an insulin depot, a dosage unit and a glucose sensor. The measurement of the actual glucose concentration in blood is still an unsolved problem. Two methods are described for an electroanalytical glucose sensor. Under the interfering action of amino acids and urea in-vitro measurements show an error of between 10% and 20%. (4 refs.)

63630 AES investigations of chemical composition of some alkali compounds. P.Dolizy, F.Grolier (Lab. d'Electronique et de Phys. Appl., Limeil-Brevannes, France).

Surf. & Interface Anal. (GB), vol.5, no.1, p.4-12 (Feb. 1983).

Auger electron spectroscopy is used as a quantitative and qualitative tool to investigate solid surfaces. Conventional quantitative analyses are based on the comparison of the Auger signal from the sample to that from pure standard. A detailed analysis of peak shape of Auger signal shows that the upper part of the derived Auger line (lower energy side) is strongly related to the chemical bonding whereas the lower part (high energy side) is nearly insensitive to the chemical effects. A calibration method for quantitative Auger spectro-

scopy based on the amplitude variation of the LVV Auger transitions of one element as a function of its chemical bonding within the compound is described. This method takes into account sample 'matrix' effects as well as all kinds of instrumental effects on the measured Auger signal. It has also been shown that AES can be used to make successful chemical analyses on alkali antimonides. A direct relation between electronic charge transfer between atoms and Auger peak shape has been observed, it is used to relate photoelectric quantum yield of SbK_x compound to the ionicity of the Sb-K bond. (33 refs.)

63631 Foundations, models and judgement of ionisation-smoke-detectors. I. Introduction and operating method. G.Meyer (Friedrich Merk-Telefonbau GmbH, Munchen, Germany).

Tech. Mess. (Germany), vol.50, no.3, p.93-7 (March 1983). In German. Describes the principle of smoke-sensitive I-chambers and introduces a theoretical model for the derivation of I-V-characteristics. With simple approximations the effect of influence quantities is discussed. A summary of various criteria for judging ionisation-smoke-detectors is presented. (no refs.)

63632 The application of plasma mass spectroscopy to plasma etching. K.M.Eisele (Fraunhofer-Inst. für Angewandte Festkörperphys., Freiburg, Germany).

Vak.-Tech. (Germany), vol.32, no.2, p.48-52 (March 1983). In German.

The mass spectrometer as used for residual gas analysis is often employed to gain insight into plasma processes, for instance when sputtering or plasma etching. In Plasma etching the gases used are of complex, mostly molecular structure and sometimes mixtures of several gases, which are excited and partially fractured in a glow discharge. The mass distribution of the resulting components is being changed when they pass through the ionizer which precedes the quadrupole mass filter. A plasma mass spectrometer does not require such an ionizer. It therefore does not change the composition of the constituents and provides more accurate information about the etch process. Some examples will demonstrate its application. (6 refs.)

63633 On the analysis of inhomogeneous glasses with the electron microprobe. H.Reiss, L.Horn, H.Bruhl (Sektion Chemie, Friedrich Schiller Univ., Jena, Germany).

Wiss. Z. Friedrich-Schiller-Univ. Jena, Math. Naturwiss. Reihe (Germany), vol.31, no.6, p.1131-7 (1982). In German.

There are different problems in quantitative electron microprobe analysis of microphases or crystalline inhomogeneities in glasses. The diameter of the inhomogeneities may be too small and in the case of metastable separation the distance between the droplets too low. Such problems are illustrated graphically and proved by examples. An additional error results from penetration of primary electrons in glasses, generally consisting of light elements. (3 refs.)

Proceedings of the Third International Conference on 'Vibrations at Surfaces' See Entry 59532

Three-dimensional profiling with the Sandia nuclear microprobe See Entry 59882

Imaging XPS—a new technique. I. Principles See Entry 59891

Secondary electron imaging as an aid to STEM microanalysis See Entry 59893

Using the 'C' programming language for interface control See Entry 59901

Microbeam analysis of a Commercial Advanced Gas Cooled Reactor material See Entry 60233

SIMS depth profiling studies of spene-based ceramics and glass ceramics leached in synthetic groundwater See Entry 60278

Liquid chromatography in migration studies See Entry 60318

An application of SIMS to fusion energy research determination of ion impact desorption cross sections See Entry 60392

Measurement of iodine-129 at the femtogram level by negative surface ionization mass spectrometry See Entry 60480

Laser-saturated fluorescence measurements of OH concentration in flames See Entry 60782

X-ray photoelectron spectroscopy of cadmium arachidate monolayers on various metal surfaces See Entry 60837

Two-photon ionization. Capability of lasers for trace analysis See Entry 60876

Difference-frequency as a tunable source for detection of free radicals See Entry 61223

Investigation of sintering activator distribution in refractory materials by means of an X-ray microanalyzer See Entry 61312

Mass spectroscopic study of precursors in a nitrogen-filled electrical shock tube See Entry 61601

Molecular composition of zinc-germanium diphosphide vapour See Entry 62078

Study of the vaporization of solid AIs See Entry 62081

Magnetochemical study of titanium dioxide doped with tantalum pentoxide See Entry 62545

IR reflection investigation of corrosion of optical glasses See Entry 63005

Raman spectroscopic investigations of polymethine dyes See Entry 63006

Indirect determination of the single loss function from plural scattering data See Entry 63112

Anodic oxidation of GaAs in oxygen plasma and qualitative analysis of anodic oxide films by AES and XPS See Entry 63439

Nature of the carboxylate species incorporated in anodic alumina films formed in oxalic acid solution See Entry 63470

Home resources serving to develop Auger and SIMS spectrometers for thin-film and surface analytical tests See Entry 63473

Fundamentals of the surface-analytical methods AES/SAM, ESCA (XPS), SIMS, and ISS in comparison with X-ray microanalysis and their application for material testing See Entry 63488

Stereochemical rearrangements of complexes in liquid crystals See Entry 63544

Reactions induced by ion bombardment of solid cyclohexane at 77K See Entry 63567

Hot atoms and cold facts: mysteries and opportunities in vibration-assisted surface chemistry See Entry 63585

Investigation of precipitated alumina structures by secondary-ion mass spectrometry and electron paramagnetic resonance spectrometry. III. Structure of an alumina coating precipitated on rutile titanium dioxide See Entry 63592

IR spectroscopic investigations on the adsorption of propionic acid and N_2N -dimethylformamide on SiO_2 and Al_2O_3 from the liquid phase See Entry 63607

Regional silver content of radiographic film determined by X-ray fluorescence compared with optical densitometry See Entry 63947

Feasibility of noninvasive analysis of lead in the human tibia by soft X-ray fluorescence See Entry 63948

Coal analysis by nuclear methods See Entry 64246

In-situ analysis of coal by measurement of neutron-induced prompt γ -rays See Entry 64247

Multi-element analysis of coal during borehole logging by measurement of prompt γ -rays from thermal neutron capture See Entry 64248

Nuclear geophysics in prospecting, exploration and development of oil and gas fields See Entry 64249

Advances in gamma-gamma logging See Entry 64252

82.90 OTHER TOPICS IN PHYSICAL CHEMISTRY

States of Am in aqueous solution See Entry 60582

86.00 ENERGY RESEARCH AND ENVIRONMENTAL SCIENCE

86.10 ENERGY RESOURCES AND THEIR UTILISATION

(inc. economic aspects; for nuclear engineering and nuclear power studies, see 28.00)

86.10B Fossil and other fuels

63634 Methane as the energy supply from peripheral resources coal and natural gas. L.Biondi.

Elettrotecnica (Italy), vol.69, no.12, p.1151-2 (Dec. 1982). In Italian.

The paper gives some information on work carried out in Italy. It was a study concerned with diminishing energy supplies and the problems involved in transporting energy over appreciable distances and also of storing energy sources. Much energy at present is derived from coal, hydro sources and oil and is then converted into electricity. Attention was paid particularly to the possibilities of using methane, often a by product of coal and natural gas. The transport and storing of this offers interesting possibilities and the paper states that more attention should be paid to the gasification of coal to obtain methane prior to burning as at present. Various alternative methane producing systems are mentioned, together with their basic working systems. (no refs.) G.V.D.

63635 The properties of a metal hydride fuel for use in an urban vehicle. D.H.Bradhurst, P.M.Heuer (Lucas Heights Res. Labs., CSIRO, Sutherland, NSW, Australia), H.C.Watson, E.E.Milkins, J.Edsell, W.R.B.Martin, A.Kempf.

J. Less-Common Met. (Switzerland), vol.89, no.2, p.575-83 (Feb. 1983). (International Symposium on the Properties and Applications of Metal Hydrides, Toba, Japan, 30 May-4 June 1982).

Fe-Ti-Mn alloys were evaluated for use for the storage of hydrogen fuel in a demonstration urban vehicle. The activation and poisoning characteristics of the alloys were studied with the aim of both minimizing the operating temperatures and pressures and reducing the overall weight of the fuel storage assembly. Alloy structures were studied by metallography, X-ray and neutron diffraction and electron microprobe analysis. Small amounts of magnetic Fe_2Ti impurity and an oxygen-rich phase found by these methods did not seriously affect the hydrogen capacity of the alloys. The vehicle was equipped with a four-cylinder internal combustion engine which has been successfully modified to run smoothly on hydrogen fuel. Water injection was needed for satisfactory operation at power levels in excess of 20 kW, but satisfactory operation could be achieved at lower powers by using a modified inlet valve, a dual manifold system and other modifications to the ignition, valve timing and engine tolerances. (7 refs.)

Performance comparison of 15- and 165-tpd Texaco coal gasifiers See Entry 63721

Development of hydrides for motor vehicles See Entry 63741

Accumulation of fossil fuels and metallic minerals in active and ancient rift lakes See Entry 64095

86.10D Wind energy

63636 Mathematical programming models for the economic design and assessment of wind energy conversion systems. K.A.Reinert (Granville Corp., Washington, DC, USA).

Wind Eng. (GB), vol.7, no.1, p.43-59 (1983).

System reliability is one of the important determinants of the economic and technical feasibility of wind energy conversion systems. The inclusion of storage facilities into these systems greatly increases their reliability. Recognizing this, two inter-period mathematical programming models are formulated which optimize the design of a wind energy conversion system, locating wind turbines in a number of distinct arrays, sizing a storage facility, providing rules for the operation of the storage facility, and ensuring that a pre-specified level of demand is met. In both models, the storage facility is modeled via linear decision rules. In the second model, system reliability is explicitly addressed via chance constraints, and demand is met with a given level of probability. (15 refs.)

63637 Proposal for a new design of wind power generator. H.H.Rosenbrock (Control Systems Centre, Univ. of Manchester Inst. of Sci. & Technol., Manchester, England).

Wind Eng. (GB), vol.7, no.1, p.60-3 (1983). (no refs.)

63638 Agriculture wind energy applications analysis. J.P.Wagner (Dev. Planning & Res. Associates Inc., Manhattan, KS, USA).

Int. J. Ambient Energy (GB), vol.3, no.4, p.207-12 (Oct. 1982). [received: March 1983]

Contains simulation model results for a sample agricultural wind energy application which depicts a hypothetical winter wheat and sorghum farm. (1 rel.)

86.10F Tidal and flow energy

(inc. water-wave energy)

- 63639 Hydro-electricity in India.** J.J.De Lima, H.Dickinson, H.W. Whittington (Dept. of Electrical Engng., Univ. of Edinburgh, Edinburgh, Scotland). Seventeenth Universities Power Engineering Conference, Manchester, England, 30 March-1 April 1982 (Manchester, England: Univ. Manchester Inst. Sci. Technol. 1982), 6 pp.
Although the paper is concerned with the role of hydro-electric generation, it sets this in context by reviewing briefly the contribution of other sources. The potential of India's large river system is surveyed, with the historical development of water power, present trends and future prospects. (6 refs.)

86.10H Geothermal energy

- 63640 A forecast of geothermal drilling activity.** A.J.Mansure, G.L.Brown (BDM Corp., Albuquerque, NM, USA). *Geothermal Energy (USA)*, vol.10, no.11, p.8-18 (Nov. 1982). Estimates the number of geothermal wells to be drilled in the United States for each 5-year period to 2000 AD. The report presents forecasts of the growth of geothermally supplied electric power. The report then quantifies the different types of geothermal wells needed to support the forecasted capacity. The rate of growth of electric capacity at geothermal resource areas is expected to be 15 to 25 percent per year (after an initial critical size is reached) until natural or economic limits are approached. Five resource areas in the United States should grow to significant capacity by the end of the century. The best estimates of the number of wells that must be drilled in each 5-year period to support the electric capacity are given. About 5000 geothermal wells are expected to be drilled in support of all electric power projects in the United States from 1981 to 2000 AD. The reported numbers include production, exploration, injection, and replacement wells and take into account drilling other resource areas. The Geysers area is expected to retain most of the drilling activity for the next 5 years. By the 1990s, the Imperial Valley is expected to contain most of the drilling activity with the result that half of the geothermal wells drilled in the next 20 years will be in the Imperial Valley. (19 refs.)

- 63641 L'énergie géothermique a basse enthalpie pour le chauffage des locaux** (The geothermic energy based on enthalpy for district heating). M.Villaume.

Report EUR 7802 FR, Comm. European Communities, Luxembourg (1982), 92 pp. In French. Contract 584-78 EGF.

Some of the parameters affecting geothermal energy development, principally the effect of borehole yield and temperature, and the power of the heat-pump are discussed. The effects of climate and intercore systems are noted. The production and application systems are first examined theoretically, and the effect of costs under various headings on profitability are studied. The results are presented in graphical form.

- 63642 Faisabilité technique et économique de la géothermie basse énergie en Europe** (Technical and economic feasibility of deep geothermal energy in Europe).

Report EUR 8241/I FR, Comm. European Communities, Luxembourg (1982), xiv+264 pp. In French. Contract 640-78 EGF.

The practicability of using low energy (30°C to 150°C) geothermal energy in Europe, and already exploited for 10 years in France, is examined. Investigates the possible geothermal sites, gives an inventory of potential resources and an economic balance-sheet. The applications of such sources (not suitable to power generation) in district heating, agriculture, industry and fish farming are discussed.

86.10K Solar energy

- 63643 Effect of solar gain through walls and windows on annual building heat needs.** M.G.Davies (Dept. of Building Engng., Univ. of Liverpool, Liverpool, England).

Int. J. Ambient Energy (GB), vol.3, no.4, p.181-6 (Oct. 1982). [received: March 1983]

A window with an open south facing aspect (in the United Kingdom) can admit large solar gains in cold but sunny conditions and will then reduce the need for back-up heating. In cold overcast conditions the same window will cause a bigger demand to be placed upon the heating plant. The net energy need depends upon the local climate, the comfort temperature chosen, ventilation losses and the design of the window or glazed wall. A study is reported using 50 years of jointly occurring daily values of temperature and irradiance at 53.4°N. A rank order is suggested for the effectiveness of various constructions as energy saving components. (4 refs.)

- 63644 Study of water heating by solar energy through the ground.** M.Soulas, Hladik J. (Lab. d'Energetique Solaire, Univ. d'Angers, Angers, France), G.Le Palec, M.Daguene.

Entropie (France), vol.19, no.109, p.32-5 (1983). In French.

Studies the heating of water flowing vertically through the ground the surface of which is irradiated by the incident solar flux. The authors calculate analytically the temperature profile as a function of depth and time, and compare the results with their experience. (7 refs.)

- 63645 Comparison of annual passive systems efficiencies in the Mediterranean zone.** E.Tasdemiroglu (MTA, Ankara, Turkey), F.Ramos, D.Tinaut.

Opt. Pura & Apl. (Spain), vol.15, no.3, p.115-18 (1982).

An experimental evaluation of thermal performance of a thermic accumulation wall is made with the construction of a dwelling in the 'Solar Energy Thermic Applications Center' of MTA (Marmaris). The annual energy balances of the house were established with the aid of computer simulation programs of CSIC. Finally, a comparison of annual energy balances of the CNRS solar house of Odello was made with Marmaris house, the differences between both houses being interpreted in accordance with the structural characteristic of dwellings, the geographical situation and meteorological conditions. (7 refs.)

- 63646 Economical analysis of residential solar water heating systems.** G.Barcelo, R.Urculo (Installation Engng. Consultant Office, Madrid, Spain), E.Tasdemiroglu.

Opt. Pura & Apl. (Spain), vol.15, no.3, p.147-61 (1982).

This study analyzes the economic feasibility of residential solar water heating systems. Different conventional installations, using different fuels (butane, electricity, fuel oil), are compared with solar energy installations. Three economic/technical models which include the influence of increasing fuel cost are presented and compared with other possible kinds of investments to determine the economic feasibility of the system. It is found that different economic conclusions are possible and justifiable for investment situations having differ-

ent constraints. The results of the present study would be a sufficient documental base so as to set the decisions within the alternative solutions of national energy policy. (8 refs.)

- 63647 Solar heating of a tank at an aquiculture pilot plant.** R.Palmer, J.Riera, A.Calera (Dept. de Física, EITI, Valencia, Spain), D.Tinaut.

Opt. Pura & Apl. (Spain), vol.15, no.3, p.163-7 (1982). In French.

A solar heating installation is reported in which solar energy is applied in an aquiculture pilot plant where a constant thermal level during the entire year must be maintained. By using solar storage as the heat source for the biological basin, the resulting lower storage temperatures should allow higher collection efficiencies. Description and operation of the experimental installation is discussed. (5 refs.)

- 63648 Lambertian analysis of mirrors and Fresnel lenses for solar concentration.** A.Luque, E.Lorenzo (Inst. de Energia Solar, Univ. Politécnica Madrid, Madrid, Spain).

Fourth E.C. Photovoltaic Solar Energy Conference. Proceedings of the International Conference, Stresa, Italy, 10-14 May 1982 (Dordrecht, Netherlands: Reidel 1982), p.666-70

Concentrators for extended sources useful for tracking and quasi-static applications are analysed, based on the idea that maximum energy on the collector is cast if the concentrator illuminated by the source becomes a Lambertian source. It is demonstrated that the achievement of this condition is not compatible with the condition of casting on the collector all the energy entering the concentrator. Different analysis of concentrators are presented based on these ideas. (7 refs.)

- 63649 A 500 W_{PK} photovoltaic concentrator using a glass laminated metal membrane reflector.** W.Haaf, K.Hagenlocher.

Fourth E.C. Photovoltaic Solar Energy Conference. Proceedings of the International Conference, Stresa, Italy, 10-14 May 1982 (Dordrecht, Netherlands: Reidel 1982), p.677-81

A 3 m diameter parabolic dish has been constructed. The reflector shape has been chosen such as to give a most homogeneous intensity distribution for a geometric concentration ratio of C=50. As converter a C50 generator using new monocrystalline Si concentrator cells has been developed. The system is placed in polar position and tracked by driving one axis. The generator drives a consumer water pump and feeds two batteries as a buffer storage for tracking, closed water circuit cooling, and electronic control. Outdoor tests have been started. (no refs.)

- 63650 Fluorescent planar concentrator (FPC) Monte-Carlo computer model limit efficiency and latest experimental results.** K.Heidler, A.Goetzberger, V.Wittwer (Fraunhofer-Inst. für Solare Energiesysteme, Freiburg, Germany).

Fourth E.C. Photovoltaic Solar Energy Conference. Proceedings of the International Conference, Stresa, Italy, 10-14 May 1982 (Dordrecht, Netherlands: Reidel 1982), p.682-6

A Monte-Carlo computer model for simulation and optimization of fluorescent concentrators is described. The program calculates absolute efficiencies 'ab initio'; agreement between simulated and experimental data is good. Power flow diagrams and optimization characteristics for single sheet collectors and collector stacks are discussed. It is shown that stacking of up to three sheets does not degrade the concentration ratio. For a 'realistic-ideal' three-sheet collector stack, 9% electrical efficiency at an optical concentration ratio of 10 is derived as a conservative upper limit for the conversion of solar radiation into electrical energy by a photovoltaic FPC-system. Presently the best experimental values for a right angle triangle with 400 cm² area and 3 mm thickness are 9% optical and 2% total electrical efficiency with Si-solar cells. The concentration ratio at the output edge is 2.9. For a three sheet stack an electrical efficiency of 3.1% could be reached. (11 refs.)

Second-stage concentrators—a new formalism See Entry 61254

Greenhouses on building roofs using heat from ventilating air See Entry 63654

750 suns concentrator modules using GaAs solar cells See Entry 63683

High performance evacuated solar collectors—design, applications and viability See Entry 63724

Using solar energy to heat water in low income housing See Entry 63725

Planar solar reflectors See Entry 63726

86.10N Nuclear energy

- 63651 Electricity generating costs when changing from the PWR to the APWR.** W.Seifritz, P.Wydlar (Inst. für Reaktorforschung, Wurenlingen, Switzerland).

Atomwirtsch.-Atomtech. (Germany), vol.28, no.1, p.28-31 (Jan. 1983). In German.

There has been a great deal of discussion recently about the advanced pressurized water reactor as a successor to the present line of pressurized water reactors prior to the introduction of the fast breeder line. The basic underlying idea is the rise in the conversion ratio to 0.9-0.95 by means of spectrum hardening achieved as a result of a reduced moderator fraction. Aside from all technical problems it is assumed that an advanced pressurized water reactor is technically feasible and will be licensed. For a utility company the first question arising is that of the reduction of costs of a kilowatt-hour of electricity generated in the advanced reactor as against a classic pressurized water reactor. More specifically, the point of interest is the uranium price level from which an advanced pressurized water reactor with its higher conversion ratio is able to reduce the electricity generating costs compared to a present pressurized water reactor. (5 refs.)

- 63652 World resources of natural uranium.** M.V.Ziegler, E.Bertel.

Tech. Mod. (France), vol.74, no.11-12, p.29-36 (Nov.-Dec. 1982). In French. [received: March 1983]

Uranium ore is distributed very widely (but not uniformly) throughout the world, and deposits are frequently discontinuous. Following a brief geological note, and definitions of resource categories, some tabulated figures for the principal world sources are given. The recovery efforts made in the main exploiting countries are reviewed, and the final section deals with consumption and demand, and factors affecting the market. (no refs.) J.S.

- 63653 The place for fast breeders in the French energy situation.** J.Petit, L.Vautrey (CENS, Gif-sur-Yvette, France).

Proceedings of the L.M.F.B.R. Safety Topical Meeting, Lyon-Ecully, France, 19-23 July 1982 (Paris, France: Société Française d'Energie Nucleaire 1982), p.95-101 In French.

France is poorly situated regarding indigenous supplies of fossil fuels; in 1980, 98% of oil consumed was imported, 70% of the gas and 56% of the coal. With this background, electricity generation has shown a sharp decrease in the oil fraction, a rise in nuclear and 'new' sources (solar, biomass, geothermal, wind, waves), with coal and hydro more or less the same. As recent generating costs quoted are 16, 26 and 56 centimes/kWh for nuclear, coal

and oil respectively, there is a strong economic incentive for nuclear. The programme up to 1990 envisages the commissioning of 1900 MWe PWR and 5 at 1300 MWe, and an extension of the La Hague reprocessing plant of 2 units of 800 tonnes/year capacity. From 1991 on, various options are available, with special emphasis on the fast reactor concepts Rapsodie, Phenix and Super-Phenix I. The new project embracing the Creys-Malville fast breeder reactor is of particular interest, especially as an overall generating cost of 80% of an equivalent PWR has been estimated. (no refs.) G.C.

Energy reviews. Nuclear power systems. Vol.1 See Entry 59549

86.10Z Other topics

63654 Greenhouses on building roofs using heat from ventilating air. I.F.Livchak (Inst. Pischevoi Promyshlennosti, Moscow, USSR). *Int. J. Ambient Energy (GB)*, vol.3, no.4, p.203-6 (Oct. 1982). [received: March 1983]

Argues for rational use of exhaust ventilation as a heat source for roof-mounted greenhouses which would add significantly to agricultural land resources with little adverse effect on urban life and minimum energy use. (no refs.)

86.30 ENERGY CONVERSION

86.30D Electrochemical conversion: general

(for superionic conductors, see 66.30H)

63655 Redox ion flow cell for solar energy storage. H.Cnobloch, W.Kelermann, H.Nischik, K.Pantel, G.Siemens (Siemens AG, Erlangen, Germany). *Siemens Forsch. & Entwicklungsber. (Germany)*, vol.12, no.2, p.79-84 (1983).

In redox ion cells the energy is stored in solutions of metal ion pairs at different states of oxidation, such as for example Fe^{2+}/Fe^{3+} and Cr^{2+}/Cr^{3+} . Graphite foils serve as electrodes for the conversions and they are activated with 0.2 mg Pb per cm^2 and 0.2 mg Au per cm^2 for the reaction $Cr^{2+} = Cr^{3+}$. The separation of cathode and anode is achieved by an ion exchange membrane. A completely charged cell can be loaded with a current density of more than 100 mA/ cm^2 at 0.7 V and at 30°C. (6 refs.)

86.30F Secondary cells

63656 Cross-linked polyvinyl alcohol films as alkaline battery separators. D.W.Sheibley, M.A.Manzo, O.D.Gonzalez-Sanabria (NASA, Lewis Res. Center, Cleveland, OH, USA). *J. Electrochem. Soc. (USA)*, vol.130, no.2, p.255-9 (Feb. 1983).

Cross-linking methods have been investigated to determine their effect on the performance of polyvinyl alcohol (PVA) films as alkaline battery separators. The following types of cross-linked PVA films are discussed: (i) PVA-dialdehyde blends post-treated with an acid or acid periodate solution (two-step method), and (ii) PVA-dialdehyde blends cross-linked during film formation (drying) by using a reagent with both aldehyde and acid functionality (one-step method). Laboratory samples of each cross-linked type of film were prepared and evaluated in standard separator screening tests. Then pilot plant batches of films were prepared and compared to measure differences due to the cross-linking method. The pilot-plant materials were then tested in nickel oxide-zinc cells to compare the two methods with respect to performance characteristics and cycle life. Cell test results are compared with those from tests with Celgard. (7 refs.)

63657 Electrolyte film structure on battery separator and electrode materials. H.F.Bittner, C.C.Badcock (Chem. & Phys. Lab., Aerospace Corp., El Segundo, CA, USA).

J. Electrochem. Soc. (USA), vol.130, no.2, p.259-64 (Feb. 1983). Structural properties of alkaline electrolyte films on battery electrode and separator materials are investigated. Thermodynamic principles that affect film formation are presented, and a model is developed that predicts the wetting-dewetting transition, for a network of fibers, as a function of electrolyte volume and fiber network compactness. Film characteristics on single fibers and networks of a variety of materials are studied by a laser diffraction technique and by conductivity measurements. Materials studied include nickel, cadmium, nylon, polypropylene, and Teflon. Wetting characteristics of actual separator materials are studied in a simulated battery environment. Experimental results yield good agreement with the model. (6 refs.)

Diffusivity in zinc chloride-potassium chloride electrolyte See Entry 62142

86.30J Photoelectric conversion: solar cells and arrays

63658 Use of photovoltage for electrodeposition on solar cells. V.K.Jain (Solid State Phys. Lab., Delhi, India), A.P.Kulshreshtha. *Indian J. Technol.*, vol.20, no.9, p.373-5 (Sept. 1982). [received: March 1983]

A new technique is reported for the electrolytic deposition of a metal on a solar cell. The technique does not employ an external electric bias field, but uses the internal photoinduced voltage of the solar cell itself. The experimental details of depositing silver over the existing metallized contact structure of the cell and a transparent conducting oxide coating over the entire solar cell front surface are presented. The proposed technique reduces the consumption of the processing materials and makes the fabrication procedure less expensive and simplified. (6 refs.)

63659 Photovoltaics: an alternative form of energy. R.Buhs, V.Cordes. *Ind.-Anz. (Germany)*, vol.105, no.24, p.60-3 (25 March 1983). In German. Discusses direct conversion of solar power into electric power, and describes solar cells presently available. Multicrystalline, metal/insulator/semiconductor and indium/tin oxide solar cells and cells made by vapour condensation, screen printing and ion implantation under development are discussed. System costs and generating costs (£0.30-0.90/kWh) are briefly considered. (no refs.) J.S.

63660 Tough photovoltaics for military and civil use. *Int. Power Generation (GB)*, vol.6, no.2, p.44-5 (March 1983).

Solar photovoltaic panels are an excellent source of power where silence and lack of moving parts are more important than first cost. The technique of producing solar cells from wafers of single crystal silicon is now well proven but many photovoltaic modules have been let down by poor packaging which deteriorates rapidly and allows ingress of water to the connections to the crystals causing rapid breakdown. There are signs that this state of affairs is changing, and some manufacturers have taken great pains to produce modules which are resistant to weather and unsympathetic handling. (no refs.)

63661 Thermal and mechanical properties of multilayer substrates for low-cost solar cells obtained by dry-pressing. G.Celotti (Istituto Lamel-CNR, Bologna, Italy), L.Moretini, G.Ortelli.

J. Mater. Sci. (GB), vol.18, no.4, p.1005-14 (April 1983).

A study has been made of the possibility of producing ceramic substrates for low-cost solar cells by means of the simple technology of moulding by dry-pressing. Special attention was taken to avoid adding costly materials (organic and inorganic) to the basic commercial kaolin. It emerged that the only treatment necessary was the precalcination of approximately half the powder at temperatures of 1200 to 1350°C. The various characterization techniques showed that, in spite of the simplicity of the technologies utilized, after a final firing at 1600°C, one can obtain finished products with the same thermal expansion coefficient as silicon (from ambient temperature to 800°C) and with mechanical characteristics that make the products perfectly suitable for resistance to the thermal shock, resulting from contact with molten silicon. (14 refs.)

63662 Low-cost solar power is on the horizon. B.H.Carlisle.

Mach. Des. (USA), vol.55, no.4, p.58-65 (24 Feb. 1983).

Describes the Si solar cell and discusses the growth process for single crystals of the semiconductor. The first generation of Si cells were grown using the Czochralski process, but newer techniques of crystal growth are now becoming commercial. These newer techniques are described, including semicrystalline cell casting, the dendritic web, edge-defined film-fed growth, and amorphous Si cells. (no refs.)

63663 Silicon solar cells for terrestrial applications. J.G.Grabmaier (Forschungslab., Siemens AG, München, Germany).

Naturwissenschaften (Germany), vol.70, no.3, p.127-32 (March 1983). In German.

The direct conversion of solar energy to electrical energy (photovoltaic effect) by solar cells is receiving increasing attention on the world-wide scale. Photovoltaic energy conversion offers itself to a practical and meaningful implementation in regions without a conventional energy grid. The author deals with the principles of silicon solar cells for terrestrial applications and new methods for the production of the necessary silicon. (13 refs.)

63664 Capacitance of amorphous silicon pin solar cells. H.P.Neiderer, B.Rauscher.

Phys. Status Solidi a (Germany), vol.75, no.2, p.537-45 (16 Feb. 1983).

The i-region of pin solar cells on the basis of amorphous silicon provides the carrier collection. The density of (localized) states (DOS) in the region diminishes the electric field, favors recombination and limits the collection efficiency. The low-frequency capacitance of pin diodes is indicative for the DOS. The small-signal capacitance of a pin solar cell is measured in the frequency range 0.1 to 10³ Hz for temperatures between 30 and 100°C at zero DC bias. A simple diode model is suggested. It involves the assumption of constant DOS values in the p-, i-, and n-regions. These values are determined by fitting. It is shown that low-level doping of the i-region and illumination stress significantly raise the capacitance and the DOS. (19 refs.)

63665 Cascade heterophotocells using wide-gap A^{III}B^{VI} compounds. P.A.Gashin, G.G.Dvornik, M.B.Kagan, T.L.Lyubashevskaya, A.V.Simashkevich, A.Ya.Foksha (V.I. Lenin State Univ., Kishinev, USSR).

Sov. Tech. Phys. Lett. (USA), vol.8, no.8, p.403-4 (Aug. 1982). Translation of: *Pis'ma v Zh. Tekh. Fiz. (USSR)*, vol.8, no.15-16, p.930-3 (Aug. 1982). [received: April 1983]

Reports a study of an nZnSe-pZnTe-nCdSe heterophotocell fitted with a contact structure which allows the nZnSe-pZnTe and pZnTe-nCdSe heterojunctions to be connected in separate circuits. The cascade structure was fabricated through the successive epitaxial deposition from the gas phase of ZnTe and CdSe layers on the (110) plane of single-crystal ZnSe substrates with a thickness of 0.2-0.5 mm. (6 refs.)

63666 Grain boundary effects in polycrystalline silicon solar cells. I. Solution of the three-dimensional diffusion equation by the Green's function method. N.C.Halder, T.R.Williams (Dept. of Phys., Univ. of South Florida, Tampa, FL, USA).

Sol. Cells (Switzerland), vol.8, no.3, p.201-23 (April 1983).

For the polycrystalline silicon solar cell problem, the three-dimensional diffusion equation of the minority carrier with grain boundary effects has been solved for the first time using Green's function method. New analytic expressions for the photocurrent and the dark current of an n-p junction fibrously grained cell have been derived. The present three-dimensional theory, which is an improvement over the previous one-dimensional theory, points out correctly the limiting factors of the solar cell. It has been shown that the current-voltage characteristics and the efficiency of a polycrystalline n-p junction cell are critically influenced by the grain boundary effects. (36 refs.)

63667 Grain boundary effects in polycrystalline silicon solar cells. II. Numerical calculation of the limiting parameters and maximum efficiency. N.C.Halder, T.R.Williams (Dept. of Phys., Univ. of South Florida, Tampa, FL, USA).

Sol. Cells (Switzerland), vol.8, no.3, p.225-38 (April 1983).

For pt.1 see ibid., vol.8, no.3, p.201-23 (1983). Extensive numerical calculations have been made of the photocurrent, the dark current and the fill factor for n-p junction polycrystalline silicon solar cells utilizing previously developed theory in three dimensions. Various grain boundary effects such as grain boundary recombination velocity, grain size and grain orientations were considered. It has been shown that for zero grain boundary effect the current-voltage characteristics, fill factor and efficiency approach the single-crystal limit. For polycrystalline silicon solar cells it has been demonstrated that an efficiency of about 15% could be produced with fibrously grained samples of grain size 100 μ m, recombination velocity 100 m s⁻¹ and thickness 100 μ m. (16 refs.)

63668 Diffusion length determination in n⁺-p-p⁺ structure based silicon solar cells from the intensity dependence of the short-circuit current for illumination from the p⁺ side. G.C.Jain, S.N.Singh, R.K.Kotnala (Div. of Materials, Nat. Phys. Lab., New Delhi, India).

Sol. Cells (Switzerland), vol.8, no.3, p.239-48 (April 1983).

A new method of diffusion length measurement in n⁺-p-p⁺ structure-based silicon solar cells is presented. This method exploits the strong dependence of the collection efficiency of the p-n junction on both the thickness d and the diffusion length L of the minority carriers in the p-base region when the p-n junction is separated from the illuminated surface by the base region. The cell is illuminated from the p⁺ side with monochromatic radiation and the variation in the short-circuit current density J_{sc} with the intensity P_0 is measured. The diffusion length is determined from the slope of the J_{sc} versus P_0 curve. The validity of this method is not limited to the cases of $d/L > 1$ and, in practice, it may be suitable for cells with $d/L > 0.6$. In the present case it was used to determine L in n⁺-p-p⁺ silicon solar cells with bifacial symmetry. These cells had $d/L > 2.5$ and the values of L determined by the present method showed a remarkable agreement with those determined from the photoluminescence measurement for illumination from the n⁺ side. (18 refs.)

63669 Design of antireflection coatings for textured silicon solar cells. B.L.Sopori, R.A.Pryor (Solar Energy Res. & Dev., Motorola Inc., Phoenix, AZ, USA).

Sol. Cells (Switzerland), vol.8, no.3, p.249-61 (April 1983).

The design of a thin film coating to optimize the performance of a textured silicon solar cell is described. A ray optics approach is used to determine the reflection characteristics of textured cells with a two-layer thin film coating. A generalized expression for the external quantum efficiency in terms of the given internal quantum efficiency and the coating parameters is determined. The parameters of the thin film layers, the refractive indices and the thicknesses are determined so as to maximize the integrated cell response to an air mass 2 spectrum. (7 refs.)

63670 Reactive sputtered Ta_2O_5 antireflection coatings. F.Rubio (Escuela de Ingenieros Industriales, San Sebastian, Spain), J.Denis, J.M.Albella, J.M.Martinez-Duart.

Sol. Cells (Switzerland), vol.8, no.3, p.263-8 (April 1983).

Ta_2O_5 antireflection coatings were prepared by reactive sputtering from a tantalum target in a magnetron system. The optical constants of the films were determined from reflectance and transmittance spectra in the 0.25-2.5 μm wavelength interval. The refractive index was close to 2.0 in the visible region, resulting in optimum impedance matching for silicon solar cells. The sputtered Ta_2O_5 films showed an absorption coefficient smaller than about $10^3 cm^{-1}$ for photon energies below 4 eV. Finally, sputtered Ta_2O_5 antireflection coatings were tested on silicon solar cells and were found to increase the efficiency of the cells from 9.5% to 12.9%. (14 refs.)

63671 The fill factor of a solar cell from a mathematical point of view. A.De Vos (Lab. voor Elektronica en Meettech., Rijksuniv. te Gent, Gent, Belgium).

Sol. Cells (Switzerland), vol.8, no.3, p.283-96 (April 1983).

The problem of finding the fill factor of a solar cell given the values of the network elements, i.e. the photogenerated current, the dark saturation current, the diode quality factor, the shunt resistance and the series resistance, is tackled. Cases without shunt or series losses are treated first and then cases with small shunt and series losses are considered. Most of the proposed solutions to the problem are presented in the form of infinite expressions so that the user can obtain the desired accuracy by suitable truncation of these expressions. (11 refs.)

63672 Gallium arsenide concentrator solar cells. M.Yamada, A.Kitamura (Kansai Electric Power Co. Inc., Osaka, Japan), T.Yamaguchi, M.Kawashima, K.Motoyoshi, S.Iguchi, Y.Sasatani.

Sumitomo Electr. Tech. Rev. (Japan), no.22, p.243-50 (Jan. 1983).

The GaAs solar cell is advantageous in that it can be used under highly concentrated sunlight. By using this material in concentrating photovoltaic power generation it is possible to reduce the required amount of GaAs per unit generation. The authors introduce the structure of such GaAs concentrator solar cells, an outline of their fabrication process, design of an anti-reflection coating and a grid pattern and their characteristics. (7 refs.)

63673 Development of a 1pKW photovoltaic concentrator system with silicon cells. M.Giuffrida, A.Oberli, P.Zani, G.Dionisio, G.Ramacciotti, G.Scarpi, M.Conti, P.Nason.

Report EUR 8200 EN, Comm. European Communities, Luxembourg (1982), 41 pp. Contract 456-78-1 ESI.

The authors describe the development work between January 1978 and December 1979 on the design, construction and preliminary testing of a 1 pKW photovoltaic unit with concentration ($\times 50$), passive cooling and silicon cells. The concentration system, devised in prototype form, involved cooling system optimisation, optical and tracking systems considerations as well as photovoltaic cell design. From preliminary outdoor tests an overall efficiency close to 9% has been measured, using a single subarray of 14 cells. The results of the program should be useful for the evaluation of the merits of using small concentrator type photovoltaic units in southern Europe and assist in adapting the characteristics of the photovoltaic generator to the requirements of a dependable electricity producing system ready to meet load demands at any time.

63674 Conception, analyse du systeme, realisation et experimentation d'un generateur photovoltaïque autonome de 5 kW Au Refuge des Evettes (Conception, analysis of the system, realisation and experimentation of an autonomous 5 kW photovoltaic generator at the Refuge des Evettes). B.Aubert.

Report EUR 8204 FR, Comm. European Communities, Luxembourg (1982), 48 pp. In French. Contract 463-78-1 ESF.

The results of a study carried out on the independent Photovoltaic Generator installed at the Evettes Refuge deals with the evolution of the system under working conditions. The effects of winter conditions and the precautions taken are first examined followed by a description of snow clearance and starting-up procedures (battery charging, etc.).

63675 Cellules solaires au CdTe en couches minces polycristallines. Elaboration par pulvérisation triode et transport a courte distance (CdTe solar cells in polycrystalline thin films. Elaboration for triode sputtering and short distance transport). Y.Marfaing.

Report EUR 8213 EN/FR, Comm. European Communities, Luxembourg (1982), 62 pp. Contract 436-78-1 ESF.

CdTe is a semiconductor compound which has been studied for some time because of interest in photovoltaic conversions. The author studies CdTe homojunctions and the realisation of polycrystalline CdTe thin films. In the study of homojunctions he analyses the electrical conduction mechanisms and their influence on the conversion efficiency, the photoelectric efficiency of the junction in relation to volume and surface recombination. To this aim he considers the conditions of preparation and characterisation of the junction surface layers. The possibilities of triode sputtering are explored. Co-sputtering of Cd and CdTe are investigated with a view to obtaining stoichiometric composition and control of electrical resistivity. Three references are reprinted in full in an appendix.

63676 Integrated thin film solar cell generators with higher output voltages.

Report EUR 8160 EN, Comm. European Communities, Luxembourg (1982), 57 pp. Contract 428-78-ES D/ESC-R-003-D (B).

A technology for the production of large-area integrated Cu_2S -CdS thin film solar cell generators with higher output voltages was developed. On glass substrates with an area of $14.5 \times 29 cm^2$ integrating Ag-back contacts are vacuum-deposited. The CdS-layers are produced by evaporating CdS-powder with the aid of a large-area evaporator. They are comparable in quality with those CdS-layers that are vacuum-deposited with a point-type evaporator. For the production of the Cu_2S -layers two modifications of the Cleveite wet process was found to give good results: (1) dipping the cells in a flow of Cu^{+} -ion solution and (2) spraying the Cu^{+} -ion solution to rotating CdS substrates. A glass sheet, with an integrating Au-plated copper grid, serves for front-contacting and encapsulation. The copper grid is produced in situ on the front-glass by applying screen-printing and etching techniques to a 35 μm thick copper foil, which has been laminated to the front glass with a hot

setting adhesive. The front glass and the substrate glass carrying the active layers are laminated by applying higher temperatures and pressure. (17 refs.)

63677 Etude de la technologie d'un module solaire offrant une bonne dissipation thermique (Study of the technology of a solar module that offers good heat dissipation). D.Diguet, J.Anguet.

Report EUR 8159 FR, Comm. European Communities, Luxembourg (1982), 66 pp. In French. Contract 448-78-3 ESF.

Although the encapsulation of solar cells does not considerably affect the final cost of the module in the long run considerable economies may be achieved because cheaper materials, printed circuit techniques and automated production may be used. The technologies with relevant economics and performance characteristics for such a system are studied. A theoretical analysis of the heat flow in a solar panel is appended.

63678 Etude et realisation de croissances epitaxiales de composés III-V par pyrolyse mixte d'organometalliques et d'hydrures sous pression reduite: Application a l'etude de structures de piles solaires (Study and realisation of epitaxial growth of III-V compounds by mixed pyrolysis of organometallics and hydrides under reduced pressure: Application to the study of solar cell structures). G.Gave, M.Le Metayer, M.Orgert.

Report EUR 8207 FR, Comm. European Communities, Luxembourg (1982), 22 pp. In French. Contract 193-78 IESF.

The epitaxial growth of gallium arsenide by chemical reaction in the vapour phase, using organometals under low pressure for use in solar piles has been studied. The results are reported of Hall mobility tests on the products using two doping materials. The structure of photovoltaic layers is briefly examined, and their exploitation as solar cells is described.

63679 Increase of minority carrier diffusion length under the effect of a large band gap gradient [in solar cells]. A.Bouazzi, J.Mimila Arroyo (Lab. de Physique des Solides, CNRS, Meudon, France).

In Cellules solaires constituées de couches minces de CdTe polycristallines (Solar cells made from polycrystalline CdTe thin films), 8 pp., *Report EUR 8154 EN-FR*, Comm. European Communities, Luxembourg (1982), 75 pp. Contract 206-76 ESF.

It has been shown that a device constituted by a graded-gap material in front of a p-n junction will give a high efficiency solar cell. An expected property of the graded gap material is to increase the carrier diffusion lengths, bringing the collection factor to a maximum value. Direct determination of minority carrier diffusion lengths has been performed by measuring the junction current induced in an angle-lapped graded-gap p-n junction as a laser beam (He-Ne, 12 μm diameter) is scanned along the bevel surface. CdHgTe graded-gap structures were prepared by vapor phase transportation of HgTe on CdTe single crystal in isothermal conditions. In such structures effective diffusion lengths have been shown to vary linearly with the gradient of band gap and to increase by more than ten times. As an example in n-type graded solid solutions hole effective diffusion lengths up to 11.5 microns have been measured with a gap gradient of 0.23, $10^3 eV/cm$. This result confirms the validity of the graded band gap concept and opens the way to high efficiency solar cells.

63680 Solar cells made of thin layers of polycrystalline CdTe. Y.Marfaing (CNRS, Paris, France).

In Cellules solaires constituées de couches minces de CdTe polycristallines (Solar cells made from polycrystalline CdTe thin films), 25 pp., *Report EUR 8154 EN-FR*, Comm. European Communities, Luxembourg (1982), 75 pp. In French. Contract 206-76 ESF.

Outlines some of the general characteristics of these cells, one of the most promising methods of conversion of solar energy by a photovoltaic process. Experimental evidence is presented with a theoretical analysis of optimisation with an upper coating of a CdHgTe alloy. A theoretical appraisal of the preparation of thin coatings is then given. Diagrams are given to illustrate the theoretical results which have been obtained. The mathematical theories are then presented, together with a number of graphs obtained experimentally. There are also details concerning the homojunctions. (no refs.) G.V.D.

63681 Optimisation of new types of MIS silicon solar cells. R.Van Overstraeten, R.Mertens.

Report EUR 8142 EN, Comm. European Communities, Luxembourg (1982), 44 pp. Contract 439-78-1 ESB.

Deals with grating MIS solar cells. These structures rely on the introduction of an inversion layer by the fixed charge present in the insulating oxide that has been deposited onto the silicon. The insulating oxide also serves as an anti-reflection coating on the silicon. The inversion layer-substrate junction acts as a collecting barrier for the photogenerated minority carriers. The collected carriers travel through the inversion layer; the MIS structure present under the grid connects the inversion layer with the outside world. Since the active part of MIS grating cells is not covered by metal layers, no transparent metal layers are required in these structures. In addition, a second collection mechanism is present in these cells; it is a two dimensional diffusion of the generated carriers towards the MIS grid. (21 refs.)

63682 Photovoltaic requirements estimation - A simplified method. J.W.Doane, J.B.Gresham.

Report EPRI-AP-2475, Electr. Power Res. Inst., Palo Alto, CA, USA (Feb. 1983), 140 pp.

Available from Res. Rep. Center, Box 50490, Palo Alto, CA 94303, USA. Presents a simplified, single-year analysis method for evaluating the economics of photovoltaic (PV) systems for central station applications. Details are provided of (1) a computer code developed to determine the fuel and variable operations and maintenance savings attributable to a PV system for a single year and (2) a method developed to represent PV system and module cost-performance trade-offs.

63683 750 suns concentrator modules using GaAs solar cells. E.Fanetti, C.Flores, G.Guarini, F.Paletta (CISE SpA, Milan, Italy).

Fourth E.C. Photovoltaic Solar Energy Conference. Proceedings of the International Conference, Stresa, Italy, 10-14 May 1982 (Dordrecht, Netherlands: Reidel 1982), p.671-6

In order to make experience on high concentration and check the maturity of GaAs technology, two small size modules have been fabricated. In the first module, single GaAs cells, Fresnel lens 750 suns concentrators and passive cooling are used while in the second one a spectrum split approach and active cooling are applied in order to increase the conversion efficiency. In this last case, GaAs (1.43 eV bandgap) cells are combined with GaAlAs (1.7 eV bandgap) cells and optical filters transmitting the high energy part of sunlight to the high bandgap cell and reflecting the low energy part to the other one. The characteristics of the principal components such as GaAs and GaAlAs solar cells, Fresnel lenses, spectrum splitting optical filters and heat dissipators, described as well as the performances of the two photovoltaic modules. (4 refs.)

63684 Physical limitations of present thin film solar cells. Y.Marfaing (Lab. de Phys. des Solides, CNRS, Meudon, France). Fourth E.C. Photovoltaic Solar Energy Conference. Proceedings of the International Conference, Stresa, Italy, 10-14 May 1982 (Dordrecht, Netherlands: Reidel 1982), p.688-97.

A comparison is made between the various thin film solar cells by stressing the physical factors which limit their present performances. A general diagram is drawn up on which each cell is localized by two coordinates: one is relative to photocurrent generation, the other is indicative of diode rectifying properties. These aspects are detailed by considering the diode saturation current, the electron-hole pair collection length and the curve filling factor in an unified way which makes use of reference values. The efficiency limitations are thus precisely pointed out and the possibilities of future improvements are discussed. (29 refs.)

63685 8% efficiency a-SiC:H/a-Si-H heterojunction solar cells. Y.Tawada, K.Tsuge, M.Kondo, K.Nishimura, H.Okamoto, Y.Hamakawa (Faculty of Engng. Sci., Osaka Univ., Osaka, Japan).

Fourth E.C. Photovoltaic Solar Energy Conference. Proceedings of the International Conference, Stresa, Italy, 10-14 May 1982 (Dordrecht, Netherlands: Reidel 1982), p.698-703.

An experimental investigation for the wide gap window material in the amorphous silicon solar cell is shown on methane based and ethylene based a-SiC:H. The methane based a-SiC:H/a-Si-H heterojunction solar cell shows a larger short-circuit current density than the ethylene based one. From IR absorption analysis, methane based a-SiC:H film is recognized a rather ideal amorphous SiC alloy as compared with ethylene based one. It has been found through these investigations that the chemical bonding structure is an important factor for a window material. 8% efficiency barrier has been firstly broken through with this methane based a-SiC:H/a-Si-H heterojunction solar cell. (10 refs.)

63686 Amorphous silicon solar cells produced by a consecutive, separated reaction chamber method. Y.Kuwano, M.Ohnishi, S.Nakano, T.Fukatsu, H.Nishiwaki, S.Tsuda (Res. Center, Sanyo Electric Co. Ltd., Osaka, Japan). Fourth E.C. Photovoltaic Solar Energy Conference. Proceedings of the International Conference, Stresa, Italy, 10-14 May 1982 (Dordrecht, Netherlands: Reidel 1982), p.704-8.

A consecutive, separated reaction chamber method has been developed for the fabrication of a-Si solar cells. In this method, p, i, and n layers are deposited in different reaction chambers, and the undesirable doping caused by residual dopant gases which remain in the reaction chamber can be avoided. Following various kinds of fundamental experiments, Glass/SnO₂/p(a-SiC)-i-n/Me type a-Si solar cells were fabricated by this method, and the best conversion efficiency was 8.15% with a size of 2 mm×2 mm in sunlight of AM-1. The best conversion efficiency for integrated type a-Si solar cells fabricated by this method was 6.35% with a size of 10 cm×10 cm. The integrated type a-Si solar cells are being experimentally used in battery chargers, radios, TV receivers, and a 2 kW demonstration plant. (5 refs.)

63687 Charge collection in a-Si:H solar cells. G.Muller, G.Muck, M.Simon, G.Winterling (Messerschmitt Bolkow Blohm GmbH, Ottobrunn, Germany).

Fourth E.C. Photovoltaic Solar Energy Conference. Proceedings of the International Conference, Stresa, Italy, 10-14 May 1982 (Dordrecht, Netherlands: Reidel 1982), p.709-13.

The performance of p-i-n and Schottky barrier cells is investigated as a function of intrinsic layer thickness, d_i, up to d_i=2.5 μm. The main result is that the efficiency of p-i-n/ITO cells is limited by the extraction of photo-generated holes. The hole (μ_h)-product is determined from the saturation of the photocurrent with increasing reverse bias. The d_i-dependence of the hole (μ_h)-product indicates that charge collection in a-Si:H is severely limited by surface—and interfacial effects. (7 refs.)

63688 The effect of glow discharge excitation frequency on the performance of microcrystalline Si:H thin films and devices. R.R.Gay, D.L.Morel, D.P.Tanner, D.Kanani, H.S.Ullal (ARCO Solar Inc., Chatsworth, CA, USA). Fourth E.C. Photovoltaic Solar Energy Conference. Proceedings of the International Conference, Stresa, Italy, 10-14 May 1982 (Dordrecht, Netherlands: Reidel 1982), p.714-18.

Alloys of Si and H prepared by the glow discharge decomposition of SiH₄ are being developed world-wide for use in thin-film solar cells. The present study focuses on two important aspects of this technology. The first is the effect of excitation frequency on intrinsic material properties, and the second is the influence of processing methodology on device performance. Measurements made on intrinsic materials indicate that electron mobility increases with decreasing excitation frequency. Additional measurements made on devices indicate no systematic change in hole properties with frequency, and thus the conduction band is the main material property affected by excitation frequency. Device performance is found to be very sensitive to exposing the incomplete structure to the atmosphere between layers. Further, the n-i interface is found to be sensitive to the frequency at which the intrinsic layer is deposited. The implications of these observations to device fabrication technology are discussed. (no refs.)

63689 Electrodeposited CdS/CdTe heterojunction solar cells. B.M.Basol, R.L.Rod, E.S.Tseng (Monosolar Inc., Santa Monica, CA, USA). Fourth E.C. Photovoltaic Solar Energy Conference. Proceedings of the International Conference, Stresa, Italy, 10-14 May 1982 (Dordrecht, Netherlands: Reidel 1982), p.719-26.

The latest in a series of solar cells made using electrochemical deposition is the CdS/p-CdTe heterojunction described here. The two ultrathin polycrystalline active layers were electrodeposited to yield cells with an efficiency of 7% over 0.2 cm² area. Best observed solar cell parameters were V_{oc}=0.79 V, J_{sc}=18.8 mA/cm² and F.F.=0.56 under illumination of 100 mW/cm². An improved window material should increase the efficiency of this potentially low-cost cell. (17 refs.)

63690 Thin film heterojunction CdS/Cu ternary alloys solar cells with minority carrier mirrors. M.Kwiatniak, J.J.Loferski, R.Beaulieu, R.R.Arya, E.Vera (Div. of Engng., Brown Univ., Providence, RI, USA), L.Kazmerski. Fourth E.C. Photovoltaic Solar Energy Conference. Proceedings of the International Conference, Stresa, Italy, 10-14 May 1982 (Dordrecht, Netherlands: Reidel 1982), p.727-31.

A new concept in the fabrication of thin film solar cells with a multilayer structure in which they base region contains a minority carrier mirror (MCM) is reported. The theory of heterojunctions employing CdS as a wide bandgap window and layers of CuInSe₂ and CuGaSe₂Te_{1-x} with MCM as the photovoltaically active semiconductor is presented. A first cell of this type was made by RF-sputtering the successive layers; its AMI efficiency was about 4%. (6 refs.)

63691 Large area CdS/Cu₂S thin film solar cells produced by electrophoretic deposition. T.J.Cumberbatch, I.D.McNally, E.W.Williams, D.J.Gibbons, M.Claybourn, H.Clou, P.M.G.Dickinson (Central Res. Labs., Thorn EMI plc, Hayes, England), R.Hill, N.M.Pearsall, J.Woods, G.Russell, P.C.Pande.

Fourth E.C. Photovoltaic Solar Energy Conference. Proceedings of the International Conference, Stresa, Italy, 10-14 May 1982 (Dordrecht, Netherlands: Reidel 1982), p.732-6.

Electrophoretic deposition can be used to deposit large area thin films of CdS or ZnCdS/Cu₂S thin films have also been prepared. This technique has significant advantages over more conventional procedures with deposition rates of up to 3 μm min⁻¹ achieved. Recrystallisation of the as deposited powder layer is necessary and has been achieved using both laser and thermal treatments. A pulsed dye laser has also been used to aid the formation of heterojunctions prepared by a number of vacuum and non vacuum techniques. Preliminary results from these heterojunctions are outlined. (5 refs.)

63692 Sprayed zinc-cadmium sulfide films for backwall Cu₂S/(ZnCd)S cells. V.P.Singh, M.C.Bost, J.F.Jordan, D.M.Spitzer, Jr. (Photon Power Inc., El Paso, TX, USA).

Fourth E.C. Photovoltaic Solar Energy Conference. Proceedings of the International Conference, Stresa, Italy, 10-14 May 1982 (Dordrecht, Netherlands: Reidel 1982), p.737-41.

Zn_xCd_{1-x}S films (0<x<0.5) were spready on tin oxide coated glass. Film thickness showed little variation with x; resistivity increased exponentially with x. Cu₂S/Zn_xCd_{1-x}S cells formed on these films were found to have much lower J₀, higher Voc and α, and lower Jsc than their CdS counterparts. Also, the spectral response of their short-circuit current was more sensitive to the white light bias than that of the Cu₂S/CdS cell. Photocapacitance showed a quenching band around 900 nm which accompanied an enhancement band for the Voc. (14 refs.)

63693 Large area and high efficiency a-Si:H solar cell. Y.Higaki, M.Kato, M.Aiga, Y.Yukimoto (LSI R&D Lab., Mitubishi Electric Corp., Hgjo, Japan).

Fourth E.C. Photovoltaic Solar Energy Conference. Proceedings of the International Conference, Stresa, Italy, 10-14 May 1982 (Dordrecht, Netherlands: Reidel 1982), p.745-8.

A conversion efficiency of 5.4% for a-Si:H solar cell on 10×10 cm² stainless steel substrate has been obtained. Large area a-Si:H solar cells were fabricated by the C-coupled (60×60 cm² parallel plates) glow discharge method. The stainless steel substrate were polished down to 0.2 μm maximum roughness. Boron concentration profile was measured by IMA technique. The inverted (nip/s.s) configuration is superior to normal (pin/s.s) type for a-Si:H solar cell, since boron atoms likely pile up at the interface between the substrate and the a-Si:H even though B₂H₆ gas is not introduced. The undesirable boron atoms seem to come from the susceptor or the side wall of the reaction chamber, which cannot be etched out easily. Power dissipation at the transparent conducting film, at the comb electrode, and at the bus electrode on this large area solar cell were calculated respectively. It was concluded that the loss at the bus electrode is the largest and with the reduction of its resistance, the cell performance would be improved. As a result, Voc of 0.85 V, Jsc of 11.5 mA/cm², F.F. of 0.554 and efficiency of 5.4% have been obtained. (no refs.)

63694 Stability of amorphous silicon solar cells with pin structure. W.Kruhler, M.Moller, H.Pfleiderer, R.Plattner, B.Rauscher (Res. Lab., Siemens AG, Munich, Germany).

Fourth E.C. Photovoltaic Solar Energy Conference. Proceedings of the International Conference, Stresa, Italy, 10-14 May 1982 (Dordrecht, Netherlands: Reidel 1982), p.754-8.

Solar cells made from hydrogenated amorphous Silicon with pin structure show an efficiency of up to 7.4% on 6 mm² and up to 5% on 2"×2". Degradation experiments with illumination and under forward bias in the dark, were performed. These measurements as well as capacitance and spectral response measurements show, that optically or electrically injected carriers induce recombination enhanced defect reactions, which lead to an increase of the density of states and, respectively, to a decrease of the ur-product, mainly of that of the holes. Compensation of the normally n-type i-layer by doping with Boron leads to higher cell stability due to a shifting of the Fermi level closer to midgap. The effect of different concentrations of Boron in the i-layer on its dark and photoconductivity was investigated. A maximum of photoconductivity is seen for 5 ppm. Preliminary tests on cells suggest, that the degradation can be minimized by a controlled Boron concentration of the i-layer. (7 refs.)

63695 Carrier conduction in a-Si:H solar cells. M.K.Han, P.Sung, R.Lahri, W.A.Anderson (Dept. of Electrical & Computer Engng., State Univ. of New York, Amherst, NY, USA).

Fourth E.C. Photovoltaic Solar Energy Conference. Proceedings of the International Conference, Stresa, Italy, 10-14 May 1982 (Dordrecht, Netherlands: Reidel 1982), p.759-63.

The conduction process in a-Si:H Schottky structures (I-N⁺/SS) is found to be barrier controlled at low forward bias (<0.2 V) and bulk controlled at large forward bias (>0.6 V). The i-layer shows evidence of space charge limited current conduction (SCLC) in the dark. A model incorporating these considerations has been presented to develop equations for the terminal I-V characteristics of these structures. Dark I-V characteristics of the P-I-N structure are also explained on the basis of the above model. Dark C-V characteristics of the Schottky structures also support the existence of SCLC conduction in these structures. (7 refs.)

63696 Optical optimization of amorphous silicon solar cells. W.den Boer, R.M.van Strijp (Dept. of Electrical Engng., Delft Univ. of Technol., Delft, Netherlands).

Fourth E.C. Photovoltaic Solar Energy Conference. Proceedings of the International Conference, Stresa, Italy, 10-14 May 1982 (Dordrecht, Netherlands: Reidel 1982), p.764-8.

A computer simulation study is presented to calculate the optical behaviour of thin film solar cells. Application to Schottky-barrier a-Si:H solar cells with highly reflective back contacts indicates that multiple reflections are strong for long wavelength light and can be used to improve the efficiency. Relative maxima in the AMI integrated absorption occur at certain a-Si:H film thicknesses. For a given cell configuration the optimum antireflection coating is calculated. For weakly absorbed monochromatic radiation the electron-hole pair generation rate varies periodically with distance from the front contact due to interference. Integrated over the solar spectrum interference peaks in the generation rate are reduced, but remain present near the back contact. The computer program can be easily adapted for calculations on p-i-n cells, tandem cells and multi-junction cells. (7 refs.)

- 63697 Large area hydrogenated amorphous silicon for photovoltaic application.** G.J.Smith, W.I.Milne (Cambridge Univ., Cambridge, England), P.Blackborow.
Fourth E.C. Photovoltaic Solar Energy Conference. Proceedings of the International Conference, Stresa, Italy, 10-14 May 1982 (Dordrecht, Netherlands: Reidel 1982), p.769-72.
Satisfactory production techniques for depositing hydrogenated amorphous silicon (a-Si:H) over large area remain to be developed. This paper reports the manufacture of uniform films of a-Si:H by glow discharge of silane over an area 60 cm in diameter. Electrical and optical properties and film quality are discussed. (6 refs.)
- 63698 Antimony doping in vacuum deposited thin film silicon photovoltaic cells.** C.Feldman, F.G.Satkiewicz, N.A.Blum, K.G.Hoggarth (Appl. Phys. Lab., Johns Hopkins Univ., Laurel, MD, USA).
Fourth E.C. Photovoltaic Solar Energy Conference. Proceedings of the International Conference, Stresa, Italy, 10-14 May 1982 (Dordrecht, Netherlands: Reidel 1982), p.783-7.
A method for antimony doping silicon polycrystalline thin films and single crystals has been investigated. The method is compatible with the concept of forming photovoltaic cells completely in a vacuum system. Layers of Sb_2O_3 and Si were deposited either simultaneously or sequentially through masks onto the silicon surface. Heating (e.g. 1100°C , 1 hr) in either an inert atmosphere or oxygen brought about the formation of an SiO_2 -Sb glassy layer and caused Sb to diffuse into the base silicon surface. The oxide complex is then etched off leaving n-type regions of the surface. Reactions of the layers were examined by secondary ion mass spectrometry and X-ray diffraction. (6 refs.)
- 63699 Photovoltaic performance of CdS heterojunctions on polycrystalline silicon.** E.Scafe, G.Maletta, R.Tomaciello, P.Alessandrini, A.Camanzi, L.de Angelis, F.Galluzzi (Lab. Ricerche Assorini, Monterotondo, Roma, Italy).
Fourth E.C. Photovoltaic Solar Energy Conference. Proceedings of the International Conference, Stresa, Italy, 10-14 May 1982 (Dordrecht, Netherlands: Reidel 1982), p.788-92.
New results on photovoltaic performance of n-CdS/p-Si heterojunctions are reported. Conversion efficiencies up to 11.1% for single crystal Si and 9.2% for semi-crystal Si have been obtained (without ARC and BSF) by a systematic study of CdS film doping, Silicon substrate preparation and interfacial oxide thickness. (5 refs.)
- 63700 Temperature dependence of the IV-characteristic of Cu₂S-CdS thin film solar cells and related phenomena.** G.H.Hewig, F.Pfisterer, H.W.Schock (Inst. fuer Phys. Elektronik, Univ. Stuttgart, Stuttgart, Germany).
Fourth E.C. Photovoltaic Solar Energy Conference. Proceedings of the International Conference, Stresa, Italy, 10-14 May 1982 (Dordrecht, Netherlands: Reidel 1982), p.793-7.
The temperature dependence of the IV-characteristic of Cu₂S-CdS solar cells in the dark and under various illumination conditions has been measured in the range -100 to $+100^\circ\text{C}$. The major findings are: (1) Cells processed in different ways exhibit different temperature dependences of the IV-characteristics. (2) The temperature dependence is influenced in different ways by illuminating the cells with varying monochromatic light. (3) Cells showing a strong light-effect also show a strong temperature dependence of the IV-characteristics. The population density of copper levels in the CdS region adjacent to junction is a function of temperature and of illumination and causes variation of the field strength and of the interface recombination velocity at the metallurgical junction. These mechanisms are responsible for the observed effects. (8 refs.)
- 63701 Comparison between various ion beam doping procedures and anneal techniques used in manufacturing silicon solar cells.** J.C.Muller, A.Meshi, P.Siffert (CRN, Strasbourg, France), J.Com-Nougue, C.Tessari, Jp.Dumas.
Fourth E.C. Photovoltaic Solar Energy Conference. Proceedings of the International Conference, Stresa, Italy, 10-14 May 1982 (Dordrecht, Netherlands: Reidel 1982), p.994-8.
Conventional ion implantation of phosphorus and ion incrustation (non mass separated PF_5 molecular ions), have been used to realize the N^+ layer of single crystalline silicon solar cells. Various regrowth techniques have been investigated: classical thermal treatment, laser annealing in the liquid and solid phase regimes and electron beam annealing. A systematic investigation by DLTS has allowed the determination of the optimal conditions of the post thermal treatment. Finally, large scale cells ($\geq 10\text{ cm}^2$) that have been prepared by using industrial processes and efficiencies higher than 13% have been measured for the two doping procedures. These techniques are presently applied to polycrystalline silicon from various sources. The first results obtained on solar cells elaborated with these materials, in particular the silicon under development at Laboratoire de Marcoussis are given. (12 refs.)
- 63702 Status of ion-implanted silicon solar cells.** W.Schmidt, K.-D.Rasch (AEG-Telefunken, Heilbronn, Germany).
Fourth E.C. Photovoltaic Solar Energy Conference. Proceedings of the International Conference, Stresa, Italy, 10-14 May 1982 (Dordrecht, Netherlands: Reidel 1982), p.999-1006.
Ion implantation is considered as a possible low-cost 'cold' process for junction formation in terrestrial solar cell fabrication. But it requires a subsequent implantation damage annealing step. Various annealing techniques as thermal treatment or irradiation with laser or electron beams have been applied. The results indicate for all annealing techniques lower efficiencies compared with standard diffused cells. The problems of annealing are discussed. The influence of a post-anneal heat treatment and of resistivity on the performance of pulsed electron beam annealed cells is evaluated. (13 refs.)
- 63703 Optimization of pulsed electron beam annealing process for silicon solar cells.** A.Laugier, D.Barbier, G.Chemisky (Inst. Nat. des Sci. Appl. de Lyon, Villeurbanne, France).
Fourth E.C. Photovoltaic Solar Energy Conference. Proceedings of the International Conference, Stresa, Italy, 10-14 May 1982 (Dordrecht, Netherlands: Reidel 1982), p.1007-12.
Ion implanted silicon solar cells characteristics are related to pulsed electron beam annealing parameters (PEBA). Evolution of electron beam energy deposition profile versus charging voltage and plasma field emission diode geometry is studied. By computer simulation of thermal effects it is shown that molten depth and liquid phase duration can be adjusted to yield the best ion implanted junction characteristics. Effect of heating Si wafers above 400°C before pulsing is investigated. SIMS profiling is used to determine junction profiles after PEBA in (100) phosphorus implanted silicon. PEBA solar cells characteristics are presented. (6 refs.)
- 63704 Silicon solar cells by ion implantation: E-beam and self annealing.** G.F.Cembali, R.Galloni, G.Lulli, A.Mazzone, P.G.Merli, R.Nipoti (CNR, Istituto LAMEL, Bologna, Italy), F.Zignani.
Fourth E.C. Photovoltaic Solar Energy Conference. Proceedings of the International Conference, Stresa, Italy, 10-14 May 1982 (Dordrecht, Netherlands: Reidel 1982), p.1013-17.
Two different techniques, based on ion implantation, have been experimented to obtain solar cells: a) ion implantation followed by electron beam annealing, b) self-annealed ion implantation. Silicon single crystals have been used to get a better understanding of the processes. In all cases radiation damage is annealed by a solid phase process. Solar cells tested at AM1.5 show efficiencies between 13 and 13.5% which may be compared with a 15% AM1.5 efficiency obtained by ion implantation and furnace annealing. Experimental results are compared with data obtained from a computer simulation to evaluate emitter tailoring effects. A new electron gun especially designed and set up for annealing purpose is presented. (6 refs.)
- 63705 An automated ion implant/pulse anneal machine for low cost silicon cell production.** A.J.Armini, S.N.Bunker, M.B.Spitzer (Spire Corp., Bedford, MA, USA).
Fourth E.C. Photovoltaic Solar Energy Conference. Proceedings of the International Conference, Stresa, Italy, 10-14 May 1982 (Dordrecht, Netherlands: Reidel 1982), p.1018-22.
The continuing development of a high throughput ion implanter and a pulsed electron beam annealer designed for dedicated silicon solar cell manufacture is reviewed. This equipment is intended for production of junctions in 10 cm wide wafers at a throughput up to 10 MW_p per year. The principal features of the implanter are the lack of mass analysis and defocusing utilizing electrostatic deflection. The implanted surface is annealed by liquid phase epitaxy resulting from a single burst of a large area electron beam. Cells with non-mass analyzed ion implantation have yielded AM1 cell efficiencies in excess of 15%. Pulse annealed Czochralski cells have been made with AM1 efficiencies of 13% vs. 15% for a furnace annealed group. J_{sc} is 3-4% higher for pulse annealing; V_{oc} is usually lower. Results of pulse annealing of polycrystalline materials indicate that cell performance comparable to diffusion can be obtained. (10 refs.)
- 63706 Laser processing in the preparation of high efficiency polycrystalline silicon solar cells.** E.Courcelle, E.Fogarassy, J.C.Muller, P.Siffert (CRN, Strasbourg, France).
Fourth E.C. Photovoltaic Solar Energy Conference. Proceedings of the International Conference, Stresa, Italy, 10-14 May 1982 (Dordrecht, Netherlands: Reidel 1982), p.1023-8.
Two doping processes, based on the use of high power lasers as surface localized energy sources have been employed to realize the junction on P-type polycrystalline silicon, prepared by a case technique (Wacker). These are non mass separated ion implantation, the ions being generated from PF_5 , and laser induced diffusion of Sb deposited on surface. Annealing involves either a Q-switched pulsed Ruby laser ($\lambda=0.69\text{ }\mu\text{m}$, $E=1.5\text{ J/cm}^2$) providing a larger area beam (0.8 mm) or a repetitively Q-switched, CW pumped YAG ($\lambda=0.53\text{ }\mu\text{m}$, $E=2.5\text{ J/cm}^2$) laser focused on 100 microns diameter spots scanned on large area. The properties of the doped layers have been investigated and compared to that of single crystalline silicon handled in the same way. The characteristics of solar cells were studied as a function of various parameters, such as ion implantation conditions, thickness of the dopant layers and effect of post laser thermal treatments. Cell performances under AM1 conditions are rather promising, since efficiencies up to 11% have been achieved on large grained cast silicon for large area cells. (8 refs.)
- 63707 The influence of surface texture and thermal treatment on the performance of laser-annealed silicon solar cells.** W.Sinke, D.Hoonhout, F.W.Saris (FOM-Inst. for Atomic & Molecular Phys., Amsterdam, Netherlands).
Fourth E.C. Photovoltaic Solar Energy Conference. Proceedings of the International Conference, Stresa, Italy, 10-14 May 1982 (Dordrecht, Netherlands: Reidel 1982), p.1029-33.
Single-crystal silicon cells have been made by shallow, mass-analyzed ion-beam implantation followed by Q-switched ruby-laser annealing. The influence of surface texture of the substrate, and of a thermal treatment at 400°C or 600°C during 40 min. either prior to, during or after pulsed-laser annealing on the performance of the cells has been studied. Structure and composition of implanted and annealed silicon have been investigated by Rutherford backscattering and channeling. Solar cell performance was characterized by measuring the I-V-curve. It was found that texturized surfaces are very prone to laser-induced damage as compared to non-texturized or polished surfaces. Treating the implanted silicon wafers to 400°C during pulsed-laser-annealing results in improved open-circuit-voltage, with respect to laser-annealing without substrate-heating. (5 refs.)
- 63708 Implantation of boron and boron fluoride compounds into silicon for production of solar cells.** A.Nylandsted Larsen, F.Nielsen, G.Sorensen (Inst. of Phys., Univ. of Aarhus, Aarhus C, Denmark).
Fourth E.C. Photovoltaic Solar Energy Conference. Proceedings of the International Conference, Stresa, Italy, 10-14 May 1982 (Dordrecht, Netherlands: Reidel 1982), p.1034-8.
The effects of pulsed laser irradiation on single crystalline silicon implanted with mass-separated B, BF, BF_2 , and BF_3 have been studied by channeling transmission electron microscopy, and sheet resistivity measurements. It is shown that a high implantation dose of fluorine in the surface layer causes a decrease in the threshold energy density for recrystallization. Low sheet resistivities before recrystallization is also found to correlate to the fluorine concentration. (9 refs.)
- 63709 Grain boundary photocurrent enhancement in solar cells made by laser diffusion.** G.B.Turner, D.Tarrant, D.Aldrich (Arco Solar Inc., Chatsworth, CA, USA), R.Pressley, R.Press.
Fourth E.C. Photovoltaic Solar Energy Conference. Proceedings of the International Conference, Stresa, Italy, 10-14 May 1982 (Dordrecht, Netherlands: Reidel 1982), p.1039-43.
An enhanced photocurrent has been observed at grain boundaries in solar cells made by Gas Immersion Laser Diffusion (GILD). Wafers of Wacker 'Silso' polycrystalline material were sliced from the cast block, kept in order, and subjected to different treatments. Many grain boundaries extended through three wafers. One wafer was furnace-diffused with phosphorus (850°C , 1 hr) and the next was made by the GILD method. A third wafer was heat treated, without dopant, the same as the furnace-diffused cell. Laser photocurrent scans show that many grain boundaries degrade photocurrent in cells that have been heat treated but enhance it slightly in GILDed cells. Photocurrent scans on the backs of the cells show the effect strongly amplified. Two models are presented which are consistent with these results. (4 refs.)
- 63710 Dry process for economic cell manufacturing.** J.Donon, H.Lauvray, P.Aubril, G.David, P.Loubly (Photowatt Internat. SA, Caen, France).
Fourth E.C. Photovoltaic Solar Energy Conference. Proceedings of the International Conference, Stresa, Italy, 10-14 May 1982 (Dordrecht, Netherlands: Reidel 1982), p.1044-8.
Different dry processes for cell manufacturing are under development leading to important cost reduction: plasma etching in order to remove the thin damaged layer induced during sawing with a wire saw, to etch away the oxide layer after diffusion and to open the junction on the edges, general use of screen printing in order to obtain N^+/P and $\text{N}^+/\text{P}/\text{P}^+$ structures with screen printed doping sources, to print front and back contacts (silver can be

used for the front, aluminium and silver for the back with the possibility of diffusing through the oxide and the junction when needed), to deposit the AR coating, either at the end of the process or during the junction formation. The main advantages of these dry processes using plasma etching and screen printing are: low material consumption, high throughput versus capital investment ratio, little pollution, automation capability. A preliminary economic analysis is made to show the interest of using such a process in production capacity. (no refs.)

63711 Low-cost structures and optimization of support structures.

J.Glockl, P.Helm, K.Trader.
Fourth E.C. Photovoltaic Solar Energy Conference. Proceedings of the International Conference, Stresa, Italy, 10-14 May 1982 (Dordrecht, Netherlands: Reidel 1982), p.1050-2
Presents a newly developed low-cost support structure for PV panels based on elements commonly used for fence construction. Thereafter trade-off methods to arrive at an optimization in terms of total costs for support structures have been described. (no refs.)

63712 Screen printed SIS-type solar cells.

J.N.Avaritsiotis (Univ. of Athens, Dept. of Phys., Athens, Greece), D.S.Campbell, C.Caroubalos.
Fourth E.C. Photovoltaic Solar Energy Conference. Proceedings of the International Conference, Stresa, Italy, 10-14 May 1982 (Dordrecht, Netherlands: Reidel 1982), p.1053-5
The experimental results of a feasibility study that has been under-taken in order to investigate the potentiality of the thick film technology in the fabrication of ITO-single crystal Si solar cells, are discussed. Newly developed thick film pastes, in use in the optoelectronics industry have been tried. In this structure the ITO thick film acts not only as a conducting surface layer that induces the SIS junction but also as an antireflective coating. Promising cells were fabricated employing conventional thick film apparatus that is widely used in the microelectronics industry, showing a $V_{oc}=310$ mV and a $J_{sc}=1$ mA/cm², under a total insolation of 613 W/m². Further work is necessary for the optimisation of the cell parameter. (7 refs.)

63713 An improved derivation of solar cell parameters in terms of transition probabilities.

P.T.Landsberg (Univ. of Southampton, Southampton, England).
Fourth E.C. Photovoltaic Solar Energy Conference. Proceedings of the International Conference, Stresa, Italy, 10-14 May 1982 (Dordrecht, Netherlands: Reidel 1982), p.1056-8
Using rate equation and quasi-chemical potentials, the relation $j=j_L-j_{rev}[\exp(qV/KT)-1]$ is obtained. It yields identifications for j_L and j_{rev} in terms of radiative and non-radiative transition probabilities per unit time. (3 refs.)

63714 The world's largest 12 volt single string photovoltaic module.

P.Lauwers, G.R.Smekens.
Fourth E.C. Photovoltaic Solar Energy Conference. Proceedings of the International Conference, Stresa, Italy, 10-14 May 1982 (Dordrecht, Netherlands: Reidel 1982), p.1063-4
Presents the world's largest nominal 12 Volt single string photovoltaic module ever made until today. It is a 1 m 2 module consisting of 40 semicrystalline cells, each 15 cm by 15 cm. The module delivers 72 Watt under 1000 W/m², AM-1.5 illumination. The results listed here are those of a first batch of 100 wafers processed from starting material to encapsulated module. (no refs.)

63715 Light assisted pulsed annealing of photovoltaic silicon by microwave energy.

P.Chenevier, J.Cohen, G.Kamarinos (CNRS, Enserg, Grenoble, France).
Fourth E.C. Photovoltaic Solar Energy Conference. Proceedings of the International Conference, Stresa, Italy, 10-14 May 1982 (Dordrecht, Netherlands: Reidel 1982), p.1065-7
Recommends a new method of pulsed annealing using microwave energy. This method allows annealings of sufficiently short duration (on the order of 100 ms) to operate in an ordinary clean room ambience, and to treat relatively large areas. Moreover, the total energy efficiency is far higher (up to 20 to 30%) than with a laser or electron beam. In addition, microwave generators also allow profiling the power pulse, so that the treatment can be accurately controlled. (no refs.)

Cellules solaires constituées de couches minces de CdTe polycristallines (Solar cells made from polycrystalline CdTe thin films) See Entry 59550

Impurity incorporation in RAO polysilicon layers and consequences on their electrical properties See Entry 61950

Semiconductor processing with excimer lasers See Entry 61965

Impurity diffusion in amorphous silicon and its implications for solar cells See Entry 62176

Liquid-phase epitaxial growth of ZnSe on ZnTe substrate See Entry 62283

Elimination of boron in silicon by zone melting under a high-frequency inductive plasma: role of reactive plasmas and of slag. Characterisation of photovoltaic silicon See Entry 63153

Continuous deposition of photovoltaic grade CdS sheet at the unit operations scale See Entry 63164

Deposition of cadmium chalcogenide thin films by a solution growth technique using triethanolamine as a complexing agent See Entry 63184

Critical technology limits to silicon material and sheet production See Entry 63187

The photoelectrochemical etching of TiO₂ single crystals See Entry 63445

A 500 W_{PK} photovoltaic concentrator using a glass laminated metal membrane reflector See Entry 63649

Temperature effect on phenosafranine-EDTA photogalvanic cell See Entry 63716

86.30K Photoelectrochemical conversion

63716 Temperature effect on phenosafranine-EDTA photogalvanic cell.

K.K.Rohatgi-Mukherjee, M.Bagchi, B.B.Bhowmik (Phys. Chem. Lab., Jadavpur Univ., Calcutta, India).
Electrochim. Acta (GB), vol.28, no.3, p.293-300 (March 1983).
The photogalvanic effect in phenosafranine-EDTA aqueous solution has been studied in deoxygenated solutions using platinum electrodes for both chambers, illuminated and dark, at different temperatures. For temperature variations between 20 and 49°C, the values of open circuit photovoltage V_{oc} change from 543 to 870 mV and that of steady state photocurrent I , from 1.58 to 3.24 μ A. The present results show that with increasing temperature the photovoltage and photocurrent increase linearly, the time to attain both the equilibrium values also diminishes gradually. Photovoltage and photocurrent appear only in unstirred solutions. An attempt has been made to analyse the effect of pH, light intensity and solvent to understand the temperature dependence of photovoltage. Power conversion efficiency is only 0.24 μ W

cm⁻² and solar energy efficiency 10⁻³%. The current-potential curve indicates high activation overpotential responsible for low efficiency of the cell. Calculation of thermodynamic parameters show large negative entropy for cell reaction. (18 refs.)

63717 Ceramic SrTiO₃ photoanodes: enhancement of photoactivity through donor doping.

B.Odekirk, J.S.Blakemore (Oregon Graduate Center, Beaverton, OR, USA).
J. Electrochem. Soc. (USA), vol.130, no.2, p.321-6 (Feb. 1983).
Results are reported for the photoactivity of lanthanum-doped, strongly reduced SrTiO₃ in microcrystalline ceramic form. Photoanodes of La_xSr_{1-x}TiO₃ (with x up to 0.01) were used in photoelectrochemical cells with simulated AM2 solar illumination, and aqueous electrolytes of various pH. The photoresponse was highest for strongly basic electrolytes, and 1M NaOH was used for subsequent experiments. Samples with heavy doping and strong reduction (heated at 1325K with $P_{O_2} \leq 10^{-18}$ atm, and quenched) showed good photoactivity without external bias. Impurity band formation for $x \geq 0.003$ provides an extension of the spectral response to longer wavelengths, and improves the quantum efficiency. Weakly doped samples ($x \leq 0.002$) show a modest photo-oxidation after operation in a PEC cell for several hours, but this feature is absent for large doping. No significant photodecomposition effects were seen after operation at AM2 illumination for up to 50 hr. (30 refs.)

63718 Photocathodic reactions at p-InP.

K.Uosaki, H.Kita (Dept. of Chem., Hokkaido Univ., Sapporo, Japan).
Sol. Energy Mater. (Netherlands), vol.7, no.4, p.421-9 (Jan.-Feb. 1983).
The photocurrent-potential and the capacitance-potential relations are determined for p-InP in 1 M NaOH and in 0.5 M H₂SO₄. Hydrogen evolution is the main photocathodic reaction in 1 M NaOH but a significant amount of the current leads to In deposition in 0.5 M H₂SO₄. The Tafel-like behaviour of the photocurrent-potential relation, the non-linear relation between the photocurrent and the light intensity and the photocurrent enhancement by addition of an easily reducible compound (methyl viologen) all suggest that a surface process controls the rate. Inversion layer formation is inferred from the Mott-Schottky plots. (17 refs.)

63719 Factors affecting the efficiency of chemically deposited CdSe based photoelectrochemical cells.

R.C.Kainthla, J.F.McCann, D.Haneman (School of Phys., Univ. of New South Wales, Kensington, NSW, Australia).
Sol. Energy Mater. (Netherlands), vol.7, no.4, p.491-500 (Jan.-Feb. 1983).
CdSe thin films have been deposited on titanium, nickel and stainless steel substrates by a chemical deposition technique from an aqueous solution of cadmium acetate, ammonia and sodium selenosulfate. The effects of film thickness, substrates and annealing temperature in air on the performance of CdSe based photoelectrochemical cells have been studied. Open-circuit voltages up to 728 mV have been obtained for film deposited on nickel substrates. By optimising deposition and post deposition conditions, for Ni and Ti substrates efficiencies up to 5.5% have been obtained on small (1 cm²) cells. (15 refs.)

The photoelectrochemical etching of TiO₂ single crystals See Entry 63445

86.30L Electrogasdynamic and magnetohydrodynamic conversion

(see also 52.75 Plasma devices and applications)

63720 High temperature preheating of the oxidizer for MHD combustors by direct combustion of fuel. II.

V.V.Ghia.
Rev. Roum. Sci. Tech. Ser. Electrotech. & Energ. (Rumania), vol.28, no.1, p.89-94 (Jan.-March 1983).
For pt.I see ibid., vol.27, no.4, p.467 (1982). A calculation formula is established, which states the influence of the supplementary quantity of oxygen V_{O_2} on the enrichment of the combustion air. The effect of the oxidizer high-temperature preheating on the fuels combustion is also presented. (3 refs.)

86.30Q Chemical energy conversion

(for electrochemical conversion, see 86.30D; for photoelectrochemical conversion, see 86.30K)

63721 Performance comparison of 15- and 165-tpd Texaco coal gasifiers.

G.N.Richter, J.S.Stevenson, L.S.Hollingsworth.
Report EPRI-AP-2814, Electr. Power Res. Inst., Palo Alto, CA, USA (Jan. 1983), 36 pp.
Available from Res. Rep. Center, Box 50490, Palo Alto, CA 94303, USA.
Presents the results of steady-state tests that were conducted at the Texaco Montebello 15-tpd coal gasification pilot plant. An analysis of several conditions is made, and these results, presenting representative performance information, are compared with those obtained at Ruhrkohle/Ruhrchemie's 165-tpd demonstration plant in order to obtain gasifier scale-up data. Qualitative results are also given of parametric tests conducted to determine the influence of Serox operating variables on H₂S, COS and CO₂ removal from the syngas.

86.30R Thermal energy conversion (heat engines and heat pumps)

63722 Development of a metal hydride compressor.

K.Nomura, E.Akiba, S.Ono (Nat. Chem. Lab. for Industry, Ibaraki, Japan).
J. Less-Common Met. (Switzerland), vol.89, no.2, p.551-8 (Feb. 1983).
(International Symposium on the Properties and Applications of Metal Hydrides, Toba, Japan, 30 May-4 June 1982).
The National Chemical Laboratory for Industry (NCL) model 4 chemical engine has been completed. This is a type of hydrogen compressor using LaNi₅ as the energy conversion medium. The container, consisting of 19 copper tube elements with aluminium inner fins and covered with a stainless steel heat-insulated water jacket, is filled with 18.9 mol of LaNi₅. The compressor is composed of a pair of these containers, two electrical boilers (9 kW), a circulating pump, valves and other components. The container is able to absorb 1.3 m³ (at normal temperature and pressure (NTP)) of hydrogen, and the time needed for preheating (90°C) and cooling (27°C) is less than 3 min. In the present investigation, using this container, the basic operating characteristics such as the hydrogen-absorbing and hydrogen-desorbing ability, the thermal efficiency, the heat transfer coefficient and the reaction velocity have been examined. Because of the circulating hot water (90°C: 30 l min⁻¹), the NCL model 4 compressor is able to desorb 360 l min⁻¹ (NTP) of high pressure (18-12 atm) hydrogen gas continuously in 3 min. However, this is its maximum ability under stable conditions. The overall heat transfer coefficient estimated is about 300-1200 kcal m⁻² h⁻¹ °C⁻¹. Using a plunger

pump, the NCL model 4 compressor has been combined with a reverse osmosis type of desalination apparatus, and a practical test is now under way. (5 refs.)

63723 Coefficients of performance of hydride heat pumps. T.Nishizaki, K.Miyamoto, K.Yoshida (Central Res. Lab., Sekisui Chem. Co. Ltd., Osaka, Japan).

J. Less-Common Met. (Switzerland), vol.89, no.2, p.559-66 (Feb. 1983). (International Symposium on the Properties and Applications of Metal Hydrides, Toba, Japan, 30 May-4 June 1982).

A model for calculating the coefficients of performance (COPs) is presented for a chemical heat pump which contains two metal hydrides and which consists of four reactors. Two reactors contain the first metal hydride MH_1 and the other two contain the other metal hydride MH_2 . A concept of the sensible heat exchange between the reactors containing the same hydride is introduced into the model as one of the means of improving the COP. The dependence of the COP on the various design parameters is discussed. The results of the numerical calculation show that a sufficiently flat plateau, low reactor heat capacities and a highly efficient sensible heat exchange are essential to the achievement of a high COP. (5 refs.)

86.30S Photothermal conversion

63724 High performance evacuated solar collectors—design, applications and viability. G.L.Harding, B.Window (School of Phys., Univ. of Sydney, Sydney, NSW, Australia), R.Gammon.

Int. J. Ambient Energy (GB), vol.3, no.4, p.171-80 (Oct. 1982). [received: March 1983]

The design of evacuated collectors developed in various laboratories is reviewed and the research and development work on an all-glass evacuated collector at the university is discussed in detail. Long-term comparative test data for flat plate and evacuated collectors and the projected economics of large volume manufacture of all-glass collectors indicate the viability of evacuated collectors for applications such as domestic water heating. (16 refs.)

63725 Using solar energy to heat water in low income housing. J.A.Basson (Nat. Building Res. Inst., Pretoria, S Africa).

Int. J. Ambient Energy (GB), vol.3, no.4, p.187-94 (Oct. 1982). [received: March 1983]

The Institute originally developed a pipe type integral solar water heater for use in low income dwellings. This design was subsequently adapted to suit manufacturing procedures and utilise more durable materials. The integral unit is relatively inexpensive and simple to install and operate. Its solar efficiency is high but the water in the unit cools during the night. The integral unit is inherently frost-resistant in a mild winter climate because of the large waterways and small exposed surface area. Units currently available are water and hail resistant and of durable construction. (8 refs.)

63726 Planar solar reflectors. H.F.Chiam (Res. Dept., ICI Australia Operations Pty Ltd., Melbourne, Victoria, Australia).

Int. J. Ambient Energy (GB), vol.3, no.4, p.195-202 (Oct. 1982). [received: March 1983]

A planar reflector is preferred to curved alternatives as a concentrating or augmenting device for a flat-plate solar collector. The performance characteristics of a reflector-augmented collector are reviewed. Particular emphasis is placed on the practical application of the principal results to single reflector and V-trough systems. The usefulness of highly reflective, horizontal diffuse surface to a tilted collector, and the comparative performance of a faceted reflector containing two planar segments are also discussed. (6 refs.)

63727 The effect of design parameters on thermal efficiency of collector storage wall passive systems. D.Tinaut, E.Tasdemiroglu, F.Ramos, F.Hernandez (Inst. de Optica 'Daza de Valdes', Madrid, Spain).

Opt. Pura & Apl. (Spain), vol.15, no.3, p.143-6 (1982).

The thermal performance of Trombe-Wall is studied in detail and the energy transfer fractions are calculated by computer simulation. The program is based on analytically developed correlations, the input data being measured values recorded within the period of one year. The annual variation of energy flow through the thermal wall into the building is represented by efficiency curves. From these efficiency curves, obtained as functions of both the specific construction characteristics and environmental conditions, it is possible to predict the amount of energy saving of passive system and also to determine the percentage of radiation, convection and natural thermocirculation rates. (4 refs.)

63728 Composition, optical properties and degradation modes of Cu/graded metal-carbon solar selective surfaces. S.Craig, G.L.Harding (School of Phys., Univ. of Sydney, Sydney, NSW, Australia).

Thin Solid Films (Switzerland), vol.101, no.2, p.97-113 (11 March 1983).

A detailed study is reported of the composition and properties of a production Cu/graded stainless steel-carbon selective surface which is incorporated in all-glass evacuated solar thermal collectors. The Auger depth profile, reflectance for wavelengths in the range 0.35-2.5 μm and temperature-dependent emittance for the range 100-300°C were determined for the selective surface before and after heat treatment of the collector at 500°C. The composition, carbon atom bonding states, electrical resistivity, refractive indices (wavelengths, 0.35-2.5 μm), IR transmittance (wavelengths, 2.5-16 μm) and emittance (100-300°C) for a set of homogeneous stainless steel-carbon component layers of the graded layer profile were also determined before and after heat treatment. In addition, a multilayer stack computer model based on the composition profile of the production selective surface and the comprehensive refractive index data for the set of homogeneous component layers was developed. Correlation of the experimental data for the set of homogeneous layers with alterations in reflectance for the multilayer stack resulting from the substitution or removal of component layers in the stack allowed a detailed evaluation of the factors determining production selective surface properties before and after heat treatment. A theoretical study of alternative grading profiles with a view to optimizing the solar selective properties of the surface is also discussed. (32 refs.)

63729 Optimization and microstructural analysis of cobalt-sulfide-pigmented aluminum oxide. A.Scherer, O.T.Inal (Dept. of Metall. & Materials Engng., New Mexico Inst. of Mining & Technol., Socorro, NM, USA).

Thin Solid Films (Switzerland), vol.101, no.4, p.311-28 (25 March 1983).

Porous anodic films formed on aluminum in a phosphoric acid electrolyte were used to develop selective solar coatings by double precipitation of cobalt acetate and ammonium sulfide inside the pores. The black coatings containing cobalt sulfide were then sealed in hot water and their optical, mechanical and thermal degradation properties were tested. Multiple linear regression routines were used to optimize the absorbance and emittance values and the coating formation conditions were accordingly adjusted. After optimization, the coatings were characterized by scanning and transmission electron microscopy, and thermal stability tests were performed to determine the long-term quality

of the coatings. The coatings were found to have good thermal stability up to 150°C and high adhesion strength as well as absorbances of up to 0.965 at emittances ranging from 0.15 to 0.25. (15 refs.)

63730 Results and analysis of a round robin test series using solar simulators. J.E.Moon.

Report EUR 8006 EN, Comm. European Communities, Luxembourg (1982), 53 pp. Contract ESA-G-047-UK(N).

This round robin test series using solar simulators was performed as part of a collaborative programme co-ordinated by the Commission of the European Communities to assess and develop methods of testing solar collectors within the European Community. Eight laboratories, representing seven E.C. Countries, have undertaken thermal performance tests on the Dutch (DRU) flat plate collector in their solar simulators. These results have been analysed and are presented individually for each laboratory and also collectively. As part of the analysis, the measured data has been adjusted to allow for differences in the environmental test conditions between laboratories. Conclusions are drawn which will form the basis for recommendations on testing solar collectors in solar simulators to be documented and included in the next edition of the 'CEC Recommendations for European Solar Collector Test Methods' (to be published in 1983). (5 refs.)

Implantation as a tool for performing selective materials (application to solar energy conversion) See Entry 61943

86.40 ENERGY STORAGE (SECONDARY ENERGY)

86.40C Storage in mechanical energy

63731 Compressed-air energy storage: Commercialization potential and EPR roles in the commercialization process. D.W.Boyd, O.E.Buckley, E.C.Clark.

Report EPR-EM-2780, Electr. Power Res. Inst., Palo Alto, CA, USA (Dec. 1982), 160 pp.

Available from Res. Rep. Center, Box 50490, Palo Alto, CA 94303, USA. Describes an assessment of potential roles that EPR might take to facilitate the commercial acceptance of compressed-air energy storage (CAES) systems. Detailed analyses of the market potential of utility storage technologies are provided, and interviews with representatives of key participants in the CAES market are presented. A decision analysis synthesizing much of the information about market and technology status is given.

86.40F Storage in thermal energy

63732 Development of thermal energy storage technology using metal hydrides. I.Yonezu, K.Nasako, N.Honda, T.Sakai (Res. Centre, Sanyo Electric Co. Ltd., Osaka, Japan).

J. Less-Common Met. (Switzerland), vol.89, no.2, p.351-8 (Feb. 1983). (International Symposium on the Properties and Applications of Metal Hydrides, Toba, Japan, 30 May-4 June 1982).

The rate of heat transfer is important in heat storage technology using metal hydrides because the rate of hydrogen transfer depends on the rate of heat transfer. A new metal hydride container with heat pipes which were able to transfer heat rapidly was constructed and was used to operate the heat storage system with a hydrogen flow of 1.5 l min⁻¹ between 3.5 kg beds of CaNi_2 and LaNi_2 . The metal hydride beds were located inside cylindrical heat pipes 66 cm long with an inside diameter of 4 cm. (2 refs.)

63733 Dynamic characteristics of a hydride heat storage system. M.Kawamura, S.Ono (Nat. Chem. Lab. for Industry, Ibaraki, Japan), Y.Mizuno.

J. Less-Common Met. (Switzerland), vol.89, no.2, p.365-72 (Feb. 1983). (International Symposium on the Properties and Applications of Metal Hydrides, Toba, Japan, 30 May-4 June 1982).

An Mg_2Ni hydride heat storage system for a batch polymerization reaction was designed and manufactured and its performance was investigated experimentally. A theoretical model to describe the dynamic characteristics of the hydride heat storage (HHS) system was also developed. The model predictions are in good agreement with the experimental performance of the HHS system. The temperature gain of the heat transfer medium depends strongly on the heat transfer area, the flow rate of the heat transfer medium and the heat transfer coefficient. (3 refs.)

Study of water heating by solar energy through the ground See Entry 63644

A heat storage reactor for metal hydrides See Entry 63736

Hydrogen permeability of hydride powder during the heat generation stage See Entry 63737

86.40H Storage in chemical energy

Redox ion flow cell for solar energy storage See Entry 63655

86.40K Hydrogen storage and technology

63734 Light-induced generation of hydrogen at CdS-monograin membranes. D.Meissner, R.Memming, B.Kastening (Inst. fur Phys. Chem., Univ. Hamburg, Hamburg, Germany).

Chem. Phys. Lett. (Netherlands), vol.96, no.1, p.34-7 (25 March 1983).

A new kind of membrane consisting of small particles of single-crystalline CdS embedded in a polymer film is described. In various photoelectrolysis experiments the properties of the membrane which separates a cell in two compartments were investigated. Relatively large quantities of H_2 were produced in the presence of an electron donor such as S^{2-} ions or EDTA and small quantities by direct photoelectrolysis of H_2O . This technique gives information on the role of catalysts deposited on one or both faces of the membrane. (15 refs.)

63735 A technique for analyzing reversible metal hydride system performance. P.M.Golben, E.L.Huston (Ergenics Div., MPD Technol. Corp., Wycokoff, NJ, USA).

J. Less-Common Met. (Switzerland), vol.89, no.2, p.333-40 (Feb. 1983). (International Symposium on the Properties and Applications of Metal Hydrides, Toba, Japan, 30 May-4 June 1982).

An experimental method is described which permits rapid characterization of hydride modules without requiring internal measurement of the bed temperature. The time to charge or discharge is measured as a function of the hydrogen pressure. A pressure-to-temperature transformation which relies on reversible metal hydride thermodynamics is applied to determine the bed temperature. This transformation facilitates conventional heat transfer analysis on hydride modules. Results are presented for the charging of a 0.375 in (0.95

cm) tubular hydride module. The time to 90% charge is less than 5 min when the temperature difference between the LaNi_5 bed and the external cooling water exceeds 14°C . This result compares very favorably with laboratory reactors designed for rapid heat transfer. (18 refs.)

63736 A heat storage reactor for metal hydrides. S.Wakao, M.Sekine (Tokai Univ., Kanagawa, Japan), H.Endo, T.Ito, H.Kanazawa. *J. Less-Common Met. (Switzerland)*, vol.89, no.2, p.341-50 (Feb. 1983). (International Symposium on the Properties and Applications of Metal Hydrides, Toba, Japan, 30 May-4 June 1982).
A reactor for a metal hydride heat storage system is required to have good heat transfer properties and as small a heat capacity as possible because the heat produced during the metal-hydrogen reaction is finite and its loss must be minimized. However, few theoretical studies of heat storage reactors that use finite quantities of heat have been made. The transfer of the heat of reaction in the reactor was studied theoretically and experimentally and the results are summarized. The theoretical and experimental results agreed relatively well, so that the application of the fundamental concept proposed in this paper to the design of heat storage reactors using metal hydrides which produce finite quantities of heat is justified. (1 ref.)

63737 Hydrogen permeability of hydride powder during the heat generation stage. M.Kawamura, S.Ono (Nat. Chem. Lab. for Industry, Ibaraki, Japan), S.Higano, K.Kamino. *J. Less-Common Met. (Switzerland)*, vol.89, no.2, p.359-63 (Feb. 1983). (International Symposium on the Properties and Applications of Metal Hydrides, Toba, Japan, 30 May-4 June 1982).
The permeability characteristics of a hydride powder bed were examined experimentally. Powder movement, which was assumed to be due to backward and forward flow, was observed after a number of hydriding-dehydriding cycles. When the exothermic reaction was performed at high temperatures, a pressure drop between the end point and the filter pipe appeared; however, no such pressure drop was observed at room temperature, when no reaction occurred. It is shown that the development of equipment to reduce the pressure drop is of importance in the improvement of this novel heat storage system. (4 refs.)

63738 Hydrogen storage in thin film metal hydrides. H.Wenzl, K.-H.Klatt, P.Meuffels (Inst. für Festkörperforschung, KFA Jülich, Jülich, Germany), K.Papathanassopoulos. *J. Less-Common Met. (Switzerland)*, vol.89, no.2, p.489-94 (Feb. 1983). (International Symposium on the Properties and Applications of Metal Hydrides, Toba, Japan, 30 May-4 June 1982).
Sandwich films were prepared by vapour deposition on quartz crystals or polycrystalline aluminium foil, e.g. $\text{quartz}/\text{V}(1\ \mu\text{m})/\text{Pd}(100\ \text{nm})$ and $\text{Al}(20\ \mu\text{m})/\text{Pd}(100\ \text{nm})/\text{V}(10\ \mu\text{m})/\text{Pd}(100\ \text{nm})$. The vanadium films can be hydrided almost reversibly from the gas phase within seconds to $\text{VH}_{0.5}$ at 300K and a hydrogen pressure of 1 bar and within 1 min to $\text{VH}_{1.8}$ at 300K and a hydrogen pressure of 30 bar. The known phase diagrams of the V-H_2 system were reproduced. The $\text{Al}/\text{Pd}/\text{V}/\text{Pd}$ films were used in prototype hydrogen storage containers: a 2% mass fraction of hydrogen was stored, similar to TiFe hydride storage, but a much higher heat exchange rate was attained. (5 refs.)

63739 Life properties of Ti-Mn alloy hydrides and their hydrogen purification effect. T.Gamo, Y.Moriwaki, N.Yanagihara, T.Iwaki (Central Res. Lab., Matsushita Electric Industrial Co. Ltd., Osaka, Japan). *J. Less-Common Met. (Switzerland)*, vol.89, no.2, p.495-504 (Feb. 1983). (International Symposium on the Properties and Applications of Metal Hydrides, Toba, Japan, 30 May-4 June 1982).
The effects of pressure-induced absorption-desorption cycling on the degradation properties and the hydrogen purification ability of Ti-Mn alloy hydrides were studied. The lines in the characteristic X-ray diffraction pattern were much broader and weaker in the cycled alloys but the C14 hexagonal structure was maintained and no second phase was observed. The hydrogen capacity was reduced by 30% for Ti-Mn binary alloy and by 20% for Ti-Mn multicomponent alloys after about 10000 cycles in contrast with the marked reduction observed for LaNi_5 . In some cases slight recovery could be produced by heating at 500°C for 1 h in a vacuum after cycling. Gas chromatography measurements on hydrogen released from $\text{TiMn}_{1.5}$ hydride showed that the hydrogen purity was better than 99.9999% (except for an H_2O impurity) after a purge release of only a few per cent of hydrogen when the purity of the commercial grade hydrogen absorbed by the hydride was 99.99%. It can be concluded from the results of these measurements that hydrogen purification using Ti-Mn alloy is related to two factors. The removal of N_2 , CO and CO_2 proceeds by surface poisoning (i.e. oxidation, physisorption or chemisorption), whereas the removal of CH_4 , O_2 , H_2O and Ar is controlled by surface poisoning and concentration. The hydrogen purification effect of Ti-Mn alloy hydrides showed little degradation even after a large number of absorption-desorption cycles. (11 refs.)

63740 Hydrogen storage properties of FeTi_{1+x} and $\text{FeTi}_{1+x}\text{O}_y$ flakes produced by splat quenching. M.Amano, Y.Sasaki, R.Watanabe, M.Shibata (Nat. Res. Inst. for Metals, Tokyo, Japan). *J. Less-Common Met. (Switzerland)*, vol.89, no.2, p.513-18 (Feb. 1983). (International Symposium on the Properties and Applications of Metal Hydrides, Toba, Japan, 30 May-4 June 1982).
The splat quenching method was used to produce FeTi_{1+x} and $\text{FeTi}_{1+x}\text{O}_y$ flakes in order to simplify the pulverizing process. Batches (300-1000 g) of $\text{FeTi}_{1.22}$, $\text{FeTi}_{1.23}\text{O}_{0.007}$ and $\text{FeTi}_{1.24}\text{O}_{0.04}$ flakes 0.10-0.15 mm thick were produced using a rotating water-cooled disc after arc melting the constituent metals in an argon atmosphere. The hydrogen storage properties of the splat-quenched and annealed flakes were investigated. The powders obtained by pulverizing $\text{FeTi}_{1.22}$, $\text{FeTi}_{1.23}\text{O}_{0.007}$ and $\text{FeTi}_{1.24}\text{O}_{0.04}$ flakes reacted with hydrogen even after storage for several months in a desiccator or immersion in water for several days. They can also be hydrided after an incubation period at room temperature without any heat treatment. The addition of the oxide phase produces a reduction in the incubation time. (9 refs.)

63741 Development of hydrides for motor vehicles. J.Topler, O.Bernauer, H.Buchner, H.Sauferer (Daimler-Benz AG, Stuttgart, Germany). *J. Less-Common Met. (Switzerland)*, vol.89, no.2, p.519-26 (Feb. 1983). (International Symposium on the Properties and Applications of Metal Hydrides, Toba, Japan, 30 May-4 June 1982).
The storage of hydrogen in metal hydrides is suitable for motor vehicles as well as for stationary applications. Since the metal hydrides are used both for fuel and for heat storage some interesting technical developments are possible. The development and applications of low and high temperature hydrides are reported and the solutions of some technical problems (e.g. improvement of heat transfer and hydride manufacture) are presented. (7 refs.)

63742 RNi_5 hydrogen storage compounds. J.Liu (Res. Center, Inco Alloy Products Co., Suffern, NY, USA), E.L.Huston. *J. Less-Common Met. (Switzerland)*, vol.89, no.2, p.527 (Feb. 1983). (International Symposium on the Properties and Applications of Metal Hydrides, Toba, Japan, 30 May-4 June 1982).
Summary form only given, as follows. The production of low cost RNi_5 hydrogen storage compounds requires the effective utilization of low cost rare earth mixtures and their byproducts. In this study a wide variety of commercial rare earth mixtures was used in the preparation of RNi_5 alloys which were successfully evaluated for hydriding properties. Blends of rare earth mixtures can be made to adjust hydride properties over wide ranges. The hydrogen capacity exceeded hydrogen-to-metal atomic ratios of 1.0 for all samples tested and was found to be independent of the rare earth ratios. Hydriding properties can be predicted well with linear regression equations derived from the experimental data and involving cerium, lanthanum, praseodymium and neodymium weight fractions. The desorption plateau pressure at 25°C is given by the relation; $\ln P_D = 10.60 - 5.70X_{\text{Ce}} - 10.03X_{\text{La}} - 8.46X_{\text{Pr}} - 7.40X_{\text{Nd}}$, when the rare earth weight fractions are normalized to give $X_{\text{Ce}} + X_{\text{La}} + X_{\text{Pr}} + X_{\text{Nd}} = 1$. (no refs.)

63743 Recent production of rare earth metals as hydriding materials. H.Toma, R.Ohmachi (Santoku Metal Industry Co., Kobe, Japan). *J. Less-Common Met. (Switzerland)*, vol.89, no.2, p.528 (Feb. 1983). (International Symposium on the Properties and Applications of Metal Hydrides, Toba, Japan, 30 May-4 June 1982).
Summary form only given, as follows. Gives a general view of the resources and production capacity of rare earths including misch metal and lanthanum metal for metal hydride applications. The composition and methods of producing misch metal and lanthanum metal are discussed. (no refs.)

63744 Development of a hydrogen storage system using metal hydrides. H.Suzuki, Y.Osumi, A.Kato, K.Oguro, M.Nakane (Government Industrial Res. Inst., Osaka, Japan). *J. Less-Common Met. (Switzerland)*, vol.89, no.2, p.545-50 (Feb. 1983). (International Symposium on the Properties and Applications of Metal Hydrides, Toba, Japan, 30 May-4 June 1982).
Fundamental research has been carried out on the development of the basic technology for a stationary hydrogen storage system using metal hydrides. The authors have built and tested a misch metal-nickel-manganese hydride storage reservoir (a unit cell), with an effective storage capacity of $1.6\ \text{m}^3$ of hydrogen. On the basis of the experiments, they have built and tested a stationary hydride reservoir for hydrogen storage constructed from many layers of the unit cells; this has a possible storage capacity of $16\ \text{m}^3$ of hydrogen. (5 refs.)

63745 RNi_5 hydrogen storage compounds ($\text{R} \equiv$ rare earth). J.Liu (Inco Res. & Dev. Center, Suffern, NY, USA), E.L.Huston. *J. Less-Common Met. (Switzerland)*, vol.90, no.1, p.11-20 (March 1983).
The production of low cost RNi_5 ($\text{R} \equiv$ rare earth) hydrogen storage compounds requires the effective utilization of low cost rare earth mixtures and their byproducts. A wide variety of commercial rare earth mixtures was used in the preparation of RNi_5 alloys which were successfully evaluated for hydriding properties. Blends of rare earth mixtures can be made to adjust hydride properties over wide ranges. Plateau pressures and hysteresis can be predicted well with linear regression equations involving cerium, lanthanum, praseodymium and neodymium weight fractions. The hydrogen capacity exceeded $[\text{H}]/[\text{M}] = 1.0$ for all samples tested and was found to be independent of the rare earth ratios. (14 refs.)

63746 Hydrogen absorption in $\text{La}_3\text{Ni}_{13}\text{B}_2$. F.Spada, H.Oesterreicher (Dept. of Chem., Univ. of California, San Diego, La Jolla, CA, USA). *J. Less-Common Met. (Switzerland)*, vol.90, no.1, p.1-4 (March 1983).
Reports on the hydriding properties of $\text{La}_3\text{Ni}_{13}\text{B}_2$ ($\text{LaNi}_{4.33}\text{B}_{0.67}$). Samples of differing composition were prepared to ascertain the binary stoichiometry. Compounds were prepared by induction melting the constituent elements. The samples were annealed, and then X-ray powder patterns were obtained using both $\text{CuK}\alpha$ and $\text{Cr K}\alpha$ radiation to verify phase purity. The hydrogen desorption isotherm was determined by pressure monitoring over the range 10 to 100 atm. (7 refs.)

Effective thermal conductivity of metal hydride beds See Entry 61384
Heat transmission analysis of metal hydride beds See Entry 61385
The properties of a metal hydride fuel for use in an urban vehicle
..... See Entry 63635
Development of thermal energy storage technology using metal hydrides
..... See Entry 63732
Dynamic characteristics of a hydride heat storage system See Entry 63733

86.70 ENVIRONMENTAL SCIENCE

(see also 87.60R Radioactive pollution; for oceanographic aspects, see 92.10; for hydrological aspects see 92.40; for meteorological aspects see 92.60)

86.70C Soil

63747 Effect of decreased use of lead in gasoline on the soil of a highway. D.S.Byrd, J.T.Gilmore, R.H.Lea (Dept. of Chem., Northeast Louisiana Univ., Monroe, LA, USA). *Environ. Sci. & Technol. (USA)*, vol.17, no.2, p.121-3 (Feb. 1983).
So that the effect on lead concentrations in highway soils of the mandatory use of unleaded gasoline in new automobiles could be assessed, lead concentrations in soils along US Interstate 20 in northeast Louisiana were determined in 1973, 1974, and 1979. These concentrations increased from 1973 to 1974 but decreased from 1973 to 1979. Lead in the soil moved slowly in the direction of surface water flow. Lead concentrations decreased with depth to 300 mm but then increased. The mandatory use of unleaded gasoline has decreased the lead concentrations in soils near highways. (7 refs.)

Proceedings of the Symposium on Low-Level Waste Disposal. Site Characterization and Monitoring (NUREG/CP-0028) See Entry 59537
Calculation of atmospheric-fallout concentrations on a drainage basin
..... See Entry 63758

86.70E Water

63748 Estimation of the percentage of annual groundwater recharge with bomb tritium using a cumulative mass balance method. B.C.E.Egboka (Dept. of Geol., Univ. of Nigeria, Nsukka, Nigeria), J.A.Cherry, R.N.Farvolden. *Pure & Appl. Geophys. (Switzerland)*, vol.120, no.2, p.330-47 (1982).
The bomb tritium (^3H) distribution patterns in the aquifer beneath an abandoned landfill at the Canadian Forces Base (CFB) Borden, Ontario, and in a

sandy aquifer at Whiteshell Nuclear Research Establishments (WNRE) Pinawa, Manitoba, all in Cada, were delineated in great detail. A sampling and monitoring network of multilevel samplers and bundle piezometers were used. The directions of groundwater flow were established, and the boundary between the tritiated and non-tritiated zones of the two aquifers were closely demarcated. Using a cumulative mass balance method, the ^3H input mass into the aquifers was compared with the ^3H mass in groundwater storage to estimate the percentages of annual groundwater recharge from 1953 to 1978. (12 refs.)

63749 Use of data on warm industrial effluents to study the dispersal of pollutants in rivers. V.A.Averkov, N.N.Del'vin, V.V.Pisarev, R.L.Strunze, A.K.Sukhoruchkin (Inst. of Appl. Geophys., USSR). *Sov. Meteorol. & Hydrol. (USA)*, no.1, p.65-9 (1982). Translation of: *Meteorol. & Gidrol. (USSR)*, no.1, p.82-7 (1982).

The possibility of using heated waste waters to study the dispersal of pollutants that they carry is examined. The problem posed is solved with the aid of differential equations that describe turbulent transport of matter and heat in a mixed flow within a two-dimensional watercourse. A linear relation linking the temperature and the concentration of the pollutants at each point of the stream is derived. A series of field experiments has been performed to test this relationship. (7 refs.)

63750 Water pollution in the Fukuoka area. H.Yorozu, Y.Awaya, T.Kusuda.

Technol. Rep. Kyushu Univ. (Japan), vol.55, no.4, p.329-36 (Aug. 1982). In Japanese. [received: Feb. 1983]

For the conservation of water areas and the purification of water, positive environment-planning is required. To make clear the relationship between urban development and water pollution, the water quality levels of eleven rivers in the Fukuoka area during the past twenty-one years are investigated. Water quality levels in some rivers were predicted with regression analysis, in which the objective variables, water quality indices, are BOD and $\text{NH}_4\text{-N}$, and the number of the explanation variables is fourteen. In the case of analysis with data of the three river basins, the results are not applicable to the prediction of the water quality in other river basins with different regional characteristics such as the area of urban districts, and commercial and industrial population density. In the case of analysis with data of all the river basins investigated, the water quality in each river can be predicted to some extent. In order to improve the results in this study, additional variables would be needed. (4 refs.)

63751 Some aspects of the influence of surface and ground water chemistry on the mobility of thorium in the 'Morro do Ferro' environment. N.Miekeley, M.G.R.Vale, M.Tavarez (Catholic Univ. of Rio de Janeiro, Rio de Janeiro, Brazil), W.Lei.

Scientific Basis for Nuclear Waste Management V. Proceedings of the Materials Research Society Fifth International Symposium on the Scientific Basis for Nuclear Waste, Berlin, Germany, 7-10 June 1982 (New York, USA: North-Holland 1982), p.725-33

During one year the elemental composition and some relevant physico-chemical parameters of stream water, which receives drainage water from the radioactive deposit have been measured. In addition, ground water samples from bore holes, as well as stagnant waters from trenches, and percolation waters from an old mine gallery have been analyzed. Although the data are still incomplete, the authors felt encouraged to publish preliminary results, noticing that information concerning thorium concentration in natural waters, especially ground waters, are very scarce. (12 refs.)

63752 Potential for the rapid transport of plutonium in groundwater as demonstrated by core column studies. D.R.Champ, W.F.Merritt, J.L.Young (Chalk River Nuclear Labs., Atomic Energy of Canada Ltd., Chalk River, Ontario, Canada).

Scientific Basis for Nuclear Waste Management V. Proceedings of the Materials Research Society Fifth International Symposium on the Scientific Basis for Nuclear Waste, Berlin, Germany, 7-10 June 1982 (New York, USA: North-Holland 1982), p.745-54

Examines the potential for the transport of Pu in a groundwater flow system through the use of laboratory columns prepared from 'undisturbed' horizontal cores taken from saturated zone soils adjacent to the Chalk River glass block site. The columns were spiked with ^{239}Pu , continuously eluted with groundwater from the glass block site, and the activity and physical-chemical characteristics of the ^{239}Pu in the effluent determined following various manipulations of the column elution conditions. (9 refs.)

Proceedings of the Symposium on Low-Level Waste Disposal. Site Characterization and Monitoring (NUREG/CP-0028) See Entry 59537

Need for geological characterization of low-level nuclear waste disposal sites See Entry 60250

Geotechnical measurements at the Maxey Flats, Kentucky low-level radioactive waste disposal site—lessons learned See Entry 60255

Hydrologic characterization of sites for shallow disposal of low-level radioactive wastes See Entry 60256

Techniques of groundwater investigation at proposed low-level nuclear waste disposal sites See Entry 60257

Ground-water monitoring techniques for low-level radioactive disposal sites See Entry 60258

Lessons learned in a hydrogeological case at Sheffield, Illinois See Entry 60259

Surface water considerations for low-level radioactive waste site See Entry 60260

Hydrologic and hydrodynamic aspects of low-level radioactive waste disposal to streams See Entry 60261

Effect of releases from near-surface low-level waste sites on surface water quality See Entry 60262

Some interactive factors affecting trench cover integrity on low-level waste sites See Entry 60264

Meteorology and climatology as parameters on low level waste disposal monitoring See Entry 60267

Model for near field migration See Entry 60301

Model for far field migration See Entry 60302

Leach rates of high level waste and spent fuel: limiting rates as determined by bench and bedrock conditions See Entry 60303

Aqueous phase diffusion in crystalline rock See Entry 60304

Hydrothermal conditions around a radioactive waste repository See Entry 60306

A combined analytical model for performance assessment of the waste package/geologic medium systems See Entry 60308

Ion water migration phenomena in dense bentonites See Entry 60312

Transport of actinides through a bentonite backfill See Entry 60313

Evaluation of solubility and speciation of actinides in natural groundwaters See Entry 60314

Study of radionuclide migration from deep-lying repository sites with overlying sedimentary layers See Entry 60315

A comparison of in-situ radionuclide migration studies in the Studsvik area and laboratory measurements See Entry 60316

Liquid chromatography in migration studies See Entry 60318

Studies of the mobilization of thorium from the Morro do Ferro See Entry 60319

Properties and mobilities of actinide colloids in geologic systems See Entry 60320

The migration of radionuclides with ground water. A discussion of the relevance of the input parameters used in model calculations See Entry 60321

Laboratory tests on the migration behavior of selected fission products in aquifer materials from a potential disposal site in northern Germany See Entry 60323

Modelling of the migration of lanthanoids and actinoids in ground water; the medium dependence of equilibrium constants See Entry 60324

Evaluation of radionuclide transport: effect of radionuclide sorption and solubility See Entry 60325

Radionuclide retardation during transport through fractured granite See Entry 60326

A comparative analysis of fractured and porous medium radionuclide transport See Entry 60327

Calculation of atmospheric-fallout concentrations on a drainage basin See Entry 63758

86.70G Atmosphere

63753 The interaction between air pollution dispersion and residential heating demands. F.W.Lipfert, P.D.Moskowitz, J.Dungan, J.Tichler, T.Carney (Brookhaven Nat. Lab., Upton, NY, USA).

J. Air Pollut. Control Assoc. (USA), vol.33, no.3, p.208-11 (March 1983).

Urban air pollution has traditionally been modeled using annual, or at best, seasonal emissions inventories and climatology. These averaging techniques may introduce uncertainty into the analysis, if specific emissions (e.g. SO_2) are correlated with dispersion factors on a short-term basis. This may well be the case for space heating emissions. An analysis of this problem, using hourly climatological and residential emission estimates for six US cities, indicates that the errors introduced using such averages are modest ($\sim \pm 12\%$) for annual average concentrations. Maximum hourly concentrations vary considerably more, since maximum heat demand and worst case dispersion are in general not coincident. The paper thus provides a basis for estimating more realistic air pollution impacts due to residential space heating. (8 refs.)

63754 Smog chamber studies of NO_x transformation rate and nitrate/precursor relationships. C.W.Spicer (Battelle Columbus Labs., Columbus, OH, USA).

Environ. Sci. & Technol. (USA), vol.17, no.2, p.112-20 (Feb. 1983).

An environmental chamber study of nitrogen oxide reactions is described. The aim of the investigation was to determine (1) the rate of NO_x transformation to nitrate products, (2) the environmental factors that influence the transformation rate, (3) the relationship between nitrate products and their hydrocarbon and NO_x precursors, and (4) relationships among NO_x , O_3 , and nitrates. The experiments made use of a 17-component hydrocarbon mixture designed to represent the major organic constituents of urban air. The implications and limitations of the experimental results are discussed. (23 refs.)

63755 Acid fog. B.Hileman.

Environ. Sci. & Technol. (USA), vol.17, no.3, p.117A-20A (March 1983).

Provides an account of the occurrence of acid fog. Acid fog occurs as a result of pollution. The author reports observations made in southern California that were made with a rotating arm collector. In addition to pH observations of NO_3^- , SO_4^{2-} , NH_4^+ and H^+ were also made. The observations indicate that acid fog is an important pollution phenomena and that very high acidity levels may occur away from the pollution source. Previous to these studies pollution measurements on foggy days only sample the ambient levels of gases in the air and ignored the pollution within fog droplets. (3 refs.)

63756 Gaseous tracers of Arctic haze. M.A.K.Khalil, R.A.Rasmussen (Dept. of Environmental Sci., Oregon Graduate Center, Beaverton, OR, USA).

Environ. Sci. & Technol. (USA), vol.17, no.3, p.157-64 (March 1983).

At Pt. Barrow in the Arctic, winter concentrations of CHCl_3 , CCl_2F_2 , CCl_3F , CH_2Cl_2 , C_2Cl_4 , C_2HCl_3 , CO , and CH_3Cl exceed their concentrations during other times of the year, similar to the seasonal pattern of Arctic haze. The anthropogenic halocarbons and the combustion-derived CO and CH_3Cl are produced at the same midlatitude locations as the precursors of Arctic haze and therefore serve as inert tracers of long-distance transport of pollution to the Arctic atmosphere. The best gaseous tracers of Arctic haze are entirely man-made and have atmospheric lifetimes of less than about 5 years, or their concentrations are far from equilibrium with current yearly emissions. The presence of combustion-derived gaseous pollution in the Arctic during winter agrees with independent studies showing a significant combustion-derived component in the Arctic haze aerosol. During winter faster transport of polluted air to the Arctic is partly responsible for the occurrence of Arctic haze as well as the observed excess concentrations of trace gases. (33 refs.)

63757 Numerical simulation of fog formation and liquid water content on polydisperse multi-composition aerosols due to combustion-related pollutants. R.J.Hung (Univ. of Alabama, Huntsville, AL, USA), G.S.Liaw, R.E.Smith.

J. Environ. Sci. (USA), vol.26, no.1, p.44-8 (Jan.-Feb. 1983).

Reports the results of investigations of the dynamic and microphysical processes involved in the formation of advection fog on aerosols. The effects of a polydisperse aerosol distribution and a multi-composition aerosol species on the condensation/nucleation processes are of particular interest. The results show that an aerosol population with a high particle concentration provides more favorable conditions for the formation of a denser fog than an aerosol population with a larger particle size, if the value of the total mass concentration of the aerosols is kept constant. A numerical study of the effect of the aerosol particle size distribution on the wet removal nucleation processes shows that the aerosol particle size distribution does not affect the amount of liquid water produced if the mass concentration of the aerosol particles is kept constant. (18 refs.)

- 63758 Calculation of atmospheric-fallout concentrations on a drainage basin.** V.A.Borizlov, N.I.Troyanova (Inst. of Experimental Meteorology, USSR). *Sov. Meteorol. & Hydrol. (USA)*, no.1, p.76-8 (1982). Translation of: *Meteorol. & Gidrol. (USSR)*, no.1, p.95-7 (1982).
A model that includes washing into surface waters, fixing in the soil, and contamination of bottom sediment is proposed for the behavior of pollutants of global origin in a drainage basin. The model is illustrated using the behavior of strontium-90 in the soil and rivers of the Podmoskov'e. (2 refs.)
- Proceedings of the Symposium on Low-Level Waste Disposal. Site Characterization and Monitoring (NUREG/CP-0028)** See Entry 59537
- Air quality measurements for site characterization** See Entry 60265
- Radiochemical measurements for evaluating air quality in the vicinity of low-level waste burial sites—the West Valley experience** See Entry 60266
- Meteorology and climatology as parameters on low level waste disposal monitoring** See Entry 60267
- On-site meteorological measurements for low-level radioactive waste disposal** See Entry 60268
- An air quality data analysis system for interrelating effects, standards, and needed source reductions. VII. An O₃-SO₂ leaf injury mathematical model** See Entry 63760
- Physics of remote sensing** See Entry 63761
- Possibility of using certain transitions of He-Ne and He-Xe lasers for the analysis of nitric oxide, sulfur dioxide, and higher hydrocarbons** See Entry 63762
- High-sensitivity atmospheric gas analysis based on intracavity laser detection of scattered radiation** See Entry 63763
- The NO/NO₂/O₃ photostationary state in Claremont, California** See Entry 64160
- Air quality screening model with long-term averaging** See Entry 64161
- Major ion composition and chemical associations of inorganic atmospheric aerosols** See Entry 64168
- Global distribution and southern hemispheric trends of atmospheric CCl₄F** See Entry 64189

86.70J Noise

(see also 43.50 Noise, its effects and control)

- 63759 Using the NRR to estimate the real world performance of hearing protectors.** E.H.Berger (EAR Div., Cabot Corp., Indianapolis, IN, USA). *Sound & Vib. (USA)*, vol.17, no.1, p.12-18 (Jan. 1983).
The efficacy of single number measures of hearing protector noise reduction is examined. The accuracy of such estimates is shown to be a function of both the procedure by which the single number is computed and of the assumed attenuation data from which it is computed. One such single number measure is the EPA's Noise Reduction Rating (NRR) which is intended to be subtracted from the C-weighted work-place noise levels in order to estimate the employees' A-weighted exposures. By summarizing data from over 10 studies, incorporating 1551 subjects, it is demonstrated that the principal error in using the NRR or an NRR-like number is the basic laboratory data from which the NRR is computed. Thus, utilization of a long method computation involving an octave band noise analysis and the full attenuation and standard deviation data for the protector, gains one little in terms of improving estimates of the actual protection received by industrial populations. (19 refs.)
- Proceedings of the Third International Workshop on Railway and Tracked Transit System Noise** See Entry 59530
- Influence of the time pattern of noise exposure on the acquisition of and recovery from auditory fatigue.** See Entry 63856

86.70L Measurement techniques in environmental science

- 63760 An air quality data analysis system for interrelating effects, standards, and needed source reductions. VII. An O₃-SO₂ leaf injury mathematical model.** R.I.Larsen (US Environmental Protection Agency, Res. Triangle Park, NC, USA), A.S.Heagle, W.W.Heck. *J. Air Pollut. Control Assoc. (USA)*, vol.33, no.3, p.L98-207 (March 1983).
For pt.VI see ibid., vol.30, p.662 (1980). Leaf injury data from acute and chronic exposure studies of Dare soybean were regressed against the logarithms of exposure time and O₃ and SO₂ concentrations to develop a new two-pollutant leaf injury model (which explains 88% of the variance) and to calculate the parameters of best fit for this new model and a previously developed one-pollutant model. Using the calculated parameters, the percentage of leaf surface injured over a growing season by O₃, SO₂, or both simultaneously was estimated for an ambient air sampling site located 2 miles from a coal burning power plant. For this site, the one- and two-pollutant models predicted that SO₂ effects would be negligible if SO₂ concentrations never exceeded the National Ambient Air Quality Standard (NAAQS) of 0.50 ppm, averaged over 3 h. However, calculations suggest that O₃ may injure up to 24% of Dare soybean leaf surface over a growing season even though the O₃ NAAQS of 0.12 ppm, averaged over 1 h, is never exceeded. (19 refs.)
- 63761 Physics of remote sensing.** B.L.Deekshatulu, O.P.Bajpai (Nat. Remote Sensing Agency, Secunderabad, India). *Curr. Sci. (India)*, vol.51, no.24, p.132-43 (20 Dec. 1982).
Discusses the features, of multispectral remote sensing beginning with illustrations of the typical spectral signatures of Earth features and effects of physical and biological processes on the spectral signatures. This is followed by a brief discussion on the effects of the atmosphere on remote sensing and the possible ways of correcting for them. The instrumentation for multispectral remote sensing is also discussed followed by a brief mention of the applications of remote sensing to various disciplines. The discussion is limited to the optical region of the EM spectrum i.e. 0.3 to 15 μ m which is the most exploited spectral region for remote sensing. (14 refs.)
- 63762 Possibility of using certain transitions of He-Ne and He-Xe lasers for the analysis of nitric oxide, sulfur dioxide, and higher hydrocarbons.** A.I.Popov, A.V.Sadchikhin. *J. Appl. Spectrosc. (USA)*, vol.36, no.5, p.499-501 (May 1982). Translation of: *Zh. Prikl. Spektrosk. (USSR)*, vol.36, no.5, p.727-30 (May 1982). [received: Feb. 1983]
Reports on a feasibility study of the analysis of NO, SO₂ and total higher hydrocarbons by means of a He-Ne laser ($\lambda=3.3912$ and 5.4048μ m) and He-Xe laser ($\lambda=3.3676$ and 3.9966μ m). In order to determine the feasibility

and desirability of using these lasers in the analysis of these gases, it is necessary to measure the absorption coefficients K of the radiation from the named transitions in these gases. In determining K, the authors measured the absorption of radiation of the main transitions in cuvettes of various length filled with mixtures of these gases in nitrogen. (9 refs.)

- 63763 High-sensitivity atmospheric gas analysis based on intracavity laser detection of scattered radiation.** A.P.Godlevskii, A.K.Ivanov, Yu.D.Kopytin (Inst. of Atmospheric Optics, Acad. of Sci., Tomsk, USSR). *Sov. J. Quantum Electron. (USA)*, vol.12, no.10, p.1304-7 (Oct. 1982). Translation of: *Kvantovaya Elektron., Moskva (USSR)*, vol.9, no.10, p.2007-12 (Oct. 1982). [received: April 1983]
A method of atmospheric gas analysis, based on intracavity detection of scattered radiation, is proposed and investigated. A theory of the method is developed for incoherent detection of the radiation in a laser and its possibilities are estimated. Investigations of intracavity lidar systems utilizing ruby, neodymium glass, and argon lasers are described. (12 refs.)
- 63764 On the organization of a new observing network for environmental pollution monitoring.** T.N.Zhigalovskaya, I.M.Nazarov, Sh.D.Fridman, O.S.Renne (Inst. of Appl. Geophys., USSR). *Sov. Meteorol. & Hydrol. (USA)*, no.1, p.49-55 (1982). Translation of: *Meteorol. & Gidrol. (USSR)*, no.1, p.62-70 (1982).
The advantages of using network snow surveys for a new environmental (air, surface water, soil) pollution monitoring network are pointed out. Problems of organizing the observations and using them to evaluate the pollution and forecast changes are considered. The discussion is based on five years of work in various regions of the USSR. (9 refs.)
- Measurement of iodine-129 at the femtogram level by negative surface ionization mass spectrometry** See Entry 60480

86.70Z Other topics

- Plutonium recycling scenario in light water reactors. Assessment of the environmental impact in the European Community** See Entry 59523
- Environmental information needed to license a low-level waste disposal facility** See Entry 60263
- Radionuclide retardation and release rates for oceanic sediments and clay** See Entry 60317
- Sorption of actinides in well-defined oxidation states on geologic media** See Entry 60322

87.00 BIOPHYSICS, MEDICAL PHYSICS, AND BIOMEDICAL ENGINEERING

87.10 GENERAL, THEORETICAL, AND MATHEMATICAL BIOPHYSICS

(inc. logic of biosystems, quantum biology, and relevant aspects of thermodynamics, information theory, cybernetics, and bionics)

- 63765 Inhomogeneous interfacial regions of biological systems. I. Basic differential equations and their implications.** V.S.Vaidhyanathan (Dept. of Biophys. Sci., State Univ. of New York, Buffalo, NY, USA). *J. Biol. Phys. (USA)*, vol.10, no.3, p.153-66 (1982).
On the premise that the contributions from ion-ion interaction energy terms to chemical potential of an ion in inhomogeneous regions cannot be neglected, the classical expression for electrochemical potential is modified. Resulting basic differential equations and their implications regarding ion distributions in inhomogeneous regions are presented. It is shown that a necessary consequence is the existence of a dielectric profile in inhomogeneous regions due to nonvanishing interaction energy terms of the chemical potential. (17 refs.)
- 63766 On competitive failure modes and the usefulness of a 'survival curve point of view'.** A.B.Wolbaste (Dept. of Radiation Therapy, Harvard Medical School, Boston, MA, USA). *Med. Phys. (USA)*, vol.10, no.2, p.232-6 (March-April 1983).
A number of medical phenomena may be discussed in terms of the probability of something 'surviving' as a function of time, dose, distance, etc. Employing elementary results of engineering reliability theory, the author examines the different shapes of survival curves which can arise when several modes of failure compete for the members of a homogeneous or heterogeneous population. A variety of examples of medical interest illustrate the approach. (29 refs.)
- 63767 A skeleton of physical ideas for the dynamics of complex systems.** F.E.Yates, A.S.Iberall (Crump Inst. for Medical Engng., Univ. of California, Los Angeles, CA, USA).
10th IMACS World Congress on System Simulation and Scientific Computation, Montreal, Canada, 8-13 Aug. 1982 (New Brunswick, NJ, USA: IMACS 1982), p.190-3 vol.2
Complex systems, from atomic ensembles to galactic clusters, are defined as fluid-plastic-elastic systems in which internalized atomistic time delay is large, with the consequence that interactions among parts lead to internalization of action (energy x time) and variable process delays between external inputs and outputs. Living systems are thus notably complex. The interior fields of complex systems can be described dynamically through an extended statistical mechanics and irreversible thermodynamics, in the form of an electro-magnetic-hydrodynamic field physics. Chemical reactivity (making, breaking or exchanging bonds) is subsumed in the generalized mechanics. This physical construct is applied to dynamic regulation and coordination among parts in the life forms found in the more than 300 families of flowering plants. (6 refs.)
- Use of small-angle scattering data to calculate the diameter distribution function for a system of spherical layers [biomembrane application]** See Entry 63799
- Sinusoidal voltage clamp of the Hodgkin-Huxley model** See Entry 63817
- Inhomogeneous interfacial regions of biological systems. II. Dielectric profile and ion distributions** See Entry 63820

87.15 MOLECULAR BIOPHYSICS

(see also 36.20 Macromolecules and polymer molecules)

63768 Solubility of hematoporphyrin and photodynamic damages in liposomal systems: optical and electron spin resonance studies. C.Emiliani, M.Delmelle, S.Cannistraro, A.Van de Vorst (Phys. Experimentale, Inst. de Phys., Univ. de Liege, Sart-Tilman, Belgium). *Photobiochem. & Photobiophys. (Netherlands)*, vol.5, no.2, p.119-28 (Feb. 1983).

The interaction between hematoporphyrin and egg lecithin liposomes was studied. The hematoporphyrin solubility in the lipid matrix was estimated by way of the partition coefficient which varied with lipid and sensitizer concentrations, indicating that solubilisation is a complex process. Spin labeled fatty acids were used to obtain some information about the location of maximal hematoporphyrin density within the membrane. Concerning the photodynamic damages produced by the sensitizer illumination, type I and type II mechanisms were observed but that latter amounts to more than 95%. (30 refs.)

63769 A review of some present molecular and submolecular physical concepts in biology. R.Pethig (School of Electronic Engng. Sci., Univ. Coll. of North Wales, Bangor, Wales).

J. Biol. Phys. (USA), vol.10, no.4, p.201-18 (1982).

Increasing attention is being directed towards understanding cellular processes at the molecular and submolecular levels. This article describes some of the physical concepts, such as proton transport in membrane pores and at protein-water interfaces, tunnelling processes, electronic conduction and induction effects in membrane-associated protein structures, that are currently being investigated and developed in the study of such functions as energy transduction and the passive and active transport of ions in cell membranes. (62 refs.)

63770 Protein dynamics from Mossbauer spectra. The temperature dependence. E.W.Knapp, S.F.Fischer, F.Parak (Phys. Dept. der Tech. Univ. Munchen, Garching, Germany).

J. Phys. Chem. (USA), vol.86, no.26, p.5042-7 (23 Dec. 1982).

Protein-specific dynamics reveals itself in Mossbauer spectra by a strong temperature dependence of the mean square displacement, $\langle x^2 \rangle$, of the Mossbauer nucleus. In addition, the protein dynamics may give rise to broad lines whose width and intensity also strongly depend on temperature. Both features are understood with an extension of the Brownian oscillator model which accounts for fluctuations between conformation substates mediated by transition states. The model is also capable of relating the temperature dependence of $\langle x^2 \rangle$ values obtained from X-ray investigations and Mossbauer experiments. $\langle x^2 \rangle$ values from Mossbauer experiments exhibit saturation at high temperatures. (35 refs.)

63771 Physics of ligand migration in biomolecules. P.Hanggi (Dept. of Phys., Polytech. Inst. of New York, New York, NY, USA).

J. Stat. Phys. (USA), vol.30, no.2, p.401-12 (Feb. 1983). (Proceedings of a Symposium on Random Walks and Their Application to the Physical and Biological Sciences, Gaithersburg, MD, USA, 28 June-1 July 1982).

The study of migration of ligands in heme proteins is one of the methods used to obtain information about the dynamics and function of biomolecules. An appropriate description of the kinetics involves the modeling of transport over a series of sequential barriers. Utilizing random walk theory, the physics of ligand migration enters the modeling of the kinetics on several levels of description. By use of generalized Brownian motion theory, the author develops models for biomolecular rates in presence of a frequency-dependent damping of the ligand motion. The results have the form of a modified Kramers relation. If more than one ligand moves inside a biomolecule, nonlinear blocking effects become important. The migration kinetics can then be adequately modeled by a multivariable stochastic process with nonlinear transition probabilities. Further, the author discusses the limit of validity of a description of ligand migration in terms of a set of linearly coupled deterministic rate equations. (27 refs.)

63772 Soliton excitations in deoxyribonucleic acid (DNA) double helices.

S.Yomosa (Dept. of Phys., Nagoya Univ., Nagoya, Japan).

Phys. Rev. A (USA), vol.27, no.4, p.2120-5 (April 1983).

Presents in this paper a soliton theory for the open states in deoxyribonucleic acid (DNA) and synthetic polynucleotide double helices. Kink and antikink solutions for the equation of motion of the sine-Gordon form correspond to the open states with positive and negative helicities. The energy of open form and the length of the open configuration which are theoretically estimated are in the same order with the values inferred from kinetic experimental data. (15 refs.)

63773 Adsorption of proteins in processes of interaction of polymers with blood and model solutions. A.L.Iordanskii, G.E.Zaikov.

Vysokomol. Soedin. Ser. A (USSR), vol.25, no.3, p.451-76 (March 1983). In Russian. English translation in: *Polym. Sci. USSR (GB)*

The adsorption of plasma proteins is of great importance in processes of interaction of polymers with blood. The composition of proteinated polymer surface affects the intensity of adhesion of thrombocytes and subsequent formation of the thromb. The thermodynamic aspect of adsorption is discussed. The existence of two types of adsorption of proteins is shown, one of which being characterized by essential conformational changes of strongly adsorbed globulins. The architecture and structural features of proteins on a nonphysiological surface have to determine the choice of thrombo-resistant polymeric material. (115 refs.)

Spectroscopic evidence in ϕ XYZ molecules for the three groups X, Y, Z acting as a whole, whatever the symmetry may be, in their long range interactions with the chromophore See Entry 60698

DNA-divalent metal cation interactions measured by electrophoretic light scattering See Entry 63788

87.15B Structure, configuration, conformation, and active sites at the biomolecular level

63774 Structure and function of viroids. D.Riesner (Inst. fur Phys. Biologie, Univ. Dusseldorf, Dusseldorf, Germany), G.Steger, J.Schumacher, H.J.Gross, J.W.Randles, H.L.Sanger.

Biophys. Struct. & Mech. (Germany), vol.9, no.3, p.145-70 (1983).

A review is presented. Viroids are an independent class of plant pathogens which are distinguished from viruses by the absence of a protein coat and by their unusually small size. They are single-stranded circular RNAs composed of about 360 nucleotide residues. Sequence analysis and physicochemical studies of the potato spindle tuber viroid (PSTV) have shown that, as a result of intra-molecular base pairing, viroids form a unique rod-like secondary structure which is characterized by a serial arrangement of double-helical sections and internal loops. There is no indication for an additional tertiary structure because all parts of the molecule are freely accessible to ligand interactions.

Current hypotheses about the function of viroids are discussed on the basis of their structural and thermodynamic features. The suggestion that viroid RNA has features similar to DNA has been supported by the finding that they are replicated in vitro by the DNA-dependent RNA polymerase II of the host plant. (58 refs.)

63775 A two-dimensional gas of interacting electric dipoles with hard cores: Van der Waals isotherms and their possible application in lipid phase transitions. P.A.Westhaus (Dept. of Phys., Oklahoma State Univ., Stillwater, OK, USA).

J. Biol. Phys. (USA), vol.10, no.3, p.125-51 (1982).

Calculates the thermodynamic properties of a two-dimensional fluid of hard disks with embedded dipoles. Attention is centered on the isotherms in the neighborhood of the critical point. Evaluating the canonical partition function by the 'factor cluster expansion', the author exhibits the Van der Waals loops obtained considering the exact two-body clusters. The Van der Waals isotherms can be scaled as universal functions of the parameter $\lambda = p^2/4\pi\epsilon_0 kT$, where p , r_0 , ϵ , are the dipole moment, hard core radius, and permittivity which characterize the interaction. The model is applied to the lipid phase transition found in natural and synthetic membranes. The typical critical parameters ($T_c \approx 300K$, $\pi_c \approx 50$ dyne/cm) reflect a physically reasonable value for the dipole moment of a polar head group of a lipid but a much-too-small value for the hard core radius. (17 refs.)

63776 A stochastic model for reversible pressure denaturation of chymotrypsinogen. C.W.Gardiner (Dept. of Phys., Univ. of Waikato, Hamilton, New Zealand).

J. Chem. Phys. (USA), vol.78, no.5, p.2549-56 (1 March 1983).

The relaxation rate characteristic of pressure denaturation of chymotrypsinogen is explained by a stochastic model in which both volume and shape changes are taken into account. All features of the data are explained qualitatively, though quantitative checks are not possible without more data. (8 refs.)

63777 The electronic structure of DNA related periodic polymers. P.Otto, E.Clementi (IBM Corp., Poughkeepsie, NY, USA), J.Ladik.

J. Chem. Phys. (USA), vol.78, no.7, p.4547-51 (1 April 1983).

Results of ab initio LCAO Hartree-Fock crystal orbital calculations using a minimal atomic basis set are reported for the single stranded periodic B-DNA models of cytosine, thymine, adenine, and guanine stacks and two polynucleotides with adenosine and thymidine as repeating unit, respectively. Further, the energy band structures of two poly(base pairs), poly(adenine-thymine), and poly(guanine-cytosine), representing a simple model of the B-DNA double helix are discussed. (25 refs.)

63778 Protein folding as a stochastic process. N.Go (Dept. of Phys., Kyushu Univ., Fukuoka, Japan).

J. Stat. Phys. (USA), vol.30, no.2, p.413-23 (Feb. 1983). (Proceedings of a Symposium on Random Walks and Their Application to the Physical and Biological Sciences, Gaithersburg, MD, USA, 28 June-1 July 1982).

In physiological conditions globular protein molecules assume a specific native conformation uniquely determined by its amino acid sequence. Upon environmental changes the protein molecules undergo reversible unfolding (order losing) and folding (order gaining) transitions, which is similar to the first-order phase transition. Pathways of folding have been intensively studied in the hope of deciphering the code that amino acid sequences carry as to the three-dimensional structure of proteins. A strongly simplified lattice model of proteins has been found to be a powerful theoretical tool to simulate the dynamic process of the folding and unfolding transitions. The results of the simulation indicate the existence of stochastic pathways of folding. (15 refs.)

63779 Transmission of conformational change in insulin. C.Chothia, A.M.Lesk (Lab. of Molecular Biology, Medical Res. Council, Cambridge, England), G.G.Dodson, D.C.Hodgkin.

Nature (GB), vol.302, no.5908, p.500-5 (7 April 1983).

Crystal structures of insulin contain molecules that are similar but not identical in conformation. Packed helices move relative to one another, these shifts being accommodated by motions of side-chain atoms arising from small changes in torsion angles. Such low-energy conformational adjustments can accommodate shifts of no more than ~ 1.5 Å. This limits the extent to which conformational changes can be dissipated locally, causing their transmission over long distances. (17 refs.)

63780 Facile transition of poly[d(TG)_nd(CA)_n] into a left-handed helix in physiological conditions. D.B.Hamiford, D.E.Pulleyblank (Dept. of Biochem., Univ. of Toronto, Toronto, Ontario, Canada).

Nature (GB), vol.302, no.5909, p.632-4 (14 April 1983).

Reports that the unmodified DNA polymer d(TG)_nd(CA)_n readily undergoes a transition to a Z conformation when subjected to unwinding torsional stress in ionic conditions that are close to physiological. By using a two-dimensional gel electrophoresis system, the authors have determined both the critical free energy of supercoiling that is required to initiate the transition and the free energy of supercoiling that is required to maintain this polymer in the Z form. (27 refs.)

63781 Secondary structures of proteins and peptides in amphiphilic environments (a review). E.T.Kaiser (Dept. of Chem., Univ. of Chicago, Chicago, IL, USA), F.J.Kezdy.

Proc. Natl. Acad. Sci. USA, vol.80, no.4, p.1137-43 (Feb. 1983).

Many peptides and proteins that act at lipid-water interfaces assume a unique amphiphilic secondary structure which is induced by the anisotropy of the interface. By using synthetic peptides in which these inducible amphiphilic structures have been optimized, one can show that the amphiphilic α helix is a functional determinant of representative apolipoproteins, peptide toxins, and peptide hormones. By increasing the amphiphilicity of the structurally important regions of the molecule, one can enhance the biological activity of the peptide even beyond that of the naturally occurring polypeptide. It is proposed that rigid amphiphilic secondary structures such as α helix, β sheet, or π helix will be found in most medium-sized peptides acting at membranes and lipid-water interfaces. (26 refs.)

63782 The mechanism of crystallization of proteins in an ultracentrifuge. V.V.Barynin, V.R.Melik-Adamyan (Inst. of Crystallography, Acad. of Sci., USSR).

Sov. Phys.-Crystallogr. (USA), vol.27, no.5, p.588-91 (Sept.-Oct. 1982). Translation of: *Kristallografiya (USSR)*, vol.27, no.5, p.981-7 (Sept.-Oct. 1982). [received: April 1983]

The authors develop a rapid and reproducible method of obtaining crystals of P. vitale catalase by means of ultracentrifugation. They describe a mechanism of crystallization of proteins in an ultracentrifuge, permitting choice of the optimal conditions for obtaining large crystals. (6 refs.)

Calculation of the characteristics of the conduction band for excess electrons in proteins See Entry 61035

Molecular and crystal structures of pregna-4, 16-dien-21-ol-3,20-dione acetate (16-dehydrocortexone) and pregna-1,4-dien-17 α ,21-diol-3,20-dione 21-acetate (dehydrocortexolone acetate) See Entry 61901

- Soliton excitations in deoxyribonucleic acid (DNA) double helices See Entry 63772
- Alamethicin pore formation: voltage-dependent flip-flop of α -helix dipoles See Entry 63796
- Twin crystals in *Ophrys lutea* root cells See Entry 63809
- Three-dimensional architecture of a polytene nucleus See Entry 63810
- Observation and simulation of unstained DNA images in bright field TEM See Entry 64018

87.15M Interactions with radiations at the biomolecular level

- 63783 Fluorescence spectra and decay time measurements on chlorophyll *a* and a non-aggregating analogue.** R.G.Brown, E.H.Evans, S.G.Holderness, J.Manwaring, B.May (Div. of Chem. & Biology, Preston Polytech., Preston, England). *Photobiophys. & Photobiophys. (Netherlands)*, vol.5, no.2, p.87-92 (Feb. 1983).
- The effects of water on the absorption and fluorescence intensities of chlorophyll *a* and a non-aggregating analogue in aqueous ethanol are reported. Fluorescence decay times for the latter compound in aqueous ethanol and for both compounds in the detergents dodecyl dimethylamine *N*-oxide, sodium dodecyl sulphate and Triton X-100 have also been measured. (7 refs.)
- 63784 Energy storage in the primary step of the photocycle of bacteriorhodopsin.** R.R.Birge, T.M.Cooper (Dept. of Chem., Univ. of California, Riverside, CA, USA). *Biophys. J. (USA)*, vol.42, no.1, p.61-9 (April 1983).
- A pulsed-dye laser low temperature photocalorimeter is used to study the enthalpy differences between light-adapted bacteriorhodopsin (bR₅₆₈) and its primary photoproduct (K) at 77K. A key feature of the authors' experimental method is the use of the laser-induced photostationary state as an internal reference. Analysis of the forward (bR→K), reverse (K→bR), and mixed (bR↔K) photochemical reactions were carried out to measure $\Delta H_{12} = E_K - E_{bR}$. All three experiments yielded identical values of ΔH_{12} within experimental error ($\Delta H_{12}^{ave} = 15.8 \pm 2.5$ kcal mol⁻¹). Accordingly, the primary event in the photocycle of light-adapted bacteriorhodopsin stores ~30% of the absorbed photon energy at the 568-nm absorption maximum. The authors observe that the quantum yields ϕ_1 (bR→K) and ϕ_2 (K→bR), add up to unity within experimental error: $\phi_1 + \phi_2 = 1.02 \pm 0.19$ for ϕ_1 in the range 0.28-0.33. A theoretical analysis of energy storage in K suggests that at least one-half of the enthalpy difference between K and bR is associated with charge separation accompanying chromophore isomerization. (30 refs.)
- 63785 Electrooptical behaviour of purple membrane fragments in the thin oriented film.** M.P.Petrov (Inst. of Solid State Phys., Sofia, Bulgaria), N.G.Popdimitrova. *C.R. Acad. Bulg. Sci. (Bulgaria)*, vol.35, no.11, p.1475-7 (1982).
- Reports on the electrooptical investigation of a thin oriented film of a purple membrane aqueous suspension. A planar capacitor was used consisting of two glass plates as electrodes, covered with SnO₂ and supporting the sample. The film's thickness was fixed by means of a Mylar spacer at 10 μ m. The thin SiO₂ layer was obliquely evaporated on the electrodes so as to ensure tangential boundary conditions. Regularly distributed microgrooves on the electrode surface were thus obtained. The microgrooves widths are commensurable with PM fragment sizes. Therefore, in order to ensure a good mechanical orientation, the authors introduced the suspension into the capacitor through the capillary forces. (5 refs.)
- 63786 Water proton spin-lattice relaxation behaviour in heterogeneous biological systems.** N.Niccolai, C.Rossi, E.Tiezzi (Inst. of General Chem., Univ. of Siena, Siena, Italy). *Chem. Phys. Lett. (Netherlands)*, vol.96, no.2, p.154-6 (1 April 1983).
- The water proton spin-lattice relaxation rate has been measured for a condensed 50% deuterated erythrocyte water system. Nuclear relaxation data, obtained in nonselective and selective modes, indicate that cross relaxation between erythrocyte and water protons occurs. The observed selective relaxation enhancement is interpreted in terms of intermolecular nuclear interactions modulated by motions which satisfy the $\omega\tau_c \gg 1$ condition. Selective relaxation rates are here proposed to be more sensitive to interface characteristics than the nonselective ones. (13 refs.)
- 63787 Dynamic light scattering studies of protein solutions under high pressure.** B.Nystrom, J.Roots (Inst. of Phys. Chem., Univ. of Uppsala, Uppsala, Sweden). *J. Chem. Phys. (USA)*, vol.78, no.6, pt.1, p.2833-7 (15 March 1983).
- Dynamic light scattering measurements on bovine serum albumin (BSA) at pH=4.7 ionic strength $I \approx 0.12$ M were carried out in the pressure interval 1-4000 atm and for concentrations ranging from 8-80 kg m⁻³. At moderate pressures the mutual diffusion coefficient *D* was found to decrease linearly with concentration, while at the highest pressures deviation from linearity was observed. For a given concentration, the value of *D* increases initially with pressure and passes gradually through a maximum; at higher pressures (about 1000 atm) *D* decreases with increasing pressure. The hydrodynamic radius, deduced from diffusion data extrapolated to infinite dilution, was observed to increase with pressure during the denaturation process (pressures above 1000 atm) of the protein. Upon releasing the pressure the return of *D* was not reversible. (26 refs.)
- 63788 DNA-divalent metal cation interactions measured by electrophoretic light scattering.** Kee Woo Rhee, B.R.Ware (Dept. of Chem., Syracuse Univ., Syracuse, NY, USA). *J. Chem. Phys. (USA)*, vol.78, no.6, pt.2, p.3349-53 (15 March 1983).
- The authors have used the laser Doppler technique of electrophoretic light scattering to study the electrokinetic and gross conformational manifestations of the binding of divalent cations to DNA in low-salt solutions. By electrokinetic assay, divalent ion affinities to DNA in the 5-500 μ M range increase in the order $Mn^{+2} < Co^{+2} < Mg^{+2} < Cu^{+2}$. The ELS spectra show that Cu²⁺ denatures double-stranded DNA in the 50-200 μ M concentration range, thereby augmenting the reduction in electrophoretic mobility. Counterion condensation theory correctly predicts the form of the electrophoretic mobility reduction for territorially bound ions such as Mg²⁺, but the absolute magnitudes of electrophoretic mobility predicted by an equation deduced from condensation theory overestimate the authors' experimental values. (27 refs.)
- 63789 A physical interpretation for the natural photosynthetic process.** R.Hill, P.R.Rich (Dept. of Biochem., Univ. of Cambridge, Cambridge, England). *Proc. Natl. Acad. Sci. USA*, vol.80, no.4, p.978-82 (Feb. 1983).
- The efficiency of the process of photosynthesis is shown to depend on the molecular conversion of power. This requires establishment of a discipline that is now implicit in current thought and that offers a definition of relationship between equilibrium state and power. The quantum aspect for the microscopic

process is different from the macroscopic system idealized as the heat engine and is required for the interpretation of molecular machinery. By using three postulates the ideal maximal efficiency for the molecular energy conversion is calculated from the data, which are assembled in the form of the 'Z scheme' for photosynthesis. The observed and the calculated efficiencies for a green plant are substantially in agreement. (32 refs.)

63790 Energetics of photosynthetic glow peaks. D.DeVault, Govindjee (Dept. of Physiology & Biophys., Univ. of Illinois, Urbana, IL, USA), W.Arnold. *Proc. Natl. Acad. Sci. USA*, vol.80, no.4, p.983-7 (Feb. 1983).

By postulating temperature-dependent equilibria between two or more electron carriers acting as traps for electrons or holes, it is possible to modify the Randall-Wilkins theory of thermoluminescence (see Proc. R. Soc. London Ser.A, vol.184, p.366-89, 1945) so as to explain the abnormally large apparent activation energies and apparent frequency factors observed in photosynthetic glow curves when fitted by unmodified Randall-Wilkins theory. The equilibria serve to inhibit the formation of the light-emitting excited state by withholding the needed precursor state. When the inhibition is released at higher temperature by shift of equilibrium with temperature, the rise of the glow peak can be much faster than would result from Arrhenius behavior based on the true activation energy and so appears to correspond to a higher activation energy accompanied by a larger frequency factor. From another viewpoint, the enthalpy changes, ΔH , of the equilibria tend to add to the activation energy. Similarly the entropy changes, ΔS , of the equilibria tend to add to the entropy of activation, giving the large apparent frequency factors. The positive values of ΔS needed would correspond to entropy decreases in the forward early electron transport. A comparison of the glow peaks obtained by different workers is also presented. (29 refs.)

Selective solvent suppression in ¹H FT NMR using a DANTE pulse: its application in normal and NOE measurements See Entry 59815

Sublevel decay kinetics of the triplet state of bacteriorhodopsin *a* and *b* in methyltetrahydrofuran at 1.2K See Entry 60771

Solubility of hematoporphyrin and photodynamic damages in liposomal systems: optical and electron spin resonance studies See Entry 63768

Two-dimensional deuterium NMR of lipid membranes See Entry 63798

Fluorescence of protein-treated sheep erythrocytes See Entry 63804

87.16 BIOTHERMICS

63791 Blood volume and protein responses to skin heating and cooling in resting subjects. M.H.Harrison, R.J.Edwards, L.A.Cochrane, M.J.Graveney (Royal Air Force Inst. of Aviation Medicine, Farnborough, England). *J. Appl. Physiol. (USA)*, vol.54, no.2, p.515-23 (Feb. 1983).

The effects of alterations in skin temperature on intravascular volume and protein content have been investigated in resting subjects. With a normal core temperature (*T*_{ac}) both skin cooling and skin heating caused hemoconcentration, and heating was associated with an increased rate of protein loss from the intravascular space. Raising of the skin temperature after cooling, with *T*_{ac} depressed, and cooling of the skin after heating, with *T*_{ac} raised, were associated with an immediate reversal of the hemoconcentration, and gain of protein by the intravascular space. It is concluded that intravascular volume responses to thermal stress are dependent on the skin and core temperatures obtaining immediately prior to imposition of the stress and that, in particular, a low skin temperature predisposes toward hemodilution on subsequent exposure to heat; sweating per se does not necessarily result in hemoconcentration. The association of hemodilution with augmentation of intravascular protein, and the rapidity with which extravascular protein can apparently gain entry to the intravascular space, is taken as indicating a possible direct return of protein through capillary walls. (30 refs.)

63792 Effect of temperature on regulation of breathing and sleep/wake state in fetal lambs. I.R.Moss, A.J.Mautone, E.M.Scarpelli (Pediatric Pulmonary Div., Albert Einstein Coll. of Medicine, New York, NY, USA). *J. Appl. Physiol. (USA)*, vol.54, no.2, p.536-43 (Feb. 1983).

Lamb fetuses (*n*=16) were employed to study the effect of ambient liquid temperature on behavioral (*n*=16) and recorded (*n*=8) sleep/wake states and on absolute breathing threshold and responsivity to CO₂ (*n*=8). Sleep/wake states were estimated by electroencephalogram, nuchal electromyogram, and electrooculogram, as well as by behavioral criteria ex utero. CO₂ threshold and responsivity were assessed with fetal CO₂ tests in which fetal breathing was related to increasing fetal arterial CO₂ tension (Pa(CO₂)) during CO₂ rebreathing by the ewe. The high normal CO₂ threshold of the fetus [55.7 ± 2.4 (SE) Torr] at warm 'core' temperature ($39.6 \pm 0.3^\circ\text{C}$) was lowered significantly (to 41.6 ± 1.7 Torr) by cooling and decrease of core temperature (to $37.1 \pm 0.5^\circ\text{C}$). Similarly cooling increased responsivity to CO₂ (i.e. decreased *X*-axis intercept and increased slope) of maximal intratracheal pressure (ITP), ITP 100 ms after onset of a breath, and fetal ventilatory equivalent. The increased breathing frequency with cooling was less linear. Response to cooling characteristically included (1) rapid onset of vigorous breathing movements, and (2) development of less vigorous but more regular breathing movements concomitantly with the combined reduction of skin and core temperature. (31 refs.)

63793 Unusual core temperature decrease in exercising heart-failure patients. F.G.Shellock, S.A.Rubin, A.G.Ellrodt, A.Muchlinski, H.Brown, H.J.C.Swan (Dept. of Medicine, Cedars-Sinai Medical Center, Univ. of California, Los Angeles, CA, USA). *J. Appl. Physiol. (USA)*, vol.54, no.2, p.544-50 (Feb. 1983).

Heat dissipation during exercise is presumed to be impaired in heart-failure patients due to their constricted cutaneous circulation and depressed cardiac output. The authors studied core (pulmonary artery blood) temperature and hemodynamics in 16 patients with severe heart failure who performed maximal upright incremental exercise. Skin temperatures were also measured in six of these patients during rest and peak exercise. A normal group (*n*=5) was exercised for comparison. It is concluded that heart-failure patients have an unusual core temperature decrease throughout short-term maximal exercise. This is probably caused by a redistribution of their body heat, i.e., a mixing of the core blood with the cooler contents of the cutaneous and muscle circulations. (29 refs.)

63794 Heat-induced thermotolerance expressed in the energy metabolism of mammalian cells. J.Lunec, S.R.Cresswell (MRC Cyclotron Unit., Hammersmith Hospital, London, England). *Radiat. Res. (USA)*, vol.93, no.3, p.588-97 (March 1983).

Measurements were made of the effect of heat treatment on ATP levels in control and thermotolerant populations of murine lymphoma (L5178YS) and Ehrlich ascites cells to investigate whether the development of thermotolerance is associated with an increased ability of cells to maintain energy metabolism when challenged with heat treatment. For the L5178YS cells a single heat treatment produced a rapid reduction in ATP levels. However, previously

heat treated L5178YS cells showed an increased ability to maintain ATP levels when challenged with a second heat treatment, and this ability to maintain ATP levels varied in a manner which correlated with the appearance and decay of thermotolerance seen in the parallel cell survival studies. In contrast both single and fractionated heat treatments did not reduce ATP levels in Ehrlich ascites cells. (26 refs.)

A two-dimensional gas of interacting electric dipoles with hard cores: Van der Waals isotherms and their possible application in lipid phase transitions See Entry 63775

The effect of heat and radiation on the initiation and elongation processes of DNA synthesis See Entry 63806

Variable interaction of heat and procaine in potentiation of radiation lethality in mammalian cells of neoplastic origin See Entry 63807

Recovery from heat damage in stationary and log phase diploid yeast cells under growth and non-growth conditions See Entry 63808

Hyperthermia-induced intracellular ionic level changes in tumor cells See Entry 63811

Thermal effects of laser radiation in biological tissue See Entry 63896

Temperature and adrenocortical responses in rhesus monkeys exposed to microwaves See Entry 63897

The possibilities offered by infrathermogrammetry for the diagnosis of the Raynaud phenomenon of vibrational origin See Entry 63921

Equipment for the clinical application of local microwave hyperthermia See Entry 63922

87.20 MEMBRANE BIOPHYSICS

63795 Absorbance and fluorescence changes in relation to light-scattering changes in chloroplast thylakoid membranes. S.W.Thorne, J.T.Dunice, J.A.Lee (Div. of Plant Industry, CSIRO, Canberra, Australia). *Photobiochem. & Photobiophys. (Netherlands)*, vol.5, no.2, p.71-8 (Feb. 1983).

A survey is made of Mie, Rayleigh and selective dispersive scattering of light as they relate to chloroplast thylakoid membranes. The authors show how these affect both the slow absorbance changes around 515 nm (ΔA_{515}) and fluorescence changes (ΔF_{683}) which arise from changes in salt concentrations, valencies, pH, osmolarity, or actinic light. The grana thylakoid membranes of chloroplasts are considered as a design for photoadaptation to growth-light conditions in accord with the concept of complex refractivity ($n-ik$) where refractivity (n) and absorbance (k) are interrelated over the spectrum by the Kramers-Kronig equations. (57 refs.)

63796 Alamethicin pore formation: voltage-dependent flip-flop of α -helix dipoles. G.Boheim (Lehrbereich Zellphysiologie, Ruhr-Univ. Bochum, Bochum, Germany), W.Hanke, G.Jung. *Biophys. Struct. & Mech. (Germany)*, vol.9, no.3, p.181-91 (1983).

The voltage-dependency of alamethicin pore formation is explained by a flip-flop gating mechanism of single alamethicin molecules. The energetically preferred aggregate structure is changed from antiparallel to parallel molecule orientation by membrane voltage application. The electrical field is sensed by the permanent dipole of the α -helical molecule part which spans the hydrophobic membrane core. Ion conducting pore and pore states result from electrostatic repulsion of a varying number of parallel dipoles which arrange circularly. This model is consistent with published data and with two additional experimental facts, that pore state distributions are ionic strength dependent and pore state conductances depend on ionic current direction. (33 refs.)

63797 Elastic energy stored in a membrane due to electrostriction. F.J.Blatt (Dept. of Phys. & Neurosci. Faculty, Michigan State Univ., East Lansing, MI, USA). *J. Biol. Phys. (USA)*, vol.10, no.4, p.219-22 (1982).

The elastic energy stored in a biological membrane due to electrostrictive deformation is considered, and an expression is derived that relates this energy to the change in membrane capacitance and the electrostatic energy associated with a membrane potential. Based on available evidence it is concluded that electrostriction does not make a significant contribution to the energy stored in a charged membrane system. (10 refs.)

63798 Two-dimensional deuterium NMR of lipid membranes. L.Muller, S.I.Chan (Arthur Amos Noyes Lab., California Inst. of Technol., Pasadena, CA, USA).

J. Chem. Phys. (USA), vol.78, no.7, p.4341-8 (1 April 1983).

The intrinsic linewidths of deuterium resonance in randomly oriented solids or liquid crystals can be extracted from two-dimensional NMR spectra in which spectra dispersion due to the quadrupolar Hamiltonian is removed in the indirectly detected frequency domain ω_1 . Such spectra can be obtained with a modified quadrupolar echo sequence in which the interval between the excitation and echo radio frequency pulse is rendered the second time variable. With this method, deuterium NMR linewidths have been measured in two model bilayer membranes as a function of temperature: 1-myristoyl-2-myristoyl- d_{55} -phosphatidylcholine and a 3:2 1-palmitoyl-2-palmitoyl-(16,16)- d_5 -phosphatidylcholine:cholesterol mixture. (34 refs.)

63799 Use of small-angle scattering data to calculate the diameter distribution function for a system of spherical layers [biomembrane application]. N.I.Mischchenko, L.A.Feigin (State Univ., Kiev, Ukrainian SSR).

Sov. Phys.-Crystallogr. (USA), vol.27, no.5, p.519-21 (Sept.-Oct. 1982). Translation of: *Kristallografiya (USSR)*, vol.27, no.5, p.863-6 (Sept.-Oct. 1982). [received: April 1983]

The authors consider the intensity $i(s)$ of scattering by a polydisperse system of thin spherical layers with a wide diameter distribution and a nonuniform electron density profile through the thickness of a layer. They show that up to a certain value s_1 the function $i(s)$ is closely approximated by the intensity of scattering by infinitely thin spherical shells. The value of s_1 is determined by the radius of inertia of the thickness of the layer. The authors derive an expression giving the distribution function $p(2R)$ of the numbers of layers of various diameters in terms of the intensity in a section $(0, s_1)$. (7 refs.)

Solubility of hematoporphyrin and photodynamic damages in liposomal systems: optical and electron spin resonance studies See Entry 63768

A two-dimensional gas of interacting electric dipoles with hard cores: Van der Waals isotherms and their possible application in lipid phase transitions See Entry 63775

Electrooptical behaviour of purple membrane fragments in the thin oriented film See Entry 63785

Force relaxation and permanent deformation of erythrocyte membrane See Entry 63803

Fluorescence of protein-treated sheep erythrocytes See Entry 63804

Simple computer method for evaluation of lateral diffusion coefficients from fluorescence photobleaching recovery kinetics See Entry 64004

87.25 CELLULAR BIOPHYSICS

63800 Adsorption of concanavalin A on human platelets. A.B.Bikhazi, K.M.Bitari (American Univ. of Beirut, Beirut, Lebanon). *Ann. Biomed. Eng. (USA)*, vol.10, no.5, p.219-29 (1982).

A physiological cell surface adsorption system approach is investigated on human platelets utilizing mathematical modeling. Monodispersed washed platelets are freshly collected in an isotonic buffer as a suspension utilizing a gel filtration technique. Concanavalin A is used as a glycoprotein receptor adsorbate in the adsorption studies. Three mathematical models are proposed based on simple chemical equilibrium reactions between adsorbate and cell surface receptors in an effort to explain concanavalin A-platelet surface glycoprotein interaction. Model I assumes that all receptors are undergoing simultaneous surface reactions with the adsorbate and without correlation. Model II reflects a strong correlation between the receptors, when only one receptor is active and the second receptor(s) is nothing but the combination of first receptor-adsorbate complex. Model III assumes the presence of multiple receptors on the cell surface. Only when a specific fraction of the total number of one receptor have reacted, will the other receptor(s) initiate reaction with the adsorbate. The results suggest the existence of at least three major glycoprotein receptors interacting with the lectin, and having different equilibrium constants as indicated in the adsorption isotherm. Model III seems to support best the experimental data of concanavalin A interaction with platelet surface glycoproteins. (13 refs.)

63801 Spectral characterization of photosystem I fluorescence at room temperature using thylakoid protein phosphorylation. D.J.Kyle, N.R.Baker, C.J.Artzen (Plant Res. Lab., Michigan State Univ., East Lansing, MI, USA).

Photobiochem. & Photobiophys. (Netherlands), vol.5, no.2, p.79-85 (Feb. 1983).

An analysis is presented of the spectral changes in fluorescence emission of thylakoids at room temperature associated with phosphorylation of thylakoid polypeptides. An enhancement of fluorescence above 700 nm relative to emission at 685 nm was observed on phosphorylation, and the spectral characteristics of this enhancement were similar to the fluorescence emission spectrum of an isolated PS I particle at room temperature. The changes in the 77K fluorescence emission spectra resulting from phosphorylation of the thylakoids were directly related to the spectral changes in fluorescence emission observed at room temperature. (22 refs.)

63802 Motility of mouse fibroblasts in tissue culture. W.C.Parkinson (Dept. of Phys., Univ. of Michigan, Ann Arbor, MI, USA). *Biophys. J. (USA)*, vol.42, no.1, p.17-23 (April 1983).

The growth and motion of mouse L-cells in vitro have been studied by means of time-lapse photography. In particular, the mitotic period and the motility, defined in terms of $\langle R^2 \rangle$, the mean square displacement of an ensemble of cells, have been measured as a function of temperature. The motility is a function of the phase of the cell cycle. For approximately the first one-eighth of the mitotic period the motility is well described as a random walk with persistence, the duration of the persistence being determined by the time of extension of the filopodial spindle. The temperature dependence of the diffusion constant follows the Arrhenius factor. The mitotic period, which varies exponentially as $(1/T)$, exhibits a large variance, and the time difference in replication of daughter pairs follows approximately a Poisson distribution with a mean difference of 138 min at $T=37^\circ\text{C}$. There is no evidence of mirror symmetry in the motion of daughter pairs for fibroblast cells plated in vitro in Corning tissue culture flasks. (19 refs.)

63803 Force relaxation and permanent deformation of erythrocyte membrane. D.R.Markle, E.A.Evans, R.M.Hochmuth (Dept. of Biomedical Engng., Duke Univ., Durham, NC, USA). *Biophys. J. (USA)*, vol.42, no.1, p.91-8 (April 1983).

Force relaxation and permanent deformation processes in erythrocyte membrane were investigated with two techniques: micropipette aspiration of a portion of a flaccid cell, and extension of a whole cell between two micropipettes. In both experiments, at surface extension ratios $<3:1$, the extent of residual membrane deformation is negligible when the time of extension is less than several minutes. However, extensions maintained longer result in significant force relaxation and permanent deformation. The magnitude of the permanent deformation is proportional to the total time period of extension and the level of the applied force. Based on these observations, a nonlinear constitutive relation for surface deformation is postulated that serially couples a hyperelastic membrane component to a linear viscous process. In contrast with the viscous dissipation of energy as heat that occurs in rapid extension of a viscoelastic solid, or in plastic flow of a material above yield, the viscous process in this case represents dissipation produced by permanent molecular reorganization through relaxation of structural membrane components. Data from these experiments determine a characteristic time constant for force relaxation, τ , which is the ratio of a surface viscosity, η to the elastic shear modulus, μ . (18 refs.)

63804 Fluorescence of protein-treated sheep erythrocytes. A.G.Atanassov (Inst. of Biophys., Karl Mark Univ., Leipzig, Germany), Yu.G.Atanassova, F.Pliquett.

C.R. Acad. Bulg. Sci. (Bulgaria), vol.35, no.11, p.1545-7 (1982). The binding of positively charged proteins—protamine, polylyzine, and lysozyme—with black lipid membranes increases the fluorescence intensity of the membrane bound probe 1-anilino-8-naphthalenesulphonate (ANS). Ensuing from the different properties of the phospholipid and biological membranes the authors measured the ANS fluorescence in a suspension of sheep erythrocytes treated with protamine. (6 refs.)

63805 A theoretical and scanning electron microscope study on the electrically mediated inactivation of spermatozoa. S.Mahajan, S.K.Guha, M.M.Misro (Centre for Biomedical Engng., Indian Inst. of Technol., New Delhi, India).

J. Biol. Phys. (USA), vol.10, no.3, p.113-24 (1982).

Spermatozoa are known to carry a net negative charge and have been shown to die in a DC electric field, but the cause of the lethal effect has not been explored. The authors present here an experimental and theoretical analysis of various factors likely to lead to the mortality of spermatozoa. Alterations in the spermatozoon surface complex induced by the applied current density has been identified to be the most likely cause. (16 refs.)

- 63806** The effect of heat and radiation on the initiation and elongation processes of DNA synthesis. R.C.Davis, G.T.Bowden, A.E.Cress (Dept. of Radiology, Univ. of Arizona Health Sci. Center, Tucson, AZ, USA). *Int. J. Radiat. Biol. (GB)*, vol.43, no.4, p.379-90 (April 1983).
The pH step alkaline elution and alkaline sucrose gradient techniques were utilized to evaluate alterations in DNA replication (initiation and elongation) induced by heat and low dose X-irradiation in synchronized Chinese hamster ovary cells. The initiation and elongation processes of DNA synthesis were resistant at the G₁/S boundary (4 hours after mitosis) while in mid S phase (9 hours after mitosis) DNA initiation and elongation were sensitive to X-irradiation. The initiation and elongation processes of DNA synthesis which were radiation resistant at the G₁/S boundary could be inhibited by a hyperthermia treatment (43°C for 1 hour beginning at 4 hours after mitosis). The impairment of initiation in the heated cells was maintained through late S phase while that of elongation was reversible as judged by full recovery at 15 hours after mitosis. These data suggest that the known synergistic lethality of heat and radiation may be mediated by an impairment of initiation of DNA synthesis. (26 refs.)
- 63807** Variable interaction of heat and procaine in potentiation of radiation lethality in mammalian cells of neoplastic origin. B.Djordjevic (Dept. of Radiotherapy, Mount Sinai School of Medicine, New York, NY, USA). *Int. J. Radiat. Biol. (GB)*, vol.43, no.4, p.399-409 (April 1983).
Mild hyperthermia in conjunction with procaine HCl acts as a potentiator of radiation lethality in HeLa cells, with little toxicity for unirradiated cells. The majority of irradiated cells respond extensively within a four hour period of treatment with the two agents. Potentiation of radiation lethality by the combined treatment was also found in a line of human melanoma cells, and to a lesser extent in a line of human ovarian carcinoma cells. The interaction of heat and procaine in the process of potentiation of radiation lethality was assessed from a series of radiation survival curves, with temperatures ranging from 37 to 42°C and procaine concentrations from 1 to 3 mM. The interactive factor was obtained from the ratio of the Dose Reduction Factor (DRF) due to procaine in heated cells, to the DRF due to procaine in unheated cells; a ratio larger than unity denotes interaction of heat and procaine. The largest interaction was observed when individual agents exerted only a minimal radio-potentiating effect, as if increased effectiveness of one agent pre-empted the effectiveness of the other agent. (16 refs.)
- 63808** Recovery from heat damage in stationary and log phase diploid yeast cells under growth and non-growth conditions. N.M.S.Reddy, K.B.Anjaria, V.V.Deorukhakar, B.S.Rao (Div. of Radiological Protection, Bhabha Atomic Res. Centre, Bombay, India). *Int. J. Radiat. Biol. (GB)*, vol.43, no.4, p.465-9 (April 1983).
Reports studies on the recovery from heat-induced lethal damage in yeast cells in various stages of the cell cycle. Furthermore, the authors have investigated the kinetics of recovery from sublethal heat damage under growth and non-growth conditions. The results indicate that the recovery from heat-induced lethal damage is absent in cells in all stages of division cycle, that cells recover from most of the heat induced sublethal damage both under growth and non-growth conditions, and that the recovery is faster under growth conditions than under non-growth conditions. (10 refs.)
- 63809** Twin crystals in Ophrys leuca root cells. M.Salome, S.Pais, J.Araujo-Silva, F.Carvalho-Rodrigues (Dept. de Biologia Vegetal, Lisboa, Portugal). *Microsc. Acta (Germany)*, vol.87, no.2, p.177-82 (March 1983).
Paracrystalline structures are a common feature in many biological specimens. The fact that these paracrystalline structures are crystals in shown in this paper by the appearance of crystalline associations. The twin crystals the authors report in Ophrys leuca root cells were image processed to reveal the molecular basis of the structure. A model of the twin crystals is also proposed. (6 refs.)
- 63810** Three-dimensional architecture of a polytene nucleus. D.A.Agard, J.W.Sedat (Dept. of Biochem. & Biophys., Univ. of California, San Francisco, CA, USA). *Nature (GB)*, vol.302, no.5910, p.676-81 (21 April 1983).
The three-dimensional chromosome topography in an intact nucleus has been determined using fluorescently stained Drosophila polytene chromosomes, optical fluorescence microscopy and newly developed, generally applicable, cellular image reconstruction techniques. The folding pattern is a complex mixture of parallel chromosomal segments and intertwined coils and shows extensive interaction of the chromosomes with the nuclear envelope. (39 refs.)
- 63811** Hyperthermia-induced intracellular ionic level changes in tumor cells. P.N.Yi (Dept. of Radiology, Medical Univ. of South Carolina, Charleston, SC, USA), C.S.Chang, M.Tallen, W.Bayer, S.Ball. *Radiat. Res. (USA)*, vol.93, no.3, p.534-44 (March 1983).
The intracellular content of potassium (K) ions in P815 cells decreases when the media pH is lowered, and it increases when media pH is raised. The determination of the ion content therefore requires accurate control of the medium pH. The K ion content measured both by the flame emission method and by the K analog, ⁴⁰Rb, exhibits a decline when the cells are incubated at 43°C at a fixed pH chosen between 7.4 and 6.7. The chloride content also decreases while the sodium content does not change by a significant amount. Under the same hyperthermic conditions the intracellular pH decreases by a fraction of a pH unit. Simultaneously, the cell water volume increases by 20%, as measured by tritiated water. In the final analysis, hyperthermia produces an apparent deficit in the cellular osmolarity. A possible explanation is given. (22 refs.)
- Sublevel decay kinetics of the triplet state of bacteriochlorophyll a and b in methyltetrahydrofuran at 1.2K** See Entry 60771
- Fluorescence spectra and decay time measurements on chlorophyll a and a non-aggregating analogue** See Entry 63783
- Water proton spin-lattice relaxation behaviour in heterogeneous biological systems** See Entry 63786
- A physical interpretation for the natural photosynthetic process** See Entry 63789
- Energetics of photosynthetic glow peaks** See Entry 63790
- Heat-induced thermotolerance expressed in the energy metabolism of mammalian cells** See Entry 63794
- Action potentials in macrophages derived from human monocytes** See Entry 63824
- Pulmonary microcirculatory response to localized hypercapnia** See Entry 63874
- Cellular spin resonance in rotating electric fields** See Entry 63889
- Response of multicell spheroids to 1-MHz ultrasonic irradiation: cavitation-related damage** See Entry 63894
- Cytogenetic effects of argon laser irradiation on Chinese hamster cells** See Entry 63898

- Dose-effect relationships for induction of cell inactivation and asymmetrical chromosome exchanges in three cell lines by photons and neutrons of different energy** See Entry 63900
- Demonstration of a biological effect of natural ionizing radiations** See Entry 63901
- Reciprocal translocations in ageing mice and in mice with long-term low-level ²³⁹Pu contamination** See Entry 63902
- The sequential irradiation of mammalian cells with X-rays and charged particles of high LET** See Entry 63903
- The fate of cells with chromosome aberrations after total-body irradiation and bone marrow transplantation** See Entry 63904
- Characterization of an Escherichia coli mutant (radB101) sensitive to γ and UV radiation, and methyl methanesulfonate** See Entry 63905
- Irradiation of mammalian cells in the presence of diamide and low concentrations of oxygen at conventional and at ultrahigh dose rates** See Entry 63906
- Radiobiological effects of ¹³¹I and ¹²⁵I on the DNA of the rat thyroid. I. Comparative study with emphasis on the postirradiation hypothyroidism occurrence** See Entry 63907
- Peripheral lymphocyte response to PHA and T cell population among atomic bomb survivors** See Entry 63909
- Comments on 'An assessment of the role of microdosimetry in radiobiology' by Dudley T. Goodhead [Radiat. Res. 91, 45-76 (1982)] [and reply]** See Entry 63910
- Combined flow cytometry and image cytometry of the same cytological sample** See Entry 63920
- Studying microbial growth processes with a microcomputer** See Entry 64005
- A routine flat embedding method for electron microscopy of microorganisms allowing selection and precisely orientated sectioning of single cells by light microscopy** See Entry 64010
- A versatile localization system for microscopic multiparametric analysis of cells** See Entry 64014

87.25D Biological transport; cellular and subcellular transmembrane physics

- 63812** Flickering of a nicotinic ion channel to a subconductance state. A.Auerbach, F.Sachs (Dept. of Biophys., State Univ. of New York, Buffalo, NY, USA). *Biophys. J. (USA)*, vol.42, no.1, p.1-10 (April 1983).
Nicotinic acetylcholine channels show bursts of activity where open channel currents are separated from each other by short closed periods called flickers. These flickers presumably represent transitions from the open state to the state preceding the first opening of a burst (doubly liganded, closed state). Using tissue cultured chick pectoral muscle, the authors have examined the amplitude distribution of flickers. Of those events sufficiently long to permit accurate measurement of the amplitude (~25% of all flickers), approximately two-thirds had a mean current equal to 10% of the fully open channel. The remaining one-third did appear to close completely. The subconducting flicker state is not a requisite step preceding channel opening. It is concluded that there are three types of flicker events: a short event (time constant ~0.1 ms) whose current distribution is uncertain and two longer events (time constant ~1 ms), one of which has a current ~10% of the main open state and the other of which has a current indistinguishable from zero. In contrast, the amplitude of flickers induced by the local anesthetic QX-222 is indistinguishable from zero. (24 refs.)
- 63813** Effect of tortuous extracellular pathways on resistance measurements. R.T.Mathias (Dept. of Physiology, Rush Medical Coll., Chicago, IL, USA). *Biophys. J. (USA)*, vol.42, no.1, p.55-9 (April 1983).
There are many instances in which we are limited to measuring macroscopic quantities such as a bulk flow or an average field. In biology, one is frequently interested in using such macroscopic measurements, for example, the total current from a tissue, to determine the microscopic properties of the cells or tubules of the tissue. The microstructure of the tissue will generally increase the resistance to flow over what would be measured in an unstructured medium. This paper derives a fairly general expression for the relationship between effective resistance to macroscopic flow and the specific resistance of the medium conducting the microscopic flow. This expression, called a tortuosity factor, is defined entirely in terms of measurable morphometric and geometric parameters of the tissue. (18 refs.)
- 63814** Changes in eggshell conductance after transfer of hens from an altitude of 3800 to 1200 m. H.Rahn, T.Ledoux, C.V.Paganelli, A.H.Smith (Dept. of Physiology, State Univ. of New York, Buffalo, NY, USA). *J. Appl. Physiol. (USA)*, vol.53, no.6, p.1429-31 (Dec. 1982). [received: April 1983].
Hens acclimated to an altitude of 3800 m (PB 480 Torr) were transferred to 1200 m (PB 657 Torr). Eggs were collected before departure and daily after the transfer so that changes in eggshell conductance could be studied. Over the next 2 mo eggshell conductance increased 30%, presumably to compensate for the 37% reduction (from 657 to 480 Torr) in gas diffusivity at the lower altitude. Measurements of shell thickness and number of pores in the shell allow one to calculate that most of the change in total pore area occurred by an increase in cross-sectional area of individual pores. (13 refs.)
- 63815** CO₂ diffusing capacity in isolated dog lung lobes and the role of carbonic anhydrase. T.Enns, E.P.Hill (Dept. of Medicine, Univ. of California, San Diego, La Jolla, CA, USA). *J. Appl. Physiol. (USA)*, vol.54, no.2, p.483-90 (Feb. 1983).
CO₂ diffusing capacities (DmCO₂) were measured at 22°C on 12 isolated perfused dog lung lobes before and after inhibition of lung tissue carbonic anhydrase (CA) by acetazolamide (Diamox). The hypothesis is that CA in the alveolar-capillary tissue enhances overall transport of CO₂ by converting CO₂ to HCO₃⁻ within aqueous portions of the tissue. HCO₃⁻ diffuses simultaneously with molecular CO₂, increasing the overall CO₂ flux, and then converts back to molecular CO₂ at the end of the aqueous pathway. To ensure at least partial diffusion limitation, lobes were perfused with phosphate buffer at high pH (7.7) and high flow rates. Plant CA (which is not inhibited significantly by Diamox) was added to the perfusate to provide rapid uptake of CO₂ via conversion to HCO₃⁻. After Diamox, DmCO₂ decreased 39.6%, indicating that CA does increase CO₂ transport through lung tissue. Surprisingly, DmCO₂ exceeds CO₂ diffusing capacity by only 9.3±2.1 times (without Diamox inhibition) rather than by the factor of 24 predicted by Graham's law on the basis of solubilities and molecular weights of the gases. (35 refs.)

63816 Stochastic aspects of biological locomotion. R.Nossal (Phys. Sci. Lab., Nat. Inst. of Health, Bethesda, MD, USA). *J. Stat. Phys. (USA)*, vol.30, no.2, p.391-400 (Feb. 1983). (Proceedings of a Symposium on Random Walks and Their Application to the Physical and Biological Sciences, Gaithersburg, MD, USA, 28 June-1 July 1982). Various aspects of random walks undertaken by motile bacteria and migrating leukocytes are discussed, including the motions of these cells when responding to gradients of chemoattractants. Brief reference also is made to studies of particle movements within the cytoplasm of eucaryotic cells. (39 refs.)

87.30 BIOPHYSICS OF NEUROPHYSIOLOGICAL PROCESSES

(exc. perception processes and speech)

63817 Sinusoidal voltage clamp of the Hodgkin-Huxley model. R.Fitzhugh (Lab. of Biophys., Nat. Inst. of Health, Bethesda, MD, USA). *Biophys. J. (USA)*, vol.42, no.1, p.11-16 (April 1983). A voltage clamp consisting of a sinusoidal voltage of amplitude V_1 and frequency f , superimposed on a steady voltage level V_0 , is applied to the Hodgkin-Huxley model of the squid giant axon membrane. The steady-state response is a current composed of sinusoidal components of frequencies $0, f, 2f, 3f, \dots$. The frequencies greater than f arise from the nonlinearity of the membrane. The total current is described by a power series in V_1 ; each coefficient of this series is composed of current components for one or more frequencies. For different frequencies one can derive higher-order generalized admittances characterizing the nonlinear as well as the linear properties of the membrane. Formulas for the generalized admittances are derived from the Hodgkin-Huxley equations for frequencies up to $3f$, using a perturbation technique. Some of the resulting theoretical curves are compared with experimental results, with good qualitative agreement. (5 refs.)

63818 Electrical resistance of muscle capillary endothelium. S.P.Olesen, C.Crone (Inst. of Medical Physiology, Univ. of Copenhagen, Copenhagen, Denmark).

Biophys. J. (USA), vol.42, no.1, p.31-41 (April 1983). A recently developed technique for in vivo determination of the electrical resistance of vascular endothelium in microvessels was applied to the vessels in a thin frog muscle, m. cutaneous pectoris. The technique consists of injection of current via a glass micropipette into a capillary and measurement of the resulting intra- and extravascular potential profiles with another micropipette placed at various distances from the current source. The theory of Peskoff and Eisenberg (1974) was used to handle the problems arising from distributed extravascular resistances and was experimentally shown to describe the external field satisfactorily. With this extension of one-dimensional cable theory the specific electrical resistance of arterial microvessels was $33 \Omega \text{ cm}^2$ and of venous capillaries $23 \Omega \text{ cm}^2$. The 'length constants' were 135 and 112 μm , respectively. If results from arterial and venous vessels are taken together, the ionic permeabilities at 20°C were $P(\text{Na}) = 3.9 \times 10^{-3} \text{ cm.s}^{-1}$, $P(\text{K}) = 5.7 \times 10^{-3} \text{ cm.s}^{-1}$, $P(\text{Cl}) = 5.9 \times 10^{-3} \text{ cm.s}^{-1}$ and $P(\text{HCO}_3) = 3.4 \times 10^{-5} \text{ cm.s}^{-1}$. These figures agree with figures for capillary permeability obtained in tracer experiments on whole muscle. The study bridges a gap between single capillary and whole organ techniques with the conclusion that the two different approaches lead to similar results in muscle capillaries. (42 refs.)

63819 Successive openings of the same acetylcholine receptor channel are correlated in open time. M.B.Jackson, B.S.Wong, C.E.Morris, H.Lecar (Lab. of Biophys., Nat. Inst. of Health, Bethesda, MD, USA). *Biophys. J. (USA)*, vol.42, no.1, p.109-114 (April 1983). Previous analysis of single-channel current records has shown that both the opening and closing transitions of chemically activated ion channels are operated by fast and slow kinetic processes. The fast component in the kinetics of channel opening has been interpreted as the reopening of a channel that has just closed. The fast component in the kinetics of channel closure has many possible explanations and is therefore more difficult to interpret. One can gain insight into the closing process by asking whether the lifetimes of successive openings of an acetylcholine receptor channel are correlated in open-state lifetime. Five kinetic models of channel closure are considered. Two of these models predict uncorrelated open-state lifetimes, one predicts correlated open-state lifetimes, and for two others a range of behavior is possible. Acetylcholine receptor channel data from cultured rat muscle are analyzed to show that open-state lifetimes are correlated, eliminating two models of channel gating. (20 refs.)

63820 Inhomogeneous interfacial regions of biological systems. II. Dielectric profile and ion distributions. V.S.Vaidyanathan (Dept. of Biophys. Sci., State Univ. of New York, Buffalo, NY, USA). *J. Biol. Phys. (USA)*, vol.10, no.3, p.167-177 (1982). For pt.I see *ibid.*, vol.10, no.3, p.153-66 (1982). The Taylor expansion procedure is utilized to obtain solutions of basic nonlinear coupled differential equations relating concentration profiles and electric potential profiles, under equilibrium conditions. On the basis of an assumed simple expression for the dielectric profile, solutions are obtained. Certain conclusions derived on the basis of analysis are discussed. (2 refs.)

63821 Studies on the human spontaneous electromyogram (EMyLoG). III. Spontaneous spinal cord activity of the cat relevant to the human spontaneous EMyLoG. Y.Sarica, M.Eti, C.Ertekin (Dept. of Clinical Neurology, Aegean Univ., Izmir, Turkey).

Electroencephalogr. & Clin. Neurophysiol. (Netherlands), vol.55, no.2, p.168-79 (Feb. 1983).

For pt.II see *ibid.*, vol.55, p.24-33 (1983). The spontaneous electromyogram (EMyLoG) was investigated in 16 cats, some after laminectomy and some by a percutaneous intrathecal technique similar to the human approach. Small diphasic negative-positive waves at less than 50 μV , with short durations, were consistently recorded from the posterior aspect of the spinal cord in both laminectomized and intact cats. It was demonstrated that this kind of background activity is mainly located within the posterior halves of the spinal cord and is strictly dependent on the peripheral inputs producing excitability changes in the gray matter of the posterior horn. Monophasic positive waves of larger amplitude were often recorded from the anterior halves of the spinal cord in both types of recording. (39 refs.)

63822 Thalamic rhythms in cat during quiet wakefulness and immobility. J.J.Bouyer, C.Tilquin, A.Rougeul (Lab. de Neurophysiologie Comparee, Univ. Pierre & Marie Curie, Paris, France).

Electroencephalogr. & Clin. Neurophysiol. (Netherlands), vol.55, no.2, p.180-7 (Feb. 1983).

The authors studied the cortical 'mu' rhythms in normal cats and their thalamic pacemaker. Mu (14 c/sec) activity develops when the animal is motionless, in a state of 'quiet waking'. It is distinct from other sensorimotor rhythms, with distinct cortical distributions, distinct frequencies and appearing under different behavioural and environmental conditions. The cortical mu

focus was shown to be centred within a restricted part of area SI, in the forepaw and wrist projection field. The related thalamic focus was localized in a small zone of the VP nucleus that also corresponded to the hand and wrist projection area. A coherence study confirmed the close relationship between the two foci, thalamic and cortical. After unilateral electrolytic destruction of the thalamic area, a small mu activity persisted, on the ipsilateral cortex, originating from the opposite side. After bilateral lesion of the VP foci, no mu activity could ever be recorded on either side, while the other sensorimotor rhythms were left intact. (21 refs.)

63823 Excitation-contraction coupling: role of K-activation within the transverse tubular system. J.P.Reuben, G.M.Katz (Dept. of Neurology, Columbia Univ., New York, NY, USA), P.W.Brandt, G.Suarez-Kurtz, M.S.Dekin.

Proc. Natl. Acad. Sci. USA, vol.80, no.4, p.988-92 (Feb. 1983).

Long-duration Ca action potentials induced in crustacean muscle fibers after prolonged exposure to quaternary ammonium ions are accompanied by attenuated tensions with unique time courses. The tensions have three phases. The initial phase, correlated with the upstroke of the spike, is a rapid increase in tension followed by relaxation to or near to resting level (on-tension). In the second phase, tension rises slowly as the spike plateau declines. The final phase is another rapid increase and decay in tension that is correlated with termination of the action potential (off-tension). To observe these tensions, fibers must be exposed to 50-100 mM tetrabutylammonium ion for about 1 hr or to lower concentrations for longer periods (e.g., 5 mM for 20-30 hr). To obtain a similar response in fibers treated with tetraethylammonium ion, higher concentrations or longer soaking periods, or both, are required. Because neither caffeine-induced tensions in intact fibers nor contractile protein and sarcoplasmic reticulum function in skinned fibers were modified by quaternary ammonium ions, their site of action appears to be limited to surface or transverse tubular system membranes, or both. The unique tensions can be explained by considering the mode by which quaternary ammonium ions block K channels in conjunction with a scheme in which activation of K channels within the transverse tubular system controls the driving force for influx of Ca ions. (30 refs.)

63824 Action potentials in macrophages derived from human monocytes. F.V.McCann, P.M.Guyre, J.J.Cole, J.A.G.Russell (Dept. of Physiology, Dartmouth Medical School, Hanover, NH, USA).

Science (USA), vol.219, no.4587, p.991-3 (25 Feb. 1983).

The electrical activity of macrophages derived from human blood monocytes was recorded in vitro with intracellular microelectrodes and was analyzed with computer-assisted data acquisition and analysis techniques. In cells impaled 6 to 8 days after the cultures were prepared, the resting potentials reached a maximum value of -72 millivolts. The cells were electrically excitable; spikes exhibited a slow upstroke, a fast downstroke, a discrete threshold, a large overshoot, and a brief undershoot. Repetitive firing was induced by a maintained depolarizing current. A positive relation was observed between transmembrane currents and resting potential. Voltage-current relations were nonrectifying for subthreshold current injections. Since these cells had not been treated with any specific activation factors, the electrical activity recorded is evidence for the presence of voltage-dependent inward and outward currents in the membranes of mature macrophages. (13 refs.)

Inhomogeneous interfacial regions of biological systems. I. Basic differential equations and their implications See Entry 63765

Alamethicin pore formation: voltage-dependent flip-flop of α -helix dipoles See Entry 63796

Elastic energy stored in a membrane due to electrostriction See Entry 63797

A theoretical and scanning electron microscope study on the electrically mediated inactivation of spermatozoa See Entry 63805

Flickering of a nicotinic ion channel to a subconductance state See Entry 63812

Canine thoracic electrical impedance with changes in pulmonary gas and blood volumes See Entry 63877

Comparison of electrical field plethysmography with electrical impedance plethysmography See Entry 63914

Functional imaging of the brain See Entry 63940

Laser etched bifilar fine wire electrode for skeletal muscle motor unit recording See Entry 63989

Functional stimulation—instrumentation and clinical relevance See Entry 63996

Effect of defibrillation energy on pacing threshold See Entry 63999

Effects of myocardial infarction on catheter defibrillation threshold See Entry 64000

87.32 PHYSIOLOGICAL OPTICS, VISION

63825 Effects of moderate exercise on intraocular pressure. D.R.McDaniel, C.L.Tribbey, G.S.Tobias (Southern California Coll. of Optometry, Fullerton, CA, USA).

Am. J. Optom. & Physiol. Opt. (USA), vol.60, no.3, p.154-7 (March 1983).

Intraocular pressure measurements were made on human subjects using a noncontact tonometer before and at several time intervals after moderate exercise on a bicycle ergometer. One minute after exercise, intraocular pressures were significantly decreased (by 25%) but gradually returned toward pre-exercise values in 20 to 30 min. The results confirm findings by others that physical exertion results in a transient decrease in intraocular pressures and suggest that the magnitude of the reduction and the time required for recovery are related to the severity of the exertion. (15 refs.)

63826 Ultrastructure and electric changes in donor cornea depending on the preservation time. Z.G.Takeva (Dept. of Anatomy, Medico-Biological Inst., Sofia, Bulgaria), N.G.Popdimirova, S.N.Mechkarski.

C.R. Acad. Bulg. Sci. (Bulgaria), vol.35, no.11, p.1549-52 (1982).

A study was made on the action of a moist chamber and nutritive medium, with ingredients depending on the preservation time, on the cornea potential and ultrastructure. A porcine eye cornea was used, separated and preserved in a moist chamber or in nutritive medium T-199 with ingredient Sopolcort H (250 mg l^{-1}). For the electronmicroscopic studies the material was fixed in 1% OsO_4 . After dehydration it was embedded in Durcupan ACM. The slices were prepared on ultramicrotome Reichert OH_2 , they were contrasted with uranylacetate and were observed on an electron microscope Hitachi HU 11 A. The biopotentials were measured with the help of a lamp voltmeter, the samples being placed in a plexiglass chamber constructed for the purpose. Biopotentials of 380 corneas were measured in this way. (6 refs.)

Pseudoisochromatic plate design—Macbeth or tungsten illumination? See Entry 63916

87.32C Anatomy and optics of the eye

63827 Comparison of American Optical SR-IV refractive data with clinical refractive data on a group of myopic children. T.Grosvenor, D.M.Perrigin, J.Perrigin (Coll. of Optometry, Univ. of Houston, Houston, TX, USA). *Am. J. Optom. & Physiol. Opt. (USA)*, vol.60, no.3, p.224-35 (March 1983). As a part of a 3-year Myopia Control Study being conducted at the University of Houston, 131 myopes between the ages of 6 and 15 years have been refracted by means of both the redesigned SR-IV Programmed Subjective Refractive and conventional clinical procedures. The results indicated that for the majority of subjects, the refractive data obtained by means of the SR-IV differed by no more than 0.25 D from data obtained by conventional procedures. SR-IV and clinical refractive data were also compared for a group of 30 second year optometry students, and agreement for the two methods was found to compare favorably with agreement of clinical refractive data obtained by two or more examiners. (6 refs.)

63828 Myopia development in nonhuman primates—a literature review. M.H.Criswell (Indiana Univ., School of Optometry, Bloomington, IN, USA), D.A.Goss.

Am. J. Optom. & Physiol. Opt. (USA), vol.60, no.3, p.250-68 (March 1983). Reviews and comments on the available literature dealing with myopia production in various types of monkeys and in tree shrews by experimental manipulations of their physical, visual, and/or bodily environments. The results from these studies are compared with hypotheses and models which purport to explain myopia development. Possible relations are also noted between conditions, created experimentally in myopic eyes of primates, and similar pathological states, clinically observed in certain human myopes. (71 refs.)

63829 Image quality of the human eye for eccentric entrance pupils. A.van Meeteren, C.J.W.Dunnewold (Inst. for Perception TNO, Soesterberg, Netherlands).

Vision Res. (GB), vol.23, no.5, p.573-9 (1983).

The human eye has a considerable amount of chromatic aberration and a moderate amount of spherical aberration. If a small artificial pupil is placed in front of such optics and moved away from the centre towards the periphery the chromatic aberration will result in lateral colour shifting, and the spherical aberration will cause coma. Starting from available experimental data on the chromatic aberration and the spherical aberration, modulation transfer functions (MTFs) are calculated for central and eccentric positions of small pupils placed in front of the human eye. These calculations may help to separate optical and retinal contributions to the well-known reduction of visual acuity measured with eccentric pupils. It appears that measurements with pupils smaller than 1 mm in monochromatic light can be considered optically as diffraction limited. Changes of visual acuity found in this way must be assigned to the retina. (16 refs.)

Effect of conicoid asphericity on the Tscherning ellipses of ophthalmic spectacle lenses See Entry 61252

Construction, specification, and mathematical description of aspheric surfaces See Entry 63917

A comparative study of tear evaporation rates and water content of soft contact lenses See Entry 64001

87.32E Physiology of the eye; nerve structure and function

63830 A model referenced method for the identification of evoked potential component wave forms. S.J.O'Connor, A.Tasman, R.H.Simon, M.S.Hale (Dept. of Psychiatry, Univ. of Connecticut Health Center, Farmington, CT, USA).

Electroencephalogr. & Clin. Neurophysiol. (Netherlands), vol.55, no.2, p.233-7 (Feb. 1983).

Visual evoked potentials from rat visual cortex are described as the sum of components. Each component wave form is based on a mathematical model of neural activity. The model referenced approach yields an accurate description of the evoked potential wave forms before and after administration of an anesthetic known to alter neural activity. Thus, the method is efficient, is based in neurophysiology and is sensitive to drug effect on brain activity. (15 refs.)

63831 Differences in spectral response properties of LGN cells in male and female squirrel monkeys. G.H.Jacobs (Dept. of Psychology, Univ. of California, Santa Barbara, CA, USA).

Vision Res. (GB), vol.23, no.5, p.461-8 (1983).

The spectral response patterns of single cells recorded from the lateral geniculate nucleus (LGN) of the squirrel monkey (*Saimiri sciureus*) were examined in light of recent behavioral evidence indicating that there are significant variations in visual sensitivity and color vision within this species. The principal results from an analysis of data obtained from 1084 LGN cells were that (a) a significantly higher proportion of cells showing spectrally-opponent response patterns were recorded from female subjects, and (b) the proportion of spectrally-opponent units showing RG response patterns is very much higher in females than in males. These gender-related differences in the response patterns of LGN cells are discussed in the context of the behavioral results. (26 refs.)

63832 Response vs. excitation in response-dependent and stimulus-dependent lateral inhibitory networks. D.H.Edwards, Jr. (Dept. of Biology, Georgia State Univ., Atlanta, GA, USA).

Vision Res. (GB), vol.23, no.5, p.469-72 (1983).

Response-dependent and stimulus-dependent lateral inhibitory networks may be distinguished by differences in their net response vs. net excitation functions. It is shown that the net response of a stable, response-dependent network is a monotonically increasing function of the net excitation. By contrast, the response of a stimulus-dependent lateral inhibitory network can either increase, decrease or remain constant as the net excitation of the network is increased, dependent on the relation of the inhibition to the excitation. These differences make it possible to determine that the inhibition produced by a lateral inhibitory network is stimulus-dependent if the net response of the network declines as the network excitation increases. (14 refs.)

63833 Representation of the visual streak in visuotopic maps of the cat's superior colliculus: influence of the mapping variable. J.T.McIlwain (Div. of Biology & Medicine, Brown Univ., Providence, RI, USA).

Vision Res. (GB), vol.23, no.5, p.507-16 (1983).

A series of visuotopic maps has been prepared from recordings of electrical potentials related to W-cell afferent activity in the cat's superior colliculus. These maps clearly exhibit an expected exaggeration of the representation of the upper visual field, due to tilt of the retina's visual streak in the 'position of paralysis'. This asymmetry disappears when the visual field's coordinate system is rotated by an angle equal to the tilt of the axis of the nasal streak.

Previously published maps, based on recordings from postsynaptic collicular units, have failed to reflect this tilt of the nasal visual streak, perhaps in part because the centers of unit receptive-fields are biased estimators of the retinal origin of axons terminating near a collicular recording site. (34 refs.)

63834 A new concept of retinal colour coding. W.Paulus, A.Kroeger-Paulus (Univ.-Augenlinik, Dusseldorf, Germany).

Vision Res. (GB), vol.23, no.5, p.529-40 (1983).

A theory of retinal colour coding based closely on recent anatomical and physiological results is presented. Opponent colour channels are shown to be an inevitable result of any randomly distributed retinal cone mosaic, the structure of red-green opponent colour channels remaining uninfluenced by a predominance of 'red' or 'green' cones. These findings circumvent the conflict between anatomical results with more 'green' than 'red' cones and psychophysical estimations with more 'red' than 'green' cones. The effect of receptor compression and opponent colour transformation on colour perception is investigated. Non-opponency of pure green and pure red could be attributed to receptor compression, the Bezold-Brücke phenomenon, however, to the antagonism of 'red' and 'green' cones within the receptive field surround of red-green opponent cells. The fundamental colours are estimated to be supersaturated violet, yellow-green and yellow-red. (60 refs.)

63835 Vitreal and intraretinal responses to contrast reversing patterns in the pigeon eye. A.L.Holden, Vaegen (Dept. of Visual Sci., Inst. of Ophthalmology, London, England).

Vision Res. (GB), vol.23, no.5, p.561-72 (1983).

The pattern electroretinogram (PERG) has been recorded vitreally and intraretinally in the pigeon eye. The amplitude of the PERG increases monotonically as pattern contrast is increased, with saturation of high levels. The PERG of the central yellow field has band-pass spatial tuning, with a high frequency cut-off at 8 c/deg. Time-to-peak is shortest at low spatial frequencies. Both PERG and local b-wave are small and positive-going close to the retinal surface, and large and negative-going in the inner nuclear layer. The PERG and b-wave show qualitatively similar depth profiles. (22 refs.)

A comparison of methods for measuring event-related potentials See Entry 63988

Detection of signal of rapid eye movements See Entry 64017

87.32L Light detection; adaptation and discrimination

63836 Ultraviolet sensitivity of fly photoreceptors R7 and R8: evidence for a sensitising function. R.C.Hardie, K.Kirschfeld (Max-Planck-Inst. für Biologische Kybernetik, Tübingen, Germany).

Biophys. Struct. & Mech. (Germany), vol.9, no.3, p.171-80 (1983).

Responses to continuous spectral scans in the ultraviolet (UV) have been measured intracellularly from the central retinula cells R7 and R8 in the fly (*Musca*, female). The spectral sensitivities thus obtained have a resolution limited by the bandwidth of the light supplied by the monochromator (0.3-1.5 m). One class of R7 cells, classified as 7y (Kirschfeld et al. 1978) shows three conspicuous peaks of sensitivity at 337, 355 and 373 nm. The underlying R8 cells (8y) also show three peaks but at slightly shorter wavelengths—334, 350, and 369 nm, coinciding with those seen in the peripheral photoreceptors R1-6 (Gempeler et al. 1980; Kirschfeld et al. 1982). Another class of R7 cells (7p) showed a spectral sensitivity function with a single peak at 330 nm. The underlying R8 cells (8p) also show a single-peaked function with maximum at 460 nm. The results are interpreted as providing evidence for the hypothesis that UV sensitivity in 7y and 8y cells is conferred by a UV absorbing sensitising pigment similar to that demonstrated in R1-6 cells. The spectra of both 7p and 8p cells can be simply interpreted as deriving directly from the absorption of a rhodopsin with the appropriate λ max. (24 refs.)

63837 Discrete visual defects in pearl mutant mice. G.W.Balkema, N.J.Mangini, L.H.Pinto (Purdue Univ., West Lafayette, IN, USA).

Science (USA), vol.219, no.4588, p.1085-7 (4 March 1983).

The mutant mouse pearl, characterized by its hypopigmentation, has a specific function defect in a sensory system—the retina. The intact pearl mouse has reduced sensitivity in the dark-adapted condition. Normal sensitivity is restored by isolation and superfusion of the retina with bicarbonate-buffered Ringer solution, suggesting that the retinal expression of the pearl mutation depends on a diffusible substance. The pearl phenotype is described as a possible model for human congenital stationary night blindness. (25 refs.)

63838 Scotopic sensitivity to ON and OFF stimulus transients. P.W.Russell, T.G.Wheeler (Dept. of Ophthalmology, School of Medicine, Univ. of Louisville, Louisville, KY, USA).

Vision Res. (GB), vol.23, no.5, p.525-8 (1983).

The luminance of a large diffuse field, viewed peripherally, was temporally modulated near absolute detection threshold. The field luminance either increased abruptly and decreased gradually (ON stimulus) or increased gradually and decreased abruptly (OFF stimulus). For all wavelengths shorter than 620 nm, sensitivity to the ON stimulus was greater than to the OFF. The spectral sensitivity curves obtained indicate that rods and/or their associated neural pathways are more sensitive to ON stimulus transients than to OFF. (16 refs.)

Sensitivity to countermodulating gratings following spatiotemporal adaptation See Entry 63844

Suprathreshold spatiotemporal response characteristics of the human visual system See Entry 63845

Visual detection of objects against backgrounds of nonuniform luminance See Entry 63846

87.32N Colour detection; adaptation and discrimination

63839 Densitometric measurement of human cone photopigment kinetics. V.C.Smith, J.Pokorny (Eye Res. Lab., Univ. of Chicago, Chicago, IL, USA), D.van Norren.

Vision Res. (GB), vol.23, no.5, p.517-24 (1983).

The radiance response function for steady state bleaching lights and the regeneration of the cone visual photopigments were measured using the continuous recording densitometer described by v. Norren and v.d. Kraats (see *ibid.*, vol.21, p.897-905, 1981). Measurements made on 5 deuteranopes, 1 protanope and 2 color-normal observers were similar. The radiance response function was steeper than the function predicted by a simple first-order kinetic equation. For a measured density (ca. 0.3) the authors evaluated whether high stray light (ca. 47.5%) and high two-way optical density (ca. 1.3) could account for the deviation from the prediction of a first-order equation. Such a model was rejected because these parameters predicted different estimates of the time course of regeneration for different test wavelengths (554 and 605 nm). Statistical analysis of the regeneration data revealed a highly significant non-linearity. A model in which the rate of regeneration

increases as the proportion of bleached photopigment decreases is required to explain both the radiance function and the regeneration data. (15 refs.)

- Differences in spectral response properties of LGN cells in male and female squirrel monkeys See Entry 63831
 A new concept of retinal colour coding See Entry 63834
 Small and moderate color differences. IV. Color-difference-perceptibility ellipses in surface-color space See Entry 63841
 A proposal of new standard deviate observers See Entry 63842
 Determination of visual threshold contrasts by means of achromatic and colored test objects See Entry 63847

87.32S Psychophysics of vision, visual perception, binocular vision

63840 Contrast sensitivity in albinotic patients. D.S.Loshin, R.A.Browning (Univ. of Houston, Coll. of Optometry, Houston, TX, USA).

Am. J. Optom. & Physiol. Opt. (USA), vol.60, no.3, p.158-66 (March 1983). Vertical and horizontal grating contrast sensitivity functions (CSF) were measured on eight albinotic patients. Several of these patients also had CSF measurements performed through their telescopic aids. For all the patients, the horizontal grating CSF was more sensitive than the vertical grating CSF. Although there are many pathological problems that could result in this sensitivity difference (high astigmatism, neural modification, etc.), the authors propose that in this case, the nystagmoid eye movements are the main causative factor. Through the telescopic aid, the CSF resolution acuity and peak sensitivity increased. The increase in resolution was somewhat less than would be predicted based on magnification. The increase in sensitivity is believed to be the result of stimulation of more sensitive peripheral retina. This increase in sensitivity is an added benefit to these patients corrected with low vision aids. (19 refs.)

63841 Small and moderate color differences. IV. Color-difference-perceptibility ellipses in surface-color space. D.C.Rich, F.W.Billmeyer, Jr. (Dept. of Chem., Rensselaer Polytech. Inst., Troy, NY, USA). *Color Res. & Appl. (USA)*, vol.8, no.1, p.31-9 (Spring 1983). For pt.III see AIC Color 77, Hilger, Bristol, p.495-8, 1978. Moderate (0.5-1.5 CIELAB units) color differences in surface colors were scaled visually to obtain color-difference-perceptibility ellipses. The ellipse orientations appeared to be independent of the size of the color differences over the range indicated, and were consistent with literature results obtained with visual colorimeters. In the vivid greenish yellow region, the experimental ellipse orientation agreed with the Munsell spacing but not with the orientation of the CIELAB ellipse. In the deep greenish blue region, the experimental ellipse orientation agreed better with the results of Wyszecki and Fielder (1971) than with the orientation of the MacAdam PGN ellipse. (26 refs.)

63842 A proposal of new standard deviate observers. Y.Nayatani (Osaka Electro-Communication Univ., Osaka, Japan), K.Takahama, H.Sobagaki. *Color Res. & Appl. (USA)*, vol.8, no.1, p.47-56 (Spring 1983). The method of singular-value decomposition analysis of matrices is used to analyze the 20 color-matching functions of Stiles's observers. It is confirmed that the 20 color-matching functions are well reconstituted by the first three decomposed components. A new deviate observer is derived from the first decomposed component. It is shown that the new deviate observer can be used well in the computation of observer-metamerism indices. Furthermore, an optimized deviate observer is developed by modifying the color-matching functions of the new deviate observer slightly. Both the new and the optimized deviate observer give a basis for the further study of the evaluation of observer metamerism. (13 refs.)

63843 Time thresholds for increments and decrements in luminance. W.H.Ehrenstein, L.Spillmann (Neurologische Universitätsklinik, Freiburg, Germany). *J. Opt. Soc. Am. (USA)*, vol.73, no.4, p.419-26 (April 1983). Time thresholds, i.e. the minimal durations necessary to just detect a change in brightness, were measured for light increments and decrements of a 1° test spot centered on a background of 20°. Background luminance varied from -1 to 3 log td and retinal eccentricity from 0° to 50°. Step size ranged from 0.04 to 1.5 log units and was the same in absolute units for both directions. Two types of stimuli were used: Type A, in which increments and decrements emerge from the same uniform background, and Type B, in which increments are the same as in Type A but decrements consist of a brief interruption of the test spot. Type A stimulation resulted in similar time thresholds for increments and decrements or, under some conditions, slightly shorter decrement thresholds. Type B stimulation resulted in similar thresholds for foveal vision. However, with increasing step size, decreasing background luminance, and increasing eccentricity, the time threshold for the decrement progressively exceeded that for the increment (up to 80 msec). This difference is attributed to different rise and fall times of the photoreceptor response as well as to Troxler's effect. (54 refs.)

63844 Sensitivity to countermodulating gratings following spatiotemporal adaptation. D.O.Bowker, U.Tulunay-Keesey (Dept. of Ophthalmology, Univ. of Wisconsin, Madison, WI, USA). *J. Opt. Soc. Am. (USA)*, vol.73, no.4, p.427-35 (April 1983). Contrast sensitivities to countermodulating gratings were measured with a two-alternative temporal forced-choice procedure following adaptation to a static grating of the same spatial frequency, a homogeneous flickering field of the same temporal frequency, or a countermodulating grating of identical spatial and temporal frequencies. At high spatial frequencies, the temporal-frequency content of the adaptation was not critical, that is, a countermodulating adaptation grating was only slightly more effective at raising threshold than was a static adaptation grating. At low spatial frequencies, the sensitivity to countermodulating test gratings could not be reduced by either a high-contrast stimulus matching the test in the spatial domain only or by one matching the test in the temporal domain only. Adapting to a high-contrast stimulus matching the countermodulating test grating in both spatial- and temporal-frequency domains was effective at reducing test sensitivity for one observer but not for another. (54 refs.)

63845 Suprathreshold spatiotemporal response characteristics of the human visual system. D.O.Bowker (Dept. of Ophthalmology, Univ. of Wisconsin, Madison, WI, USA). *J. Opt. Soc. Am. (USA)*, vol.73, no.4, p.436-40 (April 1983). The apparent contrasts of suprathreshold stationary gratings, countermodulated gratings, and homogeneous flickering fields were assessed with a contrast-matching procedure. Results show that, as stimulus amplitude is increased relative to threshold, variations in apparent contrast with spatiotemporal-frequency content become much less pronounced. In other words, the contrast-matching functions are more uniform across both spatial and temporal frequency at levels of contrast well above threshold. These data are interpreted in terms of a compensatory stage in the visual system that varies

its gain characteristics according to the detectability of the stimulus. (17 refs.)

63846 Visual detection of objects against backgrounds of nonuniform luminance. V.N.Martynov, B.I.Shkurskii. *Sov. J. Opt. Technol. (USA)*, vol.49, no.7, p.406-9 (July 1982). Translation of: *Opt.-Mekh. Prom.-st. (USSR)*, vol.49, no.7, p.6-9 (July 1982). [received: April 1983]

On the basis of a model of a visual analyzer as an optimum system for receiving optical signals, a method of estimating the threshold luminance difference for the visual detection of arbitrarily shaped objects against a background of nonuniform luminance has been developed and verified experimentally. (5 refs.)

63847 Determination of visual threshold contrasts by means of achromatic and colored test objects. N.P.Travnikova, A.S.Malyshova, L.V.Sergeeva, L.I.Chernikova.

Sov. J. Opt. Technol. (USA), vol.49, no.7, p.410-12 (July 1982). Translation of: *Opt.-Mekh. Prom.-st. (USSR)*, vol.49, no.7, p.9-12 (July 1982). [received: April 1983]

The threshold contrasts are determined for colored test objects having an angular size of 80-100' at background luminances of 10-150 cd/m². It is shown that the average values of the threshold for the disappearance and appearance of the colored object images are almost identical to the corresponding values of achromatic objects. (2 refs.)

63848 A geometrical theory of scaling in the sensory system with several inputs and a single output. R.Takiyama (Kyushu Inst. of Design, Fukuoka, Japan).

Trans. Inst. Electron. & Commun. Eng. Jpn. Part A (Japan), vol.J66A, no.1, p.16-23 (Jan. 1983). In Japanese.

To investigate the psychophysical functions which characterize the sensory system with several inputs and a single output, the author constructs the Riemannian state space spanned by several physical continua as well as the corresponding psychological continuum, and defines psychophysical functions as geometrically invariant quantities in the space. By introducing a certain fundamental metric based on the difference thresholds, the allowable psychophysical functions are derived. Applying this formalization, some psychophysical laws in vision are examined. It is shown that Stiles' and Abney's laws are derived as allowable functions provided that Weber's and Ekman's laws hold. (19 refs.)

63849 Visual correspondence problem in apparent moving patterns. K.Shoji, Y.Arakawa (Faculty of Engng., Utsunomiya Univ., Utsunomiya, Japan).

Trans. Inst. Electron. & Commun. Eng. Jpn. Part A (Japan), vol.J66A, no.1, p.86-92 (Jan. 1983). In Japanese.

Perceived correspondence between successive frames was investigated in right-angled trapezoids ranging in shape from right-angled triangle to square. At appropriate timing, the 1st pattern presented was presented horizontally and then 2nd pattern presented with orientational disparity, ranging from 0° to 360°. The results of the psychological experiment demonstrate the existence of competing mental tendencies to preserve the rigid structure of an object and to traverse a minimum transformational path. In order to verify this existence, a model of correspondence decision making was constructed. The computational outputs of this model fit the experimental data approximately. (9 refs.)

63850 Light and dark bars: contrast discrimination. G.E.Legge, D.Kersten (Dept. of Psychology, Univ. of Minnesota, Minneapolis, MN, USA). *Vision Res. (GB)*, vol.23, no.5, p.473-83 (1983).

Contrast increment thresholds were measured for light and dark bars as a function of the base contrast of the bars. The bars were superimposed on a uniform field of 340 cd/m². They had either rectangular or Gaussian luminance profiles, varied in width from 0.1° to 10°, and in duration from 10 to 200 msec. For the 200-msec presentations, the resulting contrast discrimination functions all had approximately the same shape when contrast was defined as $(L_{max} - L_{min}) / (L_{max} + L_{min})$, and closely resembled corresponding results for sine-wave gratings. The similarity in shape of contrast discrimination functions for light and dark bars is attributed to a retinal nonlinear intensity transformation. The 10 msec contrast discrimination functions differed from the 200-msec functions in ways that can be explained by differences in temporal integration. (42 refs.)

63851 Spatial frequency masking and Weber's law. D.J.Swift, R.A.Smith (Vision Res. Labs., Univ. of New Hampshire, Durham, NH, USA). *Vision Res. (GB)*, vol.23, no.5, p.495-505 (1983).

The threshold masking effect of one simultaneously presented grating upon another was studied as a function of mask contrast and frequency. The masking function typically obeys Weber's Law with method-of-adjustment psychophysics, and typically does not with forced-choice. This apparent discrepancy was studied in some detail. It is suggested that thresholds can be set with at least two different criteria, depending upon experimental conditions. When the mask is unfamiliar, it functions as noise and detection occurs at a constant signal/noise ratio, which yields Weber's Law. When the mask is highly familiar, its masking effect is less and obeys a power law. This power-law masking appears to represent and inherent non-linearity of the visual system. (32 refs.)

63852 Exposure duration affects the sensitivity of vernier acuity to target motion. M.J.Morgan, R.J.Watt (Dept. of Psychology, Univ. Coll. London, London, England), S.P.McKee.

Vision Res. (GB), vol.23, no.5, p.541-6 (1983).

Threshold vernier acuity was measured under different conditions of target movement and exposure duration. In the case of a simple two-line vernier target, image motion up to about 3 deg/sec had little effect upon threshold for a briefly exposed (150 msec) target, which is relatively poor even for a stationary stimulus, but produced a decrement in acuity for a continuously exposed stimulus. This finding was repeated in a second experiment, which used a centroid cue to vernier offset, and which compared the effects of horizontal and vertical orientation. It is suggested that image motion and reduced exposure duration restrict the proportion restrict the proportion of the light spread function that can be usefully sampled by the neural networks responsible for hyperacuity. (14 refs.)

63853 Practice improves adults' sensitivity to diagonals. M.J.Mayer (Univ. of California, Santa Cruz, CA, USA). *Vision Res. (GB)*, vol.23, no.5, p.547-50 (1983).

Adults who were initially less sensitive to a diagonal, 10 c/deg sinusoidal grating, practised detecting it for 3000 yes-no signal detection trials. Following practice all observers had improved their relative sensitivity to the diagonal and most were as sensitive to the diagonal as to cardinal (horizontal or vertical) orientations. Practising a cardinal axis, on the other hand, caused no improvement in sensitivity unless the pre-practice threshold for that orientation was elevated with respect to other orientations. Three hypotheses are proposed to account for the improved sensitivity. The results are also related

to the typical pattern of adult anisotropic contrast sensitivity which favors the cardinal orientations. (21 refs.)

63854 Non-astigmatic children's contrast sensitivities differ from anisotropic patterns of adults. M.J.Mayer (Univ. of California, Santa Cruz, CA, USA).

Vision Res. (GB), vol.23, no.5, p.551-9 (1983).

Monocular contrast thresholds were estimated for horizontal (H), vertical (V) and left and right diagonal 10 c/deg sinusoidal gratings for non-astigmatic children (4:10-11:2 yr) and adults using yes-no signal detection (YN) methods. Some children were also tested with two-interval forced-choice (2IFC). Younger children were less likely to have the typical adult pattern of anisotropic sensitivity, favoring H and V, while 10-11-yr-olds had more adult-like anisotropy. Within all age groups patterns of anisotropy varied considerably. Deviation of adults from the typical pattern may be related to small amounts of astigmatism in their untested eyes. 4- and 5-yr-olds were confused by 2IFC. For children 6 yr and older, 2IFC and YN threshold estimates were equivalent, but 2IFC required less testing time. (20 refs.)

63855 Measurement of factors affecting VDU readability. S.Bennett, G.Trapani (Polarizer Div., Polaroid Corp., Norwood, MA, USA).

Electronic Displays '82 and Information Display Systems, London, England, 5-7 Oct. 1982 (Buckingham, Bucks., England: Network Exhibition 1982), 14 pp.

The authors have measured contrast enhancement on three different VDUs with each of four different contrast enhancement filters. The contrast enhancement filters were of different types; circular polarizing, mesh, neutral isotropically absorbing, and spectrally selective isotropic absorbing. The results indicate that any of the four filters is useful in enhancing contrast where the contrast is being reduced by nonspecular reflections. The improvement in contrast for the case where the brightness of the reflections is about equal to the signal runs about 100% (e.g. the contrast with a filter is about double what it is without a filter). For specular, or near-specular reflections, the circular polarizing filter has a clear margin of superiority, enhancing contrast by the order of tenfold, while the other filters remain about as effective as they are for nonspecular reflections. (15 refs.)

87.34 AUDITION

63856 Influence of the time pattern of noise exposure on the acquisition of and recovery from auditory fatigue. R.Hetu (Ecole d'Orthophonie et d'Audiologie, Univ. de Montreal, Montreal, Quebec, Canada).

Rev. Acoust. (France), vol.15, no.63, p.211-15 (1982). In French.

Temporary threshold shift (TTS) is related to the time pattern of noise exposure in a relatively complex fashion. This relationship essentially involves the on-fraction, the period of intermittency and the sound level during noise bursts and quiet intervals. Data from recent studies on the influence of the exposure parameters and more specifically of their mutual interactions is reviewed. Original data are presented on the effect of the interaction between the on-fraction and the period of intermittency on the growth of TTS and also on the effect of the ambient sound level on the recovery from TTS. The predictability of TTS is examined in the context of both laboratory and real life conditions. The implications for the time-intensity trade-off in occupational noise exposure limits and for administrative control of exposure is discussed. (35 refs.)

63857 Auditory nerve-brain stem evoked potentials in cats during manipulation of the cerebral perfusion pressure. H.Sohmer, M.Gafni, K.Goitein, P.Fainmesser (Dept. of Physiology, Hebrew Univ., Jerusalem, Israel).

Electroencephalogr. & Clin. Neurophysiol. (Netherlands), vol.55, no.2, p.198-202 (Feb. 1983).

In order to study the effects of various degrees of cerebral ischemia on the auditory nerve-brain stem evoked potentials (BAEP), the cerebral perfusion pressure (CPP), defined as the difference between mean arterial blood pressure (MAP) and intracranial pressure (ICP), was systematically manipulated in anesthetized, paralyzed and ventilated cats. The CPP was varied by decreasing MAP, either by hemorrhage or by the infusion of a vasodilating drug, and elevating ICP by infusion of mock CSF into the cisterna magna, or by MAP depression and ICP elevation simultaneously. The EEG and BAEP became isoelectric far below the range of autoregulation of cerebral blood flow (CBF) so that the brain stem auditory pathway is still capable of generating its electrical response (BAEP) at very low CBF. This is paradoxical since these same regions of the brain have been shown to have the highest levels of regional metabolism as shown by their very high local cerebral blood flow and local glucose utilization. (8 refs.)

63858 Post-stimulatory effects on the auditory brain stem response: partial-masking and enhancement. A.K.Ananthanarayan, G.M.Gerken (Callier Center for Communication Disorders, Univ. of Texas, Dallas, TX, USA).

Electroencephalogr. & Clin. Neurophysiol. (Netherlands), vol.55, no.2, p.223-6 (Feb. 1983).

The auditory brain stem response (ABR) was recorded in human subjects using the stimulus configuration of a tone-on-tone forward-masking paradigm, but with all stimuli at suprathreshold levels. A masking stimulus preceded, by Δt msec, the probe stimulus which elicited the ABR. The latency vs. Δt functions for waves III and V were essentially parallel to each other and were interpreted in terms of a partial forward-masking effect, possibly originating in the cochlea. Likewise, the amplitude function for wave III showed varying degrees of decrement as a function of Δt that was also compatible with a partial forward-masking interpretation. In contrast, wave V showed an amplitude increment relative to the unmasked wave that was maximal for Δt values of 15 and 45 msec. The amplitude increment in wave V was termed enhancement and was interpreted as a central process governed by the timing of sound sequences. (17 refs.)

63859 Measurement and analyzing of fatigue by the use of the newly devised acoustical method in comparison with the optical method of fatigue analysis by the flicker fusion technique. S.Kondo (Hitachi Ltd., Tokyo, Japan).

J. Acoust. Soc. Jpn. (Japan), vol.38, no.12, p.764-73 (Dec. 1982). In Japanese.

According to the acoustical method, a 2 kHz pure tone that travels with a duration of 20 msec followed by another tone of the same frequency is given as the acoustical stimulus, and the time interval between the two is adjusted in such a way as to bring about psychological fusion of the two tones, each subject being asked to give his differential threshold value τ_m . The subject's differential threshold value ϕ_m of the flicker fusion technique is also obtained. The analysis of the relation between the degree of fatigue and τ_m and ϕ_m indicates that τ_m and ϕ_m are both related to the degree of fatigue and that the τ_m and the ϕ_m stand almost in the reverse relation to each other as to the fatigue degree. Factors that contribute to τ_m or ϕ_m are analyzed and the degree of their contribution is determined by the quantification theory. τ_m and

ϕ_m have generally negative correlation coefficients to each other, but as to the fatigue state, they stand to each other in positive relations. The average τ_m per day of the week and the frequency of incidence of fatigue per day of the week stand in correlational relations to each other, but the correlation coefficients of τ_m are greater for young adolescents while those of ϕ_m tend to be greater for older people. (14 refs.)

63860 Psychological study on L_{eq} as a measure of loudness of various kinds of noises. S.Namba, S.Kuwano (Osaka Univ., Toyonaka, Japan).

J. Acoust. Soc. Jpn. (Japan), vol.38, no.12, p.774-85 (Dec. 1982). In Japanese.

The application of L_{eq} as a measure of loudness of various noises is investigated. Nine kinds of noise sources, -aircraft noise, super express train, noise, train noise, road traffic noise, speech, music, impulsive noise, artificial level-fluctuating noise and steady noise-are used as stimuli. The duration is about 10 sec except impulsive noise. Four kind levels are used in each noise source, therefore 36 stimuli are contained in a stimulus series. They are presented in random order and their loudnesses are judged by magnitude estimation. As a result of the experiment, it is found that L_{eq} can be used as a good measure of the loudness of various noises as a first approximation. Strictly speaking, however, there is a slight, but systematical deviation from L_{eq} in PSE's of some noise sources. This fact suggests that it is necessary to add some factors to L_{eq} in order to decide the permissible levels of these noise sources. (60 refs.)

63861 Two-component hearing sensations produced by two-electrode stimulation in the cochlea of a deaf patient. Y.C.Tong, R.C.Dowell, P.J.Blamey, G.M.Clark (Dept. of Otolaryngology, Univ. of Melbourne, Parkville, Victoria, Australia).

Science (USA), vol.219, no.4587, p.993-4 (25 Feb. 1983).

Dissimilarities in perception elicited by stimulation with two electrodes were estimated. A two-dimensional spatial configuration was found to be suitable to represent the dissimilarity data, and the two dimensions could be interpreted as corresponding to the position of the apical and basal electrode of the two-electrode combination. A speech-processing strategy that converts acoustic, first and second formants to two-electrode stimulation is proposed. (12 refs.)

63862 Temporal selectivity in the central auditory system of the leopard frog. G.Rose, R.R.Capranica (Cornell Univ., Ithaca, NY, USA).

Science (USA), vol.219, no.4588, p.1087-9 (4 March 1983).

Amplitude modulation is a predominant temporal feature in many vocal signals. The leopard frog, *Rana pipiens*, has a class of neurons in the central auditory system that respond selectively to particular rates of amplitude modulation; these neurons can be characterized by a temporal tuning curve. Such selectivity is absent in the peripheral auditory system. This type of transformation may be fundamental in processing temporal information in the vertebrate sensory nervous system. (15 refs.)

87.36 SPEECH

(see also 43.70 Speech communication)

63863 On the DC component of the human voice. S.Okamura (Faculty of Electro-Communications, Univ. of Electro-Communications, Chofu, Japan).

Trans. Inst. Electron. & Commun. Eng. Jpn. Part A (Japan), vol.166A, no.1, p.95-6 (Jan. 1983). In Japanese.

The human voice has been processed in the audible frequency range. The DC component, the very low frequency portion produced by the air flow, was found to be related to the shape of the vocal organ. This component will provide additional information on prosodic features. (1 ref.)

87.38 MECHANO- AND CHEMIO-CEPTIONS

(inc. biosonic generation, detection and guidance)

63864 Intrapulmonary CO_2 receptor discharge at different levels of venous PCO_2 . R.D.Tallman, Jr., F.S.Grodins (Dept. of Biomedical Engng., Univ. of Southern California, Los Angeles, CA, USA).

J. Appl. Physiol. (USA), vol.53, no.6, p.1386-91 (Dec. 1982). [received: April 1983]

It has been suggested that avian intrapulmonary CO_2 -sensitive receptors (IPC) may be capable of affecting ventilation in response to changes in lung CO_2 load. The purpose of this study was to record IPC discharge activity in spontaneously breathing ducks when venous Pco_2 was elevated or lowered from resting levels. This was accomplished using an extracorporeal venovenous blood bypass circuit, which included a 0.8-m^2 silicone membrane blood oxygenator. Adult male Pekin ducks were anesthetized and tracheostomized. Single-unit activity was recorded from 42 IPC. During venous CO_2 loading, there was no difference in the average IPC discharge from control despite an increase in the rate of CO_2 excretion (V_{CO_2}) to twice the resting level. Venous CO_2 unloading decreased V_{CO_2} by one-half but did not significantly affect inspiratory IPC discharge and resulted in only a small increase in expiratory discharge. In contrast, inhalation of 3% CO_2 greatly reduced inspiratory discharge. Reflex adjustments in tracheal flow appear to be responsible for maintaining IPC discharge at control levels when venous Pco_2 changes. (18 refs.)

63865 Sensation of inspired volume in normal subjects and quadriplegic patients. A.F.DiMarco, D.A.Wolfson, S.B.Gottfried, M.D.Altose (Dept. of Medicine, Case Western Reserve Univ., Cleveland, OH, USA).

J. Appl. Physiol. (USA), vol.53, no.6, p.1481-6 (Dec. 1982). [received: April 1983]

To investigate the influence of respiratory muscle tension and feedback from rib cage receptors, the sensation of inspired volume was compared in normal subjects and quadriplegic patients during active breathing, with and without the addition of an inspiratory resistive load, and during passive ventilation produced by a tank respirator. In separate trials, volume sensation was assessed using tests of magnitude estimation and volume reproduction. The mean exponents and standard errors for the magnitude estimation of inspired volume in normal subjects were 1.32 ± 0.08 , 1.24 ± 0.06 , and 1.23 ± 0.09 during passive, active, and loaded breathing, respectively. These values were not significantly different from one another, nor were there any differences between normal subjects and quadriplegics. It is suggested that the upper airway receptors are not essential for volume sensation. The intensity of the sensation of a given inspired volume may depend on the level of the central nervous system motor command and/or on the tension developed by the diaphragm. (16 refs.)

63866 Central and peripheral chemoreceptor inputs to phrenic and hypoglossal motoneurons. E.N. Bruce, J. Mitra, N.S. Cherniack (Dept. of medicine, Case Western Reserve Univ., Cleveland, OH, USA).

J. Appl. Physiol. (USA), vol.53, no.6, p.1504-11 (Dec. 1982). [received: April 1983]

The hypothesis that phrenic and hypoglossal responses to progressive hypercapnia differ qualitatively because of the CO_2 -related drive inputs to their respective motoneuron pools are different was tested. The relative contributions of carotid sinus and central chemoreceptor inputs to hypoglossal and phrenic responses during hyperoxic hypercapnia were determined by comparing the two nerve activities during rebreathing runs done either before and after bilateral carotid sinus nerve (CSN) section, or without and with cooling of the intermediate, I(s), area on the ventral surface of the medulla. The studies were performed on chloralose-anesthetized, vagotomized, paralyzed cats. Cooling of the I(s) area impaired phrenic responsiveness to hypercapnia more than hypoglossal responsiveness, whereas CSN section had the opposite effect. Thus phrenic nerve response was more dependent on central chemoreceptor input than was the hypoglossal response, but hypoglossal response was more dependent on carotid sinus chemoreceptor input. It is concluded that the phrenic and hypoglossal motoneuron pools each receive a different functional input from both the medullary and the carotid sinus chemoreceptors. (23 refs.)

87.40 BIOMAGNETISM

(inc. magnetocardiography)

Two-dimensional deuterium NMR of lipid membranes See Entry 63798

87.45 BIOMECHANICS, BIORHEOLOGY, BIOLOGICAL FLUID DYNAMICS

63867 Simulation analysis of interatrial transposition of venous return (Mustard's operation). E.H. Blackstone (Dept. of Surgery, Univ. of Alabama, Birmingham, AL, USA), V.C. Rideout, D.L. Beduhn.

Ann. Biomed. Eng. (USA), vol.10, no.5, p.193-218 (1982).

Transposition of the great arteries is functionally corrected by Mustard's operation, an operation in which the atrial septum is removed and the resulting common atrial chamber repartitioned by a baffle to transpose venous return to the heart. To better understand the new physiology, a physically-based mathematical model of the infant circulation following Mustard's operation was developed and studied with the aid of computer simulation. The model reproduces certain clinical observations, including the tendency for mean pressure in both atria to be equal early postoperatively and for the pressure waveform to exhibit a steep y-descent in the systemic venous atrium. Simulation studies suggest that the mechanism for the former is transbaffle pressure coupling resulting from dynamic motion of the baffle; the mechanism for the latter is limitation of the extent of such baffle excursions. Dynamic volume of the two atria is found in the model to change according to the relative performance of the two ventricles, and stiffening the baffle leads to pressure waveforms characteristic of a small, noncompliant atrium. Mechanisms for venous 'obstruction' and decompression were also studied. The baffle and its movements, however, have little effect upon cardiac output in the model, leaving unexplained the clinical observation of low output early postoperatively. (23 refs.)

63868 Mathematical studies on particle paths in an aneurysm. H. Florian, K. Perktold, K. Gruber (Inst. für Math., Tech. Univ. Graz, Graz, Austria).

Biomed. Tech. (Germany), vol.28, no.4, p.83-90 (April 1983). In German.

The experimental visualization of streamline patterns by the injection of contrast material is useful under conditions of steady flow. In the case of pulsatile flow, however, complicating problems occur. In these cases appropriate mathematical methods provide useful results for particle paths. The authors use the results of their earlier calculations of pulsatile flow through an aneurysm model. Particle paths are examined quantitatively and compared for the physiological and an idealized pulse. The starting points and starting time are varied. The results demonstrate the time-dependent development, shift and disappearance of vortices during a pulsatile cycle and provide hints on zones of stasis. This is a significant factor in thrombogenesis. (9 refs.)

63869 Effects of velocity jumps on blood flow in large arteries. V.K. Sud (Dept. of Biophys., All India Inst. of Medical Sci., New Delhi, India), G.S. Sekhon, R.K. Mishra.

J. Biol. Phys. (USA), vol.10, no.3, p.179-86 (1982).

When a human being experiences a sudden velocity change, the blood flow is disturbed. A theoretical analysis to predict the effects of sudden velocity changes on blood flow in large arteries is presented. The situation is modelled as a one-dimensional flow problem in a viscoelastic tube where the fluid viscosity convective term in the equation of motion and nonlinearity in the elastic modulus of the tube wall are neglected. The governing equations of the model are solved by the Laplace transformations. The computed results show that relatively high blood pressures, capable of harming circulation, are produced even by relatively moderate velocity jumps. (5 refs.)

63870 Is the arterial pulse a soliton? S. Rowlands (Faculty of Medicine, Univ. of Calgary, Calgary, Alberta, Canada).

J. Biol. Phys. (USA), vol.10, no.4, p.199-200 (1982).

The recent discovery of arterial smooth muscle contractions which are synchronized with the activity of the right atrial pacemaker in the rabbit heart gives support to the hypothesis that the arterial pulse wave is a soliton. The hypothesis is amenable to experimental tests. (11 refs.)

63871 Pulmonary blood flow distribution in panting ostriches. J.H. Jones (Percy FitzPatrick Inst. of African Ornithology, Univ. of Cape Town, Rondebosch, S. Africa).

J. Appl. Physiol. (USA), vol.53, no.6, p.1411-17 (Dec. 1982). [received: April 1983]

Ostriches (*Struthio camelus*) are the only birds known that can increase post-dead space ventilation during severe heat stress without experiencing hypocapnia and respiratory alkalosis. To determine whether this phenomenon occurs due to redistribution of pulmonary blood flow during panting, thus creating an extreme ventilation-perfusion (\dot{V}/\dot{Q}) imbalance, the distributions of pulmonary blood flow in ostriches at rest (15°C) in a severe panting (45°C) were determined using radioactively labeled microspheres. Blood flow distribution at rest was greatest in the neopulmo [$18\% > \text{mean pulmonary blood flow (MPBF)}$] and the cranial ($23\% > \text{MPBF}$) and distal ($12\% > \text{MPBF}$) regions of the paleopulmo. During panting blood flow was not shunted around the lung, and flow to the neopulmo decreased to MPBF, became more homogeneous along the cranio-caudal axis, and remained nonhomogeneous along the medio-lateral axis. The results suggest that the observed decrease in gas exchange during panting is probably due primarily to shunting

of the increased ventilation around the parabronchial exchange region rather than to alterations in the patterns of \dot{V}/\dot{Q} within the lung. (44 refs.)

63872 A Starling resistor regulates cerebral venous outflow in dogs. J.M. Luce, J.S. Huseby, W. Kirk, J. Butler (Div. of Respiratory Diseases, Univ. of Washington School of Medicine, Seattle, WA, USA).

J. Appl. Physiol. (USA), vol.53, no.6, p.1496-503 (Dec. 1982). [received: April 1983]

This investigation was undertaken to determine whether a Starling resistor or venous waterfall effect exists between the sagittal sinus and the cerebral veins such that increases in sagittal sinus pressure (Pss) do not abolish cerebral venous outflow and examine two possible contributions of extracranial venous valves in regulating outflow. Anesthetized dogs were subjected to positive end-expiratory pressure (PEEP) before and after intracranial pressure (Pic) was elevated by inflation of an epidural balloon. It is concluded that a Starling resistor between the sagittal sinus and the cerebral veins regulates cerebral venous outflow when Pss is increased by PEEP and other maneuvers that raise superior vena caval pressure (Pscv). The waterfall maintains cerebral venous pressure and Pic at normal levels when Pscv and Pss are reduced. Extracranial venous valves are not essential to this mechanism. (12 refs.)

63873 Surface tension-surface area curves calculated from pressure-volume loops. T.A. Wilson (Dept. of Aerospace Engng. & Mech., Univ. of Minnesota, Minneapolis, MN, USA).

J. Appl. Physiol. (USA), vol.53, no.6, p.1512-20 (Dec. 1982). [received: April 1983]

An energy analysis and data from the literature on the relation among surface area, recoil pressure, and lung volume are used to calculate the surface tension-surface area curves corresponding to pressure-volume loops. The energy analysis has been described earlier (see *ibid.*, vol.50, p.921-6, 1981). It is based on the assumption that the tissue structure of the lung constitutes a conservative mechanical system and hence that pressure-volume hysteresis. Unlike previous methods of calculating surface tension from recoil pressure, this method does not rely on the assumption that the tissue component of recoil in the air-filled lung is the same as recoil pressure of the saline-filled lung at the same lung volume. The calculated values of surface tension decrease to less than 2 dyn/cm as surface area decreases along the deflation limb of the pressure-volume curve. Surface tension increases very steeply with surface area on the inflation limbs, reaching a limiting value of just under 30 dyn/cm. The shape of the surface tension-surface area curves, unlike the shape of the curves calculated by previous methods, is similar to the shape obtained on surface tension balances for fluid extracted from lungs. (14 refs.)

63874 Pulmonary microcirculatory response to localized hypercapnia. T. Koyama, M. Horimoto (Res. Inst. of Appl. Electricity, Hokkaido Univ., Sapporo, Japan).

J. Appl. Physiol. (USA), vol.53, no.6, p.1556-64 (Dec. 1982). [received: April 1983]

Anesthetized bullfrogs were examined to study the effects of localized hypercapnia on the red blood cell (RBC) velocity in pulmonary alveolar microvessels on the exposed lung surface. Before and after the exposure of a small area of the lung surface 6 mm in diameter to a hypercapnic gas mixture, the region was exposed to CO_2 -free control gas. The RBC velocity was measured by the use of a laser Doppler microscope. Both mean flow velocity (MV) and pulsatile amplitude (PA) were determined from the resulting flow velocity contour. Responses of pulmonary microvessels to hypercapnia were examined by measuring the vessel diameters with an ocular microscope of the microscope while gas mixtures were applied to a 1-mm-diameter region of the surface. During hypercapnia both MV (2.31 ± 0.27 mm/s) and PA (0.54 ± 0.15 mm/s) in the alveolar arterioles ($\phi = 64 \pm 14 \mu\text{m}$) were reduced, each reaching a minimum (2.01 ± 0.24 and 0.43 ± 0.19 mm/s, respectively) prior to gradual returns to their initial values. After reintroduction of the control gas, the values of MV and PA approached initial values more rapidly. In capillaries MV (1.44 ± 0.18 mm/s) and PA (0.28 ± 0.06 mm/s) decreased to 1.25 ± 0.10 and 0.15 ± 0.05 mm/s, respectively. The maximum reduction of PA (-44.6%) therefore clearly exceeded that of MV (-12.4%) in capillary flow. (19 refs.)

63875 Attenuation of hypoxic pulmonary vasoconstriction by pulsatile flow in dog lungs. T.J. Gregory, J.C. Newell, T.S. Hakim, M.G. Levitzky, N. Sedrak (Center for Biomedical Engng., Rensselaer Polytech. Inst., Troy, NY, USA).

J. Appl. Physiol. (USA), vol.53, no.6, p.1583-8 (Dec. 1982). [received: April 1983]

Pulmonary arterial pressure was measured in isolated lower lobes of dog lungs perfused in situ at several flows during ventilation with 95% O_2 -5% CO_2 and with 3% O_2 -5% CO_2 . Pulsatile perfusion was provided by a piston pump, and steady perfusion was provided by a roller pump, and steady perfusion was provided by a roller pump. The slope of the pressure-flow curve was 16.1 ± 1.6 Torr $\cdot \text{l}^{-1} \cdot \text{min}$ at all flows between 200 and 800 ml/min during 95-5 ventilation and increased to 19.4 ± 3.7 in hypoxia. When flow was 600 ml/min, with 95-5 ventilation, mean arterial pressure was 16.2 ± 1.2 Torr in steady flow and was unchanged at 15.0 ± 1.0 Torr in pulsatile flow. At the same flow during hypoxic ventilation, mean arterial pressure was 16.2 ± 1.2 Torr in steady flow and was unchanged at 15.0 ± 1.0 Torr in pulsatile flow. At the same flow during hypoxic ventilation, mean arterial pressure increased to 27.9 ± 2.4 Torr ($P < 0.01$) when flow was steady but only to 19.3 ± 1.6 Torr ($P < 0.01$) when flow was made pulsatile. Thus hypoxia increased perfusion pressure by a nearly parallel shift of the pressure-flow curve to higher pressures, and this change was smaller in pulsatile than in steady flow. (22 refs.)

63876 Comparison of hemodynamic responses to static and dynamic exercise. G.R. Bezucha, M.C. Lenser, P.G. Hanson, F.J. Nagle (Biodynamics Lab., Univ. of Wisconsin-Madison, Madison, WI, USA).

J. Appl. Physiol. (USA), vol.53, no.6, p.1589-93 (Dec. 1982). [received: April 1983]

Eight healthy male adults (25-34 yr) were studied to compare hemodynamic responses to static exercise (30% MVC in leg extension), static-dynamic exercise (one-arm cranking, 66 and 79% $\dot{V}_{\text{O}_{2\text{max}}}$), and dynamic exercise (two-leg cycling, 58 and 82% $\dot{V}_{\text{O}_{2\text{max}}}$). One-arm cranking and two-leg cycling at similar relative \dot{V}_{O_2} demands resulted in nearly identical increases in mean arterial pressure (Pa) due to different contributions of cardiac output (Q) and total peripheral resistance Q and the arteriovenous O_2 difference varied as a function of \dot{V}_{O_2} regardless of the mode of exercise (static or dynamic). On the other hand, the heart rate response, which accounted for increased Q in the exercises containing a static component, and Pa varied with mode of exercise. Any generalized scheme of cardiovascular control during exercise must account for the potential influence of dynamic and static components of the exercise. (18 refs.)

63877 Canine thoracic electrical impedance with changes in pulmonary gas and blood volumes. R.M.Smith, B.A.Gray (Dept. of Medicine, Univ. of Oklahoma Health Sci. Center, Oklahoma City, OK, USA).

J. Appl. Physiol. (USA), vol.53, no.6, p.1608-13 (Dec. 1982). [received: April 1983]

Transthoracic impedance (Z) was evaluated as an index of total lung liquid content at constant lung gas volume (LGV). Rapid changes in pulmonary blood volume (PBV) were produced in anesthetized, paralyzed, closed-chest dogs with the airway occluded at functional residual capacity. Changes in PBV produced by inflation of balloons on catheters positioned in the left atrium (LA) or inferior vena cava (IVC) were estimated from the changes in chest wall recoil pressure, using the chest wall as a plethysmograph after calibration with changes in LGV. Whereas Z increased linearly with decreases in PBV (1-6 ml/kg) produced by the IVC balloon ($\Delta Z/\Delta PBV = -0.43$ ml/kg, $r = -0.81$), Z did not change significantly with increases in PBV (1-6 ml/kg) produced by the LA balloon. These observations indicate that changes in PBV are not the primary determinant of changes in Z and raise the possibility that other hemodynamic events are more important. (23 refs.)

63878 Airway smooth muscle mechanics: reduced activation and relaxation. U.Kromer, N.Stephens (Dept. of Physiology, Univ. of Manitoba, Winnipeg, Manitoba, Canada).

J. Appl. Physiol. (USA), vol.54, no.2, p.345-8 (Feb. 1983).

Reduced activation of skeletal muscle fibers at below-optimal lengths has been reported before. The authors studied tracheal smooth muscle (TSM) as a model of airway smooth muscle to see whether such a phenomenon existed in smooth muscle also; they found that active length-tension curves at normal and raised Ca^{2+} concentrations were significantly different. This indicated reduced activation of the TSM at below-optimal lengths. This reduction was in addition to that arising from the length-tension effect. The authors also studied the mechanics of relaxation in TSM and noted that in afterloaded isotonic tension records the time course of TSM relaxation appeared to closely follow that of the isometric contraction at all loads. In this it differed markedly from relaxation in skeletal muscle where the time courses of relaxation at different loads differed from each other and from that of the isometric muscle. (15 refs.)

63879 Decay of inspiratory muscle pressure during expiration in anesthetized cats. W.A.Zin, L.D.Pengelly, J.Milic-Emili (Dept. of Physiology, McGill Univ., Montreal, Quebec, Canada).

J. Appl. Physiol. (USA), vol.54, no.2, p.408-13 (Feb. 1983).

In six spontaneously breathing anesthetized cats (pentobarbital sodium, 35 mg/kg) the authors studied the antagonistic pressure developed by the inspiratory muscles during expiration (Pmus). This was accomplished in two ways: (1) with the authors' previously reported method (see *ibid.*, vol.52, p.1266-71, 1982) based on the measurement of changes in lung volume and airflow during spontaneous expiration, together with determination of the total passive respiratory system elastance and resistance; and (2) measurement of the time course of changes in tracheal pressure after airway occlusion at end inspiration, up to the moment when the inspiratory muscles become completely relaxed. The agreement between the two methods is generally good, both in the amplitude of Pmus, and in its time course. The authors also applied the first method to spontaneous expirations through added linear resistive loads. These did not alter the relative decay of Pmus. Thus in anesthetized cats the braking action of the inspiratory muscles does not decrease when expiratory resistive loads are added, i.e., when such braking is clearly not required. (20 refs.)

63880 High-frequency oscillations via the pleural surface: an alternative mode of ventilation? H.E.Ward, J.H.T.Power, T.E.Nicholas (School of Medicine, Flinders Univ. of South Australia, Bedford Park, Australia).

J. Appl. Physiol. (USA), vol.54, no.2, p.427-33 (Feb. 1983).

High-frequency oscillatory ventilation (HFOV) of low amplitude was applied to the pleural surface of the isolated rat lung (IPL) perfused at 10 ml.min⁻¹ with Krebs bicarbonate containing 4.5% albumin (hematocrit 34%). Lung volume was held constant by a continuous positive airways pressure (CPAP) of 5 cmH₂O. Varying CPAP from 2 to 15 cm H₂O did not affect O₂ uptake. Tidal volume (V_T) was estimated with an impedance pneumograph, and it bore a direct linear relationship to the amplitude of both the loudspeaker input signal and the pressure change in the chamber up to 30 Hz; V_T was inversely proportional to the frequency (f). However, at a constant loudspeaker input of 10 V, minute expired ventilation (\dot{V}_E) remained constant (mean 104 ml.min⁻¹) as f increased from 5 to 30 Hz. Hemoglobin saturation increased by more than 80% during HFOV of 5-40 Hz and amplitude of 10 V, the maximum O₂ uptake being 14.6 ml O₂ per 100 ml perfusate. Whereas dead space was approximately 335 μ l, a V_T of less than 40 μ l could effect normal O₂ uptake, suggesting that bulk flow is playing only a minor role in gas exchange. HFOV for 60 min (CPAP 5 cm H₂O) did not affect the amount of alveolar surfactant compared with conventional ventilation at the same mean airway pressure. It is concluded that normal O₂ uptake can be maintained by applying HFOV to the pleural surface of the IPL held at constant volume. (26 refs.)

63881 Dynamic response of local pulmonary blood flow to alveolar gas tensions: analysis. B.J.B.Grant, A.M.Schneider (Dept. of Medicine, Univ. of California, San Diego, La Jolla, CA, USA).

J. Appl. Physiol. (USA), vol.54, no.2, p.445-52 (Feb. 1983).

It has been reported that left lower lobe pulmonary blood flow (Q) and alveolar CO₂ decrease then oscillate in a progressively damped manner when the lobar inspirate is changed from pure O₂ to N₂. This damped oscillatory response of lobar Q is abolished by maintaining lobar CO₂ constant. The authors set out to develop the simplest mathematical model that can simulate these experimental results by using techniques derived from control theory. Different models were tested. The simplest model that predicts the experimental data incorporates an exponential decrease of lobar Q to local alveolar hypoxia (time constant 3 min) and a damped oscillatory response of lobar Q to local alveolar hypocapnia. The response to hypocapnia has two components: a vasodilator effect possibly related to intracellular [H⁺] and a vasoconstrictor effect possibly related to changes of molar CO₂. Both these components (time constants of 4.8 min) interact with each other by cross-coupled elements (time constants of 4.8 min). This model can be used to forecast results so that its validity can be tested by experiment. (27 refs.)

63882 Effects of high-frequency oscillatory ventilation on vagal and phrenic nerve activities. G.C.W.Man, S.F.P.Man, C.T.Kappagoda (Dept. of Medicine, Univ. of Alberta, Edmonton, Alberta, Canada).

J. Appl. Physiol. (USA), vol.54, no.2, p.502-7 (Feb. 1983).

This study was undertaken to define the mechanism for the respiratory inhibition observed during high-frequency oscillatory ventilation (HFOV). The effects of HFOV on the activities of single units in the vagus (Vna) and phrenic nerves (Pna) were examined in pentobarbital-anesthetized dogs. The animals were either ventilated by intermittent positive-pressure ventilation (IPPV) with and without positive end-expiratory pressure (PEEP), or by

HFOV at a frequency of 25 Hz and pump displacement volume of 3 ml/kg. In 13 vagal units the Vna was much higher during HFOV than during IPPV or airway occlusion at a matched airway pressure. Ten units in the phrenic nerves were examined, and Pna (expressed as bursts/min) was attenuated by HFOV in all of them. In four of them, the effect of cooling the vagi to 8-10°C on Pna was examined, and it was found that HFOV failed to alter the Pna. It is concluded that 1) HFOV stimulates the pulmonary vagal afferent fibers continuously and to a degree greater than that due to static lung inflation and increased airway pressure and 2) the increased vagal activity during HFOV probably causes phrenic nerve activity inhibition. (18 refs.)

63883 Breathing He-O₂ shifts the lung pressure-volume curve of the dog. N.Berend, K.L.Christopher, N.F.Voelkel (Pulmonary Physiology Unit, Nat. Jewish Hospital & Res. Center, Denver, CO, USA).

J. Appl. Physiol. (USA), vol.54, no.2, p.576-81 (Feb. 1983).

To determine whether breathing a mixture of 80% He-20% O₂ affects the lung pressure-volume (PV) curve, eight anesthetized paralyzed dogs were studied in a volume-displacement plethysmograph. Static PV curves on air were compared with PV curves obtained after equilibration with He-O₂. The He-O₂ PV curves were significantly shifted upward by an average of 5% total lung capacity. There was no change in compliance, indicating that the shift was due to lung expansion rather than a change in elasticity. Pretreatment of the dogs with cyclooxygenase inhibitors abolished the PV shift with He-O₂. Four dogs had PV curves recorded on air and a mixture of O₂, SF₆ and Ne, a gas mixture with the same density as air but with 45% greater viscosity. The PV curve shift was even greater than observed with He-O₂ and could again be virtually abolished with a cyclooxygenase inhibitor. These results suggest that breathing a high-viscosity gas mixture results in alveolar duct dilatation due to the release of a prostaglandin bronchodilator. This may need to be taken into account in the analysis of flow augmentation with He-O₂. (26 refs.)

63884 Shock absorption of meniscectomized and painful knees: a comparative in vivo study. A.S.Voloshin (Dept. of Engng. Sci. & Mech., Iowa State Univ., Ames, IA, USA), J.Wosk.

J. Biomed. Eng. (GB), vol.5, no.2, p.157-61 (April 1983).

The principles of a noninvasive measurement of the shock absorbing capacity of the knee are presented. Accelerometry, which has been proven to be a useful tool for noninvasive measurements in biomechanical investigation, was employed for quantitative evaluation of the knee's shock absorbing capacity by registration of bone vibrations resulting from gait. Results of the experiments show that both patients with painful knee and patients after meniscectomy suffer from insufficient shock absorbing capacity of the knee. It was found that the shock absorbing capacity of a normal knee is about 20% higher than that of a pathological one. The results indicate that while meniscectomy may reduce pain, instability, swelling, etc. in an injured knee, it cannot improve its reduced shock absorbing capacity, which eventually will lead to development of degenerative osteoarthritis. It seems that the pain syndrome is a biological reaction to severe repetitive overloading of the knee. (27 refs.)

63885 Bubble dissolution physics and the treatment of decompression sickness. T.D.Kunkle (Los Alamos Nat. Lab., Los Alamos, NM, USA), E.L.Beckman.

Med. Phys. (USA), vol.10, no.2, p.184-90 (March-April 1983).

The treatment of decompression sickness often involves both recompressing the victim and administering hyperbaric oxygen in the hope of more rapidly dissolving the bubbles which cause this malady. Although many hundreds of such treatments are conducted each year in the United States alone, the underlying physical principles governing the dissolution of such bubbles are not well understood and only empirically tested. In this paper, the authors present a mathematical theory of bubble dissolution that is verified by comparison with laboratory experiments. This theory suggests that the commonly employed treatment techniques would be only marginally effective, and that in many situations the bubbles that cause the disease cannot be adequately dissolved using existing techniques and facilities. (15 refs.)

63886 A comparison of the SACH and single axis foot in the gait of unilateral below-knee amputees. N.E.Doane, L.E.Holt (Faculty of Health Professions, Dalhousie Univ., Halifax, Nova Scotia, Canada).

Prosthet. & Orthotics Int. (Denmark), vol.7, no.1, p.33-6 (April 1983).

The gait patterns of unilateral below-knee amputees wearing prostheses with either a SACH foot or a single axis foot were compared. A temporary below-knee prosthesis was fabricated for each subject using plaster of paris and Plastazote for the socket, a pylon and an artificial foot. Eight subjects were filmed at two separate sessions, one in which the SACH foot was worn on their prosthesis and one with the single axis foot on their prosthesis. Measurements of the normal leg with a SACH foot on the prosthetic limb were compared with measurements of the normal leg with a single axis foot on the prosthesis. Measurements of the prosthetic leg with both devices were also compared. A one tailed t test ($p < .05$) was used to determine statistical significance of the results obtained in six measurements of lower limb joint angles and on the percentage of time of gait cycle for stance and swing phase of the prosthetic leg. Discussion centres on the interpretation of the results from both statistical and clinical points of view. Major differences (excepting the ankle at foot-flat) between the prosthetic devices were not found. (11 refs.)

63887 Effects of alignment variables on thigh axial torque during swing phase in AK amputee gait. G.Ishai, A.Bar (Julius Silver Inst. for Biomedical Engng., Technion, Haifa, Israel), Z.Susak.

Prosthet. & Orthotics Int. (Denmark), vol.7, no.1, p.41-7 (April 1983).

It is suggested that a major source of discomfort for above-knee amputees during the swing phase of walking is the thigh axial torque (TAT) transferred at the stump-socket interface. The relation between TAT and variations in its six relevant alignment adjustments has been investigated. A computerized routine has been established which indicates optimum choice of alignment setting, based on minimal TAT peaks. Feasibility for attenuating swing phase TAT has been demonstrated in three simulated patterns of amputee gait. As a conclusion, it is suggested that a useful clinical tool could be based on the presented alignment optimisation procedure and may be expanded to include other factors associated with swing and stance phase comfort and performance. (6 refs.)

63888 An innovations approach to cardiac hemodynamics modeling. A.-H.Rashwan, A.S.Ahmed (Systems & Biomedical Engng. Dept., Faculty of Engng., Cairo Univ., Giza, Egypt).

System Modeling and Optimization. Proceedings of the 10th IFIP Conference, New York, USA, 31 Aug.-4 Sept. 1981 (Berlin, Germany: Springer-Verlag 1982), p.869-77

A new approach to the problem of modeling the blood vessels attached to the heart, especially the pulmonary artery, is presented. The analyses are based on a dynamic nonlinear compartmental model that describes the transfer of pressure energy between two sites in that vessel. The system kernels are represented by two paths; each path contains a nonlinear network in cascade with linear dynamics followed by a nonlinear transformation. The first path

reflects the dynamic compliance of the vessel under pulsatile action. The second path represents the variations of input impedance along the cardiac cycle. An experiment with (20) patients was performed to validate the model output especially in cases with aneurysm. (16 refs.)

- Force relaxation and permanent deformation of erythrocyte membrane See Entry 63803
- Effects of moderate exercise on intraocular pressure See Entry 63825
- Sensation of inspired volume in normal subjects and quadriplegic patients See Entry 63865
- On-line analysis of the femoral artery flow velocity waveform and its application in the diagnosis of arterial disease See Entry 63912
- Comparison of electrical field plethysmography with electrical impedance plethysmography See Entry 63914
- Monitoring of movement with radio frequency transducers See Entry 63915
- Simulation of the organ blood flow in computer γ -scintigraphy See Entry 63934
- Characterization of the oscillometric method for measuring indirect blood pressure See Entry 63986
- The human tibia: static testing in bending by an in vivo method See Entry 63987
- Nonlinear fluid systems identified by random noise input See Entry 63990
- A new method for measurement of respiratory resistance See Entry 63991
- Time series methods in the monitoring of intracranial pressure. II. Comparative study and initial assessment See Entry 63992
- Static response of a simple piezoelectric load cell [biomechanical applications] See Entry 63993
- Complications of and improvements to breathing circuit monitors for anesthesia ventilators See Entry 63994
- A device to quantify passive resistance to motion of the leg See Entry 63995
- A pressure curve monitor for intratracheal jet ventilation See Entry 63997
- Studies on the stress behaviour in the bone/cement interface in total hip replacement See Entry 64002
- Adaptive microcomputer control of an artificial knee in level walking See Entry 64003
- A new system for ventilating with high-frequency oscillation .. See Entry 64006
- A feedback system to control blood flow in dog lung lobes See Entry 64007

87.50 BIOLOGICAL EFFECTS OF RADIATIONS

(inc. effects of fields)

- 63889 Cellular spin resonance in rotating electric fields. M.Mischel, A.Voss, H.A.Pohl (Dept. of Phys., Oklahoma State Univ., Stillwater, OK, USA). *J. Biol. Phys. (USA)*, vol.10, no.4, p.223-6 (1982). Cells and certain other electrically polarizable objects can be seen to spin when in a rotating electric field. When a rotating field (from four Pt electrodes) is applied over a frequency range of 500 to 75000 Hz, living cells exhibit two or three response peaks, whereas dead cells exhibit only one response peak. Yeast (*Saccharomyces cerevisiae*) exhibit two peaks. The nature of these cellular spin resonances is under active study. (7 refs.)
- 63890 Biological effects of neutron radiation and their implications for the nuclear power industry. J.A.Dennis (Nat. Radiological Protection Board, Leeds, England). *Nucl. Energy (GB)*, vol.22, no.2, p.87-93 (April 1983). Stimulated by biophysical theories of the action of radiation on the cells of mammalian tissues, research on the effects of neutrons has been interpreted as implying that neutron radiation is about 60 times more effective than gamma radiation for the induction of tumours in rodents and for shortening their lives. This contrasts with the assumption made for protection purposes that it is only about ten times as effective. However, the same experiments can be interpreted also as implying that gamma radiation at the dose rates encountered in the workplace is five to ten times less effective than is generally assumed. Taken together these observations suggest that the real risks to humans from neutrons are comparable with the assumed risks from X- and gamma radiation. Further data are required to confirm these observations and their interpretation, and in the short term there is no need to change the current practices of radiological protection as regards neutron radiation. Nevertheless, it might be wise for long-term planning purposes to anticipate a reduction in the maximum permissible fluences of neutrons by a factor of about 3. (42 refs.)
- 63891 Tumor induction in BALB/c female mice after fission neutron or γ irradiation. R.L.Ullrich (Biology Div., Oak Ridge Nat. Lab., Oak Ridge, TN, USA). *Radiat. Res. (USA)*, vol.93, no.3, p.506-15 (March 1983). Describes the dose-response relationships for tumor induction after neutron irradiation in female BALB/c mice, with emphasis on the response in the dose range 0 to 50 rad. Tumors induced after radiation exposure included ovarian tumors, lung adenocarcinomas and mammary adenocarcinomas. For comparison the dose response for induction of these tumors after ^{137}Cs γ irradiation were also examined. As previously described for the female RFM mouse, the data for ovarian tumor induction after neutron and γ irradiation were consistent with a threshold model. For lung and mammary tumors the dose-response curve after neutron irradiation appeared to 'bend over' in the dose range 10 to 20 rad. The factors responsible for this bend-over and their relative contributions to the overall form of the dose-response relationship are not presently known. However, these data strongly indicate that extrapolation from data above 50 rad could result in a significant underestimate of risks. Further, it is clear that current models of neutron carcinogenesis are inadequate, since such a bend-over is not predicted at these low dose levels. (11 refs.)
- Reevaluations of Dosimetric Factors, Hiroshima and Nagasaki. Proceedings of a Symposium See Entry 59542
- Dose-effect relationships for induction of cell inactivation and asymmetrical chromosome exchanges in three cell lines by photons and neutrons of different energy See Entry 63900
- The utilization of time-dose-fractionation models in the planning of tumor radiotherapy See Entry 63932

87.50B Interactions of biosystems with radiations

- 63892 Optical polarization properties of the diffraction spectra from single fibers of skeletal muscle. Y.Yeh, B.G.Pinsky (Dept. of Appl. Sci., Univ. of California, Davis, CA, USA). *Biophys. J. (USA)*, vol.42, no.1, p.83-90 (April 1983). The diffraction spectra of laser light from single fibers of skeletal muscle exhibit a large degree of optical depolarization. When the linearly polarized incident laser source is oriented at polarization angles between $0 < \theta < \pi/2$ rad with respect to the fiber axis, the diffracted light is elliptically polarized. These results show that the phase angle of the ellipse rotates by as much as 20° when the fiber is stretched from 2.4 to 3.8 μm . To further ascertain that the observed phenomenon is diffraction related, an experimental monitoring the spectra of scattered light in between diffraction orders showed this signal to be significantly more linearly polarized. These results suggest that the degree of elliptical polarization of the diffraction spectra is a sensitive probe of A-band dynamics, including changes of the anisotropic S-2 elements. (22 refs.)
- Absorbance and fluorescence changes in relation to light-scattering changes in chloroplast thylakoid membranes See Entry 63795

87.50C Bioacoustics (sonic and ultrasonic effects on living matter)

- 63893 Safety criterion for pressure wave. Liang Zhi-an, Feng Jun-ming (Shanghai Inst. of Physiology, Acad. Sinica, Shanghai, China), Meng Zhao-hui, Ye Si-mao, Cheng Ming-kun, Zhou Yong-shen, Li Xing-qi, Song Fu-zhi, Wang Zheng-guo, Zheng Shi-gang. *Acta Acust. (China)*, vol.7, no.6, p.372-9 (Nov. 1982). In Chinese. A safety criterion for the pressure wave generated by artillery and other explosive weapons was worked out by a joint research scheme consisting of (1) making a detailed study of the physical properties of such waves and, through animal experiments, revealing the rules that govern their damaging effect; (2) finding out the principal parameters of the pressure wave that determine the condition and degree of damage and formulating a safety margin for the tested animals in terms of these parameters; (3) determining the pressure wave tolerance difference between the human body and that of the tested animal through a number of well controlled contrast experiments and then (4) drafting a preliminary safety criterion on the basis of (3) for the verification of its reliability and fitness in actual cases of exposure. (17 refs.)
- 63894 Response of multicell spheroids to 1-MHz ultrasonic irradiation: cavitation-related damage. P.G.Sacks, M.W.Miller, R.M.Sutherland (Dept. of Radiation Biology & Biophys., Univ. of Rochester, School of Medicine & Dentistry, Rochester, NY, USA). *Radiat. Res. (USA)*, vol.93, no.3, p.545-59 (March 1983). The response of EMT6/Ro single cells and multicell spheroids (150-800 μm diameter) to 1-MHz ultrasonic radiation was determined for intensities of 0.5 W/cm² for 1-5 min. Damage was assessed by evaluating both lysis and survival of individual spheroid cells, growth of whole spheroids, and the physical integrity of whole spheroids by histological and scanning electron microscopic techniques. The surviving fraction of spheroid cells was higher than that of single cells, and several of the intensity-duration combinations showed a statistically significant correlation between resistance to ultrasound and increased spheroid size. This resistance with size was also found in spheroid growth experiments. Histological sections showed that both peripheral and internal damage occur. The relationship damage to studies of effects on tissues and possible therapeutic use of nonthermal ultrasound are discussed. (20 refs.)
- Distortion of finite amplitude ultrasound in lossy media See Entry 61334

87.50E Bio-optics (effects of microwaves, light, laser and other electromagnetic waves)

- 63895 In vivo photoacoustic spectra of *Raphanus* and *Tradescantia* leaves taken at different chopping frequencies of the excitation light. C.Buschmann (Botanisches Inst., (Pflanzenphysiologie), Karlsruhe. Univ. Karlsruhe, Germany), H.Prehn. *Photobiochem. & Photobiophys. (Netherlands)*, vol.5, no.2, p.63-9 (Feb. 1983). By varying the modulation frequency of the excitation light, spectra of the different cell layers can be taken. According to the theory of Rosenzweig and Gersho (J. Appl. Phys., vol.47, p.64-9, 1976) photoacoustic spectra are received from deeper inside the sample when the chopping frequency is decreased. By increasing the modulation frequency of the excitation light, the chlorophyll and carotenoid bands for the *Raphanus* leaves become smaller; for the *Tradescantia* leaves a long wavelength chlorophyll peak disappears leaving two maxima of the flavonoids contained exclusively in the epidermis. (13 refs.)
- 63896 Thermal effects of laser radiation in biological tissue. L.Cummins (Dominican Santa Cruz Hospital, Santa Cruz, CA, USA), M.Nauenberg. *Biophys. J. (USA)*, vol.42, no.1, p.99-102 (April 1983). A theoretical model is presented that simulates the thermal effects of laser radiation incident on biological tissue. The multiple scattering and absorption of the laser beam and the thermal diffusion process in the tissue are evaluated by a numerical technique that is well suited for microcomputers. Results are compared with recent empirical observations. (14 refs.)
- 63897 Temperature and adrenocortical responses in rhesus monkeys exposed to microwaves. W.G.Lotz, R.P.Podgorski (Naval Aerospace Medical Res. Lab., Naval Air Station, Pensacola, FL, USA). *J. Appl. Physiol. (USA)*, vol.53, no.6, p.1565-71 (Dec. 1982). [received: April 1983] To determine if the endocrine response to microwave exposure was similar in a primate to that reported for other animals, rectal temperature and plasma levels of cortisol, thyroxine (T_4), and growth hormone (GH) were measured in rhesus monkeys exposed to 1.29 GHz microwave radiation. Exposures were carried out under far-field conditions with the monkey restrained in a chair. Incident power densities of 0, 20, 28, and 38 mW/cm² were used, with corresponding specific absorption rates of 0, 2.1, 3.0, and 4.1 W/kg. Blood samples were taken hourly via an indwelling jugular venous catheter over a 24-h period before, during, and after an 8-h exposure. Rectal temperature increased an average of 0.5, 0.7, and 1.7°C for the three intensities used. No changes in T_4 or GH were observed. Cortisol levels were increased during exposure to 38 mW/cm². It was concluded that the temperature and adrenocortical responses to microwave exposure of the rhesus monkey are similar to the corresponding responses of other animals. (20 refs.)

63898 Cytogenetic effects of argon laser irradiation on Chinese hamster cells. M.Nakajima (Inst. of Medical Electronics, Univ. of Tokyo, Tokyo Japan), M.Fukuda, T.Kuroki, K.Atsumi.
Radiat. Res. (USA), vol.93, no.3, p.598-608 (March 1983).
The cytogenetic effects of argon laser light on V79 Chinese hamster cells were studied. Irradiation with a defocused continuous beam from an argon laser at doses of 100 to 400 J/cm² had dose-related cytostatic and cytotoxic effects. Cell cycle analysis by flow cytofluorometric measurement indicated that argon laser irradiation induced a temporary block at the G2+M phase. The survival curve after laser irradiation was exponential without an initial shoulder and the D₀ value (34% lethal dose) was calculated as 170 J/cm². A significant increase in sister chromatid exchange was observed after laser irradiation. Laser irradiation also induced chromatid and chromosome aberrations, most of which were breaks and gaps. These chromosomal changes are probably not an artifact of the experimental procedures such as the use of phenol red and antibiotics or spontaneously emitted UV light. No mutation at the Na⁺/K⁺-dependent ATPase locus was induced by argon laser irradiation. Although the mechanism by which an argon laser beam induced cytogenetic damage remains to be investigated, the possible involvement of hyperthermia seemed to be excluded. (26 refs.)

87.50G Ionizing radiations (u.v., X-ray, gamma-ray; particle radiation effects)

63899 Mathematical model of normal tissue injury in γ -beam therapy. S.A.Belov, F.M.Lyass, R.G.Mamin, E.I.Minakova, S.A.Raevskaya.
Med. Radiol. (USSR), vol.28, no.3, p.75-80 (March 1983). In Russian.
A model of normal tissue injury as a result of exposure to ionizing radiation is based on an assumption that the degree of tissue injury is determined by the degree of destruction by certain critical cells. The dependence of the number of lethal injuries on a single dose is expressed by a trinomial, obtained as a result of processing the experimental data. Quantitative correlations have been obtained for the skin and brain. They have been tested using clinical and experimental material. The results of the testing point to the absence of time dependence in irradiation courses of up to 6 weeks' duration. Correlation with an irradiation field has been obtained for the skin. Time lag blurring time dependence within a certain range of courses, and the presence of a true regeneration component dependent on the volume irradiated are considered. Proceeding from such an understanding of injury-regeneration processes it is concluded that the concept of isoeffectivity of irradiation courses is conditional. Volume-time fractionation is a promising direction in the development of radiation therapy. (9 refs.)

63900 Dose-effect relationships for induction of cell inactivation and asymmetrical chromosome exchanges in three cell lines by photons and neutrons of different energy. J.Zoetelief, G.W.Barendsen (Radiobiological Inst., TNO, Rijswijk, Netherlands).
Int. J. Radiat. Biol. (GB), vol.43, no.4, p.349-62 (April 1983).
The impairment of clonogenic capacity as well as the induction of dicentric and centric rings by different types of radiation was investigated in three lines of mammalian cells (R-1,M; RUC-2 and V-79). The experiments were performed with cells in plateau phase cultures which contain 70-80 per cent of cells in the G₀ or prolonged G₁ phase of the cell cycle. They were irradiated with ¹³⁷Cs gamma rays, 300 kV X-rays or 0.5, 4.2 or 15 MeV neutrons. The different types of cells show an appreciable variation in sensitivity to induction of both types of effect, being greatest for 0.5 MeV neutrons, intermediate for 4.2 and 15 MeV neutrons and least for photons. The dose-response relationships for both types of effect were analysed for neutrons in terms of a linear dose coefficient only, while the results for photons required analysis in terms of linear and quadratic coefficients. The effectiveness per unit of dose for cell inactivation is greater than that for induction of dicentric and centric rings by factors of about 4 to 7. However, dicentric and centric rings constitute only a fraction of the chromosome aberrations. Maximum r.b.e. values of about 12 at low doses were obtained for 0.5 MeV neutrons. (17 refs.)

63901 Demonstration of a biological effect of natural ionizing radiations. A.Conter, D.Dupouy, H.Planet (Lab. de Biologie Medicale, Univ. Paul Sabatier, Toulouse, France).
Int. J. Radiat. Biol. (GB), vol.43, no.4, p.421-32 (April 1983).
The blue-green alga, *Synechococcus lividus*, was grown under various levels of radiations. Shielding of cultures with lead resulted in a lower cell growth rate; the reduction disappeared when a normal radiation level was restored in the lead chamber. Irradiations from a thorium source at a dose-rate 14 times higher than that of natural irradiation stimulated the growth of the algae. These results are a new demonstration of a biological effect of background radiations. (16 refs.)

63902 Reciprocal translocations in ageing mice and in mice with long-term low-level ²³⁹Pu contamination. F.Pachierotti, U.Andreozzi, A.Russo, P.Metalli (Div. of Phys. & Biomedical Sci., ENA, Roma, Italy).
Int. J. Radiat. Biol. (GB), vol.43, no.4, p.445-50 (April 1983).
Single intravenous injections of 185 Bq monomeric ²³⁹Pu were given to male mice, and the frequency of primary spermatocytes with reciprocal translocations, determined 724 days after treatment, was not significantly different from that of age-matched untreated controls. These old animals showed significantly higher aberration frequencies than young adults. The data therefore show that for low initial activity and very long retention time the possible cytogenetic effects of incorporated nuclide does not change the age-related pattern of increase of spontaneous chromosome aberrations. Considerations of the main variables involved in the induction of cytogenetic effects of incorporated plutonium, based on literature data, indicate that the initial injected activity, the estimated total accumulated average organ dose, and the retention time interact in a complex way; as far as can be seen at present, the effects seem to be dependent mainly on the initial activity at short times after contamination, while the retention time appears to be predominant in the case of long-term observations. (17 refs.)

63903 The sequential irradiation of mammalian cells with X-rays and charged particles of high LET. R.P.Bird, M.Zaider, H.H.Rossi, E.J.Hall (Dept. of Radiology, Inst. of Cancer Res., Columbia Univ. Coll. of Physicians & Surgeons, New York, NY, USA), S.A.Marino, N.Rohrig.
Radiat. Res. (USA), vol.93, no.3, p.444-52 (March 1983).
Chinese hamster V79 cells, synchronized in late-S phase, were irradiated with high-LET charged particles or X-rays, or exposed sequentially to a single dose of charged particles followed by graded doses of X-rays. The charged-particle irradiations consisted of deuterons (LET, 50 keV/ μ m) or ³He ions (96 or 160 keV/ μ m). The survival data obtained following the sequential irradiations show a synergistic effect compared with exposure to the low-LET radiation. An enhancement ratio is defined in order to quantify this effect. On the basis of this concept the present data show an enhanced interaction effect as the LET of the primary dose is increased or the size of this dose is increased.

The data are also discussed in terms of a recent theoretical formulation which predicts synergism as a result of the interaction between the sublethal damage produced by the two radiations. (12 refs.)

63904 The fate of cells with chromosome aberrations after total-body irradiation and bone marrow transplantation. F.Carbonell, A.Ganser, T.M.Fliedner, R.Arnold, B.Kubanke (Dept. of Clinical Physiology & Occupational Medicine, Univ. of Ulm, Germany).
Radiat. Res. (USA), vol.93, no.3, p.453-60 (March 1983).
Cytogenetic studies were done on bone marrow cells and peripheral lymphocytes of four patients (three with acute nonlymphocytic leukaemia, one with aplastic anaemia) at various intervals up to 861 days after total-body X-irradiation (TBI) at doses between 4.5 and 10 Gy (450-1000 rad) followed by syngeneic or allogeneic bone marrow transplantation. Whereas no radiation-induced aberrations could be found in the bone marrow, apart from a transient finding in the patient with the lowest radiation dose, aberrant metaphases were seen in the peripheral lymphocytes of three patients in the range from 2.5 to 46% even at 861 days after the exposure. There were no demonstrable aberrations related to TBI in the only patient developing graft-versus-host disease. The dicentric yield as determined in the aberrant metaphases with 46 centromeres ranged between 3.4 \pm 1.3 and 4.9 \pm 0.4. In one patient it was demonstrated by BldR-labeling that after 10 Gy (1000 rad) TBI the surviving and heavily damaged lymphocytes can go into cell cycle and reach at least the third mitosis. The percentage of aberrant cells diminished by about 25% at each mitotic division. (30 refs.)

63905 Characterization of an Escherichia coli mutant (radB101) sensitive to γ and UV radiation, and methyl methanesulfonate. N.J.Sargentini, K.C.Smith (Dept. of Radiology, Stanford Univ. School of Medicine, Stanford, CA, USA).
Radiat. Res. (USA), vol.93, no.3, p.461-78 (March 1983).
After N-methyl-N'-nitro-N-nitrosoguanidine mutagenesis of Escherichia coli K-12 (xthA14), an X-ray-sensitive mutant was isolated. This sensitivity is due to a mutation, radB101, which is located at 56.5 min on the E. coli K-12 linkage map. The radB101 mutation sensitized wild type cells to γ and UV radiation, and to methyl methanesulfonate. When known DNA repair-deficient mutants were ranked for their γ -radiation sensitivity relative to their UV-radiation sensitivity, their order was (starting with the most selectively γ -radiation-sensitive strain): recB21, radB101, wild type, polA1, recF143, lexA101, recA56, uvrD3, and uvrA6. The radB mutant was normal for γ - and UV-radiation mutagenesis, it showed only a slight enhancement of γ - and UV-radiation-induced DNA degradation, and it was \sim 60% deficient in recombination ability. The radB gene is suggested to play a role in the recA gene-dependent (Type III) repair of DNA single-strand breaks after γ irradiation and in postreplication repair after UV irradiation for the following reasons: the radB strain was normal for the host-cell reactivity of γ - and UV-irradiated bacteriophage λ ; the radB mutation did not sensitize a recA strain, but did sensitize a polA strain to γ and UV radiation; the radB mutation sensitized a uvrB strain to UV radiation. (31 refs.)

63906 Irradiation of mammalian cells in the presence of diamide and low concentrations of oxygen at conventional and at ultrahigh dose rates. E.P.Clark, H.B.Michaels, E.C.Peterson, E.R.Epp (Dept. of Radiation Medicine, Massachusetts General Hospital, Boston, MA, USA).
Radiat. Res. (USA), vol.93, no.3, p.479-91 (March 1983).
The response of cultured CHO cells to ultrahigh-dose-rate radiation (\sim 10⁹ Gy/sec) has been previously studied extensively using the thin-layer cell-handling technique developed in the authors' laboratory. These experiments have recently been extended to studies with diamide, which, unlike the other sensitizers tested, acts primarily as a shoulder-modifying rather than a dose-modifying agent in hypoxic mammalian cells. The data reported indicate that diamide is active as a sensitizer at ultrahigh dose rates in a manner similar to that observed at conventional dose rates, and does modify the shape of the breaking survival curve observed with low concentrations of oxygen. (20 refs.)

63907 Radiobiological effects of ¹³¹I and ¹²⁵I on the DNA of the rat thyroid. I. Comparative study with emphasis on the postirradiation hypothyroidism occurrence. H.Abdel-Nabi (Dept. of Radiology, Ohio State Univ., Columbus, OH, USA), J.A.Ortman.
Radiat. Res. (USA), vol.93, no.3, p.525-33 (March 1983).
One of the major disadvantages of the use of ¹³¹I in the treatment of thyrotoxicosis is the development of hypothyroidism. Alternatively, ¹²⁵I has been proposed for thyrotoxicosis therapy, and was thought to be preferable to ¹³¹I because of the short range of its emitted soft electrons. Several studies have shown ¹²⁵I to be as effective as ¹³¹I in the treatment of thyrotoxicosis, and equally likely to produce hypothyroidism. This work compared the radiobiological effects of ¹³¹I and ¹²⁵I given in doses to deliver the same amount of radiation to the rat thyroid gland. These effects were studied by in vivo determination of single-strand DNA breaks by alkaline sucrose gradient sedimentation using the DABA fluorescent technique to detect the DNA. Serum T₄ and TSH concentrations and percentage T₃ uptake were determined by RIA. The incidence of hypothyroidism following ¹³¹I and ¹²⁵I therapy was found to be the same (10% in each group). The extent of DNA damage following ¹²⁵I therapy was greater than the damage induced by a larger dose of ¹³¹I. (36 refs.)

63908 Quantitative changes in the arterial blood gases of mice following localized irradiation of the lungs. D.W.Siemann (Experimental Therapeutics Div., Univ. of Rochester Cancer Center, Rochester, NY, USA), R.P.Hill.
Radiat. Res. (USA), vol.93, no.3, p.560-6 (March 1983).
The arterial pH and partial pressures of oxygen (PaO₂) and carbon dioxide (PaCO₂) were evaluated in LAF 1 mice 15 and 38 weeks after localized irradiation of the animals' thoraxes. Graded radiation doses of 900 to 1200 rad were administered. These doses resulted in 0 to 100% lethality by 26 weeks (180 days) after irradiation. At 15 weeks after treatment mice receiving radiation doses which would subsequently result in lethality (by 180 days) exhibited significant reductions in their PaO₂ and elevations in their PaCO₂ values, respectively. However, there was no clear dose-response relationship between blood gas values and radiation dose, which may reflect the animals' ability to compensate for their poor blood gas exchange by an increased breathing frequency. At 38 weeks after irradiation the blood gas values were abnormal in mice from groups which had normal blood gas values at Week 15 (and no fatalities by Week 26) but in which animal deaths had occurred between Weeks 26 and 38. These data therefore indicated (i) that abnormal blood gas values occurred in the mice prior to fatalities resulting from the acute radiation pneumonitis syndrome and (ii) that mice surviving the initial radiation pneumonitis phase could still succumb to progressive pulmonary toxicity which was reflected by the increasing levels of animal lethality and altered blood gas tensions at the later times. (26 refs.)

63909 Peripheral lymphocyte response to PHA and T cell population among atomic bomb survivors. M.Akiyama (Immunology Lab. Radiation Effects, Res. Found., Hiroshima, Japan), M.Yamakido, K.Kobuke, D.S.Dock, H.B.Hamilton, A.A.Awa, H.Kato.

Radiat. Res. (USA), vol.93, no.3, p.572-80 (March 1983).

The percentage of T lymphocytes of atomic bomb survivors showed no change as a function of age or exposure dose. The percentage of T cells was slightly lower in malignant-tumor patients than in the control group, but was significantly higher in the group with chromosomal aberrations than in the control group. The percentages of phytohemagglutinin (PHA)-induced transformation of peripheral lymphocytes decreased significantly with age in the rad control group and the 200+rad exposure group, particularly so in the latter. The malignant-tumor group also showed lower percentages of PHA-induced transformation of lymphocytes of the chromosomal-aberration group were significantly depressed as compared with that of the control group. (36 refs.)

63910 Comments on 'An assessment of the role of microdosimetry in radiobiology' by Dudley T. Goodhead [*Radiat. Res.* 91, 45-76 (1982)] [and reply]. H.H.Rossi, A.M.Kellerer (Dept. of Radiology, Coll. of Physicians & Surgeons, Columbia Univ., New York, NY, USA), D.T.Goodhead.

Radiat. Res. (USA), vol.93, no.3, p.613-25 (March 1983).

A review of Goodhead dealt with a perspective of the evolving role of microdosimetry in the study of radiation effects in mammalian cells. The review was confined to the site concept. In this paper Rossi and Kellerer make a number of criticisms of Goodhead's review. In reply Goodhead refutes these criticisms. (46 refs.)

Radiation hormesis, public health, and public policy: a commentary See Entry 59583

The effect of heat and radiation on the initiation and elongation processes of DNA synthesis See Entry 63806

Variable interaction of heat and procaine in potentiation of radiation lethality in mammalian cells of neoplastic origin See Entry 63807

Tumor induction in BALB/c female mice after fission neutron or γ irradiation See Entry 63891

Evaluation of the efficacy of radiation therapy by means of a rated standard dose (RSD) under various conditions of irradiation See Entry 63929

The utilization of time-dose-fractionation models in the planning of tumor radiotherapy See Entry 63932

Prevention of radiation injuries during multifractionation in radiation therapy See Entry 63933

Dosimetric substantiation of mean fractionation during irradiation of bone metastases of breast carcinoma See Entry 63964

87.60 MEDICAL AND BIOMEDICAL USES OF FIELDS, RADIATIONS, AND RADIOACTIVITY

(see also 28.80 Nuclear radiation technology, including shielding)

87.60B Sonic and ultrasonic radiation

63911 Measurements of the human anterior chest wall by ultrasound and estimates of chest wall thickness for use in determination of transuranic nuclides in the lung. T.J.Sumerling, S.P.Quant (Nat. Radiological Protection Board, Chilton, Didcot, England).

Radiat. Prot. Dosim. (GB), vol.3, no.4, p.203-10 (1982).

The low energy photons on which the *in vivo* detection of plutonium isotopes and americium-241 is based are severely attenuated in body tissues. To assess the activity of these radionuclides in the lungs by external measurements it is severely attenuated in body tissues. To assess the activity of these radionuclides in the lungs by external measurements it is necessary to estimate or measure the thickness of tissues overlying the lungs. It is also desirable to distinguish between muscle and adipose tissues in the chest wall because of the difference in their attenuation properties. Diagnostic ultrasound machines developed for medical use are suitable for this purpose. Ultrasonic measurements of chest wall thickness have been made at the authors' laboratory since 1978. This paper summarizes their experience of these measurements and describes their present procedure for making the measurements. The concept of 'equivalent muscle chest wall thickness' is introduced and a method for calculating the parameter is given. Both chest wall thickness and equivalent muscle chest wall thickness have been found to correlate well with Quetelet's Index (weight divided by height squared). Residual correlations with other parameters have been examined. Empirical formulae are given that can be used to predict the chest wall thickness and equivalent muscle chest wall thickness of a subject of given weight, height and age. (14 refs.)

63912 On-line analysis of the femoral artery flow velocity waveform and its application in the diagnosis of arterial disease. T.J.Fulton, W.A.P.Hamilton, J.C.Graham, V.C.Roberts (Dept. of Biomedical Engng., King's Coll. Hospital, Medical School, London, England).

J. Biomed. Eng. (GB), vol.5, no.2, p.151-6 (April 1983).

Analysis of the instantaneous peak velocity waveform obtained from the common femoral artery can be used to provide an objective assessment of arterial disease in the leg. The calculation of waveform indices pulsatility index and rise time together with principal component analysis has been found to be the ideal method by which to assess the flow data on-line. (19 refs.)

63913 Human navigation by sound. A.D.Heyes (Dept. of Psychology, Univ. of Nottingham, Nottingham, England).

Phys. Technol. (GB), vol.14, no.2, p.68-75 (March 1983).

Discusses the development of electronic travel aids for the blind, considering in particular the use of IF and US devices. Problems associated with focusing, resolution and ranging are discussed and three methods of modulation are considered—pulse modulation, pulse repetition modulation and frequency modulation. Methods used for information processing and display are also discussed. As examples, the Sonic Guide (an FM ultrasonic aid) and the Sonic Pathfinder (a prototype pulse echo ultrasonic aid) are described. (7 refs.)

87.60D Electric and magnetic fields (d.c. and pulsed)

63914 Comparison of electrical field plethysmography with electrical impedance plethysmography. S.K.Guha, S.Anand (Centre for Biomedical Engng., Indian Inst. of Technol., New Delhi, India).

Ann. Biomed. Eng. (USA), vol.10, no.5, p.231-9 (1982).

As a means for assessing cardiac function, electrical field plethysmography (EFP) has been shown to have some features quite different from electrical impedance plethysmography (EIP). Here the two techniques are compared by using the two systems simultaneously on a subject and also with independent

use in different electrode configurations. The results conform with the view that EIP is related primarily to volumetric changes of the aorta, whereas EFP is affected predominantly by changes in cardiac dimensions and orientation. Because of this difference, the standard time differential formula used for EIP is not applicable for the computation of cardiac output from the EFP waveforms. An alternative method of computation based on the amplitude of the EFP waveform is suggested. (9 refs.)

63915 Monitoring of movement with radio frequency transducers. K.M.Jackson (Phys. Dept., Guys Hospital Medical School, London, England).

J. Biomed. Eng. (GB), vol.5, no.2, p.117-24 (April 1983).

Two approaches to the problem of monitoring human movement using radio frequency transducers are described. A simple two dimensional solution can monitor movement restricted to one plane, whilst a three dimensional transducer (linked to a computer), can follow movement in any plane. In both cases, by measuring the magnetic field produced by a set of small coils powered with high frequency current it is possible to calculate their relative displacement. If the coils are attached to the surface of the human body they can thus be used as a monitor of human movement. (9 refs.)

87.60G Laser beams, microwaves, and other electromagnetic waves

(inc. NMR; for X-rays and gamma-rays, see 87.60J)

63916 Pseudoisochromatic plate design—Macbeth or tungsten illumination? G.M.Chioran, J.E.Sheedy (Ohio State Univ., Coll. of Optometry, Columbus, OH, USA).

Am. J. Optom. & Physiol. Opt. (USA), vol.60, no.3, p.204-15 (March 1983).

Three sets of pseudoisochromatic plates were evaluated by photometry and calorimetry. The luminance contrast between the figure and background was measured and compared with a contrast detection threshold. The chromaticity coordinates of the figure and background were evaluated on the basis of how closely they approached a dichromatic line of confusion. The separation of the coordinates of the figure and background are a measure of the severity of the defect for which the plate tests. The plates were evaluated under both Macbeth (C) and tungsten (A) illuminants; two sets of plates were found to be better designed for tungsten illumination. (19 refs.)

63917 Construction, specification, and mathematical description of aspheric surfaces. G.Smith, D.A.Atchison (Dept. of Optometry, Univ. of Melbourne, Parkville, Australia).

Am. J. Optom. & Physiol. Opt. (USA), vol.60, no.3, p.216-223 (March 1983).

Rotationally symmetrical aspheric surfaces of spectacle lenses are constructed as either 'zonal aspherics' or 'continuous aspherics'. Zonal aspherics consist of annular zones surrounding a central zone with each zone being nominally spherical with progressively lower surface power the farther the zone is from the surface vertex. Aspheric surfaces are often specified by the radial drop in surface power from the center to the edge of the lens (e.g., Welsh Four-drop), but for assessment purposes the surface shape must be specified more precisely. The formulas for the description of continuous aspherics can be manipulated into different forms. Mathematical descriptions are given or developed which will enable theoretical assessment of the performances of all lenses with rotationally symmetrical aspheric surfaces. (5 refs.)

63918 Clinical nuclear magnetic resonance imaging. G.M.Bydder (Royal Postgraduate Medical School, London, England).

Br. J. Hosp. Med. (GB), vol.29, no.4, p.348-56 (April 1983).

This review considers the following topics: instrumentation; general aspects of NMR imaging; normal appearances; vascular disease of the brain; white-matter disease of the brain; cerebral tumours; paediatric neurological disease: the heart; the abdomen; the retroperitoneum and pelvis; future developments. (38 refs.)

63919 Initial clinical evaluation of whole body nuclear magnetic resonance (NMR) tomograph. I.R.Young, D.R.Bailes, M.Burl, A.G.Collins, D.T.Smith (Central Res. Labs., Thorn-EMI Ltd., Hayes, England), M.J.McDonnell, J.S.Orr, L.M.Banks, G.M.Bydder, R.H.Greenspan, R.E.Steiner.

J. Comput. Assisted Tomogr. (USA), vol.6, no.1, p.1-18 (Feb. 1982).

[received: April 1983]

A nuclear magnetic resonance (NMR) imaging system is described, and preliminary results from its clinical use are presented. The properties and detection of the magnetisation due to hydrogen protons are outlined, and a rotating frame is introduced to describe the motion of the magnetisation. Radiofrequency (RF) pulses are used to rotate the magnetisation, and slice selection is achieved using a 90° RF pulse and a magnetic field gradient. Data acquisition and image reconstruction are explained. Three scanning sequences are described: repeated free induction decay (FID), inversion-recovery, and spin-echo. These sequences produce images whose pixel values have different dependencies on hydrogen proton density, T_1 and T_2 . Inversion-recovery images shows striking differentiation between grey and white matter in the brain. The absence of bone artifact is a significant advantage over X-ray computed tomography in the posterior fossa where rapid repeated FID sequences can also be used to demonstrate flow effects. The considerable soft tissue contrast available with NMR is of value in demonstrating disease within the liver where T_1 appears to be a sensitive but relatively nonspecific diagnostic parameter. High resolution scans are of value in demonstrating the adrenal gland and spinal cord. (7 refs.)

63920 Combined flow cytometry and image cytometry of the same cytological sample. H.J.Tanke, A.M.J.Van Driel-Kulker, C.J.Cornelisse, J.S.Ploem (Dept. of Histochem. & Cytochem., Univ. of Leiden, Leiden, Netherlands).

J. Microsc. (GB), vol.130, pt.1, p.11-22 (April 1983).

Flow cytometry and image cytometry, two measuring techniques in the field of analytical cytology, can be used sequentially on the same cytological sample. Cells stained with a fluorochrome for the determination of, for example, DNA or RNA content are first analysed in suspension by flow cytometry. The results of the fluorescence analysis of the individual cells are presented after data processing as frequency histograms of the DNA or RNA content of all the cells of the sample. In these histograms certain cell populations such as those with an increased DNA content are defined and these are then selected for further investigation. This is achieved by sorting cells of interest into centrifugation buckets by means of electrostatic deflection of the droplets containing such cells. Sorted cell populations are then centrifuged on to glass slides and stained according to the acriflavine Feulgen-SITS staining procedure, a quantitative method for DNA and protein. Image cytometry of these stained cells is performed with a computer controlled television based image analysis system (LEYTAS). With this system abnormal cells with elevated DNA content or increased chromatin contrast are automatically detected, thereby eliminating almost all artefacts and normal cells. Subsequently detected objects are stored in grey-value memories after the automated analysis for visual examination by the cytologist. The possibilities of combined flow cytometry and image cytometry are illustrated in typical examples in the field of cervical, bladder and mammary cytology. (15 refs.)

63921 The possibilities offered by infrathermogrammetry for the diagnosis of the Raynaud phenomenon of vibrational origin. T.Kakosy, M.Orosz, J.Boczan.

Meres & Autom. (Hungary), vol.31, no.2, p.76-9 (1983). In Hungarian.

The authors have carried out an infrathermogrammetric examination of the hands on several healthy individuals, on people working under hand-arm vibration conditions and on others, suffering from Raynaud syndrome of non-vibrational origin, before and after cold-provocation. Five types of the infrathermogrammetric picture of the hands can be separated. The article describes characteristic features of these types and their diagnostic value. Application is recommended for aptitude tests of workers under vibrational effect, before employment and for periodic medical examinations. (6 refs.)

63922 Equipment for the clinical application of local microwave hyperthermia. B.M.Southcott (Dept. of Radiotherapy & Surgery, Charing Cross Hospital, London, England), P.B.Dunscombe, K.Gammampila, A.J.Stacey. *Med. Phys. (USA)*, vol.10, no.2, p.224-7 (March-April 1983).

The desirable features of equipment intended for the clinical application of local microwave hyperthermia are identified and the design of a machine incorporating these features is described. An assessment of the technical aspects of the performance of the equipment is given. (12 refs.)

63923 Microfluorometer for medical studies. G.V.Papayan, I.Ya.Barskii, V.V.Titov, S.S.Safinulina, V.V.Shchedrunov, O.E.Lebedev, Yu.A.Grukhin, V.V.Gushch.

Sov. J. Opt. Technol. (USA), vol.49, no.7, p.438-40 (July 1982). Translation of: *Opt.-Mekh. Prom.-st. (USSR)*, vol.49, no.7, p.34-6 (July 1982). [received: April 1983]

A microfluorometer is described that is intended for the simultaneous recording of two bands of the natural luminescence of biological specimens. The instrument is used to measure the luminescence intensity of biopsy specimens during endoscopic examination of patients as well as surgically removed material. The obtained results have shown promise for using the instrument in clinics to diagnose tumoral diseases. (3 refs.)

63924 CO₂ laser scalpel. K.Atsumi (Univ. of Tokyo, Tokyo, Japan), M.Nakajima, A.Ihara, K.Yoshida, K.Ono, J.Hiramoto, K.Sunago, S.Take-naka.

Sumitomo Electr. Tech. Rev. (Japan), no.22, p.260-3 (Jan. 1983).

Reports on the development of a CO₂ laser scalpel that has the following improved features: (1) easy-to-handle waveguide and control console; (2) suitable for a wide range of operations; and (3) highly safe system. In order to achieve these features, an improved waveguide, a handpiece with interchangeable tips, and a control console were developed. (3 refs.)

63925 Two-dimensional reconstructions from one-dimensional data by maximum entropy. S.Sibisi (Dept. of Appl. Math. & Theoretical Phys., Univ. of Cambridge, Cambridge, England).

Topical Meeting on Signal Recovery and Synthesis with Incomplete Information and Partial Constraints, Incline Village, NV, USA, 12-14 Jan. 1983 (Washington, DC, USA: Opt. Soc. America 1983), p.FA11/1-4

The maximum entropy method (MEM) is a powerful information-theoretic approach to the inversion of many types of data in science and engineering. It has been used for reconstructing positive images in such areas as radio astronomy, medical tomography, plasma diagnostics and crystallography. Practical data are always corrupted by noise and are usually incomplete: for example, there may be missing projections or missing Fourier components. Also the instrumental response function may be incompletely known. These factors can lead to severely ill-posed inversion problems. The author applies the method here to Fourier transform nuclear magnetic resonance. (10 refs.)

Effect of conicoid asphericity on the Tscherning ellipses of ophthalmic spectacle lenses See Entry 61252

Functional imaging of the brain See Entry 63940

A versatile localization system for microscopic multiparametric analysis of cells See Entry 64014

87.60J Corpuscular radiation and radioisotopes

(inc. X-rays and gamma-rays)

63926 The implementation of a radiotherapeutic plan for patients with oral tumours in the moving field irradiation regimen. M.A.Kalinichenko, T.V.Khazova.

Med. Radiol. (USSR), vol.28, no.3, p.19-21 (March 1983). In Russian.

The authors propose an original means of the control of marking out and alignment for the implementation of a radiotherapeutic plan in the moving field irradiation regimen for patients with oral tumours. The purpose of the method is to get a cross-sectional tomogram of the zone under study and a one-time representation of the fluctuation center on it in accordance with the radiotherapeutic plan and marking out. To realize this goal a metal needle was used fixed on the tube of the tomograph X-ray tube in the plane that goes through the tube focus and pivotal axis round a patient. (6 refs.)

63927 The formation of dose distributions in combined radiotherapy of patients with endometrial carcinoma. R.E.Khachatryan, A.A.Gabelov, S.M.Vatnitskii.

Med. Radiol. (USSR), vol.28, no.3, p.22-5 (March 1983). In Russian.

The authors consider some features of the dose distribution of fields of a complex shape in γ -beam irradiation using γ -therapeutic units and electron linear accelerators in the complex of combined radiotherapy of patients with endometrial carcinoma. The authors have performed a comparative analysis of calculated and experimental results characterizing dose fields in the utilization of individually selected forming matrices and standard splitting units. It has been shown that the utilization of the forming matrices makes it possible to optimize γ -beam irradiation with a necessary screening of a primary tumour focus and a preset level of dose exposure in the pelvic lateral parts of zones of regional metastases. Spatial dose distribution with the help of matrices gives an opportunity to use intense intracavitary irradiation with high energy sources using an Agat-B unit. (5 refs.)

63928 Computerized program of the calculation of dose distribution formed with γ -radiation intracavity linear sources. V.F.Minenko, A.I.Golubovsky, I.G.Tarutin.

Med. Radiol. (USSR), vol.28, no.3, p.43-6 (March 1983). In Russian.

One can achieve a high precision in the dosing of a session of intracavity radiotherapy by rapid computation of the treatment time necessary for obtaining a certain dose in a pathological focus, taking account of the location of radiation sources in the irradiation. The authors have developed an algorithm and drawn up a program for the computer ES-1022 to calculate a dose rate in any point of an irradiated volume from the system of γ -radiation sources oriented arbitrarily in space. As part of a hard- and soft ware dosimetric complex, the program calculates the treatment time by a set dose. The program makes it possible to calculate the dose distribution in any present plane (up to 4 planes at a time) of an irradiated volume. (8 refs.)

63929 Evaluation of the efficacy of radiation therapy by means of a rated standard dose (RSD) under various conditions of irradiation. V.F.Minenko. *Med. Radiol. (USSR)*, vol.28, no.3, p.57-9 (March 1983). In Russian.

In the evaluation of efficacy or while comparing various irradiation schemes with the help of the RSD concept one should consider the effect of various conditions of the patient's irradiation (energy, a field size, dose rate, etc.) on the biological efficacy of adsorbed energy. The radiobiological effect of various irradiation schemes should be evaluated by a common scale; therefore factors altering dose biological efficacy should be considered within the limits of the same RSD formula. The incorporation in the RSD formula of an empirical expression of RBE dependence on the dose rate within the range of 0.13-300 Gh/hr. and factors of the dependence of dose biological efficacy on its spatial distribution (energy, a field size) allows one not only to consider more correctly changes in the dose for the patient's irradiation from session to session but also makes it possibly to apply it to fractionated and protracted irradiation schemes. (10 refs.)

63930 The choice of geometric parameters in the optimization of irradiation of cancer patients. A.G.Strakh, I.G.Tarutin.

Med. Radiol. (USSR), vol.28, no.3, p.59-62 (March 1983). In Russian.

The authors have devised an algorithm and made a program of 2-stage optimization of irradiation conditions. First the geometric parameters of irradiation are selected (field sizes, their number, a tangential shift of the field axis) proceeding from the peculiarities of the position of tumors, vital organs and tissues in space in respect to a source for each irradiation direction. Dose optimization is done in the 2nd stage. Doses are calculated on the basis of empirical expressions for the distribution of a dose of single γ - and inhibition radiation beams up to 42 MeV. Tissue inhomogeneity and surface curvature are taken into consideration by means of corrections. (6 refs.)

63931 The utilization of computer in the planning of radiotherapeutic volume for patients with oral tumors. T.V.Khazova, A.I.Strashinin, E.S.Dianina, E.A.Kuznetsov.

Med. Radiol. (USSR), vol.28, no.3, p.62-6 (March 1983). In Russian.

A series of dose maps have been obtained on the basis of typical isodose maps for moving irradiation of patients with oral tumors, the doses being selected with the help of a specialized computer and dose calculation program for computer ES 1020: in the main cross-sectional plane going through a tumor and in parallel planes 1 cm above and below from the main plane within the limits of an irradiation field +1 cm, dose fields have been formed in the sagittal (parasagittal) plane extending through the center of a tumor. (3 refs.)

63932 The utilization of time-dose-fractionation models in the planning of tumor radiotherapy. A.S.Pavlov, K.N.Kostromina, V.S.Datsenko, M.A.Fadeeva, A.L.Bocharov.

Med. Radiol. (USSR), vol.28, no.3, p.80-3 (March 1983). In Russian.

New methods of the fractionation of preoperative γ -beam therapy for breast carcinoma and intracavity irradiation of cervical cancer patients with ²⁵²Cf fast neutron sources have been devised and tested on the basis of the cumulative radiation effect and the system of time-dose-fractionation factors. In the selection of regimens for the intracavity irradiation fractionation, one should take into account the relative biological effectiveness of the type of radiation equal to 5 by the criterion of a direct response of a tumor within the 20-30 s γ -Cf relative biological effectiveness. Taking account of the short half-life of ²⁵²Cf source, fractionation schemes should be corrected from the view-point of the system of TDF factors not less than once in 2-3 mos. (11 refs.)

63933 Prevention of radiation injuries during multifractionation in radiation therapy. K.I.Zholkivier, I.F.Zevrieva.

Med. Radiol. (USSR), vol.28, no.4, p.3-6 (April 1983). In Russian.

A radiobiological substantiation of a method of multifractionation and a review of the results of its clinical application are presented. The authors have developed a method to calculate a cumulative radiation effect and the TDF factor in radiation therapy with multiple dose fractionation in the form of several sessions daily. This method can be used to prevent the radiation-caused complications. (25 refs.)

63934 Simulation of the organ blood flow in computer γ -scintigraphy.

B.N.Dmitriyev, I.V.Misochko, A.P.Kolgin, S.L.Kovarskii, S.V.Andronov.

Med. Radiol. (USSR), vol.28, no.4, p.28-31 (April 1983). In Russian.

The determination of the relative blood flow in organs is sometimes of greater diagnostic importance than the estimation of respective absolute indices. A detailed analysis of indispensable mathematical calculations is presented. The authors propose an algorithm and optimum sequence of calculations of relative organ perfusion using computer. The paper can be of wide applied importance. (1 ref.)

63935 PETT VI: a positron emission tomograph utilizing cesium fluoride scintillation detectors. M.M.Ter-Pogossian, D.C.Ficke, J.T.Hood, Jr. (Edward Mallinckrodt Inst. of Radiology, Washington Univ. School of Medicine, St. Louis, MO, USA), M.Yamamoto, N.A.Mullani.

J. Comput. Assisted Tomogr. (USA), vol.6, no.1, p.125-33 (Feb. 1982). [received: April 1983]

The authors designed and built a positron emission transverse tomograph (PETT VI), designed specifically for fast dynamic studies in the human brain and for cardiac studies in experimental animals. The scintillation detectors incorporated into this device are fitted with cesium fluoride crystals, selected because their short fluorescence decay allows the use of a short coincidence resolving time with a concomitant reduction of unwanted random coincidences. PETT VI utilizes four rings of 72 detectors simultaneously yielding seven tomographic sections. The short coincidence resolving time of the system permits rapid data acquisition for attenuation corrections and clinical dynamic studies with data acquisition times of less than a minute. (13 refs.)

63936 Dynamic computed tomography through interpolation. H.C.Lee, C.H.Leung (Dept. of Electrical Engng., McGill Univ., Montreal, Quebec, Canada).

J. Comput. Assisted Tomogr. (USA), vol.6, no.1, p.134-40 (Feb. 1982). [received: April 1983]

A method is proposed to reduce the requirement on the scanning speed for dynamic computed tomography of relatively fast moving objects such as the heart. From the projections measured at different times, a set of optimal projections is computed for reconstructing the image at any specified time within a permissible interval. In the method, the corresponding characteristic features of the measured projections at the same viewing angle are matched optimally by a nonlinear transformation. The matched projections are then used in an interpolation procedure to compute the projections required at the specified time. The method has been tested with mathematical phantoms that undergo partial expansion, contraction, and translational motion. The results show that the proposed method can provide acceptable images from data collected at scanning speeds that would otherwise produce severely blurred images by conventional methods. (15 refs.)

- 63937 Technical aspects of digitization X-ray image processing, especially digital subtraction angiography.** M.Pfeiler, P.Marhoff (Siemens AG, Erlangen, Germany). *Electromedica (Germany)*, vol.51, no.1, p.20-31 (1983). Digital subtraction angiography (DSA) has opened up numerous new diagnostic possibilities and enables a considerable increase in objective and subjective image quality. The authors make some observations on the subject of image quality, with special reference to the important criterion 'signal-to-noise ratio'. (15 refs.)
- 63938 'Native' computed tomography: a new radiological approach of the herniated lumbar disk.** M.Stienon, D.Baleriaux, L.Jeanmart (Inst. Brodet, Brussels, Belgium). *J. Belge Radiol.*, vol.65, no.5, p.449-54 (1982). In French. Describes the native-CT technique (thin slices, direct enlargement) and the normal anatomy of the lumbar vertebra. The authors demonstrate the semiology of the lumbar discal hernia in CT, either lateral or on the midline. Thirteen patients were surgically treated, out of a series of 26 examinations, and all of them confirmed the CT diagnosis. The advantages of native-CT are discussed: noninvasive method, simplicity of application, and ability to demonstrate other lesions that can clinically mimic a herniated disk. These characteristics allow CT to be the first choice technique of examination when a lumbar discal hernia is suspected, the more invasive techniques being reserved for patients with negative or noncontributive CT, or when another intraluminal pathology is suspected. (15 refs.)
- 63939 Single photon emission computerized tomography: a new dimension in nuclear medicine-system characterization.** L.A.A.Mortelmans, M.J.K.De Roos, P.Suetsens (Acad. Ziekenhuis St. Rafael, Leuven, Belgium). *J. Belge Radiol.*, vol.65, no.5, p.455-63 (1982). Single photon emission computerized tomography (SPECT), as a counterpart of the CAT scan, provides new diagnostic capabilities in nuclear medicine. Using a rotating gamma camera, studies may be performed with gamma emitting tracers using the conventional dose. A computer creates sections in several planes (horizontal, frontal, sagittal, oblique) by a filtered back projection method from 64 injections. A technical description of the apparatus and the basic principles of the reconstruction method are provided. The following performance characteristics of the SPECT system are reported: resolution in the transaxial plane, sensitivity, slice thickness, attenuation correction, lesion contrast, and alignment check. Notwithstanding the poor constant resolution (15-20 mm), an enhancement in contrast resolution is obtained that results in a higher diagnostic detection rate. Stability of the axis of rotation, excellent field uniformity correction, and camera-table alignment are required for the production of artefact free images. (9 refs.)
- 63940 Functional imaging of the brain.** F.A.Jolesz (Dept. of Radiology, Harvard Medical School, Boston, MA, USA). *Med. Instrum. (USA)*, vol.17, no.1, p.59-62 (Jan.-Feb. 1983). New neurophysiological methods such as 2-deoxy-D-glucose (2DG) autoradiography have stimulated rapid changes in emission imaging with radionuclides. It has been recognized that general imaging concepts and methods can be applied to many interactions of waves, particles, or fields within the body. X-ray computed tomography, single-photon emission computerized tomography, positron emission tomography, and nuclear magnetic resonance imaging have the potential to enable one to visually observe biochemical events and physiological processes in the brain, where one's knowledge is limited and one's eagerness to understand function is the greatest. (6 refs.)
- 63941 Physical aspects of a rotational total skin electron irradiation.** E.B.Podgorsek, C.Pla, M.Pla, P.Y.Lefebvre, R.Heese (Dept. of Radiation Oncology, McGill Univ., Montreal, Quebec, Canada). *Med. Phys. (USA)*, vol.10, no.2, p.159-68 (March-April 1983). A technique for rotational total skin electron irradiation is presented in which the patient stands on a slowly rotating platform (SSD=285 cm) in a large uniform linear accelerator electron field ($E_0=3.5$ MeV). The beam is scattered by the transmission ionization chamber and by a special lead/aluminum scattering filter, and then degraded by a sheet of Lucite. A Farmer chamber is used as a patient dose monitor and a method for absolute dose calibration is presented. The field is uniform to within $\pm 5\%$ for dimensions of 180×40 cm². The surface dose for rotational therapy is equal to 45% of the maximum dose in a stationary beam. The rotating beam exhibits a dose maximum on the surface, falls to 80% at 0.5 cm and has an X-ray contamination of $\sim 4\%$. The surface dose rate is about 25 cGy/min for the rotating beam. The rotational beam percentage depth dose distributions, calculated using stationary beam information, agree well with measured data. The stationary beam exhibits a dose maximum at 4 mm in tissue, a surface dose of 93%, 80% dose at a depth of 1 cm, a practical range of 1.75 cm, and an X-ray contamination of 2.5%. The rotational total skin electron irradiation significantly reduces the patient treatment and setup time and solves the problem of beam matching, when compared to standard multiple-beam techniques. (10 refs.)
- 63942 The effects of misregistration of the projections on spatial resolution of CT scanners.** M.F.Kijewski (Dept. of Environmental Health Sci., Harvard School of Public Health, Boston, MA, USA), P.F.Judy. *Med. Phys. (USA)*, vol.10, no.2, p.169-75 (March-April 1983). Misregistration of the projections in 360° computed tomographic (CT) scanners has been found to blur the image without generating artifacts. The effects of this error were investigated by analytical methods and by reconstruction of real and simulated data. The point-spread function which results from shifting each projection by a constant distance ϵ consists of a two-dimensional impulse function surrounding a region of negative density. The locus of the impulse function is a circle for parallel-beam geometry and a sixth-order curve for fanbeam geometry. The anisotropy and position dependence of the point-spread function in fanbeam geometry have been characterized. The line-spread function due to the error in parallel-beam geometry consists of two delta functions located at $\pm \epsilon$. In fanbeam geometry, the line-spread function consists of two delta functions separated by approximately 2ϵ , with the locations of the impulses dependent on the position and orientation of the line. This error, combined with other sources of blurring, results in a system edge-response function which contains a flat region at one-half the maximum density. (26 refs.)
- 63943 The technical characteristics of matched filtering in digital subtraction angiography.** S.J.Riederer (General Electric Co. Medical Systems, Milwaukee, WI, USA), A.L.Hall, J.K.Maier, N.J.Pelc, D.R.Enzmann. *Med. Phys. (USA)*, vol.10, no.2, p.209-17 (March-April 1983). The technical characteristics of a new digital fluorographic image processing method called matched filtering are presented. This technique, a type of extensive temporal integration, takes a weighted sum of images acquired during passage of a contrast bolus through some area of interest. The weight of each image is governed by the magnitude of the contrast bolus in that image. An essential requirement of the matched filter is that its integral be zero. It is shown for equal exposure rates and typical bolus characteristics that matched filtering provides a factor of two higher signal-to-noise ratio (SNR) than conventional methods for bolus transit times of 10 s or higher. Equi-

valently, matched filtering can yield images with quality comparable to conventional digital subtraction angiography (DSA) at a factor of four less patient exposure. The SNR obtained with matched filtering is shown to be within 30% of an ideal bound. Comparisons of matched filtering to standard recursive methods and simple integration are made. Experimental canine studies are presented which compare matched filtering with conventional DSA. (16 refs.)

- 63944 A detailed experimental and theoretical comparison of the angular and energy dependencies of grid transmission.** H.Bernstein (Rancho Los Amigos Hospital, Univ. of Southern California, Downey, CA, USA), E.P.Muntz, J.Schreckendgust, D.J.Klein, K.Lee. *Med. Phys. (USA)*, vol.10, no.2, p.218-23 (March-April 1983). Grid transmission characteristics have been predicted, with good agreement demonstrated between experiment and theory. Differences between the present work and an earlier theoretical analysis have been noted. It is shown that comparison between experiment and theory can lead to a sensitive method for determining grid parameters. Generally, the derived grid parameters deviate somewhat from manufacturer supplied data. Use of the manufacturer's nominal parameters can lead to large errors in predicting grid transmission. (17 refs.)
- 63945 Transportation of short-lived positron emitters from a medical cyclotron to a remote imaging suite.** J.A.Corrêa, W.H.Buculewicz, H.W.Strauss, N.M.Alpert, G.L.Brownell, J.M.Taveras (Phys. Res. Lab., Massachusetts General Hospital, Boston, MA, USA), V.Ferrari. *Med. Phys. (USA)*, vol.10, no.2, p.228-31 (March-April 1983). This paper describes a system for the transport of compounds labeled with short-lived positron emitting isotopes from a clinical cyclotron to a remote imaging suite. The system consists of a pneumatic transport line for the sending of batch lots of radioactive material and a pressurized gas line for the continuous transmission of radioactive gases. Experimental performance of both systems has been measured and a simple model for the pressurized gas line is compared to experimental results. The radiation dosimetry and safety aspects of the systems are also discussed. (5 refs.)
- 63946 Characteristics of Mevatron 77 15-MV photon beam.** J.M.Paul, R.F.Koch, F.R.Khan, B.S.Devi (Dept. of Radiation Therapy, Northwest Community Hospital, Arlington Heights, IL, USA). *Med. Phys. (USA)*, vol.10, no.2, p.237-42 (March-April 1983). The characteristics of 15-MV photon beam of Mevatron 77 have been examined with respect to clinical parameters. Some of the characteristics of this 15-MV photon beam are different from those of similar machines used in radiotherapy. The tissue-maximum ratio values have been determined experimentally for SAD 100 cm and percentage depth dose values have been determined from tissue-maximum ratio data. It is found that the experimentally determined PDD values for SSD 80, 100, and 120 cm are within $\pm 1\%$ of the calculated data. The scatter-maximum ratio data have been calculated from the experimentally determined zero area attenuation coefficient and tissue-maximum ratio data and are presented as function of depth and radii of circular fields. The relative dose factors have been determined both for square and rectangular fields. The relative dose factor for rectangular fields depends on the two pairs of jaws differently and the maximum difference is about 1.5%. The flatness and symmetry are within the specifications set by the manufacturer. (13 refs.)
- 63947 Regional silver content of radiographic film determined by X-ray fluorescence compared with optical densitometry.** W.H.Oldendorf, M.A.Astrahan (VA Medical Center Brentwood, Los Angeles, CA, USA). *Med. Phys. (USA)*, vol.10, no.2, p.246-7 (March-April 1983). The regional silver content of radiographic film measured by X-ray fluorescence is compared to light absorption measured by a densitometer. Silver content analysis appears to permit a greater dynamic range of useful exposure levels than does light absorption densitometry. This improvement in latitude, however, is not considered great enough to warrant development of a complex system for scanning silver distribution in radiographic applications. (1 ref.)
- 63948 Feasibility of noninvasive analysis of lead in the human tibia by soft X-ray fluorescence.** L.Wielopolski, J.F.Rosen, D.N.Slatkin, D.Vartsky, K.J.Ellis, S.H.Cohn (Brookhaven Nat. Lab., Medical Res. Center, Upton, NY, USA). *Med. Phys. (USA)*, vol.10, no.2, p.248-51 (March-April 1983). A postmortem study was conducted to assess the feasibility of measuring bone lead concentrations noninvasively in vivo. Characteristic L X-rays were induced with an external source of ¹²⁵I in the superficial tibial cortex of the intact legs of six adults who had no history of occupational exposure to lead. Tibial lead concentrations in the same bones subsequently determined by flameless atomic absorption spectroscopy varied from 15 to 35 $\mu\text{g Pb/g}$ wet weight. The upper limit for the modern normal range of lead in the bone is about 25 mg Pb/g wet tissue. The linear correlation coefficient (r) between the measurements made with X-ray fluorescence and lead concentration by absorption spectroscopy was 0.90. Radiation doses of 10 mGy (1 rad) to 1 cm² of skin, with associated doses to the marrow of adjacent bone of about 0.6 mGy (60 mrad), yielded net lead fluorescence signals ranging from one to seven times the standard deviation of background. (30 refs.)
- 63949 A study of problems with inventory control of I-125 seeds.** H.L.McMurry, E.L.Chaney, M.Kirsch (Radiation Therapy Div., Univ. of North Carolina School of Medicine, Chapel Hill, NC, USA). *Med. Phys. (USA)*, vol.10, no.2, p.252-3 (March-April 1983). A stringent inventory control protocol was implemented to determine the fate of I-125 seeds used for interstitial implants. Results show where emphasis is needed to limit seed loss. (no refs.)
- 63950 Repair of the energy slit on an AECL Therac-20 accelerator.** J.Pipman, O.Carpenter (Dept. of Medical Phys., Memorial Sloan-Kettering Cancer Center, New York, NY, USA). *Med. Phys. (USA)*, vol.10, no.2, p.257-8 (March-April 1983). Instabilities in the beam symmetry of the authors' AECL Therac-20 accelerator were traced back to a minute water leak in the energy defining slit. (no refs.)
- 63951 Comments on 'Radiation leakage from electron applicator assembly on a linear accelerator' [and reply].** D.Jones (Northwest Medical Phys. Center, Seattle, WA, USA), A.J.Schneider. *Med. Phys. (USA)*, vol.10, no.2, p.259 (March-April 1983). Jones comments on a technical note by Schneider (see *ibid.*, vol.9, p.761, 1982) which identifies an important radiation leakage problem. In that note Schneider proposed a method for all but eliminating the radiation leakage. Jones says that this method did not work for him. In reply Schneider says that he was able to reduce leakage to 2-5% using this method, and that apparently the leakage is a machine specific characteristic. (no refs.)

63952 A regularized iterative algorithm for limited-angle inverse Radon transform. M. Defrise (Vrije Univ. Brussel, Brussels, Belgium), C. De Mol. *Opt. Acta (GB)*, vol.30, no.4, p.403-8 (April 1983). The tomography problem is investigated when the available projections are restricted to a limited angular domain. It is shown that a previous algorithm proposed for extrapolating the data to the missing cone in Fourier space is unstable in the presence of noise because of the ill-posedness of the problem. A regularized algorithm is proposed, which converges to stable solutions. The efficiency of both algorithms is tested by means of numerical simulations. (16 refs.)

63953 Geometric deconvolution of artifacts in limited view computed tomography. R.M. Rangayyan (Electrical Engng. Dept., Univ. of Manitoba, Winnipeg, Canada), R. Gordon.

Topical Meeting on Signal Recovery and Synthesis with Incomplete Information and Partial Constraints, Incline Village, NV, USA, 12-14 Jan. 1983 (Washington, DC, USA: Opt. Soc. America 1983), p.FA2/1-3. Limited-view image reconstruction and computed tomography suffer from a systematic geometric distortion. The authors present results of Fourier deconvolution techniques to correct the artifacts. (no refs.)

63954 Localization from projections based on detection and estimation of objects. D.J. Rossi (Schlumberger-Doll Res., Ridgefield, CT, USA), A.S. Willsky.

Topical Meeting on Signal Recovery and Synthesis with Incomplete Information and Partial Constraints, Incline Village, NV, USA, 12-14 Jan. 1983 (Washington, DC, USA: Opt. Soc. America 1983), p.FA3/1-4. An object-based probabilistic model is used in reconstructing a field from limited noisy projection measurements. The performance of maximum likelihood object location estimation is characterized. (7 refs.)

63955 Tomographic imaging with limited view angle using an expansion on a set of eigenfunctions adapted to space-limited objects. L. Garnerio (Inst. d'Optique, Univ. de Paris XI, Orsay, France), J. Brunol.

Topical Meeting on Signal Recovery and Synthesis with Incomplete Information and Partial Constraints, Incline Village, NV, USA, 12-14 Jan. 1983 (Washington, DC, USA: Opt. Soc. America 1983), p.FA4/1-4. In many radiation imaging applications, such as X-ray computerized tomography or nuclear medicine, tomographic systems have been recently developed, which image an object from an angularly restricted number of projections. It is well known that in such a case, some Fourier components are missing, and thus analytical reconstructions, such as Fourier synthesis can no longer be used. But, the algebraic methods allow one to take advantage of 'a priori' informations on the object, in order to recover the missing data. Many authors have proposed different reconstruction techniques, that combine limited projection data with a priori object information through iterative revisions in both image and transform spaces. These methods in general consume much computer time. The authors propose here a new approach of the problem, based on the fact that generally the imaged organs or objects do not fill the whole detector field. The knowledge of their boundaries allows one to find, for each class of objects of the same extent, a new set of expansion functions, which are more appropriate than a Fourier expansion. The expansion of the object distribution on this new set of functions allows the object reconstruction from projection data by a mere operation of matrix multiplication. The terms of the resulting linear system of equations are the same for each object of same extent, and so the corresponding matrix inversion has to be performed only once. (4 refs.)

63956 Linear estimation with a size constraint. M.J. Lahart (Naval Res. Lab., Washington, DC, USA).

Topical Meeting on Signal Recovery and Synthesis with Incomplete Information and Partial Constraints, Incline Village, NV, USA, 12-14 Jan. 1983 (Washington, DC, USA: Opt. Soc. America 1983), p.FA5/1-4. Correlation coefficients between spectral components of a space-limited image are calculated and used to estimate missing components. The technique is used for bandwidth extrapolation and recovery of missing views in computed tomography. (4 refs.)

63957 Bayesian approach to limited-angle CT reconstruction. K.M. Hanson (Los Alamos Nat. Lab., Univ. of California, Los Alamos, NM, USA), G.W. Weckung.

Topical Meeting on Signal Recovery and Synthesis with Incomplete Information and Partial Constraints, Incline Village, NV, USA, 12-14 Jan. 1983 (Washington, DC, USA: Opt. Soc. America 1983), p.FA6/1-4. Artifact reduction in limited-angle CT reconstruction is demonstrated by use of the Bayesian approach, which estimates an appropriate null-space contribution to the reconstruction. (8 refs.)

63958 The use of a priori information in image reconstruction from limited data. B.P. Medoff, W.R. Brody, A. Macovski (Stanford Univ., Stanford, CA, USA).

Topical Meeting on Signal Recovery and Synthesis with Incomplete Information and Partial Constraints, Incline Village, NV, USA, 12-14 Jan. 1983 (Washington, DC, USA: Opt. Soc. America 1983), p.FA7/1-4. An operator framework for limited data image reconstruction that applies to arbitrary scanning geometries and to arbitrary patterns of missing line integral data, is introduced. This framework is not based on a frequency domain interpretation, and hence can be used when the pattern of missing data does not correspond to a missing sector in the frequency domain. The operator framework allows the reconstruction algorithm to incorporate a wide class of a priori information about both the line integral data and the underlying density. (8 refs.)

63959 Incorporation of prior constraints in tomographic reconstructions from coded images. R.G. Paxman (Optical Sci. Center, Univ. of Arizona, Tucson, AZ, USA), G.R. Gindi, H.H. Barrett.

Topical Meeting on Signal Recovery and Synthesis with Incomplete Information and Partial Constraints, Incline Village, NV, USA, 12-14 Jan. 1983 (Washington, DC, USA: Opt. Soc. America 1983), p.FA8/1-4. The iterative Jacobi method is used to reconstruct 2-dimensional functions from 1-dimensional coded image data sets. The folding of prior constraints into the iterations improves the reconstructions. (no refs.)

63960 Inverse scattering reconstructions from incomplete Fourier space data. N.H. Farhat (Moore School of Electrical Engng., Univ. of Pennsylvania, Philadelphia, PA, USA).

Topical Meeting on Signal Recovery and Synthesis with Incomplete Information and Partial Constraints, Incline Village, NV, USA, 12-14 Jan. 1983 (Washington, DC, USA: Opt. Soc. America 1983), p.FA9/1-4. Shows that 3-D tomographic inverse scattering reconstruction of a scattering object is obtainable from data lying on a curved surface, rather than within a volume, of its accessed Fourier space as would ordinarily be required. (12 refs.)

63961 Deblurring and three-dimensional reconstruction from multiple linear-tomograms. S. Kawata (Dept. of Appl. Phys., Osaka Univ., Osaka, Japan), J. Sklansky.

Topical Meeting on Signal Recovery and Synthesis with Incomplete Information and Partial Constraints, Incline Village, NV, USA, 12-14 Jan. 1983 (Washington, DC, USA: Opt. Soc. America 1983), p.FA10/1-5.

The image of the tomogram obtained by a conventional X-ray tomographic machine is degraded by the superposition of motion-blurred images of non-pivotal planes. The authors introduce a method to eliminate these blurred images from a tomogram. In this method a set of tomograms, each focused on one of a set of parallel planes, are combined to form a three-dimensional reconstruction of blur-free tomograms. This approach is equivalent to the inversion of a linear system. By a mathematical analysis of linear-motion tomography, they found that linear-motion tomography is restricted to angularly-limited frequency information. An iterative matrix inversion algorithm with the constraints of nonnegativity and finite-extent is applied to the reconstruction of the plane of interest from a set of tomograms. (9 refs.)

The state and prospects in the development of the medical proton tract on the synchrocyclotron in Gatchina See Entry 60499

Elemental analysis performed with the Karlsruhe nuclear microprobe See Entry 63611

Mathematical model of normal tissue injury in γ -beam therapy See Entry 63899

Stability of optimum problem solution to determine optimum physical and technical conditions of irradiation See Entry 63966

Dosimetric characteristics of thermoluminescent detectors for inhibitory and electron radiation of a betatron BSM-25 See Entry 63968

Time dose distribution in radiation therapy planning See Entry 63970

Radiation absorbed dose estimates for positron emission tomography (PET): inert gases ^{19}Ne and ^{71}Kr See Entry 63972

Kerma transmission through steel for a p(66)Be(49) neutron beam: an update See Entry 63973

Dose calibrator response to brachytherapy sources: a Monte Carlo and analytic evaluation See Entry 63974

The application of multiple scattering theory to therapeutic electron dosimetry See Entry 63975

Absorbed dose determination for interstitial ^{125}I boost therapy See Entry 63976

Some theoretical derivations relating to the tissue dosimetry of brachytherapy nuclides, with particular reference to iodine-125 See Entry 63977

Monte Carlo estimates of specific absorbed fractions for an I-125 point source in water See Entry 63978

A new approach to CT pixel-based photon dose calculations in heterogeneous media See Entry 63979

Quantitative determination of tolerance doses for preoperative and postoperative radiotherapy of bones See Entry 63980

Surface doses for acrylic versus lead acrylic blocking trays for Co-60, 8-MV, and 17-MV photons See Entry 63981

87.60L Preparation of radioactive materials for medical and biomedical uses

63962 An $^{18}\text{O}_2$ -target for the high yield production of ^{18}F -fluoride. R.J. Nickles, R.D. Hichwa, M.E. Daube, G.D. Hutchins, D.D. Congdon (Medical Phys. Dept., Univ. of Wisconsin, Madison, WI, USA).

Int. J. Appl. Radiat. & Isot. (GB), vol.34, no.3, p.625-9 (March 1983). A high-pressure target for the production of ^{18}F -fluoride via $^{18}\text{O}(p, n)^{18}\text{F}$ is described. A small-volume chamber receives a standard 10 mL, glass test tube with a silvered interior. The $^{18}\text{O}_2$ target gas is admitted, irradiated, then retrieved without losses into a reservoir by cryogenic pumping. At 10-MeV proton energy, 150 mCi/ μA end-of-saturated-bombardment (EOSB) activities of ^{18}F are conveniently deposited on the inner surface of the target liner. This liner is removed and serves as the reaction flask for various syntheses needing precursor ^{18}F -fluoride. Production of the simple fluoralkane CH_3^{18}F has been chosen as the standard reaction, due to its clinical demand in the assessment of regional cerebral blood flow. (21 refs.)

63963 Measurement of activity yields for $^{12}\text{C}(\gamma, n)^{11}\text{C}$, $^{14}\text{N}(\gamma, n)^{13}\text{N}$, and $^{16}\text{O}(\gamma, n)^{15}\text{O}$ reactions as a function of electron beam energy and angle from the electron beam using thick target produced bremsstrahlung. H.V. Pittsgrud (Nuclear Medicine Lab., Univ. of Cincinnati Medical Center, Cincinnati, OH, USA).

Med. Phys. (USA), vol.10, no.2, p.147-54 (March-April 1983). The calculation of activity yields from practical photoneuclear target systems designed to produce short-lived positron emitting radionuclides for nuclear medicine purposes requires certain basic information. These include a knowledge of the photon source (bremsstrahlung energy spectrum and intensity as a function of angle from the electron beam) and the γ, n activation cross section of the secondary target element. A lack of adequate information concerning these parameters motivated the present study in which activity yields for the reactions $^{12}\text{C}(\gamma, n)^{11}\text{C}$, $^{14}\text{N}(\gamma, n)^{13}\text{N}$, and $^{16}\text{O}(\gamma, n)^{15}\text{O}$ were measured as a function of energy of and angle from the electron beam between 16 and 30 MeV and 0° and 30.5° , respectively. The data indicate highly complex relationships between the activity yield and the experimental variables. Also indicated are possible applications of the data to indicate the energy of an electron beam producing a given bremsstrahlung field in which activation measurements are made. (6 refs.)

87.60M Radiation dosimetry

63964 Dosimetric substantiation of mean fractionation during irradiation of bone metastases of breast carcinoma. T.G. Ratner, G.D. Monzul, L.A. Kulikov, V.G. Sakharovskaya.

Med. Radiol. (USSR), vol.28, no.3, p.11-14 (March 1983). In Russian. Proceeding from the drawing of maps with biologically ineffective percentage doses the authors provide a dosimetric substantiation of γ -beam irradiation of different parts of the bony skeleton. It has been shown that to choose a therapeutic plan in the utilization of a nonstandard scheme of fractionation, the calculation of the TDF factor by Orton's tables is safe and illustrative. By way of example maps are given of ineffective doses used in the irradiation of bone metastases in breast cancer patients with metastases to different parts of the skeleton. (7 refs.)

63965 Dose distributions of fast electrons with an energy of 7-24 MeV in the electromagnetic formation of a beam. R.S.Shambulov, G.V.Khavan, T.S.Saibekov, N.A.Azhigaliev, A.D.Shuinbekov. *Med. Radiol. (USSR)*, vol.28, no.3, p.14-18 (March 1983). In Russian. The formation of a wide beam is found necessary for a clinical application of a fast electron beam. An electromagnetic method of formation has been worked out, and dose distributions of fast electrons formed by this method have been compared in the tissue equivalent medium with those formed with the help of thin dispersion foils. The effect of some of the individual units of the forming device in these two methods has been assessed. The experiment was conducted on medical beta-trons B-15 and B-5M-25 manufactured in the USSR. The depth dose distributions of fast electrons along the beam central axis in the electromagnetic formation for electrons with an energy of 7-24 MeV are presented. It has been established that the beam intensity in the electromagnetic formation is higher than in the utilization of dispersion foils, and the depth dose distribution is also better. (6 refs.)

63966 Stability of optimum problem solution to determine optimum physical and technical conditions of irradiation. L.Ya.Klepper. *Med. Radiol. (USSR)*, vol.28, no.3, p.33-8 (March 1983). In Russian. The problem of the determination of optimum physical and technical plans of irradiation is often due to the problems of linear programming. To solve such a problem, it is necessary to calculate a matrix of conditions (dose rate in the system of distributed control points in the body during irradiation in different present directions). The author studies the influence of errors of the calculation of dose rates upon the optimum irradiation plans. It has been established that though the task of determining optimum plans is a correct one, convergence of the solution of a disturbed problem to an initial one occurs extremely slowly. The optimum values of the functionals of a disturbed problem converge more rapidly to the functional of an initial problem. The comparison of optimum irradiation plans or optimum and traditional irradiation plans seems difficult. To compare different irradiation plans, it is more convenient to use the values of a specific function (optimization criteria). (8 refs.)

63967 Regularities of the dose field formation in placing ^{252}Cf and ^{60}Co sources on the same plane. V.N.Ivanov, B.M.Vtyurin, L.F.Ivanova, Yu.R.Kondzharya. *Med. Radiol. (USSR)*, vol.28, no.3, p.38-42 (March 1983). In Russian. A computerized study was made of a change in the correlation between the sizes of an irradiated volume and the distribution of sources. Criteria have been established for the utilization of ^{252}Cf and ^{60}Co sources of different active length and design placed on the same plane. The reference dose rate and its derivatives have been chosen as the main parameters that characterize a dose field. A dosimetric analysis was performed using the data for an absorbed dose of neutrons in the tissue, taking account of the high RBE of ^{252}Cf fast neutrons, and a slight change of the local RBE value near the source. The irradiated volume was evaluated by introducing the 3 linear parameters of length, thickness and width. The results obtained are presented graphically. They are used for a dosimetric control of the clinical trials of ^{252}Cf and ^{60}Co sources in the treatment of patients with tumors of the tongue, oral cavity fundus, lip and other sites. (8 refs.)

63968 Dosimetric characteristics of thermoluminescent detectors for inhibitory and electron radiation of a betatron B5M-25. V.I.Popov, N.Ya.Motrii. *Med. Radiol. (USSR)*, vol.28, no.3, p.49-55 (March 1983). In Russian. The authors present the results of experimental and theoretical determinations of coefficients of the transition from thermoluminescent detector readings to an absorbed dose in water, and the correlation between the detector readings and the depth in a phantom for betatron inhibitory and electron radiations. Comparative measurements of absorbed doses have been made with a ferrous sulphate system and 2 dosimeters with ionization chambers. The measurement data have been confirmed theoretically, making it possible to use small-size autonomous glass detectors in clinical dosimetry including those for the direct measurement of irradiation dose patients receive, to control the results of the dosimetric planning of radiation therapy. Theoretical correlations obtained can be used for the prognosis of behaviour of thermoluminescent detectors in the fields of inhibitory radiation of high energies and arbitrary spectral composition as well as for electron spectra with energies up to 25 MeV. (13 refs.)

63969 Analytical description of dose fields from accelerated electrons. V.A.Kozlov, O.N.Denisenko. *Med. Radiol. (USSR)*, vol.28, no.3, p.56-7 (March 1983). In Russian. The authors present a simple expression describing dose fields in the water phantom from the betatron B5M-25 electron beam using the Fermi-Dirac distribution function. The peculiarity of these expressions is the utilization of parameters that reflect the main characteristics of a dose field—the depth distribution of 50% of the isodose and the projection of the zone of a dose decline along the beam axis and in its transverse cross section. The expressions proposed here could be also used for other electron accelerators. (4 refs.)

63970 Time dose distribution in radiation therapy planning. I.F.Zevrieva. *Med. Radiol. (USSR)*, vol.28, no.4, p.58-62 (April 1983). In Russian. Until recently the effect of a dose fractionation regimen was disregarded in radiation therapy planning. A method devised for the calculation of isodose maps made it possible to obtain iso-effective distributions where radiation exposures in different dose fractionation regimens are presented in the form of isoline in TDF units. The method of the calculation of iso-effective maps allowed one to analyse the effect of the procedure of the implementation of a radiotherapeutic plan and the conditions of dose rate fixing. The author cites by way of an example the calculation of a 3-field static irradiation of esophageal cancer with 5 fractions a week. All possible variants of the implementation of this therapeutic plan were studied. Daily irradiation of all the planned fields has been shown to be optimum. This conclusion is corroborated by the literature data. The absolute value of the TDF factor in the adjacent healthy organs and tissues increases noticeably using in the calculations isodose curves fixed to the dose in the focus depth as compared to fixing on the dose on the surface. Isoeffective maps can be successfully used for an analysis of clinical and therapeutic results. (9 refs.)

63971 Application of inhalation retention functions to in vivo measurement. M.H.Johnson (Knolls Atomic Power Lab., Schenectady, NY, USA), M.T.Ryan, K.F.Eckerman, K.W.Skrable. *Radiat. Prot. Dosim.* (GB), vol.3, no.4, p.197-201 (1982). Recent radiation protection recommendations place joint constraints on the annual dose equivalent from external irradiation and the annual intake of radionuclides. The inhalation intake of workers acutely exposed to photon emitting radionuclides can be estimated from measurements of activity burdens in the respiratory tract and the time dependence of retention derived from the respiratory clearance model. Functions describing the fraction of the inhaled material retained in the respiratory tract are derived and their application to evaluation of the radiological status of an exposed worker noted. (8 refs.)

63972 Radiation absorbed dose estimates for positron emission tomography (PET): inert gases ^{19}Ne and ^{77}Kr . K.J.Kearfoot (George Cotzias Lab. of Neuro-Oncology, Memorial Sloan-Kettering Cancer Center, New York, NY, USA).

Health Phys. (GB), vol.44, no.3, p.235-41 (March 1983). Detailed estimates of radiation absorbed dose based on solubility data and the distribution of body water and fat are presented for ^{19}Ne and ^{77}Kr , useful PET rCBF imaging agents. The steady-state inhalation of 75 mCi of ^{19}Ne and the bolus inhalation of 18 mCi of ^{77}Kr should result in comparable imaging statistics for typical protocols and lung radiation absorbed doses less than approx. 0.5 rad. A model for both steady-state and bolus inhalation techniques for soluble gases used for these radiation absorbed dose calculations is also presented. (18 refs.)

63973 Kerma transmission through steel for a p(66)Be(49) neutron beam: an update. R.K.Ten Haken, M.Awschalom, I.Rosenberg (Fermi Nat. Accelerator Lab., Batavia, IL, USA). *Health Phys.* (GB), vol.44, no.3, p.277-81 (March 1983). The measurements reported show that, in the design of a target shield for a therapeutic neutron beam source to be mounted on an isocentric gantry, considerable weight may be saved using 5 cm of polyethylene in place of 5 cm of steel, especially in the outer layers. Furthermore, for beam-off protection of medical personnel, the outer 2.5 cm of steel may be replaced with 2.5 cm of lead without significant loss of beam-on protection to the patient. (10 refs.)

63974 Dose calibrator response to brachytherapy sources: a Monte Carlo and analytic evaluation. J.F.Williamson (Dept. of Therapeutic Radiology, Univ. of Minnesota Hospitals, Minneapolis, MN, USA), R.L.Morin, F.M.Khan. *Med. Phys.* (USA), vol.10, no.2, p.135-40 (March-April 1983). It is well known that the dose calibrator response/unit exposure rate depends significantly upon source energy. However, investigation of ^{137}Cs , ^{192}Ir , and ^{226}Ra brachytherapy sources by empirical, analytical, and Monte Carlo techniques shows that source filtration significantly affects the calibrator reading to exposure rate conversion factor. The results demonstrate that for each clinically used filtration thickness an exposure calibrated standard source is required to establish the response of the well chamber. An interesting consequence of this analysis is that the Sievert point dose algorithm for clinical sources overestimates the dose on the order of 3% at distances of approximately 3.5 cm from the source. (19 refs.)

63975 The application of multiple scattering theory to therapeutic electron dosimetry. D.Jette (Dept. of Therapeutic Radiology, Rush-Presbyterian-St. Luke's Medical Center, Chicago, IL, USA), A.Pagnamenta, L.H.Lanzl, M.Rozenfeld. *Med. Phys.* (USA), vol.10, no.2, p.141-6 (March-April 1983). Fermi-Eyges multiple scattering theory for electrons is explained, and a general three-dimensional formalism is developed for its application to problems of therapeutic electron dosimetry. The formalism is illustrated by a number of elementary examples: a rectangular beam, an isotropic point source, and a scanning line source. (9 refs.)

63976 Absorbed dose determination for interstitial ^{125}I boost therapy. F.M.Waterman, K.A.Strubler (Dept. of Radiation Therapy & Nuclear Medicine, Thomas Jefferson Univ. Hospital, Philadelphia, PA, USA). *Med. Phys.* (USA), vol.10, no.2, p.155-9 (March-April 1983). Iodine-125 implants are being used to boost external beam treatments of unresectable pancreas and lung tumors. Calculations of the ^{125}I activity required to achieve a specific average peripheral dose are presented as a function of the average tumor dimension for spherical, ellipsoidal, and cylindrical implants. Both uniform and random seed spacings are investigated. The results indicate that the average peripheral dose is relatively insensitive to the seed distribution as well as to the seed activity. The average tumor dose is typically 20% greater than the average peripheral dose. (5 refs.)

63977 Some theoretical derivations relating to the tissue dosimetry of brachytherapy nuclides, with particular reference to iodine-125. R.G.Dale (Dept. of Medical Phys., Charing Cross Hospital, London, England). *Med. Phys.* (USA), vol.10, no.2, p.176-83 (March-April 1983). Using a Monte Carlo computer technique, tables of parameters have been derived which are of use in the dosimetry of brachytherapy nuclides in a variety of tissues and organs. From the results, it has been possible to derive relationships linking the composition of a tissue with the dose received at any location around an implanted source. Other factors, such as the relative importance of scattered radiation, spectral degradation, and integral dose, are also discussed. In particular, attention is drawn to possible dosimetric problems arising from the clinical use of ^{125}I . (26 refs.)

63978 Monte Carlo estimates of specific absorbed fractions for an I-125 point source in water. G.S.Burns, D.E.Raeside (Dept. of Radiological Sci., Univ. of Oklahoma Health Sci. Center, Oklahoma City, OK, USA). *Med. Phys.* (USA), vol.10, no.2, p.197-8 (March-April 1983). Monte Carlo estimates of eight specific absorbed fractions associated with an I-125 point source in water are presented for distances ranging from 1-10 cm. (6 refs.)

63979 A new approach to CT pixel-based photon dose calculations in heterogeneous media. J.W.Wong, R.M.Henkman (Dept. of Medical Biophys., Princess Margaret Hospital, Toronto, Ontario, Canada). *Med. Phys.* (USA), vol.10, no.2, p.199-208 (March-April 1983). The effects of small cavities on dose in water and the dose in a homogeneous nonunit density medium illustrate that inhomogeneities do not act independently in photon dose perturbation, and serve as two constraints which should be satisfied by approximate methods of computed tomography (CT) pixel-based dose calculations. Current methods at best satisfy only one of the two constraints and show inadequacies in some intermediate geometries. The authors have developed an approximate method that satisfies both these constraints and treats much of the synergistic effect of multiple inhomogeneities correctly. The method calculates primary and first-scatter doses by first-order ray tracing with the first-scatter contribution augmented by a component of second scatter that behaves like first scatter. Multiple-scatter dose perturbation values extracted from small cavity experiments are used in a function which approximates the small residual multiple-scatter dose. For a wide range of geometries tested, the authors' method agrees very well with measurements. The average deviation is less than 2% with a maximum of 3%. In comparison, calculations based on existing methods can have errors larger than 10%. (28 refs.)

63980 Quantitative determination of tolerance doses for preoperative and postoperative radiotherapy of bones. R.Datta (Dept. of Radiology, Louisiana State Univ. Medical Center, Shreveport, LA, USA), S.Saha. *Med. Phys.* (USA), vol.10, no.2, p.243-5 (March-April 1983). A method has been developed for the quantitative determination of the tolerance doses for preoperative and postoperative radiotherapy of bones in New Zealand white rabbits. The midshaft osteotomy was carried out on both ulnae

of each rabbit. Localized radiation of 2000, 3000, and 4000 rad (20, 30, and 40 Gy) was given in daily fractions of 500 rad to different groups of rabbits. The diaphyseal area of one forearm of each rabbit was irradiated and the other forearm was used as a control. After healing, the mechanical strength of each ulna was measured. The end point is defined as 'strength reduction dose-63' (SRD₆₃), i.e., the dose which would be expected to reduce the mechanical strength of the irradiated, fractured, and healed bone compared with the contralateral unirradiated diaphysis by 63%. The SRD₆₃s for preoperative and postoperative radiotherapy were 4350 rad (43.5 Gy) and 6200 rad (62 Gy), respectively, with a 500 rad (5 Gy)/fraction schedule. Through the use of the nominal standard dose (NSD) formula at 300 rad (3 Gy)/fraction and five fraction per week, these SRD₆₃s are equivalent to 5700 rad (57 Gy) and 8100 rad (81 Gy), respectively. (4 refs.)

63981 Surface doses for acrylic versus lead acrylic blocking trays for Co-60, 8-MV, and 17-MV photons. F.J.Bova, L.W.Hill (Div. of Radiation Therapy, Coll. of Medicine, Univ. of Florida, Gainesville, FL, USA). *Med. Phys. (USA)*, vol.10, no.2, p.254-6 (March-April 1983). Clear acrylic trays are commonly used on teletherapy units to support free-hand and custom-molded blocks for photon beam irradiation. While these trays have many desirable physical characteristics, they have the disadvantage of degrading the buildup region by contribution of low-energy electrons to the patient's surface. Recently, clear leaded acrylic has been introduced and suggested as a replacement for acrylic. The effect of the lead acrylic on the buildup region was investigated for cobalt-60, 8-MV, and 17-MV X-ray beams. The lead acrylic was found to decrease the surface dose compared to acrylic. Except for cobalt-60, the lead acrylic results in a higher dose than an open wire tray. (11 refs.)

63982 Calculation of low-energy neutron dose indices and depth doses in the ICRU tissue sphere. Y.-L.Shue, A.B.Chilton (Nuclear Engng. Program, Univ. of Illinois, Urbana, IL, USA). *Radiat. Res. (USA)*, vol.93, no.3, p.421-43 (March 1983). Detailed neutron dose distributions were calculated for the ICRU tissue sphere for broad, parallel beams of incident neutrons with 10 different energies ranging from thermal to 0.3 MeV. The calculation was carried out by the Monte Carlo method on the CYBER 175 computer of the University of Illinois. From these calculated data, a set of fluence-to-dose-index conversion factors, needed to establish the allowable limits for exposure to external neutron beams, was obtained. Normalized depth doses along the principal axis at depths of 0.007, 0.3, and 1.0 cm are also provided. The fluence-to-dose-index conversion factors are compared to previous conversion factors based on cylindrical phantoms, and any differences are explained. (21 refs.)

21st Annual Congress of the South African Association for Physicists in Medicine and Biology (papers in summary form only received) See Entry 59526
Reevaluations of Dosimetric Factors, Hiroshima and Nagasaki. Proceedings of a Symposium See Entry 59542

A low energy X-ray fluorescence method for high dose measurements on double emulsion photographic films See Entry 60475

Influence of light transmission on the response of LiF thermoluminescence detectors to thermal neutrons See Entry 60477

A polystyrene-water calorimeter See Entry 60478

Saturation curves of parallel-plate ionization chambers See Entry 60545

Biological effects of neutron radiation and their implications for the nuclear power industry See Entry 63890

Dose-effect relationships for induction of cell inactivation and asymmetrical chromosome exchanges in three cell lines by photons and neutrons of different energy See Entry 63900

Comments on 'An assessment of the role of microdosimetry in radiobiology' by Dudley T. Goodhead [Radiat. Res. 91, 45-76 (1982) [and reply] See Entry 63910

The formation of dose distributions in combined radiotherapy of patients with endometrial carcinoma See Entry 63927

Computerized program of the calculation of dose distribution formed with γ -radiation intracavity linear sources See Entry 63928

Evaluation of the efficacy of radiation therapy by means of a rated standard dose (RSD) under various conditions of irradiation See Entry 63929

The choice of geometric parameters in the optimization of irradiation of cancer patients See Entry 63930

The utilization of computer in the planning of radiotherapeutic volume for patients with oral tumors See Entry 63931

Characteristics of Mevatron 77 15-MV photon beam See Entry 63946

87.60P Radiation protection

(inc. radiation monitoring)

63983 Scientific and administrative bases of radiological protection. H.J.Dunster (Nat. Radiological Protection Board, Chilton, England). *Radiol. Prot. Bull. (GB)*, no.51, p.15-21 (March 1983).

Considers the question of how should, collectively, the proper level of exposure of a worker to ionising radiation be chosen. The author identifies how the scientific and social aspects of this question inter-relate, points out some of the more difficult issues and indicates a possible way forward. He considers the situation as it is today, with existing knowledge, existing problems and existing attitudes. (no refs.)

63984 Classification of radionuclides. K.B.Shaw (Nat. Radiological Protection Board, Chilton, England). *Radiol. Prot. Bull. (GB)*, no.51, p.22-3 (March 1983). Considers the classification scheme given in Annex 1 of the Euratom Directive of 15.7.80 (Off. J. Eur. Comm., no.L246/1). This classification is based on a scale of potential harmfulness. Another classification scheme, developed initially to provide numerical quantities for use in the designation of areas and in establishing quantities appropriate to the notification of incidents, is also considered (K.B. Shaw and S.A. Beach, NRPB report, to be published). (4 refs.)

21st Annual Congress of the South African Association for Physicists in Medicine and Biology (papers in summary form only received) See Entry 59526

2nd Special Symposium on the National Radiation Environment Indian Association for Radiation Protection (papers in summary form only received) See Entry 59527

Radiation and the Worker - Where do we go from Here? See Entry 59535

A simple modification to improve the energy dependence of ion chamber survey meters See Entry 60476

Biological effects of neutron radiation and their implications for the nuclear power industry See Entry 63890

Kerma transmission through steel for a p(66)Be(49) neutron beam: an update See Entry 63973

87.60R Radioactive pollution

(see also 86.70 Environmental science)

63985 ¹³⁷Cs content of deer: Savannah River Plant vs. South Carolina Coastal Plain herds. J.R.Watts, E.W.Rabon, A.S.Dicks (Savannah River Lab., E.I. du Pont de Nemours & Co., Aiken, SC, USA).

Health Phys. (GB), vol.44, no.3, p.272-4 (March 1983). The ¹³⁷Cs distribution of deer of both Savannah River Plant and the South Carolina Coastal Plain (SCCP) are qualitatively described by a log normal distribution. For the five years 1975-9 the SCCP means are higher at the 0.005 significance level for three years and at the 0.05 significance level for two years. It is postulated that the sterile, moist, sandy soils of the SCCP in combination with high water tables and some specific radionuclide-concentrating plants were the major factors resulting in high fall-winter accumulation of ¹³⁷Cs in meat of SCCP deer. (15 refs.)

Measurement of iodine-129 at the femtogram level by negative surface ionization mass spectrometry See Entry 60480

Measurements of the human anterior chest wall by ultrasound and estimates of chest wall thickness for use in determination of transuranic nuclides in the lung See Entry 63911

87.70 BIOMEDICAL ENGINEERING

63986 Characterization of the oscillographic method for measuring indirect blood pressure. L.A.Geddes, M.Voelz, C.Combs, D.Reiner, C.F.Babbs (Biomedical Engng. Center, Purdue Univ., West Lafayette, IN, USA). *Ann. Biomed. Eng. (USA)*, vol.10, no.6, p.271-80 (1982).

In this study, human subjects and dogs were used to determine the ability of the oscillographic method to indicate systolic and diastolic pressure. In the human studies, the auscultatory method was used as the reference. In the animal studies, directly recorded blood pressure was used as the reference. The ability of the sudden increase in cuff pressure oscillations during cuff deflation to indicate systolic pressure was examined and found to overestimate systolic pressure slightly in man, but more in animals. Systolic pressure was encountered when the cuff pressure oscillations were about one half of their maximum amplitude. However, in both man and animals the ratio was not constant; although the range was less in man than in animals. Diastolic pressure was encountered when cuff-pressure oscillation amplitude was about 0.8 of the maximal amplitude. This ratio for diastolic pressure was not constant over a range of diastolic pressure. The range of variability was less for man than for the dog. (13 refs.)

63987 The human tibia: static testing in bending by an in vivo method. I.D.Stein (US Veterans Administration Medical Center, East Orange, NJ, USA), G.Granik. *Ann. Biomed. Eng. (USA)*, vol.10, no.6, p.281-94 (1982).

Describes a method for static testing of the human tibia in bending in the living subject. A prototype device for carrying out the test has been fabricated. Model testing indicating that the device and model system are inherently accurate and reliable. However, the biological system is more complex, and while more than 200 tests have been conducted with perfect safety. The variability of replicate tests suggests that the method does not yet have general clinical utility. In some subjects, that variance is relatively small, possibly because they are more relaxed and perhaps also for anatomical reasons. In two subjects, postmortem tests correspond very well with antemortem tests on the tibiometer. It is concluded that with further refinements the method may have clinical potential, if only in carefully selected subjects. (11 refs.)

63988 A comparison of methods for measuring event-related potentials. E.Callaway, R.Halliday, R.I.Herning (Langley Porter Psychiatric Inst., Univ. of California, San Francisco, CA, USA).

Electroencephalogr. & Clin. Neurophysiol. (Netherlands), vol.55, no.2, p.227-32 (Feb. 1983).

Visual event-related potentials (ERPs) were recorded from 21 hyperactive children under 2 attention conditions (passive and active) and 4 doses of stimulant drug (methylphenidate). This data base was used to evaluate several methods of ERP component measurement. These methods were (1) conventional visual peak and trough selection; (2) automatic feature extraction based on peaks; (3) automatic feature extraction based on segments; (4) gross amplitude measures; (5) principal components analysis on normalized data and latency-adjusted data. No one method emerged as the best overall. Rather it is the case that different methods are best suited to different purposes, and criteria for choosing methods are outlined. (6 refs.)

63989 Laser etched bifilar fine wire electrode for skeletal muscle motor unit recording. R.M.Nelson (Dept. HHS, Nat. Inst. for Occupational Safety & Health, Morgantown, VA, USA), G.L.Soderberg. *Electroencephalogr. & Clin. Neurophysiol. (Netherlands)*, vol.55, no.2, p.238-9 (Feb. 1983).

To selectively record a limited number of skeletal muscle motor unit action potentials, a bifilar fine wire electrode was developed. Two 8 μ m fine wires were braided together, a hook formed, and ends insulated. A round beam pulsed laser etched a 5 μ m piece of insulation from each wire near the hooked end. Bipolar recordings from a select number of skeletal muscle motor units were obtained from these two uninsulated 5 μ m areas. Reactive and capacitative components for each set of electrodes were measured. These electrodes were selective in recording from 3 to 5 single motor unit action potentials at low isometric tension levels. (4 refs.)

63990 Nonlinear fluid systems identified by random noise input. E.Delavault, G.Saumont, R.Georges (Inst. Nat. de la Sante et de la Recherche Medicale, Hopital Xavier Bichat, Paris, France). *J. Appl. Physiol. (USA)*, vol.53, no.6, p.1643-9 (Dec. 1982). [received: April 1983]

The usual impedance measurement by Fourier analysis leads to undetectable errors when applied to nonlinear fluid systems where a nonlinear pressure drop $p=K.v^2$ adds to the linear pressure-flow relationship, but processing series of impedance data with various input levels allows the measurement of such systems. This new method has been tested on simulations, nonlinear resistances, and intubation tubings. It gives accurate estimates of the nonlinear coefficient K together with the true linear impedance of the measured system. This way, the usual respiratory impedance measurement may be applied to intubated patients, as the respiratory impedance of the subject can be separated from the linear behavior of the endotracheal tube or cannula. (23 refs.)

- 63991 A new method for measurement of respiratory resistance.** C.F.Shaw, S.T.Chiang, Y.C.Hsieh, J.Milic-Emili, C.Lenfant (Dept. of Physiology, Nat. Yang-Ming Medical Coll., Taipei, Taiwan). *J. Appl. Physiol. (USA)*, vol.54, no.2, p.594-7 (Feb. 1983).
A new method for measuring the resistance of the total respiratory system is presented. The method uses a device comprising a solenoid valve, a multiperforated plate, and a pneumotachograph. The multiperforated plate serves as a constant resistor (R_k) that is used to partially occlude the airway opening, thus rapidly and briefly reducing airflow during natural expiration. If it is assumed that the driving pressure remains constant during the very short period the airway is partially occluded, the respiratory flow immediately preceding the addition of R_k (V) and the flow reduction during partial occlusion (ΔV) allow calculation of the resistance of the total respiratory system. The resistance of 14 normal subjects and 18 patients with chronic obstructive pulmonary disease (COPD) was measured with this new method as well as with the body plethysmographic method: 90% of the interrupter values fell within ± 0.6 cm $H_2O \cdot l^{-1} \cdot s$ of the plethysmographic values, and all fell within ± 0.8 cm $H_2O \cdot l^{-1} \cdot s$. (11 refs.)
- 63992 Time series methods in the monitoring of intracranial pressure. II. Comparative study and initial assessment.** R.Allen (Dept. of Anaesthesia, Univ. of Leeds, Leeds, England). *J. Biomed. Eng. (GB)*, vol.5, no.2, p.103-9 (April 1983).
For pt.I see *ibid.*, vol.5, no.1, p.5-18, 1983. The primary objective of monitoring intracranial pressure (ICP) is to detect a reduction in brain compliance at an early stage in order to be able to initiate corrective therapy and thus ensure that an adequate cerebral perfusion is maintained. This paper describes studies aimed at assessing the value of several time series analysis techniques as a basis for a scheme of monitoring ICP. The theoretical foundations for this work were laid in pt.I. The paper begins with the outline of a suite of computer programs that were written to implement the techniques selected. Early results from studies with the programs are presented and the discussion is directed towards explaining practical aspects and limitations of the methods that were experienced. It is concluded that the most promising avenue for future development is the use of a dynamic linear model with a recursive parameter estimator within an adaptive framework. The direction of this future work is presented. (19 refs.)
- 63993 Static response of a simple piezoelectric load cell [biomechanical applications].** M.Lord, D.M.Smith (Bioengng. Centre, Univ. Coll. London, London, England). *J. Biomed. Eng. (GB)*, vol.5, no.2, p.162-4 (April 1983).
The design of a simple load cell is presented. The cell is based on piezoelectric methods employing charge amplification, and such a system inevitably results in DC drift. The optimization of the drift characteristics to yield quasistatic operation is discussed. (1 ref.)
- 63994 Complications of and improvements to breathing circuit monitors for anaesthesia ventilators.** J.A.McEwen, L.C.Jenkins (Vancouver General Hospital, Vancouver, Canada). *Med. Instrum. (USA)*, vol.17, no.1, p.70-4 (Jan.-Feb. 1983).
Despite significant improvements in the safety of anesthetic equipment in recent years, disconnection in the patient breathing circuit remains one of the most common types of preventable anesthetic mishaps. Many currently available breathing-circuit monitors cannot reliably detect several hazardous conditions in the breathing circuit. An improved breathing circuit monitor has been developed that reliably detects realistic simulations of many hazardous conditions. The software algorithm in this monitor stores the normal pressure waveform in the patient circuit, evaluates the ongoing waveform in terms of sets of absolute and relative criteria, and warns the operator when such criteria are not satisfied. A comprehensive technical and clinical evaluation is underway. (9 refs.)
- 63995 A device to quantify passive resistance to motion of the leg.** G.F.Harris, S.J.Larson, A.Sances,Jr., D.C.Hemmy (Medical Coll. of Wisconsin, Milwaukee, WI, USA), E.A.Millar. *Med. Instrum. (USA)*, vol.17, no.1, p.75-8 (Jan.-Feb. 1983).
A device has been developed to quantify passive resistance to motion of the leg in both ambulatory and nonambulatory subjects. This device was used to monitor the progress of 11 children with cerebral palsy, who received chronic cerebellar implants for the relief of hypertonus. (13 refs.)
- Comparison of electrical field plethysmography with electrical impedance plethysmography** See Entry 63914
- Monitoring of movement with radio frequency transducers** See Entry 63915
- Pseudoisochromatic plate design—Macbeth or tungsten illumination?** See Entry 63916
- Combined flow cytometry and image cytometry of the same cytological sample** See Entry 63920
- Feasibility of noninvasive analysis of lead in the human tibia by soft X-ray fluorescence** See Entry 63948
- A versatile localization system for microscopic multiparametric analysis of cells** See Entry 64014

87.70E Diagnostic methods and instrumentation

(see also 87.60 Medical and biomedical uses of fields, radiations and radioactivity)

- Elemental analysis performed with the Karlsruhe nuclear microprobe** See Entry 63611
- On-line analysis of the femoral artery flow velocity waveform and its application in the diagnosis of arterial disease** See Entry 63912
- Clinical nuclear magnetic resonance imaging** See Entry 63918
- Initial clinical evaluation of whole body nuclear magnetic resonance (NMR) tomograph** See Entry 63919
- The possibilities offered by infrathermography for the diagnosis of the Raynaud phenomenon of vibrational origin** See Entry 63921
- Microfluorometer for medical studies** See Entry 63923
- Two-dimensional reconstructions from one-dimensional data by maximum entropy** See Entry 63925
- Simulation of the organ blood flow in computer γ -scintigraphy** See Entry 63934
- PETT VI: a positron emission tomograph utilizing cesium fluoride scintillation detectors** See Entry 63935
- Dynamic computed tomography through interpolation** See Entry 63936
- Technical aspects of digitization X-ray image processing, especially digital subtraction angiography** See Entry 63937

- 'Native' computed tomography: a new radiological approach of the herniated lumbar disk** See Entry 63938
- Single photon emission computerized tomography: a new dimension in nuclear medicine-system characterization** See Entry 63939
- Functional imaging of the brain** See Entry 63940
- The effects of misregistration of the projections on spatial resolution of CT scanners** See Entry 63942
- The technical characteristics of matched filtering in digital subtraction angiography** See Entry 63943
- A detailed experimental and theoretical comparison of the angular and energy dependencies of grid transmission** See Entry 63944
- A regularized iterative algorithm for limited-angle inverse Radon transform** See Entry 63952
- Geometric deconvolution of artifacts in limited view computed tomography** See Entry 63953
- Localization from projections based on detection and estimation of objects** See Entry 63954
- Tomographic imaging with limited view angle using an expansion on a set of eigenfunctions adapted to space-limited objects** See Entry 63955
- Linear estimation with a size constraint** See Entry 63956
- Bayesian approach to limited-angle CT reconstruction** See Entry 63957
- The use of a priori information in image reconstruction from limited data** See Entry 63958
- Incorporation of prior constraints in tomographic reconstructions from coded images** See Entry 63959
- Inverse scattering reconstructions from incomplete Fourier space data** See Entry 63960
- Deblurring and three-dimensional reconstruction from multiple linear-tomograms** See Entry 63961
- Radiation absorbed dose estimates for positron emission tomography (PET): inert gases ^{19}Ne and ^{77}Kr** See Entry 63972

87.70G Patient care and treatment

- 63996 Functional stimulation—instrumentation and clinical relevance.** T.M.Srinivasan, K.Srinivasa Rao (Biomedical Engng. Div., Indian Inst. of Technol., Madras, India). *CSIO Commun. (India)*, vol.9, no.1, p.22-9 (Jan.-March 1982). [received: March 1983]
Functional electrical stimulation (FES) is accepted as a proven method of rehabilitation in various conditions of central and peripheral nervous system defects. Thus stimulation of cerebral and cerebellar cortex for prosthetic and postural rehabilitation, stimulation of cardiac muscles, phrenic nerve, spinal motor pool for bladder control, drop foot and related conditions etc. have become a clinical reality. The author deals with an electric peroneal brace used for correction of drop foot and clinical evaluation procedures for assessing the parameters and improvements in gait. This corrective method enables long term rehabilitation due to the apparent ability of central neurons to relearn this lost function. (11 refs.)
- 63997 A pressure curve monitor for intratracheal jet ventilation.** G.A.Baer, J.A.Malmivuo, P.P.Talonen (Electronics Lab., Tampere Univ. of Technology, Tampere, Finland). *J. Biomed. Eng. (GB)*, vol.5, no.2, p.134-6 (April 1983).
Most of the complications during intratracheal jet ventilation for laryngomicroscopy are due to the unnoticed wearing off of laryngeal muscle relaxation. Recovering laryngeal muscle function will, by slightly narrowing the size of the glottis, influence the slope of the quickly rising part of the pressure curve, when influences on maximum airway pressure are still not detectable. An electronic device incorporating the window comparator technique monitors the pressure curve and sets off an alarm before changes in maximum airway pressure or recovery of muscle strength in the forearm are detectable. The pressure curve monitor could be useful also with intratracheal jet ventilation for treating adult respiratory deficiency and with conventional ventilators during anaesthesia to detect the wearing off of muscle relaxation. (9 refs.)
- 63998 A battery powered constant current stimulator.** K.M.Jackson, H.T.Denyer (Dept. of Phys., Guy's Hospital Medical School, London, England). *J. Biomed. Eng. (GB)*, vol.5, no.2, p.165-6 (April 1983).
A versatile portable, constant current stimulator is described. The low active component count (2 CMOS integrated circuits, 5 transistors), and internal batteries make it a low cost safe design. Inadvertent false operations are detected by an LED which illuminates when the desired stimulus current has not been delivered. (no refs.)
- 63999 Effect of defibrillation energy on pacing threshold.** L.Rubin (Tuxedo Memorial Hospital, New York, NY, USA), P.Hudson, J.Driller, L.Dick, A.Villanueva. *Med. Instrum. (USA)*, vol.17, no.1, p.15-17 (Jan.-Feb. 1983).
After an episode of electrical defibrillation, periods of increased pacing threshold may cause lack of pacing in pacemaker patients. This effect is independent of the energy applied during defibrillation, although the data suggest that the most rapid return to predefibrillation pacing thresholds occurs after minimal energy countershocks. (7 refs.)
- 64000 Effects of myocardial infarction on catheter defibrillation threshold.** C.F.Babbs, R.L.Paris, W.A.Tacker,Jr., J.D.Bourland (Biomedical Engng. Center, Purdue Univ., West Lafayette, IN, USA). *Med. Instrum. (USA)*, vol.17, no.1, p.18-20 (Jan.-Feb. 1983).
Changes in ventricular defibrillation threshold following coronary occlusion were determined, using an electrode catheter designed for use with an automatic implantable defibrillator. Acute myocardial ischemia was produced without thoracotomy in 10 dogs (experimental group) by embolization with a plastic bead injected via a catheter into the left coronary artery. A control group of 4 dogs had only saline injected into the artery. Defibrillation threshold was measured at 15-min intervals from 1 hour before embolization to 2 hours after embolization. In the control group, voltage, current, energy, and impedance were unchanged after injection of saline into the coronary artery, and india ink perfusion revealed no ischemic areas. In the experimental group postembolization threshold current and energy were significantly higher than pre-embolization values: 0.47 vs. 0.40 A/kg and 1.01 vs. 0.80 J/kg, respectively ($p < 0.01$). The magnitude of the peak change in threshold current after embolization was positively correlated ($r = 0.79$) with the size of the ischemic zone, determined by weighing unstained areas after india ink perfusion. Defibrillation threshold for a catheter electrode configuration increased for at least 2 hours following onset of acute myocardial ischemia. This finding must be

- accounted for in the design and use of an automatic implantable defibrillator. (8 refs.)
- The state and prospects in the development of the medical proton tract on the synchrocyclotron in Gatchina See Entry 60499
- Bubble dissolution physics and the treatment of decompression sickness See Entry 63885
- Mathematical model of normal tissue injury in γ -beam therapy See Entry 63899
- Human navigation by sound See Entry 63913
- Equipment for the clinical application of local microwave hyperthermia See Entry 63922
- CO₂ laser scalpel See Entry 63924
- The implementation of a radiotherapeutic plan for patients with oral tumours in the moving field irradiation regimen See Entry 63926
- The formation of dose distributions in combined radiotherapy of patients with endometrial carcinoma See Entry 63927
- Computerized program of the calculation of dose distribution formed with γ -radiation intracavity linear sources See Entry 63928
- Evaluation of the efficacy of radiation therapy by means of a rated standard dose (RSD) under various conditions of irradiation See Entry 63929
- The choice of geometric parameters in the optimization of irradiation of cancer patients See Entry 63930
- The utilization of computer in the planning of radiotherapeutic volume for patients with oral tumors See Entry 63931
- The utilization of time-dose-fractionation models in the planning of tumor radiotherapy See Entry 63932
- Prevention of radiation injuries during multifractionation in radiation therapy See Entry 63933
- Physical aspects of a rotational total skin electron irradiation See Entry 63941
- Characteristics of Mevatron 77 15-MV photon beam See Entry 63946
- A study of problems with inventory control of I-125 seeds See Entry 63949
- Repair of the energy slit on an AECL Therac-20 accelerator See Entry 63950
- Comments on 'radiation leakage from electron applicator assembly on a linear accelerator' [and reply] See Entry 63951
- Dosimetric substantiation of mean fractionation during irradiation of bone metastases of breast carcinoma See Entry 63964
- Dosimetric characteristics of thermoluminescent detectors for inhibitory and electron radiation of a betatron BSM-25 See Entry 63968
- Time dose distribution in radiation therapy planning See Entry 63970
- Kerma transmission through steel for a p(66)Be(49) neutron beam: an update See Entry 63973
- Dose calibrator response to brachytherapy sources: a Monte Carlo and analytic evaluation See Entry 63974
- The application of multiple scattering theory to therapeutic electron dosimetry See Entry 63975
- Absorbed dose determination for interstitial ¹²⁵I boost therapy See Entry 63976
- Some theoretical derivations relating to the tissue dosimetry of brachytherapy nuclides, with particular reference to iodine-125 See Entry 63977
- Monte Carlo estimates of specific absorbed fractions for an I-125 point source in water See Entry 63978
- A new approach to CT pixel-based photon dose calculations in heterogeneous media See Entry 63979
- Quantitative determination of tolerance doses for preoperative and postoperative radiotherapy of bones See Entry 63980
- Surface doses for acrylic versus lead acrylic blocking trays for Co-60, 8-MV, and 17-MV photons See Entry 63981

87.70J Prosthetics and other practical applications

- 64001 A comparative study of tear evaporation rates and water content of soft contact lenses. T.H.Cedarstaff, A.Tomlinson (Indiana Univ., School of Optometry, Bloomington, IN, USA). *Am. J. Optom. & Physiol. Opt. (USA)*, vol.60, no.3, p.167-74 (March 1983). Tear evaporation rates were measured by resistance hygrometry in a group of five subjects wearing soft contact lenses ranging in initial water content from 38 to 70%. The water content of the lenses before and after wear was measured by a 'wet blot weighing' technique using a chemical balance. The placing of all types of soft lenses on the eye disrupts the tear film sufficiently to produce significant increases in evaporation. This increase in tear evaporation was not found to be related to the initial water content of the soft lens. Water lost by dehydration of the lens material made a relatively minor contribution to the increase in evaporation from the eye during lens wear. (14 refs.)
- 64002 Studies on the stress behaviour in the bone/cement interface in total hip replacement. D.Gebauer, W.Winter, H.Hager (Inst. für Sporttraumatologie, Tech. Univ. München, München, Germany). *Biomed. Tech. (Germany)*, vol.28, no.4, p.79-83 (April 1983). In German. Numerous studies on the problem of aseptic loosening in total hip replacement reveal the importance of biomechanical overloading in the interface between bone and cement. Since there are no measured data on the stresses present in the interface, the authors attempted to obtain initial information on the stress situation in the cup and the interface by means of a two-dimensional simulation model. The experiments showed that the interface is loaded by relatively high traction and shearing stresses which can be explained by the deformation of the bone-simulation model. These stresses might play a significant part in the cup-loosening process, quite apart from the shearing stresses induced by joint friction. (2 refs.)
- 64003 Adaptive microcomputer control of an artificial knee in level walking. A.Bar, G.Ishai, P.Meretsky, Y.Koren (Julius Silver Inst. for Biomedical Engng., Technion, Haifa, Israel). *J. Biomed. Eng. (GB)*, vol.5, no.2, p.145-50 (April 1983). An experimental microcomputer controlled prosthesis is discussed, where knee damping is governed by kinematic signals, picked up from both legs. The control algorithm is based on division of the walking cycle into ten stages; each stage characterized by an appropriate damping level which governs the restraining moment at the knee, as functionally required. Stage identification is carried out by the kinematic inputs. The experimental prosthesis was tested on one amputee, the first author of this paper. The control system was found

to be more advantageous than a conventional valve system in significantly reducing hip muscular effort on the prosthetic side. Gait symmetry is also improved. (10 refs.)

- Effect of conicoid asphericity on the Tscherning ellipses of ophthalmic spectacle lenses See Entry 61252
- A comparison of the SACH and single axis foot in the gait of unilateral below-knee amputees See Entry 63886
- Effects of alignment variables on thigh axial torque during swing phase in AK amputee gait See Entry 63887
- Construction, specification, and mathematical description of aspheric surfaces See Entry 63917

87.80 BIOPHYSICAL INSTRUMENTATION AND TECHNIQUES

- 64004 Simple computer method for evaluation of lateral diffusion coefficients from fluorescence photobleaching recovery kinetics. E.J.J.Van Zoelen, L.G.J.Tertoolen, S.W.de Laat (Hubrecht Lab., Internat. Embryological Inst., Utrecht, Netherlands). *Biophys. J. (USA)*, vol.42, no.1, p.103-8 (April 1983). A method is presented for the analysis of fluorescence photobleaching recovery curves. Based on the simplified kinetic expression of J. Yguerabide et al. (see *ibid.*, vol.40, p.69-75, 1982), a linearization procedure is described that permits unequivocal determination of all diffusion parameters. The presence of additional membrane flow or multiple diffusion coefficients can easily be detected by this method, and simple corrections for the presence of these alternative recovery processes can be made by the use of a regular mini-computer. The validity of the method is tested on simulated recovery curves, varying the contribution of flow, multiple diffusion coefficients, and statistical noise due to counting error. (9 refs.)
- 64005 Studying microbial growth processes with a microcomputer. K.F.Thompson, T.M.Roberts (Dept. of Chem., Bedford Coll., London, England). *Lab. Microcomput. (GB)*, vol.1, no.3, p.11-14 (Autumn 1982). Describes a system based on the Research Machines RML 380Z microcomputer to collect data on energy changes associated with microorganism growth, analyse the data, and produce output on cassette tape or line printer. Data acquisition is carried out in Z80 machine-code, while analysis is performed using BASIC programs. (no refs.)
- 64006 A new system for ventilating with high-frequency oscillation. Y.K.Ngeow, W.Miltzner (Dept. of Anesthesiology & Critical Care Medicine, Johns Hopkins Univ., Baltimore, MD, USA). *J. Appl. Physiol. (USA)*, vol.53, no.6, p.1638-42 (Dec. 1982). [received: April 1983] Describes simple high-frequency oscillation systems that incorporate a CO₂ absorber and supply O₂ on a need basis. These systems have the advantage of easy control of mean airway pressure and airway hydration and negligible loss of oscillatory tidal volume. Experiments done at constant tidal volume showed that as frequency (and hence total ventilation) increased, arterial CO₂ tension Paco₂ decreased. The fall in Paco₂ occurred until frequency reached approximately 20 Hz; above 20 Hz further increases in frequency had little or no effect on Paco₂. Because of their practical advantages the techniques described here may be quite useful in a clinical setting where an oscillator, rather than jet-type high-frequency, ventilation system is desired. (11 refs.)
- 64007 A feedback system to control blood flow in dog lung lobes. R.E.Brake, D.K.Adcock, R.L.Scott, J.C.Gabel (Dept. of Anesthesiology, Univ. of Texas Medical School, Houston, TX, USA). *J. Appl. Physiol. (USA)*, vol.53, no.6, p.1650-2 (Dec. 1982). [received: April 1983] An electromechanical feedback system has been developed to control blood flow to the lower left lung lobe of dogs. Blood flow is measured with an electromagnetic flowmeter. The feedback system compares the blood flow signal to an adjustable reference voltage and causes a motor to turn. The direction of motor rotation depends on the relative magnitude of the flow signal and the reference. The motor pushes the plunger or a syringe that is attached to a balloon in the right pulmonary artery. Inflation of the balloon causes increased blood flow to the lower left lobe. The authors have used the system to control lobe blood in three dogs. (2 refs.)
- 64008 Automated techniques for the study of lung alveolar stereological parameters with the IBAS image analyser on optical microscopy sections. J.P.Rigaut (Lab. de Biologie du Dev., UER Experimentale Biomedicale de Bobigny-Paris Nord, Bobigny, France), P.Berggren, B.Robertson. *J. Microsc. (GB)*, vol.130, pt.1, p.53-61 (April 1983). In the case of lung alveoli, the good contrast of the features allows the use of a fully automated image analysing procedure, yielding many of the desirable stereological parameters which can be estimated on optical microscopy slides: alveolar volume and surface densities, a form factor and average mean integral curvature. With the authors' program, specially designed for the IBAS image analyser (Kontron Bildanalyse, Munich, BRD), the whole automated process takes an average of 28 s per field. The image analyser-obtained stereological estimates compare well with those given by point and intersection counting methods. Some difficulties inherent in image analysers arise when measuring alveolar boundary lengths: a scheme is therefore proposed which eliminates the image-edge errors, with no sampling bias, by comparing three different frames inside each field. A solution to the problem of estimating automatically the positive and negative tangent counts, necessary for the curvature calculations, is also proposed. The authors' program has been applied routinely to the study of premature newborn rabbit lung alveoli, as part of a study dealing with an evaluation of the possibility of preventing the respiratory distress syndrome by the administration of heterologous surfactant. (32 refs.)
- 64009 The correlation of light and electron microscope observations. W.T.Perrie, D.M.Webb (Wolf Neuropathology Labs., Midland Centre for Neurosurgery & Neurology, Warley, England). *J. Microsc. (GB)*, vol.130, pt.1, p.73-7 (April 1983). A technique is described to allow electron microscopic investigation of a specific feature of a section on a glass slide. A section on a glass slide (previously treated with a silicone release agent) is processed as required for light microscopy. The section is then impregnated with Araldite and cured with an epoxy resin block on top of it. The section and block are removed from the side and viewed with a light microscope. The selected area for ultrastructural study remains under continuous observation while the block is trimmed. Semi-thin (1 μ m) sections retain the original staining for light microscopy and ultra-thin sections are stained with heavy metals in the normal manner. The authors show how an inflammatory lesion in a large area of muscle in a case of polymyositis may be quickly located and studied at the ultrastructural level. (14 refs.)

64010 A routine flat embedding method for electron microscopy of microorganisms allowing selection and precisely orientated sectioning of single cells by light microscopy. O.L.Reymond, J.D.Pickett-Heaps (Dept. de Biologie Vegetale, Univ. de Geneve, Geneve, Switzerland). *J. Microsc. (GB)*, vol.130, pt.1, p.79-84 (April 1983).

A simple method is described to embed material in resin, in the form of microscope slides, to observe it with high resolution light microscopy, to select, orient and section it for TEM. This method can be applied to many kinds of material but is particularly useful for the study of rare or tiny plant or animal microorganisms from field or culture. A diamond scribe, translucent hydrosoluble resin release agent, translucent and smooth resin stubs and a longitudinally perforated block-holder for ultramicrotome are the specific tools of this method. (11 refs.)

64011 BSE Z contrast imaging of uranium stained pores in the avian eggshell. H.Silyn-Roberts (Dept. of Zoology, Univ. of Auckland, Auckland, New Zealand).

J. Microsc. (GB), vol.130, pt.1, p.111-14 (April 1983).

A method is described for estimating the number of blocked pore channels and pore density and spatial distribution by the staining of the exterior pore openings of unobstructed pores with uranyl acetate, and identification of them using backscattered electron atomic number contrast imaging in the scanning electron microscope. (9 refs.)

64012 Enhancement of contrast in living and fixed specimens by the use of fibre optics. A.M.C.Burgess (Dept. of Anatomy & Histology, London Hospital Medical Coll., London, England).

J. Microsc. (GB), vol.130, pt.1, p.123-4 (April 1983).

A method is described which enhances the contrast of living and fixed specimens examined with the stereomicroscope. It consists of immersing the ends of flexible fibre optic light sources together with the specimen in the fluid used for examination. It is reported that not only does this method increase the contrast of living specimens but that it may also be applied to specimens being prepared as thin sections of freeze fracture surfaces for examination with the transmission electron microscope. A further method of enhancement of contrast is suggested which involves the fitting of light filters of complementary colours, one to each of the fibre optic light sources, before immersion with the specimen. (3 refs.)

64013 Measurement of cardiac pressure-length loops using an improved sonomicrometer. Accuracy and effect of respiration. K.Matre, J.Lekven (Surgical Res. Lab., Univ. of Bergen, Bergen, Norway).

J. Biomed. Eng. (GB), vol.5, no.2, p.110-16 (April 1983).

A transit-time sono-micrometer for measurement of myocardial dimensions is described. Crystals of frequencies 1-10 MHz can be used, enabling a large range of distances to be measured. The meter has two channels, operated in sequence to avoid interference between channels. By combining local muscle segment length with the left ventricular pressure in open-chest cats, the pressure-length loop for that segment was continuously displayed. A calibration procedure was developed, permitting calibration to be registered on a recorder and on a storage monitor at any time. Detailed interpretation of loops from normal and ischaemic segments of the left ventricle is presented. Variation of the loop form with respiration is demonstrated, which clearly necessitates a standardized reference point in the respiratory phase for comparing loops from two or more experimental situations. (16 refs.)

64014 A versatile localization system for microscopic multiparametric analysis of cells. H.H.Thaw, I.Rundquist, U.Johnsson, I.Svensson, V.P.Collins (Dept. of Pathology II Univ. of Linköping, Linköping, Sweden).

Microsc. Acta (Germany), vol.87, no.2, p.159-67 (March 1983).

A new, simple and relatively inexpensive electronic digital position readout (DPRO) system which can be applied to the rapid localization and recovery of microscopic material is described. It is based upon a commercially available digital position readout system which is routinely utilized by industry for small machine tools and measuring equipment. This has been mounted onto the stage of various microscopic instrumentation to provide X and Y coordinates relative to an arbitrary reference point. The integration of small computers interfaced to scanning interferometric, microdensitometric and fluorescence microscopes were used to demonstrate the reliability, versatility and ease of application of this system to problems of multiparametric measurements and analysis of cultured cells. The system may be expanded and applied to clinical material to obtain automatized, multiparametric measurements of cells in hematology and clinical cytology. (15 refs.)

64015 Biological applications of picosecond spectroscopy. E.F.Hilinski, P.M.Rentzepis (Bell Labs., Murray Hill, NJ, USA).

Nature (GB), vol.302, no.5908, p.481-7 (7 April 1983).

Technological advances in picosecond spectroscopy have permitted the mechanisms of various chemical, physical and biological processes to be elucidated and understood to a greater degree than ever before. By means of picosecond emission, absorption and Raman spectroscopy, one can probe and measure directly the transient intermediates and kinetics of primary events in complex biological processes. A description of two current types of laser systems—solid-state and synchronously pumped dye lasers—and their application to determining the primary events in the biological processes of dissociation of oxy- and carboxymyoglobin, excited-state relaxation of porphyrins and visual transduction, illustrate the power of picosecond spectroscopy. (47 refs.)

64016 A new method of scanning electron microscopy for imaging biological tissues. A.Boyd, S.A.Reid (Dept. of Anatomy & Embryology, Univ. Coll. London, London, England).

Nature (GB), vol.302, no.5908, p.522-3 (7 April 1983).

Reports a method by which histological sections mounted on glass slides can be imaged in the SEM at a resolution higher than that obtained using conventional light microscopy. The method exploits the facts that the ordinary, cheap light microscope slide is strongly cathodoluminescent, yet the standard histological (7 μ m) section is of such a mass thickness that it absorbs a significant proportion of electrons with energies (5-20 keV) usually used in biological SEM. Thus the measure of the glass cathodoluminescence signal is the measure of the electron flux passing through the specimen. (1 ref.)

64017 Detection of signal of rapid eye movements. M.Nishikawa, N.Ishii, A.Iwata, N.Suzumura (Faculty of Engng., Nagoya Inst. of Technol., Nagoya, Japan).

Trans. Inst. Electron. & Commun. Eng. Jpn. Part D (Japan), vol.J66D, no.1, p.33-40 (Jan. 1983). In Japanese.

Signals of rapid eye movements show the state of a sleeping stage called REM. Differential operations with smoothing are effective in the extraction of the signals. First, to remove noise from the data of the rapid eye movements, the authors developed a Wiener filtering method, which extracts the reciprocal phase signals of the movements. Second, they applied a correlation method, which characterized the negative correlation of the movements. The latter method was found to be useful in the signal detection of the movements. (8 refs.)

64018 Observation and simulation of unstained DNA images in bright field TEM. C.Quintana (Unité de Recherche, INSERM, Paris, France), N.Bonnet.

Ultramicroscopy (Netherlands), vol.10, no.3, p.253-61 (1982).

Images of unstained, unshadowed DNA prepared by the Kleinschmidt method have been obtained in bright field TEM with a usable contrast. Operating conditions include a strong defocus and a highly coherent illuminating beam. Observations suggest that a specific interaction exists between the nucleic acid and the carrier protein: cytochrome C. Computer simulations of beam-specimen interaction and of image formation were performed. The calculated dependence of contrast on defocus agrees qualitatively with the experimental results. The authors conclude that experiments with unstained biological specimens are feasible and are necessary (in spite of difficulties) to corroborate results obtained with stained material. (30 refs.)

Saturation transfer dispersion electron paramagnetic resonance using a balanced cavity: dynamical calibration and biological applications

.....See Entry 59808

Generation of femtosecond intense optical pulses and applications to time resolved spectroscopy

.....See Entry 61199

Trace element mapping of biological tissues using PIXE and XRF

.....See Entry 63615

Measurements of trace element concentration profiles across the diameter of human hair with micro-PIXE

.....See Entry 63616

The mechanism of crystallization of proteins in an ultracentrifuge

.....See Entry 63782

87.90 OTHER TOPICS IN BIOPHYSICS, MEDICAL PHYSICS, AND BIOMEDICAL ENGINEERING

64019 At what wavelengths should we search for signals from extraterrestrial intelligence? C.H.Townes (Univ. of California, Berkeley, CA, USA).

Proc. Natl. Acad. Sci. USA, vol.80, no.4, p.1147-51 (Feb. 1983).

It has often been concluded that searches for extraterrestrial intelligence (SETI) should concentrate on attempts to receive signals in the microwave region, the argument being given that communication can occur there at minimum broadcasted power. Such a conclusion is shown to result only under a restricted set of assumptions. If generalized types of detection are considered—in particular, photon detection rather than linear detection alone—and if advantage is taken of the directivity of telescopes at short wavelengths, then somewhat less power is required for communication at infrared wavelengths than in the microwave region. Furthermore, a variety of parameters other than power alone may be chosen for optimization by an extraterrestrial civilization. Hence, while partially satisfying arguments may be given about optimal wavelengths for a search for signals from extraterrestrial intelligence, considerable uncertainty must remain. (6 refs.)

90.00 GEOPHYSICS, ASTRONOMY AND ASTROPHYSICS

91.00 SOLID EARTH GEOPHYSICS

91.10 GEODESY AND GRAVITY

(for relations of gravity observations to tectonics and isostasy, see 91.45 Physics of plate tectonics)

64020 Time adjustment on 1983 June 30.

I.A.U. Circ. (USA), no.3790, 1 pp. (7 April 1983).

It is announced that a positive leap second will be introduced on 1983 June 30 such that the sequence of UTC second markers will be: 1983 June 30^d23^h59^m59^s, 30^d23^h59^m60^s, July 1st00^h00^m00^s. From 1982 July 1 to 1983 June 30 the difference UTC-TAI=-21^s, beginning 1983 July 1, UTC-TAI=-22^s. (no refs.)

64021 Earth measurement as part of a unified geodesy—foundations, state-of-the-art, and trends of development. G.W.Hein.

Z. Vermessungswes. (Germany), vol.108, no.3, p.93-104 (March 1983). In German.

After reviewing the main goals of geodesy, the determination of the figure of the Earth is considered mathematically within the framework of an integrated or operational model determining in one unified approach three-dimensional geocentric coordinates as well as the functionals of the gravity potential (geoid, deflections of the vertical, etc.). Current geodetic measurement techniques and new techniques likely to come into use soon are considered. The state-of-the-art of accuracy, resolution and other parameters is discussed. Trends and prospects of future geodetic technology are considered. (26 refs.)

64022 The choice of the datum of a trigonometric net for interpolation of points. K.R.Koch.

Z. Vermessungswes. (Germany), vol.108, no.3, p.104-11 (March 1983). In German.

The definition of a datum for a geodetic network in the case of a densification by additional points is discussed. The datum should be established such that the trace of the covariance matrix of the estimated coordinates of the additional points and of the points of the network connected with the additional points becomes minimal. It is shown that such a datum can be readily obtained by means of the matrix which contains a basis of the nullspace of the coefficient matrix for the model of the parameter estimation. The choice of such a datum is demonstrated by an example. (7 refs.)

Crustal deformation studies and earthquake prediction research

.....See Entry 64076

Neotectonic deformation, near-surface movements and systematic errors in US releveing measurements: implications for earthquake prediction

.....See Entry 64077

A geophysical approach to the granite batholith under the eastern Southern Uplands, Scotland

.....See Entry 64090

- Crustal structure of the Molucca Sea collision zone, Indonesia** See Entry 64097
- Discrimination of tectonic displacement from slope-dependent errors in geodetic leveling from southern California, 1953-79** See Entry 64212
- Height dependent errors in southern California leveling** See Entry 64122
- Earthquake prediction program in Japan** See Entry 64240
- Comparison of Earth rotation as inferred from radio interferometric, laser ranging and astrometric observations** See Entry 64265
- Expendable bubble tiltmeter for geophysical monitoring** See Entry 64270
- On the choice of artificial satellites by their optimal location data for studying the Earth's rotation** See Entry 64337
- Optimization of equatorial transfer orbit with due regard for atmospheric drag** See Entry 64358

91.25 GEOMAGNETISM AND PALAEOMAGNETISM; GEOELECTRICITY

64023 Annual report for magnetic observatories—1980. G.Jansen van Beek, R.L.Coles (Earth Phys. Branch, Energy, Mines & Resources Canada, Ottawa, Canada). *Geomagn. Ser. Earth Phys. Branch (Canada)*, no.23, p.1-90 (1983). In English, French.

In 1980, the Earth Physics Branch operated a network of 12 magnetic observatories. Several variation stations were also operated for parts of the year. The author describes the station sites, the instrumentation and the methods of data reduction and distribution. (15 refs.)

64024 On the resolving power of the VLF method. V.Bezvoda (Faculty of Sci., Charles Univ., Czechoslovakia), K.Segeth. *Pure & Appl. Geophys. (Switzerland)*, vol.120, no.2, p.348-64 (1982). The mathematical tools, used for the modelling of the electromagnetic field of the harmonic plane wave in the two-dimensional inhomogeneous medium (the case of *E*-polarization), are presented. Further, the resolving power of some parameters, that are measured in the VLF and VLF-R methods, is compared in the case of two vertical conductive dykes. To this aim, all the usual parameters of the VLF method and the most important parameter of the VLF-R method (ρ_n) have been chosen. Two groups of models that differ in resistivities have been considered. In each of the groups the distance of the dykes is variable. The parameters $|H_z|$, which has shown most promising in this respect, is examined also from the point of view of the sensibility to geological noise. The results of the modelling are illustrated by two examples of the results of field measurements. (15 refs.)

64025 A Fourier transform method for the interpretation of self-potential anomalies due to two-dimensional inclined sheets of finite depth extent. D.Atchuta Rao, H.V.Ram Babu, G.D.J.Sivakumar Sinha (Nat. Geophys. Res. Inst., Hyderabad, India). *Pure & Appl. Geophys. (Switzerland)*, vol.120, no.2, p.365-74 (1982). The self-potential anomaly due to a two-dimensional inclined sheet of finite depth extent has been analysed in the frequency domain using the Fourier transform. The expression of the Fourier amplitude and phase spectra are derived. The Fourier amplitude and phase spectra are analysed so as to evaluate the parameters of the sheet. Application of this method to two anomalies (synthetic and field data) has given good results. (7 refs.)

64026 Palaeomagnetism of Africa and Madagascar. A.Brock (Appl. Geophys. Unit, Univ. Coll. Galway, Galway, Ireland). In book: *Paleoreconstruction of the continents*, M.W.McElhinny, D.A.Valencio [Ed.], p.65-76. Washington, DC, USA: American Geophysical Union (1981), 194 pp.

Palaeomagnetic results from Africa have increased substantially in number since 1970 especially for the Precambrian. Noteworthy is the now very complete coverage of the Mesozoic, together with a good comparison between Madagascar and Africa which yields a paleoposition for Madagascar close to the East African coast. The Paleozoic is less well covered and much of the Karroo Supergroup remains to be sampled in detail. The Precambrian data is of very variable quality, but it helps to define the apparent polar wander path with greater certainty than previously. Many gaps remain, however, and a much higher density of data will be required. Careful multi-component studies have begun to appear and these must play an increasingly important role in the future work. (96 refs.)

64027 A review of the paleomagnetism of Australia and Antarctica. B.J.J.Embleton (Div. of Mineral Phys., CSIRO, North Ryde, NSW, Australia). In book: *Paleoreconstruction of the continents*, M.W.McElhinny, D.A.Valencio [Ed.], p.77-92. Washington, DC, USA: American Geophysical Union (1981), 194 pp.

Australia and East Antarctica were juxtaposed for the whole of Paleozoic and Mesozoic time. Post-Archean unity of the crustal nuclei that comprise the main Australian platform has been demonstrated, but insufficient Precambrian palaeomagnetic data from East Antarctica preclude confirmation of its Proterozoic reconstruction to Australia. Apparent polar wander (APW) relative to Australia is reasonably well understood for the Phanerozoic and the Proterozoic to about 2500 Myr. Problems highlighted include the resolution of APW between 2300 and 1800 Myr and between 1800 and 1700 Myr. Nor is it clear in which hemisphere Australia resided during the Early Paleozoic. A complex Mesozoic drift history for Australia has been elucidated following the recognition and discrimination between multi-component magnetisation vectors. Cenozoic APW reflects Australia's general northward drift since its separation from Antarctica 53 Myr ago. Data from the Antarctic Peninsula do not support post-Late Cretaceous oroclinal bending and show that little latitudinal movement has taken place in the last 100 Myr. (110 refs.)

64028 Phanerozoic palaeomagnetism of the Indian plate and the India-Asia collision. C.T.Klootwijk (Res. School of Earth Sci., Australian Nat. Univ., Canberra, Australia), C.Radhakrishnamurti. In book: *Paleoreconstruction of the continents*, M.W.McElhinny, D.A.Valencio [Ed.], p.93-105. Washington, DC, USA: American Geophysical Union (1981), 194 pp.

Summarizes Phanerozoic palaeomagnetic data from Peninsular and Extrapeninsular Indo-Pakistan obtained during the last decade. The data are interpreted in terms of Indo-Pakistan's drift with reference in particular to post-collisional deformation of Extrapeninsular Indo-Pakistan and south central Asia. Compilation of a Precambrian apparent polar wander path seems ambiguous because of poor age control and insufficient evidence for a primary or a secondary origin of the palaeomagnetic data. (75 refs.)

64029 Palaeomagnetism of South American rocks and the dynamic processes related with the fragmentation of western Gondwana. J.F.A.Vilas (Dept. de Ciencias Geologicas, Ciudad Univ., Buenos Aires, Argentina). In book: *Paleoreconstruction of the continents*, M.W.McElhinny, D.A.Valencio [Ed.], p.106-14. Washington, DC, USA: American Geophysical Union (1981), 194 pp.

Reliable South American palaeomagnetic data, presented during the last decade, are reviewed. These data define the different episodes of the geodynamic evolution of western Gondwana. The Palaeomagnetic and sea-floor spreading data are used to define the movements associated with the fragmentation of western Gondwana and the origin of the South Atlantic. (43 refs.)

64030 Pre-Neogene palaeomagnetism of Japanese islands (and vicinities). S.Sasajima (Dept. of Geology & Mineralogy, Kyoto Univ., Kyoto, Japan). In book: *Paleoreconstruction of the continents*, M.W.McElhinny, D.A.Valencio [Ed.], p.115-28. Washington, DC, USA: American Geophysical Union (1981), 194 pp.

A set of rigorous criteria has been applied to the Japanese pre-Neogene palaeomagnetic data to discriminate the normal palaeomagnetic data from anomalous ones which could have been influenced by various causes such as local tectonic movements, local geomagnetic anomalies and geomagnetic reversals of polarity. A set of apparent polar wander paths since Cretaceous time for southwest and northeast Honshu, the main island of Japan, has been drawn. Several anomalous palaeomagnetic poles suggest extensive tectonic movements. A plausible Cretaceous reconstruction map of Honshu is presented, along with its tectonic evolutionary history. The paleolatitudinal variation of SW Honshu since the Upper Carboniferous is obtained. (83 refs.)

64031 Palaeomagnetism of southeast and east Asia. N.S.Haile. In book: *Paleoreconstruction of the continents*, M.W.McElhinny, D.A.Valencio [Ed.], p.129-35. Washington, DC, USA: American Geophysical Union (1981), 194 pp.

The decade 1970-1979 saw the first palaeomagnetic work in southeast Asia, providing a useful constraint on palaeomagnetic reconstructions. The results enable a start to be made in defining boundaries of 'microplates' or major structural blocks in the region. Southeast and east Asia have an extremely complex tectonic history, and are a region of the world with very sparse palaeomagnetic data available. The results so far, although scattered, are sufficient to demonstrate the potential of the method for elucidating the tectonic and paleogeographic history of the region. (26 refs.)

64032 Pre-Carboniferous palaeomagnetism of Europe north of the Alpine orogenic belt. J.C.Briden (Dept. of Earth Sci., Univ. of Leeds, Leeds, England), B.A.Duff. In book: *Paleoreconstruction of the continents*, M.W.McElhinny, D.A.Valencio [Ed.], p.137-49. Washington, DC, USA: American Geophysical Union (1981), 194 pp.

Pre-Carboniferous palaeomagnetic data for Europe north of the Hercynian front and some areas within the Hercynian belt are reviewed and catalogued. A tentative apparent polar wander (APW) path for the Baltic Shield and the British Isles is presented which implies over 180° of relative polar shift in late Proterozoic and early Paleozoic time. Incorporation of Armorican data into this path implies that Armorica may have been attached to northern Europe and that any 'proto-Hercynian' ocean between this northern continent and Gondwana in the Paleozoic lay to the south of the Armorican massif. Comparisons of APW data from northern Europe and North America suggests that these areas may have been joined at least for some intervals within the late Proterozoic or early Paleozoic. (61 refs.)

64033 Pre-Cenozoic palaeomagnetism of southern Europe/Middle East. H.Wensink (Inst. voor Aardwentschappen Utrecht, Utrecht, Netherlands). In book: *Paleoreconstruction of the continents*, M.W.McElhinny, D.A.Valencio [Ed.], p.151-7. Washington, DC, USA: American Geophysical Union (1981), 194 pp.

The southern Europe-Middle East palaeomagnetic data have been divided into smaller units. In general, these smaller areas can be regarded as individual structural provinces. Palaeomagnetic studies of the Italian Peninsula, Iran and Afghanistan, Iberia and the Bay of Biscay, are reviewed. The structural evolution, of both Pannonia and south-eastern Europe is still poorly understood. (78 refs.)

64034 Palaeomagnetism of North America: a brief review. R.Van der Voo (Dept. of Geological Sci., Univ. of Michigan, Ann Arbor, MI, USA). In book: *Paleoreconstruction of the continents*, M.W.McElhinny, D.A.Valencio [Ed.], p.159-76. Washington, DC, USA: American Geophysical Union (1981), 194 pp.

An updated version of the apparent polar wander path of the North American craton is presented. Displaced terranes and possible microplates are identified which have yielded pole positions divergent from the cratonic apparent polar wander path; these displaced terranes are found on the eastern as well as the western side of the North American craton. (364 refs.)

64035 Palaeomagnetism of the Soviet Union. A.N.Khranov (All Union Oil Res., Geological Prospecting Inst., Leningrad, USSR), G.N.Petrova, D.M.Pechersky. In book: *Paleoreconstruction of the continents*, M.W.McElhinny, D.A.Valencio [Ed.], p.177-94. Washington, DC, USA: American Geophysical Union (1981), 194 pp.

Reviews the contributions Soviet palaeomagnetic researchers have made on three topics: synthesis of palaeomagnetic data on Russian and Siberian plates and surrounding areas; studies of events in tectonically active zones; and geodynamical characteristics of the palaeomagnetic field. The review is followed by a complete table of pre-Neogene valid palaeomagnetic poles from the territory of the USSR and key references for the period 1970-1979. (29 refs.)

64036 Marine magnetic anomalies from the western Philippine Sea: implications for the evolution of marginal basins. Tai-Chang Shih (Geophys. Lab., Univ. of Texas, Austin, TX, USA).

In book: *Tectonic and geologic evolution of southeast asian seas and islands*, D.E.Hayes [Ed.], p.49-75. Washington, DC, USA: American Geophysical Union (1980), v+326 pp. [0 87590 023 2]

A set of newly processed data is presented together with all available magnetic anomaly data from the West Philippine Basin. These combined data have made it possible to deduce the lineation patterns in this basin and to interpret the tectonic history of the western Philippine Sea. The correlations of magnetic anomalies agree very well with DSDP results and the inferred history of plate motions also agrees well with land geology of the area. The correlations indicate that the crust of the West Philippine Basin started to form before anomaly 25 time (~59 m.y. BP), probably at the ridge that was the southern boundary of the Pacific plate at that time. The West Philippine marginal basin, however, was probably formed by the entrapment of oceanic crust following the reorganization of plate boundaries in the Pacific about 40 m.y. BP. Spreading in this basin was active until anomaly 7A time (~26 m.y. BP). Estimates of the past plate motion and paleolatitude, from phase shifting the magnetic anomalies, suggest that the West Philippine Basin has

drifted north about 15° - 20° and has undergone clockwise rotation of about 50° - 70° since 35-40 m.y. BP. (72 refs.)

64037 Paleomagnetism of Truk Islands, eastern Carolines and of Saipan, Marianas. M.Fuller, J.R.Dunn, G.Green, Jin-Lu Lin, R.McCabe, K.Toney, I.Williams (Dept. of Geological Sci., Univ. of California, Santa Barbara, CA, USA).

In book: *Tectonic and geologic evolution of southeast asian seas and islands*, D.E.Hayes [Ed.], p.235-45. Washington, DC, USA: American Geophysical Union (1980), v+326 pp. [0 87590 023 2]

Paleomagnetic results from Miocene flows from the Truk Islands reveal stable magnetization having a declination of $+2^{\circ}$ and an inclination of $+6^{\circ}$, with an α_{95} of 6.8 and a k of 45.4. This is different from the present dipole field at the 95% confidence level. Ten sites are included in the analysis so that major departures from the true mean field direction due to secular variation should have been eliminated. The result gives an ancient latitude of 3° N with a $\pm 3^{\circ}$ confidence interval, which is consistent with proposed rotation about the Hawaiian hot spot pole at a rate of $1.3^{\circ}/10^6$ years for the past 10 million years. The directions of magnetization of flows of Eocene and Miocene age from Saipan reveal a mean direction of magnetization rotated clockwise from the present field direction. Although there are fewer results available from Saipan than from Truk, the results appear to be recording some tectonic rotation and not simply secular variation. The Marianas limestone of Pleistocene age has a direction of magnetization concordant with the present field. These results from Truk and Saipan reveal that tectonic models can indeed be tested in island arc and oceanic island environments by paleomagnetic observations. It is also clear that the paleomagnetism of such islands suffers from inadequate numbers of available sites and difficulties in establishing tectonic control. The similarity of the rotation observed at Saipan and Guam strongly suggests that tectonic models of the Marianas must account for major rotation of the southern end of the Marianas since their formation. (10 refs.)

64038 Paleomagnetic synthesis for southeast Asia: constraints on plate motions. R.D.Jarrard (Lamont-Doherty Geological Obs., Columbia Univ., Palisades, NY, USA), S.Sajima.

In book: *Tectonic and geologic evolution of southeast asian seas and islands*, D.E.Hayes [Ed.], p.293-316. Washington, DC, USA: American Geophysical Union (1980), v+326 pp. [0 87590 023 2]

Paleomagnetic data from Southeast Asia have been compiled, graded as to reliability, and compared and synthesized to investigate their usefulness in constraining models for the plate tectonic evolution of the region. Polar paths for the major plates, Pacific, Philippine, and Asian, are only approximately known at present. The Pacific plate has undergone a northward motion of 2-4 cm/y for the past 100 m.y., with little rotation. In contrast, the Philippine plate may have been rotating clockwise during the last 60 m.y., with 4-10 cm/y of northward motion (at least for the last 20 m.y.). The northeast portion of the Asian plate experienced about 25° C of clockwise rotation and negligible latitudinal shift since the Cretaceous. On the southeastern part of the Asian plate, the Malay Peninsula, West Kalimantan (Borneo), and southwestern Sulawesi yield very similar late Mesozoic poles, suggesting little subsequent differential movement between these areas and indicating about 50° of counterclockwise rotation and little latitudinal shift during the Tertiary. Paleomagnetic results from islands arcs emphasize the role of small block rotations behind trenches. (147 refs.)

Paleoreconstruction of the continents See Entry 59544

Long relaxation times in ferromagnets and their possible applications See Entry 62706

A geophysical approach to the granite batholith under the eastern Southern Uplands, Scotland See Entry 64090

The tectonic evolution of the South China Basin See Entry 64120

Evidence for Eocene oceanic crust in the Celebes Basin See Entry 64132

91.30 SEISMOLOGY

64039 Spreading of slip from a region of low friction. M.Comminou (Univ. of Michigan, Ann Arbor, MI, USA).

Acta Mech. (Austria), vol.47, no.1-2, p.65-71 (1983).

Recent models of earthquake faults involve heterogeneous slip regions along the faults. Some of this work suggests the following problem: two solids of different material properties are pressed together and sheared. Then, slip propagates asymmetrically from a region of low friction. (6 refs.)

64040 A boundary layer theory for Rayleigh waves in a porous, fluid-filled half space. M.A.Foda (Kuwait Inst. for Sci. Res., Safat, Kuwait), C.C.Mei.

Int. J. Soil Dyn. & Earthquake Eng. (GB), vol.2, no.2, p.62-5 (April 1983).

The application of Biot's poro-elasticity equations to the propagation of seismic waves in saturated rock is studied. This theory assumes that the rock is linearly elastic and that the pore fluid obeys Darcy's law. In this article a general boundary layer approximation of Biot's equation is used to study rapidly damped elastic waves in a half-space. (12 refs.)

64041 Amplification of P, SV, and Rayleigh waves by two alluvial valleys. M.Dravinski (Dept. of Mech. Engng., Univ. of Southern California, Los Angeles, CA, USA).

Int. J. Soil Dyn. & Earthquake Eng. (GB), vol.2, no.2, p.66-77 (April 1983).

A plane strain model for the amplification of harmonic waves by two alluvial valleys of arbitrary shape embedded in a half-space is investigated by using a boundary integral method. Perfect bonding between the valleys and the half-space is assumed. The displacement field is evaluated throughout the elastic medium for linearly elastic, homogeneous and isotropic materials so that the continuity conditions between the valleys and the half-space are satisfied in a mean-square-sense. Numerical results are presented for two semi-elliptical valleys for the incident plane P, SV, and Rayleigh waves for different angles of incidence (for P and SV-waves), frequency of incoming waves, and material properties of the valleys. The results indicate the following: (1) different incident waves caused different surface displacement amplification; (2) the presence of additional valleys may change the surface motion field significantly; (3) a strong ground motion amplitude appears to be very sensitive to the frequency of incoming waves and depends on material properties of the valleys and the half-space. (25 refs.)

64042 Seismicity and earthquake hazard in Trinidad and Tobago, West Indies. J.B.Sherpherd, W.P.Aspinall (Seismic Res. Unit, Univ. of the West Indies, St. Augustine, Trinidad).

Earthquake Eng. & Struct. Dyn. (GB), vol.11, no.2, p.229-50 (March-April 1983).

The two-island Republic of Trinidad and Tobago in the eastern Caribbean has enjoyed increased physical and industrial development in recent years; however, these islands have been subjected to damaging earthquakes during their history and an up-to-date risk assessment is needed. The authors examine two approaches to quantifying this problem: (a) the risk estimated pro-

babilistically using recent instrumental data and (b) the hazard inferred from regional tectonic movements. The probabilistic approach indicates that peak ground accelerations with a probability of exceedance of 10 per cent in 50 years could range from 0.23 g in Tobago to 0.36 g in North-West Trinidad. Tectonic considerations suggest that a maximum-moment earthquake occurring directly under either land mass could generate accelerations as high as 0.6 g; the probability of occurrence of such an event is estimated to be about 2 per cent in 50 years for Trinidad and about a tenth this risk for Tobago. (50 refs.)

64043 A coda-length magnitude scale for New England. M.P.Chaplin, S.R.Taylor, M.N.Toksoz (Dept. of Earth & Planetary Sci., MIT., Cambridge, MA, USA).

Earthquake Not. (USA), vol.51, no.4, p.15-22 (Oct.-Dec. 1980). [received: April 1983]

An empirical coda-length (signal duration) magnitude scale is developed to estimate magnitudes for earthquakes in New England. The formula is based on the mean signal duration, T (in seconds), measured from 45 local earthquakes and is given by: $m_b(Lg) = 2.21 \log_{10}(T) - 1.70$. For epicentral distances less than 600 km, the distance dependence is found to be negligibly small in comparison to other errors. Regional variations in signal duration suggest higher attenuation in southeastern New England than in New Hampshire. (12 refs.)

64044 The Charlevoix earthquake of 19 August 1979 and its seismo-tectonic environment. H.S.Hasegawa, R.J.Wetmiller (Earth Phys. Branch, Energy, Mines & Resources Canada, Ottawa, Canada).

Earthquake Not. (USA), vol.51, no.4, p.23-37 (Oct.-Dec. 1980). [received: April 1983]

The focal mechanism has been determined for an intermediate-magnitude earthquake in the most seismically active region in Eastern Canada. On August 19, 1979, an $m_b(Lg)$ 5.0 earthquake occurred in the Charlevoix seismic zone, under the St. Lawrence River near the town of St. Fidele and La Malbaie, Quebec. The P-wave nodal solution indicates thrust faulting on both nodal planes. From an analysis of surface wave data of the main shock, an estimate of focal depth falls in the range 6-11 km, in agreement with after-shock data. A mean value of the aftershock area is 3.5 km^2 , which is taken to represent the fault area of the main shock, and under the assumption of a circular fault, the stress drop of the main shock is estimated to be 50 bars. Because of the presence of zones of weakness in the epicentral area, the direction of maximum principal stress is only loosely constrained. (35 refs.)

64045 Field investigation and fault plane solution of the Bath, Maine earthquake of April 18, 1979. J.J.Pulli, R.R.Stewart, J.C.Johnston, K.M.Tubman, A.Michaels (Dept. of Earth & Planetary Sci., MIT, Cambridge, MA, USA).

Earthquake Not. (USA), vol.51, no.4, p.39-46 (Oct.-Dec. 1980). [received: April 1983]

On April 18, 1979 an $m_b(Lg)$ 4.0 earthquake occurred near Bath, Maine, and was followed by a number of aftershocks within five hours. A four-station temporary network was deployed around the epicenter for three days and recorded two possible aftershocks. Intensity interviews were also conducted with fifty-five residents of the area. Many residents reported observing intensity effects similar to those of historical New England earthquakes, such as booming sounds rather than low-frequency rumblings normally associated with ground shaking. Reports of unusual animal behavior prior to the earthquake were given by a number of the residents. The fault plane solution was determined for this event. (7 refs.)

64046 The Giles County, Virginia, seismic zone. G.A.Bollinger (Virginia Polytech. Inst., Blacksburg, VA, USA), R.L.Wheeler.

Science (USA), vol.219, no.4588, p.1063-5 (4 March 1983).

A well-defined seismic zone detected in Virginia has an orientation that is not related to the surrounding geologic structures. The orientation of the zone appears to be related to features below the Appalachian overthrust belt. A damaging earthquake that is important in evaluating seismic hazard in the southeastern United States may have occurred in the zone in 1897. (18 refs.)

64047 The tsunami of 23 November 1969 at Kamchatka and certain aspects of its occurrence. Yu.A.Zayakin (Petrovavsk-Kamchatskii Hydrometeorological Obs., USSR).

Sov. Meteor. & Hydrol. (USA), no.12, p.60-5 (1981). Translation of:

Meteorol. & Gidrol. (USSR), no.12, p.77-83 (1981).

A tsunami that occurred as a result of a severe earthquake in the southwestern Bering Sea is described and analyzed. The contours of the tsunami source are determined and the calculated tsunami-wave propagation times are charted. The causes of the tsunami are discussed, and it is concluded that a suspension flow formed after the earthquake and was one of the factors in the formation of the tsunami. It is proposed that the Kurile-Kamchatka tsunamigenic belt be extended northward along the continental slope to the parallel of 58° N. (9 refs.)

64048 Magnitude scale and quantification of earthquakes. H.Kanamori (Seismological Lab., California Inst. of Technol., Pasadena, CA, USA).

Tectonophysics (Netherlands), vol.93, no.3-4, p.185-99 (1983).

Despite various shortcomings, the earthquake magnitude scale is one of the most fundamental earthquake source parameters to be used for catalogs. Although use of a uniform scale is desirable, it is not always possible because of changes in instrumentation, the data reduction method and the magnitude formula, the station distribution, etc. As a result, various magnitude scales have been developed and are currently in use. Recent development in seismometry and earthquake source theories provide more quantitative source parameters than the magnitude. In order to maintain continuity and uniformity of the data, it is important to relate these magnitude scales and the new parameters. In view of this importance, relations between different magnitude scales are examined with an emphasis on the difference in the period of the waves used for the magnitude determination. Use of several magnitude scales determined at different periods provides a convenient method for characterizing earthquakes.

64049 A scheme for the classification of earthquakes. G.Purcaru, H.Berckhemer (Inst. fur Meteorologie und Geophys., J.W. Goethe Univ., Frankfurt/Main, Germany).

Tectonophysics (Netherlands), vol.93, no.3-4, p.201-2 (1983).

A schematic classification of earthquakes in terms of 'earthquake classes' developed earlier (Purcaru and Berckhemer, 1979, 1982) is further quantified and analyzed from a unified point of view. This multiple classification reflects the non-similarity of earthquakes and allows a unified systematization of departures from the similarity law with respect to the basic features characterizing the source process, i.e. 'FM': faulting mode (f), 'C': complexity (j), 'G': geometry (k), 'S': strain/stress (l), 'F': frequency content (m) and 'T': temporal (n). An earthquake can thus be represented as a 6-dimensional vector (j,k,l,m,n) and a 'reference earthquake' was introduced as representative of the class of earthquakes obeying the similarity law. The departures of the components k,l,m,n from those characterizing the class of the reference earthquake were used to introduce various classes of earthquakes, although

they have been only partially defined quantitatively. For a further quantization, the problem is resolved by prescribing adequate limits to classes on the basis of useful criteria derived from source parameter relations.

64050 Amplitude curves of seismic waves on the basis of HMS: observations, comparisons, conceptions. J.Vanek (Geophys. Inst., Czechoslovak Acad. of Sci., Prague, Czechoslovakia), N.V.Kondorskaya, I.V.Fedorova, L.Christoskov.

Tectonophysics (Netherlands), vol.93, no.3-4, p.203 (1983).

On the basis of 32 seismic stations selected in the region of the Eurasian continent, a homogeneous magnitude system (HMS) was established by the method of successive optimization of station corrections and magnitude calibrating functions. The HMS calibrating functions were constructed for longitudinal (PV, PH), shear (SV, SH) and surface (LV, LH) waves recorded by broad band instruments, and for PVs recorded by short period instruments. Dependence of periods of longitudinal, shear and surface waves on epicentral distance was derived. The detailed results are presented in a series of papers being published in the Bulgarian Geophysical Journal (for first two papers on PV, PVs, and PH see Bulg. Geophys. J., 4(2): 74-84 (1978); 7(4): 19-27 (1981)).

64051 Magnitude: the relation of M_L to m_{BLG} . R.B.Herrmann, O.W.Nuttl (Dept. of Earth & Atmospheric Sci., Saint Louis Univ., St. Louis, MO, USA).

Tectonophysics (Netherlands), vol.93, no.3-4, p.204 (1983).

The M_L or local magnitude, scale, was developed to quantify southern California earthquakes. The M_L scale is a measure of the maximum ground motion in the period range of about 0.3-1 sec, as recorded by a standard Wood-Anderson torsion seismograph. In 1973 Nuttl proposed an m_{BLG} scale for eastern North America earthquakes. The m_{BLG} scale is a measure of the ground motion caused by the vertical component of higher-mode Lg waves, of period 1.0 sec. It was set up so that it was numerically equal to m_b as obtained from 1-sec period teleseismic P-wave amplitudes, called m_{bP} . Thus the M_L and m_{BLG} scales, as defined, are independent of each other. Furthermore, the coefficient of anelastic attenuation of 1-sec period waves in California is almost an order of magnitude greater than it is in eastern North America. Observational data show that the near-field excitation of 1-sec period Lg waves by crustal earthquakes is essentially the same throughout the world for earthquakes of a given m_{bP} , after the m_{bP} is corrected for anomalous attenuation in the asthenosphere beneath the epicenter. Using this fact and an independent knowledge of the coefficient of anelastic attenuation for California earthquakes, a formula for m_{BLG} is developed for California. When this formula is applied to earthquakes occurring near the California and Utah WWSN stations, it is found that the m_{BLG} values are numerically equal to M_L as determined by Wood-Anderson seismographs, for earthquakes of magnitude 3-5.

64052 Source parameters of recent strong earthquakes in northeastern Iran from long-period surface waves. M.Niazi, H.Kanamori (TERA Corp., Berkeley, CA, USA).

Tectonophysics (Netherlands), vol.93, no.3-4, p.205 (1983).

The observed R_2 and R_3 phases of the September 16, 1978, Tabas, Iran earthquake across the IDA network are inverted to derive the gross source parameters of the main shock. The synthetic seismograms computed for the inferred source model are compared with observations. The agreement is generally good at most of the stations. However, unexpected asymmetrical observations at CMO, KIP and PFO stations in the northeast-southwest azimuthal directions are observed which cannot be explained by directivity alone. Possible factors responsible for these observations may include regional heterogeneities or the departure of fault plane from simple planar geometry. The resulting focal mechanism agrees with nearly pure reverse mechanism with a NW-SE strike. The seismic moment estimates range from 1.1 to 1.5×10^{27} dyne-cm. Starting with the geologic field data of the Qainat earthquakes of November 14, and 27, 1979, the R_2 and G_2 phases on the ultralong period instruments at Pasadena and Berkeley are analyzed to estimate their seismic source moments.

64053 Empirical magnitude and spectral scaling relations for mid-plate and plate-margin earthquakes. O.W.Nuttl (Dept. of Earth & Atmospheric Sci., St. Louis Univ., St. Louis, MO, USA).

Tectonophysics (Netherlands), vol.93, no.3-4, p.207-23 (1983).

Published values of body-wave magnitude m_b , surface-wave magnitude, M_s , and seismic moment, M_0 , for mid-plate and plate-margin earthquakes, are analyzed, to determine their inter-relationship and to develop scaling laws for earthquake spectra. All of the plate-margin earthquakes used in the study occurred near the border of the Pacific Ocean. The mid-plate earthquakes occurred in both continental plate interiors and oceanic plate interiors. The relations studied include, m_b - M_s , m_b - M_0 and M_s - M_0 .

64054 Characteristics of multiple shocks: wave pattern, extent and orientation of focal regions. I.V.Gorbulova (Inst. of Phys. of the Earth, Moscow, USSR).

Tectonophysics (Netherlands), vol.93, no.3-4, p.225-32 (1983).

A new approach to the interpretation of P and S waves, whereby the temporal process of radiation of multiple shock waves is taken into account, is suggested.

64055 Magnitudes of New Zealand earthquakes: a comparison of magnitudes calculated by different methods. A.J.Haines (Seismological Obs., Wellington, New Zealand).

Tectonophysics (Netherlands), vol.93, no.3-4, p.245-8 (1983).

Before the introduction in 1977 of new procedures for calculating the local magnitudes of New Zealand earthquakes, these were calculated using a derivative of Richter's method for Southern California. There are systematic differences between the magnitudes calculated by the two methods which are functions of position, magnitude and the types of seismometer recording the event. Usually the difference is small, though, for large earthquakes in particular, it can be close to unity. Differences of order unity are often observed between m_b values reported by the ISC and both sets of local magnitudes. There appears to be no relationship between the local magnitudes, which now allow for the nature of wave propagation below New Zealand, and those reported by the ISC.

64056 Regional relationships among earthquake magnitude scales.

D.H.Chung, D.L.Bernreuter (Lawrence Livermore Nat. Lab., Univ. of California, Livermore, CA, USA).

Tectonophysics (Netherlands), vol.93, no.3-4, p.249-50 (1983).

Various magnitude scales commonly used and the interrelationships among them are reviewed. It is shown that problems exist with all of the magnitude scales being used in the United States. When using regional catalogs, for example, it is often necessary to determine how the reported magnitudes were determined. Often such information is not available, although the potential errors are quite large.

64057 Determination of spectral properties of earthquakes from their magnitudes. R.Nortmann, S.J.Duda (Inst. fur Geophys., Univ. Hamburg, Hamburg, Germany).

Tectonophysics (Netherlands), vol.93, no.3-4, p.251-75 (1983).

Following the recommendation of the 'IASPEI Commission on Magnitudes' from 1967, P-wave magnitudes of distant earthquakes are being computed with the aid of the calibration functions of Gutenberg and Richter (1956). With the development of the instrumental seismology, especially in view of the availability of broad-band recordings, the question arises whether the functions are still adequate. In this investigation new calibration functions for P- and S-waves are presented, which are not only dependent on epicentral distance and focal depth, but also on the period of the spectral component of the wave. The determination of calibration functions is based on the currently most plausible global models for the velocity and anelasticity distribution. Taking into account the effective bandwidth of the instruments employed, eventually leads to the so-called spectral magnitudes. From the spectral magnitudes $m(T)$, the energy density spectrum $E(T)$ of the respective wave can readily be computed. The corresponding formula is $E(T) = 10^{2m(T)-1.4}$, with $E(T)$ in joules per hertz.

64058 Amplitude-periodband diagrams and amplitude spectra of teleseismic body waves. A.Plesinger, J.Vanek, C.Sobotova (Geophys. Inst., Czechoslovak Acad. of Sci., Prague, Czechoslovakia).

Tectonophysics (Netherlands), vol.93, no.3-4, p.277-88 (1983).

The relation between amplitude-periodband (APB) diagrams and Fourier spectra of teleseismic P- and S-waves was analyzed using displacement-proportional signals derived from magnetic tape records of the feedback-controlled broadband velocigraph operating at the KHC seismic station. Most Fourier spectra and all the APB diagrams of the wave groups investigated exhibit a more or less pronounced maximum and do not correspond to the shape of theoretical far-field spectra for the Brune model. Contrary to Fourier spectra, APB diagrams have an unambiguously defined level and are not influenced by truncation, incorrect zero level and other disturbing effects.

64059 Determination of a magnitude calibration function using short-period readings of PKP. G.Kowalle (Central Inst. for Phys. of the Earth, Acad. of Sci., Potsdam, Germany), B.Tittel, P.Bornmann.

Tectonophysics (Netherlands), vol.93, no.3-4, p.289-94 (1983).

On the basis of PKP-readings of the seismological station network of the GDR magnitude calibration functions were derived. Since 1975 one of these calibration functions for distances $D > 145^\circ$ is routinely used for magnitude determination at Collm-Station. Deviations from the m_b -values published by the World Date Centres are normally not larger than 0.2 magnitude units. For the distance range from 110° to 165° another calibration function was determined on the basis of USGS-data. Significant regional differences were found for calibration functions for several subduction zones, possibly indicating differences in the elastic properties and structure of the upper mantle in these regions.

64060 Normal, blue and red earthquakes—a new way of earthquake classification on the basis of body-wave magnitudes. S.J.Duda, R.Nortmann (Inst. fur Geophys., Univ. Hamburg, Hamburg, Germany).

Tectonophysics (Netherlands), vol.93, no.3-4, p.295-306 (1983).

Monochromatic magnitudes, based on P- and on S-waves, provide a means to recognize differences in the spectral contents of body-waves radiated from earthquake foci. New, synthetic magnitude calibration functions taking into account periods of waves recorded, improve the consistency of magnitude figures assigned routinely to earthquakes. First results of a world-wide regionalization of earthquakes according to their spectral character are presented. The preponderance of short-period radiation in one class of earthquakes, and of long-period radiation in another is seen.

64061 Relationships among the source parameters of earthquakes in Europe. D.Prochazkova (Geophys. Inst., Czechoslovak Acad. of Sci., Prague, Czechoslovakia).

Tectonophysics (Netherlands), vol.93, no.3-4, p.307-11 (1983).

Earthquake source parameters such as the seismic moment, the source dimension, the stress drop, the average of the relative displacement of the two sides of a fault, the seismic energy, etc. can serve as an important data base for describing the source and the seismic regime of the individual focal regions. These source parameters were calculated on the assumption that the mechanism of earthquakes can be described by a double couple, and taking into account the conclusions from the workshop of the ESC-Subcommission on Focal Mechanism in Budapest 1980 (Udias, 1980).

64062 Considerations for the body-wave magnitude determination in the Recent Earthquake Data Report of the United States Geological Survey. S.Miyamura (Oki Electric Industry Co. Ltd., Tokyo, Japan).

Tectonophysics (Netherlands), vol.93, no.3-4, p.313-18 (1983).

Discusses the implications of including m_b -determinations with periods longer than 2 or 3 seconds in the Recent Earthquake Data Reports (EDR) of the US Geological Survey. Previously these longer periods were not included. (1 ref.)

64063 Seismic triggering effect of tidal stress. Ding Zhong-Yi, Jia Jin-Kang, Wang Ren (Dept. of Geology, Peking Univ., Peking, China).

Tectonophysics (Netherlands), vol.93, no.3-4, p.319-35 (1983).

The tidal stress field of a layered, spherically symmetric Earth due to the Sun and Moon is used to investigate its relationship to the occurrence of earthquakes. For 70 severe earthquakes which occurred in or near China during the last 24 years, the tidal stress was calculated in spherical polar coordinates at the focus at the time of occurrence. The normal and tangential stress components along the slip direction on the earthquake fault plane were then found by a coordinate transformation. Coulomb's criterion of shear fracture is used to determine whether these stress components will trigger the earthquakes or not. The results show that of the 70 earthquakes, 43 have been subjected to a triggering effect and for the 18 events that occurred in north China, 14 have been triggered. It may be concluded that for shallow strike-slip earthquakes there is a significant triggering effect, while for oblique-slip and dip-slip earthquakes the tidal stress has only a small triggering effect.

64064 Spectra of the earthquake sequence February-March, 1981, in south-central Sweden. O.Kulhanek, T.Van Eck, N.John, K.Meyer, R.Wahlstrom (Seismological Dept., Uppsala Univ., Uppsala, Sweden).

Tectonophysics (Netherlands), vol.93, no.3-4, p.337-50 (1983).

On February 13, 1981 a relatively strong earthquake occurred in the Lake Van region in south-central Sweden. The shock had a magnitude of $M_L = 3.3$ and was followed within three weeks by three aftershocks, with magnitudes $0.5 \leq M_L \leq 1.0$. The focal mechanism solution of the main shock indicates reverse faulting with a strike in the N-S or NE-SW direction and a nearly horizontal compressional stress. The aftershocks were too small to yield data for a full mechanism solution, but first motions of P-waves, recorded at two stations, are consistent for the aftershocks. Dynamic source parameters, derived from Pg- and Sg-wave spectra, show similar stress drops for the main shock (2 bar) and the aftershocks (1 bar), while the differences in seismic

moment ($1.5 \cdot 10^{20}$ resp. $4 \cdot 10^{18}$ dyne cm), fault length (0.7 resp. 0.2 km) and relative displacement (0.15 resp. 0.03 cm) are significant.

64065 The spatial distribution of earthquakes, focal mechanism solutions, and subducted lithosphere in the Philippine and northeastern Indonesian Islands. R.K. Cardwell, B.L. Sacks, D.E. Karig (Dept. of Geological Sci., Cornell Univ., Ithaca, NY, USA).

In book: *Tectonic and geologic evolution of southeast Asian seas and islands*, D.E. Hayes [Ed.], p.1-35. Washington, DC, USA: American Geophysical Union (1980), v+326 pp. [0 87590 023 2]

The spatial distribution of earthquake hypocenters and earthquake focal mechanism solutions is used to estimate the three-dimensional configuration of lithosphere that is subducted beneath the Philippine and northeastern Indonesian islands and to estimate the geometry and nature of plate boundaries in the region. The data set consists of well-located hypocenters selected from seismological bulletins. Focal mechanism solutions for 134 earthquakes, including 68 new solutions, are correlated with tectonic features of the region. The Philippine region consists of an aggregate of island arcs lying between the Philippine Sea Plate and the Southeast Asian Plate. Convergence between the Philippine Islands and the eastern boundary of the Southeast Asian Plate appears to have occurred along the Manila Trench, Negros Trench, and Cotabato Trench. The lithosphere of the Celebes Basin has also been subducted along the western portion of the North Sulawesi Trench to a depth of over 200 km beneath the north arm of Sulawesi. Convergence between the Philippine Islands and the western boundary of the Philippine Sea Plate occurs along the East Luzon Trough and the Philippine Trench. (66 refs.)

64066 The nature of seismicity patterns before large earthquakes. H. Kanamori (Seismological Lab., California Inst. of Technol., Pasadena, CA, USA).

Earthquake Prediction. An International Review. Symposium on Earthquake Prediction, Mohonk, NY, USA, 12-16 May 1980 (Washington, DC, USA: American Geophys. Union 1981), p.1-19

Various seismicity patterns before major earthquakes have been reported in the literature. Although many earthquakes are preceded by all, or some, of these patterns, their detail differs significantly from event to event. In order to examine the details of seismicity patterns on as uniform a basis as possible, the author makes space-time plots of seismicity for many large earthquakes by using the NOAA and JMA catalogs. Among various seismicity patterns, preseismic quiescence appears most common, the case for the 1978 Oaxaca earthquake being the most prominent. Although the nature of other patterns varies from event to event, a common physical mechanism may be responsible for these patterns; details of the pattern are probably controlled by the tectonic environment and the heterogeneity of the fault plane. A simple asperity model is introduced to explain these seismicity patterns. (76 refs.)

64067 Precursory seismicity patterns: stalking the mature seismic gap. R.E. Habermann (Cooperative Inst. for Res. in Environmental Sci., Univ. of Colorado, Boulder, CO, USA).

Earthquake Prediction. An International Review. Symposium on Earthquake Prediction, Mohonk, NY, USA, 12-16 May 1980 (Washington, DC, USA: American Geophys. Union 1981), p.29-42

Mature seismic gaps are defined as gaps in which a possible precursor has been identified. The seismic gap hypothesis by itself provides an excellent means of narrowing spatial limits along plate boundaries within which the great earth quakes of the next several decades are expected. Seismicity rates measured teleseismically are tested as a possible indicator of maturity in the regions of eleven recent large events. (33 refs.)

64068 Seismicity and tectonics of the central New Hebrides island arc. B.L. Sacks, R.K. Cardwell (Dept. of Geological Sci., Cornell Univ., Ithaca, NY, USA), J.-L. Chatelain, M. Barazang, J.-M. Marthelot, D. Chinn, R. Louat. Earthquake Prediction. An International Review. Symposium on Earthquake Prediction, Mohonk, NY, USA, 12-16 May 1980 (Washington, DC, USA: American Geophys. Union 1981), p.93-116

The seismicity of the central New Hebrides convergent plate boundary is investigated with three sets of data: (1) large earthquakes ($M_s > 6.9$) for the past 75 years, (2) moderate-sized earthquakes ($m_b = 4.5$ and $M_s < 7.0$) during the past 20 years, and (3) small earthquakes ($m_b = 2.5$ to 4.5) located by local networks for several intervals of 1-2 months each since 1975 and continuously since mid-1978. Tectonic features are also discussed. (67 refs.)

64069 The 1906 San Francisco earthquake and the seismic cycle. W.L. Ellsworth, A.G. Lindh, W.H. Prescott, D.G. Herd (US Geological Survey, Menlo Park, CA, USA).

Earthquake Prediction. An International Review. Symposium on Earthquake Prediction, Mohonk, NY, USA, 12-16 May 1980 (Washington, DC, USA: American Geophys. Union 1981), p.126-40

The cyclic nature of strain accumulation and release in great earthquakes on the San Andreas fault appears to have modulated the historic pattern of seismicity in northern coastal California. Fedotov (1968) and Mogi (1968) recognized a similar seismic cycle accompanying great earthquakes in the subduction zones of the Western Pacific. The cycle consists of an extended period of quiescence after a major earthquake, followed by a period of increased activity that leads to the cycle-controlling earthquake and its fore-shocks and aftershocks. The reemergence of $M \geq 5$ earthquakes since 1955 within the latitudes of the 1906 surface rupture to the north of San Jose, after an extended period of quiescence following 1906, lead the authors to conclude that the region is entering the active stage of the cycle. (53 refs.)

64070 Earthquake hazard in the Hellenic Arc. M. Wyss (Dept. of Geological Sci., Univ. of Colorado, Boulder, CO, USA), M. Baer.

Earthquake Prediction. An International Review. Symposium on Earthquake Prediction, Mohonk, NY, USA, 12-16 May 1980 (Washington, DC, USA: American Geophys. Union 1981), p.153-72

The seismicity of the Hellenic arc is studied as a function of space and time by two methods. Firstly, data on large and great historic earthquakes are reinterpreted with the purpose of identifying seismic gaps along this plate boundary. The authors that the 8 great and 3 large earthquakes which occurred along the Hellenic arc between 1805 and 1926 can be interpreted as shallow sources along the plate boundary. Based on macroseismic data the authors propose approximate locations and size of these earthquakes. It appears that the entire Hellenic plate boundary can be considered to be a seismic gap of class 1, 2, and 3 depending on the segment. Secondly, a systematic analysis of the shallow seismicity (< 100 km) showed that the rate decreased by about 80% in the western third and portions of the eastern third of the arc. Combining the seismic gap and the seismicity rate data suggest that ruptures of about 120 ± 40 km lengths ($M = 7.3/4 \pm 1/2$) may be expected to occur along the Hellenic plate boundary near 22.5 to 23.5° E and 26.5 to 27.5° E between now (1983) and 1990. (49 refs.)

64071 A review of geological evidence for recurrence times of large earthquakes. K.E. Sieh (Div. of Geological & Planetary Sci., California Inst. of Technol., Pasadena, CA, USA).

Earthquake Prediction. An International Review. Symposium on Earthquake Prediction, Mohonk, NY, USA, 12-16 May 1980 (Washington, DC, USA: American Geophys. Union 1981), p.181-207

The geological record of the past several thousand years contains valuable information for evaluating the earthquake potential of the Earth's major fault systems. Geologists have begun to characterize past and, presumably, future behavior of active faults and recurrence intervals for large earthquakes by studying 1) uplifted marine terraces, 2) fault-scarp morphology, 3) physiographic features offset along faults, and 4) faulted or otherwise deformed young sediments. (97 refs.)

64072 Repeat time of great earthquakes along simple plate boundaries. L.R. Sykes, R.C. Quittmeyer (Lamont-Doherty Geological Obs., Columbia Univ., Palisades, NY, USA).

Earthquake Prediction. An International Review. Symposium on Earthquake Prediction, Mohonk, NY, USA, 12-16 May 1980 (Washington, DC, USA: American Geophys. Union 1981), p.217-47

Repeat times of large earthquakes are obtained for 12 segments of simple plate boundaries of the convergent type and three of the transform type for which two or more large shocks are known to have occurred at nearly the same place. Repeat time is related not only to the relative plate velocity but also to the geometry of the rupture zone. The data support the time-predictable model wherein the time interval between two large shocks is proportional to the displacement in the preceding event. When the time interval between two previous large shocks in an area is known and the ratio of their displacements can be determined, the time interval between the last large shock and a future earthquake can be estimated with much greater accuracy. An application of this calibrating technique to six regions in which three or more shocks are known to have occurred is presented. (100 refs.)

64073 Great detachment earthquakes along the Himalayan Arc and long-term forecasting. L. Seeber, J.G. Armbruster (Lamont-Doherty Geological Obs., Columbia Univ., Palisades, NY, USA).

Earthquake Prediction. An International Review. Symposium on Earthquake Prediction, Mohonk, NY, USA, 12-16 May 1980 (Washington, DC, USA: American Geophys. Union 1981), p.259-77

Examines the surface effects of great Himalayan earthquakes, and infers the extent of the associated ruptures. Some spatial and temporal constraints on the next great earthquakes are to be inferred from the reconstruction in space and time of the previous ruptures. The tectonic model is discussed. (73 refs.)

64074 Specification of a soon-to-occur seismic faulting in the Tokai District, central Japan, based upon seismotectonics. K. Ishibashi (Internat. Inst. of Seismology & Earthquake Engng., Ibaraki, Japan).

Earthquake Prediction. An International Review. Symposium on Earthquake Prediction, Mohonk, NY, USA, 12-16 May 1980 (Washington, DC, USA: American Geophys. Union 1981), p.297-332

The 'Tokai earthquake' expected in the Tokai district, the Philippine Sea coast of central Japan, is the most important target now in the Japanese earthquake prediction program. Its long- and short- prediction efforts are among the most advanced cases in the world. The author reviews in detail the long-term prediction research of this earthquake and presents the most probable fault model. The expected event is considered an interplate earthquake due to the underthrusting of the Philippine Sea plate beneath southwest Japan at the Nankai-Suruga trough. (165 refs.)

64075 Long- and intermediate-term seismic precursors to earthquakes—state of the art. M. Reyners (Lamont-Doherty Geological Obs., Columbia Univ., Palisades, NY, USA).

Earthquake Prediction. An International Review. Symposium on Earthquake Prediction, Mohonk, NY, USA, 12-16 May 1980 (Washington, DC, USA: American Geophys. Union 1981), p.333-47

Rikitake [1975, 1979] has made a thorough classification of earthquake precursors, both seismic and nonseismic. The author concentrates on research carried out since 1977, with special reference to false alarms and negative results. (113 refs.)

64076 Crustal deformation studies and earthquake prediction research. W. Thatcher (US Geological Survey, Menlo Park, CA, USA).

Earthquake Prediction. An International Review. Symposium on Earthquake Prediction, Mohonk, NY, USA, 12-16 May 1980 (Washington, DC, USA: American Geophys. Union 1981), p.394-410

Geodetic measurements have diverse applications in studies related to earthquake hazard mitigation and prediction. The author considers three areas where such measurements are particularly useful: first, in the assessment of long-term earthquake hazard; secondly, in monitoring for possible precursory crustal deformation; and thirdly, in constraining the mechanism of stress build up and release in the brittle crust. (48 refs.)

64077 Neotectonic deformation, near-surface movements and systematic errors in US leveling measurements: implications for earthquake prediction. R. Reilinger, L. Brown (Dept. of Geological Sci., Cornell Univ., Ithaca, NY, USA).

Earthquake Prediction. An International Review. Symposium on Earthquake Prediction, Mohonk, NY, USA, 12-16 May 1980 (Washington, DC, USA: American Geophys. Union 1981), p.422-40

Reviews some factors that must be considered when attempting to extract tectonic information, especially those relevant to earthquake prediction, from historic leveling observations. Evidence on the extent and nature of systematic errors nontectonic movements, and tectonic deformation (both earthquake related deformation and tectonic movements unassociated with earthquakes) from US leveling measurements is presented. Specific criteria to help recognize suspect movements are developed and illustrated by application to a reevaluation of certain southern California leveling results of particular interest in earthquake prediction. (51 refs.)

64078 A preliminary analysis of reported changes in ground water and anomalous animal behavior before the 4 February 1975 Haicheng earthquake. D. Qidong, J. Pu (Inst. of Geology, State Seismology Bur., Beijing, China), L.M. Jones, P. Molnar.

Earthquake Prediction. An International Review. Symposium on Earthquake Prediction, Mohonk, NY, USA, 12-16 May 1980 (Washington, DC, USA: American Geophys. Union 1981), p.543-65

Examines the spatial and temporal distributions of some 570 reports of changes in ground water and 670 reports of anomalous animal behavior in the three months before the Haicheng earthquake (4 February 1975, $M = 7.3$). These changes and anomalies were reported from a very large area, extending more than 150 kilometers in nearly all directions from the epicenter with no concentration near it. There are suggestions (1) of correlations in time and space of the two types of anomalies with the ground water changes preceding the aberrant animal behavior by a day or two, (2) of a greater concentration of reports near major active faults than far away from them, and (3) of migrations in time of the area in which there were frequent observations. The

data suggest that some animals may have responded to a shaking of the ground due to foreshocks and others may have sensed changes in the ground water. (9 refs.)

- Earthquake Prediction. An International Review. Symposium on Earthquake Prediction** See Entry 59541
A seismic refraction line along the axis of the southern Piedmont and crustal thicknesses in the southeastern United States See Entry 64085
The lithosphere in the Central-eastern Mediterranean area See Entry 64091
Crustal structure of the Molucca Sea collision zone, Indonesia See Entry 64097
Crustal structure across the Mariana island arc See Entry 64098
An asperity model of large earthquake sequences See Entry 64123
Variations in geologic structure along the Sunda fore arc, northeastern Indian Ocean See Entry 64139
Numerical integration method for seabed response to water waves See Entry 64144
Earthquake prediction program in Japan See Entry 64240

91.35 EARTH'S INTERIOR STRUCTURE AND PROPERTIES

64079 Leg 82 of the International Program of Ocean Drilling (IPOD): normal or abnormal ocean crust on the Mid-Atlantic Ridge; Geochemical properties. H.Bougault (Centre Océanologique de Bretagne, Brest, France), S.Cande, W.Mills, D.Curtis, R.Neuser, D.Christie, M.Rideout, J.Etoubleau, N.Drake, J.Brannon, B.Weaver, D.Echols, M.Clark, J.M.Khan, I.Hill. *C.R. Seances Acad. Sci. Ser. II (France)*, vol.296, no.1, p.97-102 (10 Jan. 1983). In French.

On Leg 82, the Glomar Challenger sampled the Ocean crust at nine sites west and southwest of the Azores Triple Junction. Shipboard analysis for key trace elements showed that the relationship between chemical characteristics of basalts and geodynamics are not as simple as predicted by some pre-cruise hypotheses. Preliminary results (example: enriched basalts and depleted basalts recovered in the same hole) allow the prediction that onshore studies (example: isotopes of Sr, Nd and Pd) will provide important information for fundamental geochemistry, magmatic processes and mantle heterogeneity. Additional highlights were the discovery of serpentinite and altered gabbro at three sites at shallow depth; the recovery of an almost complete sediment section from Oligocene through early Pleistocene; the discovery of sea-water underpressure in the basement 35 My old. (17 refs.)

64080 **Io-U dates of a coral formation from the last interglacial age on the Brazilian coast. Use of ^{232}Th as a tracer.** M.Bernat (Univ. de Nice, Nice, France), L.Martin, A.Bittencourt, G.V.Boas. *C.R. Seances Acad. Sci. Ser. II (France)*, vol.296, no.3, p.197-200 (24 Jan. 1983). In French.

Four coral samples taken in a quarry near the town of Ilheus (Bahia State, Brazil) analyzed by an α spectrometry method for ^{230}Th and uranium isotopes (using ^{229}Th and ^{232}U as tracers) gave a mean age of 123500 years. These first dates confirm the general stability of the Atlantic coast since that time. (13 refs.)

64081 **A reference section of the oceanic crust: leg 83 of the International Program of Ocean Drilling (IPOD) near the Costa Rica rift, eastern Pacific Ocean.** R.N.Anderson (Lamont-Doherty Geological Obs., Palisades, NY, USA), J.Honnorez, C.Laverne. *C.R. Seances Acad. Sci. Ser. II (France)*, vol.296, no.4, p.281-6 (31 Jan. 1983). In French.

Drilling during IPOD leg 83 has established the most complete reference section to date through the upper oceanic crust. For the first time, a drilling has reached the dike-zone and metamorphosed basalt. (7 refs.)

64082 **Gneissic intercalations within a tectonic unit from the Piedmont Ophiolite Nappe in the Western Alps: Record of a subducted continental margin?** U.Pognante. *C.R. Seances Acad. Sci. Ser. II (France)*, vol.296, no.5, p.379-82 (7 Feb. 1983). In French.

A tectonic unit from the Piedmont Ophiolite Nappe is distinguished by the association of calc-schists (schistes lustrés) with albite gneiss of continental origin and with manganese-rich quartzites. This association and the Alpine H.P. evolution suggest that the unit described represents the product of large scale transpositions in subduction environment of a part of the thinned apulian (?) continental margin bordering the Piedmont-Ligurian ocean basin. (10 refs.)

64083 **The allochthony of the 'Zone des Diapirs' in Northern Tunisia.** V.Perthuisot, H.Rouvier (Ecole Normale Supérieure Lab. Geologie, Paris, France). *C.R. Seances Acad. Sci. Ser. II (France)*, vol.296, no.5, p.393-6 (7 Feb. 1983). In French.

It is impossible to accept the allochthony of the whole diapir zone and the recent age of the Triassic extrusions. The ancient and permanent connections between each diapir and its sedimentary surroundings are proved by field evidence and confirm the ante-alpin age of the most extrusive structures. (16 refs.)

64084 **Discovery of a new nappe from the north-east in the Parnassus zone (Greece).** P.-J.Combes (Univ. des Sci. et. Tech. du Languedoc, Montpellier, France). *C.R. Seances Acad. Sci. Ser. II (France)*, vol.296, no.5, p.397-400 (7 Feb. 1983). In French.

An important klippe between Arachova and Davlia belongs to a thrust sheet coming from the northern Parnassus margin, south of Tithorea. This was probably drawn to the Parnassian substratum when the pelagonian nappe overthrust, but only after the beotian nappe appeared. Later a transverse sinistral fault with the uplift of the septentrional region induced the Arachova klippe break-down and its translation to the east. (7 refs.)

64085 **A seismic refraction line along the axis of the southern Piedmont and crustal thicknesses in the southeastern United States.** A.E.Kean, L.T.Long (School of Geophys. Sci., Georgia Inst. of Technol., Atlanta, GA, USA).

Earthquake Not. (USA), vol.51, no.4, p.3-13 (Oct.-Dec. 1980). [received: April 1983]

Arrival times of Pn and Sn phases from southeastern United States earthquakes listed in the Earthquake Data Reports from July 1970 to June 1977 show a scatter of 2 seconds. In contrast, the Pq phase arrivals show a scatter of only 0.5 seconds. The difference in scatter was interpreted as indicating variation in the depth to the Moho. In order to evaluate Moho depths, a detailed refraction line and crustal model were developed along the axis of the Southern Piedmont Province from central Georgia across South Carolina.

Accurately located recent earthquakes and explosions occurring and recorded along the axis of the Southern Piedmont Province were used to define the travel time curves. Crustal thicknesses in the southeastern United States are computed from Pn-Pg times by comparison to the Southern Piedmont crustal model. Moho depths were measured for the mountains of north Georgia, eastern Tennessee and western North Carolina. (9 refs.)

64086 **Uranium disequilibrium dating of phosphate deposits from the Lau Group, Fiji.** K.K.Roe, W.C.Burnett (Dept. of Oceanography, Florida State Univ., Tallahassee, FL, USA), A.I.N.Lee. *Nature (GB)*, vol.302, no.5909, p.603-6 (14 April 1983).

Uranium-series methods of absolute age determinations were first applied to fossil coral reefs and more recently to fossil bone, marine apatite and insular apatite. Past sea level stands, climatic conditions, primary productivity, and other factors are thought to be influential in the deposition of avian guano and subsequent insular phosphorite formation. Some deposits appear to have formed during high stands of the sea while others may be related to glacial epochs. The authors report an attempt to determine the absolute age of two phosphate deposits in the Lau Group, Fiji, by uranium-series disequilibrium techniques, in order to assist in the evaluation of their origin in terms of known palaeoclimatic information. (28 refs.)

64087 **Rates of sedimentation, and stratigraphical completeness.** J.C.Tipper (Dept. of Geology, Univ. College Galway, Galway, Ireland). *Nature (GB)*, vol.302, no.5910, p.696-8 (21 April 1983).

The most obvious result of sedimentation processes is the change in the thickness of accumulated sediment with time. Whenever the net change over a period of time is positive, a record is left of a sedimentation system's existence, a stratigraphical section. For the stratigrapher, the problem that such a section poses is to determine the detailed correspondence of thickness to time: for the sedimentologist, the problem is to infer the nature of the parent sedimentation system, and to estimate its parameters. A simple stochastic model is used to: (1) illustrate some basic stratigraphical results of elastic sedimentation processes; (2) offer an explanation for the commonly cited systematic decrease of mean sedimentation rate with increasing time span; and (3) assess the concept of stratigraphical completeness. (8 refs.)

64088 **Noble gas constraints on the layered structure of the mantle.**

I.Kaneoka (Geophys. Inst., Univ. of Tokyo, Tokyo, Japan).

Nature (GB), vol.302, no.5910, p.698-700 (21 April 1983).

Several chemical models of mantle structure have been proposed based on isotopic data such as Sr, Nd, Hf and Pb in volcanic rocks from both oceanic and continental areas. The most popular of these are two chemical models of the vertically-layered mantle: (1) that it is a depleted mantle from which mid-oceanic ridge basalt (MORB) is derived and (2) that it is a fertile mantle from which a mantle plume may arise. However, these models are almost always based on solid elements, such as Sr, Nd, Hf and Pb isotopes, and do not fully reflect the noble gas data. Because noble gases are liable to be lost from the solid Earth when a mantle differentiation occurs on a global scale in the upper mantle, the data on noble gas isotopes could give constraints on the structure of the mantle that differ from those by solid element isotopes. Based on a consideration of $^3\text{He}/^4\text{He}$ and $^{40}\text{Ar}/^{36}\text{Ar}$ ratios of recent samples, the author argues that the observed data suggest that mixing occurs between the source materials of a mantle plume and of MORB. The data seem to favour the model which assumes that the source of a typical mantle plume is deeper than that of MORB. (15 refs.)

64089 **Mantle eclogite and carbonate as sources of sodic carbonatites and alkalic magmas.** A.H.Treiman, E.J.Essene (Dept. of Geological Sci., Univ. of Michigan, Ann Arbor, MI, USA).

Nature (GB), vol.302, no.5910, p.700-3 (21 April 1983).

At mantle pressures, partial melts of peridotite + CO_2 are carbonate-rich, but contain insufficient sodium to form most carbonatites and associated silicate magmas. A possible source rock is eclogite, and extrapolations from experiments suggest that eclogite + CO_2 will coexist with melt along geotherms of low heat flow. Thermochemical calculations yield high carbonate activities, and imply that the melt is carbonatitic. The melt can be modelled in the system jadeite-calcite- CO_2 and will, on emplacement, form mineral assemblages characteristic of a wide range of alkalic rocks. The tectonic settings of carbonatites are consistent with an origin as partial melts of eclogite + carbonate + CO_2 under areas of low surface heat flow, and suggest that carbonatite emplacement is not related to mantle hotspots. (39 refs.)

64090 **A geophysical approach to the granite batholith under the eastern Southern Uplands, Scotland.** E.Lagios (Seismological Lab., Athens Univ., Athens, Greece), R.G.Hipkin.

Pure & Appl. Geophys. (Switzerland), vol.120, no.2, p.375-88 (1982).

From interpretation of the Bouguer gravity and aeromagnetic anomalies in south-east Scotland it is concluded that a massive granite batholith underlies the greater part of the eastern Southern Uplands. The granite model which was computed earlier from gravity anomalies in the Tweeddale area fits the observed magnetic anomalies closely, if a normal magnetization of 0.095 A m^{-1} is assigned, similar to values found for exposed local granites. Further gravity modelling shows that, apart from the Tweeddale Lammermuir Fault. A model for the East Lothian volcanics was computed from their electromagnetic anomalies, then their gravitational effect was combined with that estimated for the Devonian and Carboniferous sediments and the result stripped off the observed gravity field. The residual gravity anomalies were used to generate a two-dimensional model for the granite north of the Lammermuir Fault. The expected tectonic consequences of a massive granite batholith in the eastern Southern Uplands are studied. (21 refs.)

64091 **The lithosphere in the Central-eastern Mediterranean area.** G.Calcagnile (Istituto di Geodesia e Geofisica, Univ. di Bari, Bari, Italy), F.D'Ingo, P.Farrugia, G.F.Panza.

Pure & Appl. Geophys. (Switzerland), vol.120, no.2, p.389-406 (1982).

The lithosphere beneath the central-eastern Mediterranean area has been investigated by inversion of the regional dispersion relations derived from analysis of surface waves. It is possible to distinguish several types of crust with average S-wave velocities in the range 3.0-3.8 km/sec, and thicknesses varying from a minimum of about 30 km, which corresponds to the Apennines, Crete and Otranto Channel regions, to a maximum of about 51 km beneath the Ionian Sea, which can be considered as a submerged continent. Associated with these crustal features, large lateral variations have been detected in the lithosphere thickness which varies from a minimum of about 30 km corresponding to the Tyrrhenian Sea and south of Crete to a maximum of about 130 km corresponding to south-eastern Alps and north-central Greece, while the sub-Moho S-wave velocity varies in the range 4.2-4.8 km/sec. The constraint furnished by the results to the geological-tectonic setting of the investigated area, characterized by the continent-continent collision between Africa and Europe, is pointed out. (46 refs.)

64092 Primitive helium in diamonds. M.Ozima, S.Zashu (Univ. of Tokyo, Tokyo, Japan).

Science (USA), vol.219, no.4588, p.1067-8 (4 March 1983).

Thirteen diamond stones from various unspecified mines in South Africa were analyzed for the isotopic ratio of helium-3 to helium-4. Values of the ratio ranged from less than 10^{-7} to $(3.2 \pm 0.25) \times 10^{-4}$. The latter value is higher than the primordial helium-3/helium-4 ratio meteorites and close to the ratio for the solar-type helium. Such extremely high values may represent primitive helium that evolved very little (that is, showed very little increase in radiogenic helium-4) since the formation of the Earth. (9 refs.)

64093 Timing and chemistry of igneous events associated with the Southern Oklahoma Aulacogen. M.C.Gilbert (Dept. of Geological Sci., Virginia Polytech. Inst. & State Univ., Blacksburg, VA, USA).

Tectonophysics (Netherlands), vol.94, no.1-4, p.439-55 (1983). (Conference on the Processes of Planetary Rifting, St. Helena, CA, USA, 3-5 Dec. 1981).

Igneous activity in the Southern Oklahoma Aulacogen of North America was concentrated in the early rifting stages of aulacogen development. The time span over which liquids rose may not have exceeded 50 m.y. and certainly terminated before the Upper Cambrian. Igneous activity began with three basaltic liquids, stratigraphically identifiable but perhaps not all distinct genetically. This was followed by one large rhyolitic-granite episode of A-type character. One final basaltic event ended the activity. All the basaltic types seem to be tholeiitic showing more kinship with either the older, Proterozoic North American Midcontinental Rift or the northern part of the Cenozoic Rio Grande Rift, than the Cenozoic East African Rift. Two major uplifts occurred: one between the earlier basalts and the rhyolite, and one much later, after all igneous activity was over, in the Pennsylvanian.

64094 The Morton-Black hypothesis for the thinning of continental crust—revisited in western Afar. P.Mohr (Dept. of Geology, Univ. Coll., Galway, Ireland).

Tectonophysics (Netherlands), vol.94, no.1-4, p.509-28 (1983). (Conference on the Processes of Planetary Rifting, St. Helena, CA, USA, 3-5 Dec. 1981).

Geological observations along the western margin of Afar show that the Morton-Black model, in which thinning of upper continental crust at a nascent continental margin is accomplished through block faulting and tilting, is not wholly applicable. Rather, dikes are concentrated into swarms, suggestive of important direct dilatation. Faults are concentrated into sets, within which no block-tilting steeper than 45° is observed. Therefore attenuation of the Afar margins requires a significant role for processes other than block tilting, and in some margin sectors the transition from continental to neo-oceanic crust may be relatively abrupt.

64095 Accumulation of fossil fuels and metallic minerals in active and ancient rift lakes. E.I.Robbins (US Geological Survey, Reston, VA, USA).

Tectonophysics (Netherlands), vol.94, no.1-4, p.633-58 (1983). (Conference on the Processes of Planetary Rifting, St. Helena, CA, USA, 3-5 Dec. 1981).

A study of active and ancient rift systems around the world suggests that accumulations of fossil fuels and metallic minerals are related to the interactions of processes that form rift valleys with those that take place in and around rift lakes. The deposition of the precursors of petroleum, gas, oil shale, coal, phosphate, barite, Cu-Pb-Zn sulfides, and uranium begins with erosion of uplifted areas, and the consequent input of abundant nutrients and solute load into swamps and tectonic lakes. Hot springs and volcanism add other nutrients and solutes. The resulting high biological productivity creates oxidized/reduced interfaces, and anoxic and H_2S -rich bottom waters which preserves metal-bearing organic tissues and horizons. Postdepositional processes in rifts include high heat flow and a resulting concentration of the organic and metallic components that were dispersed throughout the lakebeds. Postdepositional faulting brings organic- and metal-rich sourcebeds in contact with coarse-grained host and reservoir rocks. A suite of potentially economic deposits is therefore a characteristic of rift valleys.

64096 Geothermal resources of rifts: a comparison of the Rio Grande Rift and the Salton Trough. C.A.Swanberg (Teledyne Geotech. Garland, TX, USA).

Tectonophysics (Netherlands), vol.94, no.1-4, p.659-78 (1983). (Conference on the Processes of Planetary Rifting, St. Helena, CA, USA, 3-5 Dec. 1981).

The Rio Grand Rift and the Salton Trough are the best developed rift systems in the United States and both share many features common to rifts in general, including geothermal resources. These two first have different tectonic and magmatic histories, however, and these differences are reflected in the nature of their geothermal resources. The Salton Trough is a well developed and successful rift. Quaternary silicic magmatization has occurred and several of the geothermal resources are associated with recent rhyolitic intrusions. Localized upper crustal melting is a distinct possibility and there is increasing speculation that very high temperature ($>300^\circ\text{C}$) geothermal fluids may underlie a large portion of the central trough at depths in excess of 4 km. Low temperature geothermal resources associated with shallow hydrothermal convection are less common. In contrast, the Rio Grande Rift is less well developed. The geothermal resources within the Rio Grande Rift do not correlate well with these young basalts. Rather, the quality of geothermal resources are low temperature ($<100^\circ\text{C}$) and result from forced hydrothermal convection which discharges at constrictions within or at the end of the major sedimentary basins. High temperature resources are less common.

64097 Crustal structure of the Molucca Sea collision zone, Indonesia. R.McCaffrey, E.A.Silver (Earth Sci. Board, Univ. of California, Santa Cruz, CA, USA), R.W.Raitt.

In book: *Tectonic and geologic evolution of southeast asian seas and islands*, D.E.Hayes [Ed.], p.161-77. Washington, DC, USA: American Geophysical Union (1980), v+326 pp. [0 87590 023 2]

Seismic refraction profiles run within the Molucca Sea of eastern Indonesia reveal a thick, low-velocity layer (collision complex) which is inferred to be the source of the large negative free air gravity values associated with this arc-arc collision zone. Thicknesses of low-density material of up to 15 km beneath 2 km of water can account for the free air gravity anomaly, which reaches values as low as -230 mGal. Complex travel time curves and high seismic attenuation are characteristic of refraction profiles run within the Molucca Sea collision complex. The collision complex can be interpreted as being composed of two distinct constant velocity layers. The overall similarity between travel time curves coupled with anomalous travel times on the scale of a few kilometers suggests the internal structure of the collision complex to be that of blocks with dimensions of the order of several tens of kilometers embedded in a deformed matrix showing a continuous and nearly linear increase in compressional velocity with depth. (27 refs.)

64098 Crustal structure across the Mariana island arc. S.L.LaTraille, D.M.Hussong (Inst. of Geophys., Univ. of Hawaii, Honolulu, HI, USA).

In book: *Tectonic and geologic evolution of southeast asian seas and islands*, D.E.Hayes [Ed.], p.209-21. Washington, DC, USA: American Geophysical Union (1980), v+326 pp. [0 87590 023 2]

Crustal structure across the Mariana island arc system from the Pacific plate to the Mariana Trough has been determined from 26 explosion seismic refraction profiles along a 750-km east-west line at 18°N latitude. In the northern Mariana Basin, old Pacific plate crust east of the Mariana Trench has an average thickness of 7 km, but unusually thick layers have seismic velocities of 3.1-4.3 and 5.3-5.9 km/s. The thick upper layers with low seismic velocities may be a result of midplate seamount volcanism related to the nearby Magellan seamounts. On the western side of the trench, thick sequences of low-velocity fore arc material (3.3-4.3 km/s) are found. The uppermost sediments decrease in thickness toward the trench, whereas underlying rocks with velocities between 3.5 and 5.8 km/s increase in thickness toward the trench. A relatively continuous layer with velocities from 6.1 to 6.5 km/s occurs across the entire fore arc at a depth of about 7 km. Moho velocities were not detected beneath the fore arc. In the Mariana Trough, an actively extensional back arc basin, the crust is laterally heterogeneous but in general has low seismic velocities and an average total thickness of only about 5 km. The crust may thin toward the center of the basin, where attenuation of seismic energy increases. The young back arc basin crust has seismic velocity structure similar to that found in slow-spreading midoceanic ridges. (32 refs.)

64099 1980 update of heat flow in the east and southeast Asian seas. R.N.Anderson (Lamont-Doherty Geological Obs., Columbia Univ., Palisades, NY, USA).

In book: *Tectonic and geologic evolution of southeast asian seas and islands*, D.E.Hayes [Ed.], p.319-26. Washington, DC, USA: American Geophysical Union (1980), v+326 pp. [0 87590 023 2]

Heat flow in the marginal basins of east and southeast Asia either agrees with heat predicted for the basin's age from lithospheric cooling plate models or is highly variable (order-of-magnitude variations over tens of kilometers). However, marginal basins do have large depth versus age discrepancies in comparison to those of midoceanic ridge-generated lithosphere. Thus this elevation difference must be caused not by thermal contrasts but by dynamic or density variations unrelated to the geothermal structure of the lithosphere. Heat flow in the arc-trench gap is much more complex than was previously thought, the accretionary prism having low heat flow and the fore arc basin having considerably higher heat flow. (30 refs.)

Tectonic and geologic evolution of southeast asian seas and islands See Entry 59545

Volume dependence of melting temperature at high pressure and its relation to a new dimensionless quantity See Entry 62064

A forecast of geothermal drilling activity See Entry 63640

Marine magnetic anomalies from the western Philippine Sea: implications for the evolution of marginal basins See Entry 64036

Paleomagnetism of Truk Islands, eastern Carolines and of Saipan, Marianas See Entry 64037

Paleomagnetic synthesis for southeast Asia: constraints on plate motions See Entry 64038

The spatial distribution of earthquakes, focal mechanism solutions, and subducted lithosphere in the Philippine and northeastern Indonesian Islands See Entry 64065

Crustal deformation studies and earthquake prediction research See Entry 64076

Neotectonic deformation, near-surface movements and systematic errors in US relieving measurements: implications for earthquake prediction See Entry 64077

Variations of the temperature, melt composition and water pressure during olivine crystallization in oceanic rocks from the Piton Fournaise volcano (Reunion Island, 1966 eruption) See Entry 64100

Surface deformation in volcanic rift zones See Entry 64101

The petrology and tectonics of Recent volcanism in the central Philippine Islands See Entry 64102

Geochemistry and K/Ar ages of volcanics dredged in the Philippine Sea (Mariana, Yap, and Palau Trenches and Parece Vela Basin) See Entry 64103

Primitive arc volcanism and a boninite series: examples from Western Pacific island arcs See Entry 64104

Dating on the extensive tectonism in the North-Aegean region (Greece): palynologic data See Entry 64105

The role of rifting in the tectonic development of the midcontinent, USA See Entry 64108

Geologic and geochemical evidence for the nature and development of the Middle Proterozoic (Keweenaw) Midcontinent Rift of North America See Entry 64109

Origin of the Oslo Graben in relation to the Hercynian-Alleghanian orogeny and lithospheric rifting in the North Atlantic See Entry 64110

Active versus passive continental rifting: evidence from the West African rift system See Entry 64111

Tectonic and geologic evolution of the Espanola basin, Rio Grande rift: structure, rate of extension, and relation to the state of stress in the western United States See Entry 64112

Continental rift jumps See Entry 64113

The chemical and thermal evolution of rifts See Entry 64114

Major stages of rifting evolution in the Earth's history See Entry 64115

The tectonic evolution of the South China Basin See Entry 64120

Discrimination of tectonic displacement from slope-dependent errors in geodetic leveling from southern California, 1953-79 See Entry 64121

Height dependent errors in southern California leveling See Entry 64122

An asperity model of large earthquake sequences See Entry 64123

Var and Pailon canyons (Southern Alps Margin-Western Mediterranean): a Quaternary origin through sliding See Entry 64127

Evidence for Eocene oceanic crust in the Celebes Basin See Entry 64132

The structure and evolution of the Central Basin Fault, West Philippine Basin See Entry 64133

Morphology and shallow structure of the lower trench slope off Nias Island, Sunda Arc See Entry 64135

Evolution of back arc spreading and arch volcanism in the Philippine Sea: interpretation of Leg 59 DSDP results See Entry 64137

Continental rifting and porphyry-molybdenum occurrences in the Oslo region, Norway See Entry 64138

Variations in geologic structure along the Sunda fore arc, northeastern Indian Ocean See Entry 64139

Earthquake prediction program in Japan See Entry 64240

Interpretation of SIR-A Seasat and Landsat coregistered data over Algerian plays See Entry 64242

- Coal analysis by nuclear methods See Entry 64246
- In-situ analysis of coal by measurement of neutron-induced prompt γ -rays See Entry 64247
- Multi-element analysis of coal during borehole logging by measurement of prompt γ -rays from thermal neutron capture See Entry 64248
- Measurement of the thermal neutron absorption cross section of rock samples See Entry 64251
- Advances in gamma-gamma logging See Entry 64252
- Airborne γ -ray spectrometry in uranium exploration. Principles and current practice See Entry 64254
- Determination of the concentration of uranium in soil and stream sediment samples using a high resolution energy-dispersive X-ray fluorescence analyser See Entry 64258
- Uranium isotopic disequilibrium in ground water as an indicator of anomalies See Entry 64259
- A universal gamma-gamma method for simultaneous determination of rock and ore properties See Entry 64260
- The combination of multi-element neutron activation analysis and multivariate statistics for characterisation in geochemistry See Entry 64261
- Mineral exploration of the sea bed by towed sea bed spectrometers See Entry 64262

91.40 VOLCANOLOGY

64100 Variations of the temperature, melt composition and water pressure during olivine crystallization in oceanic rocks from the Piton Fournaise volcano (Reunion Island, 1966 eruption). A.Sobolev (Acad. of Sci., Moscow, USSR), R.Clocchiatti, P.Dhamelincourt. *C.R. Seances Acad. Sci. Ser. II (France)*, vol.296, no.4, p.275-80 (31 Jan. 1983). In French.

An optical thermometry study of melt inclusions trapped in olivine phenocrysts obtained from the Piton Fournaise volcano shows that these minerals crystallized in the temperature range of 1240 to 1195°C \pm 10°C with a simultaneous change of the melt composition (MgO content from 9 to 7.6% wt). It is also noticed that the observed rise of the homogenization temperature with the duration of experiments and the simultaneous oxidation of the melt can be inferred as direct signs of water existence in the basalt system. Water occurrence in the CO₂ bearing coexisting fluid and melt inclusions was proved using a Raman laser microprobe. The spectra were obtained at a temperature near the critical point of H₂O and the p(H₂O)/p(CO₂) ratio was measured. (16 refs.)

64101 Surface deformation in volcanic rift zones. D.D.Pollard, P.T.Delaney, W.A.Duffield, E.T.Endo, A.T.Okamura (US Geological Survey, Menlo Park, CA, USA).

Tectonophysics (Netherlands), vol.94, no.1-4, p.541-84 (1983). (Conference on the Processes of Planetary Rifting, St. Helena, CA, USA, 3-5 Dec. 1981). The principal conduits for magma transport within rift zones of basaltic volcanoes are steeply dipping dikes, some of which feed fissure eruptions. Elastic displacements accompanying a single dike-like emplacement elevate the flanks of the rift relative to a central depression. Concomitant normal faulting may transform the depression into a graben thus accentuating the topographic features of the rift. If eruption occurs the characteristic ridge-trough-ridge displacement profile changes to a single ridge, centered at the fissure, and the erupted lava alters the local topography. To investigate this process the authors compute the elastic displacements and stresses in a homogeneous, two-dimensional half-space driven by a pressurized crack that may breach the surface. A derivative graphical method permits one to estimate the three geometric parameters of the dike and the mechanical parameter from a smoothly varying displacement profile. Direct comparison of measured and theoretical profiles may be used to estimate these parameters even if inelastic deformation, notably normal faulting, creates discontinuities in the profile.

64102 The petrology and tectonics of Recent volcanism in the central Philippine Islands. A.F.Divis (Environmental Sci. Associates, Wheat Ridge, CO, USA).

In book: *Tectonic and geologic evolution of southeast asian seas and islands*, D.E.Hayes [Ed.], p.127-44. Washington, DC, USA: American Geophysical Union (1980), v+326 pp. [0 87590 023 2]

Recent volcanism in the central Philippines occurs along two principal north-south chains. The eastern Bicol chain probably results from subduction in shallow dipping zone associated with the Philippine Trench. An older, more steeply dipping zone tends northward from the Sulu (Sibutu-Basilan) arc to northwestern Luzon and has tholeiitic, calc-alkaline, and shoshonitic eruptive centers which may be the result of subduction in the Manila and Sulu trenches. The Bicol chain and the western Zambales-Zamboanga chain erupt lavas which are principally pyroxene-hornblende andesites. Phreatic eruptions of alkaline-andesite affinity occur along an east-west zone in central Luzon that may be a 'leaky transform fault' joining the most active portions of the Philippine and Manila Benioff zones. Systematic trace element variations within and between the Bicol and Zambales-Zamboanga volcanic arcs suggest an origin by partial melting of the subducted slab with secondary crustal contamination and crystal fractionation having only a minor role in magma evolution. A 'pseudoisochron' relationship between ⁸⁷Sr/⁸⁶Sr and ⁸⁷Rb/⁸⁶Sr yields an apparent age of approximately 51.8 m.y. It is inferred that this relation may be derived by sequential anatexis of mineral phases showing isotopic disequilibrium. Regional zonation of trace elements in lavas parallels that reported for subduction zone depth variation in porphyry copper, molybdenum, and tin deposits in southwestern North America and the Andes. (49 refs.)

64103 Geochemistry and K/Ar ages of volcanics dredged in the Philippine Sea (Mariana, Yap, and Palau Trenches and Parece Vela Basin). L.Becallava, G.Macciotta (Istituto di Petrografia, Univ. di Parma, Parma, Italy), C.Savelli, G.Serri, O.Zeda.

In book: *Tectonic and geologic evolution of southeast asian seas and islands*, D.E.Hayes [Ed.], p.247-68. Washington, DC, USA: American Geophysical Union (1980), v+326 pp. [0 87590 023 2]

Volcanic rocks dredged from inner and outer walls of the Mariana, Yap, and Palau trenches show different petrogenetic affinities related to different original tectonic settings. From the Pacific side of the trenches, either ocean floor tholeiites, generated at diverging plate margins, or ocean island tholeiites and alkali basalts, probably related to off-ridge volcanism, have been recovered. Dredge hauls from Yap and Palau near-shore trench walls yielded volcanic rocks belonging to island arc tholeiite and calc-alkalic series, respectively. From the near-shore slope of the Mariana Trench, in addition to island arc magmatic products (boninites, andesites, and low-Ti basalts), tholeiitic and transitional basalts possibly generated during interarc spreading were also found. The constant presence in the inner trench walls of island-arc-

interarc-derived products can be attributed to a progressive consumption, by subduction, of faulted blocks from the leading edge of the overriding island arc plate. From a general reconstruction of the volcanic events in the area it appears that the inception of interarc spreading for the Parece Vela Basin and Mariana Trough took place after the magmatic activity ceased in the respective remnant arcs and long before a new island arc volcanism started to the east. (102 refs.)

64104 Primitive arc volcanism and a boninite series: examples from Western Pacific island arcs. A.Meijer (Dept. of Geosci., Univ. of Arizona, Tucson, AZ, USA).

In book: *Tectonic and geologic evolution of southeast asian seas and islands*, D.E.Hayes [Ed.], p.269-82. Washington, DC, USA: American Geophysical Union (1980), v+326 pp. [0 87590 023 2]

Recent drilling, dredging, and field studies have delineated an unusual series of high Mg, low Ti lavas in several western Pacific island arcs. Included in this series are olivine-bronzite andesites long known as boninites. On the basis of their distinctive chemical characteristics, the high Mg, low Ti lavas are discussed as a separate magma series—the boninite series. Relative to the arc tholeiite series, rocks of the boninite series are enriched in refractory elements such as Mg, Ni, and Cr, are depleted in the high-field-strength ions Ti, Zr, Y, and rare-earth elements, and are generally higher in primary volatile contents. In the Mariana and Bonin arcs, Late Eocene to Oligocene boninite series lavas are invariably associated with older lavas of the arc tholeiite series. Field and laboratory studies suggest the arc tholeiite and boninite series magmas were derived from the mantle wedge overlying the Mariana-Bonin subduction zone. Melting of the wedge, driven by the introduction of a fluid phase exsolved from the subducted lithosphere, initially produced arc tholeiite series magmas and, later, less voluminous boninite series magmas. The production of boninite series magmas apparently requires unusually high geothermal gradients in the mantle overlying a subduction zone. (77 refs.)

The spatial distribution of earthquakes, focal mechanism solutions, and subducted lithosphere in the Philippine and northeastern Indonesian Islands See Entry 64065

Crustal structure across the Mariana island arc See Entry 64098

Tectonic and geologic evolution of the Espanola basin, Rio Grande rift: structure, rate of extension, and relation to the state of stress in the western United States See Entry 64112

Evolution of back arc spreading and arch volcanism in the Philippine Sea: interpretation of Leg 59 DSDP results See Entry 64137

Expendable bubble tiltmeter for geophysical monitoring See Entry 64270

A comparison of volcanic eruption processes on Earth, Moon, Mars, Io and Venus See Entry 64408

91.45 PHYSICS OF PLATE TECTONICS

64105 Dating on the extensive tectonism in the North-Aegean region (Greece): palynologic data. N.Lyberis (Lab. de Geodynamique, Univ. Paris VI, Paris, France), J.Sauvage.

C.R. Seances Acad. Sci. Ser. II (France), vol.296, no.1, p.107-10 (10 Jan. 1983). In French.

The North Aegean trough and the associated subsiding basins are the most relevant features of the North Aegean area. Their occurrence is due to an extensive tectonic phase posterior to the compressive phase of the Middle Miocene. Palynologic analysis of samples taken from two adjacent islands (Samos and Thasos) allow an upper Miocene age to be given for the opening of the North Aegean trough. (16 refs.)

64106 Prospect for numerical information on finite rock strain from the separation of magnetic anisotropy components. L.Daly, B.Henry (Lab. de Geomagnetisme, Saint-Maur, France).

C.R. Seances Acad. Sci. Ser. II (France), vol.296, no.2, p.153-6 (17 Jan. 1983). In French.

A method permitting the separation of low field susceptibility anisotropies (i) from ferrimagnetics, and (ii) from the matrix, was proposed previously in the case where principal axes are identical. This method is extended to the general case. It consists of analysing anisotropies on neighbouring specimens of a sample; the differences are due to a variation of respective percentages of the two mineralogical parts, whereas the strain rate is constant. An application is given, in which data on the isothermal remanent magnetization anisotropy allow the checking of the validity of the method, which opens up the prospect for calibrating finite strain in rocks. (10 refs.)

64107 Initial premises for construction of a mathematical model of island arc formation. M.A.Ivakhnenko (Inst. of Cybernetics, Acad. of Sci., Ukrainian SSR).

Sov. Autom. Control (USA), vol.15, no.3, p.80-4 (May-June 1982). Translation of: *Avtomatika (USSR)*, vol.15, no.3, p.81-4 (May-June 1982). [received: April 1983]

Examination of the lineaments of the Earth's surface, including the island arcs, leads one to conjecture that they were formed by wave process. Measurements of distances between such lineaments and midocean ridges, followed by statistical processing of the results, verifies the wave theory. The nature of these waves is similar to that of wind waves, but the role of wind is played by the flow of the mantle material. Mechanical and chemical waves can also participate in this process, and this should be taken into account in construction of a model of the process of formation of island arcs. (7 refs.)

64108 The role of rifting in the tectonic development of the midcontinent, USA. G.R.Keller (Dept. of Geological Sci., Univ. of Texas, El Paso, TX, USA), E.G.Lidiak, W.J.Hinze, L.W.Braile.

Tectonophysics (Netherlands), vol.94, no.1-4, p.391-412 (1983). (Conference on the Processes of Planetary Rifting, St. Helena, CA, USA, 3-5 Dec. 1981).

Recent studies have proposed the existence of several major ancient rift zones in the midcontinent region of North America. Although the dating of some of these rifts are subject to question, an analysis of these 'paleo-rifts' reveals three major episodes of rifting: Keweenaw (~1.1 b.y. BP), Eocambrian (~600 m.y. BP), and Early Mesozoic (~200 m.y. BP). The extent of these events, documents that rifting has played a major role in the tectonic development of the midcontinent region. This role goes well beyond the initial rifting event because these features display a strong correlation with Paleozoic basins and a strong propensity for reactivation. Even though the importance of rifting can be established, recognition of rifts and delineation of their complexities remain a major problem which requires more study.

64109 Geologic and geochemical evidence for the nature and development of the Middle Proterozoic (Keweenaw) Midcontinent Rift of North America. J.C.Green (Geology Dept., Univ. Minnesota, Duluth, MN, USA).

Tectonophysics (Netherlands), vol.94, no.1-4, p.413-37 (1983). (Conference on the Processes of Planetary Rifting, St. Helena, CA, USA, 3-5 Dec. 1981).

General models of active continental rifting must take into account the large plateau basalt provinces, many of which have been precursors of or associated

with continental breakup. The Keweenaw (Middle Proterozoic) Midcontinent Rift (MCR) of North America, 2300 km long, is one such major continental rift, but it aborted before significant crustal separation was achieved. These plateau-basalt rifts, including the MCR, differ from the East African type in being dominated by broad subsidence rather than rift valleys, tholeiitic flood basalts rather than alkalic central volcanoes, and large positive gravity anomalies. Geologic and geophysical evidence is reviewed which contradicts some recent models which have been proposed for the development of the MCR.

64110 Origin of the Oslo Graben in relation to the Hercynian-Alleghenian orogeny and lithospheric rifting in the North Atlantic. M.J. Russell, D.K. Smythe (Dept. of Appl. Geology, Univ. of Strathclyde, Glasgow, Scotland).

Tectonophysics (Netherlands), vol.94, no.1-4, p.457-72 (1983). (Conference on the Processes of Planetary Rifting, St. Helena, CA, USA, 3-5 Dec. 1981). The contemporaneous extrusion of basalts in the Oslo Graben and intrusion and dolerites in northern Britain and southern Sweden at ~295 Ma calls for a common explanation. Two hypotheses are investigated: (1) the Graben and dykes resulted from extensional stresses associated with progressive lithosphere separation to the northwest of Europe in the Late Carboniferous; (2) the dykes, and therefore the Graben, were related in the same way to oblique collision of plates in the Hercynian orogeny which was developing to the south.

64111 Active versus passive continental rifting: evidence from the West African rift system. J.G. Fitton (Grant Inst. of Geology, Univ. of Edinburgh, Edinburgh, Scotland).

Tectonophysics (Netherlands), vol.94, no.1-4, p.473-81 (1983). (Conference on the Processes of Planetary Rifting, St. Helena, CA, USA, 3-5 Dec. 1981). The West African rift system comprises the Cretaceous Benue trough and the Tertiary to Recent volcanic Cameroon line. The two features are remarkably similar in shape and size and may be superimposed perfectly by rotating one with respect to the other by 7° about a pole in Sudan. Three stages in the geological history of the system are postulated. (1) The Benue trough was produced by lithosphere stretching as one arm of an RRR triple junction during the early stages of the opening of the South Atlantic. (2) At about 80 Ma (Santonian) a short-lived period of clockwise rotation interrupted the otherwise anticlockwise rotation of Africa and decoupled the lithosphere from the asthenosphere. The hot zone in the asthenosphere beneath the Benue trough thus became displaced relative to the lithosphere and moved to a new position beneath Cameroon and the Gulf of Guinea. (3) Anticlockwise rotation and asthenosphere-lithosphere coupling were restored allowing the hot zone to manifest itself as the Cameroon line.

64112 Tectonic and geologic evolution of the Espanola basin, Rio Grande rift: structure, rate of extension, and relation to the state of stress in the western United States. M.P. Golombek, G.E. McGill, L. Brown (Lunar & Planetary Inst., Houston, TX, USA).

Tectonophysics (Netherlands), vol.94, no.1-4, p.483-507 (1983). (Conference on the Processes of Planetary Rifting, St. Helena, CA, USA, 3-5 Dec. 1981). The Espanola basin of the Rio Grande rift began as a broad crustal down-warp in latest Oligocene time. The localized early faulting ended before the filling of the central Espanola basin was completed about 10 m.y. ago. Movement on faults that define the present western margin of the Espanola basin began ~10 m.y. ago. Jemez Mountain volcanism, in the western Espanola basin, also began at about this same time. West tilting of up to 30° occurred due to movement along pervasive N-trending intrabasin faults about 7.5 m.y. ago in conjunction with continued movement along the western border faults. Volcanism continued after this tilting, forming many of the large volcanic constructs of the Jemez Mountains. Regional uplift of the entire northern Rio Grande rift began ~7 m.y. ago. Movement on the Pajarito fault zone began about 5 m.y. ago and continues to the present. This fault zone defines the western margin of the Velarde graben. A change in the last principal stress direction from WSW-ENE to WNW-ESE that occurred throughout the western United States about 10 m.y. ago coincides with a roughly 3.5 times increase in the rate of extension, preferential development and movement of N- to NE-trending normal faults, and a few degrees of clockwise rotation of rocks in the western Espanola basin. Accelerated uplift of the northern Rio Grande rift also occurred at about this time indicating that activity in the entire Rio Grande rift was modulated by this change in extension direction ~10 m.y. ago that appears related to Pacific-North American plate interactions.

64113 Continental rift jumps. C.A. Wood (NASA Johnson Space Center, Houston, TX, USA).

Tectonophysics (Netherlands), vol.94, no.1-4, p.529-40 (1983). (Conference on the Processes of Planetary Rifting, St. Helena, CA, USA, 3-5 Dec. 1981). Continental rift jumps, analogous to jumps of oceanic spreading ridges, are here proposed to be common. Good examples exist in Iceland and Afar (both transitional from ridge to rift jumps), West Africa (Benue Trough and Cameroon Volcanic Line), and Kenya. Indeed, the Kenya rift appears to have jumped c. 100 km eastward c. 10 m.y. ago and is currently jumping further to the east. Possible jumps exist in the Baikal rift, the Limagne-Bresse rift pair, and parallel to ancient continental margins. Continental rifts jump distances that are approximately equal to local lithosphere thickness, suggesting that jumped rifts are controlled by lithosphere fracturing, but there appears to be no reason for the fracturing except migration of hot spots.

64114 The chemical and thermal evolution of rifts. D.K. Bailey (Dept. of Geology, Univ. of Reading, Reading, England).

Tectonophysics (Netherlands), vol.94, no.1-4, p.585-97 (1983). (Conference on the Processes of Planetary Rifting, St. Helena, CA, USA, 3-5 Dec. 1981). Any concept of the development of continental rifts requires the integration of observations on lithosphere structure, movements, and magmatic geology, with the ore customary geologic and geophysical evidence. Timing is crucial, and only the magmatism can chronicle the chemical and thermal changes in the underlying mantle. Control of the activity by older structures in the lithosphere is clear from the repetition of alkaline magmatism, which marks the release of gas-charged magmas from deep sources repeatedly tapped by reopening of lesions in the continental plate. Frequently this activity is found in ancient cratons where it perforates deeply eroded sections of granulites, themselves highly depleted in volatiles and presumably indicating a similar condition in the underlying mantle. This activity pattern, the abundance of volatiles and incompatible elements, and the capricious volcanic distributions, are explicable if the continental lithosphere acts as a template through which volatiles are channelled from the Earth's interior.

64115 Major stages of rifting evolution in the Earth's history. E.E. Milanovsky (Geological Dept., Moscow State Univ., Moscow, USSR).

Tectonophysics (Netherlands), vol.94, no.1-4, p.599-607 (1983). (Conference on the Processes of Planetary Rifting, St. Helena, CA, USA, 3-5 Dec. 1981). Linear extensional rift and rift-like structures have been generated many times during various periods of the Earth's history since early times. These structures have varied with time, however, in scale, morphology, formations,

paragenesis of tectonic features, regularity of distribution, and evolution. The author distinguishes and considers five major stages of rifting. They are: Katarchean-Archean, early Proterozoic, late Proterozoic, Paleozoic, and Mesozoic-Cenozoic.

64116 Computer fitting of continents. A.M. Hurley (British Nat. Oil Corp., Glasgow, Scotland), A.G. Smith.

In book: *Paleoreconstruction of the continents*, M.W. McElhinny, D.A. Valencio [Ed.], p.5-11. Washington, DC, USA: American Geophysical Union (1981), 194 pp.

Reviews methods of fitting continents using morphological contours together and provides a bibliography of relevant publications. (35 refs.)

64117 Pre-Cenozoic palynology and continental movements. E.M. Truswell (Bur. of Mineral Resources, Canberra, Australia).

In book: *Paleoreconstruction of the continents*, M.W. McElhinny, D.A. Valencio [Ed.], p.13-25. Washington, DC, USA: American Geophysical Union (1981), 194 pp.

Reviews developments in palynology, through the years 1970-79 as these relate to pre-Tertiary plate motions and continental positions. Discussion is restricted to those organic-walled microfossils of plant origin that are extracted after conventional recovery methods involving the maceration of rock samples with hydrochloric and hydrofluoric acids. As such, it encompasses the pollen and spores produced by terrestrial plants, and the resting cysts of marine algae—the dinoflagellates and acritarchs. (109 refs.)

64118 Paleozoic paleogeography. A.M. Zeigler (Dept. of Geophysical Sci., Univ. of Chicago, Chicago, IL, USA).

In book: *Paleoreconstruction of the continents*, M.W. McElhinny, D.A. Valencio [Ed.], p.31-7. Washington, DC, USA: American Geophysical Union (1981), 194 pp.

Reviews the available regional and world-wide reconstructions of the topography and bathymetry of the Paleozoic periods. A number of syntheses are available which show the continents in pre-Pangaea configurations. These use paleoclimatic, biogeographic and tectonic arguments to supplement the paleomagnetic data regarding the locations of the continents. Although a diversity of opinion has been expressed with respect to the orientation and even the east-to-west order of the continents, the maps of various authors share much in common. Doubtless, many of the finer details of Paleozoic plate relationships will be determined in the next few years as a number of groups are currently working on the topic. (33 refs.)

64119 Arctic seafloor structure and tectonic evolution. J.F. Sweeney (Dept. of Energy, Mines & Resources, Ottawa, Canada).

In book: *Paleoreconstruction of the continents*, M.W. McElhinny, D.A. Valencio [Ed.], p.55-64. Washington, DC, USA: American Geophysical Union (1981), 194 pp.

The age and present structure of much of the Arctic Basin has remained a mystery largely because of the unusual nature of many features of the seafloor and the lack of adequate geophysical data coverage over most of the ocean. This situation is rapidly changing as the results of several Arctic geophysical studies become known. It is now believed the Arctic Basin was created during Early Cretaceous time by the rotation of northern Alaska and the Chukotsk Peninsula away from northern Canada. The rotation may have been initiated by stress produced in the Arctic by the opening of the North Atlantic ocean. Geophysical and geological evidence from Arctic Canada and north of Alaska suggests that the North American margin of Canada Basin was created by rifting during Early Cretaceous time. (75 refs.)

64120 The tectonic evolution of the South China Basin. B. Taylor, D.E. Hayes (Lamont-Doherty Geological Obs., Columbia Univ., Palisades, NY, USA).

In book: *Tectonic and geologic evolution of southeast Asian seas and islands*, D.E. Hayes [Ed.], p.89-104. Washington, DC, USA: American Geophysical Union (1980), v+326 pp. [0 87590 023 2]

The analysis of new and previously existing magnetic data has made it possible to identify a symmetric pattern of seafloor spreading in the South China Basin; this spreading was active from the mid-Oligocene to the Early Miocene (32-17 m.y. BP). The observed trend of magnetic lineations is approximately east-west, and the position of the relict spreading center coincides closely with the east-trending linear chain of seamounts near 15°N. The pattern of identifiable anomalies is confined to the eastern half of the basin. Magnetic quiet zones occur landward of the slope-basin boundary of the China and Reed-Bank Block margins. The quiet zone boundary is associated with a characteristic free-air gravity minimum and probably marks the location of the transition from oceanic to continental crust. Bore hole stratigraphic data from both the China shelf and the Reed Bank support the authors' conclusions regarding the timing of rifting and spreading indicated by the magnetic lineations. The eastern most extension of the Palawan Trough subduction zone is probably defined by the Uluang Fault. Northern Palawan was most likely attached to the Reed-Bank Block and the China Margin prior to the mid-Oligocene. The western third of the South China Basin is still poorly surveyed, but limited data suggest that there is a major change in spreading fabric in the southwestern corner of the basin. (45 refs.)

64121 Discrimination of tectonic displacement from slope-dependent errors in geodetic leveling from southern California, 1953-79. R.S. Stein (Lamont-Doherty Geological Obs., Columbia Univ., Palisades, NY, USA).

Earthquake Prediction. An International Review. Symposium on Earthquake Prediction, Mohonk, NY, USA, 12-16 May 1980 (Washington, DC, USA: American Geophys. Union 1981), p.441-56

Jackson et al. (1980) contend that leveling before 1964 suffers from the accumulation of elevation-dependent errors in excess of one part in ten thousand times the topographic height difference (dH), or greater than 100 mm over 1000 m of relief. The contention of Jackson et al. is probed by a number of independent tests on 1100 km of levels carried out between 1953 and 1979 within the uplifted region. (24 refs.)

64122 Height dependent errors in southern California leveling. D.D. Jackson, W.B. Lee, C.-C. Liu (Dept. of Earth & Space Sci., Univ. of California, Los Angeles, CA, USA).

Earthquake Prediction. An International Review. Symposium on Earthquake Prediction, Mohonk, NY, USA, 12-16 May 1980 (Washington, DC, USA: American Geophys. Union 1981), p.457-72

For many profiles in southern California, the tilts inferred from repeat leveling data are strongly correlated with slopes. The ratio of tilt to slope at short wavelengths is nearly equal to that for long wavelengths, suggesting that the correlation results from height dependent systematic errors. A careful analysis of leveling data for southern California suggests to the authors that the reported aseismic uplift (Castle et al., 1976, 1977) can be more plausibly explained as the result of nontectonic effects including systematic leveling errors. (25 refs.)

64123 An asperity model of large earthquake sequences. T.Lay, H.Kanamori (Seismological Lab., California Inst. of Technol., Pasadena, CA, USA).

Earthquake Prediction. An International Review. Symposium on Earthquake Prediction, Mohonk, NY, USA, 12-16 May 1980 (Washington, DC, USA: American Geophys. Union 1981), p.579-92.

The variation in maximum rupture extent of large shallow earthquakes in circum-Pacific subduction zones is interpreted in the context of the asperity model of stress distribution on the fault plane. Four fundamental categories of behavior are observed. These are: (1) the Chile-type regular occurrence of great ruptures spanning more than 500 km; (2) the Aleutians-type variation in rupture extent with occasional ruptures up to 500 km long, and temporal clustering of large events; (3) the Kurile-type repeated failure over a limited zone of 100-300 km length in isolated events; and (4) the Marianas-type absence of large earthquakes. Southern Chile, Alaska, Southern Kamchatka, and possibly the Central Aleutians are grouped in the first category. The parameters governing large earthquake development are clarified. Interpretation of the four categories in terms of asperity distribution and interaction permits some inferences of the nature of stress distribution in particular zones. (70 refs.)

Paleoreconstruction of the continents See Entry 59544

Tectonic and geologic evolution of southeast Asian seas and islands See Entry 59545

A review of the paleomagnetism of Australia and Antarctica See Entry 64027

Phanerozoic palaeomagnetism of the Indian plate and the India-Asia collision See Entry 64028

Paleomagnetism of South American rocks and the dynamic processes related with the fragmentation of western Gondwana See Entry 64029

Pre-Neogene paleomagnetism of Japanese islands (and vicinities) See Entry 64030

Paleomagnetism of southeast and east Asia See Entry 64031

Pre-Carboniferous paleomagnetism of Europe north of the Alpine orogenic belt See Entry 64032

Pre-Cenozoic paleomagnetism of southern Europe/Middle East See Entry 64033

Paleomagnetism of the Soviet Union See Entry 64035

Marine magnetic anomalies from the western Philippine Sea: implications for the evolution of marginal basins See Entry 64036

Paleomagnetism of Truk Islands, eastern Carolines and of Saipan, Marianas See Entry 64037

Paleomagnetic synthesis for southeast Asia: constraints on plate motions See Entry 64038

The Charlevoix earthquake of 19 August 1979 and its seismo-tectonic environment See Entry 64044

The spatial distribution of earthquakes, focal mechanism solutions, and subducted lithosphere in the Philippine and northeastern Indonesian Islands See Entry 64065

Seismicity and tectonics of the central New Hebrides island arc See Entry 64068

The 1906 San Francisco earthquake and the seismic cycle See Entry 64069

Repeat time of great earthquakes along simple plate boundaries See Entry 64072

Great detachment earthquakes along the Himalayan Arc and long-term forecasting See Entry 64073

Specification of a soon-to-occur seismic faulting in the Tokai District, central Japan, based upon seismotectonics See Entry 64074

Crustal deformation studies and earthquake prediction research See Entry 64076

Neotectonic deformation, near-surface movements and systematic errors in US revealing measurements: implications for earthquake prediction See Entry 64077

Gneissic intercalations within a tectonic unit from the Piedmont Ophiolite Nappe in the Western Alps: Record of a subducted continental margin? See Entry 64082

The allochthony of the 'Zone des Diapirs' in Northern Tunisia See Entry 64083

Discovery of a new nappe from the north-east in the Parnassus zone (Greece) See Entry 64084

The lithosphere in the Central-eastern Mediterranean area See Entry 64091

Timing and chemistry of igneous events associated with the Southern Oklahoma Aulacogen See Entry 64093

The Morton-Black hypothesis for the thinning of continental crust—revisited in western Afar See Entry 64094

Accumulation of fossil fuels and metallic minerals in active and ancient rift lakes See Entry 64095

Geothermal resources of rifts: a comparison of the Rio Grande Rift and the Salton Trough See Entry 64096

Crustal structure of the Molucca Sea collision zone, Indonesia See Entry 64097

Crustal structure across the Mariana island arc See Entry 64098

1980 update of heat flow in the east and southeast Asian seas See Entry 64099

Surface deformation in volcanic rift zones See Entry 64101

The petrology and tectonics of Recent volcanism in the central Philippine Islands See Entry 64102

Geochemistry and K/Ar ages of volcanics dredged in the Philippine Sea (Mariana, Yap, and Palau Trenches and Parece Vela Basin) See Entry 64103

Primitive arc volcanism and a boninite series: examples from Western Pacific island arcs See Entry 64104

Evidence for Eocene oceanic crust in the Celebes Basin See Entry 64132

The structure and evolution of the Central Basin Fault, West Philippine Basin See Entry 64133

Morphology and shallow structure of the lower trench slope off Nias Island, Sunda Arc See Entry 64135

A seismic reflection study of faulting in the Mariana fore arc See Entry 64136

Evolution of back arc spreading and arch volcanism in the Philippine Sea: interpretation of Leg 59 DSDP results See Entry 64137

Continental rifting and porphyry-molybdenum occurrences in the Oslo region, Norway See Entry 64138

Variations in geologic structure along the Sunda fore arc, northeastern Indian Ocean See Entry 64139

91.50 MARINE GEOLOGY AND GEOPHYSICS

64124 Vertical sedimentation units in a barrier island washover fan. S.P.Leatherman (Geography Dept., Univ. of Maryland, College Park, MD, USA), A.T.Williams.

Earth Surf. Processes & Landforms (GB), vol.8, no.2, p.141-50 (March-April 1983).

Overwash is a major component of a barrier island's response to high energy conditions. Examination of the 19-20 March, 1975, storm deposits at Assateague Island, showed that an overwash sequence could be divided into sedimentation units. Interpretation depends upon defining textural and mineralogical combinations that can be logically ordered as a vertical sequence. If the sequence is depositional and formed from a single material, normal grading usually results; if polymineralogical and erosionally truncated, inverse grading with a top layer of heavy minerals can be formed via an in situ sorting process dependent on disturbance depth and overwash influence. (12 refs.)

64125 Systematic monthly morphologic variation of Assawoman Inlet: nature and causes. R.Slingerland (Dept. of Geosci., Pennsylvania State Univ., University Park, PA, USA).

Earth Surf. Processes & Landforms (GB), vol.8, no.2, p.161-9 (March-April 1983).

Assawoman Inlet, Virginia, USA, representative of small mesotidal barrier island tidal inlets exhibits systematic variations of sediment volume among certain of its morphologic elements. Sediment volume variations were calculated from topography-bathymetric maps of the inlet system, as surveyed on 11 occasions at approximately monthly intervals by a fathometer, and plane table and alidade. Of 36 pairings among nine morphologic elements, seven show statistically significant Pearson Product Moment Correlation Coefficients. The southern ramp margin shoals are negatively correlated with the southern beach face and the northern ramp margin shoals are negatively correlated with the northern beach face on the northern spit. The southern and northern ramp margin shoals themselves are negatively correlated. Some other erosional and depositional phenomena were studied. (16 refs.)

64126 Preliminary estimates of intertidal limestone erosion, One Tree Island, southern Great Barrier Reef, Australia. S.T.Trudgill (Dept. of Geography, Univ. of Sheffield, Sheffield, England).

Earth Surf. Processes & Landforms (GB), vol.8, no.2, p.189-93 (March-April 1983).

Estimations of surface lowering of 0.2-3.8 mm a⁻¹ were gained from measurements of pedestal heights under sedentary organisms. The role of erosion by chitons, estimated at 0.2-2.9 mm a⁻¹ for home scars and 0.2-0.7 mm a⁻¹ for grazing, and other bioerosive organisms, is briefly discussed. (18 refs.)

64127 Var and Pailion canyons (Southern Alps Margin-Western Mediterranean): a Quaternary origin through sliding. F.Guillocheau (Univ. de Bretagne, Brest, France), G.Pautot, J.M.Auzende.

C.R. Seances Acad. Sci. Ser. II (France), vol.296, no.1, p.91-6 (10 Jan. 1983). In French.

A morphological analysis of the Baie des Anges (Nice) Seabeam map has been carried out in order to investigate the genesis of the Var and Pailion submarine canyons. From the identification of the morphological units at different scales it is possible to propose a model for the formation of the canyons. The Var and Pailion canyons are interpreted as being cut in a deep-sea fan presently being destroyed by mass wasting processes. The structural framework exhibits an orthogonal fault system which plays a prominent role in the spatial distribution of the canyons and the sliding areas. The age of these canyons is thought to be Quaternary. (7 refs.)

64128 Acoustical classification of sea floor sediments. Meng Jin-sheng, Guan Dian-hua (Inst. of Acoustics, Acad. Sinica, Peking, China).

Acta Acust. (China), vol.7, no.6, p.337-43 (Nov. 1982). In Chinese.

Discusses the classification of seabed sediment using normally incident, high frequency sound pulses. A number of investigators used reflectivity of sound on the sea bottom and other quantities as features for classification of sediment types. The authors suggest a new feature which is independent of reflectivity and roughness of the seabed. The authors feature is extracted from relative form of echo envelope, it strongly correlates to attenuation of sound in sediments. The attenuation of sound is nearly proportional to frequency and at the authors frequency (120 kHz) the attenuation in different sediments varies over a tenfold range. In order to avoid the influence of surface backscattering, they used a directive transducer put near to the bottom. In the laboratory a Bayes classification was carried out by computer, and a fairly high success rate was achieved. (22 refs.)

64129 Bathymetric and oceanographic applications of Kalman filtering techniques. R.F.Brammer, R.P.Pass, J.V.White (Analytic Sci. Corp., Reading, MA, USA).

IEEE Trans. Autom. Control (USA), vol.AC-28, no.3, p.363-71 (March 1983).

Ocean currents and seamounts (underwater mountains) can be mapped by analyzing data from satellite radar altimeters. The paper describes the application of kalman filtering techniques to the analysis of such data acquired during the SEASAT mission. The altimeter data are modeled as samples from autoregressive random processes. Based on these models, matched filters are used to detect the characteristic nonstationarities in the altimeter data caused by seamounts and ocean currents such as the gulf stream. The geostrophic velocities of detected ocean currents are then estimated using Kalman smoothers. A useful formula is derived, which expresses the error power spectrum of the optimal fix lag smoother as a function of the lag and the error spectra of the optimal filter and the optimal infinite-lag smoother. (15 refs.)

64130 Microcomputer-aided analysis of hydroacoustical receiver signals. H.-D.Melzer, E.Muller (Sektion Tech. Elektronik, Wilhelm-Pieck-Univ., Rostock, Germany).

MSR (Mess. Steuern Regeln) (Germany), vol.26, no.3, p.150-4 (March 1983). In German.

The application of adaptive receiver structures for hydroacoustical sediment detection and identification requires microcomputer-aided signal processing in order to obtain on-line the a priori information necessary for optimization of the receiver equipment and to determine the interesting object parameters. The determination of the significant process parameters and indices for a specific tracking situation is carried out by an extensive analysis of the disturbed tracking signals reflected by the sea bed. (5 refs.)

64131 Sea-bed geology goes up the mountains. S.McCutcheon.*New Sci. (GB)*, vol.97, no.1346, p.510-13 (24 Feb. 1983).

By drilling into the mountains on Cyprus geologists are hoping to learn more about the sea bed. The highest rocks on the island, it seems, once lay deep beneath the sea. The author describes the activities of an informal group of earth scientists known as the International Crustal Research Drilling Group (ICRDG). (no refs.)

64132 Evidence for Eocene oceanic crust in the Celebes Basin. J.K.Weisel (Lamont-Doherty Geological Obs., Columbia Univ., Palisades, NY, USA).In book: *Tectonic and geologic evolution of southeast asian seas and islands*, D.E.Hayes [Ed.], p.37-47. Washington, DC, USA: American Geophysical Union (1980), v+326 pp. [0 87590 023 2]

Marine magnetic lineations identified as anomalies 18-20 (42-47 m.y. BP) are mapped striking approximately N65°E in the southwestern part of the Celebes Basin. Middle to late Eocene crustal ages inferred from the lineations are compatible with ages predicted from observed basement depths and heat flow. Subduction of unknown amounts of Celebes Basin crust long its margins at the presently active North Sulawesi and Cotabato trenches and possibly at the Sulu island arc during the Oligocene prevents a determination of the total duration of crustal accretion and original geographic extent of the crust in the basin. Analysis of magnetic anomaly shapes suggests little net change in latitude since the Eocene, but whether the basin has rotated during this time remains unresolved. While the Celebes Basin results are compatible with paleomagnetic measurements from Upper Cretaceous rocks in southwestern Borneo, distinctly different paleomagnetic results from the West Philippine Basin (also the Eocene age) indicate large relative displacement between the two marginal basins since the Eocene. By interpolation between observed crustal ages, heat flow, and basement depths from the South China and Celebes basins in Oligocene age is suggested for the Sulu Basin. (31 refs.)

64133 The structure and evolution of the Central Basin Fault, West Philippine Basin. S.D.Lewis, D.E.Hayes (Lamont-Doherty Geological Obs., Columbia Univ., Palisades, NY, USA).In book: *Tectonic and geologic evolution of southeast asian seas and islands*, D.E.Hayes [Ed.], p.77-88. Washington, DC, USA: American Geophysical Union (1980), v+326 pp. [0 87590 023 2]

Bathymetric and seismic profiler data were used to investigate the morphological and structural nature of the Central Basin Fault. The Central Basin Fault (CBF), a spreading ridge that was active during the early Tertiary, is composed of a series of ten echelon ridges and troughs whose individual trends are 280°-285°, while the regional trend of the large-scale zone of rough topography is more nearly 300°. Cross-strike offsets of linear deeps suggest the presence of several fracture zones. The CBF can be divided into three provinces on the basis of sediment distribution, morphology, and structural style. The southeastern province from the Palau-Kyushu Ridge to about 132°E is a region of rough basement topography that is elevated 600-800 m above the surrounding basin floor. Local deeps contain faulted and/or folded sediments up to 0.9 s in thickness. From 132°E to 128°E the central province is characterized by very rough basement topography and thin (<0.1 s) sediment cover. West of 128°E and CBF exhibits more subdued basement topography, which is often buried under thick sediments. Faulting is less frequent than in the southeast region, and east of 126°E the morphologic character of the CBF is lost. Strike-slip and normal faults with trends roughly parallel to the CBF can be recognized in the areas of the CBF where thick and well-stratified sediments are present to serve as markers for fault offset. Much of the observed faulting probably represents rejuvenation of the CBF as an active tectonic feature, following a late Eocene cessation of seafloor spreading. (20 refs.)

64134 Quaternary sedimentation processes in the South China Basin as revealed by echo-character mapping and piston-core studies. J.E.Damuth (Lamont-Doherty Geological Obs., Columbia Univ., Palisades, NY, USA).In book: *Tectonic and geologic evolution of southeast asian seas and islands*, D.E.Hayes [Ed.], p.105-25. Washington, DC, USA: American Geophysical Union (1980), v+326 pp. [0 87590 023 2]

Quaternary sedimentation throughout the South China Basin has been predominantly by downslope processes (e.g. turbidity currents and mass wasting). No evidence for sediment redistribution by thermohaline (contour) currents is observed. The seafloor of the basin returns eight discrete types of bottom echoes on 3.5 kHz echograms. These are all similar to echo types observed previously in the Atlantic Ocean. Various echo types reveal near-bottom sedimentation processes active within the basin as well as the distribution of coarse (silt/sand) sediment within the uppermost sea floor. A qualitative correlation is observed between relative abundance of bedded silt/sand in piston cores and three echo types. A large (~25000 km²) field of migrating sediment waves (echo type IIC) occurs on the down-bending seaward wall of the Manila Trench and parallels the trench floor for 450 km. The regional setting and sediments of these waves indicate that they have been formed by turbidity currents flowing southward along the Manila Trench floor. (55 refs.)

64135 Morphology and shallow structure of the lower trench slope off Nias Island, Sunda Arc. D.E.Karig (Dept. of Geological Sci., Cornell Univ., Ithaca, NY, USA), G.F.Moore, J.R.Curry, M.B.Lawrence.In book: *Tectonic and geologic evolution of southeast asian seas and islands*, D.E.Hayes [Ed.], p.179-208. Washington, DC, USA: American Geophysical Union (1980), v+326 pp. [0 87590 023 2]

The lower third of the slope between the Sunda Trench and Nias, on the trench slope break, was surveyed in detail as part of the Seatar Sumatra Transect. Oblique subduction of early Tertiary oceanic crust, which is overlain by 2-3 km of Nicobar Fan strata and by a trench wedge less than 500 m thick, has produced an accretionary prism with linear ridges and troughs. The lowermost trench slope is convex upward. Across the steepest decrease in slope, 20-30 km from the trench, there is an increased ridge spacing and a pronounced increase in the thickness of slope sediments. The basal ridge is uplifted along a thrust fault that dips 20°E beneath the arc and has several kilometers of horizontal displacement. Less than half the total convergence occurs on this basal thrust, with most of the remainder distributed across the steep basal slope. Very little convergence is absorbed across the rest of the trench slope, where large slope basins have developed. These basins are filled with several kilometers of turbidites that define arcward rotating sediment wedges rather than synclines. (65 refs.)

64136 A seismic reflection study of faulting in the Mariana fore arc. C.L.Mrozowski, D.E.Hayes (Lamont-Doherty Geological Obs., Columbia Univ., Palisades, NY, USA).In book: *Tectonic and geologic evolution of southeast asian seas and islands*, D.E.Hayes [Ed.], p.223-34. Washington, DC, USA: American Geophysical Union (1980), v+326 pp. [0 87590 023 2]

Extensive geophysical and geological data have been collected across the Mariana arc trench system. Part of these data are analysed and a preliminary map of shallow structures in the Mariana fore arc is presented. Water depth in the study area increases from 2400 m near the base of the north-trending Mariana Ridge (arc) complex in the west to about 420 m at the trench-slope

break. The sediment-smoothed seafloor is frequently offset across fault scarps. Scarp heights range from 10 to 250 m. Seismic reflection data show that sediment reflectors and basement are also offset across the faults. The faults are high-angle; normal motions have occurred on them, but strike-slip motions have not been detected. Two structural provinces that are parallel to the arc have been identified. A broad western province is marked by thick stratified sediments above an eastward-shoaling volcanic basement. The basement is characterized by overlapping diffraction hyperbolae on unmigrated MCS profiles. Major faults and horst blocks are present. An eastern province rests on the crest of a fore arc volcanic ridge and is characterized by thin sediments and many small normal faults with down-dropped blocks toward the trench. (28 refs.)

64137 Evolution of back arc spreading and arch volcanism in the Philippine Sea: interpretation of Leg 59 DSDP results. R.Scott (Dept. of Geology, Texas A&M Univ., College Station, TX, USA), L.Kroenke.In book: *Tectonic and geologic evolution of southeast asian seas and islands*, D.E.Hayes [Ed.], p.283-91. Washington, DC, USA: American Geophysical Union (1980), v+326 pp. [0 87590 023 2]

During the evolution of marginal basins and remnant arcs in the Philippine Sea both back arc spreading and arc volcanism are episodic. The early stage of back arc spreading of the Parece Vela Basin had little or no associated arc volcanism, and the last period of West Mariana Ridge arc volcanism occurred after Parece Vela Basin back arc spreading had ceased. Probable back arc spreading in the West Philippine Basin occurred between about 52 and 37 m.y. ago. Tholeiitic volcanism on the Palau-Kyushu arc may have persisted from about 42 to about 29 m.y. ago. Cessation of this volcanism coincided roughly with the sundering of the old Palau-Kyushu arch down its magmatic axis, thus initiating back-arc spreading of the new Parece Vela Basin. The Parece Vela period of back arc spreading continued from 30 m.y. ago to sometime between about 18 and 14 m.y. ago. West Mariana calc-alkalic arc volcanism was superimposed upon the old rifted fore arc of the extinct Palau-Kyushu arc between 20 and 9 m.y. ago. Again, the cessation of arc volcanism coincided with the sundering of the arc and initiation of back arc spreading of the Mariana Trough. Modern calc-alkalic arc volcanism resumed on the Mariana arc about 15 m.y. ago, roughly at the time of initiation of Mariana Trough spreading. A lack of volcanism during subduction is an unanswered petrological enigma. (52 refs.)

Tectonic and geologic evolution of southeast asian seas and islands See Entry 59545**Radionuclide retardation and release rates for oceanic sediments and clay** See Entry 60317**Marine magnetic anomalies from the western Philippine Sea: implications for the evolution of marginal basins** See Entry 64036**Leg 82 of the International Program of Ocean Drilling (IPOD): normal or abnormal ocean crust on the Mid-Atlantic Ridge; Geochemical properties** See Entry 64079**Rates of sedimentation, and stratigraphical completeness** See Entry 64087**Crustal structure across the Mariana island arc** See Entry 64098**1980 update of heat flow in the east and southeast Asian seas** See Entry 64099**Geochemistry and K/Ar ages of volcanics dredged in the Philippine Sea (Mariana, Yap, and Palau Trenches and Parece Vela Basin)** See Entry 64103**The tectonic evolution of the South China Basin** See Entry 64120**Variations in geologic structure along the Sunda fore arc, northeastern Indian Ocean** See Entry 64139**Field evaluation of some sand transport models** See Entry 64140**Numerical integration method for seabed response to water waves** See Entry 64144**Mineral exploration of the sea bed by towed sea bed spectrometers** See Entry 64262**Laser-acoustic measurements for remotely determining bathymetry in shallow turbid waters** See Entry 64264**91.60 PHYSICAL PROPERTIES OF ROCKS AND MINERALS****Variations of geomechanical properties** See Entry 60254**Geotechnical measurements at the Maxey Flats, Kentucky low-level radioactive waste disposal site—lessons learned** See Entry 60255**Diffusion in crystalline rocks** See Entry 60299**Diffusion in the matrix of granitic rock. Field test in the Stripa mine** See Entry 60299**Migration in a single fracture** See Entry 60300**Leach rates of high level waste and spent fuel: limiting rates as determined by backfill and bedrock conditions** See Entry 60303**Aqueous phase diffusion in crystalline rock** See Entry 60304**Modeling approach to determine short- and long-term thermal and thermomechanical effects of waste emplacement in a repository in basalt** See Entry 60307**Radionuclide retardation during transport through fractured granite** See Entry 60326**Long relaxation times in ferromagnets and their possible applications** See Entry 62706**Prospect for numerical information on finite rock strain from the separation of magnetic anisotropy components** See Entry 64106**Sea-bed geology goes up the mountains** See Entry 64131**Measurement of the thermal neutron absorption cross section of rock samples** See Entry 64251**91.65 GEOPHYSICAL ASPECTS OF GEOLOGY, MINERALOGY AND PETROLOGY****64138 Continental rifting and porphyry-molybdenum occurrences in the Oslo region, Norway.** H.K.Schonwandt, J.S.Petersen (Dept. of Geology, Aarhus Univ., Aarhus, Denmark).In book: *Tectonic and geologic evolution of southeast asian seas and islands*, D.E.Hayes [Ed.], p.223-34. Washington, DC, USA: American Geophysical Union (1980), v+326 pp. [0 87590 023 2]

The overall structure of the Oslo rift-system can be viewed as the result of interference between a N-S trending Permian fault system and a regional NE-SW trending Precambrian shear-zone. The formation of the Oslo Rift system apparently reflects a passive continental rifting which was gradually

succeeded by considerable igneous activity. Important porphyry-molybdenum mineralization in the Oslo region is associated with shallow level magmatism in the Glitrevann and Hurdal areas. Molybdenum mineralization of the Oslo province is closely associated with highly differentiated alkali granites which possess striking similarities to Mo-related granites of the Colorado Mo province and evolved Rapakivi- or A-type granites usually considered to be typically associated with bimodal magmatism of crustal extension and continental rifts.

64139 Variations in geologic structure along the Sunda fore arc, northeastern Indian Ocean. G.F. Moore, J.R. Curran, D.G. Moore (Geological Res. Div., Scripps Instn. of Oceanography, La Jolla, CA, USA), D.E. Karig. In book: *Tectonic and geologic evolution of southeast asian seas and islands*, D.E. Hayes [Ed.], p.145-60. Washington, DC, USA: American Geophysical Union (1980), v+326 pp. [0 87590 023 2]

The great lateral extent of the Sunda Arc allows variations in several geological parameters to be observed along the arc. Subduction varies from nearly perpendicular off Java to highly oblique off Burma. The thickness of sediments entering the subduction zone ranges from greater than 5 km in the northwest to less than 1 km in the southeast. Geologic variations along the arc produce corresponding changes in trench-slope structures. In the north, thick sediments of the Bengal and Nicobar fans are scraped off the descending oceanic plate and accreted in discrete gentle fold units bounded by imbricate thrusts. The lower trench slope is characterized by a ridge and trough morphology, with slope sediments filling the troughs. In the south, no clear internal structure can be observed between landward dipping reflectors that have been interpreted as imbricate thrust faults, suggesting that deformation is more intense in the south than in the north. The ridge and trough morphology is less pronounced than in the north. This difference is interpreted in structural style as mainly being due to a decreasing strain rate at the trench from south to north, caused primarily by the increase in thickness of sediments entering the trench and secondarily by a slower perpendicular component of subduction in the north. (36 refs.)

Tectonic and geologic evolution of southeast asian seas and islands See Entry 59545

A geological case history: lessons learned at Sheffield, Illinois See Entry 60252

Geotechnical and geomechanical parameters required for characterization of sites See Entry 60253

Variations of geomechanical properties See Entry 60254

Geotechnical measurements at the Maxey Flats, Kentucky low-level radioactive waste disposal site—lessons learned See Entry 60255

Lessons learned in a hydrogeological case at Sheffield, Illinois See Entry 60259

Dissolution of evaporites and its possible impact on the integrity of the Waste Isolation Pilot Plant (WIPP) New Mexico, USA See Entry 60290

Deformation-dissolution potential of bedded salt, Waste Isolation Pilot Plant site, Delaware Basin, New Mexico See Entry 60291

Mineralogical and geochemical factors influencing the final disposal of HLW in the Stassfurt Halite See Entry 60292

Gas production and liberation from rock salt samples and potential consequences on the disposal of high-level radioactive waste in salt domes See Entry 60293

Thermomechanical in-situ experiments and finite element computations See Entry 60294

Sorption of actinides in well-defined oxidation states on geologic media See Entry 60322

Uranium disequilibrium dating of phosphate deposits from the Lau Group, Fiji See Entry 60406

Accumulation of fossil fuels and metallic minerals in active and ancient rift lakes See Entry 64095

The petrology and tectonics of Recent volcanism in the central Philippine Islands See Entry 64102

Geochemistry and K/Ar ages of volcanics dredged in the Philippine Sea (Mariana, Yap, and Palau Trenches and Parece Vela Basin) See Entry 64103

Primitive arc volcanism and a boninite series: examples from Western Pacific island arcs See Entry 64104

91.90 OTHER TOPICS IN SOLID EARTH GEOPHYSICS

64140 Field evaluation of some sand transport models. N.H. Berg (Forest Service, US Dept. of Agriculture, Berkeley, CA, USA), *Earth Surf. Processes & Landforms* (GB), vol.8, no.2, p.101-14 (March-April 1983).

Fluorescent tracer procedures were used to monitor the movement of three commercially purchased sands in a natural dune environment. Results were compared with estimates of transport rates from three theoretical models. Estimates from models by Bagnold (1941) and Hsu (1971) were larger by as much as one order of magnitude than the rates observed in the tracer study. The model of A.A. Kadib (1965) provided closer correspondence to observed transport rates for medium sand (mean diam. 0.653 mm) but underestimated rates for coarse sand (mean diam. 0.992 mm). (34 refs.)

64141 Sorted stripes on Sub-Antarctic Kerguelen Island. K. Hall (Geography Dept., Univ. of Natal, Pietermaritzburg, S. Africa), *Earth Surf. Processes & Landforms* (GB), vol.8, no.2, p.115-24 (March-April 1983).

Observations of sorted stripes at nine different localities on sub-Antarctic Kerguelen Island are presented. The study sites range from 25-600 m above sea level and are of varying aspect. It is found that there is a strong relationship between stripe orientation and the wind direction, to the extent that at one locality stripes were oriented across a slope. Stripe width was seen to increase with altitude, and, in addition, the coarse stripe was dominant at lower elevations and the fine stripe at higher elevations. At one site a secondary set of stripes was observed to occur within the fine stripe of a primary larger set. On a trachyte plug there was evidence of lateral squeezing in the formation of the stripes. A number of minor observations pertaining to the possible mechanism of stripe formation are given. (33 refs.)

64142 Flood-related channel change in an arid-region river. W.L. Graf (Dept. of Geography, Arizona State Univ., Tempe, AZ, USA), *Earth Surf. Processes & Landforms* (GB), vol.8, no.2, p.125-39 (March-April 1983).

A review of 112 years of change in the channel of the Salt River, central Arizona, USA, shows that this arid-region river has a main-flow channel that has migrated laterally up to 1.6 km (1 mi) in response to flood events. Maps

showing locational probabilities indicate that along the channel zones of relative locational stability alternate with zones of relative instability at a 3.2 km (2 mi) interval. Construction of upstream reservoirs has reduced sediment input into the main river but has not controlled floods. The channel width has not changed except for moderate fluctuations around mean values; the main-flow channel has incised approximately 6 m (20 ft) over most of the 48 km (30 mi) study reach during six recent floods. Gradient has remained unchanged. During floods bed material was mobilized to a depth below the original bed level that was greater than the height of the water surface above the original bed. Calculations based on tractive force indicate a threshold discharge of instability that is equal to the flow with a five-year return interval. The river exhibits remarkable stability with respect to gradient and sinuosity, irrespective of water and sediment discharges, but horizontal channel location exhibited selective instability. (31 refs.)

64143 Spatial variation in solutional denudation and soil moisture over a hillslope hollow. R.W. Crabtree (School of Geography, Univ. of Leeds, Leeds, England), T.P. Burt.

Earth Surf. Processes & Landforms (GB), vol.8, no.2, p.151-60 (March-April 1983).

A spatial pattern of relative solutional denudation is described for a hillslope hollow and adjacent spurs at Bicknoller Combe, Somerset. The pattern was obtained from a network of micro-weight loss rock tablets emplaced in the soil. The results show that the hollow is the main locus of solutional denudation. The soil moisture distribution over the hollow indicates that it is a transmission zone for acid soil water percolating from the adjacent spurs to the saturated wedge at the base of the hollow. The wetter acid soils in the hollow are responsible for the relatively higher solutional denudation taking place in the hollow. (21 refs.)

Rates of sedimentation, and stratigraphical completeness See Entry 64087

Vertical sedimentation units in a barrier island washover fan See Entry 64124

Systematic monthly morphologic variation of Assawoman Inlet: nature and causes See Entry 64125

Preliminary estimates of intertidal limestone erosion, One Tree Island, southern Great Barrier Reef, Australia See Entry 64126

Channel width—drainage area relations in small basins See Entry 64152

Friction and heat exchange between air and surface in the presence of sand, salt, and ice-particle transport See Entry 64219

92.00 HYDROSPHERIC AND ATMOSPHERIC GEOPHYSICS

(for marine geology and geophysics, see 91.50)

92.10 PHYSICS OF THE OCEANS

(see also 43.30 Underwater sound)

64144 Numerical integration method for seabed response to water waves. T. Yamamoto (Rosenstiel School of Marine & Atmospheric Sci., Univ. of Miami, Miami, FL, USA).

Int. J. Soil Dyn. & Earthquake Eng. (GB), vol.2, no.2, p.92-100 (April 1983). The problem of continuously layered seabed response to water waves is solved by numerically integrating the displacement stress vectors. It is found that the commonly used approximation by discrete homogeneous multi-layers causes stress discontinuities at the interfaces between the sublayers and may invite serious errors in stability analyses of foundations. The numerical integration theory is verified with good accuracy by wave tank experiments on the motions and wave damping by clay beds. The numerical calculations of motions of the Mississippi Delta clay bed by the present theory give much smaller displacements of bed compared to the results from the quasi-static analyses by discrete homogeneous multi-layer approximations. A criterion for choosing between total stress analysis and effective stress analysis is also proposed. (31 refs.)

64145 Generation of topographic vortices and their possible effect on formation of productive zones in the ocean. Yu.N. Golubev, P.D. Lomakin, L.V. Cherkasov (Acad. of Sci., Ukrainian SSR).

Dopov. Akad. Nauk UkrSR. Ser. A (USSR), no.2, p.25-8 (1983). In Ukrainian.

Investigates the generation of topographic eddies and their influence on the formation of a zone of higher biological productivity in the region of the Ob bank (Antarctic sector of the Indian Ocean). (3 refs.)

64146 The M2 oceanic tide recovered from Seasat altimetry in the Indian Ocean. P. Mazzega (CNES/GRGS, Toulouse, France).

Nature (GB), vol.302, no.5908, p.514-16 (7 April 1983).

Seasat altimeter data, which provide measurements of the instantaneous ocean level, are used to create a model of the M2 oceanic tide in the Indian Ocean. This approach avoids the assumptions introduced in the hydrodynamical tide models and take advantage of a regular distribution of the data over the whole ocean. The hydrodynamical and empirical models that have been proposed for this ocean exhibit strong discrepancies, particularly in the deep ocean so that the use of altimeter data is of particular interest. The author investigates a new method to obtain the amplitude and phase of M2 in a large region. The validity of the model is checked using synthetic data and by comparison with tide gauge data. (25 refs.)

64147 Relaxation processes for internal waves in mesoscale flow. K.M. Watson (Marine Phys. Lab., Scripps Instn. of Oceanography, San Diego, CA, USA).

Proc. Natl. Acad. Sci. USA, vol.80, no.4, p.1144-6 (Feb. 1983).

A dynamical 'test-wave' model has been developed to study transport phenomena within oceanic internal wave fields. This model is extended to describe effects of a mesoscale flow field on internal wave transport. Previous work with weak-interaction perturbation theory has suggested a substantial enhancement due to mesoscale currents. Extension to the strong-interaction regime in the present paper suggests a relatively small effect due to mesoscale interactions. (9 refs.)

64148 Experimental study of volume scattering function of particles suspended in water. S. Sugihara (Oceanographic Instrumentation Lab. Inst. Sci. & Chem. Res., Saitama, Japan), M. Kishino, N. Okami.

Phys. Pap. Inst. Phys. & Chem. Res. (Japan), vol.76, no.4, p.96-9 (Dec. 1982).

Very strong light scattering in the backward region is not unusual even for natural sea water, and phytoplankton plays an important role on the enhancement of the back-scattering. Phytoplankton role on the enhancement of the back-scattering. Phytoplankton wall structure is responsible for the enhancement in back-scattering by phytoplankton. Vertically and horizontally

polarized components of volume scattering function might supply important information for the study of the interaction between light and particles. Vertical and horizontal components of volume scattering function for the cultures of *Chaetoceros socialis*, and *Skeletonema costatum* were therefore measured with a scatterometer. A polarizer was inserted between the light source and sample cell. Both components were recorded at every 5° interval in an angular range of 20° to 150°. (3 refs.)

64149 Objective analysis of Northern hemisphere ocean surface temperatures. A.N.Bagrov, N.N.Kozhevnikova (Hydrometeorological Sci. Res. Center, USSR).

Sov. Meteorol. & Hydrol. (USA), no.12, p.54-9 (1981). Translation of: *Meteorol. & Gidrol. (USSR)*, no.12, p.69-76 (1981).

A scheme for objective analysis of the ocean surface temperature field on the Northern Hemisphere that uses an optimum-interpolation procedure is described. The analysis is based on ship observations accumulated over five days. The data are put through climatic and horizontal control. The scheme is run on a BESM-6 computer in FORTRAN. The results are put out at the nodes of a 2.5X2.5-degree grid that covers the entire Northern Hemisphere (except for land areas and circumpolar regions). Recommendations toward further improvement of the results are given. (8 refs.)

64150 Planetary waves of seasonal origin in the ocean. A.A.Kutalo (Hydrometeorological Sci. Res. Center, USSR).

Sov. Meteorol. & Hydrol. (USA), no.1, p.56-60 (1982). Translation of: *Meteorol. & Gidrol. (USSR)*, no.1, p.71-7 (1982).

The correspondence between observed features of the water temperature distribution in the northeast Atlantic to those predicted by hydrodynamic modelling of the ocean is analyzed. It is concluded that the medium-scale organization of the temperature field is based on oceanic planetary waves of seasonal origin. (13 refs.)

64151 Vertical coherence of semi-diurnal tidal currents on the 1970 hydrophysical test range in the Atlantic. V.N.Bol'shakov, S.K.Gulev, A.S.Matygin (All Union Sci. Res. Inst. of Hydrometeorological Information World Data Center, USSR).

Sov. Meteorol. & Hydrol. (USA), no.1, p.61-4 (1982). Translation of: *Meteorol. & Gidrol. (USSR)*, no.1, p.78-91 (1982).

More than a million current-vector measurements have been processed. The variation of semi-diurnal-current coherence in the vertical establishes that the semi-diurnal currents above and below the density-discontinuity layer are independent. Below the 200-meter depth, in the layer in which the Vaisala frequency varies smoothly, the scale of the vertical coherence is estimated to be 900 meters. (8 refs.)

Topics in Ocean Physics. Proceedings of the International School of Physics, 'Enrico Fermi', Course LXXX See Entry 59539

Coupled mode solution for a cylindrically symmetric oceanic waveguide with a range and depth dependent refractive index and a time varying rough sea surface See Entry 61338

Geometric dispersion of acoustic signals propagated in a deep ocean channel See Entry 61339

A cautionary note on the use of range-dependent propagation models in underwater acoustics See Entry 61340

Optimum frequency of propagation in shallow water environments See Entry 61341

The tsunami of 23 November 1969 at Kamchatka and certain aspects of its occurrence See Entry 64047

Uranium disequilibrium dating of phosphate deposits from the Lau Group, Fiji See Entry 64086

Vertical sedimentation units in a barrier island washover fan See Entry 64124

Systematic monthly morphologic variation of Assawoman Inlet: nature and causes See Entry 64125

Acoustical classification of sea floor sediments See Entry 64128

Microcomputer-aided analysis of hydroacoustical receiver signals See Entry 64130

Quaternary sedimentation processes in the South China Basin as revealed by echo-character mapping and piston-core studies See Entry 64134

Regime of the Filchner-Ronne ice shelves, Antarctica See Entry 64155

Laser-acoustic measurements for remotely determining bathymetry in shallow turbid waters See Entry 64264

Measurement of flow velocities in the ocean with a laser Doppler hydrometer See Entry 64271

A remote recording unit for floated automatic water level recording systems See Entry 64272

92.20 INTERDISCIPLINARY ASPECTS OF OCEANOGRAPHY

Preliminary estimates of intertidal limestone erosion, One Tree Island, southern Great Barrier Reef, Australia See Entry 64126

Generation of topographic vortices and their possible effect on formation of productive zones in the ocean See Entry 64145

Experimental study of volume scattering function of particles suspended in water See Entry 64148

Possible limits on the composition of the Archaean ocean See Entry 64238

92.40 HYDROLOGY AND GLACIOLOGY

64152 Channel width-drainage area relations in small basins. M.J.Carragher (Univ. of Salford, Salford, England), M.Klein, J.R.Petch. *J. Hydrol. Processes & Landforms (GB)*, vol.8, no.2, p.177-81 (March-April 1983).

The measurement of stream channels in basins less than 3 km² shows compound relations between width and area. Break points in the relations may be attributed to the changing contribution of rapid storm flow and to the effect of bed material size. (8 refs.)

64153 The measurement of watertable levels in structured clay soils by means of open auger holes. A.C.Armstrong (Ministry of Agriculture Fisheries & Food, Cambridge, England).

Earth Surf. Processes & Landforms (GB), vol.8, no.2, p.183-7 (March-April 1983).

In structured clay soils, water levels in open auger holes (dipwells) respond to water movement through macropores and may mask the existence of drier zones either at depth or within beds. Variability between replicated dipwells expresses the small scale variation in the soil, and statements about soil water

regimes should be made in statistical terms. Suitably replicated dipwells give sufficiently precise measurements of mean watertable position for studies of soil water regimes. (19 refs.)

64154 Transport equations for heat and moisture in the soil and their application to boundary layer problems. U.Sievers, R.Forkel, W.Zdankowski (Inst. fur Meteorologie, Johannes Gutenberg-Univ., Mainz, Germany).

Contrib. Atmos. Phys. (Germany), vol.56, no.1, p.58-83 (1983).

The methods of irreversible thermodynamics are used to obtain a consistent set of transport equations for heat and moisture in the soil. It is found that the empirical diffusion laws for moisture are in harmony with the requirements of the linear Onsager theory. The new set of prognostic equations is subjected to thermodynamic filtering and is then coupled to a model of the atmospheric boundary layer. Extensive calculations are carried out to determine the influence of soil type and moisture on the atmospheric state. (22 refs.)

64155 Regime of the Filchner-Ronne ice shelves, Antarctica. G.deQ.Robin, C.S.M.Doake, H.Kohnen, R.D.Crabtree, S.R.Jordan, D.Moller (Scott Polar Res. Inst., Univ. of Cambridge, Cambridge, England).

Nature (GB), vol.302, no.5909, p.582-6 (14 April 1983).

Seismic, radio-echo, TWERLE balloon and oceanographic data of the Filchner-Ronne ice shelves are analysed. A large thin area in the central Ronne ice Shelf is found to differ from the morphology of the Ross and Filchner ice shelves. This area is partly filled by basal saline ice, which can be attributed to regional regelation caused by oceanic circulation. (34 refs.)

64156 River flows as dissipative systems. V.I.Nikora (Odessa Hydrometeorological Inst., Odessa, USSR).

Sov. Meteorol. & Hydrol. (USA), no.12, p.66-9 (1981). Translation of: *Meteorol. & Gidrol. (USSR)*, no.12, p.84-8 (1981).

The 'flow-mobile channel' system is considered from the premises of dissipative-structure theory. It is shown that the minimum energy dissipation principle proposed by M.A. Velikanov is consistent with the fundamental Prigogine-Glensdorf principle of minimum entropy production as applied to river hydraulics. (8 refs.)

64157 Spatial correlation functions of maximum discharge volumes in mountain rivers. M.A.Mamedov (State Univ., Baku, Azerbaijan SSR).

Sov. Meteorol. & Hydrol. (USA), no.12, p.70-3 (1981). Translation of: *Meteorol. & Gidrol. (USSR)*, no.12, p.89-93 (1981).

The spatial structure of the fluctuations of maximum discharge volume in mountain rivers is investigated. In view of the influence of topography in determining the maximum volumes of mountain rivers, the spatial correlation function is represented as the dependence of the pair correlation coefficients on the square root of the product of the distance between the drainage-basin centers times the difference between the average elevations of the basins. The homogeneity of the spatial correlation function is estimated. (5 refs.)

64158 Long-term forecasting of high water levels at ice dams on the Angara at Kamenska. V.N.Karnovich, T.V.Kuleshova (Sci. Res. Inst. of Hydraulic Engng., USSR).

Sov. Meteorol. & Hydrol. (USA), no.12, p.83-5 (1981). Translation of: *Meteorol. & Gidrol. (USSR)*, no.12, p.105-7 (1981).

The results of an analysis of ice-damming factors and a procedure for long-term forecasting of high water levels at ice dams on the Angara River at Kamenska are set forth. (4 refs.)

64159 Determination of the rate of development of morphological formations in river channels from indirect criteria. A.A.Levashov (Leningrad Hydrometeorological Inst., Leningrad, USSR).

Sov. Meteorol. & Hydrol. (USA), no.1, p.79-81 (1982). Translation of: *Meteorol. & Gidrol. (USSR)*, no.1, p.97-9 (1982).

Field determinations of sandbar reshaping rates are reported. A method is proposed for determining the ages of morphological formations from various natural criteria. (1 ref.)

Need for geological characterization of low-level nuclear waste disposal sites See Entry 60250

Geotechnical and geomechanical parameters required for characterization of sites See Entry 60253

Variations of geomechanical properties See Entry 60254

Geotechnical measurements at the Maxey Flats, Kentucky low-level radioactive waste disposal site—lessons learned See Entry 60255

Hydrologic characterization of sites for shallow disposal of low-level radioactive wastes See Entry 60256

Techniques of groundwater investigation at proposed low-level nuclear waste disposal sites See Entry 60257

Ground-water monitoring techniques for low-level radioactive disposal sites See Entry 60258

Lessons learned in a hydrogeological case at Sheffield, Illinois See Entry 60259

Surface water considerations for low-level radioactive waste site See Entry 60260

Hydrologic and hydrodynamic aspects of low-level radioactive waste disposal to streams See Entry 60261

Effect of releases from near-surface low-level waste sites on surface water quality See Entry 60262

Dissolution rate of salt domes on the basis of interpretation of measured salinity profiles See Entry 60289

Migration in a single fracture See Entry 60300

Model for near field migration See Entry 60301

Model for far field migration See Entry 60302

Leach rates of high level waste and spent fuel: limiting rates as determined by backfill and bedrock conditions See Entry 60303

Aqueous phase diffusion in crystalline rock See Entry 60304

Permeability monitoring technique of the near-field and far-field interface of underground openings See Entry 60305

Hydrothermal conditions around a radioactive waste repository See Entry 60306

A combined analytical model for performance assessment of the waste package/geologic medium systems See Entry 60308

Evaluation of solubility and speciation of actinides in natural groundwaters See Entry 60314

Study of radionuclide migration from deep-lying repository sites with overlying sedimentary layers See Entry 60315

A comparison of in-situ radionuclide migration studies in the Studsvik area and laboratory measurements See Entry 60316

- Studies of the mobilization of thorium from the Morro do Ferro** See Entry 60319
- Properties and mobilities of actinide colloids in geologic systems** See Entry 60320
- The migration of radionuclides with ground water. A discussion of the relevance of the input parameters used in model calculations** See Entry 60321
- Laboratory tests on the migration behavior of selected fission products in aquifer materials from a potential disposal site in northern Germany** See Entry 60323
- Modelling of the migration of lanthanoids and actinoids in ground water; the medium dependence of equilibrium constants** See Entry 60324
- Evaluation of radionuclide transport: effect of radionuclide sorption and solubility** See Entry 60325
- Radionuclide retardation during transport through fractured granite** See Entry 60326
- A comparative analysis of fractured and porous medium radionuclide transport** See Entry 60327
- Estimation of the percentage of annual groundwater recharge with bomb tritium using a cumulative mass balance method** See Entry 63748
- Use of data on warm industrial effluents to study the dispersal of pollutants in rivers** See Entry 63749
- Water pollution in the Fukuoka area** See Entry 63750
- Some aspects of the influence of surface and ground water chemistry on the mobility of thorium in the 'Morro do Ferro' environment** See Entry 63751
- Potential for the rapid transport of plutonium in groundwater as demonstrated by core column studies** See Entry 63752
- A preliminary analysis of reported changes in ground water and anomalous animal behavior before the 4 February 1975 Haicheng earthquake** See Entry 64078
- Accumulation of fossil fuels and metallic minerals in active and ancient rift lakes** See Entry 64095
- Sorted stripes on Sub-Antarctic Kerguelen Island** See Entry 64141
- Flood-related channel change in an arid-region river** See Entry 64142
- Spatial variation in solutional denudation and soil moisture over a hillslope hollow** See Entry 64143
- The global temperature trend in the Cenozoic** See Entry 64239
- Interpretation of SIR-A Seasat and Landsat coregistered data over Algerian playas** See Entry 64242
- Uranium isotopic disequilibrium in ground water as an indicator of anomalies** See Entry 64259
- Tracer techniques in hydrology** See Entry 64263
- Expendable bubble tiltmeter for geophysical monitoring** See Entry 64270
- A remote recording unit for floated automatic water level recording systems** See Entry 64272

92.60 METEOROLOGY

(see also 43.28 Aeroacoustics and atmospheric sound)

- 64160 The NO/NO₂/O₃ photostationary state in Claremont, California.** R.E.Shetter, D.H.Stedman, D.H.West (Univ. of Michigan, Ann Arbor, MI, USA). *J. Air Pollut. Control Assoc. (USA)*, vol.33, no.3, p.212-14 (March 1983). Seventeen days of detailed measurements of NO, NO₂, O₃, HNO₃ and the frequency of NO₂ photolysis—(NO₂)—were carried out in Claremont, CA, in September 1980. Under conditions when the rate of change of NO concentration is small, there must be a balance between formation and loss processes. In the classical photostationary state this balance is between NO₂ photolysis: NO₂+hv→NO+O and reaction with ozone: NO+O₃→NO₂+O₂. The results show that the latter reaction with ozone is inadequate to balance the formation step; a significant contribution is required from another NO oxidation process, possibly peroxy radical oxidation. If so, the inferred concentration of peroxy radicals shows a diurnal variation, peaking around solar noon. (20 refs.)
- 64161 Air quality screening model with long-term averaging.** D.Golomb, S.Batterman, J.Gruhl (MIT, Cambridge, MA, USA). *J. Air Pollut. Control Assoc. (USA)*, vol.33, no.3, p.215-19 (March 1983). A simple screening model is presented for estimating maximum ground level concentrations of air pollutants from single elevated buoyant sources of emissions. The model, which incorporates plausible error margins, is based on the Gaussian dispersion formula. Maximum longer-term (3, 8, 24 h) concentrations are estimated using a joint probability analysis of the persistence of meteorological worst case events. (9 refs.)
- 64162 Return-stroke electromagnetic fields of oblique lightning channels.** G.Becker, H.Volland (Radioastron. Inst., Univ. of Bonn, Bonn, Germany). *Contrib. Atmos. Phys. (Germany)*, vol.56, no.1, p.1-13 (1983). The resonant wave guide model of lightning currents simulating return strokes (R strokes) has been extended to oblique but straight lightning channels. In this model discrete resonant wave modes are generated. Only the first mode is dominant, while higher order modes can be neglected in a first approximation. The electromagnetic field of R strokes has been calculated at various distances from the source. (10 refs.)
- 64163 On the influence of nonlinear wave-wave interaction in a 3-D primitive equation model for sudden stratospheric warmings.** K.Rose (Inst. fur Meteorologie, Freie Univ. Berlin, Berlin, Germany). *Contrib. Atmos. Phys. (Germany)*, vol.56, no.1, p.14-41 (1983). In order to numerically simulate sudden stratospheric warmings, two versions of a 3-D primitive equation model are developed, one with and one without nonlinear wave-wave interaction terms. Six model runs were performed. A qualitative discussion of the wave propagation shows that wave transience rather than interaction at critical lines is involved in the reversal of the polar westerlies. (19 refs.)
- 64164 A radiation model using hourly meteorological data with results from GATE.** M.A.Atwater (TRC Environmental Consultants Inc., East Hartford, CT, USA), J.T.Ball. *Contrib. Atmos. Phys. (Germany)*, vol.56, no.1, p.42-57 (1983). A solar and infrared flux model that includes partial cloudiness is applied to data from GATE Phase III. Flux convergence profiles were computed from the surface to 350 mb for infrared, solar and net radiation. (36 refs.)

- 64165 On the influence of meteorological parameters on extinction and mass size distributions in the urban aerosol of Vienna.** R.Pirich, H.Horvath (Inst. fur Experimentalphys., Univ. Wien, Wien, Austria). *Contrib. Atmos. Phys. (Germany)*, vol.56, no.1, p.84-93 (1983). During the winters of 1979/80 and 1980 extinction coefficients were measured with a telephotometer and mass size distributions with a low pressure cascade impactor in the urban area of Vienna, Austria. The dependence of extinction on relative humidity is analysed. (20 refs.)
- 64166 On single station forecasting: sunshine and rainfall Markov chains.** K.Fraedrich, K.Muller (Inst. fur Meteorologie, Freie Univ. Berlin, Berlin, Germany). *Contrib. Atmos. Phys. (Germany)*, vol.56, no.1, p.108-34 (1983). Probabilities of weather states are predicted by first order Markov chains using single station data only. Two examples of weather phenomena are discussed which are particularly suited for short range forecasting: daily sunshine measurements and the rainfall combined with three hourly past weather observations at Berlin-Dahlem. Two probability forecasts are distinguished, both of which start from an initial observation. Finally it is shown how the diurnal cycle can be included in the Markov chain forecasts. (21 refs.)
- 64167 Doppler-SODAR measured variation of mean and turbulent wind field during PUKK.** C.Wamser (Max-Planck-Inst. fur Meteorologie, Hamburg, Germany), W.J.Muller. *Contrib. Atmos. Phys. (Germany)*, vol.56, no.1, p.135-46 (1983). Some interesting structures of nonstationary processes within the coastal boundary layer, measured by a three-component monostatic Doppler-SODAR during the field experiment PUKK close to the North Sea coast are presented. A short description of the system and an illustration of typical SODAR-profiles are given. Finally, frequency distributions of wind direction and velocities at different heights derived from nearly 1500 SODAR profiles during PUKK are compared with corresponding simultaneous SODAR-measurements at the nuclear power plant at Esensham, about 40 km south of the PUKK SODAR-station. (12 refs.)
- 64168 Major ion composition and chemical associations of inorganic atmospheric aerosols.** R.M.Harrison, C.A.Plo (Dept. of Environmental Sci., Univ. of Lancaster, Lancaster, England). *Environ. Sci. & Technol. (USA)*, vol.17, no.3, p.169-74 (March 1983). Atmospheric aerosols were sampled and analyzed for H⁺, NH₄⁺, Ca²⁺, Mg²⁺, Na⁺, K⁺, SO₄²⁻, Cl⁻ and NO₃⁻. Gaseous ammonia was also measured. The analyses demonstrated that these ions are the main constituents of the particulate water-soluble fraction of the aerosols sampled. Ion balance studies showed that the main compounds present were (NH₄)₂SO₄, NH₄NO₃ and NH₄Cl in polluted aerosols and NaCl and MgCl₂ in maritime aerosols. Backward air mass trajectories for collected samples indicated that NH₄Cl is primarily produced locally, NH₄NO₃ has a local to medium-distance origin, and (NH₄)₂SO₄ has been transported over long distances. The observations were made in rural England. (30 refs.)
- 64169 Finite-amplitude stability of a zonal shear flow.** A.G.Burns, S.A.Maslowe (Dept. of Maths, McGill Univ., Montreal, Quebec, Canada). *J. Atmos. Sci. (USA)*, vol.40, no.1, p.3-9 (Jan. 1983). Considers the stability of a zonal shear flow $\bar{u}=\tanh y$ in the framework of the β -plane approximation. The objective of this study is to determine the effects of nonlinearity on the stability of the flow by perturbing about the known linear neutral solution obtained by Howard and Drazin and, independently, by Lipps. The procedure employed is a weakly nonlinear approach which leads to the familiar amplitude evolution equation of Stuart-Watson theory. The 'Landau constant', i.e. the coefficient of the nonlinear term, turns out to be positive. Thus, nonlinearity is found to be destabilizing. Despite the fact that the linear solution is regular, critical point singularities are encountered in all higher order terms of the perturbation streamfunction expansion. (15 refs.)
- 64170 On the predictability of quasi-geostrophic flow: the effects of beta and baroclinicity.** G.K.Vallis (Scripps Inst. of Oceanography, La Jolla, CA, USA). *J. Atmos. Sci. (USA)*, vol.40, no.1, p.10-27 (Jan. 1983). The equilibrium statistics and predictability properties of one-and two-layer quasi-geostrophic flow are examined with the aid of a numerical model. The effect of beta in one-layer flow is to slow the transfer of energy into larger scales and to increase the predictability. In two-layer flow, when beta is zero, energy enters the system via baroclinic instability of the mean flow at very large scales and most energy transfer is confined to low wavenumbers. When beta is nonzero, energy enters at higher wavenumbers (in baroclinic modes mainly) before cascading preferentially to lower wavenumber zonal barotropic modes. The predictability of two-layer flow is not significantly altered by beta, because beta increases the range of wavenumber over which significant nonlinear energy transfer occurs. The predictability times of the long waves are found to be always larger than those of the short waves, even when the initial error is spread evenly across wavenumbers. Reducing the mean baroclinicity increases the predictability time. (26 refs.)
- 64171 The amplification and capture of atmospheric solitons by topography: a theory of the onset of regional blocking.** T.Warn, B.Brasnett (Dept. of Meteorology, McGill Univ., Montreal, Quebec, Canada). *J. Atmos. Sci. (USA)*, vol.40, no.1, p.28-38 (Jan. 1983). The problem of long, quasi-geostrophic baroclinic waves interacting with topography is shown to reduce to an inhomogeneous, damped Korteweg-de Vries equation. The soliton perturbation theory of Karpmann and Maslow (1977, 1978) and Kaup and Newell (1978) is then used to examine the qualitative aspects of the interaction of travelling solitons with topography. The perturbation theory suggests and numerical experiments confirm that under certain conditions incident solitons can be simultaneously amplified and stalled by topography—a process which can be interpreted as a transition to a regional blocking configuration. (24 refs.)
- 64172 The role of latent heat release in baroclinic waves—without β -effect.** C.-M.Tang, G.H.Fichtl (Fluid Dynamics Branch, NASA/Marshall Space Flight Center, AL, USA). *J. Atmos. Sci. (USA)*, vol.40, no.1, p.53-72 (Jan. 1983). Develops the analytical theory of two-level quasi-geostrophic baroclinic waves without β -effect aimed at understanding the role of latent heat release on the development of baroclinic waves. When the release of latent heat is introduced with pseudo-adiabatic ascent and dry adiabatic descent, the width a of the ascending region is different from the width b of the descending region and, furthermore, a static stability-vertical velocity correlation results in the mean state thickness increasing with time. However, the basic state shear is defined a priori, independent of the perturbations, in the formulation of the stability problem. Integro-differential equations for the perturbations are developed. Due to the mass continuity constraint, the unstable waves in the dry and moist regions are stationary in a frame of reference which translates with the mean zonal wind at the middle level, and the growth rate in the moist region is equal to that in the dry region, the same as in the dry model. Latent heat release is shown to cause a significant change in the structure of the

waves such that large departure in the horizontal heat transport from dry atmospheric values can occur. (24 refs.)

64173 The evolution of a Rossby-wave packet in a three-dimensional baroclinic atmosphere. Q.-C.Zeng (Geophys. Fluid Dynamics Program, Princeton Univ., Princeton, NJ, USA).

J. Atmos. Sci. (USA), vol.40, no.1, p.73-84 (Jan. 1983).

The development of an individual quasi-geostrophic disturbance in a three-dimensional baroclinic atmosphere is investigated by using a wave-packet representation and the WKB method. The results obtained indicate that the development of a Rossby-wave packet in the upper level of the atmosphere depends on the packet's structure and location with respect to the zonal flow, whether the zonal flow is stable or not. The wave packet develops (decays) if the three-dimensional rays are directed up-gradient (down-gradient) in the zonal flow. All characteristics of the wave packet are changing with time. The spatial scale or the three-dimensional wavelength of the developing (decaying) wave packet increases (decreases). The maximum amplitude of the developing (decaying) Rossby-wave packet moves toward (out from) the jet region, if the zonal flow is stable. Unlike a single normal mode, most wave packets cause considerable divergence of momentum and heat flux; hence there exists strong interaction between a Rossby-wave packet and the zonal flow. (28 refs.)

64174 A conservation law for small-amplitude quasi-geostrophic disturbances on a zonally asymmetric basic flow. D.G.Andrews (Dept. of Atmospheric Phys., Univ. of Oxford, Oxford, England).

J. Atmos. Sci. (USA), vol.40, no.1, p.85-90 (Jan. 1983).

A quadratic conservation law is derived for small-amplitude quasi-geostrophic disturbances on a wavy basic state. The law may be useful for describing the three-dimensional propagation of disturbances on time-averaged flows. This parallels the use of the generalized Eliassen-Palm theorem in the description of waves propagating on zonally-averaged flows. (17 refs.)

64175 Simulations of nocturnal drainage flows by a q^2 turbulence closure model. T.Yamada (Los Alamos Nat. Lab., Los Alamos, NM, USA).

J. Atmos. Sci. (USA), vol.40, no.1, p.91-106 (Jan. 1983).

Nocturnal drainage flows observed over a nearly two-dimensional ridge called Rattlesnake Hills near Richland, Washington, are simulated by using a simplified turbulence closure model in which only turbulence kinetic energy and turbulence length scale equations are solved prognostically. The present model is slightly simpler than a level 2.5 model which has been extensively used in previous simulations of various atmospheric boundary layer phenomena. Wind and temperature profiles computed by the present model are generally in excellent agreement with observations made by towers erected on the slope of Rattlesnake Hills. Strong coupling between the mean and turbulence variables is also demonstrated. (28 refs.)

64176 Growth of aqueous solution droplets of HNO_3 and HCl in the atmosphere. P.V.N.Nair, P.V.Joshi, U.C.Mishra, K.G.Vohra (Div. of Radiological Protection, Bhabha Atomic Res. Centre, Bombay, India).

J. Atmos. Sci. (USA), vol.40, no.1, p.107-115 (Jan. 1983).

Computed values of equilibrium sizes and composition of uncharged and charged aqueous solution droplets of HNO_3 and HCl at 25°C , relative humidities from 5 to 101%, and solute vapor activities from 10^{-4} to 10^1 are presented. Threshold concentrations for heteromolecular nucleation of HNO_3 and HCl at 40, 30, 20, 10, 0, and -10°C are also given as a function of the relative humidity. It is shown that atmospheric concentrations of HNO_3 and HCl can participate in nucleation at temperatures below 20°C and relative humidities above 98%. The nature of the nucleation of HNO_3 and HCl in the atmosphere including ion-induced nucleation for which there is no threshold and some of the available experimental results are discussed. (28 refs.)

64177 A theoretical determination of the capture efficiency of small columnar ice crystals by large cloud drops. J.K.Lew, H.R.Pruppacher (Dept. of Atmospheric Sci., Univ. of California, Los Angeles, CA, USA).

J. Atmos. Sci. (USA), vol.40, no.1, p.139-45 (Jan. 1983).

A theoretical model has been formulated to study by numerical techniques the efficiency E with which columnar ice crystals grown at temperatures between -3 and -8°C are captured in a cloud by relatively large, supercooled cloud drops. The ice crystals studied had lengths L of $15 \leq L \leq 240$ μm and diameters D of $1.5 \leq D \leq 240$ μm , and L/D values of 1.0, 3.0 and 10.0. The specific gravity of the ice crystals was assumed to be 0.92 and 0.5 g cm^{-3} . The cloud drops had Reynolds numbers of 10, 30, 100, 200, 300 and 400, corresponding to the drop radii r_d of 100, 165, 300, 416, 510 and 591 μm in air at 900 mb and -6°C . A few computations were made for 500 mb and -10°C . The ice crystals were assumed to have three typical, yet fixed, orientations with respect to the drop, in an attempt to take into account, in an idealized manner, the different orientations a columnar ice crystal assumes as it moves around a falling drop. (19 refs.)

64178 Measured collection efficiencies for cloud drops. K.V.Beard, H.T.Ochs, III (Illinois State Water Survey, Champaign, IL, USA).

J. Atmos. Sci. (USA), vol.40, no.1, p.146-53 (Jan. 1983).

The collection efficiency has been measured for 15 size pairs of relatively uncharged drops in over 400 experimental runs. The results indicate that collection efficiencies fall in a narrow range of 0.60 to 0.70 even though the collector drop was varied between 63 and 100 μm radius and the collected drop from 11 to 26 μm radius. The measured values of collection efficiencies were consistently below collision efficiencies based on calculations using rigid sphere hydrodynamics. The coalescence efficiencies computed from the ratio of the theoretical collision efficiencies to the measured collection efficiencies were between 0.6 and 0.8. The data show fair agreement with previous coalescence model results. Grazing trajectory collisions are considered. (31 refs.)

64179 Homogeneous and isotropic turbulence on the sphere. G.J.Boer (Canadian Climate Centre, Downsview, Ontario, Canada).

J. Atmos. Sci. (USA), vol.40, no.1, p.154-63 (Jan. 1983).

The assumption that the streamfunction for two-dimensional nondivergent flow on the sphere is a homogeneous and isotropic random field is used to obtain a variety of results for the study of large-scale atmospheric turbulence. These results differ somewhat from those for Cartesian geometry. It is shown that the necessary and sufficient condition that the turbulent flow be homogeneous and isotropic is the statistical independence of the spherical harmonic expansion coefficients of the streamfunction and the dependence of the variance of the expansion coefficients only on the wavenumber n . The homogeneity and isotropy of the vorticity field and of the velocities along and perpendicular to the geodesic connecting points on the sphere follows. The usual zonal and meridional velocity components on the sphere are anisotropic although, at a point, these velocity components are uncorrelated and have equal amounts of kinetic energy. (19 refs.)

64180 Large-scale two-dimensional turbulence in the atmosphere. G.J.Boer, T.G.Shepherd (Canadian Climate Centre, Downsview, Ontario, Canada).

J. Atmos. Sci. (USA), vol.40, no.1, p.164-84 (Jan. 1983).

Global FGGE data are used to investigate several aspects of large-scale turbulence in the atmosphere. The approach follows that for two-dimensional,

nondivergent turbulent flows which are homogeneous and isotropic on the sphere. Spectra of kinetic energy, enstrophy and available potential energy are obtained for both the stationary and transient parts of the flow. Nonlinear interaction terms and fluxes of energy and enstrophy through wavenumber space are calculated and compared with the theory. A possible method of parameterizing the interactions with unresolved scales is considered. Two rather different flow regimes are found in wavenumber space. The high-wavenumber regime is dominated by the transient components of the flow and exhibits, at least approximately, several of the conditions characterizing homogeneous and isotropic turbulence. This region of wavenumber space also displays some of the features of an enstrophy-cascading inertial subrange. (26 refs.)

64181 Hail growth in a three-dimensional cloud model. J.-L.Xu (Nat. Center for Atmospheric Res., Boulder, CO, USA).

J. Atmos. Sci. (USA), vol.40, no.1, p.185-203 (Jan. 1983).

A hailstone growth model is developed. The changes in hailstone density due to varying riming densities are considered. The contributions of evaporation to melting as well as wet growth (which cannot be neglected when the cloud temperature is approximately 0°C) are taken into account. A detailed heat balance equation is used in calculating the surface temperature of the hailstone. Detailed terminal velocity equations are applied in this model. Data of air velocities, liquid water contents, and temperature were obtained from the three-dimensional dynamic model developed by Clark. Embryos were released at each point in a subgrid of $21 \times 22 \times 17$ grid points within the dynamic model domain. Seven runs were made with various parameters: embryo radii of 0.10, 0.20 and 0.25 μm ; embryo densities of 0.4×10^3 and 0.9×10^3 kg m^{-3} ; and cloud droplet concentrations of 500 and 10^6 and 1000×10^6 m^{-3} . (33 refs.)

64182 A relationship between hailstone concentration and size. L.Cheng, M.English (Alberta Res. Council, Edmonton, Alberta, Canada).

J. Atmos. Sci. (USA), vol.40, no.1, p.204-13 (Jan. 1983).

Hailstone size distributions have been determined from 41 time-resolved hailstone samples collected at the ground from seven storms that occurred in Alberta in the summer of 1980. Most size distributions were found to quite closely fit an exponential function of the form $n(D) = n_0 e^{-\lambda D}$. In studying variations in n_0 and λ , it was found that a relationship exists between the two. In particular, correlation coefficients of ~ -0.9 were found when least-squares linear regressions were fitted to the values of $\log n_0$ versus $\log \lambda$. For Alberta storms, therefore, n_0 can be expressed in terms of λ as $n_0 = 115 \lambda^{3.63}$, and hail size distributions can be expressed in terms of the single parameter λ as $n(D) = 115 \lambda^{3.63} e^{-\lambda D}$. From an examination of hail size distributions from one storm that occurred in Switzerland, it appears likely that similar relationships can be determined for hailstorms from other regions. (21 refs.)

64183 Theory of equilibrium temperatures in radiative-turbulent atmospheres. K.-N.Liou, S.-C.S.Ou (Dept. of Meteorology, Univ. of Utah, Salt Lake City, UT, USA).

J. Atmos. Sci. (USA), vol.40, no.1, p.214-29 (Jan. 1983).

A thermodynamic model has been developed for the determination of the temperature profile based on the balance of radiative and turbulent fluxes. In the context of a one-dimensional case, it is shown that the temperature field is governed by a first-order differential-integro equation involving temperature to the fourth power. In conjunction with the temperature profile determination, parameterization programs for the transfer of broadband thermal infrared and solar fluxes in inhomogeneous atmospheres are developed. In addition, the vertical transport is parameterized using a first-order closure scheme with the eddy thermal diffusion coefficients derived from known theories or from available data. By virtue of an efficient perturbation technique devised for the solution of the thermal equilibrium temperature, it is shown that the simulated temperatures compare well with those of a standard atmosphere employing climatological water vapor, ozone and cloud profiles. Simulations using the steady-state one-dimensional model also reveal that high clouds will produce warming everywhere in the atmosphere whereas middle and low clouds will generate cooling as noted by several previous investigators. (34 refs.)

64184 Some improvements and complements to the infrared emissivity algorithm including a parameterization of the absorption in the continuum region. L.Garand (Recherche en Prevision Numerique, Dorval, Quebec, Canada).

J. Atmos. Sci. (USA), vol.40, no.1, p.230-44 (Jan. 1983).

Infrared heating rate calculations with the emissivity formulation are improved by developing simple methods to minimize the effects of the two main sources of error: 1) the use of the strong-line approximation; 2) the neglect of temperature variations along the optical path. When compared to band-by-band calculations, the resulting new scheme maintains a 5% accuracy on cooling rates, and errors generally less than 2 W m^{-2} on fluxes. The most recent band parameters of McClatchey et al. (1973) are used in the band-by-band calculations, including measured data for the vibration-rotation bands. Another novel aspect of the new scheme is the treatment of 'e-type' absorption, which is a very important effect in hot humid air near the ground. An implicit parameterization is developed which allows for 'e-type' absorption in the pre-tabulated transmission functions, and so requires no computational overhead. (20 refs.)

64185 Stationary waves in the winter stratosphere: seasonal and interannual variability. A.K.Smith (Geophys. Program, Univ. of Washington, Seattle, WA, USA).

J. Atmos. Sci. (USA), vol.40, no.1, p.245-61 (Jan. 1983).

Monthly average satellite and conventional data are used to determine the zonal mean wind and stationary waves 1 and 2 in the northern winter stratosphere for January 1973 through February 1977. Wave propagation is diagnosed with the aid of the Eliassen-Palm flux and the refractive index squared. Interannual variability in zonal mean wind and stationary wave amplitudes is greatest during the second half of winter (January-March), partially as a consequence of the irregular occurrence of major sudden warmings during those months. Both the seasonal trend and the interannual variability of the amplitude of wave 1 reflect variations in zonal mean wind, and the corresponding refractive index. The wave 1 amplitude maximum in the upper stratosphere occurs on the cyclonic side of the zonal jet, and its variability during mid-winter months is controlled primarily by refractive index variations associated with variations in the meridional curvature of the wind profile. During each year studied, a mid-winter minimum in wave 1 amplitude occurs at and above 1 mb as a consequence of a mid-winter curvature maximum. (40 refs.)

64186 Baroclinic instability of the summer mesosphere: a mechanism for the quasi-two-day wave? R.A.Plumb (CSIRO Div. of Atmospheric Phys., Aspendale, Australia).

J. Atmos. Sci. (USA), vol.40, no.1, p.262-70 (Jan. 1983).

Observations of the 'quasi-two-day' wave are reviewed and it is concluded that the weight of evidence indicates that the wave is a solstitial phenomenon, with maximum amplitudes in low latitudes of the summer mesosphere. It is

suggested that the properties of this wave and of a similar wave found in a numerical model of the middle atmosphere may be consistent with an origin via baroclinic instability of the easterly jet in the summer mesosphere. This suggestion is supported by the results of a stability analysis of a one-dimensional model of the summer mesospheric flow. (36 refs.)

64187 VHF radar observations in the stratosphere and mesosphere during a stratospheric warming. R.Rutser, P.Czechowsky, G.Schmidt (Max-Planck-Inst. für Aeronomie, Katlenburg-Lindau, Germany), K.Labitzke, J. Atmos. & Terr. Phys. (GB), vol.45, no.2-3, p.161-8 (Feb.-March 1983). For the first time the SOUSY-VHF-Radar (lat. 52°N, long. 10°E, Germany) was used to carry out measurements during a minor and major stratospheric warming in February and March 1980, respectively. Echoes have been received from the stratosphere up to an altitude of about 30 km continuously during day and night, whereas echoes from the mesosphere were restricted to the daytime and occurred sporadically at different heights within the altitude range from 60 to 90 km. The three-dimensional velocity vector has been derived from Doppler measurements made in three different antenna beam directions with a height resolution of 1.5 km. The resulting variation in height and time of the observed stratospheric and mesospheric wind speed and direction is discussed with respect to the stratospheric warming and compared with results obtained during undisturbed conditions. (11 refs.)

64188 Experiment of artificial lightning triggered with rocket. K.Horii (Dept. of Electrical Engng., Nagoya Univ., Nagoya, Japan). Mem. Fac. Eng. Nagoya Univ. (Japan), vol.34, no.1, p.77-112 (May 1982). In English. [received: March 1983] Experiments on artificial lightning triggered with a rocket pulling up a grounded wire has been carried out. The purposes of this experiment were to investigate the mechanism of the lightning discharge including predischARGE phenomena, and to develop a technique for protection from the hazards of lightning discharges. Though lightning has not been triggered in summer, 32 lightning flashes were triggered in winter at Hokuiriku, the north coast of Japan. The peak value and the duration of the discharge current, the electric field intensity at the ground, the altitude of the rocket, and other variables were measured, and relations between them discussed. The mechanism of lightning discharge was made clear from optical observations and the measurement of currents. Long gap discharges between bobbins in air and the ground were successfully performed three times. The surge voltages induced on power lines were measured and the shielding effect of the overhead grounded wire to the test line was confirmed. (18 refs.)

64189 Global distribution and southern hemispheric trends of atmospheric CCl₃F. P.J.Fraser, P.Hyson, I.G.Enting, G.I.Pearman (Div. of Atmospheric Phys., CSIRO, Aspendale, Victoria, Australia). Nature (GB), vol.302, no.5910, p.692-5 (21 April 1983). The spatial and temporal variability of the tropospherically inert tracer, trichlorofluoromethane (CCl₃F), has been simulated using a global atmospheric transport scheme and known release and photolytic data. The observational data are taken from the Geophysical Monitoring for Climatic Change (GMCC) global network, from the Pacific north-west (PNW) USA and South Pole, and from the CSIRO southern hemispheric stations at Cape Grim, Tasmania, and Mawson, Antarctica. A current CCl₃F atmospheric lifetime of 75 yr is obtained. The observations suggest that small, residual errors may exist in the CCl₃F release data. (25 refs.)

64190 Solar irradiance study. A.Pons, A.Corrans (Inst. de Optica, Madrid, Spain). Opt. Pura & Apl. (Spain), vol.15, no.3, p.119-28 (1982). In French. A new kind of solar radiometer has been constructed for the continuous measurement of solar irradiance. Using the experimental measurements, a theoretical expression is proposed as closer to real direct solar spectral irradiance in Madrid, on clear days. The experimental data also provide information on the content and size distribution of atmospheric aerosols at the time of measurements. (21 refs.)

64191 Solar radiation values received on a horizontal surface in Spain. F.Tena, D.Tinaut, A.Casanovas (Facultad de Fisicas, Univ. de Valencia, Valencia, Spain). Opt. Pura & Apl. (Spain), vol.15, no.3, p.129-42 (1982). In French. Employing linear correlations between measured values of insolation and solar irradiation, there have been deduced for a period of about 20 years the solar radiation values for 73 different places of the Peninsular part of Spain. Also the maximum and minimum values have been deduced for such a period, evaluating the total dispersions, and the mean deviations. In this way an estimation of future perspectives is possible. (9 refs.)

64192 Dynamics of the atmospheric boundary layer during the 1980 total solar eclipse. S.Sethu Raman (Atmospheric Sci. Div., Brookhaven Nat. Lab., Upton; NY, USA). Proc. Indian Natl. Sci. Acad. Part A, vol.48, suppl.3, p.187-95 (Oct. 1982). (Symposium on the Total Solar Eclipse of 16 February 1980, New Delhi, India, Jan. 1981).

An atmospheric boundary layer experiment was conducted at Raichur, India, to study the variations in the surface shear stress, heat flux and the meteorological processes that take place during a total solar eclipse. Interesting results were observed regarding the evolution of the planetary boundary layer. Changes in atmospheric stability from unstable to stable to unstable were observed during different phases of the eclipse. Downward propagation of negative heat flux associated with decreasing scales of convective eddies was also observed during the eclipse. (2 refs.)

64193 Total solar eclipse of 16 February 1980 and the vertical profiles of atmospheric parameters in the lowest 200 m. V.Ramesh Babu, J.S.Sastry (Nat. Inst. of Oceanography, Goa, India). Proc. Indian Natl. Sci. Acad. Part A, vol.48, suppl.3, p.196-201 (Oct. 1982). (Symposium on the Total Solar Eclipse of 16 February 1980, New Delhi, India, Jan. 1981).

Vertical profiles of air temperature, wind and humidity at Raichur, India (16°12' and 77°21'E), in the lowest 200 m of the atmosphere are presented for the period 15-18 February 1980. The effect of the total solar eclipse on 16 February 1980 is seen in the lowering of air temperature in the entire air column. This effect persisted for a few hours. (2 refs.)

64194 Meteorological parameters near the Earth's surface along the path of totality during the total solar eclipse of 16 February 1980. S.K.Das, S.M.Kulshrestha, K.Chatterjee, C.K.Chanderasekharan (India Meteorological Dept., Instruments Div., New Delhi, India). Proc. Indian Natl. Sci. Acad. Part A, vol.48, suppl.3, p.202-8 (Oct. 1982). (Symposium on the Total Solar Eclipse of 16 February 1980, New Delhi, India, Jan. 1981).

The instruments divisions at New Delhi and Pune of the India Meteorological Department planned an exhaustive programme to take frequent dry bulb and wet bulb temperature measurements at 14 observatories, including experimental stations at Gadag and Raichur, along the path of totality on 15, 16 and 17 February, 1980. The frequency of observations was stepped up between

1530 and 1630 IST when readings were taken at 2 minutes interval. These measurements taken at the 14 observatories have been analysed. Soil surface temperatures recorded at Gadag on 15, 16 and 17 February 1980 have also been plotted, analysed and presented. Sunshine duration record of 16 February 1980 of Gadag has also been discussed in the paper. (no refs.)

64195 Solar eclipse of 16 February, 1980—its effect on meteorological parameters. K.Mohanakumar, S.Devanarayanan (Dept. of Phys., Univ. of Kerala, Trivandrum, India). Proc. Indian Natl. Sci. Acad. Part A, vol.48, suppl.3, p.209-16 (Oct. 1982). (Symposium on the Total Solar Eclipse of 16 February 1980, New Delhi, India, Jan. 1981).

A study of the meteorological parameters across the penumbral and umbral regions during the 16 February 1980 Indian total solar eclipse has been made. Surface pressure, air temperature, soil surface temperature and relative humidity measurements made at Trivandrum, which had 80 per cent obscuration, Hyderabad which was almost in the totality path, Calcutta which had 96 per cent obscuration and New Delhi 65 per cent eclipse are discussed. It was found that the surface pressure was not much affected by the eclipse. The air temperature measured at a height of 1.2 m above the ground showed a decrease of 2.8°C at Trivandrum, 3.1°C in Calcutta and 2.7°C at Hyderabad. Soil surface temperature fell by 16.3°C at Trivandrum on the eclipse day. An increase in relative humidity was found as the eclipse advanced, reaching the highest value just after the final contact. (8 refs.)

64196 Measurements of meteorological parameters at the lowest layers of the atmosphere during total solar eclipse of 1980. R.K.Kankane, B.K.Hazra, A.B.Sarkar (Meteorological Office, Pune, India). Proc. Indian Natl. Sci. Acad. Part A, vol.48, suppl.3, p.217-23 (Oct. 1982). (Symposium on the Total Solar Eclipse of 16 February 1980, New Delhi, India, Jan. 1981).

Observations of various meteorological parameters, viz. wind speed, wind direction at two levels 3.0 and 13.5 m, air temperature at four levels 0.3, 3.0, 6.5 and 13.5 m, soil surface temperature and atmospheric pressure were made at Raichur (77°21'E, 16°12'N) during the total solar eclipse of 16 February 1980. Sensitive photo-electric anemometers and potentiometric windvanes were used for measuring wind speed and direction, sensitive linear bead thermistors were used for measuring temperature, a differential capacitor transducer was used for the measurement of atmospheric pressure. The above parameters were continuously and automatically recorded on strip chart recorders. (2 refs.)

64197 A study of change in the atmospheric properties during solar eclipse of 16 February 1980. R.K.Kapoor, B.B.Adiga (Health Phys. Div., Bhabha Atomic Res. Centre, Bombay, India), S.P.Singal, S.K.Agarwal, B.S.Gera. Proc. Indian Natl. Sci. Acad. Part A, vol.48, suppl.3, p.224-33 (Oct. 1982). (Symposium on the Total Solar Eclipse of 16 February 1980, New Delhi, India, Jan. 1981).

Monostatic sodar and a number of meteorological sensors were used to study variations in the atmospheric boundary layer at Delhi (28°6'N, 77°2'E) and Tarapur (19°50'N, 72°41'E) during the solar eclipse of 16 February 1980. The atmospheric instability (atmospheric mixing and turbulence) and solar UV component were found to have been reduced below normal values during the solar eclipse period. The atmosphere at no time became stable and the sodar echograms did not show the presence of wave motion (undulations) before, during or after the solar eclipse at either of the two places. (5 refs.)

64198 Radiometric observations of solar eclipse over New Delhi on 16 February 1980. M.K.Raina, G.S.Uppal, R.Chadha (Radio Sci. Div., Nat. Phys. Lab., New Delhi, India). Proc. Indian Natl. Sci. Acad. Part A, vol.48, suppl.3, p.234-7 (Oct. 1982). (Symposium on the Total Solar Eclipse of 16 February 1980, New Delhi, India, Jan. 1981).

A study has been made of the effect of the solar eclipse of 16 February 1980 on solar microwaves at 11 GHz and atmospheric water vapour measurements at 22.235 GHz. Radiometers at 11 GHz in the absorption mode and 22.235 GHz in the emission mode were operating simultaneously at the National Physical Laboratory, New Delhi. As the eclipse progressed in its path, a fall in the microwave emission from the Sun was observed. At the time when there was maximum obscuration over New Delhi, a fall of 6 dB was observed. On the other hand, the water vapour measurements by another Radiometer at 22.235 GHz working in the emission mode and looking at the zenith showed a marginal increase of around 10 to 15K over the sky level during the period of eclipse. (4 refs.)

64199 Atmospheric pressure perturbations during total solar eclipse on 16 February 1980. P.K.Kunhikrishnan, B.V.Krishna Murthy (Space Phys. Div., Vikram Sarabhai Space Centre, Trivandrum, India). Proc. Indian Natl. Sci. Acad. Part A, vol.48, suppl.3, p.238-53 (Oct. 1982). (Symposium on the Total Solar Eclipse of 16 February 1980, New Delhi, India, Jan. 1981).

Pressure variations recorded at three stations situated in the penumbral region during the total solar eclipse on 16 February 1980 have been analysed to study eclipse induced effects, if any. By statistical analysis, it has been established that the eclipse has produced pressure perturbations observable at the ground level. (11 refs.)

64200 Boundary layer studies conducted at Gadag during the total solar eclipse of 16 February 1980. K.Chatterjee, C.K.Chandrasekharan, V.P.Verma (Instruments Div., India Meteorological Dept., New Delhi, India). Proc. Indian Natl. Sci. Acad. Part A, vol.48, suppl.3, p.254-9 (Oct. 1982). (Symposium on the Total Solar Eclipse of 16 February 1980, New Delhi, India, Jan. 1981).

Special meteorological observations during the period covering total solar eclipse of 16 February 1980 were arranged at Gadag (Lat. 15°24'N, Long. 75°38'E) which lay in the path of totality of the eclipse to study the changes occurring in the lower boundary layer. Wind speed, wind direction, temperature and humidity instruments were installed on a micro meteorological tower at four levels 1.2 m, 3.3 m, 6.5 m and 13.5 m meter above ground and the observations were continuously recorded on strip chart recorders. (no refs.)

64201 Variations in atmospheric electrical parameters during solar eclipse. S.Nizamuddin, R.Ramanadham, A.M.Rao (Dept. of Meteorology & Oceanography, Andhra Univ., Waltair, India), M.K.Khera, B.A.Makhdomi, A.R.Rafiqi, B.N.Raina, V.Reddy Mukku, R.K.Goel, P.P.Pathak, J.Rai, N.C.Varshneya. Proc. Indian Natl. Sci. Acad. Part A, vol.48, suppl.3, p.263-70 (Oct. 1982). (Symposium on the Total Solar Eclipse of 16 February 1980, New Delhi, India, Jan. 1981).

Results of solar eclipse observations conducted at Nagarampalam near Vishakhapatnam ($\lambda=7.723^\circ\text{N}$, $\phi=148.65^\circ\text{E}$ geomagnetic) are presented. Observed variations in atmospheric conductivities, potential gradient, and air Earth current are explained by correlating them with the variations in the solar wind flux on the Earth (as a result of eclipse by the Moon) and the resulting change in atmospheric ionization. Observations by previous workers, of a different pattern of variation in conductivity during solar eclipse at high

latitudes, have also been explained on the same theoretical basis. While there are marked solar eclipse changes in atmospheric electrical parameters, no definite effects on meteorological parameters have been observed. (6 refs.)

64202 Measurements of atmospheric electricity parameters during the total eclipse of 16 February 1980. G.P.Srivastava, V.Srinivasan, A.K.De (Instruments Div., Meteorological Office, Pune, India).

Proc. Indian Natl. Sci. Acad. Part A, vol.48, suppl.3, p.271-9 (Oct. 1982). (Symposium on the Total Solar Eclipse of 16 February 1980, New Delhi, India, Jan. 1981).

Continuous recordings of atmospheric potential gradient, polar conductivities and positive and negative ion densities were made close to the ground during the total solar eclipse of 16 February 1980 at Raichur, India ($72^{\circ}21'E$, $16^{\circ}12'N$). Measurements of positive and negative electrical conductivities were also made on a 15 m high tower simultaneously. A few low level potential gradient soundings were made close to the eclipse time to study the vertical distribution of potential gradient at lower troposphere. The results are compared with the measurements taken two days before and two days after the eclipse. The instruments used are described. (4 refs.)

64203 Variation in solar energy intensity during total solar eclipse of 16 February 1980. U.K.Chaturvedi, S.K.Agrawal, N.Rajan, R.Bhanja, A.K.Nigam (Dept. of Phys., Banaras Hindu Univ., Varanasi, India).

Proc. Indian Natl. Sci. Acad. Part A, vol.48, suppl.3, p.280-3 (Oct. 1982). (Symposium on the Total Solar Eclipse of 16 February 1980, New Delhi, India, Jan. 1981).

All the solar energy trapping systems become inactive in a belt hundreds of kilometers wide for a period of hours during a total solar eclipse. This inspired the authors to measure the changes in the intensity of the sunlight during the total solar eclipse of 16 February 1980 at Puri (India). Puri is situated at $19.85^{\circ}N$, $85.80^{\circ}E$. It was only 10 km north to the middle line of the totality path of the eclipse. The intensity of the sunlight during the eclipse was measured by a CEL Suryamapi. The intensity of the sunlight at Puri sea beach decreased from 76 mW cm^{-2} to 0.01 mW cm^{-2} at the peak of totality. The temperature of the environment at the site was also measured by a sensitive alcohol thermometer. The temperature variation from $29^{\circ}C$ to $24^{\circ}C$ was observed during the same period. The sea became more violent and the wind velocity increased significantly during the total solar eclipse. (1 ref.)

64204 Determination of ozone from eclipse observations of $O_3(a^1\Delta_g)$ dayglow. V.V.Agashe, S.M.Rathi (Dept. of Phys., Univ. of Poona, Pune, India).

Proc. Indian Natl. Sci. Acad. Part A, vol.48, suppl.3, p.284-92 (Oct. 1982). (Symposium on the Total Solar Eclipse of 16 February 1980, New Delhi, India, Jan. 1981).

Observations of 1270 nm dayglow radiance of molecular oxygen during the total solar eclipse of 16 February 1980 have been described. Rate equations for production and loss of $O_3(a^1\Delta_g)$ have been used together with observed data to examine the changes in the concentration of ozone during the eclipse. It is found that ozone concentrations increased during the eclipse. At 66 km altitude, the ozone concentration increased by more than a factor of two at the mid-eclipse time over its prevailing value at first contact. (18 refs.)

64205 VLF/LF detection of ionization changes and wave motions in the middle atmosphere associated with the February 1980 total solar eclipse. Y.V.Ramanamurthy, S.C.Garg, M.V.S.N.Prasad, A.Hamid (Nat. Phys. Lab., New Delhi, India).

Proc. Indian Natl. Sci. Acad. Part A, vol.48, suppl.3, p.293-301 (Oct. 1982). (Symposium on the Total Solar Eclipse of 16 February 1980, New Delhi, India, Jan. 1981).

Based on VLF/LF radio observations, the first evidence of wave motions in the middle atmosphere associated with the total solar eclipse of 16 February 1980 is presented. The ionospheric effect on 16 kHz radiowaves monitored at New Delhi (path mid point $47.4^{\circ}N$, $29.6^{\circ}E$) manifested itself as a precursor corresponding to a decrease followed by the main increase in height of reflection because of loss of electrons due to recombination in the partially eclipsed lower D-region. Succeeding this main effect, there was a phase overshoot due to rather complex aeronomical processes. Soon after the appearance of the precursor, small periodic fluctuations in the phase are observed. The VLF paths (12.8 kHz, La Reunion-New Delhi; 12.3 kHz, Tsushima Island-New Delhi) crossing the path of totality showed larger phase retardations compared to the 16 kHz Rugby-New Delhi path which is far away from the path of totality. (23 refs.)

64206 Atmospheric gravity waves produced by solar eclipses—a review. K.Davies (Nat. Sci. Found., Washington DC, USA).

Proc. Indian Natl. Sci. Acad. Part A, vol.48, suppl.3, p.342-55 (Oct. 1982). (Symposium on the Total Solar Eclipse of 16 February 1980, New Delhi, India, Jan. 1981).

Reviews the theoretical and experimental bases for gravity wave production resulting from cooling produced by the Moon's shadow. Theoretically, it is reasonable to expect waves from the low shock after propagation in a dispersive and anisotropic atmosphere and that focusing should be expected from the eclipse geometry. Experimental evidence from the eclipses of 7 March 1970 in North America, 30 June 1973 in Africa and 23 October 1976 in Australia leave doubts as to whether such waves have been observed. (40 refs.)

64207 Evidence of atmospheric gravity waves in the wake of the eclipse shadow. R.Venkatachari, A.K.Saha, C.V.Subrahmanyam (Radio Sci. Div., Nat. Phys. Lab., New Delhi, India), S.K.Chatterjee.

Proc. Indian Natl. Sci. Acad. Part A, vol.48, suppl.3, p.370-4 (Oct. 1982). (Symposium on the Total Solar Eclipse of 16 February 1980, New Delhi, India, Jan. 1981).

An attempt was made to obtain evidence of atmospheric gravity waves at ground level and at ionospheric height during the total solar eclipse of 16 February 1980. The observations were made with two microbarographs located at Hyderabad (maximum obscuration 99 per cent) and at Delhi (65 per cent), a 10 MHz Dopplometer located at Calcutta receiving ATA, Delhi and an ionosonde at Delhi. Wavelike disturbances could be distinguished in the Hyderabad microbarograph and in the Dopplometer records that would tend to suggest that gravity waves were originating from the region of totality. No clear evidence of wave motion could be detected at Delhi on the microbarographs or in the ionograms. (10 refs.)

64208 Infrared visibility prediction by statistical methods. A.Court, G.-Y.Lin, S.Zetsche (California State Univ., Northridge, CA, USA).

Pure & Appl. Geophys. (Switzerland), vol.120, no.2, p.203-10 (1982).

This study attempts to find statistical methods of predicting infrared visibility (IRV), as calculated from hourly meteorological observations from a North Atlantic weather ship. Simple and multiple regressions expressing IRV as a function of its component weather variables, and exponential data transformations, for time lags of 1 to 24 hours, gave R^2 values from 0.68 (1-hour lag) to 0.09 (24-hour lag). These have limited predictive power for lags up to 6 hours, almost none for longer lags. Two-category discriminant analysis, using class breaks at 2 km or 10 km is of little use, due to uneven data distribution. Possibly more promising would be an application of Machine

Output Statistics ('MOS'), used routinely for temperature forecasts, to this problem. (3 refs.)

64209 A study of energy conversion in the wave number domain. U.S.Singh (Dept. of Geophys., Banaras Hindu Univ., Varanasi, India).

Pure & Appl. Geophys. (Switzerland), vol.120, no.2, p.211-17 (1982). Energy conversions from potential to kinetic energy have been studied for a part of the Northern Hemisphere in the wave number domain. The vertical distribution of energy conversions were examined and the results have been compared with the other's observational results as well as that of forecast models. (15 refs.)

64210 A study of energy, generation and conversion over North America. U.S.Singh (Dept. of Geophys., Banaras Hindu Univ., Varanasi, India).

Pure & Appl. Geophys. (Switzerland), vol.120, no.2, p.218-28 (1982). The energy conversion between potential and kinetic energy and the generation of available potential energy are computed over North America. The relative contribution from each latitude belt within the region, for each field, have been discussed. (19 refs.)

64211 Meridional transport of sensible heat in contrasting monsoon activity: spherical harmonic analysis. S.T.Awade, S.M.Bawiskar (Indian Inst. of Tropical Meteorology, Pune, India).

Pure & Appl. Geophys. (Switzerland), vol.120, no.2, p.229-48 (1982).

A spherical harmonic analysis is made of the grid point values of geopotential heights at 700 mb and 300 mb levels for the months of April to August for the years 1967 and 1972. The year 1967 is a good monsoon year and 1972 is bad monsoon year in India. Meridional transport of sensible heat is obtained in wave number domain using spherical harmonic coefficient at the 500 mb level for $m=1$ to 10 and $n=m=0$ to 10, where m represents the wave number round the globe and $n-m$ gives the numbers of zero points from north pole to south pole excluding the poles themselves. Large northward transports of sensible heat in the month of May and in the monsoon months at the subtropics are characteristics of bad monsoons. Wave 1 transports sensible heat southward (for $n-m=0$) and wave 2 transports sensible heat northward (for $n-m=4$). Strengthening of wave 1 is conducive to good monsoon year and strengthening of wave 2 is conducive to bad monsoon year. (19 refs.)

64212 Correlation functions of rainfall field and their application in network design in the tropics. D.A.Mooley, P.M.Mohamed Ismail (Indian Inst. of Tropical Meteorology, Pune, India).

Pure & Appl. Geophys. (Switzerland), vol.120, no.2, p.249-60 (1982).

The study examines the correlation function of tropical monsoon rainfall on monthly, seasonal and annual time scales and obtains the relationship between this function and the distance. The area selected for study is Vidarbha with a fairly dense network of rain gauges. Vidarbha is a meteorological sub-division of the state of Maharashtra in India. Utilizing the relationship between the correlation function of the rainfall field and the distance, the errors of optimum interpolation of rainfall at a point have been computed by applying the method of optimum interpolation by Gandin (1970). Relationships between rain gauges for a specified tolerable error in interpolation has been estimated for each of the periods. (10 refs.)

64213 Areal extent and vertical structure of radar weather echoes at Montreal. R.R.Rogers, M.K.Yau (Dept. of Meteorology, McGill Univ., Montreal, Quebec, Canada).

Pure & Appl. Geophys. (Switzerland), vol.120, no.2, p.273-85 (1982).

A large sample of radar data from the period May-August 1976 was analyzed provide information on the total area coverage of precipitation echoes at 1-km steps in altitude ranging from 2 km up to 10 km. A transformation based on known statistics of surface rainfall rate was employed to express this information in terms of the probability of certain reflectivities being exceeded at a randomly chosen point at a given altitude. The same data base was used to construct a family of average vertical profiles of precipitain reflectivity. The profiles were conditioned by the reflectivity value at the lowest level (2 km), thus providing a basis for estimating the reflectivity aloft, given the low level of surface rainfall rate. (15 refs.)

64214 The removal of particulate matter from the atmosphere: the physical mechanisms. F.Prodi (Osservatorio Geofisico, Univ. di Modena, Modena, Italy), F.Tampieri.

Pure & Appl. Geophys. (Switzerland), vol.120, no.2, p.286-325 (1982).

The removal of particulate matter from the atmosphere has been examined in the light of the physical mechanisms involved, with a view of the theoretical and experimental results available in the literature. While the wet and dry removal are usually separately discussed, it has been decided to give evidence of the fundamental mechanisms which are active in both processes. A number of them, such as the inertial impaction, the phoretic and electrostatic collection, can be expressed through the equation of motion of the individual particle. Other mechanisms, such as Brownian and turbulent deposition, and incorporation by nucleation, require a description in terms of the behaviour of a population of particles. Finally, the problem of the superposition of the different mechanisms in the actual removal processes is considered. (56 refs.)

64215 Comparison between the results of a one-dimensional model and those of stratospheric measurements for CH_4 , H_2O and nitrogen oxides. R.Borghi (Office Nat. d'Etudes et de Recherches Aérospatiales, Chatillon, France), D.Cariolle, A.Girard, J.Laurent, N.Louisnard.

Rev. Phys. Appl. (France), vol.18, no.4, p.229-37 (April 1983).

Simultaneous measurements of stratospheric trace gases have been obtained by infrared absorption spectrometry at sunset and sunrise. They are compared with the results of a 1-D photochemical model. This comparison points out: for water vapour marked discrepancies between some measured profiles and the profile of the 1-D model; the observed variations are, at least partly, due to horizontal transport and cannot be explained by this model; a good agreement between measured and calculated vertical column abundance of NO_2 at sunset and sunrise. (17 refs.)

64216 Aerosol mode of ball lightning. V.Ya.Aleksandrov, E.M.Golubev, I.V.Podmoshenskii.

Sov. Phys.-Tech. Phys. (USA), vol.27, no.10, p.1221-4 (Oct. 1982). Translation of: *Zh. Tekh. Fiz. (USSR)*, vol.52, no.10, p.1987-92 (Oct. 1982). [received: April 1983]

A model is proposed for ball lightning in which the active material is in a condensed state consisting of three-dimensional filamentary structures suspended in air. The submicron filaments are built up by the action of the electric field from charged particles and droplets formed in corona shells in linear lightning channels and are capable of participating in oxidation reactions. Reactions are assumed to be initiated by microscopic discharges during neutralization of various types of charged particles. The model gives a satisfactory explanation for the basic properties of ball lightning (why its shape remains constant, how it moves, how much energy it contains) and accounts for various mechanisms by which the energy is dissipated. (14 refs.)

- 64217 48- and 60-hour surface air temperature forecasting.** A.I.Snitkovskii (Hydrometeorological Sci. Res. Center, USSR). *Sov. Meteorol. & Hydrol. (USA)*, no.12, p.1-7 (1981). Translation of: *Meteorol. & Gidrol. (USSR)*, no.12, p.5-13 (1981).
A procedure for forecasting temperature lows 48 hours ahead and temperature highs 60 hours ahead on the basis of the model output statistics (MOS) concept with the aid of regression equations is proposed. (2 refs.)
- 64218 Relation between time and space intervals in numerical weather forecasting.** V.M.Kadyshnikov, V.M.Ryazantseva (Hydrometeorological Sci. Res. Center, USSR). *Sov. Meteorol. & Hydrol. (USA)*, no.12, p.8-16 (1981). Translation of: *Meteorol. & Gidrol. (USSR)*, no.12, p.14-24 (1981).
The wave energy propagation velocity is part of Courant's criterion, which links the time and space steps in explicit forecasting schemes. It is shown that in a polytropic hydrostatic atmosphere, the horizontal velocity of the baroclinic case is near the corresponding barotropic value, and that wave energy does not propagate vertically. Therefore, the time step depends only on the horizontal resolution of the model. Its independence of the vertical resolution is also confirmed by calculations. (9 refs.)
- 64219 Friction and heat exchange between air and surface in the presence of sand, salt, and ice-particle transport.** O.K.Zakharova (State Hydrological Inst., USSR). *Sov. Meteorol. & Hydrol. (USA)*, no.12, p.26-9 (1981). Translation of: *Meteorol. & Gidrol. (USSR)*, no.12, p.36-40 (1981).
Relationships are obtained for the heat transfer and drag coefficients on a level two meters above the surface by solving a system of equations of motion and heat combustion with terms that describe the presence of saltating sand, salt, and ice particles $3\text{--}6 \times 10^{-4}$ meters in diameter in the air stream. These coefficients increase with wind velocity and are approximately twice as large in moderate winds and three times as large in a hurricane as compared to the case in which the air stream does not transport particles. (5 refs.)
- 64220 Radiation modification of turbulent clouds.** R.Kh.Almaev, L.P.Semenov (Inst. of Experimental Meteorology, USSR). *Sov. Meteorol. & Hydrol. (USA)*, no.12, p.34-41 (1981). Translation of: *Meteorol. & Gidrol. (USSR)*, no.12, p.46-55 (1981).
The intensity fluctuations of modifying layer radiation that occur during dispersal of turbulent clouds are investigated. Expressions for the fluctuation variance of intensity level are obtained in the geometric-optics approximation by the method of smooth perturbations. It is shown that fluctuations of the real and imaginary dielectric-constant components of the medium being dispersed partially offset the intensity fluctuations. The profile changes of the average characteristics of the cloud medium being dispersed that result from saturations of the radiation acting on the medium are calculated. (10 refs.)
- 64221 Aspects of mass transfer in collisions of water drops of noncomparable size.** S.M.Kontush, A.V.Kolpakov (Odessa State Univ., Odessa, USSR). *Sov. Meteorol. & Hydrol. (USA)*, no.12, p.42-6 (1981). Translation of: *Meteorol. & Gidrol. (USSR)*, no.12, p.56-60 (1981).
An experimental procedure for the study of the phenomenon of partial coalescence of colliding drops is described, and results of experiments are reported. The experiments were performed with drops having radii 50 to 150 microns, which collided with target drops with radii 500 to 1500 microns, with the velocity varying in the range 20 to 200 cm/sec. Functional relationships linking the parameters of the drops before and after the collisions are obtained and the partial-coalescence mechanism is clarified. (12 refs.)
- 64222 Calculation of vertical turbulent heat fluxes in the marine atmospheric surface layer of tropical latitudes.** T.F.Masagutov (Inst. of Experimental Meteorology, USSR). *Sov. Meteorol. & Hydrol. (USA)*, no.12, p.47-53 (1981). Translation of: *Meteorol. & Gidrol. (USSR)*, no.12, p.61-8 (1981).
A relationship for the energy-exchange coefficients as functions of flow characteristics and the roughness of the sea surface is derived in explicit form from analysis of observational data on the structure of turbulence in the marine atmospheric surface layer that were obtained in GATE-69, BOMEX-69, and GATE-74 and on several other expeditions. The results are used to construct an improved scheme for calculation of heat, moisture, and momentum fluxes from the results of standard meteorological observations. (23 refs.)
- 64223 Year-to-year variations of Northern hemisphere zonal atmospheric circulation over a five-year period.** G.E.Vaindiner, T.L.Mukhina, V.P.Gladilina, L.L.Kazakova (Hydrometeorological Sci. Res. Center, USSR). *Sov. Meteorol. & Hydrol. (USA)*, no.12, p.80-2 (1981). Translation of: *Meteorol. & Gidrol. (USSR)*, no.12, p.102-4 (1981).
The variations of the zonal atmospheric circulation intensity in the Northern Hemisphere during the period from 1 January 1976 through 31 March 1981 are analyzed. Daily values of the zonal circulation indices on the 700 and 500 mb pressure surfaces in the North hemisphere were used as initial data. The results may be of interest for explanation of certain weather phenomena. (8 refs.)
- 64224 Use of probability methods to investigate the rate of Northern Hemisphere westerly air transport.** G.V.Gruza, V.T.Radyukhin (All Union Sci. Res. Inst. of Hydrometeorological Information World Data Center, USSR). *Sov. Meteorol. & Hydrol. (USA)*, no.1, p.1-9 (1982). Translation of: *Meteorol. & Gidrol. (USSR)*, no.1, p.5-15 (1982).
The temporal succession of westerly air transport intensities in the Northern Hemisphere as characterized by the daily values of Blinova's circulation index (CI) at the 500 mb level is analyzed. It is shown that the statistically significant coupling between successive CI values vanishes after seven days in winter and after four days in summer. (17 refs.)
- 64225 The dynamics of the nonstationary atmospheric front.** G.I.Shapiro (Inst. of Oceanology, Acad. of Sci., USSR). *Sov. Meteorol. & Hydrol. (USA)*, no.1, p.10-16 (1982). Translation of: *Meteorol. & Gidrol. (USSR)*, no.1, p.16-23 (1982).
A three-dimensional nonstationary hydrodynamic model of an atmospheric front is proposed in the approximation of a two-layer stratified, viscous, incompressible rotating fluid. The simplifications used are a small angle of inclination of the frontal surface to the horizon and a small inertial force in the momentum balance equation. An equation that describes the evolution of the frontal surface is derived and analyzed. (10 refs.)
- 64226 Mesoscale structure of an occluded front over the center of the European USSR from special measurements.** B.M.Matkovskii, N.P.Shakina (Inst. of Experimental Meteorology, USSR). *Sov. Meteorol. & Hydrol. (USA)*, no.1, p.17-24 (1982). Translation of: *Meteorol. & Gidrol. (USSR)*, no.1, p.24-33 (1982).
Rawinsonde and aircraft sounding data and high meteorological mast measurements are used to analyze the mesoscale structure of an autumn occluded frontal system over the center of the European USSR. Typical features of mesoscale occlusion structure are designated. The distribution of

the heat and moisture fluxes in the lower 300 meters of the atmosphere is discussed. (13 refs.)

- 64227 Two classes of low-variance schemes of solution of the advection equation.** E.E.Kalenkovich, I.V.Cholakh (West Siberian Regional Sci. Res. Inst., USSR). *Sov. Meteorol. & Hydrol. (USA)*, no.1, p.25-30 (1982). Translation of: *Meteorol. & Gidrol. (USSR)*, no.1, p.34-40 (1982).
Two classes of schemes for the advection equation are examined. Theoretical and experimental comparisons are made with the familiar Crank-Nicholson, Lax-Wendroff, and Gadd schemes. It is shown that the schemes proposed in this paper give smaller phase errors and reduce variance as compared with the other schemes. They may find applications in weather forecasting problems and problems in the general circulation of the atmosphere. (6 refs.)

- 64228 Interaction of clouds with the surrounding aerosol medium.** I.P.Mazin (Central Aerological Obs., USSR). *Sov. Meteorol. & Hydrol. (USA)*, no.1, p.42-8 (1982). Translation of: *Meteorol. & Gidrol. (USSR)*, no.1, p.54-61 (1982).
It is shown that the interaction of clouds with the surrounding atmosphere results in a transformation of the atmosphere's aerosol characteristics. The concentration of fine aerosol particles (AP) decreases and the size and composition spectra of the AP and their vertical distribution undergo transformations. As a result, the size spectrum of the cloud particles also varies with time: the drops consolidate and their concentration decreases, with an increased probability that the cloud will turn to ice at subfreezing temperatures. The efficiencies of these processes are evaluated, and the processes studied may play an important role in the formation of clouds and precipitation. (9 refs.)

- 64229 An atmospheric vertical temperature profile measurement by detecting infrared on board.** M.Ishido (Faculty of Engng., Kobe Univ., Kobe, Japan), K.Kan, M.Toyoda. *Trans. Soc. Instrum. & Control Eng. (Japan)*, vol.19, no.1, p.48-54 (Jan. 1983). In Japanese.
Describes an attempt to obtain the vertical temperature profile of the atmosphere by measuring the vertical infrared-radiation profile of CO₂ gas on board a rocket. While the rocket was ascending and descending through the atmosphere, the vertical profile of 15 μm band infrared radiation of CO₂ gas was measured by an infrared-radiation detection instrument. Then, making an approximation that the atmosphere has a layer structure composed of 0.6 km height, and using the iterative approximation method, the vertical temperature profile was obtained from the vertical infrared-radiation profile. The results agree fairly well with those of the CIRA model (1972) although there are some discrepancies. (11 refs.)

- Proceedings of the Symposium on Low-Level Waste Disposal. Site Characterization and Monitoring (NUREG/CP-0028) See Entry 59537
- Exploration of the Polar Upper Atmosphere. Proceedings of the NATO Advanced Study Institute See Entry 59540
- Atmospheric pressure waves generated by solar eclipses See Entry 59559
- Meteorology and climatology as parameters on low level waste disposal monitoring See Entry 60267
- On-site meteorological measurements for low-level radioactive waste disposal See Entry 60268
- High resolution absorption cross section measurements and band oscillator strengths of the (1,0)-(12,0) Schumann-Runge bands of O₂ See Entry 60742
- Experimental investigations of fluctuations of optical signals and disturbances in the atmosphere See Entry 61091
- The dependence of sound extinction on the parameters of thermal turbulence in the atmospheric boundary layer See Entry 61335
- The interaction between air pollution dispersion and residential heating demands See Entry 63753
- Acid fog See Entry 63755
- Gaseous tracers of Arctic haze See Entry 63756
- Numerical simulation of fog formation and liquid water content on polydisperse multi-composition aerosols due to combustion-related pollutants See Entry 63757
- An air quality data analysis system for interrelating effects, standards, and needed source reductions. VII. An O₃-SO₂ leaf injury mathematical model See Entry 63760
- High-sensitivity atmospheric gas analysis based on intracavity laser detection of scattered radiation See Entry 63763
- Transport equations for heat and moisture in the soil and their application to boundary layer problems See Entry 64154
- The effect of tropospheric aerosols on the Earth's radiation budget: a parameterization for climate models See Entry 64231
- Photoelectric observations of shadow bands during 16 February 1980 total solar eclipse from Japal-Rangapur observatory See Entry 64237
- Possible limits on the composition of the Archaean ocean See Entry 64238
- Laser measurements of the stratospheric ozone layer See Entry 64243
- Laboratory evaluation of an airborne ozone instrument that compensates for altitude/sensitivity effects See Entry 64244
- A simple and inexpensive method for measuring integrated light energy See Entry 64245
- Atmospheric laser spectrometer with an external cavity mirror See Entry 64267
- Monte Carlo simulation of small air-mass showers See Entry 64269
- Mapping fields of the meteorological elements given at the nodes of a latitude-longitude grid See Entry 64273
- The MMR-06-M meteorological rocket and its instrument package for measurement of density, temperature, wind, and electron concentration See Entry 64274
- On the extraction of atmospheric turbulence parameters from radar backscatter Doppler spectra. I. Theory See Entry 64279
- Mesospheric turbulence intensities measured with a HF radar at 35°S. II See Entry 64280
- Correlation of seasonal structural transformations of the F region of the ionosphere and the circulation in the stratosphere See Entry 64309
- Condensation nuclei events at 30 km and possible influences of solar cosmic rays See Entry 64334
- Solar irradiance variations. I. Analysis of modeling techniques and intercomparison of ground-based data See Entry 64448

92.60S Climatology

64230 A water vapor-energy balance model designed for sensitivity testing of climatic feedback processes. R.G.Gallimore (Dept. of Meteorology, Univ. of Wisconsin, Madison, WI, USA).

J. Atmos. Sci. (USA), vol.40, no.1, p.39-52 (Jan. 1983).

A zonal mean water vapor-energy balance (WEB) model is formulated to assess feedback interactions of the hydrologic cycle and lapse rate with the radiative fluxes, snow-dependent albedo and transport mechanisms. The WEB model is designed for comparative study and integration of many sensitivity experiments in which changes in feedback processes are introduced through variation in parameters and/or parameterizations. Specific processes in the model include 1) an explicit hydrologic cycle with the predicted atmospheric water vapor used in the determination of the solar and longwave fluxes; 2) a land albedo and surface energy budget dependency on explicit model calculations of snowfall, snow melt and snow accumulation; 3) a lapse rate dependency for the longwave emission, sensible heating and mean energy transport; and 4) separate specification for mean and eddy energy and water vapor transports. The effects of a reduced solar constant are considered. (48 refs.)

64231 The effect of tropospheric aerosols on the Earth's radiation budget: a parameterization for climate models. J.A.Coakley, Jr., R.D.Cess (Nat. Center for Atmospheric Res., Boulder, CO, USA), F.B.Yurevich. *J. Atmos. Sci. (USA)*, vol.40, no.1, p.116-38 (Jan. 1983).

Guided by the results of doubling-adding solutions to the equation of radiative transfer, the authors develop a simple technique for incorporating in climate models the effect of the background tropospheric aerosol on solar radiation. Because the atmosphere is practically nonabsorbing for much of the solar spectrum the effects of the tropospheric aerosol on the reflectivity, transmissivity and absorptivity of the atmosphere are adequately accounted for by the properties of a two-layered system with the atmosphere placed above the aerosol layer. The two-stream and delta-Eddington approximations to the radiative transfer equation then provide reasonably accurate estimates of the changes brought about by the aerosol. Furthermore, results of the doubling-adding calculations lead to a simple parameterization for the distribution of absorption by the aerosol within the atmosphere. Using these simple techniques, the authors calculate the changes caused by models for the naturally occurring tropospheric aerosol in a zonal mean energy balance climate model. The cooling influences of N₂O, methane and CO₂ pollutants are studied. (51 refs.)

uranium disequilibrium dating of phosphate deposits from the Lau Group, FijiSee Entry 64086

The global temperature trend in the CenozoicSee Entry 64239

Exploring the Martian arcticSee Entry 64412

92.65 ATMOSPHERIC OPTICS

(see also 42.00 Optics)

64232 Some features of the day-time astroclimate on Terskol peak. V.I.Troyan.

Astrometriya & Astrofiz. (USSR), no.47, p.80-3 (1982). In Russian.

About 50% of days per year on Terskol peak are suitable for observations of the Sun. A preliminary estimation of solar seeing is made. (8 refs.)

64233 Scattering matrix of nonspherical particles. Yu.A.Aleksandrov, V.P.Tishkovets.

Astrometriya & Astrofiz. (USSR), no.48, p.37-43 (1983). In Russian.

Expressions are obtained for the light scattering matrix of the nearly spherical, homogeneous and isotropic particles of random orientation. The numerical calculations of the elements of this matrix for certain particle shapes are given. (8 refs.)

64234 On isoplanatism by the arrival angles for light rays in telescopes. I.G.Kolchinskii.

Astrometriya & Astrofiz. (USSR), no.48, p.43-52 (1983). In Russian.

The formulas of Fried (1966, 1976, 1979) and those of the author for estimating sizes of isoplanatism regions by the arrival angle for the light rays in telescopes are compared with results of measurements of correlation between the image motions of stars on small angle distances. It is concluded that the Fried formula leads to underestimation of the sizes of isoplanatism regions. Possible reasons for this fact are discussed. (21 refs.)

64235 The usefulness of a bulk refractive index for the calculation of the scattering properties of mixtures of aerosol particles at wavelength 530 nm. L.Lederer, H.Quenzel, E.Thomalla (Meteorologisches Inst., Univ. Munchen, Munchen, Germany).

Contrib. Atmos. Phys. (Germany), vol.56, no.1, p.94-107 (1983).

The optical properties of a mixture of aerosol particles are based on its size distribution and the complex refractive indices of the individual particles. This paper considers the extent to which a bulk refractive index can be used to describe the scattering properties of particle polydispersions. The bulk refractive index is calculated from the volume fractions of the components, assuming external mixture. (21 refs.)

64236 Atomic nitrogen emissions from photodissociation of N₂. C.Y.R.Wu, J.K.Chen, D.L.Judge (Dept. of Phys., Univ. of Southern California, Los Angeles, CA, USA).

J. Geophys. Res. (USA), vol.88, no.A3, p.2163-9 (1 March 1983).

Cross sections for the production of N I emissions at 1412, 1493, and 1743 Å and the undispersed fluorescence in the range 1050-1800 Å produced through photodissociative excitation of N₂ have been determined at selected intense atomic emission lines and throughout the synchrotron radiation continuum from 400 to 620 Å. The neutral excited atomic nitrogen fragments are produced through direct dissociation processes as well as predissociation from the well-known two-electron excited Rydberg states. The yield for photodissociative excitation processes is found to have the same magnitude as that for photodissociative ionization processes reported by other investigators. The Doppler shifts of the excited atomic fragments have been calculated, and the relevance to atmospheric observations is discussed. (32 refs.)

64237 Photoelectric observations of shadow bands during 16 February 1980 total solar eclipse from Japal-Rangapur observatory. A.Bhatnagar, D.B.Jadhav, R.M.Jain, R.N.Shelke, S.P.Purohit (Vedhsala Udaipur Solar Obs., Udaipur, India), R.V.Bhonsle, R.Pratap.

Proc. Indian Natl. Sci. Acad. Part A, vol.48, suppl.3, p.260-2 (Oct. 1982). (Symposium on the Total Solar Eclipse of 16 February 1980, New Delhi, India, Jan. 1981).

Intensity fluctuations of shadow bands observed photoelectrically during total solar eclipse of 16 February 1980 are reported. Power spectrum analysis indicates that significant power appears at frequencies 0.32 and 0.58 Hz, thus corresponds to periods of 3 and 1.7 seconds. (no refs.)

Photon-noise limitations in wave-front-folding interferometrySee Entry 59833

Intracavity laser spectrometer with a dispersive resonator using F₂⁻ color centers in a LiF crystalSee Entry 59863

High resolution absorption cross section measurements and band oscillator strengths of the (1,0)-(12,0) Schumann-Runge bands of O₂See Entry 60742

Experimental investigations of fluctuations of optical signals and disturbances in the atmosphereSee Entry 61091

Physics of remote sensingSee Entry 63761

Some improvements and complements to the infrared emissivity algorithm including a parameterization of the absorption in the continuum regionSee Entry 64184

Variation in solar energy intensity during total solar eclipse of 16 February 1980See Entry 64203

Infrared visibility prediction by statistical methodsSee Entry 64208

Radiation modification of turbulent cloudsSee Entry 64220

The effect of tropospheric aerosols on the Earth's radiation budget: a parameterization for climate modelsSee Entry 64231

Investigating mirages with an astronomical telescopeSee Entry 64268

Atmospheric scattering effects on ground-based measurements of thermospheric windsSee Entry 64281

92.90 OTHER TOPICS IN HYDROSPHERIC AND ATMOSPHERIC GEOPHYSICS

64238 Possible limits on the composition of the Archaean ocean. J.C.G.Walker (Dept. of Atmospheric & Oceanic Sci., Univ. of Michigan, Ann Arbor, MI, USA).

Nature (GB), vol.302, no.5908, p.518-20 (7 April 1983).

It has been suggested that the partial pressure of carbon dioxide in the terrestrial atmosphere was larger in the past than it is at present. It is worth considering whether the geological record is in any way inconsistent with the proposed high partial pressures of carbon dioxide. The author examines the potential impact of high carbon dioxide partial pressure on ocean chemistry and ask what constraints are imposed by the known record of chemical sedimentation through time. The evidence consists of the persistence throughout almost the entire sedimentary rock record of calcium carbonate and sulphate precipitation. The methods of Holland (1976) are used to set limits on the composition of the water from which precipitation occurred. (31 refs.)

64239 The global temperature trend in the Cenozoic. I.I.Borzenkova (State Hydrological Inst., USSR).

Sov. Meteorol. & Hydrol. (USA), no.12, p.17-25 (1981). Translation of: *Meteorol. & Gidrol. (USSR)*, no.12, p.25-35 (1981).

The results of paleotemperature determinations made by oxygen-isotope analysis of the remains of marine planktonic and benthic microfauna are generalized, along with results of paleobotanic analyses of fossil flora from the Cenozoic (the last 60-65 million years). Analysis of these materials indicates a progressive lowering of temperature over the entire period at all latitudes in both hemispheres. Against the background of the general cooling trend, there have been two warming periods (the Eocene and Early Miocene maxima) that are observed at all latitudes. The Southern Hemisphere glacial cover formed about 15-11 million years ago, while the Northern Hemisphere remained ice-free until the middle of the Pliocene (3-3.5 million years ago). Seasonal Arctic Basin ices may have existed throughout the entire Pliocene (4.5-5.0 million years ago), while the permanent ice cover formed no earlier than 0.8-0.9 million years ago. (30 refs.)

Topics in Ocean Physics. Proceedings of the International School of Physics, 'Enrico Fermi', Course LXXXSee Entry 59539

Exploration of the Polar Upper Atmosphere. Proceedings of the NATO Advanced Study InstituteSee Entry 59540

93.00 GEOPHYSICAL OBSERVATIONS, INSTRUMENTATION, AND TECHNIQUES

93.30 INFORMATION RELATED TO GEOGRAPHICAL REGIONS

Tectonic and geologic evolution of southeast asian seas and islandsSee Entry 59545

A geological case history: lessons learned at Sheffield, IllinoisSee Entry 60252

Geotechnical measurements at the Maxey Flats, Kentucky low-level radioactive waste disposal site—lessons learnedSee Entry 60255

Lessons learned in a hydrogeological case at Sheffield, IllinoisSee Entry 60259

Dissolution of evaporites and its possible impact on the integrity of the Waste Isolation Pilot Plant (WIPP) New Mexico, USASee Entry 60290

A comparison of in-situ radionuclide migration studies in the Studvik area and laboratory measurementsSee Entry 60316

Studies of the mobilization of thorium from the Morro do FerroSee Entry 60319

Evaluation of radionuclide transport: effect of radionuclide sorption and solubilitySee Entry 60325

Effect of decreased use of lead in gasoline on the soil of a highwaySee Entry 63747

Estimation of the percentage of annual groundwater recharge with bomb tritium using a cumulative mass balance methodSee Entry 63748

Water pollution in the Fukuoka areaSee Entry 63750

Some aspects of the influence of surface and ground water chemistry on the mobility of thorium in the 'Morro do Ferro' environmentSee Entry 63751

The interaction between air pollution dispersion and residential heating demandsSee Entry 63753

Acid fogSee Entry 63755

Gaseous tracers of Arctic hazeSee Entry 63756

- Calculation of atmospheric-fallout concentrations on a drainage basin See Entry 63758
- Paleomagnetism of Africa and Madagascar See Entry 64026
- A review of the paleomagnetism of Australia and Antarctica See Entry 64027
- Phanerozoic palaeomagnetism of the Indian plate and the India-Asia collision See Entry 64028
- Paleomagnetism of South American rocks and the dynamic processes related with the fragmentation of western Gondwana See Entry 64029
- Pre-Neogene paleomagnetism of Japanese islands (and vicinities) See Entry 64030
- Paleomagnetism of southeast and east Asia See Entry 64031
- Pre-Carboniferous paleomagnetism of Europe north of the Alpine orogenic belt See Entry 64032
- Pre-Cenozoic paleomagnetism of southern Europe/Middle East See Entry 64033
- Paleomagnetism of North America: a brief review See Entry 64034
- Paleomagnetism of the Soviet Union See Entry 64035
- Marine magnetic anomalies from the western Philippine Sea: implications for the evolution of marginal basins See Entry 64036
- Paleomagnetism of Truk Islands, eastern Carolines and of Saipan, Marianas See Entry 64037
- Paleomagnetic synthesis for southeast Asia: constraints on plate motions See Entry 64038
- Seismicity and earthquake hazard in Trinidad and Tobago, West Indies See Entry 64042
- A coda-length magnitude scale for New England See Entry 64043
- The Charlevoix earthquake of 19 August 1979 and its seismo-tectonic environment See Entry 64044
- Field investigation and fault plane solution of the Bath, Maine earthquake of April 18, 1979 See Entry 64045
- The Giles County, Virginia, seismic zone See Entry 64046
- The tsunami of 23 November 1969 at Kamchatka and certain aspects of its occurrence See Entry 64047
- Source parameters of recent strong earthquakes in northeastern Iran from long-period surface waves See Entry 64052
- Magnitudes of New Zealand earthquakes: a comparison of magnitudes calculated by different methods See Entry 64055
- Relationships among the source parameters of earthquakes in Europe See Entry 64061
- Considerations for the body-wave magnitude determination in the Recent Earthquake Data Report of the United States Geological Survey See Entry 64062
- Seismic triggering effect of tidal stress See Entry 64063
- Spectra of the earthquake sequence February-March, 1981, in south-central Sweden See Entry 64064
- The spatial distribution of earthquakes, focal mechanism solutions, and subducted lithosphere in the Philippine and northeastern Indonesian Islands See Entry 64065
- Seismicity and tectonics of the central New Hebrides island arc See Entry 64068
- The 1906 San Francisco earthquake and the seismic cycle See Entry 64069
- Earthquake hazard in the Hellenic Arc See Entry 64070
- Great detachment earthquakes along the Himalayan Arc and long-term forecasting See Entry 64073
- Specification of a soon-to-occur seismic faulting in the Tokai District, central Japan, based upon seismotectonics See Entry 64074
- Neotectonic deformation, near-surface movements and systematic errors in US leveling measurements: implications for earthquake prediction See Entry 64077
- A preliminary analysis of reported changes in ground water and anomalous animal behavior before the 4 February 1975 Haicheng earthquake See Entry 64078
- Leg 82 of the International Program of Ocean Drilling (IPOD): normal or abnormal ocean crust on the Mid-Atlantic Ridge; Geochemical properties See Entry 64079
- Io-U dates of a coral formation from the last interglacial age on the Brazilian coast. Use of ^{235}Th as a tracer See Entry 64080
- A reference section of the oceanic crust: leg 83 of the International Program of Ocean Drilling (IPOD) near the Costa Rica rift, eastern Pacific Ocean See Entry 64081
- Gneissic intercalations within a tectonic unit from the Piedmont Ophiolite Nappe in the Western Alps: Record of a subducted continental margin? See Entry 64082
- The allochthony of the 'Zone des Diapirs' in Northern Tunisia See Entry 64083
- Discovery of a new nappe from the north-east in the Parnassus zone (Greece) See Entry 64084
- A seismic refraction line along the axis of the southern Piedmont and crustal thicknesses in the southeastern United States See Entry 64085
- Uranium disequilibrium dating of phosphate deposits from the Lau Group, Fiji See Entry 64086
- A geophysical approach to the granite batholith under the eastern Southern Uplands, Scotland See Entry 64090
- The lithosphere in the Central-eastern Mediterranean area See Entry 64091
- Timing and chemistry of igneous events associated with the Southern Oklahoma Aulacogen See Entry 64093
- The Morton-Black hypothesis for the thinning of continental crust—revisited in western Afar See Entry 64094
- Geothermal resources of rifts: a comparison of the Rio Grande Rift and the Salton Trough See Entry 64096
- Crustal structure of the Molucca Sea collision zone, Indonesia See Entry 64097
- Crustal structure across the Mariana island arc See Entry 64098
- 1980 update of heat flow in the east and southeast Asian seas See Entry 64099
- Variations of the temperature, melt composition and water pressure during olivine crystallization in oceanitic rocks from the Piton Fournaise volcano (Reunion Island, 1966 eruption) See Entry 64100
- The petrology and tectonics of Recent volcanism in the central Philippine Islands See Entry 64102
- Geochemistry and K/Ar ages of volcanics dredged in the Philippine Sea (Mariana, Yap, and Palau Trenches and Parece Vela Basin) See Entry 64103
- Primitive arc volcanism and a boninite series: examples from Western Pacific island arcs See Entry 64104
- Dating on the extensive tectonism in the North-Aegean region (Greece): palynologic data See Entry 64105
- The role of rifting in the tectonic development of the midcontinent, USA See Entry 64108
- Geologic and geochemical evidence for the nature and development of the Middle Proterozoic (Keweenaw) Midcontinent Rift of North America See Entry 64109
- Origin of the Oslo Graben in relation to the Hercynian-Alleghenian orogeny and lithospheric rifting in the North Atlantic See Entry 64110
- Active versus passive continental rifting: evidence from the West African rift system See Entry 64111
- Tectonic and geologic evolution of the Espanola basin, Rio Grande rift: structure, rate of extension, and relation to the state of stress in the western United States See Entry 64112
- Continental rift jumps See Entry 64113
- Arctic seafloor structure and tectonic evolution See Entry 64119
- The tectonic evolution of the South China Basin See Entry 64120
- Discrimination of tectonic displacement from slope-dependent errors in geodetic leveling from southern California, 1953-79 See Entry 64121
- Height dependent errors in southern California leveling See Entry 64122
- An asperity model of large earthquake sequences See Entry 64123
- Vertical sedimentation units in a barrier island washover fan See Entry 64124
- Systematic monthly morphologic variation of Assawoman Inlet: nature and causes See Entry 64125
- Preliminary estimates of intertidal limestone erosion, One Tree Island, southern Great Barrier Reef, Australia See Entry 64126
- Var and Pailion canyons (Southern Alps Margin-Western Mediterranean): a Quaternary origin through sliding See Entry 64127
- Evidence for Eocene oceanic crust in the Celebes Basin See Entry 64132
- The structure and evolution of the Central Basin Fault, West Philippine Basin See Entry 64133
- Quaternary sedimentation processes in the South China Basin as revealed by echo-character mapping and piston-core studies See Entry 64134
- Morphology and shallow structure of the lower trench slope off Nias Island, Sunda Arc See Entry 64135
- A seismic reflection study of faulting in the Mariana fore arc See Entry 64136
- Evolution of back arc spreading and arch volcanism in the Philippine Sea: interpretation of Leg 59 DSDP results See Entry 64137
- Continental rifting and porphyry-molybdenum occurrences in the Oslo region, Norway See Entry 64138
- Variations in geologic structure along the Sunda fore arc, northeastern Indian Ocean See Entry 64139
- Field evaluation of some sand transport models See Entry 64140
- Sorted stripes on Sub-Antarctic Kerguelen Island See Entry 64141
- Flood-related channel change in an arid-region river See Entry 64142
- Spatial variation in solutional denudation and soil moisture over a hillslope hollow See Entry 64143
- Generation of topographic vortices and their possible effect on formation of productive zones in the ocean See Entry 64145
- The M2 oceanic tide recovered from Seasat altimetry in the Indian Ocean See Entry 64146
- Planetary waves of seasonal origin in the ocean See Entry 64150
- Vertical coherence of semidiurnal tidal currents on the 1970 hydrophysical test range in the Atlantic See Entry 64151
- Regime of the Filchner-Ronne ice shelves, Antarctica See Entry 64155
- Long-term forecasting of high water levels at ice dams on the Angara at Kamenka See Entry 64158
- The NO/NO₂/O₃ photostationary state in Claremont, California See Entry 64160
- A radiation model using hourly meteorological data with results from GATE See Entry 64164
- On the influence of meteorological parameters on extinction and mass size distributions in the urban aerosol of Vienna See Entry 64165
- On single station forecasting: sunshine and rainfall Markov chains See Entry 64166
- Doppler-SODAR measured variation of mean and turbulent wind field during PUKK See Entry 64167
- Major ion composition and chemical associations of inorganic atmospheric aerosols See Entry 64168
- Simulations of nocturnal drainage flows by a q^2 turbulence closure model See Entry 64175
- A relationship between hailstone concentration and size See Entry 64182
- Experiment of artificial lightning triggered with rocket See Entry 64188
- Solar irradiance study See Entry 64190
- Solar radiation values received on a horizontal surface in Spain See Entry 64191
- Dynamics of the atmospheric boundary layer during the 1980 total solar eclipse See Entry 64192
- Total solar eclipse of 16 February 1980 and the vertical profiles of atmospheric parameters in the lowest 200 m See Entry 64193
- Meteorological parameters near the Earth's surface along the path of totality during the total solar eclipse of 16 February 1980 See Entry 64194
- Solar eclipse of 16 February, 1980—its effect on meteorological parameters See Entry 64195

- Measurements of meteorological parameters at the lowest layers of the atmosphere during total solar eclipse of 1980 See Entry 64196
- A study of change in the atmospheric properties during solar eclipse of 16 February 1980 See Entry 64197
- Radiometric observations of solar eclipse over New Delhi on 16 February 1980 See Entry 64198
- Atmospheric pressure perturbations during total solar eclipse of 16 February 1980 See Entry 64199
- Boundary layer studies conducted at Gadag during the total solar eclipse of 16 February 1980 See Entry 64200
- Variations in atmospheric electrical parameters during solar eclipse See Entry 64201
- Measurements of atmospheric electricity parameters during the total eclipse of 16 February 1980 See Entry 64202
- Variation in solar energy intensity during total solar eclipse of 16 February 1980 See Entry 64203
- Determination of ozone from eclipse observations of $O_2(a^1\Delta_g)$ dayglow See Entry 64204
- VLF/LF detection of ionization changes and wave motions in the middle atmosphere associated with the February 1980 total solar eclipse See Entry 64205
- Evidence of atmospheric gravity waves in the wake of the eclipse shadow See Entry 64207
- A study of energy, generation and conversion over North America See Entry 64210
- Correlation functions of rainfall field and their application in network design in the tropics See Entry 64212
- Areal extent and vertical structure of radar weather echoes at Montreal See Entry 64213
- Mesoscale structure of an occluded front over the center of the European USSR from special measurements See Entry 64226
- Some features of the day-time astroclimate on Terskol peak See Entry 64232
- Photoelectric observations of shadow bands during 16 February 1980 total solar eclipse from Japal-Rangapur observatory See Entry 64237
- Earthquake prediction program in Japan See Entry 64240
- Interpretation of SIR-A Seasat and Landsat coregistered data over Algerian playas See Entry 64242
- Laser measurements of the stratospheric ozone layer See Entry 64243
- Prevailing wind at heights of 80-100 km at various longitudes during the winter and spring periods of 1976-1977 See Entry 64282
- Changes in the field intensity of radio signals and noise during the total solar eclipse of 16 February 1980 in relation to ionospheric radio wave propagation See Entry 64302
- Multi-station monitoring of short and medium wave broadcast circuits during solar eclipse of 16 February 1980 See Entry 64303
- Ionospheric radio effects of the solar eclipse on 16 February 1980 See Entry 64304
- Effects of solar eclipse on shortwave transmissions See Entry 64305
- Ionospheric absorption changes in 11.8 MHz radio propagation during the total solar eclipse of 16 February 1980 See Entry 64306
- Solar eclipse effects on the lower ionosphere See Entry 64307
- AI absorption measurements during the total solar eclipse of 16 February 1980 See Entry 64308

93.55 INTERNATIONAL ORGANIZATIONS, NATIONAL AND INTERNATIONAL PROGRAMS

- 64240 Earthquake prediction program in Japan. K.Mogi (Earthquake Res. Inst., Tokyo Univ., Tokyo, Japan).
- Earthquake Prediction. An International Review. Symposium on Earthquake Prediction, Mohonk, NY, USA, 12-16 May 1980 (Washington, DC, USA: American Geophys. Union 1981), p.635-66
- The first 5-year earthquake prediction project was started in 1965, just after the Niigata earthquake of 1964, and the project has been growing at a steady rate (Kanamori, 1970; Ha-iiwara, 1975; Rikitake, 1976). The project consists of three categories. The first is various observations for long-term prediction, such as geodetic surveys and seismic observations. The second is various observations for short-term prediction, such as continuous observations of crustal deformation. The third is various fundamental studies, such as rock fracture experiments. Major topics of earthquake prediction are in the past 10 years in Japan are discussed in some detail. (84 refs.)
- A radiation model using hourly meteorological data with results from GATE See Entry 64164

93.85 INSTRUMENTATION AND TECHNIQUES FOR GEOPHYSICAL RESEARCH

- 64241 Probe experiment for measurement of plasma parameters and ion drift velocities in the ionospheric plasma onboard the Intercosmos-Bulgaria 1300 satellite. K.Serafimov, L.Bankov, M.Gusheva, T.Ivanova, V.Markov, S.Chapkunov, I.Kutiev, V.Genov (Central Lab. for Space Res., Sofia, Bulgaria).
- Acta Astronaut. (GB)*, vol.9, no.10, p.637-40 (Oct. 1982). [received: March 1983]
- Describes a complex of probe instruments designed for the equipment: ID-1, P-6, P-7 and DIET-2 to define the local plasma parameters. The instruments measure: electron temperature, electron density, ion temperature, ion density, ion energy distribution, mass ion composition, complete ion drift vector 0.1 to 5 km/s and ion density variations within the range 0.50-100%. (2 refs.)
- 64242 Interpretation of SIR-A Seasat and Landsat coregistered data over Algerian playas. P.Rebillard (Jet Propulsion Lab., Pasadena, CA, USA), J.-L.Bailais.
- C.R. Seances Acad. Sci. Ser. II (France)*, vol.296, no.1, p.103-6 (10 Jan. 1983). In French.
- Comparison of coregistered SIR-A, Seasat and Landsat data over playas located in Algeria shows that the radar backscatter is highly sensitive to the roughness and moisture of the chotts. Linear objects perpendicular to the radar illumination direction are easier to detect than the ones parallel to it. A sand cover detected on the Landsat scene but not seen on the radar images may have been penetrated by microwaves. (4 refs.)

- 64243 Laser measurements of the stratospheric ozone layer. J.Werner, K.W.Rothe, H.Walther (Sektion Phys., Univ. Muenchen, Garching, Germany). *Laser & Optoelektron. (Germany)*, vol.15, no.1, p.17-21 (March 1983). In German.

An excimer laser is used to investigate the stratospheric ozone layer from the summit of the Zugspitze in the Alp Mountains. The radiation of the XeCl laser itself is strongly absorbed by ozone; the non-absorbed reference line—necessary for the differential absorption method—is generated by stimulated Raman scattering. After a short summary of the method, the lidar system is described and some preliminary results are presented. The feasibility of using the system for monitoring stratospheric aerosol layers from volcanic eruptions is demonstrated. (15 refs.)

- 64244 Laboratory evaluation of an airborne ozone instrument that compensates for altitude/sensitivity effects. G.L.Gregory, C.H.Hudgins, R.A.Edahl,Jr. (Langley Res. Center, NASA Hampton, VA, USA).
- Environ. Sci. & Technol. (USA)*, vol.17, no.2, p.100-3 (Feb. 1983).
- One problem encountered in the use of air-quality instrumentation on aircraft is the variation of instrument sensitivity with pressure as the result of altitude changes of the aircraft. Many instruments experience sensitivity changes as much as a factor of 2 at altitudes of 6 km. Discussed are recent modifications to a chemiluminescent (ethylene) ozone detector that allow the instrument to automatically compensate for pressure/sensitivity effects. The modification provides automated mass flow rate control for both the sample and ethylene gas flows. During simulated altitude changes (300 m/min from mean sea level to 3-km altitude), flow rates were controlled to within 3% of the set point. Laboratory data are summarized. (3 refs.)

- 64245 A simple and inexpensive method for measuring integrated light energy. T.J.Sullivan, M.C.Mix (Dept. of General Sci., Oregon State Univ., Corvallis, OR, USA).
- Environ. Sci. & Technol. (USA)*, vol.17, no.2, p.127-8 (Feb. 1983).
- The ozalid technique is a simple and inexpensive method for measuring integrated sunlight energy in the field for periods up to a maximum of 1 day. The authors describe a modification of the ozalid technique that makes it suitable for long-term light measurements. Data from the modified ozalid meter were calibrated against an Eppley Precision Spectro Pyranometer. (1 ref.)

- 64246 Coal analysis by nuclear methods. C.G.Clayton, M.R.Wormald (Appl. Nuclear Geophys. Group, AERE, Harwell, England).
- Int. J. Appl. Radiat. & Isot. (GB)*, vol.34, no.1, p.3-22 (Jan. 1983).
- Reviews the use of low-energy X-rays, γ -rays and neutron interaction techniques for coal analysis in applications which range from borehole logging to on-line analysis in coal preparation plants and in coal-burning power stations. Neutron-induced prompt γ -ray analysis provides an exciting prospect for the future as it allows direct on-line measurement of the concentrations of all the major elements in coal coupled with the indirect determination of ash content and calorific value. (19 refs.)

- 64247 In-situ analysis of coal by measurement of neutron-induced prompt γ -rays. M.R.Wormald, C.G.Clayton (Appl. Nuclear Geophys. Group, AERE, Harwell, England).
- Int. J. Appl. Radiat. & Isot. (GB)*, vol.34, no.1, p.71-82 (Jan. 1983).
- In general, neutron-induced prompt γ -ray techniques provide the possibility of a total elemental analysis of the major elements in a material provided that γ -ray production cross-sections are adequate and account can be taken of perturbations in neutron flux arising, for example, from variations in density, moisture content and in the concentrations of elements which can be regarded as neutron poisons. A method is described which allows a total elemental analysis of coal by measurement of γ -ray spectra from fast and thermal neutron interactions and which are independent of variations in neutron flux in the material. (11 refs.)

- 64248 Multi-element analysis of coal during borehole logging by measurement of prompt γ -rays from thermal neutron capture. C.G.Clayton, A.M.Hassan, M.R.Wormald (Appl. Nuclear Geophys. Group, AERE, Harwell, England).
- Int. J. Appl. Radiat. & Isot. (GB)*, vol.34, no.1, p.83-93 (Jan. 1983).
- The performance of borehole logging equipment is described which is based on a ^{252}Cf neutron source and measurement of the spectra of thermal neutron capture γ -rays from most of the important elements in coal. It is shown that although a high statistical counting accuracy can be obtained for several elements in a measuring period of about 5 min, the derived concentrations are limited by the low capture cross-section of carbon. It is concluded that it is strongly preferable to employ a high energy neutron source, such as $^{241}\text{Am-Be}$, so as to include oxygen in the analysis and to obtain a higher precision of measurement for all the other elements. (11 refs.)

- 64249 Nuclear geophysics in prospecting, exploration and development of oil and gas fields. E.V.Karus, Yu.S.Shimelevich (All-Union Res. Inst. of Geophys., Moscow, USSR).
- Int. J. Appl. Radiat. & Isot. (GB)*, vol.34, no.1, p.95-117 (Jan. 1983).
- Nuclear-geophysics investigations are widely and successfully used in prospecting, exploration and development of oil and gas fields. These methods are most efficient in the further exploration of producing oil fields, the control of oil-and-gas field development and in the calculation of reserves of large oil and gas fields. Specific nuclear-geophysical methods (conventional and spectrometric γ -logging, γ - γ logging, neutron logging, pulsed neutron logging and its modifications, nuclear magnetic resonance logging), techniques of application, examples of resolved problems and the specification of down-hole equipment are discussed in this review. (34 refs.)

- 64250 Stochastic approach to the pulsed neutron logging methods. J.A.Czubek (Inst. of Nuclear Phys., Krakow, Poland).
- Int. J. Appl. Radiat. & Isot. (GB)*, vol.34, no.1, p.119-28 (Jan. 1983).
- Neutron emissions from a steady state neutron source (of the α -Be or ^{252}Cf types) can be treated as a white noise stochastic process. In the rock space, according to different neutron well-logging methods, different types of radiation resulting from nuclear reactions between the source neutrons and the nuclei of the rock elements appear. The resulting radiation is in this case the shot noise process. By doing the time cross correlation between the input (white noise) and the output (shot noise) processes, or the auto-correlation of the output process alone, the transmission function of the system is obtained. Here the transmission function is just the die-away curve observed in all kinds of pulsed neutron logs. Experimental principles and the conditions of the correlation measurements are discussed. Nuclear reactions together with the space and time distribution of different types of radiation observed in the neutron well-logging methods are presented with a view to getting the rock nuclear parameters from the correlation methods. (12 refs.)

- 64251 Measurement of the thermal neutron absorption cross section of rock samples.** J.A.Czubek, K.Drozdzowicz, E.Krynica-Drozdzowicz, A.Igiel-ski, U.Woznicka (Inst. of Nuclear Phys., Krakow, Poland). *Int. J. Appl. Radiat. & Isot. (GB)*, vol.34, no.1, p.143-51 (Jan. 1983). A knowledge of the absorption cross section of thermal neutrons for rock materials and brines is an important factor in the quantitative interpretation of the neutron lifetime logs. A new method of measurement of that parameter is presented; it is independent of the transport cross section of the sample. The method has been checked on artificial materials and on natural brine and dolomite. The volume of the sample needed is of the order 500 cm³. (12 refs.)
- 64252 Advances in gamma-gamma logging.** J.A.Czubek (Inst. of Nuclear Phys., Krakow, Poland). *Int. J. Appl. Radiat. & Isot. (GB)*, vol.34, no.1, p.153-72 (Jan. 1983). The development of γ - γ logging methods for measuring rock density and elemental composition are presented along with the physical background of the methods and experimental results from a number of research laboratories. Some methods of tool calibration based on a semi-theoretical approach are discussed. The basic physical features of some industrial applications are given as well as some remarks about future development. (60 refs.)
- 64253 The application of Monte Carlo computations to formation analysis by neutron interactions.** L.G.Sanders (Appl. Nuclear Geophys. Group, AERE, Harwell, England). *Int. J. Appl. Radiat. & Isot. (GB)*, vol.34, no.1, p.173-98 (Jan. 1983). Monte Carlo neutron and γ -ray tracking techniques can make a major contribution to the study and development of methods for the analysis of formations by neutron interactions. Problems which arise in neutron interaction analysis and the role of Monte Carlo tracking programs are discussed. Examples are presented of some Monte Carlo studies on analysis by γ -rays from neutron interactions and on oil-well log interpretation. (6 refs.)
- 64254 Airborne γ -ray spectrometry in uranium exploration. Principles and current practice.** Q.Bristow (Geological Survey of Canada, Ottawa, Canada). *Int. J. Appl. Radiat. & Isot. (GB)*, vol.34, no.1, p.199-229 (Jan. 1983). Experiments have shown that the radioelement content of bedrock is generally reflected by that of overlying till and that areas showing broad regional enrichment of radioelement concentrations are favourable for uranium exploration. Airborne γ -ray spectrometry with equipment having typical sodium iodide detector volumes of 50 L is used to record the natural radiation intensity due to potassium, uranium and thorium by flying grids at ground clearances of about 120 m. γ -ray spectra are recorded continuously in flight with navigational data all of which is processed off-line to produce maps of radioelement distribution with concentration contours. (57 refs.)
- 64255 Borehole logging for uranium by measurement of natural γ -radiation.** P.G.Killeen (Geological Survey of Canada, Ottawa, Canada). *Int. J. Appl. Radiat. & Isot. (GB)*, vol.34, no.1, p.231-60 (Jan. 1983). Calibration facilities with model holes have been established in several countries to support quantitative borehole measurements. New high density detector materials have been evaluated and have shown to yield considerable improvements for operation in the restricted environment of the borehole. γ -ray spectral logging has become available partially as a result of spin-off from parallel developments in surface and airborne γ -ray spectrometric survey equipment. The use of the high resolution solid state detector has proceeded through a series of developments to its present availability as a commercial borehole logging service in spite of the inherent detector cooling problems. Digital measurements are replacing the earlier analog measurements, and minicomputer or microprocessor-based logging systems have enabled new data processing techniques such as inverse filtering to be implemented in real time at the site of the borehole. (125 refs.)
- 64256 Uranium logging with prompt fission neutrons.** D.R.Humphreys, R.W.Barnard, H.M.Bivens, D.H.Jensen, W.A.Stephenson, J.H.Weinlein (Sandia Nat. Labs., Albuquerque, NM, USA). *Int. J. Appl. Radiat. & Isot. (GB)*, vol.34, no.1, p.261-8 (Jan. 1983). Describes a uranium logging probe which can assay U₃O₈ concentrations as slow as 100 ppm at 0.5 m/min. The probe sends 100 pulses per second of 14 MeV neutrons (2×10^6 neutrons/pulse) into the formation surrounding a borehole, and detects prompt epithermal neutrons returning from fissioning ²³⁵U. Various models of the probe have logged hundreds of boreholes in the western United States since 1976. The neutron generator is now commercially available and the probe design is available to the public. (9 refs.)
- 64257 The operation and life of the Zetatron neutron tube in a borehole logging application.** L.A.Shope, R.S.Berg, M.L.O'Neal, B.E.Barnaby (Sandia Nat. Labs., Albuquerque, NM, USA). *Int. J. Appl. Radiat. & Isot. (GB)*, vol.34, no.1, p.269-72 (Jan. 1983). The physical assembly and electrical characteristics of a Zetatron neutron tube are described. This tube is small (38 mm diameter by 126 mm), sealed-off, pulsed deuterium-tritium accelerator. Peak output rates up to 8×10^{11} neutron/s (6×10^6 neutrons/pulse) are typical. Mean time to failure in a borehole logging application was 152 h for the bare tube and 91 h for the tube-transformer assembly. Shelf life appears to be at least 2 yr. (12 refs.)
- 64258 Determination of the concentration of uranium in soil and stream sediment samples using a high resolution energy-dispersive X-ray fluorescence analyser.** T.W.Packer (Appl. Nuclear Geophys. Group, AERE, Harwell, England). *Int. J. Appl. Radiat. & Isot. (GB)*, vol.34, no.1, p.273-81 (Jan. 1983). An energy-dispersive X-ray fluorescence analyser is described, based on a high resolution Si(Li) semiconductor detector, which is suitable for directly determining the concentration of uranium in stream sediment and soil samples. The equipment can be used in a field or base laboratory or it can be mounted in a vehicle and operated from a portable petrol generator. Matrix absorption effects, which prevail due mainly to variations in the concentration of iron and calcium in the samples, are corrected for by simultaneously measuring the intensity of Compton scattered X-rays. Rapid analysis, 130-200 s measurement time, and low limits of detection 11 ppm (95% confidence level), are consistent with the requirements of geochemical prospecting. (2 refs.)
- 64259 Uranium isotopic disequilibrium in ground water as an indicator of anomalies.** J.K.Osmond, J.B.Cowart (Geology Dept., Florida State Univ., Tallahassee, FL, USA), M.Ivanovich. *Int. J. Appl. Radiat. & Isot. (GB)*, vol.34, no.1, p.283-308 (Jan. 1983). Because of the unique elemental and isotopic properties of uranium, ground water surveys are a most appropriate approach to prospecting for surficial and secondary uranium deposits. Uranium ($4+$) is generally immobile, but in oxidising and carbonate bearing waters U($6+$) is mobile and conservative. Uranium-234 is the radiogenic daughter of ²³⁸U. The intervening α -decay event causes recoil displacements and radioactive disequilibrium between the two isotopes in open systems such as surficial aquifers. Extreme variations in dissolved uranium composition of ground waters combined with significant

variations in the ratio ²⁴U/²³⁸U are indicative of the proximity and stage of evolution of secondary deposits. (59 refs.)

- 64260 A universal gamma-gamma method for simultaneous determination of rock and ore properties.** J.Charcucinski (Inst. of Phys. & Nuclear Tech., Univ. of Mining & Metall., Krakow, Poland). *Int. J. Appl. Radiat. & Isot. (GB)*, vol.34, no.1, p.353-61 (Jan. 1983). A method for the simultaneous determination of heavy element content, density, borehole diameter and grain size is described, which is based on investigation of the changes in spectrum shape. By analysing these changes in a quantitative manner, information regarding the physical parameters of the medium can be obtained. The results of laboratory tests of the method are presented. (16 refs.)
- 64261 The combination of multi-element neutron activation analysis and multivariate statistics for characterisation in geochemistry.** J.I.W.Watterson, J.P.F.Sellschop, C.S.Erasmus, R.J.Hart (NIM-Wits Activation Res. Group, Univ. of the Witwatersrand, Johannesburg, S Africa). *Int. J. Appl. Radiat. & Isot. (GB)*, vol.34, no.1, p.407-16 (Jan. 1983). Instrumental neutron activation analysis provides an accurate method for the determination of some 20 to 40 elements in geological samples. This method has been combined with pattern recognition techniques to provide a powerful method for the study of geochemical differences and for the classification of unknown samples. Discriminant analysis, a statistical method of pattern recognition, was applied to the study of mineralisation in granites, to the classification of diamonds, to the identification of sedimentary units from the Witwatersrand and to the classification of coals from the Witbank Coalfield in South Africa. The results show that the methods can be used to identify and map the mineralised phase of the granite. In the case of the diamonds trace element signatures were found which were characteristic of the sources and these were used to classify very pure unknown samples with a high rate of success. (22 refs.)
- 64262 Mineral exploration of the sea bed by towed sea bed spectrometers.** B.W.Thomas, C.G.Clayton, V.V.C.Ranasinghe, I.M.Blair (Appl. Nuclear Geophys. Group, AERE, Harwell, England). *Int. J. Appl. Radiat. & Isot. (GB)*, vol.34, no.1, p.437-49 (Jan. 1983). Marine mineral deposits and the subsequent need for in-situ analytical methods of exploration are considered. Nuclear techniques based on γ -ray spectrometry offer potential for continuous surveying. In the present paper various aspects of the design and performance of both natural and neutron-induced towed γ -ray spectrometers are discussed in detail. The interpretation of elemental abundances from the measured data is of particular importance and has been investigated using laboratory experimental and computer techniques. (7 refs.)
- 64263 Tracer techniques in hydrology.** G.V.Evans (Geophys. Tracers Group, AERE, Harwell, England). *Int. J. Appl. Radiat. & Isot. (GB)*, vol.34, no.1, p.451-75 (Jan. 1983). Presents a review of the use of environmental and artificial tracers in studies of surface waters, ground waters and sediments. Both stable and radioactive substances are considered. The environmental tracers include those whose natural abundance variations allow interference of the origins, movement or depositional history of water or sediments and those whose presence in the environment is due to man's past activities. Examples of the former type are the stable isotopes of hydrogen, oxygen and sulphur, noble gases and the radioactive isotopes carbon-14 and uranium series. The latter type of environmental tracers include radioactive elements from nuclear bomb testing and fluorocarbon compounds. Artificial tracers, categorized into radioactive, acti-vable, chemical and particulate tracers are described together with their applications in flow measurement, run-off transit-time measurement, lake dynamics and ground water movement studies. Sediment movement studies are briefly described. (86 refs.)
- 64264 Laser-acoustic measurements for remotely determining bathymetry in shallow turbid waters.** G.D.Hickman, J.A.Edmonds (Appl. Sci. Technol. Inc., Arlington, VA, USA). *J. Acoust. Soc. Am. (USA)*, vol.73, no.3, p.840-3 (March 1983). A laser technique is described that has the potential for being developed into an airborne remote sensing system for bathymetric mapping of shallow-turbid waters. This hybrid system consists of an infrared CO₂ laser transmitter and a highly sensitive microphone receiver located in the air. The interaction of the laser beam with water generates acoustic signals in water having pulse widths of 20-30 μ s and a frequency spectrum peaking between 15-25 kHz. Measurements have been made from both a floating laboratory and an operating ship. These measurements were made using a 5 to 15-J CO₂ laser to generate a sound pressure level (SPL) of 185-195 dB re: 1 μ Pa in water at a depth of 1 m. Measurements made in quiescent waters recorded water depths of 20 ± 0.1 m, while the maximum water depth obtained aboard ship was 13 ± 1 m. The two major problem areas encountered were environmental noise and the angular dependence of the bottom sediment echoes as they penetrated a 'wavy' water surface. (10 refs.)
- 64265 Comparison of Earth rotation as inferred from radio interferometric, laser ranging and astrometric observations.** D.S.Robertson, W.E.Carter (Nat. Ocean Service, NOAA, Rockville, MD, USA), R.J.Eanes, B.E.Schutz, B.D.Tapley, R.W.King, R.B.Langley, P.J.Morgan, I.I.Shapiro. *Nature (GB)*, vol.302, no.5908, p.509-11 (7 April 1983). New techniques are being developed to improve the spatial and temporal resolutions achievable in measurements of the rotation vector of the Earth. Such improvements are expected to expose fine details of this rotation and to aid in understanding their physical causes. Although not yet fully developed, two of these techniques are now in routine use: radio interferometry, and laser ranging to the Moon and to artificial satellites. To assess the accuracy being achieved in the measurement of Earth rotation it is useful to compare results obtained with these different techniques (including astrometry). The authors compare results for a 400-day period from late September 1980 to December 1981, for which data from all three types of measurements are available. The authors also compare corresponding results from classical astrometric observations which demonstrate the degree of improvement in accuracy afforded by the new techniques. (9 refs.)
- 64266 Determination of the coherent and incoherent signal components of stochastic receiving signals from experimental data [soil structure].** E.Muller (Wilhelm-Pieck-Univ. Rostock, Rostock, Germany). *Nachrichtentechn. Elektron. (Germany)*, vol.33, no.3, p.118-21 (1983). In German. An estimation method for the determination of the parameters of the Rice probability density distribution function of characteristic values determined by computation from experimental data is represented and examined by means of hydroacoustic results of measurement about the soil structure. The information about coherent and incoherent signal components or the signal-to-noise ratio gained from the estimated parameters can be used as basis for an object identification or for the disturbance variable reduction. (4 refs.)

- 64267 Atmospheric laser spectrometer with an external cavity mirror.** A.P.Godlevskii, A.K.Ivanov, Yu.D.Kopytin. *Opt. & Spectrosc. (USA)*, vol.53, no.1, p.87-9 (July 1982). Translation of: *Opt. & Spektrosk. (USSR)*, vol.53, no.1, p.150-4 (July 1982). [received: April 1983]
Experimental data are given on an intracavity ruby laser spectrometer with the cavity in the actual atmosphere in a length of up to 160 m. The laser kinetics are studied under actual weather conditions in the cavity. Sensitivity and error of humidity measurement at low negative temperatures in the atmosphere are determined. (11 refs.)
- 64268 Investigating mirages with an astronomical telescope.** C.Floor (Royal Netherlands Meteorological Inst., De Bilt, Netherlands). *Phys. Educ. (GB)*, vol.18, no.2, p.80-2 (March 1983).
Some schools or colleges where astronomy is part of the science curriculum are fortunate enough to have an astronomical telescope for observing the sky at night. The instrument can, however, also be used in the day-time for the investigation of road mirages and other mirages over warm land or water. If the telescope is fitted with an adaptor to which a camera can be attached students should be able to take photographs. The author first summarises some basic principles of mirages and their formation, and then goes on to describe the photographic techniques that can be used. (4 refs.)
- 64269 Monte Carlo simulation of small air-mass showers.** H.C.Vaughan (Astronomy Dept., Iowa State Univ., Iowa State Univ., Ames, IA, USA), G.R.White, P.A.Carr. *Pure & Appl. Geophys. (Switzerland)*, vol.120, no.2, p.261-72 (1982).
The present model permits simulation of any geographic region and the symmetrical or random positioning of any number of rain gauges. The operator has the option of entering precipitation parameters: rain cell diameter, duration, rain swath length, vector angle, and precipitation amount of any number of discrete showers. In a series of computations the model generates (1) a random 'first echo' location and resulting rain swath, which is superimposed on a specific grid of rain gauges; (2) the number of rain gauges receiving a hit; and (3) the number of undetected rain events within an area. By use of a portion of the Iowa climatological rain gauge network and parameters derived from radar and rain gauge observations the model shows that only 7% of single cell showers are determined by the existing sampling grid. (8 refs.)
- 64270 Expendable bubble tiltmeter for geophysical monitoring.** J.A.Westphal, M.A.Carr, W.F.Miller (Div. of Geological & Planetary Sci., California Inst. of Technol., Pasadena, CA, USA), D.Dzurisin. *Rev. Sci. Instrum. (USA)*, vol.54, no.4, p.415-18 (April 1983).
An unusually rugged highly sensitive and inexpensive bubble tiltmeter has been designed, tested, and built in quantity. These tiltmeters are presently used on two volcanoes and an Alaskan glacier, where they continuously monitor surface tilts of geological interest. This paper discusses the mechanical, thermal, and electric details of the meter, and illustrates its performance characteristics in both large ($>10^{-4}$ radian) and small ($<10^{-6}$ radian) tilt environments. The meter's ultimate sensitivity is better than 2×10^{-8} radians rms for short periods (hours), and its useful dynamic range is greater than 10^4 . Included is a short description of field use of the instrument for volcano monitoring. (13 refs.)
- 64271 Measurement of flow velocities in the ocean with a laser Doppler hydrometer.** N.K.Shelkovnikov, V.V.Rozanov, A.S.Chirkin (M.V. Lomonosov State Univ., Moscow, USSR). *Sov. Tech. Phys. Lett. (USA)*, vol.8, no.8, p.406-8 (Aug. 1982). Translation of: *Pis'ma v Zh. Tekh. Fiz. (USSR)*, vol.8, no.15-16, p.937-40 (Aug. 1982). [received: April 1983]
Reports the first measurements of flow velocities in the ocean by the method of laser Doppler hydrometry. The measurements were taken on the eleventh voyage of the research vessels Akademik Petrovskii (January-March 1981) with the KIT-2 system, a newly developed laser Doppler system. The results show that it is possible to measure flow velocities under natural conditions in arrangements with forward scattering and backscattering of the laser beam. (4 refs.)
- 64272 A remote recording unit for floated automatic water level recording systems.** I.M.Shenderovich, L.S.Kleban (Sci. Res. Inst. of Instrumentation, USSR). *Sov. Meteorol. & Hydrol. (USA)*, no.12, p.94-6 (1981). Translation of: *Meteorol. & Gidrol. (USSR)*, no.12, p.113-15 (1981).
The design and basic technical specifications of a remote system for observing water levels in rivers, lakes, reservoirs, and inshore regions of seas and oceans are described. This system, which was developed by the Scientific-Research Institute (NII) of Instrumentation, has successfully passed state acceptance tests and has been included in the USSR State Register of Measurement Systems. (4 refs.)
- 64273 Mapping fields of the meteorological elements given at the nodes of a latitude-longitude grid.** G.S.Rivin, A.I.Kulikov (West Siberian Regional Sci. Res. Inst., USSR). *Sov. Meteorol. & Hydrol. (USA)*, no.1, p.31-7 (1982). Translation of: *Meteorol. & Gidrol. (USSR)*, no.1, p.41-8 (1982).
Algorithms are formulated and proposed for solution of four problems that arise in drawing isolines of meteorological elements specified at the nodes of a world-wide latitude-longitude grid: 1) selection of various cartographic projections; 2) plotting the isolines; 3) finding and mapping local extremes; 4) representing the contours of continents in the required projection. Computerization of the procedure for the BESM-6 and EC-1052 computers is described. Fields drawn from FGGE data are presented. (12 refs.)
- 64274 The MMR-06-M meteorological rocket and its instrument package for measurement of density, temperature, wind, and electron concentration.** D.Gaitandzhiev, H.Gernandt, A.N.Mel'nikov, I.O.Neelov, S.V.Pakhonov (Inst. of Hydrology & Meteorology of Meteorological Service of NRB, USSR). *Sov. Meteorol. & Hydrol. (USA)*, no.1, p.86-8 (1982). Translation of: *Meteorol. & Gidrol. (USSR)*, no.1, p.103-5 (1982).
Two versions of the nose cone for the small MMR-06-M meteorological rocket are reported: one is for measurement of density, temperature, and wind by the falling-sphere method, and the other for wind measurements with the aid of dipole radar reflectors and electron concentration measurements by the electrostatic-probe method. The work as performed for the 'Interkosmos' program. Design features of the instruments used are described, and nose-cone layout schemes are presented. (8 refs.)
- 64275 Microwave systems for satellite remote sensing.** W.Keydel (Inst. für Hochfrequenztech., DFLVR, Oberpfaffenhofen, Germany). *Z. Flugwiss. & Weltraumforsch. (Germany)*, vol.7, no.1, p.21-8 (Jan.-Feb. 1983). In English.
Microwaves have application to satellite remote sensing principally in active systems synonymous with radar and in passive systems synonymous with microwave radiometer. The present state of the art of such microwave systems is shown with respect to possible applications and the most important realized or planned systems are presented concerning the respective technical

data. Typical microwave results obtainable with radar or microwave radiometers respectively are presented. The advantages and disadvantages of active and passive microwave systems in comparison to each other and to optical systems briefly discussed. (4 refs.)

- 64276 Application of excimer lasers for remote sensing.** J.B.Laudenslager (Jet Propulsion Lab., California Inst. of Technol., Pasadena, CA, USA). Topical Meeting on Excimer Lasers, Incline Village, NV, USA, 10-12 Jan. 1983 (Washington, DC, USA: Opt. Soc. America 1983), p.WB1/1-4.
Discusses the applications of excimer lasers for use in laser-induced fluorescence (LIF) measurements of atmospheric gases, biologic organisms, and minerals as well as the sensing technique requirements for DIAL measurements of gases and in situ ionization of atmospheric molecules. The design requirements of the laser and detection system are also discussed. (6 refs.)
- 64277 Practical interpolation of 2-D surfaces using the Gerchberg algorithm.** M.J.Carlotto, V.T.Tom (Analytic Sci. Corp., Reading, MA, USA). Topical Meeting on Signal Recovery and Synthesis with Incomplete Information and Partial Constraints, Incline Village, NV, USA, 12-14 Jan. 1983 (Washington, DC, USA: Opt. Soc. America 1983), p.WA3/1-4.
The interpolation of 2-D wind and hydrographic surfaces is accomplished using the Gerchberg algorithm. Special emphasis is given to algorithm implementation on an array processor. Specific applications presented are: the generation of hydrographic surfaces from bathymetry data obtained from the hydrographic airborne laser sounder and the generalization of wind-flows from cloud imaging obtained from the Geostationary Operational Satellite. Experimental results obtained using a VAX 11/780 and FPS 120 array processor system are presented. (6 refs.)
- Proceedings of the Symposium on Low-Level Waste Disposal. Site Characterization and Monitoring (NUREG/CP-0028) See Entry 59537
- Geological and geophysical techniques for development of siting and design parameters See Entry 60251
- Techniques of groundwater investigation at proposed low-level nuclear waste disposal sites See Entry 60257
- Ground-water monitoring techniques for low-level radioactive disposal sites See Entry 60258
- On-site meteorological measurements for low-level radioactive waste disposal See Entry 60268
- Thermomechanical in-situ experiments and finite element computations See Entry 60294
- Permeability monitoring technique of the near-field and far-field interface of underground openings See Entry 60305
- An air quality data analysis system for interrelating effects, standards, and needed source reductions. VII. An O_3 - SO_2 leaf injury mathematical model See Entry 63760
- Physics of remote sensing See Entry 63761
- High-sensitivity atmospheric gas analysis based on intracavity laser detection of scattered radiation See Entry 63763
- Annual report for magnetic observatories—1980 See Entry 64023
- On the resolving power of the VLF method See Entry 64024
- A Fourier transform method for the interpretation of self-potential anomalies due to two-dimensional inclined sheets of finite depth extent See Entry 64025
- Determination of spectral properties of earthquakes from their magnitudes See Entry 64057
- Determination of a magnitude calibration function using short-period readings of PKP See Entry 64059
- Considerations for the body-wave magnitude determination in the Recent Earthquake Data Report of the United States Geological Survey See Entry 64062
- Prospect for numerical information on finite rock strain from the separation of magnetic anisotropy components See Entry 64106
- Bathymetric and oceanographic applications of Kalman filtering techniques See Entry 64129
- Microcomputer-aided analysis of hydroacoustical receiver signals See Entry 64130
- The M2 oceanic tide recovered from Seasat altimetry in the Indian Ocean See Entry 64146
- The measurement of water table levels in structured clay soils by means of open auger holes See Entry 64153
- Correlation functions of rainfall field and their application in network design in the tropics See Entry 64212
- An atmospheric vertical temperature profile measurement by detecting infrared on board See Entry 64229
- On the extraction of atmospheric turbulence parameters from radar backscatter Doppler spectra. I. Theory See Entry 64279
- Mesospheric turbulence intensities measured with a HF radar at 35°S. II See Entry 64280
- Atmospheric scattering effects on ground-based measurements of thermospheric winds See Entry 64281
- Ionospheric electric field pulsations: a comparison between VLF results from an ionospheric heating experiment and STARE See Entry 64291
- Incoherent scatter observations of mid-latitude sporadic-E and comments on its data analysis See Entry 64294
- The minimum detectable value of wave vector component parallel to the magnetic field of trapped cyclotron harmonic waves See Entry 64311
- Whistler observations of magnetospheric electric field in the night side plasma-sphere at low latitude See Entry 64322
- Photometric apparatus 'Duga' for investigating Polar auroras and tropical arcs from onboard the orbital station 'Salyut-6' See Entry 64349
- Total current to cylindrical collectors in collisionless plasma flow See Entry 64354

94.00 AERONOMY AND SPACE PHYSICS

94.10 PHYSICS OF THE NEUTRAL ATMOSPHERE

(for planets, see 96.30)

64278 Initial tests of an index based on AL values for modeling magnetic storm related perturbations of the thermosphere. J.S.Nisbet, C.Stehle, E.Bleuler (Dept. of Electrical Engng., Pennsylvania State Univ., University Park, PA, USA).

J. Geophys. Res. (USA), vol.88, no.A3, p.2175-80 (1 March 1983).

Very large perturbations in the thermosphere and ionosphere are induced by motions driven by heating and by electric fields in the auroral electrojet regions. Winds carry these effects to all latitudes. Because of this, thermospheric models have terms associated with magnetic activity. The Kp and Ap indices have usually been employed; however, these are poorly correlated with the temporal variations. Initial experiments are described with new indices based on the auroral electrojet indices of magnetic activity that are more directly related to the energy driving functions. The new indices are based on the time-weighted average of the auroral electrojet indices over a period rather than on instantaneous values. Comparisons are made with the 3-hour Ap index for high-latitude atomic oxygen densities under disturbed conditions. (17 refs.)

64279 On the extraction of atmospheric turbulence parameters from radar backscatter Doppler spectra. I. Theory. W.K.Hocking (Max-Planck-Inst. fur Aeronomie, Katlenburg-Lindau, Germany).

J. Atmos. & Terr. Phys. (GB), vol.45, no.2-3, p.89-102 (Feb.-March 1983).

A theory is developed for the extraction of RMS velocities of scatterer motions from spectra measured with a Doppler backscatter radar. The effects of finite beam-widths, finite pulse lengths, beam broadening, shear broadening, and other such spectral 'contaminants' are considered. It is shown that these 'contaminants' can play a major role in determining the measured spectral widths (and, equivalently, the signal fading time), and so must be properly considered if the spectral widths are to be used to extract the RMS motions of the scatterers. It is also shown that these RMS motions can be used to estimate turbulence intensities in those cases where turbulence is the dominant cause of the scatterer motions. (24 refs.)

64280 Mesospheric turbulence intensities measured with a HF radar at 35°S. II. W.K.Hocking (Max-Planck-Inst. fur Aeronomie, Katlenburg-Lindau, Germany).

J. Atmos. & Terr. Phys. (GB), vol.45, no.2-3, p.103-14 (Feb.-March 1983).

For pt.I see ibid., vol.45, no.2/3, p.89-102 (1983). In part I a theory has been developed for extraction of turbulence energy dissipation rates from spectra measured with a radar. It was shown that factors apart from turbulence contribute to the observed spectral widths, and that these factors must be considered if accurate estimates of energy dissipation rates are to be obtained. In particular, beam-width broadening and shear broadening were important. In this paper the first results obtained with this theory are presented. The results were obtained using the large HF array at Adelaide, Australia, primarily during the southern hemisphere winter of 1981. Results are consistent with rocket measurements of turbulence, with typical values varying between 0.01 and 0.2 W kg⁻¹ at 80-90 km altitude. (33 refs.)

64281 Atmospheric scattering effects on ground-based measurements of thermospheric winds. V.J.Abreu, G.A.Schmitt, P.B.Hays, J.W.Meriwether, Jr., Ca.A.Tepley (Space Phys. Res. Lab., Univ. of Michigan, Ann Arbor, MI, USA), L.L.Cogger.

Planet. & Space Sci. (GB), vol.31, no.3, p.303-10 (March 1983).

Inherent in observations of thermospheric winds from the ground with the Fabry-Perot interferometer is the assumption that the measured Doppler shift is a property of the source medium viewed by the instrumental line of sight. However, ground based airglow observations in regions of weak airglow emission near large intensity gradients may be contaminated by scattered light. Light from areas where the emission is strong can be scattered by the lower atmosphere into the field of view of the observations. Thermospheric winds deduced from the observed Doppler shifts will then show apparent convergence or divergence with respect to the site of observation. (17 refs.)

64282 Prevailing wind at heights of 80-100 km at various longitudes during the winter and spring periods of 1976-1977. N.A.Makarov (Inst. of Experimental Meteorology, USSR).

Sov. Meteorol. & Hydrol. (USA), no.12, p.30-3 (1981). Translation of: *Meteorol. & Gidrol. (USSR)*, no.12, p.41-5 (1981).

The results of synchronous meteor-radar measurements of prevailing-wind velocities made at Khabarovsk and Obninsk in 1976-1977 are reported. The data indicate similarity of the seasonal wind cycle at altitudes of 80-100 km over the Far Eastern and European regions. In addition to the seasonal trend, the prevailing-wind velocities are subject to variations with periods of 5-30 days, which correlate weakly in the data from the two stations. The lower-thermosphere wind field is observed to react sharply to winter stratospheric warming. The spring transformation at Khabarovsk was distinguished by a sharper reversal of the zonal flow and by weakening of the easterlies in April. (9 refs.)

Exploration of the Polar Upper Atmosphere. Proceedings of the NATO Advanced Study Institute See Entry 59540

Atmospheric pressure waves generated by solar eclipses See Entry 59559

Baroclinic instability of the summer mesosphere: a mechanism for the quasi-two-day wave? See Entry 64186

VHF radar observations in the stratosphere and mesosphere during a stratospheric warming See Entry 64187

Determination of ozone from eclipse observations of O₂ (a¹Δ_g) dayglow See Entry 64204

VLF/LF detection of ionization changes and wave motions in the middle atmosphere associated with the February 1980 total solar eclipse .. See Entry 64205

Atmospheric gravity waves produced by solar eclipses—a review See Entry 64206

Evidence of atmospheric gravity waves in the wake of the eclipse shadow See Entry 64207

Atomic nitrogen emissions from photodissociation of N₂ See Entry 64236

Visible continuum emission and gravity waves See Entry 64284

Horizontal velocity dispersion of medium-scale travelling ionospheric disturbances in the F-region See Entry 64297

Optimization of equatorial transfer orbit with due regard for atmospheric drag See Entry 64358

94.10Q Airglow and nightglow

64283 Tropical nightglow observations and predictions from ionospheric models. J.Christophe, G.Thuillier (Service d'Aeronomie, CNRS, Verrieres-le-Buisson, France), M.Fehrenback, Y.Sahai, G.Weill.

J. Atmos. & Terr. Phys. (GB), vol.45, no.2-3, p.137-48 (Feb.-March 1983).

To study the tropical nightglow emissions in the vicinity of the Brazilian magnetic anomaly, two balloons were flown in February 1973 and 1977 carrying photometers. The behavior in the tropical nightglow of the 630 and 557.7 nm lines is described and compared with predictions based on recent ionospheric models. Possible effects of the magnetic activity on the F₂-layer in the tropics are suggested which are not accounted for by the ionospheric models. (40 refs.)

64284 Visible continuum emission and gravity waves. A.Molina (Dept. de Fisica Fundamental, Univ. de Granada, Granada, Spain).

Planet. & Space Sci. (GB), vol.31, no.3, p.331-7 (March 1983).

Observed oscillations in the visible continuum emission (5000 Å) are studied considering the usual visible emission mechanism, NO+O (both two-body and three-body paths). Characteristic parameters of internal gravity waves are obtained using Hines' linear theory. Values of the kinetic energy density ϵ , and temperature variations $\Delta\theta$, due to gravity waves are calculated. The results ($\epsilon \sim 10^6$ cm² s⁻², $\Delta\theta \approx 4$ -9K) are in agreement with those obtained by means of different techniques reported in the literature. A similar analysis of the simultaneous green-line emission data is made and a comparison is drawn between the results obtained for both emissions. An expression relating relative brightness of continuum emission and relative perturbations of atmospheric density is proposed. (41 refs.)

64285 Equatorial depletions in the 630.0 nm airglow at Vanimo. E.H.Carman (Ionospheric Prediction Service, Australian Dept. of Sci. & Technol., Vanimo, Papua New Guinea).

Planet. & Space Sci. (GB), vol.31, no.3, p.355-62 (March 1983).

Using ground based airglow photometry, depletions in the 630.0 nm airglow were observed at Vanimo near the southern limb of the intertropical airglow arc. The results were compared with the more common properties of equatorial plasma bubbles such as depletion magnitude, cross-sectional size and East-West drift, with good agreement. In particular, airglow depletion depths ranged from 18 to 64% with a maximum loss in emission rate of 700 R₀ (55%) on a night when the maximum recorded airglow was almost 1700 R₀. This corresponds to an electron density depletion of about 1.5×10¹² el m⁻³ observed near solar maximum. It is somewhat higher than values reported near solar minimum. The airglow depletions move eastward with velocities ranging from 90 to 140 ms⁻¹. There is qualitative evidence of vertical motion and strong correlation with range type spread-F. (15 refs.)

Determination of ozone from eclipse observations of O₂ (a¹Δ_g) dayglow See Entry 64204

94.10S Aurora

Photometric apparatus 'Duga' for investigating Polar auroras and tropical arcs from onboard the orbital station 'Salut-6' See Entry 64349

94.20 PHYSICS OF THE IONOSPHERE

(for planets, see 96.30)

64286 Observations of the HF-enhanced plasma line with a 46.8-MHz radar and reinterpretation of previous observations with the 430-MHz radar.

J.A.Fejér (Max-Planck-Inst. fur Aeronomie, Katlenburg-Lindau, Germany), H.M.Ierkic, R.F.Woodman, J.Rottger, M.Sulzer, R.A.Behnke, A.Veldhuis.

J. Geophys. Res. (USA), vol.88, no.A3, p.2083-92 (1 March 1983). During 5.1-MHz HF transmissions below the F region penetration frequency by a nearby ionospheric modification facility, radar echoes coming from F region heights at a frequency of 46.8+5.1=51.9 MHz were received while a VHF radar using the 305 m spherical reflector at Arecibo was transmitting pulses coherently on 46.8 MHz. The bandwidth of the echoes was less than 10 Hz. The so-called decay line due to the parametric decay instability was expected at a frequency lower by about 300 Hz, but it was not observed. Density variations caused by the ponderomotive force resulting from the standing wave pattern at 5.1 MHz are tentatively invoked to explain the observations. Poorly understood aspects of some previous observations with the 430-MHz radar can be similarly explained. (27 refs.)

64287 Studies of the self-focusing instability at Arecibo. D.T.Farley, C.L.Hoz, B.G.Fejér (School of Electrical Engng., Cornell Univ., Ithaca, NY, USA).

J. Geophys. Res. (USA), vol.88, no.A3, p.2093-102 (1 March 1983). Precisely simultaneous radar and satellite measurements at the altitude of reflection of a strong HF heating wave above the Arecibo Observatory were made on June 7, 1977. Parametric instabilities produce strong enhancements in the plasma line and ion line incoherent scatter radar echoes. These echoes also exhibit periodic deep fading that is attributed to a self-focusing instability. This explanation was confirmed by the in situ observation of electron density fluctuations with peak-to-peak amplitudes reaching at least 3% and a spatial dependence that corresponded closely to the radar fading pattern, at least for irregularity wavelengths ranging from a few hundred meters to a few kilometers. The correspondence implies that the radar fading is associated with the convection of the density irregularities through the radar beam. (33 refs.)

64288 Density drift instabilities and weak collisions. S.P.Gary, P.A.Bernhardt, T.E.Cole (Los Alamos Nat. Lab., Univ. of California, Los Alamos, NM, USA).

J. Geophys. Res. (USA), vol.88, no.A3, p.2103-11 (1 March 1983). Describes the effects of weak collisions on the linear kinetic theory of electrostatic density drift instabilities. The model assumes a weak, uniform density gradient, a uniform magnetic field and the BGK collision operator with a modification of the local approximation to derive a dispersion equation valid at all frequencies and wave numbers. The properties of the universal and collisional density drift instabilities at maximum growth rates are presented in detail. Their thresholds in an ionospheric model, which includes ion-neutral, electron-neutral, and electron-ion collisions, are discussed and compared with the threshold of the lower hybrid density drift instability. In particular, the ionospheric conditions (plasma density $\lesssim 10^3$ cm⁻³, altitude $\gtrsim 250$ km) and maximum scale lengths necessary to excite the universal at wavelengths of the order of the ion gyroradius are presented. (28 refs.)

- 64289 A theoretical study of the high latitude F region's response to magnetospheric storm inputs.** J.J.Sojka, R.W.Schunk (Center for Atmospheric & Space Sci., Utah State Univ., Logan, UT, USA). *J. Geophys. Res. (USA)*, vol.88, no.A3, p.2112-22 (1 March 1983). The response of the polar ionosphere to magnetospheric storm inputs was modeled. During the storm the two major processes that couple the F region to the magnetosphere, namely the electric field distribution and the particle precipitation from the magnetosphere, undergo drastic modification on relatively short F region time scales. These time-dependent changes are not simply related to the F region storm time dependent changes. The lower F region responds on a time scale of only minutes to the storm associated changes in the auroral precipitating electron flux, owing to the dominance of chemistry production-loss mechanisms over transport processes. At higher altitudes in the vicinity of $h_m F_2$, the chemistry is balanced by both plasma diffusion along field lines and horizontal plasma convection, which acts to prolong the effect of the storm for many hours after it has ceased. (15 refs.)
- 64290 A dynamic model for the auroral field line plasma in the presence of field-aligned current.** H.G.Mitchell, Jr. (Sci. Applications Inc., McLean, VA, USA), P.J.Palmadesso. *J. Geophys. Res. (USA)*, vol.88, no.A3, p.2131-9 (1 March 1983). A dynamic numerical model of the plasma along an auroral field line has been developed in order to provide a vehicle for studying ionosphere-magnetosphere coupling processes. The model is a multimoment, multifluid approximation of a gyrotropic plasma consisting of three species (electrons, hydrogen ions, oxygen ions) along a segment of auroral magnetic field line extending from an altitude of 800 km to 10 Earth radii. The authors performed simulations for the case of a current-free polar wind equilibrium of the field line plasma and the case in which a large upward field-aligned current is applied to the field line. In the former case, the agreement between this model and previous static results is reasonable given the differing boundary conditions inherent in the two cases. (38 refs.)
- 64291 Ionospheric electric field pulsations: a comparison between VLF results from an ionospheric heating experiment and STARE.** M.T.Rietveld, H.Kopka, E.Nielsen, P.Stubbe (Max-Planck-Inst. fur Aeronomie, Katlenburg-Lindau, Germany), R.L.Dowden. *J. Geophys. Res. (USA)*, vol.88, no.A3, p.2140-6 (1 March 1983). Very low-frequency radio waves can be generated in the lower ionosphere by periodically modulating the conductivity, and thus natural currents, using high power HF radio waves. In conjunction with the heating facility near Tromsø, Norway, such waves have been generated and detected on the ground using two orthogonal receiving antennas so that the polarization ellipse of the VLF signal could be reconstructed. Changes in the strength and direction of the electric field driving the modulated current are reflected in variations in the size and orientation of the VLF ellipse. During a natural Pc 5 pulsation event on October 16, 1981, a close correlation was found between the VLF signal and the electric field pulsations observed by the STARE auroral radars. This work shows that VLF signals from modulated ionospheric heating experiments can provide a sensitive, high time resolution indicator of the ionospheric electric field. (9 refs.)
- 64292 Splitting and divergence of STARE auroral radar velocities.** J.D.Whitehead, H.M.Jerkic, E.Nielsen (Max-Planck-Inst. fur Aeronomie, Katlenburg-Lindau, Germany). *J. Geophys. Res. (USA)*, vol.88, no.A3, p.2147-54 (1 March 1983). A study of the power spectra of auroral radar echoes shows that they are sometimes asymmetrical. This is probably due to two waves (at different heights) having different line-of-sight velocities. The velocity splitting occurs over a limited region of space (~300 km in geographic extent) that moves toward the equator. The velocity splitting seems to be associated with divergence of the STARE drift velocities. This has been calculated and found to have significant time and space variations—much too large to be explained by magnetic field changes. The divergence is greatest at times when the power spectrum is asymmetrical and more than one velocity may be present. Several possible corrections have been tried, but none reduce the magnitude of the divergences appreciably. The authors conclude that STARE does not measure the electric field exactly and that a correction velocity of the order of 25 m s^{-1} and divergence of the order of 10^{-4} s^{-1} is required. (12 refs.)
- 64293 A simple theoretical model for calculating and parameterizing the ionospheric photoelectron flux.** P.G.Richards, D.G.Torr (Center for Atmospheric & Space Sci., Utah State Univ., Logan, UT, USA). *J. Geophys. Res. (USA)*, vol.88, no.A3, p.2155-62 (1 March 1983). A method has been developed for calculating the ionospheric photoelectron flux that uses the concept of average electron energy loss to simplify the calculation of the degraded electron spectrum. This method, which requires only a knowledge of the total inelastic electron impact cross sections, rather than a detailed knowledge of the many partial cross sections can be used for the calculation of all secondary ion and excited state production rates. It is estimated that the use of an average energy loss reduces the computation time by a factor of 10 and considerably reduces storage requirements. The simple model is designed to provide ionospheric chemistry workers with a convenient means of obtaining photoelectron spectra similar to that which is currently available for obtaining neutral densities. (25 refs.)
- 64294 Incoherent scatter observations of mid-latitude sporadic-E and comments on its data analysis.** C.J.Zamlutti (Inst. de Pesquisas Espaciais, Sao Jose dos Campos, Sao Paulo, Brazil). *J. Atmos. & Terr. Phys. (GB)*, vol.45, no.2-3, p.79-87 (Feb.-March 1983). Incoherent scatter observations of sporadic-E have been reported from measurements at Arecibo (18.3°N) in the last decade. Some important results have been achieved. They are examined in this article as a source for improving the Es study. Critical aspects of experiment design and data analysis are also considered for further experiments. (43 refs.)
- 64295 VLF ionosonde and long-distance propagation anomalies produced by galactic Cen X-4 X-ray burst in May 1979.** L.R.Piazza, P.Kaufmann (Inst. de Pesquisas Espaciais, Sao Jose dos Campos, Sao Paulo, Brazil), P.R.Pardo. *J. Atmos. & Terr. Phys. (GB)*, vol.45, no.2-3, p.121-5 (Feb.-March 1983). The galactic X-ray source Cen X-4 produced a large outburst in May 1979, measured by the Ariel-5 satellite. Low ionosphere group heights measured daily by a VLF ionosonde indicated an anomalous lowering of the effective reflection height in good correlation with the Cen X-4 burst as well as an increase in the reflection coefficient, larger for larger frequencies. Diurnal VLF phase variations in a long-distance propagation path presented nighttime 3-4° deviations from the average in some days during the Cen X-4 bursting period. The geomagnetic activity in the period covered by this investigation was low, and the results obtained are a suggested confirmation that galactic transient X-ray sources are capable of producing sufficient ionization effects to be detected as low ionosphere anomalies. (16 refs.)
- 64296 High-latitude plasma densities and their relation to riometer absorption.** M.Friedrich (Dept. of Communications & Wave Propagation, Tech. Univ. Graz, Graz, Austria), K.M.Torkar. *J. Atmos. & Terr. Phys. (GB)*, vol.45, no.2-3, p.127-35 (Feb.-March 1983). A large number of D- and E-region electron density profiles from high latitudes have been analysed. These were derived from rocket-borne wave propagation experiments and—after careful screening—arranged according to riometer absorption. Statistical profiles for various degrees of absorption, including 9 dB, were established both for day and night. Furthermore, the height region predominantly contributing to the absorption has been identified. Finally a mean variation of the density of negative ions has been derived. (23 refs.)
- 64297 Horizontal velocity dispersion of medium-scale travelling ionospheric disturbances in the F-region.** T.Shibata, T.Okuzawa (Dept. of Appl. Electronic Engng., Univ. of Electro-Communications, Tokyo, Japan). *J. Atmos. & Terr. Phys. (GB)*, vol.45, no.2-3, p.149-59 (Feb.-March 1983). Daytime observations of the horizontal velocity dispersion of medium-scale travelling ionospheric disturbances (TID) near the F_2 peak height have been carried out using an array of HF Doppler sounders in central Japan. Cross-correlation analysis of sample records has shown that the horizontal trace velocity is a decreasing function of the period of fluctuations in the range 13.3-40 min. The theoretical dispersion of the atmospheric gravity waves is also calculated using Klostermeyer's (1974) method. Comparison between the observed and the calculated results suggests the possibility that the components of the lower period of the observed velocity dispersion may be a remnant of the quasi-evanescent mode pertinent to lower-height levels. (44 refs.)
- 64298 Prediction of total electron content using the International Reference Ionosphere.** L.F.McNamara, P.J.Wilkinson (Dept. of Sci. & Technol., Ionospheric Prediction Service, Darlinghurst, Australia). *J. Atmos. & Terr. Phys. (GB)*, vol.45, no.2-3, p.169-74 (Feb.-March 1983). Comparisons are presented between the values of total content (TEC) observed at 31°S and those predicted using the Australian Ionospheric Prediction Service's version of the International Reference Ionosphere. Although discrepancies sometimes exceed 30% they are usually less than 20%. The predicted TEC values tend to be too low in daytime summer, too high in daytime winter, and have an incorrect diurnal variation during winter days. Although the predicted TEC was sensitive to the errors in the f_oF_2 values used, the major discrepancies remained. (10 refs.)
- 64299 Auroral riometer absorptions and the F-region disturbances observed over a wide range of latitudes.** L.A.Hajkowicz (Dept. of Phys., Univ. of Queensland, St. Lucia, Queensland, Australia). *J. Atmos. & Terr. Phys. (GB)*, vol.45, no.2-3, p.175-9 (Feb.-March 1983). Standard riometer data from a southern auroral station were compared with ionograms obtained at five stations positioned from sub-auroral to equatorial latitudes. The rapid onset in riometer absorption, during intense substorm activities in an equinoctial period, was associated with a sequential propagation of ionospheric disturbances deduced from the F-region parameters $h'F$ and range spread-F. The time shift between absorption maxima and extrapolated commencement times of the disturbances was consistent with the presence of large-scale travelling ionospheric disturbances (TIDs), propagating equatorwards with velocities lying typically in the range 600-900 m s^{-1} , and with a median velocity of 720 m s^{-1} . It is suggested that the onset of TIDs is associated with high-energy particle precipitation, manifested by the occurrence of auroral absorption events. The results indicate that large-scale TIDs are simultaneously generated in both hemispheres. (22 refs.)
- 64300 Generation of ionospheric irregularities by thermal-source: a new mechanism.** U.N.Das (Dept. of Maths., Gauhati Univ., Gauhati, Assam, India), A.C.Das. *Planet. & Space Sci. (GB)*, vol.31, no.3, p.311-16 (March 1983). A new mechanism for the generation of ionospheric irregularities of scale sizes of the order of 100 m or more, has been developed on the basis of a thermal energy source due to collisional current dissipation. An important role is played by the diffusion of particles along and across the magnetic field. A threshold condition for the instability has been obtained and it is shown that these irregularities can be generated in the F-region height of the auroral ionosphere when the electric field is enhanced to about 10 mV m^{-1} . (27 refs.)
- 64301 Nonlinear phenomena in laboratory and space plasmas.** A.Y.Wong (Dept. of Phys., Univ. of California, Los Angeles, CA, USA). *Phys. Scr. (Sweden)*, vol.T2, no.1, p.262-70 (1982). (1982 International Conference on Plasma Physics, Goteborg, Sweden, 9-15 June 1982). Laboratory observations of wave trapping and generation of density cavities verified quantitatively the predictions of the nonlinear Schrodinger equation. Recent observations on the resonant interactions between electromagnetic waves and ionospheric plasmas are interpreted as first tentative evidence for the existence of cavitons in the ionosphere. (7 refs.)
- 64302 Changes in the field intensity of radio signals and noise during the total solar eclipse of 16 February 1980 in relation to ionospheric radio wave propagation.** A.K.Sen, B.Saha, S.K.Trehan, S.Sekhar Dey, S.K.Saha, R.N.Dutta, S.K.Chatterjee, J.S.Sehra, M.K.Das Gupta (Centre of Advanced Study in Radio Phys. & Electronics, Calcutta, India). *Proc. Indian Natl. Sci. Acad. Part A*, vol.48, suppl.3, p.302-7 (Oct. 1982). (Symposium on the Total Solar Eclipse of 16 February 1980, New Delhi, India, Jan. 1981). Various scientific observations for the studies on the ionospheric propagation of radio signals and noise in the VLF to HF bands were made at different Indian locations in umbral and penumbral regions of the solar eclipse on 16 February 1980. Analysis of the results indicates that, in general, there is an improvement of radio propagation during the eclipse. Some evidence of travelling ionospheric disturbances apparently related to the eclipse is indicated. A peculiar absorption of signal starting even before the first contact has been observed. The results obtained are compared with other eclipse results and critically examined in the light of the current knowledge about the mechanisms of the ionospheric changes involved, including the gravity wave perturbations. (15 refs.)
- 64303 Multi-station monitoring of short and medium wave broadcast circuits during solar eclipse of 16 February 1980.** D.R.Lakshmi, B.M.Reddy (Nat. Phys. Lab., New Delhi, India), R.Chakravarthy, M.Sain. *Proc. Indian Natl. Sci. Acad. Part A*, vol.48, suppl.3, p.308-15 (Oct. 1982). (Symposium on the Total Solar Eclipse of 16 February 1980, New Delhi, India, Jan. 1981). During the 16 February 1980 total solar eclipse, several short wave and medium wave broadcasts of All India Radio were monitored at several locations on either side of the path of totality, the disposition of the stations so chosen as to locate the control points of the circuits in the totality path. Special mention may be made of the short wave transmissions at 15.25 MHz from Delhi and 9.55 MHz from Bombay which were monitored at Madras and Trivandrum. In addition, a few medium wave transmissions also were

monitored so that information can be derived on the change in the pattern of field intensity recording with change in the altitude of the control points. Ionosondes were specially pressed into operation for this event at two stations located in the totality zone. It was observed that the increase in the signal intensities during the totality is higher than the total ionospheric absorption given by the CCIR formula. This indicates that the CCIR formula underestimates the ionospheric absorption by as much as 12 dB in certain cases. (8 refs.)

64304 Ionospheric radio effects of the solar eclipse on 16 February 1980. K.G.Jani, G.Datta, D.B.Patel, K.M.Kotadia (Dept. of Phys., Gujarat Univ., Ahmedabad, India).
Proc. Indian Natl. Sci. Acad. Part A, vol.48, suppl.3, p.316-24 (Oct. 1982). (Symposium on the Total Solar Eclipse of 16 February 1980, New Delhi, India, Jan. 1981).

The solar eclipse at Karwar (14.6°N, 74°E) was total for about 2 1/2 minutes around 1540 hr IST and this place happens to be the midpoint of one-hop Colombo-Ahmedabad ionospheric radio propagation path. The field strength of radio signals on 11.8 MHz transmitted from Radio Sri Lanka and received at Ahmedabad showed an increase of about 23 dB above the normal value and the maximum of increase occurred during the totality of the solar eclipse. This effect was clearly noticed in spite of the fact that the eclipse day was magnetically disturbed. At Ahmedabad (23°N, 72.6°E) where the solar eclipse was about 75 per cent at its maximum phase around 1541 hr IST, vertical incidence A1-ionospheric radio pulse absorption on 2.2 and 1.8 MHz reduced to half of its normal value (22-25 dB) with a time-delay of about 18 minutes following the maximum phase. The above results are discussed in relation to the changes in the ionisation in the lower ionosphere and the modes of oblique path radio propagation associated with the obscuration of solar radiation during the eclipse. (10 refs.)

64305 Effects of solar eclipse on shortwave transmissions. E.P.Radhakrishnan, N.Balan (Dept. of Phys., Univ. of Kerala, Trivandrum, India), A.A.Sridhar, K.Usha Devi.
Proc. Indian Natl. Sci. Acad. Part A, vol.48, suppl.3, p.325-33 (Oct. 1982). (Symposium on the Total Solar Eclipse of 16 February 1980, New Delhi, India, Jan. 1981).

The effects of solar eclipse on long distance communications have been studied by monitoring the Delhi shortwave transmissions on 15.25 MHz at Trivandrum during the total solar eclipse of 16 February 1980. Signal strength shows a maximum enhancement of 30 dB 15 minutes before the maximum phase of the eclipse at the path mid-point. During the beginning of the eclipse the signal strength remains steady around the control day value for 20 minutes after the first contact while at the end of the eclipse it falls sharply to the control day value. Signal fading rate is very high at the beginning and at the end of the eclipse while it is very low during the maximum phase of the eclipse. Probability distribution of the signal strength exhibits a double hump during the eclipse period. The results are interpreted in terms of the possible changes in the lower ionosphere and at the reflection level by means of model computations for Delhi-Trivandrum propagation path. (12 refs.)

64306 Ionospheric absorption changes in 11.8 MHz radio propagation during the total solar eclipse of 16 February 1980. G.Rajaram, T.R.Rao, D.D.Patil (Indian Inst. of Geomagnetism, Bombay, India).
Proc. Indian Natl. Sci. Acad. Part A, vol.48, suppl.3, p.334-41 (Oct. 1982). (Symposium on the Total Solar Eclipse of 16 February 1980, New Delhi, India, Jan. 1981).

Variations in the 11.8 MHz signal strength (Colombo-Bombay propagation path) during the total solar eclipse of 16 February 1980 are interpreted in terms of possible changes in the lower ionosphere. The main features observed are a sharp rise of almost 20 dB following onset of the eclipse, followed by two distinct drops in signal strength which were separated by a brief interval of enhanced signal; a marked rise in the received signal was also noticed about an hour before first contact. The eclipse night was characterised by regular, periodic fading which is not a normal night-time feature for this propagation path. These eclipse-induced changes are discussed in the light of astronomical and ionospheric observations of this same eclipse reported by other workers. (23 refs.)

64307 Solar eclipse effects on the lower ionosphere. R.Venkatanarayana, T.S.N.Somayaji (Dept. of Phys., Andhra Univ., Waltair, India).
Proc. Indian Natl. Sci. Acad. Part A, vol.48, suppl.3, p.375-9 (Oct. 1982). (Symposium on the Total Solar Eclipse of 16 February 1980, New Delhi, India, Jan. 1981).

Short term fluctuations in ionospheric first order echo amplitude at Waltair are investigated for eclipse effects. Power spectrum analysis of short term fluctuations during the period 1500-1630 hours on 16 February 1980 when a near total solar eclipse (99 per cent) occurred showed periods with a lower cut-off period equal to 6.75 minutes significantly higher than the cut-off period of 5.25 minutes for the corresponding period on 15 February 1980 taken as the control day. The group height was found to increase from 110 km just before the eclipse to an average of 127.5 km around the middle of the eclipse period. The larger cut-off period on the eclipse day is attributed to the increase in the altitude level of region where most of the ionospheric absorption is caused. Neglecting the effect of neutral winds and assuming the absence of significant ionization at the D-region heights during a near total eclipse, it is inferred that the temperature at an altitude of about 127.5 km is significantly lowered during the eclipse. (8 refs.)

64308 A1 absorption measurements during the total solar eclipse of 16 February 1980. U.V.Girish Kumar, K.V.V.Ramana (Ionosphere & Space Res. Labs., Andhra Univ., Waltair, India).
Proc. Indian Natl. Sci. Acad. Part A, vol.48, suppl.3, p.380-7 (Oct. 1982). (Symposium on the Total Solar Eclipse of 16 February 1980, New Delhi, India, Jan. 1981).

A1 absorption measurements taken during the total solar eclipse of 16 February 1980 at a frequency of 2.4 MHz are used to obtain the temporal variation of $N_m E$ at 105 km and $R_m D$ at 75 km. The contributions from E- and D-regions to the total absorption are also computed and it is found that during the time of near totality the contributions are approximately equal. The decrease in the total absorption from the time of beginning of the eclipse to the time of minimum absorption is about 25 dB with a time lag of 9 minutes. A 30 per cent decrease in $N_m E$ and a 70 per cent decrease in $N_m D$ with time lags of 9 minutes and 19 minutes, respectively, are noted in the temporal variations of $N_m E$ and $N_m D$ during the time of eclipse. The contributions from the uniform solar disc, solar corona and active regions distributed over the solar disc to the total absorption are 45 per cent, 25 per cent and 20 per cent respectively. (7 refs.)

64309 Correlation of seasonal structural transformations of the F region of the ionosphere and the circulation in the stratosphere. V.F.Chepura (Inst. of Experimental Meteorology, USSR).
Sov. Meteorol. & Hydrol. (USA), no.1, p.38-41 (1982). Translation of: *Meteorol. & Hydrol. (USSR)*, no.1, p.49-53 (1982).

Studies the monthly-average midday values of the critical frequencies of the F₂-layer over Moscow, Leningrad, and Ottawa in the period 1958-80. The dates of the spring and fall structural transformations of the F-region over the middle Northern Hemisphere average 4-6 weeks earlier than in the stratospheric circulation. The spring restructuring of the F-region precedes that of the meteor-zone circulation by an average of two weeks. (8 refs.)

64310 Temperature of the plasmasphere determined from VLF observations at SANAÉ. A.R.W.Hughes, B.Nugent (Dept. of Phys., Univ. of Natal, Durban, S Africa).

S. Afr. J. Phys. (S. Africa), vol.5, no.4, p.123-7 (1982). A new method is employed to determine plasma temperatures in the plasmasphere. The method assumes that the plasma is in diffusive equilibrium. Electron densities at two points on each field line are used to calculate a scale height and hence the temperature of the plasma. The temperatures are determined at high altitudes where, because of low densities, conventional probe techniques do not work well. (17 refs.)

64311 The minimum detectable value of wave vector component parallel to the magnetic field of trapped cyclotron harmonic waves. T.Utsunomiya (Dept. of Electrical Engng., Nat. Defense Acad., Yokosuka, Japan).
Trans. Inst. Electron. & Commun. Eng. Jpn. Part B (Japan), vol.66B, no.1, p.155-6 (Jan. 1983). In Japanese.

Shows that the cyclotron harmonic waves trapped near the magnetic equator plane, to be received by a topside sounder spacecraft, have the minimum value for their wave vector component parallel to the magnetic field, depending on the direction of the orbit of the spacecraft. (2 refs.)

Exploration of the Polar Upper Atmosphere. Proceedings of the NATO Advanced Study Institute See Entry 59540

Numerical double layer solutions with ionisation See Entry 61661

VLF/LF detection of ionization changes and wave motions in the middle atmosphere associated with the February 1980 total solar eclipse .. See Entry 64205

Evidence of atmospheric gravity waves in the wake of the eclipse shadow See Entry 64207

Probe experiment for measurement of plasma parameters and ion drift velocities in the ionospheric plasma onboard the Intercosmos-Bulgaria 1300 satellite See Entry 64241

Tropical nightglow observations and predictions from ionospheric models See Entry 64283

Equatorial depletions in the 630.0 nm airglow at Vanimo See Entry 64285

Excitation of an electrostatic wave by a cold electron current sheet of finite thickness See Entry 64324

Quarter-wave ULF pulsations See Entry 64326

The self-focusing of whistler waves See Entry 64327

Total current to cylindrical collectors in collisionless plasma flow See Entry 64354

The influence of ionospheric refraction on radio astronomy interferometry See Entry 64394

Radio communication and sunspots See Entry 64449

94.30 PHYSICS OF THE MAGNETOSPHERE

(for planets, see 96.30)

64312 Plasma rest frame frequencies and polarizations of the low-frequency upstream waves: ISEE 1 and 2 observations. M.M.Hoppe, C.T.Russell (Inst. of Geophys. & Planetary Phys., Univ. of California, Los Angeles, CA, USA).

J. Geophys. Res. (USA), vol.88, no.A3, p.2021-7 (1 March 1983). Using magnetic field data from the dual ISEE 1 and 2 spacecraft the authors have determined the plasma rest frame frequencies and polarizations of the large amplitude low frequency (0.03 Hz) upstream waves. The monochromatic sinusoidal waves associated with 'intermediate' ion fluxes are magnetosonic waves with rest frame frequencies $\sim 0.1 \Omega_p$ and wavelengths $\sim 1 R_E$. The obliquely propagating 'shocklet' form of the waves is also predominantly in the magnetosonic mode, but occasionally also appears in the Alfvén mode. The generation of the magnetosonic mode has been explained by the well established cyclotron resonance mechanism driven by narrow reflected ion beams but the concurrent observation of Alfvén mode waves appears to require wave generation by the more isotropic diffuse ion distributions as well. (17 refs.)

64313 Solar wind deceleration and MHD turbulence in the Earth's foreshock region: ISEE 1 and 2 and IMP 8 observations. C.Bonifazi, G.Moreno (Inst. Plasma Spazio, Consiglio Nazionale delle Ricerche, Frascati, Italy), C.T.Russell, A.J.Lazarus, J.D.Sullivan.

J. Geophys. Res. (USA), vol.88, no.A3, p.2029-37 (1 March 1983). The interaction of the solar wind with ions backstreaming from the Earth's bow shock is investigated using plasma and magnetic field measurements on ISEE 1 and 2 and IMP 8 at widely separated positions in the Earth's foreshock. This technique separates temporal and spatial variations within the foreshock. It is found that the solar wind acceleration associated with backstreaming ions is correlated with the amplitude of the MHD turbulence and that the largest decelerations are seen close to the bow shock. The density of the backstreaming ion beam is strongly correlated with distance from the shock and decreases by about a factor of 3 in a distance of about 3 R_E . (26 refs.)

64314 Ions upstream of the Earth's bow shock: a theoretical comparison of alternative source populations. S.J.Schwartz, M.F.Thomsen, J.T.Gosling (Univ. of California, Los Alamos Nat. Lab., Los Alamos, NM, USA).

J. Geophys. Res. (USA), vol.88, no.A3, p.2039-47 (1 March 1983). A theoretical framework is developed for studying trajectories of ions reflected or leaked upstream from the Earth's bow shock and subject to the Lorentz force in a steady interplanetary magnetic field **B** and the $\mathbf{V} \times \mathbf{B}$ electric field. The effects of a sharp shock potential rise are included. Expressions are derived for the guiding center motion and gyromotion in a frame (the Hoffman-Teller frame) moving parallel to the shock surface with sufficient speed to transform the incident solar wind velocity into motion entirely along the interplanetary magnetic field; the appropriate equations are also provided to transform these motions back to the observer's frame. The utility of these expressions is illustrated by comparing the predicted upstream motions for four different source models for upstream ions: magnetic moment-conserving reflection of solar wind ions; specular reflection of solar

wind ions; magnetic moment-conserving leakage of magnetosheath ions; and leakage of magnetosheath ions parallel to the shock normal. (34 refs.)

64315 The oblique whistler instability in the Earth's foreshock. D.D.Sentman (Inst. of Geophys. & Planetary Phys., Univ. of California, Los Angeles, CA, USA), M.F.Thomsen, S.P.Gary, W.C.Feldman, M.M.Hoppe. *J. Geophys. Res. (USA)*, vol.88, no.A3, p.2048-56 (1 March 1983). The linear Vlasov stability properties of electron velocity distributions, similar to those observed in the upstream foreshock region in association with obliquely propagating whistler waves at approximately 1 Hz, are studied. These distributions are modeled by a sum of bi-Maxwellians with drift speeds parallel to the magnetic field B . Such distributions are found to be stable to modes with wavevectors k parallel to B but unstable to whistler waves propagating obliquely to the magnetic field. The frequencies and wavelengths of these unstable modes agree well with those of whistlers observed upstream of the Earth's bow shock. (48 refs.)

64316 Mass composition of substorm-related energetic ion dispersion events. R.J.Strangeway, R.G.Johnson (Lockheed Palo Alto Res. Lab., Palo Alto, CA, USA). *J. Geophys. Res. (USA)*, vol.88, no.A3, p.2057-64 (1 March 1983). The Lockheed ion mass spectrometer flown onboard the SCATHA (P78-2) spacecraft is used to study the mass composition of two ion dispersion events. The energy-dispersed ions are observed over the full energy range of the instrument (0.1-32 keV/q) in the noon-dusk local time sector. On one of the days, March 22 (day 81) 1979, the dispersing ions are first observed following an isolated substorm. A long period of low magnetic activity is present prior to the substorm on this day, and a decrease in Dst is observed following the first observation of the dispersing ions. On the second day studied, June 7 (day 158), 1979, the correlation between ground magnetic activity and initial observation of dispersing ions is not so clear, since the dispersion follows a period of high magnetic activity. The differences between proton and oxygen dispersion are studied. Localised injection of ionospheric plasma are responsible for the composition changes. Pitch angle studies were also made. (21 refs.)

64317 High- β theory of low-frequency magnetic pulsations. S.Migliuolo (High Altitude Obs., Nat. Center for Atmospheric Res., Boulder, CO, USA). *J. Geophys. Res. (USA)*, vol.88, no.A3, p.2065-73 (1 March 1983). The theory of low-frequency (compared to ion cyclotron) arbitrary- β modes is developed for the following system: a two-component (hot and cold) inhomogeneous plasma, and a straight inhomogeneous magnetic field. This system is taken to model the magnetosphere, near the geomagnetic equator. The stability properties of three modes are presented in detail: the drift-compressional mode (driven by pressure gradients) the firehose mode (driven by $T_{\perp} > T_{\parallel}$), and the drift mirror mode (driven by $T_{\perp} > T_{\parallel}$). Comparisons to earlier models and to one observed event are also presented. (32 refs.)

64318 Pc 1 pulsation activity at Ottawa. J.C.Gupta (Div. of Geomagnetism, Earth Phys. Branch, Energy, Mines & Resources, Ottawa, Canada). *J. Geophys. Res. (USA)*, vol.88, no.A3, p.2075-82 (1 March 1983). Pulsations in the Pc 1 period range recorded at Ottawa for three years during the IMS are analyzed to study some of their occurrence characteristics. The diurnal occurrence pattern depends on the seasons and on the prevailing magnetic activity conditions. In both cases the morning peak shifts to earlier hours and the evening peak shifts to later hours with increasing conduction (electron density) in the ionosphere. The largest number of events were recorded in the winter months and about as many in the equinoctial months. A large majority of the events are inferred to occur, at Ottawa, during the recovery phase of magnetic storms. The enhancements of Pc 1's noted at different levels of magnetic activity seem to be controlled by the location of the plasmopause and also by the propagation conditions in the ionosphere. (43 refs.)

64319 Solar wind control of the low-latitude asymmetric magnetic disturbance field. C.R.Clauer (Space Telecommunications & Radioscience Lab., Stanford Univ., Stanford, CA, USA), R.L.McPherron, C.Searls. *J. Geophys. Res. (USA)*, vol.88, no.A3, p.2123-30 (1 March 1983). The technique of empirical linear prediction filters is used to investigate the extent to which the low latitude dawn-dusk magnetic asymmetry is controlled by the dawn-dusk solar wind motional electric field V_B , and/or by substorm processes measured by the westward auroral electrojet index AL . The dawn-dusk asymmetry is measured by a new index defined as the difference between dawn and dusk deviations in the X (geomagnetic Northward) magnetic field component. The empirically determined filters obtained from this analysis provide quantitative information which characterizes the coupling processes. For example, the V_B to AL filter is a delayed pulse beginning after a delay of about 15 minutes, peaking at 60 minutes and returning to zero at 120 min. The filter has the characteristics of a low pass filter with a cutoff frequency at 10^{-4} Hz. The V_B to ASYM filter is also a delayed pulse with similar constants. (23 refs.)

64320 Convective growth rate of ion cyclotron waves in H^+ - He^+ and H^+ - He^+ - O^+ plasma. L.Gomberoff, R.Neira (Dept. de Fisica, Univ. de Chile, Santiago, Chile). *J. Geophys. Res. (USA)*, vol.88, no.A3, p.2170-4 (1 March 1983). The behavior of the convective growth rate of the electromagnetic proton-cyclotron instability is investigated in detail in a H^+ , He^+ plasma and when a third (minority) cold ion component such as O^+ is taken into account. It is shown that amplification is the result of an interplay between the cold species and the thermal anisotropy of the energetic protons. The results seem to be in good agreement with the observations performed on board GEOS 1 and 2 concerning the generation of ULF waves, below the proton gyrofrequency. It is also shown that a small amount of O^+ can strongly affect the behavior of the convective growth rate of the instability below the He^+ gyrofrequency, even far away from the O^+ stop band. (13 refs.)

64321 Satellite observations of signals from a Soviet mid-latitude VLF transmitter in the magnetic-conjugate region. V.I.Larkina, O.A.Maltseva, O.A.Molchanov (Inst. of Terrestrial Magnetism, Ionosphere & Radio Wave Propagation, Acad. of Sci., Moscow, USSR). *J. Atmos. & Terr. Phys. (GB)*, vol.45, no.2-3, p.115-19 (Feb.-March 1983). The results of the Intercoms-19 satellite experiment which receives VLF signals arriving via a magnetospheric path have been examined. The reception zone in the magnetically conjugate region (MCR) has been shown to be centred near the L-value (2.6) of the transmitter of 15 kHz radio waves. The received signals arrive at the MCR with wave normal angles to the geomagnetic field, ψ , far from the resonance cone. These results indicate an effective amplification of the signal in the magnetosphere by 10-15 dB and effective ducting of VLF waves across the equatorial plane of the magnetosphere. (14 refs.)

64322 Whistler observations of magnetospheric electric field in the night side plasma-sphere at low latitude. P.N.Khosa, M.M.Ahmad, Lal Mani (Dept. of Phys., Regional Engng. Coll., Srinagar, Kashmir, India). *Moon & Planets (Netherlands)*, vol.27, no.4, p.453-62 (Dec. 1982). Whistlers recorded at low latitude ground stations of Gulmarg, Nainital and Varanasi were used to infer the east-west component of electric field on the nightside plasmasphere at $L=1.2, 1.12$, and 1.07 during magnetic storm periods. The method of measuring electric field from the observed cross-L motions of whistler ducts within the plasma-sphere, indicated by changes in nose frequency of whistlers, is outlined. The nose frequencies of the nonnose whistlers under consideration are deduced from the Dowden-Allocock linear Q-technique. (20 refs.)

64323 Generation of Alfvén waves in an anomalous resistivity region. A.A.Arykov, Yu.P.Maltsev (Polar Geophys. Inst., Apatity, USSR). *Planet. & Space Sci. (GB)*, vol.31, no.3, p.267-73 (March 1983). Studies disturbances produced by a field-aligned current flowing through a thin layer with a finite conductivity along the magnetic field. The layer conductivity is an arbitrary function of transverse coordinates and time. It is shown that a suddenly emerging layer of the anomalous resistivity in the region of the auroral field-aligned currents leads to a generation of an Alfvén impulse with an amplitude up to 100 gammas. All electromagnetic disturbances appear to be localized inside the magnetic field tube passing through the anomalous resistivity region. An attempt to hinder the field-aligned current with an insulator does not stop the current, but forces it to flow round the insulator. (15 refs.)

64324 Excitation of an electrostatic wave by a cold electron current sheet of finite thickness. K.S.Hwang, E.G.Fontheim, R.S.B.Ong (Dept. of Atmospheric & Oceanic Sci., Univ. of Michigan, Ann Arbor, MI, USA). *Planet. & Space Sci. (GB)*, vol.31, no.3, p.285-93 (March 1983). Electrostatic waves excited by a field-aligned electron current sheet of finite thickness are investigated. The finite width of the current sheet gives rise to boundary conditions to be satisfied at the sheet edge. This results in a restriction to the number of modes which may be driven unstable. Ducted and evanescent mode solutions are obtained. It is shown that the finite thickness of the current sheet partially stabilizes the system and contributes to the coherence of the excited waves. (17 refs.)

64325 Pc1 wave generation by sudden impulses. J.V.Olson, L.C.Lee (Geophys. Inst., Univ. of Alaska, Fairbanks, AK, USA). *Planet. & Space Sci. (GB)*, vol.31, no.3, p.295-302 (March 1983). Induction magnetometer data recorded at College, Alaska have been studied for the occurrence of ULF emissions associated with sudden impulses (SI). In this study the authors surveyed three years of data (1977-1979 inclusively) and found that for the 76 SIs reported in IAGA bulletins, 32 were found to be followed by ULF emissions in the College data. While the 76 SIs occurred at all local times those which were associated with ULF emissions at College peaked in occurrence near local noon. These observations are interpreted in terms of a simple model based upon a Chapman-Ferraro double-dipole model of the magnetosphere. Using this model an estimate of field compressions associated with SIs can be made and from this the increases in the temperature anisotropy and plasma beta may be estimated. This simple model predicts maximum growth rate near noon on high latitude field lines, just inside the magnetopause. Further, inspection of growth rate curves for varying plasma anisotropy and beta leads to the conclusion that an increase in anisotropy is the primary cause of the ULF emissions observed. (15 refs.)

64326 Quarter-wave ULF pulsations. W.Allan (Phys. & Engng. Lab., DSIR, Lower Hutt, New Zealand). *Planet. & Space Sci. (GB)*, vol.31, no.3, p.323-30 (March 1983). Recent theoretical work has predicted the possible existence of 'quarter-wave' ULF pulsation resonances, in which the wave electric field has a near-node in one ionosphere and an antinode in the conjugate ionosphere. Eigenvalues are derived for quarter-wave toroidal and guided poloidal resonances for a range of L-values and plasma density distributions. From these eigenvalues, resonant periods can be obtained. Three pulsation events with anomalously long periods (when interpreted as half-waves) are examined in the light of these results. It is decided that only one event is a good candidate for quarter-wave status; this event seems likely to be a driven resonance effectively in the quarter-wave guided poloidal mode. (28 refs.)

64327 The self-focusing of whistler waves. V.I.Karpman, R.N.Kaufman (IZMIRAN, Moscow, USSR). *Phys. Scr. (Sweden)*, vol.T2, no.1, p.252-61 (1982). (1982 International Conference on Plasma Physics, Goteborg, Sweden, 9-15 June 1982). A general Schrodinger equation describing the propagation of whistler waves along the magnetic field is obtained. On the basis of this equation and the magnetohydrodynamic plasma equations supplemented by the ponderomotive force of the whistler wave field, the self-focusing of whistler waves is considered. A family of stationary solutions describing the structures of self-focused wave beams both in density crests and troughs is found. It is shown that the beam propagating in density crest decays due to the wave tunnelling. Therefore, only the density troughs may result from the well-developed self-focusing of whistler wave parallel to the magnetic field. (16 refs.)

Exploration of the Polar Upper Atmosphere. Proceedings of the NATO Advanced Study Institute See Entry 59540

A theoretical study of the high latitude F region's response to magnetospheric storm inputs See Entry 64289

A dynamic model for the auroral field line plasma in the presence of field-aligned current See Entry 64290

Temperature of the plasmasphere determined from VLF observations at SANAE See Entry 64310

Total current to cylindrical collectors in collisionless plasma flow See Entry 64354

Active plasmas near planets and stars See Entry 64371

94.40 COSMIC RAYS

94.40C Origin and propagation outside the solar system

64328 Plasma in astrophysics. R.M.Kulsrud (Plasma Phys. Lab., Princeton Univ., Princeton, NJ, USA). *Phys. Scr. (Sweden)*, vol.T2, no.1, p.177-81 (1982). (1982 International Conference on Plasma Physics, Goteborg, Sweden, 9-15 June 1982). Two examples in which plasma theory is essential to the understanding of astrophysical phenomena are presented. These are magnetic reconnection and the collisionless interaction between a population of energetic particles and a cooler gas or plasma, in particular the interaction between galactic cosmic rays and the interstellar medium. (11 refs.)

64329 Distribution of cosmic rays and magnetic field in the galactic halo under conditions of hydrostatic equilibrium. A.Ghosh, V.S.Ptusk. *Pis'ma v Astron. Zh. (USSR)*, vol.9, no.2, p.90-3 (1983). In Russian. English translation in: *Sov. Astron. Lett. (USA)*
Cosmic ray diffusion in the Galaxy is considered within the condition of hydrostatic equilibrium. It is found that the size of the halo approximately equals 10 kpc. (16 refs.)

The origin of the nonthermal radio emission in normal disk galaxies See Entry 64539

94.40H Energetic solar particles and photons

64330 Gamma astronomy of the Sun and study of solar cosmic rays. B.M.Kuzhevskii (M.V. Lomonosov Moscow State Univ., Moscow, USSR). *Sov. Phys.-Usp. (USA)*, vol.25, no.6, p.392-408 (June 1982). Translation of: *Usp. Fiz. Nauk (USSR)*, vol.137, no.2, p.237-65 (June 1982). [received: April 1983]

A detailed discussion is given of the various nuclear reactions proceeding in the Sun's atmosphere under the influence of flare-accelerated particles. The role of such reactions in formation of the line spectrum and continuum of gamma-rays from the distributed and quiet Sun is discussed. The gamma-ray fluxes in individual lines and in the continuum are estimated. The possibility of applying data on gamma-ray emission from the Sun to analysis of particle acceleration in solar flares and the conditions of their ejection into interplanetary space is analyzed. (103 refs.)

Final state branching ratio in the ^7Be decay See Entry 60139

^7Be decay scheme and the solar neutrino problem See Entry 60140

Condensation nuclei events at 30 km and possible influences of solar cosmic rays See Entry 64334

Energetics of particles accelerated in solar flares See Entry 64450

94.40L Composition and energy spectra

64331 Neutron fraction in primary cosmic rays inferred from muon charge ratio. K.Kinoshita, A.Kuwazuru (Phys. Dept., Kagoshima Univ., Kagoshima, Japan).

Prog. Theor. Phys. (Japan), vol.69, no.1, p.354-7 (Jan. 1983).
The μ^+/μ^- ratio at sea level was calculated by using detailed parameterization of the accelerator data and the quark model for K^+ production from neutron beam. Quite a large fraction ($\approx 30\%$) of neutrons in primary flux is required to explain the observed ratio, if some unknown mechanisms are not introduced. (18 refs.)

64332 Theory of cosmic ray spectra. V.N.Tsytoich (P.N. Lebedev Phys. Inst., Moscow, USSR).

Phys. Scr. (Sweden), vol.T2, no.2, p.562-70 (1982). [received: April 1983]
(1982 International Conference on Plasma Physics, Goteborg, Sweden, 9-15 June 1982).

A new theory of cosmic ray spectra is presented which predicts the energy spectra for cosmic ions and electrons $\sim 1/\epsilon$, up to the highest possible ϵ in the spectra with the value of $\gamma=3$ very close to that observed (ϵ is the particle energy). The theory shows that the He^3 cosmic ions are preferentially created as compared to He^4 cosmic ions in coincidence with observations. The theory shows that the abundance of heavy ions in cosmic rays with $Z>20$ should be two orders of magnitude larger than the abundance of these elements in usual matter with agreement to observations. The theory gives the subcosmic ray ($\ll mc^2$) spectra $\sim 1/\epsilon$ (ϵ is the kinetic energy) and gives also the increase of the abundances or nonrelativistic but superthermal He^3 ions as compared to He^4 ions, which could be used to explain the increase in the abundances of He^3 in active solar regions. There are not any ad hoc assumptions in the theory; it is based on the well established resonant wave particle interactions in turbulent plasmas and especially the radiative effects in these interactions. (16 refs.)

64333 On the nature of low-energy antiprotons in cosmic rays. F.A.Agaronyan, S.R.Kel'ner, Yu.D.Kotov.

Pis'ma v Astron. Zh. (USSR), vol.9, no.2, p.102-7 (1983). In Russian. English translation in: *Sov. Astron. Lett. (USA)*

A model of the formation of the cosmic ray antiproton spectrum in a plasma consisting mainly of electron-positron pairs ($n_+ \approx n_- \gg 10$) is considered. Additional energy losses due to Coulomb collisions in the plasma provide significant increases of the antiproton flux in the energy range ≤ 1 GeV. (19 refs.)

The role of cosmic rays in the development of particle physics See Entry 59567

Development of the cosmic ray techniques See Entry 59568

Cosmic rays and particle physics at Berkeley See Entry 59572

Evolution of chemical abundances in massive stars. II. Abundance anomalies in Wolf-Rayet stars in relation with cosmic rays and ^{22}Ne in meteorites See Entry 64479

94.40R High-energy interactions

Observation of large deviations from the Bethe-Bloch formula for relativistic uranium ions See Entry 60558

How stable is our vacuum? See Entry 64563

94.40T Muons and neutrinos

Final state branching ratio in the ^7Be decay See Entry 60139

^7Be decay scheme and the solar neutrino problem See Entry 60140

Neutron fraction in primary cosmic rays inferred from muon charge ratio See Entry 64331

94.40V Cosmic-ray effects in meteorites and terrestrial matter

64334 Condensation nuclei events at 30 km and possible influences of solar cosmic rays. D.J.Hofmann, J.M.Rosen (Dept. of Phys. & Astron., Univ. of Wyoming, Laramie, WY, USA).

Nature (GB), vol.302, no.5908, p.511-14 (7 April 1983).
Two recent observations have provided the basis for study of a relationship between solar activity and the formation of small particles in the Earth's atmosphere: the discovery of annual increases of condensation nuclei (CN) at 30 km and the detection of sulphuric acid molecules in large negative ion clusters in the 25-35 km altitude region. These observations have now led the

authors to formulate and test a model wherein CN are formed in a 'polar cloud chamber' supersaturated with sulphuric acid vapour and triggered by ionisation associated with solar flare cosmic radiation. The authors conclude that such a model provides a potential explanation of the observations. (15 refs.)

94.60 INTERPLANETARY SPACE

(see also 96.60 Solar physics)

64335 Acceleration of low-energy protons and alpha particles at interplanetary shock waves. M.Scholer (Max-Planck-Inst. fur Phys. & Astrophys., Inst. fur Extraterrestrische Phys., Garching, Germany), F.M.Ipavich, G.Gloeckler, D.Hovestadt.

J. Geophys. Res. (USA), vol.88, no.A3, p.1977-88 (1 March 1983).

Low-energy protons and alpha particles have been investigated in the energy range 30 keV/charge to 150 keV/charge associated with three different interplanetary shock waves in the immediate preshock and postshock region. The data were obtained with the Max-Planck-Institut/University of Maryland sensor system on ISEE 3. In particular, the authors studied spatial distributions in the preshock and postshock medium as measured in the spacecraft frame and after transformation into the solar wind and the shock frame of reference, respectively, the dependence of the phase space density at different energies on distance from the shock, and the form of the distribution function of both species immediately at the shock. In the preshock region particles are flowing in the solar wind frame of reference away from the shock and in the postshock medium the distribution is more or less isotropic in this frame of reference. The mechanisms responsible for particle acceleration are discussed. (48 refs.)

64336 Jovian modulation of interplanetary electrons as observed with Voyagers 1 and 2. A.W.Schardt, F.B.McDonald, J.H.Trainor (Lab. for High Energy Astrophys., NASA Goddard Space Flight Center, Greenbelt, MD, USA).

J. Geophys. Res. (USA), vol.88, no.A3, p.1989-2000 (1 March 1983).

The release of magnetospheric electrons from Jupiter into interplanetary space is modulated by the Jovian rotation period. This effect was initially discovered by Pioneer 10, and the Voyager 1 and 2 observations permit a more detailed study of this modulation. It was found that the modulation period agrees on the average with the synodic period of Jupiter (9 h 55 min. 33.12 s), but over intervals of weeks it can differ from the synodic period by several minutes. The lack of exact synchronization is attributed to changes of the plasma population in the Jovian magnetosphere. Such changes affect the magnetic field sweep-back and departure from exact corotation. However, the magnetospheric asymmetry, which is responsible for the modulation, is always re-established at the same longitude. Thus no long term departures occur from the synodic period. The Jovian modulation appears to be a persistent feature of the interaction between the solar wind and the magnetosphere, and the disappearance of the modulation away from Jupiter is attributed to interplanetary propagation conditions. (28 refs.)

Plasma rest frame frequencies and polarizations of the low-frequency upstream waves: ISEE 1 and 2 observations See Entry 64312

Solar wind deceleration and MHD turbulence in the Earth's foreshock region: ISEE 1 and 2 and IMP 8 observations See Entry 64313

Ions upstream of the Earth's bow shock: a theoretical comparison of alternative source populations See Entry 64314

The oblique whistler instability in the Earth's foreshock See Entry 64315

Multiple transonic solutions with a new class of shock transitions in steady isothermal solar and stellar winds See Entry 64368

Active plasmas near planets and stars See Entry 64371

Ion implantation phenomena in space See Entry 64375

Solar System sputtering See Entry 64409

Comparison of measurements of electromagnetic induction in the magnetosphere of Venus with laboratory simulations See Entry 64411

94.80 AEROSPACE FACILITIES AND TECHNIQUES; SPACE RESEARCH

(see also 87.65 Aerospace biophysics and medical physics)

64337 On the choice of artificial satellites by their optimal location data for studying the Earth's rotation. V.T.Taradiy, G.T.Yanovitskaya.

Astrometriya & Astrofiz. (USSR), no.47, p.76-9 (1982). In Russian.
Numerical modeling of the influence of perturbing accelerations upon the parameters of satellite motion show that the high altitude satellites are the best for studying the Earth's rotation. (3 refs.)

64338 The HIPPARCOS space astrometry mission. M.A.C.Perryman (Space Sci. Dept., ESA, ESTEC, Noordwijk, Netherlands).
Adv. Space Res. (GB), vol.2, no.4, p.51-8 (1982). (Proceedings of Symposium 4 of the COSPAR Twenty-Fourth Plenary Meeting, Ottawa, Canada, 16 May-2 June 1982).

The scientific aim of ESA's space astrometry mission HIPPARCOS is the accurate determination of astrometric data for a large number of celestial bodies. A complete survey of all stars down to about $B=8.9$ mag is presently anticipated, along with a selection of stars down to the limiting magnitude of about $B=13$ mag, chosen by virtue of their particular astrometric or astrophysical importance. At the same time a supplementary stellar catalogue, TYCHO, will be generated. This will contain astrometric data (positions tied to the HIPPARCOS system with an accuracy of 0.05 arcsec or better) and photometric data for all stars down to about $B=11.2$ mag, thus comprising some 400000 or more additional stars. A summary of the principal scientific objectives, a description of the payload, and an overview of the scientific coordination and of the processing of the scientific data is presented. (3 refs.)

64339 Planned NASA space infrared astronomy experiments. G.G.Fazio (Harvard-Smithsonian Center for Astrophys., Cambridge, MA, USA).
Adv. Space Res. (GB), vol.2, no.4, p.97-106 (1982). (Proceedings of Symposium 4 of the COSPAR Twenty-Fourth Plenary Meeting, Ottawa, Canada, 16 May-2 June 1982).

A summary is presented of the present status of the NASA space infrared astronomy program. Projects described include the Infrared Astronomy Satellite (IRAS), Small Infrared Telescope on Spacelab 2 (IRT), Cosmic Background Explorer (COBE), Shuttle Infrared Telescope Facility (SIRTF), Space Telescope (ST), and the Large Deployable Reflector (LDR). The important technical developments achieved in these programs are also discussed, as well as critical needs for future missions. (17 refs.)

64340 The Comet Halley flyby IR sounder 'IKS'. M.Arduini (Lab. de Phys. Stellaire et Planetaire, Verrieres-le-Buisson, France), J.P.Bibring, S.Cazes, M.Combes, N.Coron, J.F.Crifo, T.Encrenaz, R.Gispert, D.Harduin, J.M.Lamarre, D.Malaisé.

Adv. Space Res. (GB), vol.2, no.4, p.113-22 (1982). (Proceedings of Symposium 4 of the COSPAR Twenty-Fourth Plenary Meeting, Ottawa, Canada, 16 May-2 June 1982).

An infrared sounder is being developed in France to observe in 1986 Comet Halley from the Soviet 'VEGA' flyby probes. The instrument called 'IKS' has three measuring channels. Two of these channels will provide the spectrum of the comet emission in the spectral intervals 2.5-5.0 μ and 6-12 μ , at a constant resolution $\lambda/\Delta\lambda=50$. The third channel analyzes the comet I.R. image at a spatial frequency of about 1 arc minute⁻¹. It is hoped that (1) most primary simple molecules emitted by the nucleus will be identified; (2) the chemical composition and perhaps crystalline structure of the dust grains and ices released by the comet will be derived; and (3) the diameter of the nucleus and its brightness temperatures will be measured. (6 refs.)

64341 GIRL—the German Infrared Laboratory for Spacelab. D.Lemke (Max-Planck-Inst. Astron., Heidelberg, Germany), M.Grewing, D.Offermann, S.Drapatz, Klipping, G..

Adv. Space Res. (GB), vol.2, no.4, p.123-30 (1982). (Proceedings of Symposium 4 of the COSPAR Twenty-Fourth Plenary Meeting, Ottawa, Canada, 16 May-2 June 1982).

GIRL is a liquid helium cooled 50 cm telescope equipped with four focal plane instruments dedicated to astronomical and aeronomical observations. These instruments, a detector array, a photopolarimeter, an Ebert-Fastie-spectrometer and a Michelson-interferometer make up an 'infrared observatory'; having high sensitivity and high spectral and spatial resolution. Si:Ga-, Si:Sb-, Si:As-, Si:P-, Ge:Be-, Ge:Cu- and Ge:Ga-detectors with NEP-values as low as 3×10^{-17} W Hz^{-1/2} have been tested and will be used to cover the wavelength range 3..120 μ m. A full size 'thermal model' of the GIRL cryostat containing 300 l of superfluid helium at 1.6K has been tested at the industrial prime contractor MBB. Several new techniques for cold telescopes are used in GIRL, for instance a glass ceramics primary mirror, a low power chopping secondary and an active helium phase separator. (8 refs.)

64342 The Extreme Ultraviolet Explorer. S.Bowyer (Astron. Dept., Univ. of California, Berkeley, CA, USA).

Adv. Space Res. (GB), vol.2, no.4, p.157-65 (1982). (Proceedings of Symposium 4 of the COSPAR Twenty-Fourth Plenary Meeting, Ottawa, Canada, 16 May-2 June 1982).

The Extreme Ultraviolet Explorer (EUVE) Mission is described. The purpose of this mission is to search the celestial sphere for astronomical sources of extreme ultraviolet (EUV) radiation (100-1000 Å). The search will be accomplished with the use of three EUV telescopes, each sensitive to different bands within the EUV band. A fourth telescope will perform a high sensitivity search of a limited sample of the sky in a single EUV band. In six months, the entire sky will be scanned at a sensitivity level comparable to existing surveys in other more traditional astronomical bandpasses. A substantial number of EUV sources such as hot white dwarfs and stellar coronae are certain to be discovered given our current knowledge. More uncertain is what entirely new classes of objects will be discovered as EUV sources. A moderate resolution (~5 Å) spectroscopy option is being considered which would cover the band from 80 to 600 Å. (36 refs.)

64343 The ROSAT mission. J.Trumper (Max-Planck-Inst. für Phys. und Astrophys., Garching, Germany).

Adv. Space Res. (GB), vol.2, no.4, p.241-9 (1982). (Proceedings of Symposium 4 of the COSPAR Twenty-Fourth Plenary Meeting, Ottawa, Canada, 16 May-2 June 1982).

A primary scientific objective of the ROSAT mission is to perform the first all-sky survey with an imaging X-ray telescope leading to an improvement in sensitivity by several orders of magnitude compared with previous surveys. A large number of new sources ($\geq 10^4$) will be discovered and located with an accuracy of 1 arcmin or better. After completion of the survey which will take half a year the instrument will be used for detailed observations of selected sources with respect to spatial structure, spectra and time variability. In this mode which will be open for guest observers ROSAT will provide substantial improvement over the imaging instruments of the Einstein observatory. The main ROSAT telescope consists of a fourfold nested mirror system with 83 cm aperture having three focal plane instruments. Two of them will be imaging proportional counters (0.1-2 keV) providing a field of view of 2°, an angular resolution of $\approx 30''$ in the pointing mode and a spectral resolution $\Delta E/E \approx 45\%$ FWHM at 1 keV. The third focal instrument will be a high resolution imager (≈ 320). (15 refs.)

64344 AXAF, a permanent orbiting X-ray observatory: telescope and instrumentation plans. M.V.Zombeck (Harvard-Smithsonian Center for Astrophys., Cambridge, MA, USA).

Adv. Space Res. (GB), vol.2, no.4, p.259-70 (1982). (Proceedings of Symposium 4 of the COSPAR Twenty-Fourth Plenary Meeting, Ottawa, Canada, 16 May-2 June 1982).

The Advanced X-ray Astrophysics Facility (AXAF) now under study is to be a long-lived X-ray observatory in space. It is to be launched by the Space Shuttle, maintainable on-orbit, and retrievable for ground refurbishment. The AXAF is conceived as an X-ray telescope with 6 nested grazing incidence X-ray mirrors (with a maximum aperture of 1.2 m) and interchangeable and replaceable focal plane instruments. The optics will provide 0.5 arcsecond imagery over a several arcminute field and somewhat reduced resolution over 1 degree in the X-ray band from 0.1 to 10 keV (1.2 to 120 Å). The characteristics and expected performance of the observatory are described. (7 refs.)

64345 X-ray astronomy from the Space Shuttle. D.McCammon (Phys. Dept., Univ. of Wisconsin, Madison, WI, USA).

Adv. Space Res. (GB), vol.2, no.4, p.271-9 (1982). (Proceedings of Symposium 4 of the COSPAR Twenty-Fourth Plenary Meeting, Ottawa, Canada, 16 May-2 June 1982).

A wide variety of new X-ray instrumentation is being proposed to attack an even wider variety of astrophysical problems. It includes general-purpose instruments which, with further development and testing, may someday be part of the complement of an orbiting 'observatory' facility, such as AXAF. Other instruments promise significant and often necessary advantages for a narrower range of problems. The testing and development of all of these ideas, and in particular finding an efficient way to employ the latter class to make the observations for which they are intended, pose dilemmas for which the Space Shuttle potentially offers solutions. A discussion of possible modes for using the Shuttle and a brief sampling of new instrumentation ideas are presented. (18 refs.)

64346 Japanese satellite programs in X-ray astronomy. S.Miyamoto (Dept. of Phys., Osaka Univ., Osaka, Japan).

Adv. Space Res. (GB), vol.2, no.4, p.285-91 (1982). (Proceedings of Symposium 4 of the COSPAR Twenty-Fourth Plenary Meeting, Ottawa, Canada, 16 May-2 June 1982).

Future programs of X-ray astronomy in Japan are described. Following the Hakucho satellite, ASTRO-B and ASTRO-C are under preparation. ASTRO-B, to be launched in early 1983, is designed for the study of X-ray spectra and variability of X-ray sources. It is equipped with gas scintillation proportional counters of total area 1000 cm², one dimensional X-ray focusing collectors, transient source monitors and a gamma-ray burst monitor. ASTRO-C will be launched in 1987 to study the time variability of cosmic X-ray sources with high statistical accuracies. The main emphasis is placed not only on the accurate timing analysis of the galactic sources but on the investigation of the time variability of active galactic nuclei. This satellite will be equipped with large area, low background proportional counters of total area of about 5000 cm², an all sky monitor and a gamma-ray burst detector. (4 refs.)

64347 Instruments for X-ray astronomy. S.L.Mandelstam (P.N. Lebedev Phys. Inst., Acad. of Sci., USSR), V.G.Kurt, B.I.Valnicek, L.A.Vainstein, E.K.Sheffer, V.A.Slemzin, I.A.Zhitnik.

Adv. Space Res. (GB), vol.2, no.4, p.293-9 (1982). (Proceedings of Symposium 4 of the COSPAR Twenty-Fourth Plenary Meeting, Ottawa, Canada, 16 May-2 June 1982).

Describes instruments for galactic-extragalactic and solar X-ray astronomy. (no refs.)

64348 X-ray Timing Explorer. H.Bradt (Center for Space Res., Dept. of Phys., MIT, Cambridge, MA, USA).

Adv. Space Res. (GB), vol.2, no.4, p.315-21 (1982). (Proceedings of Symposium 4 of the COSPAR Twenty-Fourth Plenary Meeting, Ottawa, Canada, 16 May-2 June 1982).

The payload for the US X-ray Timing Explorer is currently being selected by NASA. Some of the possible instrumental capabilities and scientific objectives of the mission are described. (14 refs.)

64349 Photometric apparatus 'Duga' for investigating Polar auroras and tropical arcs from onboard the orbital station 'Salyut-6'. N.P.Petkov, M.M.Gogoshev, S.I.Sargoichev.

C.R. Acad. Bulg. Sci. (Bulgaria), vol.35, no.9, p.1229-32 (1982). In Russian.

A description and schematic circuit diagrams are given of an electrophotometric apparatus, designated 'Duga', and designed and constructed for installation on the Soviet orbiting space station, 'Salyut-6' as part of the equipment for investigation optical effects in the upper atmosphere such as the polar auroras and the tropical and equatorial arcs. The operation of the optical part of 'Duga' is based on the use of a double-filter method, whereby the spectral background around each emission line is measured by means of the change in the angle of inclination of the filter. In addition to determining the spectral characteristics of the observed atmospheric phenomena, the apparatus also enables their spatial coordinates to be recorded. Within the period May 1979 to Sept. 1980 the 'Duga' apparatus was used in about 30 sessions of observation, the results of which confirmed the validity of the observation method. (4 refs.) A.J.B.

64350 Spacecraft attitude sensing based on the Earth's radiation. L.Fraiture (European Space Operations Centre, Darmstadt, Germany).

ESA Bull. (France), no.33, p.29-36 (Feb. 1983).

Spacecraft payloads usually have to be oriented towards specific targets and in many cases very accurate attitude parameters must be calculated. The Earth itself constitutes an obvious inertial reference, and one means of determining the absolute orientation of the spacecraft's axes is to observe the Earth's radiation by means of optical sensors working at visible or, more frequently, infrared wavelengths. Some key albedo and infrared sensors used in ESRO/ESA spacecraft are surveyed pointing out that these sensors work successfully up to altitudes of 30000 km, and are considerably less complex than the alternative star sensors. (no refs.)

64351 Earth-return trajectory options for the 1985-86 Halley opportunity. R.W.Farquhar, D.W.Dunham (NASA Goddard Space Flight Center, Greenbelt, MD, USA).

J. Astronaut. Sci. (USA), vol.30, no.4, p.307-28 (Oct.-Dec. 1982). [received: March 1983]

A unique and useful family of ballistic trajectories to Halley's comet is described. The distinguishing feature of this family is that all of the trajectories return to the Earth's vicinity after the Halley intercept. It is shown that, in some cases, the original Earth-return path can be reshaped by Earth-swingby maneuvers to achieve additional small-body encounters. The Earth-return trajectory technique also provides an opportunity for a low-cost Halley sample-return mission. Dust and gas samples are collected during the high-velocity flythrough of Halley, and then returned to a high-apogee Earth orbit. Aerobraking maneuvers are used to bring the sample-return spacecraft to a low-altitude circular orbit where it can be recovered by the Space Shuttle. (16 refs.)

64352 Navigation system design for a Halley sample return mission. L.J.Wood, S.L.Craig, D.K.Yeomans, M.J.Bergam (Jet Propulsion Lab., California Inst. of Technol., Pasadena, CA, USA).

J. Astronaut. Sci. (USA), vol.30, no.4, p.329-46 (Oct.-Dec. 1982). [received: March 1983]

A ballistic sample return mission to Comet Halley was recently considered by the United States. The authors describe the navigation system and the navigation strategy which would have been employed in such a mission, assuming a launch in August of 1985, an arrival at the comet in March of 1986, and a return to Earth in August of 1989. Estimates of spacecraft comet- and Earth-relative orbit determination accuracies are presented as functions of time. Target-relative delivery accuracies for the spacecraft and associated trajectory correction maneuver requirements are presented also. (16 refs.)

64353 Position parameter estimation for slit-type scanning sensors. J.W.Fowler, E.G.Rolfé (Jet Propulsion Lab., California Inst. of Technol., Pasadena, CA, USA).

J. Astronaut. Sci. (USA), vol.30, no.4, p.385-402 (Oct.-Dec. 1982). [received: March 1983]

When a celestial source of electromagnetic radiation is detected by a slit-type scanning sensor, the position deduced for it will generally have an error whose statistical description is nongaussian. This must be taken into account in the formulation of an optimal estimation technique for these positions. The authors describe such a technique, including methods for deciding whether separate detections stem from a single common source and methods for combining multiple detections to obtain refined estimates of source positions. (8 refs.)

64354 Total current to cylindrical collectors in collisionless plasma flow. R.Godard, J.G.Laframboise (Phys. Dept., York Univ., Toronto, Canada). *Planet. & Space Sci. (GB)*, vol.31, no.3, p.275-83 (March 1983). A theory is presented for charged-particle collection by a cylindrical conducting object, such as a spacecraft or an electrostatic probe, which is moving transversely through a collisionless plasma, such as those in the upper atmosphere and space. The calculation is approximate, using symmetric potential profiles which are exact for the infinite-cylinder stationary case. Theoretical current predictions are presented for ratios of collector potential to electron thermal energy $e\phi_c/kT_e$ from 0 to -25, for ion-to-electron temperature ratios $T_i/T_e=1$ and 0.5, ratio of collector radius to electron Debye length r_c/λ_D from 0 to 100, and ratio of flow speed to ion thermal speed $S_i=U/(2kT_i/m_i)^{1/2}$ from 0 to 10. Comparisons with existing exact calculations by other authors show that none of these fulfil all of the requirements for nontrivial comparison. Appropriate parameter ranges for future exact calculations are thereby suggested. (31 refs.)

64355 Some geometric expressions for the observation by means of a spinning satellite. T.Kohno (Inst. of Phys. & Chem. Res., Saitama, Japan). *Rep. Inst. Phys. & Chem. Res. (Japan)*, vol.58, no.6, p.105-16 (1982). In Japanese.

Some spherical geometric expressions needed for the observation by means of a spinning satellite or a rocket are obtained. One needs the geometric relations between the field of view and the direction of the geomagnetic field or the location of the Earth for the observation of the radiations such as charged particles or X-rays. Further, in case of the observation of X-rays emitted from a local area of the Earth or the Earth's atmosphere, it is necessary to get the location of the point which corresponds to the line of sight in the field of view. In addition to their mathematical expressions, some calculated results for the scientific satellite 'HINOTORI' will be presented. (1 ref.)

Proceedings of Symposium 4 of the COSPAR Twenty-Fourth Plenary Meeting See Entry 59524

Space adapted cryogenics See Entry 59787

Calibration system for satellite and rocket-borne ion mass spectrometers in the energy range from 5 eV/charge to 100 keV/charge See Entry 59875

Space plasma diagnostics See Entry 61705

Probe experiment for measurement of plasma parameters and ion drift velocities in the ionospheric plasma onboard the Intercosmos-Bulgaria 1300 satellite See Entry 64241

Microwave systems for satellite remote sensing See Entry 64275

On the extraction of atmospheric turbulence parameters from radar backscatter Doppler spectra. I. Theory See Entry 64279

Mesospheric turbulence intensities measured with a HF radar at 35°S. II See Entry 64280

Atmospheric scattering effects on ground-based measurements of thermospheric winds See Entry 64281

Incoherent scatter observations of mid-latitude sporadic-E and comments on its data analysis See Entry 64294

Optimization of equatorial transfer orbit with due regard for atmospheric drag See Entry 64358

How to achieve diffraction limited resolution with large space telescopes See Entry 64379

FLUTE or TRIO: different approaches to optical arrays in space See Entry 64380

Solar radiometry: spectral irradiance measurements See Entry 64381

Solar radiometry: total irradiance measurements See Entry 64382

X-ray imaging techniques—modulation collimator and coded mask See Entry 64383

The Pinhole/Occluder Facility See Entry 64384

Atomic clocks for astrophysical measurements See Entry 64390

A navigation model for the Venusian atmosphere See Entry 64410

94.90 OTHER TOPICS IN SPACE PHYSICS

Exploration of the Polar Upper Atmosphere. Proceedings of the NATO Advanced Study Institute See Entry 59540

95.00 FUNDAMENTAL ASTRONOMY AND ASTROPHYSICS, INSTRUMENTATION AND TECHNIQUES AND ASTRONOMICAL OBSERVATIONS

95.10 FUNDAMENTAL ASTRONOMY

64356 On the catalogue of the stars positions in the NPZT programme. S.Sadzhakov, M.Dachich, D.Shaletich. *Astrometriya & Astrofiz. (USSR)*, no.48, p.58-9 (1983). In Russian. The paper deals with compilation of the catalogue of the NPZT stars in Beograd. Some characteristics of this catalogue are given. The catalogue has been already used in compiling the general catalogue of the NPZT stars by Yasuda. (no refs.)

64357 On investigation of the magnitude equation. G.A.Ivanov. *Astrometriya & Astrofiz. (USSR)*, no.48, p.59-63 (1983). In Russian. The reasons for the magnitude equation in photographic astrometry are considered. The methods are described for investigation of this error using the plates of the Kapteyn field at different hour angles taken by the double long-focus astrograph at the Main Astronomical Observatory (Kiev). The results of the determination of magnitude equation values obtained with application of a diffraction grating and without it are in good agreement. (2 refs.)

64358 Optimization of equatorial transfer orbit with due regard for atmospheric drag. V.S.Novoselov. *Vestn. Leningr. Univ. Ser. Mat. Mekh. & Astron. (USSR)*, no.1, p.92-9 (Jan. 1983). In Russian. An optimal two-impulse coplanar transfer between near-circular equatorial orbits is constructed by taking into account the atmospheric drag and Earth oblateness. (4 refs.)

Time adjustment on 1983 June 30 See Entry 64020

Comparison of Earth rotation as inferred from radio interferometric, laser ranging and astrometric observations See Entry 64265

The HIPPARCOS space astrometry mission See Entry 64338

On the effect of systematic errors of proper stellar motion on determination of solar motion parameters See Entry 64402

Variance and correlations of errors of rectangular coordinates for the selenodetic reference points See Entry 64404

Accuracy of the outer orientation in the selenodetic coordinate system See Entry 64405

Determination of the orientation angles of the selenodetic coordinates system based on the photographic positional observations of the Moon See Entry 64406

No occultations by Uranus II and Pluto See Entry 64423

Supernovae See Entry 64494

Supernovae See Entry 64495

95.10C Celestial mechanics

(for dynamics and kinematics of stellar systems, see 98.10)

64359 Theory for the motion of the four large planets. The solution TOP82. J.L.Simon (Bureau des Longitudes, CNRS, Paris, France).

Astron. & Astrophys. (Germany), vol.120, no.2, pt.2, p.197-202 (April 1983). The TOP82 solution is obtained from a theory of the four large planets which has been adjusted to the numerical integration DE200. The variables used are $a, \lambda, E, e, \omega, \Omega$. The theory includes the perturbations developed up to the third order of the masses for the four large planets. Perturbations up to the seventh order obtained by harmonic analysis, using an iterative process complete the theory for the couple Jupiter-Saturn. The comparison to an internal numerical integration over 1000 yr shows the accuracy obtained. The TOP82 solution is described and the perturbations of the four large planets by the inferior planets computed by Bretagnon (1982) and the relativistic perturbations expressed in isotropic and standard coordinates are presented. Adjustment to the numerical integration of the JPL DE200 (Standish, 1982) gives the constants of integration. The differences TOP82-DE200, over one century are given, for the four large planets, for the heliocentric longitude, the heliocentric latitude and the radius vector. Finally, the author gives the mean elements connected to the fixed J2000.0 ecliptic and the mean elements connected to the ecliptic of the date. (8 refs.)

64360 An empirical initial estimate for the solution of Kepler's equation. B.V.Sheela (Mission Operations & Planning Div., ISRO Satellite Centre, Bangalore, India). *J. Astronaut. Sci. (USA)*, vol.30, no.4, p.415-19 (Oct.-Dec. 1982). [received: March 1983]

An empirical formula is presented for an efficient initial estimate for the iterative solution of Kepler's equation. This formula is essentially a polynomial in eccentricity and mean anomaly whose coefficients have been obtained by minimizing the sum of the squared differences of the actual and calculated eccentric anomaly corresponding to a wide range of points in the $M-e$ plane. The efficiency in terms of the number of iterations for convergence is discussed along with comparisons with those of other starting formulas. (5 refs.)

Earth-return trajectory options for the 1985-86 Halley opportunity See Entry 64351

Navigation system design for a Halley sample return mission See Entry 64352

Optimization of equatorial transfer orbit with due regard for atmospheric drag See Entry 64358

Accuracy of the outer orientation in the selenodetic coordinate system See Entry 64405

A second order Jupiter-Saturn planetary theory. I See Entry 64419

The elimination of the critical terms of a first order Uranus-Neptune theory through Hori's method. I See Entry 64424

95.30 FUNDAMENTAL ASPECTS OF ASTROPHYSICS

64361 Comptonization effects in spherical accretion onto black holes. J.R.Ipser (Dept. of Phys., Univ. of Florida, Gainesville, FL, USA), R.H.Price. *Astrophys. J. (USA)*, vol.267, no.1, pt.1, p.371-83 (1 April 1983).

For spherical accretion of gas onto a black hole, dissipative heating (from magnetic reconnection, dissipation of turbulence, etc.) leads at high accretion rates to densities and temperatures at which Comptonization unavoidably plays an important role, both in determining gas temperature and in forming the emergent spectrum. The authors find approximate descriptions of some observational features of such astrophysical objects with a simple, yet justifiable, Ansatz that evades the complexities of nonlocality. A very natural connection between the ratio of luminosity to Eddington luminosity and the hardness of X-ray spectra emerges, suggesting that the observed X-ray hardness ratios of luminous sources are a consequence of those sources being more or less Eddington limited. (23 refs.)

64362 Gravitational lens effects of neutrino astronomical objects. Xu Chongming, Wu Xuejun (Dept. of Phys., Fudan Univ., Shanghai, China). *Astron. & Astrophys. (Germany)*, vol.120, no.1, pt.1, p.15-20 (April 1983). Neutrino astronomical objects are discussed as transparent gravitational lenses. The trajectory of a light ray emitted from the source which is located either outside or inside the transparent isotropic astronomical object is obtained by means of the solution of the geodesic equations. (If the source tends to infinity, the trajectory corresponds to the ordinary deflection of light by the Sun.) Furthermore, the brightness amplification ratio K is derived from the redistribution of intensity due to the gravitational lens effects. The amplification K is computed in the metric of a star of uniform density. K can reach a value of five hundred under some conditions. Finally, it is suggested that some quasars may be the sources in neutrino astronomical objects. (29 refs.)

64363 Hydrogen at high pressures and temperatures. M.Robnik, W.Kundt (Inst. für Astrophys., Univ. Bonn, Bonn, Germany). *Astron. & Astrophys. (Germany)*, vol.120, no.2, pt.2, p.227-33 (April 1983). The authors assess the degree of ionization, and equation of state of hydrogen above the dissociation temperature $T_{\text{dis}}=4.47$ eV/k. A vapour-liquid-like phase transition is found below a (second) critical point at $(T_c, \rho_c)=(1.9 \cdot 10^4 \text{ K}, 2.4 \cdot 10^{11} \text{ dyn cm}^{-2})$. At the transition, the degree of ionization changes almost discontinuously. The low-density phase is almost non-degenerate whereas the high-density phase is almost completely degenerate, i.e. can be

identified with liquid metallic hydrogen. An updated phase diagram is presented. (25 refs.)

64364 An exact solution for an isothermal gas cloud with fast differential rotation. F.Schmitz (Inst. für Theoretische Astrophys., Univ. Heidelberg, Heidelberg, Germany). *Astron. & Astrophys. (Germany)*, vol.120, no.2, pt.2, p.234-6 (April 1983). Properties of an isothermal self-gravitating gas cloud with fast differential rotation, infinite extension, a flattened density distribution, and finite central density are discussed. It is described by a simple exact solution of the equations of structure of self-gravitating and rotating gaseous masses. These are transformed to a simple differential equation which seem appropriate for search of exact solutions. Further attempts to find other exact solutions are discussed. (11 refs.)

64365 Atomic calculations for Ca XVII; UV and X-ray lines. A.K.Bhatia, H.E.Mason (Lab. for Astron. & Solar Phys., Goddard Space Flight Center, NASA, Greenbelt, MD, USA). *Astron. & Astrophys. Suppl. Ser. (France)*, vol.52, no.1, p.115-24 (April 1983). Energy levels, transition probabilities, collision strengths (distorted wave) are obtained for the configurations $2s^2$, $2s2p$, $2p^2$, $2s3s$, $2s3p$ and $2s3d$ and $2s3d$ configurations of Ca XVII. The theoretical intensity ratios for the UV and X-ray lines are compared with observed intensities in solar flare spectra. (19 refs.)

64366 Magnetohydrodynamic Universe corresponding to a Kantowski-Sachs metric. M.Bray. *C.R. Seances Acad. Sci. Ser. II (France)*, vol.296, no.4, p.221-4 (31 Jan. 1983). In French. Presents some exact solutions of the Einstein system for a MHD energy-momentum tensor generating a Kantowski-Sachs metric. (2 refs.)

64367 Accelerator simulation of astrophysical processes. T.A.Tombrello (W.K. Kellogg Radiation Lab., California Inst. of Technol., Pasadena, CA, USA). *IEEE Trans. Nucl. Sci. (USA)*, vol.ns-30, no.2, p.1169-72 (April 1983). (1982 IEEE Conference on the Application of Accelerators in Research and Industry, Denton, TX, USA, 8-10 Nov. 1982). The interaction of energetic ions with matter is responsible for many of the processes by which the elements were synthesized, energy is generated in stars, interstellar grains are destroyed, and molecules are created in space. All of these processes are amenable to simulation in the laboratory using accelerated ion beams, which allows a more comprehensive understanding of nature than one could obtain by observation alone. In addition, ion beam techniques are extremely useful in the determination of the elemental and isotopic abundances that arise from astrophysical nuclear synthesis. (20 refs.)

64368 Multiple transonic solutions with a new class of shock transitions in steady isothermal solar and stellar winds. S.R.Habbal, K.Tsinganos (Harvard-Smithsonian Center for Astrophysics, Cambridge, MA, USA). *J. Geophys. Res. (USA)*, vol.88, no.A3, p.1965-75 (1 March 1983). A new class of shock transitions are shown to arise in the transonic solutions of the steady isothermal solar wind equations when, for example, momentum deposition gives rise to multiple critical points in the flow. These shock transitions between critical solutions occur for a certain range of the parameters characterizing the momentum deposition function. In the presence of such shock transitions, the isothermal wind equations admit multiple transonic solutions, namely a continuous solution passing through an inner critical point and solutions involving a shock transition between critical solutions. These multiple transonic solutions have the same flow speed at the base but different supersonic flow speeds at infinity. The physical relevance of these properties for astrophysical systems such as the inner solar wind, extragalactic jet flows and accretion discs are discussed. (28 refs.)

64369 Electron-impact excitation of the Cameron system ($a^3\pi \rightarrow X^1\Sigma$) of CO. P.W.Erdman, E.C.Zipf (Dept. of Phys. & Astron., Univ. of Pittsburgh, Pittsburgh, PA, USA). *Planet. & Space Sci. (GB)*, vol.31, no.3, p.317-21 (March 1983). Studies the excitation of the Cameron bands of carbon monoxide ($a^3\pi \rightarrow X^1\Sigma$) by electron impact on CO and CO₂. This investigation was prompted by a recent study of the Martian airglow by Conway (1981) who concluded that the cross section for the dissociative excitation of the Cameron bands is seven times larger than the laboratory value reported by Ajello (1971a) and by a perplexing inconsistency between the optical cross section and CO($a^3\pi$) time-of-flight experiments. The present authors found that three factors have contributed to these discrepancies: (1) spectral contamination of the (1,4) Cameron band used by Ajello to normalize the entire Cameron band cross section, (2) major revisions in the magnitude of the CO($a^3\pi$) radiative lifetime, and (3) new insights into the effects of the CO($a^3\pi$) velocity distribution on the field of view of the emission experiments. The new results suggest that the calculated photoelectron fluxes in the Martian atmosphere may be too large by a factor of 3. (12 refs.)

64370 Is the local monopole flux enhanced? K.Freese, M.S.Turner (Astron. & Astrophysics Center, Univ. of Chicago, Chicago, IL, USA). *Phys. Lett. B (Netherlands)*, vol.123B, no.5, p.293-8 (7 April 1983). Dimopoulos et al. (1982) have suggested that a cloud of monopoles orbiting the Sun may significantly enhance the local monopole flux relative to the average flux in the Galaxy. The present authors have studied this scenario in detail and find that if the magnetic fields of strength $O(100 m_{16} \text{ kG})$ exist inside the Sun, then monopoles passing through the Sun can be captured into orbit, leading to a local enhancement of at most $O(50 m_{16}^2)$ (monopole mass = $m_{16} 10^{16} \text{ GeV}$). Monopoles of mass 10^{16} GeV can also be captured into orbit by passing through Jupiter, this leads to a local enhancement of $O(1.1-3)$. (12 refs.)

64371 Active plasmas near planets and stars. K.Schindler (Ruhr-Univ. Bochum, Bochum, Germany). *Phys. Scr. (Sweden)*, vol.T2, no.1, p.163-8 (1982). (1982 International Conference on Plasma Physics, Göteborg, Sweden, 9-15 June 1982). There are many processes in nature that correspond to the following scheme. During a passive quasi-stationary time-variation suddenly critical conditions are reached, which lead to the onset of an active dynamic phase. Here the terms 'passive' and 'active' indicate whether or not the process is predominantly driven by external variations. Typically, free energy is slowly accumulated during the passive phase and is rapidly released during activity. The point of onset of the active phase can usually be associated with some kind of instability or nonequilibrium condition. There is increasing evidence indicating that prominent space and astrophysics processes belong to this general class of phenomena. The author discusses relevant aspects of two major examples of such phenomena that belong to the Solar System, i.e. geomagnetic and solar activity. (36 refs.)

64372 Recent topics in physics of hot plasmas in space environment. A.Hasegawa (Bell Labs., Murray Hill, NJ, USA). *Phys. Scr. (Sweden)*, vol.T2, no.1, p.223-7 (1982). (1982 International Conference on Plasma Physics, Göteborg, Sweden, 9-15 June 1982). A brief review is presented on the subject of recent interest in physics of hot plasmas in space environment. The subjects chosen are the double layer, the reconnection of magnetic line of force, and Jupiter's magnetosphere. (34 refs.)

64373 A review of double layer simulations. R.A.Smith (Sci. Applications Inc., McLean, VA, USA). *Phys. Scr. (Sweden)*, vol.T2, no.1, p.238-51 (1982). (1982 International Conference on Plasma Physics, Göteborg, Sweden, 9-15 June 1982). A critical review of numerical simulations of plasma double layers is presented. Physical aspects of the double-layer problem are discussed, together with numerical methods appropriate to treat them. Particular emphasis is given to examining boundary conditions and their effect on the physical dynamics. Some physical processes currently thought to be important for double layers are discussed, and the simulation results are described with particular emphasis on their relation to these concepts. The review concludes with an interpretive discussion of the results, together with comments on their applicability to laboratory situations and to double layers in space. (60 refs.)

64374 A stationary free boundary problem for a circular flow with or without surface tension. H.Okamoto (Dept. of Maths., Univ. of Tokyo, Japan). *Proc. Jpn. Acad. Ser. A (Japan)*, vol.58, no.10, p.422-4 (Dec. 1982). The author considers a free boundary problem which is a model for a flow round a planet. The flow is hence circular, and the fluid is taken as perfect and irrotational. (3 refs.)

64375 Ion implantation phenomena in space. J.-P.Bibring, F.Rocard (Lab. Rene Bernas, CSNSM, Orsay, France). *Radiat. Eff. (GB)*, vol.65, no.1-4, p.159-65 (1982). (Proceedings of the First International Conference on 'Radiation Effects in Insulators', Arco, Largo di Garda, Italy, 1981). Particle-grain interactions at implantation energies occur in a large variety of astrophysical sites. The expected physical, chemical and isotopic effects are discussed, as deduced from the analyses of (i) lunar grains implanted with the solar wind ions, and (ii) terrestrial grains implanted in the lab with H, C, N, ..., ions. Special emphasis is placed on the amorphisation and the erosion of the grains, and on the synthesis of radicals and molecules within the implanted grains. Implications in planetology and astrophysics are presented. (21 refs.)

Relativistic astrophysics See Entry 59551
On the structure of space, time and field See Entry 59651
Upper limits to fermion masses in the Glashow-Weinberg-Salam model See Entry 59975
Final state branching ratio in the ^7Be decay See Entry 60139
 ^7Be decay scheme and the solar neutrino problem See Entry 60140
Radioactive ion beams for studying astrophysical nuclear reactions See Entry 60510
Atomic calculations for the Fe XX X-ray lines See Entry 60637
Arc measurements of Fe II transition probabilities See Entry 60648
Effective potential description and long wavelength structure of three-point correlations in strongly coupled plasmas See Entry 61604
Recent development in the statistical theory of high-density plasma See Entry 61612
Possibility of amorphous glassy state in astrophysical dense plasmas See Entry 62441
Plasma in astrophysics See Entry 64328
On the nature of low-energy antiprotons in cosmic rays See Entry 64333
Theory for the motion of the four large planets. The solution TOP82 See Entry 64359
Atomic clocks for astrophysical measurements See Entry 64390
Equatorial confinement of thermal plasma near the rings of Saturn See Entry 64422
First-order Fermi acceleration in solar flares as a mechanism for the second-step acceleration of prompt protons and relativistic electrons See Entry 64431
Short period coronal oscillations: observation and interpretation See Entry 64437
Investigation of damping constant for the neutral iron line profiles in undisturbed solar photosphere See Entry 64442
Mesoturbulence See Entry 64443
Spectral features of the filamentary and physically nonhomogeneous prominences. III. Structure and stratification of physical conditions See Entry 64444
QUIPS: time-dependent properties of quasi-invariant self-gravitating polytropes See Entry 64453
On the stability of rotating stellar models in general relativity theory See Entry 64454
Charged particle reaction cross sections and nucleosynthesis See Entry 64460
Oscillator strengths and Ne abundance in B stars See Entry 64468
V1343 Aquilae See Entry 64492
Loss of angular momentum in a binary system due to collisionless particles as monopoles or gravitinos: does it exceed the gravitational radiation emission in the binary system PSR 1913+16? See Entry 64498
Some nonlinear mechanisms of pulsar emission See Entry 64503
Equilibrium composition and neutrino emissivity of interacting quark matter in neutron stars See Entry 64504
Radiation processes in stellar X-ray sources See Entry 64516
Is the rapidly repetitive radiation from X-ray sources due to explosive three wave interaction? See Entry 64517
The Crab Nebula. I. Photoionization of a bright filament See Entry 64528
Far-infrared rotational transition lines of the interstellar water vapor See Entry 64535
The origin of the nonthermal radio emission in normal disk galaxies See Entry 64539
Runaway instability in accretion disks orbiting black holes See Entry 64544
The evolution of shear and gravitational wave perturbations of Friedmann models and the isotropy of the Universe See Entry 64560
The production of string loops in an expanding universe See Entry 64565

- Natural values of coupling constants and cosmological inflation in a supersymmetric model See Entry 64566
 Axions and the primordial monopole problem See Entry 64567
 The Inflationary Universe lives? See Entry 64569
 Beyond the Big Bang See Entry 64570

95.45 OBSERVATORIES

- Scattering matrix of nonspherical particles See Entry 64233

95.55 ASTRONOMICAL INSTRUMENTS

- 64376 Experience of studying the spherical and chromatic aberrations of the double wide-angle 400/2000 astrophot. S.P.Major, G.A.Ivanov, A.N.Kanivets.

Astrometriya & Astrofiz. (USSR), no.47, p.84-7 (1982). In Russian.
 Optical properties of the double wide-angle astrophot are studied. The Hartmann criterion and the colour curves of the objectives are obtained. The test plates were taken with 6 narrow-band interference filters, with 3 colour glass filters and without a filter. Two kinds of screen, namely, the Hartmann diaphragm and a screen with two splits were used. In addition to the Hartmann test the Hertzprung method was involved to study the colour curves. This purpose an objective grating with 1.67 mm diameter grating bars and with a 0.33 mm space between the bars was used. (5 refs.)

- 64377 Field errors of the photometric system of the double long-focus astrophot of the Main Astronomical Observatory the Ukrainian SSR Academy of Sciences. G.A.Ivanov.

Astrometriya & Astrofiz. (USSR), no.47, p.87-90 (1982). In Russian.
 Describes methods for determining the field error and the colour system of the double long-focus astrophot. The central part of the field with diameter 40'-50' can be used for photographic photometry. (2 refs.)

- 64378 The photometric field error of the double wide-angle astrophot of the Main Astronomical Observatory of the Ukrainian SSR Academy of Sciences. N.G.Guseva, L.N.Kolesnik, N.F.Levina.

Astrometriya & Astrofiz. (USSR), no.47, p.99-101 (1982). In Russian.
 The photometric field error has been determined for the Zeiss double wide-angle astrophot of the Golosevsky Observatory ($D=400$ mm, $F=2000$ mm). The results indicate that the field error is symmetrical with respect to the plate centre. A field of about 1.5° (5 cm) radius is free from errors. The photometric field correction depends on the photographic density E of stellar images and is the smallest for $E=0.1-0.5$. (5 refs.)

- 64379 How to achieve diffraction limited resolution with large space telescopes. F.Rodder (Univ. of Nice, Nice, France).
Adv. Space Res. (GB), vol.2, no.4, p.3-9 (1982). (Proceedings of Symposium 4 of the COSPAR Twenty-Fourth Plenary Meeting, Ottawa, Canada, 16 May-2 June 1982).

Large space telescopes cannot be made diffraction-limited at least for short wavelengths. Methods for reconstructing diffraction-limited images are reviewed including active optics, Michelson stellar interferometry, non-redundant aperture arrays, deconvolution and shearing interferometry. Expressions are given for the signal-to-noise ratio in each case and the results of laboratory simulations are presented. (14 refs.)

- 64380 FLUTE or TRIO: different approaches to optical arrays in space. A.Labeyrie (CERGA, Saint Vallier de Thiey, France), E.Savaria, G.Schumacher.

Adv. Space Res. (GB), vol.2, no.4, p.11-22 (1982). (Proceedings of Symposium 4 of the COSPAR Twenty-Fourth Plenary Meeting, Ottawa, Canada, 16 May-2 June 1982).

FLUTE and TRIO are two versions of a proposed optical interferometer, intended as a first step towards large optical arrays. The two apertures of FLUTE are linked by solid members, while TRIO relies totally upon active stabilization techniques to maintain optical coherence with three satellites serving as array components. The feasibility of utilizing solar radiation pressure for fine control is studied. A natural and periodic variation of baseline spacing can be achieved by certain orbital configurations. (10 refs.)

- 64381 Solar radiometry: spectral irradiance measurements. G.E.Brueckner (E.O. Hulburt Center for Space Res., Naval Res. Lab., Washington, DC, USA).

Adv. Space Res. (GB), vol.2, no.4, p.177-83 (1982). (Proceedings of Symposium 4 of the COSPAR Twenty-Fourth Plenary Meeting, Ottawa, Canada, 16 May-2 June 1982).

The present measurement accuracy of the solar spectral irradiance is insufficient to derive the real long-term solar spectral irradiance variability at all wavelengths. Possible error sources are discussed. A series of new second generation solar irradiance photometers are now under construction which should considerably improve these measurements. At the same time, efforts are made to improve the absolute UV calibration methods to derive a unified UV radiation scale. (7 refs.)

- 64382 Solar radiometry: total irradiance measurements. C.Frohlich (Phys. Meteorologisches Obs., World Radiation Center, Davos, Switzerland).
Adv. Space Res. (GB), vol.2, no.4, p.191-8 (1982). (Proceedings of Symposium 4 of the COSPAR Twenty-Fourth Plenary Meeting, Ottawa, Canada, 16 May-2 June 1982).

The operating principles of modern absolute radiometers are discussed and the methods of their characterization, that is the accurate determination of the uncertainties, are described. In view of this analysis, the results of the solar constant determinations of the last 6 years are reviewed and an estimate of their uncertainties given. Procedures for the strategy of future experiments are recommended. (21 refs.)

- 64383 X-ray imaging techniques—modulation collimator and coded mask. M.Oda (Inst. of Space & Astronaut. Sci., Tokyo, Japan).

Adv. Space Res. (GB), vol.2, no.4, p.207-16 (1982). (Proceedings of Symposium 4 of the COSPAR Twenty-Fourth Plenary Meeting, Ottawa, Canada, 16 May-2 June 1982).

Imaging over the hard X-ray energy band may be achieved by masking the flux with proper obstacles. The imaging modulation collimator has been developed and has been applied thus far, e.g. to produce hard X-ray pictures of the solar flare and to construct the X-ray image of the Crab Nebula up to the angular resolution of ~ 10 arcsec. Variations of the concept such as the Fourier Transform Telescope are discussed. Virtue of the modulation collimator is that high angular resolution may be achieved with a relatively simple detector system and that a wide field of view may be accommodated. Among several proposed coded masks, the techniques of Hadamard transform are discussed in some details. (15 refs.)

- 64384 The Pinhole/Occulter Facility. H.S.Hudson (Center for Astrophys. & Space Sci., Univ. of California, San Diego, CA, USA).

Adv. Space Res. (GB), vol.2, no.4, p.307-14 (1982). (Proceedings of Symposium 4 of the COSPAR Twenty-Fourth Plenary Meeting, Ottawa, Canada, 16 May-2 June 1982).

The Pinhole/Occulter Facility concept uses a remote occulting mask to provide high resolution observations of the solar corona and of astronomical X-ray sources. With coded-aperture and Fourier-transform techniques, the Pinhole/Occulter makes images at a resolution of 0.2 arc sec for 2-120 keV X-rays, using a 50-m boom erected from the payload bay of the Space Shuttle or mounted on a free-flying platform. The remote occulter also creates a large shadow area for solar coronal observations; the Pinhole/Occulter concept includes separate optical and ultraviolet telescopes with 50-cm apertures. These large telescopes will provide a new order of resolution and sensitivity for diagnostic observations of faint structures in the solar corona. The Pinhole-Occulter is a powerful and versatile tool for general-purpose X-ray astronomy. The large collecting area of 1.5 m² results in a 5 σ detection threshold of about 0.02 μ Jy for the 2-10 keV band, or about 10⁻⁵ ph/(cm²sec keV)⁻¹ at 20 keV. (20 refs.)

- 64385 Flight-time system with automatic adjustment and logic sampling of information for the Nataliya-2 telescope. D.Yu.Akimov, S.E.Belenko, Yu.D.Kotov, O.N.Romanov, V.T.Samoilenko (Inst. of Engng. Phys., Moscow, USSR).

Instrum. & Exp. Tech. (USA), vol.25, no.4, pt.1, p.828-32 (July-Aug. 1982). Translation of: *Prib. & Tekh. Eksp. (USSR)*, vol.25, no.4, p.45-9 (July-Aug. 1982). [received: April 1983]

Describes a flight-time system designated for operation in a γ -telescope; the system is characterized by automatic adjustment and logic sampling of information. The counters comprise a scintillator, lightguides, FEU-85 photomultipliers and amplifiers. The basic characteristics of the system are: flight base, 40 cm; size of the sensitive detector region, 240×240×5 mm; and suppression of the background resulting from particles moving in the opposite direction, 100-200 fold at a recording efficiency in excess of 90% for useful events. Power consumption is about 8 W. The characteristics are preserved in a wide temperature range and when the supply voltages change, owing to automatic adjustment of the delays of signal propagation in the measuring channels. (16 refs.)

- Proceedings of Symposium 4 of the COSPAR Twenty-Fourth Plenary Meeting See Entry 59524

- Photoconductive detectors for space IR astronomy See Entry 59841

- Calibration system for satellite and rocket-borne ion mass spectrometers in the energy range from 5 eV/charge to 100 keV/charge See Entry 59875

- On isoplanatism by the arrival angles for light rays in telescopes See Entry 64234

- Investigating mirages with an astronomical telescope See Entry 64268

- The Comet Halley flyby IR sounder 'IKS' See Entry 64340

- GIRL—the German Infrared Laboratory for Spacelab See Entry 64341

- The Extreme Ultraviolet Explorer See Entry 64342

- The ROSAT mission See Entry 64343

- AXAF, a permanent orbiting X-ray observatory: telescope and instrumentation plans See Entry 64344

- X-ray astronomy from the Space Shuttle See Entry 64345

- Japanese satellite programs in X-ray astronomy See Entry 64346

- Instruments for X-ray astronomy See Entry 64347

- X-ray Timing Explorer See Entry 64348

- Gamma-ray imaging with a rotating modulator See Entry 64386

- The automatic photoelectric device with a laser interferometer for measuring photographs of limbs in meridian instruments See Entry 64388

- Atomic clocks for astrophysical measurements See Entry 64390

95.65 AUXILIARY AND RECORDING INSTRUMENTS

- 64386 Gamma-ray imaging with a rotating modulator. P.Durouchoux (CENS, CEA, Gir-sur-Yvette, France), H.Hudson, G.Hurford, K.Hurley, J.Matteson, E.Orsal.

Astron. & Astrophys. (Germany), vol.120, no.1, pt.1, p.150-5 (April 1983).

A γ -ray imaging system, called a rotating modulator, is described, which allows a large area of the sky (radius $\approx 27^\circ$) to be imaged with a limiting resolution of $\leq 1^\circ$ for intense sources. It operates in the 30 keV-10 MeV energy range, and does not rely on position sensitive detection devices. It possesses a multiplex advantage which allows sky surveys to be completed in a small fraction of the time needed by a conventional collimation system. In addition, it is relatively insensitive to background fluctuations, which makes it ideally suited to satellite applications. The concept is illustrated by the results from a study of a γ -ray spectroscopy experiment. (11 refs.)

- 64387 Superconducting bolometers for IR astronomical techniques. II. Noise limitations. V.P.Kuz'kov.

Astrometriya & Astrofiz. (USSR), no.47, p.95-8 (1982). In Russian.

For pt.1 see ibid., no.42, p.90-6 (1980). Methods of decreasing the noise in superconducting bolometers and ways of increasing their detectivity are analyzed. Problems concerning the effect of the bolometer on the noise of a photodetection device are considered. A scheme is proposed to stabilize the bolometer in order to provide long integration times. (5 refs.)

- 64388 The automatic photoelectric device with a laser interferometer for measuring photographs of limbs in meridian instruments. B.A.Golovko.

Astrometriya & Astrofiz. (USSR), no.48, p.89-94 (1983). In Russian.

An automatic device for measuring photographs of the limb of a graduated circle is designed on the basis of a laser interferometer. The random error of the measurement of distances between the divisions of the circle and the index is $\pm 0.14 \mu\text{m}$ ($\pm 0.01''$). The systematic error does not exceed $\pm 0.2 \mu\text{m}$. (11 refs.)

- 64389 Characterisation of the Reticon 100×100 array. D.Mohr (High Altitude Obs., Nat. Centre for Atmospheric Res., Boulder, CO, USA).
AAS Photo-Bull. (USA), no.31, p.5, 8 (1982).

Assesses the use of a Reticon 100×100 photodiode array. The author describes some of the results from tests. Also included are the results of earlier work on film signal-to-noise done by Dick Munro in order to compare the Reticon with film. (1 ref.)

- Photometric errors induced by edge effects on hypersensitised Kodak spectroscopic plates, Type 103a-O See Entry 59866

- Reciprocity failure of hypersensitised and unhyposensitised Kodak Technical Pan Film 2415 See Entry 59867

- Calibration system for satellite and rocket-borne ion mass spectrometers in the energy range from 5 eV/charge to 100 keV/charge See Entry 59875
- GIRL—the German Infrared Laboratory for Spacelab See Entry 64341
- The ROSAT mission See Entry 64343
- AXAF, a permanent orbiting X-ray observatory: telescope and instrumentation plans See Entry 64344
- X-ray astronomy from the Space Shuttle See Entry 64345
- Japanese satellite programs in X-ray astronomy See Entry 64346
- Instruments for X-ray astronomy See Entry 64347
- Flight-time system with automatic adjustment and logic sampling of information for the Nataliya-2 telescope See Entry 64385

95.70 OTHER INSTRUMENTATION AND TECHNIQUES

(inc. clocks, frequency standards)

- 64390 Atomic clocks for astrophysical measurements.** R.F.C.Vessot, E.M.Mattison (Harvard-Smithsonian Center for Astrophysics, Cambridge, MA, USA). *Adv. Space Res. (GB)*, vol.2, no.4, p.23-31 (1982). (Proceedings of Symposium 4 of the COSPAR Twenty-Fourth Plenary Meeting, Ottawa, Canada, 16 May-2 June 1982).
- Recently developed atomic hydrogen masers have achieved stability well into the 10^{-16} domain for averaging time intervals beyond 1000 sec and future devices promise further improvements. Proposed space missions using these clocks are discussed for the measurement of the Sun's gravity field distribution and tests of gravitation and relativity including a search for pulsed low frequency (~ 0.001 Hz) gravitational waves, and orbiting VLBI stations. Estimates of system performance capability, are discussed and the accuracy capability of relativistic measurements evaluated. (12 refs.)
- 64391 Laboratory simulation of photometric light curves of the asteroids.** M.A.Barucci, R.Casaccia, M.Fulchignoni (Istituto di Astrofisica Spaziale, CNR, Frascati, Italy), R.Burchi, A.Dipaolantonio, C.Giuliani, L.Milano, F.Scaltriti, V.Zappala. *Moon & Planets (Netherlands)*, vol.27, no.4, p.387-95 (Dec. 1982).
- Reports laboratory simulations of asteroid observations obtained using a specially designed apparatus SAM (the acronym stands for System for Asteroid Models). The aim of the experiment is to assess the geometrical and physical characteristics of an asteroidal body which may affect the shape of its light curve; and, in particular, the parameters which define asteroid orientation with respect to the observer, and the shape and surface morphology of the asteroids. The design and operation of the SAM are described in some detail and the first results obtained with models having a regular shape are presented and discussed. (8 refs.)
- ASA 1000 and color too See Entry 64399

95.75 TECHNIQUES OF OBSERVATION AND REDUCTION

- 64392 Infrared speckle imaging: improvement of the method; results on Miras and protostars.** J.M.Mariotti (Istituto di Fisica Cosmica, Milano, Italy), A.Chelli, R.Foy, P.Lena, F.Sibille, G.Tchountonov. *Astron. & Astrophys. (Germany)*, vol.120, no.2, pt.2, p.237-48 (April 1983).
- After the first results obtained in 1978 and 1979, a new infrared speckle-interferometer has been built at Lyon Observatory and successfully tested during three observation runs. Improved methods of data reduction, including selection of true diffraction limited images, are presented here. Suggestions for further improvements are also done. 19 spatial spectra have been obtained for 11 sources, some of them being observed with several Position Angles and/or wavelengths. Three extremely interesting objects are discussed in detail: (a) IRC+10216 for which the ellipticity is derived at $\lambda=4.6 \mu\text{m}$. (b) The protostellar candidate GL 2591, which is marginally resolved at $4.6 \mu\text{m}$, and whose angular size is too small to account for the total luminosity of the associated molecular cloud. (c) MWC 349 for which the authors derive an upper limit, supporting the pre-planetary disk model proposed for this source. (55 refs.)
- 64393 A generalized algorithm for efficient photometric reductions.** J.Manfroid (Dept. d'Astrophys., Univ. de Liege, Cointe-Ougree, Belgium), A.Heck. *Astron. & Astrophys. (Germany)*, vol.120, no.2, pt.2, p.302-6 (April 1983).
- The authors present a generalized method applicable to the reduction of photometric observations in any well-defined system. The method is characterized by the use of practically every measurement of any non-variable star in the reduction procedure. Its main advantages are a greater accuracy and a substantial saving of observing time on extinction and standard stars. A particular case of application to the *uvby* system is detailed and discussed in an appendix. (19 refs.)
- 64394 The influence of ionospheric refraction on radio astronomy interferometry.** T.A.T.Spoelstra (Netherlands Found. for Radio Astron., Dwingelo, Netherlands). *Astron. & Astrophys. (Germany)*, vol.120, no.2, pt.2, p.313-21 (April 1983).
- A correction procedure for ionospheric refraction in radio astronomy interferometry is outlined. This correction is applied to observations made with the Westerbork Synthesis Radio Telescope and its results are discussed. It turns out that a correction for a combination of both horizontal and vertical gradients in the electron density distribution can improve the observations considerably. It is shown that this approach gives better results than would be derived by taking into account the horizontal structure of the ionosphere only. The available ionosphere data based on ionosonde observations limit the applications significantly. At present the correction can only be determined each full hour. Furthermore, since the information about the ionosphere is determined from ionosonde data it is not possible to derive reliable corrections around sunrise, when rapid changes in the vertical electron density distribution occur. (20 refs.)
- 64395 Determination of microturbulent velocity using Fraunhofer lines of Fe I.** V.A.Shemina. *Astrometriya & Astrofiz. (USSR)*, no.47, p.41-8 (1982). In Russian.
- Develops and applies a new method for determining microturbulent velocities in the solar photosphere. The method is based on different responses of equivalent widths and central depths of the Fraunhofer lines to variations in microturbulent velocity. The results of photometric microturbulent velocity determinations by various methods are described. (43 refs.)

- 64396 On the use of the false perturbation method in astronomical practice.** S.V.Pasechnik, V.V.Telnyuk-Adamchuk, A.N.Shaido. *Astrometriya & Astrofiz. (USSR)*, no.48, p.85-8 (1983). In Russian.
- The false perturbation method is discussed as applied to solution of ill-conditioned systems of linear equations. The conditionality number is shown not to be criterion for application of the method. Different procedures for determining the real eigenvalues of the normal equation matrix and a general scheme for solving the ill-conditioned equation system are suggested. (22 refs.)
- 64397 Japan-US joint VLBI experiment.** N.Kawajiri (Radio Res. Labs., Ministry of Posts & Telecommunications, Ibaraki, Japan). *J. Inst. Electron. & Commun. Eng. Jpn. (Japan)*, vol.65, no.10, p.1046-9 (Oct. 1982). In Japanese. [received: March 1983] (11 refs.)
- 64398 A posteriori spatial filtering of a short-exposure image distorted by the atmosphere.** P.A.Bakut, K.N.Sviridov, V.N.Sidelnikov, N.D.Ustinov. *Opt. & Spectrosc. (USA)*, vol.53, no.1, p.96-7 (July 1982). Translation of: *Opt. & Spektrosk. (USSR)*, vol.53, no.1, p.163-6 (July 1982). [received: April 1983]
- Proposes an approach for reconstructing the modulus and phase of the optical transfer function (OTF) $H(\omega)$ of the atmosphere-telescope system [and, consequently, of the impulse response $h(s)$ of the system] by means of statistical processing of the spatial spectra of fragments of the recorded image and by using an iteration procedure for reconstruction. (2 refs.)
- 64399 ASA 1000 and color too.** D.Dicico. *Sky & Telesc. (USA)*, vol.65, no.3, p.215-17 (March 1983).
- The author reports astronomical tests of the new Kodacolor VR 1000 35-mm colour film. Photographs of the Orion Nebula, the Pleiades, and star trails between Polaris and Cassiopeia are described. (no refs.)
- 64400 Automatic Sun observations. II. Methods of observations.** N.A.Topchilo. *Vestn. Leningr. Univ. Ser. Mat. Mekh. & Astron. (USSR)*, no.1, p.99-110 (Jan. 1983). In Russian.
- The Sun observation methods realized on the basis of computer programs worked out for RT-22 automation are presented. Their precision, advantages and defects are described. Some problems which can be solved by means of new methods are also outlined. (3 refs.)
- Comparison of Earth rotation as inferred from radio interferometric, laser ranging and astrometric observations See Entry 64265
- On investigation of the magnitude equation See Entry 64357
- Field errors of the photometric system of the double long-focus astrophot of the Main Astronomical Observatory the Ukrainian SSR Academy of Sciences See Entry 64377
- The automatic photoelectric device with a laser interferometer for measuring photographs of limbs in meridian instruments See Entry 64388
- Variance and correlations of errors of rectangular coordinates for the selenodetic reference points See Entry 64404
- Accuracy of the outer orientation in the selenodetic coordinate system See Entry 64405
- Determination of the orientation angles of the selenodetic coordinates system based on the photographic positional observations of the Moon See Entry 64406
- Stellar interferometry: diameters and effective temperatures of five giant stars See Entry 64470
- Analysis of optical imagery for Seyfert's Sextet and VV 172 See Entry 64549
- ## 95.80 ASTRONOMICAL OBSERVATIONS (LISTED BY TECHNIQUES OF OBSERVATION)
- R 66(Aeq): an LMC B supergiant with a massive cool and dusty wind See Entry 64482
- ## 95.80D Radio and radar
- Very Large Array observations of solar active regions. III. Multiple wavelength observations See Entry 64433
- Solar radio noise registrations at the Oslo Solar Observatory, 1975-81 and comments on the whole series of measurements 1954-81 See Entry 64451
- High-resolution X-ray and radio maps of the millisecond pulsar See Entry 64499
- Polarimetry of the millisecond pulsar See Entry 64500
- A high-latitude H I-clud with optical emission See Entry 64525
- Detection of HCO^+ and HCN absorption towards three galactic H II-regions See Entry 64529
- Linear polarization observations in selected celestial zones—The anticentre region See Entry 64533
- The gas distribution in the central region of the Galaxy. IV. A survey of neutral hydrogen in the region $349^\circ \leq l \leq 13^\circ$, $-10^\circ \leq b \leq 10^\circ$, $|v| \leq 350 \text{ km s}^{-1}$ See Entry 64541
- 102 MHz observations of Seyfert galaxies See Entry 64547
- VLA observations of H_2CO in DR 21 See Entry 64551
- Variability at 5 GHz in low luminosity radio nuclei of galaxies and quasars See Entry 64552
- Aperture synthesis observations of Orion B at 2.695 and 8.085 GHz See Entry 64553
- Low-frequency variability and predicted superluminal motion in 3C 147 See Entry 64555
- X-ray radio, and infrared observations of the 'rapid burster' (MXB 1730-335) during 1979 and 1980 See Entry 64556
- ## 95.80G Far infrared (bolometric, photoconductive)
- Infrared speckle imaging: improvement of the method; results on Miras and protostars See Entry 64392
- Infrared photometry of southern Wolf-Rayet stars See Entry 64478
- The nature of the cool component of the BX Monocerotis symbiotic system See Entry 64487
- Herbig-Haro 57 See Entry 64491
- Infrared photometry of the RS CVn binaries. I. TY Pyxidis See Entry 64509

- The compact H II region S235A. Observations and interpretation See Entry 64523
 X-ray radio, and infrared observations of the 'rapid burster' (MXB 1730-335) during 1979 and 1980 See Entry 64556

95.80J Photographic region (near infrared, visible, and normal ultraviolet)

- On isoplanatism by the arrival angles for light rays in telescopes See Entry 64234
 On the catalogue of the stars positions in the NPZT programme See Entry 64356
 On investigation of the magnitude equation See Entry 64357
 ASA 1000 and color too See Entry 64399
 Determination of the orientation angles of the selenodetic coordinates system based on the photographic positional observations of the Moon See Entry 64406
 Exploring the Martian arctic See Entry 64412
 Rotation properties of the high-numbered asteroids 1236 Thais and 1317 Silverta See Entry 64415
 Physical studies of asteroids. X. Photoelectric light curves of the asteroids 219 and 512 See Entry 64416
 Electrophotometry of Saturn. I. Brightness distribution along equatorial regions in the 0.346-0.595 μ m spectral interval See Entry 64420
 Saturn See Entry 64421
 No occultations by Uranus II and Pluto See Entry 64423
 Periodic Comet Tempel 1 (1982j) See Entry 64427
 Preliminary observations of velocity fields at the solar poles See Entry 64432
 Does the solar activity cycle extend over more than an 11-year period? See Entry 64435
 Dynamical behaviour of surges See Entry 64436
 Short period coronal oscillations: observation and interpretation See Entry 64437
 Investigation of nickel abundance in the solar atmosphere See Entry 64438
 Investigation of damping constant for the neutral iron line profiles in undisturbed solar photosphere See Entry 64442
 Mesoturbulence See Entry 64443
 Undisturbed chromospheric structure observed above the solar limb See Entry 64445
 Coherent scattering in the solar spectrum: survey of linear polarization in the range 3165-4230 Å See Entry 64446
 UBV photometry of FK4 and FK4 supplement stars See Entry 64457
 Model-atmosphere analysis of high-dispersion spectra of four red giants and supergiants See Entry 64465
 Linear polarization variations of six T Tauri stars See Entry 64469
 Stellar interferometry: diameters and effective temperatures of five giant stars See Entry 64470

- Radial velocity studies of cataclysmic binaries. I. KR Aurigae See Entry 64474
 Time-resolved spectrophotometry of the nova-like variable RW Trianguli See Entry 64475
 Carbon stars and the seven dwarfs See Entry 64476
 The flare activity of V780 Tau See Entry 64480
 Intrinsic colours and absolute magnitudes of selected R Coronae Borealis variables See Entry 64483
 HR 6522: a previously unknown multiperiodic delta Scuti star See Entry 64484
 On the variability of the two brightest stars in the galactic cluster IC 2391 See Entry 64485
 High speed photometry of PG0244+104 See Entry 64486
 Spectrum of 11 Cam in 1980-1981 See Entry 64489
 Nova Serpentis 1983 See Entry 64490
 KR Aurigae See Entry 64493
 Supernovae See Entry 64494
 Supernovae See Entry 64495
 Rapid rotation and stellar activity in the triple system HD 165590 See Entry 64507
 The early B-type eclipsing binary FZ CMa (HD 52942): a massive triple system See Entry 64511
 Light curves of four southern bright hitherto unknown eclipsing binaries See Entry 64513
 HD 85037: probable new eclipsing variable See Entry 64514
 Spectroscopic binary orbits from photoelectric radial velocities. XLIX. HD 80655 See Entry 64515
 An investigation of the heavily reddened young open cluster Tr 27 on the Walraven photometric system See Entry 64520
 The globular cluster NGC 6544 See Entry 64521
 Investigation of the region around the emission nebula IC 1848 See Entry 64530
 Investigation of the region around the emission nebula NGC 1499 See Entry 64531
 On interstellar light absorption in the Galaxy See Entry 64532
 The origin of the nonthermal radio emission in normal disk galaxies See Entry 64539
 OJ 287 See Entry 64543
 Light variability of the Seyfert galaxy Zw 0039.5+4003 (IV Zw 29). During 1967 through 1981 See Entry 64546

95.80M Space ultraviolet

- Identification and properties of the M giant/X-ray system HD 154791=2A 1704+241 See Entry 64462
 The ultraviolet spectrum of the supermassive object R136a. I. The mass loss rate See Entry 64471

- The spectra of late type dwarfs and sub-dwarfs in the near ultraviolet. II. Limits to variability in Mg II emission from IUE spectrophotometry See Entry 64472
 ψ^3 Piscium and the rotation-activity connexion See Entry 64473
 Coordinated Einstein and IUE observations of a disarptions brusques type flare event and quiescent emission from Proxima Centauri See Entry 64477
 The ultraviolet reddening of Be stars See Entry 64481

95.80N X-ray

- Identification and properties of the M giant/X-ray system HD 154791=2A 1704+241 See Entry 64462
 Coordinated Einstein and IUE observations of a disarptions brusques type flare event and quiescent emission from Proxima Centauri See Entry 64477
 High-resolution X-ray and radio maps of the millisecond pulsar See Entry 64499
 Rapid rotation and stellar activity in the triple system HD 165590 See Entry 64507
 X-ray radio, and infrared observations of the 'rapid burster' (MXB 1730-335) during 1979 and 1980 See Entry 64556
 Discovery of X-ray bursts from GX 3+1 (4U 1744-26) See Entry 64557

95.80Q gamma-ray and elementary particle

- V1343 Aquilae See Entry 64492

95.80S Other (inc. gravitational radiation, magnetograms, etc)

- VLF ionosonde and long-distance propagation anomalies produced by galactic Cen X-4 X-ray burst in May 1979 See Entry 64295

95.85 CATALOGUES, ATLASES ETC

- 64401 H α atlas of the northern Milky Way taken with a wide-field camera. T.Sasaki. *Astron. Her. (Japan)*, vol.75, no.11, p.311-13 (1982). In Japanese. Describes the K1420 wide-field (17°) camera, observations using various film/filter combinations, and the construction of the 1982 kyoto atlas of the northern Milky Way in H α emission. Each circular area of photographed sky is accompanied by overlays indicating SAO stars and other objects. (no refs.)
 On the catalogue of the stars positions in the NPZT programme See Entry 64356

95.90 OTHER TOPICS IN ASTRONOMY AND ASTROPHYSICS

- Proceedings of the Meeting held by The Astronomical Science Group of Ireland See Entry 59529

96.00 SOLAR SYSTEM

96.10 GENERAL, SOLAR NEBULA, AND COSMOGONY

- 64402 On the effect of systematic errors of proper stellar motion on determination of solar motion parameters. S.P.Rybka, A.I.Vatsenko. *Astrometriya & Astrofiz. (USSR)*, no.48, p.53-8 (1983). In Russian. Solar motion parameters obtained from Pulkova, Tashkent and AGK3 proper stellar motions are analyzed. The systematic errors of proper stellar motions in these catalogues resulted from differences of the estimations of solar motion parameters. (8 refs.)
 64403 The mass-independent fractionation of oxygen: a novel isotope effect and its possible cosmochemical implications. M.H.Thiemens, J.E.Heidenreich, III (Univ. of California, San Diego, La Jolla, CA, USA). *Science (USA)*, vol.219, no.4588, p.1073-5 (4 March 1983). Experimental evidence is presented which demonstrates a chemically produced, mass-independent isotopic fractionation of oxygen. The effect is thought to result from self-shielding by the major isotopic species $^{16}\text{O}_2$, but other possible mechanisms such as molecular symmetry cannot be ruled out. In a three-isotope plot, the experimentally produced fractionation line is essentially equal in slope to the observed carbonaceous chondrite mixing line. The implications for the early history of the solar system are discussed. (19 refs.)

96.20 MOON

- 64404 Variance and correlations of errors of rectangular coordinates for the selenodetic reference points. I.V.Gavrilov, A.S.Duma. *Astrometriya & Astrofiz. (USSR)*, no.48, p.64-71 (1983). In Russian. Variance and correlations of errors of the rectangular coordinates of 32 selenodetic reference points from the Consolidated catalogue is computed and analyzed. There is practically no correlation between the errors of the heteronymous coordinates of the considered point. The correlation between the homonymous coordinates of different points is either small or poorly determined. (4 refs.)
 64405 Accuracy of the outer orientation in the selenodetic coordinate system. V.S.Kislyuk. *Astrometriya & Astrofiz. (USSR)*, no.48, p.71-8 (1983). In Russian. Two sets of elements are considered for describing the absolute orientation of the selenodetic coordinate system. Errors of the Moon rotation parameters are analyzed as those affecting the accuracy of the absolute orientation of the quasi-dynamic coordinate system, the third axis of which is connected with the mean direction to the Earth. (17 refs.)

64406 Determination of the orientation angles of the selenodetic coordinate system based on the photographic positional observations of the Moon. V.S.Kislyuk, N.A.Vasilenko, R.L.Semerenco, V.B.Kollyuk. *Astrometriya & Astrofiz.* (USSR), no.48, p.78-84 (1983). In Russian. The photographic observations of the Moon against a stellar background were used for determining the orientation of the selenodetic coordinate system which is realized by the Consolidated Catalogue of 4900 basic points on the lunar surface with respect to the selenodetic coordinate system, the third axis of which is connected with the mean direction to the Earth. (13 refs.)

64407 The evolution of the Moon: a finite element approach. S.Chacko (Dept. of Geology, Rice Univ., Houston, TX, USA), J.C.De Brumaecker. *Moon & Planets* (Netherlands), vol.27, no.4, p.467-92 (Dec. 1982). Thermal convection has considerable influence on the thermal evolution of terrestrial planets. Previous numerical models of planetary convection have solved the system of partial differential equations by finite difference methods, or have approximated it by parameterized methods. The authors have evaluated the applicability of a finite element solution of these equations. The model analyses the thermal history of a self-gravitating spherical planetary body; it includes the effects of viscous dissipation, internal melting, adiabatic gradient, core formation, variable viscosity, decay of radioactive nucleides, and a depth dependent initial temperature profile. Reflecting current interest, physical parameters corresponding to the Moon were selected for the model. (41 refs.)

Ion implantation phenomena in spaceSee Entry 64375

A comparison of volcanic eruption processes on Earth, Moon, Mars, Io and VenusSee Entry 64408

96.30 PLANETS AND SATELLITES

(exc. the Moon; for celestial mechanics, see 95.10; for Earth as an astronomical body, see 91. Geophysics)

64408 A comparison of volcanic eruption processes on Earth, Moon, Mars, Io and Venus. L.Wilson, J.W.Head, III (Dept. of Geological Sci., Brown Univ., Providence, RI, USA). *Nature* (GB), vol.302, no.5910, p.663-9 (21 April 1983).

The silicate planets and satellites display a wide range of physical, chemical and atmospheric characteristics which may influence the nature of volcanism, a major geological process common to the evolution of the surfaces of these bodies. Consideration of the process of magma ascent and eruption from first principles allows predictions to be made concerning volcanic eruption styles and expected landforms and deposits on each planetary body. Examination of actual landforms and deposits in the light of these predictions leads to a better understanding of the nature of volcanic eruption processes and outlines outstanding problems. (113 refs.)

64409 Solar System sputtering. T.A.Tombrello (W.K. Kellogg Radiation Lab., California Inst. of Technol., Pasadena, CA, USA). *Radiat. Eff.* (GB), vol.65, no.1-4, p.149-58 (1982). (Proceedings of the First International Conference on 'Radiation Effects in Insulators', Arco, Largo di Garda, Italy, 1981).

The solar wind and energetic magnetospheric ions are important agents for modification of the planetary surfaces and atmospheres with which they interact. Knowledge of the details of the sputtering mechanisms involved in these interactions can help in determining the interrelation of a number of planetary processes. The author discusses several sites in the Solar System where sputtering phenomena are significant. The quantitative understanding of these examples could be extended if one had a more detailed picture of the sputtering of insulators. Recent experimental results that bear on these problems as well as the gaps in the knowledge that prevent further progress will be presented. (52 refs.)

Hydrogen at high pressures and temperaturesSee Entry 64363

96.30E Venus

64410 A navigation model for the Venusian atmosphere. P.W.Birkeland, B.G.Williams, A.S.Konopliv (Jet Propulsion Lab., Pasadena, CA, USA). *J. Astronaut. Sci.* (USA), vol.30, no.4, p.367-83 (Oct.-Dec. 1982). [Received: March 1983]

A static, exponential atmosphere model for Venus is developed using period change data from the Pioneer Venus spacecraft. The model is derived from approximately 600 passages of the spacecraft through the upper Venusian atmosphere, or almost three full circulations of the planet. The model reflects several important, known atmospheric features (diurnal bulge, layering, etc.) and confirms several observations of a more sophisticated analysis. Several new phenomena are observed. (4 refs.)

64411 Comparison of measurements of electromagnetic induction in the magnetosphere of Venus with laboratory simulations. I.M.Podgorny, E.M.Dubinin, P.L.Israelevich (Space Res. Inst., Acad. of Sci., Moscow, USSR), C.P.Sonett. *Moon & Planets* (Netherlands), vol.27, no.4, p.397-406 (Dec. 1982).

Analysis of Venera 9 and 10 data suggest a comingled excitation of the ionosphere of Venus by the time dependent component of the interplanetary magnetic field, upon which may be superimposed a contribution from the interplanetary electric field. The inductive contributions correspond respectively to generation of eddy currents and to unipolar induction. The former is suggested when the interplanetary magnetic field exhibits significant changes in intensity or orientation, but could also have contributions from fluctuations in plasma pressure expressed through the frozen-in field. The magnetic field measured near Venus by Venera 9 and 10 is considered within this framework and with respect to laboratory simulation using both conducting and insulated spheres. (27 refs.)

A comparison of volcanic eruption processes on Earth, Moon, Mars, Io and VenusSee Entry 64408

96.30G Mars

64412 Exploring the Martian arctic. D.C.Parker, C.F.Capen, J.D.Beish. *Sky & Telesc.* (USA), vol.65, no.3, p.218-20 (March 1983).

The authors describe measurements of the retreat of the Martian north polar cap during 1979 and 1980, and during 1981 and 1982. During both apparitions the polar cap retreated more quickly than at previous oppositions, and the cap that remained at the beginning of the Martian summer was unusually small. In particular the dark feature Rima Tenuis re-appeared in 1980 and 1982 for the first time since 1903. These observations suggest that the Martian climate varies on a time scale of decades, and that the two most recent northern summers have been unusually warm. A possible correlation between the climates of Mars and the Earth is discussed briefly. (no refs.)

Channels of MarsSee Entry 59552

Electron-impact excitation of the Cameron system ($a^2\pi-X^1\Sigma$) of COSee Entry 64369

A comparison of volcanic eruption processes on Earth, Moon, Mars, Io and VenusSee Entry 64408

96.30H Asteroids

64413 Structure of asteroids expected from impact experiments. A.Fujiwara. *Astron. Her.* (Japan), vol.75, no.11, p.300-4 (1982). In Japanese.

Discusses methods of firing high velocity bullets up to 10 km/s, impact destruction, velocities of single particles and self-rotation, the Hirayama families of asteroids and collisions between parent bodies. (no refs.)

64414 Statistical study of asteroids. K.Ishida, T.Mikami. *Astron. Her.* (Japan), vol.75, no.11, p.305-10 (1982). In Japanese.

Considers the number and distribution of asteroids in the Solar System. The results of the McDonald and Palomar-Leiden photographic surveys are analyzed and the distributions of asteroid orbital parameters, magnitudes, albedos, and diameters are discussed. (no refs.)

64415 Rotation properties of the high-numbered asteroids 1236 Thais and 1317 Silvetta. H.J.Schober (Inst. fur Astron., Graz, Austria), A.Schroll. *Astron. & Astrophys.* (Germany), vol.120, no.1, pt.1, p.106-8 (April 1983).

1236 Thais and 1317 Silvetta were observed photoelectrically in *UBV*, each during three nights in September 1980, using the 0.6 m Bochum telescope during ESO-time, at the European Southern Observatory, La Silla, Chile. For 1317 Silvetta a 7 h rotation period and a lightcurve amplitude of 0.40^m with primary and secondary extrema were observed. For 1236 Thais an increase in brightness was detected during three consecutive nights with $\Delta V = 0.08^m$, indicating that 1236 Thais might be a slowly spinning asteroid with a very long rotation period. For both asteroids *UBV*-colors were measured and no significant variation found. (6 refs.)

64416 Physical studies of asteroids. X. Photoelectric light curves of the asteroids 219 and 512. C.-I.Lagerkvist, L.Kamel (Astron. Observatoriet, Uppsala, Sweden).

Moon & Planets (Netherlands), vol.27, no.4, p.463-6 (Dec. 1982).

For pt.IX see ibid., vol.27, no.1, p.107-10 (1982). Composite light curves are presented for the asteroids 219 Thunelda and 512 Tarimensis. Rotation periods of 1.24^h and 0.2326^h are derived for the two asteroids, respectively. *UBV*-colours are presented for the asteroids 147, 219, 317, and 512. (5 refs.)

Laboratory simulation of photometric light curves of the asteroidsSee Entry 64391

96.30K Jupiter

64417 The problem of cooling the cold Io torus. J.D.Richardson, G.L.Siscoe (Dept. of Atmospheric Sci., Univ. of California, Los Angeles, CA, USA).

J. Geophys. Res. (USA), vol.88, no.A3, p.2001-9 (1 March 1983). The transport of ions inward from Io's orbit is first modeled on the assumption that radial diffusion is the dominant transport mechanism and then modeled with a combination of diffusive and convective transport. Included in the model are thermal as well as number density transport, radiation, ionization and pickup of local neutrals, recombination, charge exchange, and Coulomb interactions. Pure diffusive transport is capable of accounting for the dramatic inward depletion of the torus only by invoking recombination or by postulating a massive increase in the production rate of torus ions sometime prior to Voyager encounter. It is shown that radical time dependence cannot account simultaneously for the density and temperature observations. Similarly, recombination is found to be much too slow to be the cause of the observed density decrease inside of Io. The model combining convection and diffusion can reasonably match the data, but only with a diffusion coefficient 100 times less than that derived from Pioneer observations. (40 refs.)

64418 A theory of the Io phase asymmetry of the Jovian decametric radiation. K.Hashimoto, M.L.Goldstein (Lab. for Extraterrestrial Phys., NASA Goddard Space Flight Center, Greenbelt, MD, USA).

J. Geophys. Res. (USA), vol.88, no.A3, p.2010-20 (1 March 1983).

Proposes an explanation of an asymmetry in the occurrence probability of the Io-dependent Jovian decametric radiation. This asymmetry is found to arise because when Io is in the northern part of the torus, more intense Alfvén waves are generated propagating southward than northward. These waves then cause the excitation of decametric radiation in the northern ionosphere after reflection from the southern ionosphere. The asymmetry then results from the propagation time of the Alfvén wave and the bending of the magnetic field (Alfvén wing) along this trajectory. The ray paths of the decametric radiation are calculated using a three-dimensional ray-tracing program in the Jovian ionosphere. (42 refs.)

64419 A second order Jupiter-Saturn planetary theory. I. O.M.Kamel (Astron. Dept., Faculty of Sci., Cairo Univ., Giza, Egypt), A.A.Bakry.

Moon & Planets (Netherlands), vol.27, no.4, p.417-30 (Dec. 1982).

Presents a second order secular Jupiter-Saturn planetary theory through Poincaré canonical variables, von Zeipel's method and Jacobi-Radau referential. The authors neglect in the expansions terms of power higher than the fourth with respect to eccentricities and sines of inclinations. The authors assume that the disturbing function is composed of secular and critical terms only. (19 refs.)

Jovian modulation of interplanetary electrons as observed with Voyagers 1 and 2See Entry 64336

Theory for the motion of the four large planets. The solution TOP82See Entry 64359

Recent topics in physics of hot plasmas in space environmentSee Entry 64372

A comparison of volcanic eruption processes on Earth, Moon, Mars, Io and VenusSee Entry 64408

96.30M Saturn

64420 Electrophotometry of Saturn. I. Brightness distribution along equatorial regions in the 0.346-0.595 μ m spectral interval. A.P.Vid'machenko. *Astrometriya & Astrofiz.* (USSR), no.47, p.70-5 (1982). In Russian.

Photoelectric scans of Saturn's equatorial region are given for the 0.346-0.595 μ m spectral interval. The data were obtained at Majdanak Mountain on February 16, 1980 at the time of ring disappearance. The obtained brightness distributions are in good agreement with those for 1966. The limb brightness

increases with a decrease in wavelength and becomes brighter than the central region at $\lambda \leq 0.372 \mu\text{m}$. (12 refs.)

64421 Saturn. R.Suggs, R.Beebe.

I.A.U. Circ. (USA), no.3789, 1 pp. (7 April 1983).

The authors report the discovery on 1983 March 28 of a bright white cloud in Saturn's northern hemisphere. The cloud is at a planetographic latitude of $+38^\circ \pm 2^\circ$, and its west end was $10^\circ \pm 2^\circ$ east of Saturn's central meridian on March 29^h10^m36^s UT. The rotation period of Saturn at this latitude is 10^h41^m. This cloud is probably similar to the convective feature observed by the Voyager spacecraft at the same latitude and described by Smith et al. (1982). (1 ref.)

64422 Equatorial confinement of thermal plasma near the rings of Saturn.

W.-H.Ip (Max-Planck-Inst. für Aeronomie, Katlenburg-Lindau, Germany).

Nature (GB), vol.302, no.5909, p.599-600 (14 April 1983).

In the unique environment of the rings of Saturn, because of a combination of the magnetic field geometry and the meteoroid impact ionization at the ring plane, a thin plasma disk having a total thickness of no more than a few per cent of the planetary radius might exist in the vicinity of the ring system. The radial transport of this ring plasma to larger radial distances may act as an important source of the thermal plasma in Saturn's magnetosphere. The author suggests that the recent observations by the Voyager 2 Plasma Science team are not inconsistent with this scenario. (28 refs.)

Theory for the motion of the four large planets. The solution TOP82

.....See Entry 64359

A second order Jupiter-Saturn planetary theory. ISee Entry 64419

96.30T Other planets

64423 No occultations by Uranus II and Pluto. P.Maley.

I.A.U. Circ. (USA), no.3790, 1 pp. (7 April 1983).

The author reports observations of the close approach of Umbriel to Hyd-21^h64352 on 1983 March 25. No occultations were seen by an observer at Oberon, New South Wales, or by observers near Brisbane and Canberra. It is also reported that no occultation of BD+6^h2851 by Pluto was observed from Houston, Texas, during 1983 April 4^h07^m23^s to 4^h07^m51^s UT. (2 refs.)

64424 The elimination of the critical terms of a first order Uranus-Neptune theory through Hori's method. I. O.M.Kamel (Astron. Dept., Faculty of Sci., Cairo Univ., Giza, Egypt).

Moon & Planets (Netherlands), vol.27, no.4, p.407-15 (Dec. 1982).

An outline for the elimination of the critical terms of a first order Uranus-Neptune theory is presented with a stress on the application of Hori's (1966) procedure to the problem. (5 refs.)

Theory for the motion of the four large planets. The solution TOP82

.....See Entry 64359

96.50 OTHER OBJECTS IN THE PLANETARY SYSTEM

96.50G Comets

64425 Fluidization in the surface layer of cometary nuclei. I. A static layer at the fluidization threshold. L.M.Shul'man.

Astrometriya & Astrofiz. (USSR), no.47, p.62-9 (1982). In Russian.

A system of equations is derived to describe the static fluidized surface layer of a cometary nucleus. An exact solution of this system is found for the case when the layer is at the fluidization threshold. The temperature difference between the external surface of the dusty mantle and the surface of the ice under the mantle is shown not to depend on the dust layer thickness. The gas output of ice covered with a mineral mantle is shown to be three or four orders lower than that of the exposed ices. (7 refs.)

64426 Interaction between large cosmic bodies and atmosphere.

V.P.Korobeynikov (Math. Inst., Acad. of Sci., Moscow, USSR), P.I.Chushkin, L.V.Shurshalov.

Acta Astronaut. (GB), vol.9, no.10, p.641-3 (Oct. 1982). [received: March 1983]

The initial stage of movement of a large gaseous body in the Earth's atmosphere is calculated. For the Tunguska meteorite blast, the radiation and the thermal effect on the ground are computed using the multi-group spectrum approximation. Different types of trajectories of cosmic bodies having non-zero lift/drag ratio are found. (9 refs.)

64427 Periodic Comet Tempel 1 (1982j). J.-C.Merlin, J.Bortle, C.S.Morris.

I.A.U. Circ. (USA), no.3793, 1 pp. (19 April 1983).

Total visual magnitude estimates are reported for the period 1983 March 29 to April 18; the comet brightened from mag. 11.3 to mag. 10.4 during this time. (no refs.)

64428 A multi-fluid model of an H₂O-dominated dusty cometary atmosphere. M.L.Marconi, D.A.Mendis (Center for Astrophys. & Space Sci., Univ. of California, San Diego, La Jolla, CA, USA).

Moon & Planets (Netherlands), vol.27, no.4, p.431-52 (Dec. 1982).

A self-consistent multi-fluid solution of the dynamical and thermal structure of an H₂O-dominated, two-phase dusty-gas cometary atmosphere is obtained by solving the simultaneous set of differential equations representing conservation of number density, momentum and energy, together with the transfer of solar radiation in streams responsible for the major photolytic processes and the heating of the nucleus. The validity of this model, as in the earlier single-fluid ones, is restricted to the collision-dominated region where all the heavy species (ions and neutrals) are assumed to achieve a common temperature and velocity. Calculations are presented for a comet of radius 2.5 km with a dust/gas ratio of 1, at a heliocentric distance of 1 AU. (26 refs.)

The Comet Halley flyby IR sounder 'IKS'See Entry 64340

Earth-return trajectory options for the 1985-86 Halley opportunitySee Entry 64351

Navigation system design for a Halley sample return missionSee Entry 64352

96.50K Meteors, showers and meteoroids

Equatorial confinement of thermal plasma near the rings of SaturnSee Entry 64422

96.50M Meteorites, micrometeorites

Interaction between large cosmic bodies and atmosphereSee Entry 64426

Evolution of chemical abundances in massive stars. II. Abundance anomalies in Wolf-Rayet stars in relation with cosmic rays and ²²Ne in meteoritesSee Entry 64479

96.60 SOLAR PHYSICS

64429 Dynamics and spectroscopy of asymmetrically heated coronal loops. J.T.Mariska, J.P.Boris (Naval Res. Lab., Washington, DC, USA).

Astrophys. J. (USA), vol.267, no.1, pt.1, p.409-20 (1 April 1983).

Investigates numerical models of steady flows along coronal magnetic flux tubes of varying cross sectional area. The flows are induced by altering the spatial symmetry of the heating. Calculations of the ionization balance and line emission for a number of ionization stages of oxygen suggest that heating induced flows may be responsible for the redshifts seen in spectral lines formed in the network at transition region temperatures. (27 refs.)

64430 Flare loop radiative hydrodynamics. IV. Dynamic evolution of unstable semiempirical loop models. C.-H.An, R.C.Canfield, G.H.Fisher, A.N.McClumont (Center for Astrophys. & Space Sci., Univ. of California, San Diego, CA, USA).

Astrophys. J. (USA), vol.267, no.1, pt.1, p.421-32 (1 April 1983).

For pt.1 see *ibid.*, vol.265, no.1, pt.1, p.507-18 (1983). The nonlinear phase of evolution of a thermally unstable coronal loop is followed by solving numerically the time-dependent equations of gasdynamics and radiative transfer. It is found that an unstable loop evolves, by chromospheric evaporation or condensation, on the coronal conductive time scale, even if the linear growth rate of the instability is much larger. (34 refs.)

64431 First-order Fermi acceleration in solar flares as a mechanism for the second-step acceleration of prompt protons and relativistic electrons. T.Bai, H.S.Hudson, R.M.Pelling (Center for Astrophys. & Space Sci., Univ. of California, San Diego, CA, USA), R.P.Lin, R.A.Schwartz, T.T.von Rosenvinge.

Astrophys. J. (USA), vol.267, no.1, pt.1, p.433-41 (1 April 1983).

Finds that for two of the hard X-ray bursts of an energetic flare on 1980 June 27, the time profile of the hard X-rays above 235 keV is delayed by 3 s with respect to the time profiles of the lower energy X-rays and that the high energy spectrum becomes flatter with time during each of these bursts. It is argued that during this flare a second-step mechanism accelerated further some of the high-energy tail population of the first-step electrons. After estimating the acceleration rate, it is concluded that first-order Fermi acceleration operating in a closed flare loop is a very likely mechanism for the second-step acceleration. (45 refs.)

64432 Preliminary observations of velocity fields at the solar poles. L.E.Cram (Sacramento Peak Obs., Sunspot, NM, USA), B.R.Durney, D.B.Guenther.

Astrophys. J. (USA), vol.267, no.1, pt.1, p.442-54 (1 April 1983).

The 13 m Littrow spectrograph at Sacramento Peak Observatory has been used to study the Doppler shift of Fe I $\lambda 5863$ in the polar regions of the Sun over a 20 day interval. The daily observations were assembled into a polar projection of the line-of-sight velocity field. The projection shows a very clear pattern of supergranulation. When a low-pass spatial filter is run over the data, a pattern of large-scale (80-100 Mm) velocity features can be seen. Cross-correlation studies show that the supergranular pattern rotates with a synodic period of 35 days, while there is evidence that the larger features rotate with a shorter period of about 30 days. (21 refs.)

64433 Very Large Array observations of solar active regions. III. Multiple wavelength observations. K.R.Lang, R.F.Willson (Dept. of Phys., Tufts Univ., Medford, MA, USA).

Astrophys. J. (USA), vol.267, no.1, pt.1, p.455-64 (1 April 1983).

For pt.II see *ibid.*, vol.247, no.1, pt.1, p.338-47 (1981). VLA synthesis maps of the active regions AR 2505 and AR 2646 at wavelengths of 2 cm, 6 cm, and 20 cm are presented and compared with the magnetic structure of the underlying photosphere. The 20 cm radiation in terms of the bremsstrahlung of thermal electrons trapped in magnetic loops. (31 refs.)

64434 The excitation of type II radio bursts in the corona. W.J.Wagner, R.M.MacQueen (High Altitude Obs., Nat. Center for Atmospheric Res., Boulder, CO, USA).

Astron. & Astrophys. (Germany), vol.120, no.1, pt.1, p.136-8 (April 1983).

Simultaneous radioheliograph and orbital coronagraph observation of coronal transient activity shows metric type II radio emission originating early in the event, well below the visible white light transient. It is suggested that the shock which excites the type II emission is independent of the transient, in the sense that it is initiated in the low corona (probably in association with a flare) and travels through the already-existing transient disturbance with a propagation speed significantly greater than that of the front edge of the transient itself. Radio emission then results when the flare shock overtakes, first, the region of principal density pile-up along the sides of the expanding transient and only later the top of the transient. (21 refs.)

64435 Does the solar activity cycle extend over more than an 11-year period? J.-L.Leroy, J.-C.Noens (Obs. du Pic-du-Midi, Bagnères-de-Bigorre, France).

Astron. & Astrophys. (Germany), vol.120, no.2, pt.2, p.181-2 (April 1983).

The authors have analysed coronal data obtained at Pic du Midi from 1944 to 1974, searching for the latitude variation of coronal activity. According to their results the whole evolution of activity in the corona spreads over a time lapse of about 17 years in agreement with the recent work of Legrand and Simon (1981). Therefore there is increasing evidence that the duration of an activity cycle is much longer than the time interval between two consecutive cycles. (13 refs.)

64436 Dynamical behaviour of surges. G.Banos (Dept. of Astron., Univ. of Ioannina, Ioannina, Greece), H.Dara-Papamargariti.

Astron. & Astrophys. (Germany), vol.120, no.2, pt.2, p.181-4 (April 1983).

Trajectories, velocity curves as a function of height and the force, besides gravity, acting on the surge material have been determined from time sequences of Ho-filtergrams of twenty-two surges of various sizes. The trajectories are found to be helical in shape. The deceleration, which takes place after the maximum velocity has been reached, is in most cases smaller than if gravity alone were acting and is attributed to a force due to the presence of the magnetic field. (25 refs.)

64437 Short period coronal oscillations: observation and interpretation. S.Koutchmy (Inst. d'Astrophys., CNRS, Paris, France), Y.D.Zugzda, V.Locans.

Astron. & Astrophys. (Germany), vol.120, no.2, pt.2, p.185-91 (April 1983).

The result of an experiment devoted to the search of short period coronal waves using the green coronal line 5303 Å of Fe XIV are analyzed. After the

subtraction of sky aureola fluctuations, two time series of measurements performed at a 40° height over a faint facular area and small changing chromospheric features show power spectra with evidence of Doppler velocity oscillations with periods near 300 s, 80 s, and especially 43 s. However, no prominent intensity fluctuations appeared. The observed waves are considered as good candidates for being resonant Alfvén oscillations viewed at a low level through several legs of coronal arches, with a typical distance between feet being equal to the autocorrelation distance of the network and with foot-points inserted in the photosphere. A model of such an arch is subsequently computed and seems to fit quite well the observed periods and velocity amplitudes. In addition the energy flux balance is evaluated and the role of such waves in the heating mechanism of coronal arches is discussed. (25 refs.)

64438 Investigation of nickel abundance in the solar atmosphere. B.T.Babii, M.B.Griyak, I.F.Margolych, R.E.Rykalyuk. *Astrometriya & Astrofiz. (USSR)*, no.47, p.22-7 (1982). In Russian. The abundance of neutral nickel in the solar photosphere is obtained from 78 Ni I lines. The Holweger and Muller photospheric model is preferred with a microturbulent velocity of 0.9 km/s, a macroturbulent velocity of 1.5 km/s and both components being independent of depth. The damping constant is found by fitting the observed and calculated line profiles. (17 refs.)

64439 Determination of the total photospheric velocity field from the Fraunhofer lines of different elements. N.N.Kondrashova. *Astrometriya & Astrofiz. (USSR)*, no.47, p.27-31 (1982). In Russian. The amplitude of the total photospheric velocity field is determined using weak lines of different elements. The velocity field at large depth and the influence of the damping constant are studied. The Van der Waals damping constant with the correction factor $E=2.5$ does not essentially change the amplitude of the photospheric velocity field in the optical depths $-3.0 \leq \lg \tau_5 \leq -0.5$. A decrease in the velocity amplitude at large depths has not been confirmed. (16 refs.)

64440 Oscillator strengths of ionized iron lines. R.I.Kostyk, T.V.Orlova. *Astrometriya & Astrofiz. (USSR)*, no.47, p.32-4 (1982). In Russian. Solar oscillator strengths are obtained from equivalent widths of 59 ionized iron lines. The internal accuracy of the results is determined. (15 refs.)

64441 Spectral features of filamentary physically nonhomogeneous prominences. II. Hydrogen (second level excitation, ionization). N.N.Morozhenko, V.V.Zharkova. *Astrometriya & Astrofiz. (USSR)*, no.47, p.34-41 (1982). In Russian.

Hydrogen emission is studied in homogeneous and nonhomogeneous (filamentary) prominences. A plane-parallel geometry and the five-level plus continuum model of the hydrogen atoms were used to solve the transfer equations for Lyman α and continuum emission. The second level excitation degree and a relative emission measure along the line of sight are obtained. (21 refs.)

64442 Investigation of damping constant for the neutral iron line profiles in undisturbed solar photosphere. B.T.Babii, L.I.Ben'ko, R.E.Rikalyuk. *Astrometriya & Astrofiz. (USSR)*, no.48, p.3-10 (1983). In Russian. The damping constant is determined for profiles of 32 solar Fe I lines. The enhancement factor E is shown to be different for the high and low excitation potentials and varies from 2 to 6. The damping constant increases slightly with the line excitation potential and decreases with a rise in its optical depth. Formulas for describing the dependence of the damping constant on the optical depth are suggested for calculating the equivalent widths of the lines. (29 refs.)

64443 Mesoturbulence. R.I.Kostyk. *Astrometriya & Astrofiz. (USSR)*, no.48, p.10-16 (1983). In Russian. The mean square mesoturbulent velocity in the solar photosphere (the Kubo-Anderson process) is depth-independent and is equal to 1.7 km s^{-1} . The correlation length decreases with the height from 750 km ($\lg \tau = -0.8$) to 350 km ($\lg \tau = -1.7$). For the solar photosphere the equation $\xi^2 = \nu_{\text{micro}}^2 + \nu_{\text{macro}}^2$ seems to hold accurately enough. (24 refs.)

64444 Spectral features of the filamentary and physically nonhomogeneous prominences. III. Structure and stratification of physical conditions. N.N.Morozhenko. *Astrometriya & Astrofiz. (USSR)*, no.48, p.16-25 (1983). In Russian.

For pt.II see ibid., no.47, p.34-41 (1982). In the framework of models of structurally and physically inhomogeneous quiescent prominences with $n_H = \text{const}$ the intensities of H_β , He I $\lambda 3880$ and Na I ($D_1 + D_2$) lines are calculated. Comparison of these data with observations resulted in estimation of structural and physical parameters of the prominences. (23 refs.)

64445 Undisturbed chromospheric structure observed above the solar limb. R.A.Gulyaev. *Astrometriya & Astrofiz. (USSR)*, no.48, p.25-32 (1983). In Russian.

From recent results of observations of the fine chromospheric structure it follows that the low chromosphere extends up to the height about 1500 km above the solar surface. The horizontal structures observed in the emission lines of metals (Na I, Mg I, Ca I, Ba II, Sr II) are predominant. At a height more than 1500 km the spicules observed in the H, He I and Ca II lines become the predominant element. The spicules undergo transverse oscillations which appear to result from the propagation of Alfvén waves. The motionless bases of the spicules are fixed on the boundary layer between the low and upper chromospheres. (29 refs.)

64446 Coherent scattering in the solar spectrum: survey of linear polarization in the range 3165-4230 Å. J.O.Stenflo, D.Twerenbold (Inst. of Astron., ETH-Zentrum, Zurich, Switzerland). *Astron. & Astrophys. Suppl. Ser. (France)*, vol.52, no.1, p.161-80 (April 1983).

The linear polarization 10 sec of arc inside the solar limb has been recorded over the wavelength range 3165-4230 Å with the vertical spectrograph of the Kitt Peak McMath telescope. This polarization is caused by coherent resonant and fluorescent scattering in the solar atmosphere. The polarization observed in several multiplets of Fe I, as well as in 1 Ca II, 3 Mg I, and 22 Co I is affected by quantum-mechanical interference between the excited states of different total angular momenta. The CN molecule shows significant polarization, increasing to a maximum at each band head. Unexpectedly large polarization is found among others in 21 Ni I, 2 Ti II, 1 Cu I, as well as in a number of Fe I lines. The continuum polarization increases steeply with decreasing wavelength, and is generally larger than the intrinsic line polarization. (12 refs.)

64447 A variation in the mesh of the photospheric granular network with solar activity. C.J.Macris (Acad. of Athens, Athens, Greece), J.Rosch. *C.R. Seances Acad. Sci. Ser. II (France)*, vol.296, no.4, p.265-8 (31 Jan. 1983). In French.

For the period 1966-1978, a negative correlation has been found between the mean center-to-center distance of the granules and solar activity as expressed by the Wolf number or by the radio-flux at 2800 MHz. This behaviour results from a global shrinking of the histogram towards small distances when the activity increases. (11 refs.)

64448 Solar irradiance variations. I. Analysis of modeling techniques and intercomparison of ground-based data. L.Oster (Lab. for Planetary Atmospheres, NASA Goddard Space Flight Center, Greenbelt, MD, USA).

J. Geophys. Res. (USA), vol.88, no.A3, p.1953-64 (1 March 1983). Computes the full disc irradiance at 2800 MHz ("F10.7") on the basis of individual active regions (ARs) on the Sun as observed in the light of the Ca II K line at 393 nm. The solar radio emission is used as a stand-in for UV measurements from above the atmosphere, since it does not have significant calibration problems, and since day by day records are available for many years. The author illustrates in detail the techniques for parameterization of the model calculations which, with few changes, are applicable to UV measurements. In addition to the excellent overall agreement and the impressively close correspondence of day to day variations, no indication of a systematic discrepancy between model and observations over the entire 10-year period was found. Nor is there a contribution to the 2800 MHz irradiance that is not directly related to individual ARs on the Sun at any given day. (15 refs.)

64449 Radio communication and sunspots. J.Kennell (Ionospheric Prediction Service, Learmonth Solar Obs., Learmonth, Australia). *Pract. Wireless (GB)*, vol.59, no.4, p.49-53 (April 1983). Discusses sunspots and its effects on radio communication. The solar ionising radiations, the sunspot number and method of counting sunspots are considered. (no refs.)

64450 Energetics of particles accelerated in solar flares. L.G.Kocharov. *Pis'ma v Astron. Zh. (USSR)*, vol.9, no.2, p.125-7 (1983). In Russian. English translation in: *Sov. Astron. Lett. (USA)*. A method is proposed for the determination of the minimal energy of particles accelerated in solar flares, based on the observed anticorrelation between the spectral index and particle flux. The total energy of the accelerated particles is estimated. (12 refs.)

64451 Solar radio noise registrations at the Oslo Solar Observatory, 1975-81 and comments on the whole series of measurements 1954-81. O.Elgaroy, O.Hauge. *Report 54*, Univ. Oslo, Blindern, Norway (1982), 40 pp.

Observations of solar radio noise have been performed at Oslo Solar Observatory at Harestua since 1954. Since September 1973 the observing frequency has been 228 MHz. The author presents observational data for the years 1975-81. It is a continuation of Report no. 12 which covered the years 1958-59, Report no. 16 for the years 1960-64 and Report no. 48 which contained data for the period 1965-74. The description of the method of tabulation of data is almost the same as in previous reports. In 1981 the observations of solar radio noise were brought to an end. Three sunspot maxima and the two intervening minima were covered. A discussion of the whole series of measurements is undertaken. (4 refs.)

Final state branching ratio in the ^7Be decay See Entry 60139

^7Be decay scheme and the solar neutrino problem See Entry 60140

Radioactive ion beams for studying astrophysical nuclear reactions See Entry 60510

Atomic calculations for the Fe XX X-ray lines See Entry 60637

Dense and multicomponent plasmas See Entry 61618

Gamma astronomy of the Sun and study of solar cosmic rays See Entry 64330

Atomic calculations for Ca XVII; UV and X-ray lines See Entry 64365

Solar radiometry: spectral irradiance measurements See Entry 64381

Solar radiometry: total irradiance measurements See Entry 64382

Atomic clocks for astrophysical measurements See Entry 64390

Determination of microturbulent velocity using Fraunhofer lines of Fe I See Entry 64395

Automatic Sun observations. II. Methods of observations See Entry 64400

Some common peculiarities of solar and stellar magnetic fields See Entry 64459

97.00 STARS

97.10 STELLAR CHARACTERISTICS

64452 Mass loss from rotating magnetic stars: Weber and Davis revisited. K.B.MacGregor, V.J.Pizzo (High Altitude Obs., Nat. Center for Atmospheric Res., Boulder, CO, USA).

Astrophys. J. (USA), vol.267, no.1, pt.1, p.340-3 (1 April 1983). The model of Weber and Davis (1967) for the flow of a magnetically coupled wind from a rotating star is reexamined in the light of criticisms by Barker and Marlborough (1982). When differences in the respective definitions of the stellar angular velocity are reconciled, it is found that the extended theory proposed by the latter authors is equivalent to the original Weber and Davis description. (16 refs.)

64453 QUIPS: time-dependent properties of quasi-invariant self-gravitating polytropes. A.Munier, M.R.Feix (Centre d'Etudes de Limeil, CEA, Villeneuve-St-Georges, France).

Astrophys. J. (USA), vol.267, no.1, pt.1, p.344-57 (1 April 1983). Quasi-invariance, a method based on group transformations, is used to obtain time-dependent solutions for the expansion and/or contraction of a self-gravitating sphere of perfect gas with polytropic index n . Quasi-invariance transforms the equations of hydrodynamics into 'dual equations' exhibiting extra terms such as a friction, a mass source or sink term, and a centripetal/centrifugal force. The search for stationary solutions in this 'dual space' leads to a new class of time-dependent solutions, the QUIP (for quasi-invariant polytrope), which generalizes Emden's static model and introduces a characteristic frequency related to Jeans's frequency. The second order differential equation describing the solution is integrated numerically. A critical point is seen to exist for $n \neq 3$. Solutions corresponding in the 'dual space' to a time-dependent generalization of Eddington's standard model ($n=3$) are discussed. (16 refs.)

64454 On the stability of rotating stellar models in general relativity theory. L.Lindblom (Inst. of Theoretical Phys., Dept. of Phys., Stanford Univ., Stanford, CA, USA), W.A.Hiscock.

Astrophys. J. (USA), vol.267, no.1, pt.1, p.384-401 (1 April 1983). Investigates the effects of viscosity, and thermal conductivity on the stability of rotating stellar models in general relativity theory. The equations of motion for the perturbed fluid stellar model (including nonadiabatic and dissipative effects) are used to construct an energy functional for the perturbed motion

of the star. This energy is used to investigate the stability of rotating stellar models. (29 refs.)

64455 Necessary conditions for the stability of rotating Newtonian stellar models. L.Lindblom (Inst. of Theoretical Phys., Dept. of Phys., Stanford Univ., Stanford, CA, USA).

Astrophys. J. (USA), vol.267, no.1, pt.1, p.402-8 (1 April 1983).

It is shown that the positivity of a certain energy functional for the perturbations of a rotating stellar model is a necessary condition for stability. The stellar models considered are composed of viscous and thermally conducting fluid, whose equilibrium states are necessarily rigidly rotating and isothermal. The perturbations are not restricted to be adiabatic or axisymmetric. This work generalizes the results of Barston (1969, 1970) who proved an analogous necessity theorem for nonrotating dissipative fluid stellar models. (14 refs.)

64456 Stellar coronae: What can be predicted with minimum flux models? R.Hammer (Joint Inst. for Lab. Astrophys., Univ. of Colorado, Boulder, CO, USA), F.Endler, P.Ulmschneider.

Astron. & Astrophys. (Germany), vol.120, no.1, pt.1, p.141-6 (April 1983).

To determine the possible errors of various minimum flux corona (MFC) predictions, the authors compare MFC models with a grid of detailed coronal models that covers a range of two orders of magnitude in both the total amount ϕ_{M0} of coronal heating and the characteristic damping length L . For given ϕ_{M0} , the pressure at the base of the transition region has a maximum as a function of L . This maximum possible pressure is the only quantity that can be predicted with sufficient accuracy by the MFC concept. MFC predictions of the mass loss rate and of the energy losses due to stellar wind can be wrong by many orders of magnitude. The unreliable MFC formulae should be replaced by a grid of detailed models which account for the coronal dependence on L . (38 refs.)

64457 UVB photometry of FK4 and FK4 supplement stars. T.Oja (Astron. Obs., Uppsala, Sweden).

Astron. & Astrophys. Suppl. Ser. (France), vol.52, no.1, p.131-4 (April 1983).

UVB photometry is presented for 320 stars of the FK4 and FK4 Supplement catalogues. (no refs.)

64458 Molecular clouds and star formation. C.M.Walmsley (Max Planck Inst. fur Radioastron., Bonn, Germany)

Irish Astron. J., vol.15, no.3, p.161-80 (March 1982). [received: April 1983]

An overview is given of recent theoretical and observational developments relevant to star formation. In particular, some theoretical models of protostar evolution are discussed as well as current ideas concerning the causes of the collapse of a protostellar gas cloud. Observational data, relevant to the formation of low mass stars in nearby dust clouds, is reviewed. Finally, as an example of high mass star formation, recent radio and infrared observations of the Orion molecular cloud are discussed. (42 refs.)

64459 Some common peculiarities of solar and stellar magnetic fields. S.I.Gopasyuk, A.B.Severnyi.

Pis'ma v Astron. Zh. (USSR), vol.9, no.2, p.120-4 (1983). In Russian. English translation in: *Sov. Astron. Lett. (USA)*

The measured values of the ratio of magnetic field strengths in active and quiet regions on the Sun are shown to be dependent on the equivalent width of different Fe I lines. This dependence is similar to that obtained for magnetically variable stellar rotators. A possible explanation of this effect by a difference in chemical composition of quiet and active regions is proposed. (9 refs.)

64460 Charged particle reaction cross sections and nucleosynthesis. D.G.Sargood (School of Phys., Univ. of Melbourne, Parkville, Victoria, Australia).

Phys. Rep. (Netherlands), vol.93, no.2, p.61-116 (Dec. 1982).

The role of proton and α -particle induced reactions in carbon, neon, oxygen and silicon burning in massive stars is surveyed. The problems associated with determining thermonuclear reaction rates for reactions with widely spaced resonances and with closely spaced or overlapping resonances are discussed and the associated experimental approaches are reviewed. Experimental techniques which have been used in the measurement of reaction cross sections are discussed and their strengths and weaknesses are identified. Recent developments in attempts to establish reliable statistical-model codes for calculation of reaction cross sections are presented and discussed. Finally, the results of experimental tests of statistical model codes are summarised and evaluated. (92 refs.)

RAS Specialist Discussion on Astrophysical Applications of Accretion Disks (Papers in summary form only received) See Entry 59533

Relativistic astrophysics See Entry 59551

Radioactive ion beams for studying astrophysical nuclear reactions See Entry 60510

Possibility of amorphous glassy state in astrophysical dense plasmas See Entry 62441

On investigation of the magnitude equation See Entry 64357

Hydrogen at high pressures and temperatures See Entry 64363

An exact solution for an isothermal gas cloud with fast differential rotation See Entry 64364

Accelerator simulation of astrophysical processes See Entry 64367

Multiple transonic solutions with a new class of shock transitions in steady isothermal solar and stellar winds See Entry 64368

Infrared speckle imaging: improvement of the method; results on Miras and protostars See Entry 64392

A generalized algorithm for efficient photometric reductions See Entry 64393

On the effect of systematic errors of proper stellar motion on determination of solar motion parameters See Entry 64402

Chemical separation in horizontal-branch stars See Entry 64461

Identification and properties of the M giant/X-ray system HD 154791=2A 1704+241 See Entry 64462

Meridional circulation in rotating stars. V. Cooling white dwarfs See Entry 64463

Spectral line profiles from spherical shells See Entry 64464

Model-atmosphere analysis of high-dispersion spectra of four red giants and supergiants See Entry 64465

A discussion of the infrared and radio region of the calculated spectral energy distribution of O-type stars See Entry 64466

Evolution of chemical abundances in massive stars. I. OB stars, Hubble-Sandage variables and Wolf-Rayet stars. Changes at stellar surfaces and galactic enrichment by stellar winds See Entry 64467

Oscillator strengths and Ne abundance in B stars See Entry 64468

Linear polarization variations of six T Tauri stars See Entry 64469

Stellar interferometry: diameters and effective temperatures of five giant stars See Entry 64470

The ultraviolet spectrum of the supermassive object R136a. I. The mass loss rate See Entry 64471

The spectra of late type dwarfs and sub-dwarfs in the near ultraviolet. II. Limits to variability in Mg II emission from IUE spectrophotometry See Entry 64472

ψ^3 Piscium and the rotation-activity connexion See Entry 64473

Radial velocity studies of cataclysmic binaries. I. KR Aurigae See Entry 64474

Time-resolved spectrophotometry of the nova-like variable RW Trianguli See Entry 64475

Coordinated Einstein and IUE observations of a disaritions brusques type flare event and quiescent emission from Proxima Centauri See Entry 64477

Infrared photometry of southern Wolf-Rayet stars See Entry 64478

Evolution of chemical abundances in massive stars. II. Abundance anomalies in Wolf-Rayet stars in relation with cosmic rays and ^{22}Ne in meteorites See Entry 64479

The flare activity of V780 Tau See Entry 64480

The ultraviolet reddening of Be stars See Entry 64481

R 66(Aeq): an LMC B supergiant with a massive cool and dusty wind See Entry 64482

Intrinsic colours and absolute magnitudes of selected R Coronae Borealis variables See Entry 64483

HR 6522: a previously unknown multiperiodic delta Scuti star See Entry 64484

On the variability of the two brightest stars in the galactic cluster IC 2391 See Entry 64485

High speed photometry of PG0244+104 See Entry 64486

The nature of the cool component of the BX Monocerotis symbiotic system See Entry 64487

On the constancy of the period of the magnetic Ap star HD 215441 See Entry 64488

Spectrum of 11 Cam in 1980-1981 See Entry 64489

Nova Serpentinis 1983 See Entry 64490

Herbig-Haro 57 See Entry 64491

V1343 Aquilae See Entry 64492

KR Aurigae See Entry 64493

Supernovae See Entry 64494

Supernovae See Entry 64495

Supernovae. II. The aftermath See Entry 64496

On the origin of the recently discovered ultra-rapid pulsar See Entry 64497

Loss of angular momentum in a binary system due to collisionless particles as monopoles or gravitinos: does it exceed the gravitational radiation emission in the binary system PSR 1913+16? See Entry 64498

Prediction of pulsar glitch frequency based on the hard superfluid model See Entry 64501

Plasmas in superstrong pulsar fields See Entry 64502

Some nonlinear mechanisms of pulsar emission See Entry 64503

Effect of the neutron $^3\text{P}_2$ pairing on the π^0 condensation threshold in neutron star matter See Entry 64505

Temperature effect on the dynamics of neutron stars with pion-condensation See Entry 64506

Rapid rotation and stellar activity in the triple system HD 165590 See Entry 64507

The effects of sudden mass loss and a random kick velocity produced in a supernova explosion on the dynamics of a binary star of arbitrary orbital eccentricity. Applications to X-ray binaries and to the binary pulsars See Entry 64508

Infrared photometry of the RS CVn binaries. I. TY Pyxidis See Entry 64509

The combined effect of mass loss and overshooting. III. Evolutionary scenarios for massive close binaries See Entry 64510

The early B-type eclipsing binary FZ CMa (HD 52942): a massive triple system See Entry 64511

Light curves of four southern bright hitherto unknown eclipsing binaries See Entry 64513

HD 85037: probable new eclipsing variable See Entry 64514

Spectroscopic binary orbits from photoelectric radial velocities. XLIX. HD 80655 See Entry 64515

Radiation processes in stellar X-ray sources See Entry 64516

Is the rapidly repetitive radiation from X-ray sources due to explosive three wave interaction? See Entry 64517

Angular distribution of radiation from the plasma of X-ray pulsars taking into account vacuum polarization by magnetic fields See Entry 64518

Investigation of the star cluster NGC 6913 (M29) See Entry 64519

An investigation of the heavily reddened young open cluster Tr 27 on the Walraven photometric system See Entry 64520

The globular cluster NGC 6544 See Entry 64521

Observed radii and structural parameters of clusters in the SMC. II See Entry 64522

The ratio of deuterium to hydrogen in interstellar space. V. The line of sight to ϵ Persei See Entry 64524

Investigation of the region around the emission nebula NGC 1499 See Entry 64531

On the turbulent motions revealed in the Sagittarius arm by interstellar-line studies See Entry 64534

The formation of disc galaxies See Entry 64537

The origin of the nonthermal radio emission in normal disk galaxies See Entry 64539

Aperture synthesis observations of Orion B at 2.695 and 8.085 GHz See Entry 64553

Models of X-ray bursters with radius expansion See Entry 64558

97.20 NORMAL STARS (BY CLASS): GENERAL OR INDIVIDUAL

64461 Chemical separation in horizontal-branch stars. G. Michaud (Dept. de Phys., Univ. de Montreal, Montreal, Quebec, Canada), G. Vauclair, S. Vauclair.

Astrophys. J. (USA), vol.267, no.1, pt.1, p.256-70 (1 April 1983). Abundance anomalies are predicted to be produced by diffusion processes in horizontal-branch (HB) and halo Population II stars. If the outer envelope is stable enough for the gravitational settling of He to be efficient, it is shown that overabundances of heavy elements are simultaneously produced. Abundance anomalies as large as 10^{-3} to 10^{-4} are expected. Detailed calculations of selective radiative accelerations and of the time evolution of abundances are presented for C, N, O, Ca, Fe, and Sr in a series of models representative of HB stars. These abundance anomalies may be important for what is called the 'second parameter problem' in globular clusters. By detailed time dependent calculations, helium underabundances and relative overabundances of ^3He are shown to be produced well within the lifetime of stars on the horizontal branch. The implications of helium underabundances on the pulsational properties of RR Lyrae variables are discussed. The role of turbulent mixing in reducing the abundance anomalies is also discussed. (71 refs.)

64462 Identification and properties of the M giant/X-ray system HD 154791 = 2A 1704+241. M. Garcia, S.L. Balunas, R. Dossy, M. Elvis, G. Fabiano (Harvard-Smithsonian Center for Astrophysics, Cambridge, MA, USA), G. Koenigsberger, J. Patterson, D. Schwartz, J. Swank, M.G. Watson.

Astrophys. J. (USA), vol.267, no.1, pt.1, p.291-300 (1 April 1983). Identifies the Ariel V X-ray source 2A 1704+241 (=4U 1700+24=3A 1703+241) with the M3 II star HD 154791. The identification is based on a precise X-ray position determined by the HEAO 1 scanning modulation collimator and the Einstein Observatory imaging proportional counter, together with a spectrum measured by the International Ultraviolet Explorer. The ultraviolet spectrum shows strong emission of C IV $\lambda 1550 \text{ \AA}$, N V $\lambda 1238 \text{ \AA}$, and Mg II $\lambda 2800 \text{ \AA}$, which is very unusual among M giants. This is the first X-ray detection of an M giant which has a completely normal optical spectrum. The X-ray luminosity reaches orders of magnitude above the mean upper limit for the coronal X-ray flux from M giants. A plausible neutron star binary model can be constructed. (52 refs.)

64463 Meridional circulation in rotating stars. V. Cooling white dwarfs. M. Tassoul, J.-L. Tassoul (Dept. de Phys., Univ. de Montreal, Montreal, Quebec).

Astrophys. J. (USA), vol.267, no.1, pt.1, p.334-9 (1 April 1983). For pt.IV see *ibid.*, vol.264, no.1, pt.1, p.298-301 (1983). Discusses the large-scale meridional circulation and concomitant differential rotation in a cooling white dwarf that does not greatly depart from spherical symmetry. It is found that the circulation velocities are utterly negligible in the degenerate interior as well as in the thin nondegenerate envelope, where the presence of a (turbulent) viscous boundary layer allows the velocities to satisfy all of the surface boundary conditions. There are no $1/\rho$ singularities in the meridional flow. The back reaction of the circulatory currents on the overall rotation rate is not very large either, thus implying at most a mild differential rotation when departure from sphericity is small. (7 refs.)

64464 Spectral line profiles from spherical shells. R. Wagenblast, C. Bertout, U. Bastian (Landessternwarte Konigstuhl, Heidelberg, Germany).

Astron. & Astrophys. (Germany), vol.120, no.1, pt.1, p.6-14 (April 1983). Studies line profiles formed in spherical, radially thin shells. The effects of the shell dimensions and line formation parameters on the profiles are investigated and it is shown that type III P Cygni profiles can easily be formed in this framework. It is demonstrated that the apparent contradiction caused by the simultaneous presence in the spectra of YY Orionis stars of a Type III P Cygni profile at H_α and inverse P Cygni profiles at the higher Balmer lines can be resolved if the Balmer lines arise in a shell detached from the star. Some physical implications of this new picture are briefly discussed. (14 refs.)

64465 Model-atmosphere analysis of high-dispersion spectra of four red giants and supergiants. N. Kovacs (Inst. fur Theoretische Phys. und Sternwarte, Univ. Kiel, Kiel, Germany).

Astron. & Astrophys. (Germany), vol.120, no.1, pt.1, p.21-35 (April 1983). A model atmosphere analysis of three cool giants (β Cet, α Tau, α TrA) and one supergiant (ϵ Peg) is presented. Measured lines are split into high excitation lines and low excitation lines in order to test the sensitivity of the ionization balance method against deviations from LTE. Even though for iron no pronounced split can be found to occur, other elements, e.g. Mn and Ni, hint at the existence of deviations from LTE in cool giant stars. Deviations from the solar abundance pattern are found for the elements of medium atomic number. Two of the stars (α TrA and ϵ Peg) display over-abundances in barium. (51 refs.)

64466 A discussion of the infrared and radio region of the calculated spectral energy distribution of O-type stars. M. Groot, P.S. The (Astron. Inst. Anton Pannekoek, Univ. of Amsterdam, Amsterdam, Netherlands).

Astron. & Astrophys. (Germany), vol.120, no.1, pt.1, p.89-96 (April 1983). The results of numerical calculations of the emerging radiation of O-type stars having an accelerated mass outflow are presented. This radiation consists of the free-free emission from the extended gaseous envelope, superposed on the attenuated flux of the star. It is argued that the discrepancies found by various authors for the mass loss rate of O-type stars determined using observed infrared and radio fluxes are caused by an inadequate treatment of the measured infrared fluxes. (39 refs.)

64467 Evolution of chemical abundances in massive stars. I. OB stars, Hubble-Sandage variables and Wolf-Rayet stars. Changes at stellar surfaces and galactic enrichment by stellar winds. A. Maeder (Geneva Obs., Sauverny, Switzerland).

Astron. & Astrophys. (Germany), vol.120, no.1, pt.1, p.113-29 (April 1983). Evolutionary models with mass loss and a detailed study of changes in the abundances of ^1H , ^3He , ^4He , ^{12}C , ^{13}C , ^{14}N , ^{15}N , ^{16}O , ^{17}O , ^{18}O , ^{20}Ne , ^{22}Ne , ^{23}Mg , and ^{26}Mg are made for initial stellar masses of 120, 85, and 60 M_\odot . The evolution has been followed through stages corresponding to OB stars, blue supergiants, Hubble-Sandage variables and various Wolf-Rayet stages (WNL, WNE, WC, WO). The evolutionary status of the Hubble-Sandage variables is examined. The origin of the variability of the Hubble-Sandage variables is discussed in relation with the instability limit (de Jager's limit) for deep turbulent external convective zones in supergiants. Comparisons are made between the theoretical C/He, N/He, and C/N ratios and those observed by Smith and Willis (1982) and by Nugis (1982) for WNL, WNE, and WC stars. The contributions of the winds of WR star to the galactic enrichment in various elements and isotopes is estimated. (82 refs.)

64468 Oscillator strengths and Ne abundance in B stars. A. Magazzu, V. Pirronello, G. Strazzulla (Osservatorio Astrofisico di Catania, Citta Univ., Catania, Italy).

Astron. & Astrophys. (Germany), vol.120, no.1, pt.1, p.139-40 (April 1983). The scaled Thomas-Fermi method and the j - K coupling scheme are used to calculate the oscillator strengths for some Ne I lines of primary astrophysical interest, comparing them with other values given in the literature. The values appear systematically a little greater (mean difference $\approx +0.12$) than those of other sources. The Ne abundance in B stars is then discussed in the light of these results. (13 refs.)

64469 Linear polarization variations of six T Tauri stars. R. Schulte-Ladbeck (Landessternwarte, Heidelberg, Germany).

Astron. & Astrophys. (Germany), vol.120, no.2, pt.2, p.203-14 (April 1983). Linear polarization observations of the T Tauri stars RV Tau, DR Tau, SU Aur, RW Aur, V 1331 Cyg, and DI Cep are presented. Two of these stars were known to show variable polarization. The four remaining stars are also identified to be polarimetric variables. The wavelength dependence of the polarization is consistent with the presence of dust grains (with a large range of sizes) in asymmetric circumstellar envelopes. The polarization varies irregularly on a time scale down to days. Periodic variation could not be detected. For RW Aur, the trajectory of the polarization vector in the Stokes parameter plane suggests short-term mass flow variations with a fixed axis of symmetry. The intrinsic position angle of RY Tau rotates in the Stokes parameter plane with a time scale of months, indicating that we might observe scattering material orbiting around this star. (20 refs.)

64470 Stellar interferometry: diameters and effective temperatures of five giant stars. M. Faucher, D. Bonneau, L. Liechti, F. Vakili (Centre d'Etudes et de Recherches Géodynamiques et Astron., Obs. du Calern, Saint Vallier de Thiey, France).

Astron. & Astrophys. (Germany), vol.120, no.2, pt.2, p.263-8 (April 1983). In French.

The authors report angular diameter measurements of α Ari, β Gem, β Umi, γ Dra, and δ Dra, performed from November 1980 to January 1982 using the two-telescope stellar interferometer (12T) at CERGA. To determine the diameter for the equivalent uniform disk the method used is inspired by that of Michelson: it is based on a visual detection of very low contrast fringes for the largest possible baseline. A laboratory simulator of 12T observation conditions has allowed a calibration of fringe contrast measurements; it yields the minimum value of the contrast detectable by eye. The diameter of α Lyr measured by 12 T then confirms the measurement by intensity interferometry (Hanbury Brown et al. 1974a). From eight red giant angular diameters and from the computation of the bolometric fluxes of those stars, effective temperatures are determined. Good agreement is obtained with the $T_{\text{eff}} - (V-K)$ relation, established from lunar occultation diameters and infrared photometry. The authors generally find diameters smaller than from indirect or theoretical methods. (37 refs.)

64471 The ultraviolet spectrum of the supermassive object R136a. I. The mass loss rate. J.V. Feitzinger, R.W. Hunschik, T. Schmidt-Kaler (Astron. Inst., Ruhr-Universität Bochum, Bochum, Germany).

Astron. & Astrophys. (Germany), vol.120, no.2, pt.2, p.269-77 (April 1983). The short and long wave spectrum (1150-3000 \AA) of the central supermassive object in the 30 Doradus Nebula, 136a, is analyzed. The equivalent widths of the lines attributed to R136a are tabulated. The P Cyg lines of C IV, N IV, N V, He II, and Si II of the stellar wind of R136a are presented. The mass loss rate $M = 310^{-4} M_\odot/\text{yr}$ is derived from the line profiles of C IV and N V by line fitting assuming ionization equilibrium. (41 refs.)

64472 The spectra of late type dwarfs and sub-dwarfs in the near ultraviolet. II. Limits to variability in Mg II emission from IUE spectrophotometry. L. Crivellari, M.L. Franco, P. Molaro, G. Vladilo (Osservatorio Astron. di Trieste, Trieste, Italy), J.E. Beckman.

Astron. & Astrophys. Suppl. Ser. (France), vol.52, no.1, p.135-42 (April 1983).

For pt.I see *ibid.*, vol.47, no.2, p.295-317 (1982). The authors have monitored, over a period of some four years, the chromospheric h and k emission cores of the G dwarfs and sub-dwarfs β Jyi (14), ζ Tuc (5), δ Pav (5) and τ Cet (5), using the long wavelength (LWR) camera of the IUE satellite. The authors supplemented their own data with equivalent IUE archive spectra. Precise and detailed statistical examination of the data shows that no variation in h or k fluxes of less than 15% could have been detected using this technique. This limit applies, even after removing the effects of saturation, of variable gain, and (as far as practicable) of scattered light between echelle orders, and clearly applies to any astrophysical use of comparable IUE data. No flux excursions larger than this value were detected in any of the objects. (10 refs.)

64473 ψ^3 Piscium and the rotation-activity connexion. D.F. Stickland, D. Williams (Royal Greenwich Obs., Hailsham, England).

Observatory (GB), vol.103, no.1053, p.58-62 (April 1983). IUE observations of the rapidly rotating ψ^3 Psc and a number of RS CVn systems, together with data from the literature, have been studied to clarify the relationship between axial rotation and chromospheric activity. (19 refs.)

Infrared speckle imaging: improvement of the method; results on Miras and protostars See Entry 64392

Radial velocity studies of cataclysmic binaries. I. KR Aurigae See Entry 64474

Carbon stars and the seven dwarfs See Entry 64476

Coordinated Einstein and IUE observations of a disarptions brusques type flare event and quiescent emission from Proxima Centauri See Entry 64477

The flare activity of V780 Tau See Entry 64480

The ultraviolet reddening of Be stars See Entry 64481

R 66(Aeq): an LMC B supergiant with a massive cool and dusty wind See Entry 64482

HR 6522: a previously unknown multiperiodic delta Scuti star See Entry 64484

On the variability of the two brightest stars in the galactic cluster IC 2391 See Entry 64485

The nature of the cool component of the BX Monocerotis symbiotic system See Entry 64487

Spectrum of 11 Cam in 1980-1981 See Entry 64489

Herbig-Haro 57 See Entry 64491

The early B-type eclipsing binary FZ CMa (HD 52942): a massive triple system See Entry 64511

The curious case of zeta Aurigae See Entry 64512

HD 85037: probable new eclipsing variable See Entry 64514

- Spectroscopic binary orbits from photoelectric radial velocities. XLIX. HD 80655 See Entry 64515
 Radiation processes in stellar X-ray sources See Entry 64516
 Investigation of the region around the emission nebula IC 1848 See Entry 64530
 The origin of the nonthermal radio emission in normal disk galaxies See Entry 64539
 Aperture synthesis observations of Orion B at 2.695 and 8.085 GHz See Entry 64553

97.30 VARIABLE AND PECULIAR STARS

(inc. novae)

- 64474 Radial velocity studies of cataclysmic binaries. I. KR Aurigae.** A.W.Shafter (Dept. of Astron., Univ. of California, Los Angeles, CA, USA). *Astrophys. J. (USA)*, vol.267, no.1, pt.1, p.222-31 (1 April 1983).
 Presents spectroscopic observations of KR Aur which reveal the object to be a close binary system with an orbital period of 3.907 hr. This result, in conjunction with the overall spectroscopic characteristics of the object, confirm the classification of KR Aur as a cataclysmic variable. Under this assumption, masses of 0.7 and 0.48 M_{\odot} are estimated for the white dwarf and the red dwarf, respectively. The methods employed in measuring the radial velocities and in estimating the masses are discussed. (37 refs.)
- 64475 Time-resolved spectrophotometry of the nova-like variable RW Trianguli.** R.H.Kaitchuck, R.K.Honeycutt, E.M.Schlegel (Astron. Dept., Indiana Univ., Bloomington, IN, USA). *Astrophys. J. (USA)*, vol.267, no.1, pt.1, p.239-55 (1 April 1983).
 The nova-like system RW Tri has been observed with the 2.1 m telescope and the IIDS of KPNO, resulting in 200 time-resolved photometric-quality spectra. These spectra simultaneously yield continuum photometry, emission line fluxes, line profiles, and radial velocities at all phases of the 5 hour 34 minute period of RW Tri. Estimates of the orbital inclination, stellar masses, and disk size are presented. (24 refs.)
- 64476 Carbon stars and the seven dwarfs.** M.Aaronson (Steward Obs., Univ. of Arizona, Tucson, AZ, USA), E.W.Olszewski, P.W.Hodge. *Astrophys. J. (USA)*, vol.267, no.1, pt.1, p.271-9 (1 April 1983).
 Reports the discovery of carbon stars in the Leo I, Leo II, and Ursa Minor dwarf spheroidal galaxies. Such stars have now been identified in all seven of the dwarf spheroidal galaxies known to surround the Milky Way. C_2 and CN band strengths are presented; while these are well correlated with each other, there appears to be a wide range in band strength at fixed color. The number of carbon stars does not seem to be a simple function of parent galaxy luminosity, nor, by implication of metallicity. The first measured radial velocities for the Leo dwarf galaxies are also reported. (46 refs.)
- 64477 Coordinated Einstein and IUE observations of a disaripions brusques type flare event and quiescent emission from Proxima Centauri.** B.M.Haisch (Lockheed Palo Alto Res. Lab., Palo Alto, CA, USA), J.L.Linsky, P.L.Bornmann, R.E.Stencel, S.K.Antiochos, L.Golub, G.S.Vaiana. *Astrophys. J. (USA)*, vol.267, no.1, pt.1, p.280-90 (1 April 1983).
 Reports simultaneous Einstein and IUE observations of the dM5e flare star Proxima Centauri during a 5 hour period in 1980 August. A major X-ray flare was observed in its entirety with the Einstein IPC. The authors present a detailed X-ray light curve, temperature determinations during various intervals, and UV line fluxes before, during and after the flare. There is indirect evidence for a 'two-ribbon flare'-like prominence eruption. The corona of Proxima Cen is analyzed in the context of static loop models; less than 6% of the stellar surface seems to be covered by X-ray emitting active regions. (55 refs.)
- 64478 Infrared photometry of southern Wolf-Rayet stars.** A.Pitault, N.Epchein, A.E.Gomez, M.C.Lortet (Section d'Astrophys. de Meudon, Obs. de Paris, Meudon, France). *Astron. & Astrophys. (Germany)*, vol.120, no.1, pt.1, p.53-7 (April 1983).
 New JHKL photometric observations of forty-nine southern Wolf-Rayet stars are presented. After correcting the magnitudes for emission line contribution, the position of the different subtypes in a $H-K-L$ colour diagram is discussed. Except for the late type WC stars, no evidence is found for a relationship between near infrared excess and spectral type. Comparison of the observed flux distribution with the empirical model of Hartmann and Cassinelli suggests a variation from star to star in the velocity law of the wind. In the near infrared range, the different subtypes constitute heterogeneous groups. (31 refs.)
- 64479 Evolution of chemical abundances in massive stars. II. Abundance anomalies in Wolf-Rayet stars in relation with cosmic rays and ^{22}Ne in meteorites.** A.Maeder (Geneva Obs., Sauverny, Switzerland). *Astron. & Astrophys. (Germany)*, vol.120, no.1, pt.1, p.130-5 (April 1983).
 For pt.1 see *ibid.*, vol.120, no.1, p.113-29 (1983). A close comparison is made between the very anomalous abundances found in models of Wolf-Rayet stars and the excesses of several isotopic ratios in the galactic cosmic rays (GCR). Attention is paid to the dilution problem of one peculiar GCR source in the overall flux. The reliable excesses of the abundance of ^{12}C , of the isotopic ratios $^{22}\text{Ne}/^{20}\text{Ne}$, $^{25}\text{Mg}/^{24}\text{Mg}$, and $^{26}\text{Mg}/^{24}\text{Mg}$ in GCR can be remarkably well accounted for by a unique dilution factor of 1 particle originating from WR stars among 50 particles in the overall GCR flux. The author examines whether the anomalous neon component (Ne-E heavily enriched in ^{22}Ne) in some carbonaceous chondrites could originate from grains condensed in the winds of some pre-solar WC stars. WC stars appear to be important contributors to the galactic enrichment in ^{22}Ne . (48 refs.)
- 64480 The flare activity of V780 Tau.** B.R.Pettersen (Inst. of Math. & Phys. Sci., Univ. of Tromsø, Tromsø, Norway). *Astron. & Astrophys. (Germany)*, vol.120, no.2, pt.2, p.192-6 (April 1983).
 Photoelectric flare monitoring has revealed seventeen U-filter flares on V780 Tau. The flares occurred with a time spacing between 2 and 36 min (average of 14 min). Analysis of the cumulative energy distribution of the flares concludes that forty-seven per cent of the U-filter radiation from the star is generated by flare activity. This puts V780 Tau among the most active flare stars in the solar neighbourhood. In many respects V780 Tau resembles the prototype flare star system UV Cet. The majority of the flares are low energy small amplitude events that occur frequently. The data are used to test the 'reservoir hypothesis' for stellar flares, but no support is found for expected correlations between interflare spacings and the quantities of the preceding or the next flares. (10 refs.)
- 64481 The ultraviolet reddening of Be stars.** R.Schild (Harvard-Smithsonian Center for Astrophysics, Cambridge, MA, USA). *Astron. & Astrophys. (Germany)*, vol.120, no.2, pt.2, p.223-6 (April 1983).
 Following the demonstration by Schild (1978) that many Be stars have an intrinsic $(B-V)$ color excess, the author examines the ultraviolet extinction of several bright Be stars. It is found that stars having an intrinsic $(B-V)$ color excess do not have the 0.22 μ bump found in the interstellar reddening law of Bless and Savage (1972). (11 refs.)
- 64482 R 66(Aeq): an LMC B supergiant with a massive cool and dusty wind.** O.Stahl, B.Wolf, F.-J.Zickgraf (Landessternwarte, Heidelberg, Germany), U.Bastian, M.J.H.de Groot, C.Leitherer. *Astron. & Astrophys. (Germany)*, vol.120, no.2, pt.2, p.287-96 (April 1983).
 High dispersion spectroscopic groundbased and IUE observations and UBV and infrared (JHKLM) photometric observations of the peculiar emission line star R 66 (Aeq) in the LMC are discussed. From the data the authors derive a model consisting of a massive ($M=30 M_{\odot}$), luminous ($L=310^5 L_{\odot}$) B-type supergiant ($T_{\text{eff}}=12000\text{K}$, $\log g=2.0$). This star is surrounded by a dense, rather cool ($T=8000\text{K}$) expanding envelope and a circumstellar dust shell with a temperature of $T=1100\text{K}$ at its inner edge. The massive flow ($M=310^5 M_{\odot} \text{ yr}^{-1}$) has a measured maximum velocity ($v_{\text{max}}=307 \text{ km s}^{-1}$) equal to the surface escape velocity and can be characterized by a ballistic velocity law. This particular decelerated massive wind of R66 is supposed to create the favourable conditions for the formation of dust grains in its outer parts. R66 belongs to the massive ($M \geq 25 M_{\odot}$) post-main-sequence envelope objects characterized by drastic mass-loss rates of the order of a few times $10^{-5} M_{\odot} \text{ yr}^{-1}$. Although not having shown any variations, a detailed comparison revealed that R66 has many characteristics in common with S Dor variables during maximum phase. The authors give arguments that massive stars may spend about 20% of their B supergiant evolutionary phase as drastic mass losers. (30 refs.)
- 64483 Intrinsic colours and absolute magnitudes of selected R Coronae Borealis variables.** A.E.Rosenbush. *Astrometriya & Astrofiz. (USSR)*, no.47, p.17-21 (1982). In Russian.
 Analyzes observational data for S Apodis, XX Camelopardalis, V and WX Coronae Austrinae, R Coronae Borealis, Y Muscae, RT Normae, RY Sagittarii, and RS Telescopii. (21 refs.)
- 64484 HR 6522: a previously unknown multiperiodic delta Scuti star.** C.Waelkens (Obs. de Geneve, Geneva, Switzerland), P.Bartholdi. *Astron. & Astrophys. Suppl. Ser. (France)*, vol.52, no.1, p.1-12 (April 1983).
 Multiperiodic light and colour variations are reported for the F2 giant HR 6522. Since this star belongs to the instability strip, it can be classified as a δ Scuti star. The pulsation periods are 0.21712 days, 0.13885 days and 0.11160 days. From various considerations it appears that these three pulsation components can be identified with the fundamental radial mode and the second and the third radial overtones, respectively. (8 refs.)
- 64485 On the variability of the two brightest stars in the galactic cluster IC 2391.** C.Waelkens (Obs. de Geneve, Geneva, Switzerland), F.Rufener. *Astron. & Astrophys. Suppl. Ser. (France)*, vol.52, no.1, p.21-5 (April 1983).
 Short-period pulsations have been suspected for the two brightest stars of the galactic cluster IC 2391. New photometric data show that both stars are indeed variable, but on a longer time scale. For omicron Velorum, a period of 2.779 days is found, and it is shown that the existing data are consistent with this period. For HR 3467, a period of 1.553 days is derived. None of these stars varied on a shorter time scale. Possible explanations for the observed variations are discussed. (16 refs.)
- 64486 High speed photometry of PG0244+104.** B.Warner (Dept. of Astron., Univ. of Cape Town, Cape Town, S Africa). *Inf. Bull. Variable Stars (Hungary)*, no.2295, p.1 (17 March 1983).
 The author reports high speed photometry on 1982 December 18 of the cataclysmic variable candidate PG 0244+104. A light curve obtained during two hours of observations is presented; the evident photometric activity in this light curve shows the star to be a rapid variable of the cataclysmic class. In addition, the mean light level of the star corresponds to a B-magnitude of about 14.7, considerably brighter than the B-magnitude of 15.8 found by Green et al. (1982). (1 ref.)
- 64487 The nature of the cool component of the BX Monocerotis symbiotic system.** P.A.Whitelock, R.M.Catchpole (South African Astron. Obs., Cape Town, S Africa). *Inf. Bull. Variable Stars (Hungary)*, no.2296, p.1-3 (18 March 1983).
 BX Monocerotis is a peculiar variable star that at first sight appears to be a symbiotic star in which the cool component is a Mira variable: it undergoes large-amplitude light variations with a period of 1374 days, and it has a composite spectrum with very strong H I emission lines. The authors report infrared observations which indicate that the cool component of the star is not, in fact, a Mira variable. First, the infrared colours obtained from JHKL photometry on 1982 November 20 do not fall in the regions of the IR two-colour diagrams occupied by Mira variables, nor do they indicate the presence of the dust excess typical of symbiotic systems containing Mira variables. Second, the near-IR spectrum (1.2 to 2.5 μ) of BX Mon, obtained on 1983 January 28, is typical of a non-Mira M-type giant, except for the presence of Paschen- β emission. The cool component of the system appears from these observations to be a normal M5 III star. It is suggested that the strong Balmer emission lines originate in the nebulosity surrounding the binary system, and that they are excited by the hot component. The light variations are more difficult to explain: they are not typical of a semi-regular variable star, and the authors suggest that they are actually associated with the orbital motion of the binary system. (8 refs.)
- 64488 On the constancy of the period of the magnetic Ap star HD 215441.** A.Hempelmann, W.Schoneich (Astrophys. Obs. Potsdam, Potsdam, Germany). *Inf. Bull. Variable Stars (Hungary)*, no.2297, p.1-3 (18 March 1983).
 The authors briefly describe a method for determining the brightness distribution over the surface of a magnetic Ap star, and for deriving the phase angle (θ) at which the centre of the photometrically peculiar region crosses the line of sight. This method is applied to an investigation of the period of light variation of HD 215441. First the wavelength dependence of θ is determined using the light curves obtained from ten-colour photometry (Schoneich et al., 1976) and from UV photometry (Leckrone 1974). It is found that θ is constant for $\lambda > 2000 \text{ \AA}$. Second, the angle θ is computed for all the available photometric observations using the elements $JD_0=2441902.49+9.4875 E$, and the values of θ are presented as a function of time from 1960 to 1982. There is no significant variation of θ during this time, and it therefore concluded that during the last 22 years there has been no change in the period of HD 215441. (9 refs.)
- 64489 Spectrum of 11 Cam in 1980-1981.** L.S.Luud, V.A.Mineva, B.Zh.Kovachev. *C.R. Acad. Bulg. Sci. (Bulgaria)*, vol.35, no.9, p.1177-80 (1982). In Russian.
 Observations were made in late 1980 and early 1981 of the Be-type star 11 Cam with the aid of a two-metre telescope. Six spectrograms were obtained for the wavelengths 3500-5000 \AA . The most interesting absorption lines of the star were those of the Balmer series, in which is observed a significant emission through the shell of the star. The spectral characteristics of the star were determined, and the Balmer decrements as calculated from the observational

data were compared with the theoretical values. Changes in the contours of the spectral lines of H_α , H_β and H_γ during the course of a night and a 24-hour period were recorded. (7 refs.) A.J.B.

64490 Nova Serpentis 1983. T.Iijima, S.Ortolani, L.Rosino. *I.A.U. Circ. (USA)*, no.3790, 1 pp. (7 April 1983).

The authors report that spectra of Nova Serpentis 1983 covering the period 1983 March 3 to 19 show broad emission features of H, He I, He II 468.6 nm, and N III 464.0 nm; and nebular forbidden lines of [O III] at 500.6 nm and 495.9 nm. The expansion velocity from the total halfwidth of the H emission bands is 4050 km/s. The H and He emission bands are formed by two broad symmetric features with a peak separation of about 5400 km/s, and a central narrower double-peaked emission with the components separated by 530 km/s. The nova has already entered the nebular stage and the excitation is increasing: in the last spectra obtained on 1983 March 19, He II 468.6 nm is stronger than H β . (no refs.)

64491 Herbig-Haro 57. J.A.Frogel, J.A.Graham.

I.A.U. Circ. (USA), no.3792, 1 pp. (19 April 1983).

It is reported that the recently-discovered starlike object in HH 57 is a strong infrared source which radiates most of its power longward of 5 μ m. Infrared photometry of the object between 2.2 μ m and 20.0 μ m is reported. At 10 μ m wavelength the emission appears to originate in a region with a diameter <2 arcsec centred on the stellar source, which is identified with IRS 8 of Reipurth and Wamsteker (1982). The infrared colours of the object are similar to those of FU Orionis and V1057 Cygni. There is no obvious emission or absorption feature in the 10- μ m window. Images of the object obtained under conditions of sub-arcsecond seeing confirm its stellar nature. A low-resolution spectrogram shows a red and essentially featureless energy distribution. (1 ref.)

64492 V1343 Aquilae. R.C.Lamb, J.C.Ling, W.A.Mahoney, G.R.Riegler, W.A.Wheaton, A.S.Jacobson.

I.A.U. Circ. (USA), no.3793, 1 pp. (19 April 1983).

The authors report evidence for γ -ray line emission from the region surrounding V1343 Aquilae (=SS 433), as a result of observations by the HEAO-3 satellite between October 10 and November 5, 1979, and from 4 to 25 April, 1980. Two γ -ray lines are observed, at energies of 1.5 MeV and 1.2 MeV. The average intensities of the two features are 15 ± 3 photons/ m^2/s for the 1.5 MeV line, and 11 ± 2 photons/ m^2/s for the 1.2 MeV line; both features vary by a factor of about five on a time scale of days. The combined power in the lines is about 2×10^{40} J/s. The lines varied by about 40 keV over 20 days during the 1979 observations. These spectral features are explained as blueshifted and redshifted components of the 1.369 MeV line from nuclear de-excitation of ^{24}Mg to its ground state. The energy variation is consistent with the kinematic model used to interpret the optical and radio phenomena previously observed in SS 433. (no refs.)

64493 KR Aurigae. J.Bortle.

I.A.U. Circ. (USA), no.3793, 1 pp. (19 April 1983).

The author reports visual magnitude estimates for the cataclysmic binary star KR Aurigae for the epochs 1983 March 21 and April 2; the star is at about magnitude 13.5. (no refs.)

RAS Specialist Discussion on Astrophysical Applications of Accretion Disks (Papers in summary form only received) See Entry 59533

Infrared speckle imaging: improvement of the method; results on Miras and protostars See Entry 64392

Spectral line profiles from spherical shells See Entry 64464

Evolution of chemical abundances in massive stars. I. OB stars, Hubble-Sandage variables and Wolf-Rayet stars. Changes at stellar surfaces and galactic enrichment by stellar winds See Entry 64467

Linear polarization variations of six T Tauri stars See Entry 64469

The ultraviolet spectrum of the supermassive object R136a. I. The mass loss rate See Entry 64471

Infrared photometry of the RS CVn binaries. I. TY Pyxidis See Entry 64509

Light curves of four southern bright hitherto unknown eclipsing binaries See Entry 64513

HD 85037: probable new eclipsing variable See Entry 64514

Cepheids and spiral structure See Entry 64548

97.60 LATE STAGES OF STELLAR EVOLUTION

(inc. black holes)

Gravitational lens effects of neutrino astronomical objects See Entry 64362

97.60B Supernovae

64494 Supernovae. H.Kosai, Y.Kozai, R.Evans, G.Thompson, R.W.Argyle.

I.A.U. Circ. (USA), no.3789, 1 pp. (7 April 1983).

Reports the discovery on 1983 April 4 of a 13th-magnitude supernova 10" west and 20" south of the nucleus of NGC 4753. The precise position of the supernova is $\alpha=12^h49^m47.23^s$, $\delta=-00^\circ55'54.2''$ (equinox 1950.0). In addition, a precise position is given for the supernova in NGC 3044 (c.f. IAU 3787), namely $\alpha=09^h51^m08.05^s$, $\delta=+01^\circ48'45.2''$ (equinox 1950.0). The supernova is 29" east and 11" south of the nucleus of NGC 3044; its photographic magnitude on 1983 March 31 was about 15. (1 ref.)

64495 Supernovae. J.Maza, R.W.Argyle.

I.A.U. Circ. (USA), no.3792, 1 pp. (19 April 1983).

Reports the discovery on 1983 April 14 of a possible 18th-magnitude supernova 57" east and 10" south of the nucleus of the galaxy NGC 7083 ($\alpha=21^h31.8^m$, $\delta=-64^\circ07'$, equinox 1950.0), in Indus. In addition a precise position is reported for the supernova in NGC 4753, namely $\alpha=12^h49^m46.91^s$, $\delta=-00^\circ55'55.0''$ (equinox 1950.0); the photographic magnitude of the supernova on 1983 April 12 was 13.3. (no refs.)

64496 Supernovae. II. The aftermath. V.Trimble (Dept. of Phys., Univ. of California, Irvine, CA, USA).

Rev. Mod. Phys. (USA), vol.55, no.2, p.511-63 (April 1983).

Part I see *ibid.*, vol.54, no.4, p.1183-224 (1982) explored stellar evolution leading up to supernovae and observations and models of the events themselves. Part II addresses the aftermath: supernova remnants, products, and by-products, including nucleosynthesis, and the future of supernova research. Some of the important questions are: (1) How close is the association among supernova events, pulsar production, and remnant production? (2) Where does most of the energy from neutron star formation go? and (3) How do supernovae interact with the rest of the Universe, for instance in heating and stirring the interstellar medium, accelerating cosmic rays, and triggering or inhibiting star formation. (760 refs.)

The effects of sudden mass loss and a random kick velocity produced in a supernova explosion on the dynamics of a binary star of arbitrary orbital eccentricity. Applications to X-ray binaries and to the binary pulsars See Entry 64508

97.60G Pulsars

64497 On the origin of the recently discovered ultra-rapid pulsar. V.Radhakrishnan, G.Srinivasan (Raman Res. Inst., Bangalore, India).

Curr. Sci. (India), vol.51, no.23, p.1096-9 (5 Dec. 1982).

The rapid rotation rate of ~ 1.5 ms of the newly discovered pulsar PSR 1937+21 is attributed to spin-up in a long-lived mass transfer binary. Such a history leads to a prediction of a very low period derivative $\sim 6 \times 10^{-19}$ ss^{-1} for this pulsar. The gravitational radiation from this pulsar is expected to be negligible. (17 refs.)

64498 Loss of angular momentum in a binary system due to collisionless particles as monopoles or gravitinos: does it exceed the gravitational radiation emission in the binary system PSR 1913+16? D.Fargion (Istituto di Fisica, Univ. di Roma, Roma, Italy).

Lett. Nuovo Cimento (Italy), vol.36, ser.2, no.14, p.449-52 (2 April 1983).

The authors consider the gravitational drag for a massive object moving in the (almost) collisionless fluid made by magnetic monopoles: the drag mechanism may be relevant in the loss of angular momentum in binary systems; in particular for a known binary system in our Galaxy associated with pulsar PSR 1913+16 they show that a monopole number density larger than 10^{-7} cm^{-3} (as the expected solar one) may induce an energy loss comparable or even larger than the one in debt to the gravitational radiation of the system. (16 refs.)

64499 High-resolution X-ray and radio maps of the millisecond pulsar. R.H.Becker (Virginia Polytech. Inst. & State Univ., Blacksburg, VA, USA), D.J.Helfand.

Nature (GB), vol.302, no.5910, p.688-90 (21 April 1983).

Radioastronomical and X-ray observations of this object are presented. A stringent upper limit is placed on any X-ray emission from the pulsar. High-resolution multi-frequency radio maps of the region which provide the best available pulsar position are presented. The authors argue against any connection between the pulsar and the nearby extended radio emission region and comment on the constraints which the X-ray data place on the nature of the this object. (10 refs.)

64500 Polarimetry of the millisecond pulsar. D.R.Stinebring (Nat. Radio Astron. Obs., Charlottesville, VA, USA).

Nature (GB), vol.302, no.5910, p.690-2 (21 April 1983).

The millisecond pulsar PSR 1937+21 might be expected to have unique waveform and polarization properties as a result of its remarkably short period and small spin-down rate. The author presents polarization observations of the main pulse and interpulse at 1415 and 2380 MHz that have higher time resolution than previously available. The main pulse depolarizes substantially over this frequency range whereas the interpulse polarization almost doubles. There is evidence that orthogonally polarized radiation is present on the leading edge of the main pulse and the trailing edge of the interpulse and that it accounts for the $\sim 90^\circ$ difference in position angle between the main pulse and interpulse. The interpulse decreases in intensity relative to the main pulse as f^{-1} , indicating (if the trend continues to lower frequency) that the high frequency interpulse dominates the main pulse below ~ 700 MHz. The main pulse is found to consist of two closely spaced components. (11 refs.)

64501 Prediction of pulsar glitch frequency based on the hard superfluid model. N.Itoh (Dept. of Phys., Sophia Univ., Tokyo, Japan).

Prog. Theor. Phys. (Japan), vol.69, no.1, p.338-40 (Jan. 1983).

Prediction of the pulsar glitch frequency is made on the basis of the hard superfluid model for pulsar glitches. It is likely that further superglitches will be observed in some of the most rapidly decelerating pulsars in the near future. (12 refs.)

64502 Plasmas in superstrong pulsar fields. H.Herold, H.Ruder (Lehrstuhl für Theoretische Astrophys., Univ. Tübingen, Tübingen, Germany).

Phys. Scr. (Sweden), vol.T2, no.1, p.206-14 (1982). (1982 International Conference on Plasma Physics, Göteborg, Sweden, 9-15 June 1982).

The observed emission of both radio and X-ray pulsars originates from plasmas under very extreme conditions. The common property is the occurrence of huge magnetic fields of the order of 10^8 T. Concerning the complex of problems associated with radio pulsars, the authors investigate the equations governing the magnetosphere of an aligned rotator and discuss possible structures of self-consistent solutions, and deal with the accretion columns of X-ray pulsars, especially with the electron-photon interactions in hot strongly magnetized plasmas. (34 refs.)

64503 Some nonlinear mechanisms of pulsar emission. J.G.Lominadze, A.D.Pataraya (Abastumani Astrophys. Obs., Acad. of Sci., Tbilisi, Georgian SSR).

Phys. Scr. (Sweden), vol.T2, no.1, p.215-22 (1982). (1982 International Conference on Plasma Physics, Göteborg, Sweden, 9-15 June 1982).

Gives results obtained from the theory of linear and nonlinear waves propagating in relativistic electron-positron plasma with a strong external magnetic field. The possible application of these results to explain the radiation mechanism in pulsars is discussed. The nonlinear equation describing the behaviour of the amplitude profile of the waves, propagating at an angle to the external magnetic field, is studied in the low frequency region. The radiation intensity of a pulsar is calculated in terms of soliton solution of the equation. The results obtained are compared with the experimental data. Two mechanisms of formation of bunches along the magnetic field are considered. (51 refs.)

Relativistic astrophysics See Entry 59551

Supernovae. II. The aftermath See Entry 64496

The effects of sudden mass loss and a random kick velocity produced in a supernova explosion on the dynamics of a binary star of arbitrary orbital eccentricity. Applications to X-ray binaries and to the binary pulsars See Entry 64508

97.60J Neutron stars

64504 Equilibrium composition and neutrino emissivity of interacting quark matter in neutron stars. R.C.Duncan, S.I.Shapiro, I.Wasserman (Center for Radiophysics & Space Res., Cornell Univ., Ithaca, NY, USA).

Astrophys. J. (USA), vol.267, no.1, pt.1, p.358-70 (1 April 1983).

Shows that a detailed treatment of the equilibrium composition of a quark liquid is crucial to the accurate evaluation of its neutrino emissivity. When massive s-quarks are present in cold quark matter, the electron fraction Y_e vanishes above a finite baryon density n_{ex} . This results in a vanishing total

emissivity at high densities, to lowest order in kT . The phase transition at which s-quarks first appear is also studied in detail. The dependences of the composition and emissivity of quark matter on the strange quark mass m_s and QCD coupling constant (at neutron star densities) α_s are calculated. The implications for neutron star cooling calculations are discussed. (31 refs.)

64505 Effect of the neutron 3P_2 pairing on the π^0 condensation threshold in neutron star matter. F.Asai (Dept. of Phys., Osaka Univ., Osaka, Japan). *Prog. Theor. Phys. (Japan)*, vol.69, no.1, p.348-50 (Jan. 1983). Phase transition of neutron star matter into a π^0 condensate is suppressed by the neutron 3P_2 pairing. In practice this suppression brings about no significant change in the condensation threshold predicted so far. (7 refs.)

64506 Temperature effect on the dynamics of neutron stars with pion-condensation. Yu.A.Berezin, B.G.Mukanova, M.N.Fedoruk. *Pis'ma v Astron. Zh. (USSR)*, vol.9, no.2, p.116-19 (1983). In Russian. English translation in: *Sov. Astron. Lett. (USA)*. Taking into account the finite temperature of the neutron star with pion-condensation, results in increasing the star radius, and decreasing the core mass, core radius, central density and density discontinuity. (3 refs.)

Relativistic astrophysics See Entry 59551

Possibility of amorphous glassy state in astrophysical dense plasmas See Entry 62441

Supernovae. II. The aftermath See Entry 64496

Radiation processes in stellar X-ray sources See Entry 64516

Is the rapidly repetitive radiation from X-ray sources due to explosive three wave interaction? See Entry 64517

Models of X-ray bursters with radius expansion See Entry 64558

97.60L Black holes

Comptonization effects in spherical accretion onto black holes See Entry 64361

Runaway instability in accretion disks orbiting black holes See Entry 64544

White holes: cosmic energy machines See Entry 64571

97.80 BINARY AND MULTIPLE STARS

(inc. extrasolar planetary systems)

64507 Rapid rotation and stellar activity in the triple system HD 165590. R.A.Stern (Jet Propulsion Lab., California Inst. of Technol., Pasadena, CA, USA), A.Skumanich.

Astrophys. J. (USA), vol.267, no.1, pt.1, p.232-8 (1 April 1983). Reports X-ray and ultraviolet observations of the spectroscopic and visual binary HD 165590. The spectroscopic binary component has a period of 0.88^d and a near-solar spectral type. A substantial soft X-ray flux is predicted for HD 165590. This prediction is confirmed by observing an X-ray luminosity of $10^{30.6}$ ergs s^{-1} for the system. No obvious periodicities of less than 0.5^d are present in the X-ray data, although stochastic variability is present. Observations with the International Ultraviolet Explorer of transition region emission lines are consistent with the X-ray data and reveal $\sim 50\%$ variability on the time scale of days. Comparison of the results with X-ray observations of other late F and G stars demonstrates that rotation-activity scaling relations are useful as gross predictors of X-ray emission. (47 refs.)

64508 The effects of sudden mass loss and a random kick velocity produced in a supernova explosion on the dynamics of a binary star of arbitrary orbital eccentricity. Applications to X-ray binaries and to the binary pulsars. J.G.Hills (Theoretical Div., Los Alamos Nat. Lab., Los Alamos, NM, USA). *Astrophys. J. (USA)*, vol.267, no.1, pt.1, p.322-33 (1 April 1983). Calculates the probability of survival of binaries and the changes in orbital elements of those binaries that do survive as a function of the mass loss experienced in the supernova explosion and of the kick velocity given the neutron star (or black hole). This is done for the general case where the preexplosion orbit can have an arbitrary eccentricity. (27 refs.)

64509 Infrared photometry of the RS CVn binaries. I. TY Pyxidis. E.Antonopoulou (Royal Obs. of Edinburgh, Edinburgh, Scotland). *Astron. & Astrophys. (Germany)*, vol.120, no.1, pt.1, p.85-8 (April 1983). Infrared light curves of the RS CVn-type binary TY Pyxidis (HD 71737) in J, H, and K have been obtained and nearly sinusoidal light variations outside eclipse have been detected, similar to those observed in other RS CVn systems. The period of these variations is approximately equal to the orbital period of the system and their amplitude decreases with increasing wavelength. Irregular light variations have also been observed. There is no conspicuous infrared excess attributable to circumstellar emission. (11 refs.)

64510 The combined effect of mass loss and overshooting. III. Evolutionary scenarios for massive close binaries. C.Doom, J.P.de Greve (Astrophys. Inst., Vrije Univ. Brussel, Brussel, Belgium).

Astron. & Astrophys. (Germany), vol.120, no.1, pt.1, p.97-105 (April 1983). For pt.II see *ibid.*, vol.116, no.2, p.308-11 (1982). The evolution of massive close binaries is revised by taking into account overshooting from convective cores. Nine different evolutionary scenarios are presented, resulting from the introduction of an Of phase for each component. The theoretical results are compared to observations of Wolf-Rayet binaries and X-ray binaries. It is found that X-ray binaries originate from the lower mass Wolf-Rayet binaries. The existence of WR+Of stars is predicted. (46 refs.)

64511 The early B-type eclipsing binary FZ CMa (HD 52942): a massive triple system. A.F.J.Moffat (Astron. Inst., Univ. Bonn, Bonn, Germany), N.Vogt, L.P.R.Vaz, B.Gronbech.

Astron. & Astrophys. (Germany), vol.120, no.2, pt.2, p.278-86 (April 1983). New photoelectric observations in *uvby* are used to construct a light curve of this double-line eclipsing system in which two components (A,B), each of type B 2.5 IV-V, revolve in a 1.27 d orbit. Modelling of the mean light curve yields: orbital inclination $i=88^\circ$; effective temperature $T_B \approx 20,600K$ ($T_A \approx 22,000K$ assumed); stellar radii $R_A \approx R_B \approx 0.28 a$ (a is the mean orbital separation) $\approx 3.1 R_\odot$; visual luminosity ratio $L_B/L_A \approx 0.89$. Hence, A and B are nearly equal, with the primary (A) being slightly hotter and more luminous. However, a consistent solution of the light curve could be achieved only if a third body, denoted X, contributes 43% to the total flux in *u,b*, *y* and 36% in *v*. The third body manifests itself independently by periodic modulation in the times of minimum light, although it is not seen directly in the spectrum. Analysis of the 23 observed-minus-predicted times of minima, spread over 8 yr, leads to $P_X = 537$ d, $e_X = 0.56$ and $A_{AB} \sin i_X = 1.94$ AU. Photographic coude spectroscopy of the A+B components yields the masses $m_A \approx m_B \approx 5.3 M_\odot$ and orbital radii $a_A \approx a_B \approx 5.5 R_\odot$. The effective Roche-lobe radii are $\approx 4.1 R_\odot$ for each star, implying that the present A+B system is well detached. (26 refs.)

64512 The curious case of zeta Aurigae. D.Darling (Univ. of Manchester, Manchester, England).

Astronomy (USA), vol.11, no.3, p.66-70 (March 1983). Presents a general discussion on the nature of zeta Aurigae. The positions of the components on the HR diagram are discussed. Various models for the available observations are briefly discussed. (no refs.)

64513 Light curves of four southern bright hitherto unknown eclipsing binaries. C.Waelkens (Obs. de Geneve, Geneve, Switzerland), F.Rufener. *Astron. & Astrophys. Suppl. Ser. (France)*, vol.52, no.1, p.13-20 (April 1983). Photometric light curves are presented for four bright southern eclipsing binaries, that were not yet known as variable stars or for which the variability was not yet understood. HR 7464 is a probable Am star in an eclipsing binary; the known single-lined spectroscopic binary HR 7422 shows two similar eclipses, so spectra with a high resolution should reveal the secondary too; both HR 6621 and HR 5034 are early-type close binaries for which there is evidence for variations of the orbital period. In particular, HR 5034 is an evolved B3 star with an orbital period of only 1.278 day, so it could be near a contact configuration. (13 refs.)

64514 HD 85037: probable new eclipsing variable. P.Renson (Univ. de Liege, Liege, Belgium).

Inf. Bull. Variable Stars (Hungary), no.2298, p.1-3 (18 March 1983). In French.

In the course of photometric observations of the Ap star HD 83368 during December 1975 and February 1977, it was discovered that one of the comparison stars, namely the Ap star HD 85037 (=GC 13508= CoD-49°4692; spectral type A0p), was itself variable. The author describes the results of *uvby* photometry of HD 85037, and presents a *y*-band light curve. The probable period of the light variation is 1.346 days. The origin adopted for the phase is the epoch JD 2442763.00. Phase zero corresponds to a sharp minimum ($\Delta m \sim 0.09$ mag.) indicated by two of the measurements which may be due to an eclipse; there is also a possible secondary minimum at about phase 0.7. In addition there is a general small-amplitude light variation ($\Delta m \sim 0.02$ mag.) with a single maximum at about phase 0.4. The implications of these observations are discussed. (3 refs.)

64515 Spectroscopic binary orbits from photoelectric radial velocities. XLIX. HD 80655. R.F.Griffin (Cambridge Obs., Cambridge, England).

Observatory (GB), vol.103, no.1053, p.56-7 (April 1983). For pt.XLVIII see *ibid.*, vol.103, no.1052, p.17-20 (1983). The author reports radial velocity measurements and orbital elements for the M-type giant star HD 80655. (4 refs.)

64516 Radiation processes in stellar X-ray sources. S.Hayakawa (Dept. of Astrophys., Nagoya, Japan).

Phys. Scr. (Sweden), vol.T2, no.1, p.167-76 (1982). (1982 International Conference on Plasma Physics, Goteborg, Sweden, 9-15 June 1982).

Mechanisms of X-ray emission from white dwarfs and neutron stars are reviewed by paying attention to radiative transfer processes. The values of plasma parameters concerned are summarized. Comptonization processes in non-magnetic plasmas are discussed. Effects of magnetic fields on radiative transfer are considered with regard to the energy dependent pulse profiles and the spectra observed for X-ray pulsars. An observational result of the super-high luminosities of X-ray bursts in excess of the Eddington limits are presented. Difficulties in accounting for such events if the bursts are triggered by nuclear flash are mentioned. (18 refs.)

64517 Is the rapidly repetitive radiation from X-ray sources due to explosive three wave interaction? H.Wilhelmsson, L.-O.Pekkari, D.Andersson (Inst. for Electromagnetic Field Theory, Chalmers Univ. of Technol., Goteborg, Sweden).

Phys. Scr. (Sweden), vol.T2, no.1, p.271-2 (1982). (1982 International Conference on Plasma Physics, Goteborg, Sweden, 9-15 June 1982).

Several features of the rapidly repetitive radiation from compact X-ray sources are suggestive of the explosive three-wave interaction as generating mechanism. The possibility of such an explanation is discussed and it is shown that this could account for the observed energy range of the radiation as well as the observed variable burst patterns. (8 refs.)

64518 Angular distribution of radiation from the plasma of X-ray pulsars taking into account vacuum polarization by magnetic fields. A.D.Kaminker, G.G.Pavlov, Yu.A.Shibanov.

Pis'ma v Astron. Zh. (USSR), vol.9, no.2, p.108-15 (1983). In Russian. English translation in: *Sov. Astron. Lett. (USA)*

Angular distributions of X-ray radiation from a homogeneous, optically thick and strongly magnetized plasma are calculated for a wide range of photon energies and plasma number densities appropriate for the radiating regions of X-ray pulsars. Angular distributions are shown to be significantly affected by vacuum polarization. It is noted that under certain conditions there are strong changes of the beam width. (17 refs.)

RAS Specialist Discussion on Astrophysical Applications of Accretion Disks (Papers in summary form only received) See Entry 59533

VLF ionosonde and long-distance propagation anomalies produced by galactic Cen X-4 X-ray burst in May 1979 See Entry 64295

Identification and properties of the M giant/X-ray system HD 154791=2A 1704+241 See Entry 64462

ψ^3 Piscium and the rotation-activity connexion See Entry 64473

Radial velocity studies of cataclysmic binaries. I. KR Aurigae See Entry 64474

Time-resolved spectrophotometry of the nova-like variable RW Trianguli See Entry 64475

The flare activity of V780 Tau See Entry 64480

On the variability of the two brightest stars in the galactic cluster IC 2391 See Entry 64485

The nature of the cool component of the BX Monocerotis symbiotic system See Entry 64487

V1343 Aquilae See Entry 64492

KR Aurigae See Entry 64493

Loss of angular momentum in a binary system due to collisionless particles as monopoles or gravitinos: does it exceed the gravitational radiation emission in the binary system PSR 1913+16? See Entry 64498

97.90 OTHER TOPICS IN STELLAR ASTRONOMY

No occultations by Uranus II and Pluto See Entry 64423

98.00 STELLAR SYSTEMS; GALACTIC AND EXTRAGALACTIC OBJECTS AND SYSTEMS; THE UNIVERSE

98.10 STELLAR DYNAMICS

- The formation of disc galaxies See Entry 64537
Kinematics and structure of the Galaxy at high galactic latitude See Entry 64540

98.20 STELLAR CLUSTERS AND ASSOCIATIONS

64519 Investigation of the star cluster NGC 6913 (M29). E.A.Herts. *Astrometriya & Astrofiz. (USSR)*, no.47, p.58-61 (1982). In Russian. The visible density distribution is plotted using probable members of NGC 6913, selected on the basis of their proper motions. The cluster is shown to consist of the nucleus with a $5'$ radius and a corona with $32'$ radius. The photometric distance (1200 pc) and the lower limit to the cluster mass ($1 \times 10^3 M_\odot$) are estimated. (6 refs.)

64520 An investigation of the heavily reddened young open cluster Tr 27 on the Walraven photometric system. R.Bakker, P.S.The (Astron. Inst., Univ. of Amsterdam, Amsterdam, Netherlands). *Astron. & Astrophys. Suppl. Ser. (France)*, vol.52, no.1, p.27-36 (April 1983). The light of many stars in Tr 27 is strongly attenuated by a foreground dark cloud. Employing *UBV*, *RI* and *JHKLM* data of 3 stars with known spectral types, the ratio of total to selective extinction of the foreground dark cloud was determined by means of the colour-difference method. The authors use this value and photometric data on the Walraven system for the determination of the distance of Tr 27. From the turn-off point of the cluster main sequence the age of the cluster is estimated. The absolute magnitude of several interesting members of the cluster is discussed. (32 refs.)

64521 The globular cluster NGC 6544. G.Alcaino (Inst. Isaac Newton, Ministerio de Educacion de Chile, Santiago, Chile). *Astron. & Astrophys. Suppl. Ser. (France)*, vol.52, no.1, p.105-13 (April 1983).

A color magnitude diagram (CMD) for the globular cluster NGC 6544 obtained from 164 stars measured photographically. The brighter part, which includes the horizontal branch, calibrated from a photoelectric sequence of 20 stars to a limiting magnitude $V=16.6$; and a fewer fainter stars, with a Pickering-Racine wedge. The CMD suggests 'medium metallicity' traits, and the deduced reddening of $E(B-V)=0.70$, places the object at 2.9 kpc from the Sun, 0.1 kpc from the galactic plane and 6.1 kpc from the galactic center. The location of most of the very reddened stars in the NW region, suggests the presence of differential reddening in the face of the cluster. (12 refs.)

64522 Observed radii and structural parameters of clusters in the SMC. H. E.Kontizas (Astron. Inst., Nat. Obs. of Athens, Athens, Greece), M.Kontizas. *Astron. & Astrophys. Suppl. Ser. (France)*, vol.52, no.1, p.143-59 (April 1983).

For pt.1 see *ibid.*, vol.49, no.1, p.1-12 (1982). The surface density profiles and the tidal radii have been found for 23 star clusters in the SMC, by means of star counts. The core radii concentration parameters were derived by fitting theoretical models. The masses of the 'red' and 'blue' clusters, compared to those of globular clusters of our own Galaxy, were found to be systematically 10 times less massive. The 'blue' clusters, seem to have dynamical behaviour similar to the galactic globulars. (10 refs.)

ASA 1000 and color too See Entry 64399

On the variability of the two brightest stars in the galactic cluster IC 2391 See Entry 64485

Investigation of the region around the emission nebula NGC 1499 See Entry 64531

98.40 INTERSTELLAR MATTER; AND NEBULAE

64523 The compact H II region S235A. Observations and interpretation. G.Olofsson (Stockholm Obs., Saltsjobaden, Sweden).

Astron. & Astrophys. (Germany), vol.120, no.1, pt.1, p.1-5 (April 1983). The compact H II region Sharpless 235A has been mapped in the wavelength range 1.6-20 μm . The infrared radiation peaks on a stellar object which has previously been identified as the ionizing source of the nebula. The near infrared radiation exhibits roughly the same spatial distribution as the radio continuum but is an order of magnitude brighter than the expected gas emission. This is interpreted as evidence for a clumpy or filamentary structure throughout the ionized region. A new infrared source was discovered two minutes of arc north of Sharpless 235A. It coincides with a faint nebulosity proposed to be a Herbig-Haro object. (15 refs.)

64524 The ratio of deuterium to hydrogen in interstellar space. V. The line of sight to ϵ Persei. A.Vidal-Madjar, C.Laurent, C.Gry, P.Bruston, R.Ferlet (Lab. de Phys. Stellaire et Planetaire, CNRS, Verrieres-le-Buisson, France), D.G.York.

Astron. & Astrophys. (Germany), vol.120, no.1, pt.1, p.58-62 (April 1983). For pt.IV see *Astrophys. J.*, vol.229, no.3, pt.1, p.923-41 (1979). The study of deuterium in the direction of ϵ Per has revealed a time variation of the observed D I absorption feature. To explain this variation it is supposed that H I material is present in the stellar wind producing the narrow absorption features observed on the blue wing of the Lyman lines. In consequence it appears that deuterium absorption lines may sometimes be contaminated by high-velocity H I present in stellar winds. Reviewing the previously published deuterium abundance determinations, it is shown that a correlation seems to exist between the stellar luminosity class and the D/H values, the lowest D/H value corresponding to the more evolved stars. The conclusion is that the local interstellar deuterium abundance is more probably of the order of 5×10^{-6} rather than 2×10^{-5} as previously thought. (42 refs.)

64525 A high-latitude H I cloud with optical emission. W.Georgik, U.Mebold, K.Reif, P.M.W.Kalberla, L.Velden (Radioastron. Inst., Univ. Bonn, Bonn, Germany).

Astron. & Astrophys. (Germany), vol.120, no.1, pt.1, p.63-73 (April 1983). A high latitude H I cloud ($\approx 91^\circ$, $b \approx 38^\circ$) extended over several degrees on the sky with brightness temperature $T_B \approx 20\text{K}$, velocity dispersion $\approx 1.0\text{ km s}^{-1}$ and a centre velocity $v_{LSR} \approx -21\text{ km s}^{-1}$, has been observed with the 100 m telescope. The cloud is found to be in detailed positional agreement with a faint diffuse nebula visible on the red and the blue prints of the Palomar Observatory Sky Survey. Estimates of the extinction in the nebula from star

counts indicate that the ratio of H I column density to extinction is about a factor of 10 smaller than the standard value found from UV-observations. (14 refs.)

64526 Diameter distribution and Σ -D relation of SNRs in M31 and in M33. E.M.Berkhuijsen (Max-Planck-Inst. fur Radioastron., Bonn, Germany). *Astron. & Astrophys. (Germany)*, vol.120, no.1, pt.1, p.147-9 (April 1983). The $N(<D)$ -D relations for SNRs in M31 and in M33 are much flatter than expected for SNRs in the phase of adiabatic expansion. The Σ -D relations are consistent with the relation for SNRs in the Galaxy. (18 refs.)

64527 Magnetic alignment of interstellar dust grains for dominating magnetic effects. P.Cugnon (Obs. Royal de Belgique, Brussels, Belgium). *Astron. & Astrophys. (Germany)*, vol.120, no.1, pt.1, p.156-63 (April 1983). Studies the asymptotic behaviour of the degree of alignment of interstellar dust grains, when magnetic effects become greater than collisional effects. Two different shapes, spheroids and square prisms, have been considered, for different elongations and different values of the grain/gas temperature ratio. (9 refs.)

64528 The Crab Nebula. I. Photoionization of a bright filament. D.Pequignot (Dept. d'Astrophys. Fondamentale, Obs. de Meudon, Meudon, France), M.Dennefeld.

Astron. & Astrophys. (Germany), vol.120, no.2, pt.2, p.249-62 (April 1983). Stationary photoionization models are presented for a bright filament of the Crab Nebula. Charge-exchange reactions and low-temperature di-electronic recombinations are taken into account. In a first series of models, the slope of the ionizing continuum is 0.5 in the ultraviolet range and joins smoothly to the 1.1 X-ray slope around 0.5 keV. It is demonstrated that constant density and constant thermal pressure models are definitely unable to explain the observations. Satisfactory models accounting for virtually all available lines from UV to IR can be obtained if the thermal pressure in the bulk of the filament is about twice that of the outer parts; the high-excitation lines are predicted to arise from an extended zone of several arcseconds. It is confirmed that the filament should be cylinder-like rather than sheet-like. It is found that not only helium but heavy elements as well as overabundant relative to H: the abundances per nucleon are quite typical of Population I so that the initial mass of the precursor of the supernova is now allowed to be large. (51 refs.)

64529 Detection of HCO^+ and HCN absorption towards three galactic H II-regions. L.-A.Nyman (Onsala Space Obs., Onsala, Sweden).

Astron. & Astrophys. (Germany), vol.120, no.2, pt.2, p.307-12 (April 1983). HCO^+ and HCN absorption have been detected towards W49, W51, and DR 21 and a detection limit has been placed on HNC absorption towards W49. The velocities of the lines imply absorbing gas near the sources as well as in diffuse spiral arm clouds. The observations suggest that HCO^+ and HCN are abundant in low density clouds. Self absorption features and absorption in gas close to the sources show that molecular clouds can be surrounded by low density, absorbing gas, which may seriously distort the emission spectra used to derive molecular cloud parameters. (39 refs.)

64530 Investigation of the region around the emission nebula IC 1848. V.I.Voroshilov, M.D.Metreveli.

Astrometriya & Astrofiz. (USSR), no.47, p.3-10 (1982). In Russian. The B, V photometry and spectral classification of 870 O-B-A stars are used to investigate the emission nebula IC 1848. Outside the nebula the O-B2 star density is three times less than that inside the nebula. The nebula distance, 2160 pc, is evaluated from observations of the stars making a contribution to the ionization. (12 refs.)

64531 Investigation of the region around the emission nebula NGC 1499. N.B.Kalandadze, V.I.Voroshilov.

Astrometriya & Astrofiz. (USSR), no.47, p.10-16 (1982). In Russian. The B, V photometry and spectral classification near 400 O-B-A stars were used to investigate the region around the emission nebula NGC 1499. It is found that at distances 1350-1800 pc a complex of dust clouds is situated outside the main absorbing layer. The density of the O-B-A stars in this region is low. The radio flux of NGC 1499 is in agreement with the flux of ionizing radiation of ξ Per (O7 V). The photometric and trigonometric parallaxes of ξ Per give the distance of NGC 1499 as 490 pc. (12 refs.)

64532 On interstellar light absorption in the Galaxy. E.A.Nazarov, M.F.Khodychikh.

Astrometriya & Astrofiz. (USSR), no.48, p.33-6 (1983). In Russian. Mean galactic absorption is determined from the galactic latitude distribution of quasars and from the dependence of brightness of the statistically brightest objects in the QSO groups on the galactic latitude. The weighted mean of the absorption is determined in the direction of the galactic pole. (8 refs.)

64533 Linear polarization observations in selected celestial zones—The anticentre region. J.P.Vallee (Inst. Herzberg d'Astrophys., Conseil Nat. de Recherches du Canada, Ottawa, Ontario, Canada).

Astron. & Astrophys. Suppl. Ser. (France), vol.52, no.1, p.125-9 (April 1983). Observations of linear polarization have been made at a wavelength of 2.83 cm for several dozens of extragalactic radio sources, in a restricted celestial angular zone towards the galactic anticentre region. This program complements previous all-sky surveys of stronger sources, in preparation for later analyses of localized polarization effects from specific zones of our Galaxy. (7 refs.)

64534 On the turbulent motions revealed in the Sagittarius arm by interstellar-line studies. C.O.Lousto, J.C.Muzzio (Obs. Astronomico, Univ. Nacional de La Plata, La Plata, Argentina).

Observatory (GB), vol.103, no.1053, p.53-5 (April 1983). The authors use published photometric and spectroscopic results to show that the turbulent motions in the Sagittarius arm invoked to explain the interstellar-line observations for $l > 340^\circ$ extend to $l < 340^\circ$ as well. (13 refs.)

64535 Far-infrared rotational transition lines of the interstellar water vapor. H.Shibai (Inst. of Space & Astronaut. Sci., Tokyo, Japan), T.Mai-hara.

Prog. Theor. Phys. (Japan), vol.69, no.1, p.77-88 (Jan. 1983). Far-infrared rotational transition lines of H_2O vapor are calculated to predict the line intensities under the condition of interstellar molecular clouds. Fractional populations for ortho- and para- H_2O molecules are obtained by solving a statistical equilibrium equation in which the authors employ recent data of H_2O - H_2 collisional excitation coefficients. Results are shown by presenting excitation temperature and optical depth for representative transition lines. Predicted intensities of several far-infrared lines are also demonstrated for a simplified cloud model. (13 refs.)

64536 Solid and gaseous carbon allotropes in ultrahigh vacuum at 3K. C.Reale (Inst. di Fisica, Politecnico di Milan, Milan, Italy).

Port. Phys. (Portugal), vol.13, no.3-4, p.193-201 (1982). In ultrahigh vacuum at 3K (the ordinary condition of the interstellar matter) carbon can be quenched-crystallized in Al-type and A3-type phases and may also become a gas with diatomic $\text{C}\equiv\text{C}$ molecules, similar to the $\text{N}\equiv\text{N}$,

O=O and H-H molecules of the three other elements that give rise to life. (7 refs.)

- Plasma in astrophysics See Entry 64328
- Distribution of cosmic rays and magnetic field in the galactic halo under conditions of hydrostatic equilibrium See Entry 64329
- An exact solution for an isothermal gas cloud with fast differential rotation See Entry 64364
- Infrared speckle imaging: improvement of the method; results on Miras and protostars See Entry 64392
- ASA 1000 and color too See Entry 64399
- Molecular clouds and star formation See Entry 64458
- The ultraviolet spectrum of the supermassive object R136a. I. The mass loss rate See Entry 64471
- The ultraviolet reddening of Be stars See Entry 64481
- Herbig-Haro 57 See Entry 64491
- Supernovae. II. The aftermath See Entry 64496
- An investigation of the heavily reddened young open cluster Tr 27 on the Walraven photometric system See Entry 64520
- The globular cluster NGC 6544 See Entry 64521
- The formation of disc galaxies See Entry 64537
- Roche's limit in a galaxy. II. The effects of rotation See Entry 64538
- The origin of the nonthermal radio emission in normal disk galaxies See Entry 64539
- The gas distribution in the central region of the Galaxy. IV. A survey of neutral hydrogen in the region $349^{\circ} \leq l \leq 13^{\circ}$, $-10^{\circ} \leq b \leq 10^{\circ}$, $|\mu| \leq 350$ km.s⁻¹ See Entry 64541
- Dissipative structures in galaxies See Entry 64542
- VLA observations of H₂CO in DR 21 See Entry 64551
- Aperture synthesis observations of Orion B at 2.695 and 8.085 GHz See Entry 64553

98.50 THE GALAXY, EXTRAGALACTIC OBJECTS AND SYSTEMS

- 64537 The formation of disc galaxies. B.J.T.Jones (LAM Obs. de Meudon, Meudon, France), R.F.G.Wyse. *Astron. & Astrophys. (Germany)*, vol.120, no.2, pt.2, p.165-80 (April 1983). The authors describe a model for the formation of disc galaxies in which the thick disc component and central bulge are the first luminous systems to form in a non-spherical massive dark halo. The thick disc that forms is not in centrifugal equilibrium except in the central parts (the bulge) and subsequent dynamical processes give it the exponential nature of the density distribution seen now. The thin disc forms from the gas lost by stellar evolution in the thick disc and accretion of primordial gas and in this way the model provides an explanation for both the thinness of this component and the apparent universality of its exponential-type profile. The authors investigate the collapse and fragmentation of gas in non-spherical halo potentials and show that it is highly likely that a hot gaseous disc is formed, collapse to a plane occurring before angular momentum becomes important. Further analysis leads to the conclusion that the hot disc will cool and form stars on a timescale shorter than the halo radial dynamical time. This means that a hot stellar system—a thick disc—is formed. (107 refs.)
- 64538 Roche's limit in a galaxy. II. The effects of rotation. H.Robe (Inst. d'Astrophys., Cointe-Ougree, Belgium). *Astron. & Astrophys. (Germany)*, vol.120, no.2, pt.2, p.215-18 (April 1983). For pt.1 see *ibid.*, vol.97, p.182-4 (1981). The tidal effects exerted by the central part of a galaxy on a galactic cloud orbiting at a distance d from the center are examined in the presence of the gravitational effect of the galactic halo and of galactic rotation. Rotation increases somewhat the Roche limit outside which equilibrium exists. Nevertheless, the halo significantly reduces the tidal effects, especially so if the galactic concentration is low. (4 refs.)
- 64539 The origin of the nonthermal radio emission in normal disk galaxies. R.Kennicutt (Dept. of Astron., Univ. of Minnesota, Minneapolis, MN, USA). *Astron. & Astrophys. (Germany)*, vol.120, no.2, pt.2, p.219-22 (April 1983). A strong correlation exists between the total nonthermal radio flux of a spiral galaxy and its integrated H α emission line flux. The correlation is much tighter than the corresponding relationship between total radio flux and the integrated optical magnitude of a galaxy. The most straightforward interpretation of this result is that the relativistic electrons responsible for the nonthermal radio emission are produced primarily by massive young stars, not by the old disk population. (18 refs.)
- 64540 Kinematics and structure of the Galaxy at high galactic latitude. N.V.Kharchenko. *Astrosmetriya & Astrofiz. (USSR)*, no.47, p.49-58 (1982). In Russian. Using the absolute proper motions of stars in 21 selected areas, the kinematic characteristics of stellar groups in the main meridional section of the Galaxy are obtained. For these stellar groups the empirical expressions for the change of radial velocities of rotation around the galactic z-axis are found as functions of distance from the galactic plane. Relative stellar abundances of the intermediate and spherical subsystems at $z=0-1.5$ kpc as well as the space densities of late-type giants at $z=1-2$ kpc are calculated. (22 refs.)
- 64541 The gas distribution in the central region of the Galaxy. IV. A survey of neutral hydrogen in the region $349^{\circ} \leq l \leq 13^{\circ}$, $-10^{\circ} \leq b \leq 10^{\circ}$, $|\mu| \leq 350$ km.s⁻¹. W.B.Burton, H.S.Liszt (Sterrewacht, Huygens Lab., Leiden, Netherlands). *Astron. & Astrophys. Suppl. Ser. (France)*, vol.52, no.1, p.63-103 (April 1983). For pt.III see *Astrophys. J.*, vol.236, no.3, pt.1, p.779-97 (1980). Presents 21-cm observations of neutral hydrogen emission from the core of the Galaxy made over a period of several years with the 140-foot telescope of the National Radio Astronomy Observatory. The material covers the region $349^{\circ} \leq l \leq 13^{\circ}$, $-10^{\circ} \leq b \leq 10^{\circ}$, at intervals of one-half degree in both l and b . Each reduced spectrum covers the velocity range $|\mu| < 350$ km.s⁻¹ at a kinematic resolution of 5.5 km.s⁻¹ to an r.m.s. sensitivity limit ≥ 0.02 K. The data are displayed in three sets of representative maps drawn in latitude-longitude, latitude-velocity, and longitude-velocity coordinates. Anomalous features representing material in the galactic core are labelled in the appropriate figures. The authors give some summarizing taxonomic remarks concerning these anomalies. (127 refs.)

- 64542 Dissipative structures in galaxies. G.Bodifée, C.de Loore (Vrije Univ. Brussels, Brussels, Belgium). *C.R. Seances Acad. Sci. Ser. II (France)*, vol.296, no.1, p.71-4 (10 Jan. 1983). In French. It is suggested that the morphological structures of disk constituents of spiral galaxies are dissipative structures, originated by nonlinear processes operating between stars and the interstellar medium. As a consequence of the occurrence of dissipative processes in conditions far from equilibrium, spatial inhomogeneities or coherent temporal cycles may be expected to appear. (9 refs.)
- 64543 OJ 287. J.Bortle. *I.A.U. Circ. (USA)*, no.3792, 1 pp. (19 April 1983). The author reports visual magnitude estimates for the BL Lacertae object OJ 287, covering the period 1983 March 21 to April 6; the object is at about magnitude 14. (no refs.)
- 64544 Runaway instability in accretion disks orbiting black holes. M.A.Abramowicz, M.Calvani, L.Nobili (Dept. of Astrophys., Oxford Univ., Oxford, England). *Nature (GB)*, vol.302, no.5909, p.597-9 (14 April 1983). The runaway instability (very fast, 'catastrophic', mass exchange) operates in close binaries when the more massive star overflows its Roche lobe. The Roche lobe radius shrinks due to the mass exchange more rapidly than the radius of the star. The star keeps overflowing its Roche lobe and continuously loses mass. It has been found that a critical equipotential surface similar to the Roche lobe also exists in the black hole accretion disk system. The existence of this lobe is not connected with the gravity of the disk but is due to general relativistic effects in the gravitational field of the black hole alone. The authors argue that all accretion disks which overflow their Roche lobes and which have masses greater than a few per cent of the mass of the central hole are unstable with respect to runaway instability. This may be very important for quasars and other active galactic nuclei. (25 refs.)
- 64545 Double galaxies, their radial velocity measurement errors and mean mass-to-luminosity ratio. I.D.Karachentsev. *Pisma v Astron. Zh. (USSR)*, vol.9, no.2, p.67-74 (1983). In Russian. English translation in: *Sov. Astron. Lett. (USA)*. New radial velocity measurements are presented for 44 pairs of galaxies from the catalogue of isolated pairs of galaxies of the northern hemisphere by Karachentsev (1972), which have not been discussed in a previous spectra survey. Using the data for 75 galaxies, common for the author's catalogue and the sample by White et al. (1982), the absolute errors of radial velocity determinations for galaxies observed with the 6-m telescope are estimated. It is shown that the ratio of the external (absolute) error of velocity measurement to the inner one, $k=\sigma_e/\sigma_i$, changes from 1.0 to 2.1 while passing from strong emission line galaxies to objects with absorption spectra. An estimate of the mean value $k=1.4$ is obtained. (10 refs.)
- 64546 Light variability of the Seyfert galaxy Zw 0039.5+4003 (IV Zw 29). During 1967 through 1981. A.S.Sharov, V.P.Arkipova. *Pisma v Astron. Zh. (USSR)*, vol.9, no.2, p.82-5 (1983). In Russian. English translation in: *Sov. Astron. Lett. (USA)*. The light curve of the Seyfert galaxy Zw 0039.5+4003 (IV Zw 29) during the period 1967 to 1981 is given. The object shows B-variability in the range of 16.5^m-18.3^m. Light maxima were recorded in 1968, 1972 and 1980. (7 refs.)
- 64547 102 MHz observations of Seyfert galaxies. V.S.Artyukh, Yu.N.Vetukhnovskaya. *Pisma v Astron. Zh. (USSR)*, vol.9, no.2, p.86-9 (1983). In Russian. English translation in: *Sov. Astron. Lett. (USA)*. Observations of 73 Seyfert galaxies at the wavelength of 3 m have been carried out. Among them 5 Sy2 and 2 Sy1 galaxies turned out to be radio-sources. There are 6 Seyfert galaxies having scintillation components with steep spectra ($\alpha > 0.7$). The linear sizes of the components are the same as those of the compact components of distant quasars. (18 refs.)
- 64548 Cepheids and spiral structure. Yu.N.Efremov. *Pisma v Astron. Zh. (USSR)*, vol.9, no.2, p.94-101 (1983). In Russian. English translation in: *Sov. Astron. Lett. (USA)*. A difference is found between the distribution of Cepheids in the planes of the Galaxy and M31 at a distance of 10-12 kpc from the centre, this is probably due to the nearness of this distance to the corotation radius in the case of the Galaxy. It is noted that provided the width of the Carina-Sagittarius arm in the Galaxy is 2-3 kpc, this arm may turn out to be an analogue to the S4 arm in M31, which reveals a concentration of Cepheids of all periods and a transversal gradient of the youngest stellar ages. The periods of Cepheids in the Galaxy and M31 (and probably in general in other Sb galaxies) increase not toward the centre but toward the angular regions of maximal star formation rate. (37 refs.)
- RAS Specialist Discussion on Astrophysical Applications of Accretion Disks (Papers in summary form only received) See Entry 59533
- Distribution of cosmic rays and magnetic field in the galactic halo under conditions of hydrostatic equilibrium See Entry 64329
- Comptonization effects in spherical accretion onto black holes See Entry 64361
- An exact solution for an isothermal gas cloud with fast differential rotation See Entry 64364
- Multiple transonic solutions with a new class of shock transitions in steady isothermal solar and stellar winds See Entry 64368
- H α atlas of the northern Milky Way taken with a wide-field camera See Entry 64401
- The ultraviolet spectrum of the supermassive object R136a. I. The mass loss rate See Entry 64471
- Carbon stars and the seven dwarfs See Entry 64476
- R 66(Aeq): an LMC B supergiant with a massive cool and dusty wind See Entry 64482
- Supernovae See Entry 64494
- Supernovae See Entry 64495
- Observed radii and structural parameters of clusters in the SMC. II See Entry 64522
- Diameter distribution and Σ -D relation of SNRs in M31 and in M33 See Entry 64526
- On interstellar light absorption in the Galaxy See Entry 64532
- Linear polarization observations in selected celestial zones—The anticentre region See Entry 64533
- On the turbulent motions revealed in the Sagittarius arm by interstellar-line studies See Entry 64534
- Analysis of optical imagery for Seyfert's Sextet and VV 172 See Entry 64549

- Variability at 5 GHz in low luminosity radio nuclei of galaxies and quasars See Entry 64552
- Beam models for extragalactic radio sources See Entry 64554
- The production of string loops in an expanding universe See Entry 64565
- The Inflationary Universe lives? See Entry 64569

98.50K Groups, clusters, superclusters

- 64549 Analysis of optical imagery for Seyfert's Sextet and VV 172.** J.W.Sulentic (Dept. of Phys. & Astron., Univ. of Alabama, University, AL, USA), J.J.Lorre.
Astron. & Astrophys. (Germany), vol.120, no.1, pt.1, p.36-52 (April 1983).
Extensive image processing of 5 m photographs of Seyfert's Sextet and VV 172 is reported. New image processing techniques and new applications of old techniques are discussed. Six principal avenues of approach were taken in the image processing: 1. field-galaxy density analysis; 2. redshift-scaled imagery; 3. interaction morphology display and enhancement; 4. color difference imagery; 5. modeling of the VV 172 halo; and 6. image texture analysis of the spiral galaxy components of Seyfert's Sextet. The purpose of these analyses, aside from the presentation of the image processing techniques, was to evaluate the evidence for physical association of the discordant redshift components of these groups. Evidence is presented to show that the halo of VV 172, in particular, cannot be explained by the overlapping envelopes of galaxies with normal luminosity profiles. (26 refs.)
- 64550 The space correlation function of rich clusters of galaxies.** A.A.Klypin, A.I.Kopylov, P.S'ma v *Astron. Zh. (USSR)*, vol.9, no.2, p.75-81 (1983). In Russian. English translation in: *Sov. Astron. Lett. (USA)*
It is shown that the space correlation junction of Abell clusters of galaxies is approximated by the power law $\xi(r) = (50h^{-1} \text{ Mpc}/r)^{1.6}$ in the range of distances $5h^{-1} \text{ Mpc} < r < 100h^{-1} \text{ Mpc}$ ($h = H/50 \text{ km/s/Mpc}$). Results on redshift determinations for rich clusters in the region $\{r < 480 \text{ Mpc and } |b| \geq 30^\circ\}$ are used to estimate the correlation function. A considerable difference between the correlation function of clusters of galaxies and that of the galaxies themselves is difficult to explain and probably is evidence for the existence of a preferable scale of clustering. (18 refs.)

The Inflationary Universe lives? See Entry 64569

98.70 OTHER OBJECTS AND BACKGROUND RADIATIONS OF UNKNOWN ORIGIN AND DISTANCES

(for pulsars, see 97.60G)

98.70D Discrete radio sources

- 64551 VLA observations of H₂CO in DR 21.** H.R.Dickel, A.F.Lubenow (Dept. of Astron., Univ. of Illinois, Urbana, IL, USA), W.M.Goss, J.R.Forster, A.H.Rois.
Astron. & Astrophys. (Germany), vol.120, no.1, pt.1, p.74-84 (April 1983).
The H₂CO absorption at 6 cm from molecular gas in front of the radio continuum source DR 21 has been mapped with the Very Large Array with an angular resolution of 2" and a velocity resolution of 0.45 km s⁻¹. Three main velocity components are seen. Comparison of the distributions of H₂CO and other molecules indicates that for all them, the absorption is strongest in the southern part of DR 21, especially near H II region C. (16 refs.)
- 64552 Variability at 5 GHz in low luminosity radio nuclei of galaxies and quasars.** R.D.Ekers (Kapteyn Astron. Inst., Groningen, Netherlands), R.Fanti, G.K.Miley.
Astron. & Astrophys. (Germany), vol.120, no.2, pt.2, p.297-301 (April 1983).
The results of a six-year program to monitor the 5 GHz flux densities of a sample of low-luminosity compact radio components are presented. These include low-luminosity isolated compact sources in elliptical and spiral galaxies as well as the cores of extended double radio galaxies and quasars. Eight cases of definite variability and four cases of possible variability have been found. No significant difference is apparent for the variability percentages or time scales between the various types of weak sources studied in this paper and the stronger sources investigated by previous authors. The results provide marginal evidence against simple relativistic beaming explanations for high-luminosity compact sources. (38 refs.)
- 64553 Aperture synthesis observations of Orion B at 2.695 and 8.085 GHz.** J.E.Wink, W.J.Altenhoff (Max-Planck-Inst. fur Radioastron., Bonn, Germany), W.J.Webster, Jr..
Astron. & Astrophys. (Germany), vol.120, no.2, pt.2, p.322-5 (April 1983).
Interferometer observations of Orion B at 2.695 and 8.085 GHz are presented. Orion B appears to be a double source: one H II region associated with the star NGC 2024 #2 and an extended H II region surrounding the star NGC 2024 #1. This structure gives support to the model that the stars NGC 2024 #2 and #1 (of spectral type O 9.5 and B 0.5, respectively) ionize the nebula. (14 refs.)
- 64554 Beam models for extragalactic radio sources.** T.P.Ray (Univ. of Sussex, Brighton, England).
Irish Astron. J., vol.15, no.3, p.199-207 (March 1982). [received: April 1983]
The author discusses the radio spectra of radiogalaxies and also their structures and sizes. The formation of beams in the nuclei and their power sources are considered. Black hole roles are discussed. (14 refs.)
- V1343 Aquilae** See Entry 64492
- Detection of HCO⁺ and HCN absorption towards three galactic H II-regions** See Entry 64529
- Linear polarization observations in selected celestial zones—The anticentre region** See Entry 64533
- The origin of the nonthermal radio emission in normal disk galaxies** See Entry 64539
- OJ 287** See Entry 64543
- 102 MHz observations of Seyfert galaxies** See Entry 64547

98.70J Quasars

- 64555 Low-frequency variability and predicted superluminal motion in 3C 147.** R.S.Simon, A.C.S.Readhead, A.T.Moffett (Owens Valley Radio Obs., California Inst. of Technol., Pasadena, CA, USA), P.N.Wilkinson, B.Allen, B.F.Burke.
Nature (GB), vol.302, no.5908, p.487-90 (7 April 1983).
VLBI observations of 3C 147 reveal that its core is a low-frequency variable radio source which has brightened by a factor of 2 in 6 years. In combination with X-ray observations, this implies that bulk relativistic motion is taking place within the core, and leads to the prediction that 3C 147 is a member of the class of superluminal radio sources. (30 refs.)
- Gravitational lens effects of neutrino astronomical objects** See Entry 64362
- On interstellar light absorption in the Galaxy** See Entry 64532
- Runaway instability in accretion disks orbiting black holes** See Entry 64544
- Variability at 5 GHz in low luminosity radio nuclei of galaxies and quasars** See Entry 64552

98.70L IR sources

(see also 98.40 in nebulae)

- Infrared speckle imaging: improvement of the method; results on Miras and protostars** See Entry 64392
- R 66(Aeq): an LMC B supergiant with a massive cool and dusty wind** See Entry 64482
- Herbig-Haro 57** See Entry 64491

98.70Q X-ray and gamma-ray sources

- 64556 X-ray radio, and infrared observations of the 'rapid burster' (MXB 1730-335) during 1979 and 1980.** A.Lawrence, L.Cominsky, W.H.G.Lewin (Dept. of Phys., MIT, Cambridge, MA, USA), M.Oda, Y.Ogawara, H.Inoue, K.Koyama, K.Makishima, M.Matsuoka, T.Murakami, T.Ohashi, N.Shibazaki, Y.Tanaka, I.Kondo, S.Hayakawa, H.Kunieda, F.Makino, K.Masai, F.Nagase, Y.Tawara, S.Miyamoto, H.Tsunemi, K.Yamashita, T.Dashido, R.Oka, T.Ohkawa, T.Maruyama, T.Yokoyama, G.Nicholson, T.Balonek, W.A.Dent, I.S.Glass, B.S.Carter, A.W.Jones, M.J.Selby, C.Martinez Roger, C.Sanchez Magro, A.B.Giles, M.Duldig, A.Pramesh Rao, V.R.Venugopal, R.F.Haynes, D.L.Jauncey, H.Okuda, S.Sato, Y.Kobayashi, J.Jugaku, D.Backman, R.Pogge, P.E.Hodge, H.D.Aller, J.van Paradijs.
Astrophys. J. (USA), vol.267, no.1, pt.1, p.301-9 (1 April 1983).
Reports partially simultaneous observations of the 'rapid burster' (MXB 1730-335) at X-ray, infrared, and radio wavelengths, covering several hundred hours during 1979 and 1980. No infrared or radio bursts were observed. Reported radio bursts are either unreal or do not bear a simple relation to the X-ray bursts from the rapid burster. The status of the reported infrared bursts also remains ambiguous. The authors also report limits to the brightness of any persistent radio source at the position of MXB 1730-335, limits to persistent X-ray emission during an extended X-ray quiet phase, and a measurement of the infrared polarization in the direction of the X-ray source. (34 refs.)
- 64557 Discovery of X-ray bursts from GX 3+1 (4U 1744-26).** K.Makishima, K.Mitsuda, H.Inoue, K.Koyama, M.Matsuoka, T.Murakami, M.Oda, Y.Ogawara, T.Ohashi, N.Shibazaki, Y.Tanaka, F.J.Marshall (Inst. of Space & Astronautical Sci., Tokyo, Japan), S.Hayakawa, H.Kunieda, F.Makino, F.Nagase, Y.Tawara, S.Miyamoto, H.Tsunemi, K.Tsuno, K.Yamashita, I.Kondo.
Astrophys. J. (USA), vol.267, no.1, pt.1, p.310-14 (1 April 1983).
During the Hakucho observations of the galactic center region in 1980 July-August, 15 X-ray bursts were observed for the first time from a bright bulge source GX 3+1 (4U 1744-26). These bursts exhibit characteristics typical of type I cosmic X-ray bursts. No bursts, however, were observed from GX 3+1 in previous Hakucho observations conducted in 1979 and early 1980. The persistent X-ray flux of GX 3+1 in 1979-1980 was roughly half the value obtained in 1971-1978 by other observers. (22 refs.)
- 64558 Models of X-ray bursters with radius expansion.** B.Paczynski (Theoretical Astrophys., California Inst. of Technol., Pasadena, CA, USA).
Astrophys. J. (USA), vol.267, no.1, pt.1, p.315-21 (1 April 1983).
A series of models of helium shell flashes on a neutron star is presented. To make models simple, no hydrogen was present and a small nuclear reaction network was used. General relativity was fully taken into account. Variation of electron scattering opacity with temperature and density was allowed for, and it was most essential for producing hydrostatic expansion of the outer layers of models. The models which expanded had relatively large helium envelope masses, developed strong shell flashes, and displayed a double peak variation of surface temperature with time. They may help to understand some X-ray bursters. (18 refs.)
- 64559 Gamma-ray astronomy.** B.Houston, A.W.Wolfendale (Univ. of Durham, Durham, England).
Irish Astron. J., vol.15, no.3, p.181-98 (March 1982). [received: April 1983]
A brief description is given of the present status of gamma-ray astronomy, both galactic and extragalactic. More detailed attention is given to a specific question: the nature of the apparent 'γ-ray sources'. The undoubted correlation of at least some of the sources with dense clouds of gas in the interstellar medium is discussed. A new analysis of the SAS II satellite data is described and comparisons are made between the 'source catalogue' from these data with the well-known 2CG catalogue from the COS-B experiment. (19 refs.)
- Identification and properties of the M giant/X-ray system HD 154791=2A 1704+241** See Entry 64462
- Coordinated Einstein and IUE observations of a disaripans brusques type flare event and quiescent emission from Proxima Centauri** See Entry 64477
- V1343 Aquilae** See Entry 64492
- The Crab Nebula. I. Photoionization of a bright filament** See Entry 64528

98.80 COSMOLOGY

(for observational cosmology, see 98.70V; for origin and evolution of galaxy, see 98.50)

64560 The evolution of shear and gravitational wave perturbations of Friedmann models and the isotropy of the Universe. J.L.Sanz (Dept. de Física Teórica, Univ. de Santander, Santander, Spain). *Astron. & Astrophys. (Germany)*, vol.120, no.1, pt.1, p.109-12 (April 1983). Considers the evolution of shear and gravitational waves, larger than the Hubble length, in Friedmann universes. By considering a perfect fluid with a linear equation of state, $p=np$, the author obtains exact analytical solutions for the perturbations in the flat case and closed-form solutions in the open and closed cases if the content of the Universe is represented either by dust, $p=0$, or radiation, $p=1/3p$. The behaviour of the different relative quantities, during the evolution of the different models, is analyzed. The difficulty to explain the present observed universal homogeneity and isotropy unless one postulates special initial conditions is stated. (15 refs.)

64561 Anisotropic cosmology. Two energy distributions generating a conformal gravitational field associated to the Kantowski-Sachs field. M.Bray. *C.R. Seances Acad. Sci. Ser. II (France)*, vol.296, no.5, p.317-20 (7 Feb. 1983). In French. Two anisotropic space-times (MHD, pure radiation) described by a metric $ds^2 = \Omega^2 [ds^2 \text{ K.-S.}]$. (1 ref.)

64562 The impossibility of a bouncing Universe. A.H.Guth (Dept. of Phys., MIT, Cambridge, MA, USA), M.Sher. *Nature (GB)*, vol.302, no.5908, p.505-7 (7 April 1983). Petrosian (1982) has recently discussed the possibility that the restoration of symmetry at grand unification in a closed contracting Robertson-Walker Universe could slow down and halt the contraction, causing the Universe to bounce. He then went on to discuss the possibility that our Universe has undergone a series of such bounces. The authors disagree with this analysis. Sher (1980) has already shown that if a contracting Universe is dominated by radiation, then a bounce is impossible. The authors show two further results: (1) entropy considerations imply that the quantity S , which must decrease by $\sim 10^{75}$ to allow the present Universe to bounce, can in fact decrease by no more than a factor of ~ 2 ; (2) if the true vacuum state has zero energy density, then a Universe which is contracting in its low temperature phase can never complete a phase transition soon enough to cause a bounce. (3 refs.)

64563 How stable is our vacuum?. P.Hut, M.J.Rees (Inst. for Advanced Study, Princeton, NJ, USA). *Nature (GB)*, vol.302, no.5908, p.508-9 (7 April 1983). It is possible that the vacuum state we live in is not the absolute lowest one. In many spontaneously broken field theories a local minimum of the effective potential, which can be quite stable, can exist for certain parameter values. The Universe, starting at a high temperature, might have supercooled in such a local minimum. If such a metastable minimum is separated by a high enough barrier from the absolute minimum, the tunneling rate from the 'false' to the 'true' vacuum may be slow enough to not have occurred in one Hubble-spacetime volume. In that case our vacuum state might suddenly disappear if a bubble of real vacuum formed which was large enough for the bulk energy gain to exceed the surface energy density in its walls. Although the persistence of the present vacuum for 10^{10} yr implies that a spontaneous transition via tunnelling is unlikely, one can ask whether a new generation of elementary particle accelerators might trigger such an unfortunate event. The authors show that this chance, fortunately, is completely negligible since the region inside our past light cone has already survived some 10^5 cosmic ray collisions at centre of mass energies of 10^{11} GeV and higher. (7 refs.)

64564 Void in the closed Universe. K.-I.Maeda, M.Sasaki, H.Sato (Res. Inst. for Fundamental Phys., Kyoto Univ., Kyoto, Japan). *Prog. Theor. Phys. (Japan)*, vol.69, no.1, p.89-99 (Jan. 1983). The evolution of a low density spherically symmetric region, which the authors call a void, in the high density closed Universe is investigated. This void expands forever while the unperturbed region collapses finally. The enlargement factor of the void is given and the global structure of a model Universe with one void is analysed. (7 refs.)

64565 The production of string loops in an expanding universe. N.Turok (Phys. Dept., Univ. of Virginia, Charlottesville, VA, USA). *Phys. Lett. B (Netherlands)*, vol.123B, no.6, p.387-90 (14 April 1983). The production of closed loops of string in an expanding universe, and how these might later seed the process of galaxy formation is discussed. It is shown how the motion of string is damped on scales larger than the horizon, and is free beneath the horizon. In particular when two waves meet beneath the horizon it is shown how non-self-intersecting loops are produced. It is speculated that each loop leads to the formation of a single galaxy. (9 refs.)

64566 Natural values of coupling constants and cosmological inflation in a supersymmetric model. C.E.Vayonakis (Lab. de Phys. Theorique et Hautes Energies, Univ. Pierre et Marie Curie, Paris, France). *Phys. Lett. B (Netherlands)*, vol.123B, no.6, p.396-400 (14 April 1983). The range of values of the temperature dependent coupling constants in a supersymmetric model is examined and the consequences for the inflationary Universe scenario are discussed. (28 refs.)

64567 Axions and the primordial monopole problem. G.Lazarides (Rockefeller Univ., New York, NY, USA), Q.Shafi. *Phys. Lett. B (Netherlands)*, vol.124B, no.1-2, p.26-8 (21 April 1983). The inevitable existence of an intermediate mass scale in axion models is used to solve the primordial monopole problem of Grand Unified Theories. It is shown that in the case where axions provide the dark matter of the Universe a measurable magnetic monopole flux may exist in our Galaxy. (22 refs.)

64568 The future of the Universe. D.A.Dicus, J.R.Letaw, D.C.Teplitz, V.L.Teplitz. *Sci. Am. (USA)*, vol.248, no.3, p.74-85 (March 1983). A forecast is given for the expanding Universe through to the year 10^{100} . All protons will decay, galaxies will form black holes and black holes will 'evaporate'. If the Universe collapses, it may cycle. (no refs.)

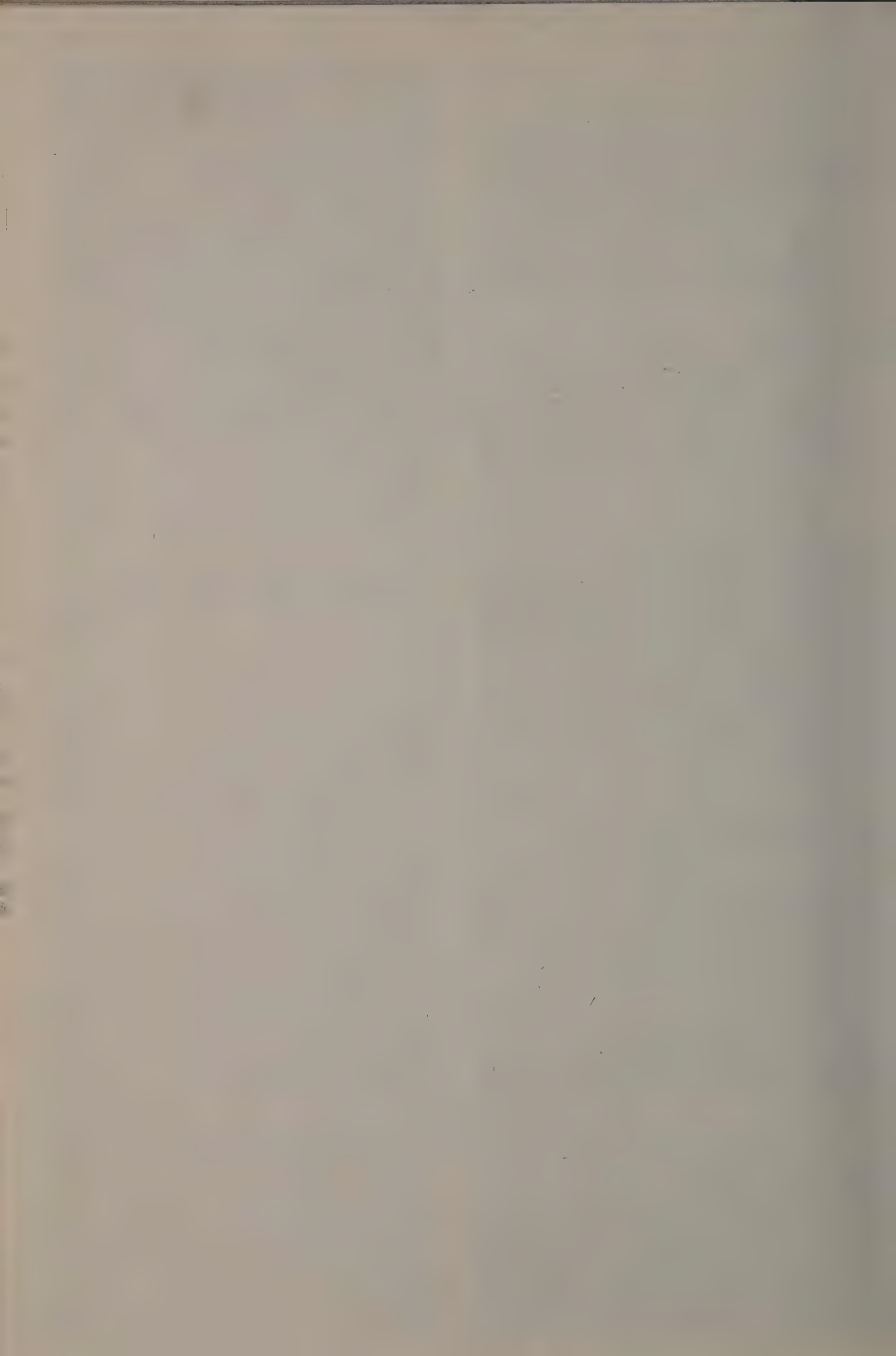
64569 The Inflationary Universe lives?. D.H.Smith. *Sky & Telesc. (USA)*, vol.65, no.3, p.207-10 (March 1983). The author discusses the cosmological implications of Grand Unified Theories, which combine the electromagnetic interaction, the weak nuclear interaction and the strong nuclear interaction. An essential element of these theories is the existence of a phase transition (spontaneous symmetry breaking) between a high-energy symmetric vacuum state and a low energy asymmetric vacuum state. In the Inflationary Universe hypothesis of Guth, this phase transition occurred during the very early history of the Universe (at $t \sim 10^{-35}$ s), and the consequent release of latent heat led to an acceleration of the expansion of the Universe and to an increase in its radius by a factor of 10^{20} to 10^{30} . Some difficulties with this model, connected with the origin of galaxies and clusters of galaxies, are discussed briefly. (no refs.)

64570 Beyond the Big Bang. A.MacRobert. *Sky & Telesc. (USA)*, vol.65, no.3, p.211-13 (March 1983). The author discusses cosmological theories related to the cause of the Big Bang and to the creation of everything from nothing. In these theories the origin of the Universe is connected with the creation of mass energy and gravitational potential energy by quantum fluctuations; these fluctuations occur either in a flat empty space or in a curved space ('superspace') that lies outside the space-time continuum of our Universe. A corollary of these theories is that our Universe is not unique; the events that created our Universe must have happened many times. Some evidence for the existence of superspace and a plurality of universes is found in the anthropic principle and in the existence of life in our Universe. (no refs.)

Relativistic astrophysics See Entry 59551
On the structure of space, time and field See Entry 59651
Upper limits to fermion masses in the Glashow-Weinberg-Salam model See Entry 59975
Magnetohydrodynamic Universe corresponding to a Kantowski-Sachs metric See Entry 64366
The formation of disc galaxies See Entry 64537
The space correlation function of rich clusters of galaxies See Entry 64550

98.90 OTHER TOPICS IN GALACTIC AND EXTRAGALACTIC ASTRONOMY

64571 White holes: cosmic energy machines. J.Narliker (Tata Inst. of Fundamental Res., Bombay, India). *New Sci. (GB)*, vol.97, no.1346, p.516-18 (24 Feb. 1983). White holes are the poor relations of black holes, neglected by the mainstream of astrophysics. The author discusses a new concept of a cosmic oscillator, however, which accords equal roles to both. (no refs.)



Author index

- Aaronson, M. + 64476
 Abakumov, G.A. + 60854
 Abakumov, V.N. + 61964
 Abashkin, V.G. + 61297
 + Abazli, H. 61874
 Abbasov, Sh.M. + 62442
 + Abdeen, A.M. 63125
 + Abdel-Ati, E. 61435
 Abdel-Malik, T.G. + 63125
 Abdel-Nabi, H. + 63907
 + Abdelhamid, M. 59767
 + Abdinov, A.Sh. 62442
 + Abdinov, D.Sh. 62437
 + Abdollahian, D. 60339
 Abdullaev, B. + 62354
 + Abdurragimov, A.A. 62695
 Abe, F. + 60072
 + Abe, F. 60082
 + Abe, M. 61689
 + Abe, Y. 60367
 + Abecasis, S.M. 60113
 Abelin, H. + 60300
 + Abeyaratne, R. 61410
 + Abiev, A.K. 62442
 + Abouchacfa, G. 61943
 Abraham, F. + 61878
 + Abraham, F.F. 62120
 + Abramov, G.L. 59760
 + Abramowicz, H. 60077
 Abramowicz, M.A. + 64544
 Abreu, V.J. + 64281
 + Abrosimov, N.K. 60499
 Abroyan, I.A. + 62339
 + Abu-Mostafa, A. 61523
 Accardi, L. 59628
 Acerbi, E. + 60497
 + Achard, J.C. 63580
 + Achard, M.F. 61779
 + Achterberg, O. 59995
 Achuthan, P. + 59671
 + Ackerman, F.J. 60276
 + Ackermann, H. 59995
 + Ackermann, M. 62790
 Ackerson, B.J. + 61544
 + Acirvos, A. 59750
 + Adachi, K. 61299
 + Adachi, M. 60107
 + Adachi, Y. 62364
 Adair, R.K. 59934
 Adamov, M.N. + 61026
 + Adams, A.R. 63039
 Adams, B.L. 61958
 + Adams, D.F. 63388
 Adams, D.J. 61746
 Adamson, M.G. + 63262
 + Adcock, D.K. 64007
 Adelberger, E.G. 60114
 + Aderholtz, M. 60033
 Adhikari, S.K. + 60155
 Adhikari, S.K. + 60065
 + Adiga, B.B. 64197
 + Adler, E.A. 61628
 Adomenas, P. + 61793
 + Adomenas, P. 62103
 Adonts, G.G. + 61602
 Aepfelbach, G. + 60789
 Afanas'ev, A.M. + 62455
 Afon'ko, E.F. + 62426
 Afsar, M.N. + 62873
 + Ageev, E.F. 62437
 Agafonova, G.A. + 61606
 Agard, D.A. + 63810
 Agaronyan, F.A. + 64333
 Agarwal, G.K. + 62351
 Agarwal, G.S. + 60676
 Agarwal, M.S. + 61705
 Agarwal, P.K. + 61826
 + Agashe, V.V. 64204
 + Agassi, D. 60676
 Ageev, A.N. + 59821
 + Ageeva, E.N. 63406
 + Aggarwal, S.K. 64197
 + Aglion, F. 60497
 + Agrawal, S.K. 64203
 Agren, J. 59748
 + Aguilar, M.G. 62802
 Aguilar-Monco, A. + 60611
 Aharoni, S.M. + 61766
 Aharony, A. 62641
 + Aharony, A. 62650
 Ahl, J.L. + 60902
 Ahlen, S.P. + 60558
 + Ahlrichs, R. 60884
 + Ahmad, M.M. 64322
 + Ahmed, A.S. 63888
 + Aifantis, E.C. 63437
 + Aiga, M. 63693
 Aihara, T. + 59777
 + Aikawa, Y. 62491
 + Aikawa, Y. 62958
 + Aivazov, M.I. + 61887
 Aizatskii, N.I. 60485
 + Akai, S. 63150
 Akasaka, K. + 62823
 + Akay, H.U. 61521
 Akenzie, K.G. + 59929
 + Akechi, K. 63213
 Akerlof, C.W. 60094
 Akesson, T. + 60074
 Akhrarov, M. + 61192
 + Aki, F. 60446
 + Akiba, E. 63722
 + Akimov, B.K. 63619
 Akimov, D.Yu. + 64385
 Akimov, V.N. + 60744
 Akimova, I.V. + 61163
 + Akita, K. 63180
 Akiyama, M. + 63909
 + Akopyan, S.Kh. 60694
 Aksenov, E.T. + 61305
 Akulin, V.M. + 60872
 Al-Ani, K.E. + 60817
 Al-Noaimi, G.F. + 61029
 + Al-Sabti, M. 60817
 Aladulesu, I. + 62068
 Alagna, L. + 63083
 Alaime, Cl. + 61172
 Alam, M.S. + 60049
 Alard, F. + 61289
 + Alario-Franco, M.A. 63538
 Albach, M. + 61048
 + Albella, J.M. 63670
 + Albers, P. 61007
 + Alberti, G. 62320
 Albeverio, S. (ed.) 59543
 Albinet, G. + 62216
 + Albrecht, A.C. 59849
 + Albrecht, C. 60437
 Albrecht, D. + 62005
 + Albrecht, D. 61999
 + Albrecht, H. 61181
 + Albrecht, H.E. 61581
 + Albrow, M.G. 60074
 Alcaino, G. 64521
 + Alcala, R. 63063
 + Alderliesten, C. 60189
 + Aldrich, D. 63709
 Aldrich, P.D. + 60706
 + Aldrich, P.D. 60709
 Aleinikov, V.L. + 61064
 + Alejandre, C. 61530
 + Alekhin, V.P. 62782
 Aleksakhin, I.S. + 60995
 Aleksandrov, A.V. + 61235
 Aleksandrov, I.V. + 61275
 Aleksandrov, I.V. + 61281
 + Aleksandrov, V.V. 63221
 Aleksandrov, V.Ya. + 64216
 Aleksandrov, Yu.A. + 64233
 + Aleksandrovich, S.V. 61887
 Alekseev, A.I. + 60681
 Alekseev, B.A. + 61709
 Alekseev, Yu. + 60436
 Alekseev-Popov, A.V. + 61115
 + Alekseeva, L.E. 63411
 + Alekseeva, Z.E. 61313
 Aleksinski, W. + 61198
 Aleshkevich, V.A. + 61247
 + Alessandria, F. 60497
 + Alessandrini, P. 63699
 + Alexander, G. 59995
 + Alexandrescu, R. 62276
 + Alfano, R.R. 60828
 Alfaro, J. + 59956
 Alferov, Zh.I. + 61193
 + Alferov, Zh.I. 61964
 Alford, P.C. + 60793
 + Algra, H.A. 63157
 Ali, A. + 61611
 Aliev, S.A. + 62437
 + Alivisatos, A.P. 62466
 Allaart, I. + 60121
 + Allain, C. 61471
 Allan, G. + 62253
 Allan, W. 64326
 Allara, D.L. + 62979
 Allard, B. + 60322
 + Allard, B. 60316
 + Allard, B. 60320
 + Allard, B. 60313
 Aliebach, J.P. 61094
 Allegra, L. + 63453
 + Allen, B. 64555
 Allen, D.M. + 63440
 + Allen, G.R. 61630
 + Allen, J.L. 61323
 Allen, P. + 60033
 + Allen, P.D. 60170
 Allen, R. 63992
 + Allen, R. 62759
 Allen, R.M. 59893
 + Aller, H.D. 64556
 + Allia, P. 62608
 + Allison, J. 60031
 + Allison, J. 60059
 + Allnatt, A.R. 62178
 Almaev, R.Kh. + 64220
 + Almedeh, S. 60074
 Almeida, J.R.L.de. 60074
 + see de Almeida, J.R.L.
 Alonso, J.A. + 60962
 + Alonso, J.A. 60975
 Alonso, J.L. + 60012
 + Alpert, N.M. 63945
 Alpgrad, K. + 60073
 + Al'shiti, V.I. 62024
 + Alster, J. 60204
 Alt, H.W. + 61536
 Altenberger, A.R. + 62141
 + Altenhoff, W.J. 64553
 Altman, A. + 60203
 Altman, S.L. + 61914
 + Altose, M.D. 63865
 Al'tshuler, B.L. + 62430
 + Al'tudov, Yu.K. 61069
 Altun, Z. + 60675
 Alvarez, E. + 59947
 Alvarez, O. 60027
 Alvarez-Cuenca, M. + 61547
 Alvarez-Estrada, R.F. + 61271
 + Aly, A.A. 63125
 Alyabina, N.A. + 62302
 Amaldi, E. 59577
 Amano, M. + 63740
 Amaral, M.H. + 62900
 + Amaya, K. 62600
 Amblard, M. + 60368
 Amelichkin, V.I. + 60493
 + Amelinckx, S. 61742
 Amemiya, H. 61665
 + Amemiya, M. 62714
 + Amemiya, M. 62712
 Amenda, W. + 60471
 Amer, A. + 59907
 + Amerik, Yu.B. 61830
 Ametistov, Ye.V. 62197
 Amoureux, J.P. + 62883
 + Amoureux, J.P. 62107
 + Amouroux, J. 63153
 + Amtenbrink, M. 63211
 + Amtenbrink, M. 63194
 Amthauer, G. + 62866
 Amusya, M.Ya. + 60745
 Amzil, H. + 62456
 An, C.-H. + 64430
 An Ying + 59913
 Anand, J.D. + 60060
 + Anand, S. 63914
 Ananthanarayan, A.K. + 63858
 Andel, Ivan. see van Andel, I.
 Andersen, J.G.M. + 60338
 Andersen, L.H. 60945
 + Andersen, L.H. 60965
 + Andersen, P. 60474
 + Andersen, S.A. 60474
 + Andersen, V. 60474
 Anderson, B.D. + 60179
 Anderson, B.D. + 60099
 + Anderson, E.W. 60083
 + Anderson, E.W. 60042
 + Anderson, E.W. 60070
 Anderson, H.L. 59569
 + Anderson, R. 61381
 Anderson, R.N. 64099
 Anderson, R.N. + 64081
 Anderson, R.Y. 60291
 + Anderson, S. 60756
 + Anderson, W.A. 63695
 Andersson, D. + 61661
 + Andersson, D. 64517
 Andersson, G. + 60301
 + Andersson, K. 60322
 + Andersson, K. 60316
 + Andersson, K. 60320
 + Andersson, K. 60313
 Ando, K. + 62760
 + Ando, K. 61270
 + Ando, K. 62942
 + Ando, K. 63182
 + Ando, T. 60446
 + Andoh, H. 62714
 + Andra, W. 62754
 Andre, J.M. + 62355
 Andreev, A.A. + 63458
 Andreev, N.F. 61227
 Andreev, V.I. + 62402
 Andreeva, N.V. + 63183
 Andrei, N. + 62551
 + Andreozzi, U. 63902
 + Andrew, R. 62297
 + Andrews, D. 60049
 Andrews, D.G. 64174
 Andrews, D.R. + 63424
 Andrews, L. + 60713
 + Andrews, M.C. 60935
 + Andriess, A.M. 61297
 Andrievskii, R.A. + 63204
 Andrievskii, R.A. 63247
 + Andronov, S.V. 63934
 Angelini, L. + 60061
 Angelini, L. + 60071
 Angelis, G.F.de. 61069
 + see de Angelis, G.F.
 Angelis, L.de. see de Angelis, L.
 + Angert, N.B. 63138
 + Angles, M. 63127
 Anglister, J. + 60724
 + Anguet, J. 63677
 Anh Nguyen Nam. 60077
 + see Nguyen Nam Anh
 Anisimova, G.P. + 60646
 Anisimova, G.P. + 61014
 + Anjaria, K.B. 63808
 Ankem, S. + 63355
 + Ankenbrandt, C. 60083
 + Ankenbrandt, C. 60042
 + Ankenbrandt, C. 60070
 + Anliker, P. 60730
 Annoni, H. 61460
 Ansari, M.A. + 62193
 Anson, C.E. + 63108
 + Ansoorge, R.E. 60073
 + Antic, E. 61867
 + Antiochos, S.K. 64477
 Anton, A.B. + 62259
 + Anton, A.B. 63099
 + Anton, A.B. 63590
 Antonetti, A. + 61199
 Antoniadis, I. + 59908
 Antonini, M. + 61994
 Antonini, M. + 61995
 Antonini, M. + 61975
 + Antonini, M. 60281
 + Antonoff, M.M. 62598
 Antonopoulou, E. 64509
 + Antonov, A.V. 62781
 + Antonov, V.N. 63085
 Antoshchuk, A.I. + 63222
 Anzai, S. + 62563
 + Aoiz, F.J. 63527
 Aoki, H. 62360
 + Aoki, M. 62283
 'Aoki, T. 60234
 + Aono, Y. 63080
 Aoyama, S. + 59928
 Apanasenko, A.L. + 63064
 Apel, W. + 62385
 Apenko, S.M. + 59984
 Apokin, V.D. + 60086
 Applequist, J. 59584
 Aragon, R. + 63146
 + Arai, H. 60910
 Arai, J. + 62862
 + Arai, K.I. 62787
 + Arai, M. 62628
 Arai, S. + 62704
 + Arai, S. 61150
 + Arai, Y. 60504
 + Arakawa, M. 61772
 + Arakawa, Y. 63849
 + Arakelyan, A.Z. 63020
 Aramaki, S. 59979
 + Araseki, H. 60149
 + Arasly, D.G. 62437
 Araujo, C.B.de. 63809
 + Araujo-Silva, J. 63809
 Arb, H.P.von. see von Arb, H.P.
 + Arbey, H. 61348
 + Arbey, H. 61488
 + Arbey, H. 61494
 Archakov, Yu.I. + 62851
 Archakov, Yu.I. + 63467
 + Ardelean, I. 62547
 Arduini, M. + 64340
 + Arend, H. 62836
 + Argyle, R.W. 64494
 + Argyle, R.W. 64495
 + Argysakis, P. 59691
 Arickx, F. + 60158
 + Arik, M. 59929
 Arisawa, T. + 60677
 Aristov, Yu.V. + 61055
 Arkhipov, V.V. + 59853
 + Arkhipova, V.P. 64546
 Armand, G. + 63116
 + Armbruster, J.G. 64073
 + Armbruster, P. 62005
 Armigliato, A. + 63624
 Armini, A.J. + 63705
 Armour, E.A.G. 61023
 Armstrong, A.C. 64153
 + Armstrong, R.L. 62686
 Armstrong, T.R. + 60405
 Arnold, G.W. 61992
 Arnold, G.W. + 60282
 + Arnold, G.W. 60284
 + Arnold, R. 63904
 + Arnold, R. 60077
 + Arnold, W. 63790
 + Arntzen, C.J. 63801
 + Aroca, C. 62576
 + Aronov, A.G. 62430
 Arora, P.K. + 63509
 Arrott, A.S. + 62623
 Arroyo, J.Mimila. see Mimila Arroyo, J.
 Arsenin, V.V. 61681
 Arsenjeyva, I.P. + 63252
 Artem'ev, M.I. + 63477
 + Artur, X. 59582
 Artukh, V.S. + 64547
 Aruchamy, A. + 62492
 Arunkumar, K.A. + 62959
 Arushanov, E.K. + 62324
 Artunyan, O.S. 59846
 + Arvieux, J. 60206
 + Arya, R.R. 63690
 Arykov, A.A. + 64323
 Asada, Y. + 62294
 + Asadov, Kh.A. 62488
 Asahi, N. 62285
 Asai, F. 64505
 + Asakura, T. 61099
 + Asano, A. 62283
 Asano, H. + 62282
 Asano, Y. + 61092
 + Asano, Y. 60072
 + Asano, Y. 60082
 + Asch, L. 62848
 + Asghar, M. 60097

- Bernasconi, J. + 59693
 + Bernasek, S.L. 63100
 Bernat, M. + 64080
 + Bernauer, O. 63741
 + Berne, B.J. 60627
 Bernede, J.-C. + 62513
 + Bernhardt, P.A. 64288
 Bernheim, M. 61046
 Bernheim, R.A. + 60769
 + Bernreuter, D.L. 64056
 Bernshein, M.L. + 63328
 Bernshteyn, M.L. + 63332
 + Bernshteyn, M.L. 63312
 Bernstein, A.M. + 60130
 + Bernstein, E.M. 60934
 Bernstein, H. + 63944
 + Bernstein, R.B. 63527
 Beroual, A. 61556
 + Berrington, K.A. 60991
 Berry, B.S. + 63339
 + Berry, L.A. 61678
 Berry, R.S. 60689
 + Berry, S. 60508
 Berry, S.D. + 60965
 + Bersohn, R. 60860
 + Bersuker, I.B. 60778
 + Bertel, E. 63652
 Berthier, Y. + 59555
 + Berthoud, G. 60368
 + Bertl, W. 60203
 + Bertout, C. 64464
 + Bertozzi, W. 60179
 + Bertrand, D. 60073
 Bertrand, J. + 59629
 + Bertrand, J. 61172
 + Berty, J. 62418
 + Beshenko, S.I. 62419
 Besmenova, T.N. + 61261
 Beshpalov, P.A. 61680
 + Bessa Sousa, J. 62645
 Betancourt, O. 61685
 + Bethke, S. 60031
 + Bethke, S. 60059
 + Betsofen, S.Ya. 63311
 Bevaart, L. + 62562
 Beveren, E. van
 see van Beveren, E.
 Bewersdorff, A. + 62218
 Bewick, A. + 62986
 Beysens, D. 61569
 + Bezruk, L.I. 61832
 Bezucha, G.R. + 63876
 Bezuglov, A.A. + 63436
 Bezдова, V. + 64024
 Bhagavatula, V.A. + 61290
 Bhandari, C.M. + 62191
 + Bhanja, R. 64203
 Bharadwaj Shyamala
 see Shyamala Bharadwaj
 + Bharali, A. 61563
 Bhasu, V.C. Jyothi. see Jyothi
 Bhasu, V.C.
 + Bhat, S.N. 62139
 Bhatcja, S.K. 61817
 Bhatia, A.K. + 64365
 + Bhatia, A.K. 61701
 + Bhatia, A.K. 60637
 Bhatnagar, A. + 64237
 + Bhatnagar, A.K. 62389
 Bhatta, N. + 61406
 Bhattacharjee, A.K. + 62534
 + Bhattacharjee, J.K. 62031
 Bhattacharya, D.K. 61396
 + Bhonsle, R.V. 64237
 + Bhowmik, B.B. 63716
 Biagi, S.F. + 60068
 + Bialkowska, H. 60077
 + Bianconi, A. 62953
 Biasi, R.S. de
 see de Biasi, R.S.
 Bibber, K. Van
 see Van Bibber, K.
 + Bibic, N. 62511
 + Bibler, N.E. 60282
 + Bibring, J.P. 64340
 Bibring, J.-P. + 64375
 Bichuya, A. 63466
 Bideau, D. + 59731
 Biedermann, G. + 60324
 + Bieganski, P. 62512
 Bielski, A. + 60658
 + Bigelow, N. 62819
 + Bigham, C.B. 60519
 + Bijker, R. 60120
 Bikhbaev, V.B. + 62481
 Bikhchantaev, I.G. + 63544
 Bikhazi, A.B. + 63800
 Biler-Sirotkina, S.N. 63331
 + Bilger, G. 63177
 Billard, J. 61784
 + Billmeyer, F.W., Jr. 63841
 + Billour, P. 60085
 Bilyk, A. 60227
 Binder, K. + 62658
 Bingrong Zhang + 62700
 Biondi, L. 63634
 Biran, B. + 59664
 + Birattari, C. 60497
 + Birch, D.J.S. 63031
 Birkner, E. + 63505
 + Bird, R.B. 61769
 Bird, R.P. + 63903
 + Birdy, R. 62557
 Birge, R.R. + 63784
 Birgersson, L. + 60299
 Birkeland, P.W. + 64410
 Birman, A.Ya. + 61173
 Biscarel, J. + 60369
 Biscarel, J. + 60385
 Bischel, W.K. + 60732
 Bischel, W.K. + 60733
 Bischof, C. + 63491
 Bishop, A.R. + 59718
 Bissinger, G. + 60899
 + Bissinger, G. 60966
 + Bissinger, G. 60967
 + Bistriclik, J.A. 60208
 Biswas, D.J. + 61188
 + Biswas, S.N. 60060
 + Bitar, K.M. 63800
 Bitran, M. 59866
 + Bittencourt, A. 64080
 Bittner, H.F. + 63657
 Bityutskaya, L.A. + 62386
 + Bivens, H.M. 64256
 Bjorken, J.D. 60089
 + Bjorklund, G.C. 59852
 + Black, G. 60732
 + Black, J.E. 62261
 + Blackmore, P. 63697
 + Blackmore, E. 60204
 Blackstone, E.H. + 63867
 + Blair, I.M. 64262
 Blair, M.F. 61495
 Blair, M.F. 61496
 + Blakemore, J.S. 63717
 + Blamey, P.J. 63861
 Blanchard, P. 59630
 Blanchard, P. + 60406
 + Bland, L.C. 60202
 Blanken, H.J. Den
 see Den Blanken, H.J.
 + Blanpied, G.S. 60213
 Blatt, F.J. 63797
 + Blaugrud, A.E. 61063
 Bleaney, B. + 62816
 + Bleuler, E. 64278
 Bliman, S. + 60972
 + Blinc, R. 62829
 + Blinc, R. 62836
 + Blinov, L.M. 62102
 + Blinov, V.M. 63417
 + Blobel, V. 59995
 Block, R.C. + 60521
 + Blok, J. 60362
 Blomberg, M. + 63516
 Blomquist, J. + 60978
 Blondeau, R. + 61152
 Bloomfield, L.A. + 60657
 Bloomquist, D.D. + 59832
 + Blue, W.K. 60528
 Blum, E.B. + 60500
 + Blum, N.A. 63698
 Blumen, A. + 59702
 + Blumenthal, N.C. 62813
 Blumich, B. 60757
 Blumich, B. + 59810
 Blumich, B. + 60702
 + Bluthner, K. 59800
 + Boas, G.V. 64080
 + Bobak, W. 61110
 Bobbio, S. + 60449
 + Bobkowski, R. 60658
 Bobyrev, V.A. + 63149
 Bocanek, L. + 62930
 + Boccard, N. 62652
 + Bocharov, A.I. 63932
 + Bocharov, A. 62512
 + Bochenek, A. 63051
 Bokharev, A.E. + 63051
 + Bochko, A.V. 63220
 + Bochkov, B.G. 62893
 Bochkov, O.E. + 62877
 Bochove, E. 61241
 Bock, H. + 61966
 + Bock, R.B. 60066
 + Bocklin, J. 60033
 + Bockmann, K. 60537
 + Bockmann, K. 60073
 + Boczan, J. 63921
 Bodak, O.I. + 61859
 + Bodak, O.I. 63265
 Boddington, T. + 62187
 Bodiffe, G. + 64542
 + Bodunova, V.N. 59853
 Boekema, C. 62871
 Boer, F.R. de
 see de Boer, F.R.
 Boer, F.W.N. de
 see De Boer, F.W.N.
 Boer, G.J. + 64179
 Boer, G.J. + 64180
 Boer, W. den
 see den Boer, W.
 + Boesten, L. 59995
 + Boeva, L.M. 61111
 + Bogatin, D.E. 62115
 Bogatov, A.P. + 61197
 + Bogatski, A.V. 61903
 + Bogdanic, N. 63228
 + Bogdanova, N.F. 63277
 + Bogdansk, M. 60085
 + Bogdali, H. 60074
 Bogomolnii, R.A. + 63582
 + Bohanan, R.E. 60429
 Bohandy, J. + 63034
 Bohaty, L. + 63151
 Bohaty, L. + 61897
 Boheim, G. + 63796
 + Bohm, H.-J. 60884
 Bohm, M.C. 62333
 + Bohm, R.K. 60902
 + Bohr, J. 62269
 + Boikova, E.I. 63138
 Boiti, M. + 59624
 Boiy, A. + 62103
 Bojarski, N.N. 61324
 + Bojowald, J. 60189
 Bokang Sun. see Sun Bokang
 + Bokarev, V.V. 63045
 Bokhan, P.A. + 61128
 Boklen, R. 63481
 Bokor, J. + 61229
 + Bokor, J. 63283
 Bokshitskii, M.N. 63383
 + Boldyrev, A.I. 60565
 + Boldyrev, V.V. 63221
 + Bolger, J. 60206
 Bollinger, A.B. + 64046
 Bolotin, A.G. + 60593
 + Bolotin, V.A. 60593
 Bolotin, V.V. 61455
 + Bolotina, E.N. 60777
 Bol'shakov, V.N. + 64151
 Bol'shov, L.A. 62132
 + Bolton, P.R. 60088
 + Bolton, R. 60204
 + Bolvin, M. 60376
 Bom, V.R. 60530
 + Bommannavar, A.S. 62854
 Bomsdorf, H. + 60773
 Bond, P.D. 60095
 Bond, V.P. (ed.) 59542
 Bondar, A.E. + 60535
 Bondarenko, L.I. + 61622
 Bondar, V.D. + 62427
 Bondyev, V.E. + 60801
 + Bonefacie, A. 63208
 Bong-Heup Kim + 62503
 Bonifazi, C. + 64313
 Bonjour, E. + 61983
 + Bonneau, D. 64470
 + Bonnet, L. 61172
 + Bonnet, N. 64018
 + Bonsignori, G. 60121
 Boom, R. + 63581
 + Boonbrahm, P. 61776
 + Booth, C.N. 60073
 + Booth, J.G. 62548
 Boothby, R.M. + 61986
 Boozer, A.H. 61605
 Bordi, F. + 60024
 Borg, J. + 60243
 Borg, J. + 61997
 Borge, M.J.G. + 60654
 Borghi, R. + 64215
 + Boris, J.P. 64429
 Borisanova, L.M. + 61833
 + Borisenko, V.G. 63320
 Borisevich, N.A. + 60844
 Borisov, A.B. 62614
 + Borisov, N.S. 60086
 Borkakoti, A.K. + 61563
 Borkowska-Bruncka, J. + 60736
 + Borland, C.J. 61522
 + Bormann, P. 64059
 + Bormontov, E.N. 62386
 Bornaia, J. 59813
 Borneas, M. 59649
 + Bormann, P.L. 64477
 + Borod'ko, Ju.G. 60845
 Borovich, B.L. + 61138
 + Borovikov, V.S. 63362
 Borshchan, V.S. + 62228
 Bortle, J. 64493
 Bortle, J. 64543
 + Bortle, J. 64427
 Bortolani, V. + 63098
 Borzenkova, I.I. 64239
 Borzilov, V.A. + 63758
 + Bos, A.J. 63615
 Bos, A.J.J. + 63616
 + Bos, A.J.J. 63614
 Bosch, A. Ten. see Ten Bosch, A.
 + Boscher, D. + 60697
 + Boschitz, E.T. 60206
 + Bose, K. 63400
 Boskovic, S. 63240
 + Bosmans, L.D. 61554
 Bosu, B. + 62852
 + Bost, M.C. 63692
 + Boswell, J. 60213
 + Botner, O. 60074
 Bott, J.F. + 63523
 Bott, T.R. + 59778
 Bottcher, C. + 60857
 + Boturov, K. 61829
 Bouazzi, A. + 63679
 Bouchairi, B.El.
 see El Bouchairi, B.
 + Boucher, D. 60707
 + Boucher, J.P. 62570
 + Bouchet, D. 61808
 Bouffard, S. + 62404
 Bougault, H. + 64079
 + Boulaud, D. 60377
 + Boulon, G. 63023
 + Bouma, W.J. 60567
 + Bourgojn, J.C. 62373
 + Bourgojn, J.C. 62376
 + Bourland, J.D. 64000
 + Bourne, F.R. 60223
 + Bourquin, M. 60068
 Bousgarbes, J.-L. + 61510
 Bouyer, J.J. + 63822
 Bova, F.J. + 63981
 Bovet, C. + 60548
 + Bovier, C. 61939
 + Bowden, G.T. 63806
 + Bowdery, C. 60031
 + Bowdery, C. 60059
 + Bowen, K. 63615
 + Bowers, E.J. 59583
 + Bowers, M.T. 63525
 Bowler, D.O. 63845
 Bowker, D.O. + 63844
 Bowman, J.D. + 60204
 + Bowman, J.D. 59936
 + Bowman, J.M. 60903
 Bowyer, S. 64342
 + Boyd, D.A. 61677
 Boyd, D.W. + 63731
 Boyd, R.D. 61382
 + Boyd, R.W. 61228
 Boyde, A. + 64016
 Boyles, C.A. 61338
 Bozang Li. see Li Bozang
 + Bozler, C.O. 63172
 Bracci, L. + 59967
 Brach, E.J. + 59856
 + Bradbury, A. 62716
 Bradbury, M.H. + 60304
 Bradhurst, D.H. + 63635
 + Bradley, E.B. 62959
 Bradlow, S. + 59727
 + Bradshaw, A.M. 62982
 + Bradshaw, A.M. 63103
 Bradt, H. 64348
 + Braester, C. 60306
 + Bragg, N.L. 60469
 Braid, I.J. + 62272
 + Braile, L.W. 64108
 + Brait, B. 62686
 Brake, R.E. + 64007
 + Bramble, D. 60944
 Brammer, R.F. + 64129
 + Bramon, A. 60093
 + Brand, H. 63552
 Brand, W.A. + 60833
 + Brandas, E. 59605
 + Brandemark, U. 63516
 Brandt, D. 61608
 + Brandt, P.W. 63823
 + Brandt, S. 59995
 + Brankoff, K. 60944
 + Brannon, J. 64079
 + Brasniet, B. 64171
 Bratashevskii, A.S. + 60164
 Bratko, D. 61755
 Bratman, V.L. + 61062
 Bratus', V.Ya. + 62807
 Brauer, P. 63598
 Brauer, P. + 63597
 Brauer, P. + 63604
 + Brauer, P. 63605
 Braun, F. + 60456
 Braune, K. + 60075
 Braune, K. + 60078
 + Braunstein, R. 62962
 + Bray, L.A. 60311
 Bray, M. 64366
 Bray, M. 64561
 + Breakstone, A. 60075
 + Breakstone, A. 60083
 + Breakstone, A. 60042
 + Breakstone, A. 60070
 + Bredas, J.L. 62355
 Bredikhin, V.I. + 63003
 + Breger, P. 61609
 + Breinig, M. 60965
 Bremaecker, J.C. De
 see De Bremaecker, J.C.
 Bremer, F. + 60218
 + Brennan, J.G. 60940
 + Brenner, A.E. 60083
 + Brenner, A.E. 60042
 + Brenner, A.E. 60070
 + Brenner, D.M. 60812
 + Brenner, D.S. 60111
 + Brestovansky, D.F. 63164
 + Brevet, W. 60188
 + Breuer, K. 61800
 Breuker, H. + 60054
 Bricault, P. + 60183
 Brice, D.K. + 61659
 + Brickmann, J. 61041
 Bricogne, G. 61730
 Briden, J.C. + 64032
 Briels, W.J. + 60885
 Bries, M. + 62053
 Briggs, R. 61578
 Brink, L. + 59923
 + Brion, C.E. 61001
 Briscoe, B.J. + 63336
 Bristow, Q. 64254
 + Bristowe, P.D. 61930
 Brittain, R.D. + 61019
 + Britten, A.J. 60068
 Broadbridge, P. 59673
 + Brobakken, K. 60066
 Brochard, F. + 61770
 Brock, A. 64026
 Brocke, W.A. + 60450
 + Brocken, M.G.M. 62205
 Brodsky, M.B. 62730
 + Brody, H. 60074
 + Brody, W.R. 63958
 + Broeckhove, J. 60158
 + Broer, R. 62262
 Broglia, R.A. + 60100
 + Bromer, H. 62812
 Bron, D.I. + 63404
 Broniatowski, A. + 62373
 + Bronner, W.E. 62143
 Bronshtein, D.Kh. 63216
 Brook, R.J. + 63198
 + Brooks, H.L. 61598
 + Broser, J. 62998
 Brosius, P.R. + 63174
 Brossmann, U. + 60423
 + Brousseau, M. 62344
 + Brown, D. 62961
 + Brown, F.B. 63515
 + Brown, G.L. 63640
 + Brown, H. 63793
 + Brown, L. 60139
 + Brown, L. 64112
 + Brown, L. 64077
 Brown, M.D. + 60940
 + Brown, M.D. 60952
 + Brown, M.K. 60202
 Brown, P.J. + 62548
 + Brown, P.J. 62698
 Brown, R.E. + 60215
 + Brown, R.E. 60182
 Brown, R.G. + 63783
 + Brown, R.J.C. 62825
 + Brown, R.M. 60068
 + Brown, V.L. 60130
 + Brownell, G.R. 63945
 + Browning, R.A. 63840
 + Brownstein, S. 59813
 Bruce, A.J. + 63077
 Bruce, E.N. + 63866
 + Bruce, J.A. 62492
 Bruckner, V. + 62450
 + Bruckner, W. 60078
 Bruckshaw, J. + 60559
 Brudnyi, V.N. + 62434
 Brueckner, G.E. 64381
 + Bruggner, R.M. 60521
 + Bruhl, H. 63033
 + Bruhl, H. 63633
 + Brukman, V.Ya. 61261
 Brumback, D.V. + 60914
 + Brun, M.Ya. 63485
 + Brun, T.O. 62383
 + Brunet, J.M. 60085
 Brunetti, R. + 62421
 Brunner, G. 60973
 + Brunol, J. 63955
 + Brunol, J. 61106
 + Brusch, M. 59588
 + Bruskov, V.A. 61859
 + Bruskov, V.A. 61892
 + Bruston, P. 64524
 + Bruyere, J.C. 62449
 Bryant, F.J. 61940
 Bryantseva, T.A. + 62287
 Brzezinska, J. + 63234
 Brzezinski, B. + 61017
 Bubenshchikov, A.S. + 63263
 + Buculewicz, W.H. 63945
 Buchdahl, H.A. 61253
 + Buchet, J.P. 60636
 Buchet-Poulizac, M.C. +
 60636
 Buchl, K. + 60472
 Buchmuller, W. + 60022
 + Buchner, H. 63741
 + Buck, R.P. 62143
 Buck, U. + 60923
 Buck, U. + 60922
 Buckingham, A.D. + 59850
 + Buckley, O.E. 63731
 + Buckley, S. 61975
 Bucksbaum, P.H. + 63283
 + Bucksbaum, P.H. 61229
 Buculei, M. + 61447
 Buda, J. + 61930
 Budtov, V.P. 61036
 Budtov, V.P. 62063

- Buerger, M.J. 61729
 Buffa, R. 61130
 +Buffam, C. 60073
 +Bugai, A.A. 62807
 +Bugge, L. 60066
 Buhs, R. + 63659
 Buj, J. 60402
 Bukaluk, A. 62185
 Bukhalova, G.A. + 63272
 Bukhman, A.B. + 59839
 Bukhman, A.B. + 61214
 Bukhshtaber, V.M. + 60337
 +Bukowski, Z. 62609
 Bulanin, M.O. + 60843
 +Bulanyi, M.F. 62807
 +Bulatova, L.V. 63458
 Bullett, D.W. 62336
 Bullock, R.E. + 60238
 +Bulot, J. 62416
 +Bullough, R. 61957
 Bultel, C. + 62014
 +Bunce, G. 60081
 +Bunce, G. 60087
 Bunde, R. 60419
 Bunker, G. 59765
 +Bunker, S.N. 63705
 Bunkin, F.V. + 63553
 +Bunkin, F.V. 63149
 Burak, Ya.V. + 62938
 +Buran, T. 60066
 Burattini, E. + 62913
 +Burchi, R. 64391
 +Burekhardt, H. 60068
 +Burd, M. 62962
 +Burdenski, S. 60958
 Bures, M. 61648
 +Burg, A.B. 60712
 +Burger, J. 59995
 Burger, L. + 60343
 +Burger, W.J. 60213
 Burgess, A.M.C. 64012
 +Burgess, D.R., Jr. 62257
 +Burgermeyer, W. 60188
 +Burie, J. 60707
 +Burke, B.F. 64555
 Burke, J.E. + 63244
 +Burkert, V. 60074
 +Burkert, V. 60054
 +Burkhard, M. 63114
 Burkholder, H.C. 60309
 +Burl, M. 63919
 +Burleson, G.R. 60202
 +Burling, P. 62634
 +Burnage, H. 61537
 +Burnasheva, V.V. 61889
 Burnel, S. + 61493
 +Burnett, D.S. 63612
 +Burnett, W.C. 64086
 Burns, A.G. + 64169
 Burns, F.C. + 60837
 +Burns, F.C. 63071
 +Burns, F.L. 60310
 Burns, G.S. + 63978
 Burns, W.G. + 60280
 Burns, W.G. + 63594
 Burns, W.S. + 60508
 +Burrow, L. 60073
 +Burrill, R. 62567
 +Burriss, J., Jr. 60821
 +Burt, T.P. 64143
 +Burton, C.H. 62575
 Burton, W.B. + 64541
 Burtshev, E.V. + 62896
 +Busch, J.R. 61255
 Buschmann, C. + 63895
 +Buschow, K.H.J. 62381
 Buskens, J. + 60534
 Bussemmer, P. + 62907
 +Bussiere, J.F. 63339
 +Busygin, V.M. 62112
 +Butcher, R.J. 61126
 +Buti, T.N. 60179
 Butkovskii, A.V. 61196
 Butler, C.C. 59571
 +Butler, J. 60083
 +Butler, J. 63872
 +Butler, J. 60042
 +Butler, J. 60070
 +Butler, L. 60804
 +Butter, K.D. 62489
 +Butterworth, G.J. 60420
 Butto, C. + 62418
 +Button, K.J. 62873
 Butusov, M.M. + 59836
 +Butusov, M.M. 61107
 Buxerolle, M. + 60477
 +Buxton, L.W. 60704
 +Buyers, W.J.L. 62686
 Buys, J.A.H.M. + 62192
 +Buzuglova, G.N. 63436
 +Buzzo, A. 60066
 Byalik, O.M. + 62372
 Bychkov, Yu.I. + 60644
 Bydler, G.M. 63918
 +Bydler, G.M. 63919
 +Bykov, Yu.A. 63223
 +Bykova, N.G. 60652
 Bykova, O.G. + 60652
 +Bykovskii, Yu.A. 61069
 Bylander, D.M. + 62329
 +Byoung-Joon Koh 60333
 Byrd, D.S. + 63747
 Bytva, I.M. + 60824
 +Bywater, S. 59813
 +Cable, J.W. 62383
 +Cable, M.D. 60112
 Cadoret, R. + 63170
 +Cadoret, R. 63169
 +Caffarelli, L.A. 61536
 Cai, B.C. + 61919
 +Cai, B.C. 62020
 Caie, A. + 63442
 Caillard, D. + 63342
 +Calage, Y. 61880
 +Calage, Y. 61882
 Calareso, W. + 61508
 Calagnoli, G. + 64091
 Calderwood, J.H. 62884
 Calef, D.F. + 63531
 +Calémczuk, R. 61983
 +Calera, A. 63647
 Callaway, E. + 63988
 +Callaway, J. 60986
 Callear, A.B. + 60806
 +Caljeja, F.J.B. 63384
 Calogero, F. + 59556
 +Calvani, M. 64544
 +Calvert, J.M. 60233
 +Calvert, S.F. 60445
 Calvi, G. + 60187
 +Calvo, M.L. 61271
 Cam Hoang Ngoc
 see Hoang Ngoc Cam
 +Camagni, P. 61994
 +Camagni, P. 61995
 +Camanzi, A. 63699
 +Cameron, D.G. 60716
 +Cameron, S. 60804
 Caminiti, R. 61756
 +Camon, J. 60497
 +Campanini, R. 60075
 +Campargue, R. 60697
 Camparo, J.C. + 60655
 +Campbell, D.S. 63712
 Campbell, E.J. + 60704
 +Campbell, E.J. 60701
 +Campbell, E.J. 60706
 +Campbell, E.J. 60705
 +Campbell, J.H. + 60276
 +Campbell, S.J. 62564
 +Campbell, S.J. 62621
 +Campet, G. 63560
 Campion, A. 62973
 +Campos, J. 60654
 Campos, R. De Azeredo
 see De Azeredo Campos, R.
 Can, C. + 60634
 Camus, P. 60506
 +Can, C. 60964
 +Cande, S. 64079
 +Candell, R.C. 64430
 Cannata, F. + 60154
 Canning, N.D.S. + 62965
 +Cannistraro, S. 63768
 Cao Chang-qi 59940
 +Capel, H.W. 62677
 +Capellmann, H. 62548
 +Capen, C.F. 64412
 Capitelli, M. + 61716
 +Cappuccio, G. 62913
 +Capranica, R.R. 63862
 Carbonell, F. + 63904
 Carboni, G. + 61027
 Card, C.J. 60360
 +Card, C.J. 60365
 Cardegna, P.A. + 62163
 +Cardello, T. 60083
 +Cardello, T. 60042
 +Cardello, T.R. 60070
 +Cardman, L.S. 60491
 +Cardon, F. 63445
 Cardwell, R.K. + 64065
 +Cardwell, R.K. 64068
 +Carewska, M. 63238
 Cariens, W.S. 59590
 Carinena, J.F. + 60210
 +Cariolle, D. 64215
 +Carlin, R.L. 62594
 +Carlin, R.L. 62672
 +Carlini, R. 59936
 Carlisle, B.H. 63662
 Carlotto, M.J. + 64277
 Carlsen, L. + 60318
 +Carlson, J.B. 60185
 +Carlson, P. 60073
 +Carlson, P.J. 60066
 +Carlson, T.A. 60674
 Carman, E.H. 64285
 +Carneiro, K. 62403
 +Carney, T. 63753
 +Carosio, R. 60533
 +Carossi, R. 60074
 +Caroubalos, C. 63712
 +Carpenter, O. 63950
 Carr, J.A. + 60209
 +Carr, M.A. 64270
 +Carr, P.A. 64269
 +Carr, R. 60870
 Carragher, M.J. + 64152
 Carre, A. + 63450
 +Carreras, B.A. 61693
 Carrick, P.G. + 60719
 Carrigan, P.H., Jr. 60261
 +Carroll, J.E. 61153
 Carruthers, P. 59986
 +Carter, A.A. 60068
 +Carter, B.S. 64556
 +Carter, J.R. 60068
 Carter, M.W. + 60265
 +Carter, S.L. 60675
 +Carter, W.E. 64265
 +Cartwright, D.J. 60911
 Cartwright, K. 60252
 +Carvalho-Rodrigues, F. 63809
 +Casaccia, R. 64391
 +Casal, H.L. 60716
 +Casalbuoni, R. 60024
 +Casalino, C. 60749
 +Casasnovas, A. 64191
 Casey, M. + 61187
 +Casiraghi, A. 63626
 +Casleton, K.H. 60902
 +Cassagnou, Y. 60212
 +Cassel, D.G. 60049
 +Casselman, C. 60376
 +Casselman, C. 60377
 +Castagnede, B. 62009
 +Castaing, B. 62206
 +Castelain, M. 62883
 +Castiglioni, M. 60498
 +Castleman, A.W., Jr. 60859
 Castoldi, M. 60552
 +Castro, E.A. 59606
 Caswell, W.B. 60250
 Catara, P. + 60098
 +Catchpole, R.M. 64487
 Cates, M. + 63123
 Catlow, C.R.A. + 59766
 +Caudano, R. 62265
 +Caudano, R. 63096
 +Caurier, E. 60158
 +Causton, L. 60066
 Cazaux, J. + 59900
 +Cazes, S. 64340
 +Cebollada, F. 62583
 +Cecchetto, E.V. 60278
 Cecil, F.E. 61700
 Cedarstaff, T.H. + 64001
 Celarier, E.A. + 59711
 Celasco, M. + 62687
 Celentano, G. + 60424
 Celenza, L.S. + 60117
 Celenza, L.S. + 60053
 Celotti, G. + 63661
 Cembali, G.F. + 63704
 +Ceotti, S. 59665
 Cercignani, C. 61570
 +Cerny, J. 60112
 +Cervic, D. 63241
 +Cerrina, F. 60622
 Cesare, N. De. see De Cesare, N.
 +Cess, R.D. 64231
 +Ch Uihlein 62365
 Chabal, Y.J. + 62252
 +Chaban, E.E. 62252
 +Chaban, N.G. 62157
 +Chaban, V.N. 61431
 Chacko, S. + 64407
 +Chackraburty, D.M. 61894
 +Chadha, R. 64198
 +Chadwick, K. 60049
 Chai Zhikuan 62129
 +Chaikovskii, E.F. 61278
 +Chaikovskii, S.Z. 63454
 +Chakrabarti, B.K. 62653
 Chakrabarti, J. 59987
 Chakrabarty, C. + 63448
 +Chakrabarty, D.K. 62854
 +Chakrabarty, P.K. 60670
 +Chakrabarty, A.K. 61095
 Chakrabarty, D. + 63380
 +Chakravarty, R. 64303
 Chakravarti, A.N. + 62326
 Chakravarty, J.G. + 61418
 +Chalasinska-Macukow, K. 61105
 +Chalot, J.F. 60546
 +Chambat, M. 61459
 Chamberlain, J.M. + 63037
 Chamberlin, R.V. + 62602
 +Chamorro, Yu.K. 61282
 Champ, D.R. + 63752
 +Champion, M. 61565
 Chan, C.T. + 62330
 Chan, R.K.-C. + 60222
 +Chan, S.I. 63798
 +Chanderasekharan, C.K. 64194
 Chandiramani, K.L. 61344
 +Chandler, D. 60628
 +Chandra, G. 59790
 +Chandra Shekar, B. 61507
 Chandrasekharaiyah, M.S. 63275
 +Chandrasekharaiyah, M.S. 62128
 +Chandrasekharan, C.K. 64200
 Chandrasekharan, E. + 61545
 +Chandrasekharan, V. 60621
 +Chaney, E.L. 63949
 Chang, B. + 60906
 +Chang, C.C. 60196
 +Chang, C.S. 63811
 Chang, C.T. 61668
 +Chang, C.Y. 59995
 Chang, D. 59959
 Chang, L.C. + 61378
 +Chang, R.K. 62955
 +Chang, R.K. 62985
 Chang, Y.C. 60260
 +Chang, Y.K. 62429
 +Chang Hyo Kim 60221
 +Chang Hyun Chung 60221
 +Chang Shu-ren 62055
 +Chang Sun Kang 60242
 +Chang Xi-zhen 60168
 Chang-de Gong
 see Gong Chang-de
 +Chang-Hi Hong 62503
 Chang-qi Cao
 see Cao Chang-qi
 Changzhi Guo
 see Guo Changzhi
 Channell, P.J. 59589
 +Chant, N.S. 60213
 +Chantrell, R.W. 62716
 +Chao, D. 62911
 Chao Shen-Chang
 see Shen-Chang Chao
 +Chapkunov, S. 64241
 Chaplin, M.P. + 64043
 Chapline, G.F. 59661
 Chapman, J.E. + 61287
 Chapman, J.N. + 62702
 Chapman, M.A.V. + 63294
 +Chapman, N.A. 60328
 Chappert, J. 62841
 +Chappey, B. 62155
 +Chappey, B. 62108
 +Chapuis, G. 62836
 +Chapurin, T.E. 60139
 Charbucinski, J. 64260
 +Charil, J. 61148
 Charles, R.G. + 60340
 +Charles, S.W. 62716
 +Charlier, A. 60358
 +Charpin, M.C. 63153
 Charvolin, J. 61777
 Chassagne, G. + 61943
 +Chatelain, J.-L. 64068
 +Chatillon-Colinet, C. 63580
 Chatterjee, K. + 64200
 +Chatterjee, K. 64194
 Chatterjee, P. 62522
 +Chatterjee, S.K. 64302
 +Chatterjee, S.K. 64207
 +Chatterjee, U.K. 61188
 +Chattopadhyay, G. 62128
 Chaturvedi, U.K. + 64203
 Chatnyan, R.M. + 63379
 +Chau-Jy Lin 62323
 +Chaudhuri, A.K. 62517
 +Chaudhuri, T.K. 63184
 +Chauveau, J. 60049
 +Chavel, P. 61106
 +Chaves, M.R. 62900
 Chebotkevich, L.A. + 62764
 +Chekrenev, A.S. 60539
 +Chelli, A. 64392
 Chelveyohann, M. 62480
 +Chemisky, G. 63703
 +Chen, A. 60049
 +Chen, H.S. 62635
 +Chen, J.K. 64236
 Chen, L.J. + 63318
 Chen, P.J. 62894
 +Chen, T.T. 62985
 +Chen, Y. 63063
 +Chen, Z.X. 62876
 Chen Cunli 62495
 Chen Guang-hua + 63075
 Chen Guanghua + 63065
 Chen Kaimao + 62484
 Chen Limin + 60505
 Chen Mao-Hsiung
 see Mao-Hsiung Chen
 +Chen Shi 59913
 Chen Tian-iun
 see Tian-iun Chen
 Chen Tu
 see Tu Chen
 +Chen-Geng 61337
 Chen-hao Wang
 see Wang Chen-hao
 Chenery, J.A. + 63507
 Chenevier, P. + 63715
 +Cheng, C.H. 61462
 +Cheng, H.C. 63318
 Cheng, L. + 64182
 Cheng, L.J. + 62457
 +Cheng, L.J. 62375
 +Cheng Ming-kun 63893
 Cheng-Li Wu + 59911
 Cheng-li Wu + 60118
 Cheng-Ming Fou + 60951
 +Chepelev, Yu.L. 63138
 Chepelev, V.P. 63215
 Cherpura, V.F. 64309
 Cherdron, W. + 60373
 Chermakhin, V.A. 63405
 +Cherenkov, M.G. 63073
 Cherkashin, V.V. + 61844
 +Cherkasov, A.S. 60827
 +Cherkasov, E.V. 62993
 +Cherkasov, L.V. 64145
 +Chermette, H. 63032
 +Chern, S.S. 61462
 +Chernenko, I.M. 62937
 +Chernenko, N.L. 63423
 +Cherniack, N.S. 63866
 +Chernikov, A.M. 61420
 +Chernikov, Yu.L. 62678
 +Chernikova, L.I. 63847
 Chernov, E.A. 61215
 +Chernukha, N.A. 62034
 +Chernykh, N.Yu. 61263
 Chernykh, E.V. 60560
 +Cherry, J.A. 63748
 +Chervenkov, V.D. 60531
 +Chervonobrodov, S.P. 62896
 +Chesters, M.A. 63108
 +Chesters, M.A. 62965
 Cheung, S.T. + 60819
 Cheung Wan Yee
 see Wan Yee Cheung
 +Chevalley, J.-L. 60073
 +Chevallier, P. 61882
 Cheveigne, S. de
 see de Cheveigne, S.
 Chhi-Chong Wu + 62323
 Chia, S.P. + 59973
 Chiam, H.F. 63726
 +Chiang, K.S. 61304
 Chiang, S. + 62966
 +Chiang, S.T. 63991
 +Chicouche, A. 62490
 +Chien, C.L. 62607
 Chien-fan Yu + 63121
 +Chigrinov, V.G. 61796
 Chih-Chong Chou + 62974
 +Chihara, M. 61129
 +Chikama, T. 61149
 Chikova, N.V. 61400
 +Child, M.S. 60865
 +Child, M.S. 60690
 +Chilingaryan, Yu.S. 62914
 +Chilton, A.B. 63982
 +Chin, Y. 60488
 Chinellato, V. + 61993
 +Chinn, D. 64068
 Chino, C.B. 61356
 Chioran, G.M. + 63916
 Chipot, M. + 63279
 Chirita, S. 61411
 Chirkina, A.P. + 63148
 +Chirkina, A.S. 64271
 +Chirkina, A.S. 61236
 +Chirkina, A.V. 63360
 +Chistoserdov, Yu.P. 61364
 Chistyakov, P.N. 61723
 +Chistyakov, V.I. 63320
 Chiu, C.W. + 60712
 Chiu, D.M. 62447
 Chiu, H.Y. + 63557
 +Chizhik, S.P. 62131
 Chizhov, S.M. + 61891
 +Choi, B.H. 63534
 +Choi, H.J. 60248
 +Choi, H.K. + 61177
 Choi Jung In
 see Jung In Choi
 +Cholakh, I.V. 64227
 +Chong, D.P. 60835
 Chong-en Wu + 60141
 Chong-shou Gao
 see Gao Chong-shou
 Chongming Xu
 see Xu Chongming
 +Choo, W.K. 63288
 +Chopov, V. 63110
 +Chopra, D. 63088
 Chopra, K.L. + 63078
 Choquet-Bruhat, Y. + 59554
 Chor Wong + 62247
 Chothia, C. + 63779
 +Chou, Y.T. + 62020

- +Chou, Y.T. 61919
 Chou Chih-Cong 61919
see Chih-Cong Chou
 Chou Kuang-chao+ 60018
 +Chou Kuang-chao 62525
 Choudhary, N.V. + 62029
 +Choudhary, D.M. 59826
 +Choudhuri, P.K. 61418
 Choudhuri, S.K.Roy *see* Roy
 Choudhuri, S.K. 61418
 +Chourasia, N.C. 62505
 Chow, T.S. 62106
 +Chowdary, B.V.R. 62162
 Chowdhury, K. + 59789
 +Chraplyvy, A.R. 61286
 Chrien, R.E. 60522
 +Chrien, R.E. 60111
 Christensen, P.H. + 62731
 +Christie, D. 64079
 +Christie, J.M. 61924
 Christillin, P. 60171
 +Christman, S.B. 62252
 Christoffel, K.M. + 60903
 Christophe, J. + 64283
 +Christopher, K.L. 63883
 +Christophorou, L.G. 61713
 +Christoskov, L. 64050
 Chrzanoski, J. + 62881
 Chtaib, M. + 62265
 Chu, C.K. 61694
 +Chu, K.H. 60338
 +Chu, M.S. 61627
 Chu, Y.Y. + 60176
 Chu, Y.Y. + 60186
 +Chu, Y.Y. 60111
 Chuang, T.J. 63587
 +Chuang, T.J. 62224
 Chuanzheng Yang *see* Yang
 Chuanzheng 62339
 +Chudnovskii, F.A. 62339
 Chui, S.T. + 62646
 +Chui, B.V. 60086
 +Chui, L.S. 60854
 +Chustov, K.V. 63345
 +Chustov, K.V. 61834
 Chukalkin, Yu.G. + 61978
 +Chukhovskii, F.N. 61735
 Chul Lee Un *see* Un Chul Lee
 +Chulkov, V.V. 61600
 +Chun, H.-U. 62317
 Chun Hee-Young *see* Hee-Young Chun
 +Chung, C. 60111
 Chung, D.H. + 64056
 Chung, P.S. + 61304
 +Chung, Y.H. 63313
 Chung Chang Hyun *see* Chang Hyun Chung
 Chung Moon Ki *see* Moon Ki Chung
 +Chung-I Tan 59926
 +Chupka, W.A. 60768
 +Chupp, T.E. 60140
 +Churaev, N.V. 62210
 +Churaev, N.V. 61479
 +Churda, D.A. 60508
 +Churcher, C.D. + 63010
 +Churchill, J.N. + 62315
 +Chushkin, P.I. 64426
 +Chutov, Yu.I. + 61601
 +Chuyanov, V. 60436
 +Chuyanova, V.A. 61709
 Ciaccio, A.D. *see* Di Ciaccio, A.
 +Cianguar, G. 60196
 Ciavola, G. + 63126
 Cierjacks, S. 60518
 +Chai, V. 61920
 +Cimmino, S. 63348
 Cipolla, S.J. + 60947
 Cirafo, S. + 63260
 Ciric, I.R. 61051
 +Cirkel, H.-J. 61190
 Citrin, P.H. + 63134
 Citrin, P.H. + 63133
 +Cizewski, J.A. 60185
 +Claessens, M. 60885
 +Claesson, G.O. 60075
 Claire, A.D. *see* Le Claire, A.D.
 +Clark, C.E. 63731
 Clark, G.P. + 63906
 Clark, E.F. + 62691
 +Clark, G.M. 63861
 +Clark, M. 64079
 +Clark, M. 60934
 +Clark, N.A. 61544
 Clark, R.E.H. + 60996
 +Clarke, D. 60031
 +Clarke, D. 60059
 Clary, D.C. 60879
 Clauer, C.R. + 64319
 Clausen, A.M. 61597
 +Claussen, N. 63239
 +Claverie, J. 63560
 +Clawson, C.W. 60208
 +Claybourn, M. 63691
 Clayton, C.G. + 64248
 Clayton, C.G. + 64246
 +Clayton, C.G. 64262
 +Clayton, C.G. 64247
 +Cleary, J.G. 60340
 +Cleeman, L. 60129
 +Clegg, T.B. 60501
 +Cleveland, W. 60074
 +Clelland, R.C. 59583
 +Clementi, E. 63777
 +Cledenin, J.E. 60088
 Clerke, E.A. + 62119
 Clerke, E.A. + 62031
 +Cleveland, C.L. 62268
 +Clifford, S.F. 61084
 +Cline Love, L.J. 60814
 +Clocchiatti, R. 64100
 +Clow, H. 63691
 Clyne, M.A.A. + 63541
 Cnobloch, H. + 63655
 Coakley, J.A., Jr. + 64231
 Coble, R.L. 63199
 Cocco, G. + 61809
 +Cocco, G. 61806
 +Cocco, G. 61807
 +Coccorese, E. 60449
 +Cochran, J.F. 62809
 +Cochrane, L.A. 63791
 +Cockayne, D.J.H. 61922
 +Cocke, C.L. 63617
 +Cocke, C.L. 63115
 +Cockerill, D. 60074
 Codazzi, D. + 61537
 +Cofta, H. 62796
 +Cogger, L.L. 64281
 +Coghen, T. 60033
 Cohen, B.I. 61696
 Cohen, B.I. + 61617
 +Cohen, J. 63715
 +Cohen, J.B. 63432
 Cohen, J.S. + 61028
 Cohen, L.H. + 62204
 +Cohen, M.L. 62318
 +Cohen, N. 63523
 +Cohen, R.H. 61617
 Cohen-Addad, J.P. + 62827
 +Cohen-Solal, G. 61946
 Cohen-Tenoudji, F. + 61360
 +Cohn, S.H. 63948
 Cole, H. 60225
 +Cole, J.J. 63824
 +Cole, T.E. 64288
 +Colella, N. 60043
 Coleman, M.M. + 62999
 +Coles, R.L. 64023
 +Coley, A. 59653
 +Colijn, P.F. 63452
 +Collet, J. 62344
 Collet, P. 59719
 +Colling, C.N. 62074
 +Collins, A.G. 63919
 Collins, A.T. + 63038
 +Collins, J.C. 60056
 +Collins, L.A. 60996
 +Collins, M.A. 59727
 +Collins, M.T. 60178
 +Collins, V.P. 64014
 +Collyer, K. 60460
 +Colson, S.D. 60715
 +Colson, S.D. 60768
 Colson, W.B. + 61166
 +Com-Nogue, J. 63701
 +Comanici, N. 62276
 +Combe, P. (ed.) 59543
 +Combes, M. 64340
 Combes, P.-J. 64084
 +Combs, C. 63986
 +Combs, S.K. 60473
 Comby, G. + 60546
 +Cominsky, L. 64556
 Comminou, M. 64039
 Conde, O. + 61760
 Condon, J.B. 63536
 +Congdon, D.D. 63962
 +Conklin, W.C. 60265
 Conlon, T.W. 60232
 Connell, G.A.N. + 62759
 +Connerade, J.P. 60980
 +Connor, J.A. 60840
 +Conrad, H. 63103
 Conrads, H. 60524
 Conradt, R. + 60295
 Conte, F. 60387
 Conter, A. + 63901
 +Conti, M. 63673
 Continantino, M.A. 62636
 +Contreras, R.H. 60592
 +Cook, B.D. 61334
 Cook, J. + 60197
 +Cook, J.P.D. 61001
 +Cook, R.F. 61908
 Cook, R.J. 60683
 Cook, P.I.H. 60421
 Coon, D.D. + 59843
 Cooper, D. + 60529
 +Cooper, D. 60455
 +Cooper, D.M. + 62865
 +Cooper, J. 63059
 +Cooper, M.D. 60204
 Cooper, P.S. + 60083
 +Cooper, P.S. 60042
 +Cooper, P.S. 60070
 +Cooper, T.M. 63784
 Coppa, G. + 61288
 Coppi, B. 60401
 +Coqblin, B. 62534
 +Cordes, V. 63659
 +Cordier, G. 61854
 Cordier, J.J. + 60425
 +Cords, D. 60031
 +Cords, D. 60059
 Corkill, R.W. + 59641
 +Cormack, A.N. 59766
 +Cormier, T.M. 60201
 +Cornelisse, C.J. 63920
 Cornell, M.C. + 61598
 +Cornet, A. 62344
 +Cornet, F. 60093
 +Coron, N. 64340
 Correia, J.A. + 63945
 +Correll, F.D. 60182
 Corrigan, E. + 59904
 +Corrigan, G. 60033
 +Corrons, A. 64190
 +Corset, J. 62988
 +Cortial, H. 60448
 +Cosman, E.R. 60198
 +Cosman, E.R. 60199
 +Cossart, D. 60805
 Cossart-Magos, C. + 60805
 +Costantino, U. 62320
 +Cot, L. 62087
 Cotter, D. 61284
 Cotterman, B.W. + 59563
 Cottet, F. + 62028
 +Cottier, L. 60758
 +Cottigame, W.B. 60209
 +Cottigame, W.B. 60202
 +Coulaf, H. 62224
 Couillaud, B. + 61232
 +Coulon, R. 61585
 +Coupland, M. 60066
 Courcelle, E. + 63706
 Court, A. + 64208
 +Courtine, P. 61846
 Courtois, D. + 60698
 Cousins, D.R. + 61982
 Cousins, D.R. + 60277
 Cousson, A. + 61874
 +Couture, M. 61054
 Coutures, J. + 61867
 +Coutures, J.-P. 61867
 Couvreur, G. + 59586
 +Cowart, J.B. 64259
 Cowley, R.A. 62603
 Cox, P.A. + 63101
 +Cox, P.T. 60041
 +Cox, P.T. 60081
 +Cox, P.T. 60087
 Coze, J. *see* Le Coze, J.
 +Crabtree, R.D. 64155
 Crabtree, R.W. + 64143
 +Cragg, D.M. 62673
 Craig, S. + 63728
 +Craig, S.L. 64352
 Craigie, N.S. + 59957
 Cram, L.E. + 64432
 Crasemann, B. 60612
 Crawford, E.S. + 63137
 +Crawley, H.B. 60075
 +Creedon, J.M. 61675
 Cremoux, B. *see* de Cremoux, B.
 +Crenn, A.P. 61273
 +Cress, A.E. 63806
 +Cresswell, S.R. 63794
 +Crest, J.P. 62456
 +Criegee, L. 59995
 +Crifo, J.F. 64340
 Crighton, D.G. 61346
 +Crjns, F. 60533
 Crisa, N. 62414
 Crissman, J.M. + 63363
 Criswell, M.H. + 63828
 Crivellari, L. + 64472
 +Crocker, M.J. 61363
 +Crone, C. 63818
 +Crooks, D.D. 63369
 +Crosley, D.R. 60788
 +Cross, L.E. 62897
 +Cross, L.E. 62876
 +Cross, R.J. 60887
 +Crowe, K.M. 60208
 Crowne, F.J. 62359
 +Csapes, Z. 60594
 +Csorna, S.E. 60049
 Cugnon, P. 64527
 Cukier, R.I. 59696
 Cukier, R.I. + 63520
 Culkowski, W.M. 60267
 +Cullen, T. 60319
 Cumberbatch, T.J. + 63691
 Cummins, L. + 63896
 Cunli Chen *see* Chen Cunli
 +Cureton, C.G. 60793
 +Curl, R.F., Jr. 60719
 +Curry, J.R. 64135
 +Curry, J.R. 64139
 Current, M.I. + 61989
 Curtin, M.W. + 60193
 +Curtis, D. 64079
 Curtiss, C.F. + 61769
 +Curtiss, L.A. 60725
 +Curtosky, R.E. 60008
 +Cuzzocrea, P. 60943
 +Cverna, F.H. 60204
 Cygler, J. + 60971
 Czech, E. + 61854
 +Czechowsky, P. 64187
 Czekaj, S. + 61702
 Czerlinski, G.H. 62693
 Czubek, J.A. 64250
 Czubek, J.A. 64252
 Czubek, J.A. + 64251
 +Da Hsuan Fang 59911
 +Da Hsuan Feng 60118
 +da Silva, M.F. 60939
 +Dachich, M. 64356
 Daenner, W. 60422
 +Dagan, S. 60074
 +Dagdigian, P.J. 60842
 +Dagenhart, W.K. 60528
 +Daguenet, M. 63644
 +Dahl-Jensen, E. 60074
 +Dahl-Jensen, I. 60074
 +Dahme, W. 61027
 Dahmen, U. + 63297
 +Dahmen, U. 63298
 +Dahmen, U. 63296
 Dai Dao-sheng *see* Dao-sheng Dai
 Dai Hai-Lung *see* Hai-Lung Dai
 +Dai Yuan-ben 59913
 +Dai Yuan-ben 60018
 +Daimaruya, M. 61440
 Dale, R.G. 63977
 d'Alencon, M. + 60448
 +Dalgaro, A. 60604
 Dalitz, R.H. 59573
 +Dallavalle, G.M. 60075
 Daly, L. + 64106
 d'Ambrumenil, N. + 62637
 +Damgaard, G. 60074
 Damuth, J.E. 64134
 +Dan, N. 63350
 Danan, H. + 62754
 +Danby, C.J. 63510
 Dance, B. 61179
 +Dang Phuc Ly 61470
 +Dangor, A.E. 60483
 +Dangwal, G.C. 60786
 +Danhelka, J. 60829
 Daniel, D.E. 60253
 +Daniel, R.A. 60491
 +Danielou, R. 61906
 Danielson, P. 61291
 Danileiko, M.V. + 61212
 Danileiko, Yu.K. + 61211
 +Danilov, O.B. 61251
 +Danilov, S.N. 61279
 Danilov, V.A. + 61118
 Danilov, V.V. + 63558
 +Dao-sheng Dai 62688
 +Daou, J.N. 62026
 +Dara-Papamargariti, H. 64436
 +Dargel, L. 62749
 Darling, D. 64512
 Darmanyan, A.P. 60791
 +Darque-Ceretti, E. 61970
 Darweh, J.W. + 59636
 +Das, A.C. 64300
 Das, A.N. + 62084
 Das, A.N. + 62085
 +Das, B.P. 60616
 +Das, G. 60213
 Das, S.K. + 64194
 Das, U.N. + 64300
 +Das Gupta, M.K. 64302
 +Das Gupta, S. 60162
 +Dasgupta, A. 61919
 Dasgupta, C. + 62666
 +Dashchuk, P.N. 61722
 Dashevskii, V.G. + 61038
 +Dashevskii, V.G. 61037
 +Dashedo, T. 64556
 +Dashuk, P.N. 61136
 Dastidar, K.Rai *see* Rai Dastidar, K.
 Dastidar, T.K.Rai *see* Rai Dastidar, T.K.
 +Date, H. 61441
 +Datsenko, V.S. 63932
 +Datta, G. 64304
 +Datta, K. 59617
 Datta, R. + 63980
 Datz, S. 60933
 +Daube, M.E. 63962
 +Daubechies, I. 59634
 Dauge, I.I. + 62000
 +Daum, H.J. 59995
 +Davankov, V.A. 60776
 +Davenas, J. 61943
 David, F. + 61653
 +David, G. 63710
 Davidovic, M. + 61763
 Davidson, A. + 59964
 Davidson, R.C. + 61165
 +Davidson, R.C. 61168
 Davies, B.M. + 63109
 Davies, I. + 59631
 Davies, K. 64206
 Davies, M.G. 63643
 +Davies, M.J. 63041
 Davies, R.A. + 62477
 +Davies, R.A. 62485
 +Davies, S. 63615
 Davis, A. + 60822
 +Davis, A.M. 62184
 +Davis, D.G. 60066
 +Davis, L. 61883
 Davis, R.C. + 63806
 Davis, S.N. 60256
 +Davoli, I. 62953
 Davydovskii, V.Ya. + 61641
 Dawes, W.N. + 61576
 +Dawson, H.R. 60950
 Dawson, J.M. 61692
 +Day, P. 62552
 Day, W.A. 59595
 +d'Azy, O.B. 60797
 +De, A. 64202
 +de Almeida, J.R.L. 62539
 de Angelis, G.F. + 59931
 +de Angelis, L. 63699
 +de Araujo, C.B. 61175
 De Azeredo Campos, R. + 59654
 +de Bellefon, A. 60085
 de Biasi, R.S. + 62720
 +de Boer, F.R. 63581
 +de Boer, F.W.N. 60134
 +De Bremacker, J.C. 64407
 +De Cesare, N. 60943
 +de Cheveigne, S. 62236
 +de Cremoux, B. 61152
 de Falco, D. + 59708
 +de Falco, D. 59931
 de Gennes, P.G. + 61764
 +de Gennes, P.G. 61770
 +de Geyer, A. 63600
 De Gregorio, S. + 59720
 +de Greve, J.P. 64510
 +de Groot, M.J.H. 64482
 +de Jong, J.J. 60381
 +de Jonge, W.J.M. 62192
 +de Jonge, W.J.M. 62625
 +de Jongh, L.J. 62567
 +de Jongh, L.J. 62381
 +de Jongh, L.J. 62601
 +De Koromay, V. 60305
 +de Laat, S.W. 64004
 de Lary, B. + 62080
 de Leon, N. + 59610
 de Lima, J.J. + 63639
 +de Loore, C. 64542
 De Loos, T.W. + 62075
 +de Martinis, C. 60497
 +de Martino, S. 59708
 De Mestre, N. + 61553
 De Micheli, M. 61267
 +De Mol, C. 63952
 +De Paola, R.A. 63588
 +de Pape, R. 61880
 +de Pape, R. 61882
 de Prunelle, E. 60624
 +De Roos, M.J.K. 63939
 +de Siena, S. 59708
 +de Tendler, R.H. 62165
 de Vate, J.F. *see* van de Vate, J.F.
 +de Vorst, A. *see* van de Vorst, A.
 De Vos, A. 63671
 +de Wit, B. 59664
 +De Young, R.J. 61143
 Deal, D. + 62962
 Dean, P.J. + 62365
 +Dean, P.J. 63036
 DeBell, K. 59728
 +DeBotton, N.R. 60088
 Debray, E. + 62155
 +Debray, E. 62108
 +DeCain, D.M. 63174
 +Deck, L. 60041
 +Deck, L. 60081
 +Deck, L. 60087
 Decken, C.B. *see* von der
 der Decken, C.B. 61669
 +Decoste, R. 61669
 Dednam, C. + 60137
 +Dedonder, J.-P. 60154
 Deehr, C.S. (ed.) 59540
 Deekshatulu, B.L. + 63761
 +Deenen, J. 59586
 DeFrise, M. + 63952
 +Degasperis, A. 59556
 +Degauque, J. 62682

- + Degtyarev, L.S. 60760
 Degtyareva, V.F. 62096
 + Dehmer, J.L. 60509
 + Dehmer, J.L. 60832
 + Dehmer, J.L. 60877
 + Dehmer, P.M. 60832
 + Dehmer, P.M. 60877
 Deini, W. 59840
 Deiters, U.K. 62051
 Dejardin, P. 62249
 + Dekin, M.S. 63823
 + Dekkers, H.P.J.M. 60795
 + Dekkers, H.P.J.M. 60796
 + Dekkers, H.P.J.M. 62912
 + Deksnis, E. 60527
 + Del Bene, J.E. 60580
 + Del Moral, A. 62592
 + Delamar, F. 59555
 + Delaney, P.T. 64101
 Delavault, E. 63990
 Delbourgo, R. 59922
 DelBruno, J.J. 60921
 + Delcroix, P. 63416
 + Delgado, R.L. 60797
 + Doli, E. 63149
 Delineshev, S.P. 61039
 Dell'Antonio, G.F. 59668
 + Delmas, A. 61943
 + Delmelle, M. 63768
 + Delrie, J.P. 62265
 + Del'vin, N.N. 63749
 + Demaison, J. 60707
 Demant, J.T. 60479
 + Dement'ev, A.S. 61244
 Dement'ev, E.N. 60496
 + Demers, Y. 60663
 + Demeschik, A.M. 61219
 Demianski, M. 59551
 + Demichev, V. 60436
 + Demidov, V.I. 60957
 + Demidova, G.N. 62500
 Demin, S.A. 63345
 Demiralp, M. 59604
 Demiryont, H. 63162
 Demont, P. 62137
 Demuth, J.E. 63093
 + Demuth, J.E. 63107
 + Dem'yanets, L.N. 61890
 Den Blanken, H.J. 60771
 den Boer, W. 63696
 den Doel, C.P. van
 see van den Doel, C.P.
 + den Hollander, W.T.F.
 59694
 + Deneuville, A. 62449
 + Denis, J. 63670
 Denis, V. 62443
 + Denisenko, O.N. 63969
 + Denisov, S.I. 62692
 + Denker, J. 62819
 + Dennefeld, M. 64528
 Dennis, J.A. 63890
 Denno, K. 60214
 + Dent, W.A. 64556
 + Demyer, H.T. 63998
 + Deorukhakar, V.V. 63808
 + DePoort, G.L. 60264
 Deptula, A. 63237
 + Deptula, A. 63238
 der Avoird, A. van
 see Van der Avoird, A.
 der Decken, C.B. von see von
 der Decken, C.B.
 der Eerden, J.P. van
 see van der Eerden, J.P.
 der Geer, C.A.J. van
 see van der Geer, C.A.J.
 der Hiede, J.A. van
 see Van der Hiede, J.A.
 der Hoek, B. van see van der
 Hoek, B.
 der Klink, J.J. van
 see van der Klink, J.J.
 der Lee, T. van
 see Van der Lee, T.
 der Linden, W.H. van
 see van der Linden, W.H.
 der Ploeg, J.P.M. van see van
 der Ploeg, J.P.M.
 der Pluym, J. van see van der
 Pluym, J.
 Der Schaaf, P.J. van
 see Van Der Schaaf, P.J.
 der Voo, R. van see Van der
 Voo, R.
 + Derado, I. 60076
 D'Erasmus, G. 60532
 + Derenchuk, V. 60559
 Derentowicz, H. 60395
 + Derikum, K. 59995
 Derkacheva, L.D. 63569
 + Derkits, C. 60584
 Dermawan, H. 60180
 + Derynatin, A.I. 61220
 Derouard, J. 60930
 Deryagin, A.V. 62709
 + Deryugin, I.A. 61243
 Desai, R.C. 61242
 + Desai, R.C. 62120
 deSantis, A. 63007
 + Descamps, M. 62107
 + Descamps, N. 61950
 + Descamps, P. 59818
 + Descotes, G. 60758
 + Deshmukh, B.T. 61951
 + Desjardins, R.L. 59856
 + Deslattes, R.D. 59899
 DeSmet, D.J. 63067
 Destrade, C. 61785
 Destuynder, P. 61451
 + Desvignes, J.M. 62773
 + Detyanenko, G.E. 62372
 + Deumens, E. 60158
 Deutsch, C. 61618
 Deutsch, J.P. 60143
 Devallette, M. 61864
 + Devanarayanan, S. 64195
 + Devare, H.G. 62868
 DeVault, D. 63790
 + Devaux, P.F. 59808
 + DeVchand, C. 59904
 Devdariani, A.Z. 60957
 + Deveau, B. 63036
 + Devezas, T.C. 62720
 + Devi, B.S. 63946
 Devi, K. Usha. see Usha Devi,
 K.
 + Deville, J.P. 61950
 + Devlin, T. 60041
 + Devlin, T. 60081
 + Devlin, T. 60087
 + Devonport, C.P. 60806
 Devoret, M. 62616
 + Devries, P.L. 60898
 + Dewar, R.L. 61643
 + DeWette, F.W. 62260
 + DeWitt, J.W. 60049
 + DeWitt-Morette, C. 59554
 Dey, S. Sekhar
 see Sekhar Dey, S.
 + Dhameincourt, P. 64100
 Dhara, A.K. 59672
 Dharmadurai, G. 62199
 + Dharmadwark, S.R. 62128
 + Dhawan, S.K. 60088
 Dheer, P.N. 62530
 Dhez, P. 61257
 + di Bartolomeo, A. 63237
 + di Bartolomeo, A. 63238
 + di Ciaccio, A. 60074
 + Di Vita, P. 61288
 + Diamond, J.J. 60606
 Dian-hua Guan
 see Guan Dian-hua
 + Dianina, E.S. 63931
 + Dianov, E.M. 59839
 + Dianov, E.M. 61214
 Dicicco, D. 64399
 Dick, B. 61224
 + Dick, L. 63999
 Dickel, H.R. 64551
 + Dickinson, H. 63639
 + Dickinson, P.M.G. 63691
 + Dicks, A.S. 63985
 + Dickinson, D.P.E. 62865
 + Dicus, D.A. 64568
 + Diepen, G.A.M. 62111
 + Dietrich, G. 60031
 + Dietrich, G. 60059
 + Dietrich, U. 62907
 + Dietz, R.E. 59898
 Dietz, R.E. 63092
 + Dieulin, M. 60634
 Diffenderfer, R.N. 60587
 Diffenderfer, R.N. 60842
 + DiGiacomio, N.J. 60662
 Diguett, D. 63677
 + Dikanov, S.A. 62797
 DiLella, D.P. 60728
 + Dillard-Bleick, M. 59554
 + Dillingham, R. 60948
 DiMarco, A.F. 63865
 Dimiduk, D.M. 63257
 + Dimitrijevic, T. 62511
 Dimitrov, D.P. 60783
 + Dimza, V.I. 62478
 + Dineykhin, M. 59961
 Ding Zhong-Yi 64063
 + D'Ingeo, F. 64091
 + Dingus, M.L. 62204
 + Dionisio, G. 63673
 + Dipaloantonio, A. 64391
 + Dirochka, A.I. 63059
 Dischoeck, E.F. van
 see Van Dischoeck, E.F.
 + Dissado, L.A. 62888
 + Distefano, G. 60981
 + Dil, P. 60241
 + Dittmann, P. 60059
 Dittich, H.G. 60426
 Dittich, H.-G. 60428
 + Dittus, F. 60537
 + Divine, R.R. 60365
 Divis, A.F. 64102
 + Divnich, N.P. 61219
 Dixit, S.N. 60669
 Dixon, M.W. 60223
 + Dixon, W.T. 61030
 Djafari-Rouhani, B. 62233
 Djaloies, A. 60189
 + Djaloies, A. 60104
 + Djajou, M. 61451
 Djordjevic, B. 63807
 + Diott, D.D. 62954
 + Dmitrenko, L.A. 63003
 Dmitriyev, B.N. 63934
 + Dmitriev, V.G. 61200
 Dmitriev, V.M. 63270
 Dmitriev, V.M. 63271
 Dmitrieva, I.K. 60882
 + Dmitrieva, V.B. 61261
 Dmitrieva, Zh.N. 61449
 + Dmytrakh, I.H. 63493
 + Do-Yul Kang. 63308
 + Doake, C.S.M. 64155
 Doane, J.W. 63682
 Doane, N.E. 63886
 + Dobatkina, T.V. 63264
 Dobierewska-Mozzrymas,
 E. 62512
 Dobrik, A.V. 63314
 Dobrokhoto, V.G. 63584
 Dobromyslov, A.V. 63343
 Dobrya, V.I. 63461
 Dobryshchik, P. 60588
 + Dobrzhynski, L. 62233
 Dobson, B. 60840
 + Dock, D.S. 63909
 + Doddrell, D.M. 59812
 + Dodgson, K. 61032
 + Dodonov, A.I. 62006
 + Dodson, G.G. 63779
 + Dodson, G.W. 60043
 Doel, C.P. van den
 see van den Doel, C.P.
 + Doern, F.E. 60278
 Dogaru, I. 61706
 Doggett, J.N. 60407
 Doi, A. 63495
 + Dolg, M. 60568
 Dolganov, V.K. 62095
 + Dolgikh, G.V. 63343
 Dolizy, P. 63630
 + Dollet, J. 63413
 Dolma, V.A. 62436
 Dolman, B.G.S. 62352
 Domanskii, A.I. 61888
 Domb, C. 59697
 Dombey, N. 59962
 Domen, S.R. 60478
 + Dominguez, P.H. 62865
 + Dominguez, B. 60229
 + Dominici, D. 60024
 Dommelen, L.L. van
 see van Dommelen, L.L.
 Donaldson, M.T. 61426
 Donnachie, A. 60067
 Donon, J. 63710
 Donovan, R.J. 63524
 Donsker, M.D. 62350
 Doom, C. 64510
 Dordor, P.P. 62459
 + Dore, C. 60068
 + Dore, J.C. 61767
 + Dore, J.C. 61768
 + Dori, L. 63624
 Dornmann, J.L. 62719
 + Dornmann, J.L. 62633
 + Dornmann, J.L. 62725
 Dornhaus, R. 62987
 + Doroba, K. 60075
 + Doroba, K. 60083
 + Doroba, K. 60042
 + Doroba, K. 60077
 + Doroba, K. 60070
 + Doron, A. 60204
 Doronin, I.V. 63303
 Dorp, J.H. van
 see Van Dorp, J.H.
 Dorset, D.L. 61823
 + Dorset, D.L. 61816
 + Doughty, B.M. 60969
 + Doumeric, J.P. 62459
 + Dousson, S. 60972
 + Dovesi, R. 61907
 Dovletov, K. 62412
 + Dowden, R.L. 64291
 Dowell, D.H. 60178
 + Dowell, R.C. 63861
 + Dosey, R. 64462
 + Doyama, M. 62156
 Doyle, B.L. 63617
 Doyle, B.L. 59882
 + Doyle, B.L. 61659
 + Drake, G.W.F. 60615
 + Drake, N. 64079
 + Dran, J.C. 60243
 + Dran, J.C. 61997
 + Drapatz, S. 64341
 Dravinski, M. 64041
 Drchal, V. 62358
 + Drees, J. 60054
 + Dreizler, H. 60707
 Dremov, S.S. 61276
 Drew, J. 60787
 + Drexhage, K.H. 61174
 + Dreze, C. 60663
 Driel-Kulker, A.M.J. Van see
 Van Driel-Kulker, A.M.J.
 + Drifford, M. 63600
 + Drijard, D. 60075
 + Driller, J. 63999
 Dritis, M.E. 63264
 Droegge, A.T. 60739
 Drogenik, M. 63248
 Drotning, W.D. 62007
 + Drozd, P.I. 62915
 + Drozdowicz, K. 64251
 + Drozhdin, S.N. 62893
 Drozhkov, Yu.P. 62933
 Druck, U. 61904
 + Druz', I.I. 61259
 + Du Ning. 63075
 + Du Ning. 63065
 Du-chum Tao
 see Tao Du-chum
 + Dubinin, E.M. 64411
 Dubler, F. 62471
 Dubois, L.H. 63094
 + DuBois, R.D. 60937
 Dubov, V.S. 60907
 + Dubrovina, I.N. 61978
 Dubrovskii, G.V. 61590
 + Dubrulle, A. 60707
 Duc Tran Minh
 see Tran Minh Duc
 + Ducas, A. 61232
 + Ducas, L.R. 62356
 + Duchemin, J.P. 61152
 Duckhwan Lee 59849
 Ducruet, A.M. 59768
 Ducrops, C. 61478
 + Duda, P.M. 62077
 Duda, S.J. 64060
 + Duda, S.J. 64057
 + Dudenkova, A.V. 61163
 + Dudko, P.P. 63307
 + Duerdorth, I.P. 60031
 + Duerdorth, I.P. 60059
 Dufay, M. 60871
 + Dufayard, J. 60930
 + Duff, B.A. 64032
 + Duff, B.G. 60066
 + Duffield, W.A. 64101
 + Duffy, J.A. 63077
 Duffresne, J. 60376
 + Dufton, P.L. 60991
 + Dufty, J.W. 61588
 Duggan, J.J. 60901
 + Duggan, J.L. 60935
 + Duggan, J.L. 60938
 + Duif, A.M. 62637
 Dujuardin, G. 60743
 Duke, C.B. 63585
 + Duke, G. 59618
 + Dukes, C. 60041
 + Dukes, E.C. 60081
 Dukhovnyi, A.M. 61119
 + Dukova, E.D. 61934
 + Duldig, M. 64556
 + Duma, A.S. 64404
 + Dumas, J.P. 63701
 + Dumas, P. 62988
 Dumont, C. 62032
 Duncan, R.C. 64504
 + Dungan, J. 63753
 + Dunham, D.W. 64351
 + Duniec, J.T. 63795
 + Dunina, L.P. 63478
 Dunken, H. 62920
 + Dunken, H. 62277
 Dunlap, B.J. 60589
 + Dunlop, A. 61910
 + Dunn, J.R. 64037
 + Dunnnewold, C.J.W. 63829
 + Dunning, T.H., Jr. 61006
 + Dunscombe, P.B. 63922
 Dunster, H.J. 63983
 Duong Pham Hong
 see Pham Hong Duong
 Duparc, O.H. 62225
 + Duparc, O.H. 62233
 + Dupuyre, R. 62827
 + Dupuy, D. 63901
 + Dupre, D.B. 61778
 Dupre, J. 61134
 + Dupuy, C. 61943
 Durand, G. 61783
 Durand, J. 62087
 Durand, J. 62817
 + Duraud, J.P. 61998
 Durban, D. 61477
 + Durney, B.R. 64432
 Durouchoux, P. 64386
 Durr, D. 59705
 Durr, U. 61158
 Dusen Huang
 see Huang Dusen
 + Dushevskii, I.V. 63461
 + Dusseau, J.M. 62499
 Duszczek, J. 63203
 Duthoo, D. 60427
 + Dutil, R. 61004
 + Dutta, R.N. 64302
 Duvankov, N.I. 63601
 Duyneveldt, A.J. van
 see van Duyneveldt, A.J.
 Duzevic, D. 63253
 + Dvornik, G.G. 63665
 + Dworkin, J. 60041
 + Dworkin, J. 60081
 + Dworkin, J. 60087
 + D'yachenko, A.I. 62524
 D'yachenko, N.G. 62453
 + Dyadyusha, G.G. 63558
 + D'yakova, A.N. 61828
 Dybkov, V.I. 63468
 Dyck, D. van see Van Dyck,
 D.
 + Dyer, M.J. 60733
 + Dygdal, R. 60658
 + Dykstra, C.E. 60603
 + Dymoke-Bradshaw,
 A.K.L. 60483
 Dysthe, K.B. 61638
 + Dyu'dya, S.V. 63079
 Dzevic, D. 63208
 Dzhamaev, S.S. 63220
 + Dzhurayev, T.D. 63265
 Dziil'ski, K. 60767
 Dzurda, W. 63060
 + Dzurisin, D. 64270
 Dzygadlo, Z. 61398
 + Eanes, R.J. 64265
 + Early, T.A. 59809
 Easteal, A.J. 61757
 Easwar, N. 62118
 + Eaves, L. 63039
 + Ebel, H. 59891
 + Ebel, M.F. 59891
 + Eberhard, A. 61967
 + Eberhardt, P. 59875
 Eberhardt, W. 60870
 + Eberly, J.H. 60668
 + Eberth, J. 60129
 Ebralidze, T.D. 61112
 Ecer, A. 61521
 + Echols, D. 64079
 Eck, J. van see van Eck, J.
 Eck, J.S. 60200
 Eck, R. 63317
 Eck, T. van see Van Eck, T.
 + Eckart, B. 60073
 + Eckert, B.M. 61675
 + Eckerman, K.F. 63971
 + Eckhardt, V. 60076
 + Eckhaus, M. 60043
 + Eckstein, J. 63171
 + Edahiro, T. 61237
 + Edahl, R.A., Jr. 64244
 + Edelman, B. 60081
 + Eden, J.G. 60873
 Ederer, D.L. 60509
 Ediger, M.D. 60619
 + Ediger, M.N. 60873
 + Edmonds, J.A. 64264
 + Edsell, J. 63635
 Edwards, C.J.C. 61032
 Edwards, C.J.C. 61033
 Edwards, D.H., Jr. 63832
 Edwards, D.M. 62335
 + Edwards, D.M. 62549
 + Edwards, G.R. 63341
 Edwards, J.G. 61202
 Edwards, J.G. 60547
 + Edwards, P.J. 63390
 + Edwards, R.J. 63791
 + Edwards, R.T. 60081
 Eerden, J.P. van der
 see van der Eerden, J.P.
 Eesley, G.L. 59851
 Eesley, G.L. 62981
 + Efendiev, S.M. 62913
 + Efendieva, I.M. 63015
 Efimov, A.V. 63373
 Efimov, Yu.Ya. 60723
 + Efremenko, N.M. 61710
 Efremov, V.A. 61120
 Efremov, Yu.N. 64548
 Egami, N. 63395
 Egami, T. 61812
 + Egami, T. 62715
 Egashira, M. 62833
 Egobka, B.C.E. 63748
 + Edgell, R.G. 63101
 Egerton, R.F. 59896
 Eghtesadi, K. 61349
 + Egorov, V.N. 63073
 Egorov, Yu.P. 63325
 + Eguchi, T. 61799
 Eguiluz, A.G. 62234
 Ehrenstein, W.H. 63843
 + Ehrlich, R. 60049
 + Eichler, R. 60031
 + Eichler, R. 60059
 + Eichner, H. 60188
 Eides, M.J. 59954

- Einfeldt, J. + 62146
 + Einterz, C.M. 60620
 + Einzinger, R. 63185
 Eisele, K.M. 63632
 + Eisenberg, F.G. 61568
 Eisenbud, M. + 60319
 + Eiss, N.S., Jr. 63374
 Ekbote, S.N. + 62528
 Ekers, R.D. + 64552
 + Eknoyan, O. 63179
 + Ekspong, G. 60073
 Ektesabi, A. Motamed
 see Motamed Ektesabi, A.
 El Banhaw, Y. + 63550
 + El Bouchairi, B. 62513
 + El Masri, Y. 61172
 + El-Sayed, M.A. 63035
 El-Shorbagy, K.A. 61497
 Elander, N. + 60631
 + Elander, N. 59605
 + Elderfield, D.J. 62673
 Elgaroy, O. + 64451
 + Elias, J. 60083
 + Elias, J. 60042
 + Elias, J. 60070
 + Eliezer, Z. 63432
 Eliseev, A.A. + 60731
 + Eliseev, P.G. 61197
 + Elkin, M.D. 60777
 + Elliger, C.A. 60716
 + Elliger, C.A. 61018
 + Ellis, H.W. 61713
 + Ellis, K.J. 63948
 + Ellrodt, A.G. 63793
 Ellsworth, W.L. + 64069
 Ellwanger, U. 59662
 Elsaber, W. + 61151
 + Elsen, E. 60031
 + Elsen, E. 60059
 Elser, V. + 60685
 + Elston, S.B. 60965
 + Elston, S.B. 60508
 Eluskov, E.P. + 63286
 + Elvis, M. 64462
 Elworthy, K.D. + 59746
 Embleton, B.J.J. 64027
 Emeh, G.G. 59669
 Emel'yanov, V.I. + 62903
 + Emets, Yu.P. 63768
 Emiliani, C. + 63768
 Emmons, H.W. 63554
 Emmons, R.W. + 63543
 Emsley, J. + 60585
 + Emsley, J.W. 60752
 Emtsev, V.V. + 61968
 Enckevort, W.J.P. van
 see van Enckevort, W.J.P.
 + Enorenaz, T. 64340
 + Enderby, J.E. 61761
 + Endler, F. 64456
 + Endo, E.T. 64101
 + Endo, H. 63736
 Endo, T. 62406
 Endo, T. + 61246
 + Endo, Y. 60720
 Endoh, Y. + 62729
 + Endoh, Y. 62554
 + Engelke, F. 62835
 + Engelke, H. 60295
 + Engelking, P.C. 60739
 Engelmann, A.R. + 60592
 England, W.B. 60572
 + Englert, F. 59664
 + English, M. 64182
 + Enikolopyan, N.S. 62419
 + Enikolopyan, N.S. 63547
 Enns, T. + 63815
 + Eno, L. 60906
 + Entel, P. 62535
 + Enting, I.G. 64189
 + Enz, U. 63157
 Enzhi Hu see Hu Enzhi
 + Enzmann, D.R. 63943
 + Epechtin, N. 64478
 + Epp, E.R. 63906
 + Erasmus, C.S. 64261
 + Erb, J. 60428
 Erb, W. + 59822
 + Erben-Russ, M. 60861
 Erdman, P.W. + 64369
 + Erell, A. 60204
 Eremenko, A.S. + 61137
 Eremenko, V.N. + 63259
 Eremenko, V.N. + 62121
 Erem, M.V. + 62379
 Erenko, A.A. + 62345
 Erhard, G. 63431
 + Erichen, I.V. 61408
 Erission, I.E. 61483
 + Erikson, T. 60312
 + Erkin, V.M. 60531
 + Erkkila, B.H. 60185
 Erley, W. + 63104
 + Ermakov, A.E. 63286
 + Ermakov, A.E. 62710
 Ermakov, V.L. + 62830
 + Ermakova, N.V. 59836
 Ermolenko, A.S. + 62580
 Ermoshkin, A.N. + 63026
 + Erniyazov, Kh. 62412
 + Ernst, V. 61846
 Erokhin, L.I. + 63619
 + Erokhin, N.S. 61622
 Ershov, N.N. + 63043
 + Erskine, J.L. 63109
 + Erskine, J.L. 62260
 + Ertekin, C. 63821
 + Erwin, R.W. 62635
 Esaki, S. + 61386
 + Escalig, B. 62014
 Eshechenko, R.N. + 63344
 + Eshekabilov, N.B. 60679
 Eskin, S.M. + 63139
 + Eskreyes, A. 59995
 + Esmond, J.R. 60742
 Espriu, D. + 59999
 + Essene, E.J. 64089
 Esteve, J.M. + 60980
 + Esteve, D. 62616
 + Eti, M. 63821
 + Etoubleau, J. 64079
 + Eulenberg, G. 60133
 + Evangelou, I. 60073
 Evangelou, S.N. + 62549
 Evans, D.J. 61476
 + Evans, E.A. 63803
 + Evans, E.H. 63783
 + Evans, G.F. 62886
 Evans, G.V. 64263
 Evans, J. + 61009
 Evans, J.W. + 63497
 + Evans, J.W. 61549
 + Evans, R. 64494
 + Evans, S. 63137
 + Evans, W.A.B. 62208
 + Evans, W.M. 60074
 + Evarestov, R.A. 63026
 Even, U. + 60800
 + Everett, D.H. 62703
 + Evvard, M.O. 62642
 + Evseev, B.A. 61887
 + Evtukh, A.A. 63055
 + Ewing, G.E. 60718
 Ewing, R.C. + 60285
 + Ewing, R.C. 60287
 + Extermann, P. 60068
 Eyal, Y. 60286
 Ezawa, Z.F. + 59950
 + Ezekiel, S. 60856
 + Ezhov, V.F. 60751
 Farag, M.M. + 60409
 Farang Liu see Liu Farang
 Fargion, D. 64498
 Farhat, N.H. 63960
 Faris, W.G. 59632
 Farkas, D. 62172
 Farkas, D. 63464
 Farley, D.T. + 64287
 + Farmer, R.J. 59922
 Farquhar, R.W. + 64351
 + Farrow, R.C. 60851
 + Farrugia, P. 64091
 Farthing, J.W. + 60928
 + Fartunin, V.I. 63373
 + Farvolden, R.N. 63748
 Farynski, A. + 60396
 + Fassler, D. 63006
 Faucher, M. + 64470
 + Faulkner, R.G. 63294
 + Faupel, F. 62153
 + Fawcett, J.L. 61148
 + Fayer, M.D. 60619
 Fazekas, P. + 62535
 + Fazely, A. 60099
 + Fazely, A. 60179
 Fazio, G.G. 64339
 Fazylyanov, R.Kh. 59827
 + Feagin, J.M. 60146
 Fedchenko, I.I. + 59678
 + Fedin, V.P. 61212
 + Fedirko, V.N. 63457
 Fedorenko, A.I. + 61925
 + Fedorenko, S.Z. 63409
 + Fedorov, A.A. 61682
 + Fedorov, A.A. 61710
 + Fedorov, V.V. 63465
 + Fedorov, Yu.A. 61420
 + Fedorov, Yu.F. 61306
 + Fedorov, Yu.M. 62951
 + Fedorova, E.G. 63261
 + Fedorova, I.V. 64050
 + Fedorovich, L.P. 63360
 + Fedoruk, M.N. 64506
 + Fedoruk, G.A. 62919
 + Fedosejevs, R. 61655
 + Fedulov, A.P. 62145
 Fedyanin, V.K. 62572
 + Fehlmann, R. 61937
 + Fehrenbach, W. 60358
 + Fehrenbach, M. 64283
 Feibelman, P.J. 61056
 + Feigin, L.A. 63799
 Feinberg, D. + 62038
 Feinberg, G. + 60894
 + Feist, J.H. 60455
 + Feist, R. 61592
 Feitzinger, J.V. + 64471
 + Feix, M.R. 64453
 + Fejer, B.G. 64287
 Fejer, J.A. + 64286
 + Felakawa, L. 60203
 + Feld, R. 61893
 + Feld, R.H. + 60272
 + Feld, S.Ya. 61275
 + Feld, S.Ya. 61281
 Felderhof, B.U. 62905
 Feldman, C. + 63698
 + Feldman, G. 60178
 + Feldman, W.C. 64315
 + Felst, R. 60031
 + Felst, R. 60059
 Fen Lu see Lu Fen
 + Feng, M.Y. 62387
 Feng Da huan
 + Feng Da huan Feng
 + Feng Jun-ming 63893
 + Feng Ren-fa 60168
 Feng Zhechuan + 62311
 + Fenochka, B.V. 63224
 + Ferey, G. 61880
 + Ferey, G. 61882
 Ferguson, J. + 60740
 + Ferguson, T. 60049
 + Ferlet, R. 64524
 + Ferdinand, J. + 60377
 + Ferdinand, J. 60376
 Fernandez, F.M. + 59606
 Fernandez, J.F. 62542
 + Ferragina, C. 63083
 + Ferrari, V. 63945
 Ferreira, J.R. Faleiro
 see Faleiro Ferreira, J.R.
 + Ferreira Marques, R. 60537
 + Ferrell, R.A. 62031
 + Ferri, D. 60324
 + Ferro, D. 62081
 + Ferroni, S. 60066
 + Ferry, P.J. 60443
 + Fertman, D.E. 60557
 + Fesser, K. 59718
 + Fetisov, V.P. 63455
 Fetter, C.W., Jr. 60257
 + Feuillade, C. 60857
 + Feuring, K. 60424
 Feyder, G. + 62033
 + Fichtl, G.H. 64172
 + Ficke, D.C. 63935
 Ficker, T. 60586
 + Fiddy, M.A. 61096
 + Fidler, J. 63110
 Fiechter, S. + 63171
 Fiedler, O. 61579
 Fiedler, O. + 61580
 Field, R.W. + 60797
 + Field, R.W. 60804
 + Field, R.W. 60780
 Fields, C.A. + 60134
 Fields, C.A. + 60106
 + Figueiras, J.A. 61416
 + Figueiras, J.A. 61417
 + Filimonov, V.N. 63312
 + Filimonov, V.S. 63183
 + Filin, V.G. 62343
 + Filinskii, A.V. 61026
 Filipchenko, A.S. + 62370
 + Filipek, S. 62393
 Filippov, A.T. 60006
 + Filippov, G.A. 63256
 + Filippov, Yu.S. 61641
 + Fillo, J.A. 60416
 + Filonenko, A.D. 61532
 + Finch, A. 62080
 + Findley, G.L. 61209
 Fink, P. + 63605
 + Fink, P. 62277
 Fink-Finowicki, J. 62950
 + Finkel, A.G. 62104
 Finkelmann, H. + 62922
 Finkman, E. 62334
 + Finn, J.M. 60179
 + Fionova, L.K. 61931
 Fiorani, D. + 62725
 Fiorani, D. + 62633
 + Fiorani, D. 62719
 + Fiorentini, G. 59967
 + Fioshina, M.A. 63601
 + Firatli, A.C. 63236
 + Firestone, A. 60075
 + Firey, B. 62260
 + Firsov, D.A. 61279
 + Firsov, D.A. 62934
 + Firsov, V.V. 60868
 Fischer, B.E. + 61999
 Fischer, D.A. + 62239
 Fischer, G. + 60875
 + Fischer, H.G. 60075
 + Fischer, O. (ed.) 59553
 + Fischer, R. 62521
 + Fischer, S.F. 60918
 + Fischer, S.F. 60918
 + Fischermeister, H. 63210
 Fisher, D.S. + 62207
 Fisher, G.B. + 63102
 + Fisher, G.H. 64430
 + Fisher, M.E. 59749
 + Fisk, Z. 62091
 + Fittipaldi, I.P. 61803
 + Fittipaldi, I.P. 62660
 Fitton, J.G. 64111
 Fitzhugh, R. 63817
 Flad, J. + 60568
 Flageolet-Daniel, C. +
 62056
 + Flahaut, J. 61865
 + Flahaut, J. 61862
 Flamant, P.H. + 61206
 + Flamant, P.H. 60775
 + Flanders, B.S. 60536
 + Flegontov, Yu.A. 61066
 + Flenner, J.P. 61357
 + Flerov, V.B. 62006
 + Flerova, S.A. 62877
 + Fletcher, I.W. 60928
 + Fliechtstein, J. 63143
 + Fliedner, T.M. 63904
 Fliege, E. + 60707
 Flint, B.K. 61262
 Flint, C.D. + 62992
 Floor, C. 64268
 Flor, G. + 60457
 Floratos, E. + 59903
 + Floratos, E. 59908
 + Florence, A.L. 60361
 + Flores, C. 63683
 Flores, R.A. + 59975
 Florian, H. + 63868
 Flowers, K.D. 61339
 + Flukiger, R. 60428
 + Flygar, W.H. 60701
 + Flynn, G.W. 60902
 + Flytzanis, N. 62036
 Foda, M.A. + 64040
 + Fofanov, A.A. 63205
 + Fogarassy, E. 63706
 + Fojas, C. + 61473
 + Foksha, A.Ya. 63665
 + Folkesson, B. 60978
 + Foll, H. 63152
 Follner, H. + 61896
 Fomichev, A.A. + 63021
 + Fomichev, V.N. 60751
 + Fomin, V.I. 61449
 + Fong-Tom, R.A. 60088
 + Fonseca, A.C. 60155
 Fontaine, B. + 61133
 Fontaine, J.P. + 60345
 Fonte, G. + 59619
 + Fonte, R. 60212
 + Fontheim, E.G. 64324
 Foonasne, T. + 60717
 Ford, P.C. + 60839
 Ford, W.K. + 60566
 + Forester, B. 61133
 + Forkel, R. 64154
 Fornace, S. 61616
 Fornasini, M.L. + 61857
 Forrest, M.A. + 63250
 Forrest, M.A. + 63441
 + Forster, J.R. 64551
 Fortes, M.A. + 62213
 + Fortin, X. 63086
 + Fortune, H.T. 60202
 Foster, C.A. + 60473
 + Foster, C.C. 60099
 + Foster, C.C. 60179
 Foster, C.G. + 61427
 + Foster, F. 60031
 + Foster, F. 60059
 Foster, J.B. 60259
 + Fotakis, C. 63524
 + Foti, G. 63126
 + Foti, G. 61991
 + Foti, G. 63567
 + Fotiev, A.A. 62133
 + Fou, T.S. 60951
 Fou Cheng-Ming
 see Cheng-Ming Fou
 + Foucher, P. 61785
 + Foulkes, E.J. 63036
 Foulon, M. 62107
 Fowler, J.W. + 64353
 + Fowler, R.F. 62208
 Fox, R.F. 59713
 Fox, R.F. 59744
 + Foy, R. 64392
 Fraedrich, K. + 64166
 + Fraenkle, H. 60527
 + Frahm, A.A. 63161
 + Frahm, R. 61886
 Fraiture, L. 64350
 Franca, E. Penna
 see Penna Franca, E.
 + Franchini, A. 63098
 Franck, E.U. 62073
 Francke, K.P. + 61181
 + Franco, M.L. 64472
 + Frandsen, P. 60074
 + Franke, G. 59995
 + Frankel, S. 60074
 Franklin, J. 60046
 Fraser, C.M. + 59966
 Fraser, J.S. + 60523
 Fraser, P.J. + 64189
 + Fraser, S. 59711
 Frasnayak, V.M. + 61875
 + Frati, W. 60074
 Fratucllo, G. + 62608
 + Frauenfelder, H. 59936
 + Frazer, M.E. 61326
 + Fredin, L. 60721
 Fredrikze, H. 60617
 + Freed, J.H. 62819
 Freed, K.F. + 59698
 + Freed, K.F. 63520
 + Freeman, D.E. 60742
 + Freeman, R. 59816
 + Freeman, R.R. 60500
 + Freeman, R.R. 61229
 Froese, K. + 64370
 + Freise, H. 60075
 Frei, H. + 63521
 + Freistenstein, B. 63152
 Freitas, P.P. + 62645
 Freller, H. 63167
 + French, K.A. 60073
 + Frenkel, T. 59816
 + Freslon, H. 60382
 Fretter, W.B. 59572
 Freund, H.P. 61167
 + Freund, P. 60076
 + Frey, R.W. 60078
 Friar, J.L. + 60166
 Friberg, P.O. 61432
 Fricke, D.K. + 63446
 + Fridman, A. 60049
 + Fridman, Sh.D. 63764
 + Friebele, E.J. 61805
 + Fried, B.D. 61628
 + Fried, M. 61936
 + Fried, S. 60317
 + Friedberg, S.A. 62593
 + Friedlaender, F.J. 62778
 Friedlander, E.M. + 60195
 + Friedman, A. 61536
 + Friedman, A. 60317
 + Friedman, B.R. + 63000
 + Friedman, H.L. 62141
 + Friedman, M. 59879
 Friedrich, M. + 64296
 Friedt, J.M. + 62861
 Fries, P.H. + 61748
 Friesel, D.L. + 60536
 + Frieze, W.E. 62239
 + Frigh, W.R. 61093
 + Fripiat, J.J. 62822
 Frisch, M.J. + 60580

- Frisch, M.J. + 60567
 Frischkorn, H.J. + 63114
 + Frischkorn, H.J. 63113
 + Fritsch, G. 61223
 + Fritsch, R. 60456
 Fritsche, H.-G. 62472
 Fritsche, H.-G. + 62473
 + Fritzer, H.P. 62546
 + Froehner, K.H. 62428
 Frogel, J.A. + 64491
 Frohlich, C. 64382
 Frohlich, J. + 59722
 + Frohlich, R. 61897
 Frohling, W. + 60748
 + Frohling, W. 60335
 + Frois, B. 60183
 + Fronts, K. 61156
 + Frucholz, R.P. 60655
 Fu-zhi Song, see Song Fu-zhi
 Fuchikami, N. 62577
 Fuchuo Pu, see Pu Fuchuo
 + Fuchs, W. 61581
 Fuda, M.G. 60153
 + Fujii, A. 62563
 + Fujii, H. 61099
 + Fujii, T. 62795
 + Fujii, T. 62792
 Fujiki, S. + 62643
 Fujimori, H. + 62789
 + Fujimori, H. 62293
 + Fujimori, H. 62728
 + Fujimori, H. 62431
 + Fujimoto, F. 63159
 Fujimoto, Y. + 61530
 + Fujimoto, Y. 59928
 + Fujino, Y. 62293
 + Fujioka, A. 60468
 + Fujioka, M. 60504
 + Fujioka, T. 61142
 Fujisaka, H. + 59716
 Fujisaka, H. + 59715
 + Fujisawa, N. 61490
 Fujita, F.E. 61461
 + Fujita, H. 61102
 + Fujita, H. 62017
 + Fujita, J. 61614
 + Fujita, M. 60468
 + Fujita, N. 63595
 Fujita, T. + 61315
 + Fujita, T. 63349
 Fujiwara, A. 64413
 Fujiwara, H. + 62295
 + Fukai, Y. 62366
 Fukamichi, K. + 62565
 + Fukamichi, K. 62566
 + Fukase, T. 62399
 + Fukatsu, T. 63686
 + Fukatsu, T. 62069
 + Fuks, M.I. 61067
 + Fukuda, A. 61772
 + Fukuda, A. 61258
 + Fukuda, M. 61147
 + Fukuda, M. 63898
 + Fukuda, Y. 60849
 + Fukui, Y. 60072
 + Fukui, Y. 60082
 + Fukusako, S. 61505
 Fukushima, S. 59723
 Fukushima, S. + 62188
 Fukushima, S. + 62189
 Fukushima, S. + 62190
 Fukutome, H. + 60596
 Fukuyama, T. + 59655
 + Fukuzawa, F. 63117
 + Fulchignoni, M. 64391
 Fuller, C.R. 61345
 Fuller, M. + 64037
 Fulton, B.R. + 60201
 Fulton, T.J. + 63912
 Funaki, Y. 62030
 Funck, E. + 60555
 + Fundamenskii, V.S. 61902
 Funfschilling, J. + 63028
 + Fung, P.C.W. 59625
 + Furrer, A. 62381
 + Furrer, A. 62573
 + Furubayashi, T. 62874
 + Furuya, H. 62166
 + Furuya, K. 62551
 + Furuya, K. 61150
 + Furuyama, M. 60434
 + Fyfe, W.S. 60279
 + Gadzhiev, S.M. 63518
 Gadzuk, J.W. + 62268
 Gaete-Garretton, L. + 61333
 + Gaete-Garretton, L. 61332
 + Gafni, M. 63857
 + Gafurov, R.B. 61814
 Gagarin, S.G. + 60640
 Gagne, J.M. + 60663
 + Gago, J. 60085
 + Gaididei, Yu.B. 62346
 + Gailloud, M. 60068
 + Gainutdinov, I.S. 62303
 Gaiser, J. + 60966
 + Gaiser, J. 60899
 Gaitsandzhiev, D. + 64274
 + Galaez, A.A. 62501
 + Galakhov, V.R. 63286
 + Galanov, E.K. 59820
 + Galashev, A.E. 61753
 + Galavura, T.Ya. 63223
 + Gal'dikas, A. 62464
 Galetti, D. + 60122
 + Galik, R. 60049
 Galison, P. + 60034
 Galkowski, A. + 61674
 Gall, H.L. see Le Gall, H.
 Gall, L.N. 59876
 + Gallagher, A. 60633
 Gallagher, T.F. + 60929
 + Gallagher, T.F. 60667
 + Gallagher, T.F. 60673
 Gallego-Juarez, J.A. + 61332
 + Gallego-Juarez, J.A. 61333
 Gallimore, R.G. 64230
 + Galloni, R. 63704
 + Galluzzi, F. 63699
 Galtsov, D.V. + 59644
 Galushko, I.M. 63281
 + Galvaleshko, N.P. 61875
 + Galvao, R.M.O. 61615
 + Gamali, E.G. 61672
 + Gammampila, K. 63922
 + Gammion, R. 63724
 Gamo, T. + 63739
 Gan Zizhao + 62362
 Ganapathy, K. + 60762
 + Ganapathy, S. 62823
 Ganapol, B.D. + 61389
 + Gancheva, T.St. 61818
 + Ganci, P. 60049
 Gane, P.A.C. + 61787
 + Ganesan, V. 61492
 Gang Xu, see Xu Gang
 Gangal, A.D. 60064
 Gangopadhyay, P. + 60960
 + Ganguly, N.K. 60115
 Ganin, Yu.G. + 61903
 Ganina, N.V. + 62301
 + Ganser, A. 63904
 + Ganssaue, E. 60195
 + Gantmakher, B.F. 60593
 + Gao, H. 61502
 + Gao, R.W. 62724
 Gao Chong-shou + 60000
 Gao Chong-shou + 60026
 Gao Chong-shou + 60020
 Gaponov, S.V. + 63161
 Gaponov, S.V. + 61671
 Garabedian, G. + 60374
 Garand, L. 64184
 Garaschuk, V.P. + 61191
 Garcia, J. + 62626
 + Garcia, L. 61693
 Garcia, M. + 64462
 Garcia, N. 62977
 Garcia, N. + 63122
 Garcia-Colin, I.S. 59596
 + Garcia-Sole, J. 62802
 + Garde, A.M. 60389
 Gardiner, C.W. 63776
 + Gardner, P.J. 62080
 + Gardner, W.L. 60528
 + Garg, M.L. 60131
 + Garg, S.C. 64205
 + Garin, Sh.N. 62006
 Garland, D.A. + 60763
 + Garner, C.D. 60840
 + Garner, C.D. 60839
 Garner, L. + 63955
 + Garnier, J.P. 62056
 Garnier, P. + 62135
 + Garoff, S. 62971
 + Garpmann, S.I.A. 60075
 + Garren, L. 60049
 Garrett, B.C. + 61006
 Garrett, J.C.P. + 60332
 Garrett, S. 62195
 Garrido, M.S. 59643
 Garside, B.K. + 61155
 Garside, J. + 63142
 + Garulli, A. 63624
 Gary, S.P. + 64288
 + Gary, S.P. 64315
 Garzaroli, F. 60389
 Gasanly, N.M. + 62044
 Gasanov, I.S. + 61070
 Gashin, P.A. + 63665
 + Gasic, M. 63230
 + Gasic, M. 63229
 Gaskell, T. + 61762
 + Gaspar, M. 61233
 Gaspar, R. 60576
 Gasparotto, M. + 60451
 + Gasparoux, H. 61785
 + Gasperin, M. 61874
 + Gast, T. 63474
 Gatehouse, B.M. + 61872
 + Gates, J.A. 63589
 Gatignon, P. 61331
 + Gatto, R. 60024
 Gaucher, P. + 61846
 + Gaudaen, J. 60073
 Gaudriot, L. + 61348
 Gault, F.D. + 60055
 + Gaune-Escard, M. 62117
 + Gautheron, B. 61900
 Gauthier, D.J. + 61228
 Gauthier, S. 62236
 Gauthier-Manuel, B. + 61471
 + Gauyacq, D. 60768
 Gave, G. + 63678
 + Gaveau, M.A. 60697
 + Gavela, M.B. 59947
 Gavrilin, N.I. + 62500
 + Gavrilov, F.F. 63056
 Gavrilov, G.M. + 61952
 Gavrilov, I.V. + 64404
 Gavrilov, L.F. + 63056
 Gavrilov, V.E. + 61251
 + Gavrilova, N.D. 62893
 Gavriluk, A.V. + 62768
 + Gavriluk, B.V. 62937
 Gavriluk, V.I. + 62937
 Gavra, S.P. + 60777
 + Gaw, J.F. 61044
 Gay, R.R. + 63688
 + Gaylord, T.K. 61072
 + Gayoso, J. 60591
 + Gazit, D. 59879
 + Gazquez, J.L. 60611
 Gebauer, D. + 64002
 + Gebauer, H.J. 60076
 Gebczak, M. + 61186
 Gebhardt, U. + 63629
 + Gedberg, M.G. 63304
 Geddes, L.A. + 63986
 + Gee, C.N.P. 60068
 Geer, C.A.J. van der 61787
 see van der Geer, C.A.J.
 Gefen, Y. + 62650
 + Gehler, S. 60323
 Gehlig, R. + 62415
 + Geich-Gimbel, C. 60033
 + Geich-Gimbel, C. 60073
 + Geim, K. 63152
 + Geiss, J. 59875
 + Geist, W. 60075
 Gekht, R.S. 62941
 + Gel'd, P.V. 62171
 + Gelfand, J. 60921
 Gell-Mann, M. 59580
 Gely, M.-H. + 61910
 Gemperle, A. + 61920
 gen. Schieck, H. Paetz 61920
 see Paetz gen. Schieck, H.
 + Gence, J.-N. 61564
 + Genkin, G.M. 61062
 Gennad'ev, V.M. + 61841
 Gennaro, M.C. + 60749
 Gennes, P.G. de 61920
 see de Gennes, P.G.
 + Genossar, J. 62413
 + Genov, V. 64241
 + Gentile, T. 60049
 + Gentry, W.R. 60958
 + Genzel, H. 59995
 + George, B. 63416
 George, T.F. + 60898
 + Georges, R. 63990
 Georgiev, N.N. + 63382
 Georgieva, I.Ya. + 62586
 Georgiev, W. + 64525
 + Gera, B.S. 64197
 Gerard, A. 61319
 Gerard, P. + 61906
 + Gerasimov, S.I. 61469
 Gerasimov, V.I. + 63372
 + Gerdnyukov, L. 60533
 Gergely, G. 63473
 + Gerhardt, H. 60657
 + Gerke, Ch. 59995
 + Gerken, G.M. 63858
 German, R.M. 63200
 + Gernsey, K. 61221
 + Gernandt, H. 64274
 + Gerosa, A. 60382
 + Gersch, H.U. 60159
 Gershman, R.L. + 63309
 + Gersten, J.I. 60828
 + Gersten, J.I. 62971
 Geshire, M. + 61268
 + Geusic, M.E. 61043
 + Geveluk, S.A. 61115
 Geyer, A. de 61115
 see de Geyer, A.
 Ghadekar, S.R. + 61951
 + Ghatak, K.P. 62326
 + Ghedira, M. 61884
 Ghia, V.V. 63720
 Ghicimetti, A.G. + 59875
 + Ghijsen, J. 63096
 + Ghodgaonkar, A.M. 60890
 Ghosh, A. + 61095
 Ghosh, A. + 64329
 + Ghosh, A.S. 60998
 + Ghosh, B. 62084
 + Ghosh, B. 62085
 + Ghosh, K.K. 62326
 + Ghosh, P.K. 61611
 + Giacomelli, G. 60075
 Giancarlo Jug. 62667
 + Giacinto, P.V. 61757
 Gibb, T.C. 62842
 Gibbons, D.J. 61207
 + Gibbons, D.J. 63691
 + Gibbons, J. 59621
 + Gibilaro, C. 62986
 Gibson, I.P. + 61767
 + Gibson, P.N. 61994
 + Gibson, P.N. 61995
 + Gibson, P.N. 60281
 + Gibson, W.M. 60068
 + Gidlund, J. 60300
 Gies, H. 60292
 + Giese, C.F. 60958
 + Gijssen, M. 60073
 + Gilad, S. 60213
 Gilbert, R.C. 64093
 Gilbert, M.G. 63501
 Gilbody, H.B. 61699
 + Gilchriese, M.G.D. 60049
 Gildenblat, G. + 62498
 + Giles, A.B. 64556
 Gilev, S.D. + 59805
 Gilinski, M.M. + 61527
 Gill, R.L. + 60111
 + Gillot, B. 62279
 Gilman, J.P. + 63526
 + Gilman, R. 60202
 + Gilmore, J.T. 63747
 + Gimpel, R.W. 60195
 + Gindi, G.R. 63959
 Ginester, A. La 61621
 see La Ginester, A.
 Ginzburg, V.L. 61621
 + Giovanetti, K. 60043
 + Girard, A. 64215
 + Girard, P. 62499
 + Girdzhunaitis, D. 61793
 Girel, S. 62948
 Girish Kumar, U.V. + 64308
 + Girnyak, M.B. 64438
 Girotti, H.O. + 59620
 + Gispert, R. 64340
 Gitterman, B.P. + 61725
 + Gittelman, B. 60049
 Gitterman, M. + 62113
 Giuffrida, M. + 63673
 + Giuliani, C. 64391
 G. Klipping, see Klipping, G.
 G. Knop, see Knop, G.
 Glad, A.S. 60458
 + Gladiola, V.P. 64223
 Gladishevskii, R.E. + 61852
 Gladkii, V.V. + 62902
 + Gladkikh, N.T. 62131
 + Gladyshevskii, E.I. 61892
 + Gladyshevskii, E.I. 61902
 + Glaid, J.L. 63097
 + Glaid, J.L. 63100
 + Glass, I.S. 64556
 Glass, N.E. + 62226
 + Glasser, R.G. 59995
 Glazunov, V.N. + 61719
 + Glek, R.I. 63429
 + Glen, J.W. 62160
 + Glendinning, I. 60031
 + Glendinning, I. 60059
 Glikman, L.G. + 61065
 Glinchuk, K.D. + 61948
 Gliner, R.E. 63358
 + Glinski, J. 62953
 Glockl, J. + 63711
 + Gloeckler, G. 64335
 + Glukhova, L.K. 63251
 + Gluzman, N.G. 62461
 + Gmeiner, R. 62317
 Go, N. 63778
 + Gobel, E.O. 61151
 Gocksch, A. + 59985
 Godard, R. + 64354
 + Goddard, M.C. 60031
 + Goddard, M.C. 60059
 Goddard, N.J. 59901
 + Goddard, P.A. 62691
 + Goddard, W.A. III. 62232
 Godlevskii, A.P. + 63763
 Godlevskii, A.P. + 64267
 Godmanis, I.T. + 63019
 + Godovskii, Yu.K. 61832
 Godzhaev, E.M. + 62411
 + Godzhaeva, F.M. 62411
 + Goedicke, K. 63158
 Goeke, K. + 60216
 + Goel, R.K. 64201
 + Goerlach, U. 60074
 + Goetzberger, A. 63650
 + Goffe, D. 60697
 Gogolev, Yu.A. + 61259
 Gogonea, S. 61550
 + Gogoshev, M.M. 64349
 + Goitein, K. 63857
 Gokhale, B.G. + 60639
 + Gokiel, R. 60075
 Gola, D. + 60188
 + Golant, V.E. 61710
 Golben, P.M. + 63735
 + Gold, L.P. 60769
 + Goldbeck, R.A. 60620
 + Goldberg, A.B. 63022
 + Goldberg, M. 60049
 Gold'berg, Yu.A. + 62497
 + Goldberg, W.I. 62118
 Golden, K.I. 61604
 Golden, W.G. + 59859
 + Goldman, I.D. 60169
 + Goldman, L.M. 61631
 Goldman, S.P. + 60615
 + Goldschmidt-Clermont, Y. 60533
 Gol'dshtein, R.V. + 61454
 + Gol'dshtein, V.Ya. 63309
 Goldstein, G.R. + 60092
 + Goldstein, M.L. 64418
 + Goldstein, S. 59705
 + Goldstein, S. 60377
 Golciewska-Herrmann, A. 61403
 + Golkowska, A. 59762
 Gollub, J.P. 61486
 Golomb, D. + 64161
 + Golomb, O.L. 60824
 Golombek, M.P. + 64112
 Golovinskii, P.A. + 60671
 Golovko, B.A. 64388
 Golovko, M.F. + 61754
 Golovko, M.F. + 61745
 Goltzman, M.F.L. 59951
 Goltsev, A.V. 62651
 + Gol'tsev, A.V. 63002
 + Golub, L. 64477
 + Golub, L.V. 62372
 Golubenko, I.V. + 61298
 + Golubev, A.A. 63628
 Golubev, A.V. + 60531
 + Golubev, E.M. 64216
 Golubev, Yu.M. + 61131
 Golubev, Yu.N. + 64145
 Golubnichi, P.I. + 61532
 Golubovic, L. 59752
 + Golubovskii, Yu.M. 61266
 + Golubovskii, Yu.A. 63928
 Golyaev, Yu.D. + 61200
 Gumberoff, L. + 64320
 + Gomes, A.S.L. 61175
 + Gomes, W.P. 63445
 + Gomez, A.L. 64478
 Goncalves, L.L. + 62539
 + Goncharenko, Yu.M. 60086
 + Goncharov, A.F. 62044
 + Goncharov, L.A. 61952
 + Gondo, Y. 62783
 + Gondo, Y. 62794
 + Gondo, Y. 62757
 + Gong Chang-de 59725
 Gonnard, P. 61947
 Gonschorek, W. + 61893
 Gonser, U. 62840
 Gonser, U. + 62790
 + Gonser, U. 62431
 + Gonzalez, D. 62567
 + Gonzalez, D. 62592
 + Gonzalez, D. 62626
 + Gonzalez, D. 62594
 + Gonzalez, D. 62672
 + Gonzalez, J.M. 62583
 + Gonzalez-Caballero, F. 63563
 + Gonzalez-Oliver, C. 61307
 + Gonzalez-Sanabria, O.D. 63656
 + Good, R.H., Jr. 60052
 + Goodell, P.D. 61567
 + Goodger, E.M. 61393
 + Goodhead, D.T. 63910
 + Goodhead, P.J. 60405
 + Goodhead, P.J. 60410
 + Goodman, L. 60878
 + Gopal, E.S.R. 62621
 Gopasuy, S.I. + 64459
 + Gopel, W. 63106
 Gorbani, I.S. + 62078
 + Gorbics, M. 60075
 Gorbunov, A.V. 61962
 Gorbunov, Yu.A. + 63371
 Gorbunova, I.V. 64054
 Gordelii, V.I. + 61050
 + Gordienko, V.M. 60241
 + Gordon, H. 60074
 + Gordon, J.C. 60068
 + Gordon, J.G. II. 62991
 + Gordon, R. 63953

- +Gordon, R.J. 63522
Gordon, S. + 60355
+Gordon, W. 62516
+Gorelowa, L.L. 63337
Gorenstein, M.I. + 59989
+Gornostaevo, S.V. 61710
Gornyi, M.B. + 60666
+Gorobets, Yu.I. 62692
Gorodtsha, L.V. + 62465
+Gorokhova, E.I. 61835
+Gorse, C. 61716
+Gorshkov, V.G. 60751
+Gorshkova, O.V. 61955
Gorton, E.K. + 61127
+Gorton, P.J. 61127
+Goryachev, Yu.M. 62396
+Goscinski, O. 60631
+Goshchitskii, B.N. 61978
+Gosling, J.T. 64314
+Goss, D.A. 63828
+Goss, W.M. 64551
+Gossanyi, A. 60343
+Goswami, G.K. 59642
Gotaas, J.A. + 62383
Goto, H. + 62364
Goto, M. + 62788
Goto, T. + 60997
Goto, T. + 62826
+Goto, T. 60955
+Gotow, K. 60213
+Gottardi, V. 61193
+Gottfried, S.B. 63865
Gottlieb, H.P.W. 61355
Gottschalk, B. 60549
Gottschalk, T.D. 59996
+Gottwald, E. 60900
Goudard, G. + 60883
Gougeon, P. + 61868
Gough, T.E. + 60924
+Goulart Rosa, S., Jr. 62662
Gounand, F. + 60667
Gouzeur, J. + 62773
+Govindjee 63790
+Gowda, B.H.L. 61492
Goy, P. + 61122
+Goy, P. 61121
+Goyal, A. 60060
Grabmaier, J.G. 63663
Grabmaier, J.G. + 63152
+Gracco, V. 60066
Gradin, P.A. 63387
+Gradwell, A.J. 61819
Graf, W.L. 64142
+Graham, J.A. 64491
+Graham, J.C. 63912
+Graham, N.B. 62068
+Graham, W.G. 60934
+Gralla, B. 62179
+Gram, P.A.M. 60206
+Gramain, J.C. 63566
Gramatikov, D.D. + 63243
+Gramigna, F. 60532
Granatkin, Yu.A. + 63364
+Grandolfo, M. 62913
+Granik, G. 63987
Grankin, I.M. + 61367
+Granovskii, A.B. 62402
+Grant, A. 60033
+Grant, A. 60533
Grant, B.J.B. + 63881
+Grant, I.P. 60616
Grant, J.L. 60255
+Grant, P.J. 60140
Grashilin, V.A. + 60550
+Grasmuck, J.P. 61358
+Grassler, H. 60033
+Grasyuk, A.Z. 61192
+Grats, Yu.V. 59644
+Graveney, M.J. 63791
+Gray, B.A. 63877
Gray, G.T., III + 63401
+Gray, L.J. 62322
Gray, R.H. 59823
+Gray, R.J. 60068
Gray, T.J. + 60964
Gray, T.J. + 63115
+Gray, T.J. 60506
+Gray, T.J. 63617
+Gray, T.J. 60948
+Grebchenko, M.F. 61796
+Grebchenko, V.G. 62396
+Grebneva, V.S. 61798
+Grebnyi, V.G. 61719
Grechov, V.V. 63128
+Greco, R. 63348
Gregor, R.B. + 60287
+Green, G. 64037
+Green, J. 60049
Green, J.C. 64109
+Green, W.V. 60235
+Greenburg, S.L. 59562
Greene, B.J. 60851
+Greene, P.D. 63039
+Greene, S.J. 60202
+Greenspan, R.H. 63919
+Gregg, J.F. 62816
Gregorio, S.De. 62839
see De Gregorio, S.
- Gregory, E.A. + 60917
+Gregory, E.A. 60911
+Gregory, G.K. 60756
Gregory, G.L. + 64244
Gregory, T.J. + 63875
Greidanus, F.J.A.M. + 62381
+Greig, D. 61819
+Greisukh, G.I. 61107
Grenier-Loustalot, M.F. + 60758
+Grens, J.Z. 60276
+Grenthe, I. 60324
+Gresham, J.B. 63682
+Greskovich, E.J. 61568
Greve, J.P.de. 60457
see de Greve, J.P.
- +Grewing, M. 64341
+Grey, I.E. 61872
Gribnikov, Z.S. 62935
+Gribov, Yu. 61709
+Grice, R. 60901
+Griem, H.R. 61607
Griffin, R.F. 64515
Griffiths, H. 60538
+Grigo, M. 62146
Grigorenko, Yu.M. + 61401
+Grigor'ev, E.I. 60337
Grigorovich, N.M. + 60722
Grigorovich, V.K. + 63365
+Grigoryan, R.A. 61138
Grigoryants, V.V. + 61280
Grigoryants, V.V. + 61282
+Grigoryeva, L.K. 62131
+Grigull, R. 59995
Grimes, N.W. + 61885
Grimley, T.B. 62237
Grimley, T.B. + 60607
+Grimm, R.C. 61643
+Grimm, W. 62585
+Grin, Yu.N. 61892
Grinberg, H. + 59733
+Grinberg, Ya.Kh. 62122
+Grinberg, Ya.Kh. 62127
Grinchenko, B.I. 61135
Grinstein, G. + 62665
Grisaru, M.T. + 59938
Griscom, D.L. + 61805
Grisenti, R. + 59881
Grisham, R.R. + 60391
Grishchenko, E.K. 61366
+Grishin, S.A. 63357
Gritskov, P.F. 63484
+Grobler, R. 60041
+Grobler, R. 60081
+Grobler, R. 60087
Groblicki, R. 59615
+Grodins, F.S. 63864
+Grodskii, S.A. 61200
Grodzins, L. 62843
+Groenenboom, P.H.L. 60381
+Groeneveld, K.O. 63114
+Groeneveld, K.O. 63113
+Groeneveld, K.O. 60965
+Groesbeck, D.E. 61534
Grogorovich, V.G. + 63305
+Groh, W. 60949
Grolemond, D.L. + 63088
+Grolleire, F. 63630
+Gromenko, V.M. 61532
+Gronbeck, B. 64511
Groot, M. + 64466
Groot, M.J.H.de. 60355
see de Groot, M.J.H.
- +Gropen, O. 60629
+Grosch, M. 59854
+Gross, H.J. 63774
+Gross, M. 61122
+Gross, M. 61121
Grosvenor, T. + 63827
Grover, J.R. + 60812
+Grozhih, V.A. 61793
Gruber, H. + 62546
+Gruber, H. + 62433
+Gruber, K. 63868
+Grubler, W. + 60165
+Gruen, D.M. 60717
+Gruen, D.W.R. + 62879
+Gruen, D.W.R. + 62880
+Grubh, J. 64161
+Gruhn, Ch. 60075
+Grukhin, Yu.A. 63923
Grum, F. + 59829
+Grummer, F. 60216
Grundy, R.E. 59745
+Grunewald, M. 59690
+Gruno, J. 60324
+Gruppen, C. 59995
Gruza, G.V. + 64224
Gruzdov, P.F. + 60583
+Gry, C. 64524
+Gryaznevich, M.P. 61682
+Gryaznevich, M.P. 61710
+Gryaznevich, V.P. 61131
+Gryaznov, V.M. 63584
+Gryaznov, V.M. 63583
Gryffroy, D. + 62839
+Grygoruk, L. 60395
- +Gryn', Yu.M. 61852
Grzegorzewski, B. + 61088
+Grzetic, V. 61008
+Gu Yi-ming. 62532
Guadagnini, E. 60036
+Guan Dian-hua. 64128
Guang-hua Chen. 62381
see Chen Guang-hua
Guangfu Zheng. 62381
see Zheng Guangfu
Guanghua Chen. 62381
see Chen Guanghua
Guansheng Zhang. 62381
see Zhang Guansheng
+Guarini, G. 63683
+Guarino, N. 60457
Gubanov, A.I. + 62337
+Gubanov, V.A. 62579
Gubenko, S.I. 63408
Gubenko, S.I. + 63410
Gubskii, A.L. + 62338
+Gudcl, H.U. 62943
+Gudkov, A.A. 63161
+Guemas, L. 62405
Guenault, A.M. + 62201
+Guenther, D.B. 64432
Guerra, F. + 59633
Guga, K.Yu. + 62422
+Gugelot, P.C. 60078
Guha, S.K. + 63914
+Guha, S.K. 63805
+Guida, J.A. 60049
+Guidi, G. 63295
Guilhott, J. + 61357
+Guilhot, J.P. 61351
+Guillaud, J.P. 60066
Guillocheau, F. + 64127
+Guinet, C. 62236
Guittard, M. + 61865
+Guittard, M. 61862
Gujrati, P.D. 59738
Guk, Yu.N. + 62171
+Gulei, G. 63330
+Gulev, S.K. 64151
+Gulis, I.M. 60825
Gulyaev, R.A. 64445
+Gumen, N.M. 63409
+Gummarson, O. 63118
Gunsner, W. + 62805
+Gunsner, W. 62634
+Gunsner, W. 62642
Gunther, L. + 62598
Gunther, L. + 62179
+Guo, B.J. 62778
Guo, T.C. + 62885
+Guo, W.W. 62885
+Guo, Y. 60088
Guo Changzhi + 61145
Guo Han-ying + 59637
+Guo Han-ying. 59638
+Guo Han-ying. 59645
+Gupta, G.P. 62865
Gupta, J.C. 64318
Gupta, J.R. + 61500
+Gupta, M. 62398
Gupta, M.K.Das. 62398
see Das Gupta, M.K.
Gupta, R.N. + 61525
Gupta, R.Sen. 62398
see Sen Gupta, R.
Gupta, S.Das. 62398
see Das Gupta, S.
+Gupta, S.K. 62528
+Gupta, U. 62212
+Gupta, Y. 60359
+Gupta, Y.K. 59639
Gurevich, S.A. + 61156
+Gurevich, Ya.B. 63377
+Guriev, E.A. 62369
+Gurinovich, G.P. 60824
Gurker, N. + 59891
Gurov, V.M. + 61944
+Gurushov, A.P. 63268
+Gurvitz, S.A. 60154
+Gusdal, I. 60559
Guseinov, F.Kh. + 62060
+Guseinov, R.K. 63330
+Guseinov, S.M. 62411
Gusev, A.G. + 62303
+Gusev, M.Yu. 62781
Gusev, Yu.L. + 59863
Guseva, N.G. + 64378
+Gusheva, V.V. 63923
+Gusheva, M. 64241
+Gus'kov, S.Yu. 61672
Gust, W. + 62170
Gustafson, G. 60091
+Gustav, K. 63499
+Gustav, K. 60597
Gusynin, V.P. + 59925
Gusynin, V.P. + 59988
Guterman, A. + 60196
+Gutermuth, P.G. 60231
Guth, A.H. + 64562
+Guth, H. 61904
+Guthrie, J.T. 61819
+Gutowksi, J. 62998
+Gutsev, G.L. 60845
+Guyon, E. 61471
- Guyon, P.M. + 60852
+Guyonnet, J.L. 60077
+Guyre, P.M. 63824
Guzenko, G.A. 61081
+Guzman, A.M. 62755
+Gyimesi, J. 62182
- Ha Tae-Kyu. 62396
see Tae-Kyu Ha
+Ha Vinh Tan. 62929
Haaf, W. + 63649
+Haaker, R.F. 60285
+Haaker, R.F. 60287
Haar, D.ter. see ter Haar, D.
+Haas, Y. 60863
Haasnoot, C.A.G. 59815
Habash, J. + 61869
Habbal, S.R. + 64368
Habery, F. + 63144
+Haberko, K. 64324
Habermann, R.E. 63637
Habersbergerova, A. + 60356
Hackett, P.A. + 60680
Haddon, R.C. + 60577
Hadermann, J. + 60315
+Haddi, D. 60573
+Haensel, R. 61886
Hafez, M. + 61520
Hage Hassan, M. 59587
+Hagenlocher, K. 63649
+Hagenmuller, P. 61864
+Hager, H. 64002
+Haggmark, L.G. 61659
Hagmann, S. 60968
+Hague, P. 60246
+Haguenauer, M. 60534
+Hahn, T.S. 61679
+Hahn, B. 60076
Hai-Lung Dai. 60858
+Hai-Lung Dai. 60780
+Haidt, D. 60031
+Haidt, D. 60059
Haigh, J. 60741
+Haigh, R.C. + 60510
Haile, N.S. 64031
Haines, A.J. 64055
Haisch, B.M. + 64477
Hajkowicz, L.A. 64299
Hakamatsuka, Y. + 62887
Haken, R.K.Ten. 62396
see Ten Haken, R.K.
+Hakim, T.S. 63875
+Hakomori, K. 61574
Hakonsen, T.E. + 60264
Halas, S. + 63625
Haldane, F.D.M. 62674
Halder, N.C. + 63666
Halder, N.C. + 63667
+Halderson, D. 60209
+Halderson, J. 60066
+Hale, M.S. 63830
+Halfpenny, P.J. 63542
Halb, B. + 62573
+Hall, A.L. 63943
Hall, D.G. + 62214
+Hall, E.J. 63903
+Hall, E.L. 62184
+Hall, G.D. 60332
+Hall, J.M. 60506
+Hall, J.M. 60964
+Hall, J.M. 60948
Hall, K. 64141
+Hall, M.B. 60605
Hall, R.B. 60807
+Hall, T.J. 61096
+Hallgren, A. 60074
+Halliday, R. 63988
+Halling, A.M. 60049
+Halperin, B.I. 62432
+Halperin, W.P. 62203
+Halperin, B.L. 62247
Halperin, V. 59695
+Halsey, G.D. 62215
Halzen, F. + 60016
+Hama, H. 60504
Hamada, S. + 63480
Hamadto, S.A. 61208
+Hamakawa, Y. 63685
Hamano, K. + 63231
+Hamanoue, K. 60820
+Hamdani, Y. 60073
Hamdi, H. + 62449
+Hamelin, J. 60427
+Hamid, A. 64205
+Hamilton, H.B. 63909
+Hamilton, W.A.P. 63912
+Hamilton, W.O. 59771
+Hamiuddin, M. 63212
+Hamman, J. 62633
+Hamman, J. 62632
Hammer, R. + 64436
+Hammond, P. 61045
- +Hamstad, M.A. 63347
Hamstra, J. 60288
Han, K.H. + 63289
Han, M.K. + 63695
Han Ki In. see Ki In Han
Han Kim Moo. 62396
see Moo Han Kim
+Han Ruqi. 62362
Han-Min Jin. 62396
see Jin Han-Min
Han-xin He. see He Han-xin
Han-ying Guo. 62396
see Guo Han-ying
+Hanawa, K. 63213
+Handa, M. 62188
+Handa, M. 62189
+Handa, M. 62190
+Handler, R. + 60041
+Handler, R. 60081
+Handler, R. 60087
+Hane, K. 60997
Hanecek, G. + 62181
Haneda, K. + 62856
+Haneda, K. 62719
+Haneman, D. 63719
Haner, D.A. + 60775
Hang-sheng Wu. 62396
see Wu Hang-sheng
Hanggi, P. 63771
Haniford, D.B. + 63780
+Hanke, P. 60075
+Hanke, W. 63796
+Hankey, W.L. 61508
Hankiewicz, E. + 63570
+Hannakam, L. 61048
Hannington, S. 61285
Hanqu Li. see Li Hanqu
+Hansch, T.W. 60657
+Hansen, J.D. 60066
+Hansen, J.-P. 61748
+Hansen, K.H. 60074
+Hansen, S.G. 61043
Hansen, U. 60348
Hansma, P.K. 62270
+Hanson, A.O. 60491
Hanson, K.M. + 63957
+Hanson, P.G. 63876
Hantsche, H. 63488
+Hanuschik, R.W. 64471
+Hara, K. 60072
+Hara, K. 62295
+Hara, K. 60082
+Hara, K. 62531
+Hara, M. 61258
Hara, Z. + 63213
+Harada, S. 63495
Haran, M.E. + 61334
+Hardekopf, R.A. 60215
+Hardekopf, R.A. 60182
+Hardie, D. 63490
+Hardiman, M. 62602
+Harding, G.L. + 63724
+Harding, G.L. 63728
+Harduin, F. + 61779
+Harduin, D. 64340
+Hardy, N.D. 61819
Hare, A.S. + 63592
+Hare, T.M. 63233
+Hariharan, P.C. 60571
+Hariharan, R. + 61572
+Harmalkar, A. + 60561
+Harmer, A.L. + 61307
+Harmon, B.D. 62046
+Harmony, M.N. 60711
+Haroche, S. 61122
+Haroche, S. 61121
+Harper, J.M.E. 63174
+Harper, R.W. 59936
+Harries, D.R. 61986
Harrington, J.A. + 61293
+Harrington, P.J. 60836
+Harrington, R.F. 61047
+Harris, C.B. 62466
+Harris, G.F. + 63995
+Harris, I.R. 61009
+Harris, M. 60074
+Harrison, H.R. 63146
Harrison, J.G. 60564
Harrison, J.G. 60889
Harrison, M.H. + 63791
Harrison, R.M. + 64168
+Harsh, V.R. 60088
+Hart, R.G. 63453
+Hart, R.J. 64261
+Hartfield, U. 60054
Hartig, G. 59753
+Hartill, D.L. 60049
Hartmann, M. + 63549
+Hartmann, M. 63548
Hartmann-Boutron, F. 62533
Haruyama, Y. + 63117
+Haseda, T. 62599
Hasegawa, A. 64372
+Hasegawa, A. + 63568
+Hasegawa, A. + 60766
+Hasegawa, A. 61634
+Hasegawa, A. 59795

- Hasegawa, H.S. + 64044
Hasegawa, K. + 60128
+ Hasegawa, M. 62786
+ Hasegawa, R. 62809
+ Haselmaier, H. 62546
+ Haseltin, H.H. 60528
+ Hashi, T. 61246
+ Hashiguchi, M. 61528
+ Hashimoto, H. 59895
Hashimoto, K. 60205
Hashimoto, K. + 64418
Hashimoto, K. + 61927
Hashimoto, K. + 63335
+ Hashimoto, O. 60096
+ Hashimoto, T. 62295
+ Hassan, A.M. 64248
Hassan, M.Hage
 see Hage Hassan, M.
+ Hassard, J. 60049
+ Hassler, H. 63167
+ Haste, G.R. 61678
Hastings, P.W. + 60808
Hassuyama, H. + 60502
Hata, J. + 60616
+ Hata, N. 62496
Hatakeyama, R. + 61652
+ Hatakeyama, S. 63535
Hatcher, C.R. 60226
Hatheway, A.W. 60251
+ Hatlee, M.D. 59685
Hatta, S. + 62722
Hattori, S. + 63392
+ Hattori, S. 60997
+ Hattori, S. 60955
Haubenreich, P.N. + 60429
Haueter, R.L. + 60354
Haufe, A. + 62341
+ Hauge, O. 64451
+ Hauge, R.H. 60721
Hauser, A. + 62943
+ Haussuhl, S. 63151
+ Haussuhl, S. 62010
+ Haussuhl, P.E. 60112
Hautiojarvi, P. + 61979
+ Haverkamp, H. 60408
+ Hawker, K.E. 61342
+ Hay, J.E. 61515
+ Hayakawa, K. 62284
+ Hayakawa, M. 62784
Hayakawa, S. 64516
+ Hayakawa, S. 64556
+ Hayakawa, S. 64557
+ Hayama, F. 62711
+ Hayashi, K. 62784
Hayashi, M. 60993
Hayashi, M. 61714
Hayashi, M. + 61512
Hayashi, M. + 61599
+ Hayashi, M. 60766
+ Hayashi, M. 62855
+ Hayashi, Y. 62712
Hayden, B.E. + 62982
+ Hayden, B.E. 63103
+ Hayes, D.E. 64133
+ Hayes, D.E. 64136
+ Hayes, D.E. 64120
Hayes, D.E. (*ed.*) 59545
+ Hayes, J.R. 63039
+ Haygarth, J.C. 62917
+ Haynes, C.V. 62001
+ Haynes, R.F. 64556
Hayot, F. 59998
+ Hays, P.B. 64281
+ Hayter, J.B. 62715
Hayward, P.J. + 60278
+ Hayward, P.J. 60279
Hazi, A.U. + 60584
+ Hazra, B.K. 64196
Hazra, C.C. + 59965
+ He Han-xin 60063
+ He Yuchuan 62944
+ Head, J.W. III. 64408
Headley, T.J. + 60284
+ Heagle, A.S. 63760
Healzer, J.M. + 60339
+ Heath, B.A. 62498
+ Heaven, M. 60801
+ Heaven, M. 61217
+ Hebrald, D. 62206
Hecht, K.T. + 59612
+ Heck, A. 64393
+ Heck, B. 60074
Heck, D. + 63611
+ Heck, T. 60129
+ Heck, W.V. 63760
Hecke, H.Van
 see Van Hecke, H.
+ Hecker, S.S. 62088
+ Heckman, H.H. 60195
+ Heddle, D.W.O. 61180
Hedges, R.M. Jr. + 60688
Hedin, F. + 60383
Hee-Yong Chun + 60333
Heermann, D.W. + 62058
+ Heese, R. 63941
Hefang Hu + 62147
Heffernan, D.M. + 61123
Heffer, E.F. 59933
+ Heftler, U. 60900
Hehenkamp, T. + 62153
Heidberg, J. + 62256
Heidberg, J. + 62983
+ Heiden, M. 60075
+ Heidenreich, J.E. III
 64403
Heidler, K. + 63650
Heikkinen, D.W. + 60511
+ Heimdahl, P.D. 59563
Heimendahl, M.von
 see von Heimendahl, M.
Hein, G.W. 64021
+ Heinen, H.-J. 63609
Heinrich, B. + 62809
+ Heinrich, B. 62623
+ Heinrich, Ch. 60188
Heinrichs, J. 59679
+ Heintze, J. 60031
+ Heintze, J. 60059
+ Heinz, W. 60430
+ Heinzmann, G. 60031
+ Heinzmann, G. 60059
+ Heiser, C. 60944
+ Heisig, U. 63158
+ Helava, H.I. 61675
+ Helfand, D.J. 64499
+ Helgaker, P. 60066
+ Helgeson, U. 60978
+ Hellenbrand, K.H. 60031
+ Hellenbrand, K.H. 60059
+ Heller, E.J. 59610
+ Heller, K. 60041
+ Heller, K. 60081
+ Heller, K. 60087
+ Helfeld, T. 59842
+ Helion, A. 61348
Heller, E. + 61860
+ Hellings, B. 62246
+ Hellings, B. 62231
Helm, H. + 60830
+ Helm, P. 63711
+ Helms, C.R. 62278
+ Helten, H.J. 60188
+ Helton, F.J. 61627
Hemlati, S. + 61810
+ Hemmerich, J. 60527
+ Hemminger, J.C. 62974
+ Hemmy, D.C. 63995
Hempelman, A. + 64488
+ Hempstead, M. 60049
+ Henderson, D. 61202
+ Henderson, G. 60705
Hendow, S.T. + 61222
+ Hendricks, M. 63511
+ Hendrie, D.L. 60196
+ Henig, E.-Th. 63218
+ Henke, B.L. 59898
+ Henkelman, R.M. 63979
+ Henneberg, K.-H. 63597
+ Henneberger, K. 62341
+ Hennings, D. 63246
+ Hennings, M.C. 63603
Henrick, R.F. 61340
+ Henry, B. 64106
+ Henry, J.Y. 62601
+ Hepp, V. 59995
Heras, C.A. + 60113
Heras, E.Las. *see* Las Heras, E.
+ Herault, A. 60383
+ Herber, 60376
+ Herbert, D.C. 62365
+ Herd, D.G. 64069
Herman, M.F. + 60627
Herman, Z.S. 60562
Hermel, W. + 63249
+ Hermel, W. 63209
+ Hermesen, T. 59621
+ Hernandez, F. 63727
Hernando, A. + 62583
+ Hernandez, B. 62696
+ Herring, R.I. 63988
Herold, H. + 64502
+ Herr, W. 60075
+ Herren, F. 60740
Herring, G.C. + 61582
Herrmann, J. + 62100
Herrmann, R.B. + 64051
+ Herrup, D. 60049
+ Hersec, S. 61152
Herts, E.A. 64519
Hertz, J.A. 62638
+ Hertzberg, R.W. 63419
+ Hervouet, C. 60377
+ Herzog, S. 62277
+ Hess, S. 61531
+ Hesse, J. 59897
+ Hetherington, E.L.R.
 60556
Hetu, R. 63856
+ Hetzrog, D.W. 60043
+ Heuer, P.M. 63635
+ Heuer, R.D. 60031
+ Heuer, R.D. 60059
+ Hevesi, I. 63149
+ Hevesi, I. 62918
Hewett, D.W. 61697
Hewig, G.H. + 63700
Hewish, N.A. + 61761
Hey, J.D. + 61609
Heyes, A.D. 63913
+ Heyman, F.F. 60066
Hezel, R. 61996
Hiabara, T. + 61308
+ Hichwa, R.D. 63962
Hickey, R.J. + 59583
Hickman, G.D. + 64264
+ Hicks, H.R. 61693
+ Hicks, R. 60049
+ Hida, K. 59732
Hidaka, Y. + 62776
+ Hidaka, Y. 62756
Hidalgo-Alvarez, R. + 63563
Hiede, J.A.Van der
 see Van der Hiede, J.A.
+ Hieple, R. 63143
Hieu Nguyen Van
 see Nguyen Van Hieu
+ Higa, O. 60453
Higaki, Y. + 63693
+ Higan, S. 63737
+ Higashi, K. 62697
+ Higgins, J.S. 62129
+ Hilal, M. 60428
Hilczner, B. + 62904
Hild, R. + 61104
+ Hildenbrand, D.L. 61019
Hileman, B. 63755
Hilinski, E.F. + 64015
+ Hilke, H.J. 60074
+ Hill, E.P. 63815
Hill, F.B. + 61008
+ Hill, I. 64079
+ Hill, J.M. 59743
+ Hill, L.W. 63981
Hill, R. + 63789
+ Hill, R. 63691
+ Hill, R.J. 61084
Hill, R.M. + 62888
+ Hill, R.P. 63908
Hiller, C. + 63528
+ Hilliard, J.E. 61932
+ Hilliard, R.K. 60380
+ Hillier, I.H. 60840
+ Hillier, I.H. 60839
Hillis, D.L. + 61678
Hills, J.G. 64508
+ Hilpert, Th. 60444
Hilsdorf-Marotta, A.M. +
 61615
+ Himdy, A.El. 60634
+ Himpfel, F.J. 62469
Hinnerichs, T.D. + 63375
+ Hinz, W.J. 64108
+ Hinzmann, G. 63006
Hioe, F.T. 59701
+ Hioki, S. 60432
+ Hioki, S. 60434
+ Hipkin, R.G. 64090
Hippensteel, S.A. + 59779
Hipp, K.W. 62271
+ Hirabayashi, M. 63393
+ Hiraga, K. 61850
+ Hirai, S. 62712
+ Hirakawa, K. 62821
Hiramatsu, K. + 62410
+ Hiramoto, J. 63924
+ Hirano, K.I. 61676
Hirata, F. + 61759
Hirata, K. 59978
Hirata, K. 59980
+ Hirata, T. 62909
+ Hiroi, H. 60378
+ Hirokane, J. 62770
Hirono, M. + 60841
Hirooka, Y. + 61660
+ Hirose, K. 62789
+ Hirota, E. 60720
+ Hiroyoshi, H. 62596
Hirsch, J.E. + 62357
+ Hirsch, P. 61922
+ Hirst, L.L. 62617
+ Hirst, L.L. 62618
+ Hirtz, P. 61152
+ Hisatake, K. 62863
+ Hisatake, K. 62723
+ Hiscock, W.A. 64454
+ Hladik, J. 63644
+ Hnilica, K. 60358
+ Hnizdo, V. 60197
Ho, J.W. + 63432
Ho, Y.K. + 60986
+ Ho Tso-hsiu 60000
+ Ho Tso-hsiu 60026
Hoai Le Kong
 see Le Kong Hoai
Hoang Ngoc Cam + 62929
+ Hobbs, L.W. 60235
Hobert, H. + 63599
+ Hochmuth, R.M. 63803
+ Hochstrasser, R.M. 61224
+ Hochstetler, W.H. 60278
Hocking, W.K. 64279
Hocking, W.K. 64280
+ Hodge, P.E. 64556
+ Hodge, P.E. 64476
Hodges, D.H. + 61438
Hodges, F.N. + 60311
+ Hodgkin, D.C. 63779
+ Hodoscek, M. 60573
+ Hoefl, J. 60779
+ Hoehn, M.V. 60105
Hoek, B.van der. *see* van der
 Hoek, B.
+ Hoening, C.L. 60276
+ Hofer, H. 60537
+ Hofer, P. 63597
+ Hoff, A.J. 60771
Hoffbauer, M.A. + 60958
+ Hoffman, D.K. 63497
+ Hoffmann, A. 62998
Hoffmann, B. + 63246
Hoffmann, F.M. + 63588
Hoffmann, H. + 62739
+ Hoffswell, R.A. 60491
Hofman, M. + 61272
Hofmann, A. 62196
+ Hofmann, D. 60965
+ Hofmann, D. 63114
Hofmann, D.J. + 64334
Hofmann, G. + 59842
+ Hofmann, M. 60859
+ Hofmann, P. 63105
+ Hofmann, W. 60075
+ Hofmeister, F. 60456
+ Hogan, L.M. 61843
Hogarth, C.A. + 63014
+ Hogg, C.S. 63121
+ Hogarth, K.G. 63698
+ Hohenocker, H. 60465
Hoiniks, J. + 60884
+ Hokyo, J. 62775
+ Holappa, L.E. 62110
Hole, J. + 63539
Holden, A.L. + 63835
+ Holderness, S.G. 63783
Holevo, A.S. 59557
+ Holian, B.L. 61751
Hollander, W.T.F.den
 see den Hollander, W.T.F.
+ Hollinger, G. 62469
+ Hollingsworth, L.S. 63721
+ Hollins, R.C. 61087
Holman, M. 60217
+ Holmes, B.S. 60755
Holmes, J.A. + 61693
+ Holmes, R. 60508
+ Holmstrom, F.E. 62315
+ Holmstrom, S. 62246
Holt, K.von. *see* von Holt, K.
+ Holt, L.E. 63886
Holt, R.C. 60346
+ Holten, D. 60792
+ Holtet, J.A. (*ed.*) 59540
+ Holtkamp, D.B. 60209
+ Holzapfel, W.B. 62960
Holzenkammer, E. + 62521
+ Holzer, R. 60358
+ Holznerr, S. 60049
Honda, N. + 62775
+ Honda, N. 63732
Honda, S. + 62770
Honda, S. + 62510
+ Honda, S. 62747
+ Hondros, E. 59555
+ Honekamp, J.R. 60355
+ Honeycutt, R.K. 64475
Hong, D.K. + 59972
+ Hong, W.K.W. 61349
Hong Chang-Hi
 see Chang-Hi Hong
Hong Duong Pham
 see Pham Hong Duong
Hongdu Liu. *see* Liu Hongdu
+ Hongo, K. 61058
+ Hongru Zhai 62700
Honmura, R. + 61803
+ Honnorez, J. 64081
+ Hood, J.T., Sr. 63935
+ Hoonhout, D. 63077
+ Hooper, J.E. 60074
+ Hooper, R.M. 63542
+ Hope, G.A. 62493
Hopf, F.A. 61169
Hopkins, J.B. + 60913
Hoppe, B. + 62617
Hoppe, B. + 62618
Hoppe, M.M. + 64312
+ Hoppe, M.M. 64315
+ Horbatsch, M. 59636
Horgan, C.O. + 61410
Hori, T. 59660
+ Hori, S. 63299
Horiguchi, T. + 62659
Hori, K. 64188
+ Horikawa, T. 63394
+ Horiki, M. 61981
+ Horimoto, M. 63874
Horinaka, H. + 62891
+ Horioka, K. 60526
Horiuchi, S. 61741
+ Horn, K. 62222
+ Horn, L. 63633
+ Hornbogen, A. 62475
Horneber, A. 60274
Horsdal-Pedersen, E. +
 60963
+ Horsfield, N. 63424
+ Hortacsu, M. 59929
+ Horvath, H. 64165
+ Horwitz, J.S. 60620
Horwitz, L.P. + 59616
Horwitz, L.P. + 60038
+ Horwitz, N. 60049
Hosaka, T. 63391
+ Hoshen, J. 59691
Hoshi, Y. + 62765
+ Hosogane, N. 60461
+ Hosogane, N. 60470
+ Hosoto, N. 62729
+ Hosoto, N. 62861
+ Hosoyama, K. 62701
+ Hosper, R. 60073
Hosten, B. + 62009
+ Hosur, R.V. 61031
+ Hotai, K. 62784
Hotier, F. + 63169
+ Hotier, F. 63170
+ House, W.A. 63604
Houshun Tang
 see Tang Houshun
+ Houska, C.R. 62289
Houston, B. + 64559
+ Houston, J.E. 60853
Houtte, D.Van
 see Van Houtte, D.
+ Hovestadt, D. 64335
Hovestreydt, E. + 61873
+ Howard, A.E. 60711
+ Howard, J. 62272
Howe, P.S. + 59939
Howe, P.S. + 59952
Howell, C.R. + 60175
+ Howells, W.S. 61761
+ Howes, B.D. 62575
+ Howlett, S.P. 63198
+ Howton, C. 61195
+ Hrbejk, J. 63588
+ Hsiao, C.C. 61462
+ Hsieh, T. 63526
+ Hsieh, Y.C. 63991
Hsu, J.P. 59591
Hsu, Y. + 62398
Hsu Shu-En
 see Shu-En Hsu
Hsuan Fang Da
 see Da Hsuan Fang
hsuan Feng Da
 see Da huan Feng
+ Hsueh-Ying Teng 61526
Hu, Z. + 61350
+ Hu Enzhi 61146
Hu Hefang. *see* Hefang Hu
Hu Ting-Yung
 see Ting-Yung Hu
Hu Wenzhong + 62732
+ Huang Dusen 63439
+ Huang Nan 60505
Huang Shanxiang 63165
+ Huang Shisheng 63065
Huang Tao + 60019
Huber, D.L. 59692
Huber, D.L. 62910
+ Huber, M. 59555
Huberman, B.A. 59709
Hubert, A. 62772
+ Hubert, A. 62585
+ Hubert, P. 60145
+ Hubner, K. 63019
+ Huchaby, D.A. 62241
+ Hudgins, C.H. 64244
+ Hudson, B.S. 60726
+ Hudson, H. 64386
Hudson, H.S. 64431
+ Hudson, P. 63999
Hudson, R.L. + 59676
Huenekens, J. + 60633
Huestis, D.L. + 60738
+ Huestis, D.L. 60830
+ Huetz-Aubert, M. 60697
+ Huetz-Aubert, M. 62137
+ Huffel, H. 59666
+ Hugentobler, E. 60076
+ Hughes, A.E. 60280
Hughes, A.R.W. + 64310
Hughes, B.D. + 59686
+ Hughes, G. 60031
+ Hughes, G. 60059
+ Hughes, H.P. 63130
+ Hughes, V.W. 60088
+ Hugla, M. 60369
+ Hugla, M. 60385
+ Huguet, M. 60424
Hui-sheng Wang
 see Wang Hui-sheng
+ Huiskamp, W.J. 62881
Huiskens, F. + 60364
+ Huiskens, F. 60922
+ Huiskens, F. 60923
+ Hukin, D.A. 62897
+ Hulien, D. 61199
+ Hulliger, F. 61877
Hulsing, H. + 62597

- +Hummel, J. 62996
 Humphreys, D.R. + 64256
 Hung, R.J. + 63757
 Hunt, B.R. + 61093
 +Hunt, C.P. 63090
 +Hunter, R.O., Jr. 61195
 Hunter, S.R. + 61713
 Hunter, T.F. + 63576
 Hulton, D.E. + 60859
 Huot, J.-P. + 61488
 Huot, J.-P. + 61494
 Hurdequint, H. + 62803
 +Hurford, G. 64386
 Hurley, A.M. + 64116
 +Hurley, K. 64386
 +Hurst, J.E., Jr. 63556
 +Husby, J.S. 63872
 +Husing, K. 60129
 +Hussaini, M.Y. 61519
 Hussey, C.D. 61292
 +Hussla, I. 62256
 +Hussla, I. 62983
 +Hussong, D.M. 64098
 Hustad, P.A. + 60254
 +Huston, E.L. 63735
 +Huston, E.L. 63742
 +Huston, E.L. 63745
 +Huston, E.L. 61568
 Hut, P. + 64563
 +Hutchinson, G.D. 63962
 +Hutchinson, M.H.R. 61187
 +Huth, B.G. 62703
 Hutson, J.M. + 60866
 +Hutson, J.M. 60865
 Huttemann, P. + 60459
 Huu Tinh Nguyen
 see Nguyen Huu Tinh
 Huxley, P. + 60891
 Hwang, K.S. + 64324
 +Hyde, P.J. 63612
 +Hyde, S.T. 61908
 Hyo Kim Chang
 see Chang Hyo Kim
 +Hyodo, M. 62245
 +Hyson, P. 64189
 Hyun Chung Chang
 see Chang Hyun Chung
 +Iachello, F. 60120
 Iandelli, A. 61855
 Ibach, H. 62238
 +Ibach, H. 63104
 +Ibarra, M.R. 62592
 +Iberall, A.S. 63767
 Ibdadpo, T.A. + 61820
 Ibraev, N.Kh. + 60823
 +Ibragimova, I.S. 63015
 Ibrahim, S.R. 62008
 +Ichihara, I. 61010
 +Ichihara, M. 61972
 Ichikawa, M. + 62284
 Ichimaru, S. 61612
 Ichimaru, S. + 62441
 Ichimaru, M. + 60184
 +Ide, S. 62820
 +Idemitsu, K. 62166
 +Idogaki, T. 62670
 +Idogawa, T. 59761
 +Ilerkic, H.M. 64286
 Igaki, H. 63393
 +Igarashi, K. 60954
 +Igarashi, Y. 59993
 +Igel, G. 60568
 +Igielski, A. 64251
 Ignatenko, V.G. 61529
 +Ignativ, M.I. 63333
 +Ignatova, I.A. 63366
 +IgoKemenes, P. 60068
 +Iguchi, S. 63672
 +Iguchi, Y. 60072
 +Iguchi, Y. 60082
 +Ihara, A. 63924
 +Ihm, Y.E. 62388
 Iida, K. 62742
 Iijima, T. 61132
 Iijima, T. + 64490
 Iishi, K. + 62045
 +Iiyoshi, A. 61698
 +Ikawa, K. 63276
 Ikeda, K. + 63393
 +Ikeda, K. 62069
 +Ikeda, K. 60191
 +Ikeda, Y. 62629
 Ikegami, T. + 61147
 +Ikemura, T. 62820
 +Ikoma, T. 62364
 +Ikuse, H. 63595
 +Ikuta, T. + 62762
 +I'in, S.I. 63378
 +I'in, U.Yu. 62478
 I'in, V.N. + 61419
 +I'inskii, K.L. 63381
 +Iliopoulos, J. 59903
 +Illigmann, A. 59806
 Ilonca, Gh. + 62547
 Imachi, M. + 59918
 Imada, M. + 59732
 +Imai, K. 60432
 +Imai, S. 61353
 +Imamov, R.M. 62455
 +Imamura, N. 62734
 +Imamura, N. 62738
 Imanishi, A. + 60553
 +Imazato, J. 62627
 +Imbert, C. 59845
 +Imhof, R.E. 63031
 +Imoto, S. 60334
 Imperatori, P. + 62081
 +Imrie, D.C. 60066
 +Imry, Y. 62640
 In Choi Jung
 see Jung In Choi
 In Han Ki. see Ki In Han
 Inaba, S. + 60955
 +Inal, O.T. 63729
 +Inami, D. 62783
 +Inami, D. 62794
 Inami, T. + 59949
 Ingram, C.H.Q. + 60206
 Inotakis, N. + 60335
 +Inisheva, L.A. 62705
 +Inkin, V.D. 60484
 +Inkson, J.C. 62485
 +Innocenti, P.G. 60075
 +Inokuchi, H. 63129
 Inomata, K. + 62786
 Inoue, F. + 62733
 +Inoue, F. 62745
 +Inoue, H. 64556
 +Inoue, H. 64557
 Inoue, M. + 62795
 +Inoue, M. 59716
 +Inoue, M. 62792
 +Inoue, M. 63030
 +Inoue, S. 63397
 Inoue, T. + 61203
 +Insolia, A. 60098
 Ioffe, B.L. 60002
 +Iogansen, L.V. 61277
 +Iolin, E.M. 62853
 +Ionkina, N.P. 63304
 Iordanskii, A.L. + 63773
 +Iori, I. 60532
 Ip, W.-H. 64422
 +Ipravich, F.M. 64335
 Ipson, J.R. + 64361
 Iqbal, Z. + 63069
 +Irgens-Defregger, A. 60918
 Irie, T. + 61439
 +Irmancinik, L. 63248
 Isacks, B.L. + 64068
 +Isacks, B.L. 64065
 +Isakov, V.N. 61280
 Ishai, G. + 63887
 +Ishai, G. 64003
 Ishibashi, K. 64074
 Ishibashi, M. + 59761
 Ishida, K. + 64414
 Ishido, M. + 64229
 Ishigame, M. + 62997
 Ishigure, K. + 63595
 Ishii, K. + 60910
 Ishii, N. + 61804
 +Ishii, N. 64017
 Ishii, T. + 62587
 +Ishii, T. 60553
 Ishikawa, J. + 60503
 Ishikawa, J. + 59877
 +Ishikawa, M. 59732
 +Ishikawa, T. 62656
 Ishikawa, Y. + 62628
 +Ishikawa, Y. 62554
 +Ishikawa, Y. 62627
 +Ishimatsu, T. 60504
 +Ishimoto, H. 62874
 +Ishio, S. 62751
 +Ishio, S. 62752
 +Ishio, S. 62581
 +Ishio, S. 62152
 +Ishizaki, Y. 60109
 Ishizuka, M. + 62751
 +Ishizuka, M. 63395
 +Ishizukhametov, M.Z. 60540
 Isikawa, Y. + 62697
 +Isakova, Z.D. 61065
 Ismail, P.M. Mohamed
 see Mohamed Ismail, P.M.
 +Israelelevich, P.L. 64411
 +Itagaki, Y. 59874
 +Ito, M. 60049
 +Ito, S. 62507
 +Ito, T. 63736
 Itoh, A. + 62745
 +Itoh, A. 63117
 +Itoh, A. 62733
 Itoh, H. + 60305
 Itoh, J. + 62863
 Itoh, K. + 59833
 Itoh, M. 61752
 Itoh, N. 64501
 Itoh, Y. + 60927
 Itsumi, M. 62519
 Ivakhnenko, M.A. 64107
 +Ivanchuk, D.F. 62372
 +Ivanov, A.K. 63763
 +Ivanov, A.K. 64267
 Ivanov, D. + 61708
 Ivanov, G.A. 64357
 Ivanov, G.A. 64377
 +Ivanov, G.A. 61280
 +Ivanov, G.A. 61282
 +Ivanov, G.A. 64376
 Ivanov, L.P. + 62779
 Ivanov, S.A. + 61794
 Ivanov, S.A. + 61795
 +Ivanov, S.I. 63055
 Ivanov, S.V. + 63359
 Ivanov, V.B. 62708
 Ivanov, V.N. + 63967
 +Ivanova, L.F. 63967
 +Ivanova, S.A. 63476
 +Ivanova, T. 64241
 +Ivanovich, M. 64259
 +Ivanyukovich, G.A. 63620
 +Ivashchenko, A.I. 62304
 +Ivashintsova, V.L. 61266
 Ivashkin, Yu.A. + 61911
 Ivashishin, O.M. + 63324
 Ivchenko, E.L. + 62921
 +Ivkin, V.G. 61711
 +Ivoilov, N.G. 62870
 Iwade, Y. + 60954
 +Iwaki, M. 63447
 Iwaki, T. 63591
 +Iwaki, T. 63739
 +Iwakura, C. 63562
 +Iwama, Y. 62753
 +Iwama, Y. 62514
 Iwamoto, T. + 63166
 +Iwamoto, T. 61299
 +Iwamura, S. 63155
 +Iwanaga, H. 61972
 Iwanicki, T. + 60430
 Iwanowski, R.J. + 61158
 Iwasaki, M. + 61528
 Iwasaki, M. + 60192
 +Iwata, A. 64017
 Iwauchi, K. + 62629
 +Iwazaki, A. 59950
 +Iyetomi, H. 62441
 Iyi, N. + 61881
 +Izen, J.M. 60049
 Izumo, K. + 60149
 Jaaskelainen, T. 61079
 +Jaccard, R. 63419
 Jach, K. 61673
 +Jach, K. 60395
 Jackson, D.D. + 64122
 +Jackson, J.E. 60223
 Jackson, K.M. 63915
 Jackson, K.M. + 63998
 Jackson, M.B. + 63819
 Jackson, M.R. + 62184
 +Jackson, T. 60460
 Jacob, C. 61518
 Jacob, I. 62048
 +Jacobi, K. 62469
 +Jacoboni, C. 62421
 +Jacoboni, C. 62632
 Jacobs, G.H. 63831
 +Jacobs, G.K. 60325
 Jacobs, S. + 60015
 Jacobsen, T. + 60069
 +Jacobson, A.S. 64492
 Jacobson, S.H. + 62150
 +Jacobsson, A. 60312
 +Jacques, J. 61785
 Jacquet-Francillon, N. + 60271
 +Jacquet, B. 60972
 Jacquot, C. + 61005
 +Jadhav, D.B. 64237
 Jae Won Mok. see Won Mok Jae
 +Jae-Hwan Kim 63308
 +Jaffe, R.L. 60926
 +Jaffe, R.L. 60835
 Jaffrey, D. 63489
 Jagannathan, E. 63610
 Jain, G.C. + 63668
 +Jain, K.K. 62882
 +Jain, R.M. 64237
 Jain, V.K. 63062
 Jain, V.K. + 63658
 Jakab, L. + 61265
 Jakani, M. + 63560
 +Jakeways, R. 61819
 Jakubik, A.T. + 60305
 +Jakubovics, J.P. 62682
 Jalochoowski, M. 62307
 +James, C. 60081
 +James, C. 60087
 +James, D.R. 61713
 James, M.B. + 63427
 Jamet, J.P. + 61905
 Jandt, O. + 60431
 Jani, K.G. + 64304
 Janis, V. + 59613
 Jankiewicz, Z. + 61184
 Jankiewicz, Z. + 61110
 Jankiewicz, Z. + 61185
 Jansson, T. 61295
 Janot, C. + 63416
 +Jansen, A.G.M. 62637
 +Jansen, J. 60206
 Jansen van Beck, G. + 64023
 +Jantsch, W. 62428
 Japaridze, G.I. + 59916
 +Jarlskog, G. 60074
 +Jarmie, N. 60215
 +Jarmie, N. 60182
 +Jaroniec, M. 63604
 Jarosinski, J. 63551
 Jarrard, R.D. + 64038
 Jarrold, M.F. + 63525
 +Jarvis, P.D. 59922
 Jasbir Singh + 60131
 +Jaskulke, R. 61580
 +Jaulmes, S. 61865
 +Jauncey, D.L. 64556
 +Jawahery, A. 60049
 Jayadevan, N.C. + 61894
 Jayasuriya, K.D. + 62621
 +Jeanmart, L. 63938
 +Jechart, I. 61628
 Jee, R.D. 59848
 +Jeffreys, P. 60074
 +Jehn, H. 62124
 Jellinek, J. + 63533
 +Jen, S. 62398
 Jena, S.N. 60029
 +Jenkins, L.C. 63994
 +Jennings, B.K. 60162
 Jennings, H.M. 63219
 +Jenny, B. 60165
 Jensen, B.S. 60321
 +Jensen, D.H. 64256
 Jensen, E.S. + 63136
 Jensen, F.B. + 61341
 Jensen, H.E.Skovgard
 see Skovgard Jensen, H.E.
 Jensen, K.E.Lindstrom
 see Lindstrom Jensen, K.E.
 +Jensen, P.B. 60474
 +Jensen, R.R. 62168
 +Jensen, T. 60074
 +Jerick, H.M. 64292
 +Jernigan, R.L. 59707
 +Jerome, D. 62404
 +Jeske, U. 60426
 +Jeske, U. 60428
 +Jesus, A.P. 60939
 Jette, D. + 63975
 J.Hladik. see Hladik J.
 +Jia Han-Kang 64063
 +Jia Lal. 61559
 Jia Li. see Li Jia
 Jian-guo Shen. see Shen Jian-guo
 Jian-min Liu. see Liu Jian-min
 Jiang Ping. 62327
 +Jibaly, M. 60049
 Jieh-shan Wang + 61607
 Jimbo, M. + 62746
 Jin Han-Min. 62750
 Jin Min Kim + 59974
 +Jin Sicong. 59912
 Jin-Kang Jia. 60325
 see Jia Jin-Kang
 +Jin-Lu Lin. 64037
 Jin-sheng Meng. 59773
 see Meng Jin-sheng
 Jin-Soo Song. 59773
 Jinchang Mao. 60271
 see Mao Jinchang
 +Jo, M. 62263
 Jockwer, N. 60293
 Joffe, A.S. 59781
 Joffly, S. 60156
 Johannsen, P.-G. + 62960
 Johannsen, S.D. + 60258
 +Johansson, E.K. 60066
 +John, N. 64064
 +John, P. 60680
 John Manley, R.St.
 see St. John Manley, R.
 +Johnsson, U. 64014
 Johnson, B.M. + 60507
 +Johnson, B.M. 60934
 +Johnson, B.R. 62819
 +Johnson, C.E. 62865
 +Johnson, D. 60073
 +Johnson, D. 60533
 +Johnson, D.J. 61820
 Johnson, D.L. 62099
 Johnson, D.L. 63193
 +Johnson, D.L. 62035
 Johnson, E.G., Jr. 61216
 +Johnson, G.L. 60713
 +Johnson, J.D. 61751
 +Johnson, J.R. 62114
 +Johnson, K.H. 62377
 Johnson, M.B. + 60211
 Johnson, M.H. + 63971
 +Johnson, R.C. 60167
 +Johnson, R.G. 64316
 +Johnston, J.C. 64045
 +Johnston, T.W. 61669
 Johri, V.B. + 59642
 Jolesz, F.A. 63940
 +Jolibois, B. 61878
 +Jon-and, K. 60073
 +Jonas, J. 62822
 +Jones, A.C. 63041
 Jones, A.D.W. 63147
 +Jones, A.W. 64556
 Jones, B.J.T. + 64537
 Jones, D. + 63951
 +Jones, D. 60981
 +Jones, D.W. 60649
 Jones, F.R. + 63442
 Jones, H.W. 60574
 Jones, J.H. 63871
 +Jones, K. 60934
 +Jones, K.W. 60507
 +Jones, L.M. 64078
 +Jones, M. 60760
 Jones, M.L. + 60969
 Jones, P.L. + 60900
 Jong, J.J.de. see de Jong, J.J.
 +Jong Tai Lee. 60220
 Jonge, W.J.M.de
 see de Jonge, W.J.M.
 Jongh, L.J.De. see De Jongh, L.J.
 +Jonsson, B. 61848
 Joong Yoo Kun
 see Kun Joong Yoo
 Jordan, D.L. + 61087
 +Jordan, J.F. 63692
 +Jordan, S. 60373
 +Jordan, S.R. 64155
 Jordan, T.F. 59623
 +Jorge, M.I.B. 63038
 Jorgensen, P. + 60575
 +Jortner, J. 60800
 Joshi, G.C. + 60786
 +Joshi, P.V. 64176
 +Joshi, S.P. 61525
 +Joshua, M. 62118
 +Jouffrey, B. 59887
 Jouve, H. + 62685
 Jouvot, C. + 60919
 +Jovic, D. 61763
 Joyce, J.M. + 60967
 +Joyce, J.M. 60899
 +Joyce, J.M. 60966
 +Joyeux, D. 61106
 +Joziasse, J. 60381
 +Judd, R.L. 61387
 +Judek, B. 60195
 +Judge, D.L. 64236
 +Judy, P.F. 63942
 Jue-lian Shen
 see Shen Jue-lian
 Juer, J.W. + 59910
 Jug, K. + 63517
 Jug Giancarlo. see Giancarlo Jug
 +Jugaku, J. 64556
 +Julien-Pouzol, M. 61865
 Jun-hua Xu. see Xu Jun-hua
 Jun-ming Feng
 see Feng Jun-ming
 +Jung, G. 63796
 Jung, P. 60411
 +Jung, W. 60389
 +Jung In Choi. 60352
 Jung-Do Kim + 60220
 +Justiniano, E. 63617
 Jutamulia, S. + 61099
 +Jyothi Bhasu, V.C. 60607
 +Kaae, J.L. 60238
 +Kabanov, A.N. 61311
 +Kablambaev, B.A. 61720
 Kablukovskaya, M.A. + 63417
 Kaburagi, M. + 62654
 +Kachmar, B.F. 63465
 +Kachru, R. 60667
 +Kachru, R. 60673
 +Kachur, P.S. 61423
 Kadmenskii, V.G. + 62502
 +Kado, H. 60031
 +Kado, H. 60059
 +Kadono, R. 62627
 +Kadotani, K. 60446
 Kadura, P. 61842
 Kadyrakunov, K.B. + 61959
 Kadyshnikov, V.M. + 64218

- Kaemmer, N. + 61363
 Kafafi, Z.H. + 60721
 + Kagan, G.E. 62171
 + Kagan, H. 60049
 + Kagan, M.B. 63665
 + Kagan, N.B. 63444
 + Kagarwal, C.V. 63448
 Kagawa, T. 60613
 + Kagaya, C. 63395
 + Kagaya, H.-M. 62136
 + Kahl, T. 60076
 Kahle, H.G. + 62553
 + Kahle, H.G. 62597
 Kahn, W.K. + 61296
 Kaige Wang see Wang Kaige
 Kaimeo Chen see Chen Kaimeo
 Kaiming Zhang see Zhang Kaiming
 Kainthla, R.C. + 63719
 + Kaiser, A. 60295
 + Kaiser, E.T. + 63781
 + Kaiser, W. 61174
 + Kaiser, W. 60918
 Kaitechuk, R.H. + 64475
 Kajantie, K. 60025
 + Kajiyama, K. 61935
 Kajzar, F. + 61226
 + Kako, F. 61629
 Kakosy, T. + 63921
 Kakuno, K. + 62783
 Kakuno, K. + 62794
 + Kakuno, K. 62757
 Kakurai, K. + 62560
 + Kakusho, O. 61352
 + Kalachev, I.B. 63364
 Kaladze, T.D. + 61663
 Kalandadze, N.B. + 64531
 + Kalandarishvili, K.G. 61193
 + Kalberla, P.M.W. 64525
 Kalbitzer, S. + 62176
 Kalebek, A. 61686
 Kalenkovich, E.E. + 64227
 + Kalippiann, P. 59946
 Kalinichenko, M.A. + 63926
 Kalinin, D.I. 61732
 + Kalinin, S.V. 61139
 Kalinin, Yu.E. + 62782
 + Kalinov, V.S. 61204
 + Kalinowski, J. 62953
 Kalita, V. + 63186
 + Kallaev, S.N. 62902
 Kalman, C.S. + 60017
 + Kalman, Gy. 60944
 + Kalvius, G.M. 62848
 + Kaluzhnyi, V.M. 61109
 + Kalani Singh 61560
 + Kamardina, F.D. 63477
 + Kamarinos, G. 63715
 Kambe, K. 61740
 Kambe, T. + 61517
 + Kambe, T. 60468
 + Kamel, L. 64416
 Kamel, O.M. 64424
 Kamel, O.M. + 64419
 + Kamernitskii, A.V. 61901
 + Kamifukumoto, H. 59716
 + Kamimori, T. 62788
 + Kamimura, K. 59655
 Kamin, V.A. + 63074
 + Kaminaka, N. 62520
 Kaminker, A.D. + 64518
 + Kamino, K. 63737
 Kaminskii, A.A. + 63020
 Kaminskii, A.S. + 63042
 Kamioka, H. 59786
 + Kamiya, H. 60446
 + Kamiya, M. 62295
 + Kamorina, G.I. 63222
 + Kamyschenko, V.D. 60557
 + Kan, K. 64229
 + Kanai, H. 60512
 Kanamori, H. 64048
 Kanamori, H. 64066
 + Kanamori, H. 64123
 + Kanamori, H. 64052
 + Kanamori, J. 62654
 + Kanamori, Y. 63117
 + Kanani, D. 63688
 + Kanayama, T. 62777
 + Kanazawa, H. 63736
 Kanazawa, I. + 62156
 + Kanda, Y. 60502
 + Kandaswamy, J. 60049
 Kandaurova, G.S. + 62766
 + Kane, J.R. 60043
 + Kaneko, S. 62082
 Kaneko, T. + 59651
 + Kaneko, Y. 60927
 Kancl, G.I. 61452
 Kaneoka, I. 64088
 + Kanetkar, S.M. 60279
 + Kaneyoshi, T. 61803
 Kang Chang Sun see Chang Sun
 Kang Do-Yul see Do-Yul Kang
 + Kanivets, A.N. 64376
 Kankane, R.K. + 64196
 Kannan, A. + 60476
 + Kannari, F. 61142
 + Kano, T. 61141
 + Kanshaya, L.M. 63027
 + Kantor, L.M. 63406
 Kanunnikov, V.N. 60495
 + Kanzaki, J. 60031
 + Kanzaki, J. 60059
 Kao, Y.C. + 63179
 + Kapachinskaya, O.G. 63148
 + Kapilow, D.A. 63092
 + Kapitza, H. 59995
 + Kaplan, T. 62322
 Kapoor, R.K. + 64197
 + Kappagoda, C.T. 63882
 + Kappel, R. 59711
 + Kapsov, A.V. 61454
 + Kaputkina, L.M. 63328
 + Kaputkina, L.M. 63332
 Kapuy, E. + 60594
 + Karabanova, V.P. 62768
 Karachentsev, I.D. 64545
 + Karagodov, A.I. 60647
 Karagodova, T.Ya. + 60647
 + Karagozov, E.S. 63359
 + Karant, Y.J. 60195
 + Karasev, S.P. 60164
 + Karasik, A.Ya. 59839
 + Karasik, A.Ya. 61214
 Karasyov, V.E. + 63050
 + Karbushev, N.I. 61233
 + Kareva, N.T. 63378
 Karig, D.E. + 64135
 + Karig, D.E. 64065
 + Karig, D.E. 64139
 + Karimov, M.F. 62766
 + Karinskii, S.S. 62502
 Karl, G. 60045
 Karlik, I.Ya. + 63040
 Karlin, D.L. + 60499
 Karlov, N.V. + 63573
 + Karlov, N.V. 60872
 + Karlova, E.K. 63573
 Karlsson, B. + 62917
 + Karlsson, B. 59757
 + Karlstrom, G. 61848
 + Karlyshev, Yu. Ya. 60550
 + Karnatak, R.C. 60980
 Karnicka-Moscicka, K. + 63076
 Karnovich, V.N. + 64158
 + Karntaler, H.P. 61923
 + Karpinskas, S.C. 62481
 + Karpinski, L. 60396
 Karpman, V.I. + 64327
 + Karpov, S.B. 59807
 Karpov, S.Yu. + 62305
 + Karpov, V.A. 61249
 + Karpov, V.V. 60824
 + Karpov, V.Yu. 63370
 + Karpukhin, S.N. 61137
 + Karpushin, V.A. 59869
 + Kartheuser, E. 62033
 + Kartmazov, G.N. 63458
 Kartuzhanskii, A.L. + 61109
 + Karunasiri, R.P.G. 59843
 Karus, E.V. + 64249
 Karwat, H. 60349
 + Karyayev, V.N. 62487
 Kasai, Y. + 62663
 + Kaskhelkin, V.V. 61419
 + Kashiwabara, K. 61938
 + Kaskhali, A.D. 61835
 + Kasova, I. 61920
 + Kasperidus, G. 59993
 + Kass, R. 60049
 Kasteleyn, P.W. + 59694
 + Kasten, A. 62597
 + Kasten, A. 62553
 + Kastenig, B. 63734
 + Kastner, R. 62474
 Kastner, S.O. + 61701
 Kasuya, K. + 60526
 + Kasuya, T. 60794
 Katanic-Popovic, J. + 63230
 + Kataria, S.K. 60097
 + Katase, A. 60502
 Katayama, T. + 62744
 Katayama, T. + 61811
 Katila, T. + 62846
 + Kato, A. 63744
 + Kato, H. 63909
 + Kato, M. 63395
 + Kato, M. 63693
 Kato, S. + 60926
 Kato, T. 60729
 + Kato, T. 61981
 + Katsuki, H. 62313
 Katsumata, K. 62574
 + Katsumata, K. 62631
 + Katsura, S. 62643
 + Katsura, S. 62661
 + Katsuyama, Y. 62220
 + Katz, B. 60875
 + Katz, G.M. 63823
 + Katz, W. 62498
 + Katznelson, E. 59616
 + Katznelson, E. 60038
 Kaufman, A.N. 61633
 + Kaufman, J.J. 60571
 + Kaufman, R.N. 64327
 + Kaufmann, P. 64295
 Kaul, R.K. 59991
 Kaupilla, W.E. + 60983
 Kaur Ravinder see Ravinder Kaur
 Kavalyauskene, G.S. + 62451
 + Kavaya, M.J. 61206
 + Kaveh, M. 62477
 + Kawabata, S. 60031
 + Kawabata, S. 60059
 Kawabe, R. + 60372
 + Kawabe, S. 59918
 + Kawaguchi, K. 62861
 + Kawahata, K. 61614
 Kawai, E.-I. 60057
 + Kawai, M. 60184
 + Kawai, M. 60453
 Kawajiri, N. 64397
 Kawakami, N. + 62123
 + Kawakami, N. 62550
 + Kawakami, S. 61269
 + Kawakubo, T. 61775
 + Kawamura, K. 60954
 + Kawamura, K. 62555
 Kawamura, M. + 63737
 Kawamura, M. + 63733
 Kawamura, Y. + 59874
 + Kawanishi, K. 62733
 + Kawanishi, K. 62745
 Kawasaki, A. + 63150
 + Kawasaka, H. 63160
 Kawasaki, K. + 61485
 Kawasaki, K. + 62544
 Kawasaki, T. 62541
 + Kawasaki, T. 60461
 + Kawashima, M. 63672
 Kawashima, S. + 61562
 + Kawasumi, S. 62313
 Kawata, S. + 63961
 + Kay, H.F. 61885
 Kaysser, W.A. + 63211
 Kaysser, W.A. + 63214
 + Kaysser, W.A. 63194
 + Kazachenko, O.V. 63628
 + Kazakova, L.L. 64223
 Kazakova, N.I. + 63406
 Kazama, N.S. + 62728
 Kazama, N.S. + 62293
 + Kazama, N.S. 62789
 + Kazandzhian, B.I. 63269
 Kazanski, A.K. + 60977
 + Kazarinov, Yu.M. 60086
 + Kazeko, G.P. 61138
 + Kazemski, L. 63690
 Ke Wu see Wu Ke
 Kean, A.E. + 64085
 Kear, M.J. + 60460
 Kearfoot, K.J. 63972
 + Keck, D.B. 61290
 Kee Woo Rhee + 63788
 Kehrl, W. 63210
 Kehr, K.W. 59704
 + Keiller, B. 63108
 + Keith, V. 62201
 Keizer, J. 61472
 Kekalo, I.B. + 62694
 Keller, G.R. + 64108
 + Keller, J. 60611
 + Kellner, A.M. 63910
 + Kellermann, W. 63655
 + Kellogg, R.G. 59995
 + Kelly, H.P. 60675
 + Kelly, J. 60179
 + Kelly, T.J. 62062
 + Kel'ner, S.R. 64333
 + Kelso, M.T. 59782
 Kemmer, N. 59579
 Kemp, N.H. 61509
 + Kemper, K.W. 60197
 + Kemper, P.R. 63525
 + Kempf, A. 63635
 + Kenefick, R.A. 60508
 + Kenefick, R.A. 60936
 Kenjo, A. 59791
 Kenkre, V.M. 59688
 Kenkre, V.M. + 62342
 Kennard, C.H.L. + 61883
 + Kennedy, C.J. 62201
 + Kennedy, J.H. 62494
 Kennell, J. 64449
 Kennicutt, R. 64539
 + Kenny, J.E. 60914
 + Kenyon-Gjerpe, I. 60066
 Kerchov, F. see Vanden Kerchov
 + Kerimov, I.G. 62695
 Kerimova, T.G. + 63053
 + Kermod, J.P. 63302
 Kern, R. + 62431
 Kerner, W. 61644
 Kerr, R.G. 60393
 + Kerr, W.C. 59718
 Kerslick, G.S. + 60483
 + Kerstan, F. 62450
 + Kersten, D. 63850
 Kersten, O. + 62895
 Kertesz, J. + 63196
 + Kervailshvili, P.D. 61952
 Keshavan, S.Y. 61466
 Kesmodel, L.L. + 63589
 + Kessler, G. 60074
 Kessler, E.G., Jr. + 59899
 + Kessler, S. 61104
 + Ketel, T.J. 60075
 + Ketel, T.J. 60078
 Ketley, I.J. + 60618
 + Ketsle, G.A. 60823
 + Ketterson, J.B. 62203
 + Keune, W. 62864
 + Keung, W.-Y. 60016
 + Kevan, L. 62801
 Keydel, W. 64275
 Keyes, T. + 59710
 + Keady, F.J. 63781
 + Kezhenis, A.P. 62462
 + Khaav, A.A. 63001
 + Khachaturov, B.A. 60086
 + Khachaturov, B.A. 60542
 + Khachaturov, B.A. 60541
 Khachatryan, R.E. + 63927
 + Khairtdinov, K.A. 61197
 + Khakimov, A.A. 63087
 + Khallameida, D.D. 62435
 Khalatnikov, I.M. + 59712
 + Khalfauji, R. 62773
 Khalil, M.A.K. + 63756
 + Khaliqov, Kh.Ya. 63268
 + Khan, F.M. 63974
 + Khan, F.R. 63946
 + Khan, J.M. 64079
 Khan, P. + 60998
 + Khandekar, D.C. 59672
 Khang Nguyen van see Nguyen van Khang
 + Khankov, S.I. 61189
 Khanna, S.K. 62012
 + Khanna, V.D. 63432
 + Khannolainen, A.K. 61316
 Khanra, B.C. 62242
 + Kharambura, S.B. 62427
 Kharchenko, N.V. 64540
 + Kharkova, A.M. 63259
 + Kharlamov, A.I. 61849
 + Kharlamova, E.Ya. 63291
 + Khasenov, M.U. 61140
 Khatri, S.S. + 63024
 + Khatsinskaya, I.M. 63411
 + Khavan, G.V. 63965
 + Khavan, I.O. 63325
 Khazheeva, Z.I. + 61901
 Khazov, T.V. + 63931
 + Khazova, T.V. 63926
 + Khara, M.K. 64201
 Khiet Tu see Tu Khiet
 + Khil'kevich, I.F. 63321
 + Khmel'niitskii, D.E. 62430
 + Khodon, Ya.I. 61423
 Khodakov, E.E. 62767
 + Khodos, G.B. 60843
 + Khodyachuk, M.F. 64532
 + Khodyayev, V.D. 62299
 Khodzhaeva, V.L. + 61798
 + Khodolenko, A.L. 59698
 Khomenko, O.A. + 63321
 + Khomich, A.V. 63017
 + Khomitskii, Yu.N. 63420
 Khorev, A.I. + 63311
 Khosa, P.N. + 64322
 Khramov, A.N. + 64035
 Khristich, E.E. + 61312
 + Khromozhkin, V.V. 63204
 + Khromov, I.E. 60846
 + Khursudyan, M.A. 62914
 Khvastantsev, L.G. + 62438
 Ki Chung Moon see Moon Ki Chung
 + Ki In Han 60352
 Kicevic, D. + 63229
 + Kicevic, D. 62430
 Kichigin, D.A. + 62335
 + Kido, H. 60240
 + Kido, T. 63117
 Kieffer, J.C. + 61669
 + Kienle, P. 60161
 Kijewski, M.F. + 63942
 Kilcup, G. + 59981
 + Kileinikov, G.I. 60531
 Killeen, J. 61695
 Killeen, P.G. 64255
 + Killian, T. 60074
 + Kilp, T. 60790
 + Kim, B.F. 63034
 + Kim, C.O. 62388
 Kim, D. 60792
 + Kim, I.S. 63290
 + Kim, J. 59972
 + Kim, J. 59974
 + Kim, J.E. 59972
 + Kim, J.E. 59974
 + Kim, N. 60072
 + Kim, N. 60082
 + Kim, S.K. 59969
 Kim, T.K. + 62388
 Kim Bong-Heup see Bong-Heup Kim
 Kim Chang-Hyo see Chang-Hyo Kim
 Kim Jae-Hwan see Jae-Hwan Kim
 Kim Jin Min see Jin Min Kim
 Kim Jung-Do see Jung-Do Kim
 Kim Moo Han see Moo Han Kim
 Kim Tae Woon see Tae Woon Kim
 Kimel'bat, V.I. 59764
 Kimoto, H. + 60432
 + Kimoto, H. 60434
 Kimura, I. + 62670
 Kimura, K. 63537
 + Kimura, S. 61881
 + Kimura, T. 60461
 + Kimura, T. 59919
 + Kimura, T. 60470
 + Kimura, Y. 62136
 Kincaid, R.H. + 62241
 + Kindrat, M.M. 61849
 King, D.A. 62251
 + King, D.A. 63105
 King, G.B. + 61593
 + King, N.S.P. 60204
 + King, R.W. 64265
 Kingston, A.E. + 60991
 Kini, K.A. 62523
 Kinoshita, K. + 64331
 + Kinoshita, K. 60049
 Kinoshita, T. 60044
 + Kinsey, J.L. 60692
 + Kinsey, J.L. 60780
 + Kinzel, W. 62658
 + Kinzhibalo, V.V. 63264
 + Kiontke, S. 60054
 + Kipatsi, H. 60322
 + Kipatsi, H. 60313
 + Kirakawa, K. 62606
 + Kirchner, H.O.K. 61915
 Kirichenko, N.A. + 59862
 + Kirichenko, N.A. 63149
 + Kirichenko, N.A. 63553
 + Kirichenko, N.A. 63573
 Kirichenko, Yu.A. + 62198
 Kirichenko, Yu.A. + 61375
 + Kirichok, P.P. 63223
 + Kirikov, V.A. 62902
 + Kirilenko, V.V. 63270
 + Kirilenko, V.V. 63271
 Kirillova, L.G. 63145
 + Kirin, A. 63208
 + Kirk, W. 63872
 + Kirmaier, C. 60792
 + Kirmenskii, A.P. 62870
 + Kirovskaya, I.A. 62483
 + Kirsch, M. 63949
 Kirsch, W. + 59739
 + Kirscheid, K. 63836
 + Kirschfeld, K. 60066
 + Kirsei, V.I. 61191
 Kirste, B. + 62834
 + Kirtley, J.R. 62968
 + Kirzhnits, D.A. 59984
 Kiselev, N.G. 61108
 + Kiselev, V.V. 63356
 + Kiselev, V.V. 63362
 + Kiseleva, N.V. 63003
 + Kishi, Y. 63180
 Kishimoto, M. + 62714
 + Kishimoto, W. 61440
 + Kishinami, K. 61379
 + Kishino, M. 64148
 + Kisiel, A. 63076
 Kisly, P.S. + 63225
 Kislyuk, V.S. 64405
 Kislyuk, V.S. + 64406
 Kiss, L.I. 59775
 Kiss, S.J. + 63241
 Kisslinger, J. + 60433
 Kisslinger, L.S. + 60004
 + Kisslinger, L.S. 60005
 + Kistiakowsky, V. 60049
 + Kita, E. 62858
 + Kita, H. 63299
 + Kita, H. 63718
 Kitagawa, H. + 61102
 Kitagawa, S. + 60834
 + Kitajima, K. 63080
 Kitakado, S. 60021
 + Kitamura, A. 63672
 + Kitamura, T. 63562
 + Kitaoka, S. 62714
 Kittrell, C. + 60804
 + Kiyama, M. 62860
 + Kiyokawa, T. 60367
 + Kiziah, R.R. 60202
 + Kjaer, J. 62269
 + Kjems, J.K. 62573

- + Kjems, J.K. 62010
+ Klabunovskii, E.I. 62115
Klafter, J. + 59735
+ Klassen, N.V. 60971
+ Klatt, K.H. 63738
Klauder, J.R. + 59634
+ Kleban, L.S. 64272
+ Klein, A. 60136
+ Klein, D.J. 63944
+ Klein, H. 60033
+ Klein, J. 60139
+ Klein, J. 62236
+ Klein, M. 64152
+ Klein, M.L. 62039
+ Klein, M.L. 62092
+ Klein, M.P. 63582
Klein, W. 59751
+ Klein, W. 62058
+ Kleinhans, H.D. 62100
+ Kleinman, L. 62329
+ Kleinsasser, A.W. 63174
Kleintjens, L.A. 62072
Kleinwächter, P. + 60159
Kleman, M. 61802
Kleman, M. + 61791
+ Klemperer, W. 60750
+ Klemperer, W. 60734
+ Klepp, K. 61873
Klepper, L.Ya. 63966
+ Klerk, M. 63246
+ Kleshechev, A.S. 63329
+ Kliger, D.S. 60620
+ Kligshtein, M.S. 61828
+ Klimchuk, M.A. 60892
Klimenko, V.N. + 63197
Klimontovich, Yu.L. 61591
Klimovitch, S.U. + 60551
+ Klimovskii, I.I. 61139
+ Klinger, L.M. 62173
+ Klinger, O.E. 63226
+ Klingshirn, C. 62940
Klink, J.J. van der
+ see van der Klink, J.J.
+ Klipping, C. 64341
+ Klockars, C.E. 60316
Klootwijk, C.T. + 64028
Klopov, B.A. + 61573
Klose, S. + 61800
+ Klostermann, K. 63599
+ Klotz, C.E. 60833
Klotsman, S.M. 62149
+ Klotz, D. 60323
+ Klovning, A. 59995
+ Kluge, E.E. 60075
Kluwick, A. + 61551
Klypin, A.A. + 64550
+ Klyuch, A.S. 63332
+ Klyukov, A.G. 61311
+ Kmetko, E.A. 61851
Knapp, E.W. + 63770
Kneipp, K. + 63006
+ Knies, G. 59995
Knight, A.E.W. + 60816
+ Knight, A.E.W. 60815
Knize, R.J. 60656
Knoll, G.F. 60515
Knop, W. + 62552
+ Knop, G. 60054
+ Knops, H.J.F. 61836
Knops, R.J. + 61404
+ Knupfer, W. 60133
+ Knuyt, G. 60417
Knystautas, E.J. 60946
Kobayashi, A. 60014
+ Kobayashi, H. 61058
Kobayashi, K. + 61843
Kobayashi, K. + 62491
+ Kobayashi, M. 63029
+ Kobayashi, N. 60927
+ Kobayashi, N. 61384
+ Kobayashi, N. 61385
Kobayashi, R. + 61490
Kobayashi, T. 61371
+ Kobayashi, T. 60031
+ Kobayashi, T. 60059
+ Kobayashi, T. 62786
+ Kobayashi, T. 60461
+ Kobayashi, T. 61240
+ Kobayashi, T. 61689
+ Kobayashi, Y. 64556
Kobe, D.H. 60645
+ Kobuke, K. 63909
Koch, K.R. 64022
+ Koch, M.E. 60803
Koch, R.A. + 61342
+ Koch, R.F. 63946
Koch, S.W. + 62120
Kochan, B. + 62486
Kocharov, L.G. 64450
Kochelap, V.A. + 61144
Kockelmann, H. + 59834
+ Kocsanyi, L. 61265
+ Kocur, P.M. 60938
Kodaira, J. + 60058
Koel, B.E. + 62264
+ Koene, B. 60534
+ Koenen, F.T.M. 60467
Koenig, W. 60161
+ Koeningberger, G. 64462
Kogan, E.M. + 62506
Koh, E.Ya. + 60700
Koh Byoung-Joon
+ see Byoung-Joon Koh
+ Kohgi, M. 62628
Kohiki, S. + 59883
+ Kohlhaase, A. 60923
+ Kohne, J. 62296
+ Kohnen, H. 64155
Kohno, T. 64355
Kohno, T. + 60107
+ Koike, M. 60208
Koike, Y. + 62399
+ Koike, Y. 60182
Koima, M. + 62152
+ Koizumi, M. 62587
+ Koizumi, N. 62629
Kojima, H. + 60434
+ Kojima, H. 62856
+ Kojima, H. 60432
Kojima, N. 61583
Kok, R.A. + 60605
+ Kokott, Th. 60073
Kokubo, T. + 62909
+ Kokushkin, A.M. 61194
+ Kolar, D. 63539
Kolar, D. (ed.) 59538
+ Kolchin, A.G. 61682
+ Kolchin, A.G. 61710
Kolchinskii, I.G. 64234
+ Kolesnik, L.I. 63051
+ Kolesnik, L.I. 63042
+ Kolesnik, L.I. 64378
+ Kolesov, S.A. 63478
Kolezhuk, K.V. + 62919
+ Kolgin, A.P. 63934
+ Kollotzek, H. 60431
+ Kollyuk, V.B. 64406
+ Kolmeder, C. 60918
+ Kolmykov, V.I. 63462
+ Kolokolov, N.B. 61606
+ Kolokolov, N.B. 61721
+ Kolokolov, N.B. 60957
+ Kolomenskii, E.A. 60163
+ Kolosov, Yu.N. 61069
Kolotetz, H. + 60435
+ Kolpakov, A.V. 64221
Koltun, D.S. 60119
Koma, A. + 63091
+ Komamiya, S. 60031
+ Komamiya, S. 60059
+ Komarov, A.D. 61683
+ Komarov, I.V. 60977
+ Komatsu, K. 62783
+ Komazaki, Y. 61384
+ Komle, A.A. 61117
Komminos, Y. + 60609
+ Komoda, T. 62751
+ Komornicki, A. 60926
Komorowski, L. 61847
+ Kompa, K.L. 60861
+ Kompanets, I.N. 62504
+ Konczol, S. 59774
Kondepudi, D. + 63500
Kondo, I. + 60461
+ Kondo, I. 64556
+ Kondo, I. 64557
+ Kondo, I. 60470
Kondo, K. + 61772
+ Kondo, K. 60072
+ Kondo, K. 60088
+ Kondo, K. 61698
+ Kondo, K. 60082
+ Kondo, M. 63685
+ Kondo, O. 61528
Kondo, S. 63859
+ Kondorskaya, N.V. 64050
Kondrashova, N.N. 64439
+ Kondratenko, A.N. 61657
+ Kondzhary, Yu.R. 63967
+ Konenko, I.R. 62115
Kong Hoai Le
+ see Le Kong Hoai
+ Konig, F. 60442
+ Konig, V. 60165
Konin, A.M. 62439
Koningsveld, R. + 62111
Konishi, S. + 60394
+ Konishi, S. 62164
+ Konnov, B.A. 60499
Kono, H. + 60687
Kononov, E.Ya. 61704
+ Konopliv, A.S. 64410
+ Kononov, I.P. 61213
+ Kononov, O.G. 60164
Konrad, R. + 62076
+ Konstantinov, I.I. 61798
+ Konstantinov, I.I. 61830
Konstantinov, V.B. + 61264
Konstantinova, A.F. + 62924
Konsulova, M. 59801
Kontizas, E. + 64522
+ Kontizas, M. 64522
+ Kontorov, M.D. 60514
Kontush, S.M. + 64221
+ Konvisar, P.G. 61200
Konyakin, I.A. + 61260
+ Kooijman, S. 60066
+ Kooijman, W. 60467
+ Koonin, S.E. 60142
Kopelman, R. + 59691
Kopinga, K. + 62625
+ Koppa, H. 64291
+ Kopp, C. 61537
Koppen, P.A.M. van
+ see van Koppen, P.A.M.
+ Koppitz, B. 59995
+ Kopylov, A.I. 64550
+ Kopytin, Yu.D. 63763
+ Kopytin, Yu.D. 64267
Korber, C. + 63278
Korchkov, V.P. + 63163
+ Kordova, I.R. 60761
+ Koren, Y. 64003
+ Koreneva, L.G. 60761
+ Koreneva, N.A. 61280
+ Koreneva, N.A. 61282
+ Korhonen, M.A. 61933
+ Korn, G. 61181
Korneeva, N.N. + 63329
Korner, A. + 61923
+ Korner, A. 61915
Korneta, W. + 62763
+ Kornienko, A.A. 62379
+ Kornilov, M.Yu. 60760
Korobeynikov, V.P. + 64426
+ Korol', E.N. 61022
+ Korolikhin, V.V. 63003
Korompay, V.D.
+ see De Korompay, V.
+ Korostelin, Yu.V. 61163
Koroteev, N.I. + 61234
+ Korotkov, N.A. 63463
Korshunov, L.G. + 63423
Korten, M. 60462
+ Korthaus, E. 60294
Korzunin, G.S. + 62705
Kosai, H. + 64494
+ Koschar, P. 63114
+ Koschar, P. 63113
+ Koseck, K. 60054
Koseki, H. + 62105
Koshchenko, V.I. + 62122
Koshchenko, V.I. + 62127
Koshchev, V.I. + 63409
Koshiba, M. + 61329
+ Koshiba, M. 60031
+ Koshiba, M. 60059
Koshizuka, N. + 61270
+ Koshizuka, N. 62760
+ Koshizuka, N. 62942
+ Koshizuka, N. 63182
+ Koshkarev, D.G. 60492
Kosic, T.J. + 62954
+ Kosmac, T. 63239
+ Kosmyna, M.B. 61278
+ Kosoburd, T.P. 61097
+ Kossanyi, J. 63560
+ Koster, R. 60294
+ Kostic, E. 63241
+ Kostikov, Yu.P. 62545
+ Kostina, I.V. 63367
Kostogorov, E.P. + 61595
+ Kostrotsa, S.A. 61140
+ Kostrotsa, T.V. 63458
+ Kostromina, K.N. 63932
+ Kostov, Yu.A. 61709
+ Kostov, Yu.A. 61682
+ Kostov, Yu.A. 61710
Kostyk, R.I. + 64443
Kostyk, R.I. + 64440
+ Kostyukova, E.P. 63367
+ Kosulin, N.S. 61845
+ Koszykowski, M.L. 60848
+ Kotadia, K.M. 64304
+ Kotai, E. 61936
+ Kotani, T. 63140
Kotecky, R. + 59740
Kothari, N.C. + 61240
Kotkis, M.A. + 63412
+ Kotmann, F. 60537
+ Kotnala, R.K. 63668
+ Kotoh, K. 60240
+ Kotomin, E.A. 63026
Kotov, Yu.A. + 60482
+ Kotov, Yu.D. 64333
+ Kotov, Yu.D. 64385
+ Kotova, M.A. 63003
Kotsarenko, N.Ya. + 61061
+ Kottis, Ph. 63012
+ Kottis, Ph. 63033
+ Koumoto, K. 62878
Kounnas, C. + 60007
+ Kouri, D.J. 63497
Koutchmy, S. + 64437
+ Kouvel, J.S. 62383
+ Kouvel, J.S. 62803
+ Kovachev, B.Zh. 64489
Kovacs, N. 64465
+ Koval', V.P. 63420
+ Koval'chuk, M.V. 62455
+ Koval'chuk, Yu.V. + 61963
+ Koval'chuk, Yu.V. 61964
+ Koval'chuk, Yu.V. 61193
Kovalev, N.F. + 61067
Kovaleva, A.D. + 63479
+ Kovarskii, S.L. 63934
+ Kovash, M.A. 60179
+ Kovba, L.M. 61891
+ Kovtonyuk, N.F. 61117
+ Kovtun, A.P. 62338
Kowalle, G. + 64059
Koyama, F. + 61150
+ Koyama, J. 61315
Koyama, K. + 62600
+ Koyama, K. 64556
+ Koyama, K. 64557
Koyama, T. + 63874
Koyamada, Y. + 61302
+ Kozai, Y. 64494
Kozak, J.J. + 59685
+ Kozhevnikova, N.N. 61419
+ Koziarkiewicz, W. 61702
Kozin, G.I. + 61213
+ Kozina, G.S. 63059
Kozlov, I.M. + 60539
+ Kozlov, M.G. 60751
+ Kozlov, P.V. 63373
+ Kozlov, S.M. 62198
Kozlov, V.A. + 63969
+ Kozlov, V.A. 59839
+ Kozlov, V.A. 61214
+ Kozlov, Yu.I. 61722
Kozlova, O.G. + 61934
+ Kozlovskii, I.V. 60172
Kozlovskii, V.I. + 61114
+ Kozlovskii, V.I. 61163
Kozma, L. + 63218
+ Kozmenko, M.V. 63505
+ Kozmutza, C. 60594
+ Kozmyrev, A.F. 63487
+ Kozmyrev, A.N. 61682
+ Kraft, C.S. 62755
+ Kraynovich, D. 60864
Krakowski, M. + 61049
Kranbuehl, D.E. + 63011
+ Krappukhin, V.V. 63444
+ Krasevec, V. 63248
+ Krasevec, V. 63253
+ Kraskinski, J. 61228
Krasenko, T.I. + 62133
+ Krasnozhoz, A.I. 63311
+ Krasovitskii, V.V. 61666
Krasutskii, P.A. + 60760
+ Krath, H. 63036
Krause, M.O. + 60622
+ Krause, M.O. 60674
+ Kraushaar, J.J. 60106
+ Krauskopf, K. 60319
Krauth, H. + 60437
+ Krautz, E. 62433
+ Kravchenko, T.V. 61815
Kravchenko, V.A. + 62276
Kree, P. 59932
+ Krehbiel, H. 60031
+ Krehbiel, H. 60059
+ Krehnick, D.L. 60049
+ Kretschmar, K. 63103
+ Kretzer, H. 60188
Kreutz, E.W. + 62470
+ Krikland, J.P. 61731
Krishan, J. + 62882
+ Krishna Murthy, B.V. 64199
+ Krishnan, R. 63310
+ Krishnan, R. 62727
+ Kristhal, M.A. 63454
+ Kristjansson, K.S. 63576
Kritchman, E.M. 61254
Krivandina, E.A. 61840
Kriven', V.A. 61415
+ Krivitskii, V.P. 61849
Krivoglas, M.A. + 62050
+ Krivonogov, G.S. 63332
+ Kroeger, R. 60074
+ Kroenke, L. 64137
Kroger, W. + 61581
+ Kroger-Paulus, A. 63834
Krogh, J. von
+ see von Krogh, J.
+ Kroh, J. 63570
+ Krokmal', Yu.D. 62877
+ Kroll, D.M. 62059
Kromer, U. + 63878
+ Kroner, F. 60533
Krongauz, V.G. + 63027
Krongauz, V.V. + 63529
+ Krouse, H.R. 63625
+ Krug, A.D. 60307
Kruglov, S.I. + 61316
+ Kruglyak, N.E. 61765
Kruhl, W. + 63694
Krumin', A.E. + 62478
+ Krummacker, S. 60870
+ Krumphold, R. 63249
Krus, L.W. + 60229
+ Krut, A.A. 61109
+ Kryachko, V.V. 62502
Kryder, M.H. + 62755
+ Kryknanov, I.A. 63444
+ Krymova, A.I. 63569
+ Krynicka-Drozdzowicz, E. 64251
+ Krystek, M. 59822
Kryszewski, M. + 63031
+ Kryuchkov, A.N. 63547
+ Kryukov, N.N. 61401
Kryukova, I.V. + 61160
Kryukova, I.V. + 61161
+ Kryzhanovskii, B.P. 61189
+ Krzhivitskaya, S.N. 62412
+ Krzyzanowski, Z. 61182
Kuang-chao Chou
+ see Chou Kuang-chao
+ Kubanek, B. 63904
+ Kubasta, E. 61980
Kubiak, G.D. + 63556
Kubo, H. + 62606
+ Kubo, H. 62821
+ Kubota, T. 63029
+ Kubota, Y. 60049
Kucherenko, E.S. 63280
+ Kucherenko, V.F. 63314
Kuczyński, G.C. 63195
+ Kudashchev, S.R. 63479
+ Kudasov, B.G. 60493
+ Kudin, B.G. 63382
+ Kudo, K. 62889
+ Kudrevatikh, N.V. 62709
+ Kudrinskii, J. 62358
+ Kudryavtsev, Yu.N. 63621
+ Kudryavtseva, G.P. 63412
+ Kudykina, A.A. 62919
Kudzin, Yu. + 62831
+ Kudzin, A.Yu. 62877
+ Kuhn, G. 62309
Kuhn, J.H. + 60062
+ Kucharev, A.V. 61305
Kukharskii, A.A. 62994
+ Kukimoto, H. 63166
+ Kukimoto, H. 62906
+ Kuklin, R.N. 62131
+ Kuklin, V.M. 61657
Kukolich, S.G. + 60709
+ Kukolich, S.G. 60706
+ Kukolich, S.G. 60710
+ Kukolich, S.G. 60708
Kulagin, S.A. + 63044
Kulakovska, B. + 63559
Kuleev, I.G. 62397
+ Kuleshov, A.P. 62275
+ Kuleshova, T.V. 64158
Kulhanek, O. + 64064
+ Kuliev, A.A. 62060
Kuliev, B.B. + 63268
+ Kuliev, E.M. 63268
Kulieva, N.A. + 62061
+ Kulikov, A.I. 64273
+ Kulikov, A.V. 60499
+ Kulikov, L.A. 63964
+ Kulish, V.V. 61642
+ Kulskarni, V.D. 61572
+ Kulshburg, A. 63173
+ Kulshreshtha, A.P. 63658
+ Kulshreshtha, S.M. 64194
Kulsrud, R.M. 64328
Kulsrud, R.M. + 61679
+ Kumagai, K. 63399
+ Kumahara, T. 60468
+ Kumamoto, K. 61142
+ Kumar, A. 62193
Kumar, D. + 61209
Kumar, U.V. Girish
+ see Girish Kumar, U.V.
+ Kumazawa, M. 59795
Kumeda, M. + 62286
+ Kumeda, M. 61804
+ Kumozaki, K. 62792
Kun Joong Yoo + 60221
+ Kundt, W. 64363
Kunhikrishnan, P.K. + 64199
+ Kunieda, H. 64556
+ Kunieda, H. 64557
+ Kunii, Y. 61623
Kunimatsu, K. 62989
Kunkle, T.D. + 63885
Kunne, L.D. + 62475
+ Kuno, Y. 62627
+ Kuno, K. 61412
+ Kunselman, A.R. 60043
Kunz, S.D. + 59819
+ Kunze, R.C. 60455
Kuo, V.W.C. + 63319
Kuo, Y.C. + 62724
Kuo-Ho Yang. 59622
+ Kuiperman, W.A. 61341
Kupshchuk, P. + 60527
+ Kurabayashi, T. 62292
Kuramoto, F. + 63080
+ Kuramoto, K. 62875
+ Kuratov, A.A. 61844
Kurbatov, G.A. + 62034
+ Kurbatov, G.A. 62995
Kurbatov, L.N. + 63059
+ Kuryumov, A.V. 63220
Kurganov, A.A. + 60776
+ Kurihara, K. 60461
+ Kurihara, K. 60470
+ Kurihara, T. 62156
Kuriki, K. + 61623
+ Kurita, S. 63066
Kuritsyn, A.M. + 59872
+ Kuroda, H. 61620
Kuroda, K. + 61129

- +Kuroda, K. 61799
+Kuroiwa, K. 61147
+Kurokawa, S. 60072
+Kurokawa, S. 60082
Kuroki, T. 62820
+Kuroki, T. 63898
+Kuropatkin, Yu.P. 60493
+Kurtz, V.G. 64347
+Kurtz, H. 60631
+Krumi, T. 63451
+Kusao, K. 59883
+Kush, G.G. 63256
+Kushnir, M.A. 63045
+Kuska, R. 62181
Kusno, D. 60051
+Kuster, E.J. 62268
+Kusuda, T. 62510
+Kusuda, T. 62770
+Kusuda, T. 62747
+Kusuda, T. 63750
Kutalo, A.A. 64150
+Kutiev, I. 64241
Kuwahara, H. 61149
+Kuwahara, K. 62508
+Kuwano, S. 63860
Kuwano, Y. 63686
+Kuwazuru, A. 64331
+Kuze, E. 61772
+Kuze, E. 61258
+Kuzenkova, M.A. 63225
Kuzhevskii, B.M. 64330
Kuzii, V.V. 61744
Kuz'kov, P.P. 64387
Kuzmenko, N.E. 60703
+Kuz'min, A.M. 61892
+Kuz'min, G. 63505
+Kuz'min, S.S. 61117
+Kuz'min, Yu.E. 61140
Kuznetsov, A.A. 62275
Kuznetsov, A.P. 59603
Kuznetsov, A.V. 61687
+Kuznetsov, A.V. 61711
+Kuznetsov, E.A. 63931
+Kuznetsov, V.I. 62276
+Kuznetsov, V.P. 60482
+Kuznetsov, Yu.V. 60557
+Kuznetsov, L.A. 60703
Kvande, H. 62079
Kvantov, M.A. 62545
+Kvitsinskii, V.A. 60664
Kwan, T.J.T. 61164
Kwiatniak, M. 63690
+Kydon, D.W. 62824
Kyle, D.J. 63801
+Kyogoku, T. 63535
+Kyun-Kook Shin 60333
Kyuntse, I.A. 62832
- +La Ginester, A. 63083
La Marche, P.H. 62003
Laaksonen, L. 60563
Laarif, A. 61900
Laat, S.W. 60438
see de Laat, S.W.
Labbeyrie, A. 64380
Labit, M. 61358
+Labitze, K. 64187
+Labzovskii, L.N. 60751
+Lach, J. 60083
+Lach, J. 60042
+Lach, J. 60070
+Lackas, W. 59995
Ladde, G.S. 63777
+Ladik, J. 63777
Ladik, J.J. 62328
+Ladvishchenko, Yu.M. 60843
Lafon, A. 59682
+Lafraimboise, J.G. 64354
Lagerkvist, C.-I. 64416
Lagios, E. 64090
Lagne, J. 59602
+Lagrez, A. 61000
+Lagunas-Solar, M.C. 60177
Lahart, M.J. 63956
+LaHoz, C. 64287
+Lahri, R. 63695
Lai Wu-yan 62384
+Lain, L. 63524
Lakshmanan, M. 59946
Lakshmi, D.R. 64303
+Lakshmikumar, S.T. 62161
+Lakshminarasimha, C.S. 61712
Lal Jia 64322
+Lal Mani 63925
+Lam, C. 62003
+Lamarre, J.M. 64340
+Lamb, R.C. 64492
Lambert, D.K. 59860
- Lambert, J.M. 60182
+Lambert, M. 61782
Lambiotte, J.J. 61519
Lami, A. 60990
+Lamintsev, V.G. 63330
+Lampert, R.A. 60793
+Lamsa, J.W. 60075
+Lan, Y.Y. 61624
+Lancaster, J. 60559
Land, D.J. 60952
+Land, D.J. 60940
Landers, R. 62280
+Landman, U. 62268
Landsberg, P.T. 63713
+Landschoff, P.V. 60067
Landstrom, O. 60316
Lane, B. 61168
+Lane, L.J. 60264
+Lane, N.F. 60987
Lane, P.L. 60410
Lanch, M.Yu. 61336
+Lang, A.R. 61922
+Lang, G. 62852
+Lang, H. 60323
Lang, K.R. 64433
+Lang, R.S. 60471
+Langen, J. 60054
+Langer, J.M. 62158
Langer, J.S. 62057
Langevin, Y. 61998
+Langevin, Y. 60243
+Langevin, Y. 61997
Langhoff, S.R. 60835
+Langhoff, S.R. 60604
Langkilde, F.W. 60799
Langley, R.A. 61658
+Langley, R.B. 64265
+Langridge-Smith, P.R.R. 60913
+Lanier, R.G. 60185
+Lanjesse, J. 63414
Lans, J.v.d. 60033
+Lanske, D. 60033
+Lantratov, S.V. 61200
Lanyi, P. 63209
+Lanzl, L.H. 63975
+Laperashvili, T.A. 62497
+Lapeyre, D. 59887
+Lapicicella, A. 61914
+Lapicki, G. 60935
Lapidus, E.M. 62501
+Laplace, G. 61878
+Laplanché, G. 62144
+Lapshin, V.P. 63373
Largy, B.de de Largy, B.
Larkina, V.I. 64321
Larsen, A.Nylandstedt
see Nylandstedt Larsen, A.
Larsen, A.Nylandstedt
Larsen, E.W. 61388
+Larsen, J.T. 60397
Larsen, R.I. 63760
+Larson, S.J. 63995
+Larsson, R. 60978
+Larsson, S.A. 60316
+Larue, R. 60183
+Las Heras, E. 60975
+Lashkui, A.V. 62324
+Laskar, A.L. 62163
Lasser, R. 60412
+Lashchukina, V.A. 60844
+Laszewski, R.M. 60491
LaTraille, S.L. 64098
+Lattke, H. 63578
+Lattuada, M. 60187
Latyshev, A.N. 63045
+Latyshev, V.P. 63314
Latz, R. 63113
+Latz, R. 63114
+Lau, B.W. 62388
+Lau, K.H. 59995
+Lau, K.H. 61019
Laubacher, D.B. 60105
+Laube, B.L. 62955
+Laube, B.L. 62985
Laude, F. 60270
+Laude, L.D. 62297
Laudenslager, J.B. 64276
Laugier, A. 63703
+Launay, J.C. 63560
+Launay, J.P. 60249
+Laurendeau, N.M. 60782
+Laurent, C. 64524
+Laurent, J. 64215
+Laurikainen, P. 60083
+Laurikainen, P. 60042
+Laurikainen, P. 60070
+Laurvay, H. 63710
+Lauvray, H. 63153
Laursen, P. 63714
Laux, L. 60781
Lavallard, P. 62347
Laverie, M. 60388
+Laverne, C. 64081
LaVerne, J.A. 63572
+Lavigne, P. 61669
+Lavollee, M. 60797
+Lavrentev, F.F. 63307
- +Lavrienko, I.A. 63217
+Law, C.K. 61586
Law, K.Y. 63049
+Lawande, S.V. 59672
+Lawless, W.N. 62874
Lawrance, W.D. 60815
Lawrence, A. 64556
Lawrence, D.M. 59560
+Lawrence, J.M. 62091
+Lawrence, M.B. 64135
Lawson, A.C. 61856
Lay, T. 64123
+Lazarev, P.G. 63463
Lazarides, G. 64567
+Lazarus, A.J. 64313
Lazarus, M.S. 63443
+Lazin, V.I. 60540
Lazzarini, A.J. 60199
+Lazzarini, A.J. 60198
Le Claire, A.D. 62180
+Le Coze, J. 63266
+Le Gall, H. 62773
Le Kong Hoai 63518
+Le Metayer, M. 63678
Le Page, Y. 61879
+Le Palec, G. 63644
+Le Roy, R.J. 60866
+Le Yaouanc, A. 59907
+Lea, R.H. 63747
+Leach, S. 60805
+Leach, S. 60743
+Leach, S. 62142
+Leadbetter, A.J. 61787
Leal, F.A.M. 61175
+Leask, M.J.M. 62816
Leatherman, S.P. 64124
Lebed, B.M. 62706
Lebedev, A.A. 59798
+Lebedev, O.E. 63923
+Lebedev, S.S. 61247
+Lebedev, S.V. 61710
+Lebedev, V.V. 59712
Lebedev, Yu.N. 62288
+Lebedeva, T.P. 61211
+Lebedeva, V.V. 60652
Leblanc, M. 61880
Leblanc, M. 61882
+Lebo, C. 60099
+Lebowitz, J.L. 59705
+Lebrun, M. 60143
+Lecar, H. 63819
Leccia, F. 60145
+Leclercq, R. 63144
+Leclercq, J. 60331
Lecomte, G.V. 62613
Lederer, L. 64235
+Lederer, P. 61905
+Ledoux, I. 61226
+Ledoux, R.J. 60198
+Ledoux, R.J. 60199
+Ledoux, T. 63814
Leduc, M. 60665
Lee, A.I. 59743
+Lee, A.I.N. 64086
+Lee, C.W. 61731
+Lee, D.M. 62819
Lee, D.N. 63313
Lee, H.C. 63936
+Lee, J.A. 63795
Lee, J.K. 61627
+Lee, K. 63944
Lee, K.C. 61758
+Lee, K.C. 62955
+Lee, L.C. 64325
+Lee, L.C. 60867
+Lee, P.A. 62432
Lee, R.A. 61073
Lee, R.A. 61074
Lee, R.A. 61075
Lee, S. 60224
+Lee, S.A. 61582
Lee, T. Van der
see Van der Lee, T.
+Lee, W.B. 64122
Lee, Y.E. 62109
+Lee, Y.T. 60864
+Lee, Z.H. 59788
Lee Duckhwan
see Duckhwan Lee
Lee Jong Tai
see Jong Tai Lee
Lee Tong-Nyong
see Tong-Nyong Lee
Lee Un Chul
see Un Chul Lee
Lee Young Whan. see Young Whan
+Leenen, M. 60054
Leeuwen, W.F. van
see van Leeuwen, W.F.
+Lefebvre, J. 62107
+Lefebvre, P.Y. 62014
+Lefebvre, J.M. 63941
+Legeay, V. 61318
Legendre, R. 61498
+Leger, A. 62236
Legge, G.E. 63850
+Legon, A.C. 60701
- +Legon, A.C. 60704
+Legostaev, Yu.L. 63284
+Legrain, R. 60212
+Legros, C. 61357
+Lehmann, E. 59995
+Lehmann, K.K. 60734
Lehnhoff, T.F. 60307
+Lehraus, I. 60533
+Lei, W. 60319
+Lei, W. 63751
Lei Lin
see Lin Lei
+Leiferov, B.M. 63042
+Leigh, J.R. 60200
Leigh, K.M. 60246
+Leighy, J.E. 63262
Leipold, M.H. 63187
+Leitch, M. 60204
+Leite, J.R.R. 61175
+Leitherer, C. 64482
+Leitner, G. 63249
Leksikov, A.A. 62951
+Lekven, J. 64013
+Lelong, C. 63414
+Leloup, C. 60448
+Lemanska-Bajorek, A. 62158
Lemke, D. 64341
Lemke, H. 62367
+Lemmon, R.P. 59564
+Lena, P. 64392
+Lenfant, C. 63991
Lengfeller, H. 62996
+Lenglet, W.J.M. 63616
Lenke, D. 62479
+Lennert, P. 60031
+Lennert, P. 60059
+Lenser, M.C. 63876
Lenthe, J.H. van
see van Lenthe, J.H.
+Lenzen, G. 60054
Leon, N.de. see de Leon, N.
+Leonhardt, H.W. 63491
+Leonov, A.I. 62545
+Leopold, D. 60296
Leppert, M. 59772
Leppington, F.G. 59599
Leroy, J.-L. 64435
+Lescure, S. 61451
+Leshchenko, V.T. 61837
+Leshina, T.V. 63506
+Lesko, A.M. 63779
+Lesko, K.T. 60140
+Leskovich, V.I. 61160
+Lesser, P.M.S. 60953
+Lester, T.W. 61593
+Leszczynski, J. 60588
+Letaw, J.R. 64568
Letnik, D.A. 62458
Leung, A.Y.T. 61436
+Leung, C.H. 63936
Leuven, P. Van
see Van Leuven, P.
+Levandovskiy, V.V. 62707
Levashov, A.A. 64159
+Levchenko, N.M. 62198
+Levelut, A. 62900
Levelut, A.M. 61786
+Levelut, A.M. 61779
+Levenson, M.D. 61242
+Leventhall, H.G. 61349
+Lever, D. 60304
+Levesque, D. 61690
Levi, D. 59588
+Levi-Setti, R. 62003
+Levin, E.S. 62171
+Levin, F.S. 60566
+Levina, N.F. 64378
+Levine, R.D. 60692
Levinson, H.J. 62984
Levintov, I.I. 60028
+Levites, I.I. 63404
+Levititzky, M.G. 63875
+Levshin, L.V. 60823
+Levshin, L.V. 60826
+Levy, D.H. 60914
+Levy, F. 62405
+Levy, L.P. 62819
Levy, M. 62791
+Levy, M. 61372
Levy, P.M. 62804
+Levy, Y. 59845
Lew, J.K. 64177
+Lewendel, B. 59995
+Lewin, W.H.G. 64556
+Lewis, F.A. 62393
+Lewis, F.A. 62062
Lewis, S.D. 64133
+Lezdin, A.E. 60659
+Lhiaubet, G. 60377
+L'Homme, A. 60377
+Li Bozang 62536
Li Hanqiu 62363
+Li Jia 62332
Li Ling-fong
see Ling-fong Li
Li Sai-Ping. see Sai-Ping Li
+Li Xing-qi 63893
+Li Zu Yu 60532
+Liang Yan Sun 62283
- Liang Zhi-an 63893
+Liao Xianbing 61146
+Liao, G.S. 63757
+Libeyre, P. 60425
+Libeyre, P. 60427
+Liboff, R.L. 61123
+Lichtenstadt, J. 60203
+Lichtenhaler, R.N. 62075
+Lidiak, E.G. 64108
Lidorenko, N.S. 62131
+Lieberberg, D.H. 62066
+Liebert, L. 61791
+Liebertz, J. 61897
+Liebertz, J. 63151
+Liebmann, R. 62618
+Liechlin, L. 64470
+Liem Phan 62918
+Lifshits, V.G. 62764
+Light, J.C. 60905
Lightfoot, P.D. 63510
Likhitshtein, A.I. 62579
Lill, J.V. 60905
+Lillestol, E. 59995
+Lilley, J.S. 60201
+Lim, C.S. 59949
Lima, J.J. De
see De Lima, J.J.
Limin Chen. see Chen Limin
Lin, A.M.T. 60084
Lin, C. 61283
+Lin, G.-Y. 64208
+Lin, L.S. 62020
+Lin, R.P. 64431
+Lin, S. 62911
+Lin, S.H. 60687
Lin, W.H. 61325
Lin Chau-Jy
see Chau-Jy Lin
Lin Jin-Lu. see Jin-Lu Lin
Lin Lei 61773
Lin Zhao-hua
see Zhao-hua Lin
+Lincot, D. 61946
+Lindau, I. 63135
Lindblom, L. 64455
Lindblom, L. 64454
+Lindeman, T.G. 60859
Linden, W.H. van der
see van der Linden, W.H.
Linders, P.W.J. 59884
+Lindgren, B. 60714
+Lindgren, O. 59923
+Lindh, A.G. 64069
+Lindroos, V.K. 61933
+Lindsay, D.M. 60763
Lindstrom Jensen, K.E. 60289
+Lineberger, W.C. 60855
+Ling, J.C. 64492
Ling Ye
see Ye Ling
Ling-fong Li 59960
+Linh, V. 61861
+Linke, M. 59840
+Linsky, J.L. 64477
+Linsse, L. 60534
+Lionnet, D. 60425
Liou, K.-N. 64183
+Liou, M.K. 60953
+Lipari, P. 60049
Lipatov, Yu.S. 61774
+Lipatov, Yu.S. 61765
+Lipatov, Yu.S. 61830
+Lipichin, N.N. 63455
Lipfert, F.W. 63753
+Lipovskii, A.A. 61305
Lipovsky, R. 62059
+Lipsikh, S.I. 59989
+Lisin, A.N. 63422
+Lissitskaya, L.A. 63322
+Lisutskaya, D. 60074
+Liszt, H.S. 64541
Little, C.A. 60263
+Little, F.E. 60177
+Littlewood, T.M. 61598
+Litunovskii, R.N. 61682
+Litunovskiy, R.N. 61709
+Litunovskiy, R.N. 61710
+Litunovskiy, R.N. 61711
+Litunovskiy, R.N. 61687
+Litvinov, I.A. 61832
+Litvin-Staszewska, E. 62370
+Liu, C.-C. 64122
+Liu, C.S. 61624
Liu, J. 63742
Liu, J. 63745
Liu, L.C. 62007
+Liu Farang 62732
+Liu Hongdu 62311
+Liu Jian-min 59725
Liu Qun-L
see Quan-L. Liu
Liu Wenming 62332
Liu Wing-Ki
see Wing-Ki Liu
+Liu Zhi 63065
+Liu Zuwei 59912
+Livage, J. 62416
Livchak, I.F. 63654

- Lizon-Tati, J. 59787
 +Lloyd, J.R. 61378
 +Lo Russo, S. 61993
 Lobanov, A.N. + 61724
 +Lobanov, V.V. 62171
 +Lobanovich, E.F. 62455
 +Lobashev, V.M. 60163
 +Locans, V. 64437
 +Locardi, B. 61806
 Locatelli, M. + 61395
 Lochart, T.J. 60268
 +Lodding, A. 62170
 +Lode, W. 61467
 +Lodge, K.W. 61914
 +Loebinger, F.K. 60031
 +Loebinger, F.K. 60059
 +Loehrke, R.I. 61482
 +Loehrke, R.I. 61383
 +Loferski, J.J. 63690
 Loftus, D. + 62142
 +Logan, C.M. 60511
 Logan, J. + 63530
 Logginov, A.S. + 61157
 +Logginov, A.S. 62779
 Loginov, Yu.Yu. + 62112
 +Loginova, R.G. 62302
 +Logunov, A.V. 63366
 Lohmann, A.W. + 61076
 Lohmann, A.W. + 61052
 +Lohner, T. 61936
 +Lohnert, H. 60455
 Lohneysen, H.von
 see von Lohneysen, H.
 +Lohse, T. 60075
 Loidl, A. + 62010
 Loiko, N.N. + 62298
 +Lomakin, P.D. 64145
 +Lomdahl, P.S. 59718
 Lominadze, J.G. + 64503
 +Londer, Ya.I. 61724
 Lone, M.A. + 60519
 +Long, L.T. 64085
 Long, S.R. + 60836
 Longgren, K.E. + 61637
 +Longgren, K.E. 61629
 Loo, B.H. 62975
 Loore, C.de. *see de Loore, C.*
 Loos, T.W.De.
 see De Loos, T.W.
 Lopes, J.S. + 60939
 Lopez, E. + 62576
 +Lopez, J. 62253
 +Lopez, J. 61395
 +Lopez, M. 62087
 Lorant, S.J.St.
 see St. Lorant, S.J.
 +Lord, D. 59856
 Lord, M. + 63993
 Lorenc, J. 62086
 +Lorents, D.C. 60830
 +Lorenzo, E. 63648
 +Lorin, C. 60369
 +Lorre, J.J. 64549
 +Lorstad, B. 60074
 +Lortet, M.C. 64478
 +Los, J. 60897
 +Losev, V.F. 60644
 Loshin, D.S. + 63840
 +Loshinskii, A.M. 63051
 Lotz, W.G. + 63897
 +Loutat, R. 64068
 +Loubly, P. 63710
 +Loubriat, M. 60382
 +Louer, D. 61871
 +Louer, M. 61871
 +Louie, S.G. 62330
 +Louis, W.C. 60068
 +Lounisard, N. 64215
 Loulguere, J.C. + 59845
 Lousto, C.O. + 64534
 +Loutfy, R.O. 63049
 Love, L.J.Cline.
 see Cline Love, L.J.
 +Love, W.F. 61290
 +Lovell, D. 61520
 +Loveluck, J.M. 62671
 +Lovey, E.C. 63293
 +Lovisetto, L. 60451
 Low, J.J. VI + 62232
 +Lowenstein, J.H. 62551
 +Lower, K. 63226
 +Lowndes, R. 60066
 Loyd, D.H. + 60950
 Lozhechnikov, O.B. 63191
 +Lozinskiy, M.E. 62832
 +Lozovik, Yu.E. 62354
 +Lozovik, Yu.E. 59984
 Lozoviy, Ya.B. 62274
 Lu, P.Y. + 60828
 +Lu Fen. 62363
 Lu Yu.
 see Yu Lu
 +Lubatti, H.J. 60077
 +Lubatti, H. 60074
 +Lubecka, M. 62749
 +Lubell, M.S. 60088
 +Lubenow, A.F. 64551
 Lubensky, T.C. 62098
 Lubitz, K. 63245
 +Lubnin, E.N. 63411
 +Lubonski, J. 63186
 +Lucas, J. 60585
 +Lucas, K. 62148
 +Lucci, A. 61809
 Luce, J.M. + 63872
 Lucht, R.P. + 60782
 Luckas, M. + 62148
 +Luckner, F. 64048
 +Ludlam, T. 60074
 +Ludwig, E.J. 60501
 +Luft, G. 63629
 Lugoviy, P.S. + 61431
 Lugovoi, V.N. 61225
 +Luhrsens, W. 59995
 +Luk, B. 60041
 +Luk, K.B. 60081
 +Luk, K.B. 60087
 Lukas, W. + 62117
 +Lukashenko, V.I. 60664
 Lukaszewski, M. 62872
 +Lukin, A.A. 62707
 +Luklinska, Z.H. 60405
 +Lukoshyus, I.P. 61244
 +Luk yanchuk, B.S. 63149
 +Luk yanchuk, B.S. 63553
 +Luk yanchuk, B.S. 63573
 +Luk yanchuk, B.S. 59862
 +Luk yanchuk, N.G. 61903
 Lukanov, S.I. + 60694
 +Luk yanova, L.N. 62324
 +Luk yanova, V.I. 63620
 +Lull, G. 63704
 Lunardini, V.J. 61377
 Lundberg, B. 60081
 +Lundberg, B. 60041
 +Lundberg, B. 60087
 +Lundby, A. 60066
 Lundqvist, B.I. + 62246
 +Lundqvist, B.I. 62231
 Lunec, J. 63794
 +Lungershausen, T. 61223
 +Lunt, S. 60473
 +Lunt, S. 63576
 +Lupin, V.A. 61430
 Luppi, J. + 60904
 Luque, A. + 63648
 +Lush, G.J. 60066
 +Luton, J.N. 60429
 +Lutskii, V.N. 62515
 +Lutz, P.J. 63164
 +Lutze, W. 60285
 Luud, L.S. + 64489
 Lux, F. + 60737
 Ly Dang Phuoc
 see Dang Phuoc Ly
 +Lyadskaya, G.A. 63344
 +Lyakhov, N.Z. 63221
 +Lyakhova, M.B. 62707
 +Lyalina, N.M. 61829
 +Lyaly, V. 60368
 +Lyapin, A.I. 61944
 +Lyass, F.M. 63899
 Lyberis, N. + 64105
 +Lynch, A.C. 59796
 +Lynch, J.F. 62114
 +Lynch, V.E. 61693
 Lynden-Bell, R.M. + 62039
 Lynds, L. + 61020
 Lynn, J.W. + 62635
 +Lynn, K.G. 62239
 +Lyov, J.P. 61635
 +Lysenko, M.G. 62811
 +Lyskovich, A.B. 62427
 +Lytle, F.W. 60287
 +Lytle, F.W. 63081
 +Lyubasheskaya, T.L. 63665
 Lyubimov, V.N. + 62024
 Lyubushkin, V.A. + 63618
 +Lyubushkina, L.M. 63618
 +Lyus, M.L. 60838
 Lyuttsau, V.G. + 63367
 +Lyutyi, E.M. 63333
 McCarthy, I.E. + 60984
 McCarthy, M.F. + 61413
 +McCarthy, R.J. 60179
 +Macciotta, G. 64103
 +McClellan, M.R. + 63097
 +McClelland, R.W. 63172
 +McCliment, E. 60083
 +McCliment, E. 60042
 +McCliment, E. 60070
 McClintock, F.A. + 61912
 +McClure, D.S. 63022
 +McClymont, A.N. 64430
 McConnell, K.G. + 59767
 +McCorkle, D.L. 61713
 +McCown, A.W. + 60873
 +McCubbin, N.A. 60074
 McCutcheon, S. 64131
 +McDaniel, D.R. 63825
 +McDaniel, F.D. 60935
 +McDaniel, F.D. 60938
 +McDermid, I.S. 60775
 +McDonald, A.B. 59936
 Macdonald, D.D. + 60248
 +McDonald, F.B. 64336
 +McDonald, I.R. 62039
 +McDonald, J.D. 62083
 +McDonnell, M.J. 63919
 +Macdowell, A.A. 60839
 +Macdowell, C.A. 62823
 McElhinny, M.W. (ed.)
 59544
 McEwen, J.A. + 63994
 MacEwen, S.R. + 63472
 +McFall, W.D. 62393
 +McFarlane, R.A. + 61183
 McFee, R. 61589
 +McFeely, F.R. 63097
 McGary, M.C. + 61362
 McGee, T.J. + 60821
 +McGill, G.E. 64112
 +McGlynn, S.P. 61209
 McGraw, R. + 63602
 MacGregor, K.B. + 64452
 +McGrew, V. 61397
 +McGrew, J.B. 60110
 McGuire, J.H. 60970
 Machac, J. 61154
 +Macharashvili, G.G. 60086
 Machta, J. 59689
 McHugh, S. + 60359
 +Maciel, G.E. 59809
 +McIlrath, T.J. 60821
 +McIlwain, A. 60559
 McIlwain, J.T. 63833
 +McInally, I.D. 63691
 +McKay, R.A. 61030
 +McKay, W.W. 60049
 +McKee, J.S.C. 60559
 McKee, S.G. + 62062
 +McKee, S.P. 63852
 +McKellar, B.H.J. 60166
 +McKenzie, C.D. 63613
 +Mackenzie, J.D. 62147
 +Mackenzie, R. 60073
 McKeon, D.G.C. + 59971
 McKinley, I.G. + 60326
 +McKinley, I.G. 60328
 Mackowiak, M. + 62825
 +MacLachlan, J. 60083
 +MacLachlan, J. 60042
 +MacLachlan, J. 60070
 McLaren, A.C. + 61908
 +McLerran, L. 60025
 +McLerran, L. 59983
 +McMahan, A.K. + 62093
 +McMahan, M.A. 63527
 +McMullin, W.A. 61165
 McMurphy, H.F. + 63949
 McNamara, L.L. + 64298
 +Macovski, A. 63958
 +McPherron, R.L. 64319
 +MacQuenn, R.M. 64434
 +McRae, E.G. 63092
 +Macri, M. 60066
 Macris, C.J. + 64447
 MacRobert, A. 64570
 +MacRobert, A.J. 63541
 +Macropoulos, V. 63172
 +McTague, J.P. 62269
 +McVey, J.K. 60811
 +McVoy, K.W. 60161
 Mada, J. + 62758
 +Madden, R.P. 60509
 +Mader, H. 60773
 +Mader, R. 60099
 +Mader, R. 60179
 +Mader, T.E. 60509
 +Madi, A. 62312
 Madix, R.J. 63586
 +Madsen, V.A. 60130
 +Madsen, V.A. 60180
 +Madurga, V. 62583
 +Maeda, A. 62188
 +Maeda, A. 62189
 +Maeda, A. 62190
 +Maeda, H. 60468
 +Maeda, K. + 63627
 +Maeda, K.-I. + 64564
 +Maeda, O. 60468
 Maeder, A. 64467
 Maeder, A. 64479
 +Maehata, Y. 62746
 +Magat, L.M. 63287
 Magazzu, A. + 60650
 Magazzu, A. + 64468
 +Magee, C.W. 61937
 +Magennis, J.P. 62062
 Maggiore, C.J. + 63612
 +Maggs, M.N. 60073
 +Magione, E. 60098
 +Magnum, J.P. 60377
 +Magomedbekov, E. 61007
 Magro, C. Sanchez
 see Sanchez Magro, C.
 Mahajan, S. + 63805
 +Maher, J.V. 62118
 Mahishi, J.M. + 63388
 Mahmood, S. 60050
 +Mahoney, J. 60196
 +Mahoney, W.A. 64492
 Maidagan, J.M. + 60974
 +Maier, J.K. 63943
 +Maier, J.P. 60805
 Maier, K.H. + 60185
 Maier, W. + 62940
 +Maihara, T. 64535
 +Maikov, V.G. 63287
 +Maier, C. 59808
 Mainardi, F. 59598
 +Maiorov, N.I. 61566
 +Maissa, P. 62101
 Maiti, C.R. 61394
 Maitland, G.C. + 61596
 +Maix, R.C. 60444
 Majani, C. + 63238
 +Majani, C. 63237
 Majewski, W.A. 59855
 +Majling, J. 61888
 +Major, S. 63078
 Major, S.P. + 64376
 +Makalkova, N.A. 63483
 Makarov, N.A. 64282
 Makarov, Yu.N. 61625
 +Makarova, L.I. 62419
 +Makeev, M.V. 61959
 +Makhdomi, B.A. 64201
 Makhmudov, M.M. + 63265
 Makhutov, N.A. + 63360
 +Makhutov, N.A. + 63476
 +Makhutov, N.A. 63422
 +Maki, A. 60072
 +Maki, A. 60082
 +Maki, H. 61938
 Maki, K. + 63451
 +Makino, F. 64556
 +Makino, F. 64557
 +Makino, Y. 62784
 Makishima, K. + 64557
 +Makishima, K. 64556
 +Makita, T. 63292
 +Makita, Y. 62892
 +Maksimishin, M.D. 63429
 +Maksimov, A.B. 63407
 Maksimov, S.B. + 61430
 Maksimovich, G.G. + 63333
 Maksimovich, G.G. + 63457
 +Maksimovskii, S.N. 62298
 +Maksiova, L.V. 61430
 Maksymowicz, L.J. + 62749
 +Malaise, D. 64340
 +Malanotte Rizzoli, P. 59539
 Malbert, M. + 63127
 +Maldutis, E.K. 61244
 +Malet, J.C. 60376
 +Malet, J.C. 60377
 +Malet, J.C. 60383
 +Maletta, G. 63699
 Maley, P. 64423
 +Maleyran, R. 60548
 Malinov, L.S. + 63291
 +Malinskii, Yu.M. 61832
 +Maliek, J. 61088
 +Malley, M.M. 60798
 Mallow, J.V. + 59562
 +Malmhall, R. 62748
 +Malmvuo, J.A. 63997
 +Malnev, V.N. 60700
 Malou, P. + 62108
 +Malou, P. 62155
 Malov, V.V. + 61277
 Malozemoff, A.P. + 62640
 Malozemoff, A.P. + 62566
 +Malozovskii, Yu.M. 62422
 +Malthete, J. 61785
 Mal'tsev, I.M. 61256
 +Maltsev, Yu.P. 64323
 +Maltseva, O.A. 64321
 Malyarzh, E.M. + 60172
 +Malyshcheva, A.S. 63847
 +Malysheskiy, V.A. 63284
 Malyukov, B.A. + 62300
 +Malyutenko, V.K. 62422
 Mamedov, A.M. + 63015
 Mamedov, M.A. 64157
 +Mamedov, Sh.S. 63053
 +Mamin, B.P. 63899
 +Mamko, R.G. 61849
 Mamyana, A.L. + 61839
 Man, G.C.W. + 63882
 +Man, S.F.P. 63882
 Manara, A. + 60281
 +Manara, A. 61975
 +Manara, A. 61994
 +Manara, A. 61995
 +Manaud, J.-P. 61864
 +Mandelbrot, B.B. 62650
 Mandelstam, S.L. + 64347
 +Maneche, G. 60922
 +Manfrinetti, P. 63260
 Manfrodi, J. + 64393
 +Mangini, N.J. 63837
 Mani Lal.
 see Lal Mani
 Manicham, J. + 61643
 +Manley, O.P. 61473
 Manley, R.S. John
 see St. John Manley, R.
 +Mann, J.B. 60996
 +Mann, L.G. 60185
 +Mannelli, I. 60074
 Mano, H. 62604
 Manocha, A.S. + 63514
 +Manohar, A. 59981
 +Manson, J.R. 63116
 +Manson, S.T. 60937
 Mansure, A.J. + 63640
 +Mansuripur, M. 62759
 Mansurov, G.M. + 62916
 +Mantsch, H.H. 60716
 +Manuaba, A. 61936
 +Manuilov, M.V. 62228
 +Manwaring, J. 63783
 +Manykin, E.A. 62455
 +Manz, J. 63528
 +Manzo, M.A. 63656
 +Mao, C.-L. 60088
 +Mao Jinchang. 62484
 +Mao-Hsiung Chen. 62323
 Maouche, B. + 60591
 Maple, M.B. (ed.) 59553
 +Mar, A. 63577
 +Maradudin, A.A. 62234
 +Maradudin, A.A. 62226
 +Maradudin, A.A. 62235
 +Maranon, J. 59733
 +Marathe, V.R. 62557
 +Marcelja, S. 62879
 +Marcelja, S. 62880
 +March, N.H. 60962
 +March, N.H. 61757
 +March, R. 60081
 Marchal, A. + 60247
 +Marchal, G. 63416
 Marche, P.H.La.
 see La Marche, P.H.
 +Marchenko, I.M. 63223
 Marchenko, S.N. 62611
 Marchetti, M.C. + 61588
 +Marchik, I.I. 62706
 Marciano, W.J. + 59963
 Marconi, M.L. + 64428
 +Marcott, C. 60781
 +Marcus, J. 61884
 +Marcus, P. 59555
 +Marcus, R.A. 60848
 +Marder, T.E. 63483
 +Mardirosova, I.V. 63272
 +Marenikov, S.I. 59863
 +Marfaing, J. 61801
 Marfaing, Y. 59550
 Marfaing, Y. 63675
 Marfaing, Y. 63680
 Marfaing, Y. 63684
 Margerie, J. 61159
 +Marghita, D. 61447
 +Margolin, H. 63355
 +Margolin, H. 61927
 +Margolin, H. 63335
 +Margolych, I.F. 64438
 +Margrave, J.L. 60721
 +Marhoff, P. 63937
 +Mari, C.M. 63626
 Marichin, V.A. + 63351
 +Maricq, M. 60917
 Maricq, M.M. + 60911
 Marine, W. + 61801
 +Marinelli, M. 61961
 Marinerio, E.E. 59858
 Marinkovic, Z. + 62186
 +Marino, S.A. 63903
 +Marinos, C. + 62822
 Mariotti, J.M. + 64392
 Mariska, J.T. + 64429
 Mark, E.van.
 see van Mark, E.
 Mark-Markowitch, M. + 60413
 +Markin, V.G. 60337
 Markle, D.R. + 63803
 +Markou, A. 60074
 Markov, A.V. + 61926
 +Markov, V. 64241
 +Markovich, V.L. 61734
 +Markus, F.A. 61097
 Marletta, G. + 62320

- + Marletta, G. 61991
 + Marletta, G. 63567
 + Marlow, W.H. 63602
 + Marmet, P. 61004
 + Maron, Y. + 61063
 + Maroncelli, M. 60716
 + Maroni, V.A. 60725
 + Marowsky, G. 60738
 + Marples, J.A.C. 60280
 Marques, R. Ferreira
 + see Ferreira Marques, R.
 + Marriner, J. 60083
 + Marriner, J.P. + 60042
 + Marriner, J.P. 60070
 + Marsaglia, E.A. 62698
 + Marsh, H. 63250
 + Marsh, H. 63441
 + Marsh, W.R. 63594
 + Marshall, A.F. 61808
 + Marshall, F.J. 64557
 + Marshall, J.M. 62417
 + Marshall, R. 60031
 + Marshall, R. 60059
 + Marston, P.L. 61083
 + Martellini, M. 59657
 + Martenson, H. 62049
 + Martelot, J.-M. 64068
 + Marti, T. 60076
 + Marti-Lopez, L. 61090
 + Martikainen, H.O. + 61933
 + Marti, F. 61669
 + Martin, J.J. 62016
 + Martin, J.L. 61199
 + Martin, J.L. 63342
 + Martin, J.P. 60697
 + Martin, L. 64080
 + Martin, P. 61906
 + Martin, P. 60081
 + Martin, R.L. 60614
 + Martin, R.L. 61028
 + Martin, R.M. 62091
 + Martin, W.B. 63635
 + Martinelli, F. 59739
 + Martinelli, G. + 59927
 + Martinez, J.P. 59887
 + Martinez Roger, C. 64556
 + Martinez-Duart, J.M. 63670
 + Martinez-Mekler, G.C. 61029
 + see De Martinis, C.
 Martino, S. de
 + see de Martino, S.
 + Martinuzzi, S. 62456
 + Martoff, C.J. + 60208
 + Martone, R. 60449
 + Martinus, Z. 62443
 + Marty, A. 61016
 + Martynenko, A.F. 63409
 + Martynov, A.F. + 62780
 + Martynov, V.N. + 63846
 + Maruyama, T.N. 63163
 + Maruyama, T. 64556
 + Maruyama, Y. 60677
 + Marx, G. 60296
 + Maryasova, V.I. 63506
 + Masagutov, T.F. 64222
 + Masai, K. 64556
 + Masden, B.F. 61693
 + Mase, A. 61614
 + Mase, S. 59780
 + Mashchenko, V.E. + 63017
 + Mashkova, E.S. 62006
 + Mashovets, T.V. 61968
 + Masiello, P.J. 60342
 + Maslakov, G.V. 61313
 + Maslennikov, V.L. + 61306
 + Maslujk, V.A. 63197
 + Maslowe, S.A. 64169
 + Masoero, A. 62687
 + Mason, H.E. + 60637
 + Mason, H.E. 64365
 + Masri, Y. El
 + see El Masri, Y.
 + Masson, A. 59555
 + Massouh, S. + 61939
 + Masters, A.J. 59710
 + Masuda, K. 61953
 + Masuda, K. 60446
 + Masuda, S. 62263
 + Masumoto, T. 62565
 + Masumoto, T. 62701
 + Masuya, H. 62752
 + Matafonov, V.N. 60086
 + Matalon, M. + 61586
 + Mateescu, D. 61422
 + Mateev, V.K. 60703
 + Matera, R. + 60414
 + Matera, R. 60409
 + Mather, D.J. 60246
 + Mathews, G.J. 60510
 + Mathias, R.T. 63813
 + Mathieu, J. 61564
 + Matis, H.S. 60204
 + Matisov, B.G. 60666
 + Matkovskii, B.M. + 64226
 + Matre, K. + 64013
 + Matrosov, Yu.I. + 63312
 + Matsubara, F. 62591
 + Matsuda, A. 62496
 + Matsuda, S. 60453
 + Matsuda, T. 60553
 + Matsuhata, H. + 61799
 + Matsui, H. + 61981
 + Matsumoto, K. + 62082
 + Matsumoto, M. 61308
 + Matsumoto, S. + 61938
 + Matsumoto, T. 62711
 + Matsumura, H. 60031
 + Matsumura, H. 60059
 + Matsuo, Y. + 63292
 + Matsuo, M. + 60453
 + Matsuo, M. 62765
 + Matsuo, M. 60849
 + Matsuo, M. 64556
 + Matsuo, M. 64557
 + Matsuo, T. + 63058
 + Matsushita, S. 62737
 + Matsuta, K. 62818
 + Matsutera, H. 62776
 + Matsutera, H. 62756
 + Matsutera, H. + 62496
 + Matsura, M. + 62125
 + Matsuyama, M. + 62169
 + Matsuzaki, I. + 61775
 + Matsuzawa, H. + 60512
 + Matte, J.P. 61669
 + Matteson, J. 64386
 + Matteucci, G. + 59894
 + Matthews, C.G. + 63068
 + Matthews, R. 60533
 + Mattis, D.C. 59737
 + Mattison, E.M. 64390
 + Mattison, H. 63471
 + Matulenko, Yu.A. 60086
 + Matulenko, Yu.A. 60542
 + Maturana, G. + 59659
 + Matuszek, J.M. 60266
 + Matveenko, E.V. 61160
 + Matveev, A.N. 61247
 + Matveev, A.V. + 61249
 + Matygin, A.S. 64151
 + Matyushenko, L.A. 62586
 + Matzke, H. + 61990
 + Maurer, R.J. 60936
 + Maurer, W. 60430
 + Maurette, M. 60243
 + Maurette, M. 61997
 + Maunton, A.J. 63792
 + Mautz, J.R. + 61047
 + May, B. 63783
 + May, J.R. 60429
 + May, P. 60406
 + Mayer, F.J. + 60397
 + Mayer, M.J. 63853
 + Mayer, M.J. 63854
 + Mayer-Borricke, C. 60189
 + Mayer-Borricke, C. 60104
 + Mayerhofer, J. 63173
 + Mayes, T.W. 59564
 + Mayes, W.H. 61362
 + Mayhew, M. 60680
 + Maza, J. + 64495
 + Mazin, I.P. 64228
 + Mazo, R.M. 61059
 + Mazurak, L.P. 61423
 + Mazzega, P. 64146
 + Mazzetti, P. 62687
 + Mazzoldi, P. 61993
 + Mazzone, A. 63704
 + Mead, R.D. 60855
 + Meakin, P. 63008
 + Mebold, U. 64525
 + Mechkarski, S.N. 63826
 + Meder, M.R. + 60102
 + Medoff, B.P. + 63958
 + Medvedev, M.V. 62676
 + Medvedev, V.G. 59820
 + Medvedko, A.S. 60496
 + Meek, J.T. 60836
 + Meerschaut, A. 62405
 + Meeteren, A. van
 + see van Meeteren, A.
 + Megy, R. 62595
 + Mehan, R.L. 62184
 + Mehnert, W. 60054
 + Mehta, R. + 60935
 + Mehta, R. + 60938
 + Mei, C.C. 64040
 + Mei-quan Wu
 + see Wu Mei-quan
 + Meier, G. 62908
 + Meier, K. 60031
 + Meier, K. 60059
 + Meier, S. 63609
 + Meijer, A. 64104
 + Meinke, R. 60073
 + Meisel, M.W. 62203
 + Meisels, G.G. 63526
 + Meisels, G.G. 63572
 + Meissner, D. + 63734
 + Meitzner, G. + 63081
 + Meixner, C. 60527
 + Mejane, A. 60377
 + Mekhed, G.N. 63364
 + Mekhtiev, A.Sh. 62488
 + Melekhin, V.N. + 61726
 + Melekhova, T.F. 63221
 + Melentiev, L.A. (ed.) 59549
 + Melik-Adamyani, V.R. 63782
 + Meliksetian, A. + 60357
 + Melissinos, A.C. 60049
 + Melikadze, R.G. 62131
 + Melkumov, A.N. + 61814
 + Melkumova, E.Yu. 59644
 + Melkus, W. 60455
 + Mel'nikhenko, A.S. 61913
 + Mel'nik, B.A. 61771
 + Melnik, I.G. 61959
 + Melnik, N.N. 62044
 + Mel'nik, V.I. 63054
 + Mel'nikov, A.N. 64274
 + Mel'nikov, L.Yu. 61144
 + Melnikov, V.V. + 60994
 + Melroy, O.R. + 62143
 + Melton, B.F. + 59564
 + Melzer, H.-D. + 64130
 + Memming, R. 63734
 + Menakhin, L.P. 61724
 + Mencke, D. 61584
 + Mende, G. + 62489
 + Mendes, R. Vilela
 + see Vilela Mendes, R.
 + Mendis, D.A. 64428
 + Meneas, S. 62716
 + Menez Soares, D. 62291
 + Meng Jin-sheng + 64128
 + Meng Zhao-hui. 63893
 + Menrath, P. 60145
 + Menon, M.M. + 60528
 + Men'shikov, K.A. 59890
 + Menzheres, G. Ya. + 61828
 + Menzies, R.T. 61206
 + Mercier, J. 61884
 + Merer, A.J. 60719
 + Meretsky, P. 64003
 + Meriani, S. 61806
 + Meriani, S. 61807
 + Meriwether, J.W., Jr. 64281
 + Merkinishin, G.V. 59838
 + Merklin, J.F. 61593
 + Merkulov, V.A. 61409
 + Merkulov, V.S. 62947
 + Merli, P.G. 63704
 + Merlin, J. 62394
 + Merlin, J.-C. + 64427
 + Merlini, A.E. 60498
 + Merlini, D. 62668
 + Meron, M. 60507
 + Meron, M. 60934
 + Merritt, W.F. 63752
 + Mertens, R. 63681
 + Merts, A.L. 60996
 + Merzbacher, E. + 60146
 + Meschanin, A.P. 60086
 + Meshkov, E.E. 61573
 + Mesli, A. 63701
 + Messemmer, G. + 60438
 + Messemmer, G. 60447
 + Messier, J. 61226
 + Metastayer, M.D. 60049
 + Mestechkin, M.M. + 60590
 + Mestkovsky, S.G. 61250
 + Mestre, N. de
 + see De Mestre, N.
 + Metal', A.S. 61719
 + Metalli, P. 63902
 + Metayer, M.L. 60996
 + see Le Metayer, M.
 + Metelitsa, O.N. + 61060
 + Metras, F. 60758
 + Metreveli, M.D. 64530
 + Metsch, B.C. 60133
 + Metson, J.B. + 60279
 + Meuffels, P. 63738
 + Meunier, G. 61864
 + Meunier, S. + 61565
 + Meusemann, H. + 60408
 + Meyer, B. 63086
 + Meyer, C. 61134
 + Meyer, F. 60074
 + Meyer, G. 63631
 + Meyer, H. 59995
 + Meyer, H. 62204
 + Meyer, H.J. 59995
 + Meyer, K. 64064
 + Meyer, K.P. 62904
 + Meyer, M. 63607
 + Meyer, O. 59995
 + Meyer, P.P. 60632
 + Meyer, W.T. 60075
 + Mezei, F. 62634
 + Mezei, M. 61749
 + Mezey, G. 61936
 + Mich, D.A. 60920
 + Michael, H.R. 60374
 + Michaels, A. 64045
 + Michaels, H.B. 63906
 + Michailov, G.M. + 60845
 + Michailovits, L. + 62918
 + Michalopoulos, D.L. 61043
 + Michaud, G. + 64461
 + Michel, D. + 62835
 + Michel, J.A. + 61639
 + Micheli, M. De
 + see De Micheli, M.
 + Michelsen, N. 61347
 + Michelsen, U. 59995
 + Michi, J. 60799
 + Micocci, G. + 62424
 + Middleton, R. 60139
 + Midukov, V.Z. + 63190
 + Miedema, A.R. 63581
 + Miekeley, N. + 63751
 + Miekeley, N. 60319
 + Migliuolo, S. 64317
 + Migoni, R. 62165
 + Migus, A. 61199
 + Migus'kina, Z.A. 61313
 + Mihailescu, I. 62276
 + Miham, K. 61042
 + Mikaciani, A.L. 61117
 + Mikami, T. 64414
 + Mikhailov, G.V. + 62344
 + Mikhailov, V.Yu. 61200
 + Mikhailovskiy, A.B. 61663
 + Mikhailov, M.S. + 63346
 + Mikhailskii, S.N. 63223
 + Mikhitarian, V.M. + 61162
 + Mikhijev, V. 63252
 + Mikitishin, S.I. 63340
 + Mikkelsen, D.R. 60391
 + Miklave, A. 60925
 + Mikuchenis, V.F. + 62462
 + Milano, L. 64391
 + Milanovsky, E.E. 64115
 + Milazzo, M. 60941
 + Mildebrath, M. 60947
 + Miles, S.L. + 63100
 + Miley, G.K. 64552
 + Milic-Emili, J. 63991
 + Milic-Emili, J. 63879
 + Milkins, E.E. 63635
 + Millar, E.A. 63995
 + Miller, D.R. 63123
 + Miller, G.A. + 60005
 + Miller, G.A. 60004
 + Miller, G.E. 60821
 + Miller, H.E. 60429
 + Miller, H.G. + 60103
 + Miller, I.E. 62201
 + Miller, J.C. + 63522
 + Miller, J.P. 60208
 + Miller, J.P. 60043
 + Miller, K.J. 60015
 + Miller, M.W. 63894
 + Miller, P.D. 60935
 + Miller, R.D.C. 59953
 + Miller, R.E. 60924
 + Miller, R.H. 60088
 + Miller, T.A. 60801
 + Miller, T.A. 61217
 + Miller, W.F. 64270
 + Miller, W.H. 63528
 + Mills, D.L. 62261
 + Mills, D.M. 60500
 + Mills, H.E. 60031
 + Mills, H.E. 60059
 + Mills, R. + 62322
 + Mills, R.L. + 62066
 + Mills, W. 64079
 + Milne, W.I. 63697
 + Milora, S.L. 60473
 + Milosavljevic, M. + 62511
 + Milosevski, M.I. 63243
 + Milostene, C. 60533
 + Mil'vidskii, M.G. 63051
 + Mil'vidskii, M.G. 62301
 + Mil'vidskii, M.G. 62305
 + Milyutin, E.R. + 61091
 + Mimila Arroyo, J. 63679
 + Min Kim Jin
 + see Jin Min Kim
 + Minakova, E.I. 63899
 + Minamisono, T. + 62818
 + Minchinton, A. + 61001
 + Mindak, M. 61184
 + Minehart, R.C. 60213
 + Minenko, V.F. 63929
 + Minenko, V.F. + 63928
 + Mineva, V.A. 64489
 + Ming Zhong Wang 60048
 + Ming Zhong Wang + 59902
 + Ming-kun Cheng
 + see Cheng Ming-kun
 + Mingay, D.W. 60137
 + Minh Duc Tran
 + see Tran Minh Duc
 + Minh-Tho Nguyen 63511
 + Miniewicz, A. + 59797
 + Min'kov, A.V. 62050
 + Minogin, V.G. 60660
 + Minogin, V.G. 60661
 + Minota, T. 61517
 + Minowa, M. 60031
 + Minowa, M. 60059
 + Mints, I.I. 63288
 + Minyaev, O.A. 61682
 + Minyaev, O.A. 61710
 + Minyaev, O.A. 61687
 + Minyaev, V.N. 61709
 + Mirabal, M. 62296
 + Mirabel, P. 62056
 + Miranda, R.M. 62213
 + Miransky, V.A. 59925
 + Miransky, V.A. 59988
 + Mirin, D.N. 63040
 + Mirochnick, A.G. 63050
 + Mironov, A.V. + 61205
 + Mironov, S.L. 61035
 + Mirosevic-Anzulovic, M. 63228
 + Mirti, P. 60749
 + Mischanuch, B.G. + 61022
 + Mischel, M. + 63889
 + Mischke, R.E. 60206
 + Mischke, R.E. 59936
 + Miserey, F. + 63057
 + Missev, L. 60895
 + Mishchenko, A.P. 63583
 + Mishchenko, N.I. + 63799
 + Mishin, D.D. + 62707
 + Mishin, S.A. 61726
 + Mishkin, E.A. 61530
 + Mishra, P.C. 63517
 + Mishra, R.K. 63869
 + Mishra, S.N. + 62868
 + Mishra, U.C. 64176
 + Misiuk, A. 63188
 + Mischko, I.V. 63934
 + Misra, M. 62306
 + Misra, U.D. 60639
 + Misro, M.M. 63805
 + Misroli, G.F. 59894
 + Mistry, N.B. 60049
 + Mitaray, S. 62309
 + Mitchell, D.J. 62214
 + Mitchell, G.E. 60174
 + Mitchell, G.E. 61802
 + Mitchell, G.R. + 63122
 + Mitchell, H.G., Jr. + 64290
 + Mitchell, I.V. 60941
 + Mitin, A.V. 62867
 + Mitkin, R.B. + 59869
 + Mitra, J. 63866
 + Mitra, S. + 62557
 + Mitra, T.K. 62348
 + Mitrokhovich, N.N. + 63455
 + Mitsuda, K. 64557
 + Mitsuishi, N. + 61010
 + Mittemeijer, E.J. 63452
 + Mitzner, W. 64006
 + Miura, M. 62045
 + Miura, M. 61850
 + Miura, Y. + 62874
 + Miwa, H. 62605
 + Mix, M.C. 64245
 + Miyagi, M. + 61269
 + Miyaji, K. 59770
 + Miyake, O. + 60378
 + Miyako, Y. 62630
 + Miyama, T. + 62792
 + Miyama, T. 62795
 + Miyamoto, K. 63723
 + Miyamoto, N. + 62661
 + Miyamoto, S. 64346
 + Miyamoto, S. 64556
 + Miyamoto, S. 64557
 + Miyamura, S. 64062
 + Miyashita, S. 60072
 + Miyashita, S. 60082
 + Miyata, H. 60072
 + Miyata, H. 60082
 + Miyata, M. 61538
 + Miyatake, H. 60504
 + Miyachi, T. 62891
 + Miyazaki, K. + 60770
 + Miyazaki, M. 61811
 + Miyazaki, M. 62744
 + Miyazaki, T. + 62723
 + Miyazaki, T. 62697
 + Miyazaki, T. 62699
 + Miyazawa, S. + 59707
 + Mizoguchi, R. + 61352
 + Mizoguchi, T. 62722
 + Mizrahi, S.S. 60122
 + Mizuno, M. + 62403
 + Mizuno, T. 60248
 + Mizuno, Y. 63733
 + Mizuta, M. 63166
 + Mizuta, M. 62906
 + Mizutani, U. 62125
 + Mizutani, U. 62514
 + Mjaskinova, L.P. 63351
 + Mjohls, U. 61638
 + Mjornmark, U. 60074
 + Mkhitarian, V.M. + 59847
 + Mkrtchyan, V.S. 61887
 + Mnatsakanyan, P.S. 60544
 + Mobed, N. + 60162
 + Mobius, K. 60748
 + Mochinaga, J. 60954
 + Mochizuki, O. 60468
 + Mochizuki, T. + 60398
 + Mockler, M. + 63047
 + Mocnik, I. 63248
 + Modelli, A. 60981
 + Modest, M.F. + 61390
 + Modis, T. 60068

- + Moeller, J.A. 60528
 + Moerl, L. 62972
 Moffat, A.F.J. + 64511
 + Moffet, A.T. 64555
 Mogi, K. 64240
 + Mohamed Ismail, P.M. 64212
 Mohan, L.R. Ram
 see Ram Mohan, L.R.
 Mohan, V.K. + 61515
 Mohanakumar, K. + 64195
 + Mohanty, R. 61209
 Mohapatra, R.N. + 59970
 Moharam, M.G. + 61072
 Mohr, D. 64389
 Mohr, P. 64094
 Moi, L. + 61121
 + Moi, L. 61122
 + Moinester, M.A. 60204
 + Moiseev, V.N. 63457
 + Moissa, E.G. 61828
 Moity, J. 60648
 Moizhes, B.Ya. + 62482
 Mok Jae Won. *see* Won Mok Jae
 + Mokrushina, E.N. 59821
 Mol, C.De. *see* De Mol, C.
 + Molaro, P. 64472
 + Molchanov, O.A. 64321
 + Molchanov, V.A. 62006
 Molfino, P. + 60439
 Molina, A. 64284
 Molinari, A. 61414
 + Molinari, G. 60439
 + Moller, D. 64155
 + Moller, M. 63694
 + Moller, R. 60074
 + Mollrud, R. 60066
 + Molnar, P. 64078
 Molotskii, M.I. + 62371
 + Molzon, W. 60074
 Mom, V. 61825
 + Monceau, P. 62405
 + Moncrieff, D. 60840
 Mondal, A. + 63184
 Mondal, A. + 63181
 Mondrus, I.N. 60486
 + Moneti, G.C. 60049
 + Monich, E.A. 60542
 + Monin, Yu.I. 60514
 + Monnerie, L. 63048
 + Monod, P. 62803
 Monson, P.A. + 61758
 + Montano, P.A. 60774
 Montes, C. 61654
 Montgomery, D. 61489
 Montixi, G. + 61585
 Montmitonnet, P. + 61970
 + Montroll, E.W. 59686
 + Montroll, E.W. 59706
 + Monzul', G.D. 63964
 Moo Han Kim + 60242
 Mooley, D.A. + 64212
 Moon, J.E. 63730
 Moon Ki Chung + 60353
 Moons, F. + 60415
 + Moore, C. 61040
 + Moore, C.F. 60202
 + Moore, D.G. 64139
 + Moore, D.T. 61255
 + Moore, G.F. + 64139
 + Moore, G.F. 64135
 + Moore, R.S. 60213
 + Mora, P. 61653
 Moral, A.Del. *see* Del Moral, A.
 + Morales, A. 60145
 + Morales, J. 60145
 + Morato, L. 59633
 + Moravcsik, M.J. 60092
 + Morawski, H. 61049
 + Moreau, V.P. 62115
 + Moreau, D. 60454
 + Moreira, J.M. 62401
 + Morel, D.L. 63688
 + Moreno, G. 64313
 + Morettini, L. 63661
 Morgan, J.R. + 63035
 Morgan, K. + 60754
 Morgan, M.J. + 63852
 + Morgan, P.J. 64265
 Morgan, W.L. + 60982
 + Morgan-Pond, C. 62804
 Morgenstern, I. 62647
 + Morgulis, L.M. 61926
 + Morgunova, N.N. 63406
 + Mori, K. 63166
 Mori, M. + 59780
 + Mori, S. 60072
 + Mori, S. 60082
 Mori, T. + 62017
 Mori, T. + 63299
 + Mori, T. 61909
 + Mori, T. 63306
 + Moriarty, J.A. 62093
 Morigaki, K. 62837
 + Morimoto, K. 60088
 Morin, P. + 62622
 + Morin, P. 62645
 + Morin, R.L. 63974
 + Morinaka, A. 61092
 + Moreneau, R. 62416
 + Morishima, I. 60834
 + Morishita, E. 61385
 + Morishita, I. 62806
 + Morita, S. 60910
 + Morita, S. 60109
 + Morita, T. 62659
 + Moriawaki, Y. 63739
 + Moriyama, K. 60461
 + Moriyasu, K. 60077
 + Morjan, I. 62276
 + Mork-Morkenstein, P. 60350
 + Mornacchi, G. 60075
 Moro, G. + 61743
 + Morokuma, K. 60926
 + Moron, J.W. 62181
 + Moronesi, M. 60369
 + Moroni, A. 60532
 Morozhenko, N.N. 64444
 Morozhenko, N.N. + 64441
 + Morozov, B.I. 63222
 Morozov, N.V. + 61111
 Morozov, V.A. + 60880
 Morozova, N.K. 63016
 + Morris, C.E. 63819
 + Morris, C.L. 60202
 + Morris, C.S. 64427
 + Morrish, A.H. + 62717
 + Morrish, A.H. 62856
 + Morrish, A.H. 62584
 + Morrish, A.H. 62858
 + Morrison, D.R.O. 60033
 + Morrison, G.R. 62702
 Morrison, H. + 60784
 + Morrow, F. 60049
 Morse, M.D. + 60915
 Mortelmans, L.A.A. + 63939
 Morup, S. + 62857
 + Morup, S. 62731
 + Moruzzi, V.L. 62566
 Morvan, D. + 63153
 + Moscowitz, A. 60781
 + Moscovy, A.J. 63037
 + Moser, H. 63023
 + Moser, J. 62848
 + Moser, P. 62026
 + Moser, U. 60076
 + Moser, U.F. 60088
 Moses, H.E. 59627
 + Mosher, R.A. 62956
 + Moskala, E.J. 62999
 + Moskalova, M.A. 63072
 + Moskovits, M. 60728
 + Moskowitz, P.D. 63753
 + Moslehi, B. 61294
 + Moss, B. + 61816
 + Moss, B. 61823
 Moss, I.R. + 63792
 + Moss, R.E. 60618
 Moszner, N. + 63548
 + Motamed Ektebbi, A. 60503
 + Motaweh, H.A. 63125
 Motegi, H. + 62875
 Motizuki, K. + 62624
 + Motizuki, K. 62619
 + Motorin, V.I. 62065
 + Motoyoshi, K. 63672
 + Motril, N.Ya. 63968
 + Mouli, J.C. 62029
 Mountfield, K.R. + 62395
 + Moussa, F. 61782
 Movaghar, B. + 59690
 + Mozelev, A.A. 60484
 + Mozgova, N.N. 62462
 + Mozhaiskaya, V.S. 61248
 + Mozin, I.V. 61709
 + Mozin, I.V. 61711
 Mrozowski, C.L. + 64136
 + Mschliel, G.E. 59814
 + Muchlinski, A. 63793
 + Muck, G. 63687
 Muckerman, J.T. + 60690
 Mudher, K.D. Singh
 see Singh Mudher, K.D.
 Mudholkar, V.M. + 61309
 + Muhlemann, P. 60068
 + Muhlenweg, U. 60323
 + Muhlestein, L.D. + 60380
 + Muhlestein, L.D. 60379
 + Muirhead, E.G. 60170
 + Mukai, S. 62166
 + Mukamel, D. 62665
 + Mukanova, B.G. 64506
 + Mukerjee, A.K. 63347
 + Mukerji, J. 63380
 + Mukherjee, A. + 59930
 + Mukherjee, D. 63400
 + Mukherjee, H.M. 62326
 + Mukherjee, S.B. 60423
 + Mukhina, T.L. 64223
 Mukhopadhyay, S. + 62348
 Mukku, V.Reddy
 see Reddy Mukku, V.
 Mulder, C.A.M. + 62677
 + Mulkens, H. 60073
 + Mullani, N.A. 63935
 + Muller, A. 60949
 + Muller, C.H., III. 60798
 + Muller, D. 61195
 Muller, E. 61739
 Muller, E. 64266
 + Muller, E. 64130
 Muller, G. + 63687
 + Muller, G. 62218
 Muller, H. + 63596
 + Muller, H. 62471
 + Muller, H. 63446
 + Muller, H. 62473
 + Muller, H. 62474
 Muller, J. + 60629
 + Muller, J.B. 59897
 Muller, J.C. + 63701
 + Muller, J.C. 63706
 Muller, K. + 62446
 + Muller, K. 64166
 Muller, L. + 63798
 + Muller, L. 60076
 + Muller, R. 59840
 + Muller, R. 60294
 + Muller, Th. 60073
 + Muller, W.J. 64167
 Mulokozi, A.M. + 62124
 + Munarova, T.B. 63346
 + Munch, U. 62277
 + Mund, C. 63629
 + Munday, D.J. 60073
 Munier, A. + 64453
 + Munir, G. 60730
 + Munoz-Yague, A. 62308
 Munson, L.F. + 60365
 + Muntanyu, F.M. 62436
 + Muntz, E.P. 63944
 Muntzing, L.M. 60351
 Muradov, V.G. + 63621
 + Muradova, O.N. 63621
 + Murai, S. 63150
 + Murakami, H. 62156
 + Murakami, K. 59864
 + Murakami, T. 63393
 + Murakami, T. 64556
 + Murakami, T. 64557
 + Murakami, T. 60109
 + Murakami, T. 63399
 + Murali, N. 61365
 + Muramatsu, K. 62669
 + Muramoto, K. 61379
 + Muramoto, T. 61246
 + Murata, H. 62045
 + Murata, H. 61850
 + Murav'ev, A.I. 63461
 + Murav'ev, A.I. 63346
 + Murav'ev, A.V. 62174
 + Muromtsev, A.V. 62853
 Murota, T. 60013
 + Murphy, E.G. 60460
 + Murphy, P.G. 60031
 + Murphy, P.G. 60059
 Murphy, T. 59909
 Murray, A.M. + 60710
 Murray, C.A. 62266
 Murray, J.J. + 62250
 + Murrell, J.N. 60891
 Murrieta, H.S. + 62802
 Murso, H. + 60296
 Murthy, B.V. Krishna
 see Krishna Murthy, B.V.
 + Murthy, K.S. 62134
 Murthy, N.S. + 59826
 Murthy, S.Narasimha
 see Narasimha Murthy, S.
 Murty, K.L. + 61984
 Mushailov, E.S. + 62833
 + Musher, S.L. 62065
 + Musho, M.K. 59685
 + Musilova, J. 62930
 Musil, K. + 60649
 + Mustaev, P.T. 62501
 + Mustafa, M. 61596
 Muthukumar, M. 59700
 + Mutoh, H. 62733
 + Mutoh, T. 61698
 Muzhevika, A.S. + 63483
 + Muzinich, I.J. 59963
 + Muzzio, J.C. 64534
 + Myashita, S. 60088
 + Myatt, G. 60033
 Myers, S.M. 60390
 + Myhra, S. 60277
 + Myhra, S. 61982
 + Myrheim, J. 60066
 + Myrtle, K.G. 62809
 + Mys'kiv, M.G. 61902
 + Mysnik, A.I. 60086
 Mytsyk, B.G. + 62899
 + Nachinov, V.A. 62764
 Nagai, H. + 62815
 Nagai, K. + 61368
 + Nagai, M. 60236
 + Nagai, M. 60446
 + Nagakura, M. 62704
 + Nagamine, K. 62627
 + Nagano, H. 62527
 + Nagaoka, M. 59726
 + Nagaraj, V.T. 61438
 + Nagarajan, M.A. 60194
 Nagarathna, H.M. + 60774
 + Nagasawa, A. 63292
 + Nagase, F. 64556
 + Nagase, F. 64557
 Nagase, Y. + 62069
 Nagashima, K. 60329
 Nagasubramanian, G. + 62493
 + Nagata, S. 62862
 Nagaya, K. 61433
 + Nagiev, A.B. 62411
 Nagle, D.E. + 59936
 + Nagle, F.J. 63876
 Nagler, S.E. + 62686
 + Nagpal, K.C. 62528
 Najdich, Yu.V. + 63217
 + Naidu, M.S. 61712
 + Naidu, P.R. 62029
 Naidyuk, Yu.G. + 62349
 + Naik, P.K. 59793
 + Naik, V.W. 60476
 + Nail, T. 60185
 + Nair, K.P.R. + 60779
 + Nair, P.V.N. + 64176
 + Nair, S. 60308
 + Nair, S.V. + 62168
 + Naito, A. 62823
 + Naito, F. 60553
 Naitoh, M. + 61440
 Najjar, Y.S.H. + 61393
 + Naka, M. 62431
 + Nakada, M. 62563
 + Nakada, T. 60075
 + Nakagami, T. 61149
 + Nakagawa, Z. 63231
 + Nakahara, M. 62140
 Nakahara, S. + 63438
 + Nakai, R. 63150
 Nakai, Y. + 63398
 + Nakai, Y. 63013
 + Nakajima, K. 63180
 Nakajima, M. + 63898
 + Nakajima, M. 63924
 + Nakamae, K. 62711
 + Nakamura, E. 62875
 Nakamura, H. + 62283
 + Nakamura, H. 63394
 Nakamura, I. + 61538
 + Nakamura, K. 62282
 + Nakamura, K. 63013
 + Nakamura, S. 63627
 Nakamura, T. + 62555
 + Nakamura, T. 60927
 + Nakamura, T. 62874
 + Nakamura, T. 62958
 + Nakamura, Y. 62283
 + Nakamura, Y. 62561
 + Nakamura, Y. 62741
 + Nakamura, Y. 61629
 + Nakane, M. 63744
 Nakanishi, H. + 59749
 Nakanishi, K. 62655
 + Nakanishi, K. 61747
 + Nakanishi, M. 62531
 + Nakano, I. 60072
 + Nakano, I. 60088
 + Nakano, I. 60082
 Nakano, K. 60116
 Nakano, N. + 61620
 Nakano, R. + 63160
 + Nakano, S. 63686
 Nakano, Y. 59717
 Nakano, Y. + 61549
 + Nakao, T. 62757
 + Nakashidze, G.A. 62497
 Nakatsuji, H. 60569
 Nakawaki, Y. 59977
 + Nakayama, T. 60461
 + Nakazawa, K. 62286
 + Nalbantyan, O.G. 61839
 Nam Anh Nguyen
 see Nguyen Nam Anh
 + Namazov, A.D. 62695
 Namba, S. + 63860
 + Namba, S. 59874
 Namsrai, Kh. + 59961
 Nan Huang. *see* Huang Nan
 + Nanai, L. 63149
 + Nanda, V.S. 62054
 Nandi, R.N. + 60711
 + Nandi, S. 59973
 + Nanis, L. 62142
 Nanopoulos, D.V. + 59663
 + Naou, M. 62765
 + Nappi, A. 60074
 Napravnik, J. + 60241
 + Narain, S. 59646
 + Narang, R.S. 63542
 Narasaki, N. + 62889
 Narasimha Murthy, S. + 61503
 + Narayan, J. 62429
 Narayana, M. + 62801
 Narayana, N.Venkata
 see Venkata Narayana, N.
 Nardulli, G. 59937
 Narita, S. + 63029
 + Narlikar, A.V. 62528
 Narlikar, J. 64571
 + Naroska, B. 60031
 + Naroska, B. 60059
 + Naruse, Y. 60394
 + Naruse, Y. 62164
 + Nasako, K. 63732
 Nascimento, M.A.C. 60600
 Nasibov, A.G. + 63330
 + Nasibov, A.S. 61163
 + Nasibov, A.S. 61114
 + Nason, P. 63673
 + Nasonov, N.N. 63079
 + Nassar, M. 61435
 Nasryov, K.A. + 60850
 + Natanzon, Ya.V. 62121
 + Nateprov, A.N. 62324
 + Nath, A.K. 61188
 + Nauenberg, M. 63896
 + Nauman, R.V. 61209
 + Naumov, N.Yu. 61726
 + Navaneth, G.N. 61361
 + Navarro, R. 62567
 + Navarro, R. 62592
 + Navarro, R. 62626
 + Navarro, R. 62594
 + Navarro, R. 62672
 Navneet + 62445
 Navratil, G.A. + 61640
 Nayatani, Y. + 63842
 Nayfeh, A.H. + 61435
 + Naylor, P.D. 63101
 Nazarathy, M. 59835
 + Nazareno, V.A. 60163
 Nazarov, E.A. + 64532
 + Nazarov, I.M. 63764
 + Nazaryan, E.Kh. 61968
 Naze Tjotta, J. + 61343
 Nazmy, M.Y. 63402
 Neagle, W. + 63593
 + Neb, D.K. 62041
 + Nebbia, G. 60532
 + Nechaev, Yu.S. 63263
 + Nedelec, O. 60930
 + Neel, P. 59818
 + Neelov, I.O. 64274
 + Neganov, A.B. 60086
 + Neira, R. 64320
 Neklyudov, I.M. + 61988
 + Neklyudova, O.V. 63573
 + Nellen, B. 60033
 + Nelson, D.D., Jr. 60888
 Nelson, D.R. 61789
 + Nelson, G.W. 63500
 Nelson, L.S. + 62077
 Nelson, R.M. + 63989
 + Nelson, R.S. 60280
 Nemashkii, B.A. + 60181
 + Nemchinskii, V.A. 61717
 + Nemchinskii, V.A. 62482
 Nemkovich, N.A. + 60825
 Nemoshkalenko, V.V. + 61849
 Nemoshkalenko, V.V. + 63085
 + Nenadovic, T.M. 62511
 + Nenner, I. 60852
 + Nepochatkh, Yu.V. 61367
 + Nepokoichitskii, G.A. 62779
 + Neratoom, B.V. 60381
 + Nerenberg, M.A. 61547
 Neretnieks, I. 60303
 + Neretnieks, I. 60300
 + Neretnieks, I. 60301
 + Neretnieks, I. 60299
 + Neretnieks, I. 60302
 + Neretnieks, I. 60298
 + Neri, F. 59985
 + Neronov, V.A. 63221
 + Nersisyan, A.A. 59916
 + Nesbitt, H.W. 60279
 + Nesmelov, E.A. 62303
 + Netter, H. 62996
 Neuberger, J. + 62467
 Neufeld, H. 60032
 + Neukammer, J. 60623
 + Neumann, B. 59995
 + Neumann, L. 60241
 + Neumann, N. 59842
 + Neumann, W. 60129
 + Neuser, R. 64079
 + Nevolin, V.N. 61069
 + Newcomb, J. 60948
 + Newell, J.C. 63875
 + Newhouse, J.S. 59691
 + Newman, D.J. 62578
 Newman, J.S. 60364
 Newman, R.N. 60366

- Newmarch, J.D. 59585
 Newmarch, J.D. 59611
 Newsum, J.M. + 62554
 + Newstein, M. 61124
 + Newton, J.M. 63427
 + Newton, M.D. 63530
 + Nevzal, J. 61272
 + Ngai, K.L. 59687
 Ngocow, Y.K. + 64006
 Ngoc Cam Hoang
 see Hoang Ngoc Cam
 Nguyen, D.H. + 60379
 N'Guyen, H. Tran
 see Tran N'Guyen, H.
 Nguyen, T.K. + 60454
 Nguyen Huu Tinh 61781
 + Nguyen Huu Tinh 61785
 Nguyen Minh-Tho
 see Minh-Tho Nguyen
 Nguyen Nam Anh + 60895
 + Nguyen Van Hieu 62929
 Nguyen van Khang 61399
 Ni Wei-Tou, see Wei-Tou Ni
 Niaz, M. + 64052
 Nicolai, N. T. 63786
 + Nicholas, T. 63375
 + Nicholas, T.E. 63880
 + Nichols, D.G. 60258
 Nicholson, D.R. 61647
 + Nicholson, G. 64556
 + Nicholson, J.R.S. 62691
 Nickles, P.-V. + 61223
 Nickles, R.J. + 63962
 + Nicklow, R.M. 62046
 Nicolai, A. 60452
 + Nicolai, H. 59664
 Nicolai, L.I. + 62165
 + Nicolaides, C.A. 60609
 + Nicolas, J. 61867
 + Nicoletti, F. 61993
 + Nidaev, E.V. 61959
 + Niehaus, A. 63503
 Nieke, H. 61071
 Nielsen, A. Nordkov
 see Nordkov Nielsen, A.
 + Nielsen, B.S. 60074
 + Nielsen, E. 64291
 + Nielsen, E. 64292
 + Nielsen, F. 63708
 Nielsen, M. + 62269
 Niesen, L. 62844
 + Niessen, A.K. 63581
 + Niewisch, J. 60078
 + Nigam, A.K. 64203
 + Nigam, K.D.P. 61474
 + Nigam, K.D.P. 61475
 + Nigam, K.M. 61474
 + Nimi, T. 61938
 + Nikiforova, E.V. 61449
 + Nikishin, A.V. 62305
 + Nikishov, N.A. 63328
 + Nikitin, A.S. 62303
 + Nikitin, L.P. 63040
 Nikitin, V.I. 63494
 + Nikitin, Yu.P. 60011
 + Nikitina, G.A. 61189
 + Nikogossyan, V.R. 61162
 + Nikolaenko, V. 60533
 + Nikolaev, G.N. 61138
 + Nikolaev, V.N. 61211
 + Nikolaeva, V.P. 61838
 Nikolaevskii, E.S. + 59915
 + Nikolaich, A.Ya. 60625
 + Nikolaev, A.A. 60514
 Nikora, V.I. 64156
 + Nikotin, O.P. 60539
 + Nikulin, Yu.A. 62369
 + Nilsson, A. 60074
 + Nilsson, B.E.W. 59923
 Ning Du, see Du Ning
 + Nipoti, R. 63704
 + Nirmal Singh 60131
 Nisbet, J.S. + 64278
 + Nischik, H. 63655
 + Nishi, K. 63451
 Nishibayashi, S. + 63397
 + Nishida, N. 62874
 + Nishihara, H. 61315
 + Nishihara, H. 62625
 + Nishihara, Y. 61811
 + Nishihara, Y. 62744
 Nishijima, M. + 62263
 Nishikawa, M. + 64017
 Nishikawa, M. + 60240
 + Nishikawa, O. 63299
 + Nishikawa, T. 63495
 Nishimura, H. 60490
 + Nishimura, K. 63685
 Nishimura, S. 61424
 Nishimura, S. 61448
 + Nishina, K. 60336
 + Nishinaga, T. 62410
 + Nishino, Y. 62927
 Nishioka, H. + 60167
 Nishioka, M. 59650
 Nishiyaki, T. 63154
 + Nishiyaki, H. 63686
 + Nishiyama, K. 62627
 Nishiyama, S. 60123
 + Nishiyama, S. 62889
 Nishizaki, T. + 63723
 + Nishizawa, A. 61614
 Nishizawa, J. + 62292
 Nisitani, H. + 63396
 + Nitsche, R. 63171
 + Nitschke, C. 62479
 + Nitta, T. 63058
 + Nitti, L. 60061
 + Nitti, L. 60071
 Nitzan, A. + 59681
 + Nitzan, A. 62150
 + Nitzan, A. 62971
 Niwa, Y. 59601
 Nizamuddin, S. + 64201
 + Nizkoulos, V.B. 60499
 + Nizzoli, F. 63098
 + Nobili, L. 64544
 + Noda, T. 61042
 + Noens, J.-C. 64435
 Nogues, J.L. 60273
 + Nogues, M. 62633
 Noid, D.W. + 60848
 + Noid, D.W. 60690
 + Noid, D.W. 60886
 + Nojiri, Y. 62818
 + Nolle, E.L. 62298
 + Nolte, G. 59897
 + Nolte, G. 60965
 + Nolte, M. 60129
 + Nollting, F. 63504
 Nomura, A. + 61141
 Nomura, K. + 63722
 Nomura, N. + 62520
 Nonnenmacher, T.F. +
 59618
 + Nordberg, E. 60049
 + Nordby, P.L. 61743
 + Nordlander, P. 62246
 + Nordkov Nielsen, A.
 60474
 + Norem, J. 60081
 Norfolk, D.J. + 63579
 Norman, E.B. + 60140
 Norren, D.van
 see van Norren, D.
 + Norskov, J.K. 62246
 + North, A.M. 63031
 + Northrup, C.J.M. 60282
 + Northrup, C.J.M. 60284
 Nortmann, R. + 64057
 + Nortmann, R. 64060
 + Nose, H. 62294
 Nose, S. + 62092
 Noskova, T.N. 59873
 + Nosov, A.A. 61841
 Nossal, R. 63816
 + Norkin, A.B. 63329
 Noto, K. + 59788
 + Novak, I. 60838
 + Novakovic, B. 63207
 Novgorodtsev, A.B. 61068
 Novik, V.K. + 62893
 + Novikov, A.A. 63014
 + Novikov, A.G. 61280
 + Novikov, M.A. 63003
 + Novikov, N.N. 63251
 + Novikov, V.A. 61261
 + Novikov, V.A. 62434
 + Novikova, T.S. 61527
 + Novokhatskii, V.V. 61243
 + Novomlinskii, L.A. 62095
 Novoselov, V.S. 64358
 + Novozhilov, V.E. 60540
 + Nowak, A. 60396
 + Nowakowski, W. 61110
 Nowik, I. 62845
 Nowinski, J.L. 61429
 + Nowogrocki, G. 61878
 + Noyan, C. 63432
 Nozaki, H. + 62558
 + Nozaki, M. 60031
 + Nozaki, M. 60059
 + Nozaki, T. 60031
 + Nozaki, T. 60059
 + Nozdrav, V.F. 62932
 + Nozuchi, H. 62891
 Nshanian, Y.S. + 61425
 + Nugent, B. 64310
 + Numata, T. 62946
 + Nunez-Lagos, R. 60145
 + Nunez-Regueiro, M.
 61395
 + Nunnemann, A. 60789
 + Nurani, A.P. 62633
 + Nurieva, K.M. 63015
 + Nurullaev, Y.G. 62442
 + Nurushev, S.B. 60086
 + Nurushev, S.B. 60542
 + Nuttall, H.E. 60308
 + Nuttall, H.E. 60327
 Nuttli, O.W. 64053
 + Nuttli, O.W. 64051
 + Nuyts, J. 59904
 + Nuzzo, R.G. 62979
 Nyberg, C. + 63095
 Nyden, M.R. 60579
 Nyden, M.R. + 60578
 Nyenhuis, J.A. + 62778
 + Nygaard, K.J. 61598
 + Nyilas, A. 60428
 + Nyilas, A. 60437
 Nylandsted Larsen, A. +
 63708
 + Nylandsted Larsen, A.
 60555
 + Nylund, K. 61980
 Nymán, L.-A. 64529
 Nystrom, B. + 63787
 + Obara, M. 61142
 Obata, T. + 59656
 + Oberti, A. 63673
 + O'Brien, E.V. 63588
 + O'Brien, F. 60043
 + Obukhov, A.E. 60761
 + Obynochyn, A.A. 63506
 + Ocheret, N.P. 63272
 + Ochsi, H.T. 62784
 + Ochs, H.T. III 64178
 O'Connell, J.K. + 60987
 + O'Connor, S. 60714
 O'Connor, S.J. + 63830
 Oda, M. 64383
 + Oda, M. 64556
 + Oda, M. 64557
 Oda, Y. + 62527
 + Odajima, A. 62105
 + Odaka, S. 60031
 + Odaka, S. 60059
 + Oddo, J.M. 60374
 Odekrick, B. + 63717
 + Odelius, H. 62170
 + Odian, A. 60073
 Oehme, K.-L. + 62828
 + Oelert, W. 60189
 + Oelert, W. 60104
 Oelke, W.C. + 59771
 Oelgart, G. + 61971
 + Oertel, H., Jr. 62218
 Oertel, W. + 62277
 Oeschler, H. F. 60212
 Oesterle, B. 61542
 + Oesterreicher, H. 62588
 + Oesterreicher, H. 62644
 + Oesterreicher, H. 63746
 Offenberger, A.A. + 61655
 + Offermann, D. 64341
 + Offermann, P. 60269
 + Offermann, P. 60283
 + Ogata, A. 60468
 + Ogawa, S. 61811
 + Ogawa, Y. 62313
 + Ogawara, Y. 64556
 + Ogawara, Y. 64557
 + Ogden, R.W. 61408
 + Oger, L. 59731
 + Ogg, M. 60049
 Ogita, H. + 63315
 Ogo, Y. + 62927
 + Ogo, Y. 63350
 + O'Grady, B.V. 63524
 O'Grady, K. + 62716
 Oguchi, T. + 62615
 + Oguchi, Y. 60453
 + Oguma, M. 60239
 + Ogura, I. 61129
 + Oguro, K. 63744
 Ogurtsov, I.Ya. + 60778
 + Oh, D.J. 61984
 + Oh, S. 60559
 + Ohara, Y. 60453
 + Ohashi, T. 64556
 + Ohashi, T. 64557
 Ohashi, Y. 63352
 Ohba, Y. + 62906
 + Oheda, H. 62496
 + Ohga, T. 60453
 + Ohira, H. 61412
 + Ohkawa, T. 64556
 Ohkoshi, M. + 62747
 + Ohkoshi, M. 62510
 + Ohkoshi, M. 62770
 Ohkubo, M. 60440
 + Ohkubo, M. 60556
 + Ohkubo, M. 60446
 + Ohkura, M. 62284
 + Ohmachi, R. 63743
 Ohmachi, Y. + 63154
 + Ohmichi, T. 62188
 + Ohmichi, T. 62189
 + Ohmichi, T. 62190
 Ohmori, Y. + 61237
 + Ohmura, T. 59883
 Ohnishi, K. + 59864
 + Ohnishi, M. 63686
 + Ohno, K. 62874
 + Ohno, N. 63013
 Ohsawa, M. F. 62990
 + Ohshima, T. 60553
 + Ohta, S. 62563
 + Ohta, T. 61485
 + Ohta, T. 62718
 + Ohtani, A. 62599
 Ohtsuka, Y. 61078
 + Ohtsuka, Y. 59833
 + Ohtsuki, H. 60453
 + Ohya, N. 61981
 + Ohya, Y. 61512
 Ohyama, T. 62420
 Oikawa, H. 62175
 Oja, T. 64457
 + Ojeda-Castaneda, J. 61052
 + Ojeda-Castaneda, J. 61076
 + Oka, R. 64556
 + Oka, T. 60772
 + Okabayashi, K. 63403
 + Okabe, M. 63306
 Okabe, Y. + 63447
 Okada, I. 63176
 + Okada, K. 60398
 + Okada, M. 61562
 + Okada, M. 61329
 Okada, T. + 63394
 Okada, Y. 61917
 + Okami, N. 64148
 Okamoto, H. 64374
 + Okamoto, H. 63685
 + Okamoto, I. 62431
 + Okamoto, I. 62699
 Okamoto, K. 62761
 + Okamoto, K. 62295
 + Okamoto, S. 62491
 + Okamura, A.T. 64101
 + Okamura, M. 62399
 Okamura, S. 63863
 Okamura, Y. + 62178
 + Okhotnikov, O.G. 61197
 Okiji, A. + 62550
 + Okiji, A. 62663
 + Okiji, A. 62123
 + Okinaka, Y. 63438
 + Okorochkov, A.I. 62924
 Oksanich, A.P. 61928
 + Okuda, H. 64556
 + Okuda, H. 61691
 + Okuda, M. 60997
 Okuda, T. + 62942
 Okuda, T. + 63182
 + Okuda, T. 62760
 + Okuda, T. 61270
 + Okuma, K. 62788
 Okuno, H. + 62509
 + Okuno, H. 60553
 + Okuno, T. 62496
 Okuri, Y. + 63350
 + Okushi, H. 62496
 + Okuzawa, T. 64297
 Okwamoto, Y. 59670
 Olabandji, S.O. + 60233
 Oldendorf, W.H. + 63947
 Olefiord, I. + 63471
 + Oleinik, G.S. 63220
 + Olekhovich, A.I. 61734
 Olekhovich, N.M. + 61734
 Olesen, S.P. + 63818
 Olinger, B. + 62094
 + Oliveira, C.G. 59654
 + Oliver, L. 59907
 Oliveri, S. + 61557
 Oliveri, E. + 62662
 + Ol'khovik, G.A. 63623
 Olofsson, G. 64523
 Olofsson, U. + 60320
 + Olofsson, U. 60322
 + Olofsson, U. 60313
 Olsen, J. + 60570
 + Olsen, J. 60575
 + Olsen, J.M. 59995
 + Olsen, L.H. 60074
 + Olsen, S.L. 60049
 Olson, J.V. + 64325
 Olson, R.E. 60976
 + Olsson, J. 60031
 + Olsson, J. 60059
 + Olsson, M.G. 60015
 + Olaszewski, E.W. 64476
 O'Mahony, J.R. 60403
 + O'Mahony, J.R. 60404
 + Omar, A.R. 60200
 + Omel'yanenko, I.F. 63409
 + Omote, Y. 62713
 + Onchi, M. 62263
 Ondrey, G. + 60860
 + O'Neal, M.L. 64257
 + Oneda, S. 60003
 + O'Neill, L.H. 60031
 + O'Neill, L.H. 60059
 Ong, N.P. + 62353
 + Ong, R.S.B. 64324
 + Onishi, K. 63395
 + Onishi, K. 62736
 + Ono, K. 63924
 + Ono, S. 63595
 + Ono, S. 63733
 + Ono, S. 63737
 + Ono, S. 63722
 + Onodera, A. 62599
 + Onodera, H. 62701
 + Onopko, D.E. 60745
 + Onuchin, A.P. 60535
 + Oomens, A.A.M. 60467
 + Ophel, T.R. 60200
 Opitz, C. + 62474
 + Opitz, C. 63596
 Oppenheim, R. + 60088
 + Oppenheim, U.P. 61206
 Oprysko, M.M. + 63527
 + Orbach, R. 62602
 + Ord, J.L. 63067
 + Ord, J.L. 63068
 O'Reilly, J.M. + 62956
 + Oren, Y. 60074
 + Oren, Y. 60533
 + Orera, V.M. 63063
 + Orestova, L.M. 63327
 + Orgeret, M. 63678
 + Orihara, H. 60109
 + Orito, S. 60031
 + Orito, S. 60059
 + Orlova, A.O. 61934
 + Orlova, T.V. 64440
 + Orlyukas, A.S. 62462
 + Ormont, A.B. 62287
 + Orosz, M. 63921
 + Orr, J.S. 63919
 Orrit, M. + 63033
 + Orrit, M. 63012
 + Orsal, E. 64386
 + Orszag, A. 61199
 + Orszag, S.A. 61519
 + Ortelli, G. 63661
 + Ortmann, J.A. 63907
 + Ortolani, S. 64490
 + Osada, M. 61981
 + Osadko, I.S. 63044
 Osaka, A. + 61813
 Osaka, T. + 62892
 + Osborn, M.K. 60808
 Osborne, A.R. (ed.) 59539
 + Osborne, J.L. 60140
 + Oshima, H. 59656
 + Oshima, K. 63595
 + Oshkaderov, S.P. 63324
 Osipenko, V.G. + 63460
 + Osiv, P.N. 61457
 Osmond, J.K. + 64259
 + Osokin, D.Ya. 62830
 Osten, H.-J. + 59806
 Oster, L. 64448
 + Osterfeld, F. 60180
 + Ostertag, C. 62170
 Ostreiko, V.N. + 62678
 + Ostroumenko, A.P. 61278
 + Ostrovskaya, G.V. 61963
 + Ostrovskaya, N.F. 63220
 + Ostrovskii, V.L. 60778
 + Ostrovskii, Yu.I. 61111
 + Osugi, J. 62140
 + Osumi, Y. 63744
 + Osumi, Y. 62718
 + Oswald, H. 60188
 Oswald, P. 61481
 + Osyka, E.I. 63223
 Ottaviani, G. 63334
 + Otten, D. 60923
 + Otterlund, I. 60075
 Ottinger, C. + 60961
 Ottinger, H.C. 59729
 Otto, A. + 62967
 + Otto, A. 62267
 Otto, P. + 63777
 + Otwinowski, S. 60078
 + Ou, S.-C.S. 64183
 + Oualid, J. 62456
 + Ouchi, Y. 61258
 + Oudar, J. 59555
 + Ovchinnikov, B.M. 63628
 + Ovchinnikov, I.V. 63564
 + Ovchinnik, A.E. 63064
 Overend, J. 62978
 + Overend, J. 60781
 + Overill, R.E. 60585
 + Overseeth, O. 60041
 + Overseeth, O.E. 60081
 + Overseeth, O.E. 60087
 Overstraeten, R. Van
 see Van Overstraeten, R.
 + Ovsyannikov, N.P. 61841
 + Ovsyannikov, M.I. 62302
 Owen, D.R.J. + 61416
 Owen, D.R.J. + 61417
 Owen, J.F. + 62985
 + Owen, J.F. 62955
 + Owens, A. 62859
 + Oxtton, J.A. 63108
 Ozaki, J. + 61015
 Ozawa, K. + 62752
 Ozer, M. 59968
 Ozgovic, W. + 63266
 Ozima, M. + 64092
 + Ozisik, M.N. 61541
 Ozkul, C. 61077
 + Ozolins, D.A. 60995

- + Pac, P.V. 59969
 + Pacaud, F. 60271
 Pacchierotti, F. + 63902
 Pace, M.D. + 60755
 + Pacifico, M. 60369
 Pack, R.T. 60881
 Packer, T.W. 64258
 Paczynski, B. 64558
 + Padezhnova, E.M. 63264
 + Paduio, J. 61868
 + Paetz gen. Schieck, H. 60188
 + Paetzold, R. 63505
 + Paetzold, R. 60737
 + Paganelli, C.V. 63814
 + Paganini, C. 60497
 Page, Y.Le. *see* Le Page, Y.
 + Pages, M. 61874
 + Pagnamenta, A. 63975
 + Pagni, P.J. 63555
 Pahuja, O.P. + 62054
 + Pais, S. 63809
 + Pajunen, P. 60904
 + Pak, G.T. 61197
 + Pak, N.K. 59929
 Pakhomov, P.M. + 61831
 + Pakhomova, N.E. 63477
 + Pakhomov, S.V. 64274
 + Pakulov, S.N. 62799
 Pal, P.K. 61511
 + Palacio, F. 62567
 + Palacio, F. 62594
 + Palacio, F. 62672
 + Palazotto, A.N. 63375
 Palec, G.L. *see* Le Palec, G.
 + Palenzona, A. 63260
 + Palenzona, A. 61857
 + Paletta, F. 63683
 Palewski, T. + 62609
 Palfalvi, I. 59758
 + Palffy, L. 61172
 Palinkas, J. + 60944
 + Palkin, V.Yu. 61601
 Palm, R.E. 60370
 + Palmadesso, P.J. 64290
 Palmer, A.W. + 59796
 + Palmer, D.A. 60088
 + Palmer, I.G. 63369
 Palmer, R. + 63647
 Palmour, H. III + 63233
 + Pambrun, C. 63048
 + Pambrun, R. 63234
 Panaccione, L. 60463
 + Panactov, V.P. 62768
 Panasyuk, V.V. + 63493
 + Panda, L. 60088
 + Pande, P.C. 63691
 + Pandey, G. 60784
 Pandey, J.D. + 62212
 Pandey, P.K. + 62969
 Pandey, S.N. + 59639
 + Pandiarajan, K. 60762
 + Pandya, D.K. 63078
 + Pandya, N.C. 62505
 Panella, M. 60464
 + Pania, V.S. 60535
 + Panissod, P. 62817
 + Pan'kevich, N.V. 61952
 + Pankov, E.D. 61260
 Panov, B.F. 61539
 + Panov, L.I. 62396
 Pansu, B. + 62083
 + Pant, D.D. 60786
 + Pantaleo, A. 60532
 + Pantel, K. 63655
 Pantelev, G.V. + 63073
 + Pantelev, V.A. 62174
 + Pantelev, V.S. 59828
 + Panteleo, A. 60187
 + Panter, M. 60075
 + Panvini, R.S. 60049
 + Panza, G.F. 64091
 Paola, R.A. De. *see* De Paola, R.A.
 + Papathanassopoulos, K. 63738
 Papathodorou, G.N. + 60725
 Papayan, G.V. + 63923
 + Pape, K.H. 59995
 Pape, R.de. *see* de Pape, R.
 Pappa, C.de. 62632
 + Pappas, M. 61425
 + Pappay, S.V. 63469
 Paradijs, J.van. *see* van Paradijs, J.
 + Parak, F. 63770
 Paramonov, V.F. 59680
 + Parashar, R.S. 62530
 + Parcell, E.W. 61127
 + Pardo, G. 63563
 + Pardo, P.R. 64295
 + Parenyuk, I.A. 61875
 + Parfenov, B.G. 63360
 + Parfenov, L.B. 60086
 + Parfenova, N.I. 63583
 + Parfenova, N.I. 62115
 + Parida, M.K. 59965
 + Paris, P.J. 61639
 + Paris, R.L. 64000
 + Parish, A.T. 59796
 + Park, R.E. 61155
 Park, S.C. + 63353
 + Parkanyi, T. 60343
 Parker, D.C. + 64412
 Parker, D.T. 59792
 Parker, F.L. 60262
 Parker, F.T. + 62588
 Parker, F.T. + 62644
 + Parker, R.J. 60585
 + Parkes, T. 61553
 + Parkhomchuk, V.V. 60496
 + Parkhurst, G. 60049
 Parkin, S.S.P. + 62698
 Parkinson, W.C. 63802
 + Parkinson, W.H. 60742
 + Parmenter, C.S. 60810
 + Parmenter, C.S. 60810
 + Parr, A.C. 60509
 + Parr, A.C. 60832
 + Parr, R.G. 60578
 Parrinello, M. + 62090
 + Parris, P.E. 62342
 + Parry, G.W. 60389
 + Parry, R.F. 60112
 + Partamyan, Kh.V. 61162
 + Partamyan, Kh.V. 59847
 + Parthasaradhi, K. 60936
 + Parthasarathy, G. 62161
 + Parthe, E. 61873
 + Pascual, P. 59999
 Pasechnik, S.V. + 64396
 + Pasechnik, S.V. 62932
 Pashchenko, V.P. + 63223
 + Pashinkin, A.S. 63139
 + Pasquale, G. 60369
 + Pass, R.P. 64129
 + Passi, J.N. 60060
 Pasturel, A. + 63580
 Pastusiak, W. 62380
 + Pasushenkov, A.G. 62707
 Paszti, F. 61936
 + Pataraya, A.D. 64503
 + Patau, J.-P. 63127
 + Pate, B.B. 63135
 Patel, A.R. + 62505
 + Patel, D.B. 64304
 + Patel, N.B. 62280
 + Pathak, K.N. 62351
 Pathak, L. + 61365
 + Pathak, P.P. 64201
 + Patil, D.D. 64306
 + Patterson, J. 64462
 + Paty, M. 60077
 Paul, J.M. + 63946
 Paul, P. + 60481
 Pauling, L. 60601
 Paulus, W. + 63834
 + Pauronov, M. 63564
 Pauthenet, R. 62556
 + Pautot, G. 64127
 + Pavicevic, M. 63252
 + Pavlenko, A.V. 61305
 + Pavlishin, I.V. 61220
 Pavlov, A.S. + 63932
 + Pavlov, G.G. 64518
 + Pavlov, S.A. 61336
 Pavlov, Yu.A. 62612
 + Pavlova, L.F. 63584
 + Pavlova-Grishina, N.S. 61901
 + Pavlovskii, A.I. 61725
 + Pavlovskii, D.A. 61277
 + Pavlovskii, V.K. 61312
 + Pavlychev, A.A. 60745
 + Pawlaczky, C. 62904
 + Pawlikowski, J.M. 62486
 Paxman, R.G. + 63959
 + Paxman, R.G. 61100
 + Payne, L.E. 61404
 Payne, M.C. + 62485
 Payne, S.A. + 63022
 Pazzderskii, V.A. 62936
 + Pazinich, L.M. 59799
 + Pearce, B.K. 60223
 + Pearce, G.F. 60031
 + Pearce, G.F. 60059
 + Pearman, G.I. 64189
 + Pearsall, N.M. 63691
 + Pearson, W.B. 61860
 + Pececi, R.D. 60022
 Pechenkin, V.A. 61960
 + Pechersky, D.M. 64035
 + Pecheux, J. 61510
 Pechukas, P. 59609
 + Pecora, R. 60726
 + Pecseli, H. 61636
 + Pecseli, H.L. 61637
 + Pecseli, H.L. 61635
 + Pednekar, S. 60248
 Pedrini, C. + 63032
 Pedziwiatr, A.T. + 61858
 Peemoeller, H. + 62824
 + Peercey, P.S. 61949
 + Peercey, P.S. 63617
 + Pegg, D.T. 59812
 + Pegg, D.T. 59817
 + Pegg, D.T. 60753
 + Pehl, R.H. 60536
 Peisakhson, I.V. + 61263
 Peiter, A. + 61467
 + Pejovnik, S. 63248
 + Pejovnik, S. (ed.) 59538
 + Pekkar, L.-O. 64517
 + Pelc, N.J. 63943
 + Pelek, L.N. 62460
 + Pelissier, J. 61977
 + Peliti, L. 62463
 + Pellat, R. 61653
 + Pellegri, P. 61172
 + Pellicoro, M. 60061
 + Pellicoro, M. 60071
 + Pellin, M.J. 60717
 + Pelling, R.M. 64431
 + Pells, G.P. 61973
 + Pells, G.P. 61974
 + Pelton, A.D. 63267
 Pel'tis, S.P. + 61444
 + Pelzbauer, Z. 63351
 Pelzer, N. + 60231
 + Pempinelli, F. 59624
 Pendley, R.D. + 60718
 + Pene, O. 59907
 + Pengelly, L.D. 63879
 + Penin, I.A. 62298
 Pen'kovskii, A.I. 59831
 + Penland, C. 61342
 + Penna Franca, E. 60319
 Pennington, M.R. 59992
 + Penrose, J. 60277
 + Pepin, H. 61669
 Peppmiller, P.L. + 60948
 + Pepper, M. 62477
 + Pepper, M. 62485
 Pequignot, D. + 64528
 Peralta-Fabi, R. + 61480
 Peracaci, R. + 59648
 + Perchaskii, V.K. 61859
 + Percheron-Guegan, A. 63580
 + Perchonok, R. 60049
 + Perdrix, M. 60956
 Perelygin, L.S. + 60892
 + Perervey, V.M. + 63462
 + Pereyra, R.A. 62088
 + Perez, J.F. 62662
 + Perfuno, A. 60414
 + Perillo, E. 60943
 Perino, S.C. + 62278
 + Perktold, K. 63868
 Perlt, H. 60079
 Perrie, W.T. + 64009
 + Perrier, J. 60068
 + Perrign, D.M. 63827
 + Perrign, J. 63827
 Perrin, C. + 61870
 + Perrin, D. 60085
 Perrot, F. + 62368
 Perry, B.N. + 61124
 Perry, J.W. + 60691
 Perryman, M.A.C. 64338
 Pershin, V.K. + 61797
 Persson, B.N.J. 62229
 Persson, B.N.J. 63111
 Persson, M. + 62231
 + Persson, M. 62246
 + Persson, O. 60316
 Perthuisot, V. + 64083
 Pesch, J.A. 59804
 Pessnelle, A. + 60956
 Pesquera, L. + 59714
 + Pessine, F.B.T. 60863
 + Pestrikov, D.V. 60496
 + Petch, J.R. 64152
 + Petel, M. 60546
 + Petermann, G. 63582
 + Peters, P.E. 60276
 Peters, P.J.M. + 61182
 + Petersen, A. 60031
 + Petersen, A. 60059
 + Petersen, J.S. 64138
 + Petersen, P. 60081
 + Petersen, P. 60087
 + Peterson, E.C. 63906
 Pethig, R. 63769
 + Pethrick, R.A. 63031
 Petit, J. + 63653
 + Petit, J.C. 60243
 + Petit, J.C. 61997
 Petkov, N.P. + 64349
 Peto, G. 63156
 + Petrenko, P.V. 63434
 Petrenko, V.F. + 62160
 Petric, B. + 63228
 + Petric, N. 63228
 + Petropoulos, J.H. 62183
 + Petrosyan, A.A. 62914
 + Petrosyan, P.G. 62487
 + Petrov, A.E. 62298
 + Petrov, K.I. 62157
 Petrov, M.P. + 63785
 + Petrov, N.N. 61725
 + Petrov, V.K. 59989
 + Petrov, V.V. 61978
 + Petrov, Yu.N. 62276
 Petrova, A.I. 60908
 + Petrova, E.M. 63197
 + Petrova, G.N. 64035
 + Petrovic, V. 63207
 + Petrovich, F. 60209
 + Petrovikh, Y. 60533
 + Petrovskii, V.N. 61213
 + Petrun'kin, V.Yu. 61305
 Petrushin, N.V. + 63366
 + Pettenkofer, C. 62267
 + Petter, W. 61877
 Pettersen, B.R. 64480
 + Pettersson, L. 63516
 Pettinger, B. + 62972
 + Pettitt, B.M. 61759
 Petukh, M.L. + 63622
 + Petukhov, A.V. 60652
 Petukhov, B.V. 62018
 + Petukhov, V.A. 63569
 Peturaud, P. + 60344
 + Peturaud, P. 60385
 + Petyukevich, V.V. 61280
 Petzow, G. + 63194
 + Petzow, G. 63211
 + Petzow, G. 63214
 Peyrou, C. 59567
 + Pfannes, H.-D. 62864
 + Pfeffer, D. 60017
 Pfeiler, M. + 63937
 Pfeuty, P.M. + 63546
 + Pfister, C.E. 59722
 + Pfisterer, F. 63700
 Pfeleiderer, H. + 63664
 + Pfeleiderer, H. 63694
 + Pham Hong Duong. 62347
 Phan Liem. *see* Liem Phan
 + Phillips, D. 60793
 + Phillips, D.S. 60235
 Phillips, R.T. 63070
 + Phillips, S.B. 59971
 + Phillips, W. 60043
 Philpott, M.R. + 62991
 Phuoc Ly Dang. *see* Dang Phuoc Ly
 + Piaceente, V. 62081
 Pian, J. + 59608
 + Pianarosa, P. 60663
 + Piasetzky, E. 60203
 + Platt, U. 60382
 Piazza, L.R. + 64295
 Piccioni, O. 59574
 + Piche, M. 61669
 + Pichola, W. 61184
 + Pichola, W. 61185
 + Pichugin, A.T. 63457
 Pickering, N.C. 61354
 + Pickett, G.R. 62201
 + Pickett-Heaps, J.D. 64010
 + Picraux, S.T. 61659
 + Piela, L. 62355
 + Piemontese, L. 60548
 + Piersanti, C. 62083
 + Pierazzini, G. 60074
 + Pigeolet, A. 62297
 + Pigeon, M. 60369
 + Pignataro, S. 62320
 + Pignataro, S. 63567
 + Pigoury, M. 63414
 Pijkeren, D.van. *see* van Pijkeren, D.
 Pikuz, S.A. + 60909
 + Pilkington, R.S. 60765
 + Pillai, P.K.C. 62445
 + Pillay, R.G. 62868
 Pillet, P. + 60673
 + Pilling, M.J. 60756
 + Pilling, M.J. 60822
 + Pillsticker, M. 60435
 + Piloyan, S.G. 61602
 Piltungrud, H.V. 63963
 Pilyankevich, A.N. + 63469
 + Pilyankevich, A.N. 63220
 Pilyankevich, E.A. + 61834
 + Pimenova, A.Z. 63359
 + Pimental, G.C. 63521
 + Pimentel, B.M. 60122
 Pinas, G.J. + 62235
 + Pinchuk, V.M. 62372
 + Pincus, P. 61764
 + Pines, A. 62814
 Ping Jiang. *see* Jiang Ping
 + Pini, M.G. 62569
 + Pinsky, B.G. 63892
 + Pinto, L.H. 63837
 + Pion, A. 60368
 Piotrowski, K. + 62684
 + Piotrowski, K. 62681
 Pipkin, F.M. + 59755
 + Pipkin, F.M. 60049
 + Piples, L. 60350
 Pipman, J. + 63950
 + Pireaux, J.J. 62265
 + Pireaux, J.J. 63096
 Pirich, R. + 64165
 + Pirogov, Yu.A. 61064
 Pirouz, P. + 61922
 + Pirozhkov, A.N. 60163
 + Pirronello, V. 63126
 + Pirronello, V. 60650
 + Pirronello, V. 64468
 Pisani, C. + 61907
 + Pisarev, V.V. 63749
 Pisent, G. 60148
 + Pisipati, V.G.K.M. 62097
 + Piskunov, A.K. 61722
 + Pitatlev, G.V. 60664
 Pitault, A. + 64478
 + Pitt, A.D. 63036
 + Pivovarov, L.N. 61266
 + Pizio, O.A. 61754
 + Pizio, O.A. 61745
 + Pizzo, V.J. 64452
 Pizzuto, A. 60441
 + Pla, C. 63941
 + Pla, M. 63941
 + Placci, A. 60548
 + Placidi, M. 60548
 + Planet, H. 63901
 + Platonov, N.S. 63569
 + Plattner, R. 63694
 + Plaut, R.H. 61426
 Pleshakov, V.F. 61733
 + Pleshakov, S.A. 61235
 Plesinger, A. + 64058
 + Plesko, S. 62822
 Plessis, P. + 61004
 + Plewinsky, B. 60296
 + Plews, M.J. 62961
 + Pliquet, F. 63804
 + Plo, C.A. 64168
 + Plo, M. 60145
 Ploc, R.A. 62219
 Ploeg, J.P.M.van der. *see* van der Ploeg
 + Ploem, J.S. 63920
 Ploshkin, V.V. + 63456
 + Plotnikov, A.E. 61959
 Plotnikov, A.I. + 61420
 + Plotnikov, M.A. 63085
 Plotnikov, V.S. + 59857
 + Plotzki, I. 63605
 + Plotzki, I. 62275
 Plumb, R.A. 64186
 + Plunkett, R. 60049
 Pluyko, V.A. + 60135
 Pluym, J.van der. *see* van der Pluym, J.
 Pnevmatikos, St. + 62036
 + Po Tso-hsiu. 60020
 Postranciou, A. + 59905
 Postrand, I. 62970
 Postrand, I. + 62267
 Podgaisskii, M.S. + 63407
 + Podgornov, A.A. 62228
 Podgorny, I.M. + 64411
 Podgorsak, E.B. + 63941
 + Podgorsak, E.B. 60545
 + Podgorski, R.P. 63897
 Podio-Guidugli, P. 61405
 + Podmoshenskii, I.V. 64216
 + Podolskii, V.N. 61601
 + Podsvirov, O.A. 62339
 + Podval'nykh, G.S. 63222
 + Poe, R.T. 63534
 Poeltl, D.E. + 60811
 + Pogarev, D.E. 62316
 + Pogge, R. 64556
 Pognante, U. 64082
 Pogosyan, A.R. + 62454
 + Pogson, S. 60559
 + Pohl, H.A. 63889
 + Pohlmann, B. 59690
 + Polirier, P. 59856
 + Pokhil, Yu.A. 63307
 Pokhmurskii, V.I. + 63465
 Pokleba, A.K. + 60651
 + Pokorny, J. 63839
 + Pokrovskii, A.N. 61891
 + Pokrovskii, V.A. 61022
 + Pokrovskii, Ya.E. 63042
 Pokrowsky, P. + 59852
 + Polato, P. 61993
 Poliakoff, E.D. + 60832
 + Polikarpov, S.S. 61194
 + Poling, R. 60049
 + Politiowicz, P.A. 59685
 + Polivanov, V.V. 61311
 Pollak, E. + 60630
 + Pollak, E. 63532
 + Pollanen, L. 61979
 Pollard, D.D. + 64101
 Pollard, H.F. 62023
 Pollock, W.J. + 63490
 + Polokhov, V.N. 63428
 Polovina, G.P. 63084
 + Poltavets, V.N. 60590
 + Polubotko, A.M. 62337
 + Poluektov, I.A. 62504
 Polyakov, A.A. + 62925
 + Polyakov, A.Ya. 61955
 + Polyakov, B.I. 60854
 + Polyakov, D.G. 63040
 + Polyakov, M.I. 61189
 + Polyakov, N.E. 63506
 + Polyakov, V.A. 63221
 + Polyakova, I.A. 62957
 + Polyakova, V.P. 63583
 + Polyanskaya, T.A. 62487

- Richards, P.G. + 64293
 + Richards, P.G. (ed.) 59541
 + Richards, R.H. 61576
 + Richards, P.L. 62966
 + Richards, P.L. 62984
 Richards, P.M. 59703
 Richards, R.W. 61821
 + Richards, R.W. 62068
 + Richardson, D. 60460
 Richardson, J.D. + 64417
 + Richardson, J.L. 61166
 + Richert, J. 59675
 + Richter, A. 60133
 Richter, D. 62047
 + Richter, G.J. 63629
 Richter, G.N. + 63721
 Richter, H. + 60269
 Richter, W. + 59800
 + Rickus, E. 62470
 + Rideau, G. 59629
 Ridener, F.L., Jr. + 60052
 + Rideout, M. 64079
 + Rideout, V.C. 63867
 Riebold, W.L. + 60350
 Riederer, S.J. + 63943
 + Riegler, G.R. 64492
 + Riera, J. 63647
 + Ries, G. 60428
 + Rieseberg, H. 60031
 + Rieseberg, H. 60059
 Riesenr, D. + 63774
 + Riestler, J.L. 60077
 + Riese, R.P. 59756
 Rietveld, M.T. + 64291
 Rigaut, J.P. + 64008
 + Rigby, D. 61032
 + Rigby, D. 61033
 + Riggi, F. 60187
 + Righetti, G.B. 60451
 + Rijndoudt, E. 60448
 Ripkema, J.J.M. + 61836
 + Rikalyuk, R.E. 64442
 Riklund, R. + 61034
 + Rimmer, A.B. 60055
 + Rinkondi, F. 60075
 + Rinkyavichyus, V.S. 62451
 Rinneberg, H. + 60623
 + Rioux, C. 60183
 Risbud, S.H. + 63274
 + Riski, K. 62846
 Risset, J.C. 59724
 Ristic, M.M. 63192
 + Ristic, M.M. 63252
 + Ristic, M.M. 63243
 + Ristic, M.M. 63207
 + Ristic, M.M. 63242
 + Ristic, M.M. (ed.) 59538
 + Ristic, R.I. 63142
 + Ristinen, R.A. 60106
 Ritchie, B.G. + 60213
 Ritby, M. + 59605
 + Ritter, R.C. 59755
 + Ritter, T. 60936
 + Ritter, T. 59938
 + Riva, F. 59938
 + Rivarola, R.D. 60974
 Riveiro, J.M. + 62582
 + Riveiro, G. 62582
 Rivin, G.S. + 64273
 Rizzetta, D.P. + 61522
 + Rizzo, A. 62424
 Rizzo, T.G. 60023
 Rizzoli, P. Malanotte
 + see Malanotte Rizzoli, P.
 Roadman, R.E. + 61482
 Robbins, E.I. 64095
 Robe, H. 64538
 Robert, J.L. + 62499
 Robert, M. 62211
 Roberts, B.L. + 60043
 + Roberts, J. 62142
 + Roberts, K.J. 63542
 Roberts, K.V. 61619
 + Roberts, T.M. 64005
 + Roberts, V.C. 63912
 + Robertson, B. 64008
 Robertson, D.S. + 64265
 + Robillard, L. 61507
 Robin, G. de Q. + 64155
 Robinson, I.K. 62221
 Robnik, M. + 64363
 + Rocard, F. 64375
 Rocheleau, R.E. + 63164
 + Rochester, C.H. 63593
 Rochester, G.D. 59570
 + Rock, D. 60077
 + Rock, J.W. 63442
 + Rockwell, D. 61484
 + Rod, R.L. 63689
 + Roddie, A.G. 60547
 Roddier, F. 64379
 Rodier, N. + 61862
 + Rodkiewicz, C.M. 61525
 + Rodnyi, P.A. 63043
 + Rodriguez, J.-F. 63279
 + Rodriguez, M.A. 59714
 + Rodriguez, S. 62033
 Rodriguez, V.D. + 63063
 Rodriguez Roldan, A.-M. + 61871
 Rodygin, L.V. + 61171
 Roe, K.K. + 64086
 + Roessel, F. 60315
 + Rogachev, V.I. 63222
 Rogacheva, N.N. 61446
 Roger, C. Martinez
 + see Martinez Roger, C.
 + Rogers, P.S.Z. 63612
 Rogers, R.R. + 64213
 + Rognien, T.D. 61617
 + Rogutskii, I.S. 61969
 Rohatgi-Mukherjee, K.K. + 63716
 + Rohlf, J. 60049
 + Rohrig, N. 63903
 + Rohsenow, W.M. 61376
 + Rohwer, K. 62805
 + Roiron, G. 60534
 + Rojo, J.A. 62567
 + Rojo, J.A. 62592
 + Rojo, J.A. 62626
 + Rokita, E. 63611
 Rokos, I.A. + 59837
 + Rokosova, L.A. 59837
 Roldan, A.-M. Rodriguez
 + see Rodriguez Roldan, A.-M.
 + Rolf, E.G. 64353
 + Roll, U. 62170
 + Romain, J.P. 62028
 Romalis, N.B. 61456
 + Roman, Th. 60442
 Romander, C.M. + 60361
 + Romanenko, Yu.V. 61722
 Romaniv, O.N. + 63421
 Romano, S. + 61848
 + Romanov, A.A. 63458
 + Romanov, E.S. 62870
 Romanov, G.S. + 61718
 + Romanov, O.M. 63425
 + Romanov, O.N. 64385
 + Romanov, Yu.F. 61264
 + Romanova, N.G. 61263
 Romanovskii, Yu.R. 61330
 + Romanyuk, N.A. 62899
 + Romelt, J. 63528
 + Romig, A.D., Jr. 62020
 Romo, W.J. 60160
 Ron, S. + 63532
 + Ronconi, F. 62608
 Ronfard-Haret, J.C. + 63566
 Rong Tang Ma
 + see Ma Rong Tang
 + Ronzhin, A.I. 60542
 + Ronzhin, A.I. 60541
 Roos, M.J.K. De
 + see De Roos, M.J.K.
 + Roos, P.G. 60213
 + Root, J. 63787
 Rosa, S. Goulart, Jr.
 + see Goulart Rosa, S., Jr.
 + Rosatelli, F. 60439
 Rosato, E. + 60943
 + Rosch, J. 64447
 Rose, G. + 63862
 Rose, K. 64163
 + Roseler, J. 62341
 Rosen, G. 59945
 Rosen, G. 60010
 + Rosen, J.F. 63948
 + Rosen, J.M. 64334
 + Rosen, S.L. 60354
 + Rosenberg, E.I. 60070
 + Rosenberg, I. 63973
 Rosenberg, L. 59635
 + Rosenberg, M. 63144
 Rosenberg, Z. + 62413
 + Rosenblum, S.S. 60208
 Rosenbrock, H.H. 63637
 Rosenbush, A.E. 64483
 + Rosenfeld, C. 60049
 + Rosenthal, Y. 60413
 Roseninge, T.T. von
 + see von Roseninge, T.T.
 + Roser, H.W. 60165
 Roshan, N.R. + 63583
 + Rosinberg, M.L. 61690
 + Rosino, L. 64490
 + Roslyakov, I.N. 63462
 Rospenik, M. + 60735
 + Ross, D.A. 60007
 Ross, D.K. 62526
 + Ross, D.K. 61009
 + Ross, J. 63498
 + Ross, R.T. 60533
 Ross-Murphy, S.B. + 63496
 + Rossat-Mignod, J. 62601
 + Rossat-Mignod, J. 62642
 + Rosselet, L. 60074
 + Rosselet, Ph. 60068
 + Rosset, R. 63603
 + Rossi, A. 59682
 Rossi, B. 59568
 + Rossi, C. 63786
 Rossi, D.J. + 63954
 Rossi, H.H. 63910
 + Rossi, H.H. 63903
 + Rossi, L. 60497
 + Rossi, L. 60066
 + Rossi, U. 61288
 + Rossky, P. 61759
 Rossler, K. + 63578
 Rossmanith, H.-P. 61428
 Rossmanith, H.-P. 61450
 + Rosso, E. 60074
 + Rost, A. 62895
 + Rost, M. 59995
 + Rostoker, N. 60494
 + Rostovtsev, V.S. 62371
 + Roszak, S. 60571
 + Roth, M. 62005
 Rothe, A. 59754
 + Rothe, K.W. 64243
 + Rothschild, M. 60862
 + Rothschild, M. 60874
 Rothschild, W.G. + 60684
 + Rots, A.H. 64551
 + Rottger, J. 64286
 + Roubaud, G. 60475
 + Roucau, C. 62405
 + Rouet, A. 59905
 + Rougeul, A. 63822
 Rouna Sun
 + see Sun Rouna
 + Rousseau, J. 60697
 + Routledge, I.A. 63440
 + Rouver, H. 64083
 + Rowe, D.M. 62191
 + Rowe, P. 60031
 + Rowe, P. 60059
 Rowlands, S. 63870
 Rowlinson, J.S. 62071
 Roy, A.K. + 62653
 + Roy, C.L. 62467
 + Roy, D.M. + 60310
 + Roy, P. 59930
 + Roy, R. 60183
 Roy, R.J. Le
 + see Le Roy, R.J.
 + Roy, S.K. 62653
 Roy, S.R. + 59646
 + Roy Choudhuri, S.K. 61406
 + Rozanov, N.N. 62916
 + Rozanov, V.B. 61672
 + Rozanov, V.V. 64271
 + Rozanski, K. 61198
 Rozendaal, H.C.F. + 63452
 + Rozenfeld, M. 63975
 Rozenman, G.I. + 63138
 + Rozet, J.-P. 60508
 + Rozhda, A.F. 62580
 + Rozhdvestenskaya, I.V. 61892
 Rozhkov, B.K. 59870
 Rozhkov, B.K. 61101
 + Rozhkov, V.V. 63079
 Rozhkoval, E.V. + 63425
 + Rozmus, W. 61655
 Ruan Tunan + 59912
 + Ruan Tunan. 59902
 + Rubakha, V.I. 63003
 Rubbo, M. + 63141
 Rubel, A. 61535
 Rubin, L. + 63999
 + Rubin, S.A. 63793
 + Rubinacci, G. 60449
 Rubio, F. + 63670
 + Rubio, J.O. 62802
 + Rubinsk, V.I. 60957
 + Rucinski, G. 60049
 + Rud, V.D. 63190
 + Rudakoff, G. 62828
 + Rudakoff, G. 63545
 + Rudakoff, G. 63608
 + Rudakoff, G. 63606
 + Rudd, J.M. 62809
 + Ruder, H. 64502
 Rudkovskaya, L.M. + 63273
 Rudman, P.S. + 61567
 + Rudoi, Yu.N. 62811
 + Rudolph, W. 60944
 Rudra, P. + 62610
 + Ruedl, E. 60409
 + Ruf, J.A. 60254
 + Rufener, F. 64485
 + Rufener, F. 64513
 + Ruff, G.A. 60929
 + Ruhs, N. 60465
 Ruibys, G. + 62440
 + Rukhadze, A.A. 61233
 + Rukman, G.I. 62402
 + Rumble, E. 60224
 + Rumyantsev, S.I. 63459
 + Rumynskaya, I.G. 60735
 + Rundquist, I. 64014
 + Runge, S. 60956
 Ruoff, P. + 63513
 Ruqi Han
 + see Han Ruqi
 + Rurukin, A.N. 61213
 + Rusanov, K.V. 61375
 + Rusandbrooke, J.G. 60073
 + Rushton, K.C. 60246
 Rusin, P.I. + 60256
 + Rusov, I.G. 63371
 + Rusov, V.A. 61201
 + Russell, C.T. 64313
 + Russell, C.T. 64312
 + Russell, G. 63691
 + Russell, J.A.G. 63824
 + Russell, J.W. 62986
 + Russell, L.M. 59779
 Russell, M.J. + 64110
 Russell, P.W. + 63838
 + Russell, T.W.F. 63164
 + Russo, A. 63902
 Russo, S. Lo
 + see Lo Russo, S.
 + Rustamov, S.R. 61200
 Ruter, R. + 64187
 + Ruzhnikov, V.A. 61707
 + Ryabchenko, S.M. 62831
 + Ryabov, G.A. 60499
 + Ryabov, S.E. 63574
 Ryabtsev, A.N. 60635
 + Ryabyshv, A.M. 63456
 + Ryan, M.T. 63971
 + Ryan, P.M. 60528
 + Ryan, T.L. 60429
 + Ryazantseva, V.M. 64218
 + Rybakov, Yu.L. 59889
 + Rybalko, V.F. 61988
 Ryberg, R. 63540
 Rybka, S.P. + 64402
 Rye, R.R. + 60853
 + Rykalin, V.I. 60542
 + Rykalyuk, R.E. 64438
 + Rykhlov, A.F. 61264
 + Rykov, A.A. 63558
 Ryppal, K. + 61635
 + Ryppal, K. 61638
 + Rysakov, V.M. 61055
 + Rytz, D. 62901
 + Ryzkin, B.S. 61156
 + Ryzhi, V.I. 61744
 Ryzhikov, V.D. + 60543
 Rzewski, K. + 60668
 Sa Ban-hao + 60063
 + Saarikko, H. 60033
 + Saarikko, H. 60073
 + Saarikko, T. 60073
 + Sachenko, V.P. 62338
 + Sachs, F. 63812
 Sacks, P.G. + 63894
 + Sadchikhin, A.V. 63762
 Sade, M. + 63293
 + Sadeghi, N. 60930
 Sadhu Singh 61468
 + Sadoff, A.J. 60049
 + Sadovskii, C.M. 60808
 Sadykhov, R.Z. + 62695
 + Sadykov, N.M. 61837
 Sadzhakov, S. + 64356
 Saegusa, N. + 62584
 Saegusa, N. + 62588
 + Saethre, L.J. 60629
 Saez-Puche, R. + 63538
 + Safinya, K.A. 60929
 + Safinya, K.A. 60667
 + Safinula, S.S. 63923
 + Safonova, M. 60436
 + Safronova, U.I. 60651
 + Saftic, B. 62296
 + Saga, R. 59777
 + Sagaradze, V.V. 63423
 + Sagatelyan, D.M. 61118
 + Sagawa, N. 60372
 Sagdeev, R.Z. + 63506
 + Sagitov, S.I. 62504
 + Saha, A.K. 64207
 + Saha, B. 64302
 + Saha, R.L. 63400
 + Saha, S. 63980
 + Saha, S.K. 64302
 + Sahai, Y. 64283
 + Sahalos, J.N. 61053
 + Sahi, K. 63144
 + Sahm, P.R. 62218
 + Sahota, M. 61819
 + Sai, A.S. 62938
 Sai-Ping Li + 59983
 + Saibekov, T.S. 63965
 + Saidashev, I.I. 62487
 + Sain, M. 64303
 + St. John Manley, R. 59885
 + St. Loran, S.J. 60088
 + Saint-Gaudens, M. 60270
 + Saint-Gregoire, P. 62087
 Saiteevsky, B. 60386
 + Saito, A. 62737
 + Saito, G. 63129
 + Saito, H. 61379
 + Saito, N. 62628
 Saito, T. + 62630
 Saito, Y. 62538
 Saito, Y. + 61042
 + Saito, Y. 61141
 + Saitta, B. 60033
 + Sakabe, S. 60398
 + Sakai, N. 59949
 + Sakai, T. 61614
 + Sakai, T. 63732
 + Sakai, Y. 61538
 + Sakamoto, A. 61302
 Sakamoto, Y. + 61850
 Sakata, K. 63018
 + Sakata, K. 63397
 + Sakharov, N.V. 61682
 + Sakharov, N.V. 61710
 + Sakharovskaya, V.G. 63964
 + Sakita, B. 59956
 + Sakena, G.D. 60670
 + Sakumoto, H. 62713
 + Sakurai, A. 61512
 + Sakurai, K. 60643
 Sakurai, Y. + 62736
 + Sakurai, Y. 62156
 + Sakurai, Y. 62509
 + Sakurai, Y. 62946
 + Sakurai, Y. 62737
 + Saelev, E.Yu. 63053
 + Salam, A. 59647
 Salamandra, G.D. + 61566
 Salazar, J.M. + 63384
 Salerno, J.P. + 63172
 + Saletskii, A.M. 60826
 Salikhov, K.M. + 60759
 + Salje, E. 62415
 + Salzman, V.M. 62488
 Salmon, R. + 61861
 + Salmon, R. 63560
 + Salomon, E.B. 60509
 Salome, M. + 63809
 + Salomone, A. 60497
 Salone, V. 61555
 + Salpietro, E. 60424
 Salter, P.F. + 60325
 + Salva, H. 62405
 + Salvan, F. 61801
 + Salvatore, F. 60324
 + Salzborn, E. 60949
 + Salzburger, H. 60437
 Salzmann, P. + 62585
 + Samakhotina, N.K. 62412
 Samarin, B.A. + 63435
 + Samarina, A.M. 63463
 + Sambandham, M. 59683
 + Samoc, M. 63028
 + Samoc, M. 59797
 + Samoilenko, V.T. 64385
 + Samoilova, I.A. 62919
 + Samokhov, V.A. 63270
 + Samokhov, V.A. 63271
 Samokhvalov, M.A. 62476
 + Samoto, T. 62775
 + Samoylov, A.I. 63366
 + Samoylov, S. 61492
 + Sampoli, M. 63007
 + Samson, A.V. 60995
 Samuel, S. 59906
 + Samulenis, V.I. 62462
 Samulski, E.T. + 61778
 Sanborn, J.B. 60228
 + Sances, A., Jr. 63995
 Sanchez, C. + 62416
 + Sanchez, M.C. 62582
 + Sanchez, P. 62576
 + Sanchez Magro, C. 64556
 + Sandberg, C.J. 63146
 + Sandberg, C.J. 62630
 + Sander, I. 59840
 + Sanders, J.M. 60936
 Sanders, L.G. 64253
 Sandholm, S.T. + 60847
 + Sandmann, W. 60472
 + Sandner, W. 60667
 + Sandorfi, A.M. 60178
 + Sandrock, G.D. 61567
 + Sandrock, G.D. 61568
 + Saneyoshi, K. 62863
 Sangani, A.S. + 59750
 + Sanger, H.L. 63774
 + Sanglet, E. 60631
 + Sanjeevaiah, B. 60678
 + Sannabhadri, R.S. 59790
 + Sannes, F. 60049
 + Sannikov, N.I. 63436
 Sano, H. 60979
 + Sano, S. 61368
 Sano, T. + 60367
 + Sano, T. 61660
 + Sanochkin, Yu.V. 61715
 + Sansonetti, P. 61289
 Santhanam, S. + 62517
 + Santoro, G. 63098
 + Santos, E. 59714
 + Santroni, A. 60066
 + Sanyal, S.P. 62041
 Sanz, J.L. 64560
 + Saparov, Kh. 61401
 + Saage, V.F. 63040
 + Saperstein, D.D. 59859
 + Sapetski, A.N. 63573
 + Sapetski, A.N. 59862
 + Sapper, J. 60423
 + Sarangi, S. 59789
 Sarantsev, V.P. + 60484
 Saraswathy, V. + 60606

- + Saraykin, A.I. 60086
 Sargentini, N.J. + 63905
 + Sargoichev, S.I. 64349
 Sargood, D.G. 64460
 Sarica, Y. + 63821
 + Saris, F.W. 63707
 + Sarkadi, L. 60944
 + Sarkar, A.B. 64196
 + Sarkar, U. 59965
 + Sarkisov, Yu.A. 61306
 Sarkisyan, L.A. 60489
 + Sarma, B.K. 62203
 Sarmiento, E.F. + 62660
 + Sarmiento, P.R. 61803
 + Sarode, F.A. 61810
 + Sarott, F.-A. 63069
 Sarraf, S.P. + 61631
 Sarraf, V.I. + 63256
 + Sarraf, V.I. 63316
 Sartori, G. 59942
 + Sarvarov, F.S. 60759
 + Sarylova, M.E. 63583
 + Sasa, Y. 63627
 + Sasai, M. 60596
 Sasajima, S. 64030
 + Sasajima, S. 64038
 + Sasaki, M. 64564
 Sasaki, T. 64401
 + Sasaki, T. 60409
 + Sasaki, Y. 63740
 + Sasaki, Y. 61237
 + Sasaki, Y. 62581
 + Sasao, N. 60088
 + Sasatani, Y. 63672
 + Sass, B. 60474
 + Sass, S.L. 61930
 + Sastry, J.S. 64193
 Sastry, S.B.S. + 63202
 Sathish, S. + 62529
 + Sathkiewicz, F.G. 63698
 Sato, A. + 61909
 + Sato, A. 60031
 + Sato, A. 60059
 + Sato, A. 63299
 + Sato, H. 64564
 + Sato, H. 62778
 + Sato, J. 63160
 Sato, K. + 62945
 + Sato, K. 62697
 + Sato, K. 63315
 + Sato, K. 62946
 + Sato, M. 59950
 + Sato, M. 60378
 + Sato, M. 62752
 Sato, N. + 63129
 + Sato, N. 61652
 + Sato, S. 64556
 + Sato, S. 63535
 Sato, T. + 63276
 Sato, T. + 61691
 + Sato, T. 62927
 Satoh, K. + 60488
 + Satoh, M. 63399
 + Satoh, T. 62565
 Satou, M. + 63159
 + Satsunkevich, V.D. 63622
 + Sattar-zade, I.S. 62061
 + Sattar-zade, I.S. 63518
 + Sattarov, D.K. 61298
 + Sau, J. 60134
 Sauerbrey, R. + 60831
 + Sauers, I. 61713
 + Sauerwein, R. 60054
 + Sauerfer, H. 63741
 + Saumon, G. 63990
 + Saunders, B.J. 60068
 Saunders, V.R. + 60608
 Saude, A. + 61776
 Saupé, A. + 62908
 + Saute, M. 61012
 + Sauvage, J. 64105
 + Sauvajol, J.L. 62883
 + Sauvajol, J.L. 62107
 + Savaria, E. 64380
 Savchenko, A.K. + 62515
 + Savchuk, O.U. 62898
 + Savelli, C. 64103
 + Savinkova, V.L. 61709
 + Savinkina, M.A. 63221
 + Savitski, B.A. 61925
 Savitsky, E.M. + 62115
 + Savitsky, E.M. 63583
 + Savostyanova, T.P. 62115
 Savruk, M.P. + 61457
 + Savukins, A.Yu. 61013
 Savula, Ya.G. 61402
 + Savushkin, A.F. 61173
 Savvak, G.I. + 63224
 Savvakis, C. + 62183
 + Savvin, V.V. 61298
 + Savytchev, V.V. 63277
 + Sawa, S. 61268
 + Sawa, T. 62786
 + Sawaguchi, T. 62820
 + Sawamoto, H. 59795
 + Sawicka, B.D. 62849
 Sawicki, J.A. + 62849
 Sawicki, M. 60152
 Saxena, A.K. + 61475
 Saxena, A.K. + 61474
 + Sayer, B.G. 60754
 Sayers, C.M. 62013
 Sazonov, V.N. + 60846
 Scafe, E. + 63699
 + Scalapino, D.J. 62357
 + Scallitri, F. 64391
 + Scalan, M.J. 60840
 + Scarinci, G. 61807
 + Scarpelli, E.M. 63792
 + Scarpi, G. 63673
 + Scarr, J.M. 59995
 Schaaf, P.J. Van Der
 ... see Van Der Schaaf, P.J.
 + Schablitzky, D. 60054
 + Schachinger, L. 60081
 + Schader, J. 63114
 + Schader, J. 63113
 + Schaefer, H.F., III. 61044
 Schaefer, J. + 61030
 + Schaefer, J. 60922
 + Schaefer, J. 60923
 Schaefer, J.A. + 63106
 + Schaeren, R. 60537
 + Schafer, H. 61854
 + Schaff, W.J. 62374
 Schamel, H. 61662
 Schardt, A.W. + 64336
 Scharf, B. 60610
 Schastlivtsev, V.M. + 63284
 Schattschneider, P. + 63110
 + Schatz, G.C. 62969
 + Schauer, M.M. 60965
 + Schechter, D.E. 60528
 + Schechter, J.M. 59948
 + Scheingraber, H. 60770
 + Schewe, M.W. 63278
 + Schen, G. 60448
 Scherer, A. + 63729
 Scherer, G.J. + 60734
 Scherer, G.W. 61463
 + Schermann, J.P. 61000
 + Scheurer, H. 60406
 Schieck, H. Paetz gen.
 ... see Paetz gen. Schieck, H.
 Schiewer, E. + 60275
 + Schiffrin, L. 61809
 + Schiffmacher, G. 61867
 + Schiffer, G. 59619
 Schild, R. 64481
 Schiller, S. + 63158
 Schilling, R. + 59737
 Schindler, K. 64371
 + Schindler, R.H. 60074
 Schippers, P.H. + 60796
 Schippers, P.H. + 62912
 Schippers, P.H. + 60795
 + Schirato, P. 60068
 + Schirmacher, W. 59690
 + Schistad, B. 60074
 + Schistad, B. 60066
 + Schiwietz, G. 60965
 Schlachter, A.S. + 60949
 + Schlegel, E.M. 64475
 Schleicher, K.T. + 62317
 + Schlenk, B. 60944
 + Schlenker, C. 61884
 Schlenzig, K. 59785
 Schlesinger, Z. + 62230
 Schlosser, Ch. + 62812
 + Schlott, N.E. 63071
 + Schmalz, T.G. 60905
 Schmatko, K.-J. + 61190
 Schmeisser, D. + 63107
 Schmeisser, D. + 62469
 + Schmeisser, D. 63093
 Schmelz, H. 63235
 + Schmelzbach, P.A. 60165
 + Schmelzer, N. 62146
 + Schmid, P. 60033
 + Schmidt, B. 62489
 + Schmidt, D. 59995
 + Schmidt, G. 62895
 + Schmidt, G. 64187
 + Schmidt, J. 61372
 + Schmidt, J.E. 62398
 + Schmidt, K.H. 60355
 + Schmidt, R.L. 59794
 Schmidt, W. + 63702
 + Schmidt-Bocking, H. 60965
 + Schmidt-Kaler, T. 64471
 + Schmieder, G. 62940
 + Schmitt, D. 62622
 + Schmitt, G.A. 64281
 Schmitz, F. 64364
 + Schmitz, N. 60033
 + Schneekloth, U. 60031
 + Schneider, A.J. 63951
 + Schneider, A.M. 63881
 Schneider, F. 61688
 + Schneider, G.M. 62100
 + Schneider, G.M. 62076
 + Schneider, G.M. 61592
 + Schneider, M. 61639
 Schneider, W. 61546
 Schneider, W.R. 59747
 + Schneider, W.R. 59693
 + Schnicke, G. 60054
 + Schnorrenberg, W. 60188
 + Schobert, H. 60159
 Schober, H.J. + 64415
 + Schock, H.W. 63700
 + Schoenfeld, H. 60389
 Scholer, M. + 64335
 + Scholz, R. 61971
 + Scholz, R. 62904
 Schommers, W. 61594
 + Schoneich, W. 64488
 + Schongren, F. 60459
 + Schonhammer, K. + 63118
 Schonhense, G. 59888
 + Schoning, J. 60218
 Schonwandt, H.K. + 64138
 Schopf, E. + 61976
 Schopohl, N. + 62202
 + Schosser, C.L. 62954
 + Schreckengost, J. 63944
 + Schreiber, D. 62703
 + Schreiner, F. + 60317
 + Schreiner, H. + 63206
 + Schreiner, H. 63167
 + Schriber, S.O. 60330
 + Schrobilgen, J. 60754
 + Schroder, H.P. 60103
 + Schroll, A. 64415
 + Schuijlenburg, H. 60534
 + Schuler, K.P. 60088
 + Schulte, R. 60033
 Schulte-Ladbeck, R. 64469
 + Schultz, J. 63450
 + Schultz, A.I. 62446
 + Schulz, B. 63549
 Schulz, P.A. + 60855
 + Schulz, S.W. 62317
 + Schulze, W.A. 62876
 + Schumacher, G. 64380
 + Schumacher, J. 63774
 + Schumann, B. 62309
 + Schunk, R.W. 64289
 + Schuresko, D.D. 60473
 + Schurr, J.M. 63009
 Schutte, F.-J. + 61221
 + Schutz, B.E. 64265
 + Schwartz, D. 64462
 + Schwartz, G.P. 63094
 + Schwartz, M. 63000
 + Schwartz, R.A. 64431
 Schwartz, S.J. + 64314
 + Schwarz, H. 61896
 Schwarz, R. + 60085
 Schwarz, U. + 60443
 + Schwarz, U. 60459
 + Schwingruber, M.R. 60314
 Schweizer, K.S. + 60628
 + Schwendeman, R.H. 60847
 Schwiager, H. + 61464
 Schwingler, J. 59581
 + Scoppola, E. 59720
 Scott, A.M. 61238
 Scott, A.M. 61239
 + Scott, D.K. 60193
 + Scott, D.M. 60016
 + Scott, M.D. 63137
 Scott, R. + 64137
 + Scott, R.L. 64007
 Scrocco, M. 63131
 + Scudieri, F. 61961
 Seager, C.H. 62409
 Seah, M.P. + 63090
 + Seaman, L. 60359
 Sean, P.N. + 62035
 + Seals, C. 64319
 + Sechi-Zorn, B. 59995
 + Seconi, G. 60981
 + Sedat, J.W. 63810
 + Seddon, K.R. 60756
 + Sedrank, N. 63875
 Seebler, L. + 64073
 + Seely, M.L. 60088
 + Segal, G.A. 60606
 + Segall, R.L. 60277
 Segessmann, A. + 60444
 + Segeth, K. 64024
 + Segeth, W. 60132
 Sehr, P.A. + 59808
 + Sehra, J.S. 64302
 Seidel, M. + 59854
 + Seiden, J. 62595
 Seidl, P.A. + 60202
 + Seidman, D.N. 61989
 Seifritz, W. + 63651
 + Seiler, F. 60165
 Seilmeier, A. + 61174
 + Seiranyan, K.B. 63020
 + Seitz, H. 62570
 + Sekhar Dey, S. 64302
 + Sekhon, G.S. 63869
 Seki, H. 62976
 Seki, N. + 61505
 Sekiguchi, M. + 60096
 + Sekiguchi, T. 62683
 + Sekine, M. 63736
 + Sekine, Y. 62069
 + Sekoguchi, K. 61386
 + Selby, M.J. 64556
 + Seleznev, A.G. 61845
 Seliger, J. + 62836
 Seliger, J. + 62829
 Seligman, T.H. + 59943
 + Selke, W. 62658
 + Selkin, A.V. 62921
 + Sell, P.-J. 62218
 + Sella, C. 62719
 Sellers, R.M. 63571
 + Sellin, I.A. 60965
 + Sellin, I.A. 60508
 Sellinschegg, D. 60230
 + Sellschop, J.P.F. 64261
 + Sellyey, W.C. 60491
 + Semenchinskii, S.G. 59799
 + Semenok, K.N. 61889
 + Semenkikh, N.T. 59872
 Semenov, A.E. + 62993
 + Semenov, L.P. 64220
 + Semenov, R.I. 60646
 + Semenov, R.I. 61014
 + Semenov, V.K. 60542
 + Semenov, V.K. 60541
 Semenov, V.N. + 63411
 + Semenova, A.S. 61815
 + Semerenko, R.L. 64406
 + Semiletov, S.A. 62299
 + Semiletov, S.A. 62287
 + Semlyen, J.A. 61032
 + Semlyen, J.A. 61033
 + Semyannikov, A.A. 63261
 Sen, A.K. + 64302
 + Sen, A.K. 61640
 + Sen Gupta, R. 60959
 Senapati, H. + 62161
 + Senatorov, A.K. 61214
 + Sengers, J.V. 62031
 + Sengers, J.V. 62119
 + Senjanovic, G. 59970
 + Senno, H. 62726
 + Sens, B. 61174
 Sentman, D.D. + 64315
 + Septier, A. 63057
 + Sera, K. 60910
 Serafimov, K. + 64241
 + Serafini, L. 60497
 + Seraphin, B.O. 62917
 + Serdobol'skaya, O.Yu. 62228
 + Serdyukov, V.I. 59863
 Sereda, Yu.S. 59667
 + Seregina, L.N. 62851
 + Sergeev, V.I. 62515
 + Sergeev, V.L. 60895
 + Sergeeva, L.V. 63847
 + Sergent, M. 61868
 + Sergent, M. 61870
 + Sergienko, A.I. 62345
 + Sergot, P. 63048
 Serikov, A.V. 61656
 Sermadras, P. + 60249
 + Serri, G. 64103
 + Serughetti, J. 61943
 + Serughetti, J. 61939
 Serykh, V.P. 61728
 Seshadri, S.R. 62223
 Seshan, K. + 62854
 + Seshu Bai, V. 59802
 + Sesma, J. 60210
 + Sesny, R. 60368
 + Setegien, A.S. 63422
 Sethu Raman, S. 64192
 + Setser, D.W. 63514
 Settles, G.S. + 61526
 + Severyny, A.B. 64459
 + Sevin, D. 60956
 + Seyboth, P. 60076
 + Seyerlein, J. 60076
 Seznec, R. + 61318
 Shaaban, A.H. + 61541
 + Shabel'nikov, V.P. 61022
 + Shablygin, M.V. 61831
 + Shablygin, M.V. 61815
 Shadrachev, E.V. + 63459
 + Shafeev, G.A. 63149
 Shaffer, G.W. 61300
 + Shafi, Q. 64567
 + Shafranosh, I.I. 60995
 + Shafron, S.M. 60934
 Shafter, A.W. 64474
 + Shaido, A.N. 64396
 Shaikevich, I.A. + 62915
 Shaka, A.J. + 59816
 Shakalov, F.E. + 62483
 + Shakarov, H.O. 63261
 Shakhanova, G.V. + 63485
 + Shakhovets, K.G. 61682
 + Shakhovets, K.G. 61710
 + Shakhovtsov, V.I. 61969
 Shakhovtsova, S.I. + 61969
 + Shakin, C.M. 60053
 + Shakin, C.M. 60117
 + Shakina, N.P. 64226
 + Shalagin, A.M. 60850
 + Shaleitch, D. 64356
 Shalit, H. + 62015
 + Sham, T.K. 60870
 + Sham, T.K. 63443
 Shamanaeva, L.G. 61335
 Shambulov, R.S. + 63965
 + Shandil, R.G. 61500
 + Shaner, J.W. 62094
 Shanin, V.I. 61310
 + Shanina, B.D. 62807
 Shank, C.V. 61176
 + Shantharama, L.G. 63039
 Shanzhang Huang
 ... see Huang Shanzhang
 + Shapiro, E.I. 60593
 Shapiro, G.I. 64225
 + Shapiro, I.I. 64265
 + Shapiro, S.L. 64504
 + Shapkin, P.V. 61163
 Shapovalov, V.I. + 63370
 + Shapovalova, G.Ya. 63460
 + Shapovalova, T.P. 63139
 Sharafutdinov, G.Z. 61465
 Sharan, V.B. 63046
 Sharifov, M.Kh. + 63323
 Sharipova, S.Kh. 61443
 Sharma, B.K. 62130
 + Sharma, C.S. 59608
 + Sharma, G.K. 61309
 Sharma, H.V. + 62407
 + Sharma, N. 62882
 + Sharma, P. 62992
 + Sharma, S.P. 59639
 + Sharmazan, I.V. 63404
 Sharov, A.S. + 64546
 + Sharp, A.R. 62824
 + Sharp, R.T. 59943
 Shaskov, D.P. + 63428
 Shatashvili, N.L. + 61649
 + Shatwell, R.A. 59850
 + Shaumeyer, J.N. 61502
 + Shaver, I.Kh. 63027
 Shaverdyan, B.S. + 59921
 Shaw, C.F. + 63991
 Shaw, K.B. 63984
 Shaw, M.P. + 61985
 Shaw, M.S. + 61751
 + Shaw, P.M. 60246
 + Shchagina, N.M. 62902
 Shchedrin, G.S. 63475
 + Shchedrunov, V.V. 63923
 + Shchegoleva, N.N. 63287
 Shchegoleva, T.V. 63300
 + Shchelokov, R.N. 63270
 + Shchelokov, R.N. 63271
 + Shchelokov, R.N. 63050
 + Shchennikov, V.V. 62461
 + Shcherbakova, N.I. 61089
 Shcherbakova, M.E. + 63482
 + Shcherbinin, P.P. 61707
 + She, C.Y. 61582
 Shea, J.A. + 60708
 + Sheaff, M. 60041
 + Sheaff, M. 60081
 + Sheaff, M. 60087
 Sheddalkar, V.P. + 62139
 + Sheedy, J.E. 63916
 Sheela, B.V. 64360
 + Sheffer, E.K. 64347
 + Sheffield, S.A. 59832
 + Sheftel, E.N. 63365
 + Sheftel, E.N. 63305
 Sheibid, D.W. + 63656
 Sheikh, A.W. + 59790
 + Sheindlin, B.E. 63454
 + Shek, M.L. 63135
 Shekar, B. Chandra
 ... see Chandra Shekar, B.
 + Shekhter, L.N. 63263
 + Sheline, R.K. 60185
 + Shelke, R.N. 64237
 Shelkovnikov, N.K. + 64271
 Shellock, F.G. + 63793
 + Shemet, V.V. 61282
 Sheminova, V.A. 64395
 Shen, D.F. + 62946
 + Shen, S.F. 61491
 + Shen, Y.R. 60864
 + Shen Jian-guo. 60009
 + Shen Jue-lian. 62384
 Shaffer, G.W. 61300
 + Shafi, Q. 64567
 + Shafranosh, I.I. 60995
 + Shafron, S.M. 60934
 Shafter, A.W. 64474
 + Shaido, A.N. 64396
 Shaikevich, I.A. + 62915
 Shaka, A.J. + 59816
 Shakalov, F.E. + 62483
 + Shakarov, H.O. 63261
 Shakhanova, G.V. + 63485
 + Shakhovets, K.G. 61682
 + Shakhovets, K.G. 61710
 + Shakhovtsov, V.I. 61969
 Shakhovtsova, S.I. + 61969
 + Shakin, C.M. 60053
 + Shakin, C.M. 60117
 + Shakina, N.P. 64226
 + Shalagin, A.M. 60850
 + Shaleitch, D. 64356
 Shalit, H. + 62015
 + Sham, T.K. 60870
 + Sham, T.K. 63443
 Shamanaeva, L.G. 61335
 Shambulov, R.S. + 63965

- +Shestak, A.F. 62065
 +Shesterikov, S.A. 61419
 Sheshopalov, V.E. 63430
 Shetter, R.E. + 64160
 +Sheveleva, A.S. 62453
 +Shewmon, P.G. 62022
 Shi Chen. *see* Chen Shi
 Shi Songyao. *see* Songyao Shi
 Shi-gang Zheng. *see* Zheng Shi-gang
 Shi-kun Wang. *see* Wang Shi-kun
 Shiba, H. + 62589
 +Shiba, K. 60677
 Shibai, H. + 64535
 +Shibanov, Yu.A. 64518
 +Shibata, M. 63740
 +Shibata, N. 61972
 Shibata, T. + 64297
 +Shibata, T. 62744
 +Shibata, T. 60453
 +Shibazaki, N. 64556
 +Shibazaki, N. 64557
 +Shibayeva, L.S. 63547
 +Shibuya, K. 61299
 +Shida, Y. 60096
 Shields, F.D. 62248
 Shields, L. 62340
 +Shiffrin, S.S. 61926
 Shiga, M. + 62561
 +Shigematsu, T. 62864
 Shigenaka, N. + 63306
 Shih, C.C. 59736
 Shih Tai-Chang. *see* Tai-Chang Shih
 +Shiho, M. 60468
 +Shiino, K. 60553
 Shikama, T. + 61973
 +Shilnikov, V.I. 63015
 Shilov, V.V. + 61765
 +Shilov, V.V. 61774
 +Shilov, V.V. 61830
 +Shilova, M.V. 63074
 +Shima, H. 63495
 +Shimada, M. 62587
 Shimada, S. + 60236
 +Shimelevich, Yu.S. 64249
 +Shimizu, F. 60643
 Shimizu, K. 61086
 +Shimizu, R. 62762
 +Shimizu, T. 61804
 +Shimizu, T. 62286
 +Shimizu, Y. 61623
 +Shimshock, R.P. 62917
 +Shin, M.C. 63313
 Shin Kyun-Kook. *see* Kyun-Kook Shin
 Shinar, R. + 62494
 +Shindo, Y. 60378
 Shinjo, T. + 62860
 +Shinjo, T. 62729
 +Shinjo, T. 62861
 +Shinmura, H. 61660
 +Shinoda, Y. 63154
 +Shinohara, I. 61827
 +Shinohara, M. 62874
 +Shinozuka, T. 60504
 +Shint, Ya.O. 61876
 +Shintani, Y. 63155
 Shinzato, S. + 62508
 Shirae, K. + 62721
 +Shiraga, H. 60398
 Shirai, H. + 61058
 +Shiraishi, K. 63480
 +Shirasaki, M. 62862
 +Shiro, Y. 62045
 Shisheng Huang. *see* Huang Shisheng
 +Shishkina, M.V. 61798
 +Shishova, T.A. 60995
 Shitov, V.G. + 61107
 Shiue, Y.-L. + 63982
 +Shivakumar, G.K. 62505
 Shivamoggi, B.K. 61645
 Shivamoggi, B.K. + 61624
 Shivaram, B.S. + 62203
 +Shkal'kova, G.V. 61248
 +Shklyarskii, O.I. 62349
 +Shkurskii, B.I. 63846
 +Shlesinger, M.F. 59686
 +Shlesinger, M.F. 62027
 Shlishchenskii, B.E. + 61313
 +Shlosman, S.B. 59740
 +Shmakova, E.S. 62288
 +Shmal'ko, A.V. 61278
 +Shmartsev, Yu.V. 62995
 +Shmartsev, Yu.V. 62487
 +Shmatov, V.T. 63343
 +Shmid, M. 60111
 +Shmyt'ko, I.M. 62095
 Shohoji, N. 62116
 +Shoidin, S.A. 61113
 Shoji, K. + 63849
 Shoji, K. + 62245
 Shope, L.A. + 64257
 +Shorygin, P.P. 60880
 +Shouji, M. 62737
 Shouxian Fang. *see* Fang Shouxian
 +Shpak, M.T. 61212
 +Shpak, M.T. 63054
 +Shpakovskaya, L.P. 61925
 +Shraiber, V.M. 60735
 Shrouf, T.R. + 62897
 +Shteinberg, M.M. 63288
 +Shstessl, E.A. 61595
 Shtrikman, S. + 62639
 Shu-En Hsu. + 63341
 Shu-ren Chang. *see* Chang Shu-ren
 +Shubakov, V.S. 63435
 Shubin, A.A. + 62797
 Shubina, A.K. + 63487
 +Shuimakov, A.D. 63965
 +Shukurov, T. 60844
 +Shukurov, R.I. 63323
 Shul'man, L.M. 64425
 +Shur, L.N. 59915
 +Shur, Ya.S. 63287
 +Shurshalov, L.V. 64426
 Shuryak, E.V. 59994
 Shuryak, E.V. 59997
 Shushakov, V.D. + 61845
 +Shushakova, T.V. 61845
 +Shushpanov, O.E. 61275
 +Shushpanov, O.E. 61281
 +Shuvalov, L.A. 62902
 +Shuvalov, L.A. 62829
 +Shuven Yang. 61296
 +Shvartsman, E.I. 62396
 +Shvartsman, L.A. 63320
 Shvets, V.A. 59878
 +Shvinderman, L.S. 62173
 Shyamala Bharadwaj. *see* Shyamala Bharadwaj
 +Shyu, C.M. + 62128
 +Shyu, C.M. 62375
 +Shyu, C.M. 62457
 Si-mao Ye. *see* Ye Si-mao
 Siao Fang Sun. + 62911
 +Sibener, S.J. 63121
 +Sibille, F. 64392
 Sibisi, S. 63925
 +Sicart, J. 62499
 +Siciliano, E.R. 60204
 +Siciliano, E.R. 60211
 Sicking, G. + 61007
 Sicong Jin. *see* Jin Sicong
 +Siddles, R.M. 60917
 +Sidel'nikov, S.B. 63371
 +Sidel'nikov, V.N. 64398
 +Sidis, V. 60897
 +Sidorenko, F.A. 61844
 +Sidorin, A.V. 61211
 +Sidorin, K.K. 62034
 +Sidorov, V.A. 62438
 +Sidorov, V.A. 63189
 +Sidorova, L.I. 63426
 +Siebert, H.W. 60068
 +Siegbahn, P. 63516
 +Siegbahn, P.E.M. 60602
 Siegel, E. 62258
 Siegrist, T. 61877
 Sieh, K.E. 64071
 +Siehs, J. 61966
 +Siekmann, S. 62218
 Siemann, D.W. + 63908
 +Siemann, R.H. 60500
 +Siemens, G. 63655
 Siena, S.de. *see* de Siena, S.
 +Sievers, A.J. 62230
 Sievers, U. + 64154
 +Siffert, P. 63706
 +Siffert, P. 63701
 +Sigarev, A.A. 63072
 +Sigaud, G. 61779
 Sigelle, M. + 63143
 Siggia, E. 61501
 +Sikdar, M.K. 62610
 Sikora, R. 63255
 +Silbey, R. 59735
 +Silivra, A.A. 61061
 +Silk, J.D. 60196
 +Sil'nikova, E.F. 63326
 Silva, M.F.da. *see* da Silva, M.F.
 +Silva, N.P. 62664
 +Silver, E.A. 64097
 +Silverman, A. 60049
 Silvi, B. + 60621
 Silyn-Roberts, H. 64011
 +Simakin, A.V. 63149
 +Simard, R.L. 60354
 +Simas, A.M. 60561
 +Simashkevich, A.V. 63665
 Simhan, R.G. 62159
 +Simic, V. 62186
 Simik, A. 60466
 +Simin'kovich, V.N. 63421
 Simizu, S. + 62593
 +Simoes, T.J.M. 59620
 Simon, J.C. + 61148
 Simon, J.L. 64359
 +Simon, M. 63687
 Simon, R. + 59794
 +Simon, R.H. 63830
 Simon, R.S. + 64555
 Simonius, M. 59935
 +Simonov, A.P. 60854
 +Simonov, V.I. 61901
 +Simonov, Yu.A. 61903
 +Simons, D.G. 60940
 +Simons, D.G. 60952
 +Simpson, C.J.S.M. 63507
 +Simpson, C.J.S.M. 60917
 +Simpson, C.J.S.M. 60911
 Simpson, D.W. (ed.) 59541
 +Sinfelt, J.H. 63081
 +Singal, S.P. 64197
 +Singh, I. 62407
 Singh, J. 62037
 +Singh, M.M. 63448
 Singh, R.K. + 62041
 Singh, S. 59830
 +Singh, S.N. 63668
 Singh, U.S. 64209
 Singh, U.S. 64210
 Singh, V.P. + 63692
 Singh Bani. *see* Bani Singh
 Singh Jasbir. *see* Jasbir Singh
 Singh Kamal. *see* Kamal Singh
 +Singh Mudher, K.D. 61894
 Singh Nirmal. *see* Nirmal Singh
 Singh Sadhu. *see* Sadhu Singh
 Sinha, G.D.J. Sivakumar
 +Sinha, G.D.J. 62306
 +Sinita, L.N. 59863
 Sinke, W. + 63707
 +Sinyakov, G.N. 60767
 +Sipatov, A.Yu. 61925
 +Sirugue-Collin, M. (ed.) 59543
 +Sisakyan, E.V. 59862
 +Sisakyan, I.N. 61118
 +Siscoe, G.L. 64417
 +Sistenich, K. 60111
 +Sitenko, Yu.A. 59925
 +Sitenko, Yu.A. 59988
 +Sitz, G. 63556
 +Sitzer, M.R. 61477
 +Sivakumar Sinha, G.D.J. 64025
 +Sivasegaram, S. 63550
 Six, J. + 59582
 +Sixel, P. 60533
 +Sixou, P. 62101
 Skagius, J. + 60298
 +Skard, J.A. 59995
 +Skasyskii, Ya.K. 61114
 Skell, P.S. + 63519
 Skelton, D.F. + 61731
 Skinner, E.K. + 62001
 +Skinner, R.F. 63579
 +Skjelving, G. 60066
 +Sklangsky, J. 63961
 +Sklenarc, A.M. 60357
 +Skobelev, I.Yu. 60909
 Skoblo, A.V. + 63478
 Skolnick, M.S. + 63036
 +Skolnick, M.S. 62365
 +Skopinov, S.A. 61797
 +Skorbin, A.D. 62881
 +Skorczakowski, M. 61185
 +Skorova, A.V. 61901
 +Skovgard Jensen, H.E. 60474
 +Skrable, K.W. 63971
 +Skrabkov, O.V. 60931
 Skribanowitz, G. 59868
 Skripov, V.P. + 61753
 +Skripov, V.P. 62209
 +Skritskii, V.L. 62462
 +Skriver, H.L. 62046
 Skrynnchenko, Yu.M. + 63361
 +Skrczcanowski, W. 61702
 +Skubic, P. 60049
 +Skubic, P. 60081
 +Skubic, P. 60087
 Skubis, A. 59825
 +Skuja, A. 59995
 +Skumanich, A. 64507
 Skvarka, P. 60219
 Slaby, J. + 61105
 +Sladkin, D.N. 63948
 Slaus, I. 60147
 +Slaus, I. 60182
 +Slemzin, V.A. 64347
 Slingerland, R. 64125
 +Slobodrian, R.J. 60183
 Slonczewski, J.C. 62774
 +Slonskii, I.V. 62938
 +Slough, J. 61640
 S.L. Varghese. *see* Varghese, S.L.
 +Smaardyk, J.E. 60371
 +Smalley, R.E. 60913
 +Smalley, R.E. 60915
 +Smalley, R.E. 61043
 +Smart, R.St.C. 60277
 +Smeets, P.H.M. 60467
 +Smekens, G.R. 63714
 +Smerd, P.G. 60389
 +Smetannikov, A.S. 61718
 +Smialowska, S. 60248
 +Smirnitkii, V.B. 61193
 +Smirnitkii, V.B. 61963
 +Smirnov, A.Ya. 61204
 +Smirnov, E.N. 61725
 +Smirnov, E.V. 60086
 +Smirnov, L.S. 61959
 Smirnov, M.A. + 63378
 +Smirnov, V.M. 61138
 +Smirnov, V.P. 61711
 +Smirnov, Yu.M. 60994
 Smirnova, A.P. + 63288
 +Smirnova, A.V. 61458
 +Smit, H.C.D. 60384
 +Smit, A.C. 63336
 Smith, A.G. 59867
 +Smith, A.G. 64116
 +Smith, A.H. 63814
 +Smith, A.J. 61869
 Smith, A.K. 64185
 Smith, A.W. + 63039
 Smith, D.H. 64569
 +Smith, D.J. 62151
 +Smith, D.M. 63993
 +Smith, D.T. 63919
 Smith, E. 63385
 Smith, G. + 61252
 Smith, G. + 63917
 +Smith, G. 62074
 Smith, G.J. + 63697
 +Smith, G.P. 60788
 +Smith, H.K. 61858
 +Smith, I.W.M. 60808
 Smith, J.L. + 61851
 +Smith, J.L. 62091
 +Smith, K.C. 63905
 +Smith, K.W. 60912
 Smith, N.O. 59558
 +Smith, N.V. 63132
 +Smith, P.B. 60500
 Smith, P.V. 60132
 Smith, P.V. 62331
 +Smith, P.W. 61187
 Smith, R.A. 64373
 +Smith, R.A. 63851
 +Smith, R.E. 63757
 Smith, R.M. + 63877
 Smith, T. 63449
 Smith, V.C. + 63839
 +Smith, V.H., Jr. 60561
 +Smith, V.J. 60068
 Smith, W.E. + 61100
 +Smith, W.W. 60673
 Smits, J.W. + 63157
 Smolenaers, P.J. + 59782
 Smolin, M.D. + 62396
 +Smolin, Yu.I. 61888
 Smol'nikov, E.A. + 63327
 +Smol'skii, O.V. 61963
 +Smorgonskii, V.G. 61171
 +Smotrakov, A.V. 63273
 +Smotritskii, L.M. 60163
 +Smyth, J.R. 61872
 +Smythe, D.K. 64110
 Snavey, D.L. + 60715
 +Snegov, M.I. 60827
 +Snell, C.M. 61164
 +Snell, C.M. 62516
 +Snisarenko, E.A. 61317
 Snitkovskii, A.I. 64217
 +Snover, K.A. 60178
 +Snyder, A. 60049
 Snyder, D.T. + 60362
 Snyder, H.L. + 63008
 Snyder, R.G. + 60716
 Snyder, R.G. + 61018
 +Snykers, M. 60415
 +Soardo, G.P. 62608
 Soares, D.Menez. *see* Menez Soares, D.
 Soares, O.D.D. 59759
 +Sobagaki, H. 63842
 Sobolev, A. + 64100
 +Sobolev, A.G. 62504
 +Sobolev, N.A. 59798
 +Sobolev, Yu.V. 60163
 +Soboleva, E.M. 62504
 +Soboleva, N.F. 59776
 +Sobotova, C. 64058
 +Soderberg, G.L. 63989
 +Sodja, J. 60083
 +Soga, F. 60096
 Soh, K.S. + 59969
 +Soh, K.S. 59972
 Sohmer, H. + 63857
 Sohni, M.F. + 59658
 +Soifer, G.B. 62832
 +Soifer, V.A. 61118
 +Soinikov, Yu.A. 60823
 Soitkar, V.S. + 61361
 Sojka, J.J. + 64289
 Sokalski, W.A. + 60571
 +Sokol, R.J. 61949
 +Sokolov, I.A. 61963
 Sokolov, I.V. 60642
 +Sokol'ski, A.A. 61060
 +Soll, M. 60456
 Solmajer, T. + 60573
 +Solodov, I.Yu. 62228
 +Soloev, Yu.I. 63204
 +Soloubov, V.V. 62324
 +Solomatina, V.A. 61173
 +Solomatina, V.S. 61235
 +Solomentsev, V.I. 61311
 +Solochev, L.E. 62923
 +Solov'ev, S.P. 61889
 +Solov'eva, G.S. 60583
 +Solovyanov, V.L. 60086
 +Solov'yev, L.F. 60086
 Som, S.K. 61540
 Soma, T. + 62136
 +Somayaji, T.S.N. 64307
 Somers, L.J. 59944
 Sommer, W.F. + 60235
 +Somorjai, G.A. 62264
 Somov, A.N. + 61479
 +Sompolinsky, H. 62666
 +Sonderregger, P. 60085
 Sone, K. 63575
 +Sonett, C.P. 64411
 +Song, H.S. 60052
 Song Fu-zhi. 63893
 Song Jin-Soo. *see* Jin-Soo Song
 Song-ling Zhao. *see* Zhao Song-ling
 +Songyao Shi. 62700
 Soni, S.K. 59941
 Soni, V. 60125
 Soni, V. 60126
 Sonin, E.B. 62200
 +Sonnenchein, J. 59964
 +Sonoda, M. 61439
 +Sonomura, H. 62891
 +Sooch, S.S. 60131
 +Sood, S.K. 61500
 Soohoo, R.F. 62690
 Soos, Z.G. + 62356
 +Soper, D.E. 59982
 +Soper, D.E. 60056
 Sophy, Y. + 60382
 +Sopinskii, N.V. 62915
 Sopori, B.L. + 63669
 +Sorensen, C.M. 61593
 +Sorensen, G. 63708
 Sorensen, H. + 60474
 +Sorensen, J. 61661
 +Sorensen, S.O. 60066
 +Sorokin, A.R. 61128
 +Sorokin, I.E. 63304
 +Sorokin, P.V. 60164
 +Sorokin, V.N. 61887
 +Sosnowski, R. 60075
 +Sotnik, N. 62470
 +Souabaramayer, J. 61005
 +Soucek, V. 59613
 +Soucek, V. 59613
 +Souder, P.A. 60088
 Souga, C. 60244
 Soulas, M. + 63644
 Sousa, J.B. + 62401
 Sousa, J.Bessa. *see* Bessa Sousa, J.
 +Soussen-Jacob, J. 60684
 Southcott, B.M. + 63922
 +Southwell, W.H. 61255
 Spada, F. + 63746
 +Spadaccini, G. 60943
 +Spahiu, K. 60324
 Spalburg, M.R. + 60897
 +Spamer, E. 60133
 +Spanjer, T.G. 62689
 +Sparks, M. 61293
 Sparrow, E.M. + 61554
 Sparrow, E.M. + 61504
 Spasskii, M.N. + 63377
 +Spears, K.G. 60813
 Spears, W.R. + 60445
 +Spector, B.I. 61114
 +Spector, Ya.I. 63457
 Spencer, M.G. + 62374
 +Spencer, T. 59722
 +Spengler, J. 60075
 +Sperduto, A. 60199
 +Spersien, F. 60165
 +Sperling, L.H. 61824
 +Speth, E. 60455
 Spicer, C.W. 63754
 +Spicer, W.E. 63135
 +Spichkin, G.L. 61136
 +Spichkin, G.L. 61722
 +Spillmann, L. 63843
 +Spirov, G.M. 61725
 +Spitaten, C. 60187
 +Spitzer, D.M., Jr. 63692
 +Spitzer, H. 59995
 +Spitzer, M.B. 63705
 Spitzig, W.A. 63354
 Spoelstra, T.A.T. 64394
 Spohn, H. 59741
 +Spohr, R. 62005
 +Spohr, R. 61999
 +Spotz, M.S. 61290

- +Sprackling, M.T.62015
 +Springmann, E.60431
 +Sproue, G.D.60481
 +Spruth, J.61737
 +Spurny, F.60477
 +Spyropoulou-Stassinaki, M.60533
 +Srednicki, M.59663
 +Sridhar, A.A.64305
 +Sridhar, K.61492
 +Srinivasa Rao, K.63996
 +Srinivasan, G.64497
 Srinivasan, R.S. +61434
 +Srinivasan, S.63612
 Srinivasan, T.M. +63996
 +Srinivasan, V.64202
 +Srivastava, B.K.62193
 Srivastava, B.N.61125
 Srivastava, D.K. +60115
 Srivastava, G.P. +64202
 Srivastava, P.C. +62376
 +Srivastava, R.C.59642
 Staa, R. van.see Van Staa, R.
 +Stabler, A.60529
 +Stabler, A.60455
 Stace, A.J. +61040
 +Stacey, A.J.63922
 +Stadhouders, A.M.59884
 +Stadnik, P.E.60543
 +Stadtke, H.60350
 Staerk, H. +63565
 +Staerk, H.63504
 +Stafeev, V.I.61279
 +Stafeev, V.I.62934
 +Stafstrom, S.61034
 Stahl, O. +64482
 +Stahr, S.63151
 +Stair, P.C.62257
 +Staley, S.W.60711
 +Stals, L.M.60417
 +Stammler, M.60272
 Stangeby, P.C.61011
 Stankic, S. +62864
 Stanton, S.G. +60726
 +Stap, C.C.A.H.63616
 Stapele, R.P. van.see van Stapele, R.P.
 +Stapf, I.62124
 +Starke, E.A., Jr.63319
 +Starostin, Yu.V.62779
 +Starostin, Yu.V.62781
 +Stasel'ko, D.I.61119
 Stassis, C. +62046
 Stathopoulos, A.Y. +61974
 +Stavitskij, B.61708
 +Stazak, S.M.60873
 +Steadman, S.G.60199
 +Stedman, D.H.64160
 +Stedman, G.E.63010
 +Steel, D.G.61183
 +Steel, W.A.61758
 +Steele, J.W.60397
 +Stefan, P.M.63135
 Stefanov, S.R. +61364
 +Stefanovic, D.63252
 +Stefanovich, L.I.63004
 +Steffen, P.60031
 +Steffen, P.60059
 +Steffen, R.M.60105
 Stegeman, G.I.61303
 +Steger, G.63774
 +Steger, J.G.60264
 +Stehle, C.64278
 Stein, H. +60861
 Stein, H.J. +61949
 Stein, I.D. +63987
 +Stein, P.C.60049
 Stein, R.S.64121
 +Stein, T.S.60983
 +Steinberg, I.Z.60724
 Steinberg, V. +63552
 +Steiner, M.62562
 +Steiner, M.62560
 +Steiner, M.62552
 +Steiner, R.E.63919
 +Steiner, W.61980
 +Steinle, F.S., Jr.61523
 +Stejskal, E.O.61030
 +Stelbovics, A.T.60984
 +Stella, B.59995
 +Stelle, K.S.59939
 +Stelle, K.S.59952
 +Stencel, R.E.64477
 Stenflo, J.O. +64446
 Stenflo, L. +61170
 +Stenina, V.V.60731
 +Stenlund, E.60075
 +Stenlund, E.60078
 +Stenzel, R.L.61664
 Stenzel, W. +63103
 Stepanenko, I.A. +61683
 +Stepanescu, A.62687
 +Stepanov, A.I.61137
 +Stepanov, A.I.61201
 +Stepanov, B.M.62402
 +Stepanov, S.I.61116
 +Stepanov, S.I.63356
 Stephanowitz, R.63005
 +Stephens, K.60031
 +Stephens, K.60059
 +Stephens, N.63878
 +Stephenson, W.A.64256
 Stepina, A.I. +63426
 +Stepka, F.S.59779
 Steppov, M.N. +63422
 +Stepto, R.F.T.61032
 +Stepto, R.F.T.61033
 +Stergiou, A.60533
 +Stern, A.60413
 +Stern, J.59957
 Stern, K.H. +62290
 Stern, R.A. +64507
 Stevens, J.G.62850
 +Stevenson, D.A.61808
 +Stevenson, J.S.63721
 +Stewart, A.M.62621
 Stewart, G.M. +60809
 +Stewart, J.M.59641
 +Stewart, R.R.64045
 Steytler, D.C. +61768
 Stickland, D.F. +64473
 +Stickland, D.P.60068
 +Stiegelschmitt, A.63227
 Stienon, M. +63938
 Stinchcombe, R.B.62543
 Stine, J.R. +60886
 Stineberg, D.R.64500
 +Stirling, W.L.60528
 Stizza, S. +62953
 +Stobbs, W.M.61985
 +Stobiecki, F.62740
 Stobiecki, T. +62740
 Stock, S.R. +61932
 +Stockbauer, R.60509
 +Stockli, M.60948
 Stockli, M.P.60626
 Stoffels, J.J.60480
 +Stoffl, W.60185
 +Stojic, M.61763
 Stoletnik, I.60035
 +Stoll, H.60568
 +Stolov, A.M.61711
 +Stois, A.L.H.59884
 +Stolterfoht, N.60965
 Stolyarov, A.D.61098
 +Stolyarov, V.L.62694
 +Stolz, W.62176
 Stone, J. +61286
 Stone, J.R. +61534
 +Stone, R.60049
 +Stone, S.60049
 +Stoneham, A.M.60280
 Storck, R.60297
 +Storey, D.59910
 +Storizhko, V.E.60181
 +Storozhenko, Yu.O.60164
 +Storozhev, V.V.61280
 Strakh, A.G. +63930
 Stramska, H.62949
 Strangway, R.J. +64316
 +Strassner, A.I.63931
 +Strassner, G.60208
 +Strathdee, J.59647
 +Straub, G.K.59666
 Straumal, B.B. +62173
 +Strauss, H.L.60685
 +Strauss, H.L.60716
 +Strauss, H.L.61018
 +Strauss, H.L.60727
 +Strauss, H.W.63945
 +Strazzulla, G.63126
 +Strazzulla, G.60650
 +Strazzulla, G.64468
 +Streater, R.F.59676
 +Streit, W.B.61758
 +Streibl, B.60431
 +Streibl, N.61052
 +Streit, K.P.60068
 Streitenberger, P.62314
 +Streng, K.H.60062
 +Streubel, R.61464
 +Strigalev, V.E.61276
 Strijp, R.M. van.see van Strijp, R.M.
 +Strikovskii, M.D.61671
 Strizhak, V.A. +63356
 +Strizhak, V.A.63362
 +Strobel, P.61879
 Strominger, A.E.59958
 Strong, R.L. +62260
 +Strongin, M.60870
 +Stross, N.61551
 +Strubel, R.62277
 +Struble, G.L.60185
 +Strubler, K.A.63976
 +Struensee, R.L.63749
 +Strzelecki, L.61791
 +Strzelecki, L.62083
 +Stubbe, P.64291
 +Studenikin, V.A.59871
 +Stuke, J.62521
 +Stumbris, E.P.60593
 +Stumer, I.60074
 +Stumpfe, W.63226
 +Stuppaker, V.V.62524
 +Stupperich, K.59995
 +Stwalley, W.C.60802
 +Stwalley, W.C.60803
 +Stwalley, W.C.60888
 +Stwertka, P.M.60201
 +Su Xing Wu.63198
 Su Zhao-bin +62525
 +Su Zhao-bin.62384
 +Suarez-Kurtz, G.63823
 +Subba Ramaiah, K.63202
 +Subrahmanyam, C.V.64207
 Subramaniam, B. +63061
 Subramaniam, B. +62016
 +Sucher, J.60894
 +Suck, S.H.63543
 Sud, V.K. +63869
 Suda, S. +61385
 Suda, S. +61384
 +Suda, T.60841
 +Sudarshan, E.C.G.59948
 Sudo, S. +61698
 +Suematsu, Y.61150
 +Suenaga, T.62643
 +Suetnik, W.62990
 +Suetsugu, P.63939
 Sueyoshi, T. +62712
 Suezawa, Y. +62757
 +Suezawa, Y.62783
 +Suezawa, Y.62794
 Sugano, R. +59919
 +Sugarbaker, E.60106
 +Sugawara, H.59651
 +Sugaya, T.60072
 +Sugaya, T.60082
 Suggs, R. +64421
 Sugihara, S. +64148
 Sugimoto, H. +62366
 Sugisaki, M. +62166
 +Sugisaki, M.60240
 +Sugisaki, Y.61909
 +Sugita, N.62860
 Sugita, R.62310
 Sugiura, T. +63178
 +Sugiyama, N.61299
 Suhnel, J. +63499
 +Sujak, B.62881
 +Sukegawa, T.63178
 +Sukhodolov, B.G.62782
 +Sukhoruchkin, A.K.63749
 +Sukhorukov, A.I.59712
 +Sukigara, M.62491
 Sukkar, M.H. +62377
 +Sukstanskii, A.L.62042
 Sulentic, J.W. +64549
 +Sulkes, M.60919
 Sullivan, B.J. +60788
 +Sullivan, J.D.64313
 +Sullivan, M.60074
 Sullivan, N.S. +59818
 Sullivan, T.J. +64245
 Sultan, M. +61387
 +Sulzer, M.64286
 +Sul'zhenko, V.K.63365
 Sumerling, T.J. +63911
 +Sumida, N.61922
 +Sumita, M.62892
 +Sumitani, M.60820
 Sumiya, K. +62711
 +Sumiyama, A.62527
 Sumiyama, K. +62741
 Sun, J.C. +63534
 +Sun, K.J.61372
 +Sun Bokang.61945
 Sun Kang Chang.see Chang Sun
 Sun Liang Yan.see Liang Yan Sun
 +Sun Rouna.62129
 Sun Siao Fang.see Siao Fang Sun
 +Sunaga, K.63924
 +Sundaram, V.S.62800
 Sundararajan, G.63433
 Sundararajan, G. +62022
 +Sundholm, D.60563
 +Sung, C.C.61084
 +Sung, P.63695
 +Sunnappawar, K.P.61361
 Suo-Anttila, A. +60371
 +Supovnev, N.P.62707
 Surana, K.S.59594
 +Surkov, Yu.P.60551
 +Surman, M.63105
 +Surovnikov, M.V.62300
 +Susak, Z.63887
 +Sushin, V.N.62288
 +Sussmann, G.62002
 +Sutcliffe, L.H.60765
 +Sutera, C.M.60187
 Suthanthiraraj, S.A. +62162
 +Sutherland, R.M.63894
 Suto, M. +60867
 +Sutovskii, S.M.62916
 Sutton, R.A. +60170
 +Sutton, R.B.60043
 Suzuki, H. +63744
 +Suzuki, K.62820
 +Suzuki, K.61972
 Suzuki, M.59734
 +Suzuki, M.61102
 +Suzuki, M.61329
 Suzuki, N.62571
 Suzuki, N. +62619
 Suzuki, N. +62926
 +Suzuki, N.62624
 +Suzuki, N.62589
 Suzuki, S. +62713
 Suzuki, T.60124
 Suzuki, T.62743
 Suzuki, T. +60794
 Suzuki, Y. +62785
 Suzuki, Y. +62821
 +Suzuki, Y.60677
 +Suzuki, Y.61652
 +Suzuki, Y.59612
 +Suzuki, Y.60461
 +Suzuki, Y.62606
 +Suzuki, Y.60470
 +Suzumura, N.64017
 +Suzuki, A.60372
 +Svensson, I.64014
 +Sverdlow, L.M.60777
 +Sveshnikova, G.A.63330
 +Sveshnikova, I.N.62287
 +Svirgun, A.A.61191
 +Sviridov, K.N.64398
 Svirskaia, P. +60829
 +Svirskaia, P.63577
 Swahn, J. +60475
 +Swaid, I.62076
 +Swalen, J.D.60837
 +Swalen, J.D.63071
 Swaminathan, M.K. +61492
 +Swan, H.J.C.63793
 Swanberg, C.A.64096
 +Swank, J.64462
 +Swanson, J.G.62001
 +Swanstrom, P.60575
 +Sweeney, D.W.60782
 Sweeney, J.F.64119
 +Swierczynski, R.61674
 Swift, D.J. +63851
 Swijgenhoven, H. van.see van Swijgenhoven, H.
 +Swindell, G.E.60247
 Swol, R. van.see van Swol, R.
 +Sworakowski, J.59797
 +Syehogov, V.A.61306
 +Syehogov, V.A.63087
 +Sydyr, B.I.62460
 +Sykes, A.61684
 Sykes, L.R. +64072
 +Symons, M.C.R.60766
 +Symons, M.C.R.63568
 +Symons, T.J.M.60075
 +Symons, T.J.M.60196
 +Synorov, V.F.62386
 +Syryeva, O.N.62133
 +Szabo, G.60343
 +Szaniawski, A.63186
 +Szezekowski, M.60075
 +Szezekowski, M.62904
 +Szezycki, L.60077
 +Szezyrenyl, M.59814
 Szweczyk, A. +62681
 +Szweczyk, A.62684
 +Szilagyi, Z.62983
 Szilas, P. +62002
 +Szoplik, T.61105
 +Sztajn, J.62727
 +Szved, R.60075
 +Szydlak, J.61184
 +Szydlak, J.61185
 Szymczak, H. +62793
 +Szymczak, R.62771
 +Szymczak, R.62684
 +Szymczak, R.62681
 +Szymerska, I.62243
 +Tabanfar, S.61390
 Tabe, M. +61935
 +Tabiryani, N.V.61788
 Tabony, J. +63600
 +Tacker, W.A., Jr.64000
 +Tada, K.63150
 +Tada, K.62926
 +Tada, O.63155
 Tae Woon Kim +60352
 Tae-Kyu Ha +63511
 +Taft, C.A.62865
 Tagata, G.61437
 +Tagawa, K.62858
 Tagirov, V.I. +62488
 Taguchi, M.61613
 +Taguchi, N.60468
 +Tahir-Kheli, R.A.62544
 +Tahira, S.60468
 +Tai, S.60820
 Tai Lee Jong.see Jong Tai Lee
 Tai-Chang Shih.64036
 +Tainturier, G.61900
 +Takada, T.62860
 +Takagi, H.63535
 +Takagi, K.62082
 +Takagi, S.60192
 +Takagi, T.59877
 +Takagi, T.60503
 +Takagishi, N.61141
 +Takahama, K.63842
 +Takahashi, H.62792
 +Takahashi, K.63447
 +Takahashi, K.61813
 Takahashi, M. +62581
 Takahashi, M. +60109
 Takahashi, M. +62699
 +Takahashi, M.62739
 +Takahashi, M.62751
 +Takahashi, M.62723
 +Takahashi, M.62752
 +Takahashi, M.62683
 +Takahashi, M.62683
 +Takahashi, T.60526
 Takahashi, Y.59920
 +Takahei, K.61147
 +Takajo, S.63214
 +Takano, Y.62874
 +Takanohashi, T.63180
 Takao, M. +62726
 Takara, T. +61353
 Takashige, M. +62958
 +Takashige, M.62874
 +Takata, M.62491
 +Takayama, H.62656
 +Takebe, T.63150
 +Takeda, H.60031
 +Takeda, H.60059
 Takeda, K. +62599
 +Takeda, K.62600
 +Takeda, M.61129
 Takeda, S.61853
 +Takei, H.62628
 +Takei, H.62554
 +Takei, H.62596
 +Takekawa, S.61881
 +Takemaru, K.61689
 +Takemoto, N.61385
 +Takenaka, M.63080
 +Takenaka, S.63924
 Takeno, Y. +62753
 Takeshima, M.62423
 +Taketani, H.60107
 Takeuchi, M.62444
 +Takeuchi, S.61972
 Takeuti, Y. +61407
 Takeva, Z.G. +63826
 Takezoe, H. +61258
 Takezono, S. +63399
 Takikawa, K. +60082
 +Takikawa, K.60072
 +Takikawa, K.60088
 Takisawa, N. +62140
 Takiyama, R.63848
 +Takizawa, T.60432
 +Takizawa, T.60434
 +Takizawa, Y.61827
 +Talaga, R.59936
 +Tale, I.A.63026
 +Tallen, M.63811
 Tallman, R.D., Jr. +63864
 +Talonen, P.P.63997
 Talukdar, R. +60670
 +Taluts, N.I.63343
 +Tal'yanskii, E.B.62435
 +Tamamura, K.60468
 +Tampieri, F.64214
 Tamura, H. +63562
 Tamura, I.62649
 Tamura, I. +62855
 Tamura, S.62390
 +Tamura, Y.61302
 Tan Chung-i.see Chung-i Tan
 Tan Ha Vinh.see Ha Vinh Tan
 +Tanabe, H.60378
 Tanabe, T. +60334
 +Tanaka, A.63108
 Tanaka, E. +60574
 Tanaka, F. +62734
 Tanaka, H. +61747
 +Tanaka, I.60820
 Tanaka, K. +59726
 +Tanaka, K.62496
 +Tanaka, K.63398
 Tanaka, M. +60820
 +Tanaka, M.63480
 +Tanaka, O.61386
 +Tanaka, R.60072
 +Tanaka, R.60082
 Tanaka, S. +62738
 +Tanaka, S.62492
 +Tanaka, S.63396
 +Tanaka, T.63392
 +Tanaka, T.62683
 +Tanaka, T.62735
 +Tanaka, Y.60105
 +Tanaka, Y.64556
 +Tanaka, Y.64557

- +Tananov, A.I.63360
 +Tanbun-et, T.61150
 +Tandon, P.N.62868
 +Tandy, P.C.60179
 Tang, C.-M. +64172
 +Tang, K.61195
 +Tang, K.T.63534
 Tang, K.Y. +60810
 +Tang Houshun.63439
 Tang Ma Rong.
 see Ma Rong Tang
 +Tange, H.62788
 +Tani, N.62980
 +Tanifuji, T.61308
 +Tanigawa, Y.61407
 +Taniguchi, Y.61352
 Tanimoto, M. +62631
 Tanis, J.A. +60934
 Taniuti, T. +61634
 tani, T. +59895
 Tank, Z.Q. +61462
 Tanke, H.J. +63920
 +Tanner, B.K.62691
 +Tanner, D.P.63688
 +Tanoue, H.62777
 +Tanouti, B.63560
 Tao Du-chum.61499
 Tao Huang. *see* Huang Tao
 +Tapeley, B.D.64265
 +Taqqu, D.60537
 +Taquet, B.60448
 Taraduy, V.T. +64337
 +Tarasenko, V.F.60644
 +Tarasov, E.A.61201
 +Tarasov, E.N.62709
 Tarenkov, V.Yu. +62524
 Tarhoumi, M. +62727
 +Tarle, G.60558
 +Tarnovskii, G.V.60337
 +Tarrach, R.59999
 +Tarrago, G.61134
 +Tarrant, D.63709
 +Tartakovsky, V.K.60172
 Tarte, P. +61866
 +Tarulis, V.P.61244
 +Tarusawa, Y.62745
 +Tarutin, I.G.63928
 +Tarutin, L.G.63930
 +Tasaki, A.62858
 Tasdemiroglu, E. +63645
 +Tasdemiroglu, E.63646
 +Tasdemiroglu, E.63727
 +Tashita, K.62712
 +Tashliev, K.62412
 Taskine, A. +62110
 +Tasman, A.63830
 +Tassi, A.62537
 +Tassi, A.62590
 +Tassin, J.F.63048
 +Tassoul, J.-L.64463
 Tassoul, M. +64463
 Tata, X.R. +59948
 Tatarinov, S.I. +62104
 +Tatarov, O.O.63434
 +Tatevskii, V.M.60593
 +Tatsuyama, C.62245
 +Tavan, P.62211
 +Tavares, M.63751
 +Tavares, J.M.63945
 +Tavernier, J.60066
 Tawada, Y. +63685
 +Tawara, Y.64556
 +Tawara, Y.64557
 Taylor, B. +64120
 +Taylor, C.K.63519
 +Taylor, D.60508
 +Taylor, J.B.62250
 +Taylor, J.C. +61899
 +Taylor, K.V.60728
 Taylor, R.A. +62682
 Taylor, R.G. +60237
 +Taylor, S.R.64043
 +Tchountonov, G.64392
 +Teather, G.G.60971
 +Tegelara, P.M.H.L.62562
 Teig, L.J. +60070
 +Teig, L.J.60083
 +Teig, L.J.60042
 +Teirlinck, D.63416
 Teitel, E.I. +63287
 +Teitgen, R.61537
 +Teitler, S.59687
 +Teixeira, J.61760
 Tejedor, M. +62696
 +Tejessy, W.60533
 +Tekulia-Buxbaum, P.
 62391
 Telegin, L.S. +61236
 +Telesnin, R.V.62780
 +Telesnin, R.V.62781
 +Telesnin, R.V.62810
 +Tel'minov, E.N.60644
 +Tel'nov, V.I.60535
 +Telnyuk-Adamchuk, V.V.
 64396
 +Temam, R.61473
 Temkin, A.60989
 Tempel, A. +62309
 Ten Bosch, A. +62101
 Ten Haken, R.K. +63973
 Tena, F. +64191
 Tench, R.E. +60856
 Tendeloo, G. Van
 see Van Tendeloo, G.
 Tendler, R.H. de
 see de Tendler, R.H.
 Teng Hsueh-Ying
 see Hsueh-Ying Teng
 +Tengstal, C.G.63095
 +Tenishev, A.E.60164
 Tennakone, K.62408
 Tennakone, K. +62964
 +Tennyson, J.60885
 +Tennyson, R.C.61427
 +Tepley, C.A.64281
 +Teplitz, D.C.64568
 +Teplitz, V.L.64568
 +Teplov, P.P.61709
 +Teplov, P.P.61710
 +Teplov, P.P.61711
 +Teplov, P.P.61687
 +Teplov, V.A.63344
 +Teplyashin, L.L.61204
 +Tepore, A.62424
 ter Haar, D.61650
 Ter-Pogossian, M.M. +
 63935
 +Terada, A.62282
 +Terakura, K.62566
 Terao, K.61516
 +Terawa, Y.63451
 +Terekhov, V.N.63361
 +Tereshchenko, N.A.63423
 +Ternovskaya, M.F.61234
 +Terrissol, M.63127
 +Tertoolen, L.G.J.64004
 Teschke, O. +62291
 Teshima, T. +60003
 +Teshya, B.M.63467
 +Tetsmer, J.63612
 +Tessari, C.63701
 +Tessier, M.62727
 +Tete, C.63416
 Tetsuka, T. +61614
 +Tewordt, L.62202
 +Texist-Hervo, C.61950
 +Tezey, N.63162
 Thakur, A.N. +60878
 Thatcher, W.64076
 Thaw, H.H. +64014
 +The, P.S.64520
 +The, P.S.64466
 +Themans, B.61900
 +Theobald, F.61900
 +Theocharopoulos, P.60533
 Theoleyre, S. +62154
 Therez, F. +62490
 Thiehl, G. +63086
 Thiemens, M.H. +64403
 +Thierens, H.M.60112
 +Thiessen, J.W. (ed.). 59542
 +Thimmarayappa, H.M.
 61503
 +Thirumalai, K.60307
 Thiry, P.A. +63096
 +Thiry, P.A.62265
 +Thistlethwaite, P.60787
 +Tholence, J.L.62719
 +Tholence, J.L.62633
 +Tholence, J.L.62725
 +Thomalla, E.64235
 Thomas, B.W. +62462
 +Thomas, D.A.61824
 +Thomas, G.63266
 Thomas, G.F.59674
 +Thomas, H.J.60944
 +Thomas, J.-M.61493
 Thomas, L.H.59565
 +Thomas, M.F.62865
 +Thomas, T.D.60999
 +Thomaz, M.F.63038
 +Thompson, A.60991
 +Thompson, A.W.63401
 +Thompson, G.64494
 Thompson, I.J. +60194
 +Thompson, J.60074
 Thompson, J.D. +62091
 Thompson, K.F. +64005
 +Thompson, M.N.61704
 +Thompson, P.61885
 +Thompson, R.60237
 Thomsen, J.S.60638
 +Thomsen, K.61637
 +Thomsen, K.61636
 +Thomsen, K.61635
 +Thomsen, M.F.64314
 +Thomsen, M.F.64315
 +Thomsom, G.60087
 +Thomson, G.60081
 Thoret, J.61863
 +Thorndike, E.H.60049
 Thorne, S.W. +63795
 Thornton, P.H. +63390
 +Thoulouze, D.62206
 +Thresher, J.J.60068
 +Thron, J.60083
 +Thron, J.60042
 +Thron, J.L.60070
 Thuc, D.D. +63545
 Thuc, D.D. +63608
 +Thuillier, G.64283
 Thulke, W. +61886
 +Thulstrup, E.W.60799
 Thunvik, R. +60306
 Thurn, G. +63474
 Tian-jun Chen +59926
 +Tichina, I.I.62078
 +Tichler, J.63753
 +Tiebel, R.61221
 +Tieger, D.60043
 Tielian, G. +62944
 +Tien, C.61548
 +Tien, C.L.61391
 +Tien, C.L.61392
 +Tien, J.K.62168
 +Tiersten, H.F.61413
 +Tiezzi, E.63786
 +Tighe, W.61655
 Tikhonov, A.K. +63454
 +Tilquin, C.63822
 Tily, P.J.61577
 +Timm, U.59995
 +Timmermans, J.60534
 +Timofeev, F.N.61156
 Timoshchuk, V.I. +62710
 Tinaut, D. +63727
 +Tinaut, D.63647
 +Tinaut, D.63645
 +Tinaut, D.64191
 +Tinet, D.62822
 Ting-Yung Hu +63374
 Tinh Nguyen Huu
 see Nguyen Huu Tinh
 Tipper, J.C.64087
 +Tipping, J.62187
 +Tipton, T.60769
 +Tirozzi, B.59720
 +Tishchenko, A.V.61306
 +Tishchenko, A.V.63087
 +Tishina, E.M.61163
 +Tishkovets, V.P.64233
 +Titov, N.A.60163
 +Titov, S.A.60745
 +Titov, V.P.62121
 +Titov, V.V.63923
 +Tijova, N.M.61832
 +Tittel, B.64059
 +Tittel, F.K.60738
 +Tittel, F.K.60831
 +Tittmann, B.R.61360
 Tiwari, R. +61560
 Tiwary, S.N.60599
 Tjotta, J. *see* Naze Tjotta, J.
 +Tjotta, S.61343
 +Tkach, A.N.63421
 +Tkachenko, V.A.63222
 +Tkachev, A.N.60909
 +Tkachev, A.N.62679
 +Tkaczky, S.60077
 +Tleuzhanov, A.B.61140
 +Toba, H.62747
 +Tobazeon, R.62154
 +Tobias, G.S.63825
 +Tobin, R.C.61908
 +Tobin, R.G.62966
 +Tobin, R.G.62984
 Tobocman, W.60151
 Toburen, L.H. +60937
 Toby, B.H. +63590
 +Toby, B.H.62259
 +Toby, B.H.63099
 +Todd, A.M.M.61691
 +Todd, S.63496
 Toepel, R. +63606
 +Togami, Y.62945
 Tognetti, V. +62671
 +Tognetti, V.62569
 +Tognetti, V.62657
 +Tohda, T.63058
 Tohsaki-Suzuki, A. +60191
 +Toki, H.60193
 +Tokovoy, O.K.62145
 +Tokoz, M.N.64043
 +Tokuda, K.60910
 +Tokuda, M.61308
 Tokura, I. +61379
 +Tokuyama, T.62806
 +Tolaryia, V.N.63367
 +Tolpygo, K.B.62343
 +Tolstenko, E.V.63426
 +Tolstolutskaia, G.D.
 61988
 +Tolstykh, G.D.61336
 +Tolutis, R.62440
 +Tom, V.T.64277
 Toma, H. +63743
 +Tomaciello, R.63699
 Tomandi, G. +63227
 +Tomassello, P.60595
 Tombrello, T.A.64367
 Tombrello, T.A.64409
 +Tomlin, V.I.60825
 Tomina, K. +63155
 +Tomina, K.62563
 +Tomio, L.60155
 +Tomio, H.59895
 +Tomishima, Y.61015
 Tomita, Y. +63403
 +Tomkinson, J.62272
 +Tomlinson, A.64001
 +Tomlinson, A.A.G.63083
 +Tomokoyi, Y.61799
 Tonegawa, T.62540
 +Tonegawa, T.62654
 +Tonejc, A.M.63253
 +Toney, K.64037
 Tong, T.W. +61391
 Tong, T.W. +61392
 Tong, Y.C. +63861
 Tong-Nyong Lee61651
 +Tonkoshkur, A.S.62426
 +Tonkov, M.V.60722
 Tonomura, A.62769
 Topchilo, N.A.64400
 Topler, J. +63741
 +Topsoe, H.62857
 +Toriyama, T.62863
 +Torkar, K.M.64296
 +Torok, I.60944
 +Toronov, O.G.61606
 +Toroptseva, T.N.63573
 +Torossian, A.60425
 +Torossian, A.60427
 +Torr, D.J.64293
 +Torreao, J.R.A.60065
 +Torrini, A.61991
 +Torrini, L.63126
 +Torrini, L.61991
 +Torstenfelt, B. +60313
 +Torstenfelt, B.60322
 +Torstenfelt, B.60316
 +Torstenfelt, B.60320
 Toscano, E.H.63368
 +Tosi, M.P.61757
 +Tostevin, J.A.60167
 +Totsuka, Y.60031
 +Totsuka, Y.60059
 Toussaint, D. +60030
 +Towne, N.60491
 Townes, C.H.64019
 +Townsend, H.E.63453
 +Townsend, P.K.59939
 +Toyoda, K.59874
 +Toyoda, M.64229
 Toyoda, T. +59626
 Toyokawa, R. +60468
 +Toyota, N.59788
 Trad, A.61320
 +Trader, K.63711
 Trager, F. +62224
 +Trahern, G.60049
 Trail, C.C. +60953
 +Trainor, J.H.64336
 +Tramer, A.60797
 +Tran, M.W.61639
 +Tran, N.H.60673
 +Tran Minh Duc59900
 +Tran N'Guyen, H.62137
 +Trapani, G.63855
 Trauboth, H. +60347
 Travis, B.J. +60327
 Travnikova, N.P. +63847
 +Treado, P.A.60182
 Trefftz, E.60992
 +Trehan, P.N.60131
 +Trehan, S.K.64302
 +Treichel, R.63565
 +Treilleux, M.61943
 Treiman, A.H. +64089
 +Tremblay, A.-M.S.62216
 +Trentadue, L.60058
 +Treve, Y.M.61473
 +Tribbey, C.L.60073
 +Tribbitt, H.63825
 +Tributsch, H.63582
 +Trifonov, A.S.59821
 Trimble, V.64496
 +Trinquier, J.59887
 +Tripathi, H.B.60786
 +Tripathi, A.60670
 +Tristram, G.60085
 +Trivig, G.60941
 +Troade, J.P.59731
 +Troccaz, M.61947
 +Trofimenko, M.Yu.62453
 +Trokhimchuk, A.D.61754
 +Tropchenko, A.Yu.61264
 Tropp, J. +62813
 Trotman, D.L. +60469
 Trouve, J. +62144
 Troyan, V.I.64232
 +Troyanova, N.I.63758
 +Trubachev, A.M.59805
 Trudgill, S.T.64126
 +Truhlar, D.G.61006
 +Trukhin, A.N.63019
 +Trukhin, V.N.62925
 +Trullinger, S.E.59718
 +Truman, A.59631
 +Truman, A.59746
 Trumper, J.64343
 +Truol, P.60208
 Truswell, E.M.64117
 Trzciński, W. +61543
 +Tsai, C.C.60528
 Tsallis, C.62620
 +Tsallis, C.62660
 Tsang, J.C. +62968
 +Tsaplin, B.A.61831
 +Tsarenkov, B.V.62497
 Tsarenkov, G.V.63052
 +Tsarev, O.M.61887
 Tsane, A. Ya.60696
 +Tsendrovskii, V.A.61109
 +Tsent, E.S.63689
 +Tsubokawa, T.D.61045
 Tsidi'kovskii, I.M. +61649
 +Tsinganos, K.64368
 +Tsintsadze, N.L.61649
 Tsirkunova, S.E. +61876
 Tso-hsiu Ho. *see* Ho Tso-hsiu
 Tso-hsiu Ho. *see* Po Tso-hsiu
 +Tsuchimoto, S.62751
 +Tsuchiya, T.62887
 +Tsuchiya, Y.61775
 Tsuchiya, T. +63349
 +Tsuda, S.63686
 +Tsuge, K.63685
 Tsuji, M. +59885
 Tsujimoto, H. +62737
 +Tsujimura, A.62815
 Tsukabayashi, I. +61629
 Tsukahara, S. +62777
 +Tsukahara, S.62735
 Tsukamoto, K.63140
 Tsukamoto, T.60108
 +Tsukanov, V.G.62504
 +Tsukishima, T.61614
 Tsukruk, V.V. +61830
 +Tsukruk, V.V.61774
 +Tsunashima, S.62746
 +Tsunemi, H.64556
 +Tsunemi, H.64557
 +Tsunenari, T.63394
 +Tsono, K.64557
 Tsuru, K. +62559
 Tsuru, K. +62568
 Tsuya, N. +62787
 +Tsvetkov, V.Yu.62694
 +Tsvetyskii, V.L.61444
 Tsykalo, A.L. +61792
 Tsytoich, V.N.64040
 Tsytoich, V.N.64332
 +Tsytoich, V.N.61170
 +Tu, G.Z.59624
 Tu Chen +62748
 Tu Khiet61646
 +Tubman, K.M.64045
 +Tuck, B.62167
 +Tuleta, M.63060
 +Tulinov, B.M.61453
 +Tullborg, E.L.60316
 +Tuller, H.L.62377
 Tully, F.P.63508
 +Tully, J.C.59681
 +Tul'skii, S.A.61251
 +Tulunay-Keesey, U.63844
 Tunan Ruan
 see Ruan Tunan
 +Tunnell, L.60964
 +Tunnell, L.N.60506
 Tur, M. +61294
 +Turek, P.60189
 +Turek, P.60104
 Turkes, P.62194
 +Turkevich, L.A.62602
 +Turlet, J.M.63012
 +Turlet, J.M.63033
 +Turner, A.P.L.63472
 +Turner, D.L.60752
 Turner, G.B. +63709
 +Turner, M.F.61684
 +Turner, M.S.64370
 +Turner, P.S.60277
 Turok, N.64565
 +Turov, A.61990
 +Turov, E.A.62506
 +Turp, J.E.60756
 Tursunov, A.T. +60679
 +Tur'yanskii, A.G.62298
 +Tusche, R.63206
 +Tuszynski, J.61186
 Tuszynski, J.A. +62796
 +Tuyn, J.W.N.60475
 +Tvardauskas, G.62443
 Tway, P.C. +60814
 +Twerenbold, D.64446
 Twigg, M.E.63112
 Twizell, E.H. +61408
 +Tyapunina, N.A.61911
 +Tyler, S.K.60405
 +Tyrlirk-Held, J.63266
 Tyson, J. +62859
 +Tyurin, A.V.62453
 +Tyurina, E.G.61375
 Ubelis, A.P. +60659
 +Uchikawa, S.61689

- + Uchiki, H. 60849
 + Uchishiba, H. 62758
 Uchiyama, M. + 61574
 + Uchiyama, S. 62746
 + Uda, M. 63627
 Uddholm, P. 61412
 Uddholm, P. 61610
 + Udoev, Yu.P. 61276
 Ueba, H. 60693
 + Ueba, H. 62245
 + Ueda, S. 62286
 + Uedaira, S. 62784
 Uehara, G. + 62531
 + Uehara, T. 60432
 + Uekusa, H. 62745
 + Uemori, R. 63299
 Uemura, Y.J. + 62627
 + Ueno, T. 61528
 + Ugliengo, P. 61907
 + Uhlmann, D.R. 62067
 + Uhrmacher, M. 60078
 + Uhllein, Ch. 63036
 Uhllein Ch. *see* Ch Uhllein
 + Ujihara, K. 61222
 + Ukhanov, Yu.I. 62995
 + Ulbricht, A. 60437
 + Ullal, H.S. 63688
 + Ullaland, O. 60075
 + Ullrich, H. 59897
 Ullrich, R.I. 63891
 + Ulmanis, A. 62764
 + Ulmschneider, P. 64456
 Ul'yanov, K.N. + 61600
 + Ul'yanov, K.N. 61724
 + Un Chul Lee. 60352
 + Underhill, A.E. 62403
 Une, K. 60239
 + Unger, D.G. 59960
 Unger, D.J. + 63437
 Ungier, L. + 60999
 + Unno, H. 63178
 Unoki, H. 62089
 Unruh, K.M. + 62607
 + Uo, K. 61698
 Uosaki, K. + 63718
 Upadhyaya, G.S. + 63212
 + Uppal, G.S. 64198
 + Urai, A. 60526
 Uramoto, J. 63175
 Uray, L. + 62391
 + Urbanski, M. 59762
 + Urculo, R. 63646
 + Urunbaev, B.M. 59798
 + Urvaeva, N.L. 59836
 + Uryu, N. 62559
 + Uryu, N. 62568
 + Usha Devi, K. 64305
 + Ushakov, A.Yu. 62452
 + Ushakov, A.Yu. 62934
 + Ushioda, S. 62974
 + Ushiroda, S. 61599
 + Ushveridze, A.G. 59921
 Uskokovic, D. + 63207
 + Uskov, A.V. 62504
 + Usmanova, G.Sh. 63365
 + Usov, A.A. 61892
 + Usov, Yu.A. 60086
 + Usova, N.A. 59678
 + Ustinov, A.I. 63345
 + Ustinov, A.I. 61834
 + Ustinov, N.D. 64398
 + Ustinov, V.V. 62506
 Utsunomiya, T. 61057
 Utsunomiya, T. 64311
 Utley, C.A. 60516
 + Uvarov, V.L. 62890
 + Uvarova, T.G. 61890
 + Uyukin, E.M. 62924
 + Uyukin, E.M. 62454
 + Valenti, G. 60071
 + Valiev, L.M. 62695
 Valisalo, P. + 61397
 + Valkovic, V. 63616
 + Valkovic, V. 63614
 Valukana, L. + 63025
 + Valladas, G. 60546
 Vallascas, R. 61571
 Valle, J.W.F. 60144
 Vallee, J.P. 64533
 Vallis, G.K. 64170
 + Valnicke, B.I. 64347
 + Valyaeva, L.E. 63477
 + Valyukenas, V.-I.Yu. 62462
 + van Andel, I. 62205
 van Beek, G. Jansen *see* Jansen van Beek, G.
 + van Beelen, H. 62205
 van Beveren, E. 60037
 + Van Bibber, K. 60199
 van de Vate, J.F. + 60384
 + Van de Vorst, A. 63768
 + van den Doel, C.P. 59659
 + Van der Avoird, A. 60885
 + van der Eerden, J.P. 61836
 van der Geer, C.A.J. + 60467
 + Van der Hiede, J.A. 63615
 van der Hoek, B. + 61918
 van der Klink, J.J. + 62901
 + Van der Lee, T. 60885
 + van der Linden, W.H. 61918
 + van der Ploeg, J.P.M. 60795
 + van der Pluym, J. 60203
 + Van Der Schaaf, P.J. 63452
 Van der Voo, R. 64034
 van Dishoeck, E.F. + 60604
 van Dommelen, L.L. + 61491
 + Van Dorp, J.H. 62075
 + Van Driel-Kulker, A.M.J. 63920
 + van Duynveldt, A.J. 62562
 + van Duynveldt, A.J. 62594
 Van Dyck, D. + 61742
 + van Eck, J. 63503
 + Van Eck, T. 64064
 + van Enckevort, W.J.P. 61918
 + Van Hecke, H. 60049
 Van Hieu Nguyen *see* Nguyen Van Hieu
 + van Houtte, D. 60972
 van Khang Nguyen *see* Nguyen van Khang
 + van Koppen, P.A.M. 63525
 + van Leeuwen, W.F. 60384
 + van Lenthe, J.H. 60608
 + Van Leuven, P. 60158
 + van Mark, E. 60456
 van Meeteren, A. + 63829
 + van Norren, D. 63839
 Van Overstraeten, R. + 63681
 + van Paradis, J. 64556
 van Pijkeren, D. + 63503
 + van Ramele, H.J.F. 60467
 + Van Staa, R. 59995
 + van Staple, R.P. 63157
 + van Strijp, R.M. 63696
 Van Swijghoven, H. + 60417
 + van Swol, R. 60534
 + Van Tendeloo, G. 61742
 + van Veen, N. 60860
 van Westenbrugge, J.K. + 60381
 + van Willigen, H. 62834
 Van Wood, E. + 61255
 + van Zee, R.J. 60764
 Van Zoelen, E.J.J. + 64004
 + Vana, N. 61966
 + Vanden Kerchove, F. 63445
 + Vandenbergh, C. 60358
 + Vandenbergh, R.E. 62839
 + Vandermeeulen, W. 60415
 Vanderschaeve, G. 61921
 Vanek, J. + 64050
 + Vanek, J. 64058
 Vanichkin, P.G. + 60514
 + Vanin, V. 61107
 + Vankan, J.M.J. 62838
 + Vankatesan, C. 61438
 + Vanquickenborne, L.G. 63511
 + Varadhan, S.R.S. 62350
 Varakin, V.N. + 61021
 Varentsov, V.L. + 60751
 + Varga, Z. 62918
 + Varganov, V.A. 63332
 + Varghese, S.L. 60506
 + Varghese, S.L. 60964
 + Varisico, G. 60497
 Varisov, A.Z. 61024
 Varisov, A.Z. 61025
 Varshava, S.S. + 62460
 + Varshneya, N.C. 64201
 + Vartsky, D. 63948
 Vasan, V.S. + 60887
 + Vashishta, P. 62090
 Vasichev, B.N. + 59760
 Vasichev, B.N. + 59889
 + Vasichev, B.N. 61311
 Vasilenko, I.I. + 63420
 + Vasilenko, N.A. 64406
 + Vasiets, P.A. 61191
 Vasil'ev, A.N. + 60542
 + Vasil'ev, B.I. 61192
 + Vasil'ev, S.N. 61710
 + Vasil'ev, V.I. 61709
 + Vasil'ev, V.I. 61682
 Vasil'eva, M.A. + 61279
 Vasilevskii, M.J. + 62174
 + Vasilyev, A.N. 60086
 Vasil'yeva, E.V. + 63258
 + Vasin, A.V. 63601
 + Vassent, B. 60243
 Vasseur, P. + 61507
 + Vassiliadis, G. 60533
 Vate, J.F. van de *see* Vate, J.F.
 + Vatnitskii, S.M. 63927
 + Vatsenko, A.I. 64402
 + Vauclair, G. 64461
 + Vauclair, S. 64461
 Vaughan, H.C. + 64269
 + Vautrey, L. 63653
 Vayonakis, C.E. 64566
 + Vaz, L.P.R. 64511
 + v.d. Lans, J. 60074
 + Vecchia, P. 62913
 Vecchio, R.S. + 63419
 Vedel, J. 61670
 + Veeaman, W.S. 62838
 Veen, N. van *see* van Veen, N.
 + Vogh, E. 60343
 + Vehanen, A. 61979
 Veit, I. 61369
 Veitsman, E.V. 62217
 + Vektaris, G. 63025
 + Velasco, J. 60534
 + Velasco, B. R.M. 61029
 + Velden, L. 64525
 + Veldhuis, A. 64286
 + Velichko, I.A. 61838
 + Velichko, V.Ya. 62339
 + Velikanova, T.Ya. 63259
 + Velikova, N.G. 63270
 + Velikova, N.G. 63271
 + Velisek, J. 62126
 + Vella, E. 60074
 Velu, E. + 62595
 Venkata Narayana, N. 61558
 Venkatachari, R. + 64207
 Venkatanarayana, R. + 64307
 + Venkatesan, K. 59671
 + Venslav, Yu.M. 63404
 + Ventskovich, Z.P. 63320
 + Venturi, P. 63624
 + Venturini, V. 60497
 + Venugopal, V.R. 64556
 + Veprek, S. 63069
 + Vera, E. 63690
 Verdier, A. 60487
 + Verdier, P.H. 63011
 + Vereshchagin, Yu.A. 61844
 + Verheul, H. 63614
 Verkin, B.I. + 63307
 + Verma, A.L. 63024
 + Verma, G. 62353
 Verma, K.K. + 60802
 Verma, K.K. + 60803
 Verma, S.L. + 59793
 + Verma, V.P. 64200
 + Vernaz, E. 60270
 Vernikov, M.A. + 60793
 Verolainen, Ya.F. 59659
 Verolainen, Ya.F. + 60625
 Veroshin, A.V. + 62042
 + Veselova, T.V. 60827
 Vesna, V.A. + 60163
 Vessot, R.F.C. + 64390
 + Vetter, V.V. 62764
 + Vetschkin, I.D. 63618
 + Vetrov, V.Yu. 61794
 + Vetrov, V.Yu. 61795
 + Vetter, A.M. 60491
 Vettermann, S. + 60597
 + Vetukhnovskaya, Yu.N. 64547
 + Via, G.H. 63081
 + Viallet, P. 61016
 + Vickerman, J.C. 63592
 + Vicsek, T. 63196
 + Vidal, B. 60698
 + Vidal, C. 59682
 + Vidal, C.R. 60770
 + Vidal, M. 60076
 Vidal-Madjar, A. + 64524
 Vid'machenko, A.P. 64420
 + Vidmar, P.J. 61342
 + Vieillard-Baron, B. 63413
 + Viesti, G. 60532
 + Vietzke, E. 60418
 + Vigdorovich, E.N. 63139
 Vigier, G. + 62394
 Vigue, J. + 61012
 + Vigue, J. 60883
 + Vijayan, P.N.M.R. 60476
 + Vikhnam, V.S. 62800
 + Viksman, G.Sh. 62078
 + Viktoravichyus, V. 62464
 Viktorova, E.N. + 60827
 Viallonga, E. + 60920
 Vilas, J.F.A. 64029
 Villea Mendes, R. 59677
 + Vilok, L.V. 61815
 + Villanueva, A. 63999
 Villameur, A. 63641
 + Villeneuve, G. 62459
 + Villeneuve, G. 60127
 + Vinai, F. 62608
 Vincent, H. + 61884
 + Vinciguena, D. 60187
 + Vineyard, M.F. 60197
 Vinh Tan Ha *see* Ha Vinh Tan
 + Vinogradov, A.S. 60744
 + Vinogradov, A.S. 60745
 + Vinogradov, A.V. 63428
 + Vinogradov, E.A. 62044
 + Vinogradov, E.A. 63072
 + Vinogradov, I.P. + 60868
 + Vinogradova, M.N. 62369
 Vinokur, B.B. 63418
 Vis, R.D. + 63614
 + Vis, R.D. 63616
 Vishnevskii, N.K. + 60541
 + Vishnevskii, N.K. 60542
 Viswanathan, R. + 62257
 Vita, P.D. *see* Di Vita, P.
 Vitali, G. + 61961
 Vitiaz, P.A. 63201
 + Viticoli, S. 62633
 Vitiello, S.A.S. + 60169
 Vitkavage, D. + 63564
 Vit'ko, V.I. + 63079
 Vittori, M. + 63295
 + Vittori, A. 60098
 + Viviani, A. 60439
 + Vladilo, G. 64472
 Vladimirov, V.I. + 61916
 + Vlasov, K.B. 62710
 + Voelkel, N.F. 63883
 + Voelzl, M. 63986
 + Vogel, O. 62277
 Vogelbruch, K. + 60418
 + Vogelsberger, W. 63606
 + Voges, U. 60347
 Vogt, H. + 63609
 + Vogt, M. 63578
 + Vogt, N. 64511
 + Vogt, O. 62573
 + Voht, P. 63172
 + Vohra, K.G. 63509
 + Vohra, K.G. 64176
 Voiculescu, D. + 61422
 Voigt, K. + 63168
 + Voigt, K. 63249
 Voishvillo, N.A. + 61089
 + Voitekhova, E.A. 63583
 Voitovich, A.P. + 61204
 Voitsekhovskii, V.N. + 61838
 + Voitsenya, A.V. 63079
 Vol'fson, L.Yu. + 61311
 + Volk, C.H. 60655
 + Volk, G.P. 63217
 + Volkotrub, N.P. 62372
 Volkov, A.D. + 61707
 Volkov, A.V. + 61931
 + Volland, H. 64162
 Vollmer, O. + 60455
 + Vollmer, O. 60529
 Volokhov, V.M. + 60931
 Voloshin, A.S. + 63884
 Voloshin, S.A. + 60011
 Volovich, I.V. 59924
 + Volovik, V.D. 63055
 + Volte, A. 60085
 Volynets, F.K. + 61835
 von Arb, H.P. + 60537
 + von der Decken, C.B. 60335
 + von Heimendahl, M. 61976
 + von Holt, K. 60073
 + von Krogh, J. 60031
 + von Krogh, J. 60059
 + von Lohneysen, H. 62613
 + von Raben, K.U. 62955
 + von Rosenvinge, T.T. 64431
 Voo, R. Van der *see* Van der Voo, R.
 + Voorhees, L.D. 60263
 Vorakso, I.K.h. + 59776
 Vorchenko, A.I. 61727
 + Vorob'ev, A.A. 60499
 Vorob'ev, L.E. + 62934
 Vorob'ev, V.M. + 61657
 Vorob'ev, V.P. + 63054
 Vorob'ev, V.V. + 62679
 + Vorob'ev, Yu.D. 62764
 + Vorob'ev, L.E. 61279
 Voronenko, B.I. 63486
 Voronin, A.P. + 63221
 Voronov, A.P. + 61278
 + Voronov, V.V. 60181
 + Voronova, T.A. 63258
 Voronyuk, L.V. + 60664
 Voroshilov, V.I. + 64530
 + Voroshilov, V.I. 64531
 Vorozheikin, V.S. + 61113
 Vorst, A. Van de *see* Van de Vorst, A.
 Vos, A.De *see* De Vos, A.
 Voskresenskaya, V.I. + 61248
 + Voss, A. 63889
 Vourvopoulos, G. 60190
 Voutsas, G.P. + 61898
 + Voyekhova, E.V. 63264
 Vrestal, J. + 62126
 V.Sidis *see* Sidis V.
 + Vtyurin, B.M. 63967
 Vul, A. Ya. + 62487
 + Vulcan, W.F. 60043
 + Vul'f, L.B. 63435
 + Vulpiani, A. 62463
 + Vygovskaya, E.A. 62501
 + Vylegzhnin, B.V. 59853
 + Vylegzhnin, O.N. 63263
 + Vysotskaya, Z.P. 61831
 + Vysotsky, M.J. 59954
 + Wachsmuth, H. 60033
 + Wachtel, H. 63599
 + Wada, H. 62558
 Wada, K. + 62656
 + Wada, M. 63299
 + Wada, M. 62599
 Wada, T. + 62220
 Wadatani, M. 59914
 Wade, R.H. + 61977
 Wadsworth, J. + 63369
 + Wadi, W.R. 61028
 Waelkens, C. + 64484
 Waelkens, C. + 64485
 Waelkens, C. + 64513
 Wagenblast, R. + 64464
 + Wagner, A. 60031
 + Wagner, A. 60059
 + Wagner, A.F. 61006
 + Wagner, D.K. 62374
 Wagner, F.E. 62847
 + Wagner, H.-G. 62790
 Wagner, J.P. 63638
 + Wagner, W. 59995
 Wagner, W.J. + 64434
 + Wah, Y.W. 60083
 + Wah, Y.W. 60042
 + Wah, Y.W. 60070
 + Wahistrom, R. 64064
 Wai, H.G. + 62578
 + Waidmann, G. 60450
 + Waith, W. 60088
 + Wakabayashi, T. 60766
 Wakamatsu, S. + 60336
 Wakao, S. + 63736
 Wakao, S. + 63561
 + Wakeham, W.A. 61596
 + Wakiyama, T. 62683
 + Wakui, K. 59864
 + Wakuta, Y. 60502
 + Walch, S.P. 60602
 + Walchli, M. 60537
 + Walck, Ch. 60073
 Wald, J.W. + 60283
 Waldrner, F. 62798
 Walker, G.E. 60173
 + Walker, J.C. 62859
 + Walker, J.C.G. 64238
 + Walker, P.J. 62865
 + Walker, R.A. 62004
 + Walkiewicz, T.A. 60110
 Wallace, D.C. + 59666
 Wallace, J. + 63239
 + Wallace, W.E. 61858
 Walmisley, C.M. 64458
 Walmisley, H.L. 61561
 Walmisley, R.G. + 61808
 + Walrafen, G.E. 62963
 + Walsh, C.A. 59685

- +Walsh, C.J. 61632
 +Walsh, D.J. 62129
 +Walter, H.K. 60203
 Walter, L. 60525
 +Walter, R.L. 60175
 +Walter, W. 60831
 +Walters, W.B. 60111
 +Walters, W.S. 63594
 +Walther, H. 64243
 Walzer, U. 62064
 +Wampler, W.R. 61659
 Wamser, C. + 64167
 Wan Yee Cheung + 60768
 +Wandelt, B. 63031
 Wang, C.H. + 62928
 Wang, C.P. 61210
 Wang, M.S. + 60893
 +Wang, P.S. 63124
 +Wang, S. 61177
 +Wang, S. 61150
 Wang, S.-C. + 61548
 +Wang, W.P. 63068
 +Wang, X. 62755
 Wang, Y.Z. + 62387
 Wang, Z.Z. + 62405
 Wang Chen-hao + 61370
 +Wang Hui-sheng 63075
 Wang Jieh-shan
 ...see Jieh-shan Wang
 +Wang Kai-ge 61145
 Wang Ming Zhong
 ...see Ming Zhong Wang
 Wang Ming Zhong
 ...see Ming Zhong Wang
 +Wang Ren 64063
 Wang Shi-kun + 69638
 +Wang Shi-kun 69637
 +Wang Zheng-guo 63893
 +Wanklyn, B.M. 62691
 Wansleben, S. + 62648
 +Wapstra, A.H. 60208
 +Ward, C.P. 60073
 +Ward, D.R. 60073
 Ward, H.E. + 63880
 Ward, L. 69824
 +Ware, B.R. 63788
 +Ware, W.R. 60819
 +Warming, P. 60031
 +Warming, P. 60059
 Warn, T. + 64171
 Warner, B. 64486
 +Warnke, M. 62202
 Warren, W.S. + 61245
 Washida, N. + 63535
 +Washiyama, M. 62283
 +Wasserman, I. 64504
 +Wassermann, E.F. 62613
 Watanabe, D. + 62683
 +Watanabe, H. 63231
 +Watanabe, H. 62596
 Watanabe, I. + 63030
 +Watanabe, K. 62860
 Watanabe, M. + 61827
 +Watanabe, N. 61747
 +Watanabe, R. 63740
 Watanabe, T. + 60446
 +Watanabe, T. 60432
 +Watanabe, Y. 60031
 +Watanabe, Y. 60059
 +Watatani, S. 62711
 +Watel, G. 60956
 Waterman, F.M. + 63976
 +Watson, H.C. 63635
 +Watson, J.W. 60099
 +Watson, J.W. 60179
 Watson, K.M. 64147
 +Watson, M.G. 64462
 Watson, R.L. + 60936
 +Watt, R.J. 63852
 +Watters, J.F. 61987
 Watterson, J.F.W. + 64261
 +Watton, A. 62824
 Watts, B.R. 61929
 Watts, J.R. + 63985
 +Waugh, A.B. 61899
 +Waugh, J.S. 62293
 +Wawrzynski, J. 60658
 Weaire, D. + 63302
 Weart, S.R. 69578
 +Weaver, B. 64079
 Weaver, D.S. + 61552
 +Weaver, M.J. 62991
 +Weaver, R. 62142
 +Webb, A.W. 61731
 +Webb, D.M. 64009
 +Webber, S.E. 60818
 +Weber, D. 60049
 Weber, G. + 62279
 +Weber, G. 60073
 +Weber, G. 60031
 +Weber, G. 60059
 Weber, H. J. + 62939
 Weber, H.-W. + 61980
 +Weber, I. 63599
 Weber, J.H. 62138
 +Webster, C.R. 60775
 +Webster, W.J., Jr. 64553
 +Weckung, G.W. 63957
 +Wedler, H. 60456
 +Weeks, J.D. 62207
 +Wegener, D. 60075
 Wegner, M.W. + 61924
 +Wei, C.-Y. 61989
 Wei Zhu
 ...see Zhu Wei
 Wei-Tou Ni + 69653
 +Weidberg, A.R. 60073
 +Weiden, N. 69802
 +Weidenmuller, H.A. 60161
 +Weigel, D. 62135
 +Weigold, E. 61001
 +Weill, G. 64283
 +Weill, R. 60068
 +Weinberg, W.H. 62259
 +Weinberg, W.H. 63099
 +Weinberg, W.H. 63590
 +Weinhold, F. 60581
 +Weinkauff, A. 62648
 +Weinlein, J.H. 64256
 Weir, G.J. 61373
 +Weiss, J.J. 61690
 +Weisberg, K.-V. 60474
 +Weisenburger, S. 60275
 Weisman, R.B. 61231
 +Weiss, A. 69802
 Weissel, J.K. 64132
 Weissman-Wenocur, D.L. + 63135
 Weitz, D.A. + 62971
 +Weitz, E. 62257
 +Welch, G. 69995
 Weller, A. + 63504
 +Weller, A. 63565
 +Wells, J. 60033
 +Wells, M.R. 62816
 Wells, O.C. 69886
 Wells, R. + 63347
 +Welsh, R.E. 60043
 +Weltner, W., Jr. 60764
 Wen Zhenyi 62378
 +Weng, S.L. 60870
 Wenming Liu
 ...see Liu Wenming
 Wensink, H. 64033
 Wenzhong Hu
 ...see Hu Wenzhong
 Wenzl, H. + 63738
 +Wenzl, H. 60412
 +Werlen, M. 60088
 +Werner, F. 60435
 Werner, J. + 62428
 Werner, J. + 64243
 +Wernhard, K.L. 60033
 Wernitz, C. 60150
 +Wert, C.A. 60235
 +Wertheim, G.K. 63133
 +Wertheim, G.K. 63134
 +Wertz, D.H. 61766
 +Wesner, D. 60870
 +Wesner, F. 60456
 Wesselinowa, J.M. 62040
 Wesson, J.A. + 61684
 West, B.J. + 62027
 +West, D.H. 64160
 +West, G.B. 60520
 West, J.M. + 60328
 +West, J.M. 60326
 +West, P.C. 69952
 +West, P.C. 69658
 West, W.P. + 60798
 +Westcott, O.M. 61987
 Westenbrugge, J.K. van
 ...see van Westenbrugge, J.K.
 +Westgate, W.M. 60561
 Westhaus, P.A. 63775
 Westmacott, K.H. + 63298
 +Westmacott, K.H. 63297
 +Westmacott, K.H. 63296
 Weston, V.H. 69597
 +Westphal, H. 63168
 Westphal, J.A. + 64270
 +Westsik, J.H., Jr. 60311
 +Westmiller, R.J. 64044
 Weytens, Ch.H.L. + 62838
 Whan Lee Young
 ...see Young Lee
 +Wheaton, J.H. 60528
 +Wheaton, W.A. 64492
 +Wheeler, B.L. 62493
 +Wheeler, D. 60224
 +Wheeler, J.C. 63546
 +Wheeler, R.L. 64046
 +Wheeler, T.G. 63838
 Whelan, D.A. + 61664
 Whitaker, B.J. + 60916
 +White, G.R. 64269
 White, I.H. + 61153
 White, J.C. + 61217
 +White, J.V. 64129
 +White, R.E. 60165
 +White, R.M. 60510
 White, R.W. + 63254
 +White, T.O. 60073
 +Whitehead, J.C. 60928
 Whitehead, J.D. + 64292
 +Whitelaw, J.H. 63550
 Whitelock, P.A. + 64487
 +Whitman, R. 60081
 +Whitman, R. 60087
 Whitmore, P.M. + 62466
 +Whittaker, E.A. 69852
 Whittemore, W.L. + 60520
 +Whittington, H.W. 63639
 Whittington, S.G. 69699
 +Whitworth, R.W. 62160
 +Whyley, R. 60043
 +Wiberg, K.B. 60715
 +Wickham-Jones, C.T. 60917
 +Wickham-Jones, C.T. 60911
 +Wickramaaratchi, M.A. 63514
 Wider, G. + 61031
 Widmer, A.E. + 61937
 Wiedenmann, A. + 62634
 Wiedenmann, A. + 62642
 Wiegand, M. 60641
 Wiegart, N.J. 61703
 +Wiegmann, P.B. 69916
 Wielopolski, L. + 63948
 +Wiese, W.L. 60649
 +Wightman, T. 69829
 +Wijayanayake, R.H. 62964
 +Wilcke, R. 60049
 Wilcoxon, J.P. + 63009
 +Wilczek, F. 60030
 +Wildenthal, B.H. 60179
 +Wilderemuth, K. 69626
 +Wilhelmi, B. 62907
 Wilhelmsson, H. + 64517
 +Wilhelmsson, H. 61170
 Wilkerson, J.F. + 60501
 +Wilkinson, C. 60041
 +Wilkinson, C. 60081
 +Wilkinson, C. 60087
 +Wilkinson, P.J. 64298
 +Wilkinson, P.N. 64555
 +Williams, A.R. 62566
 +Williams, A.T. 64124
 +Williams, B.G. 64410
 +Williams, D. 64473
 Williams, D.C. 61218
 +Williams, D.F. 63028
 +Williams, E.A. 61631
 +Williams, E.W. 63691
 +Williams, I. 64037
 +Williams, J.C. 63041
 +Williams, M.B. 69718
 +Williams, R.D. + 60142
 +Williams, S.W. + 61180
 +Williams, T.M. 61986
 +Williams, T.R. 63666
 +Williams, T.R. 63667
 +Williams, W.J. 63579
 Williamson, J.F. + 63974
 Willigen, H. van
 ...see van Willigen, H.
 +Willis, W.J. 60074
 +Willisy, A.S. 63954
 +Willson, R.F. 64433
 +Wilquet, G. 60073
 Wilsch, A. + 61592
 Wilson, C.H. + 61326
 Wilson, I.R. + 62227
 Wilson, L. + 64408
 Wilson, M.W. + 60862
 Wilson, M.W. + 60874
 +Wilson, R. 60049
 Wilson, T.A. 63873
 +Wilson, W.L., Jr. 60831
 Wiltshire, M.C.K. + 62575
 +Winde, B. 61800
 +Windle, A.H. 61822
 +Window, B. 63724
 Wine, P.H. + 60785
 +Wing, N.D. 69882
 Wing-Ki Liu 61587
 +Winik, M. 60074
 Wink, J.E. + 64553
 Winnik, M.A. + 63577
 +Winnik, M.A. 60829
 +Winscom, W.J. 60748
 Winske, D. + 61677
 +Winter, G.G. 69995
 +Winter, H. 62325
 +Winter, R.G. 60203
 +Winter, R.G. 60043
 +Winter, W. 64002
 Winterborn, K.B. 60554
 +Winterling, G. 63687
 +Winther, A. 60100
 Wismontski-Knittel, T. + 60790
 Wit, B.de
 ...see de Wit, B.
 Witcomb, M.J. + 63296
 +Witcomb, M.J. 63297
 +Witcomb, M.J. 63298
 +Witherspoon, T.C. 63293
 +Witt, A.F. 63172
 Wittberg, T.N. + 63124
 +Wittek, W. 60033
 +Wittenman, W.J. 61182
 Witten, E. 69976
 +Wittig, C. 60863
 +Wittwer, V. 63650
 +Witzeling, W. 60074
 Wlodarczyk, E. 61442
 +Wlodarczyk, E. 61674
 +Wlodarczyk, E. 61543
 +Wobig, H. 60433
 Wodkiewicz, K. + 61230
 Woensdregt, C.F. 61895
 +Wohlfarth, E.P. 62639
 +Wohn, F.K. 60111
 +Wojciechowski, S. 69621
 +Wojciechowski, W. 60588
 Wojtczak, L. + 62675
 Wolbarst, A.B. 63766
 +Wolf, A. 60111
 +Wolf, B. 64482
 Wolf, G.K. 61942
 +Wolfendale, A.W. 64559
 Wolfenden, A. 63338
 Wolfer, W.G. 61956
 +Wolfson, D.A. 63865
 Wolniowicz, H. 62011
 Wolters, G.F. 60039
 Wolters, G.F. 60047
 +Wolynes, P.G. 63531
 Won, K.W. 62052
 Won Mok Jae 60582
 Wong, A.Y. 64301
 +Wong, B.S. 63819
 Wong, J.W. + 63979
 +Wong, R.L.M. 61350
 Wong Chor
 ...see Chor Wong
 Woo Rhee Kee
 ...see Kee Woo Rhee
 Wood, C.A. 64113
 Wood, E. van
 ...see van Wood, E.
 Wood, J.W. + 61096
 Wood, K.A. + 60727
 Wood, L.J. + 64352
 +Wood, M.H. 61957
 +Wood, M.I. 63507
 +Woodard, S.E. 60510
 Woodfin, R.L. 60363
 Woodhouse, N.M.J. 69917
 +Woodis, A. 60224
 +Woodman, R.F. 64286
 Woodruff, D.P. + 62222
 +Woodruff, G.L. 60140
 Woods, C. + 61195
 +Woods, J. 63691
 +Woody, B.A. 61020
 +Woody, C. 60074
 +Wooley, C.B. 61255
 +Woolfe, G. 60787
 +Woolfson, M.S. 61762
 +Woolum, D.S. 63612
 Woon Kim Tae
 ...see Tae Woon Kim
 +Wopernow, W. 62392
 +Worlitzer, K. 61221
 Wormald, C.J. + 62074
 +Wormald, M.R. 64246
 +Wormald, M.R. 64248
 Wormald, M.R. + 64247
 +Worsk, J. 63884
 Woste, L. 60876
 Wouters, J.M. + 60112
 +Woznicka, U. 64251
 +Wriedt, H. 60031
 +Wriedt, H. 60059
 +Wright, C.J. 61768
 +Wright, K. + 69757
 +Wright, P.R.S. 60533
 +Wright, R.E. 60528
 +Wrighton, M.S. 62492
 Wrigley, S.P. + 60912
 +Wrobel, J. 60395
 Wroblewska, G. 63232
 +Wroblewski, A.K. 60077
 Wu, C.H. + 69706
 Wu, C.Y.R. + 64236
 +Wu, D. 61287
 Wu, H.Y. + 61106
 +Wu, K.C. 61462
 +Wu, T.W. 63318
 +Wu, Y.S. 62387
 Wu Cheng-li
 ...see Cheng-li Wu
 Wu Chi-Chong
 ...see Chi-Chong Wu
 Wu Chong-en
 ...see Chong-en Wu
 Wu Hang-sheng + 62532
 Wu Ke + 69645
 +Wu Ke 69637
 +Wu Ke 69638
 +Wu Mei-qin 61321
 Wu Su Xing
 ...see Su Xing Wu
 Wu Xi-zhen + 60168
 +Wu Xuejun 64362
 Wu-yun Lai
 ...see Lai Wu-yun
 +Wunsch, M. 60075
 +Wunsche, H.-J. 62341
 +Wurflinger, A. 62053
 +Wurtz, D. 69690
 +Wuthrich, K. 61031
 Wyatt, D.G. 61575
 Wyatt, R.E. + 63512
 +Wyatt, R.E. 60630
 +Wyder, P. 62637
 +Wydler, P. 63651
 +Wynne, J.J. 60768
 +Wyse, R.F.G. 64537
 Wyss, M. + 64070
 +Xi-te Zheng 69926
 Xi-zhen Chang
 ...see Chang Xi-zhen
 Xi-zhen Wu
 ...see Wu Xi-zhen
 Xianbing Liao
 ...see Liao Xianbing
 Xianming Zheng
 ...see Zheng Xianming
 Xiao-ze Zhang
 ...see Zhang Xiao-ze
 +Xie Yicheng 60019
 Xin Zhou
 ...see Zhou Xin
 Xing Wu Su
 ...see Su Xing Wu
 Xing-qi Li
 ...see Li Xing-qi
 Xitong Yu
 ...see Yu Xitong
 Xixiang Xu
 ...see Xu Xixiang
 Xu, J.-L. 64181
 Xu Chongming + 64362
 Xu Gang + 63023
 Xu Jun-hua + 61337
 Xu Qingzheng
 ...see Qingzheng Xu
 +Xu Xixiang 63065
 Xu Zhenjia + 61945
 +Xue, S.T. 69995
 Xuejun Wu
 ...see Wu Xuejun
 +Yabe, T. 60398
 Yablonskii, S.V. + 62102
 +Yabumoto, T. 63160
 +Yacamán, M.J. 61736
 Yadav, R.B. 62043
 Yadav, R.B. 62869
 Yagasaki, K. 62400
 Yagi, K. + 61299
 Yaji, T. + 63066
 Yakovenko, M.G. 61445
 +Yakovlev, V.A. 61261
 +Yakovlev, V.A. 63072
 +Yakovlev, V.V. 61514
 +Yakovlev, Yu.A. 60543
 +Yakovlev, Yu.P. 62070
 +Yakovleva, I.L. 63284
 +Yakhnin, M.A. 63021
 +Yakovskii, Ch.A. 63189
 +Yamabe, T. 69726
 Yamada, C. + 60720
 +Yamada, G. 61439
 Yamada, H. + 62980
 Yamada, I. + 62806
 +Yamada, K. 60849
 +Yamada, K. 60794
 Yamada, M. + 63672
 +Yamada, M. 62596
 +Yamada, S. 60031
 +Yamada, S. 60059
 Yamada, T. 64175
 +Yamada, T. 69715
 Yamagata, T. + 62507
 +Yamaguchi, H. 60109
 +Yamaguchi, K. 62758
 Yamaguchi, M. + 62718
 Yamaguchi, S. + 61142
 +Yamaguchi, S. 62293
 +Yamaguchi, T. 63150
 +Yamaguchi, T. 63672
 Yamaguchi, Y. + 61044
 +Yamaguchi, Y. 62826
 +Yamakido, M. 63909
 Yamamoto, H. + 62701
 +Yamamoto, H. 60111
 +Yamamoto, M. 63935
 Yamamoto, S. + 69795
 +Yamamoto, S. 63315
 Yamamoto, T. 64144
 +Yamamoto, T. 60334
 Yamamoto, Y. + 63470
 +Yamamoto, Y. 60072
 +Yamamoto, Y. 60128
 +Yamamoto, Y. 60082
 +Yamamoto, Y. 62980
 +Yamanaka, K. 61203
 Yamanaka, C. 60399
 +Yamanaka, C. 60398
 +Yamanaka, S. 62765
 +Yamasaki, S. 62496
 Yamashiro, M. + 63492

- + Yamashita, K. 64556
 + Yamashita, K. 64557
 + Yamashita, M. 63398
 + Yamashita, S. 62997
 + Yamato, M. 62721
 Yamauchi, H. + 62596
 + Yamauchi, H. 62701
 + Yamauchi, H. 61092
 Yamazaki, M. 59652
 Yamazaki, S. + 63180
 Yamazaki, T. + 62514
 + Yamazaki, T. 62627
 + Yamin, P. 60081
 + Yampolskii, V.I. 63073
 Yan Sun Liang
 + Yanada, T. 62752
 + Yanagida, H. 62878
 + Yanagida, M. 61352
 + Yanagida, T. 60022
 + Yanagihara, N. 63739
 + Yanagisawa, C. 60031
 + Yanagisawa, C. 60059
 + Yang, F.M. 62387
 + Yang, K.T. 61378
 + Yang, M. 60961
 + Yang, Q.S. 61392
 + Yang, R.T. 62247
 + Yang, S.C. + 60888
 + Yang Shuanzheng 62281
 Yang Kuo-ho
 + see Kuo-Ho Yang
 Yang Shuwen
 + see Shuwen Yang
 + Yang Ying-hui 60168
 + Yang Zhen-qing + 62055
 + Yankovskii, A.A. 63622
 + Yanovitskaya, G.T. 64337
 + Yantis, G.I. 63304
 Yao, L.S. 61506
 + Yao, L.S. 61380
 Yaouanc, A.L.
 + see Le Yaouanc, A.
 + Yarema, S.Ya. 61457
 + Yaremko, Yu.I. 61091
 + Yarkony, D.R. 60587
 + Yarkony, D.R. 60842
 + Yarmolyuk, Ya.P. + 61892
 + Yarmolyuk, Ya.P. 61852
 + Yaroslavskii, I.D. 62925
 + Yaroslavtsev, V.T. 60854
 + Yaroslavtseva, V.V. 59807
 + Yarovoi, S.S. 60593
 Yartys', V.A. 61889
 + Yaryna, V.P. 60337
 + Yashinovit, C.J. 59768
 + Yastrebov, A.B. 61192
 + Yasuda, T. 60072
 + Yasuda, T. 60082
 + Yasuoka, K. 60072
 + Yasuoka, K. 60082
 + Yates, F.E. + 63767
 + Yatsenko, L.P. 61212
 + Yatsenko, S.P. + 63261
 + Yatsenko, Yu.V. 63410
 + Yatsura, O.R. 63223
 + Yatsyshen, V.V. 61080
 + Yau, M.K. 64213
 + Yavin, A.I. 60203
 Ye Ling + 62319
 + Ye Si-mao 63893
 + Yeager, D.L. 60575
 + Yeager, D.L. 60570
 + Yeates, A.T. + 62215
 + Yee, W.A. + 60620
 + Yee Cheung Wan
 + see Wan Yee Cheung
 + Yeh, Y. + 63892
 + Yeheskel, J. + 59879
 + Yen Yu-Sze see Yu-Sze Yen
 + Yeo, J.K. + 61824
 + Yeomans, D.K. 64352
 + Yessik, M. 61178
 + Yeung, H.C. 61552
 + Yi, J.J. + 63290
 + Yi, P.N. + 63811
 + Yi-cheng Zhang 59927
 + Yi-ming Gu see Gu Yi-ming
 + Yi-zhong Zhuo
 + see Zhuo Yi-zhong
 Yicheng Xie
 + see Xie Yicheng
 + Yin, M.T. + 62318
 + Ying An
 + see An Ying
 + Ying-hui Yang
 + see Yang Ying-hui
 + Yinnon, H. + 62067
 + Yli-Kauppi, J. 61979
 + Yoder, G.L., Jr. + 61376
 + Yokoyama, T. 64556
 + Yokoyama, Y. + 62735
 + Yokoyama, Y. 62760
 + Yokoyama, Y. 61270
 + Yomosa, S. 63772
 + Yoneda, H. 60526
 + Yoneda, N. 62887
 + Yonekawa, I. 60470
 + Yonekura, Y. 62863
 + Yonemura, Y. 63561
 + Yoneta, M. 61505
 + Yoneyama, H. 59918
 + Yonezawa, Y. 62286
 + Yonezu, I. + 63732
 + Yong-shen Zhou
 + see Zhou Yong-shen
 + Yoo Kun Joong
 + see Kun Joong Yoo
 + York, D.G. 64524
 + Yorozu, H. + 63750
 + Yoshida, H. + 62164
 + Yoshida, H. + 61372
 + Yoshida, H. 60394
 + Yoshida, H. 62791
 + Yoshida, H. 62615
 + Yoshida, K. 63924
 + Yoshida, K. 60453
 + Yoshida, K. 63723
 + Yoshida, K. 63447
 + Yoshida, M. + 63013
 + Yoshie, H. 62815
 + Yoshihara, K. 60820
 + Yoshii, M. 60504
 + Yoshiie, T. + 61972
 + Yoshioka, K. 60834
 + Yoshioka, M. 62751
 + Yoshimura, K. 63091
 + Yoshino, K. + 60742
 + Yoshino, R. + 60470
 + Yoshino, R. 60461
 + Yoshioka, D. + 62432
 + Yoshioka, K. + 61689
 + Yoshizawa, M. 61240
 + You-guo Qin
 + see Qin You-guo
 + You-wen Yu
 + see Yu You-wen
 + Young, D.T. 59875
 + Young, E.T. 59841
 + Young, G.R. 60199
 + Young, I.R. + 63919
 + Young, J.L. 63752
 + Young, L. + 62151
 + Young, R.J. De
 + see De Young, R.J.
 + Young, R.T. 61965
 + Young, R.T. + 62429
 + Young Whan Lee 60353
 + Yousif, R.H. 63386
 + Yu, L.J. 61776
 + Yu, Z. 60529
 + Yu, Z. 63893
 + Yu, Z.X. 60828
 + Yu Chien-fan
 + see Chien-fan Yu
 + Yu Li Zu
 + see Li Zu Yu
 + Yu Lu 62384
 + Yu Xitong 63439
 + Yu You-wen 60001
 + Yu-Sze Yen + 62814
 + Yuan, V. 59936
 + Yuan-ben Dai
 + see Dai Yuan-ben
 + Yuasa, Y. 63492
 + Yuchuan He
 + see He Yuchuan
 + Yudenich, L.S. 62344
 + Yudin, E.G. 62021
 + Yudina, T.G. 62301
 + Yuki, T. 61010
 + Yukimoto, Y. 63693
 + Yul'berdin, Yu.F. 61157
 + Yura, H.T. + 61084
 + Yurchenko, A.G. 60760
 + Yurchikov, E.E. 63286
 + Yurevich, F.B. 64231
 + Yurke, B. + 62819
 + Yurkovskaya, A.V. 63506
 + Yurtin, I.L. 62680
 + Yuzawa, M. 61328
 + Yuzhakov, V.I. 60823
 + Yuzhakov, V.I. 60826
 + Yvert, M. 60066
 + Zabil'skii, V.V. + 63316
 + Zaborov, A.V. + 62676
 + Zadra, A. 60546
 + Zagar, L. + 63226
 + Zagar, V. 62829
 + Zagar, V. 62836
 + Zagrebini, S.B. 60995
 + Zahari, M.D. + 62167
 + Zahra, A. 63266
 + Zaider, M. 63903
 + Zaikov, G.E. 63773
 + Zaitov, F.A. + 61955
 + Zajac, G. 63089
 + Zajc, W.A. 60208
 + Zak, J. 63089
 + Zakharov, N.G. 63043
 + Zakharov, V.P. + 61642
 + Zakharova, A.A. 61487
 + Zakharova, O.K. 64219
 + Zaleskaya, G.A. 60844
 + Zaleskii, V.O. + 61194
 + Zalmanzon, Yu.E. 60557
 + Zaluzny, M. 62952
 + Zamkovoi, V.I. 60760
 + Zamlutti, C.J. 64294
 + Zammitt, U. 61961
 + Zand, M. 60290
 + Zander, A.R. 60935
 + Zaneagin, V.D. 63372
 + Zangvil, A. 63274
 + Zani, P. 63673
 + Zanon, D. 59938
 + Zapas, L.J. 63363
 + Zapata, L.E. + 61143
 + Zappala, V. 64391
 + Zare, R.N. 63556
 + Zaretskii, Yu.G. 62995
 + Zaretsky, J. 62046
 + Zargar yants, M.N. + 63444
 + Zaruba, V.N. 63482
 + Zarubo, S.V. + 62369
 + Zasadych, Yu.B. 60540
 + Zashu, S. 64092
 + Zasurskaya, L.A. 61833
 + Zavalii, P.Yu. + 61902
 + Zavorotney, Yu.D. + 63004
 + Zayakin, Yu.A. 64047
 + Zayats, N.S. 61948
 + Zaychenko, S.G. 61954
 + Zboinski, J. 59797
 + Zdanovits, L. 63076
 + Zdebs'kii, O.P. + 62898
 + Zdukowski, W. 64154
 + Zecca, A. 59881
 + Zech, G. 59995
 + Zeda, O. 64103
 + Zee, R.H. + 61987
 + Zee, R.J. van
 + see van Zee, R.J.
 + Zehaf, M. 62456
 + Zehlein, H. + 60447
 + Zehlein, H. 60438
 + Zehua Zhang
 + see Zhang Zehua
 + Zeigler, A.M. 64118
 + Zel'dovich, B.Ya. + 61788
 + Zelener, M.F. + 59828
 + Zelenin, V.P. + 59807
 + Zelenka, R.L. + 61383
 + Zeman, F. + 63173
 + Zemke, W.T. 60802
 + Zemlyanski, V.M. + 61219
 + Zemskov, V.S. + 63277
 + Zenevich, V.A. 60882
 + Zeng, Q.-C. 64173
 + Zengin, D.M. 62425
 + Zenkevich, P.R. + 60492
 + Zenkov, D.I. 61725
 + Zetsche, S. 64208
 + Zevrieva, I.F. 63970
 + Zevrieva, I.F. 63933
 + Zewail, A.H. 61245
 + Zewail, A.H. 60691
 + Zhabotinski, M.E. 61280
 + Zhadanov, B.V. + 62957
 + Zhai Hongru
 + see Hongru Zhai
 + Zhan, W.S. 62387
 + Zhang, L.S. 62724
 + Zhang, X.L. + 62876
 + Zhang, Z. + 60864
 + Zhang, Z.-T. + 62878
 + Zhang Bingrong
 + see Bingrong Zhang
 + Zhang Fang-qing 63075
 + Zhang Fangqing 63065
 + Zhang Guansheng + 63439
 + Zhang Kaiming 62319
 + Zhang Xiao-ze 60063
 + Zhang Yi-cheng
 + see Yi-cheng Zhang
 + Zhang Zehua 61945
 + Zhang Zhong-ye + 60001
 + Zhao Song-ling + 61321
 + Zhao Xie-ying 61370
 + Zhao-bin Su
 + see Su Zhao-bin
 + Zhao-hua Lin + 62688
 + Zhao-hui Meng
 + see Meng Zhao-hui
 + Zharinov, A.V. + 61715
 + Zharkova, V.V. 64441
 + Zhdanovich, G.M. + 63189
 + Zhe-ying Zhao
 + see Zhao Zhe-ying
 + Zhechuan Feng
 + see Feng Zhechuan
 + Zhen-qing Yang
 + see Yang Zhen-qing
 + Zheng Guangfu + 61146
 + Zheng Shi-gang 63893
 + Zheng Xi-te see Xi-te Zheng
 + Zheng Xianming 61146
 + Zheng-guo Wang
 + see Wang Zheng-guo
 + Zhenjia Xu
 + see Xu Zhenjia
 + Zhenyi Wen
 + see Wen Zhenyi
 + Zheviakov, A.P. 61251
 + Zhi Liu
 + see Liu Zhi
 + Zhi-an Liang
 + see Liang Zhi-an
 + Zhigalovskaya, T.N. + 63764
 + Zhigun, A.P. 63478
 + Zhikuan Chai
 + see Chai Zhikuan
 + Zhilkin, V.A. + 61469
 + Zhitnik, I.A. 64347
 + Zhitnikov, Yu.V. + 61453
 + Zhizhin, G.N. + 63072
 + Zhog Wang Ming
 + see Ming Zhog Wang
 + Zhokiver, K.I. + 63933
 + Zhong Wang Ming
 + see Ming Zhong Wang
 + Zhong-Yi Ding
 + see Ding Zhong-Yi
 + Zhong-yu Ma
 + see Ma Zhong-yu
 + Zhorin, V.A. + 62419
 + Zhorin, V.A. + 63547
 + Zhou, M.L. 60176
 + Zhou, M.L. 60186
 + Zhou Xin 62536
 + Zhou Yong-shen 63893
 + Zhu Wei + 60009
 + Zhuchkov, V.M. 62021
 + Zhuchkova, L.Ya. 60776
 + Zhukova, T.B. 62369
 + Zhuo Yi-zhong 60063
 + Zhuo Yi-zhong 60168
 + Zhuravlev, D.A. 59857
 + Zhuravlev, E.N. 62500
 + Zhuravlev, S.V. + 60826
 + Zhuravlev, N.A. 63429
 + Zia, R.K.P. 62059
 + Ziada, S. + 61484
 + Ziborov, A.I. 63017
 + Zichy, J. 62026
 + Zickgraf, F.-J. 64482
 + Ziebeck, K.R.A. 62548
 + Ziegler, P.V. + 63652
 + Zielinski, P.G. + 63282
 + Zieminski, A. 60077
 + Ziessow, D. 59810
 + Ziessow, D. 60702
 + Zignani, F. 63704
 + Zigunskaya, A.V. 61282
 + Zil'berman, V.V. 61062
 + Zil'berman, A.G. 63412
 + Zilbershtein, A.Kh. + 62923
 + Zilitis, V.A. 60672
 + Zimkina, T.M. 60744
 + Zimmermann, D. + 60465
 + Zimmermann, D. 60789
 + Zimmermann, W. 59995
 + Zin, W.A. + 63879
 + Zinchenko, Zh.F. 61458
 + Zinevich, N.I. 60496
 + Zinn, W. + 62296
 + Zinovjev, G.M. 59989
 + Zinth, W. + 60918
 + Ziock, H.J. 62213
 + Ziolkiewicz, S. 62900
 + Ziolkowski, Z. 60395
 + Zipf, E.C. 64369
 + Zipper, E. 62808
 + Zivkovic, L.J.M. + 63242
 + Zizhau Gan see Gan Zizhau
 + Zobel, V. + 60129
 + Zoelen, E.J.J. van
 + see Van Zoelen, E.J.J.
 + Zoetelief, J. + 63900
 + Zokhdi, Z. 62903
 + Zola, C.L. 61534
 + Zolin, V.F. + 60761
 + Zolina, N.K. + 61066
 + Zoll, J. 60533
 + Zolotarev, V.M. 62916
 + Zolotajuk, E.V. + 62853
 + Zolotukhin, I.V. 62782
 + Zombeck, M.V. 64344
 + Zon, B.A. 60671
 + Zong-ye Zhang
 + see Zhang Zong-ye
 + Zorkii, P.M. 61833
 + Zorn, G.T. 59995
 + Zotov, A.D. + 63381
 + Zsoldos, E. 62182
 + Zu Yu Li see Li Zu Yu
 + Zubairy, M.S. 61230
 + Zubechenko, V.S. + 63434
 + Zuberik, R. 62793
 + Zubkova, S.M. + 62343
 + Zudov, O.R. 59820
 + Zugl, W. 59834
 + Zugza, Y.D. 64437
 + Zukas, E.G. + 62088
 + Zumofen, G. 59702
 + Zundel, G. 61017
 + Zunger, A. 62361
 + Zurmuhle, R.W. 60139
 + Zushi, H. 61698
 + Zuwei Liu see Liu Zuwei
 + Zverev, V.A. + 61097
 + Zvolinskii, V.P. 60761
 + Zwanzig, R. 59684
 + Zwanzig, R. 61480
 + Zweck, J. 62739
 + Zyalov, A.A. 60164
 + Zyrnicki, W. 60736
 + Zyrnicki, W. 63559
 + Zys, J. 61226
 + Zys, J. 62810
 + Zyzin, A.M. + 62781

BIBLIOGRAPHY INDEX

- ⁶⁷Zn Mossbauer spectroscopy, (59 refs.) 62846
 Abstraction vs. exchange channels in D+HCl reaction, (58 refs.) 63522
 Acoustic emission during phase transformations in alloys, (94 refs.) 63486
 Adhesion of polymers to metal surfaces, (72 refs.) 63491
 Arctic seafloor, (75 refs.) 64119
 Atmosphere aerosol loss mechanisms, (56 refs.) 64214
 Atomic spectroscopy July-December 1982, (568 refs.) 59560
 Automatic camera lens focusing systems, (57 refs.) 59869
 Back arc spreading and arc volcanism in Philippine Sea, (52 refs.) 64137
 Basic-potential method for studying crystal potential, (124 refs.) 61850
 Beta decay and the weak interaction, (103 refs.) 59577
 Boninite magma series, (77 refs.) 64104
 Charged particle reaction cross sections and nucleosynthesis, (92 refs.) 64460
 Chronology of particle physics, (165 refs.) 59582
 Conversion electron Mossbauer spectroscopy, (83 refs.) 62849
 Crab Nebula, (51 refs.) 64528
 Cyclic and linear poly(dimethyl siloxanes) study, (53 refs.) 61032
 Diffusion of substitutional impurities in iron, (75 refs.) 62175
 Disc-like molecules and mesogenic polymorphism, (90 refs.) 61785
 Earthquake precursory seismicity patterns, (76 refs.) 64066
 Earthquake seismic precursors, (113 refs.) 64075
 Effects of ionizing radiation on amorphous insulators, (52 refs.) 61805
 Electromagnetic and weak interactions in stochastic space-time, (116 refs.) 59961

Electron-atom scattering, (123 refs.)	60988	Phase space vortices and double layers, kinetic theory, (77 refs.)	61662
Enthalpies of formation of iron alloys, (186 refs.)	63581	Photoemission from surface-atom core levels, (103 refs.)	63134
Fatigue crack closure, roughness-induced, (107 refs.)	63401	Plasma double layers, (60 refs.)	64373
Formation of disc galaxies, (107 refs.)	64537	Plate tectonics of Philippines and NE Indonesia, (66 refs.)	64065
Fractionally charged ions in crystal lattices of organic ion-radical salts, (59 refs.)	61847	Polymaleic anhydride synthesis and properties, (53 refs.)	63549
Galaxy centre H I distribution, (127 refs.)	64541	Polymerisation initiated by reducing transition metal compounds, (70 refs.)	63548
High-rate sputter deposition technique, (55 refs.)	63158	Polymorphism in polar mesogens, (81 refs.)	61779
Horizontal-branch stars, (71 refs.)	64461	Polymorphism in polar mesogens, (37 refs.)	61780
Hydrocarbon chemistry in irradiated CO ₂ /CO/CH ₄ /H ₂ O/H ₂ mixtures, (66 refs.)	63579	Polymorphism in polar mesogens, (55 refs.)	61781
Hydrological techniques involving tracers, (86 refs.)	64263	Precipitation of supersaturated aluminium-base solid solutions, (128 refs.)	63300
Indian Phanerozoic palaeomagnetism, (75 refs.)	64028	Protein adsorption in polymer-blood interaction processes, (115 refs.)	63773
Infrared laser stimulated surface processes, (64 refs.)	63587	Pulsar radiation mechanisms, (51 refs.)	64503
Infrared speckle imaging of Miras and protostars, (55 refs.)	64392	QCD cornerstones, (294 refs.)	59992
Intramolecular vibrational relaxation from C-H stretch fundamentals, (52 refs.)	60809	Quantum electrodynamics, (54 refs.)	59581
Japan earthquake prediction programme, (84 refs.)	64240	Quaternary sedimentation in South China Basin, (55 refs.)	64134
Japanese palaeomagnetism, (83 refs.)	64030	Radiation hormesis, public health and public policy, (77 refs.)	59583
Langmuir turbulence, (52 refs.)	61647	Randomly mixed magnets with competing interactions, (53 refs.)	62574
Large earthquake recurrence times, (97 refs.)	64071	Reaction Hg + I ₂ - HgI + I revisited, (58 refs.)	63527
Large earthquake repeat times, (100 refs.)	64072	Retinal colour coding, (60 refs.)	63834
Light meson spectroscopy, (190 refs.)	60006	Semiclassical determination of adiabatic barriers on a three-dimensional potential energy surface, (67 refs.)	60630
Light scattering changes in chloroplast thylakoid membranes, (57 refs.)	63795	Sensitivity to countermodulating gratings following spatiotemporal adaptation, (54 refs.)	63844
Lower trench slope off Nias Island, Sunda Arc, (65 refs.)	64135	Sheared colloidal suspensions, (70 refs.)	61544
Luminance increment and decrement time thresholds, (54 refs.)	63843	Si ₃ N ₄ preparation, reaction mechanisms, (84 refs.)	63219
Lytotropic polymeric liquid crystals, (45 refs.)	61778	Solar System sputtering, (52 refs.)	64409
Magnetism of amorphous metal-metal alloys, (67 refs.)	62566	Solution of the Kondo problem, (86 refs.)	62551
Manganese halides and sulphide, electron spin resonance at 4K, (55 refs.)	60764	Spectroscopy and integral image quality, (79 refs.)	59870
Marine magnetic anomalies from West Philippine Sea, (72 refs.)	64036	Spectroscopy of vibration assisted surface chemistry, (86 refs.)	63585
Microscopic equipment, methods, applications and related topics, (875 refs.)	59561	Standard interfaces for program-modular multiprocessor systems, nuclear physics applications, (50 refs.)	60560
Molecular and submolecular physical concepts in biology, (62 refs.)	63769	Structure and function of viroids, (58 refs.)	63774
Monte Carlo simulation of solid N ₂ , (57 refs.)	61848	Sun, gamma rays and cosmic rays, (103 refs.)	64330
Mossbauer spectroscopy and magnetism, (67 refs.)	62841	Superflows and superfluidity, (105 refs.)	62200
Mossbauer spectroscopy of implanted sources, (93 refs.)	62844	Supernovae, (760 refs.)	64496
Mossbauer spectroscopy with ^{191,193} Ir, (141 refs.)	62847	Surface electromagnetic fields, (125 refs.)	61056
Mossbauer spectroscopy with actinide elements, (58 refs.)	62848	Surface enhanced Raman scattering, (62 refs.)	62959
Mossbauer studies of valence fluctuations, (57 refs.)	62845	Surface enhanced Raman spectra, (60 refs.)	62967
Multicritical phenomena in liquid crystals, (84 refs.)	62099	Surface vibration spectroscopy by atom scattering, (54 refs.)	63119
Myopia development in nonhuman primates, (71 refs.)	63828	Technicolor, (93 refs.)	59991
Na ₂ , properties, (329 refs.)	60802	Tokai District, Japan, earthquake prediction, (165 refs.)	64074
Nematic to smectic-A transition, (60 refs.)	62098	Transparent conductors, (293 refs.)	63078
Neutral-current experiments, (99 refs.)	60034	Triatomic molecules, double excited vibr. states dynamics, (52 refs.)	60688
North American palaeomagnetism, (364 refs.)	64034	Twisted chiral mesophases, (152 refs.)	61784
Nuclear waste disposal, regulations in different countries, (62 refs.)	60231	U prospecting by γ-ray borehole methods, (125 refs.)	64255
Oxygen donor in gallium phosphide, (54 refs.)	62365	Uranium extrapolation by airborne γ-ray spectrometry, (57 refs.)	64254
Paleomagnetism and plate motions in SE Asia, (147 refs.)	64038	Valence and hybrid bond orbital theory, (97 refs.)	60562
Paleomagnetism of Australia and Antarctica, (110 refs.)	64027	Vibrational energy disposal in reactions of fluorine atoms with hydrides of groups III, IV and V, (57 refs.)	63514
Paleomagnetism of Africa and Madagascar, (96 refs.)	64026	Volcanic rocks of Philippine Sea, (102 refs.)	64103
Particle simulation of plasmas, (105 refs.)	61692	Volcanoes of Earth, Moon, Mars, Io, Venus, (113 refs.)	64408

BOOK INDEX

- Adsorption on metal surfaces. An integrated approach;** J.Bernard (editor/s). [Amsterdam, Netherlands: Elsevier 1983] 59555
- Analysis, manifolds and physics. Revised edition;** Y.Choquet-Bruhat, C.DeWitt-Morette, M.Dillard-Bleick. [Amsterdam, Netherlands: North-Holland 1982] 59554
- Channels of Mars;** V.R.Baker. [Bristol, England: Adam Hilger 1982] 59552
- Elementary statistical thermodynamics. A problems approach;** N.O.Smith. [New York, USA: Plenum 1982] 59558
- Energy reviews. Nuclear power systems. Vol.1;** L.A.Melentiev (editor/s). [Chur, Switzerland: Harwood Academic Publishers 1982] 59549
- Neutron sources. For basic physics and applications;** [Oxford, England: Pergamon 1983] 59546 (introductory abstract), 60515-25
- Paleoreconstruction of the continents;** M.W.McElhinny, D.A.Valencio (editor/s). [Washington, DC, USA: American Geophysical Union 1981] 59544 (introductory abstract), 64026-35, 64116-19
- Plutonium recycling scenario in light water reactors. Assessment of the environmental impact in the European Community;** [Chur, Switzerland: Harwood Academic Publishers 1982] 59523
- Probabilistic and statistical aspects of quantum theory;** A.S.Holevo. [Amsterdam, Netherlands: North-Holland 1982] 59557
- Realism and the aim of science;** K.R.Popper. [London, England: Hutchinson 1983] 59547
- Relativistic astrophysics;** M.Demianski. [Oxford, England: Pergamon 1981] 59551
- Research and development on radioactive waste management and storage. First annual progress report of the European Community programme 1980-1984;** [Chur, Switzerland: Harwood Academic Publishers 1982] 59548
- Spectral transform and solitons: Tools to solve and investigate nonlinear evolution equations. Vol.1;** F.Calogero, A.Degasperis. [Amsterdam, Netherlands: North-Holland 1982] 59556
- Superconductivity in ternary compounds. II. Superconductivity and magnetism;** M.B.Maple, O.Fischer (editor/s). [Berlin, Germany: Springer-Verlag 1982] 59553
- Tectonic and geologic evolution of southeast asian seas and islands;** D.E.Hayes (editor/s). [Washington, DC, USA: American Geophysical Union 1980] 59545 (introductory abstract), 64036-8, 64065, 64097-9, 64102-4, 64120, 64132-7, 64139

CONFERENCE INDEX

- Low-level waste disposal, 1982;** Arlington, VA, USA, 16-17 June 1982, [U.S. Nucl. Regul. Comm.; Oak Ridge Nat. Lab] (Oak Ridge, TN, USA: Oak Ridge Nat. Lab. 1982] 59537 (introductory abstract), 60250-68
- Advanced Space Instrumentation in Astronomy;** Ottawa, Canada, 16 May-2 June 1982, [1982] 59524 (introductory abstract), 59787, 59841, 61257, 61262, 64338-48, 64379-84, 64390
- Application of accelerators in research and industry;** Denton, TX, USA, 8-10 Nov. 1982, [DOE: NSF: D.A.R.P.A.: Naval Surface Weapons Centre; NBS; et al] [April 1983] 59528 (introductory abstract), 59882, 59899, 60104, 60131, 60147, 60174-6, 60182, 60186, 60190, 60214-15, 60232-3, 60390-3, 60491, 60506-11, 60612, 60626, 60662, 60899, 60933-53, 60963-70, 60983, 60989, 61608, 61658, 61699-700, 62003, 63088, 63113-15, 63611-17, 64367
- Astronomical Science Group of Ireland May 1981 Meeting;** Cork, Ireland, 22 May 1981, [March 1982] 59529 (introductory abstract)
- Astrophysical applications of accretion disks;** London, England, 8 Oct. 1982, [April 1983] 59533 (introductory abstract)
- Axes measurement systems;** London, England, 2 March 1983, [London, England: IEE 1983] 60346
- Earthquake prediction;** Mohonk, NY, USA, 12-16 May 1980, [D.W.Simpson, P.G.Richards (editor/s), [Washington, DC, USA: American Geophys. Union 1981] 59541 (introductory abstract), 64066-78, 64121-3, 64240
- Electronic displays;** London, England, 5-7 Oct. 1982, [Buckingham, Bucks., England: Network Exhibition 1982] 63855
- Excimer lasers;** Incline Village, NV, USA, 10-12 Jan. 1983, [Opt. Soc. America; Air Force Office Sci. Res.; IEEE] [Washington, DC, USA: Opt. Soc. America 1983] 59858, 59874, 60732-3, 60738, 60830-1, 60873-4, 61195, 61217, 61965, 63283, 64276
- Exploration of the polar upper atmosphere;** Lillehammer, Norway, 5-16 May 1980, [C.S.Deehr, J.A.Holtet (editor/s), [Reidel: Dordrecht, Netherlands 1981] 59540 (introductory abstract)
- Fusion technology 1982;** Julich, Germany, 13-17 Sept. 1982, [Oxford, England: Pergamon 1983] 60405-74, 60498, 60526-9, 61686-9, 61708-11
- Grain boundaries in semiconductors;** Boston, MA, USA, Nov. 1981, [H.J.Leamy, G.E.Pike, C.H.Seager (editor/s), [New York, USA: North-Holland 1982] 62278, 62373-7, 62409, 62428-9, 62457, 63172
- High energy spin;** Westhampton Beach, NY, USA, Sept. 1982, [1982] 59565, 59902, 59934-7, 60040-8, 60070, 60080-92
- History of particle physics;** Paris, France, 21-23 July 1982, [Dec. 1982] 59566 (introductory abstract), 59567-82
- Indian radiation protection;** Bombay, India, 19-23 Jan. 1981, [March 1983] 59527 (introductory abstract)

- LMFBR safety**; Lyon-Ecully, France, 19-23 July 1982, (*European Nucl. Soc.: AINS*) [Paris, France: Societe Francaise d'Energie Nucleaire 1982] 60331, 60344-5, 60366-88, 63653
- Magnetic films and surfaces**; Yokohama, Japan, 13-16 Sept. 1982, [March 1983] 61270, 61372, 61906, 62220, 62293-6, 62508-10, 62520, 62566, 62690, 62702, 62717-20, 62728-62, 62770-7, 62791-5, 62858-64, 62944-6, 63157, 63182, 63451
- Magnetism**, Kyoto; Kyoto, Japan, 6-10 Sept. 1982, [Feb. 1983] 62506, 62682-5, 62711-16, 62725-6, 62769, 62783, 62855-7, 62942
- Magnetism**, Kyoto; Kyoto, Japan, 6-10 Sept. 1982, [Feb. 1983] 59732, 61803, 61811-12, 62089, 62125, 62192, 62387-9, 62431, 62507, 62533-4, 62538-41, 62544, 62547, 62552-5, 62559-65, 62569-72, 62574-5, 62581-5, 62589-608, 62620-43, 62654-61, 62669-73, 62686-9, 62697-701, 62721-4, 62727, 62784-90, 62798, 62803, 62809, 62816-17, 62826, 62943
- Nonlinear fluid behavior**; Boulder, CO, USA, 7-11 June 1982, [March 1983] 59596, 59709-10, 59744, 61403, 61472, 61485-6, 61501, 61531, 61544, 61569, 61588, 61769-70, 61789, 62057, 62118-19
- Nuclear waste management V**; Berlin, Germany, 7-10 June 1982, *W.Lutze* (editor/s), [New York, USA: North-Holland 1982] 60269-328, 63471, 63751-2
- Optical fiber communication, 1983**; New Orleans, LA, USA, 28 Feb.-2 March 1983, [New York, USA: IEEE 1983] 59536 (introductory abstract),
- Photovoltaic solar energy**; Stresa, Italy, 10-14 May 1982, *W.H.Bloss, G.Grassi* (editor/s), [Dordrecht, Netherlands: Reidel 1982] 61950, 62176, 62521, 63152, 63164, 63177, 63187, 63648-50, 63683-715
- Plasma physics**; Goteborg, Sweden, 9-15 June 1982, [1982] 61612, 61618, 61621, 61662, 64301, 64327-8, 64371-3, 64502-3, 64516-17
- Plasma physics**; Goteborg, Sweden, 9-15 June 1982, [1982] 59880, 60398-401, 61170, 61489, 61632-40, 61649-50, 61655, 61679-81, 62441, 64332
- Power engineering**; Manchester, England, 30 March-1 April 1982, [Manchester, England: Univ. Manchester Inst. Sci. Technol. 1982] 63639
- Processes of planetary rifting**; St. Helena, CA, USA, 3-5 Dec. 1981, (*American Geophys. Union; Lunar & Planetary Inst.; NASA; NSF*) [1983] 64093-6, 64101, 64108-15, 64138
- Properties and applications of metal hydrides**; Toba, Japan, 30 May-4 June 1982, [Feb. 1983] 60334-5, 60394, 61007-10, 61384-5, 61567-8, 62047-8, 62062, 62114-15, 62164, 62366, 63561-2, 63583-4, 63635, 63722-3, 63732-3, 63735-44
- Quantum chemistry**; Uppsala, Sweden, 13-20 June 1982, [March 1983] 59604-6, 59726, 60561-2, 60570-6, 60591-2, 60594-5, 60600, 60613, 60631, 60835, 60884-5, 61848, 61914, 62246, 62328, 62355, 62378, 63032, 63515-17
- Radiation and the worker**; London, England, 7 Jan. 1983, [March 1983] 59535 (introductory abstract),
- Radiation effects in insulators**; Arco, Largo di Garda, Italy, 1981, [1982] 59534 (introductory abstract), 60243, 61805, 61939-43, 61966-7, 61975, 61983, 61990-9, 62004-5, 63126, 63578, 64375, 64409
- Railway and tracked transit system noise**; Monument, CO, USA, 8-10 April 1981, [22 March 1983] 59530 (introductory abstract),
- Random walks and their application to physical and biological sciences**; Gaithersburg, MD, USA, 28 June-1 July 1982, [Feb. 1983] 59531 (introductory abstract), 59684-707, 62027, 62152, 63771, 63778, 63816
- Reevaluations of dosimetric factors**; Germantown, MD, USA, 15-16 Sept. 1981, (*Office Health Environ. Res.; Office Energy Res.; U.S. Dept. Energy*) *V.P.Bond, J.W.Thiessen* (editor/s), [Oak Ridge, TN, USA: U.S. Dept. Energy 1982] 59542 (introductory abstract),
- Refractory metals, hardmetals and special materials**; Reutte, Austria, 1-5 June 1981, [1982] 59762, 59795, 62007, 62053, 62077, 62079, 62390, 62882, 62927, 63167-8, 63173, 63249, 63317
- Signal recovery and synthesis**; Incline Village, NV, USA, 12-14 Jan. 1983, (*Opt. Soc. America; Air Force Office Sci. Res.*) [Washington, DC, USA: Opt. Soc. America 1983] 61082, 61730, 63925, 63953-61, 64277
- Sintering, theory and practice**; Portoroz, Yugoslavia, 7-10 Sept. 1981, *D.Kolar, S.Pejovnik, M.M.Ristic* (editor/s), [Amsterdam, Netherlands: Elsevier 1982] 59538 (introductory abstract), 63185, 63192-201, 63206-14, 63217-18, 63225-48, 63252-3
- Stochastic processes in quantum and statistical physics**; Marseille, France, 29 June-4 July 1981, *S.Albeverio, P.Combe, M.Sirugue-Collin* (editor/s), [Berlin, Germany: Springer-Verlag 1982] 59543 (introductory abstract), 59628-34, 59668-9, 59676-7, 59719-24, 59739-41, 59746-7, 59931-2, 62350, 62668
- South African health physics**; Bloemfontein, South Africa, 16-18 March 1981, [March 1983] 59526 (introductory abstract),
- Supercritical fluids: Their chemistry and application**; Cambridge, England, 13-15 Sept. 1982, [March 1983] 59525 (introductory abstract), 59794, 61592, 62051-2, 62071-6, 62111
- System modelling and optimisation**; New York, USA, 31 Aug.-4 Sept. 1981, *R.F.Drenick, F.Kozin* (editor/s), [Berlin, Germany: Springer-Verlag 1982] 63888
- System simulation and scientific computation**; Montreal, Canada, 8-13 Aug. 1982, (*IMACS: Int. Assoc. Math. Modelling; Int. Soc. Comput. Methods Eng.; et al.*) [New Brunswick, NJ, USA: IMACS 1982] 61397, 61519, 61605, 61619, 61643-4, 61685, 61693-7, 63767
- Topics in ocean physics**; Varenna, Italy, 7-19 July 1980, *A.R.Osborne, P.Malanotte Rizzoli* (editor/s), [Amsterdam, Netherlands: North-Holland 1982] 59539 (introductory abstract),
- Total solar eclipse (1980 February 16)**; New Delhi, India, Jan. 1981, [Oct. 1982] 59559, 64192-207, 64237, 64302-8
- Vibrations at surfaces**; Asilomar, CA, USA, 1-4 Sept. 1982, [15 Jan. 1983] 59532 (introductory abstract), 60693, 61020, 62229-31, 62251-67, 62965-77, 63092-109, 63118, 63540, 63556-7, 63585-90
- Vibrations at surfaces**; Asilomar, CA, USA, 1-4 Sept. 1982, [Feb. 1983] 59851, 59859-60, 62224-6, 62232-8, 62268-71, 62978-91, 63071-2, 63119-23

CORPORATE AUTHOR INDEX

- Atomic Energy Canada Ltd., Chalk River, Ont.**
Canadian accelerator breeder system development, AECL-7840. 60330
- CERN, Geneva, Switzerland**
CEDAR counters for particle identification in the SPS secondary beams: A description and an operation manual, CERN-82-13. 60548
Non-perturbative phenomena in QCD vacuum, hadrons, and quark-gluon plasma, CERN-83-01. 59994
- Comm. European Communities, Luxembourg**
Analysis and synthesis of the theoretical studies performed on the control and safety of LWR's burning plutonium fuel, EUR 8118 EN. 60358
Catalogue of facilities in Member States of the European Communities for testing the packaging of radioactive materials, EUR 8254 EN. 60247
Cellules solaires au CdTe en couches minces polycristallines. Elaboration par pulvérisation triode et transport a courte distance (CdTe solar cells in polycrystalline thin films. Elaboration for triode sputtering and short distance transport), EUR 8213 EN/FR. 63675
Cellules solaires constituées de couches minces de CdTe polycristallines (Solar cells made from polycrystalline CdTe thin films), EUR 8154 EN-FR. 59550
Conception, analyse du système, réalisation et experimentation d'un générateur photovoltaïque autonome de 5 kW Au Refuge des Evettes (Conception, analysis of the system, realization and experimentation of an autonomous 5 kW photovoltaic generator at the Refuge des Evettes), EUR 8204 FR. 63674
Criticality safety hazards arising from the transport of fissile materials, EUR 8345 EN. 60246
Development of a 1pKW photovoltaic concentrator system with silicon cells, EUR 8200 EN. 63673
Electric and photoelectric characteristics of CdTe p-n homojunctions, EUR 8154 EN-FR. 62490
Etude de la technologie d'un module solaire offrant une bonne dissipation thermique (Study of the technology of a solar module that offers good heat dissipation), EUR 8159 FR. 63677
Etude et réalisation de croissances épitaxiales de composés III-V par pyrolyse mixte d'organometalliques et d'hydrures sous pression réduite: Application à l'étude de structures de piles solaires (Study and realization of epitaxial growth of III-V compounds by mixed pyrolysis of organometallics and hydrides under reduced pressure: Application to the study of solar cell structures), EUR 8207 FR. 63678
Faisabilité technique et économique de la géothermie basse énergie en Europe (Technical and economic feasibility of deep geothermal energy in Europe), EUR 8241/I FR. 63642
Increase of minority carrier diffusion length under the effect of a large band gap gradient [in solar cells], EUR 8154 EN-FR. 63679
'Integrated thin film solar cell generators with higher output voltages', EUR 8160 EN. 63676
L'énergie géothermique a basse enthalpie pour le chauffage des locaux (The geothermic energy based on enthalpy for district heating), EUR 7802 FR. 63641
Optimisation of new types of MIS silicon solar cells, EUR 8142 EN. 63681
Recrystallization processes in amorphous and polycrystalline silicon, EUR 8141 EN. 63334
- Results and analysis of a round robin test series using solar simulators, EUR 8006 EN. 63730
Solar cells made of thin layers of polycrystalline CdTe, EUR 8154 EN-FR. 63680
- Electr. Power Res. Inst., Palo Alto, CA, USA**
Assessment of chemical processes for the postaccident decontamination of reactor coolant systems, EPRI-NP-2866. 60365
BWR refill-reflood program constitutive correlations for shear and heat transfer for the BWR version of TRAC, EPRI-NP-1582. 60338
Cleaning steam generators off-line (soaking) with chelants, EPRI-NP-2815. 60340
Comparison of COMETHE-IIIJ and FCODE-BETA fission gas release predictions with measurements, EPRI-NP-2903. 60224
Compressed-air energy storage: Commercialization potential and EPRI roles in the commercialization process, EPRI-EM-2780. 63731
Eddy-current NDE for intergranular attack, EPRI-NP-2862. 60341
Feasibility study: A new cable tray hanger concept for nuclear power plants, EPRI-NP-2910. 60223
Fire tests in ventilated rooms. Detection of cable tray and exposure fires, EPRI-NP-2751. 60364
Full-scale turbine missile concrete impact experiments, EPRI-NP-2745. 60363
General and localized corrosion of carbon and low-alloy steels in oxygenated high-temperature water, EPRI-NP-2853. 60248
Monitoring system for determining air leakage and oxygen concentrations in the secondary cycle of pressurized water reactor plants, EPRI-NP-2865. 60362
NATBWR: A steady-state model for natural circulation in boiling water reactors, EPRI-NP-2856-CCM. 60339
Performance comparison of 15- and 165-tpd Texaco coal gasifiers, EPRI-AP-2814. 63721
Photovoltaic requirements estimation - A simplified method, EPRI-AP-2745. 63682
Postaccident decontamination of reactor primary systems and test loops, EPRI-NP-2842. 60360
Results of EDF/Framatome underclad crack detection methods, EPRI-NP-2841. 60249
Review and application of the TRAC-PD2 computer code, EPRI-NP-2826. 60222
Scale model turbine missile casing impact tests, EPRI-NP-2742. 60361
Scale modeling of turbine missile impact into concrete, EPRI-NP-2746. 60359
Thermal-hydraulic code qualification: ATHOS2 and data from Bugey 4 and Tricastin 1, EPRI-NP-2872. 60342
Valve inlet fluid conditions for pressurizer safety and relief valves in Westinghouse-designed plants, EPRI-NP-2296. 60357
Waterside corrosion of zircaloy fuel rods, EPRI-NP-2789. 60389
- Hungarian Acad. Sci., Budapest**
Dual-process. A highly reliable process control system, KFKI-1983-08. 60343

- Ist. Naz. Fis. Nucl., Catania, Italy**
Are classical tachyons slower-than-light quantum particles?, INFN/AE-83/1. 59592
- Ist. Naz. Fis. Nucl., Genoa, Italy**
Doppio discriminatore leading edge (Double leading edge discriminators), INFN/TC-82/13. 60552
- Ist. Naz. Fis. Nucl., Legnaro, Italy**
Progress report on heavy ion identification by Bragg Curve Spectroscopy at the Legnaro XTU Tandem Laboratory, INFN/BE-82/4. 60532
- Ist. Naz. Fis. Nucl., Milan, Italy**
Status of the superconducting cyclotron project in Milan, INFN/TC-82/12. 60497
- Nagoya Univ., Japan**
Effect of trapped electrons on the wave-induced current, IPPJ-620. 61613
Measurement of small-scale density fluctuation in JIPP T-II plasma by millimeter and sub-millimeter wave scattering, IPPJ-619. 61614
- Nat. Bur. Stand., Washington, DC, USA**
Beam-profile measurement of laser pulses using a spatial filter to sample the hermite modes for a string of pulses, NBS-TN-1057. 61216
- Nat. Phys. Lab., Teddington, England**
Temperature control of an acousto-optic modulator in an Argon ion laser using an R.F. servo loop, NPL-DES-78. 61202
Theoretical analysis of photon drag detectors, NPL-DES-76. 60547
- Phys.-Tech. Bundesanstalt, Braunschweig, Germany**
Elektronische Einrichtungen als Teile von Messgeräten zur Mengenmessung von Fluiden (Electronic systems as a part of a measurement device for flow measurement of fluids), PTB-Me-40. 61584
- UKAEA, Culham, Abingdon, Oxon., England**
Methane formation during deuteron bombardment of carbon in the energy range of 100 to 1500 eV, CLM-R 236. 63575
Tokamak disruptions, CLM-R 233. 61684
- Univ. Lyon, France**
Fonction génératrice des facteurs isoscalaires des groupes unitaires (Generating function of isoscalar factors of unitary groups), LYCEN/8306. 59587
- Univ. Oslo, Blindern, Norway**
Solar radio noise registrations at the Oslo Solar Observatory, 1975-81 and comments on the whole series of measurements 1954-81, 54. 64451
- Univ. Oxford, England**
Tritium isotope separation using resonance radiation, OUEL-1429/82. 61011

SUPPLEMENTARY LIST OF JOURNALS

- ACM Trans. Comput. Syst. (USA)**
ACM Transactions on Computer Systems Association for Computing Machinery, 11 West 42nd Street, New York, NY 10036, USA
- Comput. Sch. (GB)**
Computers in Schools MUSE Information Office, Five Ways School, Scotland Lane, Bartley Green, Birmingham B32 4BT, England. Subscription address: Heinemann Computers in Education Ltd., 22 Bedford Square, London WC1B 3HH
- CRC Crit. Rev. Biomed. Eng. (USA)**
CRC Critical Reviews in Biomedical Engineering Formerly: *CRC Crit. Rev. Bioeng. (USA)* CRC Press Inc., 2000 Corporate Boulevard, N.W., Boca Raton, FL 33431, USA
- Inf. Process. Mach. (Czechoslovakia) - (IPRMDD)**
Information Processing Machines Academia, Publishing House of the Czechoslovak Academy of Sciences, 112 29 Praha 1, Nove Mesto, Vodickova 40, Czechoslovakia
- Radiat. Eff. Lett. Sect. (GB) - (RELDRK)**
Radiation Effects Letters Section Formerly: *Radiat. Eff. Lett. (GB)* Gordon and Breach Science Publishers Ltd., 42 William IV Street, London WC2N 4DE, England
- Vopr. At. Nauki & Tekh. Ser. Fiz. Radiats. Povrezhdenii & Radiats. Mater. (USSR)**
Voprosy Atomnoi Nauki i Tekhniki, Seriya: Fizika Radiatsionnykh Povrezhdenii i Radiatsionnoe Materialovedenie Khar'kovskii Fiziko-Tekhnicheskii Institut, AN USSR, Kharkov 108, USSR
- Vopr. At. Nauki & Tekh. Ser. Obshch. & Yad. Fiz. (USSR)**
Voprosy Atomnoi Nauki i Tekhniki, Seriya: Obshchaya i Yadernaya Fizika Khar'kovskii Fiziko-Tekhnicheskii Institut, AN USSR, Kharkov 108, USSR
- Wire Tech (USA)**
Wire Tech Formerly: *Wire Technol. (USA)* Huebner Publications Inc., 6521 Davis Industrial Parkway, Solon, OH 44139, USA

Electronic Reliability Data

A guide to selected components

Electronic Reliability Data is an accurate, up to date source of numerical data on the reliability of electronic components.

Failure Rates

Precise values are given of failures per million hours of a large number of electronic components from resistors to microcircuits.

Operational Experience

Much of the data is drawn from the analysis and evaluation of actual failures in an industrial environment.

Environmental Factors

The effect of many different environmental factors have been evaluated and their effect on failure rates determined. Such factors include:-

- Electrical stress ratio
- Temperature
- Age
- Storage

Applications

The effects of different applications have been quantified so that failure rates can be determined for the use of components in applications varying from digital computers to rocket launches.

Electronic Reliability Data provides an accurate assessment of the likely failure rate of components and is the most complete and up to date source of numerical data available. A concise guide to the subject of reliability is given and there is an extensive bibliography of over 700 references with abstracts, to the most recent literature on the subject.

Electronic Reliability Data: A guide to selected components.

Components covered: Resistors, Capacitors, Diodes, Transistors, Thyristors, Microcircuits.

225 pages, ISBN 852962 40 1 £125 (\$300 Americas only)

For further information contact:

INSPEC Marketing Department
Station House
Nightingale Road
Hitchin,
Herts. England
Tel: (0462) 53331

or

INSPEC
IEEE Service Center
445 Hoes Lane
Piscataway
NJ 08854, USA
Tel: (201) 981 0060

Librarianship and Information Studies Series

The authors in this series deal in a practical way with the problems faced by libraries and information scientists that have been the subjects of research within past years. The results of the latest research are analysed, discussed and related to real situations. Workers at centres of study of librarianship and information science will, through this series, be presented with invaluable aids to further research; librarians and information scientists 'in the field' will also find much food for thought.

1. Computer-based information services in science and technology: principles and techniques.

M. F. Lynch

96pp., 234 x 156mm, casebound, 1974, ISBN 0 901223 55 7,
£3.65 UK, \$ 9.00 Americas, £4.30 Elsewhere

This book covers the application of computers to the major information services in science and technology. Coverage is given to the problems of character representation and transformation during input; storage and output; data and record description and storage structures; and typical filehandling systems and file manipulations. The role of computer type-setting in the production of publications is described at some length, as are the characteristics and implementation of information-retrieval services.

2. Asian and African collections in British libraries: problems and prospects

A. Benewick

139pp., 234 x 156mm, casebound, 1974, ISBN 0 901223 48 4,
£6.20 UK, \$ 14.50 Americas, £7.25 Elsewhere

This book discusses the administrative problems of establishing and maintaining Asian and African collections in Britain. Particular emphasis is placed on acquisition, interlibrary co-operation, bibliographical control and finance. The impact of area collections on general library techniques, and the prospects for area collections, from the viewpoint of developing adequate national provision for them, are also discussed.

3. Languages of indexing and classification: a linguistic study of structures and functions

W. J. Hutchins

160pp., 234 x 156mm, casebound, 1975, ISBN 0 901223 68 9,
£8.00 UK, \$ 19.00 Americas, £9.35 Elsewhere

Within the broad field of information science, the problems of indexing and classification continue to occupy positions of central and crucial importance. In recent years there have been impressive developments in automated information-retrieval systems, but these have not led to any lessening of interest in indexing and classification theory, although understanding of these basic processes remains inadequate. This volume contributes to the understanding of the fundamental questions of the nature of indexing languages—how they work and why they sometimes fail. This book is an examination of the basic features of the theoretical issues of indexing and classification in terms of linguistic structures and functions, and assumes that readers have some knowledge of the languages of documentation and the problems of indexing and information retrieval.

4. Libraries for the blind: an international study of policies and practices

D. E. Schauder and M. D. Cram

152pp., 234 x 156mm, casebound, 1977 ISBN 0 901223 91 3,
£10.00 UK, \$ 23.50 Americas, £11.70 Elsewhere

This study reviews contemporary practices, policies and trends in library services for blind and partially sighted people. Most available accounts of such services have confined themselves to a particular country, reading medium or technical development. This study, however, can be said to be truly international, and extremely comprehensive. The authors, both practising librarians, present the results of research which included many visits to libraries for the blind and related organisations, from which valuable information was gained that was not readily available except by personal contact. Furthermore, their literature search extends up to 1976, resulting in an extensive bibliography. The book can be used equally as a textbook for students of librarianship, or as a guide for practising librarians.

5. Information management

D. Mason

121pp., 234 x 156mm, casebound, 1978, ISBN 0 906048 15 2,
£7.50 UK, \$ 18.00 Americas, £9.00 Elsewhere

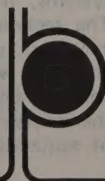
This volume is a highly practical guide to the management of industrial information services. From the premise that the information manager should take a positive approach to his company's information needs, the author discusses the managerial problems of establishing and running an information service within a company and emphasises practical techniques for their solution. Location, planning and finance are some of the topics covered. Several case-study exercises are given to underline the text, and key texts for further study are appended to each chapter. Although written primarily for industrial information managers and for new entrants into industrial information services, this volume will be of interest to all who work in, or are responsible for, information services.

Inquiries, and orders with remittances should be sent to:

Publication Sales Department, Peter Peregrinus Ltd.,
PO Box 26, Hitchin Herts. SG5 1SA, England.

Orders for the Americas should be sent to:

Peter Peregrinus Ltd.,
IEEE Service Centre, 445 Hoes Lane, Piscataway, NJ 08854, USA.



Antennas and propagation

The papers presented at the international conference on antennas and propagation have now been published as number 169 in the IEE Conference Publication series. The conference, held in London in November 1978, was sponsored by the IEE Electronics Division in association with the IEEE, the IMA, the IoP, the IERE, and URSI.

Topics covered under the main session headings are as follows:-

Antennas: arrays; adaptive antennas; reflectors and radomes; h.f. antennas; antenna measurements; v.h.f. antennas; numerical techniques, contoured beams; reflector antennas; feeds; scattering and diffraction; conformal and planar antennas; antenna theory and practice.

Propagation: remote sensing and propagation over sea surfaces; effects of ground and atmospheric irregularities on propagation from m.f. to s.h.f.; ionospheric propagation; propagation through rainfall measurements; propagation through rainfall prediction methods; scattering from hydrometeors; earth-space radio propagation.

2 parts, 136 papers, 735 pp., 297 x 210mm, photolitho,
ISBN 0 85296 195 2,
November 1978, soft covers,
£26.00 UK, \$61.00 Americas,
£30.50 Elsewhere.

Inquiries, and orders with remittances should be sent to:
Publication Sales Department,
IEE, PO Box 26,
Hitchin, Herts. SG5 1SA,
England.

Orders for the Americas should be sent to:
IEE, INSPEC/IEEE Service Centre,
445 Hoes Lane, Piscataway, NJ 08854, USA.



IEE Control Engineering Series 7

Feedback and multivariable systems

D. H. Owens

This theoretical text is concerned with the provision of an analytical and conceptual basis for the analysis and design of unity negative multivariable-output feedback-control systems by using Laplace transforms and frequency-domain techniques. Throughout the text, all system elements are assumed to be described by linear, time-invariant, deterministic state-vector models. Preliminary chapters concentrate on the basic properties of dynamical models. Feedback is introduced in the form of constant-state feedback but attention is focused on output feedback systems and system description using transfer function matrices.

Intermediate chapters discuss performance specifications and design concepts and difficulties by detailed consideration of analytical methods and numerical results for first-second-order multivariable systems, mixed-type systems and dyadic systems. The techniques are based on system decomposition and lead naturally to the general material of later chapters where a detailed treatment commutative control, characteristic loci, dyadic expansions and the inverse Nyquist array is provided plus an outline of sequential design and contraction-mapping algo-

tithms. The final chapter provides a detailed analysis of the asymptotic structure and compensation of multivariable root-loci using dynamic transformation of system inputs and outputs.

October 1978, 320pp., 216 x 135mm, casebound,
ISBN 0906048 03 6, £13.50 UK, \$31.00 Americas,
£15.50 Elsewhere.

Inquiries, and orders with remittances should be sent to:

Publication Sales Department, Peter Peregrinus Ltd.,
PO Box 26, Hitchin, Herts. SG5 1SA, England.

Orders for the Americas should be sent to:
Peter Peregrinus Ltd.,
IEEE Service Centre, 445 Hoes Lane,
Piscataway, NJ 08854, USA.



ABSTRACTS AND CURRENT PAPERS JOURNALS
SUBSCRIPTION PRICES 1983

	USA \$	UK £	ROW £	JAPAN ¥
PHYSICS ABSTRACTS (PA)	1350	540	690	462,300
2nd and subsequent copies	560	300	300	201,000
ELECTRICAL & ELECTRONICS ABSTRACTS (EEA)	1000	460	560	375,200
COMPUTER & CONTROL ABSTRACTS (CCA)	610	285	350	234,500
PA/EEA/CCA COMBINED SUBSCRIPTION	2650	1120	1430	958,100
EEA/CCA COMBINED SUBSCRIPTION	1460	650	830	556,100
CURRENT PAPERS IN PHYSICS				
Member rate	78	38	38	—
Non-Member rate	170	98	98	65,000
CURRENT PAPERS IN ELECTRICAL & ELECTRONICS ENGINEERING				
Member rate	78	38	38	—
Non-Member rate	145	80	80	53,600
CURRENT PAPERS ON COMPUTERS & CONTROL				
Member rate	78	38	38	—
Non-Member rate	145	80	80	53,600
KEY ABSTRACTS				
Member rate*	38	19	19	—
Non-Member rate	80	36	36	24,100
KEY ABSTRACTS				
EMI/PMI COMBINED	—	60	60	40,200
All Key Abstracts combined				
Member rate	250	125	125	—
Non-Member rate	580	275	275	184,200

*The Key Abstracts Member rate is available to Members of the IEE and IEEE only.

CUMULATIVE INDEXES

Cumulative indexes are available for *Physics Abstracts*, *Electrical & Electronics Abstracts* and *Computer & Control Abstracts*, for both authors and subjects. These cumulations generally cover a period of four years, with the exception of *Computer & Control Abstracts* where the initial volume covered the period 1966-68. The table below shows the prices and periods for the two types of cumulative index.

	PHYSICS ABSTRACTS		ELECTRICAL & ELECTRONICS ABSTRACTS		COMPUTER & CONTROL ABSTRACTS	
	Subject	Author	Subject	Author	Subject	Author
	£	£	£	£	£	£
1955-59	20	20	15	20	—	—
1960-64	40	17	20	12	—	—
1965-68	60	25	35	20	—	—
1969-72	—	—	72	64	48	30
1973-76	600	300	250	150	150	75
1977-80	770	450	380	250	250	120
1966-68	—	—	—	—	15	

For US\$ and Yen prices please contact the appropriate address below

ORDERING PROCEDURE

THE AMERICAS
North (including Canada), Central and South
All orders from the above areas, and orders from members of Institute of Electrical and Electronics Engineers Inc, anywhere in the world, should be sent to Fulfillment Manager, Institute of Electrical & Electronics Engineers Inc., 445 Hoes Lane, Piscataway, N.J. 08854, USA. Telephone (201) 981 0060

日本のお客様にご案内申し上げます

日本国内に於ける INSPEC の購入価格はすべて円建てとなっております。また刊行物はすべて航空便で配達されます。INSPEC 刊行物の価格、その他についてのお問い合わせは最寄りの羊取取扱専門店または輸入総代理店株式会社・エス・エンテック・カンパニー 千105東京都港区新橋1-13-12 TEL 03 (502) 6471 までご連絡ください。

REMAINDER OF THE WORLD

All remaining subscriptions should be sent to INSPEC Marketing Department, P.O. Box 26, Hitchin, Herts SG5 7RS, England. Telephone Hitchin 53331, Telex 825962, Telegrams IEE G.

OTHER INSPEC SERVICES

SDI
(Selective Dissemination of Information.)
This is a service individually tailored to the requirements and interests of the engineer or research worker. Details of information relevant to the interest profile of the individual subscriber are selected from the data being processed for the INSPEC database. Information is dispatched weekly on 150 mm x 100 mm (6" x 4") cards.

TOPICS
This is an SDI service based on standard profiles. There are over 70 subjects covering high-activity areas of research and development. This is an inexpensive card service designed to alert engineers and researchers to the availability of literature within their subject area.

MAGNETIC TAPES
Tapes containing all the information included in the INSPEC publications are issued twice monthly. They enable the larger research and development organisations to produce their own internal information and current-awareness services.

Physics Abstracts

1st July 19

Summary Classification

The full classification and contents are given at the front of the journal, followed by an **Alphabetical Index** to the subjects covered

- | | |
|---|---|
| <p>00.00 General</p> <p>01.00 Communication, Education, History and Philosophy</p> <p>02.00 Mathematical Methods in Physics</p> <p>03.00 Classical and Quantum Physics; Mechanics and Fields</p> <p>04.00 Relativity and Gravitation</p> <p>05.00 Statistical Physics and Thermodynamics</p> <p>06.00 Measurement Science, General Laboratory Techniques, and Instrumentation Systems</p> <p>07.00 Specific Instrumentation and Techniques of General Use in Physics</p> <p>10.00 The Physics of Elementary Particles and Fields</p> <p>11.00 General Theory of Fields and Particles</p> <p>12.00 Specific Theories and Interaction Models; Particle Systematics</p> <p>13.00 Specific Reactions and Phenomenology</p> <p>14.00 Properties of Specific Particles and Resonances</p> <p>20.00 Nuclear Physics</p> <p>21.00 Nuclear Structure</p> <p>23.00 Radioactivity and Electromagnetic Transitions</p> <p>24.00 Nuclear Reactions and Scattering: General</p> <p>25.00 Nuclear Reactions and Scattering: Specific Reactions</p> <p>27.00 Properties of Specific Nuclei listed by Mass Ranges</p> <p>28.00 Nuclear Engineering and Nuclear Power Studies</p> <p>29.00 Experimental Methods and Instrumentation for Elementary-Particle and Nuclear Physics</p> <p>30.00 Atomic and Molecular Physics</p> <p>31.00 Theory of Atoms and Molecules</p> <p>32.00 Atomic Spectra and Interactions with Photons</p> <p>33.00 Molecular Spectra and Interactions with Photons</p> <p>34.00 Atomic and Molecular Collision Processes and Interactions</p> <p>35.00 Properties of Atoms and Molecules; Instruments and Techniques</p> <p>36.00 Studies of Special Atoms and Molecules</p> <p>40.00 Classical Areas of Phenomenology</p> <p>41.00 Electricity and Magnetism; Fields and Charged Particles</p> <p>42.00 Optics</p> <p>43.00 Acoustics</p> <p>44.00 Heat Flow, Thermal and Thermodynamic Processes</p> <p>46.00 Mechanics, Elasticity, Rheology</p> <p>47.00 Fluid Dynamics</p> <p>50.00 Fluids, Plasmas and Electric Discharges</p> <p>51.00 Kinetic and Transport Theory of Fluids; Physical Properties of Gases</p> <p>52.00 The Physics of Plasmas and Electric Discharges</p> | <p>60.00 Condensed Matter: Structure, Thermal and Mechanical Properties</p> <p>61.00 Structure of Liquids and Solids; Crystallography</p> <p>62.00 Mechanical and Acoustic Properties of Condensed Matter</p> <p>63.00 Lattice Dynamics and Crystal Statistics</p> <p>64.00 Equations of State, Phase Equilibria, and Phase Transitions</p> <p>65.00 Thermal Properties of Condensed Matter</p> <p>66.00 Transport Properties of Condensed Matter (Nonelectronic)</p> <p>67.00 Quantum Fluids and Solids; Liquid and Solid Helium</p> <p>68.00 Surfaces and Interfaces; Thin Films and Whiskers</p> <p>70.00 Condensed Matter: Electronic Structure, Electrical, Magnetic, and Optical Properties</p> <p>71.00 Electron States</p> <p>72.00 Electronic Transport in Condensed Matter</p> <p>73.00 Electronic Structure and Electrical Properties of Surfaces, Interfaces, and Thin Films</p> <p>74.00 Superconductivity</p> <p>75.00 Magnetic Properties and Materials</p> <p>76.00 Magnetic Resonances and Relaxation in Condensed Matter; Mossbauer Effect</p> <p>77.00 Dielectric Properties and Materials</p> <p>78.00 Optical Properties and Condensed Matter Spectroscopy and other Interactions of Matter with Particles and Radiation</p> <p>79.00 Electron and Ion Emission by Liquids and Solids; Impact Phenomena</p> <p>80.00 Cross-Disciplinary Physics and Related Areas of Science and Technology</p> <p>81.00 Materials Science</p> <p>82.00 Physical Chemistry</p> <p>86.00 Energy Research and Environmental Science</p> <p>87.00 Biophysics, Medical Physics, and Biomedical Engineering</p> <p>90.00 Geophysics, Astronomy and Astrophysics</p> <p>91.00 Solid Earth Geophysics</p> <p>92.00 Hydrospheric and Atmospheric Geophysics</p> <p>93.00 Geophysical Observations, Instrumentation, and Techniques</p> <p>94.00 Aeronomy and Space Physics</p> <p>95.00 Fundamental Astronomy and Astrophysics, Instrumentation and Techniques and Astronomical Observations</p> <p>96.00 Solar System</p> <p>97.00 Stars</p> <p>98.00 Stellar Systems; Galactic and Extragalactic Objects and Systems; The Universe</p> |
|---|---|